

SPONSORED BY



SOLMAX

[Home](#)

[GRI-25](#)

[Title Index](#)

Geosynthetics 2013

We are pleased to present the electronic proceedings of Geosynthetics 2013.

The Geosynthetics 2013 plenary and technical programs included more than 140 papers assigned to 26 sessions over the three-day conference period.

Geosynthetics 2013 also featured a sold out trade show and impressive participation from our very generous sponsors. We wish to thank them for their generous financial contributions that helped make this show possible. Please be sure to visit their websites by clicking on the logos to the left.

Disclaimer: The opinions expressed and the data provided during Geosynthetics 2013 and the published Proceedings are those of the author(s) and/or presenter(s) and do not necessarily represent the opinions of the Industrial Fabrics Association International (IFAI) or any of its subsidiaries or divisions. Papers contained in these proceedings are the original work of each author. For permission to reprint any paper or presentation materials in these proceedings, please contact the authors directly or the IFAI Bookstore Manager, 1801 County Road B West, Roseville, MN 55113-4061 USA.

[CD produced by Industrial Fabrics Association International ©2013](#)

GRI - 25



Geosynthetics 2013 is the site for the 25th edition of the [Geosynthetic Research Institute](#) (GSI) conference, GRI-25.

The theme for this year's conference is "25-Year Retrospective on the Geosynthetics Industry and Glimpses into the Future."

[GRI-25 Foreword and Table of Contents](#)

April 1

Geosynthetic Materials and Properties

[Innovation in Polyolefin Resins Used in Geosynthetics Over the Past 25 Years](#)

Grace Hsuan, Drexel University

[Antioxidants for Geosynthetic Resins and Applications](#)

Joseph J. Fay, BASF Corp.

[Overview of Geomembrane Manufacturing Methods](#)

Fred Struve, Consultant

[Opportunities and Solutions, Developments and Growth of the Geomembrane Industry](#)

Gary Kolbasuk, Raven Industries

[Thermal Seaming of Polyethylene Geomembranes](#)

Mark Sieracke, Weaver Boos Consultants Inc. and Ian Peggs, I-CORP Intl.

[The Language of an Industry: Geosynthetics Testing and Measurement](#)

Sam Allen, TRI/Environmental Inc.

[Background and Development of GRI's Geosynthetics Specifications](#)

George Koerner and Robert Koerner, Geosynthetic Institute

[Geotextile Filters...25+ Years of Research and Experience](#)

Robert D. Holtz, University of Washington and Barry Christopher, Christopher Consultants

[A Brief History of Geosynthetic Drainage Media: From Rocks to SIM Tested, Patented, Strand Geometries](#)

Boyd Ramsey, GSE Lining Technology LLC

[Engineering Characteristics of Geosynthetic Clay Liners: Questions Asked and Answered Over Time](#)

Dave Daniel, University of Texas - Dallas

[Geofoam: History of the Lightweight Contender](#)

Archie Filshill, InterGEO Services

April 2

Geosynthetic Systems and Infrastructure

[A 25-Year Perspective on Waste Containment Liner and Cover System Designs](#)

Using Geosynthetics

Rick Thiel, Thiel Engineering

Reinforced Soil Walls and Slopes in Retrospect (i.e., The Good, the Bad and the Ugly)

Barry Christopher, Christopher Consultants; Robert D. Holtz, University of Washington; Ryan R. Berg, Ryan R. Berg & Assocs., Inc. and Richard P. Stulgis, Geocomp Corporation

Geotextiles in Marine Engineering: Past, Present and Future

Chris Lawson, TenCate Geosynthetics Asia

A Brief History of Heap Leaching

Monte Christie, Geo-Logic Associates and Mark Smith, RRD International Corp.

Geosynthetic Design Methods Used in Roadway Applications

Robert Koerner, Geosynthetic Institute

The Evolution of Geosynthetics in Erosion and Sediment Control

Joel Sprague, TRI/Environmental Inc.

The International Geosynthetics Society (IGS): No Borders for the Good Use of Geosynthetics

Jorge Zornberg, University of Texas- Austin

IFAI Turns 101 with 33 Years of Geosynthetic Representation

Andrew Aho, Geosynthetic Materials Association

30 Years of the Magazine Formerly known as GFR

Ron Bygness, Geosynthetics Magazine / IFAI

ASTM International Committee D35 on Geosynthetics – Looking Back Over 30 Plus Years

Dave Suits, North American Geosynthetic Society

The Geosynthetic Institute's Background and History

Bob Koerner, Geosynthetic Institute

Title Index

[A Comparison of Landfill Closure Systems](#)

[A Unique Camouflage Floating Cover](#)

[Abrasion Resistance of Geomembrane](#)

[An Innovative Use of Expanded Polystyrene Insulated Concrete Forms \(ICF\) For Geohazards](#)

[Analytical Approach of Junction Property Evaluation of Geogrids by Designing with Clamping System](#)

[Antioxidant Depletion of HDPE Geomembrane without HALS in an Extreme Environment](#)

[Beach Restoration of Coastal Town to Increase Tourism](#)

[Bending Stiffness of Geosynthetic-Reinforced Soil \(GRS\) Platform](#)

[Beneficial Impact of Polymer Treatment on the Swelling and Long-Term Hydraulic Efficiency of Ca-Bentonites Compared to the Standard Sodium Activation Method](#)

[Benefit-Cost Analysis of Geosynthetics in Water Resources](#)

[Beneficial use of Dredged Contaminated Sediments using Geotextile Tube Technology at Port in Santos, Brazil](#)

[Biofilm-Enhanced Treatment for Arctic Wastewater Stabilization Ponds Using Geotextile Substrate](#)

[Biological Clogging Resistance of Tubular Drainage Geocomposites in Leachate Collection Layers](#)

[Bituminous Geomembrane Liner at the Agnico-Eagle Mine in Kittilä, Finland](#)

[Campbell Shipyard Receives a Massive Underwater Geosynthetic Sediment Cap Adjacent to San Diego Hilton Convention Center](#)

[Case History – Geomembrane & Floating Cover System, South Australia Water Corporation, Wattle Park Potable Water Reservoir](#)

[Case History on the Use of Geonet composite in Red Willow Dam Modifications](#)

[Case History: HDPE Pipe Boot Failure due to Thermal Contraction of HDPE Pipe](#)

[Centrifuge Modeling of Geotextile Reinforced Slopes](#)

[Centrifuge Modeling of Landfill Composite Cover Systems](#)

[Cleveland Harbor, Ohio Interim Dredge Disposal Plan: Geotextile Reinforcement of Placed Dredge Fill](#)

[Comparative Evaluation of Different Aperture Geogrids for Ballast Reinforcement through Triaxial Testing and Discrete Element Modeling](#)

[Comparison of the Effect of Multifilament and Fibrile Types of Polypropylene Fibers on the Unconfined Compressive Strength of High Plasticity Clay](#)

[Confined Metallic Reinforcement Connection Tests on a MSE Wall System](#)

[Confined-Accelerated Creep Tests on Geosynthetics](#)

[Construction and 3 Years of Field Monitoring on a 12 m high Geogrid Reinforced and Lime Stabilised Noise Barrier Wall with Respect to the Stress Development in the Facing area](#)

[Deep Soil Mixed Foundation Using Geosynthetic Reinforcement for Levee Support](#)

[Design Considerations for Tall Geosynthetic Reinforced Soil Walls under Extreme Load Conditions in Mining Infrastructure](#)

[Design of Earthen Levee Strengthening with HPTRM for Hurricane Overtopping Conditions](#)

[Development of Piled Geo-wall](#)

[Development of, and Experience During, a Program for the Certification of Geoelectric Liner Integrity and Leak Location Surveyors](#)

[Dewatered and Decontaminated Disposal of Dredged Sediments Using Geotextile Bags, Containers and Tubes](#)

[Double Lining Systems: One and One Can Make Three!](#)

[Durability Studies on Coir Geotextiles](#)

[Effective Strategies for Residual Polymer and Aquatic Toxicity Testing For Dredge Slurry Dewatering](#)

[Effects of Discrete Fibers on the Stress-Dilatancy and Micromechanics of Fiber-Reinforced Sand](#)

[Electrical Leak Detection Surveys for Brine Ponds in SQM, Chile](#)

[Elevated Temperature Effects on Smooth Geomembranes - Geotextile Interfaces](#)

[Engineered Anti Erosion Works along the Banks of River Ganges](#)

[Enhancing the Performance of HDPE Geomembranes with flexible Polypropylene](#)

[Environmental Benefit of Carbon Footprint Using Geotextile Tubes](#)

[Estimating the Lifetime of Exposed Geomembranes using Thin-Film Samples and Accelerated UV Aging](#)

[Evaluating Wind Uplift for Exposed Geomembranes using Computer Modeling](#)

[Evaluation of Ethylene Vinyl Alcohol \(EVOH\) for Containment of High Concentrations of Volatile Organic Compounds in Geosynthetics](#)

[Experimental and Numerical Studies on Geocell Reinforced Sand Beds](#)

[Experimental and Theoretical Study on Interference Phenomena between the Bearing Members of Different Geogrids in Pullout Loading Conditions](#)

[Failures of Geomembrane Liners for Agricultural Waste Storage Ponds](#)

[Feasibility of MASW \(Multi-Channel Analysis of Surface Waves\) for Evaluating the Dynamic Properties of Geofoam](#)

[Finite Element Mesh Generation for Drainage Geocomposites](#)

[Flexible Pavement Performance with and without Geosynthetics: Nine year Follow-up](#)

[Flexural Behavior of Concrete Beams Reinforced With Different Types of Geogrids](#)

[Frictional Performance of Segmental Concrete Wall Units with Flexible Mechanical Connectors](#)

[Geocells Reinforced with Geogrids is the Winning Solution for Repairing Landslides in Hawaii](#)

[Geomembrane Surficial Landfill Gas Collection Systems](#)

[Geosynthetic Clay Liners - Accomplishments and disappointments, dos and donts of GCLs](#)

[Geosynthetic Opportunities Associated With Shale Gas Extraction](#)

[Geosynthetics in Drainage Systems](#)

[Geosynthetics: The Solution for Managing Nuclear Power Generation Water Supply in an Arid Environment](#)

[Geosynthetic Reinforced Soil – Integrated Bridge Systems: Successful Private Sector Case Studies over the last 20 Years](#)

[Geotextile Constriction Size and Physical and Chemical Clogging Potential](#)

[Geotextile Tube Failures](#)

[Granular Columns Reinforced with Geosynthetics: An overview of employment trends](#)

[High Density Polyethylene \(HDPE\) Lined Produced/Flow-back Water Evaporation Ponds](#)

[Implications of MSE Connection Criteria for Frictionally Connected GRS Structures](#)

[Importance of Variability in the Interface Shear Strength between Textured Geomembranes and Geocomposite Drainage Layers in Landfill Covers](#)

[Improving the Stability of High Fill Load Structures Built on Low-Strength Geosynthetic Interfaces](#)

[Influence of Textile Structure in Relationship to Filtrate Quality in Dewatering Applications Using Geotextile Containers](#)

[Influence of the Protection Used for Installation Damage in Long Term Durability of soil Reinforcement Elements](#)

[In-Situ Deformation Measurements for Geomembranes in Landfill Liners](#)

[Interface Friction Testing Between Soil and a Bituminous Geomembrane](#)

[Investigation of a Gas Bubble in Final Cover Constructed with A Geosynthetic Liner](#)

[Investigation of Temperature Variation in Soil Backfill and its Consequence to Tensile Strength of Geogrid](#)

[Laboratory Evaluation of the Performance of Geosynthetic-Reinforced Aggregate over Weak Subgrade](#)

[Lake Tahoe California Lake Shore Bluff Stabilization and Restoration](#)

[Layer Coefficient Ratio for Reinforced Pavements and the Influence of Pavement Thickness and Subgrade Strength](#)

[Leak Location Liner Performance Evaluation](#)

[Lifetime Prediction of Thin HDPE Geomembranes for the Shrimp Aquaculture Industry](#)

[Lining Systems for Shale Gas Drilling Activities](#)

[Market Impacts for Geosynthetic from the Regulation of the Storage of Coal Combustion Residuals](#)

[Microbiological Resistance Properties of Synthetic and Natural Textiles](#)

[Mine Water Treatment with Geotextile Tube System at Goldex Mine \(Val d'Or, Qc, Canada\)](#)

[Model Test of Stacked Permeable Geosynthetic Tubes](#)

[Numerical Modeling of Geogrid-Reinforced Unpaved Roadways](#)

[Numerical Simulation of Pullout Tests in Residual Clayey Silt](#)

[Observation and Numerical Modeling of MSE Test Wall Constructed Near Motorway 5C Section Drivusa-Gorica in Bosnia and Herzegovina](#)

[On the Role of Human Error in Failure of Three Geosynthetic Stabilized Earth Walls](#)

[Paving Fabric Interlayer Systems for Pavement Enhancement](#)

[Permanent Geosynthetic Wrapped Face MSE Retaining Wall](#)

[Polyester Geogrids as Asphalt Reinforcement - A Proven Technology](#)

[Prediction of Tensile Strength Behaviour of Coir Geotextiles](#)

[Preliminary Assessment of the Mechanical Properties of Recycled Expanded Polystyrene \(EPS\) Block Geofoam](#)

[Preliminary Evaluation of Thermally Induced Strains and Pressures Developed in a GRS Integrated Bridge System](#)

[Radial Load Tests for the Evaluation of Stress-Strain Relation of Geocells](#)

[Rehabilitation of Raw Water Reservoir Liner for Franklin WTP](#)

[Reinforced Soil Structures for Landfill Expansion](#)

[Remediation of Industrial Wastewater Sludge by Electrokinetic Geobox](#)

[Removing Human Error from Geomembrane Leak Location Surveys](#)

[Repeated Load Tests on Geocell Reinforced Sand Subgrades](#)

[Secondary Containment Retrofitting Using a Bituminous Geomembrane](#)

[Seismic Behaviour of Hybrid Reinforced Soil High Walls and Slopes](#)

[Seismic Performance of Mechanically Stabilized Earth Wall with Lightweight Aggregate \(LWA\) Backfill](#)

[Separation/ Stabilization Geotextiles - The Underlying Solution that we have had all along for more resilient roads](#)

[Settlement-Compensating Connection of Geomembrane to Pile Caps for Structures Developed on Old Landfills](#)

[Soil Erosion control using Coir Geotextile – A Fuzzy Logic Modeling](#)

[Specifying Allowable Geomembrane Leakage Rates Based on Available Technology](#)

[Storage of Coal Combustion Residuals with a Geosynthetic Liner - A 30 Year Forensic Study](#)

[Studies on Behaviour of Footings on Prestressed Geogrid Reinforced Granular Bed Overlying Weak Soil](#)

[Studies on Engineering Behaviour of Coir Waste Mixed Soil](#)

[Study on Geogrids for Improving Safety in Underground Mining](#)

[Subgrade Improvement for Segmental Retaining Walls](#)

[Surface Analysis of Weathered HDPE Geomembrane Studied by LSCM and FTIR Spectroscopy](#)

[Ten Years of Innovation in the Application of Piled Embankments in the Netherlands](#)

[Tensile Behavior of Triaxial Geogrid: Application of the Theoretical Method](#)

[Tensile Behavior of Triaxial Geogrid: Development of a Theoretical Method](#)

[Test Field for Monitoring Geocomposite Reinforcement behavior in a Crane Working Platform at a Wind Farm](#)

[Testing and Specifying Erosion Control Products](#)

[The Comparison and Analysis of International Tensile Test Methods and Results](#)

[The Impact of Site Conditions on the Electrical Surveying of Pond Liner Installations](#)

[The Mechanics of Filter Cake Formation on a Geotextile](#)

[The Upper Chiquita Reservoir Floating Cover and Liner](#)

[The use of a Concrete Composite for a Boat Ramp Extension](#)

[The use of Cationic Starch-Based Polymers in Geotextile Tube Dewatering Applications](#)

[Time-Dependent Impact of RECPs on Surface Water Quality](#)

[Trending Applications in Landfill Closure: Case Studies and Data on Exposed, Trenchless Covers](#)

[Unconfined Compressive Strength Behaviors of Fiber-Fly Ash-Soil Mixtures](#)

[Unique Approach to Dewatering of Mine Wastewater Residuals Using Geotextile Containers](#)

[Use of an Innovative Geocomposite to Construct a Reinforced Slope using Marginal Fill Soils in Canada](#)

[Use of Bituminous Geomembrane in Harsh Conditions](#)

[Use of Chemically Modified Geotextiles to Selectively Remove Metallic Impurities From Potable Water](#)

[Use of Coir Fiber Reinforcement Technique to Improve Strength of Cement Kiln Dust Treated Black Cotton Soil Subgrade](#)

[Use of Electronic Leak Detection System in 24/7 On-Line Mode to Control Construction and Operation of Lined CAL Lagoons](#)

[Use of Geocomposite as an Internal Drain in Levees Subjected to Seepage: Centrifuge Model Study](#)

Use of Geotextile Reinforced Slope for Containment Facility Dike

What Value of Interface Friction to Select for Geosynthetic Liner on Landfill Slopes?

CD produced by Industrial Fabrics Association International ©2013

The 25th Annual GRI Conference Proceedings

"A 25-Year Retrospective of the Geosynthetic Industry and Glimpses Into the Future"

GRI-25 Conference
Long Beach California Conference Center
on April 1-2, 2013



Editors:

George R. Koerner
Y. Grace Hsuan

Robert M. Koerner

Marilyn V. Ashley
Jamie R. Koerner

FOREWORD TO THE GRI-24 CONFERENCE

This conference focuses on the first 25 years of the geosynthetics industry insofar as its materials, properties, systems and infrastructure is concerned. Prior to that, there appeared very few extremely disconnected segments of the emerging technology at least from the perspective of written articles and papers. The earliest of these segments are the following:

- The first “pond liners” were used for reservoirs and canals in 1946
- “Net-like” drainage structures were developed and patented in 1960
- The first fabrics for soil subgrade stabilization, aka “road rugs”, were used in the late 1970’s
- “Filter fabric” applications were first reported in 1966
- “Grid-like” products were developed for soil reinforcement in the late 1970’s

Of course, the above “firsts” (with their eclectic names) have today been brought under the specific product terminology of geomembranes, geonets, geotextiles and geogrids. Together with the much more recently introduced products of geosynthetic clay liners, geofoam, geocells, and numerous geocomposites they form the technology we now know as “geosynthetics”.

This leaves the specific date of the beginning of *geosynthetics* very subjective. The earliest of conferences was in Paris in 1977, however, it focused entirely on geotextiles. This was followed by conferences in Las Vegas in 1982 and in Vienna in 1986, both predominately on geotextiles and then one in 1984 in Denver on geomembranes. The earliest books; on pond liners in 1977 and construction fabrics in 1980, were published by J. Wiley and Sons in a practical construction guide series. ASTM had its first impromptu meeting in New York City in 1977 and was focused mainly on “textiles in the ground”. The point we make is that none of these events can be considered as the beginning of the holistic technology of geosynthetics.

“Geosynthetics” as a unified and coalesced technology in its own right can arguably be dated by a series of closely dated events. They are the formation of the International Geosynthetics Society (IGS) in 1983, the publication of the magazine, GFR, also in 1983, the coalescence of the American Society of Testing Materials (ASTM) into a Geosynthetics Committee in 1985 and the formation of the Geosynthetic Research Institute (GRI) in 1986.

Thus, the beginnings of geosynthetics, per se, appears to the editors of these proceedings to be in the time frame of 1983-1986. Dating from this general time frame, we are now at the twenty-fifth of our GRI conferences and it appears to be a fitting time to reflect on the now unified technology of geosynthetics. In so doing, GRI-25 is presented as attempting to capture the past record of geosynthetics insofar as the materials involved, their myriad properties, how they are formed into systems for various major applications and the organizational infrastructure of the technology. We sincerely hope that the participants of the conference and readers of these proceedings find the efforts of the authors authoritative and reflective of the first quarter century of the technology.

Conference Organizers and Proceedings Editors
Geosynthetic Institute
475 Kedron Avenue
Folsom, PA 19033 USA

George R. Koerner
Y. Grace Hsuan

Robert M. Koerner

Marilyn V. Ashley
Jamie R. Koerner

ACKNOWLEDGMENTS

The Geosynthetic Institute (GSI) is an umbrella organization which encompasses all facets of geosynthetic materials. The five sub-institutes focus on research, education, information, accreditation and certification. A conference such as this one contains all of these activities. Clearly, research is being presented. Obviously, the effort is meant to be educational. Additionally, these proceedings form an information outlet which is available to all who are interested. Lastly, the important issues of accreditation and certification influence all of our undertakings.

The institute itself is open to all organizations involved or interested in geosynthetics. This includes government (federal, state and local) agencies, facility owners, designers, consultants, testing laboratories, quality assurance organizations, resin and additive suppliers, manufacturers, manufacturer's representatives, contractors, installers, and research institutes. Recent categories of Affiliated Organizations and Associate Members have been added to facilitate international outreach and to include state regulatory agencies, respectively. Information is available on our Home Page at <www.geosynthetic-institute.org> or from the editors of these proceedings. We wish to acknowledge and thank all of the GSI members and associate members for their support of our endeavors. The current organizations (in the order in which they joined the institute) and their representatives are as follows. Current Board of Director members are identified accordingly.

Full Members of the Geosynthetic Institute

GSE Lining Technology, Inc. - *Boyd Ramsey*
AECOM - *Kevin McKeon/Ken Bergschultz/John Trast*
U.S. Environmental Protection Agency - *David A. Carson*
E. I. DuPont de Nemours & Co., Inc. - *John L. Guglielmetti/David W. Timmons*
Federal Highway Administration - *Silas Nichols/Daniel Alzamora*
Golder Associates Inc. - *Mark E. Case/Tim Bauters*
Tensar International Corporation - *Mark H. Wayne [BoD]*
Colbond Geosynthetics - *Richard Goodrum*
Geosyntec Consultants - *Steve Poirier*
Syntec Corp. - *Aigen Zhao*
LyondellBasell Industries - *Fabio Ceccarani/Melissa Koryabina*
TenCate Geosynthetics - *John Henderson/Chris Lawson*
CETCO - *Chris Athanassopoulos/James T. Olsta*
Huesker, Inc. - *Steven Lothspeich/Dimiter Alexiew*
NAUE GmbH & Co. KG - *Kent von Maubeuge [BoD]*
Propex - *Steve Thaxton/Judith Mulcay*
Fiberweb, Inc. - *Brian H. Whitaker*
NTH Consultants, Ltd. - *Rick Burns*
TRI/Environmental Inc. - *Sam R. Allen [BoD]/C. Joel Sprague*
U. S. Army Corps of Engineers - *David L. Jaros [BoD]*
Chevron Phillips Co. - *Lili Cui [BoD]*
URS Corp. - *John C. Volk/Ronald H. Hager*
Solmax Géosynthétiques - *Robert Denis*

Envirosource Technologies, Inc. - *Douglas E. Roberts*
CARPI Tech BV - *Alberto M. Scuero/John A. Wilkes*
Civil & Environmental Consultants, Inc. - *Daniel Tolmer/Anthony W. Eith*
Agru America, Inc. - *Paul W. Barker/Markus Haager/Dee Strong*
Firestone Specialty Products - *Jeff Pankonie/Bill Tippins/Christa K. Petzke*
Waste Management Inc. - *Greg Cekander/John Workman [BoD]*
GeoComp/GeoTesting Express - *W. Allen Marr/Richard P. Stulgis*
GEI Consultants - *Michael A. Yako*
GSE Chile, S.A. - *Mauricio Ossa*
Atarfil, S. L. - *Mario Garcia Girones/Emilio Carreras Torres*
Republic Services Inc. - *Joe Benco/Tony Walker*
GSE Europe - *Stefan Baldauf/Catrin Tarnowski/Peter Riegl*
InterGEO Services Co. - *Archie Filshill/Phil McGoldrick*
Raven Industries, Inc. - *Gary M. Kolbasuk*
CTI and Associates, Inc. - *Te-Yang Soong/Kevin Foye*
Advanced Earth Sciences, Inc. - *Kris Khilnani/Suji Somasundaram*
Carlisle Syntec, Inc. - *Randy Ober/Krista Gonzalez/Julie Sitch/Matt Leathermann*
EPI, The Liner Co. - *Daniel S. Rohe/Mark Wolschon*
Geo-Logic Associates - *Monte Christie*
Weaver Boos Consultants, Inc. - *Mark Sieracke [BoD]*
Aquatana (Pty) Ltd. - *Piet Meyer*
Jones Edmunds, Inc. - *Donald E. Hullings*
The Mannik & Smith Group, Inc. - *John S. Browning III/Francis J. Biehl*
Plásticos Agrícolas y Geomembranas, S.A.C. - *Jhoana Carolina Diaz Martinez*
Afitex-Texel - *Pascal Saunier*
EVAL Americas (Kuraray) - *Robert Armstrong*
In-Line Plastics/GeoProducts - *Mark Williams/Marlyn Waltner*
Bombay Textile Research Institute - *A. N. Desai*
BASF Corporation - *Joseph J. Fay/Ralph Maier*
Watershed Geosynthetics LLC - *Michael Ayers*
ThermaGreen - *Tim Walter/Blu Alexander/Ken vander Velden*
Maccferri - *Massimo Ciarla/Pietro Rimoldi*
Jones & Wagener (Pty) Ltd. - *Anton Bain*

Affiliated Organizations of the Geosynthetic Institute

FGSI-Korea (FITI) - *Jeonhyo Kim/H.-Y. Jeon*
GSI-Taiwan (NPUST) - *Chiwan Wayne Hsieh [BoD]*

Associate Members of the Geosynthetic Institute

Delaware Solid Waste Authority - *Anne Germain*
Nebraska Department of Environmental Quality - *Michael Behrens*
New York State Dept. of Environmental Conservation - *Robert J. Phaneuf*
Maine Department of Environmental Protection - *David E. Burns*
New York State Department of Transportation - *Robert Burnett/James Curtis*
California Water Resource Control Board - *Leslie Graves/Nadine Langley*
New Jersey Dept. of Environmental Protection - *Michael J. Burlingame*

Pennsylvania Dept. of Environmental Protection - *Steve Socash*
Florida Dept. of Environmental Protection - *Richard B. Tedder*
U.S. Bureau of Reclamation - *Jay Swihart/Peter Irely*
Michigan Dept. of Environmental Quality - *Margie Ring/Xuede (Dan) Qian*
Environment Agency of the United Kingdom - *Rob Marshall*
Florida Dept. of Transportation - *Mario Paredes*
National Resources Conservation Center - *Stephen D. Reinsch*
Virginia Dept. of Environmental Quality - *Donald Brunson*
Massachusetts Dept. of Environmental Protection - *Paul Emond*
Philadelphia Water Department - *Vahe Hovsepian*
Oak Ridge National Laboratory (c/o Savannah River Remediation LLC) - *Amit Shyan*

GRI-25 Conference
Long Beach, California, Conference Center – April 1-2, 2013

	<u>Page</u>
Foreword	i
Acknowledgements	ii
Program	v

Geosynthetic Materials and Properties: Moderator, Y. (Grace) Hsuan

1.1	Innovation in Polyolefin Resins Used in Geosynthetics Over the Past 25 Years <i>Grace Hsuan (Drexel University)</i>	1
1.2	Antioxidants for Geosynthetic Resins and Applications <i>Joseph J. Fay (BASF)</i>	9
1.3	Overview of Geomembrane Manufacturing Methods <i>Fred Struve (Consultant)</i>	27
1.4	Opportunities and Solutions, Developments and Growth of Geomembrane Industry <i>Gary Kolbasuk (Raven Industries)</i>	42
1.5	Thermal Seaming of Polyethylene Geomembranes <i>Mark Sieracke (Weaver Boos Consultants, Inc.) and Ian Peggs (I-CORP Intl.)</i>	65
1.6	The Language of an Industry: Geosynthetics Testing and Measurement <i>Sam Allen (TRI/Environmental, Inc.)</i>	82
1.7	Background and Development of GRI’s Geosynthetics Specifications <i>George Koerner/Robert Koerner (Geosynthetic Institute)</i>	92
1.8	Geotextile Filters... 25+ Years of Research and Experience <i>Robert D. Holtz (University of Washington) and Barry R. Christopher (Christopher Consultants)</i>	110
1.9	A Brief History of Geosynthetic Drainage Media: From Rocks to SIM Tested, Patented, Strand Geometries <i>Boyd Ramsey (GSE Environmental LLC)</i>	130
1.10	Engineering Characteristics of Geosynthetic Clay Liners: Questions Asked and Answered Over Time <i>Dave Daniel (University of Texas – Dallas)</i>	136
1.11	Geofoam: History of the Lightweight Contender <i>Archie Filshill (InterGEO Services)</i>	160

Geosynthetic Systems and Infrastructure: Moderator, George R. Koerner

2.1	A 25-Year Perspective on Waste Containment Liner and Cover System Design Using Geosynthetics <i>Rick Thiel (Thiel Engineering)</i>	169
2.2	Reinforced Soil Walls and Slopes in Retrospect (i.e., The Good, The Bad and the Ugly) <i>Barry Christopher (Christopher Consultants), Robert D. Holtz (University of Washington), Ryan R. Berg (Ryan R. Berg & Assocs., Inc.) and Richard P. Stulgis (Geocomp Corporation)</i>	212
2.3	Geotextile in Marine Engineering: Past, Present and Future <i>Chris Lawson (TenCate Geosynthetics Asia)</i>	240
2.4	A Brief History of Heap Leaching <i>Monte Christie (Geo-Logic Associates) and Mark Smith (RRD International Corp.)</i>	265
2.5	Geosynthetic Design Methods Used in Roadway Applications <i>Robert Koerner (Geosynthetic Institute)</i>	288
2.6	The Evolution of Geosynthetics in Erosion and Sediment Control <i>Joel Sprague (TRI/Environmental, Inc.)</i>	323
2.7	The International Geosynthetics Society (IGS): No Borders for the Good Use of Geosynthetics <i>Jorge Zornberg (University of Texas-Austin)</i>	342
2.8	IFAI Turns 101 with 33 Years of Geosynthetic Representation <i>Andrew Aho (Geosynthetic Materials Association)</i>	358
2.9	1983-2013: 30 Years of the Magazine Formerly Known as GFR <i>Ron Bygness (Geosynthetics magazine/IFAI)</i>	362
2.10	ASTM International Committee D35 on Geosynthetics – Looking Back Over 30 Plus Years <i>Dave Suits (North American Geosynthetics Society)</i>	368
2.11	The Geosynthetic Institute’s Background and History <i>Robert Koerner (Geosynthetic Institute)</i>	375

INNOVATION OF POLYOLEFIN RESINS USED IN GEOSYNTHETICS OVER THE PAST 25 YEARS

Y. G. Hsuan

Department of Civil, Architectural and Environmental Engineering, Drexel University, Philadelphia, PA USA

ABSTRACT

Polyolefin is the most widely used polymer for the manufacturing of geosynthetics and will be focused on in this paper. Over the past 25 years, the advance of polyolefin resins is significant and has contributed to the innovative development of new catalysts and modern design of the polymerization process. For example, polyethylene with bimodal molecular weight distributions can achieve an ultra-high stress crack resistance and impact resistance. For polypropylene, new copolymers produced by reactor granule technology can reach flexibility and impact resistance beyond some of the rubbery elastomers. This paper briefly summarizes the new catalysts and polymerization processes used to produce modern polyolefin resins.

INTRODUCTION

By definition, geosynthetics are defined as planar products manufactured from polymeric material used with soil, rock, earth or other geotechnical engineering related material as an integral part of a human-made project, structure, or system. Thus, polymers are the essential part (≈ 97 wt. %) of all geosynthetic products and their properties are related accordingly. The majority of geosynthetics (including polyolefins) are made from thermoplastic polymers which can be processed through an extruder into specifically designed products. Table 1 shows the polymers commonly used in geosynthetics. To varying degrees, polyethylene (PE) and polypropylene (PP) are the two dominant types of polymer for geomembranes (GM), geotextiles (GT), geonets (GN), geopipe (GP), geogrids (GG) and geocomposites (GC).

The four most widely used polymers: PE, PP, PET and PVC, are sometimes referred to as commodity plastics which are used in large volume in many commercial market. The basic polymerization processes of these types of polymers are relatively well defined but vary by the technologies patented by each chemical company. Galli and Vecellio (2004) summarized that PE and PP have growth steadily for the past 50 years. In 2003, 65 vol. % of the total plastics were PE and PP. They also emphasized that the growth of PE and PP was driven by the development of catalysts and polymerization technologies, as illustrated in Table 2. Polymers with high performance properties were produced stimulating new engineering products. Geosynthetic materials are one of the technologies that benefits from those new innovations and has evolved accordingly, for example, the development of HDPE geomembranes with high stress crack resistance and highly flexible PP geomembranes. In this paper, the innovative new developments in PE and PP resins used in geosynthetics over the past 25 years will be described.

Table 1 – Types of polymers used to manufacture geosynthetics, Koerner (2012)

Geosynthetic	Types of Polymers	Estimated Percentage in Usage
Geomembranes	Polyethylene (PE)	80%
	Polypropylene (PP)	10%
	Polyvinyl chloride (PVC)	10%
	Ethylene polyethylene diene terpolymer (EPDM)	3%
	Chlorosulfinated polyethylene (CSPE)	2%
Geotextiles	Polypropylene (PP)	90%
	Polyethylene (PE)	5%
	Polyethylene terephthalate (PET)	5%
Geogrids	Polyethylene terephthalate (PET)	50%
	Polypropylene (PP)	30%
	Polyethylene (PE)	20%
Geonets	Polyethylene (PE)	100%
Geopipe (Smooth and corrugated)	Polyethylene (PE)	50%
	Polyvinyl chloride (PVC)	30%
	Polypropylene (PP)	20%
Geocomposites	Polypropylene (PP)	60%
	Polypropylene (PE)	38%
	Polyamide (PA)	2%

Table 2 – New Development in Catalysts and Polymerizations

Year	Catalysts	Year	Polymerization
1955	Ziegler-Natta	1977	Union Carbide LLDPE process
1968	High yield δ -MgCl ₂ supported catalysts for PE	1982	Spheriopol Process for PP
1975	High yield δ -MgCl ₂ supported catalysts for PP		

POLYETHYLENE

As seen in Table 1, polyethylene (PE) is perhaps the most widely used polymer in geosynthetics, as it is in many consumer products. PE is a unique polymer with a large range of densities, from 0.890 g/cc to 0.960 g/cc. There are two types of polymerization from which two different polyethylene molecular structures are created. The conventional process uses high pressure and relative high temperature to initiate free radical reactions, generating highly branched polyethylene chains; see Fig. 1(d). The density of this type of polyethylene is relative low and thus is categorized as Low Density Polyethylene (LDPE). The second process which became commercialized in the late 1960's utilizes catalytic polymerization at low pressure and temperature, generating linear polyethylene chains; see Fig. 1(a). Because of the linear

structure, this type of PE can achieve a very high density due to a high fraction of crystallized domains. However, the high crystallinity limits many potential applications for the polymer due to its relatively high brittleness, tendency to cracking, and generally low compliance. By introducing co-monomers to the polymerization process, the co-monomer can graft onto the linear polymer chains forming a short branches (Bobsein and Seeley, 1994). The branch length is governed by the co-monomer type which is an α -olefin, such as butene, hexene, octene, etc. On the other hand, the branching frequency directly influences the density of the PE with greater branch frequency leading to lower density; see Fig. 1. This results in a wide range PE resins with different densities. The linear PE is categorized into four groups based on the density range according to ASTM D883, as shown in Table 3.

Table 3 – Polyethylene density classification according to ASTM D883

Category	Abbreviation	Density range (g/cc)
High Density Polyethylene	HDPE	>0.941
Medium Density Polyethylene	MDPE	0.926 – 0.940
Linear Low Density Polyethylene	LLDPE	0.919 – 0.925
Low Density Polymer	LDPE	0.910 – 0.925

Note: LDPE is the highly branched type of polyethylene

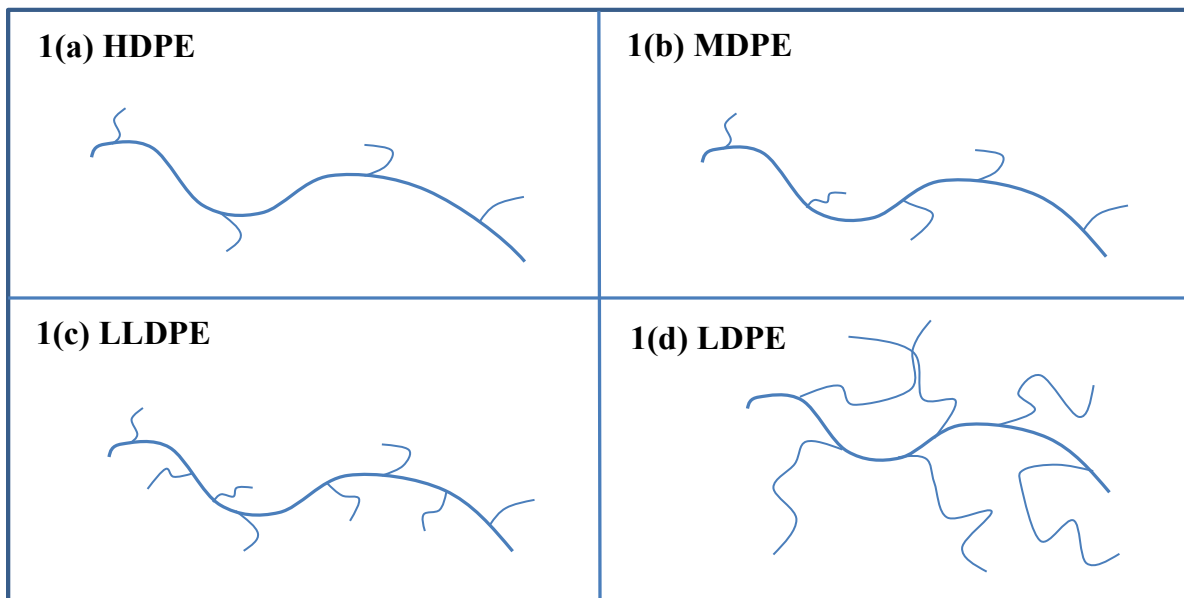


Figure 1 – Four types of polyethylene with respect to its branching length and frequency. (heavy line = carbon polymer chain, light lines = chain branches)

In the last 25 years, the advances in PE polymerization technology and catalysts have produced a series of polyethylenes with different molecular weight distributions yielding a variety of performance properties. There are three types of catalysts: Ziegler-Natta, supported metal oxides (Phillips type of catalysts), and metallocenes (Rodriguez, 1996).

- (i) Ziegler-Natta Catalysts and Phillips Type of Catalysts: These two types of catalysts have multiple reactive sites differing in reactivity. Polyethylene being generated from these catalysts consists of a broad molecular weight distribution and long polymer chains. Furthermore, the comonomer branches tend to concentrate in the short polymer chains reducing the lubricating effect during the product extrusion process.
- (ii) Metallocenes: These catalysts have a single active site, enabling them to generate polymers with narrow molecular weight distribution. Also the comonomer branches are uniformly distributed. With well controlled molecular weight and comonomer type, a PE with high crystallinity and high elastic property can be created.

The progression toward high performance PE resin is reflected in the advance of PE pressure pipes, particular in the enhancement of stress crack resistance and creep resistance. In the 1980's the highest pressure rated PE pipes were certified to sustain internal pressure of 80 MPa at 20°C for 50 years. They were designated as PE80. The PE80 resins are polymerized using either Ziegler-Natta catalysts or Phillips processes in a single reactor, as described above. The resin possesses a broad molecular weight distribution curve and the short chain branching tends to concentrate in the shorter polymer chains. In past ten years, a new type of high performance polyethylene resin, PE100, was developed and is currently being used in high pressure PE pipes. Pipes made from this resin can sustain 100 MPa at 20°C for 50 years which is 20 MPa higher internal pressure than the PE80. Such enhancement is contributed by the new bimodal PE resin. The uniqueness of PE100 bimodal resin is that the short chain branching is concentrated on the longest polymer chains and thus lowers the crystallinity and increases the probability of tie molecule formation. The stress cracking resistance of PE100 can well exceed 1000 hours using the PENT test (ASTM F1437) and similar improvement should also be expected in the notched constant tensile load (NCTL) test (ASTM D5397) as used in the geosynthetic industry. Furthermore, high creep rupture strength and rapid crack propagation are also afforded. Forcing the short chain grafting onto the longest polymer chains, the bimodal resin must be produced via the polymerization process in a reactor rather than melt blending in the extruder. This is because phase separation can take place during the melt mixing when blending two resins with large difference in molecular weight distributions (Moreno et al., 2012). There are two types of polymerization processes used to create bimodal PE resins with the desired short branching distribution:

- (i) Two stage polymerization runs a specific single catalyst through two sequential reactors (Alt, et al., 2001). This process has a much higher cost than the single reactor process that is used to polymerize PE80.
- (ii) Single stage polymerization uses a new catalyst. Currently it is possible to polymerize PE100 in a single reactor (DesLauriers et al., 2005).

In summary, there are three types of molecular weight distribution curves with different short chain branching distributions which vary between a broad molecular weight polymer and a bimodal molecular weight polymer. This can be seen in Figure 2.

Polyethylenes used for geosynthetics are made from the polymerization process yielding PE80 (Bobsein and Seeley, 1994). Each type of geosynthetics (such as GM, GG, or GN) uses

different PE resins with specific melting index and density to optimize the extrusion processing and to comply with performance requirements. For unique applications that require extremely high stress crack resistance and creep resistance, PE100 resin can be used to manufacture a geosynthetic product that meets extremely high engineering performance demands.

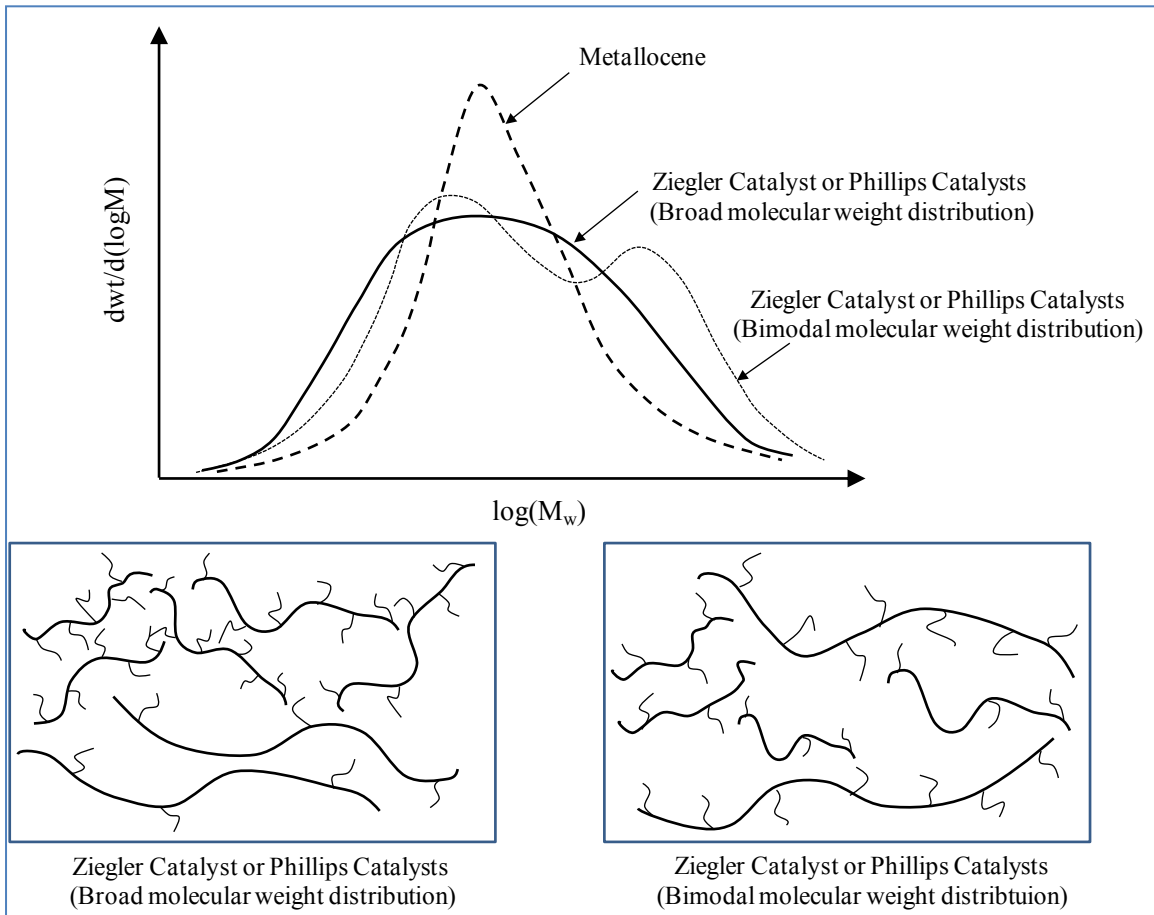


Figure 2 – Schematic diagrams to illustrate three types of molecular weight distribution curves and corresponding short chain branching distribution curves.

POLYPROPYLENE

Polypropylene (PP) is similar to polyethylene as a type of polyolefin which is composed of carbon and hydrogen atoms in the molecular structure. The difference, however, is that a pendant methyl (CH_3) group is attached to every other carbon atom along the polymer chain. The location of the methyl group with respect to the zigzag conformation of the polymer chain creates three types of PP: atactic, isotactic, syndiotactic. In an atactic, the methyl group is randomly distributed along the polymer chain. Isotactic PP has the methyl group positioning along one side of the polymer chain. A regular alternative arrangement of methyl groups characterizes the syndiotactic PP. The three types are shown in Figure 3. It is the regular structure of the isotactic type that allows PP to be crystalline.

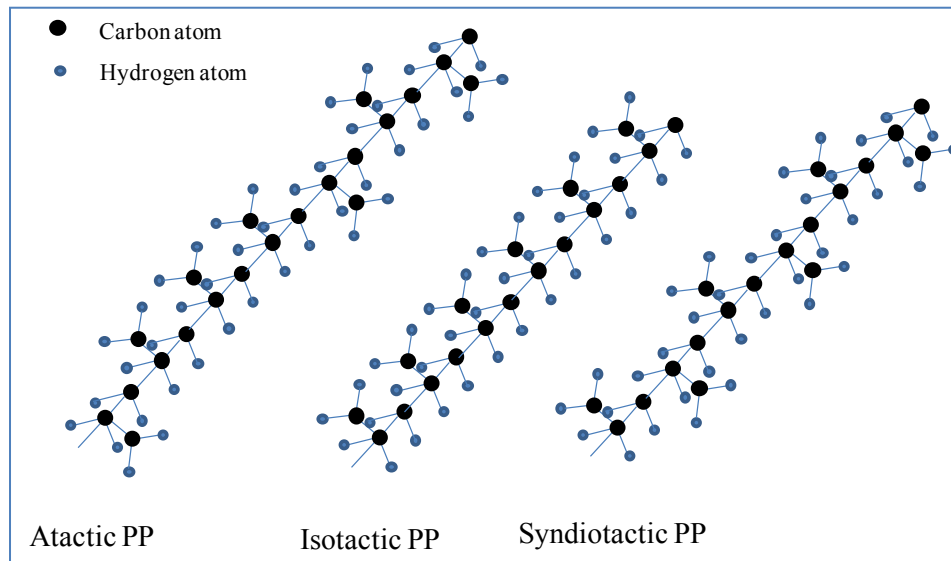


Figure 3 – Three types of tacticity of PP.

Prior to the invention of Ziegler-Natta catalytic polymerization, only amorphous atactic PP was produced which had very limited engineering applications. In 1954, Giulio Natta successfully created isotactic PP using Ziegler catalysts and recognized the significance of catalyst architecture, particularly surface chemistry. Goodall (1986) categorized the progress of PP into three generations based on the percentage of isotactic PP being generated. The first and second generations are based on TiCl_3 catalyst yielding 90-95 wt% to 96-97wt% of isotactic PP respectively. The third generation, which has been applied to produce commercial PP since 1980, utilizes MgCl_2 as the supporting catalyst. Although the percentage yield of isotactic PP is lower than the first generation, ranging from 90 to 95 wt%, the weight percentage of polymer generated increases almost 1000 fold for a unit gram of catalyst.

Isotactic PP is used in geosynthetics, including geotextiles, geogrids, and geocomposites as shown in Table 1. As a homopolymer, isotactic PP however possesses a relatively high glass transition temperature (100°C) and high rigidity, and thus it is not an ideal polymer for manufacturing flexible geomembranes. On the other hand, the propylene based copolymer synthesized using reactor granule technology (RGT) has created a new type of geomembrane classified as flexible polypropylene (or fPP) geomembranes. RGT was developed by Himont/Montecatini's during 1980s using the superactive MgCl_2 /Ziegler-Natta catalysts. The final polymer is spherical particles with interior morphology to be either "onion shaped" or porous (Galli, 1994). Such processes can eliminate the pelletization step of the resin. In the meantime, advanced polymerization processes make it possible to produce PP copolymer with a much higher impact resistance in an effective and economic way. The two internationally known processes are Spheripol and Catalloy, as shown in Figure 4. Spheripol processes use liquid monomers mixed with catalyst components in the loop reactor to create homopolymer which is then fed into a gas phase reactor to generate co-polymers. In the Catalloy process, different types of olefinic monomers are introduced during the polymerization of propylene, generating multiphase polymer alloys (Bigiavi, et al., 2005).

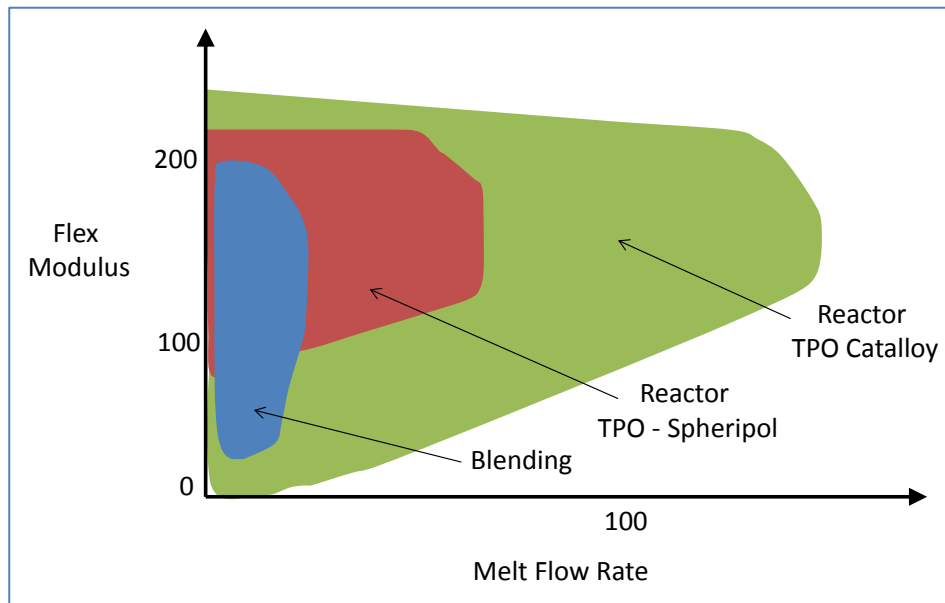


Figure 4 – Flexural Modulus of different thermoplastic olefins (TPO), (Galli, 1994).

CONCLUSION

Over the past 25 years, the innovation in polyolefin polymerization has greatly enhanced the performance of many geosynthetics. In particular, polyolefin geomembranes have benefited the most. HDPE geomembranes can possess enhanced properties although they require a delicate balance, such as crystallinity and stress cracking. The new bimodal PE100 resin can provide excellent stress crack resistance as well as high chemical resistance. For fPP geomembranes, a variety of polypropylene based copolymer resins can be used depending on the required engineering properties.

ACKNOWLEDGEMENT

Dr. Hsuan is supported by National Science Foundation as the Director of Structural Materials and Mechanics Program in the Civil, Mechanics, and Manufacturing Division. Any opinions, findings, and conclusions or recommendations expressed in this paper are those of the author and do not necessarily reflect the views of the National Science Foundation.

REFERENCES

- Alt, F.P., Bohm, L.L., Enderle, H.F., Berthold, J. (2001), “Bimodal Polyethylene – Interplay of Catalyst and Process”, *Macromol. Symp*, 163, pp. 135-143.
- Bigiavi, et al. (2005), “Polypropylene – The Technology”, *Polypropylene Handbook*, 2nd Edition, Pasquini, N. Ed., published by Basell Polyolefins, 584 pages.

Bobsein, R.L. and Seeley, R.B. (1994), "Polyethylene Polymerization by Slurry Technique", 8th GRI Conference, Geosynthetic Resins, Formulations and Manufacturing, edited by Hsuan, Y.G. and Koerner, R.M., PP. 1-6.

DesLauriers, P.J., et al., (2005), "A Comparative Study of Multimodal vs. Bimodal Polyethylene Pipe Resins for PE-100 Applications", *Polymer Engineering and Science*, pp. 1203-1213.

Galli, P. (1994), "The Breakthrough in Catalysis and Processes for Olefin Polymerization: Innovative Structures and a Strategy in the Materials area for the 21st Century", *Progress in Polymer Science*, Vol. 19, pp. 959-974.

Galli, P. and Vecellio, G. (2004), "Polyolefins: The Most Promising Large-Volume Materials for the 21st Century", *Journal of Polymer Science: Part A: Polymer Chemistry*, Vol. 42, 394-415

Goodall, B.L. (1986), "The History and Current State of the Art of Propylene Polymerization Catalysts", *J. of Chemical Education*, Vol. 63, No. 3, pp. 191-195.

Koerner, R.M. (2012), Designing with Geosynthetics, 6th Edition, Vol. 1 and 2.

Moreno, J., von Grieken, R., Carrero, A., and Paredes, B. (2012), "Bimodal Polyethylene for Pipe Applications Obtained by Chromium Oxide/Metallocene Binary Catalysts", *Proceedings of Intl. Plastics Pipes Conference XVI, Barcelona, Spain, September*.

Rodriguez, F. (1996), Principles of Polymer Systems, 4th Edition, published by Taylor and Francis, Washington, DC. 690pg.

ANTIOXIDANTS FOR GEOSYNTHETIC RESINS AND APPLICATIONS

Joseph J. Fay and Roswell E. King III
BASF

ABSTRACT

Polyolefins are intrinsically susceptible to oxidative degradation. Depending upon the polymer type, processing conditions and end use requirements, a variety of antioxidants may be added to the polymer to provide stability and protection against oxidation. For geomembranes, geonets, geogrids and other geosynthetic materials, it is important to protect the polymer during manufacturing processes as well as during storage and installation to prevent degradation which could affect the durability of the final product. For materials designed for long term use, antioxidants are needed to provide stability and to prevent premature product failure. There are several types of antioxidants which can be employed to improve the stability of geosynthetics that may be subjected to thermally and/or photolytically initiated degradation. A brief review of antioxidant types, mechanisms and application test data relevant to geosynthetics is presented.

INTRODUCTION

Polyolefins are used in numerous applications due to the wide spectrum of properties that can be designed into the polymer through current polymerization technologies and the broad variety of manufacturing processes that can be used to convert these polymer resins into finished products. Polyolefins are produced on a huge scale. Worldwide polyethylene capacity exceeds 50 million tons and polypropylene capacity exceeds 20 million metric tons (Wigotsky, 1994) attesting to their prolific use. Additives, of one type or another, are incorporated into nearly every pound of polyethylene and polypropylene produced to improve the performance of these polymers.

Geosynthetics are but one of the many highly specialized applications in which polyolefins are used. Geosynthetics, which may be geotextiles, geomembranes, geogrids, etc., are also used in a wide array of applications. The application area spans a multitude of uses in environmental, transportation and geotechnical engineering. Typical functions include separation, reinforcement, filters, drains and barriers (Suits, 1994). Amongst the multitude of polyolefin products, polymer stabilization principles transcend product line boundaries and often play an integral role in the development and use of such products.

In geosynthetic applications, stabilizer additives (antioxidants) are incorporated (melt compounded) into the polymer during manufacture. Antioxidants (AO's) are used to protect the polymer during melt processing as well as to protect the finished product from the negative effects of oxidation (Klemchuck and Horng, 1984). Oxidation, which results from either thermally or photolytically initiated chemical reactions in the presence of oxygen, degrades the polymer and reduces physical properties, thereby altering the suitability of the material for the intended application. It is important to consider a broad range of properties when selecting a material to meet regulatory and design standards. These properties include tensile properties,

tear and puncture resistance, as well as numerous endurance properties such as chemical resistance, and creep and stress relaxation, in addition to others (Cadwalader, et al., 1992). Stabilizers, when used judiciously, can effectively counter the tendency of the polymer to oxidize and can significantly increase the service life of the material (Schmidt, et al., 1984).

ANTIOXIDANTS

In the absence of stabilizing additives, polyolefins are prone to degrade via oxidative mechanisms as depicted in the auto-oxidation cycle, Figure 1. Polymer degradation may be initiated by polymerization catalyst residues, heat or shear which initiate chain scission in the polymer, generating free radical species. Oxygen reacts readily with the unstable, reactive carbon centered radical to form a peroxy radical. This oxygen centered radical species then abstracts a hydrogen atom from the surrounding polymer to form a hydroperoxide and create yet another carbon centered radical species. The resultant hydro peroxide can be decomposed to yield two additional oxygen centered radical species. The polymer carbon centered radical can react with oxygen to continue the cycle. As this radical generation is geometric in nature, a significant radical flux can be generated which can severely transform and ultimately degrade the polymer. Even at ambient conditions, unstabilized polymers are found to degrade, as evidenced by changes in color, physical properties and melt flow properties during storage. Ultimately, without the interruption of the free radical auto-oxidative chemistry, the polymer is oxidized to the point of discoloration, brittleness, crazing, cracking or chalking and product failure.

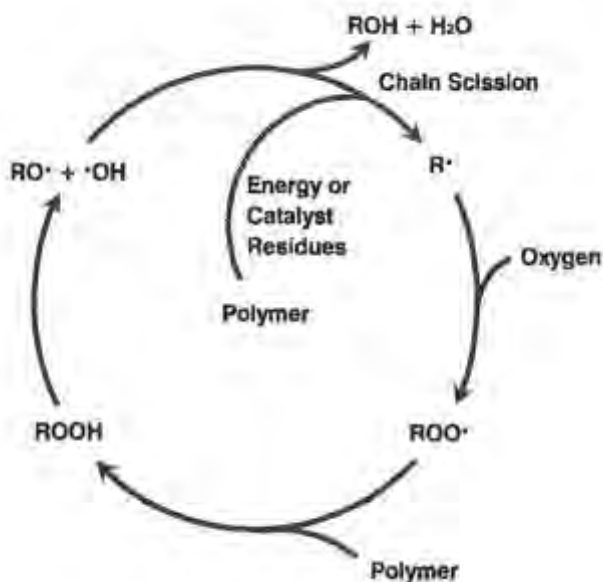


Figure 1. Auto-oxidative cycle.

Similarly, hydroperoxides, which may be formed during processing or as a result of auto-oxidation, are unstable toward UV energy and can be photolytically cleaved, generating radical species much in the same way that they are generated by thermal processes. Photo-oxidative degradation is depicted in Figure 2.

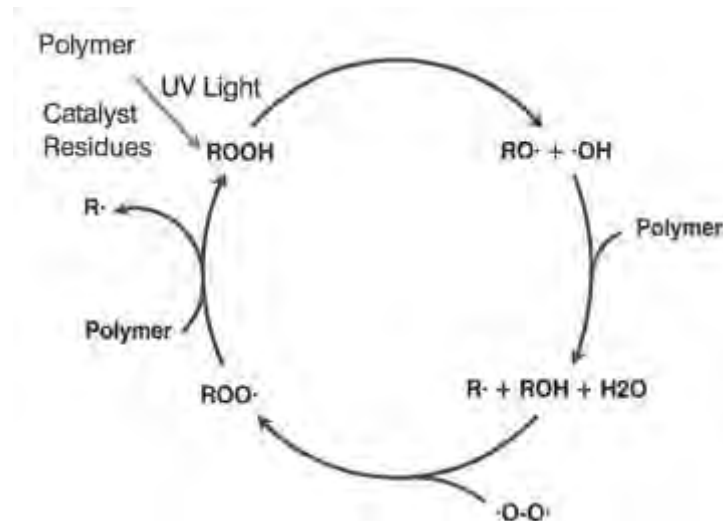


Figure 2. Photo-oxidative degradation pathways.

Antioxidants that are useful in polymer applications are generally classified by the mechanism in which they act as stabilizers during degradation. Primary oxidants provide stabilization by trapping or deactivating free radical species after they are formed. Secondary antioxidants decompose hydroperoxides, which may otherwise be transformed into free radical species, into non-radical species thereby inhibiting the formation of radicals. For each of these two categories, there are a few major classes of chemistries which are commercially significant. Antioxidants referred to herein are listed in Table 1.

PRIMARY ANTIOXIDANTS

This general class of antioxidants is capable of interrupting free radical processes by donating labile hydrogen atoms to the free radicals. These hydrogen donating antioxidants slow down oxidation by sacrificially competing with the polymer for free radicals, thereby decreasing the extent to which the polymer is transformed or degraded. Of course, the antioxidant is preferentially oxidized and if sufficient radicals are being generated in the system, the antioxidant may be entirely consumed and eventually rendered ineffective.

Heat, shear and UV light can initiate the formation of radical species. However, certain antioxidants, by the nature of their molecular structure, are more or less capable of reacting with radical species depending upon the conditions during which the radicals were generated.

Hindered Phenolic Antioxidants

The chemistry of phenolic antioxidants has been extensively reviewed (Pospisil, 1991; Pospisil, 1988; Scott, 1993) and consequently, will not be discussed in detail here, other than to describe how they can be used in practice. Phenolic AO's are incorporated into the polymer to stop the chemistry associated with the free radicals by first donating hydrogen atoms to interrupt the auto-oxidation process. Phenolics typically react with oxygen centered free radicals, and consequently, can interrupt the auto-oxidation cycle depicted in Figure 3. The resulting phenoxy

radical is thermodynamically more stable than the oxygen centered free radical. This is due to the resonance delocalization of the radical around the phenyl group, Figure 4.

Table 1. Key to Referenced Stabilizers

Code		Commercial Example
AO-1		Irganox [®] 1076
AO-2		Irganox [®] 1010
P-1		Irgafos [®] 168
MD-1		Irganox [®] MD 1024
HALS-1		Tinuvin [®] 770
HALS-2		Tinuvin [®] 622
HALS-3		Chimassorb [®] 944
HALS-4		Chimassorb [®] 119

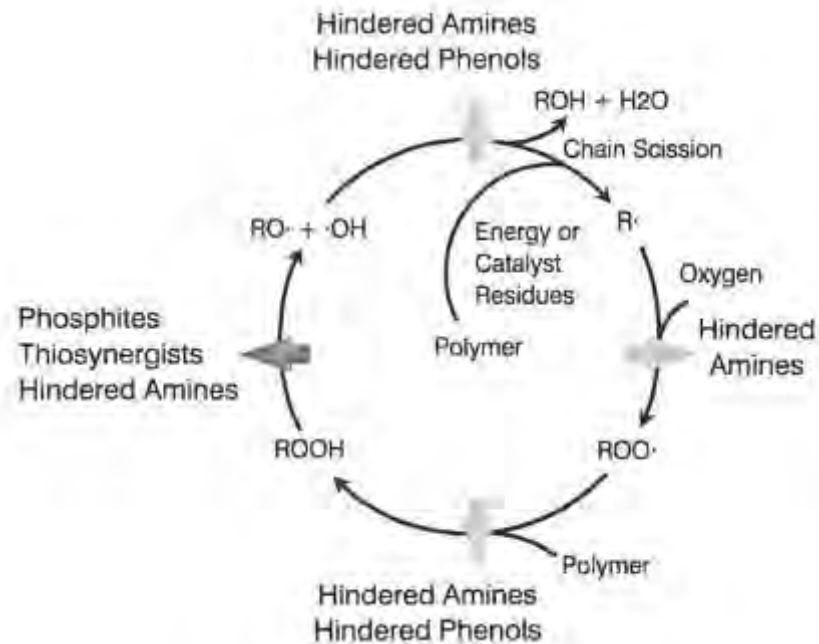


Figure 3. Autocatalytic thermo-oxidation cycle depicting points at which various stabilizers are effective.

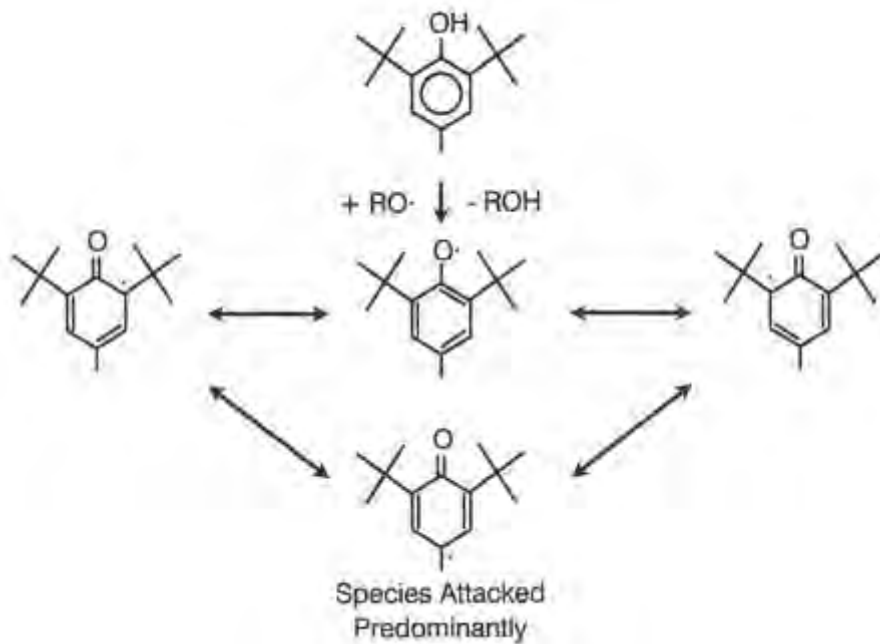


Figure 4. Initial stabilization reactions of phenolic antioxidants and resonance stabilization of the free radical.

Phenolic AO's, depending upon the specific molecular structure, are capable of donating hydrogen atoms, undergoing rearrangement reactions, and further reacting with free radicals until they are no longer reactive towards radical species. This total consumption of the phenolic is typically undesirable due to the generation of color bodies, especially in unpigmented and lightly pigmented systems. Co-additives, such as trivalent phosphorous compounds and scavengers for acidic catalyst residues, are commonly used in combination with the phenolic to improve overall performance.

Figure 5 illustrates the significant improvements in long term heat aging (LTHA) that are obtained with the addition of AO-1 and AO-2 to polypropylene.

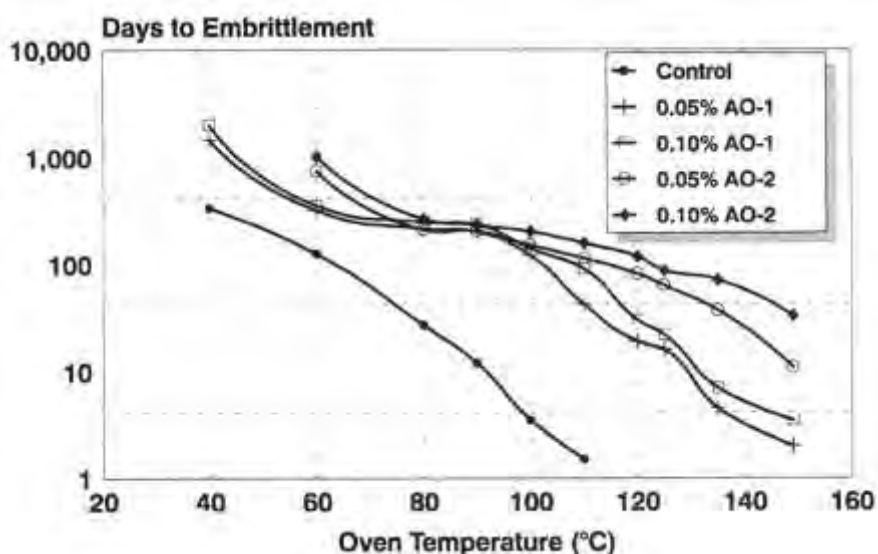


Figure 5. Phenolic antioxidants can significantly improve the oxidative stability over a broad temperature range in Polypropylene homopolymer containing 0.1% calcium stearate, 120 μm film.

Hindered Amines

This class of antioxidants is historically associated with light stability since they are extremely effective at protecting polyolefins from the damaging effects of ultraviolet radiation (Gugumus, 1990). However, hindered amines are also useful as primary antioxidants as they are also capable of scavenging free radicals, albeit at lower temperatures (less than 135°C). The most common hindered amine is based on the 2,2,6,6-tetramethylpiperidine functions group. The antioxidant behavior of hindered amines is illustrated in Figure 6. The hindered amines differ fundamentally from hindered phenols in that the hindered amine mechanism is a cyclical and regenerative (Klemchuk and Gande, 1989; Carlsson, et al., 1979; Denisov, 1989). Only when undesirable side reactions take place is the hindered amine rendered ineffective. It has also been proposed (Dulog and Bleher, 1986) that hindered amines are capable of decomposing hydroperoxides, further broadening the mechanisms for stabilization.

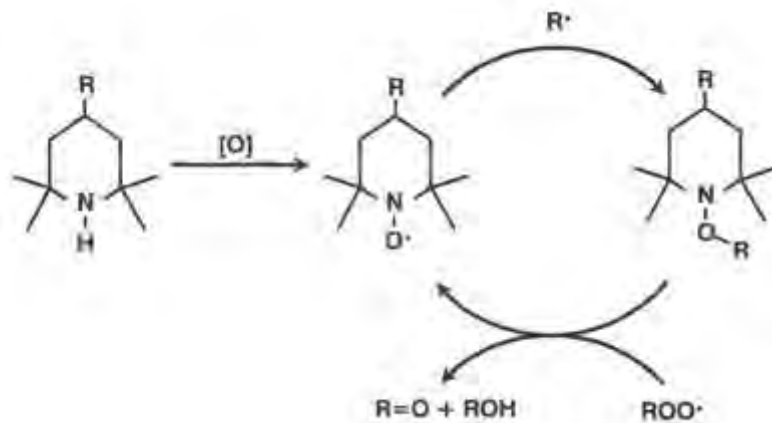


Figure 6. Stabilization mechanism for HALS depicting regenerative, cyclic process of radical scavenging.

Nevertheless, hindered amines efficiently interrupt the auto-oxidation chain reaction, Figure 3, via mechanisms which may involve reactions with carbon and oxygen centered radicals, as well as decomposing peracids or hydroperoxides (Gugumus, 1993). Regardless of the specific mechanisms involved, hindered amines provide excellent performance as stabilizers at lower temperatures as long term thermal stabilizers (Gijsman, 1994; Drake, et al., 1992) in addition to their recognized efficacy as light stabilizers (Gugumus, 1994). HALS-1, HALS-2 and HALS-3 are typical hindered amine light stabilizers which can be used to provide UV stability for geosynthetics during storage and installation, where UV exposure can potentially damage the product. Representative performance of HALS is illustrated in Figure 7.

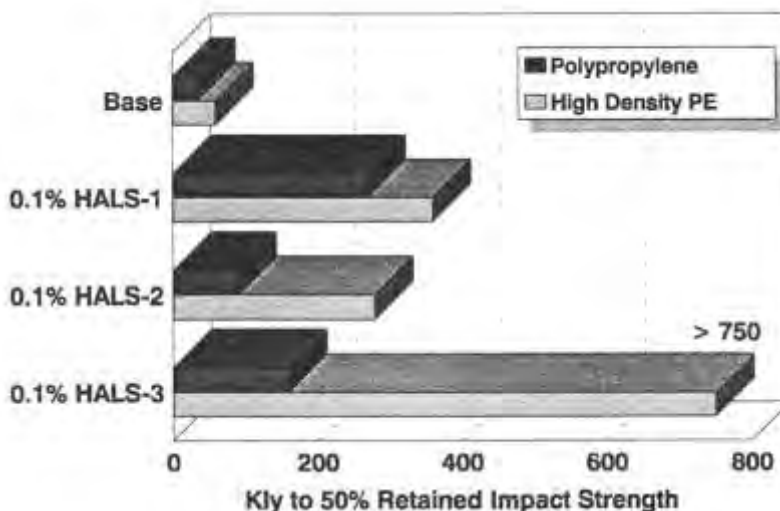


Figure 7. Light stability of PP and HPE, PP contains 0.05% AO-2/0.05% P-1 and 0.1% Ca stearate; Ziegler HDPE contains 0.025% AO-1, 0.5% TiO₂ and 0.1% Ca stearate. 2 mm plaques, Florida 45 degree south exposure.

As mentioned above, it should be clearly stated that the antioxidant capability of hindered amines proceeds most efficiently at temperature below 135°C, but preferably below 120°C where performance is much more effective, Figure 8. Consequently, hindered amines should not be considered as melt processing stabilizers. In practice, after melt compounding most polymers are not typically exposed to such high temperatures during end use applications. For those that are exposed to high temperatures, other combinations of antioxidants can be used, such as those based upon phenolic and thiosynergists which are discussed below.

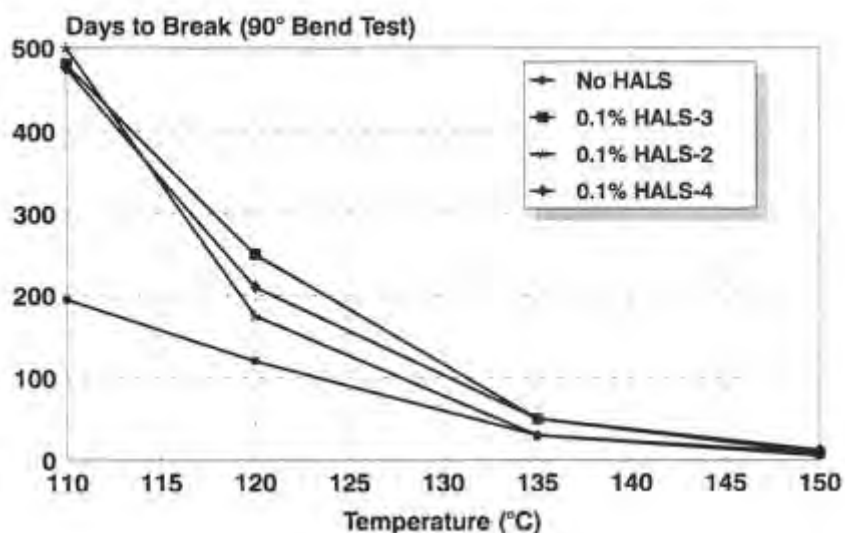


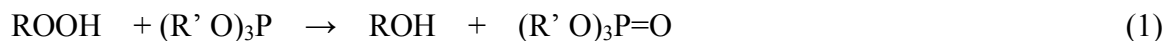
Figure 8. HALS provide thermal stability at temperatures below 135°C in polypropylene homopolymer containing 0.10% P-1/0.05% AO-1 and 0.05% calcium stearate; oven aging of 40 mil plaques.

SECONDARY ANTIOXIDANTS

One of the most damaging species in the auto-oxidation process is the hydroperoxide moiety, ROOH as illustrated in Figures 1 and 2. Under elevated temperatures, hydroperoxides decompose via a hemolytic cleavage to yield two free radicals. This step is representative of the catalytic nature of auto-oxidation. The destruction of the hydroperoxides which continually build up in the polymer, is essential in protecting the polymer. Most commercially available peroxide decomposers are based on trivalent phosphorus compounds and divalent sulfur compounds.

Phosphites: Trivalent Phosphorus Compounds

The chemistry of phosphites and phosphonites has been reviewed (Pobedimskii, et al., 1980; Schwetlick et al., 1987). In essence, a P(III) compound reacts stoichiometrically with hydroperoxide, ROOH, to produce an alcohol, ROH, with the simultaneous oxidation of P(III) to P(V), as shown in Equation 1.

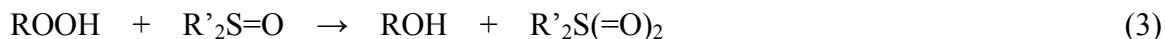
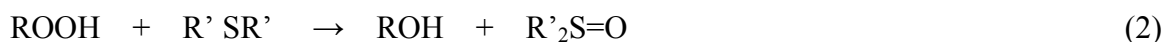


This reaction occurs during melt compounding and extrusion of the polymer. However, at ambient temperatures, the reaction is very slow. This increases the importance of the hindered amines mentioned above, which are capable of decomposing hydroperoxides at temperatures below 120°C to 135°C.

Phosphorus (III) compounds may also react with free radicals (Schwetlick, 1987). However, the contribution of this chemistry is secondary in comparison to hydroperoxide decomposition.

Thiosynergists: Divalent Sulfur Compounds

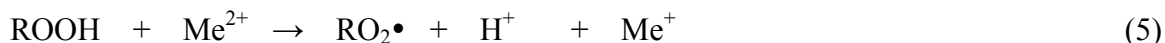
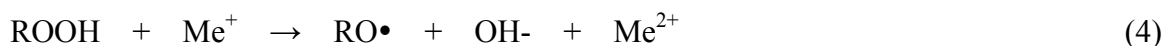
Dialkyl thiodipropionate esters, such as distearyl thiodipropionate (DSTDP) and dilauryl thiodipropionate (DLTDP), are more commonly referred to as thiosynergists. The chemistry of S(II) compounds has also been reviewed (Kulich and Shelton, 1991; Armstrong, et al. 1979; Armstrong, et al., 1975). Thiosynergists react similarly to phosphorus compounds in that hydroperoxides are transformed into alcohols, with concomitant oxidation of S(II) to S(IV) as shown below.



The chemistry does not stop with the formation of the sulfone (Equation 2) or sulfoxide (Equation 3). Elimination reactions result in the formation of sulfonic and sulfonic acids, which can further decompose to sulfur dioxide and sulfur trioxide. Fortunately, these sulfur transformation products are also very effective at decomposing hydroperoxides and contribute to polymer stabilization. As a result of these additional reactions, thiosynergists can react with more than one equivalent of hydroperoxide species. However, these decomposition products can have a negative effect on the ability of hindered amines to function as antioxidants or light stabilizers, which is discussed below.

METAL DEACTIVATORS

Polymers that come into contact with metals of low oxidation potential, such as copper or iron, are susceptible to oxidation from the metal catalyzed decomposition of hydroperoxides, as shown in Equations 4 and 5.



One way to avoid the negative influence copper on autooxidation is to use metal deactivators (Muller, 1990). Metal deactivators are typically designed to contain hydrazide or amine functional groups that can complex with the metal, providing stabilization. Metal deactivators, such as MD-1, also include a phenolic antioxidant as part of the molecular structure to provide antioxidant performance as well.

EFFECT OF TEMPERATURE

Figure 9 summarizes the temperature ranges over which the major classes of antioxidants are effective. Phenolic antioxidants have the broadest applicability as they function over the broadest range of temperatures. Note that thiosynergists, in combination with a phenolic antioxidant, are effective at providing thermal stability at elevated temperatures, but that they do not provide stabilization during melt processing. On the other hand, phosphites only provide melt processing stability and are not effective antioxidants at lower temperatures. Hindered amines, as mentioned above, are most effective at temperatures below 135°C. For many applications, it is necessary to use a combination of two or more antioxidants to provide the needed stabilization.

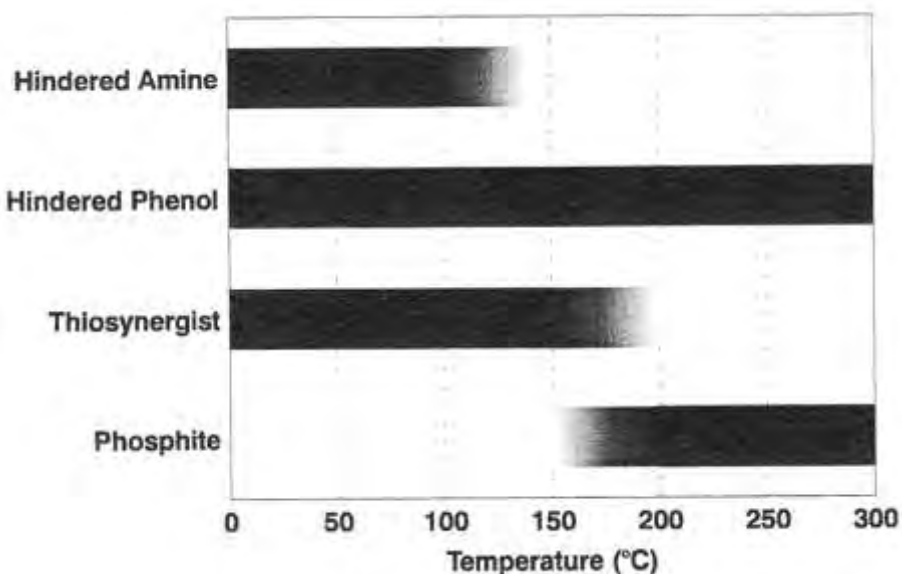


Figure 9. Effective temperatures for stabilizers.

SYNERGISTIC MIXTURES OF ANTIOXIDANTS

When used alone, neither phosphites nor thiosynergists are capable of providing complete melt processing and thermal stability of the polymer. However, in combination with a phenolic antioxidant, the performance of these binary systems is typically better than the sum of the performance levels of each additive. This is known as synergism.

For example, blends of a phenolic antioxidant and a phosphite are very useful for melt compounding of polyolefins (Zinke, et al., 1980) and engineering polymers (Muller and Schwarzenbach, 1982). When both additive classes are used together, the combination of hydroperoxide scavenging (phosphite) and free radical scavenging (AO) probably results in more effective stabilization. As a result, a lower total radical flux occurs and there are fewer radicals to degrade the polymer and to deplete the additives. However, if the phosphate is entirely consumed at the end of the polymer processing, it has done its share of work. Also, consumption of the phosphite also preserves more of the phenolic antioxidant for long term thermal stability.

In Figure 10, the combined use of P-1 and AO-2 results in an increased concentration of AO-2 in the polymer following multiple pass extruder compounding. For geosynthetic applications, preservation of the antioxidant, which provides long term thermal stability, is very important.

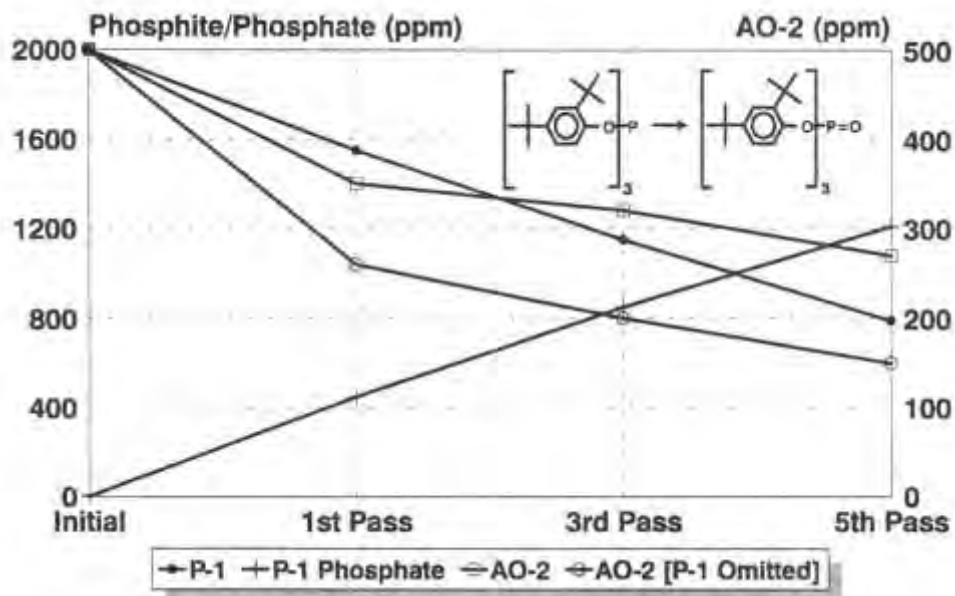


Figure 10. Effect of using P-1 on AO-2 concentration. HDPE containing 0.05% AO-2 and 0.2% P-1; multiple extrusion at 260°C.

Similarly, blends of phenolic antioxidants with thiosynergists provide exceptional long term thermal stability to polyolefins. Although thiosynergists provide no activity during melt processing, they do provide excellent performance as a hydroperoxide decomposer during long term thermal aging. Combined with the free radical scavenging capability of the phenolic AO's, superior formulations can be established.

ANTAGONISTIC MIXTURES OF ANTIOXIDANTS

While mixtures of antioxidants can be synergistic, they may also be antagonistic. For instance, if one wanted to ensure long term thermal stability and light stability, one might use a combination of phenolic antioxidant and thiosynergist for thermal stability and a hindered amine for light stability. Unfortunately, the oxidation products of the sulfur compound can be quite acidic. The acidic species from the sulfur transformation chemistry can react with the hindered amine (which is basic) to form a salt. This salt formation prevents the hindered amine from entering into the free radical scavenging cycle (Kikkawa, et al., 1987). Figures 11 and 12 document the negative effects of polypropylene and polyethylene UV stability that may be obtained when combinations of thiosynergists and hindered amines are used together. While significant reductions in UV stability and thermal stability may be observed, additional research has shown that the extent of antagonism is both variable and unpredictable. By varying both the total concentration of the additives and their ratio, it is possible to devise a formation in which the antagonistic effects are minimized.

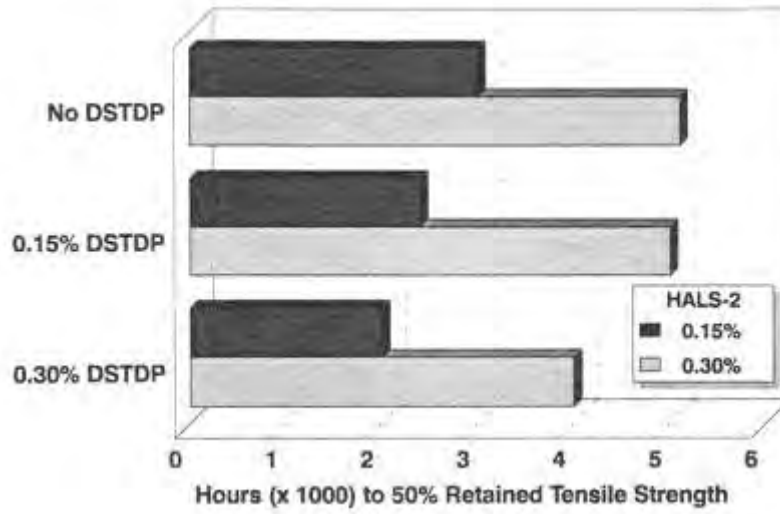


Figure 11. Effect of thiosynergists of UV stabilized polypropylene homopolymer; Xenon Weather-O-Meter exposure.

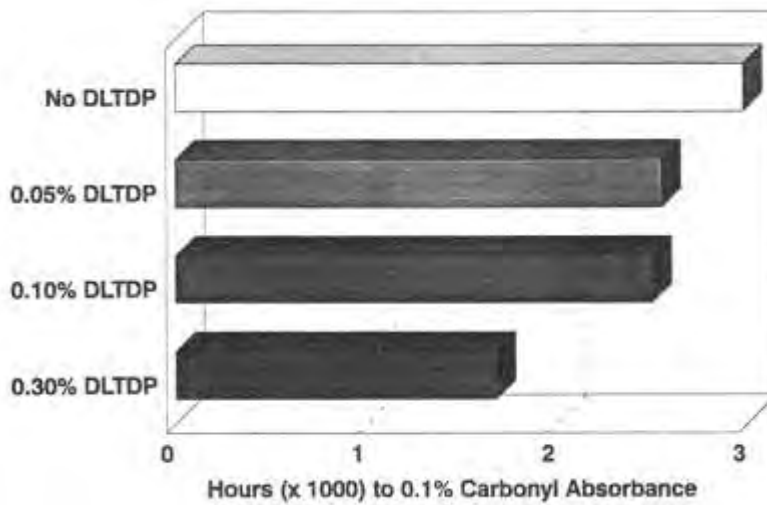


Figure 12. Effect of thiosynergists on UV Stabilized Ziegler high density polyethylene containing 0.15% HALS-1; Xenon Weather-O-Meter exposure.

CARBON BLACK

Carbon black is commonly compounded into polymers as both a pigment and a UV stabilizer (Mair, 1967; Walldner, et al., 1950). As UV stabilizer, carbon black can be quite effective, though at concentrations where UV protection is significant, processing can be adversely affected. The use of combinations of HALS and carbon black can be an effective way to reduce the amount of carbon black contained in the formulation which may improve processing and long term thermal stability, Figure 13. HALS-2 is generally preferred for carbon black applications. While carbon black is beneficial for UV stability, it may be detrimental with respect to thermal stability, as evidenced by the results of an oven aging test and measured embrittlement times, Figure 14. Again the use of HALS-2 or HALS-3 is an effective means of improving the thermal stability in carbon black pigmented applications. For geosynthetics that are carbon black pigmented, surface temperatures as high as 80°C (175°F) have been measured on exposed surfaces in the field (Cadwallader, 1988).

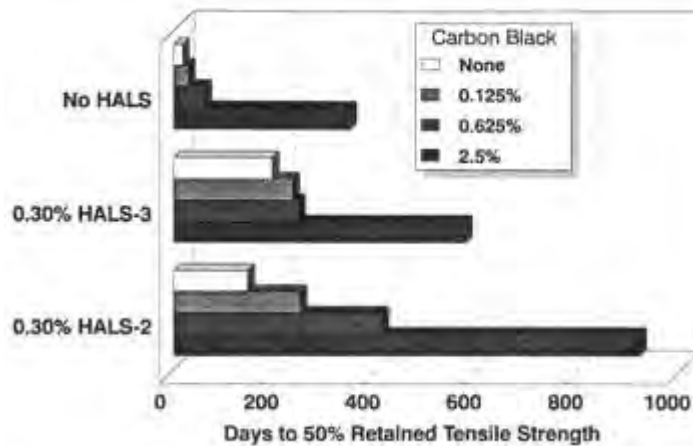


Figure 13. HALS effectiveness in PP homopolymer containing 0.1% P-1/0.1% AO-2 and 0.1% calcium stearate; Vulcan 9 carbon black; Xenon Arc Weather-O-Meter exposure 2 mm films.

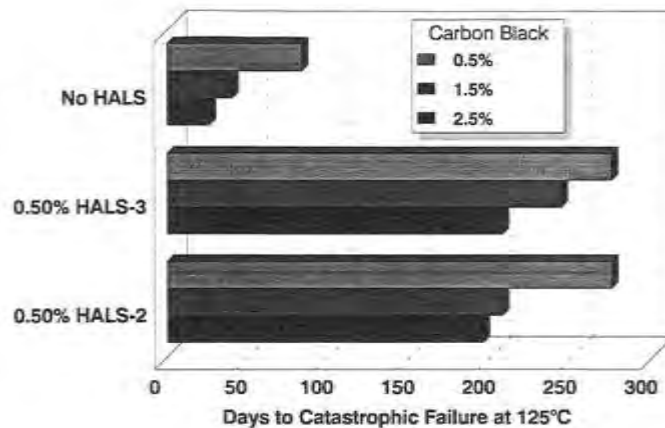


Figure 14. HALS effectiveness in PP homopolymer containing 0.1% P-1/0.1% AO-2 and 0.1% calcium stearate. Oven aging of 2 mm films; Vulcan 9 carbon black.

ACCELERATED AGING TESTS

In order to evaluate the thermal stability of polymeric materials, accelerated aging tests are often employed. This is necessary as the rate of oxidation at ambient temperatures for well stabilized polymers can be excruciatingly slow, especially with respect to the time frame for product development. As a result, testing at elevated temperatures is favored for it reduces the time needed for evaluation. Ideally, the accelerated test should be based upon correlations with actual performance. However, as suitable correlations may not always exist which account for all of the specific variables, one should proceed carefully with accelerated testing.

Oxidation induction times (OITs) and long term heat aging (LTHA) are common evaluation methods which are used to assess the thermal stability of polymers, and the effectiveness of antioxidant systems. OIT tests are typically done above the melting point of the polymer which does not reflect end use conditions, but testing can be completed in minutes or hours. Comparatively, LTHA tests are done below the melting point and are more relevant to end use conditions, but test times can be on the order of months or years.

In evaluating the performance of AO-1 and AO-2, the latter also in combination with P-1, by both OIT and LTHA, significant differences were noted between the two test results, Figure 15. Phosphites do not contribute to thermal stability, as the LTHA results show, except when the consumption of primary antioxidant during melt processing is decreased by the presence of P-1. However, significant increases in OIT were observed. To the casual observer the addition of P-1 would appear to provide a significant boost to LTHA. Most likely, the boost in OIT is due to the test being conducted in an oxygen rich environment where hydroperoxides are generated. Additionally, the high testing temperature allows the phosphite to contribute to the increased OIT values. Although this might seem like a good way to meet an OIT specification, in reality, the enhanced OIT results may be quite misleading as a predictor of actual performance. Similarly, in Figure 16, the correlation between OIT's and embrittlement times (from LTHA) is also poor when different pigments are evaluated. Several papers have recently addressed the topic of OIT testing (Cadwallader, 1988; Pauquet, et al., 1993; Todesco, 1992).

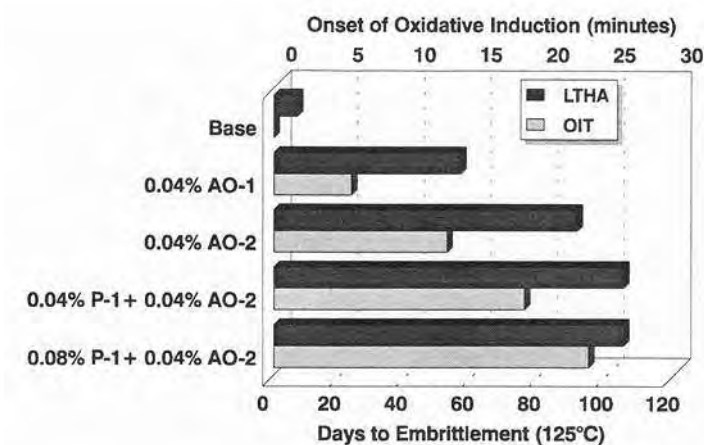


Figure 15. Comparison of LTHA and OIT data for a CRO₃/SiO₂ catalyzed high molecular weight high density polyethylene; oven aging on 125 mil plaques, OIT on 11 mil films at 200°C in O₂ on preoxidized AI pans.

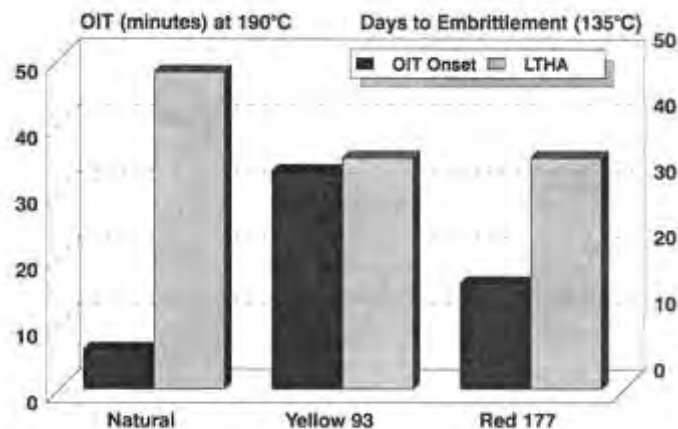


Figure 16. Lack of correlation between OIT and LTHA for polypropylene homopolymer containing 0.10% P-1/0.5% AO-2, 0.3% HALS-1, 0.05% calcium stearate and 0.5% pigment.

CONCLUSION

Antioxidants play an integral role in the development of polyolefin products. The inherent instability of polyolefins towards both thermal and photolytic degradation is such that without the incorporation of stabilizing additives, it is unlikely that polyolefin geosynthetic materials would be suitable for long term applications. Although antioxidants are very effective in most applications, certain combinations of additives have been found to have either synergistic or antagonistic effects on one another. Careful selection of appropriate additives and use levels that do not result in overstabilization and excessive cost need to be balanced with the need to manufacture and install materials which will withstand the environment to which they are subjected. The use of hindered amines as primary antioxidants offers a new choice in the selection of stabilizers to provide long term stability.

Continuous developments in polyolefin catalysis and the ever increasing demands that are required for both existing and new applications continue to push the limits of existing polymer stabilizers. However, polymer additives research and development has led to the recent development of enhanced systems and new products to meet the expanding needs of the geosynthetic industry as well as for others (Davis, 1994; Handreck, 1994; Horsey, et al., 1994; Drake and Cooper, 1993).

ACKNOWLEDGEMENTS

The authors would like to recognize the contribution of Ciba Additives Development and Applications Laboratories in Ardsley, NY and Basle, Switzerland and are grateful for permission from Ciba Additives to publish this article.

REFERENCES

Armstrong, C., Plant, M. A. and Scott, G. (1975), "Mechanisms of Antioxidant Action: The Nature of the Redox Behaviour of Thiodipropionate Esters in Polypropylene," *Eur. Polym. J.*, Vol. 11, pp. 161-171.

Armstrong, C., Husbands, M. J. and Scott, G. (1979), "Mechanisms of Antioxidant Action: The Antioxidant-Active Products Formed from the Dialkyl Thiodipropionate Esters," *Eur. Polym. J.*, Vol. 15, pp. 241-248.

Cadwallader, W. M. (1988), "Accelerated Aging of High Density Polyethylene Geomembranes: A Novel Approach," *Proc. Ind. Waste Conf.*, Vol. 42, pp. 419-428.

Cadwallader, M. W., Anderson, J. D. and Messmer, D. (1992), "Geosynthetics: High Technology Landfills," *Solid Waste and Power*, Vol. 6, No. 6, pp. 28-34.

Carlsson, D. J., Garton, A. and Wiles, M. M. (1979), "The Photo-Stabilization of Polyolefins," *Development in Polymerization Stabilization*, Elsevier Applied Science Publishers, London, Vol. 1, pp. 19-259.

Davis, L. (1994), "Compatibility of Flame Retardant and UV Stabilization Packages for Polypropylene Fiber," *The Future of Fire Retarded Materials: Applications and Regulations*, Fire Retardant Chemicals Assoc., pp. 1-22.

Denisov, E. T. (1989), "Mechanisms of Regeneration of Hindered Nitroxyl and Aromatic Amines," *Polym. Degrad. Stab.*, Vol. 25, pp. 209-215.

Drake, W. O., Gugumus, F., Bonora, M., Canova, P., Zweifel, H., Pauquet, J.-R. and Todesco, R. V. (1992), "Hindered Amine Stabilizers Used as Hindered Amine Thermal Stabilizers," *14th Ann. Conf. Adv. Stab. Degrad. Polym.*, Lucerne, Switzerland.

Dulog, L. and Bleher, R. (1986), "The Reaction of Nitroxyl Radicals with Hydroperoxides," *Makromol. Chem.*, Vol. 187, pp. 2357-2367.

Gijsman, P. (1994), "The Mechanism of Action of Hindered Amine Stabilizers (HALS) as Long Term Thermal Stabilizers," *Polym. Degrad. Stab.*, Vol. 43, pp. 171-176.

Gugumus, F. (1990), "Light Stabilizers," *Plastic Additives*, 3rd Ed., Oxford University Press, New York, Chapter 3.

Gugumus, F. (1993), "Re-Evaluation of the Stabilization Mechanisms of Various Light Stabilizer Classes," *Polym. Degrad. Stab.*, Vol. 39, pp. 117-135.

Gugumus, F. (1994), "Mechanisms of Thermooxidative Stabilization with HAS," *Polym. Degrad. Stab.*, Vol. 44, pp. 299-322.

- Handreck, D. R. (1994), "New Hindered Amine Stabilizers for Polyolefins," *Property Enhancement with Modifiers and Additives*, SPE RETEC, New Brunswick, NJ, pp. 103-114.
- Horse, D., Leggio, A. and Reinicker, R. (1994), "Hindered Amine Light Stabilizers (HAS)/Pigment Interactions – HAS Structural Effects on Color Strength," *Effects of Plastics*, SPE RETEC, Oakbrook, IL, pp. 209-216.
- Kikkawa, K., Nakahara, Y. and Ohkatsu, Y. (1987), "Antagonism Between Hindered Amine Light Stabilizers and Sulfur-Containing Compounds," *Polym. Degrad. Stab.*, Vol. 18, pp. 237-245.
- Klemchuk, P. P. and Horng, P. L. (1984), "Perspectives on the Stabilization of Hydrocarbon Polymers Against Thermo-Oxidative Degradation," *Polym. Degrad. Stab.*, Vol. 7, pp. 131-151.
- Klemchuk, P. P. and Gande, M. (1989), "Stabilization Mechanisms of Hindered Amines," *Makromol. Chem., Macromol. Symp.*, Vol. 28, pp. 117-144.
- Kulich, D. M. and Shelton, J. R. (1991), "Organosulfur Antioxidants: Mechanics of Action," *Polym. Degrad. Stab.*, Vol. 33, pp. 397-410.
- Mair, H. J. (1967), "Polyathylen al Werkstoff zum Isolieren von Hochspannungskabeln," *Kunststoffe*, Vol. 57, p. 930.
- Muller, H. (1990), "Metal Deactivators," *Plastics Additives*, 3rd ed., Oxford University Press, New York, Chapter 2.
- Mueller, H. and Schwarzenbach, K. (1982), U.S. Patent No. 4,360,617.
- Pauquet, J. R., Todesco, R. V. and Drake, W. O. (1993), "Limitations and Applications of Oxidative Induction Time (OIT) to Quality Control of Polyolefins," *Proc. 42nd Int. Wire & cable Symp.*, IWCS, Eatontown, NJ, pp. 77-85.
- Pobedimskii, D. G., Mukmeneva, N. A. and Kirpinchnikov, P.A. (1980), "Organophosphorus Stabilizers: Efficiency and Mechanisms of Action," *Dev. Polym. Stab.*, Vol. 20, pp. 125-184.
- Pospisil, J. (1973), "Transformations of Phenolic Antioxidants During the Inhibited Oxidation of Polymers," *J. Pure Appl. Chem.*, Vol. 36, pp. 207-232.
- Pospisil, J. (1988), "Mechanistic Action of Phenolic Antioxidants in Polymers – A Review," *Polym. Degrad. Stab.*, Vol. 20, pp. 181-202.
- Pospisil, J. (1991), "The Key Role of Antioxidant Transformation Products in the Stabilization Mechanisms – A Critical Analysis," *Polym. Degrad. Stab.*, Vol. 34, pp. 85-109.

Schmidt, R. K., Young, C. and Hewitt, J. (1984), "Long Term Field Performance of Geomembranes – Fifteen Years' Experience," *Proc. Int. Conf. Geomembranes*, Ind. Fabr. Assoc Inc., St. Paul, MN, Vol. 2, pp. 60-65.

Schwetlick, K., Pionteck, J., Konig, T and Habicher, W. D. (1987), "Organophosphorus Antioxidants-VIII. Kinetics and Mechanism of the Reaction of Organic Phosphites with Peroxyl Radicals," *Eur. Polym. J.*, Vol. 23, No. 5, pp. 383-388.

Scott, G. (1993), Atmos. Oxid. Antiox., Elsevier Publ. Co., Amsterdam.

Suits, L. D. (1994), "Geotextiles," Encycl. Chem. Technol., 4th Ed., Vol. 12, Wiley-Interscience, New York, 503-511.

Todesco, R. V. (1992), "Recent Advances in Stabilization of Polyethylene: Co-Additives," *Proc. SP '92 Polyethylene World Congress*, Zurich.

Walldner, V. T., Clarke, W. J., Decoste, J. B. and Howard, J. B. (1950), "Weathering Studies on Polyethylene: Wire and Cable Applications," *Ind. Eng. Chem.*, Vol. 42, pp. 2320.

Wigotsky, V. (1994), "Polyolefins: Chemical Reawakenings," *Plast. Eng.*, Vol. 50, No. 7, pp. 14-17.

Zinke, H., Lorinz, H. J. and Linhart, H. (1980), U.S. Patent No. 4,187,212.

OVERVIEW OF GEOMEMBRANE MANUFACTURING METHODS

Fred Struve
Houston, TX

ABSTRACT

This paper describes the current manufacturing methods and equipment used for the most commonly installed geomembranes. They are the polyolefins, mainly high density polyethylene (HDPE), linear low density polyethylene (LLDPE), but also flexible polypropylene (fPP). The most significant differences between competing manufacturing methods are also presented.

1.0 POLYMER INTRODUCTION

Geomembranes, used for pollution control, water conservation, aquaculture, heap leach mining, etc., are a necessary and vital part of human endeavors to progress, conserve valuable resources and yet protect the environment.

While there are several methods used to manufacture geomembranes there are also certain applications which require very specific properties. For instance handling fluids at high temperature, or having resistance to particular chemically aggressive substances are common situations. However, the vast majority of applications are excellently served by the family of polyolefin based thermoplastic resins and copolymers.

The polyethylene resin family is made up, generally, of “commodity” resins with remarkably good resistance to an enormous range of common chemicals. The specific resins commonly used for geomembrane manufacture are selected with the major goal of optimizing longevity, chemical resistance; mechanical properties; environmental stress crack resistance; processability; availability; and price. The final selection is, understandably a compromise.

A few very general observations about the polyethylene polyolefin polymers are:

1. Higher density, improves chemical resistance, but reduces stress crack resistance.
2. Polyethylene copolymers of either hexene or butene are currently most commonly used.
3. Lower density improves flexibility and ability to deform when subjected to the deformation that subgrade settlement requires (for instance when used to cap landfills)
4. Relatively broad-molecular-weight distribution imparts improved melt strength which is important for product made from the circular die (aka blown-film) processes. The flat die extrusion processes is not as sensitive to the molecular weight distribution properties of polymers.
5. Relative ranking of prices of common copolymers are; butene-lowest, then hexene, and then octene.
6. The newer single-site-catalyst product costs and properties are not addressed in this document.

2.0 MANUFACTURING INTRODUCTION

Two manufacturing methods are in use for producing the wide width (typically 7.5 to 8.5 m wide), thick (typically 0.75 to 2.50mm thick) geomembranes in common usage

They are produced by extruding molten polymer through either circular dies or flat dies. The terms “round” for circular and “flat” will be used consistently throughout the balance of this paper.

Both methods have virtually identical requirements for “generic” items like:

- Raw material delivery, storage and handling equipment.
- Electricity and other utilities
- Extrusion equipment.
- Cooling capacity and heat exchangers.
- Material handling equipment ahead of the winder.
- Winding and finished roll handling equipment.
- Finished product storage and shipping facilities.

However they differ significantly in how the molten polymer, delivered by the extruder(s) is converted into a continuous web, and cooled, before ending up at the winder, to be wound into rolls, and stored/shipped.

The term “web” will be used consistently throughout the balance of this document instead of terms like geomembrane, sheet or flexible membrane liner.

Viewing typical facilities of both methods one would observe that:

3.0 DIE FLAT MANUFACTURING FACILITY

The flat production facility would have a typical industrial height building and a fairly long almost horizontal web path between the die area and the winder equipment (some 20 m). Such a facility is shown in the photographs of Figure 1.



(a) Control panel used in manufacturing



(b) Example of a large (8.0 in.) diameter extruder

Figure 1. Photographs of flat die web manufacturing.



(c) Sheet existing the counter rotating rollers

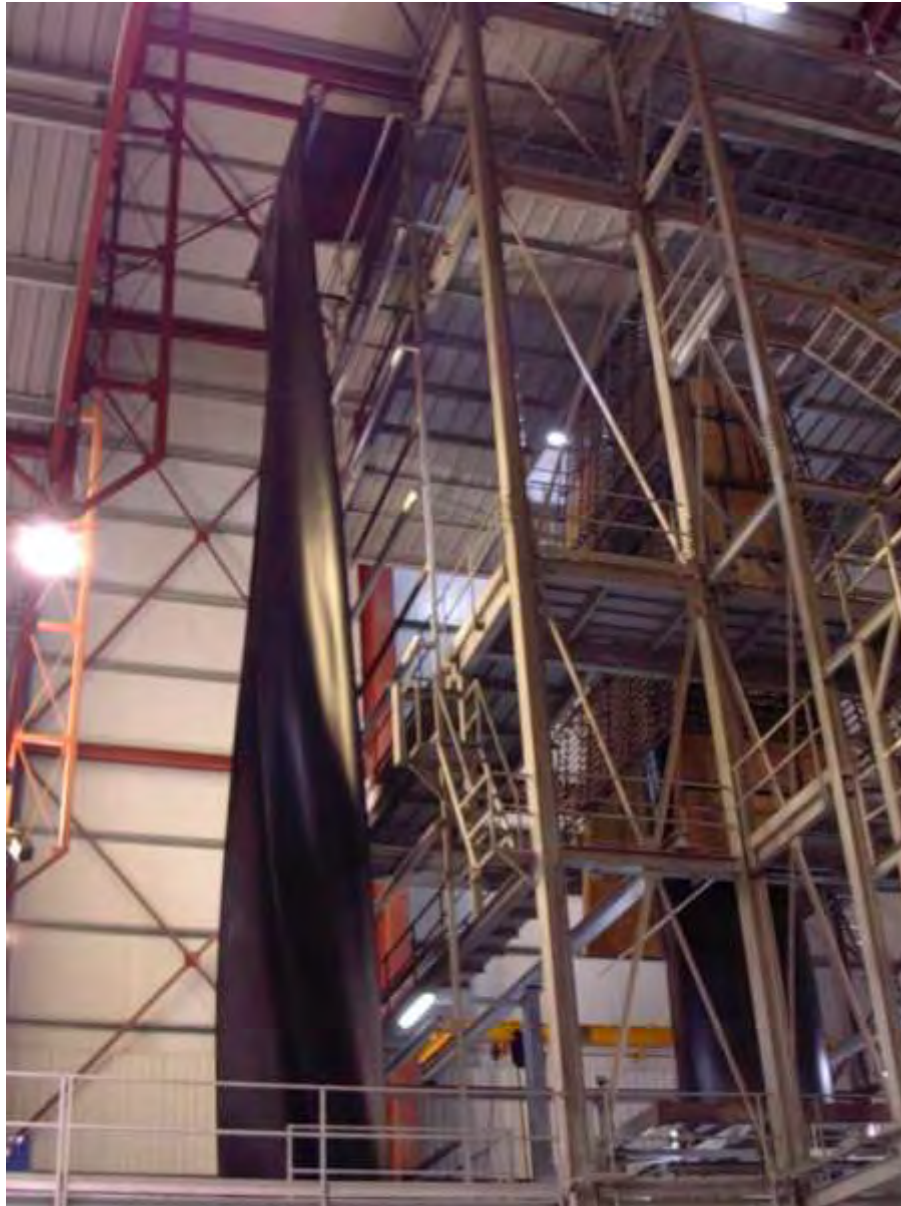


(d) winder is part of a flat die production facility although it could just as well be used for round die production.

Figure 1 (cont.). Photographs of flat die web manufacturing.

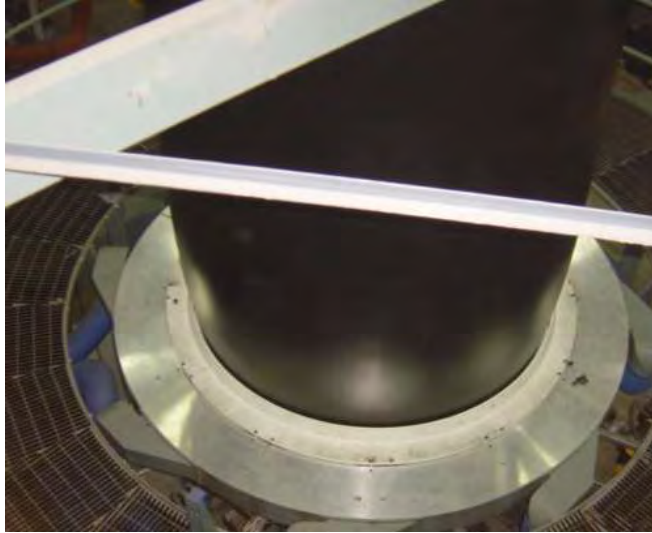
4.0 ROUND DIE MANUFACTURING FACILITY

The round production facility would have a smaller footprint than the flat facility, but have a tower some 25m high directly over the die area. The web from a round die starts as a tube which is drawn up vertically into the high tower and then on its way down the tower it is slit and handled as web of width equal to the circumference of the originally extruded tube. This means that a round facility requires a “custom” high tower bay. Such a facility is shown in the photographs of Figure 2.



(a) Tower used in production

Figure 2. Photographs of round die web manufacturing.



(b) Sheet exiting the round die moving upward

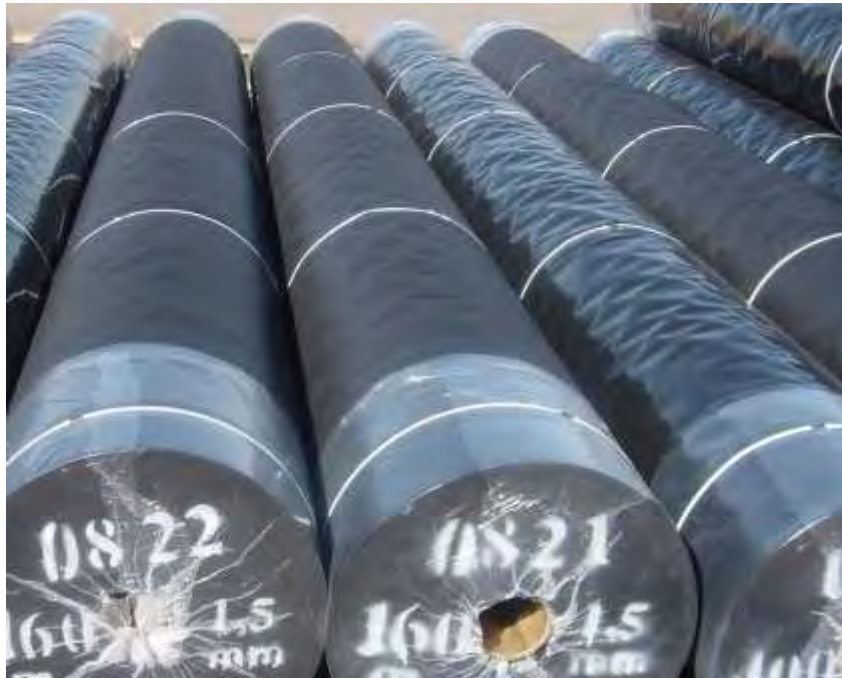


(c) Cylinder coming down from tower

Figure 2 (cont.). Photographs of round die web manufacturing.



(d) Cut cylinder entering accumulator



(e) Rolls, ready for shipment, from either method

Figure 2 (cont.). Photographs of round die web manufacturing.

5.0 SPECIFIC FEATURES OF, AND DIFFERENCES BETWEEN, FLAT AND ROUND WEB PRODUCTION

This section addresses the design, features and detail differences between flat and round dies, as well as web handling and cooling directly after the polymer exits the die. This is the “heart” of the differences between the two methods.

The intention is to introduce only sufficient information to make sense of the limitations (advantages and disadvantages) of both technologies and to assist end-users when evaluating how well their end-product requirements would be met by one or the other. It is also to assist manufacturers in the process of selecting production equipment to meet their projected market requirements.

5.1 *Polymer Exit from the Die*

Flat: The molten polymer exits horizontally from a straight slit in a die.

Round: The polymer exits vertically upward from a circular slit in a die.

5.2 *Polymer Internal Flow Path in the Die*

Flat: The polymer passage in a flat die has complex profile to ensure that the pressure drop from the central polymer entrance to the center of the slit (some 450mm) is the same as that to each edge of the slit (some 3,500mm)

Round: The polymer is fed into the die centrally and has symmetrical and equal distribution to the die exit.

Discussion: For “normal” production of smooth sheet from polymers with rheology close to the design parameters of the extrusion die this difference is of little or no consequence

5.3 *Multilayer Coextrusion Capability*

Flat: Feed Block Coextrusion: A comparatively “simple” multilayer die block ahead of the flat die entrance can layer polymer from different extruders which then passes through the die as a “sandwich”; see Figure 3.

Manifold die coextrusion: In this case two or more completely separate dies are bolted together so that each has its own entrance and flow path, and they are configured to come together near the exit slit.



Figure 3. Die configuration for a three layer flat die web.

Round: Coextrusion is accomplished by “nesting” two or more dies together coaxially. This is comparatively straight forward as they are all concentric and symmetrical. Here too the different flows come together near the exit slit; see Figure 4.

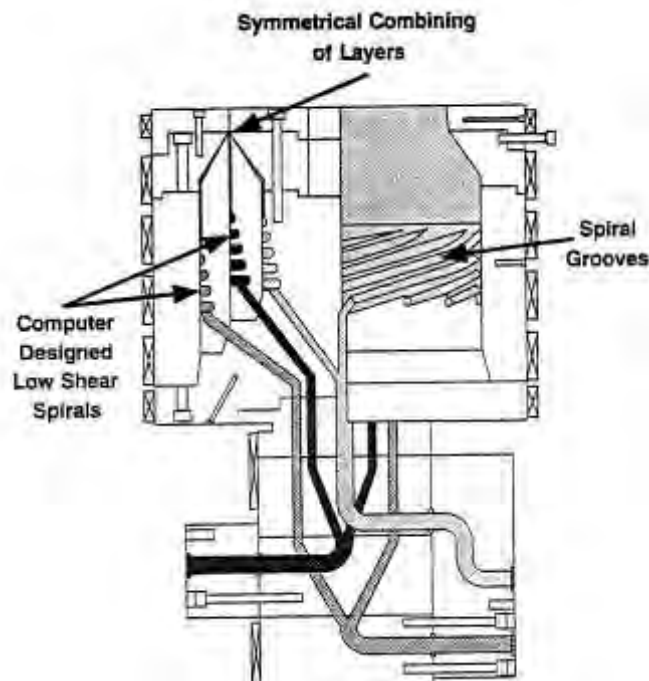


Figure 4. Die configuration for a three layer round die web.

Discussion: For die block coextrusion, if the rheologies (viscosity) of the polymers in the different layers are not closely matched, the three layers will not distribute evenly across the width. The less viscous material will flow more easily towards the edges and the more viscous polymer will seek the “easiest” way out along the shorter pathway towards the center of the exit slit, resulting in a variable “sandwich” across the width of the web.

Manifold die coextrusion would eliminate this problem, however manifold dies are extremely costly, and I am unaware of any having been made anywhere near the width of interest for geomembrane webs.

Round coextrusion dies are also more expensive than monolayer dies as they are literally multiple dies nested together concentrically, however the machining of such dies is readily achieved on normal (but large) vertical lathes and milling machines. Many of these coextrusion dies of the sizes of interest have been made.

5.4 Thickness Control

Flat: Excellent thickness control by either manually or automatically adjusting bolts, which deflect the lip if the exit slit of the die, can be achieved (+/- 1%, or better). Changes of web thickness from say 2mm to 1.5mm are achievable. However, it requires stopping the line and adjusting the internal “choker bar” to suit the new requirement, see Figure 5.



Figure 5. Typical “flex-lip” flat die detail.

Round: Deforming the exit slit of a round die in the same way as done on flat dies is not possible. Various indirect methods of controlling thickness are used (adjusting cooling air flow and/or velocity) are used, but with limited success on dies of the sizes of interest, and web thicknesses of interest. New, clean, round dies can readily be expected to produce webs within +/-5% of nominal thickness. Changes of thickness from say 2mm to 1mm can be done “on the fly” with no downtime and only a few meters of transition “scrap”.

Discussion: Webs made from round dies will almost certainly require more raw material per unit area, than those made from flat dies in order to maintain a given thickness specification. A single anomalous “low” area of very limited width (die line) results in increasing the thickness of the entire web to bring that one line above the minimum specification.

5.5 Webs with Enhanced Friction Properties (“Textured” Product)

To achieve improved friction along the sloping sides of landfills impoundments and canals, the rather extreme “slipperiness” of the surface of polyethylene webs must be “roughened” in some way. Methods in use are listed as follows:

5.5.1 Embossing the surface. This method physically creates a surface pattern of some sort, by forcing the web between a set of rigid metal rolls which have had the desired pattern engraved on their surfaces. The web typically has to be quite soft (at high temperature) for this process to be successful. If not hot “enough” undesirable and unacceptable stresses are impressed into the web. If “too hot” the desired sharp definition of the pattern is lost as the polyethylene exhibits a memory of sorts and the pattern will “shrink” back and loose its definition. This is an “in-line” process. In addition it is extremely difficult/impossible to emboss web less than 1.5mm thick, see Figure 6.

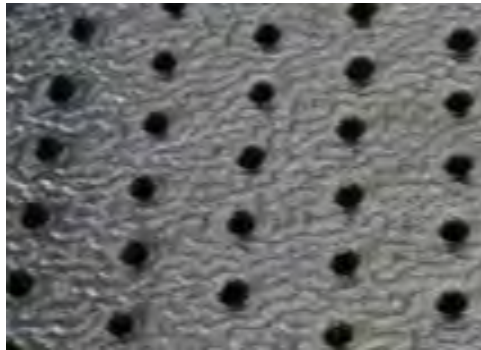


Figure 6. Embossed web surface.

5.5.2 Spray-on. This is an additional “out of line” process in which a roll of smooth surfaced web is unwound and passed under a series of nozzles which spray droplets of very hot molten polymer onto the web. Being a secondary process, this is costly. It is also slow and “messy”. Providing droplets with sufficient heat content to melt into and bond with the web, as well as retain some desirable sharpness for enhanced friction is problematic, see Figure 7.

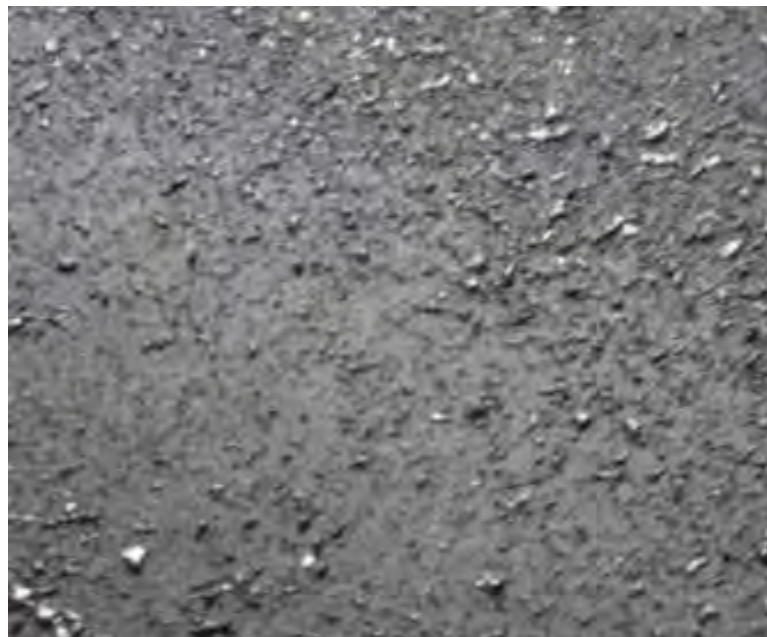


Figure 7. Spray-on web surface.

5.5.3 Injection of non polluting gas (typically nitrogen) into the surface layer(s) of a three layer coextruded web. On exiting the die, the gas expands. The polymer is too soft to allow bubbles to form and remain as discrete bubbles (as in foamed “clam shell” fast food take-out containers), instead the bubbles burst and smear on/in the surface layer(s) creating a distressed rough surface with enhanced friction properties. Gas injection into the melt for this process must be controlled accurately. Too much gas results in larger bubbles forming and intruding into the center (core) layer resulting ultimately in “pin holes” through the web, see Figure 8.



Figure 8. Injection-of-gas web surface.

5.5.4 Foaming and or nucleating agents in the surface layers of a web. These have been tried and found to make controllable “good looking” textured surfaces. This approach is unusable for two reasons: Firstly, all the added chemicals are not 100% activated so that when subsequently welding webs together, which requires heating of the surfaces in some manner, further activation occurs and results in defective welds; Secondly, in hazardous waste landfills, leachate is very carefully analyzed and the presence of “stray” chemicals can result in such a facility being shut down. As a result, there is no photograph of this type of surface pattern.

Flat: As previously noted, manifold dies have not been considered “reasonable” for the subject web widths and thicknesses. Further the widely differing path lengths from die entrance to slit exit in these dies results in different “bubble” formation from gas injection, resulting in a totally unsatisfactory overall web surface. To date gas injection is a non-starter.

Spray coating the smooth sheet is one option used by some.

Embossing is also used by some. The embossing rolls required are costly and will be discussed later in the section on web cooling and handling.

Round: The inherent symmetry of these dies is ideal for even distribution and control of multilayer structures. The vast majority of textured product is manufactured by round multilayer gas injection lines.

Commentary: The height of the friction enhancing protrusions above the base web (asperities) is specified, and checked, as an index test, during manufacturing. This “asperity height” specification is being raised and methods other than gas injection, are finding it increasingly difficult to meet the newer specifications.

5.6 Cooling the Web After it Exits the Die and Production Rate

Flat: When producing a smooth web, the molten polymer exiting the die slit is in close proximity to the nip of a set of cooling rolls, and the web is essentially deposited onto the lower roll. (Hence there is no need for high melt strength polymers). The thickness of the web is determined by the die. The web is just “kissed” (or “polished” in production terminology) in the nip of the two rolls. Undue pressure on the web at this stage results in differences in orientation and undesirable stress patterns frozen into the web. The web wraps around the middle roll and then around the top roll. These rolls are internally cooled and impressive examples of engineering design (and cost!), balancing strength (to minimize sagging over their considerable span) and maintaining an even temperature across the full width as well as good heat transfer performance (as this is where/how the web is cooled).

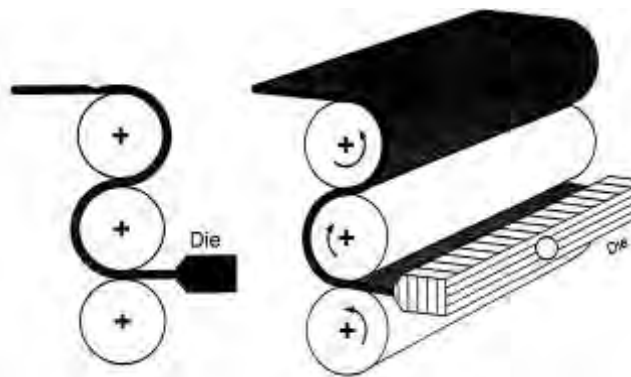


Figure 9. Manner of the web exiting the die.

Considering the span and mass of these rolls sagging/bending over their unsupported width is unavoidable. To compensate for this such rolls are sometimes “crowned”. However, irrespective of any and all schemes to cope with this issue it cannot be eliminated. This is the reason that there is a definite limit to how close to each other the rolls can be run (for thinner web production). A 1.0 mm web thickness is below or at the limit, and setting the roll clearances at this limit is, in fact, very risky, for if the rolls touch each other their plated and finely ground surfaces are marred, requiring difficult removal, re-machining, and re-plating.

To make a textured web by the embossing method requires at least the lower and middle rolls to have the required pattern engraved in them. Also changing from smooth to embossed production requires removal of one set of rolls and installation of the other; or separate dedicated production lines. The temperature control of the rolls is no trivial matter in all cases, but in the case of embossed web production, the production rate has to be decreased to achieve satisfactory product.

Round: As the web (in tubular form) is drawn vertically away from the die slit it is cooled by chilled air being blown against it from highly sophisticated and accurately machined air rings, both externally and internally. It is here that it becomes clear that broader molecular weight distribution polymers are necessary for the, as yet, “unfrozen” web to be strong enough to accept the machine direction pulling (tension) force as well as the impact of the cooling air.

Discussion: Since the web from a flat die is “dropped” onto the cooling surface, which cools the web by conduction (much more efficient than impingement and convection by air cooling), it is possible to operate extruders at higher temperature and high throughput rates, almost without regard to the lack of physical integrity of the “as extruded” web. Truly stellar production rates (~2,800 kg/hr) have been achieved on flat die extrusion lines.....Provided (there is always a caveat) the web is in the thickness range of 1.5mm to 2.0mm and smooth (not textured). Hypothetically if one had a huge and consistent need for product in this range, a flat die line would serve very well.

The most modern round die lines top out at rates of approximately 1,800kg/hr. They are very versatile with the ability to change thickness from less than 1mm to 2.5mm “on the fly” and to change to/from smooth to textured production “on the fly” also with very little transition scrap. Clearly they are best able to respond quickly to multiple differing customer needs.

5.7 Drawdown, Orientation and Dimensional Stability

Polymer exiting the die slit of both flat and round dies is thicker than the final web thickness. This is the result of shrinkage due to the phase change from the molten to the solid state, as well as shrinkage due to the coefficient of thermal expansion/contraction and reduction of temperature as the web cools from extrusion temperature to room temperature.

Further than the temperature effects, mechanical effects are in play. The web is drawn away from the die at a higher speed than that at which it exits the die....reducing its thickness and orienting it in the machine direction (MD) in both cases, see Figure 10.

Flat: As the web cools it is not restrained in any way (other than some minimal friction between it and the rolls) in the cross machine direction (XMD). Operators of flat die lines must control the line speed versus the die exit speed (extrusion rate) differential very carefully to avoid imparting an excessive amount of MD orientation to the web. This manifests itself later in the field when there is a tendency for the web to shrink in the MD when in the hot sun or when being welded. There are specifications and quality control tests to check the dimensional stability property of product.

Round: In addition to the MD drawdown, the extruded web-tube is inflated slightly by pressurized air to a diameter slightly larger than the actual die slit diameter which draws the web down in the XMD as well. (The ratio of the two diameters is known as the “Blow-up Ratio” or BUR). Webs made on round die lines generally exhibit evenly balanced MD and XMD orientation, comfortably within dimensional stability specification.

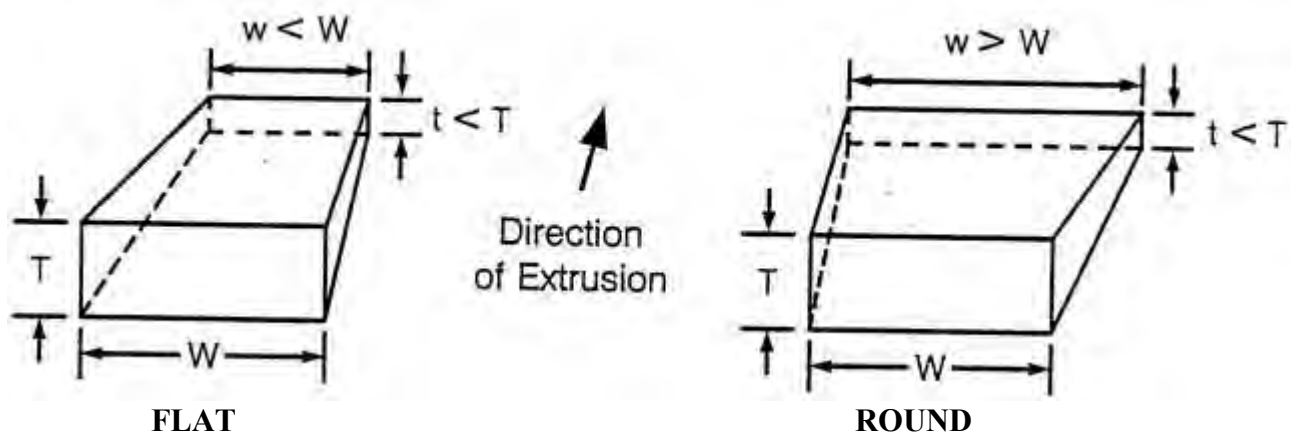


Figure 10. Depiction of the differences in web orientation flat vs. round.

6.0 SUMMARY AND CONCLUSIONS

The manufacturing methods described in this overview are, in principle, those that were in use in the general plastics industry 25 years ago. However their use to produce geomembranes was not common then. Stretching the time line from the 25 year central theme of this retrospective conference to 30/35 years, the following four developments highlight arguably the four most significant developments in the unique geomembrane-branch of the plastics manufacturing industry.

1. In the late 1970's Gundle Plastics, in South Africa demonstrated to the world that it was possible to make wide sheet up to 2.5mm thick from a large diameter round die. Before then, 0.5mm was generally considered the upper limit. This has become the most widely used manufacturing method.
2. During the 1980's bold geomembrane companies pushed machinery manufacturers of flat die equipment to make equipment that could produce the uncommonly wide thick sheet, suitable for geomembranes.
3. In the late 1980's the very important issue of Environmental Stress Cracking of geomembranes came under intense scrutiny driven by the EPA and GRI. The response, and developments made by the polymer industry, to improve this property were (and still are ongoing) extremely significant.
4. The development of geomembranes with enhanced surface friction characteristics, in the 1980's, and their subsequent acceptance by the design engineering community, was (is) also a significant event in the industry.
5. The innovative development of providing a smooth edge on textured sheet which greatly assisted the improvement of field welding quality.

Geomembrane manufacturers continue to develop new and better ways to make their products, many of them proprietary, but advancements to the basic "old" ways are continuously being made.

OPPORTUNITIES AND SOLUTIONS, DEVELOPMENT AND GROWTH OF THE GEOMEMBRANE INDUSTRY

Gary Kolbasuk
Raven Industries, Sioux Falls, SD, USA

ABSTRACT

Polymeric or synthetic hydraulic barriers (geomembranes) have been used in civil engineering applications for over 50 years. Spurred on first by the need to contain water for agricultural and potable water use and then by the need to protect water from pollutants, geomembranes went through an initially slow developmental and acceptance process. As environmental pollution pressures grew, interest and research in geomembranes as a solution accelerated. Eventually, action by regulatory agencies such as the US EPA, brought about rapid growth in geomembrane use and technology. This paper provides a short overview of this history.

INTRODUCTION

A relatively short paper such as this cannot do justice to the history of geomembrane development and use. As with geotextiles and some other geo-materials, there is enough information to write a book. What this paper attempts to do is to give the reader a flavor of what the industry was, how it grew and what it has become today. All materials and activities are not exhaustively covered. The focus is on the major products and activities in the industry.

Because of my background, this paper has a slightly different perspective than the other papers in this symposium in that I have spent most of my career working for manufacturers of geosynthetics and have never worked in academia. Wearing a manufacturing hat, I'm sure, has colored my view of the world and causes my priorities to be a little different than those of a professor, a regulator or a practicing engineer. Based on that perspective, this paper touches on not only the technical developments of geomembranes, but also the business climate, moods of the industry and some of the monetary motivations that caused the industry to change and grow. Also, while I have spent time working in the international market, the bulk of my experience is in the North American market and the information here reflects that bias.

Geomembranes came into use as a result of a growing world population putting increasing demands on our ever more precious water resources. Man's activities were polluting those resources at an alarming rate. Natural materials such as compacted clay and manmade inorganic materials such as concrete did not perform well enough and / or were too expensive to use in some applications.

ASTM's definition of a geomembrane is an essentially impermeable geosynthetic composed of one or more synthetic sheets. That bland description, while accurate, does not convey a picture of what a geomembrane is and does. In its simplest form, a geomembrane is a synthetic hydraulic barrier used to contain water and/or pollutants, keep water and/or pollutants out of a clean environment, act as a gas barrier or be a physical barrier in an aquatic environment.

Geomembranes have had a profound impact on the quality of life in developed countries and is improving the quality of life in developing countries. Society depends on geomembranes to contain hazardous waste byproducts in landfill, to control odors from industrial processing ponds, to collect gas generated in landfills, to preserve and convey potable water, to grow food in aquaculture applications, to waterproof dam faces, to control effluents in sewage treatment plants and to provide enjoyment from applications such as golf course ponds, decorative fish ponds and even the magic fountains at the Bellagio in Las Vegas.

PERIODS OR PHASES OF GEOMEMBRANE MARKET GROWTH

Cutting up the history of geomembranes into periods is somewhat artificial in that there are no real boundaries. The periods and dates I have selected are useful only in trying to organize a picture of the market and technology developments. Others, I'm sure, would divide up the history differently. But I think this is a useful exercise in setting the stage for the rest of the paper and organizing the information.

Phase I. Experimenting and Learning

The first phase of geomembrane history starts in the early 1950's as scientists and engineers started to explore the potential use of synthetic materials in civil engineering and agricultural applications. The research was basic in nature, finding out what these materials could do, how they could be used and how well they held up. Publications of this research made information available to a wider audience and supported acceptance and slow growth.

With some large chemical companies promoting the use of their materials and smaller fabricators, distributors and construction companies looking to make some money in a new field, a number of materials found progressive acceptance until in the late 1960's liner use became widespread. The growth in use, and lack of structure in the industry, brought about the need for standardization and specifications which opens the second period of geomembrane growth.

Phase II. Recognition and Growth

The second phase begins around 1970, plus or minus a couple years. Recognition began in the form of several standards being written for lining materials including three ASTM specifications, one each for polyvinyl chloride (PVC), polyethylene (PE) and butyl sheeting for pond, canal and reservoir lining. These standards were both material specifications as well as test procedures for some of the tests.

As the recognition phase continues, these materials began to find their way into environmental applications. State and federal regulations began to require flexible membrane liners (FML's) fueling an increase in liner use. Many new manufacturers and installers entered the market.

This period draws to a close as the geomembrane manufacturers, users and regulators gathered under the umbrella of the National Sanitation Foundation to provide a much needed consensus specification for a broad range of liners, bringing legitimacy to the industry, paving the way for the next phase of growth.

Phase III. Geo-Era, Technology and Prosperity

Of any of the dates for the beginning and ending of a phase of geomembrane history, for me, 1983 is the most solid. This is the start of the Geo-Era. 1983 is the year that Joe Fluet coined the term geosynthetics from which the rest of the geo-terms were created. Standard specifications and test methods were being written, technical publications were being born, industrial organizations being formed.

This phase was the most active of any stage, with the fastest growth in not only market size, but in new product development, testing technology, raw material technology and education. It was a fast paced fun time that slowly ended as the industry matured.

Phase IV. Mature Phase

This phase sort of sneaks up on the industry. It does not happen in a single year but is the slow maturing of the industry. Little business becomes big business. Small business, wild, shoot from the hip entrepreneurs that thrive in fast growing markets are replaced by more formal big business professionals (not always a different person, but certainly a major change in demeanor and focus). Broad scope, intensive research and learning is replaced by more limited focused areas of research and refinement of information. Innovation and high margins are replaced by commodity pricing and cost cutting. Custom job specifications are replaced with standard specifications (well, maybe someday). The excitement and enthusiasm of double-digit growth is replaced with running a day-to-day business with low single digit growth at best.

This does not mean that working in geomembranes is boring or that there is nothing left to learn or no new innovations to be made. Geomembranes are a very important product and the market place has enough stimulus to maintain interest. New products are being developed, but things are happening at a slower pace than before. The market place is not driving rapid change. For those who have been in the industry for 20 years, 30 years or more, some look back, sigh, and reflect on just how much fun they had back then and, by comparison, how life is now a little less exciting. Of course, I'm sure the changes in accepted business entertainment practices had nothing to do with that.

THE LIFE HISTORY OF SYNTHETIC GEOMEMBRANES

Trying to decide on how to organize the body of this paper caused me considerable consternation. There is an individual history to each of the materials as well as many other segments of industry history. There is enough information to write a long paper on each of the lining materials themselves. Rather than address each of their histories individually from start to end, I cover them in segments using the above four phases.

My apologies to the many people that have made extensive contributions to the geomembrane industry that I have neglected to mention in this paper. Since this is a paper and not a book, I have intentionally limited the details in order to provide an overview of the history of geomembranes.

PHASE I. EXPERIMENTING AND LEARNING

The early history of geomembranes no doubt has many starts in different places, but the best known is the early work of Mike Hickey at the Bureau of Reclamation and Dr. C. W. Lauritzen at Utah State University. Motivated by preserving valuable water resources in the western United States, they experimented with natural materials, concrete, flexible PVC, polyethylene, rubber sheeting, asphaltic products and other waterproofing sealants. Without the addition of a synthetic hydraulic barrier, many canals, ponds and reservoirs lost up to 50% of their water through seepage to the groundwater. This water was not necessarily lost from use, but was not available where needed and additional expense was needed to drill wells and recover the water.

Their experimentation resulted in a number of publications in the 1950's and 1960's that started the education process and began to make potential users aware of an alternative to natural materials and concrete. Some of the early titles of papers by Lauritzen et. al. are "Butyl Fabrics as Canal Lining Materials" (1953), "Ways to Control Losses from Seepage" (1955), "Plastic Film for Controlling Seepage Losses in Farm Reservoirs" (1956) and "Linings for Irrigation Canals" (1963). Some early papers by Hickey include "Evaluation of Plastic Films as Canal Lining Materials" (1957), "Report on Installation of Experimental Plastic Membrane Canal Lining Material" (1957) and "Plastic Film Cut Off and Canal Lining" (1959). The focus is clearly on water preservation and a basic understanding of how polymeric films and sheets could be used.

As this period progressed, on the business side of the equation, far away from the research, early manufacturing of plastic geomembranes was done or encouraged by large chemical companies that saw an opportunity to sell pounds. They were creating products and looking for a market for them. A chemical company or a manufacturer converting the raw materials into a liner sold to local distributors who they trained in solvent welding or taping who in turn trained the contractors. The distributors sold a variety of products and would sell whatever they could to whoever was willing to buy.

There was probably less concern than there should have been about whether the products were appropriate for some of the applications where they were used. Installers in the field typically were unaware of technical aspects of the products they were installing and just went out and "winged it" (in the words of an early installer). Installations were done on rocky subgrades and other horrible situations without giving it much thought. Stone backfill was frequently placed on the liners without cushion fabrics to prevent puncture. Many failures paved the way for the CQA companies that sprung up later. Engineering firms were involved, specifying materials, but much of the information they had to work with is what was supplied to them by the distributor representatives.

PVC

I do not know which material was used first for hydraulic containment so I will start with flexible PVC film and sheet since it grew to represent a large portion of the early geomembrane market. PVC is normally a rigid material, but when plasticizers are compounded into it, it becomes flexible and has improved low temperature properties. Flexible PVC's use in the

United States started in the 1930's and its first hydraulic containment application was swimming pools. In 1952, Union Carbide Corporation looked at the hydraulic containment market as a place with the potential to move some serious pounds of plastic.

The early PVC geomembranes had several attributes that made them very desirable and is what helped their use grow over other materials. They were very flexible which let them conform to irregular surfaces easily. They had a fairly low modulus, which let them stretch to conform to point stresses such as gravel. They had good puncture resistance and relatively good tear resistance for an unreinforced material. PVC sheet was easily fabricated into large sheets using chemical or heat welding. Also, important as its physical properties, PVC films and sheets were easily joined in the field with chemical methods such as solvent bonding or bodied solvent bonding.

As with all the materials, there were many failures that made learning possible. Animal activity, human activity and mother-nature in acts as violence such as debris carrying gulley washers down PVC lined canals challenged the liners. The early PVC films used by the Bureau of Reclamation were 0.2 mm (8 mils) thick. As the need for durability during installation and use became apparent, the thickness of the PVC liners continued to increase until 0.5 mm (20 mil) PVC was standard for more demanding applications and 0.75 mm (30 mil) was available for those wanting to be sure they were using a liner that would stand up to abuse.

Even though the market was growing, it was not growing fast enough to hold Union Carbide's interest and in 1962 they got out of the fabrication business. Charlie Staff, who had been working at Union Carbide on the PVC market, left the company and founded a company with his brother Ed that would eventually become Staff Industries. The Staff brothers were successful in their endeavor and helped shape the early PVC geomembrane manufacturing market.

Toward the end of the "experimenting and learning" phase, attention began shifting from pond, canal and reservoir linings to pollution concerns. Preventing pollution of ground water from brine ponds and other chemical storage ponds were becoming more of a concern. PVC was used to line new ponds, retrofitted into existing but cracked concrete storage facilities and being used in floating cover applications to protect potable water from bird droppings and other airborne contamination.

Polyethylene

In the 50's and 60's, polyethylene found limited use in hydraulic applications in the United States, primarily pond and canal linings. The polymer used in that period was conventional, high pressure, low density polyethylene (LDPE), suitable because of its flexibility. LDPE, not to be confused with linear low density polyethylene (LLDPE), has poor tear strength and did not fare well.

High density polyethylene (HDPE) geomembrane production and use originated in Germany in the late 1960's with Schlegel. Early high density polyethylene geomembranes consisted of narrow sheets of polyethylene laid down end to end on a hot roll, the roll indexing and then another layer being laid down on the hot roll, slightly overlapping the first sheet. In this way, a

long, wide sheet with cross direction fused overlaps was created. This type of geomembrane was successfully used, and continued to be used into this century. Since the sheet had irregular thickness due to the overlaps, an in between the sheets extrusion welding process was developed to join sheets of material on site.

Chlorosulfonated Polyethylene

Chlorosulfonated polyethylene (CSPE) was manufactured by DuPont and sold under the trade name of Hypalon. CSPE began being used in the mid-1960s in both unreinforced and reinforced forms. Reinforcement was typically a polyester scrim.

Black CSPE liners had an advantage over PVC in that CSPE had good UV resistance and was suitable for exposed applications. The reinforcement aided the material in holding up in high stress applications such as steep slopes and floating covers. CSPE saw limited use in this period but became a dominant lining material later.

Asphaltic Materials

Asphaltic or bituminous liners fall under the geosynthetic classification since they contain a synthetic reinforcement layer and many contain a polymeric film. Modern bituminous geomembranes look much more like geomembranes than did the first products in the market.

One of the very first synthetic liquid containment lining systems was an asphaltic product made by Gulf State Asphalt. They took the cutout tabs from making asphalt shingles, ran them through an extruder, reinforced them with fiber and made 4' by 12' planks. They were welded on site with hot asphalt. The finished liner was then frequently painted with a silver paint. The City of Phoenix used the product to line the inside of concrete water tanks.

W. R. Meadows, started in the 1950's. Meadow Mat was an 1/8" thick asphalt core board with a plastic 8 mil PVC film suspended between two layers of felt that had a weather coating on top of it. It was a seven element construction for pond linings and canals which sold until mid 70s. It was sold as 4' wide pieces 8' to 50' long. Joining was also with hot asphalt on overlapped pieces or they were butted against each other and gusset strips 6 to 8" wide covered the joints and were then hot moped in place.

These liners found use in military applications, potable water storage and brine storage ponds in the Houston chemicals industry. Because of the weight, it was expensive to ship, handle and install. But it was the only game in town until the more traditional geomembranes came along.

PHASE II. RECOGNITION AND GROWTH

Recognition and appreciation for the performance of flexible membrane liners is what spurred the growth during this period. Growth means business opportunities and more people and companies jumping on the wagon. Proliferation also means more choices as companies attempted to differentiate themselves based on product properties and / or cost. Those

attempting to use these materials felt the need for some organization and set about to write the first consensus standards for the products and their installation.

The American Society of Agricultural Engineers, after a number of years of work, wrote a specification on installation (AP340.1). In 1972 the American Society for Testing and Materials (ASTM) generated ASTM Standard D3083 for Flexible PVC Plastic Sheeting for Pond, Canal and Reservoir Lining; Standard D3020 for polyethylene and ethylene copolymer sheeting; and Standard D3254 for butyl rubber sheeting. These specifications provided an easy reference for the novice being introduced to these materials and helped add legitimacy to lining material use for water containment applications.

The Bureau of Reclamation was key in the development and acceptance of geomembranes. People like Bill Morrison and Ron Frobel continued the work of Lloyd Timblin at the Bureau and expanded the use in the western US for water containment.

But it was the United States Environmental Protections Agency (US EPA) that forced the technical growth of geomembranes that paved the way for the tremendous growth in the use of geomembranes in the third period of this history of geomembranes. Robert (Bob) Landreth was a significant force in the United States in this period and the next in providing not only Office of Research and Development (ORD) funding for a broad range of research projects, but also providing his leadership, ethics and insights across the many disciplines and interests that made up the industry.

Much of the increase in geomembrane use in the next phase came from environmental applications, fueled by the US EPA, which began supporting the use of geomembranes in the bottom of hazardous waste storage facilities. On July 6, 1982, the US EPA promulgated regulations that contained the following statement.

Prevention (via geomembranes), rather than minimization (via compacted clay liners), of leachate migration produces better environmental results in the case of landfills used to dispose of hazardous wastes. A liner that prevents rather than minimizes leachate migration provides added assurance that environmental contamination will not occur.

That statement highlights the recognition of value that geomembranes brought to environmental protection technology.

This activity was not limited to the United States nor was the United States working by itself. Klaus Stief was leading Germany along a similar direction that required the use of thick geomembranes in hazardous waste landfills. In fact, HDPE lining technology was developed in Germany and brought to the US.

Finally, I would be remiss if I failed to mention the mining industry in this paper. While mining does not hold the same interest for the public as pollution and the need for potable water, the use of geomembranes in mining applications certainly got the attention of mines, geomembrane manufacturers and engineers. Rising metal prices in the 1970's along with the abundance of low

grade ores, prompted the use of geomembranes in heap leach pads, solution ponds and evaporation ponds. And with the large size of many mining applications, mines came to represent a significant percentage of geomembrane use.

PVC

PVC's growth continued steadily during this period, being supported more and more by environmental needs. An example of PVC recognition by regulatory agencies is in 1977, prompted by an increase in drilling for oil in northern Michigan, the state of Michigan passed a requirement that reserve pits for the drilling mud be lined with 0.5 mm (20 mil) PVC. This and other regulatory activities brought new companies into the market. PVC found itself as the solution to many other environmental problems such as capping landfills, closing unlined facilities and in ponds at wastewater treatment plants.

As the market grew and there became more competition, quality improvements were made. Companies like Watersaver, Palco, EPI and Staff fabricated and installed PVC liners along with Hypalon and other lining materials. They were responsible for promoting the materials, improving factory seaming processes and improving overall product quality.

Even though PVC was not viewed as UV resistant or very chemical resistant, in most applications PVC performed very well and was relatively inexpensive. Toward the end of this period, PVC was king and life was good for those in the PVC liner business. By 1983, PVC had almost 50% of the geomembrane market (percent of area installed).

Polyethylene

As mentioned earlier, thick polyethylene geomembrane technology started in Germany with Schlegel. Heiner Hammer was a driving force responsible for many of the developments at Schlegel. With their new technology they tackled lining the Garling industrial waste site. From the experience at Garling, other landfills and ponds, Dr. Knipschild published the first product and installation specifications.

In South Africa around 1978, Clifford Gundle became aware of Schlegel, and was intrigued by the potential for large projects with polyethylene liners. Gundle was in the blown film and recycling business and was making construction and agricultural film up to 0.25 mm in thickness. Some of these were being used in what we would consider geomembrane applications, liners for irrigation ponds. They had been working with polyethylene since the 1960's, but not in geomembranes and they were interested in getting into the thicker liner market.

Gundle offered to supply Heiner Hammer (who was no longer with Schlegel) and his South African partner, to make a 1.5 mm HDPE liner for a large oil storage facility in South Africa. Gundle had an 1800 mm diameter die but had no idea how to make a 1.5 mm thick material. The HDPE they used at the time was a real HDPE with a density in the 0.960 range. To make it usable in geomembrane applications, they alloyed the HDPE with ethylene vinyl acetate (EVA). While they had a raw material with workable physical properties, they were not having any luck

making the heavy gauge material because the molten polymer was too weak to hold itself up during the extrusion process. Fred Struve came up with the idea of using an internal mandrel (cooling can) to hold the bubble up and stabilize the sheet. It worked and they were into the beginning of what I would consider to be main-stream polyethylene production.

Having made the sheet, the challenge of consistently making good welds was in front of them. Gundle was familiar with a variety of welding technologies but none worked as well as they would have liked. That is when Fred Struve invented his extrusion welder with the mixing tip that agitated the extrudate and surface of the sheet to make reliable welds. With that, they were in the business and ready to expand to the United States.

As a side note, today's standard width polyethylene geomembrane originated with that mandrel. They wanted to ship product by rail and two rolls 6.86 meter wide (22.5') would fit in a standard open top rail car. Once the mandrel was made, they had no options to make other sizes without making new mandrels. So they stuck with that size and brought it to the United States when they opened a plant in Houston.

Schlegel was first to enter the US HDPE geomembrane market. They started selling their liners out of a Houston facility in 1977 and started production there about 1979. Schlegel was the dominant player in the world thick (2.0 and 2.5 mm) HDPE liner market at the time.

Gundle started operations in the US in 1982, in part, because of the impending US regulations requiring the use of lining materials. They initially took the position of being a manufacturer only and relied on installation companies like Serrot to do the installations.

Schlegel and Gundle started the polyethylene geomembrane market in the United States and had the immense task of not only making and selling the materials, but educating the end users, installers and engineers on the material's properties and proper use. By comparison to even just a few years later, they were dealing with a very unsophisticated customer base, and were learning fast themselves

While Gundle and Schlegel started the HDPE geomembrane market, there were many other players that had a significant roll in shaping the market. Large chemical companies, the manufacturers of the resins used to make the liner, had a large economical and liability interest. They provided state of the art research facilities and technical assistance. Engineering firms provided innovative designs. Entrepreneurial installers developed installation techniques and made the roll goods into functioning facilities.

Chlorosulfonated Polyethylene

Hypalon, along with PVC dominated the geomembrane market during most of this period. When someone said liner, many people thought Hypalon. Manufactured in relatively narrow sheets, it was easy to fabricate into wide panels for easy field installation. Like PVC, it was flexible and easy to solvent weld. With the added benefit of long term UV stability, it took over the exposed geomembrane markets such as ponds, emergency containment liners and floating covers.

Hypalon was not without its weaknesses. It was not chemically resistant as some other so called specialty geomembranes of the time. It was more expensive than most other materials. It tended to cross-link or cure with time, making repairs increasingly difficult. There were occasional blistering problems, particularly in floating covers. Solvent welding became more difficult as the temperature dropped. With PVC's better pricing and HDPE's better chemical resistance, Hypalon began losing market share in 1981.

Bituminous

During the last period, bituminous (asphalt) geomembranes were thick, heavy chunks of material whose installation was very labor intensive. As the other polymeric geomembranes became proven, these slabs were replaced by lighter weight geotextile impregnated, modified asphalts. They continued to be a built up technology containing several functional layers. This product was more popular in Europe than the United States.

Chlorinated Polyethylene (CPE)

Chlorinated polyethylene (CPE) and CPE alloy liners were popular for a few years particularly in exposed applications. It was used in both reinforced and unreinforced forms. It tended to have good UV and chemical resistance along with reasonable flexibility. In 1980, approximately 12,000 square meters of CPE was used in the Mt. Elbert Forebay impoundment. That installation alone was about 10% of the entire North American geomembrane market that year. Being chemically in-between PVC and Hypalon, it found use as a transition strip between the two materials.

Ethylene Interpolymer Alloy (EIA)

The first ethylene interpolymer alloy geomembrane was developed in 1975 as a coated fabric by a company making plastic coated fabrics for a variety of non-civil engineering applications. The first installation of an EIA geomembrane took place in 1976. EIA was developed in response to the need for more a more petroleum resistant liner than the CPE products being used. This product, in several variations, has been successful in substantial niche markets from its introduction through today.

Other Polymeric Geomembranes

This period saw considerable experimentation with polymer types, thermoplastic and rubber compounds. Several were of significance for a period of time, but never became main stream. For that reason, they will not be discussed here.

PHASE III. GEO-ERA, TECHNOLOGY AND PROSPERITY

I picked 1983 for the start of the third period because of all the notable activity that year. 1983 saw a number of engineers who were becoming the leaders of the industry organizing technical information and industry interactions. This period is marked by the coming of age of

geomembranes and related products. NSF published Standard 54 on Flexible Membrane Liners. The International Geosynthetic Society (IGS) was formed in 1983. The Geotechnical Fabrics Report (GFR), the first industry publication, started to be printed. Joe Fluet coined the term Geosynthetics from which the rest of the geo-terms were formed. Sponsored by the US EPA, J.P. Giroud started giving courses on geosynthetics in the United States. The first conference on geomembranes was being organized for 1984. 1984 saw the birth of the Journal of Geotextiles and Geomembranes. Manufacturers of geomembranes were pushing education of users, regulators and engineers on how to specify and use their products. Geomembrane use was just starting a rapid growth in environmental applications. Construction quality assurance (CQA) also became an area of rapid growth as everyone grappled with quality problems, failures and how to prevent them.

Wow, what a year! Still, geomembrane use in North America was just a small fraction of what it would be just a few years later. Figure 1 shows the value in millions of dollars of geomembrane sales in North America. 1983 sales were only half of what they would be in 1984 and growth continued at a brisk pace for many years.

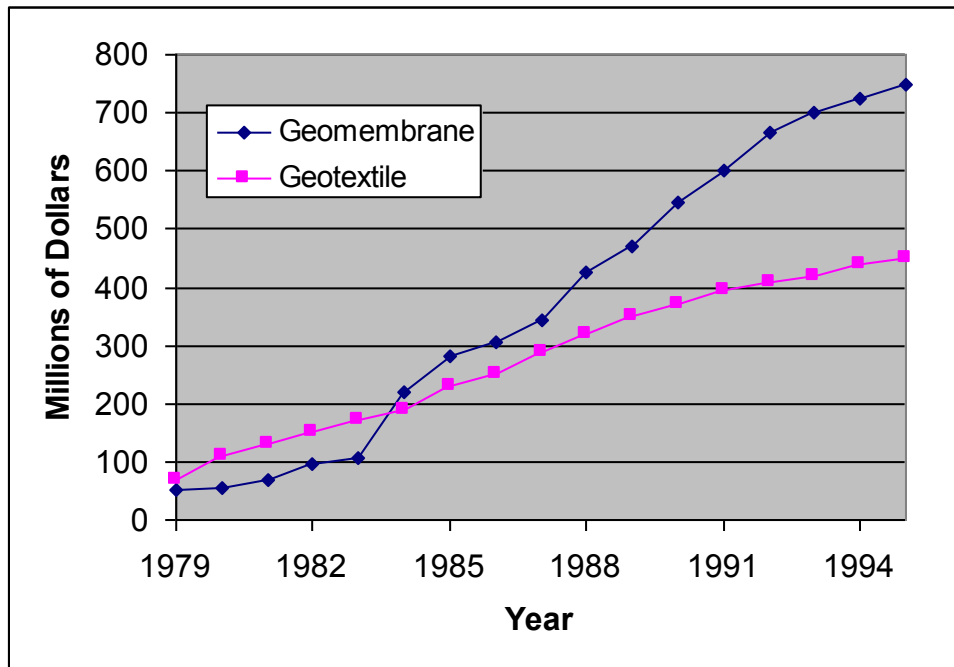


Figure 1. Estimated geosynthetic market in North America.

During 1983 and the following years, the engineering and construction world as a whole learned about and started using geomembranes in more applications than ever. The products, the specifications and many of the designs were still fundamental in nature and were changing as people learned more about geomembranes, how to use them and what their shortcomings were. In 1985, Dr. Robert Koerner formed the Geosynthetics Research Institute (GRI) and a geomembrane manufacturer was the first company to step up to the plate, cut a check and become a member. In 1986, Dr. Koerner published the first edition of “Designing with Geosynthetics”, “the” textbook on geosynthetics design worldwide for almost 20 years.

As this period continued into the late 1980's and early 1990's, in the area of polyethylene geomembranes, friction sheet and a variety of coextruded products came to market. The significance of stress crack resistance forced resins for HDPE geomembranes to change. VLDPE appeared in the market place. Performance tests came to the forefront of test development.

Information and direction came from many organizations. ASTM committee D35 tackled the enormous needs of the industry for standard test methods. Technical Guidance came fast and furious through the EPA. Of the many very informative and useful EPA technical guidance documents, one in particular needs to be mentioned. Some of us refer to it as the bible of early geomembrane research and chemical compatibility. It is the Lining of Waste Containment and Other Impoundment Facilities by Matrecon written by Henry Haxo. It houses much of the early research that led to the US EPA specifying geomembranes for containing pollutants.

Even with these efforts, there was still a need for more research, more standard test methods and more professional guidance. GRI provided methods and specifications that ASTM could not develop or develop fast enough. The forceful, focused technical leadership from Bob, Grace and George at GRI brought the entire geosynthetic industry together and deserves much credit for the growth of the industry.

And that leadership was desperately needed. Manufacturers, while training many engineers and installers in the use of geosynthetics, also spent a fair amount of effort fighting each other. Specification wars were rampant. One up-man-ship, touting one's products while smashing the competition did so much damage that some engineers, regulators and users lost faith in any of the products. Specifications were written by manufactures as marketing tools. Specifications being written by engineers were sometimes performance and design based, but often were only a copy of a manufacture's specification. As this period comes to an end, NSF 54 was losing credibility due to neglect and opened the door for GRI specifications.

Duel Track Hot Wedge Welding

I start this section out with a discussion of welding technology instead of the materials because of the importance of welding in the successful use of geomembranes. In talking about geomembranes I frequently think about the as manufactured sheet or the finished installation. A whole lot of stuff goes on in between the two. Design, site preparation, deployment, welding and finishing off the construction are all key phases of a successful geomembrane installation. Welding is sometimes viewed as material specific, but one welding technique can be applied to most all thermoplastic geomembranes, wedge welding.

The reason for focusing on wedge welding is that it has become the preferred method of welding for many engineers and geomembrane installation owners. Wedge welding joins two sheets of plastic by passing the sheets over a heated wedge that melts the two surfaces and joins them with pressure to make a seal. No outside adhesives or chemicals are introduced. When using duel track welders, an air channel is formed between the two seals, which can be pressurized with air to check seam continuity. The process is mechanically controlled with the operator(s)

monitoring the welder functions and making sure the sheet edges going through the welder are clean. This type of welder has shown a high rate of success and is capable of consistently making good welds.

Hot wedge welding did not originate in the geomembrane industry. It was developed by a Mr. Kurylec in Czechoslovakia in 1947 for welding linoleum. In 1978, Sarnafil of Switzerland developed their version of the welder for polyethylene geomembranes and received a patent for it in 1982.

Clark Gunness, working for Sarnafil, introduced wedge welding to John Hardison of National Seal Company (NSC) in the early 1980's, granting NSC the right to use the welder for geomembranes. Even though NSC supposedly had exclusive rights to use the welder for geomembranes, Sarnafil was not enthusiastic about enforcing their patent and other companies began using the welding technology.

Clark Gunness was very active in spreading the use of wedge welding. He worked with Columbia Lining Systems in Calgary, Alberta one of the first companies to use the dual track welder. They developed a wide channel, high pressure test to really challenge the integrity of the seam, not just its continuity. Clark started developing his own welder, the Resicon R88 in 1981. It was a small welder compared to the Sarna and NSC welders and was designed to fit under the seat in commercial aircraft. In 1985, he started selling the welder commercially and their use became fairly widespread by 1988.

In Germany, the Bundesanstalt für Materialforschung und Prüfung (BAM) required both wedge welding and on-board data acquisition with respect to welding conditions such as welding speed, wedge temperature, pressure, etc.. Jack Donaldson and myself carried the technology a step further and developed the "Smart Mouse" welder. Not only did the welder monitor the welding conditions, it also controlled the speed of the welder to respond to changes in liner temperature during the course of making a weld.

In spite of an EPA conference on the subject in 1993, the smart mouse did not catch on for a couple reasons. First it cost about three times more than a normal welder. It had greater maintenance costs because of the technology. And lastly, it did not eliminate cutting holes in the liner every 500 feet because it could not eliminate weld failures. Contamination such as soil or moisture in the weld was not detected or controlled by the welder. Still, a lot was learned as a result of the research and some of the infrared sensors for sheet temperature and auto speed controls did find their way into production equipment.

PVC

The North American PVC industry grew and was prosperous, peaking out during the late 80s and early 90s. Even though the PVC lining industry was growing and doing well during that time, the rate of growth was only a small fraction of that being experienced on the polyethylene side of the industry.

The marketing, research and training done by the polyethylene manufacturers supported engineers and regulators with what they wanted, information they could hang their hats on, advance the state of practice and write specifications and regulations that they could justify with data. The PVC manufacturers, fabricators and installers did not jump on the technology band wagon and provide the same kinds of data and did not pursue education of engineers and regulators anywhere near the same extent as the polyethylene industry. The PVC group spent more effort complaining. As a result, polyethylene products became the material that was written into more and more specifications and regulations. By the time the PVC industry recognized what was happening, it was too late.

PVC technology was not stagnant during this period. The quality of plasticizers improved. In the early stages, dioctyl phthalate (DOP) was the predominate plasticizer used. During the end of this period, DOP started being replaced by less migratory plasticizers such as diisodecyl phthalate DIDP.

While the technology was available, not much dual track wedge welding was being done with PVC geomembranes, maybe none in the US. It is thought that some Canadian PVC geomembrane installers were using wedge welders in the 80's. EPI was the first US PVC installer to attempt to embrace wedge welding to at least a limited degree in the early 90's. The main driving force for using wedge welding on PVC at the time was to extend the installation season, being able to weld in cool conditions in the early spring and late fall without tents and other such measures.

Polyethylene

While I refer to this period as the Geo-Era, in the geomembrane market, it can easily be referred to as the polyethylene era. Polyethylene geomembrane producers stepped up to the plate and blasted the geomembrane market wide open with aggressive marketing to end users, design engineers and regulators. Not only did their efforts propel polyethylene use over other types of geomembranes, they also accelerated the widespread use of geomembranes as a solution for environmental and water quality problems.

The industry also had the help of some researchers and regulators that saw the inertness or chemical resistance of high density polyethylene as a distinct advantage in the lining of hazardous waste landfills. Work published by Dr. Hans August and others in Germany showed HDPE to be the only material to stand up to the wide variety of chemicals being placed in hazardous industrial landfills at the time. Similar work funded by the USEPA had Henry Haxo developing chemical compatibility procedures and comparing the available lining materials. When that testing started in the early 80's there were many types of liners being used and evaluated and not much PE. By the late 80's polyethylene was the material of choice, not just because of good performance in the chemical compatibility tests such as EPA method 9090, but also because the polyethylene suppliers participated more in the testing.

But life was not a walk in the park for the polyethylene industry. There were many problems to be solved. In that group was friction, or the lack of it. As many people learned the hard way, walking on a wet, three to one, polyethylene lined slope frequently resulted in an unexpected

quick trip to the bottom of the slope. If personal embarrassment and an occasional broken leg was the only issue with smooth PE geomembranes, textured geomembranes may never have been developed. As it turns out, heavily loaded wet soil and waste does not like to stay put on a steep polyethylene lined slope either. Neither does a heavily loaded polyethylene liner like to stay put on a wet slope. Failures occurred at both interfaces and the industry needed to provide a solution.

One of the most studied failures and one that forced friction sheet into production was the 1988 slope failure at the Kettleman Hills Waste Landfill in California. 490,000 m³ of waste was involved. The landfill design was state of the art, incorporating multiple geomembranes, drainage layers, cushion layers and a compacted clay liner. Failure occurred at more than one interface. The primary failure was at the clay-geomembrane interface. Byrne, et. al, published one of several papers analyzing the failure.

One of the first structured geomembranes (referred to as friction or textured in the US) was developed in Germany by Agru in the late 80's. It had 5 mm tall spikes embossed on the surface. Subsequently, several variations were developed with ribs and other protrusions by Agru and others.

Not everyone thought the first alternative to smooth polyethylene sheet was good enough. Besides being dangerous to fall on, the large dramatic structures significantly reduced the materials tensile strength and elongation at break. Even though HDPE is not designed to be used past its yield point of about 13%, some engineers did not like the dramatic change in properties.

One of Schlegel Lining Technology's customers, BFI, encouraged them to develop an alternative. In the US in the late 1980's, SLT developed a friction sheet by adding a spray on PE coating that was fairly well adhered, but not well enough to seriously reduce the tensile properties at break.

National Seal Company (NSC) developed yet another textured sheet, a smooth sheet coated with a thin foamed layer of polyethylene. The Foam bubbles broke open during the coating operation yielding a rough textured surface. Like the SLT sheet, this textured sheet retained more of the smooth sheet tensile at break properties and was one of the most aggressive textures on the market.

Gundle purchased their second blown sheet line in 1986. This line had coextrusion capabilities and the extruders were designed for injection of nitrogen in the outside two layers. In this way, they made a textured sheet. As the plastic came out of the die, the bubbles being stretched broke open and cooled to make a rough surface. There were many problems with this product early on (holes in the sheet, globs of foamed material sticking to the die then sloughing off onto the sheet, poor consistency, etc.). It eventually became the industry standard as the process was improved to make a better product and it proved to be the least expensive way to make a textured sheet.

With all the choices available in textured sheet and geosynthetic clay liners (use instead of compacted clay in some instances), the USEPA with the cooperation of Waste Management and the manufacturers, set up a long-term slope stability evaluation in Cincinnati. There were 14

instrumented, full scale tests performed on 2:1 and 3:1 slopes. Three of the 2:1 slopes failed. The failures along with the non-failures provided valuable information for future designs.

Another major problem was stress crack resistance. The resins used for many of the early HDPE geomembranes were hand-me-downs from the gas pipe industry. These were real HDPE resins with densities of 0.940 to 0.945. While they may have worked well for pipe, they did not stand up to the abuse taken as part of a PE lining system. Most of the failures occurred at welds that were overheated, distorted, over ground or somehow made with a stress concentrating defect.

The industry responded by making stress crack performance improvements such as lowering the density of the polyethylene resin being used. It was necessary to take the density down below 0.940 g/cm³, the lower boundary set by ASTM for HDPE (0.940 being a somewhat arbitrary number). Since HDPE was already engrained in the industry as a product, no one wanted to change the product name to medium density polyethylene liners. So the industry definition of HDPE was changed to a finished sheet density of at least 0.940 using a polyethylene with a density of at least 0.932 g/cm³. (The carbon black, used for UV resistance, brings the density up about 0.008 to 0.012 g/cm³).

While everyone realized that the stress crack resistance of the products needed to be improved and lowering the density was a good way to go, more factors effect stress crack resistance than density (average molecular weight (MW), MW distribution, distribution of comonomer on the polymer backbone, distribution of the comonomer across the different MW molecules, comonomer type, processing conditions, stabilization and so on). So a quantitative test was needed to measure the stress crack resistance of HDPE geomembranes. The “bent strip” testing being used was useless since all the materials in use had good enough stress crack resistance to stress relax before failing.

Dr. Grace Hsuan of GRI developed the notched constant tensile load (NCTL) test to differentiate materials. The test avoided the stress relaxation interference of the bent strip and had short enough failure times to be used as a quality control test (not as short as the industry would have liked, but short enough to be practically useful). By evaluating the NCTL properties of many liners, some that failed and many that did not, a specification was arrived at that is still the standard today.

Many properties were evaluated and tests developed for geomembranes in this period, often with a focus on polyethylene. Lifetime assurances were addressed with oxidation induction time (OIT), carbon black content, carbon black dispersion, air oven aging and UV aging. Durability and resistance to puncture were evaluated with large-scale hydrostatic tests and multi-axial tensile.

But some roadblocks were introduced to new innovation. One that appeared that has not gone away is viewing thickness as a performance property. Many industries have gone to better performing and more expensive grades of polyethylene to get better performance and offset the raw material cost increase by down-gauging, making a thinner product. Since thickness was viewed, at least in practice, as a performance property, minimum thickness is almost always the first property listed in a material specification.

There were some exceptions. For instance, even though HDPE was a dominant lining material, linear low density polyethylene (LLDPE) began growing in applications such as caps where its flexibility and ability to conform to moving subgrades was viewed as positive. Being a cap, it was not perceived to need the same chemical resistance as a primary bottom liner. LLDPE was not specifically addressed in the regulations and was, by default, allowed to be thinner than HDPE in some applications such as landfill liners.

Then very low density polyethylene showed up with even better extensional properties. It did not have the UV or chemical resistance of HDPE or even LLDPE but provided some unique properties. NSC patented a coextruded liner with a VLDPE core and HDPE skins so as to get the most flexibility and the best UV and Chemical resistance in one sheet.

Flexible Polypropylene

Flexible Polypropylene (fPP) geomembranes appeared on the market in the early 1990's. The resin was made with a "Catalloy" process that allowed a high percentage of ethylene-propylene rubber (EPR) to be co-polymerized with polypropylene in the reactor. This very flexible material did not resemble standard, stiff polypropylene and made an early splash in the market in both reinforced and unreinforced forms despite its high cost. By 1993, several papers had been written on the use of fPP geomembranes.

The fPP took some market away from polyethylene. It was more flexible than even VLDPE (but not as flexible as PVC). It also had better stress crack resistance than HDPE and was thought to be a good alternative for black liquor lagoons at pulp mills.

fPP took a big chunk out of the Hypalon market. It had better cold weather properties than Hypalon. It was easier to install and repair after having aged. It was easily wedge and hot air welded. It was processed on the same extrusion equipment as polyethylene and other reinforced geomembranes. Even though it cost a lot compared to PE, it was less expensive than CSPE.

Chlorosulfonated Polyethylene

Hypalon continued to lose market share during this period, being replaced more and more by polyethylene and, toward the end of the period, by fPP. CSPE had its niche markets where it dominated, such as floating covers, but polyethylene made inroads there as well and fPP was coming on strong. Still, Hypalon had a good piece of the market during this period.

PHASE IV. MATURE PHASE

Of all the dates I have selected for the phases of geomembrane growth, this is the least well defined. The beginning of this phase could be defined by a change in the growth of the market. It could be defined by a change in market profitability. It could be defined by an onset of mergers and acquisitions. It could be defined by a reduction in funds available for research and product development. It might be defined by a reduction in attendance at industry conferences and symposiums.

But it cannot be defined by an end to the need to learn, develop new products, develop new designs, develop new installation procedures, write new standards, conduct more research or find interesting topics to disagree on. After all, we still, still had not succeeded in one of the most fundamental tasks of all. One of the most annoying, counterproductive procedures that continues to haunt the industry. Taking a perfectly good geomembrane installation with good dual track wedge welds and cutting a three foot long hole over a foot wide every 500 feet. So there was definitely work yet to be done.

For the sake of attaching a general date, I would say we had progressed well into this phase by the mid-1990's and will use 1994 as year one.

Based on my description of this phase of geomembrane life, you might think that there is nothing to write about. While I claim the industry entered a mature phase, I said nothing about it entering a grave. New product development and research was alive and well. New spray on bituminous and polyurea geomembranes were introduced. Very flexible polypropylene geomembrane applications were growing. New coextruded PE products were coming to market.

The Bureau of Reclamation (Jack Haynes, Jay Swihart, Alice Comer) began monitoring the Deschutes lining project to evaluate geomembranes in rough sub grade irrigation canals (installed in 1991-1993). A workshop was held in Berlin at the BAM to work through the differences in philosophy of landfill design and construction. The International Association of Geosynthetic Installers (IAGI) was formed in 1995 to provide a voice for the installers.

Also in the period, signs of the mature stage show themselves in the merger of SLT and Gundle to form GSE. Bob Landreth sadly retires long before we wanted him to. Long after it outlived its usefulness, the once hallmark of the industry, but now outdated NSF 54 on FML's is withdrawn.

Welding

Refinement and continuous improvement is a necessary part of the "mature phase". Wedge welding continues, more than ever, to be the preferred method of making field welds in thermoplastic liners. Since the smart mouse could not stop failures or reduce the number of destructive field seam tests, the effort changed to smart people as the answer. This approach is two fold. The first is taking seam samples wisely, not just at fixed intervals. The other is to better educate and train the people making the seams.

The first effort to reduce the number of destructive seams through a variable sampling rate came from the Geosynthetics Institute GRI GM-14 guide for "Selecting Variable Intervals for Taking Geomembrane Destructive Seam Samples Using the Method of Attributes", adopted in 1998. This guide attempts to reward successful welding efforts on a job site by reducing the test frequency and it penalizes poor welding with more frequent testing.

IAGI approach the people side by setting up a certification program for welding technicians. An experience technician can go through training, take a written exam and take a hands on exam to

be certified. This program kicked off in 2002 for polyethylene geomembranes and in 2004 for reinforced geomembranes. IAGI is trying to convince engineers to specify certified technicians as a requirement and has published a White Paper on “Improving Geomembrane Installations.”

PVC

The PVC market began shrinking in this phase of geomembrane history and continues to shrink slowly today. PVC is not technically as accepted by much of the engineering and regulatory community today as polyethylene is. PVC is not a bad material and there are not many material failures. There is just a perception issue with many regulators and engineers. Many engineers can't get what they want from the material, such as the consistency of dual track field welds with air channel testing. While some material is being wedge welded today, much of it is still chemically welded. Technically, the manufacturers have not done enough to improve the perception of their product.

My opinion and the opinion of several people from the PVC side of the business that I spoke with as part of gathering information for this paper is that if the PVC industry had pursued a similar, aggressive marketing, education and technology strategy as the polyethylene industry did, the PVC geomembrane share of the market would have been and would still be much larger.

Processing and compounding improvements have been made but the manufacturers do not advertise or promote those changes. In compounding PVC, mixtures of plasticizers and stabilizers can be used to make products for different applications. South American and European manufacturers make different products for buried vs unburied applications.

There are those in the PVC FML industry that are actively working for improvement. The industry did join together to form the PVC Geomembrane Institute (PGI) for conducting research, publishing technical information on PVC geomembranes, writing a standard specification for PVC geomembranes and offering an opportunity to address the technical needs of the engineers and owners. They continue to investigate ways to improve PVC specifications such as adding a requirement for a minimum plasticizer molecular weight.

Dan Rohe and Mark Wolschon are heading up two ASTM PVC task groups. The first is an attempt to write a consensus ASTM standard specification for PVC geomembranes, something even the polyethylene industry has been shy to do. The other is a dual track weld air channel test to evaluate the peel strength of a seam to eliminate the need to cut holes every 500 feet in field seams. Hats off to them for their efforts.

For the foreseeable future, there will continue to be a need for the PVC geomembranes. It has advantages and it has a place. But it will not be on par with PE products. PE is entrenched and is inexpensive. PVC continues to do better in South America than the US.

Polyethylene

The changes that took place in the polyethylene geomembrane industry during the previous period were amazing. At the beginning of the period, it was a small specialty market that was

not well known. By the end of the period, incredible advances were made in products and technology. Equally amazing to those who took polyethylene through that period is how by the beginning of this period, polyethylene geomembranes had become a commodity product, sold by the pound as unenthusiastically as PVC pipe is sold at a home improvement store.

Technology advances were still being made at a fairly brisk rate in materials, extrusion technology, welding, installation and design. But the market had become so large that the only way the manufacturers could service it was selling standard product in mass. This has served to limit new product development for smaller niche areas by major manufacturers. Since higher raw material costs cannot be easily passed on, new materials like metallocenes are very slow to enter the market.

Flexible Polypropylene

Flexible polypropylene use grew quickly during the early part of the period and had 5% of the geomembrane market by 1995. Its high cost compared to polyethylene and PVC limited its use to places where its combination of flexibility, chemical resistance, UV resistance and ease of wedge welding allowed it to compete on performance.

There were several failures early on as the industry learned how to properly design with and use the product. Some aging concerns still have to be fully addressed at the writing of this paper and continue to be under investigation.

Hypalon

Through the early 90's Hypalon's share of the market rapidly declined and was down to only 5% of the North American market by 1995. Flexible polypropylene was rapidly replacing it. DuPont, eventually walked away from the market, not in that they quit selling the raw materials to the industry, but in that they quit promoting its use. Hypalon geomembranes are still made and installed but represent only a small amount of current geomembrane use.

Bituminous Geomembranes

A number of companies continue to make bituminous geomembranes. Their use in Europe is still fairly strong and represent over 10% of geomembrane use. Their use in North America is less than 2% of the geomembrane market but may be growing. They have a 30 year history of use and find their way into a variety of applications including waterproofing dam faces, pond liners, canals and transportation.

EPDM

Ethylene propylene diene terpolymer (EPDM) is not a new polymer or new to geomembranes but is seeing some new life in civil engineering applications. EPDM was introduced in 1963 but saw most of its use in single ply roofing products. EPDM was used in geomembrane applications in the US, but like the bituminous geomembranes, it has found more use

internationally. The exception is the home and business decorative pond market, where EPDM enjoys over 90% of the market.

EPDM is a very flexible, versatile material with good UV resistance. Because it is a fully cured rubber, it cannot be heat welded and must be glued or taped together in the field if the project is larger than what can be factory supplied. Since installation does not require any specialty equipment, EPDM is well suited to small applications. That said, it has been used in landfill caps larger than 4 hectares (10 acres).

FUTURE PHASE

I don't claim to be able to predict the future but there are a few observations I would like to make. The world population continues to grow. Land, air and water requirements for that population continue to grow. The world continues to get more polluted, not less. The rates may have been reduced dramatically in many parts of the world and the impact of select pollutants may have been reduced, but pollutants as a whole continue to spread. Popular talk about global warming is starting to be replaced by discussions of solar dimming, the reduction of sunlight reaching the earth's surface due to air borne pollutants and increased cloud cover.

Geomembranes are an important tool in conveying water, holding water, covering water, protecting water by containing hazardous materials, being a hydraulic barrier in purification processes and being a gas barrier, preventing air pollutants from escaping. Their need will not diminish during the foreseeable future. As the demand placed on geomembranes get greater, I believe new polymers will find their way into geomembranes. The polymers used today are good polymers and, for the most part are inexpensive. Many other polymers have barrier properties superior to the most common polymers being used in geomembranes today (and they cost more). Want a glimpse of the available technology, just take a look at what is going on in the booming industry of food and medical packaging. I can see five, seven and more layer coextruded geomembranes with polymers like polyamide, ethylene vinyl alcohol, polyester and other barrier materials being used in conjunction with polyethylene. We may even see breathable geomembranes that let moisture through but contain pollutants.

Through these challenges of the future and changes that are certain to come, sound research, active industry interaction and education of new and existing engineers and scientists will be needed to provide direction and high-quality information. The leadership provided by the Geosynthetic Institute, its associated institutes, Robert Koerner, George Koerner, Grace Hsuan, others at Drexel University, and many others in the industry will be invaluable in keeping us on track and focused on the key issues.

ACKNOWLEDGEMENTS

Fred Rohe and Fred Struve for their contributions from their memories and guidance in writing this paper.

REFERENCES

- Byrne, R. J., et. al., (1992), "Cause and Mechanism of Failure of Kettleman Hills Landfill", Proceedings of Conference on Stability and Performance of Slopes and Embankments II, ASCE, pp 1-23.
- Daniel, David E., et. al, (1998), "Slope Stability of Geosynthetic Clay Liner Test Plots", Journal of Geotechnical and Geoenvironmental Engineering, pp 1.
- Donaldson, J., Kolbasuk, G. M., (1993) "Summary of Experience With NSC Data Acquisition Welders", Geosynthetic Liner Systems: Innovations, Concerns, Designs, pp 1-5.
- Frobel, R. K. et. al., (1999), "EPDM Geomembrane Caps, Commercial Landfill", Geotechnical Fabrics Report, October/November, pp 36-41.
- Giroud, J. P., (2002), "Geosynthetics in perspective – 1983-1987," Geotechnical Fabrics Report, June / July, pp. 10-15.
- Gourc, Jean-Pierre, (1994), "1994 Mercer Lecture: Geosynthetics and Environmental Engineering", Proceedings of the 8th GRI Conference, pp. 279-???
- Haxo, Henry, (1988), "Lining of Waste Containment and Other Impoundment Facilities", EPA/600/2-88/052.
- Kays, W. B. (1977), "Construction of Linings for Reservoirs, Tanks, and Pollution Control Facilities", John Wiley & Sons, 379 pages.
- Knipschild, F., (1994), "Guidelines for the Installation of Geomembranes for Ground Water Protection in West Germany", International Conference on Geomembranes, Denver, U.S.A., pp 227-231.
- Koerner, R. M., (1990), Designing with Geosynthetics, 2nd Ed., Prentice Hall, 652 pages.
- Koerner, R. M., (1997), Designing with Geosynthetics, 4th Ed., Prentice Hall, 761 pages.
- Landreth, Robert E., (1993), "Proceeding of the Workshop on Geomembrane Seaming: Data Acquisition and Control"
- Landreth, Robert E., (1984), "The Role of Flexible Membrane Liners in Support of RCRA Regulations", International Conference on Geomembranes, Denver, U.S.A., pp. 21-23.
- Materials and Technologies, (2004), "Bituminous Geomembranes", GFR, June/July, pp. 22-24
- Nobert, J., (2003), "Geomembrane Specifications: How Did We End Up Here?", GRI-17 Conference Proceedings, pp. 143-162.

Peggs, I., (2002), "Geosynthetics in Perspective: 1993-1997", GFR, September, pp 10-15.

Schoenbeck, M., "Performance of Chlorosulfonated Polyethylene Geomembranes after Long Term Weathering Exposure, pp. 136-151

Staff, Charles E., (1984), "The Foundation and Growth of the Geomembrane Industry in the United States", International Conference on Geomembranes, Denver, U.S.A., pp. 5-8.

Stuart, Waugh, (1984), "Quantifying the Geomembranes Market in North America – Past, Present and Future", International Conference on Geomembranes, Denver, U.S.A., pp. 47-48.

THERMAL SEAMING OF POLYETHYLENE GEOMEMBRANES

Mark Sieracke, Principal, Weaver Boos Consultants
Ian Peggs, President, I-Corp International

INTRODUCTION

Seaming is the need to join geomembrane so as to create water tight containment. It is far superior to shingling and overlap! Seaming-either factory or field-is required on all large scale installations.

Discussion will primarily focus on polyethylene seaming since it has become the most common (but not exclusive) geomembrane for waste containment and related waterproofing applications. A retrospective review going back 25 years takes us to 1988 which was shortly after the double track wedge welder became well established in North America. Much had happened before then, as summarized below.

THE EARLY DAYS OF POLYETHYLENE SEAMING

It is understood from Clifford Gundle that the first joints in large deployment areas of High Density Polyethylene (HDPE) geomembranes were made in South Africa by Allan Lever using interlocking pipe sections buried in anchor trenches (Figure 1).

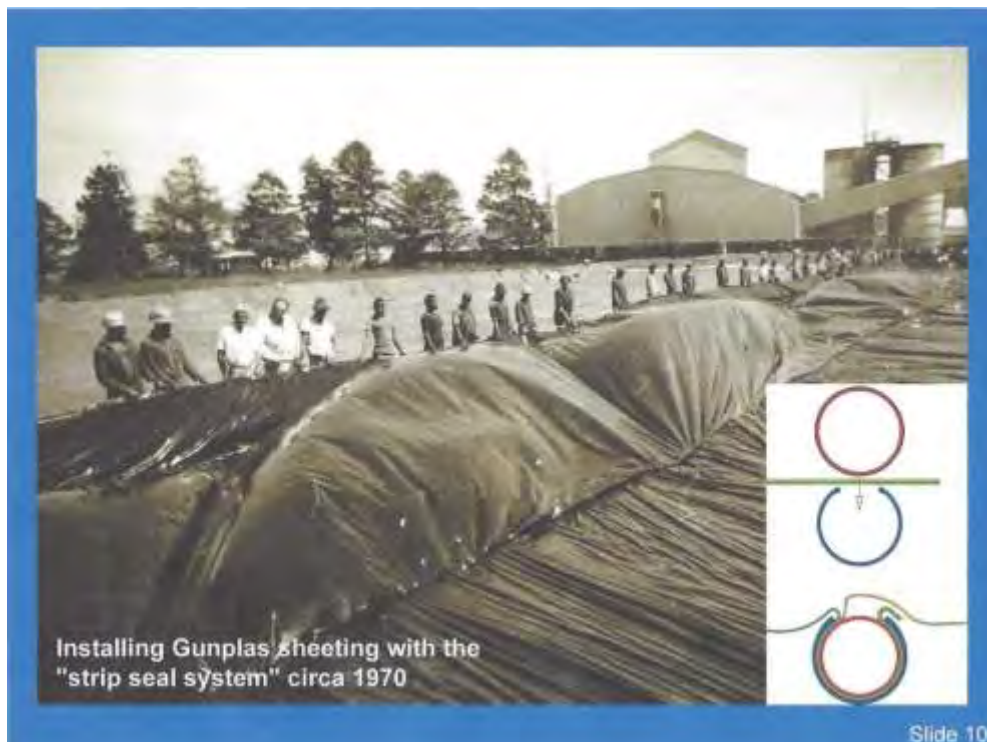


Figure 1. First polyethylene seam (Courtesy Clifford Gundle).

However it did not take long for the handheld rotary head extruder (Figure 2) developed by Fred Struve to appear on the scene to provide a more water tight seam taking advantage of the ability to reheat and extrude polyethylene materials onto the seam area.

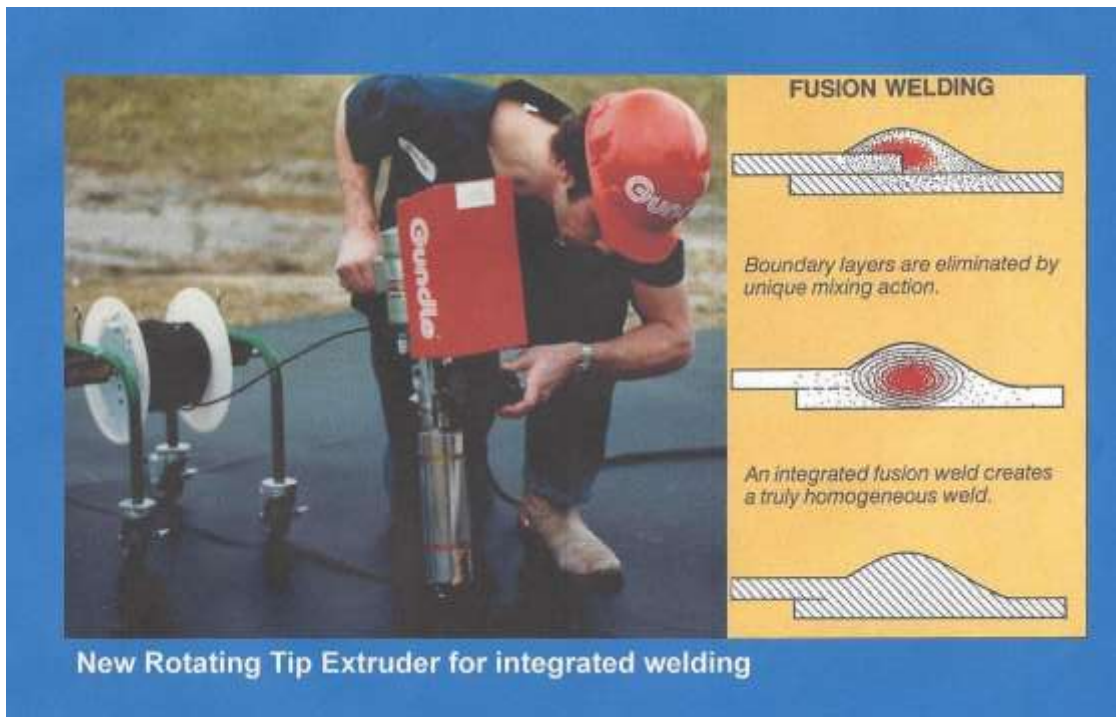


Figure 2. Rotary head extrusion welder (courtesy Clifford Gundle).

At the same time Heiner Hammer of Schlegel Lining Technology in Germany was building a geomembrane manufacturing machine (Figure 3) that consisted of an indexing heated drum about 2 m diameter on which approximately 450 mm wide strips of HDPE were extruded transversely. The drum was rotated sufficiently for the next transverse strip to be laid overlapping the previous strip by about 30 mm and bonding to it while it was still hot. This process was not considered “factory seaming”, it was the process to create a continuous long roll of geomembrane up to 10 m wide was made consisting of cross-roll strips (Figure 4).



Figure 3. Schlegel's indexing drum geomembrane machine (courtesy Catrin Tarnowski).



Figure 4. Thirty year old Schlegel HDPE geomembrane with frequent horizontal welds.

Field welds for the Schlegel liners were made using a large ice-cream cart size extruder on wheels (Figure 6) loaded with HDPE pellets that extruded a bead of resin about 35 mm wide between the overlapped sheets.



Figure 6. Schlegel Lap welding machine (courtesy Catrin Tarnowski).

On the whole, the transverse overlaps made in the factory on the Schlegel geomembrane performed extremely well but the edge of the overlap area was quite susceptible to stress cracking in hot/cold environments – a function of the early pipe grade high density resins and the weld geometry. Stress cracking was first identified by Peggs and Little in 1985 (Procor Inc., private report)

The Schlegel lap extrusion weld for field installations was replaced by the rotary head extrusion welder (Figure 2) developed by Fred Struve at Gundle as the primary welding technique for several companies.

INTRODUCTION OF WEDGE WELDING

In the early 1980s Sarna (Switzerland) had developed an automated single track wedge welder for welding roofing membranes. Clark Gunness became the US representative for Sarna (and Sarnafill membrane) and introduced the fusion welder to National Seal Company. National Seal, via Hans Poetsch Sr., worked with Sarna to build a patented welding machine. However, Pfaff in Germany had already built (~1980) and patented such a wedge welding machine and claimed patent infringement. However, the upshot was that Sarna, NSC, and Pfaff all worked together on the worldwide development of the double track hot wedge welding machine, (see Figure 7).

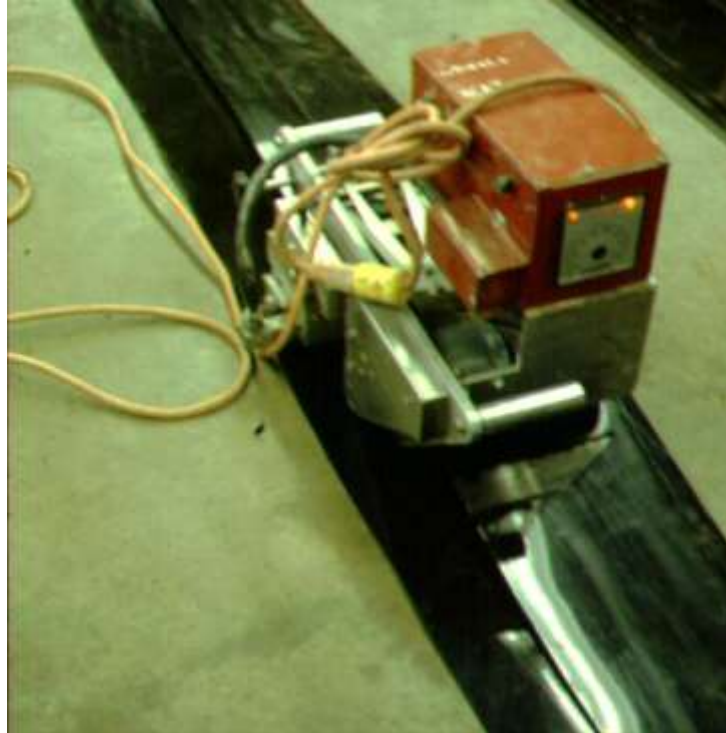


Figure 7. Example of an early wedge welding machine.

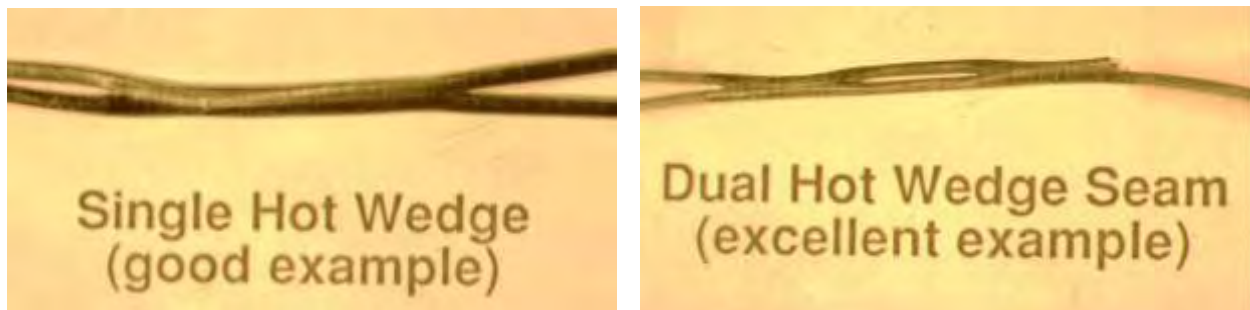


Figure 8. Cross sections of wedge welds.

In the 1980's, National Seal began was an installer/fabricator using the wedge welder for both factory fabrication of large panels as well as for field seams. National Seal eventually began manufacturing large rolls of geomembranes and use the wedge welder for field installations.

There was a time when different installers were using different welding techniques leading to variations in quality, inspection techniques and testing approaches. Eventually, the double track wedge welder evolved into the primary production welding device for polyethylene geomembranes and the same technology has now been adopted for PVC and other geomembranes. Of course, extrusion welding of polyethylene geomembranes is still being used for repair and detail work.

Double track wedge welding provided the advantage of automation, two parallel weld tracks and an efficient non-destructive testing procedure.

Different versions of wedge welding, both single track and double track, are used for a variety of geomembrane types and a variety of thicknesses. It is not uncommon to see wedge welders used on geotextiles as an alternative to sewing.

In 1996 Leister, primarily building hot air welding machines, introduced a combined hot wedge/hot air machine which combines the best of both worlds/welds. The hot air would contribute to annealing any induced stresses at the edges of the weld.

Over the years there have been advances in the construction of the wedge welder itself with different frames, different materials for the wedge and increased equipment durability. However, the concept of wedge welding has remained the same.

Even though the wedge welder provided an option for more consistent seaming and more efficient non-destructive testing, there were still seam quality issues with wedge welding. Consensus was that wedge welding is still better than any type of extrusion welding. There are, however, human and environmental variables that could impact the quality of a seam such that destructive testing is still justified.

To address some of these variables, there has been improvement in the equipment and certification programs for the welders. Over the years, there has been significant improvement in the seaming quality, however, we continue to take destructive tests every 500 feet and repair the hole with an inferior welding technique.

To address some of the variables, the concept of “smart welders” with data acquisition for evaluation of the seaming process was evaluated and tried by one installer. The USEPA organized a workshop on “Geomembrane Seaming: Data Acquisition and Control” in 1993 (EPA/600/R-93/112). Although the smart welder is a regulated requirement in Germany, parts of Europe and South East Asia, they have not been adopted in North America. The goal of the smart welder was to raise confidence in the consistent quality of the seam leading to elimination or reduction of the non-destructive testing requirement. Both the cost and the sensitivity of the electronics of a smart welder required an offsetting savings in the testing costs. This concept was never fully adopted and the smart welder was simply not adopted.



Figure 8. Example of Smart Welder.

MICROSTRUCTURE OF WELDS

Little has been written on the microstructure of HDPE geomembrane welds, an understanding of which is necessary to understand their performance and durability. Figure 9 shows a cross section of an extrusion weld. This weld would be better if it had a smooth surface profile.

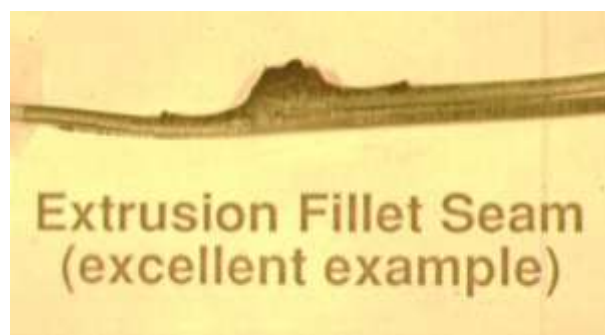


Figure 9. Cross section of extrusion weld.

Figure 10 shows a schematic cross section of the microstructure of an extrusion weld

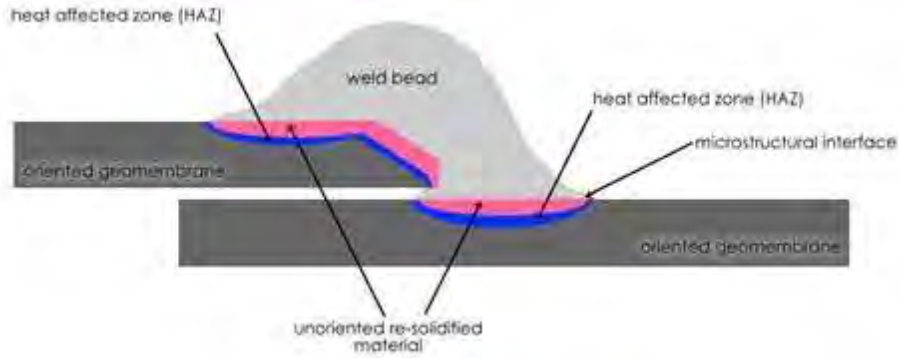


Figure 10. Schematic of extrusion weld.

The thermal energy in the extruded weld bead should be sufficient to melt the surface layers of both geomembranes such that the molten bead and molten geomembrane mix together, cool, and solidify. Therefore the Melt Indices of the extrudate and geomembrane materials should be similar. When the surface of the geomembrane is melted its oriented microstructure (resulting from extrusion) is lost such that when it solidifies the melted and solidified material effectively becomes isotropic in structure. Adjacent to that layer is a heat affected zone (HAZ) which has not been melted but which has been heated to some degree which will affect the oriented microstructure, perhaps increasing crystallinity somewhat.

The slope of the interface between melt solidified and heat affected material, and the width of the heat affected zone may act as an internal “notch” to initiate stress cracking. Figure 11 shows how a craze, the precursor of a stress crack, is initiated at an angle, possibly the gradient of the melt solidified and HAZ interface, just under the edge of the weld bead. Steep gradients will provide a larger notch effect than a shallow gradient. In this respect the annealing effect of a hot air environment in addition to a heated wedge may be beneficial to the long term mechanical durability of the weld.

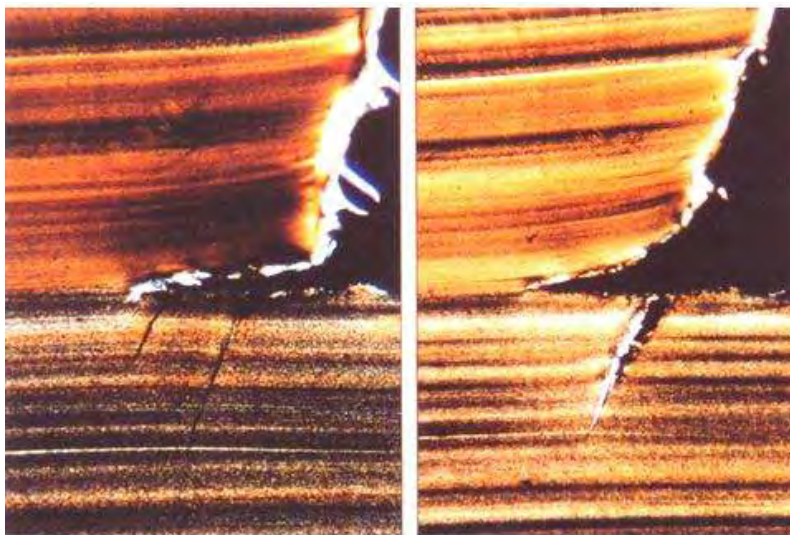


Figure 11. Craze becomes stress crack in geomembrane just below edge of weld bead.

It is for the reasons mentioned above that it is necessary to measure shear elongation in seam tests to ensure that the geomembrane at the edge of the weld has not been overheated, oxidized and embrittled.

Similar microstructural features occur and can be seen at the edge of a wedge weld at the root of the squeeze-out bead (Figure 12). In addition, when viewed with crossed polarizing filters the residual stress distributions are identified by the different colors.



Figure 12. Thin slice cross section at root of squeeze-out bead in a fusion weld viewed with crossed polarizing filters.

When a peel test is done on a poorly bonded fusion weld and separation occurs, in some HDPEs crazes can again be initiated in the separated surfaces (Figure 13). If a uniaxial tensile test is performed on such a crazed seam the break stress can be reduced about 70%. Hence the reasons for limiting the amount of peel separation in a peel test.



Figure 13. Crazes initiated in peel separated surface (arrowed). Squeeze-out bead to left.

Microstructural features have also been found useful in investigating separation in plane breaks in fusion welds. The first occurrence of separation-in-plane (SIP) was reported by Peggs in 1985. Figure 14 shows the striated microstructure that enabled the geomembrane to be delaminated by hand along the white bands. Clearly, in this case, there was a problem in uniformly dispersing the carbon black additive.

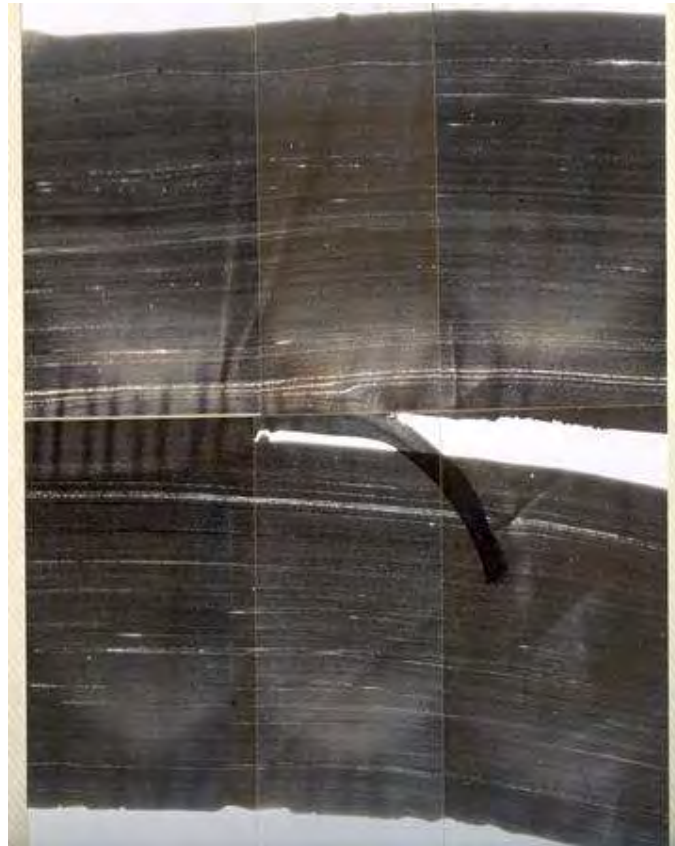


Figure 14. Striated microstructure resulting in SIP along the white lines.

Figure 15 shows a seam in which SIP occurred in a peel test.

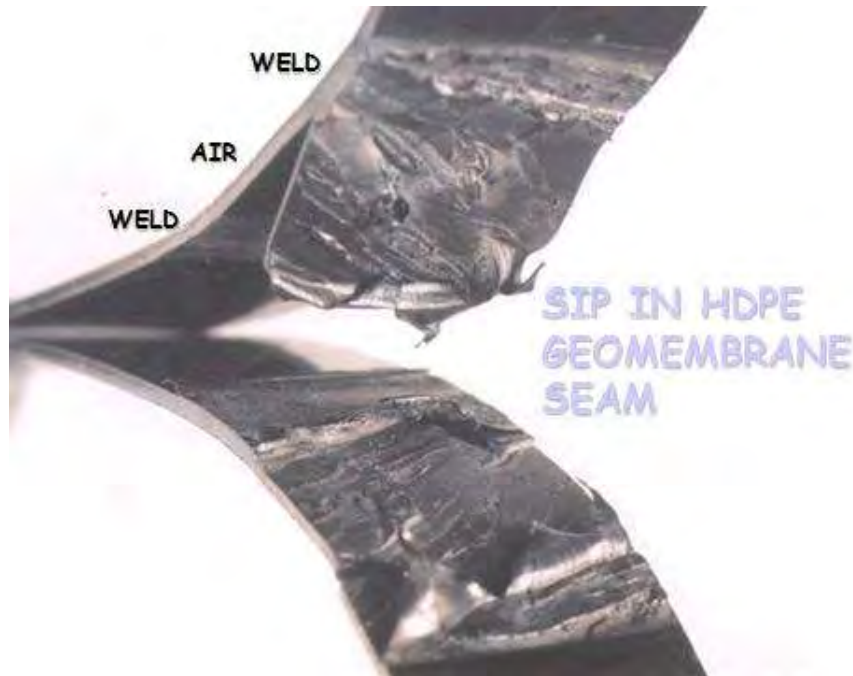


Figure 15. SIP in peel test specimen.

A number of papers (Struve 2003, Smith 2001) have been written about the cause of SIP. The most common cause is thought to be the use of an additive package with an incompatible masterbatch carrier resin. However, the issue essentially remains unresolved and is the subject of the recent GRI white paper #25 “The Separation-In-Plane (SIP) Mode of Failure When Testing Geomembrane Seams“. (2012). GRI does not consider SIP to be a problem provided the seam peel strength requirement is met.

SEAM TESTING

We are all familiar with destructive seam peel and shear strength testing to assess seam bond strength. However, for the reasons mentioned above, Peggs (1996) and Thiel (2013), believe it more appropriate to measure shear elongation and peel separation and, in fact, to almost ignore strength values. Geomembrane strength values are a function of geomembrane thickness. Why is the strength so critical when the weld interfaces we are trying to evaluate are the same for all thicknesses? They actually do not tell us very much about bond quality. The strengths are an indicator of potential damage to the base geomembrane-not a measurement of bond quality of the two geomembrane sheets.

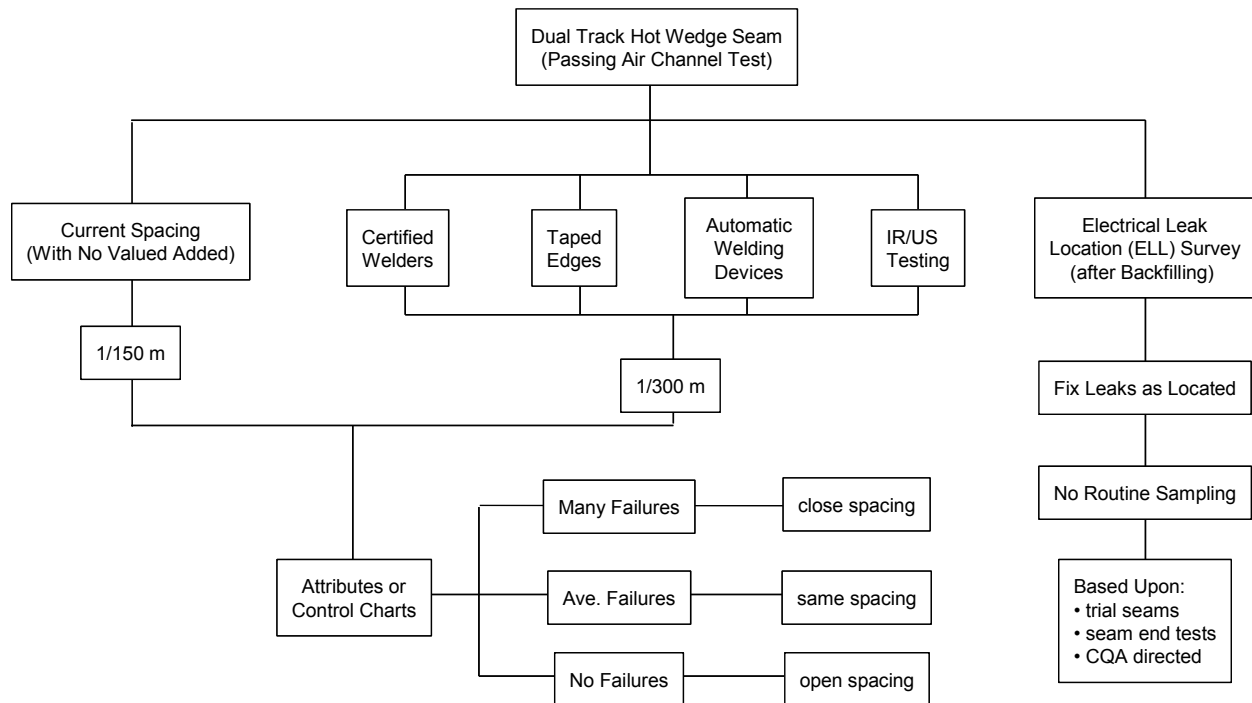
When five specimens are tested in shear and peel modes it is still not unusual to see specifications that allow one of the five to fail for acceptance of the complete seam sample. This is a 20% failure rate of a critical liner parameter which surely should not be acceptable. It is proposed that all ten specimens meet specifications of ductility at break and no peel separation

FUTURE DEVELOPMENTS/NEEDS

The two main objectives for the future still remain as they have been for many years:

- Develop a confidence level in the weld that will eliminate the need to cut holes in good seams for destructive peel and shear testing and having to make repairs using three times the length of an acknowledged inferior extrusion welded seam, and
- New techniques/methodologies to nondestructively evaluate 100% of a weld.

A strategy to increase the confidence in the weld quality to modify the destructive test frequency has been available from GRI and has been successfully used on projects and in CQA plans.



Probably the two most relevant technologies for non-destructive testing are ultrasonic and infrared thermography. The ultrasonic pulse-echo technique, essentially for thickness measurements, was first proposed for use in Germany in 1992 (Müller 2013 personal communication). In 1996 the use of ultrasonics was no longer required although some CQA firms continued to use it. In 2009 the use of ultrasonics was issued as a standard by the BAM Institute. It requires three thickness measurements on fusion seams every 10 m. With their certified HDPE resins, certified geomembranes of 2.5 mm thickness, certified welding machines, and certified welding personnel, they have found that a reduction in thickness of 0.3 to 0.8 mm from the total nominal pre-weld thickness of 5.00 mm is indicative of proper thermal energy input, welding speed, and nip roll pressure to produce an effective weld. An intermediate signal from the weld interface is indicative of an inadequate weld. Clearly, such a parameter is not necessarily appropriate for thinner materials, different resins, and different welding machines. Nor does it provide 100% coverage of a weld length.

In addition, a flat-ended transducer is required to make full firm contact with the weld surface which can be done on fusion welds but not on extrusion welds. This presents a limitation for ASTM D7006 “Standard Practice for Ultrasonic Testing of Geomembranes” for evaluating seams. The requirement for a consistent uniform pressure can also be a problem on seams in a wrinkled liner.

One hundred percent coverage on both fusion and extrusion welds can potentially be achieved if a pitch-catch technique (shadow method) is used in which the ultrasonic pulse is induced in the liner on one side of the weld, the signal passed through the weld interface, and is picked up at the other edge of the weld in the other liner using continuous contact roller transducer probes (Figure 16). Figure 17 shows the change in signal as the quality of the weld changes. However, there still remains the practical problem of variation in transducer contact pressure at wrinkles. This may be avoided by more recent “Airscan” probes that do not require contact with the geomembrane, but no work has been done in this area yet.

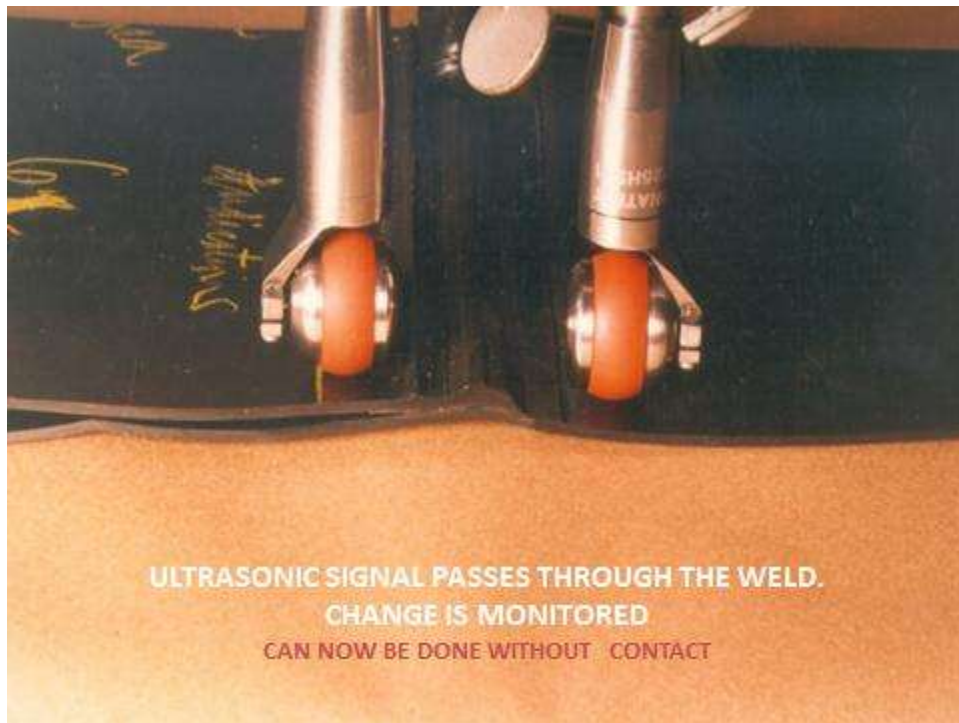


Figure 16. Pitch-catch ultrasonic geometry using roller transducer probes.

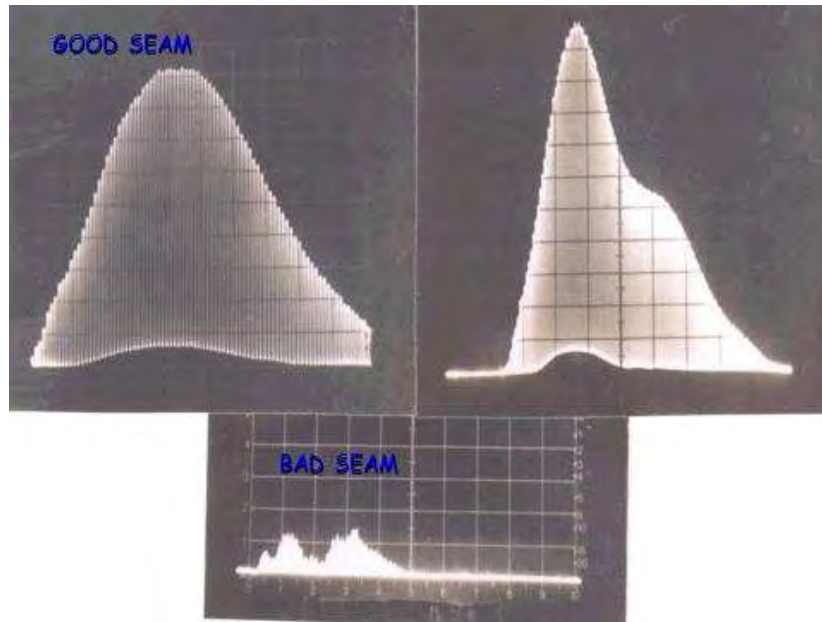


Figure 17. Ultrasonic signal after passing through various weld interfaces.

It is interesting to note that the first GRI geomembrane standard GRI-GM1 was “Seam Evaluation by Ultrasonic Shadow Method“, issued in 1986.

Coletanche bituminous geomembranes with their wide overlapping seams are frequently 100% tested by an array of pulse-echo transducers in a liquid-filled drum that is rolled along on top of the overlap seam (Figure 18). A continuous contour plot of weld interface quality (Figure 19) is obtained.



La Galaube Dam - October 2000
COLETANCHE NTP3 – Automatic control of seams by CAC 94

Figure 18. Ultrasonic inspection of bituminous geomembrane seam.
Multi-transducer housing arrowed (courtesy Bernard Breul).

Details of measurement results with

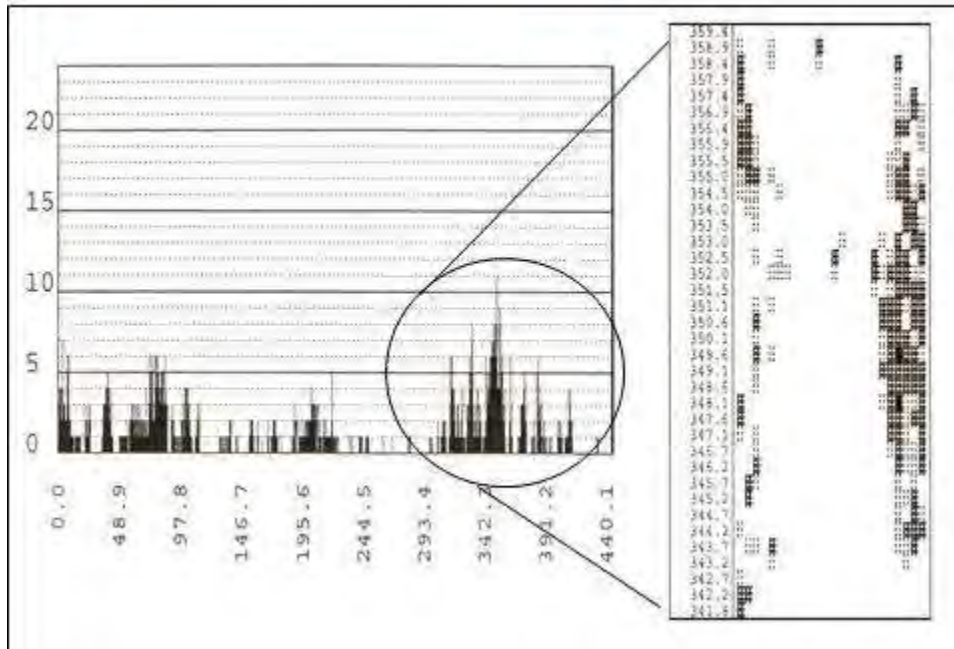


Figure 19. Display of ultrasonic data. (courtesy Bernard Breul).

Infrared thermography may be a better option for assessment of 100% of seam quality. In this non-contact technique the surface of the weld is flash-heated with a pulse of IR energy then the surface of the weld is monitored using an IR camera, for a second or two, for temperature changes. Where the weld is well-bonded the surface temperature decreases as heat is conducted down through the weld. At poor weld interfaces and where there are internal flaws the surface remains at a higher temperature due to the poor conduction of heat across the weld interface. Figure 20 shows a plan view thermogram of a double track seam at a location where the speed of the welding machine was changed. The two weld tracks are different and differences can be seen along the length of each track. Red represents a hot surface and a poorer weld while green/blue is a cooler surface and a better quality weld. Peel tests were performed on the left and right sections of each weld track and the only specimen that peeled was from the red section of the bottom track.

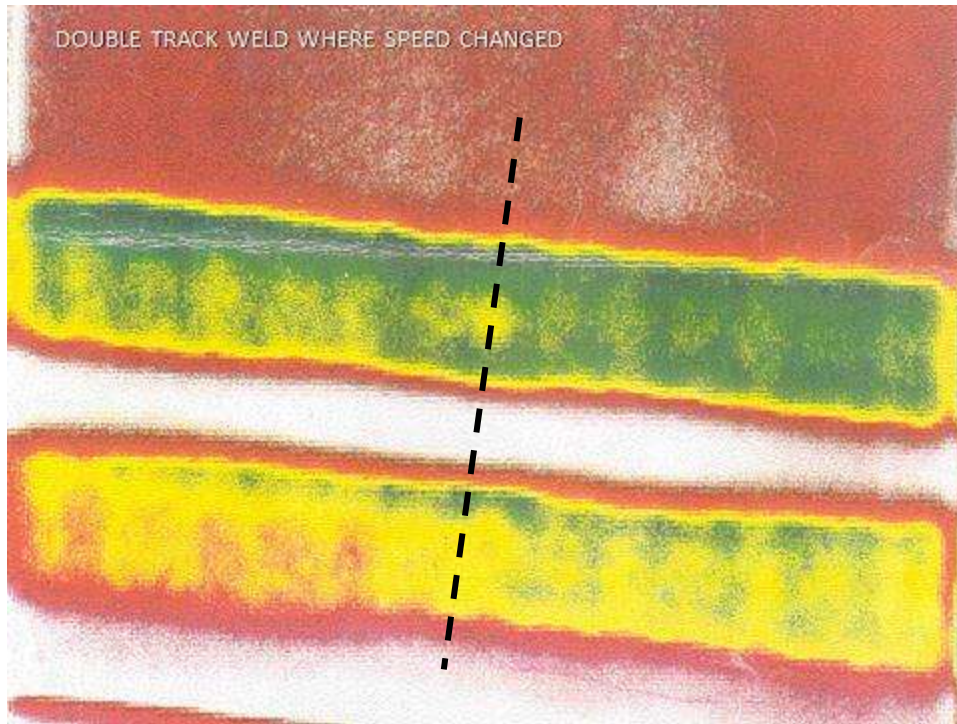


Figure 20. Plan view of double track weld at location (dotted line) where welder speed was changed.

Ultimately, such a monitoring system could be appended to a welding machine to interrogate the weld immediately after welding, and with appropriate feedback to adjust the welding machine parameters to allow for changes in liner temperature caused by passing clouds and wind etc. The interesting challenge, of course, is to identify what features of the weld thermogram are acceptable, for not all features will be critical to the performance of the weld.

However, and to be realistic, if smart welders are not considered necessary, the addition of a sophisticated weld quality interrogation technique is even less likely to be implemented. On the other hand if, after trial weld calibration, there was no requirement for destructive testing and even no requirement for nondestructive air pressure and vacuum box testing, there may be some hope for this technology.

CONCLUSIONS

The seaming of polyethylene geomembranes has evolved from a simple mechanical connection to applying a hot extrudate to a controlled automated fusion welding process. In addition, this fusion welding process has also allowed for an efficient method to non-destructively test the welded seam.

The quality of the equipment and available certification of welders and CQA inspectors have all been instrumental in the improvements made and the quality of geomembrane seams. However, we still continue to having failing destructs. Regardless of the advances we have made, we still

need to make sure the equipment is operating properly, the seam area is clean and dry, we understand the variations in melt flow index between the geomembranes we are welding and we need to keep looking for new ways to test seams to change the status quo of cutting out the seams for purely statistical reasons.

REFERENCES

Müller, V., (2013), personal communication.

Peggs, I.D. (1985) “Why Quality Control? A Graphic Case History”, Geotechnical Fabrics Conference, Cincinnati, 1985.

Peggs, I.D., (1996) “A Reassessment of HDPE Geomembrane Seams Specifications” Geosynthetics Applications Designs and Construction”, Proceedings of EuroGeo1, Balkema, Netherlands, pp 693-695.

Smith, M., (2001) “Comments on Geomembrane Seam Testing”, Mining Record Magazine, July/August, 2001.

Struve, F., (2003) “Separation in Plane (SIP)”, GFR Magazine Vol. 21, No. 2, March 2003, pp 24-25.

Thiel, R., (2013), personal communication.

THE LANGUAGE OF AN INDUSTRY: GEOSYNTHETICS TESTING AND MEASUREMENT

Sam Allen
Vice President, TRI/Environmental, Inc.

ABSTRACT

Geosynthetics testing activity has been a pillar of the geosynthetic industry’s history and experience. Success and challenges in laboratory measurements continue to be strongly related to both industry growth and its struggles. While ASTM and ISO are critical to permanent standards development and distribution, the Geosynthetic Institute has also played a vital role in promoting excellence in laboratory testing protocols and practice.

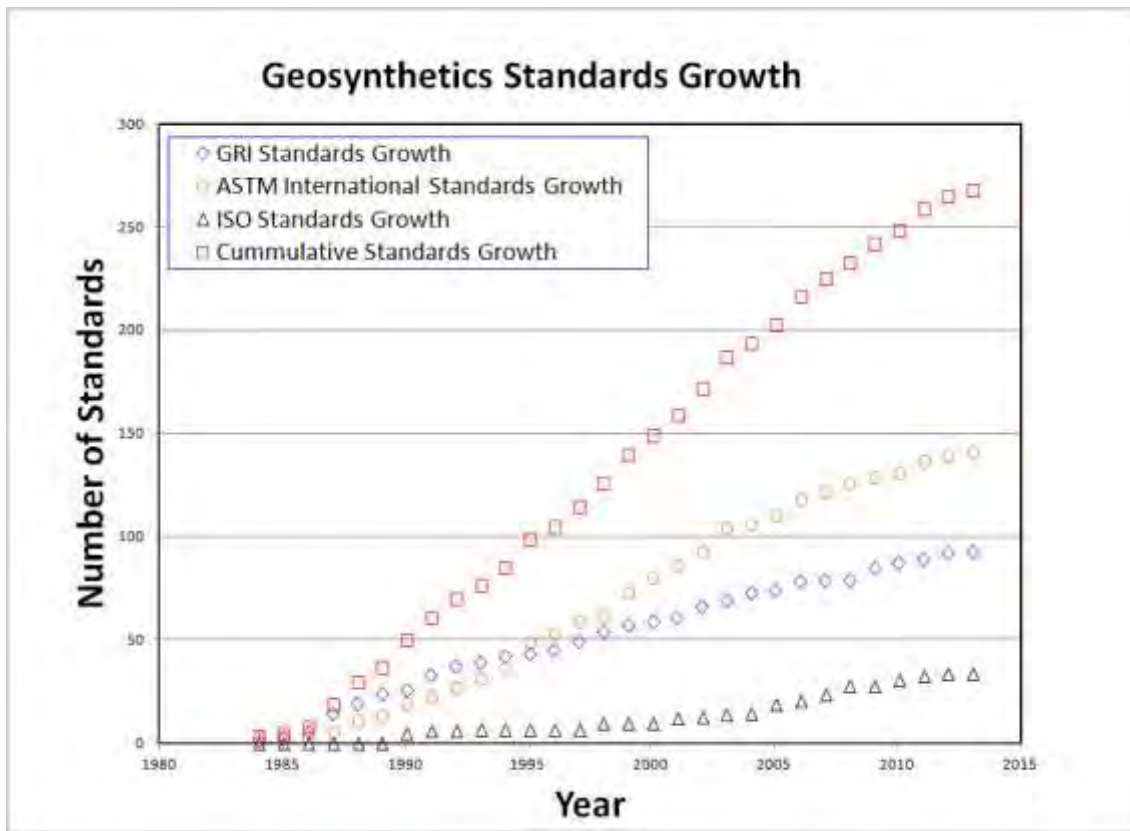


Figure 1: Growth of Geosynthetic Standards

INTRODUCTION

Successful geosynthetic laboratory testing provides objective measurements for material manufacturing, engineering design, product purchasing, dispute resolution, etc., etc. The industry’s core functioning depends on geosynthetic product measurement in every aspect of its operation. Testing alone is not relevant unless performed in accordance with agreed upon standards and norms thereby facilitating transparent manufacturing quality control, independent

third-party quality assurance and, most significantly, standardized international material specifications which opens up the opportunity for free and fair competition. The growth of geosynthetic materials standards over many years has been both impressive and directly linked to our industries general growth. Figure 1 shows the historical growth in geosynthetics standards.

GEOSYNTHETIC TESTING – EARLY CHALLENGES

Testing efforts in the geosynthetics community have played an integral part on the economic and technical growth of our industry. In the early days of geosynthetic product development (and the endless battle for product acceptance) manufacturers, specifiers and regulators relied heavily on borrowed test procedures from other industries, many developed by the general plastics and textile industries. Emergency laboratory testing technicians seeking to digest established ASTM test procedures were left disconcerted when the standard's text did not include the term geosynthetics nor their idiosyncrasies.

Additionally, unique features of geosynthetic materials often necessitated the modification of borrowed standards to accomplish the measurement of a relevant property. The geomembrane industry used only a very small portion of the relatively broad test procedure ASTM D638, *Standard Test Method for Tensile Properties of Plastics*, while taking great liberties with modifications not included in the standard. In addition, geonet compression strength was observed in accordance with ASTM D1621, *Standard Test Method for Compressive Properties Of Rigid Cellular Plastics*, while resulting features of load displacement curves were not always described by the standard. This left the reporting lab uncertain as to what information to record and report. Many more examples of inappropriate (aka, misfit) tests and the resulting confusion existed. What followed was a variety of loosely documented industry modifications that invited laboratory variability, apples-to-oranges product comparisons, and weak (if not completely) inappropriate material specifications.

This very real handicap to industry growth was countered in many significant ways by the Geosynthetic Research Institute (GRI), the first and legacy institute of what is now the Geosynthetic Institute. While the ASTM Committee D35 on Geosynthetics (as an outgrowth of Committee D13 on Textiles) was formed in 1984 and initiated the first development of geosynthetic specific test procedures, the GRI accelerated this process by leading the way in many needed and urgent measurement procedures described in GRI standards. For example, the needed design support test for geotextile filters, *Geotextile Filter Performance via Long Term Flow (LTF) Tests*, was the first published GRI geotextile test procedure, GRI GT1, in 1986. GRI-GG1 in 1987 on geogrid junction strength was (and for an additional 25-years) very controversial. GRI-GM1, *Seam Evaluation by Ultrasonic Shadow Method*, presented a summary of non-destructive seam evaluation techniques based on acoustic technologies. These and many other GRI test procedures worked in concert with D35 Committee work to expedite the needed and urgent response to a geosynthetics industry hungry for standardized test procedures.

This heritage of the Geosynthetic Institute and its robust commitment to geosynthetic measurement continued with the Geosynthetic Accreditation Institute (GAI). As previously described, the early geosynthetic testing laboratory experience with borrowed test procedures and newly developed and implemented measurement protocols was difficult and challenging.

The truth that all testing facilities were not meeting the challenge with equivalent success required an effort to establish a standard not only for testing procedures, but also for geosynthetic laboratory operation. The GAI was formed in 1995 and was the result of direct industry request to the GSI for a program that would credential testing laboratories active in geosynthetics testing. Unlike other accrediting services the GAI focused on a testing-centric approach making sure that equipment and procedure practiced in a geosynthetics testing laboratory were correct. An on-site audit by a testing practitioner as well as annual proficiency testing assures a robust and challenging GAI program.

GEOSYNTHETICS TEST METHODS DIRECTLY LINKED TO INDUSTRY GROWTH

The geosynthetics industry has always been, and will always be, an industry of measurement. Geosynthetic products, their properties, their applications, their technical benefits, their economic benefits, their environmental benefits, are all most powerfully expressed through the expression of measurement. When the geosynthetics industry has embraced the standardization of measurement procedure and expression, our materials and their acceptance (indeed their requirement) have followed. Conversely, when we have struggled with a variety of competing or non-standard measurements, our geosynthetic materials have continued to be a me-too or an uncertain “option”.

An example of measurement success is realized in the expression of stress crack resistance. In the early 1980’s, the use of high density polyethylene (HDPE) in geomembranes was often defined, mostly by competitive material lobbies, by the concern for the material’s resistance to slow crack growth under stress. This very real phenomenon involved the material’s response under stress as a time dependent, but certain, crack development through the geomembrane rendering it inconsequential as a barrier material. To make matters worse, the measurement of stress crack resistance at the time was performed in general accordance with ASTM D 1693, *Standard Test Method for Environmental Stress-Cracking of Ethylene Plastics*, which required excessively long test durations. The test often required 1500 hours to articulate a minimum resistance to this property and associated compliance to a given specification. Even if a specimen passed the specification, ongoing stress relaxation made the test less challenging with increasing test time.

The following years saw the HDPE geomembrane industry foster a steady pulse of newer improved resins articulated through newer more aggressive test procedures. Fully replacing ASTM D 1693 is the notched constant tensile load (NCTL) stress crack test, described in the Appendix of ASTM D 5397, *Standard Test Method for Evaluation of Stress Crack Resistance of Polyolefin Geomembranes Using Notched Constant Tensile Load Test*, shown in Figure 2. The benefits of an industry pursuing what could have been a “poison pill” have included a more meaningful and faster test procedure as well as wider material acceptance. Instead of negating HDPE as a successful geomembrane material, the robust standardized response to the concern over stress crack resistance contributed to a regulatory code requiring HDPE geomembranes in many containment applications.



Figure 2: ASTM D 5397, Appendix – Notched Constant Load Stress Crack Testing

Conversely, while geosynthetic applications in roadway design and improved performance have long been documented, required use of geosynthetics in roads has yet to be practiced or even suggested in many parts of the world. One of the many reasons is the persistent search for a standardized measurement, an agreed upon test or proof, that provides both the user community with confidence in the investment and an even playing field for geosynthetic manufacturers striving for product acceptance. While there have been dozens of large scale field studies and numerous synthesis reports summarizing field experience, the missing fundamental, so important to our materials and their use, is an accepted measurement that is worthy of this application. Recent efforts have focused on design and design parameters, helping to focus on needed measurements and worthy test procedures to provide design inputs. Even these approaches, however, are varied internationally and suggest a long road to international standardization. Again, the agreed upon, standardized measurement of geosynthetic performance has yet to be realized in this application, and the industry's sluggish growth results.

GEOSYNTHETIC TESTING AS MARKET CONTRIBUTION

The advantages of geosynthetic test development and standardized measurement of properties, accompanying the resulting culture of geosynthetic use, has always been a part of our history. The well told story of the 1988 Kettleman Hills landfill failure illustrates the need for and contribution of responsive testing. The Kettleman failure plane between a compacted clay liner and a HDPE smooth geomembrane helped to usher in a new era of shear strength characterization. The resulting evaluation of geosynthetic interfaces day-lighted the relatively weak geosynthetic interfaces involved in landfill slope design. The forensic effort to model the failure between the smooth HDPE geomembrane and the compacted clay liner was first attempted via the use of traditional 2.8 in. round and 2.0 in. square shear boxes, routinely used for the measurement of internal strength of soils. However, due partly to the use of non-

representative clay moisture contents, and also the need for measurement of resistance at large displacement values, the crucial need for large-scale interface friction testing was realized. Large scale friction testing of geosynthetic interfaces demonstrated that available shear strengths under high loads were often described by friction angles less than 10 degrees. Significantly, the use of larger scale, 300 mm square friction boxes explained the Kettleman Hills failure and contributed to the development and performance expression of textured geomembranes. Today, ASTM D 5321, *Standard Test Method for Determining the Shear Strength of Soil-Geosynthetic and Geosynthetic-Geosynthetic Interfaces by Direct Shear*, and ASTM D 6243, *Standard Test Method for Determining the Internal and Interface Shear Resistance of Geosynthetic Clay Liner by the Direct Shear Method* are in universal use.



Figure 3: ASTM D 5321/D 6243 Large-Scale Friction Test

In addition to assisting the industry in developing new materials fostering improved slope stability, the friction test also contributed many laboratory test developments including the accordion pillow for normal load application, soil and GCL clamps providing both hydration and dewatering of absorbent and compressible materials, and a host of tools to verify and document the veracity of load application. Hard lessons learned included the need for proper clamping and the use of displacement rates assuring drained test conditions.

In addition to interface friction, the investigation of other geosynthetic-soil interaction properties has been an ongoing effort for the geosynthetic testing community. From scale affects of applied test equipment to the proper handling of fine grained soils and large aggregates, the testing of geosynthetic interaction properties has been the subject of detailed standardization efforts. This category of testing has been characterized by “art” as well as standard operating procedure. The challenge has been to standardize the art practiced by the experienced “good” laboratories into detailed test procedures put into widespread practice.

The segmental block reinforced soil wall marketplace was partially propelled by robust connection testing of the block to geosynthetic reinforcement connection. This test is standardized in ASTM D 6638, *Standard Test Method for Determining Connection Strength Between Geosynthetic Reinforcement and Segmental Concrete Units (Modular Concrete Blocks)*. The sister to this test is the interaction properties of the geosynthetic within the reinforced soil zone. Pull-out testing was developed for this purpose and is now standardized in ASTM D6706, *Standard Test Method for Measuring Geosynthetic Pullout Resistance in Soil*.

Measured test results assisted the design engineer in realizing cost effective, aesthetically pleasing, engineered civil structures. However, early attempts at good quality measurements included negotiating with inconsistent block, varying grid rib thickness and a range of connection designs including frictional, looped and pinned mechanical connections. Repetitive testing experience and transparency regarding test preparation helped to provide a much needed feedback loop to the manufacturing industry to propel both the improvement of testing techniques and the growth of the technology of geosynthetic reinforced soil walls and slopes.

GEOSYNTHETIC TESTING PLANTS SEEDS OF CHANGE

Geosynthetic test procedures have sometimes been the seeds of change in the way a technical challenge was perceived or a traditionally practiced measurement was performed. This is certainly true with larger scale friction testing discussed previously. It is also certainly true with the development and standardization of the accelerated test methods, such as the Stepped Isothermal Method (SIM).

SIM

While this approach was first described in a GRI test procedure, its current standardized form is documented in ASTM D6992, *Standard Test Method for Accelerated Tensile Creep and Creep-Rupture of Geosynthetic Materials Based on Time-Temperature Superposition Using the Stepped Isothermal Method*. The birth of this test was related to the challenge associated with creep-rupture testing of coated polyester (PET) geosynthetic reinforcement products. Due to the relatively low temperature dependence of PET relative to other polymers and the inherent variability within a product, the observed creep rate at a given load was often found to be less than the creep rate observed at an even higher load. This, of course, did not make sense. The solution was found in a new perspective of the well established but largely unused (in the geosynthetics industry at the time) practice of strain shifting, the process of time-shifting recorded strain data at a given test temperature to overlap with recorded strain data from a higher temperature. The details of SIM have been described in many technical papers, but it is accurate to report that by using a single specimen test, thereby avoiding specimen-to-specimen variability, SIM literally provided a valid short-cut to the traditional strain-shifting process resulting in months if not years of creep-rupture testing being accomplished in a few days time. Because this was so unusual and difficult to absorb, much of the early standardization work focused on non-technical negotiations with various users and regulators. This very necessary and appropriate exercise in defense of a testing technology propelled its use not only in the geosynthetics industry throughout its robust product development, but also other geosynthetics-related industries such as plastic pipe. SIM fostered the keen awareness that not all high tenacity

polyesters are created equal and not all manufacturing techniques are as stressful as others to the final produced product.

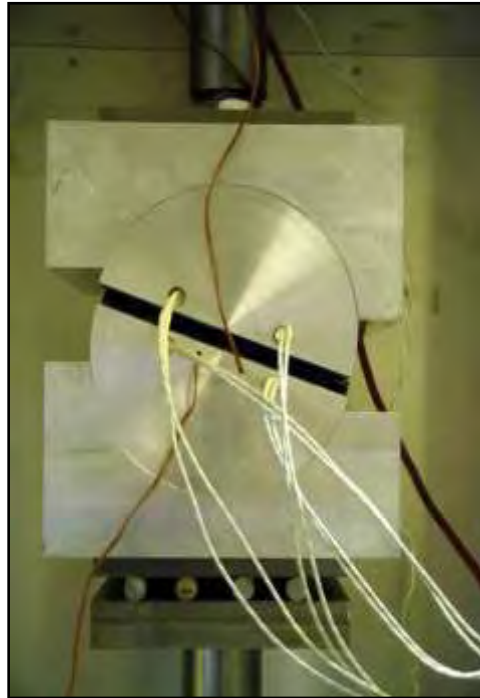


Figure 4: Compressive Creep as Measured Under Shear Loading in Accordance with ASTM D 7361

SIM also fostered new and still increasingly frequent discussion of compression creep behavior of geosynthetic drainage products. The technology of SIM has proven very effective at significantly reducing the time necessary to identify or confirm the creep reduction factor of geonets and geocomposites. ASTM D7361, *Standard Test Method for Accelerated Compressive Creep of Geosynthetic Materials Based on Time-Temperature Superposition Using the Stepped Isothermal Method*, describes the relevant test procedure. Compressive SIM also contributed to new engineered drain structures and continues to foster newer measurement tools in the geosynthetic drain industry including thickness dependent transmissivity testing.

Leak Detection

Other test procedures representing significant industry change include the suite of ASTM test procedures describing electrical resistivity testing used for leak detection in geomembrane containment applications. They are as follows.

- D6747, *Standard Guide for Selection of Techniques for Electrical detection of potential Leak Paths in Geomembranes*
- D7002, *Standard Practice for Leak location on Exposed Geomembrane using Water Puddle System*
- D7703, *Standard Practice for leak Location on Exposed Geomembranes Using the Water Lance System*

- D7007, *Standard Practice for Electrical methods for Locating Leaks in Geomembrane Covered with Water or Earth Material*
- D7240, *Standard Practice for Leak Location using Geomembranes with an Insulating Layer in Intimate Contact with a Conductive Layer via Electrical Capacitance Technique (Conductive Geomembrane Spark Test)*



Figure 5: ASTM D7002 Leak Detection Testing

These procedures set the stage for aggressive adoption of this technology for unequaled quality assurance of installed geomembrane systems, and protection of our environment. For example Abigail Beck of the TRI-CORP Liner Integrity Center recently reported the following information for over thirty landfill expansions using modern construction methods and regulatory driven CQA programs:

- Landfill cells without a liner integrity survey have an average leakage rate of 13.3 gpad.
- Landfill cells that have performed a dipole method survey have an average leakage rate of 7.6 gpad
- Landfill cells that have performed both bare geomembrane and dipole method surveys have an average leakage rate of 1.2 gpad

The technology described in these procedures and practiced in the field continues to change the way we think about construction quality assurance of installed geomembrane systems, encouraging and fostering the highest achieved work effort.

Pore Size Distribution (PSD)

While the global geosynthetics industry copes with a very inconsistent practice of employing a wide range of geotextile opening size measurement procedures, the standard of pore size distribution testing, described in ASTM D 6767, *Standard Test Method for Pore Size Characteristics of Geotextiles by Capillary Flow Test*, is gaining warranted attention. This direct measurement of opening sizes based on measured pore pressures holds the promise of greatly simplifying the measurement of not only opening sizes but also water and air permeability. ASTM Committee D35 held a workshop in January 2013 outlining recent test equipment improvements, PSD correlation to other opening size test procedures and the PSD test result benefit a more robust filtration design. Also of note were reports of how PSD testing has been used forensically to explain unexpected material performance when AOS testing or permittivity testing has not been responsive.

It is now clear that the success of PSD will have implications for the practice of using AOS, COS, FOS, permittivity and air flow test procedures, inviting a significantly reduced measurement regime for geotextile filtration properties. Its implication to existing hydraulic design methods promises to see renewed analyses in this regard.



Figure 6: ASTM D 6767 PSD Test Apparatus

GEOSYNTHETIC TESTING LESSONS LEARNED

It is clear that geosynthetic testing has played a vital role in our narrative, facilitating commerce, developing products, establishing specifications and answering questions. Along the way the testing industry itself has learned a few key lessons that are expected to remain relevant. Two of the most universal of these lessons are as follows.

- 1) Testing is Humility: The best laboratory is one that experiences the full force of system failure including wrong procedure, awkward technique, inappropriate equipment, careless or ignorant process, etc., etc. There is always something to learn and nothing can ever replace the “burn” of tough experience. We simply never know enough. Materials always follow universal laws ...until they don't. Discomfort is key to a robust, alert and active geosynthetic measurement activity.
- 2) Laboratory Testing is Messy: Indeed, the best testing experience is only achieved with a lot of testing! Throughout his book *Outlier's*, the author Malcolm Gladwell often references the "10,000-Hour Rule", arguing that one of the keys to the success in any field is the performance of a specific task for about 10,000 hours. This is certainly true for geosynthetics testing work with its significant variety of materials, test procedures and awareness requirements. And in addition to test performance, a good working geosynthetic laboratory is full of non-testing activity such as sample preparation, equipment calibration, equipment maintenance, environmental control, document management, electronic system maintenance, customer interaction and audit responses just to name a few.

CONCLUSION

The geosynthetics testing industry relies upon a strong and relevant testing community in every aspect of its activity. Testing procedures and the standardization effort behind them has been of historical significance to the broad arc of geosynthetic industry experience, and will continue to be relevant to our future growth. Geosynthetic properties, performance expectations, new application efforts and their place in the family of construction materials will be largely defined by a responsive and successful testing industry relying on the language of measurement.

REFERENCES

- Beck, Abigail (2012). "A Statistical Approach to Minimizing Landfill Leakage", SWANA, Washington D.C. Conference Proceedings.
- Beck, Abigail (2012). "How Much Does my Landfill Leak?" Waste Advantage Magazine, December Issue.
- Gladwell, Malcolm (2008). *Outliers*. Little, Brown and Company. pp. VII–IX. ISBN 978-0-316-01792-3.

BACKGROUND AND DEVELOPMENT OF GRI's GEOSYNTHETICS SPECIFICATIONS

Robert M. Koerner and George R. Koerner
Geosynthetic Institute, Folsom, PA USA

ABSTRACT

When the National Sanitation Foundation ceased servicing and distributing its NSF #54 specification for geomembranes in 1991, the task fell upon the Geosynthetic Research Institute (GRI)* for continuation. With a bit of trepidation we started on HDPE but only after considerable in-house research was undertaken, particularly on stress crack resistance and oxidative induction time. After the specification was finalized in 1997, LLDPE followed in 2000 and then fPP in 2002. Upon investigating a number of fPP failures the fPP specification was withdrawn followed by a major in-house research project on exposed durability and then reinstated in 2009. Scrim reinforced polyethylene specifications were adopted between 2003 and 2009 for fPP, LLDPE and MDPE as well as for EPDM both nonreinforced and scrim reinforced. The seaming specification for all of the polyolefins was adopted in 2002.

Other specifications were developed where the need was evidenced. The geotextile tube specification in 1999, geotextile cushion specification in 2002 and 2004, geotextile separators specification 2004 and 2008, and the GCL specification in 2005. Current efforts are focused on a geocell specification.

Other possible geosynthetics specifications for geogrids, geonets/geonet composites and turf reinforcement mats have not been successful to date although many draft versions have been attempted.

In spite of the lack of a complete set of specifications, however, it is felt (and sincerely hoped) that the GRI geosynthetic materials specifications have brought a considerable amount of order to an otherwise turbulent scene. While some manufacturers are understandably reluctant to enter such efforts, the specifying community is certainly pleased with the results to date as evidenced by their widespread use. We will certainly continue to maintain and update the existing specifications and attempt to get the draft efforts into final approved status.

*The Geosynthetic Research Institute (GRI) was formed in 1986. From that time forward, all standards (specifications, guides, practices and test methods) have been prefixed GRI and continue to the present. The superseding Geosynthetic Institute (GSI) was formed in 1995 with GRI being one of its five subsidiary institutes.

BEGINNINGS

Of the various and ever-growing applications for geosynthetic materials in the late 1970's and 1980's three groups envisioned the need for generic specifications. They were the U.S. Army Corps of Engineers (COE) for hydraulically related geosynthetics, the Federal Highway Administration (FHWA) together with the American Association of State Highway and Transportation Officials (AASHTO) for transportation related geosynthetics, and the U.S. Environmental Protection Agency (EPA) for waste containment related geosynthetics. The first two groups (COE and FHWA/AASHTO) developed their generic specifications "in-house" with the majority of input coming from federal and state agency personnel. The third group (EPA) relied almost exclusively on those in private industry which had a vested interest in the outcome. It is this third group focusing on geomembranes which eventually was replaced by GSI's research arm, the Geosynthetic Research Institute, in becoming involved in the specification process.

The Resource Conservation and Recovery Act of 1976 gave the U. S. EPA the authority to control hazardous substances from cradle-to-grave. Between this time and the land disposal restrictions for hazardous wastes (commonly called Subtitle "C"), considerable research at many academic institutions was undertaken regarding barriers to contain both liquid and solid wastes. Most significant was the work of Anderson, et al. (1981) who used 100% neat chemicals to permeate different clay soils in fixed wall permeameters. The (now obvious) result was shrinkage of the clay soil test specimens such that rapid flow occurred through the clay specimen and into the effluent. This undesirable feature of clay liners caused the EPA to promulgate the following regulations on July 6, 1982:

"Prevention (via synthetic membrane liners); rather than minimization (via clay liners), of leachate migration similarly produces better environmental results in the case of surface impoundments used to dispose of hazardous wastes. A liner that prevents rather than minimizes leachate migration provides added assurance that environmental contamination will not occur."

The synthetic membrane liners in the above regulation were renamed by federal and state personnel to flexible membrane liners, or FML's, and are fully embedded in environmental regulations to date. Obviously, the above situation stimulated the growth of the FML (aka, geomembrane) industry and many *proprietary specifications* (for both thermoplastic and thermoset resin types) became immediately available.

The task of putting some order and control to the situation fell to EPA's National Environmental Research Center in Cincinnati, Ohio and specifically to its Chief, Robert E. Landreth. He co-opted the National Sanitation Foundation (NSF) to convene groups of individuals from the liner community to generate *generic specifications* within each specific resub type. Included were personnel from public health, users and industry groups which eventually developed the NSF #54 set of generic specifications (1983, 1985, 1990 and 1991). The following geomembrane materials and their seams were included:

- Polyvinyl Chloride (PVC)

- Polyvinyl Chloride-Oil Resistant Grade (PVC-OR)
- Chlorinated Polyethylene (CPE) Unsupported
- Chlorinated Polyethylene (CPE) Supported
- Polychloroprene (CR) Unsupported
- Polychloroprene (CR) Supported
- High Density Polyethylene (HDPE) Non-Textured
- Ethylene-Propylene Diene Terpolymer (EPDM)
- Epichlorohydrin Polymers (CO)
- Chlorosulfonated Polyethylene (CSPE)
- Chlorosulfonated Polyethylene-Low Water Absorption (CSPE-LW)
- Thermoplastic Nitrile-PVC Oil Resistant Grade (TN-PVC)
- Ethylene Interpolymer Alloy (EIA)
- Chlorinated Polyethylene Alloy (CPE-A) Unsupported
- Chlorinated Polyethylene Alloy (CPE-A) Supported

Subsequent to 1991, however, the committee did not meet and NSF then decided not to continue the effort in light of their many other activities. Since the Geosynthetic Research Institute was well established by now, its resin and geomembrane focus groups suggested that GRI should become involved. More specifically those geomembranes no longer used should be eliminated, newer geomembranes should be added, and all of the physical, mechanical and endurance properties should be updated to current ASTM and GRI standard test methods. This ongoing activity fell to the Geosynthetic Research Institute (GRI) which was somewhat of a “stretch” since it was a new activity (other than research, per se) which would challenge our negotiating and people-oriented skills. That said, GRI was indeed a logical choice for crafting specifications since all possible tests were conducted in-house which is a great asset insofar as credible data is concerned. Furthermore, the laboratory accreditation program, handled by George Koerner, was operational and challenges to the data that was generated were minimal.

THE GRI GM13 SPECIFICATION FOR HDPE (SMOOTH AND TEXTURED) GEOMEMBRANES

High density polyethylene (HDPE) manufacturers began operations in the Houston, Texas area in 1982. Within the next 10-years this material in various thicknesses was used for the base liner of solid waste landfills and liquid surface impoundments on a regular basis. The only generic specification was according to NSF #54 and it needed drastic revision. Two items were in dire need of updating and/or replacing; stress crack resistance and durability criteria. Perhaps most importantly was the assessment of stress crack resistance which used ASTM D1693 (the bent strip test) in the NSF #54 specification. On several occasions materials which passed this laboratory test subsequently failed in the field, Hsuan 1998 and 2000. As a result, we were awarded an EPA contract to look into the matter and Grace Hsuan was the principal investigator. Over the subsequent 7-8 years she developed the notched constant tension load (NCTL) test and its single point variation per ASTM D5397. The research was a coordinated effort with most of the sheet manufacturers and resin suppliers. Ultimately, the research effort had the effect of eliminating some ten resins from use in manufacturing HDPE geomembranes. Figure 1 presents this situation which also served the purpose of setting a minimum value for use in the eventual specification. For the single point version of the test, the original specification

value was originally set at 200 hours and subsequently increased to 300 hrs. The effect of this new test method and its numeric value was to virtually eliminate stress crack failures of HDPE geomembranes in the field.

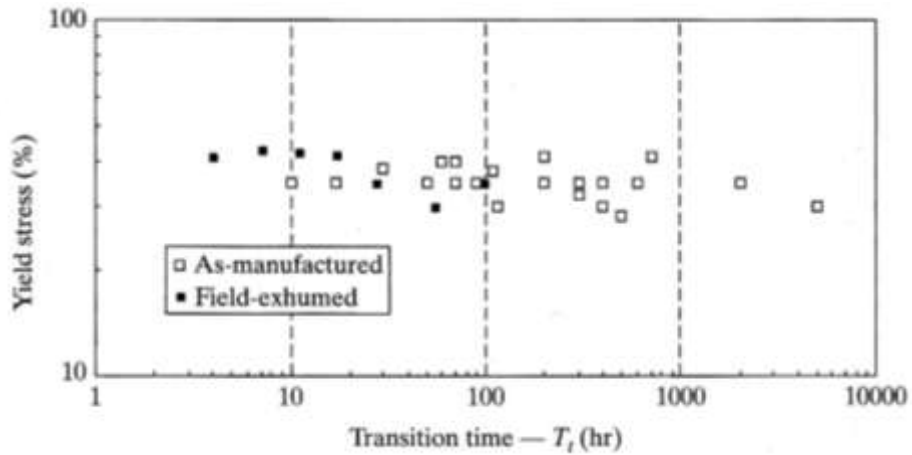


Figure 1. Ductile-to-brittle transition points for 21 virgin geomembranes and 7 field-retrieved geomembranes (after Hsuan 1998, 2000).

In a parallel effort we were awarded a second EPA contract to estimate the durability, aka to predict field service life, of HDPE under buried conditions such as beneath a solid waste landfill. This 10-year effort, based on laboratory modeling using time-temperature superposition and then subsequent Arrhenius modeling, indicated that the lifetime of HDPE consisted of three distinct stages as shown in Figure 2.

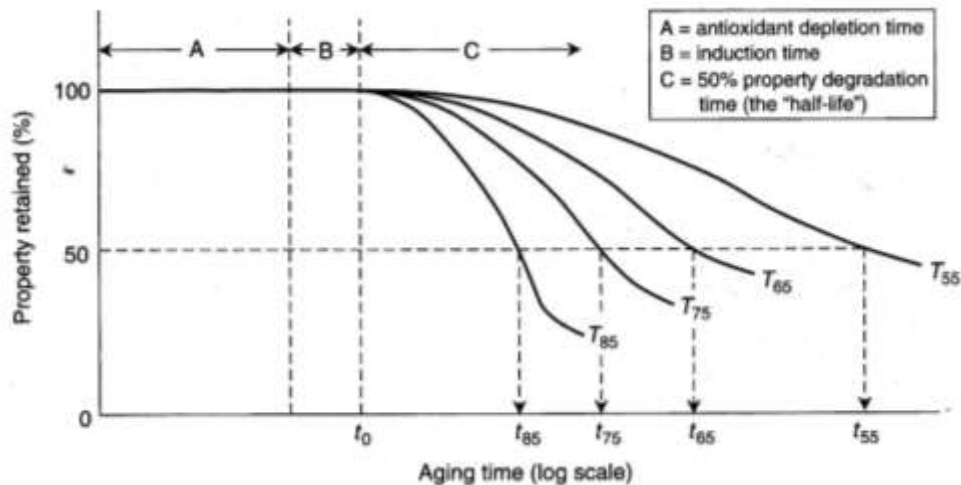


Figure 2. Lifetime stages of polyolefin geomembranes (Koerner, et al., 1990).

These stages were subsequently quantified as given in Table 1. In it can be seen that Stage A, the antioxidant depletion time for HDPE at 20°C, is slightly over 200 years. Fortunately, the antioxidants in an HDPE formulation can be indirectly challenged using the oxidative induction

time (OIT) test, either standard or high pressure, and can thereby be included in a generic specification. These two issues, stress crack resistance and oxidative induction time, led directly into the formation of our first generic specification that being for HDPE smooth and textured geomembranes.

Table 1 – Lifetime Prediction of a Nonexposed HDPE Geomembrane as a Function of In-Situ Service Temperature (Koerner, 2012)

In Service Temperature (°C)	Stage “A” (years)			Stage “B” (GSI data) (years)	Stage “C” (Ref. 43) (years)	Total Prediction* (years)
	Standard OIT	High Press. OIT	Average OIT			
20	200	215	207	30	208	445
25	135	144	140	25	100	265
30	95	98	97	20	49	166
35	65	67	66	15	25	106
40	45	47	46	10	13	69

*Total = Stage A (average) + Stage B + Stage C

At a December 13, 1998 meeting in Philadelphia, work began in earnest on a table of required test methods, values and frequency of testing. In the group were resin producers: Rex Bobsein of Phillips, Nolan Edmonds of Novacor, Phil Dunaway of Solvay, Frank Nagy of Mobil, Adel Haddad of Quantum, Pam Maeger of Chevron, and geomembrane manufacturers: Fred Struve/Bill Walling of Gundle, Gary Kolbasuk/George Zagorski of NSC, Jim Nobert/George Yazdani of Poly-Flex, Bob Otto of Serrot, Dave Eakin of S.D. Ent.

Following this meeting, intense testing was performed by all of these organizations in assessing the stress cracking performance of their materials via the new ASTM D5397 notched constant tensile load (NCTL) test. In addition, the standard and high-pressure OIT initial values and subsequently after oven ageing and ultraviolet fluorescent exposure were major durability items worked on by all. Note that both stress cracking and OIT performance are both resin and additive related, thus the large group of resin producers was extremely active, and the geomembrane manufacturers as well. Simultaneous with the durability criteria development was the physical and mechanical property development. Here the geomembrane manufacturers played the major role, as did George Koerner, in evaluating and homogenizing the data into a single set of acceptable values. It should be noted that many nominally significant tests which were in the NSF #54 specification were purposely omitted. They were as follows:

- volatile loss
- dimensional stability
- coefficient of linear expansion
- resistance to soil burial
- low temperature impact
- bent strip ESCR test
- wide width tensile
- water vapor transmission
- water absorption

- ozone resistance
- modulus of elasticity
- hydrostatic resistance
- tensile impact
- multi-axial burst

After three meetings and countless telephone calls among the parties involved, the HDPE specification tables were completed. Text was then added and agreed upon by the two focus groups. The complete draft specification was then sent to the general membership for comments, and there were many. The focus groups then assessed these comments and agreed to the final specification. It was launched June 27, 1997, under the title:

GRI-GM13, Standard Specification for “Test Methods, Test Properties, Testing Frequency for High Density Polyethylene (HDPE) Smooth and Textured Geomembranes”. Subsequently, this specification has had eleven minor revisions.

For additional detail see Hsuan and Koerner (1997, 1999) and Koerner (2008).

THE GRI-GM17 SPECIFICATION FOR LLDPE (SMOOTH AND TEXTURED)

The same two focus groups involved in the HDPE specification transitioned directly into the development of a lower density polyethylene specification. This was initially called very low density polyethylene (VLDPE), which was a bad idea of Bob Koerner, but then relabeled more appropriately as linear low density polyethylene (LLDPE). Some major differences between it and the HDPE specification are as follows:

- tensile yield strength and elongation are not required for LLDPE, only break strength and elongation
- 2% modulus as a maximum value is required so as to ensure flexibility
- initial OIT values are the same as HDPE however, lower percentages are required after oven aging and ultraviolet exposure
- a large three-dimensional axi-symmetric break strain test is required

This last test method was developed so as to simulate out-of-plane deformation of geomembranes and was originated by Koerner, et al. (1990). They unfortunately used a very high pressurization rate of 6.9 kPa/min. This was then copied as the default pressurization rate in the current ASTM D5716 test method. It is presently felt to be much too fast to give a representative performance value for the various geomembrane materials. Additional work is presently ongoing to observe slower pressure rates thereby allowing stress relaxation of the molecular structure to occur during the test. The LLDPE specification was adopted on April 3, 2000, under the title:

GRI-GM17, Standard Specification for “Test Methods, Test Properties, Testing Frequency for Linear Low Density Polyethylene (LLDPE) Smooth and Textured Geomembranes”. Subsequently, this specification had nine minor revisions.

THE GRI-GM18 SPECIFICATION FOR fPP GEOMEMBRANES (NONREINFORCED AND SCRIM REINFORCED)

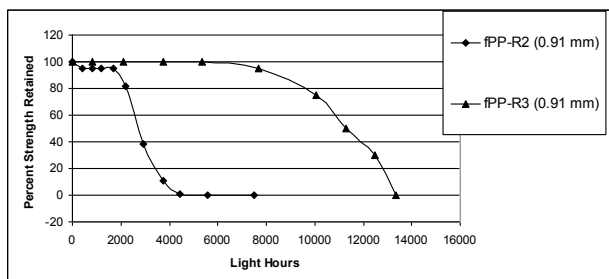
Having both HDPE and LLDPE specifications ongoing, we felt that the third polyolefin geomembrane, namely flexible polypropylene, would be similar. Considerable overlap was indeed the case in physical and mechanical properties for unreinforced fPP, however, a new set of test methods and test values were needed for the scrim reinforced types, namely, for fPP-R. This was accomplished by considerable in-house testing and also testing by different focus groups of GSI members. The polyethylene groups now transitioned to polypropylene resin suppliers and sheet manufacturers. They included the main resin producer Bob Butala/Stan Bialowas of Basell; the geomembrane manufacturers Chris Taylor of Carlisle, Joe Kalbas/John Heathcote of Firestone and consultants Ron Frobel and John Cowland.

We unfortunately (as was to be seen) extended the OIT values for the polyethylene specifications to the durability criteria for polypropylene. The original fPP specification was adopted on February 18, 2002, under the title:

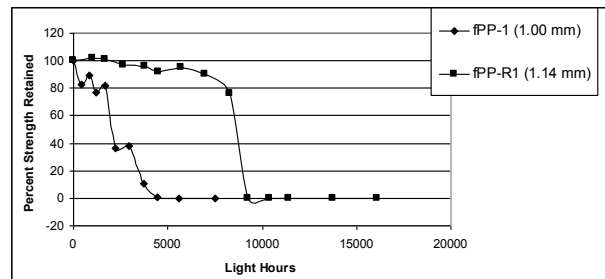
GRI-GM18, Standard Specification for “Test Methods, Test Properties, and Testing Frequencies for Flexible Polypropylene (fPP and fPP-R) Nonreinforced and Reinforced Geomembranes”.

Within a year of its adoption we had a fPP field failure which unfortunately passed our OIT durability criteria. Several other failures occurred subsequently and this specification was temporary suspended on May 3, 2004 and then withdrawn on January 22, 2007, due to concerns about OIT being able to predict long-term durability. Apparently, the antioxidant depletion mechanism characterized by OIT tests in HDPE and LLDPE geomembranes is more complicated and less reliable for fPP geomembrane formulations.

An intense research program followed using the fluorescent ultraviolet light weathering devices (ASTM D5238) subjecting samples until their halflife occurred in either strength or elongation. Using a correlation factor from four field failures (see Figure 3 and Table 2 where 1.0 year in a hot climate equals 1200 light hours at 70°C) we used a 20,000 light hour criterion as being the minimum acceptable durability value. The resulting exposed lifetime predictions using this protocol for fPP and most other commonly used geomembranes are given in Table 3. The GRI GM18 specification was reinstated on March 20, 2009. It has had six minor revisions.



(a) Two field failure sites in West Texas



(b) Two field failure sites in Southern California

Figure 3. Ultraviolet incubation times versus strength retained for four archived fPP geomembranes taken from field failures sites; Koerner, Koerner and Hsuan (2012).

Table 2 - Laboratory-to- Field Correlation Factor (using ASTM D7238 @ 70°C); GRI (2012)

Method	Thickness (mm)	Field (yrs.)	Location	Lab halflife (lt. hr.)	Correlation Factors (lt. hrs./1.0 yr.)
fPP-1	1.00	≈ 2	W. Texas	1800	900
fPP-R1	1.14	≈ 8	W. Texas	8200	1025
fPP-R2	0.91	≈ 2	So. Calif.	2500	1250
fPP-R3	0.91	≈ 8	So. Calif.	11200	1400
					1140 (ave.)

Table 3 - Predicted Geomembrane Lifetimes Based on 50% Reduction of Strength and/or Elongation; Koerner, R. M., Koerner, G. R. and Husan, Y. G. (2012)

Geomembrane Type	Nominal thickness (mm)	Applicable Specification	50% reduction* (light hours)	Predicted lifetime (years)
fPP	1.00	GRI-GM18	40,000	33
HDPE	1.50	GRI-GM13	≈ 60,000	≈ 50
LLDPE	1.00	GRI-GM17	40,000	33
EPDM	1.14	GRI-GM21	37,000	30
PVC-N.A.	0.75	ASTM D7171	8,000	7**
PVC-Euro	2.50	proprietary	38,000	32

*Using ultraviolet fluorescent weathering devices at 70°C set at 340 nm wavelength and 0.78 W/(m²-nm) irradiance for a daily cycling of 20 hours light and 4 hours dark with condensation.

**Only recommended for “buried applications”.

THE GRI-GM22 SPECIFICATION FOR PE-R EXPOSED GEOMEMBRANES

The GM22 specification is focused on lightweight scrim reinforced polyethylene geomembranes used for temporarily exposed conditions. It covers 0.2, 0.3 and 0.5 mm thickness sheet. The resin density is unspecified with the exception that it must be 0.930 g/cc or greater. High pressure OIT is required of 1000 min. and a minimum of 50% strength and elongation retained is required after 10,000 light hours in fluorescent light exposure per ASTM D7238 at 70°C. The specification was adopted on November 9, 2006 under the title:

GRI-GM22, “Test Methods, Required Properties and Testing Frequencies for Scrim Reinforced Polyethylene Geomembrane Used in Exposed Temporary Applications”. It has had one revision. It has had two minor revisions.

THE GRI-GM25 SPECIFICATION FOR LLDPE-R GEOMEMBRANES

This specification for scrim reinforced linear low density polyethylene (LLDPE-R) geomembrane could well have been coupled to GRI-GM17, but several members wanted it to be separate. Different, however, is that the thickness categories of 0.61, 0.91, and 1.14 mm are

coupled with serviceability commentary of standard, moderate and severe conditions, respectively. The commonality of the sheet properties to GM17 and the scrim properties to GM18 is to be expected. The specification was adopted on September 18, 2009 under the title:

GRI-GM25, “Test Methods, Required Properties and Testing Frequencies for Reinforced Linear Low Density Polyethylene (LLDPE-R) Geomembranes”. It has had four minor revisions.

THE GRI-GM21 SPECIFICATION FOR NONREINFORCED AND REINFORCED EPDM GEOMEEMBRANES

The only non-polyolefin geomembrane specification we have is for the thermoset polymer ethylene propylene diene terpolymer, or EPDM. The specification covers both nonreinforced and scrim reinforced types in several thicknesses. The physical and mechanical tests and required properties follow the polyethylene and polypropylene specifications but the durability criteria are different. After oven aging and ultraviolet light exposure (either Xenon arc or fluorescent tube devices) percents retained for strength and elongation of the nonreinforced types are required. For the scrim reinforced types, a bend test was developed and at a 7X magnification no surface cracking can be observed. This specification was adopted on October 27, 2003 under the title:

GRI-GM21, “Test Methods, Required Properties and Testing Frequencies for Ethylene Propylene Diene Terpolymer (EPDM) Nonreinforced and Scrim Reinforced Geomembrane”. It has had four minor revisions.

THE GRI-GM19 GEOMEMBRANE SEAM SPECIFICATION

The NSF #54 specification included seam test requirements with each of the respective sheet resin types. We decided to have a separate seam specification since we were dealing almost exclusively with polyolefins, the exception being EPDM which is totally different in its seaming requiring adhesive bonding or an adhesive tape.

As with accepted practices, the relevant seam tests for the polyolefins were shear and peel for both fusion and extrusion welding of the various sheets. The first issue raised by several specifiers was why require 90% of the sheet strength in shear and only 62% of the sheet strength in peel? These values stemmed from Henry Haxo of Matrecon (1988) who performed the earliest EPA research on the topic. As found by Struve and Koerner (2005), however, when the parent unseamed sheet is pulled over a 90° rod (as in the peel seam test) its strength decreases significantly compared to the standard linear tension mode. It is such that 62% of the sheet in the peel test compared to the standard tension test mode is about 90% of the sheet in a similar mode. Thus, the 90% in shear and 62% in peel are reasonably logical values for a seam specification. That said, the general agency and specifying engineer’s concern over seam strength (as contrasted to seam uniformity and consistency) was felt to be somewhat excessive. For this reason the GRI-GM19 specification values are somewhat lower than most specifications based on the above percentages. We felt that this lower strength approach was somewhat justified based on the leak location data of Table 4. Here it was seen that only 6.32% of

geomembrane holes in the field were caused by the welding of the seams. Conversely, the balance of the holes were in the sheets themselves. This leads one to conclude that perhaps our general focus for quality assurance purposes should be more than simply testing geomembrane seams?

Table 4 – Holes in Geomembranes Located by the Electrical Leak Location Method; Nosko and Touze-Foltz (2000)

(a) Location of Holes

No. of Holes	Flat Floor (1)	Corners and Edges (2)	Under Drainage Pipes (3)	Pipe Penetrations (4)	Other (5)
4194 100%	3261 77.8%	395 9.4%	165 3.9%	84 2.0%	289 6.9%

(b) Cause of Holes vs. Size of Holes

Size of Holes (cm ²)	Stones	%	Heavy Equip.	%	Seam Welds	%	Cuts	%	Worker Directly	%	Total
<0.5	332	11.1	-	-	115	43.4	5	8.5	195	-	452
0.5-2.0	1720	57.6	41	6.3	105	39.6	36	61.0	105	84.4	2097
2.0-10	843	28.2	117	17.9	30	11.3	18	30.5	36	15.6	1044
>10	90	3.0	496	75.8	15	5.7	-	-	-	-	601
Amount	2985		654		265		59		231		4194
Total	71.17%		15.59%		6.32%		1.41%		5.51%		100%

The GRI-GM19 seam specification addresses the required strength and related properties of thermally bonded polyolefin geomembranes; in particular, high density polyethylene (HDPE), linear low density polyethylene both nonreinforced (LLDPE) and scrim reinforced (LLDPE-R) and flexible polypropylene both nonreinforced (fPP) and scrim reinforced (fPP-R). It became available on February 18, 2002 under the title:

GRI-GM19, “Seam Strength and Related Properties of Thermally Bonded Polyolefin Geomembranes”. It has had six minor revisions, one of which addressed the separation-in-plane (SIP) mode of failure. In this regard SIP is acceptable if the seam passes all other criteria of the specification.

THE GRI-GT12 GEOTEXTILE CUSHION SPECIFICATION

This specification was prompted by two facts; namely, that holes in geomembranes are primarily made from stone punctures (71.17% according to Table 4b) and that no available geotextile specification addressed very high mass per unit area (weight) geotextiles. These

cushioning (or protection) geotextiles are invariably needle punched nonwoven polypropylene fabrics.

The variation in mass per unit area as indicated in the specification is from 340 to 4000 g/cc. Using this range of geotextile weights mechanical tests were conducted in-house leading to grab tensile strengths and elongations, as well as tear and puncture resistance test. Since puncture behavior is at the heart of the material’s performance in a cushioning specification three alternative puncture tests are allowed. The pin puncture (ASTM D4833) is the standard, but pyramid puncture (ASTM D5494) and CBR puncture (ASTM D6241) are possible alternatives. Figure 4 shows the interesting interrelationships between the three puncture tests.

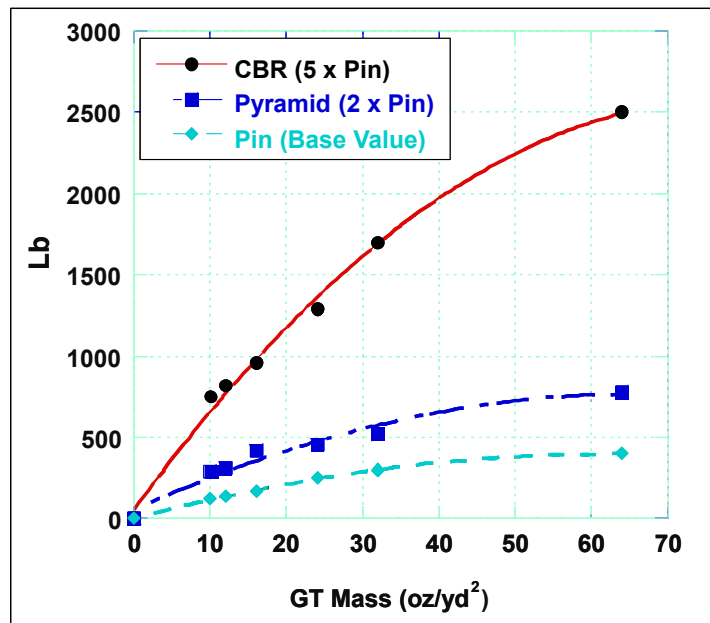


Figure 4. Puncture test method interrelationships for needle punched nonwoven geotextiles.

The specification is listed as GRI-GT12(a) “ASTM Version” and titled “Test Methods and Properties for Nonwoven Geotextiles Used as Protection (or Cushioning) Materials”. The ASTM version was approved on February 8, 2002 and has had two minor revisions to date.

Subsequent to the ASTM test methods being exclusive to the specification we were requested to have an alternative ISO test method which was developed accordingly via George Koerner’s correlation testing.

The equivalent specification is listed as GRI-GT12(b) “ISO Version” under the same title, but with only one puncture method that being ISO 12959. The ISO version was approved on March 10, 2004 and one revision has been made to date.

THE GRI-GCL3 SPECIFICATION FOR GEOSYNTHETIC CLAY LINERS

This specification covers geosynthetic clay liners (GCLs), describing types of tests, the specific test methods, minimum and sometimes maximum values, and the minimum testing frequencies. Geosynthetic Clay Liners (GCLs) are also called Clay Geosynthetic Barriers (GBR-Cs). There are two general categories of GCLs covered in this specification: internally reinforced and nonreinforced. Within each of these categories there are geotextile related, polymer coated geotextile related, and geomembrane/geofilm related types.

Being one of our most complicated specifications due in large part by the large variation in the manufactured products, there are separate test methods for the clay component itself, geotextiles themselves, and the geomembrane/geofilm themselves. Then there are also tests required for the manufactured composite material. In crafting the specification there were many specific issues most of which required considerable compromise for the different manufacturers (primarily Kent von Maubeuge of NAUE and Jim Olsta of CETCO) and the authors in convening the group. They were as follows:

- mass per unit area of geotextiles
- scrim component within geotextiles
- geofilm thickness
- mass per unit area of bentonite
- peel strength of the composite
- permeability testing of geomembranes and geofilm related GCLs
- maximum alkaline liquid permeability
- broken needles in manufactured product
- minimum field overlap distance
- GCL wrapping material and thickness

Further discussion on each of these items is available in Koerner (2010). That said, there are still three unsettled issues which are being investigated. They are swell index, moisture content and alkalinity permanent. Commentary on each follows.

It is generally known that high quality field deposits of sodium bentonite are becoming more scarce and more costly to excavate, transport and process from their geologic origin. That said, the bentonite in some GCL's is presently a "peptized" calcium bentonite which introduces sodium ions into the bentonite structure. Such processing can change the swell index which is presently set at 24 ml/2g. The current value is under review and discussion.

The as-manufactured moisture content of the bentonite in different GCL's is an active point of disagreement among manufacturers and users. The range of values is from 10% to 40%, which is obviously enormous. To simply take the average of all manufactured products serves no one and is therefore not an option. The specification lists the value as being "both site-specific and product-specific and is currently being evaluated".

Presently the alkalinity permeant required in the specification is a 0.1 M CaCl₂ solution. This arbitrary value is quite contentious. Efforts are ongoing to evaluate other permeants, such

as different leachates (from landfills, shale gas operations and coal combustion residuals), to see if a more typical alkaline permeant can be used.

The specification has been finalized as of May 16, 2005 under the designation GRI-GCL3 and is titled “Test Methods, Required Properties, and Testing Frequencies of Geosynthetic Clay Liners (GCLs)”. It has had two minor revisions to date.

THE GRI-GT10 SPECIFICATION FOR GEOTXTILE TUBES

Not covered in the FHWA/AASHTO specification for commonly used geotextiles is one designated for geotextile tubes. This specification covers high strength geotextile index test properties for subsequent use to form coastal and riverine structures in the form of a soil filled geotextile tubes. The specification sets forth a set of minimum physical, mechanical and hydraulic properties that must be met, or exceeded by the geotextile being manufactured. In a few cases, a maximum value is specified. The specification covers not only the main geotextile tube, but also the scour apron(s), if so required in the design. Also the numeric tables are in categories for “aggressive” conditions or Class 1 and for “typical” conditions or Class 2. The manufacturers group which interacted in the crafting of the specification was Tom Stevens and John Henderson of TenCate, Tom Collins of Huesker and Gary Willibey of Propex.

Perhaps the greatest item of concern was the tension testing of the high strength geotextiles in this specification. Such testing is highly dependent on the grip type vis-à-vis the strength of the fabric and its seams. A special guide was crafted in this regard, GRI-GT9, and in Table 5 the various grip types for different strength geotextiles are readily seen.

Table 5 – Recommended Grip Types for Wide Width Testing of Geotextiles and Their Seam Connections, see GRI-GT9 for Details

Grip Type	Examples or Description	Ultimate Wide Width Tensile Strength (± 25%)	
		kN/m	lb/in
(1) standard	<ul style="list-style-type: none"> • mechanical • serrated surfaces • commonly available 	< 50	< 300
(2) special	<ul style="list-style-type: none"> • air or hydraulic activated • special friction or shaped surfaces • many have a keeper behind grips 	< 90	< 500
(3a) wedge	<ul style="list-style-type: none"> • mechanical • serrated • epoxy/soft metal 	< 180	< 1000
(3b) split barrel	<ul style="list-style-type: none"> • internal keeper 	< 180	< 1000
(4) roller	<ul style="list-style-type: none"> • capstan type • internal keeper 	unlimited	unlimited

This specification was adopted on September 27, 1999 under the title of: “Test Methods, Properties and Frequencies for High Strength Geotextile Tubes Used as Coastal and Riverine Structures”. It was revised one time since its inception.

THE GRI-GT13 SPECIFICATION FOR GEOTEXTILE SEPARATORS

In general, we do not craft generic specifications in cases where another credible group has the topic covered. This is certainly the case for the AASHTO M288 specification on commonly used geotextiles in the transportation industry. In it geotextile separation between subgrade soil and stone base aggregate is covered insofar as required test methods and properties are concerned. That said, the installation survivability classifications of Class 1, 2 or 3 geotextiles are listed but left open to the specifier as to how to differentiate between them. We have had many questions in this regard. Table 6 following is the essential contribution that our specification brings to the user. The class of geotextile is completely defined insofar as the construction site conditions and proposed installation equipment are concerned.

One other addition to this specification is that both ASTM and ISO versions are available with their respective test method designations.

These two specifications GRI-GT13(a) – ASTM Version and GRI-GT13(b) – SI Version are titled “Test Methods and Properties for Geotextiles Used as Separation Between Subgrade Soil and Aggregate” and they were adopted in 2004 and 2008 respectively. The ASTM version has seen two minor revisions since adoption.

Table 6 - Required Degree of Survivability as a Function of Subgrade Conditions, Construction Equipment and Lift Thickness
 (Class 1, 2 and 3 Properties are Given in the AASHTO M288 Specification;
 Class 1 + Properties are Higher than Class 1 but Not Defined at this Time)

	Low ground-pressure equipment ≤ 25 kPa (3.6 psi)	Medium ground-pressure equipment > 25 to ≤ 50 kPa (>3.6 to ≤ 7.3 psi)	High ground-pressure equipment > 50 kPa (> 7.3 psi)
Subgrade has been cleared of all obstacles except grass, weeds, leaves, and fine wood debris. Surface is smooth and level so that any shallow depressions and humps do not exceed 450 mm (18 in.) in depth or height. All larger depressions are filled. Alternatively, a smooth working table may be placed.	Low (Class 3)	Moderate (Class 2)	High (Class 1)
Subgrade has been cleared of obstacles larger than small to moderate-sized tree limbs and rocks. Tree trunks and stumps should be removed or covered with a partial working table. Depressions and humps should not exceed 450 mm (18 in.) in depth or height. Larger depressions should be filled.	Moderate (Class 2)	High (Class 1)	Very High (Class 1+)
Minimal site preparation is required. Trees may be felled, delimited, and left in place. Stumps should be cut to project not more than ± 150 mm (6 in.) above subgrade. Fabric may be draped directly over the tree trunks, stumps, large depressions and humps, holes, stream channels, and large boulders. Items should be removed only if placing the fabric and cover material over them will distort the finished road surface.	High (Class 1)	Very high (Class 1+)	Not recommended

*Recommendations are for 150 to 300 mm (6 to 12 in.) initial lift thickness. For other initial lift thicknesses:

- 300 to 450 mm (12 to 18 in.): reduce survivability requirement one level;
- 450 to 600 mm (18 to 24 in.): reduce survivability requirement two levels;
- > 600 mm (24 in.): reduce survivability requirement three levels

Note 1: While separation occurs in every geotextile application, this pavement-related specification focuses on subgrade soils being “firm” as indicated by CBR values higher than 3.0 (soaked) or 8.0 (unsoaked).

Source: Modified after Christopher, Holtz, and DiMaggio (1984)

OTHER GRI GENERIC SPECIFICATIONS

Admittedly, our track record for other geosynthetic specifications has not been good. There is indeed a demand by the user/specifier community, however, product variation for some geosynthetics is so great and entrenched interests are so compelling that many are in draft form and not yet finalized. They are as follows:

- Specification for Uniaxial Geogrids in Permanent Reinforcement Applications, e.g., Reinforced Walls and Steep Soil Slopes (18 revisions to date)
- Specification for Biaxial Geogrids in Reinforcement Applications, e.g., Pavements, Foundations and Bases (9 revisions to date)
- Specification for Biplanar Geonets and Geonet Composites (countless revisions to date)
 - Approach A – No Transmissivity
 - Approach B – With Transmissivity Values
 - Approach C – With Transmissivity Values and Default Reduction Values
- Specification for Turf Reinforcement Mats (4 revisions to date)

SUMMARY AND CONCLUSIONS

In 1991 when the National Sanitation Foundation ceased servicing and distributing its NSF #54 specifications for geomembranes we had no idea that GSI/GRI would become so involved since then and apparently into the future as well. To be sure, it is a most difficult process to craft a credible generic specification for a given category of geosynthetic material. If required test properties are too low then utility to the regulator, owner, designer and specifier is compromised, and if too high then constraints to the resin/additive supplier, manufacturer and sales representatives are unacceptable. Indeed a realistic “middle ground” is necessary on the part of all involved and particularly for the negotiator; that being GSI/GRI in the case of these specifications.

Upon reflection, however, there are several powerful reasons why GSI/GRI should be involved in crafting of generic geosynthetic specifications.

1. The membership of the institute is open to all segments of the industry. Regulators, owners, consultants, testing laboratories, resin suppliers, additive suppliers, manufacturers/representatives and contractors/installers are all involved which has the decided advantage that at the end of the process one has arrived at an industry-wide specification.
2. From its very inception in 1986 GRI has been developing and distributing detailed test methods. Therefore, if a specification calls for a new test method we can develop it almost immediately in comparison to the extremely long times for ASTM and ISO. Afterward, such a GRI test method can be transitioned to ASTM (or ISO) as have been 26 of them to date.
3. By virtue of the institute’s Laboratory Accreditation Program we can perform every ASTM, ISO and GRI test method that is known to exist. Thus, *opinion* in the negotiations is minimized and *factual data* is maximized. Even further, it is difficult to

criticize the in-house data since we are the deciding laboratory in proficiency testing as well as in countless conflict-resolution decisions.

4. The monetary issue is largely non-existent since GSI does not do independent laboratory testing or consulting. Of course, it is the member organizations who initiate, interact and approve the specifications, however, there are many cases where non-GSI organizations have had meaningful input to the process.
5. The specifications are completely free to anyone with an interest in using them. They are on the open section of our website at www.geosynthetic-institute.org/spec.htm and it is always the most recent revision that is presented.
6. Each of the specifications on our website is accompanied by a power point tutorial showing all of the test methods and the numeric values required.
7. We are not offended in any way if users of our generic specifications modify them for site-specific applications so long as the modifications are appropriately designated. In this regard, revisions (if common) are an excellent indication to us that the matter or item should be re-investigated.

In conclusion, the crafting of generic specifications by GSI/GRI was never in our original “business plan” but we are glad to have embarked on the venture. While negotiations were and are often contentious, we at the institute have been made better and we certainly hope that the geosynthetics industry as a whole has been properly guided as well.

ACKNOWLEDGEMENTS

We sincerely thank all of our sponsoring organizations. Without them, GSI/GRI simply could neither happen nor exist. This paper is part of the activity ongoing at the institute. The current GSI member organizations and their contact members are given on the institute website at www.geosynthetic-institute.org. Board of Director members are identified accordingly.

REFERENCES

Anderson, D. C., Brown, K. W. and Green, J. (1981), “Organic Leachate Effects on the Permeability of Clay Liners,” Proc. National Conference on Management of Uncontrolled Hazardous Waste Substances,” HMCRI, Silver Springs, MD, Oct. 28-30, pp. 233-229.

Christopher, B. R., Holtz, R. D. and DiMaggio, J. A. (1984), *Geotextile Engineering Manual*, U.S. DOT, FHWA Contract No. DTFH 61-80-C-00094.

Hsuan, Y. G. (2000), “Data Base of Field Incidents Used to Establish HDPE Geomembrane Stress Crack Resistance Specification,” Jour. of Geotextiles and Geomembranes, Vol. 18, No. 1, February, pp. 1-22.

Hsuan, Y. G. (1998), “Data Base of Field Incidents Used to Establish HDPE Geomembrane Stress Crack Resistance Specification,” Proc. GRI-12 Conference on Lessons Learned from Geosynthetics Case Histories, GII Publ., Folsom, PA, pp. 153-176.

Hsuan, Y. G. and Koerner, R. M. (1997), "GRI Finalizes Its First Specification," GFR, Vol. 15, No. 7, September, pp. 17-19.

Hsuan, Y. G. and Koerner, R. M. (1999), "Rationale and Background for the GRI-GM13 Specification for HDPE Geomembranes," Proc. Geosynthetics '99, IFAI Publ., Roseville, MN, pp. 385-400.

Koerner, R. M. (2010), "Generic Specification for GCL Manufacturing Quality Control; Details and Unsettled Issues," Proc. 3rd International Conference on Geosynthetic Clay Liners, Würzburg, Germany, SKZ Publ., pp. 333-340.

Koerner, R. M. (2008), "Celebrating a Decade of GSI/GRI Polyolefin Specifications," Geosynthetics, Vol. 26, No. 3, June/July, pp. 46-47.

Koerner, R. M. (2012), Designing With Geosynthetics, 6th Edition, Xlibris Publ. Co., 915 pgs.

Koerner, R. M., Halse, Y. G. and Lord, A. E. (1990), "Long-Term Durability and Aging of Geomembranes," Proc. Waste Containment Systems," Geotech. Special Publ., ASCE, pp. 106-134.

Koerner, R. M., Koerner, G. R. and Hsuan, Y. G. (2012), "Lifetime Prediction of Laboratory UV Exposed Geomembranes: Part I – Using a Correlation Factor," GRI Report #42, GSI, Folsom, PA, 36 pgs.

Koerner, R. M., Koerner, G. R. and Hwu, B.-L. (1990), "Three Dimensional, Axi-Symmetric Geomembrane Tension Test," Proc. Geosynthetic Testing for Waste Containment Applications, STP 1081, Ed. R. M. Koerner, ASTM, pp. 170-184.

Matrecon, Inc. (1988), "Lining of Waste Containment and Other Impoundment Facilities," EPA/600/1-88/052, U. S. EPA, Cincinnati, OH, September, ≈ 1000 pgs.

National Sanitation Foundation (1983, 1985, 1990, 1991), NSF Standard 54, "Flexible Membrane Liners," Ann Arbor, MI, ≈ 60 pgs. (depreciated)

Nosko, V. and Touze-Foltz, N. (2000), "Geomembrane Liner Failure: Modeling of Its Influence on Contaminant Transfer," Proc. EuroGeo 2, Bologna, Italy, pp. 557-560.

Struve, F. and Koerner, G. R. (2005), "Behavior of HDPE Sheet and Seams Subjected to a 90° Tensile Test," Proc. GRI-18 Conference on Geosynthetics R & D, Geo-Frontiers, Austin, TX, pp. 4345-4351.

GEOTEXTILE FILTERS--25+YEARS OF RESEARCH AND EXPERIENCE

Robert D. Holtz
University of Washington

Barry R. Christopher
Roswell, Georgia

ABSTRACT

The paper is a personal memoir of the Authors' experiences as consultants and researchers on geotextile filters. The paper outlines the work leading to the development of the FHWA Geotextile Filter Design Criteria in 1983-1985. Experiences at Purdue University and the University of Washington on the determination of the pore size distribution of geotextiles is recounted, as is the work on developing a filter criteria based on measured pore sizes. Finally, the development of a flexible wall gradient ratio device for determining the gradient ratio of fine grained soils is described and some test results with the device are presented.

INTRODUCTION AND SCOPE

Geotextiles have been an attractive alternative to graded granular filters from their earliest days. Of course engineers wanted to use the Terzaghi graded granular filter criteria, but how does one determine the grain size distribution of especially a nonwoven geotextile? Wovens were a bit simpler; i.e., the size of the openings between the filaments could be related to the grain sizes of the protected soil.

The title of this paper is a bit misleading, because we begin our review in the late 1950s; however we wanted to provide a little background for our involvement with geotextile filters. Because this article emphasizes research and development work done at STS Consultants, Purdue, and at the University of Washington, it is personal and not intended to be a comprehensive review. Several books and articles are available that give a much more complete review of the entire spectrum of research on geotextile filters including those which did not perform as anticipated (e.g., Koerner and Koerner, 2013).

BEFORE THE FHWA GEOTEXTILE ENGINEERING MANUAL

In an obituary we prepared about Robert J. Barrett, we called him the "Father of Geotextiles" (Holtz and Christopher, 1990), because in the late 1950s he first had the idea to use a fabric to replace graded granular filters in erosion control revetments (Barrett, 1960). Bob Barrett's employer, Carthage Mills, sponsored some laboratory development work at Soil Testing Services, Inc. of Northbrook, Illinois, starting in 1957. Silvio Pollici, a laboratory engineer at STS, developed a soil-fabric permeameter (Pollici et al., 1961-1969) that was later refined and standardized as the Gradient Ratio test by C. C. Calhoun (1972) of the US Army Corps of Engineers. About the same time, Barrett convinced the Corps to do some large-scale field tests to really prove the efficacy of geotextile filters under armor stone on the inland waterway in Florida.

That work was the basis for much of the design, testing methods, installation procedures, and material specifications that we use today for geotextile filters in erosion control revetments.

When Christopher joined STS Consultants in 1977 as a project and laboratory engineer, he of course learned about the early work at STS for Carthage Mills, and he did some basic laboratory tests on geotextile permeability and filtration. Bob Barrett, who was changing companies to help a new European manufacture (Nicolon) to enter the US market, approached Christopher shortly after he joined STS to repeat the gradient ratio tests they had previously performed on these new geotextiles. Shortly after completion of that work, Carthage Mill's retained Christopher to evaluate ten of their early geotextile filter projects, document project performance, and perform field evaluation for case histories on selected projects (e.g., see Christopher, 1983). These early projects had a significant influence on Christopher's future work in geosynthetic filters as well as his dedication to advancing geosynthetics technology in general.

After Barrett's pioneering efforts, there were a few others involved in the development of geotextiles for drainage and filtration (see e.g., Agershou, 1961). In Europe during the 1970s, pioneering work on geotextile filters was done by H. J. M. Ogink (1975) at the Delft Hydraulics Laboratory in Holland, H. J. List (1973) at the Federal Hydraulics Bureau in Germany, and Alan McGown and David Sweetland (1973) at Strathclyde University in Scotland. About the same time, some European polymer and textile manufacturers interested in developing alternative markets for their products came in the US and Canada through their North American subsidiaries or through licensing agreements. The most notable research in the US at that time was by Dan Marks and Bob Carroll; their work is now classic (see Marks, 1975; Rosen and Marks, 1975; and Carroll, 1983).

The first research sponsored by FHWA began in 1977 at Oregon State University (Bell and Hicks et al., 1980 and 1982). (Holtz was on the board of advisors and acted as a reviewer-consultant for this project.) The OSU research focused on the evaluation of existing and the development of new test methods and procedures for determining the engineering properties of geotextiles, including those appropriate for filtration and drainage design.

In the late 1970s, specifications for all geotextile applications including filtration, drainage, and erosion control, were not generic nor were they often based on sound engineering research or experience. The FHWA realized that to improve practice, state highway engineers would need formal training in geotextile engineering. The first FHWA geosynthetics courses were developed and taught by Professor T. Allan Haliburton of Oklahoma State University, who unfortunately passed away after only a few courses were taught.

The authors were awarded the second contract in 1983, and part of our charge was to update Haliburton's draft course materials (Haliburton, Lawmaster, and McGuffey, 1981) into the *Geotextile Engineering Manual* (Christopher and Holtz, 1985). We were not particularly happy with their treatment of geotextile filters, although to be fair, we used many of their concepts and construction procedures. It was during this rewrite that we developed what became known as the FHWA Geotextile Filter Design Criteria. This criteria was further refined after 1983-1985 in the FHWA Geosynthetic Design and Construction Guidelines of 1989, 1996, and 2008. The 1996 version was turned into a textbook published by BiTech (Holtz, Christopher, and Berg, 1997).

THE FHWA GEOTEXTILE FILTER DESIGN CRITERIA

We began by reviewing and summarizing all the previous work we could find on geotextile filters, including the STS reports mentioned above (Pollici, et al., 1960-1969). We also found the books by Cedergren (1977), Koerner and Welsh (1980), and Rankilior (1981), as well as the proceedings of a few early conferences and symposia, very helpful in providing case histories and some design procedures. Three early conference proceedings were particularly noteworthy: the 1977 Paris *International Conference on the Use of Fabrics in Geotechnics*, the *First Canadian Symposium on Geotextiles* in Calgary (1980), especially the paper by Bell (1980), and the 1982 *Second International Conference on Geotextiles*, in Las Vegas. We also reviewed those earlier papers and reports on geotextile filters and filtration mentioned above (Barrett, Pollici, Calhoon, Marks, Carroll, Ogink, List, McGown and Sweetland, Bell et al.), as well as the US Army Corps of Engineers (1977) *Guide Specification for Engineering Fabrics*. Finally the papers by McKeand (1977), McGown (1978), Schober and Teindl (1979), Lawson (1982), Hoare (1982), and Giroud (1982) were especially influential.

Our discussion of geotextile filters began with a summary of the properties of both graded granular materials as well as geotextiles required for filtration and drainage. We also discussed the problem of a grain size versus pore size distribution of the filter, and we discussed the influence of fiber size, fabric structure, and porosity of the geotextile. Most of this summary is still valid today.

Although Haliburton, et al. (1981) mentioned the criteria for critical nature of the project and severity of the soil and hydraulic conditions, they did not emphasize them for design. During our rewrite, we included these conditions, as defined by Carroll (1983), as a formal part of the design process. These conditions are summarized in Table 1, because we believe they are not only very important for filtration and drainage design, but they can apply as well to virtually all aspects of civil engineering design.

Table 1 - Guidelines for Evaluating the Critical Nature or Severity of Drainage and Erosion Control Applications (after Carroll, 1983)

A. Critical Nature of the Project		
<u>Item</u>	<u>Critical</u>	<u>Less Critical</u>
1. Risk of loss of life and/or structural damage due to geotextile failure:	High	None
2. Repair costs versus installation costs of feature:	>>>	= or <
3. Evidence of geotextile clogging before potential catastrophic failure:	None	Yes
B. Severity of the Conditions		

<u>Item</u>	<u>Severe</u>	<u>Less Severe</u>
1. Soil to be protected:	Gap-graded, pipable, or dispersible	Well-graded or uniform
2. Hydraulic gradient:	High	Low
3. Flow conditions:	Dynamic, cyclic, or Pulsating	Steady state

In reviewing the background and comments in the GEM during the preparation of this paper, it is quite remarkable that we apparently had such a clear understanding of all the factors that influence soil retention, permeability, and filtration characteristics of geotextiles in 1983. For example, we noted that no single evaluation technique can be used to determine all of the factors, conditions, and intended uses of a geotextile filter, and thus design must consider site-specific conditions, especially in critical design situations. And this is still true today.

We should also mention an NCHRP study performed by Koerner and Koerner (1994), in which they evaluated 91 sites with 84 involving some type of edge drain installations around the US. Many of these cases were failures or had experienced problems. They took soil and geotextile samples, performed appropriate tests, and applied several design criteria to see which procedures would have predicted the observed performance. We quote: "It was determined that the currently used Federal Highway criteria are excellent predictors (i.e., design methods) in all cases. These criteria should be disseminated to the widest possible audience and utilized accordingly."

The FHWA Criteria performed the best of all procedures, never once predicting success when a failure had occurred. In four successful cases, however, it predicted failures, which in effect means the criteria is conservative, something that designers of geotextile filters should really appreciate.

RESEARCH AT PURDUE AND UW ON THE PORE SIZE DISTRIBUTION OF GEOTEXTILES

The work at Purdue University on determining the pore size distribution (PSD) was largely based on a considerable amount of previous work using mercury intrusion porosimetry (MIP) to measure pore sizes in concrete, compacted and stabilized soils, and other materials. For example, Holtz had supervised the PhD work of C. H. Juang on the PSD of sand-clay mixtures (Juang and Holtz, 1986a, b, and c). Could a similar technique using MIP be used for nonwoven geotextiles? If this would work, then we could design geotextile filters based on their pore sizes.

About that time Christopher became involved with Chemie Linz, a nonwoven manufacturer, and it seemed reasonable to approach them for some funding to investigate this technique. A letter proposal was sent to Mr. Gerhard Werner, the lead engineer with Chemie Linz, and he checked with André Rollin at École Polytechnique in Montréal, who at that time, had done the most work on the PSD of nonwovens. André had used image analysis for his investigations, he did not believe MIP would be feasible for geotextiles, and he advised against

funding the proposal. So Holtz approached Joe Luna who at that time was an engineering manager with Hoescht-Celanese and he was willing to fund a post-doctoral student S. Prapaharan to do some preliminary analysis with MIP. It worked quite well, as we reported in Prapaharan, Holtz, and Luna (1989). In addition to MIP, Prapa was able also to do some comparative image analyses, and we showed that even with compression up to about 50% of the ASTM thickness, the PSD was essentially unaffected. Figure 1 shows the PSD diagrams as determined using MIP as well as image analysis.

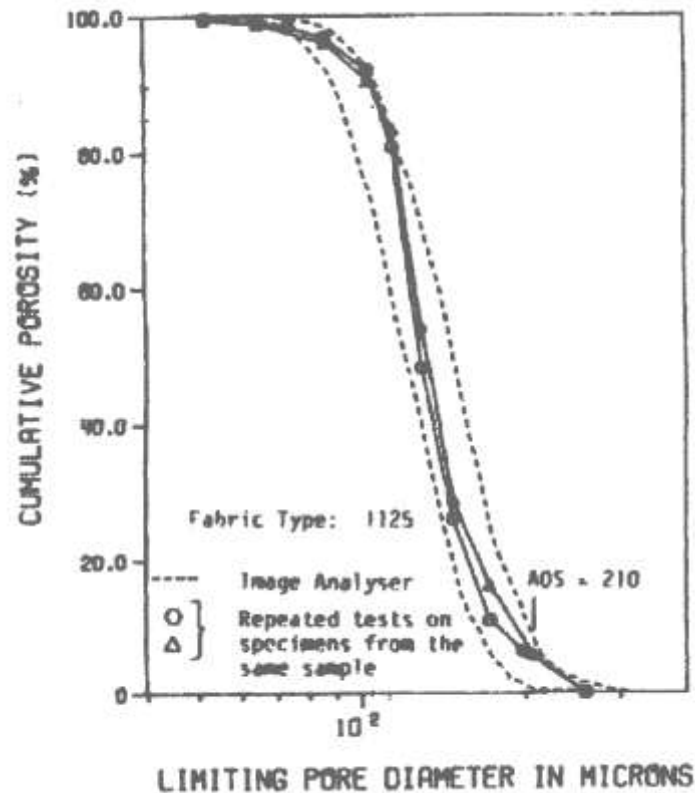


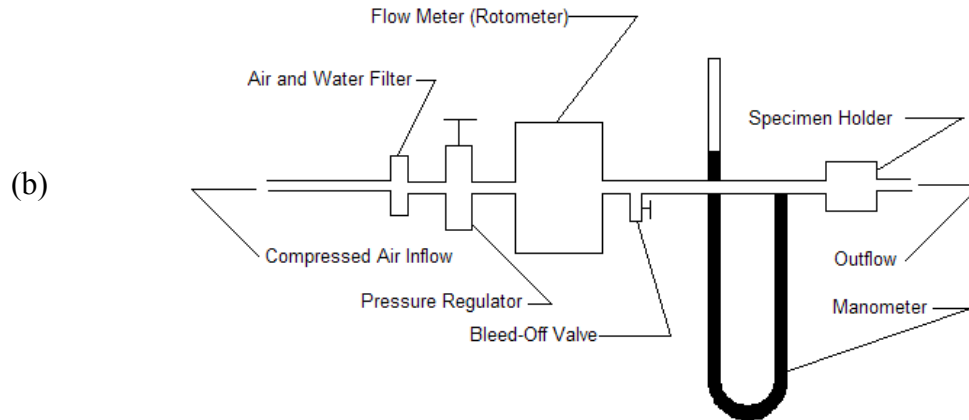
Figure 1. Comparison of MIP and image analysis on a nonwoven polyester (from Prapaharan, Holtz, and Luna, 1987).

As part of his PhD research at the University of Washington, Gregory Fisher showed that the critical pore size in filter behavior was the *constriction* pore size, and that this was true for both geotextiles as well as graded granular filters. He also developed a design method for geotextiles based on the PSD. To determine the pore size distributions of the filters, he also used the “bubble point method,” not the MIP, to determine the PSD of both woven and nonwoven geotextiles (Fisher, 1994).

Why the bubble point method (BP)? Well, for one thing, the BP method measures the constriction pore size as well as the distribution of pores in geotextiles. We also think it measures the true pore size, but that is subject to some debate. And finally, the BP method provides a direct relationship with the hydraulic conductivity of the geotextile, which is also very useful for filter design. Most of these issues are discussed at length in Fischer and Holtz (1991) and Fischer, Holtz and Christopher (1993, 1996a and b).

Figure 2a is a schematic diagram of the BP apparatus and Fig. 2b is a photograph of the apparatus Fischer used.

(a)



(b)



Figure 2. (a) Schematic diagram, and (b) photograph of the bubble point test equipment (from D'Hondt, 2005).

Recognizing that comparative research was needed to support these findings, Christopher encouraged Dr. Shobia Bhatia of Syracuse University to perform additional research to confirm the validity of using the BP method. Bhatia and her student (and now her colleague) Jennifer Smith evaluated various test methods for determining the pore size characteristics of geotextiles including sieving methods, the BP method and MIP techniques (Bhatia and Smith, 1994 and 1996, and Bhatia et al., 1996).

Based on this early research, Christopher initiated an ASTM task group to develop a standard test method for the determination of the PSD of geotextiles and relate PSD to filtration performance. In 2002, ASTM standardized the BP test procedure for determining the pore size characteristics of geotextiles (ASTM D-6767-02).

Fischer (1994) had suggested that some additional work was necessary to improve the BP method, because there were still some questions regarding the fluid used in the test, the shapes of the pores, and whether the pores were constructed upon entrance or exit. This additional work

was done by UW student Douglas P. D'Hondt. He drilled holes of various sizes corresponding to the AOS of geotextiles (70 to 850 μm) into specimens of PVC, aluminum, and HDPE; some of the solids had single holes, one with a countersink, while others had multiple holes and a range of hole sizes. He then used water and mineral oil as the BP test fluids. Details of these tests and the results are described in D'Hondt (2005). Principal conclusions are the following:

1. Specimens should be oriented with the air pressure applied in an upward direction, especially for large pore sizes.
2. BP procedures is accurate even when the pores are not perpendicular to the plane of the specimen
3. BP test was repeatable, especially on nonwovens and wovens with smaller holes. However, it does not reliably replicate the AOS values reported by manufacturers.
4. The accuracy of the BP method is dependent on the contact angle used: ASTM D-6767 should be modified to allow different contact angles for different test fluids and polymers.
5. D-6767 should also be able to account for temperature variations and the possibility of compressed specimens of thick nonwovens.

As part of D'Hondt's research, we cooperated with Prof. Ahmed Aydilek of the University of Maryland, who at that time was also doing research on the PSD of geotextiles, but using image analysis. Figure 3 presents a comparison of some of the results determined by Aydilek, D'Hondt, and Holtz (2007).

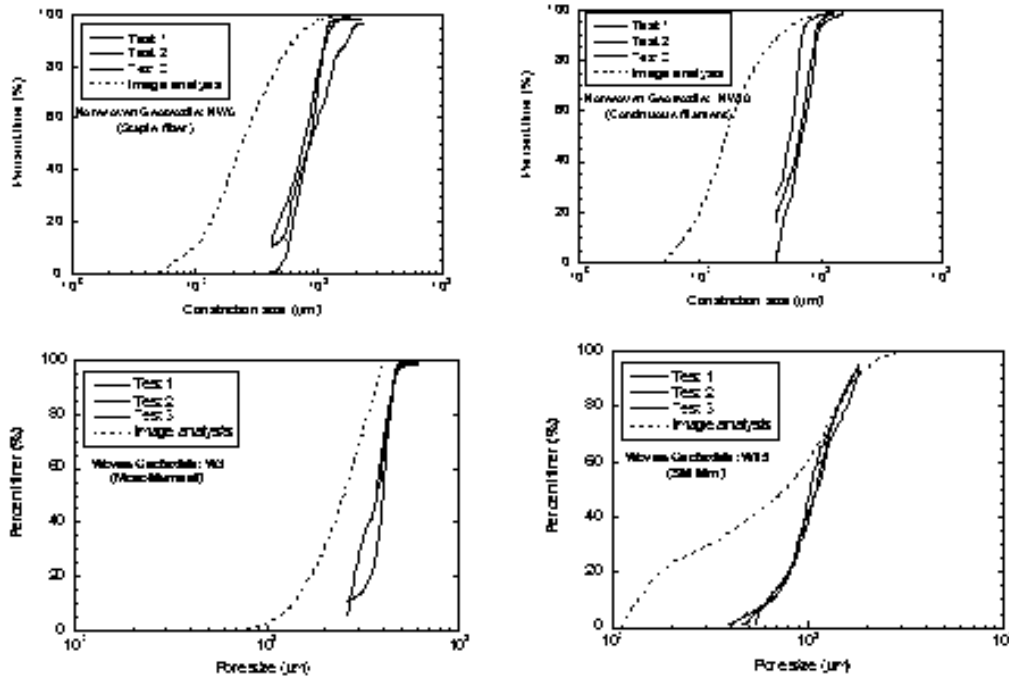


Figure 3. Comparison of the PSDs or CSDs (constriction pore size distributions) of four geotextiles determined by the BP method as well as image analysis (Aydilek, D'Hondt, and Holtz, 2007).

Some of the conclusions of Aydilek et al. (2007) and Aydilek et al. (2008) are as follows:

1. The O_{95} of wovens by image analysis is approximately equal to the AOS of the same geotextiles as determined by ASTM D 4751
2. The bubble point O_{95} for nonwovens is not the same as the AOS.
3. ASTM D 6767 for the bubble point test is the best available test to determine constriction sizes of nonwoven geotextiles

Other researchers who have advanced the use of BP for determining the PSD of geotextiles include David Elton (e.g., Elton, et al., 2007, and Elton and Hayes, 2008) and Karen Henry (Henry and Patton, 1998). ASTM Committee D-35 is currently updating the BP standard considering all of this research, especially recommendations related to the pore fluid.

RESEARCH AT UW ON THE GRADIENT RATIO TEST

The gradient ratio test discussed at the beginning of this paper was standardized by ASTM in 1990 (ASTM D 5101), largely because of the diligence of Don Shanklin and the support of the USDA, Soil Conservation Service laboratory. However, the test tended to produce variable results and additional work to refine the test was needed.

Filtration research at the University of Washington by Gregory Fischer and others was largely influenced by a summary of research needs on geotextile filters at that time, as described by Christopher, Holtz, and Fischer (1993). Because Fischer was a practicing consulting geotechnical engineer, he also wanted to study some of the broadly graded glacial tills that are common in the Seattle area. The local geotechnical consulting community assumed that “Geotextiles don’t work in our soils, because our soils are different!”

Fischer started with a critical review of all previous work on graded granular filters, and then on geotextile filters. The work on granular filters was summarized by Fischer and Holtz (1996).

For the long-term flow tests, Greg used the Gradient Ratio (GR) Test because it was an established ASTM standard (D-5101) that is fairly straightforward to run, and the apparatus is simple and inexpensive. Furthermore, measurements of the gradient could be made at several locations in addition to the standard locations of 25 mm and 50 mm. It was also possible to collect any fines that might happen to pass the filter, and it can accommodate relatively large flow rates anticipated in the soils he tested. Mare (1994) also conducted some long term GR tests to complement Fischer’s work. A critique of the GR test is in Fischer, Holtz, and Christopher (1994).

The grain size distributions for the two glacial till soils tested are shown in Fig. 4, while Fig. 5 is a photo of four of the GR devices used. The soils were tested at very low densities to enhance filter clogging. Water filters were utilized to insure that any decrease in flow rate observed was due clogging of the geotextiles and not due to contaminants in the water. To aid in the saturation of the soil specimens, CO₂ was used to displace the air in the voids. Because the tests were expected to take several weeks, an algaeicide was also used. Table 2 lists the four geotextiles tested along with some of their characteristics.

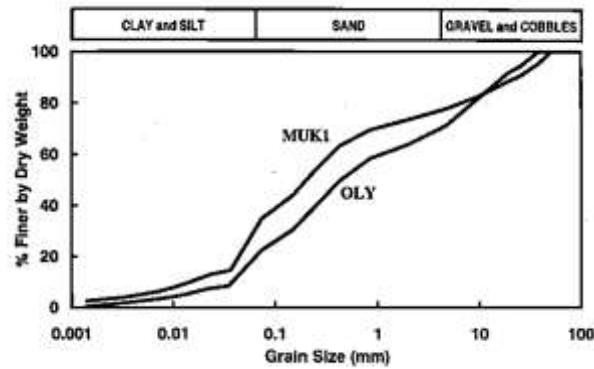


Figure 4. Grain size distributions of two broadly graded glacial till soils from the Seattle area (Fischer, 1994).



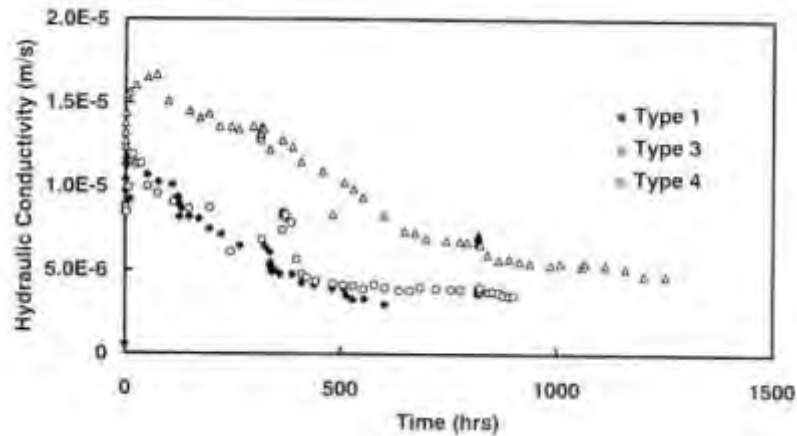
Figure 5. Gradient Ratio test equipment used by Fischer (1994).

Table 2. Geotextiles Tested by Fischer (1994) and Mare (1994).

Geotextile type	Polymer	type	Mass/unit area (g/m ²)	AOS (mm)
Needlepunched nonwoven	polypropylene	Continuous filament	281	0.12-0.21
Needlepunched nonwoven	Polyester	Continuous filament	254	0.12-0.21
Heatbonded nonwoven	polypropylene	Continuous filament	213	0.08
Multifilament woven	polypropylene	Continuous filament	220	0,21

Examples of some of Fischer's (1994) and Mare's (1994) results are shown in Fig. 6. Additional long term filtration results were reported by Fischer, Mare, and Holtz (1999).

a)



b)

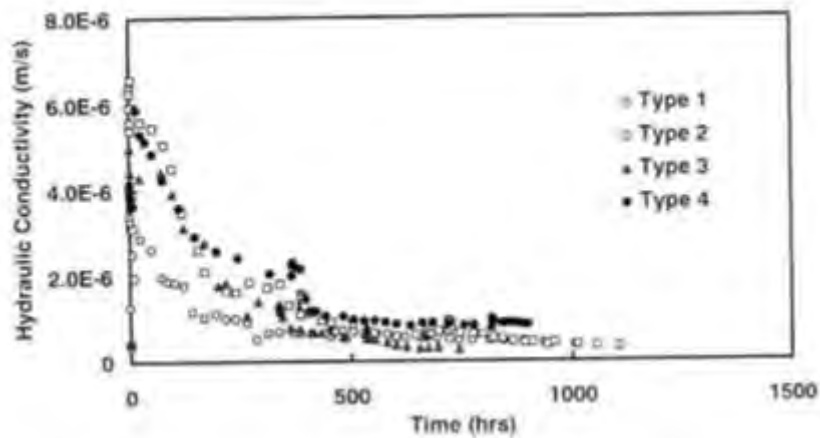


Figure 6. Long-term GR filtration tests on soils (a) OLY, and (b) MUK1 (after Fischer, 1994, and Mare, 1994).

Some of the practical implications of our filtration research are that the Seattle area glacial soils are not really that different. It is possible to design a successful geotextile filter for them by using the FHWA filter criteria (Christopher and Holtz, 1983), although a GSD of the soils to be filtered is required—no surprise there—as are filtration tests for critical designs (Table 1).

ASTM used this research, along with that of others, to update the gradient ratio test standard in 2001.

Other research in the last 25 years on filtration performance using the gradient ratio tests should also be recognized. Mark Wayne working with Bob Koerner evaluated the long-term

filtration performance versus current design practice (Wayne and Koerner, 1993). Studies by Jonathan Fannin on cyclic GR testing (Fannin and Srikongsri, 2007) is especially noteworthy. We are also aware that GR tests have been performed by practicing engineers to assess the most appropriate geotextile(s) for critical applications, and we hope their work will influence fellow engineers to use this best practice.

Development of Filter Criteria Based on PSD

Fischer (1994) also developed a design procedure based on the pore size distribution of geotextiles. This procedure was described by Fischer, Christopher, and Holtz (1990) and Holtz (1992).

Development of the FWGR

One of the more important developments by the UW group is the flexible wall gradient ratio test (FWGR). The test and its development were first reported by Harney and Holtz (2001) in a paper based on Michael Harney's MSCE thesis (Harney, 2001). The FWGR is basically a combination of the standard GR test with the flexible wall permeameter (ASTM D-5084), as shown conceptually in Fig. 7. The test was developed to overcome some of the disadvantages of the two conventional filtration tests, the GR and the hydraulic conductivity ratio (HCR, ASTM D-5567) tests. Specimens can be saturated using backpressure; stress conditions can be controlled during testing; and piping along the walls can be eliminated. Thus the FWGR should be more appropriate than the GR alone for soils with appreciable fines. These advantages were also shown by Henry and Holtz (2003).

FWGR specimen preparation is no more complex than that required for conventional triaxial testing, and only minor modifications or upgrades to existing flexible wall permeameter equipment were necessary. Two required modifications were the development of a latex membrane with pressure ports (Fig. 8) and a flexible wall permeameter cell base with multiple pressure lines. Rather than trying to apply backpressure to standpipe manometers, we also built a pressure transducer manifold (Fig. 9) with multiple transducers for measuring the head at different elevations above the geotextile specimen. The FWGR is evaluated identically to the GR, as shown in the equation

$$F G \equiv G \equiv \frac{i_{soil}}{i_{soil+filter}}$$

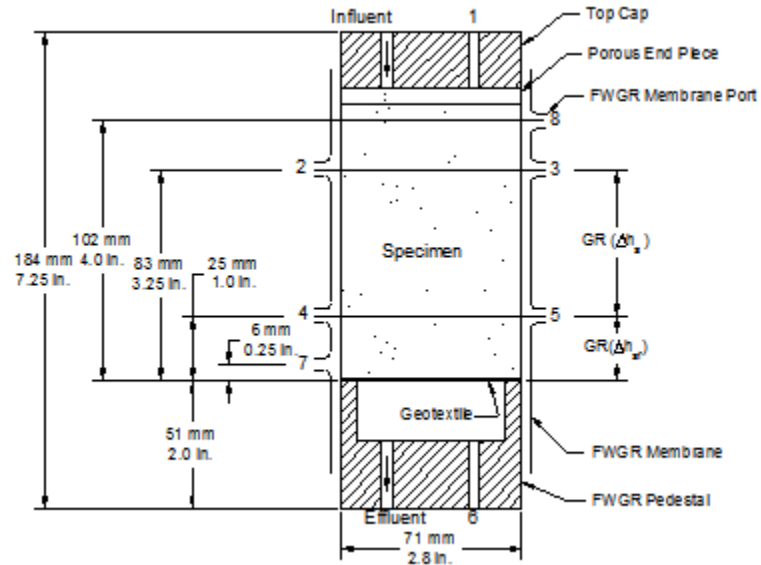


Figure 7. Basic concept of the FWGR; also shown are the locations of head measurement ports.



Figure 8. FWGR 71 mm diameter latex membrane with pressure ports.

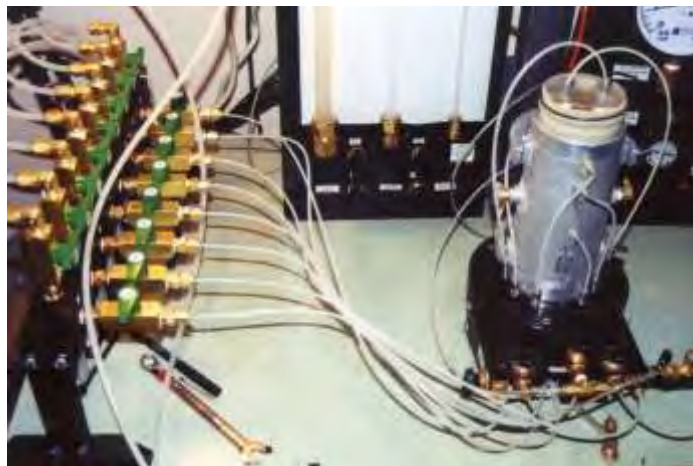


Figure 9. FWGR specimen in mold and pressure transducer manifold.

Typical results from Harney (2001), Bailey (2004), Bailey, Harney, and Holtz (2005), and Harney, Bailey, and Holtz (20??) are summarized in the following paragraphs. First, a comparison of the FWGR and GR test results are shown in Fig. 10.

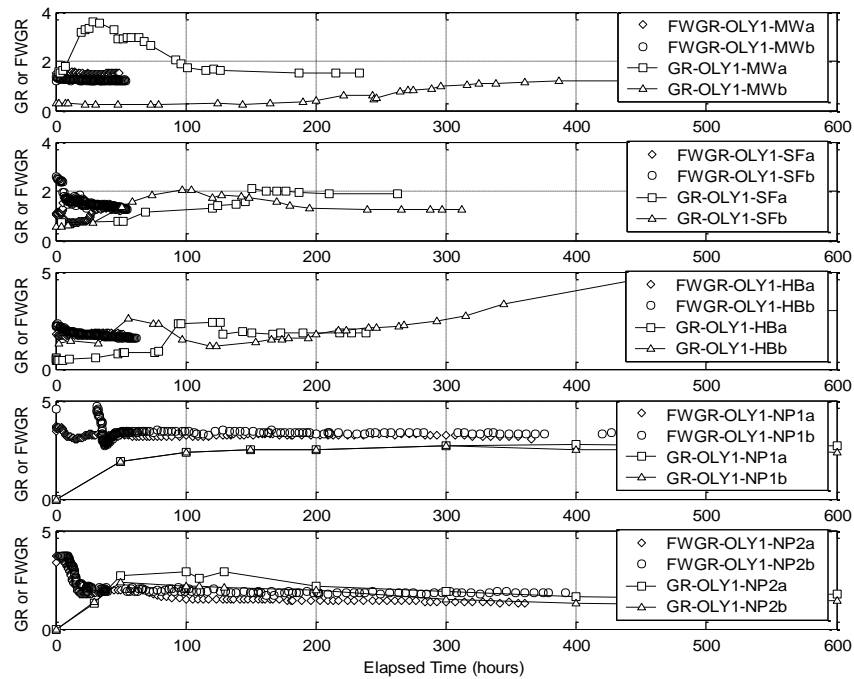
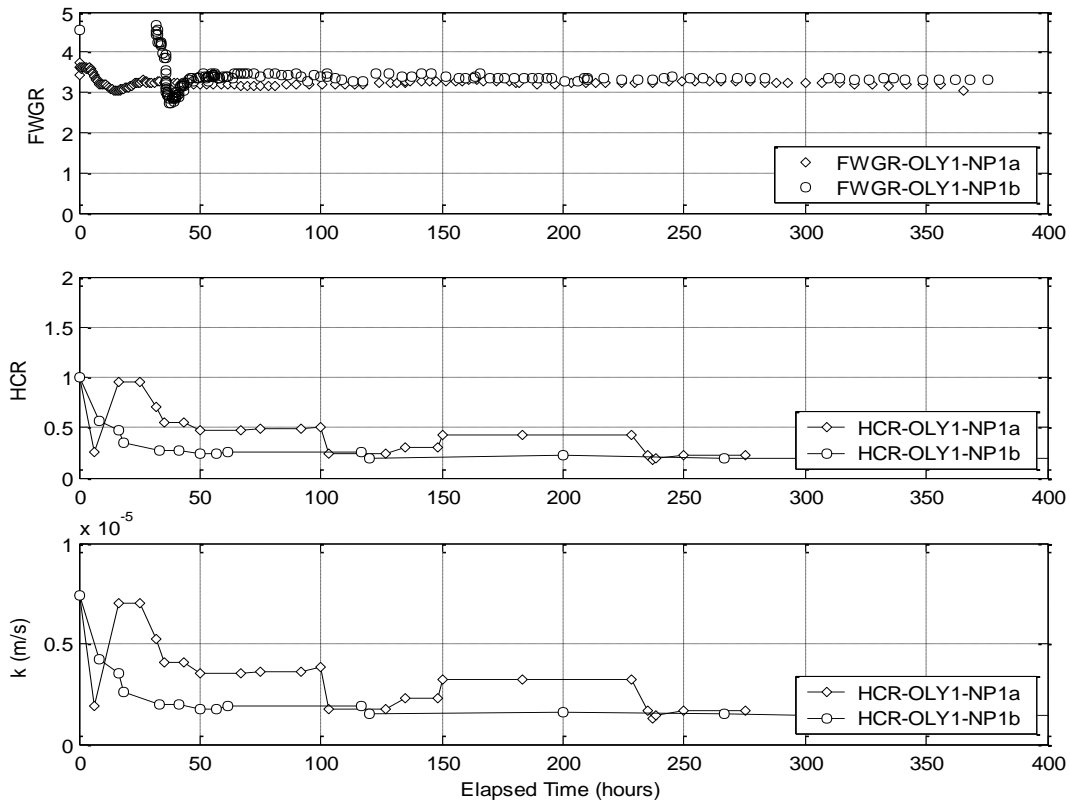


Figure 10. Comparison of FWGR and GR test results on the OLY soil (Fig. 4) and the geotextiles in Table 2.

Figure 11 compares results of FWGR and HCR tests and FWGR and GR tests on a needle-punched nonwoven.

A)



B)

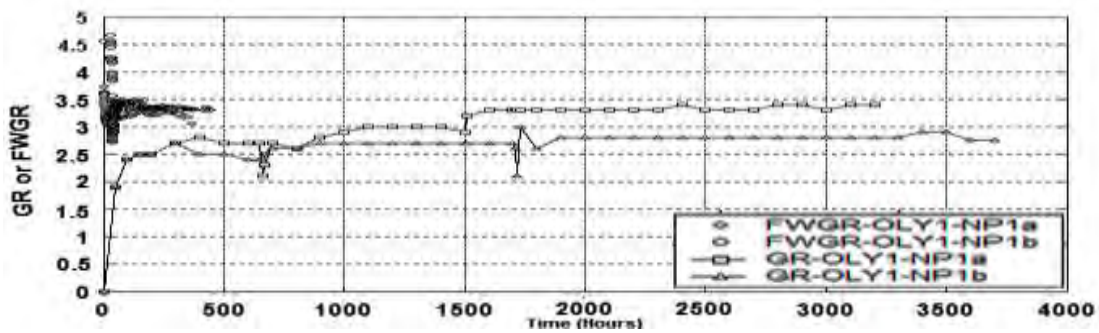


Figure 11. Comparison of (a) FWGR and HCR test results with (b) FWGR and GR test results, all on a needle punched nonwoven (NP1).

Results of similar comparative tests on another nonwoven, a slit-film woven, and a monofilament woven are shown in Harney (2001), Bailey (2004), Bailey, Harney, and Holtz (2005), and Harney, Bailey, and Holtz (20??). All these test results indicate that the two tests give very similar results, that the FWGR test is repeatable, and that it stabilizes much faster than the GR tests. These tests were performed on well-graded granular soils, soils that typically are difficult to

test in the conventional GR apparatus. For the two soils tested, the FWGR gives more reliable results than the HCR test, and it provides a reliable and repeatable direct determination of the soil and system hydraulic conductivity.

FINAL REMARKS

In his 2008 Terzaghi Lecture, Jean-Pierre Giroud made two, at first glance, rather surprising assertions:

1. Geosynthetics are the single most important development in civil engineering in the 20th Century; and
2. Because of our research on geotextile filters, we now have a better understanding of Terzaghi's graded granular criteria.

The summary of our research and development experience with geotextile filters summarized in this paper validates both statements. On the other hand, we are confident that PSD will dominate geosynthetic designs of the future and that the design of geosynthetic filters will advance well beyond the basic graded granular filter criteria.

REFERENCES

- Agershou, H.A. (1961) "Synthetic Material Filters in Coastal Protection," *Journal of the Waterways, Port, Coastal, and Oceans Division*, ASCE, Vol. 87, No. WW1, pp. 111-123.
- Aydilek, A. H., D'Hondt, D., and Holtz, R. D. (2007) "Comparative Evaluation of Geotextile Pore Sizes Using Bubble Point Test and Image Analysis," *Geotechnical Testing Journal*, ASTM, Vol. 30, No. 3, pp. 173-181; Response to Discussion, Vol. 31, No. 4, pp. 370-371.
- Aydilek, A. H., D'Hondt, D., and Holtz, R. D. (2008) Response to discussion of "Comparative Evaluation of Geotextile Pore Sizes Using Bubble Point Test and Image Analysis," *Geotechnical Testing Journal*, ASTM, Vol. 31, No. 4, pp. 370-371.
- Bailey, T. D. (2004) "Measurement of Geotextile Filtration Behavior Using the Gradient Ratio Test, the Hydraulic Conductivity Ratio Test and the Flexible Wall Gradient Ratio Test," MSCE Thesis, University of Washington.
- Bailey, T. D., Harney, M. D., and Holtz, R. D. (2005), "Rapid Assessment of Geotextile Clogging Potential Using the Flexible Wall Gradient Ratio Test", *Proceedings of the GRI-18 Conference*, Austin, Texas (CD-ROM), ASCE.
- Barrett, B. (1966), "Use of Plastic Filters in Coastal Structures," *Proceedings of the 10th International Conference on Coastal Structures*, Tokyo, Japan, pp. 1048-1067.
- Bhatia, S. K., and Smith, J. L., 1994, "Comparative Study of Bubble Point Method and Mercury Intrusion Porosimetry Techniques for Characterizing the Pore-Size Distribution of Geotextiles," *Geotextiles and Geomembranes*, Vol. 13, pp. 679-702.

Bhatia, S.K., and Smith, J.L. (1996). "Geotextile characterization and pore-size distribution: part II, a review of test methods and results." *Geosynthetics International*, Vol. 3, No. 2, pp. 155-180.

Bhatia, S.K., Smith, J.L., and Christopher, B. . (1996). "Geotextile Characterization and Pore Size Distribution: Part III. Comparison of Methods and Application to Design", *Geosynthetics International*, IFAI, Vol. 3, No. 3, pp. 301-328.

Bell, J. . (1980) "Design Criteria for Selected Geotextile Installations," *Proceedings of the First Canadian Symposium on Geotextiles*, Calgary, Alberta, pp. 35-57.

Bell, J. . and Hicks, . G. (1980) "Evaluation of Test Methods and Use Criteria for Geotechnical Fabrics in Highway Applications," *Interim Report* for the US Federal Highway Administration by the Transportation Research Institute, Oregon State University, Corvallis, Report No. FHWA/RD-80/021.

Bell, J. . and Hicks, . G. (1982) "Evaluation of Test Methods and Use Criteria for Geotechnical Fabrics in Highway Applications," *Final Report* for the US Federal Highway Administration by the Transportation Research Institute, Oregon State University, Corvallis (Draft).

Calhoun, C. C. (1972), "Development of Design Criteria and Acceptance of Specifications for the Plastic Filter Cloth," Technical report 5-72-7, US Army Corps of Engineers Waterways Experiment Station, Vicksburg, Mississippi.

Carroll, R.G. (1983) "Geotextile Filter Criteria", *Transportation Research Record 916*, Transportation Research Board, pp. 46-53..

Cedergren, H. R. (1977) *Seepage, Drainage, and Flow Nets*, Second Edition, Wiley.

Christopher, B. ., 1983, "Evaluation of Two Geotextile Installations in Excess of a Decade Old", *Transportation Research Record 916*, Transportation Research Board, Washington, D.C., pp. 79-88.

Christopher, B. R. and Holtz, R. D. (1985) *Geotextile Engineering Manual*, U.S. Federal Highway Administration, Washington, D. C., FHWA-TS-86/203, 1044 pp.

Christopher, B. R. and Holtz, R. D. (1989) *Geotextile Design and Construction Guidelines*, U.S. Federal Highway Administration, National Highway Institute, Washington, D.C., Report No. FHWA-HI-90-001, 297 pp.

Christopher, B. ., Holtz, . D. and Fischer, G. . (1993) "Research Needs in Geotextile Filter Design", *Filters in Geotechnical and Hydraulic Engineering*, Proceedings of the First International Conference "Geo-Filters '92", Karlsruhe, Germany, J. Braums, M. Heibaum, and U. Schuler, editors, Balkema, pp. 19-26. (Also published as "Potrzeba Badan Projektowania Filtrów z Geotekstyliów", in *Geotechniczne Aspekty Skladowania Odpadow*, Seminar Proceedings, Gdansk, Poland, 1994, Vol. I, pp. 245-252.)

D'Hondt, D. P. (2005) "An Investigation of the Pore Size Distribution of Geotextiles and Other Materials by the Bubble Point Method," MSE Thesis, University of Washington.

Elton, D. J., and Hayes, D. W., 2008, "The Significance of the Contact Angle in Characterizing the Pore Size Distribution of Geotextiles," *Geosynthetics International*, Vol. 15, No. 1, pp. 22-30.

Elton, D. J., Hayes, D. W., and Adanur, S., 2007, "Bubblepoint Testing of Geotextiles: Apparatus and Operation," *Geotechnical Testing Journal*, Vol. 30, No. 1, pp. 9-16.

Fannin, R.J. and Srikongsri, A. (2007) *Geotextile filters in cyclic flow: test results and design criteria*, Proceedings of Geosynthetics 2007, Washington, D.C., Jan.16-19, 2007, pp.170-185., IFAI.

Fischer, G. . (1994) "The Influence of Fabric Pore Structure on the Behavior of Geotextile Filters," PhD dissertation, University of Washington, 502 pp.

Fischer, G. ., Christopher, B. . and Holtz, . D. (1990) "Filter Criteria Based on Pore Size Distribution", Proceedings of the Fourth International Conference on Geotextiles, Geomembranes, and Related Products, The Hague, The Netherlands, Vol. 1, pp. 289-294.

Fischer, G. . and Holtz, . D. (1991) Discussion of "Comparative Studies of Different Porometry Determination Methods for Geotextiles", by L. Van der Sluys and W. Dierickx, *Geotextiles and Geomembranes*, Vol. 10, No. 4, pp. 379-381.

Fischer, G. ., Holtz, . D. and Christopher, B. . (1993) "A Critical review of Geotextile Pore Size Measuring Methods", *Filters in Geotechnical and Hydraulic Engineering*, Proceedings of the First International Conference "Geo-Filters '92", Karlsruhe, Germany, J. Braums, M. Heibaum, and U. Schuler, editors, Balkema, pp. 83-90.

Fischer, G. ., Holtz, . D., and Christopher, B. ., (1996a) "Evaluating Geotextile Flow Reduction Potential Using Pore Size Distribution", *Geofilters '96 Comptes rendus/Proceedings*, Montréal, Québec, Canada, J. Lafleur and A. L. Rollin, Editors, École Polytechnique Montréal, pp. 247-256.

Fischer, G. R., Holtz, R. D., and Christopher, B. R., (1996b) "Evaluating of Geotextile Pore Structure", *Recent Developments in Geotextile Filters and Prefabricated Drainage Geocomposites, ASTM STP 1281*, S. K. Bhatia and L. D. Suits, editors, American Society for Testing and Materials, pp. 3-18.

Fischer, G. R. and Holtz, . D. (1996) "A Critical review of Granular Soil Filter Retention Criteria", *Geofilters '96 Comptes rendus/Proceedings*, Montréal, Québec, Canada, J. Lafleur and A. L. Rollin, Editors, École Polytechnique Montréal, pp. 409-418.

Fischer, G. R., Maré, A. D., and Holtz, . D. (1999) "Influence of Procedural Variables on the Gradient Ratio Test", *Geotechnical Testing Journal*, ASTM, Vol. 22, No. 1, pp. 22-31.

Giroud, J.-P. (1982), "Filter Criteria of Geotextiles," *Proceedings of the 2nd International Conference on Geotextiles*, Las Vegas, IFAI., Vol. 1, pp. 103-108.

Giroud, J.-P. (2008) "Criteria for Geotextile and Granular Filters," 44th Terzaghi Lecture, presented in New Orleans, March.

- Halliburton, T. A., Lawmaster, J. D., and McGuffey, V. C. (1981) "Use of Engineering Fabrics in Transportation Related Applications," Final Report DTFH-80-C-00094 for FHWA, Haliburton Associates, Stillwater, Okla.
- Harney, M. D. (2001) "Measurement of Geotextile Filter Clogging Potential Using the Flexible Wall Gradient Ratio Test," MSCE Thesis, University of Washington.
- Harney, M. D. and Holtz, R. D. (2001) "Flexible Wall Gradient Ratio Test", *Proceedings of Geosynthetics Conference 2001*, Portland, Oregon, Industrial Fabrics Association International, pp. 409-422.
- Harney, M. D., Bailey, T. D., and Holtz, R. D. (20??) "Clogging Potential of Geotextile Filters Using the Flexible Wall Gradient Ratio Test", *Geotechnical Testing Journal*, ASTM (submitted, reviewed, and accepted, pending required changes that were never completed.)
- Henry, K. S. and Holtz, R. D. (2003) "Long Term Gradient Ratio Tests," *Proceedings of the Two Rivers Conference--56th Canadian Geotechnical Conference and 2003 NAGS Conference*, Winnipeg, Manitoba, Canada (6 pp. on compact disc).
- Henry, K. S., and Patton, S., 1998, "Measurement of the Contact Angle of Water on Geotextile Fibers," *Geotechnical Testing Journal*, Vol. 2, No. 1, pp. 11-17.
- Hoare, D. J. (1982) "Synthetic Fabrics as Soil Filters: A Review," *Journal of the Geotechnical Engineering Division, ASCE*, Vol. 108, No. GT10, pp.
- Holtz, R. D. (1992) "Filter Criteria Based on Pore Size Distribution", discussion session on filtration, *Proceedings of the 4th International Conference on Geotextiles, Geomembranes and Related Products*, The Hague, The Netherlands, Vol. 3, pp. 1051-1052.
- Holtz, R. D. and Christopher, B. R. (1990) "In Memoriam of Robert J. Barrett (1924-1990)", *Geotechnical News*, Vol. 8, No. 3, pp. 41.
- Holtz, R. D., and Christopher, B. R. (1994), "Filtration Behavior of Broadly Graded, Cohesionless Tills", *Proceedings of the Fifth International Conference on Geotextiles, Geomembranes, and Related Products*, Singapore, Vol. 1, pp. 659-662.
- Holtz, R. D., Christopher, B. R., and Berg, R. R. (1996) *Geosynthetic Design and Construction Guidelines*, U.S. Federal Highway Administration, National Highway Institute, Washington, D. C., Publication No. FHWA-HI-95-038, 396 pp.
- Holtz, R. D., Christopher, B. R., and Berg, R. R. (1997) *Geosynthetic Engineering*, BiTech Publishers, Vancouver, British Columbia, Canada., 451 pp.
- Holtz, R. D., Christopher, B. R., and Berg, R. R. (2008) *Geosynthetic Design and Construction Guidelines*, U.S. Federal Highway Administration, National Highway Institute, Washington, D. C., Publication No. FHWA-NHI-07-092, 592 pp.
- Juang, C. H. and Holtz, R. D. (1986a) "A Probabilistic Permeability Model and the Pore-sized Density Function", *International Journal for Numerical and Analytical Methods in Geomechanics*, Vol. 10, pp. 543-553.

Juang, C. H. and Holtz, . D. (1986c) "A Note on Preparation of Specimens of Non-Cohesive Material for Mercury Intrusion Porosimetry", *Geotechnical Testing Journal*, ASTM, Vol. 9, No. 3, pp. 154-155.

Juang, C. H. and Holtz, . D. (1986b) "Fabric, Pore Distribution, and Permeability of Sandy Soils", *Journal of Geotechnical Engineering*, ASCE, Vol. 112, No. 9, pp. 855-868. (On the GED Awards Committee list of 10 best geotechnical papers, 7/86-6/87.)

Koerner, . M. and Koerner, G. . (2013) "Geotextile Filter Failures: Examples and Lessons Learned," Robert D. Holtz Symposium at 2013 Geocongress, San Diego, Calif., GeoInstitute of ASCE, (in publication).

Koerner, . M. and Koerner, G. . (1994) "Long-Term Performance of Geosynthetics in Drainage Applications," NCHP report 367, National Cooperative Highway Research Project, Transportation Research Board, Washington, DC., 54 p.

Koerner, R. M. and Welsh, J. P. (1980) *Construction and Geotechnical Engineering Using Synthetic Fabrics*, Wiley, 267 pp.

Lawson, C. . (1982) "Filter Criteria for Geotextiles," *Journal of the Geotechnical Engineering Division*, ASCE, Vol. 108, No. GT10, pp_1300-1317.

List, H. J. (1973) "Untersuchungen von Instalatar Belastungen Kunststoffe-Filter für den asserbau," *Mittelungsblattt der Bundesanstalt fur asserbau*, No. 35.

Maré, A. D. (1994) "The Influence of Gradient atio Testing Procedures on the Filtration Behavior of Geotextiles," MSCE Thesis, University of ashington.

Marks, B. D. (1975) "The Behavior of Aggregate and Fabric Filters in Subdrainage Applications." Research Report, Dept of Civil Engineering, University of Tennessee.

McGown, A. (1978) "The Properties of Nonwoven Fabrics Presently Identified and Being Important in Public orks Applications", Congress Papers from *Index 78*, Session 1, Civil Engineering, European Disposables and Nonwovens Association (EDANA), Amsterdam, pp. 1.1.2.

McGown, A. and Sweetland, D. B. (1973) "Fabric Screen ese arch and Development," University of Strathclyde, Report, Dept of Civil Engineering.

McKeand, E. (1977) "Behavior of Nonwoven Fabric Filters in Subdrainage Applications," *Proceedings of the International Conference on the Use of Fabrics in Geotechnique*, Paris, Vol. II, pp. 171-176.

Ogink,H. J. M. (1975) "Investigations on the Hydraulic Characteristics of Synthetic Fabrics," *Publication No. 146*, Delft Hydraulics Laboratory, Delft, The Netherlands.

Prapaharan, S., Holtz, . D. and Luna, J. D. (1989) “Pore Size Distribution of Nonwoven Geotextiles”, *Geotechnical Testing Journal*, ASTM, Vol. 12, No. 4, pp. 261-268.

Pollici, S. J., Baker, C. N., and Gnaedinger, J. P. (1961, 1962, 1964, 1965, 1967, and 1969) Unpublished Laboratory Soil–Fabric Permeability and Filtration Evaluation Reports Performed on Carthage Mills Geotextiles by STS Consultants, Ltd., Northbrook, Illinois.

Proceedings of the *First Canadian Symposium on Geotextiles* (1980) Canadian Geotechnical Society, Calgary, Alberta.

Proceedings of the *International Conference on the Use of Fabrics in Geotechnics* (1977): National Laboratoire des Ponts et Chaussées, Paris, France

Proceedings of the *Second International Conference on Geotextiles* (1982) Industrial Fabrics Association International, Las Vegas, Nevada.

Rankilor, P. R. (1981) *Membranes in Ground Engineering*, Wiley, 377 pp.

Rosen, W. J. and Marks, B. D. (1975 "Investigation of Filtration Characteristics of a Nonwoven Fabric Filter" Transportation Research Record 532, Transportation Research Board, Washington, DC.

Schober, W. and Teindl, H. (1979) "Filter–Criteria for Geo-textiles," Proceedings of the Seventh European Conference on Soil Mechanics and Foundation Engineering, Brighton, England.

US Army Corps of Engineers (1977) *Civil Works Construction Guide Specification for Plastic Filter Fabric*, Corps of Engineer Specification No. CW-02215, Office of the Chief of Engineers, Washington, DC.

ayne, M.H., and Koerner, .M., 1993, “Correlation Between Long-Term Flow Testing and Current Geotextile Filtration Design Practice” *Proceedings of Geosynthetics '93*, IFAI, Vol. Vol. 1, Vancouver, British Columbia, Canada, 501-517.

A BRIEF HISTORY OF GEOSYNTHETIC DRAINAGE MEDIA: FROM ROCKS TO SIM TESTED, PATENTED, STRAND GEOMETRIES

Boyd Ramsey
GSE Environmental LLC

In the beginning, there were rocks...after that; there was sand...but then!

I would believe that most of you have attended a “Mercer” lecture during your attendance at a conference or tradeshow. Frank Brian Mercer (O.B.E.) was a prolific British engineer. Born in 1927, he did groundbreaking work in multiple fields and his accomplishments include the primary basic invention of both geonets and geogrid materials.

Mercer’s work in Britain resulted in the creation of Netlon Corporation in the USA and the issuing of US patent 2919467 titled: “Production of Net-like Structures” on January 5, 1960. This patent addresses the general production of geonets used today, although the level of sophistication has advanced dramatically, as one would expect.

The commercialization of the geonet and geocomposite materials was taken up by “Netlon” in Britain and in the United States, the Minnesota based company “Wood Conversion Products” began to be involved in the manufacture of these materials. This organization later changed its name and is more popularly known as “Conwed Ltd.” An early schematic of a geonet production line (from “Austin”) is pictured here:

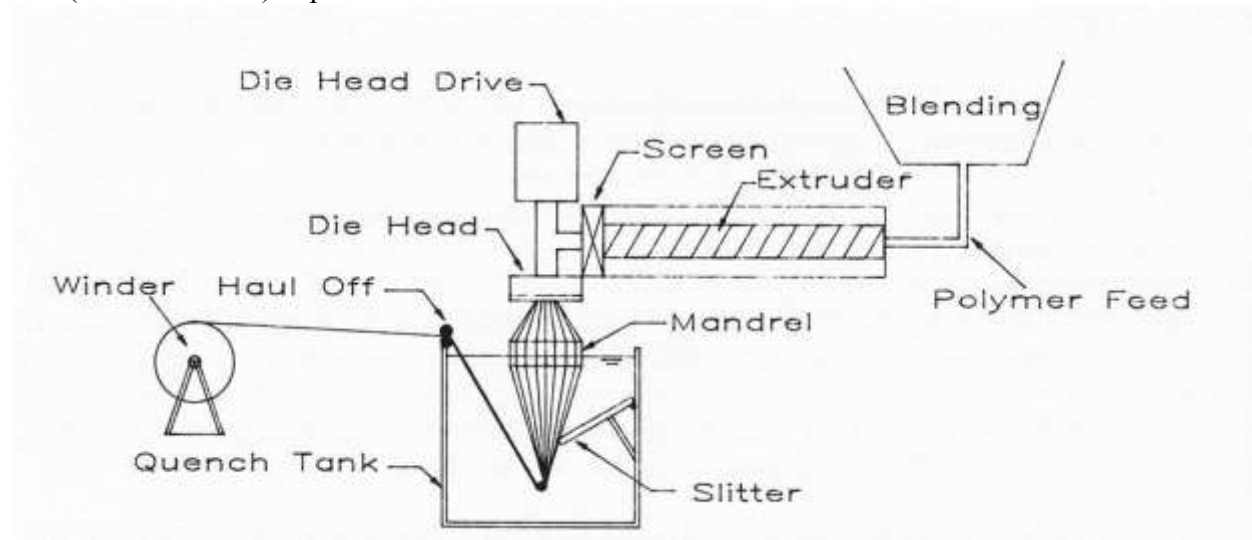


Figure 1. Schematic view of geonet production line.

In one of the first major “field tests” of these materials, in 1987, Tony Eith and the leadership and staff of the Geosynthetic Institute conducted an examination of a geonet installation. A section of a commercial landfill was constructed with a geonet collection system and was evaluated in the “real-world” environment by application of ~2600 liters (700 gallons) of water and subsequent measurement of the timing and quantity of materials collected at the sump. This testing was repeated with multiple and increasing overburden loads of municipal waste with

depths of near zero (essentially unfilled), 14 meters (46 feet) and 28 meters (92 feet). The measurements allowed the calculation of a field transmissivity and accurate validation of the flow rates and response times of the system. Obviously the system performed well, or we would not be discussing this 25 years later. To quote from the conclusions; ” *The full scale flow test results of a geonet leak detection system illustrated in this paper indicate that geonets are effective in their liquid transmissivity capabilities and can function as designed and intended.*”

It was obvious that to be effective in most applications the geonet would need some filtration media to protect the net from clogging, thus the creation of geotextile – geonet laminates that are commonly known as geocomposites. The vast majority of those used today are manufactured with needle punched nonwoven polypropylene geotextiles as filtration media, commonly 6 or 8 ounce per square yard (200 to 270 grams per square meter), although it should be stated that several companies hold patents and have developed technology to laminate other fabric types with differing filtration properties. Additionally, recognition should be given to past usage of polyester fabrics as filtration media. In the early 1990’s polyester was the fabric of choice primarily due, to ease of lamination. Subsequently polyester became over-priced for the geosynthetic marketplace and has fallen out of common usage.

Also, a few words must be given to the bonding of the geonet and geotextile materials. The original production lines used flame bonding where the geonet was exposed to open flame. Advancements in technology led to what is described as “wedge” lamination, where the surface of the geonet is exposed to a heated wedge or metal plate. In both cases, the geotextile is then exposed immediately to the heated surface of the geonet and light pressure is then used to assure sufficient bonding takes place.

In 1993 Tenax began production in the United States, Tenax (now Syntec) has a well-deserved reputation for innovation in this field and pioneered several important product design and application engineering concepts over the years.

At the 8th GRI conference in 1994, Richard Austin of Netlon presented a paper titled: “The manufacture of Geonets and Composite products” in which he described the manufacturing process for geonet and geocomposite production in some detail. This was an excellent foreshadowing of the technical issues that would surround the testing, performance requirements and engineering of these materials. To quote one section of the paper:

“By using different size dies, die slots and mandrels, and changing the rotation of the dies, a wide variety of different net products can be manufactured using the above process”.

He went on to discuss net geometry, rib sizes, references to both to “straight strand” configurations and increasing net thicknesses. In the Quality Assurance portion of the paper, he discussed compressive creep, thickness dependent transmissivity, temperature dependent transmissivity, interface variability, geotextile intrusion, peel strengths and interface frictional performance. A photograph of several current geonet varieties is below:

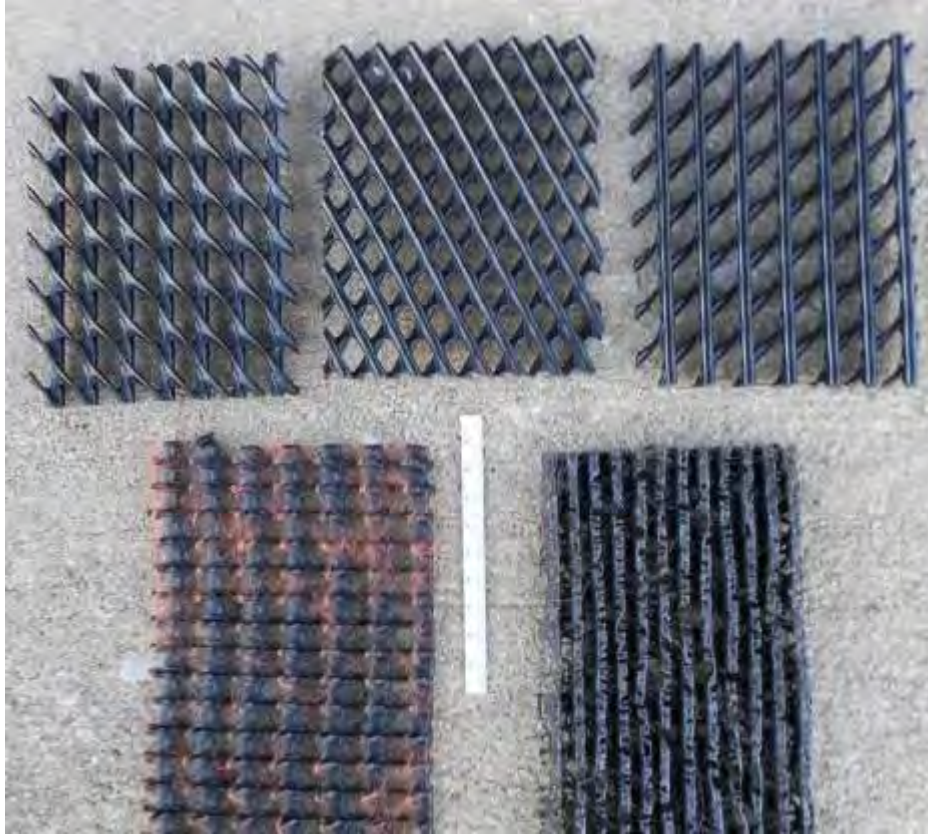


Figure 2. Various types of geonet drainage cores currently in use.

At the 13th GRI conference held in 1999, Pietro Rimoldi of Tenax was charged with predicting the future of geonet and geocomposite products. Predictions are always a difficult task. He laid out the case for the substitution of geocomposite for sand, an argument that many of us are still presenting today and he covered nearly all of today's "selling points" with the only real new advantage being the "green" value of geocomposite materials. He correctly pointed out the issue of low "shipment density"; one can only cover a small area with the contents of a standard shipping container of geocomposite materials. He accurately predicted growth of product types, and consolidation within the industry. He also did a great job of predicting additional applications in earthen and concrete dams, transportation and other infrastructure applications as well as introducing the concept of cusped geonets and other strand geometries.

The late 1990's and early 2000's were a period of many innovations within this marketplace and during this period, the race to the patent office was rejuvenated. Nearly all of these advances were made in pursuit of the same common goal; to get the highest flow rate (transmissivity) for the longest time (in-service duration) with the minimum amount of material. This fairly simply stated goal however, resulted in a rich and complex range of designs invoking variation in a very broad range of geonet characteristics. Most critical in this author's opinion were and are strand shape, geonet thickness, geonet strand orientation and materials (geonet and geotextile) composition.

In 2000, the publication *Geosynthetics International* devoted a special issue (Volume 7, Nos. 4-6, 2000) to liquid collection systems. Authors included J.P. Giroud, Jorge Zornberg, Aigen Zhao, Rudy Bonaparte, Ennio Palmeira, Gregory N. Richardson, Rick Thiel and others. This publication summarized the engineering foundation for the use and performance of these materials and explored concepts such as thickness dependent flow, radial performance, hydraulic transmissivity equivalency between geosynthetic and granular liquid collection layers and others. In 2001, the Geosynthetic Institute published GRI–GC8, Determination of the Allowable Flow Rate of a Drainage Geocomposite (2001). This document provided guidance and documented the application of reduction factors to assure that the real-world performance of these systems would have both adequate flow rates and sufficient longevity.

Another important milestone was the publication in GFR magazine (now Geosynthetics Magazine) of a multipart article and associated discussions on the engineering of lateral drainage systems. These articles and engineering advances were authored by Gregory N. Richardson, J.P. Giroud, and Aigen Zhao. The principle article was titled “Lateral Drainage Design Update” and was presented in two parts in the January /February and March 2002 issues of GFR.

In 2004, Dhani Narejo and Sam Allen outlined an accelerated procedure to measure compressive creep properties of geonet and geocomposites using the Stepped Isothermal Method (SIM). This concept became embodied in ASTM D7361, Standard Test Method for Accelerated Compressive Creep of Geosynthetic Materials Based on Time-Temperature Superposition Using the Stepped Isothermal Method and is used widely today to determine the long term performance characteristics of these materials and assist in engineering design.

At the GRI-22 conference held in 2009 in Salt Lake City, an important paper, which the author believes deserves more attention, was jointly presented by Bob and George Koerner. The paper, titled: “Geocomposite Drainage Material Connections and Attachments” addresses the termination constructions and the flow of liquids out of these types of products and into piping; a critical aspect of the installations that has been occasionally overlooked to significant consequences.

In 2011 Sam Allen published an article in Geosynthetics magazine titled “Accelerated flow testing of geosynthetic drains” that summarized the state of the practice in evaluations and predictions of the behavior of these materials.

A final word should also be included regarding market size. Over the past decades, several individuals, and organizations have tracked the size and growth of the geonet and geocomposite marketplace; while the general goals have been the same, the methodologies and specific details of these efforts have differed and some details have been lost to the vagaries of history. In overview, the market for geocomposite drainage products (geonets and accompanying geotextiles) roughly doubled between 1999 and 2004 to a total of approximately 67 million pounds per year. Since 2004, the market has not quite doubled again and the latest market estimate for geocomposite products (including geotextiles) is approximately 125 million pounds per year.

The level of sophistication from Dr. Mercer's era has increased substantially; details such as initial flow rate, reduction factors to accommodate various types of clogging and intrusion, effects of thickness changes, benefits of specific strand geometries and geotextile variations and other factors are regularly addressed. Standardized test protocols and techniques are available and can be used to reliably compare materials performance and to predict the long term behavior of materials. In short, geocomposites have passed the "look at this new stuff" era and are aging well into an innovative material with a well-defined and engineered performance.

REFERENCES

Allen, S., "Accelerated flow testing of geosynthetic drains". June, 2011, Geosynthetics Magazine.

ASTM D7361, Standard Test Method for Accelerated Compressive Creep of Geosynthetic Materials Based on Time-Temperature Superposition Using the Stepped Isothermal Method, West Conshohocken, Pennsylvania, USA.

Austin, R. A., "The Manufacture of Geonets and Composite Products," *Proc. GRI-8 on Geosynthetic Resins, Formulations and Manufacturing*, IFAI, 1995, pp. 127–238.

Eith, A. W. and Koerner, R. M., "Field Evaluation of Geonet Flow Rate (Transmissivity) Under Increasing Load," *J. Geotextiles and Geomembranes*, Vol. 11, Nos. 5-6, 1992, pp. 153–166.

Geosynthetic Institute, GRI Standard GC8, Standard Guide for Determination of the Allowable Flow Rate of a Drainage Geocomposite, Folsom, Pennsylvania, USA.

Giroud, J.P. et.al, Special Issue On Liquid Collection Systems, Geosynthetics International, (Volume 7, Nos. 4-6, 2000).

Hardin, K.Z. and Ramsey, B. U.S. Patent 6,802,672

Heathcote, D. et.al. U.S. Patent 7,470,094

Ianniello, P.J., Capra, G. and Zhao, A. U.S. Patent 6,802,669

Koerner, R. M. (2012), *Designing With Geosynthetics*, 6th Edition, Xlibris Publ. Co., 914 pgs.

Koerner, R. M. and Koerner, G. R., "Geocomposite Drainage Material Connections and Attachments," *Proc. GRI-22 Conference*, Salt Lake City, UT, GSI Publ., Folsom, PA, 2009, pp. 57–65.

Mercer, F.B. U.S. Patent 2,919,467

Narejo, D. and Allen, S., "Using the Stepped Isothermal Method for Geonet Creep Evaluation," *Proc. EuroGeo3, Munich, Germany, 2004*, pp. 539-544.

Ramsey, B. and Narejo, D., "Using Woven and Heat-Bonded Geotextiles in Geonets Geocomposites," *Proc. GeoFrontiers, GSP 130-142, ASCE, 2005 (on CD)*.

Richardson, G. et.al, "Lateral Drainage Design Update". Geotechnical Fabrics Report, V20, N1 and 2, Jan. /Feb. and March 2000, (now Geosynthetics Magazine).

ENGINEERING CHARACTERISTICS OF GEOSYNTHETIC CLAY LINERS: QUESTIONS ASKED AND ANSWERED OVER TIME

David E. Daniel

University of Texas at Dallas, Richardson, Texas USA

ABSTRACT

Geosynthetic clay liners (GCLs) evolved from subsurface waterproofing materials that are manufactured in small panels and typically affixed to the earthen backfill side of basement walls. A transformative event occurred when GCLs were first used in a waste containment application in the mid 1980's. Soon thereafter, intensive research was launched to investigate and document the engineering characteristics of GCLs. A number of specific questions about GCL behavior were asked and answered, though nearly all issues will continue to benefit from further research. New questions will be posed and answers developed as new materials evolve and new applications are explored.

In the late 1980s and early 1990s, the cost and practical advantages of GCLs compared to compacted clay liners quickly became evident. As a result, the use of GCLs in waste containment applications grew rapidly. Today, GCLs are widely used and are an important element not only in waste containment applications but in various other sealing and waterproofing uses, as well.

The main technical and engineering issues regarding GCLs can be grouped into seven broad categories: (1) hydration of GCLs; (2) hydraulic properties of bentonite in GCLs; (3) composite action of GCLs with a geomembrane; (4) stability of GCLs on slopes; (5) the physical integrity of GCLs; (6) transport of chemicals through GCLs and the equivalency of GCLs to compacted clay liners; and (7) advances in materials and designs.

This paper traces understanding of engineering characteristics over time for a few key parameters. At the close of the paper, the author looks forward regarding future uses of GCLs. He would like to see more use of bentonite sandwiched between two geomembranes, more use of a protective layer beneath GCLs to mitigate impact of any unforeseen puncture and to limit diffusive migration of chemicals, more consideration of site-specific conditions in GCL design, better management of wrinkles in geomembranes that overlie GCLs, and more considered use of GCLs for some near-surface applications.

INTRODUCTION

Geosynthetic clay liners (GCLs) evolved from subsurface waterproofing materials that were manufactured in the early 1960s and are still in widespread use today. The thin waterproofing panels typically measure roughly 2.4 m by 1.2 m in length and width, and are

affixed to a basement wall, which is then backfilled to cover up the panel. The bentonite in the waterproofing panel provides the desired sealing.

A transformative event occurred in the mid 1980s when GCLs were first used in a waste containment application (Schubert, 1987). Shortly thereafter, intensive, independent research was initiated worldwide to investigate and document the engineering characteristics of GCLs. In addition, the cost and practical advantages of GCLs compared to compacted clay liners quickly became apparent. The amount of GCL material used in waste containment applications grew rapidly throughout the world. This growth was driven by the significant advantages of GCLs compared to compacted clay liners, which include:

- Lower cost of GCLs in most cases;
- Much faster construction times with GCLs;
- Far less uncertainty and risk regarding schedule and cost with GCLs;
- Less volume of landfill space consumed by GCLs;
- Potentially lower hydraulic conductivity and, hence, lower seepage rates with GCLs; and
- Opportunity to engineer high-performance materials either through modification of the bentonite or design of the overall geosynthetic system.

Geosynthetic clay liners exhibit some fundamental drawbacks compared to compacted clay liners, the most significant of which are:

- Very low shear strength of hydrated bentonite;
- Because of the thinness of GCLs, vulnerability to physical damage (e.g., thinning of bentonite by stones in the subgrade, puncture, or penetration by plant roots);
- Vulnerability to chemical alterations of the bentonite that can result in a significant increase in the hydraulic conductivity of the bentonite; and
- Limited impedance to chemical diffusion due to thinness of the bentonite layer.

Over the past 25 years, a number of specific questions about GCL behavior were asked by owners/operators, design engineers, researchers, and regulatory officials. Over time, many of these questions were answered (at least partially, if not entirely) from the results of research studies, though many issues will continue benefit from further investigation, and a few are considered “hot topics” today. New questions will inevitably be posed as new materials evolve and as new applications develop.

In this paper, attention is focused on several issues as follows:

1. Hydration of GCLs.
2. Hydraulic properties of bentonite in GCLs.
3. Composite action of GCLs with a geomembrane.
4. Stability of GCLs on slopes.
5. The physical integrity of GCLs and vulnerability to damage
6. Equivalency of GCLs to compacted clay liners.
7. Advances in materials and design

At the close of the paper, the author will look forward regarding use of GCLs. He would like to see more use of bentonite sandwiched two geomembranes, more use of a protective layer beneath GCLs to mitigate impact of any unforeseen puncture and to limit diffusive migration of chemicals, more consideration of site-specific conditions in GCL design, better management of wrinkles in geomembranes, and more selective less use of GCLs in near-surface environments.

HYDRATION OF GCLs

An issue that perhaps has not been given as much attention as it should have received is the hydration of GCLs placed in contact with earth materials. Geosynthetic clay liners are manufactured using relatively dry bentonite, although in the early days of GCL manufacturing, bentonite mixed with a water-soluble adhesive in some commercial products occasionally left the factory with sufficient high water content that they underwent considerable dimensional shrinkage upon drying in the field. But for the most part, the issue with GCLs is not drying of the product but, rather, hydration of bentonite once the GCL is installed in the field.

Bentonite is an inherently hydrophilic material that has great affinity to absorb water. It is this characteristic that is one of bentonite's most unique and desirable characteristics. If given access to water in almost any form, relatively dry bentonite will absorb the water.

Water absorption or desorption, like all fluid movement, is driven by gradients in energy. Essentially, water moves from a location of higher energy to one of lower energy (or "downhill" in more simplistic terms). The pore water pressures in bentonite are strongly negative compared to atmospheric pressure. This very large "suction" pressure of relatively dry bentonite gives bentonite the ability to absorb water from almost any moisture-holding material (e.g., soil or rock). For practical purposes, except perhaps for the driest materials imaginable in nature, bentonite will absorb moisture from the adjacent material until the two materials reach equilibrium in terms of water energy.

For a given material, a relationship exists between water content and soil water potential, although the relationship may not be unique and usually depends on the wetting path, i.e., the relationship is slightly different for materials that are being wetted compared to materials that are being dried. Few engineers seem to grasp basic concepts of soil moisture potential and water content-suction relationships, perhaps because of relatively little instruction in most universities on the subject of "unsaturated soil mechanics." In any case, GCLs are sometimes placed on the subgrade with little understand as to what will happen next.

When a GCL is placed on a damp or moist subgrade with only a geotextile (at most) separating the bentonite from the subgrade, the GCL absorbs moisture from the subgrade, as indicated in Figure 1. The process can be slowed with a thicker geotextile separating the bentonite from the subgrade, but hydration will occur nevertheless. Note that the hydration time is on the order of days to weeks.

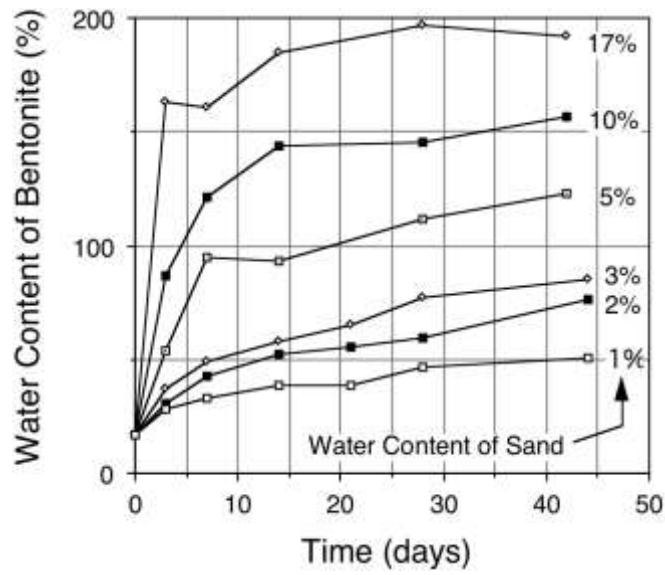


Figure 1. Water content of bentonite vs. time for geotextile-encased GCL placed on sand (Daniel, Shan, and Anderson, 1993).

When the bentonite reaches equilibrium with the adjacent soil, the equilibrium will be in terms of energy (water potential), not water content. This is seen clearly in Figure 1 where the water content of the sand is between 1% and 17% and, over time, the water content of the bentonite equilibrates between 50% and 200%. The relationship between suction and water content of bentonite can be measured in the laboratory, as shown in Figure 2. As a practical reference, it may be noted that plants wilt and die when the suction is approximately 15 bars (1 bar of pressure \approx 1 atmosphere of pressure). At a suction of 15 bars, the equilibrium water content of the bentonite is on the order of approximately 50%. At this moisture content, bentonite is moist with a shear strength similar to saturated bentonite (Daniel, Shan, and Anderson, 1993).

Several devices are available to measure soil suction. Daniel et al. (1993) used a thermocouple psychrometer, which is a relative-humidity measuring device for determining soil water potential. Southen and Rowe (2007) employed the more widely utilized axis translation technique. Beddoe, Take, and Rowe (2011) employed both high-capacity tensiometers (axis translation) and relative humidity measurements to measure the soil moisture retention curve. There exist enough published data for one to obtain at least a preliminary estimate of the relationship between soil suction and water content for the bentonite component of GCLs from published information. This aspect of GCL material behavior is reasonably well understood.

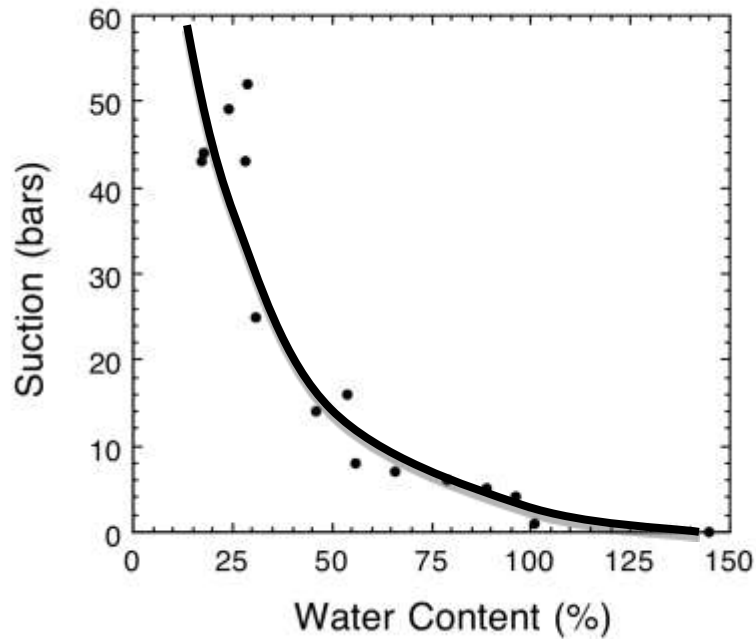


Figure 2. Relationship between soil suction and water content of bentonite in a geotextile-encased GCL (Daniel, Shan, and Anderson, 1993).

Research has pointed to some of the subtleties of soil-moisture retention. A recent investigation by Sarabian and Rayhan (2013) found that the GCL hydrates to a lesser extent if there is cyclic wetting and drying. Sarabian and Rayhan also found that the ability of the soil to conduct moisture to the GCL is important; moist, sandy soils promote more rapid conduction of water and hydration of the adjacent GCL than lower permeability, clay-rich soils. Chevrier et al. (2012) found that hydration was slowed, and moisture absorption reduced, when the process occurs at low temperature ($\approx 5^{\circ}\text{C}$). Rayhani et al. (2011) as well as Anderson, Rayhani, and Rowe (2012) report similar findings but additionally note that the method of GCL manufacture can have a significant impact on the amount of water absorbed.

In summary, with rare exception (the exception being bentonite placed in contact with exceptionally dry materials found rarely in nature), bentonite placed in contact with natural materials in the subsurface will absorb moisture from the subgrade and hydrate. In an overlapped section of GCL, with two layers of GCL, both layers hydrate (Jahangir and Daniel, 1999).

The hydration process can be essentially stopped by separating the bentonite in a GCL from the adjacent soil materials with a geomembrane (Estornell and Daniel, 1992). Water vapor may diffuse through some geomembranes, but the rate is typically extraordinarily slow especially with hydrophilic geomembranes such as HDPE that absorb little or no water.

Hydration has practical implications. For example, suppose a geotextile-encased GCL is placed on a wet subgrade and covered with a geomembrane. Within a few days, the bentonite will have absorbed water and become moist. Walking over the geomembrane could thin the bentonite where people have walked, though foot pressures are seldom large enough to cause damage. Heavier loads such as from construction equipment could do damage if the GCL is not adequately covered and protected. On the positive side, bentonite must be hydrated to achieve low hydraulic conductivity, and the hydration process can “activate” the bentonite and result in low hydraulic conductivity.

HYDRAULIC PROPERTIES OF BENTONITE IN GCLs

Permeation with Water

When the U.S. EPA approached the author in the late 1980s and initiated university-sponsored research on GCLs, he was not especially concerned with whether bentonite had low hydraulic conductivity to water because the low hydraulic conductivity of bentonite was well known. At the time, the author’s attention focused on the overlapped sections of the GCL panels. The manufacturers claimed that these overlaps “self sealed” and required no physical bonding. The author was skeptical and focused initial research on determining whether this was true.

Estornell and Daniel (1992) conducted large-scale tests and concluded that, indeed, the overlaps do self-seal if installed as recommended by the manufacturer. For some GCLs with comparatively thin geotextiles, no additional bentonite may be needed in the overlap because as the bentonite hydrates, it extrudes through the openings in the geotextiles and provides the sealing mechanism. For thicker geotextiles, extra bentonite may be needed in the overlap to provide the seal.

Numerous investigators have reported information about the hydraulic conductivity of GCLs, e.g., Shan and Daniel (1991) in the early days of GCL research. For permeation with water, the testing methods are now reasonably standardized and typically involve a flexible-wall permeameter (e.g., ASTM D-5887). The ranges of hydraulic conductivity reported are reproducible and consistent with data obtained from larger-scale tests.

A point sometimes overlooked is the influence of vertical effective stress on the hydraulic conductivity of GCLs, as shown, for instance, in Figure 3. An increase in compressive stress causes a reduction in porosity and in hydraulic conductivity.

Bentonite is well known not only for its swelling characteristics, but shrinkage properties, as well. Bentonite swells when wetted but tends to shrink and crack when dried. Boardman and Daniel (1996) conducted large-scale tests on GCLs that were allowed to desiccate underneath approximately 0.5 m of cover material. Hot air was circulated to dry the GCL *in situ*. Boardman and Daniel found that the GCLs cracked severely but, upon rehydration, swelled and completely recovered their low hydraulic conductivity when permeated with tap water.

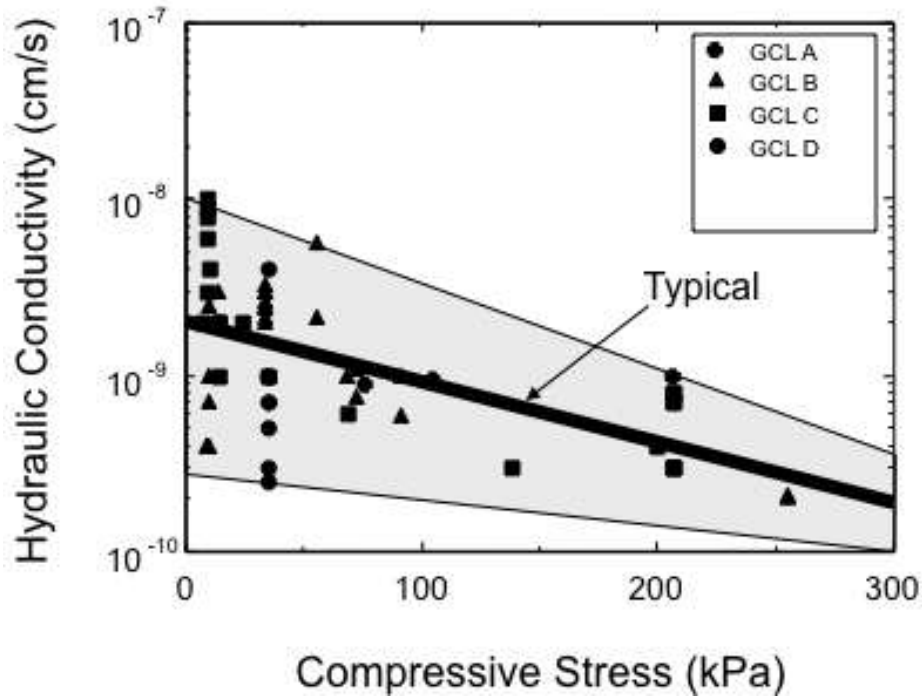


Figure 3. Hydraulic conductivities of GCLs, or the bentonite component of GCLs, as a function of effective confining stress for GCLs permeated with tap water.

Azad et al. (2011) conducted experiments involving GCLs that were configured in a composite liner system, buried, and subjected to high temperatures (39 to 45°C). Desiccation and even some cracking were noted, but upon permeation of the desiccated GCLs, little if any alteration in hydraulic conductivity was noted. The self-healing is attributed to the swelling characteristics of bentonite, absent any deleterious factor (such as chemical alteration a low confining stress) that might inhibit the swelling capacity of the bentonite.

Kraus et al. (1997) and Hewitt and Daniel (1997) investigated the effects of freeze-thaw on the hydraulic conductivity of GCLs. Both studies indicated no damage from multiple cycles of freeze-thaw. Podgorney and Bennett (2005) were concerned that the earlier studies did not extend to a sufficiently large number of freeze-thaw cycles and, thus, performed tests out to 150 freeze-thaw cycles, finding no significant change in hydraulic conductivity. Although there may be some extenuating circumstances in which repeated freeze-thaw might be of concern, these studies are an example of research addressing and largely putting to rest a question about GCLs.

Another question that has been investigated is the hydraulic integrity of GCLs subjected to deformation, such as differential settlement in a landfill cover system. LaGatta et al. (1997) conducted experiments in which a bladder was deflated beneath a large specimen of GCL that was covered with about 0.5 m of gravel. This set-up produced severe differential settlement while the GCL was being permeated, thus enabling deformation to be related directly to hydraulic conductivity. LaGatta et al. found that GCLs could withstand large differential settlement (Δ) over horizontal distance L with essentially no harmful impact on hydraulic

conductivity so long as $\Delta/L \leq 10\%$. Koerner, Koerner, and Eberle (1996) used a different methodology but found essentially identical results. These two studies reinforced one another and answered the basic question about how much deformation a GCL can withstand and maintain hydraulic integrity.

Permeation with Chemical Solutions

Much has been written about GCLs permeated with chemical solutions. Shackelford et al. (2000) provide an excellent overview. Early work by Petrov and Rowe (1997), Petrov, Rowe and Quigley (1997), and Ruhl and Daniel (1997) focused primarily on the effects of organic liquids on the hydraulic conductivity of GCLs. Work expanded to include inorganics (e.g., James, Fullerton, and Drake, 1997; and Shackelford et al., 2000).

In early work, Ruhl and Daniel (1997) permeated five different GCLs using seven permeant liquids (real and simulated waste liquids) and three hydration conditions. When dry GCLs were permeated directly with the real or simulated waste liquids, very high hydraulic conductivities were measured for a simulated leachate with high Ca^{++} concentration. Large increases were also observed when the permeant liquid entering a dry GCL was a very strong acidic or caustic solution. However, when the GCLs were first hydrated with water and then permeated with these same liquids, far lower hydraulic conductivities were observed, although the tests did not continue long enough to develop full breakthrough of the permeating liquids. In contrast, low hydraulic conductivity was observed regardless of the prehydration condition for more dilute, real-world leachates. Guyonnet et al. (2005) found similar effects but studied microstructure and gel phenomena associated with various permeant liquids and prehydration conditions.

The study by Petrov, Rowe, and Quigley (1997) was particularly significant because the investigators mention that effective confining stress could influence the susceptibility of a GCL to chemical alterations when permeated with various chemicals. Few data were presented, however. This is an area ripe for further research. The application of effective confining stress tends to compress and close any cracks or macropores that might tend to form in the bentonite from chemical alterations. For example, data in Figure 4 for a compacted clay demonstrate the potential for large compressive stress to minimize the vulnerability of clay soils to increases in hydraulic conductivity when permeated with aggressive organic liquids.

One of the challenges of hydraulic conductivity testing is the need for long testing time. Jo et al. (2005) took great care to permeate to full breakthrough and equilibrium, but testing times were up to 2.5 years and the tests required as many as 686 pore volumes of flow. Some investigators have tried to correlate the results of relatively fast and inexpensive index tests (e.g., liquid limit and swell index tests) with hydraulic conductivity results to screen bentonite for potential changes in hydraulic conductivity (Lee et al., 2005). Chung and Daniel (2008) experimented with a modified fluid loss test as a rapid indicator for effects from certain liquids. Further research is needed. However, most index tests are performed at zero effective confining stress and may have limited utility because effective confining stress may be one of the most important parameters affecting hydraulic conductivity.

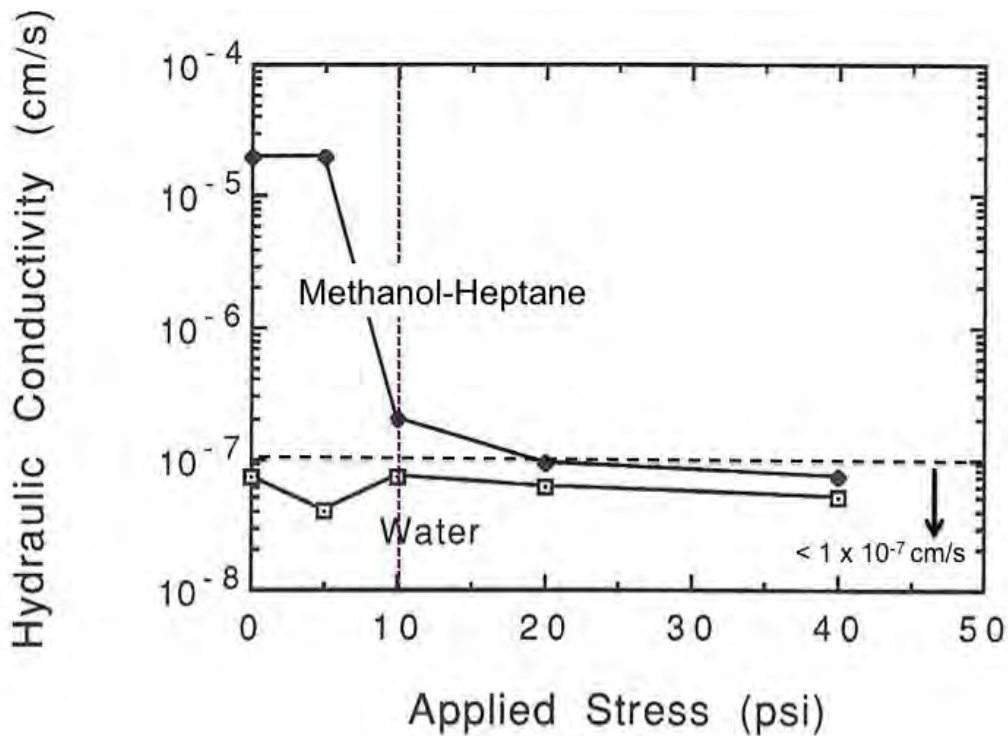


Figure 3. Effect of applied confining stress on hydraulic conductivity of a compacted clay permeated with either water or methanol followed by heptane (after Broderick and Daniel, 1990).

Shackelford, Sevick, and Eykholt (2010) provide a comprehensive assessment of the impacts of tailings liquids on the hydraulic conductivity of GCLs. The tailings liquids tested caused multiple orders of magnitude increase in hydraulic conductivity. The researchers commented on how essential it is to test the GCL with the actual liquids from a project site.

Tests on liquids from other projects (e.g., Lange, Rowe, and Jamieson, 2009b) have not always shown an adverse impact from the waste liquid. Benson, Ören, and Gates (2010) describe tests with a hyperalkaline solution, along with less aggressive solutions, and discuss some of the subtleties involved in this type of testing. Kashir and Yanful (2000) permeated a GCL with a strongly acidic mining drainage liquid and found a significant increase in hydraulic conductivity, though the effect was greatly reduced with the application of high effective confining stress. The actual chemistry of the waste liquid, and the vertical stress to which the test specimen is subjected, can have a significant effect, with the range of impact on the hydraulic conductivity ranging from nil to devastating, depending on the waste liquid.

A special case of occasional interest is the use of GCLs to retain (perhaps temporarily) spilled hydrocarbon fuels or other non-water-soluble organic liquids. Daniel, Shan, and Anderson (1993) and Jahangir and Daniel (1999) demonstrated that the ability of GCLs to retain such liquids (i.e., have a low initial hydraulic conductivity when the liquid contacts the GCL) depends almost entirely on the water content of the GCL at the time when the hydrocarbon liquid

is exposed to the GCL. At low water contents in the bentonite, the hydrocarbon passes readily through the GCL without hydrating the bentonite or causing it to swell. On the other hand, if the bentonite is hydrated with water, capillary tension at the water-hydrocarbon interface tends to exclude the hydrocarbon from even entering the GCL. Rowe, Mukunoki, and Bathurst (2006) tested a GCL that was exhumed from an actual site and exposed to multiple freeze-thaw cycles prior to permeation with jet fuel; results were consistent with other research findings.

To summarize, a tremendous amount of research has been performed on a broad range of liquids that are potentially incompatible with the bentonite component of GCLs. The testing procedures are well established (e.g., ASTM D-6766). The major variables are known. The critical importance of certain parameters such as prehydration with water is understood. The potential for Na^+ to be replaced by polyvalent cations and cause deleterious impacts on hydraulic conductivity is well documented (in fact, this was known decades earlier!). Having acknowledged this large body of knowledge, there still remain considerable uncertainties, which the author views as follows:

- Can quick, simple testing methods be developed and employed to show definitively how the water of hydration in the field at a particular site will influence the hydraulic characteristics of GCLs?
- What are the effects of vertical compressive stress on the behavior of a GCL?

Gas Permeability

The flow of gas through GCLs may be a relevant issue in some situations. Several investigators have examined gas permeability: Didier, Bouazza, and Cazaux (2000), Shan and Yao (2000), and Vangpaisal and Bouazza (2004) were among the early investigators. These studies demonstrate what one would expect: dry bentonite is highly permeable to gas, but once the bentonite absorbs enough water to cutoff continuous air-filled passages through the material, the gas permeability plummets to a very small value. In addition to moisture content, the presence of gas-permeable structure (e.g., needle-punched fibers) and the confining stress (larger confining stress produces lower gas permeability) influence the permeability of GCLs to gas.

Applications in Landfill Covers: Wet/Dry with Chemical Alteration

Melchior (1997) published the results of field tests on landfill covers that had a significant impact on the research community. Melchior found that infiltration rates through low-permeability barriers in landfill cover systems were low for the first several years and then skyrocketed following a severe summer drought. When the materials were exhumed, it was found that cracks had developed and hydraulic conductivity increased. In addition, it was discovered that calcium had replaced sodium as the exchangeable cation in bentonite, causing a significant increase in hydraulic conductivity.

Subsequent studies, primarily by Prof. Craig Benson and his team, demonstrated that wet/dry cycles tend not to be deleterious if there is no alteration of pore water chemistry, but can be very damaging if sodium is replaced by calcium or another polyvalent cation (Lin and

Benson, 2000). The same is true even with gas permeation (Bouazza, Vangpaisal, and Jefferis, 2006).

One of the most important studies was that of Meer and Benson (2007), who exhumed samples of GCLs from four landfill cover systems. At all four sites, Na^+ in the bentonite had been replaced by Ca^{++} and Mg^{++} . Hydraulic conductivities of the exhumed materials varied over 5 orders of magnitude. Meer and Benson report that, "...hydraulic conductivities on the order of 10^{-6} to 10^{-4} cm/s should be expected if exchange occurs coincidentally with dehydration, and the effects of dehydration are permanent once the water content of the GCL drops below approximately 100%." Meer and Benson (2007) as well as Benson et al (2007) note that field results demonstrate that covering a GCL with 760 mm of cover soil does not prevent ion exchange from occurring.

In an even more far-reaching investigation of GCLs exhumed from landfill covers, Scalia and Benson (2011) report that:

- "In most environments, divalent cations likely will replace the native Na^+ in GCLs deployed in composite barriers. Exchange appears to occur more rapidly and completely when the GCL is installed on a subgrade with higher water content."
- GCLs hydrated to a water content of at least 50% seemed to be less vulnerable to changes in hydraulic conductivity caused by ion replacement – one may want to design the GCL to hydrate to this water content or higher, for example, by managing the water content of the underlying or overlying material.

COMPOSITE ACTION OF GCL's WITH A GEOMEMBRANE

"Composite action" refers to the intimacy of hydraulic contact between a geomembrane and underlying low-permeability-soil material. If the geomembrane is in intimate contact with the clay material, liquid will not spread laterally at the interface between the geomembrane and clay even if there is a defect (hole, defect in seam, etc) in the geomembrane. This is the desired situation because intimate hydraulic contact minimizes seepage rates. On the other hand, if there is a highly permeable layer separating the geomembrane from the clay (e.g., layer of sand, transmissive geotextile, or gap such as an opening beneath a wrinkle in a geomembrane), liquid will spread laterally at the interface, and the seepage rate will be much larger because the area of flow through the clay material will be much larger.

Harper, Wilson-Fahmy, and Koerner (1992) performed an early study that quantified the effect of a geotextile at the interface. The results of this and other studies have demonstrated the obvious: flow is much less with intimate contact, and any horizontally transmissive stratum or material between the geomembrane and clay soil is detrimental. The key is the lateral transmissivity of the interface. Transmissivity of compressible materials, such as non-woven geotextiles, is dependent upon the compressive stress. Bouazza and Vangpaisal (2006) demonstrated that the same principles that apply to intimate contact for gas flow, as well.

The need for intimate contact between a geomembrane and clay material is well recognized in the industry (Wilson-Fahmy and Koerner, 1995), and data illuminating the technical parameters are found in various publications, e.g., Barroso et al (2006). Unfortunately, the behavior that promotes excellent hydraulic contact and outstanding composite behavior often requires thin geotextiles that plug from hydrating, swelling bentonite; in such conditions the bentonite swelling into the geotextile may “lubricate” the interface between the geotextile [particularly woven geotextiles, Vukelic, Szaots-Nassan and Kvanicka (2010)] and an adjacent geomembrane. Materials and designs that address the intimate contact problem may be creating another one: low interface shear strength. This remains an area of research opportunity.

One exacerbating factor working against good intimate contact between a geomembrane and underlying GCL is the tendency for geomembranes to wrinkle. Such wrinkles may not be compressed when backfilled (Soong and Koerner, 1998), leaving a transmissive zone between geomembrane and clay. Take et al. (2007) developed a technique to map geomembrane wrinkles from aerial photographs. Prof. Kerry Rowe’s group has documented how extensive the interconnected wrinkles can be (e.g., Chappel et al., 2012), raising further concerns about the deleterious impact of geomembrane waves and wrinkles on composite behavior with GCLs or any other type of low-permeability liner adjacent to the geomembrane.

For many years, the author has been an advocate of encasing bentonite between two geomembranes to achieve maximum hydraulic performance. Giroud and Daniel (2004) provide analytical tools to assist in calculating leakage rates through such systems. The power of such a system, if intact and undamaged, is undeniable. Even with occasional imperfections in the overlying geomembrane, so long as the underlying geomembrane remains intact, the seepage path is typically very long from entrance point in the defect to exit point, which would typically be an overlap in the GCL. Figure 5 depicts the concept.

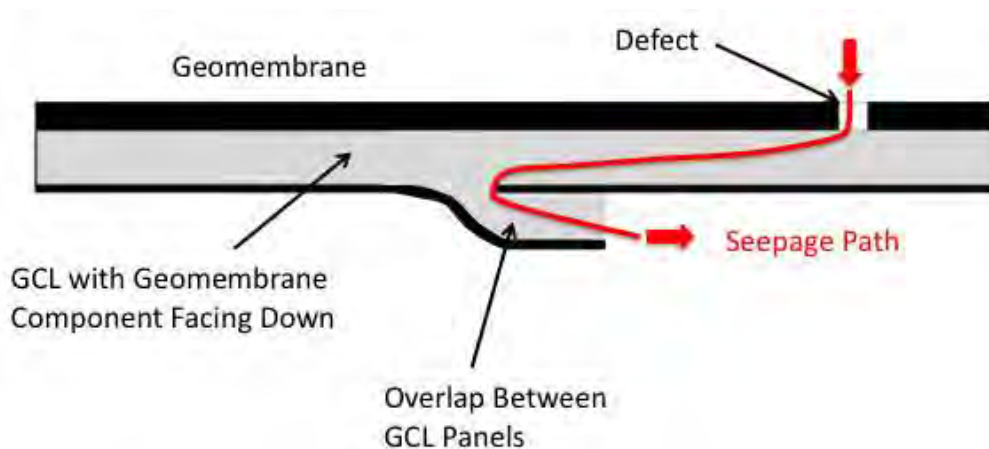


Figure 5. Concept of a geomembrane-backed GCL installed with geomembrane component facing down, and an overlying geomembrane, creating a long, tortuous seepage path through the bentonite in a manner that tends to minimize seepage.

STABILITY OF GCLS ON SLOPES.

The extraordinarily low shear strength of wet bentonite has been very well known for decades. Shan and Daniel (1991) provided some of the earliest data on shear strength of unreinforced, hydrated GCLs. Gilbert, Fernandez, and Horsfield, D.W. (1996) and Stark and Eid (1996) were among the first to publish shear strength results for internally reinforced GCLs.

For the author, the most significant experience with GCLs on slopes was the construction under EPA sponsorship of multiple test plots in Cincinnati, Ohio (Daniel et al., 1999). The project team included the author, Dr. Robert Koerner, and Dr. Rudolph Bonaparte, with guidance from the EPA project officer, David Carson. Numerous GCL industry sponsors provided materials and installation crews. Multiple test plots were constructed on 2H:1V and 3H:1V slopes, challenging not only the GCL materials but also the interface between GCLs and an overlying geomembrane. All the 3H:1V slopes remained stable for years, but two of the test plots on 2H:1V slopes exhibited failures about 2 months after construction. Failure occurred at the interface between the woven geotextile side of GCLs and a textured geomembrane. In hindsight, it was not surprising that the failures would have occurred because laboratory shear testing performed later indicated interface angles of friction near the slope angles. Gradual hydration was the reason for failure after 2 months and not immediately upon completion of construction. The findings pointed many in the industry toward use of GCLs with non-woven geotextiles on both surfaces to deliver enhanced interface strength for slope applications.

Much research has recently been performed, and continues, to investigate the internal and interface shear strength of GCLs. For example, Fox and Ross (2011) performed extensive testing on critical GCL interfaces and studied the large deformations. McCartney, Zornberg, and Swan (2009) present a database of 534 large-scale direct shear test results for interface strength test results between GCLs and geomembranes.

From the author's perspective, the key question is whether the engineering design community has the capacity to employ GCLs on slopes in a safe, cost-effective manner. For the most part, the author believes that the community has this knowledge and capacity. Testing methods are now well developed, e.g., ASTM D-6243 for direct shear testing. Experience with this type of testing is extensive, and databases have been published in the open literature. Field cases have correlated reasonably well with laboratory-measured results. Laboratory testing has helped clarify various critical parameters, such as impact of hydration, confining stress, and deformation, when in turn has pointed designers toward thinking holistically about design. There is need for further research, but from the author's perspective, the first-order questions about GCL shear strength have been asked and answered, and we are now in the process of exploring some of the finer points at issue.

PHYSICAL INTEGRITY OF GCLs

One of the issues identified early in the study of GCLs is the potential for stones or other objects to displace bentonite and thin the GCL. Koerner and Narejo (1995) studied the bearing capacity of GCLs and concluded that if a load of width B is placed a distance H above the bentonite layer (separated by a layer of sand, for instance), there was little or no thinning so long as the H/B ratio was greater than 1 to 2. Fox et al. performed independent research with similar study objectives but different technique, and came to essentially the same conclusion, i.e., there

is not much problem so long as $H/B \geq 1$ to 1.5. This general area of research is an example of a question that has essentially been asked and answered.

Several researchers have studied the penetration of gravel particles or stones into hydrated GCLs. Fox, De Battista, and Mast (2000) placed gravel with a particle size up to 50 mm directly above the GCL, and applied vertical stress. Although there was thinning beneath gravel particles, the hydraulic conductivity was within acceptable limits. Dickinson and Brachman (2006) measured the thinning of GCLs from gravel (50 mm) placed above a geomembrane/GCL composite liner. Thinning was significant without adequate protection. Dickinson, Brachman, and Rowe (2010) examined the intrusion of GCLs into a geonet, and thinning of the GCL caused by ribs in the geonet indenting the GCL. The investigators found some thinning of the GCL, but no deleterious impact on hydraulic conductivity. An object that tends to penetrate into and thin the bentonite may also tend to consolidate the bentonite into a lower-porosity, less permeability material that offsets impacts of thinning. The thinning of GCL accompanied by lateral flow of bentonite away from the thinned zone is the primary source of concern.

Shrinkage of GCLs can cause problems, independent of changes in hydraulic conductivity, such as reduction in the width of overlaps. Many variables influence the shrinkage of GCLs, as described by Rowe, Bostwick, and Take (2011).

A GCL placed at shallow depth without protection such as that afforded by an overlying geomembrane may be vulnerable to penetration by and damage from plant roots. In shallow environments, a suitable geomembrane or other barrier over the GCL may be the most effective way to prevent roots from penetrating the GCL.

EQUIVALENCY OF GCLs TO COMPACTED CLAY LINERS

In the early days of GCL use for waste disposal applications, the regulatory agencies did not know how to deal with evaluating GCLs. The very first use by Schubert (1987) involved use of a GCL that went beyond the minimum requirements – thus, there was relatively little difficulty in gaining regulatory acceptance. The real issue was whether a thick, compacted clay liner could be replaced with a GCL. As mentioned earlier, the advantages of GCLs over compact clay liners represent considerable motivation for owners.

To gain regulatory acceptance, the argument was advanced that if a GCL's performance could be shown to be equivalent to or better than that of a compacted clay liner, then the regulatory agency might approve substitution of a GCL for a compacted clay liner. Most of the attention focused on demonstrating the hydraulic equivalency of a GCL to a compacted clay liner, which must typically have a hydraulic conductivity of $\leq 1 \times 10^{-7}$ cm/s. Equivalency analysis for this factor is a straight-forward calculation of seepage quantity based on Darcy's law. Generally speaking, there was not much difficulty demonstrating this efficiency for low hydraulic heads acting on GCLs with hydraulic conductivities in the 10^{-8} to 10^{-9} cm/s range.

No standardized set of ground rules exist for how to establish equivalency.. Publications such as Koerner and Daniel (1994) may provide some guidance. The sticking point in such analyses is the set of parameters that will be considered. For example, will chemical release from

the liner be considered, even though it is not mentioned in the regulations? Because most U.S. regulations for waste containment focus almost entirely on thickness and hydraulic conductivity of the compacted clay liner, an argument can be made that such considerations are beyond the scope of the regulations and beyond the scope of an equivalency demonstration.

One of the areas in which GCLs are different from compacted clay liners is their ability to retard release of chemicals via diffusion. Diffusion is the transport of chemicals across a barrier in response to a chemical gradient. The key parameters, for a given chemical and concentration of the chemical in a landfill or lagoon, are diffusion coefficient in the barrier material (bentonite in the case of a GCL) and thickness. The thicker the barrier, the less the diffusive release. The thinness of GCLs makes them inherently a comparatively poor barrier to diffusive release, unless the chemical itself tends not to diffuse readily through bentonite. Most chemicals do diffuse through bentonite, but some species will be absorbed by bentonite and diffuse more slowly.

Lake and Rowe (2000) provide a useful primer on diffusion of inorganic elements through GCLs. Lange, Rowe, and Jamieson (2009a) provide an extensive compilation of information regarding the diffusion of metals through GCLs. Diffusion coefficients for a range of metals did not vary a great deal from one another. The techniques for measuring diffusion coefficients are well developed (Rowe et al., 2000), as are methods for analyzing diffusive transport through the bentonite component.

The diffusion of VOCs through relatively thin GCLs may be of more concern than diffusion of metals because VOCs can migrate in liquid or gaseous phase. Gaseous-phase diffusion presents a risk for transport away from many waste containment facilities. Paumier et al. (2011) investigated the impact of calcium exchange, which is known to have potentially significant deleterious impact on hydraulic conductivity, upon the rate of diffusion of VOCs through bentonite. Although there was a small change in diffusion rates for Na and Ca-rich bentonite, the impact was small and the authors note that, “The increase in the diffusion coefficient of VOCs, thus, does not seem to be of concern for the range of GCL hydraulic conductivities generated by cation exchange in this study.”

The author considers this area of research relatively mature and well developed – the primary questions relate to complexities in the system, such as coupled effects from large thermal gradients, coupled liquid/vapor transport, biological processes integrated with physical and chemical processes, and complexities from multiple landfill components, e.g., composite action of a geomembrane and GCL.

ADVANCES IN MATERIALS AND DESIGN

Over time, there have been many advances in GCL design, including use of different types of geotextiles, heat burnishing surfaces of geotextiles to strengthen the material, incorporating a geomembrane in the GCL system, and others. The creative use of geosynthetic materials will undoubtedly continue to evolve and to create even more options for GCLs.

Engineering the bentonite itself has been the subject of much research. These efforts have included study of different types of bentonites (e.g., Lee and Shackelford, 2005), additives (chemical and physical), and well as chemical alteration of bentonite. For instance, with respect to physical additives, Schmitt et al. (1977) tried adding two granular materials (expanded shale and recycled glass) to strengthen the bentonite and ameliorate the problem of low shear strength of GCLs. They found that very low hydraulic conductivity was observed in the mixtures with up to 50% additive to the bentonite, and that the additives significantly improved the shear strength of the mixture, particularly at high normal stress. It is perhaps a little surprising that, over the years, more work has not been performed to examine additives that would strengthen the bentonite, especially since low strength of hydrated bentonite is such an important issue for GCLs. Probably the practical reason is that there are other ways to deal with shear strength challenges.

Much research, proprietary and public, has been performed regarding the use of polymers as additives to bentonite, and several forms of commercial products are available with polymer additives. Polymers are discussed in the literature (e.g., Ashmawy et al., 2002; McRory and Ashmawy, 2005, and Razakamanantsoa, Barast, and Djeran-maigre, 2012). The proprietary nature of these additives makes broad conclusions difficult, other than to note that polymer additives almost always tend to reduce hydraulic conductivity to water and to improve resistance to alterations from many chemicals. Perhaps their main drawback is cost.

Organo-bentonites are another material alteration designed to minimize the vulnerability to deleterious alterations in hydraulic conductivity caused by certain chemicals. Test results typically show that the bentonite can be stabilized against degradation from permeant liquids (e.g., Lorenzetti, Bartelt-Hunt, Burns, and Smith, 2005; and Katsumi et al., 2008).

LOOKING TO THE FUTURE

As the author prepared this paper and reflected on 25 years of research on GCLs, he was struck by how much has been learned. An entire body of knowledge has been created from essentially nothing. To the many researchers, manufacturers, and design engineers, he offers sincere congratulations on a job well done. The profession has methodically identified questions, studied them, and sorted through the findings to reach conclusions. Engineering practice associated with GCLs rests on a solid base of knowledge.

As the author looks forward, several areas of change and advancement may be desirable and are offered for consideration:

1. More use of bentonite sandwiched two geomembranes (Figure 5) is encouraged. This type of liner offers the opportunity for significantly enhanced hydraulic performance compared to many other systems. The potential for enhanced performance is not just a little – the system may be orders of magnitude less permeable than a single geomembrane overlying a bentonite layer. Concerns include slope stability if the bentonite hydrates (which should occur exceedingly slowly).
2. More use of a protective layer beneath GCLs to mitigate impact of any unforeseen puncture and to limit diffusive migration of chemicals is suggested. In some ways, the

author's favorite composite liner system would be the one shown in Figure 5 underlain with perhaps 300 mm of a moderately low-permeability material (say 10^{-6} to 10^{-7} cm/s). This low-permeability material serves as a fail-safe material in case the geosynthetic liner system is punctured, and also serves to enhance diffusion impedance of the system. By using a hydraulic conductivity greater than 10^{-7} cm/s, cost can be controlled.

3. More consideration of site-specific conditions in GCL design is recommended. This suggestion is focused primarily on the hydration of the GCL and the impacts that the site-specific soils, pore fluids, and overall conditions will have on GCL performance. This issue deserves more research but, ultimately, simple methods are needed by the design engineer.
4. Better management of wrinkles in geomembranes is advised. Geomembrane wrinkles exacerbate the challenge of achieving intimate contact. It seems unwise to the author to go to great lengths to engineer a high quality GCL and then not go to great lengths to ensure intimate contact of the geomembrane with the GCL.
5. More selective less use of GCLs in near-surface environments is recommended. Experience shows that the application of vertical compressive stress tends to compress bentonite and enhance its stability. More research on this effect, particularly for permeation with chemicals, is needed. But placing GCLs near the surface with very little vertical confining stress and sometimes very little protection creates an inherently challenging situation. More thought should be given as to whether GCLs are really the best design choice in near-surface applications with very limited protection afforded the GCL.

ACKNOWLEDGMENTS

The author's early work on GCLs was supported by the US EPA without whose support so many advances in GCL knowledge and use would not have been possible. Special thanks are due to Bob Landreth, Walter Grube, and David Carson.

In the early days of the author's GCL research, several industry representatives provided critical collaboration, information, and in many cases research support. Special thanks are due to Jim Anderson, Richard Erickson, Tom Stam, Jim Olsta, and Kent von Maubeuge.

The author had the pleasure of collaborating with numerous consulting engineers on various projects, and he is grateful to all for these opportunities. Special appreciation is extended to Rudy Bonaparte, J. P. Giroud, Mario Manassero, Greg Richardson, and Rick Thiel.

None of the author's research contributions would not have been possible without the insights, creativity, and dedication of numerous graduate students working with the author. Special thanks are given to Paula Estornell, Tom Boardman, Mark LaGatta, Mark Gleason, Ben Cooley, Juniran Lai, Heather Scranton, Hsin-yu Shan, Karen Schmidt, Ashraf Jahangir, and Jin Chung.

The group of academic researchers involved in study of GCLs has been is a relatively small, close-knit group of individuals with whom the author has deeply enjoyed sharing research findings and ideas. Special thanks are extended to Bob Gilbert, Steve Wright, and Ed Kavazanjian, and Grace Hsuan.

Three individuals have had a particularly profound impact on the author's career and thinking about GCLs. The author thanks Roy Olson for teaching him a way of thinking (about bentonite and many other things), to Steve Trautwein for numerous helpful ideas for testing materials and for his superb equipment, and to Robert Koerner for his brilliant mind and deep wisdom that helped to guide the thinking and practice of not only this individual but numerous others, as well.

REFERENCES

ASTM D-5887 (2013), "Standard Test Method for Measurement of Index Flux through Saturated Geosynthetic Clay Liner Specimens Using Flexible Wall Permeameter," American Society for Testing and Materials, Philadelphia, PA.

ASTM D-6243 (2013), "Standard Test Method for Determining the Internal and Interface Shear Resistance of Geosynthetic Clay Liner by the Direct Shear Method," American Society for Testing and Materials, Philadelphia, PA.

ASTM D-6766 (2013), "Standard Test Method for Evaluation of Hydraulic Properties of Geosynthetic Clay Liners Permeated with Potentially Incompatible Aqueous Solutions," American Society for Testing and Materials, Philadelphia, PA.

Anderson, R., Rayhani, M.T., and Rowe, R.K. (2012), "Laboratory Investigation of GCL Hydration from Clayey Sand Subsoil," *Geotextiles and Geomembranes*, V. 31, pp. 31-38.

Ashmawy, A.K., El-Hajji, D., Sotelo, N. and Muhammad, N. (2002), "Hydraulic Performance of Untreated and Polymer-Treated Bentonite in Inorganic Landfill Leachates," *Clays and Clay Minerals*, V. 50, No. 5, pp. 546-552.

Azad, F.M., Rowe, R.K., El-Zein, A., and Airey, D.W. (2011), "Laboratory Investigation of Thermally Induced Desiccation of GCLs in Double Composite Liner Systems," *Geotextiles and Geomembranes*, V. 29 No. 6, pp. 534-543.

Barroso, M., Touze-Foltz, N., von Maubeuge, K., and Pierson, P. (2006), "Laboratory Investigation of Flow Rate through Composite Liners Consisting of a Geomembrane, a GCL and a Soil Liner," *Geotextiles and Geomembranes*, V. 24, No. 3, pp. 139-155.

Beddoe, R.A., Take, W.A., and Rowe, R.K. (2011), "Water Retention Behavior of Geosynthetic Clay Liners," *Journal of Geotechnical and Geoenvironmental Engineering*, V. 137, No. 11, pp. 1028-1038.

Benson, C.H., Ören, A.H., and Gates, W.P. (2010), "Hydraulic Conductivity of Two Geosynthetic Clay Liners Permeated with a Hyperalkaline Solution," *Geotextiles and Geomembranes*, V. 28, No. 2, pp. 206-218.

Boardman, B.T., and Daniel, D.E. (1996), "Hydraulic Conductivity of Desiccated Geosynthetic Clay Liners," *Journal of Geotechnical Engineering*, Vol. 122, No. 3, pp. 204-209.

Bouazza, A., and Vangpaisal, T. (2006), "Laboratory Investigation of Gas Leakage Rate through a GM/GCL Composite Liner Due to a Circular Defect in the Geomembrane," *Geotextiles and Geomembranes*, V. 24, No. 4, pp. 110-115.

Bouazza, A., Vangpaisal, T., and Jefferis, S. (2006), "Effect of Wet-Dry Cycles and Cation Exchange on Gas Permeability of Geosynthetic Clay Liners," *Journal of Geotechnical and Geoenvironmental Engineering*, V. 132, No. 8, pp. 1011-1018.

Broderick, G.P., and D.E. Daniel (1990), "Stabilizing Compacted Clay Against Chemical Attack," *Journal of Geotechnical Engineering*, Vol. 116, No. 10, pp. 1549-1567.

Chappel, M.J., Brachman, R.W.I., Take, W.A., and Rowe, R.K. (2012), "Large-Scale Quantification of Wrinkles in a Smooth Black HDPE Geomembrane," *Journal of Geotechnical and Geoenvironmental Engineering*, Vo. 138, N.6, pp. 671-679.

Chevrier, B., Cazaux, D., Didier, G., Gamet, M., and Guyonnet, D. (2012), "Influence of Subgrade, Temperature, and Confining Pressure on GCL Hydration," *Geotextiles and Geomembranes*, V. 33, pp. 1-6.

Chung, J., and Daniel, D.E. (2008), "Modified Fluid Loss Test as an Improved Measure of Hydraulic Conductivity for Bentonite," *Geotechnical Testing J.*, V. 31, No. 3, pp. 243-251.

Daniel, D.E., Shan, H.Y., and J.D. Anderson (1993), "Effects of Partial Wetting on the Performance of the Bentonite Component of a Geosynthetic Clay Liner," *Proceedings, Geosynthetics '93*, Industrial Fabrics Association International, St. Paul, Minnesota, V. 3, 1993, pp. 1483-1496.

Daniel, D.E., Koerner, R.M., Bonaparte, R., Landreth, R.L., Carson, D.A., and Scranton, H.B. (1998), "Slope Stability of Fourteen Full-Scale Field Test Plots Containing Geosynthetic Clay Liners," *Journal of Geotechnical and Geoenvironmental Engineering*, Vol. 125, No. 7, 1998, pp. 628-637.

Dickinson, S., and Brachman, R.W.I. (2006), "Deformations of a Geosynthetic Clay Liner beneath a Geomembrane Wrinkle and Coarse Gravel," *Geotextiles and Geomembranes*, V. 24, No. 5, pp. 285-298.

Didier, G., Bouazza, and D. Cazaux (2000), "Gas Permeability of Geosynthetic Clay Liners," *Geotextiles and Geomembranes*, 18: 235-250.

- Estornell, P., and Daniel, D.E. (1992), "Hydraulic Conductivity of Three Geosynthetic Clay Liners," *Journal of Geotechnical Engineering*, Vol. 118, No. 10, pp. 1592-1606.
- Fox, P.J., De Battista, D.J., and Chen, S.J. (1996), "Bearing Capacity of Geosynthetic Clay Liners for Cover Soils of Varying Particle Size," *Geosynthetics International*, Vol. 3, No. 4, pp. 447-461.
- Fox, P.J., De Battista, D.J., and Mast, D.G. (2000), "Hydraulic Performance of Geosynthetic Clay Liners under Gravel Cover Soils," *Geotextiles and Geomembranes*, Vol. 18, Nos. 2-4, pp. 179-201.
- Fox, P.J., and Ross, J.D. (2011), "Relationship between NP GCL Internal and HDPE GMX/NP GCL Interface Shear Strengths," *Journal of Geotechnical and Geoenvironmental Engineering*, V. 137, No. 8, pp. 743-753.
- Gates, W.P., and Bouazza, A. (2010), "Bentonite Transformations in Strongly Alkaline Solutions," *Geotextiles and Geomembranes*, V. 28, No. 2, pp. 219-225.
- Gilbert, R.B., Fernandez, F., and Horsfield, D.W. (1996), "Shear Strength of Reinforced Geosynthetic Clay Liner," *Journal of Geotechnical Engineering*, Vol. 122, No. 4, pp. 259-266.
- Giroud, J.P., & Daniel, D.E. (2004), "Liquid Migration in a Bentonite Layer Overlain by a Geomembrane Having Defects and Underlain by a Geomembrane," Special Issue on Geosynthetic Clay Liners, *Geosynthetics International*, Vol. 11, No. 4, pp. 311-329.
- Guyonnet, D., Gaucher, E. Gaboriau, H., Pons, C.-H., Clinard, C., Norotte, V., and Didier, G. (2005), "Geosynthetic Clay Liner Interaction with Leachate: Correlation between Permeability, Microstructure, and Surface Chemistry," *Journal of Geotechnical and Geoenvironmental Engineering*, V. 131, No. 6, pp. 740-749.
- Harpur, W.A., Wilson-Fahmy, R.F., and Koerner, R.M. (1992), "Evaluation of the Contact between Geosynthetic Clay Liners and Geomembranes in Terms of Transmissivity," *Proceedings of the 7th GRI Seminar, Geosynthetic Liner Systems: Innovations, Concerns and Designs*, Geosynthetic Research Institute, Drexel University, Philadelphia, PA, pp. 138-149.
- Hewitt, R.D., and Daniel, D.E. (1997), "Hydraulic Conductivity of Geosynthetic Clay Liners Subjected to Freeze-Thaw," *Journal of Geotechnical and Geoenvironmental Engineering*, Vol. 123, No. 4, pp. 205-313.
- Jahangir, A., and Daniel, D.E. (1999), "Containment of Oils with Geosynthetic Clay Liners using Natural Soil-Moisture for Bentonite Hydration," *Geosynthetics '99*, Vol. 1, pp. 163-180.
- James, A.N., Fullerton, D., and Drake, R. (1997), "Field Performance of GCL under Ion Exchange Conditions," *Journal of Geotechnical and Geoenvironmental Engineering*, Vol. 123, No. 10, pp. 897-902.

- Kashir, M., and E.K. Yanful (2001), "Hydraulic Conductivity of Bentonite Permeated with Acid Mine Drainage," *Canadian Geotechnical Journal*, Vol. 38, No. 5, pp. 1034-1048.
- Katsumi, T., Ishimori, H., Onikata, M., and Fukagawa, R. (2008), "Long-Term Barrier Performance of Modified Bentonite Materials against Sodium and Calcium Permeant Solutions," *Geotextiles and Geomembranes*, V. 26, No. 1, pp. 14-30.
- Koerner, R., and Daniel, D. (1994), "A Suggested Methodology for Assessing the Technical Equivalency of GCLs to CCLs," *Proceedings, Geokunststoff-Ton-Dichtungen, GTD*, H. Zanzinger (Ed.), Nurnberg, Germany, pp. 61-83.
- Koerner, R.M., and Narejo, D. (1995), "Bearing Capacity of Hydrated Geosynthetic Clay Liners," *Journal of Geotechnical Engineering*, Vol. 121, No. 1, pp. 82-85.
- Koerner, R.M., Koerner, G.R., and Eberle, M.A. (1996), "Out-of-Plane Tensile Behavior of Geosynthetic Clay Liners," *Geosynthetics International*, Vol. 3, No. 2, pp. 277-296.
- Kraus, J.F., Benson, C.H., Erickson, A.E., and Chamberlain, E.J. (1997), "Freeze-Thaw Cycling and Hydraulic Conductivity of Bentonitic Barriers," *Journal of Geotechnical and Geoenvironmental Engineering*, Vol. 123, No. 3, pp. 229-238.
- LaGatta, M.D., Boardman, B.T., Cooley, B.H., and Daniel, D.E. (1997), "Geosynthetic Clay Liners Subjected to Differential Settlement," *Journal of Geotechnical and Geoenvironmental Engineering*, Vol. 123, No. 5, pp. 402-410.
- Lake, C.B., and Rowe, R.K. (2000), "Diffusion of Sodium and Chloride through Geosynthetic Clay Liners," *Geotextiles and Geomembranes*, Vo. 18, Nos. 2-4, pp. 103-132.
- Lange, K., Rowe, R.K., and Jamieson, H. (2009a), "Diffusion of Metals in Geosynthetic Clay Liners," *Geosynthetics International*, V. 16, No. 1, pp. 11-27.
- Lange, K., Rowe, R.K., and Jamieson, H. (2009b), "The Potential Role of Geosynthetic Clay Liners in Mine Water Treatment Systems," *Geotextiles and Geomembranes*, Vol. 28, No. 2, pp. 199-205.
- Lee, J.M., and Shackelford, C.D. (2005), "Impact of Bentonite Quality on Hydraulic Conductivity of Geosynthetic Clay Liners," *Journal of Geotechnical and Geoenvironmental Engineering*, V. 131, No. 1, pp. 64-77.
- Lee, J.M., Shackelford, C.D., Benson, C.H., Jo, H.-Y., and Edil, T.B. (2005), "Correlating Index Properties and Hydraulic Conductivity of Geosynthetic Clay Liners," *Journal of Geotechnical and Geoenvironmental Engineering*, V. 131, No. 11, pp. 1319-1329.
- Lin, L.-C., and Benson, C.H. (2000), "Effect of Wet-Dry Cycling on Swelling and Hydraulic Conductivity of GCLs," *Journal of Geotechnical and Geoenvironmental Engineering*, Vol. 126, No. 1, pp. 40-49.

- Lorenzetti, R.J., Bartelt-Hunt, S.L., Burns, S.E., and Smith, J.A. (2005), "Hydraulic Conductivities and Effective Diffusion Coefficients of Geosynthetic Clay Liners with Organobentonite Additives," *Geotextiles and Geomembranes*, V. 23, No. 5, pp. 385-400.
- McCartney, J.S., Zornberg, J.G., and Swan, R.H. Jr. (2009), "Analysis of a Large Database of GCL-Geomembrane Interface Shear Strength Results," *Journal of Geotechnical and Geoenvironmental Engineering*, V. 135, No. 2, pp. 209-223.
- McRory, J.A. and Ashmawy, A.K. (2005), "Polymer Treatment of Bentonite Clay for Contaminant Resistant Barriers," *Proceedings, GeoFrontiers 2005*, GSP 142, ASCE.
- Melchior, S. (1997), "In-Situ Studies on the Performance of Landfill Caps (Compacted Clay Liners, Geomembranes, Geosynthetic Clay Liners, Capillary Barriers)," *Proceedings, International Containment Conference*, St. Petersburg, pp. 365-373.
- Paumier, S., Touze-Foltz, N. Mazeas, L, and Guenne, A. (2011), "Quantification of Volatile Organic Compounds Diffusion for Virgin Geosynthetic Clay Liners and for a GCL after Contact with a Synthetic Leachate," *Journal of Geotechnical and Geoenvironmental Engineering*, V. 137, No. 11, pp. 1039-1046.
- Petrov, R.J., and Rowe, K.R. (1997), "Geosynthetic Clay Liner (GCL) – Chemical Compatibility by Hydraulic Conductivity Testing and Factors Impacting Its Performance," *Canadian Geotechnical Journal*, V. 34, pp. 863-885.
- Petrov, R.J., Rowe, R.K., and Quigley, R.M. (1997), "Comparison of Laboratory-Measured GCL Hydraulic Conductivity Based on Three Permeameter Types," *Geotechnical Testing Journal*, Vol. 20, No. 1, pp. 49-62.
- Podgorney, R.K., and Bennett, J.E. (2006), "Evaluating the Long-Term Performance of Geosynthetic Clay Liners Exposed to Freeze-Thaw," *Journal of Geotechnical and Geoenvironmental Engineering*, V. 132, No. 2, pp. 265-268.
- Rayhani, M.T., Rowe, R.K., Brachman, R.W.I., Take, W.A., and Siemens, G. (2011), "Factors Affecting GCL Hydration under Isothermal Conditions," *Geotextiles and Geomembranes*, V. 29, No. 6, pp. 525-533.
- Razakamanantsoa, A.R., Barast, G., and Djeran-maigre, I. (2012), "Hydraulic Performance of Activated Calcium Bentonite Treated by Polyionic Charged Polymer," *Applied Clay Science*, V. 59-60, pp. 103-114.
- Rowe, K., Lake, C.B., and R.J. Petrov (2000), "Apparatus and Procedures for Assessing Inorganic Diffusion Coefficients for Geosynthetic Clay Liners," *Geotechnical Testing Journal*, 23(2): 206-214.

- Rowe, R.K., Mukunoki, T., and Bathurst, R. (2006), "Compatibility with Jet A-1 of a GCL Subjected to Freeze-Thaw Cycles," *Journal of Geotechnical and Geoenvironmental Engineering*, V. 132, No. 12, pp. 1526-1537.
- Rowe, R.K., Bostwick, L.E., and Take, W.A. (2011), "Effect of GCL Properties on Shrinkage When Subjected to Wet-Dry Cycles," *Journal of Geotechnical and Geoenvironmental Engineering*, V. 137, No. 11, pp. 1019-1027.
- Ruhl, J.L., and Daniel, D.E. (1997), "Geosynthetic Clay Liners Permeated with Chemical Solutions and Leachates," *Journal of Geotechnical Engineering*, Vol. 123, No. 4, pp. 369-381.
- Sarabian, T., and Rayhan, M.T. (2013), "Hydration of Geosynthetic Clay Liners from Clay Subsoil under Simulated Field Conditions," *Waste Management*, V. 33, No. 1, pp. 67-73.
- Scalia, J., and C.H. Benson (2010), "Hydraulic Conductivity of Geosynthetic Clay Liners Exhumed from Landfill Final Covers with Composite Barriers," *Journal of Geotechnical and Geoenvironmental Engineering*, V. 137, No. 1, pp. 1-13..
- Schubert, W.R. (1987), "Bentonite Lining in Composite Lining Systems," *Geotechnical Practice for Waste Disposal '87*, R.D. Woods (Ed.), ASCE, pp. 784-796.
- Schmitt, K.E., Bowders, J.J., Gilbert, R.B., and Daniel, D.E. (1997), "Enhanced Shear Strength of Sodium Bentonite Using Frictional Additives," *Proceedings*, International Containment Conference, St. Petersburg, pp. 355-361.
- Shackelford, C.D., Benson, C.H., Katsumi, T., Edil, T.B., and L. Lin (2000), "Evaluating the Hydraulic Conductivity of GCLs Permeated with Non-Standard Liquids," *Geotextiles and Geomembranes*, 18: 133-161.
- Shackelford, C.D., Sevick, G.W., and Eykholt, G.R. (2010), "Hydraulic Conductivity of Geosynthetic Clay Liners to Tailings Impoundment Solutions," *Geotextiles and Geomembranes*, Vol. 28, No. 2, pp. 149-162.
- Shan, H.Y., and Daniel, D.E. (1991), "Results of Laboratory Tests on a Geotextile/Bentonite Liner Material," *Geosynthetics '91*, Vol. 2, Industrial Fabrics Association International, St. Paul, Minnesota, pp. 517-535.
- Shan, H.Y., and J.T. Yao (2000), "Measurement of Air Permeability of Geosynthetic Clay Liners," *Geotextiles and Geomembranes*, 18: 251-261.
- Soong, T.-Y., and Koerner, R.M. (1998), "Laboratory Study of High Density Polyethylene Geomembrane Waves," *Proceedings*, International Conference on Geosynthetics, Vo 1, pp. 301-306.
- Southen, J.M. and Rowe, R.K. (2007), "Evaluation of the Water Retention Curve for Geosynthetic Clay Liners," *Geotextiles and Geomembranes*, V. 25, pp. 2-9.

Stark, T.D., and Eid, H.T. (1996), "Shear Behavior of Reinforced Geosynthetic Clay Liners," *Geosynthetics International*, Vol. 3, No. 6, pp. 771-786.

Take, W.A., Chappel, M.J., Brachman, R.W.I., and Rowe, R.K. (2007), "Quantifying Geomembrane Wrinkles Using Aerial Photography and Digital Image Processing," *Geosynthetics International*, Vol. 14, No. 4, pp. 217-227.

Vangpaisal, T., and Bouazza, A. (2004), "Gas Permeability of Partially Hydrated Geosynthetic Clay Liners," *Journal of Geotechnical and Geoenvironmental Engineering*, V. 130, No. 1, pp. 93-102.

Vukelic, A., Szaots-Nassan, A. and Kvanicka, P. (2010), "Extrusion of Hydrated Bentonite Through the Woven Geotextile of GCL and the Influence on GCL/GM Interface Shear Strength," *Proc. 3rd Intl. Symposium on Geosynthetic Clay Liners*, Wurzburg, Germany, pp. 241-248.

Wilson-Fahmy, R.F., and Koerner, R.M. (1995), "Leakage Rates through Holes in Geomembranes Overlying Geosynthetic Clay Liners," *Geosynthetics '95*, Industrial Fabrics Association International, St. Paul, MN, pp. 655-668.

GEOFOAM: HISTORY OF THE LIGHTWEIGHT CONTENDER

Archie Filshill
InterGEO Services, Trevoise, PA

ABSTRACT

Although geofoam has been around for over 40 years, it has not been utilized fully in the United States until the last 10 years. The growth in the US market can be attributed to the growing need to build on sites that were previously considered “unsuitable” for construction activity. Highway realignments, backfill against existing structures, increased fill over existing utilities and underground structures are examples for the recent growth of geofoam applications in the USA. In recent years, as geofoam has become more accepted, it has gained visibility in textbooks and short courses. A definition of Geofoam from “Designing with Geosynthetics” defines the product as follows: “A block or planar shaped rigid cellular foamed polymeric material used in geotechnical engineering applications.”

INTRODUCTION AND BACKGROUND

There are several materials capable of being used for geofoam applications but for the purposes of this paper, expanded polystyrene geofoam will be focused upon. Expanded polystyrene (EPS) is created by sand sized particles of styrene resins being supplied to a geofoam “molder”. The molder expands the styrene resin into small cellular spheres using pentane gas. These gas filled spheres are expanded in bulk into a mold. This mold creates relatively large blocks of polystyrene. Standard blocks sizes are approximately 1m x 1m x 2.5m.

Various types of rigid plastic foams were first developed circa 1950 and used mainly for thermal insulation. Thermal insulation properties are created by the 98% gas by volume within the expanded polystyrene. The two most commonly used foams in construction are extruded polystyrene (EXP) and expanded polystyrene (EPS). EXP is more commonly used as insulation boards in 25 to 50 mm thicknesses in foundation applications. The primary function is insulation and puncture protection of foundation waterproofing.

Today, the primary applications of geofoam include lightweight fills, compressible inclusions, thermal insulation, vibration damping, fluid transmission, and structural support. Geofoam is often capable of combining several of these functions into one application; see Figure 1.



Figure 1 - First picture author remembers seeing geofoam used in an advertisement.

TIMELINE OF MAJOR APPLICATIONS

The first geotechnical application (other than of thermal insulation) was for roadway, airfield and railroad foundations in Europe. The application was of particular interest in Scandinavia where permafrost was causing severe damage to roadways. The application used geofoam as an insulator to reduce the effects of permafrost in subgrades. Dr. G.A. Leonards, Professor of Civil Engineering at Purdue was granted a patent in 1966 for this application. Geofoam is the lightest of all the lightweight fill options from 1 to 3% of the weight of soil. A major recent application includes backfill behind bridge abutments as shown in Figure 2, so as to reduce lateral loads and/or reduce surcharge loads on underling soils.



Figure 2 – Lateral load reduction on bridge abutments (Courtesy of Geofoam Research Center).

Use in such geotechnical applications started in the 1960's. The first use of EPS in a geotechnical application in 1965 was done in Norway. To date, there have been over 500 roadway projects completed in Norway.

Late 1960s – Frost Protection was utilized in Germany

1965 – Oosterbaan, M. D. and Leonards, G. A., "Use of insulating layer to attenuate frost action in Highway Pavements", Highway Research Record No. 101, Highway Research Board, Washington, D.C., U.S.A., pp. 11-27.

1972 – First road embankment project in Norway

The Flom Bridge in Norway was the first roadway application for geofoam. The effects of permafrost and reconstruction with geofoam are shown in Figure 3.



Figure 3 – Reduction of permafrost effects at the Flom Bridge (Courtesy of Norwegian Public Roads Administration).

Early 1970s – First EPS geofoam projects in The Netherlands

Mid to Late 1970's –EPS used during the famed oil-pipeline construction in Alaska

1985 – First Abutment backfilling and road construction on soft ground in Japan

1985 – First Conference on Geofoam held in Oslo. Norway

The conference was a one day event held on June 25th sponsored by the Directorate of Roads, Norwegian Road Research Laboratory and Norwegian Plastics Federation. The title of the conference was "Plastic Foam in Road Embankments, A New Way of Solving Soft Ground Problems". There were 150 attendees, 5 papers presented and 12 case histories that reviewed the past 13 years of experiences.

1987 – First known highway use in USA, was in Durango, Colorado, on a landslide repair for Highway 120

The Colorado Highway 160 slope stabilization project between Mesa Verde National park and the City of Durango in southwestern Colorado is the earliest known use of EPS-block geofoam for slope stabilization and repair. Details of this case history can be obtained from Yeh and Gilmore (1992). The slide, covered an area of approximately 0.4 ha and involved about 8,410 cubic meters of slide material. The soils that failed were removed and the embankment was rebuilt with geofoam.

1990 – 14th Green at Coeur d' Alene Resort, Idaho

One of the more popular well known uses of geofoam, although not geotechnical, is the floating green at Coeur d'Alene Resort in Idaho; see Figure 4.



Figure 3 – A geofoam floated golf course green (Courtesy of WorldGolf.com).

1992 – The word “Geofoam” was termed within the geosynthetics industry

1994 – Second Conference on Geofoam held in Honolulu, Hawaii

An international symposium on polystyrene geofoam in below ground applications was organized by Prof. J. S. Horvath of Manhattan College. Seven papers were presented along with a field trip to a lightweight embankment.

Late 1990’s – First Levee - Torne Levee in the United Kingdom

1995 – A 217 page book by J. S. Horvath titled “Geofoam Geosynthetic” was published.

Horvath’s book includes an overview of materials, current standards, a comprehensive description of the types of geofoam products available, constituent materials, and manufacturing processes. It describes the material properties of different geofoam products in the context of geotechnical engineering applications and discusses recommendations for additional standards development and for future research.

1996 – Third Conference on Geofoam held in Tokyo, Japan

This conference had 300 attendees and 33 papers submitted. The conference was titled “International Symposium on EPS Construction Method”.

1997 – Geofoam Research Center was established.

The Geofoam Research Center (GRC) at Syracuse University was formed by Prof. Dwight Negussey. It is dedicated to research of geofoam properties, development of innovative applications, dissemination of technical information and technology transfer through education. The center has assisted manufacturers, engineers and contractors with both large and small projects. GRC has given technical seminars to state department of transport staff, consulting engineers and university audiences. Development of standards and performance verification of geofoam projects are also areas of interest of GRC. The center was established in 1997 through industry support.

1997-2001 – I-15 project Salt Lake City, Utah using 0.28 million cubic meters of geofoam

The I-15 project was a \$1.5 billion design/build project to reconstruct 27 kilometers of roadway through Salt Lake City in preparation for the 2002 Winter Olympic Games. The project required 160 MSE walls with vertical fills. Geofoam was selected to minimize settlement under the fill and eliminate damage to underground utilities; see Figure 5.



Figure 5 – I-15 lightweight fill project in Salt Lake City, Utah.

2001 – First Geofoam Bridge Approach in the USA- Buffalo Road Bridge, Warsaw, NY

A replacement bridge consisting of pre-stressed concrete box beams with a composite concrete deck having a span length of 26 m utilized expanded polystyrene (geofoam) fill and a large spread footing. This was the first use of geofoam for bridge structural support in the United States. The bridge is currently being monitored by the Geofoam Research Center.

2001 – Fourth Conference on Geofoam held in Salt Lake City, Utah
There were 160 attendees at the conference with 44 published papers.

2005 – ASTM D6817-11 Standard Specification for Rigid Cellular Polystyrene Geofoam

Abstract from ASTM D6817 - This specification presents the types, physical properties, and dimensions of rigid cellular polystyrene (RCPS) intended for use as geofoam. This specification, however, does not address the layout, placement, and workmanship for proper installation and performance of the geofoams. RCPS geofoams shall be formed by the expansion of polystyrene resin beads or granules in a molding process (EPS), or by the expansion of polystyrene base resin in an extrusion process (XPS). They may also be manufactured with reprocessed polystyrene foam (regrind). The RCPS geofoams shall meet combustibility and curing requirements and, when tested, shall adhere to physical property requirements such as dimensions and density, compressive resistance, flexural strength, and oxygen index. Final products should also meet surface damage, volume damage, and UV degradation limits.

2005 Woodrow Wilson Bridge – Route 1 Bridge Approach using 20,000 CY Geofoam

In this project, geofoam was selected as a lightweight fill so as to expedite construction of the US Route 1 bridge approach along the Washington DC beltway. Existing soft soils and underground utilities made geofoam a natural choice for Virginia Department of Transportation and the Federal Highway Administration (FHWA). The project used over 20,000 m³ of geofoam and resulted in a 10 m embankment with the roadway placed directly on top of the geofoam; see Figure 6.



Figure 6 – Rt. #1 bridge approach in Washington, DC (Courtesy of InterGEO Services).

2006 – FHWA Priority; e.g., “Market Ready Technology”

Benefits listed by the FHWA with regard to geofoam include:

- Accelerates foundation construction.
- Reduces project schedules times.

- Saves money.
- Requires limited labor for construction.
- Exerts little to no lateral load on retaining structures.
- Can be constructed easily in limited right-of-way areas and in adverse weather conditions.

2008 – FHWA New Technology; e.g., “Functional Technology”

2010 – Geofoam had been used on State DOT projects in most states in the U.S.

2011 – Fifth Geofoam Conference in Lillestrom, Norway

The two day conference was titled “Geofoam Blocks in Construction Applications”. It had 42 papers submitted and 38 papers presented.

NEW APPLICATIONS AND RESEARCH

New applications in Norway include the use of geofoam as the entire embankment fill for a temporary bridge over “quick clay” as shown in Figure 7a and detailed in Figure 7b.



Figure 7a – Temporary bridge abutment over quick-clay (Courtesy of Norwegian Public Roads Administration).

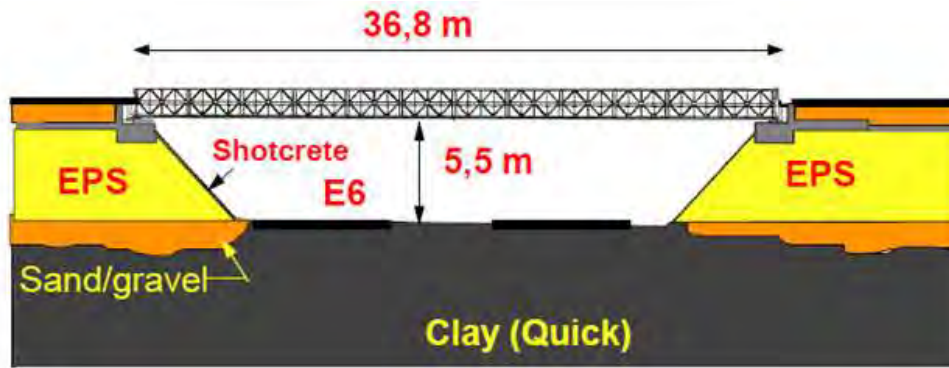


Figure 7b – Cross section of both temporary bridge abutments (Courtesy of Norwegian Public Roads Administration).

Current research on geofoam is focused on long term creep resistance and use of recycled materials. Additionally, the use of geofoam as a seismic buffer, was started in 2007 at Queens College by Richard Bathurst.

CONCLUSIONS

Although geofoam has a long successful history throughout the world, it has not been used extensively until recently in North America. As exhumed samples from early projects show excellent performance, market acceptance is growing. The interest of the technical community regarding geofoam continues to challenge its material properties so as to increase the type of applications, including high risk projects. This lightweight contender continues to prove itself 40 years after its initial introduction into the civil engineering community.

REFERENCES

Geir Refsdal, 2011 Geofoam conference

Geofoam Applications in the Design and Construction of Highway Embankments

Timothy D. Stark, David Arellano, Department of Civil and Environmental Engineering,
University of Illinois at Urbana-Champaign, Urbana, Illinois

John S. Horvath, Scarsdale, New York, Dov Leshchinsky, ADAMA Engineering, Inc., Newark,
Delaware, July 2004

Horvath, J. S. (1999), "Geofoam and Geocomb," *Proc. GRI-13 Conference*, Dec. 14-15, 1999,
GII Publ., Folsom, PA, pp. 71-104.

Horvath, J. S. (1995), *Geofoam Geosynthetic*, Horvath Engineering P.C. Publisher, Scarsdale,
NY, 217 pgs.

Koerner, R. M. (2012), *Designing With Geosynthetics*, 6th Edition (in two volumes), Xlibris
Publishing Co., Indianapolis, IN, 914 pgs.

Negussey, D. (1997), "Properties and Applications of Geofoam," Society of Plastics Engrs., 20 pgs.

Negussey, D. (2001), Slope Stabilization With Geoform, Geofoam Research Center, Syracuse University, Syracuse, NY, 126 pgs.

A 25-YEAR PERSPECTIVE ON WASTE CONTAINMENT LINER AND COVER SYSTEM DESIGN USING GEOSYNTHETICS

Richard Thiel

Thiel Engineering, Oregon House, CA USA

1. INTRODUCTION

This paper presents the perspective of one design practitioner regarding changes that have occurred in the industry over the past 25 years – particularly as related to the design of waste containment systems using geosynthetics. An effort has been made to present practical changes that have taken place in approaches to design, rather than advances in academic theory. Given the practical limitations of a single person writing an overview of this topic, there are bound to be biases in emphasis and subject matter related to the author's perspective and experience. In this regard the author asks forbearance from the readers, and welcomes any feedback from industry peers.

The author entered the field of waste containment engineering in 1986, at the very beginning of the 25-year retrospective period addressed in this paper, and his first projects were the design and evaluation of two major double-lined hazardous waste landfills, one in Illinois and one in California. It is interesting to observe that there is no significant difference between what we see looking at a set of design drawings from the Kettleman Hills Hazardous Waste Landfill project from 1987 (a detail is shown in Figure 1), and a set of drawings for a landfill design that would be produced today. We know, however, that there has, in fact, been a significant increase in the understanding we bring to current design approaches for these types of facilities, compared to the understanding we had 25 years ago. The aim of this paper is to highlight these changes in our approach to design that have taken place in the past generation.

Despite these advances over the past 25 years, important and fundamental questions continue to linger in the minds of designers, regulators, and owners, albeit tempered with greater understanding. Some examples of these persistent questions are:

- How long will these materials last?
- How much redundancy do we need?
- What should be the factor-of-safety? (or reliability?)
- Do we really need CQA?
- What kind of liner system is best, and how thick should it be?

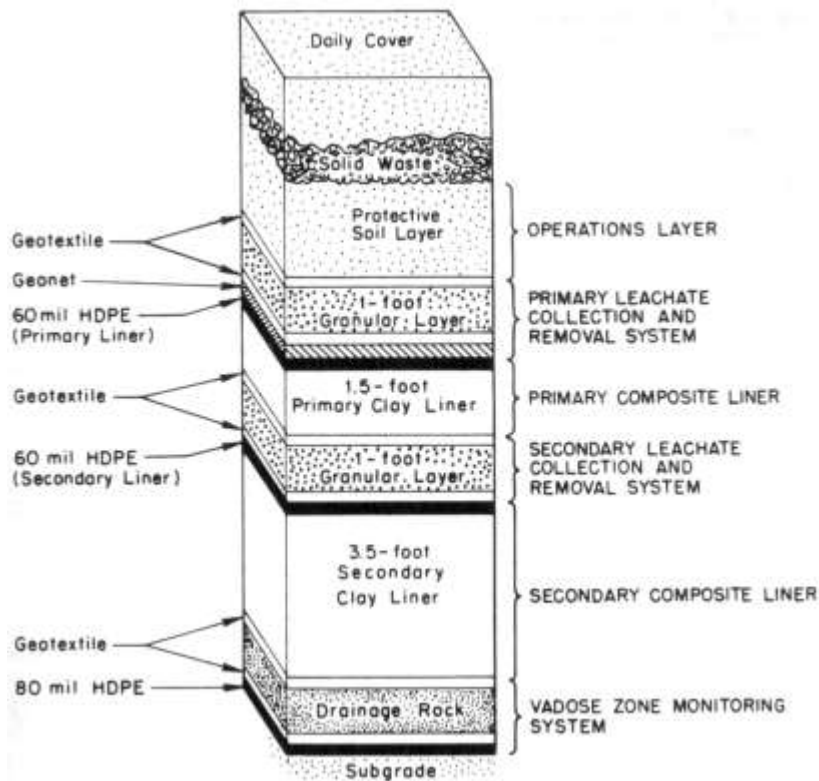


Figure 1. Detail of actual hazardous waste liner system design from 25 years ago.

2. WHAT IS A CONTAINMENT LINER SYSTEM?

What is a liner system? This is a fundamental question that deserves brief mention. In general, the author defines it as a barrier layer that has a lateral drainage layer above and/or below it, as illustrated in Figure 2. This simple concept helps us focus our discussion on the value of materials that serve as a barrier to fluids (e.g., geomembranes and GCLs), versus those that provide a transmissive layer to fluids (e.g., geonets and geocomposite drainage layers), or that serve as a protective layer for one of these two functions (e.g., a geotextile filter, or a geotextile puncture-protection layer).

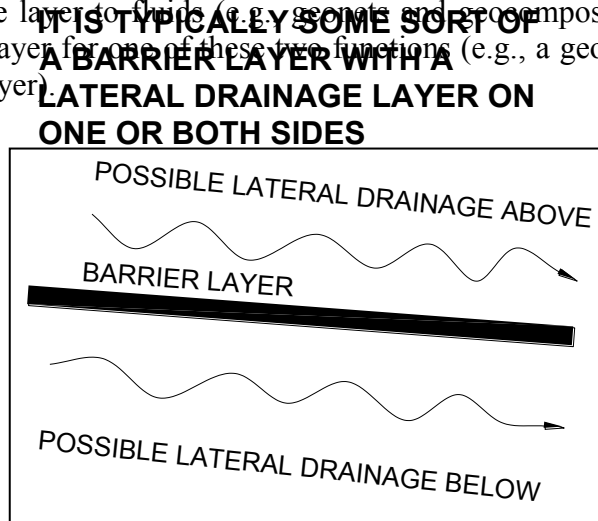


Figure 2: Schematic of author's definition of a liner system.

3. A COMMENT ON REGULATIONS GOVERNING WASTE CONTAINMENT LINERS AND COVERS IN THE USA

The containment industry is largely driven by regulations, as good regulations have proved essential for the proper long-term stewardship of our environment. Using U.S. regulations as a benchmark, we can generally say that the regulations that require liner systems for waste containment facilities came into being at the beginning of the 25-year period we are reviewing, as RCRA Subtitle C (hazardous waste) was promulgated in the early 1980's, and RCRA Subtitle D (municipal waste) in the early 1990's. These regulations essentially required single-composite bottom liners (with an extra geomembrane liner and lateral drainage layer for Subtitle C), with an overlying lateral drainage layer to collect leachate. The cover systems were also required to be single-composite liner systems. Very few changes have been made in these basic regulations since that time, other than allowing for some alternative design approaches. From this point of view, it is not surprising that a set of design drawings for a Subtitle C landfill in 1987 looks quite similar to a set of design drawings for a landfill today.

The environmental performance record of landfills constructed in the past 25 years has indeed been quite good, confirming the wisdom of the regulatory approach outlined in the 1980's. Indeed, we have definitely gotten our arms around the issues, and have them more or less contained (!). Meanwhile, as we examine new understandings gained from continued academic research, material improvements developed by manufacturers, experience gained in construction and operations, ingenious engineering solutions, lessons learned from failures, and approaches being developed by our neighbors around the world, we see definite indications that the industry has steadily advanced in its understanding over the past generation. And these improved materials, practices, and understandings will certainly continue in the next generation. Any suggestions for improvement that may be implied in this paper should by no means be considered as criticism of past implementations and approaches. Far from it. The U.S. - its industry regulators, owners, operators, engineers, technicians, contractors, and citizen-users - has done an excellent job of implementing a great infrastructure for "housecleaning" and environmental management that should be, and often is, the envy of other nations.

4. LIST OF TOPICS ADDRESSED IN THIS PAPER

To provide the reader with a quick reference of the topics that are addressed in this paper, the following list presents the order of the topics presented. Since the topics have been numbered to provide easy location, the headings before this section are included for completeness.

1. Introduction (previous to this section)
2. What is a containment liner system? (previous to this section)
3. A comment on regulations governing waste containment liners and covers in the USA (previous to this section)
4. List of topics addressed in this paper (this section)
5. Brief discussion of geosynthetic materials

6. Contaminant transport
7. Aging durability and geomembrane service life
8. Slope stability
9. Steep-slope bottom liner systems
10. Piggyback liner systems
11. Lateral drainage design
12. Details related to penetrations and attachments
13. Details related to anchor trenches
14. Exposed geomembrane covers
15. Ponds
16. Secondary containment around tanks
17. Construction, CQA, and specifications with regard to design considerations
18. Moving into the future

5. BRIEF DISCUSSION OF GEOSYNTHETIC MATERIALS

In deciding what to write about in greater detail and what to skim over with a passing reference, the author has elected to focus narrowly on specific design approaches. Several excellent papers are being presented at this conference that discuss our past generation of experience regarding different types of geosynthetic resins, additives, manufacturing methods, standards for testing, standards for specifying, and standards for installation and CQA. For this reason, geosynthetic materials in themselves are discussed only briefly in this section.

The following is a concise list of topics relative to geosynthetic materials which, from the author's perspective as a design practitioner, are significant relative to design. A check mark (✓) appears beside those topics that are described in more detail. Where there is no (✓), the reader is encouraged to review other papers from the proceedings of this conference to learn more about those subjects.

Geomembranes

A list of geomembrane-specific issues of acknowledged significance that have been addressed to a greater or lesser degree in the past 25 years, includes:

Long-term chemical compatibility: This was a major effort early on, and a lot has been learned in this regard. Early chemical immersion and index testing, which was developed by Dr. Henry Haxo, resulted in EPA Test Method 9090. That has since been superseded by ASTM D5322 and D5747 and related standards. Chemical compatibility charts are typically available from

manufacturers, and these test methods are available for testing against specific chemical environments.

Advances in resins and products. Manufacturers have been the driving force for the development of an ever more efficient and useful selection of geomembrane materials, and market dynamics have conspired to retire some of the less efficient products. A good example of this is chlorosulphonated-polyethylene (CSPE), long-marketed under the trade name of Hypalon. Initially a major player in the exposed geomembrane market, its high cost and a number of technical issues caused it to all but disappear from the North American market (though the formulation is still available from an Asian producer), and its function has largely been replaced by reinforced polypropylene (PP-R). The PP-R material suffered a temporary setback in popularity in the early 2000s as durability failures started to show up. It turned out that a number of manufacturers had skimmed on the antioxidant additive packages, but this problem has since been recognized and corrected. Another significant product development that has had a major impact on the design and use of geomembranes, and which did not exist at the beginning of our 25-year review period, was the use of textured surfaces on polyethylene geomembranes. These new surfaces provided much greater interface shear strength characteristics against various soils and other geosynthetics, which the industry has aggressively utilized ever since. These are only a few examples of numerous product developments that have occurred in association with geomembranes, and others will undoubtedly continue to be developed in the future.

Installation and seaming: There have been significant advances in our understanding of good installation and seaming practices, and of seaming equipment for thermoplastics. Perhaps the most significant development in seaming equipment was the introduction of hot-wedge welding for thermoplastic geomembranes, which took place near the beginning of our 25-year review period. Since that time, various improvements to seaming equipment have been made by different manufacturers, but the fundamentals of providing good welds have essentially remained unchanged over these past 25 years. Now as much as ever, good operator training, attentiveness, and CQA are the keys to successful welding.

Testing and specifying: Refined methods of testing and specifying have been developed through the efforts of GRI and ASTM, and the collaboration of manufacturers, designers, and testing laboratories. As an example in our industry, GRI GM13 became an industry cornerstone for specifying HDPE, and serves as an ongoing example for other materials. ASTM subcommittee D35 has developed a plethora of standards and guides for the testing and installation of geomembranes.

Wrinkles: An increased understanding of the development and control of wrinkles, and wrinkles as a design consideration. (√)

Allowable strain: An increased understanding of puncture protection and long-term durability issues. (√)

Soil cover: An increased understanding of procedures for covering with soils.

ELL surveys: An expanded use of electrical leak location (ELL) surveys on both bare and covered geomembranes.

Slope stability: An increased understanding of slope stability. (√)

The desiccation of materials underlying exposed geomembranes: An increased appreciation of the dynamics involved.

Ponds and Reservoirs: Not much fundamental change in the approach to pond design, but a refined understanding of pond design issues. (√)

Development and use of Exposed Geomembrane Covers (EGCs). (√)

Contaminant transport: An increased understanding of leakage prediction and contaminant transport. (√)

Penetration and Connection Details: Increased appreciation for details related to connections and penetrations – an area where the industry can find great room for improvement. (√)

Repairability of aged and exposed liners: We are continually learning in this area, as facilities are continually aging.

GCLs

The past 25 years could be said to be “the generation of GCLs”, since this is the period in which they were introduced and developed, and standards were established for hydraulic conductivity testing, index and performance testing, seaming, needle issues, deployment and handling, construction, and durability issues. The major technical issues that affect liner design, and which are still the subject of ongoing evaluations, include:

Product innovations: Many different types of products have been promoted that include different bentonites and different carriers, including polymer-amended bentonites.

Equivalency with compacted clays.

Cation exchange: Much attention has been given to cation exchange in bentonite for different conditions of hydration, normal loads, liquids, soils, peptized bentonite, polymer-amended bentonite, and solo GCL vs. composite vs. encapsulated GCLs.

Shear strength: An increased understanding of interface vs. internal shear strength; peak vs. post-peak; effects of different hydration methods; encapsulation. (√)

Hydration mechanisms: Advances in our understanding of the hydration of GCLs set on a subgrade; encapsulated GCLs, and the quantification of hydration mechanisms and rates (see Thiel et al., 2001).

Panel shrinkage. The issue of GCL panel shrinkage has received a lot of attention since the author first reported gaps in GCL panels that had originally been overlapped (Thiel & Richardson, 2005). Although there have been numerous published studies and great advances in our understanding of this issue since that time, the author of this paper feels satisfied that a pragmatic solution has been found, which is to simply heat-tack all fabric-based GCL seams, as described in Thiel & Thiel (2009).

Geonets and Geocomposite Drainage Layers

Geosynthetic drainage layer products have been available since the early 1980's. New products continue to be developed, which include bi-planar and tri-planar products, as well as cusped sheets, nubbed-surfaces on geomembranes that are then covered with a geotextile, and drain-tubes encapsulated in geotextiles that are offered as alternatives. Stouter materials that are able to handle long-term high loads are also available.

Laminated geotextiles that form a 'geocomposite': In the late 1980's, geonet products laminated with geotextiles were not even available, and today they are so pervasive that the term "geocomposite" is used almost synonymously to refer to a geonet laminated with a geotextile. The techniques and specification for lamination (viz. peel strength) has improved over this time, along with our understanding. (√)

Transmissivity: We have seen greatly improved understanding of how to measure and how to design, using the transmissivity offered by these products for lateral drainage in different situations. (√)

Clogging: There is lack of long-term data regarding chemical and biological clogging of these materials, especially in bottom liner applications, and we can expect that more studies and understanding will be gained in the future.

Geotextiles (specifically those related to filtration and puncture protection)

Filtration: Over the past 25 years there has been improved understanding and elucidation of the geotextile filtration function (Giroud 2010). The science and theory of geotextile filtration has been greatly advanced in terms of a better understanding of the relationship between granular and geotextile filters, the role of the hydraulic gradient in filtration, the relationships between fiber geometries, minimum thickness and porosity requirements (or the percent of open area for woven geotextiles), the effective filtration opening size, etc. That said, there may be a gap between the available knowledge base versus the actual practices used in containment engineering (this might be different in another field such as dam engineering, where filters are much more critical, JP Giroud, pers. comm.). In general, there has not been a great incentive for sophisticated filter design in landfill engineering, so any number of older standard methods or rules of thumb are often utilized in material selection in this commodity-driven market. The author tends to use Leuttich et al. (1991), which is over 20 years old, as his filter design reference.

Puncture Protection: An improved understanding and improved specification for puncture protection (cushioning) methods. Rational approaches have been developed for evaluating the effectiveness of candidate geotextiles for specific puncture-protection applications. The long-term applicability of the different approaches remains an open question, as the advocates of different views can present significant differences in their final recommendations. (√)

NWNP Manufacturing: Although the manufacturing capabilities for nonwoven needlepunched (NWNP) geotextiles allow for the creation of fairly specialized products in terms of denier size, fiber cross-sections, fiber lengths, wettability, polymer, and degree of needle punching, in North

America, these products have been, and continue to be widely commoditized using the same polymers (primarily PP in North America, though PET was formerly used and is still used in China; this is a market decision), with relatively fine 6-denier fibers. While there have been and will continue to be product innovations, the majority of products will likely continue to be offered in much the same fashion as they have for the past two decades.

Testing and specifying: Specified index and performance tests have remained relatively constant over the period, albeit with some fine tuning.

Durability. Geotextiles are used by themselves, as well as in conjunction with products such as geosynthetic drainage layers and GCLs. The long-term durability of geotextiles relative to their intended functions of providing filtration, separation, and interface shear strength is still a question of interest. Research is being conducted in this regard, and its outcomes will undoubtedly influence the practice of design in the future.

6. CONTAMINANT TRANSPORT

The goal of designing containment systems is to reduce the transport of contaminants into the groundwater to an acceptably low level for the contaminating life of the facility. Models of contaminant transport mechanisms and rates are used to make permitting and design decisions. In general, two different mechanisms of contaminant transport through landfill liners are actively discussed in today's literature: advection and diffusion. Advection, commonly referred to as 'leakage', is governed by Darcy's law, in which the flow through defects and soils is governed by the head buildup on the top of the liner system. Diffusion involves the migration of chemical constituents through intact media based on Fick's law; it is concentration-driven, independent of gravity and head conditions. Both transport mechanisms increase with an increase in temperature, so that landfill operating temperatures have a significant effect on contaminant transport. See Rowe (2005) for further discussion of these mechanisms.

The USEPA regulations for MSW landfill base liner requirements (RCRA Subtitle D as codified in 40 CFR Part 258, paragraph 258.40) are written to cover two different approaches. Paragraph 258.40(a)(1) is a performance-based standard to protect groundwater. Paraphrased, the regulation in 258.40(a)(1) states that contaminant transport through a liner system must result in no more than the specified prescriptive maximum contaminant levels stated in the regulation. This performance-based regulation requires the applicant to demonstrate, usually through the modeling of contaminant transport, that the proposed design will comply with its terms. As an alternative to the performance-based approach, paragraphs 258.40(a)(2) and (b) provide a prescriptive design basis for the liner and leachate collection system. If the prescribed design criteria are fulfilled, the design is presumed to meet the groundwater protection standards and no contaminant-transport modeling is required. These are the two well-known design standards for a single-composite liner and overlying leachate collection layer in the U.S.

The EPA (1993) provides technical background and guidance related to the Subtitle D ruling. Guidance is provided related to the contaminant transport modeling required to demonstrate compliance with the performance-based regulation, and an extensive list of computer modeling codes that were available at that time is provided in the reference. While many complex contaminant-fate-and-transport mechanisms were recognized by the EPA (1993), including

diffusion, it is interesting to note that this guidance document puts a clear emphasis on advective-only transport through the liner system. In two distinct places the guidance states that “the factor that most strongly influences geomembrane performance is the presence of defects...or penetrations of the liner.” The guidance suggests, for example, that the HELP model Version 3 (Schroeder et al., 1994), which incorporates the landmark Giroud leakage equations for composite liners (Giroud & Bonaparte, 1989, Giroud et al. 1989, and Giroud et al. 1992), should be used to estimate advective leakage through the liner, and that a model such as MULTIMED, developed by the USEPA (<http://www.epa.gov/ceampubl/mmedia/multim2/>) should then be used to evaluate the fate and transport of the leakage through the underlying hydrogeologic strata (the vadose and saturated zones) up to the defined point of compliance. Thus, for many years and even up to the present day, in many projects and many jurisdictions, contaminant transport modeling through liner systems focused exclusively on estimating the number and size of defects in the geomembrane liners, estimating the head over the geomembrane liners, and applying some form of the Giroud equation in order to estimate advective leakage through the liner system. Subsequently, significant efforts and advances in the application of the analytical and empirical equations for estimating advective flow were made in order to consider various types of overliner and underliner conditions (Giroud et al. 1997b,c), estimates of leakage and hole probabilities through double-liner systems (Giroud et al. 1997a), the effect of high head levels up to 3 m (Giroud, 1997), the effect of very large holes (Touze-Foltz & Giroud, 2005), long defects (Giroud & Touze-Foltz, 2005), the difference between the leakage rates of GCL and clay liners below geomembranes (Giroud et al., 1997d, and Rowe et al. 2004), statistical data on hole size and frequency (Marcotte et al., 2009; Forget et al., 2005; Darilek & Laine, 2001), the effects of wrinkles on calculations (Rowe, 1998), and various assumptions on the number of holes per hectare (e.g. see Giroud & Touze-Foltz, 2003). The effectiveness of these models has been confirmed, if not calibrated in hindsight, by field performance data reported by Bonaparte et al. (2002).

Although the theory and modeling ability to consider diffusion was available well before the 25-year period we review here, the author’s perception is that only in the past dozen years or so has there has more serious consideration been given to contaminant transport through liners via the mechanism of diffusion. This perception is by no means universal. A number of jurisdictions in various locations around the world may have seriously considered it earlier, and some jurisdictions do not consider it even to this day. That said, it was as recent as 2001 that the author was first required to consider diffusion as part of an alternative liner demonstration. See an interesting discussion of the state of consideration of this issue in 2002 in Giroud & Touze-Foltz (2003).

Rowe et al. (2004) suggest that under design conditions prior to termination of the operation of a leachate collection system and/or failure of a geomembrane liner, the primary transport mechanism through modern liners is usually chemical diffusion, most notably for certain organic constituents. As leachate collection systems age and clog, leachate mounding may occur. At the same time, geomembrane liners age and potentially develop more defects as they approach the end of their service life. As these ‘elderly’ system failures occur, and depending on the nature of the natural underlying hydrogeology, the issue of advective transport will become more significant. Rowe (2005) documented several cases in which diffusion resulted in measurable contaminant transport even over relatively small timeframes. Rowe et al. (2004) demonstrated

that there can be significant diffusion of certain organic compounds through geomembrane liners even while the volume of advective leakage is negligible. They further argue that calculations should be performed to assess the adequacy of a liner system combined with the underlying attenuation-layer soils, to determine if adequate environmental protection is provided over the contaminating lifespan of the facility.

Summary: It is commonly acknowledged that all liners leak, with or without geomembrane defects. The concept of composite liners is well founded, and industry feedback has vindicated the rationale for these liner systems in the results obtained by performance monitoring. At the same time, we recognize that even though we have been installing composite liners with good results for more than a generation, the lifetime of many facilities will far exceed this initial 25-year period, in terms of their operating lifetimes as well as their post-closure lifetimes.

Future: Given the modest cost impact of adding a secondary liner and leakage collection system, it is reasonable to expect that the benefits of the long-term redundancy provided by double liner systems will continue to be recognized. These systems will therefore be promoted more broadly than they already are, both for the control of advective leakage and the greater reduction in diffusion that they provide. Because of our recognition that contaminant transport risks might be a function of the age of a particular infrastructure, some of the considerations described in the next section of this paper, which addresses aging durability, will likely come into play. The inclusion of diffusion considerations in contaminant transport analyses is likely to become increasingly prevalent in the prediction of performance. Also, ELL surveys will likely become more and more of a norm in the specifications for new liner construction, in order to reduce the number of geomembrane defects that appear early in the facility life.

7. AGING DURABILITY AND GEOMEMBRANE SERVICE LIFE

The industry is indebted to the service provided by Dr. Henry Haxo for contributions he made in the mid-1980s to our understanding of the long-term compatibility between various polymers and various chemical environments. This was the beginning of our understanding of the durability of aging polymeric materials in waste environments, and there have been many advancements and studies since that time. Although other papers in this conference may touch upon some of these same topics, the author felt obliged to include those aspects of the continuing research in this area that may influence immediate design decisions.

For buried applications that are intended to be a quasi-final solution (i.e., for which there is no long-term plan to replace, upgrade, or decommission the installed liner system), there have been few studies regarding the expected lifetimes of liners, except for those used with polyethylene materials. Polyethylene is the most studied and accepted polymeric material for long-life (multi-generation) projects (see interesting discussion on this in Giroud & Touze-Foltz, 2003). Although bituminous materials could perhaps be considered long-life as well, given that they are analogous to natural asphaltic material, they have not received a fraction of the attention and market share for containment lining systems as compared to polyethylene. Other polymeric membrane materials have also been used for long-term buried applications, PVC in particular, but estimated quantifications of their lifetime and aging-durabilities are lacking, and field exhumations have turned up mixed results. Other flexible membrane liner materials, such as PP, EIA, etc. have found excellent utilization in exposed applications such as reservoirs, ponds, and

exposed secondary containment applications where there is an expectation of a finite-design lifetime on the order of one generation (i.e., 25 years, more or less). Though it would be fortuitous if some of these other materials had even longer lifetimes in service, at the present time they probably could not be used as design criteria, in the absence of more comprehensive aging-durability studies. There are a few excellent references on the selection of geomembrane materials for various uses, including Rollin et al. (2002), and Scheirs (2009). A number of attempts have been made in the past to create a selection matrix based on weighted or absolute criteria, and the author has even been involved in creating and evaluating such matrices. The author's experience with these matrices, though, is that they are too simplistic and do not usually lend themselves to an appropriate manner of evaluating materials. The best manner of evaluating materials is to clearly define the chemical, aging, and durability requirements for both long-term service and short-term construction survival. If more than one material happens to meet these requirements, then other considerations, such as cost, and the offsetting pros and cons can be used for the final selection.

Chemical compatibility aside (which is a large area in itself), prediction of the lifetime the various materials used in liners has been a holy grail from the beginning – how long will these materials last? However, the question itself requires some clarification if we are to answer it, for what does the question imply? Rowe (2012) has answered the question definitively for the industry: The lifetime of a geomembrane can be considered to have ended when it cracks so extensively that its presence as a fluid barrier is compromised on a massive basis over large areas.

Thus, to answer the question, “how long will the liner last?”, we might do better to ask: “what will cause it to crack, and what will accelerate the appearance and propagation of cracks?”

Research related to the factors that affect the service life of a polyethylene geomembrane is described in the following paragraphs. For materials other than HDPE, insufficient data is available to assess their long-term performance in buried liners or covers (NRC, 2007).

The basic chemical engineering of the resin itself. Resins that are more crystalline, and therefore more chemically resistant, tend to have a lower stress-crack resistance. To this end, a great deal of work related to the development of stress-crack resistant resins has been done in the past 25 years, with perhaps the greatest changes made in the early 1990's. As a result, the term “high-density” polyethylene is now widely recognized as being a slight misnomer, because the density of all of the major “HDPE” geomembranes produced by the various manufacturers have been lowered to the point that they are technically considered a “medium density” polyethylene material, according to strict chemical engineering definitions. Nonetheless, the term “HDPE” is so ingrained in common usage that this semantic nuance is almost universally disregarded. The defining test with regard to stress cracking is the Notched Constant Tensile Load test, developed by the Geosynthetics Institute, and now the test standard established by ASTM as D5397. Just as a point of reference: while many resins in the late 1980s had NCTL transition times of less than 100 hrs, today one can easily obtain a resin with a transition time of greater than 1000 hrs.

The anti-oxidant (AO) package in the resin formulation. The effectiveness and lifetime of the additives that serve to protect the geomembrane from oxidation have been found to be a fundamental key to the ultimate lifetime of the geomembrane. While it is difficult for civil

engineers to keep abreast of the nuances of polymer engineering, the GRI-GM13 standard guide is a good reference to use for specifying a good formulation for a geomembrane. The critical test in this regard has to do with the Oxidative Induction Time. Two tests are available that address this factor: Standard (ASTM D3895) and High-Pressure (ASTM D 5885). It appears that the High-Pressure test is much more indicative of the important anti-oxidants that contribute to long life (versus protecting against the high-temperature manufacturing process), and test values of 800 minutes are available from manufacturers.

Temperature. Temperature is a key factor in making long-term lifetime predictions for geomembranes. For example, it is estimated that the effective lifetime of HDPE at 40° C may be only 15% of its effective lifetime at 20° C (ref GRI 2010, or Rowe, 2005). Even short durations of exposure to high temperatures may significantly affect a geomembrane's lifetime (Rowe, 2012). In this regard, we would note the data from Koerner & Koerner (2006), which indicate that bioreactor landfill temperatures are significantly higher (on the order of 45-50 °C) than standard 'dry' landfill cell temperatures (on the order of 25-30 °C). Rowe (2012) also reported elevated landfill temperatures for wastes containing fly ash mixed with MSW, or wastes containing high aluminum content mixed with MSW (Stark et al., 2012a). Given the very significant effect of high temperatures on geomembrane service life, Rowe (2012) has suggested that the redundancy provided by secondary liners, considered separate from their operating temperatures, may effectively increase the service life of the overall liner system. The author would suggest that the monitoring of leachate temperatures just as they exit the landfill into sumps or pump stations can provide useful information feedback for site operators.

Allowable stresses and strains. Ongoing studies indicate that stress concentrations become the crack initiation sites for PE resins. Thus, the time-to-cracking, and the locations of cracks, will be largely influenced by the number of localized strains in the geomembrane. These types of strains may occur at all locations where gravel particles, which are present either in the subgrade or in the overlying leachate collection layer, cause the geomembrane to deform. Strains will also be found where there are wrinkles, which in North American installations are commonly prevalent in geomembranes as they are being covered. There is continuing debate and discussion regarding allowable strain level. For example an upper limit of 6-8% has been recommended by Peggs et al. (2005) and others, while the Germans are very conservative in their requirements, aiming for a design strain of 0.25% (Bishop, 1996) through the use of sand puncture-protection layers, and strict controls for the deployment-and-covering sequences used with geomembranes, in order to avoid burying wrinkles, for the reasons discussed above.

Past standard industry guidelines for allowable subgrade preparation and allowable overliner and puncture-protection materials have historically been established to promote geomembrane survivability and longevity of service. In light of ongoing research, these past standard practices were laudable and appropriate, and should be continued to be respected.

Recent research (Rowe, as yet unpublished) has shown that the highest quality subgrades are very stiff and smooth. Smoothness can be created using very well-graded materials that contain sands and silts, and even some fraction of gravel. Athanassopoulos et al. (2012b) have shown that subgrade soils that have a largely fine-grained soil matrix (e.g., clay liners) but some significant gravel content, can potentially result in significant geomembrane damage if there is

some relative movement (e.g., due to seismic shaking), but that this potential damage can be avoided if a GCL is installed between this subgrade and the overlying geomembrane.

The author has repeatedly verified in the field that almost every soil subgrade over which GCLs and geomembranes are being deployed benefits from the application of water spraying and smooth-drum rolling within a narrow window of time before the geosynthetics are deployed. In this way, the displacement of soils and rocks caused by the geosynthetic deployment activities is minimized. It may be useful to include a general requirement of this method of execution in project specifications.

Regarding puncture protection from overliner materials, the industry standard for many years, and up through the present time in the USA, has been the geotextile puncture-protection formula developed by Koerner et al. (1996), and recently updated by Koerner et al. (2010). While geotextiles that are selected based on this approach may result in materials having a mass/area of 500-1000 g/m², the approaches used by the Germans (e.g., Witte, 1997) suggest that a minimum mass/area of 3000 g/m² is required, or in a more favorable approach, that sand blankets be used. Brachman and Sabir (2012) have shown that with coarse 50 mm drainage stone, even multiple layers of heavy NWNP geotextile protection totaling 2780 g/m² may allow exceedance of the suggested allowable strain values over time periods typical of a landfill design life. This has led to the suggestion that geomembrane service life can be extended by the use of a sand layer to provide puncture protection. Brachman and Gudina (2008) arrived at similar conclusions for drainage stones of sizes of 25 mm and 50 mm. The degree of geomembrane strain can be kept lower if a finer gravel, or a more well-graded gravel, or more rounded as opposed to angular gravel is used, or if a firmer subgrade is created. We would note that the tendency towards a smaller, more well-graded gravel size is in conflict with the desire for a larger, more well-sorted gravel size to resist leachate collection system clogging. Designers thus need to weigh the trade-offs involved and provide appropriate puncture protection for a given situation. More definition can be expected in the future with regard to the use of acceptable overliner gravel sizes in conjunction with various puncture-protection strategies.

Wrinkles. The subject of wrinkles is mentioned many times in this paper, partly because they are so endemic to liner installations, and partly because they affect many aspects of the function and integrity of the liner systems. Giroud & Morel (1992) provide an excellent theoretical understanding of the cause and prediction of wrinkles for different types of geomembrane materials in different conditions. NRC (2007) makes the simple observation that “wrinkles are common in North American landfills”. In the author’s experience this is likewise true in most of the world, except for Germany, where they insist on wrinkle-free geomembrane installations. While there has been no definitive standard on the control of wrinkles in geomembranes in North American installations, research over the past 25 years has progressively shown more and more why wrinkles are undesirable. The reasons for this include strains in the geomembrane that result in accelerated stress cracking at the locations of wrinkles (Rowe 2005), greatly increased leakage potential due to the loss of intimate contact with the underlying clay or GCL liners over significant areas (Rowe 2005), the reduced effectiveness of lateral drainage layers on top of geomembrane wrinkles, and the increased potential for construction damage, because wrinkles protrude upwards into the path of grading equipment blades. Thus, the most likely places where leaks will originate are also the worst places. Daniel and Koerner (2007) indicate that “the

geomembrane must be flat when it is backfilled”, and they provide a list of proactive measures that can be taken to minimize the incidence of wrinkles. Scheirs (2009) suggests that at times, a compromise must be sought between the conflicting requirements of minimizing wrinkles while avoiding ‘trampolining’. The author’s practice in North American installations has been to set a maximum allowable wrinkle height of 2-3” (50-75 mm) during covering operations, and to use variations in daily temperatures to maximum advantage during this process. Using daily temperature as a primary control makes sense, since fundamentally, a geomembrane must be covered at or below its deployment temperature in order to achieve a wrinkle-free installation (Take et al., 2012). The question thus arises: on what basis should an acceptable wrinkle height be set? Chappel et al. (2012) showed that when the total area of wrinkles is less than 8-10% of the total area, then the maximum interconnected wrinkle length will generally be less than 200 m, which they considered an acceptable maximum length for the control of advective leakage due to random holes. At the sites that they studied, they observed that at geomembrane surface temperatures below 37 °C, the interconnected wrinkle length was typically less than 100 m. A related study by Take et al. (2012) indicates that the wrinkle height at this same temperature was estimated to be between 50-75 mm, which precisely corroborates the author’s experience-based specification. This approach cannot be taken so simply, though. If one reads the references and field studies carefully, it is actually the *onset of wrinkling to those heights* where the interconnectivity between wrinkles becomes a problem. In general, soil covering over polyethylene geomembranes needs to be halted a few hours after sunrise and can be begun again a few hours before sunset, with the exact times being specifically related to the maximum interconnected wrinkle length. Other approaches to limiting this maximum length could be as simple as placing sandbags between wrinkles to prevent their interconnection. This simple concept, however, may be not so simple to implement. We would note that these various approaches do not address the reduced service life at the locations of wrinkle. Take et al. (2012) suggest that any wrinkles with a height of 20 mm or more at the time of burial are likely to remain forever trapped, and will thus likely become sites of stress concentrations to varying degrees, depending on the particular wrinkle geometry.

Thickness. All other things being equal, thicker geomembranes will be more durable during construction, and will last longer (Rowe et al. 2010).

8. SLOPE STABILITY

Significant advances in our understanding, testing, and evaluation of slope stability have been made in the past 25 years. In landfill slope stability issues, the distinction is often made between bottom-liner stability and veneer (e.g., final cover) stability. Although the underlying geomechanics that govern stability are the same in both cases, the normal loads and sensitivities to pore pressures are vastly different, so it is useful to discuss them separately.

Bottom Liner Stability Issues

At the beginning of this paper’s 25-year retrospective period, we had a major bottom-liner failure at the Kettleman Hills landfill in 1987. This was, and still is perhaps, the largest permitted hazardous waste landfill in the world. The liner system was fairly complex, as shown in Figure 1. This event created a great awareness of slip surfaces and the need to check the slope stability in lined containment systems, and perhaps inspired more technical papers on slope stability than

any other containment project (e.g., Filz et al., 2001; or Stark and Poepple, 1994). The key lessons learned from this failure include:

- The importance of phasing and fill planning relative to slope stability. The failure would never have happened if the filling of the landfill had been performed in a proper sequence. The landfill operations essentially attempted to fill one side of a slippery bowl. If the other side of the bowl had been constructed sooner, and if the landfilling had been more balanced between the two sides, the failure would never have occurred. Since that time, this same lesson, unfortunately, has been learned the hard way at a few other major landfill projects. There is really no need for anyone else to have to learn this lesson; we can all definitely learn from this one mistake that occurred in 1987.
- Stark and Poepple (1994) used this failure to suggest to the industry that it might be good to use post-peak shear strengths on the backslopes of lined containment areas, while peak strengths may or may not be acceptable on the base areas, depending upon the seismic hazard. Ten years later, Stark and Choi (2004) elegantly refined this discussion.
- Filz et al. (2001) and Esterhuizen et al. (2001) wrote a pair of landmark papers on the progressive mobilization of shear strength in lining systems, using the Kettleman Hills failure as their case study. A similar paper was written by Reddy et al. (1996). The key lesson we can learn from these papers is that the mobilization of shear strength is not equal and uniform as is assumed by limit-equilibrium analyses. It is of overwhelming importance for practitioners to understand that the rigid-block modeling of slope stability, which is what is done in all 2-D limit-equilibrium models, does not represent the dynamics of reality. In fact, the shear strength is mobilized in a very specific localized fashion, such that all failures are essentially progressive failures. This is a significant reason why it is prudent to assume post-peak shear strengths for significant portions, especially the backslopes, of lined facilities. While the author does not advocate that slope stability analyses should use the finite-element approach in general, it is valuable for practitioners to study these references in the literature in order to gain an appreciation of the true mechanics of shear strength mobilization.

In the same vein as the lessons learned from the fill sequencing at Kettleman Hills, Smith and Giroud (2000) and Breitenbach (1997) emphasized that heap leach mining projects have also demonstrated that filling considerations for the first lift are the most important, relative to slope stability, and are typically more critical than the final fill configuration.

Based on the Kettleman Hills and similar solid waste failures, as well as numerous failures in the mining industry, it has become clear that the critical situations for slope stability risk are during construction, in the early phases of filling, and in the critical intermediate phases of filling. This concept must be borne in mind, even though many regulatory requirements have historically required only the examination of the final fill configurations to ensure slope stability. Thus, a key message for geotechnical practitioners involved in such projects is that not only do these different stages of geometry need to be modeled, but the shear strength testing for critical interfaces needs to be conducted at normal loads appropriate to these different conditions.

Peak vs. Post-Peak Strength. Partly as a result of the Kettleman Hills failure, but also because of the greater awareness and emphasis on slope stability evaluations in general, much work and many publications have been dedicated not only to understanding the shear strength characteristics of different materials and interfaces, but also to coming to grips with which shear strengths should be used relative to peak strength, post-peak strength, or residual strength. Some key publications in this regard include:

- ASTM D7702 - Standard Guide for Considerations When Evaluating Direct Shear Results Involving Geosynthetics. This recent guideline provides a very good discussion of the relevant issues related to the commissioning and interpretation of shear strength testing, and provides a good list of references that include many key related publications. This ASTM Standard reviews important issues such as the fundamental aspects of measuring and reporting shear strength using ASTM direct shear methods; evaluation of the Mohr-Coulomb envelope over appropriate normal load ranges; how to evaluate the subject of cohesion (or adhesion); how to evaluate the shear-displacement curves reported from tests; suggestions for reviewing results and test methods against historical data and published guidance; the value of inspecting specimens after testing; and multi-interface test approaches.
- For a modern reinforced GCL-geomembrane interface, and internal GCL shear strengths at moderately high normal loads, the author considers Fox and Ross (2011) to be the most comprehensive and relevant paper, as it provides useful insights on hydrated GCL shear strengths. This publication also includes references to numerous other key papers on the subject.
- In the same vein, an interesting publication on geomembrane and GCL interfaces under ultra-high normal loads, such as those that are experienced in large heap-leach facilities, was published by Athanassopoulos et al. (2012).
- A comprehensive discussion of unreinforced GCL shear strength, under both hydrated and dry (encapsulated) conditions was published by Thiel et al. (2001).
- There has been discussion of different approaches to the selection of peak versus post-peak, or even residual, shear strength parameters for use in slope stability analyses, as discussed by Thiel (2001). The Ohio EPA (2004) presented the interesting approach of requiring residual interface shears strengths for all liner systems on slopes steeper than 5%. GRI (2011) considered the selection of shear strength to be the “most-sensitive-unknown-variable” in performing stability analyses.
- When assigning post-peak shear strengths, a standard industry approach has been developed (Thiel 2001) that uses the post-peak shear strength of the interface that has the lowest peak strength. It is important for this concept to be applied for specific normal load ranges, since the lowest peak strength may shift from one interface to another under different normal load ranges. For example, for interfaces involving textured geomembranes with reinforced GCLs, it is commonly acknowledged (e.g., Athanassopoulos et al. 2012) that at increasing normal loads there comes a point at which the peak GCL internal shear strength is lower than the strength of the interface between

the textured geomembrane and the hydrated GCL. Thus, if a post-peak strength analysis were being conducted, it would be necessary to determine the normal load at which the transition from the interface to the GCL internal strength would take place.

- A number of designers and academics (e.g., Gilbert and Byrne 1996) recommend that a factor of safety greater than one be achieved in all containment system slope designs, assuming that residual strengths are mobilized along the entire slip surface. This view was later echoed by Stark and Choi (2004).

Pore Pressure. There has been an increasing recognition of the importance of considering pore pressures in landfill and heap leach stability analyses (Thiel, 2001; and Castillo et al., 2005). In its 2011 report on 20 large landfill failures, GRI found that liquids were considered a major mobilizing factor in more than half of the failures, and liquids in general were involved in all the failures. It is thus worth highlighting the fact that after gravity, pore pressures are the single most significant destabilizing element, especially for sites practicing liquid recirculation. It is known that at least one major landfill failure was caused by the aggressive recirculation of leachate (Hendron et al. 1999).

Method of Analysis. The actual methods of analysis that are used have not changed appreciably over the past 25 years. Slope stability analyses are most commonly assessed using computer programs that evaluate the limit equilibrium of a 2-D cross-section. Although 3-D and finite-element analysis methods are available, from a pragmatic point of view, the everyday stability analysis has been and will continue to be 2-D in actual practice. There are three main reasons for this, which are clearly laid out by Duncan (1996): the inherent conservatism of the practice, its ease of application, and its avoidance of errors. One aspect of this practice worth noting is that the judgement of experienced practitioners is required in order to select critical cross-sections.

Acceptance Criteria. Apart from the mechanics of selecting appropriate material properties, geometries, phreatic surfaces, and methods of analysis, the other significant decision that must be made by the geotechnical practitioner regards the acceptance criteria. Traditionally, static stability analyses were evaluated on the basis of a “factor of safety” (FS); based on the historical practices in the profession, a value of 1.5 is commonly considered acceptable. For seismic analyses (in California, for example), 25 years ago the industry was commonly using variations of a “pseudo-static” analysis that used a predetermined horizontal acceleration roughly on the order of 0.15 g, and required that $FS \geq 1.0$ under those conditions. While both of these acceptance criteria are still in use, more sophisticated and appropriate approaches have been developed in the past 25 years.

The legacy of requiring a minimum static factor of safety of 1.5 is still a relatively universal standard in the solid waste industry, although the author has noted that in many heap leach facilities, values of 1.3 are commonly accepted. The acceptance of a specific value implies a certain reliability of all of the factors that comprise the analysis, such as the geometry, shear strength parameters, and phreatic surfaces. Given that every single input going into an analysis involves some degree of uncertainty, a more intelligent manner of evaluating slope stability is based on the concept of ‘reliability’, or its inverse, namely ‘probability of failure’. The implementation of a reliability analysis was made very approachable for the industry at large by a landmark publication by Duncan (2000). In this paper, Duncan provided the tools (spreadsheet

equations) and approaches needed to create the necessary input to estimate the reliability of just about any type of engineering analysis, including slope stability. Design practitioners in all disciplines are highly encouraged to obtain this reference and follow its methods for all significant calculations. The output of the exercise will result in a “most-likely-value” factor-of-safety, as well as a reliability value (or its inverse, probability of failure). A significant benefit of this approach is that the manner in which decisions that affect slope stability are made can be easily communicated to the project sponsor, and the risks involved in making those decisions can be shared. While this approach will give both the designer and the client a feel for the sensitivities of certain parameters related to the project’s reliability, it still begs the question of what is an appropriate probability of failure. Guidance on this can be found in other industry publications, such as Whitman (1984) or D’Hollander (2002).

Seismic. Seismic analyses for landfills and leach pads have undergone significant advances. The “design earthquake” definition used in the 1980s used concepts of ‘maximum-probability’ and ‘maximum-credible’ earthquakes. With the enactment of Subtitle D in 1993, the design earthquake for permitted landfills was defined as an event that would have a “10% probability of occurrence in 250 years”. Since that time, the USGS has developed excellent online seismic hazard analysis tools, which are available at <http://earthquake.usgs.gov/hazards/>. If one inputs a latitude and longitude, the website will provide the peak ground acceleration for the selected probabilistic design event, mean and modal moment magnitudes, as well as spectral accelerations for a range of fundamental periods.

Early in the 25-year period under discussion, in addition to the pseudo-static method described above, the solid-waste industry adopted a chart-based deformation-analysis approach that was based on the use of the estimated yield acceleration and the assumed Richter magnitude of the design earthquake. This approach was based on the Newmark method (Newmark, 1965) as developed by Makdisi and Seed (1978), which is used to estimate the earthquake-induced deformation of dams and embankments. Bray et al. (1998) significantly advanced and refined this chart-based deformation concept. The most recent widely used chart-based approach is the one published by Bray and Travaserou (2007). More sophisticated approaches include performing a 1-dimensional seismic response analysis using an actual or simulated earthquake motion that is input to a computer program such as SHAKE, and performing double-integration on the acceleration vs. time response in order to estimate Newmark-type sliding magnitudes, or conducting 2-dimensional finite-element site-response analyses for actual or simulated time histories. The latter approach is typically used only in situations in which the more simplified conservative analyses do not provide acceptable results. Regardless of the method used, there is still the question of what constitutes an acceptable result. At this point, the main reference that is cited in the industry is by Seed and Bonaparte (1992), who conducted a survey of leading engineering firms, and found a general consensus that acceptable deformation under a design earthquake should be limited to no more than 150-300 mm.

Future: Going forward, the key questions relative to slope stability will continue to revolve around the selection of an appropriate shear strength and the consideration of appropriate pore pressures. Questions still remain regarding the appropriate selection of peak vs. post-peak shear strength parameters, long-term durability with regard to interface and internal shear strengths, and controls and impacts of waste saturation on stability. The importance of these issues still

remains to be fully appreciated, especially as bioreactor technology continues to expand, and as leachate collection and removal systems (LCRS's) continue to clog.

Veneer System Stability Issues

Veneer systems in landfills that might experience stability issues are those on sloped locations of final covers systems, or bottom-liner sloped areas that have a geomembrane and/or GCL barrier that is/are covered with relatively thin layers of leachate collection and/or operational soil materials during construction. Because this layer is often relatively thin compared to the slope length, these systems are commonly and conservatively treated as 'infinite slopes' from a slope stability point of view, although toe-resistance can be incorporated if desired. From this point of view, a veneer situation can be simply considered to be a block on a sloping surface.

While significant failures of landfill bottom liners may number only a couple of dozen in the past 25 years, veneer failures undoubtedly number in the hundreds. Many of these probably go unreported, and those that make the industry news-circuit are sufficient testimony that they are a significant problem. The geotechnical aspects of final cover system slope stability follow the same principles as those used for other geotechnical stability problems. What is unique and important to recognize relative to final cover systems is their sensitivity to relatively small changes in loading, slope angle, pore pressures, or shear strengths, all of which make them more susceptible to sliding failure (Thiel 2008).

While the author does not have a statistical list to quantitatively present the causes and triggering mechanisms of such failures, his familiarity with industry issues and discussions with peers over the past 25 years indicate the following reasons for veneer failures:

- Pore pressures acting at the liner interface. There are two types of pore pressures that can act at the veneer-cover interface: those from above, and those from below.
- Pore pressures above the geomembrane. The most pervasive cause of veneer failure is liquid (namely, rain) from above that percolates through the topsoils and builds up over the liner. It is easy to demonstrate that if there is no drainage layer between the geomembrane and the cover soil, the factor of safety for the stability of the soil sitting on the liner is in one stroke cut roughly in half. This is explicitly described, along with a number of design solutions, by Thiel and Stewart (1993), and in several other follow-up publications by others in the industry, such as Giroud et al. (1995b) and Koerner and Soong (1998). The main principle of the design solution is clearly to provide a dependable transmissive layer, such as gravel or a geocomposite drainage layer, between the geomembrane and the soils. The author notes that one of the changes in the industry over the past 25 years has been the elimination of the misnomer "cap-net", which was used to refer to less expensive geonets that were being promoted for landfill caps, under the perceived view that a lower level of performance would be needed in caps than in bottom liners. Analyses very often prove that the transmissivity requirements for landfill covers may significantly exceed the requirements for bottom liners due to slope stability concerns. The largest transmissivity reduction factor for these applications is typically "biological", as plant roots have been demonstrated to reduce transmissivity by 50%.

- Pore pressures below the geomembrane. Landfill gas pressures that are exerted upon the bottom surface of a cover geomembrane have caused several documented veneer-cover slope failures in the industry. Again, the design solution is to provide a lateral drainage layer below the cover system that collects and ultimately vents these pressures. The only industry design methodology published to date is that of Thiel (1998).
- Lubrication at the geomembrane interface. The author is aware of two types of “lubrication”-induced veneer failures. One is caused by the extrusion of bentonite from the woven side of a needle-punched GCL against a geomembrane. Such a failure was well-documented at a test site in Cincinnati (Daniel et al., 1998). A GCL was placed on a moist subgrade with the woven side face up, and was then covered by a geomembrane and 3 feet of soil on a 2:1 slope. Shortly after installation, two of the test plots slid. This demonstrated that bentonite extrusion from the woven side of a GCL needs to be taken into account if it is placed against a geomembrane, or perhaps that it is best to use a non-woven geotextile-based GCL against a geomembrane. The other “lubrication” failure, which was documented by Thiel (2009), involved a PVC geomembrane that slid on a nonwoven geotextile on a 4:1 slope about three months after being covered with soil. In the forensic investigation it was discovered that the condensation of moisture between the PVC geomembrane and geotextiles significantly decreased the interface shear strength, as compared to the dry interface. The lesson in this case is that interface shear tests with geomembranes should always be sprayed with water before assembling the test sandwich, because this truly replicates field conditions.
- Equipment-loading-induced failures. It has been documented that inertial forces from equipment can locally cause the peak interface strengths to be exceeded, resulting in post-peak interface strengths. Progressive failures of this type, which have eventually led to large-area slope failures, have been evaluated by the author and documented in the literature (e.g., Stark et al. 2012b, Thiel and Narejo, 2005). The lessons learned in general are that small, wide-track, low-pressure equipment should be used to spread cover soils over geosynthetics, and that the pushing of soils should be done in an uphill, not a downhill direction. Also, the failure evaluation presented by Thiel and Narejo (2005) led to a change in the industry-standard for geocomposite peel strength, which was upgraded from 0.5 pound-per-inch (ppi) to a MARV value of 1 ppi for projects in which shear strength is a critical factor.
- Simple failures due to inadequate shear strength. ‘Simple’ veneer-type failures due to inadequate interface shear strength, without any other extenuating factors, have been regularly experienced in the industry. These are typically non-dramatic and are not popularly documented because they are corrected as soon as they are discovered.
- Other. There are other types of veneer slope failures, such as veneer-reinforcement failures, that are less common and more specialized.

As with bottom-liner systems, perhaps the “most-sensitive-unknown-variable” is again the assumed shear strength parameters. In veneer cover design, it is critical for testing to be performed within the low normal load ranges under consideration. One of the most significant abuses of the interpretation of laboratory shear strength data is the cavalier backwards-

extrapolation of the cohesion intercept. This is typically a very unconservative approach that should really never be used, especially for the low normal load regimes for cover systems.

Seismic analyses for final cover systems can use the same chart-based methods described in the preceding section. The author recommends the Bray et al. (1998) reference as the most appropriate method, since it offers explicit solutions for the tops of landfills, taking into account amplification up through the waste mass.

As described in the preceding section, a significant decision that must be made by the geotechnical practitioner regards the acceptance criteria. As with bottom liners, $FS = 1.5$ is a commonly accepted basis of design for covers. As regards the allowable deformation in seismic analyses, the most germane reference is Kavazanjian (1998), who suggests that deformations of 1 m or more are allowable, as long as the responsible party is ready, willing, and funded to make repairs. If it is desired that the damage caused by the design earthquake would be relatively insignificant, then the estimated deformations should be less than 150-300 mm.

Future: Going forward, the key questions relative to veneer slope stability will continue to revolve around the selection of an appropriate shear strength and the consideration of appropriate lateral drainage layers above and below the barrier layer (viz. geomembrane). The long-term reliability of the assumed drainage layer transmissivity is also a subject of concern, as is described later, in the section 'Lateral Drainage Design'.

9. STEEP-SLOPE BOTTOM LINER SYSTEMS

As the industry has developed more confidence in liner-system construction over the past generation, and as the challenge of siting new waste repositories has become more difficult, steep-slope locations such as sidehills, canyons, and quarries have become more common disposal sites. Steep-slope bottom liner systems require special consideration not only in terms of slope stability, but also in terms of subgrade preparation, installation challenges, wrinkle management, covering, and the effects of settlement and downdrag on the liner systems. Each of these issues is discussed briefly below.

Subgrade preparation. The specifications for appropriate subgrade preparation should really be no different for a steep-slope application than they are for a flat-bottom application, and yet the achievement of a firm, smooth surface is much more difficult on a steep slope. The contractor's resourcefulness often makes it possible to successfully prepare firm, smooth surfaces on soils as steep as 1.5(H):1(V). At other times, engineered solutions such as puncture-protection layers, geofoam, or shotcrete may be in order.

Installation challenges. Installer ingenuity is required to safely deploy and seam geosynthetics on steep slopes. Special considerations include the effort to avoid overly disturbing the prepared subgrade, welding machine burnouts, CQA access, and wrinkle management. Because of the effect of gravity and daily expansion and contraction, the management of wrinkles at the toes of long slopes can be troublesome, especially for multiple layers. Often there is no good choice but to cut out the multiple layers of wrinkles and add a repair-seam near the toe of the slope. This activity is best done after the soil cover layers have been placed on the bench at the toe of the slope, so that trampolining of the lining system across the bench does not occur. For several

reasons, including the problem of wrinkles, it is advisable for benches to be installed at maximum vertical intervals of approximately 15 m.

Settlement and downdrag. Settlement and downdrag along steep-lined slopes will occur to varying degrees during initial construction, initial landfilling, and long-term waste settlement. The key questions in this regard are: “how much downdrag will occur?” and “at what degree of slope inclination does downdrag become a concern?” There has been little field monitoring and limited research on this subject. The research that has been done indicates that at a slope inclination of perhaps 2(H):1(V) or steeper, downdrag could be a significant concern (Jones and Dixon, 2005), but it could occur on flatter slopes as well, depending on the forces and the relative interface shear resistances within the liner system (Lui and Gilbert, 2003).

The occurrence and amount of downdrag that will ultimately occur is acknowledged to be a quite complex matter, and perhaps beyond our ability to accurately predict. In the design of steep slopes, the author believes it is necessary for the design to be able to accommodate downdrag without incurring any damage to the primary liner system. In the author’s opinion, protection of a steep-slope liner against downdrag damage can be accomplished in two ways. One is to provide one or more preferential slip surfaces above the primary liner. The second is to provide a veneer-reinforcement layer above the primary liner. The two methods can also be combined. For example, a slip surface consisting of a single-sided geocomposite could be deployed over a geomembrane on a steep slope (see Snow et al., 1994, as perhaps the first published example of this). The interface between the bare geonet and the geomembrane is much more slippery (i.e., has less shear resistance) than any other interface in the lining system, and will therefore slip when there is relative movement above the primary liner due to waste settlement and downdrag. In a geocomposite, the greatest stress due to interface slippage will be located near the crest of the slope, and at some point it will rip at that location. If a high-strength geotextile is anchored on the bench at this location, directly beneath the geocomposite, then as the geocomposite continues to be dragged down-slope, an ever-greater window-area of the high-strength geotextile will be exposed to the overlying soil that is engaging the downdrag forces. As this is taking place, a high-strength geotextile can provide two functions: (1) it can protect the underlying primary geomembrane from being directly exposed to the overlying soil materials, and (2) it can bear the downdrag load. Depending on the normal forces and downdrag forces, the high-strength geotextile would eventually reach its load-bearing capacity when the window of exposure reaches a certain size, and at this point the high-strength geotextile would rip. The design engineer would have to make an estimate whether or not the total amount of downdrag movement would exceed the ripping-point of the high-strength geotextile. If it was deemed probable that the downdrag movement would continue past this point, then a second layer of high-strength geotextile could be installed below the first layer, thus allowing another sequence of downdrag movement before this layer, in its turn, has its tensile strength challenged. This paper presents the first reported description of this technique; a more complete and publicized exposition is planned in the coming year.

The Future: We can expect more finite-element modeling of stresses and strains in steep-slope liner systems, and hopefully, more controlled instrumentation and reporting of actual steep slope liner systems.

10. PIGGYBACK LINER SYSTEMS

As old landfills reach their capacity and new sites become difficult to find, the practice of filling a new lined landfill against the side, or on top of, of an old existing landfill has become an attractive option that is routinely considered, and will always be a potential choice in local solid waste management plans. While these “piggyback” lateral and vertical expansion designs may not be everyday events, they will also not be rare. In addition to the typical design issues related to slope stability, the design goals for such systems are generally to allow the leachate and gas generated from the new waste mass to be effectively captured and directed to the new leachate collection and removal system, without leaching through the old waste mass that likely has a less reliable, or nonexistent leachate collection system. The collection of landfill gas from the old waste mass below the new liner system may also be an issue, but this is a separate discussion that is outside the scope of this paper.

A piggyback liner system has to be able to withstand the anticipated future total and differential settlements from the underlying waste foundation upon which it is constructed. Thus, one of the design tasks would be to model the future settlement of the waste mass upon which the piggyback liner will be installed, in order to verify that the anticipated total settlement would not result in a substandard slope (which would mean a generally established minimum of 2% of residual slope), for drainage of the new leachate collection system on the piggyback liner. Design approaches could include compacting the existing waste (which could even be as extreme as deep dynamic compaction), and steepening the slope of the existing waste using soil or non-putrescible waste, so that when it settles, there is less of a chance of it becoming too flat.

Localized differential settlements, e.g., sinkholes that might develop due “rusty refrigerators” and thus create a void in the underlying waste, can potentially be managed with ‘brute force’, i.e., a geogrid or high-strength geotextile reinforcement below the new liner system. The lateral extent of effective protection provided by subgrade reinforcement is limited to something on the order of 3 m in diameter, plus or minus, depending on the depth of the overlying new waste and the type of reinforcement selected. Original discussion and details can be found in Giroud et al. (1990), and excellent summaries are presented in a number of informative PowerPoint presentations that are available from the Geosynthetics Institute (Folsom, PA) and Koerner (1994).

11. LATERAL DRAINAGE DESIGN

The intelligent use of lateral-drainage design elements is recognized as an aspect of containment-system design that requires perhaps the most insightful and experienced engineering talent that can be brought to bear, because their impacts on slope stability and containment are so highly significant. In the world of geosynthetics, it is traditionally understood that geonets provide a lateral drainage function. Although cusped drainage panels have also been used to provide lateral drainage, their use in containment systems is relatively rare, and the author has never used them in these applications. There is one ‘nubbed-surface’ geomembrane product that, when covered with a geotextile, provides in-plane drainage, and the author has successfully used this. While some very specialized, loosely needle-punched, very-heavy denier nonwoven fabrics have been used for the lateral drainage of gases, in general geotextiles are not by themselves appropriate for lateral drainage applications.

At the beginning of the 25-year period under discussion, only a limited selection of bare bi-planar polyethylene geonets was available for geosynthetic lateral drainage materials. If a geotextile filter was needed adjacent to the geonet, it had to be deployed separately. Beginning in 1988, the ability to heat-laminate nonwoven needlepunched (NWNP) geotextiles to one or both sides of geonets was developed, and many different thicknesses and cross-sections of bi-planar and tri-planar geonets are now being offered. The heat-lamination of a geotextile to a polyethylene geonet is performed by melting the outside of the polyethylene geonet and then pressing the NWNP geotextile onto the melted surface. The lamination is actually created by the mechanical grip of the cooled polyethylene around the geotextile fibers. The hotter the melted surface, and the more pressure that is applied while it is melted, the more securely the geotextile fibers will be 'gripped' by the cooled polyethylene, though to the detriment of the geonet's transmissivity. The integrity of the lamination is measured in an index test called a 'ply-adhesion' or 'peel' test (ASTM D7005). Originally, manufacturers only specified a minimum average roll value (MARV) of 0.5 lb/inch (ppi) for this property. As described above in the section 'Veneer System Stability Issues', a couple of slope stability failures where this interface failed led to a new industry MARV of 1.0 ppi. The manufacturing control of this heat-laminated interface has greatly improved over the years, to the point where a more uniform and consistent peel strength is achieved, with less 'holidays'. The lamination of geotextiles over geonets has become so common that one rarely finds bare geonets being used anymore. The ability to laminate geotextiles not only provided a commonly needed filter against one side of the geonet, but also provided a good frictional interface against textured geomembranes on the other surface. The combination of a geotextile laminated to a geonet forms a 'geocomposite', and these have become so prevalent that the term 'geocomposite' is practically an industry synonym for this type of product, even though the term 'geocomposite' is generic and could refer to any number of geosynthetics that are combined together. In the discussion that follows, the author will use the term 'geocomposite' to intend both geonets that are laminated with geotextiles, and nubbed-geomembranes that create a transmissive layer when covered with a separate geotextile.

The most important performance property of a geonet or geocomposite is its transmissivity, which is essentially equivalent to its in-plane hydraulic conductivity multiplied by its thickness. Units of transmissivity are gallons per minute per foot of width (English units), or cubic meters per second per meter of width, which ends up being reported as m^2/s . Testing and specifying the transmissivity of geonets and geocomposites has been greatly refined and improved over the past dozen years. The most significant advance came with GRI Test Standard GC8 - Determination of the Allowable Flow Rate of a Drainage Geocomposite (Geosynthetic Institute, Folsom, PA) in 2001. In this test method, the manufactured material is tested against geosynthetic or soil super- and sub-strates that are representative of the field conditions, under normal pressures that are representative of field conditions, for 100 hrs. The material should also be tested under a gradient equal to or greater than the design gradient (never at a lower gradient), in accordance with ASTM D4716 (Test Method for Constant Head Hydraulic Transmissivity (In Plane Flow) of Geotextiles and Geotextile Related Products). The GC8 method provides that appropriate reduction factors should then be applied to the test results in order to account for long-term geotextile and soil intrusion, biological clogging, chemical clogging, and creep. Finally a global factor of safety should be applied to this value. Excellent discussions regarding this approach are provided in Giroud et al. (2000a).

A very fundamental aspect of the discussion of the use of lateral drainage layers in all applications is the fact that all design methods assume an unconfined in-plane flow. If this assumption is violated, then all the calculated benefits of lateral drainage layers in terms of reducing leakage, or reducing pore pressures to preserve slope stability, may be invalidated. To this end, Giroud et al. (2000a) has provided simple and elegant design approaches for designing the required transmissivity of the lateral drainage layers for given conditions of liquid input, slope, and drainage outlet spacing. In addition, Giroud et al. (2000b) has shown that a relatively thin geocomposite drainage layer requires a greater transmissivity than a much thicker granular drainage layer in order to obtain an equivalent flow capacity and maintain unconfined flow. Additional design equations for compound slopes, stacked double-drainage layers, and radial flow can be found in the same special publication as the Giroud et al. (2000a and 2000b) references.

Five specific areas of containment engineering design in which lateral drainage plays a major role are described below, along with advances in our understanding, and current design approaches that employ geosynthetic lateral drainage layers.

Bottom-liner primary LCRS in landfills (or “overliner” drain layer in heap leach pads). A cornerstone of the USEPA Subtitle D and C regulations is the requirement of an LCRS (which is a lateral drainage layer) that limits head buildup on the liner to a maximum of 30 cm. The initial recommendations in the 1980s for minimum required permeabilities of $1E-03$ cm/s were much too low to ensure good long-term performance, and tended to result in short- and long-term clogging. Primary landfill LCRS's clog to a significant degree over time. Rowe (2005) presents several examples and literature citations that document cases in which systems lost over 3 orders of magnitude of permeability over a 4-10 year period. Clogging is cited as being caused by the combination of biological and inorganic precipitate, with the inorganic precipitate being a long-term clog residue that is composed primarily of calcite.

A landmark paper was provided by Koerner et al. (1994), regarding large-scale drainage correction factors (DCF) for LCRS's, in which DCF was defined as the total area of the LCRS divided by the geotextile filter flow area. The extremes of this factor are $DCF = 1$, for the case in which a blanket filter covers the entire LCRS gravel collection layer, and $DCF = 24,000$, for when a perforated pipe is wrapped with a geotextile filter and all the leachate must flow through the portions of the geotextile filter that cover the perforations in the drainage pipe. An intermediate value of $DCF = 40$ might exist where the geotextile filter is wrapped around the gravel envelope immediately surrounding the leachate collection pipes. Experience has shown that relatively thin blanket filters, with $DCF = 1$, provide a leachate-treatment function that reduces the clogging of the LCRS layer (Rowe 2005), without becoming overly clogged themselves. Wrapping geotextiles around pipes or constrained areas is not recommended. Rowe & Van Gulck (2003) describe how the presence of a blanket filter performed better than no filter, and how a NWNP filter performed better than a woven filter. The author's practice is to provide a lightweight (135 g/m^2) NWNP geotextile as a compromise, thus providing a filter material that will provide the filtration/treatment benefit and will be less prone to clogging than heavier materials.

The author has found that designers use geonets and geocomposite drainage layers in primary LCRS's with caution, because of the clogging issue, and with even more caution in the case of

‘wet’ landfills in which liquids are recirculated. Even if new geocomposite drainage layers can be shown to permit a flow equivalent to that of a 30-cm-thick coarse granular system, they may have only one-tenth of the total porosity, and are therefore much more susceptible to clogging when put into service. Also, it is commonly accepted that a 60-cm-thick layer of soil material is typically required as a minimum protective layer above a geosynthetic liner prior to waste placement, so using a 30-cm -thick granular drainage layer already satisfies at least half of that requirement. If gravel drainage materials are not readily available, and there is a temptation to use geosynthetic drainage layers as the primary LCRS material, the author would still suggest providing, in general, ‘gravel windows’ that are 60-cm thick by approximately 4-m wide (the width of construction equipment) that cover the major leachate collection pipes and sump area, and a total coverage of at least 15% of the surface area of the landfill bottom.

In the future, we can expect more research related to reduction factors for clogging, and recommendations for providing greater redundancy in permeability, slope, pipe size, and spacing in LCRS’s.

Leakage detection layer in landfill bottom liner systems (secondary collection). Double-lined landfills with leakage detection layers (also called secondary LCRS) are common in the USA because they provide redundancy of environmental protection and performance feedback. Indeed, the limited feedback we have on the excellent performance of composite liner systems is mainly a result of the double-lined landfill data provided from New York landfills (Bonaparte et al., 2002).

There are generally two key design criteria for properly designed leakage collection layers: (1) provision for rapid reporting of a significant leak in the primary liner system to the secondary sump (a 24-hour detection time is commonly specified), and (2) limiting of the head acting on the secondary liner system to less than the thickness of the secondary lateral drainage layer, or less than 30 cm, whichever is less.

One of the main benefits of using a geocomposite lateral drainage layer material for the secondary collection system is that its high transmissivity is conducive to very rapid reporting of leakage to the sump. Methods of calculating the travel time of a leak through the secondary lateral drainage layer to the sump are provided in Giroud et al. (1997a) and Richardson et al. (2000), and perhaps the only reference that provides a method for calculating the head buildup on a secondary liner subjected to leakage from above is provided by Giroud et al. (1997a).

Leakage detection and management layer in a double-lined pond. The discussion later in this paper on ‘Ponds’ provides a background discussion of why on most important pond projects, double-liners with intervening leakage detection layers are used. Geosynthetic drainage layers are often used for the leakage detection and collection layers. Thiel and Giroud (2011) also discuss how it has been proven that the air space between two textured geomembranes has been successfully utilized to provide leakage detection and control in a number of pond cases.

Groundwater underdrain systems. The use of underdrains to provide hydraulic control of groundwater conditions is a standard practice in geotechnical foundation engineering. Advances made in geocomposite drainage materials over the past generation have certainly given us increased flexibility in addressing these design issues.

Final-cover lateral-drainage layer above the cover geomembrane. As described in the section ‘Veneer System Stability Issues’, the provision of a lateral drainage layer directly above a geomembrane’s final cover is often essential for maintaining the vegetative soil cover stability. The methods described by Thiel and Stewart (1993) and Giroud et al. (2000a) allow geocomposite lateral drainage layers to be properly designed to preserve the cover veneer stability. Experience has shown that it is important to maintain good outflow conditions that allow the lateral drainage layers to discharge. Freezing conditions, for example, are suspected of having precipitated localized failures due to water backup in the drainage layer (Bonaparte et al., 2002, and the author’s personal experience).

Final cover lateral-drainage layer below the geomembrane. As described above in the section ‘Veneer System Stability Issues’, providing a lateral drainage layer directly below a geomembrane’s final cover is often essential for maintaining the final cover stability, as described by Thiel (1998). Geocomposite drainage layers have been found to be perfectly suited for this application, and in addition, suited for providing gas relief and enhanced landfill gas collection. The author has also found that they provide a secondary benefit of capturing side-slope leachate seeps, which can then be directed to the toe, or to a collection gallery beneath the final cover system, and then conveniently reintroduced into the LCRS at an appropriate location.

Note on installation issues. The installation of geonets and geocomposites is relatively simple, but there are a few aspects of the process that must be performed with care to avoid defeating its intended purpose. One aspect that has historically received very little attention from manufacturers and was not addressed in the earlier literature concerns geocomposite butt seams. Butt seams require the laminated geotextile to be stripped back from the bottom of one roll and from the top of the other roll in order to provide net-to-net contact at the seam. On several jobs I have heard the installers, when asked to do this, make the ‘remarkable remark’: ‘...but we never do this’. This means that their standard practice has always been to incorrectly overlap the geocomposites with the geotextiles intact, which severely reduces their transmissivity. Only recently has this issue been correctly addressed in the literature, by Koerner & Koerner (2009). A second aspect that is often overlooked is that geocomposites have flow-directionality, with the maximum flow occurring in the machine direction. The flow capacity can be reduced between 30% and 90% in the transverse direction, depending on the type of geonet. Thus, panel placement instructions may need to be provided in the design and verified by CQA. Thirdly, the outlet condition details of geocomposites are critical for their proper long-term functioning. This issue is partly addressed by Koerner & Koerner (2009).

12. DETAILS RELATED TO PENETRATIONS AND ATTACHMENTS

Experience in the review, design, and performance of field inspections, and in the attachment of geomembrane boots and connections to structures, reveals that a wide variety of standards and approaches are employed. The execution of the details involved is very much an art of workmanship, and depends a great deal on the experience and understanding of the installer. There has historically been very little guidance in the literature regarding the fine points of specifying and implementing these critical details. The typical manufacturer’s details and guidelines are not much more than concepts that have been repeated for over two decades. Thus, there is a big difference between what we assume and expect, versus what is actually

constructed, in terms of the leak resistance of geomembrane penetrations and attachments to structures. Before 2009, the only substantive references on the subject were the ASTM Guide D6497, Standard Guide for Mechanical Attachment of Geomembrane to Penetrations or Structures, and Wells (1993). Thiel & DeJarnett (2009) touch upon some of the detailed and critical aspects that should be addressed when specifying and constructing geomembrane seals around penetrating pipes (referred to as “boots”) and attachments to structures. In addition to specific recommendations, Thiel also provides the following general recommendations as guiding principles for the design and construction of geomembrane penetrations and boots:

- Penetrations and attachments are more susceptible to leakage than a free-field geomembrane liner. Owners and designers should always be prepared to manage leakage at these locations. Critical applications should always be designed with redundancy (double liners, double boots, leakage detection layers, etc.).
- For exposed and serviceable installations, it is prudent to have a regular inspection and maintenance program for geomembrane penetrations and attachments.
- Penetrations and attachments require a great deal of care and craftsmanship to construct. Designers and CQA personnel should give extra attention to detailing and inspecting these items. Installers should develop in-house standards to assure the quality of their own installations.

Giroud & Soderman (1995a) provide guidance for the connections between a geomembrane and rigid structures, and propose a method to determine the amount of wall batter that is required to decrease the tensions and strains in the geomembranes to an allowable level. Giroud & Soderman (1995b) provide guidance for analyzing the mechanism of deformation of a geomembrane that is supported by a soil dike and is subject to differential settlement at its connection to a rigid structure.

It is clear that the subject of leak-resistant details is complex and cannot be taken for granted. The few technical guidance documents that are available related to these critical aspects of containment construction suggest that more development can be expected in the future in this area. Meanwhile, a lot of faith will continue to be put in the skill and craftsmanship of the installer.

13. DETAILS RELATED TO ANCHOR TRENCHES

Geomembrane anchor trenches are often a matter of convenience for general contractors and installers, and are probably commonly over-designed. For common types of anchor trenches where the liner system will be buried, not much has changed in the past 25 years. Good practices to consider when designing and specifying standard anchor trenches are:

- It may be good to design standard-type anchor trenches so that the geomembrane pulls out before tearing, so that more material stays intact in the undesirable event of slope movement.

- Keep anchor trench designs simple and flexible. Since they are generally for the convenience of the contractor, it may be good to allow for the contractor to suggest alternatives.
- The author believes that for double-liner systems, it is always best to seam the primary and secondary liners together in the anchor trench. This then rules out the possibility that liquids will enter the leakage detection system through this avenue.
- Backfilling in anchor trenches should be performed carefully so as not to damage the geosynthetics, and should always be done well and in a controlled fashion. Loose backfill has the potential to become water-logged, which can only create problems of various sorts.

Critical anchor trenches are required for exposed geomembranes (e.g., ponds and EGC's) or high-strength anchorage applications (e.g., reinforcement). For these applications, a more detailed engineering analysis may be necessary in order for such trenches to resist the tension forces that may develop in the geomembrane due to forces such as wind (see the next section on EGC's). Historically, most textbook methods for evaluating anchor trench pullout only considered the shear resistance along the planar surfaces of the anchor trench (e.g., the trench walls), and they assumed "frictionless rollers" at the corners. The most common approaches, such as those suggested by Koerner (1994) and Qian et al. (2002) were perceived as providing inadequate consideration of the pullout resistance around the corners of an anchor trench. The most significant advance in anchor trench design methodology in the past 25 years was proposed by Villard and Chareyre (2004). Based on a combination of analytical reasoning, finite element modeling, and laboratory testing, they recommended a design approach for L- and V-shaped anchor trenches that accounts for corner forces using the Euler-Eytelwein equation for belt-friction. The analytical methodology that they proposed is considered by the author to be far superior to any other methodologies that were previously proposed. Thiel (2010) presents a case study that provides some refinements to the Villard and Chareyre (2004) method and shows how their method could be used to optimize construction on large projects.

14. EXPOSED GEOMEMBRANE COVERS (EGCs)

Within the past 25 years, the concept of having a relatively long-term exposed geomembrane cover (EGC) has found a definite niche in real-world applications, and such installations that have been designed to last at least one generation are proving successful. A good summary of the rationale and justification for such covers is provided by Koerner (2012).

Design challenges in the installation of an EGC include: (a) providing adequate anchorage of the geomembrane so that it can resist the typically strong wind forces; (b) making sure that all important geomembrane welds are constructed so that they would only be stressed in a shear mode, and not a peel mode; (c) managing intense stormwater runoff from the exposed geomembrane area; (d) ballast for low-wind conditions; and (e) managing the large number of penetrations through the cover geomembrane that would cause localized stresses during wind storms. Exposed conditions also mean that the cover is susceptible to damage from animals (birds, deer, etc.), meteoric events (e.g., hail), vandalism, and fire. Even so, many successful and

substantial EGCs have been constructed, some now approaching 20 years old, including some in Florida and Louisiana that have survived major hurricanes.

As mentioned above, one of the largest challenges in the design of an EGC is accounting for wind loads. At high wind velocities, all geomembranes are likely to be uplifted. In this regard, Giroud et al. (1995a) presented a landmark paper that provides a method for evaluating the tension, strain, and deformation of a geomembrane that is uplifted by the wind. Zornberg and Giroud (1997) provided refinements to the original method, and Giroud et al. (1999) provided additional discussion regarding anchorage design.

15. PONDS

The primary difference between containment liner systems involving ponds versus landfills is the intentional design of the operational conditions of relatively high heads. Leakage under high head conditions will produce more consequences than it will under low heads.

Ponds are designed and constructed for many different uses; these include architectural or decorative purposes, golf courses, recreation or sport facilities, habitats, fisheries, stormwater detention, sedimentation, water storage, chemical containment, and wastewater containment. Different types of ponds can have different design criteria related to liquid containment. Most ponds are intended to contain liquids with the desirable goal of having as little leakage or infiltration to the ground as is reasonably possible. In the extreme case of chemical and strong-wastewater ponds, significant leakage to the environment is unacceptable and may also be illegal, depending on the specific circumstances. Leakage from a pond can be undesirable for the following several reasons, according to Thiel and Giroud (2011):

- Potential contamination and pollution of soils and groundwater from the leaking fluids.
- Possible underground erosion and/or formation of solution cavities, which is one type of “geotechnical damage”.
- Possible slope instability due to phreatic surface buildup below the liner, which is a second type of “geotechnical damage”.
- Potential uplifting of the liner, reducing the pond capacity and exposing the liner to mechanical damage and excessive stresses due to the pressure of gas and/or liquid present under the liner and/or to the buoyancy of the liner.
- Potential loss of valuable clean water, or potential loss of a valuable solution (in the case of chemical and production ponds).
- Potential difficulty in maintaining an acceptable liquid level, which may be important in decorative ponds, water reservoirs for recreation or sport activities, reservoirs for pump-storage stations, etc.

The basic design of pond liner systems has not substantially changed in the past 25 years. Digging holes in the ground to contain liquid is not a particularly new idea, and lining these holes with synthetic liners to reduce leakage losses has been done for over 80 years. In fact,

Koerner (1994) reports that the term '*pond liner*' was eventually superseded by the term 'geomembrane', which tells us how geomembranes were originally used. Single geomembrane liners constructed over a smooth, firm, relatively low-permeability subgrade, and covered with a ballast layer of at least approximately 30 to 60 cm, may provide a high degree of resistance to leakage, even when the geomembrane contains defects. The reason for this is that the ballast layer will generally prevent gas pressures from uplifting the geomembrane, and will maintain intimate contact between the geomembrane and the soil subgrade, thereby keeping the leakage rate at a very low level, even where there are defects in the geomembrane. Depending on the ballast type, the size of the geomembrane defects, and the degree of liquid head in the pond, the leakage rate from this type of pond can be estimated using empirical equations that are available in the literature. There are also other considerations that must be considered in the installation of soil ballast layers over pond geomembranes, such as soil type, placement method, pond volume impact, cost, and veneer stability.

Ponds that are important from a geotechnical, commercial, or environmental point of view are typically double-lined with intermediate leakage detection and collection layers. These types of ponds have been in use and have been regulated for at least the past 25 years. Thiel and Giroud (2011) describe in detail how deductive engineering and operational experience clearly show that any critical pond design using an exposed geomembrane primary liner requires a well-designed, well-monitored, and well-maintained leakage collection system if one expects the pond to function properly. Often, geosynthetic drainage layers are used. The key design features for ponds typically include (top-to-bottom) a properly anchored primary geomembrane sloped down to a sump, a lateral drainage layer that controls leakage by efficiently draining to an extraction sump, a secondary geomembrane, and a prepared foundation. Thiel and Giroud (2011) discuss four levels of leakage control, why it is important that the leakage collection layer be designed so that it has adequate transmissivity to control the head buildup in the leakage collection layer to a level that is less than the thickness of the leakage collection layer, and the concept of an Action Leakage Rate (ALR) for ponds.

Empty ponds, especially large ones, may present significant wind uplift considerations for exposed geomembranes. Anchorage for these liners can follow the methods discussed above for EGCs. The author has been involved in projects in which intermediate anchor trenches were created across the bottoms of very large ponds to manage the wind uplift.

The range of geomembrane materials used in pond applications is typically much more diverse than that used for landfills. In fact, for potable-water applications, the use of polyethylene geomembranes is in the minority, as compared to the use of other materials such as reinforced polypropylene. The manufacturers and installers of flexible geomembranes typically promote their products for pond applications because their satisfactory performance in these applications has been verified for periods of up to 20 years, and also because of the much smaller number of field seams that are needed due to the use of prefabricated panels. As with any project, specific geomembrane resins must be chosen that will provide appropriate chemical compatibility, exposure and construction durability, and repairability.

Wrinkles are often endemic to pond designs in which the geomembrane is exposed. Because of the undesirable consequences of hydrostatic forces on geomembranes that 'bridge' or 'trampoline' across the corners and toes of slopes, exposed geomembranes are often installed

with enough slack to prevent bridging in the coldest conditions. As a consequence, the exposed geomembranes in ponds typically exhibit different degrees and patterns of wrinkling during warm periods. Wrinkles that experience hydrostatic forces typically take the shape of flattened ‘fins’ protruding normal from the subgrade planar surface. The largest ‘fins’ will typically occur with HDPE geomembrane materials, because of that material’s relatively high thermal expansion coefficient, and its propensity to have larger wrinkles further apart than more flexible materials. The author is aware of at least two large pond projects in recent years (one reported by Peggs, 2012; the other not published) in which very strange cracking failures occurred at the tops of these fins. The hypothesized explanation for this is twofold: (1) the protruding exposed tips of these fins finally stress-cracked because they had experienced numerous cyclic stress-strain reversals, and (2) they had also potentially experienced localized loss of anti-oxidants at the surface, possibly exacerbated by being exposed and stretched passed the yield point at the tip of the fold. While these types of failures are rare in the author’s experience, and while numerous successful exposed HDPE-lined ponds have provided 20 or more years of service without such events, the fact that this has recently occurred twice on very large ponds is worth noting by any engineer who is considering the lining of large ponds.

16. SECONDARY CONTAINMENT AROUND TANKS

Diked secondary containment that is used to contain potential spills around the outside of fuel and chemical storage tanks is commonly provided using geosynthetic materials such as geomembranes. The use of single GCLs to provide this function has not seemed popular, probably because of the need to provide a minimum of 30 cm of overburden soil confinement on top of the GCL, and the propensity of shallow-buried GCLs exposed to variable meteoric conditions and wet-dry cycles to experience a degradation of their low hydraulic conductivity in these applications. In the author’s experience, geomembranes used in these applications are most often exposed and are not buried, with some exceptions. Because of the need for chemical compatibility with fuels and strong chemicals, the geomembrane materials typically used for this application are HDPE, reinforced ethylene-interpolymer-alloy (EIA), and thick bituminous geomembranes. Spray-on liner materials, such as polyurea, are typically the most expensive, but have also been used in these applications.

HDPE offers the advantages of lower cost, compatibility with HDPE pipe for welding boots and embedment strips, and good repairability. The disadvantage of HDPE is its expansion and contraction characteristics. Since an exposed secondary containment diked area is similar to an empty pond, as described above, numerous wrinkles are endemic to these installations. These wrinkles trap stormwater and create extra opportunities for wind damage and stress concentrations.

The advantage of reinforced EIA material is its greatly reduced expansion and contraction that is the result of its reinforcement. Its disadvantage, in the author’s experience, is that the large number of hand-welds that must be made using hot air guns and rollers seems to result in numerous small adhesion failures over time; these are essentially sites where leakage takes place.

The advantage of thick, roll-out bituminous geomembranes is that they seem very durable for foot and light equipment traffic and for maintenance activities, and are highly resistant to wind

uplift. There may be some disadvantages to these materials if exposed to chronic fuel exposure, such as drips that sometimes occur at these installations.

Numerous attachments and penetrations are endemic to these installations, which require a lot of attention to detail (see discussion on ‘Penetrations and Attachments’).

17. CONSTRUCTION, CQA, AND SPECIFICATIONS WITH REGARD TO DESIGN CONSIDERATIONS

Although there will be other papers at this conference that discuss the experience of the past 25 years related to specifications, installation, and the seaming of geosynthetics, the author feels obliged to mention a few items as they relate to design.

CQA. The author would like to acknowledge the continued need now, as much as ever, for construction quality assurance (CQA). The author’s extensive and ongoing experience in performing designs and CQA in this industry has shown that there is no less need for CQA today than there was 25 years ago.

Conformance Testing. Related to CQA, the author believes that there is a continued need for conformance testing of geosynthetic products, but that this could perhaps be done in a more intelligent manner now than it was 25 years ago. There are a number of index tests that continue to be performed with relatively high frequency that were established 25 years ago (e.g., ‘every 100,000 sq ft’). Perhaps with GAI-LAP accreditation and extensive MQC reporting, there could be relaxation of many of the industry standard requirements for certain conformance tests, and more acceptance of MQC results and manufacturer certifications. On the other hand, there are certain index and performance tests that may be more critical for design performance criteria that still require frequent testing. Depending on the project-specific requirements, these tests could include items such as peel strength for various materials, transmissivity testing, interface shear strength, oxidative induction times, and other critical properties.

ELL. This conference would not be complete without mentioning the progress that has been made in the past 25 years in the use of electrical geophysical methods to locate defects in installed geomembranes. This activity goes by various names, including electric leak location (ELL), which is the acronym used in this paper. Development of the ELL method began in 1980 at the Southwest Research Institute in San Antonio, Texas under cooperative contracts with the U.S. Environmental Protection Agency. Commercial surveys conducted on water-covered geomembranes began around 1985, and on soil-covered geomembranes around 1988, right at the beginning of the 25-year period we are discussing (Laine & Darilek, 1993). Since then, the capabilities of this method and its relatively low cost have propelled it to the forefront of the geosynthetics world as the most state-of-the-art quality-control/quality-assurance method for installed geomembranes. Required by an increasing number of regulatory boards for new landfill expansions, it is now also being applied worldwide to heap leach facilities in the mining industry.

The basic method of ELL is to connect an electrical power supply to electrodes above and below the liner, and to then detect areas where there is localized electrical current flow through leaks in the otherwise insulating liner. ELL methods are standardized by ASTM D7002; Standard

Practice for Leak Location on Exposed Geomembrane Using the Water Puddle System, and ASTM D7007; Standard Practices for Electrical Methods for Locating Leaks in Geomembranes Covered with Water or Earth Materials. The ELL method has the ability to detect defects that would not ordinarily be detected using standard CQA methods, especially those caused by placement of the initial soil layers over the top of the liner system. It has been known for some time (see Nosko et al., 1996) that most significant geomembrane damage is caused by construction machinery during the placement of earth materials on the geomembrane. Smith et al. (2007) describe specific measures that can be included in the design and specifications to enhance the electrical leak- location signal and improve the quality of the survey. For over a decade, these techniques have been part of the author's standard design practice in bottom liner systems for landfills and heap leach pads.

Experience. A general word of advice, based on our last 25 years of experience, is to recommend that an experienced, responsible party who is intimately familiar with construction procedures be involved in decisions related to design details, and to any issues related to slope stability (this could be different professionals for different parts of the design).

Along the vein of experience, a lot can be learned by studying failures that have occurred in the industry over the past 25 years. Many of the references cited in this paper contain discussions of failures with observations of useful lessons that were learned. Perhaps the largest compendium of containment-system failures of various sorts is contained in Appendix F of Bonaparte et al. (2002).

18. MOVING INTO THE FUTURE

The discussions in the preceding sections suggest that while we have come a long way, significant questions remain to be answered, and there are areas that show clear room for improvement. While regulations assume a certain static immobility once they've been established, the understandings we gain through experience never stop growing. It is only natural and desirable, then, for new understandings to eventually render existing minimum compliance regulations inadequate, and to inspire designs that are more effective and efficient.

Key items discussed in the preceding sections that could contribute to more effective designs include:

- An emphasis on high-performance, very highly stress-crack-resistant resins for geomembranes (and other geosynthetics) with more robust AO packages.
- More robust leachate collection (lateral drainage) layers.
- Greater deliberation given to long-term allowable strain in geomembranes, with greater attention given to puncture protection and wrinkle management.
- Further investigation into the long-term durability of shear strength interfaces and appropriate acceptance criteria for slope stability for the full range of bottom liners, covers, static conditions, and seismic conditions.

- More requirements with regard to monitoring the impacts of operations on liquid levels and temperatures, especially in light of the bioreactor concept.
- More consideration for shortening the post-closure care period by weighing the benefits of enhanced waste degradation and waste stabilization using anaerobic versus aerobic methods.
- More consideration of design redundancy in specific design elements (e.g., extra pipes, closer spacing) and for the design as a whole (e.g., double liner systems).
- More attention to robust details.

One might well ask: “If the industry’s performance has been so stellar in the past 25 years, why consider changing a winning game? Especially since any of the proposed so-called-improvements might lead to increased cost of construction or operations, why would we want to change?” The answers to these questions can be found in the learning process we are all engaged in. Part of this learning is the realization that our excellent track record over the past 25 years may only represent a relatively small fraction of the life legacy presented by constructed landfills. For this reason, we should continue to query the durability and aging characteristics of our designs in light of the expected duration of the operational life and post-closure care period, especially for the very large, regional facilities that are now being constructed. The recommendations in the NRC (2007) report mainly focus on increased funding and requirements for the monitoring of existing facilities, with the aim of assessing the long-term performance of engineered systems.

REFERENCES

Athanassopoulos, C., Fox, P., and Thielmann, S. (2012a), “Interface Shear Strength Testing of Geomembrane/GCL Composite Liner Systems under Ultra-High Normal Stresses”, Eurogeo 5, Valencia, Spain, September 2012.

Athanassopoulos, C., Fox, P., Thielmann, S., and Stern, A. (2012b), “Shear-Induced Geomembrane Damage due to Gravel in the Underlying Compacted Clay Liner”, Geoamericas 2012 Conference, Lima, Peru, May 2012.

Bishop, D.J. (1996), “Discussion of ‘A comparison of puncture behavior of smooth and textured HDPE geomembranes’ and ‘Three levels of geomembrane puncture protection’ by Narejo, D.B.” *Geosynthetics Int.* V3, No.3, pp 441–443.

Bonaparte, R., Daniel, D., and Koerner, R. (2002), Assessment and Recommendations for Improving the Performance of Waste Containment Systems. EPA/600/R-02/099, EPA Office of Research and Development, Cincinnati, OH, Dec 2002.

Brachman, R.W.I. and Gudina, S. (2008) "Gravel contacts and geomembrane strains for a GM/CCL composite liner", *Geotextiles and Geomembranes*, **26**(6): 448-459.

Brachman, R. and Sabir, A. (2012), “Long-Term Assessment of a Layered-Geotextile Protection Layer for Geomembranes”. *J. Geotech. Geoenviron. Eng.*

- Bray, J.D., Rathje, E.M., Augello, A.J. and Merry, S.M. (1998) "Simplified Seismic Design Procedure for Geosynthetic-Lined Solid-Waste Landfills", *Geosynthetics International*, Vol. 5, Nos. 1-2, Pages 203-235.
- Bray, J.D. and Travasarou, T. (2007). Simplified Procedure For Estimating Earthquake-Induced Deviatoric Slope Displacements, *Journal of Geotechnical and Geoenvironmental Engineering*, ASCE, Vol. 133, No. 4, April.
- Breitenbach, A.J. (1997) "Overview Study of Several Geomembrane Liner Failures Under High Fill Load Conditions." *Proc. of Geosynthetics '97*, IFAI, Vol. 2, pp. 1045-1061.
- Castillo, J, Hallman, D., Byrne, P., and Parra, D. (2005) "Dynamic Analysis of Heap Leach Pad Under High Phreatic Levels", *Proceedings of XXVII Mining Convention*, Arequipa, Peru, Sep 2005.
- Chappel, M.J., Rowe, R.K., Brachman, R.W.I. and Take, W.A. (2012). "A comparison of geomembrane wrinkles for nine field cases", *Geosynthetics International*, 19(6): 453-469.
- Daniel, D. and Koerner, R. (2007), Waste Containment Facilities : Guidance for Construction, Quality Assurance and Quality Control of Liner and Cover Systems, 2nd Edition, ASCE Press, New York, NY.
- Daniel, D., Koerner, R., Bonaparte, R., Landreth, R., Carson, D., and Scranton, . (1998). "Slope Stability of Geosynthetic Clay Liner Test Plots." *J. Geotech. Geoenviron. Eng.*, 124(7), 628–637.
- Darilek, G.T. & Laine, D.L. (2001), "Costs and benefits of geomembrane liner installation CQA," *Proceedings of Geosynthetics 2001*, IFAI, Portland, Oregon, February 12-14, 65-75.
- D'Hollander, R. (2002) "Reflections on Appropriate Reliability Values for Geosynthetic Design", *Proceedings of the GRI-16 Conference*, Dec 2002, Geosynthetic Institute Publications, Folsom, PA, pp. 75-80.
- Duncan, (2000), "Factors of Safety and Reliability in Geotechnical Engineering", *ASCE J. of Geotech & Geoenv. Engrg*, V126, N4, April, pp 307-316.
- EPA, (1993), Solid Waste Disposal Facility Criteria Technical Manual, EPA530-R-93-017, November.
- Esterhuizen, J.B., Filz, G.M., and Duncan, J.M. (2001) "Constitutive Behavior of Geosynthetic Interfaces" *J. of Geotechnical and Geoenvironmental Engineering*, ASCE, Vol. 127, No. 10, Oct., pp. 834-840.
- Filz, G.M., Esterhuizen, J.B., and Duncan, J.M. (2001) "Progressive Failure of Lined Waste Impoundments" *J. of Geotechnical and Geoenvironmental Engineering*, ASCE, Vol. 127, No. 10, Oct., pp. 841-848.
- Forget B, Rollin A.L., Jacquelin T. (2005). "Lessons Learned from 10 Years of Leak Detection Surveys on Geomembranes", *Proceed. Sardinia 2005*, Sardinia.

- Fox, P.J. and Ross, J.D. (2011), "Relationship between NP GCL Internal and HDPE GMX/NP GCL Interface Shear Strengths", *J. Geotech. Geoenviron. Eng.*, 137 (8), 743–753.
- Gilbert, R.B. and Byrne, R.J. (1996) "Strain-Softening Behavior of Waste Containment System Interfaces." *Geosynthetics International*, IFAI, Vol. 3, No. 2, pp. 181-203.
- Giroud, J.P. (2010), "Development of criteria for geotextiles and granular filters", Prestigious Lecture, Proceedings of the 9th International Conference on Geosynthetics, Guarujá, Brazil, May 2010, Vol. 1, pp. 45-64.
- Giroud, J.P (1997), "Equations for calculating the rate of liquid migration through composite liners due to geomembrane defects", *Geosynthetics International*, Vol. 4, Nos. 3-4, pp. 335-348.
- Giroud, J.P., and Bonaparte, R. (1989). "Leakage through liners constructed with geomembranes-parts I and II" *Geotextiles and Geomembranes* 8(1), 27-67, 8(2), 71-111.
- Giroud, J.P., & Morel, N. (1992), "Analysis of Geomembrane Wrinkles", *Geotextiles & Geomembranes*, Vol. 11, No. 3, pp. 255-276. (Erratum: 1993, Vol. 12, No. 4, p. 378.)
- Giroud, J.P. and Soderman, K.L., (1995a), "Design of Structures Connected to Geomembranes", *Geosynthetics International*, Vol. 2, No. 2, pp. 379-428.
- Giroud, J.P. and Soderman, K.L., (1995b), "Comparison of Geomembranes Subjected to Differential Settlement", *Geosynthetics International*, Vol. 2, No. 6, pp. 953-969.
- Giroud, J.P., & Touze-Foltz, N., 2003, "Geomembranes in Landfills: Discussion at the 7th International Conference on Geosynthetics", *Geosynthetics International*, Vol. 10, No. 4, pp. 124-133.
- Giroud, J.P. & Touze-Foltz, N. (2005). "Equations for calculating the rate of liquid flow through geomembrane defects of uniform width and finite or infinite length." *Geosynthetics International*, 12, No. 4, 191–204.
- Giroud, J.P., Khatami, A., and Badu-Tweneboah, K. (1989). "Evaluation of the rate of leakage through composite liners," *Geotextiles and Geomembranes* 8(4), 337-340.
- Giroud, J.P., Bonaparte, R., Beech, J.F., & Gross, B.A., 1990, "Design of Soil Layer-Geosynthetic Systems Overlying Voids", *Geotextiles & Geomembranes*, Vol. 9, No. 1, Elsevier, London, England, pp. 11-50.
- Giroud, J.P., Badu-Tweneboah, K., and Bonaparte, R. (1992). "Rate of leakage through a composite liner due to geomembrane defects," *Geotextiles and Geomembranes* 11(1), 1-28.
- Giroud, J.P., Pelte, T. and Bathurst, R.J. (1995a), "Uplift of Geomembranes by Wind", *Geosynthetics International*, Special Issue on Design of Geomembrane Applications, Vol. 2, No. 6, pp. 897-952.
- Giroud, J.P., Bachus, R.C., & Bonaparte, R. (1995b), "Influence of Water Flow on the Stability of Geosynthetic-Soil Layered Systems on Slopes", *Geosynthetics International*, Special Issue on

Design of Geomembrane Applications, Vol. 2, No. 6, pp. 1149-1180. (Errata, 1997, Vol. 4, No. 2, pp. 209-210.)

Giroud, J.P., Gross, B.A., Bonaparte, R. and McKelvey, J.A., (1997a), "Leachate Flow in Leakage Collection Layers Due to Defects in Geomembrane Liners", Geosynthetics International, Vol. 4, Nos. 3-4, pp. 215-292.

Giroud, J.P., Khire, M.V. and Soderman, K.L., (1997b), "Liquid Migration Through Defects in a Geomembrane Overlain and Underlain by Permeable Media", Geosynthetics International, Vol. 4, Nos. 3-4, pp. 293-321.

Giroud, J.P., King, T.D., Sanglerat, T.R., Hadj-Hamou, T., and Khire, M.V. (1997c), "Rate of Liquid Migration Through Defects in a Geomembrane Placed on a Semi-Permeable Medium", Geosynthetics International, Vol. 4, Nos. 3-4, pp. 349-372.

Giroud, J.P., Badu-Tweneboah, K. and Soderman, K.L., (1997d), "Comparison of Leachate Flow Through Compacted Clay Liners and Geosynthetic Clay Liners in Landfill Liner Systems", Geosynthetics International, Vol. 4, Nos. 3-4, pp. 391-431.

Giroud, J.P., Gleason, M.H. & Zornberg, J.G. (1999), "Design of Geomembrane Anchorage Against Wind Action", Geosynthetics International, Vol. 6, No. 6, pp. 481-507.

Giroud, J.P., Zornberg, J.G., and Zhao, A. (2000a), "Hydraulic design of geosynthetic and granular liquid collection layers," Geosynthetics International, V7, Nos. 4-6, pp 285-380.

Giroud, J.P., Zhao, A., and Bonaparte, R. (2000b), "The myth of hydraulic transmissivity equivalency between geosynthetic and granular liquid collection layers," Geosynthetics International, V7, Nos. 4-6, pp 381-401.

GRI (2010). White Paper #6, "Geomembrane Lifetime Prediction".

GRI (2011) Analysis And Critique Of Twenty Large Solid Waste Landfill Failures, GRI Report #41, authored by R.M. Koerner and C. Wong, Geosynthetic Research Institute, Folsom PA, Oct 11, 2011.

Hendron, D.M., Fernandez, G., Prommer, P.J., Giroud, J.P., and Orozco, L.F. (1999) "Investigation of the Cause of the 27 September 1997 Slope Failure at the Dona Juana Landfill" Proc. Sardinia '99 Seventh International Waste Management and Landfill Symposium, CISA, Vol. III, pp. 545-554.

Jones, D.R.V. and Dixon, N. (2005), "Landfill lining stability and integrity: the role of waste settlement," Geotextiles and Geomembranes, V23, N1, February, pp 27-53.

Kavazanjian, E. (1998). Current Issues in Seismic Design of Geosynthetic Cover Systems, Sixth International Conference on Geosynthetics, IFAI, Atlanta, GA, USA: 219-226.

Koerner, R.M. (1994), Designing with Geosynthetics, 3rd Ed., Prentice Hall, Englewood Cliffs, NJ (note: this is now available in the 6th Edition).

- Koerner, R.M. (2012), "Traditional vs. exposed geomembrane landfill covers", *Geosynthetics magazine*, V30, N5, October/November, 2012, pp 34-41.
- Koerner, G.R. & Koerner, R.M. (2006). "Long term temperature monitoring of geomembranes at dry and wet landfills." *Geotextiles and Geomembranes*, V24, No.1.
- Koerner, R.M. & Koerner, G.R. (2009) "Geocomposite Drainage Material Connections and Attachments", GRI-22 Conference, February 27, 2009, Salt Lake City, Utah.
- Koerner, R.M. and Soong, T.Y. (1998). *Analysis and Design of Veneer Cover Soils*, Sixth International Conference on Geosynthetics, IFAI, Atlanta, GA, USA: 1-23.
- Koerner, R. M., Wilson-Fahmy, R. R. and Narejo, D., (1996), "Puncture protection of geomembranes; Part III examples." *Geosynthetics International*, Vol. 3, No. 5, IFAI, St. Paul, MN, pp. 655-675.
- Koerner, R.M., Hsuan, Y.G., Koerner, G.R. and Gryger, D. (2010), "Ten year creep puncture study of HDPE geomembranes protected by needle-punched nonwoven geotextiles", *Geotextiles and Geomembranes*, V28, N6, pp 503-513.
- Laine, D.L. and Darilek, G.T. (1993), "Locating Leaks in Geomembrane Liners of Landfills Covered With a Protective Soil", *Proceedings for Geosynthetics '93 held in Vancouver, B.C. in April 1993*, IFAI, pp. 1403-1412.
- Luettich, S.M., Giroud, J.P., and Bachus, R.C. (1991), Geotextile Filter Design Manual, Report prepared for Nicolon Corp., Norcross, GA. A short version of this was also published by the same authors in the *Proceedings of the 5th GRI Seminar*, Drexel University, Dec 12-13, 1991.
- Lui, C.-N., and Gilbert, R.B. (2003), "Simplified method for estimating geosynthetic loads in landfill liner side slopes during filling," *Geosynthetics International*, V10, N1, pp 24-33.
- Makdisi, F. and Seed, H.B. (1978), "Simplified Procedure for Estimating Dam and Embankment Earthquake Induced Deformation", *ASCE J. of Geotec. Engr.*, V104, NGT7, pp 849-867.
- Marcotte M., Rollin A.L. and Charpentier C. (2009), "The importance of liner thickness and CQA implementation in landfills", *Geosynthetics 2009*, February 25-27 2009, Salt Lake City, Utah.
- Newmark, N. (1965) "Effects of Earthquakes on Dams and Embankments", *Geotechnique*, V15, N2, pp 139-160.
- Nosko V., Andrezal T., Gregor T. & Garnier P. (1996). "Sensor Damage Detection System – The Unique Geomembrane Testing Method", *Proceed. EuroGeo*, Netherlands pp 743-748.
- NRC (2007), Assessment of the performance of engineered waste containment barriers. National Research Council of the National Academies, National Academies Press, Washington, DC.

- Ohio EPA (2004). Geotechnical and Stability Analyses for Ohio Waste Containment Facilities, Geotechnical Resource Group (GeoRG), Ohio Environmental Protection Agency, Columbus, Ohio 43216-1049, Sept 14, 2004.
- Peggs, I.D. (2012), "Impact of Variable Stresses on Accelerated Stress Cracking of HDPE Wrinkles", Second Pan American Geosynthetics Conference & Exhibition, Geoamericas 2012, Lima, Peru, May, 2012.
- Peggs, I.D., Schmucker, B., and Carey, P. (2005). "Assessment of maximum allowable strains in polyethylene and polypropylene geomembranes." Proc., Geo-Frontiers 2005, Austin, Texas.
- Qian, X., Koerner, R.M, and Gray, D. (2002), Geotechnical aspects of landfill design and construction. Prentice-Hall, NJ., 717 pp.
- Reddy, K.R., Kosgi, S. and Motan, S. (1996) "Interface Shear Behavior of Landfill Composite Liner Systems: A Finite Element Analysis." Geosynthetics International, IFAI, Vol. 3, No. 2, pp. 247-275.
- Richardson, G.N., Giroud, J.P., and Zhao, A. (2000), "Design of Lateral Drainage Systems for Landfills", manual prepared for Tenax Corporation.
- Rollin, A., Pierson, P., and Lambert, S. (2002), Geomembranes, Guide de choix, Presses Internationales Polytechnique, Quebec, Canada.
- Rowe, R.K. (1998). "Geosynthetics and the minimization of contaminant migration through barrier systems beneath solid waste." Proc. 6th Int. Conf. on Geosynthetics, Atlanta, 27–103.
- Rowe, R.K. (2005). "Long-term performance of contaminant barrier systems", 45th Rankine Lecture, *Geotechnique*, **55** (9): 631-678.
- Rowe, R.K (2012). "Short and long-term leakage through composite liners", The 7th Arthur Casagrande Lecture", *Canadian Geotechnical Journal*, 49(2): 141-169.
- Rowe, R.K. and VanGulck, J. (2003) "Experimental and modeling study into clogging of leachate collection systems", Proceedings of 8th International Waste Management and Landfill Symposium, S. Margherita di Pula, Cagliari, Sardinia, Italy.
- Rowe, R.K., Quigley, R.M., and Brachman, R.W. (2004), Barrier Systems for Waste Disposal, 2nd Edition, Spon Press, London.
- Rowe, R.K, Islam, M.Z. and Hsuan, Y.G. (2010). "Effect of thickness on the aging of HDPE geomembranes", *ASCE Journal of Geotechnical and Geoenvironmental Engineering*, 136(2):299-309.
- Scheirs, J. (2009), A Guide to Polymeric Geomembranes, John Wiley & Sons, United Kingdom.
- Schroeder, P.R., Dozier, T.S., Zappi, P.A., McEnroe, B.M., Sjostrom, J.W., and Peyton, R.L. (1994). "The Hydrologic Evaluation of Landfill Performance (HELP) Model: Engineering

Documentation for Version 3," EPA/600/R-94/168b, September 1994, U.S. Environmental Protection Agency Office of Research and Development, Washington, DC.

Seed, R.B., and Bonaparte, R. (1992), "Seismic Analysis and Design of Lined Waste Fills: Current Practice," Proceedings of the Conference on Stability and Performance of Slopes and Embankments - II, ASCE Special Geotechnical Publication No. 31, pp. 1521-1545.

Smith, M.E, and Giroud, J.P. (2000) "Influence of the Direction of Ore Placement on the Stability of Ore Heaps on Geomembrane-Lined Pads", SLOPE STABILITY IN SURFACE MINING, SME, ch. 49, PP 435-438.

Smith, B.L., Darilek, G.T. & Laine, D.L. (2007), "Enhanced Geomembrane CQA Through Proper Application of Geomembrane Leak Location Surveys", Geosynthetics 2007 Conference Proceedings, Washington, DC, U.S.A. January 16-19, 2007.

Snow, M.S., Kavazanjian, E. & Sanglerat, T.R., 1994, "Geosynthetic composite liner system for steep canyon landfill side slopes", Proceedings of the International Conference on Geotextiles, Geomembranes and Related Products, Singapore, Vol. 3, pp 969-972.

Stark, T.D. & Choi, H. (2004). Peak versus residual interface strengths for landfill liner and cover design. Geosynthetics International, V11, No.6, pp. 491-498.

Stark, T.D., and Poeppel, A.R. (1994) "Landfill Liner Interface Strengths from Torsional Ring Shear Tests." J. of Geotechnical Engineering, ASCE, Vol. 120, No. 3, March, pp. 597-615.

Stark, T.D., Martin, J.W., Gerbasi, G.T., Thalhamer, T., and Gortner, R.E. (2012a), "Aluminum waste reaction indicators in a municipal solid waste landfill," ASCE JGGE, V138, N3, March, pp 252-261.

Stark, T.D., Choi, H., Lee, C., and Queen, B. (2012b), "Compacted Soil Liner Interface Strength Importance," ASCE JGGE, V138, N4, April, pp. 544-550.

Take, W.A, Watson, E., Brachman, R.W.I., and Rowe, R.K. (2012) "Thermal expansion and contraction of geomembrane liners subjected to solar exposure and backfilling", ASCE *Journal of Geotechnical and Geoenvironmental Engineering*, 138(11): 1387 – 1397.

Thiel, R. (1998) "Design Methodology for a Gas Pressure Relief Layer Below a Geomembrane Landfill Cover to Improve Slope Stability." Geosynthetics International, Vol. 5, No. 6, pp. 589-616.

Thiel, R. (2001). "Peak vs. Residual Shear Strength for Landfill Bottom Liner Stability Analyses." Proceedings, GRI-15, Houston, Texas

Thiel, R. (2008) "Slope Stability Sensitivities of Final Covers", IFAI, GeoAmericas conference, Cancun, Mexico, March 2008.

Thiel, R. (2009) "Post-Construction Landfill Liner Failure and Lessons Learned", IFAI, Geo 2009, Salt Lake City, Feb 2009.

- Thiel, R. (2010) "Optimization of Anchor Trench Design for Solar Evaporation Ponds." Proceedings for the 9th International Conference on Geosynthetics, May 2010, Garuja, Brazil.
- Thiel, R. and DeJarnett, G. (2009) "Guidance on the Design and Construction of Leak-Resistant Geomembrane Boots and Attachments to Structures", GRI Session of the IFAI-sponsored conference, Geo 2009, Salt Lake City, Feb 2009.
- Thiel, R. and Giroud, J.P. (2011) "Important Considerations for Leakage Control of Exposed Geomembrane-Lined Ponds" Proceedings of Sardinia '11 Thirteenth International Landfill Symposium, Oct. 2011.
- Thiel, R., and Narejo, D. (2005) "Lamination Strength Requirements for Geonet Drainage Geocomposites." Proceedings of the 18th Annual GRI Conference/ASCE Geofrontiers Conference, Austin, TX, January 2005.
- Thiel, R., and Richardson, G. (2005) "Concern for GCL Shrinkage when Installed on Slopes." Proceedings of the 18th Annual GRI Conference, accepted for presentation at the ASCE Geofrontiers Conference, Austin, TX, January 2005.
- Thiel, R.S. and Stewart, M.G. (1993) "Geosynthetic Landfill Cover Design Methodology and Construction Experience in the Pacific Northwest." Proceedings of Geosynthetics '93 held in Vancouver, B.C. in April 1993, pp. 1131-1134.
- Thiel, R. and Thiel, C. (2009) "GCL Shrinkage - A Possible Solution", Geotechnical Fabrics Report, V27N1, Feb-Mar 2009, pp. 10-21.
- Thiel, R.S., Daniel, D.E., Erickson, R., Kavazanjian, E., and Giroud, J.P. (2001) GundSeal Design Manual. Available from GSE, Houston, TX. September 2001.
- Touze-Foltz, N. & Giroud, J.P. (2005). "Empirical equations for calculating the rate of liquid flow through composite liners due to large circular defects in the geomembrane." Geosynthetics International, 12, No. 4, 205–207.
- Villard, P. and Chareyre, B. (2004), "Design methods for geosynthetic anchor trenches on the basis of true scale experiments and discrete element modelling." Canadian Geotechnical Journal. V41, pp. 1193-1205.
- Wells, L. (1993). "Guidance for design of watertight geomembrane attachments to concrete surfaces," Geosynthetics '93, IFAI, Vancouver, BC, Canada, pp 1119-1129.
- Whitman, R.V. (1984) "Evaluating Calculated Risk in Geotechnical Engineering", 17th Terzaghi Lecture, JGGE, ASCE, V110, N2, Feb, pp 143-188.
- Witte, R. (1997), "Practice-oriented investigations to improve geotextile protective layer systems for geomembranes with regard to their long-term protective efficacy", in Advanced Landfill Liner Systems, Edited by H. August, U. Holzloner, and T. Meggyes, Thomas Telford Publishing, Heron Quay, London, pp 270-277.

Zornberg, J.G. and Giroud, J.P., (1997), "Uplift of Geomembranes by Wind – Extension of Equations", *Geosynthetics International*, Vol. 4, No. 2, pp. 187-207 (Errata: 1999, Vol. 6, No. 6, pp. 521-522).

REINFORCED SOIL WALLS AND SLOPES: IN RETROSPECT (i.e., The Good, the Bad and the Ugly)

Barry R. Christopher
Geotechnical Engineering Consultant

Robert D. Holtz
University of Washington

Ryan R. Berg
Ryan R. Berg & Associates, Inc.

Richard P. Stulgis
Geocomp Corporation

ABSTRACT

The use of geosynthetic reinforced soil walls and slopes has grown significantly over the past 25 years. Though, surprisingly, the materials, design procedures, and construction techniques used with these structures have only modestly changed. This paper provides a historical review of many of the activities over that period of time that brought us to where we are today in the implementation and maintenance of this technology. This era started off with some of the most significant changes, with a number of suggestions for design improvement, but as with many civil engineering activities such improvements are slow to materialize. Good practices developed during this period have led to significant success in the use of geosynthetic reinforced walls and slopes as highlighted in this paper. However, a number of issues were identified during this era, primarily resulting from bad practices. In this paper, best practices are reviewed along with design improvements and current progress on implementing those improvements. The outcomes resulting from not following good practice established during this period will also be reviewed.

INTRODUCTION AND SCOPE

Geosynthetic reinforcement has been used for reinforced soil wall and slope construction in North America since the mid 1970s, although the number of early reinforced soil walls and slopes was rather small. From only a few hundred walls constructed by 1987 (Yako and Christopher, 1987), the beginning of this 25 year period, thousands of structures are currently constructed each year. This paper provides a historical review of many of the activities over that period of time that brought us to where we are today in the implementation and maintenance of this technology. Much of the early practice, before this period, was documented in Christopher and Holtz (1985) and Berg et al. (1998) provided a very good review of those early design methods, a summary of which is included later in this paper. During the 1980s, a number of advancements were made in the US practice, which are also reviewed later in this paper. While research and instrumented studies since the 1980s have supported further advancements, few have been incorporated into current design models (although current activities may soon be moving these efforts to the forefront.)

THE EARLY YEARS BEFORE THIS 25 YEAR ERA

The Federal Highway Administration (FHWA) Geotextile Engineering Manual (Christopher and Holtz, 1985) provides a summary of design methods that were available at that time for both slopes and walls and provides detailed case histories of early projects. As identified in the manual, there were no standard design methods within the public or private sector at that time. Four methods were identified for slopes and five methods were identified for walls, each having different assumptions for developing the load in the reinforcement and resistance provided by the reinforcement. There was a method developed by the US Forest Service (Steward et al., 1977) and most other methods had been developed by academic researchers or proprietary system developers. Although all of the design methods appeared to be theoretically sound and test cases were typically used to verify adequate performance, none of the design methods could be completely validated through instrumented structures (i.e., what was the actual factor of safety and corresponding uncertainty). Therefore, several different detailed design methods were included in the manual for users to evaluate with a suggestion that more than one be considered as a check.

At that time, most structures were constructed with wrapped facings, although some experiments with timber facing and full-height panels were used with geotextile reinforcement in Glenwood Canyon, Colorado in the early 1970s (Robert Barrett, personal communication). A block-face geosynthetic reinforced soil wall was constructed in the late 1970's, see Figure 1.

Another detailed report on reinforced walls and slopes was published in the 1987. The National Cooperative Highway Research Program (NCHRP) 290 Reinforcement of Earth Slopes and Embankments report (Mitchell and Villet, 1987) provides comprehensive state-of-the-art discussion on earth reinforcement principles, materials, design procedures and construction materials. Steel and geosynthetic reinforcements and



systems are addressed this report.

Figure 1. First geosynthetic reinforced soil, block-faced wall constructed in the late 1970s (Courtesy of Professor J.R. Bell)

A new geosynthetic – *geogrid* – was introduced in North America in 1982. This geosynthetic was specifically developed for soil reinforcement applications such as walls and slopes. Early wall and slope applications in North America are included in proceedings of the 1984 Polymer Grid Reinforcement Conference (Forsyth and Bieber; Busbridge; Bonaparte and Margason; Bell et al.; 1984). The first precast panel faced geogrid reinforced soil walls in North America were constructed in 1984 and 1985 (Berg et al., 1986) in the US and in 1985 in Canada (Berg et al., 1987). The tie-back wedge method of analysis with an internal lateral pressure equivalent to active Rankine was used for design of these and subsequently geogrid reinforced soil walls. Masonry wall (a.k.a., segmental retaining wall

(SRW); and, modular block wall (MBW)) units introduced in the mid 80s for construction of gravity walls were soon (i.e., 1986) combined with geosynthetics for design and construction of reinforced soil walls. Since then, the geogrid and the MBW unit manufacturers and suppliers have spurred the use of geosynthetic retaining walls.

BEHAVIOR OF REINFORCED SOIL (1983 – 1989)

The absence of a validated design standard was not only an issue with geosynthetics, but all other types of reinforced soil systems. FHWA identified eight different generic reinforcement systems, including three generic geosynthetic systems (i.e., geotextiles, geogrids and smooth plastic strips), ribbed and smooth steel strip reinforcements, bar mat reinforcements, welded wire mesh reinforcements, and woven wire (e.g., gabion) mesh reinforcements. Structures using these reinforcements were designed using completely different methods for determining both the reinforcement strength and reinforcement interaction (i.e., pullout resistance) requirements. Many of the approaches were developed by proprietary interests. FHWA had identified all of these systems under one umbrella term Mechanically Stabilized Earth walls (partly to avoid conflicts with proprietary names for wall supplier systems). Under the sponsorship of the FHWA, a study on the “Behavior of Reinforced Soil” was undertaken to verify the adequacy of existing design methods to accurately predict performance. Based on the review of existing methods, comprehensive guidelines were to be developed for evaluating and using soil reinforcement techniques considering the absence of consistent design methods and the difficulties in comparing the stability of different systems. The end product was a manual of practice for design and construction of reinforced soil structures.

The scope of the FHWA study encompassed five principal tasks:

- A review of the technology and design methods at that time, primarily based on the extensive literature study performed (by Mitchell and Villet, 1987).
- A laboratory testing program to evaluate reinforcement variables and stress distribution patterns, consisting of:
 - Reduced scale (approximately 1 m high) models.
 - Forty-seven small scale (150 mm high) centrifuge model tests.
 - Five large scale (500 mm high) centrifuge model tests.
 - Pullout tests to evaluate stress transfer and develop standard methods for obtaining design input parameters.
- Full scale, fully instrumented field tests (Figure 2) to evaluate the existing design approaches. Field models included:
 - Eight, 11 m wide by 6 m high, reinforced soil walls using steel strips, steel bar mats, geogrids, woven wire mesh and geotextiles as reinforcement. Facing systems for walls included 5 walls with concrete facing panels, 2 walls with gabion faces, and one wrapped faced wall. A privately funded ninth wall, using geogrid reinforcements and modular block facing units, was added near the end of the study.
 - Four, 15 m wide by 7.6 m high slopes constructed at 1 horizontal to 1 vertical and 1 horizontal to 2 vertical using geotextile and geogrid reinforcement.
 - Well graded sand and gravel, cobbles, and silt for reinforced fill.
 - Field pullout tests on each wall reinforcement.

- Concentrated footing type loads on select walls and embankment surcharge loading on all of the wall systems.
- Preliminary analysis of the field results along with a parametric study using the finite element method.
- Preparation of a design manual of practice (Christopher et al., 1989).



Figure 2. FHWA-Study, Instrumented walls constructed in Algonquin, Illinois by STS Consultants (from Christopher, 1993)

The data from each of the phases was primarily reviewed in relation to the goal of the project (e.g., verification of existing design techniques) and planning the next phase. During the performance of the study, it became apparent that a unified design approach for all reinforcement systems should and could be developed based on the results of the study. The results indicated that the different reinforcement systems when designed according to a unified approach, behave in a similar and predictable manner, provided that the “density” of reinforcement (amount of reinforcement per area of the reinforced section) is similar. The principal difference in performance can be attributed to the extensibility of the reinforcement, or stiffness of the reinforced soil composite.

Based on the results of the field and laboratory work, a method was advanced based on the preliminary analysis of the data (Christopher et al., 1989). The resulting design method for MSE walls was based on a stiffness approach for quantifying the lateral pressure coefficient (i.e., the stiffness of the reinforcement based on its modulus and the density of reinforcement in the reinforced soil mass). The design method provided the basis for the *Simplified Method* currently used in the AASHTO and FHWA design documents. An in-depth comparative review of the data from all phases of this study including the development of the design model is presented by Christopher (1993).

For reinforced soil slopes, a rotational limit equilibrium analysis, with the assumption that the geosynthetic reinforcement acted tangential to the failure surface, predicted well the magnitude and location of the maximum stress in the reinforcement and was determined to be a suitable method for design. This method was incorporated into both the FHWA MSE design

manual (Christopher et al., 1989), and the second edition of the FHWA geotextile design manual (Christopher and Holtz, 1989). A detailed evaluation of the design approach is presented by Christopher and Leschinsky (1991) and a reliability analysis of the procedure is presented by Cheng and Christopher (1993). FHWA also developed an Interim Guidelines for Design, Specification, & Contracting of Geogrid Mechanically Stabilized Earth Slopes on Firm Foundations (Berg, 1991).

The FHWA study recognized that both the wall and slope design methods were conservative (i.e., safe) as demonstrated by the instrumentation results. However, as noted in the report, all things considered, variability in construction procedures, fill and backfill, foundation material, and construction control would suggest only moderate changes in the design procedures at that time, and that it was more important to use this information to improve design consistency. Even though a broad range of soil types was evaluated, for these same reasons, the design guide recommended the use of select granular fill with minimum fines (< 15% finer than 0.075 mm) for wall structures. A number of recommendations were offered for improvement, several of which were related to reductions in the conservatism in the calculated tension from the standard wall design method versus measured soil values for geosynthetic reinforcements. These included use of more uniform loading such as a trapezoidal versus triangular distribution of stress in the reinforcement, use of confined stress strain for evaluation of reinforcement tension and deformation response, the influence of face stiffness on overall wall deformation, and development of composite design models (Christopher et al., 1989, also see Collin, 1986 and Christopher, 1993).

As a demonstration of the conservatism, the actual factor of safety for the FHWA-study retaining walls (i.e., removing many levels of conservatism) were evaluated by Christopher et al., 1992. Although the systems were designed for an internal factor of safety of 1.5, the geogrid wall had an actual factor of safety of 3.3 or greater, and the factor of safety for the slopes constructed with woven geotextiles and extruded geogrids had factors of safety ranging from 2.1 to 7.0. One wall constructed with a nonwoven geotextile had a design and actual factor of safety of 0.94. Although 900 mm of horizontal movement (i.e., 15% times the height of the wall) was measured near the top of the wall after construction, the wall did stop moving and did not fall down, again indicating inherent conservatism in the design approach.

FHWA was also concerned about the durability of reinforcements. Much of the early methods for calculating the allowable strength were based on reduction factors, but the factors were based on polymer durability charts (as opposed to exposure testing), some creep testing and in some cases, a factor for installation damage. Both the FHWA research report (Christopher et al., 1989) and the FHWA Geotextile Design and Construction Guidelines Manual (Christopher and Holtz, 1989) advocated a method using a similar partial reduction factor approach advanced by Bonaparte and Berg (1987):

$$LTADS = \frac{T_{ult} \times CRF}{RF_{ID} \times RF_D \times FS}$$

Where, LTADS = Long Term Allowable Design Strength
 T_{ult} = Ultimate strength of the geosynthetic

- CRF = Creep reduction factor (ratio of the creep limit strength obtained from creep test to ultimate strength)
- RF_{ID} = Reduction factor for installation damage
- RF_D = Reduction factor for polymer durability
- (Note. The creep factor is in the numerator as it was not considered to be a degradation mechanism unless that level of strength was exceeded – it was eventually moved to the bottom of the equation.)

However, there were no test standards for durability, creep or installation damage at that time and the actual longevity of the polymer was questioned by some engineers. In 1990, FHWA published a study on Durability/Corrosion of Soil Reinforced Structures (Elias, 1990) that proposed criteria for evaluating reinforcement material. The geosynthetics section was primarily based on a literature study with the exception of installation damage, where extensive field tests were performed to support information from the literature.

There were a number of well documented geosynthetic reinforced soil wall and slope case histories in the 1980's, several of which are documented in the in the Geosynthetics Case Histories (Raymond and Giroud, 1987). Summaries of 54 projects are presented by Yako and Christopher, 1987. Those reviews included project details, design information, reinforcement properties and design methodology, and, where available, instrumentation and results. Two other significant case histories were the Tucson, Arizona wall (Berg, et al., 1986), which uniquely used geogrid reinforcement connected to full height precast concrete facing, and the 15.2 m high Rainier Avenue wall (Holtz et al., 1991; Allen et al., 1991; and, Christopher et al., 1990). This second case, at the time, was the tallest reinforced soil wall in the US, and it was fully instrumented to evaluate internal and external performance. The instrumentation results from both of those walls confirmed the current conservative design models and the excellent performance of geosynthetic reinforced soil walls. In the case of the Rainier Avenue wall instrumentation results, even though the design factor of safety was 1.2, the face deformations were only about 10 mm, and post-construction creep was about one-half that amount after 9.5 months. The measured strains of the geotextile reinforcement were very small, typically about 0.5 percent; the maximum observed by only one gage was slightly more than 1 percent.

The tallest reinforced soil slope in the US was a 33.5 m structure constructed in 1987 for large scale contour land forming for the Ridgegate subdivision, La Jolla, California.

Other projects are described in a number of International and North American Geosynthetic conferences that took place in the 1980's. One very significant event was a NATO workshop in Canada where a number of international reinforced soil experts (consultants, academics and proprietary systems experts) met and reviewed the state of the art and the state of the practice (see Jarrett and McGown, 1987). Two specialty conferences also took place in 1990 that provide very good case histories and research studies of this period. One was an international specialty conference on "Performance of Reinforced Soil Structures" (McGown et al., 1990) that took place in Glasgow, Scotland. The other conference was the American Society of Civil Engineers (ASCE) conference on "Design and Performance of Earth Retaining Structures" in New York City (Lambe and Hansen, 1990).

And the best news, there were few documented failures during this period. The few that were reported were typically on test walls (e.g., the FHWA study) or connection failures in attempts to develop alternate facing systems. Those not documented in the literature include walls backfilled with fine grained soils and surficial failure of reinforced soil slopes. A harbinger of what was to come.

THE 90'S

During and after the FHWA study, several alternate wall design methods were proposed. During the late 80's AASHTO established a task group (Task Force 27) that developed design guidelines based on a literature review (e.g., Mitchell and Villet, 1987) and wall supplier input (AASHTO 1990). For geosynthetics, the tie-back wedge method of analysis was recommended, which was similar to the approach evaluated in the FHWA study and that used by geogrid manufacturers and suppliers since the mid 80s. The 1990 procedures formed the basis for the 1991 AASHTO Standard Specifications; however, geosynthetics were in a separate section from the MSE (e.g., steel reinforcement) wall section of the manual. In the 1994 AASHTO Standard Specifications, the stiffness approach was introduced as an alternate design method. However, several wall suppliers objected to using the new, more complicated stiffness method of analysis, (primarily, at least the lead author suspects that this rejection was due to the unification of the design, which took away some of their uniqueness.)

In 1994, representatives from AASHTO and FHWA met to review the methods for calculating the backfill reinforcement loads that were available at that time in the AASHTO Standard Specifications for walls. Their objective was to unify the design methods and to simplify and clarify the specifications. Full scale MSE wall case history data (i.e., from the FHWA study, as well as other instrumented structures) was reviewed, such that the method could be calibrated to the empirical data, since all of the methods available were empirical in nature. The effect of simplifications in the method, such as how vertical soil stresses are calculated and how reinforcement stiffness is considered in the design, could also be evaluated with this full scale wall data to ensure that the unified method developed had adequate accuracy. From this effort, the FHWA/AASHTO Simplified Method was developed as published by Elias and Christopher (1996/1997) and AASHTO (1997). Also, see Allen et al., 2001 for a full description of this effort along with a review of additional instrumented case histories to support the method. These changes also put geosynthetics on an equivalent level with steel reinforced soil systems in the AASHTO guidelines, as they were evaluated using the same methodology.

The durability guidelines from FHWA (Elias, 1990) were also being revisited. An extensive research program on geosynthetic durability was undertaken in the early 1990s that involved national geosynthetic specialist expertise from industry, academia, transportation agencies and consulting engineers. The objective was to gain a better understanding of the mechanisms and environments which affect the strength degradation rate of geosynthetic reinforcement, and to develop a practical methodology for comparing geosynthetic products. This program was funded as a FHWA HP&R National Pooled fund study, which was led by FHWA and Washington State DOT. The results of the test program and the degradation testing protocol were documented in the FHWA Corrosion and Degradation/Degradation of Soil

Reinforcements for MSEW and RSS (Elias, 1997). GSI also played a role in this study by validating some of the test protocol results (Koerner et al., 2006).

While the public sector was getting organized, so was industry. In 1993, the National Concrete Masonry Association (NCMA) published a design manual for segmental retaining wall (SRW) gravity and SRW-face reinforced soil walls (a.k.a. modular block walls), for use in the private sector (Simac et al., 1993). A tie-back wedge method of analysis, but with the use of Coulomb active lateral pressure and failure line for internal and external design, is used in this manual. Coulomb theory (versus Rankine theory used by FHWA and AASHTO) is used to take advantage of the beneficial effects from wall facing batter and interface friction between the reinforced fill and wall face. The manual, which covers everything from short landscape walls to taller (i.e., 20⁺ feet high in 1993) walls, also allowed for the use of less select material with up to 35% < 0.075 mm fine grained soils, if carefully evaluated and approved by a geotechnical engineer. The manual was updated in 1997. A complementary Segmental Retaining Wall Seismic Design Manual was published by NCMA in 1998 (Bathurst, 1998).

The use of up to 35% fines in the reinforced fill has been extensively discussed in each edition of the NCMA manual. Again, the scope of the manual is for a wide variety of wall uses and heights and, thus, use of finer grained soils is, and has been, acceptable for many applications. Each edition of the manual has stated that cohesionless free draining (less than 10% fines) backfill materials are preferred. However, soils with low plasticity (i.e., CL, ML, SC with $PI \leq 20$) may be used provided the following four additional design criteria are implemented:

- Proper internal drainage is installed.
- Only soils with low to moderate frost heave potential are used.
- The internal cohesive shear strength parameter, c , is conservatively ignored for stability analysis.
- The final design is checked by a qualified geotechnical engineer to ensure that the use of cohesive soils does not result in unacceptable time-dependent movement of the SRW system.

The manual editions further promote the use of granular wall fill by listing their advantages of:

- Easier to place and compact.
- Higher permeability which assists drainage.
- Greater shear strength, which reduces applied stress.
- Generally less susceptible to creep.

Assessment that the use of fine grained soils will not result in unacceptable time-dependent movement requires proper understanding of the conditions leading to wetting of the fill, the associated loss in strength and increased deformability, and the influence of pore water pressures on the internal and external loads, connection stresses, and pullout resistance.

A very good review of all of the design methods previously mentioned in this paper, as well as a wall suppliers design approach, with respect to the calculation of the loads in the reinforcement and the resistance provided by the reinforcement is included in Berg, et al., 1998.

An example is used to compare the conservatism in each approach. A somewhat unique method was used to evaluate conservatism, comparing the resistance (R) to load (L) ratio developed from each design method, which clearly shows the range of conservatism for each of the design methods as shown in Figure 3. Based on this review, the transportation specific AASHTO and FHWA procedures were shown to be more conservative (about 30% more reinforcement required) than non-transportation specific procedures such as NCMA.

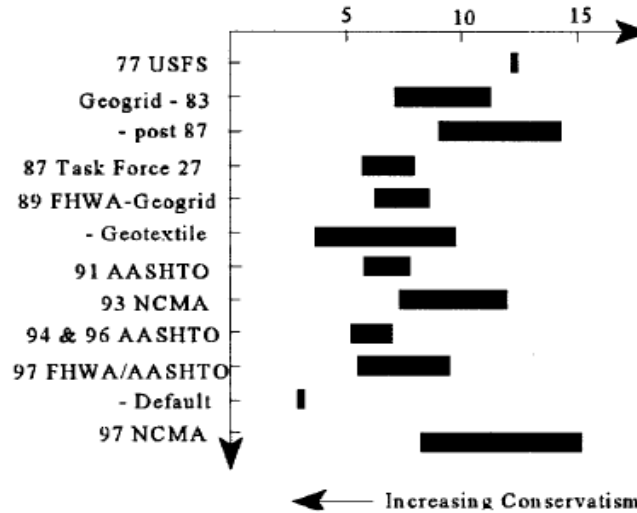


Figure 3. Resistance – Load Ratio Trends and Ranges (from Berg et al., 1998)

Another very thorough comparative review of several of the design approaches, including design details, factors of safety and reduction factors, can be found in Koerner and Soong (2000). Their evaluation includes: 1) a modified Rankine approach as illustrated by Koerner and Soong (1999), which is similar to the previously mentioned Forest Service method; 2) the FHWA 1998 approach; and the NCMA 1997 approach. In addition to the internal design for reinforcement load, they also evaluated pullout and facing connection requirements, as well as external stability design (e.g., stability against sliding, bearing capacity and overturning). Again a design example was used for direct comparison and it again clearly showed that the FHWA method was more conservative than the NCMA method for both internal and external stability, while the Modified Rankine method was about the same for tensile strength and slightly more conservative for pullout requirements than the FHWA method. They also noted that the public agencies have traditionally been more conservative than the private sector.

Reinforced soil slope design is covered in the above referenced FHWA guidelines document, as well as in the updated FHWA Geosynthetics Design and Construction Guidelines Manual (Holtz et al., 1998). A computer program, RSS, was developed by FHWA for the design and analysis of reinforced slopes following the design procedures in the reference manual (Geocomp Corporation, 1996). The FHWA manual was incorporated as the help screens within the program. These guidelines were often cited for both public and private sector work. Private sector also relied on geosynthetic manufacturers' design methods, as well as on several text books (e.g., Koerner, 1994 and Holtz et al., 1997) and commercially available software. Virtually all of the RSS design methods were based on limit equilibrium theories (e.g., slope stability approach extended to reinforced soil).

It should be noted that there were other proprietary design methods for both walls and slopes promoted during this same period, but they were not usually validated by instrumented structures, and, in some cases, were somewhat theoretically deficient. Also during this decade, there was a proliferation of wall suppliers. Remember that modular block facings (also known as segmental retaining wall units) were first used in 1985. By 1995 there were at least 10 modular block wall systems, and by the end of the 90's there were at least 10 additional systems. The number of geosynthetic walls constructed by the end of the 1990s was on the order of 25,000 in the US and 35,000 worldwide (Koerner et al., 2001). With this number of walls there were bound to be a few unsuccessful structures. Unfortunately there were more than a few, as discussed later in this section.

Before we review failures, there were a number of well documented successes, again many of which are contained in the proceedings of conferences that were held during the 90s (e.g. the 5th and 6th International Conferences on Geosynthetics, the North American Geosynthetics conferences held biannually during the 1990s and the GSI annual conferences (like GRI-25). Although all of these case histories are important in qualitatively documenting performance, several North American case histories were fully instrumented and noteworthy, as the results quantitatively verify performance and the design procedures. One of these projects is a 15.2 m high, 1H:1V geosynthetic reinforced soil slope (Salmon Lost Trail Pass) shown in Figure 4, which at the time was one of the tallest reinforced soil slopes and one of the few that had been instrumented (Zornberg et al., 1995). The structure was constructed as an FHWA experimental features project and was instrumented with inclinometers within the reinforced zone, extensometers on the reinforcement, and piezometers within and at the back of the reinforced section, and survey monitoring. The results of the instrumentation were used to verify both the design method and a new RSS slope stability program developed by the FHWA for reinforced soil slopes called RSS. Centrifuge models of this slope with instrumented reinforcement were also constructed to evaluate both the working stress and at failure conditions (Zornberg, 1994). This study confirmed the validity of the limit equilibrium approach for predicting internal failure of reinforced soil slopes.

Another project is a 15 m high, instrumented reinforced soil slope for repair of a failed slope on Pennsylvania SR54, which was reconstructed using wet, nearly saturated sandy clay type soils, the spoil from the previously failed slope (Wayne and Wilcosky, 1995). Instrumentation included deformation response of the needle punched nonwoven geotextile reinforcement and pore water pressure dissipation within the reinforced fill during construction. The pore pressure measurements confirmed that consolidation of the slope would be completed by the end of construction due to the pore water pressure dissipation provided by the in-plane drainage characteristics (i.e., transmissivity) of the geotextile.

A third, equally relevant reinforced soil structure is the 6 m high Test Wall built by the Louisiana Transportation Research Center (LTRC) (Figure 5). The test wall was constructed to evaluate the design procedure and performance of geosynthetic-reinforced structures constructed with silty-clay backfill on a soft clay foundation. The instrumentation program involved monitoring wall deformations, foundation settlements, reinforcement strains, vertical and horizontal soil stresses near the wall facing, and pore water pressures under the wall (Farrag and Morvant, 2001). The instrumentation results from the LTRC walls were also used in another

numerical modeling study to evaluate walls with poor draining backfill on soft soil (Saidin, 2007). The results of the study showed that numerical simulations (using FLAC) could predict very well the performance of geosynthetic reinforced soil walls with complex conditions including fine grained reinforced fill and foundation soils, significant settlement (over 0.2 m), and compaction and infiltration effect. The results emphasized the importance of adequate drainage under these conditions.



Figure 4. Salmon Lost Trail Pass instrumented reinforced soil slope on Hwy 93, designed by the Western Federal Lands Highway Division (FHWA) using decomposed granite soils.



Figure 5. Louisiana Transportation Research Center (LTRC) Test Wall Built with Silty-Clay Reinforced Fill over Soft Soil

There was also a significant amount of research conducted in the 1990s to improve the understanding of reinforced soil and to more thoroughly evaluate issues such as the conservatism in design, composite behavior and deformation response. The excellent performance of the Rainier Avenue wall described in the previous section led to some experimental and analytical research at the University of Washington. A plane strain in-soil test apparatus, the Unit Cell Device (UCD), was developed by PhD student S. R. Boyle to directly measure strains in the reinforcement and thus provide the soil-geosynthetic interaction moduli necessary for accurate numerical modeling of GRS. Two examples from Boyle (1995) and Boyle et al. (1996) are shown in Figures 6 and 7. Figure 6 shows some in-soil stress-strain results from UCD tests conducted at a confining pressure of 10 kPa on specimens of the Rainier Avenue sand alone and reinforced with different geotextiles. Because no other in-soil stress-strain results were available to compare with these data, Boyle (1995) also conducted a UCD test with a sheet of stainless steel as reinforcement. Its yield stress was 0.23 percent and its modulus was very close to 200 GPa. These values gave confidence that at least the measured in-soil stress-strain behavior was in the right order and approximately correct.

The results shown in Figure 7 have important implications for design. Boyle (1995) conducted a relaxation test on a specimen of the Rainier Avenue sand reinforced with a 2-layer stitch bonded polypropylene slit-film geotextile. After loading to about 4 percent strain, the load was held constant while continuing to measure the tension in the geotextile. As shown in Figure 7, strain continued, as would be expected, but most interestingly, the tension reduced (relaxation) and then all movement ceased. The specimen and reinforcement were at equilibrium under the applied stresses and no additional strains occurred as long as no additional load was applied. The same thing must happen in the field at working stresses that are well below the failure

stresses. This suggests that creep of the geotextiles in full-scale structures is not a problem because of stress relaxation. Similar results have also been shown by field measurements of real GRS walls, e.g., the Rainier Avenue Wall and a steep slope reinforced with geogrids constructed in Norway (Fannin and Herman, 1990; Fannin, 1994; and Fannin, 2001). One wonders, are the recommended default creep reduction factors really justified?

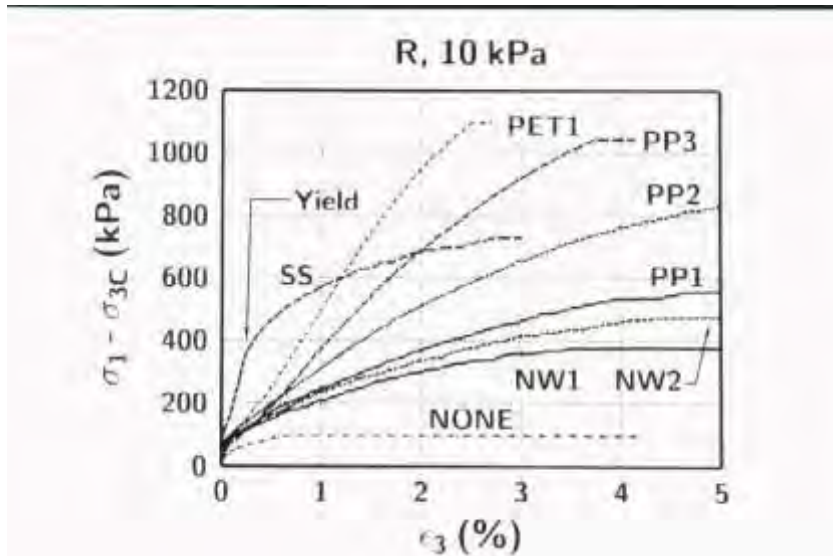


Figure 6. UCD stress-strain results on the Rainier Avenue sand at a confining pressure of 10 kPa; sand alone (NONE), two nonwoven geotextiles (NW1 and NW2), four woven geotextiles (PP1, PP2, PP3, and PET1), and stainless steel sheet (SS) (Boyle, 1995).

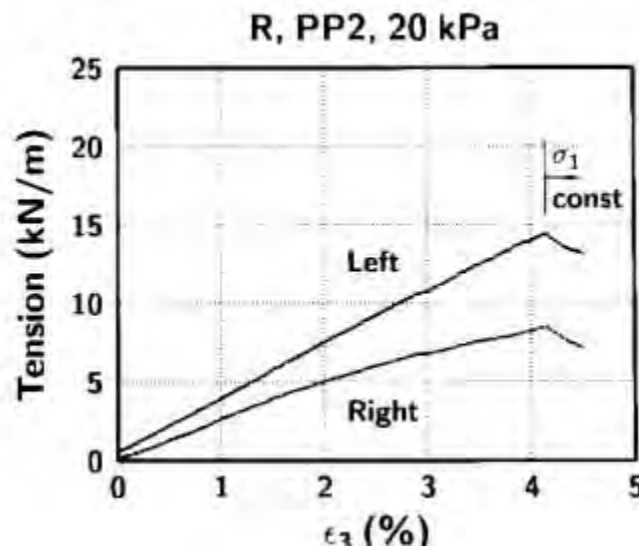


Figure 7. Results of a UCD test conducted on a specimen of Rainier Avenue sand at 20 kPa reinforced with one of the Rainier Avenue reinforcing geotextiles, a two-layer stitch bonded woven polypropylene slit-film.

A number of papers on this research are contained in the conferences previously mentioned. In addition, there were several international symposiums on this topic, including a specialty symposium in Denver, Colorado, 1991 (Wu, 1992a) and a series of conferences held annually in Kyushu starting in 1991. One of the major research undertakings during this period was the construction of full scale walls in a highly controlled laboratory environment. One such wall was constructed for the Denver, Colorado international symposium, which was fully instrumented and loaded to failure, with prediction of the failure load provided by many of the conference attendees (Wu, 1992b).

The most significant test wall program was established at the Royal Military College of Canada in the late 80s. A specially constructed 3.6 m high by 3.3 m wide by 6 m deep instrumented retaining wall test facility at the Royal Military College has been used to construct a number of full-scale walls and slopes. In the 1990s, 17 geosynthetic reinforced soil walls, two reinforced and two unreinforced soil slopes had been constructed and taken to collapse under staged surcharge loading. The results have been used to examine the accuracy of current methods of design and analysis of reinforced walls and slopes. The data has also proved useful to calibrate analytical and numerical models (Bathurst et al., 2000 and 2001; Lee et al., 1999; Lee, 2000; and Holtz and Lee, 2001). The Lee work is interesting because he first calibrated his constitutive models with field and laboratory data from the Rainier Avenue wall. He then was able to make true "Class A" predictions of wall face deflections and reinforcement strains for three RMC test walls with excellent agreement. An additional benefit of the RMC work and the Lee (2000) study was the development of the K-Stiffness method, described later.

While reinforced soil wall design is conservative, as indicated by practically all of the research, it is only conservative in relation to internal strength requirements for the reinforcement. By the end of the decade, it was apparent that the overall reinforced soil wall design with geosynthetics was much less conservative than assumed by most engineers. In a study by Soong and Koerner (1999), 26 failures were identified from the literature. However, as noted in their study, many failures go unreported. In a paper by Christopher and Stulgis (1999), based on information from engineers around the country, they indicated that the unreported failure rate could easily be on an order of magnitude greater than the reported number. A significant majority of which were in the private sector. It should be noted that many of the noted problem projects are excessive movement problems (i.e., serviceability failures). Also, most of the reported failures and most of the unreported failures that the authors are aware of typically used high fines soil for the reinforced fill and they occurred immediately following (or soon after) extensive water events (i.e., rainfall, snowmelt or flooding). Even so, 1 in 130 (i.e., 1 in 35000/260) is still well above the typical failure rates for non critical civil engineering structures (e.g., on the order of 1 in 1000 as indicated by Whitman, 1984).

This issue was getting the attention of owners. Several agencies (state and local – e.g. Dekalb County, Georgia) placed moratoriums on constructing geosynthetic reinforced soil walls and some established height restrictions (e.g., no greater than 3 m, Missouri DOT). As a result, the subject also gained interest from wall suppliers, design engineers and of course researchers, and will be discussed in the next section.

THE 2000s

In the 2000s, there were three major efforts related to design activities, including efforts to improve the current design methods, to resolve the issues with using fine grained soil, and to reduce the number of wall problems. One of those activities was to develop sufficient calibration to reduce the inherent conservatism in the FHWA/AASHTO design model. This effort was initiated through the development of resistance factors for the Load and Resistance Factor Design (i.e., limit state design) in the AASHTO 2002 interim LRFD design specifications. Although the resistance factors in the LRFD approach were backcalculated from the existing design method, that effort quantified the conservatism and uncertainty in the current design methods through an extensive review of instrumented structures (see Allen et al., 2001). There was significant resistance to the LRFD approach in the private sector, but, by end of the decade, AASHTO no longer supported the allowable stress design in the AASHTO 2002 Specifications and were on their 4th edition of the LRFD specifications (AASHTO 2007 with 2008 and 2009 interims) and the design methods in the FHWA MSE wall design guidelines had been converted to LRFD (Berg et al., 2009).

In recognition of issues resulting in poor performance of structures, the new FHWA manual also incorporated significantly more information on design details and included a series of checklists for design and various aspects of construction including drawing review, specification compliance, and construction. Another significant change was the position on drainage requirements. The FHWA manual previously indicated that the design engineer should evaluate the project conditions and determine if drainage is required. In recognition of the consequences in not following good drainage practices, **the new position recommends that adequate drainage features be required for all walls unless the engineer determines that such features are not needed for a specific project.** Along with these additions to the design manual a new course was also added to the National Highway Institute training program on inspection of reinforced soil structures.

NCMA was equally proactive, especially with respect to drainage requirements for walls; publishing a complementary Segmental Retaining Wall Drainage Manual (Collin et al. 2002). The current, 3rd edition of the NCMA Design Manual for Segmental Retaining Walls was published in 2009, and incorporates materials from the 1998 seismic and 2002 drainage manuals, and refers to the drainage manual for good drainage practice.

Three new design methods were also proposed. Based on the information from an extensive review on performance of existing structures (Allen et al., 2002; Allen and Bathurst, 2002), a newly developed lateral earth pressure method called the K_o Stiffness Method (Allen et al., 2003 and 2004) was developed and is currently being calibrated by instrumenting structures designed using that approach. An extensive treatise on MSE walls was published in the 2002 *Geosynthetics International* journal special issue on Geosynthetic-Reinforced Soil Wall Performance and Design Implications, and highlights work by Bathurst and Allen.

The second new design approach was to use an empirically derived composite model for geosynthetic reinforced soil walls integrated with bridge system (GRS-IBS). The geosynthetic reinforced soil system in this case consists of closely spaced layers of geosynthetic reinforcement and very select compacted granular fill material. IBS is a fast, cost-effective method of bridge support that blends the roadway into the superstructure. GRS-IBS includes a reinforced soil foundation, a GRS abutment, and a GRS integrated approach. This method has significant value when employed for small, single-span structures meeting the criteria described in an NCHRP Report No. 556 on its development (Wu et al, 2006).

The third method was to use the limit equilibrium analysis conventionally used for slopes to design walls (Leshchinsky et al., 2004 and Leshchinsky and Han, 2007). This method determines the distribution of required tensile resistance along each reinforcement layer such that the factor of safety on the strength of the soil is uniform everywhere within the reinforced soil mass. By optimizing the reinforcement resistance, the method reduces the reinforcing requirements and the inherent conservatism in the lateral earth pressure approach.

The 2000s also saw the movement of numerical modeling from research to practitioners, with the development of less computationally intensive, simplified programs with canned inputs for reinforcement interaction and facing elements. The ability to evaluate failure in newer models allows the methods to be used to confirm limit equilibrium solutions, in addition to providing an indication of deformation response for different conditions (e.g., see Figure 8). The down side is that they still require good characterization of all elements composing the problem and accurate modeling of the problem or else it may lead to nonconservative results, and, unlike the other empirical design methods, there is no inherent conservatism.

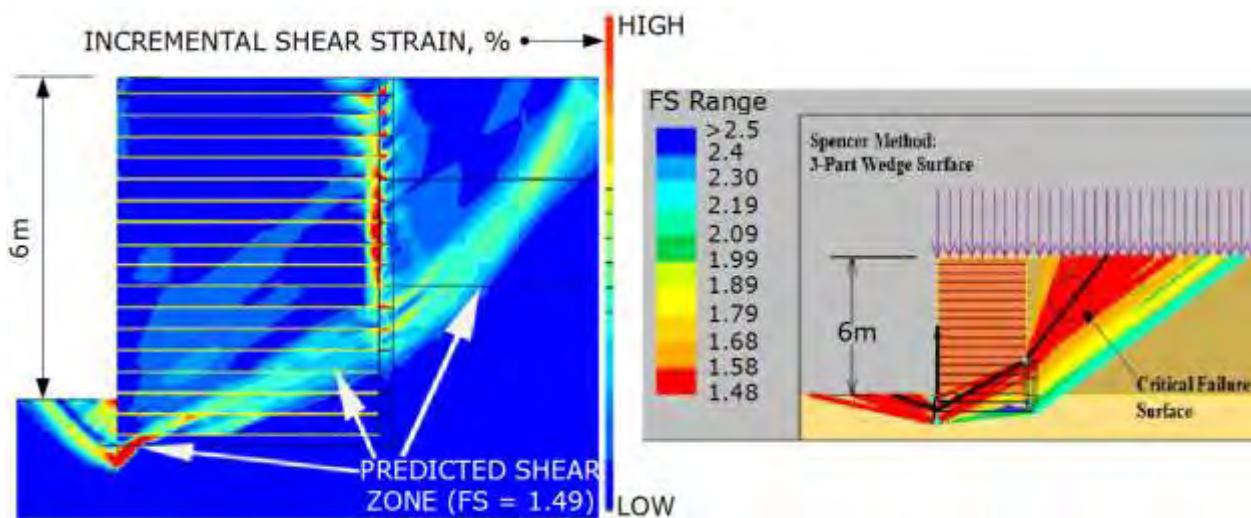


Figure 8. Comparison of a) predicted in-service shear strains and failure surface using a Finite Element Method (PLAXIS) and b) Critical failure surface obtained from a limit equilibrium solution of the same problem using ReSSA (from Christopher et al., 2005).

Another significant development this decade was the calibration of the existing earth pressure models and correspondingly the establishment of safeguards in construction to expand the use of marginal soils. Even though there were reported problems in using fine grained soils, there was also a significant rise in the cost of select granular materials. In fact, in some states MSE walls and thus also geosynthetic reinforced soil systems no longer had a cost advantage over other wall systems (e.g., concrete cantilever walls). In order to relax the more rigorous AASHTO and FHWA reinforced fill requirements, a significant public sector research project was initiated, NCHRP Project No. 24-22 "Selecting Backfill Materials for MSE Retaining Walls", with private sector (NCMA) participation, to evaluate marginal soils in reinforced soil walls.

The focus of the NCHRP 24-22 project was to develop material selection guidelines, soil parameters, testing methods, and construction specifications that would allow the use of more fine-grained backfill materials within the reinforced zone of mechanically stabilized earth (MSE) retaining walls. Figure 9 presents the layout and pertinent details of the NCHRP full-scale test walls.

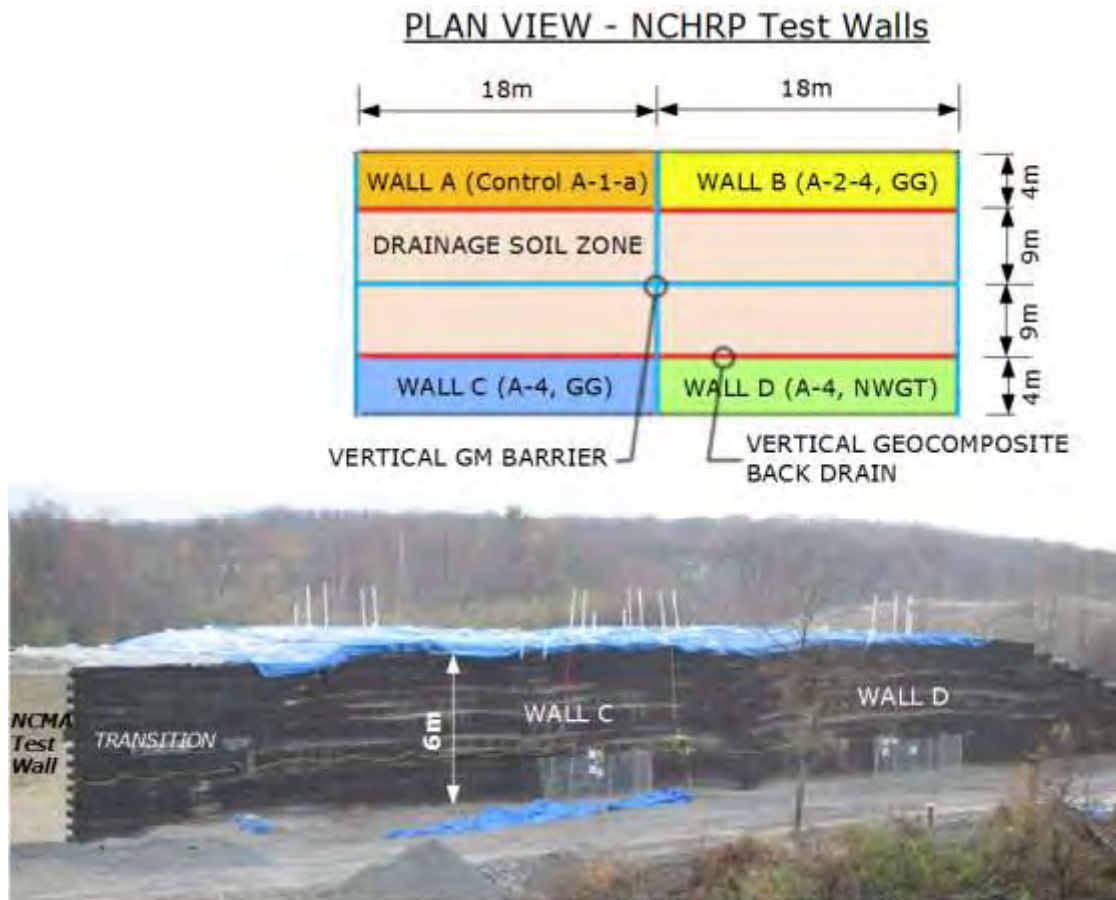


Figure 9. Full-Scale Field Test (NCHRP 24-22)

The test walls rigorously evaluated the seepage issue associated with the use of “high fines” reinforced fill. Several hydrotests were conducted over a 2-year period during which water was pumped into the drainage soil zone of each of the test walls. The test walls were fully instrumented. Most instruments were electronic and connected to automatic data logging equipment that provided data 24/7 over the two year test program.

The research clearly demonstrated that MSE structures with higher fines soils in the reinforced fill than currently allowed by AASHTO will provide excellent performance. This work demonstrates that the current AASHTO limit on maximum fines content can be increased (for walls reinforced with geosynthetic materials) from 15% to 25% subject to the following considerations:

- Soils with less than 25% fines and a Plasticity Index not greater than 6% are used.
- All potential sources of pore pressure build-up in the reinforcing zone should be addressed by the design.
- Good practices are used to control the quality of material selection and placement, as the performance of higher fines soils is more susceptible to as-placed density and moisture content than free draining materials.

As in previous decades, there were a number of published case histories in conferences and journals. Two case histories stand out as the most significant of this era. The first project is the Founders Meadows Bridge project in Colorado (Abu-Hejleh, 2000). In July of 1999, the Colorado Department of Transportation (CDOT) successfully completed the construction of the new Founders/Meadows Bridge near Denver, which is a two-span bridge over an Interstate highway supported by geosynthetic-reinforced segmental, modular block retaining walls. The reinforced soil system was designed using geogrid reinforcement to provide bridge support and to support the roadway approach embankment, which would also alleviate the common bridge approach bump problem. A comprehensive material testing and instrumentation program was conducted due to the experimental nature of this wall. Three sections were instrumented to provide information on external movements, internal soil stresses, temperatures, moisture content, and geogrid strains during various construction stages and after the structure opening to traffic. The instrumentation results to date indicate the overall performance of this structure has been satisfactory and that the design was conservative, partly attributed to the use of conservative soil strength values.

The second project is the 74 m high, 1V:1H geosynthetic reinforced soil structure constructed to extend the runway at Yeager Airport in Charleston, WV as shown in Figure 10. This is currently the tallest reinforced soil slope in North America and maybe the world. Due to the mountainous conditions, the ground surface around the airport slopes down steeply over 91 m to the surrounding Elk and Kanawha Rivers, roadways, churches, houses and other structures. In order to meet recent FAA Safety Standards, upgrades to the airport runways required extending Runway 5 approximately 150 m to create an emergency stopping apron for airplanes. Engineering evaluation indicated the reinforced slope provided the most cost effective and easiest constructed option. It has a vegetated facing that blends into the surrounding green hills of Charleston, WV. Unfortunately the structure was not instrumented, but clearly demonstrates the potential of using geosynthetic soil reinforcement to build green structures for the future.



Figure 10. 242 ft (74 m) High 1H:1V Reinforced Soil Slope for Airport Runway Extension (Lostumbo, 2009)

2010 - 2013

Well, this decade is just getting started, but there have already been some significant activities, which will clearly impact the future of geosynthetic reinforcement technology. As a result of the demonstrated performance of GRS-IBS, the technology was selected for the FHWA's Every Day Counts initiative, aimed at accelerating implementation of proven, market-ready technologies. A design manual, FHWA-HRT-11-026 (Adams et al., 2011) was developed for the implementation of the technology, which outlines design approach and construction requirements of GRS-IBS. A second document provides a synthesis report to substantiate the design method.

Over 100 bridge structures have been designed today, and a majority have been constructed, several of which have been instrumented. A comprehensive data base is being maintained. More information on the utilization of this technology can be obtained from http://www.fhwa.dot.gov/everydaycounts/technology/grs_ibs/ and an FHWA design guidance document is available at:

<http://www.fhwa.dot.gov/publications/research/infrastructure/structures/11027/index.cfm>.

A second program that was generated over the past several years is Geotech Tools, a large toolbox for the engineering and construction of earthworks and ground improvement. This was developed under the second Strategic Highway Research Program (SHRP 2) *Project R02 Geotechnical Solutions for Soil Improvement, Rapid Embankment Construction, and Stabilization of the Pavement Working Platform* by a team of university researchers from Iowa State University, Virginia Tech, and the University of Kansas and nationally recognized ground improvement consultants. It is a readily accessible web-based system that contains a catalog

with detailed information on 46 geoconstruction and ground improvement techniques, including geosynthetic reinforced soil walls and slopes as well as support technologies for soft ground support. Users will find that the value of the system is that it has collected, synthesized, integrated, and organized a vast amount of critically important information on these geotechnologies. Eight engineering tools are available for each geotechnology and include guidance for design, QC/QA methods, specifications, and cost estimating. This system can be accessed at www.GeoTechTools.org and is free to use.

Recently, AASHTO T-15 Committee, in cooperation with FHWA, formed a task force to assist in future decision making for the AASHTO LRFD specification articles related to MSE wall design. The primary purpose was to develop a strategy for addressing recognized gaps in the design specifications with regard to MSE walls and incorporating key aspects of a significant amount of research that has been developed and published in the last 5 to 10 years. This task force will provide an opportunity for leaders in the development of reinforced soil design, specifically as applied to walls, to work toward consensus on key MSE wall design issues and how they should be handled. It is envisioned that the findings and recommendations of this Task Force will help chart the future direction of the design practice in North America.

Unfortunately the ugly part of the practice continued to emerge, with the 2012 count at 141 documented cases of MSE wall failures resulting in either excessive deformation or actual collapse (Koerner and Koerner, 2012). As with previous assessments of the primary causes, inadequate or improper design and/or construction were the apparent issues. Again, the major design inadequacy appears to be the lack of proper drainage procedures and the placement of water bearing utilities (i.e., “plumbing”) within the reinforced soil zone. Based on the findings, the authors recommend shifting the utilities out of the reinforced soil zone, which is also the recommendation in the FHWA MSEW/RSS manual (Berg et al., 2009). Again, a preponderance of the failures were found to be the result of *major construction inadequacy* in the use of fine grained silty and clayey backfill soils and furthermore their inadequate placement and compaction. One other final point that was noted from the data base is that 140 of the 141 cases were in the private sector.

Other factors that often result in poor performance include inadequate global or external stability, unexpected surcharges, lack of proper inspection, poor training for workers, and little or no control of the construction by the designer. “Value engineered” or “contractor supplied” designs, with no budget for checking alternates by competent professionals can also result in poor performance. In some jurisdictions (e.g., Seattle, Washington) require GRS “wall” designs to be stamped by a registered structural engineer. Although well qualified in structural engineering practice, they may have limited experience with and knowledge of soil reinforcement principles and practices, geosynthetic reinforcements, and/or drainage issues and detailing. Furthermore, they are often not retained for construction inspection.

Large developments involving reinforced structures are a potential source of difficulties and occasional failures. There often is a disconnect between the GRS wall designer, the geotechnical engineer of record, and the site civil engineer. The lines of responsibility are often unclear and the contractual relationships fuzzy as to who is responsible for what and when. This relationship is further complicated by wall designs supplied by materials suppliers and

distributors who are not responsible for the soils, drainage, or construction. Note that in recognition of these responsibility issues, the current NCMA Design Manual for Segmental Retaining Walls (2009) now contains specific chapters on: roles and responsibilities on projects involving SRWs; design guidelines for site civil engineers; and design guidelines for project geotechnical engineer. Also note that detailed discussions on procuring, designing and constructing MSE walls to minimize problems and ensure long service life were published in a 2007-2008 series of articles in *Geosynthetics* magazine by Simac and Fitpatrick.

Clearly, fixing problems is always more expensive than proper inspection and control by the designer, but practitioners are often not adept at convincing clients of this fact. It has been estimated that the cost of fixing a failure is about ten times greater than the cost of the original design and construction! The high cost of all the ugliness mentioned above is unnecessary, costly, and potentially tragic.

IN RETROSPECT

Figure 11 provides a timeline of many of the more notable activities over the past 25 years, which have had a significant impact on the implementation and maintenance of this technology. Although there was much success over the last 25 yrs in implementing this technology, we can and should learn from the past. The following provides the retrospect of the past 25 years from the authors' perspective. We hope others can also glean additional insights from this brief history of geosynthetic reinforced soil walls and slopes. From this historical perspective, we have concluded:

1. The historical review of these activities and developments shows how far we have come in the implementation and maintenance of reinforced soil technology. Best practices were identified during this period that have led to significant success and design improvement in using geosynthetic reinforcement. A number of issues were identified that have resulted in poor performance and even failures, which could be significantly reduced by the broader application of those best practices.
2. The design methodology currently used in the design of reinforced soil structures (walls and slopes) results in structures with conservative reinforcement against internal failure.
3. MSE walls on transportation projects are generally conservatively designed using granular soils, i.e. with "low fines" soil in the reinforced zone. Private MSE walls are less conservatively designed, and use a variety of reinforced soils. The majority of walls that have performed poorly, due either to collapse or excessive deformation of the walls, are in the private sector and consisted of reinforced fill comprised of silty sand and clayey soils, with pore water pressure in these reinforced fill materials contributing to the excessive deformation or collapse of the walls.
4. Drainage - Drainage - Drainage: All designers should follow the recommendations in the FHWA design manual: All walls should include good drainage unless the engineer can prove that it is not required.

5. All designers should follow the advice of Koerner and Koerner, 2012 and the recommendations in the FHWA design manual: Keep the utilities out of the reinforced fill.
6. We should have maintained a taskforce of experts from both the private and public sector (like the AASHTO Task Force 27, the NATO group of experts, and the newly formed AASHTO T15 Taskforce) as a permanent standing body to provide a forum for review, evaluation and implementation of new design methods and provide better consistence between public and private practice.
7. The key to the future use of geosynthetics in reinforced soil lies in improved communication. Communication can best be achieved through education, and not only by academic institutions. Education is a challenge to the entire industry. Once everyone involved with MSE wall design and construction understands the issues associated with the proper use of this technology, we will indeed reach new heights in terms of the advancement and application of this technology.

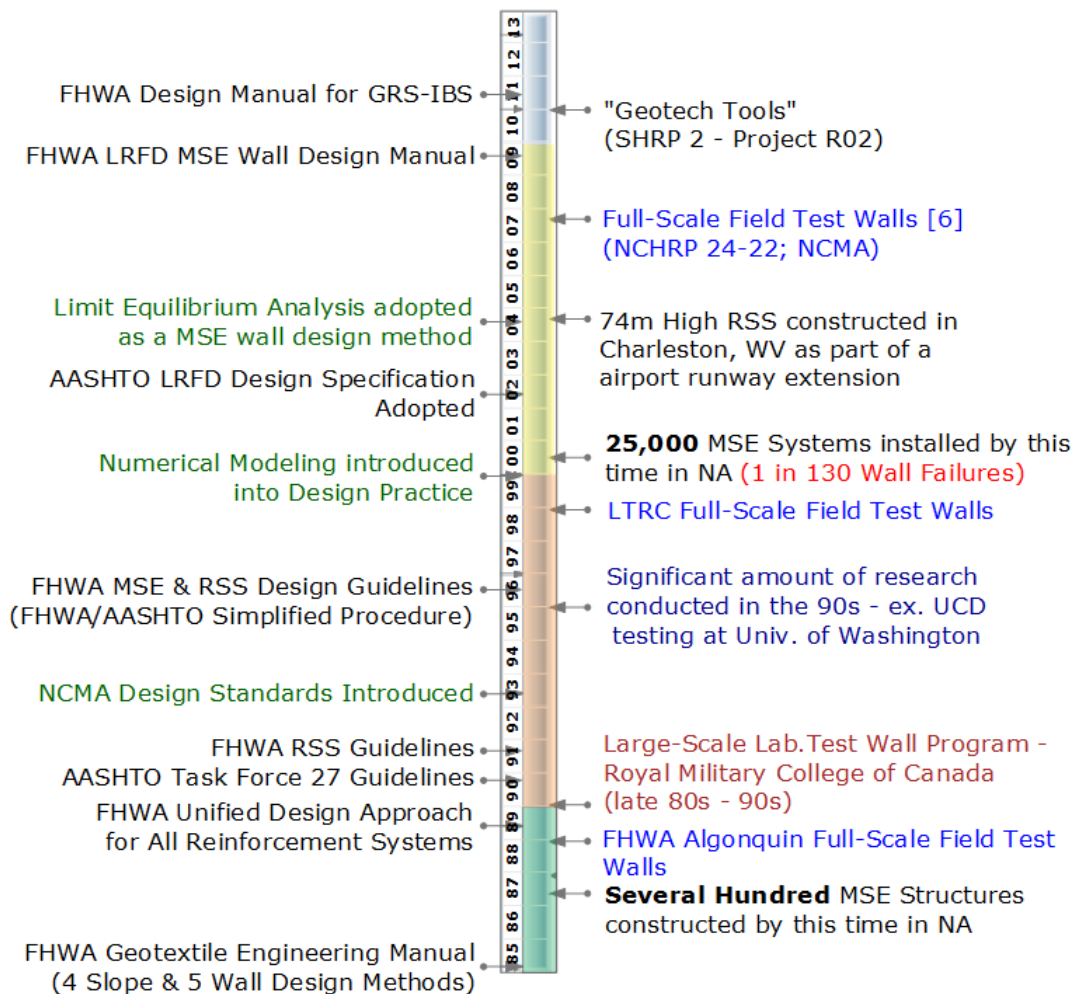


Figure 11. Timeline in the Development, Implementation and Maintenance of MSE Walls and Reinforced Soil Slopes

REFERENCES

AASHTO (1991) Standard Specifications for Highway Bridges, Fourteenth Edition, 1989 with 1990 and 1991 Interims and Commentary, American Association of State Highway and Transportation Officials, Washington, DC, USA.

AASHTO (1994) Standard Specifications for Highway Bridges, Fifteenth Edition, 1992 with 1993 and 1994 Interims and Commentary, American Association of State Highway and Transportation Officials, Washington, DC, USA.

AASHTO (1997) Standard Specifications for Highway Bridges, Sixteenth Edition, American Association of State Highway and Transportation Officials, Washington, DC, USA.

American Association of State Highway and Transportation Officials (AASHTO). 2002. *LRFD Bridge Design Specifications*, 2nd Edition, American Association of State Highway and Transportation Officials, Washington, D.C.

American Association of State Highway and Transportation Officials (AASHTO). 1999. *Interim Standard Specifications for Highway Bridges*, American Association of State Highway and Transportation Officials, Washington, D.C.

AASHTO, (2002). *Standard Specifications for Highway Bridges*, 17th Edition, American Association of State Highway and Transportation Officials, Washington, D.C.

AASHTO, (2007). *AASHTO LRFD Bridge Design Specifications*, 4th Edition, American Association of State Highway and Transportation Officials, Washington, D.C.

AASHTO (2010). *LRFD Bridge Design Specifications*, 5th Edition, American Association of State Highway and Transportation Officials, Washington, D.C.

AASHTO-AGC-ARTBA (1990) Task Force 27 Report: In Situ Soil Improvement Techniques, American Association of State Highway and Transportation Officials, Washington, DC, USA, 324p.

Abu-Hejleh, N., Outcalt, W.S., Wang, T. and Zornberg, J.G. (2000), Performance Of Geosynthetic-Reinforced Walls Supporting the Founders/Meadows Bridge and Approaching Roadway Structures Report 1: Design, Materials, Construction, Instrumentation and Preliminary Results, Colorado Department of Transportation, Report Number CDOT-DTD-R-2000-5.

Adams, M., Nicks, J., Stabile, T., Wu, J., Schlatter, W., and Hartmann, J. (2011) Geosynthetic Reinforced Soil Integrated Bridge System, Interim Implementation Guide, U.S. Department of Transportation, Federal Highway Administration, McLean, VA, Report Number FHWA-HRT-11-026, 169 p.

Allen, T.M., Christopher, B.R. and Holtz, R.D. (1991) "Performance of a 12.6 m High Geotextile Wall in Seattle, Washington", Geosynthetic-Reinforced Soil Retaining Walls, Wu, J.T.H., Editor,

Proceedings of the International Symposium on Geosynthetic-Reinforced Soil Retaining Walls, Denver, CO, pp. 81-99.

Allen, T.M., Christopher, B.R., Elias, V.E. and DiMaggio, J. (2001) Development of the Simplified Method for Internal Stability Design of Mechanically Stabilized Earth (MSE) Walls, Washington State Department of Transportation Research Report WA-RD 513.1, 2001, 108 pp.

Allen, T.M. and Bathurst, R.J., “Soil Reinforcement Loads in Geosynthetic Reinforced Walls at Working Stress Conditions”, Geosynthetics International, Vol. 9, Nos. 5-6, pp. 525-566 (2002).

Allen, T.M., Bathurst, R.J. and Berg, R.R., “Global Level of Safety and Performance of Geosynthetic Walls: An Historical Perspective”, Geosynthetics International, Vol. 9, Nos. 5-6, pp. 395-450 (2002).

Allen, T. M., Bathurst, R. J., Holtz, R. D., Walters, D., and Lee, W. F. (2003) “A New Working Stress Method for Prediction of Reinforcement Loads in Geosynthetic Walls”, *Canadian Geotechnical Journal*, Vol. 40, No. 5, pp. 976-994

Allen, T. M., Bathurst, R. J., Holtz, R. D., Lee, W. F., and Walters, D. (2004) “A New Working Stress Method for Prediction of Reinforcement Loads in Steel Reinforced MSE Walls”, *Journal of Geotechnical and Geoenvironmental Engineering*, ASCE, Vol. 130, No. 11, pp 1109-1120.

Bathurst R.J. (1998). NCMA Bathurst, R. J. (1998). NCMA Segmental Retaining Wall Seismic Design Procedure—Supplement to Design Manual for Segmental Retaining Walls, 2nd Ed., National Concrete Masonry Association, Herndon, Va.

Bathurst, R.J. and Walters, D.L. (2000), Lessons learned from full scale testing of geosynthetic reinforced soil retaining walls, GeoEng2000, Melbourne, Australia, November 2000, 14 p.

Bathurst, R.J., Walters, D., Vlachopoulos, N., Burgess, P. and Allen, T.M., “Full Scale Testing of Geosynthetic Reinforced Walls”, Invited keynote paper, *Proceedings of Geo-Denver 2000*, American Society of Civil Engineers, Edited by J.G. Zornberg and B.R. Christopher, ASCE Special Publication No. 103, Advances in Transportation and Geoenvironmental Systems using Geosynthetics, pp. 201-217 (2000).

Bathurst, R.J., Walters, D.L., Hatami, K. and Allen, T.M. (2001). “Full-scale performance testing and numerical modelling of reinforced soil retaining walls,” Special plenary lecture: International Symposium on Earth Reinforcement, IS Kyushu 2001, Fukuoka, Japan, 14 November 2001, 26 p.

Bell et al., 1984, Proceedings of the Conference on Polymer Grid Reinforcement, Institution of Civil Engineers, London, 1984.

Berg, R.R. (1991) Interim Guidelines for Design, Specification, & Contracting of Geogrid Mechanically Stabilized Earth Slopes on Firm Foundations, U.S. Department of Transportation, Federal Highway Administration, Washington DC,

Berg, R.R., Bonaparte, R., Chouery, V.C., and Anderson, R.P. (1986) "Design, Construction, and Performance of Two Geogrid Reinforced Soil Retaining Walls," *Proceedings of the IIIrd International Conference on Geotextiles*, Vienna, Austria, pp. 401-406.

Berg R.R., La Rochelle, P., Bonaparte, R., and Tanguay, L., (1987) "Gaspe' Peninsula Reinforced Soil Seawall - Case History," *Proceedings of Soil Improvement - A Ten Year Update*, J.P. Welsh, Ed., Geotechnical Special Publication No. 12, American Society of Civil Engineers, pp. 309-328.

Berg, R.R., Allen, T.M. and Bell, J.R. (1998) "Design Procedures for Reinforced Soil Walls – A Historical Perspective," Proceedings of the Sixth International Conference on Geosynthetics, Atlanta, pp. 491-496.

Berg, R.R., Christopher, B.R. and Samtani, N. (2009) Mechanically Stabilized Earth Walls and Reinforced Soil Slopes, Design and Construction Guidelines, U.S. Department of Transportation, Federal Highway Administration, Washington DC, FHWA-NHI-09-083 and FHWA GEC011, 668 p.

Bonaparte, R., and Berg R.R., (1987). "Long-Term Allowable Design Loads for Geosynthetic Soil Reinforcement," Proceedings of the Geosynthetics '87 Conference, New Orleans, LA, pp. 181-192.

Bonaparte, R. and Margason, E., "Repair of Landslides in the San Francisco Bay Area," Proceedings of the Conference on Polymer Grid Reinforcement, Institution of Civil Engineers, London, 1984, pp. 64-68.

Boyle, S. R. (1995) *Deformation Prediction of Geosynthetic Reinforced Soil Retaining Walls*, PhD Dissertation, University of Washington, 392 pp.

Boyle, S. R., Holtz, R. D., and Gallagher, M. (1996) "Influence of Strain Rate, Specimen Length, and Confinement on Measured Geotextile Strength Properties", *Geosynthetics International*, Vol. 3, No. 2, pp. 205-225.

Busbridge (1984) Proceedings of the Conference on Polymer Grid Reinforcement, Institution of Civil Engineers, London, 1984.

Cheng, S. and Christopher, B.R. (1991) "A Probabilistic Review of Geotextile Reinforced Slope Design", Proceedings of Geosynthetics '91, Vol. 1, Atlanta, GA, USA, pp. 455-468.

Christopher, B.R. and Holtz, R.D. (1985) Geotextile Engineering Manual", U.S. Department of Transportation, Federal Highway Administration, Washington DC, Report No. FHWA-TS-86/203, March 1985, 1044 p.

Christopher, B.R. and Holtz, R.D. (1989) Geotextile Design and Construction Guidelines", U.S. Department of Transportation, Federal Highway Administration, Washington DC, Report No. HI-89-050, 265 p.

Christopher, B.R. and Leshchinsky, D., "Design of Geosynthetically Reinforced Slopes", Geotechnical Engineering Congress 1991, McLean, F., Campbell, D.A. and Harris, D.W., Editors, Vol 2 of the Proceedings of the Congress sponsored by the Geotechnical Engineering Division of ASCE, Boulder, Colorado, USA, Jun 1991, pp. 988-1005.

Christopher, B.R. (1993) "Deformation Response and Wall Stiffness in Relation to Reinforced Soil Wall Design", Ph.D. thesis, Purdue University, 352 p.

Christopher, B.R., Gill, S.A., Giroud, J.P., Juran, I. Scholsser, F., Mitchell, J.K. and Dunicliff, J., (1989) "Reinforced Soil Structures, Volume I. Design and Construction Guidelines", U.S. Department of Transportation, Federal Highway Administration, Washington DC, Report No. FHWA-RD--89-043, 287 p.

Christopher, B.R., Gill, S.A., Giroud, J.P., Juran, I. Scholsser, F., Mitchell, J.K. and Dunicliff, J. (1989) "Reinforced Soil Structures, Volume II. Summary of Research and Systems Information", U.S. Department of Transportation, Federal Highway Administration, Washington DC, Report No. FHWA-RD--89-043, 158 p.

Christopher, B.R., Holtz, R.D. and Allen, T.M. (1990) "Instrumentation for a 12.6 m High Geotextile-Reinforced Wall", Proceedings of the International Reinforced Soil Conference, McGown, A., Yeo, K. and Andrawes, K.Z., Editors, British Geotechnical Society, Glasgow, Scotland, pp 73-78.

Christopher, B.R. and Stulgis, R.P. (1999) "The Future of Geosynthetics: Mechanically Stabilized Earth (MSE) Walls", Geosynthetics in the Future: Year 2000 and Beyond, GRI Conference Series GRI-13, Koerner, R.M., Koerner, G.R., Hsuan, Y. and Marilyn V. Ashley, Editors, Geosynthetic Institute, Folsom, PA, pp.172 – 182.

Christopher, B.R., Leshchinsky, D and Stulgis, R. (2005). "Geosynthetic Reinforced Soil Walls and Slopes: U.S. Perspective," Proceedings of the Conference GeoFrontiers, Geotechnical Special Publication 141, International Perspectives on Soil Reinforcement Applications, ASCE, Austin, Texas.

Collin, J.G. (1986). "Earth Wall Design", Ph.D. Dissertation, University of California, Berkeley.

Collin, J.G., Berg, R.R. and Meyers, M.S. (2002). Segmental Retaining Wall Drainage Manual, National Concrete Masonry Association, Herndon, VA, 96p.

Elias, V. (1990) Durability/Corrosion of Soil Reinforced Structures, Report No. FHWA-RD-89-186, Office of Engineering and Highway Operations, R&D, McLean, VA, 173 p.

Elias, V. (1997) Corrosion/Degradation of Soil Reinforcements for Mechanically Stabilized Earth Walls and Reinforced Soil Slopes, FHWA Report No. FHWA-SA-96-072, NTIS, Springfield, VA. 105p.

Elias, V, and Christopher, B.R., (1996 released/ 1997 publication/ 1999 updated) Mechanically Stabilized Earth Walls and Reinforced Soil Slopes, Design and Construction Guidelines, U.S. Department of Transportation, Federal Highway Administration, Washington DC, Contract No. DTFH61-93-C-000145, 367 p.

Fannin R. J. and Herman, S. (1990) "Performance Data for a Sloped Reinforced Soil Wall," Canadian Geotechnical Journal, Vol. 27, No. 5, pp. 676-686.

Fannin, R. J. (1994) "Field Observations on the Load-Strain-Time Behaviour of Geogrid Reinforcement," Canadian Geotechnical Journal, Vol. 31. No. 4, pp. 564-569.

Fannin, R. J. (2001) "Long-Term Variations in Force and Strain in a Steep Geogrid-Reinforced Soil Slope," *Geosynthetics International*, Vol. 8, No. 1, pp. 81-96.

Farrag and Morvant, 2001

Forsyth and Bieber (1984) Proceedings of the Conference on Polymer Grid Reinforcement, Institution of Civil Engineers, London, 1984.

Geocomp Corporation, 1996, RSS - Reinforced Soil Slopes Version 2.

Holtz, R.D., Allen, T.M. and Christopher, B.R. (1991) "Displacement of a 12.6 m High Geotextile-Reinforced Wall", Deformation of Soils and Displacements of Structures XECSMFE, Associazione Geotecnica Italiana, Editor, Proceedings of the Tenth European Conference on Soil Mechanics and Foundation Engineering, Florence, Italy, pp. 725-728.

Holtz, R. D. and Lee, W-F. (2001) "Internal Stability Analysis of Geosynthetic Reinforced Retaining Walls", Final Research Report, Washington State Department of Transportation, Report No. WA-RD 532.1, 458 pp.

Holtz, R.D., Christopher, B.R. and Berg, R.R., Geosynthetic Design and Construction Guidelines, U.S. Department of Transportation, Federal Highway Administration, Washington DC, Report No. HI-95-038, 1995 (revised 1998), 396 p.

Holtz, R.D., Christopher, B.R. and Berg, R.R., Geosynthetic Engineering, BiTech Publishers Ltd., Richmond, British Columbia, Canada, 1997, 452 p.

Holtz, R.D., Christopher, B.R., and Berg, R.R. (2008) *Geosynthetic Design and Construction Guidelines*, Participant Notebook, NHI Course No. 13213, FHWA Publication No. FHWA HI-95-038 (revised), Federal Highway Administration, Washington, DC.

Jarrett, P.M. and McGown, A., Editors (1987) The Application of Polymeric Reinforcement in Soil Retaining Structures, NATO Advanced Study Institute Series, Kluwer Academic Publishers.

Koerner, R. M., (1994), Designing With Geosynthetics, 3rd Edition, Prentice Hall Publication Co., Englewood Cliffs, NJ, 761 pgs.

Koerner, R. M. and Soong, T.-Y. (1999), "Geosynthetic Reinforced Segmental Retaining Walls," 17th PennDOT/ASCE Conf. on Geotechnical Engineering, Hershey, PA, 1999, 36 pgs.; also Proc. GRI-14 Conference, GII Publ., December 2000, pp. 268-297; and Journal of Geotextiles and Geomembranes, Vol. 19, No. 6, August, 2001, pp. 359-386.

Koerner, R.M. and Soong, T.Y. (2000) "Design of Drainage Systems for Segmental Retaining Walls, Proceedings of the 17th ASCE/PennDOT Geotechnical Conference, Hershey, PA, Nov. 1-3, pp. 1-38.

Koerner, R. M., Koerner, J. and Soong, T.-Y. (2001), "Earth Retaining Wall Costs in the USA," Proc. Geosynthetics Conference 2001, Portland, OR, IFAI Publishers, 2001, pp. 483-508.

Koerner, G.R., Hsuan, Y.G. and Koerner, R. M. (2006), "Long Term Monitoring of Alkalinity at the Geogrid-Block Interface at a Full Scale Segmental Retaining Wall," Proceedings of the 8th International Conference on Geosynthetics 8 ICG-Yokohama Japan Millpress Rotterdam, ISBN 9059660447, pp. 1205-1208.

Koerner, R. M. and Koerner, G. R. (2012), "A Data Base and Analysis of 141 Failed Geosynthetic Reinforced Mechanically Stabilized Earth (MSE) Walls," Proceedings 26th PA Geotechnical Conference, October 25-26, Hersey, PA, 14 pgs.

Lambe, P.C. and Hansen, L.A., Editors (1990) Design and Performance of Earth Retaining Structures, Proceedings of a Conference Sponsored by the American Society of Civil Engineers, New York, NY, USA.

Lee, W.F. (2000) Internal Stability Analysis of Geosynthetic Reinforced Retaining Walls, Ph.D. thesis, University of Washington, Seattle, WA.

Lee, W. F., Holtz, R. D., and Allen, T. M (1999) "Full Scale Geosynthetic Reinforced Retaining Walls: A Numerical Parametric Study", *Proceedings of Geosynthetics '99*, Boston, Massachusetts, Industrial Fabrics Association International, Vol. 2, pp. 935-948.

Leshchinsky, D. and Han, J. (2007) "Analytical Framework for Geosynthetic Reinforced Earth Structures: Part I – Ideal Approach," GeoDenver 2007 Geosynthetics in Reinforcement and Hydraulic Applications, Denver, Colorado, Feb. 18-21, 2007, ASCE.

Leshchinsky, D., Hu, Y., and Han, J. (2004). "Limited reinforced space in segmental retaining wall," *Geotextiles and Geomembranes*, 22(6), 543–553.

Lostumbo, J.M. (2009). "Yeager Airport Runway Extension: Tallest Known 1H:1V Slope in U.S.," *Proceedings of Geosynthetics 2009*, Salt Lake City, Utah, pp. 593-598.

McGown, A., Yeo, K. and Andrawes, K.Z., Editors (1990) Performance of Reinforced Soil Structures, Proceedings of the International Reinforced Soil Conference, the British Geotechnical Society, Glasgow, Scotland, Thomas Telford, London, 484 p.

Mitchell, J. K., and Villet, W. C.B. (1987) Reinforcement of Earth Slopes and Embankments, NCHRP Report 290, Transportation Research Board, Washington, DC., 323 pp.

Raymond, G.P. and Giroud, J.P., Editors (1993) Geosynthetics Case Histories, International Society for Soil Mechanics and Foundation Engineers, Committee TC9 on Geotextiles and Geosynthetics, BiTech Publishers Ltd, Richmond, British Columbia, 277 p.

Saidin, F. (2007) "Behavior of Geosynthetic Reinforced Soil Walls with Poor Quality Backfills on Yielding Foundations," PhD Dissertation, University of Washington, Seattle, 320 pp.

Simac, M.R., Bathurst, R.J., Berg, R.R. and Lothspeich, S.E. (1993) NCMA Segmental Retaining Wall Design Manual (First Edition), National Concrete Masonry Association, 2302 Horse Pen Road, Herndon, VA 22071-3406

Soong, T. and Koerner, R.M. (1999), Geosynthetic Reinforced and Geocomposite Drained Retaining Walls Utilizing Low Permeability Backfill Soils, GRI Report #24, Geosynthetic Research Institute, Folsom, PA, 140 p.

Wayne and Wilcosky (1995). "An Innovative Use of a Nonwoven Geotextile in the Repair of Pennsylvania State Route 54", *Geotechnical Fabrics Report*, Volume 13, Number 2.

Whitman, R.V. (1984), "Evaluating Calculated Risk in Geotechnical Engineering," ASCE Journal of the Geotechnical Engineering Division, Vol. 110, February

Wu, J.T.H., Editor (1992a), Geosynthetic-Reinforced Soil Retaining Walls, Proceedings of the International Symposium on Geosynthetic-Reinforced Soil Retaining Walls, Denver, Colorado, USA, August 1991, A. Balkema Publisher, 375 p.

Wu, J.T.H. (1992b), "Construction and Instrumentation of the Denver Test Walls," Geosynthetic-Reinforced Soil Retaining Walls, Proceedings of the International Symposium on Geosynthetic-Reinforced Soil Retaining Walls, Denver, Colorado, USA, August 1991, A. Balkema Publisher, pp. 3-20.

Wu, J.T.H., Lee, K.Z.Z., Helwany, S.B., and Ketchart, K. (2006). *Design and Construction Guidelines for GRS Bridge Abutment with a Flexible Facing*, Report No. 556, National Cooperative Highway Research Program, Washington, DC.

Yako, M.A. and Christopher, B.R., 1987, "Polymerically Reinforced Retaining Walls and Slopes in North America", The Application of Polymeric Reinforcement in Soil Retaining Structures, Jarrett, P.M. and McGown, A., Editors, NATO Advanced Study Institute Series, Kluwer Academic Publishers, pp. 239-282.

Zornberg, J.G. (1994) Performance of Geotextile-Reinforced Structures, PhD dissertation, Department of Civil Engineering, University of California, Berkeley, California.

Zornberg, J.G., Barrows, R.J., Christopher, B.R. and Wayne, M.H. (1995) "Construction and Instrumentation of a Highway Slope Reinforced with High-Strength Geotextiles", Proceedings of Geosynthetics '95, Vol. 1, Nashville, Tennessee, USA, pp. 13-28.

GEOTEXTILES IN MARINE ENGINEERING: PAST, PRESENT AND FUTURE

Chris Lawson
TenCate Geosynthetics Asia, Malaysia

ABSTRACT

Geotextiles have been used in marine engineering for over 50 years. From their early beginnings as filters in simple revetment structures geotextiles have grown to be currently used in a wide variety of different marine structures with increasing sophistication. The paper reviews the development history of geotextile revetment filters as well as highlighting the current usage of geotextiles in a wide range of marine engineering techniques. In the future, it is expected that this variety of use will increase further, along with increased sophistication as access to conventional materials becomes more difficult and environmental sustainability becomes more important.

INTRODUCTION

When Bob Barrett published his paper on the use of “plastic filters” in coastal structures in USA in 1966 (Barrett, 1966) it provoked early interest internationally in the possibility of using geotextiles (not known then by the term “geotextiles”) for coastal and marine engineering applications. While the application of (the fore-runner to) geotextiles in these structures had started in Europe in the 1950’s the Barrett paper provided the first formal reference on this subject. At the time (and over the succeeding 15 years), geotextiles faced much suspicion and skepticism, not only because of the perception that the material appeared to be made from “the same type of plastic as my children’s toys”; but also because of a lack of familiarity and performance knowledge, and a lack of rational design procedures.

Over the subsequent 45 years geotextiles have not only overcome these early obstacles, but have gone on to become integral parts of many modern marine engineering projects. Today, geotextiles are considered as standard materials in a wide variety of marine structures. Further, over the last 10 to 15 years we have witnessed a considerable increase in the sophistication of geotextile use in marine engineering projects. This combination of increasing variety and sophistication has led to many innovative marine solutions involving geotextiles.

In examining the past, present and future of geotextiles in marine engineering it is proposed to look at the past through the introduction of geotextile filters in revetment and reclamation structures which began some 40 to 50 years ago, and are considered standard practice today. For the present it is proposed to look at examples of the wide range of geotextile applications in marine engineering that currently exist. This will demonstrate not only the variety, but also the sophistication of many of these current applications. For the future, it is proposed to look briefly at some of the trends going forward in the use of geotextiles in marine engineering.

GEOTEXTILE FILTERS IN MARINE ENVIRONMENTS: 1960'S TO PRESENT

Revetment and reclamation filters

An early use of geotextiles in marine engineering was as filters in simple revetment (slope protection) structures. It is uncertain exactly when this began, but there are European propositions of use as early as the 1950's. However, this paper will take the examples of use given by Barrett (1966) from the early 1960's as the early reference examples. As stated already, Barrett's paper created interest around the world in coastal and marine engineering circles to the extent that by 1970 geotextile filters had been employed in revetments in Europe, Australia and Japan, including the USA.

The concept of using a geotextile filter in a revetment is shown in Figure 1 where the geotextile substitutes for the conventional fine and coarse filter. In the past revetments utilized multiple layers of sand, gravel and rock to create an erosion resistant surface (see Figure 1a). Each granular layer in the revetment had to be small enough to prevent the material from below being eroded while at the same time be large enough to prevent it from being eroded out of the coarser layer above. Meeting these requirements required multiple granular layers which proved expensive and difficult to install, in many cases under water.

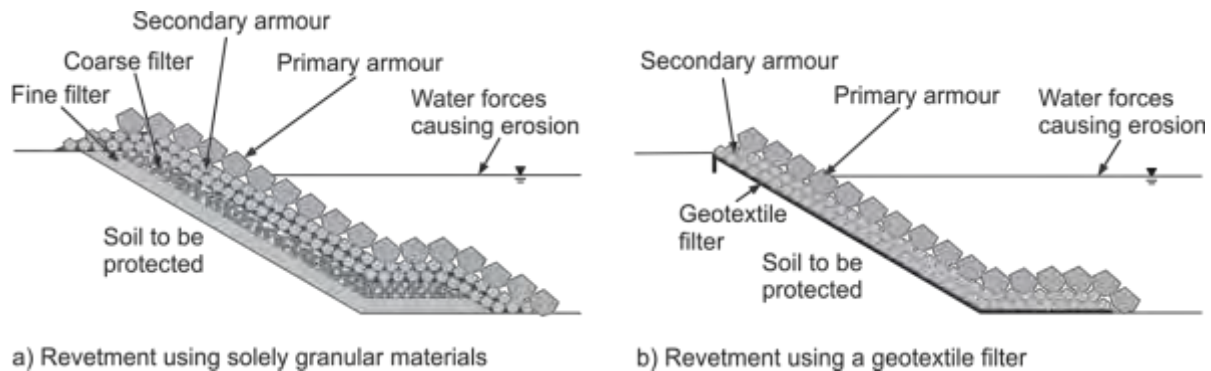


Figure 1. Revetment using solely granular materials and comparative structure using a geotextile filter.

The use of geotextile filters in revetments is very cost-effective; in fact, this has one of the highest cost-benefit ratios of any geotextile application. The geotextile has relatively fine pores which prevent the erosion of fine soils beneath it, and at the same time it is a “sheet-like” material and cannot be washed out through the coarse layers above. Thus, a single geotextile filter layer can substitute for multiple granular layers as shown in Figure 1b.

Even early in the use of geotextile revetment filters it was recognized that well-defined design criteria was necessary in order to quantify the appropriate geotextile filter properties. The geotextile had to meet specific hydraulic criteria in order to prevent soil erosion and allow free water flow. It also had to meet specific mechanical criteria in order to prevent mechanical damage. Further, it had to meet specific durability criteria in order to last for the design life of the revetment structure. Quantifying these different geotextile criteria has defined the 40 years history of geotextile revetment filter research.

The earliest research in USA on geotextile hydraulic criteria was carried out by Calhoun (1972) of the US Army Waterways Experiment Station. Besides establishing filtration limits under a unidirectional flow regime for a very limited range of soil types and geotextiles, one conclusion reached was to have a profound effect on geotextile filter selection for many years to come in the USA. This conclusion was that nonwoven geotextiles should not be used as filters because “it was difficult to determine their appropriate hydraulic properties” compared to woven geotextiles which had easily identifiable properties of Equivalent Opening Size and Percent Open Area. While there was much subsequent filter research in USA and Europe in the intervening years that demonstrated the good performance of nonwoven geotextile filters, it was not until the late 1980’s that nonwoven geotextiles were accepted as suitable revetment filter geotextiles in the USA. Even today, the requirements established by Calhoun in 1972 can be seen in some US Government (specifically US Corps of Engineers) geotextile specifications.

In Europe and the rest of the world the development of geotextile hydraulic criteria under unidirectional flows began in the mid 1970’s and continued on into the early 1990’s. These are reported in another paper by Bob Holtz delivered at this conference. Much of this work was carried out using nonwoven geotextiles and a large database of nonwoven geotextile filter performance with a wide range of soil types was built up.

Revetments are subject to a variety of hydraulic forces depending on their location. These can range from hydraulic drawdown (unidirectional flows) to water currents (surface shear flows) to waves and tides (reversing flows). The geotextile filter must be designed for the most critical hydraulic condition occurring. Much of the physical modeling that has been used to develop geotextile hydraulic criteria over the last 40 years has been carried out under unidirectional flow conditions. The reason for this is that the conditions are relatively simple to replicate in the laboratory (only a unidirectional water flow) with the equipment being relatively simple to develop and operate. Modeling wave and tide conditions (reversing flows) is much more complex, especially for revetment structures. Not only is there the complexity of varying reversing flows (disturbing forces of different wave heights and wave periods) but also the complexity of the confining effect of the weight of the revetment armor on top of the geotextile filter (stabilizing forces of the armor overburden stress). It has only been over the last 5 to 10 years that laboratory modeling equipment has been developed with the sophistication and precision to evaluate the performance of geotextile filters under reversing flow conditions. Results under reversing flow conditions published by Srikongsri (2010) show regions of different geotextile filter retention behaviour according to different external stress ratios (see Figure 2). It is interesting to note that the proposed recommended “safe” retention limit for reversing flow conditions shown in Figure 2 is virtually identical to the retention limit for unidirectional flow conditions published many times over. It would appear that the increased erosive forces caused by wave forces are counterbalanced by the added confining stress caused by the presence of the rock armor thus resulting in overall conditions very similar to that of (simpler) unidirectional flow regimes.

Early in the use of geotextile revetment filters it was recognized that mechanical criteria played a very important role in the performance of the geotextile filter. Puncturing and tearing of the geotextile during installation resulted in soil erosion and fairly quick failure of the revetment. Clearly, to perform well the geotextile filter has to resist these mechanical stresses that occur

during installation. Historically, a variety of approaches have been adopted to develop suitable mechanical criteria. These have ranged from the development of empirical relationships based on geotextile properties, e.g. Lawson (1992); to the development of empirical relationships based on energy absorption properties, e.g. Wong et al. (2002); to the development of classification systems, e.g. AASHTO (2005). Today, much is known about the mechanical criteria for geotextile revetment filters under a wide variety of installation conditions.

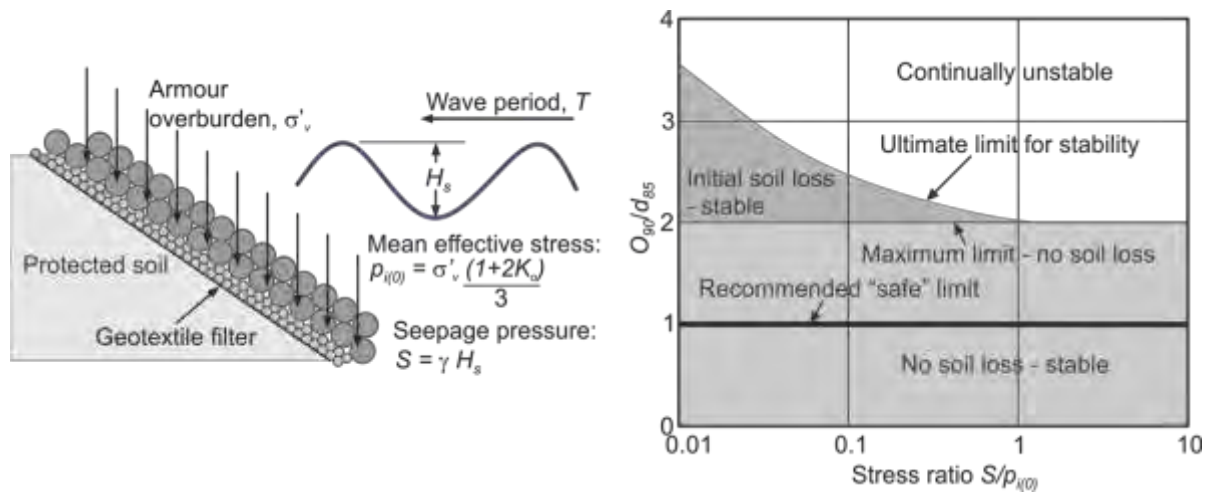


Figure 2. Geotextile filter retention criterion for waves and tides condition.
(After Srikongsri, 2010)

Early in the use of geotextile revetment filters it was recognized that durability criteria were also important requirements. Geotextiles are composed of polymers which remain very stable over long periods of time when buried in varied soil environments. However, when exposed to UV radiation these polymers oxidize, become brittle and lose elongation and strength. Clearly, to avoid this occurrence the geotextile filter must have adequate UV resistance during the revetment construction procedure and there needs to be an adequate rock covering to ensure that no UV radiation penetrates the revetment structure (to the geotextile) during its design life.

While revetment structures using geotextile filters may have been considered very novel 40 to 50 years ago, today they are standard practice, and commonly in use the world-over. We see them constructed in varied hydraulic environments and see them composed of different armor systems. By far the most common form of revetment is one that utilizes rock armor. However, revetments using geotextile filters are also constructed using concrete armor, concrete blocks and concrete forms depending on the local prevailing conditions.

The use of geotextiles as reclamation filters is also as old as that for revetment filters. Here, rather than placing the geotextile on the soil to be protected and then placing the rock armor on top, a rubble-mound containment dyke is first constructed and then the geotextile filter placed on the inside slope followed by the placement of the reclamation fill (see Figure 3). The geotextile filter prevents the placed reclamation fill from being eroded out through the rubble-mound dyke of the reclamation. This technique is normally used where water depths and water forces do not justify the placement of the fill material before the placement of the protection

layers (the protection layers must be placed before the placement of the fill material to prevent loss of the fill).

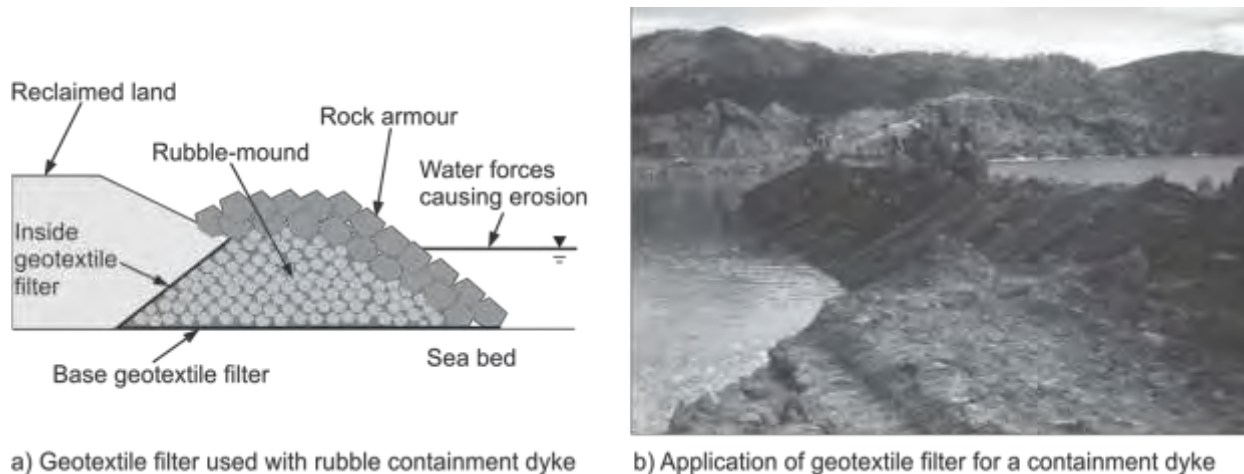


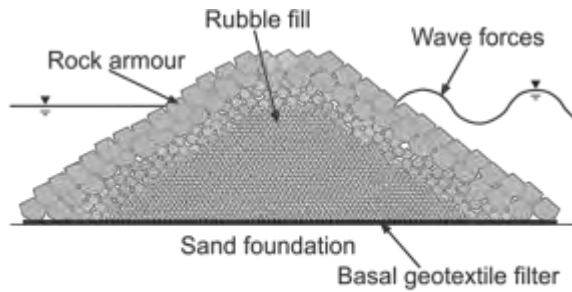
Figure 3. Geotextile filter used in conjunction with rubble containment dyke.

While the inside geotextile filter shown in Figure 3a does not have to resist rocks being dropped on it (as is the case for revetments), it does have to be robust enough to span across the rough surface of the rubble-mound dyke. This normally requires a robust geotextile filter to be used in this location. Depending on the foundation conditions a base geotextile filter may be also required beneath the containment dyke (Figure 3a). This can arise in situations where the sea bed consists of soft soils or of sand.

Basal filters beneath rubble-mound breakwaters

Where rubble-mound breakwaters are located on rock or overconsolidated clay foundations erosion across the base of and at the toes of the breakwater generally does not occur. However, if the breakwater is located on a sand foundation then erosion and scour at the toe of the breakwater and across its base can occur which may lead to undermining and instability. In these situations a geotextile filter, located across the base of the rubble-mound breakwater, is included to prevent erosion and scour of the sand foundation. The typical layout of a rubble-mound breakwater with a basal geotextile filter is shown in Figure 4a.

Depending on the location of the rubble-mound breakwater the basal geotextile filter may need to be installed at appreciable water depth and in diverse water current and wave conditions. To facilitate this, the basal geotextile filter is normally first fabricated on-land into what is known as a “fascine mattress” prior to floating to site and sinking into place. Historically, this technique was originally developed in Europe using “fascines” (brushwood) as a form of filter for the base of rubble breakwaters. With the advent of geotextile filters in the 1970’s this original technique was modified with the fascines forming a “floating skeleton” structure for the geotextile filter to facilitate the installation of the basal filter to considerable water depth. This technique has become the standard form of rubble-mound breakwater construction on sand foundations.



a) Basal geotextile filter in rubble-mound breakwater



b) Fabrication of fascine mattress on land



c) Towing fascine mattress into place



d) Sinking of fascine mattress on the seabed

Figure 4. Basal geotextile filter and fascine mattress installation technique.

The modern fascine mattress technique involves the on-land fabrication of large geotextile sheets attached to a lattice fascine (or bamboo) network, Figure 4b. The “fascine mattress” is then pulled into the water and floated to its installation location (Figure 4c) and then sunk into place on the seabed by the application of rock on top of the mattress (Figure 4d). The deployment and installation procedure normally imparts quite high tensile loads to the geotextile filter, and consequently, woven geotextiles with tensile strengths ranging from 100 kN/m to 200 kN/m are commonly used for this application. However, it should be noted that higher strength woven geotextiles have also been used.

REINFORCED SOIL STRUCTURES IN MARINE ENVIRONMENTS: 2000’S TO PRESENT

Reinforced soil structures using geosynthetics have been in use on land for almost 40 years. Today, basal reinforced embankments, reinforced slopes and reinforced retaining walls are standard forms of construction on-land, and well-recognized design Codes exist for them, e.g. BS8006-1:2010.

Over the last 10 years there has been interest in transferring the economies of reinforced soil construction achieved on-land to in-water (i.e. marine) construction. Constructing reinforced soil structures in and under water is more complex than constructing them on-land. However, with the advancement in marine construction techniques and installation accuracy marine reinforced soil structures have become a viable alternative to conventional structures.

When designing reinforced soil structures in-water two important considerations must be taken into account. First, the out-of-balance forces can be of different magnitude and second, more robust surface protection and coarser fills may be required because of the presence of external water forces. In determining the out-of-balance forces the bulk density of the reinforced fill is used for on-land calculations while the buoyant density may be used for in-water calculations, Figure 5a. This makes the out-of-balance forces in-water considerably less than on-land, and would normally mean considerably less reinforcement required for stability. However, the designer needs to consider if these conditions will remain the same over the design life of the structure. The presence of external water forces creates an erosive environment which normally requires more robust surface protection and special (more-coarse) reinforced fills than would normally be the case for on-land construction, Figure 5b. Further, external water forces may impart higher stresses on the reinforced soil structure than occurs on-land. These differences have to be taken into account at the design stage.

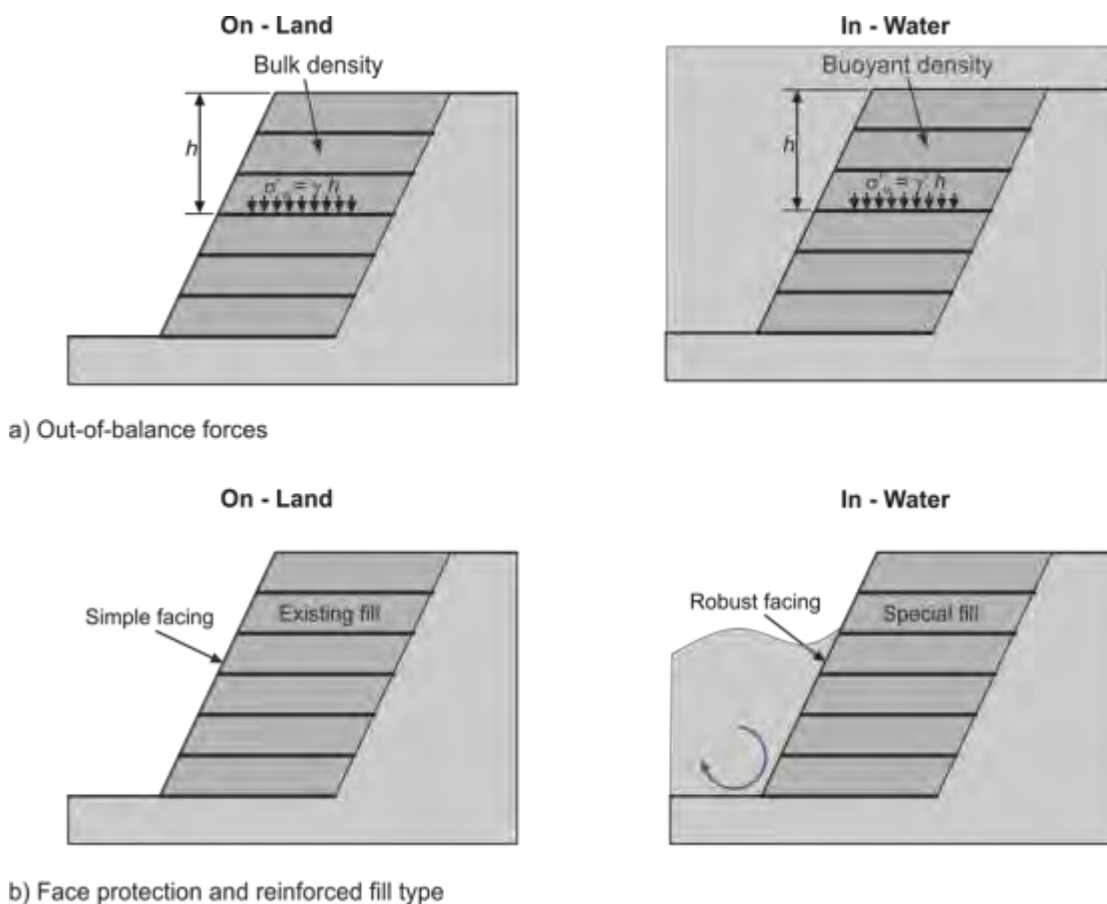


Figure 5. Two differences between on-land and in-water reinforced soil techniques.

Basal reinforced breakwaters and seawalls

To perform their function breakwaters and seawalls must maintain their shape and height. Consequently, where possible, these structures are located on stable foundations so they do not undergo deformations (change in height) over time. However, in certain situations, locating these

structures in areas of soft foundation soils may be unavoidable, especially where the precise location of the breakwater is critical.

Historically, where breakwaters and seawalls have to be located in areas of soft foundation soils the conventional construction procedure has been to first dredge the soft soil and replace it with sand-fill prior to construction of the breakwater, Figure 6a. For large breakwaters this is still the preferred procedure (or the use of a deep foundation improvement technique), however, for smaller breakwaters and seawalls the dredging of the soft foundation and its replacement with sand-fill makes the structure very expensive (in certain cases prohibitively so).

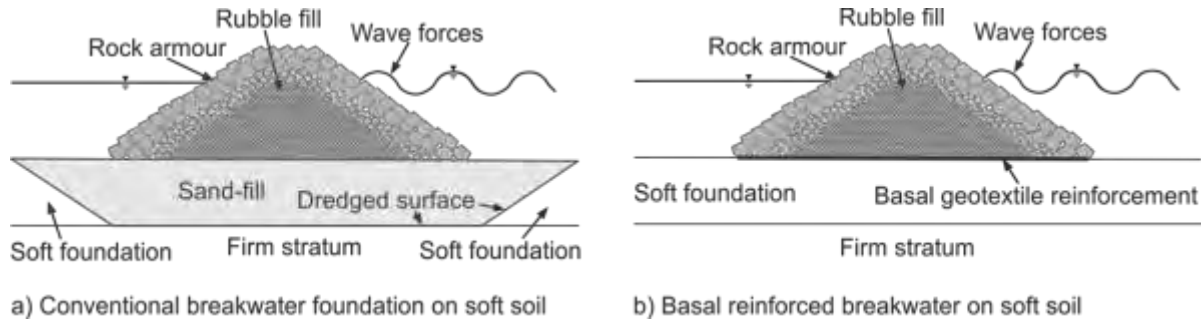


Figure 6. Comparison between a conventional breakwater located on a soft foundation and a basal reinforced breakwater or seawall.

There are two problems with constructing breakwaters and seawalls directly on soft foundation soils. First, there is the problem of stability where the soft foundation cannot support the weight of the breakwater or seawall. Second, there is the problem of settlement where the soft foundation consolidates and the height and shape of the breakwater or seawall changes. The problem of stability may be overcome by the use of basal geotextile reinforcement, Figure 6b. Here, the basal reinforcement enhances the short term stability of the breakwater until such time as the soft foundation has gained adequate shear strength to support the breakwater by itself.

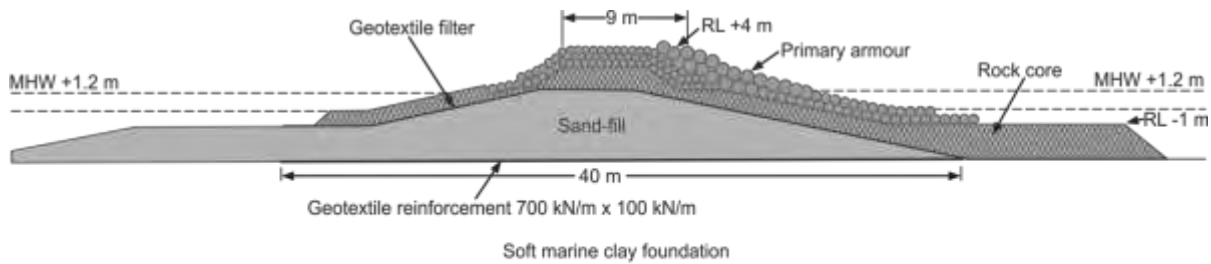
The use of basal reinforcement to enhance the stability of breakwaters and seawalls is identical to the technique used to enhance the stability of embankments on-land, and there is a long history of this (some 40 years).

Breakwaters and seawalls are designed to maintain a specific height and shape. When these structures are constructed on soft foundation soils consolidation of the soft foundation leads to settlement of the breakwater, a reduction in height and a change in shape. To prevent this performance loss either the breakwater height is over-compensated during initial construction to allow for future settlements, or subsequent placement of rock is programmed sometime after construction to maintain the design height of the breakwater.

Ameratunga et al. (2006) report on a basal reinforced seawall constructed on soft marine clay for the expansion of the Port of Brisbane, Australia. The seawall was constructed to contain dredged maintenance spoil which would then form the land area for the port expansion. A significant length of the 4.6 km long seawall was located on a very soft marine clay layer up to 30 m in thickness with an undrained shear strength as low as 5 kPa at the surface and increasing

linearly with depth. The surface of the soft marine clay layer was approximately 3.5 m below average water depth.

To ensure short term stability of the seawall basal reinforcement was included as shown in Figure 7a. The basal reinforcement used was a 700 kN/m woven polyester geotextile placed on top of the soft marine clay layer by means of a special installation barge, Figure 7b. Sand-fill was dredged and placed on top of the basal reinforcement up to mean high water level. Following this a geotextile filter was placed across the top of the sand-fill prior to placement of the rock armouring, Figure 7c. It was anticipated that settlement of the seawall would approximate 1 m so the height was over-compensated by this amount during construction.



a) Cross section through basal reinforced seawall



b) Placement of basal reinforcement and sand-fill



c) Placement of rock armour

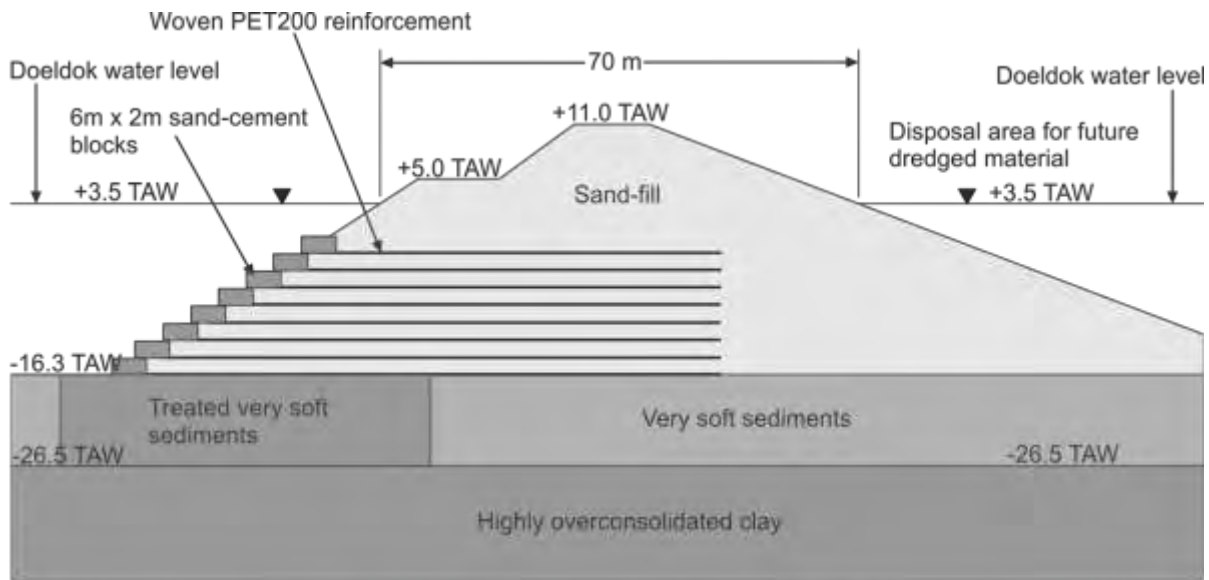
Figure 7. Basal reinforced seawall on soft foundation (After Ameratunga et al., 2006).

Reinforced slopes

While the construction of reinforced slopes in marine environments is uncommon compared to other forms of marine structures, they do nevertheless demonstrate the level of sophistication currently possible in practice. The choice of the appropriate materials and their accurate placement in water is critical to the performance of the resulting reinforced soil structure.

Van Miegheem et al. (2006) report on the design and construction of a submerged reinforced slope that formed part of a partially submerged containment dam constructed in an existing dock basin (“Doeldok”) at the Port of Antwerp, Belgium. The containment dam, shown in Figure 8a, was constructed to retain dredged spoil from port expansion and maintenance dredging operations and had a total height of 27 m, of which 19 m was constructed below water.

The major challenge for this project was that the containment dam had to be constructed on very soft sediments, of thickness approximately 9 m, in the base of the existing dock; and these could not be removed for environmental reasons. Due to the very low bearing capacity and undrained shear strength of these sediments (2 to 4 kPa), it became clear that some kind of foundation layer reinforcement was required to ensure stability of the containment dam. The solution used was to combine deep soil mixing beneath the side-slopes of the containment dam with geotextile reinforcement in the outer (steeper) slope of the dam (see Figure 8a). The inner slope of the dam was constructed with a flatter side-slope, and thus only deep soil mixing was carried out here. The combination of the two treatments at the outer slope of the dam ensured there was adequate stability during the controlled construction of the containment dam.



a) Cross section through partially submerged containment dam showing details of submerged reinforced slope



b) Fabrication of the block facing and reinforcement on land



c) Installation of the prefabricated facing and reinforcement under water

Figure 8. Submerged reinforced slope for partially submerged containment dam (After Van Miegheem et al., 2006).

Once the deep soil mixing had been carried out beneath the future side-slopes of the containment dam, construction of the dam was carried out using sand-fill placed in stages to control stability. On the outer side of the containment dam stability was maintained by using sand-cement segmental block facing units attached to layers of woven PET200 geotextile

reinforcement (200 kN/m in strength). The use of the block facing units enabled the outer side-slope to be constructed at an angle of 2.5H:1V, and also prevented erosion of the sand-fill. The use of polyester geotextile reinforcement was considered important as it would enable the geotextile to sink easily in water and thus facilitate placement. To provide the required stability, eight layers of woven PET200 geotextile reinforcement were installed at 2 m vertical spacings, and extending continuously between 65 m and 100 m into the containment dam. The fabrication of the facing blocks and the attached woven polyester reinforcement was carried out on land (see Figure 8b) prior to installation in the dock.

On the outside of the containment dam slope, the large block facings with the attached geotextile reinforcement were installed using a large capacity floating crane (see Figure 8c). Once the block facing unit had been placed under water the woven PET200 geotextile reinforcement was then completely rolled out across the sand-fill surface in one continuous sheet, to the length required, using a second floating crane. The sand-fill used for the filling operations was obtained from excavation works for the construction of a new dock nearby in Antwerp harbour. The sand was selected on the basis of its grain size distribution and fines content. The sand-fill was placed in layers 2 m thick using hydraulic filling. At each 2 m lift, the foundation was allowed to consolidate for a period of 1 to 2 months. Following this, another block facing layer was placed along with the woven PET200 geotextile reinforcement and the sand filling procedure repeated.

GEOTEXTILE CONTAINMENT IN MARINE ENVIRONMENTS: 1950'S TO PRESENT

Geotextile containment, where sand-fill is encapsulated inside a geotextile, provides a variety of effective mass-gravity protection units that are differentiated on the basis of shape and mass. The geotextile skin provides the containment strength and integrity, and prevents loss of the sand-fill. The fabrication of the geotextile skin provides the shape and size of the containment unit. The sand-fill provides the contained mass of the unit. The use of sand-fill for these units is important as it ensures a permeable unit as well as a stable unit that does not undergo volume change with time. Three types of geotextile containment units are used in marine engineering. These are geotextile bags (Figure 9a), geotextile tubes (Figure 9b) and geotextile containers (Figure 9c).

Geotextile bags, Figure 9a, are small-volume containers that are filled on land or above water and then pattern-placed either near water or below water level. They are manufactured in a range of shapes, and range in volume from 0.3 m³ to 8 m³. Geotextile tubes, Figure 9b, are tubular (sausage-shaped) containers that are formed insitu on land or in water. The tubes are filled by hydraulically pumping sand-fill into the tube. Geotextile tubes range in size from 4 m to 25 m in circumference, and up to 200 m in length for marine applications. Geotextile containers, Figure 9c, are large-volume containers that are filled in barges above water and then deposited into submarine environments. The volumes of these containers more commonly range from 100 m³ to 700 m³, although containers as large as 1,000 m³ have been installed.



a) Geotextile bags



b) Geotextile tubes



c) Geotextile containers

Figure 9. Types of geotextile containment units used in marine engineering.

Geotextile bags

Peoples' normal perception of geotextile bags is that they are the small, ubiquitous "sand-bags" seen the world-over shoring up flood defenses in times of natural calamity. These bags are small in volume ($< 0.3 \text{ m}^3$) and are not considered here. Rather, the geotextile bags covered in this paper refer to those types specifically developed for, and used in, marine engineering applications. These are larger, more-robust and durable than the conventional "sand bag". In a modern context, these larger geotextile bags started to be used for marine applications in Europe in the 1950's. At the time, these bags were manufactured from woven nylon materials and ranged in volume from 0.5 m^3 to 1 m^3 . Since that time geotextile bags have evolved to larger volume units (up to 8 m^3) of varying shapes (pillow, mattress and box shaped), along with the use of specially developed, highly resistant, geotextile skins.

For best performance it is essential that the geotextile bags be filled to maximum density and volume. This becomes more difficult as the volume of the bag increases, but can be enhanced by using water to compact the sand-fill hydraulically within the geotextile bag. Filled density and volume is important from the viewpoint of maximising stability, but it is also important from the viewpoint of minimising the effects of fill liquefaction and internal movement, and the subsequent loss of shape of the geotextile bags. To ensure the contained fill is

maintained in its dense state the geotextile skin should have adequate tensile stiffness and not undergo stretching and deformation over time.

One major advantage of geotextile bags is that these small-volume units can be used to construct marine structures that require good geometrical tolerances. This can make them preferable to large-volume units such as geotextile containers when specific slope and height tolerances are required. Another advantage of the small-volume geotextile bag units is that maintenance and remedial works can be carried out easily by replacing the failed bag(s). This is simpler than carrying out remedial works on larger-volume containment units such as geotextile containers.

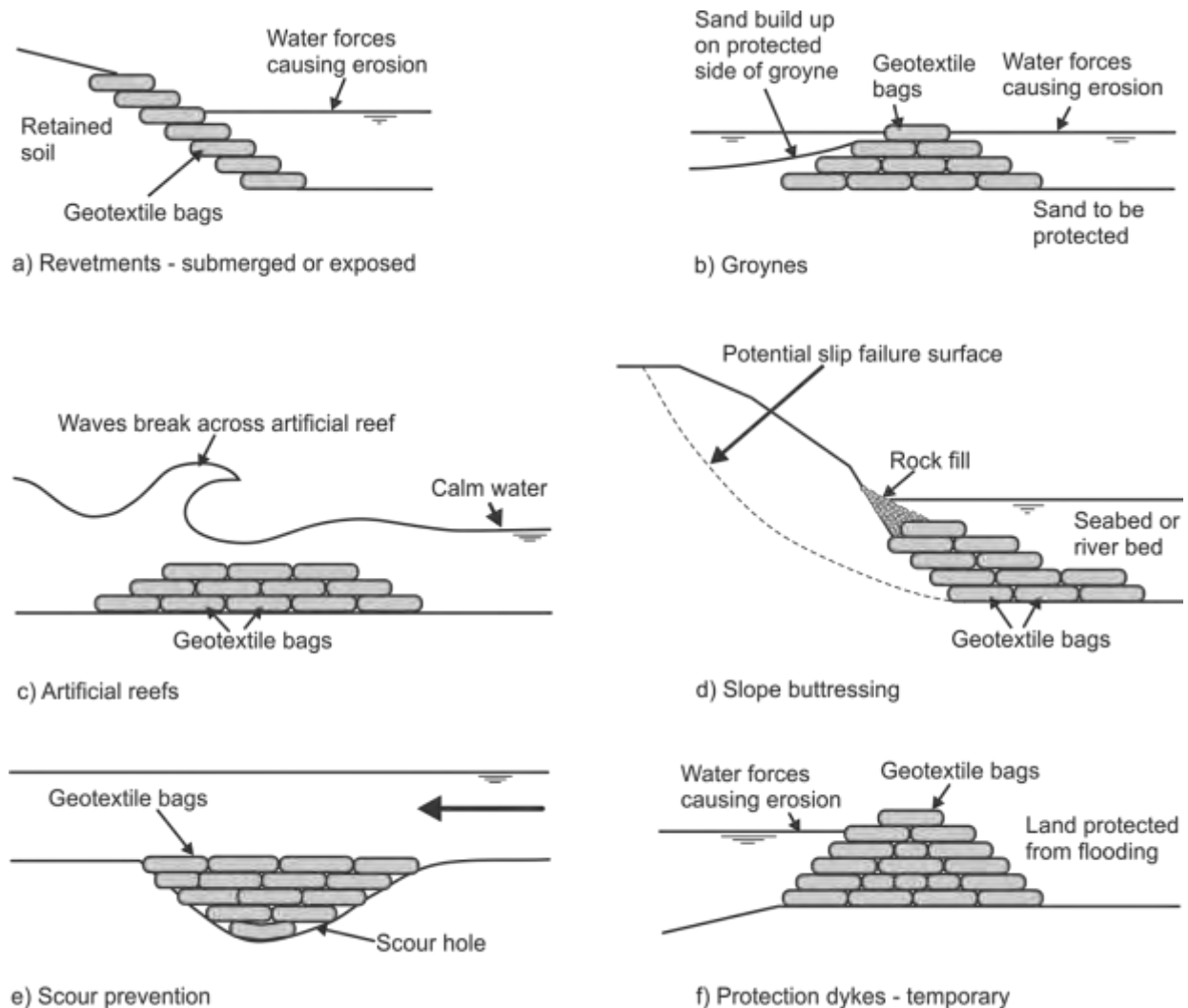


Figure 10. Applications for geotextile bags (After Lawson, 2008).

Geotextile bags are used for a range of marine applications. These are shown in Figure 10 and described briefly below. Geotextile bags are used for revetments (Figure 10a) where their contained fill is used to provide stability and prevent erosion. Geotextile bags have been used for

both submerged as well as exposed revetments (the same as geotextile tubes). Much of the details concerning geotextile bag revetments also apply to geotextile tube revetments.

Geotextile bags may be used as groynes (Figure 10b) to prevent the littoral movement of shoreline sediment. Geotextile bags can also be used to construct artificial reefs (Figure 10c). Here, the same conditions apply for geotextile bags as for geotextile containers. A major advantage of geotextile bags is that they can be installed to better geometric tolerances than relatively large-volume geotextile containers. Also, being relatively small in volume and having considerably better fill density, the geotextile bags are less prone to liquefaction from waves (or its effects) than the relatively large-volume geotextile containers.

Geotextile bags can be used to provide buttress support to an unstable slope in a hydraulic environment (Figure 10d). Here, the geotextile bags act as a mass-gravity berm providing additional restraint to the toe of the unstable slope. One advantage of geotextile bags for this application is that installation can be carried out by simple lifting equipment; thus geotextile bags can be installed at shallow water depths if necessary, unlike geotextile containers, which have to be installed at relatively greater water depth.

Geotextile bags are used as expedient means of scour prevention to prevent undermining of nearby structures (Figure 10e). They can be easily installed using simple machinery. The bags conform to the shape of the scour hole and thus provide good sealing qualities. Protection dykes (Figure 10f) are one of the original applications for geotextile bags. This expedient use of geotextile bags comprises the most basic, and common, form of geotextile containment application. However, geotextile bags may also be used for more sophisticated and substantial protection dyke structures where they may be required to perform over long periods of time. Here, the geotextile bags are required to perform in the same manner as geotextile tubes for this same application. The pattern-placement of geotextile bags forms a stable mass-gravity structure that is resistant to erosion when subjected to hydraulic forces.

While Figure 10 shows a range of marine applications for geotextile bags, by far the most common use is for revetments where the bags provide the primary armor protection. Critical to the design of geotextile bag revetments is the revetment extent and slope; local bag stability; sand stability within the bags; geotextile strength; geotextile abrasion resistance and geotextile durability. Recognized design procedures exist for geotextile bag revetments, e.g. Pilarczyk (2000), Bezuijen and Vastenbergh (2012).

Geotextile tubes

Geotextile tubes first began to be used for hydraulic and marine structures in the 1960's. These tubes (known as "Longard" tubes) were of relatively small circumference (less than 5 m) and proved of limited use due to instability problems in hydraulic environments (they did not have the required mass-gravity to resist normal hydraulic and wave forces). Longard tubes also utilized an impermeable lining inside the woven geotextile skin in order to pressurize the tube with water before introduction of the sand fill.

In a modern context, the geotextile tubes that are familiar today began to be used in the 1980's. These geotextile tubes are manufactured in much greater circumferences than the earlier

generation Longard tubes which make them very stable in hydraulic and marine environments. Also, the woven geotextile skin is permeable, enabling the water from hydraulic filling to easily pass out of the tube, with the sand-fill being retained inside.

Geotextile tubes are fabricated in the factory prior to delivery to site. Over the years since their original development much has been learned regarding the performance of these materials, the intricacies of filling them successfully, and the methodology of fabrication. The nature of the tensile loads generated in the tubes during filling and their magnitude determines the required strength of the geotextile used, the nature of the sewn seams and their location. The judicious use of high capacity seams and their location governs the level of tensile loads that can be sustained by the geotextile tube. Further, an adequate factor of safety (minimum of 3.5) should be applied to the generated tensile loads in order to arrive at a safe tensile strength for the sewn seams in the geotextile tube.

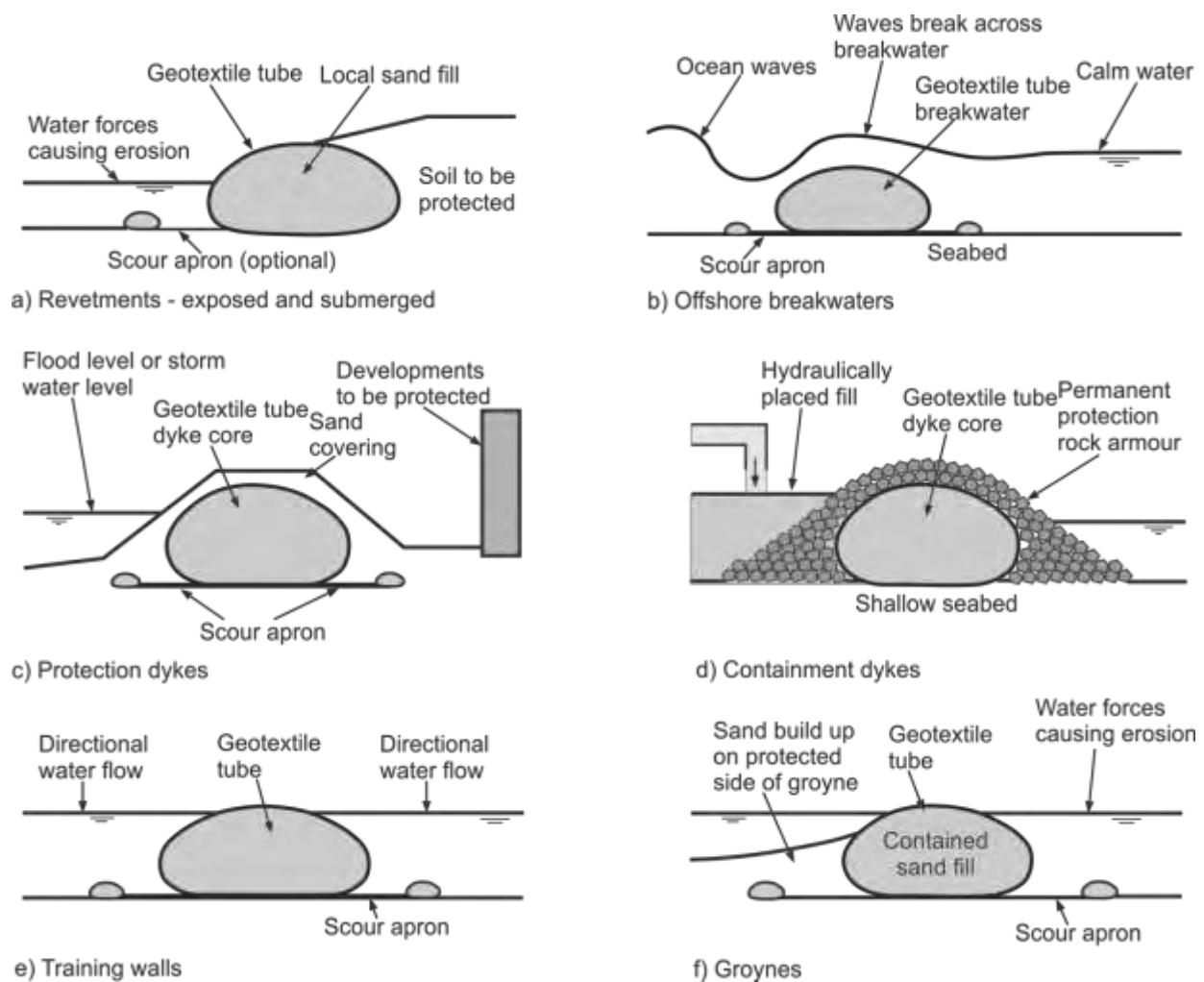


Figure 11. Applications for geotextile tubes (After Lawson, 2008).

Geotextile tubes are used for a variety of marine structures where their mass-gravity provides the primary protection. These are shown in Figure 11. Geotextile tubes are used for

revetment structures (Figure 11a), where their contained fill is used to provide mass-gravity stability. They are used for both submerged and exposed revetments. For submerged revetments the geotextile tube is covered by local soil, and is required to provide protection only when the soil cover has been eroded during periods of intermittent storm activity. Once the storm is over, the revetment is covered by soil again, either naturally or by maintenance filling. For exposed revetments the geotextile tube is exposed throughout its required design life. Scour aprons are normally included to prevent scour of the geotextile tube toe.

Geotextile tubes are also used for offshore breakwaters (Figure 11b) to prevent the erosion of shoreline developments. Here the filled geotextile tube is located a certain distance offshore in order to dissipate wave forces before they can reach the shoreline. Again, scour aprons are used beneath the geotextile tube breakwater to ensure that local erosion does not undermine the breakwater structure.

Geotextile tubes are used for protection dykes (Figure 11c), where they prevent flood and storm damage to valuable structures and real estate. Where geotextile tube protection dykes are constructed it is common to cover the geotextile tube with local soil. The geotextile tube is required to function only intermittently during storm or flood periods when the soil cover is eroded. The use of the soil cover provides several advantages to the geotextile tube core. First, it hides the geotextile tube core, thereby providing an aesthetic environment and ensuring no damage due to vandalism. Second, it protects the geotextile tube from long-term exposure to direct sunlight (UV degradation).

Geotextile tubes are used for the cores of containment dykes (Figure 11d) where water depths are relatively shallow. Here, the tube structure contains a filled reclamation area, the reclamation fill being dry-dumped or placed hydraulically. The advantage of this approach is that the same hydraulic fill used in the reclamation can also be used inside the geotextile tubes, thus avoiding the need to import granular fill for the dykes. Containment dykes constructed from geotextile tubes provide an economic alternative to other forms of construction, such as sheet-piled walls, especially where the foundation soil is soft. Where water forces dictate, and where longevity is required, rock armouring can be placed around the geotextile tube core (see Figure 11d).

Geotextile tubes are suitable for training walls (Figure 11e) where they are used to isolate and redirect water flows. Where geotextile tubes are used for training works it is common to leave the tube exposed except for major structures, where rock armour layers may be placed over it to dissipate and redirect hydraulic forces. Where the tubes are left exposed, a geotextile shroud may be used across the top of the tube, or a coating applied, to enhance its longevity in an exposed environment.

Geotextile tubes can be used as groynes (Figure 11f) to prevent the littoral movement of sediment. In most cases the geotextile tubes are left exposed, but coatings or a rock covering may be applied, depending on the circumstances and the required life expectancy.

Geotextile tubes behave as mass-gravity units when installed. Thus, the design of geotextile tube structures lends itself to the limit mode approach. Lawson (2008) has detailed the

various design limit modes for geotextile tube structures and Bezuijen and Vastenberg (2012) provide current detailed design guidelines.

Lawson (2008) reports on the construction of an artificial island using geotextile tubes for the containment dyke as part of the Incheon Grand Bridge Project in Korea. The artificial island was constructed in order to construct the bridge viaduct in the dry and was to be left in place following completion as it will later be enveloped by a large land reclamation scheme to build a new high technology city – Songdo City.

The foundation conditions where the artificial island is located consist of very soft marine clay to an approximate depth of 20 m. Further, in this area the tide range is very high, with a maximum difference in level of 9.3 m. This results in the exposure of the soft clay foundation at low tide and inundation to around +4.64 m at high tide. As a result of these difficult local conditions it was decided to construct the containment dyke for the artificial island out of geotextile tubes, as it was considered that the alternative of using sheet pile walls would not be feasible considering the low shear strength of the soft foundation and the height to which the artificial island would have to be raised to account for high tide level.

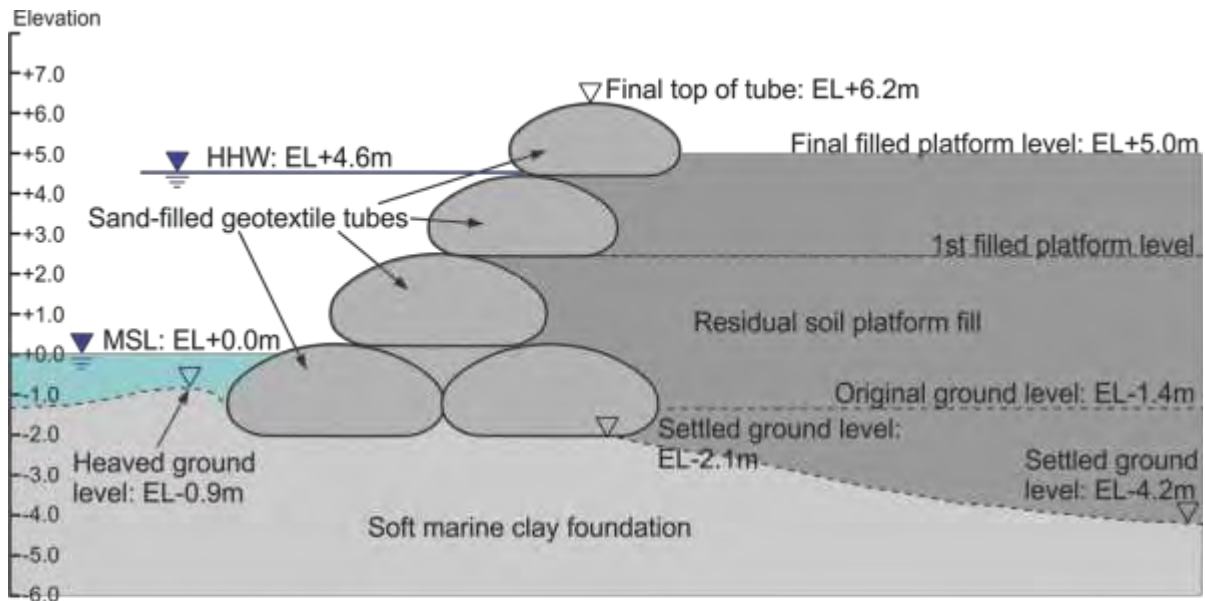
Figure 12a shows the typical cross section through the artificial island following construction. The base of the wall has two tubes side-by-side, with a third tube placed on top. Later, a fourth and fifth tube was then placed to bring the island up to the required design height. Figures 12b and c show the installation of the base geotextile tube layer. The tubes were laid out at low tide, and then at high tide the sand fill for the geotextile tubes was brought to the site by barge, mixed with water, and pumped hydraulically into the geotextile tubes.

Locally available residual soil was used for the fill material for the island, Figure 12d. Figure 12e shows the completed island with the freeway viaduct being constructed in the dry.

The performance of the geotextile tube structure on this project has been evaluated in some detail. The results show that the filled tubes themselves underwent very little deformation once filled. The structure itself has remained very stable, even allowing for an apparent heave of around 0.5 m of the soft foundation in the vicinity of the toe of the geotextile tube wall (see Figure 12a). The geotextile tube wall has settled around 0.7 m, while the centre of the island fill has settled around 2.8 m, all due to the high compressibility of the soft foundation beneath the artificial island.

Geotextile containers

Geotextile containers first started to be used in the early 1990's where it was necessary to provide "soft" offshore submarine structures that wouldn't damage ship traffic in the event of a collision. The essence of these units at that time was to provide large mass-gravity structures whose geometry was not considered to be of prime importance. Consequently, for economic reasons, this led to the deployment of large-volume containers (500 m³ to 1,000 m³) which generated high tensile loads in the containers during installation. This resulted in a relatively large proportion of failures (container ruptures) as the analysis methods and the specialist fabrication technology for these units was still in its infancy.



a) Cross section through artificial island showing settlements



b) Installing initial geotextile tube



c) Installing base geotextile tube layer



d) Final filling of artificial island



e) Construction of viaduct

Figure 12. Construction of artificial island for viaduct construction using geotextile tubes, Incheon Bridge Project, Korea.

Over the succeeding years the analysis methods, fabrication technology and installation techniques have been greatly refined. Also, there has been increased emphasis placed on the finished geometry of completed container structures. As a consequence of this the most common geotextile container units currently used range in volume between 100 m^3 and 600 m^3 .

Because of their large volume geotextile containers are installed by means of a split-bottom barge. Figure 13 shows the typical formation and installation of a geotextile container. It entails the placing and filling of the geotextile container in the split-bottom barge; the container is then sealed and the barge positioned at the correct dumping location. The split-bottom barge opens, and the geotextile container passes through, and descends through the water to the seabed. Depending on its source, the container fill may be dry-placed, wet-placed or hydraulically pumped into the container. For marine works the type of fill used is normally sand, or of sand consistency, as this doesn't change in shape once the container has been installed. More recently, cement stabilized cohesive fills have also been used.

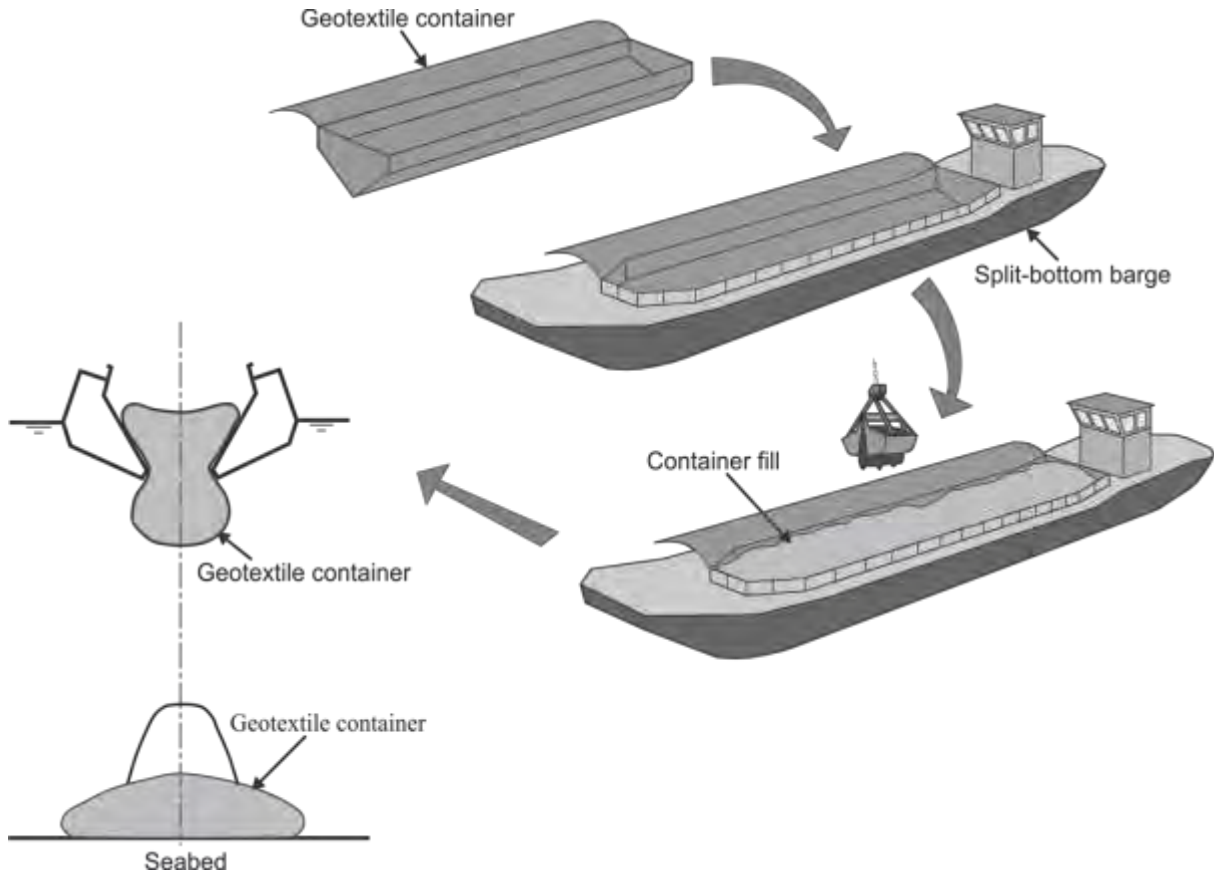


Figure 13. Installation procedure for geotextile containers (After Pilarczyk, 2000).

Geotextile containers are fabricated to fit the specific dimensions of the split-bottom barge. The tensile loads generated in the container during installation, the level of fill in the container, the tensile strength of the geotextile and the seaming technology used all govern the success of the geotextile container solution. Lawson (2008) and Bezuijen and Vastenberg (2012) provide design guidelines for geotextile containers.

The type of container shown in Figure 13 takes the form of an envelope where the container is closed and sealed once it is filled in the barge. More recently, containers of tubular shape have been used. These are hydraulically filled in the split-bottom barge, with the inlet ports sealed after filling, prior to installation of the container on the seabed. This type of

geotextile container is normally of smaller volume compared to the conventional envelope geotextile container; being between 100 m³ and 300 m³ in volume.

Figure 14 shows the range of marine engineering applications for geotextile containers. Geotextile containers are used as part of offshore breakwaters to prevent the erosion of the shoreline (Figure 14a). The technique here is the same as that for geotextile tube offshore breakwaters except that geotextile containers are used at greater water depth and a rock covering is normally placed across the top of the containers to raise the breakwater to its required height.

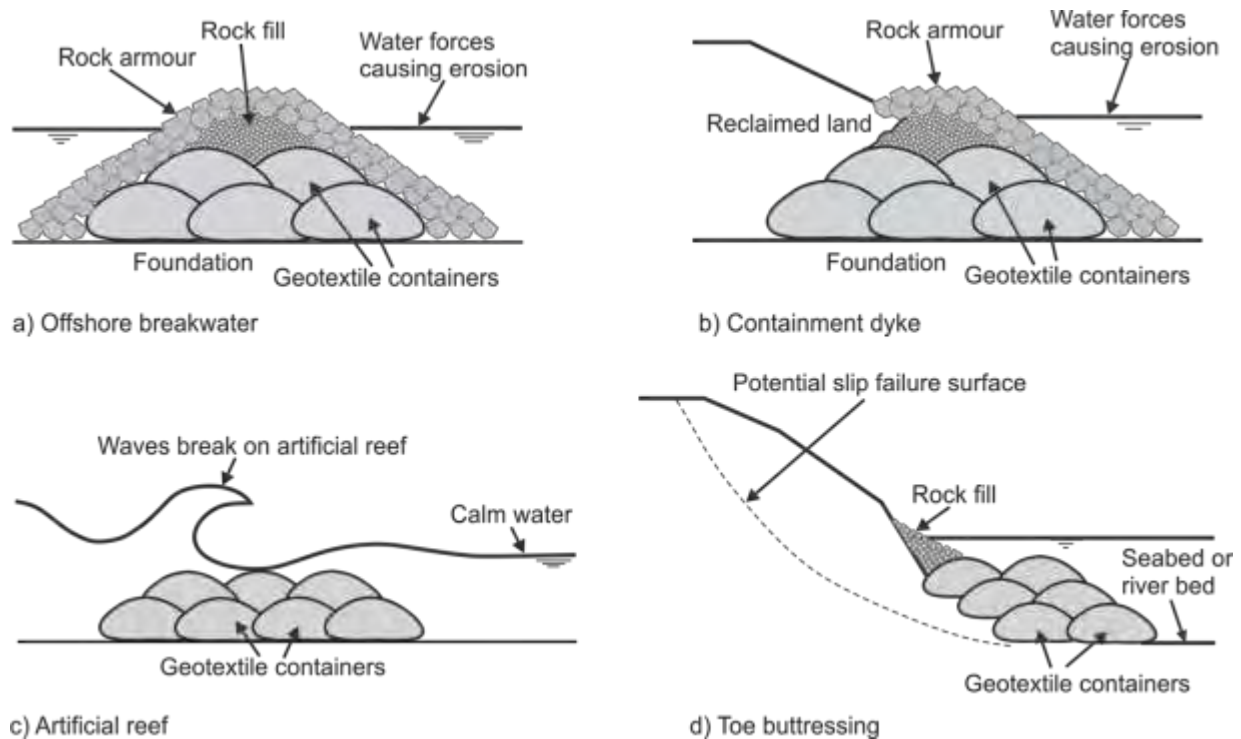


Figure 14. Marine applications using geotextile containers (After Lawson, 2008).

Geotextile containers are used for containment dykes where the water depth facilitates the placement of the containers (Figure 14b). The technique is the same as that for geotextile tubes except that the geotextile containers are used at greater water depth. A rock covering is normally placed across the top and down the outer face of the geotextile containers to raise the containment dyke above water level. Where the dyke is to remain submerged geotextile containers may be the sole units.

Geotextile containers can be used to construct artificial reefs (Figure 14c). Here, the containers provide a raised platform (a reef) that forces waves to break over the top of the reef. This prevents erosion of the protected shoreline. As well as dissipating wave energy artificial reefs also can be used to refract waves and alter the normal waveform. However, to do this successfully requires the reef to be constructed to a specific plan geometry with specific side slopes and platform height. This level of placement accuracy is normally outside the limits of large-volume geotextile container placement, and is more suited to the application of smaller-volume geotextile bags. Further, the nature of geotextile containers makes it difficult to fill them

to maximum volume and density. Consequently, it is to be expected that if the filled geotextile containers are to be exposed to continual wave activity then liquefaction of the sand fill will cause a change in shape of the exposed containers and a subsequent lowering of the surface level of the artificial reef. This then alters the shape of the waveform across the top of the reef, and thus the structure may require periodic maintenance to maintain the existing waveform.

Geotextile containers are used for the underwater buttressing of unstable slopes (Figure 14d). Here, the weight of the geotextile containers is utilized to provide a counter-weight berm for a potentially unstable slope. The advantage of using geotextile containers is that a “soft” buttress structure is provided that won’t damage shipping.

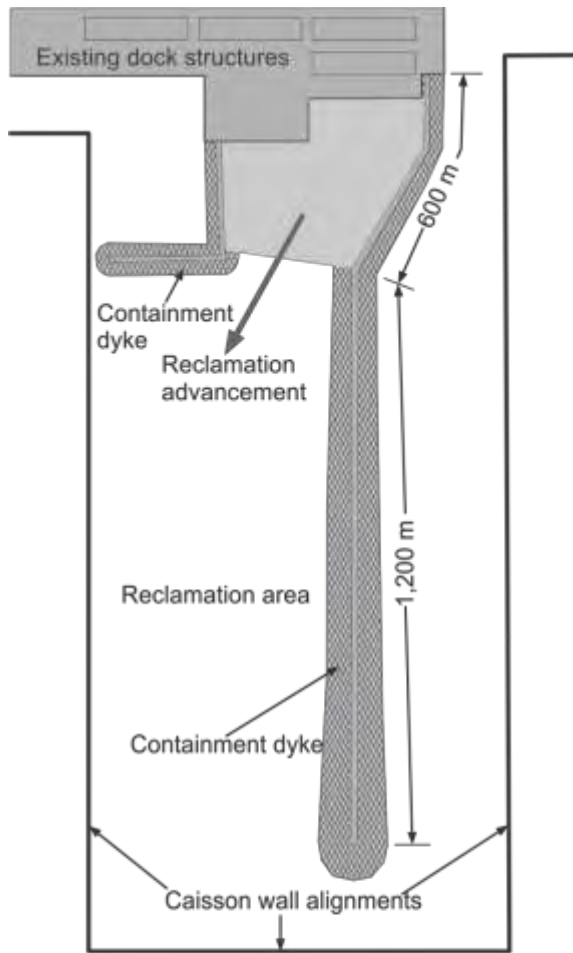
Geotextile containers are large volume mass-gravity units. At considerable water depth their placement accuracy maybe limited due to water currents etc. Consequently, geometrical tolerances are normally limited for these types of structures unless special techniques are applied.

Kamada (2010) and Chew et al. (2011) describe the construction of a temporary marine containment dyke using geotextile containers in Singapore. The containment dyke was used to retain reclamation fill and control sediment plumes with the reclamation location being close to busy shipping lanes, coral reefs and a nature reserve.

Figure 15a shows the plan layout of the reclamation works with the primary temporary containment dyke running some 1,800 m down the spine of the port reclamation area. The periphery of the reclamation consists of concrete caisson retaining walls. As the caisson wall installation progresses, the area between it and the central containment dyke was filled using locally dredged material and construction waste.

Figure 15b shows a cross section through the temporary marine containment dyke. It consists of stacked geotextile containers filled with cement mixed soil as the outer layer of the dyke. The soil fill was obtained from excavation projects on-land and in-sea in Singapore. Also, the same cement mixed soil was used for the core of the dyke between the geotextile containers. The containment dyke was constructed in water depths ranging from 5 m to 30 m. Because of local ocean currents of up to 2.5 m/s the accurate placement of the geotextile containers was considered a major issue, especially at water depths over 15 m. At all depths, container placement accuracy was required to be within 0.5 m, and the geotextile containers were not to rupture during placement.

To meet the container placement accuracy requirements and prevent container rupture during placement a specially designed installation barge was built, Figure 15c. The barge had a special container releasing cradle that could be lowered into the water enabling accurate placement and limiting the mechanical stresses on the containers. For water depths up to 15 m the releasing cradle remained at the water surface during geotextile container release, while for water depths over 15 m the releasing cradle was lowered to the appropriate depth before container release.



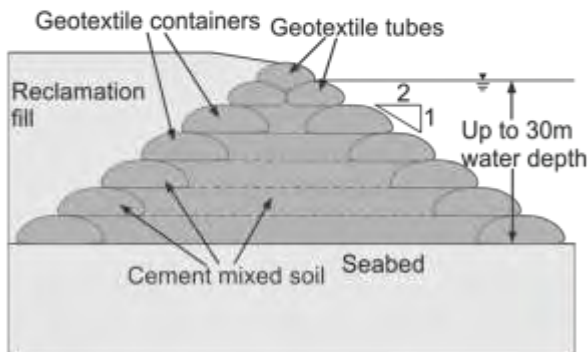
a) Plan layout of reclamation works



c) Geotextile container installation barge



d) Filled geotextile container in installation barge



b) Cross section through containment dykes



e) Geotextile tube crest of containment dyke

Figure 15. Layout of port reclamation and geotextile container installation technique.
(After Chew et al., 2011 and Kamada, 2010)

The geotextile containers used were tubular in shape and of 300 m^3 in filled volume. The method of filling the containers was as follows. The geotextile container was rolled out in the barge release cradle. A second barge was used to mix the soil fill with the appropriate amount of

cement, and then this mixture was pumped into the geotextile container in the installation barge to fill the tubular container (Figure 15d). The installation barge was then positioned using GPS, and the release of the geotextile container carried out. The procedure was then repeated. During installation an average of 6 geotextile containers were installed per day.

Near the water surface the dyke was completed by using geotextile tubes, see Figures 15b and 15e. Once this central dyke was completed reclamation fill was placed between the (progressing) caisson wall and the dyke. Later, foundation improvement techniques were applied to the reclamation fill in order to improve its strength and deformation characteristics.

THE FUTURE: 2013+?

During the last 50 years the use of geotextiles in marine engineering has evolved from simple revetment filters to a wide range of sophisticated engineered structures today. Geotextile revetment filters have evolved from being “novel” materials, and greeted with some suspicion and skepticism, 40 years ago to being standard practice today. Other geotextile techniques such as geotextile containment are also becoming standard marine engineering practice after 25 years of development. Over the succeeding years it is expected that these existing techniques will be utilized on an ever-widening scale in marine engineering as they provide very cost-effective solutions.

Over the next 10 years it is expected that access to conventional materials, e.g. sand and rock, will become much more difficult. Already we are seeing in certain regions of the world that local access to conventional materials is non-existent or prohibitively priced, and consequently, these materials have to be transported in by distances that can be over 1,000 km. In order to conserve these materials for local projects, countries have even banned the export of sand and rock to neighboring countries, which have made the cost of conventional materials very high. To alleviate this reliance on conventional materials alternative solutions and techniques have been developed, many of these utilizing geotextiles, to arrive at more cost-effective marine engineering solutions. It is to be expected that this drive for alternative solutions will become more important over succeeding years.

Also, over the next 20 years it is expected that environmental sustainability will become an important issue in marine engineering. Already the acquisition of conventional materials, such as sand and rock, are becoming difficult to source, necessitating long transport distances. This results in a large carbon footprint when using wholly conventional (i.e. granular) materials compared to solutions using geotextiles. As environmental sustainability becomes a more important issue, more emphasis will be placed on those solutions that create lower carbon footprints. Geotextile solutions are well-placed for this.

With the future direction placing more emphasis on the use of alternative materials and techniques for marine engineering, the requirement for geotextiles to have improved performance (compared to those readily available today) will become a necessity. Already, we are seeing the development of composite geotextiles to meet specific marine application requirements. As the level of marine application sophistication continues geotextiles will be

required to exhibit improved structural and durability performance compared with those in common use today.

Much of conventional marine engineering occurs near and around coastlines. While offshore engineering has existed for 50 years (associated with the offshore oil and gas industry) it has remained a very specialized engineering area. Over the last 5 years conventional marine engineering techniques have moved further offshore where it has now become synonymous with offshore engineering in many respects. This has involved the construction of marine structures in deeper water, and has required the development of sophisticated installation procedures and techniques. It is expected that this offshore sophistication will continue over the following years.

CONCLUSIONS

There has been considerable evolution in geotextile use in marine engineering over the last 50 years. In that time, early innovations in the use of geotextile revetment filters have become standard practice and there has been an ever-widening variety of geotextile solutions being used in marine engineering. This current wide variety of use has required increased sophistication in application and installation. For the future it is expected that geotextile solutions will continue to evolve in marine engineering (in terms of use and sophistication) and this will be driven by better cost-effectiveness, improved performance and environmental sustainability.

REFERENCES

AASHTO (2005), "Standard Specification for Geotextile Specification for Highway Applications, M288-05", American Association of State Highways and Transportation Organizations, Washington DC, USA.

Ameratunga, J., Boyle, P.J., Loke, K.H., Hornsey, W. and Strevens, M. (2006), "Use of Geotextiles to Overcome Challenging Conditions at the Seawall Project in Port of Brisbane", Proceedings Eighth International Conference on Geosynthetics, Yokohama, Japan, September, Millpress, Vol. 2, pp. 1085-1088.

Barrett, R.J. (1966), "Use of Plastic Filters in Coastal Structures", Proceedings Tenth International Conference on Coastal Engineering, Tokyo, Japan, pp. 1048-1067.

Bezuijen, A. and Vastenbergh, E.W. (2012), "Geosystems Design Rules and Applications", Taylor and Francis Group, London, UK.

BS8006-1:2010. "Code of Practice for Strengthened/Reinforced Fill and Other Soils", British Standards Institution.

Calhoun, C. (1972), "Development of Design Criteria and Acceptance Specifications for Plastic Filter Cloths", U.S Army Waterway Experiment Station, Vicksburg, USA.

Chew, S.H., Tan, C.Y., Loh, C.K., Lim, S.K. and Lam, J.P.W. (2011), “Design and Construction of Containment Bund Using Geotextile Tubes in Singapore”, Proceedings Fourteenth Asian Regional Conference on Soil Mechanics and Geotechnical Engineering, Hong Kong, No. 314.

Christopher, B.R. and Holtz, R.D. (1985) “Geotextile Engineering Manual”, Federal Highway Administration, Report No. FHWA-TS-86/203, Washington, USA.

Kamada, Y. (2010), “Geotextile Tube Installation Barge”, Proceedings Nineteenth World Dredging Congress, Beijing, China, September, pp. 492-504.

Lawson, C.R. (2008), “Geotextile Containment for Hydraulic and Environmental Engineering”, Geosynthetics International, Vol. 15, No. 6, Thomas Telford Ltd, UK, pp. 384-427.

Lawson, C.R. (1992), “Geotextile Revetment Filters”, Geotextiles and Geomembranes, Vol. 11, Nos. 4-6, Elsevier, pp. 431-448.

Pilarczyk, K.W. (2000), “Geosynthetics and Geosystems in Hydraulic and Coastal Engineering”, Balkema, Rotterdam.

Srikongsri, A. (2010), “A Laboratory Permeameter Study of Geotextile-Soil Retention in Cyclic Flow”, PhD Thesis, University of British Columbia, Canada.

Van Mieghem, J., Van Impe, W.F., Boone, C., Mengé, P. and Baertsoen, A. (2006), “Detailed Design, Validation of the Design and Monitoring of an Underwater Embankment Built on Dredged Material in the Doeldok”, Proceedings Thirty First PIANC Conference, Estoril, Portugal, May, pp. 1-17.

Wong, W.K., Chew, S.H., Tan, S.A. and Faure, Y.H. (2002), “Puncture Resistance of Geotextiles Against Installation”, Proceedings Seventh International Conference on Geosynthetics, Nice, France, Swets and Zeitlinger, pp. 1405-1408.

A BRIEF HISTORY OF HEAP LEACHING

Monte A. Christie, PE, GE

Mines Group Leader, Geo-Logic Associates, Grass Valley, CA USA

Mark E. Smith, PE

President, RRD International Corp., Incline Village, NV USA

ABSTRACT

Heap leaching has had wide success allowing mines to profitably recover metals from very low grade (metal content) ores that were previously uneconomical with traditional milling operations. Heap leach facilities rely on the performance of geosynthetic products to provide efficient solution recovery and environmental containment, of which a critical component is the liner system. The liner system not only functions as the barrier between the facility and open environment, but also directly affects metal recovery and thus operating revenue.

Due to skyrocketing metal prices and the resulting increased demand on reserves, mines have been pushed to more remote and difficult locations - sites are becoming more and more challenging at the same time that regulatory and community criteria is increasing around the world. In Latin America especially, where ore reserves are plentiful but terrain and climate complex, some of the challenges faced are remote areas, aggressive terrain, availability of qualified contractors and work forces, high elevation, extreme weather, as well as many others. This article explores a few of those.

HISTORY

There are two main methods for extracting metals from ore: crushing and grinding (milling) followed by either leaching or flotation (concentration), and heap leaching followed by extraction of the metal from the aqueous phase using several technologies (the most common being solvent extraction / electro-winning, or SX/EW, for copper, and either carbon absorption or zinc precipitation for gold and silver). Milling circuits require large capital investments and incur higher operating expenses (per tonne of ore processed) as compared to heap leaching, and thereby require higher feed grades to be cost effective (1 tonne equals 1,000 kg). On the other hand, milling can recover 85% to over 90% of the contained metal while heap leaching generally achieves 50% (uncrushed or run-of-mine ore) to 75% (crushed ore). Thus, low grade deposits tend to be processed by heap leaching and high grade by milling; projects with a wide range of ore grades will often have both types of recovery circuits.

The mining industry utilizes heap leach technology on a very large commercial scale for the extraction of gold, silver, copper, uranium, and on a smaller scale (pilot scale and limited commercial production) for nickel and other minerals. It is also used for nitrate, iodine and other salts. The technology requires a lined leach pad to provide containment of the ore and recovery of the leach ("pregnant" or "PLS") solutions, as illustrated in Figure 1. The heap leach facility may be designed as a conventional pad (permanent, multi-lift heap), on/off or reusable pad (dynamic heap), or a valley leach pad, depending on the site conditions and characteristics of the ore to be processed.

The actual principle of heap leaching has a long history. For example, mines in Hungary recycled copper-bearing solutions through waste dumps (the earliest form of “heaps” where non-engineered dumps) in the mid-sixteenth century, and Spanish miners percolated acid solutions through large dumps of waste rock containing very low concentrations of oxide copper on the banks of the Rio Tinto (“red river”) in 1752. By 1900, leaching operations were employing such techniques as leach/rest cycles to maximize copper recovery. Dump leaching using both acid and alkaline solutions has been practiced by uranium producers since the late 1950’s. Modern heap leaching (that is, engineered heaps, containment systems and modern metallurgical processes) of precious metal ores using the cyanidation process was originally suggested by the U.S. Bureau of Mines in 1967. The first commercial application of gold heap leaching occurred in the late 1960’s by the Carlin Gold Mining Company in northern Nevada. Cortez Gold Mines started the first large scale operation in the early 1970’s by leaching marginal grade ore (www.miningandmetallurgy.com).

In the mid-1970’s, heap leaching technology was improved in order to handle low grade, clayey deposits that were not amenable to conventional milling. The principal improvement, agglomerating of the ore, was prompted by increased exploration for low grade deposits as the price of gold increased dramatically; especially starting in about 1979 after the US liberalized the domestic gold market. Many of the deposits discovered could not be processed by the conventional heap leaching techniques because the clays or fines generated during crushing, or gauge material within the deposit, impeded uniform percolation of solution through the heaps. Pelletizing of iron ore had long used a binder-based process for binding fines to improve handling characteristics, and that agglomeration technology was adapted to gold heap leaching. Crush ore is agglomerated most commonly by pre-wetting and adding chemical binders (such as Portland cement for gold and silver ores and concentrated sulfuric acid for copper, uranium and nickel) and then mixing in a drum. This process causes the finer particles to adhere to the aggregate, and the chemical binders give those agglomerates enough strength to survive the transportation and stacking process. Agglomeration technology is applicable to most crushed ore, wastes, and milled tailings. An adaptation of tailings co-disposal technology (Leduc, et al 2004) was first commercialized at the Ruby Hill gold mine in Nevada, and subsequently tested on other projects, wherein milled ore (“pulp”) is mixed with heap leach ore and binder to create what has been called “pulp agglomeration;” this allows either a low-cost method of disposing of mill tailings (when the quantities are sufficiently low relative to the volume of heap leach ore) or the use of fine grinding to improve leaching of the higher grade ores in the heap without adversely affecting percolation.

The results of the technological improvements which have occurred throughout the 1970’s and into the 1980’s can be seen in dramatic production increases. By the mid of 1980s, production of gold from heap leaching had increased to over 30 percent of total U.S. gold production from an estimated 6 percent at the beginning of 1980s and negligible in the 1970s. Heap leaching unlocked previously uneconomic deposits by reducing both capital and operating costs, allowing grades as low as 0.5 g of gold per metric tonne of ore (gmt) to be profitably mined and processed.

Chile became the next logical place to apply the emerging technology due to its’ abundant, large copper resources, dry climate and friendly political environment. In addition to the advantages found in gold heap leaching, copper oxide deposits were simply not amenable to

conventional milling and concentration except in the rarest of cases. Heap leaching, on the other hand, was tailor-made for these deposits. Large-scale copper heap leaching began in Chile in 1980 with the Lo Aquirre project. By the early 1990's Chile had about 10 major copper heap leach projects, most using conventional lined leach pad technology. Copper heap leaching in the USA started with unlined run-of-mine leach dumps and only three lined copper heap leach pads were constructed in the USA during the 1980s. Chile is now home to most of the world's largest leach pads, measured both in containment area (several million square meters each) and contained ore tonnage (heaps with design capacity in excess of 1 billion tonnes). The average leach pad area is now over 1 million m² and projects are in the planning stages for leach pads in excess of 10 million m² in Turkey, Burma, and Africa. Essentially all of these are geomembrane lined (Breitenbach & Smith, 2006 & 2012).

This growth of copper production and heap leaching is shown below in Table 1. The importance and increase in heap leaching to now (nearly half of all copper being produced by heap leaching) shows the tremendous success of the technology. Copper heap leaching has climbed from an obscure idea in the 1980s to 40% of world copper production today.

Table 1 - Copper Production – SX/EW (heap leach) versus Concentrate (mill and smelting)

Year	SX/EW Prod. (KT Cu/year)	Concentrate Prod. (KT Cu/year)	Total Production (KT Cu/year)	SX/EW as % of total
1970	11	5,889	5,900	0.2%
1975	109	6,791	6,900	1.6%
1980	255	7,395	7,650	3.3%
1985	356	7,444	7,800	4.6%
1990	801	7,349	8,150	9.8%
1995	1,563	8,437	10,000	15.6%
2001	2,844	10,356	13,200	21.5%
2005	4,990	9,910	14,900	33.5%
2010	6,335	9,565	15,900	39.8%

HEAP LEACHING ECONOMICS

This reason for the increase in heap leaching as shown above in Table 1 can be illustrated by an example that shows how the technology not only increases ore reserves, but increases revenues as well. Consider an idealized large gold deposit as follows (gold is simpler in every aspect than copper and thus makes for a simpler example, but the fundamentals apply equally to copper and uranium):

EXAMPLE: Given the following information:

- 100M tonne high-grade gold ore reserves with an average metal content of 0.17 oz gold per tonne ore, suitable for conventionally milling;
- 100M tonne low-grade ore with an average metal content of 0.05 oz gold per tonne ore, suitable for heap leaching; and,

- 300M tonne waste (sterile and sub-economic rock that must be mined to access the high-grade ore).

In this example the low-grade ore is exclusively “internal” ore that must be mined to access the high-grade ore. In a more real-world case there would be additional “external” ore that would enlarge the overall pit limits, and different economics would apply to those tons.

Assuming the following typical operating costs, which were taken for several recent projects in South America:

- average project-life gold price \$1,700/oz;
- milling (including crushing, grinding, metal recovery and tailings disposal) at \$15/tonne of ore processed;
- heap leaching (including crushing, stacking, leaching and metal recovery) at \$8/tonne of ore processed;
- mining at \$1/tonne of rock mined (all ore and waste);
- metal recovery in the mill of 90% for the average high-grade and 93% when that grade is increased; and,
- heap leach recovery of 65% for average low-grade and 68% when that grade is increased.

SOLUTION:

The mill-only option would process the 100M tonnes of high-grade ore and produce approximately 17M oz of gold for revenue of \$16,010M after capital and operating costs. Adding the heap leach circuit would add some capital and operating costs between the mill and the heap leach, but would double the reserve to 200M tonnes of ore resulting in approximately 22M oz of gold and an increase in revenue to \$23,020M. In this example, heap leaching increased the gold reserve by 30%. Most mining companies are publicly traded and total resource - ounces “in the ground” for gold miners - is a key factor in setting their stock price. Thus, simply adding heap leaching to a company’s technology portfolio does in fact significantly increase their market capitalization.

Of course, there are some limitations with heap leaching and not all gold or copper ores can or should be heap leached. Milling, for example, has better selectivity and most poly-metallic ores such as those with both gold and copper cannot be heap leached without giving up on one or the other metal. Primary sulfide copper ores (e.g., chalcopyrite, bornite) are very difficult to heap leach with economically viable recoveries, though bio-leaching technology is being commercialized and holds promise for huge resources of low-grade primary ores; the Escondida mine in Chile is the world’s largest such heap leach, with over 4 billion tonnes of primary sulfide resource, and the La Granja project in Peru, which is under study, has nearly twice that. For alkaline (gold and silver) leaching, the presence of sulfide minerals increases reagent consumption (and thus operating costs) and can reduce recovery, making gold and silver

sulfides much less amenable to heap leaching; bio-leaching technology is also emerging to make these ores heap leach amenable and the first commercial plant is in operation near Elko, Nevada.

HEAP LEACHING TECHNOLOGY

The basic principle behind heap leaching is relatively simple. The metal from the ore is extracted using physical contact with a solvent leaching solution to dissolve the target metal (or, in some cases, salt). The impregnated solution is collected and processed to remove most of the metal, the pH and solvent concentrations adjusted and the solution recirculated to the heap. To enhance metal recovery, modern processes often use one or more of several available upgrading methods including pregnant solution recycling (recirculation of lower tenor pregnant solutions to the heap before routing to the plant for metal recovery), bio-leaching (for sulphide copper and gold ores), air injection (an emerging technology for primary sulfide copper ores) and physical alteration of the ore (e.g., crushing, agglomeration). It should be noted that while these methods generally improve the metallurgical response of the ore, they can also change its geotechnical properties (Ulrich et. al., 2003) and, in the case of bio-leaching, those changes can be time dependent and difficult to predict.

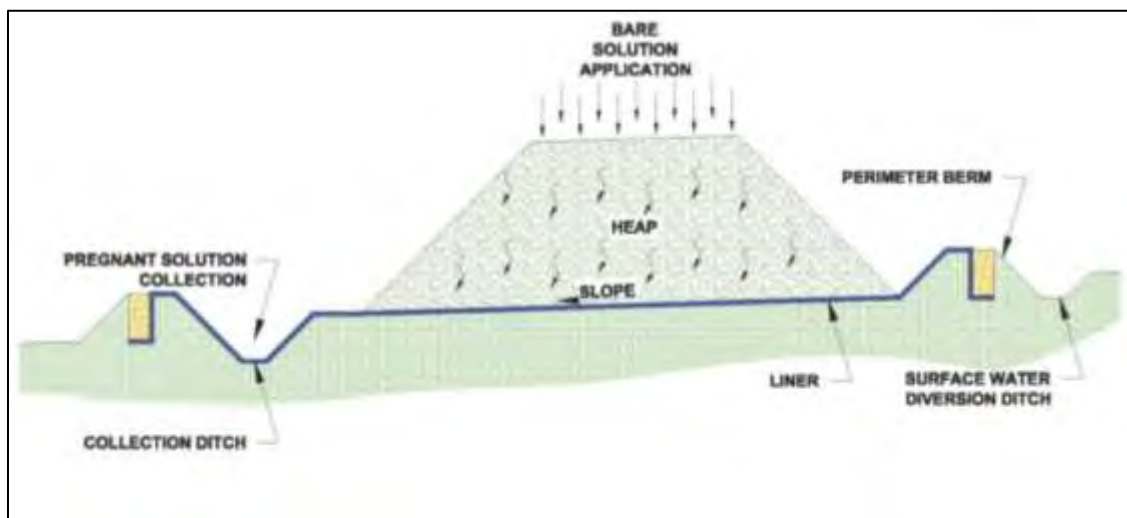


Figure 1. Heap and pad schematic.

Typical modern heaps have fill heights (ore depths) typically on the order of 100 meters, with some of the highest exceeding 160 m; heaps exceeding 240 m with 4 MPa normal stresses are in planning (Lupo, 2010). Ore is usually crushed to about the gradation of road base, but in some cases is processed without crushing (so-called run-of-mine or ROM) or only with primary crushing (nominally passing 150 to 200 mm). Ore is stacked either with trucks (and sometimes loaders) or conveyor-stacking systems in lifts ranging from less than 5 m to greater than 15 m in thickness, with about 7m being typical. Each lift is leached and then either overlain or removed and replaced. In the case of oxide copper ores, which can have very high acid consumptions, a thin inter-lift liner is usually placed before the leached lift is overlain.

There are four types of heap leach pads:

1. **Conventional or ‘flat’ pads** – relatively flat, either graded smooth or terrain contouring on gentle alluvial fans in relatively thin lifts typically between 5 m and 15 m. The ore is stacked, leached, and then overlain in a multi-stacked or permanent heap;
2. **Dump leach pads** – similar to flat pads or can include rolling terrain. The term ‘dump’ usually means that the lifts are much thicker at around 50 m and the ore very low grade and processed ROM or primary crushed only;
3. **Valley leach pads (VLPs)** – as the name suggests, these systems incorporate leach pads designed in natural valleys using either a buttress dam at the bottom of the valley, or a leveling fill within the valley. Buttress dam can be as high as 100 m but more typically are around 20 m. VLPs can be impounding, with process solution stored within the heap, or free draining; and,
4. **Dynamic heaps or on/off pads** – these are hybrid leach systems. A relatively flat pad is built using a robust liner and overliner system. Then a single lift of ore, from 4 m to 10 m thick, is loaded and leached. At the end of the leach cycle the spent ore, or ‘ripios’ in most mining literature, is rinsed and removed for disposal. The pad is then recharged with fresh ore and the process repeated for 10 to 25 years. Usually loaded with conveyers and stackers. In some cases, especially for large operations, bucket wheel excavators are used in the unloading cycle, while in others, wheel loaders and trucks are used. For on/off pads, the critical design loads for the containment system come from the ore handling equipment, not the weight of the ore. Trucks and loaders can apply wheel loads of up to 53 tonnes, with 24 tonnes being common, with considerable horizontal loading caused by braking and turning.

While the civil and geotechnical design criteria for each of these will differ depending upon site-specific constraints and ore types, the following points are universal:

- The pad should be laid out to accommodate the loading method, ore production rate, leach cycle, ultimate tonnage to be processed, surface hydrology for higher rainfall sites, closure and local topography;
- Lift heights are set to optimize recovery and for ease of operations; thicker lifts result in lower stacking costs (per tonne of ore) but longer leach cycles and, in some cases, lower metal recovery or higher reagent consumption;
- Constituents of the leach solution - water, acid or alkali, cyanide, organics, and so forth - need to be conserved as much as practical and can constitute a full 50% of total operating costs. Further, in many arid sites such as Northern Chile and Southern Peru, water availability (or lack thereof) can limit production;
- Designs must recognize the need to avoid mingling of process solutions (where applicable) and to withstand a designated storm event as well as manage the dilution created by lesser storm events. That is, small storm events are, out of necessity, mixed with pregnant solutions but larger storm events should be isolated where practical;

- The heap must be stable for both static and dynamic conditions, and geotechnical properties must include the potential for physical, chemical and biological degradation inherent in the heap leaching process. For low permeability ores especially in tropical climates, static liquefaction due to rapid stacking of either the heap or the ripios dump (for on/off pads) can also be a critical design factor. The seismic risk of these sites is often underestimated by engineers and operators more familiar with North America. Common design PGAs in Northern Chile are around 0.40g and a recent tailings dam project used 1.25g as the design event.

LINER SYSTEM DESIGN

While heap leaching is important to the mining industry for the reasons already articulated, it's important to the geosynthetics community for other reasons. Conventional milling requires a tailings disposal facility, which is a complex and important geotechnical structure and most firms engaged in the civil and geotechnical design of heap leach projects are also design tailings facilities. In the copper industry, less than 1% of the area of tailings facilities are lined with geomembranes. For gold the number is larger and increasing, but remains well under 50%. On the other hand, essentially 100% of leach pads are lined with at least one geomembrane and the average leach pad now exceeds 1M m² in lined area.

Integral to the design of the heap leach facility is the geomembrane liner system, which provides a physical barrier between the facility and open environment to contain the leach solutions. The liner system also influences the design of the solution collection system and overall stability of the facility. Liner systems for modern heap leach facilities employ a range of geosynthetic products, such as geomembrane liners, geotextiles, GCLs, geogrids, geonets, and plastic pipes to achieve the desired performance for solution containment, solution collection, and heap stability. The design of the heap leach facility and liner system is tailored to suite the unique conditions at each mine site, ore characteristics, and leaching methodology. That said, the vast majority of pad liners are either HDPE or LLDPE of 1.5 or 2.0mm thickness, often with the bottom textured and with a low permeability foundation (clay, silt or GCL).

A heap leach liner system design must consider the following (from bottom to top):

1. Foundation Layer – the suitability of local conditions not only to withstand the intended dead and live loads with acceptable deformation and stability, but to be chemically resistant to the leaching solutions in the likely event of leakage (e.g., much of Atacama Desert of Northern Chile is covered with a few meters of soils with high soluble salt contents);
2. Subdrain – some heap leach pads incorporate subdrains due to subsurface ground water conditions. This is especially true in tropical or high Andean sites, and for all valley leach pads;
3. Low-permeability layer – either a compacted soil liner or (much less commonly) geosynthetic clay liner (GCL) is usually used;
4. Geomembrane liner – a flexible membrane to act as a composite liner with the underlying low-permeability layer. Double geomembrane liners are rare but

increasing, and in some cases are required either by industry standards (e.g., impounding VLP) or local laws (for all leach pads in certain jurisdictions);

5. Overliner materials – a drainage or protective layer to facilitate draining the heap and protecting the geomembrane liner. This layer also provides physical separation between the geomembrane and the stacking or unloading equipment; and
6. Solution collection and air injection piping – pipes are needed to increase the solution collection within the gravel overliner, as well as to inject air, if needed.

These liner system details are similar to landfills with some modifications for different processes and regulatory criteria. However, while environmental containment is a key driver, so is metal recovery and reagent conservation. One main difference is the solution flow; for example, the process flow rates are much higher for heap leaching than typical landfill leachate flows. Typical irrigation rates are 10 to 15 L/hr per m² of irrigation area. Required irrigation areas are dictated by the ore processing rate, and 100,000 to 300,000 m² are common on larger projects. This results in flows of 1,000 to nearly 5,000 m³/hr. Whereas typical landfill leachate flows are on the order of 2 to 20 m³/hr. These larger flows require better solution collection (tighter pipe spacing) or heads can build up and cause instability, increase reagent consumption, impede aeration and retard metal recovery. With burial depths of 140 m to 160 m, the pipes are pushed to - and often beyond - their limits and drainage system failures are becoming more common in the industry (see Figures 2 and 3).



Figure 2. Sink hole on top of the heap at the Cerro Verde copper mine, Central Peru, which developed directly over a collapsed drainage pipe. In part because of failures like this, the Cerro Verde heap has experienced dramatic increases in the water level, to over 20 m above the liner, and some local liquefaction failures (see Figure 3).



Figure 3. Local liquefaction failure at the Cerro Verde copper heap leach, triggered by high solution levels. For scale, the benches are separated vertically by 7 m.

While the most common method of heap leaching is to continuously stack new ore over leached ore, and allow the process solutions to flow through the underlying layers, there are cases where this is impractical. The most common being acid leaching of oxide ores, which continue to consume acid even after the target metal has been extracted. This is the case with uranium, oxide copper, and nickel laterites. In these cases, thin liners are installed between each lift of ore. These so-called inter-lift liners serve the purpose of intercepting pregnant solution after it has penetrated (typically) the upper most lift of fresh ore. Since the inter-lift liners do not serve an environmental protection function, they are typically relatively thin. A small amount of leakage is acceptable as the primary cost of leakage is the value of the additional acid consumption. The use of inter-lift liners became popularized in Chile about 15 years ago and now there are perhaps a dozen major operations using this technology. One of the earliest such operations used very thin low density polyethylene (not linear low or LLDPE) with the seams sewn in a “J” fashion like a geotextile. Seepage was estimated by measuring the cumulative flow reporting to the lower inter-lift liners and the base environmental liner, and averaged about 3% of the flow over the top-most inter-lift liner. Modern systems with better quality liners and proper seaming methods report much less than 1% bypass, and 1 to 2% is commonly used for process calculations (Smith, 1996 and Smith & Welkner, 1994).

Heap leaching has been successful for gold, silver, uranium and copper and is starting to take shape for nickel laterites. Nickel laterites have three major differences from the more traditional heap leach ores: (i) the ores are more soil-like than rock-like, (ii) the reagent (sulfuric acid) consumption is dramatically higher than for copper or uranium, and (iii) the process produces a significant quantity of plant filtrate (chemical tailings) that require aggressive management and containment. A typical nickel laterite ore will consume 500 kg of concentrated acid per tonne of ore, compared to well under 50 kg for most copper and uranium ores. This

high acid consumption also correlated to significant degradation of the physical properties of the ore, and nickel laterites can experience permeability reductions of several orders of magnitude during the leaching process. This makes heap leaching very challenging and while this application has been the subject of intensive research and pilot-scale testing over the past 15 years, there has only been one small-scale commercial operation (the Murin Murin mine in Northern Australia). On the other hand, the attraction of this technology is similar to gold and copper: heap leaching offers much lower capital costs as compared to the traditional processing methods of smelting or high pressure acid leaching (HPAL), and heap leaching is metallurgically-compatible with a wider range of ore types thus increasing resources for many projects. And while heap leaching has had a robust history of success for every mineral to which it's been applied, the primary hydrometallurgical process for nickel laterites, HPAL, has had more failures than successes, some of which spectacular; recent examples include the Ravensthorpe mine (owner: Australian miner BHP) in Western Australia, which resulted in a 90% write-off of the \$3.8 billion capital investment, and the Goro mine (owner: Brazilian miner Vale) in New Caledonia, which was built at total cost of over \$6 billion, versus the original estimate of \$1.8, and has little hope of ever recuperating that investment. It's no surprise, therefore, that every major nickel producer is currently studying heap leaching and large-scale pilot plants have or are operating in Australia, Turkey, Brazil, Colombia, China and the Philippines.

HEAP CONSTRUCTION

The construction or stacking of heaps involves placement of ore in controlled, loose and relatively dry lifts stacked with face angles at the natural angle-of-repose, with set-back benches between lifts to provide stable overall slopes as well as erosion control, as shown in Figure 3. Each lift is irrigated using drip emitters or, less commonly, sprinklers (either “wobblers” or “rain bird” style impact sprinklers). Leaching is generally conducted in a few months (gold, silver, uranium and oxide copper) to about 1-1/2 years (sulfide copper and nickel laterites) leach cycles. Irrigation solutions can be either recirculated leach solutions to upgrade the metal tenor, or fresh solvents (dilute high pH cyanide for gold and silver, weak sulfuric acid for uranium and copper, and strong sulfuric acid for nickel). The longer leach cycles require larger leach pad areas, stretching some facilities to dimensions in kilometers; as an example, the 2013 expansion of the Escondida copper bio-leach facility in Northern Chile will bring the leach pad's overall dimensions to 2 km x 5 km, or 10M m². This is one of three heap leach circuits plus a traditional mill and concentrator) at the Escondida complex.

The maximum rock particle size of ore ranges from ROM (cobble and boulder sizes) to the more common crushed sand and gravel sizes (most commonly, 90% passing, or P90, of 10 mm to 25 mm). The crusher operations often include agglomeration to provide a more efficient distribution and binding of fines for improved and more uniform permeability, reduced fines migration and, ultimately, better recovery of the target metals. The individual ore lifts are offset with benches along the exterior slope for stability, but also for operations. This “loose” stacking facilities solution application and desired permeability for leaching. The bench faces are not compacted, which is opposite for landfills. Landfills are compacted as dense as practical to maximize air space utilization, increase stability and reduce long-term settlement. This is another good example of the difference in drivers between heap leaching and municipal waste landfilling. A schematic section of the exterior ore heap slope is shown in Figure 4.

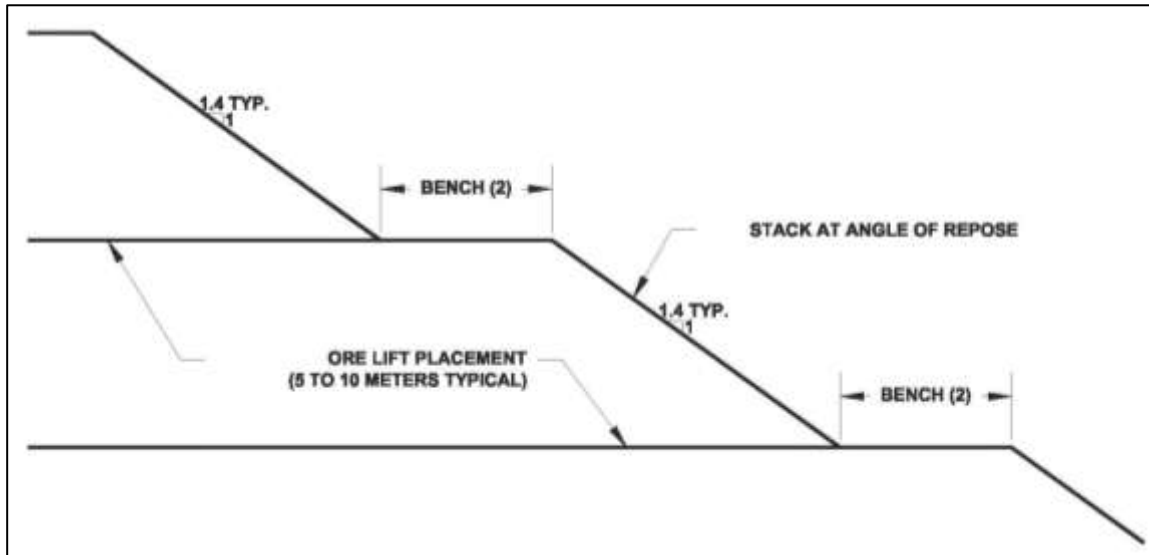


Figure 4. Typical cross section showing individual lifts and offset benches along exterior slope of heap leach pad to provide stability.

Ore is stacked a number of ways depending upon the shape of the leach pad, production rates and ore particle size. Transport to the edge of the pad can be by trucks or overland conveyor. For relatively low tonnage rate operations or those using very large particle sizes (either ROM or primary crush only, such as at Escondida), truck stacking is the most common approach. The larger the project, however, the more the economics tend towards conveyor distribution and stacking, as shown in Figure 5. This is also a less stressful way to place the ore and generally improves hydraulic performance. A method pioneered at the Mantoverde copper mine in Chile incorporates advancing the liner system at the same time as the heap is stacked, thus avoiding the need for a protective cover system to isolate the stacking equipment from the geomembrane (Figures 7 & 8). Drainage is accomplished by placing perforated pipes at relatively close spacing. This method is only suitable for well-drained ores of sufficiently fine gradation to not puncture the liner. This loose stacking of ore again facilitates the solution application by maintaining permeability of the ore without compacting it with repeated truck traffic. Pipe spacing might be as close as 2 m for higher irrigation rates or ores of modest permeability.

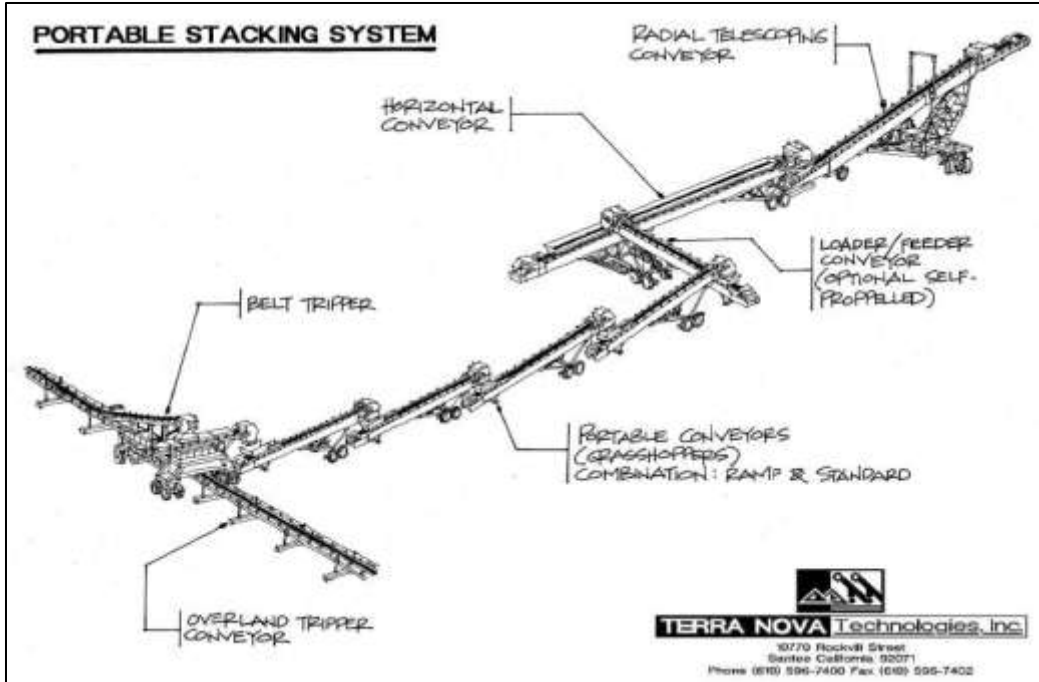


Figure 5. Portable stacking system consisting of tripper, grasshoppers, horizontal conveyors, and radial stacker.



Figure 6. View of heap leach pad being stacked with portable grasshopper conveyors.



Figure 7. Mantoverde-style liner deployment showing ore being stacked soon after liner is placed.



Figure 8. Solution collection system ready to be deployed in advance of ore stacking.

HISTORIC STABILITY PERFORMANCE

One of the earliest and best known large-scale geomembrane-related slope failures was the Kettleman Hills landfill slope failure in Northern California in 1988 (Mitchell et al. 1990). Several major landfill slope failures occurred between 1988 and 1997 in North America, Europe, Africa and South America (Koerner and Soong 1999). Several less known leach pad slope failures occurred at about the same time (1985 to 1993) at mine sites in North America, South America and Australia (Breitenbach 1997). The Northridge earthquake in Southern California in 1994 (Matasovic et al. 1995) and subsequent earthquakes in Chile and Peru in 1995 and 1996 gave some insight into the seismic behavior of high fills on geomembrane liner systems.

The historic performance of fills on geomembrane liner systems indicates that translational (lateral movement) wedge slip failures generally occur along the planar liner interface contact with soils or geosynthetic materials. However, heap failures differ from landfill failures in that the slope failure often occurs during the initial ore heap fill lift placement operations, rather than at the greater heights (Breitenbach, 2003; Smith & Giroud, 2000).

The known slope failures from weak foundation conditions beneath the liner system included a combination of one or more of the following: re-activating an existing landslide surface, thawing of frozen subgrade soils, overly wet subgrade (natural soils or underliner fills), subgrade subsidence in compressible natural soils or low density fills, and excavations at critical downgradient fill toe areas that caused unloading of toe support materials. The known slope failures from excessive hydraulic conditions above the liner system included a combination of one or more of the following: intense rain storm events, poor internal containment material drainage, excess solution application on the surface or injection into the heap (a method occasionally used for secondary recovery from low permeability ores), or solution pipeline breaks near exterior fill slopes and causing localized saturation. These high fill slope failure exceptions are rare in occurrence and can be eliminated or mitigated at the end of operations into closure. They also tend to be modest in terms of the damage they do, and rarely do they put the base liner system at risk.

For the non-miners, an interesting comparison of heap leach pads and landfills is discussed by Breitenbach & Thiel (2009).

LINER INTERFACE STRENGTHS

There is nothing particularly different in heap leach stability versus landfill stability; however, some important research has come out of heap leach design. With heaps pushing 160 meters in height and ore densities much greater than municipal solid wastes (bulk wet specific gravities of about 2.0), normal stresses on the liner system are generally much higher for leach pads than landfills. And with impounding VLPs, water levels and associated hydraulic heads on the liners can be much higher than landfills (up to 45 m).

Large-scale laboratory direct shear (LSDS) test results from studying the long-term liner performance under high loads indicate the geomembrane liner interface contact with underlying and overlying materials gains strength with time (Breitenbach and Swan 1999). The time-dependent increase in liner interface peak and residual shear strength is mainly due to two

conditions: 1) the apparent effect of high load deformations or dimpling on a micro scale in the planar geomembrane liner surface, and 2) a reduction in excess pore pressures in the low permeability base soils. The measured cohesion or apparent adhesion in the study decreased with time and were assumed to be negligible for conservative long-term liner strength conditions. Degradation of the overliner due to chemical attack can more than compensate for these increases and, thus, it's important for any testing program to consider this factor.

SEISMIC BEHAVIOR

Similar with landfills, leach pads are large earthen structures subject to an array of motions during a seismic event. Durkee, et. al. (2003) describe the seismic slope stability and deformation analyses for a heap leach facility. The performance is typically evaluated using analytical methods developed for earth embankments. In particular, pseudo-static slope stability and seismically-induced permanent deformation analyses are commonly employed. Since the anticipated time of construction and operation of a heap leach facility is relatively short at 10 to 20 years, and post-operational stability is generally less critical, pseudo-static methods are employed using the ground acceleration associated with the operational basis earthquake (OBE) to estimate the factor of safety during the working life of the heap leach. When post-operational (long-term) conditions are evaluated (e.g. reclamation, closure and post-closure), the design ground acceleration is often based on the maximum design earthquake (MDE). The higher acceleration associated with the MDE often produces pseudo-static factors of safety of less than one, therefore displacement analyses are often performed. Both the Newmark-type analysis developed by Makdisi and Seed (1978) and simplified Bray & Travasarou (2009) methods can be used to determine seismic displacements.

A case in point, with heap leach pads in high seismic areas such as Chile, Peru and Turkey, the intensity of the seismic shaking with PGAs of 0.35 (Chile, Peru) to 0.49 (Turkey) are high compared to the relatively modest values in California.

HEAP LEACHING ISSUES IN SOUTH AMERICA

Steep Terrain: Breitenbach and Smith (2012) identified some 26 valley leach pads (VLPs) in Latin America, and in the last decade 90% of those built in the world were in Latin America. VLPs, especially those with internal solution impoundments, present special design and operational considerations ranging from steep base slopes and challenging site grading to extreme ore depths (now exceeding 160m) and complex leach kinetics. The popularity of this technology stems in part from the mining boom, but it is also a result of the technology's success at projects like Barrick's Pierina gold mine in Peru (commissioned in 1998 and for the first few years of its life was the lowest cash cost gold producer in the world). There is now a blurring of the line between conventional leach pads (CLPs) and VLPs with flat pad designs now routinely incorporating steeper and variable slopes, terrain-contour grading, innovative overliner systems and other advancements pioneered on VLPs, pushing the importance of heap stability (Lupo, 2008). The identifying trait that distinguishes VLPs from CLPs is that two or three sides of the heap are contained by natural valley wall topography. This also tends to result in a relatively steep longitudinal slope (the axis of the valley), often in excess of 10% or even 20%. For this reason, VLPs commonly require a supporting buttress at the downstream toe, and this buttress can then be used to create an internal impoundment to store process solutions or extreme storm

events in the ore's available porosity. When internal ponds are used the resulting hydraulic heads can be extreme; in the case of Pierina, for example, the peak seasonal water level is about 45 m over the primary liner. In addition to increasing the leakage through the liner, this can also make the heap more vulnerable to liquefaction (static or dynamic). Leaching kinetics can also be affected, since a greater portion of the heap is saturated (or nearly saturated), and closure can be much more complex since heap rinsing and detoxification can require more time and effort, and ensuring long-term drainage a challenge (Breitenbach and Smith, 2012).

Crushing size: Metal recovery is related to crushing size, with finer particles generally allowing better recovery. With increasing metal prices the economic break-even point has moved to finer and finer particle sizes. But, finer gradations generally result in lower permeability and lower shear strength. For the same irrigation rate, lower permeability means higher degrees of saturation and, potentially, higher phreatic levels - decreasing stability and increasing the risk of liquefaction. It also means less air movement, which can retard leaching kinetics.

Liner systems: As projects are constructed in more challenging terrain, geosynthetic clay liners (GCLs) are becoming more popular, either to replace the clay underliner or to solve specific steep slope issues. Recent projects in Peru and Mexico have produced costs for compacted clay liners (CCLs) of up to \$15/m³, or \$6.00/m² for a 400mm-thick clay layer. The time to install a CCL can be on the critical path and, as any construction manager will attest, clay work is a high-risk task with cost over-runs and delays the norm. GCLs eliminate most budget and schedule risks while often providing superior leak prevention at similar costs. This is no news to landfill designers and operators, but is only recently becoming accepted in the mining industry.

Elevated temperatures: Most testing and design analyses for liner and drainage systems are performed at standard ambient temperatures of about 20°C. However, bio-leaching, the most common technology used for copper ores, can increase temperatures to at least 40°C. This increases the puncturing potential of geomembrane liners and makes polyethylene pipes more vulnerable to collapse. For example, standard dual-wall corrugated pipe behaves well under 140 m of burial at 23°C but collapses at 100 m depth when the temperature is increased to 50°C (Sinha & Smith, 2012).

Heap Drainage: The importance of heap drainage and controlling hydraulic head over the liner for heap stability cannot be overstated (Thiel & Christie, 2005). Overliner placement on steep slopes is often impractical or presents an unacceptable risk to either the liner integrity or worker safety. At other sites, suitable aggregate simply isn't available, a common problem at tropical and semi-tropical locations. In these projects an emerging technology to either replace or reduce the amount of high-quality gravel is the use of drainage geocomposites, which are cost competitive with a conventional gravel overliner. Where the stacking equipment is working on top of the active lift ("advance" stacking), a geocomposite can often completely replace the gravel overliner. For retreat stacking, where the stacker operates directly on the overliner, a geocomposite can be used for drainage and a lower-quality gravel (i.e., primary crushed ore) above that for physical separation. Cost comparisons on several projects have shown that the geocomposite system can be lower in cost to a conventional gravel overliner. This approach also

reduces construction time and lowers the risk of damage to the liner, most of which occurs when the gravel is placed (Smith & Li, 2012).

Limited Skilled Contractors: Countries with mining history (e.g., Chile) tend to have available skilled contractors for complex work items (clay, geomembrane, and dam construction). In countries with emerging mining industry, such as Argentina and Panama, this is a serious limitation that adversely affects an engineer's choice of technologies, construction schedule, and the project's success rate. Limited access to heavy earth moving equipment also slows production. During the construction of the VLP at Pierina (Peru, 1997-1998), the earthworks required five contractors and every available haul truck - 125 at peak construction. These delays strain owner schedules, increase the risk of cost overruns, delays and commissioning problems. The importance of schedules in mining is hard to overstate; the average production of a large copper mine is about 150,000 tonnes of copper annually. At current metal prices, the value of a lost day is now over \$3,000,000. And it's common for the construction manager to share in the delay-induced losses.

High Elevations: The typical copper or gold mine in Peru and Chile is at an elevation or around 4,000 m. The Pascua-Lama mine, currently under construction, straddles the Andes; the haul road exits the mine at an elevation of 5,100 m. Other than extreme weather, the issues at high altitude include (a) worker productivity, including mental clarity and increased propensity for errors, (b) worker safety and higher accident rates and the increase risk of fatalities; and (c) equipment productivity, as engines and motors require down-grading for horsepower at altitude, which means trucks move slower and pumps deliver less head, and consequently move less material. While some of this is easy to account for, such as engine and motor factoring, worker productivity and safety are often inadequately considered in planning, at considerable costs to owners, operators and contractors.

Extreme Weather: High rainfall and high altitude Andean sites add to the difficulty of construction as well as the need for design measures to divert severe peak events from inundating pads and ponds. Depending upon the site, the "dry" season may only provide a few months for construction and even then extreme events can create havoc. A case in point: one mine in Northern Sonora, Mexico, received over 490 mm of rainfall in July 2012, higher than the greatest annual rainfall on record. Such severities can cause delays in construction, damage constructed or under-construction areas, and even overtop the emergency ponds. They also increase the needed time to construct and commission in unpredictable ways. The high altitude, cold climate Andean sites offer another degree of difficulty requiring safety measures for workers and can slow productivity. Cold weather and wind can adversely affect access roads and create life-threatening conditions. Winds are stronger and more erratic at higher elevations; at Pascua-Lama winds in excess of 140 km/hr are common and the highest winds destroyed the recording station, literally ripping the station, tower and concrete footings out of the rock and tossing them down the mountain. Another Andean site had a gust of wind lift a geomembrane panel during placement, causing the technician standing on the liner to be thrown in the air and land on his head, compressing vertebrae in his neck.

Tropical and Andean projects can experience very high annual rainfall, with average annual precipitations from 1,000 mm to over 4,000 mm common. Storms can also be very intense, with peak rainfall of over 200 mm in a few hours, or 500 mm in a few days. The high

annual rainfall presents problems of surplus water, both in terms of water management, and making some construction activities very difficult or impossible (including operation of the stacking equipment as well as deploying liners). Intense storms can also damage agglomerated ore, creating impervious surfaces and zones of channeling within the heap and otherwise impede leaching. Average moisture content in the as-stacked ore can also be increased to the point of creating a risk of static liquefaction. One of the techniques almost universally used to manage high rainfall is the application of temporary geomembrane covers or “raincoats.” More specifically, a raincoat is placed over the heap to shed rainwater before it enters the process circuit. An industry review updated in 2008 found 34 heap leach projects that have used or are planning to use raincoats (Stemson, et al 2010).



Figure 9. Currently the largest use of raincoats is at the Lagunas Norte gold mine in northern Peru with approximately 30 ha installed (Sept. 2012).

Limited Knowledge: A lack of regulatory capacity in developing countries strains the local regulators faced with complex, modern projects. For example, the requirement for leak detection without the technology or what constitutes reasonable leakage rates is endemic in the developing world. Mexico allows shallow French drains, which are highly unreliable and give false confidence. Argentina, on the other hand, requires reasonably advanced leak detection (including, in some cases, double geomembrane liners) but has an expectation of zero leakage. Developing countries have limited resources and expertise for robust construction observation. Installation quality is often much lower than owner, regulator or community expectations. All of which results in higher leakage rates and corresponding higher metal loss, increased environmental risk and more regulatory intervention. The solution requires the design to

anticipate these potential shortcomings, and keep it as simple as possible. Ideally, a very high level of interaction with the affected stakeholders including in many cases educational outreach programs is required.

Remote Areas: Difficult access can affect equipment and contractor selection and can also affect recruiting for key positions, especially in a robust labor market. For example, Rio Tinto's La Granja site in Peru is only 220 km from Trujillo, a major city in Northern Peru, yet a 10 hour drive. In addition, the drug cartels have increased risks in Northern Mexico and Northern Peru and companies are placing restrictions on travel to these areas, thereby restricting experienced professionals from site visits. Many of the sites are adjacent to known drug cartels in Mexico and there are large areas in Peru and Colombia where any travel requires a military escort (on one of the authors' projects, the Peruvian military refused to provide escort!)

EMERGING TECHNOLOGIES

Electrical Leak Location (ELL): Well established in the North American landfill industry, this technology is only recently gaining traction in mining. There is already growing experience with leak testing in Peru, Argentina and Chile, and some jurisdictions are starting to make ELL surveys strongly recommended or even mandatory. Thiel, et al (2005) and Beck & Smith (2006) studied the economic benefits of this technology and found the ratio of benefit (reduced metal loss) to the cost of the surveys as high as 12 with very short payback periods. And this is before considering the harder to quantify but potentially much more important benefits of reduced environmental and social impacts.

While this technology is seeing a rapid growth in popularity among South American mining operations, a yet-to-be-tested benefit is the potential to perform routine verification of containment for on-off pads (dynamic heaps). With a conductive substrate (or a liner with a conductive bottom) and a little attention to detail, a leach pad could be surveyed for damage during each unloading cycle. It's only logical that the high benefit-cost ratio of ELL surveys on initial installations would accrue to the cyclic loading conditions of a dynamic heap. This is another way to increase profits, reduce the likelihood of failure, and improve the relationship between miners and stakeholders.

Thermal Covers: Seasonal low temperatures, especially at high altitudes, can retard leaching kinetics, extending leach cycles and reducing metal production. This is especially important for bio-leaching, where the effectiveness of the bacteria is much more susceptible to temperature than non-biological kinetics. Capturing solar radiation and reducing convection losses can add several degrees to the lowest seasonal temperatures, accelerating kinetics or adding weeks or months to the available leach time (or reducing the required leach time and thereby increasing production rates). Measurements at one pilot facility reported temperatures in the irrigation system immediately below the cover a full 35°C above ambient, which produced leach rates significantly faster than predicted from ambient temperature column tests. A large pilot test of thermal covers is currently underway in the Western United States and another is in planning in South America, both for bio-leach facilities.

Evaporative Covers: In many mining areas, including Northern Mexico, Southern Peru and much of Chile, water availability is a key issue and often a restriction. For example, in

Chile's copper district (Region 2), recent expansions at Escondida have required the construction of a large desalinization plant near Antofagasta and a 160 km pipeline - with a static head of 3,000 meters - to the mine site. Southern Peru Copper Co. is also considering desalinization for their increasing water needs. Total cost for water, including capital amortization and pumping, can exceed \$3.50/m³, and processing commonly uses 0.5 m³ or more of water per tonne of ore. Evaporation rates in the Chilean Atacama often exceed 3,000 mm/year, producing \$10.50/m² per year in the value of water lost to evaporation. Geomembrane covers can reduce evaporative losses to near zero and the payback period for these is often on the order of 1 to 2 years. There can also be considerable social benefit from taking aggressive and visible efforts to reduce water consumption in areas that have water shortages affecting agriculture and other key industries. Evaporative covers also have the benefit of reducing salt formation on top of the heaps, which can limit percolation and affect recoveries (see Figure 10).



(a) Without a raincoat



(b) With a raincoat

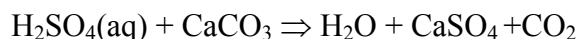
Figure 10. Nickel pilot heaps without and with raincoats, showing the reduction in evaporative salt formations. Such salts can significantly impair percolation and thereby leaching efficiencies. The salts also contain targeted metals, thus reducing recovery.

Evaporation control: Water supply is becoming one of the key areas limiting expansion of mining. In some areas, such as the Atacama and Namib deserts, water is so scarce that new projects are limited by their ability to either import (e.g., trans-national pipelines) or create (e.g., desalinization) fresh water. Limited water opens the door to spending a little money to reduce water demand in exchange for allowing higher mineral processing rates. Floating pond covers is the most obvious idea; with desert evaporation rates and high water costs, the economics pencil out even before considering other benefits like reagent consumption and reduced contamination in the final product (i.e., through dust and debris) as shown:

Floating cover installed cost: \$15 to 20/m²
Value of water savings: 3,000mm/m²/yr x \$3.50/m³ = \$10.50/m²/yr
Payback period = 17 to 23 months

Strong acid environments: Geomembrane properties are affected by strong acids, a long-known and long-avoided fact. Exactly how much the performance degrades is quite simply not well known but of course is of interest, especially with design lives now routinely exceeding 20 years and strong-acid agglomeration commonplace. Limited antidotal and even more limited laboratory data suggests some softening of HDPE & LLDPE and embrittlement of PVC and these affects are intensified at elevated temperatures. A recently completed and critically important study into this phenomenon carried out at Queen's University suggests that HDPE and LLDPE geomembranes perform well in acidic leach solutions, with OIT depletion rates slower than for MSW landfill leachates (Abdelaal, F. B., et al 2012).

ARD reduction and carbon credits: Mine wastes, including spent heap leach ore, are well known for their potential to produce acid rock drainage, a phenomenon related to the weathering of pyritic minerals and compounded by residual acids from the leach cycle. The acid then mobilizes heavy metals either in the same waste or present beneath the acid-producing wastes. The production of acid drainage requires oxygen, and unsaturated soil or clay covers do little to restrict air transport via barometric "pumping" from the top and exposed slopes. Geomembranes, on the other hand, can be excellent air barriers and installation of a geomembrane capping system can sufficiently reduce the availability of oxygen to prevent or significantly retard generation of acid. In addition to the obvious savings in long-term ARD treatment costs and the related reduction in environmental and social liabilities, for sites located in the developing world there may also be marketable carbon credits available since the neutralization of acid, whether naturally or via a treatment plant, releases vast quantities of CO₂. Consider a dump with an acid potential of 100 kg per tonne of waste; neutralization of that acid will produce carbon dioxide according to the following equation:



Thus, properly sealing the dump from oxygen and suppressing the acid reaction can produce 0.045 tonnes of carbon credits per tonne of waste. The European carbon market values these credits in the range of US\$20 to \$30 per tonne of CO₂, equating to \$0.88 to \$1.32 per tonne of waste. For a copper mine producing 25 to 100 million tonnes of spent ore annually, a fairly common range, this can make a meaningful impact to the bottom line.

CONCLUSIONS

This paper has shown the history and importance of heap leaching on the heavy metal mining industry, which in turn has shown the uses and importance of geosynthetics to mining. The heap leach projects are some of the largest users of geomembranes, by some estimates consuming 40% of all geomembrane produced, and continued uses are still being developed. The use of strong acids and bases, as well as extreme environments push the geosynthetics to their limits, but have shown to be an integral part of the mining industry's modern success.

REFERENCES

- Abdelaal, F. B., Rowe, R. K., Smith, M. E., Brachman, R. W. I. and Thiel, R. (2012), "OIT depletion of HDPE and LLDPE without HALS in extremely low pH solution," to be presented at and published in the proc of Second Pan American Geosynthetics Conference & Exhibition, Geoamericas 2012, Lima, Peru, May.
- Breitenbach, A. J. and Smith, M. E. (2012), "Design considerations for impounding valley leach pads v. conventional," Mining Engineering, Vol. 64, No. 7, pp. 49-55, July.
- Breitenbach, A. J. and Thiel, R. S. (2009), "A Tale of Two Conditions: Heap Leach Pad versus Landfill Liner Strengths"
- Breitenbach, A. J., (2003), "Improvement in Slope Stability Performance of Lined Heap Leach Pads from Design to Operation and Closure"
- Durkee, D.B., Augello, A.J., Joshi, B., and Kidd, D.A. (2003), "Seismic Slope Stability & Deformation Analyses for a Heap Leach Facility", Tailings & Mine Waste Conference.
- Leduc, Marc, Bachens, M. and Smith, M.E. (2004), "Tailings Co-Disposal™ & Sustainable Development," proceedings of the annual meeting of the Society of Mining Engineers, February.
- Lupo, J. F. (2008) "Steep Terrain Heap Leach Pad Liner System Design", The First Pan American Geosynthetics Conference & Exhibition, Cancun, Mexico
- Lupo, J. F. (2010) "Liner System Design for Heap Leach Pads", Geotextiles and Geomembranes, 28(2), 163-173
- Mining and Metallurgy,
http://www.miningandmetallurgy.com/gold/html/design_and_operation_of_heap_1.html
- Smith, M. E. (2011) "Emerging Trends in Heap Leach Containment", The Mining Record, Dec.
- Smith, M.E. and Giroud, J. P. (2000), "Influence of the Direction of Ore Placement on the Stability of Ore Heaps on Geomembrane-Lined Pads," Slope Stability in Surface Mining, Chapter 49, Society of Mining Engineers, Hustrulid, W.A., M.K. McCarter and D.J.A. van Zyl, Eds.
- Smith, M.E. and Leduc, M. (2003), "Tailings Co-disposal: Innovations for Cost Savings and Liability Reduction," The Mining Record, September.
- Smith, M.E. (1996), "Inter-life Liners in Copper Heap Leaching," The Mining Record, July.
- Smith, M.E. and Welkner, P.M. (1994), "Liner Systems in Chilean Copper Heap Leaching," SME Annual Meeting, Preprint #94-95, Albuquerque, NV, Feb. 14-17.

Stemson, M.L., Sepulveda, C. and Smith, M.E. (2010), “Water Management in Tropical Nickel Laterite Heap Leach Projects,” proceedings of II International Congress on Water Management in the Mining Industry, Santiago, Chile, June.

Thiel, R., A. Beck and Smith, M. E. (2005), “The value of geoelectric leak detection services for the mining industry,” GRI-18 Geosynthetics Research & Development in Progress.

Thiel, R. S. and Christie, M. A. (2005), “Leachate Recirculation and Potential Concerns on Landfill Stability”, North American Geosynthetic Society Conference.

Ulrich, B., Andrade, H., and Gardner, T. (2003), “Lessons Learnt from Heap Leaching Operations in South America – An Update”, The Journal of The South African Institute of Mining and Metallurgy

GEOSYNTHETIC DESIGN METHODS USED IN ROADWAY APPLICATIONS

Robert M. Koerner
Geosynthetic Institute, Folsom, PA USA

ABSTRACT

From the very beginnings of geosynthetics roadways have been a major application area. Geotextiles were used successfully on soft subgrade soils for unpaved roads since the 1970's. Geotextiles for prevention of reflective cracking in asphalt overlays began in the 1980's. Geogrids within stone base aggregate for paved and unpaved roads, as well as railroads, began shortly thereafter. Considering the tremendous amount of roadways of all types, however, many feel (the author included) that the full potential of geotextiles and geogrids in roadway applications is largely unfulfilled. One reason is perhaps because the necessary design methodology is either unavailable or overlaps the various functions that may be simultaneously occurring, i.e., a specific design methodology for each mechanism is yet to be developed and moreover accepted by the owner/regulatory community.

This paper, essentially a review of available design methods for each mechanism, purposely distinguishes between four unique functions that geosynthetics provide in roadway applications. They are the following:

1. Geotextiles and/or geogrids used for reinforcement of soft soil subgrades for unpaved roads.
2. Geotextiles used for separation on firm soil subgrades for paved and unpaved roads
3. Geogrids used for reinforcement within stone base aggregates on firm subgrades for paved and unpaved roads
4. Geotextiles or geogrids used for waterproofing or reinforcement of reflective cracking in asphalt overlays of paved roads

The state-of-the-practice insofar as design is concerned will be presented in each of these four discrete areas. The perceived status of geosynthetics in roadways and recommendations going forward will be offered as well.

1.0 INTRODUCTION AND BACKGROUND

Stabilization of unsuitable subgrade soil for the purpose of constructing a pathway, aka a roadway, dates back to 3000 B.C. with the use of split-log *corduroy* roads over peat bogs (Dewar, 1962). The ridged surfaces were filled with available soils but the deterioration of the timber and particularly its lashing was an obvious problem. Many variations on this theme ensued including tar and bitumen surfaces and then concrete, but for the purposes of this paper, the paradigm change was made in 1926 by the South Carolina Highway Department (Beckham and Mills, 1935). A heavy cotton fabric was placed on a primed soil base, hot asphalt was applied to it and then a thin layer of sand used as the wearing surface. Eight field test sites of such unpaved roads were conducted. Until the cotton fabric deteriorated, the roads were in good

condition in that there was reduced cracking, raveling and backfill failures. This project was clearly the forerunner of the separation and reinforcement functions of polymeric geosynthetics as we know them today.

It is common knowledge that the amount of present roadways is enormous. Table 2 gives some statistics in this regard. Clearly, roads are vital to our way of life and an area in which geosynthetics have made some positive strides (as will be seen) but there is much more that can and should be done. This paper focuses on the main functions offered by geosynthetics used in roadway applications insofar as what has been accomplished over the past 25-years and where we might be venturing into the future. They are geotextiles and/or geogrids used for both unpaved and paved roads, for the functions of separation, reinforcement and waterproofing.

Table 1(a) - Roads in the USA in 2008 (Federal Highway Administration)

Type	Length (kilometers)	Length (miles)
unpaved	2,132,000	1,324,000
paved with asphalt	1,451,000	901,000
paved with concrete	84,000	52,000
paved but unspecified	2,867,000	1,781,000

Table 1(b) - Roads in Selected Countries in 2009
(World Road Statistics - International Road Federation)

Country	Major Roads (Paved ?)		Secondary Roads (Unpaved ?)	
	kilometers	miles	kilometers	miles
China	97,000	60,000	3,402,000	2,113,000
Japan	61,000	38,000	1,135,000	705,000
Germany	53,000	33,000	592,000	368,000
France	21,000	13,000	931,000	578,000
United Kingdom	53,000	33,000	367,000	228,000
United States	351,000	218,000	6,183,000	3,840,000

1.1 Overview of Geotextiles or Geogrids Used for Reinforcement of Soft Soil Subgrades for Unpaved Roads

Unpaved roads (also called secondary roads, farm-to-market roads, access roads and haul roads) represent a tremendous opportunity for geosynthetics, primarily geotextiles or geogrids. The situation generally focuses on soft soil subgrades which have the geotextile or geogrid placed directly on the ground surface even with the natural vegetation remaining in place. A stone base course (of varying types and thicknesses) is placed on the geosynthetic material. No permanent surfacing (i.e., concrete or asphalt pavement) is placed on the stone. At most, the road is surfaced with quarry crusher run or chip seal for reasonable ridability. At a later time, perhaps years after settlement takes place and ruts are backfilled, a permanent surfacing may be placed if the traffic warrants such an expenditure.

This particular application has triggered the high-volume use and acceptance of geotextiles in the 1970s followed thereafter by geogrids, since calculations can be made for the thickness of stone required both without a geosynthetic and then with a geosynthetic; the difference being the thickness of stone that is saved. By determining the cost of stone saved

versus the cost of the geosynthetic, the savings in using the geosynthetic is known immediately. The particular design process used in arriving at the respective thicknesses is obviously critical and will be described later.

That said, it is important to realize that the geosynthetic must have its tensile modulus or strength mobilized via deformation of the soil subgrade. The yielding of the soil subgrade is the triggering phenomenon, allowing for geosynthetic deformation and the mobilization of its tensile properties. How much deformation is necessary with regard to the vehicular loading, the particular geosynthetic, the time it takes for adequate strength mobilization, and so on, are all pressing questions, but the deformation of the soil subgrade is critical. A soft, yielding soil subgrade is needed to mobilize the geosynthetic's strength—but how soft? In light of the tremendous variety of assessments, most transportation engineers use a broad generality which is based on the California Bearing Ratio (CBR) of the soil subgrade. The CBR test is used throughout the world and standardized accordingly; e.g., see ASTM D1883. The CBR value is a comparison of the soil's resistance to the force of a 50 mm diameter plunger at a given deformation with that of a crushed stone-base material. It is actually a percentage value, although it is rarely expressed as such. The test on the soil subgrade can be performed either at the in-situ moisture content or the soil can be saturated for 24 hr and then tested. These two conditions give rise to unsoaked and soaked CBR values, respectively. Typical values are given in Table 2 where it is seen that soaked CBR values are generally lower than unsoaked values, but the difference greatly depends on the soil type.

Table 2 - Recommended Soil Subgrade CBR Values to Distinguish Different Geosynthetic Functions in Roadway Applications

Geosynthetic Function(s)	CBR - Value	
	Unsoaked	Soaked
Separation	≥ 8	≥ 3
Stabilization*	8-3	3-1
Reinforcement and Separation	≤ 3	≤ 1

*a frequently used but poorly defined transition term that always includes separation, some unknown amount of reinforcement, and often filtration as well.

Insofar as an approximate generalization as to when geotextiles or geogrids are used for unpaved roads as a function of unsoaked CBR values of the soil subgrade strength, see Figure 1. Clearly, base course thickness reduction factors increase as soil subgrade CBR's decrease. The figure also attempts to distinguish between different types of geotextiles and geogrids. That said, it does not attempt to distinguish between individual properties within each type of geosynthetic material. It is presented here only as a guide since the more analytic and product specific approaches are offered later in this paper.

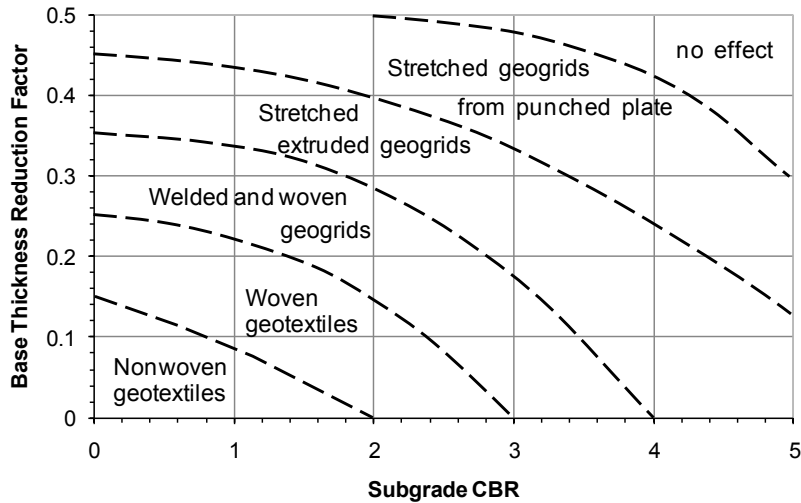


Figure 1. Reduction of roadway base course thickness using various geosynthetics. (After van Gurp and van Leest [2002])

1.2 Overview Geotextiles Used for Separation on Firm Soil Subgrades for Paved and Unpaved Roads

Irrespective of whether the road surface is unpaved or paved, the stone base will be placed directly on the soil subgrade. Depending on the site-specific circumstances, most notably the soil's stiffness and moisture regime at this interface, a gradual movement of soil up into the gravel and the associated gravel down into the soil will occur. This is shown schematically in Figure 2. As indicated, the preservation of this original boundary is necessary in order to take advantage of the full-depth effect of the stone base course. Certainly, a geotextile placed at this interface so as to preserve the integrity of the interface is a worthwhile goal. In this case the geotextile is functioning as a separation fabric and has applicability to both paved and unpaved roadway systems.



(a) Mechanism of fine soils pumping into stone base voids and prevention using geotextiles



(b) Mechanism of stone base intrusion into fine soil subgrade and prevention using geotextiles

Figure 2. Different mechanisms involved in the use of geotextiles involved in the separation function (Koerner, 2012).

1.3 Overview of Geogrids Used for Reinforcement Within Stone Base Aggregates on Firm Subgrades for Paved and Unpaved Roads

Whenever geosynthetic usage in unpaved roads is discussed, the question of the material's use in paved roads on firm subgrades often follows. To address this properly, we must focus on the general characteristics of the situation. It is most important to recognize that if the road is to be paved with concrete or asphalt immediately (i.e., during initial construction), it cannot be placed on an excessively yielding soil subgrade. If the subgrade yields, the road section will deform and the surfacing will simply crack after a few load repetitions. Many agencies put the *lower limit* of acceptable unsoaked CBR values in the range 10 to 15. As just discussed, however, the geosynthetic must deform in order to mobilize its strength, and the *upper limit* of soil subgrade strength for such mobilization as suggested in Table 2 is an unsoaked CBR of 3 to 8. This contradiction begs the question of how the geosynthetic is to reinforce if it is not significantly deformed. Advocates of a reinforcement function in paved roads on firm soil subgrades will suggest that the geosynthetic deformation around the coarse-aggregate base course (when heavily rolled) is sufficient to mobilize the geosynthetic's strength. In this regard, emphasis shifts from savings in base course thickness to increased number of traffic repetitions. Thus the shifting of design method(s) will be done accordingly.

There is, however, another reason for using a geosynthetic within the stone base. Geogrids (and to a much lesser extent geotextiles) have been placed within the stone aggregate base course for providing lateral reinforcement. A properly designed geogrid inclusion prevents the stone from horizontal migration due to the dynamic loads produced by trucks and automobiles traveling on the asphalt or concrete wearing surface. Additional details on this mechanism will follow.

1.4 Overview of Geotextiles or Geogrids Used for Waterproofing or Reinforcement in Reflective Cracking of Asphalt Overlays of Paved Roads

This leads to the fourth category of this paper on geosynthetics in roadway applications which is the use of interlayers in asphalt overlays. The resurfacing of existing pavements which have excessive cracks in them represents an ongoing and expensive task for all federal, state, local, and private organizations that own and maintain roads. Such resurfacing is usually done with asphalt (bituminous) overlays ranging in thickness from 25 to 100 mm. Particularly exasperating to the road owners (and to the users and their automobiles, as well) is when the cracks in the original pavement reflect up through the new overlay earlier than anticipated. To combat this, thicker overlays than desirable are used but at the cost of added expense, lower curb heights, and excessive weight and thickness on the subgrade system. Due in part to the magnitude of this problem and the potential opportunities that it represents, the use of geotextiles to remedy the situation has been accomplished in a number of ways. In some instances strips of geotextile have been placed over the cracks, spanning it by 150 to 600 mm on each side, and the overlay placed above. Polyester, polypropylene, and fiberglass geotextiles, as well as geogrids, have all been used in this regard. By far the major use, however, has been to place full-width geotextile sheets over the entire pavement surface, which have been waterproofed with asphalt cement or asphalt emulsion, and then overlain with the final bituminous surfacing. The goal of such a process is to either decrease the thickness of the overlay while keeping a lifetime

equivalent to not using a geotextile, or increase the lifetime of the overlay while using the same thickness as without the use of the geotextile.

A very large market for geotextiles has developed as have the installation procedures. This is shown in the successive photographs of Figure 3 and is fully described in manufacturers literature, as well as in Koerner, 2012.



(a) Filling cracks in existing bituminous pavement



(b) Spraying asphalt-based sealant over existing pavement



(c) Geotextile being placed by mechanical equipment



(d) Hot mix bituminous overlay being placed



(e) Asphalt pavement core showing the crack-arresting feature offered by the geotextile with the new overlay placed above

Figure 3. Installation procedures and equipment for using geotextiles in reflective crack prevention for bituminous overlays. (Compliments of Amoco, now Propex, Fabrics and Fibers Co.)

1.5 Overview of Paper

Using this introductory and background section of geosynthetics used in roadway applications we can readily visualize how the various mechanisms described are individually positioned within a roadway's cross section, see Figure 4. Of course, two or three areas can function simultaneously, but they will be treated separately so as to focus upon the idiosyncrasies of each.

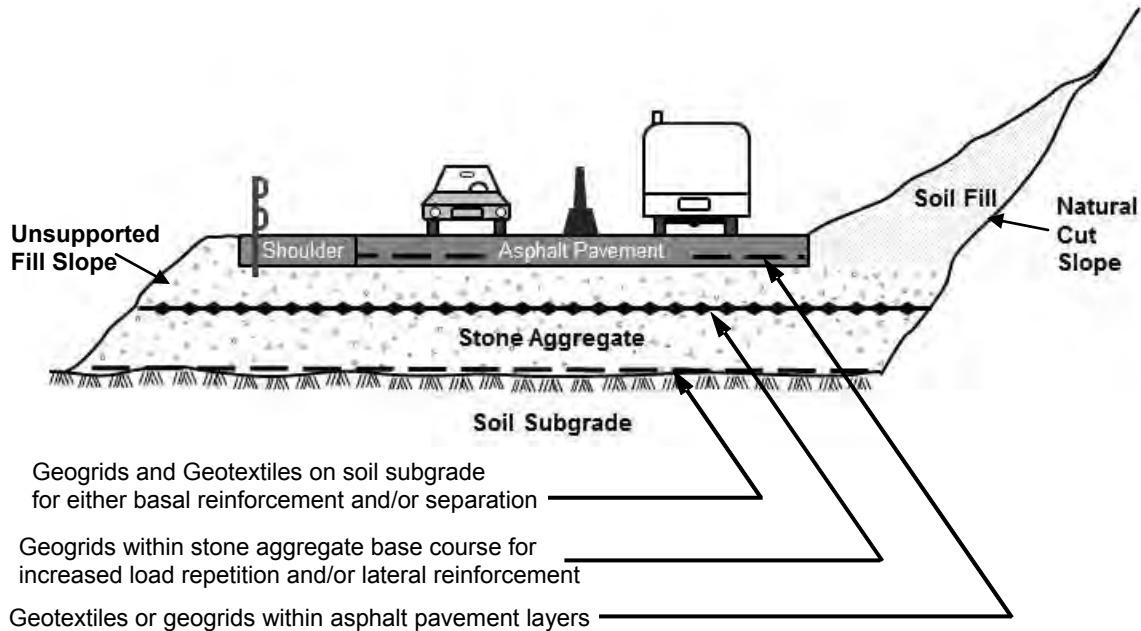


Figure 4. The four areas of geosynthetic use in road applications to be described herein.

2.0 GEOTEXTILES OR GEOGRIDS USED FOR REINFORCEMENT OF SOFT SOIL SUBGRADES FOR UNPAVED ROADS

All of the major geotextile and geogrid manufacturers have an unpaved road design method for use with their particular geosynthetics. They usually show CBR (or other soil strength values) on the x-axis and the required stone thickness (with and without a geosynthetic) on the y-axis. All result in logical behavior, with the geosynthetic providing greater savings in stone aggregate as the soil subgrade becomes weaker. Since most manufacturers have a range of products available for the reinforcement of unpaved roads, it is also seen that the heavier and stronger geotextiles and geogrids result in greater stone savings than the lighter and weaker ones. Because each manufacturer's set of curves has its own background (based on theory, laboratory work, field observation, or empirical observation), it is nearly impossible to compare one manufacturer's procedure with another. Yet the design methods have served the industry well and generally with excellent success. Their use is certainly acceptable and if only one manufacturer's products are available, its method should continue to be used. If, however, a number of geotextiles and/or geogrids are available, a method that views them on the basis of a specific, well-defined property is needed. Such a property could well be the material's tensile modulus, which is the basis of design in the procedure to follow.

Giroud and Noiray [1981] use the geometric model shown in Figure 5 for a tire wheel load of pressure p_{ec} on a $B \times L$ area, which dissipates through h_o thickness of stone base without a geotextile and h thickness of stone base with a geotextile.

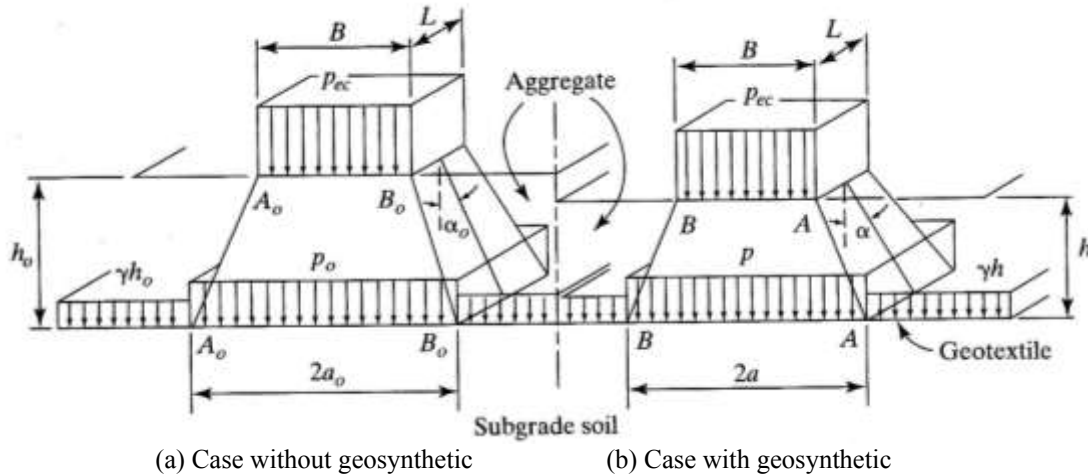


Figure 5. Load distribution by aggregate layer (after Giroud and Noiray [1981]).

This geometry results in stress on the soil subgrade of p_o (without geotextile) and p (with geotextile) as follows:

$$p_o = \frac{P}{2(B + 2h_o \tan \alpha_o)(L + 2h_o \tan \alpha_o)} + \gamma h_o \quad (1)$$

$$p = \frac{P}{2(B + 2h \tan \alpha)(L + 2h \tan \alpha)} + \gamma h \quad (2)$$

where

P = axle load, and

γ = unit weight of the stone base course aggregate.

Knowing the pressure exerted by the axle load through the aggregate and into the soil subgrade, shallow-foundation theory of geotechnical engineering can now be used. Assumed throughout the analysis that the soil is functioning in its undrained condition and thus its shear strength is represented completely by the cohesion (i.e., $\tau = c$). Thus the tacit assumption is that the soil subgrade consists of saturated fine-grained silt and clay soils. Critical in this design method are the assumptions that without the geotextile the maximum pressure that can be maintained corresponds to the elastic limit of the soil, that is,

$$p_o = \pi c + \gamma h_o \quad (3)$$

and that with the geotextile the limiting pressure can be increased to the ultimate bearing capacity of the soil, that is,

$$p^* = (\pi + 2)c + \gamma h \quad (4)$$

These assumptions reasonably agree with the earlier findings of Barenberg and Bender [1978] using small-scale laboratory tests, where on a deformation basis they found that large-scale ruts began at a $3.3c$ value with no geosynthetic reinforcement, versus a $6.0c$ value with geosynthetic (where c is the undrained soil shear strength).

Thus for the case of no geosynthetic reinforcement, Eqs. (1) and (3) can be solved to give Eq. (5), which results in the desired aggregate thickness response curve without the use of the geotextile or geogrid.

$$c = \frac{P}{2\pi \left(\sqrt{P/p_c} + 2h_o \tan \alpha_o \right) \left(\sqrt{P/2p_c} + 2h_o \tan \alpha_o \right)} \quad (5)$$

where

- c = soil cohesion,
- P = axle load,
- p_c = tire inflation pressure,
- h_o = aggregate thickness, and
- α_o = angle of load distribution ($\cong 26$ deg.).

For the case where geosynthetic reinforcement is used, p^* in equation (4) is replaced by ($p - p_g$), where p_g is a function of the tension in the geosynthetic; hence its elongation is significant. On the basis of the probable deflected shape of the geosynthetic-soil system,

$$p_g = \frac{E\varepsilon}{a\sqrt{1 + (a/2S)^2}} \quad (6)$$

where

- E = tension modulus of the geotextile or geogrid,
- ε = elongation (strain),
- a = geometric property, and
- S = settlement under the wheel.

Combining equations (2), (4), and (6) and using $p^* = p - p_g$, gives Eq. (7), where h is the unknown aggregate thickness with geosynthetic reinforcement. The geosynthetic reinforcement is represented by “E”, the tensile modulus of the specific geogrid or geotextile being considered per ASTM D4595, or equal.

$$(\pi + 2)c = \frac{P}{2(B + 2h \tan \alpha)(L + 2h \tan \alpha)} + \frac{E\varepsilon}{a\sqrt{1 + (a/2S)^2}} \quad (7)$$

With these two sets of equations, the design method is essentially complete, since both h_o (thickness without a geosynthetic) and h (thickness with a geosynthetic) can be calculated. From these two values $\Delta h = h_o - h$ can be obtained, which represents the savings in aggregate due to the presence of the geosynthetic. For convenience, however, the result can be read directly from Figure 6. This figure also considers the effects of traffic. In this case, the required thickness h' becomes $h' = h'_o - \Delta h$, which is obtainable from the curves by subtracting the two ordinate values of h'_o and Δh . Note that the effect of service lifetime takes the form of number of vehicle passages.

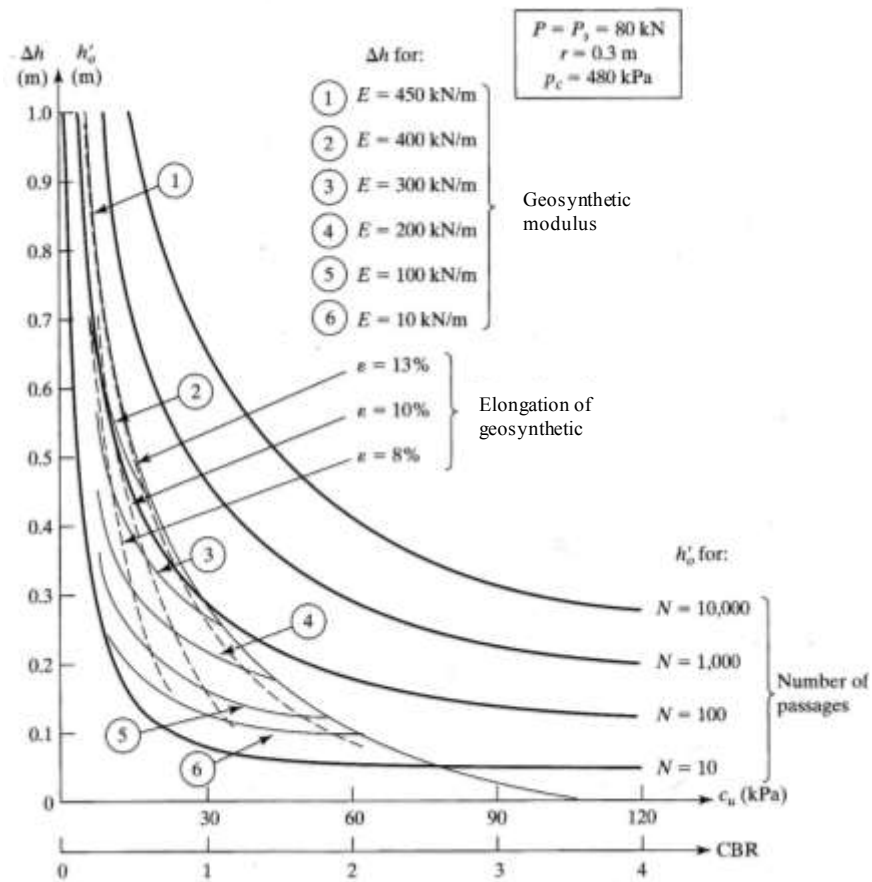


Figure 6. Design graphs for reducing aggregate thickness using a geosynthetic. Aggregate thickness h'_o without geotextile when traffic is taken into account and change in aggregate thickness (Δh) resulting from the use of geosynthetic rather than relying only on subgrade soil cohesion. (After Giroud and Noiray [1981])

It is important to recognize that in the previous design process the savings in stone aggregate can be directly compared to the cost of the geotextile or geogrid and the least costly alternative selected. Koerner (1982) presents a cost analysis of the alternatives with distance from the quarry and geosynthetic source being the major variables. This example problem and its solution follows.

Example: Given 1000 passages of a 80 kN single-axle-load vehicle with tire inflation pressure of 480 kPa; soft fine-grained soil CBR = 2.0; geosynthetic modulus $E = 170$ kN/m, and an allowable rut depth = 0.3 m. Determine the aggregate savings and do an economic analysis based on the distance the project is from the aggregate source and geosynthetic supplier, respectively, using the following data (the stone unit weight is 20 kN/m^3):

Distance (km)	Aggregate cost (dollars/kN)	Geosynthetic cost (dollars/m ²)
< 5	0.90	0.72
5-20	1.20	0.76
20-50	1.70	0.78
50-100	2.50	0.84
100-200	3.80	0.90

Solution: At CBR = 2.0 from Figure 6;

$$\begin{aligned}
 h'_o \text{ (without geotextile)} &= 300 \text{ mm} \\
 h' \text{ (with geotextile)} &= 205 \text{ mm} \\
 \Delta h \text{ (savings in stone)} &= 95 \text{ mm}
 \end{aligned}$$

Based on 20 kN/m^3 , this is a $0.020 \text{ kN/m}^2\text{-mm}$ stone thickness, which results in the following table. It is easily seen that the use of the geosynthetic reinforcement is very economical and becomes more so as the distance from the aggregate source to the project site becomes greater.

Distance from Source (km)	Aggregate total cost (dollars/kN)	Aggregate unit cost (dollars/m ² -mm)	Aggregate total cost (dollars/m ²)	Geosynthetic total cost (dollars/m ²)	Geosynthetic total savings (dollars/m ²)
<5	0.90	0.018	1.71	0.72	0.99
5-20	1.20	0.024	2.31	0.76	1.55
20-50	1.70	0.035	3/31	0.78	2.53
50-100	2.50	0.050	4/79	0.84	3.95
100-200	3.80	0.075	7.13	0.90	6.23

The Giroud and Noiray (1981) procedure just presented has been revised and upgraded for specific geogrids by Giroud and Han (2004, 2012) to include (i) an improved analytic formulation, (ii) a variable angle α_o in Figure 5, (iii) an increase in the bearing capacity factor for the reinforced case from 5.14 to 5.71, and (iv) a dimensionless parameter “k” which depends on contact area, base thickness, type of reinforcement and test method. Furthermore, k is defined as follows:

$$k = \tan \alpha_o \left(0.96 - 1.46J^2\right) \left(\frac{r}{h}\right)^{1.5} = 1.26 \left(0.96 - 1.46J^2\right) \left(\frac{r}{h}\right)^{1.5} \quad (8)$$

where

- α_o = stress distribution angle (see Figure 5)
- r = radius of tire contact angle
- h = base thickness after compaction
- J = aperture stability modulus of geogrids as determined by a laboratory test

The resulting design equation for the thickness of the aggregate base course “ h ” is as follows:

$$h = \frac{1.26(1 + k \log N)}{1 + 0.204(R_E - 1)} \left[\frac{\frac{P}{\pi r^2}}{\sqrt{\left(\frac{s}{f_s}\right) \left[1 - 0.9 \exp\left(-\left(\frac{r}{h}\right)^2\right)\right]} N_c c_u} - 1 \right] r \quad (9)$$

where

- N = number of axle passes
- R_e = modulus ratio of aggregate base to subgrade soil
- S = allowable rut depth
- f_s = reference rut depth (= 75 mm)
- N_c = bearing capacity factor
- c_u = undrained shear strength of subgrade soil
- P = individual wheel load
- k = see Eq. 8

This revised approach toward obtaining the required aggregate base thickness using geogrid reinforcement depends on “ k ”, which in-turn depends on “ J ”, the aperture stability modulus value that is obtained from a torsional rotation laboratory test. This test method, originated by Kinney (1998), has been standardized as GRI-GG9 (2004).

Some author’s commentary on this revised design procedure follows:

1. The original method used an elastic modulus as obtained from a standard wide-width tensile test which results in a stress-strain (or load-elongation) behavior of the candidate test specimen.
2. The revised method uses an elastic modulus as obtained from an in-plane torsional rotation method. As stated by Giroud and Han (2004, 2012) it is applicable to small deformation which they feel is more appropriate.
3. The modulus “ J ” in Eq. 8 generally has the dimension of “mm-kg/deg”, or equivalent, and this is used in Eq. 8 which has a constant in front of “ J ” and thus cancels the units out.

4. It should be noted that the torsional rotation method per GRI-GG9 has been used on all types of geogrids and data has been generated accordingly. The method has not been used for geotextiles although there is no reason why it could not be done in a similar manner.

Going forward, an alternative simulation test for the unpaved road application appears to the author to be the axisymmetric out-of-plane test. This test was developed by Shields, et al. (2005) for geogrids and then extended for geotextiles and geonets by Andrejack and Wartman, 2010, see Figure 7. This test has also been recently used by Wrigley, et al. (2011) who evaluated a number of geogrids and found remarkably good agreement with wide width tensile values at least up to about 2% strain. In using the above mentioned axi-symmetric out-of-plane tension test for high strength reinforcement materials failure is not likely achieved. In this regard, a modulus 2 to 4% strain is the limit depending on the strength of the geogrid or geotextile.

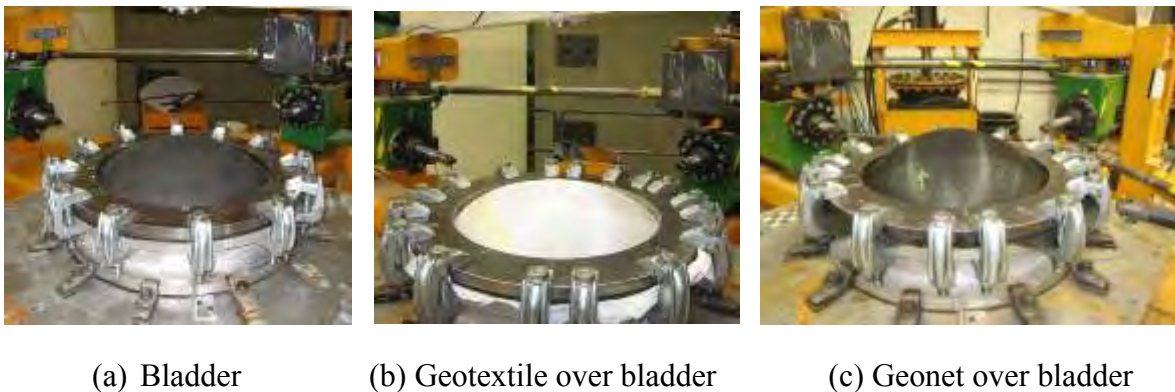


Figure 7. Axisymmetric out-of-plane tension test (after Andrejack and Wartman, 2010).

3.0 GEOTEXTILES USED FOR SEPARATION ON FIRM SOIL SUBGRADES FOR PAVED AND UNPAVED ROADS

As shown on Figure 4, geotextile separators are often placed directly on the soil subgrade in order to separate it from the overlying stone base aggregate. The twofold detrimental phenomena of loss of gravel and intrusion of soil subgrade was illustrated in Figure 2. The geotextiles being polymeric (presently the majority are polypropylene based) have sufficient durability properties such that degradation within pavement lifetime is not an issue. Of course, the geotextile must survive the installation process, but with adequate physical and mechanical properties (such as stipulated in the AASHTO M288 specification) this is readily accomplished.

Designing for separation itself, however, is elusive. Many manufacturers have guidance in that 25 to 100 mm of stone base aggregate are preserved over time by virtue of the inclusion of a geotextile separator. While this sounds reasonable to the author it is generally too subjective

for a cost-conscious and somewhat skeptical transportation engineer. That said, some limited empirical guidance is afforded by the U.S. Federal Highway Administration; see Figure 8 in this regard. Needed is either an analytic based design method or field justification based on actual long-term performance. That performance should show how long the pavement is serviceable both with and without the geotextile inclusion.

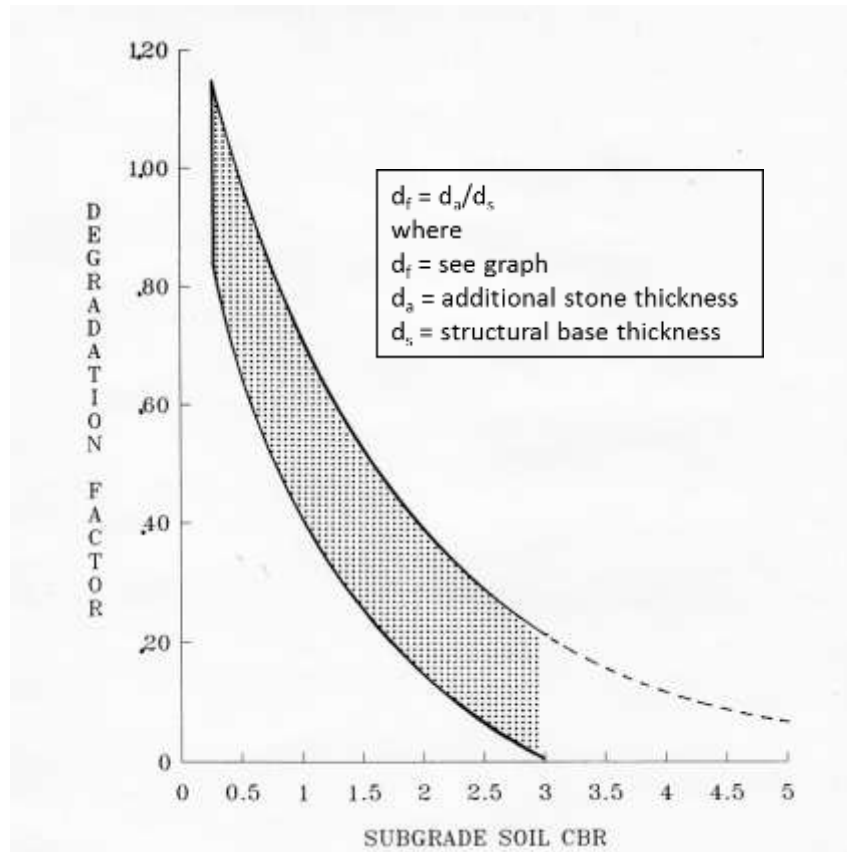


Figure 8. Reduction in stone base thickness when using a geotextile separator, adopted from FHWA (Jan. 1989).

To this end, four field sites have been prepared with and without geotextiles for an assessment over time, see Koerner (2000). These are full lane width paved road sites of approximately 100 m in length; see Figure 9. Furthermore, different geotextiles have been used at the sites to see if and how much longevity is associated with each geotextile as contrasted to the control sites at each end of the run with no geotextiles. Table 3 gives the relevant information, however, data on the performance is not yet available. It is felt to be essential to implement and evaluate as many such studies as possible in order to justify the widespread use of geotextiles as separators in paved road applications.

Table 3 – GSI Long-Term Benefit/Cost Separation Sites (Koerner, 2000)

Site	Location	Installed	Owner	Monitoring
1 a-b	Springfield, PA	June 1994	private	rut depth
2 a-f	Rt. 522, Orbisonia, PA	June 1998	PA-DOT	visual
3 a-b	I-79, Washington, PA	July 1998	PA-DOT	visual
4 a-c	Rt. 30, York, PA	June 1999	PA-DOT	crack survey



(a) Site 1 in Table 3



(b) Site 2 in Table 3



(c) Site 3 in Table 3



(d) Site 4 in Table 3

Figure 9. Field sites in Pennsylvania under investigation to evaluate geotextile performance over time in the separation function.

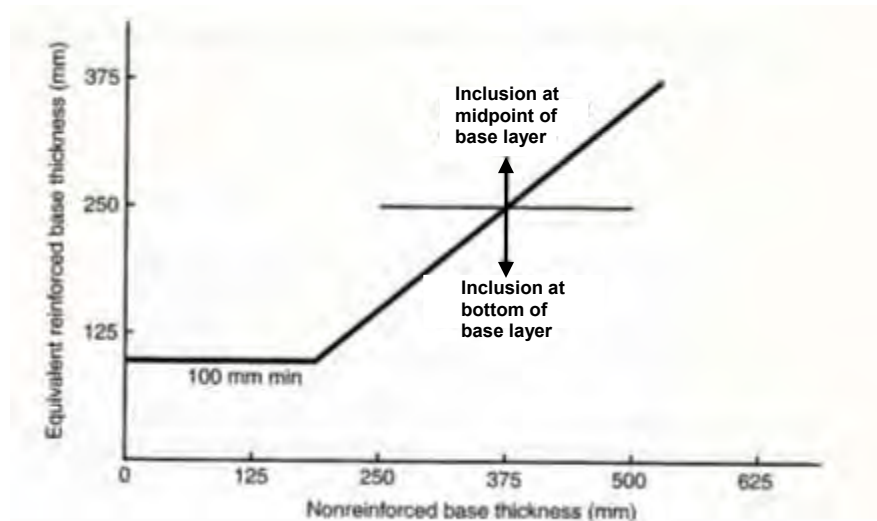


Figure 11. Geogrid-reinforced aggregate base courses for roadways using geogrids, after Carroll, et al. (1987).

4.1 Use-What-Works

Use-what-works is not as foolish as it seems since this is precisely how unpaved road applications as just explained gained acceptance, particularly from contractors who verified the considerable saving in stone base using the geosynthetic. The fundamental difference with strong soil subgrades having $CBR_{US} \geq 8$ or $CBR_S \geq 3$, however, is that the base course is typically as thin as it can possibly be even without the geogrid inclusion. For example, stone base courses as thin as 100 to 150 mm are regularly used for asphalt paved roads and further reductions are simply not viable. Of course, for major roads and interstate highways the stone base courses become thicker. At any rate, a very different mindset is suggested for justification of the inclusion of the geogrid. This, the author and others believe, is better rideability (less rutting) and/or longer service lifetime (for direct cost savings). That said, this use-what-works approach toward selecting a geosynthetic is completely judgmental and is not felt to be a design method, per se.

4.2 The CBR Cover Design Method

The CBR Cover Design Method noted on Figure 10 is essentially for unpaved roads wherein separation, stabilization and reinforcement are the primary function and are related to the soil subgrade's CBR-value. Recall Table 2 in this regard. Again, however, the lower values of CBR are simply not viable when the base course is paved so the "unpaved road technique" is not applicable for this type of paved road situation.

4.3 The AASHTO Method

The AASHTO Method was based on a major experimental road test conducted in the 1960's resulting in the 1993 AASHTO Design Guide. The essence of the method is to calculate an overall structural number (SN) that is indicative of the required total pavement thickness for proper serviceability. It is solved using a nomograph based on the following equation.

$$\log W_{18} = Z_R \times S_O + 9.36 \times \log(SN + 1) - 0.2 + \frac{\log \frac{\Delta_{psi}}{2.7}}{0.4 + \frac{1094}{(SN + 1)^{5.19}}} + 2.32 \log M_R - 8.07 \quad (10)$$

where

- W_{18} = 18 kip design equivalent single axle loads (ESAL's)
- Z_R = standard reliability level
- S_O = standard deviation
- Δ_{psi} = allowable loss in serviceability
- M_R = resilient modulus for the geosynthetic being considered
- S_N = structural number as follows:

$$SN = (a \times d)_{hma} + (a \times d \times m)_{base} + (a \times d \times m)_{subbase} \quad (11)$$

where

- a = coefficient of relative strength
- d = thickness of each layer
- m = modifier for moisture in the system

In order to introduce geosynthetics into the above design process, there are two options. The *first option for increased W_{18} or EASL's* is based on a TBR-value as defined below, Berg, et al. (2000)

$$TBR = N_R / N_U, \text{ and} \quad (12)$$

$$W_{18-rein} = (TBR)(W_{18-unrein}) \quad (13)$$

where

- TBR = traffic benefit ratio
- N_R = load cycles to reach a given rut depth (reinforced)
- N_U = load cycles to reach the same rut depth (unreinforced)
- $W_{18-rein}$ = ESAL's for the reinforced case
- $W_{18-unrein}$ = ESAL's for the unreinforced case

Shukla (2002) suggests that TBR values are from 1.5 to 10 for geotextiles and 1.5 to 70 for geogrids. That said, the entire procedure is based on resilient modulus laboratory testing using a specific candidate geotextile or geogrid.

The *second option for reduced base course thickness* is based on a BCR-value defined as follows:

$$BCR = T_R / T_U \quad (14)$$

where

- BCR = base course reduction factor
- T_R = base course thickness for the reinforced case
- T_U = base course thickness for the unreinforced case

This value is then applied to the SN equation (but only on the base course layer), as shown below.

$$d_{base(R)} = \frac{SN_u - (a \times d)_{hma} - (a \times d \times m)_{subbase}}{BCR(a \times m)_{base}} \quad (15)$$

where

- $d_{base(R)}$ = reduced base course thickness due to the reinforcement
- SN_u = structural number corresponding to the unreinforced W_{18} value

There have been several field studies which have been focused on verification of the above procedure, particularly those of Abd El Halim, et al. (1983), Miura, et al. (1990) and Webster (1992). In general, BCR improvements are suggested to range from 20% to 40%, however, all assessments are specific to the reinforcement materials being considered and the resulting resilient modulus testing conditions.

4.4 The NCHRP Method

The NCHRP method is presently called the mechanistic-empirical (M-E) method and it attempts to incorporate geometry, all pavement materials (including the specific geosynthetic material), traffic climate and associated laboratory generated properties. Characterizing the candidate geosynthetic are its laboratory generated static and cyclic moduli. Different confidence levels can also be inferred in using the process which is diagrammatically shown in Figure 12.

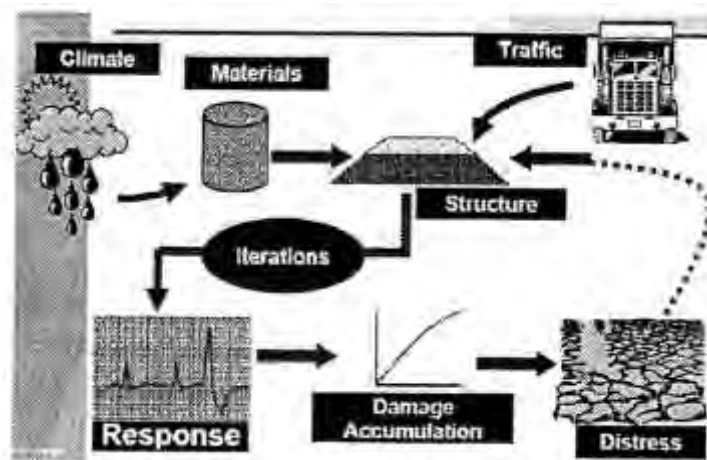


Figure 12. Flowchart for M-E Design (NCHRP 2004).

While some researchers feel that the M-E method is more appropriate than the AASHTO method (Al-Qadi, 2008), both rely heavily on measuring laboratory physical and mechanical properties. Even more importantly is the correlation of those laboratory evaluations to field performance which has been “spotty”, at least based on GSI’s unpublished field sites. In this regard it should be noted that small savings in aggregate thickness, as in paved roads, are very sensitive to laboratory test values. This is unlike the unpaved road aggregate savings situation which is less affected by changes in laboratory test values. The reader is referred to the NCHRP (2004) guide manual for details.

4.5 The Lateral Reinforcement Approach

As the name implies, the lateral reinforcement approach should be considered for assessing the pavement’s lifetime and service performance and also to assess the controlling mechanism involved. To the author, and others, longitudinal cracking of asphalt pavements is widespread in flat shoulder locations or those which are built-up fill areas; note the unsupported left side of Figure 4. Conversely, in areas which are in cut situations and have lateral restraint, as in the supported right side of Figure 4, such longitudinal cracks are at a minimum or altogether absent. Such observations strongly suggest to the author, and others, that the stone aggregate base course is laterally moving in a somewhat unrestricted manner in flat or unsupported fill shoulder situations. When the overlying bituminous pavement starts to lose its ductility (in as little as a few years), the movement of the original stone aggregate support results in such longitudinal pavement cracking as shown in Figure 13. It is shown in a more aggressive stage adjacent to a stream in Figure 14.



Figure 13. Longitudinal pavement cracking on unrestrained (left) pavement edge and none on curb retained (right) pavement edge.



Figure 14. Major longitudinal cracking causing traffic diversion.

Certainly, a properly aperture sized geogrid within the stone aggregate base course should prevent or minimize this occurrence. In addition to determining the tensile stress-strain properties of the geogrid (both static and dynamic), is the junction, or node, stiffness and/or strength. These concepts were first introduced by Kinney (1998) who showed the actual phenomenon by filming stone particle movement from a plexiglass bottomed box by a moving wheel load. In so doing the individual stone particles moved outward from the wheel load (as expected) and also moved slightly forward as well. The resulting elliptic spiral motion, which dissipated with distance from the wheel load, was greatly diminished by the inclusion of a geogrid.

Kinney then devised an in-plane torsional rotation test to quantify the geogrid's resistance to such applied torque values. The test is available as GRI-GG9 and is shown in plan and elevation as Figure 15. This concept of lateral reinforcement of the aggregate particles within the stone base course is considered by the author as being worthwhile to pursue (for firm soil subgrade situations) in the future.



Figure 15. Plan and elevation view of the test apparatus for in-plane torsional rigidity determination of bidirectional geogrid stiffness per Kinney (1998) and GRI-GG9 test method (2004).

5.0 GEOTEXTILES OR GEOGRIDS USED FOR WATERPROOFING OR REINFORCEMENT OF REFLECTIVE CRACKING OF ASPHALT OVERLAYS IN PAVED ROADS

The resurfacing of existing pavements that have excessive cracks in them represents an ongoing and expensive task for all federal, state, local, and private organizations that own and maintain roads. Such resurfacing is usually done with bituminous overlays ranging in thickness from 25 to 100 mm. Particularly exasperating to the road owners (and to the users and their automobiles as well) is when the cracks in the original pavement reflect up through the new overlay earlier than anticipated. To combat this, thicker overlays than desirable are used but at the cost of added expense, lower curb heights, and excessive weight and thickness on the subgrade system. Due in part to the magnitude of this problem and the potential market that it represents, the use of geosynthetics to remedy the situation has been attempted in a number of ways. In some instances strips of geotextile or geogrid have been placed over the cracks, spanning them by 150 to 600 mm on each side, and the overlay placed above. Polyester, polypropylene, and fiberglass geosynthetics have all been used in this regard. Alternatively, a major use has been with full-width geotextile sheets which have been waterproofed with asphalt cement or asphalt emulsion, over the entire pavement surface, and then overlaid with the final bituminous surfacing. In all cases, the goal is to either decrease the thickness of the overlay

while keeping a lifetime equivalent to not using a geosynthetic, or to increase the lifetime of the overlay while using the same thickness as without the use of the geosynthetic. It should be noted that this technique is used only for deteriorated existing bituminous pavements, not for cracked Portland-Cement concrete pavements. The significantly sharper edges of concrete would generally puncture and tear the geosynthetics used in this application.

That said, a clear-cut primary function is difficult to identify. It probably involves either the reinforcement from one side of the existing cracks to the other (via the geotextile's tensile strength), or moisture-proofing against water moving through the existing cracked pavement and into the subgrade via the impregnation of the geotextile with asphalt cement or asphalt emulsion. Since either function is possible; both design concepts will be described.

5.1 Full Lane Width Lightweight Geotextiles (or Geogrids) Using a Reinforced Based Design

The key to the reinforcement-based design of geotextiles and also geogrids in reflective crack prevention in bituminous pavement overlays is the effectiveness as determined by laboratory testing or by experience. Quantitatively, it is defined as follows:

$$FEF = \frac{N_r}{N_n} \quad (16)$$

where

- FEF = fabric effectiveness factor,
- N_r = number of load cycles to cause failure in the geotextile reinforced case, and
- N_n = number of load cycles to cause failure in the nonreinforced case.

Values of FEF vary widely when based on laboratory tests (as they usually are), the range being from 2.1 to 15.9; see Murray (1982). Upon having this value, however, design can be approached by a number of procedures. Majidzadeh, et al. (1982), use a mechanistic design procedure influenced by both rutting (distortion) and fatigue (cracking). Another approach, however, is merely to modify existing asphalt overlay design methods. In this regard the design traffic number (DTN), upon which overlay designs are based, can be modified as follows:

$$DTN_r = \frac{DTN_n}{FEF} \quad (17)$$

where

- DTN_r = design traffic number in the geotextile reinforced case,
- DTN_n = design traffic number in the nonreinforced case, and
- FEF = fabric effectiveness factor.

Using the Asphalt Institute's overlay design procedure (1977) the specifics are as follows:

1. Determine the soil subgrade strength value as represented by its CBR value.
2. Determine the initial traffic number (ITN). This is a combination of each vehicle's weight and respective number of load repetitions based on traffic counting.

3. Determine the adjustment factor for the desired design period and estimate traffic annual growth rate.
4. Multiply the ITN by the adjustment factor to obtain the design traffic number DTN for use in the thickness design chart.
5. Use Figure 16 (or equivalent) to determine the full-depth asphalt-to-pavement thickness, t_{An} , needed for the design subgrade strength value, the DTN , and the selected design period.
6. Determine the effective thickness, t_e , of the existing pavement.
7. The thickness of asphalt concrete overlay required, then, is equal to $t_{An} - t_e$.
8. This process is repeated for the geosynthetic-reinforced case using Eq. 17, which results in a thickness t_{Ar} .
9. The resulting two thicknesses (nonreinforced and geosynthetic-reinforced) are then compared ($t_{An} - t_{Ar}$) to note the savings in asphalt overlay thickness since the base thickness is the same in both cases. See Koerner (2012) for a numeric example using this method.

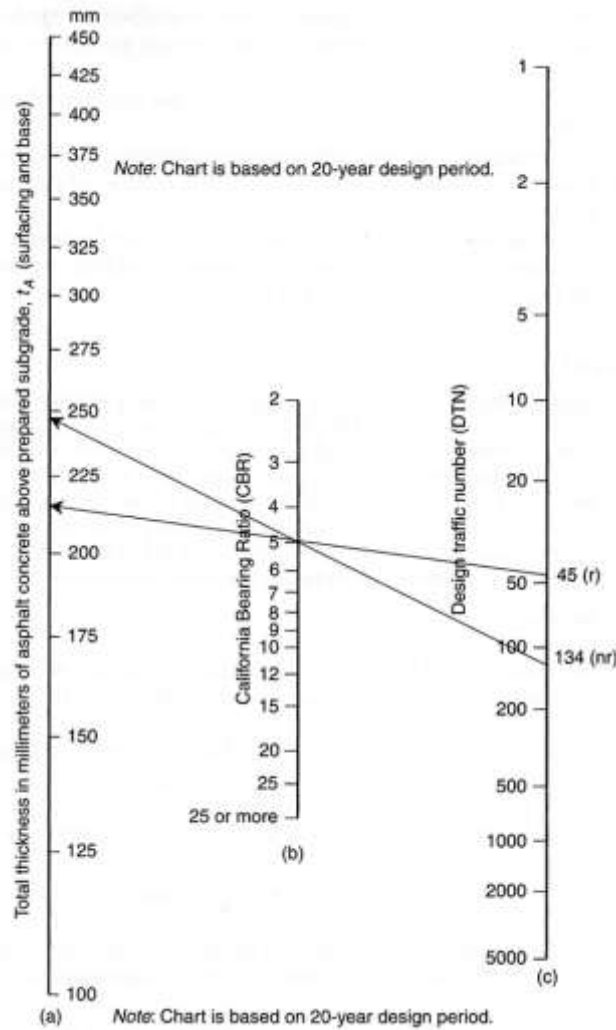


Figure 16. Thickness requirements for asphalt pavement structures using unsoaked subgrade soil CBR, after Asphalt Institute (1977). Arrows indicate a typical design wherein approximately 30 mm of overlay is saved using the reinforcing geosynthetic.

5.2 Full Lane Width Lightweight Geotextiles Using a Waterproofing Based Design

Again using the Asphalt Institute's techniques (1977), one can develop an alternate design procedure for geotextiles (this procedure only applies to geotextiles) used in asphalt overlay situations; this time using an approach based on a waterproofing hypothesis. This concept should not come as a surprise since adequate subgrade drainage of pavements has long been suspected as being the key factor for extending conventional pavement lifetimes. Cedegren (1989), clearly illustrates this type of improved pavement lifetime. The particular procedure to be used, adopted from Bell (1983-85), utilizes field-measured rebound deflections of the existing pavement system along with the design guide of Figure 17. The individual steps in the design are as follows:

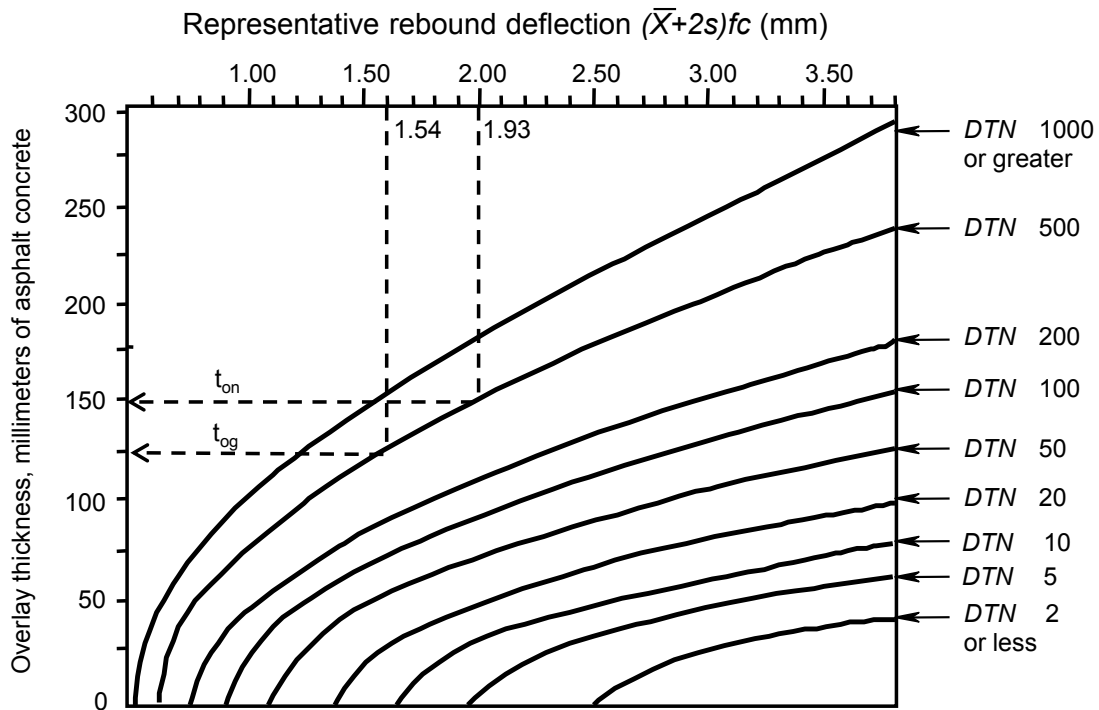


Figure 17. Asphalt overlay thickness required to reduce pavement deflection from a measured to a design deflection value (a rebound test), after Asphalt Institute (1977). Arrows indicate a typical design wherein 30 mm of overlay is saved using the waterproofing geotextile.

1. Determine the representative rebound deflection.
2. Determine the initial traffic numbers (*ITN*). It is a combination of each vehicle's weight and respective number of load rejections based on traffic counting.
3. Determine the initial traffic number adjustment factor for the desired design period.
4. Multiply the *ITN* by the *ITN* adjustment factor to obtain the *DTN* for use in the overlay thickness chart.
5. Enter the overlay thickness chart at the representative rebound deflection and move down vertically to the curve representing the *DTN* (interpolate if necessary). Move horizontally to the overlay thickness scale and read the thickness of overlay required.

6. For the case of a geotextile included in the pavement cross-section and of it being suitably waterproofed, one can appropriately modify the representative rebound deflection (RRD) equation as follows:

$$RRD = (\bar{X} + 2s)fc \quad (18)$$

where

- \bar{X} = arithmetic mean of measured Benkelman beam deflection values,
- s = standard deviation,
- f = temperature adjustment, and
- c = critical period adjustment factor, which is largely influenced by moisture in the subgrade system.

7. The design process is then repeated as with the non-geotextile case, and the resulting two thicknesses are compared to note the savings in asphalt overlay using the geotextile. In this case it is again 30 mm (as with the reinforcement assumption). See Koerner (2012) for a numeric example using this method.

5.3 Commentary on Previous Two Subsections

This topic of crack reflection prevention in bituminous pavement overlays illustrates the dilemma of assessing the primary function that the geosynthetic serves. Using two completely different hypotheses (one based on reinforcement and the other based on waterproofing), two completely different designs can be developed. It simply begs the question of where the truth actually lies. For geotextiles it could be either, for geogrids it is reinforcement. For geotextiles, it might be a combination of the two phenomena working together! In general, however, it is felt that field reports are definitely on the positive side. Based on geotextile experiences to date, the following recommendations are offered:

- For those states that are using proprietary or competition-limiting specifications for geotextiles, the adaptation of Texas DOT specifications for use is encouraged.
- Prior to placement of a geotextile overlay system, the condition of the existing roadway should be documented. When an unstable roadway is suspected, deflection tests are recommended. While limiting deflection values have yet to be established for geotextile systems, it is important that data be obtained that could assist in their eventual evaluation.
- Since all geotextiles presently being marketed are not equivalent in physical properties, agencies should conduct the tests identified in the Texas DOT specification, including the asphalt retention test, so as to develop documentation that may be useful later in assessing relative geotextile performance.
- Rather than placing the geotextile on the cracked existing pavement, construct an asphalt leveling course first so as to provide a relatively unblemished surface for applying the tack coat and the geotextile. This will assure more complete and uniform impregnation of the geotextile by the tack coat and will also assist in determining the type of tack coat to be used and the proper application rate.

- For pavement rehabilitation projects that include pavement widening with new asphaltic concrete overlays, geotextiles placed longitudinally over the shoulder-pavement and/or widening joint should be considered. The Maine DOT (1994) has had success in this regard. Both longitudinal and transverse joints were retarded significantly when using a high strength geotextile directly spanning the cracks in question.
- Over jointed Portland-cement concrete pavements, no evidence has been provided to support placing a geotextile system across the full roadway width in a continuous mat. Instead, the use of heavy-duty geotextile materials in strips over transverse and pavement edge joints and cracks is presently recommended. A summary report by the U.S. Army Corps of Engineers (Alhrich, 1986) on this particular application of geotextiles has arrived at similar conclusions.

5.4 Use of High Strength Geotextiles or Geogrids Spanning Transverse and Longitudinal Pavement Cracks

The use of high strength geosynthetics to retard and minimize reflective cracking within old pavements from propagating through newly placed asphalt overlays is a related topic of great interest. Results of laboratory testing by Molenaar and Nods (1996) suggest the use of a power law to calculate the rate of crack propagation through the new overlay thickness:

$$\frac{dc}{dN} = AK^n \quad (19)$$

$\frac{dc}{dN}$ = crack propagation rate per number of load cycles,
 K = stress intensity factor, and
 A, n = experimentally obtained constants.

The following numeric example illustrates how Eq. 19 can be used in the prediction of overlay lifetime without, and then with, different types of geogrids and a geotextile.

Example: A 100 mm asphalt overlay is to be placed on top of a severely cracked pavement having a firm base. The DTN for the pavement is 100,000 load repetitions (cycles) per year. The combined overlay, existing asphalt layer and base profile, yields a design stress intensity factor (K) of 10 N/mm^{1.5} and constants A of 1.0×10^{-8} and n of 4.3. **(a)** Calculate the average rate of crack growth of the new asphalt overlay. At a full-propagation failure assumption, what is the lifetime (in terms of number of cycles and years) of the new asphalt overlay without reinforcement? **(b)** Redo the problem using the inclusion of various geosynthetic reinforcement materials with A values as follows:

nonwoven geotextile: $A_{GT} = 0.50$ ($A_{\text{non-reinf.}}$)—author estimate
polypropylene geogrid: $A_{PP} = 0.35$ ($A_{\text{non-reinf.}}$)—author estimate
polyester geogrid: $A_{PET} = 0.33$ ($A_{\text{non-reinf.}}$)—Molenaar and Nods (1996)
fiber glass geogrid: $A_{FG} = 0.25$ ($A_{\text{non-reinf.}}$)—author estimate

Solution: (a) Using the power law of Eq. (19), the crack propagation rate is calculated, from which the number of cycles and lifetime are obtained. The crack-propagation rate for the nonreinforced case is:

$$\begin{aligned} \frac{dc}{dN} &= AK^n \\ &= 1 \times 10^{-8} \times (10)^{4.3} \\ &= 0.0002 \text{ mm/cycle} \end{aligned}$$

from which the number of load cycles (non reinforced) is:

$$\begin{aligned} N &= \frac{T}{(dc/dN)} \\ &= \frac{100}{0.002} \\ &= 500,000 \text{ cycles or 5 years} \end{aligned}$$

(b) Using the various modified *A*-values for different types of geosynthetic reinforcement gives rise to the table below.

Reinforcement	Crack Growth Rate (mm/cycle)	Lifetime (cycles/years)
None	2.0×10^{-4}	500,000/5
Geotextile	1.0×10^{-4}	1,000,000/10
PP geogrid	0.7×10^{-4}	1,400,000/14
PET geogrid	6.6×10^{-5}	1,500,000/15
FG geogrid	5.0×10^{-5}	2,000,000/20

The technique is very intriguing and warrants additional research in this important roadway engineering application.

6.0 SUMMARY AND RECOMMENDATIONS

This retrospective paper on geotextiles and geogrids used in roadway applications has attempted to cover in as concise a manner as possible, the different geosynthetic functions applicable to typical roadway cross-sections. The main reason being that the overall status of roadway deterioration is so enormous and yet vastly undercapitalized upon from a geosynthetics perspective. The situation seems to be at a point where the relatively short lifetimes of pavement systems are unfortunately expected to be the norm. In the author's opinion, geotextiles and geogrids hold the key to longer pavement lifetimes as well as better serviceability of the roadway system itself. This is not meant to criticize the asphalt, concrete, or stone base courses being used, however, it is meant to criticize the nonuse of geosynthetic materials. Of course, the cost of the pavement system will somewhat increase, but the tradeoff of longer lifetimes and/or less stone base or asphalt surfacing will usually result in a net benefit/cost increase. Furthermore,

and in terms of sustainability, a large net saving of many tons of CO₂ per highway project will be realized, see Miner and Davis (2011) in this regard.

The paper is presented in four very discrete and independent sections while recognizing that interactions are present in some cases. This method of presentation is done in order to focus on specific design methodologies and field performances whenever available. The four different independent sections are summarized as follows; recall Figure 4:

In Section 2.0, geotextiles and/or geogrids are used for reinforcement when placed on soft soil subgrades of unpaved roads where the focus is on stone base aggregate saved by inclusion of the geosynthetic material.

It is felt that this topic has the best formulated analytic procedure of all that are treated in this paper. The Giroud-Noiray (1981) development is analytically viable using basic geotechnical engineering principles. The result is a design nomograph which can be readily used to determine the amount of stone base necessary without a geosynthetic and then with a geosynthetic. The difference is, of course, the thickness of stone base saved.

Important in using this procedure is that the specific geosynthetic to be used (geotextile or geogird) is represented by its elastic modulus obtained from a standardized wide-width tensile test resulting in a stress vs. strain, or load vs. elongation, test. Its applicability to all geotextiles and geogrids is an important feature.

Giroud-Han (2004, 2012) have revised this method to include improvements in the analytic equations resulting directly in the required stone base thicknesses. They also changed the test method for characterization of the geosynthetic being used. Now the recommended test method is an in-plane torsional rotation test and even further the available data is only valid for two specific types of manufactured biaxial geogrid. This particular test does not appear to the author to simulate the actual field behavior or the downward pyramidal force diagram upon which the method is based. Of course, the required modulus could be taken from a more representative test method. In this regard the author favors a large scale axisymmetric pressure test which is available and is currently being standardized.

In Section 3.0, geotextiles are placed directly on soil subgrades for the purpose of long-term separation of it and the overlying stone base course thus providing better rideability of the surface in both paved and unpaved roads.

Conceptually, stone base particles punching down into the subgrade soil and the subgrade soil migrating upward into the stone base is easy to visualize. The softer the subgrade soil, the more aggressive is the phenomenon. Both reduced stone base thickness and its loss of drainage capability are expected and often seen after excavation. Yet, to analytically formulate the situation remains for the future. It is indeed worthwhile since the low cost geotextile being used need only to replace about 25 mm of stone base to justify itself.

In Section 4.0, reinforcement geogrids are placed within the stone base aggregate of paved and unpaved roads on firm subgrade soils to either result in increased traffic or to

prevent the stone base aggregate from lateral movement thus preserving serviceability for longer lifetime.

There are numerous design methods that have been developed for this particular application. They are generally (not always) based on the increased number of equivalent single axle loads (ESAL's) that the reinforced stone base will provide over the nonreinforced stone base. Included are the CBR Cover Design Method, the AASHTO Method (1993), the NCHRP Method (2004), the M-E method (2004) and other related research efforts of which there are many.

For major highways with thick stone base courses, and even with subbase courses, the geogrid's inclusion can produce increased traffic repetitions or even save on stone base thickness. However, for the much more common roadways with only 100 to 200 mm of stone base overlain with 50 mm of asphalt, further reductions in stone base thicknesses are not likely in the author's opinion. Indeed, more traffic load repetitions are a worthwhile goal but to justify the increased cost of the geogrid reinforcement for this purpose is a difficult "sell" to many transportation engineers.

On the other hand, an analytic procedure for the *lateral reinforcement mechanism* has not been developed. Yet, there is ample field evidence that longitudinal cracking of asphalt paved roads is commonplace. Kinney, et al. (1998) have shown the behavior in laboratory demonstrations and in so doing developed the in-plane torsional rigidity test which is an excellent simulation. Needed are design methodologies indicating how a geogrid within the stone base restrains its lateral movement and subsequent distortion and cracking of the overlying asphalt pavement. Then the elastic modulus from the in-plane torsional rigidity test can be appropriately used.

In Section 5.0, geotextiles or geogrids used for waterproofing or reinforcement are placed on deteriorated asphalt roadway surfaces as a interlayer for subsequent asphalt resurfacing so as to provide lower cost or longer lifetime.

Whether the proper mechanism of reinforcement or waterproofing is more correct is uncertain, however, for this application both have a design methodology available for use. There are also many reports of field performance with excellent results in moderate and warm climates. There are, however, reported issues in cold climates. Many moderate and warm climate states use the application of full-width light weight geotextiles on a routine basis. It is indeed a worthwhile and mature application.

That said, other techniques of using high strength geotextiles or geogrids over transverse and longitudinal cracks as well as full width geogrids are still in the analytic development stage. Of course, at a higher unit cost than lightweight geotextiles the need for deterministic performance becomes more necessary.

In conclusion and in order to capture the author's thoughts and recommendations for these four geotextile and geogrid roadway applications, Table 4 is offered.

Table 4 – Status and Recommendations of Geosynthetic Use in Roadway Application

GS Location (see Figure 4)	GS Type	Function	Analytic Design Status	Field Verification Status	Owner Acceptability
Beneath Stone Base	GT or GG	Reinforcement	Excellent	Excellent	Excellent
Beneath Stone Base	GT	Separation	Poor	Good	Nominal
Within Stone Base • vertical stresses • horizontal stresses	GG GG	Reinforcement Reinforcement	Good Poor	Poor Good	Reasonable
Above Existing Pavement Surface	GT GG	Waterproofing Reinforcement	Good Emerging	Reasonable Good	Good

where GS = geosynthetic, GT = geotextile and GG = geogrid

Readily seen is that both analytic design and field verification need improvement before geotextile and geogrid use in roadway applications become standardized and fully accepted by the transportation community. An integrated analytic design **and** field performance verification is necessary for certain aspects of all four of the categories shown in Table 4. Only then can economic justification be relied upon which leads to confident acceptance. Since geotextile and geogrid potential is so great in pavement applications, such an integrated approach seems necessary and will, in due course, be implemented.

ACKNOWLEDGEMENTS

This paper is made available through financial assistance of the Members, Affiliated Members and Associate Members of the Geosynthetic Institute (GSI). We sincerely thank them in this regard. See our website at www.geosynthetic-institute.org for their identification and contact persons.

REFERENCES

Abd El Hamim, A. O., Haar, R. and Chang, W. A. (1983), “Geogrid reinforcement of asphalt pavements and verification of elastic layer theory,” Transportation Research Board, RRBR No. 949, pp. 55-65.

Ahlich, R. C. (1986), “Evaluation of asphalt rubber and engineering fabrics as pavement interlayers,” GL-86-34, Vicksburg, MS, U. S. Army Corps of Engineers.

Al-Qadi, I. L., Dessouby, S. H., Kevon, J. and Tutumleur, E. (2008), “Geogrids in flexible pavements; validated mechanisms,” Jour. Transportation Research Board, No. 2045, Washington, DC, pp. 102-109.

American Association of State Highway and Transportation Officials (1993), AASHTO Guide for design of pavement structures, Washington, DC.

Andrejack, T. L. and Wartman, J. (2010), “Development and interpretation of a multi-axial tension test for geotextiles,” Jour. Geotextiles and Geomembranes, Vol. 28, No. 8, pp. 559-569.

Asphalt Institute (1977), "Asphalt overlays and pavement rehabilitation," MS-17, College Park, MD.

ASTM D1883, Standard test method for CBR (California Bearing Ratio) of laboratory compacted soils.

Barenberg, E. J. and Bender, D. A. (1978), "Design and behavior of soil-fabric-aggregate systems," Proc. 57th Annual Meeting, TRB, Washington, DC.

Beckham, W. K. and Mills, W. H. (1935), "Cotton fabric reinforced roads," Engr. News-Record, Oct. 3, pp. 453-455.

Bell, J. R., Jr. (1983-85), Designing with Geosynthetics, unpublished course notes of R. M. Koerner and J. R. Bell.

Berg, R. R., Christopher, B. R. and Perkins, S. W. (2000), "Geosynthetic reinforcement of the aggregate base/subbase courses of flexible pavement structures," GMA White Paper II, IFAI, Roseville, MN, 176 pgs.

Carroll, R. G. Jr., Walls, J. G. and Haas, R. (1987), "Granular base reinforcement of flexible pavements using geogrids," Proc. Geosynthetics '87, IFAI, pp. 46-57.

Cedegren, H. R. (1989), Seepage, Drainage and Flow Nets, New York, Wiley, 475 pgs.

Dewar, S. (1962), "The oldest roads in Britain," *The Countryman*, Vol. 59, No. 3, pp. 547-553.

Giroud, J.-P. and Han, J. (2012), "The Giroud-Han design method for geosynthetic reinforced unpaved roads," *Geosynthetics Magazine*, Vol. 30, No. 1, February/March, pp. 40-49.

Giroud, J.-P. and Han, J. (2004), "Design method for geogrid-reinforced unpaved roads: Part 1, Development of design method, pp. 775-786 and Part 2, Calibration and applications, *Journal of Geotechnical and Geoenvironmental Engineering*, ASCE, Vol. 150, No. 8, pp. 787-797".

Giroud, J.-P. and Noiray, L. (1981), "Design of geotextile reinforced unpaved roads," *Jour. Geotechnical Eng. Div., ASCE*, Vol. 107, No. GT9, pp. 1233-1254.

GRI Standard Test Method GG-9 (2004), "Torsional behavior of bidirectional geogrids when subjected to in-plane torsion," Geosynthetic Institute, Folsom, PA, 6 pgs.

Kinney, T. C., Abbot, J. and Schuler, J. (1998), "Benefits of using geogrids for base reinforcement with regard to rutting," in *Stabilization on Geosynthetic*, TRB, Vol. 1611, Washington, DC, pp. 86-96.

Koerner, G. R. (2000), "Geotextile separation study," *GFR Magazine*, Vol. 18, No. 3, June/July, pp. 14-21.

Koerner, R. M. (1982), Discussion on Giroud and Noiray paper previously cited.

Koerner, R. M. (2012), Designing With Geosynthetics, 6th Edition (in two volumes), Xlibris Publishing Co., Indianapolis, IN, 914 pgs.

Majidzadeh, K., Luther, M. S. and Skylut H. (1982), "A mechanistic design procedure for fabric-reinforced pavement systems," Proc. 2nd Intl. Conf. on Geotextiles, August, IFAI, pp. 529-534.

Miner, J. and Davis, L. (2011), "Going green with textile interlayers; how to comply with pavement preservation," Proc. GRI-24 Conference, Dallas, TX, GSI Publ., Folsom, PA, pp. 8-27.

Miura, N., Sakai, A., Taesiri, Y., Yamanouchi, T. and Yasuhara, K. (1990), "Polymer grid reinforced pavement on soft clay grounds," Geotextiles and Geomembranes, Vol. 9, No. 1, pp. 99-123.

Molenaar, A. A. A. and Nods, M. (1996), "Design method for plain and geogrid reinforced overlays on cracked pavements," Proc. 3rd RILEM Conference, E * FN Spon., pp. 311-320.

Murray, C. D. (1982), "Simulation testing of geotextile membranes for reflective cracking," Proc. 2nd IGS Conference, IFAI Publ., pp. 511-516.

National Cooperative Highway Research Project (2004), "Guide for mechanistic-empirical design of new and rehabilitated pavement structures," NCHRP Project 1-37A, Washington, DC.

Personal communication from Maine Department of Transportation, 1994.

Reck, N. C. (2009), "Mechanistic-empirical design of geogrid reinforced paved flexible pavements," Proc. Jubilee Symposium on Polymer Geogrid Reinforcement, A. McGown, Ed., pp. 73-78.

Shields, M. K., Sprague, C. J., Gilbert, R. B. and Allen, S. R. (2005), "Bending Stiffness Index Test for Geogrid Reinforcement of Pavement Base Material," Proc. Geo-Frontiers Congress, ASCE GeoInstitute.

Shukla, S. K. (2002), "Geosynthetics and their applications," Thos. Telford Publ. Lty, 425 pgs.

The Asphalt Institute (1977), "Asphalt overlays and pavement rehabilitation," Manual Series No. 17 (MS-17), College Park, MD, November.

Theyse, H. L., DeBear, M. and Rust, F. C. (1996), "Overview of the South African mechanistic pavement design analysis method," 75th TRB Meeting, Washington, DC, Paper No. 961294.

van Gurp, C.A. P. and van Leest, A. J. (2002), "Asphalt pavements on soft soil," Proc. 9th Intl. Conf. on Asphalt Pavements, ISAP, Copenhagen, Denmark, pp. 1-18.

Webster, S. L. (1992), "Geogrid reinforced base courses for flexible pavements for light aircraft: test section construction, behavior under traffic, laboratory tests, and design criteria," final report, DOT/FAA/RD-92/25, U. S. Department of Transportation and Federal Aviation Administration, 91 p.

Wrigley, N. E., Zheng, H. and Yuan, S. P. (2011), "The confinement effect of different geogrids – 3," Proc. Geo-Frontiers 2011, ASCE, Reston, VA, pp. 2163-2172.

Zornberg, J. G. and Gupta, R. (2010), "Geosynthetics in pavements: North American contributions," Proc. 9th IGS, Brazil, pp. 379-398.

THE EVOLUTION OF GEOSYNTHETICS IN EROSION AND SEDIMENT CONTROL

C. Joel Sprague
TRI/Environmental, Inc., Greenville, SC

ABSTRACT

Much of the development of geosynthetics technology in environmental applications has been in response to government regulations. This is certainly true for geosynthetics used in erosion and sediment control. Geosynthetics continue to replace traditional materials such as soil and stone in performing important engineering functions in erosion and sediment control applications while simultaneously introducing greater versatility and cost-effectiveness. Geosynthetics are widely used as a “carrier” for degradable materials to the enhancement of vegetative establishment; as nondegradable materials to extend the erosion control limits of vegetation or soil; as primary slope or channel linings; as components in silt fences and turbidity curtains; and as a component in an ever growing array of sediment retention devices.

Along with the introduction of geosynthetics into this wide range of applications has come the need for industry-wide initiatives to promote their correct use and new test methods to characterize them. All of which, are a “work in progress”.

THE NEED FOR EROSION AND SEDIMENT CONTROLS

Much of the development of geosynthetics technology related to erosion and sediment control applications has been in response to government regulations. A progression of regulatory actions has brought a national focus on erosion and sediment control, including:

- Amendments to the Federal Water Pollution Control Act (1985) - eliminating discharge of any pollutant to navigable waters.
- The Clean Water Act (1987) - requiring National Pollution Discharge Elimination System (NPDES) Permits for large construction sites. More recently, NPDES regulation of construction activities on one or more disturbed acres of land became effective on February 16, 2012 . . . though numeric turbidity limits have been stayed!
- Intermodal Surface Transportation Efficiency Act (1991) - requiring erosion control guidelines for all federal-aid construction projects. This led to AASHTO’s “Erosion and Sediment Control in Highway Construction,” in Volume III, Highway Drainage Guidelines (1992). This has subsequently been made a regulatory document.
- Coastal Zone Act Reauthorization Amendments (1990) - requiring measures to control non-point sources of pollution in coastal areas.

The centerpiece of regulatory action has been the NPDES permitting process, which is required for construction activities. An NPDES permit requires a Storm Water Pollution Prevention Plan (SWPPP) that must include both the technical basis used to select the pollution control practices (a.k.a., best management practices or BMPs) to avoid increasing the historical amount of sediment in water and the maintenance of each sediment and erosion control measure.

Why Geosynthetics?

Geosynthetics have proven to be among the most versatile and cost-effective ground improvement materials. Their use provides the following advantages over traditional materials:

- *Lighter, Easier to Handle, More Durable* - Geosynthetics are comprised of plastic.
- *Verifiable Material Quality Control* - Geosynthetics are manufactured in controlled environments under standard operating conditions.
- *Easier Construction Quality Control* - Often the installation procedure for geosynthetics is as simple as rolling out and securing in place as opposed to concrete or rock being constructed in place and subject to variations caused by weather, handling and placement.
- *Real Cost Savings* - Geosynthetics are typically less costly to purchase, transport and install than are aggregates or subcontractor-dependent systems.
- *Technical Superiority* - Geosynthetics are engineered materials optimized for performance.
- *Easier Construction* - Geosynthetics can be installed quickly, providing the flexibility to construct during short construction seasons, breaks in inclement weather, or without the need to demobilize and remobilize the earthwork contractor.
- *Material Availability* - Numerous geosynthetic suppliers and ease of shipping insure competitive pricing and availability of materials.
- *Enhanced Sustainability* - Studies have shown significantly lower CO₂ generation than with natural soil or rock.

What do Geosynthetics do in Erosion and Sediment Control Applications?

Geosynthetics replace traditional materials such as soil and stone in performing important engineering functions, and thus can be selected via a “design-by-function” methodology as prescribed by Koerner (2012). While traditional applications of geosynthetics perform more common in-ground functions such as separation and filtration, geosynthetics used in erosion and sediment controls are used on the soil surface. As such, they introduce the following unique functions according to ASTM D5819:

- *Containment* - A geosynthetic provides containment when it encapsulates or surrounds materials such as sand, rock, and fresh concrete.
- *Dynamic Filtration* . . . A geosynthetic performs the dynamic filtration function when the equilibrium geotextile-to-soil system allows for adequate liquid flow with limited soil loss across the plane of the geotextile over a service lifetime compatible with dynamic flows.
- *Screening* . . . A geosynthetic, placed across the path of a flowing fluid (ground water, surface water, wind) carrying particles in suspension, provides screening when it retains some or all soil fine particles while allowing the fluid to pass through. After some period of time, particles accumulate against the screen, which requires that the screen be able to withstand pressures generated by the accumulated particles and the increasing pressure from accumulated fluid.
- *Surface Stabilization* . . . A geosynthetic, placed on a soil surface, provides surface stabilization when it restricts movement and prevents dispersion of surface soil particles subjected to erosion actions (rain, wind), often while allowing or promoting vegetative growth.

- *Vegetative Reinforcement* . . . A geosynthetic provides vegetative reinforcement when it extends the erosion control limits and performance of vegetation.

EROSION AND SEDIMENT CONTROL MATERIALS

Geosynthetics, as well as natural materials, are used extensively in erosion and sediment control systems such as:

- Temporary, degradable materials for the enhancement of vegetative establishment;
- Long-term, nondegradable materials to extend the erosion control limits of vegetation or soil;
- Primary slope or channel linings;
- Silt fences and turbidity curtains;
- Components in sediment retention devices.

A large construction site may have several different erosion and sediment control materials depending on location (i.e., slopes vs. channels), flow conditions (i.e., sheet vs. concentrated), and regulatory requirements.

Erosion Control Systems

There are two categories of erosion control systems: The first is termed temporary or degradable and the second is termed long-term or nondegradable. There are numerous types of materials within these categories according to Zoghi, et al, (2000). Temporary degradable systems include conventional loose mulches, as well as, hydraulic mulch geofibers (HMG), erosion control netting (ECN), open weave meshes (ECM), erosion control blankets (ECB), and fiber roving systems (FRS). The long-term systems include conventional sod and riprap, as well as, turf reinforcement mats (TRM), fabric formed revetments (FFR), geocellular confinement systems (GCS), gabions (G), and articulating concrete blocks (ACB). ECNs, ECMs, ECBs, and TRMs commonly contain geosynthetic components and are classified as rolled erosion control products, or RECPs. Other geosynthetic systems include FFRs and GCSs.

The advantages and disadvantages of the various systems are detailed in Tables 1 and 2. The relative performance of permanent systems is presented in Table 3, and the relative installed costs of the various erosion control systems is presented in Table 4. Following are brief descriptions of each system.

Hydraulic Mulch Geofibers (HGM) – Hydraulic mulch is commonly used as an alternative to loose straw mulch. It consists of short organic fibers, such as paper, straw, wood, coconut, or cotton, mixed with water in a tank (usually with seed) and sprayed over the bare soil. As it dries it forms a thin mulch layer, yet it is still susceptible to the wash and wind-blown problems associated with loose fiber mulches. A more stable matrix can be created by incorporating a tackifier or adhesive in the mixture that, after drying, is stable when re-wetted by rainfall.

Erosion Control Netting (ECN) – Erosion control netting is typically polyolefin biaxially-oriented process (BOP) mesh. ECNs are used for anchoring loose fiber mulches. They are rolled out over the seeded and mulched area and stapled or staked in place.

Open Weave Meshes (ECM) – Open weave meshes are woven of organic “twines” of jute or coir or polyolefin yarns. Organic ECMs typically are 0.25 to 0.50 in. thick and have 1 inch or larger square uniform openings. Polyolefin meshes are considerably thinner with smaller openings. All meshes are very flexible, promoting intimate ground cover, though they do not provide full ground coverage. Organic meshes also absorb water, which can help maintain soil moisture.



Figure 1 – ECM Applied Over Straw



Figure 2 – ECM on Hillside

Erosion Control Blankets (ECB) – Erosion control blankets are organic fiber filled “blankets” consisting of straw, wood (excelsior), or coconut fibers sewn to or between synthetic (or organic) nettings. ECBs provide a thick (up to 0.5 in.) full coverage of mulch which better absorbs rainfall impact and retains moisture. The nettings add strength to help ECBs resist erosive forces. Their useful life is limited to durability of the organic fibers.



Figure 3 – ECBs Come in Many Varieties



Figure 4 – ECB (left) vs. HMG (right)

Fiber Roving Systems (FRS) – Fiber roving systems use fibrillated, or split, yarns that are fed off spools and continuously fed from the spools through a special air gun and uniformly applied over a seeded soil surface. A randomly laid mat of continuous strands results and provides a high percentage of ground cover. A tackifier is then sprayed on top of the FRS to firmly anchor it to the soil. FRS can conform to almost any geometry.

Turf Reinforcement Mats (TRM) – TRMs are thick mattings composed of fused or stitched polymer nettings (often filled with polymeric fibers), randomly laid monofilaments, or yarns woven or tufted into an open, dimensionally stable mat. The dimensional stability produces a somewhat stiffer, but much stronger mat. These flexible, synthetic mats are designed to be used in conjunction with topsoil and seed or turf to create strong, durable and continuous soil-root-mat matrices which can provide more than twice the erosion protection of plain grass alone.



Figure 5 – TRMs are Polymer Structures



Figure 6 – TRMs are Used in Channels

Fabric Formed Revetments (FFR) – Fabric formed revetments take advantage of low-cost, durable, synthetic fabrics to produce three-dimensional forms for casting concrete slabs. By pumping a very fluid fine-aggregate grout into a fabric envelope consisting of two layers connected by tie-chords or by interweaving at points, a concrete mattress can be constructed in minutes. FFRs provide the durability of rigid linings, such as cast-in-place concrete or asphaltic concrete, and the flexibility and permeability of riprap or gabion systems.

Geocellular Confinement Systems (GCS) – Geocellular confinement systems, often called geocells, are made of strips of polymer sheet or geotextile connected at staggered points so that, when the strips are pulled apart, a large honey-comb mat is formed that can be filled with soil, rock or concrete. Geocell thickness (depth) typically ranges from 2 in. to 12 in. A GCS is effective at assuring that surface soil is retained on a slope.



Figure 7 – FFR Installed in Wave Zone



Figure 8 – GCS “Honeycomb” Structure

Gabions (G) – Gabions are compartmented rectangular containers made of galvanized steel hexagonal wire mesh and filled with hand-sized stone. In highly corrosive conditions a polyvinyl chloride coating is used over the galvanized wire. Gabions are more flexible, durable and permeable than rigid structures and more stable than loose rock.

Articulating Concrete Blocks (ACB) – Articulating concrete block (ACB) revetments are interlocking cellular concrete blocks, with varying amounts of open area within or between blocks, underlain by a filtration geotextile. The blocks can be assembled into mats either at the factory or on site with or without cables running through them. The blocks are held on the slope by anchors placed at the top of the slope and/or friction between the slope and the blocks. ACB revetments provide the porosity, flexibility, vegetation encouragement, habitat enhancement, and ease of installation of rolled RECPs and the nonerodibility, self-weight, and high shear resistance of rigid linings.

Table 1 – Some Potential Advantages and Disadvantages of Temporary, Degradable Erosion Control Systems

SYSTEM	POTENTIAL ADVANTAGES	POTENTIAL DISADVANTAGES
Loose Mulches	Lowest cost Well accepted High installation rate Moderate sediment yield Moderate vegetative density	Very temporary (< few weeks/months) No concentrated flows Dusty Requires anchoring (crimping, tackifier) May require noxious weed certification
Hydraulic Mulch Geofibers (HMG)	Low cost Well accepted High installation rate Moderate sediment yield Moderate vegetative density	Very temporary (< few weeks/months) Very low or no concentrated flows
Erosion Control Netting (ECN)*	More effective than tackifier (if properly anchored)	Temporary (1-2 yrs.) More costly than tackifier Netting may interfere w/ maintenance (if inadequately anchored)
Open Weave Meshes (ECM)*	Low to moderate cost Moderate sediment yields Moderate vegetative density Moderate moisture absorption	Temporary (1-2 yrs.) Low flows only Not complete ground cover Moderate moisture absorption
Erosion Control Blankets (ECB)*	Low to moderate cost Easy to install Good moisture absorption Very low sediment yield Very good vegetative density	Temporary (1-3 yrs.) Low to moderate flows Netting may interfere with maintenance (if improperly manufactured or inadequately anchored)
Fiber Roving Systems (FRS)*	Low to moderate cost High subgrade conformance Very low sediment yield Very good vegetative density	Temporary (1-2 yrs.) Low to moderate flows only Special equipment required

**Commonly composed partially or completely of geosynthetics.*

Table 2 – Some Potential Advantages and Disadvantages of Long-term, Nondegradable Erosion Control Systems

SYSTEM	POTENTIAL ADVANTAGES	POTENTIAL DISADVANTAGES
Sod	Immediate vegetation and its associated benefits	May need irrigation Risk of dying before establishment High costs Limited to turf grasses
Turf Reinforcement Mats (TRM)*	Moderate costs Long-term (indefinite) Moderate to high flows Encourages infiltration Mod. to high vegetative density Extends the limits of vegetation Flexible over differential settlement	Low to moderate sediment yields during unvegetated stage Requires vegetative establishment for effective long-term performance
Riprap	Long-term (maintenance req'd) Moderate to high flows Encourages infiltration Low to moderate sediment yield (when underlain by a geotextile)	Moderate to high cost Possible negative aesthetic/safety impact Difficult to install on steep slopes Low vegetative density Often unstable, especially w/o geotextile
Other Hard Armor Systems**	Long-term (indefinite) Moderate to very high flows Low to moderate waves Low to moderate sediment yields Range of fill materials Durable and low maintenance	High to very high costs None to delayed vegetation establishment None to low vegetation density May prevent infiltration Special deployment/equipment req'ts

**Commonly composed partially or completely of geosynthetics; **Including: Fabric Formed Revetments, Geocellular Confinement Systems, Gabions, Articulating Concrete Blocks*

Table 3 - Typical Erosion Control System Performance Limits

BMP	Limiting Shear (psf)
Mechanically or Hydraulically Applied Seeding	< 0.5
Mechanically or Hydraulically Applied Mulching	< 0.5
Meshes and Nets	0.5-1.5
E.C. Blankets	1.5-3.0
Fiber Roving	1.0-2.0
Natural Vegetation	up to 2.0
Sod	0.4-3.7
Turf Reinforcement	2.0-11.0
Geocellular Confinement	10
Fabric Formed Revetments	2.2-24
Riprap (6" to 18" thick)	2.5-5.0
Gabions (6" to 18" deep)	35
Interlocking Block Mats	4.4-25

Geosynthetics in bold. Conversions: ft/s = m/s x 3.28; psf x 47.88 = Pa

Table 4 - Costs of Erosion Control Systems

Erosion Control System*	Approx. Cost per Square Yard – Installed***
Dry-Blown and Hydraulic Mulching	\$0.50 - \$1.00
Meshes and Nets	\$0.50 - \$1.00
E.C. Blankets	\$1.00 - \$1.50
Fiber Roving	\$1.50 - \$3.00
Sod	\$2.00 - \$3.00
Turf Reinforcement	\$4.00 - \$7.00
Hard Systems**	\$15.00 - \$60.00

Geosynthetics in bold. * Excludes subgrade preparation, soil amendments and seeding operations.

** Includes Geocellular Confinement, Fabric Formed Revetments, Riprap, Gabions, Interlocking Block Mats.

*** Cost is very sensitive to freight and labor rates.

Sediment Control Systems

In general, the benefits of geosynthetic sediment control systems over traditional structures, such as rock checks and sediment traps, include: minimal labor required to install; low cost; highly efficient in removing sediment; very durable and sometimes reusable. The performance of sediment control systems typically depends on the proper selection and deployment of sediment retention devices (SRDs). SRDs, such as silt fences, typically cause the following to happen:

- The SRD initially screens silt and sand particles from runoff.
- A soil filter is formed adjacent to the upstream face and reduces the ability of water to flow through the fence.
- This leads to upstream ponding, which serves as a “stilling” basin to collect suspended soils from runoff water.

To perform satisfactorily as an SRD, the geotextile component must have properly sized openings, which initiate the formation of a soil filter. Also the strength and storage capacity of the SRD must be adequate to contain the volume of water and sediment anticipated during a major storm. Hydraulic loading during a storm event is commonly the primary loading considered.

Other SRDs include turbidity curtains and fiber rolls. Turbidity curtains are reusable floating panels of geotextile or geomembrane that prevent water-polluting sediment from shore-side construction or off-shore filling and dredging operations from moving off-site. The top edge of each curtain contains floats and weights are attached to the lower edge of the curtain to keep it vertical in the water. Fiber rolls are three-dimensional rolls of organic fibers contained within a tubular netting or geotextile structure. They are commonly used as ditch checks or slope interrupters.



Figure 9 – Silt Fence



Figure 10 – Wattles in Channels



Figure 11 – SRD Protecting Inlet



Figure 12 – Turbidity Curtain

Emerging Erosion and Sediment Control Technologies

Biotechnology – Probably the hottest topic in erosion control today is “biotechnology”, or the maximum use of vegetation. This technology appeals to environmentalists and engineers, alike, because it looks good and brings the many benefits of vegetation to bear on the problems of erosion and water quality. This is also why geosynthetic-containing RECPs are steadily gaining in popularity. RECPs nurture and support vegetation that, by itself, is often fragile, costly and labor-intensive to construct.

Geotextile Tubes and Containers – Very large geotextile containers filled with dredged material have re-gained popularity in the past decade because of their simple placement and construction, cost effectiveness and minimum impact on the environment. These containers are hydraulically or mechanically filled with a variety of dredged material types, including fine-grained materials. Containment of dredged material in geotextile tubes, bags or other large containers, filled in place or filled in large bottom dump hopper barges and dumped below water has helped solve several difficult construction problems. Dike construction using long, sometimes continuous, tubes in wetlands, subdivision and perimeter dikes in dredged material disposal areas, under

water stability berms, containment of contaminated materials, island construction, barrier island breach repair and structural scour protection are examples of projects that could not have been completed without use of geotextile containment systems.



Figure 13 – Biotechnology for Shoreline



Figure 14 – Geotextile Tube / Groin

Anchored Geotextiles and Geonets – An anchored geonet presents a good example of an emerging development in biotechnical stabilization, specifically for stabilization of sandy slopes and coastal landforms. The anchored geotextile or geonet is made of a fabric or net which is stretched over and pulled down tightly on the ground surface and is secured in place by means of anchors inserted through and fastened to the geotextile.

3D Cement/Fabric Composites – Unique 3-dimensional cement/fabric composites are replacing traditional concrete in some erosion control applications. Cement mix is trapped within a flexible 3D fabric structure. There may be a waterproof layer on one side. The composite can be hung vertically, laid in trenches, or cut and formed into shapes to create a durable layer of concrete, all without the need for molds or mixers. It can be installed in the rain and other wet conditions. The fabric is wetted to activate the cement, and within 24 hours, the product has cured to 80% strength. The fabric structure reinforces the concrete and reduces cracking, while using up to 95% less concrete than conventional methods.



Figure 15 – Anchored Geosynthetic



Figure 16 – 3D Cement/Fabric Composite

INDUSTRY EFFORTS

The first attempts to promote the erosion and sediment control industry were by the International Erosion Control Association (IECA) in the 1980s. The IECA even set up a committee (Committee C) to look into test methods to characterize the ever expanding products being introduced. Within a few years, the IECA determined that because of liability issues surrounding the setting up of standards, the standardization effort was better undertaken by ASTM. As a result, members of Committee C became some of the strongest initiators of efforts to energize and formalize meetings of manufacturers to develop, draft, and standardize test methods. These efforts fueled two industry-wide initiatives:

- The Erosion Control Technology Council (ECTC), an industry group driven by manufacturers, and
- ASTM D18.25 and D35.05, Subcommittees on Erosion and Sediment Control, where other interest groups (i.e. engineers, regulators, researchers) where other industry partners could contribute to the standardization effort.

In 1994, the Erosion Control Technology Council (ECTC), an organization of rolled erosion control product (RECP), hydraulically applied erosion control product (HECP), and sediment retention fiber roll (SRFR) manufacturers commissioned a program to identify and establish a common terminology and to develop standardized index and performance tests for the characterization of erosion control and sediment retention products containing natural materials. In January 1997, a manual of common terminology and recommended index testing standards (*ECTC Technical Guidance Manual: TASC 00197*) was issued to the industry. Then, in the late 1990s, ECTC once again commissioned a new class of test – this time it was bench-scale performance tests – that focused on testing an erosion control product along with a default soil system under carefully controlled “standard” conditions. The project included the development of bench-scale (i.e. small-scale) laboratory tests for slope erosion, channel erosion, vegetation enhancement, and biodegradability.

Subsequent to each of these development efforts, there have been coordinated efforts to work through the ASTM International to achieve consensus standardization of both erosion control and sediment retention test procedures. This work continues within ASTM Subcommittee D18.25, “Erosion and Sediment Control Technology” and Committee D35, “Geosynthetics.” Over the past decade, ASTM has released several new standard test methods for turf reinforcement mats (TRMs) and erosion control blankets (ECBs) that have been eagerly adopted. New standard test methods for Sediment Retention Devices have also been released, though their adoption has been slower.

Though both ECTC and ASTM began their erosion control efforts with a primary focus on RECPs, the ASTM effort quickly evolved to include biotechnology, various hard armor systems, and sediment retention devices. The ECTC remained focused on RECPs until around 2006 when it, too, began addressing HECPs and then, more recently sediment retention fiber rolls (SRFRs).

ASTM has struggled to make significant progress in standardizing HECP test methods, though the effort continues. It appears proprietary interests make consensus building difficult.

Finally, it should be noted that the IECA has just in the last year re-initiated its effort to pursue erosion and sediment control standards. It has formed that Standards and Practices (S&P) Committee, including subcommittees focusing on terminology, sediment control testing, sediment control design, and turbidity testing. The IECA S&P Committee plans to funnel it's efforts into ASTM for eventual consensus standardization.

QUALITY CONTROL, QUALITY ASSURANCE AND PERFORMANCE TESTING

As noted in the previous section, the industry recognized early on that with so many new types of erosion control products (many incorporating geosynthetics), and their associated new applications, has come a need for new relevant tests to properly characterize them. Basic index tests are typically needed to assure manufacturing quality control. Not only are these tests useful for manufacturing quality control, but when used on the same materials deployed in bench-scale and large-scale performance tests, they serve to “bench-mark” the performance results to specific material properties. Not surprisingly, a variety of performance tests have been developed over the years to answer design questions regarding performance among different products and product categories.

Since 2003, the National Transportation Product Evaluation Program (NTPEP) has provided a program for independent testing of RECPs. The program has included both index tests and bench-scale “indexed performance” tests. The goal of the program is to minimize duplicative testing of erosion control products done by individual State Departments of Transportation (DOTs) by providing a process where manufacturers and suppliers submit their products to the NTPEP for independent index and bench-scale testing. The results of the testing are then shared with participating DOTs. The results of the testing may be used for assessing product conformance to material specifications. Further, the testing results provide quantitative material data necessary for placing specific products on, or removing specific products from a DOT's qualified products list (QPL). The NTPEP program is intended to serve as a nationwide quality assurance (QA) program for the DOTs.

Additionally, in 2009, NTPEP began offering independently verified large-scale erosion control performance testing to complement on-going index and bench-scale testing. NTPEP (2011) describes the purpose and rationale for exclusive use of standardized test procedures in the programs.

While standardized tests for geotextiles – which are used in many SRDs – have been available for decades, new tests have been needed for RECPs. The following section details the tests that have developed and are generally used to characterize RECPs and SRDs.

Index Testing

Index tests are standard tests that may be used for manufacturing quality control and to compare the relative material properties of several different RECPs. Quality Control tests are index tests which are performed on a production basis to evaluate product integrity, quality, continuity, and the impact of changes in production methodology on product properties. Quality

control test results can be reported with statistical relevance when they are run with sufficient frequency. Recently, ASTM D4354, “Standard Practice for Sampling of Geosynthetics for Testing”, has been revised to include appropriate sampling frequencies to achieve a 95% confidence level for RECP quality control, quality assurance, and conformance testing. Following are the index test methods used for RECPs:

- Mass per Unit Area: ASTM D 6475, “Standard Test Method for Measuring Mass per Unit Area of Erosion Control Blankets”;
- Mass per Unit Area: ASTM D 6566, “Standard Test Method for Measuring Mass per Unit Area of Turf Reinforcement Mats”.
- Thickness: ASTM D 6525, “Standard Test Method for Measuring Nominal Thickness of Permanent Rolled Erosion Control Products”.
- Tensile Strength: ASTM D 6818, “Standard Test Method for Ultimate Tensile Properties of Turf Reinforcement Mats”.
- Light Penetration: ASTM D 6567, “Standard Test Method for Measuring the Light Penetration of a Turf Reinforcement Mat (TRM)”.
- Water Absorption: ASTM D 1117 Section 5.4 and ECTC-TASC 00197, “Standard Guide for Evaluating Nonwoven Fabrics – Absorptive Capacity Test (for Larger Test Specimens)”.
- Specific Gravity: ASTM D 792, Method A, “Standard Test Methods for Density and Specific Gravity (Relative Density) of Plastics by Displacement”.

Following are index test methods used for SRDs:

- Mass per Unit Area: ASTM D 5261, “Standard Test Method for Measuring Mass per Unit Area of Geosynthetics”;
- Thickness: ASTM D 5199, “Standard Test Method for Measuring Thickness of Geosynthetics”. Note: Many SRDs are 3-dimensional products (i.e. wattles, bales, etc.), thus non-standard procedures are currently used to measure such things as density (or unit weight per length) and circumference.
- Tensile Strength: ASTM D 4595, “Standard Test Method for Measuring the Wide-width Tensile Strength of Geosynthetics”;
- Permittivity: ASTM D 4491, “Standard Test Methods for Water Permeability of Geotextiles by Permittivity”.
- Apparent Opening Size (AOS): ASTM D 4751, “Standard Test Method for Measuring the Apparent Opening Size of Geosynthetics”.
- Percent Open Area (POA): Corps of Engineers protocol CW02215.
- Ultraviolet Stability: ASTM D 4355, “Standard Test Method for Deterioration of Geotextiles by Exposure to Light, Moisture and Heat in a Xenon Arc Type Apparatus”. The exposed specimens are typically tested for retained strength in accordance with ASTM D 6818. Note: Since accelerated tests have not shown a consistent correlation to outdoor exposures, ASTM’s D 5970, Standard Test Method for Deterioration of Geotextiles from Outdoor Exposure is also used.

Bench-Scale Testing

Bench-scale “indexed” performance tests are a class of tests that have been developed to focus on testing the RECP/soil system or SRD/water system under carefully controlled “standard” conditions. Bench-scale tests have been developed for slope erosion, channel erosion, and vegetation enhancement for RECPs and for filtration efficiency and flow for SRDs. Bench-scale tests do not reflect product installation techniques or site conditions to which these materials are typically subjected. Therefore the results of these tests may not be indicative of a RECP’s or SRD’s actual field performance. Following are the bench-scale test methods used for RECPs:

- Slope Erosion and Runoff Reduction: ASTM D 7101, “Standard Index Test Method for Determination of Unvegetated Rolled Erosion Control Product (RECP) Ability to Protect Soil from Rain Splash and Associated Runoff under Bench-Scale Conditions”.
- Permissible Shear and Channel Erosion: ASTM D 7207, “Standard Test Method for Determination of Unvegetated Rolled Erosion Control Product (RECP) Ability to Protect Sand from Hydraulically-Induced Shear Stresses under Bench-Scale Conditions”.
- Germination/Vegetation Growth: ASTM D 7322, “Standard Test Method for Determination of Rolled Erosion Control Product (RECP) Ability to Encourage Seed Germination and Plant Growth under Bench-Scale Conditions”.

Following are the bench-scale test methods used for SRDs:

- Filtration Efficiency and Flow: ASTM D 5141, “Standard Test Method for Determining Filtering Efficiency and Flow Rate of the Filtration Component of a Sediment Retention Device Using Site-Specific Soil”.
- Horizontal Permeability: Many SRDs are three-dimensional, and therefore cannot be tested for clear water flow (a.k.a. permeability or flow rate) using standard procedures that have been developed for planar materials. To fill the gap, a “horizontal permeability” test has been developed that exposes the SRD to a constant head of clear water on one side.

Large-Scale Testing

Large-scale performance tests have been developed to simulate expected field conditions to report performance properties of “as installed” RECPs. Large-scale tests have been developed for slope erosion and channel erosion. The channel erosion test may be conducted un-vegetated or vegetated. Performance of RECPs relies not only on material properties but also on the installation techniques. Products are installed on the test slope or channel per manufacturer installation recommendations. The results of these tests are more indicative of actual field performance of RECPs and are acceptable for use in design calculations. Following are the large-scale test methods used for RECPs:

- Slope Erosion: ASTM D 6459, “Standard Test Method for Determination of Rolled Erosion Control Product (RECP) Performance in Protecting Hillslopes from Rainfall-Induced Erosion”.

- Channel Erosion: ASTM D 6460, “Standard Test Method for Determination of Rolled Erosion Control Product (RECP) Performance in Protecting Earthen Channels from Stormwater-Induced Erosion”.

The most unique thing about SRD’s is that, typically, for them to be very effective in retaining sediment they must also impound most of the runoff. Conversely, for them to freely pass runoff, they have to be allowed to pass a significant amount of sediment. Neither of these extremes is usually preferred, so the user has to determine the proper balance of retaining sediment while permitting seepage. Following are the large-scale test methods used for SRDs that are used to quantify the “balance” of retention and flow provided under standard conditions:

- ASTM D 7351, “Standard Test Method for Determination of Sediment Retention Device Effectiveness in Sheet Flow Applications”.
- ASTM D 7208, “Determination of Temporary Ditch Check Performance in Protecting Earthen Channels from Stormwater-Induced Erosion”.
- ASTM’s WK11340, is a derivation of ASTM D 6459, Large-scale Slope Erosion Testing, but permits a flatter slope and calls for a lighter rainfall.
- ASTM D 7351 can be modified to better simulate the runoff being more concentrated and potentially having a lower sediment load as may be applicable to inlet protection.
- Another modification to the D 7351 protocol that has been proposed is the Texas Transportation Institute’s (TTI) Sediment Control Device (SCD) performance testing facility to focus on evaluation of roadside SCDs.

Some of the unique standardized tests are shown in the following figures.



Figure 17 - ASTM D 6818, Tensile Testing

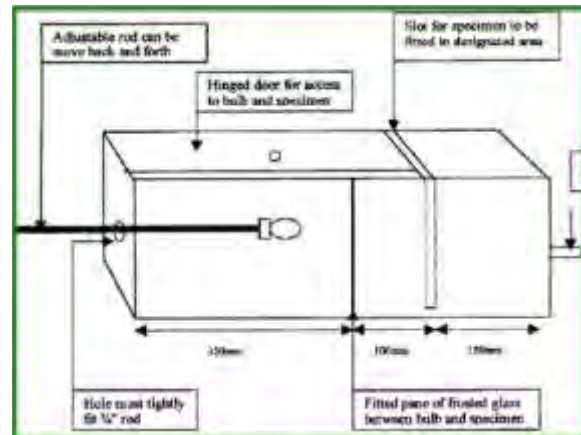


Figure 18 - ASTM D 6567, Light Box for % Light Penetration



Figure 19 - ASTM D 7101, Rainfall



Figure 20 - ASTM D 7207 Hydraulic Shear



Figure 22 - ASTM D 5141



Figure 21 - ASTM D 7322 Germination Testing



Figure 23 - ASTM D 5141 Test Close-up



Figure 24 - ASTM D 6459 Slope Testing

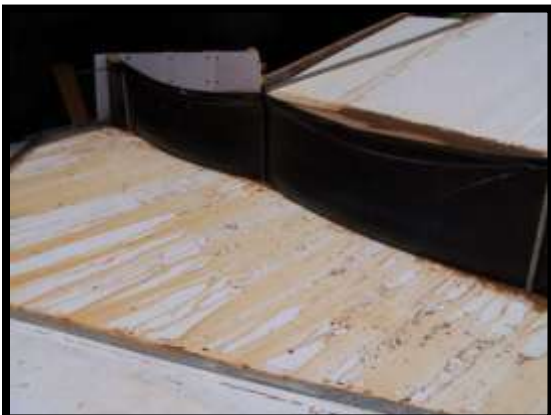


Figure 26 - ASTM D 7351 with Silt Fence



Figure 25 - ASTM D 7351 SRD Testing



Figure 27 - ASTM D 6460 Channel Testing



Figure 28 - ASTM D 7208 Check Testing



Figure 29 - ASTM D 7208 Close-up

EXISTING INDEPENDENT DATA AND MATERIAL SPECIFICATIONS

Independent RECP and SRD Data

While relatively little independent data on SRDs exists, the opposite is true for RECPs. Thanks largely to the NTPEP program mentioned earlier, much independent data on a wide range of products is available at www.ntpep.org. Sprague and Sprague (2013) have summarized the available NTPEP data and proposed associated specifications.

Generic RECP and SRD Specifications

The most widely circulated “generic” specifications for RECPs are the categorizations presented by the ECTC (2006) and the Federal Highway Administration’s FP-03 (2003). These specifications include both temporary and permanent RECPs, and reflect different performance levels based on functional longevity, C-Factor, and Permissible Shear from large-scale testing. An update of the ECTC specification is expected in the coming months.

Unfortunately, there are no widely circulated “generic” specifications for SRDs. Thankfully, the IECA Committee on Standards and Practices is working toward developing specifications, but developing test methods is their initial focus.

CONCLUSIONS

Geosynthetics continue to replace traditional materials such as soil and stone in performing important engineering functions in erosion and sediment control applications while simultaneously introducing ever greater versatility and cost-effectiveness. Geosynthetics are commonly used along with temporary, degradable materials for the enhancement of vegetative establishment; as long-term, nondegradable materials to extend the erosion control limits of vegetation or soil; as primary slope or channel linings; and as components in silt fences and turbidity curtains and an ever growing array of sediment retention devices.

Industry-wide initiatives are well underway to promote the correct specification and use of geosynthetics in erosion and sediment control. This includes efforts to facilitate more

comprehensive quality systems in manufacturing and better measurements of performance via new and better test methods. All of this is indeed a “work in progress”.

REFERENCES

ECTC (2006), “ECTC Standard Specification for Temporary Rolled Erosion Control Products,” Erosion Control Technology Council, www.ectc.org.

ECTC (2006), “ECTC Standard Specification for Permanent Rolled Erosion Control Products,” Erosion Control Technology Council, www.ectc.org.

FHWA (2003), “Standard Specifications for Construction of Roads and Bridges on Federal Highway Projects”, FP-03(U.S. Customary Units), U.S. Department of Transportation, Federal Highway Administration.

Koerner, R. M. (2012), Designing with Geosynthetics, 6th Edition, Xlibris, Corp.

NTPEP (2011), “ECP User Guide,” National Transportation Product Evaluation Program, AASHTO, www.ntpep.org.

Sprague, C.J. and Sprague, J.E. (2013), “Testing and Specifying Rolled Erosion Control Products,” Proceedings of Geosynthetics 2013, Long Beach, IFAI.

Zoghi, M., Sprague, J., and Allen, S (2000), Emerging Materials for Civil Infrastructure: State of the Art, Chapter 3: Emerging Geomaterials for Ground Improvement, Edited by Lopez-Anido, R.A., Naik, T.R., Fry, G.T., Lange, D.A., and Karbhari, V.M., ASCE.

THE INTERNATIONAL GEOSYNTHETICS SOCIETY (IGS): NO BORDERS FOR THE GOOD USE OF GEOSYNTHETICS

Jorge G. Zornberg, Ph.D., P.E.

Professor, The University of Texas at Austin, Austin, Texas, USA

President, International Geosynthetics Society (IGS)

ABSTRACT

Over its 30 years of existence, the International Geosynthetics Society (IGS) has grown enormously, both in the number of members and in the scope and impact of its activities. Today, the IGS has over 3,000 members, including over 150 corporate members and 350 student members. During this period, the IGS organized a remarkable number of international conferences and regional (continental) conferences as well as hundreds of national (chapter) conferences. In addition, it has formed chapters in 38 countries or groups of countries, and implemented numerous educational, technical and outreach programs. This paper provides an overview of the history of the IGS, its standing within the context of international learned societies, an overview of its chapters, of its conferences and of ongoing initiatives aimed at providing continued advancement of geosynthetics.

INTRODUCTION

2013 marks the 30th anniversary of the International Geosynthetics Society (IGS). Over its 30 years of existence, the IGS has grown remarkably. As of January 2013, the IGS consists of 3,135 members, including 2,620 individual members, 356 student members, and 159 corporate members. The IGS chapters, which are somewhat equivalent to the member societies of other international societies, were initiated with pioneer chapters in western Europe, North America and eastern Asia, but subsequently spread out to the rest of the world, including South America, Africa, and eastern Europe.

During this period, the IGS has accomplished the organization of seven international conferences, thirteen regional (continental) conferences, and hundreds of national (chapter) conferences. In addition, current counts show IGS chapters in 38 countries or group of countries, with several other countries currently in the process of establishing new chapters. The society has established awards programs with emphasis on rewarding technical excellence, it has implemented numerous educational programs, compiled educational material, prepared terminology documents in multiple languages, sponsored student programs, and organized numerous outreach programs, to name a few of its activities and achievements. To provide a context to the IGS trajectory in fostering the good use of geosynthetics worldwide, this paper provides an overview of the history of the IGS, its standing within the context of international learned societies, an overview of the chapters of the IGS and a summary of its successful conference series. In addition, the

paper provides an overview of the current structure of the IGS, its operating units and a few examples of ongoing initiatives.

The information in this paper is an updated and expanded version of information partially presented by the author as part of the “President’s Corner” series of articles published in *IGSNews*, the Newsletter of the IGS.

AN OVERVIEW OF THE THIRTY YEAR-HISTORY OF THE IGS

The organization of early international conferences on geosynthetics (or “fabrics” at the time) provided the forum for discussions on the formation of an international society. An early international conference on the use of “Fabrics” in geotechnics was held in Paris, France, in 1977. However, the concept of an international society, which will later become the IGS, was only formulated in 1980 (Giroud 2008). Subsequently, during the Second International Conference on Geotextiles held in Las Vegas, USA in 1982, the formation of the IGS was explicitly discussed. Finally, the “International Geotextile Society,” as it was named at the time, was officially founded on November 10, 1983 with Charles Schaerer (Switzerland) as its President. This founding of the society initiates the 30 year-timeline shown in Figure 1.

The timeline highlights **important milestones** in the history of the society (see Figure 1, in pink). At the time of the society’s founding in 1983, the “G” in the IGS acronym originally corresponded to “Geotextiles,” but the growth of the scope of the society activities was reflected in 1994 when the IGS Council approved changing the society’s name into the International “Geosynthetics” Society. As also shown among the milestones in the figure, access to the highly regarded “Geotextile & Geomembranes” technical journal was added as a benefit to the IGS membership early in the history of our society (in 1987), becoming the first official journal of the IGS. A second and equally prominent technical journal, “Geosynthetics International,” became an official IGS journal in 1994. The availability of two technical journals is good evidence of the high emphasis of the IGS on the dissemination of information. It is notable that these two journals have been consistently ranked among the best journals in the field of geotechnical engineering.

Outreach to young members in our discipline has received special focus throughout the history of the IGS, with key milestones being the establishment of student membership in 1990 and the implementation of unique student awards programs since 2000. A fresh and equally relevant milestone is the creation by the IGS Council of the its Young Members Committee in December 2012, which aims at facilitating and promoting the active participation of young members (under 35 years old) in technical geosynthetics activities and the operation of the IGS.

More recent milestones in the history of the IGS include the formation of the IGS Technical Committees (TCs), approved by the IGS Council in 2010 as well as the implementation of Council Operating Units that include not only IGS Council

Committees but also Council Task Forces. Also in 2010, the IGS Council approved a statement for the Core Purpose of the IGS, a 4-year operations plan, and a long-term Big Audacious Goal. In 2011, the office of the IGS Secretariat Manager was relocated to South Florida (in Jupiter, FL), after a long, productive operation of the IGS secretariat activities from Easley, South Carolina. Also in 2011, and following approval by the IGS Council, the IGS accepts invitation by the Federation of International Geo-Engineering Societies (FedIGS) to join this Federation as its first non-founding member. Finally, and on the verge of preparation of this article (January 2013), the total IGS membership exceeded the mark of 3,000 IGS members, which probably deserves a place as a milestone in the 30 year-timeline (approximately 100 members per year over the existence of the IGS).

Also shown in the timeline are the **international conferences** organized by the IGS (see Figure 1, in blue). As discussed subsequently in this paper, the international conferences, along with the regional and chapter conferences, are vital forums to discuss the continuous advancement and transfer of information regarding geosynthetics. Changes in the name of the international conferences reflect the growth of our discipline, from the first international conference (preceding the formation of the IGS) “on the Use of Fabrics,” to international conferences “on Geotextiles,” to international conferences on “Geotextiles, Geomembranes and Related Products,” to (since 1998) international conferences on “Geosynthetics.”

The international conferences also represent important landmarks in the affairs of the IGS as they are the setting of its quadrennial general assemblies, where change in the council and elected officers of the IGS occurs. The presidency of Schaerer, appointed by the first IGS Council in 1983, was followed by seven subsequent presidents which, following a procedure probably unique among international learned societies, were all elected by direct vote of each one of the IGS members. They include J.P. Giroud (USA, 1986-90), Kerry Rowe (Canada, 1990-94), Colin Jones (UK, 1994-98), Richard Bathurst (Canada, 1998-2002), Daniele Cazzuffi (Italy, 2002-04), Fumio Tatsuoka (Japan, 2004-10) and, as of May 2010, Jorge G. Zornberg (USA).

Finally, the timeline also shows a number of important **“first” occasions/events** in the history of the IGS (see Figure 1, in yellow), starting with the formation of the first IGS Council in 1983. The first issue of the IGS Newsletter (IGSNews) was published in 1985 and has been regularly published since then. The first of the current 38 chapters of the IGS was the Japanese chapter, approved by the IGS Council in 1985. With the increasing relevance of the geosynthetics discipline and of the activities of the IGS came the opportunity of recognizing excellence. Accordingly, as shown in the timeline, the first Honorary membership was awarded in 1989 (to Prof. Masami Fukuoka), the first series of IGS Awards was presented in 1990 (to J.E. Fluet and E.R. Steinle) as was the first Young IGS Member Achievement Award (to R. Jewell), the first Mercer Lecture was awarded in 1992 (to Prof. R.M. Koerner), the First Giroud Lecture (also awarded to Prof. R.M. Koerner) was presented in 1998, the first IGS Service Award (to Prof. D. Elton) was presented in 2001, and first IGS Achievement Awards were presented in 2006 in recognition to exemplary service to an IGS chapter.

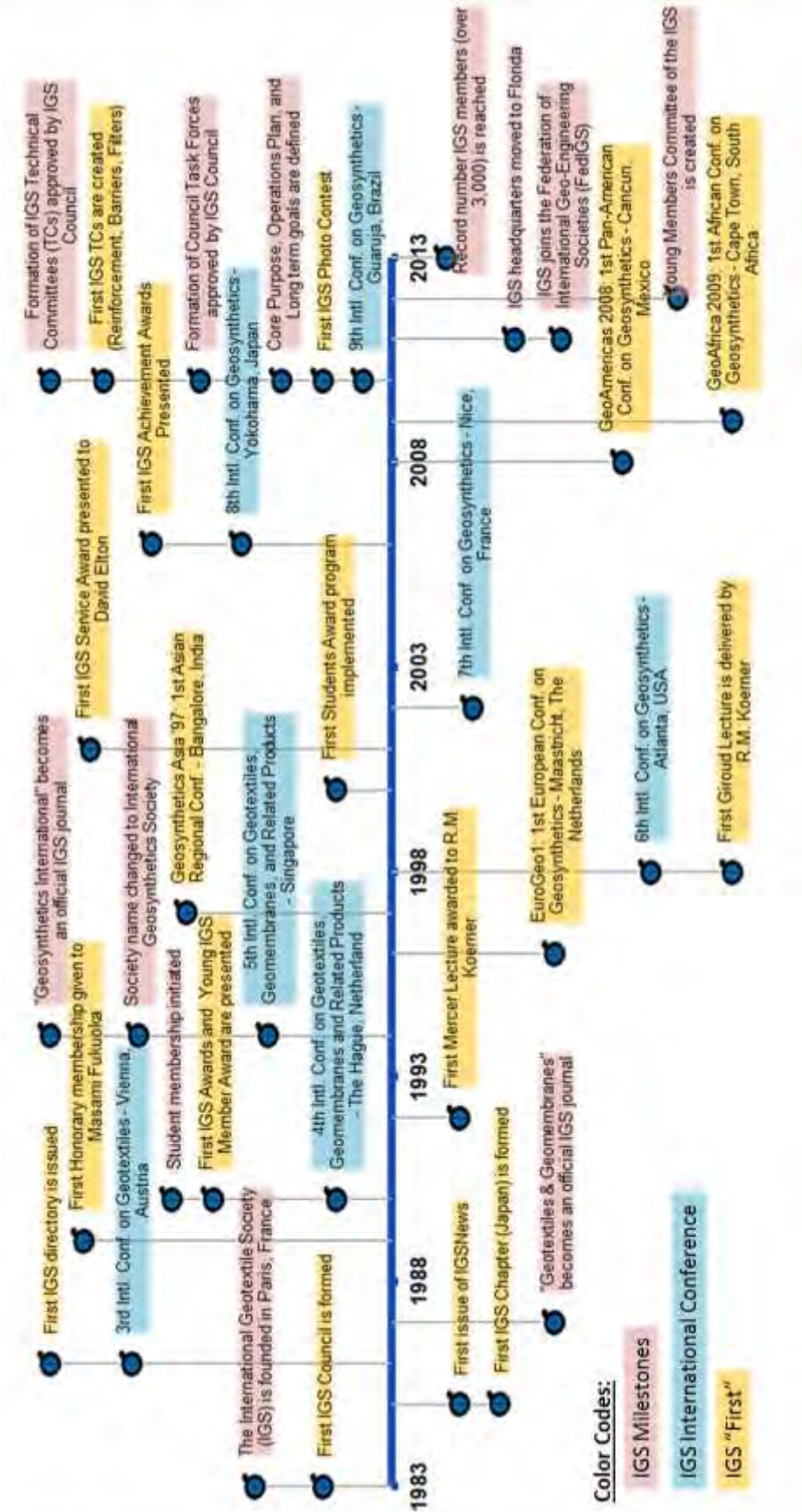


Figure 1: Overview of the thirty year-history of the IGS.

While the formation of the IGS was partly triggered by the forum of geosynthetic experts organizing international conferences (two of which preceded the creation of the IGS), it was the IGS that subsequently triggered the organization and successful implementation of other regional, specialty, and national geosynthetic conferences. Noteworthy among them are the series of IGS regional conferences, which are also organized also every four years (two years apart from the International Conferences). The European regional conferences (EuroGeo series) was launched in 1996 (Maastrich, the Netherlands), the first Asian Regional conference (Geosynthetics Asia series) was held in 1997 (Bangalore, India), the Pan-American Regional conferences (GeoAmericas series) were initiated in 2008 (Cancun, Mexico), and the African Regional conferences (GeoAfrica series) launched in 2009 (Cape Town, South Africa). A more recent IGS “first” also shown in Figure 1 includes the First IGS Photo Contest in 2010, which received over 140 entries of photos documenting the good use of geosynthetics worldwide. Finally, and also in 2010, the IGS Council approved the creation its first Technical Committees (TCs) on Soil Reinforcement, Barrier Systems and Filtration all initiated in 2010.

Throughout its 30 years of existence, the army of volunteers that have served the IGS Council, its chapters, its committees, and its conferences has and continues to make a significant difference towards an expanded, good use of geosynthetics worldwide.

THE IGS IN THE INTERNATIONAL ARENA

The IGS occupies a special place among the international learned societies with focus on Geotechnical, Environmental, and Hydraulic Engineering. A current initiative of the IGS is that of increasing the connection to international sister societies. Some important steps have been recently taken in this direction, which will enhance the coordination and collaboration of the IGS with four important International Sister Societies, namely:

- the International Society of Soil Mechanics and Geotechnical Engineering (ISSMGE),
- the International Society of Rock Mechanics (ISRM),
- the International Association for Engineering Geology and the Environment (IAEG), and
- the International Commission for Irrigation and Drainage (ICID)

The interaction with ISSMGE, ISRM, and IAEG is product of the recent decision of the IGS to accept the invitation to join the Federation of the International Geo-Engineering Societies, or FedIGS (Zornberg 2011). This Federation includes these three founding member societies and now the IGS as the very first non-founding member international society invited to join. Joining FedIGS will bolster the IGS objective of increased connections to sister international organizations. Specifically, the IGS now has a direct channel of communication with three of the most relevant International Geo-Societies.

Table 1 provides a comparison of the membership, as well as the number of chapters and technical committees, of the IGS with that of the ISSMGE, ISRM and IAEG as self-

reported by the various organizations in May 2012. The number of individual members of the IGS is an order of magnitude smaller than that of ISSMGE but on the same order of magnitude as the individual membership of the ISRM and IAEG. On the other hand, the IGS includes a healthy corporate membership, which exceeds (often significantly) the number of corporate members of our sister geo-societies. The table also compares the number of chapters (or member societies) among the different international sister societies. As shown in the table and discussed later in this paper, the presence of the IGS around the globe is increasing with the continued increase in its number of chapters. The IGS is now represented on all the continents with its 38 chapters, which is comparable to the number of national groups of international sister societies. In addition, the IGS has initiated the implementation of Technical Committees (TCs). While this number is comparatively small (TCs on Soil Reinforcement, Barrier Systems, and Filtration), the IGS TCs are expected to grow rapidly and to provide significant opportunities for collaboration with the ISSMGE and other sister societies.

Table 1. Number of chapters, committees and membership of the IGS and some International Sister Societies

	ISSMGE	ISRM	IAEG	IGS
Number of National Groups or Chapters	86	48	55	38
Number of Individual Members ^(*)	18,323	5,992	2,900	2,976
Number of Corporate Members	21	125	0	159
Number of Technical Committees	24	9	10	3

(*) Includes student members

Another important development involving the relationship of the IGS with International Sister Societies is the Memorandum of Understanding recently signed between the IGS and the International Commission for Irrigation and Drainage (ICID). The IGS Officers met with the Board of ICID in October 2010, and set the base for a process that ended in October 2011 with the signing of the Memorandum of Understanding. The International Commission on Irrigation and Drainage (ICID) was established in 1950 as a Scientific, Technical and Voluntary Not-for-profit Non-Governmental International Organization (NGO) with headquarters in New Delhi, India. The Commission is dedicated to “enhancing the worldwide supply of food and fiber for all people by improving water and land management and the productivity of irrigated and drained lands through appropriate management of water, environment and application of irrigation, drainage and flood management techniques.” ICID has a consultative status with the United Nations Economic and Social Council (ECOSOC), United Nations Educational, Scientific and Cultural Organization (UNESCO), and the World Meteorological Organization (WMO). Since the mission of ICID is to stimulate and promote the development of new technologies worldwide for achieving sustainable irrigation and drainage technologies, the cooperation with IGS is expected to lead to guidelines and policies that acknowledge the benefits of geosynthetics in important hydraulic projects.

In addition to these collaborative efforts with international sister societies, the IGS has formalized its relationship with standard organizations, including TC 221 of the

International Standards Organization (ISO) and TC 189 of the European Committee of Standardization (CEN). Collaborative efforts are currently being planned the various international sister societies and international standard organizations, which are expected to promote the advancement of geosynthetic technologies in multiple areas of engineering.

NO BORDERS FOR THE GOOD USE OF GEOSYNTHETICS I: THE IGS CHAPTERS

2012 was an active year regarding increasing the portfolio of chapters in the IGS, and by the time of its meeting on December 12, 2012 (12-12-12) in Bangkok the IGS Council concluded the year with the approval of four new chapters in four continents (Kazakhstan, Ghana, Iran, and Colombia). This represents an increase in the number of IGS chapters of over 10%. These new additions, which brought the total number of chapters in the Society to 38, provide good evidence of the healthy and continued growth of the IGS.

The addition of each new chapter provides the IGS with the opportunity not only to the newcomer by extending our ongoing technical activities into new geographic areas, but also to existing IGS chapters who receive additional stimulus to their ongoing activities. A good example is the recent opportunity to initiate a program aimed at providing educational material on geosynthetics to professors in the universities of some of our youngest chapters. The IGS response to this need is expected to lead to a broad initiative focused on undergraduate education on geosynthetics. This initiative will certainly benefit young and mature chapters alike.

The concept of IGS chapters developed soon after the founding of the IGS. During its 30 year-timeline, the number of IGS chapters has grown remarkably. Figure 2 shows the chronology of the formation of IGS chapters. As shown in the figure, the number of chapters has been increasing at a significantly high (and reasonably steady) rate of over one chapter per year; 1.25 chapters per year, to be more precise. As previously mentioned, Japan took the initiative of formalizing the very first chapter of the IGS in 1985. This initiative was soon followed by North America (NAGS) and the United Kingdom, which formed the first chapters in the Americas and Europe in 1986 and 1987, respectively. New chapters were continuously added to the IGS ranks and, by 1993 (the 10th anniversary of the IGS), a total of 10 chapters were already operating across Asia, Europe, and North America. By the end of the second decade in the life of the IGS, a total of 24 chapters had been formed (now in all continents). And by 2012, the number of IGS Chapters had reached 38 as a result of a continued focus on increasing the presence of the IGS and of geosynthetics to all regions.

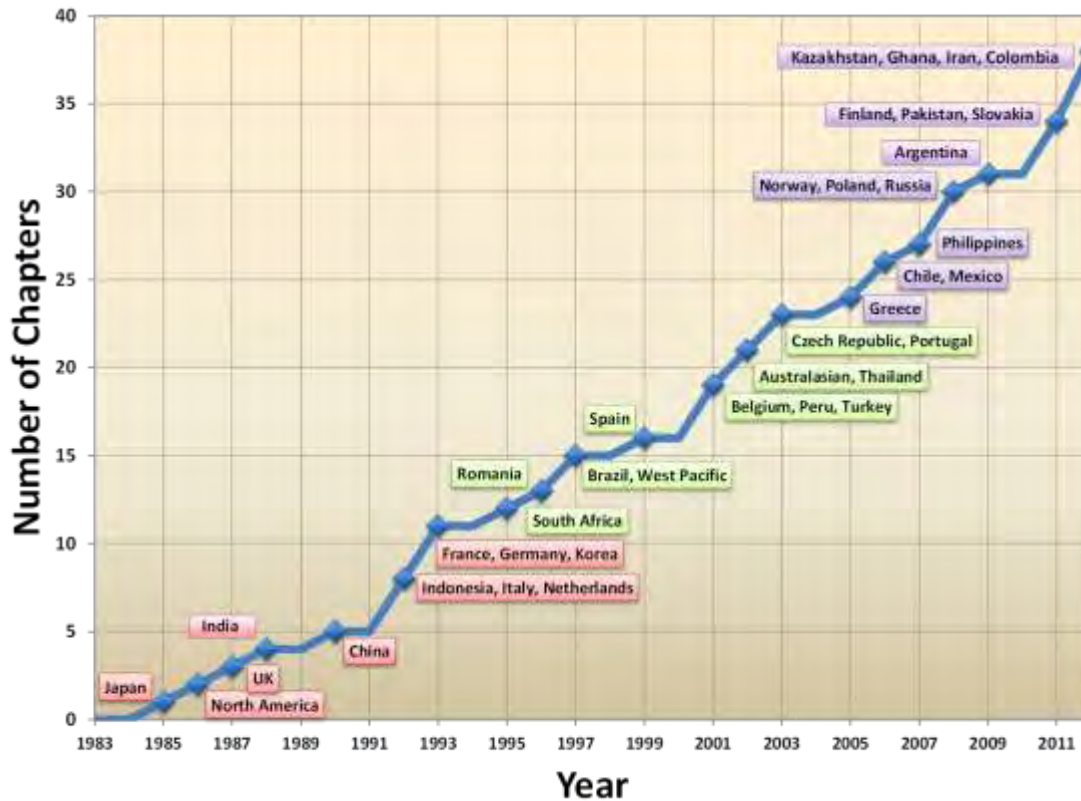


Figure 2: Chronology of the formation of IGS Chapters.

Figure 3 shows the world presence of the IGS in the form of IGS Chapters. As mentioned, during the first decade of the IGS, chapters were created in western Europe, North America and eastern Asia (countries shown in red in Figure 3). They correspond to regions in the world where the geosynthetics market is now mature regarding the currently traditional applications involving geosynthetics. During the second decade of the IGS, new chapters spread out to the rest of the continents, including South America, Africa, and Oceania (countries shown in green in Figure 3). This second generation of chapters includes growing economies in the world where the geosynthetics industry is probably still finding its acceptance by governmental agencies but that now counts with a solid group of professionals educated on geosynthetics. Indeed, many of the most spectacular projects involving geosynthetics have been constructed in some of these countries. Finally, during the third decade of the IGS, new chapters have been formed in areas such as eastern Europe, central Asia, and Latin America (countries shown in purple in Figure 3). This third generation of chapters includes countries where the geosynthetics market is mostly in the emerging stage and where technology transfer, which should be sensitive to local practices and economic conditions, may lead to a significant increase of the geosynthetics market.

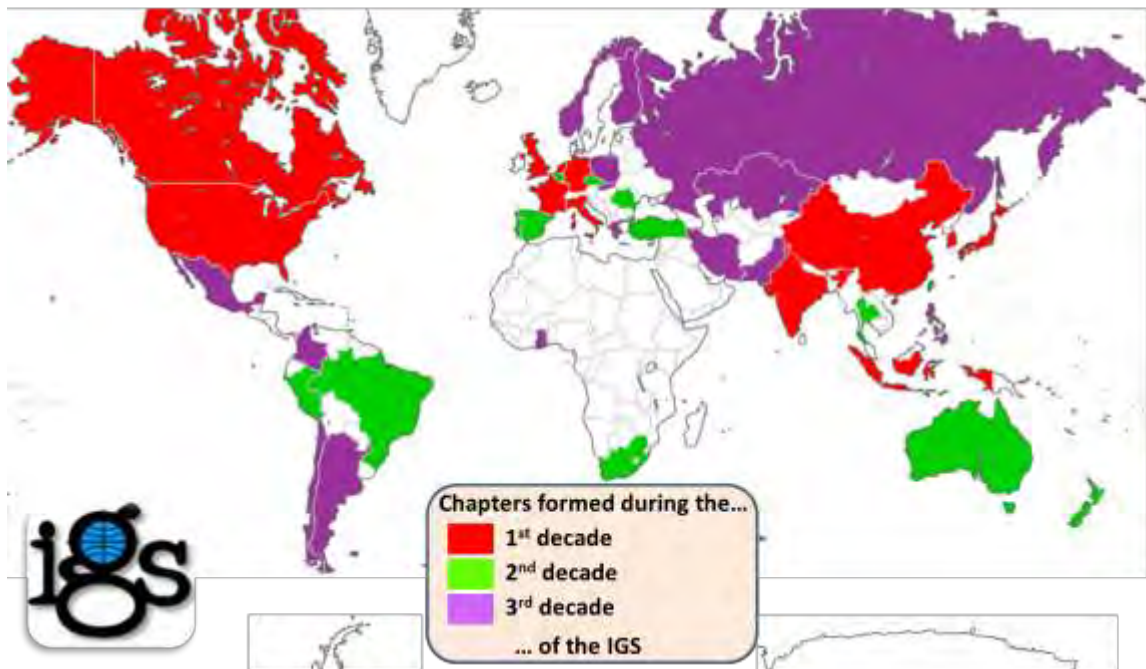


Figure 3: Chapters formed during the three decades-history of the IGS.

The number of technical activities conducted by the many IGS chapters is, simply, impressive. Starting in 2008, new guidelines were developed by the IGS to facilitate the communication and summary of the important chapter activities. The heart of this new approach is the completion by the IGS chapters of a new Standard Reporting Form. These reports have highlighted a truly impressive number of technical activities organized by the IGS chapters. These activities include, to name a few, multi-lingual national conferences, educational programs aimed at regulators, student initiatives and a healthy number of professional meetings. Ongoing initiatives being implemented at the IGS level to directly benefit the individual IGS Chapters include support to the development of online chapter membership web pages, nomination of chapter members in the various technical committees of the IGS, participation in the student awards program of the IGS, involvement in the technical program of the IGS Regional Conferences, and participation in the various ongoing educational initiatives of the IGS.

NO BORDERS FOR THE GOOD USE OF GEOSYNTHETICS II: THE IGS CONFERENCES

The Conferences of the IGS have played a remarkable role in the development of geosynthetic products and its applications. Much of the information on material properties, testing methods, applications and design approaches that we use in geosynthetics engineering has been vetted through these conferences. Of particular importance are the **International Conferences** of the IGS, which are held every four years. This series of conferences has been a premier outlet of, and in many cases has

indeed triggered, many of the advances in geosynthetics. Figure 4 illustrates the location of the various international conferences (see yellow stars, with the corresponding conference number). As illustrated in this figure, the international conferences of the IGS have been well distributed throughout the globe. The first International Conference was held in Paris (France), in 1977, and was followed by the 1982 conference in Las Vegas (USA), the 1986 conference in Vienna (Austria), the 1990 conference in The Hague (Netherlands), the 1994 conference in Singapore, the 1998 International Conference on Geosynthetics (ICG) in Atlanta (USA), the 2002 ICG in Nice (France), the 2006 ICG in Yokohama (Japan), and the most recent 9th ICG held in Guarujá (Brazil) in 2010.

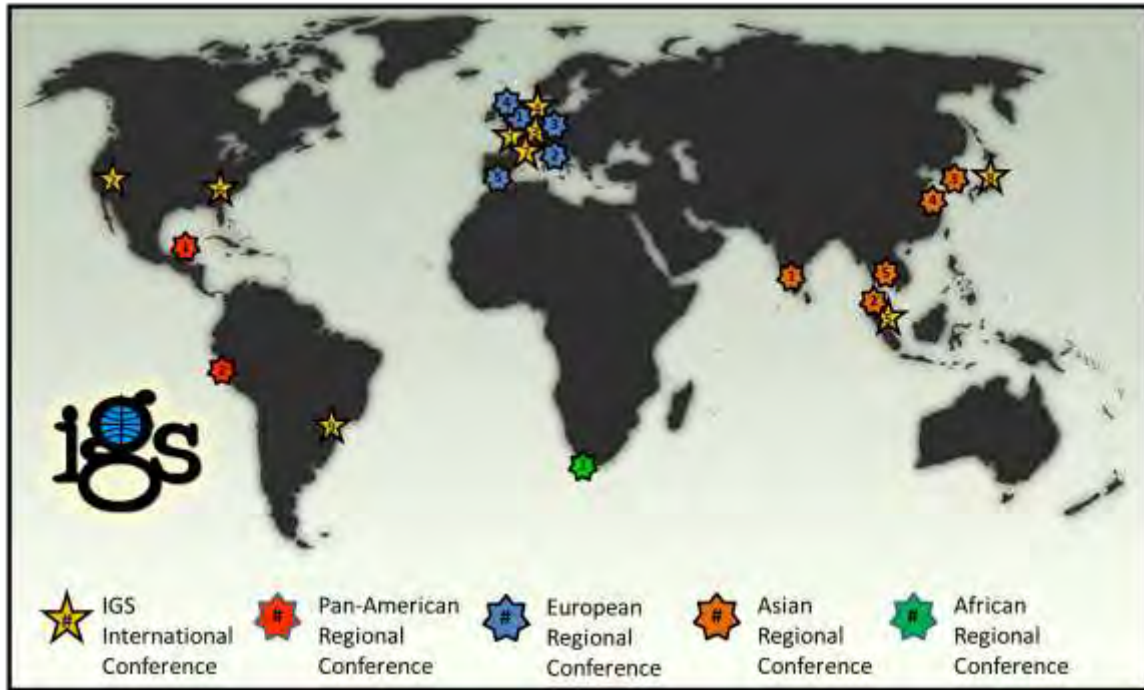


Figure 4: Past International and Regional Conferences of the IGS.

(Note: the number in each symbol corresponds to the sequence in each series of conferences)

In addition to the international conferences, **Regional Conferences** of the IGS have been organized in Europe, Asia, the Americas, and Africa. As with the international conferences, the series of IGS regional conferences are organized every four years, generally 2 years after the international conferences. Figure 4 also shows the location of the previous regional conferences of the IGS. The European Regional Conferences on Geosynthetics (“EuroGeo” series of conferences) include the 1996 EuroGeo1 in Maastricht (Netherlands), the 2000 EuroGeo2 in Bologna (Italy), the 2004 EuroGeo3 in Munich (Germany), the 2008 EuroGeo4 in Edinburgh (UK) and the 2012 EuroGeo5 in Valencia (Spain). The Asian Regional Conferences on Geosynthetics (“Geosynthetics Asia” series of conferences) include the 1997 conference in Bangalore (India), the 2000 conference in Kuala Lumpur (Malaysia), the 2004 conference in Seoul (South Korea), the 2008 conference in Shanghai (China), and the 2012 conference in Bangkok (Thailand). The Pan-American Regional Conferences on Geosynthetics (“GeoAmericas” series of conferences) started in 2008 with GeoAmericas 2008 in Cancún (Mexico), which was

followed by the recent 2012 Conference in Lima (Peru). Finally, the African Regional Conferences on Geosynthetics (“GeoAfrica” series of conferences) is the newest series of regional conferences of the IGS, having started in 2009 with GeoAfrica 2009, which was held in Cape Town (South Africa).

The venues for many of the **upcoming conferences** of the IGS have already been selected. Figure 5 shows the locations of the upcoming IGS International and Regional Conferences on Geosynthetics. The next of these conferences will be the much-anticipated Second African Conference on Geosynthetics, GeoAfrica 2013. The conference will take place in Accra, Ghana, on November 18-20, 2013. With important infrastructure needs in Africa and impressive projects address them in areas such as mining and transportation, we anticipate that major opportunities to the advancement of geosynthetics will spring from this important African event. As also shown in the figure, the next international conference, the 10th International Conference on Geosynthetics (10ICG) will be held in Berlin from 21 to 25 September 2014. The conference will take place in direct connection with the 33rd Baugrundtagung (German Soil Mechanics Conference). As the Baugrundtagung expects over 1,200 participants, great synergy and interaction is anticipated between these events, especially in the co-organized, co-located exhibition. The overlapping of lectures from both events will also attract many additional experts from the geotechnical and geosynthetics professions.



Figure 5: Upcoming International and Regional Conferences of the IGS.

(Note: the number in each symbol corresponds to the sequence in each series of conferences)

As noted, three of the conferences of the current cycle of IGS Regional Conferences took place in 2012, including the Second Pan-American Geosynthetics Conference

(GeoAmericas 2012), held in Lima, Peru, the Fifth European Geosynthetics Conference (EuroGeo5) held in 2012 in Valencia, Spain, and the Fifth Asian Geosynthetics Conference (Geosynthetics Asia 2012) held in Bangkok, Thailand. Each one of these conferences concluded with the announcement of the venues for the next series of conferences. The IGS is extremely pleased with the full suite of upcoming (2016) IGS Regional Conferences. As also shown in Figure 5, they are scheduled to take place in Miami, USA (GeoAmericas 2016, 11-13 April 2016), Istanbul, Turkey (EuroGeo6, 25-29 September 2016), and New Delhi, India (Geosynthetics Asia 2016, November 2016). Finally, the IGS Council in its meeting of 12-12-12 has already selected the venue for the subsequent (2018) International Conference on Geosynthetics (11ICG), which will be held in Seoul, South Korea in September 2018. Even though many IGS activities will take place until this event, we are looking forward to what will certainly become another landmark in the history of geosynthetic developments.

In addition to the series of International Conferences, and the multiple series of Regional Conferences organized under the umbrella of the IGS, the chapters of the IGS regularly organize **national conferences** on Geosynthetics. They attract significant local participation and provide a remarkable forum for transference of knowledge on geosynthetics. Inspection of the IGS calendar of events in the IGS website (www.geosyntheticssociety.org) includes the listing of many of these well-established events. For example, in this Spring 2013 the French Chapter of the IGS will be holding Rencontres Géosynthétiques 2013 (Dijon, France April 09-11, 2013). This will be the 9th conference of this series in France and corresponds to one of the many series of national conferences on geosynthetics organized regularly by the chapters of the IGS.

The organizing committees of each one of these upcoming IGS International, Regional, and National Conferences on geosynthetics are planning well-integrated technical programs that will include innovative technical sessions, discussion panels, and educational components. Each one of them will certainly provide unique opportunities to share experiences, knowledge, advances, and opportunities related to geosynthetics and affiliated technologies.

CURRENT STRUCTURE OF THE IGS OPERATING UNITS

The governing body of the IGS is its Council, a body of 24 representatives elected for the most part by direct vote of the IGS membership at large. The leadership of the IGS Council includes five IGS Officers: the IGS president, vice-president, and immediate past president, who are elected directly by the IGS members, as well as the IGS secretary and treasurer, who are appointed by the IGS Council. Considering the significance of communications and bold goals of the IGS, the IGS Council approved a new structure of Operating Units aimed at facilitating communications and implementing tasks effectively (Zornberg 2010). Figure 6 shows the structure of the current (2013) IGS Operating Units. Compared to the structure of previous IGS Councils, the new structure involves comparatively fewer Council Committees but it now includes a number of formal Task Forces. Under the new structure the Council Committees, which typically meet before the

meeting of the IGS Council, evaluate relevant issues and make recommendations for consideration by the Council. On the other hand, Task Forces involve a small number of members who will typically meet after the council with the objective of implementing the new council decisions. In addition, a new track of Technical Committees was approved by the IGS Council. Unlike the Council Committees and Council Task Forces, the schedule of the meetings of Technical Committees does not necessarily conform to that of the IGS Council.

The chairpersons selected by the IGS Council to lead each one of the Council Committees, Council Task Forces and Technical Committees are also shown (in parenthesis) in Figure 6. The group of Committee Chairs form an Operating Unit that meets regularly in order to facilitate implementation of activities that bridge across multiple committees. The Financial Committee, the only committee required by the IGS bylaws, provides advice on financial matters to the IGS council.

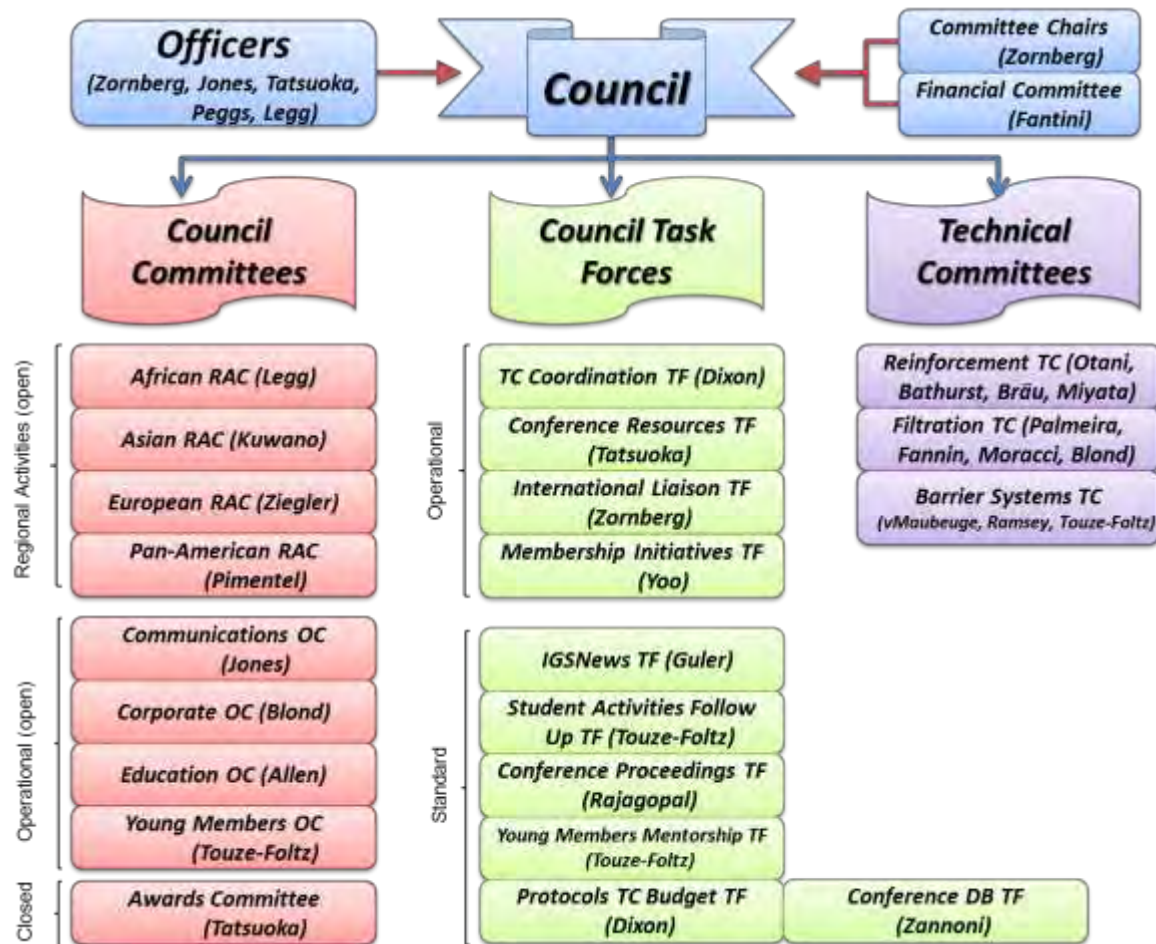


Figure 6: Structure of the Council Committees, Council Task Forces and Technical Committees of the IGS Council.

(Note: Chairpersons of the various Operating Units are shown in parenthesis)

The Council Committees of the IGS Council include a group of Regional Activities Committees, the charge of which includes promoting the activities and presence of the IGS in a given region, helping with the formation of new IGS Chapters, assisting in the organization of regional conferences of the IGS, and facilitating the distribution in the region of material to promote technical and educational events that will benefit the geosynthetics discipline. These are open committees, so representatives of the IGS chapters are encouraged to participate in the meetings and activities of these committees. Another group of committees involve the Operational Committees of the IGS Council, which are also open for participation by any IGS member. These include the Communications Committee, which is tasked among other activities to compile each issue of *IGSNews*, the Corporate Committee, which serves the needs of the corporate membership of our Society, the Education Committee, which has generated a wealth of educational documents at multiple levels and in multiple languages over the years, and the brand new Young Members Committee, which aims at facilitating the activities of the new generation of IGS members. Finally, the Awards Committee is a closed committee serving the IGS Council in identifying and recognizing the most deserving technical contributors to our industry.

While individual members of the IGS Council have diligently worked to accomplish a myriad of important activities, recent experiences have indicated that tasks are often implemented more effectively when the effort is organized under formal Task Forces of the IGS Council. A number of these Task Forces conduct continued operations. This includes the TC Coordination Task Force, which aims at organizing the new Technical Committees of the IGS, the Conference Resources Task Force, focused on consolidating the rich experience gained so far in IGS conferences, the International Liaison Task Force, which focuses on the interaction with our sister learned societies, and the Membership Initiatives Task Force, which aims at evaluating issues related to the characteristics and number of IGS members. In addition, a number of additional Task Forces are short-lived, with an expected completion of their activities in approximately one year. These include the Task Forces on *IGSNews*, Student Activities, Conference Proceedings, Young Members Mentorship, Budget Protocols, and Conference Database. These Operating Units have been assigned well-defined tasks, which are expected to be completed and delivered to the Council by the time of the next meeting of the IGS Council.

A new addition to the structure of Operating Units of the IGS Council is the set of Technical Committees (TCs) of the IGS. This includes three TCs: Soil Reinforcement, Filtration, and Barrier Systems. The leaders of these new TCs initiated their operation after having compiled proposals that were approved by the IGS council and outlined the possible activities of these TCs. These possible activities include interacting with conference organizers to lead technical sessions at upcoming conferences, with designers to produce technical documents, with academics to offer short courses, and with special emphasis on young professionals who are expected to stimulate the use of geosynthetics among the new generation of engineers.

INITIATIVES OF THE IGS

It is a daunting task to document the many initiatives of the IGS, as they are so many. Consequently, and for illustration purposes, this section summarizes two of these many initiatives. One of them is a well-established, continued effort. The second one is a new initiative.

One of the many **well-established initiatives** of the IGS relates to high-level dissemination of information on geosynthetics, which is a core mission of the IGS. This is well accomplished by the two official technical journals of the IGS: “*Geotextiles and Geomembranes*” and “*Geosynthetics International*.” “*Geotextiles and Geomembranes*” is published six times per year by Elsevier. Under the leadership of Kerry Rowe as Editor, the journal aims at increasing general awareness, prompting further research and assisting in the establishment of international codes and regulations about geosynthetics. “*Geosynthetics International*” is published six times per year by Thomas Telford. Under the leadership of Richard Bathurst as Editor and J.P. Giroud as chair of the Editorial Board, the journal covers research, behavior, performance analysis, testing, design, construction methods, case histories and field experience regarding geosynthetics. The IGS is very proud by the very high impact factor of its two journals, which constitute an excellent example of a well-established activity of the IGS that serves the IGS membership and the geosynthetics community at large. The editors and editorial boards of these two journals have been certainly driven by the same enthusiasm that has driven the rest of the IGS leadership. It should be emphasized that access to these two journals is free for IGS members with direct download available through the IGS website. This is among the most important direct benefits of the IGS membership.

A good example of one of the **new initiatives** of the IGS is the pilot program being initiated to address the educational needs in the country of one of our youngest chapters: Argentina. Specifically, the “Educate the Educator” (indeed, “Educando al Educador,” as the course will be in Spanish) will take place in Villa Carlos Paz, Argentina, from May 26 to 28, 2013. This is a good example of a joint effort between an IGS Chapter (IGS-Argentina in this case) and the IGS (through its Pan-American Activities and Education Committees). The focus of this program is on undergraduate education with the overall goal that every civil engineering student graduating from a civil engineering program in Argentina will have received a basic exposure to geosynthetics. The goal is perhaps a simple, one hour-long exposure class, but offered to every single civil engineering undergraduate student in the country. As part of this effort, 30 civil engineering professors will receive a fellowship that will cover expenses to participate in a premier training program on geosynthetics. This pilot program will benefit from the involvement of the Argentinean Council on Civil Engineering Curriculum (CODIC), an agency that has encouraged the development of this educational program. A terrific precedent of training civil engineering professors exists as a training program was previously implemented in North America over fifteen years ago (Elton 1996). After over 15 years since the excellent experience in North America, education on geosynthetics at the undergraduate level remains a current, worldwide need. The IGS is not alone in recognizing this important need. Indeed, the Geosynthetic Institute (GSI),

with its major educational arsenal on geosynthetics, and the Geosynthetic Materials Association (GMA), with its capability of mobilizing the geosynthetics industry, are equally engaged in promoting basic geosynthetic education. The opportunity exists for significant synergism in this undergraduate educational effort.

FINAL REMARKS

With the IGS now completing three decades of existence, the challenges and opportunities involving the dissemination of geosynthetics knowledge continue to be significant. Indeed, the role of the IGS in this dissemination is expected to continue to grow, and it is the intention of the IGS to tailor the assistance to the various geosynthetics interest groups according to their specific needs. A remarkable characteristic of the IGS has been its capability to evolve while, at the same time, always maintaining a clear aim at its core purpose, which is **“to provide the understanding and promote the appropriate use of geosynthetic technology throughout the world.”**

REFERENCES

- Elton, D.J. (1996) Professor Training Course Fits a Need, *Geotechnical Fabrics Report*, Vol. 14, No. 3, April, pp. 50-52.
- Giroud, J.P. (2008). “The Origins of the IGS and a Challenge for the Future.” *IGSNews*, Vol. 24, No.3, November, pp. 3-7.
- Zornberg, J.G. (2010). “The Strategic Goals of the IGS.” *IGSNews*, Vol. 26, No. 2, July, pp. 2-3.
- Zornberg, J.G. (2011). “Relationship of the IGS with our International Sister Societies.” *IGSNews*, Vol. 27, No. 3, November, pp. 2-4.

IGS CONTACT INFORMATION

For additional information of the various initiatives of the IGS, please visit the IGS website at www.geosyntheticssociety.org or contact the IGS Secretariat Manager via email at igssec@geosyntheticssociety.org.

IFAI TURNS 101 WITH 33 YEARS OF GEOSYNTHETIC REPRESENTATION

Andrew Aho, Director, Technical Markets, IFAI

In 2013 the Industrial Fabrics Association International (IFAI) celebrates its 101st year. The association had humble beginnings when 14 members met at the Brown Palace Hotel in Denver on September 12, 1912. Today, IFAI, with 1800 member companies, is the largest trade association representing suppliers, end product manufacturers and service providers of industrial fabrics.

The association began as the National Tent & Awning Association representing the canvas and awning manufacturers in the central part of the United States. Today, IFAI represents 12 distinct special interest groups or market segments. These special interest groups include the original tent and awning markets and now extend into highly technical markets such as safety and geosynthetics.

At the start, the mission of the trade association was to set standard weights and pricing for products made of canvas. A mission like that today would likely end in criminal and civil prosecution of the trade association leadership. The initial group was formed to combat the price setting policies of the cotton mills that supplied the raw materials for the canvas manufacturing industry. Eventually, the association would expand to include the cotton suppliers.

The first president of the association was A.H. Rawitzer of the Scott-Rawitzer Manufacturing Company of Omaha, Nebraska. The association grew rapidly and by 1915 it needed an official office to coordinate its activities. It had elected as its second president W.K. Jacobs, who owned the Minnesota Tent & Awning Company in St. Paul, Minnesota. W.K. Jacobs sited the office of the association in the same building as his business. The association headquarters remained in downtown St. Paul until 1997 when moved into its current location in Roseville, Minnesota, a first ring suburb of St. Paul.

Also in 1915, the association started publishing the *National Tent and Awning Manufacturer's Review* which has morphed into today's IFAI's flagship publication *Specialty Fabrics Review*. The first employee of the association was James E. McGregor, hired as both the editor of the Review and the executive secretary of the association. He remained in those positions for 37 years. McGregor wrote an editorial in each issue he published. In the 1930s some of his editorials had nothing to do with the fabric industry. Some took aim at the rubber stamp congress, radicals and a subject current today, the federal deficit. By the 1950s McGregor's editorials seemed obsessed with communism, including Stalin and tips on how to spot a Communist.

During McGregor's tenure, the membership continued to grow. In 1936 the membership expanded to include the truck cover and boat cover manufacturers. However, in the 1940s synthetic fibers such as rayon and nylon challenged canvas in the marketplace. The association continued to be a canvas organization. In 1957, companies from Canada joined the association and the association added International to its name – Canvas Product Association International.

(Today, IFAI has members in more than 50 countries.) Polyester became part of the market in the 1960s. The association was no longer just for canvas manufacturers and in 1966 the Review changed its name to the Industrial Fabric Product Review. With the advent of polypropylene and acrylics in the 1970s and more synthetic based fibers in the 1980s the association remained stubborn and kept canvas in its name until 1981 when it was changed to Industrial Fabric Association International.

With the growth in synthetics, many market segments or divisions were formed at IFAI. In 1980 IFAI formed the Geotextile Division, representing the manufacturers of geotextiles. In 1982 IFAI organized the Second International Conference on Geotextiles in Las Vegas, Nevada. IFAI began publishing *GFR* magazine (now *Geosynthetics* magazine) with the first issue in the summer of 1983. Geosynthetics have been an important part of IFAI ever since. IFAI has organized or co-organized thirteen geosynthetic conferences since 1982 and published the conferences proceedings.

Demand for geomembranes has increase due to regulation of hazardous and solid wastes and the end of open dumping of waste in the United States in the late 1970s and early 1980s. The industry needed a place for trade association activities and in 1983 IFAI formed the Geomembrane Division. Activities of both the Geotextile and Geomembrane Divisions were related to the development of specifications and technical issues related to the materials. The Geotextile Division worked with the American Association of State Highway and Transportation Officials (AASHTO) and academic, state and federal representatives to develop and revise the AASHTO M288 geotextile specifications. The Geomembrane division focused on the new RCRA regulations and specifications for liners used in waste containment.

In 1997 the members of the two divisions voted to change the direction of the association to one of marketing geosynthetics and move away from the specification and technical issues. That year IFAI merged the Geotextile and Geomembrane Divisions to form the Geosynthetic Materials Association (GMA). Joe Luna of Colbond was the initial chairman of the GMA Executive Committee. Other members were Gary Willibey of Amoco Fabrics and Fibers Co., Marc Theisen with Synthetic Industries, Dave Clarke with TC Mirafi, Giovanni Capra of Tenax and Monte Thomas of TNS Advanced Technologies. IFAI assigned staffer Danette Fettig as the managing director. Ms. Fettig continued managing GMA until 2004.

By 1998 GMA had 37 members companies including producers of geogrids and geocells. That year GMA developed its first website www.gmanow.com. Maccaferri joined the GMA Executive Council later in 1998 and Massimo Ciarla proposed the development of GMA Mexico. Oscar Couttollenc was contracted to represent GMA Mexico from his office in Mexico City.

Even though the association looked to a move away from specifications and technical issues it remained embroiled in the development of specifications for geotextiles and geogrids. The AASHTO subcommittee on Materials Technical Section E4 Task Force on Geogrid/Geotextile Specifications requested that GMA help develop further a specification for Geotextiles and a separate specification for Geogrids. The issue was very controversial due to the proprietary nature of the brands and materials. The result was the development of a White Paper rather than

a specification. In July of 1998 GMA presented AASHTO with the White Paper: *Geosynthetics In Pavement Systems Applications*. A further attempt to move away from technical issues was unsuccessful when the same AASHTO committee requested the industry make another attempt to develop a specification for geogrids. Again the result was a report known as GMA White Paper II: *Geosynthetic Reinforcement of Aggregate Base/Subbase Course of Pavement Structures*, published in June 2000.

In 2000, *GFR* magazine became the official magazine of GMA and remains today with the new name *Geosynthetics*.

Term limits required GMA to replace Joe Luna as chairman of the GMA Executive Council. Giovanni Capra was elected chair in 2001 and for two two year terms ending in 2005. Under Giovanni Capra's guidance GMA continued to build on the membership growth enjoyed under Joe Luna. The membership was now at 45 and included the majority of manufacturers and large distributors of geosynthetics. The Executive Council grew to eight members by adding GSE represented by Ernie English. The market segments were represented by focus groups based on products. GMA continued to focus on market promotion and education. GMA contracted with TRI to develop a *Geosynthetics Handbook*.

There remained need for technical presence within GMA. In 2003 discussions with Dr. Bob Koerner began regarding becoming the "technical arm" of GMA.

By 2004 GMA had gained significant membership and an aggressive agenda. It was clear that GMA needed additional staff time from IFAI. IFAI made a commitment to provide additional staff expertise to GMA. At the same time, Chairman Capra began an initiative to develop a long term strategic plan for GMA. The plan identified the need to compete with traditional construction materials at a policy level within the U.S. government. It also recognized the need for more education regarding the proper use of geosynthetics. In 2005, Andrew Aho was hired as the managing director of GMA. During that year, Ernie English replaced Giovanni Capra as chairman. After a short time as chair, Ernie English resigned due to work commitments at GSE and John Henderson from TenCate was elected chairman.

GMA began a search for a lobbying firm that could help GMA affect government policy to help preserve and grow the geosynthetic market in the United States. GMA hired Kemp Partners and the Whitmer and Worrall lobbying firm to represent the industry in Washington, D. C. The Kemp Partners firm was led by Jack Kemp the former congressman and vice presidential candidate. For the first time, the industry had full time representation in Washington, D.C. along with a very high profile name associated with it.

The second need identified by GMA's strategic plan was more education regarding the proper use of geosynthetics. Technical information was very much needed in the market place. Since the GMA plan was to promote the industry and shy away from technical issues that had caused disruption in the membership, GMA looked to Dr. Bob Koerner and the Geosynthetic Institute and concluded the discussion begun in 2003 by contacting with them to provide technical assistance to the market place through the GMA Techline. After a slow start in 2005, the Techline has become a robust educational tool for anyone with technical questions regarding

geosynthetics. The Geosynthetic Institute team have fielded thousands of technical questions through gmatechline@ifai.com.

John Henderson led GMA from 2005 to June 2011. During his tenure GMA's government relations program matured. The successful efforts to get the Government Accountability Office (GAO) to complete a study of geosynthetics as an innovative material in transportation applications began at that time. The government relations activities were a very attractive recruiting tool and GMA's membership doubled by 2007 and now boasts 80 member companies. In addition, a major accomplishment during this time was the development of the AASHTO/NTPEP audit program for manufacturers of geotextiles used by state DOTs. The program also requires that the prime manufacturer's name or numerical I.D. is printed on the fabric.

Boyd Ramsey of GSE became chairman when Henderson's terms ended. Boyd Ramsey took the lead in fashioning GMA's position on coal ash waste, ensuring that geosynthetic liners in coal ash disposal sites were included in the two regulatory options put forth by the Environmental Protection Agency (EPA). GMA has been a strong supporter of the legislative solutions moving through congress regarding coal ash waste.

The GMA government relations program has been very successful at the federal level, with a list of congressional champions. GMA is now leveraging that success at the state and local level. The GMA State and Local initiative began in the fall of 2012. The initial target states are Tennessee, Ohio and Illinois. GMA members and lobbyists have been meeting with state DOTs to promote the AASHTO audit and printing program. GMA is also connecting with the Governors' offices and the road builder associations to promote the use of geosynthetics. Meetings are also held with the state EPAs to promote GMA's position regarding coal ash waste. Education and government relations will continue to be the focus of GMA's activities. All but a few manufacturers are members of GMA. GMA developed a program for distributors, and today a third of the members are distributors of geosynthetics. Membership also includes testing firms and equipment manufacturers. GMA has strong relationships with the Geosynthetic Institute, the International Geosynthetics Society (IGS), Fabricated Geomembrane Institute (FGI) and North American Geosynthetics Society (NAGS), and often invites those organizations to participate in GMA lobby days and presents a united front as we educate congress and federal agencies.

The geosynthetics industry will remain an important part of the business activities of IFAI. IFAI will continue its philosophy of hosting conferences with partners to expose related industries to geosynthetic materials. The Geosynthetics 2013 conference includes co-locating with the Southwest Geotechnical Engineers Conference and GRI 25. In 2015 IFAI will co-locate with International Erosion Control Association (IECA) in Portland, Oregon. The annual IFAI EXPO has included geosynthetics in its programming and has begun to draw both attendees and exhibitors to the EXPOs. IFAI's magazine *Geosynthetics*, and its associated website, is the premier source of case studies of geosynthetics applications, as well as the source of the array of geosynthetic products which are featured in the annual *Specifiers Guide*. GMA will continue to represent the industry to congress and federal regulatory agencies as well as at the state and local level.

30 YEARS OF THE MAGAZINE FORMERLY KNOWN AS *GFR*

Ronald W. Bygness

Geosynthetics magazine, Industrial Fabrics Association International, Roseville, Minn., USA

ABSTRACT

This article is on the formation and background of *Geosynthetics* magazine (formerly *GFR*) and reviews some of the many highlights over its 30-year history. It also sheds insights into its host institutions; the IFAI and GMA. Its success as the worldwide magazine of, and about, the geosynthetics industry is assured. Furthermore, it is well positioned to continue this leadership position well into the future.

INTRODUCTION

In 1915, the Industrial Fabric Association International's precursor—the National Tent & Awning Association—started publishing the *National Tent & Awning Manufacturer's Review*, which has morphed into the current IFAI flagship publication, *Specialty Fabrics Review*.

With the growth in the manufacturing and distribution of synthetic materials, additional market segments (divisions) were formed at IFAI. In 1980, IFAI established the Geotextile Division, representing the manufacturers of geotextiles. In 1982, IFAI organized the Second International Conference on Geotextiles in Las Vegas, Nevada. IFAI has organized or co-organized 13 geosynthetic conferences since 1982 and has published the conferences' proceedings.

IFAI began publishing the *Geotechnical Fabrics Report*—quickly referred to as simply *GFR* (now *Geosynthetics* magazine)—with its first quarterly issue in the summer of 1983. *Geosynthetics* have been an important part of IFAI ever since. The magazine is now celebrating its 30th anniversary.

Also in 1983, IFAI formed the Geomembrane Division. Activities of both the Geotextile and Geomembrane Divisions were related to the development of specifications and technical issues related to the materials. The Geotextile Division worked with the American Association of State Highway and Transportation Officials (AASHTO) and academic, state, and federal representatives to develop and revise the AASHTO M288 geotextile specifications. The Geomembrane Division focused on new regulations and specifications for liners used in waste containment as specified in 1976's [Resource Conservation and Recovery Act](#) (RCRA) plus several added RCRA amendments in the 1980s.

In 1997, IFAI merged the geomembrane and geotextiles divisions into the Geosynthetic Materials Association (GMA), and assigned former *GFR* editor Danette Fettig as the managing director. Fettig continued managing GMA until 2005.

In 2000, *GFR* magazine became the official magazine of the Geosynthetic Materials Association (GMA) and remains so today with the magazine's new name, *Geosynthetics*. *Geosynthetics* is also the official publication of the North American Geosynthetics Society (NAGS).

In mid-2005, Andrew Aho was hired as the managing director of GMA. Later that year, Ron Bygness was named the new editor of the magazine formerly known as *GFR*, with his first issue—February/March 2006—redesigned and retitled *Geosynthetics*.

GMA looked to Dr. Bob Koerner and the Geosynthetic Institute (GSI), and concluded discussions that had started in 2003, by contracting with them to provide technical assistance to the marketplace through the “GMA Techline.” After a slow start in 2005, the Techline has grown into a robust educational tool for anyone with technical questions regarding geosynthetic materials and their many applications. The GSI team has fielded thousands of technical questions through gmatechline@ifai.com, with selections of Techline Q-and-A regularly reprinted in *Geosynthetics* magazine.

Geosynthetics flourished following its name change and comprehensive redesign in 2006, growing from 36 pages in eight 2005 issues, to 56 pages per issue in five 2006 bimonthly magazines, and up to 64 pages per issue in 2010. The December/January issue continued each year as the annual *Specifier's Guide*.

The *Geosynthetics* magazine website launched in mid-2009, offering geosynthetics and geotechnical news, educational papers, print magazine content, feature stories, electronic archives, and association news from GMA, NAGS, GSI, and numerous other organizations and sources. IFAI's magazine, *Geosynthetics*, and its associated website, is today a premier source of case studies of geosynthetics applications, as well as the source of the array of geosynthetic products, applications, and services that are featured in the annual *Specifier's Guide*.

Five snapshots of the 30-year history of “The magazine formerly known as *GFR*” follow, with one of the five chronological segments featured in each of the 2013 issues of *Geosynthetics* magazine.

THE BEGINNINGS: 1983-1988

1983: The first issue of a new quarterly magazine called *Geotechnical Fabrics Report* is published by the St. Paul, Minn.-based Industrial Fabrics Association International (IFAI). The editor is Michael E. Coughlin ... Byline contributors in the premiere issue are Bruce Lamberton, J.P. Giroud, Robert Carroll Jr., and A.S. Balasubramaniam. The editor also recognizes industry experts as technical article reviewers: Dick Bell, Joe Fluet Jr., Bob Koerner, and Giroud ... Also in 1983, the Geomembrane Division is formed at IFAI.

1984: June 20-24—IFAI cosponsors the International Conference on Geomembranes in Denver, Colo. ... *GFR* notes that on Nov. 8, 1984, two days after his re-election, President Ronald Reagan signed H.R. 2867, The Hazardous and Solid Waste Amendments of 1984, amendments that mandate double liner systems in hazardous-waste landfills (Subtitle C).

1985: Joan R. Haglund is the new editor and *GFR* switches from a quarterly to a bimonthly publishing schedule ... June 4-5—The first geotechnical conference concentrating on both geotextiles and geomembranes is held in Cincinnati, Ohio ... In the November/December 1985 issue, *GFR* introduces the “Product Reference Guide & Directory” (later to become the “Specifier’s Guide”).

1986: The Austrian postal administration issues a stamp featuring a roll of light-brown nonwoven geotextile in commemorating the 3rd International Conference on Geotextiles (3ICG), held in Vienna ... *GFR* reports that Superfund amendments from the U.S. Congress change the size of the trust fund and how it is replenished as well as the criteria for selecting sites ... in January, the American Society on Geosynthetics (ASG) is formed ... Giroud is elected president of the International Geosynthetics Society (IGS) ... the Geosynthetic Research Institute (GRI) is founded and incorporated ... Koerner, the GRI director, publishes the first edition of *Designing With Geosynthetics*.

1987: *GFR* switches to a bimonthly, except monthly in November and December, with the December issue devoted to the “Product Reference Guide & Directory” ... The Geomembrane Division suggests changes for the EPA’s “Manual of Procedures and Criteria for Inspecting the Installation of Flexible Membrane Liners.”

1988: The Geotextile Division publishes a brochure featuring the history of the geosynthetics industry covering polymers, applications, and specifications ... *GFR* reports on the EPA releasing new regulations for the operation of municipal solid-waste landfills (Subtitle D) ... *GFR*’s Product Reference Guide is renamed the “Specifier’s Guide.”

AN INDUSTRY EVOLVING: 1989-1994

1989: *GFR* reports that EPA regulations now require leak-detection systems along with secondary containment linings... the September/October issue includes an IFAI marketing research article, “Geotextile Market Report: An Industry Evolving,” which charts annual production in millions of square yards: 1985 (210 msy), 1986 (235 msy), 1987 (264 msy), 1988 (297 msy), 1988 forecast (333 msy), and 1990 projected (369 msy).

1990: Danette Fettig begins a 16-year career at IFAI, starting as the *GFR* editor ... In an interview with *GFR*, newly elected IGS president R.Kerry Rowe challenges the industry to “disseminate knowledge concerning the benefit and correct use of geosynthetics to a broader range of potential uses and to encourage the development of new and innovative products and applications.”

1991: *GFR* notes the founding and incorporation of the Geosynthetic Institute (GSI) ... IFAI’s Geotextile Division starts a Washington Liaison Committee with a goal of expanding geotextile acceptance and use in federal projects.

1992: *GFR* reports that the Geotextile Division’s government relations Liaison Committee met with members of the U.S. House Public Works and Transportation Committee’s Surface

Transportation Subcommittee to promote the use and value of geotextile materials in maintaining the nation's infrastructure. Several representatives say they have never heard of geosynthetics.

1993: The magazine's 10th anniversary is marked with a cover makeover that highlights the letters *GFR* in red ... *GFR* now has 14,000 subscribers ... *GFR* writes about industry growth slowing as municipalities put off work on landfills after the EPA's ruling on Subtitle D is put on hold.

1994: *GFR*'s annual "Specifier's Guide" is available on disk for the first time ... 1994 is the first of five years for the Educate the Educators program—the "Professor Training Course for Geosynthetics" is the brainchild of Barry Christopher and courses are conducted during five summer sessions at Auburn (Alabama) University, from 1994 to 1998. Geosynthetics courses are offered today at more than 60 universities, up from only six in 1994.

ONWARD WITH A FEW BUMPS: 1995-2000

1995: *GFR* covers Geotextile Division's ongoing fight against the EPA's proposal to include geotextiles as a product that can be manufactured with recovered materials ... after five years as editor, Danette Fettig moves into a marketing position at IFAI and Dawn Sawvel is named *GFR* editor ... Austria-based Polyfelt (later acquired by Royal TenCate) ceases U.S. operations, leaving 75 people out of work and 5-6 million pounds of geotextiles stockpiled in its warehouse.

1996: After a year in IFAI marketing, Fettig returns to the geo world as the geosynthetics division's staff director as well as conference coordinator for Geosynthetics'97 in Long Beach and 6ICG (1998) in Atlanta, Georgia... GSI's Robert Koerner is awarded the 1996 Terzaghi Lectureship, presented by ASCE's Geo-Institute ... Two interesting items in the 1996 *GFR* calendar: Sept. 30–Oct. 2, the first EuroGeo conference—EuroGeo1 in Maastricht, Netherlands; and "Legal issues and the geosynthetics manufacturer"—a seminar held during the 1996 IFAI Expo in Atlanta.

1997: *GFR* reports that the American Association of Transportation Officials (AASHTO) is asking IFAI's geosynthetic's divisions to develop specifications for geosynthetics in pavement-subbase reinforcement.

1998: IFAI announces that its geotextile and geomembrane divisions are merging into a single Geosynthetic Materials Association (GMA)... With funding, sponsors, and attendees getting harder to arrange, the class of 1998 is the finale for the Educate the Educators program at Auburn University.

1999: *GFR* covers the EPA's accelerated plan for toxic contamination cleanup at facilities that generate, store, treat, or dispose of hazardous material—1999 projections are 200 cleanup sites per year until at least 2005 ... GMA is named the representative geosynthetic trade association to the National Transportation Product Evaluation Program (NTPEP) ... GMA opens an office in Mexico City.

2000: Maria de Lurdes Lopes from Portugal and GMA managing director Danette Fettig from the U.S. are the first women elected to the IGS Council ... *GFR* reports on the largest geomembrane footprint project in North America—301 acres at Florida gypsum stack site.

AN ANNIVERSARY AND A NEW DIRECTION: 2001-2005

2001: *GFR* notes that the U.S. Congress passed a \$32.9 billion bill for federal highway programs... An artificial reef is constructed with geotextile containers filled with sand to help slow erosion of Surfer's Paradise in Narrowneck, Australia on Australia's Gold Coast ... ASCE's 2001 "Report card for America's infrastructure" hands out below-average grades, specifically referencing *an aging bridge network* (five years before the I-35 bridge collapsed in Minneapolis).

2002: *GFR* reports that the American Society of Testing and Materials (ASTM) is changing its name to ASTM International ... *GFR* celebrates its 20th anniversary with a four-part history lesson by authors J.P. Giroud (June/July issue), Greg Richardson (August), Ian Peggs (September), and Robert Koerner (October/November) ... Daniele Cazzuffi elected IGS president at 7ICG in Nice, France.

2003: Former associate editor, Chris Kelsey, is named *GFR* managing editor ... in *GFR* industry news, NTPEP launches a new program to help state DOTs prequalify rolled erosion control products ... *GFR* publishes its third Spanish-language issue ... IFAI announces plans to partner with ASCE's Geo-Institute for its 2005 biennial geosynthetics conference—Geo-Frontiers-2005 in Austin, Texas.

2004: A March *GFR* article recaps the U.S. University Council on Geotechnical Education and Research workshop in Atlanta ... *GFR's* compilation, "Designer's Forum—Vol. 1 (1997-2003)" now available ... Geosynthetic Research Institute (GRI) approves two new standards—GT12b (nonwoven geotextiles as protection material) and GT13 (geotextiles as separation between subgrade soil and aggregate) ... A landmark article, "Lessons Learned from Failure: Landfill Covers" by Gregory Richardson and K.L. Pavlik, is published in the October/November issue of *GFR*.

2005: A watershed year for the geosynthetic industry's trade association and its magazine—Andrew Aho is hired as the new managing director of GMA, *GFR* undergoes vigorous internal redesign efforts with Vol.24, No.1 (February/March 2006), and Ron Bygness comes onboard as the new editor of *Geosynthetics* (née *GFR*) magazine ... Aho and Bygness are inaugurated at their first geosynthetics conference, NAGS 2005/GRI-19, Dec. 14-16, in Las Vegas, Nevada.

NEW DIRECTIONS: 2006-2012

2006: *GFR* officially becomes *Geosynthetics* with the publication of the February/March 2006 issue ... *Geosynthetics* reports on the Bowman Road bridge in Defiance County, Ohio—the first U.S. bridge to use the Geosynthetic Reinforced Soil / Integrated Bridge System promoted by the Federal Highway Administration (FHWA) ... *Geosynthetics* announces that GMA will offer a new level of membership for geosynthetics distributors.

2007: The year debuts with the Geosynthetics 2007 conference in Washington, D.C. and at the event, *Geosynthetics* highlights geosynthetic materials in expanding the infamous I-5/805 “Merge” in Southern California ... *Geosynthetics* reports on GMA’s contracting with a Washington, D.C. lobbying firm to implement the association’s government relations program.

2008: “In the Lab” returns as an occasional column in *Geosynthetics* ... *Geosynthetics* runs a classic case history, with Bill Hawkins of Fiberweb and GSI’s George Koerner unearthing a 1972 geotextile installation ... editor Bygness unleashes his “three-corner stool” program—trade association (GMA), publication (*Geosynthetics*), and industry conference management (IFAI’s biennial geosynthetics conferences since 1982)—in the magazine’s August editorial, “We are all in this together.”

2009: *Geosynthetics* wins gold and silver medals for Best Technical Article from the Minnesota Magazine and Publications Association ... J.P. Giroud elected to the National Academy of Engineering ... a new recurring column continues in *Geosynthetics*—featuring questions-and-answers from the GMA Techline.

2010: www.geosyntheticsmagazine.com gets support from the print magazine, with the “On the Web” column in every issue ... the December 2008 coal-ash disaster in Kingston, Tenn., continues to fuel nationwide discussions by the EPA for coal-ash containment with mandatory linings and groundwater monitoring ... a clarion call for the 20-teen years—“sustainability”—is spreading like wildfire as the GSI column asks, “Are We Missing the Sustainability Boat?”

2011: Boyd Ramsey elected chairman of GMA’s Executive Council, replacing two-term chair, John Henderson ... *Geosynthetics* launches its two-year Sustainability Series, with content provided by GRI-24 papers presented at GeoFrontiers-2011 in Dallas ... Old-timer Series—“Recalling early days of shear testing” by Allan Breitenbach—concludes with Part 3... GeoFrontiers-2011 hailed as the best geosynthetics conference since, well, since GeoFrontiers-2005 in Austin, Texas.

2012: IFAI’s Steve Warner steps down and is replaced as president/CEO by Mary Hennessy... “Giroud-Han design method” gets a two-part update and explanation by the well-known authors... It’s everywhere—“To frack or not to frack,” asks *Geosynthetics*’ August editorial—as controversial oil and gas recovery methods spread across North America.

CONCLUSION

As with the industry itself, *Geosynthetics* magazine has an interesting history, likewise with ups and downs, plenty of highlights along with a few forgettable lowlights during its 30-year publishing history. The magazine formerly known as *GFR* moves into its fourth decade with the ongoing objectives of serving, informing, educating, and learning from the geosynthetics community. It has been a good 30-year run. And the future of *Geosynthetics*—the industry and the magazine—look bright indeed.

ASTM INTERNATIONAL COMMITTEE D35 ON GEOSYNTHETICS – LOOKING BACK OVER 30 PLUS YEARS

L. David Suits
Executive Director, North American Geosynthetics Society

February 2014 will be the 30th anniversary of ASTM International Committee D35 on Geosynthetics. But it had its beginning in the Fall of 1977 when a group of seventy plus persons gathered in a crowded hotel room in New York City in response to a questionnaire to determine interest in test standardization for these new engineering materials then known as filter fabrics. That was just one of the commonly used names for geotextiles that included construction cloth, construction fabrics, stabilization fabrics, erosion control fabrics and many more names that described their intended use. The questionnaire was distributed to fabric manufacturers, DOT and other government agency engineering departments, civil and geotechnical engineering consulting firms, and the civil and geotechnical engineering departments at universities across the U.S. A. It was early in 1978 when, as a result of this meeting, ASTM organized subcommittee D13.61 on filter fabrics under Committee D13 on Textiles. Trudy Raumann from Monsanto deserves the credit for getting this group organized and setting it on its way.

When thinking of other persons involved in this initial effort, too many names come to mind to list all of them for fear of leaving some out. When the subcommittee was formed four subsections were set-up. In addition to section leaders and the subcommittee chairperson a subcommittee secretary was appointed. Those taking on these initial leadership positions were: Tudy Raumann (Monsanto), subcommittee chair; Paul Miller, subcommittee secretary (US Army Corps of Engineers); John Ball (University of Alabama), followed by L. David Suits (then of the NYSDOT), section on permeability and filtration chair; Dana Toups (Carthage Mills), followed by Robert G. Carroll Jr. (then of CFMC-Mirafi), section on endurance properties chair; Dick Van Scoy (DuPont), followed by Bennett Baird (DuPont) shortly after its formation, section on mechanical properties chair; and Marshall Silver (University of Illinois and STS Consultants), followed by Barry Christopher (then of STS Consultants), section on nomenclature chair.

In 1980 it was realized that there was limited participation from the geotechnical community in the work of subcommittee D13.61. To try and encourage more participation from this area a joint subcommittee between Committee D13 on Textiles and D18 on Soil and Rock was formed. The subcommittee carried the designation D13.61/D18.19 on Geotextiles and Related Products. Ballots on draft standards went through both subcommittees and both Main committees. Administering joint ballots and resolving negatives proved to be a nightmare. Following discussions with Committee D13, Committee D18, and ASTM Headquarters, and with agreement from all three, ASTM Committee D35 on Geotextiles and Related Products was officially formed in February of 1984 at the Town and Country Hotel in San Diego, CA. Barry Christopher, then of STS Consultants, was named chair. In 1985, after further discussion between D18 and D35, the geomembrane subcommittee under D18 was moved to D35.

As of the writing of this paper membership in Committee D35 has grown from those 70 plus persons meeting in New York City to 316 members.

In order to ensure continued participation from the geotechnical community, the D35 bylaws originally required that it meet for both of its semi-annual meetings in conjunction with the meetings of Committee D18. The bylaws have since been revised to require that only one of the semi-annual meetings be held with D18. However, the Committee still continues to hold both meetings the same week as D18.

Since the beginning in the crowded hotel room in 1977 there have been 70 meetings of Committee D35 and its predecessors. These have been held all over the US and Canada. They include: New York City (2); Philadelphia, PA (1); Washington, DC (1); Charlotte, NC (1); Atlanta, GA (7); Chicago, IL (1); Orlando, FL (3); Phoenix, AZ (3); Kansas City, KS (1); Kansas City, MO (1); Cincinnati, OH (1); St. Louis, MO (3); Louisville, KY (2); New Orleans, LA (3); Los Angeles, CA (1); San Diego, CA (4); San Francisco, CA (2); Ft. Lauderdale, FL (2); Coco Beach, FL (1); Tampa, FL (3); Albuquerque, NM (2); Toronto, Canada (3); Baltimore, MD (2); Denver, CO (4); San Antonio, TX (2); Montreal, Canada (1); Memphis, TN (1); Las Vegas, NV (1); Atlantic City, NJ (1); Seattle, WA (1); Reno, NV (2); Norfolk, VA (2); Dallas, TX (1); Salt Lake City, UT (1); Costa Mesa, CA (1); Vancouver, Canada (1); Anaheim, CA (1); Jacksonville, FL (1).

As the number of polymer products for geotechnical related applications grew, the scope of D35 encompassed many of these new materials and their testing technology. The D35 subcommittee on terminology developed a definition for the term “geosynthetic,” which received Committee approval. In 1989, D35 received ASTM approval to change its name to ASTM Committee D35 on Geosynthetics.

Realizing that in order to develop standards for the various test methods of interest there needed to be some guidance on how to sample these materials to ensure test results that were indicative of the materials. That is the test results needed to be statistically valid. The first standard to receive D35 approval was Practice D4354, Practice for the Sampling of Geotextiles for Testing. This has since been renamed to Practice for Sampling of Geosynthetics for Testing. Shortly after D4354 was approved Method D4355, Test Method for Deterioration of Geotextiles from Exposure to Ultraviolet Light and Water (Xenon-Arc Type Apparatus) was approved. These approvals took place in 1984 shortly after D35 became a Main Committee. In 1985 D35 activities were focused on diverse array of property tests; Suits, et al., 1985.

These included among others:

D35.01 - Mechanical Properties

Grab Tensile Strength

Wide Strip Tensile

Puncture Test

Trapezoid Tear

Diaphragm Bursting Strength Test Method

D35.02 – Endurance Properties

Abrasion Resistance
Creep Behavior
Chemical Resistance
On-Site Protection and Handling

D35.03 – Permeability and Hydraulic Conductivity

Apparent Opening Size
Gradient Ratio (Soil-Geotextile System Performance)
In-place Transmissivity (Underload)
Permittivity Underload
Thickness

As of the writing of this paper there are 155 approved D35 standards. They include test methods, guides, practices, and specifications. They appear in ASTM International Volume of Standards 4.13.

Many of the first standards that were being worked on were adaptations of existing ASTM Committee D13 textile standards. Revisions were made to incorporate the needs of the geotechnical community. They were primarily index property standards such as trapezoid tear, grab tensile, mass per unit area, thickness, and pin puncture. Standards that were directly related to the needs of the geotechnical community, yet still considered as index property tests included geotextile permittivity, the apparent opening size of geotextiles, unconfined tension creep of geosynthetics, mineral stabilizer content of bituminous geomembranes, and geonet breaking force among many.

As work progressed in developing the index property standards it was realized that there was a need to start developing standards which would help to evaluate the performance of the geosynthetics. While some of the following may be considered as quasi-performance, they are closer to performance than index properties. These include filtration efficiency of geotextiles, wide width tensile strength, pullout resistance, vertical compression of geocomposite pavement panel drains, geotextile clogging potential, long term creep, and interface shear, among many. One of the difficulties with performance tests is that they may require a long time to complete. An example is determining the long term creep characteristics of a geosynthetic. The method for accelerated compressive creep of geosynthetic materials based on time-temperature superposition using the stepped isothermal method allows the determination of the very long time creep characteristics (1000-10,000 hours) in a relatively short period of time.

To assist in the use of the test standards a number of guides and practices have also been developed by D35. Examples of these, besides the sampling one mentioned above, include practices for determining the 2% secant modulus for polyethylene geomembranes, evaluating the deterioration of geotextiles from outdoor exposure, quality control of geosynthetic clay liners, determining the specification conformance of geosynthetics and the installation of geocomposite pavement drains. Examples of guides which have been developed include selection of test

methods for prefabricated vertical drains, acceptance testing requirements for geonets and geonet drainage composites, the storage and handling of geosynthetic clay liners, the mechanical attachment of geomembranes to penetrations and structures, the identification, storage and handling of geosynthetic rolls and samples, and the use of expanded polystyrene geofoam in geotechnical projects, among several others.

The last area of standardization that the committee started to work in was the development of standard specifications for the various geosynthetic materials. While there was an initial resistance to move into this area it was realized that in order to complete the loop in standards development, this was a necessary step to take. Examples of specifications developed thus far include circular-knit geotextile for use in subsurface drainage applications, geocomposites for pavement edge drains and other high flow applications, prefabricated bituminous geomembranes used as canal and ditch liners, non-reinforced PVC geomembrane seams, non-reinforced PVC geomembranes used in buried applications, geosynthetic alternate daily covers, and rigid cellular polystyrene geofoam.

For those who may not be familiar with the ASTM International protocol for developing and approving standards a brief summary follows. In D35 each subcommittee has a number of task groups (TG) which work on individual standards. Once agreement has been reached in the TG, the draft is sent to a subcommittee ballot. Each individual member of the subcommittee receives a ballot and can vote on the draft. While each organization that is represented on the committee can have as many members on the committee as they want, only one member has the official vote. There must be a 60% return of official votes for the ballot to be valid. That said any negative vote or comment received from any individual member has to be addressed and resolved. Once all issues are addressed and resolved at the subcommittee level, the draft is sent to a Main Committee ballot. The same protocols rule at this level as at the subcommittee level. Due to space limitations this paper cannot go into the specifics of how resolution can be made, but in summary the following actions can be taken: 1) Agree with the voter and re-draft the standard and re-ballot; 2) After discussion with the negative voter explaining why the draft is written as it is, the voter may withdraw his/her negative vote; 3) The negative voter may be found non-persuasive for a valid technical reason. In this instance the recommendation must be upheld at the subcommittee and/or Main Committee; 4) The decision may be made that the issues are too numerous or complex and the draft withdrawn from consideration. While this may sound like a cumbersome procedure, it insures that all concerns are heard and addressed in a fair manner resulting in the best standard that can be developed at that time.

Since its very beginnings the activities of D35 and its predecessors have received excellent administrative support from ASTM staff at all levels. These include: Jim Thomas, current President of the Society, who served as the D13 Staff Manager when the activities first got underway; Ken Pearson, current Senior Vice President of Operations, served as the staff manager to D18 when D18 first was involved; Bob Morgan, the current Staff Manager to D18; Janet Bove, the first Staff Manager to D35; Jamie Kerr, past Staff Manager to D35; Bob Held, past Staff Manger to D35, Pat Picariello, past Staff Manager to D35; Christi Sierk, past Staff Manger to D35; and Katerina Koperna, current D35 Staff Manager.

Besides staff support, ASTM has assisted D35 in standards development through various one hour training workshops which are available to all ASTM International members. One particular training opportunity is a two day leadership workshop, while open to all ASTM International members, has assisted D35 members to become leaders within the Committee and their respective organizations.

One of the primary activities of the Committee beyond standards development has been technology transfer through informal workshops and formal symposia. The first years of D13.61 and D13.61/D18.19 were filled with workshops where technical and marketing people shared their activities and needs in the area of testing. These workshops have provided, and continue to provide, excellent exchange of practices and concepts. Since the establishment of Committee D35 there have been countless committee sponsored “workshops” focusing on specific geosynthetic issues. These workshops bring together interested D35 and non-D35 members to accelerate resolutions to difficult technical issues and advance the understanding of difficult methodologies in geosynthetic standards development.

Since its organization in 1984 D35 has sponsored ten formal symposia. Nine of these have resulted in a formal Standard Technical Publication (STP) of the papers presented. These symposia include:

1985 – Los Angeles, CA – Joseph Fluet, Organizer and STP Editor; “Geotextile Testing and the Design Engineer (STP 952 – 11 papers)

1989 – Orlando, FL – Ian Peggs, Organizer and STP Editor; “Geosynthetics: Microstructure and Performance (STP 1076 – 13 papers)

1990 – Las Vegas, NV – Robert M. Koerner, Organizer and STP Editor; “Geosynthetic Testing for Waste Containment” (STP 1081 – 26 papers)

1993 – San Antonio, TX – Robert G. Carroll, Jr. and Jonathon Cheng, Organizers and STP Editors; “Geosynthetic Soil Reinforcement Testing Procedures” (STP 1190 – 17 papers)

1995 – Denver, CO – Shobia Bhatia and L. David Suits, Organizers and STP Editors; “Geotextile Filters and Prefabricated Drainage Geocomposites” (STP 1281 – 15 papers)

1996 - Atlanta, GA – Larry Well, Organizer and STP Editor; “Testing and Acceptance Criteria for Geosynthetic Clay Liners (GCLs)” (STP 1308 – 18 papers)

1999 – Memphis, TN - Peter Stevenson, Organizer and STP Editor; “Grips, Clamps, and Strain Measurements” (STP 1379 – 12 papers)

1999 – Seattle, WA – Jim Goddard, John Baldwin, L. David Suits Organizers and STP Editors; “Testing and Performance of Geosynthetics in Subsurface Drainage,” jointly

sponsored by D35, D18 and the Transportation Research Board Committees on Subsurface Drainage, and Geosynthetics (STP 1390 – 9 papers)

2003 – Denver, CO - Robert Mackey and Kent Von Maubeuge, Organizers and STP Editors; “Advances in Geosynthetic Clay liner Technology: 2nd Symposium” (STP 1466 – 10 papers)

2012 – San Diego, CA – Kent Von Maubeuge, Organizer and STP Editor; “Current and Future Practices for the Testing of Multi-Component Geosynthetic Clay Liners” (There has been no STP number assigned as of the writing of this paper.)

The real progress of the D35 standards development has come from the many members who have taken on a personal objective to achieve the development of a standard. Some have accomplished this many times through the past three decades. The highest award given out by ASTM to recognize outstanding contributions to the Society is the Award of Merit. Committee D35 has had nine recipients of this award. They include: L. David Suits (1986), Robert Carroll (1987), Jack Hodge (1988), Barry Christopher (1990), Ronald Frobel (1992), Robert Koerner (1994), Robert Mackey (2003), James Goddard (2009), and Sam Allen (2010). Along with the award goes the title of Fellow of ASTM.

The Committee has recognized many others through Committee sponsored awards for their work in developing D35 standards. The names are too numerous to try and list here.

The current Committee Officers and Technical Subcommittee Chairs are:

Chairman – Robert Mackey

1st Vice Chairman – Tim Bauters

2nd Vice Chairman – James Goddard

Recording Secretary – Mark Wolschon

Membership Secretary – James Olsta

Subcommittee D35.01 on Mechanical Properties – Joel Sprague, chairman

Subcommittee D35.02 on Endurance Properties – George Koerner, chairman

Subcommittee D35.03 on Permeability and Filtration – Dave Suits, chairman

Subcommittee D35.04 on Geosynthetic Clay Liners – K. Von Maubeuge and J.P. Kline – co-chair

Subcommittee D35.05 on Erosion Control – Vacant as of the writing of this paper.

Subcommittee D35.10 On Geomembranes – Gary Kolbasuk – chairman

Past chairmen of D35 include: Barry Christopher (1984-1989); L. David Suits (1990-1995; 1998-2003); David Wyant (1996-1997); Sam Allen (2004-2009); Robert Mackey (2010-present).

In an effort to help people become familiar with the D35 standards the committee has been offering a one day short course highlighting many of our standards that are published in the ASTM International Book of Standards. These sessions have been offered over the last several years at the geosynthetics conferences held in North America.

The D35 Committee has been excellent doorway for those new to the geosynthetic field, allowing them to learn the latest technical knowledge and make professional contacts within geosynthetic organizations. Many of the current experts and leaders within the geosynthetic field have started their careers and found opportunities for growth and leadership through their involvement within D35.

In conclusion: As new geosynthetics and new applications are developed, the work of D35 will continue. However, it will not only continue in the development of new standards, but in maintaining the current standards to keep them relevant to the needs of the geosynthetics community. All ASTM International standards must be reviewed at least every five years, and actions taken to; 1) reapprove as is; 2) revise to bring them up to date with current practices at the time, or; 3) withdraw as no longer relevant.

ACKNOWLEDGEMENTS

The author wishes to thank Robert G. Carroll, Jr., Barry Christopher and Robert Mackey for providing reviews and suggestions for this paper.

REFERENCES

Suits, L. D., Carroll, R. G. and Christopher, B. "ASTM Geotextile Committee Testing Update", Geotechnical Testing Journal, GTJODJ, Vol 6, No. 4 , Dec 1985, pp. 191-198.

THE GEOSYNTHETIC INSTITUTE'S BACKGROUND AND HISTORY

Robert M. Koerner
Geosynthetic Institute, Folsom, PA USA

ABSTRACT

Most histories of people, places and things (like organizations) are chronologically subdivided between watershed events. This history of the Geosynthetic Institute is written along similar lines. The very sporadic beginnings in the late 1970's until 1986 is the first section to be described. Indeed, the year 1986 was pivotal in a number of ways. The second period from 1987 to 1998 was most important in establishing ourselves as the premier geosynthetics research and development organization on a national and international basis specializing on all types of geosynthetics and in all of their myriad applications. The third period from 1999 to the present represents a segue from the institute being focused completely on R & D, to related activities such as broad-based information, professional education, laboratory accreditation, inspection certification, along with the requisite R & D projects.

Now after these 35-years we approach the fourth period which is indeed the future. In this regard we offer some "musings" as to what it might portend for GSI and by association for geosynthetics in general.

INTRODUCTION

This paper reviews about 35-years of involvement in the area now known as geosynthetics materials and applications in discrete stages. They are as follows:

- 1.0 The beginnings through 1986 which include personal events leading to the formation of the Geosynthetic Research Institute within Drexel University
- 2.0 The time from 1987 through 1998 in which we mainly performed federal agency (U.S. EPA and U.S. FHWA mainly) projects and established ourselves accordingly.
- 3.0 The time from 1999 to the present in which we reconfigured ourselves to a full-service institute servicing its membership to the maximum extent possible.
- 4.0 The future beyond 2013 which is, of course, conjecture but will likely bring about entirely new applications areas (using existing or yet-to-be-developed products and materials) and is indeed exciting. We will use our "crystal-ball" to anticipate such activities. Only the future will tell how close we come to these predictions.

1.0 BEGINNINGS THROUGH 1986

Bob Koerner having received his doctoral degree in Geotechnical Engineering from Duke University in 1968, at age 35, started his academic career at Drexel University later than most beginning assistant professors. The Dean of Engineering at Drexel at the time, George Dieter, more than suggested that he get his research activity in high-gear and without delay. This was done over the next approximately ten years working in multiple (but unconnected) areas of deep

foundations, powder metallurgy, pharmaceutical powders, coal briquetting, acoustic emission monitoring, soil grouting, ground penetrating radar, and eventually pond liners and filter fabrics. Bob published over a hundred technical papers in this ten-year period before geosynthetics (many with U.S. EPA sponsorship under John Brugger and many co-authored with physics colleague Art Lord) and rose through the academic ranks to full professor in 1975.

The last two items in the above list of project areas came about from several consulting projects; namely, an architectural pond liner and a clogged geotextile erosion control mattress. This latter situation eventually generated several papers on geosynthetics in the late 1970's. The activity also stimulated a small research collaboration with Frank Ko of the Philadelphia College of Textiles and Science which resulted in more technical papers and the development of some specialized laboratory testing equipment.

In this same time frame Bob was also inviting speakers to make classroom presentations and two were memorable; Bill Witherow of Carlisle Rubber Co. and Bill Regan of Mirafi, Inc. (now TenCate Geosynthetics Inc.). They both gave informative in-class presentations to his graduate foundations course and opened up in his mind the opportunities within the emerging technology.

The real break came, however, when a Wiley Book Company editor Dan Morris asked Joe Welsh, a grouting contractor colleague, to write a small nomograph on construction fabrics. Joe didn't have time but suggested that Bob did. Bob initially thought that there wasn't enough published information on the topic but shortly thereafter the proceedings of the 1977 Paris Conference on the "Use of Fabrics in Geotechnics" became available. Bob called Dan and said that we would indeed write such a book. Thus, the 1980 first book on the subject became available; see Figure 1. It was an instant success and the phone "simply never stopped ringing".

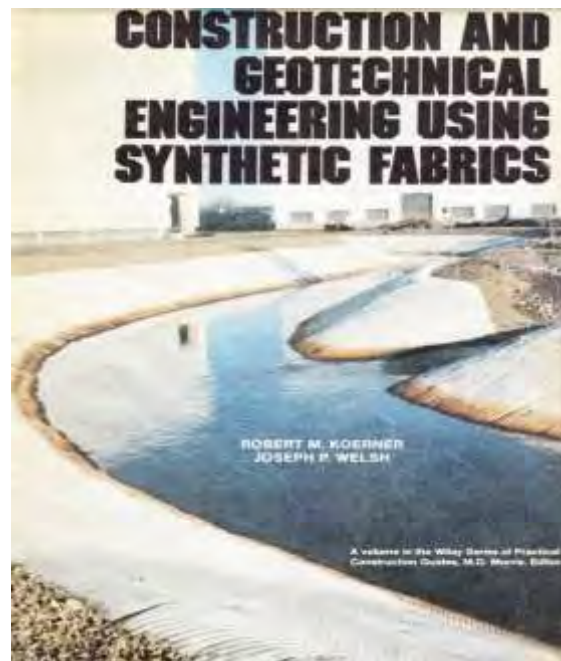


Figure 1. The first book on geosynthetics (Koerner and Welsh, 1980).

The impact of the book was so strong that all other research was halted and full concentration focused on this emerging area. Industrial contracts from Crown Zellerbach, Tensar, Mirafi and DuPont were the first of many and very soon a small research group was formed at Drexel. At this time the group was working out of the soils laboratory at Drexel which was well equipped soils-wise since Bob had developed a three-term graduate level soils laboratory sequence. As with all soils labs, they are inherently dirty and a somewhat clean area was desired for this new polymer related work. Also, there was no privacy and other facility and students had no inhibition of “borrowing” from our well-stocked equipment and hardware. In 1982, the small group moved into an enclosed room (about 30 by 20 feet) within the structures laboratory. The structures facility were not happy by this intrusion, but we had research money and were not to be denied; see Figure 2.

Yet, not all was smooth-sailing. Allen Halliburton of Oklahoma State University reviewed the book shown in Figure 1 with the awkward comment that “here is the salad, but where is the meat-and-potatoes”. Of course, this type of challenge led to a better and more comprehensive book which was stimulated by conversation with Dick Bell of Oregon State University and Jean-Pierre Giroud of Woodward-Clyde Consultants (now URS Corp.). In 1984, we had just finished team-teaching a course on what was now known as geosynthetics at the University of Wisconsin. The idea that was proposed was to put together a joint set of notes which would form the basis of a new book. As it turned out, Jean-Pierre was discouraged by his company and Dick was having difficulty in finishing his federal highway grant on geotextiles. Therefore, Bob persisted alone and in 1986 published the first edition of the meat and potatoes textbook, “Designing with Geosynthetics”. Four major items converged with its publication in 1986. First, in this pivotal year of 1986, Drexel’s President, William Gaither, called together the engineering faculty to encourage the faculty to develop centers and institutes, as opposed to doing independent consulting. Bob jumped on the opportunity and posed to him that we needed unique and automatous space (which was readily located) to which he countered that we weren’t to get him in trouble and no financial assistance was to be forthcoming from Drexel, i.e., we had to do it on our own!

Second, we moved from our one-room operation in the main engineering building to the West Wing of the Rush Building on Drexel’s campus, see Figure 3. The group consisted of Bob Koerner, Grace Hsuan (then an Assistant Professor of Civil Engineering and fortunately for us a polymer expert), Art Lord (a Professor of Physics and long-time faculty colleague), Marilyn Ashley (who started as Drexel’s civil engineering department secretary shortly after high school in 1973 and moved and then remained with us throughout our total experience), a new employee named Paula Koerner as a clerk/accountant, and a superb group of graduate research assistants including (most of all) George Koerner then working on his doctoral research.

Third, is that we incorporated as the Geosynthetic Research Inc. on August 12, 1986 (to be modified into Geosynthetic Research Institute on March 3, 1989 and eventually to the Geosynthetic Institute on December 16, 1991).



(a) The room's identification plaque



(b) R.A. student John Bove entering the laboratory



(c) R. A. student George Koerner performing a direct shear test



(d) Colleague Grace Hsuan performing a permittivity test

Figure 2. First geotextile/geomembrane laboratory; i.e., a room at Drexel in 1982.



(a) Three floors plus a basement



(b) New employee Paula Koerner in 1986



(c) The third floor hydraulics laboratory

Figure 3. Home of GRI in the West Wing of the Rush Building on Drexel's campus from 1986 to 1998.

Fourth, with the brand-new *Designing With Geosynthetics* book we “went on the road” teaching two-day courses. Manfred Hausmann of Australia was on sabbatical leave and handled the Drexel courses for Bob, and Paula did all of the logistics (books, slide trays, hotels, registration, lunches, breaks, etc., etc.) in the following cities.

1. September 4-5, 1986, Washington, DC
Sheraton, New Carrollton, MD
2. September 17-18, 1986, Atlanta, GA
Sheraton, Century Center I-85
3. September 23-24, 1986, Raleigh, NC
Sheraton, Crabtree, SC US 70W
4. October 8-9, 1986, Dallas, TX
Sheraton Grand at DFW Airport
5. October 14-15, 1986, Houston, TX
Sheraton Town & Country I-10
6. October 29-30, 1986, San Francisco, CA
Sheraton Airport, Burlingame
7. November 3-4, 6, Los Angeles, CA
Sheraton Industry Hills
8. November 19-20, 1986, Chicago, IL
Sheraton North Shore, Northbrook
9. November 24-25, 1986, St. Louis, MO
Sheraton Plaza I-270

All of these two-day courses were well attended and helped immeasurably in establishing GRI in the eyes of the fledgling geosynthetics communities. Most notable was the San Francisco course in which Bob Landreth of the U.S. Environmental Protection Agency and Henry Haxo of Metrecon Inc. were in attendance. This gave us not only credibility but also access to EPA funding. In turn, conducting the various projects brought involvement with the consulting and manufacturing communities with the eye of eventually forming a consortium of member companies.

By the end of 1986 all of the pieces of the institute were in place to be acted upon accordingly.

2.0 TIME FRAME FROM 1987 THROUGH 1998

This eleven-year period is subdivided accordingly to major activities undertaken as the Geosynthetic Research Institute, or GRI, functioning out of the West Wing of the Rush Building on Drexel University’s campus; recall Figure 3.

2.1 Formal Courses at Drexel

According to Drexel’s definitions, “centers” are focused on research only, while “institutes” perform research and also have an associated curriculum. Being an institute, we crafted a master’s degree program specializing in geosynthetics engineering. It consisted of ten, three-credit, term long courses in geosynthetics and it was complimented by electives and math

requirements. Additionally, theses on geosynthetics topics were often selected by the students as electives.

Table 1 – Master of Science in Civil Engineering – Special Program in Geosynthetics Engineering

Fall	Winter	Spring
1. Geosynthetic I (CIVE 650) (geosynthetics overview and geotextiles)	Geosynthetics II (CIVE 651) (geogrids, geonets and geomembranes)	Geosynthetics III (CIVE 652) (GCLs, geopipes and geocomposites)
2. Polymer Properties (CIVE 790) (physical, chemical and mechanical properties)	Polymer Processing (CIVE 791) (polymerization and processing of geosynthetics)	Polymer identification (CIVE 792) (chemical test methods and fingerprinting of geosynthetics)
3. Math Requirement	Math Requirement	Perspectives in Geosynthetics (CIVE 790-571)
4. Elective Sequence I	Elective Sequence I	Elective Sequence I
5. Elective Sequence II	Elective Sequence II	Elective Sequence II

Bob Koerner taught the Geosynthetics I, II, II and Perspectives courses while Grace Hsuan taught the three polymer related courses. The program was quite popular and many of the students taking this program have made their careers in geosynthetics, a fact of which we are very proud. Incidentally, Paula Koerner was given her nickname “GeoMom” from this group of students during this period of time.

2.2 Funded Research

Obviously, these students functioning as research assistants (or R.A.’s) needed financial sponsorship and we were fortunate in soliciting grants from several federal agencies (mainly the U.S. EPA) and others as well. Table 2 presents the main contracts in this regard.

Table 2 – Major Sponsored Research Projects

Sponsor	Topic	Date	Co-PIs with Bob	Amount
EPA	Geomembrane Lifetime	1983-86	A. E. Lord	\$ 190,000
EPA	Geosynthetics in Landfills	1987-92	A. E. Lord	450,000
EPA	Biological Clogging of Filters	1988-93	G. R. Koerner	600,000
EPA	Stress Cracking of HDPE	1989-93	Y. G. Hsuan	600,000
NCHRP	Performance of GS Drains	1990-93	G. R. Koerner	500,000
PaDOT	Geogrid Design Methods	1991-92	R. Wilson-Fahmy	50,000
EPA	QA/QC of Geosynthetics	1992-93	D. E. Daniel	80,000
EPA	Performance of Landfills	1993-00	D. E. Daniel and R. Bonaparte	1,000,000
NSF	Lifetime Prediction of GSs	1994-01	Y. G. Hsuan	170,000

The heavy funding from the U.S. Environmental Protection Agency is noteworthy in the previous table and it was due to our close association with Robert E. Landreth. Bob was the Chief of the Municipal Solid Waste and Residuals Management Branch of EPA located in Cincinnati, Ohio. Our association was very close since we represented the engineering counterpoint to Henry Haxo (a research chemist) who did all of the early research on

geomembranes and their compatibility to various leachates. After Henry retired, GRI “inherited” the bulk of EPA’s solid waste landfill research activity. In addition to the research, there were numerous EPA conferences and workshops in EPA’s headquarters in Cincinnati; all of which we had a heavy commitment. They included, but were not limited to, the following:

- Two conference workshops on geomembrane installation
- Two conference workshops on QA/QC of geosynthetics
- Three conference workshops on geosynthetic clay liners
- Two traveling seminars to all ten EPA Regions

Regarding this last item, some additional detail is warranted due to its importance in spreading the research and related technology to the regulatory community. The following description is taken from a paper by Greg Richardson (then with S & ME, Inc. and later a consulting engineer) entitled “GRI – The Beginnings” written and delivered at a 2004 Symposium Honoring the Research Achievements of Robert M. Koerner at Drexel University and published accordingly.

“After completion of the EPA design manual in the fall of ’87, Bob and Greg were asked to prepare a portion of a manual for a training course to be held in each of the EPA regions. These courses were free to attend and open to EPA staff, state regulators, engineers, owners, etc. The course format was quickly established: David Daniel of the University of Texas at Austin would present clay liner design and placement considerations, Bob Landreth would discuss chemical compatibility of liners, Greg would discuss liner design, final cover design, and liner inspection, while Bob discussed leachate collection and long-term considerations. During the summer of ’88, courses were held in San Francisco, Seattle, Dallas, Chicago, Denver, Kansas City, Philadelphia, Atlanta, New York, and Boston. With attendance ranging from 400 to over 600, we were overwhelmed with the response.

EPA monitored the effectiveness of the courses by having the audience rate the speakers and provide comments. While Dave, Bob, and Greg had comparable weighted averages for scores, Greg alone attracted the outliers. Each night, as we flew to the next course, Dave and Bob would read to our fellow passengers selected comments from the outliers regarding Greg. With such comments as “should not be allowed in public”, “a danger to the global environment”, etc., Greg relied on bourbon to counter the stares of fellow passengers. Comments too obscene to be read were passed from aisle to aisle; the lack of in-flight movies was not noticed by anyone except Greg.

Allowing two years for the dust to settle, Bob Landreth organized a second national course series focused of landfill closures. This was precipitated by the significant number of Superfund and CERCLA closures of sites contaminated by historic industrial/municipal actions. Paul Schroeder (of the U.S. Army Corps of Engineers) joined our team to discuss the HELP model but proved to be ineffective at deflecting the outliers from Greg. As we moved from Atlanta, Philadelphia, Boston, Dallas, Kansas City, Denver, Newark, Chicago, Seattle, and Oakland during the summer of 1990, Bob and Dave presented “Outliers – Part II” to the traveling public.

Approximately 10,000 people attended these two series of national EPA courses and for most this was their first exposure to geosynthetics and landfill design procedures. Even more than a decade later, it is rare to meet with a regulatory group regarding a landfill that someone in the group has not attended one of these courses.”

The importance of these two series of twenty lectures cannot be overstated. It put all of us speakers (and with it GRI) in the spotlight with respect to landfill, surface impoundment and waste pile design and construction. Figure 4 shows the group, but doesn’t nearly show the camaraderie and sheer joy we had being together and thus becoming life-long fiends.

2.3 Technical Research Publications

With extremely active and ongoing academic courses and research projects, the usual academic *publish or perish* mantra was very easy to embrace. We looked forward to spreading-the-word of this quite new field of geosynthetics. In order to form a contrast within the various time-frames of this paper we group the various publications accordingly; see the shaded portion of Table 3.

Here it is seen that the publications increased dramatically after the 1979-1986 time period in all of the different categories. Of course, almost everything was new and the various requests were abundant. After this intermediate period from 1987 to 1998, the activity remained strong, but a clear shifting from journal articles to proceedings papers is noted. People wanted the information as soon as possible and the peer-review scrutiny of journal articles simply took too long.

Table 3 – General Statistics on GRI/GSI Geosynthetic Publications

Type	1979-1986	1987-1998	1999-2012
Books, Proceedings, and Major Reports	2	32	38
Journal Papers and Keynote Papers	7	63	26
Conference Proceedings Papers	20	65	108
Major Articles and Proprietary Reports	10	62	112
TOTALS	39	222	284



Robert E. Landreth; U. S. EPA



Davie E. Daniel; Univ. Texas at Austin



Robert M. Koerner; Drexel Univ. & GRI



Gregory N. Richardson, S & ME, Inc.

Figure 4. Team of speakers at the 1988 and 1990 U. S. EPA region workshops on liner and cover systems.

2.4 Professional Courses

Since very few universities and colleges teach even a single course in geosynthetics (at its peak only 15 did so and considering that there are about 600 engineering universities and colleges in America that's only 3.3%), professional courses ranging from 4 hours to 3 days duration were regularly offered and invariably well received. Using the time increments described in this paper, the following table applies.

Table 4 – General Statistics on GRI/GSI Geosynthetics Professional Courses

Sponsor	1979-1986	1987-1998	1999-2012
Professional Organizations	14	21	4
Conference Organizations	2	6	6
GRI/GSI Hosted	4	45	66
Agencies	1	40	3
Universities	2	11	2
Companies	5	24	2
Others	2	1	2
TOTALS	30	148	85

The most active time period was from 1987-1998 when 148 geosynthetics courses were presented. Within this period only 45 of the 148 (30%) were offered at GRI since we were quite constrained space-wise. This changed dramatically in the next time period when we moved to new facilities with conference space and better all-around logistics. Also noted is that we were invited to speak at many state agencies, no doubt stemming from the U.S. EPA seminars mentioned earlier. Other than those estimated 10,000 people, a crude guess is that we reached an additional 5,000 participants with the above listed courses.

2.5 The GRI/GSI Consortium

Having such a close association with federal agencies like EPA, it was somewhat natural that the entire geosynthetics community would be interested in us. Thus, the idea of forming a consortium was discussed with, among others, Greg Richardson who greatly encouraged the idea. A visit to the Textile Research Institute at Princeton University gave the idea of creating a very broad institute including agencies, owners, designers, testing laboratories and manufacturers, and eventually resin/additive suppliers, and contractors/installers as well. While some of the generated data and research findings would not be to the liking of all groups, once decided upon everyone would be *onboard*. We decided to start beginning in 1987 with an initial membership fee of \$15,000 per year (\$10,000 per year afterward) and had an immediate response. Organizations joining in the first year were as follows:

1. Gundle (now GSE)
2. Soil and Materials, Inc.
3. U.S. EPA
4. Polyfelt (now TenCate)
5. Waste Management Inc.
6. Hoechst Fabrics Co.
7. Browning Ferris Ind. (now WMI)
8. Monsanto Inc.
9. E. I. duPont Co.
10. Golder Assoc.
11. Mirafi (now TenCate)
12. Tensar Inc.
13. U. S. FHWA

To date, we have had 119 member organizations (of which 53 have remained throughout) and an additional 18 associate members which are state or federal agency related. The latter are at the reduced membership rate of \$1,000 per year whereas membership is now at \$10,000 per year and has never been increased! A current listing of the membership is on our website at www.geosynthetic-institute.org. Needless to say, we are deeply appreciative of this past and ongoing member and associate member support.

In this time period from 1987 through 1998 considerable structure to the institute's operations was being formed:

- A home page was developed and maintained.
- Annual meetings were held.
- Focus groups of like-minded organizations were formed and held accordingly.
- GRI Standards for test methods, guides, practices and specifications were developed.
- Separate specification group meetings were held.
- Traveling seminars to member locations were regularly given.
- A quarterly Newsletter/Report was generated.
- An annual GRI conference was formed.

2.6 The GRI Conferences and Proceedings

Since research results should be available to the members as soon as possible, an annual research conference was initiated in 1986. For the first sixteen years it was held at a nearby Philadelphia hotel, but eventually it went to various locations-of-opportunity where other events were being held. Different from other conferences, the idea of having a specifically targeted conference theme was implemented. Thus, the GSI conferences have always been a tutorial-of-sorts, and included presentations from all member organizations, not only GRI personnel. Conferences to date and their themes have been as follows:

GRI-1 (1987)	“Soft Soil Stabilization Using Geosynthetics”
GRI-2 (1988)	“Durability and Aging of Geosynthetics”
GRI-3 (1989)	“The Seaming of Geosynthetics”
GRI-4 (1990)	“Landfill Closures: Geosynthetics, Interface Friction and New Developments”
GRI-5 (1991)	“Geosynthetics in Filtration, Drainage and Erosion Control”
GRI-6 (1992)	“MQC/MQA and CQC/CQA of Geosynthetics”
GRI-7 (1993)	“Geosynthetic Liner Systems: Innovations, Concerns and Designs”
GRI-8 (1994)	“Geosynthetic Resins, Formulations and Manufacturing”
GRI-9 (1995)	“Geosynthetics in Infrastructure, Enhancement and Remediation”
GRI-10 (1996)	“Field Performance of Geosynthetics and Geosynthetic Related Systems”
GRI-11 (1997)	“Field Installation of Geosynthetics”
GRI-12 (1998)	“Lessons Learned from Geosynthetic Case Histories”
GRI-13 (1999)	“Geosynthetics in the Future: Year 2000 and Beyond”
GRI-14 (2000)	“Hot Topics in Geosynthetics I: Bioreactors, GCLs, SRWs, Industry Issues”
GRI-15 (2001)	“Hot Topics in Geosynthetics II: Peak/Residual, RECMs, Installation, Concerns”

- GRI-16 (2002) “Hot Topics in Geosynthetics III: Probability, Landfill Uses, Poor Backfill, Concerns”
- GRI-17 (2003) “Hot Topics in Geosynthetics IV: MSE Properties, Geotextile Tubes, Challenges, Opportunities”
- GRI-18 (2004) “Geosynthetics Research and Development In-Progress”
- GRI-19 (2005) “Sessions on Low Permeability Backfill Soils, Heap Leach Systems and Various Hot Topics”
- GRI-20 (2007) “Use of Geosynthetics to Combat or Mitigate Acts of Terrorism and/or Natural Disasters”
- GRI-21 (2008) “Geosynthetics in Agriculture and Aquaculture”
- GRI-22 (2009) “It’s All in the Details”
- GRI-23 (2010) “Geosynthetic Materials Durability: Field and Laboratory Experiences”
- GRI-24 (2011) “Optimizing Sustainability Using Geosynthetics”
- GRI-25 (2013) “25-Year Retrospectives on the Geosynthetic Industry and Glimpses Into the Future”

The GRI Conferences (consisting mainly of GRI personnel and GRI member speakers) were always action-packed, informative, innovative and dynamic. The core group assembling and coordinating them are shown in Figure 5a. The conference proceedings form a data base of great value and, while not widely distributed, have us referencing the information on a regular basis. Among stand-out events were the hospitality sessions with the largest shrimps imaginable (thanks to National Seal Corp.) and the after-conference critique of all speakers with a grading system that sometimes boarded on *brutal*. The reviewers were invariably the best-in-the-business.

The brochure from the first GRI Conference in 1987 on “Soft Soil Stabilization Using Geosynthetics” follows, along with a photograph taken during the associated field trip.



Figure 5a. Bob Koerner, Paula Koerner, Grace Hsuan, Marilyn Ashley, Jamie Koerner, George Koerner and Te-Yang Soong taking a break from GRI conference organizing.

Very Soil Soil Stabilization Using High Strength Geosynthetics

Thursday, October 22, 1987

Friday, October 23, 1987

- 6:00 Registration**
Creeese Student Center, 32nd and Chestnut Streets, Philadelphia, PA
Lobby of Room 101
- 9:00 Welcoming Remarks**
- Dr. R. W. Schneider, VP Research, Drexel University
 - Dr. R. E. Woodring, Dean of Engineering, Drexel University
- 9:15 Session I - Design**
- J. Fowler, Corps of Engineers, Vicksburg, MS
"Overview and Perspectives"
 - R. M. Koerner, Drexel University, Philadelphia, PA
"Current Design Methods"
 - R. K. Rowe, University of Western Ontario, Ontario, Canada
"Finite Element Methods"
 - J. F. Beech, GeoServices Inc., Boynton Beach, FL
"Time-Dependent Strength Behavior"
 - Short Papers and Open Forum
- 12:30 Lunch**
- 1:30 Session II - Details**
- F. Ko, Drexel University, Philadelphia, PA
"Seaming and Joining Methods"
 - R. D. Holtz, Purdue University, W. Lafayette, IN
"Vertical Strip Drains"
 - A. E. Lord, Jr., Drexel University, Philadelphia, PA
"Centrifuge Methods"
 - G. N. Richardson, Soil and Material Engineers, Inc., Raleigh, NC
"Testing and Monitoring"
 - Short Papers and Open Forum
- 4:00 Actual Testing of High Strength Fabrics and GRI Open House**
- 7:30 Dinner**

- 8:00 Session III - Manufacture and Construction**
- P. Pisseeuw, Enka, b.v., Holland
 - G. Willibey, Nicolon Corp., Atlanta, GA
 - B. Myles, ICI, England
 - R. Mattox, Tensar Corp., Atlanta, GA
 - Short Papers and Open Forum
- 11:30 Session IV - Field Trip (with Box Lunch)**
- B. Ulbell, S. Fritzing, Corps of Engineers - Overview of Wilmington Harbor Project
- 12:15 Session IV - Field Trip**
- R. V. Locurcio, LTC Corps of Engineers, Philadelphia, PA
(Bus to Wilmington, Delaware to view installation of sewn 1500 lb/in (260 kN/m) fabric placed off a floating barge in 10' (3 m) deep water with a dike built on top of it. Project is 3.2 miles (5.2 km) long and 600' (180 m) wide with strip drains for accelerated consolidation. Truly a fantastic project! Return bus to Philadelphia International Airport or Sheraton Hotel.)

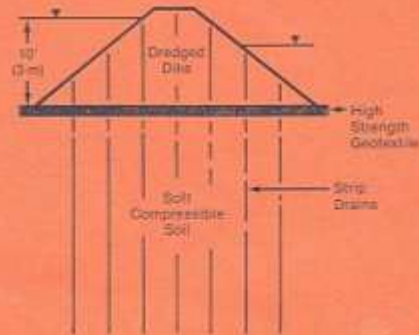


Figure 5b. Bao-Lin Hwu, John Bowders, Bob, COE Inspector and Jack Fowler at Wilmington Harbor field trip during the first GRI conference.

2.7 The GRI Proprietary Reports

In trying to attract and maintain members, we felt that something of proprietary value should be offered. In this regard R & D reports, which are only accessible on the password protected portion of our website, seemed worthwhile. These reports are purposely kept out of general circulation for at least two years and then only disseminated on a piecemeal basis. They are as follows:

1. March 20, 1988, "Environmental Stress Cracking of HDPE Geomembranes Seams and Related Studies"
2. December 7, 1988, "A Quantification and Assessment of Installation Damage to Geotextiles"
3. June 27, 1989, "Biological Clogging of Geotextiles Used as Landfill Filters"
4. June 21, 1990, "The Photo-Initiated Degradation of Seven Nonwoven Needle Punched Geotextiles"
5. October 1, 1990, "Finite Element Modeling of Soil-Geogrid Interaction with Application to the Behavior of Geogrids in Pullout Loading Condition"
6. June 18, 1992, "Parametric Evaluation of Primary Leachate Collection System Behavior Using the "HELP" Model"
7. December 9, 1992, "Geotextile Specifications for Transportation Applications: GRI's Second Survey"
8. December 9, 1992, "Stability Analysis of Multilined Slopes in Landfill Applications"
9. June 24, 1993, "Stress Cracking Behavior of HDPE Geomembranes and its Prevention"
10. July 27, 1993, "Experimental Puncture Behavior of HDPE Geomembranes Without, Then With, Various Protection Materials"
11. August 10, 1993, "A Survey of State Municipal Solid Waste (MSW) Liner and Cover Systems"
12. June 22, 1994, "FEM Behavior of Analysis of Plastic Pipe at High Normal Stresses"
13. September 26, 1994, "Design Methodology for Geomembrane Protection Materials"
14. February 3, 1995, "Drainage to Retaining Structures Using Geocomposite Sheet Drains: The State-of-the-Practice in the USA"
15. July 5, 1995, "Leachate Clogging Assessment of Geotextile and Soil Landfill Filters"
16. December 11, 1995, "Long Term Durability of HDPE Geomembranes Part I - Depletion of Antioxidants"
17. June 17, 1996, "Behavior of Waves in High Density Polyethylene Geomembranes"
18. December 9, 1996, "Cover Soil Slope Stability Involving Geosynthetic Interfaces"
19. June 17, 1997, "The Design of Drainage Systems Over Geosynthetically Lined Slopes"
20. June 18, 1998, "Earth Retaining Wall Costs in the USA"
21. December 7, 1998, "A Survey of Solid Waste Landfill Liner and Cover Regulations: Part I - USA Status"
22. December 18, 1998, "Analysis and Critique of Ten Large Solid Waste Landfill Failures"
23. March 30, 1999, "A Survey of Solid Waste Landfill Liner and Cover Regulations: Part II - World Wide Status"
24. July 30, 1999, "Geosynthetic Reinforced and Geocomposite Drained Retaining Walls Utilizing Low Permeability Backfill Soils"

25. December 20, 2000, "Installation Guide for Drainage Materials Associated With Segmental Retaining Walls (SRWs)"
26. August 1, 2001, "Field Monitoring and Laboratory Study of Geosynthetics in Reinforcement Applications"
27. January 9, 2002, "Internal Drainage of Low Permeability Backfill Soils of Geosynthetic Reinforced Earth Walls"
28. August 7, 2002, "A GRI White Paper on the Questionable Strategy of Soil-Only Landfill Covers" [Comment; white papers now form a core publication effort for the institute]
29. September 30, 2003, "Selected Papers on the Design Decision of Using Peak versus Residual Shear Strengths"
30. June 14, 2005, "Direct Shear Database of Geosynthetic-to-Geosynthetic and Geosynthetic-to-Soil Interfaces"
31. July 17, 2006, "Status of Adoption and Use of the AASHTO M288 Geotextile Specification Within U.S. State Departments of Transportation"
32. January 12, 2007, "GRI's Third Survey of Solid Waste Landfill Liner and Cover Systems: Part I - USA Status"
33. February 27, 2007, "Translational Failure Analysis of Solid Waste Landfills Including Seismicity"
34. October 24, 2007, "GRI's Third Survey of Solid Waste Landfill Liner and Cover Systems: Part II - Worldwide Status"
35. September 12, 2008, "Symposium Papers on Vegetated MSE Berms at Landfills"
36. October 15, 2008, "Inadequate Performance of Geotextile Filters Under Difficult and Challenging Field Conditions"
37. November 4, 2008, "Geosynthetic Supported Base Reinforcement Over Deep Foundations"
38. December 16, 2009, "A Data Base and Analysis of Geosynthetic Reinforced Wall Failures"
39. April 1, 2010, "Remediation of Excessively Deforming MSE Retaining Walls"
40. June 23, 2010, "On the Prevention of Failures of Geosynthetic Reinforced Mechanically Stabilized Earth (MSE) Walls and Recommendations Going Forward"
41. October 27, 2011, "Analysis and Critique of Twenty Large Solid Waste Landfill Failures"
42. January 3, 2012, "Lifetime Prediction of Laboratory UV Exposed Geomembranes: Part I - Using a Correlation Factor"

3.0 TIME FRAME FROM 1999 TO PRESENT

By 1999, the Geosynthetic Research Institute was well recognized nationally and internationally primarily as a research and development institute within, or associated with, an academic institution, namely Drexel University. However, the membership wanted more than R & D studies which invariably relied on students. Remember, the main goal of students is to finish and get on with their lives. The desirable *new dimensions* required a broadening of personnel and activities which brings into focus the third phase of this retrospective paper.

3.1 Legal Arrangements

Regarding various incorporations the following took place:

- August 12, 1986 “Geosynthetic Research Inc.” in Delaware (abandoned April 15, 2012)
- March 3, 1989 “Geosynthetic Research Institute” in Delaware
- December 16, 1991 “Geosynthetic Institute” in Delaware
- September 8, 1993 GSI Granted IRS 501 (C)(3) Status (i.e., we are a nonprofit tax-free organization)

In addition, trade (service) marks were acquired for the interrelated institutes now under a new configuration, i.e.,

- “Geosynthetic Research Institute”,
- “Geosynthetic Information Institute”,
- “Geosynthetic Education Institute”,
- “Geosynthetic Accreditation Institute”,
- “Geosynthetic Certification Institute”,

and, if ever needed, “The Journal of Geosynthetics”. This provided for the expanded structure of the institute as shown in Figure 6.

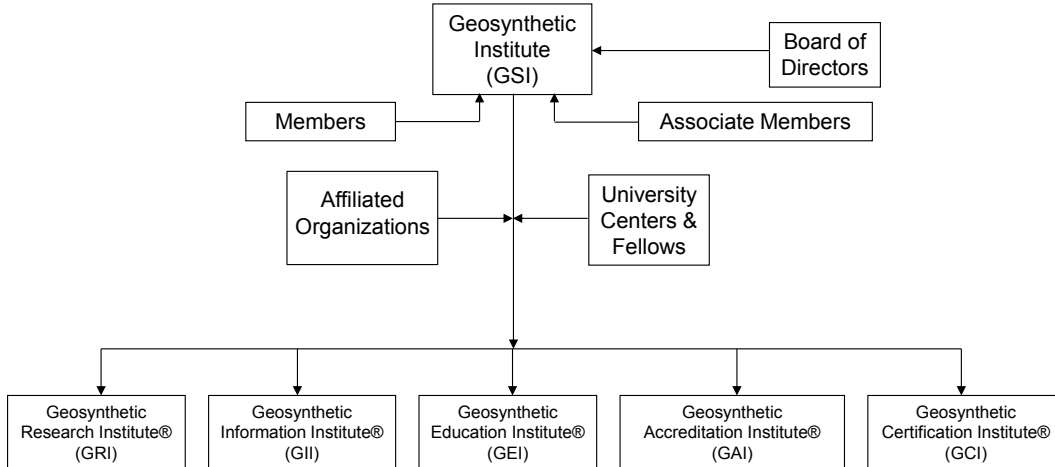


Figure 6. The organizational structure of the Geosynthetic Institute.

This organizational structure required a number of actions which took place immediately upon its formation. First, Bylaws were needed and they were developed and published on January 1, 1996. They have been slightly revised five times since then. Second, the Bylaws required a nine-person Board of Directors (BoD) which was selected on the basis of established focus groups plus acknowledgement of the growing international member organizations. Each BoD member serves for three years and the three groups of three are staggered annually. BoD members can repeat themselves. The names of the BoD members to date follow and we wish to gratefully acknowledge their service and guidance to the organization.

Table 5 – History of the GSI Board of Directors

	1996	1997	1998	1999	2000	2001	2002	2003	2004
AGENCY	D. Jaros	D. Jaros	D. Jaros	D. Jaros	D. Jaros	D. Jaros	D. Jaros	D. Jaros	D. Jaros
OWNER	D. Spikula	D. Spikula	D. Spikula	D. Spikula	R. Jones	T. Eith	T. Eith	T. Eith	T. Eith
CONSULTANT	L. Overmann	L. Overmann	D. Stulgis	D. Stulgis	D. Stulgis	D. Stulgis	D. Stulgis	D. Stulgis	D. Stulgis
RESIN	P. Maeger	P. Maeger	P. Maeger	R. Bobsein	R. Bobsein	R. Bobsein	R. Bobsein	R. Bobsein	R. Bobsein
GM/GCL	F. Struve	B. Torres	B. Torres	B. Torres	B. Ramsey	B. Ramsey	B. Ramsey	J. Olsta	J. Olsta
GT/GG	J. Paulson	J. Paulson	J. Paulson	J. Paulson	J. Paulson	G. Willibey	G. Willibey/ M. Theisen	M. Theisen	B. Ramsey
INTERNATIONAL	P. Rimoldi	P. Rimoldi	P. Rimoldi	P. Rimoldi	P. Rimoldi	P. Rimoldi	K. von Maubeuge	K. von Maubeuge	K. von Maubeuge
AT-LARGE	S. Allen	S. Allen	S. Allen	S. Allen	S. Allen	S. Allen	S. Allen	S. Allen	S. Allen
AT-LARGE	G. Kolbasuk	G. Kolbasuk	G. Kolbasuk	G. Kolbasuk	G. Kolbasuk	G. Kolbasuk	D. Suits	D. Suits	D. Suits

	2005	2006	2007	2008	2009	2010	2011	2012	2013
AGENCY	D. Jaros	D. Jaros	D. Jaros	D. Jaros	D. Jaros	D. Jaros	D. Jaros	Dr. Jaros	D. Jaros
OWNER	T. Eith	T. Eith	T. Eith	T. Eith	T. Eith	T. Eith	T. Eith	T. Eith	J. Workman
CONSULTANT	D. Stulgis	D. Stulgis	D. Stulgis	D. Stulgis	D. Stulgis	D. Stulgis	D. Stulgis	M. Sieracke	M. Sieracke
RESIN	R. Bobsein	R. Bobsein	R. Bobsein	P. Oliveira	P. Oliveira	P. Oliveria	R. Bobsein	R. Bobsein/ L. Cui	L. Cui
GM/GCL	J. Olsta	G. Kolbasuk	G. Kolbasuk	G. Kolbasuk	G. Kolbasuk	G. Kolbasuk	G. Kolbasuk	T. Rafter	T. Rafter
GT/GG	B. Ramsey	B. Ramsey	B. Ramsey	B. Ramsey	B. Ramsey	B. Ramsey	B. Ramsey	B. Ramsey	M. Wayne
INTERNATIONAL	K. von Maubeuge	K. von Maubeuge	K. von Maubeuge	K. von Maubeuge	K. von Maubeuge	K. von Maubeuge	K. von Maubeuge	K. von Maubeuge	K. von Maubeuge
AT-LARGE	S. Allen	S. Allen	S. Allen	S. Allen	S. Allen	S. Allen	S. Allen	S. Allen	S. Allen
AT-LARGE (then Intl. 2)	D. Suits	M. Sieracke	M. Sieracke	M. Sieracke	W. Hsieh	W. Hsieh	W. Hsieh	W. Hsieh	W. Hsieh

Third, the need and desirability of federal and state regulatory agencies was felt to be imperative. Discussions among the BoD eventually came to the conclusion that full membership at \$10,000 per year was not feasible, so a greatly reduced fee of \$1,000 was decided upon. To date, we have attracted six federal agencies, eleven state environmental agencies, four state transportation agencies and two city agencies. They are indeed welcome and their presence and collective inputs are very meaningful in every respect.

Fourth, it was recognized that geosynthetics are international (Geosynthetics-Without-Borders?) and that the institute's personnel and logistics are limited, so a special category of "Affiliated Organizations" was created. These are international government or academic institutes that are desirous of our information and wish to create a GSI-affiliated organization within their own country. Of course, all of our intellectual knowledge can be translated and used accordingly. To date, we have a GSI-Korea under the FITI Testing and Research Institute (Jeongyho Kim) and INHA University (Han-Yong Jeon), and also a GSI-Taiwan under the National Pingtung University of Science and Technology (C. Wayne Hsieh). Both are sincerely appreciated and very active.

Fifth, we have the ability to co-opt and coordinate activities with other universities on an as-required basis. To date, we have been involved with a research effort on plastic pipe with Drexel University (Grace Hsuan) a reinforced wall activity with the University of Delaware (Dov Leshchinsky) and a hydraulic structure waterproofing activity with the University of Texas at Austin (Jorge Zornberg). This activity is greatly augmented by the awarding of GSI Fellows which will be described later.

3.2 GSI's New Home

Operating from the West Wing of Drexel's Rush Building was not really suited for a rigorous plastics-related R & D institute and to the new activities which we planned; for example,

- it had erratic room air conditioners,
- it had no humidity control,
- it had regular squirrel-invasions,
- the security was poor (we had one burglary which Bao-Lin Hwu thwarted),
- it required lugging equipment up and down four flights of stairs,
- communications were difficult,
- there was no room for growth, and
- our rapidly growing neighbor, the College of Information Sciences, wanted us out!

It was really time for us to go and Jamie Koerner (George's wife) was perfect for finding us an off-campus home. Located beyond city limits and only four miles from the Philadelphia International Airport it was the former MRI center of a local hospital. Substantially built with a lot of potential laboratory space George Koerner reconfigured the entire building's 5000 sq. ft., single story building. The reception area for Marilyn Ashley was nicely configured as well as an adjacent area for Paula Koerner and Jamie Koerner. There is a perfect sized conference room capable of hosting up to 22-people and the final arrangements couldn't have been better if we had designed the building from scratch. It even has properly zoned space for expansion. Figure 7 shows photographs of our GSI home.



(a) Our street approach sign



(b) Parking and front entrance



(c) Marilyn Ashley at her pivotal position



(d) Bob lecturing in conference room

Figure 7. GSI's new home in Folsom, Pennsylvania.

3.3 Ongoing Research Activities at GSI

Research and development will always be a core activity of GSI and a number of projects have been carried-over to our new home. That said, our ideal research project is one which takes many, many years. Short term projects using standardized test methods are invariably shifted to the member consulting companies or testing laboratories. Research projects presently ongoing are the following. Note the estimated durations which are well beyond the time frame for graduating students.

- In-situ temperature monitoring of geomembrane liners and covers at both dry and wet landfills (15 years and ongoing).
- Flow behavior of leachate collection systems and fully degraded waste (7 years and recently concluded)
- Ultraviolet exposure of all types of geosynthetics in laboratory weathering devices (10 years and ongoing)
- Alkalinity between masonry blocks in MSE walls (7 years and ongoing)
- Forensic analysis of MSE wall failures and their remediation (12 years and ongoing)
- Forensic analysis of landfill failures (10 years and ongoing)
- Forensic analysis of geotextile filtration situations (15 years and ongoing)
- Forensic analysis of veneer slope slides (10 years and ongoing)
- Forensic analysis of all types of geosynthetic materials failures (30 years and ongoing)
- In-situ behavior of exposed geogrids of flexible faced MSE landfill berms (projected time is 50+-years)

An additional comment with respect to research has to do with the crafting of generic specifications for various classes of geosynthetics. This is a most difficult task since most companies seek conformance to their particular products while other groups seek ultimate safety against the unknowns. This middle ground balancing act has been reasonably successful with eleven complete specifications and another six in-progress. Those that have been adopted are available free on the institute's website. George Koerner describes details in a companion paper in these proceedings.

3.4 Ongoing Information Activities at GSI

From print-to-electronic formats, information generated from institute activities are split between that available to the general public and that available only to members. In fact, the institute's website (developed and maintained by Marilyn Ashley) is configured in this manner. Everyone (members and nonmembers) can access the open part at www.geosynthetic-institute.org, which has the following menu.

Members

- GSI Members
- GSI Affiliates
- Associate Members
- Focus Groups
- Meetings

Education

- Courses
- Available CDs
- GSI Fellows

Research

- Current Projects
- Technical Papers

Accreditation

- Introduction
- Application
- Accredited Labs
- Test Methods

Information

- Specifications
- Guides and Practices
- White Papers
- Newsletters
- GMA Techline
- GSI Member Links
- Buy Publications

Certification

- Geosynthetics/Compacted Clay Liners
- MSE Walls, Berms and Slopes

Contact Us

- Dr. Robert M. Koerner
- Dr. George R. Koerner
- Dr. Grace Hsuan
- Mrs. Paula Koerner
- Mrs. Jamie Koerner
- Ms. Marilyn Ashley

To go further one needs a members-only password. When you get into this section the following information is presented.

- GRI Standards (≈ 90)
- GRI Proprietary Reports (42)
- Citations of GRI Technical Papers (325)
- GSI Annual Meeting Notes
- Links to the Geosynthetics World
- Keyword Search for Literature
- Example Problems (from DwG book)
- Frequently Asked Questions (FAQs)

Note that the *links* section in the open part of the website is to GSI members, whereas the *links* section in the password protected section is to the entire geosynthetics world

The *Keywords Section* contains about 30,000 citations of the majority of the geosynthetics literature published in English. It's quite easy to use provided that you have a specific topic or area in mind. This is the section of the website that we (and others we are told) use the most used in our daily activities.

An interesting mechanism to broadcast information that is generally quite opinion-based is that of a *White Paper*. GSI has a special section of the home page devoted to this type of information outlet. There are presently twenty white papers, available to everyone, and they are of two types. One type is technical related (written by Bob and George Koerner) and the other is survey related (assembled by Jamie Koerner). These white papers are frequently visited and sometimes even referenced in technical papers which make us somewhat apprehensive. One has

to question the appropriateness of the action since many are opinion-based and all are without peer review. Nevertheless, they have served our needs as well as others quite nicely.

3.5 Ongoing Education Activities at GSI

Education, in its various forms is at the heart of all technologies and geosynthetics are no exception. That said, education has many forms. The 42-GRI Reports mentioned in Section 2.7 could easily be mentioned here as well. The 263 courses listed in Section 2.4 are directly related to education and now, more often than not, they are hosted at GSI where we can accommodate up to 22-people. Most are one-day long and having our laboratory in-house we (George and Bob) can go back-and-forth between lectures and related test demonstrations. It is a very effective format.

Obviously, power point presentations follow along with all projects and are shared with the membership. They number about 150 and most are about one hour in length. Some of the more current topics, like shale gas plays and coal combustion residuals, have short voice-overs on the individual slides.

All of these presentations are candidates for on-line webinars. Currently, eight are offered on a semiannual basis hosted by the American Society of Civil Engineers (ASCE). Their format is a noon to 1:00 PM presentation followed by 30 minutes of questions and answers. Some of these webinars have had as many as forty companies on line for the event.

Certainly the capstone of the institute’s education effort is embodied in the book titled “*Designing With Geosynthetics*”. Its sixth edition was published in 2012 and this latest version is available in hardback, or softbound and e-book. There is also a 1230 power point CD entitled “Instructors Guide”. The history of the various editions follows:

Table 6 – Publication History of the **Designing with Geosynthetics** 2012 Book

Edition	Published	Pages	Sales
First	1986	424	3197
Second	1990	652	2645
Third	1994	783	4686
Fourth	1998	761	5460
Fifth	2005	796	3500
Sixth	2012	914	?

Since 2008, GSI has been awarding graduate fellowships to students worldwide for conducting geosynthetics research. The criteria are as follows:

- Student must be pursuing a doctoral degree
- Student must be researching a geosynthetic topic
- Student must be approved by advisor or administrator

Table 7 gives the history of the program to date and many of the students have received second and third year funding as well.

Table 7 – GSI Graduate Student Fellowships

	Name	University	Advisor	Topic
<u>2008-2009 A.Y.</u>				
1-08	Michael McGuire	Virginia Tech University	George Filz	Reinforced pile supported embankments
2-08	Connie Wong	Drexel University	Grace Hsuan	Specification for corrugated HDPE pipe
3-08	Axel Ruiken	RWTH Aachen University	Martin Ziegler	Geogrid behavior in MSE systems
4-08	Elena Kapogianni	National Technical University of Athens	Michael Sakeilaniou	MSE slopes under seismic conditions
5-08	Xiaoming Yang	University of Kansas	Jie Han	Geocell behavior in aggregate bases
<u>2009-2010 A.Y.</u>				
1-09	Anil Bhandari	University of Kansas	Jie Han	Geogrids under dynamic loading
2-09	Brent Robinson	North Carolina State University	Mo Gabr	GT/GG behavior in lime stabilized soils
3-09	Ioanna Tzavara	University of Crete	Yiannis Tsompanakis	Seismic design for MSE reinforced walls
4-09	Majid Khabbazian	University of Delaware	Victor Kaliakin	GS reinforced stone columns
<u>2010-2011 A.Y.</u>				
1-10	Tanay Karademir	Georgia Tech	David Frost	Elevated temperature effects on strength
2-10	Jing Ni	University of Wollongong	Buddhima Indraratna	PVDs under cyclic loads
3-10	Bret Lingwall	University of Utah	Steven Bartlett	GS protection of buried pipes
4-10	Carmen Franks	University of Maryland	Ahmet Aydilek	GS filters for urban storm water runoff
<u>2011-2012 A.Y.</u>				
1-11	Ryan Corey	University of Kansas	Jie Han	GS protection of buried pipelines
2-11	G. Hossein Roodi	University of Texas at Austin	Jorge Zornberg	Pavement lifetime using field data
3-11	Felix Jacobs	RWTH Aachen University	Martin Ziegler	Geogrid reinforced soil behavior
4-11	Mahmound Khachan	Syracuse University	Shobba Bhatia	Deflocculants for geotextile tubes
<u>2012-2013 A.Y.</u>				
1-12	Chuangi Wang	University of Memphis	David Arellano	Properties of Recycled Expanded Polystyrene
2-12	Xunchang Fei	University of Michigan	Dimitrios Zekkos	Biodegradation of Geotextiles
3-12	Jitendra K. Thakur	University of Kansas	Jie Han	Recycled Asphalt Used in Geocells

3.6 Ongoing Accreditation Activities at GSI

The Geosynthetic Accreditation Institute-Laboratory Accreditation Program (GAI-LAP) was initiated following numerous requests to accredit the operations of testing laboratories within the geosynthetic community. The program is intended to monitor geosynthetic laboratory capability. The program goal is to accredit geosynthetic testing laboratories for performing consensus standardized test methods insofar as equipment, documentation and testing protocol. *It is important to note that this program is not meant to certify individual test results.*

The program was first requested by state and regional environmental regulators, during a series of courses taught nationally in 1988 (on liner systems) and again in 1990 (on cover systems). Subsequently, a survey of GSI member organizations listed the lack of geosynthetic laboratory accreditation as a severe shortcoming of the industry.

After a Pittsburgh meeting with a number of third-party testing laboratory owners on April 20, 1994, we framed the Geosynthetic Accreditation Institute-Laboratory Accreditation Program (GAI-LAP) around two international known standards; ISO 9000 and ISO 17025. Although the GAI-LAP models itself after these standards it does not profess to be affiliated with ISO or any other accreditation organization. Rather, the program is a hybrid one tailored to the immediate needs of the geosynthetic testing community.

It is felt that the GAI-LAP has a threefold effect on geosynthetic testing. *First*, it gives credibility to those laboratories that are properly equipped and prepared to do the respective tests. *Second*, by omission, it eliminates those laboratories that are not equipped to do specific tests. *Third*, as an ancillary benefit it requires laboratories to prepare a quality manual, write test-specific standard operating procedures and prepare test reports for each test method for which accreditation is desired.

The intent of the GAI-LAP is to prevent errors and inaccuracies by following an approved plan and utilizing standard procedures. By so doing, it is hoped that the funds expended in geosynthetic testing are being spent with clear objectives in mind. The intent of this endeavor is to have a system in place that will aid communication and be accompanied by a paper trail of documentation. The program is rigorous in comparison to the current state-of-the-practice in geosynthetics laboratory testing. It should be mentioned that despite its voluntary nature, competitive pressures may make accreditation seem like a necessity. This is particularly true for laboratories that do federally funded work or who are involved with international work.

The success of the program far exceeds our initial expectations. Driving home from the Pittsburgh meeting, Grace Hsuan, George Koerner and Bob Koerner anticipated about ten laboratories in the program and currently we have 49! They are 11-third party labs, 32-manufacturers quality control labs (which we never envisioned joining the program), four research institute labs, and two government labs. As shown in Figure 8, Synthetic Industries, Inc. was the first manufacturers quality control lab to join the program. There are a possible 280 geosynthetic test methods (ASTM, ISO and GRI Standards) that can be accredited and the average of the present 49 laboratories in the program is thirty.



Figure 8. Ceremony in 1996 at Synthetic Industries, Inc. plant for the first accredited manufacturing QC lab. (Ted Koerner, Leonard Chill and Bob)

The core of the program is to send samples to the accredited labs for specific tests to evaluate their proficiency in having results fall within two standard deviations ($\pm 2\sigma$) of the mean value (μ) of the material. The data base is kept by George Koerner who expertly directs the entire effort. Additionally, an on-site visit to each lab is required every five years and these visits have provided excellent training for the respective laboratories and their technicians. Additionally, one of the major outgrowths of the GAI-LAP program is the settling of “conflict resolution” issues between laboratories with different test results for the same tests. This issue occupies much of George Koerner’s time in reaching a consensus.

Needless to say, the program is an outstanding success and far beyond our initial expectations.

3.7 Ongoing Certification Activities at GSI

GSI now has two separate inspector certification programs. One (begun in 2006) focuses on QA/QC of field inspection of waste containment geosynthetics and compacted clay liners. The other (begun on Dec. 1, 2011) focuses on MSE Wall, Berm and Slope field inspection. They are both similar in that a perspective candidate must conform to the following:

- Be recommended by a professional engineer who knows, and can attest to, at least six months of acceptable experience performing CQA activities with either geosynthetic liner or cover systems or MSE walls, berms, or slopes using geosynthetic reinforcement.

- Submit a completed application and be approved by the Geosynthetic Certification Institute to take the exam.
- Must successfully pass a written examination (70% of the questions is the passing grade) proctored by GCI or a GCI designated organization and graded by the Geosynthetic Certification Institute to become a certified inspector.
- Must pay a one-time fee which covers a five-year period upon completion of the above items. The fee is \$500 for five-years of certification.

Program #1 - Inspection of Liner Systems for Waste Containment Facilities

This program now in its sixth year has been received, and in some cases required, by solid waste owners, state regulators, and design consultants for proper QCA in field installation of both geosynthetic materials and compacted clay liners. The statistics to date are as follows.

Table 8 – Inspection Certification Test Results - 2006-2012

Year	Geosynthetic Materials		Compacted Clay Liners		Commentary
	No. of people taking exam	No. of people failing exam	No. of people taking exam	No. of people failing exam	No. of people failing both exams
2006	141	5 (3%)	128	12 (9%)	2 (1.5%)
2007	82	11 (13%)	73	12 (16%)	7 (8.5%)
2008	95	25 (26%)	89	20 (22%)	13 (14%)
2009	36	7 (19%)	36	2 (5%)	2 (6%)
2010	59	12 (20%)	54	7 (13%)	5 (8%)
2011	54	6 (11%)	53	3 (6%)	1 (2%)
2012	34	5 (15%)	28	3 (11%)	3 (9%)
TOTAL	501	72 (25%)	461	59 (13%)	33 (7%)

The 5-year renewal period for those having taken the exam in 2006 is ongoing and about 60% have renewed accordingly. This is felt to be encouraging from our perspective.

Program #2 - Inspection of MSE Walls, Berms and Slopes

The official launch of this program was on December 1, 2012 with a course and the examination afterward. There are now thirty persons certified by GCI for the inspection of MSE Walls, Berms and Slopes.

While a field inspector cannot require proper design or instruct a contractor how to build the structure, flaws can be identified for possible design modification or mitigation action. Furthermore, and at minimum, construction practices can be observed and corrected if inadequate or improper. It will be interesting to see if this program has a positive impact in stemming the large number of MSE structure failures that we are presently confronted with.

4.0 MUSINGS ON GSI'S FUTURE

To accurately predict the future one must be both observant and lucky. Yet, the exercise is considered worthwhile by many organizations since in one's busy daily routine we rarely take time to project our thoughts forward. That said, the attempt will be made to suggest GSI's future in the context of research, information, education, accreditation and certification.

4.1 Future Research Activities

GSI's research has been, and will likely be in the future, decidedly "mission-oriented". As such, it is based on actual problems and related concerns. To do research for the sake of research itself or because a piece of laboratory equipment is idle is simply not justifiable in our opinion. There are simply too many meaningful field problems to be solved. Projects we envision to be ongoing or for the future are as follows;

- long-term field behavior of liner and cover systems,
- long-term field behavior of filtration and drainage systems,
- long-term field behavior of exposed geosynthetics,
- evaluation of long-term behavior of various infills within GCL's
- laboratory based lifetime prediction of exposed geosynthetics,
- evaluation of additive behavior (primarily antioxidants) in various geosynthetic material formulations
- evaluation of plasticizer and/or filler behavior in various geosynthetic material formulations
- evaluation of the use of recycled plastic in noncritical geosynthetic applications
- forensic analyses of all types of geosynthetic and geosynthetic-related system failures,
- effect of different alkalinity and oxidation levels on long-term behavior of geosynthetic materials,
- ongoing development and publication of GRI standards, test methods, guides, practices and specifications,
- development and initial test screening for new products developed by member organizations,
- developing data bases of inadequately performing geosynthetics and geosynthetic related systems, and
- other tasks and projects as suggested by the GSI member organizations.

4.2 Future Information Activities

Some commentary on the information value of conferences is in order. In the past, such conferences have been of major benefit for geosynthetics (and all other areas as well) in providing technical information, exhibits, networking among individuals, and opportunities for meetings of all types. Yet current economic and time constraints appear to be working against this mode of activity. Increased travel and lodging costs, high conferences and exhibit fees, solicitation of quality papers, time away from work, time away from family, etc., etc. all appear to be stressing the generic conference-type of activity. If this is a somewhat accurate

perspective, then what is available (now, or in the future) to provide a replacement for these traditional conferences?

Clearly, teleconferencing, and as an extension video teleconferencing, is how multi-national corporations are currently operating. This can be formatted for specific topics of technical orientation and even extended to business topics as well.

Somewhat related are company websites which are information-related vehicles that have also obviated print copy of brochures, leaflets, hand-outs, and related hard copy documents. Their ease of immediate updating is a tremendous asset. This trend will obviously continue and will (hopefully) be made more user-friendly and appealing. IT-people will very likely facilitate this in the near future.

The future status of technical articles of all types (including geosynthetics) is “dicey”. Clearly, hard copy is being greatly diminished. For example, the universally used and valued Journal of Mathematics by Elsevier Publishing Company costs university libraries \$23,000 per year! The geosynthetics industry currently has two excellent journals, one of which is completely electronic and the other moving in this direction. A users search for a particular article, however, is only as good as the keyword search engine can provide. That said, online reading (and understanding) of technical papers is, at the best, unwieldy in its reading and particularly its comprehension. However, there is simply no turning back in this regard.

This trend is now unnervingly moving into complete textbooks! The two volume sixth edition of “*Designing With Geosynthetics*” is now available as an e-book. It costs a paltry \$3.70 per volume (\$7.40 total). Incidentally, the previous 5th edition sells for \$300! Yet, to scroll from the index through the two volume 915-page book is tedious to say the least. If in the future, some voice command should be able to lead one directly to, for example, “axi-symmetric tension results of geogrids”, it would be a major breakthrough. Perhaps in the future?

4.3 Future Education Activities

Obviously we will continue to develop and provide power point presentations on all aspects of geosynthetics and geosynthetic related systems. Directly related is the offering of webinars which has just recently been started. We see a real future in this regard, not only for the education value, but also for the necessity of maintaining professional registration. While our offerings are currently on behalf of ASCE we envision many other possible hosts, IGS, NAGS, IFAI, GMA, ISSMGE, ASTM, ISO, etc. While interaction is not presently available, webinars are indeed cost-effective educational vehicles. In the future, however, an interaction feature will no doubt be available and perhaps even video.

This interactive feature will then allow our present one-day courses to be beamed live from GSI including laboratory demonstrations and actual test-by-test training. In this same regard, it is certainly possible to have every geosynthetic test method to be put on dedicated section of our website so as to illustrate proper laboratory procedures and training for laboratory technicians.

The national educational trend of distance learning is presently proliferating at a tremendous rate within all universities. Complete degree-granting curricula can be accessed and obtained on-line without ever going to the university campus, per se. This type of educational outreach is considered to be sufficient adaptable to present a geosynthetics course and it is only a matter of time for its development and implementation. In this regard, initial discussions are ongoing.

4.4 Future Accreditation Activities

The currently laboratory accreditation program of the institute has been extremely successful (thanks to George Koerner and the associated laboratories), but why should GSI stop at laboratory accreditation? Various segments of the geosynthetics industry which might be candidates for future accreditation are the following;

- manufacturing companies and technicians (currently provided by ISO 9000 or 14,000)
- installation companies and technicians (currently provided by the IAGI organization)
- design organizations (devoid of anything except the designers professional integrity)

This last item has been often requested in the past. Since so few civil engineering graduates have had any exposure to geosynthetics they are essentially all novices to the field. Note that there are 10,000 civil engineering graduates in America each year and like amount worldwide. Their lack of insight into the nuances of different geosynthetics and how they function can lead to naive and indeed dangerous designs, plans and specifications. GSI has often been challenged to develop a program of accrediting design consultants who are generating geosynthetic-related plans and specifications. By virtue of an interview and examination a professional engineering designation in “geosynthetic engineering” could be developed and implemented.

In a similar regard, we hope that the member organizations confide in us to the extent of peer-review of their information. Of course, this aspect of peer-review has been ongoing for project plans and specifications of many projects in the past. We hope this continues into the future. It is often surprising how a different set of eyes can pick out items which might become problematic or even disastrous. Of course this requires both confidence in us and rapid response. The institute will continue to provide such service as requested of its members.

4.5 Future certification activities

To “accredit” is one thing, to “certify” is quite another. At the least, certification implies complete compliance to what is claimed and, as such, carries both insurance and legal implications. In this regard, to certify products, designs, installations, etc., is beyond the institutional or financial capabilities of GSI.

On the other hand, to certify others to properly implement specific activities of their doing is felt to be reasonable. In this regard, two current GSI certification programs are ongoing and felt to serve a vital need; namely,

- inspectors certification for installation of geosynthetic and compacted clay liners for waste containment systems, and
- inspectors certification of geosynthetic reinforced mechanically stabilized earth walls, berms and slopes.

Other similar certification programs that could be developed in the future would focus on “waterproofing of hydraulic systems”, “geosynthetics in mining and minerals extraction technologies”, “geosynthetics in aquaculture and agriculture applications”, “geosynthetics in radioactive materials encapsulation”, and related (somewhat futuristic) applications.

4.6 Summary

Looking to the future, we hope that GSI is appropriately positioned for expansion and integration into various diverse activities. Not only are the materials themselves capable of transition and modification, but the systems utilization has the utmost flexibility to be directed toward new and challenging applications. As such, our present configuration seems to be flexible enough to provide a pathway into the future as is illustrated on Figure 9 following.

ACKNOWLEDGEMENTS

We sincerely thank all of our sponsoring organizations. Without them, GSI simply could never have happened nor prospered in the positive manner that it has done over these initial 25-years. This paper is a description of the activity that has been ongoing at the institute during this time period. The current GSI member organizations and their contact members are on the institute website at www.geosynthetic-institute.org. Board of Director members are identified accordingly.

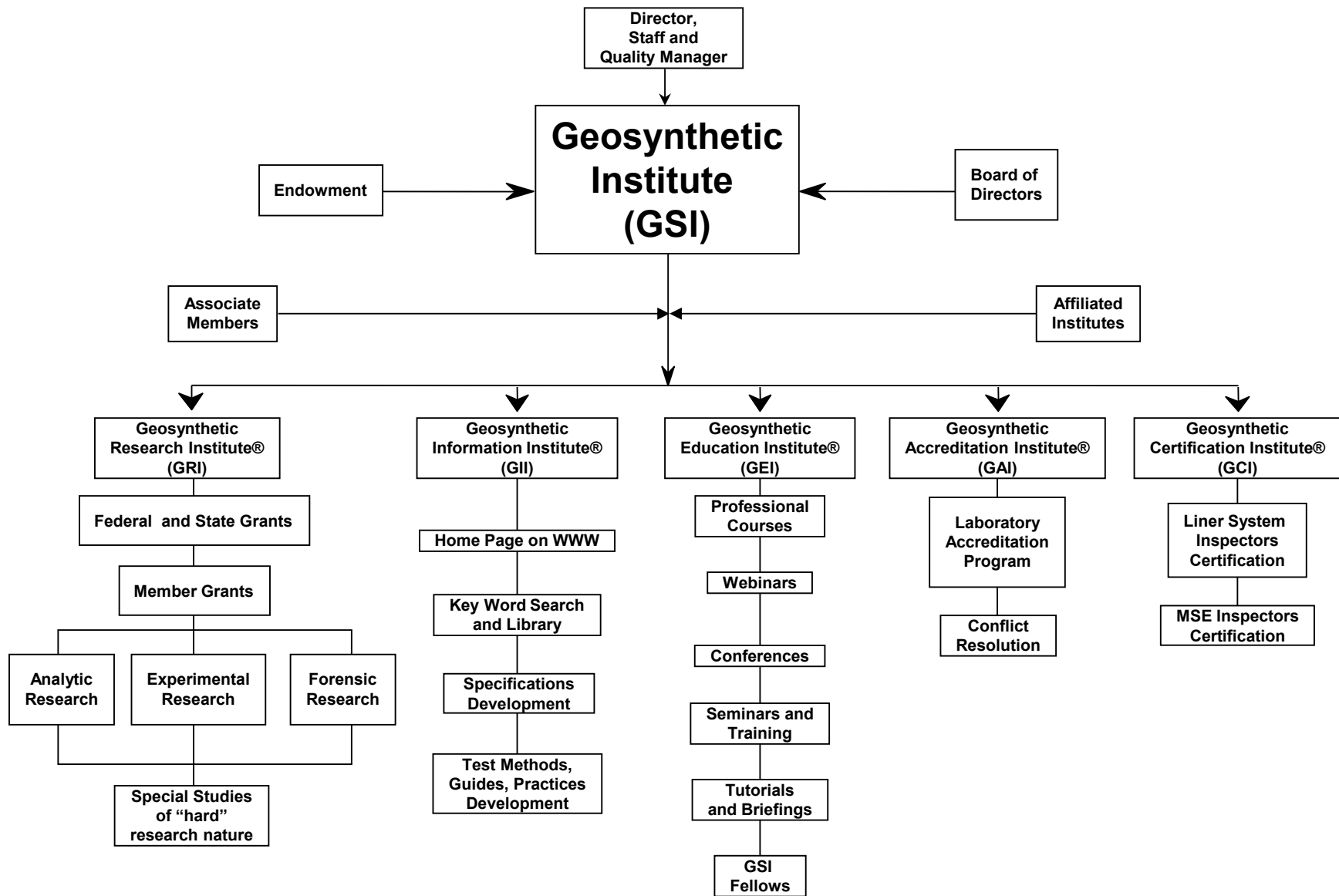


Figure 9 – Current structure of GSI with its operational capabilities

A Comparison of Landfill Closure Systems

David Beben, P.E., Project Engineer, HDR Engineering Inc., david.beben@hdrinc.com
Kanishka Perera, Ph.D., P.E., Project Manager, HDR Engineering Inc., kanishka.perera@hdrinc.com
Mark Roberts, P.E., Vice President, HDR Engineering Inc., mark.roberts@hdrinc.com

ABSTRACT

Each year thousands of acres of municipal solid waste (MSW) landfills are capped with a traditional USEPA Subtitle D landfill prescribed cover system comprised of a geomembrane liner, drainage layer and a protective and ballasting soil cover layer overlain with grass. However, alternatives to the traditional soil/geomembrane final cover are currently being designed, permitted and installed around the United States due to superior environmental performance, increased stability, secondary use applications and decreased cost. These innovative alternative cover systems also can offer lower construction cost, lower post-closure maintenance, ease of inspection, verification of performance, and low erosion. These aspects are compared and contrasted for three alternative MSW landfill cover systems: evapotranspiration (ET) covers, synthetic turf geomembrane covers and exposed geomembrane covers (EGCs). These cover systems are evaluated on the criteria of ease of permitting, infiltration rate, longevity, aesthetics, environmental impacts, regional suitability, construction and post-closure care costs, compatibility with on-site systems, and proposed end uses. HDR Engineering has utilized a performance-based approach to landfill cover system design and continues to successfully implement it for differing state regulatory frameworks in lieu of the Subtitle D-prescribed system. Using this approach to the USEPA's thirty-year post closure care period enables the regulatory community to rely less on prescriptive closures with a diminishing post-closure care fund over time to that of a performance based cap with sufficient funds available for repairs and even replacement based either on savings and/or secondary use revenue generation.

1. INTRODUCTION

Final cover systems are an essential component of a closed landfill's long-term environmental controls. Subtitle D of the Resource Conservation and Recovery Act requires that the final cover system must have an infiltration, or barrier, layer with a hydraulic conductivity equal to, or less than, that of the bottom liner system, a protective and ballasting layer comprised of 18-inches of soil fill to minimize infiltration, overlain with six-inches of topsoil to sustain vegetation, and a healthy stand of grass to reduce erosion. However, the USEPA also establishes in 62 FR 40710 that state administrators have the regulatory authority to approve alternative final cover designs that can meet or exceed specific engineering performance characteristics of the prescribed system. It explains that an alternative to the final cover can be approved if the permittee can show that the permeability of the infiltration layer can be met by an equivalent reduction in infiltration, and the protective cover layer can be replaced with a system that can be shown to reduce erosion and continues to protect the long-term performance of the infiltration layer. In modern landfill systems the infiltration layer is typically a geomembrane, a geosynthetic clay liner or a clay layer, and the protective cover layer often consists of soil and an underlying lateral drainage medium such as a geonet/geotextile or sand.

Landfill owners have researched alternatives to the prescriptive final cover system for a several reasons. One is that imported soil can be costly when a suitable soil source is not located near the project site. Second, the soil/geomembrane system can be prone to veneer-type failures, where the final cover system components slide down the sideslope. Final cover systems are particularly prone to veneer failures if the underlying drainage component between the protective cover and the impermeable geomembrane does not perform as designed for one or a combination of performance complications associated with Subtitle D closures. Third, the installation of a cover system cause greenhouse gas emissions, particularly from the soil borrow process, hauling vehicles and equipment pushing soil upslope at steep 4:1 or 3:1 slopes. Lastly, the maintenance operations during the post-closure care period of a Subtitle D prescribed cap typically require ongoing turf and soil maintenance for the entire system to perform as designed consisting of frequent mowing, water, fertilizer, top soil replacement, erosion control, and sedimentation basin maintenance.

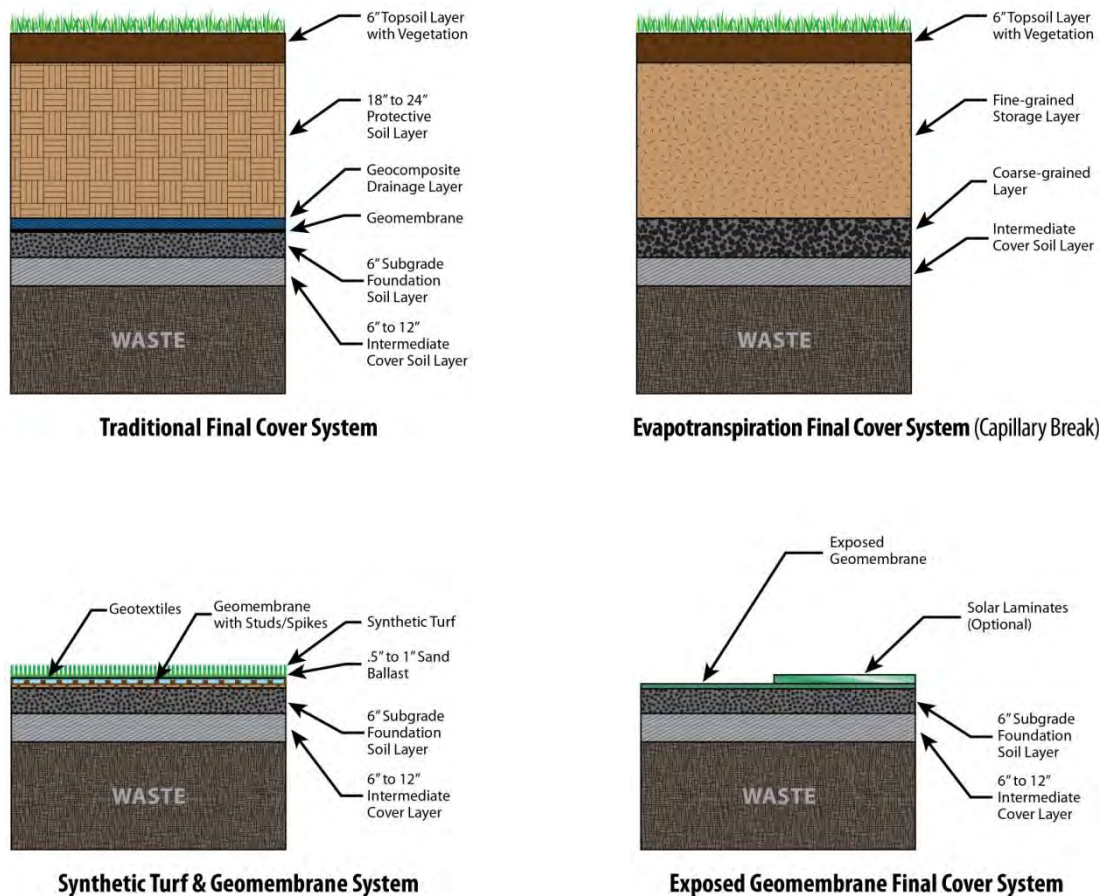


Figure 1 Final Cover System Profiles

2. EVAPOTRANSPIRATION COVER

Evapotranspiration (ET) cover systems, also called water balance or monolithic covers, are designed to minimize infiltration of precipitation into waste by increasing surface runoff, soil moisture storage and evapotranspiration. The ET cover is comprised of a two to four foot soil cap supporting local plant species. Unlike the other alternative final cover options, the ET cover does not contain geosynthetics and is the only alternative considered for this analysis with an entirely vegetated cover. Additionally, ET covers rely on the water removal capabilities of uptake of moisture via plant transpiration and evaporation.

An ET cover is the most prevalent alternative to the Subtitle D landfill final cover system in western states with dry climates with low rainfall amounts. Texas, for instance, has several constructed ET cover systems. The Texas Commission of Environmental Quality (TCEQ) has published a guidance document (RG-494) which specifies less than 4 mm of percolation into the waste mass per year during the 30-year period of record. Currently, TCEQ plans to monitor three test site projects near Dallas, San Antonio and Houston to determine the appropriate approval mechanisms for ET covers. California has dozens of evapotranspiration covers in arid and semiarid regions of the state.

The following is listing of advantages and disadvantages of the ET cover compared with a prescribed Subtitle D cap and the other two alternate cover systems:

Advantages

- No geosynthetics are required.
- Landfill gas venting systems may not be necessary.
- This option has the lowest stormwater water runoff volume of the three alternatives.
- A low maintenance vegetated cover system that can be integrated with surrounding natural landscape.

Disadvantages

- Secondary uses may be limited such as solar power which would require rigid solar panels and frames, and concrete footings/slabs which could limit the ET cover performance features by affecting its evapotranspiration and water storage properties.
- Vegetation will experience an establishment period which can last several months to years and includes high landscaping maintenance activities that could include intense watering, fertilizer, erosion control, and re-seeding/planting . The cover system will be vulnerable to wind and rain erosion during this period.
- The post-closure care costs are higher than the synthetic turf and EGC alternatives due to the continued cover maintenance.
- Fertilizers and amendments are short-lived and will likely require re-applications.
- Significant soil quantities are required..
- Greenhouse gas emissions are the highest of the three alternative options.
- Unanticipated localized waste exposure is most likely to occur of the three alternative options.

3. SYNTHETIC TURF AND GEOMEMBRANE COVER SYSTEM

A recent addition to innovative final cover systems for landfills is synthetic turf which utilizes a studded LLDPE or HDPE geomembrane in conjunction with synthetic turf attached to woven geotextile. The synthetic turf system provides low maintenance costs and protection to the final cover geomembrane and underlying geotextile. The synthetic turf is typically green but can be manufactured in other colors. In contrast with an EGC, the synthetic turf does not require horizontal and vertical anchoring at discrete intervals and instead sand ballast is provided. The ballast is typically comprised of 1/2 to 1 inch thick sand layer (D_{50} approximately 0.6 mm) and assists with protection from long-term UV exposure, shear stress from light equipment and wind uplift. Synthetic turf was first installed as a landfill final cover system in 2008 in Louisiana. Since then, the system has been permitted and installed at landfills in Texas, California, Missouri, Pennsylvania, Florida and Georgia.

The following is listing of advantages and disadvantages of the ET cover compared with a prescribed Subtitle D cap and the other two alternate cover systems:

Advantages

- Less geosynthetic anchoring and/or pinning is required than typical exposed geomembrane cap (EGC) designs.
- A solar array comprised of rigid-type panels with concrete foundations is being installed in California.
- Post-closure maintenance costs (erosion, mowing, and fertilizer) are less than a Subtitle D or ET cover system.
- High interface friction and low chance for veneer stability issues when compared to a Subtitle D cover system.
- Less UV exposure of the geomembrane when compared to the EGC. Weatherometer ASTM G147(02) tests performed on the exposed portion of the yarn shows less than 10 percent tensile strength loss after 20 years. Additional UV exposure tests on the synthetics turf are ongoing.
- Conforms to various slopes and transitions and performs better than Subtitle D or ET on steep slopes
- Pro-rated 20+-year material warranty available

Disadvantages

- More stormwater runoff when compared to a Subtitle D or ET cover system.
- Erosion of ballast sand by wind and rain could make the cover system vulnerable against wind uplift under extreme conditions. Limited sand ballast and turf repair is expected in the post-closure period.
- Material creep could occur appearing like "loose carpet" and requiring specialized repairs
- Synthetic turf is currently a patented technology and therefore not competitively priced.
- Emergency gas vents in addition to passive vents or active wells are recommended.
- Sand ballast may be expensive if not locally available.
- Not yet authorized as a landfill final closure in most states.
- Unable to confirm the integrity of the barrier layer (geomembrane) with visual inspections.
- Slippery on steep slopes

4. EXPOSED GEOMEMBRANE COVER (EGC)

An exposed geomembrane cover system utilizes a single geomembrane layer over a prepared earthen subgrade. These cover systems contain no soil or vegetation and thus have a cost savings at closure and during the post-closure period of the landfill. EGC's have been utilized in the United States using HDPE, LLDPE, scrim-reinforced polypropylene, EPDM and other proprietary resin formulas for geomembranes. The EGC system does not have the potential for veneer slope-type failures (i.e. sliding of cover components) that can occur on a Subtitle D or synthetic turf cover systems. The EGC is anchored into the landfill utilizing trenches and/or pins designed to counter balance wind uplift forces.

EGC's have been permitted and installed as landfill closures in Louisiana, Florida, Delaware, Georgia, New York and Texas. The performance criteria of exposed geomembrane caps include UV resistance, seamability, seam durability, chemical resistance, puncture resistance, stress-strain characteristics, and interface friction. UV degradation has been noted as the most important property in exposed conditions. A multitude of UV exposure tests have been performed on geomembranes and the body of work and example projects are more extensive than synthetic turf. In research described in GRI's White Paper #6, HDPE geomembrane that has been exposed to accelerated aging via UV light has performed well. The study has estimated an HDPE lifetime of 36 years and testing at 70°C (158°F) is still ongoing. In other research, standard oxidative induction time and high pressure oxidative induction time tests have been performed to determine the antioxidant properties of the exposed HDPE and LLDPE geomembrane.

LLDPE rely on antioxidants (carbon black and other stabilizers) for their resistance to UV radiation. The nature of the LLDPE resin and its formulation is very similar to HDPE. Because LLDPE has a lower density, hence lower crystallinity, than HDPE, it has the effect of allowing oxygen to diffuse into the polymer structure more quickly and therefore reduce its lifetime when compared to HDPE (Koerner et. al, 2005). Past experience with exposed geomembranes in other industries and technical research has shown that polyethylene geomembranes that are manufactured with a sufficient level of stabilizers and antioxidants have excellent UV resistance and lifetimes much greater than the industry-standard time span of 20 years.

The following is a listing of advantages and disadvantages of the EGC cover compared with a prescribed Subtitle D cap and the other two alternate cover systems

Advantages

- Flexible solar panel arrays have been installed and are currently producing power. Fixed-frame solar arrays are possible similar to the synthetic turf solar panels.
- Accelerated aging tests indicate that HDPE manufactured per GRI-GM13 has a predicted lifetime greater than 36 years. GSE recently introduced a line of high-performance geomembranes that have superior endurance properties than typical 60-mil HDPE.
- HDPE geomembrane cost is competitively priced (based on resin prices) and commercially available.
- Post-closure costs (erosion, mowing, and fertilizer) are less than a Subtitle D or ET cover.
- Access to the landfill beneath the EGC is less cumbersome than the synthetic turf or Subtitle D cover systems.
- No veneer slope stability issues.
- Can confirm geomembrane integrity and make repairs relatively easily compared to synthetic turf or Subtitle D caps in which the barrier layer integrity cannot be confirmed and inspecting and repairing is difficult.
- UV exposure tests are indicating life-spans of greater than the standard 30-year Subtitle D post-closure care period.
- Not susceptible to shifting soils or erosion for long-term performance of ballast conditions or infiltration conditions
- Pro-rated 20+year material warranty available

Disadvantages

- Anchoring into the soil/waste is required increasing the capital cost and construction time. An alternative to anchor trenches are tension pins which are installed at discrete horizontal intervals and vertical depths. The EGC is connected to the pins to provide required counter balancing forces during wind uplift.
- More vulnerable to damage by hail, wind and other externalities than the other alternatives.
- Not yet authorized as a landfill final closure in most states.
- The most UV exposure to the geomembrane compared to other alternative final cover options.
- More stormwater runoff when compared to a Subtitle D or ET cover system.
- One landfill EGC final cover has been permitted and constructed in Louisiana. Regulatory approval for the EGC as final cover is pending in Texas and Georgia.
- Emergency gas vents in addition to passive vents or active wells are recommended similar to synthetic turf.

5. COST COMPARISON OF FINAL COVER SYSTEM ALTERNATIVES

Table 1 summarizes the costs of an example subject landfill located in West Texas – a region with arid climate conditions and in a state which has approved alternate final cover systems. This West Texas landfill has compared its currently permitted final cover system with each of the three alternatives presented above. These costs do not include engineering, permitting, quality assurance and certification that will occur during all installations. Additionally, the costs do not incorporate post-closure water quality monitoring, leachate management and general professional services.

Table 1. Budgetary Cost Comparison of Final Cover System Alternatives

	Permitted Subtitle D Cover System	Evapotrans- piration Cover (2.5-ft. Thick)	Closure Turf [®]	EGC
Closure Construction				
Construction Costs (\$/acre)	\$160,000 ¹	\$91,300 ¹	\$93,502 ²	\$75,000 ^{3,1}
Total Construction Cost (25- acre closure)	\$4,000,000	\$2,282,500	\$2,337,552	\$1,875,000
Post-Closure Final Cover Maintenance				
Vegetation Maintenance including fertilizer, mulch application, watering (\$/acre)	---	\$400	---	---
Stormwater System and Erosion Maintenance (\$/acre)	\$350	\$300	\$70	---
Geomembrane Maintenance (\$/acre)	\$25	---	\$100	\$150
General Inspections (\$/acre)	\$50	\$50	\$50	\$50
Total Annual Post-Closure Care (25-acre closure)	\$10,625	\$18,750	\$5,500	\$5,000
Total 30-Year Post-Closure Care (25-acre closure)	\$318,750	\$562,500	\$165,000	\$150,000

Notes:

1. Costs for permitted closure, EGC and ET cover systems are based on a unit cost of \$18 per cubic yard based on soils from an off-site borrow source approximately one mile from the site. Costs for gas vents (permit system), maintenance period (ET cover) and stormwater control are included.
2. Closure Turf construction cost is based on manufacturer's budgetary cost of \$2/square foot. Additional costs for gas vents, ballast sand and stormwater control are included the unit price.
3. EGC construction cost is based on a GSE's budgetary cost of \$0.55/square foot for green GSE High Performance Geomembrane. Additional cost for anchor trenches, gas vents, backfill soil and stormwater control are included the unit price.
4. Permitted closure system cost is based on geomembrane and geocomposite at \$0.50/sf and 0.55/sf, respectively.

6. SOLAR POWER GENERATION POTENTIAL

The development of solar power generating arrays on closed landfill final covers is an emerging technology. By generating renewable energy on closed sites, landfill owners are reclaiming land that would otherwise have limited post-closure use. Landfills with solar generating arrays will be able to accomplish a number of goals including post-closure period cost savings, the sale of renewable energy, lowering off-site energy purchases and providing an image of sustainability. The characteristics and costs of the two types of panel systems are discussed.

6.1 Photovoltaic Laminate (PVL) Solar Panels

Photovoltaic laminate (PVL) thin-film solar panels have been used in roofing, landfill EGC's and other applications. These panels are lightweight, flexible, easy to install and do not require an expensive concrete ballasting structure. The PVL's have been formulated to be exceptionally durable by encapsulation in UV-stabilized polymers. These panels have not been installed with synthetic turf or ET cover systems. As previously mentioned, a flexible solar array was constructed at the Tessman Road Landfill in San Antonio, Texas. Other EGC projects with flexible solar laminates have been installed in the country including a 1-MW array at the Hickory Ridge MSW Landfill in Atlanta, Georgia.

Construction cost and electrical revenue from a 250-kW solar panel array are discussed. A Xunlight XR36 PVL is selected with nameplate wattage of 300 watts per panel. Therefore, an array of 860 panels will provide 250 kW of direct current power. Based on previous EGC solar designs with a gentle slope and no liner penetrations, it is estimated that this array will require a 2.5-acre area of EGC. The kilowatt hours provided to the utility grid will vary in the field due to hours of sunlight, temperature, angle to the sun, and the efficiency of the conversion from direct current to alternating

current. Given these parameters, material and installation cost of a 250-kW array encompassing a 2.5-acre area will cost over \$1.2 million, produce 341 MWh of electricity in the first year and generate approximately \$27,000 of electrical revenue in the first year, assuming \$0.08/kWh electricity buy back cost.

6.2 Monocrystalline or Polycrystalline Solar Panels

Rigid solar panels (monocrystalline or polycrystalline) are most commonly installed on shallow (<5% grade) landfill slopes. In comparison to PVL's, the rigid panel have higher UV conversion efficiency, are more competitively priced and are able to be installed at an angle which maximizes incoming solar radiation. However, they are the heaviest and require a rigid frame mounting system.

A rigid-type solar array can be installed in conjunction with synthetic turf. A 1-MW system comprised of approximately 2,000 panels will soon be installed at the Crazy Horse Landfill in Salinas, California and another large array is planned in Connecticut. The rigid solar panels will be mounted on non-penetrating concrete footings and a metal frame will interconnect the panels to provide stability. The articulated frame is designed to prevent resistance to landfill differential settlement. Rigid-type solar panels can also be installed in EGC applications with racks welded directly to the geomembrane. A racking system welded directly to an EGC is used on a steep sideslope EGC at the Biosphere project in Arizona. If traditional ballasted racks are used in which concrete footings or foundations are incorporated in concert with an EGC, then the ballasted racks will require an isolation design that allows uplift conditions to occur without impacting the solar system.

A 250-kW array of rigid solar panels was also considered for comparison to a PVL array. Based on information from a similar landfill site, a 250-kW array will require 1.5 acres of landfill space, 40% of the footprint required by PVL's. A 250-kW array size was selected for comparison since it provides a good scale-able factor for expansion. A manufacturer provided a cost of \$5 to \$6/W for construction and installation which is greater than the cost for PVL's. The installation costs for crystalline solar panels can vary significantly and prices have recently declined due to competition from Chinese solar panel manufacturers. In the report "Tracking the Sun IV" by the Berkley National Laboratory, the PVL systems were slightly less expensive for systems >100 kW; however, the authors cautioned that there was a poor sampling of PVL systems. Given these parameters, a 250 kW area encompassing an 1.5-acre area will cost over \$1.5 million, produce 371 MWh of electricity in the first year, and generate approximately \$30,000 of electrical revenue in the first year, assuming \$0.08/kWh electricity buy back cost.

6.3 Solar Array Cost Comparisons

Table 2 is a summary table of the costs for a PVL versus a rigid-panel array. These costs are budgetary estimates based on project and will need to be re-visited for the site-specific conditions. We note that solar panel manufacturers will typically provide a guarantee of power generation over 20 years; for instance, Xunlight guarantees that their PVL product will retain 80% of its power-generating capacity after 25 years.

Table 2. Budgetary Cost Comparison of Solar Power Generating Arrays

	Photovoltaic Laminates	Rigid Solar Panels
Area of Final Cover Required for 250- kW Array	2.5 acres	1.5 acres
Electrical Generation from 250-kW Array for Initial Year	341 MWh	371 MWh
Electrical Revenue for the Initial Year	\$27,000	\$30,000
Capital Cost of 250-kW Array	\$1,200,000	\$1,500,000

Notes

1. Electrical generation was determined through the National Renewable Energy Laboratory's PVWatts calculator (<http://www.nrel.gov/rredc/pvwatts/>) and assuming a 0.705 DC/AC derate factor.
2. The capital costs of 250-kW arrays were from Xunlight and Closure Turf, LLC. Additional costs were added for contingency and electrical interconnection.
3. The revenue from a 250-kW array is based on a \$0.08/kWh buy back price. This price can be increased due to incentives from the local power authority and grants.

7. CONCLUSIONS

Three innovative alternative landfill cover systems were evaluated on the basis of ease of permitting, infiltration rate, longevity, aesthetics, environmental impacts, regional suitability, construction and post-closure care costs, compatibility with on-site systems, and proposed end uses. These systems if designed and installed properly have performance equal

to or greater than a prescribed USEPA Subtitle D landfill cover system. ET cover system provides advantages in arid and semiarid regions when soil is readily available and relatively inexpensive. EGC and synthetic turf systems provide advantages in less greenhouse gas emissions during construction, little to no soil and less post-closure care maintenance. A cost comparison among the traditional prescribed Subtitle D cover system and three alternatives indicate that the Subtitle D system is the most expensive, followed by the ET cover, the synthetic turf and the EGC systems. Each of the three alternative cover systems have the capability of installing solar power generating arrays to provide the closed site with a beneficial reuse option.

REFERENCES

- Grassie, Norman and Gerald Scott. *Polymer Degradation and Stabilization*. Cambridge University Press. 1985.
- J.L. Richards and Associates, Ltd. "Trail Waste Facility Landfill Optimization/Expansion Project, EA/EPA Document Appendices M-P." March 2002.
- Koerner, Robert M. *Designing with Geosynthetics, 5th Edition*. Pearson, Prentice Hall. 2005.
- Koerner, Robert M., Y. Grace Hsuan and George R. Koerner. "Geomembrane Lifetime Prediction, Unexposed and Exposed Conditions". GRI White Paper #6, June 7, 2005, updated February 2011.
- Qian, Xuede, et. al. *Geotechnical Aspects of Landfill Design and Construction*. Prentice Hall. 2002.
- "Revisions to Criteria for Municipal Solid Waste Landfills; Final Rule and Proposed Rule," 62 Federal Register 145 (29 July 1997), pp. 40707-40713.
- Sadlier, M. and Frobel, R. "Geomembrane Properties – A Comparative Perspective", presented at the *GeoEnvironment Conference*, Melbourne, Australia, November 1997.

A Unique Camouflage Floating Cover

Andrew Mills, Layfield Environmental Systems Corp, USA, amills@layfieldgroup.com
Stephen Roades, Burke Industries Inc., USA, steveroades@burkeindustries.com
David Ott, Layfield Environmental Systems Corp, USA, dott@layfieldgroup.com

ABSTRACT

The 41-year-old Santa Ynez Reservoir in Pacific Palisades, CA was an open water reservoir until recently when the Los Angeles Department of Water and Power (LADWP) covered it to conserve water, decrease water contamination, and change from chlorine to chloramines. The reservoir is on 9 acres of land and is approximately 70 feet deep. When full it holds 117 million gallons of potable water and serves both Pacific Palisades and the Highlands. A unique aspect of this project was the requirement to develop a custom color to address the aesthetic requirements demanded by the local community. This paper outlines the development of this custom colored cover material and the details of manufacture, fabrication, and installation.

1. INTRODUCTION

1.1 Santa Ynez Reservoir

The Santa Ynez Reservoir is tucked between two mountains in the Topanga State Park just north of Santa Monica, CA. The reservoir is overlooked by thousands of homeowners in an upscale neighborhood. The surrounding community was very concerned with the change in the appearance of the reservoir as it is a visual focal point for most of them.

To meet the stringent visual requirements set forth by the community, the LADWP worked with the material supplier and the installer to find a custom material color that would blend in with the surroundings. The material supplier proposed the use of a Chlorosulphonated Polyethylene (CSPE) cover material in a special mottled green camouflage color. They produced several large samples in different color combinations. After a thorough review by the community council and the local homeowners a green/black camouflage color was chosen.



Figure 1: The completed reservoir blends nicely with its surroundings.

The Reservoir was completed in time to bring it back online for Southern California's fire season. The community expressed their approval of the final appearance of the project, and LADWP added another covered potable water reservoir to their portfolio.

1.2 Background

The approval process for this project started in 2002 with a floating cover originally proposed for installation in 2006. The upgrade to the reservoir was part of a response to the US Environmental Protection Agency's (USEPA) Stage 2 Disinfectants and Disinfection Byproducts Rule (S2DBPR 2006) and the Long Term 2 Enhanced Surface Water Treatment Rule (LT2ESWTR 2006). These two rules were delayed in their release until 2006, which in turn delayed the Santa Ynez project.

LADWP chose to address the S2DBPR rule by switching from chlorine disinfectant to a chloramine disinfectant. This change reduced undesirable disinfection by-products (DBPs). DBPs are also reduced by adding an opaque floating cover as sunlight can react with disinfection chemicals to form undesirable by-products. A floating cover also addressed the LT2ESWTR surface treatment rule as the cover effectively isolates the stored water from surface run-off and rainwater.

With the choice to add a floating cover made, the next steps were to choose a material and to obtain approval from the local community.

2. COVER SELECTION

2.1 Material Selection

Chlorosulphonated Polyethylene (CSPE) was originally chosen as the cover material. CSPE has been used successfully in municipal reservoir service for other covers in California and has shown excellent longevity and performance. CSPE was also available with a 30-year warranty against normal weathering. Finally, CSPE was available in a variety of colors, all with extended weathering resistance. This selection of colors would be the key to moving this project forward.

Geomembrane and floating cover materials are not known for their wide selection of colors. In order to achieve long term UV protection the standard color is usually black. Black pigments - the most common being carbon black - provide excellent UV protection to thermoplastic geomembrane and floating cover materials. As soon as you move away from black the UV resistance falls off rapidly. CSPE is unusual in that it is a thermoplastic at the time of manufacture but then crosslinks in service to become a thermoset rubber product. As the material crosslinks it becomes more resistant to chemical attack and more resistant to UV degradation. This means that CSPE can be stabilized in a range of colors much more easily than regular thermoplastic geomembrane and floating cover materials. The manufacturer of the CSPE had developed a wide range of colors in the roofing industry, and this color palette was brought in to satisfy the aesthetics of this job.

2.2 Aesthetics

For 41 years the reservoir provided a visual focal point in the hills across from the Pacific Palisades community. The community association was very sensitive to the reservoir's appearance and had participated in a number of aesthetic upgrades over the years. Some of these aesthetic upgrades included specific plantings above the reservoir and in the dam face to make the area appear more natural. The color of the service road had also been chosen to better blend with the surroundings.



Figure 2 and 3: Naturalized concrete slope above the reservoir. Construction (left) and finished slope (right).

One of the most unique aesthetic features was a protected slope area above the reservoir. Surface run-off from rainstorms and rainwater infiltrating under the graded slope had washed out a section of the slope. The damaged section of the slope was replaced with a compacted soil-cement fill. PVC pipe sub-drains were installed to remove infiltrating rainwater and concrete surface drains for run-off. Although the soil-cement slope face was effective, it did not meet with

the aesthetic requirements of the community association. The solution was to create a rockscape that closely matched the surrounding area (Figures 2 and 3). The construction of this rockscape occurred at the same time as the new floating cover installation.

2.3 Color Selection

Choosing a cover with the active participation of the local community association was a very different experience. The first success was identifying that a cover could be used at all. It is a credit to LADWP staff that they were able to make the case for a floating cover in the first place. The next step then was to choose a color.

Initially the CSPE manufacturer sent a selection of colors for review. From these initial color swatches a selection was chosen. From these initial colors selections 10-ft by 20-ft samples were prepared and arrayed on the slope behind the reservoir for the community to observe and rate. In reviewing these samples it was felt that a multi-color arrangement would be preferable to a solid color and that a dark green with a mottled appearance might work.

2.4 Multi-Color Membrane

The CSPE manufacturer had available a rubber calendaring operation that essentially allowed them to “hand-make” specific colors and materials. By adding pieces of different material colors into the rubber at the last stage of mixing they were able to create a material with random streaks of color in an overall uniform shade. This is very similar to the multi-color patterns seen in resilient vinyl flooring. If the color is added early in the mixing stages it will be uniform; by adding different colors late in the mixing stages a series of streaks can be prepared.

Samples of the multi-color material were prepared for the community association and finally, after many samples and extensive consultation, a dark green material with black streaks was chosen. In the July/August 2011 issue of Land and Water the manufacture was quoted as saying, “The floating cover has been constructed of CSPE geomembrane panels that have been produced with a one-of-a-kind mix of black and green coloring in each panel. The color mix creates a large-scale camouflage that helps the entire reservoir mimic the changing shades of the hills and vegetation.” (Roades, 2011)

3. CONSTRUCTION

After draining the reservoir between October 2009 and May 2010, the old inlet/outlet tower and pipeline were demolished, and the asphalt concrete liner, which had served the reservoir well, was repaved (Figure 4 and 5). New pipelines and appurtenances were then installed and the facility filled. Then, in October 2010 the reservoir was drained again to enable the last phase of reconstruction. This included installation of the floating cover (work which began in January 2011).

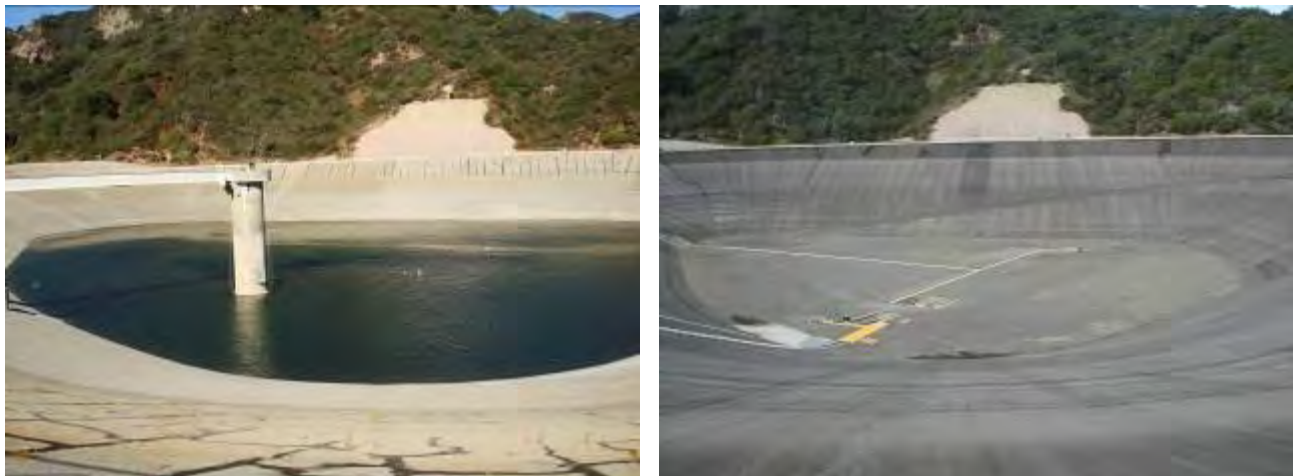


Figure 4 and 5: Original reservoir (left) and after removal of tower and new asphalt concrete lining (right). Note the original concrete faced slope at back.

4. COVER MANUFACTURE

The cover was truly a hand-crafted one-of-a-kind material. Manufacture starts with blending of the ingredients. These ingredients travel through a number of blenders until they are fully dispersed into a batch of material that has the approximate consistency of cookie dough. About 50 lbs of this rubber dough are put onto a two-roll mill where they are heated and blended into a soft semi-molten state. An operator manipulates the rubber on the mill for a pre-set period, folding the material back and forth, until the material is blended and the colors are smooth and well-dispersed. Then the rubber batch is dropped onto a table and taken to the next two-roll mill. This second mill makes sure that all the materials are up to temperature before being fed into the calendar.

In the manufacture of this unique cover material 50 lbs batches of dark green material were laid out onto a table after the first mill, and three pieces of black were placed onto the rough sheet. This was then rolled back up and then transferred



Figure 6 and 7: Feeding CSPE into the two-roll mills. Mill #1 on left, Mill #2 on right. Tan CSPE shown.

to the second mill. On the second mill the operator did not blend the material but let the black form streaks in the surface. When the streaks had reached the right consistency the rubber batch was dropped onto a table and taken to the calendar to be fed into the machine.

The calendar squeezes the rubber batch into a thin film and then presses it onto the support fabric. The 45-mil material made for this project consisted of a 17-mil coating on both sides of a support fabric. The final product maintained a consistent color throughout the project. If you look at the pictures of the reservoir you can see that the color did not vary considerably from batch to batch.

5. COVER FABRICATION

The custom material was shipped to the fabricator's facilities in El Cajon, California, which is near San Diego. It is up to the fabricator/installer to create the drawings and layout details that will convert the designer's intent into a finished floating cover.

There are two guidelines that are followed for the design of floating covers in California. The first is M25 Floating cover guideline (AWWA 2000). The second is the CA/NV Floating Cover Guideline (AWWA 1999). The fabricator/installer prepared the cover drawings for this project as seen in Figure 11.

Because this reservoir was lined with an asphalt concrete liner, a chafer strip was used to prevent wear on the underside of the cover. The chafer strip is made from the same material as the floating cover and extends about 2/3 of the way down the slope. As the cover moves up and down in response to water level



Figure 8: Installing a 35-ft-wide fabricated panel.

changes, the chafer strip prevents wear against the asphalt concrete.

The fabrication step allows specialty materials, such as this specially colored material, to be made into large panels, thus reducing the need for field welds. (Prefabricated panels are prepared in the controlled conditions of the factory, which eliminates weather risk on fabrication seams. By using prefabricated cover panels, field installation times are reduced and overall seam quality improves.)

This fabricator has a unique ability to make prefabricated panels up to 36 ft wide without folds using a specially designed 36-ft-wide winder. Eliminating folds in prefabricated panels reduces wrinkling for a smoother appearance. The chafer strip panels were folded and fabricated into smaller bundles; however, the cover panels used the wide roll technique to make panels 35 ft wide.

Prefabrication welding was accomplished using hot wedge welders. The welders are uniquely set up with 3-inch-wide wedges and adjusted so that there is no flap left on either the top or the bottom of the seam. Welding the seam down completely on both sides of the weld makes it easier to clean the cover when it is in service.

Panels were prefabricated according to a predetermined plan. Each fabricated panel was wrapped in a protective wrapper and numbered to match the installation plan.

6. COVER INSTALLATION

Cover layout is detailed in Figure 11. The cover design is a defined-sump style that follows the design outlined in US patent 3,991,900. In this design a series of floats and weights are attached to the surface of the cover and create channels to collect rainwater. Pumps in these channels remove the rainwater and pump it off the cover.

Cover installation began in January 2011 and was completed later that year. The first component installed was the chafer strip. This was placed on the asphalt liner and secured to the top of the slope using a small concrete wall and batten bars. Sand tubes and sand bags held the chafer strip in place against wind uplift until the cover was placed on top.

The cover material was then placed on top of the chafer strip and extended across the bottom of the reservoir. The cover material must be completely placed to reduce the risk of rain delays before proceeding with detail work. Once the cover material is placed and tested the detail work can begin. Details included the floats and weights that create the defined sumps, as well as hatches and vacuum relief vents.



Figure 9 and 10: Chafer strip installation (left). Cover panels being installed (right).

A defined sump floating cover uses a series of floats and weights to create channels in the surface so that water can be removed. The floats are made from expanded polyethylene foam. This foam is then protected from UV damage by wrapping with the same material as the floating cover. These float covers are laid out and welded to the surface of the cover after the cover is completed and tested. The floats are typically 9 ft long, 6" thick, and 12" wide on the floor and 3' long x 6" thick x 12" wide on the slopes.

The weights in the bottom of the sump channels are sand tubes. A doubled section of CSPE material is first welded down the middle of the channels where the sand tube will rest in service. This is the highest wear area of a floating cover. This is where dirt and debris will accumulate and it needs to be protected. Once this wear strip is placed a series of straps are welded to the cover; these hold the sand tubes in place. The sand tubes are 5 ft long and are 5 inches in diameter on the floor and 3 ft long by 5 inches in diameter on the slopes. The sand tubes are made from the same material as the floating cover. They are also perforated so that there is no air in the tube that will work against the weight of the sand.

The layout of the floats and weights is adjusted based on the final layout of the pond. Because the seams in the final cover may vary slightly from their planned positions on the drawings, the final layout of floats and weights must be adjusted to the as-built dimensions of the cover.

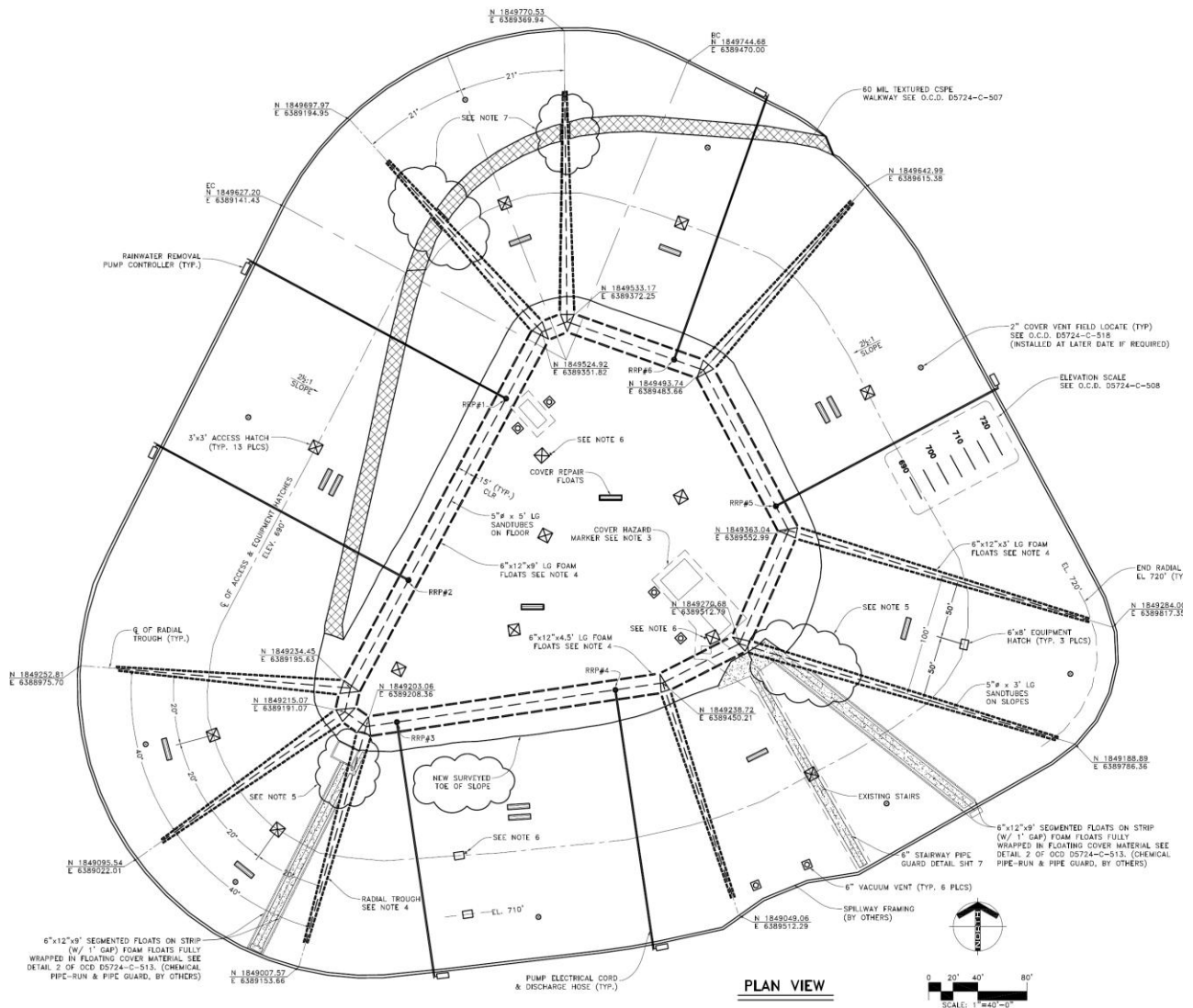


Figure 11: Layout design for the defined-sump floating cover.

The distance between float channels controls channel depths when the reservoir is full. On Figure 11 the distance between channels can be seen to be wider at the bottom of the reservoir and then tapering to the top of the reservoir. There is less slack to account for at the top of the reservoir so the channels are not as deep. This design has been worked out by experience and results in a smooth, flat cover at all operating levels.

Finally, there is an overflow spillway on the top of the reservoir that protects the cover against inadvertent overflows. This spillway was originally designed to have a stainless steel flap that would move out of the way during an overflow. The design was modified and the overflow flap constructed from CSPE material and sand tubes to minimize flap weight and

provide an efficient operation. A stainless steel frame was constructed and set into the concrete spillway. The chafer strip was then connected to the inside bottom of the frame while the cover was brought up over the frame and draped down the back. The draped section is then weighted with sand tubes to prevent the flap from opening unless there is an overflow.



Figure 12: View of the overflow swale.

7. CONCLUSION

The Santa Ynez floating cover project was an example of a standard cover that required non-standard attention to aesthetics and color. The final project is an attractive part of the local landscape while providing additional protection to drinking water in the area. The ability to select a “handmade” color on this project helped the local water department get the buy-in from the community they needed so that they could go ahead with the functional improvements needed. CSPE materials are one of the few geosynthetic barrier materials used for floating covers that has a broad color palette while maintaining long term UV resistance.

ACKNOWLEDGEMENTS

We would like to acknowledge the following organizations and their participation in this project:

Los Angeles Department of Water and Power
Burke Industries Inc.
Layfield Environmental Systems Corp.



Figure 13: The completed project filled and in service. Note the road colors, rock texture above reservoir, plantings on the slopes below the reservoir, and the mottled color of the floating cover.

REFERENCES

- Burke, N. Kutnewsky, D. Price, V. Gerber, D. (1976). Reservoir cover and canalizing means, US Patent #3,991,900, US Patent and Trademark Office, Alexandria, VA, USA.
- Roades, S. (2011). Under Cover Operations, *Land and Water July/Aug Issue*, Land and Water Inc., Fort Dodge, USA
- Flexible Membrane Covers and Linings for Potable Water Reservoirs (2000), American Water and Waste Water Association, Denver CO, USA.
- Reservoir Floating Cover Guidelines (1999). California –Nevada Section of the American Water and Waste Water Association, Rancho Cucamonga, CA, USA

Abrasion Resistance of Geomembranes

G. R. Koerner, Ph.D., P.E., CQA, Geosynthetic Institute, USA, gkoerner@dca.net

R. M. Koerner, Ph.D., P.E., NAE., Geosynthetic Institute, USA, robert.koerner@coe.drexel.edu

M. R. Koerner, Geosynthetic Institute, USA, maxkoerner@comcast.net

ABSTRACT

There are many critical applications where geomembranes can be subjected to abrasion, e.g., linings of tunnels, canals, reservoirs, pumped storage facilities, etc. In this sense abrasion is the ongoing process of scuffing, scratching or rubbing away of the surface exposed material. Abrasion can be intentionally imposed by an abrasive material in a controlled process or by abuse in an uncontrolled manner.

This paper reports on the abrasion resistance behavior of five commonly used geomembranes, i.e., HDPE, LLDPE, fPP, PVC and EPDM. The laboratory method used was the Taber abrasion device per ASTM D4060 wherein weight loss, strength retained and elongation retained were measured as a function of rotation cycles. Both dry and saturated conditions were evaluated.

In general the softer geomembranes, as measured by their durometer, abrade more readily than the stiffer ones. Thus, HDPE was the least abraded and EPDM the most. Regarding mass loss, the amount of abrasion under dry conditions was greater than under saturated conditions. This finding was reversed with strength retained and elongation retained in that the saturated conditions were slightly more severe than the dry conditions. This was unexpected and is puzzling yet the data is consistent in this regard. As anticipated, the coarser abrasion disk was more severe than the medium abrasion disk for all of the variables evaluated.

1. ABRASION TESTING

There are a large number of standardized abrasion test devices and procedures. Some of these are the following:

- Crockmeter Abrader
- Fully Abrasive Tester
- Sliding Block Abrader
- Transverse Abrader
- Gakushen Head Abrader
- Hexbr Flex Abrader
- Taber Abrasion Tester

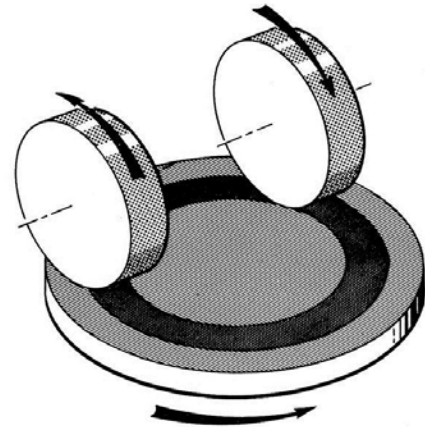
All are designed as accelerated abrasion test devices but none are applicable to all materials and to different abrasion scenarios. In this regard, they are application specific; see Koerner and Bove (1989), Rigo and Cazzuffi (1991), Cancelli and Cazzuffi (1994), Mullen-Rochholz (1996), Alexander (1998), Ossa (2005) and Koerner (2012) who have evaluated abrasion of various geosynthetic materials. Of the above group, we have arbitrarily selected the Taber Abrasion Tester for evaluation of the geomembranes in this study. Perhaps the major reason for doing so is its adaptability for containing, positioning and evaluating smooth geomembrane surfaces.

Taber Abrasion is a test device and procedure to determine a selected material's resistance to abrasion. The abrasion phenomenon can be difficult to quantify and compare by itself that is why weight loss is often used to evaluate its effect. The original weight of a test specimen is measured, the test specimen is then placed in the abrasion tester; a load is placed on top of the abrader wheel and it is allowed to spin for a specified number of revolutions. The final weight is taken and the abrasion weight loss calculated. The load and abrading wheel can be adjusted for softer or harder materials. Abrasive damage is also judged numerically by the change in tensile properties of test specimens removed from the abraded material. Strength and elongation percentage retained between the abraded and unabraded specimen is measured via the appropriate tensile tests for the various geomembrane types. This ASTM test method (D4060) is similar to ISO 3537 and ANSI/SAE Z26.1, Test 17.

The Taber abrasion device used for this study is shown in Figure 1a. A schematic of the device during motion is shown in Figure 1b. Fundamental in conducting the tests are the applied weight on the rotating wheels and the type and texture of the abrasion wheels themselves. These are shown in Figures 1c and 1d, respectively. For the tests conducted in this study, we used a 1.0 kg weight throughout and used both CS-10 (medium) and CS-17 (coarse) abrasion disks.



a) GSI's Taber abrasion device



b) Schematic of Taber mechanism



c) Different abrasion weights



d) Different abrasion wheels

Figure 1. Details of the Taber abrasion device.

2. DETAILS OF TABER ABRASION TESTING

To generate useful data, abrasion specimens must be flat. This is done one of two ways depending on the rigidity of the specimens. This is via a ring clamp specimen holder or threaded ring specimen holder. The threaded ring specimen holder was used in our case because all five geomembranes tested were rigid and tough enough to not undergo warping while being clamped and abraded in this manner. A neoprene rubber substrate served as the flexible material on the standard specimen platen with a 100 grit emory paper used in conjunction with the clamp ring. The neoprene substrate is standard procedure and the emory paper prevents any stretching and wrinkling.

Figures 1a and 1b show the test conditions in the “dry” condition. Thus a vacuum is applied continuously during the test. This is to prevent wheel surface change during the test that may become clogged due to the pick-up of plastic or other materials from test specimens. Such residue must be cleaned at frequent intervals. The abrasive effort cannot be subject to variation due to changes in the abrasive characteristics of the wheel during testing. Figure 2 shows a photograph of an abraded specimen with a stencil of how tensile specimens are cut from the abraded samples. As noted in Figure 1b, the abrasion simulates a skidding action about the specimen. With one wheel moving forward and the other in reverse as the specimen rotates on the platen in a counter clockwise manner. It is interesting to note that the track left on the specimen is somewhat wider than a wheel width.



Figure 2. Abraded specimen with tensile test outlines for strength and elongation retained properties.

A replicate set of all test specimens was also subjected to a saturated abrasion testing by equipping the Taber abrasion device with a rimmed specimen holder as seen in Figure 3. This is useful to determine the effect of absorbed and/or surface moisture on abrasion resistance of the test specimen. It should be made clear that saturating the samples during the abrasion exposure might be quite different than exposing them to flowing water.



Figure 3. Reconfigured specimen holder so as to provide for saturated conditions.

3. DETAILS OF GEOMEMBRANES TESTED

For this study we selected five different geomembranes that are commonly used in the applications listed in the abstract. They are high density polyethylene (HDPE), linear low density polyethylene (LLDPE), flexible polypropylene (fPP), Polyvinyl Chloride (PVC) and Ethylene Propylene Diene Monomer (EPDM). All were smooth surfaced and were about the same thickness between 0.75 and 1.20 mm. They conformed to international specification as first quality material. The corresponding specifications for each geomembrane are as follows;

- HDPE, GRI Test Method GM13, Standard Specification for Test Methods, Test Properties and Testing Frequency for High Density Polyethylene (HDPE) Smooth and Textured Geomembranes
- LLDPE, GRI Test Method GM17, Standard Specification for Test Methods, Test Properties and Testing Frequency for Linear Low Density Polyethylene (LLDPE) Smooth and Textured Geomembranes
- fPP, GRI Test Method GM22, Standard Specification for Test Methods, Test Properties and Testing Frequency for flexible polypropylene (fPP) Smooth and Textured Geomembranes
- PVC, ASTM D7176, Standard Specification for Non-Reinforced Polyvinyl Chloride (PVC) Geomembranes Used in Buried Applications

- EPDM, GRI Test Method GM23, Standard Specification for Test Methods, Test Properties and Testing Frequency for Ethylene Propylene Diene Monomer (EPDM) Geomembranes.

Each of the materials used in this investigation went through the complete set of physical, mechanical, and endurance tests cited in the respective specifications. The results of this testing are given in Table 1.

Table 1. Geomembranes evaluated in the abrasion testing of this study.

Geomembrane Type	Specification Designation	Nominal Thickness (mm)	Compounded Density (g/cc)	Durometer Shore Type D (hardness)	Comments
HDPE	GRI-GM13	1.0	0.942	50	passed all criteria
LLDPE	GRI-GM17	1.0	0.930	46	passed all criteria
fPP	GRI-GM22	0.75	0.949	33	passed all criteria
PVC	ASTM D7176	0.75	1.20	29	slightly low mol. wt. plasticizer
EPDM	GRI-GM23	1.15	1.32	27	passed all criteria

4. RESULTS OF THIS STUDY

The five geomembranes listed in Table 1 were all evaluated under dry and saturated conditions in the Taber abrasion device at cycles of 10, 100, 1000 and 5000 rotations with both the CS-10 (medium) and CS-17 (coarse) abrasion discs. Upon conclusion of the testing of each specimen, the following three properties were measured;

- mass (weight) loss in mg from the original test specimen's mass,
- strength retained as a percentage of the original strength, and
- elongation retained as a percentage of the original elongation.

Regarding strength and elongation testing, the ASTM test method used for the geomembranes was according to the designated specification. In this regard, HDPE, LLDPE and fPP used ASTM D6693, PVC used D882 and EPDM used D412. The results from this testing program are given in Tables 2a, b and c for the dry conditions and Tables 3a, b and c for the saturated conditions.

Table 2. Mass loss, strength retained and elongation retained for Taber abrasion testing in the "dry" condition.

(a) Dry mass loss (mg) Taber adhesion (ASTM D4060) results for five geomembranes under 1 kg load for various durations and abrasive disks

Cycles GM Type	Abrasion Disk CS-10 (Medium)				Abrasion Disk CS-17 (Coarse)			
	10	100	1000	5000	10	100	1000	5000
HDPE	0.4	0.8	10.4	33.0	0.2	2.8	4.3	46.2
LLDPE	0.3	1.4	14.3	32.1	1.2	1.4	6.5	42.0
PVC	0.7	6.1	26.0	58.8	0.6	5.6	29.3	69.2
fPP	0.3	0.5	14.8	60.5	0.8	2.9	8.7	68.2
EPDM	1.2	7.3	52.1	218.7	2.7	8.8	51.9	278.9

(b) Dry percent strength retained after Taber adhesion testing (ASTM D4060) for five geomembranes under 1 kg load for various durations and abrasive disks

Cycles GM Type	Abrasion Disk CS-10 (Medium)				Abrasion Disk CS-17 (Coarse)			
	10	100	1000	5000	10	100	1000	5000
HDPE	95	94	90	91	98	85	87	85
LLDPE	98	90	88	86	97	96	95	94
PVC	94	93	99	94	96	93	90	88
fPP	98	89	91	89	93	90	91	90
EPDM	95	93	86	86	98	87	81	77

(c) Dry percent break elongation retained after Taber adhesion testing (ASTM D4060) for five geomembranes under 1 kg load for various durations and abrasive disks

Cycles GM Type	Abrasion Disk CS-10 (Medium)				Abrasion Disk CS-17 (Coarse)			
	10	100	1000	5000	10	100	1000	5000
HDPE	95	91	88	86	92	90	87	85
LLDPE	100	92	88	86	95	98	92	86
PVC	92	92	100	92	93	87	87	86
fPP	98	90	90	87	94	99	91	90
EPDM	94	95	89	87	97	90	85	81

Table 3. Mass loss, strength retained and elongation retained for Taber abrasion testing in the “saturated” condition.

(a) Saturated mass loss (mg) Taber adhesion (ASTM D4060) results for five geomembranes under 1 kg load for various durations and abrasive disks

Cycles GM Type	Abrasion Disk CS-10 (Medium)				Abrasion Disk CS-17 (Coarse)			
	10	100	1000	5000	10	100	1000	5000
HDPE	0.9	1.8	2.2	12.4	0.9	2.4	4.5	17.8
LLDPE	0.5	1.6	2.5	13.4	1.0	2.3	8.0	25.1
PVC	1.3	5.3	9.8	23.9	1.2	2.2	11.9	60.9
fPP	0.5	1.3	11.4	25.8	0.5	1.8	14.9	33.3
EPDM	1.8	3.0	19.5	51.3	1.7	6.5	42.8	100.7

(b) Saturated percent strength retained after Taber adhesion (ASTM D4060) results for five geomembranes under 1 kg load for various durations and abrasive disks

Cycles GM Type	Abrasion Disk CS-10 (Medium)				Abrasion Disk CS-17 (Coarse)			
	10	100	1000	5000	10	100	1000	5000
HDPE	95	96	90	81	98	79	85	81
LLDPE	99	92	92	89	98	95	91	83
PVC	94	99	92	89	99	94	94	91
fPP	93	97	98	98	95	96	96	97
EPDM	96	90	83	75	96	85	88	73

(c) Saturated percent break elongation retained after Taber adhesion (ASTM D4060) results for five geomembranes under 1 kg load for various durations and abrasive disks

Cycles GM Type	Abrasion Disk CS-10 (Medium)				Abrasion Disk CS-17 (Coarse)			
	10	100	1000	5000	10	100	1000	5000
HDPE	97	93	87	85	92	86	90	84
LLDPE	97	95	93	88	93	96	91	79
PVC	99	100	96	86	98	97	89	84
fPP	88	79	85	81	99	87	85	87
EPDM	100	88	86	74	92	83	85	76

5. DISCUSSION

Some general observations of the abrasion data shown in Table 2 (dry conditions) and Table 3 (saturated conditions) are that the data is reasonably “well behaved” insofar as the effect of number of abrading cycles. In this respect the dry condition mass loss shown in Table 2a increases exponentially going from 10 through 5000 cycles. In a like manner, the saturated condition mass loss in Table 3a is also exponentially increasing but significantly less so than with the dry specimens. Of course, this is logical to expect and was anticipated. Furthermore, since the applications envisioned invariably involve water, the saturated condition tests are probably closer to reality. Also seen in the comparisons of mass loss in Tables 2a and 3a, the CS-17 (coarse) abrasion disk is indeed more aggressive than the CS-10 (medium) abrasion disk by approximately 15 to 50%. Again this is an anticipated outcome. Clearly seen in this mass loss data is

that the ordering from lowest to highest is in direct proportion to the hardness of the various geomembranes. In this regard, recall the Shore hardness durometer values in Table 1. Perhaps the outlier in this uniformity is the EPDM geomembrane which is only slightly lower than PVC and fPP in durometer but is significantly higher in its mass loss at all cycles. This may be due to a change in the type of failure which was atypical in that small particles were being pulled from the gradually abrading surface. That said, the saturated mass losses are significantly lower than the dry mass losses and these, the saturated, values are probably more indicative of realistic geomembrane applications.

Regarding the strength retained values in Table 2b (dry conditions) and Table 3b (saturated conditions) the data shows a decrease with increasing number of abrasion cycles. However, the change is nowhere as drastic as with mass loss and is also somewhat less consistent. There also appears to be a relative sharp decrease in the 5000 cycle data over that of 1000 cycles. One other important feature of the strength retained data is that it was as great, or even greater, in the saturated tests than in the dry test. This finding was quite unexpected, but it occurred in most of the five geomembranes evaluated.

Finally, the elongation retained values of Tables 2c (dry conditions) and Table 3c (saturated conditions) trend extremely close to the strength retained values discussed previously. This comment refers to the elongation retained decreases being somewhat linearly decreasing with number of cycles rather than exponential as with the mass loss, but also with the close agreement of mass loss with decreasing durometer. Lastly, the fact that the elongation retained was lower under saturated conditions (Table 3c) than with dry conditions is again a surprise for which we have no answer. In this regard, the data must speak for itself.

6. SUMMARY AND CONCLUSIONS

The Taber abrasion device and testing protocol has been available for decades. In this regard it seems very well suited for testing geomembranes, yet there is a lack of experimentation in this regard. When abrasion of geomembranes are at issue, as in the applications mentioned in the abstract, it is felt that Taber abrasion should be a candidate test method. In fact, there is no generic specification that we know of which requires abrasion resistance. If this eventually occurs we recommend that the Taber device be specified and used accordingly. The test is, however, clearly an index test and the data is best considered when used in comparison to other like data.

In conclusion, five commonly used smooth surface geomembranes were evaluated in dry and saturated conditions. Under abrasion cycles from 10 to 5000 with two different abrasion disks (medium and coarse), the data obtained showed the following trends.

- Increasing cycles produced greater mass loss, less strength retained and less elongation retained.
- The mass loss data exhibited an exponential trend, whereas the strength and elongation retained were closer to a linear trend with increasing abrasion cycles.
- There was a clear trend of mass loss, strength retained and elongation retained with durometer of the five geomembranes evaluated; the harder the surface, the lower were the changes in values. In this regard the ordering from least-to-greatest changes was HDPE, LLDPE, PVC, fPP and EPDM.
- A major discrepancy in the anticipated trends, however, was when testing under dry conditions the mass loss was greater than when testing with saturated conditions, while with strength retained and elongation retained the wet conditions produced the greater changes. This was a most pronounced trend with both strength retained and elongation retained values being close to one another and mass loss being far greater in changes from as-received values and in the opposite direction.

ACKNOWLEDGEMENTS

This paper is made available through financial assistance of the Members, Affiliated Members and Associate Members of the Geosynthetic Institute (GSI). We sincerely thank them in this regard. See our website at www.geosynthetic-institute.org for their identification and contact persons.

REFERENCES

- Alexander, W. A. (1998). Abrasion properties of geotextiles subjected to dynamic loading, *Proc. 6th ICG*, Atlanta, IFAI Publ., pp. 1161-1164.
- Cazuffi, D., Puccio, M. and Venesia, S. (1983). Essai de resistance a l'abasion de membranes, feuilles et revetments pour des ouvrages hydrauliques, *C.R. Colloque sur l'Etancheite des Ouvrages Hydrauliques*, Paris February, pp 57-88.

- Cancelli, A. and Cazzuffi, D., (1994). Environmental aspects of geosynthetic application in landfills and dams, *Proc. 5th Int'l Conf. I*, Singapore, Special Volume, pp. 55-96.
- Rigo, J-M and D. A. Cazzuffi, (1991). Test standards and their classification, *Geomembranes - Identification and Performance Testing*, Edited by A.L., Rollin and J.M., Rigo, Rilem report 4, Chapman and Hall, The University Press, Cambridge, Great Britain, pp 47.
- Koerner, R.M., 2012. *Designing with Geosynthetics*, 6th ed., Volumes 1 & 2, Xlibris Corporation, Bloomington, Indiana, USA.
- Koerner, G. R. and Bove, J. A., (1989). Inspection of HDPE geomembrane installations, *Proc. Geosynthetics '89*, San Diego, IFAI Publ., St. Paul, MN, pp. 70-83.
- Muller-Rochholz, J. (1996). Abrasion testing of geosynthetics, *Proc. of Geosynthetic Applications*, Balkema Publ. Rotterdam, pp. 1061-1064.
- Ossa, M. (2005). Geomembranes used in heap leach SX-EW mining: a manufacturer's perspective" *Proc. GRI-19*
- Cazuffi, D., Puccio, M. and Venesia, S. (1983). Essai de resistance a l'abasion de membranes, feuilles et revetments pour des ouvrages hydrauliques, *C.R. Colloque sur l'Etancheite des Ouvrages Hydrauliques*, Paris February, pp 57-88.

An Innovative Use of Expanded Polystyrene Insulated Concrete Forms (ICF) for Geohazards

Bret N. Lingwall, PhD, PE, Kleinfelder, Inc, USA, blingwall@kleinfelder.com
Steven F. Bartlett, PhD, PEm University of Utah, USA, Bartlett@civil.utah.edu

ABSTRACT

Pipelines are damaged by permanent ground displacement (PGD) resulting from faulting, land-sliding, or liquefaction. Insulated concrete forms (ICFs), a product constructed of two slabs of rigid polystyrene foam, separated by plastic brackets, can be used in trenches as a compressible inclusion to reduce PGD pipeline damage. The initial rigidity and relative compressibility at large stress levels make ICFs a candidate for protecting underground pipelines undergoing PGD. The imposed pipe distress from PGD is reduced by lowering the resistance to pipe movement. ICFs, when placed in the trench, can perform this function; accommodating the horizontal movement between the pipe and the soil, reducing the imposed stress on the pipe. Full and bench scale tests were performed to define this interaction, soil-ICF-pipe non-linear springs required for pipeline design were developed. The results for the ICF-soil system shows a significant reduction in pipeline stress for the case where the pipeline undergoes PGD.

1. INTRODUCTION

The concept of using Expanded Polystyrene (EPS) Geofoam as a "compressible inclusion" between walls or foundation elements and a soil mass was conceptualized about 20 years ago (Horvath 1995, 2005). These publications explore this concept by simple numerical analyses and conceptual models for estimating the developed static earth pressures against buried structures using Geofoam inclusions. Yoshizaka and Sakanoue (2003) investigated Geofoam as a method to reduce lateral force-displacement relationships for buried pipelines. They found a 33 to 60% reduction in the lateral soil-pipe forces when Geofoam was used as light-weight trench backfill for pipe undergoing horizontal displacement. However, Yoshizaka and Sakanoue (2003) did not place Geofoam in the sidewalls of the trench, but used it as a light-weight cover to reduce vertical loads. More recently, Choo et al. (2007) explored the use of Geofoam as a cover system for buried steel pipelines subjected to vertical fault offset. They used centrifuge testing of scaled models to show the benefits of EPS as a light-weight material in reducing pipeline stresses undergoing vertical offset. Choo et al. (2007) demonstrated that the light-weight cover application of Geofoam can assist in reduction of pipeline damage, but they did not address the compressible inclusion effects of the Geofoam cover in reducing the stresses, particularly for horizontal offset problems.

Considerable work has been done for the case of rigid steel pipelines undergoing horizontal offset from strike-slip faults, liquefaction-induced lateral spread and slope failure. Newmark and Hall (1975), Wang and Yeh (1985), and Kennedy et al. (1979) developed solutions for the stresses and strains imposed on a steel pipeline by permanent ground displacements (PGD). For horizontal PGD and its impact to pipelines, ASCE (1984), MCEER (1999) and American Lifeline Alliance (ALA) (2005) recommend using the Newmark and Hall (1975), Kennedy et al. (1979) and Finite Element Method (FEM) approaches for evaluating vertical movements. ASCE, MCEER and ALA recommend that FEM and elastic methods are best suited for horizontal movements and are applicable to cases where the pipeline is buried sufficiently deep so as not to reach ground surface. In addition, ASCE, MCEER and ALA recommend using Trautmann and O'Rourke (1985) soil-pipe springs.

Perhaps numerical modeling offers the best method of evaluating complex soil/pipe interactions. FEM has been used extensively to model horizontal permanent ground deformations and their effects on buried steel pipelines (Takada, 2001 and Desmond et al., 1995). Recently, Karamitros et al. (2007) used the FEM to develop a strike-slip model for pipelines crossing active faults based on the earlier work of Wang and Yeh (1985) and Kennedy (1979). Trautmann and O'Rourke (1985) demonstrated that lateral and vertical movements of pipes through soil are essentially the same as for flat anchor plates undergoing lateral or vertical movements in soils. Their findings were confirmed by Cheuk et al. (2005). The objective of both Trautmann and O'Rourke and Cheuk et al. was to develop soil-pipe interaction Winkler springs for FEM modeling. The Winkler (1867) spring approach is based on developing relations that assume the soil and structure will interact as a non-damped uncoupled spring. Soil spring constants are generally dependent upon the sectional configuration and the dimensions of an underground structure, rigidity of soil deposits, direction of loading and boundary conditions (Matsubara and Hoshiya 2000). These springs are often non-linear, and research on Geofoam shows that soil-EPS-pipe interaction can be modeled with non-linear springs (Lingwall 2011).

Insulated Concrete Forms (ICFs) are proposed to be used as a compressible inclusion for laterally displacing pipes due to PGD. The compressible nature of the EPS foam material forming the slab sides of the ICF, coupled with the void between the slabs separated by only thin plastic clips, provide the potential to reduce the non-linear soil-pipe interaction spring stiffness and strength. This research develops the non-linear spring needed for pipeline design for PGD. The non-linear springs are developed through a combination of laboratory testing, bench scale pipe-ICF testing, and full scale pipe-ICF-soil testing with a laterally displacing pipe.

2. ICF FOAM MATERIAL

ICFs are constructed by separating two EPS slabs by a set of plastic clips. The plastic clips are spaced along plastic brackets, which are glued to the EPS slabs. The plastic clips separate the EPS slabs 152 to 304 mm depending on manufacturer and vendor. In this case, 152 mm long clips were used. The brackets are spaced 204 mm apart. The slabs are 304 mm in assembled thickness, and run 1.2 to 2.4 m in length. An ICF with two clips per bracket is shown in Figure 1. The edges of the EPS slabs have rabbited edges for stacking ICFs on top of one another for foundation wall construction.

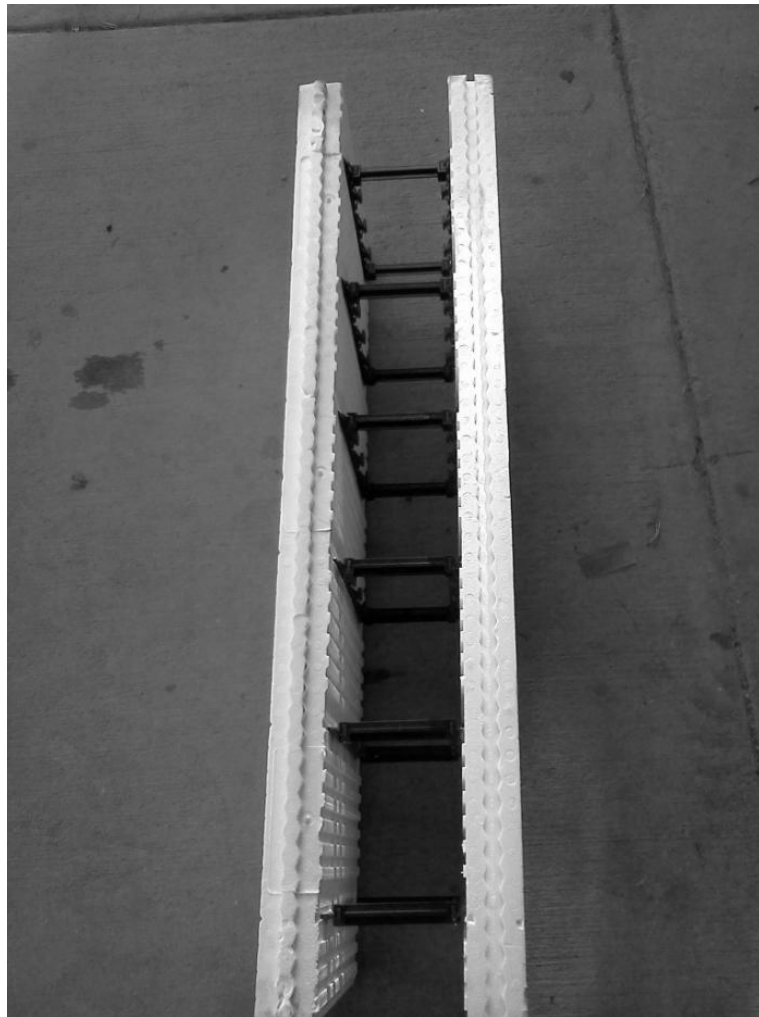


Figure 1. ICF with 2 plastic clips in place on each bracket

Samples of the ICF foam material were trimmed using a hot wire cutter for specimen testing of the foam. Samples were trimmed to 2 mm cubes, matching the specimen size for Geofom in ASTM D6817. Specimens were measured to have a density of 24 kg/m³. This compares to the minimum specified density of EPS 22 from ASTM D6817 (22 kg/m³). 7 specimens were tested in uniaxial compression to approximately 80% vertical (axial) strain. The compressive resistance at 1% strain was found to be approximately 79 kPa, 5% strain of 132 kPa, and 10% strain of 144 kPa. These compressive resistances compare well to EPS 22 from ASTM D6817, as well as the specimen testing for EPS 22 from

Lingwall (2011). Figure 2 shows the compression test stress:strain curves for all 7 specimen tests as well as typical curve for EPS 22. It should be noted that the specimens were taken from 4 different ICFs from different production batches obtained from local ICF contractors. The foam material is shown to be variable, though the shape of the different stress:strain curves are similar for all specimens. The foam material shows extreme strain hardening after approximately 50% strain.

ICF Foam Material Compression Tests

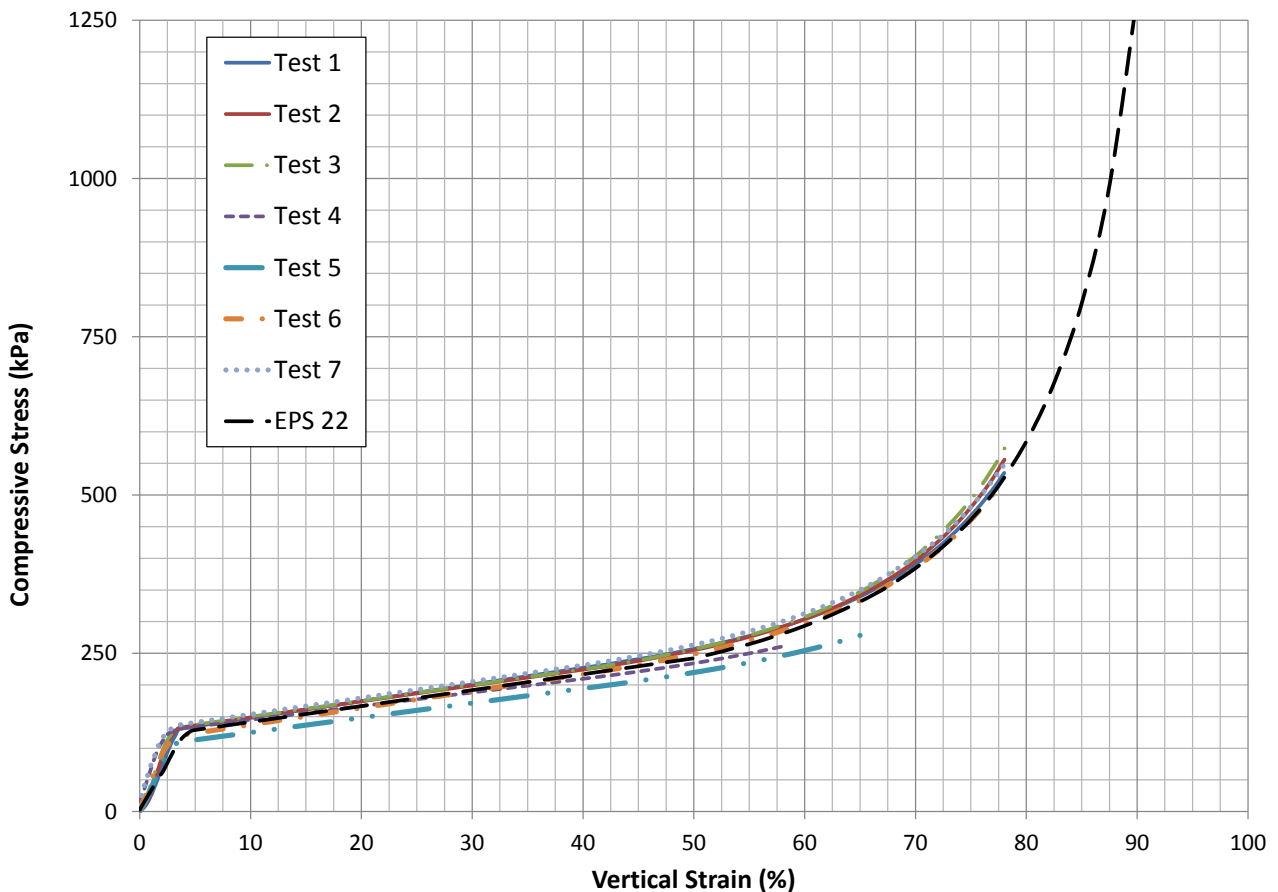


Figure 2. Stress:Strain relationships for ICF foam material and comparison with EPS22

The strength of an ICF when placed against a laterally displacing pipe will be governed by the tensile strength of the foam slab. Lingwall (2011) showed that in pipe-EPS22 interaction Geofomo has tensile strengths of 95.7 to 191.5 kPa. ASTM D6817 specifies a minimum flexural strength of 239.4 kPa.

3. ICF-PIPE INTERACTION TESTS

Once the foam material was characterized, the next step in developing non-linear springs is bench scale testing. Bench scale testing performed involved placing a 406 mm long section of ICF against grade X60 rigid steel pipe. In this case, the pipe had an outer diameter of 89 mm (3.2 mm pipe wall thickness). The pipe and ICF were pushed together slowly, with forces and displacements measured. The resultant force-displacement relationship is the non-linear spring. This directly measured the complex behavior of the ICF as a system with foam, brackets, and clips interacting with the rigid pipe. The pipe was rigid in comparison with the ICF, though it did have some flexibility. The pipe is supported for 90 mm at the middle of its length. The top of the ICF was pushed by a 6.4 mm thick steel plate.

The ICF was pushed into the pipe in two configurations. The first configuration was pipe parallel to the plastic brackets and clips. This means that the resistance to pipe movement was completely dependent on foam slab rigidity and tensile strength. The second configuration was pipe perpendicular to the plastic brackets and clips. In this case, the resistance to pipe movement depended on both the rigidity of the foam slab and the stiffness and strength of the plastic clips.

Figure 3 shows the ICF and pipe at the end of interaction testing in a pipe parallel configuration, and that the foam slabs experience tensile failure at the point of pipe contact. Figure 4 shows the resultant force:displacement relationships for pipe-ICF interaction using 6, 8, or 10 plastic clips for the 304 mm wide, 406 mm long, section of ICF.

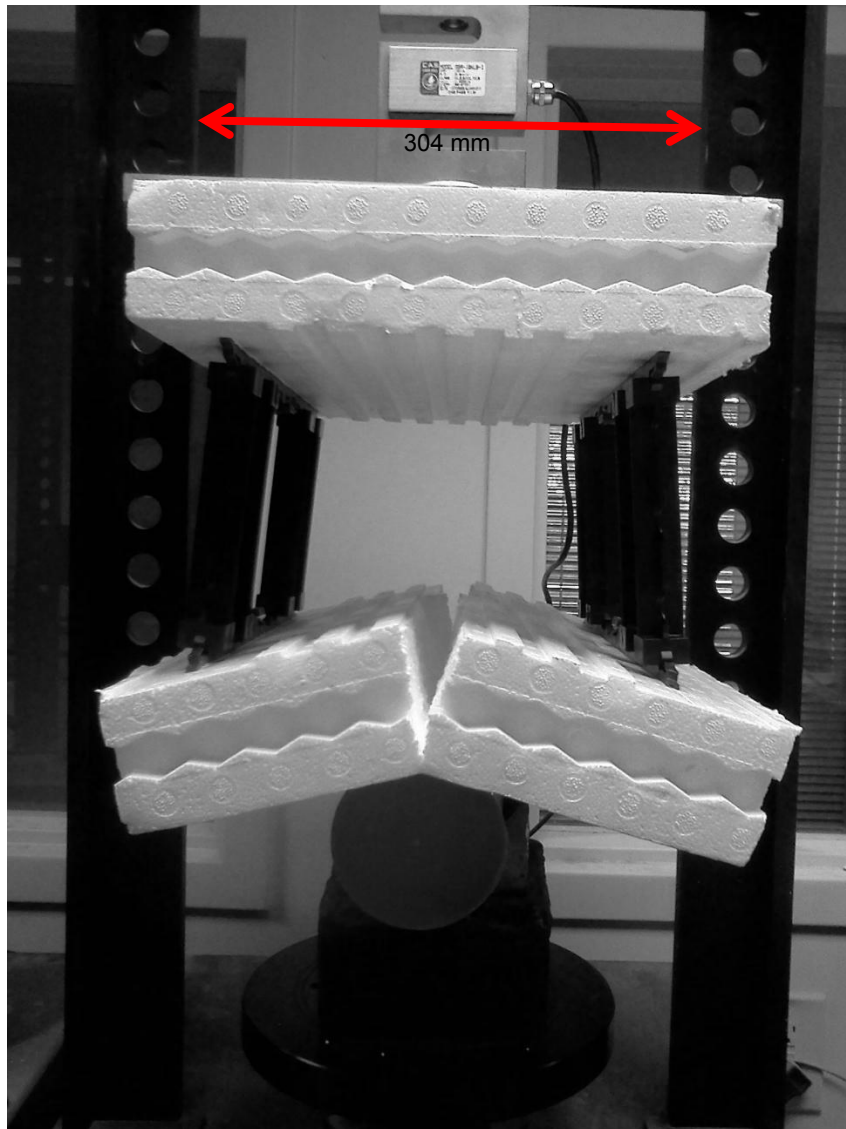


Figure 3. ICF after pipe interaction testing with rigid pipe

Figure 4 demonstrates that the pipe parallel condition produces almost no resistance to pipe movement. EPS22 resists movement many times more than the pipe parallel condition. This configuration is deemed too soft for realistic construction and pipe design. The results for the pipe perpendicular tests show less resistance to pipe movement than the EPS 22 block, but within a more reasonable range of resistances.

The resistance and stiffness shown in Figure 4 should not be used directly for design. The actual buried pipe system is backfilled with soil, and the ICF pushes against the compliant backfill and/or trench side wall. This introduces more complexity to the actual design non-linear spring. Also, construction and installation of an ICF trench system requires a separation material to keep backfill and debris from entering the void between the ICF slabs. If backfill or debris enters the void, the system could perform differently.

ICF-Pipe Interaction Tests

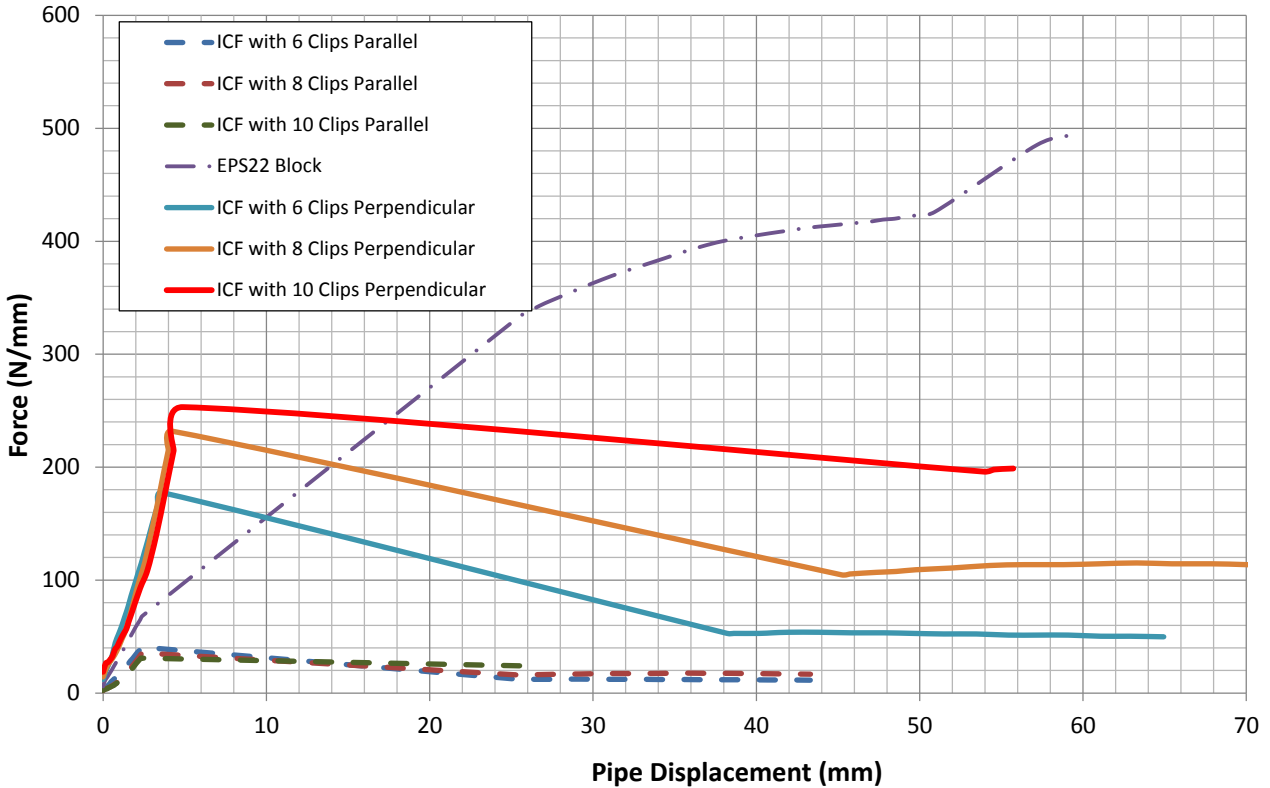


Figure 4. ICF pipe interaction test results showing forces at pipe displacements

4. FULL SCALE PIPE-ICF TEST

A test using a 171.5 mm OD pipe was conducted to obtain the force-displacement behavior (non-linear spring) for an ICF system with complete sand backfill. For this test, the pipe was pushed laterally in a trench box into an ICF, with sand surrounding the pipe and ICF. This test was done to explore the benefits of using ICFs as a compressible inclusion against a pipe undergoing horizontal displacement. The primary goal the research described in this section was to measure the reduction in stress on the pipe for the various cases and to later use this information for numerical modeling and design using the resultant non-linear spring information from testing. This full-scale experiment was conducted at the University of Utah's Department of Civil and Environmental Engineering in the fall of 2010.

4.1 Experimental Set-Up

A contained test system (i.e., trench box) was locally manufactured for the experimental program. This test system included a loading device, reaction system (i.e., box) for the load device, a test chamber for the soil-ICF-pipe interaction testing, and the necessary instrumentation for measurements.

The box's overall dimensions are: 5.33 m long, 1.83 m wide and 1.83 m high (Figure 6). The box was constructed of 6.4 mm thick steel plates. The horizontal load capacity of the box is approximately 112 kN. Both ends of the trench box were reinforced and braced with structural steel angle and channel sections to withstand the forces involved in the experiments. The end walls of the trench box were heavily reinforced to minimize the reaction deflections of the ram against the wall. A reinforced door was constructed on one end, which allowed side entry into the box. The top of the box was left open, this allowed for sand to be placed in the box from above.

Internally, the trench box is divided into two chambers by a rigid 10 mm steel partition wall. The first, or smaller, chamber houses the actuator and is 2.13 m long, as measured internally from the end wall to the partition wall. In the smaller chamber, the actuator reacts internally against the end wall of the steel box. Three struts extended from the actuator, through the partition wall, into the second chamber. Stiffeners were added to the struts to prevent any vertical

movement. Thus, the actuator imposes the purely horizontal force on the pipe via these steel struts that extend into the second chamber. Both chambers were 1.83 m wide.

The second, or larger, chamber is 3.2 m long and houses the pipe, geofoam and sand backfill used in the test program. It was filled with sand and/or EPS geofoam according to preselected configurations. In this chamber, the 171.5 mm O.D. steel pipe was welded onto the struts. This allowed sand to be placed around the pipe in the second chamber, and the pipe to be pushed laterally into the ICF and backfill system. The center of the pipe rests 457 mm above the bottom of the box, which produces a height to pipe diameter ratio (H/D) of 10. Sand backfill 1.7 m thick was placed above the pipe, giving the pipe a field stress condition.

The actuator used in this test program utilized a MTS electronic control and data acquisition system. The actuator has a maximum capacity of 445 kN with a maximum stroke of 150 mm. The maximum displacement rate for the ram is 3 m per minute. The ram is powered by a MTS pneumatic pump with computer controlled manifold and servo. Feedback for the system is through the displacement transducer and the tests were done as displacement controlled tests. (The system is capable of cyclic testing though this capability was not utilized in this test program.) Several types of measurements were taken during the test program. The total load applied to the pipe by the actuator was measured by a single load cell. The displacement of the actuator, as it pushed the pipe into the backfill material was measured with a displacement transducer. Vibrating wire and resistant base total earth pressure cells were placed in the backfill to measure the horizontal and vertical stresses that developed in the sand backfill mass. Both the load cell and the displacement transducer were calibrated prior to their use in the subsequent test program.

Sand was imported to the test for backfill. This clean sand was processed before delivery for a consistent gradation throughout the material. All fines were non-plastic, and the gradation is shown in Figure 5. Sand was used for backfill due to the low variability in its gradation, ease of placement, and consistent compaction. Sand was compacted in 304 mm loose lifts with a hand operated vibratory plate compactor to a dry unit weight of 15.7 kN/m³, (16.1 kN/m³ total unit weight). Compaction was tested on each lift with a nuclear density gauge.

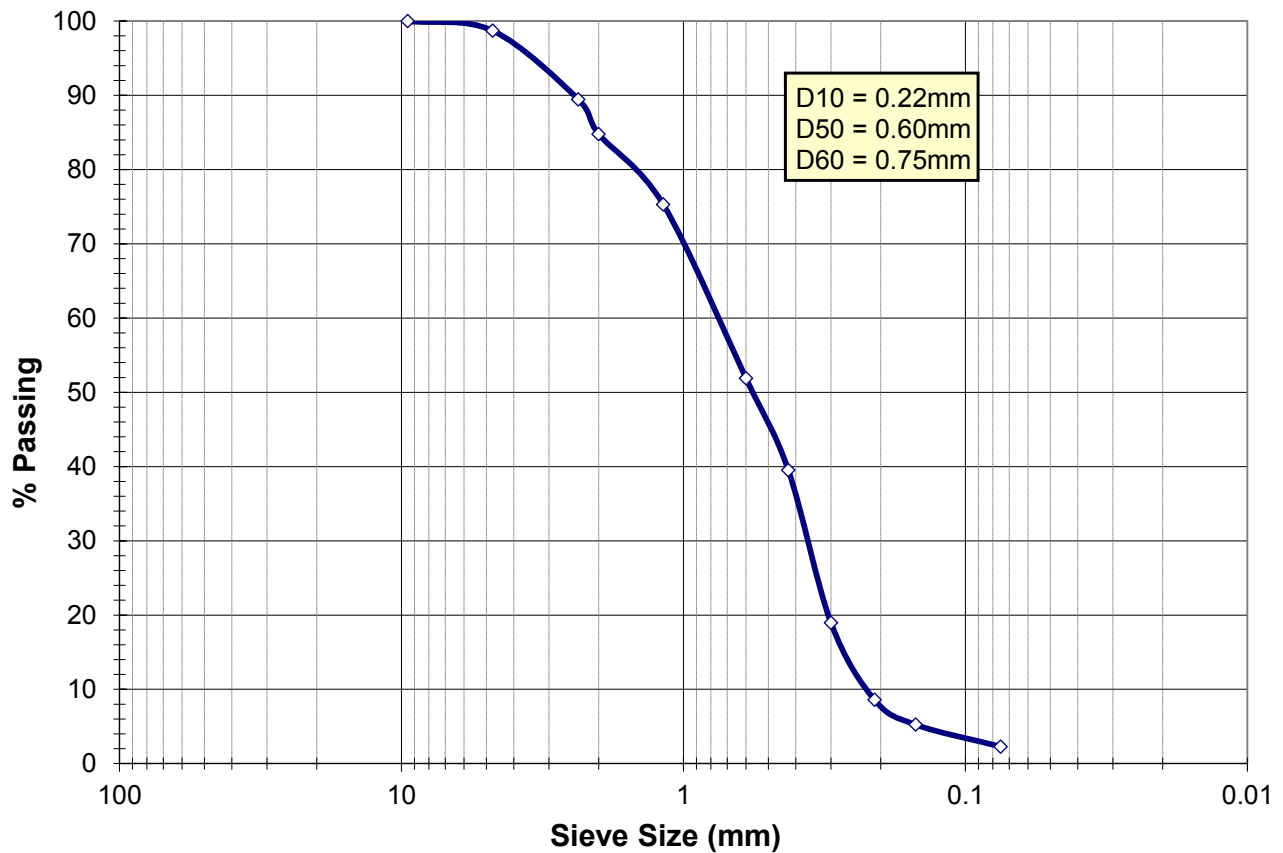


Figure 5. Grain size distribution for sand backfill in full scale ICF-pipe test

In parallel with the full scale ICF-pipe interaction test, a baseline full-scale lateral pipe movement test was performed using only sand backfill. This baseline provides a comparison to the ICF test, and shows improvement over traditional backfill systems. The baseline case of sand only backfill was run first. Full details of the comparison baseline case are in Lingwall (2011).

The test procedure for both sand baseline and ICF backfill tests began with placing two layers of smooth plastic sheeting along the steel walls of the experimental box. Between the layers of plastic a friction reducing thin layer of silicon lubricant was applied. This lubricant, in conjunction with two layers of plastic, reduced edge effects, and better simulated a plane-strain situation. As such the data collected was interpreted as plane strain. This is similar to the approach used by Trautman and O'Rourke (1985) and Cheuk et al. (2005). The Trautmann and O'Rourke study is the basis for current design non-linear springs used in pipeline design for PGD. This test does not seek to revolutionize the pipeline design procedures, but update it with new information for a new backfill system. The ICF was then assembled as shown in Figure 1. The test was chosen to run in a pipe-perpendicular to plastic strut configuration based on the testing presented in section 3 of this paper. The ICF was wrapped in 2 layers of plastic to prevent sand backfill from flowing into the void between the foam slabs. The ICF was placed along side the pipe, and sand was backfilled around both.

After backfilling of the box, the actuator was displaced slowly (25 mm/min), with continuous data collection. The actuator was displaced until the threshold of 111 kN was reached on the load cell, or a maximum horizontal pipe displacement of 152 mm. After completion of displacement, the test is stopped. Data collection backed up, and the pipe retracted to its initial position. The box is then emptied, and the ICF exhumed for inspection and qualitative examination of its failure.

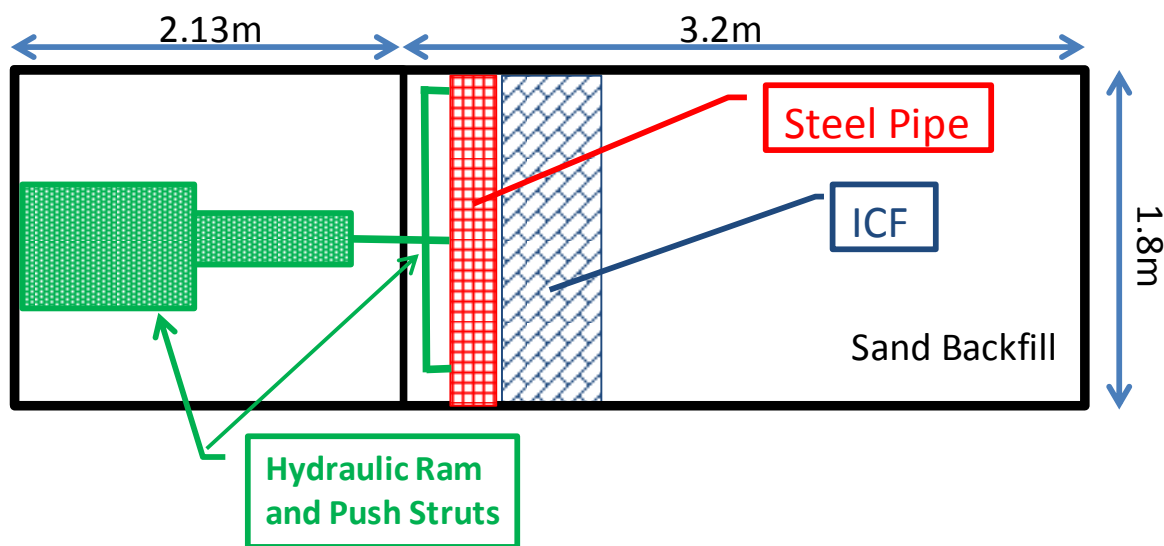


Figure 6. Full scale test apparatus schematic in Plan View

4.2 Full Scale Test Results

The force-displacement relationships measured during lateral pipe movement during both tests are shown in terms of force per unit length in Figure 7. The sand backfill test maximum pipe resistance was measured to be 50 kN/m at 57 mm of displacement. The curve is approximately linear until a measured load was reached of 10 kN/m at 0.4 mm of displacement. After that, the sand backfill test experienced a non-linear force:displacement relationship. The pipe resistance reduced after the peak to a residual value of 47 kN/m by 76 mm of pipe movement.

The measured peak force of the ICF backfill test was 29.5 kN/m at 21 mm of pipe movement. After this point, the plastic struts yielded in the test, at the same time the entire ICF began to push back into the sand backfill. A complex behavior occurred, with plastic struts and brackets bending, stretching, and yielding, with foam slabs failing in tension, with some compression of the material at the point of contact, while the entire ICF is pushed into the sand backfill. This behavior is similar to the behavior observed in the bench scale testing. This complex behavior is demonstrated in Figure 7 by the seemingly erratic behavior after yield. This complex behavior continued until the end of the test also seen in the exhumed ICF shown in Figure 9. The peak load of the ICF was 40% less than the loose sand backfill baseline, while the ICF also had softer system stiffness. This shows that the non-linear spring for an ICF backfill system is softer and less stiff than sand backfill system. This reduces potential pipe distress due to PGD. The results of the two full scale tests

were normalized as shown in Figure 8 by the depth below ground surface, unit weight of the surrounding backfill soil, and the projected contact area of the pipe. This unit-less presentation of the data is for easier comparison with the recommendations in ASCE, ALA, and MCEER as well as the original lateral pipe tests in loose sand from Trautmann and O'Rourke (1985). The required stiffness and strength for pipeline design can be taken from Figures 6 and 7.

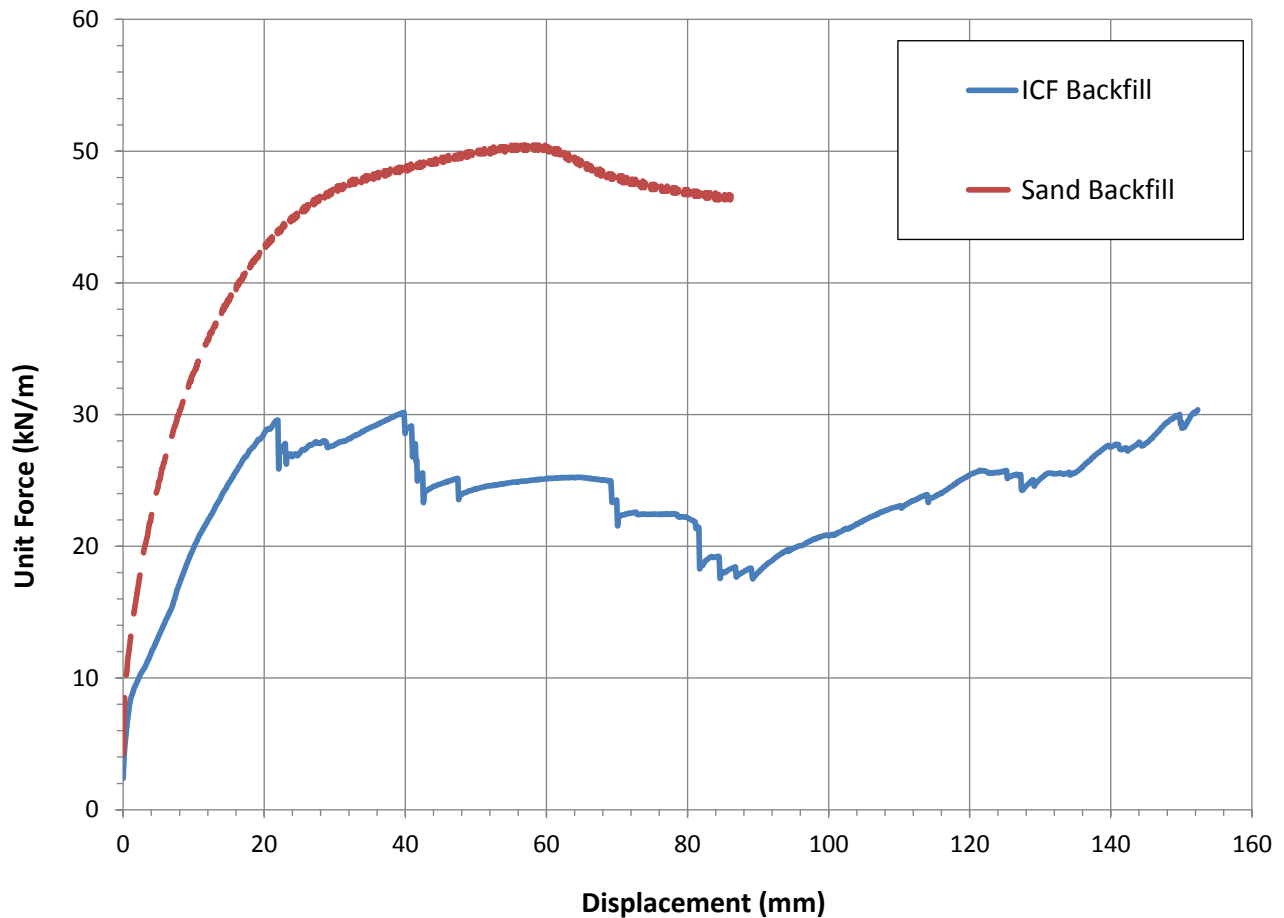


Figure 7. ICF-Pipe full scale test results comparing with sand only backfill

After completion of the ICF backfill test, the ICF was exhumed from the sand backfill for examination. This exhumed ICF is shown in Figure 9. The pipe was loaded against the shown ICF foam slab down the center of the ICF. The displacing pipe loaded the ICF and caused it to crack down the middle as shown. The plastic struts and clips bent, yielded, but only in a few cases experienced ultimate failure. The foam material that was between the plastic struts and the pipe compressed significantly from an initial thickness of over three mm to a final thickness of less than 12.5 mm. Thus, the ICF foam slab experienced localized strains of 85% and greater. The foam slab opposite pipe contact showed little distress. The majority of the distress at that slab occurred at the plastic struts where the clips attached.

The results of the ICF test are dependent on the number of clips used between the foam slabs. If more clips are to be used in the ICF than used in this test (2 per bracket), then the results should be scaled similar to the difference in strength between the pipe perpendicular tests shown in Figure 4. The sand backfill was loose, and retesting with denser sands, different soils, and layered systems can result in differing non-linear springs. Site specific testing and design is recommended for situations where ICFs are proposed to protect pipelines in place from PGD.

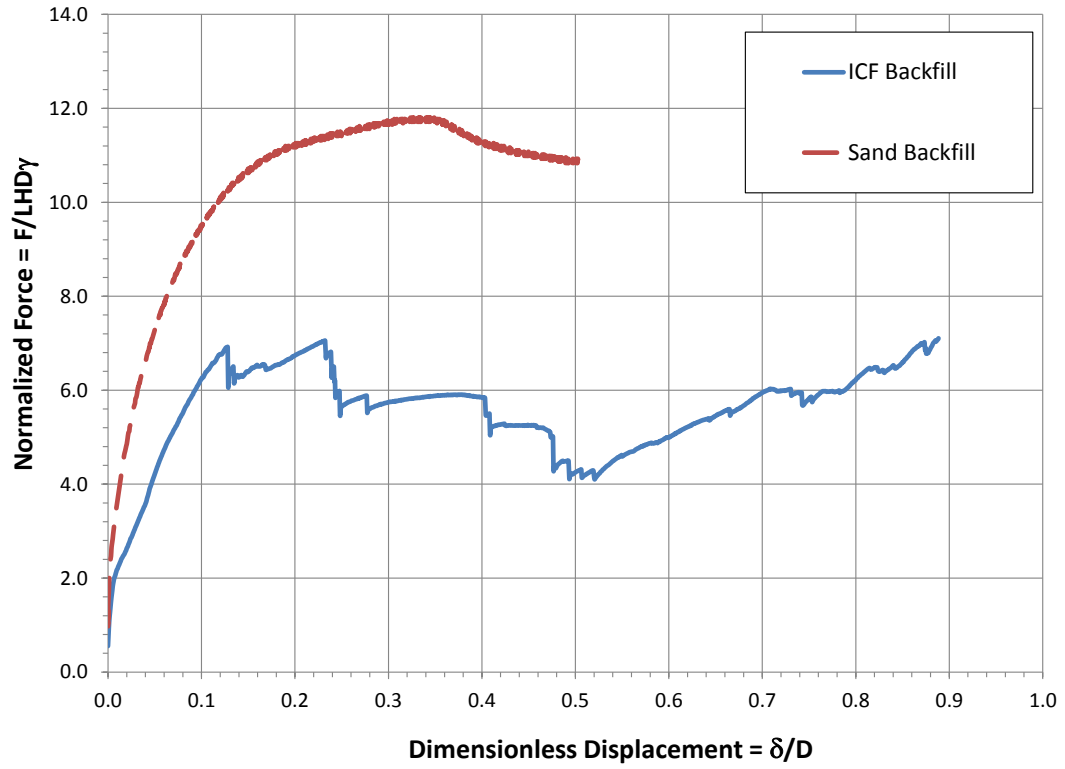


Figure 8. Normalized ICF-Pipe full scale test results including comparison with sand only backfill



Figure 9. Exhumed ICF after full scale ICF-pipe test

5.1 Conclusions

The use of ICFs for geohazard reduction was investigated in this study by use of ICFs as compressible inclusions against pipelines undergoing permanent ground displacements from faulting, landslides, or lateral spreading. The foam material for the ICF was tested in compression for developing design non-linear springs for pipeline design with an ICF backfill. The foam material compared well to EPS 22, a grade of EPS Geofoam. Sections of ICF were then tested in direct contact with a displacing pipe, varying the number of clips and orientation of the pipe with respect to the plastic brackets that hold the separation clips in the assembled ICF. The pipe parallel bracket orientation was found to be too weak for reliable pipeline design. The number of clips used in ICF assembly affects the resistance to pipe movement. Full scale tests with a pipe and sand backfill in plane strain conditions were then conducted. The resultant full scale non-linear springs can be used for pipeline design. The loose sand only backfill baseline test compared well to previously published non-linear springs from the geotechnical literature. The ICF backfill test (with loose sand surrounding ICF and pipe) showed 40% less resistance to lateral pipeline displacement as well as a less stiff response. ICFs can thus be used for protection of pipelines at fault crossings or other areas of PGD. Site specific testing and design is recommended since these tests used only one grade of ICF from one manufacturer and used loose sand as the material through which the pipe was laid. Differing soils and ICFs, as well as differing geometries, can produce differing results.

ACKNOWLEDGEMENTS

The authors wish to thank Evert Lawton and Aurel Trandafir for their support of the full scale testing, and Kleinfelder Inc. for the use of its materials testing laboratory equipment and geotechnical instrumentation.

REFERENCES

- American Lifeline Alliance (ALA), (2005), *Guidelines for the Design of Buried Steel Pipelines*, July 2001, ASCE, Reston VA, USA.
- ASTM D6817. Standard Specifications for Rigid Cellular Polystyrene Geofoam. *American Society for Testing and Materials*, West Conshohocken, Pennsylvania, USA.
- American Society of Civil Engineers (ASCE), (1984). *Guidelines for the Seismic Design of Oil and Gas Pipeline Systems*, Technical Council on Lifeline Engineering, Committee on Gas and Liquid Fuel Lifelines, ASCE, Reston, VA, USA.
- Cheuk, C.Y. White, D.J. and Bolton, M.D. (2008). Deformation mechanisms during uplift of buried pipes in sand, *Journal of Geotechnical and Geoenvironmental Engineering*, ASCE, 134:154-163.
- Choo et.al (2007) Remediation for buried pipeline systems under permanent ground deformations, *Soil Dynamics and Earthquake Engineering*, Elsevier, 27:1043-1055.
- Horvath, J.S. (1995). *Geofoam Geosynthetic*. Horvath Engineering, PC, New York, NY, USA.
- Horvath, J.S. (2005). Expanding the use of Expanded Polystyrene (EPS) Geofoam in Practice, Boston Society of Civil Engineers Section/American Society of Civil Engineers Geo-Institute 2005 Geotechnical Engineering Seminar, Waltham, MA, U.S.A.
- Karamitros, D.K., Bouckovalas, G.D., and Kouretzis, G.P. (2007). Stress Analysis of Buried Steel Pipelines at Strike-slip Fault Crossings, *Soil Dynamics and Earthquake Engineering*, Elsevier, 27:200-211.
- Kennedy, R.P., Darrow, A.C., Short SA. (1979). Seismic design of oil pipe systems, *Journal of Technical Councils of ASCE*, 105:119-134.
- Kennedy, R.P., Kincaid, R.H. (1983). Fault crossing design for buried gas oil pipelines. *Pressure Vessels and Piping*, ASME, 77:1-9.
- Lingwall, B.N. (2001). Development of an Expanded Polystyrene Geofoam Cover System for Pipelines at Fault Crossings, PhD Dissertation, University of Utah, UT, USA.
- Matsubara, K., and Hoshiya, M. (2000). Soil Spring Constants of Buried Pipelines for Seismic Design, *Journal of Engineering Mechanics*, ASCE, 126:76-83.
- Multidisciplinary Council on Earthquake Engineering Research (MCEER), (1999). *Response of Buried Pipelines Subject to Earthquake Effects*, MCEER Monograph No. 3, MCEER, Buffalo, NY, USA.
- Newmark, N.M., Hall, W.J. (1975). Pipeline design to resist large fault displacement, *Proceedings of U.S. National Conference on Earthquake Engineering*, EERI, Ann Arbor, MI, USA, 1:416-425.
- Vougioukas, E.A., Theodossis, C., Carydis, P.G. (1979). "Seismic analysis of buried pipelines subjected to vertical fault movement." *Journal of Technical Councils of ASCE*, ASCE, 105:432-441.
- Wang, L.R., Wang L.J. (1995). Parametric study of buried pipelines due to large fault movement, *ASCE TCLEE Monograph 6*, ASCE, 6:152-159.
- Winkler, E. (1867). *Die lehre von elastizität und festigkeit*, H. Dominicus, Prague, Czech Rep.
- Yoshizaka, K., and Sakanoue, T. (2003). Experimental Study on Soil-Pipeline Interaction Using EPS Backfill, *Pipelines 2003*, ASCE, Baltimore, USA, July 2003, 1:1126-1134.

Analytical Approach of Junction Property Evaluation of Geogrids by Designing with Clamping System

H.Y. Jeon, Y Jin, Division of nanosystem engineering, Inha University, Korea(Rep.), hyjeon@inha.ac.kr

ABSTRACT

Geogrids are used as reinforcement materials with a significant mutual effect on the surrounding soil. This mutual effect can be explained by friction between the soil and geogrid surface, as well as the transfer of passive resistance of the cross direction rib to the geogrid machine direction rib via the junction to accommodate the load of the soil. Therefore, geogrids should have sufficient junction strength to maintain the mutual effect with the surrounding soil. In general, the junction strength is calculated using the conversion equation recommended in GRI GG-2. On the other hand, the GRI GG-2 test has inherent weakness in not being able to consider the scale effect of geogrid specimens. Recently, a newly developed multi-clamp was used to test the junction strength. This method gives the junction strength considerable scale efficiency in a better way. In this study, a range of test conditions including the junction number, strain rate and specimen length, were examined to determine their effect on the junction strength. The normalized geogrid junction strength was calculated. The data was used to assess the optimization conditions for the testing multi-junction strength. The results demonstrate the suitability of using the multi-junction strength test considering the scale effect.

1. INTRODUCTION

Textile geogrids are representative reinforcement materials consisting of connected parallel sets of intersecting ribs with an aperture of sufficient size to allow strike-through of the surrounding soil, stone or other geotechnical materials. Therefore, a geogrid is a matrix like material with large open spaces called apertures between the ribs, which are typically 10 to 100 mm, and are known as longitudinal and transverse ribs [1]. The network structure of a geogrid has a stronger interaction with the adjacent soil than other sheet type reinforcements. In general, the interaction between the soil and geogrid is divided into 3 terms; (a) friction between the geogrid and adjacent soil, (b) soil to soil friction in direct contact with apertures and (c) passive resistance of the cross direction ribs of geogrids. Geogrids impose loads due to friction of the cross direction rib surface to the soil and the transfer of passive resistance of the cross direction ribs through the junction with the mechanical direction rib. Therefore, adequate junction strength is needed to carry the induced force. GRI GG-2 with a "T" shaped specimen is used widely. This method can determine the single junction strength, junction efficiency, and geogrid junction strength. The initial values of the single-junction strength and junction efficiency are obtained directly from the test results. On the other hand, this method assumes a linear relationship between the junction strength and junction number. The geogrid junction strength is calculated using the conversion equation recommended in GRI GG-2 [2]. Most of the geosynthetics employed in civil engineering are used as tensile members, and are subject to an assessment of their tensile strength by taking a specimen of a wide width. Therefore, more reliable test methods that include the scale effect are needed. The current trend in the assessment of the tensile strength of geosynthetics involves tensile strength tests on a specimen with a width as wide as possible. This technique can provide more accurate and reliable test data, considering the scale effect of a specimen. This paper proposes a multi-junction test method to assess the geogrid junction strength by considering the aperture size scale effect.

2. EXPERIMENTAL

2.1 Preparation of Geogrid

Polyethylene-terephthalate (PET) filament woven and warp knitted geogrids with polyvinyl chloride (PVC) coating were used. Table 1 lists the specification and physical properties of geogrids.

Table 1. Specifications of the geogrids.

Geogrid	Raw Material /Coating Agent	Number of ribs (/m)	Mechanical properties	
			Ultimate Strength (ton/m)	Elongation at Break (%)
W-GG-1	PET/PVC	47	6	12
W-GG-2	PET/PVC	38	10	12
WK-GG-1	PET/PVC	42	6	12
WK-GG-2	PET/PVC	38	10	12

2.2 Single and Multi-Junction Tests

The testing apparatus shown in Fig. 1 (a) is used mainly for assessing the single junction strength of a geogrid according to the GRI GG-2. The test method uses a clamping fixture that grips the transverse ribs of the geogrid immediately adjacent to and on each side of the longitudinal rib. The lower portion of the longitudinal rib is gripped in a standard clamp. Each clamp is mounted in a tensile testing machine, where the test specimen is pulled apart.

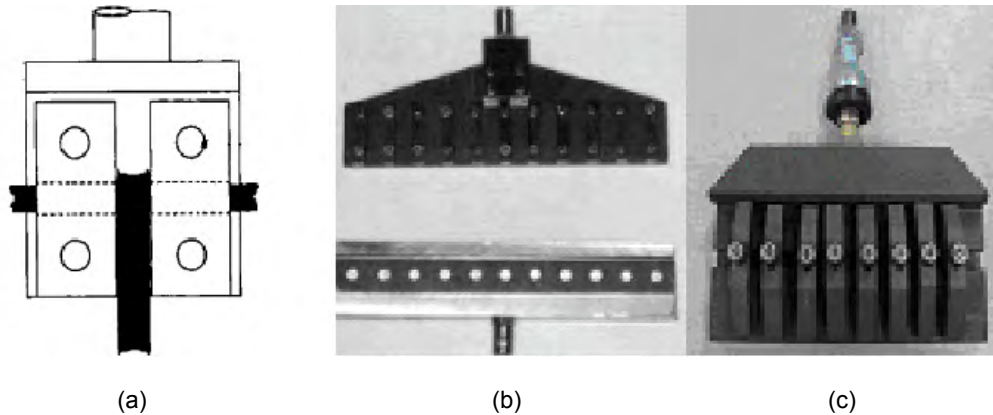


Figure 1. Overview of the junction test clamp (a) single junction test clamps (b) old designed multi-junction clamp (c) newly designed multi-junction clamp

In this study, a single-junction test was carried out using multi-junction clamp device. From the test results, the geogrid junction strength and junction efficiency (standard) was calculated using the following equations (eq. 1~3).

$$J_{rib} = \sum_{i=1}^n J_i / n \quad (1)$$

$$J_{grid} = (J_{rib}) (n_{junction}) / w \quad (2)$$

$$E_{junction} = (J_{rib} / T_{rib}) \times 100 \quad (3)$$

where, J_{rib} =single-junction strength (average);
 J_i =single junction strength of each junction (experimental value);
 n = the total number of test specimens;
 J_{grid} = the geogrid junction strength per unit width;
 $n_{junction}$ = the number of junctions in a unit width; w = unit width (typically 1 m or 1 ft);
 $E_{junction}$ = the junction efficiency; and
 T_{rib} = the tensile strength of single rib (GRI GG-1).

Previous studies [3-4] employed an old designed multi-junction clamp to test the geogrid junction strength (Fig. 1 (b)). The basic concept for this equipment was to widen the single junction test clamp and the point-to-point length was

determined by the aperture size of the test conditions. For the old designed multi-junction test, the point-to-point length and width of the clamp was 25 mm and 280 mm, respectively. The upper clamp had 11 gripping points for the junctions and the lower clamp was a flat type with 11 gripping points. Using the modified method, the geogird junction strength should be more reasonable than that obtained from the single junction test. On the other hand, this type of clamp is only suitable for testing geogrids with an aperture size of 25 mm. A newly developed multi-clamp was used recently to test the junction strength. This is composed drawing a multi-junction grip. The clamp is composed of a set of single grips in parallel. The pitch of the clamp grips can be adjusted freely. The total number of restraining grips is 9. In the lower part, a normal type rib clamp was used. Fig. 2(c) shows the newly designed multi-junction clamp with 8 grips. The experimental results are reported in terms of the multi-junction strength per specific number of ribs. The geogrid junction strength per unit width was calculated using the following equations (Eq. 4~6):

$$J_{\text{multi-rib}} = \sum_{i=1}^n J_{i\text{-multi}}/n \quad (4)$$

$$J_{\text{grid}} = \frac{(J_{\text{multi-rib}})(n_{\text{junction}})}{(W)(n_{\text{test}})} \quad (5)$$

$$E_{\text{junction}} = (J_{\text{grid}} / T_{\text{wide-width}}) \times 100 \quad (6)$$

where $J_{\text{multi-rib}}$ = the junction strength of a specimen width with i number of junctions (average);
 $J_{i\text{-multi}}$ = the each junction's junction strength width with i number of junctions (experimental value);
 n = the total number of test specimens;
 J_{grid} = the geogird junction strength per unit width;
 n_{junction} = the number of geogird junction per unit width;
 W = the unit width (typically 1m or 1 ft);
 n_{test} = the number of junction in the tested specimen;
 T_{grid} = the geogrid tensile strength per unit width.

To evaluate the effectiveness of the newly developed multi-junction testing apparatus and test conditions (strain rate, specimen length and junction numbers), a multi-junction clamp was employed to determine the junction strength with a test speed of 20, 50 and 100 mm/min under ambient conditions. 1~8 rib specimens were gripped in the clamps and the gauge length was 50mm, 100mm and 150mm. The single junction test samples were prepared according to the GRI-GG 2 test method and the test process was performed according to the ASTM D4595 for the united test condition. Multi-junction tests have been used under the same testing conditions and procedures, as ASTM D4595 except for the clamp devices.

2.3 Single and Wide-width Tensile Tests

Single and wide-width tensile strength test conditions were used according to the ASTM D4595 test method. A roll grip clamp was used in this test. Table 2 lists the total test conditions. The test data was compared with those of the junction tests.

Table 2. Test condition

Properties	Single junction test	Multi- junction test	Single tensile test	Wide-width tensile test
Scale effect	Unconsidered	considered	Unconsidered	Considered
Strain rate (mm/min)	70 (20, 50, 100)	70 (20, 50, 100)	70	70
Specimen width	1 rib	1~8rib (200 mm)	1 rib	200 mm
Specimen length (mm)	300 (50, 100, 150)	300 (50, 100, 150)	300	300

3. RESULTS AND DISCUSSION

3.1 Optimization of Geogrids Multi-Junction Strength Evaluation

Table 3 lists the test results of the single junction strength classified according to the grip position. In the GRI GG-2 test method, the upper grip position is as close as possible to the vertical center rib. This newly developed test method recommends that the upper grip position be in the middle of the vertical center rib. The single junction strengths tested using the new developed methods were lower than those tested according to the GRI GG-2 for woven and warp knitted geogrid. The elongation values displayed an opposite trend to the strength. GRI GG-2 determines the specimen under ideal conditions to examine the maximum junction strength. On the other hand, in soil, the cross rib of the geogrids suffers from variable curvature ribbing, and the center bearing rib is at the peak of the curvature. Therefore, gripping the center of the cross rib is more appropriate for representing the actual utilizing conditions. Nevertheless, the junction test is an index test, not a performance text, even if it is adjusted from one junction to 8 junctions.

Table 3. Single-junction test results according to the grip position.

Geogrid	Value	20 mm/min		50 mm/min		100 mm/min	
		GRI	New	GRI	New	GRI	New
W-GG-1	J_{single} (kgf)	12.0	11.4	12.5	11.6	13.6	12.8
	Elongation (mm)	2.2	2.4	2.5	2.8	2.5	2.7
W-GG-2	J_{single} (kgf)	19.2	18.5	19.8	18.8	20.4	19.7
	Elongation (mm)	3.9	4.1	4.2	4.3	4.2	4.7
WK-GG-1	J_{single} (kgf)	28.2	27.1	30.1	27.5	28.5	27.7
	Elongation (mm)	6.1	6.3	5.8	6.7	5.9	6.3
WK-GG-2	J_{single} (kgf)	39.1	37.7	39	38	39.6	38
	Elongation (mm)	7.0	7.4	6.4	7.4	6.6	7.0

Similar to the single junction test, the mean junction strength per rib and the geogrid junction strength per unit width were also calculated using multi-junction test results. Firstly, geogrids with 1-8 junctions were tested and the curves of the junction strength to the number of junctions were plotted. Secondly, normalized values of the junction strength were calculated for each sample. Fig. 2 shows the junction strength plotted as a function of the number of junctions in different specimen lengths. The junction strength obtained at different lengths showed no change in junction strength at the rupture point because woven and warp knitted materials contained a PET filament. Therefore, to derive precise data, the same conditions except for the specimen length were summarized and analyzed.

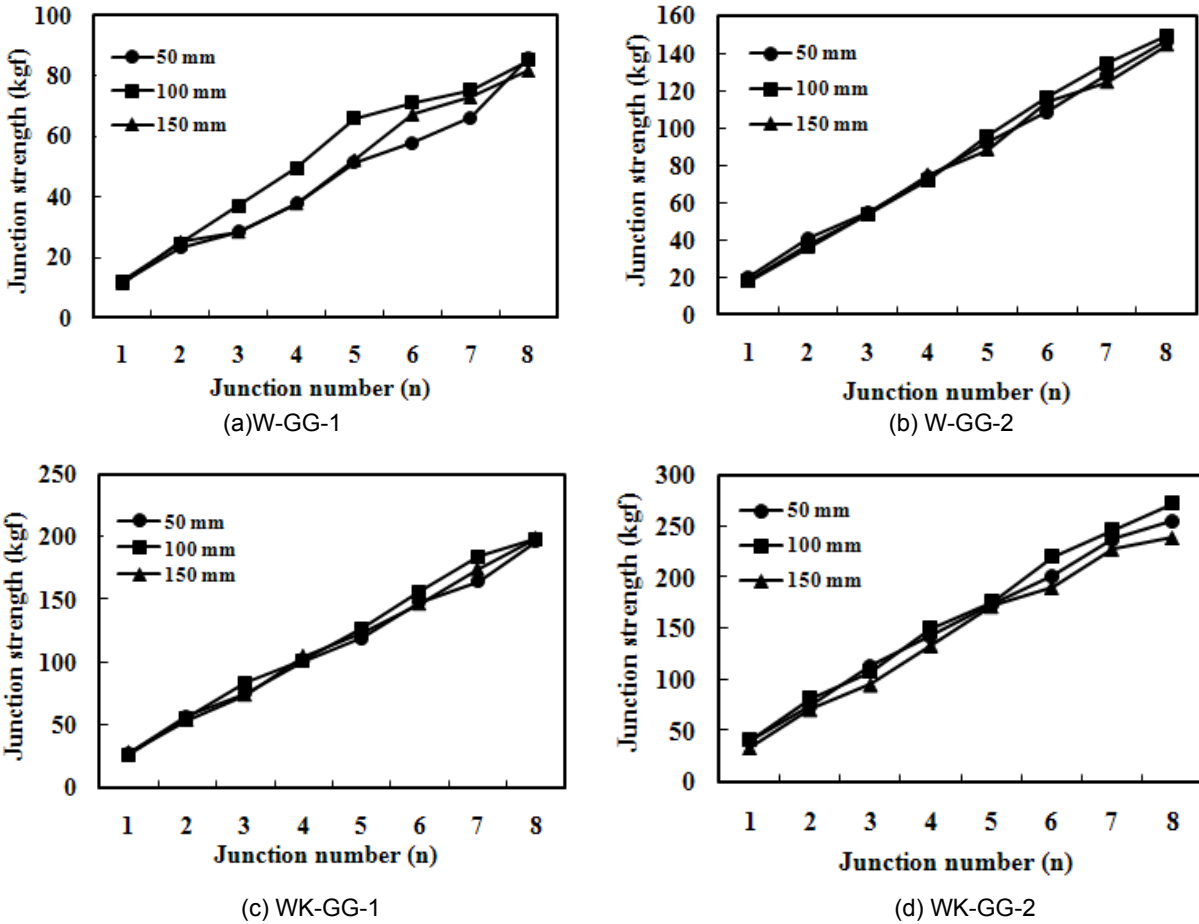
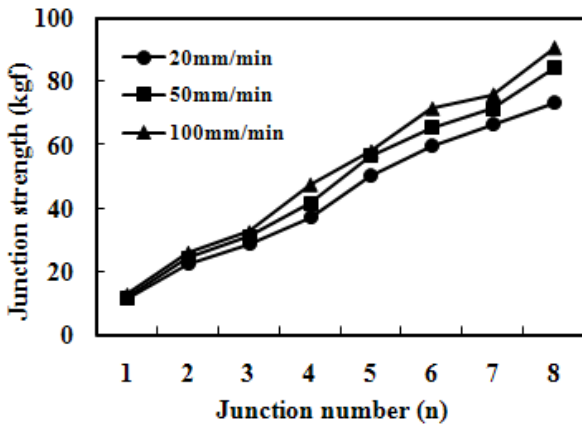
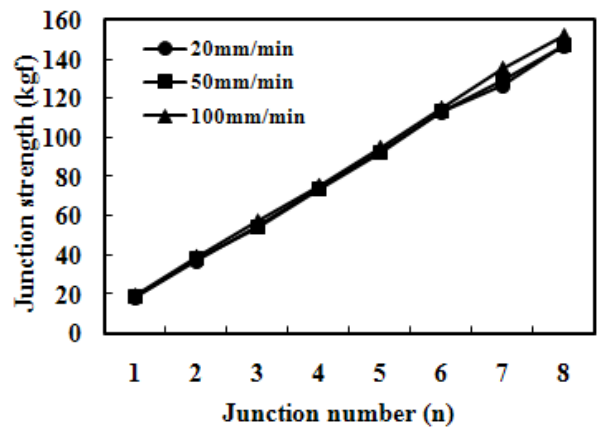


Figure 2. Regression analysis of the junction strength as a function of the number of junctions at different specimen lengths for geogrids.

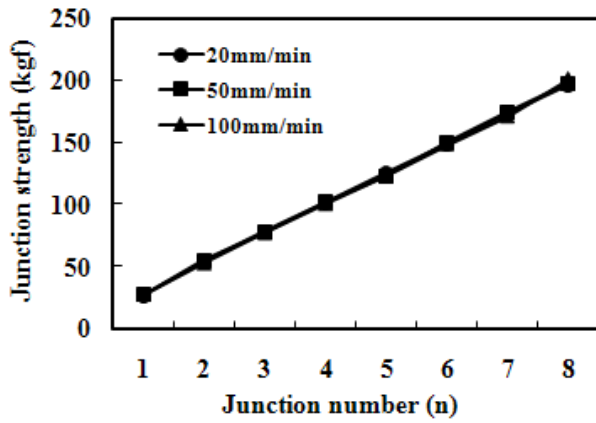
Fig. 3 show the regression analysis results of the number of junctions as a function of the junction strength with the strain rate of geogrids. All the plots were divided uniformly and the curves showed a similar trend. Therefore, the data has good reliability. The junction strength increased linearly with the number of junctions. This difference was attributed to the scale effect and variation in the difference in manufactured products. Fig. 4 shows the relationship between the number of junctions and normalized junction strength with the strain rate of the geogrid. The woven geogrid junction strength depends strongly on the junction number, whereas the strength does not change significantly if the number of junctions is increased to three or more. Fig. 5 shows that the woven geogrids show residual strength over the peak strength. When the woven geogrid junctions were pulled out, the load-strain curve was just drawn by each member value mathematically, and the peak point appearance was not affected by any member over the peak strength. When the junction number was more than 3, their mutual-effect almost reached equilibrium and the data was stabilized. The woven geogrid junction strength increased with the strain rate due to a pulling-out mechanism. The abrasion force also increased with increasing strain rate. The multi-junction test indicated that a woven geogrid specimen with more than 3 junctions can provide reliable data of the junction strength with the scale effect taken into consideration. For warp knitted geogrids, each normalized value decreased lineally, whereas the junction number increased. This is because the warp knitted geogrid has no residual strength. Therefore, when the multi-junction strength was tested, the point peak can be determined provided at least one of the junctions is broken up. The strain rate had no effect on the warp knitted type. From this review, normalization of the junction strength is more reasonable with increasing number of junctions for a warp knit geogrid. Therefore, the junction width should be as wide as possible to consider the sufficient scale effect.



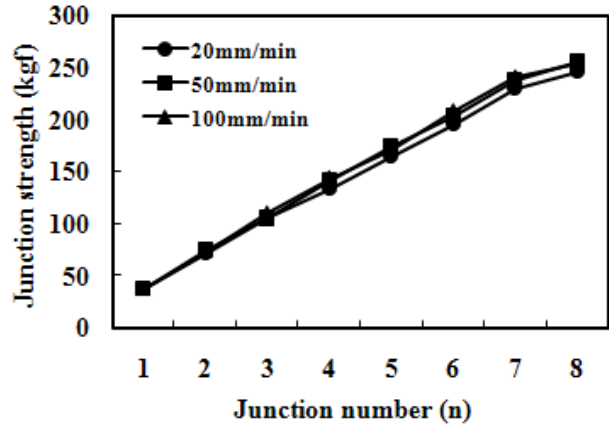
(a) W-GG-1



(b) W-GG-2

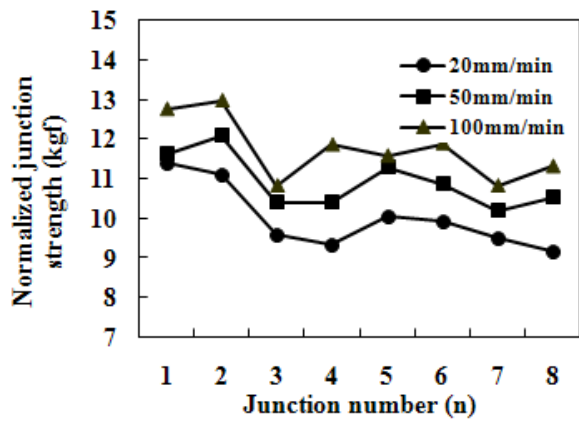


(c) WK-GG-1

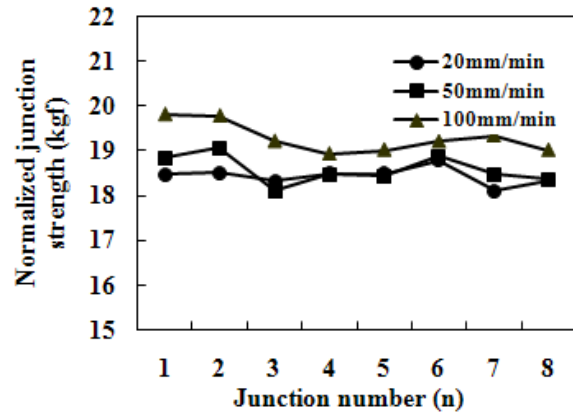


(d) WK-GG-2

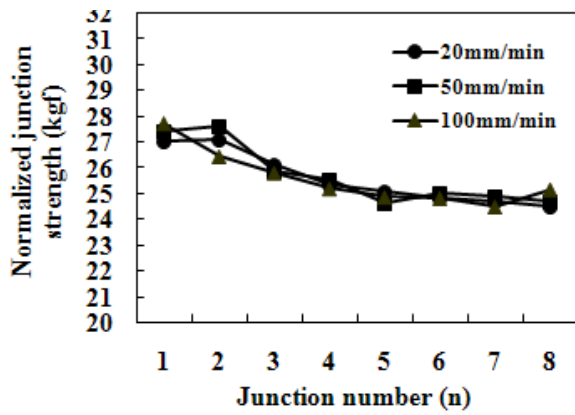
Figure 3. Regression analysis of the junction strength as a function of the number of junctions versus at different strain rates for geogrids.



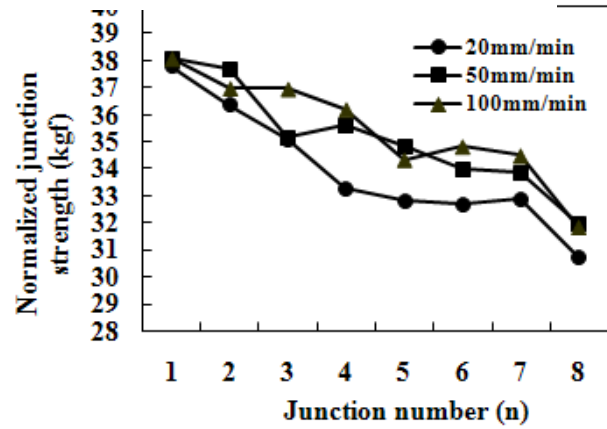
(a) W-GG-1



(b) W-GG-2



(c) WK-GG-1



(d) WK-GG-2

Figure 4. Relationship between the normalized junction strength and the number of junctions at different strain rates.

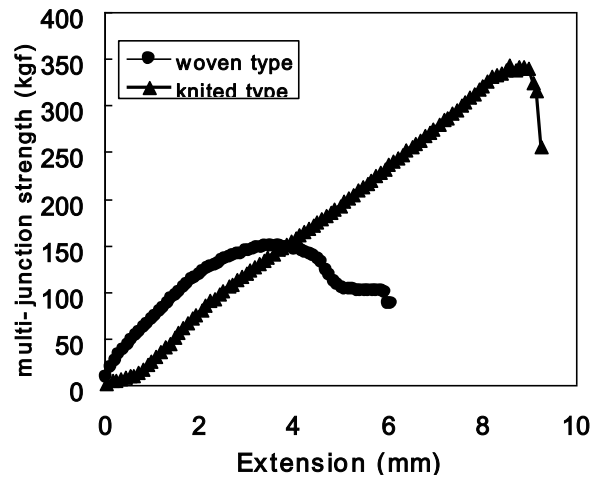


Figure 5. Typical load-extension curves of the multi-junction test

3.2 Analysis of Tensile Property and Junction Property for Geogrids

Table 4 lists the results of the multi-junction test proposed in this study. The mean and standard deviation of the test results were also calculated. The data deviation was uniform, and the maximum and minimum value have been selected and discarded to derive reliability data.

The results of the single and multi-junction tests were compared with those of the single and wide-width tensile tests. (Table 5). Equations 1, 2 and 3 were used to calculate the geogrid junction strength and junction efficiency (standard). These calculated values were compared with the values from the multi-junction strength test calculated from Equations 4, 5 and 6 (proposed). The multi-junction test values were lower than the single-junction test values due to the scale-effect. The scale-effect exists in both tensile and junction tests. On the other hand, a comparison of the results of the single tensile test and wide-width tensile test revealed a slight change because of the stable tensile strength and handling process. The scale effect in the junction test was much lower than the tensile test particularly the warp knitted geogrid. This was attributed to the single-junction strength data of the product distribution being more disordered than the single tensile test. Moreover, the multi-junction clamp has a greater tendency to error during handling. Therefore, multi-junction tests result in a large decrease in strength.

Table 4. Results of the multi-junction strength test.

Test no.	W-GG-1		W-GG-2		WK-GG-1		WK-GG-2	
	Strength (kgf)	Strain (%)	Strength (kgf)	Strain (%)	Strength (kgf)	Strain (%)	Strength (kgf)	Strain (%)
1	122	3.32	159	3.72	245	8.25	249	7.07
2	111	3.55	163	4.1	260	8.58	252	7.11
3	118	3.41	154	4.04	265	9.31	259	7.36
4	125	3.45	152	3.95	272	9.45	257	7.32
5	110	2.94	169	4.36	272	8.49	246	8.18
6	123	3.19	175	3.75	289	9.1	258	7.44
7	113	3.44	167	4.34	271	8.61	271	7.73
8	118	3.66	170	3.58	277	9.9	222	6.08
9	108	4.29	169	4.14	289	9.24	242	6.95
10	105	3.51	175	4.03	279	8.99	251	7.26
AVERAGE	115.7	3.5	166.3	4.0	273.6	8.9	253.3	7.3
SD ¹	5.68	0.40	6.72	0.29	9.1	0.49	6.61	0.38

¹SD is standard deviation.

Table 5. Results of the tensile and junction test.

Geogrid	$T_{\text{single-rib}}$ (T/m)	$T_{\text{wide-width}}$ (T/m)	$T_{\text{scale effect}}$	$J_{\text{single-rib}}$ (T/m)	$J_{\text{wide-width}}$ (T/m)	$J_{\text{scale effect}}$
W-GG-1	7.6	7.9	1.04	0.56	0.54	0.97
W-GG-2	13	12.8	0.98	0.86	0.79	0.92
WK-GG-1	8	7.8	0.97	1.43	1.29	0.9
WK-GG-2	12.8	13.1	1.02	1.52	1.2	0.79

Table 6. Junction efficiency of geogrids.

Value	Geogrid			
	W-GG-1	W-GG-2	WK-GG-1	WK-GG-2
E_{single}	7.4	6.6	17.9	11.9
$E_{\text{wide-width}}$	6.84	6.2	16.5	9.2

Table 6 lists the junction efficiency derived from Equations 3 and 6. The multi-junction test values were slightly lower than the single junction test values due to the scale effect of the multi-junction test, which is larger than wide-width tensile test. Moreover, the multi-junction test method can be more accurate in representing the junction efficiency than the single-junction test considering the scale effect.

4. CONCLUSION

Junction strength of warp knitted geogrid decreased with increasing number of junctions, whereas the woven geogrid had a similar value for 3~8 junctions except for a decrease of up to 3 junctions. The junction strength of woven geogrid increased with increasing strain rate, whereas the strain rate had no effect on the warp knitted geogrid. The specimen length did not affect the junction strength. Similar to the tensile test, the geogrid junction strength determined from the multi-junction test was lower than that from the single junction test due to the scale effect of the specimen. The geogrids junction strength and junction efficiency can be evaluated using the geogrids multi-junction test method considering the scale effect. The clamp width should be as wide as possible for a warp knitted geogrid to hold the maximum number of junctions, and a clamp width with a holding capacity of 3 junctions is needed for a woven geogrid.

REFERENCES

- Koerner, R.M., (2005). *Designing with Geosynthetics*, 5th Edition, Person, Education Inc., Upper Saddle River, NJ, USA.
- GRI, GRI Test Method GG-2, (2002). *Geogrid Junction Strength*, Geosynthetics Research Institute, Drexel University, PA, USA.
- Jeon, H.Y., Yuu, J.J. (2003). "Assessment of junction strength of geogirds by a multi-junction test method", *Polymer Testing*, 22, pp. 267-274.
- Jeon, H.Y., Yuu, J.J. (2000). "Test method of wide-width geogrid junction strength", *Proceedings of the 1st China International Geosynthetics Conference*, Shanghai, pp. 188-197.

Antioxidant Depletion of HDPE Geomembrane Without HALS in an Extreme Environment

Fady B. Abdelaal, GeoEngineering Centre at Queen's-RMC, Queen's University, Canada,
fady.badran@ce.queensu.ca

R.Kerry Rowe, GeoEngineering Centre at Queen's-RMC, Queen's University, Canada,
Kerry@civil.queensu.ca

ABSTRACT

High density polyethylene (HDPE) geomembranes (GMBs) play the primary role in composite liner systems used as hydraulic barriers. Performance of this function is contingent on how long the GMB remains intact without developing more than a limited number of holes during construction. The main source of long-term hole formation in liners is cracking that occurs after degradation of the polymer. This long-term effect will occur after the GMB has lost the protection of antioxidants and have become vulnerable to degradation (e.g., oxidation) and a consequent failure can occur even at low over burden stresses. The rate of antioxidant depletion and geomembrane degradation is a function of its compatibility with exposure media and this should be assessed for each type of exposure to ensure that there will be adequate liner durability and long-term performance. HDPE GMBs are now widely used in applications involving extremely high pH such as certain heap leach applications and mining ponds, the Bayer process, low-level radioactive waste and brine ponds. These applications involve the exposure of the liner to pH between 9.0 and 14.0. Although the durability of HDPE GMBs has been extensively investigated in the last two decades, there is a paucity of research into the performance of HDPE GMBs in these high pH solutions. To investigate the durability of HDPE GMBs in these environments with high pH, an extensive study was initiated looking at pH, GMB type, antioxidant package and GMB thickness on the service life of GMB in mining applications. In this paper, antioxidant depletion rates for geomembrane incubated in a solution with a pH = 13.5 are presented and a preliminary extrapolation to field temperature is provided. Results from standard OIT test are presented for a geomembrane without hindered amine light stabilizers (HALS).

1. INTRODUCTION

1.1 Geomembrane Durability

Geomembranes (GMB) are typically used in many environmental applications acting as a hydraulic barrier layer. High density polyethylene (HDPE) with density $\geq 0.941 \text{ g/cm}^3$ (ASTM D883) and linear low density polyethylene (LLDPE) with density between 0.919 and 0.925 g/cm^3 (ASTM D883) are the most commonly used PE GMBs in modern geoenvironmental applications. Typically GMBs are formulated from 94-98% PE resin, 2-3% carbon black, and 0.25-3% antioxidants and additives (Koerner et al. 2005). Chemical and environmental exposure of the GMB can cause various degradation mechanisms such as physical degradation, chemical degradation, biological degradation, ultraviolet degradation, degradation by swelling, degradation by extraction, oxidative degradation and thermal degradation (Haxo and Nelson 1984; Sangam and Rowe 2002). Performance of a GMB is contingent on how long the GMB remains intact without developing more than a limited number of holes during construction. The main source of long-term hole formation in liners is cracking that occurs after degradation of the polymer.

According to Hsuan and Koerner (1998), HDPE pass through three distinct stages during its service life. In Stage I; HDPE will start to lose its antioxidants either physically (due to volatilization and solvent extraction) or chemically consumed by free radicals. The depletion of antioxidant increase with time, reaching residual values that is not sufficient to protect the GMB. In the Stage II, the HDPE can resist degradation for some time after depletion of antioxidant (Stage I) without any measurable reduction in its physical properties. In the last stage (Stage III), degradation of the polymer takes place and a change in its physical properties is measurable. The end of the service life is defined when a specific property (e.g. tensile property per ASTM D5397; Melt index (MI) per ASTM D1238; stress crack resistance (SCR) per ASTM D5397) degrades with time to reach 50% of its initial (or specified) value.

1.2 Heap Leaching Applications

Heap leaching is a common geoenvironmental application for GMBs. Heap leaching is a mining technique where mineral ores (most commonly metallic) are crushed and staked in heaps on a lined pad. The heaps are usually irrigated with an acid or a base (based on the ore type and mineral) to extract the mineral from the ore in relatively short times. The leached solution which contains the dissolved mineral is called the pregnant leach solution (PLS). The PLS, which is characterized by its extreme pH and high metal concentration, is collected to be processed for mineral extraction.

Copper, uranium and nickel heap leaching are examples of acidic PLS where sulfuric acid is used in the irrigation of the heap. This results in an extremely low pH PLS that is in contact with the GMB. The pads are usually lined with a composite liner having, in addition to the GMB primary liner, a low hydraulic conductivity soil acting as a secondary liner such as compacted clay liner (CCL) or geosynthetic clay liner (GCL).

HDPE GMBs are now widely used in applications involving extremely high pH such as certain heap leach applications, mining ponds, the Bayer process and brine ponds. These applications involve the exposure of the liner to pH between 9.0 and 14.0. According to Kappes (2002) leaching gold and silver from their ores are similar where diluted sodium cyanide is used to dissolve the metals without dissolving other metals like copper and zinc. To reduce the mobilization of other minerals, the solution is maintained at pH of 9.5 to 11 by adding lime. In addition to mining applications, GMBs can be relied on to provide containment in stabilized hazardous solid waste landfills and low-level nuclear waste landfills. Low-level radioactive waste typically has a high pH in the range of 9-12.5 and has low concentrations of radioactive elements (Abdelaal et al. 2011).

Although the durability of HDPE GMBs has been extensively investigated in the last two decades, there is a paucity of research investigating the performance of HDPE GMBs in high pH solutions. Thus, to investigate the durability of HDPE GMBs in such environments with high pH, an extensive study was initiated looking at pH, GMB type, antioxidant package and GMB thickness effects on the service life of GMB in mining applications. The full test matrix together with the chemistry of the tested solutions is provided in Abdelaal et al. (2011). In this paper, antioxidant depletion rates for a 1.5 mm HDPE GMB incubated in a solution with a pH=13.5 are presented.

2. EXPERIMENTAL INVESTIGATION

GMB coupons (190 mm by 100 mm) were incubated in 4 liter glass containers separated with 5mm glass rods. The GMB tested is a 1.5mm HDPE (Table 1) where its additives package does not contain hindered amine light stabilizers (HALS) as previously indicated by Rowe et al. (2010b). GMB coupons are immersed in three different immersion solutions (Table 2) and incubated in forced air ovens at different temperatures. The temperatures used in this study are 75, 85, and 95°C allowing the accelerated ageing of the GMB in order to obtain antioxidant depletion times in convenient testing time frames. The use of the 95°C temperature was adopted after the findings of Rowe et al. (2010a) that showed consistent antioxidants depletion rates at 95°C together with the lower temperatures without changing in the depletion mechanism for both water and synthetic municipal solid waste (MSW) leachate.

Table 1. Index properties of the virgin geomembrane examined in this study.

Property	method	Values
Nominal thickness (mm)	ASTM D5199	1.5
Std-OIT (minutes)	ASTM D3895	100 ± 2.0 ¹
HP-OIT (minutes)	ASTM D5885	273 ± 16
Suspected HALS ²	--	No
Crystallinity (%)	ASTM E794	48
Density	ASTM D1505	0.947
Melt flow index (g/10min)	ASTM D1238	14.3 ± 0.8
Single point stress crack resistance (SCR) (hours)	ASTM D5397	840 ± 220 ⁵
Strength at yield MD ³ (kN/m)	ASTM D6693	27.0 ± 1
Strength at break MD (kN/m)	ASTM D6693	46.0 ± 5.0
Strain at yield MD(%)	ASTM D6693	24.0 ± 2
Strain at break MD (%)	ASTM D6693	825 ± 80
Strength at yield XD ⁴ (kN/m)	ASTM D6693	29.0 ± 0.5
Strength at break XD (kN/m)	ASTM D6693	44.0 ± 6.0
Strain at yield XD(%)	ASTM D6693	19.0 ± 0.4
Strain at break XD(%)	ASTM D6693	830 ± 95

¹Virgin OIT presented here differs from that reported in Rowe et al 2010 (a,&b) due to ageing of the roll in room temperature between the time of their tests and these tests;

²Hindered Amine light stabilizers;

³MD: Machine direction;

⁴XD: Cross machine direction;

⁵Based on a strength at yield in XD of 29kN/m. Additional replicates were tested since Abdelaal et al. (2011; 2012) resulting in a slightly higher average SCR reported here than in those earlier publications.

The chemical composition for the high pH solution presented in this study is simulating extreme pH of the PLS for gold, silver, aluminum heap leaching and low-level radioactive waste leachates. For safety reasons, both cyanide found in gold and silver PLS and radionuclides found in low-level radioactive waste leachate were excluded from the extreme high pH solution simulated in the current study. The selected chemistry of the high pH solution used (Table 2) represent the low metal concentrations found in the low-level radioactive waste to minimize the precipitation of the salts at such extremely high pH.

Table 2. Chemistry of the immersion solutions used in the current study

Analyte	Water ¹	MSW leachate ³	Solution pH=13.5 ⁴
pH	~7.0	~6.0	13.5
Aluminum	<1.0	0.0013	0.30
Ammonium	--	0.00073	--
Cadmium	<0.025	--	--
Calcium	0.10~0.30	--	--
Cobalt	<0.02	0.031	0.03
Copper	<0.2	0.01	10.3
Iron	<0.05	0.4	0.01
Lead	<0.03	--	--
Lithium	--	--	--
Magnesium	<0.05	--	3.0
Manganese	<0.05	0.163	--
Nickel	<0.3	0.111	0.08
Potassium	0.2~0.6	--	200
Sodium	1.0~1.6	0.086	27590
Zinc	<0.01	0.011	0.02
Chloride	--	--	--
Sulphate	--	3.04	311
Surfactant ²	--	5ml/l	--

¹ Reverse osmosis water; also used as water an in the preparation of MSW leachate and Solution 1.

² IGEPAL Ca-720

³ Calculated from Rowe et al. (2010b)

⁴ Abdelaal et al. (2011) calculated values

3. RESULTS AND DISCUSSIONS

3.1 Antioxidant Depletion Results

A differential scanning calorimeter (DSC) was used to obtain the standard oxidative induction time (Std-OIT) for the GMB specimens in accordance to ASTM D3895. Since the GMB presented in the current study does not have HALS, Std-OIT was solely used as an indicative tool for the antioxidant depletion stage. A first order exponential decay relationship (Hsuan and Koerner 1998) is used to depict antioxidant depletion rates in terms of Std-OIT depletion:

$$\text{Std-OIT}_t = (\text{Std-OIT}_o) e^{(-st)} \quad [1]$$

or, by taking the natural logarithm on both sides:

$$\ln(\text{Std-OIT}_t) = -st + \ln(\text{Std-OIT}_o) \quad [2]$$

where Std-OIT_t is the standard OIT remaining at any time t (min), Std-OIT_o is the initial standard OIT (min), s is the antioxidant depletion rate (month^{-1}), and t is the ageing time (month).

The variation of $\ln(\text{Std-OIT})$ with incubation time at 75, 85 and 95°C is presented in Figure 1 for a 1.5mm HDPE GMB (Table 1) in solution with pH = 13.5 (Table 2). The relation between $\ln(\text{Std-OIT})$ and time is fitted via linear regression, complying with the OIT depletion data previously presented in different immersion solutions for different GMBs by various investigators (Hsuan and Koerner 1998; Gulec et al. 2004; Rowe and Rimal 2008 a & b; Rowe et al. 2008; Rowe et al. 2009; Rowe et al. 2010 a, b & c; Abdelaal et al. 2011,2012). The slopes of the linear regressions, presented in Table 3, are the antioxidant depletion rates at different temperatures. For the incubation duration presented (4.5 months), full antioxidant depletion (to residual Std-OIT values) was achieved only at 95°C. Nevertheless, fitting the early data

obtained at 85 and 75°C would result in a conservative (shorter) estimate of antioxidant depletion time than fitting the data at the full depletion of antioxidants as demonstrated by Rimal and Rowe (2009). Consequently, predictions of antioxidant depletion stage at field temperatures presented in the next part, based on the conservative antioxidant depletion rates estimated at 75 and 85°C should result in shorter, hence more conservative, antioxidant depletion times at field temperatures. These estimates will be upgraded as more data comes available.

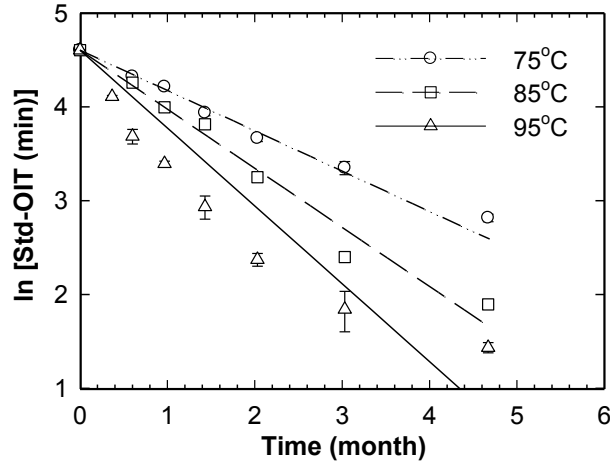


Figure 1. Antioxidant depletion rates (Std-OIT) for solution with pH=13.5 at three elevated temperatures.

Table 3. Antioxidant depletion rates for immersion in solution pH=13.5 at different temperatures.

Temperature (°C)	Antioxidant depletion rate (s) (month ⁻¹)
95	0.83
85	0.63
75	0.43

3.2 Antioxidant Depletion Predictions at Field Temperatures

A time temperature superposition technique (Arrhenius model) was used to extrapolate the antioxidant depletion rates at site specific temperatures. The Arrhenius equation, as presented by Hsuan and Koerner (1998) can be written as:

$$s = A \exp(-E_a / (RT)) \quad [3]$$

or, by taking the natural logarithm on both sides:

$$\ln s = \ln(A) - (E_a/R) (1/T) \quad [4]$$

where s = antioxidant depletion rate (month⁻¹), E_a = activation energy (J.mol⁻¹), R = universal gas constant (8.314 J.mol⁻¹.K⁻¹), T = absolute temperature (K), and A = a constant often called the collision factor.

The antioxidant depletion rate(s) at three elevated temperatures presented in Table 3 are used to establish the Arrhenius plot (Figure 2). Arrhenius equation for the HDPE GMB incubated in a solution of pH=13.5 is presented in Figure 2. Table 4 shows the predicted antioxidant depletion times at a potential range of field temperatures based on the Arrhenius equation presented in Figure 2. The antioxidant depletion stage is predicted to be 1.8 and 4.0 years at 60 and 40°C, respectively.

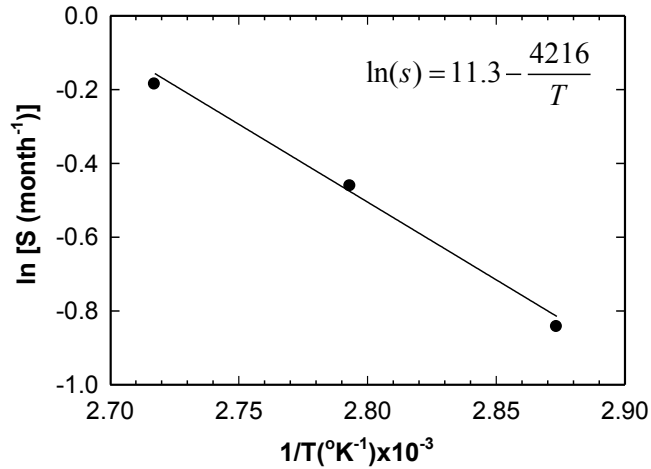


Figure 2. Arrhenius Plot of the antioxidant depletion for GMB immersed in solution pH=13.5

Table 4. Antioxidant depletion rates for immersion in solution pH=13.5 at different temperature.

Temperature (°C)	Antioxidant depletion time (years)
60	1.8
50	2.6
40	4.0

3.3 Antioxidant Depletion at Different Incubation Solutions

Figure 3 shows the antioxidant depletion at 85°C in solution with pH=13.5, water (Rowe et al. 2010a) and MSW synthetic leachate (Rowe et al. 2010b). The chemical compositions together with the pH of the three incubation solutions are presented in Table 2. It can be seen that the antioxidant depletion rates in MSW leachate is the fastest followed by solution with pH=13.5 then water. Table 5 shows the antioxidant depletion rates in different incubation solutions at 85°C. The depletion rate in MSW leachate and water is 1.8 and 0.4 times the depletion rate in solution with pH=13.5, respectively.

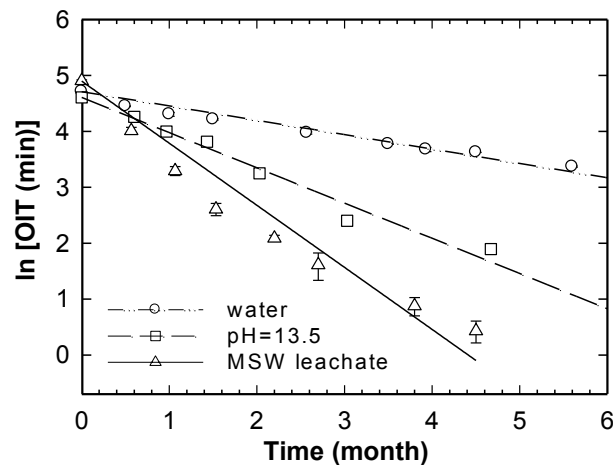


Figure 3. Std-OIT depletion for 1.5mm HDPE GMB in different immersion fluids at 85°C (data in water and MSW leachate are from Rowe et al. 2010a and Rowe et al. 2010b, respectively).

Table 5. Antioxidant depletion rates for immersion in solution pH=13.5 at different temperature (antioxidant depletion rates in water and MSW leachate are from Rowe et al. 2010a and Rowe et al. 2010b, respectively).

Incubation solution	Antioxidant depletion rate (s) (month ⁻¹)
Solution pH=13.5	0.63
Water	0.26
MSW leachate	1.11

4. CONCLUSIONS

Preliminary results were presented in this paper for antioxidant depletion from a 1.5mm high density polyethylene geomembrane in a solution with a pH = 13.5 representing extreme pH seen in some of heap leach pads applications, Bayer process, brine ponds and low-level radioactive waste landfills. The results are compared with those for immersion in water and synthetic municipal solid waste landfill leachate. Based on the testing duration presented in this paper, the following preliminary conclusions have been reached:

- The predicted antioxidant depletion times (Stage I of service life) was about 1.8 years at 60°C, 2.6 years at 50°C and 4.0 years at 40°C,
- The antioxidant depletion in solution with pH=13.5 was faster than water but slower than synthetic municipal solid waste landfill leachate. Antioxidant depletion rates in MSW leachate and water is 1.8 and 0.4 times the depletion rate in solution with pH=13.5, respectively, at 85°C.

The results presented in the current study only apply for the specific HDPE GMB without HALS tested in the immersion solutions presented. As indicated by Rowe and Rimal (2008b) and Rowe et al. (2010c), immersion testing is very extreme and the depletion rate in a real liner application is likely to be much slower (by a factor of 2.9-3.4 at various temperatures) than in the immersion tests. Also these times only represent the first stage of the ageing of the GMB and not the full service life. More testing is underway to investigate a wider range of pHs on different GMBs (LLDPE and HDPE) providing more indicative results on the compatibility of different GMBs in a range of solutions relevant to heap leaching, Bayer process, brine ponds and low-level radioactive waste applications. The full set of results will be published in a subsequent papers when they have been run a sufficient time to draw firm conclusions.

ACKNOWLEDGEMENTS

The research presented in this paper was funded by the Natural Science and Engineering Research Council of Canada (NSERC) and used equipment provided by funding from the Canada Foundation for Innovation (CFI) and Ontario Ministry of Research and Innovation. The authors are grateful to their industrial partners, Solmax International, Terrafix Geosynthetics Inc, Ontario Ministry of Environment, the Canadian Nuclear Safety Commission, AECOM, AMEC Earth and Environmental, Golder Associates Ltd., Knight-Piesold, and the CTT group for their participation in, and contributions to, the overarching project; however the opinions expressed in the paper are solely those of the authors. The authors are especially appreciative of the value of discussions with Rod McElroy, Senior Metallurgist AMEC Mining and Metals, Rick Thiel and Mark Smith.

REFERENCES

- Abdelaal, F.B., Rowe, R.K., Smith, M.E. and Thiel, R. (2011). OIT Depletion in HDPE GMBs used in contact with solutions having very high and low pH, *Pan-Am CGS Geotechnical conference*, Toronto, ON, Canada.
- Abdelaal, F.B., Rowe, R.K., Smith, M., Brachman, R.W.I. and Thiel, R. (2012). Antioxidant depletion from HDPE and LLDPE geomembranes without HALS in and extremely low pH solution, *2nd Pan American geosynthetic conference and Exhibition, Geoamericas 2012*, Lima, Peru.
- ASTM D883-11 Standard Terminology Relating to Plastics, *American Society for Testing and Materials*, West Conshohocken, Pennsylvania, USA.
- ASTM D1238 Standard Test Method for Flow Rates of Thermoplastics by Extrusion Plastometer, *American Society for Testing and Materials*, West Conshohocken, Pennsylvania, USA.
- ASTM D1505. Standard Test Method for Density of Plastics by the Density-Gradient Technique, *American Society for Testing and Materials*, West Conshohocken, Pennsylvania, USA.
- ASTM D3895 Standard test method for oxidative-induction time of polyolefins by differential scanning calorimetry, *American Society for Testing and Materials*, West Conshohocken, Pennsylvania, USA.

- ASTM D5397 Standard Test Method for Evaluation of Stress Crack Resistance of Polyolefin GMBs Using Notched Constant Tensile Load Test, *American Society for Testing and Materials*, West Conshohocken, Pennsylvania, USA.
- ASTM D5885. Standard Test Method for Oxidative Induction Time of Polyolefin Geosynthetics by High-Pressure Differential Scanning Calorimetry, *American Society for Testing and Materials*, West Conshohocken, Pennsylvania, USA.
- ASTM D6693 Standard Test Method for Determining Tensile Properties of Nonreinforced Polyethylene and Nonreinforced Flexible Polypropylene GMBs, *American Society for Testing and Materials*, West Conshohocken, Pennsylvania, USA.
- Gulec, S. B., Edil, T. B. and Benson, C. H. (2004). Effect of acidic mine drainage on the polymer properties of an HDPE geomembrane. *Geosynthetics International*, 2 (11): 60-72.
- Haxo, H. E. and Nelson, N.A. (1984). Factors in the durability of polymeric membrane liners, *Proceedings of the international conference on geomembranes*, IFAL, Denver, Colorado, USA, 2: 287-292.
- Hsuan, Y. G. and Koerner, R. M. (1998). Antioxidant depletion lifetime in high density polyethylene GMBs. *ASCE Journal of Geotechnical and Geoenvironmental Engineering*, 124: 532-541.
- Kappes, D.W. (2002). Precious Metal Heap Leach Design and Practice, *Kappes, Cassidy & Associates*, Reno, Nevada, <http://www.kcareno.com>.
- Koerner, R. M., Hsuan, Y. G., and Koerner, G. R. (2005). GMB lifetime prediction: unexposed and exposed conditions. *GRI White Paper # 6*, Geosynthetics Institute, Pennsylvania, USA.
- Rimal, S. and Rowe, R.K. (2009). Diffusion modelling of OIT depletion from HDPE geomembrane in landfill applications, *Geosynthetic International*, 16(3):183-196.
- Rowe, R.K. (2005). Long-Term Performance of Contaminant Barrier Systems, 45th Rankine Lecture, *Geotechnique*, 55 (9): 631-678.
- Rowe, R.K. and Abdelaal, F.B., Islam, M.Z., and Hsuan Y.G. (2010a). The strange effect of increasing temperature in accelerated ageing of HDPE GMBs immersed in liquids, *9th International Conference on Geosynthetics*, Guarujá, Brazil, 793-798
- Rowe, R.K, Islam, M.Z. and Hsuan, Y.G. (2010b). Effect of thickness on the ageing of HDPE GMBs, *ASCE Journal of Geotechnical and Geoenvironmental Engineering*, 136 (2): 299-309.
- Rowe, R.K., Islam, M.Z., Brachman, R.W.I., Arnepalli, D.N. and Ewais, A. (2010c). Antioxidant depletion from an HDPE GMB under simulated landfill conditions, *ASCE Journal of Geotechnical and Geoenvironmental Engineering*, 136 (7): 930-939.
- Rowe, R.K. and Rimal, S. (2008a). Ageing of HDPE GMB in three composite liner configurations, *ASCE Journal of Geotechnical and Geoenvironmental Engineering*, 134 (7): 906-916.
- Rowe, R.K. and Rimal, S. (2008b). Depletion of antioxidant from HDPE GMB in a composite liner, *ASCE Journal of Geotechnical and Geoenvironmental Engineering*, 134 (1): 68-78.
- Rowe, R.K, Islam, M.Z., and Hsuan, Y.G. (2008). Leachate chemical composition effects on OIT depletion in HDPE GMBs, *Geosynthetics International*, 15 (2): 136-151.
- Rowe, R.K., Rimal, S. and Sangam, H.P. (2009). Ageing of HDPE geomembrane exposed to air, water and leachate at different temperatures, *Geotextiles and Geomembranes*, 27 (2) 131-151.

Beach Restoration of Coastal Town to Increase Tourism

A. H. Diaz, Geomembranas y Geosinteticos SA de CV, Mexico, D.F.
Coauthors –E. Trainer& T. Stephens, TenCate Geosynthetics. Pendergrass, Georgia.
A. Arriaga-Noguez, Geomembranas y Geosinteticos SA de CV. Mexico, D.F.



ABSTRACT

This paper describes the use of Geotextile tubes for shoreline protection of a coastal town, to increase economical activities. The project was originated from serious erosion of an entire coastline, a situation which worsened in 2007 with the Cold Front #4, causing severe losses in buildings and major lagoons that represent an important aquaculture production source. From this event the authorities took emergency measures to stem the damage, by developing a first stage recovery in 2008 with the installation of Geotextile tubes to protect 300 linear meters of the coastline. In February 2012 was developed a second stage of more than 2,000 linear meters of Geotextile tubes.

Once this second stage was completed, the area faced strong winds and high waves of Tropical storm Ernesto in July 2012, where over the more than 2 km of protection, scour was observed only at the junction between two tubes. Due to the effective performance of this Technology in the present case, we conclude that the success in coastal protection and recovery of the beaches is related to the Geotube® Technology units manufacture processes, design characteristics and installation process.

1. INTRODUCTION

For centuries major storm events have battered shorelines and coastal areas. It is not only the size of the storm that leads to extensive damage, but the combination of sustained winds, rain, and flooding. Controlling and fighting the power of water is a daunting task, but geotextile containment technology is a proven, cost-effective method for a variety of shoreline protection and marine construction projects for defense against major storm events.

Geotextile tubes prevent storm damage and protect the environment through the building of custom marine structures. The installation of geotextile containers can be temporary or permanent, and in most cases the structures are invisible to the coastal environment. The technology involves the fabrication of a large container made of a specially engineered textile, which is filled with sand and buried within the shoreline. During installation, the geotextile container is filled to a specific design height that provides protection to adjacent coastal areas. The geotextile container holds the sand in place which prevents erosion and property damage during major storm events.

In Mexico these natural phenomena have caused serious damage in coastal areas, one of the regions with major erosion losses is the state of Tabasco, where Federal authorities have begun construction of several kilometers of sand dune core using geotextile tubes to prevent sand erosion and flooding of a small town, Sanchez Magallanes. The coastal area of Cardenas, Tabasco, has lost over a kilometer of beachfront due to the effects of climate change over the last 25 years.

The sand dune structure using geotextile tubes is designed to prevent further erosion along the shore, especially in summer when strong winds and large waves are particularly damaging to seaside communities. Many local residents have fled further inland due to the increasing erosion of shoreline.

2. LOCATION

The village of Andrés Sanchez Magallanes is a fishing port of 6200 inhabitants, located in the municipality of Cárdenas, in the Mexican State of Tabasco. It is located 137 km northwest of Villahermosa, the Statecapital and 87 km from the municipal seat, Cárdenas (Fig. 1).By its population and commercial activity, Sanchez Magallanes is the second population on importance of the municipality, only after the municipal seat, the city of Cárdenas.

The main economic activity in the community is fishing of oysters and crab, which is complemented with the livestock and tourist activity in holiday seasons. The system of lagoons "Carmen-Pajonal- La Machona" is where the main oyster's farms are located, which places the village as the main producer of oysters at the national level.Tourists come mostly from the municipal seat and the nearby state capital of Villahermosa. The main attractions of the town are the beaches of the bar of Santa Anna, the Spa "EnsueñodelTropico" (Dreams of the Tropic), the nearby lagoons system of El Carmen, La Machona and Pajonal, as well as the island El Pajal, where several species of birds nest.

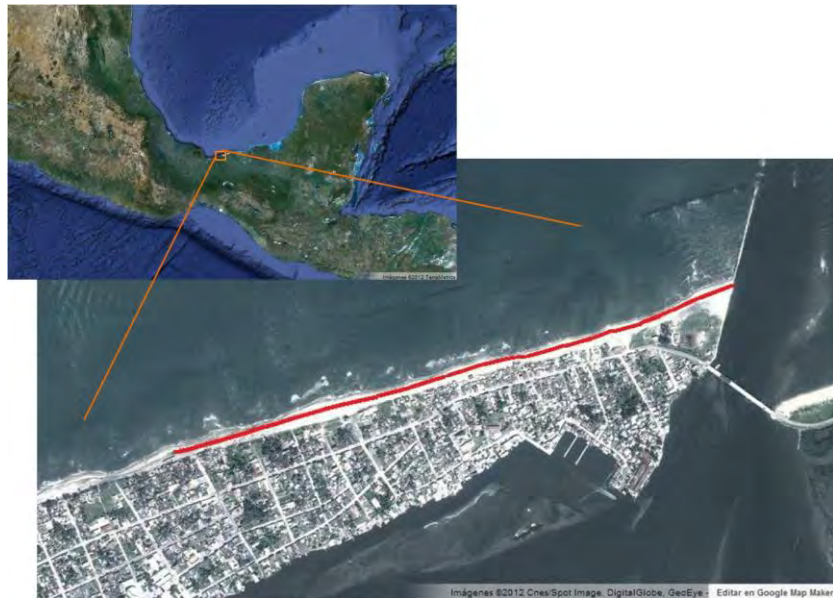


Figure 1. Sanchez Magallanes location in the state of Tabasco, where were built 2 jetties and submerged breakwaters in the late 80's early 90's.

3. THE CHALLENGE

The villagefaces a serious problem of marine erosion. This problem has made many of its residents relocateto other areas.The marine erosion problem is caused by the effects of climate change, but also by the residents not maintaining thenatural barriers, mangrove and sand dunes, which are a major factor in coastal protection.

In this area of the coast of Tabasco, coastal current is predominantly from east to west, having an inversion of the littoral transport of short duration in the so-called "windy" season or "Nortes".

In the late 80's early 90's twojetties were built on the coast of Sanchez Magallanes. A structure like that placed on the coast,creates an obstacle to the current, and sand from the east side was intercepted by the east Jetty, being held in near-total form. The missing natural power of sand from the opposite side, since the waves and tide conditions remain the same, there is no compensation of the sand that is transported running down, or to the west, so the beach line recedes.

Proof of this is the fact that periodically the breakwater on the eastern side has required to be extended and on the opposite side has needed extends the built-in.Beach erosion that occurs immediately neighboring the west jetty of the port of Sanchez

Magallanes aside, even after building the four docks parallel to the coast, and the Jetty of close in the West end with Concrete bags elements, should not be viewed as something unusual. This because firstly by the fact that experience in other similar work carried out not only on the coasts of our country, but in other parts of the world, has shown that achieve a proper restitution of the original Beach line usually take awhile, between four to eight years.

Secondly, and this is the most important thing, is that prior to the construction of the jetties, initiated its construction by stages already for several decades, the regime of littoral drift of sand transported by the effect of currents generated by the action of the waves and tides was responsible for maintain a dynamic balance, being the sand carried by these currents removed in a certain place by the effect of the power at a certain given site, compensated by which was transported from upstream.

Because as described previously, the only way to avoid the occurring erosion on the part in question, while the work of the docks parallel to the coast retains the low volume of sand that manages to outflank the nose of the jetties, is resorting to a process of artificial feeding of restitution of the beach sand. Artificially supplied sand must be an almost total stop of the beach reverse process while the separate coastal jetties allow the deposit of sand carried naturally as a result of flanking the nose of the West jetty.

4. COASTAL PROTECTION AND RECOVERY OF THE BEACHES

4.1 Cold Front #4, October 2007.

In 2007, from October 20 to 23th 2007, the coast line of Sanchez Magallanes, suffered a strong involvement of the coastline by the action of the Cold Front #4 with gusts of up to 130 km/h and waves of up to 10m.

This event dramatically intensified the process of loss of sand in the West side, both due to the increase of the sea level, product of the tide, winds and the intense waves, being affected some buildings close to the beach as well as some other structures. During the visit to the site after this meteorological phenomenon was a setback in the almost uniform reduction of the coast line on the order of five meters approximately along three kilometers of the coast (fig. 2).



Figure 2. Heavy damage by erosion from the Cold Front #4 October 2007

The damages caused by the Cold Front #4 were not limited to the Sanchez Magallanes coast. The Cold Front #4 was also responsible for the flood of Villahermosa (the state capital) of that year, the biggest event of this type in decades. To solve

the emergency situation in Sanchez Magallanes the authorities decided to install 300m of Geotextile tubes to protect the central part of the town and stop erosion (fig. 3).

The installation took place in the month of January of 2008. Units of Geotextile tubes, with circumferences of 7.6m, lengths of 18m with mechanical ports (GP8) and conventional ends were used for the construction of a new sand dune 20m from the wet beach, almost at the footing of the remaining houses. The units were designed to achieve heights from 1.5m to 1.8 with a minimum safety factor of 3.4.



Figure 3. The units were covered with sand (from a nearby mine) to protect them against the traffic of villagers and visitors over them and vandalism.

The contractor (Control de Erosion) filled the units using sand pumps and the material used was taken from the ocean floor.

4.2 Sanchez Magallanes in 2008- 2011.

During this period, the wave action and the erosion destroyed almost 104 houses. The erosion along the Spa Ensueño del Tropicó demolished homes, businesses and public buildings.

Unfortunately for the local inhabitants, the tourist activity (locals and strangers) have to go to the nearby beach called Bahía Acapulquito, located in the Ejido San Rafael at the East part of the municipality far from Sanchez Magallanes.

Also the erosion created new challenges. Because of the destruction of the sand dunes the sea waves start getting very close and eventually (if nothing is done) will join lagoons El Alacrán and El Manatinero with the ocean; even mentioned that there is already evidence that that has happened in the past "windy season" in the Manatinero lagoon where sea water got into the lagoon.



Figure 4. Eventually sand has been deposited naturally favoring the beach recovery

In that regard, the local authorities emphasized that "we cannot allow that to happen because it puts at risk an entire ecosystem of the lagoon complex Carmen-Pajonal - La Machona by the effects of salinization of the water and that it would even extend to other areas of the municipality as "Costa Chica", to the detriment of fishing, the oysters, the agriculture and animal husbandry."

Therefore a new Coastal Line protection project became of vital importance not only for the inhabitants of the town and port of Sánchez Magallanes, San Rafael, El Alacrán and Sinaloa, among others that are located in the coast and whose properties are threatened by the advance of the Mexico Gulf.

The units installed in 2008 were under continue follow up by the local authorities and were proposed as the best method to protect the coastal line. During these 3 years the units withstand the forces of the ocean. Only one of the units was damaged by vandalism in the month of May of 2010. The remaining material of that unit was used by the local people to create small shelters and protection for their houses (fig. 4).

4.3 Sanchez Magallanes 2011-2012.



Figure 5. After 3 years Geotextile tubes installed in 2008 withstood the force of strong waves, by these Geotube® Technology were proposed as the best method to protect the coastal line.

In September 13 of 2011 the Direccion General de Puertos Mexicanos, the office of the Federal Government in charge of the ports and coastal structures started the bidding process LO-009000986-N34-2011, for the "Construction of the beach protection structures of Sanchez Magallanes". The project was designed to protect 2.1 km of the coast of Sanchez Magallanes from the jetty (called La Punta) to the local cemetery using Geotextile tubes (fig. 6).

The federal executives argued that the project is a rescue comprehensive since on the one hand is intended to revive the tourist, gastronomic and commercial activity in Sánchez Magallanes port, but also the protection certainly will prevent a sea join the lagoons because this complex Carmen-Pajonal - Machona Lagoon is the pillar of the oysters, activity of which depend on thousands of families. Also the protection of the beach will guarantee to the residents that their properties already will not be taken by the sea and therefore they regain their value.

Prior to this announcement, several meetings occurred between the engineers of Puertos Mexicanos and G&G, domestic representative of TenCate Geosynthetics in Mexico to analyze the problem and define the basis for the licitation. There were no doubts about the use of Geotextile tubes after the performance shown by these units at the site for several years.



Figure 6. There were installed 77 Geotextile tubes to attain the total longitude of 2,303.85 linear meters from the existing breakwater to the local cemetery along all the coastal line.

The characteristics of the Geotextile tubes designed for this project were:

- Textile Tube: 77 units of 27m each made of Geotextile tensile strength of a 180 x 180 kN/m accordingly to ASTM D 4595, polypropylene, sand color. Circumference: 7.6m. Also the units had Flat End® technology and mechanical (GP8®) ports.
- Scour Apron: made of Geotextile tensile strength of a 70 x 86.3 kN/m accordingly to ASTM D 4595, polypropylene, black, and 5.18m wide with one anchor tube of 1.2m of circumference. The scour aprons had to be attached to the units at the factory.

Due to the fact that some units would be laid on areas where house and other buildings existed before, a nonwoven needle punch Geotextile were considered as a protection. The fabric selected was Mirafi® 1100N CBR Puncture Strength 3.11kN accordingly to ASTM D 6241 (Fig. 7)

Mechanical Properties	Test Method	Geotextil Type 1	Geotextil Type 2
Wide Width tensile Strength (at ultimate) MD/ CD	ASTM D4595	78.8 / 109.4	1026 / 1026
Wide Width Tensile Elongation (%)	ASTM D4595	20	20
Factory Seam Strength KN/m	ASTM D4884	70	582
Apparent Opening Size (AOS) mm (US Sieve)	ASTM D4751	0.43 (40)	30 (0.60)
Water Flow Rate (l/min/m ²)	ASTM D4491	813	813
UV Resistance(% strength retained after 500hrs)	ASTM D4355	80	70
Mass/ Unit Area (g/m ²)	ASTM D5261	585	949

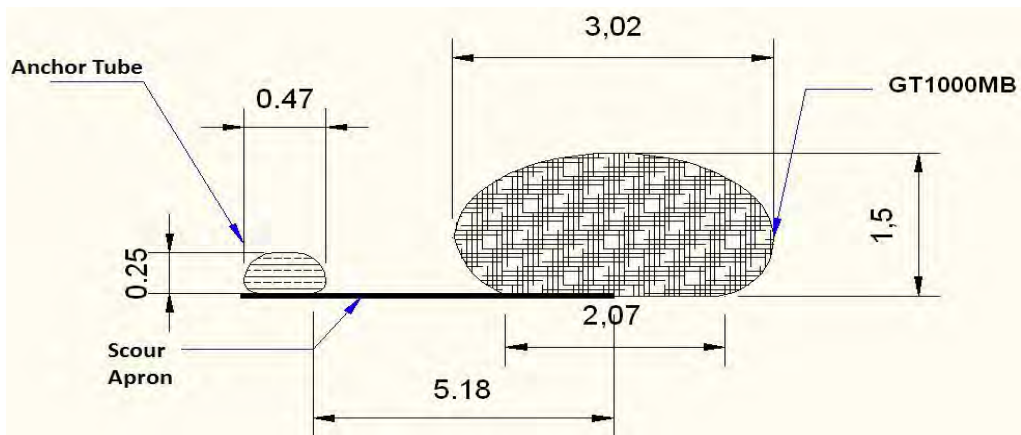
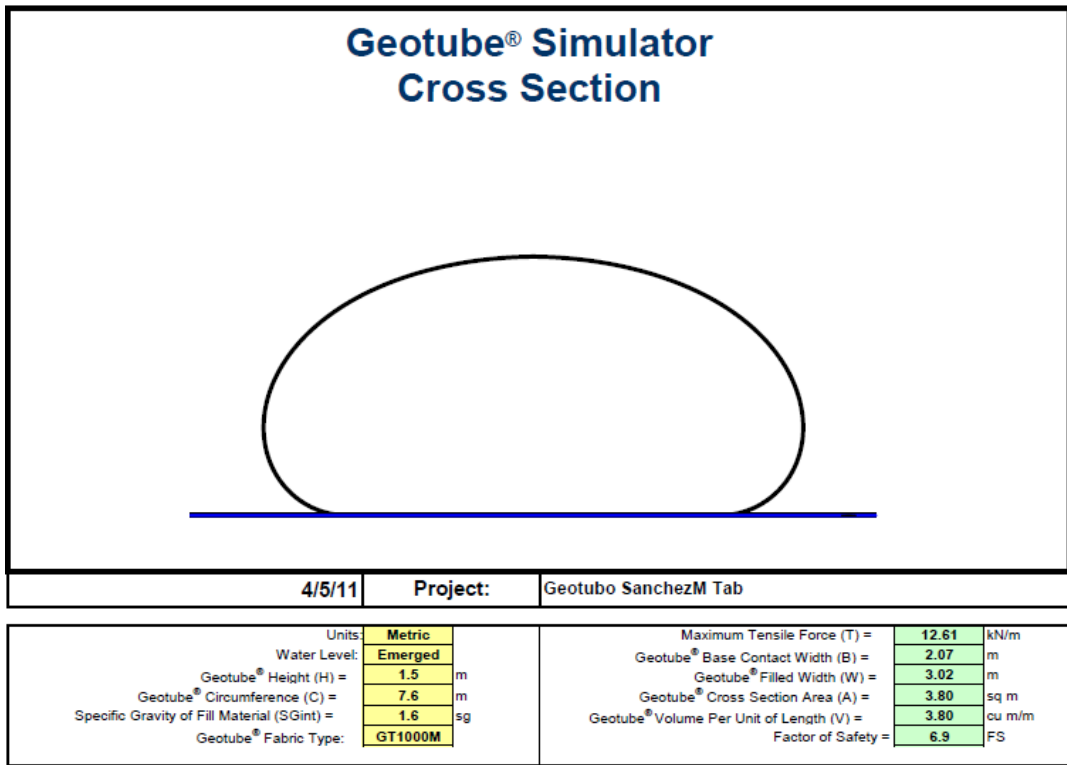


Figure 7. Characteristics of scour apron, anchor tube and geotextile tubes installed

The contract was awarded to Control de Erosion in December 2011 and the installation was set for the beginning of February 2012.

The installation project:

a) Demolition: Concrete structures were observed to demolish, being mostly of abandoned houses and remains of tourist restaurants and the Spa facilities. For the implementation of this concept pneumatic equipment such as a compressor of high pressure with a breaker hammer were used. The debris resulting of the process was moved to an authorized disposal site.

b) Cleaning and Leveling: Shall be carried out cleaning and leveling of the site through the use of mechanical equipment (backhoe or similar), to meet the lines and project levels. The place where the Geotextile tube units were placed will be aligned using metallic posts which placed default namespaces so that the tube will be laid in the places according to the blueprints. It should be noted that the area must be clean and free from any material with cutting edges, glass or any material that can affect damage materials (Fig. 8).

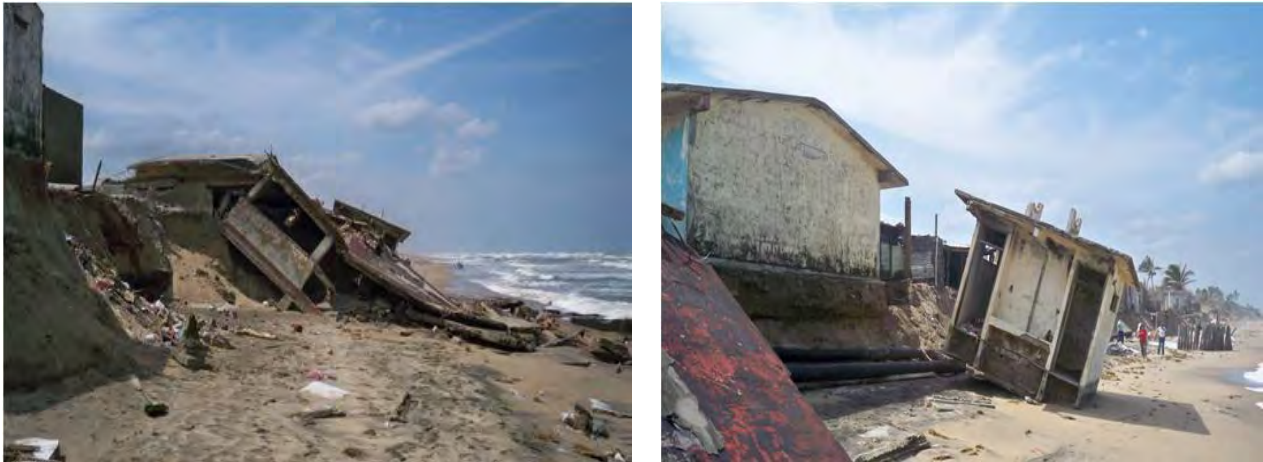


Figure 8. In the place, there was a lot of debris, resulting from the intense coastal erosion

c) Topobatismetrics of the work zone. There will be the work of topobatismetrics in the area of extraction of sand for the volumes of work and monitoring of the same, in order to correlate the project data with the data from the date of the construction of that work, likewise in the beach area will take place the lifting and topographic stroke to delimit levels and lines of project.

d) Protection Geotextile: It is fabricated according to measure indicating the project section, so local labor is used in combination with the workmanship specializing, work to run are as follows; (a) extends the roll of geotextile which is supplied with a width of 4 metres approximately, (b) is cut with extreme care to be attached through the use of a machine sand bag seamer, uses nylon cord and occur two seams to ensure that you do not remove, (c) sewing once the mantle of the geotextile is seam tube anchoring or ballast in accordance with draft which will be filled with sand hydraulically injected once they are already in the final project site. Once it is ready, they have to be rolled up and transported to the site of placement through the use of unskilled labor.

e) Installation and filling the units. Once the surface where the unit is going to be laid, the Textile tube with its scour apron is placed and aligned in the desired place. The process is executed in two stages. The first one uses a Toyo Pump of 30 HP. The pump fills most of the volume of the unit at high pressure. Sand is taken from the ocean floor. A diver in the ocean moves the nozzle of the pump like and extracts the sand. In the second stage or "finishing" the unit a Toyo Pump of 7.5HP is used to fill the last part of the units. The volume of each unit is approximately 117.8m³. The process to fill each unit takes 3.5 hours in average (Fig. 9)

f) Backfilling of the void between the Geotextile tubes units and the sand dune. The process was executed using the Toyo Pumps. Care should be taken in order to prevent erosion in the footing of the units where no scour protection exists.



Figure 9. Installation and filling of Geotextile tubes

5. RESULTS

In early August 2012 the coast of Sanchez Magallanes suffered the effects of Hurricane Ernesto. This phenomena crossed the Yucatan Peninsula from the Mexican Caribbean where were observed maximum sustained winds of 110 km /h with gusts of 120 km /h. It was observed that along the more than 2,000 linear meters of Geotextile tubes installed on the coastal line, only in one zone was observed scour between the joint of 2 units.

This scour has seen before when wave driven water overtopped the Geotextile containers and in returning to the ocean accumulated at one point undermining the tube and scour apron which resulted in erosion of the sand to a depth equal to the tube height. To solve the problem, a new tube of the same circumference, length and height as the original structure must be installed with a scour apron under the location of the new tube.

Despite this event of strong marine erosion along all Geotextile tubes line, it was clearly observed the retention of sand over the structure, which propitiates the beach recuperation and protection against future events of natural phenomena.



Fig. 10 Scour aprons in operation



Fig. 11 Retention of sand behind the protection line with Geotube® Technology

ACKNOWLEDGEMENTS

We are grateful to Eng. Mauricio Porraz of Erosion Control Company responsible of the geotextil tubes installation for the information shared. Also to Eng. Celso Morales and Arq.Arturo Perez Castro from the Federal Coordination of Ports and Merchant Marine in México.

Bending Stiffness of Geosynthetic-reinforced Soil (GRS) Platform

Christopher M. Gemperline, P.E., U.S. Bureau of Reclamation, USA, cgemperline@usbr.gov

ABSTRACT

Understanding the homogenous bending stiffness of geosynthetic reinforced soil (GRS) beams and platforms can aid in the design of civil structures that span unstable or compressible soil and subsurface pipe conduits. Despite the increasing use of GRS, GRS beams and platforms bending behavior has received little attention. GRS beams and platforms are typically composed of alternating layers of geosynthetic reinforcement and soil, resting on soft or unstable soil, and are competently supported on either end. This investigation evaluates composite or "homogenized" mass bending stiffness resulting from the inclusion of geosynthetic reinforcement in GRS. Analyses are performed using the two dimensional FEM and the Winkler foundation model. The research consists of two primary analyses. The first was a parametric study to ascertain the influential parameters contributing to the bending stiffness. The second investigated the effect of reinforcement spacing and the number of layers on the GRS stiffness. The research concludes that bending resistance is best gained by decreasing the spacing between reinforcement layers and using higher strength soils. Increasing reinforcement tensile strength also increases bending resistance, but the affect was ancillary to the spacing and soil stiffness. The GRS beams numerically modeled for this study exhibited similar displacement behavior to the Winkler foundation model, indicating that the bending behavior of GRS beams can be analyzed using methods that apply to fundamental concepts of beam bending theory.

1. INTRODUCTION

Geosynthetic-Reinforced Soil (GRS) is a soil mass that is reinforced by compacting layers of soil between horizontal layers of geosynthetic sheets. Over the past two decades, GRS has been employed in the construction of many types of earth structures, including retaining walls, bridge abutments, embankments, slopes, roadway, and shallow foundations. GRS structures have many distinct advantages over their conventional counterparts. GRS structures are typically more ductile, more flexible (hence more tolerant to differential settlement), more adaptable to low quality backfill, easier to construct, require less over-excavation, and are more economical. Among the various applications of GRS, the GRS platform has received little attention. A GRS platform is typically composed of alternating layers of geosynthetic reinforcement resting on soft or unstable soil and competently supported on either end. A GRS is a soil mass that is strengthened to restrain the development of tensile strain in the direction of bending. Since soil is weak in tension, suppression of tensile strain is an effective means to increase the bending stiffness of soil that will otherwise develop significant tensile strain. The inclusion of geosynthetic reinforcement therefore effectively improves the engineering behavior of the composite mass, or in other words improves the material properties. Civil engineering structures constructed on soft or unstable soils are likely to experience considerable settlement. Minimal displacements for most civil engineering applications are desired to maintain stability, structural integrity, serviceability, and durability. Design of structures such as roadways, railways, tanks, walls, slopes, pipelines, and buildings, on soft soils where the structure will impose a significant load over a large area, have employed a variety of techniques to minimize displacement. Traditional measures can be environmentally unsound, as well as cost, labor, and schedule prohibitive. Over the past decade the use of geosynthetic-reinforced soil (GRS) platforms to improve resistance of the underlying foundation soil against the applied loads or to transfer structural loads to more competent soils has gained popularity. A better understanding of GRS bending stiffness can be applied to design of civil works that require spanning undesirable soils. Bending stiffness is an important consideration for projects that have a small tolerance for movement such as rail roads, and pipelines. GRS platforms have also been extensively used to bridge over unstable soils and have also been effectively used to bridge areas that are susceptible to settlement when subsurface ice lenses melt following placement of fill soils. The ability to estimate the improved bending stiffness of GRS platforms will provide valuable insight in the design of GRS structures subjected to bending. This research investigated the improved bending stiffness of a GRS platform foundation using the Finite Element Method (FEM) and the Winkler foundation model. The objectives, method of research implemented for this study, a summary of results, and a proposed relationship to more conveniently estimate bending stiffness of GRS platforms are discussed.

1.1 Objectives

This study investigated the bending stiffness of a GRS platform using the Winkler Foundation model with two primary objectives. The first objective was to investigate effects of various parameters of a GRS platform on the bending stiffness of the GRS composite and the applicability of beam theory. The second objective was to develop a preliminary relationship for estimating the bending stiffness of GRS platforms.

Both objectives utilize numerical modeling to investigate the composite bending behavior of GRS beams. The Winkler Foundation model was used in this study to verify the FEM used to determine the vertical displacement at the base of GRS beams and then used again to estimate the composite bending stiffness of GRS beams. The first objective instituted a parametric study to analyze the effects that the amount of geosynthetic reinforcement, the tensile modulus of geosynthetic reinforcement, and the modulus of elasticity of soil used to construct GRS beams (E_b) have on composite bending stiffness. The second objective examined the relationship between the bending stiffness of a composite GRS beam and reinforcement spacing. This was achieved by varying the number of layers, which changes the geometric moment of inertia. Classical elastic bending theory establishes that the bending stiffness remains constant with added layers i.e. E_b multiplied by moment of inertia remains constant. The bending deflections determined from the FEM were compared to the bending deflections determined using the Winkler Foundation analytical model with known moduli of elasticity to estimate a composite bending modulus of elasticity for a GRS beam. A preliminary relationship between geosynthetic reinforcement spacing and bending modulus of elasticity is proposed.

1.2 Method of Research

This study examines GRS beams in pure bending where normal stresses in the GRS member remain below the yield strength and Hook's law applies. In other words, herein the GRS beam is treated as a uniform composite elastic material. Deformations of an elastic beam are caused by the bending moment measured by the curvature of the neutral surface. Curvature is defined as the reciprocal of the radius of curvature ρ , and has been shown to be related to the bending moment (M), modulus of elasticity (E), and moment of inertia (I) by equation 1 in the elastic range.

$$\frac{1}{\rho} = \frac{M}{EI} \quad [1]$$

Equation 1 defines bending stiffness or resistance to bending as being dependent on modulus of elasticity (E) and the moment of inertia (I). (EI) is commonly referred to as the bending stiffness. Classical bending theory suggests the deformed shape of a loaded beam remains constant as reinforcement layers are added to a beam such that EI remains constant. This study reveals that GRS generally follow this concept when applied to the Winkler Foundation model.

Numerical models of a simply supported geosynthetic-reinforced soil beam on an elastic foundation were created and analyzed using a FEM program. The models developed for the parametric study, the first portion of this study, evaluated the effects of geosynthetic reinforcement tensile modulus, soil modulus of elasticity, and the reinforcement spacing on the bending stiffness of GRS beams and platforms with the assumption of elasticity. Models developed in the second portion of this study evaluated the GRS beams and platforms bending stiffness with varying geometric moment of inertia to reinforcement spacing. A simply supported beam on an elastic half space was chosen for this study because, the widely used Winkler foundation analytical solution can be used to facilitate verification of the numerical model and provide a convenient way to estimate bending stiffness in a graphical manner. The Winkler foundation treats beams and platforms as flexible and the soil upon which they rest as a bed of springs. An elastic constant of the springs is referred to as the coefficient of subgrade reaction (k_f). A Winkler solution is appropriate because this study is limited to two dimensional bending and displacements. The Winkler model is further discussed in subsequent sections. The two dimensional modeling implies a unit platform or beam width. Because this study is concerned with the composite or "improved material" bending behavior of GRS beams or platforms, the geometric moment of inertia was determined using rectangular cross-sections with a unit width. A FEM software program that features a boundary condition that can be defined by a spring constant, which is a fundamental principal used by the Winkler foundation model, was selected.

2. FINITE ELEMENT MODEL AND VERIFICATION OF MODEL

A two dimensional FEM was used for modeling a beam composed of soil and geosynthetic reinforcement. The model was verified by comparing it to the analytical solution developed from the Winkler model. This section briefly describes the Winkler foundation and justifies the material parameters used in this analysis.

This study directly compares a GRS finite element beam to the Winkler foundation model which is a widely used analytical solution to an elastic beam on an elastic foundation. The displacements resulting from the loading conditions in this study are assumed to be small enough that shear, tensile and compression failure will not develop, therefore the FEM modeling conducted in this investigation assumes perfectly elastic soil properties. This is a simplification of true field condition because soil is not linear elastic and for intents and purposes does not resist tension; however, this assumption allows for direct comparison to the Winkler foundation model which although not precise, provides an accurate portrayal of the effect geosynthetic reinforcement has on soil beams. Future work could perhaps involve laboratory and field study in conjunction with FEM modeling to develop a more precise GRS beam analytical solution.

A two dimensional FEM model was used to model beams composed of soil and geosynthetic reinforcement. The FEM model was verified by comparing it to the analytical solution developed from the Winkler model. The verification process is described in subsequent sections of this paper. A plane-strain, FEM model was created to represent a simply supported beam on soft soil. The soft soil was modeled as equally spaced springs that resist load vertically, but not vertical. A 3-meter long 1/2-m thick non-reinforced beam was modeled using elastic parameters. GRS beam models developed for analysis were composed of linear elastic elements with structural beam elements interbedded at pre-determined horizontal spacing. The range of GRS beam geometry was selected to be similar to that used in a case study investigating the performance of a geosynthetic reinforced pile supported highway embankment presented by Liu (Liu, et al., 2007).

Finite elements were 2.5 cm by 2.5 cm quadrilaterals with 4 nodes. This analysis did not incorporate any type of staged construction or self-weight effects; therefore the incorporation of unit weight was not necessary. The bottom beam elements were connected to a bed of "springs," which are defined by a spring constant (k_s) equivalent to what is known as the modulus of subgrade reaction (k_f) when used to represent soil. One spring was located at the corner of each of the bottom row of elements of the beam. The beams analyzed in this study were subjected to a 250 kPa uniformly distributed vertically applied load across the full length of the beam as depicted in Figure 1. This loading was chosen because it resulted in discernible displacements near the beam midpoint making it easy to use graphical techniques described later and also because it avoids large deformations that would typically be associated with shear failure.

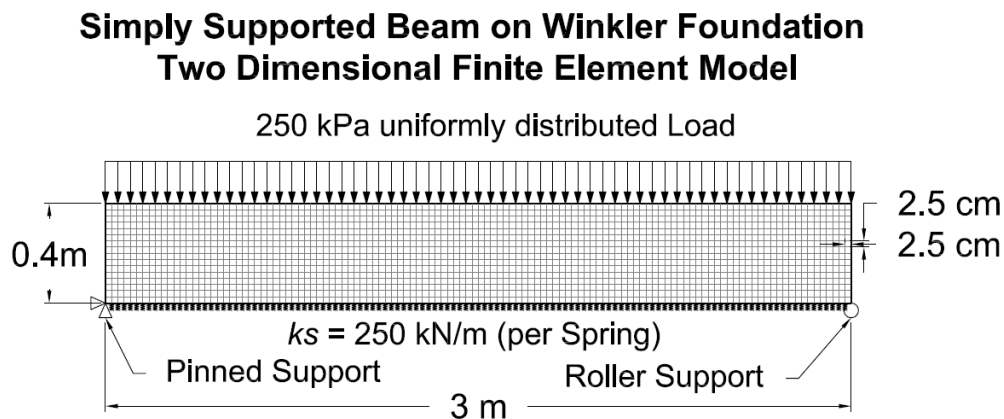


Figure 1. Two Dimensional Finite Element Model.

2.1 Winkler Foundation Model for Beams on an Elastic Foundation

Many models have been proposed to represent the half space response beneath structures (Scott, 1981) however, the spring model first suggested by Euler and further developed and used by Winkler is the most widely used and is commonly referred to as the Winkler foundation. The Winkler Foundation model was used in this study to verify the FEM model used to determine the vertical displacement at the base of GRS beam and then used again to estimate the composite or "improved material" bending stiffness of GRS beams. Many mathematical relationships have been pre-determined for a variety of Winkler foundation conditions and, conveniently presented by a number of authors (Young, 1989). The relationship between the vertical pressure (P) acting on a solid surface, and the vertical deflection (y) is given by the equation:

$$P = k_f y \quad [2]$$

k_f has been referred to by many names such as the coefficient of subgrade reaction, the subgrade modulus, and the modulus of subgrade reaction, but it is fundamentally the foundation soil stiffness. The Winkler solution models foundation soils as vertical springs with a single value (k_f). The Fem models the foundation as an elastic half-space defined by two constants, such as modulus of elasticity (E) and poisons ratio (ν). Obtaining precise comparisons between the one parameter Winkler model and a two parameter FEM model is difficult. Variations or improvements on the spring model have been suggested however, the complexity of the analysis increases rapidly for foundation models that incorporate more variables and features than those represented in the Winkler model. A soil subgrade is generally neither homogeneous nor isotropic. Even if the same soil is uniform for a considerable depth, the increasing overburden pressure with depth causes the soil to stiffen with depth. For this reason it seems reasonable to represent the foundation soil with something more suitable than the Winkler model. However, many other attempts at more precise mathematical solutions of a beam on elastic foundations become very complex and remain open to significant debate of accuracy. The Winkler model was utilized in this study for its convenience and history of successful use and for that reason a spring

boundary condition was implemented as the beam foundation in the numerical modeling. By selecting a foundation composed of vertical springs in the FEM model, direct comparisons of the results could be made to solutions of the Winkler model solved for known stiffness. The general solution to deflection of a flexible beam on a Winkler foundation is

$$w = C_1 \cos \beta x + C_2 \sin \beta x e^{\beta x} + (C_3 \cos \beta x + C_4 \sin \beta x) e^{-\beta x} \quad [3]$$

Where C_1 through C_4 are constants determined by the end and loading conditions and the parameter β has the dimensions length $(L)^{-1}$ and includes the properties of the foundation soil and the beam. The general solution describes the deflected shape of the beam between loading points and end constraints. The coefficients (C_1 , C_2 , C_3 , and C_4) are determined based on the end constraints and loading conditions or the “boundary conditions”. Specific solutions have been solved for many end conditions and loading schemes and tabulated for implementation in spreadsheets (Young, 1989). Deflection along the length of the beam is determined by using the method of super-position. A simple supported uniformly distributed load across the entire length of a beam was selected for this analysis because it was considered an idealized representation of a beam supported on the ends and soft soil between.

2.2 Material Properties

This section discusses the material properties that were selected to define the properties of elements in the FEM models. These values are considered realistic based on typical soil and geosynthetic properties used for GRS. The material properties presented in this section are considered the “base properties” and used for the majority of the models developed for this study; however, they were varied in the parametric study portion of the investigation to better understand which properties have the most influence on the bending stiffness of GRS beams.

Poisson’s ratio (ν) is defined as the ratio of the horizontal strain (ϵ_h) to the vertical strain (ϵ_v). Typical values of ν for silts and sands range from 0.2 for loose materials to 0.4 for dense material. Values for saturated clays vary from about 0.4 to 0.5. The theoretical maximum value for saturated clay undergoing no volume change when stressed is 0.5. For the purposes of this study variation of Poisson’s ratio is expected to have negligible influence and was assumed to be 0.3 for both the foundation and beam soils.

The purpose of this study focuses on the deflection of a beam composed of soil and geosynthetic reinforcement, therefore the mechanism occurring between the beam and the soft soil was not considered in significant detail. Consequently, the soil foundation material was modeled in a simplified way by vertical springs so that the beam deflection could be directly compared to the Winkler model. The stiffness of the foundation soil (k_f) depends on the compressibility of the soft soil and links the settlement (y) to the vertical stress. If a foundation of width B is subjected to a load per unit area of (p) it will undergo a settlement. From Equation 2 it can be seen that the units of k_f is Force (F)/Length $(L)^{-3}$. The value of the coefficient of subgrade reaction is not constant for a given soil, but rather depends on several factors, such as the length and width of the foundation, and also the depth of embedment, modulus of elasticity of the soil, poisson’s ration, and thickness of the soil unit. Since the modulus of the elasticity of the composite reinforced beam is unknown for this analysis an estimation of k_f with minimal beam properties was needed. Vlasov and Leontiev proposed the following relationship for a plane stress condition (Scott, 1981):

$$k_f = \frac{E_f}{(1 - \nu_f^2)} \frac{\nu B}{2} \quad [4]$$

The only beam property is width. ν has the dimensions L^{-1} and expresses the rate at which vertical displacement decays with depth. For most practical purposes ν can be assumed to be equal to one. The U.S. Bureau of Reclamation has published compression characteristics for various re-compacted soil types classified by the unified soil classification system (U.S. Bureau of Reclamation, 1998). This resource was used for selecting reasonable estimations for E_f to be used in Equation 4. Low plastic soils (CL) range from 4.6 to 2.8 percent compression at 100 psi. A value of 3.5 percent strain at 100 psi was selected as a representative value for the foundation soil. Since $E = \sigma/\epsilon$, then $E_f = 100 \text{ psi} / 3.5\% \cong 20,000 \text{ kPa}$. Assuming a ν_f of 0.3 and $B = 1 \text{ m}$ for a two dimensional plain strain analysis, then substituting E_f of 20,000 kPa into Equation 4 gives $k_f \cong 10,000 \text{ kN/m}^3$.

The FEM model consists of a beam resting on a bed of springs as shown on Figure 1, which requires a spring constant (k_s) for the springs that, exerts a constant reactionary force to the bottom of the beam and that is equivalent to the modulus of subgrade reaction. k_f is defined by the units of F/L and the k_s is defined with units of F/m³ therefore, the equivalent k_s for a given k_f can be found by using the area of the bottom of the plain strain finite element. For this study elements were 0.025 m long and the beam was assumed to be 1m in width for the plain strain condition. The k_s value is then found to be $10,000 \text{ kN/m}^3 (0.05 \text{ m}^2) = 500 \text{ kN/m}$

Silty sand with gravel (GM-SM) soils are typically recommended for use when constructing a geosynthetic soil mass and therefore, used to estimate reasonable FEM input parameters for the soil platform matrix. A linear elastic model was

chosen for the soil elements in this study for its direct correlation with the analytical Winkler Foundation model. For a linear-elastic model, there is no yield value defined. Using the U.S. Bureau of Reclamation published compression characteristics, for various soil types. The median value of 1.2 percent strain at 100 psi was selected as a representative value for the foundation soil. Since $E = \sigma/\epsilon$, $E_b = 100 \text{ psi} / 1.1\% \cong 57,000 \text{ kPa}$.

Beam elements were used to simulate geosynthetic tensile reinforcement. The beam element used in the FEM software for this study was formulated using the conventional Bernoulli beam theory. This beam element requires the slope, as well as the lateral displacement, to be continuous within the element. Each node associated with a beam element is given a rotational degree-of-freedom in addition to the two displacement degrees-of-freedom. The tensile modulus selected for this analysis is based on values for commonly used material published by a reputable geogrid manufacture. The tensile modulus at 1 percent strain is 547 kN/m in the machine direction and 773 kN/m in the cross machine direction. The cross machine value was chosen as the base value assuming the strongest direction would be oriented across the beam span. The structural member used to model reinforcement was selected to resist tension and the interface with the soil was fully bonded. The baseline material parameters are summarized Table 2

Table 2. Model Verification Input Parameters Summary Table.

	Winkler Model	Finite Element Model
Modulus of subgrade reaction (k_f)	10,000 kN/m ³	N/A ²
Spring Constant (k_s)	N/A	250 kN/m
Modulus of elasticity (E_b)	57,000 kPa	57,000 kPa
Poisson's ratio of the beam soil (u_b)	N/A	0.3
Beam Length (L)	3m	3m
Beam Thickness (h)	0.5m	0.5m
Soil Behavior Model	Linear Elastic ¹	Linear Elastic
Support Condition	Simply Supported	Simply Supported

Notes: 1) Assumption of the Winkler Method
2) N/A denotes not applicable to the method

A graphical comparison between the Winkler model and the FEM model was made. The calculated deflection at the bottom of the FEM model aligns very closely with the calculated deflection of the Winkler model at the bottom of a beam. This verification indicates that the FEM models developed to include geosynthetic reinforcement can reasonably be compared to the results of the Winkler model and used to better understand the GRS bending behavior.

2.3 Graphical Estimation of GRS beam composite Modulus of Elasticity

Several vertical displacement curves were developed with the analytical Winkler model using various moduli of elasticity for the beam. The results of the FEM simulation program were then compared to the Winkler model results to estimate an equivalent modulus of elasticity. Figure 2 illustrates how this was done. The vertical displacement measured in the FEM model is plotted with square points along with several gray Winkler model vertical displacements that were calculated using the same geometric shape as the FEM model beam but representing various moduli of elasticity. Symmetry is assumed between the ends of the beam and therefore only half of the beam deflections are shown here, this allows for an expanded view of the plots enabling a more precise estimation of composite modulus of elasticity. The FEM model vertical displacement results could then be compared to the graphical solutions of Winkler foundation to estimate a composite modulus of elasticity of the FEM GRS model. For the example presented in Figure 2 the FEM curve falls where it is anticipated the Winkler curve representing a modulus of elasticity equal to 150,000 kPa would be located. Hence, 150,000 KPa is selected to be a comparable representation of the modulus of elasticity for the GRS.

The FEM model boundary conditions at the ends of the platform are a little different from those used for the Winkler model. The Winkler model assumes a simple support whereas the FEM constrains lateral movement of the reinforcement. Restraining the lateral movement of the reinforcement prevents the ends of the beam from tipping inward, as is characteristic of simply supported beams Figure 3. For this reason the vertical displacement of the GRS FEM model does not match exactly to the simply supported Winkler. This deviation is most notable near the support where the FEM curve has a flatter shape. Even though, the end conditions modify the beam somewhat, a simply supported Winkler end condition still provides a good fit to the FEM as illustrated in Figure 2 by the good agreement with the vertical displacement determined at the bottom of the beam. This deviation from the Winkler solution represents a deviation from common beam theory. In this example, and in subsequent comparisons, the modulus of elasticity is estimated by best fitting predicted FEM and Winkler displacements at the midpoint and one third of the beam span length. It should be noted that this catenary effect is an added benefit that improves the performance of GRS beams and platforms and support structures.

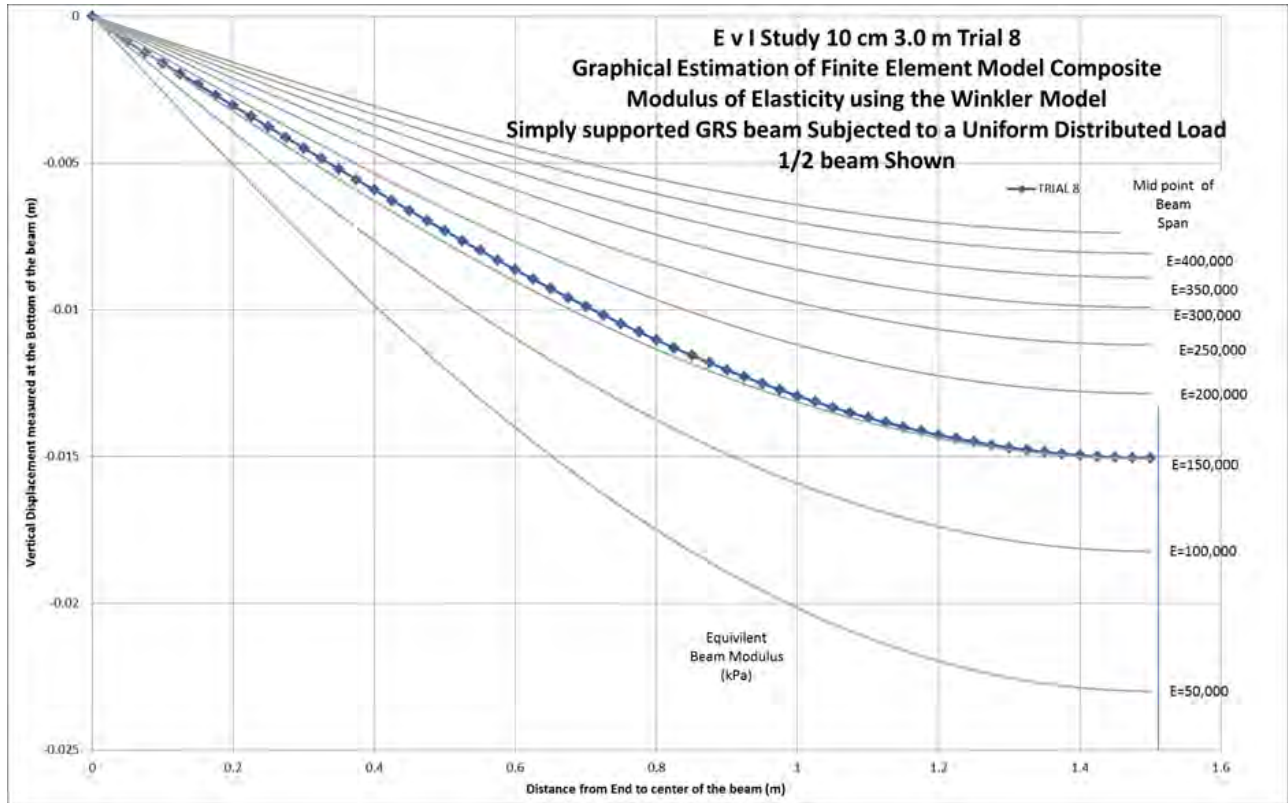


Figure 2. Example of how composite GRS beam modulus of elasticity was estimated

Simply Supported Beam on Elastic Foundation Two Dimensional Winkler Model Reinforced Deformation Sketch

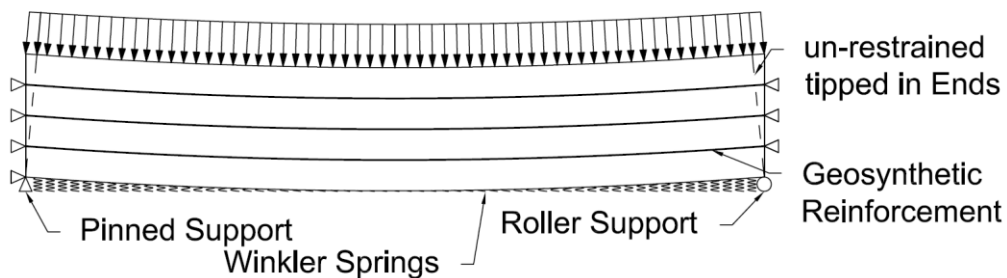


Figure 3. Sketch illustrating difference in end conditions for a GRS beam compared to a non-reinforced simply supported beam. The dashed end lines indicate the “tipped in ends” that are characteristic of simply supported beams. The solid end lines restrained by the boundary condition illustrate how the reinforcement restrains this movement

3. PARAMETRIC STUDY

The first objective of this study was to conduct a parametric in which modulus of elasticity, geosynthetic reinforcement and the number of layers geosynthetic reinforcement was varied to observe the effect each parameter has on the composite bending stiffness of a GRS platform. The Winkler model was used for estimating the lateral displacement of the flexible GRS beams on soil. It is important to remember that the Winkler foundation model makes the simplifying assumptions, that the platform is linear elastic and the foundation soil reacts as vertical springs.

The moment of inertia was kept constant in the parametric study while the geosynthetic reinforcement stiffness, soil modulus of elasticity, and the vertical spacing of reinforcement were varied as summarized in Table 3. The composite

modulus of elasticity for the trials was estimated using the graphical method described previously. A summary of the parametric testing program and the estimated moduli of elasticity is summarized in Table 3.

Table 3. Parametric FEM Modeling Program and Results Summary

Trial Number	Modulus of Elasticity x cross-sectional area of the geosynthetic reinforcement (EA)	Modulus of Elasticity of the beam Soil (E_b)	Number of Equally Spaced geosynthetic Reinforcement Layers at	Beam Length (m)	Estimated Modulus of Elasticity (kPa)
1	750 kPa	57,000 kPa	4	3.0	300,000
2	375 kPa	57,000 kPa	4	3.0	300,000
3	1500 kPa	57,000 kPa	4	3.0	340,000
4	750 kPa	37,000 kPa	4	3.0	200,000
5	750 kPa	77,000 kPa	4	3.0	375,000
6	750 kPa	57,000 kPa	2	3.0	250,000
7	750 kPa	57,000 kPa	8	3.0	375,000
8*	N/A	57,000 kPa	N/A	3.0	57,000

N/A denotes not applicable

*Note: Trial 8 was not modeled with reinforcement; rather it was used for verification of the FEM and comparison

The results presented in Table 3 of the parametric study show that reinforcement in general has a significant influence in GRS beam and platform bending stiffness. This is indicated by obvious difference in vertical displacement between Trial 8 which is un-reinforced versus the other trials. The results indicate that modulus of elasticity of the soil and the reinforcement spacing significantly influence in GRS beam. Increasing and decreasing the modulus of elasticity of the soil 10,000 kPa changed the composite modulus of elasticity 75,000 kPa and 100,000 kPa respectively. Increasing and decreasing the number of layers by two layers changed the composite modulus of elasticity 75,000 kPa and 50,000 kPa respectively. Fabric tensile stiffness had the least effect on the composite bending modulus of elasticity. Increasing and decreasing the fabric tensile modulus by factors of two changes the GRS beam modulus of elasticity 40,000 kPa and zero.

Some deviation from the Winkler solution is caused by the catenary boundary condition selected for the FEM model as discussed previously. The particular solution to the Winkler model represents a simple support at the beam ends. Unlike this, the FEM restrained the fabric layers from horizontal movement at the beam end. This resulted in slight differences in Winkler and FEM deflected shapes, especially near the support. Another effect that may have caused the variance from the Winkler model is that the structural members used to model the geosynthetic reinforcement were only allowed to resist tension and not compression, therefore, the composite E is not likely uniform from top to bottom of beam and the location of the neutral axis is dependent on the internal stresses developed from bending, which changes with beam location. These conditions do not constitute a variation from beam theory, but they do challenge creation of a closed-form analytical solution. Furthermore, because numerical modeling is complicated and time consuming, a simplified approach is justified.

4. STUDY OF MODULUS OF ELASTICITY IN RELATION TO MOMENT OF INERTIA

The second objective of this study was to examine the bending stiffness of GRS beams by analyzing the relationship between modulus of elasticity determined by the graphical method describe in Section 3 and the geometric moment of inertia of the beam. GRS beams of consistent spacing and material properties were modeled with varying moments of inertia. The moment of inertia was varied by addition of alternating layers of soil and geosynthetic reinforcement, which subsequently increased the cross-sectional height. Figure 4 presents sketches that illustrate the cross sectional areas of the beam configurations modeled for this portion of the study. The geometric rectangular moment of inertia of a GRS cross-section is defined by equation 5.

$$I = \frac{bh^3}{12} \quad [5]$$

Base (b) was assumed to be equal to 1-meter reflecting a two dimensional finite element analysis and use of the metric system of units. Height (h) was varied with the number of equally spaced GRS layers. Geometric modulus of elasticity was determined using the same graphical method described in section 3 and does not account for the varying stiffness of the soil and reinforcement.

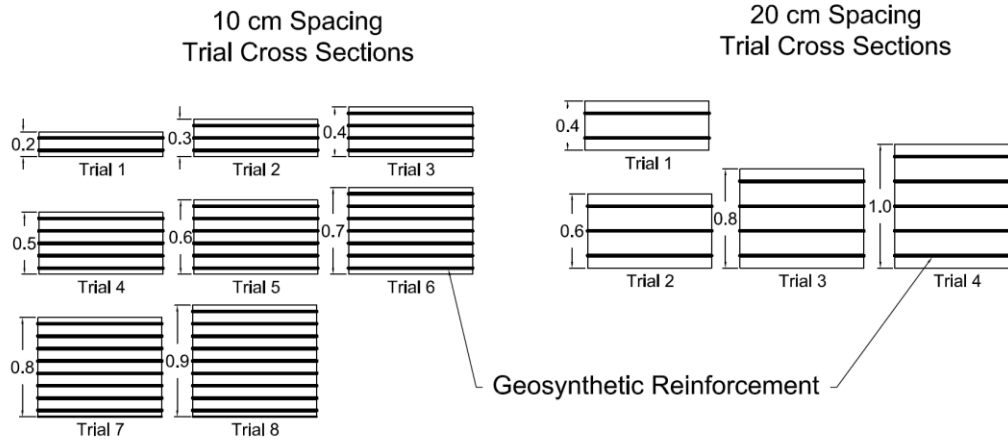


Figure 4. Sketch illustrating the cross sections of the varied FEM modeling program using varied moments of Inertia

The FEM model results for the GRS beam sections in Figure 4 are plotted with a set of Winkler beam solutions for a similar homogenous beam to graphically determine a modulus of elasticity for the GRS beam using the methods presented in Section 3. The modulus of elasticity was determined for three conditions 1) matching deflection at 1/3 the beam length, 2) matching deflection at midpoint (1/2 the beam length) and 3) visually best fitting the entire deflected shape of the FEM model to a Winkler solution.

It is evident from the results that beams with smaller geometric moments of inertia have larger differences between the estimates of modulus of elasticity at 1/2 and 1/3 of the beam length. For this reason, there is less confidence when estimating modulus of elasticity for beams with moments of inertia less than 0.005 m^4 using the graphical method applied in this study. There is less variation in the estimated moduli of elasticity for moments of inertia greater than 0.005 m^4 . This effect may be an indication that GRS beams require a minimum number of layers to develop a composite effect.

A Winkler platform exactly conforms to conventional pure beam bending mechanics so the deformed shape of the beam would be the same for all combinations of E and I having a constant product (C) ($EI=C$), all other parameters being equal. Hence, for pure beam bending, a linear relationship is expected for $1/E$ and I ($I=C(1/E)$). Taking the log of both sides of this relationship and rearranging, the pure bending relationship between I and E can be expressed as a linear relation between logarithms of I and E [$\log(I) = -\log(E) + C2$]. However, it is observed in Figure 6 that the relationship that develops from the FEM models is not linear, but rather log-linear. This is not a reflection of the FEM failing to comply with beam theory, rather, it is a consequence of not estimating the conventional moment of inertia of composite beams sections i.e. by implementing the parallel axis theorem on a transformed section. This was done so that a relationship could be developed to estimate a composite material stiffness enhancement. Some deviation from the Winkler solution is evident by the slight differences in the deformed shapes of the Winkler solution and the GRS Beam FEM. The reasons for these differences have been discussed.

Simplification of the calculation of the modulus was necessary to develop a useful relationship between modulus of elasticity and geometric moment of inertia for GRS beams with moments of Inertia greater than 0.005 m^4 or beam thicknesses of 0.4 m. Discussion of the relationship and restrictions follow.

Figure 5 a) and b) show the estimated moduli of elasticity versus geometric moment of inertia for the trials conducted. Moments of inertia greater than 0.005 m^4 were modeled for GRS beams having 10 cm and 20 cm reinforcement spacing respectively. Beam spans of 3.0 m and 3.5 m are presented separately with a best fit line.

The moduli of elasticity for the different beam spans appear to converge with increasing moments of inertia indicating beam span has less of an effect for GRS beams with larger moments of inertia or higher cross sections. This is intuitively understandable since thick short beams bend less and the effect of beam stiffness would become less significant.

As expected from the observations made in the parametric, study reducing the spacing of reinforcement layers provides an increase in modulus of elasticity as indicated in Figure 6 a) and b). This also, is intuitively explained since the beam becomes stiffer with addition of reinforcement. Figure 6 a) and b) show how the 10 cm reinforcement spacing improves the modulus of elasticity and consequently bending stiffness for both span distances modeled for this study. Once again, this effect appears to diminish somewhat with an increase in beam thickness therefore the benefit of closely spaced reinforcement increases with greater spans.

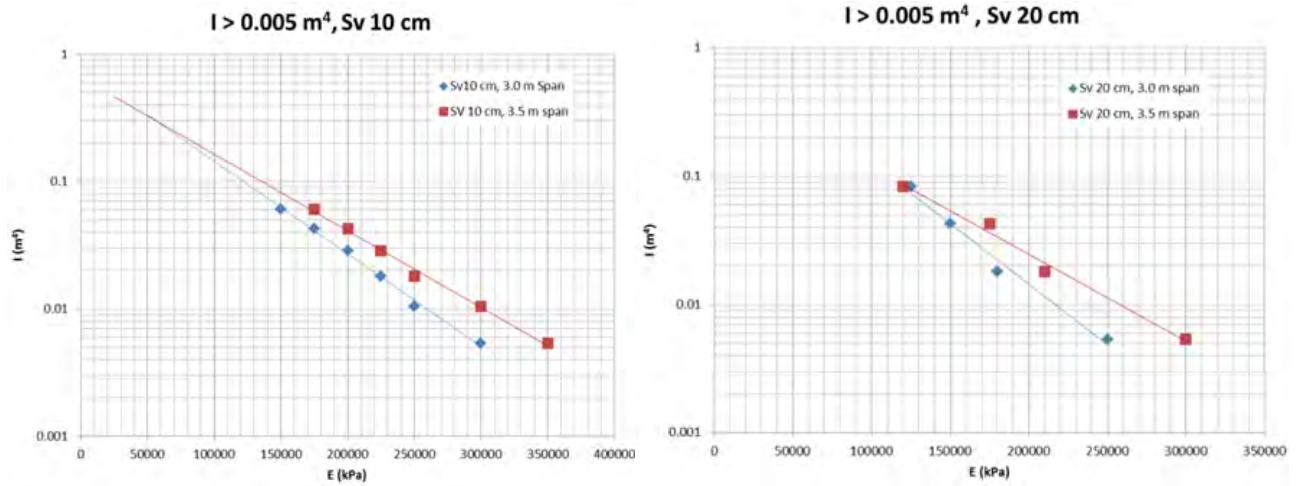


Figure 5. Estimated moduli of elasticity versus moment of inertia for the trails conducted with moments of inertia greater than 0.005m⁴. Figures a) and b) are the results of the 10cm and 20 cm reinforcement spacing. Lines were best fit to 3.0 m and 3.5 m span data.

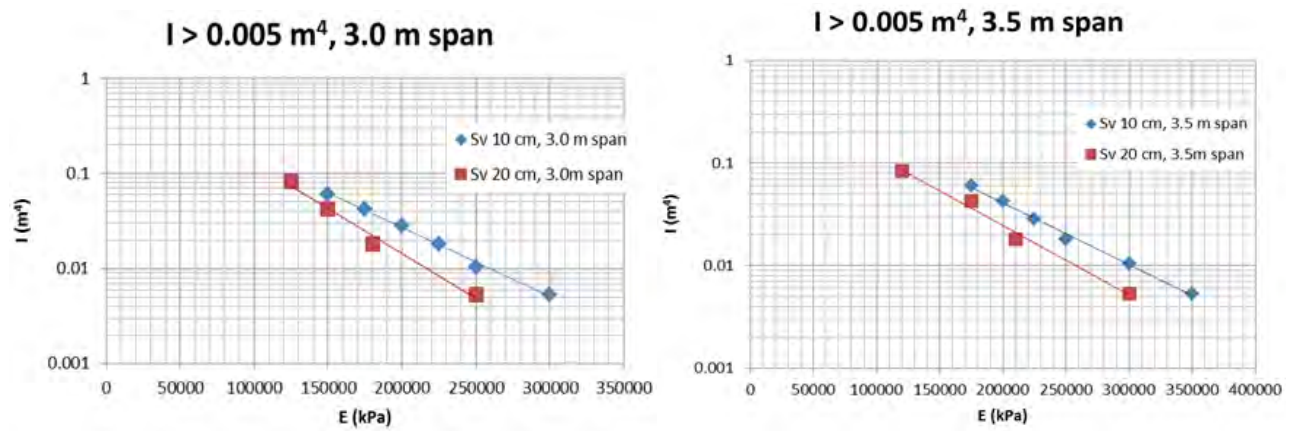


Figure 6. Estimated moduli of elasticity of versus moment of inertia for the trails conducted with moments of inertia greater than 0.005m⁴. Figures a) and b) compare the results of 10cm and 20 cm reinforcement spacing to the different span lengths modeled for this study.

The results from this portion of the study verify that the bending stiffness of GRS beams is largely a function of reinforcement spacing and geometric moment of inertia. The results also indicate that the span to beam height ratio has an ancillary effect. The beam span to length ratio is not evaluated further in this study, however it should be considered for future study.

4.1 Proposed S_v Composite E Relationship

A relationship between geosynthetic reinforcement spacing and the modulus of elasticity is developed here using the data above. A relationship to estimate modulus of elasticity for a given spacing is proposed based on the observation that E increases with I and converges to a single point. The relationship is presented in equations 6, 7, and 8.

$$E = \frac{\log(I) - b}{m} \quad [6]$$

$$m = -1 \times 10^{-7} S_v - 5 \times 10^{-6} \quad [7]$$

$$b = \log(I') - m E' \quad [8]$$

Where E is in units of kPa; S_v is to be the units of centimeters; and I' and E' are the moment of inertia and modulus of elasticity converge and have the units of m^4 and kPa respectively. For the GRS beam modeled in this portion of the study the I' and E' values were found to be $0.27329 m^4$ and $44,444 kPa$ respectively. Based on the results of the parametric study, I' and E' are expected to be a function of the material properties. The parametric study results demonstrate that the geosynthetic reinforcement tensile strength has a minimal effect on the bending stiffness. For this reason, the modulus of elasticity of the soil matrix is anticipated to have the most influence on I' and E' . Additional study could develop a relationship between the I' and E' making the relationship presented in this study applicable to additional soil types.

5. SUMMARY AND CONCLUSIONS

Geosynthetic-Reinforced Soil (GRS) is a soil mass that is reinforced by incorporating horizontal layers of geosynthetic sheets. A better understanding of GRS bending stiffness is expected to improve GRS design and application related to embankments on soft foundations, or negative batter GRS walls. This study investigated the bending stiffness of a GRS platform on a Winkler foundation with two primary objectives. The first objective was to investigate effects of various parameters of a GRS platform on the bending stiffness of the GRS composite and evaluate the applicability of beam theory. The analysis indicated that bending resistance is best gained by decreasing the spacing between reinforcement layers and using higher strength soils. Increasing reinforcement tensile strength had some effect upon bending resistance, but its affect ancillary to the spacing and soil modulus of elasticity parameters.

Some deviation from the Winkler solution is caused by the different boundary condition selected for the FEM model. Unlike a simply supported beam that the Winkler Model is based upon, the FEM restrained the fabric layers from horizontal movement at the beam end. This resulted in slight differences in Winkler and FEM deflected shapes, especially near the support. Another effect that may have caused the variance from the Winkler model is that the structural members used to model the geosynthetic reinforcement were only allowed to resist tension and not compression, therefore the composite E is not likely uniform from top to bottom of the beam and the location of the neutral axis is dependent on the internal stresses developed from bending, which changes with beam location. These conditions do not constitute a variation from beam theory, but they do challenge creation of a closed-form analytical solution. Furthermore, because numerical modeling is complicated and time consuming, A method of approximating the improved bending stiffness based on key parameters was the second objective. The relationships among geosynthetic reinforcement spacing, modulus of elasticity and geometric moment of inertia were examined. Based on limited analyses, the relationship appears to be functional for estimating a composite bending stiffness of GRS platforms with properties and dimensions within the ranges used for this study.

ACKNOWLEDGEMENTS

The author would like to acknowledge the support of his Wife, Chantal and his two sons Brady and Rowan for their patience and understanding of time missed with them in pursuit of this research. The author would also like to thank his advisor Jonathan T.H. Wu, PhD. and Father Mark C. Gemperline, PhD. for the support and mentoring they have provided throughout his engineering career. The industry sponsors are, MCG Geotechnical Engineering, Inc., University of Colorado, Denver, and the U.S. Department of the Interior, Bureau of Reclamation, USA.

REFERENCES

- Liu, H. L., et al. (2007). Performance of Geogrid-Reinforcement and Pile-Supported Highway Embankment over Soft Clay: Case Study. 2007. pp. 1483-1493.
- Scott, Ronald. (1981). Foundation Analysis. Englewood Cliffs, NJ : Prentice-Hall, 1981.
- U.S. Bureau of Reclamation. (1998). Earth Manual Part 1. Denver, CO : United States Government Printing Office, 1998.
- Young, Warren C. (1989). Roark's Formulas for Stress and Strain Sixth Edition. New York, NY : McGraw-Hill Book Company, 1989.

Beneficial Impact of Polymer Treatment on the Swelling and Long-Term Hydraulic Efficiency of Ca-bentonites Compared to the Standard Sodium Activation Method

G. Di Emidio, PhD, Laboratory of Geotechnics, Ghent University, Belgium, gemmina.diemidio@gmail.com
R. D. Verastegui Flores, PhD, Laboratory of Geotechnics, Ghent University, Belgium
A. Bezuijen, PhD, Laboratory of Geotechnics, Ghent University, Belgium

ABSTRACT

The hydraulic conductivity of Geosynthetic Clay Liners for the confinement of waste disposal facilities, mainly depends on the hydraulic conductivity of the core bentonite clay encased between the two geotextiles. Sodium bentonite clays are widely used for Geosynthetic Clay Liners due to their low hydraulic conductivity to water. Calcium bentonites are low cost and readily available. On the other hand, the hydraulic conductivity of calcium bentonites is higher compared to that of sodium bentonites. This study compares the impact of the treatment of calcium bentonite with an anionic polymer, Sodium Carboxymethyl Cellulose (Na-CMC) with HYPER clay technology, to the standard sodium activation treatment of calcium bentonites. The swelling ability and the hydraulic conductivity of a calcium bentonite to CaCl_2 solutions was compared to the hydraulic conductivity of sodium activated bentonite and polymer treated bentonite. Test results showed the beneficial effect of the anionic-polymer treatment on the swelling and hydraulic performance of the clay analyzed.

1. INTRODUCTION

Leachate from landfills may contain harmful substances for the environment and for the human health. The spread of these substances is prevented by the use of hydraulic barriers such as Compacted Clay Liners (CCLs) and Geosynthetic Clay Liners (GCLs). GCLs are factory – manufactured clay liners consisting of a thin layer of bentonite encased by geotextiles or glued to a geomembrane, may be mechanically held together by needling, stitching, or chemical adhesives. High quality bentonites, like sodium bentonite, are used in GCLs. Sodium bentonite clays are widely used because of their low hydraulic conductivity to water and favorable swelling properties (Mitchell, 1993; Shackelford et al., 2000; Egloffstein, 2001; Bouazza, 2001). However, these type of clay may be not readily available, expensive and prone to cation exchange in the long term. For these reasons there is a tendency to prefer low quality, less expensive and readily available calcium bentonite clays enhanced by treatment with sodium activation. However, exposure to high concentrations of organic or inorganic compounds, largely present in landfill leachates, can change the clay fabric, of natural-sodium or sodium-activated bentonites, increasing their hydraulic conductivity (Norrish, 1954; Mitchell, 1993). Another critical disadvantage of the sodium activation is the consequent formation of calcium carbonate precipitates into the soil. This calcium carbonate may re-dissolve during contact with a dilute permeant, releasing calcium ions that exchange with sodium in the clay (Guyonnet et al., 2005). This exchange leads to obliteration of the beneficial low permeability, and to the development of a more permeable clay.

To overcome these problems, modified clays have been recently introduced in barrier applications to improve their chemical resistance to aggressive permeants (Kondo, 1996; Onikata et al., 1996, 1999; Flynn and Carter, 1998; Schroeder et al., 2001; Ashmawy et al, 2002; Simon and Müller, 2005; Lorenzetti et al., 2005; Filippi et al., 2007; Betega de Paiva et al., 2008; Mazzieri et al., 2010; Katsumi et al., 2008; Di Emidio, 2010a&b; Bohnhoff & Shackelford, 2010; Palomino, 2010; Scalia et al., 2011; Malusis et al., 2011). In view of pollutant containment applications, it is of great interest to evaluate the potential benefits of these treated clays, by analyzing their hydraulic behaviour, investigating the mechanisms through which the amendments can improve the sealing capacity of a clay, to highlight the more suitable treatment technique and to further investigate the weaknesses of the available treatments with the aim of future advancements and improvements.

2. MATERIALS

In this study three materials are compared: a natural calcium bentonite (CaB), the same CaB sodium activated (SA CaB) and the same CaB treated with the HYPER clay technology (HCaB). The latter treatment method consists of mixing the base clay with a polymeric solution (containing 8% - by weight of clay - of Sodium Carboxymethyl Cellulose, Na-CMC) with a mechanical stirrer for 30 minutes. This slurry is then oven dried at 105° C for 16 hours. After drying, the HYPER (CaB) clay is ground first manually using a mortar and pestle and then mechanically using a Retsch Mortar Grinder RM 200. This treatment method can also be applied to other types of clay with different polymer dosages (Di Emidio, 2010b).

Some properties of the materials tested here are listed in Table 1.

The electrolyte solutions used in this investigation are deionized water, KCl and CaCl₂ solutions with different concentrations. The deionised water was used as base solution for the HYPER clay and electrolyte solutions preparation. The deionized water was produced using a water purification system PURELAB Option-R 7/15. The electrical conductivity of the deionized water was EC=0.0039 mS/cm, the pH = 7.57, and the redox potential was Eh=293 mV. The electrolyte solutions were used to test the swelling and the hydraulic conductivity of the materials. The solutions were prepared by dissolving different concentrations of KCl and CaCl₂·2H₂O (>99.7% pure) in deionised water. Some properties of the solutions are listed in Table 2.

Table 1. Characteristics of tested soils (CaB=calcium bentonite; SA CaB=sodium activated calcium bentonite; HCaB=HYPER CaB clay).

Characteristics	CaB	SA CaB	HCaB
Swell index (ml/2g)	12	19	42
Specific gravity	2.5	2.5	2.2
Liquid limit (-)	309.53	414.16	831.60
Plastic limit (-)	64.03	64.83	199.39
Plasticity Index (-)	245.50	349.33	632.21
Smectites - Mica (%)	82 - 0	82 - 0	82 - 0
Quartz - Opal (%)	2 - 0	2 - 0	2 - 0
Feldspars (%)	2	2	2

Table 2. Chemical properties of the electrolyte solutions.

Solution	Concentration [M]	EC [mS/cm]	Salinity [-]	pH [-]	Eh [mV]
Deionized water		0.0039	0.0	7.57	293
KCl	0.0001	0.0142	0.0	6.45	258
	0.001	0.143	0.0	6.22	243
	0.01	1.392	0.5	6.261	304
	0.1	12.760	7.3	6.59	324
CaCl ₂	0.0001	0.0253	0.0	6.35	297
	0.001	0.251	0.0	7.28	330
	0.005	1.211	0.4	6.56	262
	0.01	2.220	0.9	6.69	238
	0.1	18.540	11	6.77	260

3. METHODS

The tests performed on the three samples were: (1) swell index test using various electrolyte concentrations and valence; (2) the swell pressure test and (3) the hydraulic conductivity test using a 5 mM Calcium Chloride solution. The swell index tests were performed to have a qualitative evaluation of the impact of various electrolyte solutions with different concentrations (0.0001 M up to 0.5 M) and valences (K⁺¹ and Ca⁺²). The swell pressure tests were executed to prepare the samples for the hydraulic conductivity test and also to overcome some limitations of the swell index test for the qualitative evaluation. These limitations can be caused by turbidity of the solutions during the experiment and/or macropores formation that could false the results (see Fig. 2 in Section 4).

3.1 Swelling Tests

Swell index tests were performed on the untreated CaB calcium bentonite clay, the sodium activated clay and the HYPER clay following the ASTM D5890. The bentonites were oven dried at 105° C. After drying, the bentonites were ground using a mortar and pestle until 100% passed the #200 mesh U.S. standard sieve. 90 ml of the testing solutions were poured into a 100 ml graduated cylinder. Two grams of sieved bentonite were poured in the aqueous solutions in 0.1 g increments. After the 2 g were added, the remaining 10 ml solution was poured to fill the cylinder to the 100 ml. This additional solution was also used to rinse any particle of bentonite adhered to the internal sides of the cylinder. After 16 hours of hydration period, the final temperature and the volume of swollen bentonite were measured.

Swell pressure tests were also performed on the untreated CaB, the sodium activated clay and the HYPER clay. The swelling pressure test apparatus used consists of a stainless steel ring (7.1 cm diameter) accommodated in a one-dimensional cell (similar to a standard oedometer cell) located in a frame provided with a load cell connected to a computer. The specimen was prepared by spreading a thin layer of dry clay (0.45 g dry bentonite/cm²) into the stainless steel ring placed into the oedometer cell. The aim of this procedure was to obtain samples that represent the bentonite core of a standard GCL with typical dry bentonite per unit area of 0.45 g/cm². After assembling the sample was inundated with the testing solution (CaCl₂ 5 mM). For these powder samples a fixed height (h=0,665 cm) was chosen to obtain a similar initial porosity (with a dry unit weight of 6.65 kN/m³) for all samples. The swelling pressure was measured by the load cell keeping the height of the sample constant. The achievement of a steady maximum swelling pressure was chosen as termination criteria. The CaB sample was dismantled from the swell pressure setup after 7 days, the Sa CaB sample after 10.5 days and the H CaB sample after 5 days.

3.2 Hydraulic Conductivity Test

As mentioned above, thin clay specimens were prepared for the hydraulic conductivity tests in the swell pressure setup, with the purpose of simulating the bentonite core of a standard GCL hydrated with the testing solution (CaCl₂ 5 mM) in order to test the hydraulic efficiency of non pre-hydrated samples. The hydraulic conductivity tests were performed in flexible wall permeameters. The tests were executed with a hydraulic gradient of about 55 and an average effective stress of 30 kPa. This effective stress was chosen in order to simulate an extreme condition, such as the lowest effective stress expected in a landfill cover. In case the effective stress is increased (to represent, for instance, a landfill base liner), the hydraulic conductivity will decrease accordingly (Petrov and Rowe, 1997).

The samples chosen for the hydraulic conductivity tests were: the calcium bentonite as base material, the sodium activated bentonite and the HYPER clay calcium bentonite, in order to compare the beneficial effects of the two treatments. A 5 mM CaCl₂ permeant solution was chosen in order to study the effect of cation exchange on the hydraulic conductivity of the clays analyzed.

4. RESULTS

This section shows the results of the experimental work on the calcium clay treated with two enhancement methods: the standard sodium activation and the novel HYPER clay technology that consists, as seen above, in a treatment with an anionic polymer. First, the swell index test results will be shown to have a qualitative indication of the impact on the treated and untreated clays of various electrolyte solutions with different concentrations and valences. There is, in fact, a well-known inverse relationship between the swell index and the hydraulic conductivity of bentonite clays (Jo et al., 2001), therefore it can give an idea of the potential hydraulic behavior of a soil. Then swell pressure test results will be shown, these tests were useful to overcome some limitations encountered in the swell index tests (e.g. due to macropore formation) and to prepare the samples from a powder to a simulated GCL disc, for the hydraulic conductivity test. Finally the results of these hydraulic conductivity tests will also be illustrated. The samples for the hydraulic conductivity tests were first hydrated with the permeant solution in the swell pressure setup to represent the worst case scenario (direct permeation with electrolyte solution without pre-hydration with water).

Figure 1 shows the swell index of the materials versus concentration of the KCl and CaCl₂ solutions used. As shown in the figure, the swell index of the treated clays was higher compared to that of the untreated calcium bentonite clay. The HYPER clay showed a higher swell index compared to both the untreated clay and the sodium activated clay for KCl solutions 0.0001 M up to 0.5 M. For CaCl₂ solutions from 0.0001 M up to 0.01 M (which is similar to a typical maximum pore water content that may be expected, Lin & Benson, 2005) the HYPER clay showed a higher swell index compared to the untreated clay. For concentrations of CaCl₂ higher than 0.05 M the swell index of the three clays was comparable. This result indicates that the HYPER clay treatment could potentially perform better compared to the sodium activation. For concentrations of CaCl₂ between 0.005 M and 0.01 M it was observed an unusual behavior for the sodium activated clay: a card house structure with marked macropores was detected (Figure 2-left); this behavior was highlighted with a letter "M" in Figures 1 and 2-right on the columns that showed this phenomenon. The card house structure with marked macropores evidently produced false measurements of the swell index of the sodium activated clay within that range of concentrations. To overcome this limitation and to represent the actual swelling performance of the clays, a one-dimensional swell pressure test was performed using a 0.005 M CaCl₂ solution. The swell pressure test, in fact, is not expected to be affected by this type of macropores formation, because of the mechanisms that govern the swell pressure phenomenon: when hydrated, the bentonite clay adsorbs a large amount of water molecules and ions; as a consequence a swell stress is raised by this water entering the pores among montmorillonite particles and the interstitial layers in individual montmorillonite crystals, leading to an increase in volume and manifested as a stress on the surrounding materials. On the other hand, the macropores formation, in the swell index test, leads to an increase in volume (due to the structure and the presence of macropores), but do not raise the interstitial stress between clay layers and on the surrounding materials. The results of the swell pressure are given in Figure 2 and 3. The swell pressure of the HYPER

clay is higher compared to that of the sodium activated clay in the 0.005 M CaCl_2 solution, in contradiction with the misleading swell index test results that showed an apparent opposite behavior due to the macropore formation (Figure 2-right). Figure 3 clearly shows the variation of the swell pressure for the three clays with time. As expected, both treated clays showed a higher swell pressure compared to the untreated calcium clay. As shown in the Figure 2-right, the swell pressure of the HYPER clay was higher compared to that of the sodium activated clay, overcoming the technical limitations of the swell index test observed and suggesting the potential higher hydraulic performance of the HYPER clay.

Figure 4 shows the hydraulic conductivity of the three clays vs. time. As expected, the hydraulic conductivity of both treated clays were lower than that of the untreated clay due to the typical thinner diffuse double layer between clay platelets in the calcium bentonite. Besides, Figure 4 also shows that the hydraulic conductivity of the HYPER clay was lower than that of the sodium activated clay, indicating a higher performance of the HYPER clay not only in terms of swelling ability (as seen above) but also in terms of hydraulic conductivity. These results were in good agreement with swelling tests results. As expected, the higher the swell pressure, the lower the hydraulic conductivity of the materials tested. The reference hydraulic conductivity to deionized water of a natural sodium-bentonite is of the order of $6.4\text{E-}12$ m/s (see Di Emidio, 2010a). The hydraulic conductivity to CaCl_2 5mM of the HYPER clay shown in Figure 4 is of the same order ($7.8\text{E-}12$ m/s after 1,5 Pore Volumes of flow) whereas the hydraulic conductivity to CaCl_2 5mM of the sodium activated clay was half order of magnitude higher ($3.04\text{E-}11$ m/s after 5 Pore Volumes, PV). The hydraulic conductivity of the calcium clay after 25 PV of flow is $1.52\text{E-}10$ m/s. The lower hydraulic conductivity of the HYPER clay is due to its thicker diffuse double layer (DDL) that is maintained in the long term due to the irreversible adsorption of the polymer into the clay (Di Emido, 2010b). The polymer, in fact, intercalates between the clay particles maintaining the interlayer open and adsorbing lots of immobile water molecules and ions. This phenomenon restricts the pore space available for the flow and causes tortuous flow pathways, which is typical of dispersed structured low permeable clays. Given that the thickness of the adsorbed layer is inversely related to the ions concentration and valence, bentonites are particularly sensitive to changes in the composition of the pore fluid. In particular, electrolyte solutions with high valence (such as the CaCl_2 solution used in this work) cause the thickness of the diffuse double layer to collapse and therefore the hydraulic conductivity to increase.

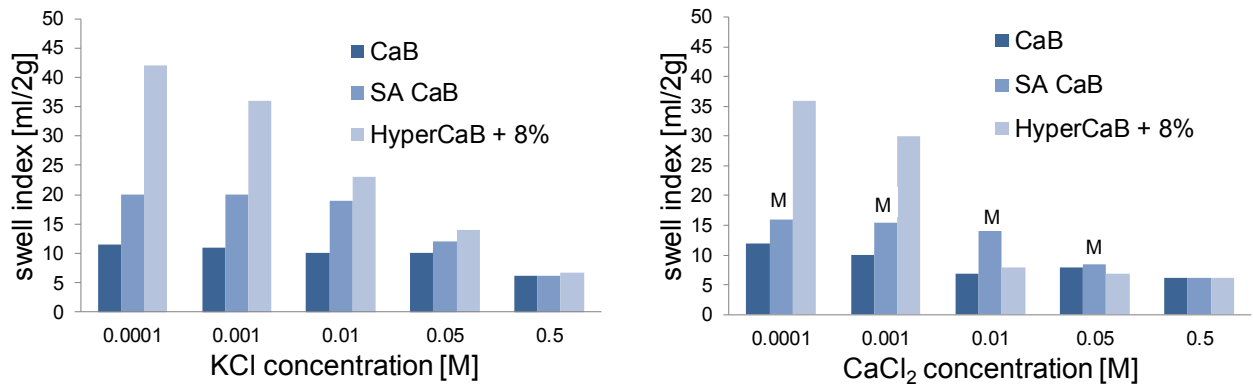


Figure 1. Swell index in KCl and CaCl_2 solutions of the untreated calcium bentonite (CaB), of the sodium activated CaB and of the CaB treated with the HYPER clay technology using 8 % CMC by dry weight (HYPER CaB clay 8%)

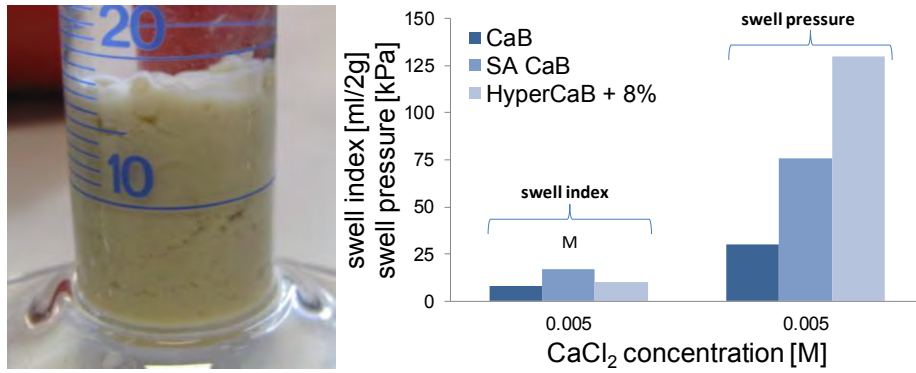


Figure 2. At the left: macropore formation in the swell index test of the sodium activated clay in a 0.005 M CaCl₂ solution. At the right: swell pressure vs. time of the untreated calcium bentonite (CaB), of the sodium activated (SA) CaB and of the CaB treated with the HYPER clay technology using 8 % CMC by dry weight (HYPER CaB clay 8%).

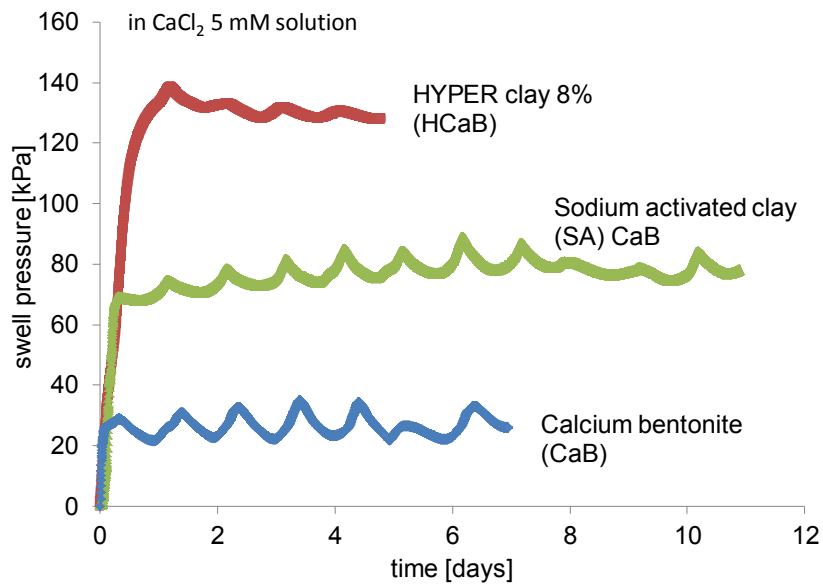


Figure 3. Swell pressure vs. time of the untreated calcium bentonite (CaB), of the sodium activated CaB and of the CaB treated with the HYPER clay technology using 8 % CMC by dry weight (HYPER CaB clay 8%).

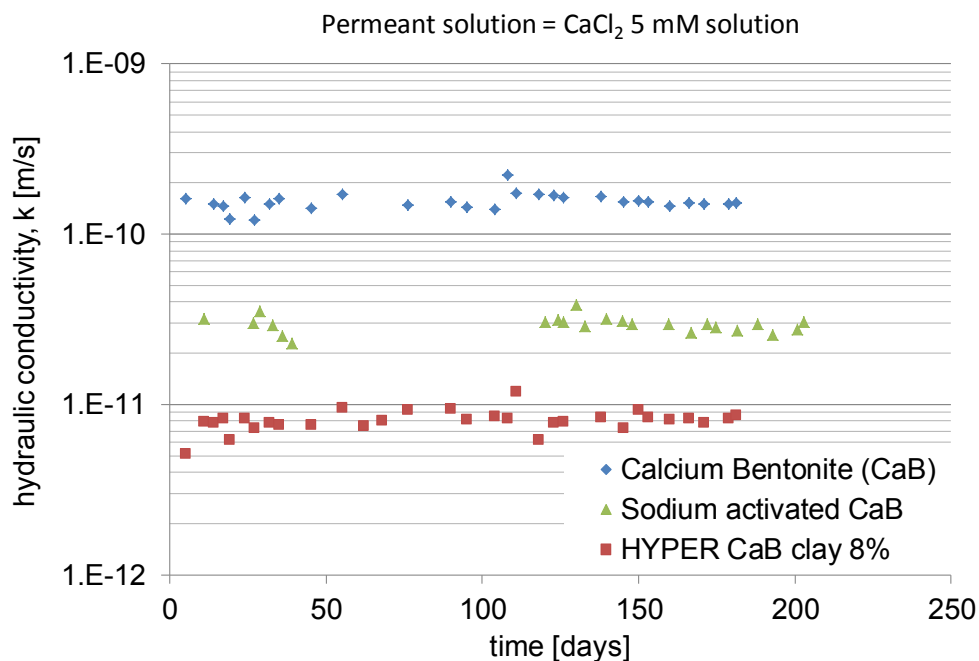


Figure 4. Hydraulic conductivity to CaCl₂ 5 mM solution of the untreated calcium bentonite (CaB), of the sodium activated CaB and of the CaB treated with the HYPER clay technology using 8 % CMC by dry weight (HYPER CaB clay 8%).

5. DISCUSSION SECTION

The swelling ability of the treated clays was quantified by means of standard swell index test and swelling pressure tests. Both showed that the treatment with the anionic polymer studied here improved the swelling ability of the untreated clay compared to the sodium activation method. The swell index test of the sodium activated clay showed some limitations in its accuracy due to the macropore structure of the clay in contact with CaCl₂ solutions. The macropores formed lead to a card house structure with an apparent high swell index. On the other hand, the swell pressure test was not affected by this phenomenon. Therefore, the swell pressure provided more reliable information on the swelling ability of the clays. Hydraulic conductivity tests were conducted on untreated calcium bentonite clay, sodium activated clay and polymer treated clay. As expected, the hydraulic conductivity of the untreated clay was the highest due to a compressed double layer thickness. The hydraulic conductivity of the HYPER clay was the lowest. The low hydraulic conductivity of the HYPER clay is due to its thick diffuse double layer (DDL) which is maintained in the long term. Further research is in progress to confirm these results for higher concentrations of the permeant solution (such as CaCl₂ 10 mM and 100 mM).

ACKNOWLEDGEMENTS

The authors acknowledge ir. Jolien Seuryck and Mr. Jan Van Der Perre for the help provided for the experiments.

REFERENCES

- Ashmawy, A. K., El-Hajji, D., Sotelo, N. and Muhammad, N. (2002). Hydraulic performance of untreated and polymer-treated bentonite in inorganic landfill leachates., *Clays and Clay Minerals*, 50(5): 546–552.
- Betega de Paiva, L., Morales, A.R., Valenzuela Díaz, F.R. (2008). Organoclays: Properties, preparation and applications. *Applied Clay Science*, Elsevier, 42: 8–24.
- Bohnhoff, G.L. & Shackelford, C.D. 2010. Global Geoenvironmental Engineering Challenges. *The First US-India Workshop on Global Geoenvironmental Engineering Challenges*. November 7, New Delhi, India.
- Bouazza, A. (2001). Geosynthetic clay liners, *Geotextiles and Geomembranes*, Elsevier 20: 3–17.
- Di Emidio, G. (2010a). Hydraulic and Chemico-Osmotic Performance of Polymer Treated Clays, *PhD thesis*, ghent University.
- Di Emidio, G. (2010b). Clayey barriers. *Patent Pending: PCT/EP2011/064542, WO2012/025564 A1*.

- Egloffstein, T. A. (2001). Natural bentonites-influence of the ion exchange and partial desiccation on permeability and self-healing capacity of bentonites used in gcls, *Geomembranes and Geotextiles*, Elsevier 19: 427–444.
- Filippi, S., Mameli, E., Marazzato, C. and Magagnini, P. (2007). Comparison of solution-bleeding and melt-intercalation for the preparation of poly(ethylene-coacrylic acid)/organoclay nanocomposites., *European Polymer Journal*. Elsevier, 43(5): 1645–1659.
- Flynn, B. N. and Carter, G. C. (1998). Waterproofing material and method of fabrication thereof. *US 6537676B1*
- Guyonnet, D., Gaucher, E., Gaboriau, H., Pons, C.-H., Clinard, C., Norotte, V., Didier, G. (2005). Geosynthetic Clay Liner Interaction with Leachate: Correlation between Permeability, Microstructure, and Surface Chemistry, *Journal of Geotechnical and Geoenvironmental Engineering*, ASCE, 131(6): 740-749.
- Jo, H., Katsumi, T., Benson, C. H. and Edil, T. B. (2001). Hydraulic conductivity and swelling of non-prehydrated gcls permeated with single species salt solutions, *Journal of Geotechnical and Geoenvironmental Engineering*, ASCE 127(7): 557–567.
- Katsumi, T. (2010). *Geosynthetic Clay Liners for Waste Containment Facilities*, Bouazza and Bowders eds., Chapter 4.
- Katsumi, T., Ishimori, H., Onikata, M. and Fukagawa, R. (2008). Long-term barrier performance of modified bentonite materials against sodium and calcium permeant solutions, *Geotextiles and Geomembranes*, 26: 14–30.
- Kondo, M. (1996). Method of activation of clay and activated clay. 5573583
- Lin, L.-C. and Benson, C.-H. (2005). Effect of wet-dry cycling on swelling and hydraulic conductivity of GCLs. *Journal of Geotechnical and Geoenvironmental Engineering*, ASCE, 126(1): 40-49.
- Lorenzetti, R. J., Bartelt-Hunt, S. L., Burns, S. E. and Smith, J. A. (2005). Hydraulic conductivities and effective diffusion coefficients of geosynthetic clay liners with organobentonite amendments, *Geotextiles and Geomembranes*, 23 (2005) 385400 23: 385–400.
- Malusis, M., McKeehan, M.D., LaFredo, R.A. 2010. Multiswellable bentonite for soil-bentonite vertical barriers. *Proceedings of the sixth International Congress on Environmental Geotechnics*, 6th ICEG, November 8-12, New Delhi, India
- Mazzieri, F., Di Emidio, G. and Van Impe, P. O. (2010). Diffusion of CaCl₂ in a modified bentonite: impact on osmotic efficiency and hydraulic conductivity, *Clays and Clay Minerals*, 58(2): 351-363.
- Mitchell, J. (1993). *Fundamentals of Soil Behaviour*, John Wiley & Sons.
- Norrish, K. (1954). The swelling of montmorillonite, *Transactions Faraday Society*, 18: 120–134.
- Onikata, M., Kondo, M. and Kamon, M. (1996). Development and characterization of a multiswellable bentonite, in M. K. ed. Balkema Rotterdam (ed.), *Environmental Geotechnics*, pp. 587–590.
- Onikata, M., Kondo, M., Hayashi, N. and Yamanaka, S. (1999). Complex formation of cation-exchanged montmorillonites with propylene carbonate: Osmotic swelling in aqueous electrolyte solutions., *Clays and clay minerals*. Vol. 47, No.5,672-677. 47(5): 672–677.
- Palomino, A.M. (2010). Polymer-enhanced geomaterials for use in geoenvironmental applications, *The First US-India Workshop on Global Geoenvironmental Engineering Challenges*. November 7, New Delhi, India.
- Petrov, R. J. and Rowe, R. K. (1997). Geosynthetic clay liner (gcl) – chemical compatibility by hydraulic conductivity testing and factors impacting its performance, *Canadian Geotechnical Journal*, 34: 863–885.
- Scalia, J., Benson, C.H., Edil, T.B., Bohnhoff, G.L., Shackelford, C.D. 2011. Geosynthetic Clay Liners containing bentonite polymer nanocomposite. *Proceedings of the Geo-Frontiers 2011 Congress*, Dallas, Texas.
- Schroeder, C., Monjoie, A., Illing, P., Dosquet, D. and Thorez, J. (2001). Testing a factory-prehydrated gcl under several conditions, in CISA (ed.), *Proceedings Sardinia 2001, 8th International Waste Management and Landfill Symposium*, Cagliari, Italy, Vol. 1.
- Shackelford, C. D., Benson, C. H., Katsumi, T., Edil, T. B. and Lin, L. (2000). Evaluating the hydraulic conductivity of gcls permeated with non-standard liquids, *Geotextiles and Geomembranes*, Elsevier 18: 133–161.
- Simon, F. G. and Müller, W. W. (2005). Standard and alternative landfill capping design in germany, *Environmental Science and Policy*, Elsevier 7(4): 277–290.

Benefit-Cost Analysis of Using Geosynthetics in Water Resources

M. Goldenberg, P.E., CETCO, USA, mgold@amcol.com

ABSTRACT

Increased water main breaks, leaking water reservoirs, and a lack of investment in infrastructure has left America's network of water systems in disrepair, warranting a D-minus grade from the American Society of Civil Engineers (ASCE, 2009). As certain regions of the United States, particularly the southwest, face water shortages, the need to rebuild the nation's water infrastructure is becoming increasingly important. This paper will present a cost-benefit analysis of constructing a composite liner system (geomembrane in combination with a GCL) to the expected savings in dollars from water saved. To evaluate their effectiveness in limiting water leakage, liner systems with and without an underlying GCL will be evaluated using tools commonly used in the landfill industry. Discount cash flow calculations indicate that the cost to construct a more robust liner will result in a net savings compared to the projected price of water lost over time from deteriorating reservoirs or those designed without a supporting low permeability secondary barrier.

1. INTRODUCTION

Funds for infrastructure are often seen as discretionary, especially during difficult economic times. Unfortunately, this lack of funding leads to deteriorating roads and bridges, water main breaks, leaking reservoirs, and so forth. This not only causes inconveniences in terms of roadway congestion, it can be more devastating in terms of a faulty bridge or a failed water reservoir. A lack of investment in the maintenance of current infrastructure can result in much greater costs in the future when the road, bridge, or water containment structure fails altogether. The importance of America's infrastructure is often understated - in terms of current and future economic investment, safety, and in the case of fresh drinking water, preserving a valuable limited resource.

According to the World Water Organization, the world's water consumption rate is doubling every 20 years, which is twice the rate of population growth (WWO, 2010). Further, it is projected that by the year 2025 water demand will exceed supply by 56% (WWO, 2010). The agriculture industry consumes between 75 and 90 percent of a region's available water supply (WWO, 2010). According to the Natural Resources Defense Council (NRDC), climate change will also have a significant impact on the sustainability of water supply in the coming decades (NRDC, 2010). A study by Tetra Tech for the NRDC found that more than 1,100 countries will face higher risks of water shortages by 2050 as a result of global warming. And more than 400 of these countries will face extremely high risks of water shortages (NRDC, 2010).

Economics would indicate that the price of water would increase in the coming years as the supply of fresh drinking water decreases. It is important to note that the current price of water in the United States is much less than several other developed countries, and this price is likely to increase in the coming years to cover the expenses necessary to repair the current water infrastructure and develop new infrastructure to sustain the resource. For example, Germany is currently paying \$1.91 for a cubic meter of drinking water. The United States is paying just \$0.51 for the same amount. Using tools that are commonly used in the landfill industry with reasonable assumptions, the total amount of water lost through compacted clay and geosynthetic lined systems can be approximated. From this methodology, the total cost of water lost can be calculated, and a cost-benefit analysis of installing a more robust geosynthetic system will be evaluated.

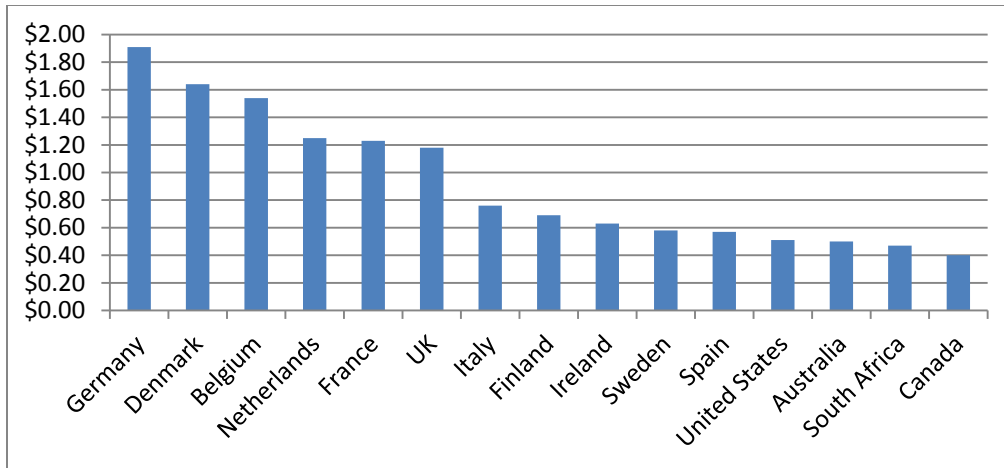


Figure 1. Fresh water price comparison in developed countries in U.S. dollar per m³ (American Water Works Company, September 2011).

Several options are available for lining water containment structures, including natural soil barriers and manufactured geosynthetics. For the purposes of this study, the following liner systems will be reviewed: traditional compacted clay liners, geosynthetics such as geomembranes and geosynthetic clay liners (GCLs), and composite liners, which include the combination of a geomembrane and an underlying soil layer or a GCL. Cost/benefit analysis on concrete liners were evaluated in the past (Zornberg and Webber, 2003). The study concluded that a geomembrane-concrete composite liner was more effective at reducing seepage as compared to concrete alone, 95% reduction as compared to 70% reduction. For the purposes of this paper, the goal is to maximize performance while minimizing cost. Accordingly, concrete will not be discussed further due to its significantly higher price in materials, hauling, and labor, as compared to soil and geosynthetic lined systems. The goal of this evaluation is to demonstrate a cost-benefit analysis of a properly installed geosynthetic system as compared to the price of lost water.

2. COMPACTED CLAY LINERS AND GEOSYNTHETICS

Compacted clay liners have been historically used to minimize infiltration in several applications, including water and wastewater reservoirs, landfills, and mining sites. Off-site borrow sources of clay or silt soils are often required to construct a low-permeability compacted soil liner. Significant upfront investigation is necessary to properly characterize the extent and the quality of the soil at the borrow source. In the landfill industry, the standard for a clay liner requires a hydraulic conductivity of 1×10^{-7} cm/sec and a thickness of 0.6 meters (2 ft) for sufficient performance. Depending on the availability of quality soil, the cost of excavating and hauling clay can be substantial, especially if distances are significant. Further, compacted clay can be difficult to install, with considerable variability in quality, which can lead to preferential flow pathways through the clay matrix (Rogowski, A.S., USEPA, 1990). Additionally, compacted clay liners can be susceptible to freeze-thaw cycling, with evidence of increased permeability due to its effects (LaPlante and Zimmie, 1992). For these reasons, a compacted clay liner would typically be installed in combination with a separate overlying geomembrane.

Because the topic of this paper is related to water containment, the geosynthetics that contribute to reducing water infiltration include geomembranes and Geosynthetic Clay Liners (GCLs). Drainage geocomposites can be used as well, often as leak detection layers in a double lined system. Several options exist for geomembranes, with the most popular being HDPE, LLDPE, PP and PVC. Each type of geomembrane has its own advantages and disadvantages, which are outside the scope of this paper and should be evaluated on a site-specific basis. Geomembranes are practically impermeable when intact; however, they are also prone to punctures due to installation damage. Giroud and Bonaparte (1989) presented field data on defect sizes and frequencies that were obtained from construction quality assurance and control (CQA and CQC) programs and forensic analysis for landfills and surface impoundments. They found that typical causes of defects in geomembranes include discontinuous seams, seam failures, damage from construction equipment, and puncturing by stones found in the adjacent soil. Although certain geomembranes may be more prone to punctures than others, it is reasonable and conservative to assume that at least some defects will occur with even the most stringent quality assurance and quality control program. Giroud and Bonaparte (1989) recommend using a frequency of one defect for every 4,000 m² of geomembrane and a defect area of 1 cm² for design purposes. Although these recommendations were based on landfill applications, it is reasonable to assume similar conditions for water containment structures utilizing geomembrane liners.

Various types of GCLs exist on the market. The most frequently specified are needle-punched reinforced GCLs - where the fibers from the cover geotextile are needlepunched through a layer of sodium bentonite clay to the opposite base geotextile. Geosynthetic clay liners that contain sodium bentonite between two geotextiles are typically characterized as “standard” GCLs, and are certified to maximum hydraulic conductivity values of 5×10^{-9} cm/sec, when tested in accordance with ASTM D 5887. The low GCL permeability is attributed to the low hydraulic conductivity of the sodium bentonite clay. As the bentonite hydrates, it swells and creates a tortuous flow path for water. Because standard GCLs are thin, typically 0.7 cm, increased water depths would result in high hydraulic gradients, which would translate into higher flow rates through the liner. Because of this, standard GCLs would not be recommended as standalone liners for liquid depths greater than 30 cm (1 ft). In these cases, the GCL should be used as a part of a composite liner (with an overlying geomembrane), or a composite GCL (geomembrane-laminated) can be considered as well. Geomembrane-laminated GCLs can be used as stand-alone liners in ponds or smaller water reservoirs. These types of GCLs are typically recommended for water depths that are less than 5 meters (16 ft). Because the seams of a geomembrane-backed GCL are simply overlapped, high water pressure can exacerbate the flow rate through the seams. A separate welded geomembrane overlying a standard GCL typically results in optimal hydraulic performance.

3. COMPOSITE LINERS

Geomembranes have been successfully used in countless liquid containment applications. Nonetheless, because of their thin structure they are susceptible to damage. While an intact geomembrane is virtually impermeable, minor damage can lead to a high leakage rate, especially when high hydraulic heads are being contained, and the underlying subgrade is porous. Much research has been devoted to measuring and minimizing leakage due to geomembrane defects (Weber CT, 2008; Giroud, 1997). Weber and Zornberg (2005) studied the application of geomembranes in dam construction. The study concluded that one should not expect the geomembrane to be fully impervious. This was attributed to a geomembrane being susceptible to installation damage and long-term service. Thorough construction quality control (CQA) can limit the number and size of geomembrane defects. However, even the most stringent CQA would not find the smallest punctures, which can lead to increased water losses. Nosko and Touze-Foltz (2000) used an electrical damage detection system to evaluate geomembrane damage during installation for over 300 landfill sites totaling more than 3,250,000 m². The study resulted in 4,194 defects detected, or approximately one defect per 800 m². It should be noted that defects can also occur post construction. During filling operations, as pressure increases, stones in the underlying subgrade can puncture a geomembrane.

Fukuoka (1986) and Brown et al. (1987) also investigated leakage through geomembrane defects. Fukuoka (1986) conducted large-scale permeameter tests to investigate leakage through defects in a reservoir liner for heads up to 40 m. Brown et al. (1987) conducted smaller scale permeameter tests to measure leakage through defects in liners for heads up to 1 m. Both authors concluded that a gap between the underlying soil and geomembrane contributed to significant increases in leakage where defects in the geomembrane occurred. Flow would occur laterally along the interface between the soil and geomembrane, as well as into the underlying soil layer. This research provided an initial understanding that the quality of contact between the geomembrane and the underlying soil or GCL can have a significant outcome on the overall leakage rate.

Further research by Giroud (1997) led to empirical equations for calculating leakage through composite liners with geomembrane defects. The equations are derived based on the understanding that the flow through a composite liner system (where a geomembrane overlies a low permeability soil or GCL) will depend on size of the geomembrane defect, the hydraulic head on top of the liner system, the hydraulic conductivity of the underlying soil or GCL, the thickness of the underlying soil or GCL, and the quality of contact between the geomembrane and the underlying low permeability soil or GCL layer, as shown in Figure 2. According to Giroud (1997) “in the case of a GCL, good contact conditions may be assumed because GCLs are usually installed flat, and because the bentonite slurry that may exude from a hydrated GCL contributes to establishing a close contact between the geomembrane and the GCL, provided sufficient compressive stress is applied.” Touze-Foltz and Giroud (2003) refined these empirical equations to more accurately predict liner leakage for three types of defects (circular defects, defects of circular length, and damaged wrinkles) and three types

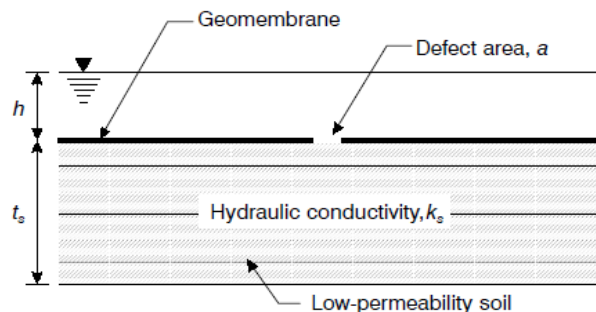


Figure 2. Variables in Giroud's Equation (Giroud, 1997).

of contact conditions (excellent, good, and poor). The Touze-Foltz and Giroud equations only apply to relatively low hydraulic heads of less than 3 meters.

Weber (2008) conducted a series of hydraulic conductivity tests for geomembrane-only liners, geomembrane-compacted clay liners, and geomembrane-GCL liners under high hydraulic heads – up to 45 meters. Using existing equations by Giroud (1997) and Touze-Foltz and Giroud (2003), Webber (2008) developed equations for calculating leakage through geomembrane-compacted clay and geomembrane-GCL liners under high hydraulic heads. To evaluate the accuracy of existing equations used to predict leakage through geomembrane-only liners, Webber conducted geomembrane-only hydraulic conductivity tests, with a high permeability sand layer beneath the geomembrane. These results were evaluated using Bernoulli's equation for flow through an orifice, as recommended by Giroud and Bonaparte (1989). Webber (2008) concluded that these equations are valid for estimating flow through a geomembrane defect over a sand layer; however, the accuracy of the equation depended on the coefficient C, which can vary with the hydraulic head. The results of Webber's testing program are shown in Figure 3. The geomembrane-GCL and geomembrane-compacted clay liners performed very similarly as would be expected when quality clay (with an average hydraulic conductivity of 8×10^{-7} cm/sec in this case) is placed beneath a geomembrane. The geomembrane-only tests had leakage rates that were several orders of magnitude greater than the geomembrane/GCL and the geomembrane/CCL liners, which is consistent with the calculations in this study.

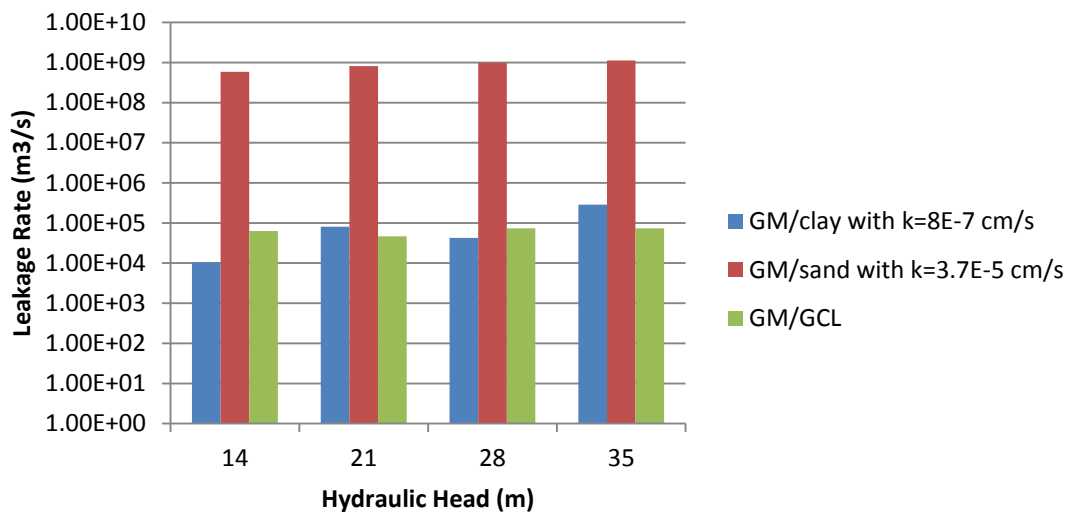


Figure 3. Results from experimental program by Webber, 2008.

4. BENEFIT/COST ANALYSIS FOR LINERS

To limit additional variability, Giroud's equations (Giroud, 1997) were used to calculate the leakage rate for the composite liner systems in this study. These equations are used regularly in the landfill industry, and are proven in their accuracy. As mentioned above, a drawback of using Giroud's equations for this study is the limited hydraulic head of 3 meters. Although this hydraulic head is not representative of field conditions, which are well over 100 meters in some instances, the end result is believed to be similar when comparing the effectiveness of one liner system to another. Darcy's Law was used to calculate the leakage through the compacted clay liner.

For the calculations in these analyses, the soil subgrades were assumed to be 0.3 meters (1 foot) thick at the specified hydraulic conductivities. The soil hydraulic conductivities ranged between 1×10^{-5} m/sec and 1×10^{-7} m/sec, with a most likely value of 1×10^{-6} m/sec. Because these hydraulic conductivity values are high (several orders of magnitude higher than the controlling liner component – the geomembrane) the end result would be the same considering greater soil thicknesses. The compacted clay component was assumed to be 0.6 meters thick with hydraulic conductivity values ranging between 1×10^{-9} m/sec and 1×10^{-7} m/sec due to the expected field variability of clay liners (Rogowski, USEPA, 1990). The GCL hydraulic conductivity values ranged between 3×10^{-11} m/sec and 1×10^{-10} m/sec, conservatively. The geomembrane defect diameters ranged from 0.0016 m to 0.05 m for each composite liner option. The number of defects in the geomembrane ranged between 2.5 to 25 per hectare for the GCL option and between 5 and 50 per hectare for the geomembrane-only option. This assumption is reasonable because the GCL acts as a geomembrane cushion in addition to a low permeability barrier. The contact coefficient

between the geomembrane and the GCL was 0.21, while the contact coefficient between the geomembrane and the soil was 1.15, as recommended by Giroud (1997). According to a study on dams titled Mission 2012 - Clean Water by the Massachusetts Institute of Technology, the average life of a dam is 50 years. The calculations in this study assume an interest rate of 10% over the 50 year period. As discussed in the introduction, the price of water can also vary. These calculations used a range between \$0.51/m³ (current price of water in the United States) and \$1.91/m³ (highest current price in developed countries), with a most likely value of \$0.92 (the average price in developed countries). The price may increase in time, which would work in favor of a potentially more expensive liner system that minimizes water losses.

Many of the parameters used to calculate the value of a composite liner system are highly variable. For this reason, a statistical approach was taken to find the probability that the benefit-to-cost ratio of constructing various liner systems was greater than one. The technical and economic effectiveness of the three liner systems were compared by comparing ratios of the net present or discounted life-cycle costs (e.g., NPV_{clay}/NPV_{GM/GCL} and NPV_{GM/soil}/NPV_{GM/GCL}). Using the method in Duncan (2000), the ratios were calculated for the most likely values (MLV), MLV plus one standard deviation, and the MLV minus one standard deviation. The values used for this study are shown in Table 1. Assuming a normal distribution, the probability that the discounted cost ratio would be greater than one was calculated. The results of these calculations found that, in most cases, it would be economically beneficial to construct a geosynthetic composite (GM/GCL) liner in lieu of compacted clay or a geomembrane-only liner. The probability that the discounted cost of a geomembrane-only liner would exceed the discounted cost of a geosynthetic composite liner is 100% when the underlying soil has a hydraulic conductivity of 1x10⁻⁶ m/sec. When the hydraulic conductivity of the underlying soil is an order of magnitude less permeable (1x10⁻⁷ m/sec), the probability decreases slightly to 93%. Comparing the discounted cost of a compacted clay liner to the discounted cost of a geosynthetic composite liner, the probability decreases to 82%. These calculations indicate that although geosynthetic liner systems may initially require a higher capital cost to construct, these costs are most likely offset by the improved performance (i.e., reduced leakage and saved water). Table 1 shows the range and most likely values of the variables used.

Table 1. Variable Input Parameters.

Variable	Units	HCV	MLV	LCV	σ
Head	m	3	3	3	
Defect Diameter	m	0.05	0.01	0.0016	0.008
Price of Water	\$/m ³	\$1.91	\$0.92	\$0.51	\$0.233
GM/Soil					
Variable	Units	HCV	MLV	LCV	σ
Contact Quality Factor		1.15	1.15	1.15	
Number of installation defects per hectare		50	25	5	7.5
Installed Cost of GM/Soil	\$/ha	\$84,162	\$67,048	\$49,934	\$5,705
Soil Hydraulic Conductivity	m/sec	1.00E-05	1.00E-06	1.00E-07	1.7E-6, 6.8E-7
Cost of Recoverable Water Lost	\$/ha/yr	\$1,883,258	\$60,970	\$837	
Clay (No GM)					
Variable	Units	HCV	MLV	LCV	σ
Hydraulic Conductivity	m/sec	1.00E-07	1.00E-08	1.00E-09	1.7E-08, 6.8E-09
Installed Cost of CCL	\$/ha	\$77,129	\$68,458	\$58,303	\$3,138
Cost of Recoverable Water Lost	\$/ha/yr	\$361,403	\$17,408	\$965	
GM/GCL					
Variable	Units	HCV	MLV	LCV	σ
Contact Quality Factor		0.21	0.21	0.21	
Number of installation defects per hectare		25	12.5	2.5	3.8
GCL Hydraulic Conductivity	m/sec	1.00E-10	5.00E-11	3.00E-11	1.2E-11, 3.4E-11
Installed Cost of GM/GCL	\$/ha	\$148,326	\$114,097	\$79,868	\$11,410
Cost of Recoverable Water Lost	\$/ha/yr	\$683	\$73	\$4	

Notes:

All costs in US\$

MLV = Most Likely Value, LCV = Lowest Conceivable Value, HCV = Highest Conceivable Value

σ = Standard Deviation. In general, standard deviations were calculated using $\sigma = (HCV - LCV)/6$, as recommended by Duncan (2000). In selected cases, such as the infiltration rates through the ET cap, this method resulted in a negative value for $MLV - \sigma$, indicating a skewed distribution. In these cases, two standard deviation values were used: for the lower bound, σ_1 was calculated using $0.68 \times \mu$ (Harr, 1987); for the upper bound, σ_2 was calculated using Duncan (2000).

5. SENSITIVITY ANALYSIS

The chosen values for hydraulic conductivities, number of defects, sizes of defects, and installed material costs were taken from historical research and CETCO's database. Although these values are believed to represent typical field conditions as accurately as possible, they are highly variable and should be evaluated on a site by site basis. For instance, the above calculations assume an interest rate of 10%. Increasing the rate to 12% will result in a decreased probability of 70% for the geomembrane/GCL liner to have a lower discounted cost than the compacted clay liner. The clay and underlying soil hydraulic conductivities are significant variables that can affect the outcome of these calculations. For instance, if the clay is assumed to be ideal, with little or no long-term deterioration, with hydraulic conductivity values of 1×10^{-9} m/s (MLV), 1×10^{-10} m/s (LCV), and 1×10^{-8} m/s (HCV), and leave all the other variables unchanged, the compacted clay liner becomes much more favorable, with a probability of 94% of having a lower discounted cost than the geosynthetic composite liner. Conversely, using the Benson (2007) data, which shows significant deterioration over time, with hydraulic conductivity values of 1×10^{-7} m/s (MLV), 1×10^{-8} m/s (LCV), and 1×10^{-6} m/s (HCV), and leave all the other variables unchanged, the geosynthetic composite liner becomes much more favorable, with a probability of having a lower discounted cost than the compacted clay of 100%. The same would apply to the geomembrane-only liner – if the underlying subgrade is naturally low permeability soil, the geomembrane-only option would be more favorable. These are just a few examples of the parameters specific to each liner system that can affect the calculated discounted cost ratios. Accordingly, it is recommended that when evaluating different liner options, the analysis above, as described by Duncan (2000), be performed using site-specific values to ensure that the option with truly the best technical and economic value (i.e., lowest discounted cost) is selected.

6. SUMMARY AND CONCLUSIONS

As certain regions in the United States and elsewhere face water shortages, the need for a sustainable solution increases. One aspect of this solution should include more robust liner systems to preserve the fresh water that is currently available. Several liner options are available – including concrete, compacted clay, geosynthetics, and combinations of these. This study evaluated a composite liner with a geomembrane in combination with an underlying GCL, a geomembrane by itself (over a porous soil), and a compacted clay liner. Example calculations found that in most cases it would be economically beneficial to construct a geosynthetic composite liner in lieu of a compacted clay liner or a geomembrane-only liner, despite the potentially greater short term material cost. As the price of water increases, this conclusion is further validated because of the decreased water loss with a more robust liner. Based on the calculations presented in this paper, the probability that the discounted cost of a geomembrane-only liner would exceed that of a geomembrane-GCL composite liner is between 93% and 100%, depending on the permeability of the soil beneath the geomembrane. The probability that the discounted cost of a compacted clay liner would exceed that of a geomembrane-GCL liner is 82%. These results support the use of a more robust, potentially more costly liner system to decrease long-term water leakage rates. It is recommended that this type of analysis be performed for site specific projects, as certain variables can greatly affect the performance of various liner systems.

It is also important to note that additional costs not taken into consideration in this study include those associated with obtaining additional fresh water where the existing water may be lost. For instance, the cost to locate, pump, and treat fresh water can be substantial. Countries such as Israel, India, Aruba, Australia, and several others are already forced to produce at least some fresh water via desalination, a process that is significantly more expensive than typical water treatment methods, generally more than twice as much (NY Times, July 2012). The energy required to desalinate water is substantial, and many environmentalists object to the method, which they say greatly contributes to global warming. The power needed to remove the salt from seawater accounts for 60 to 70 percent of the cost of desalination (NY Times, July 2012).

REFERENCES

- American Society of Civil Engineers (ASCE), 2009. <<http://www.infrastructurereportcard.org>>
Benson, C., Sawangsuriya, A., Trzebiatowski, B., and Albright, W. (2007). Post-Construction Changes in the Hydraulic Properties of Water Balance Cover Soils, *J. Geotech. and Geoenvironmental Eng.*, 133(4), 349-359.

- Brown, K.W., Thomas, C.J., Lytton, R.L., Jayawickrama, P. and Bahrt, S. (1987). "Quantification of leak rates through holes in landfill liners." *Rep. No. EPA/600/2-87/062*, US EPA, Cincinnati, OH.
- Duffy, M. (2011). White Paper - The value of Water. American Water Works Company. <www.amwater.com>.
- Duncan, J.M. (2000). "Factors of Safety and Reliability in Geotechnical Engineering," *Journal of Geotechnical and Geoenvironmental Engineering*, Vol. 126, No. 4, pp. 307-316.
- Fukuoka, M. (1986). "Large scale permeability test for geomembrane-subgrade system." *Proc. 3rd Int. Conf. on Geotextiles*, Vienna, Austria, pp. 917-922.
- Giroud, J.P. and Bonaparte, R. (1989). "Leakage through liners constructed with geomembranes – Parts I and II." *Geotextiles and Geomembranes*, 8(1) and 8(2), pp. 27-67 and 71-111.
- Giroud, J.P. (1997). "Equations for calculating the rate of liquid migration through composite liners due to geomembrane defects." *Geosynthetics International*, 4(3-4), pp. 335-348.
- LaPlante, C. M. and Zimmie, T.F. (1992). "Freeze/Thaw Effects on the Hydraulic Conductivity of Compacted Clays." *Transportation Research Board '92*, Washington, D.C., 71st Annual Meeting.
- Natural Resources Defense Council. 2010. <<http://www.nrdc.org/globalwarming/watersustainability/index.asp>>.
- New York Times on the Internet. 2012. The New York Times. 9 Jul. 2012. <<http://www.nytimes.com>>
- Nosko, V. and Touze-Foltz, N. (2000). "Geomembrane liner failure: Modelling of its influence on contaminant transfer." *Proc. 2nd European Conference on Geosynthetics*, Vol. 2, Bologna, Italy, pp. 557-560.
- Rogowski, A.S. (1990). "Relationship of Laboratory-and Field-Determined Hydraulic Conductivity in Compacted Clay." *Rep. No. EPA/600.S2-90-025*, US EPA, Cincinnati, OH.
- Thiel, R., Beck, A., and M.E. Smith (2005), "The Value of Geoelectric Leak Detection Services for the Mining Industry", *Geo-Frontiers 2005*.
- Touze-Foltz, N. and Giroud, J.P. (2003). "Empirical equations for calculating the rate of liquid flow through composite liner due to geomembrane defects." *Geosynthetics International*, 10(6), pp.215-233.
- Webber, C.T. (2008). "Leakage through Defects in Geomembrane Liners under High Hydraulic Heads." Unpublished doctoral dissertation, University of Texas, Austin, TX.
- Weber, C.T., and Zornberg, J.G. (2005). "Use of GCLs to Control Leakage through Geomembrane Defects under High Hydraulic Heads." *Proceedings of the NAGS 2005 Geosynthetics Conference*, North American Geosynthetics Society, Las Vegas, NV, December 14 – 16, pp. 1 - 8 (CD-ROM).
- Weber, C. T., and Zornberg, J. G. (2005). "Leakage through Liners under High Hydraulic Heads." *Geosynthetics Research and Development in Progress, Eighteenth Geosynthetic Research Institute Conference (GRI-18)*, Austin, Texas, January 26 (CD-ROM).
- World Water Organization. 2010. <http://www.theworldwater.org/water_facts.php>.
- Zornberg, J.G., and Weber, C.T. (2003). "Geosynthetics Research Needs for Hydraulic Structures" *Proceedings of the Seventeenth Geosynthetic Research Institute Conference, Hot Topics in Geosynthetics IV*, Las Vegas, Nevada, December 15-16, pp. 183-197.

Beneficial Use of Dredged Contaminated Sediments Using Geotextile Tube Technology at a Container Port In Santos, Brazil

T. Stephens TenCate Geosynthetics, USA, t.stephens@tencate.com

L. C. Q. C. Melo, University of São Paulo, São Paulo, Brazil. leo@allonda.com

M. M. Futai, Department of Soil Mechanics, University of São Paulo, São Paulo, Brazil. futai@usp.br

ABSTRACT

A large container and bulk cargo terminal is being constructed in the Port of Santos, Brazil. When completed the terminal will be the largest private owned port facility in Brazil with over 600,000 m² dedicated to container storage. To development the site, large quantities of imported fill would be required in addition to dredging and disposal off site of large volumes of contaminated sediments. In total this was a significant cost to develop the site. Allonda and TenCate engineers developed an alternative solution based on using the dredged contaminated sediments to be dewatered and contained on site in large geotextile tubes. This material would be environmentally secured permanently within the geotextile tubes over which the container storage yard would be constructed. Additionally, this solution would eliminate 600,000 m³ of imported fill and disposal offsite of the same volume of contaminated sediments. The alternative design greatly reduced the construction cost.

1. INTRODUCTION

Empresa Brasileira de Terminal Portuarios S.A. (Embraport) is an 848,000 m² container and bulk port terminal, being constructed in the Port of Santos, Brazil. This is an undertaking of Odebrecht Transportation in partnership with Dubai World Ports and Coimex. When completed, the Embraport terminal facility will not only be the largest private owned port facility in Brazil with over 600,000 m² dedicated to container storage, but it will be the largest in South America. Also, the terminal will be able to turn over 20 million TEU (units equivalent to a 20' containers) and 2 billion liters of bulk liquids per year. Total investment when completed will be \$1.15 billion/USD. The terminal is located on the north shore of the Estuario de Santos opposite the City of Santos in the State of Sao Paulo in an area that is primarily within a tidal flat zone.

To construct the terminal bulk and container storage area, more than 1.5 million m³ of fill would be required to be imported to achieve a platform level of +3.5 meters. The import of fill represented a major financial impact for the Embraport owners. In addition, 600,000 m³ of contaminated sediments was required to be, dredged from the entrance channel and turning basin of the terminal, dewatered, and disposed in an offsite facility, adding to the major cost of the site development. In total this put at risk the financial model for the project.

Allonda, the TenCate representative in Brazil, and TenCate engineers developed an alternative solution based on beneficial use of the contaminated dredged sediments. The solution was to use large (36.5m) circumference geotextile tube units to contain and dewater the contaminated sediments within onsite dewatering cells. The dewatering cells would be under the proposed container storage area, over which final fill and pavement section would be placed. The implementation of this solution would be to environmentally secure and contain the dewatered contaminated sediments within the fill section of the terminal, and reduce by 30% the required import of offsite fill material. The result would be to greatly reduce the construction cost and salvage the project financial model.

To proceed, major design considerations must be overcome. These included; 1) the ability of the geotextile tube system to contain and dewater contaminated sediments in a secure environment, 2) to treat all of the effluent and to return this effluent back to the native environment without any impact, 3) to provide a stable platform on which to store ocean containers stacked up to 7 layers high, and 4) to construct a site with a 40 plus year design life

This paper will address the design, modeling, field instrumentation, geotextile tube installation and dewatering operation, and effluent treatment required for the project. In addition this paper will present the economic impact of the beneficial use of contaminated dredged sediments for this project.

2. BACKGROUND

In 2007 Embraport was granted a Brazilian federal license to develop the site for the terminal and port facility. The initial survey and soil borings indicated that more than 50% of the site was in the tidal flats with an elevation between -1.0 and

+1.0. (See Fig. 1) All of the proposed terminal area was located over approximately 22 to 25 meters soft to medium sandy silt. To achieve the design platform elevation of 3.5m and to account for anticipated settlement, it was calculated that 1.5 million m³ of select fill must be imported to achieve the design platform elevation. Additionally, the environmental impact study identified more than 600,000 m³ of contaminated sediments were overlaying the sandy area of turning basin and entrance channel. As a condition of the construction license, it would be required that Emraport would remove and dispose in an upland secure facility all of the contaminated sediments that must be removed. Given the cost of these two requirements, the owners of Emraport contacted Allonda and TenCate engineers to submit a conceptual design incorporating geotextile tube technology to determine if this could be employed to help reduce some of the site development cost.



Figure 1 Location of Emraport Terminal

3. CONCEPT OF OPTIONAL DESIGN

Engineers proposed a conceptual design that consisted of impermeable berms to be installed around the perimeter of the site to an elevation of +4.5m with internal berms installed to an elevation of +2.5m to divide the site into several areas to act as geotextile tube dewatering cells. A woven geotextile separator would be placed on the mud surface within the cells over which a 0.5 m thick layer of gravel would be placed to act as a drainage blanket to convey the effluent from the geotextile tube to an internal channel. (See Figure 2)

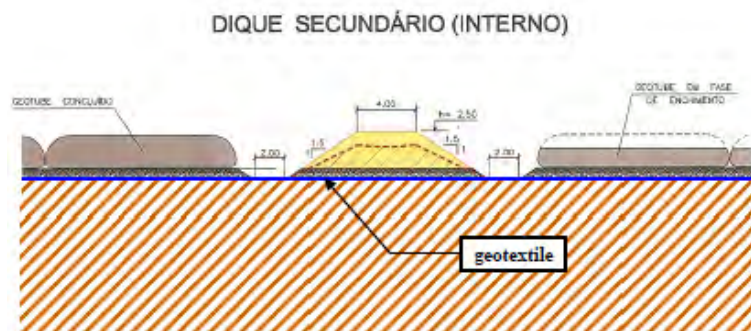


Figure 2 Geotextile Tube with Internal Berm

Large geotextile tube units (36.5m cir. X 65m long) of a high strength woven monofilament by fibrillated tape woven engineered textile would be installed. (See Table 1 for the Geotextile Tube Mechanical and Hydraulic Properties) The 600,000 m³ of contaminated sediments from the turning basin and entrance channel would be hydraulically dredged and pumped to the geotextile tubes. In-line, an organic polymer would be injected to flocculent the solids and binding the contaminants to the soil particles. The effluent would be filtered thru the pores of the geotextile tube, collected in the

perimeter channels, and pumped to an onsite water treatment plant for secondary treatment to precipitate any heavy metals or other solids, to neutralize to a pH of 7 and then to release back to the natural environment.

Table 1 Geotextile Tube Mechanical and Physical Properties

Mechanical Properties	Test Method	Unit	Minimum Average Roll Value	
			MD	CD
Wide Width Tensile Strength (at ultimate)	ASTM D4595	kN/m (lbs/in)	78.8 (450)	109.4 (625)
Wide Width Tensile Elongation	ASTM D4595	%	20 (max.)	20 (max.)
Factory Seam Strength	ASTM D4884	kN/m (lbs/in)	70 (400)	
CBR Puncture Strength	ASTM D6241	N (lbs)	8900 (2000)	
Apparent Opening Size (AOS)	ASTM D4751	mm (U.S. Sieve)	0.43 (40)	
Water Flow Rate	ASTM D4491	l/min/m ² (gpm/ft ²)	813 (20)	
UV Resistance (% strength retained after 500 hrs)	ASTM D4355	%	80	

Filtration Properties	Test Method	Unit	Typical Value
Pore Size Distribution (O ₅₀)	ASTM D6767	Micron	80
Pore Size Distribution (O ₉₅)	ASTM D6767	Micron	195

Once all of the geotextile tubes within each cell have been filled, an overburden of up to 8 ton/m² would be applied to facilitate settlement. The settlement would be monitored and when stability the overburden would be removed and placed on the adjoining cell to repeat the process. (See Figure 3.)

By adopting this design, it was estimated that the cost of the site development could be reduced by 20% to 30%. Thus it was attractive to the owner who agreed to fund site testing to validate assumptions of the Concept of the Optional Design.

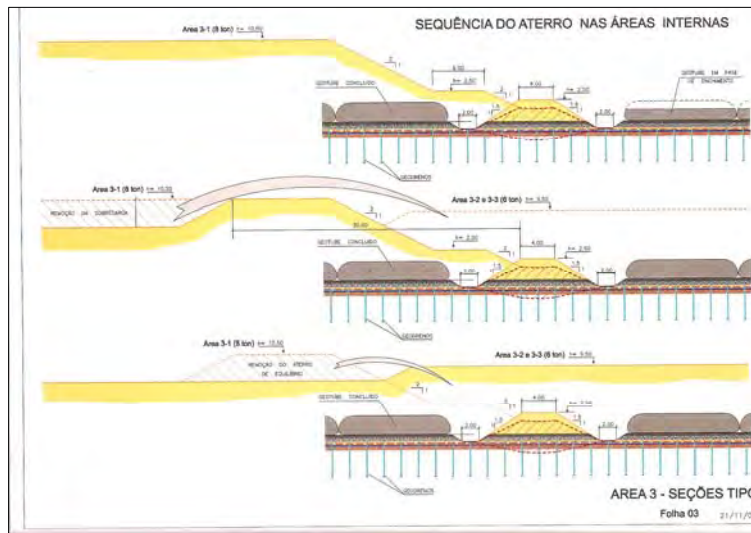


Figure 3 Geotextile Tube Overburden Placement Sequence

4. SITE TESTING AND MODELING

The first major questions that had to be answered were the settlement amount the rate of settlement. This would be based on the amount of fill that had to be placed over specific areas for container and bulk storage to achieve the design platform elevation. In some areas the fill would be as much as 4.5m thick. In 2008, to accurately forecast the settlement amounts and rates, a 150m by 75m test section was constructed at the most forward location of the fill section. (See Figure 4.) Different areas of the test section were loaded with the different overburden amounts that duplicate actual designed overburden amounts for the areas of the container and bulk storage. The settlement of each section was monitored over time to develop a curve that can be expected during the site construction.



Figure 4 Field Settlement Test Conducted in 2008

The second question that had to be answered was the consolidation that could be achieved when the contaminated sediments were contained and dewatered inside the geotextile tubes. To answer this question, a number of GDT model test were conducted using samples of the contaminated sediments taken from the ship berth area, the turning basin, and from the entrance channel. These test determined that 65% dewatered solids could be achieved within the geotextile tubes within 30 days after completing the geotextile tube filling. The GDT model testing also provided the information to select the type of polymer for the contaminated sediments, the dosage of polymer required to maintain the optimum dewatering performance, and to forecast the quality of the effluent that could be obtained during the dewatering phase.

5. CONSTRUCTION

Following the site and model testing, the final design was performed and construction started in 2010. The perimeter berm and internal dewatering cells were completed in 2011 and the first of 280 geotextile tubes 36.5m cir. X 65m long were installation and dredging started. Dredging was conducted using a 45 cm cutter head pumping to the geotextile tube units at a rate of 1,400 m³/hr. The dewatering contractor designed and managed the geotextile tube dewatering operation including the dredge manifold system, the automated polymer make down and injection system, and the effluent water treatment plant. Each geotextile tube was filled multiple times to a height of 2.2 m and allowed to dewater. The final dewatered height for all tubes was approximately 1.8 m. Each geotextile tube contained approximately 2,145 m³ after dewatering.

The effluent water from the geotextile tube units drained into a collection basin from which it was pumped to a water treatment basin. The pH of the effluent water was raised to precipitate dissolved solids. Next the water was transferred to a second basin where the water was naturalized, filtered thru activated carbon filters then released back into the environment.

After the geotextile tube units within each cell reached 65% solids following dewatering, a gravel drainage media was placed over the top of the tubes and then the overburden up to 8 ton/m² was placed over the gravel (See figure 5).



Figure 5 Drainage Layer and Overburden Placement March 2012

When all of the 600,000 m³ of contaminated sediments have been dredged into the geotextile tubes and the overburden consolidation phase completed, the container storage area paved section will be installed. (See Figure 6)

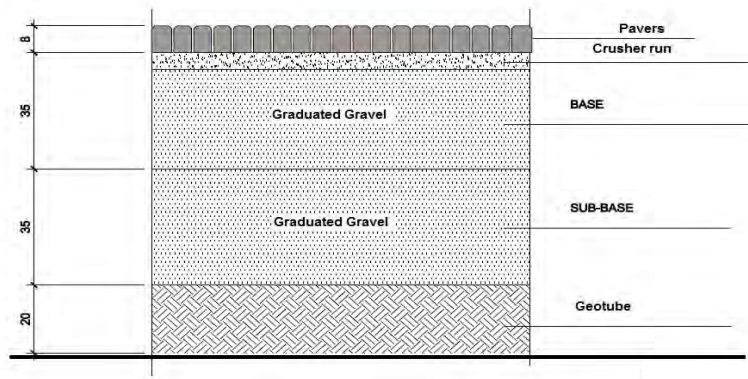


Figure 6 Pavement design

Figure 7 provides a rendition of the site when pavement has been completed in the winter of 2013.



Figure 7 Project When Completed 2013

6. CONCLUSION

The Embraport project is still under construction and will not be completed until late 2013. However, the dredging and dewatering of 600,000 m³ of contaminated dredging has been completed. The actual field results of the percent solids achieved and volume reduction correlate to the GDT modeling that was conducted prior to the start of dredging. The drainage blanket and overburden placed over the dewatered geotextile tubes has been completed and settlement of the site after placement of the overburden is consistent with the settlement results of the test section installed in 2008. Effluent from the geotextile tubes was maintained during and after the dewatering phase. The treatment and discharge back into the natural environment was monitored for the entire time of the process. The returned water was well below the standards required by the environmental permit. The reduction of importing 600,000 m³ of fill material to achieve the designed platform elevation has been achieved by the use of the dredged contaminated sediments from the turning basin and entry canal.

Therefore, it can be concluded that the beneficial use of contaminated sediments using geotextile tubes can be achieved, that modeling tools are available that can accurately forecast the results of the use of geotextile tubes, and total project savings are achievable when utilizing this technology.

Biofilm-enhanced Treatment for Arctic Wastewater Stabilization Ponds Using Geotextile Substrate

Evan Bridson-Pateman, Graduate Student, Dalhousie University, Canada, evan.bp@dal.ca
Rob Jamieson, PhD, P.Eng, Dalhousie University, Canada, jamiesrc@dal.ca
Craig Lake, PhD, P.Eng, Dalhousie University, Canada, craig.lake@dal.ca

ABSTRACT

Communities of the territory of Nunavut, Canada are facing potential changes to their wastewater discharge standards, as is the rest of the country. Remoteness and low populations create issues in implementing conventional treatment systems in these communities. Wastewater stabilization ponds are the most common treatment method, but berms constructed from thawed, coarse-grained local till result in continuous wastewater exfiltration. This study examines the potential for a geotextile biofilter retrofit to existing berms to treat wastewater as it exfiltrates.

Previous research suggests the suitability of geotextiles as a substrate for biological growth and filtration, however the effects of cold temperature on these biofilters is not fully understood. This study found that at 10°C, removal efficiencies were 40-80% for biological oxygen demand, 80% for total suspended solids, and 1-log for *Escherichia coli*. Maximum treatment performance was achieved fastest under the condition where large volumes of wastewater have passed through the filter.

1. INTRODUCTION

New wastewater treatment regulations from the federal government of Canada will have an impact on many Canadian municipalities, but those in remote areas of northern Canada face unique challenges. The entire territory of Nunavut, Canada has only 25 communities outside its capital city, with an average population of approximately 1,050. Some consist of as few as 130 people (Government of Nunavut, 2011). Communities in the Northern Territories of Canada also have small tax bases to fund infrastructure projects and must find innovative ways to meet wastewater treatment regulations imposed by the federal government. Even more challenging in terms of infrastructure development is that these communities are only serviced by air or sea transportation linkages. As such, deliveries of construction materials and machinery can only occur in optimum weather conditions, at high cost.

The most common form of wastewater treatment in these northern communities is the use of wastewater stabilization ponds (WSP) constructed from local till, and are often designed to rely on frozen soil berms to retain the wastewater. WSPs have been shown to effectively reduce effluent concentrations of biological oxygen demand (BOD₅), total suspended solids (TSS) (Saqqar and Pescod, 1995), and ammonia nitrogen (NH₄-N) (Pano and Middlebrooks, 1982). Furthermore, a 2-log reduction in fecal coliform bacteria is common (Polprasert et al., 1983). Many of the berms used to construct WSPs in these northern areas exhibit excessive seepage and low retention times due to the use of local sandy till in berm construction (Bölter, et al. 2006). The low retention times can diminish treatment (Meron et al., 1965) which may create challenges in complying with water quality regulations. Environment Canada's *Wastewater Systems Effluent Regulations* were released in 2012 and require maximum effluent concentrations of 25 mg/L for TSS and BOD₅, and less than 1.25 mg/L of NH₄-N (Environment Canada, 2012a). Bacterial discharge limits are typically evaluated on a case-by case basis.

The treatment performance of exfiltrating WSPs could be improved by a retrofit in two ways: (i) reducing the seepage through the berms, and (ii) providing a further polishing step to the exfiltrating water. One economical way to retrofit existing WSPs is through the use of geosynthetics such as geotextiles, since reconstructing the lagoons with imported clay material is economically impractical. Geotextiles can provide a medium for biofilm growth and hence provide potential biofiltration treatment. Although geotextiles are traditionally used in drainage filtration, research has shown their potential in wastewater treatment applications. In South Carolina, hanging-bag geotextile filtration of fresh liquid manure and lagoon sludge was used to accomplish 60 to 90% removal of TSS and 26 to 65% removal of NH₄-N (Baker et al. 2002). In Philadelphia, bench-scale experimentation with two-filter geotextile columns removed 91 to 97% of TSS and BOD₅, and 90% of NH₄-N in septic tank effluent (Yaman et al., 2005). This was confirmed at full-scale by Hu and Gagnon (2006), showing that using geotextile filters in recirculating biofilters resulted in 77% removal of TSS, 95% removal of BOD₅, 96% removal of NH₄-N, as well as 2.2 log removal of fecal coliforms. In addition to their use as direct filters of wastewater, there is evidence that geotextiles can be used as effective filters when used as baffles in sedimentation tanks. Municipal wastewater (with commercial, industrial and residential sources) was filtered using a tank with geotextile baffles and resulted in average removal efficiencies of 95% for TSS, 92% for

BOD₅, and 97% for NH₄-N (Korkut et al., 2006). If used within a WSP berm the biofilm that forms on the geotextile could also provide a reduction in hydraulic conductivity, which will result in increased retention times in the WSP. Palmeira et al. (2008) have shown hydraulic conductivity decreases in geotextiles by up to 4 orders of magnitude in 90 days via biological clogging.

Unfortunately, the effect of temperature on this type of treatment process is unknown, as all of these experiments were conducted at room temperature. In the arctic study area for this research, depending on latitude, communities have only 2 to 3 months per year with temperatures above 0°C, and average temperatures between -3°C and 11°C for those months (Environment Canada, 2012b). Studies on other types of biological filters have showed that biomat development was retarded at lower temperatures (Ratkowsky et al. 1982) and that treatment performance was reduced (Moll et al., 1999). Presumably, biological activity on the geotextile will be similarly affected by temperature.

The objective of this research is to examine the influence of temperature on the treatment of WSP effluent with geotextiles. This work is part of a larger study examining the temporal development of biofilm on geotextile biofilters within the time and temperature constraints of an arctic summer.

2. MATERIALS AND METHODS

2.1. Wastewater

The wastewater used within all experiments was collected from the outlet of the primary treatment unit of the Timberlea Wastewater Treatment Plant near Halifax, Nova Scotia. The effluent quality at this location is similar to the quality of effluent for an arctic WSP during the summer treatment season (Krkosek et al. 2012). During the experiments, wastewater was collected on a weekly basis and transported to Dalhousie University. Table 1 shows the average, and typical range of parameter values within the raw wastewater used in the experiments described below. Although it has undergone primary sedimentation, this water does not yet meet Environment Canada's regulations.

Table 1. Quality of influent wastewater

	a) Trial 1			
	NH ₄ -N (mg/L)	BOD ₅ (mg/L)	TSS (mg/L)	<i>E. coli</i> (CFU/100mL)
Mean	33.0	61.4	52.7	2.63E+05
Min	13.1	18.8	23.0	7.78E+02
Max	42.0	129.4	95.5	1.89E+06
St. Dev	8.5	43.3	25.8	6.60E+05

	b) Trial 2			
	NH ₄ -N (mg/L)	BOD ₅ (mg/L)	TSS (mg/L)	<i>E. coli</i> (CFU/100mL)
Mean	40.0	61.2	69.3	2.87E+05
Min	27.7	0.0	52.0	6.67E+03
Max	49.4	103.3	109.6	6.46E+05
St. Dev	6.8	29.4	18.2	2.29E+05

2.2. Geotextile Biofiltration Columns

Acrylic columns were designed to examine the filtration of wastewater by the geotextiles. The columns employed the approximate dimensions specified in ASTM D1987 – 07. The split column secures a 10 cm diameter geotextile coupon over gravel, simulating a geotextile placed over a lagoon berm. An O-ring provided the seal to prevent leakage. A dimensioned drawing of the column is shown in Figure 1.

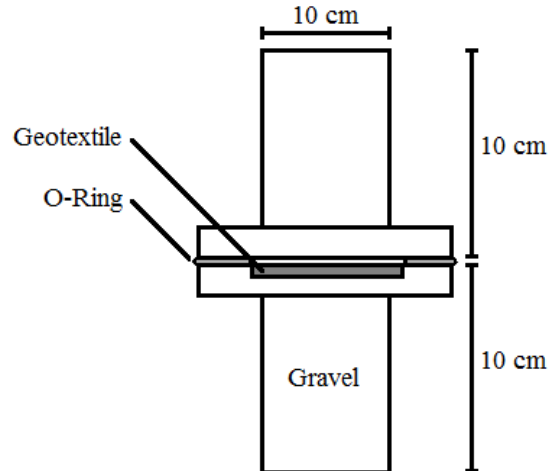


Figure 1. Geotextile Biofiltration Column

The experimental setup (see Figure 2) involved creating a “distributor” tank at a static height to keep a constant head of wastewater above the columns. Overflowing “receptacle” tanks were placed at adjustable heights to keep a constant head of water below the columns. This setup allowed for constant head hydraulic conductivity testing of the geotextile at various times during the biofiltration experiments. The apparatus was constructed in a refrigerated room at Dalhousie University. Temperature in this room was kept constant at 10°C to reflect the maximum average air temperature of an arctic summer.

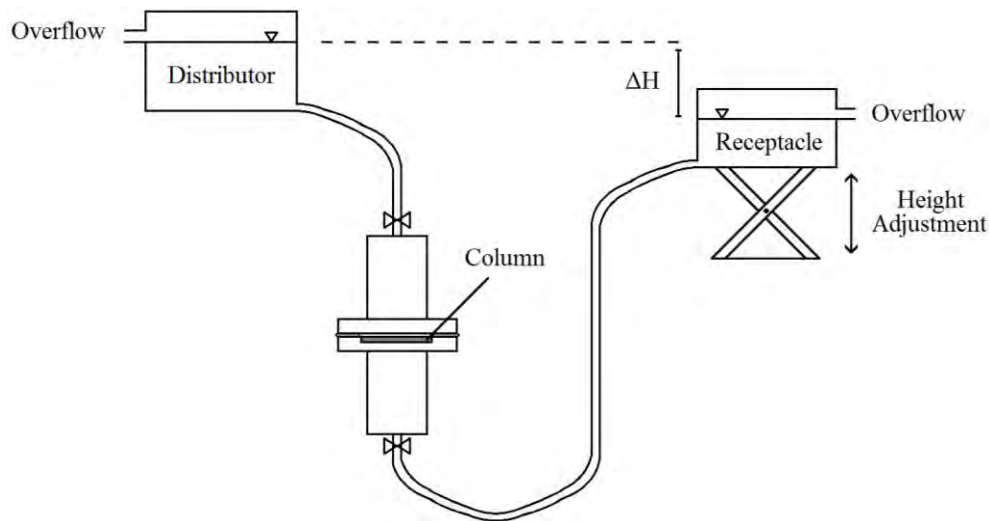


Figure 2. Experimental Set-up

2.3. Geotextiles

Several different nonwoven, continuous filament geotextiles were chosen as the substrate for biofiltration. Yaman et al. (2005) showed that nonwoven, continuous filament geotextiles resulted in more biomass growth per unit area than both woven and stapled nonwoven geotextiles. This was confirmed by Korkut et al. (2005), with nonwoven continuous filament growing the most biomass.

Two nonwoven continuous filament geotextiles were supplied by Terrafix®. The first (product number 400R) was labeled with a ‘4,’ had an apparent opening size (AoS) of 0.212 mm, and a dry weight of 23.7 g/cm². The second (product number 600R) was labeled with a ‘6,’ had an AoS of 0.15 mm, and a dry weight of 33.9 g/cm². The geotextiles were installed in the columns above a 10 cm bed of 6 mm minus gravel. In total, six columns were used: ‘4A’ and ‘4B’ (duplicates of 0.212 mm AoS geotextile); ‘6A’ and ‘6B’ (duplicates of 0.15 mm AoS geotextile); and ‘gA’ and ‘gB’ (duplicates without geotextile, using gravel bed only)

2.4. Trial 1: Semi-Stagnant Condition

Influent wastewater was sampled and analyzed for a suite of water quality parameters. The wastewater was placed into each experimental column for one week (under no flow conditions), then drained through the geotextile where the leachate was analyzed for the same water quality parameters. After draining, the hydraulic conductivity of the geotextile was measured by allowing raw wastewater through the filter in accordance with the constant head procedure outlined in ASTM D1987 – 07. New raw wastewater was then added to the column and procedure was repeated. Trial 1 was run for three months; the approximate length of an arctic summer.

2.5. Trial 2: Continuous Permeation

For the second trial, a scenario where wastewater continuously permeates from the WSP was simulated. First, water quality parameters of the influent wastewater were measured, followed by permeation of the raw wastewater through each column at a rate of 1 to 2 mL/s. After 1.5L of raw water flowed through each geotextile (the equivalent volume of the column), the leachate parameters were again measured to discern any change that occurred across the geotextile.

After wastewater quality analysis, hydraulic conductivity was measured by allowing raw wastewater through the filter in accordance with the constant head procedure outlined in ASTM D1987 – 07. Finally, raw wastewater was again allowed to flow through the geotextile at a rate of 1-2 mL/s until a total of approximately 10L passed each column every week. Measurement of water quality parameters and hydraulic conductivity occurred once per week for three months. Due to space limitations, hydraulic conductivity test results are not reported in this paper.

2.6. Sample Analysis and Data Processing

All samples were analyzed at Dalhousie University following procedures from *Standard Methods for the Examination of Water and Wastewater* (Clesceri et al. 1998). Water quality parameters analyzed included BOD₅ (Std. Method 5210B) and TSS (Std. Method 2540D). NH₄-N concentrations were determined with TNT 832 kits from HACH Canada. In addition, samples were analyzed for *Escherichia coli* (*E. coli*) using membrane filtration onto m-ColiBlue24 culture media from HACH Canada.

Paired *t*-tests were performed to compare water quality before and after passing through the column. Paired *t*-tests were also performed to compare the average of the two duplicates of each geotextile (0.212mm, 0.15mm) with the average of the "gravel only" (gA + gB) columns.

3. RESULTS AND DISCUSSION

3.1. NH₄-N

Average effluent NH₄-N concentrations and percent reductions during Trial 1 are shown in Table 2. It could not be shown with statistical significance that there was any reduction in NH₄-N concentrations between the influent and effluent in any of the columns. There were also no apparent temporal trends in treatment performance. Similarly, in Trial 2, there was no statistically significant difference between influent and effluent NH₄-N concentrations, and no change in performance over time. Average effluent NH₄-N concentrations and percent reductions during Trial 2 are shown in Table 2. Effluent NH₄-N concentrations exceeded regulatory values for the entirety of both experiments.

Table 2. Average effluent ammonia concentrations (mg/L)

	Trial 1					
	4A <i>n</i> = 10	4B <i>n</i> = 10	6A <i>n</i> = 8	6B <i>n</i> = 9	gA <i>n</i> = 9	gB <i>n</i> = 9
Mean	38.3	40.0	39.1	40.1	39.8	40.1
Min	23.7	25.2	22.6	25.2	25.3	24.3
Max	48.2	49.3	50.7	49.5	52.1	49.0
St. Dev	7.2	7.8	8.7	7.6	8.1	7.6

	Trial 2					
	4A <i>n</i> = 7	4B <i>n</i> = 8	6A <i>n</i> = 8	6B <i>n</i> = 8	gA <i>n</i> = 7	gB <i>n</i> = 7
Mean	35.4	32.2	33.6	34.0	31.7	30.3
Min	23.9	13.4	13.9	18.6	12.7	12.4
Max	48.4	41.1	44.4	46.9	48.3	48.2
St. Dev	7.7	9.2	10.6	7.8	12.0	11.8

Note: *n* = number of samples

Negligible changes in ammonium concentrations are most likely attributed to less nitrifying bacteria growth at low temperatures (Hwang & Oleszkiewicz, 2007). However, ammonia oxidation by these bacteria may have been impeded by another factor. Water with high BOD₅ sitting stagnant for seven days in a column (Trial 1) will create an anoxic environment, leaving less dissolved oxygen available to nitrifiers.

3.2. BOD₅

Average effluent BOD₅ concentrations and percent reductions during Trial 1 are shown in Table 3. All columns from Trial 1 produced a statistically significant reduction in BOD₅ concentrations between the influent and effluent. However, t-tests confirmed only the 0.212mm AoS geotextile removed more BOD₅ than the gravel layer alone. BOD₅ removal rates in Trial 1 did not change markedly with time.

Table 3. Average effluent biological oxygen demand concentrations (mg/L) and percent reductions

	Trial 1					
	4A <i>n</i> = 8	4B <i>n</i> = 8	6A <i>n</i> = 8	6B <i>n</i> = 8	gA <i>n</i> = 8	gB <i>n</i> = 8
Mean	32.6	33.5	37.1	37.3	40.3	40.3
Min	14.3	16.5	10.5	12.0	14.3	12.8
Max	64.0	53.6	72.7	75.0	64.0	72.0
St. Dev	14.6	11.6	18.1	18.2	15.2	17.7
% Reduction	48%	45%	43%	41%	37%	40%

	Trial 2					
	4A <i>n</i> = 6	4B <i>n</i> = 7	6A <i>n</i> = 7	6B <i>n</i> = 7	gA <i>n</i> = 7	gB <i>n</i> = 7
Mean	33.1	31.1	33.6	31.7	25.3	26.5
Min	7.5	4.5	6.0	9.4	7.5	3.8
Max	106.0	109.0	107.0	106.0	106.0	109.0
St. Dev	36.8	35.9	37.5	33.5	35.8	37.1
% Reduction	40%	35%	31%	17%	48%	50%

Note: *n* = number of samples

Similarly, in Trial 2, effluent water quality was significantly better than influent, as shown by the % reductions in Table 3. Again, it could not be shown with confidence that either geotextile removed more BOD₅ than the gravel layer alone. However, BOD₅ removal rate was observed to increase in all columns over time, as shown in Figure 3. This may be due to increased clogging of the gravel, either by physical filtration of solids (section 3.3), or by biological growth. Although average BOD₅ concentrations only exceed the regulatory limits by <10 mg/L, after 80L had flowed through the filters, effluent BOD₅ concentrations were consistently below 25 mg/L.

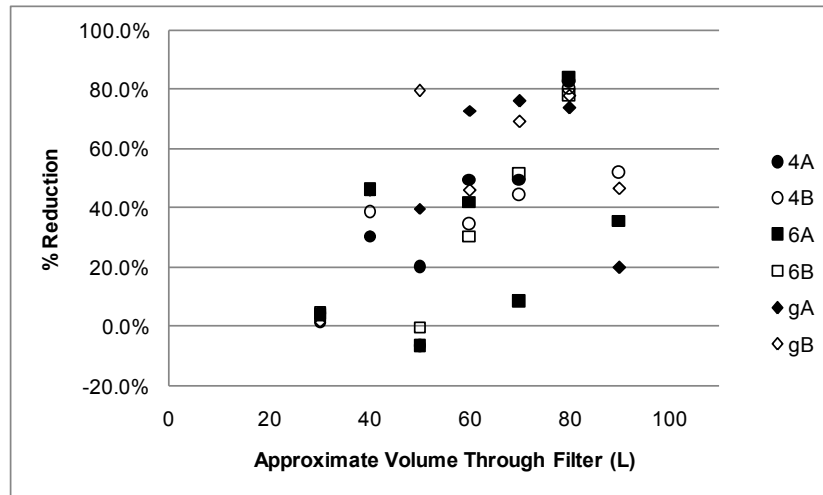


Figure 3. Trial 2 percent reduction in biological oxygen demand concentration over time

3.3. TSS

Average effluent TSS concentrations and percent reductions during Trial 1 are shown in Table 4. All columns showed a statistically significant reduction in TSS concentrations between the influent and effluent. Both the 0.212mm and 0.15mm AoS geotextiles removed significantly more solids than the gravel layer alone. TSS removal rate improved with time, to a maximum of 80% after week 9, as shown in Figure 4. Average effluent concentrations for all geotextile columns were below the regulatory limit of 25 mg/L with the exception of one 6A replicate. The gravel columns exceeded regulations on average.

Table 4. Average effluent total suspended solid concentrations (mg/L) and percent reductions

	Trial 1					
	4A <i>n</i> = 10	4B <i>n</i> = 10	6A <i>n</i> = 8	6B <i>n</i> = 9	gA <i>n</i> = 9	gB <i>n</i> = 9
Mean	16.9	24.6	26.2	24.3	31.8	30.4
Min	8.6	10.1	9.3	9.4	15.8	16.0
Max	28.5	48.8	75.3	53.3	115.0	101.3
St. Dev	6.1	12.2	20.7	14.0	30.3	25.4
% Reduction	75%	64%	63%	64%	65%	56%

	Trial 2					
	4A <i>n</i> = 6	4B <i>n</i> = 7	6A <i>n</i> = 7	6B <i>n</i> = 7	gA <i>n</i> = 7	gB <i>n</i> = 7
Mean	17.7	17.8	16.9	17.7	22.3	19.6
Min	9.7	8.7	7.7	7.7	12.0	5.5
Max	50.5	54.7	48.0	53.6	55.2	62.8
St. Dev	16.1	16.5	15.4	16.0	14.9	19.6
% Reduction	60%	61%	61%	62%	48%	53%

Note: *n* = number of samples

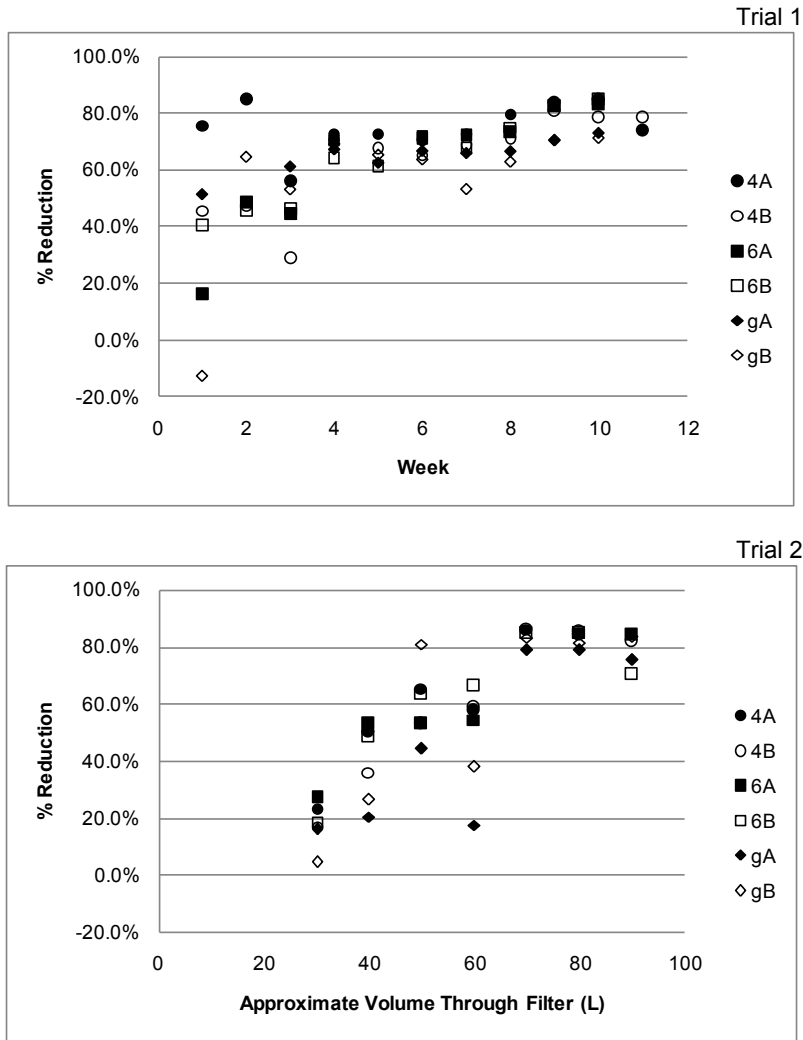


Figure 4. Percent reduction in total suspended solid concentration over time

Percent reduction of TSS concentrations in Trial 2 also improved with time, reaching a stable 80%, as shown in Figure 4. This happened at week five, and is likely due to the larger volumes of water passing through the filter, causing channels through the geotextile to constrict faster. Like Trial 1, all columns showed a statistically significant reduction in TSS concentrations between the influent and effluent. Effluent from all columns met Environment Canada's regulations.

It was also shown with 95% confidence that the geotextiles outperformed the gravel. However, removal of TSS in the gravel columns approached that of the geotextile columns as time progressed. This is likely due to biomat growth on the gravel in both types of columns gaining a more prominent effect by the end of the trials. Effluent concentrations and percent reductions are shown in Table 4.

3.4. *Escherichia coli*

Average effluent *E. coli* concentrations in Trial 1 are shown in Table 5. All columns showed a statistically significant reduction in *E. coli* concentrations between the influent and effluent. Only the 0.212mm AoS geotextiles removed significantly more bacteria than the gravel layer alone. *E. coli* removal rate in all columns was approximately one order of magnitude over the 12 week experiment for Trial 1.

Table 5. Average effluent *Escherichia coli* concentrations (CFU/100mL) and log-reductions

	Trial 1					
	4A	4B	6A	6B	gA	gB
	n = 10	n = 10	n = 10	n = 10	n = 10	n = 10
Mean	1.44E+04	2.37E+04	2.73E+04	2.51E+04	3.23E+04	2.80E+04
Min	2.00E+03	1.00E-01	3.89E+03	4.00E+03	3.00E+03	4.00E+03
Max	4.27E+04	8.89E+04	1.00E+05	6.67E+04	1.33E+05	5.50E+04
St. Dev	1.36E+04	2.53E+04	2.72E+04	1.86E+04	3.62E+04	1.72E+04
Log Reduction	1.26	1.57	1.01	1.00	0.99	0.84

	Trial 2					
	4A	4B	6A	6B	gA	gB
	n = 7	n = 7	n = 8	n = 8	n = 6	n = 6
Mean	2.23E+05	2.53E+05	1.71E+05	2.16E+05	1.73E+05	2.19E+05
Min	2.44E+03	2.17E+03	1.11E+02	1.11E+02	2.22E+03	1.56E+03
Max	1.46E+06	1.63E+06	1.27E+06	1.62E+06	9.89E+05	1.27E+06
St. Dev	5.44E+05	6.07E+05	4.43E+05	5.66E+05	4.00E+05	5.16E+05
Log Reduction	0.11	0.02	0.10	0.14	0.05	0.10

Note: *n* = number of samples

By contrast, in Trial 2, no statistically significant differences between influent and effluent were observed. This is likely due to less time in the column (2.5 min vs. 1 week) for *E. coli* die-off to occur. The low log-reduction is shown in Table 5. Additionally, no significant differences were observed between the geotextile and “gravel only” columns.

4. SUMMARY AND CONCLUSIONS

To evaluate the applicability of geotextile as a biofilter substrate addition to wastewater stabilization ponds in the arctic, two scenarios were considered. Trial 1 simulated water contained in the WSPs for a one week period. Trial 2 simulated spring thaw followed by continuous exfiltration of water through the WSP berms. Both cases considered geotextiles without any existing biofilm prior to testing. Residential wastewater that had undergone sedimentation was used as raw influent to simulate the water quality in WSPs of Nunavut.

Two nonwoven, continuous filament geotextiles were tested, with apparent opening sizes (AoS) of 0.212mm and 0.15mm. In Trial 1, significantly better BOD₅, TSS, and *E. coli* removal was observed by these two geotextiles than tests on gravel alone. Of the two, the 0.212mm AoS geotextile outperformed gravel alone on more occasions than the 0.15mm AoS. The reason for this is unknown, as the two geotextiles performed similarly in Trial 2. With further study, it is anticipated that more corroborating evidence will be observed showing little difference between the two AoSs. Trial 2, significantly better treatment by the geotextile alone was observed.

In terms of TSS removal, efficiencies of up to 80% were observed in both trials. However, this removal rate was reached quicker for Trial 2 when more water passed through the filters per week. From the start of Trial 1, BOD₅ removal reached its average value of 42%, and remained relatively constant over the course of the study. In comparison, for Trial 2 BOD₅ removal improved with time, starting low, but ultimately reaching values between 60% and 80%. Limited results were observed from both ammonia and bacteria removal. No significant ammonia treatment was observed in either trial. Minor *E. coli* removal was observed in Trial 1 only.

Overall, the geotextiles provided the final polishing necessary to reduce TSS concentrations below the 25 mg/L maximum. Additionally, the gravel itself appears to contribute to the polishing effect, reducing effluent BOD₅ concentrations below 25 mg/L, after biomat growth and clogging occurs. However, effluent NH₄-N concentrations never fell below regulatory maximums. Further treatment for ammonia is necessary to avoid non-compliance.

Although some polishing effect by the geotextile was observed, it is important to note that this study was performed at 10°C. As previously noted, temperature has a considerable effect on biological activity (Ratkowsky et al. 1982, Moll et al., 1999). As such further study should be conducted at the overall summer average (5°C) and summer minimum average (1°C) air temperatures of a Nunavut summer (Environment Canada, 2012b). It should be also noted that

future studies by the authors are considering the influence of existing biomat formation on the geotextiles for a variety of potential operating conditions. Before recommending geotextile implementation in WSPs, the authors need the results of field-scale studies planned in a controlled environment at Dalhousie University.

ACKNOWLEDGEMENTS

Funding for this research was provided by the Government of Nunavut and NSERC. A special thanks to Brian Kennedy and Ray Dubé at Dalhousie University for their technical assistance in constructing and maintaining the columns and apparatus, and Rick Lowe at Halifax Water.

REFERENCES

- ASTM D1987 – 07. Standard Test Method for Biological Clogging of Geotextile or Soil/Geotextile Filters, American Society for Testing and Materials, West Conshohocken, Pennsylvania, USA.
- Baker, K.B., Chastain, J.P., and Dodd, R.B. (2002). Treatment of lagoon sludge and liquid animal manure utilizing geotextile filtration. ASAE Meeting, Paper No. 024128, St. Joseph, MI.
- Bölter, M., Blume, H-P. and Wetzell, H. (2006). Properties, Formation, Classification and Ecology of Arctic Soils: Results from the Tundra Northwest Expedition 1999 (Nunavut and Northwest Territories, Canada), *Polarforschung*, Deutschen Gesellschaft für Polarforschung, 73:89-101.
- Clesceri, L.S., Greenberg, A.E. and Eaton, A.D., eds. (1998). *Standard Methods for the Examination of Water and Wastewater*, 20th Ed. American Public Health Association, the American Water Works Association and the Water Environment Federation, Washington DC, USA.
- Environment Canada (2012a). Wastewater Systems Effluent Regulations, Department of Justice, from <http://laws-lois.justice.gc.ca/PDF/SOR-2012-139.pdf>.
- Environment Canada (2012b). Canadian Climate Normals 1971-2000, National Climate Data and Information Archive, from http://www.climate.weatheroffice.gc.ca/climate_normals/index_e.html.
- Government of Nunavut (2011). Nunavut Population Estimates by Region and Community, 1996 to 2011, Population Estimates and Projections, Nunavut Bureau of Statistics, from <http://www.eia.gov.nu.ca/stats/index.html>.
- Hu, Z. and Gagnon, G.A. (2006). Impact of filter media on the performance of full-scale recirculating biofilters for treating multi-residential wastewater, *Water Research*, 40: 1474-1480.
- Hwang, J.H. and Oleszkiewicz, J.A. (2007) Effect of cold-temperature shock on nitrification, *Water Environment Research*, Water Environment Federation, 79:964-968.
- Korkut, E.N., Martin, J.P. and Yaman, C. (2006). Wastewater treatment with biomass attached to porous geotextile baffles, *Journal of Environmental Engineering*, ASCE, 132: 284-288.
- Krkosek, W.H., Ragush, C., Boutilier, L. Krumhansl, K., Gagnon, G.A., Jamieson, R.C. and Lam, B. (2012). Treatment performance of wastewater stabilization ponds in Canada's far north, *15th International Conference on Cold Regions Engineering*, CSCE, Québec City, PQ, Canada.
- Meron, A., Rebhun, M. and Sless, B. (1965). Quality changes as a function of detention time in wastewater stabilization ponds, *Journal (Water Pollution Control Federation)*, Water Environment Federation, 37:1657-1670.
- Moll, D.M., Summers, R.S., Fonseca, A.C. and Matheis, W. (1999). Impact of temperature on drinking water biofilter performance and microbial community structure, *Environmental Science & Technology*, American Chemical Society, 33:2377-2382.
- Palmeira, E.M., Remigio, A.F.N., Ramos, M.L.G. and Bernardes, R.S. (2008). A study on biological clogging of nonwoven geotextiles under leachate flow, *Geotextiles and Geomembranes*, International Geosynthetic Society, 26:205-219.
- Pano, A. and Middlebrooks, E.J. (1982). Ammonia nitrogen removal in facultative wastewater stabilization ponds, *Journal (Water Pollution Control Federation)*, Water Environment Federation, 54:344-351.
- Polprasert, C., Dissanayake, M.G. and Thanh, N.C. (1983). Bacterial Die-off Kinetics in Waste Stabilization Ponds, *Journal (Water Pollution Control Federation)*, Water Environment Federation, 55:285-296.
- Ratkowsky, D.A., Olley, J., McMeekin, T.A. and Ball, A. (1982). Relationship between temperature and growth rate of bacterial cultures, *Journal of Bacteriology*, American Society for Microbiology, 149:1-5.
- Saqqar, M.M. and Pescod, M.B. (1995). Modeling the performance of anaerobic wastewater stabilization ponds, *Water Science and Technology*, 31:171-183.
- Yaman, C., Martin, J.P. and Korkut, E. (2005). Use of layered geotextiles to provide a substrate for biomass development in treatment of septic tank effluent prior to ground infiltration, *Journal of Environmental Engineering*, ASCE, 131: 1667-1675.

Biological Clogging Resistance of Tubular Drainage Geocomposites in Leachate Collection Layers

Blond E., eng., SAGEOS / CTT Group, St-Hyacinthe, Quebec, Canada, eblond@gcttg.com
 Fourmont S., AFITEX, Champhol, France, sfourmont@draitube.net
 Saunier P., AfiteX-Texel, Ste Marie, Canada, psauhier@draitube.net

ABSTRACT

Although drainage geocomposites are frequently used for rainwater drainage or gas collection system in landfill covers, their application in leachate collection layers is rather limited. The authors believe that a key limitation to their use in leachate collection is a lack of knowledge of their sensitivity to biological clogging, and its consequence on the capacity of the Leachate collection layer (LCL) to meet landfill regulations prevailing in the US and Canada. In the first section of this document, a literature review was conducted of the actual drainage needs applicable to the LCL. This review led to the conclusion that leachate flow potentially reaching the LCL over the lifespan of a “dry tomb” landfill is significantly lower than what is required in the early stages of its life. This observation allowed for a larger tolerance to biological clogging of a drainage geocomposite if combined with a granular drainage layer meeting reasonable requirements with respect to biological clogging resistance. In the second section of this paper, the long term performance of tubular drainage geocomposites was investigated. Fresh leachate originating from a class 2, non-hazardous landfill located in the center of France, was circulated through a tubular drainage geocomposite during an eighteen months’ time period under anaerobic conditions, without any observation of clogging. In the third section of this paper, the results are analyzed and interpreted. Based on this research and analysis, it is suggested that the tested tubular drainage geocomposite could replace a fraction of the granular drainage layer of a Leachate Collection System (LCS) in a dry tomb landfill.

1. INTRODUCTION

Drainage geocomposites are used with an increasing frequency by landfill designers to substitute granular materials, especially in landfill covers. However, drainage geocomposite installations on the base of the landfill as a drainage component of the Leachate Collection System (LCS) are rather limited. The authors believe that a key limitation to their use on this particular location is a lack of knowledge of their sensitivity to biological clogging, among other fears and design challenges associated to the relatively harsh operating conditions at this location (i.e., high stress combined with potentially aggressive leachate). However, redesigning the drainage layer in order to permit partial replacement of the granular by a drainage geocomposite could represent a significant cost saving of high quality granular drainage materials, which can be expensive when they must be hauled in from distant quarries to the landfill, and also voluminous when compared to drainage geocomposites. Using geocomposites would therefore increase the waste storage capacity of the landfill and reduce the number of trucks, thus decreasing the carbon footprint of the landfill. Therefore, the installation of drainage geocomposites as a component of LCS in landfills is an alternative approach with both economic and environmental benefits.

The primary objective of the study was to validate that a tubular drainage geocomposite would not clog within 18 months, while exposed to fresh circulating leachate in a condition similar to what would be experienced in-situ and could therefore be used as a partial replacement of gravel in the design of leachate collection layer (LCS) at the bottom of landfills. The secondary objective was to assess landfill regulations in the US and Canada to determine if replacement of a fraction of the drainage layer by this tubular drainage geocomposite (Figure 1) would meet regulatory requirements.

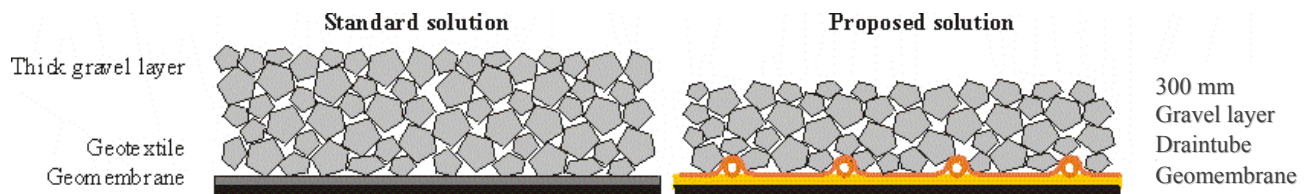


Figure 1. Typical and Proposed LCS Design cross section

2. PERFORMANCE REQUIREMENTS

2.1 Regulatory Requirements

The head of leachate on the lining system and the thickness of the drainage layer are the two requirements which are commonly described in the various regulations prevailing throughout North-America.

In the vast majority of the cases, LCS must be designed to maintain the leachate head on the liner to 0.3 m or less. Landfills in EPA-approved jurisdictions must have a state or tribe approved performance design (EPA 1993). In the EPA-approved solid waste program in the State of California, a blanket LCS is required for a Class II municipal solid waste landfill, which the LCS must ensure no buildup of hydraulic head on the liner, but the thickness of the LCS is not specified (Title 27, California Code of Regulations).

In Canada, landfill regulations are mandated by provinces or territories, not the federal government. In some jurisdictions (i.e. Alberta), leachate head must be monitored, but there is no specified limit or design requirements for LCS thickness, thus no regulatory limits on the use of geocomposites in the LCS (Government of Alberta 2010). In Newfoundland, the LCS must be a minimum of 0.3 m in thickness plus a 0.375 m cushion layer between the LCS and the waste, with a maximum leachate head of 0.3 m (Government of Newfoundland and Labrador 2010). In the province of Ontario, the combination of the primary LCS and the cover must maintain leachate head on the liner at 0.3 m or less for a service life of 100 years and the infiltration rate through the final cover is required to be equal to or greater than 0.15 m/year (Ontario Regulation 232/98). This forced infiltration means that there will be leachate generation long after installation of the final cover, thus a continued potential for leachate generation, and therefore biological clogging.

As a consequence, the potential replacement of a fraction of the granular drainage layer by a geocomposite with sufficient hydraulic performances can be considered to be feasible for landfills located in jurisdictions which do not prescribe a minimum thickness of the drainage layer. Another factor that could potentially present some restrictions to this design is the prescribed design life of the LCL, i.e. under the Ontario regulation, which could require further investigations.

In order to assess that the hydraulic capacity of the drainage layer (0.30 m of gravel including the drainage geocomposite) will be sufficient to meet the performance requirement (maximum head of leachate of 0.30 m), it is necessary to:

- Identify the required capacity of the drainage layer; and
- Predict the long term behavior of the drainage layer (i.e. creep and clogging).

2.2 Hydraulic Requirements - Review of the Quantity of Leachate Predicted in the Literature

The key hydraulic design criteria for LCS systems are that the head on the liner needs to be smaller than the prescribed value (typically 0.3 m) and that the liquid thickness in the LCS be less than the thickness of the drainage layer thickness throughout the entire design life of the landfill. Typically the McEnroe equations are used to determine the liquid supply rate in the LCS system. The majority of the North American designers probably use the HELP model which uses the McEnroe equations as well. The more recent literature recommended double-checking the HELP model calculations with approximate solutions with Giroud's Equation (1992, 1995).

As an alternative design approach to predict leachate generation rates, Bellenfant (2009) states that there are two stages to consider; while the cell is being filled (~1 to 5 years), and after the final cover is installed (10's to 100's of years).

During the first stage, the quantity of leachate which is generated is the greatest, because there is no final cover and all the rainfall reaches the waste. Additional parameters have been identified as influencing the volume of leachate collected from the LCS:

- More evaporation will take place when there is thicker waste, therefore reducing the quantity of leachate reaching the LCS (Bellenfant, 2009);
- Techniques used in the operation of the landfill will change the quantity of water penetrating the waste, and also the leachate generated (i.e., type of daily covers, slopes).

The LCA model (SITA, Creed, EIA, 1998) provides an estimation of the quantity of leachate collected from the LCS relative to the precipitation, considering the number years that a cell has been in operation and the presence – or not – of a cover:

- 0 to 18 months with no cover, 20% of the precipitation quantity;

- 18 months to 5 years with no cover, 6.6% of the precipitation quantity;
- 5 to 10 years with no cover, 6.5% of the precipitation quantity;
- 10 years + with a geomembrane cover: 0.2% of the precipitation quantity.

Although the amount of water collected from the LCS is almost as much as the precipitation during the first weeks or months of operation when there is little or no waste in the cell, it rapidly decreases after only 18 months. Moreover, once a low permeability cover has been installed, the quantity of leachate to be drained by the leachate collection layer will be an insignificant fraction of what it was during its first weeks of operation. As a consequence, it is reasonable to consider that the LCS is a critical component of the lining system during only the first few years that the landfill is in operation if the landfill final cover is designed to allow only a nominal amount of precipitation to enter the landfill.

It is thus possible to state that even if the performance of a drainage layer designed to absorb the rainfall in a given area is reduced to 20% of its initial capacity after 18 months, it will still fulfill its function and meet regulatory requirements as a LCL when the landfill is operated in the conditions considered in the LCA model. The same approach can be used to state that a sufficient performance would be offered by a LCL presenting as little as 0.2% of its initial capacity following installation of a geomembrane final cover.

These numbers appear promising considering the observations reported by Rowe (2005), which suggest that clogging of the gravel layer can occur after a period of time that can vary between a decade to a century, depending on the design of the LCS and the properties of the leachate.

2.3 Long Term Performance of Geocomposite Drainage Layers

Among the issues which have to be considered in the design of LCS, creep, and biological/chemical clogging are among the key factors as outlined by GRI GC8, which is widely used in North America for the design of drainage geocomposites.

$$FS = \frac{\theta_{allow}}{\theta_{req'd}} \quad (1)$$

With

$$\theta_{allow} = \frac{\theta_{100}}{RF_{CR} \cdot RF_{CC} \cdot RF_{BC}} \quad (2)$$

where θ_{100} is the transmissivity measured in accordance with ASTM D4716 (after 100 hours seating time with in-situ conditions), and the RF are Reduction Factors addressing:

- RF_{CR} = creep deformation;
- RF_{CC} = chemical clogging;
- RF_{BC} = biological clogging.

Besides the creep, chemical, and biological clogging potential, the GRI GC8 approach also indirectly includes other limiting factors such as geotextile intrusion by requiring consideration as a reference value the transmissivity measured after 100 hours under in-situ conditions which reproduces geotextile intrusion.

However, the reduction-factor approach developed in GRI GC8 focuses solely on the drainage geocomposite itself and its long term performance, not as a component of a LCS. Issues such as the length of the design life used to determine these reduction factors are not clearly defined in the GRI GC8 standard, and could generate divergent interpretation of their significance. Moreover, it was not possible for the authors to identify any published scientific justifications for these proposed values in the GRI-GC8 standard, which have been discussed in-depth by several authors including Zhao et al. (2012).

Although the preferred approach to the design of drainage geocomposites may vary depending on the application and assumptions considered, there is a broad acceptance regarding the fact that creep and biological / chemical clogging are the key factors affecting the performance of drainage geocomposite used in LCS and that an improvement of existing design guidance would be welcomed.

Although biological and chemical clogging are likely to occur in every type of product, one of the strengths of tubular drainage geocomposites is the shape of the core and its ability to resist very high stresses while confined in soil. Saunier et al. (2010) have observed that the transmissivity of tubular drainage geocomposites was not affected by normal load or

creep up to normal stresses as high as 2500 kPa and test durations up to 100 hours. It was concluded that the creep reduction factor in GRI GC8 can be neglected as long as the product is confined in soil. As a consequence, it is suggested that biological and chemical clogging can be considered to be the only factors which are likely to affect the performance of tubular drainage geocomposites.

2.4 Leachate Composition

Several landfill leachate characteristics should be considered for proper evaluation of the performance of any product in contact with leachate. The nature of waste may change tremendously depending on local regulations, existence of recycling programs, wealth of the community and other factors. As a consequence, observations made on a given landfill may be applicable only to very similar landfills, but cannot be generalized to any type of landfill.

- Leachate composition;
- Age of the leachate;
- Temperature, which influences the growth of biomass; and
- Anaerobic conditions to reflect the conditions prevailing in the bottom of a landfill.

The leachate characteristics considered here is located in Section 3.2, Experimental Set-Up.

3. INVESTIGATION

3.1 Scope

The study was conducted on a landfill identified as 'class 2' under the French designation, which describes sites designed to receive municipal solid wastes and non-hazardous industrial wastes. For this type of landfill, the waste includes a significant fraction of organic matter resulting of normal human activity and is thus known to develop biologically active leachate.

3.2 Experimental Set-Up

Two tubular drainage geocomposites were tested, and compared to gravel. These consist of a series of 25 mm diameter perforated corrugated pipes sandwiched between two layers of non-woven polypropylene geotextiles (Figure 2). The upper geotextile (in contact with the granular drainage layer above), is composed of special fibers made with silver ions acting as a biocide agent (ACB filter).

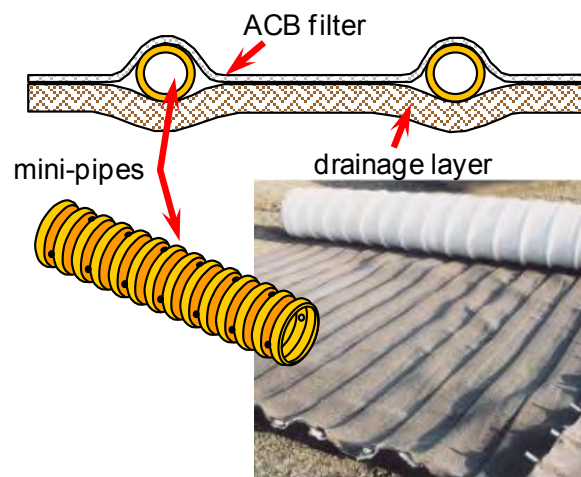


Figure 2. Tested tubular drainage geocomposite

Issues related to leachate composition outlined above have been taken into account in the experimental design. Transportation to a laboratory to run a laboratory-controlled experiment was not considered to be a realistic option as the change of properties of the leachate would be too significant; it was thus decided to bring the experimental setup to the landfill. The test temperature was controlled within a range of 20 to 30°C considering that only the first two years of

service are of interest to the authors. Although it is known that the temperature at the bottom of landfills can exceed this value after several years of service (Rowe et al. 2006, Koerner and Koerner 2006), the selected temperature range was considered to be as close as possible to service conditions in the LCS during the first two years of activity at the bottom of the landfill.

The test cell design was developed in order to observe the clogging potential of both the filter and core (perforated pipes) of the geocomposite. The test cells were installed in a building located near the perimeter of the landfill, close to a leachate sump, where fresh leachate could be easily pumped and injected into the test cells. The building was maintained at a temperature of $25\pm 5^\circ\text{C}$ year round in order to maintain a biological activity of a similar nature than what is likely to be experienced by the geosynthetic drainage products at the bottom of landfill during their first years of operation. Preservation of anaerobic conditions was ensured by the design of the test cell, which was achieved by positioning the outflow weir above the top of the cell to submerge the interior of the cell in leachate, and relatively small diameter pipes were used to inject the leachate into the cells. The leachate was circulated through a gravel layer first, then through the geocomposite, and collected through the exit of the pipe on one end of the cell, (Figure 3). Although the tested product is not sensitive to normal load, a normal load in the range of 100 kPa was used to represent conditions at the base of a landfill cell within 18 months of operation. The normal load was achieved by controlling the compression of calibrated springs (Figure 4).

3.3 Leachate Injection

The system used to control injection of a fixed quantity of leachate in the conditions of the test is described as follows:

1. A large volume of leachate was pumped into a 'buffer reservoir' located above the cells, then allowed time to equilibrate with room temperature.
2. The first series of electro-valves were opened simultaneously to allow flow of the leachate from the buffer reservoir into smaller calibrated reservoirs, each equipped with a valve to control the leachate to a fixed volume.
3. A second series of electro-valves were opened to permit flow of the leachate into the test cell a short time after stabilization of the second step.

One standard pump was needed to inject leachate into the 'buffer reservoir'. The pump and the electro-valves were controlled using timers. Overall, this system allowed injection of one liter of leachate into the test cells ten times per day, (at a frequency of 144 minutes), which was considered sufficient to maintain a constant supply of nutrients to the micro-organisms likely to develop into the system, while maintaining the test conditions.

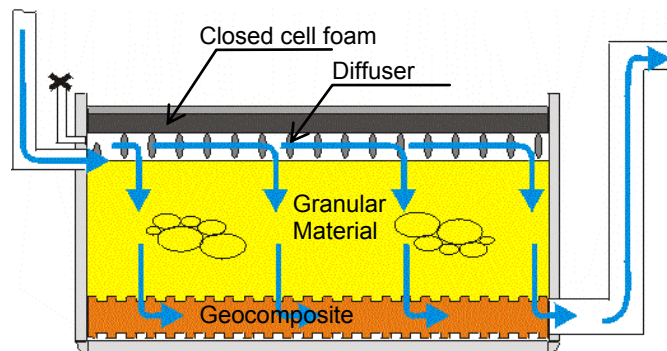


Figure 3. Cross section of a test cell



Figure 4. Control of the 100 kPa normal stress

3.4 Monitoring Technique

As mentioned at the beginning of this paper, this project involved a collaborative effort from the landfill owner, a geosynthetics manufacturer and a laboratory. In addition to the supply of the test area, the personnel available on-site was used for periodic control of the experiment, as well as to perform simple measurements and to report their observations to the laboratory.

The monitoring technique was designed to ensure the performance of this approach. As the objective of the project was to observe a lack of clogging after 18 months, a simple measurement of the time needed for leachate to percolate through the system under fixed conditions was adopted. A container was thus installed in parallel to the pipe used to inject the leachate. A falling head infiltration test was then performed using the same path as the one used by the leachate itself. Although this technique cannot be used to quantify potentially minor adverse effect of the leachate on the system, the blocking of any component of the system can be easily detected.

Figure 5 presents the system used to monitor the infiltration rate. The time needed for the water to enter the system was measured by observation of the water level traveling between the lines marked 'H₀' and 'H₁'. An infiltration rate was calculated, expressed as the velocity of the water entering the cell, under an average head of 0.15 m (0.15 m being half of the allowable head according for many regulations). From these observations, a clogging index was defined as the ratio between the infiltration rate at a given time, and the initial infiltration rate.

3.5 Experimental Program

Three configurations were tested, and each was replicated three times for a total of nine test cells. Two out of the three configurations involved tubular drainage geocomposites with anti-bacterial filters (Table 1). The third configuration was involving only gravel (Figure 6). The gravel was selected according to the current regulatory requirements prevailing in France: crushed gravel, sieved between 20 and 40 mm. An overview of the complete test set-up is presented in Figure 7.

Table 1: Tested geocomposite properties

	Standard	type 'A'	type 'B'
Test cell number		1, 4, 7	3, 6, 9
Mass per unit area of the filter (g/m ²)	EN 9864	160	240
Mass per unit area of the cushion (g/m ²)	EN 9864	800	800
In-plane transmissivity ($\sigma = 400 \text{ kPa}$, $i=0.1$, m ² /s)	ISO 12958	$5,7 \times 10^{-4}$	$5,7 \times 10^{-4}$
Antibacterial treatment		Embedded, non-leachable silver ions	

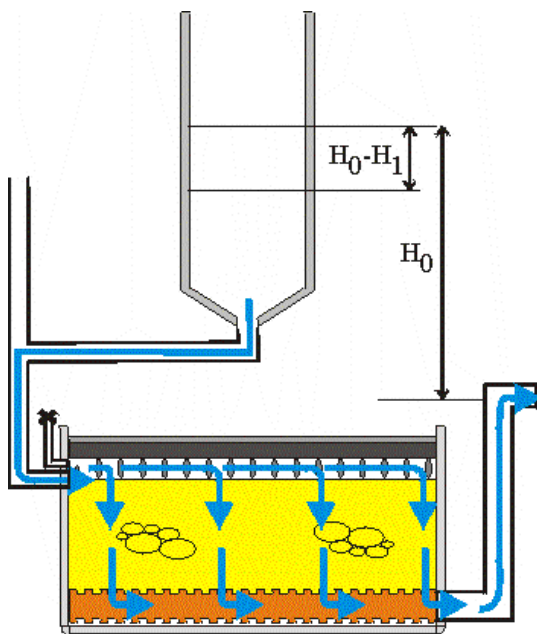


Figure 5. Periodic monitoring system.



Figure 6. Gravel (dimensions of the cell: 250 mm x 250 mm)

4. OBSERVATIONS

No significant clogging could be detected using the technique described above. At the end of the test, the cells were dismantled to observe the quantity of biomass accumulated in the system and to proceed with observations, measurement of the pore volume, and weighing the quantity of biomass accumulated in the gravel.

4.1 Clogging

Figure 8 presents the change of the clogging index with time for each of the three configurations. After 18 months, it was observed that none of the systems had lost their efficiency, with a 'clogging index' in the range of 3 to 5.



Figure 7. View of the 9 cell test apparatus

4.2 Residual Volume of Voids in the Gravel

In order to determine the residual porosity at the end of the test, the quantity of water that freely flowed out of the saturated cells was collected and compared to the total volume of the inside of the cell. It was found that the measured void volume ranging from 27% to 34% for all three drainage types, demonstrating the presence of a significant amount of voids in the granular drainage layer (Table 2).

4.3 Weight of Biomass and Fine Particles Trapped into the Components

After measurement of the volume of voids, the accumulated biomass and minerals trapped into the system were collected at the end of the project using the following procedure:

- Gravel and test cell were washed in clear water;
- Biomass in the water was filtered from water on a geotextile;
- Wet biomass was weighed;
- Biomass was dried in the air, at room temperature;
- Dry residual material was weighed.

The corresponding measurements are presented on Table 2. It can be observed that a significant amount of biomass has developed into and immediately above the geotextiles (cushion component of the tubular drainage geocomposite), which is consistent with previous observations of clogging (Rowe 2005).

Table 2: Measurements conducted after testing

	Cell #	Void ratio %	Mineral particles		Biomass	
			In the gravel Kg/m ²	On the geocomposite Kg/m ²	In the gravel Kg/m ²	On the geocomposite Kg/m ²
Type A	1	34%	0.288	1.472	6.016	5.856
	4	33%	0.736	1.696	6.912	6.464
	7	27%	0.672	1.696	7.040	5.408
Gravel	2	30%	0.608	0.800	4.832	4.448
	5	32%	0.480	0.896	5.344	7.104
	8	30%	0.736	0.992	5.184	5.184
Type B	3	33%	0.256	1.456	5.696	6.448
	6	34%	0.640	1.808	6.464	6.352
	9	30%	0.928	2.064	6.656	6.160

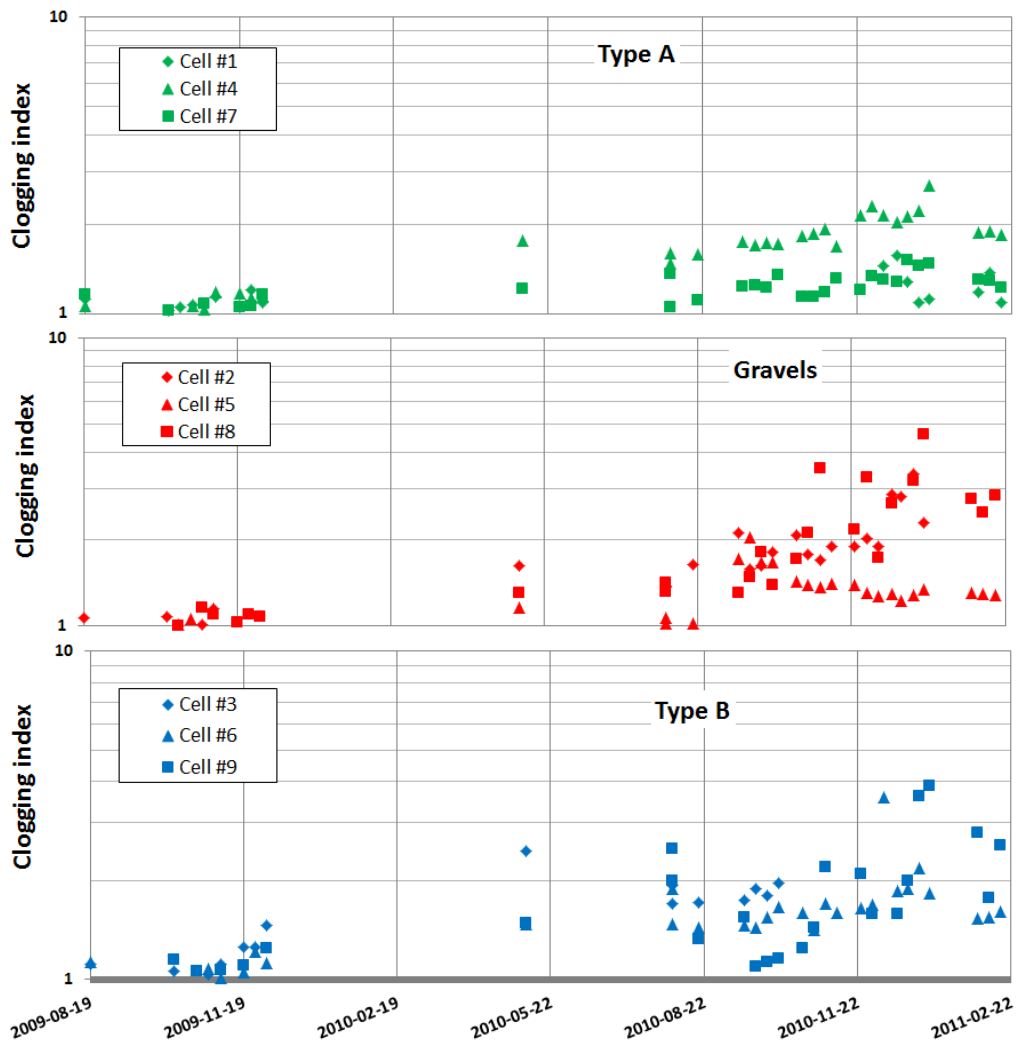


Figure 8. Clogging index

4.4 Visual Observations

Although a shiny black film of biomass could be observed in the gravel and as well as on the geotextile of the tubular drainage geocomposite, connected void spaces were still existent, allowing water to flow through the gravel and the geocomposite. These observations were consistent within the entire set of experiments ran. No visual evidence of

buckling or damage of the pipes arising from the combination of leachate exposure and normal load could be observed. Examples of the dismantled drainage components are presented in Figures 9, 10, and 11.

5. DISCUSSION AND CONCLUSIONS

A thorough literature review was conducted regarding the regulatory required and actual drainage capacity of the LCS over the life of a “dry tomb” landfill. This literature review led to the conclusion that leachate flow potentially reaching the leachate collection layer of a “dry tomb” landfill is significantly less at the end of its lifespan, than what is required in the early stages of its lifespan. This particular observation allowed for some flexibility regarding the long term performance of geocomposite drainage layers with respect to chemical and biological clogging. Specifically, the highest anticipated leachate supply rates are anticipated during the early stages of the landfill; while once the final cover is installed the anticipated leachate supply rates have significantly dropped off.

This particular observation is basically in line with the second component of this research; which shows that although clogging increases over time; the drainage media may not completely clog, thus still allowing the reduced leachate supply to be removed from the bottom liner and meeting the set goals of maintaining the hydraulic head below the prescribed threshold (typically 0.3 m).



Figure 9. Gravel in cell 8.



Figure 10. Side view of the geocomposite in cell 4 (type A).



Figure 11. Side view of the geocomposite in cell 7 (type A).

On the other hand, experimental confirmation was presented herein that a tubular drainage geocomposite incorporating a geotextile treated with silver ions as a biocide agent can remain functional for up to 18 months, when exposed to leachate in representative conditions as what would be present at the bottom of a LCS in an active landfill classified as ‘class 2’ (municipal solid waste and non-hazardous industrial waste) under the French regulation. Both styles of tubular drainage geocomposites and the gravel used as the control did not experience complete clogging to the point they would be no longer functional after 18 months of testing. However, it was not possible to detect any statistical difference in clogging between the various configurations due to the preferred monitoring strategy.

Based on these considerations, it is possible to conclude that replacement of 0.50 m of gravel by a tubular drainage geocomposite and 0.30 m of gravel represents a solution which can meet the performance-based regulatory requirements related to LCSs in dry tomb landfills in many jurisdictions, with the following assumptions:

- The system composed of the drainage geocomposite + gravel layer is designed to fulfill the drainage requirements prevailing at the initial stage of the life of the landfill, when mainly rainfall water is to be drained, and
- The 0.30 m gravel layer is designed to fulfill the drainage requirements prevailing after 18 months, which is only a fraction of the initial requirements.

ACKNOWLEDGEMENTS

The authors wish to thank Dr. Melissa Chappel, Ph.D. (CTT Group), for fruitful discussions regarding regulatory requirements related to drainage layer performance requirements prevailing on the North American Market.

REFERENCES

- Bellenfant G. (2009). Modélisation de la production de lixiviat en centre de stockage de déchets ménagers, Thèse de doctorat présentée à l'INPL, 178 pages.
- California Code of Regulations, Title 27, Environmental Protection—Division 2, Solid Waste.
- Environmental Protection Agency (1993) Criteria for Solid Waste Disposal Facilities : A Guide for Owner's/Operators (EPA-530-SW-91-089).
- Fourmont S., Bloquet C., Haddani Y. (2008). Partial replacement of the granular layer at the bottom of a landfill: short and long term monitoring of drainage geosynthetics. EuroGeo 4, United Kingdom, 6 pages.
- Giroud, J. P., Zhao, A., Tomlinson, H. M. & Zornberg, J. G. (2004). Liquid flow equations for drainage systems composed of two layers including a geocomposite. Geosynthetics International, 11, No. 1, 43–58
- Government of Alberta (2010). Standards for Landfills in Alberta, Government of Alberta.
- Government of Newfoundland and Labrador (2010). Guidance Document: environmental Standards for Municipal Solid Waste Landfill Sites, Government of Newfoundland and Labrador, St. John's.
- Koerner, G.R., Koerner, R.M. (2006). Long term temperature monitoring of geomembranes at dry and wet landfills. *Geotextiles and Geomembranes* 24:72-77.
- NF EN 9864 (2005). Géosynthétiques - Méthode d'essai pour la détermination de la masse surfacique des géotextiles et produits apparentés.
- NF EN ISO 12958 (2010). Géotextiles et produits apparentés - Détermination de la capacité de débit dans leur plan
- GRI Standard-GC8 (Standard guide for determination of the allowable flow rate of a drainage geocomposite, 2001).
- Ontario Ministry of the Environment (1998). Landfill standards: a guideline on the regulatory and approval requirements for the new or expanding landfill sites, Ontario Ministry of the Environment, Ontario Regulation 232/98. The Queen's Press, Toronto.
- Schroeder, P.R., Dozier, T.S., Zappi, P.A., McEnroe, B.M., Sjostrom, J.W. and Peyton, R.L. (1994), "The Hydrologic Evaluation of Landfill Performance (HELP) Model: Engineering Documentation for Version 3", EPA/600/R-94/168b, U.S. Environmental Protection Agency, Risk Reduction Engineering Laboratory, Cincinnati, OH.
- Rowe R.K. (2005). Long term performance of contaminant barrier systems, *Géotechnique* 55: 631-678.
- Saunier P., Ragen W., Blond E. (2010). Assesment of the resistance of Draitube drainage geocomposites to high compressive loads. *9th International Conference on Geosynthetics*, Brazil.
- Zhao A., Blond E., Recalcati P. (2012). Drainage Geonet Composites and Performance Assessment. EuroGeo 5, Valencia, Spain (in press).

Bituminous Geomembranes Liner at Agnico-Eagle Mine in Kittilä, Finland

Bertrand Breul, Axter Coletanche Montréal Canada, BBreul@axtercoeltancehe.com
Bernard Breul, Axter Coletanche, Irvine USA, Breul@eirnet.com

ABSTRACT

This paper discusses the reason behind the choice of a bituminous geomembrane to line two process-water ponds at the Agnico-Eagle gold mine in Kittilä, Finland. The Kittilä Mine lies within the Arctic Climatic Region (150 km north) where daylight reaches a minimum of 1 hour per day in winter and a maximum of 24 hours in summer with an average annual temperature of zero degrees Celsius. The paper describes the mine in general, reviews the regulatory framework for the liner system, and provides details about design, construction and Construction Quality Assurance activities and the benefits associated with the bituminous geomembrane liner such as the use of large aggregate under and above with no cushion geotextile, flexibility of schedule, and the possibility to install in cold weather.

1. INTRODUCTION

1.1 Background

Kittilä Gold Mine is operated and owned by Agnico-Eagle Mines Ltd headquartered in Toronto (Ontario, Canada). This mine is the second mine located the northern region of Finland. Environmental permission for the mine operations was granted by Northern Finland Environmental Permit Authority in 2002. Mining started its operations with an open pit with an anticipated depth of 150 m. After 3 years of pit mining, underground mining via ramp access will begin with a target depth of 450 m. The Kittilä mine in northern Finland is approximately 900 kilometers north of Helsinki and 40 kilometers from Kittilä (Figure 1).



Figure 1: Location

Key numbers about the mine include

- Area 860 ha
- Annual ore mining (Suurikuusikko deposit) 1,000,000 tons
- Annual waste rock mining 4,000,000 tons
- Annual gold production 5 tons
- Roads 4 km
- Pipelines. 15 km

The mine opened in the summer of 2008 and has an estimated lifetime of 15 years.

1.2 Weather

The Kittilä Mine lies within the Arctic Climatic Region (150 km north) where daylight reaches a minimum of 1 hour per day in winter and a maximum of 24 hours in summer. Temperatures are cold (Figure 2), with an average mean monthly temperature in July of 15 °C and in January of -15 °C. The mean annual air temperature at the site is approximately 0 °C. Winds are moderate and generally from the west. Average wind speeds are about 25 km/hr.

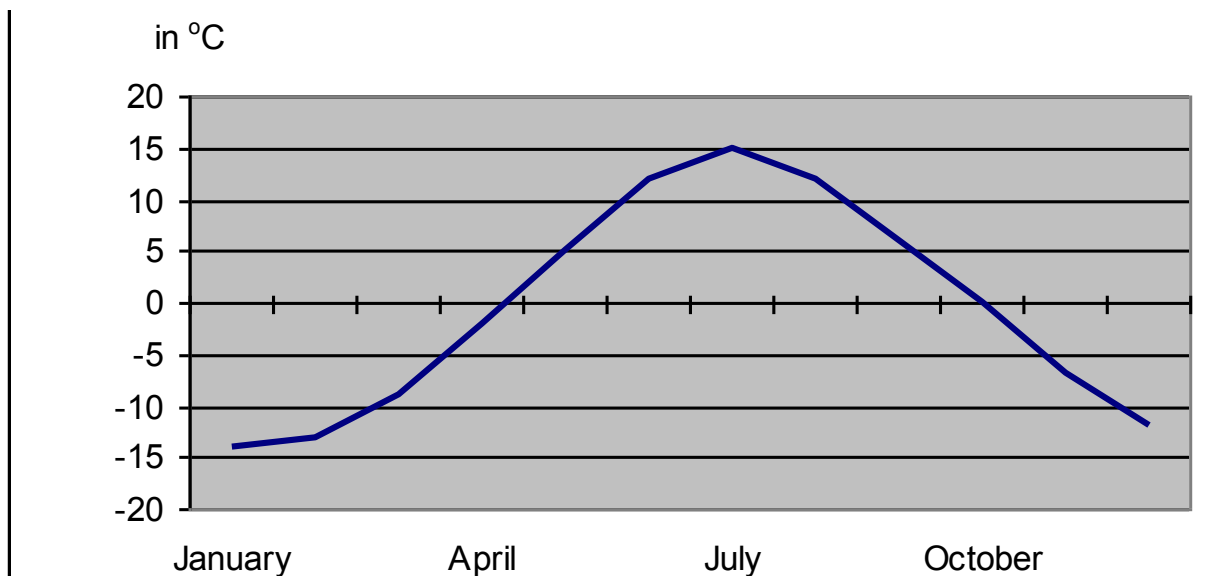


Figure 2: Average Monthly Temperatures in Kittilä

As shown on Figure 3 precipitation averages over 50 mm per month with rain generally occurring between May and October. Figure 3 also shows that it rains or snows almost half of every month. As shown on Figure 2 and 3, the warmest period is between June and September, but it is the wettest too.

Weather conditions are therefore not conducive to the deployment of geosynthetics which typically requires dry weather and relatively warm temperatures for proper seaming.

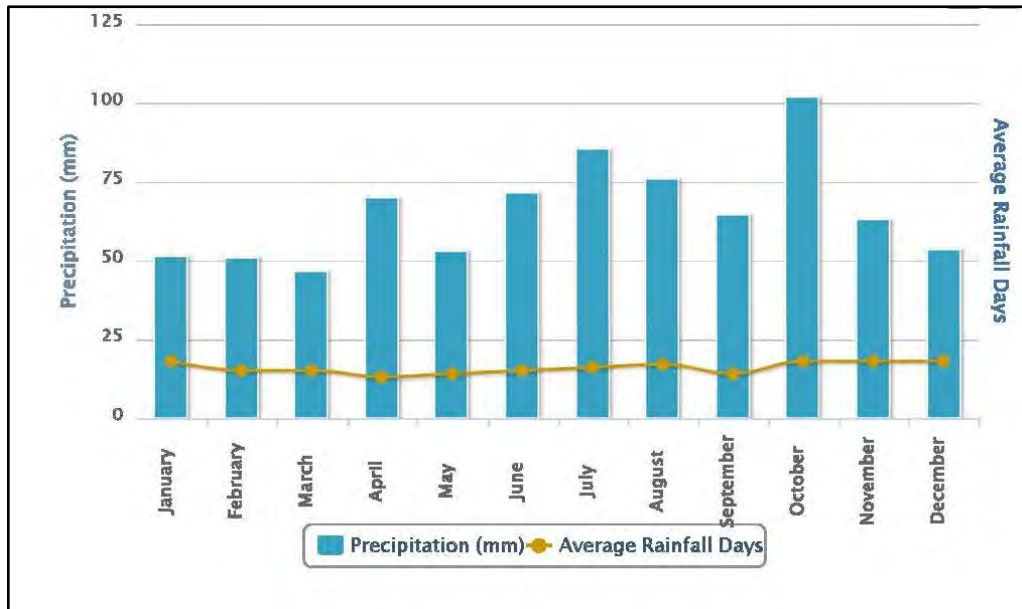


Figure 3: Average Monthly Precipitation Totals in Kittilä

2. PROJECT

2.1 Purpose

The mine facility plan calls for a small and a large pond for a combined area of 54 hectares to receive the process water from the gold processing plant. Water from the ponds is then recirculating back to the process. So the water circulation is practically a closed system. As part of the environmental permit for the mine, a watertight liner was required by the Finnish Ministry of Environment.

2.2 Schedule

The two ponds (Figure 4) had to be lined by the fall of 2008. However the construction season for earthwork runs from June to November. Prior to June the ground is frozen and cannot be excavated and after November very low temperature, snowfall, and darkness limit work. It was decided to excavate and line the ponds in two phases:

- Phase 1 in 2007: excavate and line the smaller pond and excavate and begin lining the bottom of the larger pond.
- Phase 2 in 2008: finish lining bottom and slopes of the larger pond.

The work went in accordance with the schedule and the ponds were finished lining by the fall of 2008 and are currently being used by the mine.



Figure 4: Aerial view of the two ponds

2.3 Design

The design of the ponds called for an excavation surrounded by dikes to get the required volume. The cross section of the dam consists of a core built with blasted rock with particle size up to 600 mm in diameter. The water side of the dike was covered with a layer of blasted rock but with a maximum diameter of 300 mm itself and protected by a layer of gravel not exceeding 55 mm in diameter. This last layer was compacted using an excavator equipped with a compacting plate (Figure 5) to provide a smooth surface with no ruts. The dikes were designed to function like a zoned dam built with material recovered from the mining operation. A 1 meter thick sealing layer was then placed on the bottom of the pond. The sealing layer consist of the excavated moraine rolled and compacted exhibiting a saturated hydraulic conductivity less than 5×10^{-8} m/s. The ponds were then lined with a geomembrane as discussed in the next section.

The concept behind the zone cross section and varying grain size is for the dike to perform like a drain should leakage occur an reduce the risk for piping failure or catastrophic flow though the large pores of the 600 mm rock if the dikes were built only with this size rocks



Figure 5: Compaction of side slopes

2.4 Liner System

The project was initially designed with a polymeric geomembrane (HDPE or LLDPE) but the client expressed interest in switching to a bituminous geomembrane to line the ponds at Kittilä because:

- It can be installed at temperatures as low as -30 degrees Celsius which was a critical element with respect to schedule when considering the construction season in Lapland and the fact that it was anticipated that construction would extend until October to make the deadline imposed by the mine for use of the ponds.
- It can be installed in moist/humid connections
- It can be installed directly over the sealing layer and does not require a protective sand layer or cushion beneath. This provided a time and cost savings.
- It has a low thermal expansion coefficient so the geomembrane does not expand (i.e. wrinkles) or contract throughout the day when temperature varies. Therefore the geomembrane lays flat on the ground (Figure 6) and provides in combination with low permeability moraine a very efficient composite liner system meeting the requirements of the permit for water tightness.



Figure 6: Liner on bottom of pond – note absence of wrinkles

In order to optimize the cost for the design of the liner system a 3.5 mm-thick bituminous geomembrane was used on the bottom and a 4.0 mm-thick bituminous geomembrane thicknesses was used on the slopes

The design based on using a bituminous geomembrane was subject to regulatory review and a public survey to obtain approval from the local to the national agencies. The approval was granted in three months.

2.5 Bituminous Geomembrane

The structure of the bituminous geomembrane used, is shown on Figure 7 and consists of

- A non-woven polyester long fiber geotextile with a mass per unit area of 200 to 400 g/m²,
- A glass fleece reinforcement which provides stability during fabrication and contributes to the strength of the geomembrane,
- A bituminous mastic consisting of a blown 100/40 pen bitumen, and filler. This mastic impregnates the whole structure and give the waterproofness of the product and ensure the longevity in protecting the non-woven geotextile and the high resistance of the product,
- A Terphane film bonded to the underside when the membrane is hot, which prevents penetration of the membrane by plant roots, and
- A coating of fine sand on the upper surface to provide a greater traction on slopes, giving greater operator safety by any kind of weather even in case of snow and security, and increases protection from the degrading effects of UV radiation.

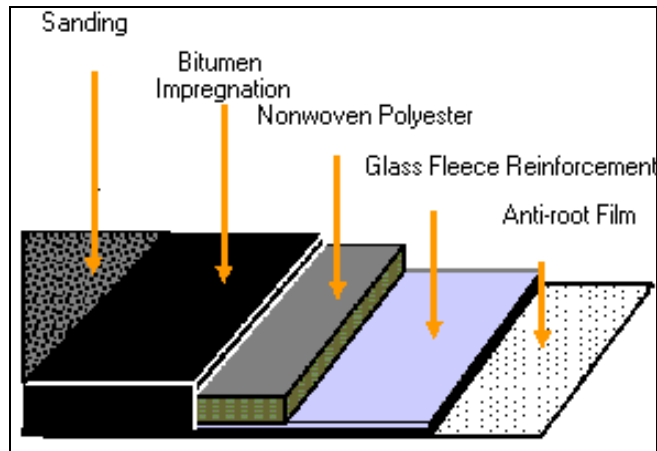


Figure 7: Schematic cross-section of bituminous geomembrane

This manufacturing system results in a geomembrane with a long life expectancy due to its resistance to high levels of mechanical stress and negligible ageing characteristics. Grades range in thicknesses from 3.5 mm up to 5.6 mm.

3. CONSTRUCTION

The installation was completed by a local company (Destia Oy) based in Helsinki (Finland) hired as the general contractor. Its business area is primarily the planning, construction, upkeep and maintenance of roads. Destia Oy, with no previous experience in laying bituminous geomembrane, installed the bituminous geomembrane in the ponds and provided the Quality Control testing and reporting after being trained by a supervisor of the manufacturer.

3.1 Installation

For the preparation of the support two workers removed sharp gravel and natural organic fill from the surface with rakes while another operated a compactor. Installation of bituminous geomembrane is similar to that of all other geomembranes using spreader bar hooked to excavator. The difference is that a hydraulically controlled spreader bar is used to control deployment of the bituminous geomembrane on the slopes. The hydraulically controlled spreader bar allows rewinding the geomembrane if too much is unrolled. Two workers unroll the geomembrane and one other operates the excavator. Two welders were needed to weld the joints and one assistant to roll and seal the joints after welding (Figure 8).

In essence a crew of 6 to 8 people is all that is needed to prepare the subgrade and deploy the bituminous geomembrane

On average, approximately 5 000 m²/day of bituminous geomembrane were installed with two welding teams,



Figure 8: Welding of adjacent panels of bituminous geomembrane

3.2 Quality Controls

One lab technician from the general contractor was trained by the supervisor of the distributor to follow the quality control plan all along the work. This technician was completely dedicated to this work. All seam testing and destructive samples were documented daily and recorded in a computer-generated report.

Ultrasound testing (Figure 9) was used to monitor quality of the total width of the seam on the project. The quality of the seam is essential for any geomembrane. The Ultrasound testing probe is used to check the entire 20 cm width of the seam. Ultrasound waves are able to detect imperfections in the seam and to measure the width of the defect.

Any defect was repaired by placing a patch over the defective area.



Figure 9: Ultrasound testing

4. CONCLUSION

The choice of bituminous geomembrane was validated by a successful construction of the two ponds. The use of bituminous geomembrane provided several benefits at the Kittilä mine. The most important were:

- Ability to work in cold wet weather which allowed the ponds to come on line on time and did not affect opening of the mining operations.
- Cost reduction since local materials were used for bottom and slopes. There was no need for a fine sand or cushion layer under the geomembrane
- Installation by the general contractor rather than a specialty subcontractor. This gave a better control of the schedule which was a critical element of the project.

Campbell Shipyard Receives a Massive Underwater Geosynthetic Sediment Cap Adjacent to San Diego Hilton Convention Center

Rich Sack, P.E., TenCate Geosynthetics, USA, r.sack@tencate.com

ABSTRACT

A site known as Campbell Shipyard adjacent to the Hilton San Diego Convention Center in Downtown San Diego, California has been used for over 100 years for industrial activities that included commercial fishing ships and naval ship repair early on and eventually moved to a petroleum tank farm, municipal refuse incinerator and gas manufacturing and waste facility. In the 1990s, the shipyard lease expired and a massive cleanup of the site soon began. After many years, the port completed cleanup of the above water portions of the site, but found it too expensive to test and safely remove all of the 37,000 SM (9.2 acres) of polluted sediments hidden below the water's surface on the bay floor. Engineers decided to create a massive underwater permanent cap over the contaminated soils. At the heart of this mammoth size underwater cap is a high strength woven geotextile panel that was created with a unique blend of both polypropylene and polyester fibers (to yield a specific gravity greater than water) that sinks. The geotextile rolls were sewn into massive panels and fitted with PVC encased rebar that were deployed directly from a moving sectional barge using GPS tracking to assure proper over-lap and location of adjacent panels.

1. INTRODUCTION

The Port of San Diego was required by the California Regional Water Quality Control Board (RWQCB) to clean up below water polluted sediments at the former Campbell Shipyard. Campbell Shipyard is an extremely highly visible sight located along the San Diego Convention Center in San Diego, California, as shown in Figure 1. Initially, it was proposed to simply dredge (remove) all of the contaminated material from the underlying surface of the 37,000 SM (9.2 acres) of the bay (a massive undertaking). Unfortunately, the removal of all the contaminated sediment would cause instability to many existing structures in and along the bay and be too costly to remove (due to the highly variable elevation changes of the polluted sediments). The demolition and removal of many of the old structures brought even more sediment up to the surface – (almost doubling the sediment quantities in some areas) adding to the quantity of the contaminated sediments. The Port found that capping the contaminated sediments using a composite layer of high strength woven geotextile, gravel, rock and sand was the best option to control the contaminated sediments.



Figure 1. Project Site

2. CAP DESIGN

2.1 Project Overview

The contaminated unconsolidated sediments were found to have an undrained strength of 48.8 to 488 kilograms per square meter (10 to 100 pounds per square-foot). Wang et al. (2006). The cap to be placed over the contaminated sediments consisted of several layers – each placed individually. The high strength woven geotextile panel was to be deployed directly from a floating sectional barge and laid out directly onto the bay surface. The high strength woven geotextile panel was placed at the bottom of the cap to maintain separation between the existing contaminated bay sediments and the layers of gravels and sand to be placed on top of the geotextile. The high strength woven geotextile panel also helped increase the bearing capacity of the underlying sediments – so thicker lifts could be placed while constructing the cap layer. The increase in bearing capacity helped reduce the risk of mud waves (sediments displacement in a wave shape adjacent to the fill loading area). With the decrease risk of mud waves occurring, the use of the high strength woven geotextiles allowed the maximum lift placement to increase from 15.3 cm to 30.6 cm (double the lift thickness) – speeding up the overall construction process. Wang et al. (2006).

2.2 Sediment Cap Cross-Section

The sediment cap was designed with a single high strength woven geotextile panel placed directly over the contaminated sediment. Some of the very soft areas had a composite layer of gravel and high strength woven geotextile over the existing sediment. A 61 cm thick layer of sand was then placed directly over the geotextile panel. The sand layer was designed to act as a fine filter that allows water pressure to be released, while sediment gets trapped deep within the layer. A 30.5 cm thick layer of gravel was then placed over the sand layer. The gravel layer acted as a transitional interface between the sand layer and the final layer. A final 61 cm thick layer of armor rock was placed over the gravel layer to resist erosion from underwater currents and boat prop thrust. Wang et al. (2006). A cross-section of the sediment cap is shown in Figure 2.

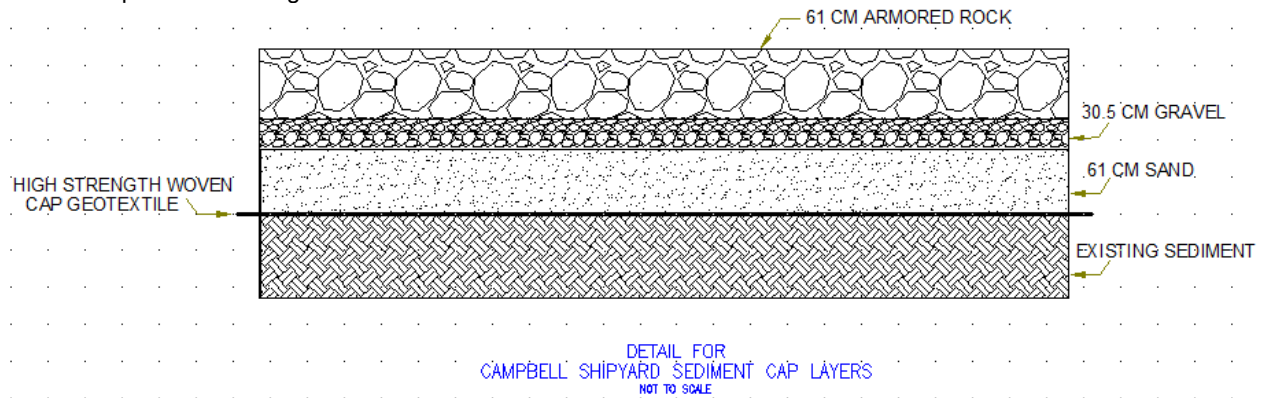


Figure 2. Sediment Cap Cross-Section

2.3 Habitat Restoration Cap

A 6,475 SM (1.6 acres) portion of the site was developed for habitat restoration. The habitat restoration zone consists of a 30.5 cm layer of well graded sand that is used to contain any contaminated sediments; the same high strength woven panel used in the other areas of the site to contain the underlying sand layer and block any contaminated sediments from escaping to the upper habitat layer; a 61 cm layer of non polluted ocean sediments mixed with sand sediments; and a final living layer of eelgrass to support ocean wildlife.

2.4 Geosynthetic Properties

Typical woven geotextiles used for subgrade stabilization are manufactured from polypropylene due to their stable weave, resistance to installation damage, high UV resistance and strength properties. The high strength woven cap geotextile had several physical requirements: high strength was required to help improve bearing capacity of the overall cap section; robust fibers that resist installation damage during deployment and during rock/sand placement; and a construction weave pattern that remains stable without tearing, unraveling, or sliding open holes when rebar is attached to it during deployment. Typical polypropylene geotextiles have a specific gravity less than ocean water, therefore it floats. A fabric that is too buoyant, such as polypropylene, would be too difficult to intimately lay over the changing contours of the bay floor without floating upward off the surface. A high strength geotextile that met the required physical requirements and uses a blend of polyester and polypropylene fibers was manufactured specifically for the project that

would have an overall specific gravity greater than 1.0 (sinks in water). The high strength woven geotextile chosen for use on this project was manufactured with a specific gravity of 1.075. This sinking geotextile will remain in place more easily than a polypropylene geotextile or geogrid and not float away from the bay floor once installed.

The final requirement of the high strength woven geotextile was high water flow rate (high permittivity). The high strength geotextile was required to pass large volumes of water through its surface, so that pore water pressure doesn't build under the sediment cap – reducing the risk of armor rock displacement.

The project engineer required that the high strength woven cap geotextile be sewn into very large panels that were approximately 13.7 M wide and 274 M long to reduce the number of overlaps. To meet the panel width requirements for the project, three rolls of fabric, that were approximately 4.7 M wide and 274 M long, were each sewn together by the fabrication department of the manufacturer prior to being shipped out onto site. The large panels were then re-rolled onto the sectional barge's roller for easy deployment. Figure 3 shows the high strength woven panel seam. Figure 4 shows the panel roller aboard the sectional barge.

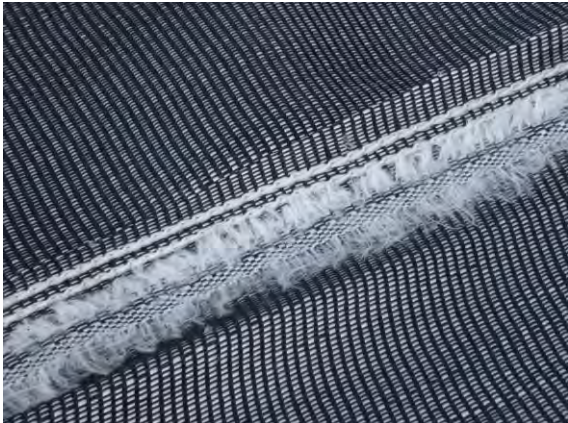


Figure 3. High Strength Woven Panel Seam.



Figure 4. Roller on Barge with Panel.

Some key physical properties of the high strength woven geotextile used in the cap construction are shown in Table 1.

Table 1. PET/PP Woven Cap Geotextile Panel

Mechanical Properties	Machine Direction	Cross-Machine Direction
Ultimate Tensile Strength (kN/m)	105.1	113.8
Tensile Strength at 5% (kN/m)	52.5	57.8
Ultimate Factory Seam Strength (kN/m)	58.3	
Specific Gravity	1.1	1.1
Water flow rate (l/m ² /min)	2241	

3. CAP CONSTRUCTION

3.1 Project Overview

All of the protrusions such as large debris, large rocks and pier column remnants that may penetrate through the cap were removed to create a somewhat flat surface before placement of the high strength woven cap geotextile panel. The massive high strength woven panels were rolled up and brought out to a floating sectional barge. The 13.7 M wide panels were deployed directly from the moving sectional barge. To keep the panel from folding over on itself and being pushed aside by underwater currents, No. 4 rebar that was placed in sealed PVC pipe (to protect it from salt water corrosion) was zip tied onto the panel at approximately 9.1 M intervals. The zip ties had to be pushed through the fabric panels and around the rebar by hand. The rebar was attached across the width of the panels as it came off the roller, before deployment into the water, as shown in Figure 5. The fabric panels remained dimensionally stable and did not allow the zip ties with rebar to slide threads over and cause open holes in the panel.



Figure 5. Rebar Attached to Woven Panel Being Deployed.

An I-beam was attached to the leading edge of the high strength woven panels and carefully lowered onto the ocean floor by a large crane, as shown in Figure 6. The I-beam served as an anchor for the panel. Once the I-beam was in place on the ocean floor, the barge would move back slowly (by pulling off from a series of anchors located outside the panel area) unrolling the panel onto the sea floor.



Figure 6. I-beam Attached to Cap Panel.

The centerline of each panel placement was used to position adjacent panels and assure proper overlap of the panels. Figure 7 shows the barge's onboard GPS tracking and location plotting of the panels as they are deployed.

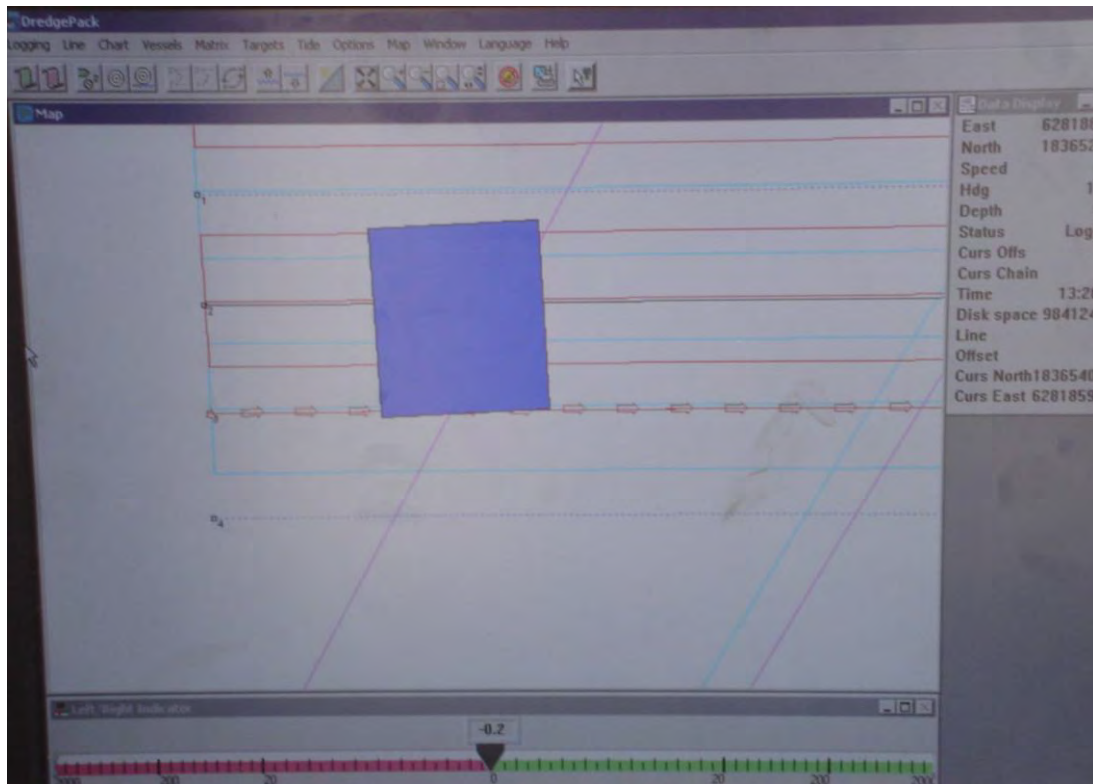


Figure 7. GPS Tracking of Panel Placement

4. CONCLUSIONS

Campbell Shipyard sediment capping project was a highly visible environmental cleanup project. The project was performed under high levels of scrutiny and regulation. The high strength woven geotextile panels increased the underlying sediment bearing capacity – allowing twice the thickness in lift thickness to be placed and cutting the fill placement time in half. The capping project was completed successfully in 2007 and the high strength woven geotextile panel was installed with great flexibility and has performed perfectly in both the sediment cap system and the eel grass habitat system area as well. A total cost of more than \$72 million has been spent on the entire Campbell Shipyard project area, including: demolition and dredging; all above and below water environmental cleanup; capping; site preparation, and construction of a large parking facility to accommodate further development. O'Connor et al. (2006). As of today, the system is still functioning perfectly.

ACKNOWLEDGEMENTS

We wish to acknowledge the Port of San Diego, design engineering firm Anchor Environmental, Weston Solutions, and material supply services of TenCate Geosynthetics distributor Triumph Geo-Synthetics Inc. in Anaheim, California.

REFERENCES

- O'Connor, S., Whelan, M., Bygness, R. (2006). San Diego Bay Gets an Underwater Facelift. *Geosynthetics Magazine*, Volume 24, Number 5, 16 - 23.
- Wang, T.S., Whelan, M., Keith, D., Verduin, J., and Brown, P. (2006). Design of the Campbell Shipyard Sediment Remediation Project. *WEDA XXVI and Texas A&M's 38th Annual Dredging Seminar*, San Diego, California, USA, 309 - 321.

Case History –Geomembrane & Floating Cover System, South Australia Water Corporation, Wattle Park Potable Water Reservoir

Brian W. Fraser, Layfield Group Limited, Vancouver, British Columbia, Canada
Paul Vince, South Australia Water Corporation, Adelaide, South Australia, Australia
Alex Gersch, Fabtech, Wingfield, South Australia, Australia

ABSTRACT

As part of a water security review to address severe drought conditions, South Australia Water Corporation (Owner) identified the need for several essential infrastructure projects which included an upgrade to the Wattle Park potable water reservoir. The Wattle Park reservoir, with an 84 million litre (22 million gallon) capacity, required a new geomembrane liner and floating cover system. At prior storage and treatment reservoirs using normal levels of chlorination for a disinfectant, the Owner had experienced premature failures with certain liner and cover materials. Based on the operational importance of the Wattle Park project, a new performance specification for the geomembrane and floating cover material was developed. Meeting this specification required a specially stabilized and formulated geomembrane. This paper addresses the technical review criteria for selecting a new geomembrane as well as a number of project challenges and techniques used by the contractor related to the installation of a new liner and floating cover.

1. INTRODUCTION

Around 2003, South Australia began experiencing severe drought situations which impacted water supplies, and resulted in strict water restrictions being enforced in many regions of the State. As part of a 2010 strategic review of its water security, the South Australia Water Corporation (Owner) identified the need to proceed with several essential water management infrastructure projects. Among these, included was an important upgrade to the Wattle Park potable water storage reservoir that provides drinking water to the City of Adelaide, the capital of South Australia. The Wattle Park water storage reservoir, with an 84 million litre (22 million gallon) capacity, required a new 14,500 m² (156,000 ft²) geomembrane liner and



Figure 1: Wattle Park Potable Water Reservoir Floating Cover nearing installation completion stage

14,500 m² (156,000 ft²) geomembrane floating cover system. The reservoir which was originally constructed in 1929, was concrete lined. After leaks in the concrete reservoir resulted in local flooding, a Chlorosulphonated Polyethylene (CSPE) liner and floating cover was installed in 1986. In 2010, independent material testing conducted on behalf of the Owner determined that the CSPE geomembrane had only 10% remaining of its original retained tear strength. This created a

number of safety and performance concerns, which resulted in the Owner prohibiting any walking on the cover system required for maintenance purposes until a new floating cover system could be commissioned. In 2010 the Owner and its consultant undertook a technical review process of geomembranes that would be suitable for the Wattle Park reservoir liner and floating cover.

2. MATERIAL SELECTION

The material selection for the geomembrane and floating cover was a critical component of the Wattle Park project. SA Water has vast experience with floating covers as a result of operating eighteen (18) cover systems from the period of 1986 to 2010. The two main materials previously used for these floating covers included Reinforced Polypropylene (RPP) and CSPE. At a number of sites using normal levels of chlorination, the Owner had experienced premature failure and lower than expected service life of the covers specific to the use of RPP. It was determined by the Owner that these failures were likely linked to chemical degradation of the material when exposed to chlorinated water. The Owner co-authored and published a 2011 technical paper on the deterioration of flexible polypropylene liners and covers (Moore et al. 2011). Based on these past material problems, SA Water performed a detailed technical review of available industry lining materials. Their intent was to source a more fortified geomembrane technology that could be used for both liners and floating covers. A fortified geomembrane is defined as a product heavily treated with stabilizers providing enhanced heat, UV stability and chemical resistance (Schiers, J 2009). The Owner specifically targeted material endurance properties including high pressure oxidative induction time (HP OIT) normally tested in accordance with ASTM 5885. The GRI GM 17 (Geosynthetic Research Industry) industry standard specifies 400 minutes of HP OIT. The Owner also required long term weathering capabilities and paid particular attention to the ultra violet (UV) protection and long term weathering capabilities of the material. The objective was to specify a geomembrane and floating cover material with a 25 year weathering warranty and proven resistance to chlorinated potable water. The Owner required proven testing and certification on the geomembranes chemical resistance for chlorine and UV resistance. The geomembrane and floating cover materials also needed to be fit for purpose in terms of suitable mechanical properties including sufficient tensile, elongation, puncture, and flexibility properties. Another important requirement was for the material to be potable water compliant and meet both the National Sanitation Foundation NSF/ANSI Standard 61 Drinking Water System Components (NSF/ANSI Standard 61) and the Australian and New Zealand standards for testing of products for use in contact with drinking water (AS/NZS 4020:2005).

Layfield (Manufacturer) submitted performance specifications on its Enviro Liner[®] 6040^{HD} (Polyolefin Alloy) geomembrane as well as material samples required for independent third party testing and verification. This specific geomembrane is a polyolefin alloy product and is categorized as a fortified material as a result of being produced from a highly stabilized formulation with an advanced UV antioxidant (AO) package. The materials endurance properties include a 2,000 minutes HP OIT and 90% tensile strength retention after 30,000 hours of accelerated UV testing in accordance to ASTM D4329. Table 1 below illustrates a number of the polyolefin alloy properties in comparison with GRI GM 17.

Table 1. Geomembrane Material Properties Comparison

HD Performance Properties	ASTM	Polyolefin Geomembrane	GRI GM 17
Thickness (min. ave)	D 5199	40 mils (1.00 mm)	40 mils (1.00 mm)
Tensile Strength at Break	D638 /D6693	191 ppi (33.5 N/mm)	152 ppi (27 (N/mm)
Elongation at Break	D638/ /D6693	1200%	800%
Puncture Resistance	D 4833	70 lbs (311 N)	56 lbs (250 N)
Critical Cone Height	D 5514	1.97 inches (50 mm)	N/A
Flexibility – Cycles without Cracking	D 6182	> 8000	N/A
Axi-Symmetric Break Resistance -% (min.)	D 5617	50%	30%
High Pressure OIT(min .ave)	D 5885	> 2000 mins	400
UV Resistance - Strength Retained	D 4329 30,000 hrs	90%	N/A
Certifications (Potable Water)			
NSF 61		Pass	N/A
AS/NZ 4020		Pass	N/A
Ozone Resistance 100 pphm @ 40°C	D 1149	No Cracks Observed	N/A

In addition to material specifications and samples, the Manufacturer submitted additional accelerated stress crack testing performed previously on its Polyolefin Alloy geomembrane with chlorine following ASTM D1693 for Environmental Stress Cracking of Ethylene Plastics. This testing protocol included immersing the geomembrane to a 1% (by volume) solution of sodium hypochlorite or the equivalent to 10,000 parts per million (ppm) at a constant fluid temperature of 50°C(122°F). The

conclusion of this testing indicated that the polyolefin alloy geomembrane retained over 800 minutes of HP OIT after 1,000 hours of immersion with no noticeable surface cracking. This helped provide the Owner with additional assurance of the geomembranes strong chemical resistance to chlorine as a disinfectant in a longer term geomembrane and floating cover application. The Manufacturer also submitted testing and a published technical paper (Mills, 2009) on its geomembrane which completed 30,000 hours of accelerated UV testing. This testing demonstrated the polyolefin alloy geomembrane retained over 90% of the materials tensile strength after 30,000 hours of accelerated UV weathering testing in accordance to ASTM D 4329.

Based on the Polyolefin Geomembranes performance specifications and the Owners testing verification, the Manufacturer's material was specified for the Wattle Park project.

3. RESERVOIR LINER & COVER

Fabtech (Contractor) an experienced liner contractor based out of Adelaide, South Australia was awarded the design, supply and installation contract for the Wattle Park containment project. The Contractor had previous fabrication and installation experience working with the manufacturer's polyolefin geomembrane including floating cover applications which proved to be a valuable asset on the project. The scope of work for the Contractor included removing the existing CSPE liner and cover, repairing the concrete reservoir surface, fabrication and the installation of a new 14,500 m²(156,000 ft²) polyolefin geomembrane liner and design, fabrication, and installation of a 14,500 m²(156,000 ft²)floating cover. A leak detection system was also designed and installed by the Contractor utilizing the existing concrete lined reservoir as the secondary liner. This required the concrete expansion joints to be sealed using a flexible epoxy to ensure any leakswere contained and did not seep into the subgrade. A penetration through the concrete floor was made to access the redundant sub grade drainage system below the concrete lined storage. A 316 stainless steel grate and collection sump was installed to transfer any leakage to a monitoring and inspection sump outside the main reservoir. Overtop of this stainless steel grate a 10mm HDPE (0.4") plate was installed to prevent the liner from penetrating into the grate and becoming damaged. The slopes of the concrete reservoir were lined with a 550 grams/ m² (16 oz/ yd²) non woven geotextile to act as both a protective cushion and as a leakage flow path on the slope walls. The floor of the reservoir was lined with a geocomposite drainage layer and an additional layer of 550 grams/m² (16 oz/ yd²) geotextiles cushion to provide sufficient flow rate and protection to the liner so it would handle the 9.5 meter (31.2 ft) of fluid head pressure. The Contractor also supplied and installed electric mixers and an upgraded electrical perimeter security fence.



Figure 2: 130 Ton crane used to remove old liner

The project faced a number of challenges including very tight site access impacting the removal of the old liner and cover system, as well as installation of the new containment system. To help address the tight space constraints, the Contractor incorporated in-depth project management controls ensuring the sequencing of all suppliers and subtrades were properly planned and stayed on schedule. The contractor also prefabricated as much of the system components as possible including the slope sections of the liner and floating cover. The reservoir was situated in a major urban neighborhood resulting in required noise control, enhanced safety systems and traffic management. The crest of the dam varied between 1.5m (4.9 ft) wide and 3.6m (11.8 ft) with an electrical security fence on a concrete parapet wall at the top of the reservoir, and a chainmesh security fence on the outside of the crest. To facilitate removal of the old CSPE liner and cover and to prepare for the installation of the new geomembrane the electrical security fence was removed. The condition of the concrete surface could not be properly assessed until sections of the liner and cover were cut out and moved manually to inspect the surface. At this point in the project it was determined that

mechanical equipment with a contact surface pressure of less than 100kPa (14.7 psi) could be safely used without damaging the concrete surface. Two Bobcats were winched down the 1:2 side slopes and used to bundle the old geomembrane into 500kg (1,102 lbs) bundles. To achieve the reach required to remove the old material a 130Ton (286,600 lbs) crane was employed positioned on the edge of the storage to lift 6Ton(13,440 lb) loads from the basin floor into waiting dump trucks which transported the used CSPE to an approved landfill site. In total 120 Tones (264,554 lbs) of material were removed.

The new floating cover system incorporated a central plate cover design which was required to address the size of cover, depth of the reservoir, batter gradient, and awkward configuration of the storage reservoir. The design required a primary and secondary ballast system. The primary ballast consisted of 200mm (7.9") diameter sand tubes around the 5 sides of the central plate system which provided the necessary tension in the cover system. The primary ballast line was designed to be 1.0m (3.28 ft) deep at top water level with 1.9m (6.2') between the paired floats. The secondary ballast made of 150mm (5.9") diameter sand tubes were installed in the corners and at the structures to take up excess material and enhance drainage. Another project challenge was the existing inlet configuration to the reservoir. There were 2 inlet points consisting of a single pipe at the northern end, and 3 pipes at the southern end of the reservoir. The pipes were surface mounted and encased in concrete. As a result, the cushion layer, liner, and cover all had to be installed up and over the structures. The cover design required a secondary ballast to help tension and control the excess material. To help reduce installation time and construction cost the Contractor prefabricated the slope panels for the geomembraneliner and floating cover. Site field welding was required for the floor section and the central plate cover system due to depth of the reservoir and access constraints. To ensure weld seam integrity, all factory and field seams were completed in accordance with the Manufacturer's recommended seem strength values of 12.2 N/mm (70 ppi) in accordance with ASTM D6392.



Figure 3: Geomembrane being installed over Geotextile

The storm water removal system was designed to handle record levels of daily rainfall as recorded by the Australian Bureau of Meteorology in a twenty four hour period with a redundancy factor of 33%. This was achieved by using three individual submersible stainless steel pumps that were fixed in pump wells located on floating platforms in different sections of the primary ballast lines which divided the cover roughly into thirds. The pumps have integral level switches for automatic operation and are permanently connected with isolators at the ring beam. The level switches are set to operate when the ballast lines have 300mm (11.8") of water, and are set to stop operation with 150mm (5.9') of water in the ballast line. The pumps are connected via flexible PVC hoses and non return valves, to HDPE pipes laid beside the walkways to additional connection points at the ring beam. The storm water is discharged to the natural local water course adjacent the main reservoir.

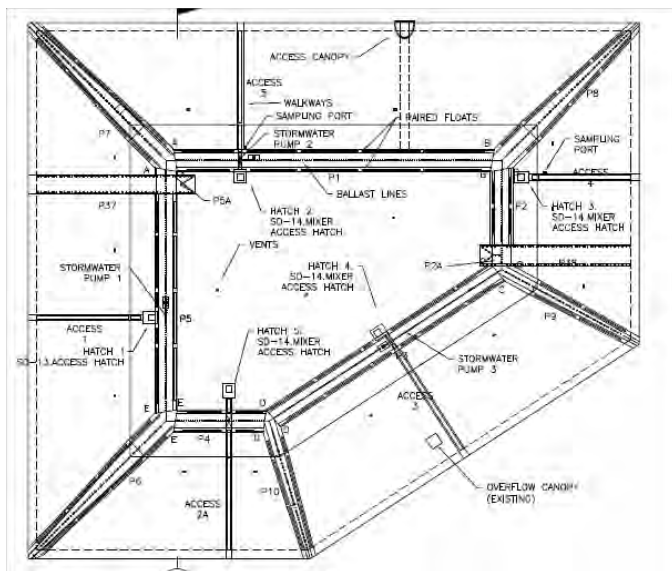


Figure 4: Plan view of Storm Water Pumps & Hatches

The design, manufacture and testing of the containment system was required to conform to (AS/NZS 1170) (AS NZS 1657). The central plate cover system incorporated a design closely following the AWWA California-Nevada Section Reservoir Floating Cover Guidelines.

During installation of the liner, the geomembrane was progressively electrically leak tested and was verified to be leak free by the contractor. The floating cover at completion was then hydrostatic tested and also confirmed to be leak free. The liner and cover system then went through a final disinfectant treatment which was a requirement for potable

4. CONCLUSION

The installation of the new geomembranes and floating cover system commenced on December 14, 2011, with the liner installation completed including electrical leak detection testing on January 2012. The new floating cover installation commenced on January 13, 2012 with completion of the cover system including all surface ancillaries on February 2, 2012.

The hydrostatic testing of the cover was concluded in late February 2012. The project was completed on time and on budget. This project highlights advancements being made with today's geomembrane technology through the use of improved film extrusion, high performance prime grade resins and advanced UV/AO additive packages. It also demonstrates the design, fabrication and installation capabilities available today in the Australia geomembrane market. In conclusion, the project's success can also be accredited to excellent communication, cooperation and experience from all parties involved to design, manufacture, and construct an important potable water storage containment project.



Figure 5: Cross view of completed floating cover showing tensioning of the cover and surface apparatus



Figure 6: Aerial view of completed Wattle Park Floating Cover System

ACKNOWLEDGEMENTS

The authors would like to thank and acknowledge Greg Moore of Moore Consulting Technology who was an active contributor in this project as part of the sourcing and qualification of materials, and with the development of the geomembrane and floating cover material specification.

REFERENCES

- ASTM D 5890-95. Standard Test Method for Determining the Integrity of Non Reinforced Geomembrane Seams Produced Using Thermo-Fusion Methods, *American Society for Testing and Materials*, West Conshohocken, Pennsylvania, USA
- ASTM D 6392. Standard Test Method for Determining the Integrity of Nonreinforced Geomembrane Seams Produced using Thermo-Fusion Methods, *American Society for Testing and Materials*, West Conshohocken, Pennsylvania, USA.
- ASTM D1693 - 12 Standard Test Method for Environmental Stress-Cracking of Ethylene Plastics, *American Society for Testing and Materials*, West Conshohocken, Pennsylvania, USA.
- ASTM D5885 - 06 Standard Test Method for Oxidative Induction Time of Polyolefin Geosynthetics by High-Pressure Differential Scanning Calorimetry, *American Society for Testing and Materials*, West Conshohocken, Pennsylvania, USA.
- Moore, G., Shiers, J. and Vince, P., (2011). Deterioration Of Flexible Polypropylene Reservoir Liners and Covers In Contact With Potable Water
- American Water Works Association, "AWWA Standard for Disinfection of Water Storage Facilities, ANSI/AWWA C652," Denver CO.
- National Sanitation Foundation, "NSF/ANSI Standard 61 Drinking Water System Components" Ann Arbor MI.
- Council of Standards Australia, AS/NZS 4020:2005 standard for Testing of products for use in contact with drinking water
- Schiers, J. (2009)., A Guide to Polymeric Geomembranes: A Practical Approach (Wiley Series in Polymer Science), 2009 Edition.
- Mills, A. (2001)., "The Effects of Chlorine on Very Low Density Thermoplastic Olefins", Geo-Frontier © and ASCE, Conference 2011
- Mills, A., Martin, M. and Sati, R (2009). Long-Term Weathering Stability and Warranty Implications for Thin Film Geomembranes, Proceedings of Geosynthetics 2009, Salt Lake City, Utah, USA.
- GRI Test Method GM 17. Test Methods, Test Properties and Testing Frequency for Linear Low Density Polyethylene (LLDPE) Smooth and Textured Geomembranes, Geosynthetic Industry, Folsom, Pennsylvania, USA.

Case History on the Use of Geonet Composite in Red Willow Dam Modifications

Peter R. Irey, Bureau of Reclamation, Denver, Colorado USA, PIrey@usbr.gov
Jack Gagliardi, P.E., Bureau of Reclamation, Denver, Colorado USA, JGagliardi@usbr.gov
Derek Wittwer, P.E., Bureau of Reclamation, Denver, Colorado USA, DWittwer@usbr.gov

ABSTRACT

The Bureau of Reclamation constructed Red Willow Dam in 1962. In 2009 sinkholes were found on the downstream face and upon further investigation cracks associated with the sinkholes were found. The solution was to use a geonet composite layer on the upstream side of a new chimney filter/drain. This geonet composite would provide three beneficial functions: secondary filter and drain to the primary chimney filter/drain; span any cracks to prevent filter from falling into cracks; and prevent propagation of new cracks across the new chimney filter system. In addition, the geonet composite will be used as the primary filter/drain above the 10,000-year flood level. Red Willow dam will be the first Reclamation dam to use such a large quantity of geonet composite drainage material (48,000 m²) in this manner. This case study covers the design of the geonet composite, positive and negative aspects of using the geonet composite, and construction techniques.

1. INTRODUCTION

Red Willow Dam and Hugh Butler Lake, completed in 1962, are features of the Frenchman-Cambridge Division of the Pick-Sloan Missouri Basin Program. The dam is located on Red Willow Creek, a tributary of the Republican River, approximately 10 miles north of McCook, Nebraska. The reservoir is primarily used for storing irrigation water, but also provides flood control benefits. Red Willow Dam is a modified homogeneous earthfill embankment constructed from silt of low plasticity. A 1.5 meters thick sand and gravel drainage blanket extends 34 meters downstream from the embankment centerline to the downstream toe where a gravel enveloped corrugated metal pipe toe drain exists. There is no cutoff trench beneath the dam and the embankment rests on windblown foundation soils, which were stripped of vegetation, pre-wetted, and compacted before constructing the embankment.

1.1 Flaws in the Embankment

During a site investigation in 2009, sinkholes were found on the downstream face near the outlet works. Upon further investigation several cracks were found on the downstream face of the dam. The outlet works and spillway conduits located at the right abutment of the dam were reportedly founded on competent Ogallala foundation. Immediately left of the outlet works the firm foundation dives steeply, so the majority of the dam is not founded on firm material. The valley fill to the left of the outlet works consists of both sands and silts, with the upper portion being mostly silt. It appears that the valley silts may be either loess or at least partially reworked loess, as they have low densities and settlement characteristics similar to that of the Peorian Loess. Severe differential settlement of the dam during and after original construction was thought to have caused the tension cracks in the embankment immediately adjacent to the outlet works and original diversion channel.

The compressible foundation silts comprising the valley fill showed settlements of up to 1 meter directly adjacent to the outlet works. The foundation above and adjacent to the outlet works conduit was shaped in a manner that would promote arching, with a 1:1 slope into the valley. This unfavorable geometry creates the potential for low stress conditions and tension cracks. These factors combined with the extremely brittle and erodible nature of the embankment and foundation soils (silts with an average plasticity index of 3) made the embankment susceptible to both cracking and erosion. On October 21, 2009, the first of several sinkholes were discovered on the downstream face of Red Willow Dam along and near the alignment of the outlet works. Further investigations revealed the presence of cracking in the embankment above the outlet works conduit and other areas along the downstream face of the dam.

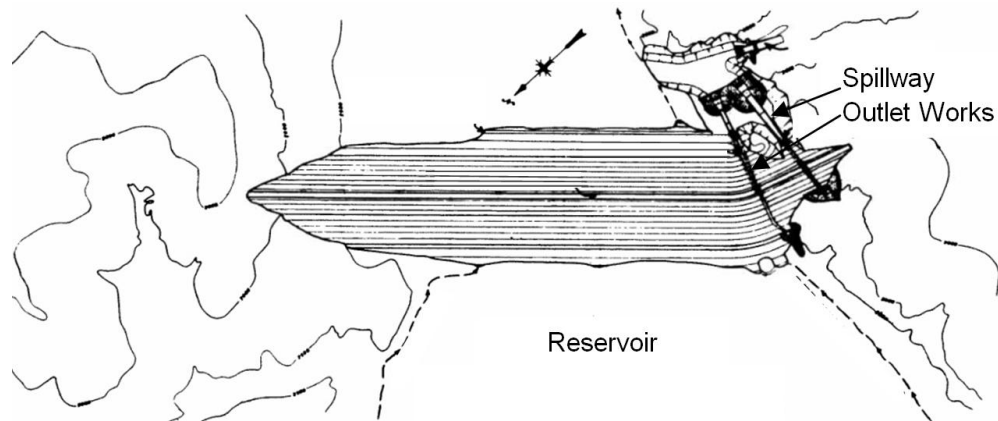


Figure 1. General plan of dam.

The potential for cracks extending through the embankment are a major concern when the embankment is made of a highly erodible material and does not have an existing filter that intercepts these cracks downstream of the embankment. Case histories suggest that the most likely potential failure mode under normal operations is internal erosion through the embankment. Furthermore, case history data suggests that close to half of embankment internal erosion failures have been associated with penetrating conduits. This type of potential failure mode is the most significant concern at Red Willow Dam given the number of cracks in the embankment that were identified near the outlet works conduit and previous issues with particle transport through undertrains at the outlet works stilling basin. Therefore, modifications were determined to be necessary in order to reduce the risk of internal erosion through the embankment.

Modifying the existing foundation to limit further settlement and cracking of the dam and/or providing a cut-off wall through the embankment was not economical due to the significant depth of bedrock beneath the majority of the embankment and the high costs associated with cutoff wall construction. Therefore, an alternate solution to address cracking and the potential for internal erosion would be to install a two-stage filter downstream of the existing embankment. The filter would ensure that existing or new cracks could not erode the embankment leading to severe seepage and ultimately failure of the dam.

2. EMBANKMENT MODIFICATIONS

Twenty three alternatives to address dam cracking were highlighted by a Reclamation design team covering a wide spectrum of concepts that included downstream filters and drains, cutoff walls, filter trenches, geo-net composite filters, upstream geomembranes, and/or various combinations of these concepts (Corrective Active Study, 2010). Among these alternatives the most cost effective and technically acceptable modifications were the alternatives that had some type of two stage or single stage filter with a berm and buttress downstream of the existing dam. Using a geonet composite as a primary filter was initially suggested, but quickly determined to be inappropriate for a federal dam, per Federal Emergency Management Agency, FEMA. According to the FEMA filter manual (2011), geotextiles cannot be used: where inspection or repair of the material is not possible, in locations critical to the safety of the dam, and as a component that could potentially lead to failure of the dam. As the design process continued and cost estimates were calculated it was determined that the most economical and state-of-the-art design would be to install a two-stage chimney filter and drain system in the downstream portion of the dam to prevent migration of fines through existing cracks that could lead to an internal erosion failure. In addition, a geonet composite would be placed upstream of the chimney filter as discussed later. Downstream of the filter, a berm and buttress would be installed to equal the reservoir pressure to prevent a blowout on the downstream face assuming full reservoir head from an open crack that extends all the way to the chimney filter/drain. Final design modifications for Red Willow Dam are shown in Figure 2.

The modified embankment depicted in Figure 2 represents the final design modifications for Red Willow Dam where Zone 1 material is fine grained material with more than 15 percent passing the 200 μ m sieve, Zone 2 material is C33 fine aggregate filter sand with less than 2 percent passing the 200 μ m sieve, and Zone 3 material is C33 number 67 coarse aggregate (ASTM C33/C33M). A geonet composite layer is rarely, if ever, used in Federal dams; therefore the design and specification of this layer played a major role in the final design process.

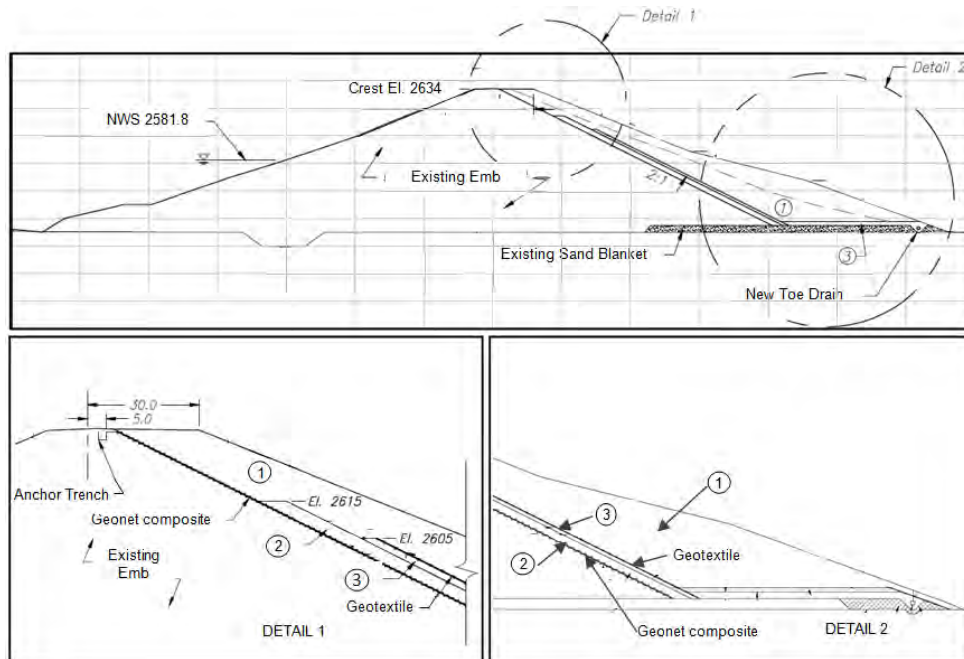


Figure 2. Modified embankment section and details.

2.1 Geo-net Composite Design

As mentioned previously, Reclamation rarely uses geosynthetic materials in embankment dam modifications. Typically only two types of geosynthetics have been used by Reclamation: geomembranes used on the upstream face or as a reservoir lining to reduce seepage and geotextiles to separate incompatible materials. Using a geomembrane upstream of the embankment was initially proposed for Red Willow Dam but was judged to be inadequate for reducing the risk for internal erosion through the embankment due to concerns with seepage flows entering the embankment below the bottom of the upstream geomembrane. Alternative configurations for the geomembrane were evaluated to intercept the seepage path but; they would have reduced storage below acceptable reservoir operations and/or required underwater placement of a geomembrane. Reclamation needed an economic solution that would help reduce the expense of importing filter materials for what likely would have to be a relatively wide chimney drain to provide both drainage and mitigate cracks in the embankment.

A double sided geonet composite was one of many solutions considered. The design team also considered using only a heavy weight geotextile, a single sided geonet composite, or only a geonet. All of these options were believed to provide significant risk reduction related to embankment cracking concerns. The decision to use a double-sided geonet composite for the modification was based on engineering judgment and lengthy discussions regarding positive and negative factors for using different geonet composite combinations. Listed below are some of the factors discussed when choosing the double sided geonet composite:

- The double sided geonet composite provides additional crack spanning ability across an open crack when compared to a single layer of geotextile or a single sided geonet composite.
- The geotextile protects the net from contamination during construction of the downstream filter and berm.
- The design only specifies a chimney sand filter being installed up to the 10,000 year flood reservoir water surface (RWS). Above this elevation a double-sided geonet composite would act as the primary filter and drain. Using a double sided geonet composite below the 10,000 year flood RWS eliminates transitioning to a different layer.
- There is a possibility that the void space in the annulus of the drain portion of the geo-net could be a repository for fines that migrated through the upstream geotextile fabric. This space was determined to be insignificant when using a biaxial geonet sandwiched between two geotextiles. The geotextiles are expected to fill the majority of the geonet void space once overlying fill is compacted over the geonet composite. Also, a thick,

heavy weight (540 g/m² with smaller AOS) upstream layer of geotextile reduces the potential for embankment fines migrating into the geonet.

- A negative factor for using double sided geonet composite is; if the excavated surface is not smooth the double sided geonet composite may not conform to the excavated slope, possibly creating a repository for fines.
- For all options, there is a potential for blinding or clogging of the geotextile; which could lead to excessive hydraulic pressures and high exit gradients behind the filter. Using a double sided geonet composite could allow for additional drainage capabilities providing better relief for potential excessive hydraulic pressures.

The double sided geonet composite was designed with a 200 mil (5mm) geonet inserted between a heavy weight 540 g/m² non-woven needle punched geotextile, and a light weight 200 g/m² non-woven needle punched geotextile. Since seepage through the embankment has never been measured or observed at Red Willow Dam, theoretical gradients were calculated above the 10,000 year flood RWS where the material will act as the primary filter. Below the 10,000 year flood RWS the geonet composite was placed upstream of a two stage filter to prevent filter sand from falling into cracks and to assist in collecting any seepage passing through the embankment. The two stage filter is expected to handle excessive seepage flows that surpass the drainage capacity of the geonet composite.

In addition, retention and permeability criteria for the two geotextiles were considered. The heavy weight geotextile was designed to be placed upstream of the geonet against fine grained embankment material and the light weight geotextile was designed to be placed downstream of the geonet against zone 2 filter sand. Design calculations used for retention assumed that the apparent opening size, AOS, of the geotextile would be less than two to three times the D₈₅ of the base materials. The term D₈₅ refers to particle size of the fine grained material, as determined by gradations, where 85 percent of the particles pass. The AOS of the upstream geotextile was specified to be less than or equal to 0.15 mm (#100 sieve) which is approximately 2.5 times the average D₈₅ of the embankment material at Red Willow Dam. The AOS of the downstream geotextile was specified to be less than or equal to 0.212 mm which will be adequate to retain the chimney filter sand.

Reclamation also verified the impact the geonet composite would have on the stability of the embankment and estimated the flow capacity for the geonet composite above the 10,000 year flood RWS. The geonet composite was modeled in the embankment stability analysis as a thin layer with a friction angle of 14 degrees. Laboratory tests were not conducted to verify the interface friction angle between the zone 1 soil and geonet composite. However, research conducted by the Geosynthetic Institute, GSI, (Koerner et al. 2005) showed significantly higher interface friction angles for geotextiles and geonet composites against cohesionless soils. Therefore, the designers felt confident that the strength was not being overestimated. Flow capacity of the geonet composite was also not verified with laboratory testing, but conservative values of transmissivity were used to calculate an equivalent gravel layer. Transmissivity was estimated from values provided by the manufacturer but reduced to account for the intrusion of geotextile into the flow path and reduction of flow from the possibility of lower gradients (Bamforth 2008). Even with these reductions the geonet composite was determined to provide the same amount of flow as a 60 centimeter wide gravel drain.

2.1.1 Installation Specifications

Physical properties for all components of the geonet composite material were specified to ensure the material performed adequately after installation. The geonet was to be comprised of 5 mm thick High Density Polyethylene (HDPE) with a tensile strength greater than 800 g/mm. Specifying a 5 mm thick geonet ensured that a reasonable flow could pass through if seepage occurred and that the material will not tear if the geonet composite has to span cracks up to 2.5 cm wide in the embankment. Similarly, physical properties were specified for both types of geotextile. The specification having the biggest impact was that the tensile strength should be greater than 70 percent after 14 days of continuous ultraviolet, UV, exposure. Specific procedures for installation and protection of the geonet composite were not detailed in the specification but were left for the contractor to decide. However, several manufacture guidelines were consulted to ensure that installation met the design intent.

Specifications were outlined describing preparation of the subgrade beneath the geonet composite. If the excavated surface beneath the geonet composite is not relatively smooth then air gaps could exist for fines to migrate into. Also, large displacements in the subgrade could place excessive tensile strength causing the material to tear. The surface was to undergo foundation inspection and approval by Reclamation before installation of the geonet composite. To achieve approval the contractor had to create a firm surface that was reasonably even and smooth, and free of offsets, abrupt indentations, and protruding materials greater than 3.8 cm. The surface was also to be void of any erosion damage and any cracks greater than 1.25 cm must be repaired before installation of geonet composite was to proceed.

To ensure surface erosion of the embankment from rainfall did not take place it was specified that the geonet composite be placed over the entire slope before installing the downstream chimney filter and berm. It was assumed the geonet

composite material would provide some level of protection to the excavated slope from erosion due to rainfall. Along with placing all of the geonet composite before constructing the filter and berm, the material had to be placed transverse to the crest, machine direction running down the embankment, with any horizontal joints located in the bottom third of the embankment. Installing the panels in this direction insured that all horizontal joints were closer to the toe of the filter where the highest overburden stresses are acting. Typically, the longest roll length a manufacture will produce is 60 meters but the downstream slope required several rolls greater than 60 meters. Specifications for seaming the geonet composite required the contractor to overlap the side by side joints of the geonet a minimum of 15 centimeters and the end to end joints were required to overlap a minimum of 30 centimeters. Along the joints the geotextile portion of the composite would be sewn or continuously welded. The geonet was overlapped to allow the panels to be tied together; the net was tied at 60 centimeter intervals for side to side joints and at 30 centimeter intervals for end to end joints. Only the most critical specifications to the design were included in this paper due to space limitations.

3. CONSTRUCTION

Construction for Red Willow Dam modifications began in the spring of 2012. The Contractor began by stripping the topsoil from the embankment and excavating 300,000 cubic meters from the downstream embankment slope. Next the existing toe drain was removed and replaced by a modern 30 centimeter diameter HDPE perforated toe drain. Once the toe drain was complete the Contractor began placing drain material over the existing sand blanket (see Figure 2) then geonet composite material was placed in panels on the downstream slope. The contractor acquired 58,500 square meters of geonet composite to place on the entire downstream face of the excavated surface. This required ordering 215 rolls of geonet composite; each roll was 3.7 meters wide and approximately 60 meters long. After a large portion of the geonet composite was installed, the chimney filter and berm were started.

3.1 Construction Issues

As discussed in the installation specifications section it was crucial for the Contractor to create a relatively smooth foundation to place the geonet composite material. The embankment surface had significant surface erosion and vegetation growth, because of the long duration between the original embankment excavation and the preparation for the geonet prior to its installation. Initially after excavating the downstream embankment the Contractor used a dozer to smooth the exposed embankment. Transverse passes were made going up and down the 2H:1V embankments slope. Crew members were then utilized to further smooth the surface using rakes. Small shrubs and other debris had to also be removed from the surface by the crew members, as shown in Figure 3.



Figure 3. Approved and unapproved subgrade below geonet. (Courtesy of Jack Gagliardi)

The contractor elected to install the geonet composite using their own crew. Using a relatively inexperienced crew meant that the geotextile could potentially be exposed to over 14-days of UV rays. A field test was conducted to see how many days the 200 g/m² geotextile could be subjected to UV rays before 30 percent of the tensile strength was lost. Three strips of geotextile were staked and sand bagged at the top of the excavated slope. Samples were taken every 7 days all the way up to 45 days and tested by Reclamation and the contractor's private quality control laboratory. Results from this trial revealed that the Contractor could leave the geotextile exposed to UV rays for a maximum of 30 days.

The contractor began placing the geonet composite on the left abutment moving across to the right abutment over the spillway and outlet works conduit. Geonet composite production rate averaged between 4 to 6 rolls per day initially but increased to 11 rolls a day after installation efficiencies were developed and an additional crew of four was added. Construction of the downstream filter and berm could not keep up with the placement of geonet composite. Therefore, a thin layer of sand was used to protect the top layer of geotextile from UV damage. The contractor originally tried dumping the sand from the crest with the intent for the sand to slide down the 2:1 slope. Complications occurred when the Contractor tried dumping the sand directly on top of the geonet composite from side dump trucks. The geonet composite was torn due to the excessive force exerted on the geonet composite by dumping the sand all at once. Also, the sand did not freely spread down the slope so crew members had to use rakes to spread the material down the 70 meter long slope. As a result of the unsuccessful efforts the contractor developed a system utilizing a telebelt (extending conveyor system) to spread sand over the entire slope as shown in figure 4. The telebelt was able to operate from the crest and toe of the embankment. This allowed almost the entire slope to be covered with sand and only a small portion, midway up the embankment, needed to be spread using hand labor.



Figure 4. Telebelt spreading sand over the geonet. (Courtesy of Jack Gagliardi)

After constructing a 60 cm wide and 90 cm deep anchor trench along the downstream edge of the crest; rolls of geonet composite were unrolled from the crest down to the toe of the excavated embankment. A long steel bar was attached to a skid-steer which secured the roll on top of the crest as two crew members pulled the geonet composite down the slope. A second roll was then unrolled down the slope parallel to the first. Each roll was manufactured with 30 centimeters of geotextile extending beyond the geonet on each edge. This posed minor difficulties when trying to fold and weld the excess geotextile underneath the geonet composite. So after rolling out the second geonet composite roll the bottom edge of the geotextile on the second panel was cut flush with the geonet. Next, two crew members worked their way down the slope making sure the panels lay relatively parallel and overlapped by 15 centimeters. After the geonet composite was deployed down the slope the bottom outside edge of the geotextile was staked to the embankment. Stakes (into the bottom geotextile) were used to anchor the material to the embankment so the wind did not lift the fabric, stakes were found to work better than sand bags on the steep slope. After the panels were secured the crew members began welding the bottom layer of geotextile. Another crew member followed tying the geonet together every 1.5 meters. Then another member was used to weld the top geotextile together. Welding of the geotextile was completed using electric heat guns powered by a gas generator located on the crest. Once this system was developed and perfected a crew of five members placed an average of 11 rolls per day. Due to relatively slow production rates the contractor was given approval from Reclamation to not seam the bottom geotextile and to only overlap the adjacent panels. Overlapping was only approved between stations 16+00 and 30+00 where no cracks had been identified in the embankment.



Figure 5. Shows sequencing of installation of geonet composite rolls.

As the contractor continued to work toward the center of the embankment where the slope length exceeded the roll length, a single roll of geonet composite could not extend to the toe of the excavated slope. At this point partial rolls of geonet composite had to be added at the bottom, which necessitated the need for horizontal (end-to-end) seams. Horizontal seams were constructed in a similar manner to vertical seams except the geonet had to be overlapped by 30 cm and tied together every 15 centimeters and the seams were staggered to eliminate any continuous horizontal seams. Constructing horizontal seams drastically decreased production rates. Therefore, the contractor added an additional crew to work entirely on horizontal seams. Typically, only 4 to 5 horizontal seams were completed in one day. Horizontal seams not only required additional overlap and closer ties but geotextile had to be manually peeled away from the geonet composite to accommodate the 30 cm of geonet overlap required.

The number of horizontal seams might have been reduced if a panel layout was prepared before ordering the geonet composite material. This would mean that each panel would be made to the correct length and less cutting and splicing would be needed. However, this would mean each roll would have to be labeled and shipped in a specific order. This would require organizing the rolls onsite so that they can be accessed when needed for installation. Also, some cost savings might have occurred if the contractor had ordered longer rolls of geonet composite for a majority of the dam. Then rolls would only have to be cut reducing the number of horizontal seams; however this would lead to more wasted material. Horizontal seams are both costly and undesirable from a design perspective since they introduce another potential weakness in the geonet composite. Note, rolls longer than 60 meters may have been limited due to the weight and size of the roll and shipping requirements but avoiding/limiting horizontal seams is recommended.



Figure 6. Installation of geonet composite panels and horizontal seams.

Inconsistencies and defects in the geonet composite caused additional production issues for the contractor. During the manufacturing process geonet roll widths can vary by ± 15 centimeters. According to the manufacturer this is unavoidable and caused as the material cools at different rates. The manufacturer also had issues bonding two different geotextile densities to the geonet. The $540\text{g}/\text{m}^2$ non-woven needle punched geotextile required additional heat to bond to the geonet. This additional heat caused melting of the geonet and holes in the lighter geotextile on some panels. Patching the lighter geotextile was easily completed by the manufacturer before shipping to the construction site. However, the geonet cannot be patched. The melted geonet caused some difficulty with tying adjacent panels together, as shown in figure 6. However, the combination of melted geonet along with varying roll widths was addressed by adding additional ties. These types of inconsistencies and defects caused additional installation time that the Contractor had not anticipated. If the same density of geotextile had been bonded to the geonet some of these defects might have been avoided. Also, specifying a larger geonet that could withstand the heat necessary to bond a $540\text{g}/\text{m}^2$ geotextile to both sides could have helped reduce some defects. However, the larger geonet would result in a larger void between the geotextile which the designers did not want.



Figure 6. Melted geonet at the edge of a geonet composite roll.

4. CONCLUSION

Reclamation does not typically use geosynthetics in embankment dams, especially for filtration, but the use of geonet composite material beneath the chimney filter at Red Willow Dam was specified as a result of the design intent discussed above. The geonet composite ensures that the chimney filter will not fall into any existing or new cracks, will serve as a layer to prevent mitigation of existing cracks into the chimney filter, acts as a primary filter and drain above the 10,000 year flood RWS, and reduces the cost of importing additional filter/drain material. Several design and construction factors were presented in this paper that will hopefully encourage the use of geonet composite. Key components presented in this case history were the discussion of the specifications and installation processes. Not including detailed installation procedures in the specifications allowed Reclamation and the contractor to work together and overcome any unforeseen issues. This saved time and allowed for a better installation. Additionally, protecting the large quantity of exposed geotextile from UV rays was crucial and the contractor's methods of using a thin sand layer was demonstrated to be very efficient. The issues encountered during construction of this modification can hopefully be avoided in the future. Geosynthetics will continue to be used for different applications and it is hoped that the results from this case history will allow embankment dam designers to consider these materials in their design and help increase construction efficiency.

ACKNOWLEDGEMENTS

The authors would like to acknowledge all of the individuals that helped ensure the construction and design of the geonet composite was possible. This includes: several designers and peer reviewers, the Reclamation construction crew that helped inspect the installation and ensure that the design requirements were achieved, and the contractor and manufacturer who made the installation possible.

REFERENCES

- ASTM C 33/C33M. Standard Specification for Concrete Aggregates, *American Society for Testing and Materials*, West Conshohocken, Pennsylvania, USA.
- Corrective Action Study Preferred Alternatives Red Will Dam (2010), United States Department of Interior, Bureau of Reclamation, Denver, CO, USA.
- Filters for Embankment Dams - Best practices for Design and Construction (2011), Federal Emergency Management Agency, Washington, DC, USA.
- Bamforth, A. (2008) In-Plane Flow Capacity Testing Of Geocomposite Drains Using Soft Platens and High Stresses, EuroGeo4, Edinburgh, Scotland, United Kingdom, Paper number 275.
- Koerner, G.R and Narejo, D. (2005), Direct Shear Database of Geosynthetic-to-Geosynthetic and Geosynthetic-to-Soil Interfaces, Geosynthetic Research Institute, GSI Report #30, Folsom, PA, USA.

Case History: HDPE Pipe Boot Failure Due to Thermal Contraction of HDPE Pipe

Padovani, A.C., P.E., Geosyntec Consultants, USA, apadovani@geosyntec.com; Minch, M.J., P.E., Geosyntec Consultants, USA, mminch@geosyntec.com; and Hunt, C.E., P.E., Geosyntec Consultants, USA, chunt@geosyntec.com.

ABSTRACT

High-density polyethylene (HDPE) pipe boots are typical in landfill construction where leachate collection pipes need to be extended from within containment areas, towards storage ponds, tanks, or treatment facilities located outside of the containment system. The installation of a pipe boot creates a fixed point for the pipe at the location of the penetration. The remaining length of the attached pipes, which can be subject to thermal expansion and contraction cycles, can range from several hundred to thousands of meters. For typical pipe lengths, the potential deformation due to expansion and contraction can vary between several centimeters to several meters, depending on changes in temperature and length of exposed pipe. For this case history, a large temperature differential combined with over one hundred meters of unrestricted length of pipe led to an observed permanent pipe deformation of approximately 0.25 meters. The resulting tensile stress was responsible for the failure of the pipe boot at the end of the pipe alignment and subsequent release of fluid outside the containment area. To account for the potential for pipes to undergo expansion and contraction deformations during construction, several measures are recommended during the design process: 1) verification of expansion and contraction potential of exposed pipes based on expected temperatures during, and after, construction and length of pipes, 2) specifying pipe construction sequence in the construction documents to reduce pipe movements during construction, and 3) boot designs that include a flexible connection to allow pipe movements to be isolated from the boot itself.

1. INTRODUCTION

In landfills, geomembrane pipe boots are sealing elements whose purpose is to prevent leaks of leachate or gas at the penetration of a relatively rigid pipe through a relatively flexible geomembrane. Standard geomembrane pipe boots consist of several or all of the following elements, depending on the containment system configuration:

- 1) pipe to be booted,
- 2) primary geomembrane (from containment system),
- 3) boot (comprised of a geomembrane sleeve and apron),
- 4) silicon sealant,
- 5) stainless steel band clamps, and
- 6) extrusion welds.

There are two types of pipe boots prevalent in landfill construction projects: 1) field-fabricated or 2) pre-fabricated. Generally, small projects choose to install field-fabricated boots to ensure that they achieve a good fit based on conditions in the field that may be hard to determine in advance. Pre-fabricated boots are generally used in projects where the pipes to be booted have large diameters or where construction tolerances are tight enough that field variances are anticipated to be within the tolerance of the pre-fabricated boot.

Although pre-fabricated boots can be easier to install in the field if conditions are within design tolerance, they tend to be much more expensive than field-fabricated boots. In addition, field-fabricated boots can be made to accommodate as-built conditions, as the Contractor can cut each element of the boot to the dimensions needed in the field. For these reasons, field-fabricated boots are more commonly used.

2. TYPICAL DESIGN

A typical field-fabricated pipe boot consists of a geomembrane sleeve which is welded both to the pipe that will penetrate the containment system, as well as a geomembrane apron which is, in turn, welded to the containment system geomembrane, thus creating a flow barrier. In some cases the geomembrane sleeve is welded directly to the pipe. Alternatively, the sleeve can be sealed to the pipe using a flexible sealant and steel band clamps. Once the geomembrane sleeve is attached to the pipe, the sleeve is then welded to the geomembrane apron, which is then finally

welded to the geomembrane layer of the containment system, thus creating a completely contained system. A typical field-fabrication detail for geomembrane liner pipe penetration used in landfill construction is shown in Figure 1.

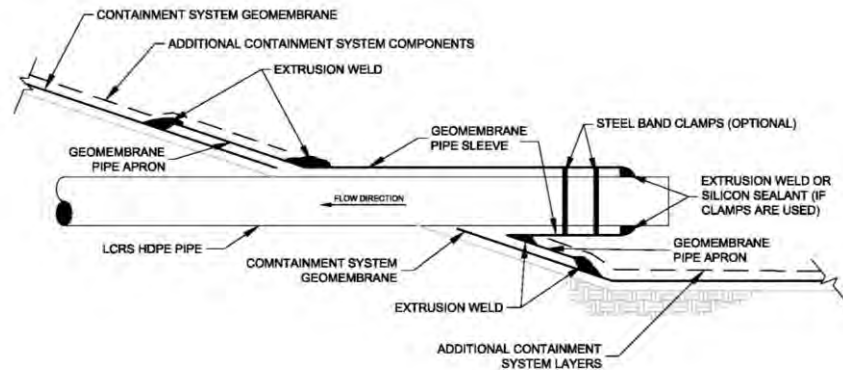


Figure 1. Typical pipe boot detail for single-containment landfill cell.

3. EXPANSION AND CONTRACTION POTENTIAL OF HDPE PIPES

HDPE is susceptible to expansion/contraction as a result of temperature variations. The coefficient of thermal expansion for unrestrained HDPE pipes is approximately 10 times that of metal or concrete. As a result large changes in HDPE pipe lengths may be observed due to temperature fluctuations.

Typical HDPE pipes used for landfill applications meet the properties of material designations PE3408 or PE3608. For such materials, the coefficient of thermal expansion typically ranges from 1.8 to 2.2×10^{-4} meters/meters-°Celsius (m/m-°C) [ISCO Industries and Performance Pipe, 2012]. Based on the equation for the theoretical change in pipe length for an unrestricted pipe,

$$\Delta L = L \cdot \alpha \cdot \Delta T, \quad [1]$$

where L corresponds to the pipe length, α to the coefficient of thermal expansion for the pipe material, and ΔT to the temperature differential. The range of α above implies that for a pipe length of 100 meters, we can expect a deformation (i.e., elongation or contraction) of approximately 0.18 to 0.22 meters, for every 10°C variation in temperature. In reality, some friction will exist between the pipe and adjacent materials, therefore deformation will be reduced, resulting in tensile or compressive stresses within the pipe. The estimated potential deformation therefore corresponds to a maximum deformation limit.

A closer look at the three variables contained in Equation 1 shows that for any project, the designer only has control over one of these three factors. The coefficient of thermal expansion is an intrinsic property of the material and varies little from one manufacturer to another. If temperature changes are solely due to climate, the designer has very little control over the maximum potential temperature differential. For unrestricted pipe length, the designer has control by using anchors along the way that can limit the stresses developed on the pipes, and hence the potential deformation, by reducing the length of pipe which can be affected by temperature variations.

4. CASE HISTORY: PIPE BOOT FAILURE OBSERVATIONS

4.1 Site Conditions

The site for this case history is an active landfill in the United States that has been in operation for many years. It is located in a region which experienced typical temperature differentials of 18 °C during the construction season (i.e., summer to early fall). During the day temperatures range between 26 to 35°C, but at night the temperatures can drop into the 10 to 16°C range.

4.2 Existing Cell and Pipe Boot Design

Due to field constraints, new waste containment cells at the site have been built upgradient from future cells. The result of this construction sequence is that leachate generated from new cells flows towards the low point in the cell, where a leachate conveyance pipe is booted through the containment system and then discharged beyond the cell into a tank or leachate pond (see Figure 2).

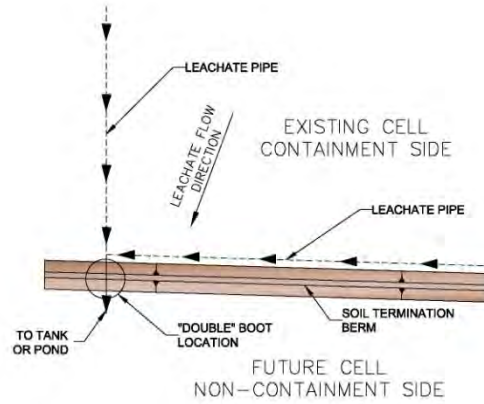


Figure 2. Leachate pipes configuration relative to pipe boot location.

With the future cell adjacent to the upgradient cell, the pipe boot is designed as a permanent feature for the cell, as it cannot readily be removed during construction of the future cell while maintaining leachate containment. As a result of this, the pipe penetration was designed as a “double” pipe boot, wherein both the upgradient containment side of the leachate pipe, as well as the downgradient non-containment side is booted through the containment system (see Figure 3). The “double” pipe boot provides a connection of the pipe to the geomembrane apron, which in turn is connected to the containment system geomembrane. Note however that the containment system geomembrane is located below the pipe penetrations to keep leachate from escaping the containment system in the event of a leak. The leachate pipe is converted to a double-containment pipe after it exits the geomembrane footprint on the downgradient non-containment side.

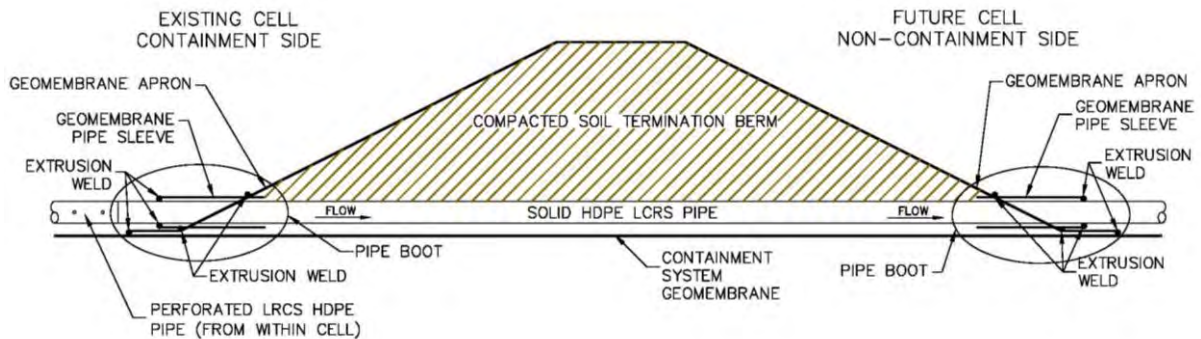


Figure 3. “Double” pipe boot schematic.

4.3 Failure Observations

During construction of a new landfill cell that would tie to the existing upgradient cell, a construction quality assurance (CQA) technician noted that there was ponded fluid on the downgradient non-containment side of the existing pipe boot. Additionally, the geomembrane apron around the pipe boot appeared to have been compressed (pulled) towards the upgradient containment side of the pipe boot (see Figure 4).



Figure 4. Containment system geomembrane and geomembrane apron around downgradient non-containment side of pipe boot upon discovery of ponded fluid.

A closer look at the pipe boot on the downgradient non-containment side revealed that the weld between the pipe sleeve and the surrounding geomembrane apron had been broken and the compacted soil within the “double” boot appeared to be saturated. Given the condition of the downgradient non-containment side of the pipe boot, it was decided that the in-place soil and waste would be excavated from the area above the pipe boot on the containment side in order to assess the condition of that boot. Figure 5 illustrates the condition of the pipe boot on the containment side, where the weld between the pipe sleeve and the geomembrane apron was broken and the booted pipe, along with its geomembrane sleeve, had moved approximately 0.25 meters away from its original location.



Figure 5. Observed displacement between original pipe boot weld location and final post-failure weld location (the knife and the finger are pointing to the two sides of the original weld).

4.4 Failure Causation Analysis

Once the condition of the pipe boot on the containment side was carefully documented, it became evident that the weld connecting the pipe sleeve to the geomembrane apron had been subjected to significant tensile stress. The failure causation analysis was therefore focused on potential sources for the tensile forces that ruptured the weld and pulled the pipe sleeve and geomembrane apron apart. As part of this evaluation, photos and daily records from the original construction of the existing cell were reviewed in order to establish the timeline of events for the installation of the existing pipe boots.

Several potential causes of the damage were considered including improper pipe welding procedures and damage by heavy equipment, but were dismissed due to the observed mode of failure. During initial cell construction, as verified by the construction photos, the entire length (approximately 180 meters) of leachate pipe was exposed and unrestrained after connection to the pipe boot. Estimates of potential thermal deformation for the pipe were then developed based on the method previously described. Using a typical site temperature differential of 18°C and the HDPE coefficient of thermal expansion of 2.2×10^{-4} m/m-°C, a maximum potential pipe deformation of approximately 0.7 meters was computed. Given the mode of failure, and the magnitude of the displacement observed in the field, we concluded that thermal deformation was the most likely cause of failure.

4.5 Modified Pipe Boot Design

The failure of the existing pipe boot was an obvious indicator that the design had to be modified prior to the construction of the new pipe boot for the new cell. Based on the results of the failure mode analyses, the first thing that was evaluated for the new design was the maximum potential thermal deformation that could be experienced by the proposed leachate pipe configuration within the new cell. With the large resulting value, similar to the 0.7 meters calculated for the existing cell, the design of the new pipe boot was focused primarily on how to isolate the movement of the leachate pipes from the pipe boot itself in order to keep the pipes from exerting tension or compression forces on the pipe boot.

Figure 6 shows the approach developed to isolate the two incoming leachate pipes from the segment of the pipe that would be booted. As shown, the new design incorporates a pipe sleeve to encase both segments of the main leachate pipe, as well as a distance between the two ends of the leachate pipes within the sleeve, to allow the pipes to freely move during the installation process. By removing a segment of the main leachate pipe, two main objectives are achieved: (1) the two segments are now given extra space, in the event that they experience thermal expansion/contraction, and (2) the length of unrestricted pipe attached directly to the pipe boot is reduced from over 100 meters, to less than two meters, thus reducing the maximum potential thermal deformation that could be experienced by that segment of booted pipe to approximately one centimeter.

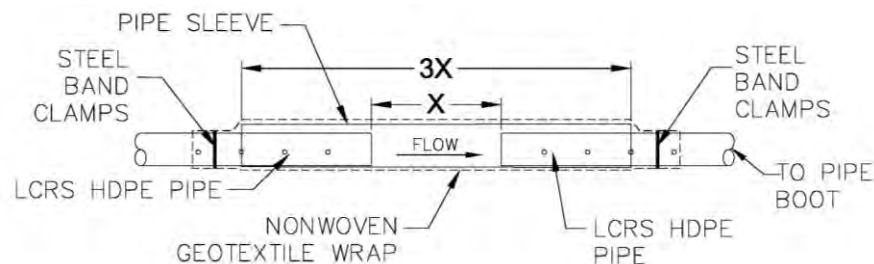


Figure 6. Schematic view of new pipe sleeve for leachate pipes on the containment side.

The revised design in Figure 6 shows a distance of "X" to separate the two ends of the leachate pipes within the sleeve, and a total pipe sleeve length equivalent to three times the value of "X". The value of "X" should be based on the estimated maximum deformation potential due to thermal expansion/contraction on the longest section of potentially exposed pipe that would otherwise be in contact with the pipe boot. The authors recommend that the distance "X" be estimated conservatively.

4.6 New Pipe Boot Construction

In addition to the new pipe sleeve design, modified field installation procedures are recommended to ensure that the new system is constructed as designed and that all aspects of the design can be verified prior to covering the boot with drainage gravel and the operations layer soil for the new landfill cell. A step-by-step sequence of construction was developed for the pipe boot and adjacent features that was added as a note on the construction drawings for the new

cell, alongside the sketch of the new pipe sleeve design. The step-by-step description included actions to be taken not only by the contractor, but also by the construction quality assurance (CQA) manager in the field. The new sequence of events included the following steps:

- 1) mark the two segments of leachate pipe to be inserted inside the pipe sleeve with 0.3-m markings starting at the edges to be inserted inside the sleeve;
- 2) slide the edges of the leachate pipes inside the pipe sleeve;
- 3) verify the distance between the edges of the leachate pipes inside the sleeve, by using the markings on the leachate pipes;
- 4) install geotextile wrap around the pipe sleeve and a portion of the leachate pipe inserted into the sleeve, and secure in place with band clamps;
- 5) place drainage gravel and operations soil everywhere along the new cell, except at the location of the new pipe sleeve and geotextile; and
- 6) verify the location of the leachate pipe within the sleeve, based on the pipe markings, and backfill the area above the sleeve with the drainage gravel and the operations layer if the distance between the edges of the leachate pipes within the pipe sleeve are found to be satisfactory; otherwise, remove the geotextile wrap, and pipes within the sleeve, cut a portion of the pipes to be inserted in the sleeves and return to step 2, proceeding through the steps as before.

The established sequence allows the CQA manager the opportunity to verify that the leachate pipes within the sleeve have enough space between them prior to burial to accommodate significant subsequent displacement. At the same time, by verifying this space just prior to burial (i.e. constraining) of the pipe, the potential for movement from thermal expansion and contraction is greatly reduced.



Figure 7. Leachate pipes and pipe sleeves configuration prior to geotextile wrap, pipe boot welding and local trench backfilling.

Figure 7 illustrates the constructed pipe sleeves (with markings) for each of the two leachate pipes that connect in the vicinity of the pipe boot. In the picture, soil can be seen in the background, which illustrates that all areas of the cell, including the trenches, were backfilled with drainage gravel and operations layer soil, as required, except for those areas directly above the new pipe sleeves. Once the distance between the two edges of the leachate pipes within the pipe sleeve was verified by the CQA manager, the area above the sleeves was backfilled and the final pipe boot inspection and work was completed.

5. CONCLUSIONS

Field conditions, including temperature fluctuations, are different for every site and can vary significantly depending on the time of the year when projects are built. The potential for pipe deformations due to thermal expansion and contraction of pipes should become a routine consideration when designing with HDPE pipes, even when the pipes will be buried. In addition to evaluating the buckling, crushing, and ring-deformation strength for the planned pipes, designers should consider all potential scenarios where expansion and contraction for a length of pipe can have an impact on other elements of the design. In addition, given the importance and critical nature of features such as pipe boots, special attention should be given to both the design and the construction of such elements to protect them from damage and ensure their proper performance in the field. If potentially affected, the construction sequence of critical elements should be specified on the construction drawings to provide assurance that pipe movements will be accommodated by the structure.

ACKNOWLEDGEMENTS

The authors would like to acknowledge the help of the skilled field technicians for the referenced case history, who were instrumental in detecting the original failure, properly documenting the original cell construction, and ultimately monitoring the construction of the new cell to ensure that the modified construction sequence and design were properly implemented. We would also like to recognize the mentorship provided by Dr. Hari Sharma during the initial evaluation of the failure, and subsequent re-design effort.

REFERENCES

ISCO Industries, LLC (2012). www.isco-pipe.com.
Plastic Pipe Institute (1992). Report TR-3, Above Ground Applications for Polyethylene Pipe, Washington, D.C.

Centrifuge Modelling of Geotextile Reinforced Slopes

AKLIK, P. Phd., Universität für Bodenkultur, Vienna, Austria, pelinaklik@gmail.com
WU, W., Universität für Bodenkultur, Vienna, Austria, wei.wu@boku.ac.at

ABSTRACT

Geotextile is being increasingly used for slope reinforcement. The failure mechanisms are important to make safe and economic design of geotextile reinforced slopes. Centrifuge modelling is a powerful tool for physical modelling of reinforced slopes and offers the advantage to observe the failure mechanisms. In this paper, we report a series of model tests on geotextile reinforced slope with three different slope inclinations of 65, 75, and 85 degrees in a geotechnical centrifuge. The aim is to identify the possible failure mechanisms. All reinforced slope models have the same height of 270mm. Dry sand was used in the experiments. The model box was subjected to increasing centrifugal acceleration until failure occurred. Photographs of the slope models were taken in flight with a digital camera and the deformations were evaluated with Particle Image Velocimetry (PIV).

1. INTRODUCTION

Geosynthetic-reinforced slopes and walls became very popular in recent years because of their financial, technical, ecological advantages. A wide range of geotechnical problems can be investigated using physical modeling techniques. Centrifuge modelling has become a successful technique in geotechnical engineering for studying the stability of prototype slopes. In order to replicate the gravity induced stresses of a prototype structure in a geometrically 1/N reduced model, it is necessary to test the model in a gravitational field N times larger than that of prototype structure (Viswanadham and König, 2009). Substantial research demonstrated the effectiveness of centrifuge modelling for studying the behaviours of geosynthetic reinforced walls and slopes, as reported by Porbaha & Goodings (1994, 1996), Zornberg et al. (1997; 1998a,b), Zornberg & Arriaga (2003), Viswanadham & Mahajan (2007), Chen et al. (2007) and Viswanadham & König (2004, 2009).

However, researches on slope with different slope angles are very rarely mentioned in the literature. In this paper, a series of reinforced slope models with a slope inclination of 65, 75, and 85 degrees were tested in a geotechnical centrifuge. The aim is to identify the possible failure mechanisms. Moreover, a technique called Particle Image Velocimetry (PIV) is used in this research to reveal the failure mechanisms of the geotextile reinforced slopes.

2. MODEL DESIGN

2.1 Centrifuge

The geotechnical centrifuge at Universität für Bodenkultur (BOKU) in Vienna was manufactured by Trio-Tech, USA and was put into operation in 1990 with partial financial support from the Austrian Science Foundation (Trio-Tech 1988). The centrifuge has the following components: a swinging basket, a balancing counterweight, a DC motor and aerodynamic enclosure. It is equipped with 56 electrical slip rings for process control and data acquisition. By using the dual platforms, two models can be tested at the same time. However, it is usual to have only one swinging basket carrying a model, while a balance weight is loaded on the other platform. The technical specifications of the centrifuge are listed in Table 1 and illustrated in Figure 1.

Table 1. Technical specifications of the centrifuge.

Diameter of the centrifuge [m]	3.0
Radius of the swinging basket [m]	1.3
Maximum angular velocity [1/min]	400
Maximum radial acceleration [g]	200
Maximum model weight [kg]	90
Maximum model height [cm]	56

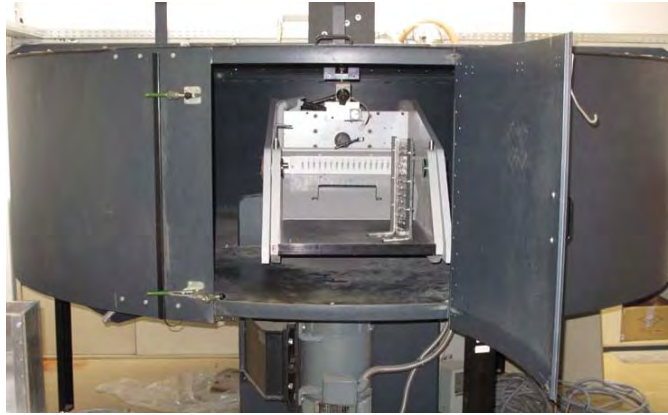


Figure 1. Photo of the centrifuge and its swinging basket.

2.2 Model Box

The model box (Figure 2) has the dimensions of 440mm*400mm*155mm in depth. A transparent Plexiglas plate with a thickness of 30mm was used on one side of the box to enable digital images to be taken during the experiment. The other walls of the box were aluminum plates with a thickness of 15mm.

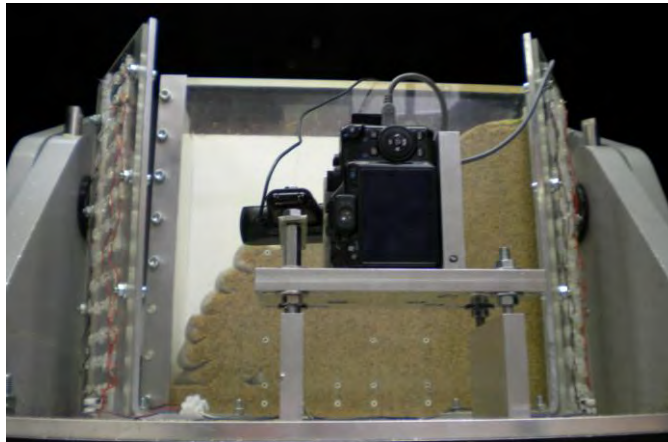


Figure 2. Geotextile reinforced slope model with a digital camera in the front and LED lights on the left and right sides.

2.3 Slope Model

Reinforced slope models have three different slope inclinations of about 65, 75, and 85 degrees. The geotextile reinforced slopes had the same height of 270mm and was built on a 40mm of soil layer of the same properties. Only half of the slope was modelled.

The model textile is an interlining. Six layers, seven layers and eight layers of model textile with a length of 200mm were placed in the geotextile reinforced slope models having 65, 75, and 85 degrees respectively.

2.4 Soil

The soil used in the experiments was uniform coarse sand (Table 2), Standard Sand II (DIN 1164/58). The tests were accomplished under dry conditions. The sand was inserted from a height of approximately 10 cm, not compacted and therefore in a loose condition.

Table 2. Properties of soil (Ferstl 1998).

Specific weight	ρ_s [g/cm ³]	2.644
Density range	ρ_{min}, ρ_{max} [g/cm ³]	1.44 – 1.65
Void ratio	e_{min}, e_{max}	0.607 – 0.844
Coefficient of uniformity		1.4
Friction angle	Φ [°]	34
Cohesion	c [kN/m ²]	0

2.5 Instrumentation

The displacement of the geotextile reinforced slope models was measured by PIV (White et al. 2001; 2003). For this purpose, a 14.7 MP Canon G10 digital camera was used to obtain high resolution digital images of the sand grains behind the Plexiglas wall. Black dots surrounded by white circles were applied to the Plexiglas, and were used as reference points for monitoring displacements within the soil. Two panels of 33 LED lights were used on both sides of the model box for lighting the centrifuge during the experiment. A laptop computer was mounted close the rotating axis of the centrifuge and connected to the main computer in the control room to save the photos during centrifuge test.

2.6 Method

The soil displacement analysis was carried out with GeoPIV8 software, developed by White & Take (2002). The first image was divided into a grid of test patches. Each test patch consists of a sample of the image matrix of size 20 * 20 pixels and the images were captured in 6 s intervals until the failure of the slope model. The recorded photographs were used to reveal the failure mechanisms of the slope after the experiment.

3. RESULTS

The results of PIV analysis of geotextile reinforced slopes are given in Figs. 3-5. In all the figures, X and Y coordinates are the lengths of the slopes in cm. Figure 3 is the geotextile reinforced slope with a slope inclination of 65 degrees. As seen from Fig. 3, the failure is occurred along the surface of the slope. Figure 4 is the slope having an inclination of 75 degrees. It can be easily seen from Fig. 4 that the shear band is occurred clearly starting in the middle of the slope and extending to the surface of slope. Figure 5 is the steepest slope with an inclination of about 85 degrees. Two shear bands were seen easily from Fig. 5 and the surface deformation of this slope has the highest values of all three models.

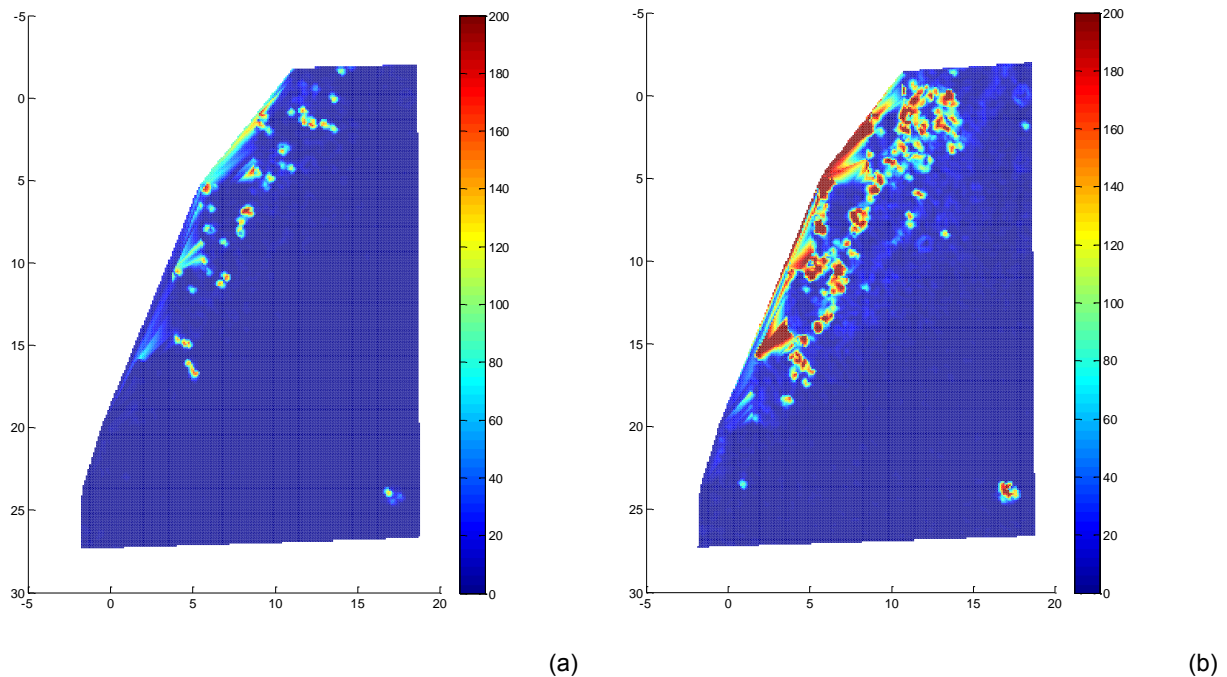


Figure 3. Pre (a) and post (b) failure mechanisms of geotextile reinforced slope with an inclination of 65 degrees.

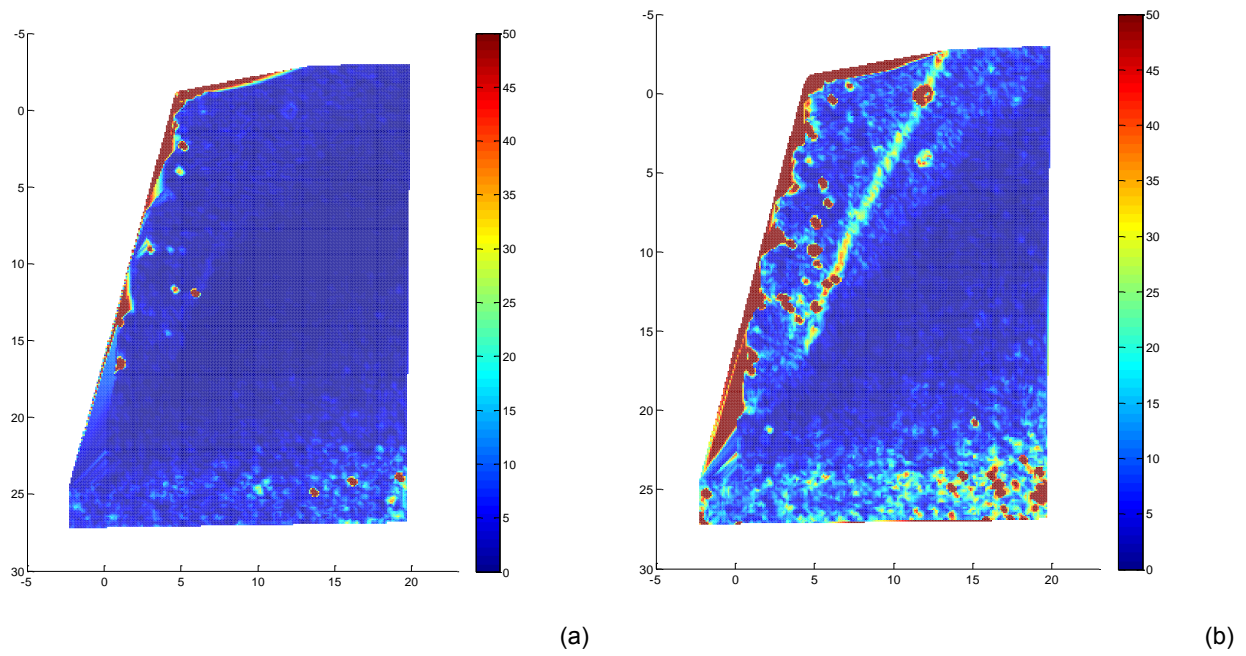


Figure 4. Pre (a) and post (b) failure mechanisms of geotextile reinforced slope with an inclination of 75 degrees.

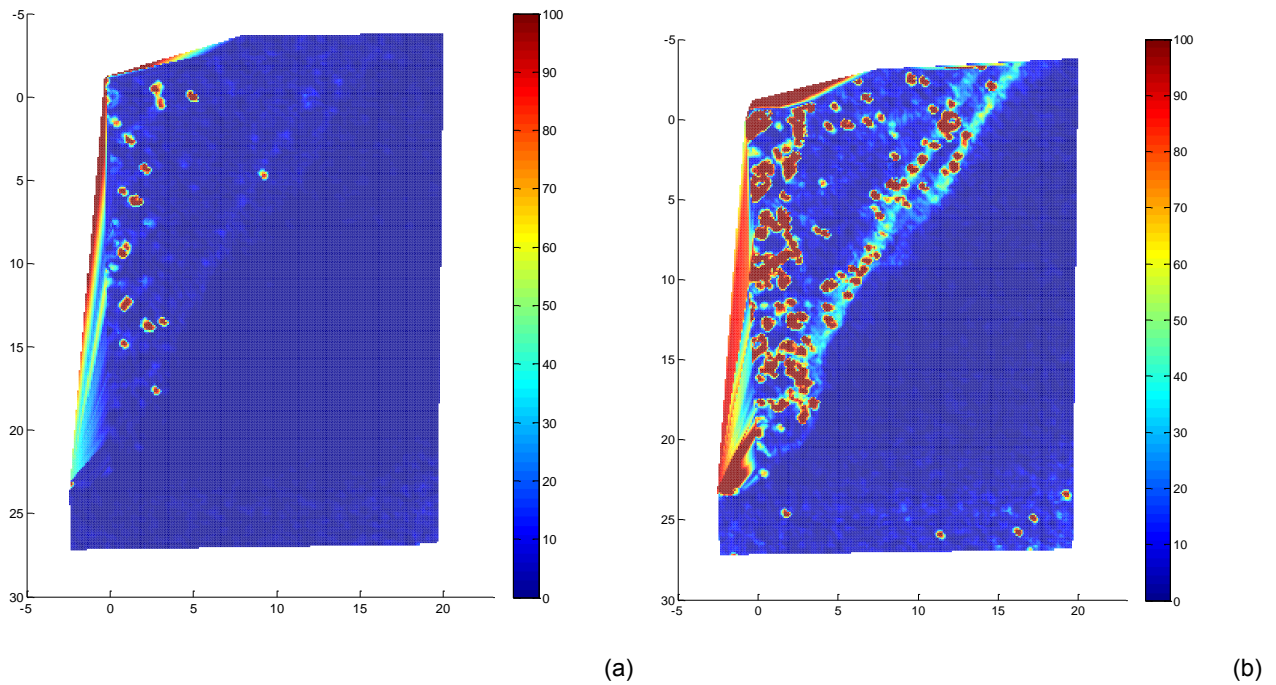


Figure 5. Pre (a) and post (b) failure mechanisms of geotextile reinforced slope with an inclination of 85 degrees.

4. CONCLUSIONS

- ✓ The required acceleration at slope failure decreases with increasing slope inclination.

- ✓ Slope failure is dictated by the tensile strength of geotextile rather than by pullout when geotextile is intersected by the failure surface.
- ✓ Failure of the centrifuge models was characterized by shear surfaces and initiated at midheights of the slopes.
- ✓ PIV is an efficient tool to instrument the slope failures in a geotechnical centrifuge.

ACKNOWLEDGEMENTS

The work of the first author is supported by the Otto Pregl Foundation for Geotechnical Fundamental Research.

REFERENCES

- Chen, H.-T., Hung, W.-Y., Chang, C.-C., Chen, Y.-J. & Lee, C.-J. 2007. Centrifuge modelling test of a geotextile-reinforced wall with a very wet clayey backfill. *Geotextiles and Geomembranes* 25 (6), 346–359.
- Porbaha, A. & Goodings, D.J. 1994. Geotextile reinforced cohesive slopes on weak foundations. *Proc. International Conference Centrifuge 94*, Singapore, 623-628.
- Porbaha, A. & Goodings, D.J. 1996. Centrifuge modeling of geotextile-reinforced cohesive soil retaining walls. *Journal of Geotechnical and Geoenvironmental Engineering*, Vol.122, No.10, 840-848.
- Take, W.A. 2003. *The influence of seasonal moisture cycles on clay slopes*. PhD dissertation, University of Cambridge Engineering Department, UK.
- Trio-Tech 1988. Technical proposal for a geophysical test centrifuge model 1231. Trio-Tech International, San Francisco, CA.
- Viswanadham, B.V.S. & Konig, D. 2004. Studies on scaling and instrumentation of a geogrid. *Geotextiles and Geomembranes*, Vol 22, 5, 307-328.
- Viswanadham, B.V.S. & Konig, D. 2009. Centrifuge modeling of geotextile-reinforced slopes subjected to differential settlements. *Geotextiles and Geomembranes*, Vol 27, 77 - 88.
- White, D.J. 2002. *An investigation into the behaviour of pressed-in piles*. PhD dissertation, University of Cambridge Engineering Department, UK.
- White, D. & Take, A. 2002. GeoPIV: Particle Image Velocimetry (PIV) Software for use in Geotechnical Testing. Cambridge, UK.
- White, D.J., Take, W.A. & Bolton, M.D. 2001. Measuring soil deformation in geotechnical models digital images and PIV analysis. *10th International Conference on Computer Methods and Advances in Geomechanics*, Tuscan, Arizona, 997-1002.
- White, D.J., Take, W.A & Bolton, M.D. 2003. Soil deformation measurement using particle image velocimetry (PIV) and photogrammetry. *Géotechnique* Vol.53, No.7, 619-631.
- Zornberg, J.G. & Arriaga, F. 2003. Strain distribution within geosynthetic-reinforced slopes. *Journal of Geotechnical and Geoenvironmental Engineering*, Vol.129, No.1, 32-45.
- Zornberg, J.G., Mitchell, J.K. & Sitar, N. 1997. Testing of reinforced slopes in a geotechnical centrifuge. *Geotechnical Testing Journal*, Vol.20, No.4, 470-480.
- Zornberg, J.G., Sitar, N. & Mitchell, J.K. 1998. Performance of geosynthetic reinforced slopes at failure. *Journal of Geotechnical and Geoenvironmental Engineering*, Vol.124, No.8, 670-683.
- Zornberg, J.G., Sitar, N. & Mitchell, J.K. 1998. Limit equilibrium as basis for design of geosynthetic reinforced slopes. *Journal of Geotechnical and Geoenvironmental Engineering*, Vol.124, No.8, 684-698.

Centrifuge Modeling of Landfill Composite Cover Systems

P.V. Divya¹, Research scholar, IIT Bombay, India, pv.divya.nair@iitb.ac.in

B.V.S Viswanadham², Professor, IIT Bombay, India, viswam@civil.iitb.ac.in

J.P. Gourc³, Professor, LTHE, University of Joseph-Fourier, France; gourc@ujf-grenoble.fr

ABSTRACT

Geomembranes are one of the commonly used geosynthetic in landfill cover systems. Even though, geomembranes are widely used as a part of composite barriers in landfill cover systems, studies pertaining to its behavior at the onset of differential settlements are very limited. Considering the advantage of centrifuge modelling technique to achieve identical stress-strain behavior in model and prototype, centrifuge modelling technique was adopted in the present study to examine the deformation behavior of geomembrane at the onset of differential settlements. Two types of geomembranes with different thicknesses and tensile stiffness were modelled. The stiffness of geomembranes was found to have significant influence in the deformation behavior of composite barriers. The upward or downward thrust exerted by the geomembrane on the clay barrier was more for stiffer and thicker geomembrane. The mobilization of downward thrust exerted by the deformed geomembrane layer in a composite barriers acts like a fictitious overburden pressure and helps in maintaining sealing efficiency of clay-based composite covers. The downward thrust exerted by geomembrane on barriers suppresses the formation of cracks due to differential settlements.

1. INTRODUCTION

In modern landfills, geomembranes (GM) are considered to be one of the most commonly used geosynthetic in landfill construction and are laid above the clay barrier of cover systems. The geomembranes used in landfill covers must be able to withstand substantial strains due to settlement of the waste and must resist penetration by construction equipment, rocks, and roots. High-density polyethylene (HDPE), linear low-density polyethylene (LLDPE), polypropylene (PP) and polyvinyl chloride (PVC) are the most common materials for GM in final covers. LLDPE geomembranes have greater ability to maintain their integrity under localized differential settlements without puncturing, tearing, or cracking than HDPE geomembranes; because of their flexibility, higher tensile break elongation, higher puncture resistance and particularly suitable to landfill cover applications (Scheirs, 2009; Islam et al. 2011).

Geomembranes are generally available in 6 - 15 m roll widths, making field seaming a very large endeavour. The seams should obviously not leak, but in addition, they should also be physically strong and maintain their integrity over a long period of time. Quality-control testing is typically performed on geomembrane barriers after installation to verify the integrity of the installed GM overlying clay barriers (composite barriers). Regardless of all the precautions taken while manufacturing, transportation, handling, storage and installation; defects in geomembranes in the form of wrinkles, holes, installation defects particularly at seams are widely reported (Rowe, 2005; Bouazza and Vangpaisal, 2006; Take et al. 2007). The main property of a seam is that it must ensure a continuous seal between two geomembrane sheets to prevent liquid or gas to escape through the impervious layer installed in landfills. Consequently discontinuity, unbonded areas and lack of adhesion between the geomembrane sheets must not be found within a seam (Rollin and Fayoux, 2005).

Differential settlements of landfill covers are inevitable in municipal solid waste landfills due to the biodegradation and settlement of underlying waste (Reddy et al. 2009; Sivakumar Babu et al. 2010) and in low level radioactive landfills due to the toppling of cover due to the voids present between waste containers (Gourc et al. 2010). Differential settlement studies of clay barriers have been reported by several investigators by performing full-scale model tests and centrifuge model tests (Jessberger and Stone, 1991; Scherbeck and Jessberger, 1993; Viswanadham and Jessberger, 2005; Gourc et al. 2010; Rajesh and Viswanadham 2011). Zhu et al. (2009) reported the differential settlement and degree of wrinkling in a geomembrane around a circular structure. The studies pertaining to the deformation behavior of composite barriers subjected to differential settlements in a centrifuge are very limited. Very recently, Divya et al. (2012) reported the influence of intact geomembrane layer on the hydro-mechanical behavior of landfill covers by varying thickness of the clay barrier by performing centrifuge model tests.

Centrifuge model tests were used to study the deformation behavior of barriers in the present study due to the practical difficulties and time delay in performing full-scale model tests and also due to the limitations of reduced scale model tests for simulating stress dependant phenomena. Hence, the motivation behind this study is primarily to evaluate the deformation behavior and sealing efficiency of composite barriers subjected to differential settlements in a geotechnical centrifuge. In the present study, an attempt has been made to study the influence of geomembrane stiffness on the

performance of composite barriers at the onset of differential settlements. However, the influence of stiffness of geomembrane was studied only using seamed low stiffness geomembrane. Centrifuge model test with low stiffness and continuous geomembrane is beyond the scope of this paper.

2. CENTRIFUGE MODEL TESTS

2.1 Centrifuge Equipment

A 4.5 m radius large beam centrifuge available at IIT Bombay was used for conducting centrifuge model tests. The centrifuge capacity is 2500 kN with a maximum payload of 25 kN at 100 g and at higher acceleration of 200 g the allowable payload is 6.25 kN. Centrifuge modeling technique was essential in the present study to simulate identical stress conditions in the model barrier as that of in the prototype. This can be achieved by subjecting a model reduced by 1/N to N times acceleration due to gravity in a controlled environment (where N = scale factor or g-level). The centrifuge model tests reported in the present study were conducted at 40 gravities (N = 40).

2.2 Model Geomembranes

Model geomembranes were selected from a number of commercially available polyethylene sheets by measuring their thickness (ASTM D6988) and by conducting tensile tests following the sample dimensions and procedure outlined in ASTM D6693. Two model geomembranes were selected with different thickness and stiffness. The stiffer geomembrane is referred herein as GM1 and weaker geomembrane as GM2. The thickness (t_{mg}) of GM1 is 0.135 mm and of GM2 is 0.05 mm in model dimensions. The thickness of the selected geomembranes GM1 and GM2 correspond to 5.4 mm and 2 mm thickness in the prototype respectively, at 40 gravities. The scaling considerations for modelling geomembranes were explained in Divya et al. (2012). Based on the scaling considerations for geomembranes, linear dimensions of the geomembrane (length and thickness of the geomembrane) and the tension developed in the geomembrane per unit width are to be reduced by 1/N times that of corresponding prototype values. The value of initial stiffness for GM1 is 480 kN/m and for GM2 is 280 kN/m in prototype dimensions at 40g. The ultimate tensile stress (kN/m²) for GM1 was 28148 kN/m² and ultimate tensile strain (%) was 450%. The corresponding values for GM2 were 21569 kN/m² and 52%.

2.3 Barrier Soil

Model clay barrier material was selected in such a way that it represents the bandwidth of properties of clay used in landfill covers (Benson et al. 1999). Out of the various combinations tried, a blend of kaolin and sand in the ratio of 4:1 (i.e. 80:20) by dry weight was selected as a model clay barrier material. The liquid limit of the model soil was 38% and plasticity index was 16%. The maximum dry unit weight was 15.9 kN/m³ and the corresponding OMC was 22% (according to standard Proctor compaction). Average value of coefficient of permeability of the model soil barrier at maximum unit weight and optimum moisture content was found to be 4.39×10^{-9} m/s and at 5% wet of optimum, it was found to be 4.23×10^{-9} m/s. The value of coefficient of permeability of the model barrier material is well within the range usually adopted for constructing barriers.

2.4 Model Test Package and Test Procedure

A strong box with front side made with Perspex sheet and back and rear side made with well machined stainless steel plates with stiffeners was used to prepare the model composite barrier. The dimensions of the strong box were 720 mm in length, 450 mm in breadth and 440 mm in height. Motor based differential settlement simulator (MDSS) was used to induce the settlements at 1 mm/min to the model barrier. A settlement rate of 1 mm/min at 40 g is equivalent to 36 mm/day in the field. This settlement rate may not be realistic when projected to the prototype dimensions but to some extent these settlement rates represent localized depressions and or sudden collapse of waste container or ground subsidence in waste disposal sites (Qian et al. 2002; Keck and Seitz, 2002; Gourc et al. 2010). The details of the MDSS system were explained by Rajesh and Viswanadham (2009). It works on a simple mechanism in which the rotational movement of the motor shaft is converted to translational movement of the central platform through a screw jack and series of gears. The MDSS system consists of a central support system and two side support system on either sides of central support system with a hinged plate resting on central support system symmetrically. Figure 1 shows the model test package used in the present study for carrying-out centrifuge tests.

A thin layer of white petroleum grease was applied to reduce the friction and adhesion between the inner walls of the container and soil layers. Model clay barrier of 15 mm (0.6 m) was prepared on top of pre-drained 30mm coarse sand layer followed by 30mm fine sand layer and separated by thin filter papers. These layers are used to induce smooth continuous differential settlements to the overlying barrier and to avoid stress concentration at the onset of differential settlements. They are referred herein as sacrificing layers. After the clay barrier of required thickness was prepared, geomembrane was placed on the top without any wrinkles. Water tight seal made-up of a thick bentonite paste was

applied all along the sides of the clay barrier and thereafter bunds were constructed along the sides to retain water during centrifuge tests. It also helps to simulate the lateral extent of the geomembrane (i.e. geomembrane covering large areas) in the field. Discrete markers were embedded 5mm below the top surface of the model clay barrier at 20mm centre to centre and also on the geomembrane.



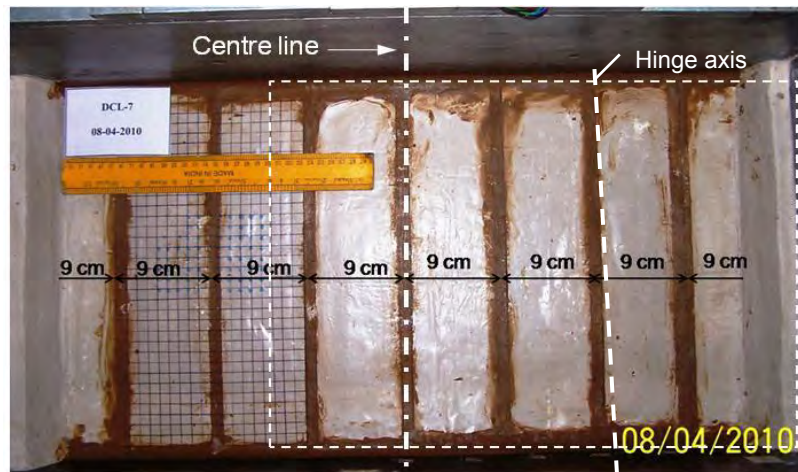
Figure 1. Model test package for centrifuge tests

The availability of an intact geomembrane layer covering large area of landfill is not practical. Geomembranes are available to a maximum roll width of 10 m. There are different techniques used for seaming of the joints like welding, use of adhesives, chemical fusion etc. The seamed joints can act as continuous geomembrane, if properly seamed. However, there can be a possibility of slippage or tearing at joints especially when the landfill cover is subjected to differential settlements. Subsequently, this leads to reduction in actual stiffness of the geomembrane.

In the present study, an attempt has been made herein to study the effect of seams (or stiffness) on the sealing efficiency of composite barriers. Also, the influence of stiffness of geomembranes on the deformation behaviour of composite barriers was also addressed. The model geomembrane sheet was cut in to 8 pieces and an overlap of 10 mm was provided such that the centre to centre distance of each GM piece is 90mm, as shown in Fig. 2. This was done to have one of the overlaps exactly along the hinge axis of the differential settlement simulator. The geomembrane sheets were overlapped in the laying direction and the joints were sealed with bentonite paste. The geomembrane type was varied, keeping the thickness of the clay barrier, overlapping of geomembrane sheets and overburden pressure as constant (Model: DCL9). The details of model preparation with intact or continuous geomembrane and its deformation behaviour are explained in Divya et al. (2012).

An overburden of 25kN/m^2 was induced with the help of fine sand layer of 27mm thickness at a dry unit weight of 15kN/m^3 and a calculated quantity of water was added so that it forms 10mm free standing water on the sand surface. Various sensors, like pore water pressure transducers (PPTs) to measure leakage through the model composite barrier and linear variable differential transformers (LVDTs) to obtain deformation profiles of the composite barriers at the onset of differential settlements were used in the present study. One digital photo camera was mounted along with the model

to view the front elevation which helps to monitor the crack development across the barrier. Also, a CCD video camera was placed on the top, to view the portion of top surface of the model and to register the depletion of water level retained on the top of the barrier during the centrifuge test. The centrifuge tests were conducted by maintaining a constant angular velocity of 93 revolutions per minute (rpm) so that 40 gravities were maintained within the clay barrier. A maximum central settlement a_{max} of 25 mm was induced which corresponds to 1 m in prototype dimensions. After attaining a maximum central settlement of 25mm, motor of MDSS was turned off and then centrifuge was initiated to stop. Differential settlement may be characterized by the distortion level a/l , which is defined as central settlement a , over a horizontal distance l where the settlement becomes negligible or by settlement ratio a/a_{max} . Limiting distortion level a_{lim}/l is defined herein as the ratio of central settlement at which a drastic change in water volume above barrier was observed to the influence length l . In the present study an influence length l of 200mm in model dimensions was used.



a) Before test



b) After test (only right hand side)

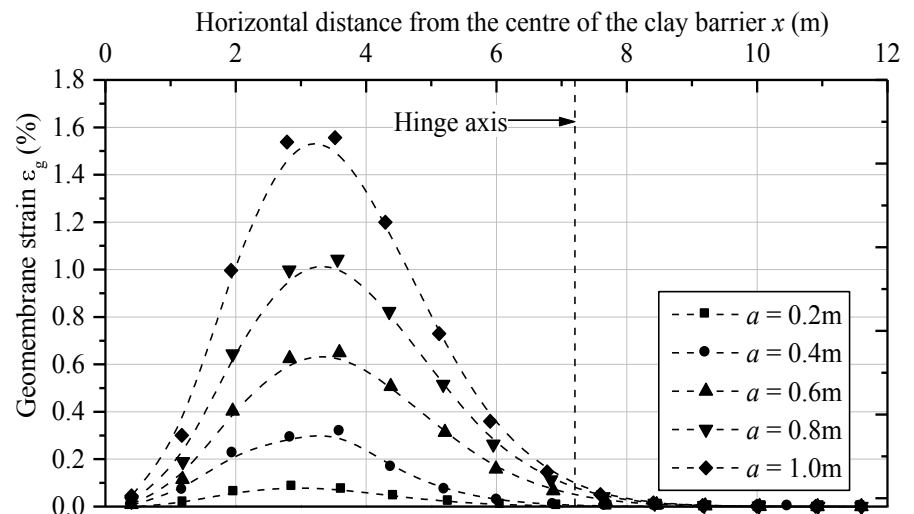
Figure 2. View of geomembrane layer with seams for Model: DCL7.

3. ANALYSIS OF TEST RESULTS AND DISCUSSION

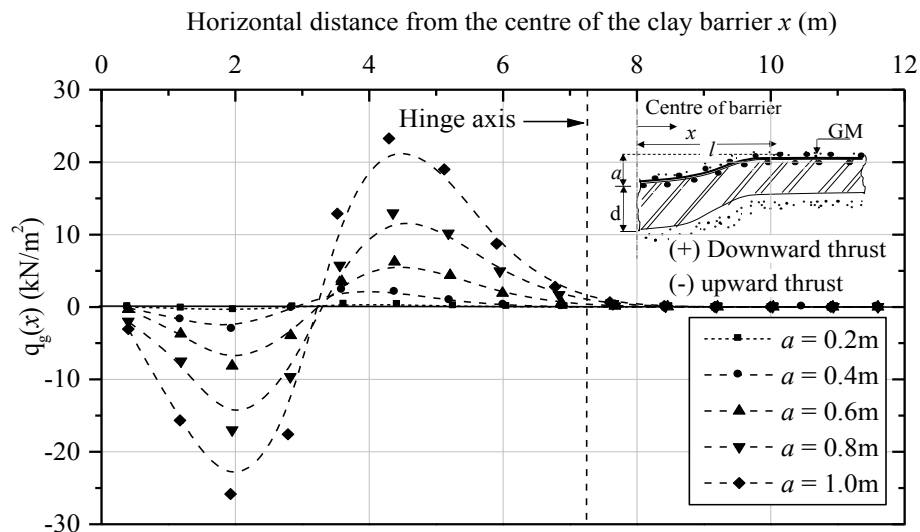
The co-ordinates of the markers on the geomembranes were obtained after performing digital image analysis of the photographs of front elevation of model composite barriers captured by the front digital photo camera at different settlement stages. Coordinates of the pre-determined permanent markers were used to standardize the image to be digitized. The error involved in digitizing the permanent markers i.e., standardizing the image can be obtained from the GRAM++ software (GRAM++, 2004). Once the error is within the tolerable limit (kept as $\pm 0.055\text{mm}$, for all the images and for all centrifuge tests), digitization of the discrete markers i.e. markers embedded on soil and markers glued on

geomembrane was carried-out. A deformation profile was fitted for the marker positions at various central settlement values. Strain distributions along the geomembrane layer at the onset of differential settlement was computed using the combined bending and elongation method proposed by Tognon et al. 2000 for geomembranes. Strain in the geomembrane along its length was computed by using $\epsilon_g(x) = \epsilon_{lg}(x) \pm \epsilon_{\kappa g}(x)$. The elongation strain $\epsilon_{lg}(x)$ in the geomembrane was obtained from the deformation profile of geomembrane, $w_g(x)$ as $[(1 + [w_g'(x)]^2)^{1/2} - 1]$. The curvature strain in geomembrane $\epsilon_{\kappa g}(x)$, was obtained from the neutral layer coefficient $R_g = 1/2$, curvature of geomembrane $\kappa_g(x)$ and thickness of geomembrane t_g as $R_g \cdot \kappa_g(x) \cdot t_g$, where x is the horizontal distance from center of the composite barrier. The curvature strain in geomembrane was negligible due to small thickness of geomembrane.

Further by using: (i) computed strain distributions along the geomembrane layer and (ii) the curvature of the deformed geomembrane layer and (iii) stiffness of the GM, the vertical thrust exerted by the geomembrane layer in the cover system was calculated by using membrane theory (Espinoza, 1994). The thrust distribution is calculated as $q_g(x) = J_g \cdot \epsilon_g(x) \cdot \kappa_g(x)$. Where, J_g is the stiffness of geomembrane in kN/m and this was obtained from the tensile load-strain curve of geomembrane GM1 and GM2 used in the present study. Figure 3 shows the typical variation of $\epsilon_g(x)$ and $q_g(x)$ along the horizontal distance from the centre of the composite barrier.



a) Geomembrane strain $\epsilon_g(x)$



b) Thrust exerted by the geomembrane $q_g(x)$

Figure 3. Typical variation of $\epsilon_g(x)$ and $q_g(x)$ along the composite barrier for model DCL6.

The variation of maximum downward thrust with distortion level a/l and settlement ratio a/a_{max} is shown in Fig. 4. The downward thrust, q_g exerted by geomembrane layer on the clay barrier at the zone of maximum curvature was found to increase with an increase in distortion level and the increase was more beyond a distortion level of 0.075 and settlement ratio of 0.6 and found to depend upon the stiffness of the geomembrane layer. It is clear from the curve that, the stiffness of geomembrane is an important parameter which decides the performance of composite clay barrier.

The value q_{gmax} for GM1 without any overlaps for model DCL6 is 23 kN/m² at distortion level of 0.125. This implies that a total downward thrust is of the order of 48 kN/m² (this includes overburden pressure of 25 kN/m² in the form of cover) is acting at the zone of maximum curvature of the clay barriers. For model DCL7 provided with similar type of geomembrane, GM1; but with seams the total downward thrust is around 45 kN/m². However, the value of q_{gmax} for model DCL9 provided with a weaker geomembrane GM2, was found to be relatively lower than GM1. This indicates that the stiffer geomembrane can exert more downward thrust on to the clay barrier surface at the onset of differential settlements.

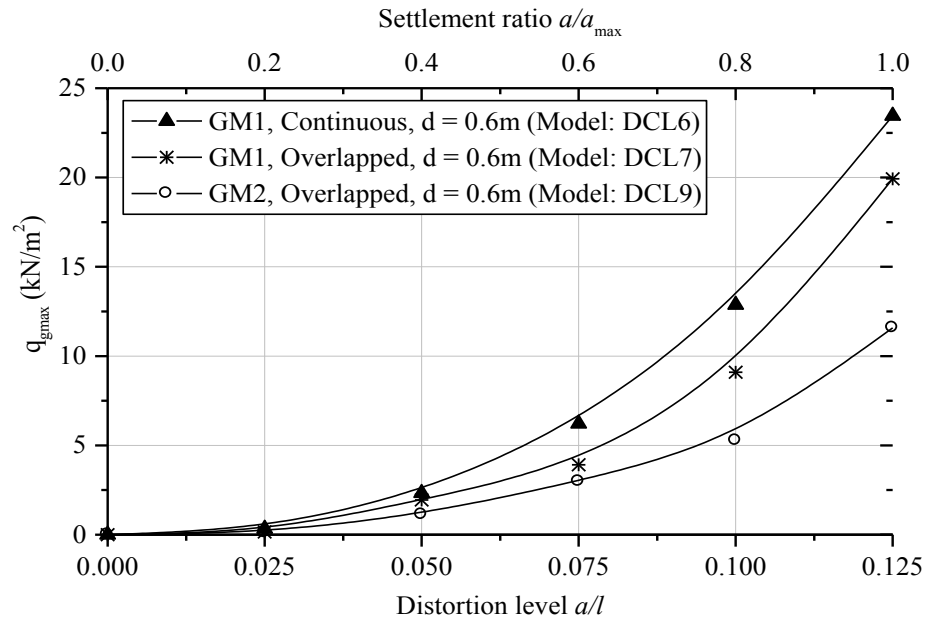


Figure 4. Variation of maximum downward thrust exerted by geomembranes

The hydraulic performance of the composite barrier can be obtained by measuring the change in height of water inundated on the top of barrier using PPTs. Volume per unit width of water is obtained by performing the numerical integration of the area under measured water profile. The height of the water along the width of the container is taken as identical to the measured value at the mid width of the container. The total volume of water above the clay barrier is twice the volume of water computed for one-half sections, which is the product of volume per unit width of water to the width of the container. Ratio of initial volume of water v_0 and volume of water at any instance v_a to the initial volume of water v_0 is defined as the infiltration ratio IFR.

Figure 5 shows the variation of infiltration ratio with distortion level and settlement ratio for composite barriers with continuous and overlapped geomembranes. Based on the variation of infiltration ratio with distortion level registered for models DCL7 and DCL9, a limiting distortion level of the order of 0.09 - 0.1 was observed, as shown in Fig. 5, irrespective of the type of geomembrane and the corresponding strain at breakthrough, ϵ_b was of the order 1.54-1.6%. The limiting distortion level was determined by back tangent method from the curve showing the variation of infiltration ratio with distortion level and settlement ratio. This indicates that the presence of seams along the length of the geomembrane (especially at the zone of the maximum curvature) can affect the sealing efficiency of a clay-based landfill composite covers.

Further, in order to understand the relative displacements of geomembrane seams provided at the zone of maximum curvature (i.e. at hinge axis) or in the tension zone, displacement vectors of markers on either side of hinge axis with and without geomembrane overlaps were compared for different settlement stages. Figure 6 presents variation of $(\Delta s/s)$ with a/l and a/a_{max} . As shown in the inset of Fig. 6, the distance between two markers is s mm initially at $a/l = 0.0$ at 40g. Subsequently, with an increase in distortion level, distance between the same markers change to $(s+\Delta s)$ mm; wherein $(s+\Delta s)$ mm includes both horizontal and vertical component of distances. A very limited increase in $(\Delta s/s)$ was registered

for model DCL6 with increasing distortion level and settlement ratio. In the case of a geomembrane with overlaps or improper joints, an adequate care was taken while selecting markers stuck to geomembrane sheets. The value of $(\Delta s/s)$ for distortion level 0.1 and settlement ratio 0.8 correspond to only 0.045-0.048. However, a steep increase in $(\Delta s/s)$ with an increase in distortion level was noted for model DCL7. The value of $(\Delta s/s)$ for model DCL7 at distortion level of 0.08 is 0.135.

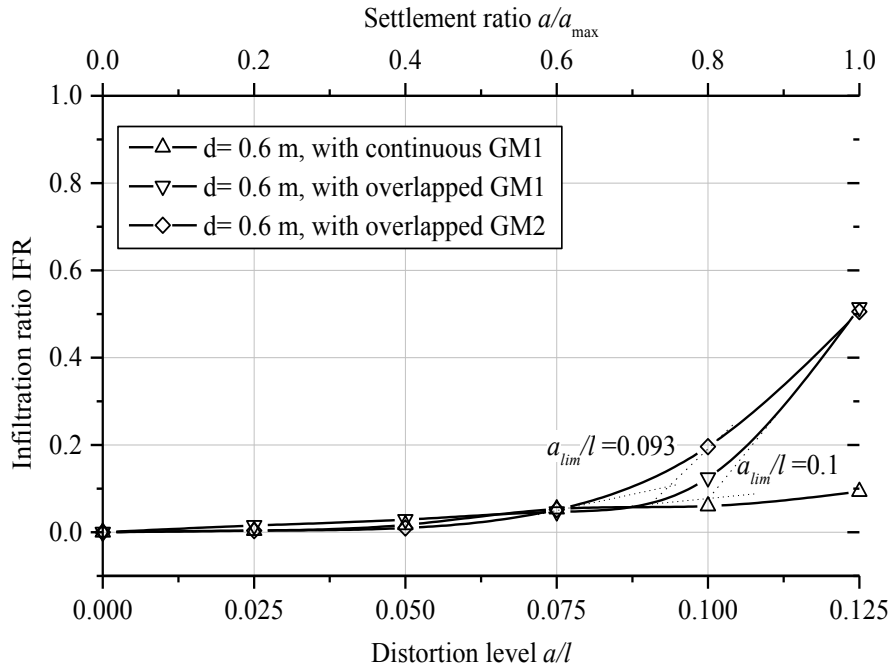


Figure 5. Variation of infiltration ratio with a/l and a/a_{max} for composite barriers

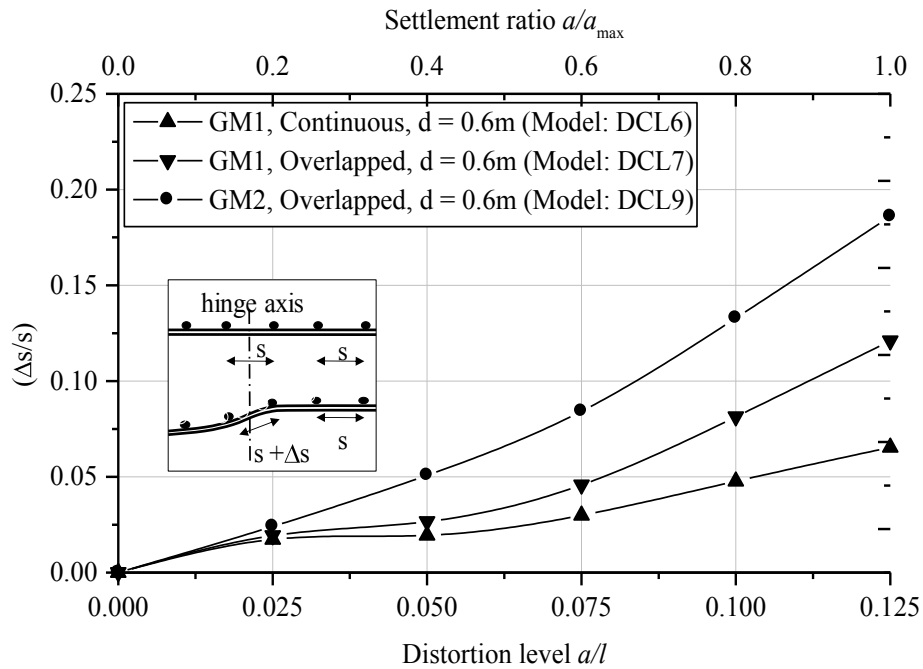


Figure 6. Variation of $(\Delta s/s)$ with a/l and a/a_{max} for barriers with continuous and seamed geomembrane

Even with a stiffer and thicker geomembrane, for a clay barrier provided with geomembrane overlaps the relative displacements in the tension zone are found to be clearly evident. This increase in $(\Delta s/s)$ for centrifuge models with

geomembrane resulted in an increase in infiltration ratio at the onset of a limiting distortion level $a_{lim}/l = 0.1$. However, till models are subjected to distortion level of 0.1, sealing provided by means of thick bentonite paste along geomembrane seams have restrained changes in infiltration ratio. Observations made during post-test investigation concur with the trend presented in Fig. 6 and can be clearly seen in Fig. 2b also. This explains the observed variation of IFR for model with weaker GM layer (GM2).

Figure 7 shows the cross-section of composite barriers at the end of centrifuge tests. The crack widths were increased in the case of composite barrier provided with overlapped geomembrane especially with weaker geomembrane compared to composite barrier provided with continuous geomembrane. The average crack width was 48 mm and 60 mm in prototype dimensions for barriers with overlapped GM1 and GM2 respectively. However with continuous geomembrane layer GM1, the crack widths were reduced to 36 mm. Though full-depth cracks were observed to occur in clay barriers, the presence of geomembrane helped in restraining catastrophic water breakthrough at the onset of differential settlements. Though catastrophic water breakthrough was not observed for composite barriers, full-depth cracks were observed to occur in clay barrier layer of composite barriers. Hence relying solely on the geomembrane presence to minimize crack formation in clay covers may be risky when defects in geomembranes occur. It will be interesting to explore the possibility of adoption of strengthening techniques to reduce the crack formation for clay barriers along with the provision of geomembranes which maintain the sealing efficiency of barrier at the onset of differential settlements.

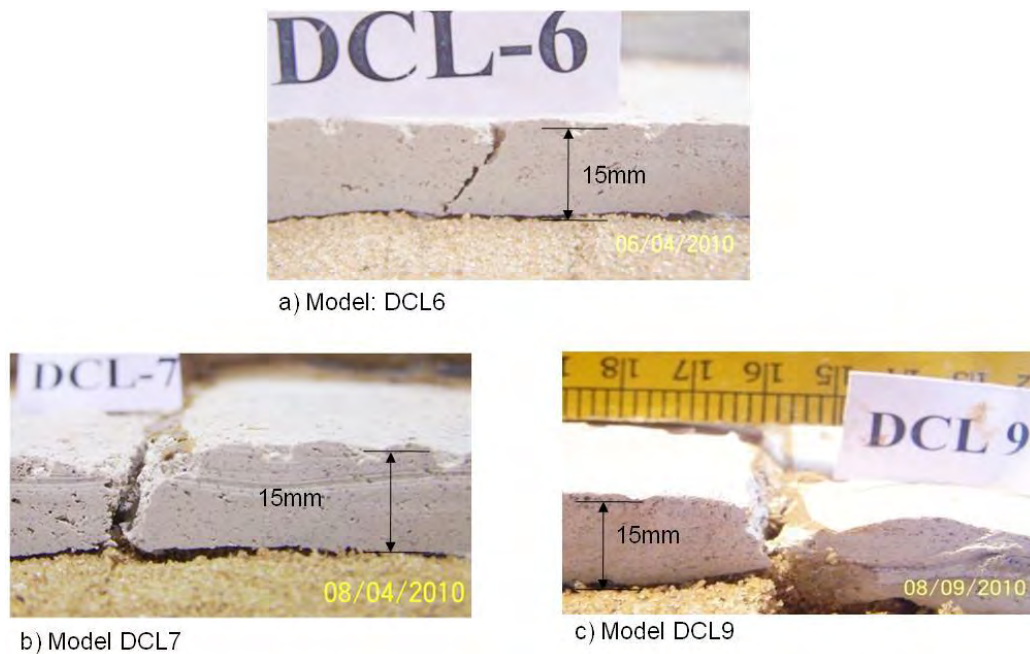


Figure 7. Cross section of clay barriers after centrifuge tests at the zone of maximum curvature.

4. CONCLUSIONS

Performance of composite barriers at the onset of differential settlements was studied by conducting a series of centrifuge model tests. Tests were also conducted using continuous geomembrane layer as well as seamed geomembranes. Two types of geomembranes with different stiffness were used. The analysis and interpretation of centrifuge test results indicate that observed response of a clay-based landfill cover with a geomembrane layer at the onset of differential settlement is attributed to the mobilization of downward thrust, q_g at the zone of maximum curvature. It was found to depend upon the stiffness of the geomembrane layer. It is very interesting to note that deformed geomembrane induces a downward thrust on the surface of the clay barrier. With an increase in distortion level the magnitude of downward thrust was observed to increase. This implies that the presence of geomembrane imposes a fictitious overburden on the surface of clay barrier of landfill composite cover subjected to differential settlements. This could be one of the reasons for not observing water breakthrough through the composite barrier at the onset of differential settlements and was found to sustain large distortion levels. The present study shows the significant influence of geomembrane in maintaining the hydraulic sealing efficiency of landfill cover system even after subjecting distortion level equal to 0.125. When seams are provided for the GM layer, the sealing efficiency of composite barriers was found to get affected after attaining a distortion level of 0.1.

ACKNOWLEDGEMENTS

This research was supported by the Indo-French Collaboration for Advanced Research (IFCPAR) and their support is highly acknowledged. The writers profusely thank the staff at the National Geotechnical Centrifuge Facility (NGCF), Indian Institute of Technology Bombay, Powai, Mumbai - 400 076, India for their active involvement during the course of the study.

REFERENCES

- ASTM D 6988(2008). Standard Guide for Determination of Thickness of Plastic Film Test Specimens. *American Society for Testing and Materials*, Philadelphia, Pa.
- ASTM D 6693 (2004). Standard Test Method for Determining Tensile Properties of Nonreinforced Polyethylene and Nonreinforced Flexible Polypropylene Geomembranes. *American Society for Testing and Materials*, Philadelphia, Pa.
- Benson, C.H., Daniel, D.E., Boutwell, G.P. (1999). Field performance of compacted clay liners, *Journal of Geotechnical and Geoenvironmental Engineering*, ASCE 126: 390–403.
- Bouazza, A. and Vangpaisal, T. (2006). Laboratory investigation of gas leakage rate through a GM/GCL composite liner due to a circular defect in the geomembrane, *Geotextiles and Geomembranes*, 24: 110–115.
- Divya, P.V., Viswanadham, B.V.S. and Gourc, J.P. (2012). Influence of Geomembrane on the Deformation Behaviour of Clay-based Landfill Covers, *Geotextiles and Geomembranes*, 34, 158-171.
- Espinoza, R.D. (1994). Soil-geotextile interaction: Evaluation of membrane support, *Geotextiles and Geomembranes*, 13(5), 281-293.
- Gourc, J.P., Camp, S., Viswanadham, B.V.S., Rajesh, S. (2010). Deformation behaviour of clay cap barriers of hazardous waste containment systems: full-scale and centrifuge tests. *Geotextiles and Geomembranes*, 28(3), 281-291.
- GRAM ++ (2004). <http://www.csre.iitb.ac.in/gram++/>
- Islam, M.Z., Gross, B.A., Rowe, R.K., 2011. Degradation of Exposed LLDPE and HDPE Geomembranes: A Review. In: *Geo-Frontiers 2011*. ASCE. Special Publication No. 201, 2065-2072 (CD-ROM).
- Jessberger, H.L., Stone, K.J.L. (1991). Subsidence effects on clay barriers, *Geotechnique*, 41(2) 185-194.
- Keck, K. N., Seitz, R. R. (2002). Potential for Subsidence at the Low-Level Radioactive Waste Disposal Area. INEEL/EXT-02-01154, Idaho National Engineering and Environmental Laboratory, U.S. Department of Energy.
- Qian, X., Koerner, R. M., Gray, D. H. (2002). Geotechnical aspects of landfill design and construction, *Prentice Hall*, New Jersey, USA, pp. 431-436.
- Rajesh, S., Viswanadham, B.V.S. (2009). Evaluation of geogrid as a reinforcement layer in clay based engineered barriers, *Applied Clay Science*, 46(2) 153-165.
- Rajesh, S. Viswanadham, B.V.S. (2011). Hydro-mechanical behavior of geogrid reinforced soil barriers of landfill cover systems, *Geotextiles and Geomembranes*, 29(1) 51-64.
- Reddy, K. R., Hettiarachchi, H., Parakalla, N. S., Gangathulasi, J., and Bogner, J. E. (2009). Geotechnical properties of fresh municipal solid waste at Orchard Hills Landfill, USA, *Waste Management.*, 29: 952–959.
- Rollin, A and Fayoux D. (2005). Geomembranes-Identification and Performance Testing, *Report of Technical Committee 103-MGH*, A.Rollin and J.M.Rigo (Eds.), Chapman and Hall, pp.51- 66.
- Rowe, R. K. (2005). Long-term performance of contaminant barrier systems. *Géotechnique*, 55(9), 631–678.
- Sivakumar Babu, G. L., Reddy, K. R., Chouskey, S. K., Kulkarni, H. (2010). Prediction of long-term municipal solid waste landfill settlement using constitutive model. *Practice Periodical of Hazardous, Toxic, and Radioactive Waste Management*. ASCE, 14(2), 139–150.
- Scheirs, J. (2009). A Guide to Polymeric Geomembranes: A Practical Approach. *John Wiley & Sons Ltd.*, West Sussex, UK, pp. 596.
- Scherbeck, R., Jessberger, H.L. (1993). Assessment of deformed mineral sealing layers. Sarsby, R.W. (Ed.), *Waste Disposal by Landfill: Proceedings of the Symposium Green'93*, Geotechnics Related to the Environment, Bolton, U.K, A. A. Balkema, Rotterdam, pp. 477-486.
- Take, W. A., Chappel, M. J., Brachman, R. W. I. & Rowe, R. K. (2007). Quantifying geomembrane wrinkles using aerial photography and digital image processing, *Geosynthetics International*, 14(4), 219–227.
- Tognon, A.R., Rowe, R.K., Moore, I.D. (2000). Geomembrane strain observed in large-scale testing of protection layers. *Journal of Geotechnical and Geoenvironmental Engineering*, ASCE, 126(12), 1194-1208.
- Viswanadham, B. V. S., and Jessberger, H.L. (2005). Centrifuge modeling of geosynthetic reinforced clay liners of landfills, *Journal of Geotechnical and Geoenvironmental Engineering*, ASCE, 131(5), 564-574.
- Zhu, B., Gao, D., Chen, Y.M. (2009). Geomembrane tensions and strains resulting from differential settlement around rigid circular structures, *Geotextiles and Geomembranes*, 27(1), 53–62.

Cleveland Harbor, Ohio Interim Dredge Disposal Plan: Geotextile Reinforcement of Placed Dredge Fill

Eugene N. Lenhardt, P.E., U.S. Army Corps of Engineers (Buffalo District),
Eugene.n.lenhardt@usace.army.mil

ABSTRACT

The available capacities of the Cleveland Harbor confined disposal facilities (CDFs) are reaching the point where hydraulic placement of dredged material is no longer feasible and will reach the minimum 2 foot containment free-board by the end of 2014. A new disposal facility will not be available until at least 2018. Therefore, in order to provide interim dredge material disposal capacity from 2015 - 2018 the existing CDFs will require dredged material to be stacked in the facilities above the original containment dike crest height. Imposed loading from the stacked dredged fill has raised some global stability concerns. A number of alternative stabilization schemes were investigated including the use of geotextile reinforcement in combination with wick drains. This presentation/paper discusses the results of the engineering analysis performed using geotextile reinforcement as part of a stabilization method.

1. INTRODUCTION

The U.S. Army Corps of Engineers (USACE), Buffalo District dredges the Cuyahoga River in Cleveland, Ohio on an annual basis to maintain adequate depth for commercial shipping. These dredged sediments are not suitable for disposal in Lake Erie and are required to be placed in a confined disposal facility (CDF). The sediments are mechanically dredged into scows, transported to the CDF, and ultimately placed by hydraulic method. At the present time there are three disposal facilities available for disposal of dredged sediments in Cleveland Harbor. These facilities are identified as CDF 9, CDF 10B and CDF12 with locations shown in Figure 1.

The available capacity of the CDFs are reaching the point where hydraulic placement of the dredged material is no longer feasible and will reach the minimum 2 foot free board by the end of the 2014 dredging season. A new disposal facility will not be available until at least 2018. In the interim period 2015-2018, it is proposed to stack dredged material by mechanical means in each CDF above the original crest height of +14 ft (4.3 m) above low water datum (LWD) for CDF 10B and CDF 12 and +12 ft (3.7 m)LWD for CDF 9.

The stability of the CDFs' perimeter rubble mound containment dikes is of critical importance to insure public safety and to insure that dredge sediments placed in the CDFs do not spill into Lake Erie. A geotechnical stability analysis was performed to determine the effects of stacking dredge material above the original CDF containment dike crest height with respect to over all global stability and local (internal) stability. Several alternative stabilization measures were investigated including the use of geotextile reinforcement in combination with foundation wick drains. The remainder of this presentation centers on the geotechnical analysis performed using geotextile reinforcement to obtain a stable stacked fill configuration for each CDF.



Figure 1 - Confined Disposal Facility (CDF) Locations

2. DREDGE MATERIAL STACKING OPTIONS

Approximately 1,000,000 (765,000 m³) cubic yards (CY) of dredged material will be placed in the CDFs for the years 2015-2018. CDF 9 is located on property owned by the City of Cleveland and CDF 12 is located on property owned by the Cleveland Port Authority. CDF 10B is currently owned by the U.S. Army Corps of Engineers. To cover any potential problems with respect to obtaining lease agreements with the city of Cleveland or the Cleveland Port Authority for CDFs 9 and 12 various stacking options were investigated based upon assumptions made with respect to the availability of the aforementioned CDF properties.

2.1 Option No.1 (CDFs 9, 10B, and 12 Are All Available)

The assumption made for this option is that all three (3) CDF properties will be available for placement of 250,000 CY (191,000 m³) of dredge material annually. Splitting the annual dredge quantity between each of the 3 CDFs and considering the aerial space available in each CDF results in a final dredge fill stack height of +20 ft (6.1 m) LWD at the

end of year 2018. These results include maximum dredge fill heights of 6 feet (1.8 meters) for CDF 10B and CDF 12 and 8 feet for CDF 9.

2.2 Option No.2 (CDF 12 No Longer Available, Placement in CDFs 9 and 10B)

The assumption made for this option is that a lease from the Cleveland Port Authority could not be obtained for CDF 12 therefore, the annual dredge quantity of 250,000 CY (191,000 m³) will be split between CDF 10B and CDF 9. This results in a stacked dredged fill height of +24 ft (7.3 m) LWD at the end of year 2018 or maximum fill heights above the original CDF crest elevations of 10 feet (CDF 10B) and 12 feet (CDF 9).

2.3 Option 3 (CDF 9 and CDF 12 No Longer Available, Place in CDF10B and Upland Landfill)

The assumption made for this option is that a lease from the City of Cleveland could not be obtained for CDF 9 nor a lease obtained from the Port Authority for CDF 12. The annual dredge quantity of 250,000 CY will be split for placement into CDF 10B and an unspecified upland landfill. At the end of year 2018 the dredged fill in CDF10B will be stacked to +28 feet LWD or 14 feet above the original CDF crest height.

2.4 Option 4 (CDF 9 and CDF 12 No Longer Available, Place All 1,000,000 CY into CDF 10B)

The assumption made for this option is to place all 1,000,000 CY (765,000 m³) for the years 2015-2018 into CDF10B. The maximum dredge fill height at the end of year 2018 is dependent upon the stacked fill height that is geotechnically stable which is estimated to be +44 feet (13.4 m) LWD.

3. FAA RESTRICTIONS (BURKE LAKEFRONT AIRPORT)

Burke Lakefront Airport is located immediately adjacent to CDFs 9, 10B, and 12 (Figure 1). The Federal Aviation Administration (FAA) mandates airspace restrictions around the runways for aircraft safety. These restrictions complicate the stacked dredge filling operations in that the dredge fill stack heights cannot exceed the FAA safety restrictions and must be placed within a vertical prism established by the FAA. Thus, as a result of these restrictions only part of the CDF foot print is available for the stacking of dredged fill.

4. SUBSURFACE CONDITIONS

The CDF rubble mound containment dikes are founded on the Lake Erie bottom sediments which have a top layer that consists of about 9 feet (2.7 m) of very soft organic silt (OL, Unified Soils Classification System) and Silty Clay (CL). Underneath the recent deposits are stiffer glacial lake deposits consisting of grey medium stiff to stiff Silty Clay (CL) with embedded pebbles. The stacked dredged fill will be placed on previously placed hydraulically dredged fill of variable composition consisting of very loose silty sand (SM), very soft organic clay (OH) and Silty Clay (CL,CH). The previously placed dredged fill material composition varies within each CDF depending upon where the hydraulic dredge discharge pipe was located. Coarser material (sand, gravel) is located near the outlet of the pipe while finer grained material settles out with distance from the end of the pipe.

4.1 Subsurface Conditions CDF 12 and Foundation Problems in "S Curve" Area

Of the 3 CDFs, the foundation conditions along the south side of CDF 12 are the most problematic. Figure 2 is the boring plan and location of geologic soil profile A-A which is presented in Figure 3. As shown in this profile the underlying previously dredged fill and recent lake deposits consists of fine grained sediments classified as organic clay (OH), silt (OL), and clay (CH) with standard split spoon penetration resistances of 0 blows/ft.

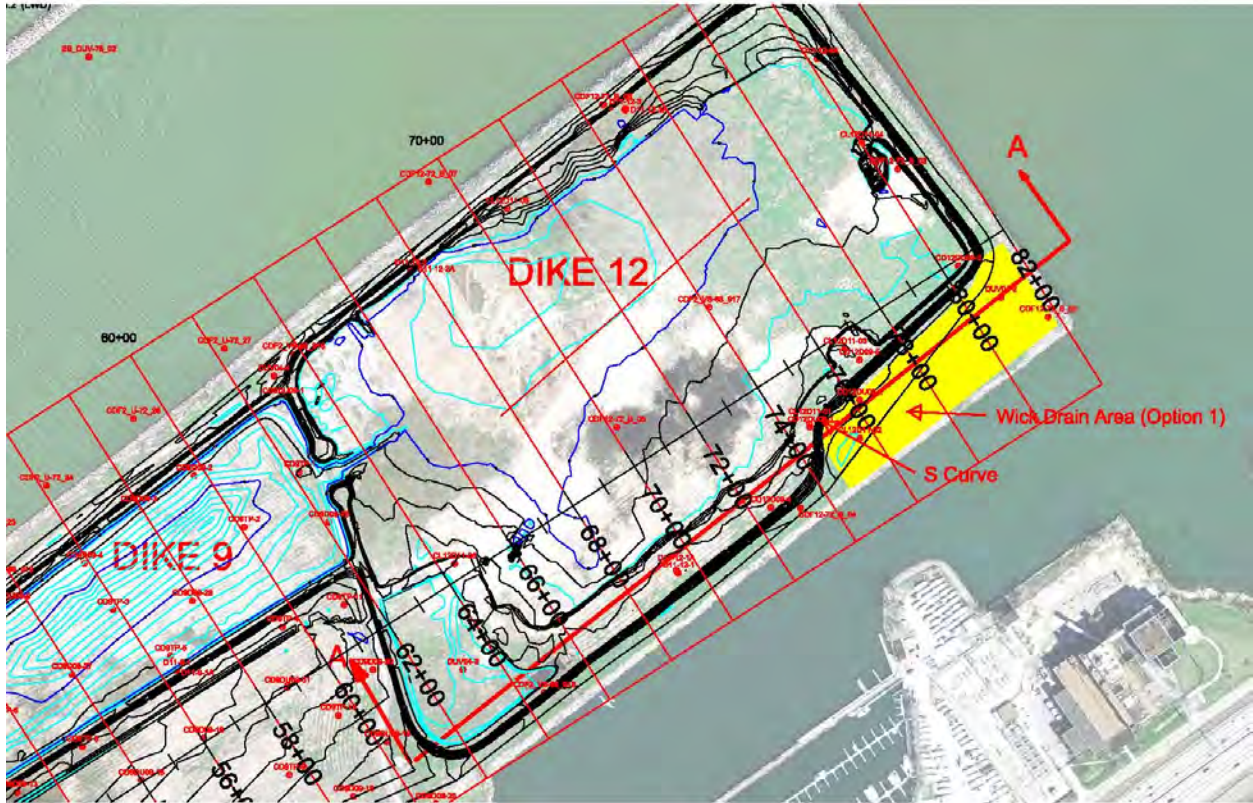


Figure 2 – Boring Plan CDF 12

To provide additional disposal capacity in CDF 12 a raised phase 1 dike was constructed in 2008. The phase 1 containment dike had a maximum crest elevation of +18 feet (5.5 m) LWD increasing the maximum potential capacity by 4 feet (1.2 m). Due to the poor foundation conditions along the south side of CDF 12 geotextile reinforcement was incorporated into the design of the containment dike. A typical section for this portion of the containment dike is presented in Figure 4 which shows that the geotextile reinforcement extended across the main portion of the containment dike and ended at the start of the flanking stability berms. During construction a portion of the south dike called the “S Curve” area experienced failure in which it appeared that the main dike and foundation had translated towards the center of the CDF and tension cracks formed at the toe of the main dike in the lake side stability berm. After the failure occurred test pits were dug into the phase 1 dike to determine the depth and location of the geotextile reinforcement. After the test pits were dug it was observed that the reinforcement had settled as much as 4 feet (1.2 m) from its initial placement location. The actual cause of the failure could not be determined but it is believed that if the reinforcement had been extended further out into the stability berm the failure may have been prevented.

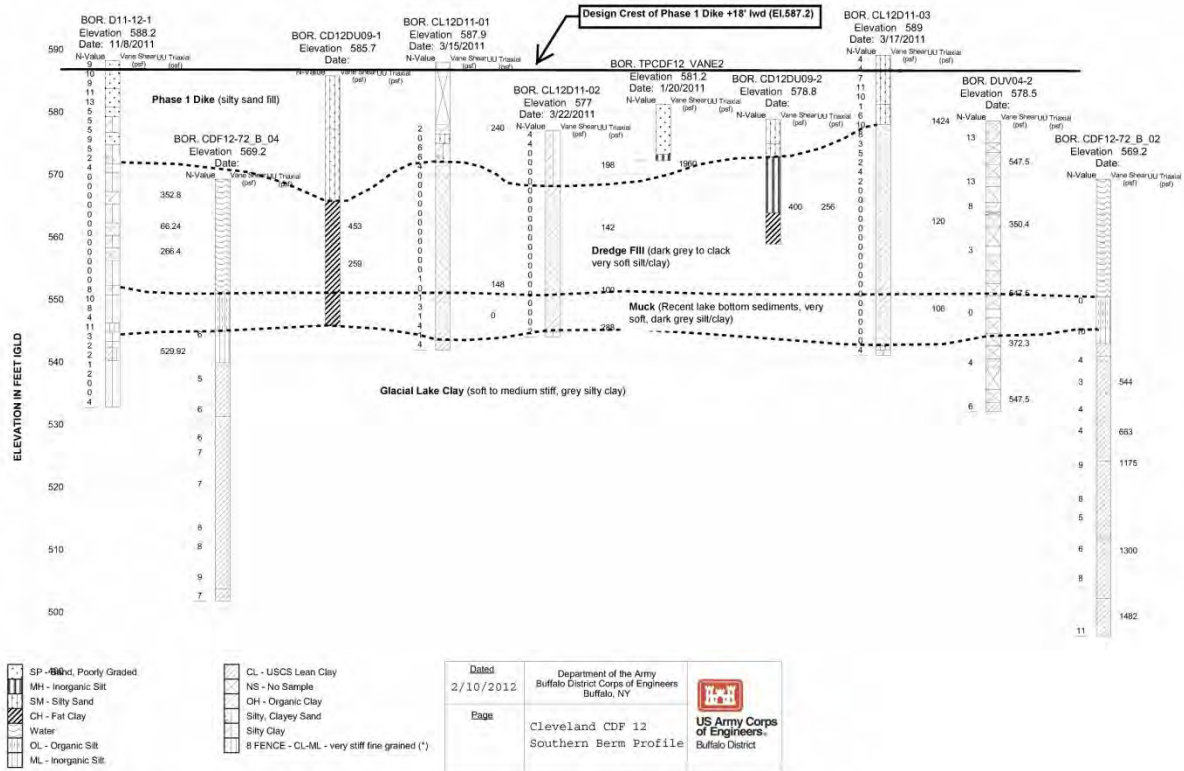


Figure 3 – Geologic Profile A-A, CDF 12

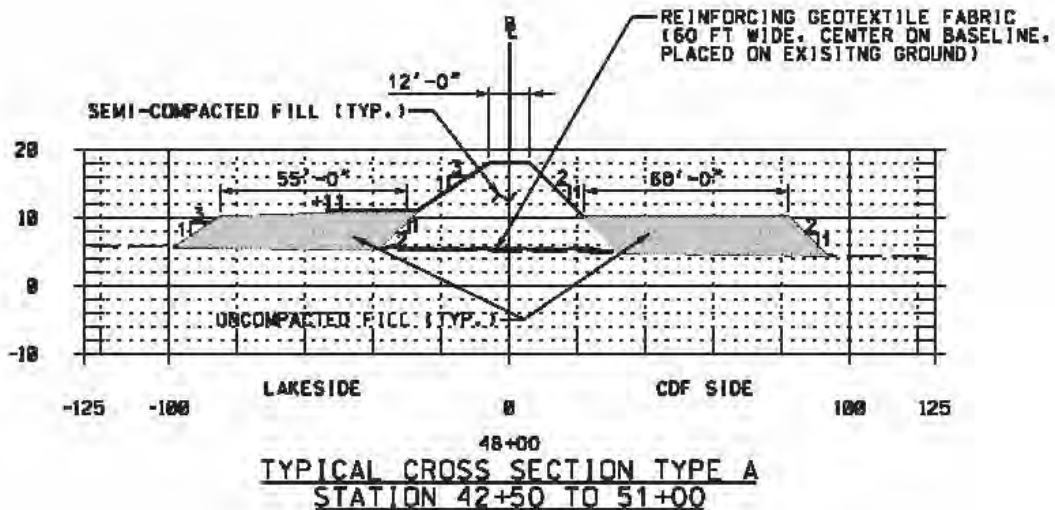


Figure 4 – Phase 1 Dike Typical Section (S Curve Area)

Shown in Figure 5 are graphical plots of the laboratory undrained shear strengths and excess pore water pressures obtained from piezometers installed along the southern side of CDF 12 after the phase 1 dike construction was completed. The graphic plot reveals that the foundation undrained shear strengths decrease with depth varying from about 350 psf (16.8 kPa) near the water table (lake level +1.5 ft (0.5 m) LWD) down to 100 psf (4.8 kPa) at the original lake bottom (-18 ft LWD). Excess pore water pressures increased with depth from about 700 psf (4.8 kPa) near the lake

level to 1,450 psf (69.4 kPa) near the bottom of the recent lake deposits at about -25 ft (-7.6 m) LWD. The excess pore water pressures in the foundation are most likely due to the imposed loads from the phase 1 dike construction which reduces the effective stresses in the foundation and thus reduces the undrained shear strengths.

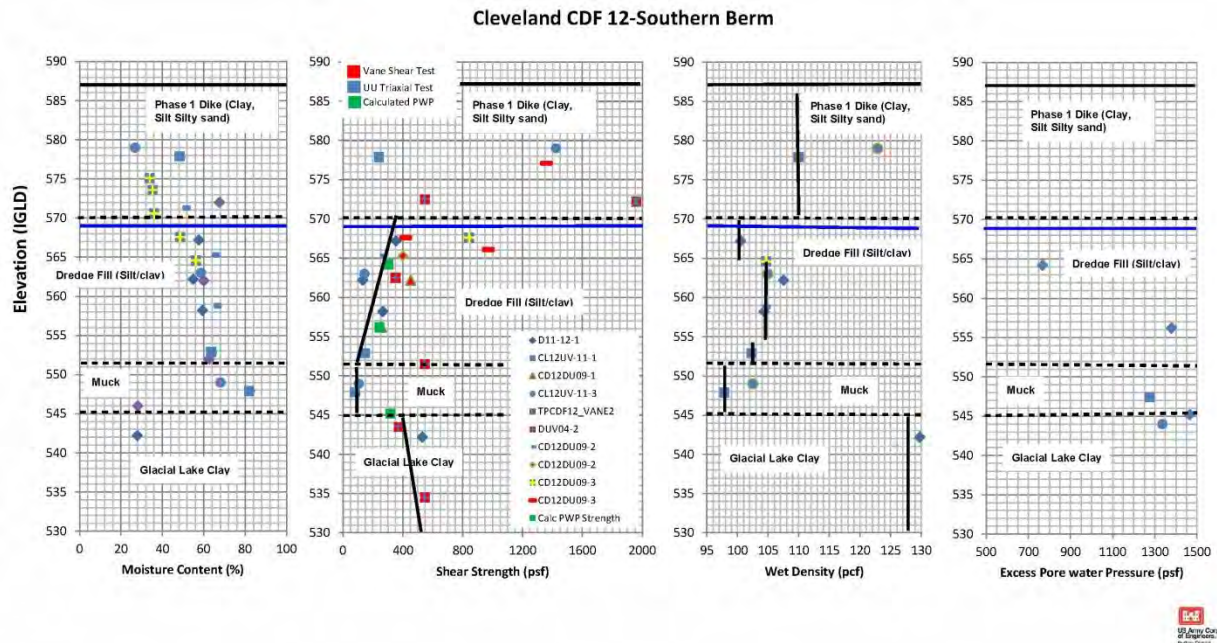


Figure 5 – Graphic Plot of Shear Strength, Moisture Content, Density and Excess Pore Pressures

5. CDF 9 PHASE 1 DIKE RAISING

In 2010 the CDF 9 was raised to +15 feet (4.6 m) LWD to provide additional dredge fill capacity. Prior to construction the ground surface was at +7feet to +9 feet (+2.1 m to +2.7 m) LWD. Thus the raised containment dikes varied from 6 to 8 feet (1.8 m to 2.4 m) in height depending upon the preconstruction ground surface elevation. Considering the lessons learned from the CDF 12 S Curve Dike failure the geotextile reinforcement was extended further out into the stability berms to force the failure to go around the fabric. The fabric was extended until the critical failure surface met an acceptable factor of safety of 1.4 (disposal side) and 1.5 (airport runway side). Presented in Figure 6 is the stability section for the south containment dike (airport runway side) which shows the critical failure surface, computed factor of safety of 1.508, and geotextile reinforcement. During construction and up until the present time there has been no evidence of any failure of these containment dikes despite similar foundation shear strengths as the CDF 12 S curve area. Thus, it appears that this design approach worked for CDF 9 Phase 1 dike raising.

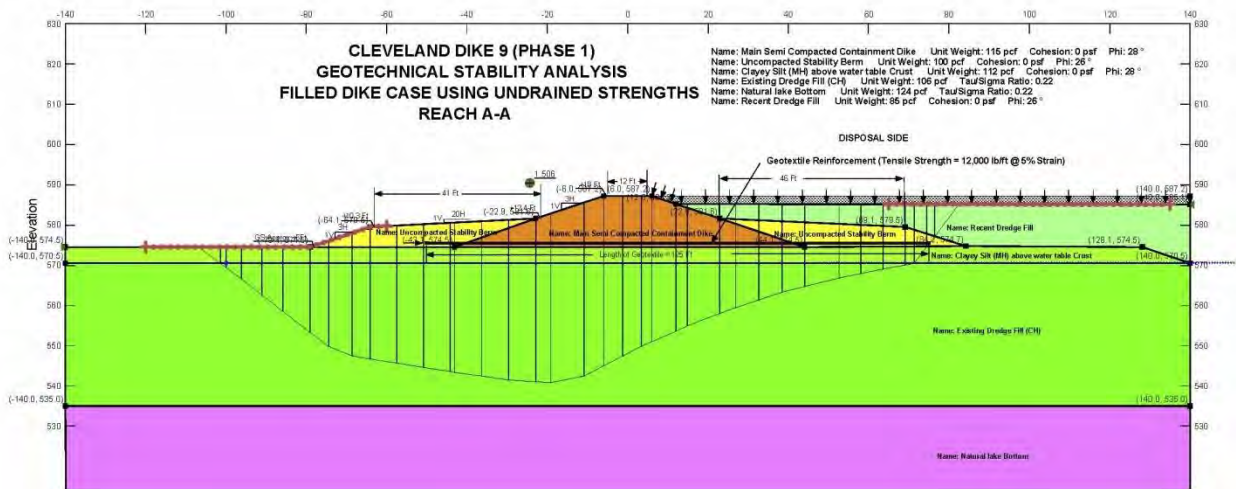


Figure 6 – CDF 9 Geotextile Reinforcement Stability Section

6. GEOTEXTILE REINFORCEMENT DESIGN APPROACH FOR 2015-2018 DREDGE STACKING

The 2015-2018 option No.4 alternative plan (all 1,000,000 CY (765,000 m³) of dredge fill placed in CDF 10B) results in the highest stacked fill height (to +44 ft (13.4 m) LWD) of all of the alternative options. Thus, this option requires the most extensive use of geotextile reinforcement and wick drains. The focus of the remainder of this presentation is the geotextile design approach used for this option. The other options also include geotechnical reinforcement at CDFs 9 and 12 but are not as extensive as the reinforcement used in CDF 10B.

6.1 Wick Drain Design CDF 10B

A cost effective method to improve the foundations undrained shear strength is to install vertical wick drains. Wick drains alleviate excess pore water pressures, increase the foundation effective stress and, therefore increase the undrained shear strength. A vertical wick drain system requires the installation of a drainage pad to transport water collected by the wick drain away. The amount of excess pore water pressure to be dissipated by the wick depends on the elevation of this drainage pad with respect to static water level (i.e. lake level). Since the ground surface in the in each of the CDF's will be above lake level after hydraulic dredging ends in 2014 (+12 ft to +16 ft or +3.7 m to +4.9 m LWD), the wick drains will have limited capability in reducing excess pore water pressures as the drainage pad would have to be placed above these elevations. Thus, full dissipation of excess pore water pressures is not possible using wick drains. However, by placing surcharge fill or by controlling the rate of dredge fill stacking the recovery of excess pore water pressures in the foundation induced by the fill will increase effective stress and thus increase shear strength.

To sufficiently increase the foundation undrained shear strengths as a result of implementing a wick drain system, specific drain pattern spacing is required in order to obtain the necessary consolidation.

The required drain spacing was determined using the computational procedure contained in Federal Highway Administration Report FHWA/RD-86, August 1986. The coefficient of consolidation and permeability of the dredge fill was obtained from laboratory consolidation tests performed as part of this study. Results of the wick drain analysis using the above referenced computational procedure requires a drain spacing of about 10 feet (3.1 m) to obtain the required strength gain and consolidation within a 1 year period. The estimated foundation strength gain was then input into the Slope/W computer model as a spatial strength function to determine the factor of safety against failure of the containment facility as a result of the imposed loads from the stacked dredged fill.

6.2 Geotextile Reinforcement Design CDF 10B

There are several references available for designing geotextile reinforcement for embankments built on soft foundations. The following two references were used for the design of geotextile reinforcement for the Cleveland CDFs: (a.)

“Geosynthetic Engineering”, Robert D. Holtz, Barry R. Christopher and, Ryan R. Berg, 1997 AND (b.) Army Technical Manual TM 5-818-8, “Engineering Use of Geotextiles”, July 1995. Both of these publications outline three possible modes of embankment failure and required stability analysis required for the design of geotextile reinforcement:

1. Bearing Failure
2. Rotational Failure
3. Lateral Spreading

The focus of this presentation is on the rotational aspect of potential foundation failure. The computer software model Slope/W (Geoslope International, Ltd) was used as the computational tool for designing the geotextile reinforcement for this mode of failure. This computer model uses limit equilibrium analysis to determine the factor of safety against failure and determines the required geotextile strength (tensile) and anchorage embedment requirements needed to obtain the minimum required factor of safety against failure. The computer model has two alternative methods on how the geotextile reinforcement is included in the stability calculations by flagging a check box option for the reinforcement as “factor of safety Dependent”, Yes or No. If the selection option is “No”, then the reinforcement forces used in the analysis are *allowable* forces and are not divided by the factor of safety calculated during stability analysis. If the selected option is “Yes” then the reinforcement forces used in the analysis are *ultimate* forces, and are divided by the factor of safety calculated in the slope stability analysis. The “No” option was used in this analysis which means that the specified tensile strength used in the computer model is the allowable strength. In addition to the allowable strength a limiting strain is specified for the geotextile that is compatible with the foundation strain developed under the mobilized shear forces. This strain was selected to be 5% as appropriate which is the limiting tensile force divided by the geotextile secant modulus (E_s).

When using the Slope/W computer model to design the geotextile reinforcement either of the two following components control the calculated resisting forces and thus computed factor of safety: (a.) Geotextile anchorage or bond resistance to prevent fabric pullout, (b.) Tensile strength of fabric to resist driving forces. In Slope/W the required bond length is indicated by a red box around the reinforcement. Graphically, if the red box occurs within the lateral extent of the fabric and behind the critical failure surface then the fabric tensile strength controls the computed factor of safety. If the factor of safety is less than the minimum required then the fabric tensile strength would have to be increased until an acceptable factor of safety is obtained. If the red box occurs at the end or beyond the lateral extent of the fabric then bond resistance controls the factor of safety. In this case the resisting fabric force is limited to the computed bond resistance in the stability calculations. If the factor of safety is less than the required minimum then the fabric bond length has insufficient anchorage and must be increased until an acceptable factor of safety is obtained. Another aspect to consider in designing the geotextile reinforcement is the potential for failure around the lateral extent of the fabric. This is what may have occurred at the CDF 12 S curve containment dike failure. The design only considered resistance offered by the fabric strength but did not consider the potential that failure could occur around the fabric. Evidence of this is the development of tension cracks just beyond the lateral extent of the fabric. The CDF 9 Phase 1 Dike raising and the current 2015-2018 stacking geotextile design considers this aspect of design and extended the fabric out until suitable factors of safety of the critical failure surface around the fabric was obtained.

Figure 7 shows the location of the CDF10B option No.4 dredge fill stack fill stacking to +44 ft (13.4 m) LWD using geotechnical reinforcement for stabilization. Note that wick drains are used in combination with the reinforcement to provide the necessary stabilization. The use of wick drains as opposed to geotextile reinforcement is more cost effective (\$7.50/SY or \$8.97/m²) installation as opposed to \$15.00/SY or \$17.95/m²) and thus would be the preferred alternative. However, wick drains have a time component associated with their application. Wick drains are used to consolidate the underlying soft fine grained foundation which increases the foundation effective stresses and thus undrained shear strength. However, the consolidation process is a time dependent process with the length of time dependent upon the wick drain spacing. Even with controlled rate of filling (staged construction) practical use wick drains would require a minimum of several months of consolidation to occur until the foundation has gained sufficient strength needed to support the imposed stacked loads. Therefore geotextile reinforcement is necessary in order to provide stability until the wick drains provide enough consolidation and thus foundation strength gain needed to support the imposed stacked fill loads. The CDF 10B Option 4 (Fill to +44 ft or +13.4 m LWD) design analysis indicated that 4 layers of high strength geotextile reinforcement (allowable tensile strength of 14,500 lbs/ft (210 KN/m) at 5% strain) was needed until the stack fill height reached a height of +24 ft (7.3 m) LWD after which enough foundation consolidation and strength gain was obtained by using wick drains to support the final stacked fill height of +44 ft (13.4 m) LWD. A final design cross showing the lateral extent of the wick drains and the geotextile reinforcement is shown in Figure 11.

7. CONCLUSIONS

The available capacity of the Cleveland CDFs are reaching the point where hydraulic placement of the dredged material is no longer feasible and will reach their original intended capacities by the end of 2014 . A new disposal facility will not

be available until at least 2018. In the interim period 2015-2018 it is proposed to stack dredge material by mechanical means in each CDF above their original design crest heights. Stacking this fill raises concerns with respect to both internal and global stability of the original rubble mound containment dikes. The application of geotextile reinforcement in combination with wick drains was investigated to obtain a stable configuration of the rubble mound containment dikes. A previous raising of CDF 12 in 2008 used geotextile reinforcement. However, failures occurred in the "S Curve" area where very weak fined grained dredge fill foundation and Lake Bottom occurs. It appeared that this failure may have occurred around the lateral extent of the geotextile reinforcement. The design analysis only considered the resistance offered by the fabric strength but did not consider the potential of failure around the fabric. Tension cracks that developed beyond the lateral extent of the fabric provide possible evidence of failure around the fabric. CDF 9 was raised in 2010 in similar fashion but as a lesson learned from the CDF 12 failure designed the fabric considering this aspect of design. To date results of this design approach have been positive with no noted failures occurring during construction up to present time.

When using computer models such as Slope/W or any other similar type limit equilibrium computer models to design geotextile reinforcement, 3 design aspects must be considered: (1.) Fabric must have enough tensile strength to prevent failure thru the fabric, (2.) The fabric must have enough anchorage or bond length to prevent pull out from driving loads and, (3.) the fabric must be extended enough to force the failure around the fabric until a sufficiently high factor of safety is obtained. This same design approach was used in the current dike stacking design analysis.

The use of wick drains to stabilize the stacked fill is the most cost effective and preferable method of stabilization. However, wick drains have a time component associated with their use. Wick drains are used to consolidate the soft fine grained foundation which increases the foundation effective stresses and thus shear strength. However, the wick drains need to be in place for at least several months before the foundation gains enough strength to be able to support the imposed stacked fill loads by themselves. In order to provide stability in the interim geotextile reinforcement is needed. Thus the combination of wick drains and geotextile reinforcement was used in the current analysis to stack dredge fill for the Cleveland 2015-2108 disposal period.

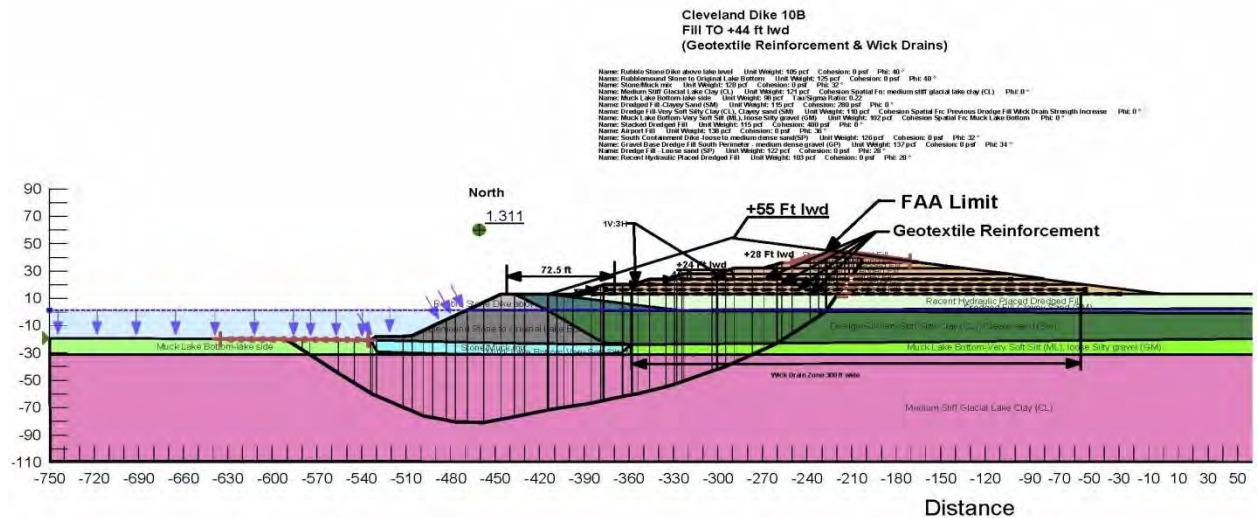


Figure 7 – CDF 10B Option 4, Geotextile Reinforcement Stability Section

**Cleveland Dike 10B
 Fill TO +44 ft lwd (Option 4)
 (Geotextile Reinforcement & Wick Drains)**

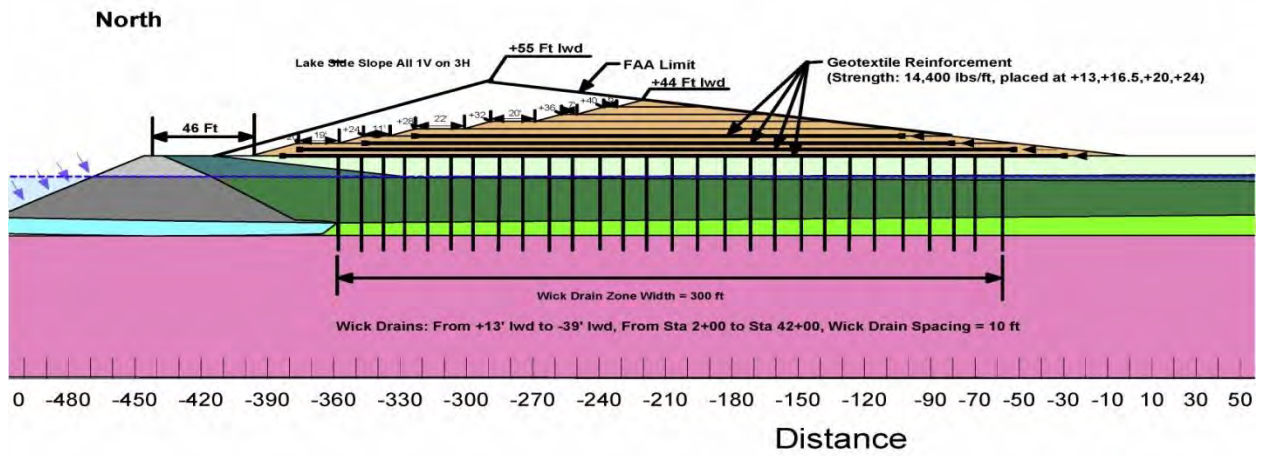


Figure 8 – CDF 10B Option 4, Final Design Section

Comparative Evaluation of Different Aperture Geogrids for Ballast Reinforcement through Triaxial Testing and Discrete Element Modeling

Yu Qian, University of Illinois at Urbana-Champaign, USA, yuqian1@illinois.edu
Debakanta Mishra, University of Illinois at Urbana-Champaign, USA, dmishra2@illinois.edu
Erol Tutumluer, University of Illinois at Urbana-Champaign, USA, tutumlue@illinois.edu
Jayhyun Kwon, Tensar International, USA, jkwon@tensarcorp.com

ABSTRACT

Geogrids are commonly used in transportation applications for stabilization and reinforcement due to their higher tensile strengths compared to geotextiles as well as the stiffness improvement they provide through arresting and interlocking granular particles in the geogrid apertures. Influenced by many factors, such as the aperture shape and size of geogrid, the degree of interlocking contributes significantly to the reinforcement benefit of geogrid for improving the performance of any geogrid reinforced system. This paper describes recent research efforts at the University of Illinois focused on conducting permanent deformation testing of geogrid reinforced ballast specimens using a large-scale triaxial test device. As part of the very preliminary evaluations, two different geogrids with rectangular and triangular aperture shapes were studied for reinforcement benefits of cylindrical specimens compacted and prepared with uniformly graded ballast sized aggregate materials. To further investigate the geogrid reinforcement mechanisms, an aggregate image-aided numerical modeling approach based on Discrete Element Method (DEM) was also adopted with the capability to create actual ballast aggregate particles as three-dimensional polyhedron elements having the same particle size distributions and imaging quantified average aggregate shapes and angularities. Preliminary results from both laboratory experiments and DEM simulations indicated that geogrids with triangular apertures performed more effectively in arresting particle movements through improved interlock.

1. INTRODUCTION

Geogrids are geosynthetic polymeric materials having large openings, i.e. apertures. They have been successfully used for decades in highway pavement applications, e.g., subgrade stabilization and base reinforcement. Geogrids have also been used in railroad track structures for stabilization and reinforcement purposes, especially for ballast reinforcement. Ballast is an essential layer of the railroad track structure, primarily provides drainage and load distribution. The benefit of geogrids in railway applications mainly comes from the interlocking between ballast particles and the geogrids. The degree of interlocking between geogrids and aggregate particles depends upon many factors, such as: aggregate gradation and shape properties, geogrid types and properties, compaction effort during installation, and loading conditions. Large scale triaxial tests or cyclic plate loading tests have been traditionally performed in the laboratory to evaluate the individual effects on the ballast behavior (Suiker et al. 2005, Brown et al. 2007, Anderson and Fair 2008, Aursudkij et al. 2009, Indraratna et al. 2010). Rectangular aperture geogrids with tensile strength properties in both machine and cross-machine directions have been commonly studied and recognized as useful materials that can effectively reduce the permanent deformation accumulation in the ballast under repeated loading (Bathurst and Raymond 1987, Shin et al. 2002, Raymond and Ismail 2003, Indraratna et al. 2006, Brown et al. 2007, Qian et al. 2011a). Recently, geogrids with triangular aperture shapes have also been introduced and studied for performance improvements of geogrid reinforced transportation systems (Qian et al. 2011b, Qian et al. 2012).

This paper describes preliminary findings from a research study recently initiated at the University of Illinois with the objective to conduct permanent deformation testing of geogrid reinforced ballast specimens using a large scale triaxial test device and model the micromechanical interlock behavior of geogrid-aggregate systems. Both rectangular and triangular aperture shaped geogrids were initially tested for permanent deformation behavior using a large scale triaxial testing device. To further investigate the geogrid reinforcement mechanisms, a numerical modeling approach based on Discrete Element Method (DEM) was also adopted with the capability to create actual ballast aggregate particles as three-dimensional polyhedron elements having the same particle size distributions and imaging quantified average shapes and angularities. This paper will present the laboratory test and the DEM simulation results for ballast specimens reinforced with the rectangular and triangular aperture geogrids under repeated loading.

2. REPEATED LOAD TRIAXIAL TEST OF BALLAST SPECIMENS

2.1 The University of Illinois Triaxial Ballast Tester (TX-24)

A large scale triaxial test device (The University of Illinois Triaxial Ballast Tester or TX-24) has recently been developed at the University of Illinois for testing specifically ballast size aggregate materials. The test specimen dimensions are 30.5 cm (12 in.) in diameter and 61.0 cm (24 in.) in height. The acrylic test chamber has dimensions of 61.0 cm (24 in.) in diameter and 122.0 cm (48 in.) in height. An internal load cell (Honeywell Model 3174) with a capacity of 89 kN (20 kips) is placed on top of the specimen top platen. Three vertical LVDTs are placed around the cylindrical test specimen at 120-degree angles between each other to measure the vertical deformations of the specimen from three different side locations. Another LVDT is mounted on a circumferential chain wrapped around the specimen at the mid-height to measure the radial deformation of the test specimen. Figure 1 shows the picture of a compacted and instrumented ballast specimen assembled inside the acrylic chamber ready to be transported to the loading frame.

The permanent deformation tests reported in this paper were conducted at a constant confining pressure of 34.5 kPa (5 psi) and the deviator stress applied was 172.3 kPa (25 psi). The repeated loading pattern was realistic field haversine load pulse with loading time of 0.4 seconds and 0.6-seconds of rest period between two loadings as shown in Figure 2.



Figure 1. Compacted ballast specimen with instrumentation assembled inside the acrylic chamber ready to be tested using the University of Illinois Triaxial Ballast Tester (TX-24)

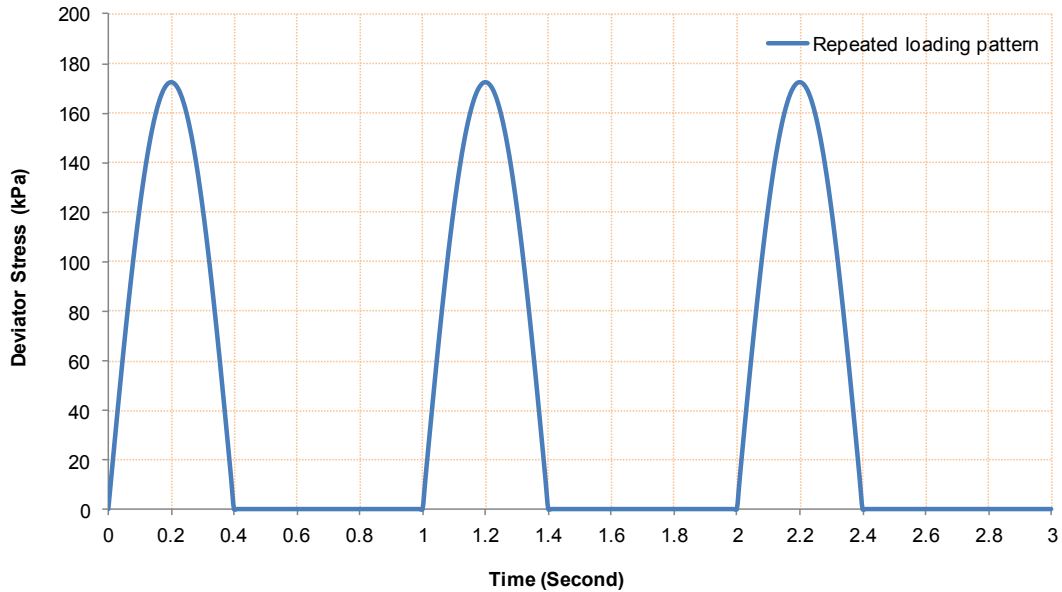


Figure 2. Repeated loading pattern used in permanent deformation tests to closely resemble field train loading

2.2 Ballast Specimen Preparation

The ballast material used in the permanent deformation tests was a clean limestone having 100% crushed aggregates. Figure 3 shows the gradation properties of the ballast material which adequately met the AREMA No.24 gradation requirements. Besides the grain size distribution, aggregate shape properties, especially the flat and elongated (F&E) ratio, the angularity index (AI), and the surface texture (ST) index, are key indices quantified by the recently enhanced University of Illinois Aggregate Image Analyzer (UIAIA) (Rao et al. 2002). One full bucket of the ballast material was scanned and analyzed using the UIAIA to determine the values of the F&E ratio, AI, and the ST index. These shape indices were then used as the essential morphological data to generate ballast aggregate particle shapes as 3D polyhedrons, i.e., individual discrete elements utilized in the ballast DEM model (see Figure 4). Table 1 lists the gradation properties and the average values of the limestone ballast shape UIAIA indices used in the DEM simulations.

An aluminum split mold was used to prepare the ballast test specimens. Three layers of a latex membrane, with a total thickness of 2.3 mm, were fixed inside the split mold and held in place by applying vacuum to prepare each specimen in layers. A thin layer of geotextile was placed on top of the base plate to prevent clogging of the vacuum port in the base plate. Approximately 68 to 73 kg (150 to 160 lbs) of ballast material was poured into the mold evenly in four lifts, with each lift compacted approximately 15-cm (6-in.) high. Each layer was compacted using a 27.2-kg (60-lb.) electric jack hammer for about 4 seconds. After compaction of the first two lifts, one layer of geogrid was placed carefully in the middle of the test specimen. At the end of placing all four lifts, each test specimen was checked for the total height and leveling of the top plate. The void ratios computed were consistently around 0.68. Figure 5 shows the photos of the geogrids tested. The detailed properties of the geogrids are given in Table 2. Figure 6 shows the aluminum split mold (on left) and the compacted ballast specimen (on right) ready for instrumentation assembly and subsequent testing.

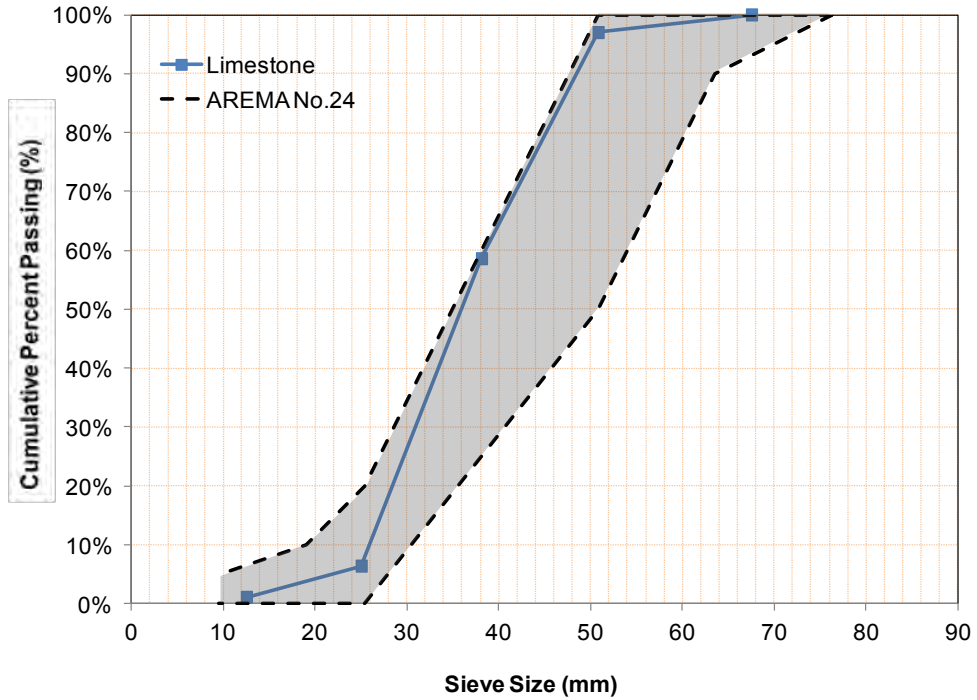


Figure3. Particle size distribution of limestone ballast aggregate compared to AREMA No. 24 specifications

Table 1. UIAIA based imaging shape properties of limestone ballast material

Angularity Index (AI) in degrees	Flat & Elongation (F&E) Ratio	Surface Texture (ST)	Coefficient of Uniformity, Cu	Coefficient of Curvature, Cc
440	2.3	2	1.46	0.97

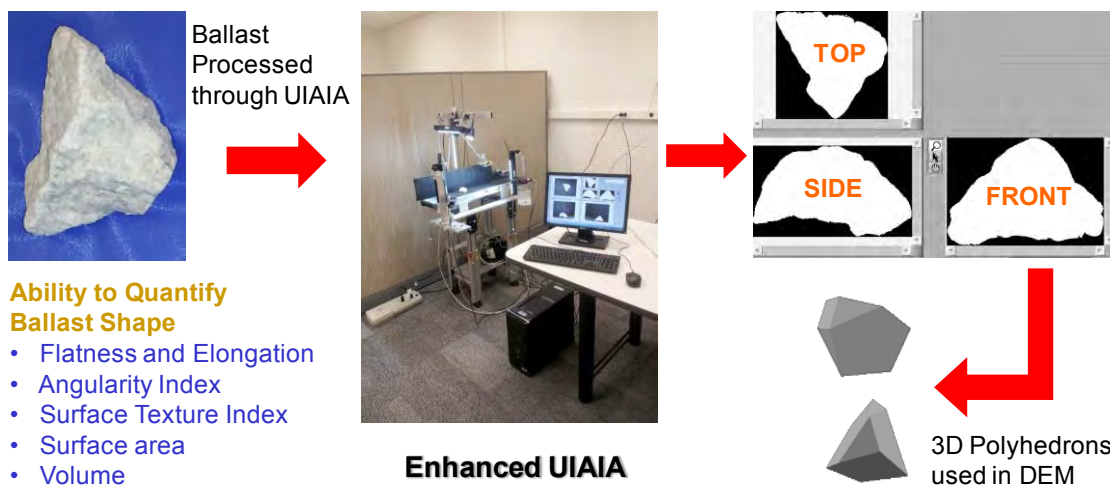
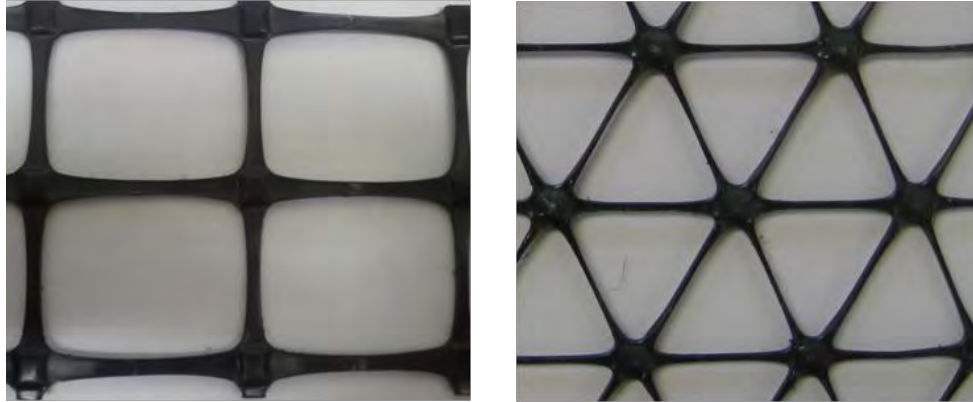


Figure4. Conceptual approach for aggregate imaging based railroad ballast discrete element model simulations



(a) Rectangular aperture geogrid (b) Triangular aperture geogrid

Figure 5. Geogrids used for ballast reinforcement in large scale triaxial tests

Table 2. Dimensions and Properties of Rectangular and Triangular Aperture Geogrids

Index Properties	Aperture Dimensions (mm)			
	Machine Direction	X-Machine Direction	Longitudinal	Diagonal
Rectangular Ap. Geogrid	46	64		
Triangular Ap. Geogrid			60	60
Minimum Rib Thickness		1.27		2.40
Mechanical Properties	Rectangular Aperture Geogrid		Triangular Aperture Geogrid	
Junction Efficiency (percentage)		93		93
Aperture Stability Modulus (m-N/deg)		0.58		
Radial stiffness (kN/m@0.5% strain)				350

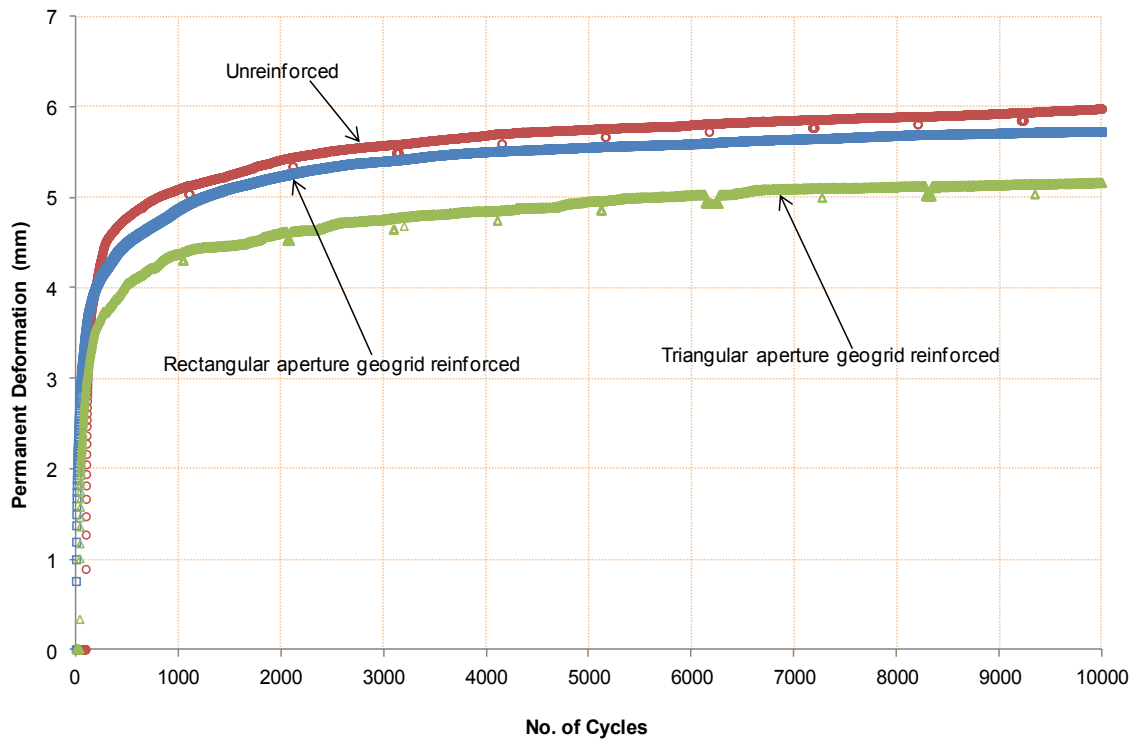


(a)

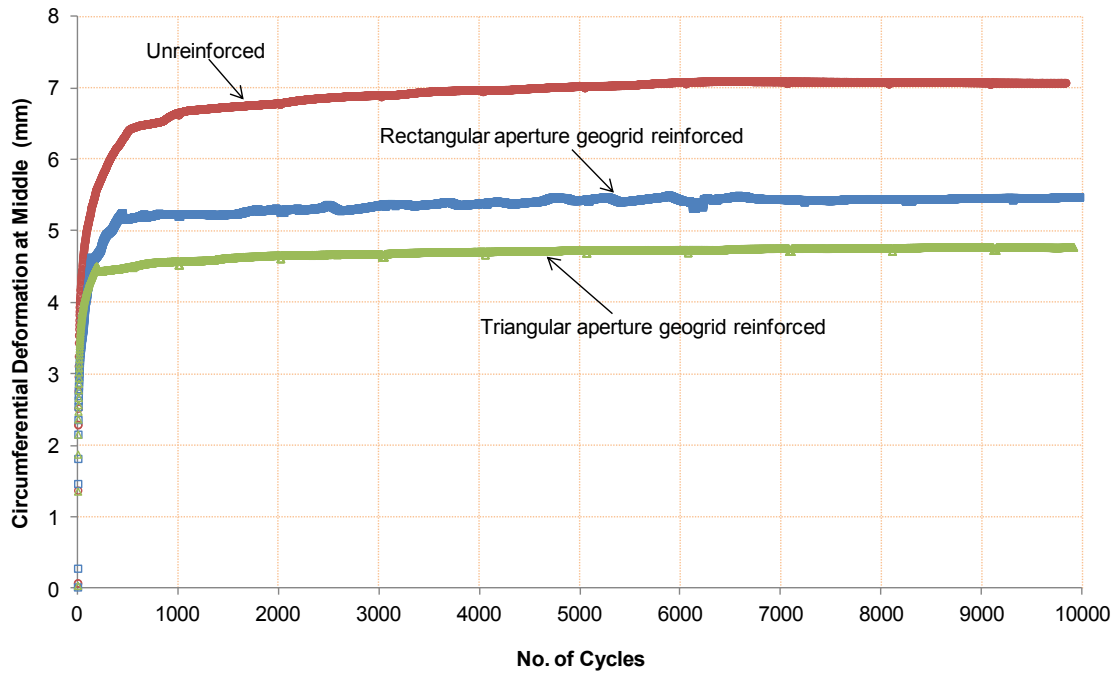


(b)

Figure 6. Pictures showing (a) Aluminum split mold used for specimen preparation, and (b) Compacted ballast specimen confined using vacuum inside three latex membranes



(a)



(b)

Figure 7. (a) Permanent axial deformations of ballast specimens; (b) Circumferential deformations of ballast specimens

2.3 Experimental Results

Figure 7 presents the preliminary results of the ballast permanent deformation tests performed in the laboratory for up to 10,000 cycles. For the first several hundreds of loading cycles, the permanent deformation and circumferential deformations increased rapidly, which was primarily due to the initial rapid “shakedown” of the ballast material. After around 1,000 loading cycles, the permanent deformation accumulated much slower and became relatively stable and so did the circumferential or radial/horizontal deformations. All the unreinforced and geogrid reinforced test specimens accumulated similar magnitudes of permanent deformation during the first one hundred load cycles and this was primarily due to the fact that geogrids were not yet fully mobilized at that time. With a single layer of geogrid placed in the middle of the test specimen, the geogrid reinforced test specimens accumulated less permanent deformation compared to the unreinforced case as the load cycles increased. When the reinforced test specimens accumulated certain amount of deformation, the geogrid’s reinforcement effect was fully mobilized and the interlock between geogrid and aggregate particles prevented further specimen bulging. This caused the specimen to stiffen and made it more resistant to deformation accumulation upon further loading. Triangular aperture geogrid reinforced test specimen accumulated the smallest permanent deformation compared with the unreinforced as well as the specimen with rectangular aperture geogrid. This indicates the triangular aperture geogrid better arrested aggregate movement with improved interlocking in all horizontal directions which can be confirmed from circumferential or radial/horizontal deformations, which happen to be of similar magnitude. Note that the triangular aperture geogrid also has thicker ribs and much higher radial stiffness when compared to the rectangular one (see Table 2). After 10,000 loading cycles, the permanent deformation for the unreinforced test specimen was 5.98 mm, the permanent deformation for the test specimen with rectangular aperture geogrid was 5.72 mm, and the permanent deformation for the test specimen with triangular aperture geogrid was 5.17 mm, respectively.

3. SIMULATION OF REPEATED LOAD TRIAXIAL TEST USING THE DISCRETE ELEMENT METHOD (DEM)

3.1 DEM Model Preparation

To investigate the mechanism of interlock and how this minimizes particle movement and causes local stiffness increase through friction and interaction of ballast particles with geogrid, a numerical modeling approach was adopted based on the Discrete Element Method (DEM) combined with image analyses of tested aggregate particles for size and shape properties. Compared to other research studies focusing on simulating triaxial tests by DEM, which often use spherical elements or element clusters (Indraratna et al. 2010, Lu and McDowell. 2010), the image-aided DEM simulation approach developed at the University of Illinois has the capability to create actual ballast aggregate particles as three-dimensional polyhedron elements having the same particle size distributions and imaging quantified average shapes and angularities. Ghaboussi and Barbosa (1990) developed the first polyhedral 3D DEM code BLOKS3D for particle flow; and Nezami et al. (2006) enhanced the program with new, fast contact detection algorithms. Tutumluer et al. (2006) combined the DEM program and the aggregate image analysis together to simulate the ballast behavior more accurately and realistically by using polyhedral elements regenerated from the image analysis results of ballast materials. This DEM approach was first calibrated by laboratory large scale direct shear test results for ballast size aggregate application (Huang and Tutumluer 2011). The calibrated DEM model was then utilized to model strength and settlement behavior of railroad ballast for the effects of multi-scale aggregate morphological properties (Tutumluer et al. 2006, 2007). More recent applications of the calibrated DEM model investigated ballast gradation (Tutumluer et al. 2009) and fouling issues (Tutumluer et al. 2008, Huang and Tutumluer 2011) that are known to influence track performance. A successful field validation study was also conducted with the ballast DEM simulation approach through constructing and monitoring field settlement records of four different ballast test sections and then comparing the measured ballast settlements under monitored train loadings to DEM model predictions (Tutumluer et al. 2011). The effect of geogrid aperture shape was recently studied by this DEM approach (Qian et al. 2011a).

Similar to the laboratory repeated load triaxial tests conducted for studying permanent deformation trends, comparative performance evaluations were also targeted for unreinforced and geogrid reinforced ballast specimens through DEM model simulations. The goal was to investigate the effects of different aperture shaped geogrids on the effectiveness of interlocking and the overall performance of the geogrid reinforced ballast. Considering the rather long DEM simulation run times that would be required for modeling the complete permanent deformation tests, the DEM simulations in this study were intended for only a small number of 100 load cycles deemed to be sufficient to enable practical comparisons of the ballast triaxial tests with or without geogrid for effectiveness within reasonable computation time. At the same time, the DEM simulation results would still help to qualitatively evaluate the influence of different aperture shapes of geogrids.

To simulate large scale repeated load triaxial compression tests using the DEM approach, the first challenge is to model the membrane which holds the specimen upright and applies the chamber confining pressure on it during testing. Previous modeling studies used rigid boundaries and chains of circular or spherical particles to simulate the membrane (Bardet 1994, Iwashita and Oda 2000, Markauskas and Kacianauskas 2006, Wang and Tonon, 2009). Lee et al. (2012)

recently used rigid rectangular cuboid discrete elements positioned in a cylindrical arrangement to simulate a flexible membrane with BLOKS3D. A similar approach was used in this study. A total of 96 rectangular cuboid discrete elements (in eight-layers) were used to form a cylindrical chamber to confine the ballast specimen as shown in Figure 7. Each layer had 12 equal size elements and the dimension of each single element was 20.32 cm (8 in.) long, 10.16 cm (4 in.) wide, and 7.62 cm (3 in.) high. These membrane elements were only allowed translational movement in radial direction. Rotation and translation movement in other directions were restricted to replicate the deformation of membrane. Note that these elements were required to have certain thickness to avoid any gap between adjacent layers when differential radial displacements between them were relatively large. Similarly, the elements were also allowed to have sufficient lengths to overlap adjacent elements to keep the circular chamber closed during simulation of triaxial tests. No contact detection was performed between these elements to allow for each element to move freely, independent of neighboring elements. The friction between the membrane elements and the ballast particles in contact with them was ignored during the DEM simulations. For the unreinforced ballast specimen, after the membrane was formed, around 500 particles were poured into the cylinder and the top platen was placed on top of the specimen to compact the ballast specimen to the same initial density under 34.5 kPa (5 psi) confining pressure as achieved in the laboratory experiment. For the geogrid reinforced ballast specimens, after the membrane was formed, about 500 particles were also poured into the cylinder in two different sets following the same gradation and shape properties of the actual ballast particles. In between, a sheet of geogrid element was generated in the middle of the ballast specimen as shown in Figure 8. The geogrid element has the same dimensions as the geogrid used in experimental study but is rigid and cannot deform. When the ballast specimen in the DEM simulation was prepared as in the similar condition as the laboratory test specimen, the repeated loading was applied to the top platen.

3.2 DEM Simulation Results

Figure 9 presents the accumulated permanent deformations as predicted by the DEM simulations for up to 100 load cycles. The deformation values at the 100th load cycle were 10.32 mm for the unreinforced case, 9.42 mm for the rectangular aperture geogrid reinforced case, and 7.97 mm for the triangular aperture geogrid reinforced case, respectively. As the purpose of the DEM simulations was to qualitatively investigate the relative performance of geogrids with different aperture shapes, due to the long DEM run times associated with each loading case, the DEM simulations for the permanent deformation predictions here considered only up to 100 cycles of the load application. Although the permanent deformations for the first hundred load cycles were somewhat similar for the unreinforced and different geogrid reinforced specimens during the laboratory testing (see Figure 7), with better control in compaction during specimen preparation in DEM simulations and the significantly high number of aggregate particle contact forces computed and checked for global granular assembly equilibrium at each iterative time step, a relatively low number of initial load cycles, such as 100 achieved here for three different simulation cases studied, was deemed to be sufficient for identifying the main reinforcement mechanisms and interlocking trends also identified in the experiments. Clearly, with DEM simulations of only up to 100 load cycles, the differences among the different ballast triaxial tests were apparent.

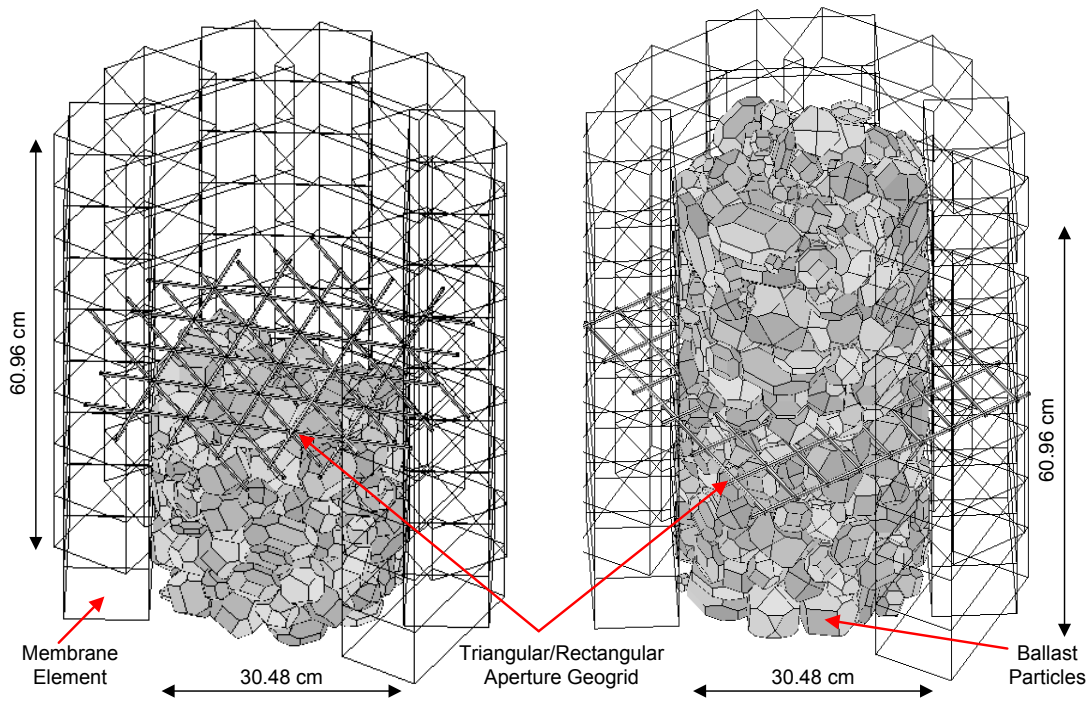


Figure8. Flexible membrane, geogrids with different apertures and ballast specimenformed in DEM simulations

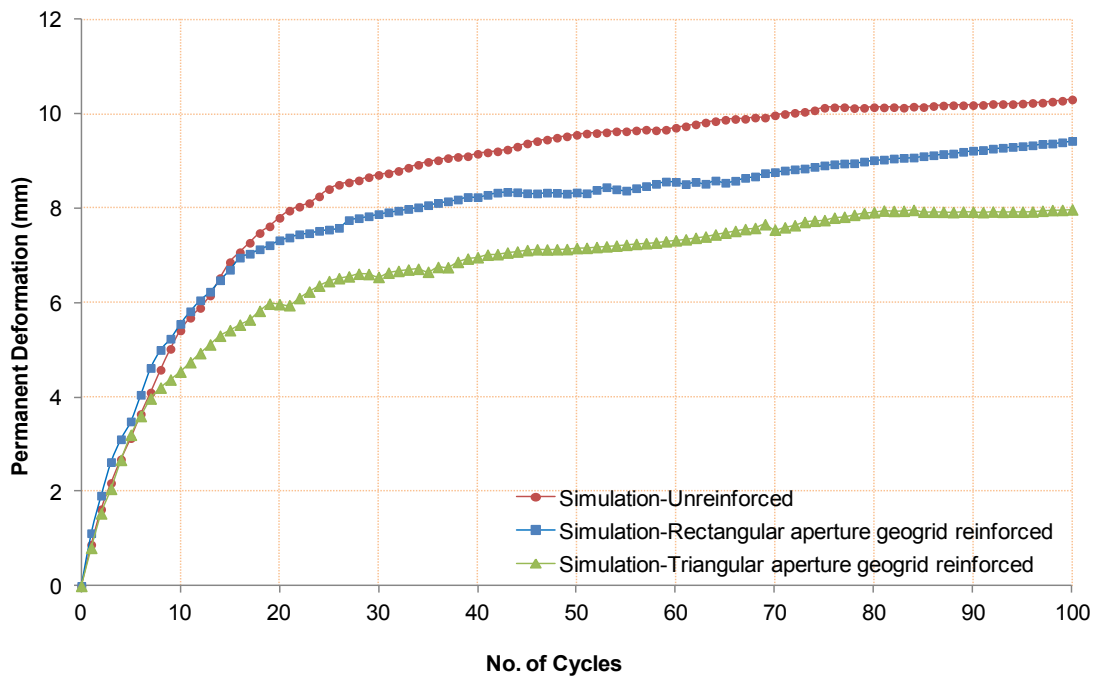


Figure9. Predicted ballast permanent deformation trends from DEM simulations with and without geogrid cases

The geogrid reinforced ballast specimens similarly yielded less permanent deformations compared to the unreinforced ballast specimen. The rectangular aperture geogrid did provide considerable reinforcement, but the triangular aperture geogrid with more uniform reinforcement in all horizontal directions provided the most significant improvement as indicated in Figure 9. These results from DEM simulations agree well with the trends observed in the

laboratory experiments. It is interesting to note that the first five DEM simulation load cycles also yielded similar magnitude deformations (approximately 4 mm) for all the unreinforced and geogrid reinforced test specimens, which means the geogrids were not fully mobilized yet. However, as the load cycles increased, the triangular aperture geogrid started to show improvement at around the 8th loading cycle during the simulation, while, the rectangular geogrid started to take effect at around the 16th loading cycle (see Figure 9). Again, the DEM simulations were intended to qualitatively compare the relative performances of geogrids with different aperture shapes using the minimum computational time. The intention has never been to match the predicted permanent deformation rates or the magnitudes at the different load cycles with the experimental results directly.

4. CONCLUSIONS

This paper focused on the permanent deformation behavior of geogrid reinforced ballast specimens as obtained from a large scale repeated load triaxial test device in the laboratory with both rectangular and triangular aperture geogrids. Further, the goal has also been to demonstrate the applicability of a repeated load triaxial testing and aggregate particle imaging based three-dimensional (3-D) numerical modeling approach, based on the Discrete Element Method (DEM), for studying geogrid-aggregate interlock reinforcement mechanism. Based on the very preliminary testing with limited data for two geogrids, the following conclusions can be drawn from this study:

1. The large scale triaxial device dedicated for testing ballast size aggregate materials developed at the University of Illinois was used successfully to investigate the permanent deformation behavior of ballast specimens under repeated loading with and without geogrid reinforcement. Both rectangular and triangular aperture geogrids were found to effectively reduce the permanent deformation accumulations of ballast materials. Triangular aperture geogrid with uniform resistance in all horizontal directions yielded the lowest permanent deformation.
2. The aggregate imaging based DEM simulation platform developed at the University of Illinois could model the repeated load triaxial tests for permanent deformation behavior of ballast specimens. Both confinement and applied deviator stress conditions on the cylindrical ballast specimens with and without geogrid reinforcement could be properly applied to investigate the interlock mechanism and micromechanical interactions between geogrids and aggregates.
3. Both the laboratory experiments and the DEM model simulations of the repeated load triaxial tests, for significantly lower number of load repetitions applied compared to the 10,000 load cycles applied in the laboratory experiments, gave similar benefits of using geogrids. The triangular aperture geogrid had better performance than rectangular aperture one in arresting particle movement in the lateral direction to yield the lowest vertical permanent deformation. More studies are needed to fully investigate aperture shape effects on the overall geogrid reinforcement mechanism.
4. The DEM simulation platform, currently being further developed, has the potential to be a quantitative tool to predict the ballast-geogrid interactions. This methodology has the potential for quantifying individual effects of various geogrid products.

ACKNOWLEDGEMENTS

The authors would like to acknowledge Tensar International, Inc. for providing the geogrids studied. The help and support of James Pforr, Research Engineer at the Illinois Center for Transportation (ICT) and Mr. Hasan Kazmee, PhD student at the Department of Civil and Environmental Engineering (CEE) at UIUC with the laboratory triaxial tests are greatly appreciated.

REFERENCES

- Anderson, W.F. and Fair, P. (2008). Behavior of Railroad Ballast under Monotonic and Cyclic Loading. *Journal of Geotechnical and Geoenvironmental Engineering*, ASCE, 134(3):316-327.
- Aursudkij, B., McDowell, G.R., and Collop, A.C. (2009). Cyclic Loading of Railway Ballast under Triaxial Conditions and in a Railway Test Facility. *Granular Matter*, (11):391-401.
- Bardet, J. P. (1994). Observations on the Effects of Particle Rotations on the Failure of Idealized Granular Materials. *Mechanics of materials*, 18(2):159-182.
- Bathurst, R. J. and Raymond, G. P. (1987). Geogrid reinforcement of ballasted track. *Transportation Research Record*. No. 1153: 8-14.
- Brown, S. F., Kwan, J. and Thom, N. H. (2007). Identifying the key parameters that influence geogrid reinforcement of railway ballast. *Geotextiles and Geomembranes*, 25(6):326-335.
- Ghaboussi J. and Barbosa R. (1990). Three-dimensional Discrete Element Method for Granular Materials. *International Journal for Numerical and Analytical Methods in Geomechanics*, (14): 451-472.

- Huang H., and Tutumluer E. (2011). Discrete Element Modeling for Fouled Railroad Ballast. *Construction and Building Materials*, (25): 3306–3312.
- Indraratna, B., Khabbaz, H., Salim, W. and Christie, D. (2006). Geotechnical properties of ballast and the role of geosynthetics in rail track stabilisation. *Journal of Ground Improvement*, 10(3): 91-102.
- Indraratna, B., Thakur, P.K., and Vinod, J.S. (2010). Experimental and Numerical Study of Railway Ballast Behavior under Cyclic Loading. *International Journal of Geomechanics*, ASCE, 10(4):136-144.
- Iwashita K., and Oda M. (2000). Micro-deformation Mechanism of Shear Banding Process Based on Modified Distinct Element Method. *Powder Technology*, 109(1-3):192-205.
- Lee, S. J., Hashash, Y.M.A., and Nezami E.G. (2012). Simulation of Triaxial Compression Test with Polyhedral Discrete Elements. *Computers and Geotechnics*, in press.
- Lu, M. and McDowell, G.R. (2010). Discrete Element Modelling of Railway Ballast under Monotonic and Cyclic Triaxial Loading. *Geotechnique*, 60(6):459-467.
- Markauskas D. and Kacianauskas R. (2006). Compacting of Particles for Biaxial Compression Test by the Discrete Element Method. *Journal of Civil Engineering and Management*, 12(2):153-61.
- Nezami E.G., Hashash, Y.M.A., Zhao D., Ghaboussi J. (2006). Shortest Link Method for Contact Detection in Discrete Element Method. *International Journal for Numerical and Analytical Methods in Geomechanics*, 30(8):783-801.
- Qian, Y., Tutumluer, E., and Huang, H. (2011a). A Validated Discrete Element Modeling Approach for Studying Geogrid-Aggregate Reinforcement Mechanisms. *Geo-Frontiers 2011*, ASCE Geo-Institute, March 13-16, Dallas, Texas.
- Qian, Y., Han, J., and Pokharel, S.K., and Parsons, R.L. (2011b). Stress analysis on triangular aperture geogrid-reinforced bases over weak subgrade under cyclic loading - an experimental study. *Journal of the Transportation Research Board*, No. 2204, Low-Volume Roads, Vol. 2, *Proceedings of the 10th International Conference on Low-Volume Roads*, July 24–27, Lake Buena Vista, Florida, USA, 83-91.
- Qian, Y., Han, J., and Pokharel, S.K., and Parsons, R.L. (2012). Performance of Triangular Aperture Geogrid-Reinforced Base Courses over Weak Subgrade under Cyclic Loading. *Journal of Materials in Civil Engineering*, in press.
- Rao, C., Tutumluer, E. and Kim, I.T. (2002). Quantification of Coarse Aggregate Angularity Based on Image Analysis. *Transportation Research Record*. No. 1787, 193-201.
- Raymond, G. and Ismail, I. (2003). The effect of geogrid reinforcement on unbound aggregates. *Geotextiles and Geomembranes*, 21(6): pp.355-380.
- Shin, E. C., Kim, D. H. and Das, B. M. (2002). Geogrid-reinforced railroad bed settlement due to cyclic load. *Geotechnical and Geological Engineering*, 20:261-271.
- Suiker, A. S. J., Selig, E. T., and Frenkel, R. (2005). Static and Cyclic Triaxial Testing of Ballast and Subballast. *Journal of Geotechnical and Geoenvironmental Engineering*, ASCE, 131(6): 771-782.
- Tutumluer, E., Huang, H., Hashash, Y.M.A., and Ghaboussi, J. (2006). Aggregate Shape Effects on Ballast Tamping and Railroad Track Lateral Stability. *In Proceedings of the AREMA Annual Conference*, Louisville, Kentucky, USA, September 17-20.
- Tutumluer, E., Huang, H., Hashash, Y.M.A., and Ghaboussi, J. (2007). Discrete Element Modeling of Railroad Ballast Settlement. *In Proceedings of the AREMA Annual Conference*, Chicago, Illinois, September 9-12.
- Tutumluer, E., Huang, H., Hashash, Y.M.A., and Ghaboussi, J. (2009). AREMA Gradations Affecting Ballast Performance Using Discrete Element Modeling (DEM) Approach. *In Proceedings of the AREMA Annual Conference*, Chicago, Illinois, September 20-23.
- Tutumluer, E., Huang, H., Hashash, Y.M.A., and Ghaboussi, J. (2008). Laboratory Characterization of Coal Dust Fouled Ballast Behavior. *In Proceedings of the AREMA Annual Conference*, Salt Lake City, Utah, September 21-23.
- Tutumluer, E., Qian, Y., Hashash, Y.M.A., Ghaboussi, J., and David, D.D. (2011). Field Validated Discrete Element Model for Railroad Ballast. *In Proceedings of the AREMA Annual Conference*, Minneapolis, Minnesota, September 18-21.
- Wang, Y. and Tonon, F. (2009). Modeling Triaxial Test on Intact Rock Using Discrete Element Method with Membrane Boundary. *Journal of Engineering Mechanics*, 135(9):1029-1037.

Comparison of the Effect of Multifilament and Fibrile Types of Polypropylene Fibers on the Unconfined Compressive Strength of High Plasticity Clay

Yuksel Yilmaz, Ph.D., Gazi University, Turkey, yyuksel@gazi.edu.tr
Kemal Karatas, B.Sc., Gazi University, Turkey, kemal221287@hotmail.com

ABSTRACT

An experimental program was undertaken to investigate the effects of discrete multifilament and fibrile types polypropylene fibers on the unconfined compressive strength behavior of clayey soil. Both type of fibers used in three different lengths (6.0mm, 12.0mm, and 19.0mm) and three fiber dosages (i.e. 0%, 0.5%, 1.0% and 2.0% by dry weight of soil). At first, compaction characteristics of the untreated soil were evaluated at standard compaction energy. Using compaction characteristics of untreated soil various fiber-soil mixtures were composed, and their unconfined compression test were carried out after 1-, 7-, and 28-days curing periods. The obtained test results indicated that the effect of fiber dosage on the unconfined compressive strength behavior is superior to the effect of fiber length and fiber type.

1. INTRODUCTION

Fine grained soils with high plasticity are not desirable for use as a structural support unless their engineering properties are improved. For many years, extensive research has been carried out on the usability of some additives (e.g. lime, cement, fly ash, cement kiln dust, chemicals, enzymes, fibers, etc.) to improve the quality and/or stability of fine grained soils.

The effect of randomly oriented discrete fibres on the engineering behavior of coarse grained soils mainly by means of strength increase is well studied. On the other hand there are a few studies on the effect of randomly oriented discrete fibres alone (not in combination with other additives such as cement, fly ash, etc.) on the geotechnical behavior of fine grained soils (Maher and Ho, 1994; Nataraj and McManis, 1997; Miller and Rifai, 2004; Mollamahmutoglu and Yilmaz, 2009; Viswanadham et al. 2009a; Viswanadham et al., 2009b; Jiang et al. 2010; Senol, 2011; Plé and Lê, 2012). In these attempts the performance of fibres on the strength characteristics of fine grained soil is incomplete and needs to be researched further.

In the present investigation, the effect of multifilament and fibrile types polypropylene fibers, fiber dosages and fiber lengths on time-dependent unconfined compressive strength behavior has been investigated.

2. PROPERTIES OF MATARIALS

2.1 Clay

The physical properties of the clay including particle size distribution, consistency limits and specific gravity were determined in accordance with (ASTM D 422-63), (ASTM D 4318) and (ASTM D 854), respectively. Based on Casagrande plasticity chart (ASTM D 2487), the soil was classified as high plasticity (CH) clay. Some of the basic characteristics of the clay are summarized in Table 1.

Table 1. Some of the physical characteristics of Ankara clay

Basic characteristics and descriptions	Value
Passing No. 200 (75 μ m) U.S. standard sieve (%)	80.2
Liquid Limit, LL (%)	97
Plastic Limit, PL (%)	28
Plasticity Index, PI (%)	69
Specific gravity, G _s	2.72
USCS Soil Class	CH

2.2 Fiber

Multifilament and fibrille polypropylene fibers with three different lengths were used in the study. 6.0mm, 12.0mm, and 19.0mm long fibrillated Multifilament polypropylene fibers are denoted as M06, M12 , M19, and fibrille polypropylene fibers are denoted as F06, F12 , F19 respectively.

Table 3. The physical characteristics of the fibres (Ployfibres, 2009)

Properties	Fibrillated polypropylene fibre	Multifilament polypropylene fibre
Appearance	Fully oriented collated fibrillated (network) form	Fully oriented multifilament fibrous form
Content	100% virgin homopolymer Polypropylene(C ₃ H ₆)N	100% virgin homopolymer Polypropylene(C ₃ H ₆)N
Compliance	ASTM C 1116-1997 Type III	ASTM C 1116 1997 Type III
Color	Transparent	Transparent
Density (g/cm ³)	0.91	0.91
Tensile strength (MPa)	400	700
Young Modulus (MPa)	2,600	3,500
Elongation at yield, %	15 %	20 %
Softening point (°C)	150	150
Melting point (°C)	160	160
Solubility in water	Insoluble	Insoluble
Hazardous ingredients, %	Nil	Nil
Acid/Alkali resistance	Stable	Stable
Abrasion resistance	Stable	Stable
Biologic durability	Stable	Stable

3. COMPOSING FIBER-CLAY MIXTURES

The mixture design of fiber amended clay samples were based on dry weight percentages of fiber in the clay matrix. The proportions of dry mass of fiber to dry mass of clay were chosen as 0% (fiberless), 0.5%, 1.0% and 2.0% based on the literature (Jadhao and Nagarnaik, 2008; Kumar et al., 2007).

4. DETERMINATION OF LABORATORY COMPACTION CHARACTERISTICS

Maximum dry unit weight of clay was achieved by applying an energy level of 600 kN-m/m³, which is equivalent to the (ASTM D 698-00a, 2006), the recommended standard compactive effort. The compaction curve of the clay is shown in Fig. 1. The maximum dry unit weight and optimum water content of the clay are 13.4 kN/m³ and 29.8%, respectively. The optimum moisture content and maximum dry unit weight of pure clay were also used to prepare samples for strength tests of fiber-clay mixtures for all fiber inclusions.

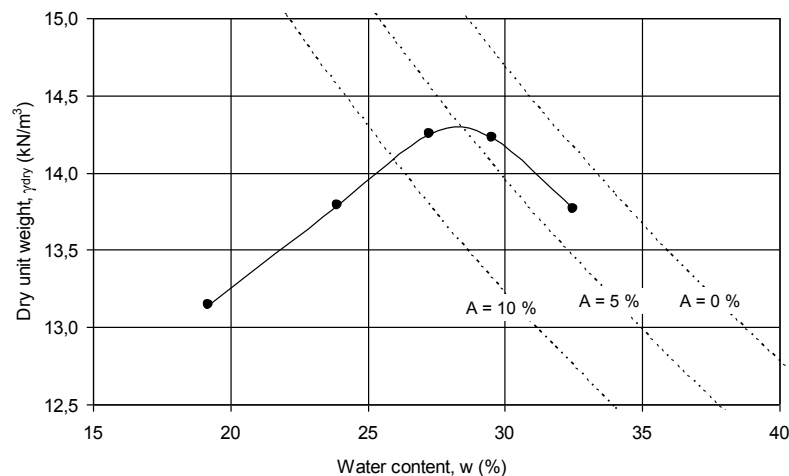


Figure 1. Standart Proctor compaction curve of the pure clay

5. PREPARATION OF FIBER-CLAY SAMPLES FOR STRENGTH TESTS

The fiber was mechanically mixed with the dry clay prior to the compaction until homogenous mixtures were obtained. A compaction mold was used to prepare cylindrical compacted samples of various fiber-clay mixtures at optimum water content and maximum dry unit weight during sample preparation. The compaction mold was designed for unconfined compression and triaxial testing specimens with a height-to-diameter ratio of 2.01. The compaction mold apparatus was made of stainless steel, and split into two parts longitudinally.

Before compaction, the inner surface of the split mold was lightly lubricated to prevent the sample from being damaged while removing it from the compaction mold. Next, the mold was assembled and a soil sample was poured into the mold in three equal layers. Each layer was compacted to a height of 33.5 mm using a stainless steel tamp with a base diameter of 49.50 mm to achieve the desired maximum dry unit weight before placing the next layer. After placing the last layer, the top and bottom end-rings of the compaction mold were unfastened. Finally, the two longitudinal split parts were removed from one another, and the cylindrical sample was gently released. All specimens measured as 50.0 mm in diameter and 100.50 mm in height.

Following compaction at optimum moisture content using standard compactive effort, the fiber stabilized soil samples were stored in sealable plastic containers to prevent moisture loss in a moist room (relative humidity above 70%) at room temperature until the day of testing. As discussed previously, the optimum moisture content and maximum dry unit weight of clay were also used to prepare samples for strength tests of fiber-clay mixtures.

6. UNCONFINED COMPRESSIN TESTS

Unconfined compression tests were performed on the specimens using strain controlled application of the axial load in accordance with ASTM D 2166 standard (ASTM D 2166-00, 2006). The strain rate was kept constant at 0.5 mm/min throughout the testing program.

Unconfined compressive strength (UCS) of the compacted untreated clay samples and fiber-clay samples, for various fiber contents, fiber types and fiber lengths, were plotted with reference to curing periods in Figures 2, 3 and 4. Figures 2, 3 and 4 reveal that UCS of the compacted untreated clay samples decreases slightly with curing period. From Fig.2 it is seen addition of fiber decreases the UCS. Comparing the effect of fiber type and length on the UCS of the fiber-clay mixtures, Fig. 2 shows that for Fiber/Clay = 0.5% mixture and Fiber/Clay = 2.0% mixture, F06 (fiber with 6 mm length) and F19 (fiber with 19 mm length) exhibit the highest UCS, respectively. Fig. 2 also shows the effect of fiber type on the UCS in such a way that for M type fibers as the length of fiber increases the UCS of the fiber-clay samples slightly increases. On the other hand, for F type fibers there is no such a certain relationship between the length of fiber and the UCS. From Figs. 2, 3 and 4 it is seen that as the curing time increases some of the fiber-clay mixtures exhibit higher UCS than those of the untreated clay samples. From Figs. 2, 3 and 4 it is also clear that as the fiber percent in the mixture increases, for example Fiber/Clay = 2.0% mixtures, the longer the fiber the higher the UCS.

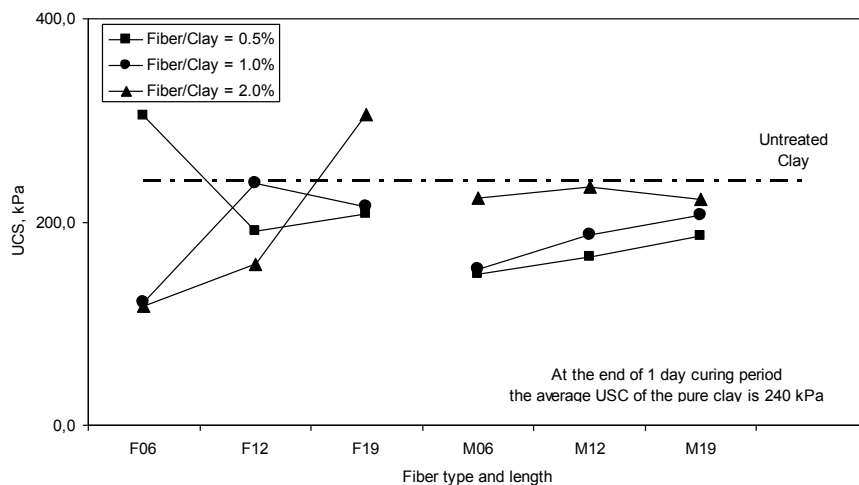


Figure 2. Variation of USC of the Fiber-Clay mixtures with type and length of fibers for 1 day curing period

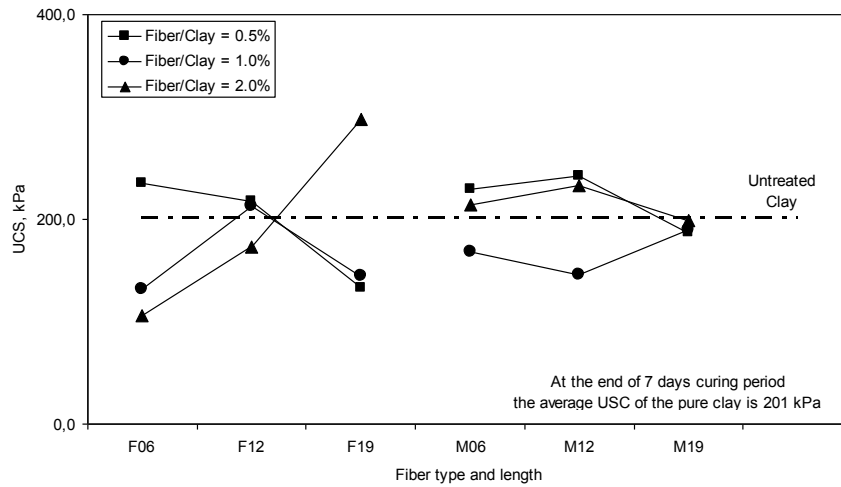


Figure 3. Variation of USC of the Fiber-Clay mixtures with type and length of fibers for 7 days curing period

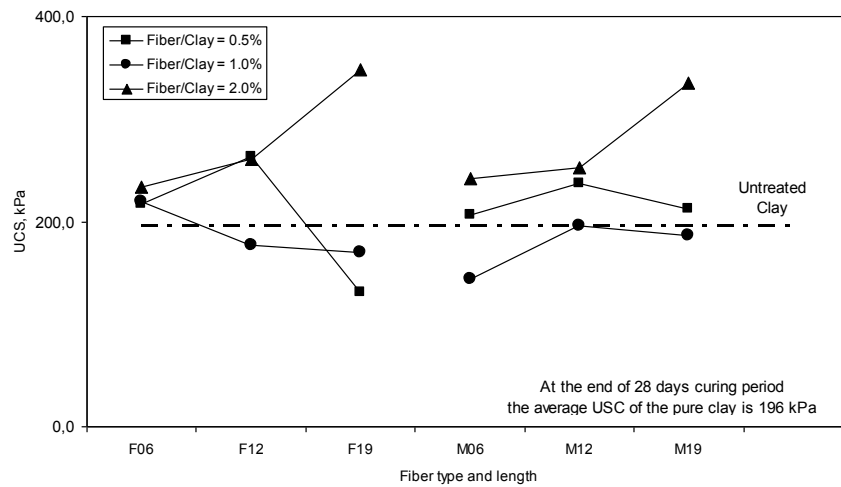


Figure 4. Variation of USC of the Fiber-Clay mixtures with type and length of fibers for 28 days curing period

7. CONCLUSIONS

Fiber-clay mixtures were composed by using high plasticity clay, multifilament (M type) and fibrile (F type) types polypropylene fibers at various proportions. The effect of fiber content and length on the strength characteristics was evaluated at the end of various curing periods. The following conclusions were drawn from this experimental study.

- 1) Addition of any type of fiber (M type and F type) with different dosages and various lengths (except 2.0% F19 and 0.5%M06) decreases the USC for 1 day curing period. As a general tendency it may be stated that for 1 day curing period addition of fiber reversely affected the UCS performance of the clay.
- 2) F19 sample (fibrile polypropylene fiber, length 19 mm with Fiber/Clay= %2.0) gives the highest increase USC at all curing periods. As a general conclusion it may be stated that primarily the percentage of fiber in the mixtures controls the UCS not the length of the fiber.
- 3) For small dosage of fibers, although the effect of length on the UCS is not clear for F type fibers, for M type fibers it is seen that as the length of the fiber increases the UCS also tend to slightly increase. For long periods of curing time the effect of type of fibers on the UCS is similar for 19 mm long fibers and Fiber/Clay= %2.0 mixtures.

ACKNOWLEDGMENTS

Financial support for this work was partially provided by Gazi University Scientific Research Project Grant No. BAP 06/2011-03.

REFERENCES

- ASTM D 422-63. Standard Test Method for Particle-Size Analysis of Soils. *Annual Book of ASTM Standards*, West Conshohocken, Pennsylvania, USA.
- ASTM D 698-00a. Standard Test Methods for Laboratory Compaction Characteristics of Soil Using Standard Effort (12,400 ft-lbf/ft³ (600 kN-m/m³)). *Annual Book of ASTM Standards*, West Conshohocken, Pennsylvania, USA.
- ASTM D 854-02. Standard Test Method for Specific Gravity of Soil Solids by Water Pycnometer. *Annual Book of ASTM Standards*, West Conshohocken, Pennsylvania, USA.
- ASTM D 2166-00. Standard Test Method for Unconfined Compressive Strength of Cohesive Soil. *Annual Book of ASTM Standards*, West Conshohocken, Pennsylvania, USA.
- ASTM D 2487-00. Standard Practice for Classification of Soils for Engineering Purposes (Unified Soil Classification System). *Annual Book of ASTM Standards*, West Conshohocken, Pennsylvania, USA.
- ASTM D 4318-00. Standard Test Methods for Liquid Limit, Plastic Limit, and Plasticity Index of Soils. *Annual Book of ASTM Standards*, West Conshohocken, PA, Pennsylvania, USA.
- Jadhao, P.D. and Nagarnaik, P.B. (2008). Influence of polypropylene fibres on engineering behavior of soil-fly ash mixtures for road construction. *Electronic Journal of Geotechnical Engineering*, v 13 C.
- Jiang, H., Cai, Y. and Liu, J. (2010). Engineering Properties of Soils Reinforced by Short Discrete Polypropylene Fiber, *Journal of Materials in Civil Engineering*, 22(12), 1315–1322.
- Kumar, A., Walia, B.S. and Bajaj, A. (2007). Influence of fly ash, lime, and polyester fibres on compaction and strength properties of expansive soil. *Journal of Materials in Civil Engineering, ASCE*, 19(3): 242-248.
- Maher, M.H. and Ho, Y.C. (1994). Mechanical-properties of kaolinite fiber soil composite, *Journal of Geotechnical and Geoenvironmental Engineering*, 129 (2): 81–1393.
- Miller, C.J. and Rifai, S. (2004). Fiberreinforcement for waste containment soil liners, *Journal of Environmental Engineering*, 130 (8): 981–985.
- Mollamahmutoglu, M. and Yilmaz, Y. (2009). Investigation of the effect of a polypropylene fiber material on the shear strength and CBR characteristics of high plasticity Ankara clay. BCR2A'09, Champaign, Illinois, USA, Paper No: 21.
- Nataraj M.S. and McManis, K.L. (1997). Strength and deformation properties of soil reinforced with fibrillated fibers, *Geosynthetics International*, 4 (1): 65–79.
- Plé, O. and Lê, T.N.H. (2012). Effect of polypropylene fiber-reinforcement on the mechanical behavior of silty clay, *Geotextiles and Geomembranes*, 32: 111-116.
- Ployfibres, (2009). Polyfibres analysis certificate, *Ployfibres Micro Reinforcement Fibres Catalogue*, Polipropilen Elyaf® Industry and Trade Co.
- Senol, A. (2011). Effect of fly ash and polypropylene fibres content on the soft soils, *Bulletin of Engineering Geology and the Environment*, 71 (2):379-387.
- Viswanadham, B.V.S., Phanikumar B.R. and Mukherjee Rahul, V. (2009a). Swelling behaviour of a geofiber-reinforced expansive soil, *Geotextiles and Geomembranes*, 27 (1): 73–76.
- Viswanadham, B.V.S., Phanikumar B.R. and Mukherjee Rahul, V., (2009b). Effect of polypropylene tape fibre reinforcement on swelling behaviour of an expansive soil, *Geosynthetics International*, 16 (5): 393-401.

Confined Metallic Reinforcement Connection Tests on a MSE Wall System

L.G. Schwarz, Johns Creek, GA USA, schwarz.lois@yahoo.com
B.R. Christopher, Christopher Consultants, Roswell, GA USA, barryc325@aol.com
T.P. Taylor, T&B Structural Systems, Inc., Fort Worth, TX USA, tom.taylor@tbssus.com

ABSTRACT

Large-scale static tension pullout tests were performed on two different metallic reinforcement connection systems embedded in gravel to compare the performance of the connections and to determine the effect of confinement pressure on the system load capacity. The metallic reinforcement elements were connected to full-scale reinforced concrete wall panels. One system consisted of a loop anchor and crimp connector with wide bar mat soil reinforcing and the other system consisted of a dual plate shaft (DPS) anchor and TAB connector with a discrete-strip bar mat soil reinforcing. The stabilized earth wall elements were confined in aggregate base material placed at a compactive effort of 95% modified Proctor (ASTM D1557). Three different overburden pressures ranging from 6.7 kN/m² to 73 kN/m² (140 psf to 1525 psf) were applied to the confined elements corresponding to wall heights of 0.3 m to 3.4 m (1 ft to 11 ft). Beyond the embedded connection, the section of reinforcement with transverse bars was isolated from the aggregate base material to prevent interaction with the soil and corresponding reduction in load at the connector. A controlled and increasing axial tensile force was applied to the free end of the reinforcing element. Instrumentation measured continuous displacement at the connector and the end of the reinforcing element until failure. This paper reviews test procedures and the instrumentation used to monitor the load and deformation response of different system components during full-scale laboratory testing. Test results are presented in terms of load and serviceability failure states as compared to AASHTO design requirements.

1. INTRODUCTION

Mechanically stabilized earth wall (MSEW) systems comprised of precast segmental concrete facing panels and inextensible metallic grid-type soil reinforcements (as shown in Figure 1 and Figure 2, respectively) are governed by applicable design and construction criteria in AASHTO LRFD Bridge Design Specifications (AASHTO 2010a), AASHTO LRFD Bridge Construction Specifications (AASHTO 2010b), and the FHWA guidelines for the Design and Construction of Mechanically Stabilized Earth Walls and Reinforced Soil Slopes (FHWA 2009).

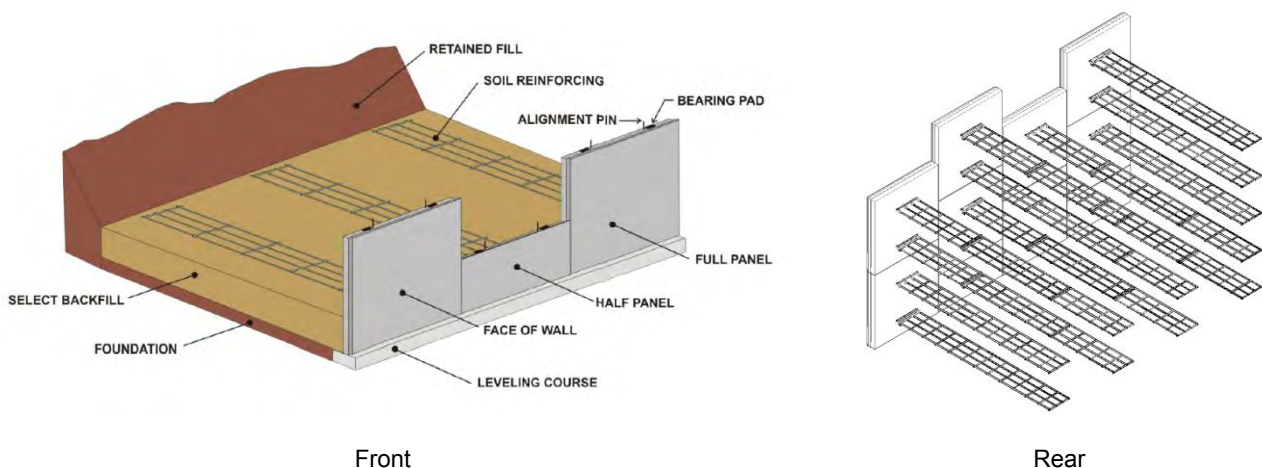


Figure 1. Isometric view of MSEW System-1 showing front and rear faces.

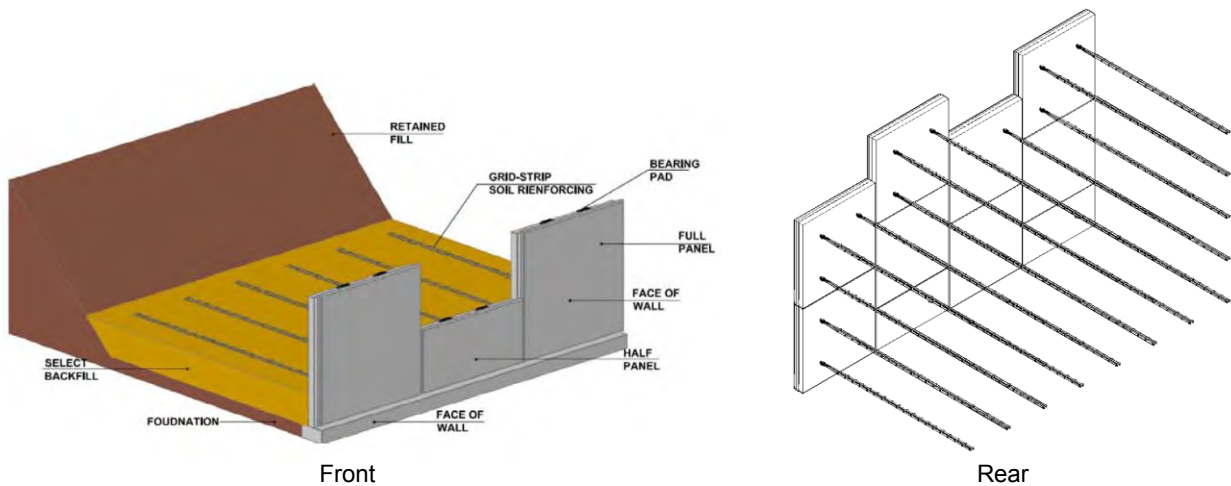


Figure 2. Isometric view of MSEW System-2 showing front and rear faces.

The basic difference in various MSEW systems is the type of reinforcements and their connections to the facing elements. Currently, evaluation of the facing connection component for design purposes involves performing unconfined tensile testing on single anchor elements embedded in concrete face panel segments. In accordance with AASHTO (2010a) requirements, evaluation of the deformation response at the connector is not required. However, the deformation of the connector required to lock up and continue to support the load is of interest as it can be used to evaluate anticipated lateral movement. In addition, a test on a single connector does not evaluate the distribution of stress over multiple connectors typically required to engage and fully mobilize the strength across welded wire reinforcements. Finally, unconfined tests do not provide an evaluation of confinement induced by overburden stress on connection systems in MSEW, which may influence both the deformation response and ultimate strength of the connection system.

The study presented herein involves full-scale laboratory testing of the complete connection system with confinement in suitable backfill material at three different overburden pressures to determine the effect of confining pressure on the connection response of the MSEW system. The complete setup for each connection type is shown schematically in Figure 3. The metallic reinforcement was isolated from the backfill with a sleeve placed beyond the embedded connection to prevent interaction with the backfill and corresponding reduction in load at the connector. Instrumentation was attached to the connection elements, as well as at the rear of the reinforcement, to monitor deformation with increasing tensile load. The soil reinforcing was extended beyond the rear of the confining box to create a free end where the force system could be attached. The tests were performed by applying an axial tensile force to the free end of the reinforcing element.

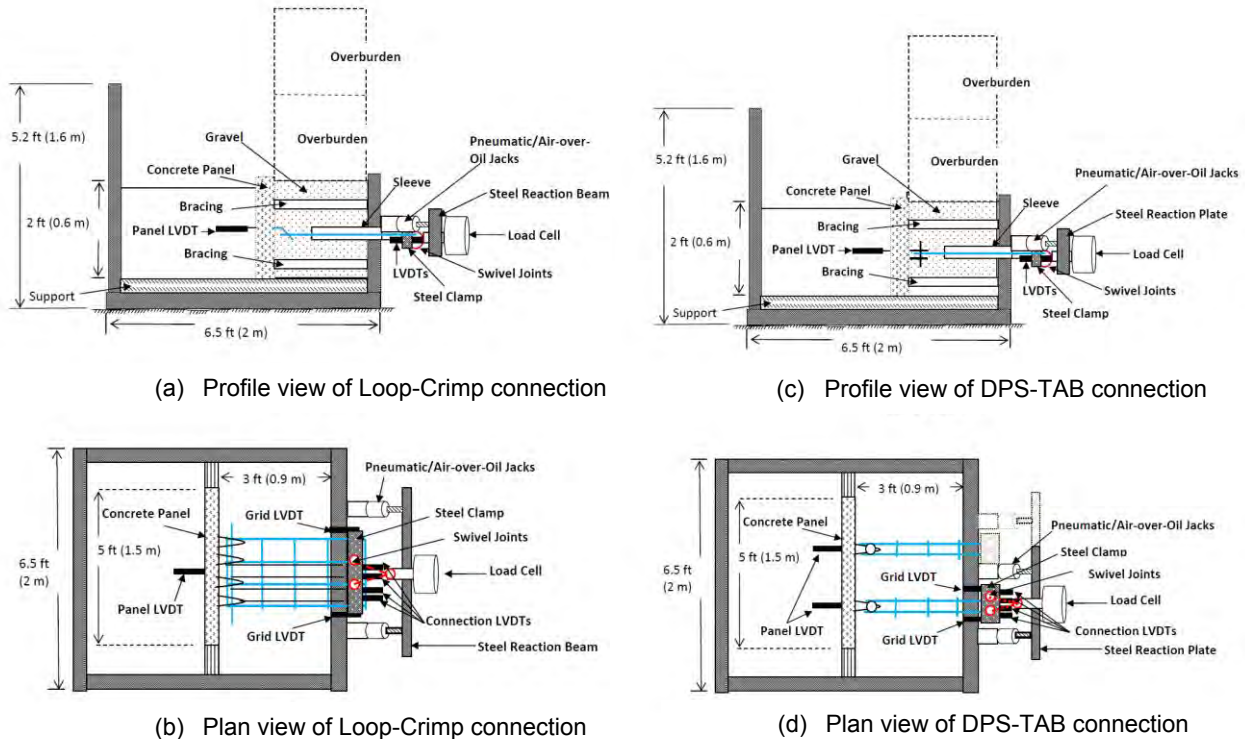


Figure 3. Test setups for Loop-Crimp system and DPS-TAB system in the GTX Stabilization box.

2. LABORATORY TESTING PROGRAM

2.1 Materials

The primary components of the mechanically stabilized earth walls (MSEWs) evaluated for this study include galvanized welded-wire grid-type reinforcing elements, rectangular precast reinforced concrete facing panels, galvanized steel connectors cast into the facing panel, steel connector elements, and select granular backfill. Standard precast panels having a face area of 2.3 m^2 (25 ft^2) and a thickness of 150 mm (6 in.) were used in the laboratory testing study. Metallic connection components are cast into the panel and used to secure the end of the soil reinforcement to the panel. In typical MSEW construction, standard panels and half-size panels are placed in the first course and special size panels are placed in the top course to match the required design and grade variations.

Two different types of MSEW systems were evaluated in this study. The first system consisted of a loop anchor and crimp connector (Loop-Crimp). This Loop-Crimpsystem consisted of 457 mm (18 in.) wide soil reinforcing (SR) elements of welded metallic grids that contained four 150 mm (6 in.) spaced longitudinal wires and 305 mm (12 in.) spaced transverse wires. The SR welded wire grids consisted of longitudinal and transverse wires of equal diameter with designations of W11 x W11, W15 x W15, and W20 x W20 corresponding to wire diameters 9.5 mm (0.374 in.), 11.1 mm (0.437 in.), and 12.8 mm (0.504 in.), respectively. The second system consisted of a dual plate shaft anchor (DPS) and TAB connector. The TAB connector is welded to narrow two-wire discrete-strip reinforcement. The yield strength of the steel wire in both systems is 450 mPa (65 ksi). The nominal tensile strength for the loop connector was equal to 290 MPa (42.3 ksi) which represents 65 percent of yield. The nominal tensile strength of the TAB connector was equal to 336 MPa (48.8 ksi) which represents 75 percent of yield. The difference in percent yield conforms to AASHTO requirements for systems with multiple point connections and single point connections, respectively.

2.1.1 Loop-Crimp Connector System

The Loop-Crimp system evaluated in this series of tests consisted of a four-wire grid-type SR element with 150 mm (6 in.) longitudinal wire spacing and 305 mm (12 in.) transverse wire spacing. The SR element is fabricated with a "V" shaped crimp placed in the longitudinal bars of the welded wire grid reinforcement directly behind the lead transverse wire for connection to the facing panel.

The reinforced concrete facing panels for the Loop-Crimp connection system are cast with a minimum of four loop anchors symmetrically placed and extending from the back face. The loop anchors are fabricated from a single 9.5 mm (0.375 in.) diameter (W11) wire into a series of four parallel loops. The end of the loop is deflected downward at a 45° angle over a length of 51 mm (2 in.). The soil reinforcement is connected to the panel by engaging the longitudinal V-crimped end of the SR element into the parallel looped panel anchor. The SR element is joined to the panel anchor by passing a 610 mm (24 in.) steel connection pin made of 9.5 mm (0.375 in.) diameter (W11) wire through the passages created at the interface of each of the crimped ends and downwardly deflecting panel anchor ends. A photo of the connection system setup for laboratory testing is shown in Figure 4(a). After the connection is made, the soil reinforcement is tensioned in order to remove any slack at the connection and seat the crimp into the loop. Failure to remove the slack will cause the connection to deform more under load.

2.1.2 Dual Plate Shaft Anchor and TAB Connector System

The dual plate shaft (DPS) anchor and TAB connector system consists of a narrow two-wire discrete-strip soil reinforcing (SR) element sometimes referred to as a grid-strip. The discrete-strip consists of two 9.5 mm (0.375 in.) diameter (W11) longitudinal bars that are spaced at 51 mm (2 in.) and with 76 to 100 mm (3 to 4 in.) wide 9.5 mm (0.375 in.) diameter (W11) transverse bars that are resistance welded to the longitudinal bars at their intersection and at a 150 mm (6 in.) interval spacing. A special forged metal TAB is resistance welded to the lead end of each of the longitudinal bars for connection to the concrete facing panel. The lead end of the TAB consists of a flat 38 mm (1.5 in.) wide by 9.5 mm (0.375 in.) thick steel plate that contains a 14 mm (0.562 in.) diameter central bolt hole. The terminal end of the TAB consists of a 16 mm (0.625 in) shaft that contains special longitudinal grooves and serrations.

The reinforced concrete wall facing panel for the DPS–TAB connection system is cast with at least one DPS anchor extending from the back face. The DPS anchor consists of two forged steel parallel 9.8 mm (0.375 in) thick flat plates extending 50 mm (2 in.) at its exposed end, and converges into a 16 mm (0.625 in.) diameter and 130 mm (5 in.) long shaft that terminates into a perpendicular 44 mm (1.75 in.) disk that is embedded into the face panel. The dual plates of the DPS anchor each have a centrally located 14 mm (0.562 in.) diameter aligned bolt hole. The discrete-strip is attached to the DPS anchor by passing the TAB end between the parallel plates so the bolt holes align and is secured from removal using a 12.7 mm (0.5 in.) diameter A325 bolt and nut. The DPS-TAB system is designed to rotate in the horizontal plane and deflect in the vertical plane without adding additional stress to the connection. Shown in Figure 4(b) is the DPS-TAB connection setup in the laboratory.



(a) Loop-Crimp connection

(b) DPS–TAB connection

Figure 4. Photos of full-scale connection systems in laboratory.

2.1.3 Aggregate Base Material

The aggregate used as backfill material was poorly graded gravel with sand (GP). It was classified as A-1-a based on gradation analysis and according to the AASHTO system. Modified Proctor compaction tests (ASTM D1557) performed on the gravel determined a maximum density of 21.3 kN/m³ (135 pcf) at an optimal moisture content of 6%. Applying an oversize correction factor the maximum dry density was determined to be 23.2 kN/m³ (148 pcf) at 3.9% optimal moisture. For the connection tests, the gravel was compacted to approximately 95% of the oversize corrected maximum dry density value with moisture at optimum to slightly higher than optimum.

3. FULL SCALE TESTING

3.1 Test Section Construction and Procedures

Confined (i.e., soil) static tensile connection tests were conducted in the GTX Stabilization Box as was previously shown schematically in Figure 3 for the Loop-Crimp connection and the DPS-TAB connection system. Each connection test involved applying an axial tension force to the free end of the metallic grid or discrete-strip SR element that extended from the back end of the box. Wire extensometers were used to monitor movements of the connection and the embedded portion of the metallic SR element. The extensometer wires were encased in small metal tubes to prevent friction on the wire. Each extensometer wire was connected to a low voltage linear displacement transducer (LVDT) on one end and to the connection or the SR element on the other end. The length of the SR that contained transverse wires was isolated from the backfill using a sleeve to prevent interaction and corresponding reduction in load at the connector. The isolation sleeves were designed to allow the reinforcement to move freely. Shown in Figure 5 are photos of the sleeve assembly. Displacement was monitored using LVDTs connected to the wire extensometers. The LVDTs provide continuous readings of displacement in the direction of the applied load during testing.



Figure 5. Photos of DPS-TAB connections and discrete-strip with sleeve enclosure.

Three overburden pressures were applied to the confined connection. For the purpose of discussion, they will be referred to as low, mid and high. Low overburden pressure corresponds to an average of 6.7 kN/m^2 (140 psf) and was attained by placement of a 300 mm (1 ft) thick layer of compacted gravel onto the connection and the SR element. Mid overburden pressure of 37 kN/m^2 (775 psf) was attained by placement of a 300 mm (1 ft) thick layer of compacted gravel onto the connection followed by stacking dead weight on top of the gravel layer. High overburden pressure corresponding to 73 kN/m^2 (1525 psf) was attained using the same method as the mid overburden pressure and the stacking of additional dead weight on top of the gravel layer as shown in Figure 6.

Two 180 kN (20 ton) pneumatic/air-over-soil jacks with a steel reaction beam were used to apply the pullout force. The jacks were interconnected to provide simultaneous loading. The SR element specimens were gripped in a steel clamp that was attached to the pullout piston using swivel connections. The swivel connections allow for adjustment in the case where SR elements do not exit the box exactly straight. The axial tensile force was measured by a calibrated load cell attached to the pullout piston. The horizontal displacement at the rear of the SR element was monitored outside the box by two LVDTs (one on each side) mounted to the longitudinal bars. In addition, LVDTs were positioned on the outside of the front face of the segmental concrete panel to monitor possible movement of the panel in the direction of the applied tensile load.

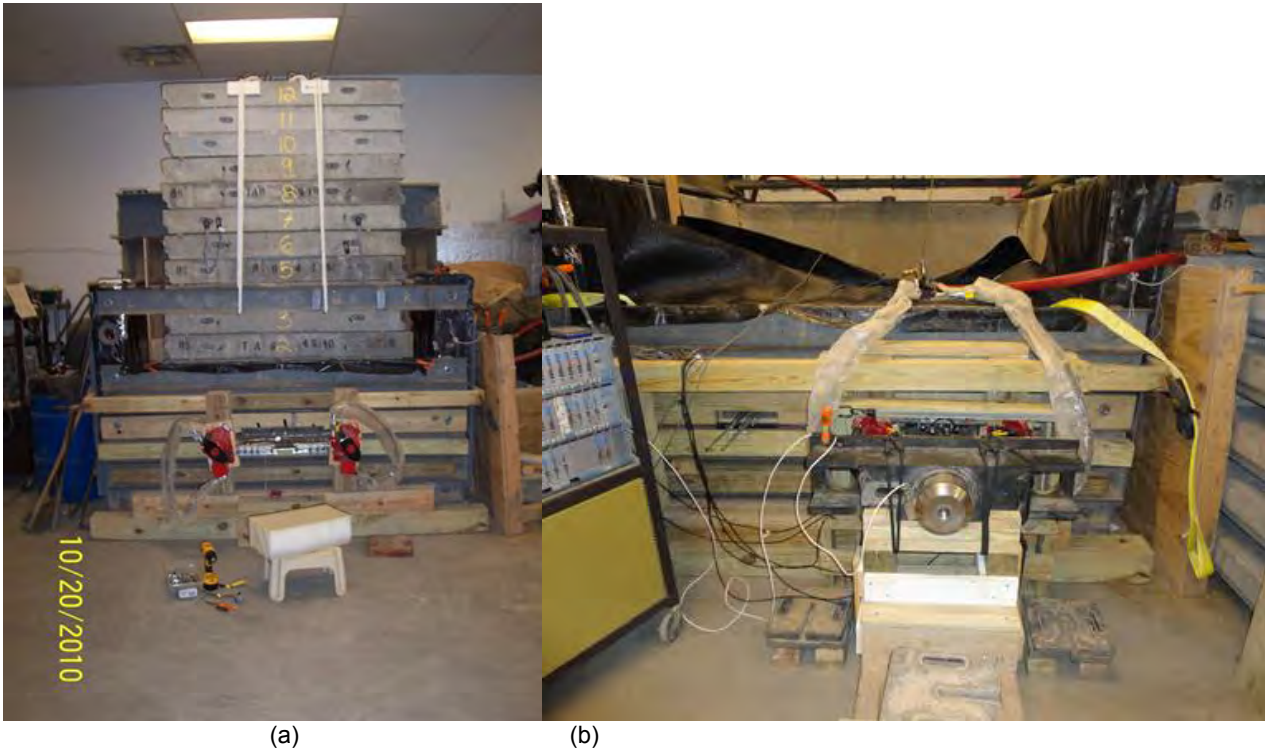


Figure 6. Full-scale confined connection laboratory test setup for (a) Loop-Crimp connection test with high overburden pressure of 73 kN/m^2 (1525 psf) and (b) DPS-TAB connection test with low overburden pressure of 6.7 kN/m^2 (140 psf).

3.2 Test Section Results

The laboratory confined connection test results for the Loop-Crimp connection and the DPS-TAB connection system are shown in Table 1. The peak load is the maximum axial tension load applied to the connection system at failure or termination of the test. The applied vertical load is the overburden pressure. Movement corresponds to displacement measured at the rear of the metallic grid using wire extensometers connected to LVDTs on the longitudinal bars. Additional measurements on where movement occurred in each element of the connection was collected and provided to the supplier for optimizing the design of the connection system.

For the Loop-Crimp connection the peak tensile load values measured during testing ranged from 103.6 to 109.5 kN (23.3 to 24.6 kips) for W11 x W11 grid, 133.0 to 159.1 kN (29.9 to 35.8 kips) for W15 x W15 grid, and 142.2 to 203.6 kN (32.0 to 45.8 kips) for W20 x W20 grid. Failure of the connection tests for the W11 x W11 and W15 x W15 metallic grids were due to longitudinal bar tension failure as exhibited in the post-test exhumed connection shown in Figure 7. Tests that terminated before failure showed no observable damage to the concrete panel. The connection tests on the W20 x W20 metallic grid failed by pullout of the loop connectors from the concrete prior to reaching 19 mm (0.75 in.) of deformation.

The peak tensile load values measured during testing of the DPS-TAB connection ranged from 82.2 to 94.3 kN (18.5 to 21.2 kips) and tend to increase slightly with confining stress as shown in Table 1. With the exception of one test, the DPS-TAB connection system exhibited structural failure of the concrete panel or the test was terminated before 19 mm (0.75 in.) of deformation was reached. For all DPS-TAB connection scenarios, no shear failure of the bars or bolts was evidenced, however the connection bolts deformed.

Table 1. Confined connection laboratory test results.

Reinforcement / Connector, <i>Element Failure</i>	Load at 19 mm Movement, kN (lb)	Peak Tensile Load, kN (lb)	Movement at Peak Load, mm (in.)	Applied Vertical Load, kN (lb)	Overburden Pressure, kN/m ² (psf)
Loop Anchor - Crimp Connection					
W11 x W11 grid / loop† <i>Type C Failure</i>	45.0 ^a (10,124 ^a)	103.6 ^a (23,299 ^a)	31.8 ^a (1.25 ^a)	3.7 (840)	6.5† (136†)
W11 x W11 grid / loop <i>Type A Failure</i>	86.8 (19,518)	105.5 ^b (23,740 ^b)	29.6 ^b (1.16 ^b)	3.7 (840)	6.7 (140)
W11 x W11 grid / loop <i>Type A Failure</i>	95.4 (21,466)	109.5 (24,647)	32.1 (1.26)	20.7 (4,650)	37.1 (775)
W15 x W15 grid / loop <i>Type A Failure</i>	128.2 (28,849)	133.0 (29,926)	20.2 (0.80)	3.7 (840)	6.6 (139)
W15 x W15 grid / loop <i>Type C Failure</i>	134.6 (30,290)	152.0 ^b (34,198 ^b)	35.6 ^b (1.40 ^b)	20.7 (4,650)	37.1 (775)
W15 x W15 grid / loop <i>Type A Failure</i>	123.2 (27,727)	159.1 (35,805)	38.0 (1.50)	40.7 (9,150)	73.0 (1,525)
W20 x W20 grid / loop <i>Type B Failure</i>	63.4 (14,029)	147.8 (33,257)	28.2 (1.11)	3.7 (840)	6.6 (139)
W20 x W20 grid / loop <i>Type C Failure</i>	100.8 (22,684)	163.8 ^b (36,844 ^b)	28.1 ^b (1.11 ^b)	3.7 (840)	6.7 (140)
W20 x W20 grid / loop <i>Type B Failure</i>	83.2 (18,709)	142.2 (31,995)	23.1 (0.91)	20.7 (4,650)	37.1 (775)
W20 x W20 grid / loop <i>Type B Failure</i>	121.4 (27,307)	203.6 (45,822)	40.6 (1.60)	20.7 (4,650)	37.1 (775)
W20 x W20 grid / loop <i>Type A & B Failures</i>	92.7 (20,857)	197.0 (44,334)	38.9 (1.53)	40.7 (9,150)	73.0 (1,525)
DPS – TAB Connection					
GS11 strip / DPS-TAB <i>Type C Failure</i>	na	82.2 (18,484)	5.8 (0.23)	3.7 (840)	6.7 (140)
GS11 strip / DPS-TAB <i>Type B Failure</i>	na	88.8 (19,980)	5.8 (0.23)	3.7 (840)	6.7 (140)
GS11 strip / DPS-TAB <i>Type B Failure</i>	na	94.2 (21,192)	na na	20.7 (4,650)	37.1 (775)
GS11 strip / DPS-TAB <i>Type B Failure</i>	na	94.3 (21,219)	11.5 (0.45)	20.7 (4,650)	37.1 (775)
GS11 strip / DPS-TAB <i>Type C Failure</i>	na	93.4 (21,012)	10.5 (0.41)	40.7 (9,150)	73.0 (1,525)
GS11 strip / DPS-TAB <i>Type C Failure</i>	na na 88.5 (19,920)	92.7 ^c (20,852 ^c) 94.0 (21,159)	12.8 (0.50) 22.9 (0.90)	40.7 (9,150)	73.0 (1,525)

Type of Element Failure: A: *Longitudinal wire(s) sheared*

B: *Panel Failed*

C: *No Failure – Test terminated*

Notes: † Panel loops were at slightly different height than other panels

^a Panel moved during test; movement value shown reflects adjustment

^b Test was stopped before actual peak may have occurred

^c Instrumentation malfunction

na – not available



Figure 7. Photos of excavated Loop-Crimp connection after full-scale laboratory testing with confinement.

4. DISCUSSION OF RESULTS

The test results found that the nominal tensile strength of the Loop-Crimp connection system exceeded the nominal strength at the connection. In the W20 x W20 metallic grid test, notwithstanding the connection was unable to be observed at the design strength level, the tensile loads at failure were well above the design strength requirements such that the concrete still had significant reserve resistance compared to the nominal strength of the connection.

Calculations in accordance with LRFD design for the allowable tension (T_{al}) load for 75-year design life are determined by the following relationship:

$$T_{al} = n \cdot A_c \cdot \phi_y \cdot F_y \quad [1]$$

Where, n is the number of longitudinal bars, A_c is the area of longitudinal bar after degradation, ϕ_y is the resistance factor, and F_y is the yield strength of the steel bars.

For purposes of comparison, the maximum design tension load for a 75-year design life for the Loop-Crimp connector using LRFD and a resistance factor of 0.65 is equal to 60.0 kN (13.5 kips) for W11 x W11 grid, 85.8 kN (19.3 kips) for W15 x W15 grid and 119.1 kN (26.8 kips) for W20 x W20 grid. As shown in Table 1, the ultimate tensile strength of the Loop-Crimp connection system tested exceeds the LRFD values for each corresponding metallic grid.

The maximum design tension load for a 75-year design life for the DPS-TAB connector system using LRFD and a resistance factor of 0.75 is equal to 34.7 kN (7.8 kips). As shown in Table 1, the ultimate tensile strength of the DPS-TAB connection system tested exceeds the LRFD value.

The reported test results also provided a measurement of the load at 19 mm (0.75 in.) deformation, which is the limiting deformation for pullout tests (FHWA 2009). This deformation represents a serviceability limit state rather than a strength limit state. The laboratory test results can be used to conservatively estimate the connection capacity for the Service I limit based on a reduction in the load factor from $\gamma = 1.35$ for the Strength I limit state to $\gamma = 1.0$ for the Service I limit state (AASHTO 2010a). Therefore, the factored load is equal to a 26 percent reduction (equivalent to a reduction in the load factor from 1.35 to 1.00) in the nominal load at the loop connector. The laboratory test results indicate that all final test results exceeded this requirement at 19 mm (0.75 in.) of measured deformation.

Consideration of the DPS-TAB connection design using LRFD and a reduced load factor for the Strength I limit state to the Service I limit state, the factored load is equal to a 35 percent reduction in the allowable load at the connector. Laboratory test results for the DPS-TAB connections show that the reduced loads range from about 53.3 to 61.3 kN (12.0 to 13.8 kips) for the confining stresses used with the system and exceed the calculated maximum design tension load of 34.7 kN (7.8 kips) by a factor of 2.3 to 2.8.

Presented in Figure 8 is the measured deformation at peak tensile load for each of the connection systems tested in relationship to the applied normal load (overburden pressure). The peak tensile load for each test is shown at the top of each bar in the graph and connection scenarios are grouped by normal load. The graph demonstrates that increasing

confinement pressure increases the peak tensile load. By comparison of the two different types of connections, consideration of the number of connection points in each test influences to some degree the measured peak load and is dependent on the extent of non-linear loading at each connection element (i.e., loop or dual plate shaft). Further, the data reflects that ridged single point connectors do not deform under load as compared to multiple single point connectors. This demonstrates even distribution of stress at the connection for a single point connector and possible uneven stress distribution at a multiple point connector.

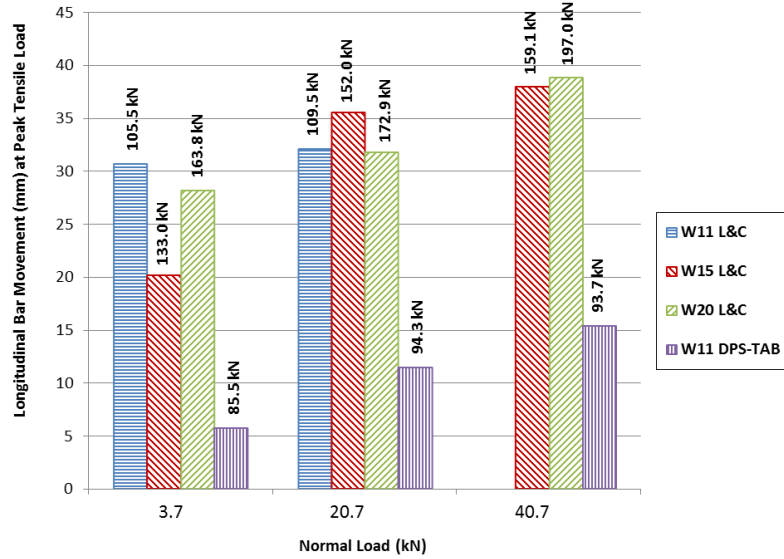


Figure 8. Deformation at Peak Tensile Load vs Normal Load.

The peak tensile loads measured during confined connection system testing and the corresponding trend lines for each test series of reinforcement type and normal load are presented in Figure 9(a). Data points enclosed in circles represent tests that did not experience bar shear failure or panel failure and were terminated. Shown in Figure 9(b) are the serviceability tensile loads measured for each Loop-Crimp connection test at 19 mm (0.75 in.) of movement and corresponding trend lines compared to the peak tensile loads.

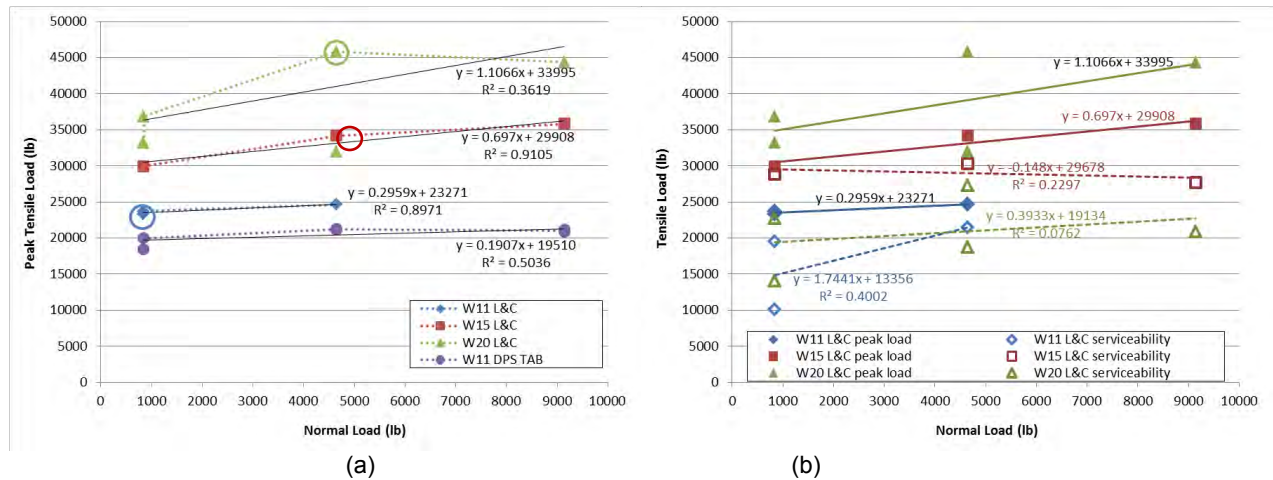


Figure 9. Measured Tensile Load vs Normal Load in terms of (a) peak tensile load and (b) serviceability tensile load.

5. CONCLUSIONS

Based on the limited confined connection tensile testing defined and discussed herein, the following conclusions can be advanced.

1. Full scale connection tests can be performed on MSEW connection systems and provide an evaluation of the influence of confinement as well as the influence in ultimate strength resulting from load distribution across multiple connectors in welded wire reinforcing systems.
2. By measuring the deformation response of the connector under confined conditions, a good assessment can be made on the various components of the connector that contribute to panel deformation and an assessment of stress in the reinforcement at serviceability limits can be made.
3. Rigid single point connectors deform less under load than systems that contain multiple connection points.
4. According to AASHTO, the limiting deformation target value is 19 mm (0.75 in.) for pullout tests. This is a serviceability limit state and not a strength limit state that is required for evaluating connection capacity.

ACKNOWLEDGEMENTS

The authors wish to acknowledge T&B Structural Systems, Inc. for their financial support in the performance of this study, GeoTesting Express, Inc. and their laboratory staff for their performance of the testing program and Geocomp Corporation for their contribution to the instrumentation of the test section.

The metallic reinforcement connection systems described as the Loop-Crimp system and DPS-TAB system with the discrete-strip soil reinforcing element used in the laboratory testing results reported herein, are US and foreign patented designs and methods of connection by T&B Structural Systems, Inc., with additional patents pending by T&B Structural Systems, Inc., and the discrete-strip is trademarked as Grid-Strip[®] in the US.

REFERENCES

- AASHTO (2010a). *LRFD Bridge Design Specifications, 5th ed.*, American Association of State Highway and Transportation Officials, Washington, D.C.
- AASHTO (2010b). *LRFD Bridge Construction Specifications, 3rd ed.*, American Association of State Highway and Transportation Officials, Washington, D.C.
- ASTM D1557. Standard Test Methods for Laboratory Compaction Characteristics of Soil Using Modified Effort, *American Society for Testing and Materials*, West Conshohocken, PA, USA.
- ASTM D6706. Standard Test Methods for Measuring Geosynthetic Pullout Resistance in Soil, *American Society for Testing and Materials*, West Conshohocken, PA, USA.
- ASTM D6638. Standard Test Methods for Determining Connection Strength Between Geosynthetic Reinforcement and Segmental Concrete Units, *American Society for Testing and Materials*, West Conshohocken, PA, USA.
- ASTM E488. Standard Test Methods for Strength of Anchors in Concrete and Masonry Elements, *American Society for Testing and Materials*, West Conshohocken, PA, USA.
- FHWA (2009). *Mechanically Stabilized Earth Walls and Reinforced Soil Slopes, Design and Construction Guidelines*, authors: Berg, R.R., Christopher, B.R., and Samtani, N. U.S. Department of Transportation, Federal Highway Administration, Washington, D.C., FHWA NHI-10-024 Vol I, NHI-10-025 Vol II, and as FHWA GEC011, 684p.

Confined-accelerated Creep Tests on Geosynthetics

F. A. N. França, Ph.D., São Paulo State University, Brazil, franca@dec.feis.unesp.br
F. P. B. Avesani, MSc. student, University of São Paulo, Brazil, franpba@sc.usp.br
B. S. Bueno, Ph.D., University of São Paulo, Brazil, bsbueno@sc.usp.br
J. G. Zornberg, Ph.D., P.E., University of Texas at Austin, USA, zornberg@mail.utexas.edu

ABSTRACT

The creep behavior of geosynthetics usually characterized by standard tests which present two main concerns: they are time-consuming and may not consider the possibly significant effect of soil confinement. Several approaches have been presented in the technical literature in order to address each of these aspects, but only independently. Recently, a new apparatus was developed in order to conduct confined-accelerated creep tests using geosynthetics and both concerns were addressed simultaneously. This paper presents a new set of creep tests conducted under different conditions with the new equipment. A biaxial geogrid and a nonwoven geotextile were used in these tests, which comprised creep rupture and creep deformation ones, both in in-isolation and in-soil conditions. The results highlight the importance of both using elevated temperatures to expedite the determination of geosynthetics creep behavior and studying the effect of soil confinement in both creep test types (creep rupture and creep deformations tests).

1. INTRODUCTION

The creep behavior of geosynthetics commonly plays an important role in the computation of the design tensile strength of these materials when used in reinforced soil structures. Among the reduction factors used to define this parameter, the one related to creep of geosynthetics usually presents the highest values (Koerner, 2005). The reduction factor due to creep behavior is quantified by conducting standard tests (ASTM D 5262), in which in-isolation specimens are subjected to a continuing and constant force while their elongation is measured. These tests are performed under controlled temperature and relative humidity conditions. In addition to the determination of the design tensile strength, creep strains obtained from such tests may be used to evaluate the reinforced soil structure behavior prior to its construction. Therefore, it can be noticed that the geosynthetics standard creep tests are used to define both the design strength and the behavior in such type of geotechnical structure.

Geosynthetics standard creep tests have been widely used to quantify the creep behavior of geosynthetics materials, mainly due to its simplicity. However, this type test presents two main concerns. Firstly, it is time-consuming, with test duration reaching 10,000 hours. Secondly, the configuration used in standard tests does not consider the possibly significant effect of soil-geosynthetic interaction (soil confinement). Together, these aspects may lead to expensive test sets and conservative results.

Geosynthetics creep response may be accelerated by conducting standard creep test at elevated temperatures (Bueno et al. 2005). These tests are commonly referred as accelerated creep tests. The creep strains at the reference temperature (e.g. room temperature) are inferred by calculations based on time temperature superposition techniques and their results. Therefore, several in-isolation accelerated creep tests with different specimens must be performed at the same load, yet at different temperatures. This set of test results is used to compose a creep master curve, which represents the creep response of the geosynthetic at the reference temperature and reaches greater times than those used in each accelerated test. This method is very well established in the technical literature. Several studies have been reported using accelerated creep tests to define geosynthetics creep response (Jeon et al., 2002; Zornberg et al., 2004; Bueno et al., 2005; Jones and Clark, 2007; Tong et al., 2009; Yeo et al., 2009). In addition, Thornton et al. (1998) proposes a new approach for evaluating tensile creep behavior of geosynthetics by means of accelerated tests, which is described by ASTM D 6992. This new method is based on increasing the test temperature in stages, which reduces the implications of material variability in the test results.

Soil confinement may have a great influence on the stress-strain behavior of geosynthetics. This aspect is usually referred to different mechanisms that restrict fibers and yarns relative movements (Elias et al., 1998). Thus, it is expected that the soil confinement effect on stress-strain behavior of geosynthetics is more substantial in geosynthetic materials manufactured with elements (fibers and yarns) which are free to move or adjust their position within the geosynthetic matrix (e.g. nonwoven geotextiles). Accordingly, geogrids are commonly considered as an example of the geosynthetic materials which stress-strain behavior is not affected by soil confinement. The geogrid ribs are not allowed to change position while loaded due to the strength of their connections. In addition, woven geotextile are generally considered as intermediary materials in this regard. Despite these stress-strain behavior pattern is frequently reported in the technical

literature, Elias et al. (1998) emphasize the importance of defining the influence of soil confinement concerning this aspect in every geosynthetic prior to real structure construction. This suggestion was based on test results in which the stress-strain behavior of a woven geotextile was dependent on soil confinement. Conversely, Boyle et al. (1996) reported a set of tests in which samples of woven geotextiles stress-strain behavior was not affected by soil confinement.

The soil-geosynthetic interaction may restrain creep strains while a continuing and constant load is applied to a geosynthetic specimen. In fact, the creep behavior of geosynthetics is commonly reported to be similar to that mentioned for their stress-strain behavior. This aspect is related to the second concern of standard creep tests (lack of soil confinement). Creep tests conducted in special chambers with in-soil specimens are more likely to address this concern. This approach was pioneered by McGown et al. (1982) and several recent studies in which other types of equipment were used are reported in the technical literature (Costa, 2004; Mendes et al., 2007; Ding, et al., 2009; Kamiji et al., 2009). Although there are a vast number of available publications, a standard approach to perform in-soil creep tests was not established so far.

Confined creep tests using geosynthetics are commonly reported using three different loading systems. Firstly, as presented by McGown et al. (1982), the specimen is loaded by means of clamps attached to a portion of the specimen located outside the testing chamber, while normal stresses are applied. The second type of loading system applies a vertical stress over the confining soil and, at the same time, the testing chamber side walls are allowed to move laterally. This produces a soil horizontal strain due to the vertical stress application. This type of equipment was used by Costa (2004) and Kamiji et al. (2009). A third type of confined creep test on geosynthetics has also been reported. This includes tests conducted with pullout testing equipment in which the load is maintained constant during the pullout test, while normal stresses are applied (Elias et al., 1998).

Each type of creep tests loading systems represents a different location of the geosynthetic material inside the reinforced soil mass. The first one, in which the specimen is loaded by means of clamps (external loading), may be used to characterize the creep behavior of the portion located in the passive zone, where insignificant soil mass movement is noticed. The portion in the active zone of the reinforced soil mass is more likely to be represented by means of creep tests in which the soil is allowed to deform laterally during the test and the load is transmitted by soil-geosynthetic interaction. Finally, creep tests using pullout testing equipment may represent the region at the end of the geosynthetic reinforcement inside the passive zone. A similar description was reported by Palmeira and Milligan (1989) regarding the mechanisms of interaction in reinforced soil structures.

Both elevated test temperature and in-soil specimen approaches have been successfully reported in the technical literature, but only independently. Regarding this, França (2012) fully presents a new device capable of conducting simultaneously confined and accelerated creep tests. This equipment was developed in the Laboratory of Geosynthetics of the School of Engineering of the University of São Paulo at São Carlos and was firstly presented in França and Bueno (2010). Further descriptions are presented in França et al. (2011) and França and Bueno (2011). Improvements have been added to this new equipment concerning the loading system. In addition, further tests were performed with both a biaxial polyester geogrid and a polyester nonwoven geotextile. This paper presents a brief description of the new device and the improvement provided to its loading system. Moreover, the results of additional tests are presented and discussed.

2. NEW CREEP TESTING EQUIPMENT

The main objective of the new creep testing equipment development was to simultaneously address both main concerns of conventional creep tests. Therefore, it comprises several systems which are responsible for confining the specimen in soil, elevate the temperature, apply the continuing and constant load, measure specimen elongation and acquire data from the tests. Figure 1 presents a general view of the new equipment with the main components.

The testing procedure consists of positioning a 200 mm wide geosynthetic specimen (1100 mm long) into the upper portion of the testing chamber (400 mm wide, 400 mm long and 200 mm high). This part of the chamber is filled with soil in order to reproduce soil-geosynthetic interaction. A thermocouple is installed in this procedure to measure the temperature nearby the specimen, which is considered as the test temperature. The lower portion houses three electrical resistances and a second thermocouple and is also filled with soil to improve heat transfer to the upper portion. The thermocouple in the lower portion controls the temperature of the electrical resistances. A pressurized air bag is placed over the top of the soil fill and is used to apply normal stresses up to 150 kPa. The chamber lid is attached to its walls and provides the reaction necessary to reach such values. Finally, a polystyrene cover surrounds the testing chamber to prevent heat loss during elevation of test temperature.

Both side walls of the upper portion of the testing chamber are provided with apertures wide enough (5 mm) to allow the specimens to reach the outer roller grips. The grips are connected to dead weights by steel cables. Thus, dead weights

are used to apply the continuing and constant load to specimens during creep tests. Besides, a set of pulleys is used to multiply to load that reaches the specimen by a factor approximately equal to 5.7. The loading system also comprises two load cells to register the load in each side of the specimens.

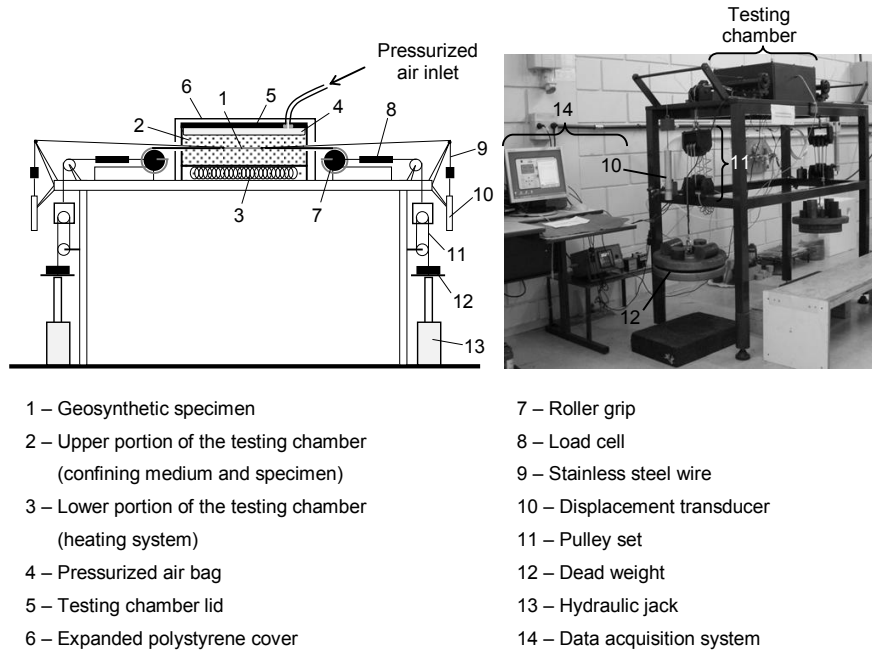


Figure 1. Main elements of the new creep testing equipment (França et al., 2012).

Two hydraulic jacks were used in the first version of the new equipment to apply creep load in a constant, smooth, proper way. Hence, the loading process should be performed by two operators at the same time. As a result, some tests presented different load rates in each side of the specimen. Concerning this, a new loading system was implemented to the equipment developed by França (2012). It consists of a steel beam that simultaneously supports the dead weight from both sides of the equipment. Then, an electrical rotor controls the downward movement of the beam, providing a smooth and homogenous loading rate in both sides of the specimen. Loading rate can be programmed by means of an automated controller. Figure 2a illustrates the new apparatus implemented to the loading system of the new creep testing equipment, while Figure 2b presents the load level during the first five minutes of a confined-accelerated creep test performed with a nonwoven geotextile loaded to 70% of its ultimate tensile strength (UTS). This test was conducted at 36.2°C and with normal stress equal to 50 kPa.

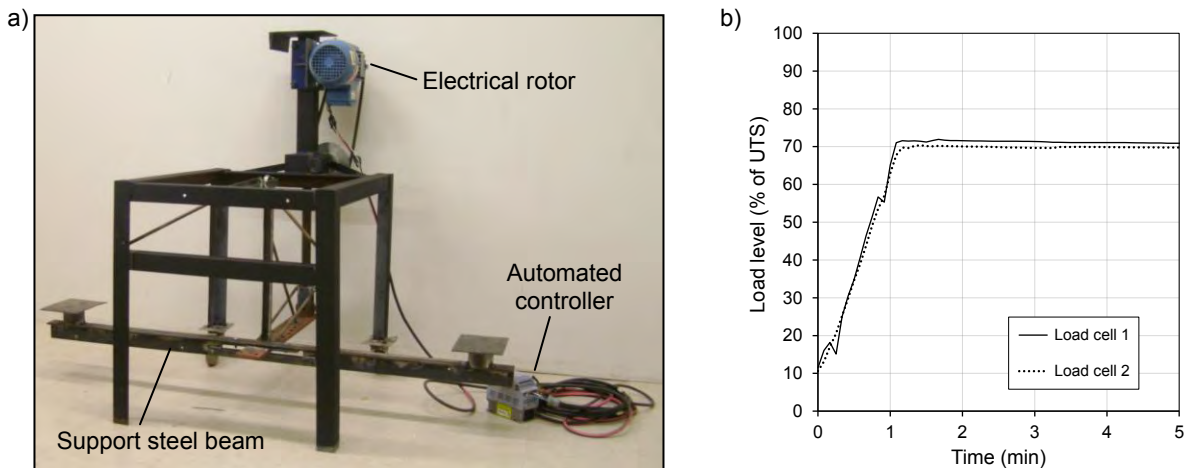


Figure 2 – New apparatus implemented to the loading system of the new creep testing equipment: a) General view; b) Load level during the first five minutes of a confined-accelerated creep test performed with a nonwoven geotextile.

The new equipment requires 1,100 mm long geosynthetic specimens. However, the specimen preparation procedure consists of reinforcing the outermost portions with a two-component adhesive in order to result in two rigid, smooth surface regions. Consequently, only the central segment (100 mm long and 200 mm wide) is subjected to creep deformations during the tests. This segment is reported as “length of interest” in this paper. At the end of the specimen preparation procedure, two pieces of stainless steel wires are attached and glued in the length of interest of the specimens. They are connected to displacement transducers in order to measure the displacement of each of these two points. Then, specimen elongation is computed by the sum of both values divided by the initial distance between them.

The new creep testing equipment is also provided with an automated data acquisition system. It is responsible for registering reading from thermocouples, load cell and displacement transducers.

3. CREEP TESTS

The new creep testing equipment was used in three different types of tests: confined, accelerated and confined-accelerated. Tests with in-soil specimens conducted at room temperature are referred as confined creep tests. On the contrary, tests conducted with in-isolation specimens and under elevated temperature are named accelerated creep tests. Finally, tests in which both measures were used simultaneously are entitled confined-accelerated creep tests in this paper. Besides, creep tests conducted under the regulations presented by ASTM D 5262 are referred as conventional creep tests and were performed in order to characterize geosynthetics creep behavior regarding the current practice. The following sections describe the materials used and the tests performed during this study. Moreover, the results from such tests are presented and discussed.

3.1 Geosynthetic Materials and Chamber Fill

Two different geosynthetic materials were used in the creep tests presented in this paper: a nonwoven geotextile and a biaxial geogrid. Both geosynthetic materials were manufactured with polyester fiber. Table 1 summarizes the main characteristics of each geosynthetic material.

Table 1. Characteristics of tested geosynthetic materials.

Characteristics	Nonwoven geotextile	Biaxial woven geogrid
Manufacturing process	Needle punched	Woven
Predominant polymer	Polyester	Polypropylene
Mass per unit area (g/m ²)	263 (6.1%) ¹	N/A ²
Aperture size (mm)	N/A ²	35.0
Nominal thickness (mm)	2.8 (5.6%) ¹	N/A ²
Tested direction	Cross-machine direction	Machine direction
Short-term tensile strength (kN/m)	14.11 (12.4%) ¹	19.72 (1.9%) ¹
Elongation at rupture (%)	68.12 (9.34%) ¹	9.6 (4.4%) ¹

¹the numbers in parentheses correspond to the coefficient of variation computed in each parameter.

²non-applicable.

Confined and confined-accelerated creep tests were performed with testing chamber filled with a dry poorly graded sand sample, classified as SP according to USCS system. Its coefficient of uniformity and coefficient of curvature were equal to 1.01 and 0.72, respectively. Maximum dry density of 16.7 kN/m³ and minimum dry density of 15.0 kN/m³ were found for the sand sample used as confining medium. The sand was used with density equal to 45% of its maximum dry density. Direct shear tests at this condition resulted in peak friction angle equal to 34.4° and residual friction angle equal to 27.5°.

3.2 Tests Performed

Firstly, the creep behavior of both geosynthetic materials were determined by means of conventional creep tests (ASTM D 5262). In fact, the geogrid was not subjected to other types of creep tests so far in this research. The nonwoven geotextile was also used in accelerated, confined and confined-accelerated creep tests. Tests with in-soil specimens were performed under normal stress of 50 kPa. Accelerated and confined-accelerated creep tests were conducted under different test temperatures. Note that some tests were performed until specimens rupture (creep rupture tests). Table 2 summarizes the characteristics of the creep tests presented in this paper.

Table 2. Characteristics of creep tests.

Type of creep test	Nonwoven geotextile			Biaxial woven geogrid	
Conventional	20 to 60% of UTS ¹ 1000 h; Room temperature			20 to 50% of UTS ¹ 80 to 95% of UTS ¹ 100 h; Room temperature	
Accelerated	50% of UTS ¹ 112 h; 35.1°C	---	---	---	---
Confined (50 kPa) ²	50% of UTS ¹ 160 h; 26.0°C	70% of UTS ¹ 131 h; 24.1°C	80% of UTS ¹ 160 h; 24.4°C	90% of UTS ^{1,3} 0.78 h; 24.5°C	---
Confined-accelerated (50 kPa) ²	50% of UTS ¹ 131 h; 36.9°C	70% of UTS ¹ 191 h; 36.9°C 265 h; 47.7°C 464 h; 59.1°C ³	80% of UTS ^{1,3} 17.5 h; 36.5°C	---	---

¹Ultimate tensile strength from short-term tensile test.

²Confining pressure applied during the test.

³Creep rupture test.

3.3 Creep test results and analysis

Nineteen creep tests are presented in this paper. Among them, ten tests were conducted with the new creep testing machine developed by França (2012). Despite geosynthetics creep curves are commonly plotted as specimen elongation versus time in logarithmic scale, the effects of temperature and soil-geosynthetic interaction in creep strains are not clearly identified since this representation reflects both initial and creep strains. On the contrary, Zornberg et al. (2004) proposed a creep curves representation in which only the creep strain of the specimens are used. In this plot, the creep strains are plotted versus the logarithm of the ratio between the current time and the time at the end of load application. Moreover, the slope of the resulting line indicates the rate of creep strain occurrence during the tests, which is designated as creep index (T_α). Hence, creep index values can be used to indicate the effect of any parameter in creep strains of any geosynthetic material. Due to this aspect, the representation suggested by Zornberg et al. (2004) was used in the analysis of the creep tests presented in this paper.

3.3.1 Nonwoven Geotextile

Different creep test types were performed with the nonwoven geotextile. Initially, tests conducted at conventional conditions and at 50% of the ultimate tensile strength (UTS) in non-conventional conditions were used to quantify the geotextile creep behavior regarding creep deformations. Figures 3a and 3b present the results obtained in conventional creep tests with specimens subjected to 20 to 60% of UTS and in creep tests under both conventional and non-conventional conditions with specimens loaded to 50% of UTS, respectively. Note that a few points are represented in this plot in order to make it clearly. However, data acquisition was performed with one minute intervals. This measure was used in every plot presented in this paper.

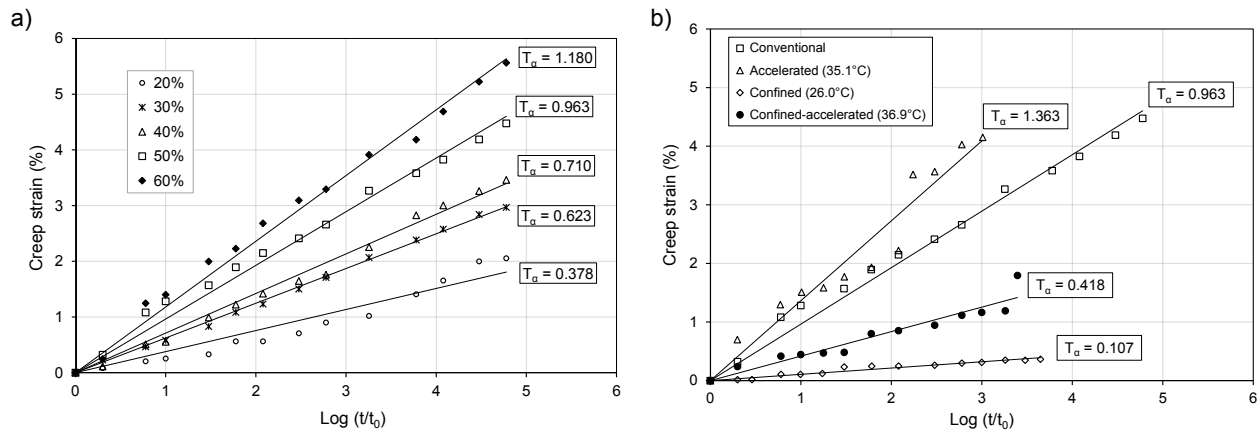


Figure 3 – Results from creep tests conducted with the nonwoven geotextile: a) Conventional creep tests with specimens subjected to load levels from 20 to 60% of UTS; b) Creep tests under both conventional and non-conventional conditions with specimens subjected to 50% of UTS.

Unsurprisingly, nonwoven geotextile creep index values are proportional to the load applied to the specimen during the test. The relationship between load levels and creep index values is approximately linear, with slope equal to 0.019 (coefficient of determination of 0.98). Regarding the specimens subjected to 50% of UTS, the nonwoven geotextile creep behavior was found to be highly affected by soil confinement in the tested conditions. A normal stress of 50 kPa was able to reduce the creep index to approximately 11% of the value obtained in the conventional condition. Note that both tests were performed at room temperature. A similar trend was found at elevated temperatures; however, the creep index change was slightly less significant. Creep index value in confined-accelerated creep test (36.9°C) was approximately equal to 30% of the one obtained in accelerated creep test (35.1°C).

Creep strain reduction due to creep reached significant levels at room temperature. Note that the creep index obtained in the confined test with the specimen loaded to 50% of UTS is smaller than the one found at conventional conditions with the specimen subjected to 20% of UTS. It indicates the high influence of soil confinement in this geotextile creep behavior. However, it is important to mention that this condition cannot be extrapolated for every nonwoven geotextile in every condition. At elevated temperature, creep index reduction was not as substantial as found at room temperature. Besides, different loading systems may induce unlike behavior, as reported by Elias, et al. (1998) and Costa (2004).

In addition to the tests described so far in this paper, a new set of tests was performed at 70, 80 and 90% of UTS with geotextile in-soil specimens. It was used to characterize the geosynthetic creep rupture behavior in confined condition. Firstly, a creep rupture confined test at 90% of UTS was performed, which caused specimen rupture approximately after 47 minutes (0.78 h). It was followed by two confined creep tests with specimens loaded to 80% of UTS, at room temperature and with temperature equal to 36.5°C. The specimens rupture did not occur in the test conducted at room temperature (until 160 h) and took place after 17.5 h at elevated temperature. Finally, four creep tests were performed with in-soil specimens loaded to 70% of UTS (at room temperature and at temperature values equals to 36.9, 47.7 and 59.1°C). The rupture only occurred at the highest temperature after 464 h.

The set of creep tests conducted with in-soil specimens loaded to 70 and 80% of UTS at elevated temperature (confined-accelerated creep tests) was interpreted in order to establish the creep master curves for each load level. Additionally, the confined creep test at 90% of UTS was used to determine the time to rupture at this load level. Figure 4a presents the creep master curves for specimens loaded to 70 and 80% of UTS. Moreover, Figure 4b presents the creep rupture curve found with this set of tests.

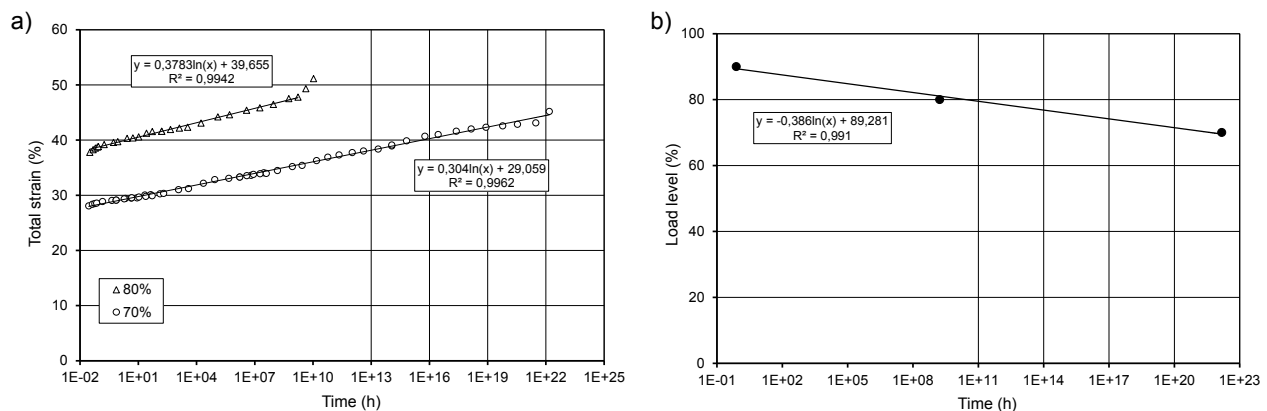


Figure 4 – Results from confined creep tests conducted with the nonwoven geotextile: a) Creep master curves for specimens loaded to 70 and 80% of UTS; b) Creep rupture curve obtained with in-soil specimens.

Creep rupture curves are used to determine the reduction factor due to creep behavior. This parameter is considered in the computation of the geosynthetics tensile design strength. Note that the reduction factor due to creep obtained with the tests performed so far would reach lower values than those suggested in the technical literature (1.5 to 3.0). For instance, the reduction factor obtained from the data presented in Figure 4b is equal to 1.20 for a service life of 50 years. However, it is important to mention that this computation is based on one single set of tests and comprises preliminary results with this geosynthetic material. Further tests are predicted to be conducted with the nonwoven geotextile using in-isolation specimen. As a result, the creep behavior at higher load levels (70 to 90% of UTS) with in-isolation specimens will be compared with that found with in-soil ones.

3.3.2 Biaxial Woven Geogrid

The biaxial woven geogrid was subjected to fewer creep tests in this research. In fact, only conventional creep tests have been performed so far. These tests were used to evaluate both creep deformations, with specimens loaded from 20 to

50% of UTS, and to determine the creep rupture curve, with specimens subjected to loads from 80 to 95% of UTS. Figures 5a and 5b presents the plots from each set of tests

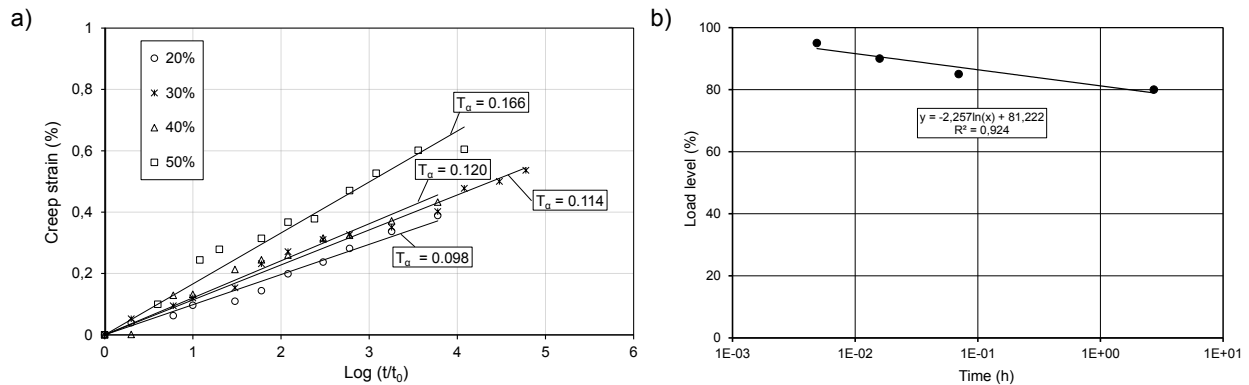


Figure 5 – Results from creep tests conducted with the biaxial woven geogrid: a) Conventional creep tests with specimens subjected to load levels from 20 to 50% of UTS; b) Conventional creep rupture curve obtained with specimens subjected to loads from 80 to 95% of UTS.

The creep index was found to be proportional to the load level, as expected for any geosynthetic material. According to the creep rupture curve, the reduction factor due to creep would be approximately 1.9 for a service life of 50 years. However, it is important to notice that this value refers to an approximate prediction since it is based on very few tests and the extrapolation process exceeded the recommended standard of one order of magnitude (ASTM D 5262).

Further tests are predicted to be conducted with the geogrid. Firstly, these tests will comprise complimentary creep rupture tests with in-isolation specimens and confined creep rupture tests using in-soil specimens. Tests with specimens loaded to lower load levels will be accelerated by elevating the test temperature. Thus, creep master curves will be established and time to rupture will be determined at these load levels. Creep rupture tests will be followed by confined creep tests at lower load levels in order to determine the effect of soil-geogrid interaction on the geosynthetic creep behavior.

4. CONCLUSIONS

This paper presented a brief description of the creep testing equipment developed by França (2012) to conduct simultaneously confined and accelerated creep tests on geosynthetics. It was also presented an additional improvement, which was implemented to its loading system. A nonwoven polyester geotextile and a biaxial woven geogrid were subjected to different creep test series. The following conclusions are drawn from the present study:

- The influence of soil-geosynthetic interaction in creep strains of the nonwoven geotextile was found to be very significant at both room and elevated temperature. Creep index values were reduced to 11 and 30% of those found with in-isolation specimens at room temperature and at 35.1°C, respectively.
- Creep rupture tests conducted using nonwoven geotextile specimens under confined condition led to reduction factors due to creep considerably lower than those usually applied in geotechnical structures design. However, this aspects still requires further investigation.
- Preliminary creep tests using biaxial woven geogrid indicated an expected creep behavior for this geosynthetic material (creep index was proportional to load level).
- A conventional creep rupture curve was suggested for the biaxial woven geogrid. Despite it was based only on four load levels, extrapolation of this curve led to recommended values.
- The new creep testing equipment performance was improved by adding the new loading system. It was able to apply the creep load at a constant rate on both sides of the specimen simultaneously;
- Further tests are predicted with both the nonwoven geotextile and the biaxial woven geogrid. Additional creep tests with other geosynthetic materials are also predicted in order to develop a larger data base regarding in-soil creep behavior of different types of geosynthetics.

ACKNOWLEDGEMENTS

The authors would like to express their gratitude to the State of São Paulo Research Foundation (FAPESP), to Coordination for the Improvement of the Higher Education Personnel (CAPES), and to National Counsel of Technological and Scientific Development (CNPq) for the financial support to this research.

REFERENCES

- Boyle, S. R., Gallagher, M. and Holtz, R. D. (1996). Influence of Strain Rate, Specimen Length and Confinement in Measured Geotextile Properties, *Geosynthetics International*, 3(2): 205-225.
- Bueno, B.S., Constanzi, M.A. and Zornberg, J.G. (2005). Conventional and Accelerated Creep Tests on Nonwoven Needle-Punched Geotextiles, *Geosynthetics International*, 12: 276-287.
- Costa, C. M. L. (2004). *Time Dependent Deformations in Geotextile Reinforced Soil Walls*. Ph.D. Dissertation, University of Sao Paulo, São Carlos, Brazil (in Portuguese).
- Ding, J., Tong, J. Zhou, W. (2008). Test Study on the Confined Creep Features of HPDE Geogrid in Sand, *EuroGeo4*, IFAI, Edinburgh, Scotland.
- Elias, V., Yuan, Z., Swan Jr., R. W. and Bachus (1998). *Development of Protocols for Confined Extension/Creep Testing of Geosynthetics for Highway Applications*. FHWA-RD-97-143, McLean, VA, USA.
- França, F.A.N. and Bueno, B.S. (2010). Creep behavior of geosynthetics using confined-accelerated tests. *Nineth International Conference on Geosynthetics*, IGS, Guarujá, Brazil.
- França, F.A.N., Bueno, B.S. and Zornberg, J.G. (2011). New equipment to conduct confined-accelerated creep tests on geosynthetics, *14th Pan-American Conference on Soil Mechanics and Geotechnical Engineering*, ISSMGE, Toronto, Canada.
- França, F.A.N. and Bueno, B.S. (2011). Creep behavior of geosynthetics using confined-accelerated tests, *Geosynthetics International*, 18-5: 242-254.
- França, F.A.N. (2012). *New equipment to conduct confined-accelerated creep tests on geosynthetics*. Ph.D. Dissertation, University of Sao Paulo, São Carlos, Brazil (in Portuguese).
- Jeon, H. Y., Kim, S. H. and Yoo, H. K. (2002). Assessment of Long-Term Performances of Polyester Geogrids by Accelerated Creep Test, *Polymer Testing*, 21: 489-495.
- Jones, C. J. F. P. and Clarke, D. (2007). The Residual Strength of Geosynthetic Reinforcement Subjected to Accelerated Creep Testing and Simulated Seismic Events, *Geotextiles and Geomembranes*, 25: 155-169.
- Kamiji, T., Bueno, B. and Costa, C. (2009). Nonwoven Geotextiles: Evaluation of Behavior in Confined Creep Tests, *EuroGeo4*, IFAI, Edinburgh, Scotland.
- Koerner, R.M. (2005). *Designing with Geosynthetics*, Prentice Hall, Upper Saddle River, NJ, USA.
- McGown, A., Andrawes, K. Z. and Kabir, M. H. (1982). Load-Extension Testing of Geotextiles Confined in Soil, *2nd International Conference on Geosynthetics*, IFAI, Las Vegas, Nevada, USA, 3: 793-798.
- Mendes, M. J. A., Palmeira, E. M. and Matheus, E. (2007). Some Factors Affecting the In-Soil Load Strain Behaviour of Virgin and Damaged Nonwoven Geotextiles, *Geosynthetics International*, 14: 39-50.
- Palmeira, E. M. and Milligan, G. W. E. (1989). Scale and other factors affecting the results of pull-out tests of geogrids buried in sand, *Géotechnique*, 39: 511-524.
- Tong, J., Gong, B. and Liu, J. (2009). An Experimental Study on the Creep Behaviour of Geogrids at Different Temperature, *EuroGeo4*, IFAI, Edinburgh, Scotland.
- Thornton, J. S., Allen, S. R., Thomas, R. W., and Sandri, D. (1998). The Stepped Isothermal Method for Time-Temperature Superposition and its Application to Creep Data on Polyester Yarn, *6th International Conference on Geosynthetics*, IFAI, Atlanta, Georgia, USA, 2: 699-706.
- Yeo, S., Hsuan, Y. G. (2009). Evaluation of Stepped Isothermal Method Using Two Types of Geogrids, *EuroGeo4*, IFAI, Edinburgh, Scotland.
- Zornberg, J. G., Byler, B. R. and Knudsen, J. W. (2004). Creep of Geotextiles Using Time-Temperature Superposition Methods, *Journal of Geotechnical and Geoenvironmental Engineering*, 130: 1158-1168.

Construction and 3 Years of Field Monitoring on a 12 m High Geogrid Reinforced and Lime Stabilised Noise Barrier Wall with Respect to the Stress Development in the Facing Area

Lars Vollmert, BBG Bauberatung Geokunststoffe GmbH & Co. KG, Germany, lvollmert@bbgeo.com
Jörg Klomp maker, BBG Bauberatung Geokunststoffe GmbH & Co. KG, Germany, jklomp maker@bbgeo.com
Chris Quirk, NAUE America, Inc., USA, cquirk@naue.com

ABSTRACT

In the course of site development a 12 m high and 350 m long noise barrier wall is constructed at an existing hill slope. A construction method with the use of onsite available cohesive soils, which is improved by using mixed binders and Polyester-geogrids in connection with a steel mesh facing element was chosen. The steel mesh facing elements are connected to the geogrid via frictional interaction. During the design process the lateral pressure on the facing has been calculated according to the German design guideline for geosynthetic reinforcements, EBGEO 2010, by using a reduced active earth pressure. The construction is accompanied by an extensive monitoring program. The available test results achieved for the facing area of the construction show very low deformations of the facing, low earth pressures and a very low rate of stress of the geogrids as well as of the steel mesh facing elements.

1. INTRODUCTION

These days geosynthetic reinforced soil structures belong economically to the most attractive construction methods due to their flexibility and versatility. Also under the ecological point of view, as e. g. CO₂ reduction, further positive impulses for this type of application can be expected in future. DIN 1054:2005 as national document, DIN EN 14475 as document for execution as well as the revision of EBGEO 2010 as design standard for geosynthetic reinforcements are corresponding state-of-the-art standards in Europe and even used in Asia due to the link to Eurocode 7 (EC7) in order to safeguard the constructions.

In the case of this presented construction (Figure 1), design and verification elements of the revised EBGEO have been implemented. The type of construction and design, first measurement results and numerical analysis on the wall have already been documented by Ilchmann et al. (2009), Pries & Meshkinghalam (2010) and Vollmert et al. (2010). Actual measurements show a slight increase of strain and stress values based on up to now three circles of years.

2. PROJECT

2.1 Survey

In the course of development measures for a residential area the installation of a noise protection wall is planned. This construction consists of a reinforced earth wall and a piled noise barrier on top of the construction. As a result of its hillside situation (compare Figure 3) the total height of the construction is partly more than 18 m with an inclination of the facing of 70°.



Figure 1. View in construction phase (without piled noise protection wall).

2.2 Construction Material

During the profiling of the construction site of the residential area soil has been excavated in a significant amount. This should be used as building material for the reinforced earth wall. This building material mainly consists of loess, loess clay, residual clay and cohesive fluvial soils, i.e. cohesive soils with differentially high sand contents. The in-situ soil on the construction area was mixed with binders (lime-cement-stabilization) on site, transported to the installation location and installed by compacting layers (Figure 2).



Figure 2. Construction site.

The required shear parameters ($\varphi \geq 27.5^\circ$ and $c \geq 10 \text{ kN/m}^2$) have been achieved and verified by shear box tests. Also the required compaction, especially in the facing area of the system, has been observed carefully.

The facing of the geosynthetic reinforced soil structure consists of welded, specially aluminium galvanized steel wire mesh (square, 100mm x 100mm). A corresponding erosion control mat made of a synthetic monofilament is used in front of the elements.

Geogrids with a high extensional stiffness are used as reinforcing elements. For economic reasons and to improve the reliability of the construction (danger of mixing up different grid types in the case of a similar visual appearance of the product) only two geogrid types, in this case Secugrid[®] 200/40 R6 and Secugrid[®] 40/40 Q6, are installed. The design strength according to EBGEO, taking creep, installation damage, $\text{pH} = 12.5$ and a partial factor of safety for material of 1.4 into consideration, is given to 87.3 kN/m (Secugrid[®] 200/40 R6) resp. 17.5 kN/m (Secugrid[®] 40/40 Q6). For the chosen reinforcing type of Polyester, long-term tests have been performed at high pH-values of up to $\text{pH} = 12.5$ as a high sensitivity against hydrolysis is known for products made by multifilament yarns. It has been found in these tests that using monolithic bars in combination with certain Polyester raw materials is much less sensitive, so that just a reduction by approx. 15% had to be taken into account for a life time of 120 years.

The connection between the front element and the geogrid is realised by friction without additional measures and verified by static design.

3. GEOTECHNICAL VERIFICATION

3.1 Structure

The proofs are performed in analogy to Eurocode 7 according to DIN 1054:2005-01 and EBGEO using the partial safety factor concept. Simplified, the verification of the stability of the geosynthetic reinforced soil structure is carried out in three steps:

- proof of reinforced soil structure
 - internal stability (two-part wedge failure mechanism, circular slip circles)

- external stability (sliding, bearing failure, eccentricity)
- proof of ground failures of the complete system (wall and fill)
 - slice method according to Bishop, where the circular slip circles can intersect with parts of the geosynthetic reinforced soil structure
- proof of earth pressure on facing

3.2 Steel Mesh Facing

The earth pressure affecting the facing has been reduced according to Pachomow et al. (2007). Therefore the dimensions of the steel mesh facing elements could have been reduced and the connection geogrid/front element has been carried out as to friction. The comparative earth pressure measurements (as documented as follows) show that the calculation approaches for the earth pressure have been on the safe side. In the meantime this process has been included into the design recommendations of EB GEO.

3.3 Serviceability

In the run-up the ground expert has forecasted settlements in a range of up to 30 cm. In the soil body of the geosynthetic reinforced soil structure itself the settlements might be up to approximately 1 cm for each layer. Thus, during the construction it was planned to carry out settlement and deformation measurements in order to confirm the forecasts and to be able to adjust them, if necessary.

4. CONSTRUCTION WORK

Before installation of the geogrids an accurate formation level had to be prepared for the front elements in the front area. Afterwards the geogrids were installed up to the leading edge of the front elements, whereupon the layers were cut by using an angle grinder.

During an effective construction time of approximately 2 months the company Nacken Landschaftsbau with their average staff of 7 workers installed or moved, respectively, approximately 25,000 m³ of prepared soils resulting from the construction site, 25,000 m² geogrid, 4,000 m² steel grid front elements as well as 300 m³ of half-gabions with a long arm excavator and a wheel-type loader. The compaction was carried out in three steps with a tamper in the front area between the bars of the steel grid elements, vibrating plate up to approximately 1 m distance to the front and a single drum vibrating roller.

5. MONITORING

5.1 Purpose

For the design of reinforced soil bodies, which can be regarded as compound system due to their small layer distances, the question must be raised how to determine the earth pressure on the facing. Evaluations of literature and comparative calculations of Pachomow et al. (2007) clearly show - depending on the flexibility of the facing elements - a reduced horizontal stress - compared to the active earth pressure - at the facing of a reinforced soil construction. Due to this fact the active earth pressure can - resulting from the compound effect of the reinforced soil structure - be reduced by 30% in the case of facing systems which are restrictedly deformable according to DIN EN 14475:2006.

For cohesive soils with continuously increasing shear strengths only few experiences are available. As for the use of inferior construction materials which require the use of binders another increase can be expected as to the economic point of view, and additional validation of the above mentioned design approaches is required. Moreover a structurally engineered and complex constructive connection of the facing elements with the geogrids can be omitted under consideration of the reduced horizontal strengths.

Thus, the instrumentation focuses upon the facing area of the construction. It is the aim to determine the dynamics at a facing element and the subsequent reinforcement layer depending on the construction progress and the time-dependent development of the shear behaviour of the soils.

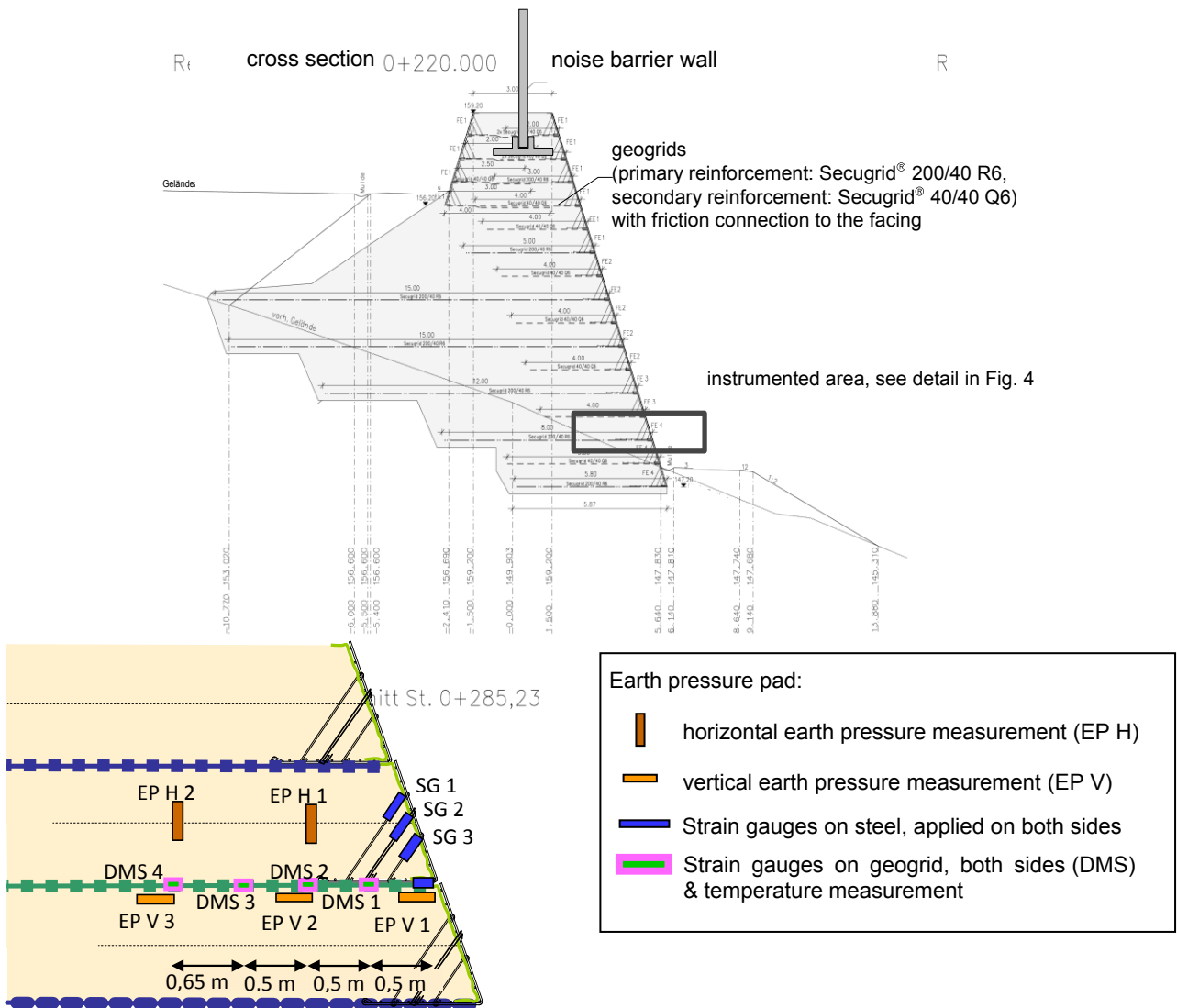


Figure 4. Instrumentation of the measuring cross-section.

5.2 Measurement Concept

The measurement concept which has been established (Figure 4) allows a determination of the horizontal stress affecting the facing by means of an instrumentation of the steel mesh facing element. For the strains measured at the geogrid the influence of the thermoplastic properties (curing process with corresponding heat development, creeping, relaxation) remains partly undetermined and must be completed in the following by means of corresponding laboratory test results.

Moreover it is necessary to carry out earth pressure measurements in order to be able to register the influence and the effect of the formation of restraints and arches (see Pachomow et al., 2007) between two reinforcement layers as well as the vertical strains and thus the load distribution in the facing area. This measurement concept has been realized by the tBU - Institut für textile Bau- und Umwelttechnik GmbH & Co. KG, Greven, Germany.

For the realization of this measurement concept the following detectors are used:

- earth pressure cell (Glötzi)

- strain gauge (HBM)
- temperature sensor

In order to guarantee the long-term monitoring of the construction complex preliminary tests had been carried out in the laboratory before the detectors were installed. The preliminary tests were carried out under hindered simulated environmental conditions as e.g. an increased water pressure of up to 3 m water column on the applied strain gauges. For the strain measurements on the steel wire and the geogrid, different strain gauges - suitable for each subsoil / strains - were used. Both strain gauge types were carried out as temperature and deformation compensated full bridges. The measured value acquisition was carried out by means of a carrier wave amplifier. Also undisturbed samples were obtained from the soil during installation to measure the shear strength at predefined time steps.

6. RESULTS STATUS 2011

6.1 Deformation Measurements

The settlement and deformation measurements which have been carried out up to now show:

- Settlements in the soil body already occurred during the construction phase with values of predominantly < 1 cm per layer. The settlements could be balanced already during the construction process by means of corresponding corrections.
- In analogy to the vertical deformations only very low horizontal deformations could be detected at certain levels (W01 up to W15 in Figure 5), which were within the measuring tolerance and which did not increase with the rising installation height.
- The settlements in the subsoil were clearly below 30 cm. Already at the end of December 2008 only just minor settlements in the range of millimeters were detected. It can be assumed that the decisive settlements have been subsided.

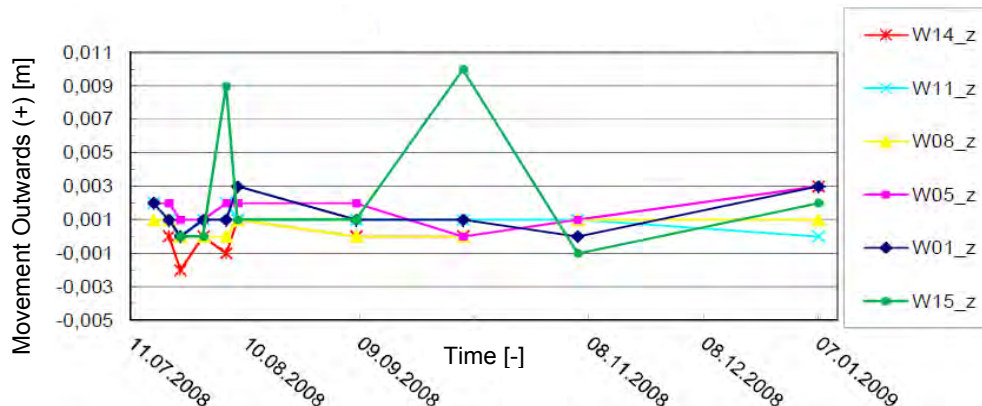


Figure 5. Horizontal Deformations (Layer 1 to 15).

6.2 Earth Pressure (Figure 6)

For the earth pressure cell (EP V1, EP V2 and EP V3) corresponding absolute values were measured immediately after installation of the respective covering. The proceeding covering did not lead to another increase for the cell which was placed near the facing area. The obtained values for all three cells were within a range which was expected. However, a reduction towards the facing area could be determined.

The horizontal strain gauges show at first - together with the increase of the coverage during the construction phase - a continuous increase up to 20 kPa in both gauges before a continuous decrease occurred in the front gauge down to approx. 10 kPa after finalization of all earth works.

6.3 Temperature

Figure 7 shows the measured temperature, located at the strain gauges of the geogrids. It can be seen quite clearly that the temperature gradient changes during the cycle of a year. The changes of the gradients are less significant with increasing coverage with soil.

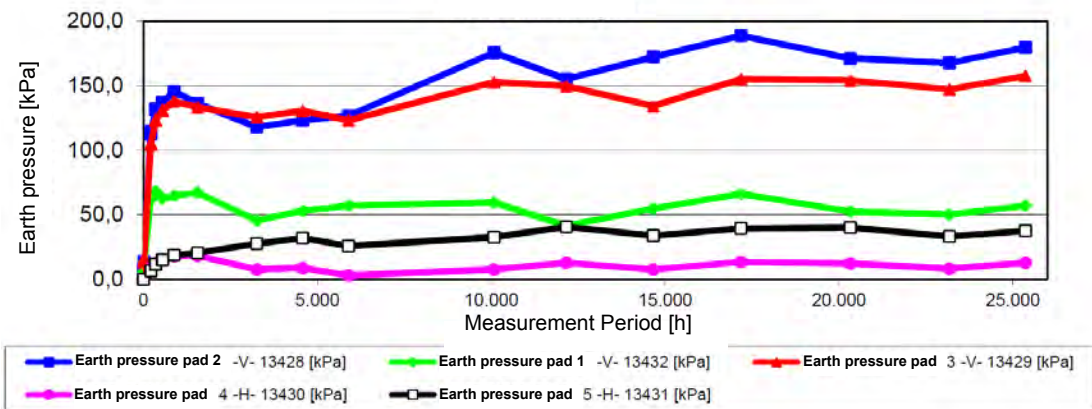


Figure 6. Earth pressure measurements.

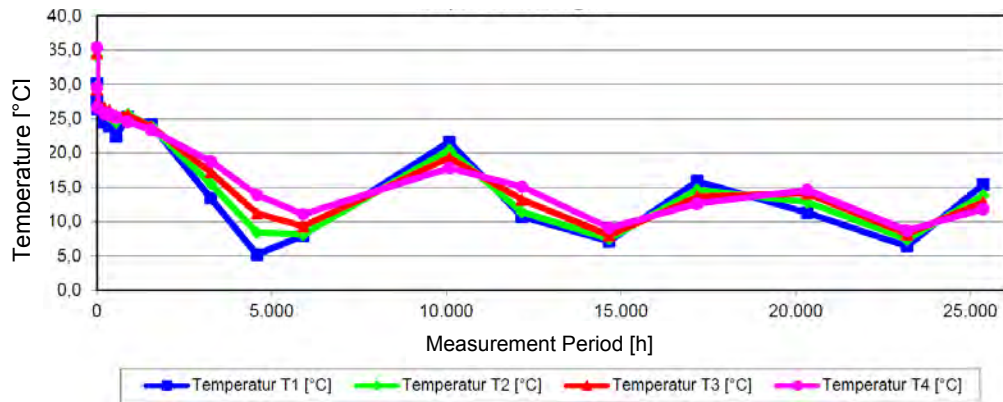


Figure 7. Temperature.

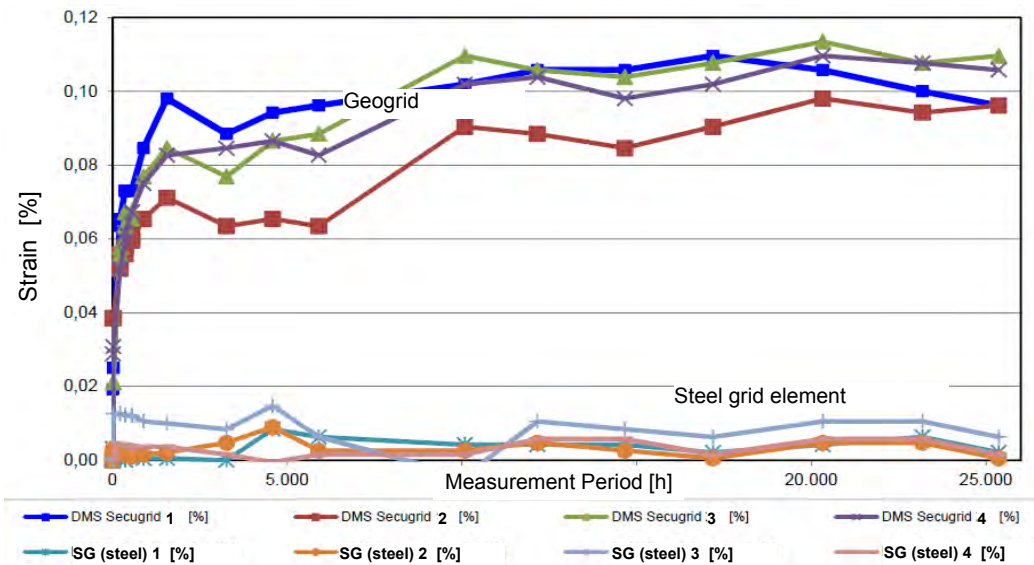


Figure 8. Strain measurements on geogrid and steel mesh facing element.

6.4 Strains of the Geogrids

Figure 8 shows the measured strains in the geogrid. All strain gauges are temperature-normalised, so these values are real strain. For the instrumented product Secugrid 200/40 R6 an absolute tensile strength value of 3.5 kN/m was achieved - assuming a linear-elastic behavior without consideration of the thermoplastic material influences. With time, a slight increase can be found.

6.5 Steel Strains

In analogy to the elongation of the geogrid also the steel tensile strengths for elongations < 0.01 % remain low.

7. EVALUATION OF TEST RESULTS

Within the framework of the preliminary evaluation of the results the measured earth pressure strains were checked as to their plausibility. The values which were obtained directly after installation were verified with the values after the first fill and construction levels. Compared to the expected values the test values show qualitatively as well as quantitatively a good correlation - without any further corrections. Especially noticeable are:

- the very low horizontal strains of less than 5 kPa in the front earth pressure cell and the
- tendency to unitize the vertical stresses (relocation of the vertical stresses to the front area).

Besides the very low total level of the operational demands of the geosynthetics also the good correlation of the above mentioned tensile strength of average 3.5 kN/m together with the horizontal stress of less than 10 kN/m measured in the first strain gauge is noticeable.

Involving the horizontal stress derived from the steel mesh facing element and the very low horizontal deformation which was determined by means of the geodetic measurement it can be noted that the horizontal stresses in the facing area apparently remain very low despite increased vertical stress rates. Compared to the ratio of the active earth pressure approach, horizontal stresses are strongly reduced also under consideration of the specific soil properties with a high cohesive percentage of the shear strength.

8. CONCLUSIONS AND FUTURE PROSPECTS

For the noise protection barrier located on a slope very low horizontal deformations could be detected. These deformations correlate qualitatively very well with the small strains in the reinforcement and the very small tensile strength which affects the steel mesh facing element. The approach of the reduced earth pressure by 30% which has been used - according to EBGeo 2010 - could thus be verified also for fill material with strong cohesive properties. For this construction the approach is still clearly on the safe side for the currently measured strains and stresses.

Besides the calculative verification of the earth pressure distribution especially the long-term monitoring of the tensile forces affecting the steel mesh facing element remain interesting, because the influences resulting from weather and thermal fluctuations could - near to surface - possibly result in a loosening and stress relocation. The instrumentation is dimensioned for a long-term monitoring of the construction.

ACKNOWLEDGEMENT

The authors appreciate the financial and technical support by NAUE GmbH & Co. KG, which enabled this technical study.

REFERENCES

- DIN 1054, Edition: 2005-01. Subsoil – Verification of the safety of earthworks and foundations – supplementary rules to DIN EN 1997-1, *Deutsches Institut für Normung e.V.*, Berlin, Germany.
- DIN EN 14475, Edition: 2006-04. Execution of special geotechnical works - Reinforced fill; German version, *Deutsches Institut für Normung e.V.*, Berlin, Germany.
- EBGeo - *Recommendations for Design and Analysis of Earth Structures using Geosynthetic Reinforcements (2011)*. Translation of the 2nd German Edition. Published by the German Geotechnical Society (Deutsche Gesellschaft für Geotechnik e.V., DGGT). ISBN: 978-3-433-02983-1. Verlag Ernst & Sohn, Berlin.

- Eurocode 7: Geotechnical design – Part 1: General rules; German version EN 1997-1:2004 + AC 2009.
- Ilchmann, C., Urbanski, D. and Vollmert, L. (2009). Ausführung und messtechnische Begleitung eines 12 m hohen Lärmschutzwalls, 11. *Informations- und Vortragstagung über „Kunststoffe in der Geotechnik“*, München.
- Pachomow, D., Vollmert, L. and Herold, A. (2007). Der Ansatz des horizontalen Erddrucks auf die Front von KBE-Systemen, 10. *Informations- und Vortragstagung über „Kunststoffe in der Geotechnik“*, München.
- Pries, J. and Meshkinghalam, S. (2010). Prognose und Verifizierung von zeitlich veränderlichen Spannungszuständen an der Außenhaut einer KBE-Konstruktion, 31. *Baugrundtagung der Deutschen Gesellschaft für Geotechnik*, Beiträge der Spezialsitzung „Forum für junge Geotechnik-Ingenieure“, München.
- Vollmert, L., Urbanski, D., Recker, C. and Ehrenberg, H. (2010). Execution and field measurements of a 12 m high reinforced and lime stabilized noise protection wall, 9th *International Conference on Geosynthetics (9ICG)*, Guarujá, Brazil.

Deep Soil Mixed Foundation Using Geosynthetics for Levee Support

B. C. Baillie, P.E., M. ASCE, Huesker Inc., USA, brian@hueskerinc.com

ABSTRACT

The construction and design of flood protection levee embankments within coastal areas has become a focal point for infrastructure management. The levee systems are usually constructed over soils with very poor bearing capacity due to their proximity to flood plains. These foundation soils create issues with long-term settlement, changing the protection height and creating the need to periodically build the levee back to the design height. In order to reduce settlements and the maintenance required to preserve design height protection, a deep foundation is required for load transfer. Deep soil mixing (DSM) has become a popular deep foundation solution for just this type of geotechnical issue. Deep soil mixing is a technique used to create cement/soil bonded columns that are utilized as end load bearing elements. The columns are used to bridge the soft foundation soils and create a semi rigid foundation for support of the levee embankment. This solution was recently used by the Corp of Engineers in New Orleans for a protection levee. For this project, a high strength geosynthetic was incorporated into the design and installed over the columns. This paper will outline the considerations necessary for geosynthetic inclusion within deep soil mixed foundations. With the proper use of reinforcement, these applications can become even more efficient in time and cost vs. unreinforced.

1.0 INTRODUCTION

Deep soil mixing has grown very popular as a soft soil foundation support solution. This construction method is used to increase bearing capacity, stabilize global failure planes and mitigate liquefaction. The key advantages of DSM installations over other solutions are cost, time, over excavation disposal and construction vibration during installation. The columns created for levee embankments are designed to reduce settlements, removing the need for staged construction and providing immediate protection at required design height. The levee can be constructed to design heights immediately providing protection much faster than other ground improvement techniques.

The installation method employs rotor tilling a cementitious material into the existing soil down to a designed bearing depth. The cement is carried to the auger shaft or shafts and into the surrounding soil by either hydraulic or pneumatic methods. The moisture content of the soil will dictate which carrier method is appropriate. Both methods however do create an excess mix of soil / cement or soil / water / cement depending on the carrier method. The volume of this excess slurry is dependent on mix design, column area and carrier method.

The constructed columns can be installed in either individual or interconnected forms. Interconnected or overlapping columns are used to form a wall or panel. The increased density of column area can provide greater bearing capacity or reinforce failure planes occurring along the outer edge of the levee.

The use of geosynthetic reinforcement for a piled or column foundations is not uncommon and the available design models have been studied, Stewart & Filz, 2005. This paper will not discuss the different design models but will instead focus on geosynthetic reinforcement selection variables specific to DSM projects. Geosynthetic reinforcement provides a high tenacity mechanism for efficient load transfer to the columns. This load transfer platform allows for reductions in the required area replacement ratio or required column density (Lawson 1992, Russell and Pierpoint 1997, Kempton et al. 1998, Han and Wayne 2000, Han and Gabr 2002) (cited in Stewart & Filz, 2005). The use of reinforcement can also reduce the required column density on the outer portion of the levee embankment used to intersect failure plains for what is called edge stability. The common design and construction approach used on DSM projects for edge stability is incorporating overlapping rows of columns or panels. The additional shear area and strength provided by the panels helps intersect these failure planes providing the necessary design stability. With the use of reinforcement, its tensile strength can be used to offset this failure mode. Another benefit is the minimization of bending forces acting on the columns.

There are many benefits in using geosynthetic reinforcement for levee's supported by DSM columns. In order to use synthetic material in this application however, certain application specific details must first be understood. This paper will discuss reinforcement variables that need to be considered before use within DSM embankment or levee structures.

2.0 SLURRY ENVIRONMENT AND HYDROLYSIS

In order to understand the variables that control reinforcement selection, the environment in which it is placed must first be discussed. The construction process for DSM columns produces an excess volume of treated soil or slurry which collects at the surface during installation. The volume of the slurry is controlled by the mix design, column diameter and depth. This excess slurry is collected and spread across the column / embankment interface within direct contact of the geosynthetic reinforcement. The slurry environment, due to the cement constituent, has a negative effect certain types of reinforcements. The cement added during the mixing process increases the pH of the slurry. This increase is dependent on soil properties and the amount of cement added, which does vary based on project specific needs. Although the extent of pH increase will vary, its effect on the reinforcement and how it governs the design process is always present.

The nominal pH range for geosynthetics commonly used in geotechnical applications is between 4 and 9. Any environment outside this range subjects certain reinforcements to hydrolysis and permanent loss of strength. The amount of hydrolysis and strength loss increases greatly as the pH increases, especially above a pH of 10. Above this level, hydrolysis inflicts exponential damage to the reinforcement and greatly affects the intended design performance and possibly the project itself. The consequence of pH variations outside nominal application ranges has been studied, Testing Protocols for Oxidation and Hydrolysis of Geosynthetics FHWA-RD-97-144 July 1999. The effect of hydrolysis on geosynthetics is measured as a percentile of ultimate strength loss per time. Per the results of this test, the unit for time is one year. Depending on the pH range within the reinforced zone, the rate of reinforcement deterioration can be very dramatic and detrimental to design for long term projects.

In order to verify the pH within the reinforced zone on a DSM project recently, three random tests were done. The data for these tests are in Figure 1. These tests were conducted on the reclaimed slurry at various areas along the foundation axis and within the area of reinforcement installation. All three tests indicated an average pH of 11.2. This pH level is well outside the nominal range for standard reinforcement applications and needs to be observed within the design procedure.

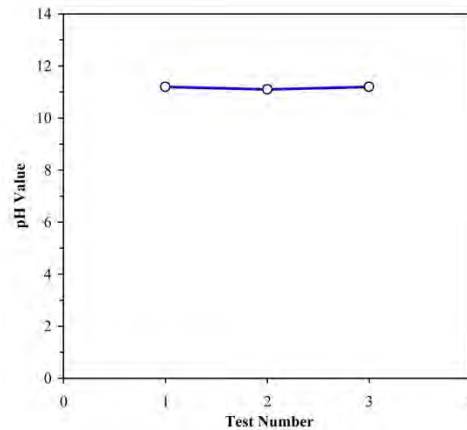


Figure 1. pH testing of DSM slurry

In order to choose the appropriate reinforcement type, the effect of the high pH environment on the base polymer needs to be understood. Both polypropylene (PP) and High Density Polyethylene (HDPE) have a pH range between 2 and 13 without loss of strength. Another reinforcement polymer type within the tested range is Polyvinyl Alcohol (PVA). PVA has a pH range between 2 and 12.5 without loss of strength and minor reductions beyond this boundary. The final and most popular reinforcement, due to availability and high strength, is Polyester (PET). PET has a normal design range between a pH of 4 and 9. Within this range on either side of pH = 7, there are small reductions in strength and they are usually taken into account during design procedures with a factor of safety for chemical and biological degradation. The reduction of strength usually utilized is between 1.05 and 1.1 and is taken directly off of the ultimate tensile strength available. But, with a tested pH environment of 11.2, this reduction is much higher. The referenced FHWA paper has tested reduction factors for coated PET reinforcements within environments outside the typical 4 to 9 range. Based on this data for a pH of 11.2, the calculated strength loss is expected to be around 0.8% per year. So, with this reduction in place, a 75 year design life can expect a 60% reduction in ultimate strength while a 100 year design has its strength reduced by 80%. These reductions should also be used before the long term performance analysis is done to properly

predict material performance. The use of PET reinforcements on DSM projects can be done, but without proper design procedures the actual strength available can be drastically underestimated.

3.0 REINFORCEMENT SELECTION AND STRAIN COMPATIBILITY

Another important variable for the proper selection of reinforcement on DSM levee projects is strain compatibility. The analysis of strain compatibility between the soils being reinforced and the material acting as the tensile reinforcement has been studied, Jewell, R.A. (1996), Zornberg, J.G. (2002) et al. As stated earlier, this paper will not discuss reinforced column design methodology. But the input for the soils contribution to arching between installed columns is universal and this is where the analysis for strain compatibility needs to be evaluated.

During the design procedure, the input for embankment or levee fill materials has a great effect on the overall efficiency and cost for the project. The designer has a choice to either use peak or residual shear strengths for the levee clay fill. The most common approach is to use peak values due to the efficiency in design it produces. A problem exists when the available long term strength in the reinforcement is not also properly analyzed for its compatibility to retain design strength at the utilized deformation limit for the intended design life.

On the same DSM project where pH was evaluated, a study of the clay embankment fill was also done. This data can be seen in Figure 2. The available peak shear strength of the clay was found to be 455 psf with 33° of internal friction. The residual strength results of the same clay were 90 psf with 16° of internal friction. The testing also yielded the amount of displacement at peak which was at around 2%. The clay tested was Corp of Engineers approved levee material and could be viewed as indicative results for most approved levee clays. These results easily show why using the peak values create a much more efficient design. But, if peak shear properties are used, there are certain performance related properties for the reinforcement that must be reviewed to ensure proper compatibility performance.

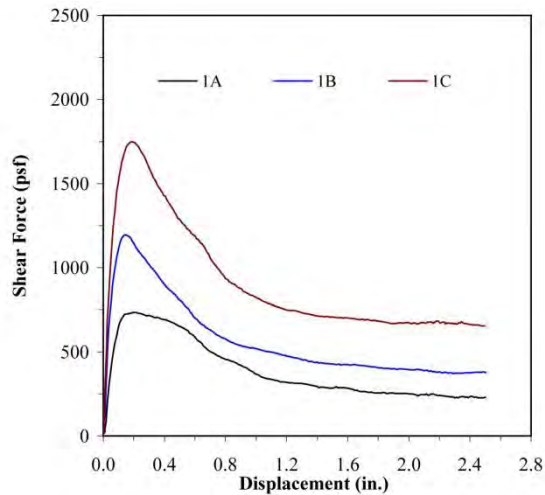


Figure 2. Direct shear test of approved levee clay

All of the previously reviewed polymers used for geosynthetic reinforcement behave much differently under load. This is especially true for long term strain analysis. All these materials will strain under load. How much so depends on certain factors like polymer type, manufacturing and magnitude of load per maximum allowable tensile capacity. The latter is expressed as a percentile of ultimate tensile strength, UTS, based on the allowable strain per time. As the design life of the structure increases, the amount of allowable UTS available decreases in relation to strain limitations. When a designer calculates the required tensile strength for reinforcement, they must then assign an expected time frame for the structure. This timeframe along with peak or residual shear displacement data will guide the designer into selecting the correctly compatible reinforcement.

The load handling ability of a selected reinforcement must be studied to ensure proper compatibility with the design variables used for time and soil shear displacement. In order to calculate the available strength within the reinforcement at strain limits per time, testing is required and can be accomplished using ASTM D-6992. This test procedure, known as the Stepped Isothermal Method or SIM, creates strain data as a function of expected design time and can be used to predict long-term strain behaviors. The data gathered, Figure 3, can then be used to calculate the UTS required for a specific manufacturers reinforcement based on project specifics.

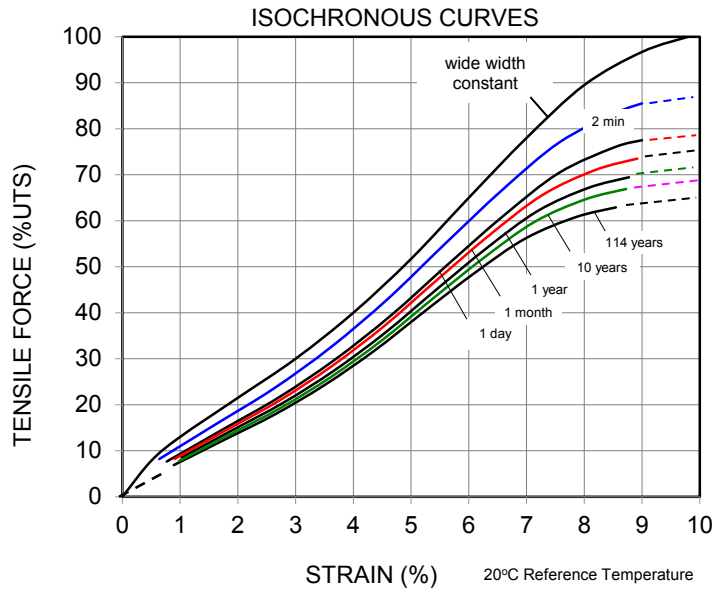


Figure 3. SIM results for one type of reinforcement

The data in Figure 3 is a sample of a SIM test for one manufacturer's polymer product type. With this data, the designer can match the displacement range of the clay with the appropriate reinforcement strain. The expected time frame for structural performance is also used to finalize the UTS reduction calculation. If a peak shear of 3% is used based on site specific data and the structure is expected to perform no less than 100 years, then the test data indicates a maximum allowable UTS of 20% for this specific material. A common misconception is the use of fast, wide width tensile tests to achieve the same selection process. If a designer was to use a short-term, wide width constant rate test, based on 3% strain, the results are much different. With the same design information, using a short-term testing analysis, the allowable UTS is now 30%. This difference becomes larger with other polymer types. The function of time is very important and needs to be review for each manufacturer's reinforcement. Short-term strain data will not properly align soil deformation with the required tensile strength at compatible strain rates with typical DSM foundation design lives.

4.0 CONCLUSION

The improvement and upgrading of floodplain protection levees and embankments has become a focal point for costal management agencies. The use of Deep Soil Mixed, DSM, columns has proven to be a cost effective solution for embankment support. The semi rigid columns provide foundation stability creating a flood protection system capable of staying at design protection heights with reduced maintenance requirements.

The use of geosynthetic reinforcement on DSM projects has the ability to create a more efficient and cost effective design. Reinforcement can decrease the area replacement ratio required by design and provide embankment edge stability. The use of reinforcement for edge stability can reduce or eliminate the need to increase column density along the outer edge. Localized column separation may also be minimized with the reinforcement acting as a binding tensile platform.

In order to utilize the benefits derived by geosynthetic reinforcement, special attention must be given to the selection process. The DSM construction process creates a high pH environment within the reinforced zone and over the installed columns. The high pH does degrade certain polymeric reinforcements reducing available design strength over time. The longer the design life, the more strength loss accumulates possibly affecting the stability of the entire system. Steps can be taken to evaluate the reinforced environment and account for proper strength reduction.

In order for the reinforcement and embankment soils to act as a cohesive unit, there must be compatible strains between the two materials. During the design process, the use of peak or residual shear strengths for the embankment clays will dictate what the allowable strain in the reinforcement will be. The maximum allowable strain within the reinforcement must also be examined with reference to time. The design life of the structure places great importance on understanding how the reinforcement reacts to designed tensile loads over time, especially long periods of time. Reviewing available test data will help correctly estimate the required reinforcement tensile strength to account for polymer and

manufacturing variability's. If all these factors are reviewed and employed in design, the use of DSM columns for the foundational support of levee systems over poor soils can provide a cost effective solution for long-term protection.

REFERENCES

- ASTM 6992. Standard Test Method for Accelerated Tensile Creep and Creep-Rupture of Geosynthetic Materials Based on Time-Temperature Superposition Using the Stepped Isothermal Method, *American Society for Testing and Materials*, West Conshohocken, Pennsylvania, USA.
- Han, J. and Gabr, M. A. (2002). Numerical Analysis of Geosynthetic-Reinforced and Pile-Supported Earth Platforms over Soft Soil. *Journal of Geotechnical and Geoenvironmental Engineering*, (128) 1, 44-53.
- Han, J., and Wayne, M. H. (2000). Pile-Soil-Geosynthetic Interactions in Geosynthetic Reinforced Platform/Piled Embankments over Soft Soil. Paper No. 000777, Presentation at 79th Annual *Transportation Research Board Meeting*, Washington D.C.
- Jewell, R. 1996. Soil reinforcement with geotextiles. *CIRIA Special Publication 123*, Thomas Telford, pp. 332.
- Kempton, G., Russell, D., Pierpoint, N. D., and Jones, C. J. F. P. (1998). "Two- and Three-Dimensional Numerical Analysis of the Performance of Piled Embankments." *Proceedings, 6th International Conference on Geosynthetics*, 767-72.
- Lawson, C. R. (1992). "Soil Reinforcement with Geosynthetics." *Applied Ground Improvement Techniques, Southeast Asian Geotechnical Society (SEAGS)*, 55-74.
- Russell, D., and Pierpoint, N. (1997). "An assessment of design methods for piled embankments." *Ground Engineering*, (30) 11, 39-44.
- Stewart, M. E. & Filz, G. M. (2005). Influence of Clay Compressibility on Geosynthetic Loads in Bridging Layers for Column-Supported Embankments. *GSP 131 Contemporary Issues in Foundation Engineering*.
- Zornberg, J.G. 2002. Peak versus residual shear strength in geosynthetic-reinforced soil design. *Geosynthetics International*, vol. 9, No. 4, 301-318.

Design Considerations for Tall Geosynthetic Reinforced Soil Walls Under Extreme Load Conditions in Mining Infrastructure

Sachin Mandavkar, M.Tech, Maccaferri Inc., USA, sachin@maccaferri-usa.com
Nageshwarreddy "Reddy" Karnati, P.E., Maccaferri Inc., USA, reddy@maccaferri-usa.com
Ghislain Brunet, M.B.A., P.Engg, Maccaferri Inc., USA, gbrunet@maccaferri-usa.com

ABSTRACT

Since the early 1970s, Geosynthetic materials have been developed and used as reinforcement in earth-retaining structures. Since then, the use of Geosynthetic's as reinforcing material for reinforced soil structures has proven to be economically attractive based on the many thousands of mechanically stabilized earth (MSE) retaining walls and reinforced soil slopes (RSS) successfully completed.

Mines, unlike other facilities usually require tall earth retaining structures. In recent years, these solutions are frequently used within the mining sector, with excellent results because of their technical and economic characteristics proven in many structures such as retaining walls along primary crushers, dams and tailing deposit containment areas.

The performance of reinforced soil retaining structures have demonstrated that they are often an optimum solution for mining structures compared to traditional retention solutions, combining structural strength, flexibility, versatility and cost effectiveness.

1. INTRODUCTION

Soil reinforcement has been used since prehistoric times for improving soils. The use of straw to improve the quality of mud or clay bricks dates back to early human history. Tree trunks and branches have been used to strengthen buildings with mud walls. Examples include bamboo and tree branches which have been used as soil reinforcement in China for over 1,000 years and along the Mississippi River in the 1880s. Other examples include wooden pegs used in England for the control of erosion and landslides. Natural soil reinforcement can also be achieved by the growth of plant roots. Reliable long term performance using natural materials however is questionable.

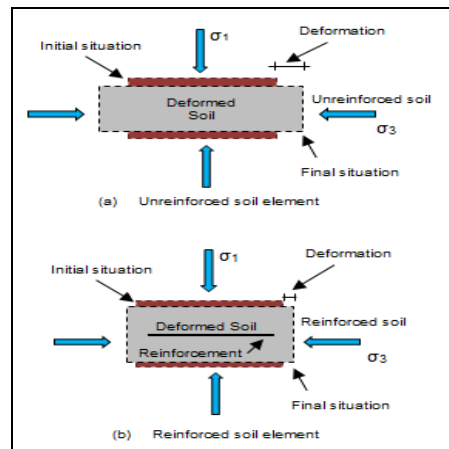


Figure 1. Deformation of a soil with and without reinforcement.

Modern methods of soil reinforcement for the construction of containment barriers were pioneered by the French architect and engineer, Henri Vidal in the early 1960s. His research led to the invention and development of the "Reinforced Earth System", in which steel straps are used as soil reinforcement. The first wall using this technology in the United States was built in 1971 in California.



Figure 2. Reinforced Soil in Malaysia (1979).

The first documented structure featuring a combination of gabions and reinforced soil was built in Sabah, Malaysia in 1979. A near vertical gabion fascia was anchored back into the ground with steel straps. This 14m high structure supports a stretch of highway between Kota Kinabalu and Sinsuran (Figure 2). Due to this success, the same solution was adopted in other sections of the highway over the subsequent years.

Seeking to ensure continuous reinforcement in the horizontal plane, a system was developed and the individual steel straps were replaced with continuous panels of hexagonal double twisted steel wire (DTSW) mesh. A panel of mesh ensures continuous longitudinal reinforcement is developed, not only by friction against the wire section, but interlock between the mesh and the soil and mechanical interlock between the particles of soil material. This is due to the large size of the mesh apertures in relation to the diameter of the wire, resulting in an overall increase in the efficiency of the reinforcement compared to reinforcement materials that provide frictional resistance alone. Corrosion resistance and structural durability is provided by heavy galvalume galvanization (Zinc/ Aluminum alloy) with an additional polymer coating. This experience enabled the optimization of a hybrid product using hexagonal double twist steel wire mesh along with extensible geosynthetic reinforcements offered the technical performance required, yet which was as simple as possible to install. The combination is well suited for use in heavily loaded/tall structures where elongation of the reinforcement is possible and requires flexibility to tolerate lateral deformations and is aptly suited in mining applications.

2. DESIGN OF DTSW MESH/GEOSYNTHETIC REINFORCEMENT SYSTEM REINFORCED WALLS

Gabion fascia DTSW mesh/Geosynthetic reinforcement system reinforced soil walls are designed and sized considering limit equilibrium analysis using a coherent gravity structure approach to check the overall stability of the structure. The types of checks considered are external stability, internal stability and combined stability. Stability checks for reinforced soil walls with vertical face is made by assuming the reinforced soil mass acts as rigid body with earth pressures (Figure 3) developed on vertical pressure plane arising from the back end of the reinforcements.

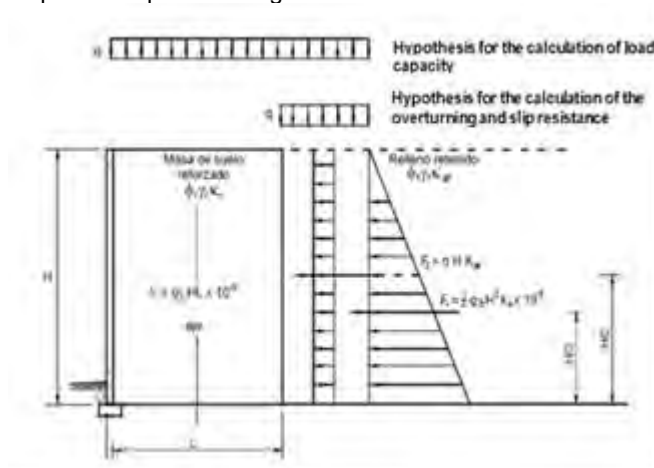


Figure 3. Earth Pressures for External Stability checks: Horizontal Back slope with Traffic Loads.

External stability checks (Figure 4) involves the checks for overall stability of reinforced mass against four potential external failure mechanisms:

- a) Sliding
- b) Overturning
- c) Bearing capacity
- d) Global Stability

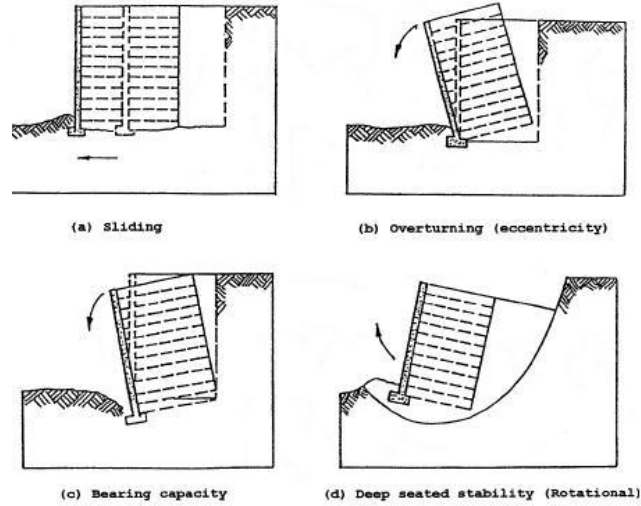


Figure 4. External Stability Checks.

Internal Stability checks involves evaluating potential (Figure 5) slip surfaces within the reinforced soil mass for 'rupture'(Figure 5a) of the reinforcement and 'pull out'(Figure 5b) of the reinforcement from the reinforced backfill material.

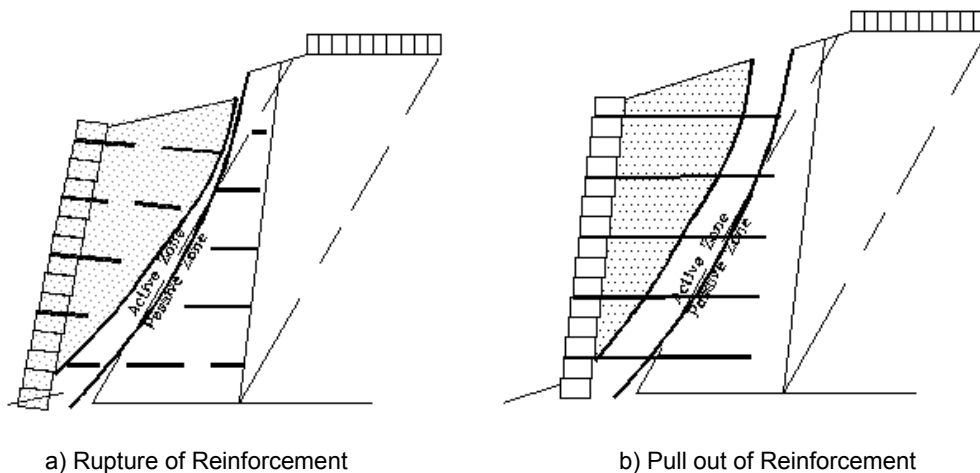


Figure 5. Internal Stability Checks.

Geogrid rupture failures can be typically overcome by selecting a stronger geogrid or adjusting the grid configurations within the structural backfill. A pull-out failure indicates that there is insufficient transfer of load from the available geogrid length into the compacted backfill. To overcome this, either the geogrid bond length is increased, or the backfill is changed to one with improved characteristics, thereby increasing geogrid-soil interaction to generate the required pull-out resistance.

The design safety factors for external stability and internal stability must meet the minimum required for the specific project considerations.

The critical failure surface is considered for reinforced soil walls with extensible reinforcement type. Despite being made from steel, hexagonal double twist steel wire mesh is considered to be “Extensible” reinforcement (Chapter 2.4.2 Manual Design Reinforced Soil Walls of the U.S. FHWA FHWA-NHI-10-024). Using this design methodology, the minimum geogrid length required to avoid pull-out of the reinforcement is calculated using the following formula:

$$L_e \geq \frac{T_{\max}}{\phi F^* \alpha \sigma_v C R_C} \quad [1]$$

Where:

- L_e : Embedded length of the reinforcement beyond the rupture surface
- T_{\max} : Maximum factored tensile load in the reinforcement
- Φ : Pullout resistance factor for reinforcement
- F^* : Pullout friction factor
- α : Scale effect correction factor (=0.8)
- σ_v : Unfactored vertical stress at the reinforcement level within the resistant zone
- C : Reinforcement surface area geometry factor
- RC : Reinforcement coverage ratio factor (=1 for continuous reinforcement)

The calculations for external and internal stability of the hybrid system can be performed within any readily available software packages, including the MacSTARS software which was exclusively developed to analyze the stability analysis of DTSW reinforcement and Geosynthetic reinforced soil structures and slopes which include tensile strength reinforcement elements. It also enables users to conduct stability analyses using the limit equilibrium method and can also consider situations without reinforcement within the backfill/slope.

3. DTSW MESH/GEOSYNTHETIC REINFORCEMENT SYSTEMS IN MINING PROJECTS

Growth in the mining sector in recent years has led to increase in demand for different types of construction methods for the various types of works within a mine; roads, containment walls, primary crushers, dams and dewatering areas and hoppers.

The use of DTSW Mesh/Geosynthetic reinforcement system reinforced structures within mines has had great success not only because of its technical and economic characteristics but because of its ease of construction, utilizing unskilled labor. This important feature can generate jobs for people living in communities near the mine, thereby generating a positive social impact and enhanced mine-community relationships

3.1 Retaining Walls Within Mining Facilities

Within mines there is often the need to create large level platforms to accommodate camps, offices, industrial facilities and so on. DTSW mesh/ Geosynthetic reinforcement system reinforced soil walls and slopes have been used extensively to make these areas stand steeper, withstand greater loads and optimize space. Often the availability of on-site structural backfill can make these solutions very cost effective.



a) Retaining wall in “Poderosa” mine ($h_{\max} = 10.0\text{m}$ - Peru). b) Floating Area in Cerro Verde mine ($h_{\max} = 12.0\text{m}$ - Peru).



c) Floating Area in Cerro Verde mine ($h_{\max} = 12.0\text{m}$ - Peru).

Figure 6. DTSW mesh/ Geosynthetic reinforcement System for Retaining Walls in Mines.

3.2 Hoppers and Crusher Installations

DTSW mesh/ Geosynthetic reinforcement system structures are used to create a level difference between two areas. These can have vertical or near vertical faces to minimize the land-take / footprint of the facility. Hoppers or crushers can be installed within the DTSW mesh/ Geosynthetic reinforcement system structure. Mined material is taken to the upper terrace and unloaded into the hopper/crusher. DTSW mesh/ Geosynthetic reinforcement systems (often complimented with high strength geogrids such as Paralink, with strengths up to 1350kN/m) can accommodate the high loads from mine dump trucks and other vehicles.



a) "Orcopampa" mine ($h_{\max} = 9.0\text{m}$ - Peru).



b) "Orcopampa" mine ($h_{\max} = 9.0\text{m}$ - Peru).

Figure 8 DTSW mesh/ Geosynthetic reinforcement System and hopper installation.

3.3 Retaining walls on Access Roads

Most mines are in remote locations and often access roads have to be constructed. Many of these require retaining walls to stabilize slopes, as well as bridges or river defenses.



Figure 9. DTSW mesh/ Geosynthetic reinforcement System for access road to the "Antamina" mine (Peru)



Figure 10. DTSW mesh/ Geosynthetic reinforcement System platform bridge abutment Doe Run mine (Peru)

3.4 Tailings Deposits

Tailings materials left over after the separation of the valuable portion from the uneconomic portion of an ore, generally contain a mixture of soil, minerals, water and rock.

These tailings are often stored in areas known as a tailings or sedimentation ponds. Due to space constraints, the pond walls can become tall and need to be designed appropriately. DTSW mesh/ Geosynthetic reinforcement System has been frequently used to construct these retaining structures, due its speed of construction and reduced structural footprint requirement. A further cost benefit can be realized if structural backfill to the DTSW mesh/ Geosynthetic reinforcement System can be sourced from waste materials from the mine site; crushed waste material, or overburden has been used in the past.



a) "Sinaycocha" mine ($h_{\max} = 8.0\text{m}$ - Peru).



b) "Poderosa" mine (Peru).



c) "Yauricocha" mine ($h_{\max} = 21.0\text{m}$ - Peru).



d) "Ares" mine ($h_{\max}=8.0\text{m}$ - Peru).

Figure 11. DTSW mesh/ Geosynthetic reinforcement System Tailings Deposit in mines.

3.5 Primary Crushers

These large structures are part of the concentration facilities within the mine and crush the mined material to predetermined dimensions for further processing. The large mine dump trucks deposit the mined ores into the top of the crusher. Access to the top of the crusher and the maneuvering yard is provided by ramps and tall retaining walls. Reinforced soil is ideally suited to accommodating the high loads applied by these vehicles.



Figure 12. DTSW mesh/ Geosynthetic reinforcement System for walls for access to the primary crusher Alto Chicama ($h_{\max} = 23.50\text{m}$ - Peru).

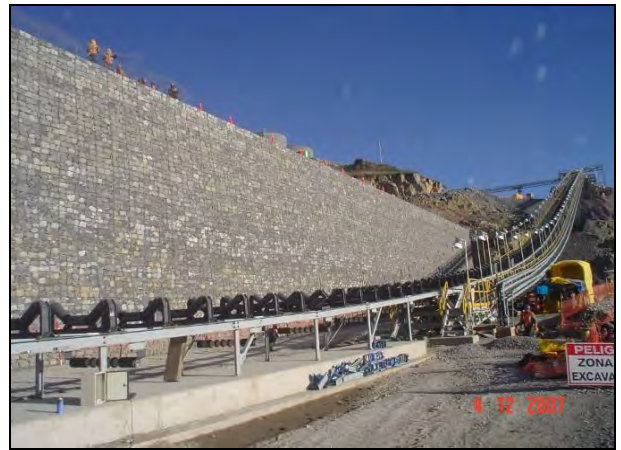


Figure 13. DTSW mesh/ Geosynthetic reinforcement System walls providing access to the primary crusher. Gold Fields ($h_{\max} = 16.50\text{m}$ - Peru).



Figure 14. DTSW mesh/ Geosynthetic reinforcement System rockfall embankment for protecting the primary crusher and conveyor belts ($h_{\max} = 20.00\text{m}$ - Peru).

4. SUMMARY AND CONCLUSIONS

Soil reinforcement uses proven technology and is ideally suited to the demands of the modern mine. With the latest generation of geogrids and soil reinforcement systems, these structures are suitable for numerous mine applications including retaining walls, rockfall protection embankments and within mine infrastructure. DTSW mesh/ Geosynthetic reinforcement System provides a cost effective and rapid to install alternative to traditional solutions. These benefits can be further enhanced when the design process determines that site-won materials are suitable for use as structural backfill.

Due to the significance of these structures, the reliability and pedigree of the selected soil reinforcement system should be a pre-requisite for mine owners and operators.

REFERENCES

- FHWA-NHI-10-024, (Nov 2009): "Design & Construction of Mechanically Stabilized Earth Walls and Reinforced Soil Slopes – Volume 1"
- HITEC Terramesh®, (2002) "Evaluation of the Maccaferri Terramesh® System Retaining Wall".
- Koerner, R.M., 2012. *Designing with Geosynthetics*, 6th ed., Volumes 1 & 2, Xlibris Corporation, Bloomington, USA.
- ASTM A975, Standard Specifications for Double-Twisted Hexagonal Mesh Gabions and Revet Mattresses (Metallic-Coated Steel Wire or Metallic Coated Steel Wire with Poly (Vinyl Chloride) (PVC) Coating), *American Society for Testing and Materials*, West Conshohocken, Pennsylvania, USA.
- British Board of Agreement, Roads and Bridges Certificate No 00/R119 "Maccaferri Terramesh® System for Reinforced Soil Embankments"
- Ing,H. Egoavil and Showan M. Reinforced Earth Wall Terramesh Systems in Mining Projects, Congress Theme:*Rock mechanics and Geotechnical Applications*

Design of Earthen Levee Strengthening with HPTRM for Hurricane Overtopping Conditions

Lin Li, PhD, P.E., Department of Civil and Environmental Engineering, USA, lin.li@jsums.edu
Farshad Amini, PhD, P.E., Department of Civil and Environmental Engineering, USA, famini@jsums.edu
Yi Pan, Department of Civil and Environmental Engineering, USA, panyi21@yahoo.com.cn

ABSTRACT

Overtopping of earthen levees produces fast-flowing, turbulent water velocities on the landside slope that can damage the protective grass covering and expose the underlying soil to erosion. In this study, the design of an innovative levee strengthening technique – High Performance Turf Reinforcement Mat (HPTRM) is developed based on true full-scale flume tests conducted during overtopping conditions simulating waves or combined wave and storm surge. As the grass roots grow through the open space of HPTRM, roots become entwined within the turf reinforced mat. The interlocking between roots and HPTRM can enhance the resistance against hydraulic and shear forces created by high water flow hydraulic condition. Flow velocity, shear stress and average overtopping velocity on landward-side slope and levee crest are measured and calculated. This paper presents new equations for hydraulic overtopping parameters, and design guidelines for combined wave and surge overtopping conditions.

1. INTRODUCTION

Overtopping of the earthen levees may occur during the periods of flood due to insufficient freeboard. The most problematic case involves the levee being overtopped by both surge and waves when the surge level exceeds the levee crest elevation with accompanying wave overtopping (Akkerman et al. 2007, Hughes and Nadal 2009). Overtopping of earthen levees produces fast-flowing, turbulent water velocities on the landside slope that can damage the protective grass covering and expose the underlying soil to erosion (Sills et al. 2008). Hurricane Katrina caused catastrophic overtopping and extensive damage to the levee system that surrounds the New Orleans (Briaud et al. 2008, Ubilla et al. 2008). Post-Katrina investigations revealed that most earthen levee damage occurred on the levee crest and landward-side slope as a result of either wave overtopping, storm surge overflow, or a combination of both (ASCE 2007). Hence, the crest and landside slopes of those levees that are at risk of overtopping must be protected with some type of strengthening method such as turf reinforcement, soil strengthening, or hard armoring. The levee strengthening systems should resist the forces of fast-flowing, turbulent water that has overtopped the levee crest. High performance turf reinforcement mat is one of the strengthening systems that can be used on the crest and landward-side of earthen levee.

HPTRM is one of the most advanced flexible armoring technologies available today for severe erosion challenges. The HPTRMs are three-dimensional TRMs joined at the intersections of randomly oriented nylon filaments with high tenacity polyester geogrid reinforcement at low strains. As shown in Fig. 1a, nearly 95% of space is open in this material. As the grass roots grow through the open space of HPTRM, roots become entwined within the turf reinforced mat (Fig. 1b). The interlocking between roots and HPTRM can enhance the roots resistance against hydraulic life and shear forces created by high water flow hydraulic erosion. A specific gravity of nylon in the HPTRM more than 1.0 ensures that the HPTRM will not float under any hydraulic condition. The geogrid reinforcement in the HPTRM can help soil stabilization mechanically by taking over when extreme conditions exist (Goodrum 2011). This paper addresses the hydraulic design of HPTRM-strengthened earthen levees on the crest and land-side slope during the combined wave and surge overtopping. The performance of HPTRM is investigated by true full-scale overtopping hydraulic model in Large Wave Flume (LWF) at the O.H. Hinsdale Wave Research Laboratory (HWRL) of Oregon State University.

2. FULL-SCALE TESTS OF COMBINED WAVE AND SURGE OVERTOPPING

A vegetated HPTRM system was developed over a six-month period in the southern climate. With a uniform distribution of seeding spread over the mat, daily watering and weekly mow of the grass were conducted in Mississippi. The height of grass was over 0.15 m before the full-scale overtopping tests. The full-scale tests were conducted in the LWF of the HWRL. The dimensions of the LWF and the levee model are shown in Fig. 2. The HPTRM system was built into a steel tray, which was put into the test section before the tests. The gap between the tray and the side wall of test section was sealed with lumber.



(a) Detailed structure

(b) Vegetated HPTRM system

Figure 1. Illustrations of HPTRM system: (a) Details of the three-dimensional structure of HPTRM mat. Polyamide filaments thermally fused at the intersections and polyester fibers interwoven as geogrid interlock. U-Shaped pin is used to fix the HPTRM mat on clay, and (b) vegetated HPTRM system. The open space of HPTRM allows roots grow through and entwined with the HPTRM to reinforce the plant roots.

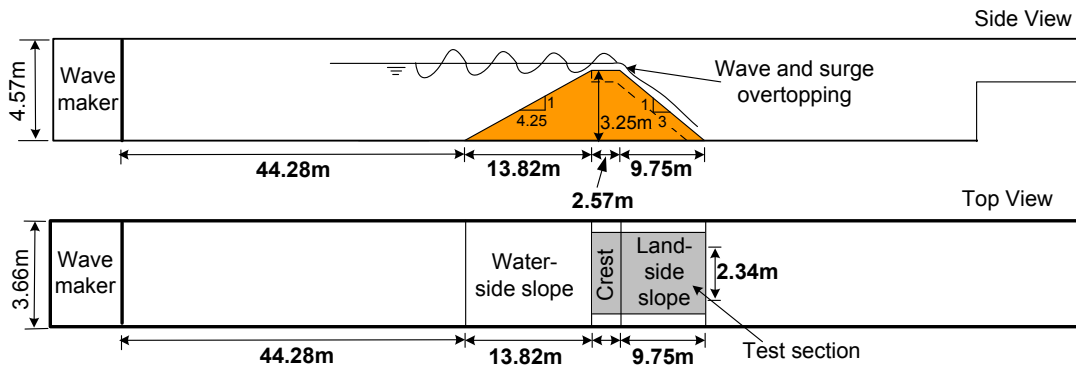


Figure 2. Profile view of the large wave flume and location of levee embankment.

Eight Acoustic Doppler Velocimeters (ADVs) were installed above the levee crest and the land-side slope to measure the x-component (parallel to the levee crest or slope) of flow velocity. Six acoustic range finders were employed to measure the flow thickness at the levee crest and the land-side slope. Based on the capability of the piston wave maker, nine combined wave and surge cases with different conditions were designed. The surge heights were in the range of 0.096 m to 0.317 m, and the significant wave heights ranged from 0.527 m to 0.908 m. The durations of each trial ranged from 10 min. to 90 min. In all the tests, irregular wave time series realization was generated conforming to the idealized TMA spectrum. Data collection started at the same instant the wave board was activated, and collection continued until the wave board stopped. Time series of water surface elevation data at five wave gauges and six acoustic range finders, and eight ADVs at were collected at a 50-Hz rate. All data were recorded for post-experiment processing. Details of hydraulic experiments can be found in Pan et al. (2012a, 2012b).

3. RESULTS

3.1 Steady Overflow Discharge

The time series of flow thickness and time series of flow velocity at the middle of the levee crest were used to estimate the time series of steady overflow discharge, q_s . Based on the formula of Henderson (1966), the steady overflow discharge can be calculated using the following equation:

$$q_s = 0.415(g)^{1/2}(-R_c)^{3/2} \quad [1]$$

where q_s is steady overflow discharge ($m^3/s-m$), g is gravity acceleration constant, R_c is freeboard (m), defined as vertical distance between the still water elevation and crest elevation. During the overflow or overtopping condition, R_c is

negative. In Eq. 1, the constant of 0.415 is smaller than Henderson's value of 0.5443 (Henderson 1966). This may be explained by the fact that the value given by Henderson (1966) is based on the assumption that minimal frictional energy losses exist along the crest and land-side slope. On HPTRM-strengthened levee crest and land-side slope, the frictional energy losses are not negligible due to the grass. Thus the frictional energy losses are the reason why the steady overflow discharge is smaller than Henderson's estimation.

3.2 Average Overtopping Discharge

The time series of flow thickness and time series of flow velocity at the middle of the levee crest were used to estimate the time series of overtopping "apparent" discharge, q_{ws} , for each test. Averages were calculated for data points 2000 to 260,000 (5160 s at 50-Hz rate). Fig. 3 shows the dimensionless combined wave and surge average overtopping discharge versus the relative freeboard for 9 tests. The measurements show a nice trend with increasing relative freeboard except for the two points with relative freeboard $-R_c/H_{m0} < 0.3$. The solid line is the best-fit empirical equation for the data points $-R_c/H_{m0} < 0.3$ given by the following equation:

$$q_{ws}/g^{1/2}/H_{m0}^{3/2} = 0.0053 + 0.378(-R_c/H_{m0})^{1.58}, \quad -R_c/H_{m0} < 0.3 \quad [2]$$

where q_{ws} is average overtopping discharge ($m^3/s\cdot m$), H_{m0} is energy-based significant wave height (m), dimensionless R_c/H_{m0} is the ratio of freeboard (R_c) and the significant wave height based on energy spectrum (H_{m0}). It reflects the proportional relationship between surge overflow and wave overtopping in the combination of surge and wave. Relative freeboard is an important parameter in the study of wave overtopping.

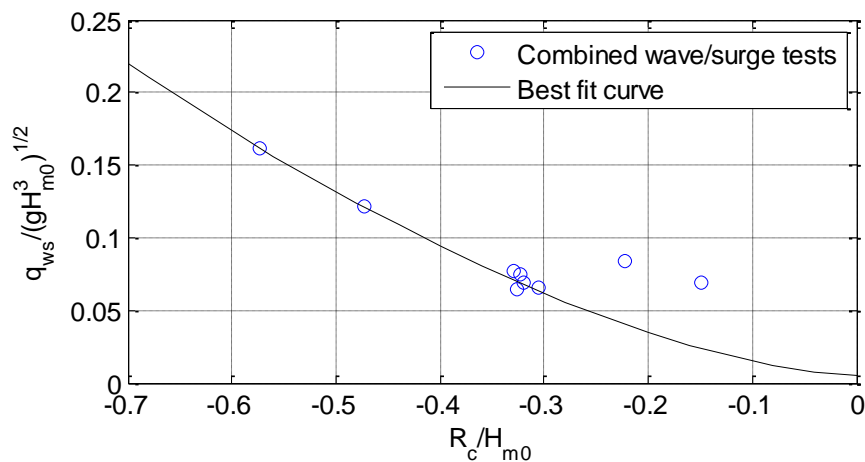


Figure 3. Dimensionless combined wave/surge average discharge versus relative freeboard

The best-fit equation had a correlation coefficient of 0.9868 and an RMS percent error of 0.0049. Hughes and Nadal (2009) concluded that peak spectral wave period (T_p) had negligible influence in the determination of q_{ws} . Based on their recommendation, the peak wave periods of the tests trials were set around 7 s to obtain a larger wave force and more severe erosion on the levee. Similarly, the peak wave period was not considered in the estimation of q_{ws} . Similar to other empirical equations, application of Eq. 2 is limited to the range of tested parameters. In particular, seaside levee slopes different from 1V:4.25H could influence the wave overtopping, but seaside slope effects should decrease as surge level increases.

Based on the value of the ratio q_{ws}/q_s , combined wave and surge overtopping cases with $-R_c/H_{m0} > 0.3$ can be summarized as surge-dominated cases. In surge-dominated combined wave and surge overtopping cases, the ratio q_{ws}/q_s is approaching unity. The combined wave and surge overtopping cases in which $-R_c/H_{m0} < 0.3$ can be summarized as wave-dominated cases. In wave-dominated combined wave and surge overtopping cases, the ratio q_{ws}/q_s increases sharply when R_c/H_{m0} approaches zero.

3.3 Flow Parameters on the Land-Side Slope of the HPTRM Strengthened Levee

Steady overflow on the steep land-side slope is supercritical with slope-parallel velocities increasing down the slope until a balance is reached between the momentum of the flow and the frictional resistance force of the slope surface. Flow down the land-side slope caused by combined waves and surge overtopping is unsteady and more complicated and thus needs more parameters to analyze.

The average flow thickness perpendicular to the slope, d_m , was calculated at the land-side slope starting with data point 2000 and continued to the end of the time series. The average flow thickness d_m on land-side slope can be described as:

$$d_m = 0.384(g\sin\theta)^{-1/3} q_{ws}^{2/3} \quad [3]$$

where d_m is average flow thickness (m), θ is angle of levee land-side slope to horizontal.

The mean flow velocity equation becomes the following:

$$v_{ws} = 2.6(g\sin\theta q_{ws})^{1/3} \quad [4]$$

where v_{ws} is mean flow velocity along the land-side slope (m/s).

The constants in Eq. 3 and Eq. 4 are related to the slope roughness, and the equations are strictly only applicable for landward side slopes of 1V:3H having armoring layer of HPTRM. The constants in Eq. 3 and Eq. 4 are close to the constants in Hughes and Nadal equations (2009) based on 25-to-1 scale laboratory tests on earthen levee, which is consistent with the description of Hughes and Nadal (2009) that the friction factors for grass levee slopes should not be much different from those of their experiments. Schüttrumpf and Oumeraci (2005) noted that friction factor is an influential parameter for wave-only flows over levees and dikes. More work is needed to determine appropriate representative friction factors for a range of slope roughness.

After several attempts using dimensionless combinations of the wave height, wave period, and steady surge discharge, the best empirical result for the wave front velocity was the relationship:

$$v_w = 4.33(gq_{ws})^{1/3} \quad [5]$$

where v_w is wave front velocity along the land-side slope (m/s). With the estimated q_{ws} given by Eq. 2, Eq. 5 can be used to obtain reasonable estimates for wave front velocity v_w . But application of Eq.5 is limited to the range of tested parameters.

4. CONCLUSIONS

A full-scale experiment of combined wave and surge overtopping of a trapezoidal levee cross section strengthened with HPTRM system was conducted to study the hydraulic overtopping parameters and design guidelines. Time series of various flow parameters associated with overtopping discharge and flow field on the land-side slope were estimated. The surge overflow discharge and average overtopping discharge in surge-dominated cases and wave-dominated case are presented. The mean flow thickness, mean flow velocity and wave front velocity associated with the unsteady flow field on the land-side levee slope were examined, and equations were developed based on the time series of flow thickness at measuring points on the land-side slope. Empirical equations for the mean flow thickness and mean flow velocity were expressed in terms of the slope angle and average overtopping discharge. The empirical equations are based on full-scale laboratory tests, which is the only way to test HPTRM on a levee embankment section with a seaside slope of 1V:4.25H and a land-side slope of 1V:3H. The equations associated with unsteady flow on the land-side slope may not be applicable for levees having different slopes.

ACKNOWLEDGEMENTS

This research was funded by the Department of Homeland Security-sponsored Southeast Region Research Initiative (SERRI) at the Department of Energy's Oak Ridge National Laboratory. The conclusions in this paper are solely those of the authors and do not necessarily reflect the opinions or policies of DHS. Endorsement by DHS is not implied and should not be assumed. Thanks are extended to Tim Maddux of the Oregon State University, Richard Goodrum of Colbond, Inc. and, Michael Robenson, Kevin Spittle, and Jessie Clark of Profile Products for their support during the experiments.

REFERENCES

- Akkerman, G.J., Bernardini, P., van der Meer, J., Verheij, H., and van Hoven, A. (2007). Field tests on sea defences subject to wave overtopping. *Proc. Coastal Structures*, Venice, Italy, July 2-4.
 ASCE Hurricane Katrina External Review Panel. (2007). *The New Orleans Hurricane Protection System: What Went*

- Wrong and Why?* American Society of Civil Engineers, Reston, Virginia. 92 pp.
- Briaud, J.L., Chen, H.C., Govindasamy, A.V., and Storesund, R. (2008). Levee erosion by overtopping in New Orleans during the Katrina Hurricane. *Journal of Geotechnical and Geoenvironmental Engineering*, ASCE,134: 618-632.
- Goodrum, R. (2011). A Comparison of sustainability for three levee armoring alternatives. *Optimizing Sustainability Using Geosynthetics*, the 24th Annual GRI conference Proceedings, edited by Koerner, G.R., Koerner, R. M., Ashley, M. V., Hsuan, G. Y., and Koerner J., R., Dallas, Texas, March 16, 2011, 40-47.
- Henderson, F. M. (1966). *Open channel flow*. New York, NY: MacMillian Publishing Co., Inc.
- Hughes SA, Nadal NC, Laboratory study of combined wave overtopping and storm surge overflow of a levee. *Coastal Engineering* 2009:56: 244–259.
- Pan, Y., Li, L., Amini, F., and Kuang, C.P. (2012a). Full scale HPTRM strengthened levee testing under combined wave and surge overtopping conditions: Overtopping hydraulics, shear stress and erosion analysis. *Journal of Coastal Research*, in print.
- Pan, Y., Li, L., Amini, F., and Kuang, C.P. (2012b). Comparison of the hydraulic performances of three levee-strengthening systems and hydraulic equivalency analysis between steady and intermittent overtopping. *Journal of Waterways, Coastal and Ocean Engineering*, ASCE, in print.
- Sills, G.L., Vroman, N.D., Wahl, R.E., and Schwanz, N.T. (2008). Overview of New Orleans levee failures: Lessons learned and their impact on national levee design and assessment. *Journal of Geotechnical and Geoenvironmental Engineering*, ASCE,134: 556-565.
- Ubilla, J., Abdoun, T., Sasanakul, I., Sharp, M., Steedman, S., Vanadit-Ellis, W., and Zimmie, T. (2008). New Orleans levee system performance during Hurricane Katrina: London Avenue and Orleans Canal South. *Journal of Geotechnical and Geoenvironmental Engineering*, ASCE,134: 668-680.

Development of Piled Geo-wall

Takashi Hara, Gifu University, Japan, t_hara@gifu-u.ac.jp
Shinichiro Tsuji, MAEDA KOSEC CO., LTD., s_tsuji@mdk.co.jp
Masaki Yoshida, MAEDA KOSEC CO., LTD., yoshida@mdk.co.jp
Kazuhide Sawada, Gifu University, Japan, sawada@gifu-u.ac.jp

ABSTRACT

The aim of this study is to develop a new type soil structure, Piled Geo-wall, which can be applied to diverse structures as substitute for concrete ones and contribute to reasonable and sustainable development of infrastructures. This study consists of several experiment studies, full scale static and impact loading tests and a dynamic centrifuge model test, and proposal of a simple design method that can reproduce the experiments' results. The experimental studies and the performance of the proposed structure have already published, hence, proposal of a simple design model and the reproducibility of the experiments' results with using the proposed design model are presented in this paper.

1. INTRODUCTION

The high ductility of soil structure reinforced by geogrid is well known, as is the possibility of building independent soil wall. The independent reinforced soil wall has been applied to such diverse structures as rock-fall protection walls, mud and snow avalanche protection walls and the suchlike. Since it can be built using existing soil at the construction site if it is compactable one, they are being used ever more frequently as one of economic and CO2 reducible structures. At present, however, the adoption of the spread foundation for the independent reinforced soil wall makes the design too wide for application to narrow construction sites, such as beside mountainous road. If a narrow independent reinforced soil wall as like as RC wall with using pile foundation is achieved, it could be widely applied. And it can also be substitute for concrete ones and contribute sustainable development.

Therefore, a new type of independent reinforced soil wall with inserting piles into the Geo-wall body, as shown in Figure 1, which is referred to "Piled Geo-wall or PGW" in this paper, has been developed. The practicability of Piled Geo-wall to diverse structures has been already confirmed from three experimental studies with full-scale static and impact loading tests and a dynamic centrifuge model test (25G) were carried out in the past years (Hara et al. 2010 and 2012).

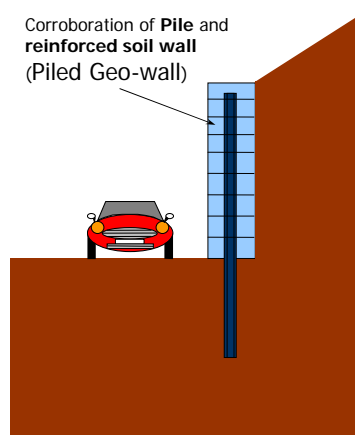


Figure 1. Image of Piled Geo-wall (PGW).

Recognizing the practicability, a study on simple design model that can reproduce the experiments' results has been conducted. In this paper, because of paper limitation, the proposed simple external stability model in the study and the reproducibility of the proposed model with respect to the experiments' results are presented.

2. PROPOSAL OF SIMPLE EXTERNAL STABILITY MODEL

Piled Geo-wall was devised from an assumption regarding the interaction between pile and Geo-wall body, which the Geo-wall body with high ductility is possible to transmit lateral forces to the piles despite occurrence of large relative displacement between the pile and the Geo-wall body as shown in Figure 2. Hence, in the design, the responses of the pile and the Geo-wall body have to be estimated respectively. Figure 3 shows the proposed simple estimation model of the responses of the pile and the Geo-wall body of Piled Geo-wall

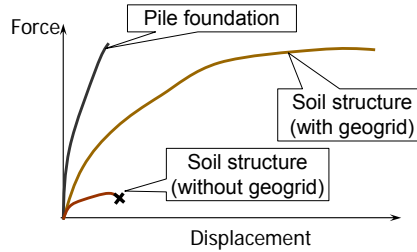


Figure 2. Interaction image between pile and Geo-wall.

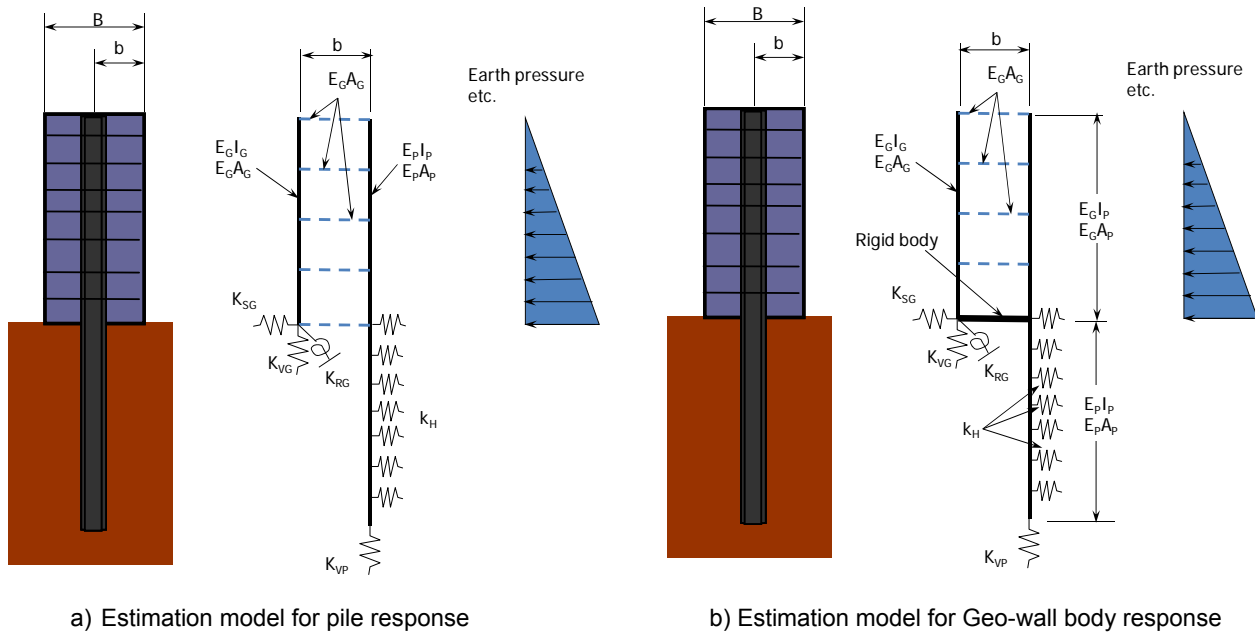


Figure 3. Fundamental external stability model.

Where, $E_P I_P$, $E_G I_G$: flexural stiffness of pile and Geo-wall (kNm^2/m), $E_P A_P$, $E_G A_G$: compressional stiffness of pile and Geo-wall (kNm^2/m), $E_G I_P$: extent without considering flexural stiffness of pile, k_H : elasto-perfectly plastic spring constant of horizontal subgrade reaction (kN/m) set from Eq. 1, the limited value of k_H is passive earth pressure, K_{VG} : elasto-perfectly plastic spring constant of vertical subgrade reaction beneath the Geo-wall body (kN/m) set from Eq. 2, the limited value of K_{VG} is ultimate bearing capacity, K_{SG} : elasto-perfectly plastic spring constant of horizontal shear reaction beneath the Geo-wall body (kN/m) set from Eq. 3, the limited value of K_{SG} , S_{\max} , is set from Eq. 4, K_{RG} : elasto-plastic rotation spring constant beneath the Geo-wall body (kN/rad) set from Eq. 5, the limited value of K_{RG} is determined by the ultimate bearing capacity, K_{VP} : elasto-perfectly plastic vertical spring constant beneath the pile (kN/m) set from Eq. 6, the limited value of K_{VP} is the ultimate bearing capacity of pile, k_h and k_v : coefficients of horizontal and vertical subgrade reaction (kN/m^3) in normal time or seismic situation, which are estimated from Specifications for Highway Bridges Part IV (JRA, 2012), D : pile diameter (m), d_u : unit depth, namely 1.0m, A_G and A_P : cross section areas of the Geo-wall body and the pile (m^2), c and ϕ : cohesion and shear resistance angle of foundation ground (kPa and rad)

$$K_H = k_h \cdot D \cdot d_u \quad [1]$$

$$K_{VG} = k_v \cdot A_G \quad [2]$$

$$K_{SG} = 1/3 \cdot k_v \cdot A_G \quad [3]$$

$$S_{max} = c \cdot A_G + \sigma \tan \phi \quad [4]$$

$$K_{RG} = k_v \cdot b \quad [5]$$

$$K_{VP} = k_v \cdot A_P \quad [6]$$

3. REPRODUCIBILITY OF PROPOSED DESIGN MODEL WITH RESPECT TO EXPERIMENTAL STUDIES

3.1 Full Scale Static Loading Test

The summary of the static loading test of Piled Geo-wall is shown in Figure 4, and the test Piled Geo-wall was built as follows; (1) Pile installing: H steel piles (H-300x300x10x15) of 6.0m in length are installed in 4.0m into the ground. (2) Setting of steel face member and installing of geogrid at each layer: steel face members were set on the both side of Geo-wall and a geogrid was installed at one layer. In the construction of Piled Geo-wall, a geogrid with holes located in the piles was installed through the piles, as shown in Figure 5-a). (3) Installing of longitudinal additional geogrid at each layer: the additional geogrid was installed on the loading side of piles, as shown in Figure 5-b), in order to transmit the load to the piles from the Geo-wall body smoothly. (4) The executions of each layer, 0.5m in thickness, were repeated until that the Geo-walls, 2.0m in height, were completed.

In this test, two jacks set at 1.0m in height to give static horizontal load. And the horizontal load is transmitted to the Piled Geo-wall as a distributed pressure through a H steel (H200 x 200 x 8 x 12), a steel plate of 0.12m and an EPS of 0.5m thickness. Therefore, triangle distribution pressure was loaded to the design model in the response analysis.

The test was performed to both Piled Geo-wall and normal Geo-wall without pile though; the test carried out to Piled Geo-wall is described in this paper.

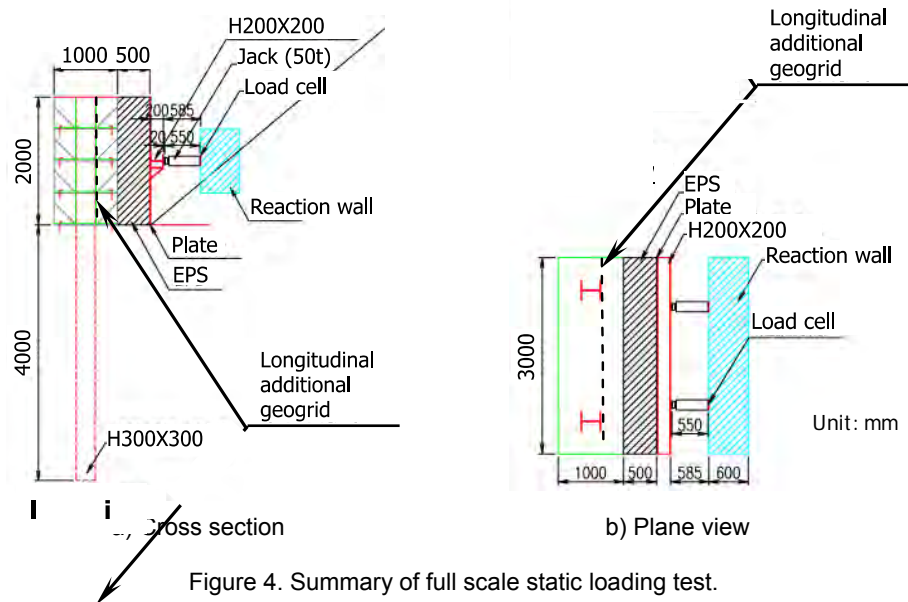


Figure 4. Summary of full scale static loading test.



a) Installing of steel face member and geogrid b) Installing of longitudinal additional geogrid

Figure 5. Building of Piled Geo-wall.

Figure 5 shows the results of dynamic penetration tests converted to N value of standard penetration test (SPT) as the ground condition of the test. In the response analysis, the result of PD-2 obtained at the vicinity point of the target Piled Geo-wall was referred.

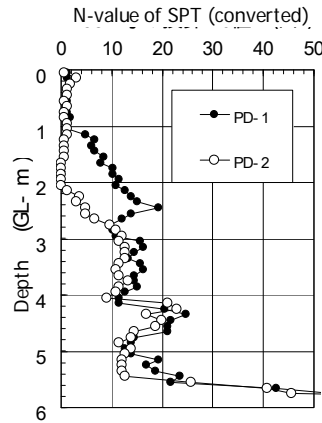
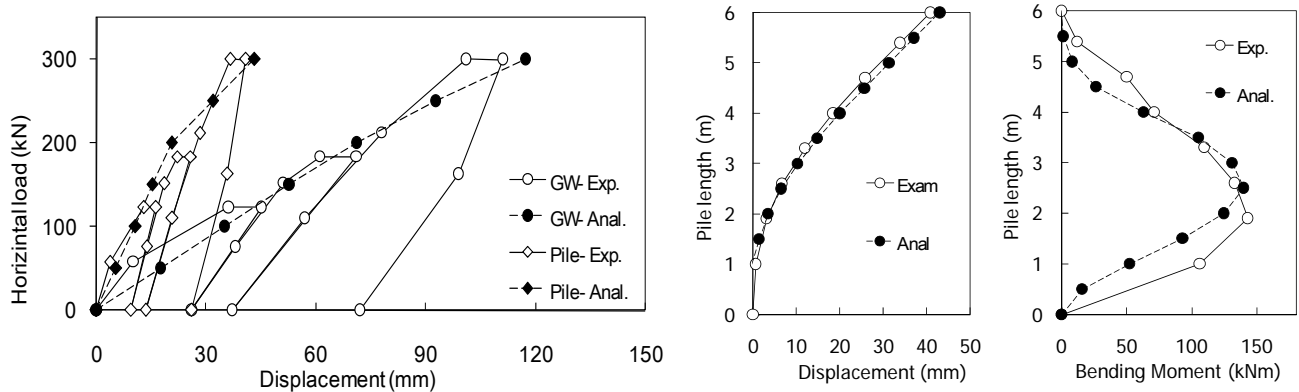


Figure 5. Ground condition.

Figure 7-a) shows the analysis results of the relationship between static load and displacement of Piled Geo-wall, top of the pile and Geo-wall body, which are compared with measured value from the test. And Figure 7-b) shows comparisons with the analysis results of maximum response of pile and measured ones from the test.

According to the results, it is confirmed that the proposed model can reproduce the response of the Piled Geo-wall and the interaction between pile and Geo-wall body as previous assumption as shown in Figure 2.



a) Relative displacement between pile and Geo-wall

b) Maximum response of pile

Figure 7. Comparison with experiment's results and analyzed ones.

3.2 Dynamic Centrifuge Model Test

Figure 8 shows the summary of the dynamic centrifuge test (25G) of Piled Geo-wall. The test was performed to both Piled Geo-wall and normal Geo-wall without pile, as shown in Figure 8-a), though, the test carried out to Piled Geo-wall is described in this paper. Figure 8-b) shows the transverse section of the Piled Geo-wall test model. In the building of Piled Geo-wall test model, installing of normal geogrid and longitudinal additional geogrid were executed as the same as real building as shown in Figure 8-c). Fig. 8-d) shows the input earthquake wave converted to actual scale.

Slope ground was made up of cement-stabilized soil and, the soil of the embankment and the Geo-wall body was compacted with density control. Geotechnical and structural parameters converted to actual scale are presented on Table.1 and 2, respectively.

Table 1. Geotechnical parameter.

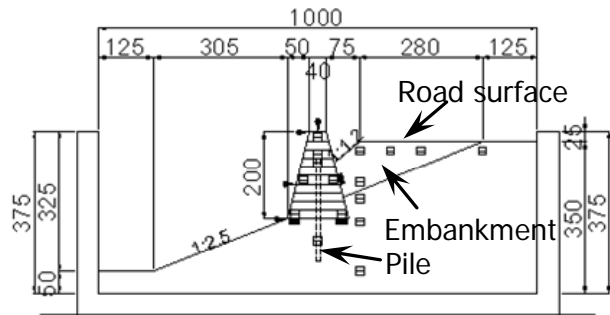
	E_0 (kPa)	c (kPa)	ϕ (deg)
Slope	3.26×10^5	55	0
Embankment	3.0×10^4	0	40
Geo-wall	3.0×10^4	0	40

Table 2. Structural parameter.

	E (kPa)	A (m ² /m)	I (m ⁴)
Pile	2.0×10^8	4.79×10^{-3}	2.04×10^{-4}
Geogrid	8.0×10^5	1.0×10^{-3}	-



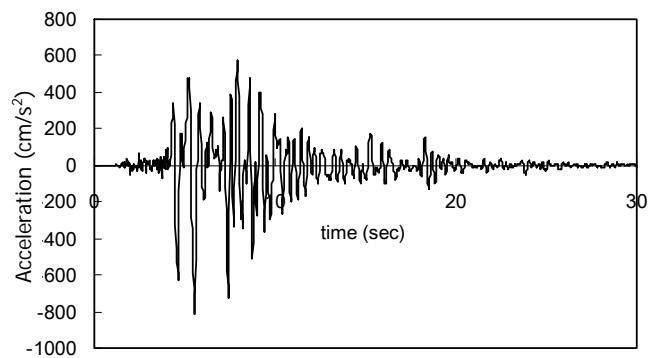
a) Centrifuge model



b) Transverse section



c) Geogrid installing



d) Input earthquake

Figure 8. Summary of dynamic centrifuge test (25G).

Because recognizing of dynamic interaction between structure and surrounding ground is necessary in order to design the structure by static analysis, dynamic interaction between the Piled Geo-wall and the embankment, transition of pile response and earth pressure at the embankment side of the Piled Geo-wall at the time that the maximum pile response was obtained are shown in Figure 9-a) to c).

According to the results, the antiphase between the response of Geo-wall body at 5th layer (the part with inserting pile) and ones of embankment and Geo-wall body at 10th layer (the part without inserting pile) is confirmed, as shown in Figure 9-d). And the states of inertia forces and earth pressure acting on the embankment side of Piled Geo-wall body at the time that the maximum pile response was obtained were confirmed, as shown in Figure 9-e).

Figure 10-a) shows the comparisons of analyzed maximum pile responses from the confirmed load states and obtained ones from the experiment. And the comparison of analyzed maximum Geo-wall body response and obtained one from the experiment is shown in Figure 10-b).

From these results, it could be confirmed that the proposed estimation model can reproduce well the actual maximum response of the pile and Geo-wall body.

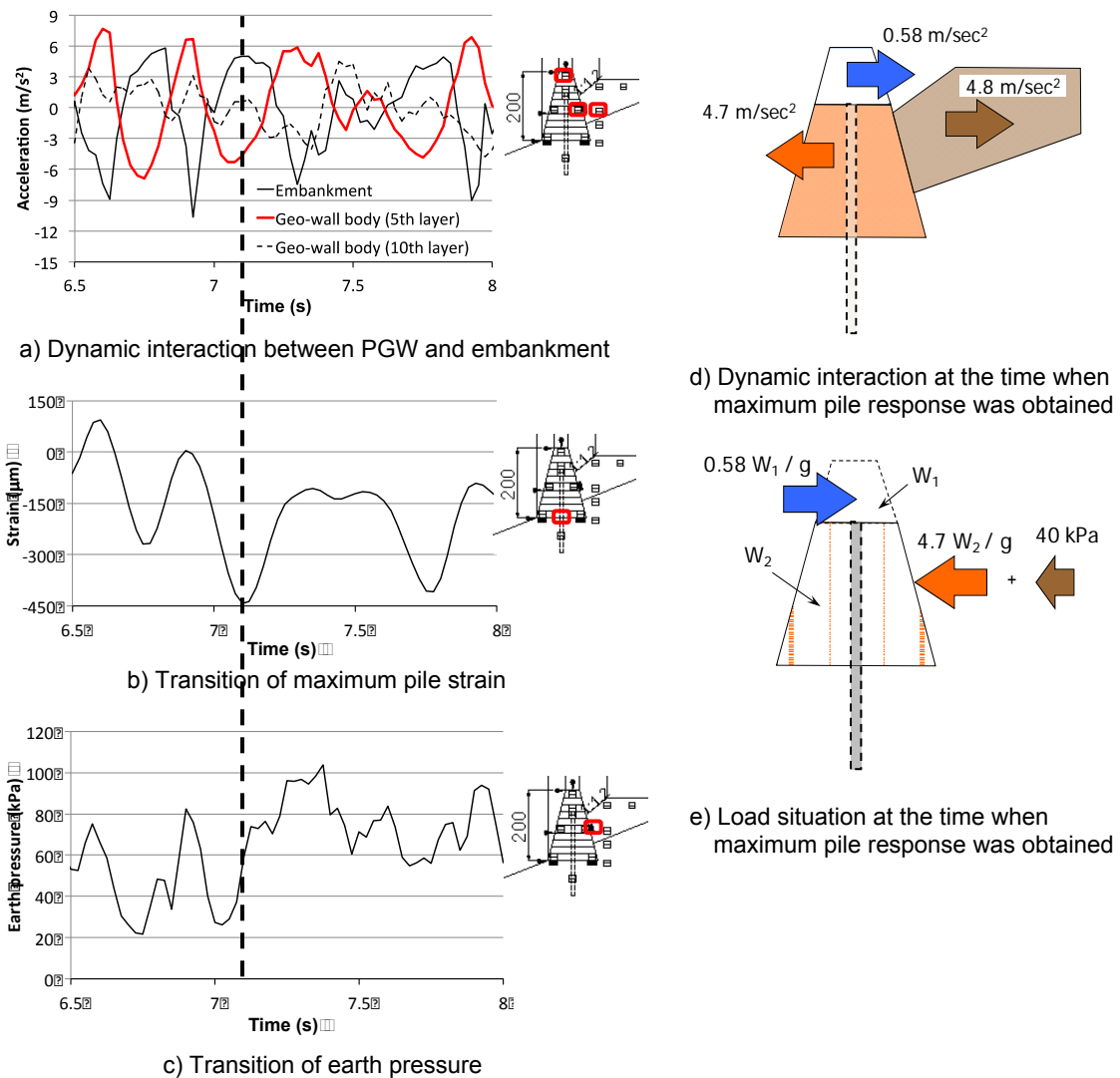


Figure 9. Dynamic responses of PGW and embankment.

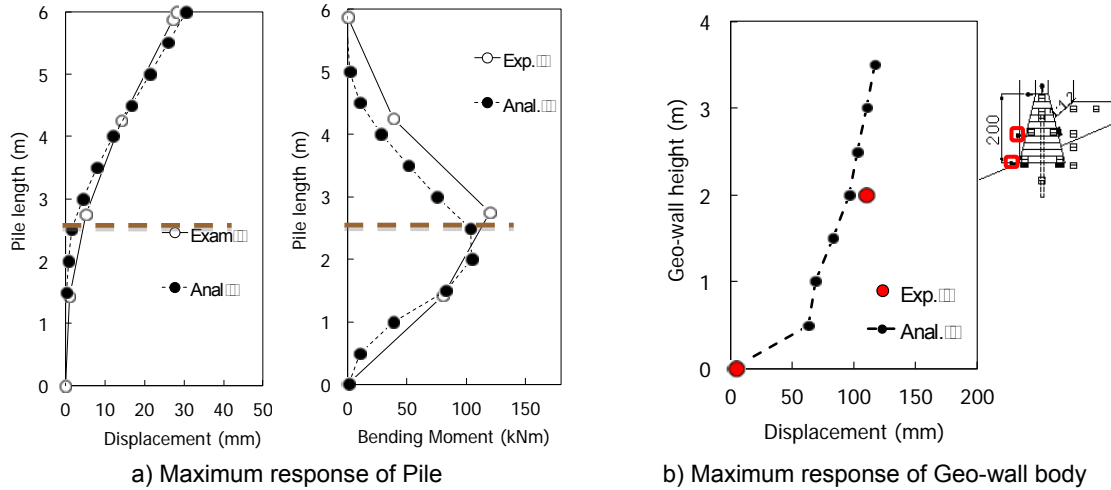


Figure 10. Comparisons of analyzed results and obtained ones from the experiment.

3.3 Full Scale Impact Loading Test

3.3.1 Static load Evaluation of Impact Load

Static load evaluation of impact load is important in case of estimation of the response of Piled Geo-wall receiving the impact load by the static analysis. Therefore the evaluation method was assumed in this study. Figure 11 shows the assumed evaluation procedure of design static load from impact-load.

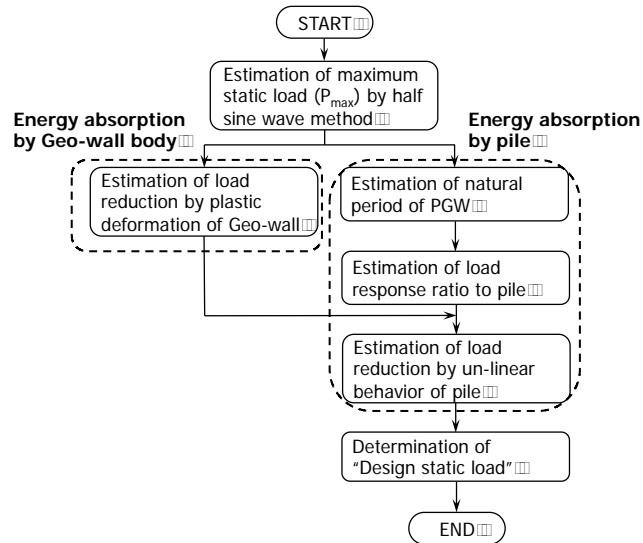


Figure 11. Evaluation procedure of design static load from impact load.

Where, the maximum static load (P_{max}) based on half sine wave method is estimated by Eq. 7. In this equation, m is mass, V_0 is initial velocity (m/sec) at the time of the rock-fall impact to the Geo-wall body, which is predicted by Eq. 8, T is sustaining period (sec) of the impact by PGW, which is assumed as 0.07sec from the experiments, g is G-force, h is falling height of the rock fall

$$P_{max} = \frac{\pi \cdot m \cdot V_0}{T} \quad [7]$$

$$V_0 = \sqrt{2 \cdot g \cdot h} \quad [8]$$

Energy absorption by Geo-wall body was assumed that the difference between entire energy and absorption energy by pile estimated from inverse analysis with using proposed model.

Load response ratio to pile expresses reduction (or amplification) effect of transmitting load to pile. It is well known that the response reduces if the structure with long natural period receives the impact load with short impact period; in contrast, the response amplifies if the structure with short natural period receives the impact load with comparative long impact period. Therefore, the coefficient considered the characteristics in case of using load estimated from half sine curve method was proposed from the past study (Clough et al. 1975). According to the study, the border of reduction and amplification of the response is said to be the case that the ratio of impact period of road and natural period of structure is about 0.26.

And finally, the design static load (P_D) is determined from the load reduction, which is estimated by equivalent energy method (Newmark et al. 1960) of both elastic and elasto-plastic analyses with using the proposed external stability model.

3.3.2 Test Results and Reproducibility of the Proposed Design Model

The impact-loading test of Piled Geo-walls is shown in Figure 12-a). In this paper, the results of two impact-loading tests to actual scale models, one is adopted in the static loading test (PGW-1) shown in Figure 4 and another is a new one (PGW-2), which the piles are installed at outside of Geo-wall as shown in Figure 12-b), are targeted.

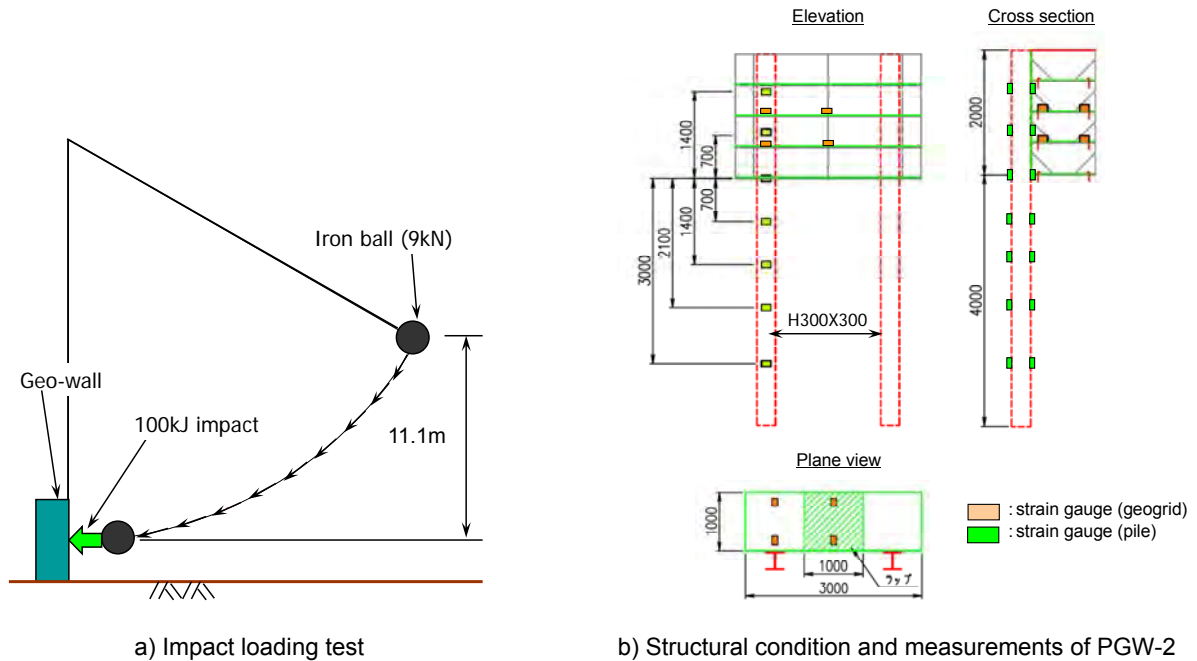


Figure 12. Summary of impact loading test.

Figure 13 show the maximum pile responses of PGW-1 and 2, respectively. According to the results, it can be confirmed that the proposed external stability model reproduces well ones obtained from the experiments. Where, it is no wonder that analyzed pile top displacements match up to obtained ones because the energy absorption of Geo-wall body was determined from inverse analysis of pile, however, the high reproducibility of the proposed model can be confirmed from the distribution in depth of the displacement and the bending moment of piles

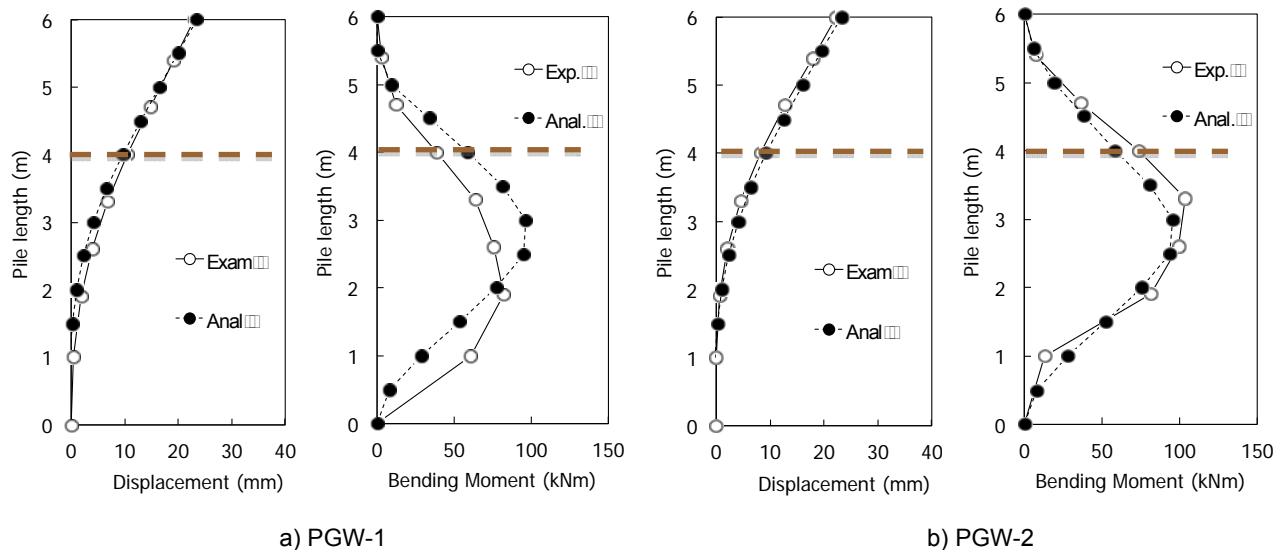


Figure 13. Maximum pile responses.

4. CONCLUSIONS

The contents of this paper are concluded as follows;

- Simple external stability model of Piled Geo-wall for practical design was proposed
- The practicability of the proposed design model was confirmed from good reproducibility of real responses obtained from full-scale static and impact loading tests, and a dynamic centrifuge model test
- In the response analysis on Piled Geo-wall in static load situation (a full scale static loading test), high reproducibility of interaction between pile and Geo-wall body by using the proposed design model was confirmed
- In the response analysis on Piled Geo-wall in seismic situation (a dynamic centrifuge model test), high reproducibility of the maximum response of pile and Geo-wall body deformation by using the proposed design model were confirmed
- In the response analysis on Piled Geo-wall in impact load situation (a full scale impact loading test) for design on rock-fall protection structure, an evaluation procedure on assumption of design static load from impact one was also proposed and its practicability was confirmed from good reproducibility of the maximum pile response by using the proposed procedure and design model

The following issues, however, have to be studied to apply the proposed model to more wide condition of Piled Geo-wall.

- Validity of the proposed model to design on larger scale (width, height) Piled Geo-wall than the test ones
- Practicability of the proposed model to the design on Piled Geo-wall with using steel-pipe pile or multiple rows' piles
- Improvement of static load conversion procedure from impact one as being able to apply to diverse conditions of Piled Geo-wall

Meanwhile, simple internal stability model has been also studied; it will be presented after more verification of validity.

REFERENCES

- Hara, T., Tsuji, S., Yashima, A. and Sawada, K. (2010). Independent reinforced soil structure with pile foundation, *Journal of SOILS AND FOUNDATIONS*, Japan Geotechnical Society, Vol.50, No.5: 565-571
- Hara, T., Tsuji, S., Yoshida, M., Ito, S. and Sawada, K. (2012). Experimental development of new type reinforced soil wall, *International Journal of GEOMATE*, The GEOMATE International Society, Vol. 2, No.2 (Sl. No.4): 213-218
- Japan Road Association (2002). *Specifications of highway bridges (Part IV: Substructures)*, Japan Road Association, Tokyo, Japan
- Clough, R.W. and Penzien, J. (1975). *Dynamics of structures*, McGraw-Hill, New York, NY, USA.
- Newmark, N.M. and Veletson, A.S. (1960). Effect of inelastic behavior on the response of simple systems to earthquake motions, *2nd WCEE*, Tokyo, Japan: 895-912

Development of, and Experiences During, a Program for the Certification of Geoelectric Liner Integrity and Leak Location Surveyors

I.D. Peggs, I-CORP INTERNATIONAL, Inc., Ocean Ridge, FL, USA, icorp@geosynthetic.com
A. Beck, TRI-Environmental, Inc., Austin, TX, USA, abeck@tri-env.com
S. Allen, TRI-Environmental, Inc., Austin, TX, USA, sallen@tri-env.com
A.J. Shah, TRI-Austin, Inc., Austin, TX, USA, Ashah@tri-austin.com

ABSTRACT

The successful performance of geoelectric geomembrane liner integrity and leak location surveys requires a knowledge of the boundary conditions and limitations of the related technologies. If not properly performed optimistic results – no leaks – will be obtained. As the requirements for the implementation of this technology became required by liner design/ CQA engineers and regulators there was a recognized need for appropriate education and certification of the engineering community to help ensure that effective surveys are performed. In this paper we describe the development of such an educational and certification program.

1. INTRODUCTION

The geoelectric method of locating leaks in geomembrane liners was essentially developed simultaneously by three separate groups in the early/mid-1980s: 1) Daren Laine and Glen Darilek at Southwest Research Institute, San Antonio, Texas, USA; 2) Vladimir Nosko of Sensor spol. s.r.o., Bratislava, Slovakia, and 3) Dan Boryta at Foote Mineral Co, Santiago, Chile. The technology started to be adopted by engineers and regulators in the late 1980s and early 1990s for both construction quality assurance (CQA) of newly installed liners and problem leak location in functioning systems. In this paper the former will be referred to as liner integrity surveys (LIS) and the latter as leak location surveys (LLS). Each group developed its own proprietary package of equipment until Leak Sensors Inc. acquired a patent and equipment from Foote Mineral Co and started to lease equipment to somewhat trained operators. This equipment was for surveying liners covered by liquids and for exposed liners. Shortly thereafter Allied Associates in the UK started to sell equipment for surveying soil-covered liners. Subsequently, the Foote patent ran out, Leak Sensors was shut down, and Allied Associates concentrated more on their base geophysical testing equipment. Thus, there came the opportunity in the early 2000s for others to manufacture packages of equipment made available to CQA engineers, facility owners, and liner installers. However, along with that opportunity, came the responsibility for those using the equipment to perform quality surveys, the main concern being that if done improperly an optimistic result would be obtained – no leaks. Therefore, it was felt necessary for there to be a training course and certification program for those wanting to apply the technology which was, by this time, clearly capable of improving the performance of geomembrane lining systems as the final stage of a CQA program. This is evidenced by the fact that several states now require LIS as the final stage of CQA for a primary liner, and New York State will soon require it for secondary liners as well. Therefore, the authors decided to put a training course and certification program together.

2. PROGRAM PHILOSOPHY

The philosophy behind the program was simply that it was better for there to be some kind of training program than no program at all and that surveyors, facility owners, and regulators would recognize such a program. There was no attempt to present this as a formal national program. It was, in fact, based on similar programs introduced by manufacturers of welding machines for welding HDPE pipe a few years earlier.

3. COURSE CONTENT

3.1 General Education

It was first decided that there should be two components to the course, general education and practical certification, but that the latter would include the former. Nominally one day was allocated for classroom instruction. The topics covered include:

- Electricity 101
- Geomembrane liner leak statistics
- Theory and boundary conditions
- Liner design considerations to facilitate effective surveys
- GCLs and conductive geomembranes and geotextiles – advantages and disadvantages
- Case histories
- Standards and specifications
- Equipment
- Field procedures
- Business development

A second day is devoted to small scale survey work in test cells (Figures 1 to 3) using the variations on the basic technique; exposed liner surveys, soil-covered liner surveys, and water-covered surveys

3.2 Water Test Cell (Figure 1)

The water cell, approximately 2 m wide by 23 m long, with water about 200 mm deep, contained a single white surface HDPE geomembrane placed on a GCL (geosynthetic clay liner). The intent of the GCL was to prevent flow of water through the necessary holes in the liner so the students would not see the general locations of the holes from water seeping out from underneath the cell. While the GCL would effectively prevent the holes from actively leaking it would not prevent the flow of current through the holes. An artificial calibration/sensitivity test hole 1.5 mm in diameter could be placed in the water and connected directly to the power supply or connected to an electrode in the soil at the side of the cell to include soil subgrade in the circuit as would occur with a real hole.

There are two holes in the liner for the students to locate.



Figure 1. Water-covered liner test cell.

3.3 Soil Test Cell (Figure 2)

The soil test cell is one roll width wide (~6.5 m) and 23 m long. It has a single liner and is covered with about 200 m of stony soil. It contains about 5 holes of different sizes and types.

In one case a confident group requested that over lunch a new hole be placed in the liner for them to find. A 3 mm diameter hole was made. They could not find it. The instructor could not find it. The soil was removed and there was the open hole. On closer examination it was noted that the puncturing tool had made a cavity in the subgrade soil such that there was no conductive pathway from soil over the liner to soil under the liner through the hole. The electrical circuit was incomplete. When the cavity was filled with soil and soil replaced on top of the liner the hole was easily detected. A very good lesson learned!



Figure 2. Soil-covered liner test cell with calibration/sensitivity test flags.

3.4 Exposed test cell (Figure 3)

This cell is the same size as the soil cell, but is built on a slope so a reservoir of water can be maintained at one end. It is double lined to exclude the subgrade from the electrical circuit under holes in the primary. The cell is divided into thirds along its length. Along one third the primary liner is conductive geomembrane with transverse fusion and extrusion welds. The remaining two thirds have a non-conductive primary geomembrane. Underneath one half of the nonconductive sheet (one third of the total width) is a GCL. Under the final third is a conductive geotextile. Therefore, the impacts of different substrates can be assessed.



Figure 3. Exposed liner test cell.

The students are divided into three groups so that all three cells can be used at the same time with each group performing calibration/sensitivity test procedures, finding real holes, and generally experimenting with “what if” practices. Thus each group spends about 2.5 hr on each technique. In the soil cell students flag the location(s) of the hole(s) which are then excavated to see who is closest.

Since the first course in 2004 approximately 275 people have attended the education component held twice per year in the spring and fall. Attendees have come from Canada, Chile, Peru, Mexico, UK, Finland, Israel, Australia, Ghana and South Africa. The course has been taken on the road to New York, Canada (2), Houston, the Philippines, and the UK.

3.5 Certification

Those candidates seeking full certification undergo a one-day field audit on one of their production surveys, usually, but not always, their first. This requires a full calibration/sensitivity test procedure, and a continuing production survey. At the end of the day a closed book written test is undergone. There are 40 multiple choice and essay-type questions in the written test and 90 minutes are allowed to answer them. The multiple choice questions may have more than one correct answer. A point is given for each correct answer, but one point is deducted for each wrong answer. Maximum points are 151 and passing mark is 50. The highest score to date is 83. Twenty six surveyors have been certified, approximately half of those that have applied.

4.0 FIELD EXPERIENCES

As in most production surveys almost all field audits have included problems that have provided a challenge to the surveyor. Probably the most complex was a double lined pond on a mine site that had metal catwalks from shore to floats in the water with underwater pipes and pumps hanging from the floats. Leaked water was removed from the leak detection system (LDS) between the liners via a pipe penetrating the secondary liner leading to a monitoring manhole. The surveyor carefully considered the isolation of water in the pond and surrounding earth from water in the LDS, the material of the leaked water removal pipe, and the material of the manhole (HDPE or concrete). And if the manhole was concrete was the inside coated, and was the standing water entering the manhole from above or under the water in the manhole, and if above, was it a constant stream or was it dripping. There can be many points to consider before determining that an effective survey can be performed on any lining system. This facility features in a series of questions in the written test. Surveyors have found it necessary to wet gravel and to bury the injector electrode in a lens of sand in gravel. In a number of cases calibration/sensitivity testing has worked well when the artificial hole has been connected directly to the power supply, indicating that the equipment is functioning correctly. However, when soil is included in the circuit a leak signal is not generated. This is usually an indication of a lack of isolation between the water/ soil above the liner and the conductive subgrade and requires the surveyor to seek such features and to remedy them. It is often a haul road that requires cutting to solve the problem.

In one case in which the surveyors found it necessary to wet the cover soil a haul road was not a major problem to sensitivity testing but did generate increasing background signals close to the road. A persistent blip in the signal near the road caused the surveyors to thoroughly examine that location and they eventually agreed that there was a hole in the liner. The general contractor said that simply was not possible at that location. The soil cover was removed and there was a significant tear in the liner.

The ability to perform geoelectric liner surveys requires a basic knowledge of electricity but more importantly requires the ability to think logically about all the components in the lining system and their impacts on the location of the current return (ground) electrode and on the completion of an electrical circuit. Clearly some people can do this while others cannot and this is usually quite apparent during the day in the test cells. Some people, when they are audited performing a survey have difficulty in putting all the layers together to determine if there is a complete circuit and, if there is no current flow, which layer could be causing the problem. Others have great difficulty in coping with the exam-type environment of the written test.

In one case, audits were performed during a water survey but the candidates had difficulty in transferring the survey principles to the soil-covered liner questions in the written test. Since all lining systems have their own unique features it is important to ensure that the surveyor has this analytical capability.

What has been noted is that those people who do not take the course have more difficulty in performing surveys than those who do attend. This gives credibility to the need and value of both the education and certification components of the program.

To ensure the program maintains its relevance it is guided by an advisory board of respected industry experts in related fields.

5. SUMMARY

The education and certification components of the course appear to be achieving their objectives of promoting liner integrity and leak location technologies, identifying their requirements and limitations, and of developing a cadre of capable and competent liner integrity and leak location survey practitioners.

Dewatered and Decontaminated Disposal of Dredged Sediments Using Geotextile Bags, Containers and Tubes

G. R. Koerner, Ph.D., P.E., CQA, Geosynthetic Institute, USA, gkoerner@dca.net
R. M. Koerner, Ph.D., P.E., NAE., Geosynthetic Institute, USA, robert.koerner@coe.drexel.edu
W. Huang, Ph.D., Rutgers University, USA, whuang@envsci.rutgers.edu

ABSTRACT

The use of geotextile bags, containers and tubes has progressed over the past 30-years from sand filling to the dewatering of river and harbor sediments and, as described in this paper, to the decontamination of those sediments when they are polluted. Unfortunately, such pollution is the case for approximately 5% of sediments dredged annually in the United States.

After reviewing the enormity of the situation, various classifications of geotextile flexible forming systems are presented. A performance test, called the pillow test, is described and used in the evaluation of flocculants which are included to efficiently dewater fine grained silt and clay sediments. Such flocculants are critical so as to minimize the negative effects of filter cake buildup on the inside of the geotextile forming systems. The paper then addresses several decontamination possibilities aimed at encapsulating the contaminants within the dewatered sediments allowing for nonpolluted effluent removal. In this regard, examples of the efficiency of charcoal are presented along with estimated costs.

1. OVERVIEW AND BACKGROUND

The amount of sediment carried by rivers and streams into downgradient harbors, estuaries and deltas is enormous by any standard. The U. S. Army Corps of Engineers (NDC, 2012) in maintaining navigable depths has dredged about 115 M m³ of sediments in the first half of 2012 and this does not include private dredging. Of the total amount of dredged sediments, it is estimated by the Corps of Engineers that approximately 5% are polluted by various contaminating species. For example, there were eleven Superfund sites where the cost of removal and remediation exceeded \$50M (U.S. EPA, 2008) with one (the Fox River site) estimated to cost \$490 M (U.S. EPA and WDNR, 2007). The estimate for remediating 58 M m³ of contaminated sediment in the Great Lakes region ranges from \$1.5 B to \$4.5 B depending on the type of remediation selected (Great Lakes Regional Collaboration, 2005 and Nadeau, et al., 2009).

Coupling the nation's watershed pollution status and the continued necessity of dredging, a safe and efficient disposal strategy is necessary and this is the topic of this research program and paper. Of the various available strategies, the use of flexible geotextile bags, containers and tubes to not only dewater the dredged sediments but also to decontaminate them as well is the ultimate goal. By dewatering we mean to decrease the water content of the dredged material to a point where handling by standard earth-moving equipment is possible. By decontamination we mean the chemical bonding of the pollutants to the dewatered sediments (which are mainly fine grained silt and clay soils) within the geotextile flexible form thereby leaving the expelled effluent in a pollution-free and acceptable status. This combined dewatering and decontamination can be performed at the dredging site, adjacent to it, or contained within a nearby landfill.

After describing the various geotextile containment strategies, the paper describes the pillow test which will be used for experimentation, various flocculants (also called coagulants) for dewatering and reducing filter cake buildup, and lastly decontamination additives vis-à-vis specific types of sediment pollutants.

2. GEOTEXTILES AS FLEXIBLE FORMS

Textile fabrics in the form of bags, filled with soil of various types, and then tied off at the top, aka *sand bags*, have been used for centuries. While natural fibers degraded rapidly, the advent of polymer fibers increased the bag's lifetime substantially. Such bags were extended into *containers* at the Mission Dam in Canada (Terzaghi and Lacroix, 1964). Their task was to seal the end of a sheet pile cutoff wall to the sloping and irregular surface of the adjacent rock abutment. A fabric container, wide at the top and narrow at the bottom, filled with cement grout was proposed but first a 5 m high prototype was built. This was considered successful and the concept was used accordingly for the actual 45 m high structure.

Rather than using discrete bags or containers of finite length, tubes of unlimited length can also be used. Flexible sand-filled tubes were made as early as 1957, but initially they were not very successful. Eventually in 1967, a patent was granted to a Danish firm, Aldek A. S., in conjunction with the Danish Institute of Applied Hydraulics. Alidek's system was developed further in 1970 (Zirbel, 1975).

Since that time the area of geotextile tubes has developed considerably to the point where extremely long and large diameter prefabricated geotextile tubes are currently being used. The use of sand filled geotextile tubes for coastal erosion control systems is an ongoing and accepted practice. Furthermore, the infill material for all categories of geotextile flexible forms now varies from hard cementitious materials to contaminated fine grained soils and industrial waste sediments. A suggested categorization is given in Table 1 and examples of the three geotextile flexible form categories are given in Figures 1(a,b,c).

Table 1. Approximate dimensions of geotextile flexible fabric form applications.

Category	Length	Length/Circumference Ratio
Geotextile Bags	0.3-7 m (1-20 ft.)	0.2-2
Geotextile Containers	5-30 m (15-100 ft.)	0.5-10
Geotextile Tubes	15-100 m (50-300 ft.)	5-30



a) Large geotextile bags for coastal erosion control (compl. NAUE).



b) Geotextile containers for removal of harbor sediment (compl. TenCate)



c) Geotextile tubes for harbor sediment dewatering (authors)

Figure 1. Examples of geotextile flexible forming systems.

3. GEOTEXTILE TYPES AND PERFORMANCE TESTING

The geotextile type used in the fabrication of bags, containers and tubes varies considerably. While the decision is usually initiated by the designer, installer, and/or contractor it must eventually be agreed upon by the owner or agent doing the purchasing. The first, and obvious, criterion is to select a geotextile which provides for a successful project. This involves one which can be successfully installed and seamed, does not burst during filling, and meets the owners expectation for adequate serviceability and appropriate long-term durability. The second, and also obvious, criterion is that the cost of materials and the installation must be minimized. Hence, the all important ratio of “benefit/cost” must be maximized.

Regarding the geotextile type and as a broad generality, small geotextile bags are often woven slit-film fabrics while larger bags are often made from needle-punched nonwoven fabrics. On the other hand, geotextile containers and tubes are usually high-strength woven (or occasionally knit) fabrics. In this latter regard, the Geosynthetic Institute has a specification listing various physical, mechanical, hydraulic and endurance properties for both geotextile tubes and their associated scour aprons under both aggressive and typical conditions (GRI-10, 2001).

The performance of the selected fabric with respect to its infill and site-specific conditions can be assessed over time or can be predicted on the basis of laboratory testing. Insofar as large scale laboratory testing is concerned there are many options, but two seem to be most common. They are the *hanging bag test* and the *pillow test*. Both are the subject of a recent paper; see Koerner and Koerner (2009) from which the following is taken.

The hanging bag test was originated by Jack Fowler of the U. S. Army Corps of Engineers in the mid-1990’s (Fowler, 1995). It was eventually formalized as a standard in 2004 (GRI-GT14). There have been several papers written about the test which are generally favorable insofar as fabric selection is concerned, e.g., Zofchak (2001), Bezuijen, et al. (2007), Koerner and Koerner (2006) and Liao and Bhatia (2006).

The test uses a candidate fabric sewn into a cylindrical form and further sewn at the bottom. The top of the bag is left open. Several aspects of the test are shown in Figure 2 including a sand slurry being poured into the top of such a bag, water flowing out of the fabric at the bottom, some passing fine sand in the pan, and the residual soil in the bag after it was cut open.

The alternative pillow test was originated by Tom Stephens of Ten Cate about 2005 (Ten Cate Geosynthetics, Inc., 2007) and formalized as a standard in 2009 (GRI-GT15). The only somewhat related references in the open literature

are the work of Bhatia and her students at Syracuse University who developed and conducted research on a similar test which they called the pressure filtration test (Bhatia and Liao 2004; Satyamurthy et al. 2008; and Satyamurthy, et al. 2009). Hydraulic pressures were measured and quantitative data produced but the laboratory configuration was different than the field simulated pillow test to be described in this paper.

The pillow test per GRI-GT15 uses the candidate fabric prefabricated into the shape of a pillow from which a flanged connector and a calibrated vertical standpipe is attached. The fabric enclosure is quite small and the amount of slurry needed per test is much less than with the hanging bag test. More importantly, hydraulic head (easily converted to inlet pressure) can be monitored over time resulting in a quantitative assessment of the system including the specific effects of the fabric, slurry, and its additives. A pillow test in progress is shown in Figure 3.



a) Sand slurry being placed in a hanging bag



b) Water exiting bottom of the hanging bag



c) Fine sediment (\leq #200 sieve) carried in the escaped effluent



d) Dewatered, but still moist, sand remaining in the cut-open bag

Figure 2. Hanging bag test using a sand slurry infill.



a) Bottom and top of pillow



b) Complete test setup



c) Incremental slurry position within column



d) Effluent escaping the pillow

Figure 3. Pillow test in-progress using a fine grained silty clay slurry.

Upon performing many comparison tests between the two methods, Koerner and Koerner (2009) arrive at the following conclusions:

“The hanging bag test is relatively large, cumbersome, and difficult to perform. It is also very qualitative in its performance. Conversely, the pillow test is quite the opposite in every respect. Importantly, the pillow test allows for flow rate measurements under varying hydraulic head, i.e., inlet pressures, which is quite valuable in quantitatively assessing fabric types, their filter cake behavior, flocculent effects, and the potential for using decontamination additives when handling polluted sediments. In this regard, the authors favor the pillow test over the hanging bag test.”

4. CHEMICAL FLOCCULANTS (OR COAGULANTS) FOR DEWATERING DREDGED SLURRIES

Most river and harbor sediments are fine grained silts and clays which are readily adaptable to aqueous suspension in the form of a dredged slurry. Dredging is a well advanced technology whereby large quantities can be pumped and transported from the removal site to its disposal destination, which in our case is within a geotextile bag, container or tube. The fundamental issue that arises, however, is that the pressure of the slurry must be contained by the fabric and of course its seams as well. Seams are typically the weak points in these fabric enclosures. Furthermore, the higher the pressure the quicker is the expulsion of water and the more efficient the entire process. With sand or gravel as the infill this is straightforward, but with silts and clays it is problematic insofar as the formation of a *filter cake* progressively built up on the inside of the fabric. This filter cake becomes thicker and more dense with continued pumping time and pressure and in so doing decreases its permeability, greatly limiting the entire infilling process; see Figure 4.



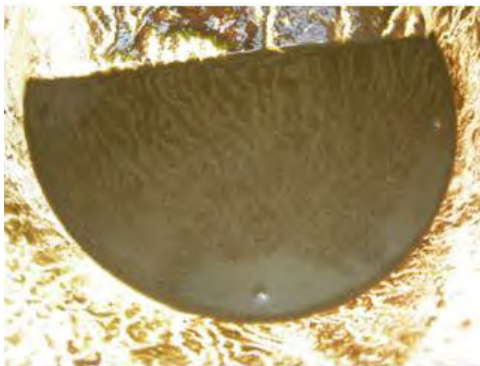
a) Filter cake buildup of sediment fines inside fabric bag enclosure



b) Close-up of the filter cake

Figure 4. Example of filter cake buildup inside a fabric during dewatering.

In order to minimize the adverse effects of this filter cake, chemicals are added to the dredged slurry during pumping. One group consists of standard chemicals (e.g., lime, alum and ferric chloride) and a second group consists of synthetic polyelectrolytes (e.g., polyacrylamide, acrylamide copolymers and others). The goal of these additives is visually illustrated in Figure 5.



a) Before using flocculants (compl. TenCate)



b) After using flocculants (compl. TenCate)



c) Flocculated vs. non flocculated sediments

Figure 5. Examples of the effect of adding flocculation chemicals.

In order to quantify the effect of adding a flocculant to a slurry of inorganic silty clay soil (which was a CL-designation), the previously described pillow test method was used. ZegaLyte 55®, a cationic flocculant, was used for this series of tests in 0.10, 0.20 and 0.40% volume additions. The flow rate response curves of three coagulant additions compared to the inorganic clay (CL) soil with no flocculant added are shown in Figure 6. The increased flow rate is pronounced with 0.10% flocculant added, and even moreso with 0.20% flocculant. The 0.40% flocculant data showed no additional improvement (the two curves identically overlap one another) indicating that the optimal amount of this particular flocculant for this particular soil is approximately 0.20% by volume. Further refinement between the different flocculant additions requires additional testing as does different flocculants and different soil types. In this regard, it appears to the authors that the pillow test is well suited for this type of evaluation.

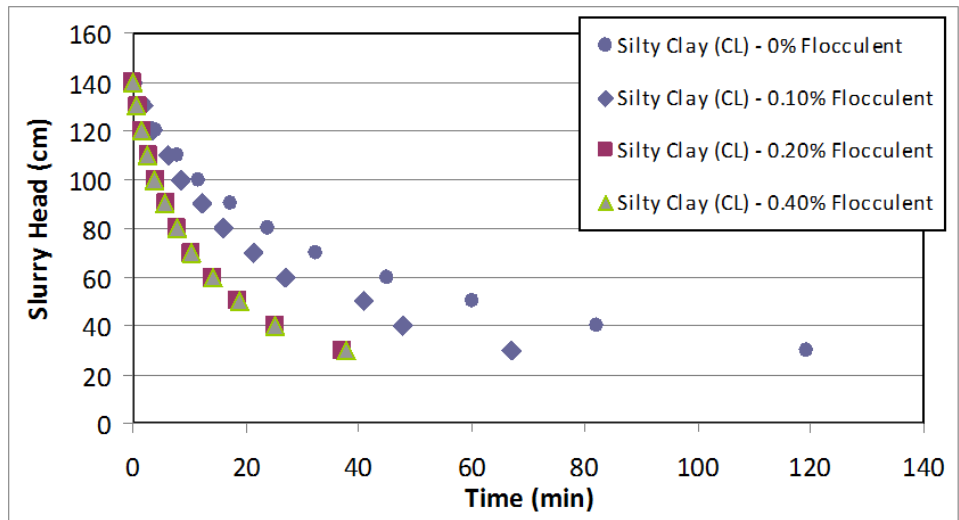


Figure 6. Effect of flocculant additives on a silty clay (CL) soil slurry (top of pillow was at 30 cm).

5. DEWATERING PLUS DECONTAMINATION

When the river and harbor sediments under consideration are contaminated, recall that the Corps of Engineers estimates that 5% of all sediments are in this condition, the situation of disposal is of major (perhaps even of controlling) importance. In this regard, the pollutants of highest frequency are as follows:

Table 2. Pollutants of highest frequency (U.S. EPA)

• Acetone	• Lead
• Aldrin/Dieldrin	• Mercury
• Arsenic	• Methylene Chloride
• Barium	• Naphthalene (Pending)
• Benzene	• Nickel
• 2-Butanone	• Pentachlorophenol
• Cadmium	• Polychlorinated Biphenyls (PCBs)
• Carbon Tetrachloride	• Polycyclic Aromatic Hydrocarbons (PAHs) (Pending)
• Chlordane	• Tetrachloroethylene
• Chloroform	• Toluene
• Chromium	• Trichloroethylene
• Cyanide	• Vinyl Chloride
• DDT, DDE, DDD	• Xylene (Pending)
• 1,1-Dichloroethene	• Zinc
• 1,2-Dichloroethane	

Using the geotextile flexible forming method in the form of bags, containers or tubes, the addition of not only a dewatering flocculant but also a decontaminant is recommended. In selecting the specific decontaminant for the precise pollutant(s) the dual concepts of solubility and adsorption are necessary to consider. The flow chart of Figure 7 illustrates the situation. In order that attachment of the pollutant to the encapsulated soil occurs, i.e., the desirable result, low solubility and high adsorption are necessary. Conversely, the pollutants will become fugitive in the escaping effluent, i.e., the undesirable result, with high solubility and low adsorption. The two intermediate strategies also illustrated but neither is optimal in this regard.

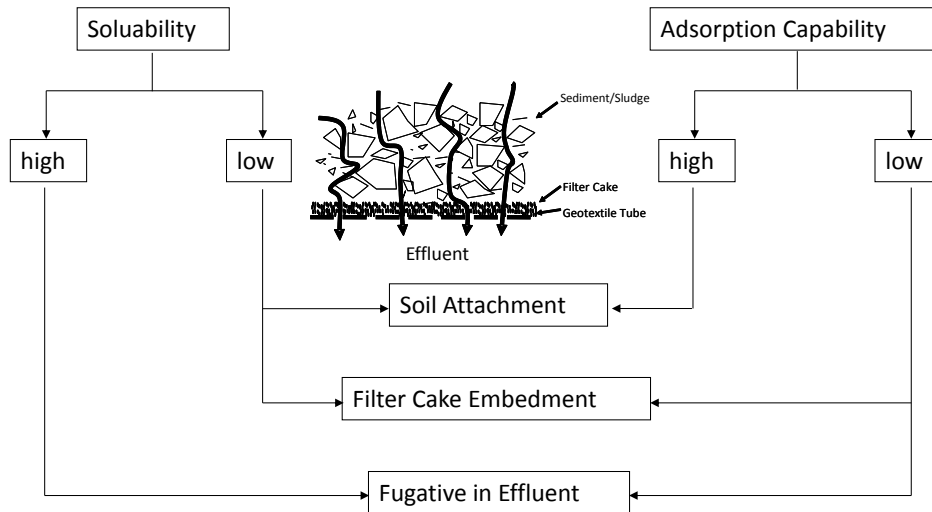


Figure 7. Alternative pathways for decontamination additives to address polluted river and harbor sediments.

The authors have considered the following decontamination additives which can be readily introduced to dredged slurries as they are filling geotextile bags, containers or tubes;

- activated carbon for removal of organic pollutants (a drinking water method),
- charcoal which is a strong sorbent for organic pollutants, or
- phosphoric rock which reacts with heavy metals to form insoluble phosphate salts.

An illustration in the form of a hypothetical example follows and uses charcoal at the rate of 5 gm/L of dredged slurry. The original contaminated slurry was 15% solids and 85% water, with a density of 1.2 kg/L, and had 100 ppm (100 mg/kg) of the following ten pollutants. The before and after dosage values are given along with the percent reductions of the individual pollutants which are all seen to be greater than 90%.

Table 3. Hypothetic example of decontamination reduction of various pollutants.

Type of Pollutant	Before (mg/L)	After (mg/L)	Reduction (%)
Polynuclear Aromatic Hydrocarbons			
Naphthalene	4.53	0.43	90.6
Fluorene	0.69	0.053	92.3
Phenanthrene	0.28	0.021	92.5
Anthracene	0.030	0.0022	92.6
Pyrene	0.077	0.0057	92.6
Benzo(a)pyrene	0.0033	0.00024	92.6
Chlorinated Chemicals			
1,2-dichlorobenzene	4.32	0.40	90.7
2-chlorobiphenyl	0.31	0.023	92.5
2,5-dichlorobiphenyl	0.063	0.0047	92.6
2,2',5,5'-chlorobiphenyl	0.0069	0.00051	92.6

Important in this regard is the cost of the added contaminant which in this case was charcoal. For the reductions illustrated in the above example, the cost at 5 gm/L is about \$1.31/m³. To achieve removal concentrations reductions of 98% or greater of the listed pollutants, the added charcoal required would be 20 gm/L thus \$5.23/m³. While such costs are far from trivial, the entire process of decontamination is critically important and can be the controlling issue insofar as the success of a project is concerned.

6. SUMMARY AND CONCLUSIONS

The flexible forming capability of fabrics lends itself to many unique situations. Nowhere is this more evident than with geotextile bags, containers and tubes used to dewater river and harbor sediments. These sediments are usually fine grained silts and clays which are dredged on an ongoing basis but unfortunately form relatively impermeable filter cake layers on the inside of the fabric enclosures. This greatly limits using high pressures and lengthens the dewatering time accordingly. As described herein, the addition of flocculants (also called coagulants), which are either standard chemicals or synthetic polyelectrolytes, serve to create flocs which increase the permeability of the filter cake thereby enhancing the process. This was shown in the paper using the pillow test method and a specific flocculent in different percentage additions.

Beyond dewatering, however, is the possibility of decontamination of polluted sediments of which there is an abundance of sites and situations. U. S. Army Corps of Engineers estimates that 5% of its dredged sediments are contaminated to varying degrees. For decontamination the additions of activated carbon, charcoal, or phosphoric rock are possible whereby the pollutants are adsorbed onto the soil particles and remain in the fabric enclosure while the effluent is decontaminated to the necessary degree. Examples of a number of polynuclear aromatic hydrocarbons and chlorinated chemicals were presented in this regard.

The geotextile bag, container and tube technology is being actively pursued by industry and the unanswered questions (primarily what type of additives and to what quantities) are presently being answered by simulated performance tests of which the authors favor the pillow test. This test was described in the paper as well as its utilization in evaluating one type of flocculating additive. The exact same test method can be used to evaluate various decontamination additives to polluted sediments and this research is presently ongoing.

ACKNOWLEDGEMENTS

This paper is made available through financial assistance of the Members, Affiliated Members and Associate Members of the Geosynthetic Institute (GSI). We sincerely thank them in this regard. See our website at www.geosynthetic-institute.org for their identification and contact persons.

REFERENCES

- Beuijen, A., Stephens, T., Trainer, E. and Chuck, F. (2007). *Ten Cate Geotube GDT Test*, Ten Cate Geosynthetics North America, Commerce, GA .
- Bhatia, S. K. and Liao, K. (2004). Overview of geotextile tube applications and research, *ICGGE-2004* (CD-ROM), ITT, Bombay, Mumbai, India.
- Fowler, J. (1995). Geotubes and geocontainers for hydraulic applications, *Proceedings Cleveland Section ASCE*, 25 pgs.
- Great Lakes Regional Collaboration (2005). Strategy to Restore and Protect the Great Lakes, December 2005.
- GRI-GT10 (2001). Test Methods, Properties and Frequencies for High Strength Geotextile Tubes Used as Coastal and Riverine Structures, Geosynthetic Institute, Folsom, Pennsylvania, USA.
- GRI-GT14 (2004). Standard Test Method for Hanging Bag Test for Field Assessment of Fabrics Used for Geotextile Tubes and Containers, Geosynthetic Institute, Folsom, Pennsylvania, USA.
- GRI-GT15 (2009). Standard Test Method for Pillow Test for Field Assessment of Fabrics/Additives Used for Geotextile Bags, Containers and Tubes, Geosynthetic Institute, Folsom, Pennsylvania, USA.
- Koerner, G. R. and Koerner, R. M. (2006). Geotextile tube assessment using a hanging bag test, *J. Geotextiles and Geomembranes*, Vol. 24, No. 2, pp. 129-137.
- Koerner, R. M. and Koerner, G. R. (2009). Performance tests for selection of fabrics and additives when used as geotextile bags, containers and tubes, *Geotextile Testing Journal*, Vol. 33, No. 3, pp. 236-242.
- Liao, K. and Bhatia, S. (2006). Evaluation on filtration performance of woven geotextiles by falling head, pressure filtration, and hanging bag tests, *Proceedings 8th IGC*, Yokohama, Japan, Millpress Publ., Rotterdam.

- Nadeau, S. C., et al. (2009). "Principles for evaluating remedial options for contaminated sediment sites, *Optimizing Decision Making and Remediation at Complex Contaminated Sediment Sites Conference*, January 8-9, New Orleans, LA.
- Satyamurthy, R., Liao, K. and Bhatia, S. K. (2008). Pressure filtration test assessment based on filtration theory, *Proceedings of EuroGeo4*, Strathclyde, Scotland, Sept. 7-10, 2008, Paper No. 296.
- Satyamurthy, R., Grzelak, M. D., Pullen, T S., Bhatia, S. K. and Kaye, P. (2009). Evaluation of geotextile tube dewatering performance of tailings using large and small scale tests, *Proceedings, Geosynthetics 2009*, Salt Lake City, Utah, IFAI Publ., Roseville, MN, pp. 428-438.
- Ten Cate Geosynthetics Inc. (2007), Product Literature, Pendergrass, NC.
- Terzaghi, K. and Lacroix, Y. (1964). Mission Dam: an earth and rockfill dam on a highly compressible foundation," *Geotechnique*, Vol. 14, No. 1, pp. 13-50.
- U. S. Army Corps of Engineers (2012), Navigation Data Center (www.ndc.iwr.usace.army.mil/dredge)
- U. S. Environmental Protection Agency (2008). *Contaminated Sediments in Superfund*, <http://www.epa.gov/superfund/health/conmedia/sediment/index.htm>
- U. S. EPA and WDNR (2007). *Record of Decision Amendment, Lower Fox River and Green Bay Superfund Site*, U. S. Environmental Protection Agency and Wisconsin Department of Natural Resources.
- Zirbel, R. (1975). Sand filled tubes used in beach protection plan, *World Dredging Marine Construction*, December, pp. 24-29.
- Zofchak, V. (2001). Performance testing of geotextile tubes, *Proceedings Geosynthetics '01*, Portland, Oregon, IFAI Publ., Roseville, MN, pp. 599-608.

Double Lining Systems: One and One Can Make Three!

Ian D. Peggs, I-CORP INTERNATIONAL, Inc., USA, icorp@geosynthetic.com

ABSTRACT

Double geomembrane lining systems have been used since 1974. That first geomembrane was made with two different materials, but since that time the same materials for each liner has become the norm. Thus the synergism of combining the best of different materials and of cancelling the disadvantages of each are not taken advantage of, thereby not achieving the maximum available performance of the superior double lining system. In this paper it is proposed we re-introduce the beneficial philosophy of using two different materials for the primary and secondary geomembranes of double lining systems, much like geomembranes and GCLs are combined to generate a better performing composite liner.

1. INTRODUCTION

As a general rule we now assume that all individual liners leak to some degree (Giroud and Goldstein, 1982) and design leakage collection and gas venting systems to deal with such leakage such that no further damage to the liner and/or subgrade occurs. However, a simple and easy solution to the negative perception of liner leakage - double lining systems - has been used for many years, but rarely is such a lining system optimized. The two geomembranes in a double lining system will, of course, likely have the same small number of flaws. However, provided the primary leakage is removed from between the two liners the secondary liner will only leak if the dribble of primary leakage passes directly over the equivalent leak in the secondary. The chances of this happening are remote (Shivashankar, et al., 1997). Thus, even though each liner may have a few flaws, the complete lining system does not leak.

However if we take this principle one step further we can perhaps optimize the performance and durability of some double lining system by using two different geomembrane materials whose performance characteristics interact synergistically to provide a combined lining system that performs better than each individually and better than double liners of the same material. In principle, this is not unlike combining a geomembrane and a geosynthetic clay liner (GCL), to generate a composite liner.

2. DOUBLE LINERS

The concept of a double liner was first presented by Giroud in 1973. The first double geomembrane liner was designed by J.P. Giroud in 1974 for a reservoir (Figure 1) in Pont-de-Claix, France (Cazzuffi et al., 2010). It consisted of a 1.5 mm butyl rubber primary liner on a bitumen-sprayed needlepunched nonwoven geotextile secondary liner with a leakage detection system (LDS) of rounded aggregate stabilized with concrete between them. It was a good example of two different lining materials complementing one another – a durable seamless uniform secondary liner on a firm compacted subgrade and a very flexible, essentially impermeable primary liner. For even more customized detail the butyl rubber was reinforced from 1 m under the water into the anchor trench so the induced stresses would be assumed by the reinforcement thereby reducing the degradation rate of the rubber. This lining system is still functioning very well. The secondary liner also prevented ground water entering the LDS and being interpreted as primary leakage.



Figure 1. Butyl rubber geomembrane bituminous geomembrane double liner constructed in 1974.
(Photo courtesy J.P. Giroud)

Many years later in 1991 the United States Environmental Protection Agency wrote “Geomembranes are not intended to be stress-bearing members, and the design should avoid stressing the material as much as possible” (United States Environmental Protection Agency, 1991, page 49). This is most important for HDPE for its susceptibility to stress cracking. Thus, that first double liner matched that requirement – the reinforced bitumen provided the flat secondary liner on a firm subgrade and the unwrinkled rubber provided the primary barrier function.

Strangely, these days we seem to have deviated from that different materials concept for double lining systems, which seems to be a missed opportunity for optimum liner performance. Most of our double lining systems in solid and liquid waste facilities are constructed with the same material, predominantly HDPE. Often the only difference between the two liners is that the secondary is thinner than the primary, it being considered as a back-up liner rather than an essential member of a sophisticated integrated high performance lining system.

Whatever the material, if both geomembranes are the same they have the same advantages and disadvantages in terms of their installation characteristics and in terms of their performance in service. This is somewhat surprising in an industry that recognizes the clear synergistic benefits of putting a geomembrane and a GCL together to make a composite liner that performs maybe three orders of magnitude better than each liner alone. It is also strange when we have available three-layer coextruded HDPE geomembranes with HDPE cores and LLDPE surface layers, or vice versa, in order to gain surface chemical resistance with increased flexibility and to blunt surface initiated stress cracks, or to minimize the potential for surface stress cracking while having a strong material. And now we have seven layer coextruded geomembranes containing a central ethylene vinyl alcohol (EVOH) layer for optimum retention of VOCs (Armstrong and Chow, 2012). Clearly, we are not optimizing our double lining systems to combine the advantages and to overcome the disadvantages of different materials, particularly in these days when many different geomembrane materials are available to us. However, a start has been made. For instance, it is generally recognized that HDPE is more suited as a basal liner where the subgrade can be well-compacted, but that LLDPE may be more suited as a landfill cap where differential settlement is more likely. That principle can be applied to double lining systems.

The intent of a landfill double lining system is for the sloping primary liner to collect, drain, and remove primary leachate. This requires a smooth flat geomembrane without wrinkles that might dam or hinder the flow of leachate. Between the

two geomembranes is a leakage detection system (LDS), often an HDPE geonet/geotextile composite that collects, drains, and removes leakage through the primary liner. The success of the double lining system is dependent upon the prevention of a hydraulic head on the secondary geomembrane. Therefore, the secondary geomembrane should also be laid flat for easy and rapid leakage removal and to prevent wrinkles from damming this flow and causing local pools that may just be in the same location as a hole in the secondary. That first double liner developed a small leak in the primary liner in 2004 which was rapidly located and repaired.

The secondary geomembrane is often placed on a low hydraulic conductivity compacted clay subgrade thereby generating a composite liner, but to achieve that synergistic composite function the geomembrane and the clay must be in intimate contact. If there are wrinkles in the geomembrane there is increased possibility of leakage occurring at the peak of the stressed wrinkles (wrinkles are not flattened by overlying soil or water) and the wrinkles allow more widespread distribution of leaked liquids. This is vastly different to the objective of the composite liner that if there is a hole in the geomembrane the local clay/GCL will be hydrated, will swell, and plug the leak. Leakage will preferentially occur along the geomembrane/clay interface until it finds a penetrable crack in the clay. A similar philosophy of parallelism applies to a double geomembrane system.

In many cases there will be a GCL under the primary geomembrane making that a composite liner which naturally requires the primary geomembrane and GCL to be in full intimate contact if maximum barrier performance is to be obtained.

Because of its broad chemical resistance HDPE is often used as a primary liner and inevitably, often by default, as a secondary liner in a double lining system. However, HDPE does have a high coefficient of linear thermal expansion that makes it difficult to install without wrinkles in locations where ambient and geomembrane temperatures are increasing during and after installation. The wrinkles preclude intimate contact with the primary clay liner, prevent rapid and effective removal of secondary leachate, and subject the HDPE geomembrane to undesirable stress when vertically compressed.

If wrinkles are not avoided when the secondary liner is installed it is difficult to place a geonet or geonet/geotextile composite LDS layer in good contact with the secondary liner. And of course it is then impossible to place a flat primary HDPE geomembrane, which itself will wrinkle, on top of two layers that are already wrinkled. All of the performance benefits we are seeking by using a double lining system are compromised. However, if good installers are cognizant of the weather conditions and can use them to advantage it is quite possible to install a good double HDPE lining system. If we install at a higher geomembrane temperature than that at which covering will occur we can theoretically build in some excess material such that at the lower temperature the liner will be flat and the covering medium will hold the liner in intimate contact with the subgrade. Of course there is the concomitant possibility that all wrinkles will not be removed or that the temperature will fall too far and bridging/trampolining will occur in corners and at the toes of slopes. No liner, particularly HDPE, should be forced into contact with the subgrade.

However, building in excess material (compensation) is much easier to talk about than to do. Ultimately it is the designer's responsibility to say how much compensation is needed because he/she knows most about the operating conditions of the liner, but mostly it is left to the installer to do the right thing.

Clearly, installing at low temperatures and allowing for covering or service at higher temperatures is another matter since wrinkles at the higher temperature cannot be avoided. Note again that wrinkles are not flattened when covered with soil or liquid.

To resolve the wrinkling concerns but to keep HDPE as the primary liner for its chemical resistance we could use a different geomembrane for the secondary liner. Clearly this should be a material with a lower coefficient of linear thermal expansion such as unreinforced PP (half the CTE of HDPE), or a reinforced geomembrane with essentially zero CTE, or even a prefabricated bituminous geomembrane. The choices are many. However, not only is CTE important so is the nature of the subgrade which may be another reason for seeking an alternative to HDPE. An unreinforced PP, PVC, or LLDPE will accommodate a rougher surface than HDPE and will be much more tolerant in the long term of the stresses associated with any differential settlement that might occur. However, if differential settlement is likely to occur one should carefully consider the break elongation of a proposed reinforced geomembrane in relation to the strain expected at any differential settlement. While traditional reinforcing scrims have break elongations of ~15%, newer scrims have break elongations close to ~40%.

The secondary liner of a double lining system probably does not need the chemical resistance of the primary. It certainly will not need the same UV resistance as the primary, unless it is to be exposed for some time before the primary is placed. And this highlights a stage in a liner's lifetime that is often ignored – the time between installation and being placed in service. It is not unknown for liners that are to be covered in service to be left exposed for 8 or 9 years before covering. A large pond HDPE liner in a windy environment was installed at low temperatures with compensation built in,

even though the liner would be covered several months later at a higher temperature. The increasing temperature generated more and larger wrinkles which were uplifted by the winds (no ballast) and blown to the downwind shore where a very large wrinkle formed and cracked after only 2 years (Peggs, 2012).

Why lay a wrinkled primary liner on top of a wrinkled secondary liner when the secondary could be laid flat? Why not use a strain resistant secondary liner that is tolerant of differential settlement, deformation, and rough subgrades and a more thermal oxidation resistant primary liner? Consider a primary liner that will better contain VOCs and a lay-flat, less costly, not-so-UV-resistant secondary liner. The combinations are virtually unlimited and can be made project specific to optimize lining system performance and durability.

Consider a MSW landfill being built in a very cold environment on a coarse gravel subgrade. It makes sense from the leachate chemistry aspect and for ease of permitting to use an HDPE primary geomembrane. This is placed on top of a primary GCL. Not only does the GCL provide a composite primary liner, it also acts as a cushion for the primary geomembrane, and with adequate moisture content allows a geoelectric integrity survey to be performed on the primary geomembrane when there is only a nonconductive geotextile/geonet/geotextile composite, often called "geocomposite", in the LDS. If the subgrade is too coarse for a secondary HDPE just meeting Geosynthetic Research Institute (GRI) standard GM13 specifications, then an HDPE with improved stress cracking resistance could be used to tolerate the surface roughness. On the other hand, if HDPE is required because of leaking leachate chemistry one could use a three layer co-extruded geomembrane with HDPE on the outside and LLDPE in the core. The HDPE would provide chemical resistance while the LLDPE would provide the flexibility to tolerate the surface roughness. And if the HDPE did start to stress crack, the cracks would be blunted and stop growing at the HDPE/LLDPE interface. While a short crack might give access of leachate to the LLDPE it would be in a very small area and not do too much damage.

One particularly interesting material combination is an HDPE primary liner with a prefabricated bituminous secondary liner. A bituminous geomembrane is relatively heavy and thick and will lay flat. It can be deployed and welded in very cold weather (-35°C). Its weight makes it more resistant than polymeric geomembranes to wind uplift. It will conform to rough subgrades, and it has a very low coefficient of linear thermal expansion. When soil is spread on top of it it does not wrinkle (Figure 2.) and it can be folded and unfolded on the ground without creasing. In a cold windy environment, such as the Arctic, it can be laid to remain flat. Welds are easily made and can be 100% nondestructively tested ultrasonically. It can make a good secondary liner.

For the primary liner engineers like to use HDPE geomembranes because many precedents have been set for its use, it has a very broad chemical resistance, and it is easier to get permitted by regulators. Regulators like HDPE, again because many precedents have been set, it requires no new thinking, and they do not have to go out on a limb to make decisions on novel materials.

Another possible option, while retaining an HDPE primary liner, is to use a more flexible (fPP, RPP, PVC, EIA, etc.) secondary liner that can be prefabricated into large panels to minimize the number of field seams for rapid installation. At the large ~350 ha (875 acre) Columbus Upground Reservoir project prefabricated panels of 1.00 mm fPP are being installed at the rate of almost 3.6 ha per day. A prefabricated secondary liner may or may not be reinforced to suit the nature of the subgrade, the potential for differential settlement, and the weather. But the ability to install a flat secondary liner exists.



Figure 2. Bituminous geomembrane. No wrinkles (top arrow). No creasing at fold (bottom arrow).

Many other examples could be provided, but it is really the principle of considering the installation, post-installation/pre-service, and in-service, requirements of the lining system that is emphasized and the realization that optimum performance may be achieved by using different materials for the primary and secondary geomembranes of a double lining system.

3. CONCLUSION

Where a double lining system is required optimum performance and maximum durability may be achieved by using different materials for the primary and secondary geomembranes. The specific materials used will be a function of subgrade quality, potential for differential settlement, installation temperature, time available for installation, temperature when line is covered, time between completion and placing in service, service temperatures, chemistry of liner content, etc.

REFERENCES

- Armstrong, R., Chow, E., (2012). Performance of Model Geomembrane with Ethylene Vinyl Alcohol (EVOH) Barrier and Value for Select Mining and Remediation Applications. Second PanAm Geosynthetics Conference & Exhibition GeoAmericas 2012, Lima, Peru.
- Cazzuffi, D., Giroud, J.P., Scuro, A. Vaschetti, B. (2010). Geosynthetic Barriers Systems for Dams, 9th International Conference on Geosynthetics, Brazil, 2010.
- Giroud, J.P. (1973). L'etancheite des Retenues d'eau par Feuilles Déroulées, Annales de l'ITBTP, 312, TP 161, December, 94-112. (in French).
- Giroud, J.P., Goldstein, J.S. (1982). Geomembrane Liner Design, *Waste Age*, Vol. 13, No. 9, September 1982, 27-30.
- Peggs, I.D. (2012). Unusual Transverse Cracking on HDPE Geomembrane Wrinkle/Whale in a Wastewater Irrigation Pond, Second PanAm Geosynthetics Conference & Exhibition GeoAmericas 2012, Lima, Peru.
- Shivashankar, M., Fluet, J.E., Reddy, D.V., (1997) Geonet Leakage Detection System Flow Patterns for Zero Leakage Estimation of Landfill Double Liner Systems, *Geosynthetics 1997*, IFAI, Long Beach, CA, USA, Vol. 1: 393-406.
- United States Environmental Protection Agency, Technical Resource Document, EPA/530/SW-91/054, Design, Construction, and Operation of Hazardous and Non-Hazardous Waste Surface Impoundments, Washington, DC, USA, June 1991, page 49.

Durability Studies on Coir Geotextiles

S Chandrakara, Professor, Department of Civil Engineering, N.I.T Calicut, India
Sreela.P.K, Assistant Professor, Department of Civil Engineering, Government Engineering College, Trichur, India

ABSTRACT

Coir geotextiles has prominent role in improving the properties of soils to utilize in pavements. Low shear strength and high compressibility, can be improved by the use of coir geo textiles. By the inclusion of coir geo textiles C.B.R value of the soil is found to be increases. One of the major deficiencies reported in using coir geotextiles is its decay. Attempts were made to improve the durability of coir geotextiles by various treatments. In this paper the results of an experimental study carried out on treated coir geotextiles with various chemicals and latex is presented. It is found that by treatment with latex durability of coir geotextiles is found to increase without causing much reduction in strength.

1. INTRODUCTION

Geo-synthetics are being increasingly used in various civil engineering applications to tackle a variety of problems. Geosynthetics may be made up of natural or synthetic materials. For the short term improvements geosynthetics with natural fibers are sometimes used. One of the popular natural geotextiles is made up of coir. Coir is 100% organic fiber which is obtained from the husk of the fruit of the coconut palm tree. It possesses the advantages of a ligno cellulose fiber .The material is not brittle, non-toxic and poses no waste disposal problems. Coir fiber has a lignin content of about 46 per cent .This strong natural fiber is also biodegradable, but at a slower rate than other natural fibers.

2. LITERATURE REVIEW

Varma et al (1986)“thermal behaviour of coir fibers” In this study the thermal characterization of naturally occurring coir fibers and modified bristle coir fibers was carried out . Balan (1995), conducted studies on “durability of coir yarn for use in geo meshes by the use of two types of coir yarns subjected to different environmental conditions. From the above study it was seen that the life of coir yarn was controlled by the type of embedment soil, climatic condition, water content, organic content and the type of coir used. The rate of degradation of coir yarn was studied in different soil environments. Sobha (1996) conducted studies on the suitability of coir felt, coir felt reinforced with nylon mesh, and combinations of coir mesh and nylon mesh. In this test the materials used to study the influence were plain coir felt, coir felt reinforced with nylon mesh and a combination of coir felt and coir mesh. Ajitha Bhasker and Mary John (1996), conducted studies using coir fabrics on improvement of subgrade for roads”. Penetration tests were carried on coir fabrics subjected to repetitive and impact loads.

Geethamma et al. (1997), conducted chemical treatments on coir fiber, to find out the effect of chemical modification, loading and orientation of fibre. Goulart et al (1999). Conducted studies on coir fibre from Brazilian north east coast on their mechanical and thermal characterization. Khalil et al. (2000) conducted studies on the effect of acetylation on interfacial shear strength between plant fibers and various matrices. Rout et al. (2001) conducted studies on “The influence of fiber treatment on the performance of coir polyester composites. Sreekala et al. (2001) conducted studies on “water- sorption kinetics in oil palm fibers” Alexander et al (2001) conducted experiments on surface characterization of natural fibers. In this study surface properties and the water up-take behaviour of modified sisal and coir fibers were examined. Not much attempts were made to enhance durability of coir geotextiles . In this paper results of an experimental study carried out on the durability of coir geotextiles on various treatments is presented. Attempts were made to treat coir yarn with different chemicals and also with latex. Durability studies conducted were restricted to certain aspects like effect of soil medium, presence of water, temperature etc.

3. MATERIALS USED FOR THE STUDY

Materials used for the study are clay, sand, coir geotextiles, natural rubber latex, and various chemicals that are required for the treatment.

3.1 Chemicals Used for Treatment

The various chemicals required for the treatment on coir are Sodium Hydroxide, Ethanol, Benzoyl Chloride, Acetic Acid, Acetic Anhydride, Sulphuric Acid, Potassium Permanganate Solution, Acetone and Dicumyl Peroxide.

Tests for identification and classification of soils and for the determination of engineering properties are done as relevant ASTM standards.

3.2 Properties of Materials

The various properties of clay determined are liquid limit 43%, plastic limit 19%, shrinkage limit 16%, Optimum moisture content (OMC) 19.5%, maximum dry density 16 k N/m³ and CBR soaked soil sample was 2%. Maximum density of sand used was 18 k N/m³ and specific gravity 2.6. The diameter of coir fibre is 16 microns and the length is 150-200mm. Density of coir fibre is 14 kN/m³ and moisture regaining capacity at 65% RH is 10-50%. The chemical compositions of coir are lignin content 45.84%, cellulose 43.44%, ash 2.22%, hemi-cellulose 0.25% and pectin and related compounds 3.3%. Properties of latex shown in the table.1

Table.1 Constituents of Natural Rubber Latex

Constituent	% Composition
Rubber particles	30-40
Protein	2-3
Water	55-65
Sterol glycosides	0.1-0.5
Resins	1.5-3.5
Ash	0.5-1.0
Sugars	1.0-2.0

3.3 Index Properties of Coir Geotextile

The index properties of the coir geo-textiles used in the experimental study is 2.5mm thickness, 9 k N/m² mass per unit area and mechanical properties such as percentage of elongation for warp is 31 and for weft is 28 also breaking strength for warp is 29 kN/mm² and for weft is 11.3 kN/mm².

4. RESULTS AND DISCUSSIONS

4.1 Chemical Treatments

Attempts were made to improve study the variation in strength of coir geotextiles by treating with various chemicals Coir geotextile yarns were dipped in chemicals for 24 hours and tested for their strength. The improvement in strength due to the chemical modifications is in the range 25-35 %. The strength is greatly affected by the concentration and the duration of treatment selected. Some of the chemicals used for treatment on Coir is harmful to the human body are dicumyl peroxide, acetic anhydride and benzoyl chloride and also these chemicals are costly and highly dangerous when handling. The sodium hydroxide treatment is less costly and harmful; but the improvement in strength is only marginal. Tensile strength behaviour of 2% Na OH treated coir yarn is presented in figure 1. It can be seen that not much improvement is achieved even after treating with 8% Na OH

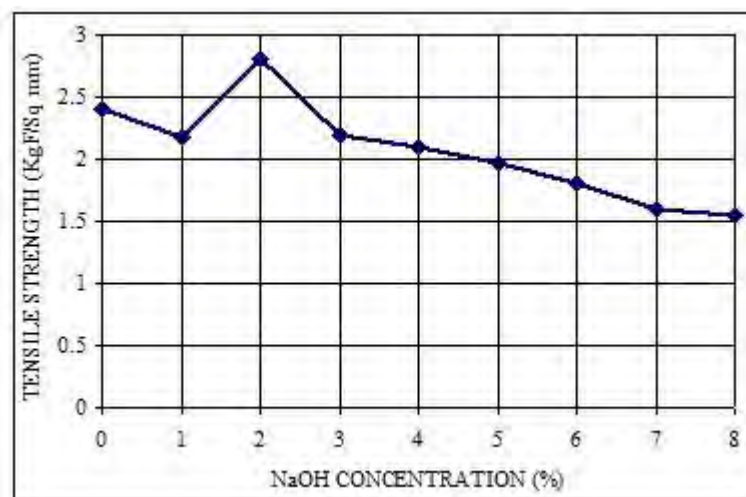


Figure.1 Tensile Strength Vs Alkali Concentration

4.2 Effect of Natural Rubber Latex Treatment

The tensile tests were carried out with untreated coir yarn and after treating with different chemicals .Results obtained are presented in Table 2 . It can be seen that the latex coating carried out on Coir yarns has improved the tensile strength about 82 % of the untreated Coir yarn. This improvement is attributed to the binding action of latex on coir.

Table.2 Improvement in Tensile Strength

TYPE OF TREATMENT	TENSILE STRENGTH (NF/ Sqm)	PERCENTAGE INCREASE IN TENSILE STRENGTH
Untreated	23	---
Alkali	28	22
Benzylation	26	15
Peroxide	31	34
Permanganate	28	21
Acetylation	27	15
Latex	42	82

4.3 Durability Studies

Coir yarn is studied by immersing the Coir yarns in different solutions and in different soil media and tensile strength was measured at regular intervals. Results obtained are presented below.

4.3.1 Influence of Submergence in Clay and Sand

It is observed that by keeping in sand, Coir was able to retain its original strength up to one month where as in clay the Coir retained its strength up to 3 months before a reduction in strength was obtained. At the end of 6 months the percentage reduction in strength of Coir in clay was 16% and in sand was 32 %. The variation of reduction in strength in sand and clay is shown in Figure 2.

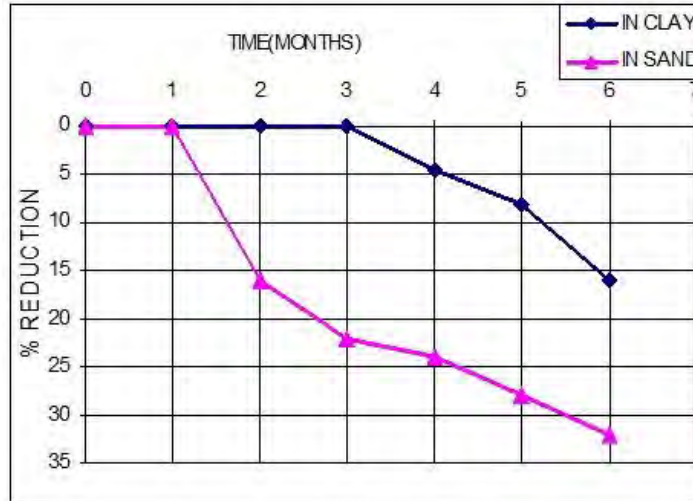


Figure.2 Reduction in Strength of Coir immersed in Sand and Clay

4.3.2 Influence of Submergence in Acidic Neutral and Alkaline Solution

Experiments were carried out to examine the strength of coir yarn in different pH medium. It is observed that at the end of 6 months the reduction in strength of Coir in acidic medium is 38 % and in alkaline medium is 45 %.The reason for the faster degradation in alkaline medium is may be the OH ions .The OH ions in the lignin content is made active by the OH negative ions in the sodium hydroxide solution which neutralize some of the lignin content in the coir, and accelerates the degradation. The degradation was found to take place in distilled water environment also. The results are presented in Figure 3.Similar tests were carried out in salt water and tap water environment. Not much change was observed.

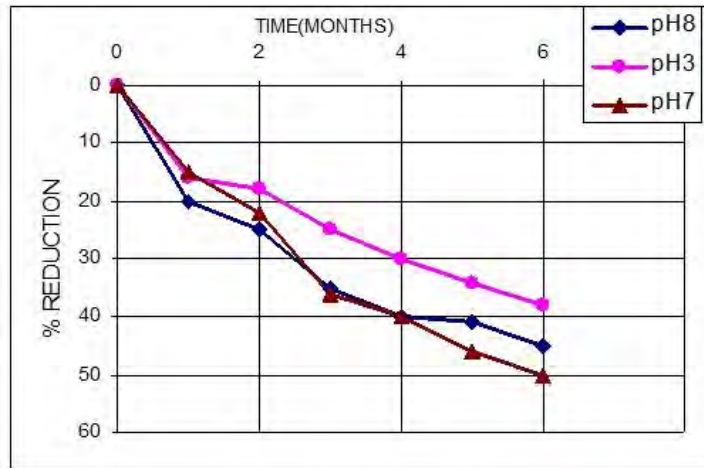


Figure.3 Reduction in Strength of Coir in Water with Different pH

4.3.3 Influence of Alternate Wetting and Drying and soaking

Tests were conducted on coir yarns subjected to alternate wetting and drying and soaking in different environment. Reduction in the strength resulting from various treatments is presented in table 3. Alternate wetting and drying was done for 10 cycles in 6 month time

Table.3 Percentage Reduction in Strength in Different Soaked Media

SOAKED MEDIA	PERCENTAGE REDUCTION IN STRENGTH AFTER 6 MONTHS
Clay	16.08
Sand	32
Salt Water	20
Tape Water	23
Distilled Water	50
Acidic Solution (pH 3)	38
Alkaline Solution(pH 8)	45
Alternate Wetting	33

4.4 Influence of Water Absorption

Untreated Coir fibers absorb much more water compared to treated fibers leading to poor mechanical properties. The alkali treatment have resulted in the removal of waxy coating on the fiber surface, as a result the cellulose components of Coir are exposed making the surface more hygroscopic. In the case of latex treated Coir a protective coating on the surface makes it water repellent, thus absorption is less. The moisture content is measured by finding the weight gain of the material. The result was shown in the Table 4.

Table.4 Water Absorption Studies

TYPE OF TREATMENT	CONDITION	MOISTURE CONTENT
Untreated	Room temperature	12%
	Fully soaked in distilled water	31%
Alkali treated	Room temperature	18%
	Fully soaked in distilled water	39%
Latex treated	Room temperature	4%
	Fully soaked in distilled water	11%

4.5 Influence of Accelerated Thermal Ageing

Accelerated tests were conducted on Coir samples for understanding its behavior.. Table 5 represents the thermal ageing results on Coir. It is observed that on increasing the temperature a reduction in strength was observed in untreated and treated coir yarns.

Table.5 Results of Accelerated Thermal Ageing

TEST TEMPERATURE	UNTREATED COIR	ALKALI TREATED COIR	LATEX TREATED COIR
	PERCENTAGE REDUCTION IN TENSILE STRENGTH		
100+1	-	-	-
125+2	60	58	30
150+2	88	83	47
175+2	100	-	64
200+2	-	100	88
250+3	-	-	100

4.6 Determination of Strength Aspects of Subgrade Using Different Treatments on Coir Geotextiles

4.6.1 CBR Test Results

CBR test is carried out on clay sample with and without treatment Coir geotextiles. Result was shown in the figure 4.

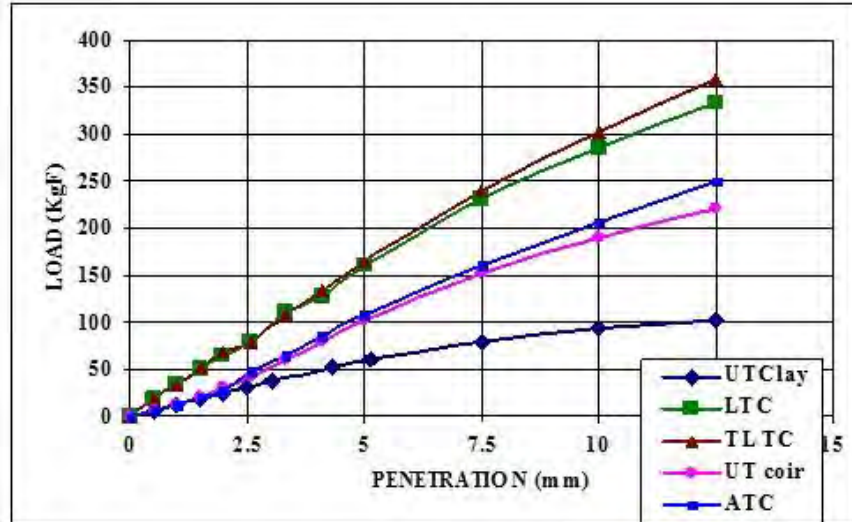


Figure.4 Load-Penetration Curve

Table.6 CBR values of soil with the use of various treated coir geotextiles

MATERIAL USED	CBR VALUE (%)
Untreated clay	2
Untreated coir	4.5
Alkali treated coir	4
Latex treated coir	7.5
Thermal-latex treated coir	7.8

The CBR value for the untreated clay is 2 % which was improved to 4.5 % by utilization of coir geotextiles. Further studies were carried out by treating coir geotextiles with various treatments for improving CBR. Alkali treated coir and the untreated coir obtains approximately the same value of CBR. The use of the latex treated coir and the thermal latex treated coir shows a significant improvement in strength that 7.5% and 7.8% respectively.

5. CONCLUSIONS

Results of the limited experimental study carried out with coir geotextiles with various treatments shows that latex treated coir geotextile shows an improvement in CBR. Results of the study indicates that coir geotextiles degrade faster in water media than in salt water media. Also in sandy soil degradation was found to be faster than in clays. In the alkaline medium the degradation was higher compared to the acidic medium. The degradation was lesser for latex treated samples compared to untreated and other chemical treated samples. From the above study it can be inferred that the latex Coir geotextile can be effectively used to improve the strength of soft clayey soils and can be effectively used as subgrade.

Reduction in strength in alkali media is attributed to change in the pH. In the alkaline media with pH 8 showed a decrease in pH and the acidic solution showed a reduction in acidity after treatment. This is due to the replacement of OH ions, contributed by the reaction between the lignin content and the solution in which the coir is immersed. The degradation of coir in sand compared to clay is due to the mechanical breakdown of the coir, when placed in contact with sand.

REFERENCES

- ASTM D 4632–86(1990) Standard Test Method for Grab Breaking Load and Elongation of geotextiles, *Annual Book of ASTM Standards*, Vol 07 ASTM International, United States.
- Ajitha Bhasker, and Mary George (2000), Role of Coir Fabrics on the improvement of Subgrade for Roads, *Proceedings of the Short Term Course on Engineering Applications of Natural Fibres*, GCE Kannur, Dec.2000: 216-230.
- Balan ,K. (1995), Durability studies on Coir yarn for uses in geo meshes , *Proceedings of the Short Term Course on Engineering Applications of Natural Fibres*, GCE Kannur, Dec.2000: 77-97.

- Geethamma, V. G., Thomas Mathew, K., Lakshmi Narayanan, R., and Sabu Thomas., (1997) Effect of Chemical Modification Loading and Orientation of Fibre, *Journal of Elsevier Science*, Vol .39, No.6-7: 1483-1491.
- Giroud, (1980), Introduction to Geotextiles and their Applications, *Proceedings First Canadian Symposium on Geotextiles*, Calgary. ,Alberta,September 3-31.
- Goulart Silva, G., .De Souza, D.A., Machado, J.C., Hourston D.J., (1999) Mechanical and Thermal Characterization of Native Brazilian Coir Fibre, *Journal of Polymer Science* , Vol .76: 1197-1206.
- Khalil, H.P.S.A., Ismail, H.D., Rozman, M.N., Ahmad, (2000). The Effect of Acetylation on Interfacial Shears Strength between Plant Fibres and Various Matrices, *Journal of European Polymer* , Vol .37: 1037-1045.
- Paul, W., Jan Ivens, Ignaas Verpoest., (2003), Natural Fibres can they replace Glass in Fibre Reinforced Plastics, *Journal of Composites Science and Technology* Vol .63: 1259-1264.
- Rout, J.,Misra , M ., Tripathy, S.S ., Nayak , S.K , Mohanty, A.K., (2001), The influence of Fibre Treatment on The Performance of Coir-Polyester Composites, *Journal of Composites Science and Technology* Vol .61: 1303-1310.
- Ramanatha Ayyar, Girish, (2000), Improvement of durability of Coir Geotextiles, *Proceedings I.G.C, Bombay*. Vol 2: 4
- Ramakrishna, G. and Sundararajan, T. (2004), Durability of natural fibres and the effect of corroded fibres on the strength of mortar, *Journal of Cement & Concrete Composites*.
- Sreekala, M.S., Jayamol George, Kumaran, M.G., Sabu Thomas, (2001), Water- sorption Kinetics in Oil Palm Fibres, *Journal of Polymer science* , Part B: Vol. 39: 1215-1223.
- Sobha.S (1996) Role of Coir Fabric in the improvement of poor Subgrades. M-Tech Thesis submitted to the Govt Engineering College Trivandrum.
- Varma .D.S,Varma.M.,Varma.I.K. (1986) Thermal behaviour of Coir fibres , *Journal of Thermochemica Acta* , Vol.108: 199-210.

Effective Strategies for Residual Polymer and Aquatic Toxicity Testing for Dredge Slurry Dewatering

Randy Wilcox, P.E., WaterSolve, LLC, USA, randyw@gowatersolve.com

Gregg E. Lebster, WaterSolve, LLC, USA

Bruce Rabe, Environmental Resources Management (ERM), USA, bruce.rabe@erm.com

ABSTRACT

Chemical conditioning is typically required to facilitate the solids and water separation in the vast majority of dredging and dewatering operations. Even with the best efforts in optimizing the chemical dose, a small fraction of the polymer may be released in the filtrate water after the dewatering operations. Site conditions and regulatory requirements specific to a particular location may dictate that aquatic toxicity testing of the discharge water be completed on individual projects.

After several products and/or combinations of products are tested in bench scale jar tests to determine the most effective products and the associated dose(s), a larger scale dewatering test is completed to determine or verify the suitability of the dewatering technology selected. The example projects discussed for this presentation utilized geotextile containers and the tests were completed accordingly. The geotextile container filtrate collected from the laboratory scale tests was subjected to a series of aquatic toxicity tests based on regulatory agency requirements.

Protocols for aquatic toxicity tests typically require acute and/or chronic toxicity test assessments on a representative sample of filtrate water after conditioned with a specified chemical. In some cases, a specific dilution with site water will be included with the procedure to simulate a mixing zone. The species selected for testing will be based on location, salinity, and other factors. It may be necessary to perform the aquatic toxicity testing using more than one chemical conditioning program.

The regulatory agency will typically approve the chemicals at the dose used in the testing. Additional toxicity testing may be required during operations. Some projects have residual polymer testing requirements. Qualitative testing is typically done in the field as a gross determination of polymer present in the water. The quantitative test is a more precise test meant to be conducted in a laboratory setting under controlled conditions.

Keywords- chemical, conditioning, regulatory, acute toxicity, chronic toxicity, whole effluent toxicity

1. INTRODUCTION

In order to effectively dewater dredged material, chemical conditioning is required. The most effective chemical conditioning program is determined by extensive bench testing. The selection of products is based on the project requirements and objectives. In many cases, two or more products are required to optimize the conditioning program.

During the dewatering operations, efforts are made to minimize the polymer use for several reasons. Even with the best efforts to optimize the use of chemical products, a small fraction of the polymer may not be captured with the solids and is released with the water. It has been demonstrated that the product will attach to any available solids in the receiving water. However, the products have toxic effects of aquatic life and any portion that is not rendered inactive by attachment to available solids has been shown to be harmful.

The material safety data sheets for the products typically contain basic ecological and toxicological information. Additional aquatic toxicity testing may be required using the water released from a simulated dewatering operation. The procedures for sample collection and testing are determined prior to testing. The products, application rates and doses are determined by testing. Samples for initial testing are collected by simulating the dewatering technique to be utilized for the specific dredging application. The aquatic toxicity tests are conducted according to the protocols prescribed by the regulatory agencies.

In certain cases, the residual polymer is measured in the filtrate water released. This measurement can be based on samples collected directly from the dewatering operation or in some cases is based on samples collected at

prescribed locations in the water body after the filtrate is released to the water body. The procedures for qualitative and quantitative testing are available to determine the presence of residual polymer and the amount of residual polymer in a specific sample.

2. CHEMICAL CONDITIONING

Based on the primary project objectives, such as dewatering efficiency, filtrate water clarity, contaminant removal or other objectives, the most effective chemical conditioning program is determined by bench testing. The sample solids concentration and other parameters are determined and required dilution is made to simulate dredge slurry with site water. The dry weight solids concentration of the dilution is also determined according to U.S. EPA Method 160.2.

Several products are evaluated in bench scale tests to determine the most effective product or combination of products to meet the project objectives. These evaluations are based on several factors including water release rate, water clarity, and flocculent appearance. These factors are used to compare the various products to isolate the most effective products and doses.

Chemicals most commonly used to enhance dewatering in dredging applications are:

1. Organic Flocculents
2. Organic Coagulants
3. Inorganic Coagulants
4. Hybrid Chemistries

The application of the chemicals is typically done by injection into the dredge line. Based on the mixing energy requirements or restrictions determined during the bench testing, the injection location relative to the dewatering mechanism can be placed. The effectiveness of the conditioning is frequently checked using a sample port placed downstream of the chemical injection. To optimize the application of chemical, the feed rate can be automatically adjusted based on variances in slurry flow rate and solids concentration.

3. AQUATIC TOXICITY TESTING

The National Pollutant Discharge Elimination System (NPDES) permitting authorities use Whole Effluent Toxicity (WET) testing program as one of the tools for achieving the Clean Water Act's prohibition of the discharge of toxic pollutants in toxic amounts. WET is defined as the aggregate toxic effect to aquatic organisms from all pollutants contained in a facility's wastewater (effluent) (54 Federal Register (FR) 23868 at 23895, June 2, 1989). WET testing methods have been developed to measure wastewater's effects on specific test organisms' ability to survive, grow and reproduce. These test methods were promulgated in 1995 and added to the list of U.S. EPA methods approved under Section 304(h) of the CWA (40 CFR 136) for use in the NPDES program.

Federal regulations establish different approaches for implementing a water quality criterion for toxicity in NPDES permits, depending on whether the criterion is expressed in a numeric or narrative form. States that have not adopted a numeric criterion for WET are expected to interpret the State narrative criterion so that the appropriate effluent limits, including any necessary toxicity numeric limits, can be established. States typically identify the method they intend to use in regulating toxics based on narrative criteria and describe how their toxics control program will protect aquatic life and attain the narrative criterion. Examples of some of the WET specific issues addressed in State toxic control programs include the following:

- how critical low flow and effluent dilution series are determined;
- receiving stream aquatic life use designations;
- frequency of monitoring;
- use of marine species or freshwater species for testing;
- sample type, test type, and biological and statistical endpoints; and
- conditions under which acute or chronic testing is required.

For the Southern Shores dredging project, treated water was discharged to a tidally influenced portion of the Dick White Bridge Channel. The State of North Carolina bases WET limitations upon the instream waste concentration (IWC) during conditions of maximum permitted effluent flow and 7Q10 receiving stream flow. The IWC for the Southern Shores project was determined to be 100 percent. In keeping with the State standard for facilities with IWC values greater than or equal to 0.25 percent, the facility was required to demonstrate that treated effluent was not chronically toxic at 100 percent.

For this application, the State required the City of Southern Shores to conduct a five concentration, pass/fail chronic toxicity test using the marine invertebrate, mysid shrimp (*Americamysis bahia*). Each of the five test concentrations consisted of 100 percent receiving water treated with a combination of water additives, bracketing the target application rate. An additional receiving water concentration without the water additives served as a negative control. A concurrent positive control consisted of aged synthetic seawater.

Per U.S. EPA Method 2002, the chronic test was conducted using 250 milliliter (mL) polypropylene containers containing 150 mL of control water or appropriate test solution. Five, seven day old test organisms were randomly introduced into each test chamber with eight replicate chambers per treatment. Organisms were fed 0.2 mL of a concentrated suspension of less than 24-hour old live brine shrimp nauplii (*Artemia* sp.) daily during the test. Organism survival was determined daily by enumerating of live mysids. Survival was defined as any body or appendage movement. At the termination of the test, mysids in each test chamber were counted, dried, and weighed to the nearest 0.01 milligram (mg).

The test was conducted at a temperature of 25 ± 1 degrees Celsius ($^{\circ}\text{C}$) under fluorescent lighting with a photoperiod of 16 hours light and 8 hours dark. Water quality measurements consisting of dissolved oxygen, pH, salinity, and temperature were performed daily on selected treatments.

Following termination of the test, statistically significant differences ($P=0.05$ or 0.01 depending on test endpoint) in mysid survival and growth were determined between the receiving water control and the various treatments. All statistical analyses were performed using the ToxCalc Version 5.0.23 software program.

To demonstrate compliance with the imposed discharge limitations, two sets of chronic toxicity tests were conducted during September 2010, on varying concentrations of Solve 3 and Solve 9330. The initial test incorporated a five concentration matrix of Solve 3 and Solve 9330 with concentrations ranging from 2.8 pounds of Solve 3 and 0.8 pounds of Solve 9330 per dry ton of product to 7.8 pounds of Solve 3 and 1.7 pounds of Solve 9330 per dry ton of product. The results from the initial exposure revealed no adverse survival effect to the five product combinations. Survival ranged from 79 to 100 percent, compared to 92.5 percent in the receiving water control (Table 1). Growth was adversely effected ($P=0.05$) in all five treatments and ranged from 0.140 to 0.247 mg per organism, compared to a control of 0.298 mg per organism (Table 1). Based on the adverse growth effects, a second set of samples were prepared and tested.

In the second set of samples, the concentration of Solve 3 was held consist at 4.5 pounds per dry product and concentration of Solve 9330 was varied from 0.16 pound to 0.8 pounds per dry product. Following the second exposure, mysid survival was again unaffected and ranged from 92.5 to 97.5 percent, compared to a receiving water control response of 95 percent (Table 2). Mysid growth ranged from 0.281 to 0.324 mg per organism; compared to a receiving water control performance of 0.336 mg per organism (Table 2). Unlike the initial test, adverse mysid growth effects ($P=0.01$) were limited to the maximum concentration of Solve 9330 of 0.8 pounds per dry ton of product. Mysid growth in the four lower concentrations of Solve 9330 was unaffected and resulted in a non-toxic response.

Table 1 - Data Summary of September 3 – 10, 2010 *A. bahia* Chronic Toxicity Test

Concentrations (lb/dry ton product)	Survival (%)	Growth Average Wt./ Organism (mg)
Laboratory Control	95	0.301
4.5 lb Solve 3 w/ 1.7 lb Solve 9330	80	0.140*
6.1 lb Solve 3 w/ 1.7 lb Solve 9330	79	0.140*
7.8 lb Solve 3 w/ 1.7 lb Solve 9330	87.5	0.188*
4.5 lb Solve 3 w/ 0.8 lb Solve 9330	95	0.247*
2.8 lb Solve 3 w/ 0.8 lb Solve 9330	100	0.240*
Receiving Water Control	92.5	0.298

* Statistically lower when compared to the control or the dilution control (P=0.05)

Table 2 - Data Summary of September 17 – 24, 2010 *A. bahia* Chronic Toxicity Test

Concentrations (lb/dry ton product)	Survival (%)	Growth Average Wt./ Organism (mg)
Laboratory Control	95	0.364
4.5 lb Solve 3 w/ 0.16 lb Solve 9330	95	0.317
4.5 lb Solve 3 w/ 0.32 lb Solve 9330	92.5	0.313
4.5 lb Solve 3 w/ 0.48 lb Solve 9330	97.5	0.298
4.5 lb Solve 3 w/ 0.64 lb Solve 9330	97.5	0.324
4.5 lb Solve 3 w/ 0.8 lb Solve 9330	95	0.281*
Receiving Water Control	95	0.336

* Statistically lower when compared to the control or the dilution control (P=0.01)

4. RESIDUAL POLYMER TESTING

When requested or required, the residual polymer can be determined according to “*Determination of the Presence of Polymer Using the Flocculation Method*”. This procedure includes qualitative and quantitative methods. The qualitative test is normally completed in the field as a gross determination of the polymer present in the sample of water. This can also be used as a comparative test for estimating the approximate quantity of residual polymer within a certain range. The quantitative test is more precise and is meant to be conducted in a laboratory setting under controlled conditions.

Initial data points are determined by using known concentrations of the flocculent and performing the test according to the method described above. The data points are then graphed and a best fit curve is added as shown in Figure 1. Samples collected are tested in the same manner and the settling times are plotted on the curve to determine the

residual polymer present. Table 2 shows the initial testing to create the data points on the left and the testing of the samples collected in the field on the right. Figure 2 illustrates the testing in a photograph showing how the settling times vary with the amount of residual polymer present.

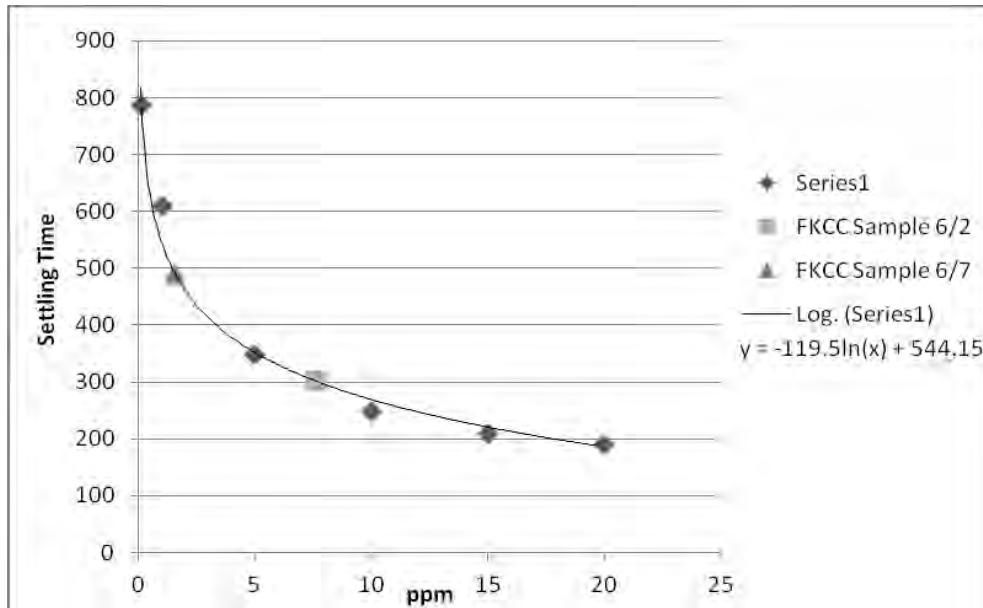


Figure 1. Residual polymer testing results

P.P.M.	Settling Time (sec)
25	158
20	190
15	209
10	248
5	348
1	609
0.1	787
0	815
FKCC Sample 6/2	302
FKCC Sample 6/7	490
FKCC Sample 6/14	>1500
FKCC Sample 6/21	>1500
FKCC Sample 6/29	>1500

Date	Settling time	PPM
6/2/2010	302	7.6 ppm
6/7/2010	490	1.56 ppm
6/14/2010	>1500	0 ppm
6/21/2010	>1500	0 ppm
6/29/2010	>1500	0 ppm

Table 2 - Data Summary of Residual Polymer Test



Figure 2. The Flocculation Method, presence of polymer increases settling rates

5. CONCLUSION

Current regulatory trends in the dredging and dewatering industry dictate that approval of dewatering chemical products is required. The regulatory agencies for individual states have variable requirements for these approvals. In order to provide the most effective products that will meet the environmental suitability standards, the type of testing presented will continue to be required. We anticipate that this specific testing will be used to satisfy the growing desire to regulate these products. With the proper testing prior to and during the project implementation, along with the use of the most effective chemical feed systems, the chemical conditioning can be optimized for dewatering dredge slurry residuals.

Effects of Discrete Fibers on the Stress-dilatancy and Micromechanics of Fiber-reinforced Sand

D. Wanatowski, Nottingham Centre of Geomechanics, Department of Civil Engineering, University of Nottingham, United Kingdom, dariusz.wanatowski@nottingham.ac.uk
S. Ud-din, Balochistan University of Engineering and Technology, Khuzdar, Pakistan
A. Marri, NED University of Engineering and Technology, Karachi, Pakistan
M.R. Hall, Nottingham Centre of Geomechanics, Department of Architecture and Built Environment, University of Nottingham, United Kingdom

ABSTRACT

The stress-dilatancy relationship plays a very important role in understanding of the mechanical behavior of granular soils. Numerous experiments on fiber-reinforced uncemented and cemented granular materials have been carried out over the last two decades. However, the effects of fiber, cement, and confining pressures on the stress-dilatancy behavior have seldom been investigated, especially at high confining pressures and at micro level. In this paper, the stress-dilatancy relations and micromechanics of fiber-reinforced uncemented and cemented sand at a wide range of confining pressures are investigated. Results obtained from drained triaxial compression tests carried out on sand with various fiber and cement contents are compared and analyzed. The effects of high confining pressure and fiber content on the stress-dilatancy behavior of cemented sand reinforced with polypropylene fibers are discussed. Scanning Electron Microscopy analysis of the effects of particle, bond and fiber damage on the stress-dilatancy behavior of the sand is presented.

1. INTRODUCTION

Numerous experiments on fiber-reinforced granular materials have been carried out by several researchers over the last two decades (e.g. Maher and Gray 1990; Michalowski and Zhao 1996; Consoli et al. 2004; Tang et al. 2007; Diambra et al. 2010; Ibraim et al. 2010; Silva dos Santos et al. 2010; Ud-din et al. 2011). However, the effects of varying fiber/cement contents and confining pressures on stress-dilatancy behavior have not been investigated very thoroughly. Furthermore, most experimental data on fiber-reinforced cemented materials have been obtained at relatively low confining pressures and at macro level. A detailed review of the literature regarding the dilation of fiber-reinforced granular materials reveals that the previous studies somehow lack detailed information on the stress-dilatancy behavior and the dilation angle of fiber-reinforced cemented soils.

The observed tendency of dense granular materials to expand in volume during drained shearing is termed as dilatancy. The physical manifestation of dilatancy was first identified by Reynolds (1885), and long afterward, Rowe (1962) introduced a stress-dilatancy theory. There are several factors that influence the dilatancy in cemented granular materials including relative density, cement content, and confining pressure (Coop and Atkinson 1993; Consoli et al. 2000, 2004, 2009, 2012; Yan and Li 2011). The volume change plays an important role in the stability of frictional materials (Bolton 1986, Lade 1988, Yu 2006). For instance, the increase in volume provides higher shear strength to geomaterials during shearing. The variation of dilatancy rate depends on the initial packing, with denser materials showing a more rapid decrease in dilatancy rate compared to loose materials. In addition, according to Yu (2006), bonding delays or prevents the tendency of soils to dilate at small strains. The effect of cement content on dilatancy has been further analyzed by Wang and Leung (2008). They found that at small strains, dilatancy is hindered by the intact bonding network that produces a web-patterned force chain. However, after yielding, the increase in the dilatancy accelerates. Moreover, they observed that the dilatancy at the peak state increases with increasing cement content. Marri (2010) and Marri et al (2010, 2012) reported a progressive suppression in the dilation of cemented sand by the gradual increase in confining pressure. According to Marri (2010) and Veiskaramia et al. (2011) a dense cemented soil exhibiting a dilative behavior at low stress levels may show a contractive behavior at higher levels of confining stress.

Since at high stresses, the suppression of dilatancy rate plays an important role in controlling the shear behavior of cemented sand, the influence of the confining pressure on the plastic properties of sand, mainly the friction and dilatancy angles are of significant importance. Moreover, the progressive suppression of dilation in cemented materials by the gradual increase in confining pressures needs to be incorporated into the design considerations and therefore, it needs further elaboration. This is because the mechanical response of cemented materials at high pressures can be significant for analysis of offshore piling, deep galleries and mine shafts, high earth dams and mechanics of oil-bearing strata. Recent developments of massive offshore constructions particularly for oil exploration have highlighted the importance of

high confining pressure, which affects design of foundations for these structures. For instance, many oil reservoirs reach depths over 1000 m subjecting naturally cemented soils to very high overburden pressures (Dalla Rosa et al. 2008). This leads to the question whether the stress-dilatancy behavior of a cemented soil at high confining pressures is similar or different from that at low confining pressures.

2. METHODOLOGY

2.1 Materials

Well-graded, medium quartz concrete sand from Sheffield in the United Kingdom, so-called Portaway sand was used as the base material for the cemented specimens. Portaway sand has the specific gravity (G_s) of 2.65, the mean grain size (D_{50}) of 0.35 mm, the coefficient of uniformity (C_u) of 2.2, and the coefficient of curvature (C_c) of 0.9. The minimum and maximum void ratios are 0.46 and 0.79, respectively, as shown in Table 1. A discrete polypropylene fiber was used as reinforcement (Figure 1). The properties of the fiber are given in Table 1.

Table 1 Index properties of sand and discrete fiber.

Properties of fiber	Values
Length, mm	22
Diameter, mm	0.023
Tensile strength, N/mm ²	0.95-1.3
Softening temperature, C	80
Density, g/cm ³	0.905
Properties of sand	Values
Effective grain size D_{10} , mm	0.19
D_{30} , mm	0.29
Mean grain size D_{50} , mm	0.39
D_{60} , mm	0.42
Uniformity Coefficient D_{60}/D_{10}	2.21
Specific Gravity, G_s	2.65
e_{max}	0.79
e_{min}	0.46



(a)



(b)

Figure 1. Discrete fibers: (a) before mixing; and (b) after mixing with sand.

2.2 High Pressure Triaxial Apparatus

A high pressure triaxial testing system, developed at the University of Nottingham (United Kingdom) in conjunction with GDS Instruments Ltd. was used for all the experiments presented in the paper. The high pressure triaxial system is

capable of testing various geomaterials including uncemented or cemented granular soils and soft rocks. The main components of the system are described by Marri (2010), Ud-din et al. (2011), Marri et al. (2012) and Ud-din (2012).

2.3 Testing Procedures

The fiber reinforced cemented and uncemented specimens (50 mm diameter and 100 mm height), were prepared by mixing sand, polypropylene fibers and/or cement. Fibers were mixed with sand prior to adding the water to achieve uniform distribution of fibers. Thorough mixing of dry materials was continued until a uniform appearance of the sand-cement mixture was obtained. For the preparation of the cemented specimens, a predetermined amount of Portland cement by weight of dry sand (5%, 10% or 15%) was added and mixed thoroughly with the sand-fiber composite. After that water was added to the mixture in accordance with the optimum moisture content of Portaway sand and further mixing was performed until a homogeneous appearance of the sand-cement-fiber mixture was achieved. The specimens were compacted in layers into a split mould to a target dry unit weight of 17.4 kN/m^3 . A thin plastic transparency sheet, cut according to the size of the mould, was used inside the mould before pouring the mix to prevent sticking the material to the walls and base of the mould. After compaction, the uncemented fiber reinforced specimens were ready for testing. However, the cemented specimens were cured for 14 days before shearing. All the specimens were saturated and isotropically consolidated to the mean effective stresses up to 20 MPa. After that the drained (CID) tests were carried out under a deformation-controlled loading mode at a constant deformation rate of 0.1 mm/min.

3. RESULTS

3.1 Homogeneity of the Mix

To investigate the mixing, distribution and homogeneity of fibers microscopically in cemented and uncemented samples, Scanning Electron Microscopy (SEM) analysis was carried out on samples before and after isotropic compression. Figure 2 shows SEM micrograph of fiber-reinforced cemented and uncemented soil samples before testing showing distribution of fibers in sand and cemented sand. It is important to note that SEM micrographs represent the qualitative information regarding the distribution as investigation is always limited to very small area and to a specific horizontal plane or to a plane of failure. The distribution of fibers which looks reasonably uniform and consistent at macro scale may not have the same level of uniformity and consistency at micro level as shown in Figure 2. It is also worth mentioning that SEM micrograph shown in Figure 2 is of about 2 mm to 5 mm wide area of the whole sample surface. In the fiber-reinforced cemented sample taken at the magnification of 50x shown in Figure 2(a), the sample was analyzed before isotropic compression and shows only the top surface of the specimen. There can be seen consistent bonding of the grains in their natural bedding plane. However, some poor bonding and cement deposition on the surface of the sand grains and fibers can also be seen. Figure 2(b) shows the SEM micrograph of fiber-reinforced uncemented sample taken at the magnification of 100x. It can be seen that fibers are distributed quite uniformly and produce a good network of fiber with sand grains. A similar distribution has also been shown by Tang et al. (2007).

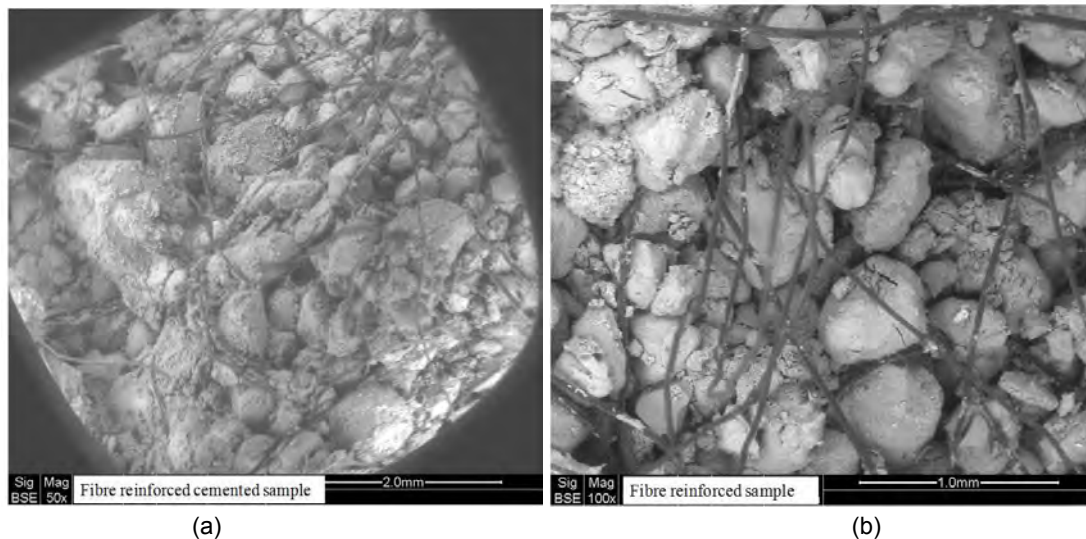


Figure 2. Fiber-reinforced samples before testing: (a) 0.5% fiber and 5% cement reinforced sample, (b) 0.5% fiber-reinforced uncemented sample.

3.2 Compaction Characteristics

The concrete sand was tested for optimum moisture and fiber contents to achieve the maximum dry unit weight. The Proctor compaction test results plotted versus both moisture content and fiber content are presented in Figures 3(a) and 3(b), respectively.

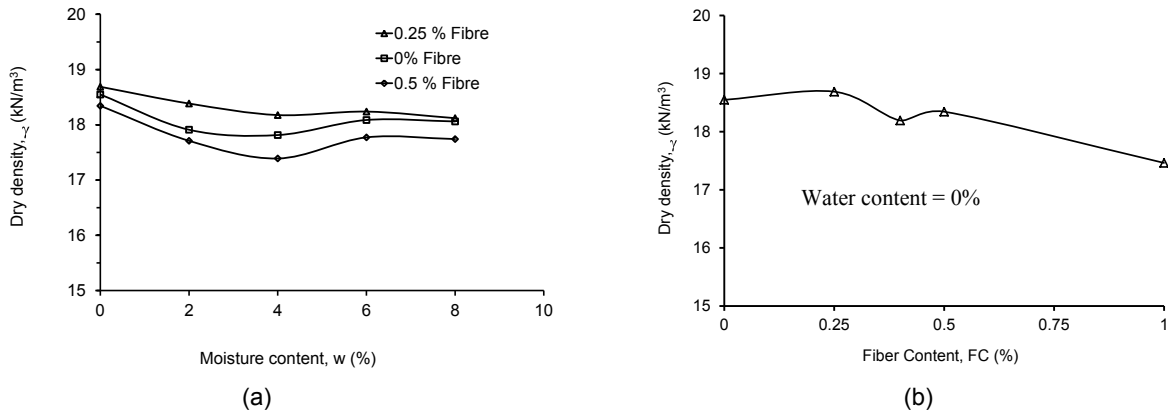


Figure 3. Results of Proctor tests on fiber-reinforced specimens.

It can be seen from Figure 3 that the clean sand exhibits two peaks in the compaction curve; one at very dry conditions, where there are no capillary tension to resist the compaction effort, and the other at the optimum moisture content, where optimum lubrication between particles occurs. Similar two peaks in the compaction curves of clean sand have been reported in the literature (e.g. Rollings and Rollings, 1996). The maximum dry density for the concrete sand is achieved at zero moisture content. Moreover, similar trends can be seen for the fiber content of 0.25% and 0.5% (see Figure 3a). It is interesting to see that the effect of fiber content is not proportional to the dry density; therefore, compaction tests were carried out for optimum fiber content as well. The optimum fiber content at zero water content was determined to be approximately 0.25% as shown in Figure 3(b).

3.3 Dilatancy Angle

The effect of addition of cement in sand can be observed in Figure 4 in which the peak dilatancy angles are plotted versus the cement content. The peak dilatancy angle is defined as the dilatancy angle when granular soil reaches its peak strength, that is $\tan \psi = -(\delta \varepsilon_v / \delta \varepsilon_q)$, where ψ = dilatancy angle, ε_v = volumetric strain, and ε_q = deviatoric strain. The increase of cement content from 0% to 2% and 5% has increased the peak dilatancy angle of sand from 14.3° to 22.61° and 32.1°, respectively. The effect of addition of fiber in sand and cemented sand can be observed in Figure 5 in which dilatancy angles are plotted for all the composites. The fibers have increased the peak dilatancy angle of uncemented sand from 1.5° to 10.17° and from 15.95° to 18.9° for cemented sand. It can be seen the effect of fiber is more significant in uncemented sand than in cemented sand.

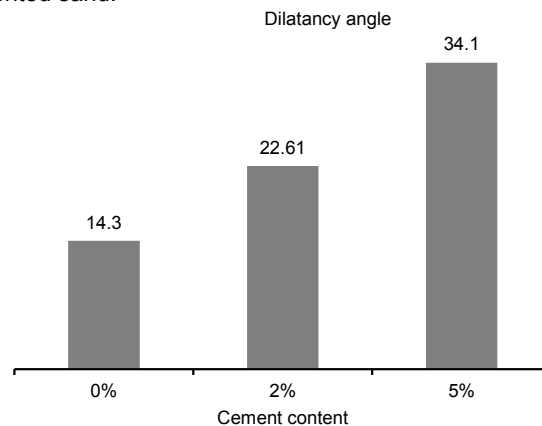


Figure 5. Effect of cement content on dilatancy angle of sand.

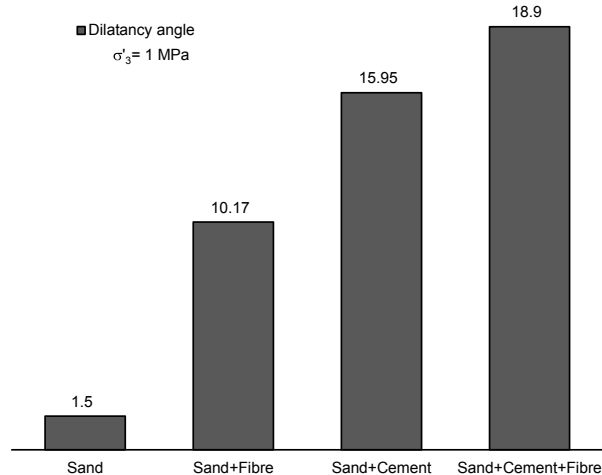


Figure 5. Effect of addition of fiber and cement on the dilatancy angle of Portaway sand.

It can be noticed from Figures 4 and 5 that peak dilatancy angles for cemented and fiber-reinforced cemented sand are relatively high. However, it should be pointed out that all the specimens were compacted to a dense state. The dilatancy in dense granular materials during shear is due to the tumbling and overriding of particles over each other. In the cemented sand there is bonding between the particles and during shear not all the bonds are being broken as was observed during SEM analysis (Ud-din et al. 2011, Marri et al. 2012). Therefore it may be presumed that for cemented sand there could be the overriding and rolling of bonded particles with significantly larger size compared to uncemented sand, which ultimately leads to higher dilatancy angles.

3.4 Effect of Cement Content and Confining Pressure on Fiber-Reinforced Cemented Sand

Some important macro scale observations of the effect of confining pressure, and cement content on the dilatancy characteristics of sand are summarized in this section. The volumetric strain curves for dense fiber-reinforced sand specimens with constant unit weight of 17.4 kN/m^3 are shown in Figure 6(a). A comparison of the effect of confining pressure reveals that the increase in confining pressure from 50 kPa to 20 MPa, results in a progressive suppression of dilation in the volumetric strain curves. This suggests that at relatively high confining pressures the significance of dilation decreases. For example, in some situations shown in Figure 6(a) the dilation may be entirely suppressed by the high confining pressure. It should be pointed out that the maximum dilation occurs at $(q/p')_{\text{peak}}$ for both fiber-reinforced cemented and uncemented sand (Marri 2010, Ud-din 2012). The points of maximum rate of dilation are identified on the effective stress ratio (q/p') versus dilatancy (D) relationships by solid circles, as shown in Figures 6(b) and 7(b).

The effect of confining pressure on the dilatational behavior of fiber-reinforced cemented sand is shown in Figure 7, which shows similar trend as that observed for fiber-reinforced sand (Figure 6). The dilatancy decreases with increasing confining pressure and axial strain to the point of maximum dilatancy increases with increasing confining pressures. The $\varepsilon_v - \varepsilon_a$ curve shows that dilation is gradually suppressed by increasing confining pressure up to 1 MPa where confining pressure overcomes the dilative behavior and totally compressive behavior can be seen at $\sigma'_3 = 4 \text{ MPa}$ and above. After comparing the responses of sand and fiber reinforced sand, as well as cemented sand and fiber-reinforced cemented sand, it can be concluded that they follow the same trend but there is more dilation and compression in fiber-reinforced materials. This additional dilation and compression observed in fiber-reinforced materials suggests that this might be entirely due to the effect of the addition of fiber.

3.5 Particle Crushing and Fiber Damage

Figure 8 shows two examples of SEM micrographs of the fiber-reinforced uncemented (Figure 8a) and cemented (Figure 8b) specimens, taken after drained shearing at the effective confining pressure of 1 MPa. A clear particle crushing in the uncemented specimen can be observed from Figure 8(a). A cement bond breakage accompanied by the particle crushing in the cemented specimen is also shown in Figure 8(b). However, only limited fiber damage in both uncemented and cemented specimens could be identified by the SEM analysis. This observation suggests that after the occurrence of particle and bond breakage, the fibers themselves could have resisted the shearing until their tensile strength was reached. In a brittle matrix composite such as the sand-cement with addition of fiber, the matrix will crack followed by gradual pull out of the ductile fiber.

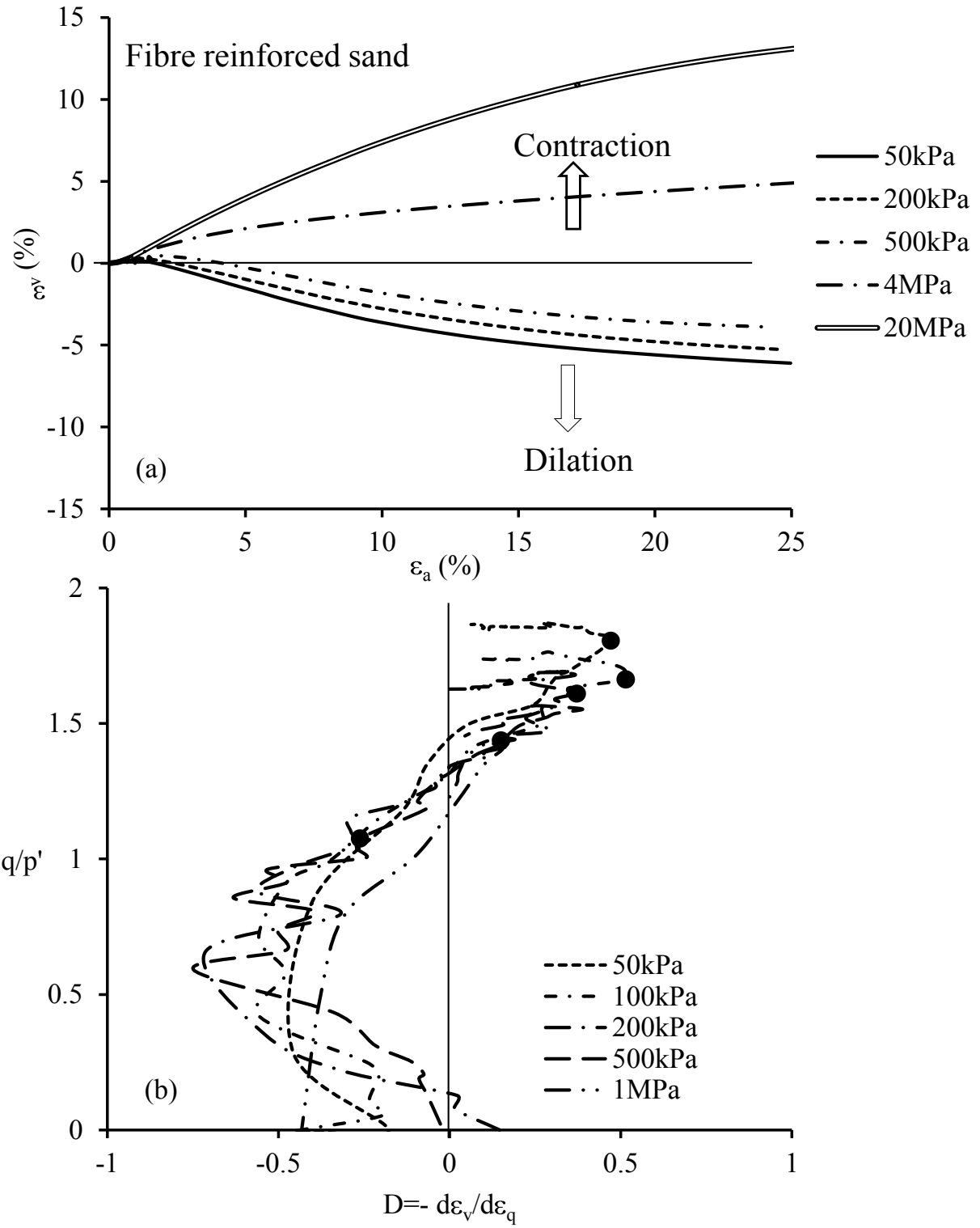


Figure 6. Dilatancy behavior of fiber-reinforced sand under varying confining pressures: (a) ϵ_v - ϵ_a , and (b) q/p' - D .

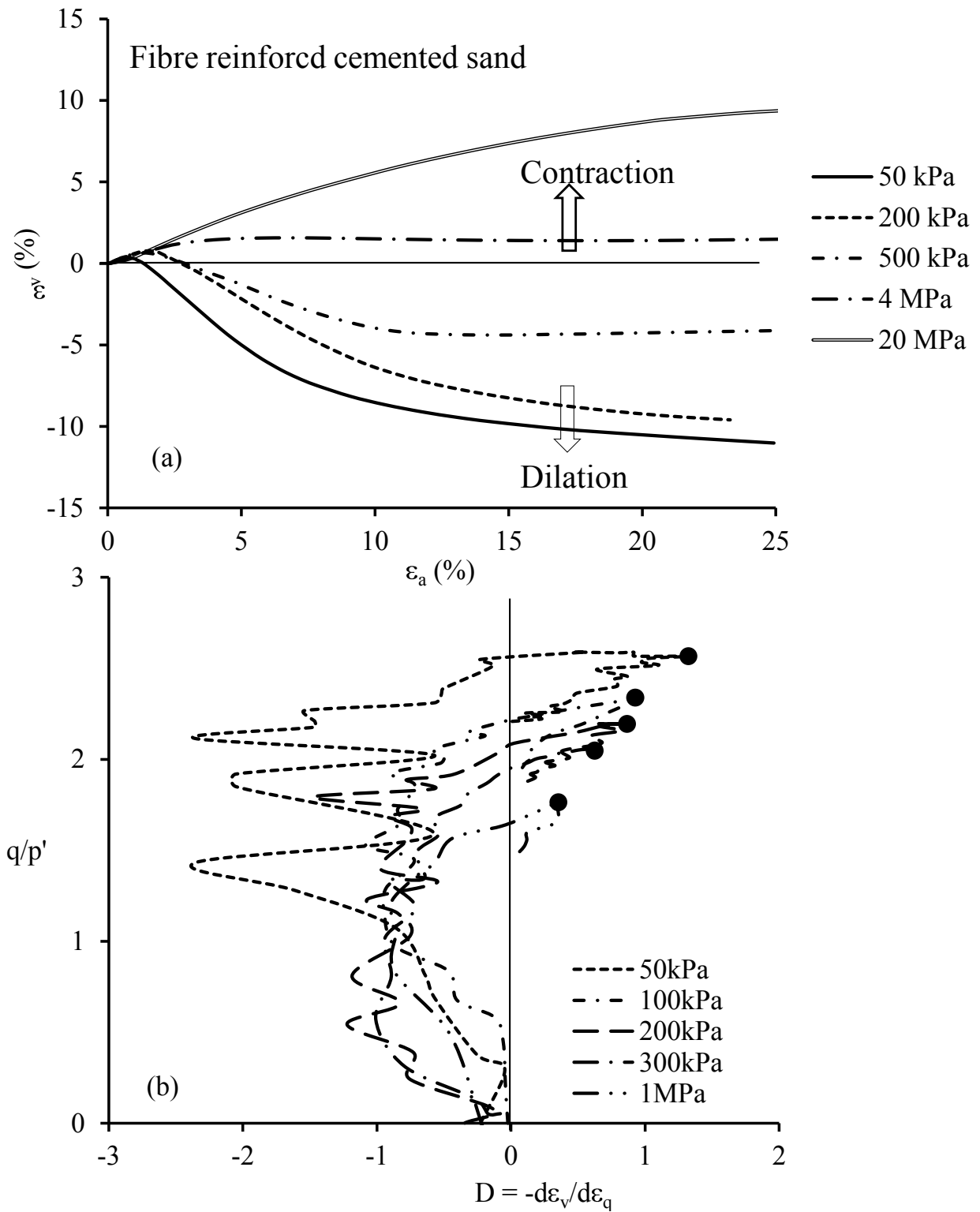


Figure 7. Dilatancy behavior of fiber-reinforced cemented sand under varying confining pressures: (a) ε_v - ε_a , and (b) q/p' - D .

It should also be pointed out that the tensile strength of the polypropylene fibres used in this study was quite high (see Table 1), so the fibres could provide a strong platform to the sand particle for rolling over when sheared to large strains. As a result, the dilation of fibre-reinforced specimens has increased significantly compared to that of unreinforced specimens. Finally, Ud-din (2012) also observed the lack of interfacial debonding at the fibre/matrix interface of the fibre-reinforced cemented specimens. Since fibres and the matrix have different Young's moduli, the interface regions have experienced minimal strains, which reduced compressibility of the specimens.

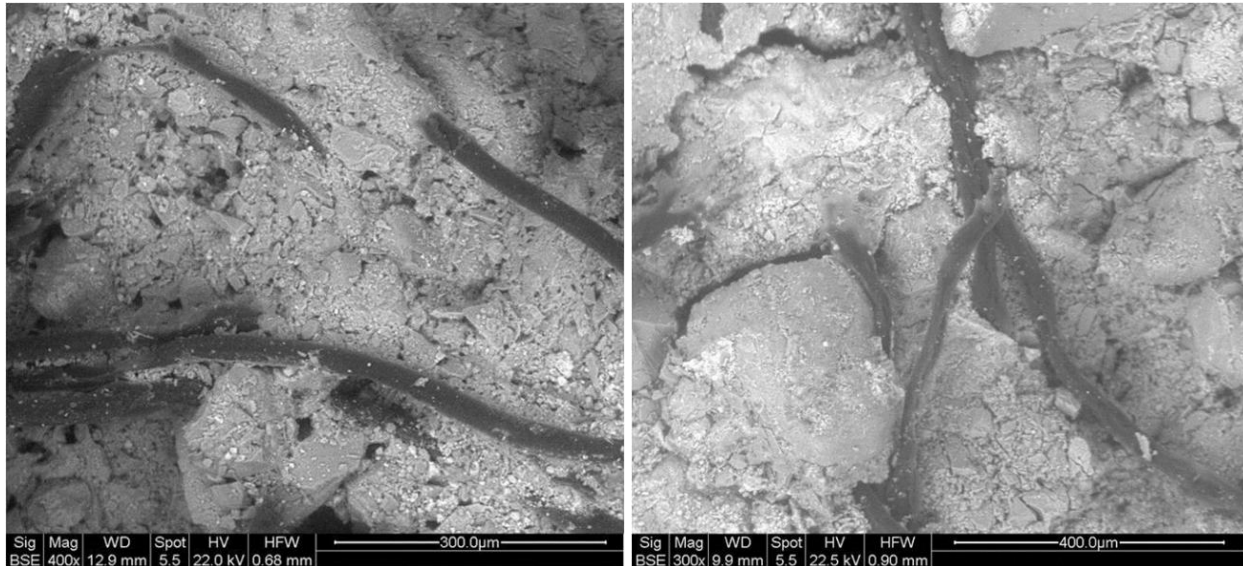


Figure 8. Examples of SEM micrographs of the fibre-reinforced specimens sheared at $\sigma_3' = 1$ MPa:
 (a) fibre-reinforced uncemented sand (0.5% fibre and 0% cement);
 (b) fibre-reinforced cemented sand (0.5% fibre and 5% cement).

4. SUMMARY AND CONCLUSIONS

In this study, drained triaxial compression tests were carried out on uncemented and cemented fiber-reinforced specimens of concrete sand with different fiber and cement contents at a wide range of confining pressures. The mechanism of dilatancy, its significance and dependence on fiber content, cement content and confining pressures was discussed. SEM analysis of selected specimens was also carried out. The results can be summarized in the following points:

1. It is challenging to achieve uniform distribution of fiber in sand specimens at microscale.
2. For uniform clean sand, it was noticed that the materials exhibit two peaks in the compaction curve; one at very dry conditions, where there are no capillary tension to resist the compaction effort, and the other at the optimum moisture content, where optimum lubrication between particles occurs. The addition of fiber has not changed the compaction characteristic of the sand. The maximum dry density was achieved at zero moisture content. The optimum fiber content for dry mix was determined to be around 0.25%.
3. The commencement of dilative behavior and the point of maximum dilatancy are fiber content, cement content, and confining pressure dependent. There is a significant effect of the addition of fiber on the response of both cemented and uncemented sand. The addition of fibers increases the dilative behavior of the composite.
4. The addition of fiber increases the dilatancy while increasing confining pressures reduces dilatancy of sand.
5. Due to addition of fiber the peak dilatancy angle increases from 1.5° to 10.17° in uncemented sand and from 15.95° to 18.9° in cemented sand. Thus, the effect of addition of fiber is more pronounced in uncemented sand compared to that in cemented sand.
6. Confining pressure affects dilative behavior of the sand. At higher pressures the effect of confinement was dominant. As a result, at the effective confining pressures higher than 1 MPa the behavior of fiber-reinforced uncemented and cemented Portaway sand was purely compressive (i.e. no dilation occurred).
7. SEM analysis revealed a significant particle crushing and bond breakage in the uncemented and cemented specimens sheared at high confining pressures. However, only limited fiber damage was identified. This suggests that the fibers provide a strong rolling platform to the sand particle during shearing to large strains,

which explains why the dilation of fiber-reinforced sand increased significantly compared to that of unreinforced specimens.

REFERENCES

- Bolton, M. (1986). The strength and dilatancy of sand. *Géotechnique*, 36(1): 65-78.
- Coop, M.R. and Atkinson, J.H. (1993). The mechanics of cemented carbonate sands. *Géotechnique*, 43(1): 53-67.
- Consoli, N.C., Rotta, G.V. and Prietto, P.D.M. (2000). The influence of curing under stress on the triaxial response of cemented soils. *Géotechnique*, 50(1): 99-105.
- Consoli, N.C., Montardo, J.P., Donato, M. and Prietto, P. (2004). Effect of material properties on the behaviour of sand-cement-fibre composites. *Ground Improvement*, 8(2): 77-90.
- Consoli, N.C., Casagrande, M.D.T., Thome, A., Dalla Rosa, F. and Fahey, M. (2009). Effect of relative density on plate loading tests on fibre-reinforced sand. *Géotechnique*, 59(5): 471-476.
- Consoli, N.C., Cruz, R.C., da Fonseca, A.V. and Coop, M.R. (2012). Influence of cement-voids ratio on stress-dilatancy behavior of artificially cemented sand. *Journal of Geotechnical and Geoenvironmental Engineering*, ASCE, 138(1): 100-109.
- Dalla Rosa, F., Consoli, N. C. and Baudet, B. A. (2008). An experimental investigation of the behaviour of artificially cemented soil cured under stress, *Géotechnique*, 58(8): 675-679.
- Diambra, A., Ibraim, E., Muir Wood, D. and Russell, A. R. (2010). Fibre reinforced sands: Experiments and modeling. *Geotextiles and Geomembranes*, 28(3): 238-250.
- Ibraim, E., Diambra, A., Wood, D. and Russell, A.R. (2010). Static liquefaction of fibre reinforced sand under monotonic loading. *Geotextiles and Geomembranes*, 28(4): 374-385.
- Lade, P.V. (1988). Effects of voids and volume changes on the behaviour of frictional materials. *International Journal for Numerical and Analytical Methods in Geomechanics*, 12(4): 351-370.
- Maher, M. and Gray, D. (1990). Static response of sand reinforced with randomly distributed fibers. *Journal of Geotechnical Engineering*, ASCE, 116(11): 1661-1677.
- Marri, A. (2010). *The mechanical behaviour of cemented granular materials at high pressures*. PhD thesis, University of Nottingham, United Kingdom.
- Marri, A., Wanatowski, D. and Yu, H.S. (2010). Drained behaviour of cemented sand at high pressures. *Proceedings of the 17th Southeast Asian Geotechnical Conference*. Taipei, Taiwan, 10-13 May 2010, 1: 17-20.
- Marri, A., Wanatowski, D. and Yu, H.S. (2012). Drained behaviour of cemented sand in high pressure triaxial compression tests. *Geomechanics and Geoenvironmental Engineering*, 7(3): 159-174.
- Michalowski, R.L. and Zhao, A. (1996). Failure of fiber-reinforced granular soils. *Journal of Geotechnical Engineering*, ASCE, 122(3): 226-234.
- Reynolds, O. (1885). On the dilatancy of media composed of rigid particles in contact; with experimental illustrations. *Philosophical Magazine, Series 5*, 20: 469-481.
- Rollings, M.P. and Rollings, R.S. (1996). *Geotechnical Materials in Construction*, McGraw-Hill, NY, USA.
- Rowe, P.W. (1962). The stress dilatancy relationship for static equilibrium of an assembly of particles in contact. *Proceedings of the Royal Society*, A269: 500-527.
- Silva dos Santos, A.P., Consoli, N.C. and Baudet, B.A. (2010). The mechanics of fibre-reinforced sand. *Géotechnique*, 60(10): 791-799.
- Tang C., Shi, B., Gao, W., Chen, F. and Cai, Y. (2007). Strength and mechanical behavior of short polypropylene fibre reinforced and cement stabilized clayey soil. *Geotextiles and Geomembranes*, 25(3): 194-202.
- Ud-din, S. (2012). *Behaviour of fibre reinforced cemented sand at high pressures*. PhD thesis, University of Nottingham, United Kingdom.
- Ud-din, S., Marri, A. and Wanatowski, D. (2011). Effect of high confining pressure on the behaviour of fibre reinforced sand. *Geotechnical Engineering, Journal of the SEAGS & AGSSEA*. 42(4): 69-76.
- Veiskaramia, M., Jahanandishb, M. and Ghahramanib, A. (2011). Prediction of the bearing capacity and load-displacement behavior of shallow foundations by the stress-level-based ZEL method. *Scientia Iranica*, 18(1): 16-27.
- Wang, Y.H. and Leung S.C. (2008). A particulate-scale investigation of cemented sand behavior. *Canadian Geotechnical Journal*, 45(1): 29-44.
- Yan, W.M. and Li, X.S. (2011). A model for natural soil with bonds *Géotechnique*, 61(2): 95-106.
- Yu, H.S. (2006). *Plasticity and Geotechnics*. Springer, New York, USA.

Electrical Leak Detection Surveys for Brine Ponds in SQM, Chile

Miguel Garcia, SQM, Chile, miguel.garcia@sqm.com
Alejandro Lara, SQM, Chile, alejandro.lara@sqm.com

ABSTRACT

SQM -- producer of lithium, iodine, nitrate and potassium salts -- operates brine evaporation ponds in various locations of the Atacama Desert, covering a total area of 42,000,000 m². High salinity of both contained liquids and subgrade, among other conditions, have posed difficulties for the performance of leak detection surveys. Solutions contained in these HDPE-lined ponds are saturated in sodium chloride and/or sodium sulfate and/or potassium chloride, and have presence of a wide gamut of other ions. Concentrations range from ~480 gpl of total salts to upwards of 720 gpl. Precipitated salts produce a layer of solution-impregnated layer as thick as 0.50 m on the floor of the ponds. Constructed on arid terrain, itself composed of up to 60% water-soluble salts, and interconnected by pumping lines, surveying of these ponds has required adaptations of equipment and technique, with satisfactory results. Difficulties faced to date are described here, as well as still-standing challenges.

1. INTRODUCTION

1.1 Geographic Location

A large producer of iodine, lithium, nitrates and potassium salts, our company operates in various locations of the Atacama Desert - the driest in the world - in the northernmost region of Chile, South America. Many of these operations include brine evaporation ponds, as well as temporary brine storage ponds.



Figure 1: Small dots show location of operations using ponds in the Atacama Desert. Ponds at each location are exposed to different environmental conditions, and present different construction, configuration, and brine composition.

1.2 Brines Origin and Composition

Brines contained in the ponds operated by the company have two major sources:

- a) Naturally-occurring brines, pumped from deposits beneath the Salar de Atacama. A significant source of lithium, potassium and nitrates, these brines are pumped to the surface for treatment and subsequent solar evaporation in ponds. Salar brines are saturated in NaCl, have a high content of Na₂SO₄, KCl and LiCl, and contain a wide gamut of other salts.
- b) Brines generated by aqueous leaching (irrigation) of caliche, a sedimentary, highly water-soluble ore, exploited as a source of iodine, nitrates and potassium. The brines are channeled and stored in HDPE ponds, treated for iodine extraction and finally pumped to evaporation ponds. These solutions are saturated in NaCl or Na₂SO₄, and have a high content of NaNO₃, KCl, MgCl₂, and a large number of other salts. Total salt content in the solutions ranges from 480 gpl when recently generated, to upwards of 720 gpl in the final stages of the evaporation process.

Table 1: Chemical analysis of leaching brines, in grams per liter (gpl).

NaCl	Na ₂ SO ₄	Other
245	145	~130

Brines generated from leaching of caliche ore may present some acidity, in which case a neutralization of the solutions is necessary before entering the evaporation pond circuit. Salar brines are mostly neutral.

From the moment they are generated at the different leaching operations, or pumped from beneath the salar, saturation in NaCl and/or Na₂SO₄ produces continuous, uninterrupted precipitation of salts during the entire process, with a wide array of chemical and mass transport equilibria. Precipitation rates and type of precipitate vary according to the composition of each solution, and are also affected by ambient temperature. This precipitation produces a floor of salts that covers the HDPE liner in every brine-holding pond in operation. The salt floor is not a continuous solid, but a porous aggregate of different salt crystals and trapped solutions.

This presence of saturated solutions, salt precipitates, mass transfer between solids and liquid, as well as ionic transport and convective flow caused by concentration and thermal gradients, produce high levels of noise that make it difficult to apply normal levels of voltage and current in electrical leak detection surveys.

1.3 Ponds

The ponds in operation vary in location, age, size, design, construction, state of repair, and attached equipment - pumps, tubing, sinks, etc.- covering a total area of 42,000,000 m² (450,000,000 ft².)

The most common characteristics of these ponds are:

- a) The liner in contact with the brines in every pond is HDPE, 1 mm thick.
- b) Most ponds have a geotextile layer under the HDPE liner.
- c) Many of the ponds have service ground wiring underneath, for use in leak detection surveys. Older ponds have no wiring.
- d) The subgrade under the geotextile layer is the desert terrain, which can be composed of 40-60% water-soluble salts.

1.4 Pond Operation

During construction, the welded seams in the HDPE liner of every pond are subject to standard quality assurance practices, such as vacuum tests. Water lance leak detection tests are also performed on recently constructed ponds, where the liner is still exposed.

After construction, most ponds are filled with different types of highly saline, chemically diverse solutions (see Table 1). Solutions are pumped from one pond to another according to their concentration, distributed in an ordered sequence, going in general from more diluted to more concentrated. This results in a sequential series – or “train” -- of ponds, interconnected by HDPE pumping lines and pumping equipment. Equipment generally includes a cement sink within the ponds.

The final result in production ponds is a low-moisture salt aggregate, which is then removed (“harvested”) by bulldozers and trucked to other facilities for further refining. Non-production ponds, which also accumulate precipitated salts, must

be cleared of salts periodically in a similar manner. Machinery movement on the salt floor during harvesting or cleaning of the ponds often damages the underlying HDPE liner.

Electrical leak detection techniques are applied in recently cleaned or harvested ponds. After the majority of the solids are removed, a salt floor always remains, and water is pumped to the pond so it covers the salt floor, in order to allow submerged-probe surveys. Most of the adjustments in equipment and technique have been made here. Surveying over the salt floor, with no added water would be preferable, but has been impracticable as of yet.

2. SURVEYING

2.1 History

Electrical leak detection surveys have been performed at our company by an external contractor – the only local provider of this service until recently – for more than a decade. A project was started in 2008 to internalize these services, involving acquisition of necessary knowledge, equipment, training and testing.

Early testing stages using standard training, equipment and technique for submerged-probe surveys were unsuccessful. Although the available equipment was adequate for use in water, with sufficiently moist subgrade (permitting ~200 V and 2 A,) it was not capable of generating usable signals in production ponds. Extensive testing was conducted to determine the magnitudes required in order to have usable readings.

2.2 Feasibility testing

It was readily apparent that the aridness and high solubility of the soil, combined with the high conductivity of the solutions, would impose electrical requirements greater than those typically sufficient during tests in training ponds filled with water. It was also apparent that the significant chemical activity within the ponds (concentration gradients, thermal convection flow) would be cause for considerable levels of noise. Thus, the first steps were measuring total resistivity of the pond/solution system, and determining the level of voltage and amperage needed in order to overcome the noise levels.

Injecting current with our power supplies yielded a voltage much lower than expected, due to the low resistivity of the system. Noise level was 1.5-1.6 V, and this high level of noise was found to distort the readings of the leak sensor.

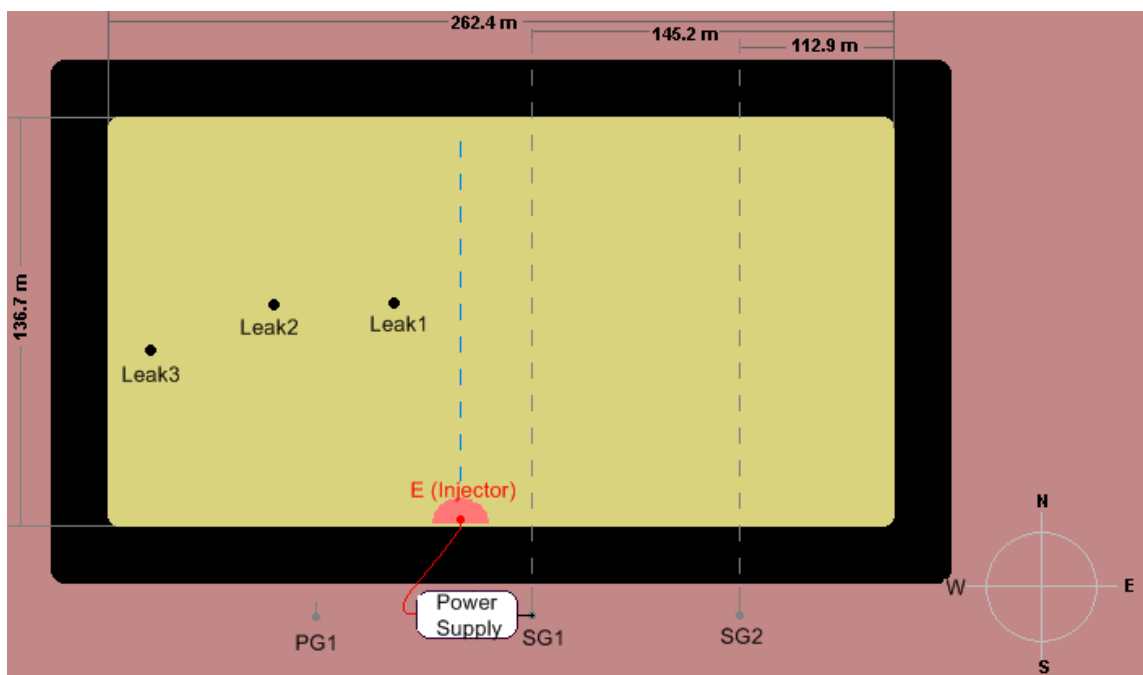


Figure 1. Component location in system, where PG1: Point Ground 1, SG1: Service Ground 1, SG2: Service Ground 2.

In order to surpass noise levels, the current applied to the system must be increased through an increase in applied voltage. Stability of the system if current is increased must be analyzed observing terrain and system resistivity. Thus, a series of voltages were applied and the resulting current was observed.

By Ohm's Law, apparent resistivity is found by:

$$R = \frac{V}{I} \quad [1]$$

Resistivity of the system with respect to the Service Ground 1 behaves linearly, which allows us to infer a constant resistivity between solution and subgrade.

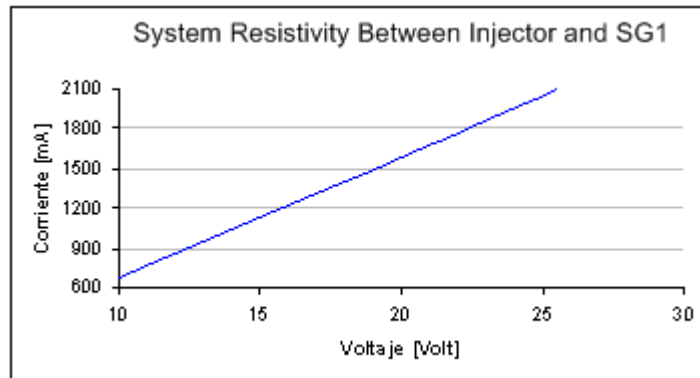


Figure 2. Observed current between Injector and SG1.

The data obtained gives an average resistivity of $R_{E-SG1} = 12.8 \Omega$.

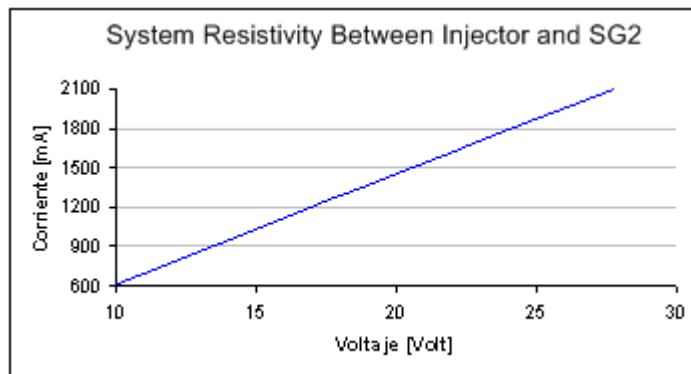


Figure 3. Observed current between Injector and SG2.

With the injector at the same position, and this time measuring between the former and service Ground 2, a linear response was also obtained, with an average resistivity of $R_{E-SG2} = 13.9 \Omega$.

A free ground point (PG1) was installed 32 m away from SG1, as shown in Figure 1, in order to determine terrain resistivity.

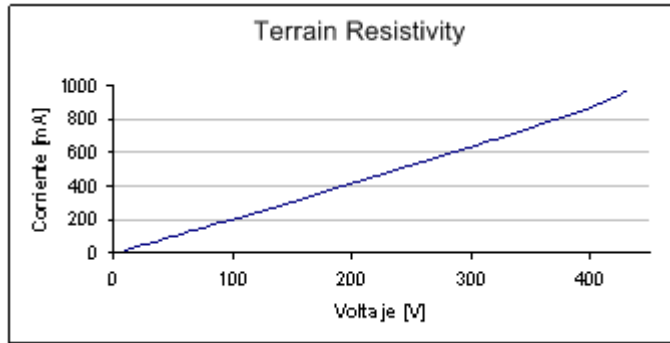


Figure 4. Observed current and voltage between PG1 and SG2.

Apparent resistivity obtained was $R_{PG1-SG2} = 492.6 \Omega$ for a 32 m distance. PG1 simulates a leak in an arbitrary point of the liner. Also relevant is to observe the resistivity between the wires under the liner.

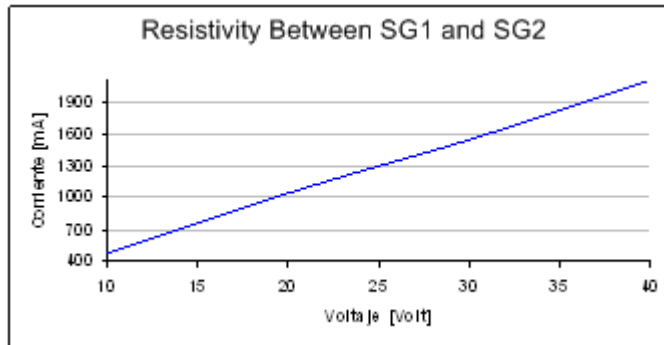


Figure 5. Observed current and voltage between service grounds1 and 2.

It was observed that resistivity is linear between service grounds, with an average $R_{SG1-SG2} = 19.3 \Omega$ at 32 m. Therefore, an external analysis of voltage and current can give the approximate location of a leak.

Low subgrade resistivity allows for high current given a relatively low potential. Of course, applying higher voltages will produce even higher currents.

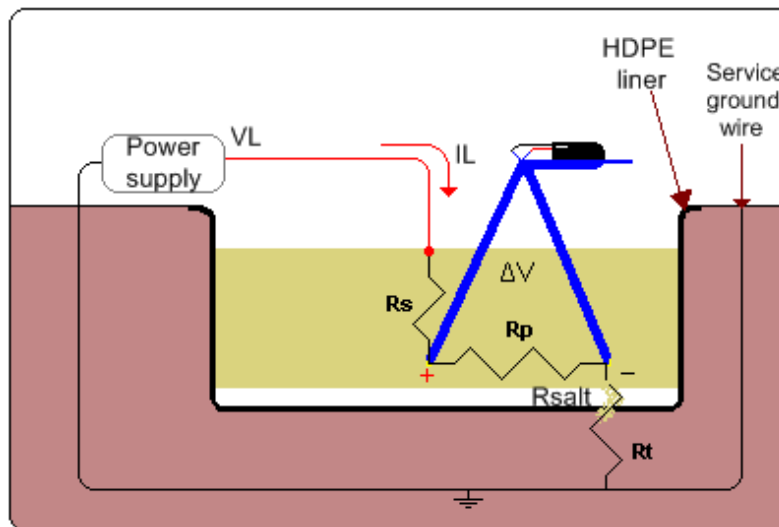


Figure 6. Electric equivalence of the system.

With data readings from the tested pond, apparent resistivity for the subgrade + solution + salt system can be calculated. We know that $R_{\text{salt}} < R_p < R_s$, and thus the leak is not detected.

From the collected data at $V_L = 20 \text{ V}$, and $I_L = 1582 \text{ mA}$:

$$R_t = 9.13 \ \Omega$$

$$R_{\text{salt}} + R_p + R_s = 3.51 \ \Omega$$

Since R_s increases with the distance from leak to positive pole of the power supply, we have:

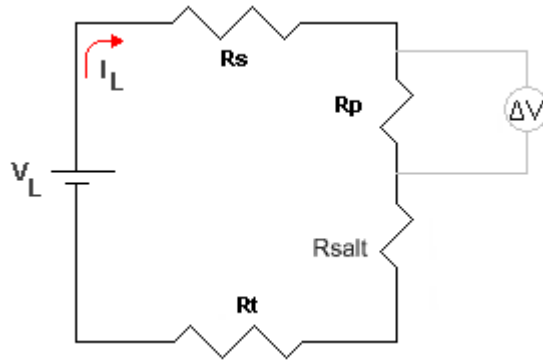


Figure 7. Schematic circuit representing the pond system.

Resistivity between probe points is dependent on solution properties, and in this case it is estimated at $0.45 \ \Omega\text{-m}$.

Therefore, applying Ohm's Law for an established current of 1582 mA and the resistivity between the electrodes, we obtain the voltage that the sensor should be reading:

$$\Delta V = R \cdot I = 0.45 \cdot 1.582 = 0.712 \text{ V} \quad [2]$$

Voltage determined in Equation 2 is within the order of the noise level detected in the tested ponds ($0.065 - 1.69 \text{ V}$). In order to surpass the noise level, a greater current is needed in the system, thus requiring a power supply capable of withstanding currents greater than 1.6 A . A larger generator, power supply and wiring were assembled, capable of producing and withstanding currents greater than 20 A .

2.3 New Equipment and Results

Tests analog to those presented in section 2.2 - resistivity of subgrade, pond/solution system and measurement of the current established between service ground wires – showed that 100 V was the voltage most adequate for stable, easily recognizable signals using the leak detector in the submerged-probe surveys. Current levels reached during surveys average 4 A , but can reach nearly 10 A in certain conditions, such as large leaks, or badly insulated cement sinks within the ponds. Power supply and wiring of the equipment used originally proved unable to withstand these amperages.

Generator, voltage regulator, AC power supply and DC converter were assembled from off-the-shelf components, with specifications adequate for sustaining currents greater than 20 A . Leak detection equipment originally acquired, including wiring and electrode rods, was replaced by the new components. Only probe electrodes and leak detector (voltmeter) were kept as part of the system.

With equipment now able to withstand the high current, signals were clearly distinguishable from the noise in the ponds, and leaks could be reliably detected, with greater success than the contracted surveyors, in less time.

Table 3: Company vs. Contractor detection leak detection results.

Voltage (V)	Current (A)	Contractor	Company	Actual
50	4.2	2	2	2
100	7	1	3	3
100	8	3	1	1
100	10	0	3	3
100	7.5	18	18	18
100	16	6	6	6

The high amperages at 100 V introduced a concern for corrosion in the stainless steel rods, and possible dissociation of the solution contained in the probe electrodes. Corrosion was detected in the rods – a reduction of 3 mm in radius for a rod originally 5 mm in radius, for 100 hours of operation at 4 to 8 A (See Figure 8). Although gasification was not detected in the solution contained in the probe's electrodes, safety procedures were implemented in order to minimize the risk of electrode explosion.

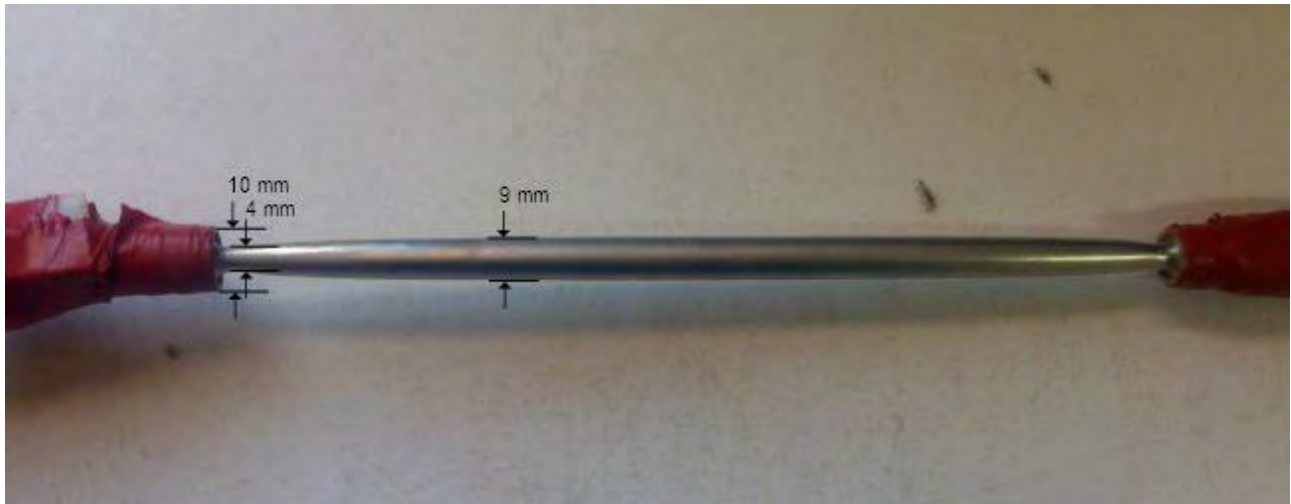


Figure 8. Corrosion in stainless steel electrode rod.

3. STILL-STANDING CHALLENGES

Modifications in equipment and technique presented here have allowed satisfactory results in submerged-probe leak detection surveys, with more accuracy and speed than previous methods.

However, submerged-probe surveys after cleaning or harvesting of ponds requires that water be pumped into the pond before the survey, over the salt floor, a time-consuming operation that would be completely avoided if the soil-probe method could be applied. However, the latter has yet to yield readable signals, and no electric current level tried with the new equipment has been able to overcome the noise. We attribute this to the highly saturated solutions trapped within the salt floor, generating an extremely conductive layer that, with the methods reported here, would require excessively high currents in order to surpass the noise levels.

4. CONCLUSIONS

Accurate, fast leak detection surveys are possible using the submerged-probe method in evaporation ponds containing highly saline brines. The current levels required to overcome noise - produced by ion transport and convective flows - surpass the capacity of "normal" electrical leak detection kits, but are achievable by carefully-assembled equipment. Leak detection on soil-over-liner is still an unsolved problem.

Elevated Temperature Effects on Smooth Geomembrane – Geotextile Interfaces

Tanay Karademir, GSI Fellow, Maltepe University, Istanbul, Turkey, tanaykarademir@maltepe.edu.tr
David Frost, F.ASCE, PE, PEng, Georgia Institute of Technology, Atlanta, USA, david.frost@ce.gatech.edu

ABSTRACT

The mechanical properties of geosynthetic materials are strongly temperature dependent. Historically, most laboratory geosynthetic interface testing has been performed at room temperature. Information today is emerging that shows how temperatures in the liner systems of landfills can be much higher due to seasonal temperature variations as well as exothermic reactions occurring in the waste body. As part of an extensive research study undertaken to investigate temperature effects on interface shear behavior, a three-component study involving surface hardness tests, single filament tensile strength tests and interface shear tests between NPNW polypropylene geotextiles and both HDPE and PVC smooth geomembranes was undertaken. A temperature controlled chamber was utilized to simulate field elevated temperature conditions. The laboratory interface shear program included tests under a normal stress level of 100 kPa and a range of test temperatures from 21 to 50 °C. Complementary geotextile single filament tensile tests were performed over the same temperature range using a dynamic thermo-mechanical analyzer to evaluate the tensile strength properties of single geotextile filaments at these elevated temperatures. The surface hardness of smooth HDPE and PVC geomembrane samples was also determined at different temperatures in this range to evaluate how temperature change affected the surface hardness as well as the interface shear behavior and strength of smooth geomembranes in combination with geotextiles. The study showed that while the tensile properties of the geotextile filaments and the geomembrane surface hardness are both reduced, the interface strength increases. Quantitative measurements provide insight into the mechanisms dictating this behavior.

1. INTRODUCTION

The behavior of an interface is a combination of the interaction behavior between the counterface materials as well as the state of the interface. In addition to mechanical surface properties such as surface roughness, the relative hardness of the counterface materials impacts the interface shear response that develops. In addition, the interaction of a material surface with that of another is also influenced by the physical and chemical properties of the materials themselves. Consequently, it is essential to thoroughly evaluate the mechanical characteristics of the materials including micro and/or macro tensile strength as well as hardness properties of counterface materials to understand their effect on interface behavior and to identify the factors controlling the shear stress-displacement response of common interfaces such as geotextile-geomembrane (Dove, 1996). Interface shear behavior at different ambient temperature conditions is not a single attribute, but a collection of performance attributes of the counterface components which requires a suite of tests to assess the engineering strength properties of the components both independently and collectively. The performance of geosynthetic layered systems during their service lifetime in terms of interface shear behavior and strength properties is of major importance in selection of geosynthetic materials (i.e. geotextiles, geomembranes) for certain geotechnical applications such as landfills.

2. THEORETICAL BACKGROUND

One of the more common composite systems that has found widespread application in geotechnical projects are those involving geotextiles and geomembranes. They are generally used as composite systems rather than as stand-alone solutions in practice due to their complimentary advantages (Koerner, 2005). The interaction behavior between geotextiles and geomembranes is a critical component in defining the interface strength governing the integrity of the overall structure as well as the stability of the constructed system. Over the past few decades, fiber-texture (i.e. geotextile-geomembrane) interaction has become an increasingly important consideration in geotechnical engineering design. Non-woven geotextiles are porous and fibrous materials that consist of irregularly oriented long filaments which vary in terms of spatial distribution, curvature, orientation, size, and mass density. Geomembranes are continuum materials which depend on properties such as tensile strength, hardness, surface roughness, and chemical constitution. Both are made from polymeric material resins and temperature has a significant effect on the physical and mechanical engineering properties such as tensile strength, modulus and hardness of polymers.

The use of geotextiles, which are fibrous pervious materials, particularly in conjunction with geomembranes which are impervious continuum materials has increased since 1980s from operating landfill examinations carried out in the past.

The employment of a geotextile layer to protect the geomembrane from damage caused by the drainage layer has been adopted as the preferred solution (Martin et al., 1984; Giroud 1984). Although these composite geosynthetic interfaces are routinely employed in landfill liners and are exposed to high elevated temperature conditions, there is very little information published in the literature to date on the influence of higher temperatures on interface shear behavior and strength characteristics of geotextiles in contact with geomembranes. The results for smooth geomembrane-NPNW geotextiles presented herein are part of a larger study aimed to fill this gap in knowledge and to show how the developed shear mechanisms and interface resistance changes with elevated temperatures. This research study in particular focused on the most common geosynthetic materials used in current North American practice when placing geotextiles in combination with geomembranes. Additionally, complementary geotextile single filament tensile tests as well as geomembrane surface hardness tests at different temperatures which provide important insight into the role of temperature in the observed behavior differences will also be summarized and discussed. These latter tests are critical for microscale analysis of elevated temperature effects on shear behavior of smooth geomembrane – geotextile interfaces.

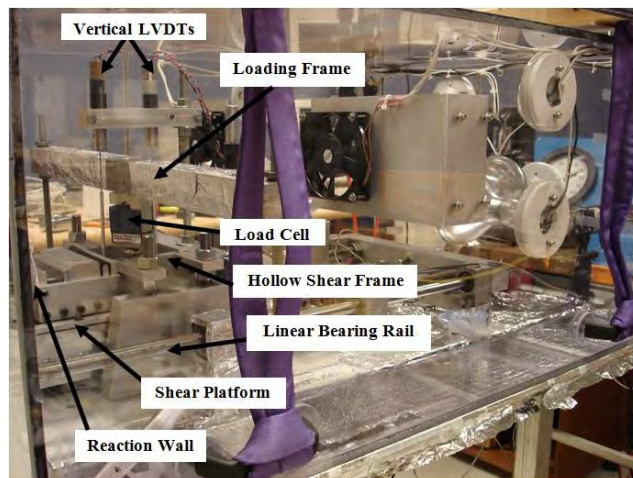
3. MATERIALS, TESTING PROGRAM AND EQUIPMENTS

A multi-phase research study was undertaken in an effort to investigate temperature effects on interface shear behavior between (a) needle punched nonwoven (NPNW) polypropylene (PP) geotextiles and both smooth high density polyethylene (HDPE) as well as smooth polyvinylchloride (PVC) geomembranes. A unique temperature controlled chamber (TCC) was developed to be utilized to simulate the field conditions at elevated temperatures and evaluate shear displacement failure mechanisms at these higher temperatures. The physical laboratory testing program consisted of multiple series of interface shear tests between aforementioned material combinations which have found widespread use in landfill applications. The two smooth geomembranes produced from different base polymers (HDPE, PVC) were tested in combination with a single staple type NPNW geotextile (mass per unit area of 270 g/m² (8 oz/yd²) per ASTM D 5261) and apparent opening size of 0.18 mm (per ASTM D 4751). High density polyethylene (HDPE) produced from formulated polyethylene resin is the most widely used geomembrane material due to its high tensile properties at low strain levels. On the other hand, polyvinylchloride (PVC) geomembranes are selected for use in infrastructure projects which require more flexibility in three dimensional performances as well as having less hardness of the geomembrane itself which can lead to enhancement of interfacial properties for combined and layered applications consisting of different material types. Force-displacement failure mechanisms developing at geotextile-geomembrane interfaces at higher temperatures were determined by imitating elevated temperature field conditions in the insulated and temperature controlled environment of the TCC. The geomembrane liner samples were sheared against the geotextile fabric specimens under a normal stress level of 100 kPa and at one of three different temperatures (21°C, 35°C and 50°C). The large displacement direct interface shear device enclosed by the TCC (Figure 1a) was utilized to measure the interface shear resistance between geotextiles and geomembranes at different elevated temperatures. In all tests, the specimens were sheared at a constant rate of displacement of 1 mm per minute over a displacement range of 60 mm.

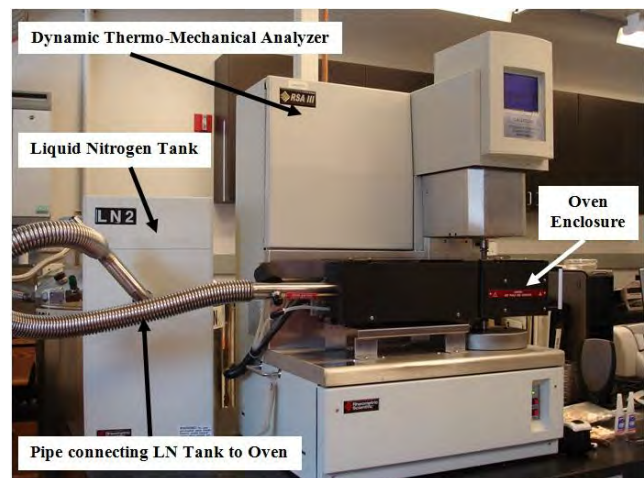
Complementary geotextile single filament tensile tests were performed at the same temperatures as the interface shear test temperatures (21°C, 35°C and 50°C) using a dynamic thermo-mechanical analyzer (DMA) (Figure 1b) to measure the micro-tensile strength properties of single NPNW-PP geotextile filaments at different elevated temperatures. A total of 45 micro-mechanical thermo-tensile tests on single geotextile filaments were conducted consisting of 15 tests at each test temperature to observe the repeatability of the developed tensile force-extension behavior as well as to see the reproducibility of filament tensile strength response at each test temperature. Single geotextile filament specimens were tested to failure using a constant-rate-of extension (CRE) type tensile testing of a predetermined gage length (i.e. initial sample length) of 12.5 mm and rate of extension of 0.125 mm/sec at different temperatures for filament specimens having an average diameter of 0.035 mm (35 µm). Using the force extension (elongation) curve (i.e. force-displacement, stress-strain), tensile strength properties including tensile strength (T_{MAX}), Young's modulus (E) (i.e. Modulus of Elasticity) were determined and their variation with temperature were evaluated.

A durometer with a constant loader test stand composed of a flexible joint system and an air damper was utilized in this study to perform surface hardness measurements of smooth geomembrane samples. This type of constant load stand maximizes repeatability of hardness tests by providing a variable speed control and a flexible joint on the load shaft to ensure complete contact with the sample material as well as to ensure consistent measurements by applying a consistent force throughout all the measurements. To investigate the variation of this index value with changing temperature for smooth HDPE as well as smooth PVC geomembranes, the Durometer with the Constant Loader Test Stand was placed in the vertical configuration of the Temperature Controlled Chamber (TCC) (Figure 1c). A total of 240 measurements were performed on HDPE as well as PVC geomembrane samples. In order to maintain consistency in measurements and to obtain accurate test results, it is required to conduct all the hardness measurements with the same speed for all the materials tested. A total of 120 measurements were taken on smooth HDPE geomembrane samples. It is recommended as good practice to take several readings and average the results by showing the variability in measurement data. A similar procedure was followed for smooth PVC geomembrane as well in which a total of 120

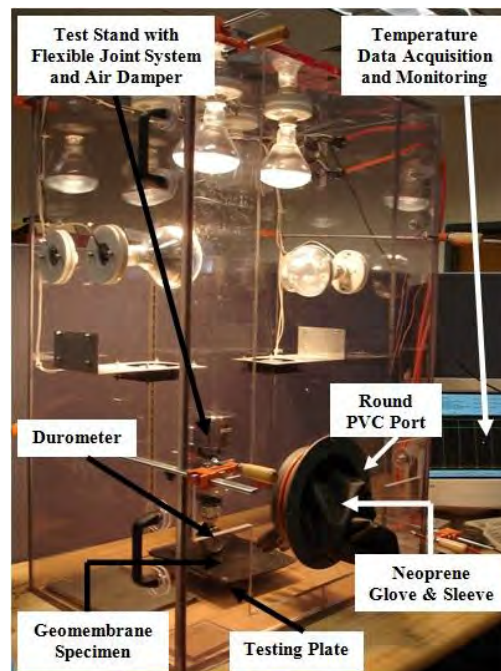
surface hardness measurements were made on geomembrane samples. The readings, in general, indicated that the variability in measurements was consistent for all the samples tested. Shore hardness measurement is a very common method used to determine surface hardness of rubber and plastic materials (i.e. polymeric materials such as geomembranes). The Shore D scale is used for relatively harder plastics and is an appropriate way of measuring surface hardness of geosynthetics (i.e. Smooth HDPE and Smooth PVC Geomembranes). Shore D Hardness (H_D) provides an index of the material surface hardness which can then be correlated to the interface friction characteristics of geosynthetic materials. As such, Shore D hardness scale, (H_D) ranging from 1 to 100 on Type D durometer gauge was an appropriate scale to attain an index value for surface hardness of these aforementioned geomembranes at different temperatures. Shore D Hardness measurements were performed according to ASTM D 2240-05 at different ambient temperatures.



a) Interface Shear Device enclosed by TCC



b) Dynamic Thermo-Mechanical Analyzer (DMA)



c) Durometer with Constant Loader Test-Stand enclosed by TCC (Vertical Configuration)

Figure 1. Testing Device and Equipments

In summary, the effects of higher temperature conditions on geosynthetic interface performance were quantified through laboratory interface shear tests at elevated temperatures in the temperature controlled chamber (TCC), fibrous material

single filament micro-mechanical tensile tests using a thermo-dynamic mechanical analyzer (DMA), and additionally through continuum material surface hardness measurements. The laboratory testing program was conducted over a range of temperature (21 °C – 50 °C) to capture variations in behavior as a function of ambient temperature.

4. TEMPERATURE EFFECTS ON SMOOTH GEOMEMBRANE – GEOTEXTILE INTERFACE SHEAR BEHAVIOR

The results of laboratory tests carried out to investigate the factors controlling the interface shear behavior and strength between smooth geomembranes and geotextiles in particular to examine the role of temperature on the interface performance developed and filament-continua interaction will be presented. The research study specifically involved in smooth high density polyethylene (HDPE) as well as smooth polyvinylchloride (PVC) geomembranes in combination with needle punched nonwoven (NPNW) fabrics. It is noted that a geomembrane liner with relatively high rigidity (smooth HDPE) as well as the one with relatively low rigidity and high flexibility/softness (smooth PVC) were selected to quantify the effects of continuum material surface hardness on the shape of the shear-displacement curve and on the magnitude of interface strength mobilized in combination with fibrous materials (geotextiles).

4.1 HDPE Smooth Geomembrane/NPNW Geotextile

The typical behavior of HDPE smooth geomembranes when sheared against NPNW polypropylene (PP) geotextiles is brittle in nature with a sharp peak and rapid transition to post-peak behavior. The stress-displacement responses of HDPE smooth geomembranes, at all temperatures tested and at 100 kPa normal stress representative of in-situ stresses typical of landfill liners, were essentially an elastic-perfectly plastic response (Figure 2a). Some post-peak softening was observed followed by a near constant large strain or residual shear stress value. The displacement required to mobilize the peak interface shear strength ranged from approximately 1 to 2 mm for the tests at temperatures ranging from 21 °C and 50 °C. The behavior of smooth HDPE geomembrane versus NPNW-PP geotextile interface can thus be described as an initial rapid increase in shear stress as soon as displacement starts followed by a peak shear stress at relatively low displacement of order of 1 to 2 mm. Additional shear displacement produced negligible to moderate reduction in shear stress. Further, the peak and post-peak (i.e. residual) interface strength values in terms of coefficient of friction, ($\tan(\delta)$) is presented in Figure 2b to display the trend with changing temperature. The post-peak strength values computed were based on shear stress values averaged over 2 mm range from 57 to 59 mm horizontal displacement. Both peak and pseudo-residual interface shear strength values increase with temperature.

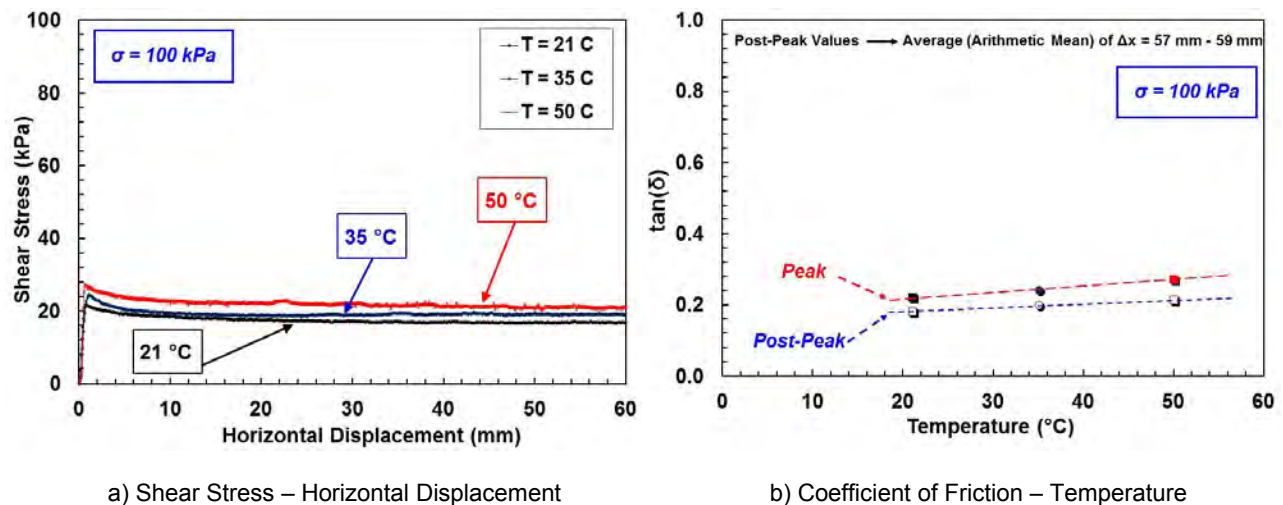


Figure 2. Smooth HDPE Geomembrane – NPNW PP Geotextile Interface

4.2 PVC Smooth Geomembrane/NPNW Geotextile

PVC geomembranes in general offer higher deformation response and increased interfacial strength and improved resistance to stress cracking as a result of their more plasticized and flexible nature. Figure 3a presents the stress-displacement responses between PVC smooth geomembrane and NPNW-PP geotextiles at 100 kPa normal stress under different ambient temperature conditions ranging from 21°C up to 50°C, and additionally, the change in peak as well as residual coefficient of friction with temperature for PVC smooth geomembrane – NPNW PP geotextile interface is shown in Figure 3b. The interface tests carried out at different elevated temperatures conditions showed similar responses in which shear displacement hardening behavior occurred after yielding in contrast to the behavior observed

with smooth HDPE geomembranes where a post-peak strain softening response developed. The tendency of PVC smooth geomembrane – geotextile interfaces to behave in this fashion was completely dependent on the differing material properties compared with HDPE liners. Additionally, the hardness reduction at higher temperatures contributed to some very minor increase in strength with increasing temperature level compared to HDPE.

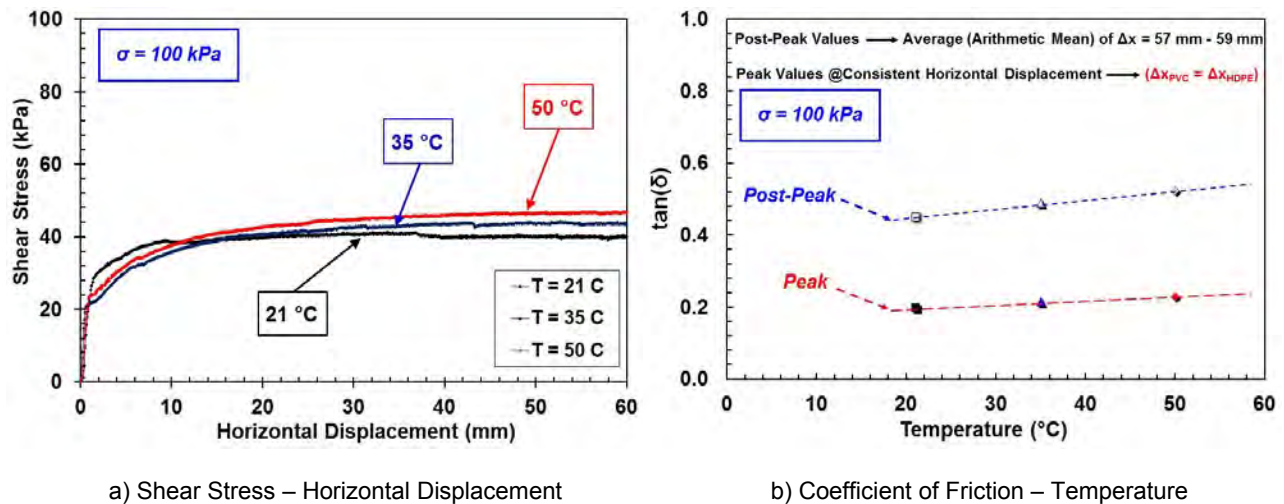


Figure 3. Smooth PVC Geomembrane – NPNW PP Geotextile Interface

As seen in Figure 3a, it is not feasible to determine distinct peak strength from the stress-displacement curve for the typical interface behavior of PVC geomembranes against NPNW geotextiles. After a rapid increase in shear stress at very small displacement (< 2 mm), a yielding type pattern occurs with displacement up to 8 mm to 10 mm displacement, and later a plastic response in terms of a slight strain-hardening behavior is observed regardless of ambient test temperature. For this reason, in the analysis of the interface results at every test temperature, the shear stress values that correspond to the shear displacements of the mobilized peak strength values of the smooth HDPE geomembrane tested were selected for the determination of the peak interface strength. Similar to the analysis process performed on the smooth HDPE test results, post-peak strength values were taken as the average of the values at shear displacements from 57 mm to 59 mm. As the interface response of the smooth PVC is plastic at different ambient temperatures, the residual shear resistances mobilized at the interface are larger than the peak strength values and results from the slight strain-hardening shear behavior observed in the smooth PVC interfaces with NPNW geotextile. In light of this, the resulting coefficient of friction values (both peak and residual) as a function of temperature were presented in Figure 3b. From the stress-displacement relationships for different ambient temperatures, the residual (post-peak) shear strengths of the PVC interface at all test temperatures were larger than the peak values. It is noted that the higher frictional resistance and the larger interface shear response in terms of stress – displacement failure envelope is related to the physical properties of the geosynthetic layered systems including hardness, stiffness, and temperature dependency which tend to alter the shear strength mobilized at the interface.

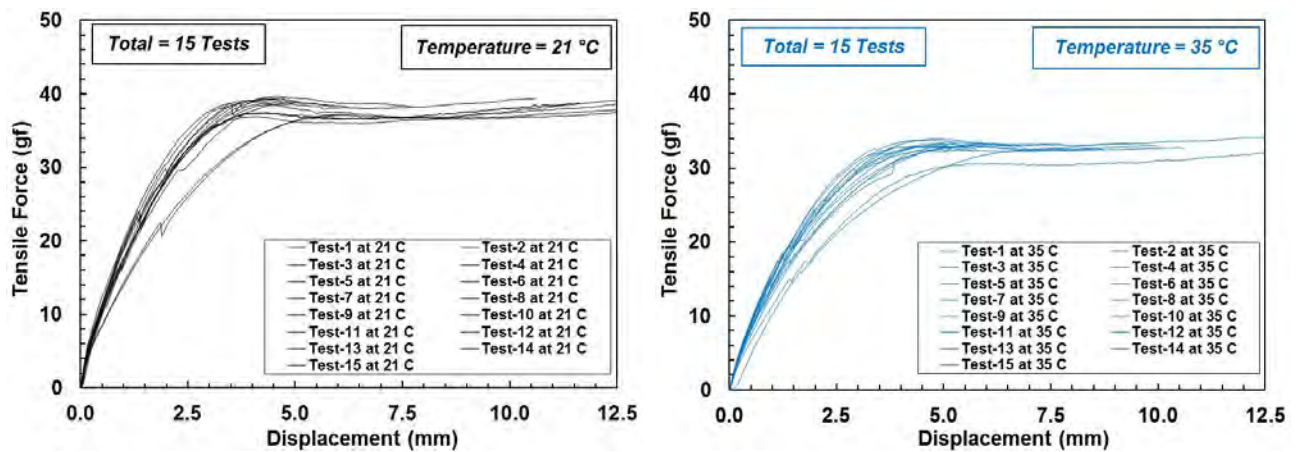
5. TENSILE PROPERTIES OF SINGLE GEOTEXTILE FILAMENTS

The single filament studies are important since the interface strength between geotextiles and geomembranes is controlled by the fabric global matrix properties as well as micro-scale characteristics of the geotextile such as filament strength and how it interacts with the geomembrane macro-topography. To this end, complementary geotextile single filament tensile tests provide insight into the role of temperature in the observed behavior differences of the individual materials. Therefore, tensile strength properties of geotextile filaments at elevated temperatures were evaluated to further understand the influence of temperature on post-peak interface shear behavior and strength. The strength of the NPNW geotextiles is related to the amount of entanglement produced by the needling and the inter-fiber friction. As such, the geotextile samples utilized in the experimental program are produced from polypropylene (PP) fibers that have more frictional surface to facilitate inter-fiber-friction leading to a relatively strong geotextile macro-structural matrix. The tensile response of the fibrous nonwoven geotextile is governed by the micro-scale (filament) and/or global-level (fabric matrix) tensile and elongation properties. In order to investigate tensile behavior and the developed “micro-scale” stress-strain response of single geotextile filaments at different temperatures, laboratory tests were performed in this study by measuring filament thermo-mechanical properties using DMA. The test temperatures between 21 °C and 50 °C were chosen to simulate the elevated temperature range expected in the field for geotechnical applications such as landfill liners.

5.1 Micro-Mechanical Thermo-Tensile Tests on Geotextile Single Filaments

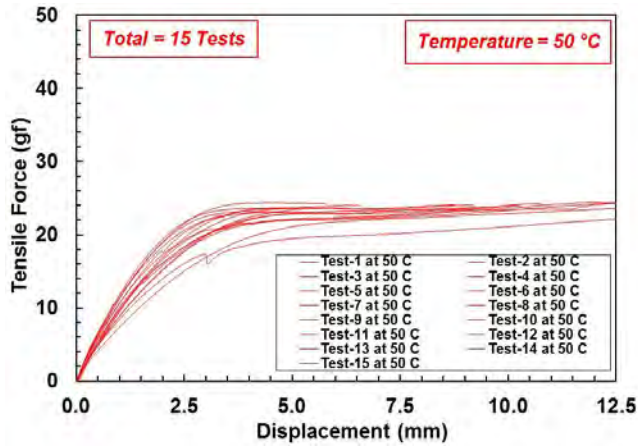
The filaments from NPNW-PP 8 oz/yd² (270 g/m²) geotextile resulted in a similar trend of tensile load-elongation response at all test temperatures such that the tensile force-displacement curve has a nonlinear elasto-perfectly plastic form in terms of stress-strain relationship (Figures 4a, 4b and 4c). The general pattern in force-elongation behavior of polypropylene filaments in tension tests can visually be portrayed in two segments: i) sharp increase to peak; and then, ii) leveling off at higher strain levels. The filaments exhibited nearly constant resistances after yielding until they reached rupture at elongations of between 70% and 120%. Before experiencing yield, the elastic portion of the curves develops with a relatively constant rate of change in tensile force with respect to displacement. The resulting force-displacement curves for lower temperature tests are located on the upper part of the load-extension space compared with force-displacement curves from higher temperature tests. In other words, the tension failure envelopes for the tested filaments diminished as the ambient temperature increased. Figure 4 presents these 45 tests in which the 15 replicate tests at each test temperature are shown in the same graph starting from the room temperature of 21 °C up to the elevated temperature of 50 °C. There is an apparent trend which can be observed in the series of graphs in Figures 4a, 4b and 4c of the tension force-displacement failure envelopes for polypropylene filament specimens diminishing as the temperature is increased. This variation in tension versus extension behavior shows the influence of temperature on force-displacement response of geotextile single filaments at micro-level.

Figure 4d presents the mean force-displacement plots during extension loading as a function of the temperature at which they were obtained. These mean curves are typical and descriptive in illustrating how the tensile behavior of single geotextile filaments at various test temperature conditions takes form. The filaments from NPNW-PP 8 oz/yd² geotextile resulted in a similar trend of tension load-elongation response at all test temperatures such that the tensile force-displacement curve has a nonlinear elasto-perfectly plastic form in terms of stress-strain relationship. The shapes of force-displacement curves for all the tests performed on filament specimens at various temperatures were in good agreement and indicated that plastic elongation behavior occurs in polypropylene filaments under tension load prior to failure of the fibers. In the tests, the tensile force increases with increasing axial extensional displacement, then, it remains almost constant during inelastic deformation of the polymeric material after passing through yielding deformation. The inelastic portions of the stress-strain curves are essentially parallel.

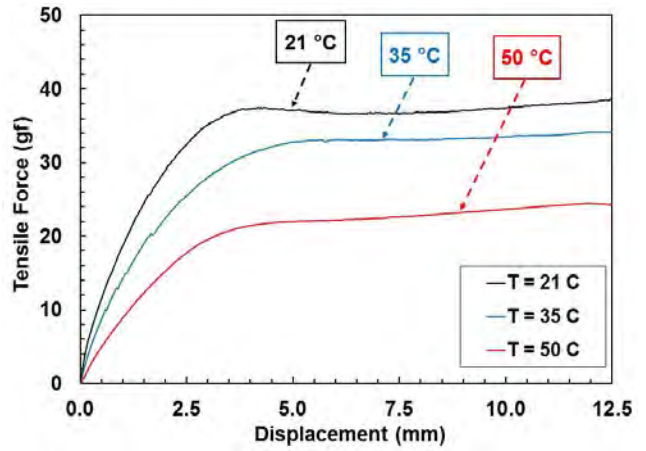


a) Force – Displacement Curves (T = 21 °C)

b) Force – Displacement Curves (T = 35 °C)



c) Force – Displacement Curves (T = 50 °C)

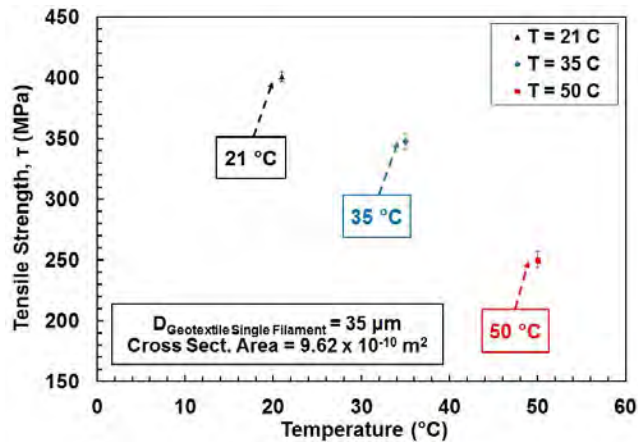


d) *Mean* Force – Displacement Curves

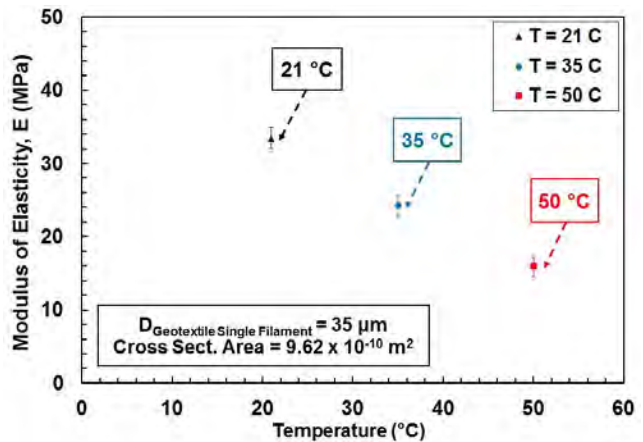
Figure 4. Tensile Force versus Elongation (Tensional Extension) Behavior for NPNW-PP Geotextile Single Filaments

One of the most important mechanical properties of polymeric materials is its tensile strength under extension force that shows the toughness and indestructibility of the material employed in the field. Since a polymer type (i.e. PP) is used as a base material to produce geotextile fibers, they do not retain tensile strength and robustness properties with temperature change to which many geotechnical engineering applications are exposed (i.e. 21 °C – 50 °C). It was observed as a result of micro-scale thermo-tensile tests on geotextile single filaments that tensile strength, (τ) for PP filaments decreased with increasing temperature with lower strength measured at higher elevated temperatures. In the experimental program temperature range (21 °C – 50 °C), the micro-tensile test at room temperature exhibited the largest toughness under extension and gave the largest tension strength value. Figure 5a shows the variation of the mean tensile strength as temperature changes.

The observed elasto-perfectly plastic force-extension behavior of PP filament specimens indicated that the fibers become stronger and stiffer as temperature decreases under tensile load application. The elastic portion of force-displacement curve rotates “clockwise” demonstrating the reduction in stiffness; hence, modulus with increasing temperature. The slope of initial linear portion of the force-displacement curves was used to compute elastic modulus (Young’s modulus). The major impact of temperature on this tensile strength property of the polymeric filaments was a reduction in stiffness (elasticity modulus) (Figure 5b).



a) Tensile Strength – Temperature



b) Modulus of Elasticity – Temperature

Figure 5. Tensile Strength Properties and Temperature (NPNW-PP Geotextile Single Filaments)

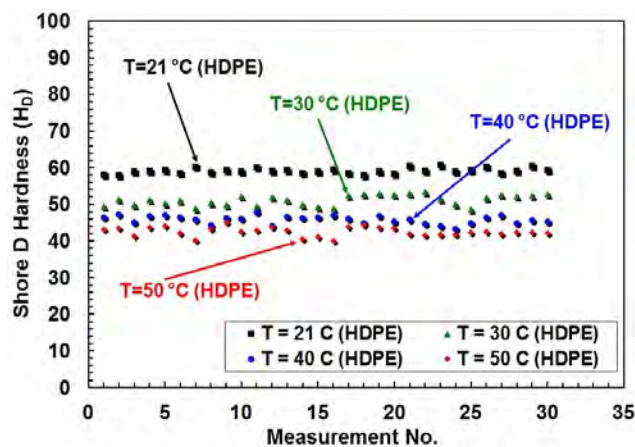
For the consequences of the thermo-mechanical tensile strength behavior of single geotextile filaments at different ambient temperatures to the global matrix level response, the total contact area involved during shearing of the

geomembranes against geotextiles depends heavily on the development of tension in the fiber and the tendency of the filament to elongate. As such the frictional resistance mobilized at geotextile versus geomembrane interfaces is heavily governed by the magnitude of the embedding of the geomembrane into the fabric matrix. This facilitates stronger interlocking between the counterface materials due to the presence of larger contact stresses at contact points at the micro-level due to reduced contact area between the different individual filaments subjected to tensional elongation. To this end, this study reported on the characterization of the tensile behavior of NPNW-PP single geotextile filaments at the “micro-scale” level to be taken into account in evaluating the interface shear behavior of fabrics (i.e. geotextiles) with continua (i.e. geomembranes) under varied temperatures. At the “micro-scale”, the tensile failure takes place due to breakage of filaments whereas at the global scale, the slippage between filaments and the structural deformation due to inherent internal geotextile void space that is governed by fabric manufacturing and fiber processing type, dominates.

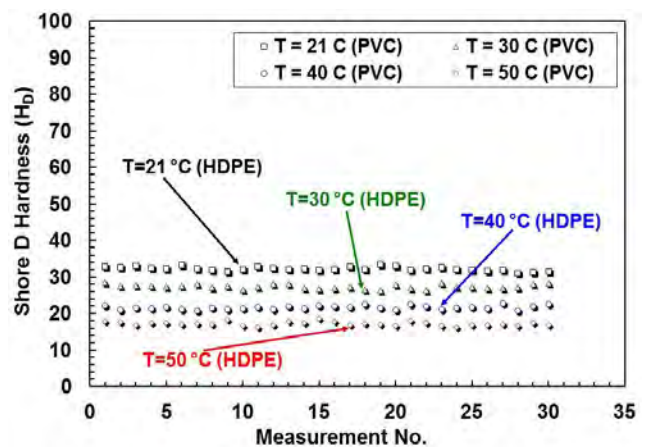
6. SURFACE HARDNESS OF GEOMEMBRANES

Hardness which depends on stiffness and viscoelastic properties of the material is defined as the resistance of a plastic material to indentation (ASTM D 2240 – 05). The peak interface strength for geotextile-geomembrane interface is mainly attributed to the geomembrane micro-texture and depends particularly on the geomembrane properties such as hardness and surface roughness. The mobilized frictional strength and the developed interface shear behavior at fabric (geotextile) – continua (geomembrane) interfaces are influenced by the surface hardness of the geomembrane, and additionally, the change in geotextile-geomembrane interface shear behavior with a change in temperature results from the relatively higher temperature dependency of geomembrane properties such as hardness (Figures 2 and 3). Geomembranes, which are polymeric continuum sheet materials comprised of a specific polymer resin, are manufactured uniformly to possess homogeneity in terms of physical and mechanical properties as well as a uniform distribution of material characteristics throughout a large lining sheet. The amount of shear resistance developed at the interface is mainly attributed to geomembrane surface pliability governed by the material hardness which can vary as a function of the ambient temperature. To this end, hardness measurements on geomembrane samples were performed to study the effect of temperature on surface hardness and interface friction of smooth high density polyethylene (HDPE) as well as smooth polyvinylchloride (PVC) geomembranes. Figures 6a and 6b present Shore D, (H_D) surface hardness measurements for both HDPE and PVC geomembranes, respectively, at temperatures ranging from 21 °C to 50 °C in 10 °C increments based on 30 readings at each test temperature to observe the repeatability of the measured surface hardness variation and material firmness behavior with increasing ambient temperature. The 30 repeat measurements at each test temperature are more than sufficient to constitute a sample population to evaluate the surface hardness change of HDPE and PVC geomembrane liners at each temperature.

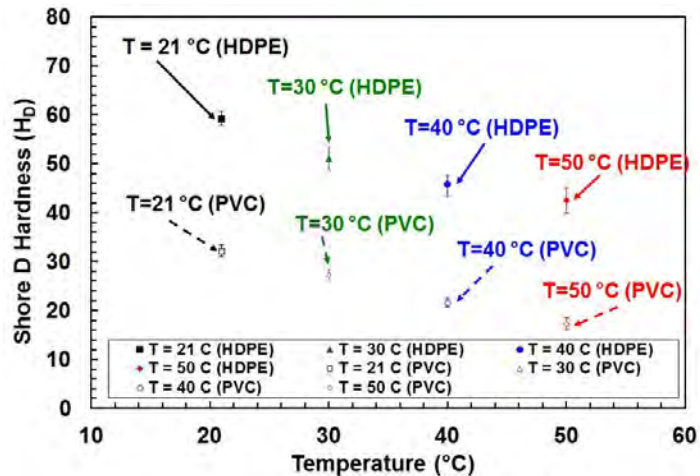
Figures 6c shows the mean values for surface hardness of both smooth HDPE and smooth PVC geomembranes measured at different temperatures (21 °C – 50 °C) with error bars showing the range and the variation in measurement data, and additionally, the change in their surface hardness with temperature. The hardness of PVC liners at all test temperatures is 0.4 – 0.5 times of the surface hardness of HDPE geomembranes; and this ratio continues in this range (0.4 – 0.5) even with increasing temperature as both the liner materials get softer and more malleable as their hardness values are reduced.



a) Repeated Hardness Measurements (HDPE)



b) Repeated Hardness Measurements (PVC)



c) The change in Surface Hardness with Temperature and the Variation/Range in Measurement Data

Figure 6. Surface Hardness and Temperature for HDPE and PVC Geomembranes

7. DISCUSSION AND CONCLUSIONS

The interface shear test results reported herein over a range of elevated temperature conditions are to capture variations in NPNW-PP geotextile – smooth HDPE or smooth PVC geomembrane interface shear behavior as a function of ambient temperature variation (T (°C)). These results were intended to provide insight into smooth HDPE or smooth PVC geomembrane – geotextile fabric interaction mechanisms at elevated temperature conditions in the field, and thus, the development of interface shear response at different temperatures.

The interface frictional resistance of both smooth HDPE or PVC geomembranes and NPNW geotextile interfaces increased with increasing ambient temperature owing to a decrease in material hardness, and hence, an increase in surface pliability of the geomembranes. It is considered that the acceleration of the polymer relaxation at elevated temperatures resulted in quick dispersion of the concentrated stresses over the interface contact area after the application of load leading to more uniform stress distribution over the entire contact surface at the interface during shear displacement. An increase in ambient temperature results in softening of the polymer and a reduction in stiffness as the temperature increases leading to greater flow of the polymeric material under a load application and greater interaction with the counterface. The peak and residual (post-peak) strength values as defined using the quantitative strength parameters including coefficient of friction, ($\tan(\delta)$) showed an increase with temperature. This is consistent with previous observations made by others of the change of frictional resistance between polymers under increasing temperature. The change of $\tan(\delta)$ over the entire range of test temperatures from 21°C up to 50°C only applies to the particular geosynthetic combinations utilized in this study.

The softer nature of PVC assists the overlying/underlying interface component to embed into the geomembrane body by forming a more intimate interface interaction as shearing progresses at each elevated temperature. As shearing progresses, the higher surface pliability of the PVC lining materials possessed at all temperatures tested, allows it to get roughened by being embedded by the counterface geotextile owing to the malleable nature of the PVC liner and this results in a larger shear resistance. The stiffer and harder nature of HDPE liners does not facilitate the counterface filament embedment into the geomembrane surface as much as the softer PVC liner. This also prevents the frictional resistance of the smooth HDPE from reaching that of the smooth PVC.

The mechanical properties of polypropylene fibers do not remain constant within the range of temperatures found in typical civil engineering applications. It was seen in the result of micro-scale thermo-tensile tests on single geotextile filaments that all filament specimens tested at different temperatures exhibited nonlinear elasto-perfectly plastic tensile behavior under extension. The tensile strength was largest at room temperature and decreased with increasing temperature. Similarly, the modulus of elasticity for polypropylene filaments decreased with increasing temperature. For the test temperatures evaluated in this study, the initial elastic modulus was the largest at room temperature.

The effects of temperature on the friction properties of geotextile versus geomembrane interfaces were examined based on surface hardness measurements at different temperatures and showed that the mobilized frictional strength at geotextile – geomembrane interfaces at different temperatures is primarily influenced by the surface hardness of the

geomembrane. In this context, the measured index value of hardness of the geomembrane surface based on a standard scale (i.e. Shore D in this case) at various temperatures provided a useful quantitative value to evaluate the shear resistance being generated at the interface of fabric – continua. Due to the differences in surface hardnesses of HDPE and PVC geomembranes, the smooth PVC exhibited higher shear stress – displacement curves than those of the smooth HDPE at all temperatures tested although both lining sheet material possess similar surface roughness characteristics. The interface tests carried out at elevated temperatures conditions for PVC liner showed similar responses in which shear displacement hardening behavior occurred after yielding in contrast to the behavior observed with smooth HDPE geomembranes where a post-peak strain softening response developed. The tendency of PVC smooth geomembrane – geotextile interfaces to behave in this fashion was completely dependent on the differing material properties compared with HDPE liners. Additionally, the hardness reduction contributed to some very minor increase in strength with increasing temperature level compared to HDPE. However, the smooth HDPE geomembrane showed a higher increase in strength with temperature for same normal stress level tested.

The experimental results and discussion presented herein have important implications for practice. In predicting the behavior of geosynthetic interfaces that are an important component of composite layered systems widely designed and employed in geotechnical applications, it is critical to consider the significant influence of operational temperature conditions on this behavior. In light of the experimental tests performed in this study and the analyses and discussion included herein, the frictional shear capacity of interfaces between geomembranes and other polymeric materials is not just influenced by the effect of temperature on the individual materials but also the effect of temperature on the combination of materials. In this context, the measured index value of hardness of the geomembrane surface based on a standard scale (i.e. Shore D in this case) at various temperatures can provide insight into how interface shear strength may change (i.e. increase or decrease) at different ambient temperature conditions compared to those determined in conventional laboratory tests conducted at standard room temperatures.

ACKNOWLEDGEMENTS

The research study reported herein was conducted in part with support from the Geosynthetic Institute through a GSI Fellowship to the first author. This support is gratefully acknowledged.

REFERENCES

- ASTM D 2240-05. (2005) Standard Test Method for Rubber Property - Durometer Hardness, *American Society for Testing and Materials*, West Conshohocken, Pennsylvania, USA.
- ASTM D 4751. (1999a; Reapproved 2004). Standard Test Method for Determining Apparent Opening Size of a Geotextile, *American Society for Testing and Materials*, West Conshohocken, Pennsylvania, USA.
- ASTM D 5261. Standard Test Method for Measuring Mass per Unit Area of Geotextiles, *American Society for Testing and Materials*, West Conshohocken, Pennsylvania, USA.
- Dove, J.E. (1996). Particle-Geomembrane Interface Strength Behavior as Influenced by Surface Topography, *Ph.D. Dissertation*, School of Civil and Environmental Engineering, Georgia Institute of Technology, Atlanta, GA, USA, 323 pp.
- Giroud, J. P. (1984). Geotextiles and Geomembranes. *Geotextile and Geomembranes*, 1(1): 5-40.
- Koerner, R.M. (2005). *Designing with Geosynthetics*, 5th ed., Prentice Hall, Englewood Cliffs, NJ, USA, p796.
- Martin, J.P., Koerner, R.M. and Whitty, J.E. (1984). Experimental friction evaluation of slippage between geomembranes, geotextiles and soils, *Proceedings of International Conference on Geomembranes*, IFAI, Denver, CO, USA, 1: 191–196.

Engineered Anti Erosion Works along the Banks of River Ganges

Chitra, R., Central Soil and Materials Research Station, New Delhi, India, chitra009@gmail.com
Manish Gupta, Central Soil and Materials Research Station, New Delhi, India, manish009@gmail.com
Murari Ratnam, Central Soil and Materials Research Station, New Delhi, India, director-csmrs@nic.in

ABSTRACT

River bank erosion is a natural process that results in the formation of the productive floodplains and alluvial terraces common to many of river systems. Events like flooding can trigger dramatic and sudden changes in rivers and streams. However, land use and stream management can also trigger erosion. Many anti-erosion techniques are used as engineered solutions to the problems. The Farakka Barrage Project (FBP), 2245 m long barrage across the River Ganga and 213 m long barrage across the River Bhagirathi, is designed to serve the need of preservation and maintenance of Calcutta Port by improving the regime and navigability of the Bhagirath-Hoogly river system. The river banks at the Farakka Barrage Project on River Ganges have been experiencing erosion, especially during floods. The protection works carried out by FBP has successfully restored the eroded banks. The paper describes the anti erosion works carried out along the banks of River Ganges and restorations of damaged banks.

1. INTRODUCTION

Rivers and their flood plains are dynamic geologic systems. Ever-changing patterns of erosion and deposition occur during the evolution of a river, especially when it begins to meander and shift its course across the cut bank of the bend, while deposition of sediment builds point bars on the inside of the meander. The shifting of meander paths occurs at varying rates, but it is generally most rapid during periods of high water. Erosion of the cut bank may attain a magnitude of centimeters or even meters per day, and streams occasionally shorten their courses dramatically by cutting across the necks of meanders. Therefore, it is unwise to build on surficial materials close to an active stream meander, even though the building sites may be higher than the flood plain.

Floods are recurrent phenomena in India from time immemorial. Almost every year some parts of the country or the other are affected by floods of varying magnitude. It is also experienced that while some parts are suffering under devastating floods, another part is suffering under drought. With the increase in population and developmental activity, there has been tendency to occupy the flood plains which has resulted in more serious nature of damage over the years.

The erosion of banks by the rivers and the consequent loss of life and property are major problems. Rivers tend to erode their beds and banks in the hilly regions resulting in the deepening and widening of rivers. When a river enters the flood plains, it shows a tendency to braid and develop number of channels causing silting of the riverbed, change in course and bank erosion. In the plains, a river shows a meandering tendency with meanders moving downstream causing erosion on the concave and deposition on the convex side and cut offs. The meanders also show a tendency to move downstream. This causes large-scale bank erosion. In deltaic reaches near the outfall into sea, the river divides itself into a number of branches resulting in bank erosion. Thus bank erosion and consequent loss of land and properties is a constant phenomenon all along the course of the river. The study of the problem and remedial measures for training of the river into the defined channel has gained importance due to increase in population pressure and want of alternative sources of livelihood for the people whose land and properties are lost to rivers.

Anti-erosion works are normally taken up only for protection of towns, industrial areas, groups of thickly populated villages, railway lines and roads where re-location is not possible on socio-techno-economic grounds, long lengths of vital embankments benefiting large areas in case retirement is not technically or otherwise feasible and agricultural lands where the cost-benefit ratio justifies such works.

Bank erosion can be minimized by adopting measures that aim at deflecting the current away from the river bank or which aim at reducing the current along the bank of the river and induce silt. The anti-erosion measures in the form of revetment or pitching along with launching apron and spurs of earth protected by armor of stones or spurs of loose stones or stones in wire-mesh crates aim at increasing resistance of the bank to erosion and deflecting the current away from the bank. These generally shift the problem in the upstream or the downstream and necessitate further works to safeguard the land against erosion.

Measures such as permeable spurs, porcupine spurs made of bamboos or of reinforced cement concrete elements reduce the velocity of flow and thus prevent erosion and induce siltation in the vicinity of the bank. Geosynthetic material

(woven geo-textile) available in various forms like big bags and tubes etc. can be filled in-site with riverbed sand to form the groynes, spurs and revetments. The dredging of the channels in the selected reaches which have silted up can be tried. Geo-web filled with concrete overlaid on geo-fabric filters in lieu of stone revetment and launching apron is also a new development.

2. EROSION CONTROL TECHNIQUES

The processes of sediment erosion, transport, and deposition may cause local and system-wide adjustments in the bed and banks of the river channel, including the migration of a river channel across the flood plain. In a natural setting, undisturbed by anthropomorphic impacts or cataclysmic events, the river is dynamic and changes occur over time as a result of these sediment processes. However, when viewed over the long term, these changes tend to fluctuate about an equilibrium condition, known as dynamic equilibrium. Disturbances to the river corridor often affect these sediment processes, and the channel may become unstable (i.e. no longer in a state of dynamic equilibrium). With time, the disturbed channel may achieve a new state of dynamic equilibrium, but viable water management activities or appropriate aquatic habitat for fish and wildlife may not be sustainable during this period of transition. Disturbances to rivers and streams can be caused by dams, water diversions, levees, roads, bridges, bank protection, removal of vegetation and woody debris, logging, grazing, gravel mining, urbanization, and recreation. There are numerous ways to control these disturbances in the river corridor and to restore fully or partially the natural processes and the dynamic equilibrium. Soil conservation practice, check dams, sediment bypass devices, and sluicing are often used to reduce sediment inflow or remove sediments from a reservoir to prolong the useful life of a reservoir.

Bank stabilization has historically been constructed on a reactionary basis in response to lateral erosion of banks from floods. The impact of bank stabilization on natural processes depends on the location of the bank relative to the channel migration zone boundaries, the rate of natural channel migration, and the material that composes the bank stabilization.

Traditional bank stabilization uses hard, angular rock that protects against the high velocities and shear stress against the bank. There are three general approaches of bank stabilization: live planting, bioengineering, and hard armoring. The best technique will depend on the size and location of the eroded bank, and the cause and severity of the erosion.

3. FARAKKA BARRAGE PROJECT

Farakka barrage was constructed across river Ganga at Farakka to divert 1135 cumecs of water into Bhagirathi River to revive it. The Bhagirathi River is one of the important spill channel, taking off from Ganga and feeding the Hoogli system which is the lifeline of this region where a large industrial complex has developed. The diverted water of 1135 cumecs to Bhagirathi – Hoogli system preserves the Kolkata Port. The Farakka Barrage Project, commissioned in the year 1975, is thus of national importance.

3.1 Meandering Behavior of River Ganges Near Farakka

River Ganges has been meandering through ages like all other alluvial rivers. Bank erosion is a common feature during the process of meandering. Ganges with its large mean discharge and a flat slope of about 1 in 20000 near Farakka, flows in a meandering state exhibiting typical behavior of a large river flowing in alluvial plains. Due to the phenomenon of meandering, the river course keeps on changing, resulting in bank erosion at different places. The comparison of the river courses in the seventies and nineties clearly indicates the progressive meandering of the river Ganges and swinging of banks causing bank erosion in the nearby regions such as Gopalpur, Aswintola, Khaskal, Panchananadpur etc. River Ganges has been meandering towards the right bank downstream of Farakka, even much before the construction of the barrage.

3.2 Anti Erosion Measures Adopted in the Past and their Efficacy

The problem of bank erosion was attempted to be tackled by construction of bull headed spurs, lowering of dip trees, construction of boulder bars during the years seventies and eighties. But none of these measures withstood the ferocity of bank erosion and got damaged after facing two or three flood seasons. The dip trees induced siltation during low floods, but during high floods, all the silt deposits were completely washed away along with dip trees.

3.3 Design Philosophy of Anti Erosion Works

The design philosophy includes the estimation of scouring potential of river which is a function of the discharge intensity and Lacey's scour depth. The fineness of river bed material is indicated in terms of silt factor which along with discharge intensity governs the Lacey's scour depth. The thickness of sloped bank pitching is determined on the basis of velocity of

flow along the bank. Similarly the thickness of launching apron is determined once the scour depth, High Flood Level and Low Water Level are known. A suitable filter is also provided below the sloped pitching and launching apron.

The design philosophy is simple but the phenomenon of bank erosion is very complex. A variety of factors and their possible combinations play a major role in causing the bank erosion. These parameters among others include river curvature, reverse/cross flows, composition of bed / bank material etc. It is for this reason the scour factor near the nose of guide builds and spurs and along the curved bends of river is taken as more as compared to that of straight reach of river.

It has been observed during bank erosion on the banks of Ganga that the whirling action of water during the flood causes the scooping out of bed material near the banks and huge landmasses on the banks just sink vertically downwards. This whirling action is an outcome of the reverse flows due to river bank curvature. Once the bed material near the bank gets scooped out because of whirling action of water, the bank becomes unstable and the soil properties of the bank material are of such type that the bank sinks vertically downwards. Hence the problem lies in identification of those places along the bank where the whirling action of water takes place so that the designed length and thickness of launching apron is suitably increased there. The eroded bed material can also be prevented from getting lifted up provided that a suitable filter is placed in position. Selection of filter material and its opening size is very important considering that at a given place on the river bed the different layers of river bed may have different soil particle size and type. When the apron gets launched then there are chances of the filter being torn apart if it does not have sufficient tensile strength. These are some of the practical difficulties in the selection of the filter material.

3.4 Farakka Barrage

The Farakka Barrage Project is designed to serve the need of preservation and maintenance of Calcutta Port by improving the regime and navigability of the Bhagirath-Hoogly river system. The increased upland supplies from Ganga at Farakka into Bhagirathi also reduces salinity in the system and ensures sweet water supply to Calcutta and surrounding areas. The rail-cum-road bridge built across the river Ganga at Farakka establishes direct road and rail communication link to the North-Eastern States. The Bhagirathi, the Feeder Canal and the Navigation Lock at Farakka form part of the Haldia-Allahabad Inland Waterway (National Waterway No. 1).

3.4.1 Principal Components of Farakka Barrage Project

The principal components of the Project are:-

- A 2245 metre long barrage across the River Ganga with rail-cum-road bridge, necessary river training works and a Head Regulator on the right side.
- A 213 metre long barrage across the River Bhagirathi at Jangipur.
- Feeder canal of 1133 cumec (40000 cusec) carrying capacity and 38.38 km. long, taken off the head regulator on the right of the Farakka Barrage.
- Navigation works such as Locks, Lock channels, Shelter basins, Control tower building, navigational lights and other infrastructure.

The jurisdiction map of the Farakka barrage project is presented in Figure 1.



Figure 1. Jurisdiction map of the Farakka barrage project

3.4.2 Activities of the Project

JURISDICTION MAP OF FARAKKA BARRAGE PROJECT

- Maintenance of Barrage and appurtenant structures.
- Anti erosion works in the original jurisdiction.
- 12.5 km u/s & 6.9 km d/s of barrage axis in the main Ganga
- 16 km d/s of Jangipur Barrage along Ganga/Padma near Moya
- Anti erosion works in the extended jurisdiction of 40 km u/s & 40 km d/s of barrage axis in the main Ganga/Padma since 2004.

3.4.3 Anti Erosion Works Executed So Far

Up stream of Farakka barrage along left bank of river Ganga:

Simultola & Birnagar area	-	Length -300m
Panchanandapur	-	Length - 4000 m
Just u/s of left guide bundh	-	Length - 220 m

3.4.4 Anti Erosion Works Being Executed Now

During the current working season, Farakka Barrage Project is presently executing the following anti erosion works.

At Birnagar – Simultala	:	870 m
At Maniakchak Ghat	:	1700 m
At Ramrampur/Arjunpur/Dhuliyani	:	700 m

Figure 2 shows a typical section of the anti-erosion work carried out at these locations.

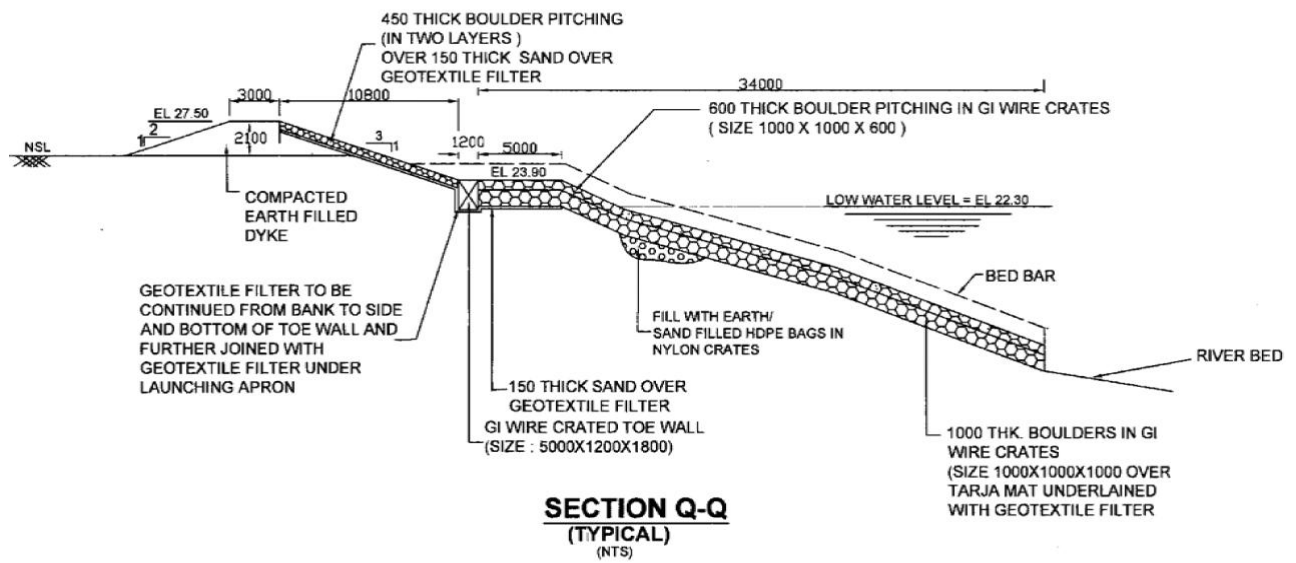


Figure 2 Typical design section of anti erosion works

3.4.5 Sequence of Anti Erosion Works

- Fixing of the Geotextile on tarza mat
- Laying of the Geotextile-tarza mat composite on the river bed
- Anchoring the Geotextile on the river bank
- Laying of two layers of boulder filled wire crates on the Geotextile-tarza mat composite



Fixing of the Geotextile on Tarza mat



Tarza mat being laid in river bed



Anchoring the Geotextile on the river bank



Laying of two layers of boulder filled wire crates on the Geotextile-Tarza mat composite

The anti-erosion works mainly involve lying of geosynthetic fabric filter under Tarza mat in water as well as on the land depending on site conditions and over that boulder filled GI wire crates of 1.6 m thickness in 34 m long apron laid/dumped to arrest scour due to high discharge intensities.

4. INVESTIGATIONS CARRIED OUT

The materials used for the protection works against the river bank erosion needs to be tested for their quality. Therefore, the Geotextiles and the GI wires which were used for the protection works at the Farakka barrage were tested at Central Soil and Materials Research Station (CSMRS).

CSMRS is a premier institute in India located at New Delhi, which deals with field and laboratory investigations, basic and applied research, and problems in geomechanics, construction materials and allied fields relevant to river valley projects within and neighboring countries viz. Nepal, Bhutan, Afghanistan etc. A well established geosynthetics material testing laboratory at CSMRS has the capability of testing woven and nonwoven geotextiles, geogrids, geonets, geomembranes, and geocomposites that are used in drainage, earthwork, erosion control, and soil reinforcement applications.

The geosynthetics laboratory is equipped with equipments that are used for evaluating the properties such as tensile strength, tearing resistance, thickness, apparent opening size, permeability, interface friction and the pull out resistance.

The Farakka barrage project authorities approached CSMRS for testing the materials used at the protection works of the eroded river banks at Farakka. A large number of Geotextile fabrics and GI wires were received at CSMRS for further testing at the laboratory.

4.1 Laboratory investigations on Geotextiles

The laboratory tests such as apparent opening size, mass per unit area, tensile strength (warp), tensile strength (weft), permeability, etc., were carried out on the geotextiles received from the projects. All these tests were carried out in accordance with ASTM standard test methods. The tests results are presented in the following table.

Table 1 Laboratory Testing on Geotextile Fabric from Farakka Barrage Project, West Bengal

Field Sample No.	Lab. Sample No.	Apparent Opening Size, Micron	Mass per Area, g/m ²	Tensile Strength (warp), kN/m	Tensile Strength (weft), kN/m	Permeability, lit/m ² /sec at 10cm head
S-3/GT	GS/2008/1	150	240.4	55.3	45.7	30.1
S-4/GT	GS/2008/2	150	241.2	55.8	44.7	30.0
S-5/GT	GS/2008/3	150	240.6	55.2	45.3	30.3
S-6/GT	GS/2008/4	150	242.5	55.5	45.1	30.6
S-7/GT	GS/2008/5	150	240.6	55.2	45.3	32.8
S-8/GT	GS/2008/6	150	242.1	55.0	45.2	31.0
S-9/GT	GS/2008/7	150	240.9	55.6	45.2	31.1
S-10/GT	GS/2008/8	150	241.3	56.1	45.5	30.5
S-11/GT	GS/2008/9	150	241.7	55.4	45.6	30.4
S-12/GT	GS/2008/10	150	242.2	55.9	46.1	30.9
S-13/GT	GS/2008/11	150	241.1	55.7	45.9	31.8
S-14/GT	GS/2008/12	150	240.8	55.1	45.4	31.5

4.2 Laboratory Investigation on GI Wire

The GI wire which is used to prepare the boulder filled wire crates, to be placed on the Tarza mat supported geotextile was subjected to the laboratory tests such as evaluation of the wrap strength of the wire, evaluation of the quantity of the zinc coating on the GI wire, evaluation of the tensile strength, , etc., as a quality control measure. This test was performed on five specimens of each 3.15 mm diameter GI wire and the average value is reported as the test value. The test results are in accordance with IS: 280-2006

4.3 Evaluation of the Quantity of the Zinc Coating on the GI Wire

The mass of zinc coating is determined as per IS: 6745-1998. The minimum zinc coating on wire of 3.15 mm diameter is taken as 80 g/m² as per IS: 4826 -1979 for light coated wire.

4.4 Evaluation of the Warp Strength of the Wire

The warp strength test was performed on five specimens per sample of the wire. The test is performed in accordance with IS: 1755-1983 and IS: 280-2006

5. CONCLUSION

The figures below show the geotextiles and GI wires used for the protection works of the river banks at Farakka barrage project.



Protection work using Geotextiles and GI wires



Slope Pitching by sand bags



Nylon Crate being dumped by boat

The protection works carried out for the river bank erosion at the river Ganges around the Farakka barrage project are somewhat simple and a highly engineered solution. While designing the protection works and choosing the products, due care has to be taken for proper design, structural integrity of the system, experienced designer and contractors who installs the system in order to avoid negative criticism.

By carrying out these protection works, the Farakka barrage project authority has restored the damaged banks of the river Ganges successfully and has imbibed a sense of security in the minds of the inhabitants of the area.

ACKNOWLEDGEMENT

The authors acknowledge the contributions of the General Manager, Farakka Barrage Project, West Bengal and his team for their valuable contribution in the preparation of this paper by way of active cooperation at the time of actual investigations and testing.

REFERENCE

- Abramson, L.W., Lee, T.S., Sharma, S., and Boyce, G.M. (1996). Slope Stability and Stabilization Methods. John Wiley & Sons: New York, N.Y.
- Abramson, L.W., Thomas, S.L., Sharma, S., Boyce, G.M. (2002). Slope Stability and Stabilization Measures, John Wiley and Sons, 2nd Edition, New York, NY.
- ASTM D 4751-2004, Test Method for Apparent Opening Size of a Geotextile.
- ASTM D 5261-1992 (2003), Test Method for Measuring Mass per unit area of Geotextiles.
- ASTM D 4595-2005, Test Method for Tensile Properties of Geotextiles by the Wide Width Strip Method.
- ASTM D 4491-2004, Test Methods for Water Permeability of Geotextiles by Permittivity.
- Freeman, G. E. & Fischenich, J. C. 2000. Gabions for Stream bank Erosion Control. U.S. Army Engineer Research and Development Center, Vicksburg, MS.
- IS: 280-2006, Indian Standard specification for Mild Steel Wire for General Engineering Purposes.
- IS: 4826 -1979, Indian Standard specification for hot-dipped galvanized coatings on round steel wires.
- IS: 1755-1983, *Indian Standard* method for wrapping test for metallic wire.

Enhancing the Performance of HDPE Geomembranes with Flexible Polypropylene

F. Ceccarani, LyondellBasell, USA; P. Goberti, LyondellBasell, Italy; M. Grazzi, LyondellBasell, Italy

ABSTRACT

Thermoplastic polyolefins (TPOs) are utilized by many industries for the production of materials that go into a variety of applications including flexible packaging, automotive components, single ply roofing membranes, and geomembranes. They are known in the geomembrane industry as “flexible polypropylene” (fPP). They are used in geomembrane applications because of their unique combination of mechanical toughness, flexibility, barrier properties, dimensional stability, and environmental resistance. Recent studies show that flexible polypropylene can be used as a HDPE/MDPE modifier to improve important properties such as flexibility, impact resistance, and environmental stress cracking resistance (ESCR). Although HDPE is widely used in a number of geomembrane applications, an improvement in certain specific properties (flexibility, impact, dimensional stability, ESCR) is often desired.

1. INTRODUCTION

1.1 Flexible Polypropylene: A Reactor-TPO

Thermoplastic polyolefins (TPOs) are polypropylene (PP) based copolymers that contain greater than 40% of a rubbery phase. In addition to being manufactured as post-reactor mechanical blends of PP and an ethylene-propylene rubber (EPR), TPOs can be produced directly in the polymerization reactors using a unique production process known as the *Catalloy* process technology. “Reactor-TPOs” produced with such technology have a unique morphology with the rubber domains very finely and uniformly dispersed within the polypropylene backbone, resulting in enhanced physical properties. These reactor-TPOs are specialty materials known in the geomembrane industry as “flexible polypropylene” (fPP). They are used due to their outstanding flexibility, puncture resistance, and impact resistance as well as their very good dimensional stability and environmental stress cracking resistance (ESCR). Being PP based materials, they have a relatively high melting point (above 140°C) and the high percentage of amorphous polymer in the composition allows these materials to maintain flexibility and impact resistance at very low temperature. Therefore fPP can often be used when very high or very low operating temperatures are expected during service life.

1.2 Typical Polyethylene Materials Used For Making Geomembranes

The three types of polyethylene (PE) that are traditionally used for producing geomembranes have different chemical structures and, consequently, different densities. High density polyethylene (HDPE) resins have densities greater than or equal to 0.941 g/cm³, medium density polyethylene (MDPE) resins have densities in the range of 0.926 to 0.940 g/cm³, and linear low density polyethylene (LLDPE) resins have densities in the range of 0.9125 to 0.925 g/cm³. HDPE is manufactured using either only ethylene as a monomer for the polymer chains (HDPE Homopolymer) or using low amounts of co-monomers (normally butene or hexene), and linear polymer chains with short-chain branches are obtained. MDPE and LLDPE are similar to HDPE but by copolymerizing the ethylene monomer with higher amounts of an alky-branched co-monomer (butene, hexene, or octene), a copolymer PE is produced in which hydrocarbon branches replace some of the hydrogen atoms bonded to the carbon atoms. The distinction between MDPE and LLDPE is a result of the degree of copolymerization, ultimately affecting the density of the polymer (the higher the short-chain branching, the lower the density), with LLDPE being significantly more flexible than MDPE and HDPE.

1.3 Weaknesses of HDPE/MDPE in Geomembrane Applications

HDPE and MDPE are widely used all over the world in a number of geomembrane applications due to their relatively low cost, good property balance, good chemical resistance and UV weathering performance, and easy processability in the blown film and flat die extrusion processes used for making geomembranes. However, an improvement in certain specific properties (flexibility, impact resistance, dimensional stability, ESCR, temperature resistance) is often desired. In fact, HDPE and MDPE are quite stiff polymers and geomembranes made with such materials tend to lack flexibility and impact resistance, especially in cold climates (for instance the Northern US and Canada) and cold environments (for instance mountainous areas), leading to potential membrane handling, installation, and durability issues. Also, polyethylene materials tend to be prone to environmental stress cracking, which is a key property in geomembrane applications.

1.4 HDPE/MDPE Property Improvement with Flexible PP

This paper investigates the properties of HDPE-fPP and MDPE-fPP blends to understand if fPP can significantly improve the weak points of HDPE/MDPE in geomembrane applications. Typical properties that are meaningful in geomembrane applications are examined for HDPE-fPP blends and compared to the properties of a 100% HDPE control and those of HDPE-LLDPE blends. In particular, test results are presented for physical properties, ESCR, weldability window, and UV weathering performance of HDPE and MDPE blended with the following two materials at both 20 percent by weight (20 wt%) and 40 percent by weight (40 wt%) incorporation levels: commercial *Catalloy* Reactor-TPO produced by LyondellBasell and commercial LLDPE produced by Polimeri Europa.

2. EXPERIMENTAL

2.1 Materials Used in this Study

2.1.1 Base HDPE and MDPE Materials

The following HDPE and MDPE commercial grades produced by LyondellBasell were used as the base PE materials for this study:

HDPE -- *Lupolen* 5021DX (density = 0.950 g/cc);

MDPE -- *Lupolen* 3721C (density = 0.937 g/cc).

2.1.2 Modifiers

The following commercial grades were used as the HDPE/MDPE modifiers:

fPP -- *Hifax* CA10A (Reactor-TPO having high EPR level; density = 0.89 g/cc);

LLDPE -- *Clearflex* FG106 (ethylene-hexene copolymer; density = 0.918 g/cc).

2.1.3 Blend Preparation

Blends were extruded using a Berstorff ZE2525 mm twin screw extruder with a strand pelletizing system. Each modifier was blended with each base PE material at levels of 20wt% and 40wt%. In order to simulate commercial geomembrane formulations and provide UV stability during the accelerated weathering test, a suitable amount of Carbon Black and UV stabilizers (HALS) were also included in each formula along with additional primary and secondary antioxidants.

2.2 Physical Property Characterization

2.2.1 Compression Molded Specimens

The physical properties listed below were measured using compression molded specimens (typical of PE materials, whereas for PP materials injection molded specimens are normally used). Specimens were molded on a COLLIN 200M press according to the ISO 293 standard.

- Melt Flow Rate (190°C/2,16kg) (ISO 1133)
- Density (ISO 1183-2)
- Coefficient of Linear Thermal Expansion (CLTE) (Internal Method)
- Flexural Modulus (ISO 178)
- Vicat Softening Point (ISO 306)
- Notched Izod Impact (ISO 180)
- Environmental Stress Cracking Resistance (ESCR) (ASTM D1693)

2.2.2 Sheet Specimens

The physical properties listed below were measured using specimens that were die cut from 1mm (40 mil) thick sheet.

- Tear Resistance (ASTM D1004)
- Puncture Resistance (ASTM D4833)
- Impact Resistance at Low Temperature (ISO 6603)
- Tensile Properties (ISO 527-3; 500 mm/min)
- Weldability Window (Internal Method)
- Accelerated UV Weathering (Internal Method)

3. RESULTS

3.1 Mechanical/Thermal Properties on Compression Molded Specimens

Test results obtained by testing compression molded specimens are reported in Table 1 and Table 2.

Table 1. Properties of HDPE-fPP and HDPE-LLDPE Blends (Compression Molded Specimens)

Physical Property	Test Method	Unit	fPP	HDPE	HDPE + 20% fPP	HDPE + 40% fPP	HDPE + 20% LLDPE	HDPE + 40% LLDPE
MFR (T=190°C; 2.16 Kg)	ISO 1133	g/10 min	0.31	0.27	0.20	0.27	0.33	0.48
Density	ISO 1183	g/cm ³	0.889	0.962	0.946	0.930	0.955	0.948
CLTE	Internal Method	m/m/°C 10-5	9.0	13.4	13.5	13.7	17.7	15.3
Izod Impact at -30°C	ISO 180	KJ/m ²	79.6	4.0	7.2	74.6	6.0	6.9
Izod Impact at -40°C	ISO 180	KJ/m ²	81.7	4.2	6.4	15.7	5.4	6.4
Flexural Modulus	ISO 178	MPa	85	1176	785	410	945	760
Vicat Soft. Temp. (9.81 N)	ISO 306	°C	55.2	125	121	96	122	117

Table 2. Properties of MDPE-fPP and MDPE-LLDPE Blends (Compression Molded Specimens)

Physical Property	Test Method	Unit	fPP	MDPE	MDPE + 20% fPP	MDPE + 40% fPP	MDPE + 20% LLDPE	MDPE + 40% LLDPE
MFR (T=190°C; 2.16 Kg)	ISO 1133	g/10 min	0.31	0.16	0.16	0.21	0.25	0.38
Density	ISO 1183	g/cm ³	0.889	0.949	0.935	0.922	0.944	0.940
CLTE	Internal Method	m/m/°C 10-5	9.0	14.5	15.6	14.5	15.7	17.7
Izod Impact at -30°C	ISO 180	KJ/m ²	79.6	5.3	26.8	87.8	7.1	10.7
Izod Impact at -40°C	ISO 180	KJ/m ²	81.7	5.7	10.4	67.0	6.4	8.4
Flexural Modulus	ISO 178	MPa	85	712	480	330	579	538
Vicat Soft. Temp. (9.81 N)	ISO 306	°C	55.2	118	111	91.5	116	112

3.1.1 Melt Flow Rate

All materials used in this study have low melt flow rate (MFR), as is typical of extrusion and blown film grades. The flowability of all the materials being fairly similar, the MFR was not significantly impacted by blending either modifier with HDPE or MDPE. Fractional MFR values were obtained and no impact on processability is expected.

3.1.2 Density

The density of the blends decreased upon modifier addition since both fPP and LLDPE have lower density than HDPE and MDPE. fPP has an even lower density than LLDPE and, therefore, a more significant decrease in density was obtained using fPP (about 3%). A lower density is beneficial because less material is needed to produce the same membrane.

3.1.3 Coefficient of Linear Thermal Expansion (CLTE)

fPP has significantly lower CLTE than PE based materials, which is why fPP is often the material of choice to minimize wrinkles when there are high temperature fluctuations during the installation of the liner. Thermal excursions can be significant between day and night or between summer and winter installation. Unfortunately, HDPE/MDPE blends with 20% or 40% fPP maintained the original CLTE with no decrease obtained. The lower a material's coefficient of linear thermal expansion, the greater its dimensional stability.

3.1.4 Izod Impact Resistance at Low Temperature

The low temperature Izod impact strength of fPP is approximately 20 times higher than that of HDPE or MDPE. Therefore a large improvement in low temperature Izod is obtained by blending in 20% and especially 40% fPP. Much smaller improvements in impact resistance are obtained by using LLDPE at either 20% or 40% as modifier.

Impact testing determines a material's toughness and resistance to puncture by impact. Impact strength is used to evaluate how much energy is required to break the impacted specimen. As geomembranes are often exposed to low temperature during servicelife (for instance, if they are installed at high altitudes or in cold climates), it is important to determine the impact performance at lower than ambient temperature.

3.1.5 Flexural Modulus

fPP is a softer and much more flexible material than either HDPE or MDPE. Test results for the materials used in this study show that fPP is about 14 times more flexible than HDPE and about 8 times more flexible than MDPE. The reduction in stiffness obtained by blending fPP at 20% is already significant (a reduction of approximately 33%), but with 40% fPP an even greater improvement is achieved (65% reduction blended with HDPE and 54% reduction blended with MDPE). While the addition of LLDPE also provides an improvement in flexibility, it is not as efficient as fPP. The stiffness reduction obtained by blending in 40% LLDPE is less than the reduction obtained by blending in only 20% fPP. The flexural modulus of the membrane material affects the ability to prefabricate large sections in the manufacturing environment. Also, a more flexible membrane will better conform to the substrate surface when the geomembrane is deployed and will be easier to install in cold climates.

3.1.6 Vicat Softening Temperature

The Vicat softening temperature of fPP is lower than that of HDPE or MDPE due to the large amount of amorphous polymer in fPP (EPR). HDPE/MDPE blends with fPP, therefore, tend to have a decreased softening temperature, which can help to broaden the material's heat welding window.

3.2 Mechanical Properties on Sheet Specimens

Test results obtained by testing sheet specimens are reported in Table 3 and Table 4.

Table 3. Properties of HDPE-fPP and HDPE-LLDPE Blends (Sheet Specimens)

Physical Property	Test Method	Unit	fPP	HDPE	HDPE + 20% fPP	HDPE + 40% fPP	HDPE + 20% LLDPE	HDPE + 40% LLDPE
Tensile Stress at Yield MD	ISO 527	MPa	7.7	25.4	18.3	14.2	21.6	18.6
Tensile Elongation at Yield MD	ISO 527	%	39.0	10.0	13.6	19.7	11.6	126
Tensile Stress at Break MD	ISO 527	MPa	22.1	20.8	30.2	29.3	27.7	29.7
Tensile Elongation at Break MD	ISO 527	%	850	747	739	805	700	690
Tensile Stress at Yield TD	ISO 527	MPa	7.0	27.7	18.1	13.1	22.7	19.3
Tensile Elongation at Yield TD	ISO 527	%	38.0	7.5	13.8	18.8	10.7	11.9
Tensile Stress at Break TD	ISO 527	MPa	22.4	15.8	16.5	23.2	21.8	30.7
Tensile Elongation at Break TD	ISO 527	%	850	310	765	795	827	830
Tear Resistance MD	ASTM D 1004	N	76	140	124	108	134	124
Tear Resistance TD	ASTM D 1004	N	74	170	146	122	156	139
Puncture Resistance	ASTM D 4833	N	252	387	372	358	394	371
Impact Strength (-30°C)	ISO 6603	N	1281	1533	1440	1483	1340	1300
Impact Failure Mode (-30°C)	ISO 6603	---	YD	YD	YD	YD	YD	YD
Impact Strength (-40°C)	ISO 6603	N	1563	1791	1677	1546	1663	1681
Impact Failure Mode (-40°C)	ISO 6603	---	YS	YD	YD	YD	YD	YD

MD = Machine Direction; TD = Transverse Direction.

Table 4. Properties of MDPE-fPP and MDPE-LLDPE Blends (Sheet Specimens)

Physical Property	Test Method	Unit	fPP	MDPE	MDPE + 20% fPP	MDPE + 40% fPP	MDPE + 20% LLDPE	MDPE + 40% LLDPE
Tensile Stress at Yield MD	ISO 527	MPa	7.7	19.0	14.7	12.0	16.4	14.9
Tensile Elongation at Yield MD	ISO 527	%	39.0	12.5	16.3	24.4	---	15.3
Tensile Stress at Break MD	ISO 527	MPa	22.1	31.6	30.7	28.7	32.1	32.1
Tensile Elongation at Break MD	ISO 527	%	850	685	738	808	722	753
Tensile Stress at Yield TD	ISO 527	MPa	7.0	20.6	14.4	11.0	17.3	15.8
Tensile Elongation at Yield TD	ISO 527	%	38.0	10.5	16.1	21.6	12.3	13.9
Tensile Stress at Break TD	ISO 527	MPa	22.4	32.4	24.8	24.7	32.3	29.5
Tensile Elongation at Break TD	ISO 527	%	850	820	751	807	820	828
Tear Resistance MD	ASTM D 1004	N	76	120	104	99	128	119
Tear Resistance TD	ASTM D 1004	N	74	139	117	104	136	127
Puncture Resistance	ASTM D 4833	N	252	362	328	312	385	356
Impact Strength (-30°C)	ISO 6603	N	1281	1432	1380	1238	1339	1400
Impact Failure Mode (-30°C)	ISO 6603	---	YD	YD	YD	YD	YD	YD
Impact Strength (-40°C)	ISO 6603	N	1563	1540	1575	1427	1584	1486
Impact Failure Mode (-40°C)	ISO 6603	---	YS	YD	YD	YD	YD	YD

MD = Machine Direction; TD = Transverse Direction.

3.2.1 Tensile Properties

The HDPE and MDPE materials used in this study have very good tensile properties, as confirmed by the tensile stress at yield and tensile stress at break test results obtained on the sheet specimens. Although fPP has lower tensile stress at yield than either HDPE or MDPE, a higher elongation at break can be obtained with fPP because of its high level of EPR. Thus, HDPE/MDPE blends with fPP have lower tensile stress at yield (between 2% and 30% lower with the addition of 20% fPP) but higher elongation at yield. fPP has tensile stress at break similar to HDPE (slightly higher) and lower than MDPE. It is interesting that for tensile stress at break, there seems to be a synergistic effect between HDPE and fPP since their blends have higher tensile stress at break than either the HDPE or the fPP alone. This could be due to a strain hardening effect. Similar results are obtained with LLDPE blends.

The tensile properties of a membrane provide practical indications about the behavior of the material when it is stretched during installation or in its service life. High tensile elongation at break demonstrates the polymer's ability to be stretched prior to break and is a key property in geomembrane applications.

3.2.2 Tear Resistance

Tear resistance is higher when the polymer has a higher degree of crystallinity, as indicated by the high tear strengths exhibited by HDPE and MDPE. As expected, tear resistance of HDPE and MDPE decreases when those materials are blended with fPP or LLDPE. Laboratory tear tests can be useful to predict a material's ability to resist tear forces and tear propagation in service.

3.2.3 Puncture Resistance

Puncture resistance of the HDPE and MDPE materials used in this study is surprisingly high-- even higher than that of fPP. Therefore, when fPP is blended in at 20%, the puncture resistance decreases a little but not significantly (about 4% with HDPE and about 10% with MDPE). Puncture resistance is especially important during installation since workers can damage the geomembrane during deployment. Also, sharp rocks can perforate the membrane from underneath and affect the integrity of the liner if the soil is not perfectly prepared.

3.2.4 Low Temperature Impact

Test results aimed at understanding the puncture impact resistance behavior of the polymers and blends used in this study were quite surprising, indicating very similar puncture impact strength for HDPE, MDPE, fPP, and their blends. Also, all samples showed ductile failure. This could be due to the specific test method that was used (ISO 6603) in which the test specimen is punctured at its center using a lubricated striker that impacts perpendicularly to the specimen surface and at high speed. This test was designed for rigid plastics and does not seem capable of discriminating between the performances of the flexible materials used in this study.

3.3 Environmental Stress Cracking Resistance (ESCR)

Test results for Environmental Stress Cracking Resistance (ESCR) according to ASTM D 1693 are reported in Table 5.

Table 5. ESCR of fPP, MDPE, HDPE, and HDPE-fPP Blends

Property	Test Method	Unit	fPP	MDPE	HDPE	HDPE + 20% fPP	HDPE + 40% fPP	HDPE + 20% LLDPE	HDPE + 40% LLDPE
ESCR (10% Igepal)	ASTM D 1693	hours	>1600	>1600	52	>1600	>1600	740	>1600
ESCR (100% Igepal)	ASTM D 1693	hours	>1600	>1600	185	>1600	>1600	>1600	>1600

Unlike PE based materials, fPP is not prone to environmental stress cracking, as confirmed in this study (ESCR > 1600 hours). The particular MDPE selected for this study also performed very well (ESCR > 1600 hours). However, the HDPE showed quite poor results at both 10% Igepal concentration (52 hours) and 100% Igepal concentration (185 hours). The addition of fPP at the 20% level was enough to dramatically improve the ESCR performance of HDPE, bringing it to the same level as 100% fPP or 100% MDPE (ESCR > 1600 hours). The addition of LLDPE also had a positive effect but not as great as fPP, since 40% addition of LLDPE was necessary to achieve the same effect as 20% fPP.

3.4 Weldability

In general fPP has a much broader welding window than PE based material due to the presence of amorphous polymer, which tends to soften and melt at lower temperatures than PE. In order to have a preliminary indication regarding whether the introduction of fPP affects the weldability of HDPE and MDPE, some sheet samples were welded with a hot wedge welding procedure using commercial equipment. Hot wedge welding is carried out by a hot wedge, which is

normally heated to a temperature of 300-500°C and pulled between the overlapping lower and upper geomembranes that need to be seamed. A system of guide rollers provides a complete surface contact between the membranes and the two separate tracks of the dual hot wedge. The surface layers of the geomembranes are melted and the two melt layers are pressed together by a squeeze roller system immediately behind the wedge. Basically, the membrane surfaces are united by the wedge-shaped arrangement and pressed together by the squeeze rollers immediately behind the wedge nose, realizing the seam. Hot wedge temperature, roller force and welding speed as well as process engineering and welding parameters can be independently controlled and adjusted to the correct values needed for the particular plastic material being used.

Seam integrity and strength were evaluated according to ASTM D 6392. This test method requires that welded specimens are subjected to both T-peel and shear tests:

- Shear tests on welded coupons can verify if there is proper elongation of the material immediately adjacent to the weld. This is useful to check if the material was adversely affected by excessive heat, scoring or over-grinding. For the materials used in this study, the shear test was considered complete once the specimen reached 50% elongation.

- The T-peel test verifies the degree of proper bonding of the weld. It was performed at a speed of 50 mm/min (as prescribed for HDPE membranes).

Pass requirements vary depending on the project and the material specification and are often determined per GRI GM19.

Based on the limited testing that was performed in this study, it is possible to summarize the results of the welding test as follows:

- fPP can be successfully welded at lower temperatures and higher speeds than HDPE/MDPE (HDPE/MDPE showed adhesion failure when welded at 400°C, while fPP could be successfully welded at high speed even at 360°C).

- The weldability window of HDPE seems to shift to lower temperatures when blended with fPP or LLDPE (HDPE could be successfully welded at 400°C when 40% fPP or 20% LLDPE were added).

- Typical HDPE welding conditions might have to be adjusted if fPP or LLDPE is blended in as a modifier.

A more thorough study would need to be executed to map the welding windows of selected HDPE-fPP blends.

3.5 Accelerated UV Weathering

Accelerated QUV aging was performed on 1 mm thick sheet specimens using an ATLAS UV 2000 apparatus and the following conditions:

- 20 hours of UV exposure with an uninsulated black panel temperature set point of 75°C (167°F), alternating with 4 hours condensation at 60°C (140°F) uninsulated black panel temperature set point.

- Irradiance level of 0.78 W/(m² nm) at 340 nm

- Exposure duration = 1000 hours

Weathering conditions were in accordance with the following two standards, which are often used for accelerated weathering tests of geomembrane formulations:

- ASTM D7238 - Standard Test Method for Effect of Exposure of Unreinforced Polyolefin Geomembrane Using Fluorescent UV Condensation.

- GRI Test Method GM13 - Standard Specification for Test Methods, Test Properties and Testing Frequency for High Density Polyethylene (HDPE) Smooth and Textured Geomembranes.

Due to equipment availability issues, the test was stopped after 1000 hours of exposure (as opposed to the 1600 hours required by GM13). For the evaluation of changes in material properties, tensile strength retention was measured, while it was not possible to measure HP-OIT retention. Test results are reported on Table 6 and Table 7.

Table 6. Tensile Stress At Break Retention after QUV Weathering of fPP, HDPE, HDPE-fPP, and HDPE-LLDPE Blends

Physical Property	Exposure Time (Hours)	Test Method	Unit	fPP	HDPE	HDPE + 20% fPP	HDPE + 40% fPP	HDPE + 20% LLDPE	HDPE + 40% LLDPE
Tensile Stress at Break	0	ISO 527	MPa	22.4	15.8	16.5	23.2	21.8	30.7
Tensile Stress at Break	500	ISO 527	MPa	21.3	16.3	14.9	24.6	17.3	32.8
Tensile Stress at Break	1000	ISO 527	MPa	20.3	16.6	14.7	19.8	16.0	17.0

Table 7. Tensile Stress At Break Retention after QUV Weathering of fPP, MDPE, MDPE-fPP, and MDPE-LLDPE Blends

Physical Property	Exposure Time (Hours)	Test Method	Unit	fPP	MDPE	MDPE + 20% fPP	MDPE + 40% fPP	MDPE + 20% LLDPE	MDPE + 40% LLDPE
Tensile Stress at Break	0	ISO 527	MPa	22.4	32.4	24.8	24.7	32.3	29.5
Tensile Stress at Break	500	ISO 527	MPa	21.3	34.2	24.2	24.1	34.7	33.0
Tensile Stress at Break	1000	ISO 527	MPa	20.3	32.6	25.1	23.1	30.9	30.8

With the exception of HDPE-LLDPE blends, all samples have good tensile strength retention. It seems, therefore, that the addition of fPP does not significantly affect the UV weathering performance of HDPE/MDPE. It must be underlined,

however, that the performance of polyolefins during the accelerated UV weathering test is highly dependent on the presence of Carbon Black in the formula, and especially on the type and amount of specific antioxidants and UV stabilizers (Hindered Amine Light stabilizers, UV Scavengers, others). The selection of a suitable stabilization package is fundamental for achieving good results during the accelerated weathering test and long-term durability during service life.

4. SUMMARY

Test results for HDPE-fPP blends and MDPE-fPP blends are presented in this paper alongside test results for HDPE-LLDPE blends and MDPE-LLDPE blends. It seems that the addition of fPP to either HDPE or MDPE provides benefits in terms of increased flexibility, improved impact resistance at low temperature, and better ESCR. While no positive effect was found on CLTE and little detrimental effect on either tear or puncture resistance was noted, a synergistic effect on tensile stress at break for HDPE-fPP blends was indicated by the data. Weldability tests seem to show that fPP addition can offer an improvement in this regard as well, but a more thorough study is needed to confirm these findings. Finally, the accelerated UV weathering test indicated that the introduction of fPP does not have a negative effect on durability if a proper stabilization package is chosen.

REFERENCES

- Koryabina M., Ceccarani F., Balow M, Paff T., and Kozlowski B. (2009). A Review of the Environmental Factors Influencing the Durability of Polyolefins, *Geosynthetics 2009*, IFAI, Salt Lake City, Utah, USA.
- Pasquini, N. (2005). Polypropylene Handbook, 2nd Edition, Hanser Publishers, Munich, Germany.
- ASTM D 638, Standard Test Method for Tensile Properties of Plastics, *American Society for Testing and Materials*, West Conshohocken, Pennsylvania, USA. [do not include year since standards are re-published every year]
- ASTM D 790, Standard Test Method for Flexural Properties of Unreinforced and Reinforced Plastics and Electrical Insulating Materials, *American Society for Testing and Materials*, West Conshohocken, Pennsylvania, USA.
- ASTM D1004, Standard Test Method for Tear Resistance (Graves Tear) of Plastic Film and Sheeting, *American Society for Testing and Materials*, West Conshohocken, Pennsylvania, USA.
- ASTM D 1238, Standard Test Method for Melt Flow Rates of Thermoplastics by Extrusion Plastometer, *American Society for Testing and Materials*, West Conshohocken, Pennsylvania, USA.
- ASTM D 1693, Standard Test Method for Environmental Stress-Cracking of Ethylene Plastics, *American Society for Testing and Materials*, West Conshohocken, Pennsylvania, USA.
- ASTM D 4439, Standard Terminology for Geosynthetics, *American Society for Testing and Materials*, West Conshohocken, Pennsylvania, USA.
- ASTM D4833, Standard Test Method for Index Puncture Resistance of Geomembranes and Related Products, *American Society for Testing and Materials*, West Conshohocken, Pennsylvania, USA.
- ASTM D 5397, Standard Test Method for Evaluation of Stress Crack Resistance of Polyolefin Geomembranes Using Notched Constant Tensile Load Test, *American Society for Testing and Materials*, West Conshohocken, Pennsylvania, USA.
- ASTM D 6392 - Standard Test Method for Determining the Integrity of Non-reinforced Geomembrane Seams Produced Using Thermo-Fusion Methods, *American Society for Testing and Materials*, West Conshohocken, Pennsylvania, USA.
- ASTM D7238, Standard Test Method for Ultraviolet Florescent Tube Device, *American Society for Testing and Materials*, West Conshohocken, Pennsylvania, USA.
- ASTM D 7613, Standard Specification for Flexible Polypropylene Reinforced (fPP-R) and Nonreinforced (fPP) Geomembranes, *American Society for Testing and Materials*, West Conshohocken, Pennsylvania, USA.
- ISO 178, International Standard, Plastics-Determination of flexural properties, *ISO*, Geneva, Switzerland.
- ISO 180, International Standard, Plastics-Determination of Izod impact strength, *ISO*, Geneva, Switzerland.
- ISO 293, International Standard, Plastics - Compression moulding of test specimens of thermoplastic materials, *ISO*, Geneva, Switzerland.
- ISO 294-1,2,3,4, International Standard, Plastics-Injection moulding of test specimens of thermoplastic materials, *ISO*, Geneva, Switzerland.
- ISO 306, International Standard, Plastics - Thermoplastic materials - Determination of Vicat softening temperature (VST), *ISO*, Geneva, Switzerland.
- ISO 527-1,2,3, International Standard, Plastics-Determination of tensile properties, *ISO*, Geneva, Switzerland.
- ISO 1133, International Standard, Plastics - Determination of the melt mass-flow rate (MFR) and the melt volume-flow rate (MVR) of thermoplastics, *ISO*, Geneva, Switzerland.
- ISO 1183-2, International Standard, Plastics - Methods for determining the density of non-cellular plastics — Part 2: Density gradient column method, *ISO*, Geneva, Switzerland.

ISO 6603-2, International Standard, Plastics - Determination of puncture impact behaviour of rigid plastics — Part 2: Instrumented impact testing, ISO, Geneva, Switzerland.

ISO 11357-1, International Standard, Plastics-Differential scanning calorimetry (DSC), ISO, Geneva, Switzerland.

GRI Test Method GM13, Standard Specification for Test Methods, Test Properties and Testing Frequency for High Density Polyethylene (HDPE) Smooth and Textured Geomembranes, *GRI*, Folsom, Pennsylvania, USA.

GRI Test Method GM18 - Standard Specification for Test Methods, Test Properties and Testing Frequencies for Flexible Polypropylene (fPP and fPP-R) Non-reinforced and Reinforced Geomembranes, *GRI*, Folsom, Pennsylvania, USA.

GRI Test Method GM19 - Standard Specification for Seam Strength and Related Properties of Thermally Bonded Polyolefin Geomembranes, *GRI*, Folsom, Pennsylvania, USA.

Environmental Benefit of Carbon Footprint Using Geotextile Tubes

M. ter Harmsel, TenCate Geosynthetics EMEA, Netherlands, M.terHarmsel@tencate.com
C.I. Jones, Sustain Ltd., United Kingdom, Craig.Jones@sustain.co.uk
T.W. Yee, TenCate Geosynthetics Asia, Malaysia, tw.yee@tencate.com

ABSTRACT

A carbon footprint is a measure of the impact that our activities have on the environment, and in particular climate change. It is the measurement of all the greenhouse gases generated by human activity including construction works, measured in units of tonnes of carbon dioxide equivalent. The lower the carbon footprint, the lesser the impact construction works have on the environment. Engineering solutions are not just compared purely on economic terms, but are beginning to be compared on carbon footprint as well. Therefore engineering solutions that protect and improve the environment are increasingly favored as opposed to those that have a negative impact to the environment. This paper describes and compares the carbon footprint of geotextile tubes alternatives versus conventional engineering solutions.

1. INTRODUCTION

Carbon footprinting as an approach is relatively new and has been developed from Life Cycle Assessment (LCA), which has been around since the late 60s. Both methods take a systematic view of the supply chain from raw material extraction through to the final disposal of the product. This approach crucially prevents decisions being made which may shift the environmental burden up and down the supply chain. The impact can be quantified as a total or can be broken down to present the results as its constituent sub-systems. The latter can be used to identify priority areas for improvements.

A product carbon footprint is an assessment of the global warming potential of a product and is also known as embodied carbon. This is often measured as a cradle to gate assessment, which includes all greenhouse gas (GHG) emissions up until the point where the product leaves the factory gate. For example raw material extraction, transportation at all stages, refining, processing and fabrication up to the product leaving its final factory gate. The boundaries of cradle to site also include the transportation up to the site of use for the product. Finally the boundaries of cradle to grave are the most holistic and include all lifecycle stages. This covers the cradle to site, usage (including operation and maintenance) and finally the end of life stage (recycling, reuse, and disposal). This study considered the cradle to grave carbon footprints of breakwater systems and sludge dewatering systems.

2. GEOTEXTILE TUBE SOLUTIONS

A geotextile tube is a closed ended tubular formed fabric unit tailored with regular filling ports. Its circumference and length may be sized specific for each project and are limited only by constraints of handling practicalities and site conditions. The geotextile tube contains the slurry mixture of solids and water that is pumped in, allows water to dissipate through the permeable fabric skin and retains solids within the geotextile tube. Geotextile tube solutions include use as structural units for marine and hydraulic engineering applications and use as containment and dewatering units for municipal, industrial, mining, agricultural and environmental dewatering applications.

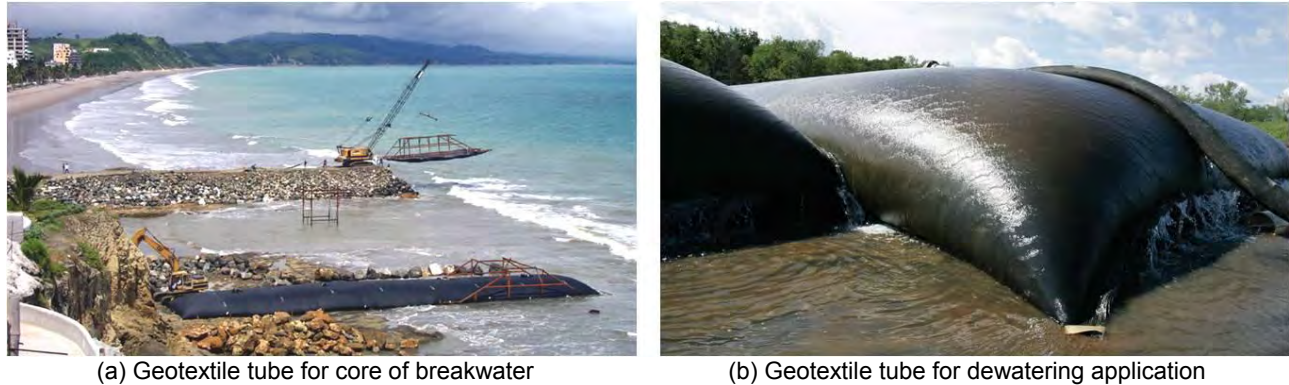
2.1 Marine and Hydraulic Engineering Applications

A geotextile tube is filled with sand to form structural unit as replacement for rock in marine and hydraulic engineering applications. Typically sand is specified as fill material for geotextile tube because it can be mixed with water to form slurry for hydraulic filling of the tube and the high permeability of sand allows the geotextile tube structural unit to be constructed rapidly with acceptable or negligible post construction deformations. Figure 1(a) shows the use of geotextile tube to replace the core of a coastal breakwater.

2.2 Dewatering Applications

Dewatering is a process operation used to reduce moisture content of sludge for a few reasons; reduction of volume to reduce cost of transportation and landfilling, reduction of excess moisture to increase the calorific value and processing cost during incineration, etc. Effectiveness is measured by percentage solids capture, dewatering rate and achievable solids content of dewatered material. Effluent water quality is also a measured success criteria, especially when in a

proposed application there is no further water treatment prior to the effluent water being released. Conventional dewatering techniques include mechanical dewatering (centrifuges, belt presses, etc.) which require high capital investment cost and natural dewatering (drying beds and sludge lagoons) which require large area of land and can be very time consuming. The performance of natural dewatering techniques is subject to the weather and the exposed sludge can emit foul odor as well as attract airborne vectors which are negative factors to the environment. Geotextile tube dewatering technology has the advantages of being able to handle very large sludge volumes, achieving very high solids capture rate, requiring low capital investment and the sludge is effectively concealed from the environment. Figure 1(b) shows the use of geotextile tube for dewatering applications.



(a) Geotextile tube for core of breakwater

(b) Geotextile tube for dewatering application

Figure 1. Geotextile tube applications

3. CARBON FOOTPRINTING METHODOLOGY

The carbon footprint was calculated by collecting data from the supply chain (primary data) and combined with literature sources (secondary data). Data was collected throughout the lifecycle which covered:

- Production of raw materials
- Transport of raw materials
- Manufacturing of the geotextiles
- Transportation to final customer
- Use
- Transport to disposal
- End of life

End of life was determined to be negligible in this study. The method used is called QuickSteps and is built upon the PAS 2050:2011 method of carbon footprinting, which is the most robust carbon footprint method to date. The main difference between these two methods is the different requirements to collect primary data from the supply chain and first tier suppliers. However the underlying principles and method requirements are otherwise the same.

The carbon footprint is measured in CO₂ equivalents (CO₂e) and all IPCC direct GHGs were included in this assessment and converted to CO₂ equivalents (CO₂e) using the latest IPCC (2007) global warming potentials (GWP). These include carbon dioxide, methane, nitrous oxide, hydrofluorocarbons (HFC), perfluorocarbons (PFC) and sulfur hexafluoride.

The exclusion from the carbon footprint is in line with accepted international standards (ISO 14040:2006 and ISO 14044:2006, and the PAS 2050:2011). This study excludes:

- Capital goods (e.g. manufacturing of vehicles, roads, buildings, machinery etc.)
- Human energy inputs to processes
- Transport of employees to and from the place of work
- Animals providing transport services
- Offsetting of emissions

The most recent data for primary data collection were used, covering a period of the calendar year in 2010. The period of GHG assessment (i.e. the temporal boundary) is 100 years, which is in line with PAS 2050:2011 and all global warming potential factors are based on a 100 year timeline.

4. CARBON FOOTPRINT COMPARISONS

Carbon footprint calculations are project specific. In many instances, geotextile tube options result in lower carbon footprints when compared with conventional solutions. A proprietary Carbon Footprint Calculator was developed for the purpose of calculating carbon footprint of and comparison between conventional and geotextile tube solutions. One comparison between geotextile tube option against conventional rock solution in marine and hydraulic engineering application and one comparison between geotextile tube option and belt press operation in dewatering application each are provided. A project case study is also described whereby the geotextile tube solution resulted in significant carbon footprint savings over the conventional solution.

4.1 Breakwater Example

In this hypothetical example a comparison is made between a breakwater built using only rock material and a breakwater built using a core consisting of stacked geotextile tube construction covered with rip-rap. This example is based on conditions applicable to the Netherlands. Figure 2(a) shows the conventional rock breakwater while Figure 2(b) shows the breakwater option with geotextile tube replaced core. Both have the same overall geometrical cross-sectional dimensions. The breakwater height is assumed as 3.3 m, with a base of 16.2 m, crown of 3 m and side slopes of 1:2. This breakwater geometry is not untypical of an inland breakwater application in the Netherlands. In Figure 2(b) three identical geotextile tube filled to height of 1.5 m are used as the core of the breakwater, replacing rock. A geotextile protection layer is used to cover the geotextile tubes before rip-rap is placed on. Both design options involved the use of a basal geotextile layer for the breakwater.

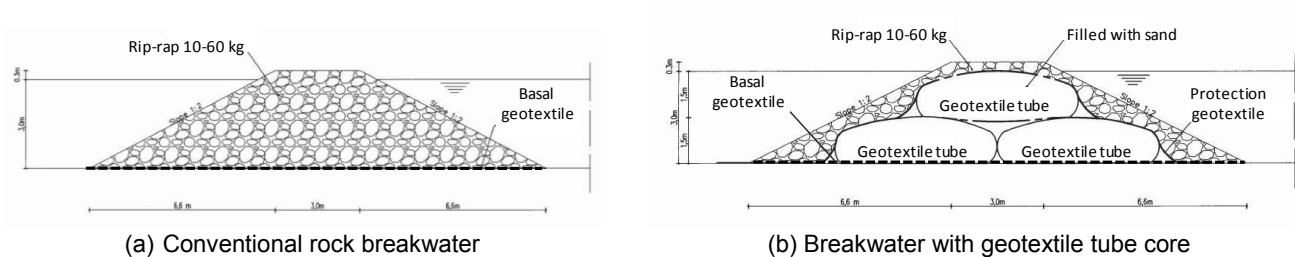


Figure 2. Breakwater details

Table 1 shows the materials, transport quantities and quantities per 100 meter of breakwater for the conventional rock only system and the alternative geotextile tube core system. The carbon footprints for both systems were determined using the proprietary Carbon Footprint Calculator. Figure 3 shows the summary of the carbon footprints per 100 meter of breakwater for the conventional rock breakwater and geotextile tube alternative. Figure 3 also shows a savings of 95 tonnes of CO₂e in carbon footprint per 100 meter when the geotextile tube system is used in replacement of the conventional rock breakwater system.

These results show that, in the context of this example, the carbon footprint of the geotextile tube solution was lower because of the lower transport emissions. This is largely a result of the lower quantity of rocks used when compared with the conventional total rock solution, due to replacement of core with geotextile tubes filled with sand. The sand was dredged onsite for this case example and the pumping energy from this operation has been included in the study. However if the sand was imported to the site the transport distance would likely be small. This is because sand is typically sourced from a local resource.

Table 1. Materials, transport distances and quantities for conventional and geotextile tube solutions for a hypothetical inland breakwater in the Netherlands.

Materials	Transport distance	Quantities per 100 meter of breakwater	
		Conventional	Geotextile Tube
Geotextile tube (4 m diameter)	150 km by road	N.A.	300 m
Sand to fill geotextile tube	Site available	N.A.	4600 tonnes
Riprap (10 – 60 kg)	1200km by sea + 50km by road	7300 tonnes	1800 tonnes
Protection geotextile (200 g/m ² nonwoven)	150 km by road	N.A.	2300 m ²
Basal geotextile (300 g/m ² nonwoven)	150 km by road	1650 m ²	1650 m ²

Breakwater Carbon Calculator Results

1. Summary Results - TenCate Geotube® System V Rock Breakwater

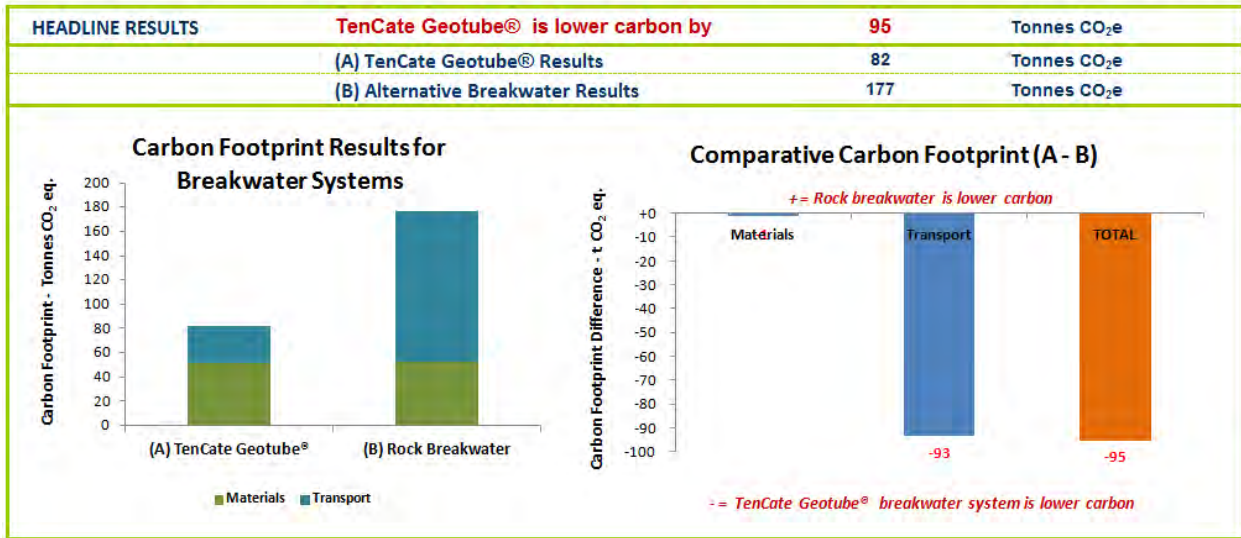


Figure 3. Summary output using proprietary Carbon Footprint Calculator

4.2 Dewatering Example

The dewatering example chosen involved a dredging project of a lake in Germany. A total of 30,000 m³ of lake sediment had to be dredged, dewatered and transported to a landfill. Two dewatering options were considered. The first option involved dewatering using a belt press system. The second option involved dewatering using geotextile tubes. The lake sediment had an in-situ solids concentration averaging 22%. Based on tests the dewatered solids concentration of 48% would be achieved for both options. In the comparison the dredging operation was not taken in account as this was similar for both options. For the geotextile tube dewatering option a dewatering platform had to be constructed first. The dewatering platform consisted of a geomembrane and a 100 mm thick layer of gravel above the liner and both materials were sourced locally within a 10 km zone. The source of energy for operating the belt press system was based on a 0.3 litre diesel generator. After the dewatering process the dewatered sludge needed to be hauled away over a distance of 30 km using 17 tonne trucks. The geotextile tube dewatering option was chosen based on both economic and carbon footprint competitiveness. The carbon footprints for both systems were determined using the proprietary Carbon Footprint Calculator. Figures 4(a) and 4(b) shows the boundaries of study for the dewatering carbon calculator of geotextile tube dewatering option and belt press dewatering option respectively. Figure 5(a) shows the carbon footprint breakdown for the geotextile tube dewatering option. Figure 5(b) shows the carbon footprint breakdown for the belt press dewatering option. For both options compared, the use of polymer as well as all related transportation activities were considered.

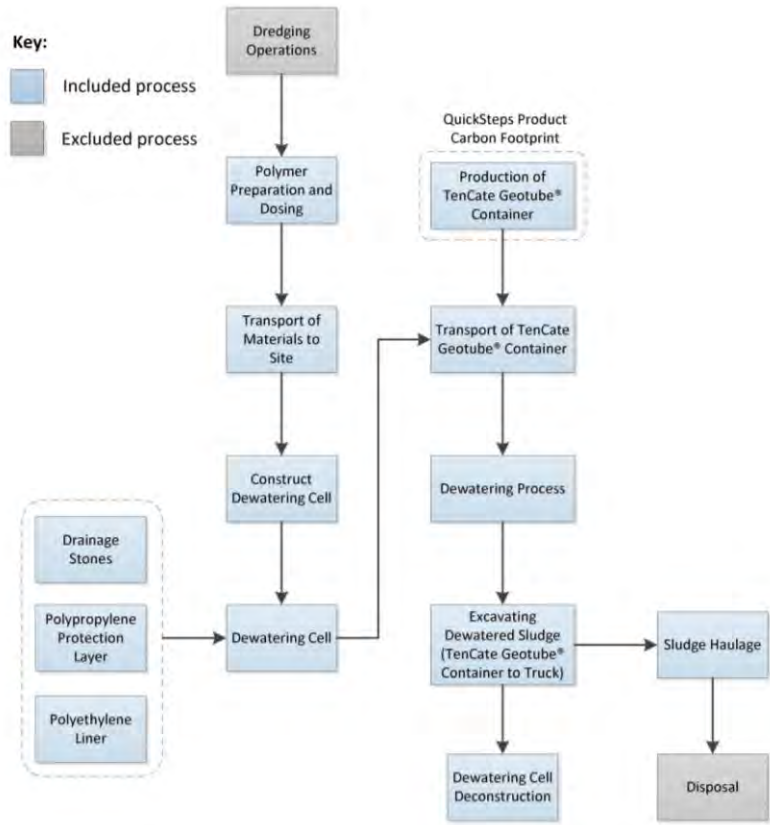
The geotextile tube dewatering option required 72 geotextile tubes of length 30.2 m and circumference of 13.7 m. The geotextile tube dewatering option had a higher cradle to site carbon footprint which comes in the form of the embodied carbon to manufacture the geotextile tubes. However the carbon footprint of the mechanical dewatering system in operation was significantly higher as a result of the electricity consumption of the mechanical system.

4.3 The Zutphen Case Study – A Combination of Dewatering and Hydraulic Engineering

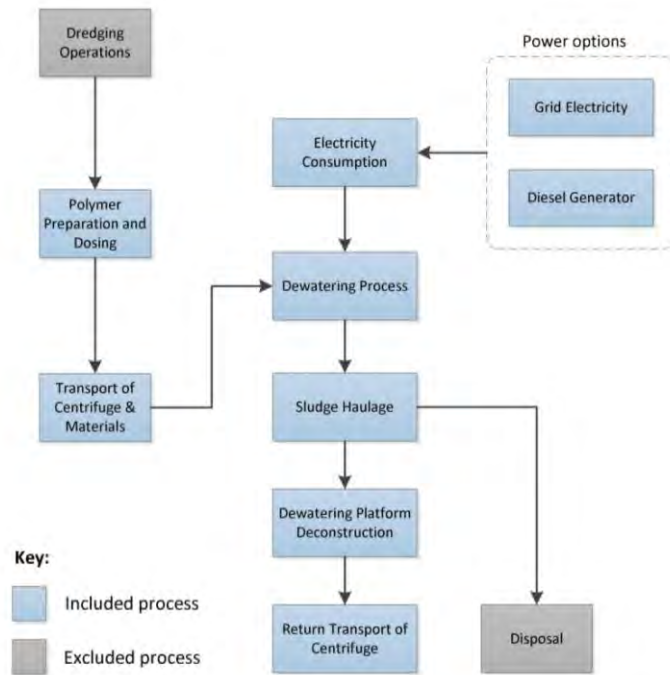
4.3.1 Background of Zutphen Project

The city of Zutphen in the Netherlands is located on River IJssel, a tributary of River Rhine. The old industrial harbour De Mars is being refurbished as part of a restoration plan of the entire industrial area. The harbour and its entrance have been neglected for many years. Fully loaded ships could only enter at high tide without grounding on the bottom of the harbour. To meet future requirements calling for access of ships with a draught of 2.8 meters, the port and the harbour entrance had to be dredged to the original depth and the riverbanks had to be restored. Without the riverbank

restoration, the harbour would again be filled with sand and sludge within a few years. Figure 6 shows the map of the Netherlands and location of Zutphen Project.

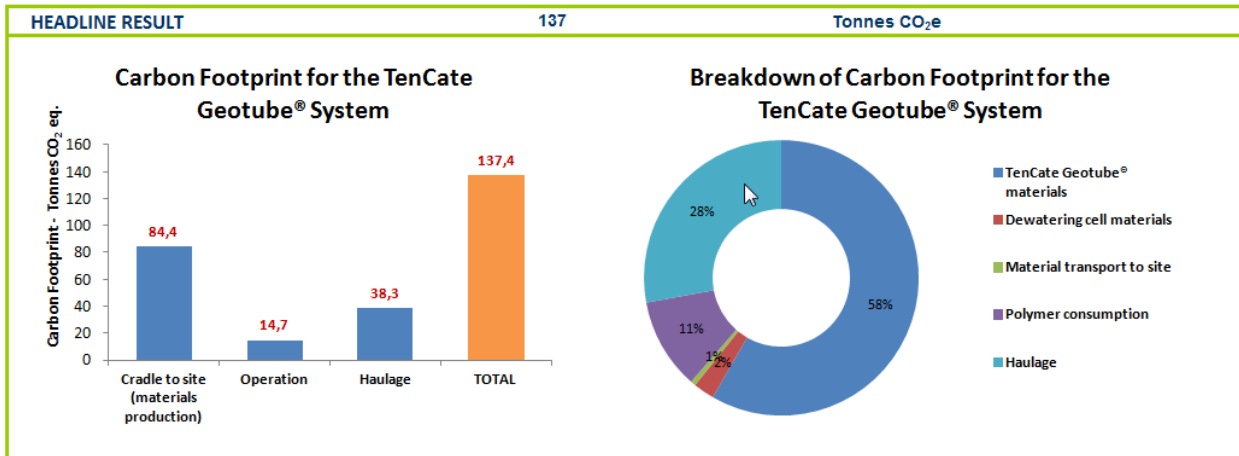


(a) Geotextile tube dewatering option

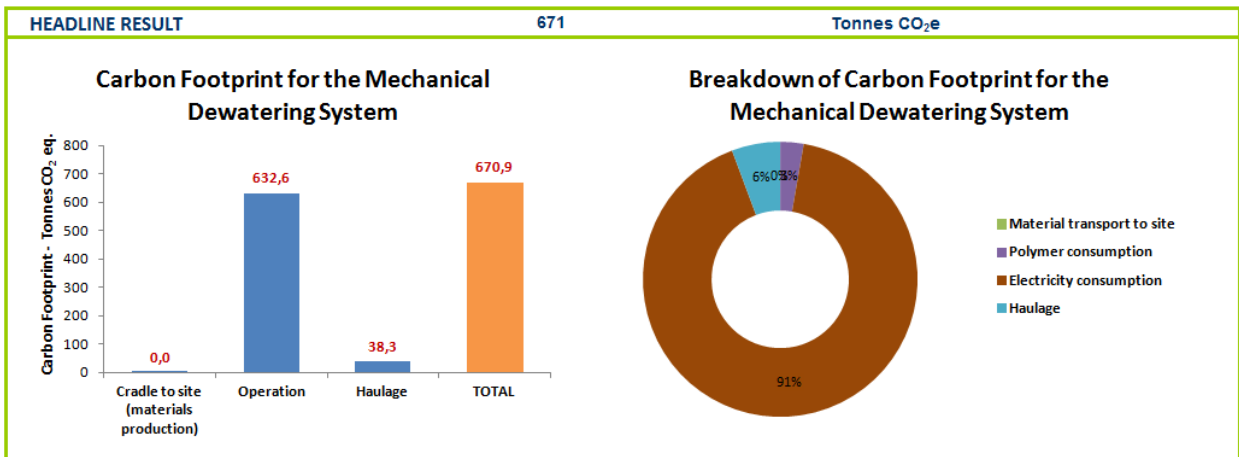


(b) Belt press dewatering option

Figure 4. Boundaries of study for the dewatering carbon calculator.



(a) Carbon footprint breakdown for the geotextile tube dewatering option



(b) Carbon footprint breakdown for the belt press dewatering option

Figure 5. Carbon footprint breakdown output using proprietary Carbon Footprint Calculator



Figure 6. Location of Zutphen Project (from Wortelboer et al. 2012).

4.3.2 The Geotextile Tube Solution

There has been a shift in strategy for the maintenance of waterways and harbours in the Netherlands in recent years. In the past the main question had been on 'how to get rid of dredged materials'. Currently, the question is more on 'where and how materials can be re-used in the most cost effective way'. In the Netherlands, contaminants in dredged materials are benchmarked by a series of designated values (Bray et al. 2001), as follows:

- Target Value (indicates the level below which risks to the environment are considered to be negligible, at the present state of knowledge)
- Limit Value (refers to the concentration at which the water sediment is considered relatively clean)
- Reference Value (is the concentration level indicating whether the dredged sediment is still fit for discharge in surface water or not)
- Intervention Value (indicates that remediation may be urgent, owing to increased risks to public health and the environment)
- Signal Value (is the concentration level of heavy metals above which the need for cleaning up should be investigated)

Dredged materials are then classified with disposal recommendations (Bray et al. 2001), as follows:

- Class 0 (below Target Value) can be spread over the land without restrictions
- Class 1 (exceeds Target Value, but is below the Limit Value) allowed to be disposed unless the soil quality is not significantly impaired
- Class 2 (does not meet the Limit Value, but is below the Reference Value) can be spread in surface water or on land, under certain conditions
- Class 3 (does not meet the Reference Value, but remains below the Intervention Value) should be stored under controlled conditions, specific requirements can be set, depending on the storage location
- Class 4 (does not meet the Intervention Value) should be contained in isolation in deep pits or on land, in order to minimise the influence on the surroundings

The Zutphen Project required both dredging and riverbank works. For the Zutphen Project, a total of 6,000 m³ of Class 2 sediment and 12,000 m³ of Class 3 sediments had to be dredged. The Class 3 contaminated sediment would have required placement in confined disposal facilities, which would have been a costly operation. The geotextile tube solution was able to solve both problems in an economical and green manner. Geotextile tube units filled with dredged sediments from the harbour were dewatered and used as replacement of imported fill material to raise the embankments to the required level. The final structure had to fulfil the geotechnical stability requirement as well as withstand the forces of River IJssel, the fastest flowing river in the Netherlands.

4.3.3 Works Execution

Figure 7 shows the aerial view of dewatering works along the riverbank. This riverbank restoration is adjacent to the harbor entrance where dredging works were carried out to increase the draught for improved navigation. Four work compartments were created, defined by sheet piles as its boundary. The compartments, each 100 m by 100 m, are aligned along the 400 m length of riverbank to be restored. The reasons for doing so were as follows:

- the sheet piles formed a barrier in which the compartments could be prepared for works,
- the sheet piles formed a barrier against River IJssel, creating a safety margin for rising water levels,
- the sheet piles contributed to the geotechnical factor of safety of the restored river bank,
- the compartments formed enclosures to serve as dewatering platforms, and
- effluent water from the tubes could be collected in the adjacent compartments and tested before it was discharged to the river in a controlled way.

The geotextile tubes were laid out and filled within within the confines of the work compartments. In each of the compartments, 4 tubes were filled on a flat surface. The geotextile tubes were sized such that they fit the confines of the compartments but at the same time maximum dewatering capacity is achieved. Figure 8 shows the filling of geotextile tube with dredged contaminated sediment within the sheet pile compartments. The tubes were filled in pairs of two with dredged material having a solids concentration of about 10%. Chemical accelerant was injected into the incoming slurry stream. The in-tube material consolidated to 65% solids concentration within 4 days. Figure 9 shows the backfilling of soil over the consolidated geotextile tube.



Figure 7. Aerial view of geotextile tube dewatering works along the riverbank.



Figure 8. Filling of geotextile tube with dredged contaminated sediment.



Figure 9. Backfilling over dewatered and stabilized geotextile tube.

4.3.4 Carbon Footprint Savings Using Geotextile Tube Solution

For the Zutphen Project a comparison of carbon footprint is made between the geotextile tube solution and that of a conventional solution. For the comparison we are only looking at the process or processes that are different between the two solutions. The conventional solution would have involved two processes, namely:

- Transportation of 12,000 m³ of Class 3 dredged contaminated sediment to the storage depot IJsselooog in the IJsselmeer for disposal
- The importation of 12,000 m³ of suitable backfill, spreading and compaction as part of the riverbank restoration works (this is the extra quantity of fill that would equal the space occupied by the dewatered sludge in the geotextile tube used for the riverbank restoration works of the adopted solution)

The geotextile solution adopted for the Zutphen Project involved only one process that was different from the conventional solution ie. use of geotextile tube and polymer as chemical accelerant for the dewatering of 12,000 m³ of Class 3 dredged contaminated sediment. Table 2 shows the carbon footprint comparisons between the geotextile tube solution and the conventional solution. These comparisons were conducted based on published carbon footprint rates (DEFRA 2010). It can be seen that an estimated savings of 83 tonnes of eCO₂ (equivalent carbon dioxide) was achieved with the adoption of the geotextile tube solution. In the context of only the compared equivalent processes, the savings for the geotextile tube solution was about 55%.

It should be noted that the storage of dredged contaminated sludge at IJsselooog involved a further carbon footprint that has not been included in the calculations. The construction, operation and final closure of the storage depot IJsselooog has a footprint and therefore the storage of 12,000 m³ of dredged contaminated sediment there would have involved a specific share of that carbon footprint. It was not possible to calculate this carbon footprint for this study due to a lack of data on the history and the future fate of the storage depot. It was therefore neglected. However this would have further tipped the balance in favor of the geotextile tube option.

Table 2. Carbon footprint comparisons between geotextile tube and conventional solutions for Zutphen Project.

Activity	Tonnes of eCO ₂	
	Conventional	Geotextile Tube
Transportation of 12,000 m ³ of Class 3 dredged contaminated sediment to IJsselooog	38	N.A.
Importation of 12,000 m ³ of suitable backfill, spreading and compaction	110	N.A.
Use of geotextile tube and chemical accelerant, and dewatering of 12,000 m ³ of Class 3 dredged contaminated sediment	N.A.	65
Total	148	65

5. CONCLUSIONS

This paper described the methodology for carbon footprinting of geotextile tube solutions and the conventional systems they replace. Two comparison examples have been given, one for marine and hydraulic application and one for dewatering application. A dredging and dewatering case study was also presented. Geotextile tube solutions appear to have more favorable carbon footprints over conventional systems in the cases presented.

REFERENCES

- Bray, R.N., Bates, A.D. & Land, J.M. (2001). Disposal of dredged material. *Dredging: A Handbook for Engineers*: Chapter 5, 89-111. Butterworth-Heinemann, Oxford, UK.
- DEFRA (2010). 2010 Guidelines to Defra/DECC's GHG Conversion Factors for Company reporting, The department for Environment, Food and rural Affairs (DEFRA).
- IPCC (2007). Climate Change 2007, *Intergovernmental Panel on Climate Change Fourth Assessment Report*, Geneva, Switzerland.
- ISO 14040:2006. Environmental management – Life cycle assessment – Principles and framework, *International Organization for Standardization*, Geneva, Switzerland.

- ISO 1404:2006. Environmental management – Life cycle assessment – Requirements and guidelines, *International Organization for Standardization*, Geneva, Switzerland.
- PAS 2050:2011. Assessing the lifecycle greenhouse gas emissions of goods and services, *British Standards Institution*, London, United Kingdom.
- Wortelboer, R.J.M., ter Harmsel, M., Zengerink, E., Westerhof, E.J. and Yee, T.W. (2012). Green environmental solutions with geotextile tubes – two case studies: Wack-Wack, Philippines and Zutphen, Netherlands, *5th European Geosynthetics Conference*, Valencia, Spain, (in print).

Estimating the Lifetime of Exposed Geomembranes Using Thin-film Samples and Accelerated UV Aging

Daniel C. Bratton, GSE Lining Technology, LLC, Houston, TX

ABSTRACT

As polyethylene geomembranes are increasingly used in exposed applications it is ever more important to quantify the lifetime of a geomembrane under these conditions. When exposed to UV radiation, free radicals are formed in the polyethylene matrix which react with the polymer chain and cause degradation. UV stabilizers and antioxidants are added to the polymer to intercept free radicals and neutralize them.

The relative concentration of additives within the polymer can be measured using the oxidative induction time (OIT). Using the Arrhenius methodology, an OIT depletion rate can be calculated. It is hypothesized that when two samples of identical formulations but different thicknesses (such as 1.5 mm against 0.125 mm) are subjected to the same accelerated UV weathering conditions that the thinner sample will have a higher OIT depletion rate. A model is proposed to quantify the acceleration factor based solely upon the difference in sample thickness.

1. INTRODUCTION

As polymer technology advances forward and plastic formulations are continuously improved, polyethylene has become increasingly practical to use in exposed engineering applications. These applications include landfill caps, solar ponds, wastewater treatment and other engineering projects that require the geomembrane to be exposed to the sun while in use. It is well established that without the proper protection, polyethylene will readily degrade when exposed to ultraviolet radiation (UV) from the sun. Extensive research has been done to discover the degradation mechanisms and the chemical reaction kinetics of degradation (Wiles and Carlsson 1980, Singh and Sharma 2007, Suits and Hsuan 2003). Moreover, practical studies have been performed to estimate the lifetime of exposed geomembranes with the use of accelerated aging (Hsuan and Koerner 1998, Sangram and Sharma 2002, Hsuan et al. 2008, Rowe et al. 2001, Accorsi 1999, Koerner et al. 2005). This study has focused primarily on the development of an empirical model that can be used to estimate the lifetime of a geomembrane using its thin-film equivalent during accelerated UV aging. The use of this model in other accelerated aging applications is discussed. The main goal is to significantly decrease the amount of time it takes to estimate the lifetime of an exposed geomembrane. Although it is not recommended to depend solely on the results of a thin-film aging test, this method can provide a lifetime estimate in a reasonable amount of time for research and product development purposes. Only by testing a full thickness sample can the prediction by the model be verified.

1.1 The Role of Antioxidants and UV Stabilizers

For the most part, it is accepted that the degradation of polyethylene when exposed to UV radiation is initiated by the formation of free radicals (Hsuan et al. 2008). These free radicals will react with oxygen to produce hydroperoxide (ROOH) groups. The formation of the ROOH group is the primary trigger for degradation. As the concentration of ROOH increases it will eventually reach a critical point where it can readily degrade with the aid of energy. The products of the ROOH degradation will then react with the polymer chain to cause degradation. Antioxidants and UV stabilizers are added to the polymer in small amounts to prevent degradation by (1) converting the free radical species to stable molecules and (2) decomposing hydroperoxides (ROOH) into stable groups rather than free radicals (Hsuan and Koerner 1998). However, antioxidants are consumed whenever they interrupt the oxidation cycle. In addition, antioxidants can migrate through the polymer and ultimately be removed by diffusion before they can serve their protective purpose. It is for this reason that the rate of antioxidant depletion is important to researchers and product developers.

The rate of the chemical reactions involved with oxidation and the formation of free radicals are increased with temperature. As the service temperature (or testing temperature) is increased, the molecules are more excited, there are more collisions, and the chance of there being sufficient activation energy for the reactions is increased. An increase in temperature also increases the antioxidant's ability to diffuse out of the geomembrane. If the temperature is increased sufficiently enough to approach the softening temperature of the polymer, then the diffusion of antioxidants out of the polymer will increase even more due to the additional amorphous regions in the polymer. An effective additive will readily react with free radicals and/or decompose hydroperoxides while also resisting diffusion out of the polymer.

1.2 Phases of Degradation

During accelerated UV aging, polyethylene geomembranes will degrade in three stages according to Hsuan and Koerner (1998): (1) depletion of antioxidants, (2) induction time, and (3) polymer degradation phase or acceleration period. The additives are in place to delay the occurrence of stages 2 and 3 and maximize the length of stage 1. Once the additives are depleted, the induction period begins. It is during this step that the concentration of ROOH begins to steadily increase until it reaches a critical point and can readily degrade. The degradation of ROOH signifies the end of the induction period and the beginning of the acceleration phase as shown in Figure 1 (Hsuan and Koerner 1998).

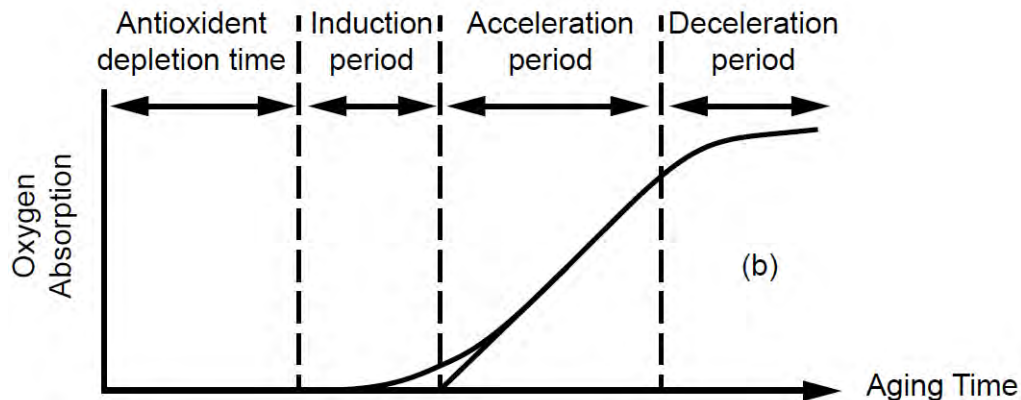


Figure 1. Phases for the oxidation and degradation of polyethylene (Hsuan and Koerner 1998)

The beginning of the induction phase can be measured by the oxidative induction time (OIT). As the OIT approaches zero it is an indication that the concentration of additives in the sample are also approaching zero. Following the end of the induction phase, the sample's progress through the acceleration phase can be measured by the change in mechanical properties, the change in rheology (melt index), or by the detection of certain functional groups that are formed by the degradation mechanisms. This study utilizes the OIT to measure the sample's progress through the antioxidant depletion phase.

1.3 Previous Aging Studies

This study was largely inspired by a previous investigation by Keegan and Ramsey (1998) which investigated the use of thin-films to compare the UV aging of samples with different levels of antioxidants and different types of UV screeners. The primary goal of Keegan and Ramsey's study was to investigate any differences during UV aging between formulations while this study was focused on deriving a relationship between the aging characteristics of thin-films and their geomembrane-thickness equivalents.

There have been a number of studies conducted on polyethylene to investigate its behavior in both accelerated aging and under field conditions. Hsuan and Koerner (1998) discussed types of antioxidants and their effect on the OIT and high pressure OIT (or HPOIT) in addition to outlining the stages of degradation as shown in Figure 1. Their study also supplied a method for antioxidant lifetime extrapolation using the OIT depletion rate which has been used in many studies since then (Sangram et al. 2002, Hsuan, et al. 2008, and Rowe, et al. 2010) and is used in this study as well. It is typically used to generate antioxidant depletion rates at several temperatures in order to extrapolate to a field temperature and estimate the time to complete antioxidant depletion under those conditions. However, these studies have mainly focused on the aging of samples of identical thickness and usually thicknesses that are typical for geomembranes such as 1.0, 1.5, or 2.0 mm. Rowe, et al. (2010) observed that the antioxidant depletion rate is not only dependent on the testing conditions, but also the thickness of the geomembrane.

1.4 The Effect of Sample Thickness

A previous study by Rowe, et al. (2010) has shown that when samples of varying thickness are exposed to identical aging conditions the OIT depletion rate increases with decreasing sample thickness. As expected, there is a strong relationship between sample thickness and the OIT depletion rate as depicted in Figure 2 below. In Rowe et al.'s study, samples of three different thicknesses (1.0, 1.5, and 2.0 mm) were immersed in a synthetic leachate at four different temperatures. For more than 12 months the samples were routinely tested for their OIT and an OIT depletion rate was calculated for each sample. Using this data, plots of the antioxidant depletion rate against the testing temperature for three sample thicknesses were produced. Figure 2 displays this same data presented in a different way. Instead of

plotting the antioxidant depletion rate against temperature at various thicknesses, the antioxidant depletion rate is plotted against the sample thickness at various temperatures and a strong linear trend is observed (R^2 was exceeding 0.94).

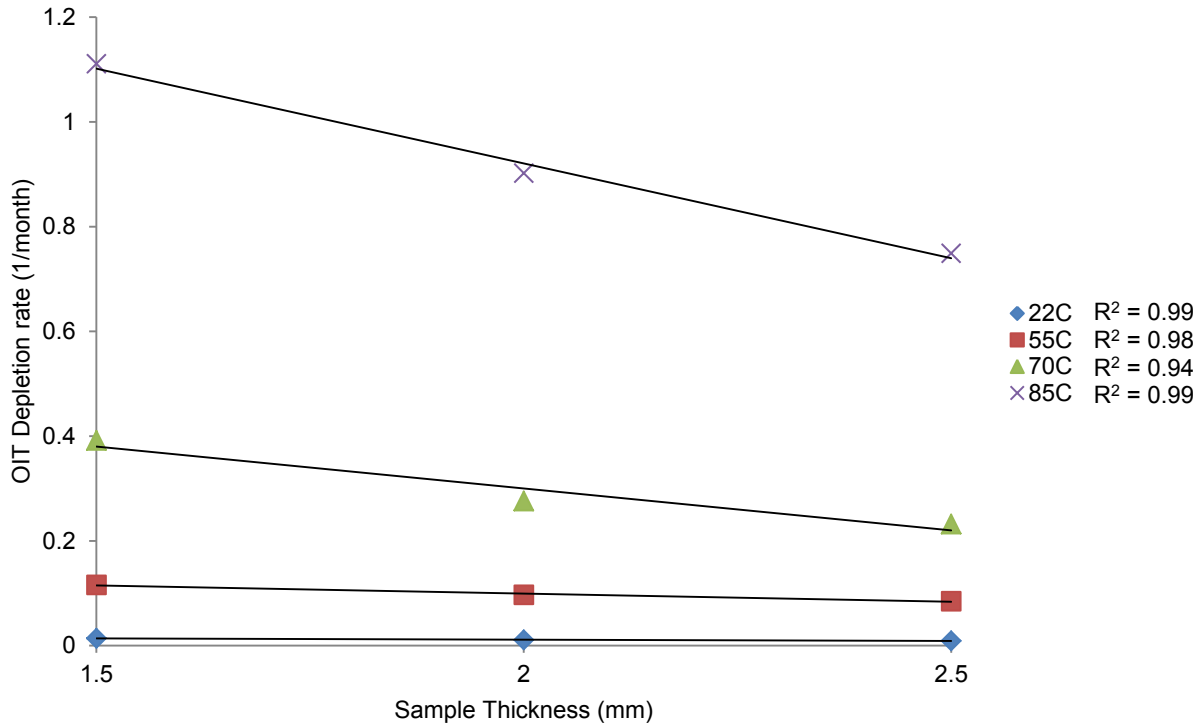


Figure 2. Data from Rowe, et al. (2011) plotted with thickness against OIT depletion rate.

Figure 2 demonstrates that the antioxidant depletion rate is strongly related to the sample thickness under identical testing conditions. This also suggests that OIT depletion rate of a thin-film could be used estimate the OIT depletion rate of a geomembrane-thickness sample. The use of thin-films is advantageous to product developers and researchers because it takes considerably less time to collect OIT depletion data.

The results published by Rowe et al. (2011) can only be used to predict the OIT depletion rate of samples that undergo the identical test method used. In order to compare the results from Rowe et al.'s test method to others, the OIT depletion rate ratio $\frac{s_H}{s_h}$ and the thickness ratio $\frac{H}{h}$ are introduced where s_H is the OIT depletion rate of a geomembrane-thickness sample, s_h is the OIT depletion rate of a thin-film sample, H is the thickness of the geomembrane-thickness sample, and h is the thickness of the thin-film sample. This way, the magnitude of difference between samples of different thicknesses is investigated and the differences between testing methods is eliminated. This is a key assumption of this study.

The thickness ratio can be compared to the OIT depletion rate ratio using the power law as shown in Equation 1 below. The constant k and power α can be determined by taking the natural log of Equation 1 and plotting $\ln \frac{s_H}{s_h}$ against $\ln \frac{H}{h}$. The slope of the resulting line is the power α and the y-intercept is the natural log of the constant k as shown in Equation 2.

$$A = kB^\alpha \text{ or } \frac{s_H}{s_h} = k \frac{H}{h}^\alpha \quad [1]$$

$$\ln \frac{s_H}{s_h} = \ln k + \alpha \ln \frac{H}{h} \quad [2]$$

The data from Rowe, et al.'s study (2010) can be used to generate values of $\frac{s_H}{s_h}$ and $\frac{H}{h}$. Three thickness ratios and OIT depletion rate ratios can be generated for the four temperatures as shown below in Table 1.

Table 1. Values used to determine the values of k and α in Equations 1 and 2 using data from Rowe, et al. (2010).

Testing Temperature (°C)	$\frac{H}{h}$	$\frac{s_H}{s_h}$
22	1.67	0.64
	1.33	0.79
	1.25	0.82
55	1.67	0.73
	1.33	0.84
	1.25	0.88
70	1.67	0.59
	1.33	0.70
	1.25	0.84
85	1.67	0.67
	1.33	0.81
	1.25	0.83

By taking the average of the values of $\frac{s_H}{s_h}$ for each value of $\frac{H}{h}$ for each temperature and then plotting the values according to Equation 2, Figure 3 is produced. The 95% confidence interval for each point is shown as error bars in Figure 3. The resulting linear trend line is shown in Equation 3 following Figure 3. Equation 4 displays the resulting power law. Theoretically, the value of k should be one (1) because two samples of identical thickness and formulation will exhibit the identical OIT depletion rate under the identical testing conditions. It is expected that the value of α be negative because the OIT depletion rate will decrease with increasing thickness. The analysis of Rowe et al.'s (2010) data yielded a value of 1.00 ± 0.13 for k and -0.86 ± 0.35 for α .

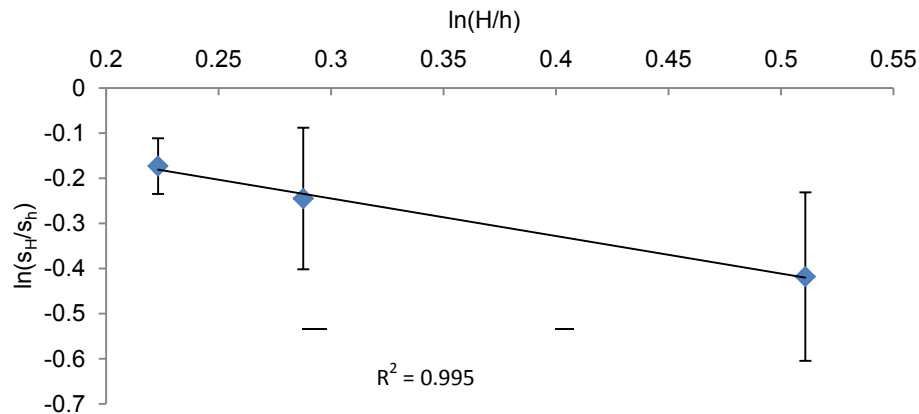


Figure 3. Linear trend line derived using Equation 2 and data from Rowe et al. (2010).

$$\ln \frac{s_H}{s_h} = (0.0046 \pm 0.13) + (-0.83 \pm 0.35) \ln \frac{H}{h} \quad [3]$$

$$\frac{s_H}{s_h} = (1.00 \pm 0.13) \frac{H}{h}^{-0.83 \pm 0.35} \quad [4]$$

Because this study utilizes the ratio between the OIT depletion rates and the ratio between the thicknesses, it is applicable across different test methods. Although samples will age differently depending on their testing conditions, the ratio between the OIT depletion rates should be the same as long as the samples are of the identical formulation and are tested in the exact same testing conditions.

In this study, UV aging was chosen because it is one of the more complex testing scenarios used for geomembranes. In addition, there is limited research published regarding the UV aging of geomembranes and it has become an increasingly important topic to the industry.

2.0 EXPERIMENTAL METHODOLOGY

2.1 Sample Preparation

All UV aging was performed in a QUV Basic ultraviolet fluorescent device which gives an irradiance of approximately $0.78 \text{ W/m}^2\text{nm}$. The UV aging was performed according to GRI GM13 (Geosynthetic Institute 2011) at a temperature of 70°C . This method incorporates a 24 hour cycle with 20 hours of UV exposure followed by a 4 hour condensation period at 60°C .

All of the samples were prepared using a lab scale calendaring line and there was some observed thickness variation in the samples (see Table 2 under thickness). Each sample was prepared according to ASTM D7238 which is shown in Figure 4. In order to avoid any interaction between the aluminum backing and the thin-film samples, a non-stabilized sample of 1.5mm HDPE was placed behind the thin-film sample.

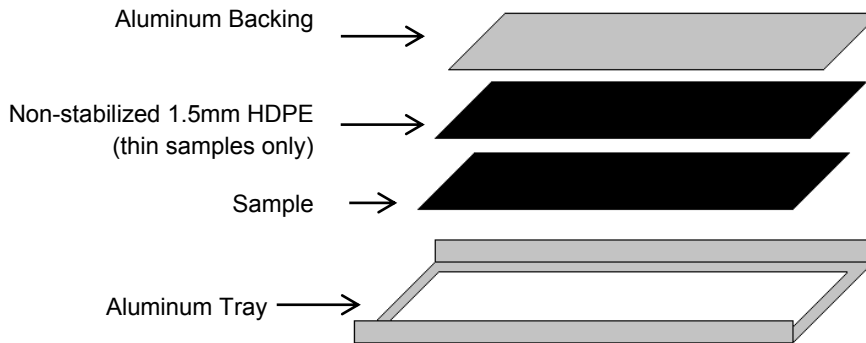


Figure 4. Sample preparation for the UV accelerated aging.

2.2 Sample Testing

Each sample was periodically taken out of the UV device and tested for its OIT according to ASTM D3895. Once an OIT value was below 10 minutes, it was assumed that the antioxidant depletion phase had ended. Each time the samples were removed from the UV device for testing they were placed back into the device randomly such that they were routinely rotated.

2.3 Calculation of the OIT Depletion Rate

As discussed in section 1.3, there are many studies that calculate an OIT depletion rate using Equations 5 and 6 below (Hsuan and Koerner 1998, Hsuan et al. 2008, Sangram and Sharma 2002). When plotting the log of the OITs against their exposure time, a linear trend is observed. The slope of the resulting line is the OIT depletion rate, s . This line can be expressed according to Equation 5 below where OIT_t is the OIT at a testing time t , OIT_0 is the initial OIT value, and s is the OIT depletion rate.

$$OIT(t) = OIT_0 e^{-st} \quad [5]$$

$$\ln OIT_t = \ln OIT_0 - st \quad [6]$$

Although the values of s have usually been calculated at various testing temperatures to extrapolate an OIT depletion rate at a desired temperature (usually a field temperature), this study used values of s calculated at two different geomembrane thicknesses in order to extrapolate and OIT depletion rate at a desired thickness.

2.4 Comparison of the Antioxidant Depletion Rates

As discussed in section 1.4, the OIT depletion rate ratio was related to the thickness ratio according to Equation 1. The OIT depletion rates of the thin-film and geomembrane-thickness samples were used to generate a value of power α . This value was compared to the value derived from data collected by Rowe, et al. (2010).

3.0 RESULTS AND DISCUSSION

3.1 Samples

Table 2 below displays the samples that were used during this study. The samples consisted of two different resins all of which had some level of thermal and UV stabilization. Two different master batches were utilized to provide four different formulations. All of the samples had 2.0 – 3.0% carbon black content. Samples with identical formulation IDs have identical formulations. There was some observed variance in the initial OIT of samples with identical formulations and it is believed that this was caused by variation in the resin lots used from sample to sample.

Table 2. Sample thickness and initial OIT information for both the thin-film and geomembrane-thickness samples.

Sample ID	Formulation ID	Initial OIT (mins)	Thickness (mils)
1	A	184	5.0±0.4
2	B	166	4.5±0.3
4	C	262	5.5±0.2
5	D	238	5.0±1.0
1*	A	257	61.3±2.0
2*	B	245	52.2±3.1
4*	C	260	48.9±2.9
5*	D	264	56.7±2.8

(*) Indicates geomembrane-thickness samples.

3.2 OIT and Calculated OIT Depletion Rates

Tables 3 and 4 display the OIT results of the samples over UV exposure time. All thin-film samples reached an OIT of 10 minutes in less than 1,678 hours. The OIT depletion rates calculated using Equation 6 for each sample are shown in Table 5.

Table 3. Measured OIT values for thin-film samples during UV exposure.
Measured OIT (mins)

UV Exposure (hrs)	1	2	4	5
0	184	166.4	262.7	237.9
337.0	47.6	45.6	159.35	123
557.0	18.4	12.95	127	88.91
902.5	6.4	11.2	23.8	51.77
1,317.0	-	-	-	-
1,678.0	-	-	3.81	9.7

Table 4. Measured OIT values for geomembrane-thickness samples during UV exposure.
Measured OIT (mins)

UV Exposure (hrs)	1*	2*	4*	5*
0	257	245	260	264
353	239	216	244	-
473	-	-	-	247
531	217	205	222	238
748	206.5	176.5	-	-
1014	188.5	132	165	-
2110	180	124	151.5	158.5

(*) Indicates geomembrane-thickness samples.

Table 5. Calculated OIT depletion rates using Equation 6.

Sample ID	Formulation ID	OIT Depletion Rate (1/hr, 10 ³)
1	A	3.76±0.87
2	B	3.14±0.33
4	C	3.31±0.09
5	D	2.32±0.25
1*	A	0.170±0.095
2*	B	0.343±0.217
4*	C	0.273±0.198
5*	D	0.250±0.072

*Indicates geomembrane-thickness samples.

Figures 5-8 display the measured OITs during UV aging for the thin-film and geomembrane-thickness samples for each formulation. As expected, the OIT depletion rates for the thin-film samples are much greater than the OIT depletion rates of the geomembrane-thickness samples.

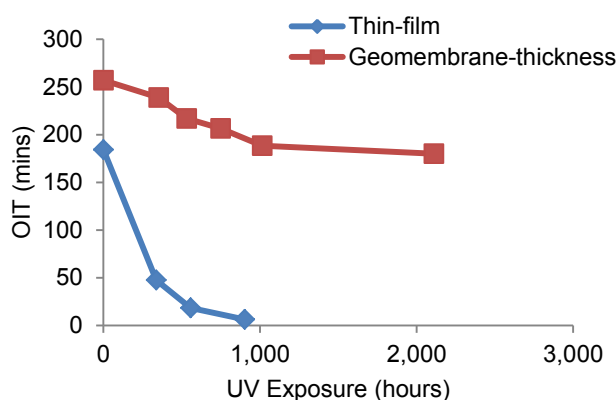


Figure 5. Measured OIT values during UV aging for formulation 1.

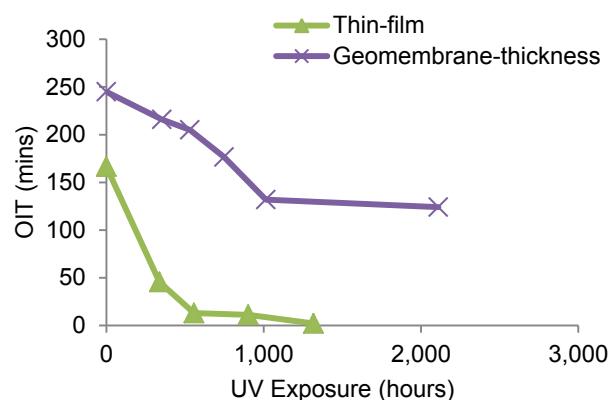


Figure 6. Measured OIT values during UV aging for formulation 2.

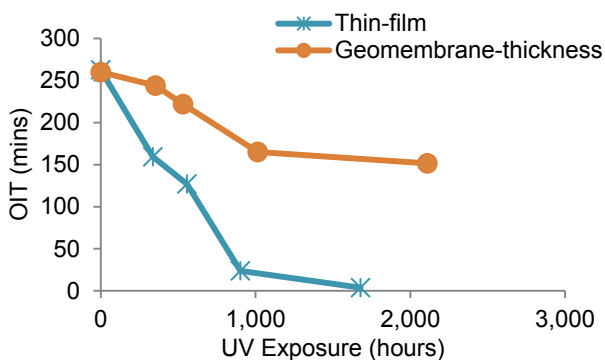


Figure 7. Measured OIT values during UV aging for formulation 4.

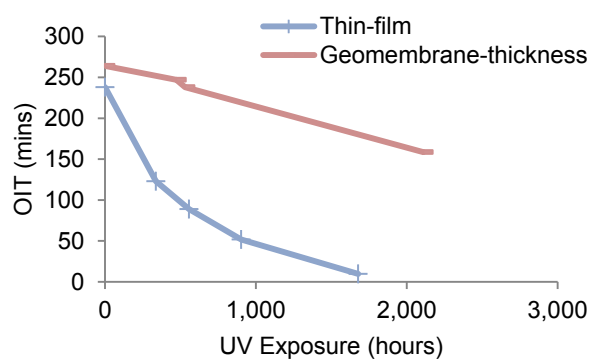


Figure 8. Measured OIT values during UV aging for formulation 5.

3.3 Calculated Values of α During UV Aging

Values for α can be calculated for each of the four formulations that were evaluated during accelerated UV aging. The value for k cannot be determined because only one value of $\frac{H}{h}$ and $\frac{s_H}{s_h}$ was produced for each formulation. As discussed in section 1.4, k is expected equal to one (1). Values for α can be calculated using Equation 7 below using a value of 1.00 for k . Table 6 displays the calculated values for α for each formulation.

$$\frac{s_H}{s_h} = (1.00) \frac{H}{h}^\alpha \quad [7]$$

Table 6. Calculated values of α for the UV aging samples using a value of 1.00 for k .

Formulation ID	α
A	-1.23
B	-0.91
C	-1.14
D	-0.92

The average value of α between the four formulations listed in Table 6 was -1.05 ± 0.34 which is comparable to the value of α that was previously calculated with Rowe et al.'s data (2011): -0.86 ± 0.35 . A preliminary F-test was conducted for the equality of variance and indicated that the variance is not statistically different between the two values of α ($P=0.0515$). A t-test assuming equal variances confirms that there is no significant statistical difference ($P=0.0621$) between the values of α calculated from Rowe et al.'s data and the data from this study.

Because the value of P (0.0515) was very close to indicating there was a significant difference between the sample variance, a t-test assuming that the variance was not equal was performed and also indicated that there was no statistical difference between the two values of α ($P=0.0688$).

A more simplified form of Equation 7 uses a value of -1 for α and a value of 1 for k and is shown below in Equation 8. Table 7 displays the estimated values of the OIT depletion rate of the geomembrane-thickness samples (s_H) using Equation 8. Table 8 displays the estimated OIT value of the geomembrane-thickness samples after 1,600 hours of UV exposure compared to the observed results.

$$\frac{s_H}{s_h} = \frac{h}{H} \quad [8]$$

By incorporating Equation 6 into Equation 8, the OIT at a desired time can be calculated directly as shown in Equation 9 where t is the desired time, h is the thin-film thickness, s_h is the OIT depletion rate of the thin-film, H is the desired thickness, OIT_t is the OIT value at time t for the desired thickness, and $OIT_{H,0}$ is the initial OIT value of the desired thickness (which can be substituted for $OIT_{h,0}$, the initial OIT of the thin-film sample, if the formulation is identical to the geomembrane-thickness sample).

$$OIT_t H = OIT_{H,0} e^{\frac{-(t)(h)(s_h)}{H}} \quad [9]$$

Table 7. Values of s_H predicted using Equation 8 for geomembrane-thickness samples.

Formulation ID	Measured values of s_h (10^3 , 1/hr)	Measured values of s_H (10^3 , 1/hr)	Estimated s_H Using Equation 8 $\alpha = -1.0$ (10^3 , 1/hr)	Percent Difference Between s_H Values $\alpha = -1.0$ (%)
A	3.75	0.170	0.306	79.5
B	3.17	0.343	0.273	20.3
C	3.31	0.274	0.372	36.0
D	2.32	0.250	0.205	18.2

Table 8. OIT values at 1,600 UV hours predicted using Equation 9 for geomembrane-thickness samples.

Formulation ID	Measured OIT value at 1,600 UV hours ¹ (mins)	Predicted OIT value at 1,600 hours UV exposure using Equation 8 (mins)	Percent difference between OIT values (%)
A	196	158	19.5
B	142	158	14.6
C	166	142	-11.8
D	177	190	-7.53

¹The value was extrapolated from measured OIT data using equation 5.

Using a value of -1 for α and a value of 1 for k , the OIT at 1,600 hours of UV exposure was predicted within 13.3% on average. In half the samples, the OIT was under predicted. For a more conservative approach, the value for α can be increased to -0.9. Using this value for α , the OIT after 1,600 hours of UV exposure is predicted within 14.7% on average and was under predicted in all four samples.

4.0 CONCLUSION

Using thin-films to estimate the OIT depletion rate of geomembrane-thickness samples can significantly reduce testing time and enable product developers and researchers to quickly estimate the aging performance of a geomembrane sample.

A strong relationship was found between the thickness of the sample and the OIT depletion rate. The OIT depletion rates are highly dependent on the test environment; therefore, a method was devised to eliminate the differences between test methods by introducing the ratio between the OIT depletion rates ($\frac{S_H}{S_h}$) and the ratio of the thicknesses $\frac{H}{h}$. By relating these two ratios using the power law as shown in Equation 1, the results can be compared across different testing methods. This study compared aging results generated by Rowe et al. (2011), which immersed samples in synthetic leachate at various temperatures, to the results of accelerated UV aging. The resulting values of α from the analysis of both data sets are statistically the same. By analyzing data from Rowe et al.'s (2011) study, α was -0.83 ± 0.35 . The α calculated in this study was -1.05 ± 0.34 .

The value of alpha can be used to estimate the OIT depletion rate of a sample of a desired thickness in any testing environment when the OIT depletion rate of a thin-film sample is known. Equation 1 can be simplified by assuming a value of -1.0 for α and 1.0 for k . When using this estimation, the OIT values after 1,600 hours of UV exposure of the geomembrane-thickness samples were estimated within 13.3%. For more conservative estimates, a value of -0.9 should be used for α . Using -0.9 for α yielded OIT estimates within 14.7% of the measured values after 1,600 hours of UV aging for the geomembrane-thickness samples.

The first 400 hours of UV aging performed on the geomembrane-thickness samples in this study was at a slightly elevated temperature from their thin-film equivalents (75°C instead of 70°C) and could be a source of error. Other sources of error include the difference in extruder residence time of the thin-film and geomembrane-thickness samples during processing. Additionally, the UV radiation is not believed to completely penetrate the geomembrane-thickness samples.

Any future work should incorporate at least three thicknesses so that a value for α and k can be estimated with a 95% confidence interval. Additional thicknesses will provide a more accurate calculation of α and k . Additionally, future studies should include several different testing methods such as oven aging and aging while immersed in liquids to confirm this study's applicability across various test methods. Multiple OITs should be taken for each formulation at each time interval to account for any error in the OIT test.

The use of thin-films could also be used to study the induction time and the acceleration phase (see Figure 1). Although this was outside of the scope of this study, thin-films could allow researchers to not only monitor the OIT depletion rate, but also the degradation of the mechanical properties. This could shed light on, as an example, the UV screening effect of different particle sizes of carbon black.

ACKNOWLEDGEMENTS

The author would like to thank Equistar Chemical Company for their support of this study.

REFERENCES

- Accorsi, J. V. (1999), The impact of carbon black morphology and dispersion on the weatherability of polyethylene, *International Wire & Cable Symposium*, Atlantic City, NJ.
- ASTM D 3895. Standard Test Method for Oxidative-Induction Time of Polyolefins by Differential Scanning Calorimetry, *American Society for Testing and Materials*, West Conshohocken, Pennsylvania, USA.
- ASTM D 7238. Standard Test Method for Effect of Exposure of Unreinforced Polyolefin Geomembrane Using Fluorescent UV Condensation Apparatus, *American Society for Testing and Materials*, West Conshohocken, Pennsylvania, USA.
- Geosynthetic Institute (2011), Test Methods, Test Properties and Testing Frequency for

- High Density Polyethylene (HDPE) Smooth and Textured Geomembranes, *Geosynthetic Institute*, Folsom, PA.
- Hsuan, G. Y., Schroeder, H. F., Rowe, K., Muller, W., Greenwood, J., Cazzuffi, D., Koerner, R. M. (2008), Long-term Performance and Lifetime Prediction of Geosynthetics, *EuroGeo4 Keynote Paper*, 1-38
- Hsuan, Y. G., Koerner, R. M. (1998), Antioxidant Depletion Lifetime in High Density Polyethylene Geomembranes, *Journal of Geotechnical and Geoenvironmental Engineering*, June: 532-541.
- Keegan, N., Ramsey, B. (1998), Accelerated Weathering Performance of White, Light Reflective Polyethylene Films and Sheet Samples, *Geosynthetics 1998*, 29-45.
- Koerner, G. R., Hsuan, G. Y. (1998), Photo-initiated Degradation of Geotextiles, *Journal of Geotechnical and Geoenvironmental Engineering*, December: 1159-1166.
- Koerner, R. M., Hsuan, Y. G., Koerner, G. R. (2005), Geomembrane Lifetime Prediction: Unexposed and Exposed Conditions, *GRI White Paper #6*, 1-9.
- Koerner, R. M., Lord, A. E. Jr., Hsuan, Y. H. (1992). Arrhenius modeling to predict geosynthetic degradation, *Geosynthetics '95 Conference Proceedings*, St. Paul, Minnesota, 921-938.
- Rowe, Kerry R., Islam, M. Z., Hsuan, Y. G. (2010), Effects of Thickness on the Aging of HDPE Geomembranes, *Journal of Geotechnical and Geoenvironmental Engineering*, February 2010: 299-309.
- Rowe, R. K., Sangram, H. P. (2002), Durability of HDPE geomembranes, *Geotextiles and Geomembranes*, 20, 77-95.
- Sangram, H. P., Rowe, R. K. (2002), Effect of exposure conditions on the depletion of antioxidants from high-density polyethylene (HDPE) geomembranes, *Can. Geotech.*, 39, 1221-1230.
- Singh, B., Sharma, N. (2008), Mechanistic implications of plastic degradation, *Polymer Degradation and Stability*, 93: 561-584.
- Suits, L. D., Hsuan, H. Y. (2003), Assessing the photo-degradation of geosynthetics by outdoor exposure and laboratory weatherometer, *Geotextiles and Geomembranes*, 21: 111-122.
- Wiles, D. M., Carlsson, D. J. (2008), Photostabilisation mechanism in polymers: a review, *Polymer Degradation and Stability*, 3: 61-72.

Evaluating Wind Uplift for Exposed Geomembranes Using Computer Modeling

Keaton Botelho, P.E., Geosyntec Consultants, USA, kbotelho@geosyntec.com,
Oliver Heynes, PhD, MMI Engineering, USA, ohaynes@mengineering.com,
Jean-Pierre Giroud, PhD, JP Giroud, Inc., USA, jpg@jpgiroud.com

ABSTRACT

The accurate calculation of wind uplift forces on an exposed geomembrane is essential for generating design requirements for the anchorage system. These requirements often largely dictate construction costs, so inaccuracies in the uplift calculation may have significant economic repercussions. Inaccuracies may occur when using generic suction factors rather than a site specific assessment using Computational Fluid Dynamics (CFD) technology. This paper presents preliminary research conducted to determine whether potential cost savings warrant more complex CFD modeling. Preliminary results comparing a two-dimensional case of an exposed geomembrane (which was used to develop generic suction factors commonly used to evaluate wind uplift) indicate the wind uplift forces calculated from a CFD model resulted in tensions that were significantly less than those using generic suction factors. Preliminary research was performed with the intention of employing CFD modeling to refine the simple prescription of generic suction factors on a site-specific basis.

1. INTRODUCTION

1.1 Objective

Giroud et al. (1995) developed and published a comprehensive analytical methodology for the various aspects of design of geomembrane exposed to wind, such as calculation of tension and strain in the geomembrane, evaluation of geomembrane deflection, and sizing of anchor trenches and benches. The methodology has been completed and refined in subsequent papers (Zornberg & Giroud 1997, Giroud et al. 1999, Giroud et al. 2006, Giroud 2009). Giroud et al. (1995) conservatively proposed that generic suction factors be used with their methodology. These generic suction factors were derived from small-scale wind tunnel testing published by Dedrick (1973, 1974a, 1974b, 1975). The wind tunnel testing was intended to replicate a reservoir with different orientations with respect to wind direction.

Herein, the analytical methodology, which is widely accepted and used, is not discussed. The purpose of this paper is essentially to show that the generic suction factors can be overly conservative and that Computational Fluid Dynamics (CFD) can be used as a method to evaluate the suction directly for a variety of different slope inclinations, orientations, lengths, and other parameters which may affect the magnitude of suction for exposed geomembranes. The paper shows that CFD modeling allows designers to predict the suction exerted by wind on an exposed geomembrane system more accurately than generic suction factors, which makes it possible to efficiently design a cost effective anchorage system.

1.2 Comparison

For the purpose of this paper, the suction was evaluated using both CFD and the generic suction factors derived by Giroud et al. (1995) from Dedrick small-scale tests. The same parameters were assumed for both approaches to provide an equal comparison of the results using both approaches. The model assumes the condition of a reservoir (negative slope inclination) located at sea level for simplification. The slope length and wind velocity were held constant and the slope inclination was adjusted from 2:1 (horizontal:vertical) to 4:1 (H:V) in 0.5:1 (H:V) increments.

2. APPLICABILITY OF CFD MODELING TO EXPOSED GEOMEMBRANES

Unlike empirical methods which are based upon relationships derived from experience, CFD is a technique that is based on the solution of Navier-Stokes equations. These equations were obtained by combining basic principles (equilibrium and continuity) with Newton's constitutive law of viscosity. Therefore, Navier-Stokes equations are the fundamental equations for analyzing the motion of Newtonian fluids. Examples include air flows over aircraft, water flow in rivers and lakes, wind dynamics on sites and many others. In all cases the fluids are governed by the same general principles which are satisfied in a CFD simulation. As computational power has increased, the use of CFD in engineering has also increased. CFD is now widely used in many industries and has been in some for almost 40 years.

A distinct advantage of CFD is the collection of data available once a simulation is complete. Contour plots of velocity, pressure, temperature or any number of variables may be produced, together with velocity vectors and streamlines. Figure 1 shows an example of a typical output from a CFD model, showing wind flow over a site. The modeling domain is approximately 1500 (length) x 900 (width) x 150 m (height) (5,000 x 3,000 x 500 ft) and the wind direction is in the length direction. The contour plot shows wind velocity magnitude, red indicating high velocity and blue low velocity. The effects of obstructions (in this case, a porous windbreak just upstream of dust piles) can be observed. In addition to the visual output which is useful for gaining general insight into flow patterns, spot measurements may also be taken anywhere in the domain of the CFD model. This is particularly useful where certain variables are critical to design – in this case, suction pressure.

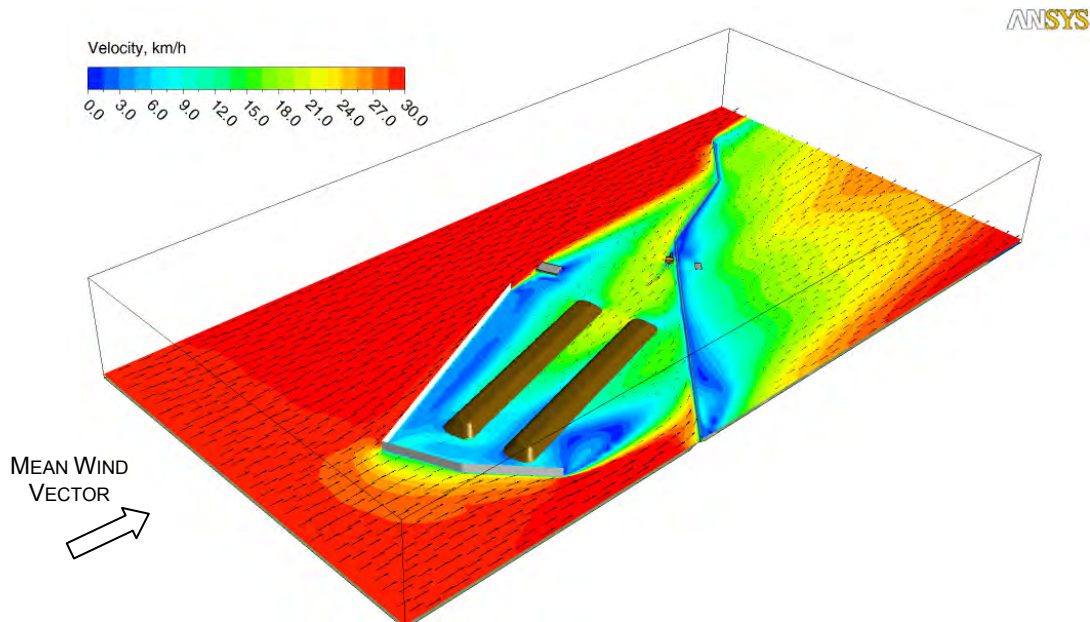


Figure 1. Example CFD Modeling Output

It is clear that the air flow over an exposed geomembrane may therefore be modeled using CFD (assuming that air behaves as a Newtonian fluid, which is a common assumption), and the output may be processed to derive the suction pressure. However, to the authors' knowledge and extent of their literature search, there are no published articles that have attempted this analysis. Application of CFD in closely related fields is common. Air flows over two- and three-dimensional hills and escarpments have been studied by Bergeles (1985), Paterson & Holmes (1993), Kim et al. (1997) and Carpenter & Lock (1999) to name a few, where the focus is often the dispersion of pollutants or the suitability of sites for wind farms. In civil engineering and architecture, CFD is often used to evaluate wind loads on buildings (see Murakami et al. (1992), Delauny et al. (1995) and Mikkelsen & Livesey (1995)), a similar problem but one where the critical parameter is not a negative uplift pressure but instead a positive face pressure. In many cases these studies include comparisons to experimental data from wind tunnels to validate the CFD model.

3. SUCTION EVALUATION

3.1 Interpretation by Giroud et al. of Wind Tunnel Tests

The generally accepted method for designing exposed geomembranes and anchorage systems has been presented in Giroud et al. (1995) and the subsequent papers mentioned above. The critical parameter is the suction factor λ which is calculated by the following equation:

$$\lambda = \frac{S}{\Delta P_{ref}} \quad [1]$$

where S is the suction pressure (positive if the pressure on the geomembrane is negative, i.e. inducing an uplift force) and ΔP_{ref} is the reference pressure, which is simply the dynamic pressure of the wind, calculated from the air density ρ and the mean wind velocity U :

$$\Delta P_{ref} = \frac{\rho U^2}{2} \tag{2}$$

Data from wind tunnel tests on small scale models of reservoirs by Dedrick (1973, 1974a, 1974b, 1975) for both windward and leeward slopes were summarized by Giroud et al. (1995) (see Figure 2, for example). These data were then simplified by Giroud et al. (1995) to be conservatively applicable to a generic slope regardless of its orientation with respect to wind direction. For the sake of simplicity, the generic slope and the adjacent horizontal areas were divided into three distinct zones, with the suction factor given at each of the three zones as:

- $\lambda = 1.0$ at the crest
- $\lambda = 0.7$ on the slope if the entire slope is considered; or $\lambda = 0.85, \lambda = 0.7, \lambda = 0.55$ for the top, middle and bottom thirds of the slope, respectively, if the slope is decomposed into three sections.
- $\lambda = 0.4$ on the bottom of the slope.

These generic suction factors are summarized in Figure 3. It is important to note that the generic suction factors given in Figure 3 are intended to be used regardless of the wind direction.

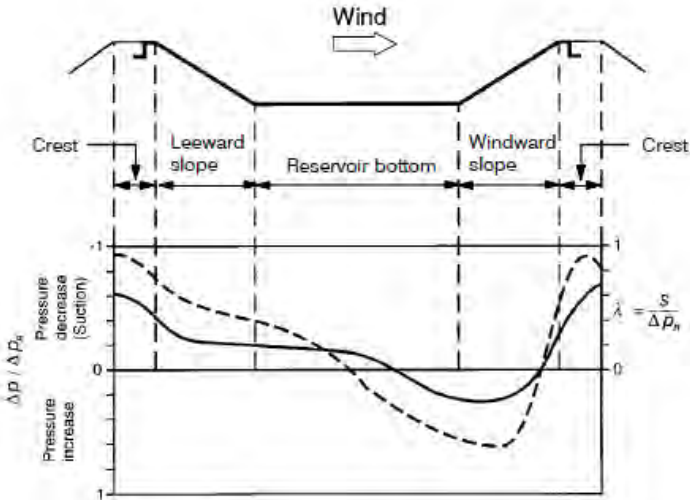


Figure 2. Pressure variation due to wind blowing past a reservoir (solid line for wind perpendicular to slope direction and dashed line for the worst case of wind at an angle) based on the work of Dedrick (1973, 1974a, 1974b, 1975). (Figure reproduced from Giroud et al. 1995)

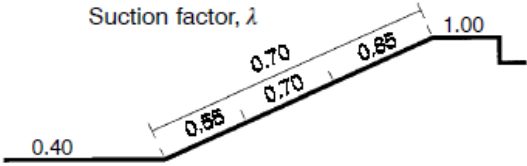


Figure 3. Generic suction factors for the worst case of wind direction as conservatively recommended by Giroud et al. (1995).

While the strength of the generic suction factors is their simplicity and conservatism, their weakness is that they do not account for parameters that are likely to have a significant impact on wind-generated suction such as slope inclination and wind direction. Furthermore, the generic suction factors do not account for other parameters that may have an

impact such as surface roughness, presence of obstructions, and complex geometries (such as benches and swales on slopes). It will be seen that the CFD method makes it possible to determine the influence of a variety of parameters on suction.

3.2 Computational Fluid Dynamics

Almost any geometry can be used with a CFD model. In this preliminary research, a two-dimensional slope was used and the slope inclination was varied from 2:1 (horizontal:vertical) to 4:1 (H:V) in 0.5:1 (H:V) increments. A view of the domain and computational mesh for the 2:1 simulation is shown on Figure 4. The computational mesh is a critical component of a CFD simulation, as the discretization of space into smaller cells on which the conservation principles are enforced provides the basis of an accurate simulation. It should be noted that the cells become smaller near the bottom boundary to accurately resolve the high velocity gradients. The labels in the figure at the mesh boundaries indicate the types of boundary conditions that were used in the simulations. A logarithmic wind velocity profile was set at the upwind (“inlet”) boundary, with the mean wind vector from left-to-right as shown in the figure. On the bottom boundary, a “wall” type boundary condition was used which enforces the no-slip condition and calculates the shear stress. The top and downwind boundaries were both set to “pressure opening” type boundaries. At these boundaries, the pressure was set to zero relative to the atmospheric pressure. This combination of boundary conditions is typical for CFD simulations of external wind flows.

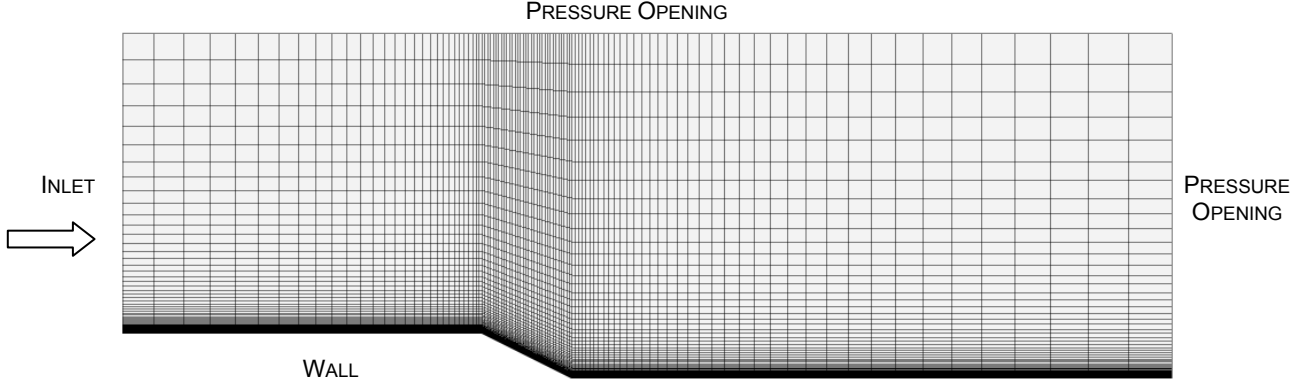


Figure 4. Typical computational mesh for a 2:1 leeward slope, with the boundary conditions marked. The mean wind vector is from left to right.

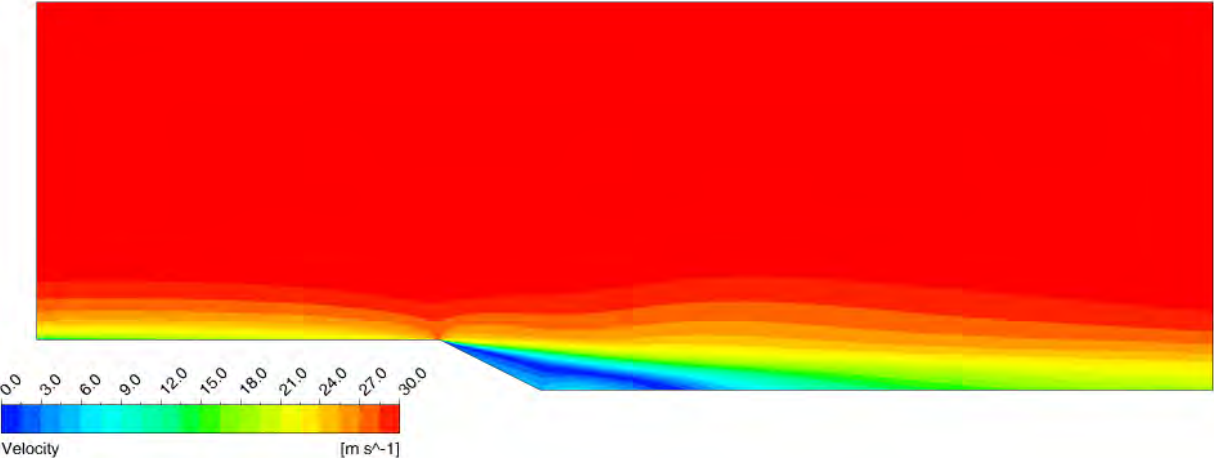


Figure 5. Contours of wind velocity for the case defined in Figure 4, showing high wind velocity (red) away from the ground and low wind velocity (blue / green) downwind of the slope.

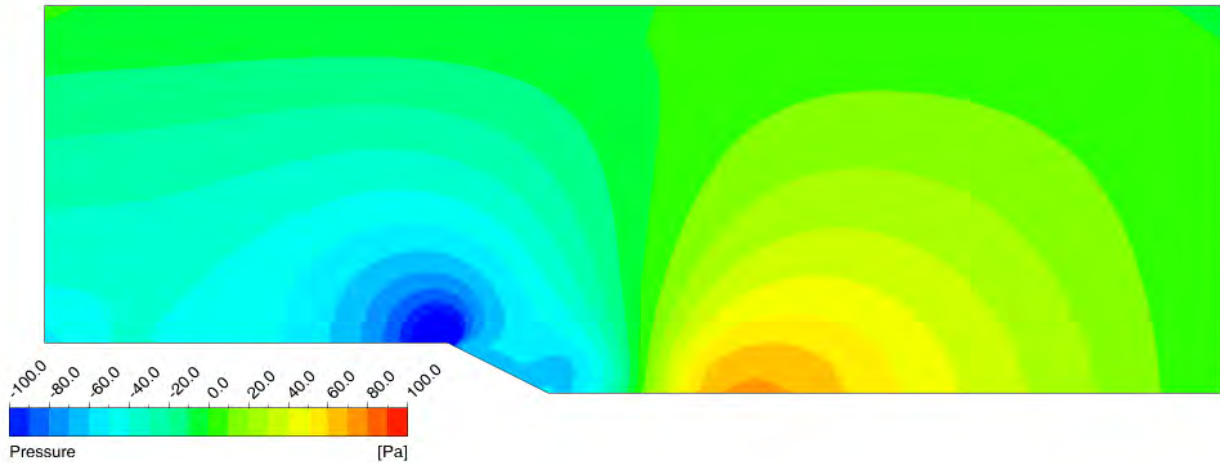


Figure 6. Contours of differential pressure (e.g. relative to atmospheric pressure) for the case defined in Figure 4.

Figure 5 shows the results from the CFD simulation for air velocity over a 2:1 leeward slope. The reference wind velocity in the simulation was set to 100 km/h. The red areas in the figure indicate air flowing at this velocity, while the blue and green areas show areas of low velocity just downstream of the slope (the wind in the figure is from left to right).

Pressure is also calculated in a CFD simulation. However, it is more useful to report the differential pressure relative to atmospheric pressure because suction is a differential pressure. For example, in Figure 6, the blue areas indicate pressures of -100 Pa or less. This is relative to atmospheric pressure, so for example if the atmospheric pressure was 101325 Pa, then the absolute pressure in the blue areas would be $101325 - 100 = 101225$ Pa.

The blue areas in Figure 6 show that a negative pressure (suction) appears on the entire face of the slope, with a greater value near the crest and gradually reducing near the bottom.

There is a quantitative difference between the results of the CFD modeling and the generic suction factors. The reference pressure ΔP_{ref} in the CFD simulation is 500 Pa (as calculated using Equation 2 with $\rho = 1.29 \text{ kg/m}^3$ and $U = 27.78 \text{ m/s} = 100 \text{ km/h}$). Therefore, suction pressures of around 60 Pa in the middle and lower thirds of the slope translate into suction factors of just over 0.1 compared to 0.70 and 0.55 for the generic suction factors recommended by Giroud et al. (1995) and shown in Figure 3. The suction pressure near the crest in the CFD simulation is approximately 100 Pa (i.e. $\lambda = 0.2$), which is far lower than the value in Figure 3 of 0.85 or 1.0.

The difference between CFD modeling and generic suction factors is even more marked when the slope inclination is reduced. The total data set from the CFD simulations is summarized on Figure 7, where the values of suction factor are plotted for the upper, mid and lower thirds of the slope. The 2:1 line (red) shows suction along the entire face, while at shallower slopes the suction on the mid-third is approximately zero and is negative on the lower third (e.g. the pressure is downwards).

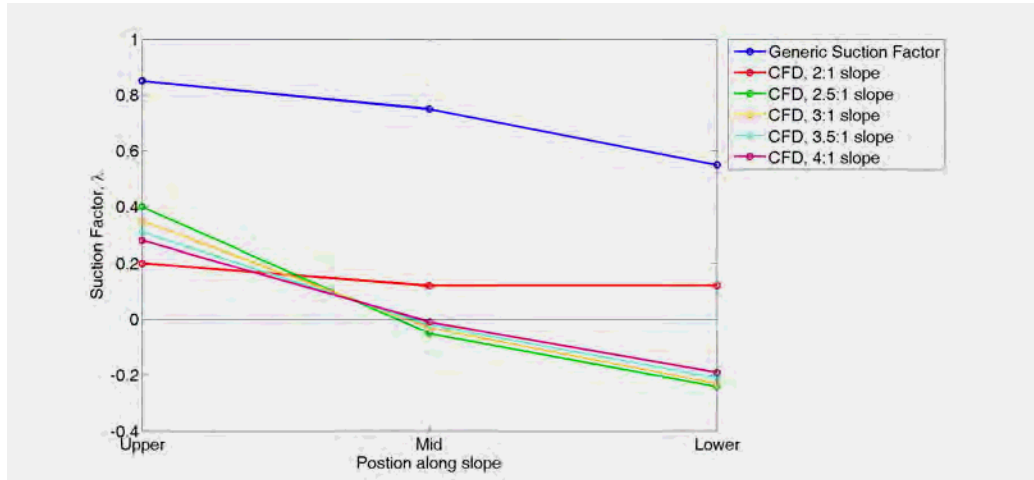


Figure 7. Comparison of Suction Factor Values

This unusual, non-linear behavior can be explained with reference to the velocity vectors on Figure 8. On the left sub-figure, the vectors for a 2:1 slope are shown. Notice that, in the low velocity areas (blue) near the ground, the vectors are pointing in the *opposite* direction to the mean wind vector – the flow has *reversed*. This is not the case for the 4:1 slope case shown on the right sub-figure on Figure 8. Here, the flow vectors all point from left to right. The two flow regimes are very different and distinct. For steep slopes, the flow is “separated” while at the shallower slopes the flow remains “attached”. Separated flow results in suction all along the face of the slope, while for attached flow the suction pressure is positive at the crest (uplift) and negative at the bottom (downward pressure).

It should be noted that the CFD results plotted in Figure 7 were obtained for wind perpendicular to the crest line since the model used was two-dimensional. In contrast, the generic suction factors (the top curve in Figure 7) correspond to the worst case for all wind orientations based on Dedrick’s tests. It is possible that part of the difference between the generic suction factors and the CFD results is due to three-dimensional effects in Dedrick’s tests where the small-scale models replicated square reservoirs with four dikes. Further investigation is needed, in particular with three-dimensional CFD models. Nevertheless, it is clear that the generic suction factors derived from the Dedrick’s experiments are extremely conservative. To assess whether a computational analysis is an economically feasible option to reduce the conservatism, we have calculated the cost impacts in the following sections.

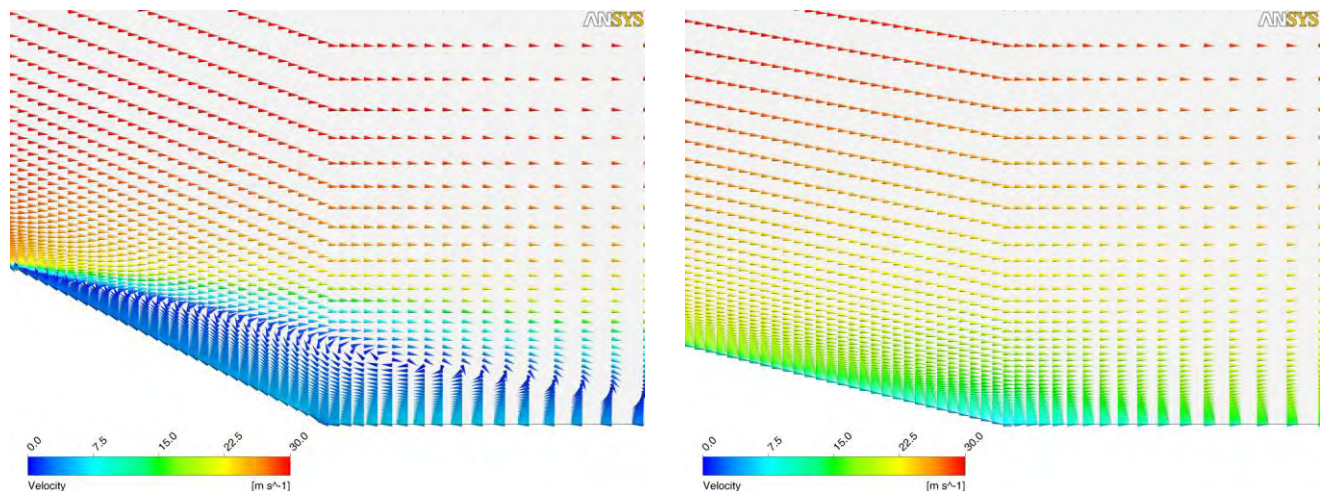


Figure 8. Contours of differential pressure (e.g. relative to atmospheric pressure).

4. TENSION COMPARISON

4.1 Objective

The suction values calculated using CFD modeling and the generic suction factors recommended by Giroud et al. (1995) were used with the analytical method by Giroud et al. (1995) to compare potential anchorage for a simplified uplift condition. The following assumptions were made to compare the two methods:

- Slope inclination = 2:1 (H:V)
- Slope height = 15 m
- Wind velocity = 100 km/h
- Elevation above sea level = 0 (i.e. assumed at sea level)
- Geomembrane mass per unit area = 1 kg/m^2
- Geomembrane assumed to have a tension-strain curve linear in its initial portion with a stiffness modulus of 450 kN/m
- Geomembrane allowable strength = 7.7 kN/m
- Suction evaluated at the crest of the slope (i.e. $\lambda = 1.0$)

The above geomembrane properties are typical properties of geomembranes that can be used in applications where the geomembrane is exposed to wind.

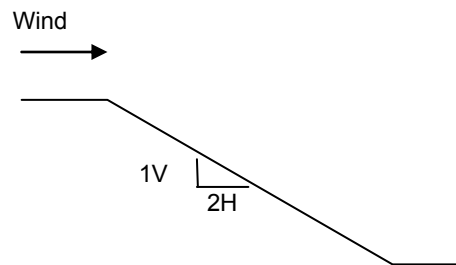


Figure 9. Tension Comparison Model

4.2 Tension Evaluation

Tension and strain in the geomembrane are linked by the following relationship, which is applicable in the initial portion of the tension-strain curve of the geomembrane which has been assumed to be linear:

$$T = J \varepsilon \quad [3]$$

Where:

- T = Tension (kN/m)
- J = Stiffness (kN/m)
- ε = Strain (%)

In the paper by Giroud et al. (1995), a simplified analytical methodology is presented for the case where the tension-strain curve of the geomembrane can be assumed to be linear. This methodology uses the normalized tensile stiffness, $J/S_e L$, where S_e is the effective suction calculated as the suction minus the weight per unit area of the geomembrane and L is the length of exposed geomembrane between two anchor trenches (also called “unsupported length”). Table 1 was generated using this simplified methodology:

Table 1. Tension Evaluation

Suction evaluation	Effective Suction $S_e^{(1)}$ (P_a)	Unsupported Length L (m)	Geomembrane Strain ϵ (%)	Geomembrane Tension T (kN/m)
Generic suction factors	416	5	1.0	4.5
	416	6	1.1	5.0
	416	7	1.3	5.9
	416	8	1.4	6.3
	416	9	1.5	6.8
	416	10	1.6	7.2
	416	11	1.7	7.7
	416	12	1.8	8.1
	416	13	1.9	8.6
	416	14	2.0	9.0
CFD	89	45	1.6	7.2
	89	46	1.6	7.2
	89	47	1.6	7.2
	89	48	1.6	7.2
	89	49	1.6	7.2
	89	50	1.7	7.7
	89	51	1.7	7.7
	89	52	1.7	7.7
	89	53	1.7	7.7
	89	54	1.8	8.1
89	55	1.8	8.1	

¹The effective suction is calculated as the suction minus the weight per unit area of the geomembrane.

Looking at the values in Table 1, the unsupported length required to develop the allowable geomembrane strength of 7.7 kN/m is approximately 5 times greater when using the suction values computed with CFD compared to the generic suction factors derived by Giroud et al. (1995) from the small-scale wind tunnel studies by Dedrick.



Figure 10. Example of exposed geomembrane anchorage (Courtesy of K. Perera, HDR)

5. POTENTIAL COST IMPACTS

A decrease in spacing for anchorage can translate to cost savings during construction. If we assume that the exposed geomembrane on a side slope is simply anchored using trenches along the slopes as shown in Figure 10, we can estimate potential cost savings by making some simple assumptions.

Table 2. Potential Cost Evaluation

Analysis Method	Trench Cost \$/m ⁽¹⁾	Slope Length m	Slope Width m	Trench Spacing m	Total Cost \$	Modeling Cost \$	Design Cost	Effective Cost \$
Generic suction factors	\$13.50	35	300	11	\$53,000	\$0,000	4,000	\$57,000
CFD	\$13.50	35	300	50	\$12,000	\$10,000	4,000	\$26,000

¹Rates for trench cost are based on experience.

The cost evaluation is overly simplified and is not intended to include all costs associated with constructing the anchor trenches or cost associated with geomembrane material. Also, the cost evaluation and the resulting cost savings would vary if some parameters (such as slope inclination) were different. This information is provided for discussion purposes and is only intended to highlight how potential cost savings can be realized. The evaluation assumes the exposed geomembrane is only anchored on the side slopes (four sides) and no horizontal or top deck anchorage is included. In reality, some horizontal anchorage could be required as well as anchorage on the top deck. Example methods for horizontal anchorage are shown in Figure 11.

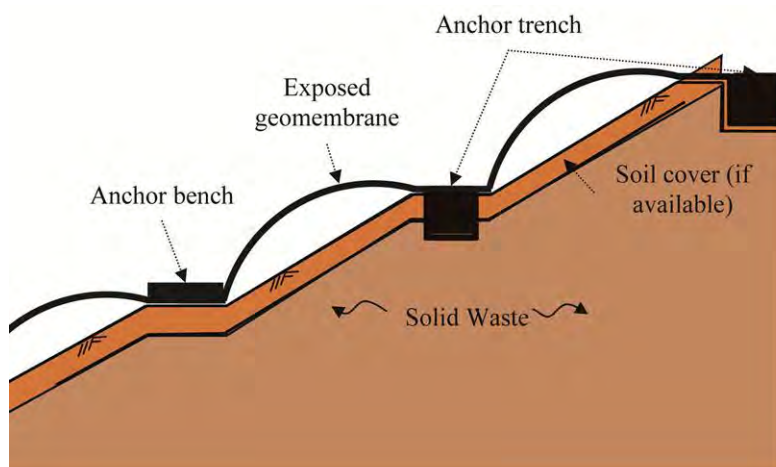


Figure 11. Example of Horizontal Anchorage (Yeo et al. 2011)

Table 2 shows a cost savings of approximately 50 percent using the simple scenario described above. Different, but still significant, cost savings would be obtained with different scenarios. Cost savings during construction would increase as the proposed project size increases. Larger projects require more anchorage than smaller projects and therefore provide more potential for cost savings when compared to the additional modeling cost associated with CFD. Cost benefits may not be realized for small and simple projects.

6. SUMMARY AND CONCLUSION

Preliminary research indicates that wind uplift forces calculated using CFD modeling produce significantly lower values of wind-generated suction than those computed using the generic suction factors recommended by Giroud et al. (1995). The CFD modeling can more accurately predict wind uplift forces allowing for less conservancy and more efficient design resulting in lower construction cost while satisfying regulatory requirements as a no method for evaluating uplift on exposed geomembranes is prescribed. However, smaller projects may not warrant more complex CFD modeling where the potential cost savings do not outweigh the additional modeling cost. Additional investigation will be undertaken to

evaluate the influence of parameters such as wind direction, presence of typical obstructions (e.g. benches), three-dimensional geometries (e.g. slopes with non-straight crest line), geomembrane surface condition, wind gusts and atmospheric turbulences. In conclusion, the analytical method published in Giroud et al. (1995) and subsequent papers for all aspects of design of exposed geomembranes (tension and strain in the geomembrane, deflection of the geomembrane, sizing of anchorages) can be used to its full potential with suction determined using CFD rather than with generic suction factors.

REFERENCES

- Bergeles, G. C. (1985). Numerical computation of turbulence flow around two-dimensional hills, *Journal of Wind Engineering and Industrial Aerodynamics*, Vol. 21, No. 3, pp. 301-321.
- Carpenter, O., & Locke, N. (1999). Investigation of wind speed over multiple two-dimensional hills, *Journal of Wind Engineering and Industrial Aerodynamics*, Vol. 81, No. 1-3, pp. 109-120.
- Dedrick, A.R. (1973). Air Pressures over Reservoir, Canal, and Water Catchment Surfaces Exposed to Wind, Ph.D. Thesis, Utah State University, Logan, Utah, USA.
- Dedrick, A.R. (1974a). Air Pressures over Surfaces Exposed to Wind, Water Harvesting Catchments, Transactions of the ASAE, Vol. 17, No. 5, pp. 917-921.
- Dedrick, A.R. (1974b). Aerodynamic Pressure Distributions over Reservoir, Canal, and Water Catchment Surfaces Exposed to Wind, *Proceedings of the 6th International Colloquium on Plastics in Agriculture*, Vol. 1, Buenos Aires, Argentina, September 1974, pp. 207-211.
- Dedrick, A.R. (1975). Air Pressures over Surface Exposed to Wind, Reservoirs, Transactions of the ASAE, Vol. 18, No. 3, pp. 508-513.
- Delaunay, D., Lakehal, D. & Pierrat, D. (1995). Numerical approach for wind loads prediction on buildings and structures. *Journal of Wind Engineering and Industrial Aerodynamics*, Vol. 57, pp. 307-321.
- Giroud, J.P., Pelte, T., & Bathurst, R.J. (1995). Uplift of Geomembranes by Wind, *Geosynthetics International*, Vol. 2, No.6, pp. 897-952.
- Giroud, J.P., Wallace, R.B., & Castro, C.J., 2006, Improved methodology for geomembrane wind uplift design, *Proceedings of the 8th International Conference on Geosynthetics*, Yokohama, Japan, September 2006, Vol. 1, pp. 225-230.
- Giroud, J.P., 2009, An explicit equation for strain in geomembrane uplifted by wind, *Geosynthetics International*, Vol. 16, No. 6, pp. 500-502.
- Kim, H. G., Lee, C. M., Lim, H. C., & Kyong, N. H. (1997). An experimental and numerical study on the flow over two-dimensional hills, *Journal of Wind Engineering and Industrial Aerodynamics*, Vol. 66, No. 1, pp. 17-33.
- Murakami, S., Mochida, A., Hayashi, Y. & Sakamoto, S. (1992). Numerical study on velocity-pressure field and wind forces for bluff bodies by $k-\epsilon$, ASM and LES, *Journal of Wind Engineering and Industrial Aerodynamics*, Vol. 41-44, pp. 2841-2852.
- Mikkelsen, A. C. & Livesey, F. M. (1995). Evaluation of the use of the numerical $k-\epsilon$ model Kameleon II for predicting wind pressures on building surfaces, *Journal of Wind Engineering and Industrial Aerodynamics*, Vol. 57, pp. 375-389.
- Paterson, D. A., & Holmes, J. D. (1993). Computation of wind flow over topography, *Journal of Wind Engineering and Industrial Aerodynamics*, Vol. 46, pp. 471-478.
- Yeo, S.-S., Johnson, R.S., & Corcoran, G.T. (2011). Alternative Anchorage Methodology for Exposed Geomembrane Installation with Flexible Solar Photovoltaic Panels, *Geo-Frontiers Congress 2011*, IFAI, Dallas, TX, USA, pp. 1463-1473.
- Zornberg, J.G., & Giroud, J.P., 1997, Uplift of Geomembranes by Wind - Extension of Equations, *Geosynthetics International*, Vol. 4, No. 2, pp.187-207. (Errata: 1999, Vol. 6, No. 6, pp. 521-522).

Evaluation of Ethylene Vinyl Alcohol (EVOH) for Containment of High Concentrations of Volatile Organic Compounds in Geosynthetics

Robert Armstrong, Kuraray America Inc., USA, robert.armstrong@kuraray.com

ABSTRACT

Geosynthetic liner systems, particularly in concrete liner applications are intended to control migration of liquids and vapor into the surrounding environment. The chemical resistance of existing geomembranes comprised of polypropylene (fPP), polyethylene (HDPE or LLDPE) could be significantly improved through use of Ethylene Vinyl Alcohol copolymer (EVOH), a random copolymer of ethylene and vinyl alcohol, which has extremely high resistance to the migration of gases, hydrocarbons and organic solvents. In select concrete liner applications the use of EVOH as part of a high barrier geomembrane (HBGM) would significantly increase the level of environmental protection and reduce potential remediation costs due to failure of liner systems. An evaluation of the performance of EVOH in containment of concentrated aromatic hydrocarbon and chlorinated hydrocarbon solvents shows EVOH can improve the volatile organic compound (VOC) barrier properties of polypropylene or polyethylene geomembranes significantly.

1. INTRODUCTION

Ethylene Vinyl Alcohol copolymer (EVOH) is a random copolymer of ethylene and vinyl alcohol, widely used to as a minor component of thermoplastic polymer composites to protect materials from oxidation and for containment of volatile organic hydrocarbons because of its outstanding barrier to gases, solvents and hydrocarbons (Lagaron et al. 2001). Typically these multilayer composites are formed by the coextrusion of multiple layers of thermoplastics into a sheet or film. Inclusion of EVOH in co-extruded geomembranes increases the capability of geomembranes to minimize the migration of gases, hydrocarbons and solvents without causing any significant changes in existing form and functionality of geomembranes (Armstrong & Chow, 2012). The use of EVOH in concrete liner solvent containment applications offers potential for significant increases in service life of the concrete liner and reduced losses of solvent from a process into the surrounding environment.

2. BACKGROUND

2.1 Use of Concrete Liners to Contain Hydrocarbons and Solvents

The majority of geosynthetic concrete liners in use are installed in relatively benign environments, such as municipal drinking water, storm water or waste water treatment systems. In certain cases however a concrete liner is challenged to contain concentrated solutions of hydrocarbons or acids. A specific example is the solvent extraction process utilized for heap leach mining of copper, in which the aqueous pregnant leach solution (PLS) is vigorously mixed with an organic solvent and selectively recovers copper from the PLS. The organic solvents used commercially in the solvent extraction step include dialkylphosphoric acids and hydroxyoximes, often in conjunction with benzene, ethylbenzene, and toluene. Effective containment of organic solvents within the solvent extraction system and prevention of offsite contamination by dilute solvents is a critical aspect of the heap leach mining process. The use of geomembranes to line concrete tanks used for solvent extraction as an alternative to stainless steel tanks has been reported, as have several failures of liners due to inadequate chemical and solvent resistance.

2.2 Properties of Ethylene Vinyl Alcohol

Several alternatives exist to improve the barrier of polypropylene and polyethylene geomembranes to organic solvents, including laminations with aluminum foil or fluorination of HDPE (Sangram & Rowe 2005), and coextrusion with polymers such as nylon or EVOH. The barrier of EVOH to a wide range of VOC's is so great that a very thin layer of EVOH within a polyethylene or polypropylene geomembrane significantly reduces diffusive migration of volatile organic compounds. A high barrier geomembrane structure containing a layer of EVOH is presented below in Figure 1. Incorporating EVOH in a HBGM would require at least three layers in a coextrusion, although five or seven layer structures would allow for optimizing the amount of EVOH at perhaps no more than 2 to 4% of the total thickness of a geomembrane. Designing and manufacturing a commercial scale multilayer cast or blown geomembrane line capable of producing a coextruded HBGM is an engineering exercise that does not require any fundamental changes or break through in coextrusion technology or practice

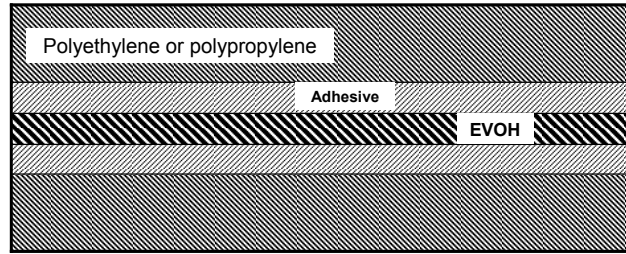


Figure 1 Model of High barrier Geomembrane (HBGM) with EVOH

EVOH has extremely good resistance to the migration of volatile organic compounds (VOC's), hydrocarbons and organic solvents, with the rate of solvent diffusion in EVOH orders of magnitude lower than in polyethylene. A large number of polymers also exhibit softening, swelling or environmental stress cracking when exposed to solvents, while EVOH retains key physical properties in the presence of organic solvents and non-ionic surfactants. As has been described by others (Park & Nibars 1993, Sangram & Rowe 2001) the migration of organic solvents through polymers such as HDPE or EVOH is a three step process of absorption or partitioning of the solvent from solution into the polymer, diffusion of the solvent through the polymer and then desorption into environment. The relationship between the mass flux due to diffusive migration and the solubility, diffusive and permeation coefficients (S_{gf} , D_g and P_g) can be stated as:

$$f = -S_{gf} D_g \frac{d_{c_f}}{d_z} = -P_g \frac{d_{c_f}}{d_z} \quad [1]$$

Where c_f = solution concentration and z = position through membrane.

Published data shows that the barrier property of EVOH to aromatic and chlorinated hydrocarbons is extremely good. Table 1 compares the permeation coefficients of a select number of solvents in EVOH and HDPE. (McWatters and Rowe, 2011 and in publication). Even under the worst case conditions for EVOH (monolayer film at 100% relative humidity), the permeation coefficients of hydrocarbon in EVOH was at least two orders of magnitude lower than LLDPE or HDPE. In previous tests of a commercial geomembrane with EVOH the permeation coefficients of the HBGM were typically three to four orders of magnitude lower than HDPE (McWatters and Rowe, 2010).

Table 1 Permeation coefficients ($\times 10^{-14}$ m²/s) of select solvents through EVOH and HDPE*

Solvent	44mol% EVOH	HDPE
benzene	3.0	1000
toluene	3.6	3000
ethyl benzene	4.4	5000
m&p xylene	5.3	6000
trichloroethylene	6.6	3400
1,2 dichlorethane	2.3	480

*Permeation coefficients in m²/s at 25ppm solvent concentration in water and 24°C

3. EXPERIMENTS

3.1 Experiment – Barrier and Physical Properties of HDPE and HDPE/EVOH Coextrusions

One litre (L) monolayer and coextrusion blow molded bottles were prepared as model solvent containment vessels, intended to mimic the function of geomembranes used as concrete liners. The bottles had a diameter of 75mm and height of 200mm, resulting in overall surface area of approximately 0.0515 sq.m. The HDPE used in the bottles was a fractional melt, high molecular weight HDPE resin typically used for agricultural chemical containers. The EVOH used was EVAL F101A, a 32 mol%, 1.6 melt Index (190°C/2160grams) EVOH supplied by Kuraray America Inc. There were three different bottle types, including a monolayer HDPE control, a six layer bottle with EVOH in the centre of the composite and finally a four layer bottle with EVOH on the inside of the bottle in contact with the solvent. The average wall thickness of the bottle was 1500 microns (60 mil) which is a typical geomembrane thickness. Table 2 below

describes the structure of each sample. The test matrix consisted of the three different bottle constructs described in Table 2 and exposed to three different solvent systems. A set of 6 bottles from each construct was filled with the three solvent solutions, sealed with a foil lined cap and exposed to a temperature of 60°C to simulate a harsh process environment.

The 3 different chemical solutions will be identified as follows:

F1 = BTEX 25 ppm = 25ppm each benzene, toluene, ethyl benzene and xylene in water

F2 = BTEX 25% = 25% by weight of benzene, toluene, ethyl benzene and xylene

F4 = TCE = 100% Trichloroethylene

The trial plan called for the weight loss of the bottles to be checked periodically for a period of two years, and that three bottles were to be removed from test between 300 and 360 days for evaluation of physical properties.

Table 2 Construction of monolayer and coextrusion blow molded bottle samples – typical sidewall thickness

Layer	6 layer coex (B1)		4 layer coex (B2)		Monolayer Control (B3)	
	Polymer	Thickness (µm)	Polymer	Thickness (µm)	Polymer	Thickness (µm)
1	HDPE	250	HDPE	900	HDPE	1500
2	HDPE regrind	400	HDPE regrind	500		
3	Adhesive Tie	50	Adhesive Tie	50		
4	EVOH	50	EVOH	50		
5	Adhesive Tie	50				
6	HDPE	700				
Total		1500		1500		1500

Throughout the balance of this paper the monolayer and coextrusion blow molded bottles that model geomembrane liners will be referred to as “B1”, “B2”, and “B3”.

The weight loss data reported is the average weight loss in grams of a set of bottles and common solvent on a given day. The weight loss experiments were conducted in a mini SHED (evaporative emissions test unit) by Intertek Inc. The experimental setup was comprised of an environmental chamber maintained at a temperature of 60°C within ±0.5°C. Each average value reported is at least four bottles (some bottles developed leaks at cap liner and were excluded from the data set). Samples were analyzed repeatedly the first month and thereafter, analysis occurred one to two times per month. The physical testing conducted to evaluate changes in physical properties of the bottles follows the general guidelines of GRI Test method GM-13 and ASTM D5747 – Standard Practice for Tests to Evaluate Chemical Resistance of Geomembranes to Liquid. Tensile testing was conducted according to ASTM D6693 Standard Test Method for Determining Tensile Properties of Non-reinforced Polyethylene Geomembranes.

4. RESULTS & DISCUSSION

4.1 Barrier Properties

After 280 days the weight loss from all bottles containing then F1 BTEX 25ppm solution was insignificant. The total weight loss for each set of samples was less than 20 grams or 2% of the average filling weight of 900 grams of aqueous BTEX solution. In the case of the F2 (25% BTEX) and F4 (100% TCE) solvents the results were significantly different. The monolayer B3 bottles failed to contain the F2 and F4 solvents, with total loss of these solvents in less than 140 days for the F2 BTEX and less than 60 days for the TCE. The weight loss data to 280 days for the F2 solvent is in Figure 2 and for the F4 solvent is in Figure 3. The weight loss from the B3 monolayer samples plateaued at just over 900 grams for the 25% BTEX solution and 1400 grams for the TCE at the point that the solvent ceased diffusing from the bottle. Based on weight loss data and surface area of the bottles, the average permeation rate of F2 BTEX was 128 grams/m².day and 485 grams/m².day for the F4 TCE from the B3 monolayer HDPE bottle. The B1 and B2 bottles with EVOH barrier showed only small weight loss over the entire 280 day period, with part of the weight loss of F2 and F4 solvents attributed to leakage at the cap liner. After 280 days the permeation rate of F2 BTEX and F4 TCE was less than 2 grams/m².day. The results of the weight loss test were as expected, with significant improvement in diffusive barrier and effective containment of concentrated solvents observed in both types of EVOH bottles. The position of the EVOH layer did not appear to have a significant effect on the barrier properties of the B1 and B2 bottles.

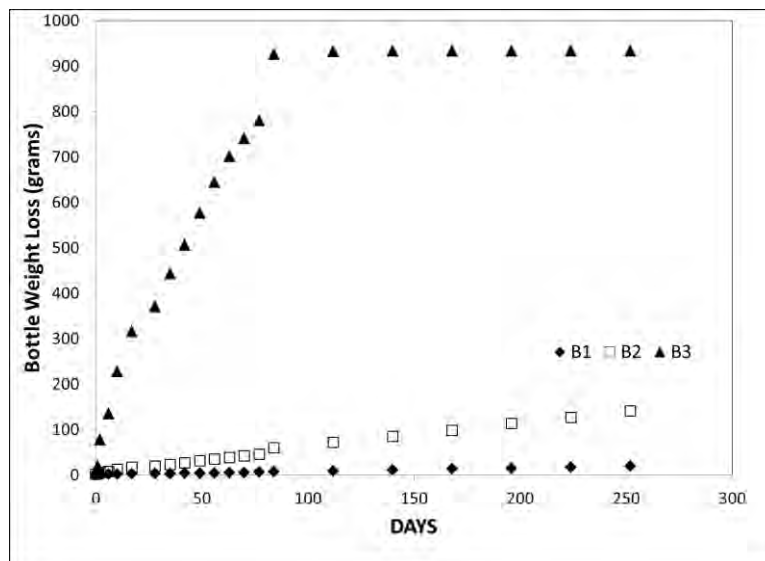


Figure 2 Weight Loss vs. Time - 25% BTEX solvent from B1, B2, B3 bottles

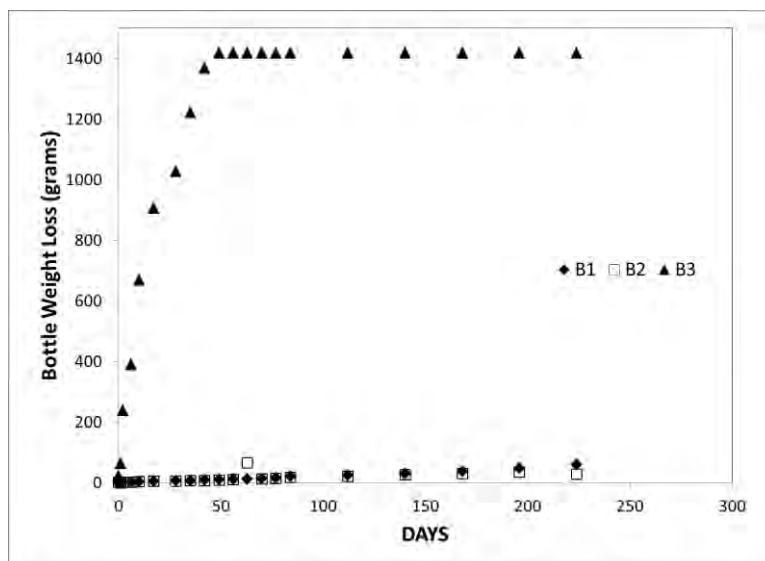


Figure 3 Weight Loss vs. Time - 100% TCE solvent from B1, B2, B3 bottles

4.2 Physical Properties

A limited evaluation of the structure and physical properties of the bottles was conducted on 3 bottles removed from each set of samples at 280 days. The physical testing was conducted as described in the experimental section and a summary of the results is presented in Table 3. A set of samples that had been reserved prior to the weight loss test were used as a control. These bottles had been stored at 20°C and 65%RH while the balance of the samples was in test. In addition to the standard GM-13 tensile properties, the modulus of each sample was measured.

The first significant result is that for the control samples the addition of EVOH to the HDPE reduces the yield strength and modulus slightly. In addition the elongation at break was significantly reduced, to a level below that required for smooth geomembranes, but still higher than that specified for textured geomembranes. It should be noted that the modulus, break and yield strength of all samples versus the control was not significantly affected by the solvents through 280 days. The second observation was the effect of moisture, solvents and position of EVOH layer on physical properties of the samples. In the case of the 25ppm BTEX solution, the B2 bottle with EVOH exposed to an aqueous solution had a high elongation at break versus the B1 bottles with EVOH layer separated from the aqueous solution by HDPE. This effect is often observed when EVOH is exposed to moisture. In the case of the 25% BTEX solution the B2

sample with EVOH layer exposed to the solvent had the lowest elongation at break, with the B2 sample showing some reduction in elongation strength, but not to the same degree. In this case the BTEX solvent mixture contained very little moisture, which caused moisture level in the EVOH layer of the B2 sample, immediately adjacent to the solvents, to drop to a lower level than that of the B1 sample, with EVOH layer separated from the solvent by a layer of HDPE. The trichloroethylene (F4) solvent had a major effect on the elongation to break of the EVOH coex samples, with elongation to break of the B1 and B2 samples exposed to TCE approaching that of the monolayer HDPE control.

To investigate the effects of the F2 and F4 solvents on the polymer structure of the samples, they were examined using Differential Scanning Calorimetry (DSC) to observe changes in melting point, Thermal Gravimetric Analysis (TGA) to detect changes in degradation temperature and Fourier Transform Infrared Spectroscopy to confirm effects of solvents on EVOH structure. The DSC analysis of melting point and enthalpy of melting showed a consistent trend of reduced melting point of the HDPE by 2 to 3°C after exposure to the F2 and F4 solvents from an average melting point of 133°C. The EVOH melting point did not change significantly after exposure to the F2 BTEX solvent mixture, but did reduce from 182°C to 178°C in samples exposed to TCE. The enthalpy of melting of the EVOH was also reduced after exposure to TCE. Observations by FTIR showed that the mol% of vinyl alcohol in the EVOH had not been reduced, so the reduction in melting point is explained by the TCE affecting the weak crystalline structure of the EVOH layer. Despite this effect on the physical properties of the EVOH, the barrier to TCE remained extremely high through 280 days at elevated temperatures.

Table 3 Physical properties of B1, B2 and B3 bottles after 280 days exposure to solvents

Properties	GM1-3	Control – No solvent			F1 – 25ppm BTEX			F2 – 25% BTEX			F4 – 100% TCE		
		B1	B2	B3	B1	B2	B3	B1	B2	B3	B1	B2	B3
Modulus (MPa)		453	400	483	499	446	476	334	445	469	367	468	482
Yield Strength (KN/m)	22	141	134	149	161	145	152	136	146	147	141	146	148
Break Strength (KN/m)	40	140	132	232	162	141	254	132	141	250	165	156	242
Yield Elongation (%)	12	15	17	16	16	17	16	21	17	17	19	17	16
Break Elongation (%)	700	180	250	660	364	380	700	110	60	710	550	550	700

*Results are the average of 5 replicates of a sample, all tested in the machine direction (MD)

In these and other tests including EVOH in a geosynthetic is observed to have a slightly negative effect on the physical performance of the geomembrane, particularly elongation to break. Further investigation of these effects and development of modified forms of EVOH is underway.

5. CONCLUSION

The barrier to dilute and concentrated aromatic and chlorinated hydrocarbons of monolayer HDPE and coextruded HDPE and EVOH model solvent containment vessels, intended to mimic the function of geomembranes used as concrete liners was evaluated over 280 days at elevated temperatures, with testing ongoing to 3 years. The diffusive barrier of monolayer HDPE to concentrated hydrocarbons was found to be practically nonexistent, while the coextruded HDPE-EVOH samples had barrier properties at least an order of magnitude lower. A limited evaluation of the key physical properties showed a reduction in elongation at break tensile properties of the HDPE-EVOH samples, which is dependent upon EVOH moisture content. EVOH offers the potential of improved VOC barrier with limited effect on key form and functional performance characteristics of concrete liners. The primary function of a geosynthetic liner is an advective and diffusive barrier to contain liquids and vapor that should not migrate into the environment. The inclusion of EVOH by coextrusion into select concrete liners intended for use with aggressive aromatic and chlorinated hydrocarbons would greatly reduce diffusive migration of VOC's, and offers potential for extended service life of concrete liner systems in aggressive environments.

ACKNOWLEDGEMENTS

The author acknowledges the contributions of Ron Rose and Edgard Chow in experiment design and execution and Steven Trener, Al Gongora and Joe Vasquez for completing the physical testing of samples.

REFERENCES

- Armstrong, R.B. 2011. Improving performance of geosynthetics for containment of volatile organic compounds through the use of ethylene vinyl alcohol (EVOH), *Proc. of Geosynthetics 2011*, Dallas, Texas, pp. .
- Armstrong, R.B. & Chow, E.A. 2012. Performance of model geomembrane with ethylene vinyl alcohol (EVOH) barrier for select mining and remediation applications, *Proc. of GeoAmericas 2012*, Lima, Peru, pp. .
- Kolbasuk, G.M. 2008. Virtually impermeable food packaging technology, geomembrane applications. 2008. *Proc. Geosynthetics 2008*, Cancun Mexico, pp. 54-63
- Lagaron, J. M.; Powell, A.K.; Bonner, J.G. 2001. *Polymer Testing*, 20/5, 569-577.
- McWatters, R.S. & Rowe, R.K. 2011. Sorption and Diffusion of BTEX through Thin-Film EVOH. *Proc of Geosynthetics 2011*, Dallas, Texas, pp. 29-39.
- Park, J.K & Nibras M. 1993. Mass flux of organic chemicals through polyethylene geomembranes. *Water Environment Research*, Vol 65(3), pp. 227-237.
- Prasad, T.V. & Brown, K.W. & Thomas, J.C. 1994. Diffusion coefficients of organics in high density polyethylene (HDPE). *Waste Management and Research*, Vol 12, pp. 61-71.
- Rowe, R.K & Sangam, H.P. 2001. Migration of dilute aqueous organic pollutants through HDPE geomembranes. *Geotextiles and Geomembranes*, Vol. 19, pp. 329-357.
- Rowe, R.K & Sangam, H.P. 2005. Effect of surface fluorination on diffusion through a HDPE geomembrane. *Journal of Geotechnical & Geoenvironmental Engineering*, 131(6), pp. 694-704.
- Rotuska, K. & Chmielewski, T. 2008, Growing role of solvent extraction in copper ores processing. *Physicochemical Problems of Mineral Processing*, 42 (2008), 29-36
- ASTM D 5747 – Standard Practice for Tests to Evaluate Chemical Resistance of Geomembranes to Liquid. American Society for Testing and Materials, West Conshohocken, Pennsylvania, USA.
- ASTM D 6693 Standard Test Method for Determining Tensile Properties of Nonreinforced Polyethylene Geomembranes. American Society for Testing and Materials, West Conshohocken, Pennsylvania, USA.

Experimental and Numerical Studies on Geocell Reinforced Sand Beds

A. Hegde, Research Scholar, Department of Civil Engineering, Indian Institute of Science, Bangalore, India-560012; Email: amarnathhegde@gmail.com ,
T.G.Sitharam, Professor, Department of Civil Engineering, Indian Institute of Science, Bangalore, India-560012; Email: sitharam@civil.iisc.ernet.in

ABSTRACT

Indian Railway has taken up the ambitious project of constructing 3300 km of new track across eastern and western corridors. The majority of these tracks will pass through the regions with poor soils including loose sands of the Indo-Gangetic belts. Hence, the experimental and numerical studies are undertaken to evaluate the suitability of geocell cellular confinement as a foundation technique for this project. This paper presents the results of the 1-g model tests performed on geocell reinforced sand bed supporting the square footing. Results show that the provision of geocell increases the ultimate bearing capacity of the sand bed by 4 times. Introduction of planar geogrid at the base of the geocell mattress not only enhances the load carrying capacity but also arrests the surface heave and prevents the footing from undergoing the rotational failure. In addition to the experimental studies, numerical study was also carried to demonstrate the simplistic approach of modeling of the geocells in FLAC^{2D}.

1. INTRODUCTION

Indian economy is one of the largest as well as the fastest growing economy in the world. In a last decade or so, India's growing economy has experienced the rise in the demand for additional transportation, infrastructure, and services. Until these days, Indian railway was playing a pivotal role in the transportation sector and was contributing to the economic success of the country. However, since last few years, Indian Railway has been facing the serious challenge to keep up the pace with country's continued economic growth and the rising demand, since all the country's high-density rail corridors are facing severe capacity constraints. Hence, to enhance the capacity, Railway ministry has undertaken the construction of Dedicated Freight Corridors across the heavy traffic networks in India. As part of this initiative, DFCCIL (Dedicated Freight Corridor Corporation of India) is constructing two corridors along western and eastern routes spanning a total length of about 3300 km (Courtesy, <http://dfccil.org>).

Much of the railway embankments and railway lines have to be constructed on the loose deposits of the Indo-Gangetic belt. In the present situation, ground improvement using vibro techniques seems to be the feasible option for the DFCCIL to strengthen the loose deposits along the proposed route. As vibro stone columns are more complex to install, it is very high time to demonstrate a new technique as an alternate to the vibro techniques. Reinforcing the soil with geocells could be one such alternative option as they distribute the load laterally. In addition, geocells are more amenable to the field applications as it is cheaper and better compared to vibro techniques. Hence, research work has been taken up with the objective of evaluating the suitability of geocell reinforcement for the construction of foundations along these railway lines.

Since last two decades, geocell reinforcement has been showing its efficacy in the field of highways and embankments. Due to its three dimensional nature, geocell offers all-round confinement to the encapsulated soil and hence leads to the improvement in the overall performance of the foundation bed. Several researchers have reported the beneficial use of 3D-reinforcements in the construction of foundations. "Broms and Massarach (1977)" adopted the metallic grid mat consisting of rectangular and triangular cells for different offshore structure. "Rea and Mitchell (1978)" and "Mitchell et al. (1979)" carried out the study on footings supported on sand beds reinforced with square shaped paper grid cells through a series of small-scale laboratory tests and observed the different modes of failure. "Guido et al. (1989)" studied the influence of number of layers of geoweb cells on bearing capacity of sand bed using laboratory model tests. Similar studies were carried out "Dash et al. (2001a)" on strip footing, "Sitharam and Sireesh (2005)" on circular footing and "Madhavi Latha and Somwanshi (2009)" on square footing by using laboratory prepared geogrid cells. "El Sawwaf and Nazer (2005)" used Unplasticized Polyvinyl Chloride (UPVC) cylinders of different diameters to study the soil confinement on circular footing. "Tafreshi and Dawson (2010)" used strips of thermo welded non-woven geotextiles as 3D cells to study the response of sand bed under static and dynamic loading.

Review of the literature reveals that the majority of the researchers have used the laboratory prepared geogrid cells instead of commercially available geocells. Since commercially available geocells are the ones, going to be used in the field, the experimental findings cannot be directly correlated with the field conditions. In the present investigation, new commercially available geocells made of polyethylene are used; which is known for its high strength and durability. Sand

collected from the Indo-Gangetic belt itself was used in the experimental program to prepare the foundation bed. The test results of the static plate load tests and the numerical simulations are discussed in this paper.

2. LABORATORY MODEL TESTS

2.1 Design of Experiments

Footing sizes were arrived as per the scaling laws suggested by “Wood (2004)”. The prototype footing was a square raft with thickness 0.5 m and width 4.5 m made up of concrete with Young’s modulus 25 GPa. For the sake of convenience, the steel footing with Young’s modulus 200 GPa was selected for the experimental studies. Considering the scaling down factor of 10, the flexural rigidities of the model and prototype footings were equated to obtain the dimensions of the model footing. The arrived size of the model footing was 150 mm width and 20 mm thickness. The sufficiently bigger size of the tank was chosen, i.e. 6 times the size of the footing (900 mm x900 mm in plan area) to keep the boundary effect minimal.

2.2 Experimental Setup

The experiments were conducted in the cast iron test tank of size 900 mm length x900 mm width x 600 mm height. The tank was fitted to the loading frame and which was connected to manually operated hydraulic jack. A square shaped steel plate with 20 mm thickness and 150mm sides was used as the model footing. The bottom of the footing was made rough by a coating thin layer of sand with epoxy glue. The load was applied on the footing through the hand operated hydraulic jack and a pre-calibrated proving ring was placed between the footing and hydraulic jack to measure the applied load. To prevent the eccentric application of the load, the ball bearing arrangement was used. Figure 1a-b represents the photographic and schematic view of the test setup.

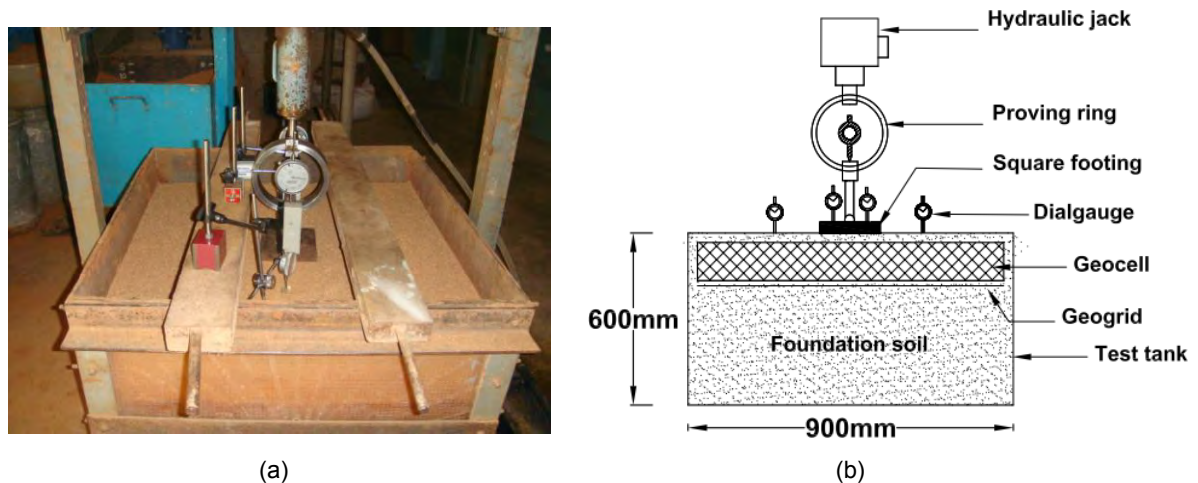


Figure 1. Test setup: (a) photographic view; (b) schematic view

2.3 Materials Used

Sand used in the investigation was dry sand with specific gravity 2.64, effective particle size (D_{10}) 0.26mm, coefficient of uniformity (C_u) 3.08, coefficient of uniformity (C_c) 1.05, maximum void ratio (e_{max}) 0.81, minimum void ratio (e_{min}) of 0.51 and angle of internal friction was (ϕ) 30° . According to Indian Standard Soil Classification System (ISSCS) the soil can be classified as poorly graded sand with symbol SP. The geocell used in the study was made up of polyethylene with a density of 0.95 g/cm^3 . The cells are 250 mm in length, 210mm in width and 150mm in depth. The thickness of the strip is 1.53 mm with cell-to-cell seam strength is 2150 N. Biaxial geogrid made up Polypropylene with aperture size 35 mm x 35 mm was used. Ultimate tensile strength of the geogrid was 20 kN/m. Figure 2 represents the tensile load-strain behavior of both geocell and geogrid used in the experiments.

2.4 Preparation of Test Bed

Firstly, the sides of the tank were coated with Polythene sheets to avoid the side friction. Pluviation technique was used to prepare the sand bed of 500 mm thickness. Before the start of the actual test, a series of trials were conducted to determine the height of fall required to achieve the desired relative density. In each trail, small aluminum cups with

known volume were placed at the different locations of the tank. A calibration chart was prepared by knowing the maximum and minimum void ratios of the sand. All the tests were conducted at a constant relative density of 65%. The height of fall required to achieve 65% relative density was directly obtained from the chart. The average density achieved in the sand bed during the pluviation was 16.08 kN/m^3 and the less than 1% difference was observed in the densities measured at the different locations of the bed. Reinforcement was placed at the predetermined depth and sand was used as the infill material. Sand was filled into the geocell pockets using the pluviation technique itself to maintain the relative density same as that of foundation bed.

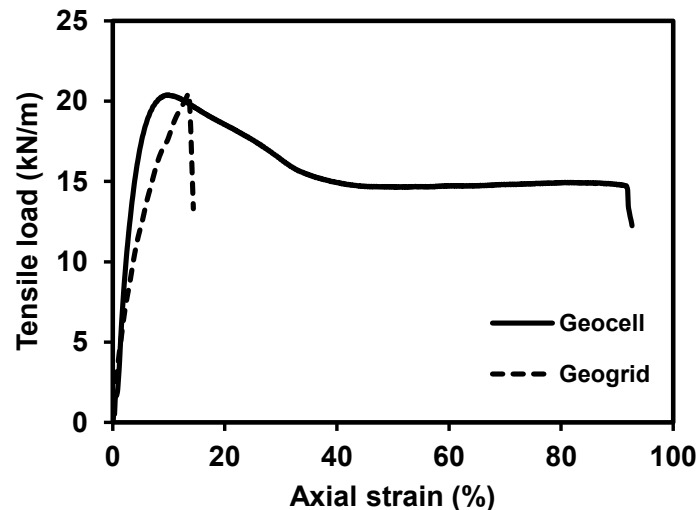


Figure 2. Tensile load-strain behavior of geocell and geogrid

2.5 Testing Procedure

Reinforcements were placed at the predetermined depth during the pluviation of sand into test tank. After preparing the sand bed of 500 mm thickness, the fill was leveled using a trowel without disturbing the density of the bed. Footing was placed at the pre-determined alignment at the surface of the sand bed. A recess was made on the top surface of the footing and a ball bearing arrangement was placed on it. The concentrated vertical load was applied on the footing with the help of ball bearing arrangement. Through the precise measurements, the footing was placed exactly at the center of the test tank in order to avoid the eccentric loading. The load applied to sand bed was measured through the pre-calibrated proving placed between the footing and the hydraulic jack. Two dial gauges (D_1 and D_2) were placed on the either side of the centerline of the footing to record the footing settlements. Another set of dial gauges (S_1 and S_2) was placed at the distance of $1.5B$ (B is the width of the footing) from the centerline of the footing to measure the deformation underwent by the fill surface. The footing settlement (S) and the surface deformation (δ) were normalized by footing width (B) to express them in non-dimensional form as S/B (%) and δ/B (%). In all the plots, settlements are reported with the negative sign and heave with the positive sign.

3. RESULTS AND DISCUSSION

3.1 Bearing Pressure-settlement Curve

Figure 3 represents the pressure settlement response for the different test conditions. For unreinforced case, failure was occurred at footing settlement of 8% of footing width. Clearly defined failure was observed in case of unreinforced bed. In case of geocell reinforcement, no clear-cut failure was observed in the pressure settlement behavior even up to the large settlement of 35% of footing width. There was a slight reduction in the slope of the pressure settlement curve at the settlement range of 22% to 24% of the footing width and after which again the slope has become constant. This nature of the curve can be attributed to the beam effect of the geocell mattress; due to its high bending and shear stiffness, geocell mattress can support the footing even after the failure of soil. The interconnected cells form a panel that acts like a large mat that spreads the applied load over an extended area, leading to an overall improvement in the performance of the foundation beds. Post test exhumation of geocell has shown the deformation in the vertical and horizontal ribs. The reason for this could be, once the soil below footing underwent the shear failure, the footing might have rested directly on the ribs of the geocell. Figure 4a-b represents photograph of the geocell before and after the tests. It was observed that the provision of the additional geogrid layer at the base of the geocell mattress further

increase the load carrying capacity as well as the stiffness of the sand bed.(i.e. flattened pressure settlement curve). Similar trends were also observed by “Dash et al. (2000 b)”.

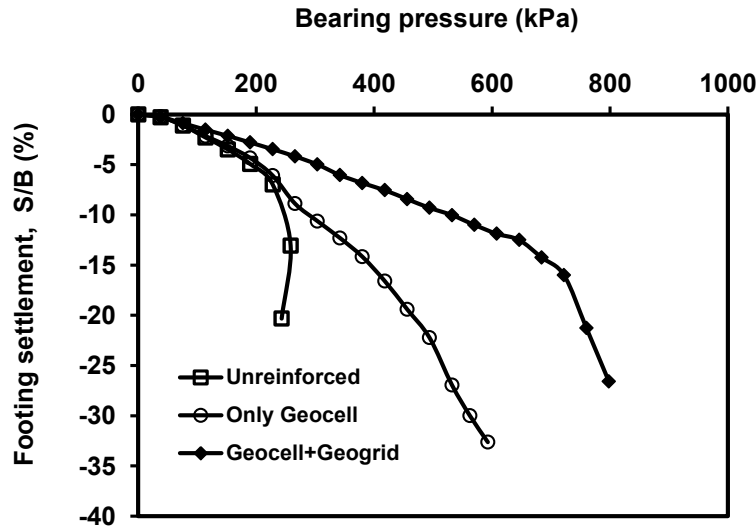
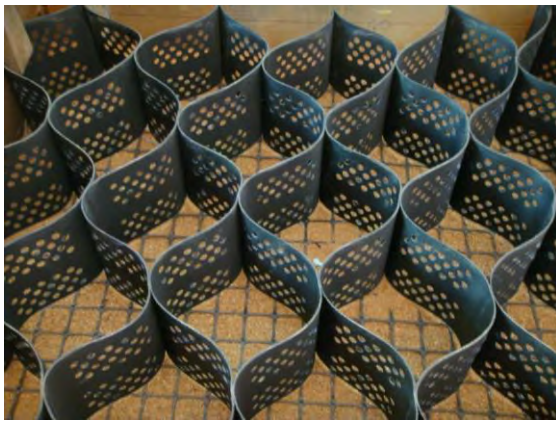


Figure 3. Variation of bearing pressure with footing settlement



(a)



(b)

Figure 4a-b. Photograph of the geocell: (a) before the test; (b) after the test

3.2 Surface Deformation

Surface deformation (settlement/heave) profiles of sand bed reinforced with different forms of reinforcement are discussed in this section. Surface deformation measurements were made through the dial gauges placed at the distance of $1.5B$ from the centerline of the footing. “Chummar (1972)” observed that the surface heaving extends up to $2B$ from the centerline of the footing for unreinforced case and with maximum heaving at a distance of $1.5B$. Generally, surface heaving can be attributed to the general shear failure of the soil mass. Figure 5 quantifies the maximum surface deformation for the different combination of reinforcements. The solid and dotted lines represent the deformation measured at the left and right side of the footing centerline. One can observe from the figure that the large difference between the solid and dotted lines. This difference is due to the rotational failure of the footing. The extent of rotation and amount of heaving was reduced in the case of the geocell reinforcement and further reduction in rotation was observed in the presence of the planar geogrid below the geocell. Interestingly, no surface heaving was observed with additional basal geogrid. From the above observation, it is evident that the combination of geocell and basal geogrid completely arrest the surface heaving and reduces the footing rotation. In addition, the planar geogrid contributes to improve the overall performance of the foundation bed by resisting the downward movement of soil due to the footing penetration. Hence, it is always beneficial to use planar geogrid layer at the base of the geocell matress.

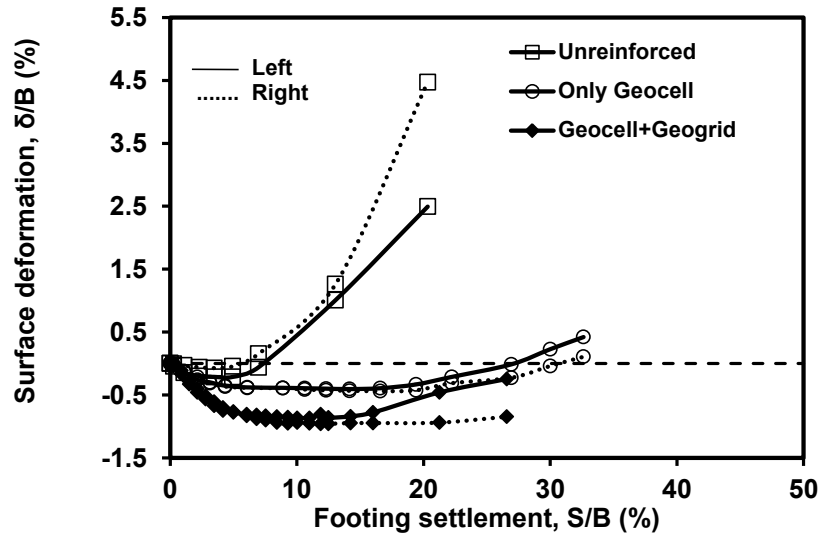


Figure 5. Variation surface deformation with footing settlement

3.3 Bearing Capacity Improvement Factor (I_f)

The increase in the bearing capacity due to the provision of the reinforcement can be measured through a non-dimensional parameter called bearing capacity improvement factor (I_f), which is defined as,

$$I_f = \frac{q_r}{q_0} \quad [1]$$

Where, q_r is the bearing pressure of the reinforced soil at the given settlement and q_0 is the bearing pressure of unreinforced soil at the same settlement. "Binqet and Lee (1975)" reported the improvement factor is similar to the bearing capacity ratio. When the ratio is beyond the ultimate bearing capacity of the unreinforced soil, the ultimate bearing capacity (q_{ult}) is used instead of q_0 . Bearing capacity improvement values for different tests are listed in Table 1.

Table 1. Bearing capacity improvement factors

Avg.S/B	Bearing capacity improvement factors (I_f)	
	Only Geocell	Geocell+Geogrid
2%	1.10	1.48
4%	1.12	1.55
6%	1.14	1.57
8%	1.25	1.83
10%	1.28	2.12
12%	1.37	2.43
14%	1.49	2.67
16%	1.63	2.88
18%	1.78	2.96
20%	1.92	3.08

3.4 Percentage Reduction in Footing Settlement (PRS)

The performance improvement of the foundation bed due to geocell reinforcement can also be quantified in terms of the reduction in the settlement of the footing using the parameter called percentage reduction in settlement (PRS), which can be defined as,

$$PRS = \left(\frac{S_0 - S_r}{S_0} \right) \times 100 \quad [2]$$

Where, S_0 is settlement of the unreinforced foundation bed corresponding to its ultimate bearing capacity (which is determined using the double tangent method), was found out to be 15% of the footing width ($S/D=15\%$). S_r is settlement of reinforced foundation bed corresponding to the footing pressure equal to the ultimate bearing pressure of unreinforced foundation bed. In the present investigation, the PRS value of 53 % was observed with only geocell case and 73% was observed with additional planar geogrid at the base of the geocell.

4. NUMERICAL STUDY

The aim of this section is to demonstrate the simplistic approach of modeling the 3-dimensional nature of geocell in 2D finite difference software called FLAC^{2D} (Fast Lagrangian Analysis of Continua in 2D). In this approach, the geocell filled with sand is modeled as an equivalent composite layer with improved strength and stiffness parameters (“Madhavi Latha and Somwanshi, 2009”). Various investigators have reported that the geocell confinement of sand induces the apparent cohesion while the friction angle remains constant (“Bathurst and Karpurapu, 1993”; “Rajagopal et al., 1999”). The induced apparent cohesion of the equivalent composite layer was calculated using the Equations (3) and (4) given by “Rajagopal et al. (1999)”. The Equation (3) is originated from the rubber membrane theory proposed by “Henkel and Gilbert (1952)”. The increase in the confining pressure ($\Delta\sigma_3$) on the soil due to the presence of geocell is given by,

$$\Delta\sigma_3 = \frac{2M\xi_c}{d} \frac{1}{1-\xi_a} = \frac{2M}{d_0} \left[\frac{1-\sqrt{1-\xi_a}}{1-\xi_a} \right] \quad [3]$$

Where, M is the secant modulus of the geocell material at axial strain ϵ_a , which is obtained from the tensile load-strain response of the geocell material at 2% axial strain and d_0 is the equivalent diameter of the geocell pocket. The increment in the apparent cohesion (C_r) due to the increase of the confining pressure is given by,

$$C_r = \frac{\Delta\sigma_3}{2} \sqrt{K_p} \quad [4]$$

Where, K_p is the coefficient of passive earth pressure. In the present study, the equivalent diameter of the geocell pocket is 0.258 m and the secant modulus (M) corresponding to 2% strain obtained from the load–strain response of the geocell material (Figure 2) was 435 kN/m. The additional confining pressure ($\Delta\sigma_3$) was calculated from Equation (3) as 34.4 kPa. Then from the Equation (4), the apparent cohesive strength of the soil composite was obtained as 30 kPa. The C_r value calculated is valid only for a single cell. Due the presence of many interconnected cells, the apparent cohesion value reduces. Rajgopal et al. (1999) observed that the reduction in C_r value is in the range of 50% to 72% of the calculated value depending upon the number of interconnected cells. In the present study, the 70% reduction in C_r value i.e $C_r=21$ kPa was used for numerical simulations. Same value of the friction angle ($\phi=30^\circ$) as that of the sand used in the experimental study was used in the simulation of sand bed and the dilation angle value of $2/3\phi$ was considered.

Elastic-perfectly plastic Mohr Coulomb model was used to model the behavior of soil. Analyses were carried out under controlled velocity loading of $2.5 \times E-5$ m/step. Only half portion of the test bed was modeled using symmetry to reduce the computational effort and the time. The FLAC^{2D} model with the details of loading and the boundary conditions are shown in Figure 6. The size of the mesh was kept same as that of the test bed used in the experimental studies. The displacement along the bottom boundary was restricted in both horizontal as well as vertical direction. The side boundaries were restrained only in the horizontal direction, while the displacements were allowed in the vertical direction. Roughness of the footing was simulated by restraining the surface nodes representing the base of the footing in the horizontal direction.

The elastic properties were obtained from the experimental pressure settlement behavior using the method proposed in the “Appendix D of the Engineering Manual: 1110-1-1904, U.S Army Corps of Engineers (1990)”. The method uses the relationship involving the slope of the pressure settlement curve, Poisson’s ratio, and equivalent diameter of the footing to determine the elastic modulus of the bed. The values found to be underestimating the ultimate bearing pressure by large extent and hence the sensitivity analyses were carried out to determine a suitable value of the elastic modulus. Table 2 presents the details of the various material properties used in the analysis. Comparisons of the pressure settlement behavior of experimental and numerical studies are presented in the Figure 7. There exist a good match between the experimental and the numerical results. However, it was found that the FLAC^{2D} overestimates the bearing pressure at higher settlements.

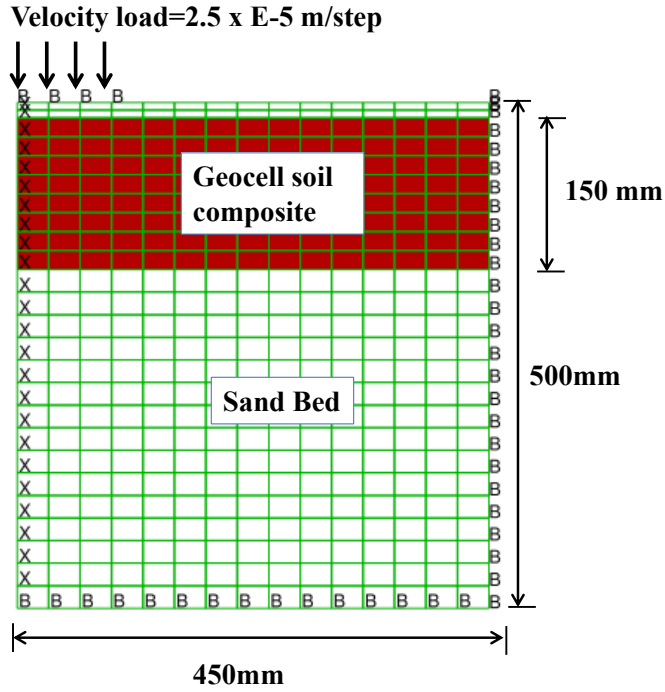


Figure 6. FLAC^{2D} model with details of loading and boundary condition

Table 2: Material properties used in the analysis

Properties	Unreinforced	Geocell reinforced	Geocell+Geogrid reinforced
Shear modulus, G(MPa)	3.1	1.25	6
Bulk modulus, K (MPa)	6.6	2.6	13
Poisson's ratio, μ	0.3	0.3	0.3
Cohesion, C (kPa)	0	21	21
Friction angle, $\phi(^{\circ})$	30	30	30
Dilation angle, $\psi(^{\circ})$	20	20	20

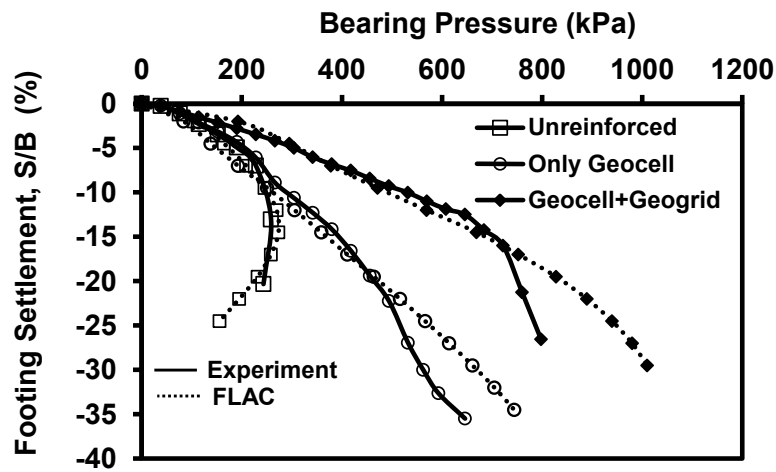


Figure 7. Comparison of experimental and numerical pressure settlement behavior

5. CONCLUSIONS

This paper has investigated the suitability of new commercially available geocells in the constructions of foundations subjected to heavy loads through stress controlled static plate load tests. In addition, the study has demonstrated the simplistic approach of modeling the 3D nature of geocell in 2D finite difference package called FLAC^{2D}. Test results suggest that the provision of geocell increases the ultimate bearing capacity of the sand bed by 4 times. Due to its high bending and shear stiffness, geocell mattress can support the footing at larger settlements and even after the failure of soil. Provision of the additional planar geogrid at the base of the geocell arrests the surface heaving and prevents the footing from undergoing the rotation failure. Hence, it is always beneficial to use planar geogrid layer at the base of the geocell mattress. By using the scaling laws suggested by “Butterfield (1999)” the results of the small-scale models tests can be extrapolated to full-scale cases. Thus, the initial studies in static condition suggest that the combination of the geocell and basal geogrid can be successfully used for the construction of foundations subjected to heavy loads. Moreover, geocells are cheaper and faster compared to vibro stone columns and hence more amenable for field applications. However, further studies are necessary to understand the behavior of geocells under repeated dynamic loadings to ascertain the suitability of geocells in the construction of foundations for railway lines. In this direction, the process of establishing the dynamic plate load test setup is in progress in the Department of Civil Engineering, Indian Institute of Science, Bangalore.

REFERENCES

- Bathurst, R.J. and Rajgopal, K. (1993). Large scale triaxial compression testing of geocell reinforced granular soils, *Geotechnical Testing Journal* 16 (3), 296-303.
- Binquet, J. and Lee, L. K. (1975). Bearing capacity tests on reinforced earth slabs, *Journal of Geotechnical Engineering Division, ASCE* 101 (12), 1241–1255.
- Broms, B.B. and Massarach, K.R. (1977). Grids mat a new foundation method. *Proceedings of 9th International Conference of Soil Mechanics and Foundation Engineering*, Tokyo, 1,433-438.
- Butterfield, R., (1999). Dimensional analysis for geotechnical engineers, *Geotechnique* 49(3), 357–366.
- Chumma, A.V. (1972). Bearing capacity theory from experimental results, *Journal of the Geotechnical Engineering Division, ASCE* 98 (12), 1257–1276.
- Dash, S.K., Krishnaswamy, N.R. and Rajagopal, K. (2001a). Bearing capacity of strip footings supported on geocell-reinforced sand, *Geotextiles and Geomembranes* 19, 235–256.
- Dash, S.K., Krishnaswamy, N.R., Rajagopal, K. (2001b). Strip footing on geocell reinforced sand beds with additional planar reinforcement, *Geotextiles and Geomembranes* 19, 529–538.
- El Sawwaf, M. and Nazer, A. (2005). Bearing capacity of circular footing resting on confined granular soil, *Journal of Geotechnical and Geoenvironmental engineering, ASCE*, 131 (3), 359-366.
- EM 1110-1-1904. *Settlement Analysis, Appendix-D*, U.S Army Corps of Engineers (1990), D6 –D8.
- Guido, V.A., Sobiech, J.P. and Christou, S.N. (1989). A comparison of texturized and non-texturized geoweb reinforced earth slabs, *Proceedings of Geosynthetics 1989*, 215-230.
- Henkel, D.J., and Gilbert, G. D. (1952). The effect of rubber membrane on the measured triaxial compression strength of clay samples, *Geotechnique* 3(1), 20-29.
- Madhavi Latha, G. and Somwanshi, A. (2009). Effect of reinforcement form on the bearing capacity of square footing on sand, *Geotextiles and Geomembranes* 27, 409-422.
- Mitchell, J.K., Kao, T.C. and Kavazanjian, Jr E. (1979). Analysis of grid cell reinforced pavement bases, *Technical Report No GL-79-8, U S Army Waterways Experiment Station*, July, 1979.
- Rajagopal, K., Krishnaswamy, N.R. and Madhavi Latha, G. (1999). Behavior of sand confined with single and multiple geocells, *Geotextiles and Geomembranes*, 17, 171–181
- Rea, C., and Mitchell, J.K. (1978). Sand reinforcement using paper grid cells, *ASCE Spring Convention and Exhibit, Preprint 3130*, Pittsburgh, PA, April, 24- 28.
- Sitharam, T.G., and Sireesh, S. (2005). Behavior of Embedded Footings Supported on Geocell Reinforced Foundation Beds, *Geotechnical testing Journal, ASTM*, Vol. 28, No. 5, 452-463.
- Tafreshi Moghaddas, S.N. and Dawson, A.R. (2010). Behavior of footings on reinforced sand subjected to repeated loading comparing use of 3D and planar geotextile, *Geotextiles and Geomembranes* 28, 434-447.
- Wood, D.M., (2004). *Geotechnical modeling, Version 2.2*. Taylor & Francis, U.K., 258-259.

Experimental and Theoretical Study on Interference Phenomena Between the Bearing Members of Different Geogrids in Pullout Loading Conditions

Calvarano, L.S., Department of Mechanics and Materials, "Mediterranea" University of Reggio Calabria, Italy, lidia.calvarano@unirc.it

Cardile, G., Department of Mechanics and Materials, "Mediterranea" University of Reggio Calabria, Italy, giuseppe.cardile@unirc.it

Gioffre, D., Department of Mechanics and Materials, "Mediterranea" University of Reggio Calabria, Italy, domenico.gioffre@unirc.it

Moraci, N., Department of Mechanics and Materials, "Mediterranea" University of Reggio Calabria, Italy, nicola.moraci@unirc.it

ABSTRACT

This paper deals with soil-geogrid interaction under pullout loading conditions. The main interaction mechanisms affecting the pullout resistance of geogrids embedded in compacted granular soils are the skin friction, between soil and reinforcement solid surface, and the bearing resistance, which develops against transversal elements.

In particular, regarding to the bearing resistance mobilized at the soil - geogrid interface, plays an important role the interference phenomena which could occur when the spacing between transversal bearing members is lower than a fixed limit, depending on the extensions of active and passive surfaces mobilized on transversal bearing members.

In order to investigate the interference phenomena, a wide CRD (constant rate of displacement) pullout test program on several extruded bi-oriented geogrids characterized by different geometry, thickness of the transverse elements and mesh size (in terms of spacing between elements) have been carried out.

Based on the pullout test results a simple theoretical method to predict the peak pullout resistance, taking into account the interference phenomena, is proposed.

1. INTRODUCTION

The use of geogrids to improve the soil mechanical behaviour has become increasingly common practice in geotechnical engineering applications. In order to analyse the internal stability of reinforced earth structures, it is necessary to evaluate the pullout resistance of reinforcement, mobilized in the anchorage zone.

The main interaction mechanisms affecting the pullout resistance of extruded geogrids are the skin friction, between soil and reinforcement solid surface, and the bearing resistance that develops against transversal elements.

Nevertheless, it is important to define the role of all the design (and test) parameters on the mobilisation of the interaction mechanisms (frictional and passive) in pullout condition, including geosynthetic length, tensile stiffness, geometry and shape, vertical effective stress (acting at the geosynthetic interface) and soil shear strength.

Experimental results carried out by the authors (Calvarano et al. 2011, Calvarano 2012) show the existence of an optimum spacing between the transversal elements which maximizes the peak pullout resistance (Figure 1).

In order to study the interference phenomena, which could occur when the distance between the bearing members decreases, the authors performed a series of pullout test on several bi-oriented geogrids (tested in transversal direction), characterized by different spacing and thickness of the bearing members, by removing some transversal bars from the same specimens.

In particular, Figure 1 shows the peak pullout resistance envelopes, in the same test conditions ($L_R = 0.90$ m and $\sigma'_v = 50$ kPa), for GGEB2 geogrid obtained varying the spacing between the transverse elements.

Therefore, when the transverse bars spacing is below the "optimum" value, the pullout response appears to be detrimentally affected by the interference phenomena between the transversal bearing members. On the other hand, when the transverse bars spacing is above the "optimum" value, the pullout resistance decreases because of the less number of bearing members that provide the passive resistance contribution to the overall pullout resistance. These

results clearly demonstrate the significant effect of the spacing between the transversal bearing elements on the peak pullout resistance of the extruded geogrids.

In the present paper, on the basis of the test results obtained by the authors (Moraci and Recalcati 2006; Moraci and Giofrè 2006; Calvarano et al. 2011, Calvarano 2012, Cazzuffi et al. 2011), in order to take into account also the interference phenomena, an extension of the theoretical method developed by Moraci and Giofrè (2006) to determine the peak pullout resistance of extruded geogrids embedded in a compacted granular soil was developed.

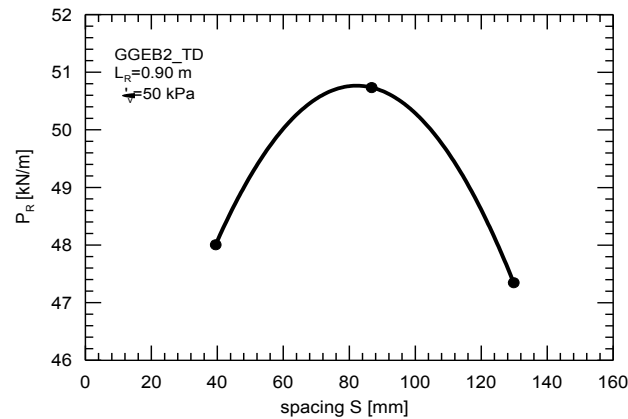


Figure 1. Effect of the transversal bars spacing on peak pullout resistance for bi-oriented geogrid specimens (Calvarano et al. 2011, Calvarano 2012).

2. EXPERIMENTAL STUDY

2.1 Test Apparatus

The test apparatus is essentially composed by a rigid steel large pullout box (1700 mm × 680 mm × 600 mm), a vertical load application system, a horizontal force application device, an internal special clamp with sleeve system, and all the required control and data acquisition instruments (Moraci and Montanelli 2000; Moraci et al. 2003; Moraci and Recalcati 2006; Giofrè and Moraci 2006).

The test apparatus is capable to produce confined failure of the geosynthetic specimen using a clamp placed inside the soil, well beyond the sleeve in order to keep the geosynthetic specimen always confined in the soil for the test duration. Friction between the soil and the side walls of the box is minimized by use of smooth Teflon films.

The equipment incorporates two sleeves near the slot at the front of the pullout box in order to avoid front wall effects as recommended by a number of researchers (Moraci and Montanelli 2000; Palmeira and Milligan 1989).

The specimen displacements are measured and recorded using inextensible steel wires connected to at least six different points along the geogrid specimen. The wires are connected to displacements transducers (Rotary Variable Displacement Transducers - RVDT) fixed to the external back side of the box. All the measurements are digitally recorded on a personal computer at defined constant time intervals.

2.2 Test Materials

The pullout tests have been performed on three PP extruded bi-oriented geogrids (named GGEB1, GGEB2 and GGEB3), tested in the transverse direction (TD) along which the geogrids carry the higher mechanical characteristics. The three geogrids show similar geometrical characteristics, in plan view, but they have different number of tensile elements, per unit width, different longitudinal rib pitch and different cross sectional shape, with main differences in rib and bar thickness.

A more detailed analysis of the transversal bar geometry has also shown a non-uniform shape with greater thickness at the rib intersection. The passive interaction mechanisms develop both at the node embossments and at the transversal bars. Therefore, the node embossment and the transversal bar geometry have been carefully determined to calculate the effective passive resistance surfaces.

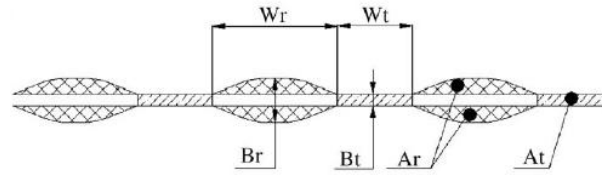


Figure 2. Schematic cross section of a generic transversal geogrid bar (Moraci and Recalcati 2006).

Figure 2 shows a schematic cross section of a geogrid bearing members that are placed transversely to the direction of pullout force. Table 1 shows the geometrical characterization of the geogrids, where W_r and B_r are the node width and thickness, respectively; S is the spacing between transversal bars in the pullout direction; W_t and B_t are the width and thickness of the bar portion between two nodes, respectively (Figure 2); A_b is the area of each rib element (including the node embossment and the bar portion between two nodes, A_t+A_r) where the bearing resistance can be mobilized. Also, per unit area of reinforcement, A_p and A_a are respectively the bearing and frictional surfaces.

Table 1. Geometrical geogrid characteristics (about symbol see Figure 2).

Geogrid	S [mm]	W_r [mm]	W_t [mm]	B_r [mm]	B_t [mm]	B_{eq} [mm]	A_b [mm ²]	A_p [mm ² /m ²]	A_a [mm ² /m ²]
GGEB1	64.54	14.98	44.34	5.73	3.88	4.43	224.3	68530	250000
GGEB2	39.48	14.81	25.84	3.76	2.90	3.29	107.1	83359	310000
GGEB3	56.92	16.24	59.49	4.95	3.72	4.02	269.7	70598	230000

A granular soil was used in these tests. The soil was classified as uniform medium sand (SP according to USCS classification system, A-3 according to CNR-UNI 10006 classification system), with grain shape from sub-rounded to rounded, uniformity coefficient U equal to 1.96, and average grain size D_{50} equal to 0.32 mm. The Standard Proctor compaction test performed show a maximum dry unit weight $\gamma_{dmax}=16.24$ kN/m³ at an "optimum" water content $w_{opt}=13.5\%$.

Direct shear tests, performed at an initial unit weight equal to 95% of γ_{dmax} (obtained at a water content of 9.3%) yield very high single values of the peak shear strength angle ϕ'_p , in the range 48° to 42° where the higher and the lower values refer respectively to the lower ($\sigma'_v=10$ kPa) and the higher ($\sigma'_v=100$ kPa) confining pressure. The shear strength angle at constant volume ϕ'_{cv} results equal to 34°.

2.3 Analysis Tests Results

Pullout tests have been carried out varying the specimen length ($L_R = 0.40, 0.90, 1.15$ m) and the applied vertical effective pressures (σ'_v was equal to 10, 25 and 50 kPa). All the tests have been performed at controlled rates of displacement (CRD) equal to 1.0 mm/min until geogrid rupture or until a total horizontal displacement of 100 mm was achieved. For all the tests, the geogrid specimens remained confined within the soil for its whole length.

The test results were analysed to define the influence of the different parameters studied (reinforcement geometry, embedded length and vertical stress) on the pullout behaviour of extruded geogrids analysed in the transverse direction (TD) and embedded in a granular soil.

The results of pullout tests for shorter and longer reinforcements are reported in Figure 3 that shows the trend of the pullout resistance versus vertical effective stresses.

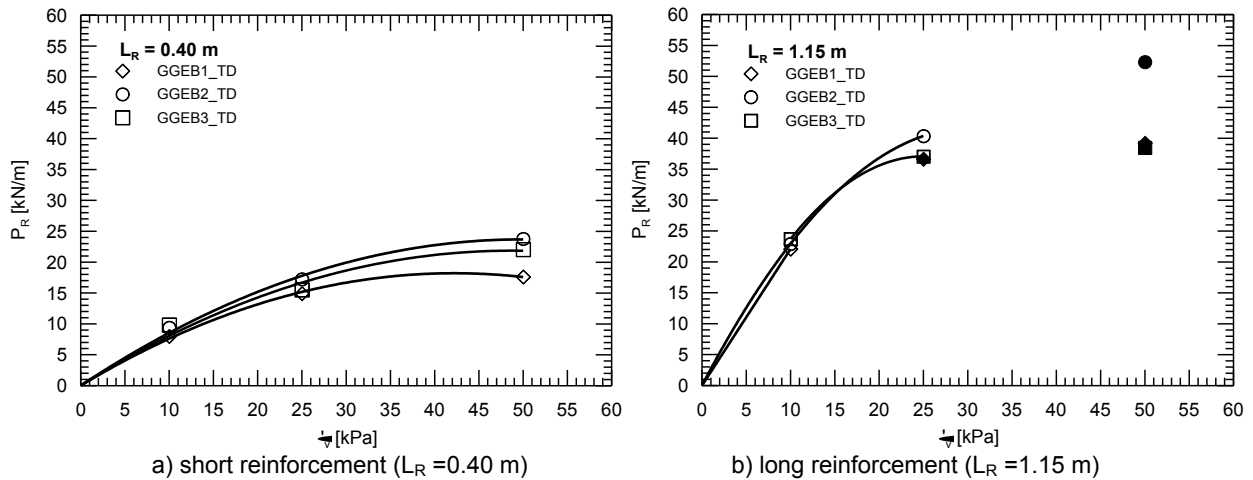


Figure 3. Peak pullout resistance envelopes varying the normal effective confining stresses for extruded bi-oriented geogrids.

When the geogrid tensile failure doesn't occur, for all bi-oriented geogrids studied and for all test conditions (L_R and σ'_v) the experimental data show a comparable values of the peak pullout resistance.

These experimental results are particularly interesting because they disagree with the comparison between the values of the overall frictional and passive surfaces on which it is possible to mobilize the interaction mechanisms. In particular, the GGEB2 geogrid is the reinforcement that has the higher values of frictional and passive surfaces when compared with the values corresponding to the GGEB1 and GGEB3 geogrids. Therefore we would expect that the GGEB2 geogrid can mobilize congruent greater values of peak pullout resistance. On the other hand the GGEB2 geogrid exhibits the lower spacing values between the transversal bearing members compared to the values measured for the GGEB1 and GGEB3 geogrids. Therefore, the comparable values of the peak pullout resistance, under the same test conditions, are due to the interference phenomena between the passive failure surfaces, that are generated in front of each bearing members, and the active failure surfaces that are generated in the unloading stress areas at the back of these bars (Palmeira 2004 and 2009).

In this case, the theoretical model developed by Moraci and Giofrè (2006) in order to determine the peak pullout resistance of extruded geogrids embedded in a compacted granular is not applicable.

3. THEORETICAL STUDY

The model proposed by Moraci and Giofrè (2006) to predict the peak pullout resistance, that takes into account the non-linearity of the envelope of rupture of fill soil and extensibility of the reinforcement, is herein modified in order to take into account the interference phenomena between transversal bearing elements.

In the proposed model is introduced a reduction factor on the passive component to take into account the interference phenomena between the extensions of active and passive surfaces mobilized between transversal bearing members. Therefore, the new theoretical expression becomes:

$$P_R = 2 \cdot C_{\alpha S} \cdot \alpha_S \cdot L_R \cdot W \cdot \sigma'_n \cdot \tan \delta + C_{\alpha b} \cdot n_t \cdot n_{tb} \cdot A_b \cdot \sigma'_b \quad [1]$$

where the symbols mean: $C_{\alpha S}$ is the reduction coefficient of geogrid area where skin friction develops (Moraci e Giofrè 2006); n_t is the number of geogrid bearing members; n_{tb} is the number of nodes in a transversal element; $A_b = A_t + A_r$ is the area of each singular module (the node embossments and portion of the adjacent transversal bar) on which the bearing resistance can be mobilized. The bearing stress σ'_b was evaluated by equation proposed by Matsui et al. (1996). Previous studies (Jewell 1985 and 1990, Dyer 1985, Palmeira and Milligan 1989; Palmeira 2004 and 2009; Calvarano et al. 2011, Calvarano 2012, Cazzuffi et al. 2011) have shown that the coefficient $C_{\alpha b}$ is primarily dependent on the geometric characteristics of the mesh reinforcement, such as the spacing and the equivalent thickness (B_{eq}) of the bearing member (Figure 4).

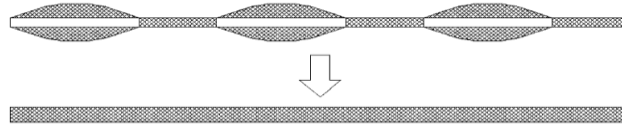


Figure 4. Assumed equivalent geometry transversal rib (Moraci and Giofrè 2006).

Palmeira and Milligan (1989), Dias (2003) and Palmeira (2009) showed that the coefficient $C_{\alpha,b}$ decreases with decreasing of the normalized spacing and suggest that the interference phenomenon can be considered negligible or absent only if the ratio $S/B > 40$. In this case, each bar of the geogrid will behave as if it were isolated. However, Palmeira and Milligan (1989) and Palmeira (2009) showed, moreover, that the interaction coefficient decreases as the number of the bars increase, and therefore decreases with the geogrid length.

Based on the above considerations $C_{\alpha,b}$ is considered as the product of two contributions:

$$C_{\alpha,b} = C_{\alpha,b1} \cdot C_{\alpha,b2} \quad [2]$$

where: $C_{\alpha,b1}$ is the of passive interference coefficient calculated in function of the spacing between bearing members, the equivalent thickness B_{eq} and in function of applied confining stress; $C_{\alpha,b2}$ is the passive interference coefficient calculated in function of the reinforcement length.

In this preliminary study $C_{\alpha,b1}$, in the range of normalized spacing studied, has the following law of variation:

$$C_{\alpha,b1} = a \cdot e^{[b \cdot (S/B_{eq})]} \quad [3]$$

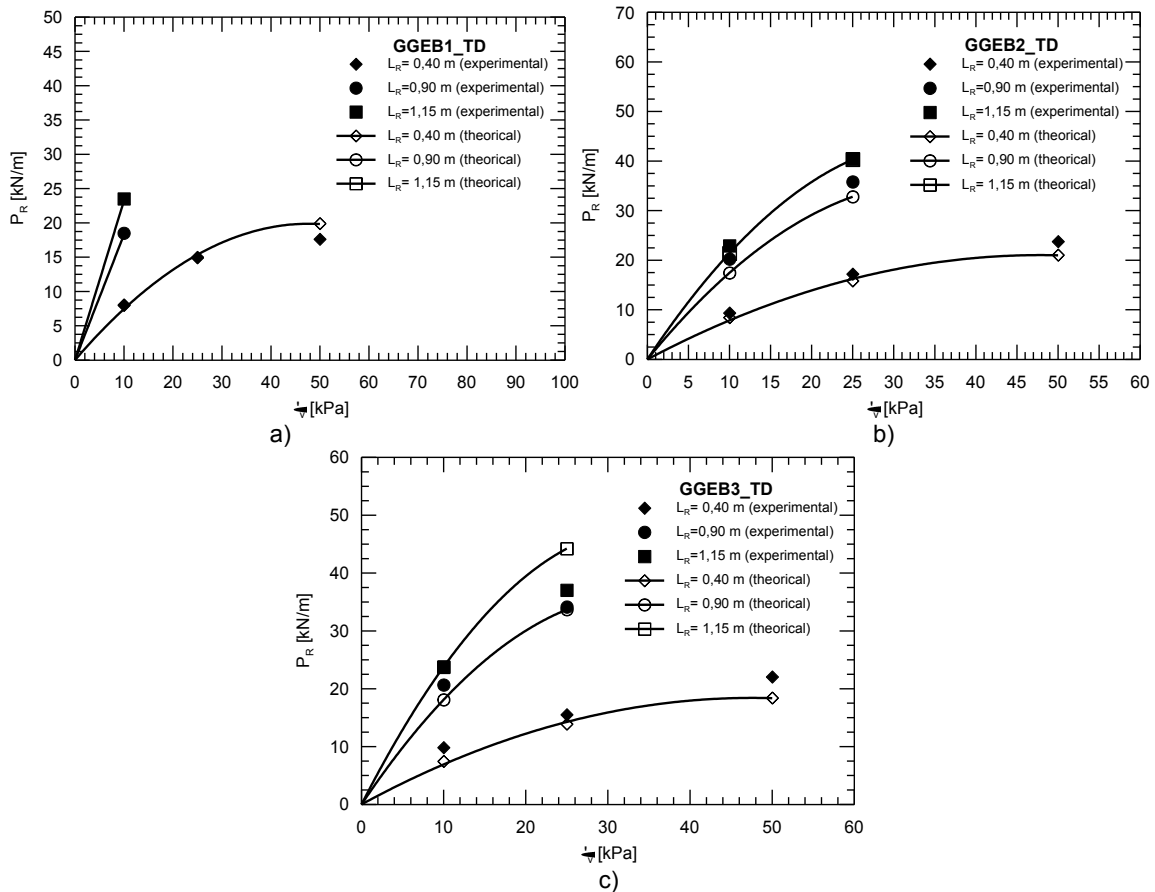


Figure 5. Comparison between experimental and theoretical values of peak pullout resistance regarding extruded bi-oriented geogrids: a) GGEB1, b) GGEB2 and c) GGEB3.

Table 2. Theoretical and experimental peak pullout resistance, P_R (kN/m), for geogrid GGEB1, GGEB2 and GGEB3.

Geogrid	Length [m]	Normal Stress σ'_v								
		10 kPa			25 kPa			50 kPa		
		P_R^{Exp} [kN/m]	P_R^{Theor} [kN/m]	P_{RS}^{Theor} [kN/m]	P_R^{Exp} [kN/m]	P_R^{Theor} [kN/m]	P_{RS}^{Theor} [kN/m]	P_R^{Exp} [kN/m]	P_R^{Theor} [kN/m]	P_{RS}^{Theor} [kN/m]
GGEB1	0.40	7.99	8.05	1.00	14.92	14.96	1.37	17.62	21.06	2.62
	0.90	18.50	18.30	1.29	-	-	-	-	-	-
	1.15	23.50	23.23	1.65	-	-	-	-	-	-
GGEB2	0.40	9.39	8.45	0.71	17.24	15.85	1.70	23.78	21.06	3.24
	0.90	20.25	17.45	1.60	35.82	32.81	3.82	-	-	-
	1.15	22.92	21.42	2.04	40.35	40.31	4.88	-	-	-
GGEB3	0.40	7.09	7.47	0.53	15.54	13.92	1.26	22.06	18.44	2.41
	0.90	20.67	18.11	1.19	34.16	33.69	2.84	-	-	-
	1.15	23.72	23.79	1.52	37.06	44.23	3.62	-	-	-

with a and b constants of the exponential function which assume different values varying σ'_v . The above constants were calibrated considering the results of the experimental tests and as upper bound $C_{\alpha b1}=1$ when $D/B_{eq} \geq 40$, the condition in which each cross bar behaves as isolated bar and therefore the interference phenomenon is irrelevant.

In particular, respectively for vertical confinement stresses of 10, 25 and 50 kPa, the constant "a" is equal to 0.1425, 0.1382 and 0.1089, while the constant "b" takes on the values of 0.0505, 0.0497 and 0.0527.

The passive interference coefficient $C_{\alpha b2}$, in the range of the lengths investigated, is a function of L_R , with the following expression:

$$C_{\alpha b2} = c \cdot L_R + d \quad [4]$$

with c and d constants of the law of linear regression equal to -0.0005 and 1.0221.

The presented comparisons (Table 2) clearly illustrate the application of the above formulation. The proposed method, for all extruded bi-oriented geogrids studied, predicts the peak experimental pullout resistances well, both for different applied vertical effective confining stresses and for different reinforcement lengths.

Table 2 reports the comparison between the peak experimental (P_R^{Exp}) and theoretical (P_R^{Theor}) pullout resistances and Figure 5 shows the comparison between experimental (closed symbols) and theoretical values (open symbols and continuous lines) of the peak pullout resistances, evaluated for the different applied vertical effective confining stresses.

In particular, where rupture confined didn't occur, for "short" reinforcements (0.40 m), the values vary between 1% and 13%, between -8% and -11% and between -24% and -13%, respectively for the GGEB1, GGEB2 and GGEB3; for the "long" reinforcements (0.90 m and 1.15 m), these differences vary about -1%, between -14% and 0% and between 0% and 19%, respectively for the GGEB1, GGEB2 and GGEB3.

On the basis of the theoretical analysis, the skin friction component P_{RS}^{Theor} represents less than 15% of the peak pullout resistance respectively for all the bidirectional geogrids.

Therefore, the comparison between theoretical and experimental results was favourable, thus confirming the suitability of the proposed approach.

4. CONCLUSIONS

The experimental results presented in this paper have shown clearly the influence of the geogrid geometry on the mechanical response of different geosynthetic reinforcements in interaction with compacted granular soil, in pullout loading condition.

Particularly, when the spacing of bearing members is lower than a fixed limit, the extensions of active and passive surfaces mobilized on transversal bearing members produce a reduction on bearing component of pullout resistance.

On the basis of experimental results, the following conclusions could be drawn:

- the increases in the bearing surface are not directly associated with increases of the mechanical response parameters if interference phenomena occur;
- the coefficient of passive interference C_{ob} proposed in the paper allows extending the previous theoretical model developed by Moraci and Giofrè (2006) also when interference phenomena, due to the proximity of the transverse bars, occur.
- the theoretical values of peak pullout resistance obtained by the proposed model are in agreement with the experimental data.
- in the case of extruded geogrids embedded in compacted uniform medium sand, the skin friction component of the peak pullout resistance is small in comparison with the bearing one. For the interfaces analysed in the research and in the test conditions used in the pullout tests the skin friction component represents less than 15% of the peak pullout resistance.

REFERENCES

- Calvarano, L. S. (2012). Comportamento di differenti geogriglie in condizione di sfilamento statico e ciclico. Ph.D. Thesis, "Mediterranea" University of Reggio Calabria, 638.
- Calvarano, L.S., Cardile, G. e Moraci, N. (2011). Influenza della geometria e della struttura del rinforzo sulla risposta meccanica all'interfaccia terreno-rinforzo in condizioni di sfilamento. *XXIV Convegno Nazionale Geotecnica "Innovazione tecnologica nell'ingegneria geotecnica"*, Naples, Italy, 2, 359-365.
- Cazzuffi, D., Calvarano, L. S., Cardile, G., Moraci, N., Recalcati P. (2011). European experience in pullout tests: The influence of geogrid's geometry and structure on interface behaviour. *Geosynthetics*, October –November 2011, 42-51.
- Dyer, M. R. (1985). Observations of the Stress Distribution in Crushed Glass with Applications to Soil Reinforcement. Ph.D. Thesis, University of Oxford.
- Jewell, R. A., Milligan, G. W. E., Sarsby, R. W. and Dubois, D. D. (1985). Interactions Between Soil and Geogrids. Proceeding from the *Symposium on Polymer Grid Reinforcement in Civil Engineering*, 18-30. Ed. Thomas Telford, London.
- Jewell, R. A. (1990). Reinforcement bond capacity. *Géotechnique* 40 (3), 513-518.
- Moraci, N. and Montanelli, F. (2000). Analisi di prove di sfilamento di geogriglie estruse installate in terreno granulare compattato. *Rivista Italiana di Geotecnica n.4/2000* (16), 5-21.
- Moraci, N., Montanelli, F. and Romano, G. (2003). Interface Pullout behaviour of geogrids embedded in compacted granular soils. *XIII European Conference on Soil Mechanics and Geotechnical Engineering*, Prague, 837-842
- Moraci, N. and Recalcati, P.G. (2006). Factors affecting the pullout behaviour of extruded geogrids embedded in compacted granular soil. *Geotextiles and Geomembranes*, 24 (22), 220-242.
- Moraci, N. and Giofrè, D. (2006). A simple method to evaluate the pullout resistance of extruded geogrids embedded in granular soil. *Geotextiles and Geomembranes*, 24 (12), 116-128.
- Palmeira, E. M., 2004. Bearing force mobilisation in pull-out tests on geogrids. *Geotextiles and Geomembranes*, 22 (28), 481- 509.
- Palmeira, E M. e Milligan, G. W. E. (1989). Scale and other factors affecting the results of pull-out tests of grid buried in sand. *Géotechnique*, 11(3), 511-524.
- Palmeira, E. M (2009). Soil–geosynthetic interaction: Modelling and analysis. *Geotextiles and Geomembranes*, 27 (5), 368-390.

Failures of Geomembrane Liners for Agricultural Waste Storage Ponds

B. Doerge, P.E., G.E., USDA-NRCS, Fort Worth, TX, ben.doerge@ftw.usda.gov,
C. Lafleur, P.E., USDA-NRCS, Fort Worth, TX, cherie.lafleur@ftw.usda.gov

ABSTRACT

The USDA-Natural Resources Conservation Service (NRCS) provides technical and financial assistance for thousands of conservation practices annually, including agricultural waste storage ponds. This paper is the outgrowth of several failures involving exposed geomembrane liners on NRCS-assisted agricultural waste storage ponds. The main points to be covered include: 1) factors responsible for failure of the liners; 2) unique requirements of agricultural waste storage facilities compared to municipal wastewater facilities and solid waste landfills; and 3) recommendations for designing constructable, cost-effective, yet robust liners for agricultural waste storage ponds.

1. INTRODUCTION

The USDA-NRCS assists with the design and construction of numerous agricultural waste storage ponds (AWSP's), primarily under its Environmental Quality Incentives Program (EQIP). A variety of pond liners are used to limit the seepage losses from the ponds, including compacted soil liners, amendment-treated soil liners, geosynthetic clay liners, and covered and exposed geomembrane liners. While most liners function satisfactorily, a number of exposed geomembrane pond liners have failed in recent years, due to a variety of causes. These failures reflect on both the harshness of the conditions which can be encountered in the setting of a commercial agricultural operation and the climbing of the learning curve associated with the implementation of a new technology.

Lessons learned from structure failures are valuable in pinpointing where improvements need to be made. To that end, this paper presents four case histories of failures of exposed geomembrane liners in AWSP's. Particular emphasis is given to the causes of failure in each case. Based on these experiences, recommendations are presented for the investigation, design, construction, and operation of AWSP's with geomembrane liners. These recommendations reflect the unique requirements and challenges associated with agricultural waste storage facilities.

2. FAILURES CASE HISTORIES

The four case histories presented below occurred on NRCS-assisted projects over the last fifteen years. All references to names and locations are omitted out of privacy considerations.

2.1 Case History No. 1

2.1.1 Project Details

Capacity of pond: 23,000 cubic meters

Liner material: Reinforced, slit-film, woven polyethylene geomembrane, 0.6 mm thick with 0.05 mm coating.

Date of construction: 1998

Time to failure: 1 year

Nature of Failure: Numerous large gas bubbles and tears in liner,

Drainage system: None.

Gas venting system: None.

The geomembrane liner was a last-minute substitution for a compacted clay liner when a suitable source of clay borrow material could not be found. The particular liner material was selected because it had been pre-approved by NRCS for use in clear water ponds, provided a pre-qualified contractor performed the installation. No quality control/quality assurance testing of the seams was performed during construction. The expertise of the installer was relied upon for quality. The seams were welded with a hand-held hot air gun and a hand roller.

During the first filling of the pond, a small bubble was observed to rise with the liquid level in the pond. It was suspected to be filled with water and dissipated as the pond filled. About nine months later, large gas-filled bubbles under the liner began to appear shortly after the pond contents were agitated for the first time (see Figure 1). Tears in the liner and floating pieces of geomembrane were also observed. Large streams of gas bubbles were observed to be escaping from

holes in the liner. The entire liner had to be removed and replaced. Inspection of the failed liner revealed numerous poorly adhered seams, burn-through, and holes along the seams.

2.1.2 Causes of Failure

Primary cause: Poor quality seams and damage to the liner during construction, leading to leakage of manure under the liner and formation of biogas bubbles.

Contributing causes: 1) inappropriate liner material used; 2) designer had no previous experience with geomembrane liners; 3) no agitation ramps or pads included in the design; 4) no quality assurance performed during construction; 5) damage to liner during agitation operations.

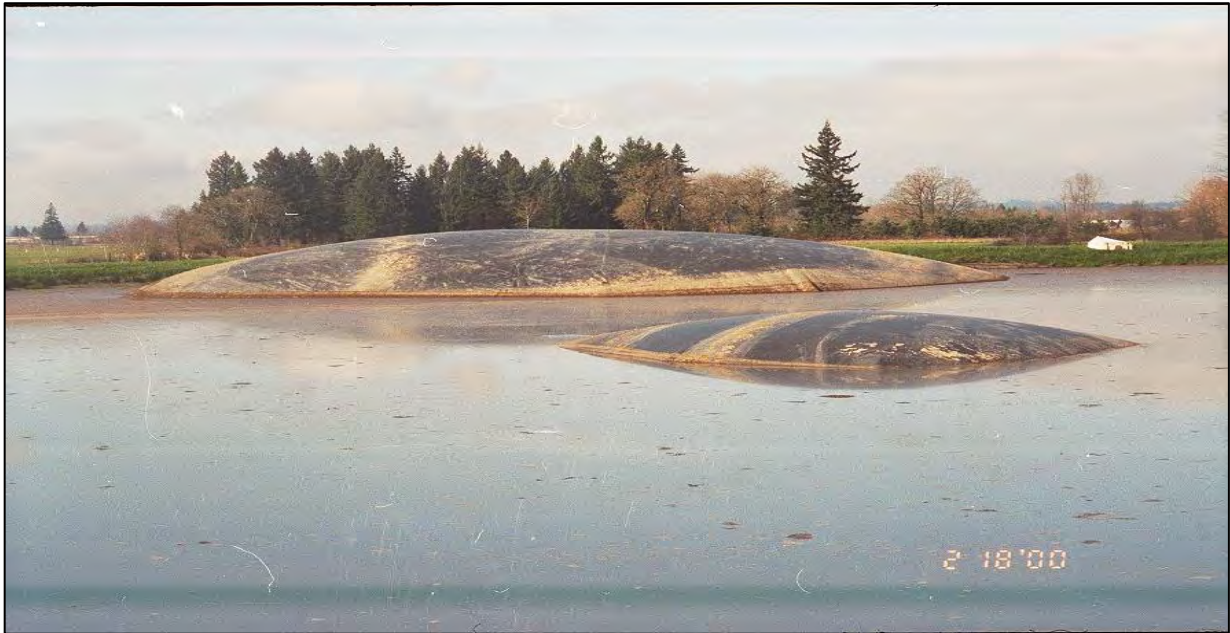


Figure 1. Large gas bubbles under geomembrane liner (Case History No. 1).

2.2 Case History No. 2

2.2.1 Project Details

Capacity of pond: 2,550 cubic meters
Liner material: Non-reinforced EPDM, 1.1 mm thick.
Date of construction: 2003
Time to failure: 2 years (initial problems); 5 years (total failure)
Nature of Failure: Numerous large gas bubbles under liner,
Drainage system: None
Gas venting system: None.

Immediately following construction, the landowner installed a series of fence posts through the liner along the top edge of the pond side slopes. Later, the landowner observed a fox scratching at the liner. It was suspected that the fox was pursuing mice that had gained access behind the liner through the holes at the fence posts. Small holes were observed in the liner and were presumably made by the fox. One of these holes was below the maximum operating level of the pond. Liquid manure is believed to have entered through this hole and accumulated behind the liner. After the first two years of operation, a single small bubble formed in the middle of the pond. The bubble was presumed to be from biogas generated by the manure that had leaked underneath the liner. The bubble went away when the pond was emptied during the summer for the following two years. The landowner apparently did not consider the bubble to be significant enough of a problem to report it to the designer. The following season, multiple bubbles appeared (see Figure 2). During the fifth year of operation, the liner was cut by the impellor of an agitation pump, presumably because it was "floating" above the bottom of the pond. The agitation and pumping were performed by a custom operator hired by the landowner. After the liner was cut, manure could flow freely under the liner and it could not be salvaged.

2.2.2 Causes of Failure

Primary cause: Animal damage, which allowed manure to leak beneath the liner and generate biogas bubbles.

Contributing causes: 1) puncturing of liner to install fence posts; 2) failure to recognize significance of gas bubbles and attempt corrective actions early on; 3) no gas venting system included in design; 4) damage to liner by agitation equipment operated by outside contractor.



Figure 2. Gas bubbles in manure storage pond Case History No. 2).

2.3 Case History No. 3

2.3.1 Project Details

Capacity of pond: 16,700 cubic meters

Liner material: Non-reinforced EPDM, 1.1 mm thick.

Date of construction: 2007

Time to failure: 1 year

Nature of Failure: Gas/water bubbles under liner,

Drainage system: Perimeter drain tile

Gas venting system: 136 g/m² nonwoven geotextile under liner with 2 percent bottom slope; flap vents on top of slope.

Design phase geologic investigations identified a perched water table in the pond area, based on redoximorphic features (mottling). The ground water level was estimated from test pits, but the pits were not left open to obtain the 24 hour water levels. A perimeter drain was included in the design to control the perched water table. During construction, sloughing occurred on portions of the pond slopes due to wet soil conditions. This wet area appeared to be a deeper seep that was separate from the upper perched water table. Air lance testing was performed to check seam quality, at the recommendation of the manufacturer. No destructive tests were run to determine the shear and peel strengths of the seams.

Approximately one year after construction, a number of large bubbles formed beneath the liner. Some bubbles were filled with liquid, as indicated by a sloshing when touched. Gas bubbles were also observed to be escaping from under the liner. After the pond was drained, an inspection of the liner revealed holes, split seams, and bubbles, along with soft, spongy soils under the liner. Three separated seams were noted.

Following the failure, twelve observation wells were installed to monitor the groundwater level fluctuation at the site. The upper perched table was found to reach levels far higher than indicated by the redoximorphic features. The perimeter drain, with a 49 m span in the narrow direction, was not capable of controlling the groundwater level under the pond.

2.3.2 Causes of Failure

Primary cause: High groundwater pressures under liner as well as split seams and holes in liner.

Contributing causes: 1) inadequate geologic investigation to determine the groundwater levels in the pond area, particularly the seasonal fluctuations; 2) inadequate drainage system under liner; 3) inadequate gas venting system under liner; 4) no destructive testing of seams was performed during construction.

2.4 Case History No. 4

2.4.1 Project Details

Capacity of pond: 7,800 cubic meters

Liner material: Non-reinforced EPDM, 1.1 mm thick.

Date of construction: 2008

Time to failure: 1.5 months

Nature of Failure: Gas bubbles under liner and tearing of liner by agitation equipment.

Drainage system: Perimeter drain tile.

Gas venting system: 0.5 m wide strips of geocomposite at 15 m spacing with 271 g/m² nonwoven geotextile under liner with 1.5 percent bottom slope; PVC pipe vents and flap vents on top of slope.

Geologic investigations identified a perched water table in the pond area, based on redoximorphic features (mottling). The ground water level was estimated from test pits, but the pits were not left open to obtain the 24 hour water levels. A perimeter drain was included in the design to control the perched water table.

The design included a gas venting system, consisting of strips of geocomposite underlain by a geotextile. The geocomposite strips were supposed to have been recessed to be flush with the ground surface, but they were not recessed, and the geotextile was laid on top of the geocomposite strips instead of underneath. The flap vent outlets for the geocomposite strips were not installed for at least a week after the liner was installed.

During the initial filling of the pond, gas accumulated in the geocomposite strips and caused them to float to the surface of the pond (see Figure 3). The PVC pipe vents were in place at this time. The presence of several larger bubbles suggested that at least some of the gas was from sources other than just the air contained within the geocomposite strips. After the bubbles had formed, the liner was cut by the agitation equipment. After the pond was drained, several seam failures were noted. Two seams in the bottom of the pond were able to be pulled apart easily by hand. Additional large bubbles under the liner were observed in the empty pond (see Figure 4). Ultimately the damaged liner was removed.



Figure 3. Gas accumulation in venting system (Case History No. 4).

2.4.2 Causes of Failure

Primary cause: inadequate gas venting system as well as leakage through seams.

Contributing causes: 1) inadequate drainage system; 2) inadequate quality control/quality assurance on seaming operations during construction; 3) gas venting system not installed as designed; and 4) damage to liner by agitation equipment.



Figure 4. Large bubbles under liner visible after emptying (Case History No. 4).

2.5 Summary – Causes of Liner Failures

The four case histories illustrate that many factors can contribute to liner failure and that multiple causes are frequently involved in a given failure. Problems can arise during all phases of the design process, including investigation, design, construction, and operation. Problems common to many of the case histories presented above include:

- Inadequate geologic investigations to determine the seasonal fluctuation of ground water in the pond area.
- Inadequate drainage and/or gas venting systems.
- Inadequate quality control/quality assurance during construction.
- Improper operation procedures.

3. UNIQUE REQUIREMENTS OF LINERS FOR AGRICULTURAL WASTE STORAGE PONDS

The design and operation of geomembrane-lined AWSP's pose unique challenges. First, geomembrane liners are much thinner than other lining materials (e.g., concrete and compacted soil) and geomembranes can be damaged relatively easily, both during and after construction. Furthermore, Koerner (2005) points out that geomembranes are more "unforgiving" than other geosynthetics in that even a small leak can produce alarmingly high leakage rates. Excessive leakage from geomembrane-lined AWSP's is an environmental concern because of the potential for pollution of ground water. It is also a functional concern. Leakage of liquid manure underneath the liner poses a serious threat to the integrity of the liner because of manure's ability to generate large amounts of biogas. Because of geomembranes' low

weight, any accumulation of gas under an exposed liner will result in harmful gas bubbles unless the liner is equipped with well functioning drainage and gas venting systems. Any error or omission in the design of these protective features can lead to rapid and total failure of the liner system. Once large gas bubbles form under the liner, it is generally considered to have failed and must be removed and replaced.

At the same time, the conditions under which AWSP's are operated can be very harsh and unpredictable. Loading, agitation, and clean-out operations can place large stresses on the liner, and these operations are typically performed by a variety of individuals who may not be fully aware of the limitations and vulnerabilities of the liner. Animals, both domesticated and wild, can also damage the liner if they have access to it.

Another major challenge relates to the economics of AWSP's. The control of seepage from AWSP's is typically mandated by state and federal regulatory agencies, and the cost of complying with these regulations is borne solely by the landowner/operator. With municipal waste water facilities and soil waste landfills, the cost of the required engineered systems can be spread out over a relatively large pool of end users. This is not the case with private farmers where the prices they receive for the commodities they produce are outside of their direct control. Therefore, it is important that the cost and complexity of liner systems for AWSP's be kept to a minimum. Elaborate, multi-layer systems like those often used in landfills are likely not economically feasible for many agricultural producers. On the other hand, liner systems for AWSP's must be sufficiently robust so that they can stand up to the operating conditions they will face over their economic life. These opposing requirements for economy and robustness must be successfully balanced to make the use of geomembranes liners for AWSP's attractive.

4. RECOMMENDATIONS FOR INVESTIGATION, DESIGN, CONSTRUCTION, AND OPERATION OF AGRICULTURAL WASTE STORAGE PONDS

Based on the insights gained from failure case histories like those presented in this paper, the following recommendations are offered for designers of AWSP's. The recommendations are separated into the followings areas: investigation, design, construction, and operation.

4.1 Investigation

Geologic investigations should be performed to characterize all subsurface conditions that could impact the performance of the liner. Such conditions include the presence of coarse-grained materials and the proximity of bedrock. It is also critical that ground water conditions be identified, including the seasonal variation of the ground water level. This information is needed to design the drainage system under the liner so that the liner will not be subjected to excess hydrostatic pressure at any time. Rising groundwater can also displace air in the soil pores and produce bubbles under the liner. Determining the seasonal high water level from redoximorphic features (mottling) alone is not adequate. The water level in boreholes and test pits should be noted, and if possible, the holes should be left open at least 24 hours to allow the water level to stabilize. Undisturbed soil samples can also be used to determine the degree of saturation. It should be noted that these water levels only show the conditions at the time of investigations. Seasonal fluctuations can be significant and may require the installation of observation wells with one or more years of monitoring.

Significant subsurface conditions are not always discovered during geologic investigations. Therefore, the designer should be present during any foundation excavations in case any differing conditions are encountered. Other inspection personnel may not be able to recognize significant changes in conditions compared to what was assumed in design. Any seepage observed within the excavation must be critically evaluated.

4.2 Design

The design of geomembrane liner systems is complex and requires specialized training and experience. Koerner (2012) states that designing pond liner systems using geosynthetics requires that the designer "buy into the whole package." This means that a number of components besides just the geomembrane are required for a geosynthetic liner system to function satisfactorily. Therefore, a geomembrane cannot simply be substituted for, say, a compacted clay liner. Other features, such as a drainage system and a gas venting system are also required, along with a full complement of quality control/quality assurance inspection and testing during construction. The case histories presented above demonstrate that incomplete understanding of these complexities on the part of the designer can result in the omission of critical features and ultimately failure of the liner. Training, expert reviews, and contracting out should be considered until in-house expertise in liner design can be brought up to an acceptable level. Designers should develop their own expertise rather than rely too heavily on manufacturer's recommendations or "experienced" installers. Manufacturers are a good source of information on their respective products, but they may not be aware of all site-specific details that may impact the overall design.

As stated above, all geomembrane liner systems should include drainage and gas venting systems. These systems should be designed assuming that some leakage will occur through the membrane. For example, Giroud and Bonaparte (1989) recommend designing the drainage system for a geomembrane based on a frequency of one 100 mm² hole per 4,000 m² of surface area. The drainage system must also be designed to maintain the ground water level below the liner. The capacity of the gas venting system should consider both gas coming from the foundation as well as gas generated by the assumed manure leakage. The gas generation potential of manure is not well defined in the technical literature and further study would be helpful. It is recommended that a continuous gas collection and transmission medium be installed under the liner, such as a nonwoven geotextile or a geocomposite (geotextile-geonet-geotextile). Closely spaced vents should be provided to facilitate the evacuation of the gas. The gas venting system should be configured so that no high spots exist where gas can be trapped.

4.3 Construction

Construction inspection personnel need to be experienced in geomembrane installation. Detailed quality control/quality assurance requirements should be developed for each project. If in-house inspection personnel do not have the required expertise, then the use of outside specialists should be considered. Seam quality should not be evaluated solely by non-destructive tests such as the air lance. Destructive samples and test strips should also be used to document seam strength. Quality assurance should also insure that all components of the project are installed as designed. Leak testing of the completed system may also be considered.

4.4 Operation

Geomembrane liners of AWSP's are subject to harsh conditions during operation which the designer must thoroughly consider during the design process. Protective features such as curbs, ramps, agitation aprons, and fences should be incorporated into the design as needed to reduce the potential for damage to the liner. The vulnerabilities of the liner should be clearly communicated to the landowner/operator in the form of a detailed operation and maintenance plan. The consequences of damage to the liner must be clearly understood all involved in the operation of the facility. The operator should be educated to be able to recognize the early signs of problems so that the designer can be notified in a timely manner and corrective action can be taken before total failure of the liner occurs. In some cases, the manure management system of the operator may make the use of an exposed geomembrane liner unadvisable, such as when the solids and liquids are not separated before storage in the pond. In such cases, an alternate lining system should be used.

REFERENCES

- Giroud, J.P., and R. Bonaparte. (1989). Leakage through liners constructed with geomembranes—Part 1. Geomembrane Liners. *Geotextiles and Geomembranes*, 8:27–67.
- Koerner, G. R. (2012). *USDA Manure Storage*, Presented on 03/29/12, East Lansing, MI.
- Koerner, R. M. (2005). *Designing With Geosynthetics*, 5th ed., Pearson Prentice Hall, Upper Saddle River, NJ, USA.

Feasibility of MASW (Multi-Channel Analysis of Surface Waves) for Evaluating the Dynamic Properties of Geofoam

Masood H. Kafash, Graduate Research Assistant, The University of Memphis, Memphis, TN;
mhssnzdh@memphis.edu

David Arellano, Associate Professor, The University of Memphis, Memphis, TN; darellan@memphis.edu

Seyed Mehrdad Hosseini, Graduate Research Assistant, The University of Memphis, Memphis, TN; shsseini@memphis.edu

Shahram Pezeshk, Professor and Department Chair, The University of Memphis, Memphis, TN;
spezeshk@memphis.edu

ABSTRACT

Expanded Polystyrene (EPS) - block geofoam has been successfully used in many civil engineering applications such as lightweight fill in roadway embankments over soft ground and in landslide stabilization and repair. Seismic loading can affect both external and internal stability of an embankment containing EPS-block geofoam. The geofoam dynamic parameters required to perform seismic analysis are the shear wave velocity, shear modulus and damping ratios. Currently, these parameters are obtained predominantly from laboratory testing such as resonant column and cyclic triaxial tests. However, laboratory tests are typically performed on small specimens and not on full-size geofoam blocks. Additionally, it is difficult to reproduce the field stresses and strains in conventional dynamic laboratory testing. Techniques such as Spectral Analysis of Surface Waves (SASW) are commonly used in geotechnical practice to measure the shear wave velocity of soils. MASW (Multi-Channel Analysis of Surface Waves) tests were performed on full-size EPS blocks to evaluate the feasibility of using geophysical techniques to measure the dynamic parameters of geofoam for use in seismic analysis. Results of the feasibility study suggest that MASW tests may be a reliable and economical procedure for determining the shear modulus of geofoam blocks.

1. INTRODUCTION

Expanded Polystyrene (EPS) - block geofoam has been successfully used in many civil engineering applications such as lightweight fill in roadway embankments (Stark et al., 2004, Arellano and Stark, 2009) over soft ground and in landslide stabilization and repair (Arellano et al., 2010; 2011b). The National Cooperative Highway Research Program Project 24-11(02), "Guidelines for Geofoam Applications in Slope Stability Projects," includes a recommended design guideline for the use of EPS-block geofoam in slope stabilization and repair and an overview of the design procedure is included in Arellano et al. (2010; 2011a&b). Figure 1 depicts the major components of an EPS-block geofoam slope system. Seismic loading can affect both external and internal stability of a slope stabilized with EPS-block geofoam. Design for external stability of the overall EPS-block geofoam slope system considers failure mechanisms that involve the existing slope material as well as failure mechanisms that involve both the fill mass and the existing slope material. Failure mechanisms that are considered for external seismic stability analysis include overall slope instability, horizontal sliding of the entire EPS-block geofoam fill mass, overturning of a vertical sided embankment, bearing capacity failure of the existing foundation earth material, and settlement of the existing foundation material. Design for internal stability considers failure mechanisms within the EPS-block geofoam fill mass. Failure mechanisms that are considered for internal seismic stability analysis include horizontal sliding between layers of blocks and/or between the pavement system and upper layer of blocks and load-bearing failure of the EPS blocks.

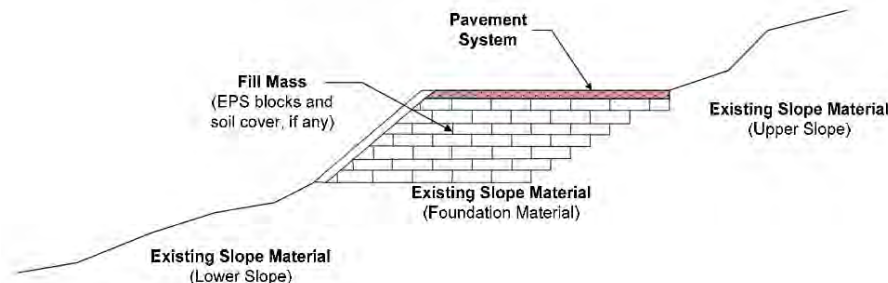


Figure 1. Major components of an EPS-block geofoam slope system (Arellano et al. 2010).

The geofoam dynamic parameters required to perform seismic analysis are the shear wave velocity, shear modulus and damping ratios. Currently, these parameters are obtained predominantly from laboratory testing such as resonant column and cyclic triaxial tests. However, laboratory tests are typically performed on small specimens and not on full-size geofoam blocks. Additionally, it is difficult to reproduce the field stresses and strains in conventional dynamic laboratory testing. Athanasopoulos et al. (1999, 2007), Duskov (1997), Trandafir et al. (2010), Athanasopoulos and Xenaki (2011), Ossa and Romo (2011) performed cyclic triaxial tests and Ossa and Roma (2011), Athanasopoulos and Xenaki (1999, 2011) performed resonant column tests to measure the dynamic properties on geofoam specimens.

The literature of the laboratory test results, indicated above, revealed that the shear modulus of EPS material is sensitive to specimen size. Duskov (1997) performed a series of cyclic uniaxial tests on cylindrical EPS specimens with a diameter of 100 mm and height of 200 mm and with a diameter of 150 mm and height of 300 mm to measure the dynamic modulus of elasticity (E_{dyn}). Dynamic modulus of elasticity is approximately twice the shear modulus based on an assumed Poisson's ratio of zero (Trandafir et al. (2010)). The density of the EPS specimens was 20 kg/m^3 . The dynamic modulus of elasticity on the smaller 100 mm diameter specimens ranged between 6.1- 8.3 MPa based on static loads ranging from 15 to 30 kPa and cyclic loads of 30 and 35 kPa. A higher modulus of 9 MPa was obtained on the larger 150 diameter mm specimen based on a test static load of 15 kPa and cyclic load of 30 kPa. Therefore, these laboratory test results indicate that the dynamic modulus of elasticity and corresponding shear modulus is dependent on specimen size.

Athanasopoulos and Xenaki (2011) developed the empirical relationship shown by Equation 1 between the shear modulus (G_0) and density (ρ) of EPS based on the results from unconfined resonant column tests on cylindrical EPS specimens with a diameter of 36 mm and height of 80 mm and with densities ranging from 10 to 30 kg/m^3

$$G_0 = 0.32\rho - 1.4 \quad (1)$$

Equation 1 provides a shear modulus of 6.28 MPa for EPS with density of 24 kg/m^3 which is significantly smaller than the shear modulus of 10.5 MPa measured by Ossa and Roma (2011) based on unconfined resonant column tests on the same EPS density, albeit with a cylindrical specimen with the same diameter but with a larger height of 89 mm. These resonant column tests results also indicate that shear modulus is dependent on the specimen size. Field or laboratory tests on full-size EPS blocks can minimize the effect of specimen size on the measured shear modulus.

Another issue with dynamic laboratory tests is the uncertainty in estimating the field stresses and strains such as estimating the in situ horizontal confining stress to incorporate in conventional dynamic laboratory tests. The confining stress used in dynamic lab tests has an influence on the shear modulus of EPS material. Ossa and Roma (2011) performed a series of resonant column tests on EPS specimens with densities ranging between 24 to 32 kg/m^3 on cylindrical samples with a diameter of 36 mm and a height of 89 mm under confining horizontal stresses of 0, 30, and 60 kPa. A higher shear modulus of 14.5 MPa was obtained under zero confining stress and a lower shear modulus of 12 MPa was obtained under a confining stress of 60 kPa based on test performed on EPS specimens with density of 30 kg/m^3 . Test results show that the shear modulus (G_0) decreases as the confining stress increases. Field tests on EPS blocks under actual field embankment configurations eliminate the need to estimate in situ stresses.

In summary, the effect of specimen size and confining stresses on shear modulus values obtained from laboratory tests can be minimized by in situ geophysical tests such as the MASW (Multi-Channel Analysis of Surface Waves) method. Geophysical techniques such as Spectral Analysis of Surface Waves (SASW) and MASW are used in geotechnical practice to measure the shear wave velocity of soils. Utilizing the Geophysical technics to evaluate the properties of different materials such as PCC slab (Bay and Stoke 1990), mortar cement (Cho 2003 and Cho & Lin 2000 & 2005), asphalt pavements (Ryden et al. 2004) have been reported several times. In this paper the feasibility of MASW testing on estimating the shear modulus of full scale EPS blocks are presented herein. A summary of the MASW procedure is subsequently provided followed by a summary of the test results and conclusions from the test.

2. MASW PROCEDURE

MASW is a geophysical test procedure which is typically used to evaluate the small strain shear wave velocity of subsurface soils. The MASW test is performed by placing geophones (typically 24) on the ground surface that record the time histories of propagating waves from an active or passive seismic source located at various distances (offset) from the sensors. Active seismic source waves are generated by hitting the ground at a specified location with a source such as a sledge hammer whereas, passive seismic source waves are generated from random sources such as nearby vehicle traffic.

In MASW testing, the seismic source is chosen based on the survey depth desired. Seismic sources with large impact energy such as the use of heavy weights can be used for deep investigations (Park (2011)). Seismic sources with lower impact energy such as the use of small balls can be used for shallow investigations (Cho and Lin (2005)). An active

seismic source consisting of a tennis ball, approximately 6.7 cm (2.64 inch) in diameter, was utilized in testing a full-size EPS block. Forty-eight 4.5 Hz geophones similar to the one shown in Figure 2(a) were placed on top of the 0.96 × 1.22 × 7.32 m (3.17×4× 24 ft) EPS block at 15.24 cm (0.5 ft) intervals as shown in Figure 3. Time histories of propagating waves were collected by dropping the ball used as the active seismic source from a height of approximately 15 cm (5.9 inch) onto the surface of the EPS block at 48 different locations or stations. At each station, the test was repeated five times, i.e., the ball was dropped five times, and for each test, the geophones recorded time histories of propagating waves.

The time histories recorded by the geophones are digitized by Geodes (Figure 2. (b)) and the digitized data is transferred to a portable laptop that contains the Geometric Seismodule Controller software™ package. The time histories of propagating waves were recorded at time intervals of 0.125 milliseconds for a duration of 2 seconds. In order to initiate the start of data collection of each test in the software, one of the following two alternatives must be specified: automatic triggering or manual triggering. In automated triggering, the start of the test is recognized by the software automatically from a trigger which is installed on the head of a sledge hammer that is used as an active seismic source and connected to the laptop computer. In manual triggering, the start of test data collection for each test is manually triggered by the person that is monitoring the data acquisition software in the laptop during the test. Since a tennis ball was used as a seismic source, the automatic triggering was not an option and the manual triggering method was used.



Figure 2. (a) 4.5 Hz geophone, (b) Geode

One objective of MASW testing is to obtain shear wave velocity profile at various locations along the block length. A shear wave velocity profile is obtained at the centerline of a series of 24 geophones aligned as shown in Figure 3. The centerline of the 24 geophones is called midsection as shown on Figure (3). Shear wave velocity profiles at other locations of the EPS block can be obtained by moving the 24 geophone series to another location along the block length to change the midsection of the 24 geophones and repeating the test. In testing the full-size EPS block, 48 geophones were utilized instead of 24 to incorporate geophones along the full length of the block to minimize the number of tests needed to obtain shear wave velocity profiles throughout the length of the block. Therefore, 48 geophones were utilized instead of 24 to obtain a two- dimensional (2D) image of shear wave velocity of the block by choosing different 24 geophones series combinations having different midsection locations along the block. The use of 48 geophones expedited the time needed to obtain shear wave velocity profile along the block compare to the time needed to obtain shear wave velocity profiles with only 24 geophones because the use of 24 geophones would require physically moving the 24 geophones after each test, which would have damaged the block as well.

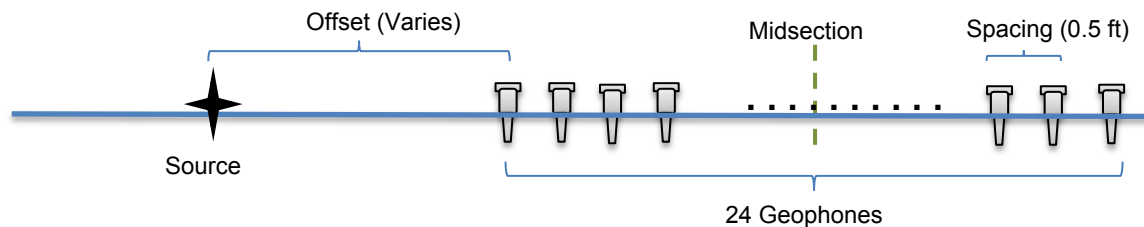


Figure 3. Source-receiver configuration for active MASW test

Noise effects such as vibrations of the data acquisition components and vibrations from random noise sources not related to the specific active seismic source used in the test, can introduce random errors in the test data.

In order to minimize noise from vibration of any data acquisition system components such as the geophone cables, connection cables and Geodes, the data acquisition system is kept away from contact with the EPS block during the tests.

In order to minimize random ambient noises that typically occur during the day the tests were also performed in the evening. Figure 4 shows the test set up for the full-size EPS22 with measured density of 20.9 kg/m³. The density was obtained from the measured weight of full-size block and the dimensions of the block. EPS 22 is designated by ASTM D6817 – 11.

The analysis used to obtain the shear modulus of the EPS block from the recorded time histories is presented next.

3. ANALYSIS

Analysis of MASW data consists of two primary steps: 1) dispersion analysis and 2) inversion analysis. An overview of each of these steps is subsequently provided.

3.1 Dispersion Analysis

The purpose of dispersion analysis is to develop a dispersion curve from the time histories recorded by the geophones. A dispersion curve is a plot of phase velocity versus frequency as depicted in Figure 5. Dispersion curves can be dispersive or non-dispersive. In dispersive curves, different frequency components of surface waves travel with different velocity and create a dispersive curve (Figure 5 (a)). For example, in soils, longer wave length (lower frequency (f_1)) penetrates greater depths which is usually in higher densities and therefore travels with higher velocity ($V_1 > V_2$) (Figure 5. (a)). If all the frequency components travel with the same velocity, the dispersion curve will be non-dispersive as a straight line (shown in Figure 5.(b)) (Park(2012)).



Figure 4. Large scale EPS block under MASW test at the University of Memphis Geotechnical Lab.

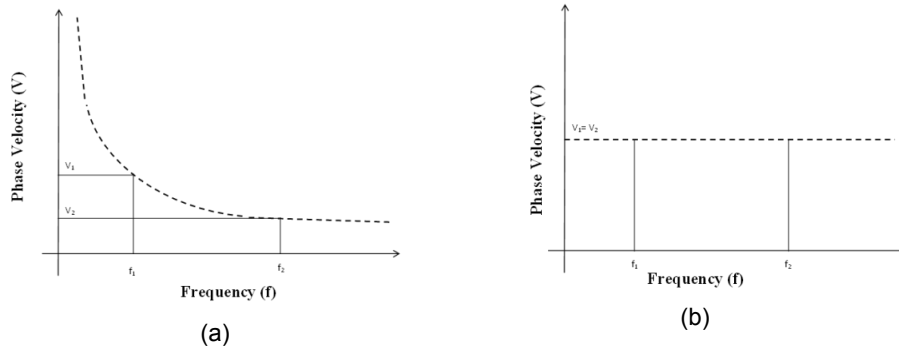


Figure 5. Phase Velocity vs Frequency for (a) dispersive curve, (b) Non- dispersive curve.

As described previously, each geophone records the time history of propagating waves for each test. Therefore, 24 time histories (traces) are recorded for each test. In order to create a dispersion curve for each test, the recorded time histories (set of 24 traces) are transformed to the frequency domain by utilizing the Fast Fourier Transformation (FFT). A band pass filter with desired corner frequencies is used to filter data for each frequency range. The filtered time histories are plotted beside each other in manner where vertical axis represents time and horizontal axis represents the offset at which, each geophone is located. By connecting the normalized peak amplitudes of all traces together, an inclined line can be drawn with a specific slope. It is possible to measure the cumulative values of time history amplitude along the slope. The slope of each line represents a unique velocity by which each frequency is travelling and is called phase

velocity. By repeating this procedure for the range of desired frequencies, a contour (dispersion curve) which represents the variation of phase velocity with frequency is generated.

Surfseis software package developed by Kansas Geological Survey is used to generate dispersion curves from the recorded time histories. The test setup configuration details, such as source location, geophone spacing, and number of tests performed at a given seismic source location, are the required software input parameters to generate the dispersion curves. In addition to the provisions previously described to minimize noise effects, the following two additional procedures were also incorporated in the analysis to minimize noise effects:

1) As described previously, at each active seismic source station, the test is repeated 5 times. A dispersion curve is developed for each test repetition at each midsection of a set of 24 geophones and the dispersion curves from the 5 repetitions of the test are stacked (summed) together to obtain a single dispersion curve to minimize noise effect that tends to influence the individual dispersion curves from each individual test.

2) As previously noted, a dispersion curve is obtained at the midsection of a set of 24 geophones for a given offset of the seismic source. Therefore, multiple dispersion curves are obtained at a given midsection location from tests that are performed at various offset locations. For example, Figure 6 provides the various test offset locations and the associated midsection location of a set of 24 geophones located at Station 11.75, which is at the center of the EPS block. Table 2 provides the offset location of each seismic source. Each offset location listed in Table 2 represents a single test. Therefore, as listed in Table 2 and as depicted in Figure 6, 13 different test offset locations are associated with the midsection location at Station 11.75. Therefore, 13 dispersion curves, one for each test offset location, are developed at Station 11.75.

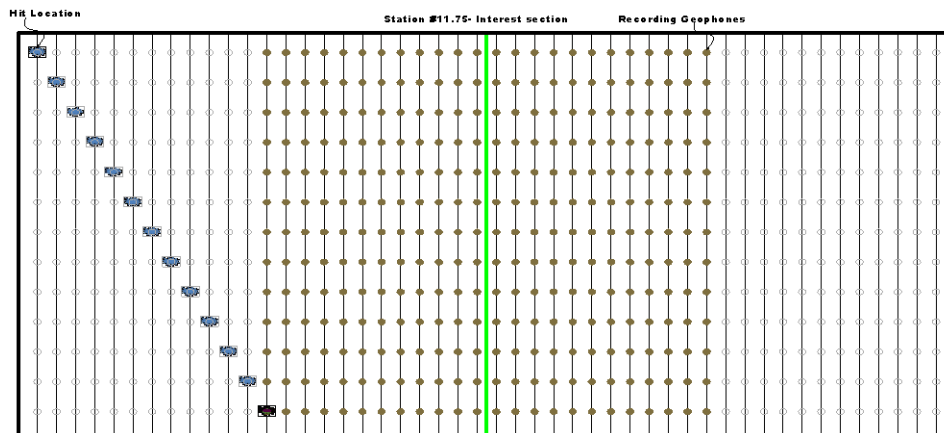


Figure 6. Geophone and test offset used to create a dispersion curve at the middle of EPS block (Station 11.75).

Table.2. Source offset combination for midsection at Station11.75

Source Location (hit) from one edge of block		Offset from the source as shown in Figure (3)	
ft	m	ft	m
0.25	0.08	6.00	1.83
0.75	0.23	5.50	1.68
1.25	0.38	5.00	1.52
1.75	0.53	4.50	1.37
2.25	0.69	4.00	1.22
2.75	0.84	3.50	1.07
3.25	0.99	3.00	0.91
3.75	1.14	2.50	0.76
4.25	1.30	2.00	0.61
4.75	1.45	1.50	0.46
5.25	1.60	1.00	0.30
5.75	1.75	0.50	0.15
6.25	1.91	0.00	0.00

Figure 7 shows the total number of dispersion curves after the two previously described procedures were performed. As shown in Figure 7, between 5 to 125 stacked dispersion curves were developed from all the tests performed on the EPS block. The stacked dispersion curves provide improved phase velocity data at various frequencies than the dispersion curves obtained from a single test.

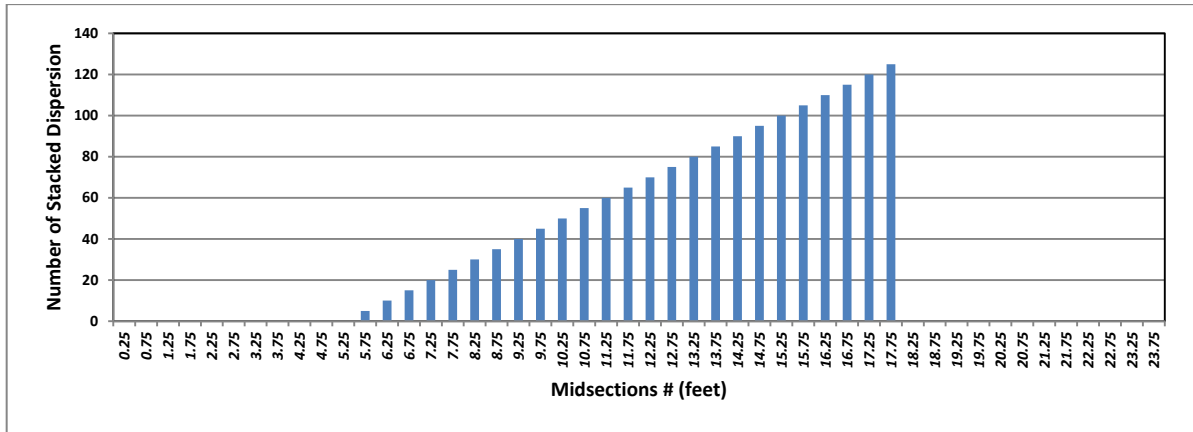


Figure 7. Total Number of stacked dispersion curve after two stacking procedures (step1 and 2) (Graphic fold)

For example, the final dispersion curve from stacking steps for Station 5.75 is shown in Figure 8. This figure shows the variation of phase velocity by frequencies and the shading represents the dominance of each phase velocity on results. Since EPS material are homogenous material, as described before, the dispersion curve are non-dispersive and show an approximately straight line. As shown in Figure 8, the dispersion curve is nearly horizontal line at frequencies greater than 70 Hz. Figure 9 shows a magnified image of the dispersion curve at frequencies greater than 70 Hz. As shown in Figure 9, the dispersion curve represents a non-dispersive wave with phase velocity constant with frequency as defined by Figure 7(b).

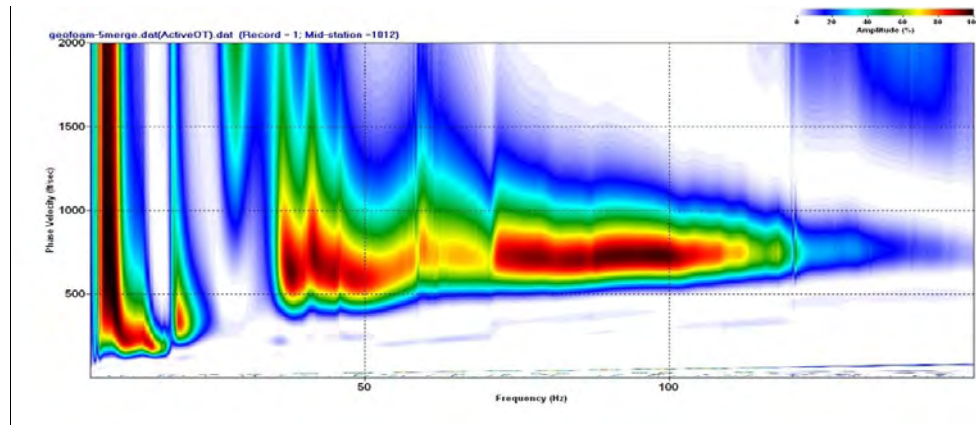


Figure 8. Dispersion curve from Surfseis for station # 5.75.

The phase velocities for various frequencies are obtained from the non-dispersive portion of the dispersion curve by connecting the highest amplitudes in this portion as shown as marked points in Figure 9. Table 3 represents the extracted phase velocities versus frequencies for this section.

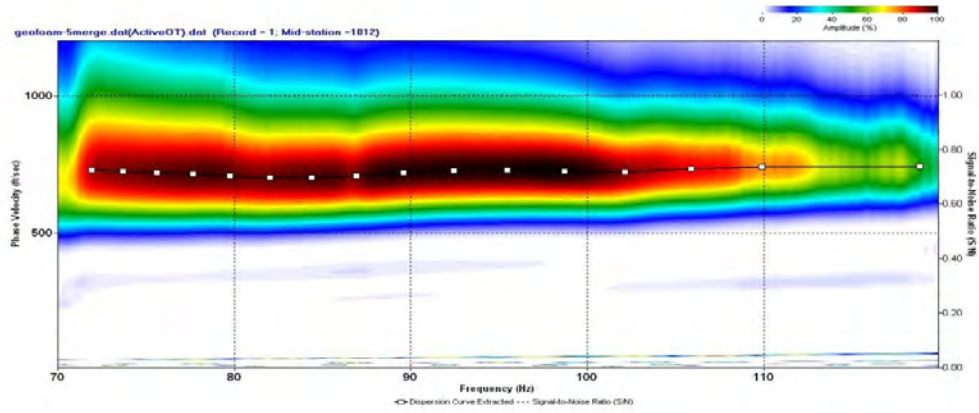


Figure 9. Extracted dispersion curve from Surfseis for station # 5.75.

This procedure is repeated for all the sections between 1.75 m (5.75 ft) and 5.41 m (17.75 ft) of EPS blocks. The dispersion curves for each station are stacked (summed) together and a combined dispersion curve for each station is used to extract the phase velocity and their corresponding frequencies.

Table 3. Extracted dispersion results.

Frequency (HZ)	Phase Velocity	
	(m/sec)	(ft/sec)
72.56	216.15	709.16
74.50	216.58	710.55
76.54	215.14	705.84
78.70	213.15	699.31
80.99	211.28	693.18
83.41	210.13	689.41
85.98	211.23	693.02
88.72	214.52	703.80
91.64	217.54	713.70
94.75	218.80	717.85
98.08	217.65	714.07
101.66	216.61	710.65
105.50	219.49	720.10
109.65	221.78	727.61
119.01	223.21	732.32

3.2 Inversion Analysis

Inversion analysis is a procedure to find the shear wave velocity profile from the experimental dispersion curves. In general the inversion is an iterative process to find a shear wave velocity profile for the experimental dispersion curve with the minimum error between theoretical dispersion curve of inverted velocity profile and experimental. In this research since the dispersion curves show a nearly straight line, the iteration to find a profile velocity is not required and the results can be estimated from the available equations related to propagating waves in homogenous media. The relationship between phase velocity (surface wave velocity (V_R)) and shear wave velocity (V_S) can be estimated from Equations (3&4) (Bay and Stokoe (1990)):

$$V_s = \frac{1+\nu}{0.862+1.14\nu} V_R \quad (3)$$

For Poisson's ratio (ν) between 0.1 and 0.3, shear wave velocity can be approximated by:

$$V_s = 1.11V_R \quad (4)$$

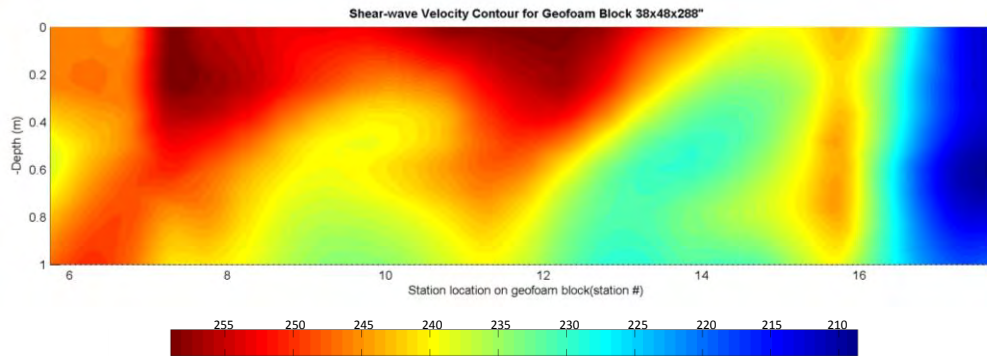


Figure 10. 2-D Shear wave velocity profile of EPS block (m/sec)

Phase velocity is converted to shear wave velocity for all the tested sections of EPS block by utilizing the Equation 4. Figure 10 depicts a 2D shear wave velocity variation within EPS block (between 1.75 m (5.75 ft) and 5.41 m (17.75 ft) of EPS blocks). This plot shows the variation of shear wave velocity by depth of EPS blocks. As shown in Figure 10, the shear wave velocity obtained from the inversion analysis varies within the block. The shear wave velocity should be the same throughout a homogenous material. However, density variations occur with a full size EPS block because of the molding process (Stark et al. 2004), which can contribute to variations in shear wave velocity within the block.

A second factor that can contribute to the variation of shear wave velocity within the block is the used inversion technics which is just based on equations related to Rayleigh wave propagation in homogeneous media. Further works to improve the inversion analysis such as utilizing the Lamb waves (Ryden et al., 2003) is recommended.

Shear modulus of material, under the small strain condition, can be calculated from the shear wave velocity from the Equation 5:

$$G = \rho V_s^2 \quad (5)$$

where,

V_s is the shear wave velocity and ρ is the density of EPS material. Measured shear wave velocities were used to calculate the shear modulus at all the section between 1.75 m (5.75 ft) and 5.41 m (17.75 ft) of EPS block by utilizing the Equation (5). Results show a shear modulus with a range of 10 to 13 MPa (1450 to 1885 psi) and an average of 12.2 MPa (1770 psi). This measured shear modulus is in the range of the shear modulus measured by Ossa and Roma (2011) from resonant column tests (10 to 16 Mpa (1450 to 2320 psi) for EPS material with density range of 24 to 32 kg/m³ (1.5 to 2 lb/ft³)) but is far from the results from resonant column tests reported by Athanasopoulos and Xenaki (2011) (2 to 8 Mpa (290 to 1160 psi) for EPS material with density range of 10 to 30 kg/m³ (0.6 to 1.9 lb/ft³)). Table 4 provides an example of calculated shear wave velocity and shear modulus at the section 5.75 with 1.75m (5.75 ft) distance from the one edge of EPS block. Results show an average shear wave velocity of 240 m/sec (787 ft/sec) and shear modulus of 11.81 MPa.

Table 4. Shear wave velocity and Shear modulus at station #5.75

Frequency (HZ)	Phase Velocity		Shear Wave Velocity		Shear Modulus, G	
	(m/sec)	(ft/sec)	(m/sec)	(ft/sec)	MPa	Psi
72.56	216.15	709.16	239.93	787.16	11.80	1711.81
74.50	216.58	710.55	240.40	788.71	11.85	1718.55
76.54	215.14	705.84	238.81	783.48	11.69	1695.84
78.70	213.15	699.31	236.60	776.24	11.48	1664.61
80.99	211.28	693.18	234.52	769.43	11.28	1635.55
83.41	210.13	689.41	233.25	765.24	11.15	1617.79
85.98	211.23	693.02	234.47	769.25	11.27	1634.80
88.72	214.52	703.80	238.11	781.21	11.62	1686.03
91.64	217.54	713.70	241.46	792.20	11.95	1733.81
94.75	218.80	717.85	242.87	796.81	12.09	1754.05
98.08	217.65	714.07	241.59	792.62	11.97	1735.61
101.66	216.61	710.65	240.43	788.82	11.85	1719.03
105.50	219.49	720.10	243.63	799.31	12.17	1765.03
109.65	221.78	727.61	246.17	807.65	12.42	1802.09
119.01	223.21	732.32	247.76	812.87	12.59	1825.46

4. CONCLUSIONS

Performance evaluation of EPS embankments under dynamic loading, such as earthquake analysis of slope stabilized with EPS blocks, depends on their dynamic properties. Shear modulus and shear wave velocity are geofam dynamic parameters required to perform seismic analysis. Understanding the behavior of EPS material under dynamic loading is a key issue in the seismic design of EPS embankments. This paper proposes the use of the MASW method to evaluate the large scale dynamic properties of EPS material. Results show an average shear modulus of 12.2 Mpa (1770 psi) for the EPS 22 with the measured density of 20.9 kg/m³ (1.3 lb/ft³).

The shear modulus measured by the MASW test shows a higher value than the reported results for EPS blocks with densities close to the tested block (20.9 kg/m³ (1.3 lb/ft³)). However, the MASW result is still in the range of the shear modulus measured by Ossa and Roma (2011) from resonant column tests (10 to 16 Mpa (1450 to 2320 psi) for EPS material with density range of 24 to 32 kg/m³ (1.5 to 2 lb/ft³)). MASW results vary greatly from the shear modulus reported by Athanasopoulos and Xenaki (2011) measured by resonant column tests (2 to 8 Mpa (290 to 1160 psi) for EPS material with density range of 10 to 30 kg/m³ (0.6 to 1.9 lb/ft³)). Further investigation by performing the resonant column test on the tested EPS block in this research is in progress.

This method can be extended to be performed on projects with EPS blocks in the field to measure the dynamic properties of the EPS material under the in-situ condition (confining and vertical pressure). Utilizing the MASW method in evaluating the dynamic properties of EPS material can provide the following potential advantages: (1) eliminate the effect of the small scale sample size on the results, (2) provide a capability to test EPS material under in-situ condition (3) provide an image of integrity of EPS blocks (4) utilize fast and economically procedures.

ACKNOWLEDGEMENTS

The authors would like to give their sincere thanks to Drew Foam Companies and Mr. Charles Tyner for providing the EPS block to The University of Memphis.

REFERENCES

- Arellano, D., and Stark, T. D. "Load bearing analysis of EPS-block geofam embankments. (2009). " *Proceedings of 8th International Conference on the Bearing Capacity of Roads, Railways and Airfields*, Champaign, IL, USA, 981-990.
- Arellano, D., Tatum, J. B., Stark, T. D., Horvath, J. S., and Leshchinsky, D. (2010). A framework for the design guideline for EPS-Block Geofam in slope stabilization and repair. *Transportation Research Record*, 2170, 100-108.

- Arellano, D., Stark, T. D., Horvath, J. S., and Leshchinsky, D. Kafash, M. H, Wang, C. (2011a). Overview of NCHRP design guideline for EPS-block Geofam in slope stabilization and repair, *4th International Conferences on Geofam Blocks in Construction Application (EPS 2011 Norway)*.
- Arellano, D., Stark, T. D., Horvath, J. S., and Leshchinsky, D. (2011b). Guidelines for Geofam applications in slope stability projects., Final report, NCHRP Project No. 24-11(02), *Transportation Research Board*, Washington, D.C.
- Athanasopoulos, G. A., Pelekis, P. C., and Xenaki, V. C. (1999). Dynamic Properties of EPS Geofam: An Experimental Investigation. *Geosynthetics International*, 6(3), 171-194.
- Athanasopoulos, G.A., Nikolopoulou, C.P., Xenaki, V.C. and Stathopoulou, V.D., (2007). Reducing the seismic earth pressure on retaining walls by EPS geofam buffers – numerical parametric study. In: D, *Proceedings of 2007 Geosynthetics Conference*, Washington, D.C., USA, 15 pp.
- Athanasopoulos, G.A., Xenaki, V.C.. (2011). Experimental investigation of the mechanical behavior of EPS Geofam under static and dynamic/ cyclic loading, *4th International Conferences on Geofam Blocks in Construction Application (EPS 2011 Norway)*.
- Bay, J.A. and Stokoe, K.H., II (1990). Field Determination of Stiffness and Integrity of PCC Slabs Using the SASW Method, *Proceedings, Conference on Nondestructive Evaluation of Civil Structures and Materials*, University of Colorado at Boulder, pp. 71-85.
- Duskov, M. (1997). Materials Research on EPS-20 and EPS-15 under representative conditions in pavement structures, *Geotextiles and Geomembranes*, 15, No. 1, 147-181.
- Kansas Geological Survey, Citing Websites. In *Software for Multichannel Analysis of Surface Waves*. Retrieved July 28, 2012, from <http://www.kgs.ku.edu/software/surfseis/index.html>
- Ossa. A., Romo. M.P. (2011), Dynamic characterization of EPS geofam, *Geotextiles and Geomembranes*, Volume 29, Issue 1, Pages 40-50.
- Park, Choon (2012). Multichannel Analysis of Surface Waves (MASW) , Short course, *2012 Geo-congress*, Oakland, Ca.
- Park, C.B., Miller, R.D., and Xia, J., (1998). Imaging dispersion curves of surface waves on multi-channel record, *68th Ann. Internat. Mtg. Soc. Expl. Geophys.*, Expanded Abstracts, p. 1377-1380.
- Ryden. N., Park. C.B., Ulriksen. P., Miller. R.D.(2003). Lamb wave analysis for non-destructive testing of concrete plate structures, *Proc Symp Appl Geophys Eng Env Probl [(SAGEEP 2003)*, San Antonio, Texas]
- Ryden. N., Park. C.B., Ulriksen. P., Miller. R.D. (2004). Multimodal approach to seismic pavement testing: *Journal of Geotechnical and Geoenvironmental Engineering*, Volume. 130, Pages 636-645.
- Stark, T. D., Arellano, D., Horvath, J. S., and Leshchinsky, D. (2004). Geofam Applications in the Design and Construction of Highway Embankments. NCHRP Web Document 65 (Project 24-11), Available at http://trb.org/publications/nchrp/nchrp_w65.pdf, Transportation Research Board, Washington, D.C.
- Hosseini, M., Pezeshk, S., Pujol, J.(2011). Reducing Uncertainties in the Velocities Determined by Inversion of Phase Velocity Dispersion Curves by Using Synthetic Seismograms, Annual meeting of the American Geophysical Union, 5-9 December, San Francisco , California.
- Hosseini, M., Pezeshk, S.(2011). Comparison of Phase Velocities and Shear-Wave Velocity Inversion Results of MASW Method Obtained by Uniform Receiver Spacing Analyzed by SurfSeis Package Software with non-uniform Receiver Spacing Analyzed by the Genetic Algorithm Inversion Scheme, Annual meeting of the Geological Society of America, 9-12 October, Minneapolis, Minnesota.
- Trandafir A.C., Bartlett, S.F., Lingwall B.F. (2010). Behavior of EPS geofam in stress-controlled cyclic uniaxial tests, *Geotextiles and Geomembranes*, Volume 28, Issue 6, Pages 514-524.
- Trandafir A.C., Erickson B.A., Bartlett, S.F., Lawton E.C. (2011). Dynamic viscoelastic properties of EPS Geofam from cyclic uniaxial tests with initial deviator stress, *4th International Conferences on Geofam Blocks in Construction Application (EPS 2011 Norway)*.

Finite Element Mesh Generation for Drainage Geocomposites

Dhani Narejo, Ph.D., P.E., GSE Environmental LLC, USA, dnarejo@gseworld.com.

ABSTRACT

Landfill cover systems invariably include a drainage layer which is most often a drainage geocomposite. The drainage design is typically based on either Darcy's Law or a combination of the law with a mass balance analysis as expressed in the "mounding equations". However, these types of analyses do not consider several site conditions including multiple soil types, anisotropy and evapotranspiration. This paper illustrates the use of a commercially available finite element software with drainage geocomposites. Simple methods, based on the published equations, were found to provide similar maximum pressure head on the liner as the finite element analysis. The pressure head was found to be very different when more than one material was involved in the drainage. The pressure head distribution along the slope and the variation of the pressure head over time were found to be of practical interest for a practicing design professional. Construction lines, drawn at 1 mm spacing, were used to define the mesh for the drainage geocomposite and a thin soil layer immediately above it. This technique appears to have resolved convergence problems for all the analyses presented in this paper. The software was found to provide an excellent representation of the sharp change in the material properties at the soil-geocomposite interface. A limited sample of conditions analyzed for this paper indicates that the finite element method can be used to solve most landfill cover seepage problems within a few hours of computer time.

1. INTRODUCTION

Landfill covers consist of a relatively thin layer of soil over an impermeable barrier. Approximately 1/2 a meter of soil, placed on a long slope, is underlain by a geomembrane and/or a geosynthetic clay liner. Stability of the cover soil is an important design concern especially with regards to the seepage and erosion resulting from rainfall. Simple methods exist for landfill cover design, and when properly implemented, are known to result in an acceptable cover system. The simplest and most popular of these methods is a veneer stability analysis that includes the effect of a maximum pressure head on the liner after a design rainfall event (Giroud et al. 1995). The pressure head is often obtained from the mounding equations of which the most popular for landfill covers are those presented by Giroud et al. (2000). Alternatively, many engineers obtain pressure head based on Darcy's Law, which yields the same results as the limit cases of the mounding equations. Such pressure head calculations are a simplified form of the reality in the field and do not consider such factors as evapotranspiration, multiple soil types, three-dimensional slopes, unsaturated flow and boundary conditions. However, the simple equations are practical and popular, as experience has shown that an acceptable landfill cover design can be obtained from these within a short time.

The finite element method of seepage analysis can also be used to obtain the pressure head distribution over the liner. Most problems can be analyzed within a few hours of computing time thanks to the power of personal computers. The finite element method does not require the simplifying assumptions of the exact solutions and, therefore, gives a more accurate prediction of the pressure head. On the other hand, certain material properties, necessary for the finite element analysis, are not required for the simple procedures. Methods do exist, however, for an estimate of the material properties based on gradation and density, and a few inexpensive tests (Th. van Genuchten et al. 1991). It is likely that in some cases a finite element seepage analysis based on even an estimate of the material properties gives more and better information than an estimate of the pressure head based on simple solutions. This paper demonstrates this by analyzing a few simple slopes with a commercially available software Hydrus 2D/3D (Simunek, et al. 2011). The problems are taken from the published literature as it is much easier and less time consuming to further explore an analysis that has been performed by others than to commence a new problem or project. The methodology presented here can be easily extended to an actual landfill cover project.

The finite element seepage analysis of unlined slopes has been reported in numerous publications (Ng & Shi, 1998; Kai & Ugai, 2004). The emphasis in this paper is on the use of drainage geocomposites in the finite element analysis as the published literature on this topic is minimal to none. Drainage geocomposites are very thin materials - only a few millimeters - with a very high hydraulic conductivity. The actual landfill cover slopes vary in dimension and can be as long as 100 meters in extreme cases. The thickness and hydraulic conductivity of drainage geocomposites is so different from the underlying and overlying materials that entering the geometry and obtaining a convergence can be difficult. The purpose of this paper is to specifically represent the geocomposite as a material - not a boundary condition - and compare the results with exact solutions. Drainage geocomposites are sometimes represented as a seepage face boundary (Iryo & Rowe, 2005) or as a drainage boundary condition. Representing drainage geocomposites as a

material, rather than a boundary, is necessary in order to obtain a pressure head distribution throughout the slope.

Based on mass conservation and Darcy's Law, Giroud et. al. (2000) derive the following equation for unconfined flow in a soil layer on a slope underlain by a barrier:

$$\lambda x = \frac{t \cos^2 \beta}{\sin \beta} - \frac{\cos^4 \beta}{\sin^2 \beta} t \frac{dt}{dx} \quad (1)$$

Where λ is a dimensionless parameter that defines the shape of the liquid surface and is given as:

$$\lambda = \frac{q_h}{k \tan^2 \beta} \quad (2)$$

In the above equations, q_h = liquid supply rate (LT^{-1}), k = coefficient of hydraulic conductivity (LT^{-1}), t = thickness of liquid (L), x = distance along x-axis (L), and β = slope angle (degrees). The authors present two limit cases of Equation 1: Equation 3 for $\beta = 0$ (i.e., $\lambda = \infty$) and Equation 4 when q_h is very small or k is very large (i.e., λ is very small).

#

$$t_{\max} = \sqrt{\frac{q_h}{k}} L \quad (3)$$

$$t_{\max} = \frac{q_h L}{k \sin \beta} \quad (4)$$

Equation 4 is the most common expression that is used to determine the required transmissivity of drainage geocomposites. For general case, where equations 3 and 4 do not apply, the authors present an approximate solution of Equation 1 as follows:

$$t_{\max} = j \frac{\sqrt{\tan^2 \beta + \frac{4q_h}{k}} - \tan \beta}{2 \cos \beta} L \quad (5)$$

Where j is defined by the authors as follows:

$$j = 1 - 0.12 \exp \left[- \left[\left(\frac{\log \frac{8q_h}{k}}{5 \sin^2 \beta} \right)^{\frac{5}{8}} \right]^2 \right] \quad (6)$$

In the above equations, t_{\max} = maximum liquid thickness, (L). Maximum pressure head, h_{\max} , is related to the maximum liquid thickness as $h_{\max} = t_{\max} \cos \beta$. Equations 3, 4 and 5 represent the expressions that are typically used in the current state-of-the-practice for the design of the landfill cover liquid collection layer. Equation 4 applies to the case of a drainage geocomposite as k is often very high for these materials resulting in a very small value of λ . Equation 5 applies to a soil drainage layer for which j value can be obtained either from Equation 6 or from a graph given by the authors. The maximum pressure head obtained from the above expressions – based on Darcy's Law and mass balance - can be compared to the maximum value obtained from a finite element analysis.

2. PROBLEM DESCRIPTION, SOFTWARE AND METHODOLOGY

The paper presents a finite element seepage analysis of several variations of a problem originally analyzed by Iryo and Rowe (2005). The published problem was first modeled exactly as described in the journal paper to ensure that the output from the software was matched the published values. Having confirmed this, four important changes were made to the model: i) the depth of the cover soil was changed to 600 mm to model a typical landfill cover soil, ii) a 5 mm thick geosynthetic drainage layer, i.e., a drainage geocomposite, was placed under the cover soil, iii) the bottom boundary

condition was changed from seepage face to no-flow to represent a geomembrane, and iv) horizontal slope length was varied from 2500 mm to 10000 mm. Iryo and Rowe modeled the original 5000 mm long by 300 mm deep slope with Seep/W software. They performed virtual experiments (no physical experiments were performed) by changing the slope angle and impingement rate (flux entering the top boundary). A 3 mm thick geotextile was modeled under the soil with a seepage face boundary under the geotextile representing flow into a geonet. The adaptation of the Iryo and Rowe problem for this paper is shown in Figure 1. It consists of a 600 mm thick soil layer underlain by a 5 mm thick drainage geocomposite which is underlain by a geomembrane. The present analysis uses the same properties for the soil and drainage material as those used by Iryo and Rowe for their soil and geotextile, respectively. Slope angle is varied between 0 and 18.4 degrees to cover a range of conditions encountered in real life landfill covers.

Hydrus 2D/3D software, version 2.01 (www.pc-progress.com) was used for the seepage analysis. The software considers both saturated and unsaturated flow and has an environmental boundary condition option that is ideal for landfill covers. For the present problem, only rainfall with no evapotranspiration was considered. The software numerically solves the Richards' equation for saturated-unsaturated flow and can be used with one-, two- and three-dimensional problems. The volumetric water content formulation of the Richards' equation is as follows:

$$\frac{\partial \theta}{\partial t} = \frac{\partial}{\partial x_i} \left[K \left(K_{ij}^A \frac{\partial h}{\partial x_j} + K_{iz}^A \right) \right] - S \quad (7)$$

Where θ is the volumetric water content (L^3L^{-3}), h is the pressure head (L), S is a sink term (T^{-1}), x_i ($i=1, 2$) are spatial coordinates (L), t is time (T), K_{ij}^A are components of a dimensionless anisotropy tensor \mathbf{K}^A and K is the unsaturated hydraulic conductivity function (LT^{-1}) given by $K(h,x,y,z) = K_s(x,y,z)K_r(h,x,y,z)$.

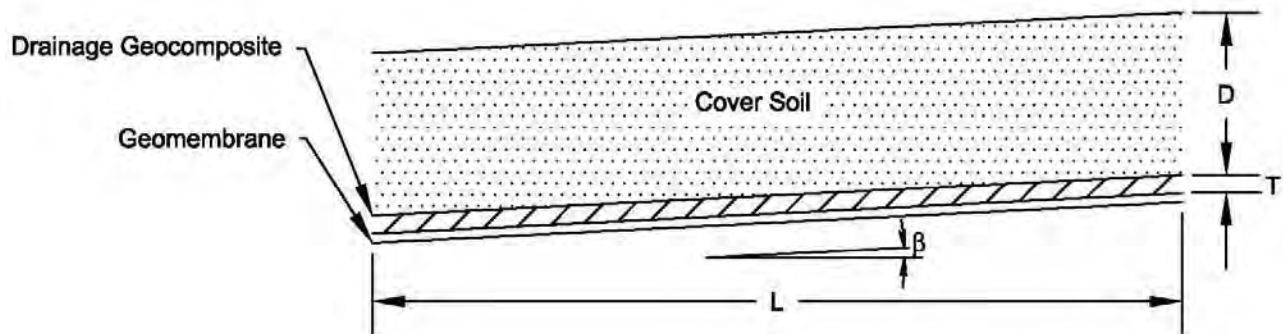


Figure 1 – Problem Modeled in the Finite Element Software.

With known boundary and initial conditions, the software solves Richards' equation using a Galerkin type linear finite element method applied to a network of triangular elements. Integration in time is achieved using an implicit finite difference scheme for both saturated and unsaturated conditions. The van Genuchten-Mualem equations with the assumption that $m=1-1/n$ were used to define water characteristic curve and the hydraulic conductivity functions. Table 1 presents the basic properties and van Genuchten parameters assumed for the materials based on the paper by Iryo & Rowe (2005). Sand and loam represent two materials with a comparatively high and low hydraulic conductivity, while the drainage geocomposite is a low transmissivity drainage geocomposite with properties similar to a thick nonwoven needlepunched geotextile.

Table 1. Basic material properties and van Genuchten parameters.

Parameter	Sand	Loam	Drainage Geocomposite
Saturated volumetric water content, θ_s , (-)	0.38	0.40	0.92
Residual volumetric water content, θ_r , (-)	0.04	0.06	0
Saturated hydraulic conductivity, K_{sat} , mm/hour	360	3.6	82800
van Genuchten parameter, a , (1/mm)	0.0072	0.00216	0.029
van Genuchten parameter, n , (-)	3.16	1.47	3.0

An environmental boundary condition with a precipitation, zero evapotranspiration and instant run-off was used for the top of the slope. The instant run-off implies that the water that does not enter the soil runs off without any head buildup at the surface. A no-flow boundary condition was used at the right and bottom of the model. The no-flow condition at the bottom represents a perfect liner with no leakage while at the right it represents a divide with a slope in the opposite direction. On the left side, a seepage face boundary condition was used. Physically, a seepage face boundary condition can be interpreted as a highly porous stone, such as in gravel drains. A uniform pressure head of -1000 mm was used for the entire domain as the initial condition representing a dry material.

The discretization of the problem of Figure 1 in the finite element software is presented in Figure 2. Construction lines parallel to the slope were used to divide the drainage geocomposite into 1 mm thick regions. Three regions of the same thickness (i.e., 1 mm) were entered immediately above the geocomposite in the cover soil. Then a triangular mesh size of 20 mm was entered for the entire domain. The result was a mesh of uniform size for the entire domain except for 8 mm thickness at the bottom of the domain where one side of the triangles was forced to be 1 mm. This mesh scheme was used after trials with several mesh refinement methods that did not work as well as the method of the construction lines. Most refinement methods resulted in a very large number of mesh elements. Very thin regions of one mm thickness were found to improve convergence significantly but convergence problems persisted nonetheless. Pressure head was found to be sensitive to the size of the mesh in the vicinity of the geocomposite.

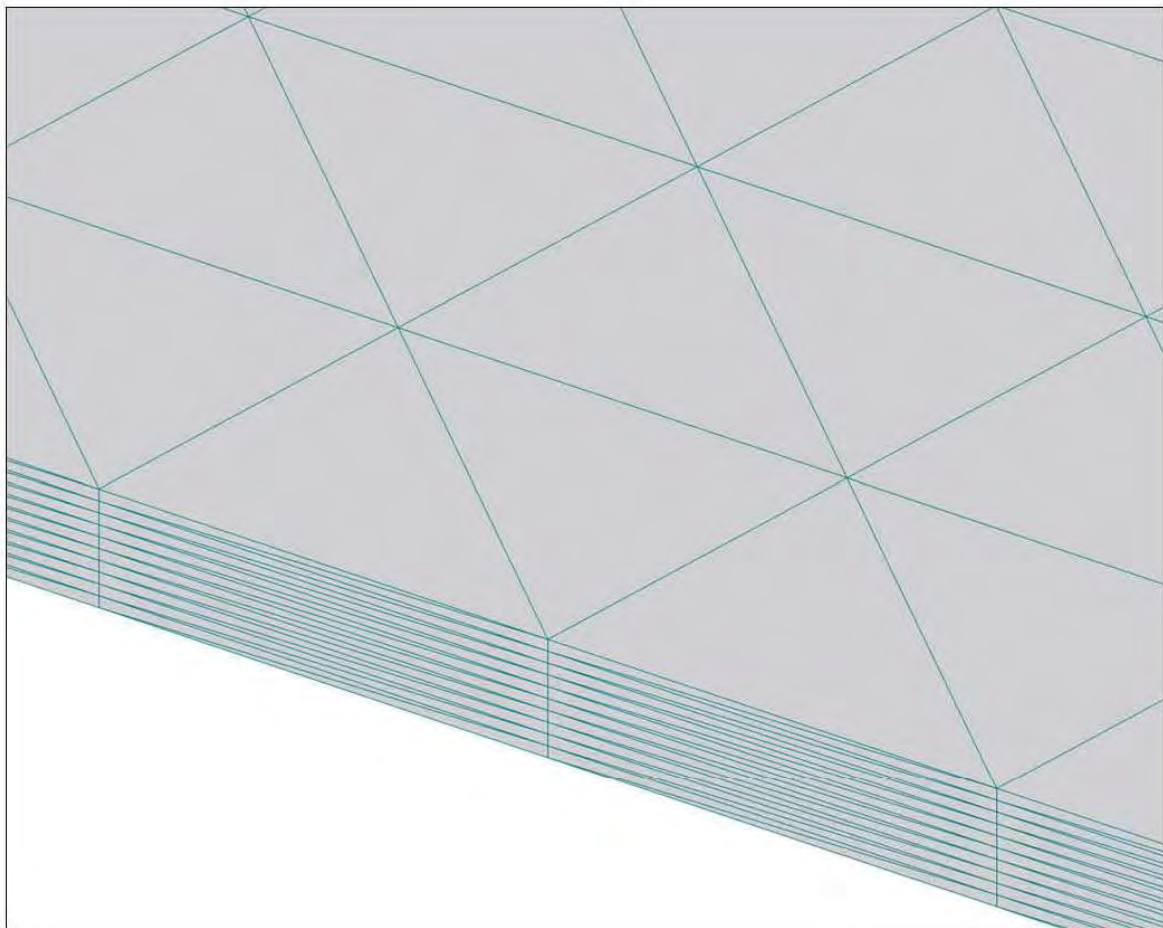


Figure 2 – Mesh Discretization Used for Geocomposite and Cover Soil (Triangle Side = 20 mm).

3. RESULTS

Table 2 presents the results of all the virtual experiments conducted for this paper. The first column represents categories, indicating the purpose of the experiments included in a specific class. For example, in Category A, the

purpose was to determine the rainfall rate that will result in a steady state pressure head of less than the thickness of the drainage geocomposite. Series C is a confirmation of the results with two different finite element software. The second column represents a sequence number of each of the runs. A total of 17 runs were performed. The third column is the slope angle which ranged from zero to eighteen degrees. Most landfill slopes are less than or equal to 3H:1V and, therefore, this was the maximum slope modeled. The fourth column represents slope length, i.e., L in Figure 1. Slope lengths were chosen arbitrarily to be 2500, 5000 and 10000 mm. Slope lengths for actual projects vary over a broad range. This paper considers slope lengths shorter than those found in practice for most projects.

Rainfall rates of 0.2, 5.9 and 30.3 mm/hour in the sixth column were determined by increasing the rainfall rate in small increments until the maximum steady state pressure head was approximately equal to the thickness of the geocomposite. Drainage is, therefore, taking place only within the geocomposite. This makes it possible to compare the results with solutions from published equations. For the last six runs, a rainfall rate of 30 mm/hour was used. Runs 1 through 8 were long enough to achieve a steady state output, referred to as SS in column 7. The last 9 runs were for 6 hours representing a 30 mm/hour probable maximum precipitation for a duration of 6 hours. Column 8 gives the maximum pressure head obtained for each of the runs. For runs 15, 16 and 17, wetting front did not reach the geocomposite. The last column shows the software used for the analyses. All runs, except #8, were performed with the software referenced above (Simunek, et al. 2011). Run 8 was performed with a different software that is often used by geotechnical engineers for seepage analysis and that was used by Iryo and Rowe for their analysis. The second software does not have an environmental boundary condition; therefore a constant flux was used for this purpose, as no evapotranspiration was considered in the analyses. This second software was used to confirm the values obtained with the primary software used in this paper.

Table 2. Maximum pressure head above the geomembrane with finite element method.

1	2	3	4	5	6	7	8	9
Series	Run No.	Slope (%)	Profile	Hor. Slope Length (mm)	Rainfall Rate (mm/hour)	Rain Duration (hrs)	Result – Max. Pressure Head (mm)	Software
A	1	0.0	Sand/GC/GM	5,000	0.2	SS	5.0	Software A
	2	5.0	Sand/GC/GM	5,000	5.9	SS	4.9	Software A
	3	18.4	Sand/GC/GM	5,000	30.3	SS	4.5	Software A
B	4	0.0	Sand/GM	5,000	0.2	SS	61.5	Software A
	5	5.0	Sand/GM	5,000	5.9	SS	417.4	Software A
	6	18.4	Sand/GM	5,000	30.3	SS	536.7	Software A
C	7	18.4	Sand/GM	5,000	5	SS	100.0	Software A
	8	18.4	Sand/GM	5,000	5	SS	102.3	Software B
D	9	0.0	Sand/GC/GM	5,000	0.2	6	-654.7	Software A
	10	5.0	Sand/GC/GM	5,000	5.9	6	-190.2	Software A
	11	18.4	Sand/GC/GM	5,000	30.3	6	2.6	Software A
E	12	18.4	Sand/GC/GM	2,500	30	6	0.8	Software A
	13	18.4	Sand/GC/GM	5,000	30	6	3.9	Software A
	14	18.4	Sand/GC/GM	10,000	30	6	226.0	Software A
F	15	18.4	Loam/GC/GM	2,500	30	6	2.6*	Software A
	16	18.4	Loam/GC/GM	5,000	30	6	2.7*	Software A
	17	18.4	Loam/GC/GM	10,000	30	6	0.0*	Software A

Notes: GM= geomembrane; GC = geocomposite; Max. = maximum, SS = steady state, Hor = horizontal, * = wetting front did not reach the drainage geocomposite in 6 hours

Design engineers typically use equations based on Darcy's Law and mass-balance to select a suitable drainage geocomposite. Some of these equations were presented in Section 1 and other similar equations are available in the literature. Equation 4 is the most popular method for calculating the required transmissivity of drainage geocomposites placed on slopes less than 90 degrees. Most of the runs presented in Table 2 were repeated with the published equations. The results are summarized in Table 3. In Table 3, the first column corresponds with the second column in Table 2 and the 2nd column corresponds to the third column in Table 2. The third and fourth columns give hydraulic conductivity of the drainage geocomposite and the cover soil, respectively. The fifth column is the effective infiltration

rate which is the lower of the hydraulic conductivity and rainfall rate. Lambda in column 6 is obtained from Equation 2. Column 7 represents the maximum pressure head obtained from equations 4, 5 or 6.

4. DISCUSSION

Runs 1 through 3 of Series A in Table 2 present pressure heads at a steady state for the rainfall rates indicated. Several iterations were performed to obtain the rainfall rate that gave the maximum pressure head approximately equal to the thickness of the drainage geocomposite. The rainfall rate required to achieve an approximate pressure head of 5 mm increases with increasing slope angle, which is to be expected. The corresponding solution with the equations is presented in Table 3 in rows runs 1 through 3. There appears to be excellent conformance between the solution obtained with the equations and that obtained with the finite element analysis. A few mm of pressure head, as represented in tables 2 and 3, does have important practical significance. The selection of the thickness of a drainage geocomposite is practically based on the pressure head, and the goal of keeping the head within the geocomposite represents real cost. The author was relieved to find this fine a conformance without much effort on the analysis. However, the comparison is based on a very small set of conditions and needs to be extended to additional slope and material characteristics. For the conditions analyzed in this paper, it is seen that the simple equations yield the same pressure head as the finite element analysis for steady state conditions when positive pressure head is within the geocomposite.

The runs in Series B show that the pressure head obtained without a drainage geocomposite is very high compared to that with the drainage geocomposite. Again, this result is as expected and the software appears to be handling the geocomposite correctly. A 5 mm thick geocomposite in the cases analyzed is found to be effective in reducing the pressure head to approximately the thickness of the drainage geocomposite. In Table 3, rows 4, 5 and 6 give the corresponding solution with the equations. The equations generally give a higher pressure head than that with the finite element analysis. The difference may be due to the unsaturated flow with the finite element analysis or approximations inherent in the exact solutions. For a uniform cover soil with no geocomposite, the current state of the practice appears to be conservative.

Table 3. Maximum pressure head above the geomembrane with published equations.

1	2	3	4	5	6	7
Run No.	Description	Drain k (mm/hour)	Cover k (mm/hour)	Infiltration (mm/hour)	Lambda	h_{max} (mm)
1	Sand/GC/GM	82800	360	0.2	∞	7.8
2	Sand/GC/GM	82800	360	5.9	0.0093	4.1
3	Sand/GC/GM	82800	360	30.3	0.0033	5.5
4	Sand/GM	NA	360	0.2	∞	117.8
5	Sand/GM	NA	360	5.9	2.143	407.4
6	Sand/GM	NA	360	30.3	0.7614	739.7
12	Sand/GC/GM	82800	360	30	0.0032	2.7
14	Sand/GC/GM	82800	360	30	0.0032	10.9
15	Loam/GC/GM	82800	3.6	3.6	0.0003	0.3
16	Loam/GC/GM	82800	3.6	3.6	0.0003	0.7
17	Loam/GC/GM	82800	3.6	3.6	0.0003	1.3

Drain = drainage geocomposite; k = hydraulic conductivity, h_{max} = maximum pressure head

In design practice the author has used software B in the past, as its results can be easily imported into slope stability analysis software. Case 8 was run only as a check on the finite element software A utilized in this paper. For software B run, a rectangular grid was used instead of the triangular grid in software A. All other model conditions were exactly the same as that with software A. The results show that both software programs give essentially the same value of maximum pressure head for the comparison case. Note that software B does not have an environmental boundary condition as

additional software must be purchased for that from the suppliers. However, a constant flux condition was used for the top boundary as no evapotranspiration was included in any of the analyses. An attempt to model the drainage geocomposite with software B resulted in convergence problems. However, with some additional practice, the author is hopeful that a drainage geocomposite can be considered as a material (not as a boundary) even within software B.

The hydraulic design of drainage layers for landfill covers is generally based on a 6-hour probable maximum precipitation (Soong and Koerner, 1997). The PMP curves are available on the Internet for the entire United States. For the rain event to be only 6 hours, the finite element analysis time discretization must be limited to six hours. Alternatively, one can apply precipitation for six hours followed by no-precipitation for some additional time. Runs in series D in Table 2 are the same as the runs in series A except that a transient condition of only 6 hours is considered. At the end of a 6-hour rainfall, the pressure head is found to be very different from that under the steady state conditions. Therefore, although the equations and the steady state finite element analyses results show good agreement, the two are very different for transient conditions. Moreover, the equations are not always conservative when the positive pressure head extends up into the cover soil. Notice a maximum pressure head of 226 mm in Run 14 in Table 2 versus 10.9 mm with equations in Table 3. Actually, a steady state pressure head of 400 mm is obtained by the finite element analysis for Run 14. The positive pressure head is now above the geocomposite and two materials are involved in drainage: sand and geocomposite. Simple equations cannot handle such a case and may significantly under-predict the pressure head if the hydraulic conductivity of the geocomposite is used in the equations. The drainage is occurring through both sand and the geocomposite and the pressure head represents this in the case of the finite element analysis. An equivalent hydraulic conductivity can be calculated and used in Equation 4. Doing this leads to a maximum pressure head of 1500 mm. Although a conservative value, this significantly over-predicts the geocomposite requirement that may be necessary to obtain a pressure head that is low enough for an adequate factor of safety against instability.

For the case of LOAM/GC/GM, the conventional design methods would indicate that a very thin drainage layer of less than 1 mm is necessary. However, the finite element analysis shows that a 6-hour storm of 30 mm/hour will not require a geocomposite as the geocomposite does not have any effect on the pressure head. A steady state analysis was not carried out for the LOAM/GC/GM cases. Cover soils with low permeability may build up significant pressure head within the cover soil while the geocomposite may stay completely dry. For example, one can review the development of the pressure head with time for Run 7 in Figure 3. The figure shows pressure head on the liner with time at about 4000 mm horizontal distance down the slope. The maximum pressure head of 250 mm occurs at about 3 hours and the steady state pressure head of 100 mm is significantly lower than this value. Depending on the storm event and material properties, maximum pressure head may occur sooner than what a steady state analysis or exact solution may show. The finite element analyses offer a valuable tool as one can track the water pressure buildup with time and adjust the design to address this.

A very important advantage of using the finite element analysis is the pressure head distribution along the liner. Figure 4 shows the steady state pressure head distribution over the liner for Run 3. It is seen that a positive pressure head is limited to only about 500 mm length of the slope which is only 1/10th of the total slope length. For the design methods currently in practice, a uniform or linear pressure head distribution is assumed over the liner for the entire slope length. The figure shows that although the maximum pressure head is nearly equal to the thickness of the geocomposite, most of the geocomposite is dry. The actual pressure distribution could have a significant effect on the factor of safety against veneer instability. In some cases, the cover soil can get saturated at the toe while rest of the slope is dry. In other cases, it may be possible for the positive pressure head to move up into the cover soil with little or no effect on the stability. Moreover, the pressure distribution can have a significant effect on the selection of the type of the geocomposite. For example, one can use a thicker or more permeable drainage geocomposite at the toe while using a thinner material farther from the toe. The finite element analysis presents an opportunity to optimize the placement of a drainage geocomposite on a slope.

5. CONCLUSIONS

A very small matrix was used to look into the possibility of the use of finite element software – The software – for seepage analysis of slopes with drainage geocomposites. The following conclusions can be drawn based on this very limited effort:

- It was seen that drainage geocomposites can be entered into the software as a material rather than a drainage boundary condition. Construction lines were used to obtain 1 mm thick triangular mesh elements for the geocomposite and a thin soil layer immediately above the geocomposite. This improved convergence significantly but convergence problems persisted.
- Convergence problems occurred when the wetting front reached the geocomposite. Additional work is necessary to develop a method to solve convergence problems so that it is very easy for a practicing geotechnical engineer to perform the analysis for a typical project.

- Simple cases showed good agreement between the finite element analysis and the published equations for the case of thin materials like drainage geocomposite. Published equations over-predict pressure head with drainage within thick cover soils. No agreement was found when more than one material was involved, such as

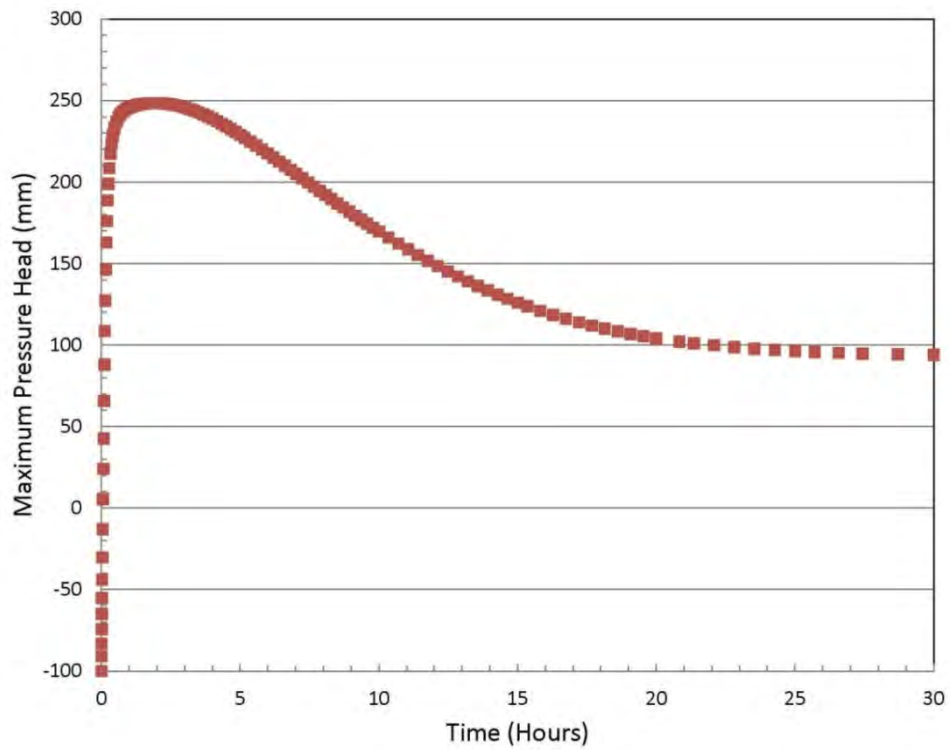


Figure 3 – Pressure Head with Time on the Liner at a Point about 1000 mm from the Toe for Run 7.

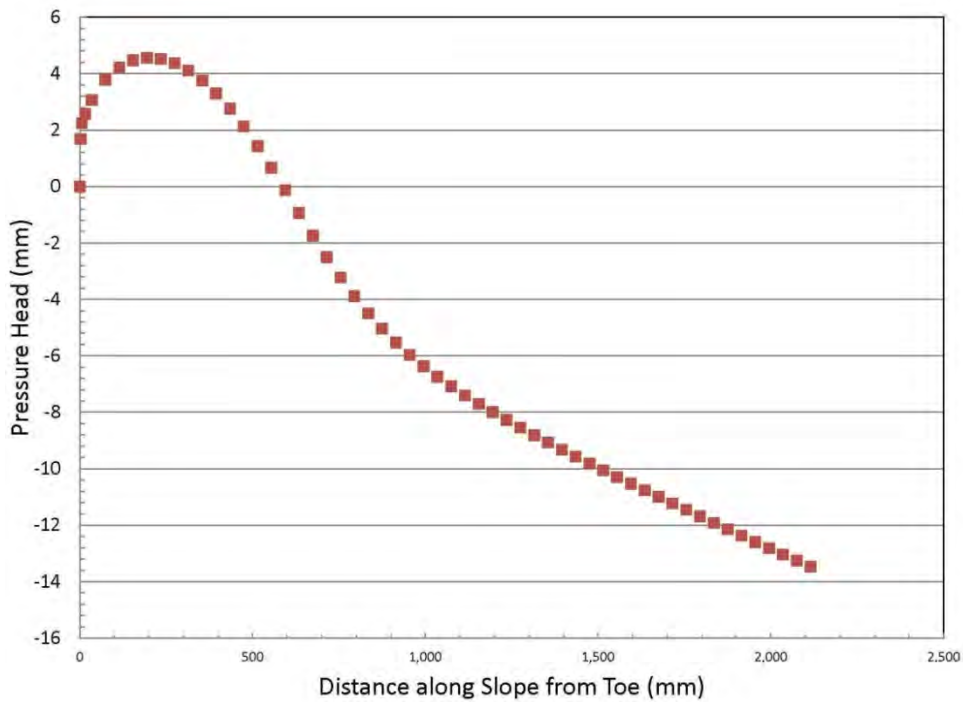


Figure 4 – Pressure Head Distribution on the Liner at Steady State for Run 3.

sand and geocomposite, or when transient conditions were analyzed, for example 6-hour rainfall.

- The pressure head distribution along the liner and with time was found to be of a significant importance for a practicing geotechnical engineer as it may affect the slope stability analysis and the material selection. Although a maximum pressure equal to the geocomposite thickness was reached, most of the geocomposite remained dry.

6. LIMITATIONS

This paper is not a comprehensive evaluation of a broad range of conditions that may occur in real life projects. Neither is it meant to be a detailed comparison of conventional design methods and finite element analysis. The objective was to see if a drainage geocomposite can be represented as a material in a finite element analysis software. This is of a significant interest for a practicing geotechnical engineer. Drainage geocomposites have a very high hydraulic conductivity and very low thickness (only a few mm). It is often difficult to include these materials in a finite element analysis. The software was found to provide consistent results. Yet only a very small range of conditions was analyzed. Moreover, no laboratory verification of the results is possible as actual physical experiments were not performed for this paper.

Drainage geocomposite was represented as a thick geotextile with properties obtained from Iryo and Rowe (2005). Real drainage geocomposites consist of a geotextile bonded to one or both sides of a geonet. A more refined representation of the drainage geocomposite with soil water characteristic curve obtained from laboratory testing is necessary. The author has initiated work on this topic but this information was not available at the time this paper was written. A more realistic soil water characteristic curve for drainage geocomposites may significantly affect the results. However, it is very likely that the software will successfully analyze a seepage problem over a broad range of conditions provided convergence problems are resolved. Convergence problems occurred in some of the cases and changing the mesh size and initial conditions resolved the problems, but it is likely that a better method exists for improving the convergence.

REFERENCES

- Cai, F. and Ugai, K. (2004). Numerical analysis of rainfall effects on slope stability. *International Journal of Geomechanics*. Vol. 4, Issue 2, pp. 69-78.
- Giroud, J.P., Bachus, R.C., and Bonaparte, R. (1995). Influence of water flow on the stability of geosynthetic-soil layered systems on slopes. *Geosynthetics International*, Vol. 2, No. 6, pp. 1149-1180.
- Giroud, J.P., Zornberg, J.G., and Zhao, A. (2000). Hydraulic design of geosynthetic and liquid collection layers, *Geosynthetics International*, Vol. 7, Nos. 4-6, pp. 285-380.
- Iryo, T. and Rowe, K.R., (2005). Hydraulic behavior of soil-geocomposite layers in slopes, *Geosynthetics International Journal*, Vol. 12, No. 3, pp. 145-155.
- Ng, C.W.W. and Shi, Q. (1998). A numerical investigation of the stability of unsaturated soil slopes subjected to transient seepage. *Computers and Geotechnics*, Vol. 22, Issue 1, 1998, pp. 1-28.
- Simunek, J., M.Th.van Genuchten, and Sejna, M. (2011). *The Hydrus Software Package for Simulating Two and Three-Dimensional Movement of Water, Heat and Multiple Solutes in Variably-Saturated Media*, Technical Manual, Version 2.0, PC Progress, Prague, Czech Republic, pp. 258.
- Soong, T.-Y. and Koerner, R.M. (1997). The design of drainage system over geosynthetically-lined slopes. GRI Report #19. Geosynthetic Institute. Kedron, PA. pp. 1-88.
- Th. van Genuchten, M., Leij, F.J., and Yates, S.R. (1991). The RETC code for quantifying the hydraulic functions of unsaturated soils. EPA/600/2-91/065. US Salinity Laboratory, US Department of Agriculture, Riverside, CA.

Flexible Pavement Performance with and Without Geosynthetics: Nine Year Follow-Up

B. A. Lacina, P.E., TenCate Geosynthetics, USA, b.lacina@tencate.com

F. S. Dull, P.E., TenCate Geosynthetics, USA, s.dull@tencate.com

ABSTRACT

A project case study was undertaken to evaluate the differential performance of asphalt surfaced flexible pavement sections in a suburban community of Raleigh, North Carolina, USA nine years after being placed in service. Pavement sections that utilized a moderate strength reinforcement geotextile at the base course - subgrade interface showed a marked improvement in durability and performance compared to other pavement sections constructed without geosynthetics in the same subdivision during the same time period. These flexible pavement sections were examined using both destructive and nondestructive evaluation methods to assess the physical differences between the geosynthetically enhanced and non-geosynthetic pavement sections.

The results of pavement coring, ground penetrating radar (GPR), falling weight deflectometer (FWD) and surface roughness measurements are presented herein. Pavement coring tests show the thickness of the pavement system layers and evaluate the layer boundaries. GPR testing results provide a larger surface cross sectional perspective into the pavement system layers in the reinforced and unreinforced sections. FWD results are presented using AREA parameters for both reinforced and unreinforced pavement sections. Pavement surface roughness assessments are presented using the mean international roughness index (MIRI) for reinforced and unreinforced pavement sections. A summary and conclusions of the pavement testing and analyses are provided at the conclusion of this report.

1. INTRODUCTION

The project site is the Cornerstone subdivision which is located approximately 16 miles to the northwest of downtown Raleigh, NC, USA (Figure 1) and is located in the Piedmont geophysical province. Soils in the Piedmont can exhibit a loss of pavement support due to the presence of mica in the typically silty or clayey sands, which causes the subgrade soils to lose strength when exposed to moisture in roadway and other geotechnical engineering applications (Christopher, *et al*, 2009). Portions of the asphalt surfaced flexible pavements named Marvino Lane and Country Trail and their intersection were constructed January, 2003 and the contractor was required by the City of Raleigh to use a biaxial strength geosynthetic and an additional 2 inches (50 mm) of aggregate base course (ABC) material for pavement support due to the poor construction conditions at the site. It was originally thought that the thickness increase was required, but the coring evaluation completed for this study indicated that this was not the case. Construction of approximately 1500 feet (460 m) of Marvino Lane and Country Trail needed to be completed during this time. Marvino Lane and Country Trail are the main collector roads that service the 300+ home subdivision and the surrounding commercial retail developments.

The contractor placed approximately 13,000 square yards (10,900 m²) of TenCate Geosynthetic's woven Mirafi® HP370 base reinforcement geotextile (Figure 2) as the biaxial strength geosynthetic required by the City. The wider roll widths than typical biaxial geogrids used in this application allowed the contractor to place the rolls over the subgrade three panels wide using the appropriate overlap on the wide collector road entering the subdivision. Use of the wider roll widths allowed the contractor to easily complete construction of the roadways on schedule. The geotextile reinforced areas of Marvino Lane and Country Trail that used the geotextile showed much less pavement distress after four years of service life than the other areas of flexible pavement completed during the prior phase without the use of a reinforcement geotextile. In addition, the traffic counts on the geosynthetic reinforced roadways are significantly higher than the traffic counts on the older roadways that showed early surface deterioration.

When the original project case study was completed in February of 2007, after approximately four years of trafficking, photos were taken of a representative area on Country Trail where the geotextile reinforcement was used as well as a section of Parkstone Drive constructed without the benefit of a geosynthetic about 6 months prior to the Country Trail section. In February of 2011, these same areas were investigated and new photos were taken noting any changes that had occurred. The sections of Country Trail and Marvino Lane where the reinforcement geotextile was installed showed no major pavement deterioration. The asphalt showed very minor surface abrasion and nothing that would indicate a deteriorating subgrade or any loss of pavement support.

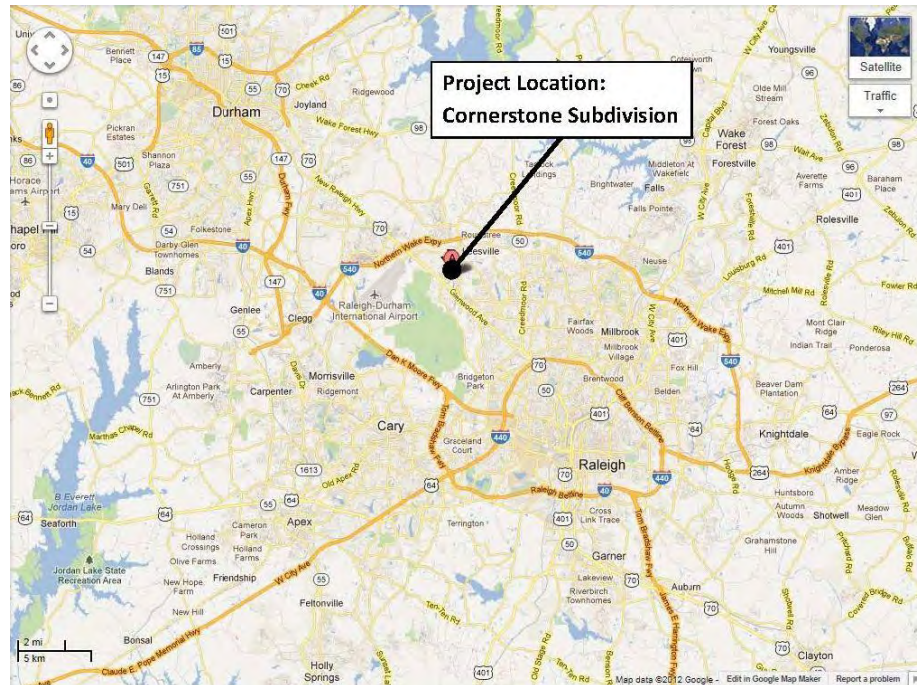


Figure 1. Project location near Raleigh, NC, USA (Google, 2012)

The Parkstone Drive area constructed without a geosynthetic had continued to deteriorate. It appeared as though a section of the pavement had been patched with a repair and areas adjacent to the repair were starting to show major signs of pavement fatigue. Another area of pavement with signs of premature deterioration was observed further into the development on Country Trail, beyond where the geotextile reinforcement was used. This part of Country Trail was constructed approximately one year after the first pavement areas that incorporated geosynthetics.



Figure 2. Pavement construction in 2003 showing placement of the woven base reinforcement geotextile.

It was also evident that the pavement sections that used the geotextile reinforcement provided a much quieter ride (less road noise) and smoother driving experience than the other pavement areas throughout the Cornerstone subdivision that did not use geosynthetics in their construction. These observations were initially considered to be significant, but were not fully understood and took some consideration to determine the appropriate analysis method(s) and their

resulting conclusions. There were some obvious difference between the geotextile reinforced pavement surfaces and the unreinforced pavement surfaces due to signs of pavement distress.



Figure 3. Conditions in 2011 on Country Trail with reinforcement geotextile and Parkstone Drive without geosynthetics.

2. ROADWAY INVESTIGATION AND EVALUATION PROGRAM

2.1 Pavement Coring Evaluation Destructive Testing on Country Trail Road: 2 Roadway Sections; 6 Cores

Six, 6 inch (150 mm) diameter pavement layer coring evaluations, including coring into the subgrade soil and to verify the existence or absence of geosynthetics in the pavement cross section, were performed by ECS Carolinas, LLP. Core testing was performed at two different locations of Country Trail Road. One location was found to have the reinforcement geotextile at the subgrade – base course interface, while the other was found to be unreinforced. A plan of the core testing locations is shown in figure 4.

A summary of the results from the coring testing report at each test location is shown in Table 1. It is evident from this testing summary that the asphalt layer thickness varied from 2 inches (50 mm) to 5 inches (125 mm) with an average of 3.4 inches (85 mm) for the unreinforced pavement areas and a uniform 2.6 inches (65 mm) for the geotextile reinforced pavement areas. Ignoring the base course thickness in the pavement repair area in coring location 1, the in-service ABC thickness varied from 4.5 inches (113 mm) to 8.5 inches (213 mm) with an average of 6.7 inches (166.7 mm) for the unreinforced pavement areas and 6.3 inches (156 mm) for the geotextile reinforced pavement areas. The unreinforced pavement areas showed much more variability in their layer thickness which is unexpected.

The pavement areas in coring locations 1 through 4 were originally constructed with no geosynthetics but coring location 1 which showed significant rutting in 2011 had a repair performed at sometime in its past, and that repair included the use of two layers of geosynthetics. This section then showed fatigue prior to the city accepting the project and the contractor had to remove and replace the failed section. The core testing shows that a light weight slit-tape woven geotextile was placed at the bottom of the repair undercut, about 22 inches (550 mm) below the pavement surface, and approximately 9 inches of compacted gravel was placed over this geotextile. Next a punched and drawn biaxial geogrid was installed and approximately 9 inches of additional compacted aggregate was placed on the geogrid. This was followed with approximately 4 inches (100 mm) of compacted hot mix asphalt (HMA). This is a repair scenario that utilizes various geosynthetic products to stabilize the gravel base aggregate represents a common repair technique used for flexible pavements constructed in the Piedmont range that show early fatigue or loose subgrade support and the results are sometimes ineffective.



Figure 4. Pavement layer core testing location on Country Trail Road in both geotextile reinforced and unreinforced pavement areas (Google 2012).

Table 1. Pavement layer summary from core testing on Country Trail Road in both geotextile reinforced and unreinforced pavement areas.

Layer Thickness (in)	Core Test Location					
	1	2	3	4	5	6
HMA	3.88	2.00	2.75	5.00	2.63	2.63
ABC	17.50	4.50	8.50	7.00	6.00	6.50
Notes	Unreinforced	Unreinforced	Unreinforced	Unreinforced	Reinforced	Reinforced
Subgrade	MH Mica	CH Mica	CH Mica	CL	ML Mica	ML Mica
Geosynthetics	Separation Geotextile at bottom of ABC				Reinforcement Geotextile	Reinforcement Geotextile
	Biaxial Geogrid at mid-gravel layer thickness					

The pavement areas in coring locations 5 and 6 were constructed with the reinforcement geotextile at the interface between the subgrade and base course as shown in Figure 2. These test locations show a good consistency between the compacted ABC thickness and HMA layers between each location. This trend of consistent layer thickness is commonly observed when flexible pavements are constructed using geotextiles. A visual summary of the layers and total thickness is shown in Figure 5.

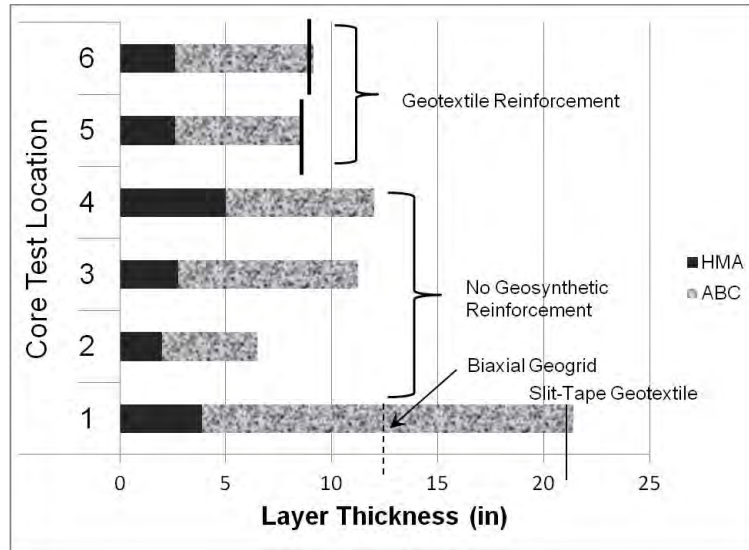


Figure 5. Pavement layer core testing result summary on Country Trail Road in both geotextile reinforced and unreinforced pavement areas.

2.2 Ground Penetrating Radar (GPR) Nondestructive Testing: Country Trail Road

GPR was performed by ECS Carolinas, LLP on two different areas of Country Trail in an attempt to verify the existence of a clear boundary created by the geotextile within the pavement cross sections. One location was found to have the reinforcement geotextile at the subgrade – base course interface, while the other was found to be unreinforced. A plan of the GPR testing locations is shown in figure 6.



Figure 6. Pavement GPR testing locations on Country Trail Road in both geotextile reinforced (Location 1) and unreinforced (Location 2) pavement areas.

Ground Penetrating Radar (GPR) nondestructive testing is a fairly straightforward technique of emitting radio waves into a substrate and measuring the reflected, refracted or absorbed waves at a receiver at the surface of the substrate. The measurements can be used to assess the subsurface materials or layers by analyzing the time taken for signals to be reflected back to the receiver. This information can then be used to determine the depth to a reflective feature or detect the absence of reflective features below the ground.

The GPR test results were obtained using Sensors and Software, Inc, Ontario, Ca Conquest GPR unit containing a 1000 MHz antenna. The GPR scans show a cross sectional image of subsurface conditions derived from reflected energy of high frequency electromagnetic waves. Reflections of these waves occur where a variation in material properties take place. For this survey, this may include the transition from the different flexible pavement system layer such as HMA to ABC, ABC to subgrade, ABC to reinforcement geotextile and reinforcement geotextile to subgrade soils.

A review and analysis of the GPR data for Location 1 on Country Trail for the pavement areas with the reinforcement geotextile are displayed in Figure 7. The results from the GPR scans display a very clear separation of layers at the transition between the HMA and ABC layers and also depth of approximately 12 inches (300 mm) that is consistent throughout the width of the roadway. We believe this layer separation is the reinforcement geotextile located between the ABC and the subgrade soils since it coincides with the approximate total flexible pavement thickness above the subgrade elevation. We are unaware of previous GPR surveys being able to locate this boundary so clearly in the past.

The significance of this result is that it shows that the pavement layers above the subgrade have maintained their as-designed thickness over the service life of the pavement to date. Early AASHTO flexible pavement design methods accounted for the lower portion of the base course aggregate intermixing with the subgrade over time (*Special Report 73*) and reducing the structural integrity of the pavement by adding approximately 2 inches (50 mm) to the final base course layer thickness. Without any consideration for reduction of tensile forces or strains at the bottom of the base course, the simple function of separation of the base course and subgrade soils has maintained the as-designed structural integrity of these reinforced pavement areas (Lacina, 2011).

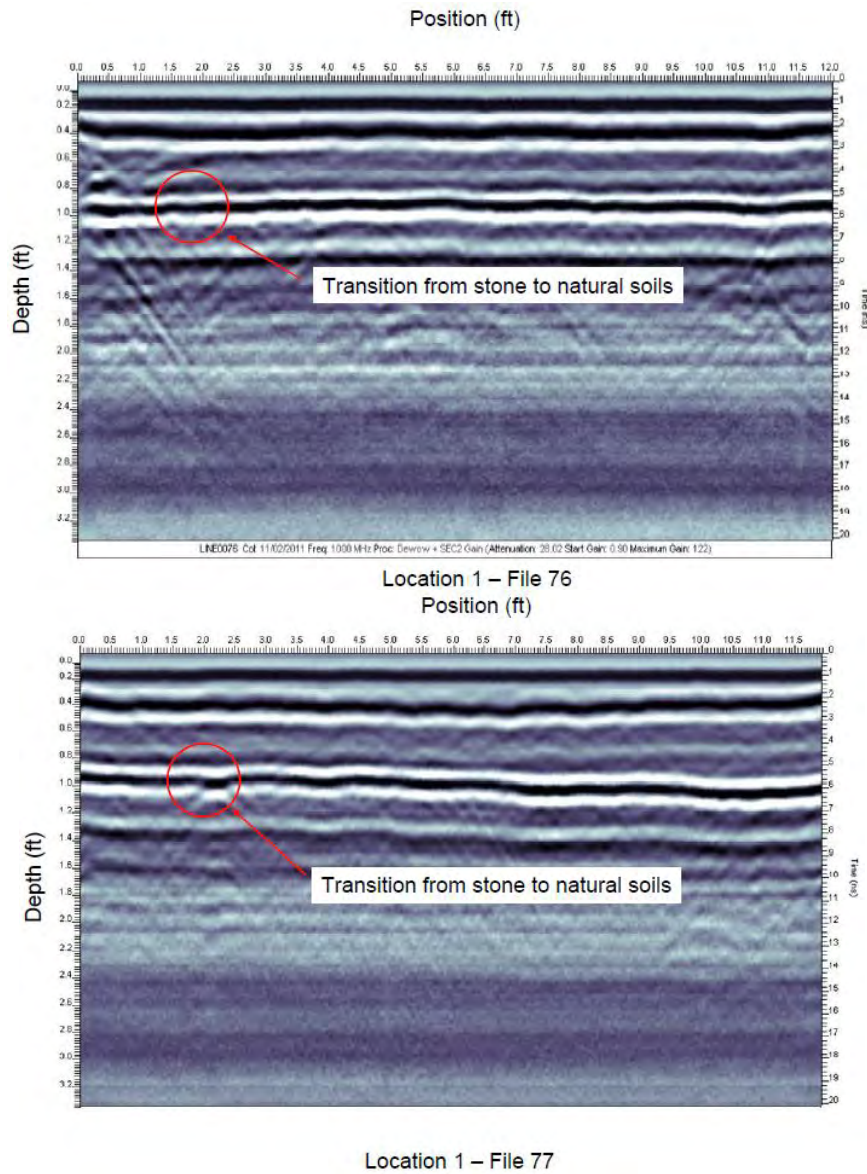


Figure 7. GPR testing image results for Location 1 on Country Trail with geotextile reinforcement.

A review and analysis of the GPR data for Location 2 on Country Trail for the pavement areas without any reinforcement geotextile shows entirely different cross sections than those in Location 1. The cross sections represented by Figure 8

show a potential separation between the ABC and subgrade soils around a depth of approximately 2.2 feet (660 mm), which transitions to a depth of approximately 12 inches (300 mm) at approximately 15 feet (4.6 m) from the curb and stays consistent along to the pavement area where the road was previously repaired.

The significance of the unclear boundary between the ABC and subgrade layers is that the current level of pavement support and structural capacity in these areas is unknown and has apparently deviated greatly from the original pavement design layer thickness. This observation is also supported by the findings of the pavement cores in test locations 2 through 4. While this GPR data supports the early AASHTO flexible pavement design recommendations to add additional base course thickness to the pavement design to compensate for aggregate loss into the subgrade over time, the actual additional thickness needed to create this compensation is unclear and would most likely be much greater than two inches.

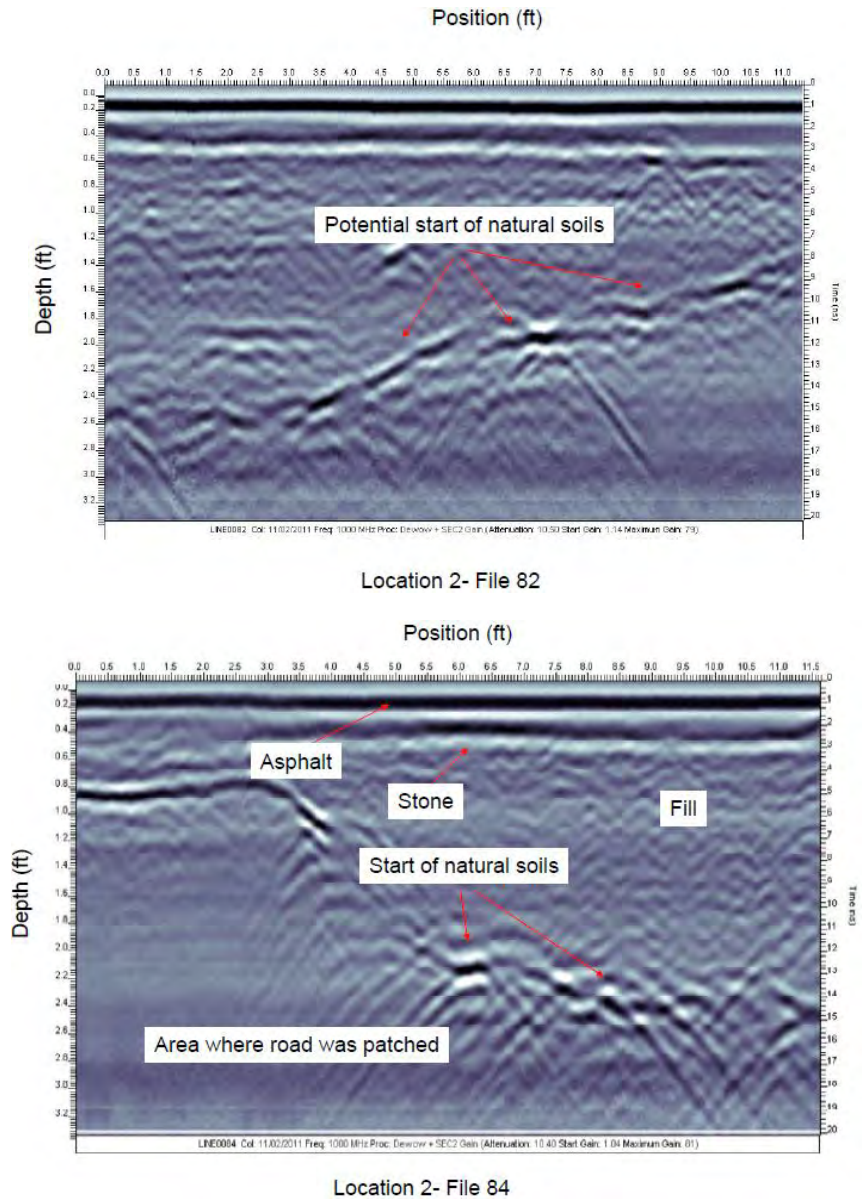


Figure 8. GPR testing image results for Location 2 on Country Trail without geotextile reinforcement.

2.3 Falling Weight Deflectometer (FWD) Nondestructive Testing: Country Trail Road and Marvino Lane

FWD tests were performed at 3 locations by TriMat Materials Testing, Inc on sections of Marvino Lane and Country Trail Road as shown in Figure 9. The presentation of testing results on Country Trail Road will be broken up into its northern

and southern portions for this FWD section of the report and in following surface roughness measurement section. The northern section of Country Trail Road was constructed without geosynthetics while the majority of the southern section was constructed using the geotextile reinforcement placed below the ABC layer.

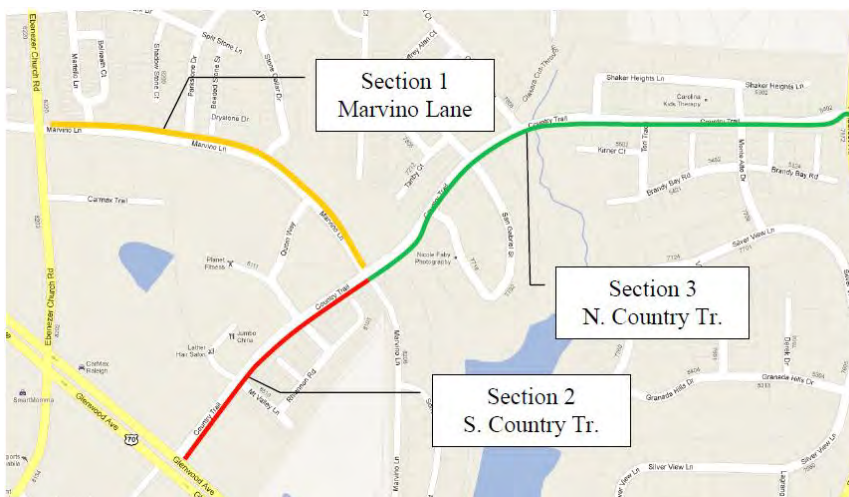


Figure 9. Falling Weight Deflectometer (FWD) nondestructive testing on Marvino Lane (Section 1); South Country Trail Road (Section 2); North Country Trail Road (Section 3).

Falling weight deflectometer (FWD) testing is a method for measuring the surface deflection of pavement surfaces and results in measurements that illustrate the deflection basin shape at the pavement surface. Deflections are measured at the center of the applied load and radially outward from the load. Deflections can be associated to pavement performance or can be used to determine the material characteristics of the in-situ pavement layers. FWD output is often presented in the form of subgrade moduli. Although layer moduli are meaningful, it can be more useful to utilize a single number as an indicator of the deflection shape.

One indicator method known as the AREA parameter characterizes the normalized area of a vertical slice taken through a deflection basin between the center of the test load, and 36 inches (0.9 m) away from the test load. Dividing the slice area by the deflection measured at the center of the test "normalizes" the AREA Parameter. The AREA is calculated using deflection measurements at 0, 12 inches (300 mm), 24 inches (600 mm) and 36 inches (0.9 m). The maximum AREA value is 36 inches and would occur when all four deflection measurements were equal, indicating that the pavement being tested would be extremely stiff (i.e. rigid pavement or thick, full-depth HMA).

The least expected AREA value is 11.1 inches (282 mm). This condition could occur only if all the pavement layers have the same elastic moduli and the pavement structure does not contribute any additional stiffness to the underlying subgrade. A low AREA value suggests that the pavement structure is not much different than the underlying subgrade material (i.e. a very stiff subgrade soil). Typical AREA values for pavements are shown in Table 2:

Table 2. AREA values for paved "Typical" roadways, North County Trail, South Country Trail and Marvino Lane.

Pavement	AREA Value (in)
Rigid	24 - 33
Thick Flexible (> 4 in, 100 mm)	21 - 30
Thin Flexible (< 4 in, 100 mm)	16 - 21
S. Country Trail, Reinforced (6,200 lb-f)	18.8
Marvino Lane, Reinforced (6,200 lb-f)	17.9
N. Country Trail, Unreinforced (6,200 lb-f)	15.3
S. Country Trail, Reinforced (8,300 lb-f)	18.9
Marvino Lane, Reinforced (8,300 lb-f)	17.5
N. Country Trail, Unreinforced (8,300 lb-f)	17.2
S. Country Trail, Reinforced (12,300 lb-f)	19.6
Marvino Lane, Reinforced (12,300 lb-f)	19.5
N. Country Trail, Unreinforced (12,300 lb-f)	17.2

As shown in Table 2 and Figure 10, the geotextile reinforced pavement areas show a higher AREA value for all three impulse loadings and this FWD testing was performed at or near the core test locations discussed in Section 2.1. All of the AREA values appear to be in the normal range for thin pavement sections and these flexible pavements have an average HMA layer thickness of = 3.2 inches (81 mm) as determined by the core testing results (Table 1). The scatter of the data points and the very low R values would indicate that the thickness of the ABC stone and pavement layer (HMA) have very little effect on the FWD deflection measurements and the AREA calculations. The core testing shows that the soil conditions encountered under the ABC layer were all similar: moist red silty-clay with trace mica. Based on the core test data, it can be assumed that the soil subgrade in all of these areas provided the same support to the overlying layers, indicating that the primary variable effecting the FWD deflection measurements is the presence of the geotextile reinforcement fabric.

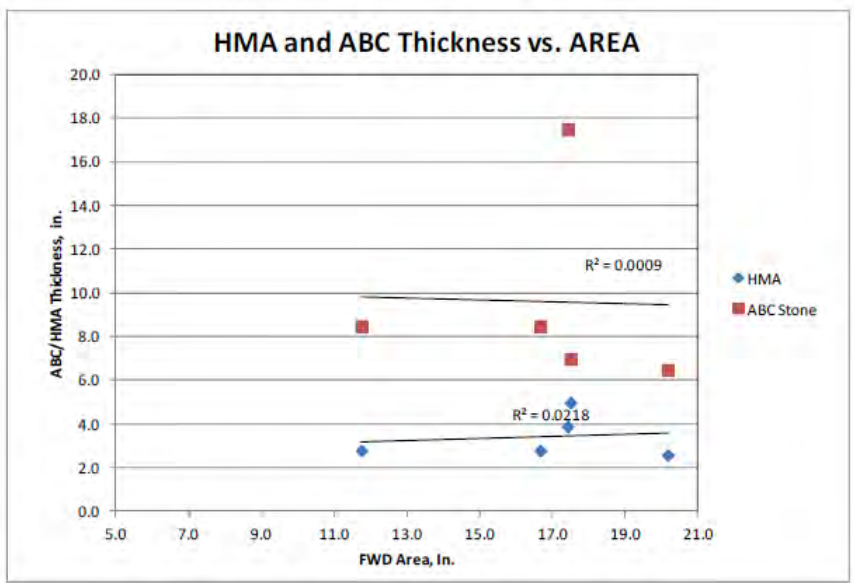


Figure 10. Correlation of AREA vs. Layer Thickness.

2.4 Surface Roughness (IRI) Nondestructive Testing: Country Trail Road and Marvino Lane

Surface roughness tests were also performed at 3 different locations at the project site by TriMat Materials Testing, Inc on sections of Marvino Lane and Country Trail Road as shown in Figure 9. The profilograph used for surface roughness testing of the pavement surface was an Ames Engineering Model 8200 high speed laser profiling device and utilizes two LMI technologies Roline 3 KHz lasers. Sampling at more than 16,000 times per second, the laser profilometers are capable of creating an exact reproduction of the road surface in digital form. Combined with on board accelerometers, the lasers are capable of producing data for any known standard of ride quality.

IRI is the International Roughness Index and measures pavement smoothness. The measurement of IRI is required for data provided to the United States Federal Highway Administration, and is covered in several standards from ASTM International: ASTM E1926 - 08, ASTM E1364 - 95(2005), and others. IRI is also used to evaluate new pavement construction, to determine penalties or bonus payments based on smoothness. The lower the calculated IRI, the smoother vehicles will ride on the pavement. The higher the IRI value, the rougher the pavement will ride.

Based on the data presented in Figure 11, the mean IRI (MIRI) ride quality on the reinforced sections of South Country Trail and Marvino Lane is better than the unreinforced section of North Country Trail. It appears that the numerous water valves located in the travel lanes on Marvino Lane affect the measured ride quality, thus yielding higher MIRI values than South Country Trail. As a reference, North Carolina Department of Transportation specifies a range of acceptable IRI values of 55-70 in/mile on new construction for US routes and Interstates.

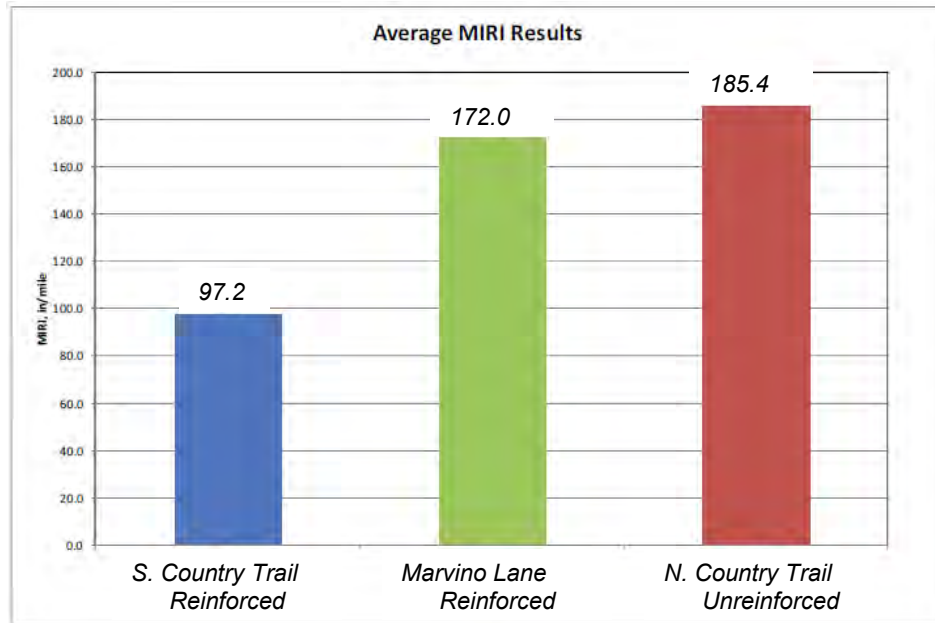


Figure 11. Mean IRI (MIRI) values for South Country Trail Road (reinforced); Marvino Lane (reinforced); and North Country Trail Road (unreinforced).

3. CONCLUSION

Flexible pavement construction was permitted by the City of Raleigh, NC over winter provided a biaxial reinforcement geosynthetic was used over the subgrade during construction. Pavement construction was made easier and proceeded faster utilizing the reinforcement geotextile. Pavement deterioration in unreinforced areas was evident early on, after only a few years in-service, which resulted in increased maintenance costs for the unreinforced pavement areas. Use of the reinforcement geotextile has increased the service life and reduced maintenance costs of the reinforced flexible pavement.

Pavement core testing showed consistent layer thickness for the HMA and ABC layers after 9 years of pavement service life in areas using the reinforcement geotextile. Core testing showed large variability in the layer thickness for HMA and ABC layers in pavement areas without geosynthetics. It also showed the presence of micaceous silt and clay subgrade soils, typical of Piedmont Geophysical Province. The stability of these unpredictable soils as subgrade material benefits greatly from the use of a reinforcement geotextile.

The GPR results from the geotextile reinforced roadway sections display a clear separation of layers at approximately 10 to 12 inches (250 – 300 mm) depth, which is consistent across the width of the roadway. The unreinforced pavement sections displayed entirely different layer thickness results and show no clear transition between the ABC and subgrade layers. They show a potential separation around a depth of approximately 2.2 feet (670 mm), which transitions to a depth of approximately 10 to 12 inches at approximately 15 feet (4.6 m) from the curb.

The FWD testing and subsequent calculated AREA values results show that the test sections constructed with the reinforcement geotextile appear to be stiffer than the unreinforced sections. The reinforced sections also appear to be performing better based on the visual evaluation as well. The use of the reinforcement geotextile has provided a stiffer roadway cross section than the comparable unreinforced pavement sections.

The average IRI measurements show that the ride quality on the reinforced section of South Country Trail is much better than the unreinforced section of North Country Trail. The average IRI measurements on the reinforced section on Marvino Lane shows a slight improvement over the unreinforced section of Country Trail and it is apparent that the measured improvement is skewed by the presence of numerous water valves in the travel lanes on Marvino Lane that can have a drastic effect on ride quality measurement. The use of the reinforcement geotextile has provided the unexpected benefits of a smoother roadway surface, which in turn improves tire rolling resistance (i.e. improved fuel economy) and improves driver comfort (i.e. improved level of service).

REFERENCES

- Christopher, B. R., Perkins, S. W., Lacina, B. A., Marr, W. A., Pore Water Pressure Influence on Geosynthetic Stabilized Subgrade Performance, *Proceedings, 2009 Geosynthetics Conference*, Salt Lake City, Utah, February 2009, *Special Report 73: The AASHTO Road Test*, HRB, National Research Council, Washington, D.C., 1962.
- Lacina, B., A, *Functions of Geotextiles Used in Roadway Base Course Construction*, AATCC Review, September / October 2011.

Flexural Behavior of Concrete Beams Reinforced with Different Types of Geogrids

F. El-Meski, Ph.D. Lecturer, Lebanese American University of Beirut, Lebanon, fme09@aub.edu.lb
G. R. Chehab, Assoc. Prof., American University of Beirut, Lebanon, gc06@aub.edu.lb
M. Harajli, Prof., American University of Beirut, Lebanon, mharajli@aub.edu.lb

ABSTRACT

The objective of this study is to investigate the performance of three geogrids of different aperture shapes and properties as reinforcement in Portland cement concrete (PCC) beams. The results from this study serve as a foundation for further investigation of using geogrids as reinforcement in thin concrete overlays. The experiment comprises of four-point bending tests conducted on unreinforced PCC beams and those with one layer of geogrid-reinforcement. The flexural behavior of the unreinforced geogrid reinforced beams for the various geogrids tested are compared. Results confirm the reinforcing benefit from the geogrids as evidenced from the load-deflection response in terms of post-cracking behavior, load capacity, crack mouth opening displacement (CMOD) and failure mode. Results also reveal a correlation between the concrete strength and the mechanical properties of the geogrid.

1. INTRODUCTION

Geosynthetics had been for long used as reinforcement and stabilization elements in various earthwork construction applications^[1]. More recently, their use as reinforcement elements has expanded into pavement systems, particularly as reinforcing elements in asphalt layers^[2,3], and as interlayers in overlay applications^[4]. Little research, however, has been conducted on their use as reinforcement in PCC overlays^[5] in pavements and other elements where steel reinforcement cannot be placed.

Geogrid has longitudinal and transverse ribs, which form apertures; a new type is launched which has triangular aperture with ribs in more directions. There are three types of geogrids used for reinforcement and interlayers: uniaxial, biaxial and triaxial (

Figure 1). Uniaxial geogrids exhibit high tensile strength in their uni-directional ribs; while biaxial geogrid ribs have tensile strengths in two directions. Tests conducted on biaxial geogrids^[1] showed that it cannot provide a uniform tensile strength when subjected to tension in different directions. It is believed that this deficiency led to the development of geogrids consisting of triangular ribs.

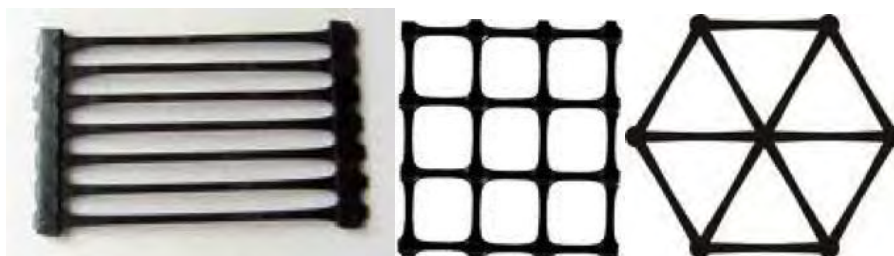


Figure 1. Uniaxial, biaxial, and triaxial geogrids

2. RESEARCH OBJECTIVE AND SCOPE

The objective of this research is to fully understand the structural behavior of reinforced beams with geogrid materials. Understanding such behavior aids in evaluating the potential of using the geogrids as reinforcement in PCC elements such as pavement overlays and identifying critical geogrid properties that impact the reinforcement effectiveness. The structural behavior will be evaluated for normal strength concrete subjected to monotonic loading. Simply supported beam specimens reinforced with one layer of either uniaxial, biaxial or triaxial geogrids are subjected to four-point bending until failure. The structural response of each is compared to that of an unreinforced

plain concrete specimen to quantify the benefits gained from geogrid reinforcement. Aspects of the behavior evaluated include the maximum load capacity, the load deflection response, crack mouth opening, flexural strength, accumulated energy absorption and mode of failure.

3. EXPERIMENTAL PROGEAM

A total of twelve beam specimens composed of 35 MPa PCC were tested. Specimen dimensions and loading details are shown in Figure 2. Specimens have a span length of 53 cm, with a triangular groove of 8 mm wide and 4.5 mm deep in the middle of the span to induce flexural failure close to the mid-span of the beam. The beams are divided into four categories: three unreinforced plain specimens used as control, three with one layer of uniaxial geogrid, three with one layer of biaxial geogrid and three with one layer of triaxial geogrid.

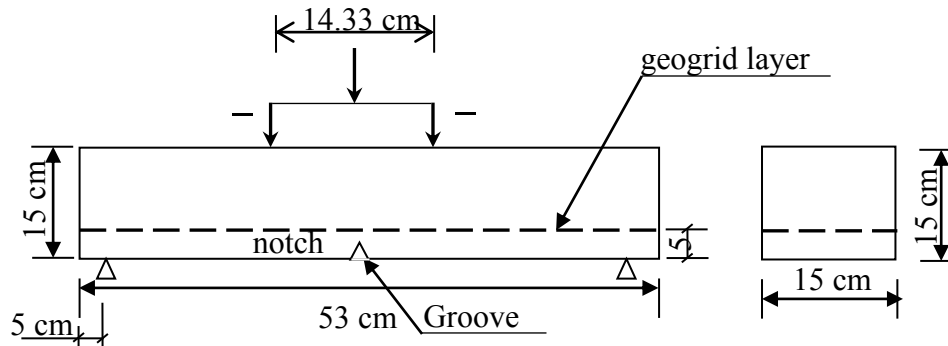


Figure 2. Typical longitudinal section showing loading position and reinforcement layout

3.1 Geogrid Properties

All three rigid geogrids used consisted of geosynthetic material but different aperture geometry and dimensions, and different mechanical properties as reported by the manufacturer, and presented in Table 1. The uniaxial type is made of high density polyethylene, while the two other types are made of polypropylene.

Table 1. Physical and mechanical properties of the geogrids used

Component (Uniaxial)	Description	Unit
Aperture Size MD	220	mm
Aperture Size TD	13/20	mm
Mass Per Unit Area	400	g/m ²
Strength at 2% Strain	17	kN/m
Strength at 5% Strain	32	kN/m
Peak Tensile Strength	60	kN/m
Yield Point Elongation	13	%
Junction Strength	50	kN/m
Long Term design Strength	28.3	kN/m

Component (Biaxial)	Description	Unit
Tensile Strength at 2% Strain	14	kN/m
Tensile Strength at 5% Strain	28	kN/m
Max Tensile Strength MD/CMD	40/40	kN/m
Elongation at Nominal Strength MD/CMD	11/10	kN/m

Index Properties (Triaxial)	Long.	Diag.	Trans.	General	Unit
Rib Pitch	40	40	-		mm
Mid-Rib depth	-	1.8	1.5		mm
Mid-Rib width	-	1.1	1.3		mm
Nodal Thickness				3.1	mm
Rib Shape				Rectangular	
Aperture Shape				Triangular	

Structural Integrity		
Junction Efficiency	93	%
Aperture Stability @ 5 kg.cm/deg	3.6	Kg.cm/deg
Radial Stiffness at Low Strain @ 0.5% Strain	300	kN/m

3.2 Specimen Fabrication

For concrete beams reinforced with one layer, a 5-cm concrete layer was first poured and compacted in the beam mold with a vibrator (Figure 3), and then the geogrid layer was carefully installed followed by layer of concrete mixture. The mixtures were consolidated to the extent possible to ensure intermixing between the concrete layers above and below the geogrid. No separation or surface voids were observed after de-molding the specimens.



Figure 3. Placing of the geogrid layer after pouring and compacting of the 5 cm concrete layer

3.3 Loading and Measurement Instrumentation

The concrete beams were subjected to flexural testing according to ASTM C78. Monotonic loading is applied through a closed-loop 100-ton servo-hydraulic universal testing machine at a constant displacement rate of 0.002 mm/sec. A 16-bit data acquisition system was used to collect data of applied actuator load, horizontal and vertical displacement at midspan, in addition to crack mouth opening displacement throughout the test until failure.

An Epsilon Model 3541 clip-on gage with 7-mm range was used for measuring the crack mouth opening displacement (CMOD). Additionally, a spring loaded LVDT was placed horizontally on one face of the beam as an added means of measuring horizontal displacement across the notch as loading was applied. A vertical spring-loaded LVDT was fixed to the bottom of the loading plate with its tip touching the specimen's bottom face at the center adjacent to the crack. The loading and instrumentation setup can be seen in Figure 4.

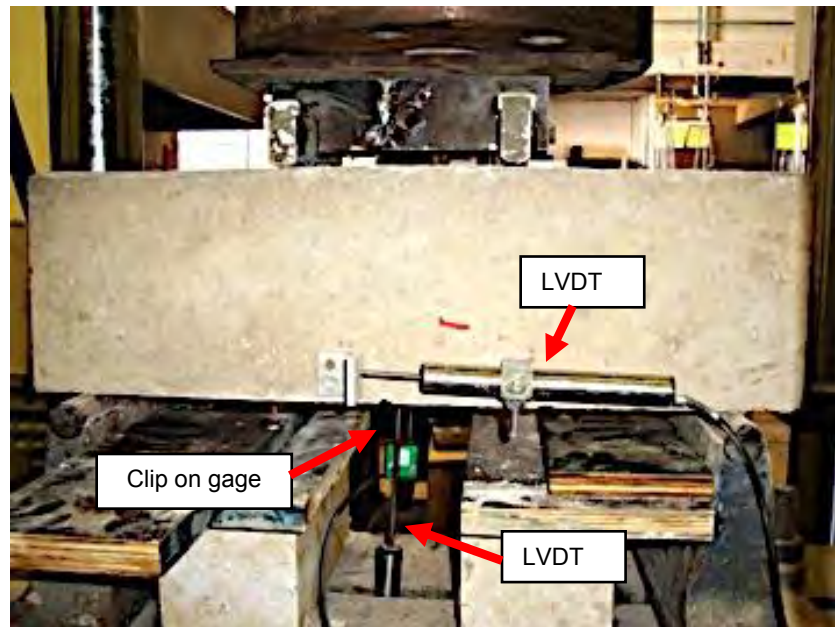


Figure 4. Testing and measurement instrumentation setup

4. RESULTS AND ANALYSIS

4.1 Load versus Vertical Displacement

The load versus vertical displacement plots for plain and reinforced concrete specimens are shown for the various geogrid types in Figure 5 through Figure 7. Figure 5(a) through Figure 5(d) present plots of the load-deflection curves for all four beam categories. Curves corresponding to the three replicates of each category are plotted separately on one graph. As seen in Figure 5(a), all three replicates of unreinforced beams fail in a brittle manner once peak load is reached, at which sudden drop in the load and eventual failure of the whole beam occur. This is expected due to absence of any reinforcement. For all reinforced specimens, both concrete and the geogrids absorb the tensile stress due to bending of the beam. Once the stress in the concrete reaches its strength value, a crack initiates in the bottom concrete layer. This leads to the inability of the concrete layer to carry any more tensile load and thus the sudden drop in load that is witnessed in the load-deformation curves. Since the geogrids' tensile strength exceeds that of concrete the load is redistributed such that it is absorbed totally by the geogrids. The slope of the load-deformation curve is now lower than the initial slope since geogrids are more ductile than concrete. Once the load reaches the strength of a rib or multiple ribs, the rib is torn and that is where a sudden drop in the load-deformation curve occurs. The load is then redistributed to other ribs and so on until all ribs are torn. At that point total failure of the specimen occurs. This phenomenon can be clearly demonstrated in Figure 6 and Figure 7, where the load-deformation curves of a representative sample for each of the geogrid-reinforced beams (uniaxial, biaxial, and triaxial) are plotted.

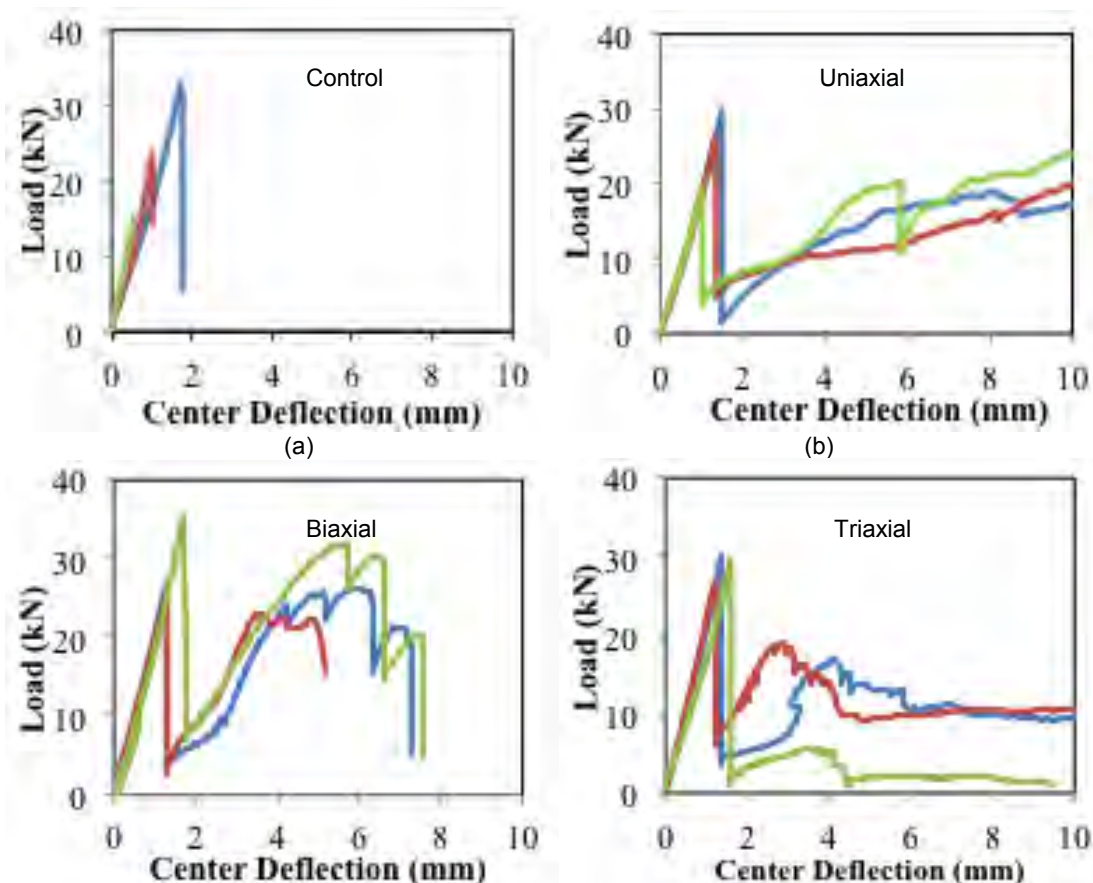
Photographs of beams during loading and after failure provide more information on the reinforcing mechanism and response of the beam under loading.

Figure 8 shows that the unreinforced beam separated into two parts directly upon failure of the concrete, while the reinforced beam remained intact as the crack initiated and cracked all the way to the top of the specimen. This is in agreement with the post-peak behavior witnessed in the load-deflection curves of reinforced beams, where load remains to be resisted after the sharp drop in load due to the concrete failure.

Figure 9 shows the extent of stretching of the uniaxial geogrid after crack opening, which explains the significant ductility observed in the load-deflection curve. **Error! Reference source not found.** reveals an excellent illustration as to why the beams reinforced with uniaxial geogrids exhibit multiple post-peaks in the load deflection curve compared to one post-peak for the biaxial and triaxial reinforced geogrids. **Error! Reference source not found.** (a) shows that failure of the geogrid occurs in the ribs, unlike the biaxial and triaxial geogrids where the failure occurs at the interface of the junction and the ribs. Hence, for the uniaxial geogrid each peak corresponds to the break of one or more ribs and hence the multiple peaks; whereas, the single peak observed for the biaxial and triaxial case corresponds to the break of the junction-rib interface.

Although all the geogrid reinforced beams had ductile post-cracking behavior, each, however, exhibited a different post-peak behavior. The beams reinforced with uniaxial geogrids exhibited the most ductility and largest load capacity. The increase in load capacity is about 30-60% compared to that of unreinforced beams, with a substantial increase in deflection ranging from 44 mm to 72 mm in compared to a deflection of 1.7mm for the unreinforced beam. The beams reinforced with biaxial geogrid showed an increase in load capacity by about 10-15% and a deformation ranging from 5 to 8 mm. On the other hand, the beams reinforced with triaxial geogrid showed an increase in load capacity by about 28% and an increase in the deflection by 10 to 20 mm.

The difference in the behavior between the three types of geogrid reinforced beam categories is attributed to the difference in the geogrids themselves, particularly: number and direction of ribs, junction characteristics, such as rigidity, width and thickness of ribs, tensile strength and stiffness, and aperture shape. For instance, the uniaxial geogrid layer in the beam consisted of seven ribs in the direction of applied tensile stress (longitudinal), with a corresponding area of 29.4 mm², the biaxial geogrid layer consisted of five ribs, resulting in an area of 17.5 mm², while the triaxial geogrid layer consisted of six ribs which resulted in an area of 14.82 mm². In addition, the junction of the uniaxial type, which is relatively rigid, was coincidentally located in the middle of the span and that might also have contributed to delaying of the rupture of the geogrid.



(c) (d)
 Figure 5. Load versus deflection curves for three replicates of beams with: a) no reinforcement, b) uniaxial geogrids, c) biaxial geogrids, and d) triaxial geogrids. Plots are for deflections up to 10 mm.

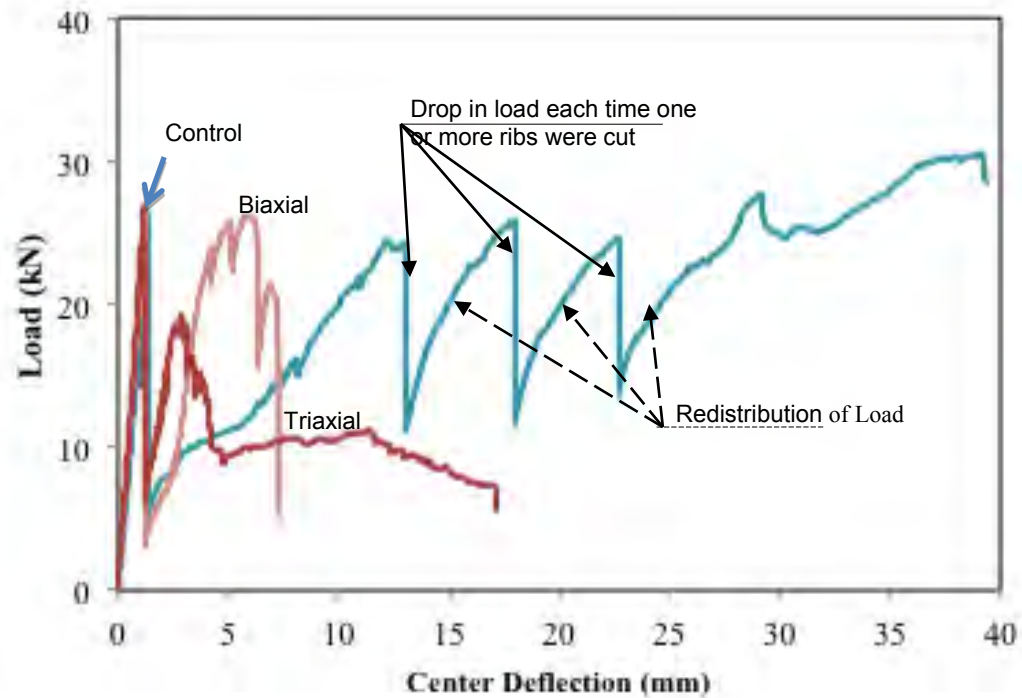


Figure 6. Representative load versus deflection curves for normal strength concrete beams and reinforced with various geogrid types.

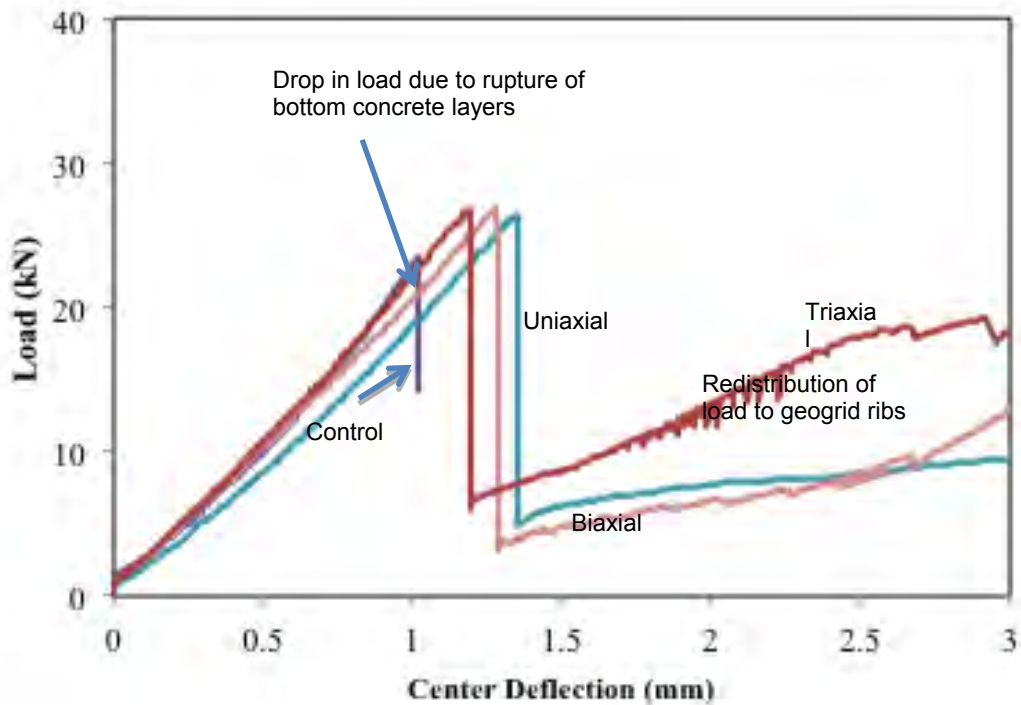


Figure 7. Representative load versus deflection for unreinforced and geogrid reinforced beams. Plots are for deflections up to 3 mm only.

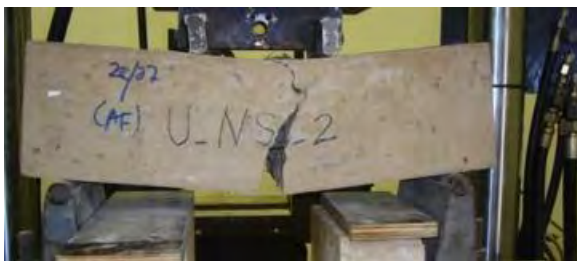


(a)



(b)

Figure 8. Failure mechanism: a) immediate brittle failure leading to specimen separation in control specimens, and b) delayed failure due to the action of the geogrids holding the specimen intact.



(a)



(b)

Figure 9. Beams reinforced with uniaxial geogrids: a) just before total failure, and b) on geogrid junction resisting load at the crack



(a)



(b)

Figure 10. Failure mode of the geogrids: a) rib failure in uniaxial geogrids, and b) failure at the junction in biaxial and triaxial geogrids

4.2 Load versus CMOD Curves

Although all beams were notched at the mid span to force a flexural crack, the cracks in some of the specimens occurred within the middle third of the span length. For those specimens, the CMOD measurements do not offer adequate insight into the effectiveness of the geogrids. A sample of CMOD data for beams reinforced with uniaxial geogrids and that failed at midspan is shown in **Error! Reference source not found.** After the initial cracking, a sudden drop in load is accompanied by a significant increase in CMOD. Then, as load is redistributed to the geogrids, CMOD increases gradually as ribs elongate until either sudden or gradual rupture of the ribs occur.

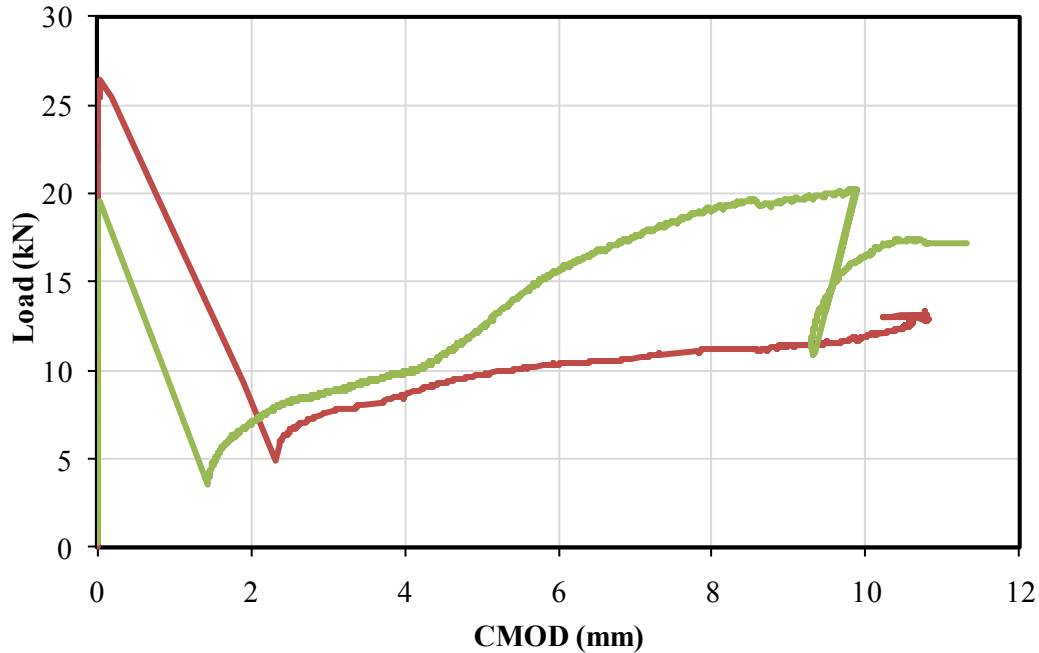


Figure 11. Load versus CMOD for normal strength concrete beams reinforced with uniaxial geogrid

4.3 Flexural Strength

According to ASTM C78, the flexural strength, which is expressed as Modulus of Rupture R , is calculated from the following formula:

$$R = \frac{Pl}{bd^2} \quad [1]$$

where:

P is the maximum total load measured, units in kN;
 l is the span length, 43 cm;
 b is the specimen width, 15 cm;
 d is the specimen height, 15 cm.

Based on the average values of three replicates, the geogrid reinforcement provides an increase in flexural strength to the concrete beams by approximately 10 to 30% for uniaxial geogrids, by 10 to 15% for biaxial, and by 25-30% for triaxial geogrids.

4.4 Fracture Energy

The area under the load-deflection curve represents the fracture energy of the concrete beams. All types of geogrid reinforcement in concrete beams lead to an increase in the fracture energy, mostly the uniaxial type.

5. CONCLUSIONS

Based on the findings of the above tests, the benefits from the use of geogrid as reinforcement for thin concrete sections can be summarized as follows:

- 1- It was noted the lack of bond between the concrete matrix and the geogrid material, caused the failure of concrete first followed by rupture of geogrids ribs.
- 2- All types of geogrid reinforcement provide a ductile post-cracking behavior, high fracture energy, high flexural strength, and large deflection.

- 3- It is worth noted that the geogrid properties have a great impact on the post-peak behavior of reinforced beams in flexure. Uniaxial geogrids with ribs aligned in the longitudinal direction yielded better performance in comparison to other types of geogrid.
- 4- Deeper notch should have been used to enforce the crack initiation at mid span

6. RECOMMENDATIONS

The inclusion of different types of geogrid in concrete beams subjected to flexural loading reveal significant improvement in the response. However, more parameters still need to be investigated such as: methods to improve the interlocking between geogrids and coarse aggregates in the concrete matrix, use of multiple geogrid layers, effects of junction location especially for uniaxial type, and behavior under cyclic loading.

ACKNOWLEDGMENTS

The authors wish to acknowledge the support of Tensar International, Tenax Corporation, and the Geoscience Company. The support of Mr. Luc Walter from Tensar is greatly appreciated. Technical help in the lab by Mr. Helmi El-Khatib and Abed El-Sheikh is also appreciated. Thanks are also due to the University Research Board at the American University of Beirut for funding this research.

REFERENCES

- Maxwell, S., Kim, W., Edil, T. B., and Benson, C.H. (2005); "Effectiveness of Geosynthetics in Stabilizing Soft Subgrades "; Report to the Wisconsin Department of Transportation.
- Webster, S.L. (1993); "Geogrid Reinforced Base Course for Flexible Pavements for Light Aircraft, Test section Construction, Behavior under Traffic, Laboratory Test Design Criteria"; Technical Report GL-93-6, U.S. Army Corps of Engineers, Waterways Experiment Station, Vicksburg, MS, USA.
- "Experimental Study on Triangular Aperture Geogrid-Reinforced Bases over Weak Subgrade under Cyclic Loading"; Yu Qian; Retrieved May 1, 2010 from <http://www.geocon.net/pdf/paper28.pdf>.
- Tang X., Palomino A., and Chehab G.R. (2008), "Laboratory Evaluation of Geogrids for Flexible Pavement Reinforcement", The First Pan American Geosynthetics Conference and Exhibition, GeoAmericas 2008 Conference Proceedings, International Geosynthetics Society.
- X.Tang, G. R. Chehab, and S. Kim; "Laboratory Study of Geogrid Reinforcement in Portland Cement Concrete"; 6th RILEM Conference on Cracking in Pavements, Chicago (2008), Pavement Cracking Mechanisms, Modeling, Detection, Testing, and Case Histories, by Al-Qadi, Scarpas and Loizos, Taylor& Francis Group, 2008 , pp. 769-778.

Frictional Performance of Segmental Concrete Wall Units with Flexible Mechanical Connectors

F.H. Ali, Department of Civil Engineering, National Defense University of Malaysia, Kuala Lumpur, Malaysia,
F.A. Salman, Department of Civil Engineering, University of Malaya, Kuala Lumpur, Malaysia.
M.Z.I. Bhuiyan, Department of Civil Engineering, University of Malaya, Kuala Lumpur, Malaysia

ABSTRACT

Segmental retaining wall (SRW) units are extensively practiced as a facing column to mechanically stabilized earth wall and bridge abutment because of its many fold advantages. Mechanical connectors are mainly used to help out unit alignment and control the wall facing batter, and it has a great effect on interface shear capacity of modular blocks. This study mainly focuses on interface shear capacity of newly and locally produced modular block units with and without shear pins. In this investigation, steel and plastic bars were used in the connection systems as shear connectors. The cavities of the blocks were not filled with gravel to minimize the number of parameters that could influence the test results. Geosynthetic inclusions were also not used at the block interface because of its influence on interface shear capacity. A series of direct shear tests were executed based on the existing ASTM and National Concrete Masonry Association (NCMA) test protocols to find out the effectiveness of steel and plastic shear pins under different normal loading conditions. Test results were outlined in the form of shear force-displacement relationship to compare the frictional performance of the blocks. Shear capacity envelopes were also plotted by using Mohr-Coulomb failure criterion to find out the angle of friction for each case. Test results revealed that the presence rigid shear pins reduce the shear capacity than a purely frictional condition and flexible shear pins increase the shear capacity.

1. INTRODUCTION

Dry-stacked columns of segmental retaining wall (SRW) units as the facing for geosynthetic reinforced mechanically stabilized earth (MSE) walls have been commonly used for about 30 years (Bathurst and Simac, 1994). Segmental retaining wall units are precast masonry concrete blocks manufactured using both types of wet and dry casting processes. The use of these types of precast concrete blocks has gained popularity in Malaysia.

Due to the discrete nature of the concrete units, facing stability is an important issue in the current design guidelines (NCMA, 1997; Elias et al., 2001) and it mainly depends on interface shear and connection failures.

Two different types of shear connection systems are mainly used in segmental retaining wall constructions to develop interlocking mechanism between successive vertical courses of units. One is built-in mechanical interlock in the form of concrete shear keys or leading/trailing lips and another one is the mechanical connector consisting of pins, clips, or wedges. Mechanical connectors are mainly used to help out unit alignment and control the wall facing batter. Bathurst and Simac (1997) reported that shear connectors (mechanical) or shear keys provide additional interface shear capacity of segmental concrete units. Ali et al. (2011) reported that the rigid (steel) and flexible (plastic) shear connectors on the interface shear capacity of segmental block system infilled with gravel.

In this investigation, steel and plastic bars were used in the connection systems as shear connectors. The cavities of the blocks were not filled with gravel to minimize the number of parameters that could influence the test results. Geosynthetic inclusions were also not used at the block interface because of its influence on interface shear capacity. To find out the performance parameters, a series of full scale laboratory tests were conducted with and without steel pins (NCMA SRWU-2, 1997; ASTM D 6916-03). Shear force-shear displacement graphs were drawn to compare performance of the infilled concrete units with and without shear pins. Shear capacity envelope graphs were also plotted by using Mohr-Coulomb failure criteria under peak and service state criteria.

2. EXPERIMENTAL PROGRAM

2.1 Segmental Concrete Unit

A newly designed segmental unit system is used in this research. The innovated concrete unit is named as I-Block due to its geometrical shape (Figure 1). The I-Blocks are wet cast masonry units made from 30N/mm² concrete, which consist of one centre web and a tail/rear flange that is extended beyond the web. The rear flange is tapered to allow the blocks to form curve walls.

I-Blocks are flat interface modular concrete blocks, which can be stacked with and without shear connectors. The maximum tapered angle of the I-Block is approximately 11.3°. I-Blocks are double open-ended units and provide a larger hexagonal hollow space in conjunction with two units, and the equivalent hole dimensions are about 450 mm in length, 257 mm in average width and 300 mm in height. Thus, I-Block promotes the increment of wall face area and also minimizes the use of concrete volume. The weight of the hollow block varies approximately 41 to 42 kg. Table 1 summarizes the physical and mechanical properties of the blocks.

2.2 Mechanical Connectors

Galvanized mild steel round bars were used in the study as a rigid mechanical connector that are generally known as shear connectors. According to the hole dimensions of the segmental concrete units, 12 mm diameter bars were selected, and the bars were cut into 125 mm in length. The physical and mechanical properties of the used round steel bars are illustrated in Table 2.

Ultrahigh molecular weight polyethylene (UHMWPE) plastic bars were used in this investigation as flexible connectors because of their toughness and flexibility. UHMWPE has also highest impact strength. White color UHMWPE round bars of 13 mm diameter were used and the parent bars of 1 m in length were cut into 100 mm in length. The physical and mechanical properties of the proposed plastic bars are given in Table 3.

2.3 Test Methodology

A general test setup for interface shear tests with I-Block system is illustrated in Figure 2. According to the test protocols (NCMA SRWU-2, ASTM D 6916-03), two layers/courses of modular block units were used for interface shear tests. The bottom course consisting of two I-Blocks was placed on platform to coincide running joint with the centerline of the horizontal actuator and braced laterally against restraining plate. The back of bottom course was fixed by using a back support beam, which was bolted with platform to stop bending of bottom course during shear testing.

Surcharge/Normal load was imposed by vertical actuator only over the top block through stiff rubber mat and simulated an equivalent height of stacked blocks. The shear/horizontal load was applied against the top course and immediately above the shear interface to minimize moment loading at a constant rate of 1 mm/min of horizontal actuator (ASTM D 6916-03). A steel plate with a gum stiff rubber mat was attached to geosynthetic loading clamp (Figure 4.9) to concentrate shearing load only over the centrally installed top block. A horizontal seating load of 0.22kN was applied to the top block to ensure close fitting of the block systems and after that the load and displacement devices were set to zero (NCMA, SRWU-2). The shear displacement and load/pressure reading were continuously measured and recorded during the tests by a data logger. The data were recorded at every 10 second interval.

Tests were continued until failure of shear resistance occurred. To check the accuracy of the test executions, three identical tests were performed at different normal loading conditions. For each test, new shear pins were used. As usually, the blocks used in the tests were new and free from any visual cracks. In order to minimize the use of new blocks for repeated tests, first time tested/used blocks (free from any damage) were reused by interchanging their positions to provide undamaged interface for subsequent testing. The used blocks were interchanged according to clockwise direction started from top block.

Mohr-Coulomb failure criterion (Eq. (1)) was used to find out interface shear capacity at ultimate strength criterion.

$$V = N \tan\lambda + \alpha \quad [1]$$

Where:

V = Interface shear capacity (kPa)

N = Normal stress (kPa)

λ = Angle of friction (deg.)

α = Apparent cohesion (kPa)

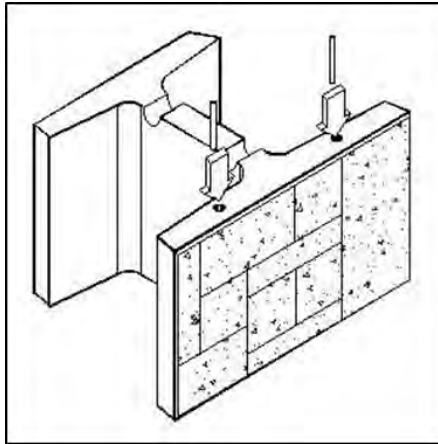


Figure 1. Schematic of I-Block showing shear connectors.

Table 1. Physical and mechanical properties of segmental concrete unit.

Property	Value
Dimensions ($W_u \times H_u \times L_u$) ¹ in mm	375x300x500
Weight (kg)	41- 42
Oven dry density (kg/m^3)	2166
Water absorption capacity (%)	7.1
Moisture content (%)	3.7
Net compressive strength (MPa)	8.0

¹ W_u = Width (Toe to heel), H_u = Height, L_u = Length (Parallel to the wall face)

Table 2. Physical and mechanical properties of steel bar.

Property	Value
Yield strength (MPa)	347
Modulus of elasticity (MPa)	200,000
Elongation (%)	34
Density (kg/m^3)	7,850
Cross section area (mm^2)	113.10

Table 3. Physical and mechanical properties of plastic bar.

Property	Value
Yield strength at 23°C (MPa)	22
Modulus of elasticity (MPa)	750
Elongation at break (%)	>300
Charpy impact strength (kJ/m^2)	No break
Density (kg/m^3)	940
Cross section area (mm^2)	127.66

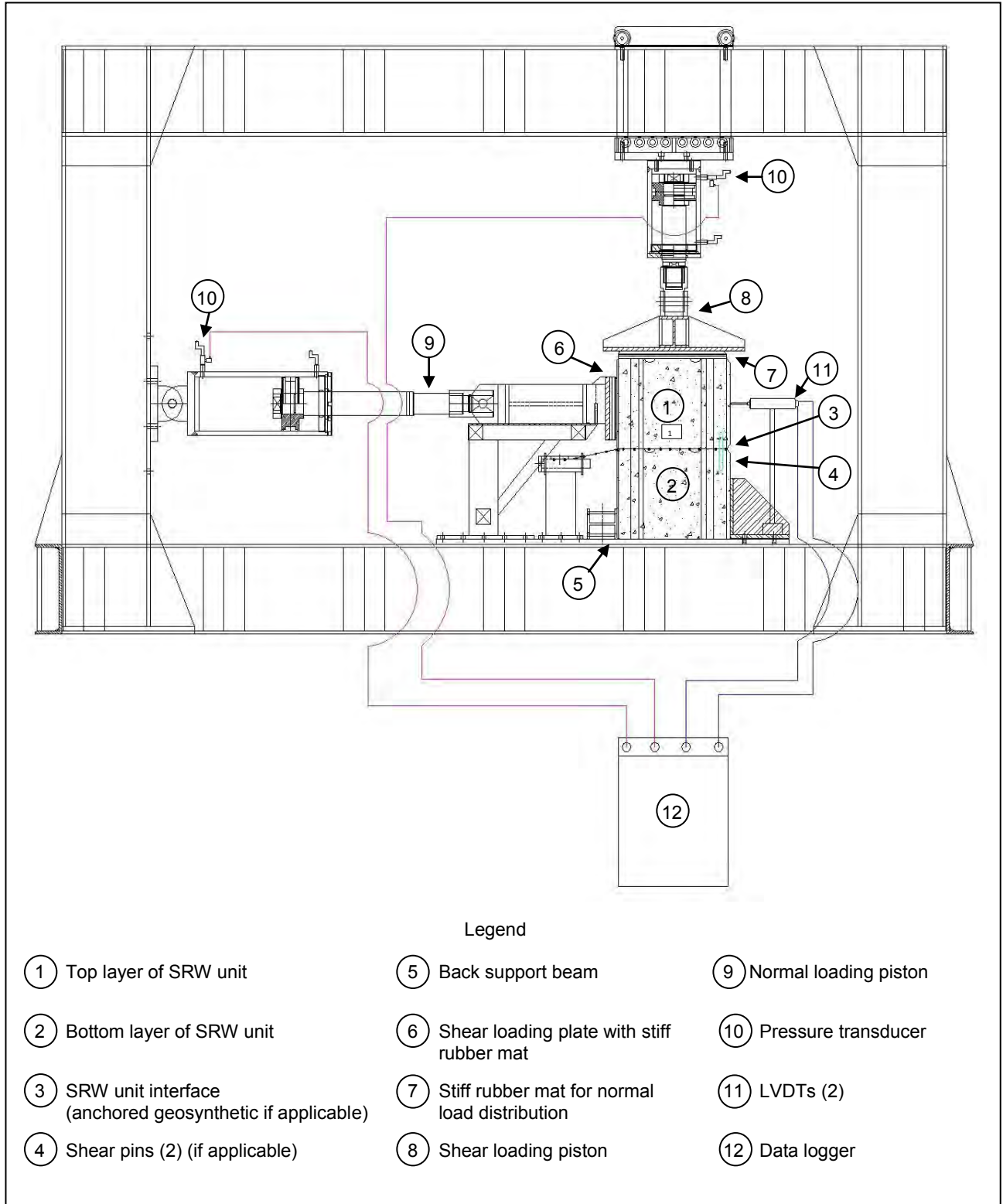


Figure 2. Generic interface shear testing arrangement.

3. TEST RESULTS AND DISCUSSIONS

The curves of Figures 3 to 5 illustrate the frictional behavior of the hollow block system for different surcharge (normal) pressures and different types of shear pins of different rigidities. The variation in normal stress increments among the test series was due to the manual controlling of normal pressure by using a pressure adjustment knob.

For the purely friction condition (without shear connectors), the curves illustrate the rapid increase of shear stresses at the early stage of load application. It may be happened due to frictional resistance of plain concrete surfaces. After reaching the maximum shear resistance, it heads towards almost a constant value with the mobilization of block.

Although, the curves show abrupt rise and fall of shear stresses with displacement for high normal stresses that may be resulted from frictional interlocking of irregular contact areas at block's interface. At the time laboratory testing, it was also observed that sudden fall of shear stresses happens due to insignificant spalling of flanges (front and rear) of top block at the interface.

The increasing patterns of shear stress at the beginning for test with plastic pins show almost similar patterns as described for purely frictional conditions but shear strength heading towards a higher maximum value with the lateral displacement and then decrease gradually with the mobilization of block. Although, the initial shear resistance is controlled by concrete-to-concrete surface friction, the presence of flexible shear pins provides additional shear resistance to the block interface. From the curves for plastic pins, it is seen that shear resistance drops gradually after a significant amount of displacement and heading towards purely frictional shear resistance. It occurs due to the pure shear failure of flexible connectors after certain amount of displacement.

For the tests with steel pins, the curve shows a typical saw-tooth pattern of shear stress after a small amount of displacement. Due to the presence of rigid pins (steel), shear stress increases sharply to a lower maximum value and then drops insignificantly. It was observed that the small drop of shear stress corresponded to the initiation of cracks at the running joints and/or insignificant spalling at flanges and joints. Due to progressive failure patterns of blocks, shear stress reaches the higher maximum value and then drops significantly (Figure 4).

The cracks at the running joints of blocks occurred due to stress concentration generated by steel (rigid) pins and propagate with displacement. In some cases, it was observed that both joints do not fail together due the block setup and block geometry. As a result, after failure of one joint shear resistance increase again and dropped permanently after complete failure of both joints (Figures 3 and 5). Due to the high stiffness, steel pin does not fail in shear but just bends slightly at high shear force.

The plots presented in Figure 6 illustrate the peak (ultimate) shear capacity envelopes for different types of shear connectors with different flexibilities. It is clear from the Figure 6 that the shear capacities of blocks with shear connectors are higher than those without shear connectors (purely frictional interface). Bathurst and Simac (1997) and Bathurst et al. (2008) reported the similar effects of mechanical interlocks or connectors on interface shear capacity for different type of block geometries. The initial peak capacity of block with steel pins is relatively higher at low surcharge pressures but the capacity significantly reduced at high normal stress than those with plastic pins. This happened due to rigidity and strength of steel pins that caused the concrete to break at small displacement (<6 mm) and reduced the area of contact significantly at high normal stress although rigid pins provided a higher apparent cohesion (normal stress-independent shear strength) than flexible plastic pins.

Shear pins are one type of mechanical connectors used to align the blocks and to provide additional interlocking to the wall system as well. If they are too rigid and strong it can damage the block at relatively small displacement and consequently reduce the interface shear capacity.

It can be said that shear pins especially flexible pins deliver more effective shear connection than purely frictional interfaces and even rigid pins (steel).

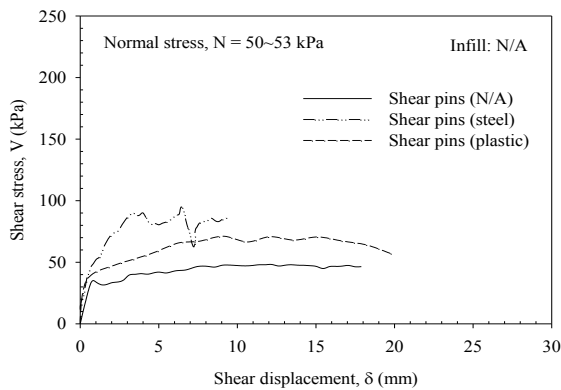


Figure 3. Shear stress versus displacement.

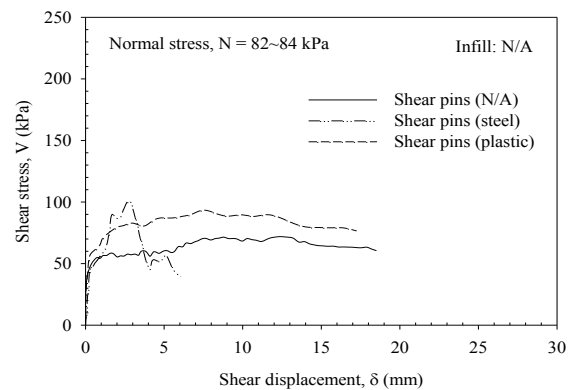


Figure 4. Shear stress versus displacement.

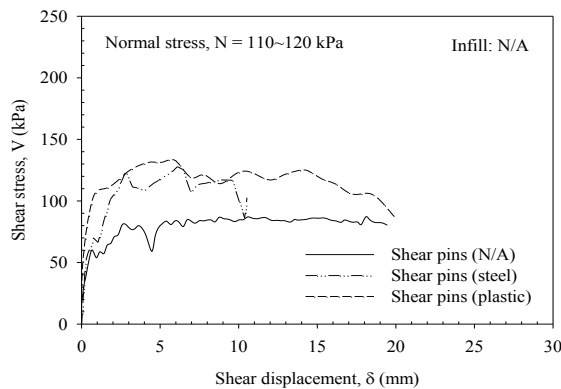


Figure 5. Shear stress versus displacement.

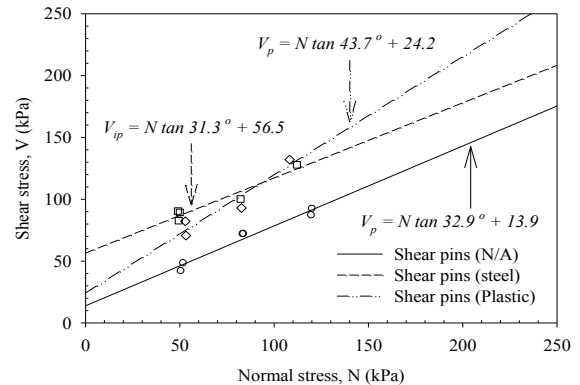


Figure 6. Shear stress versus normal stress.

4. CONCLUSIONS

Mechanical shear connectors have great influence on interface shear capacity of facing units although their principle purpose to help out unit alignment and control the wall facing batter (Bathurst and Simac, 1997 and Bathurst et al., 2008). This investigation divulges that the presence of connectors influence the interface shear capacity depending on the nature of the connectors i.e. rigid or flexible. In this study, two types of shear pins (steel and plastic) were used and the effects of the rigidity of those shear pins are summarized as follows:

- Shear pins increase the interface shear capacity of facing units by providing additional interlocking between the layers of those segmental concrete blocks.
- Steel shear pins initially increase the shear strength (initial peak capacity) than purely frictional capacity of empty block system and eventually decreased the shear strength after a small displacement.
- Flexible connectors provide higher interface shear capacity. Plastic shear pins allow the full mobilization of the interface shear capacity of the block system by failing itself in clear shear.
- The segmental block system with or without plastic shear pins easily follow serviceability criterion but the system with steel pins are unable to follow that criterion because these rigid pins breaks the block before serviceability deformation (6 mm for I-Block wall).
- Although, plastic and steel pin were used as shear transferring device in this study to provide additional interlocking for the empty block system but it is seen that plastic pin provides a better and effective shear connection to the block system in respect to shear strength and serviceability criterion.

ACKNOWLEDGEMENTS

The authors are grateful for the support provided by Soil & Slope Sdn Bhd in Malaysia. The financial support for this study was provided by a grant (Fundamental Research Grant Scheme - 2010) from the Ministry of Higher Education of Malaysia awarded to the first author.

REFERENCES

- Ali, F.H., Bhuiyan, M.Z.I. and Salman, F.A. (2011). Effects of mechanical connectors on the interface shear capacity of segmental - concrete blocks in-filled with gravel, *International Journal of Civil Engineering and Building Materials*, 1: 9-16.
- ASTM D 6916. Standard Test Method for Determining The Shear Strength Between Segmental Concrete Units, *American Society for Testing and Materials*, West Conshohocken, Pennsylvania, USA.
- ASTM D 448. Standard Classification for Sizes of Aggregate for Road and Bridge Construction, *American Society for Testing and Materials*, West Conshohocken, Pennsylvania, USA.
- Bathurst, R. J. and Simac, M. R. (1994). Geosynthetic reinforced segmental retaining wall structures in North America. Proceedings of the *Fifth International Conference on Geotextiles, Geomembranes and Related Products*, Singapore, pp.1-41.
- Bathurst, R. J., and Simac, M. R. (1997). Design and performance of the facing column for geosynthetic reinforced segmental retaining walls. In J. W. Balkema, (ed), *International symposium on mechanically stabilized backfill*. Denver, Colorado, pp.193-208.
- Bathurst, R. J., Althoff, S. and Linnenbaum, P. (2008). Influence of Test Method on Direct Shear Behavior of Segmental Retaining Wall Units. *Geotechnical Testing Journal*, 31, 1-9.
- Elias, V., Christopher, B.R. and Berg, R.R. (2001). Mechanically stabilized earth walls and reinforced soil slopes: Design & construction guidelines, FHWA-NHI-00-043, National Highway Institute, Federal Highway Administration, Washington D.C., USA.
- National Concrete Masonry Association (1997). Design manual for segmental retaining walls, 2nd ed., Herndon, Virginia, USA.
- NCMA, SRWU-2 (1997). Determination of shear strength between segmental concrete units. *National concrete masonry association* (NCMA), Herndon, Virginia, USA.

Geocells Reinforced with Geogrids is the Winning Solution for Repairing Landslides in Hawaii

Todd D. Wentworth, P.E., L.G.

AMEC Environment & Infrastructure, Bothell, WA, todd.wentworth@amec.com

Eric T. Reitter, P.E.

AMEC Environment & Infrastructure, San Diego, CA, eric.reitter@amec.com

ABSTRACT

Six landslides occurred on military service roads during a 40-day rain storm in 2006. Surface water runoff on the roads triggered embankment failures in clayey silt fill soils and saprolite. When the USACE advertised the design-build project, their conceptual repair only considered structural walls supported with vertical piles.

The selected design-build team determined that mechanically stabilized earth (MSE) walls could be constructed less expensively, quicker, and more safely than cast-in place walls resting on steel piles. The project saved \$1.5 million (approximately 50% of the project cost) by constructing MSE walls with cellular confinement (geocell) facing and geogrid reinforcement, instead of the conceptual design provided with the Request for Proposal (RFP) documents.

Geocells were selected as the MSE wall facing due to their light weight, ease of installation with relatively small construction equipment, tolerance to differential settlement, and cost compared with traditional pre-cast products and cast-in-place construction methods. Additionally, the green geocell facing blended into the lush tropical vegetation of the ravine.

1. INTRODUCTION

This design-build contract managed by the US Army Corp of Engineers (USACE) included repairing six landslides along two roads that contour down both sides of a ravine within the Wheeler Army Airfield, located in the middle of the island of Oahu, Hawaii. The six landslides occurred during the winter of 2006, during what was known as the "40 day rainstorm." During the storm, surface water from the runway and adjacent areas flowed down the roads and overfilled the storm drain system. Uncontrolled surface water flowed over the roads and down into the ravine below the roads causing severe erosion at the six sites as well as other locations.

The RFP documents included site plans with limited topography, cross-sections, photographs, and some limited geologic information. The requested repairs included constructing retaining walls, restoring the paved driving surface, adding guard rails, replacing and improving stormwater drainage controls, and replacing damaged electrical lines.

2. SITE CONDITIONS

The landslides appear to have been debris avalanches that developed into debris flows (Turner and Schuster, 1996). The failures occurred in road fill, existing colluvium on the slopes, and erosion into the native soils. The primary cause of the damage was due to uncontrolled surface water runoff causing severe erosion and hydraulic excavation. Each of the landslides were located where surface water flowed over the side of the road causing severe erosion in the embankment fill. The landslide scarps at all six sites were similar. The vertical scarps were 1.5 meters (m) to 3.7 m deep directly below the road. Hydraulic excavation had created steep gullies that drained to the main ravine. The bottoms of the gullies were 6 m to 12 m below the road and had accumulations of colluvium and slide debris within them. Photograph 1 shows the landslide scarp at Site 4.



Photograph 1. Landscape Scarp at Site 4.

2.1 Exploratory Methods

The RFP documents provided preliminary topography, borings drilled near two of the six landslides, laboratory test results of soils collected from the borings, photographs of each site, and a geologic cross-section of each site based on visual observations during a site reconnaissance. Four additional explorations were drilled on the road near the landslides that had not been drilled previously.

Drilling at the toe of the slopes was considered, but it was determined to be too difficult to drill below the steep landslide scarps in a safe manner. The main goal of drilling below the scarps was to determine the thickness of loose slide debris that would need to be removed. Since this could not be determined prior to construction, the volume of excavation and export, as well as the subgrade elevation of the walls would need to be determined during construction. This, however, was acceptable, since this was a design-build project.

2.2 Soil Conditions

The site vicinity is characterized by pahoehoe lava flows from the Koolau Volcano, known as the Koolau Basalt. Weathering of the Koolau Basalt has developed two soil types classified as saprolite and residual soil. Saprolite is a soil that exhibits relic structure of the basalt. Vesicles and joints may be visible due to color differences in the soil. The saprolite consists of stiff to hard clayey silt with variations in color and mottling. Residual soils are the result of a greater degree of weathering of the basalt so that the rock structures are no longer present. The soil is stiff to hard, brown and red, clayey silts. The Koolau Basalt and the saprolite and residual soils derived from it are known for high shear strengths (Sherrod et al., 2007).

The borings drilled at each site and the soils observed in the scarps documented road fill, residual soils, and saprolite derived from vesicular basalt. Geotechnical laboratory tests revealed that the residual soils and saprolite are generally high plasticity silt with moisture contents near their plastic limit. The laboratory strength tests results showed large variations, at least partially due to the difficulty of collecting and testing very stiff soils. Based on observations of exposed soils, drilling and sampling results, and laboratory testing, the soils possess high shear strengths. Figure 1 is a geologic cross-section from Site 4 that illustrates AMEC's stratigraphic interpretations, which was similar to all six sites.

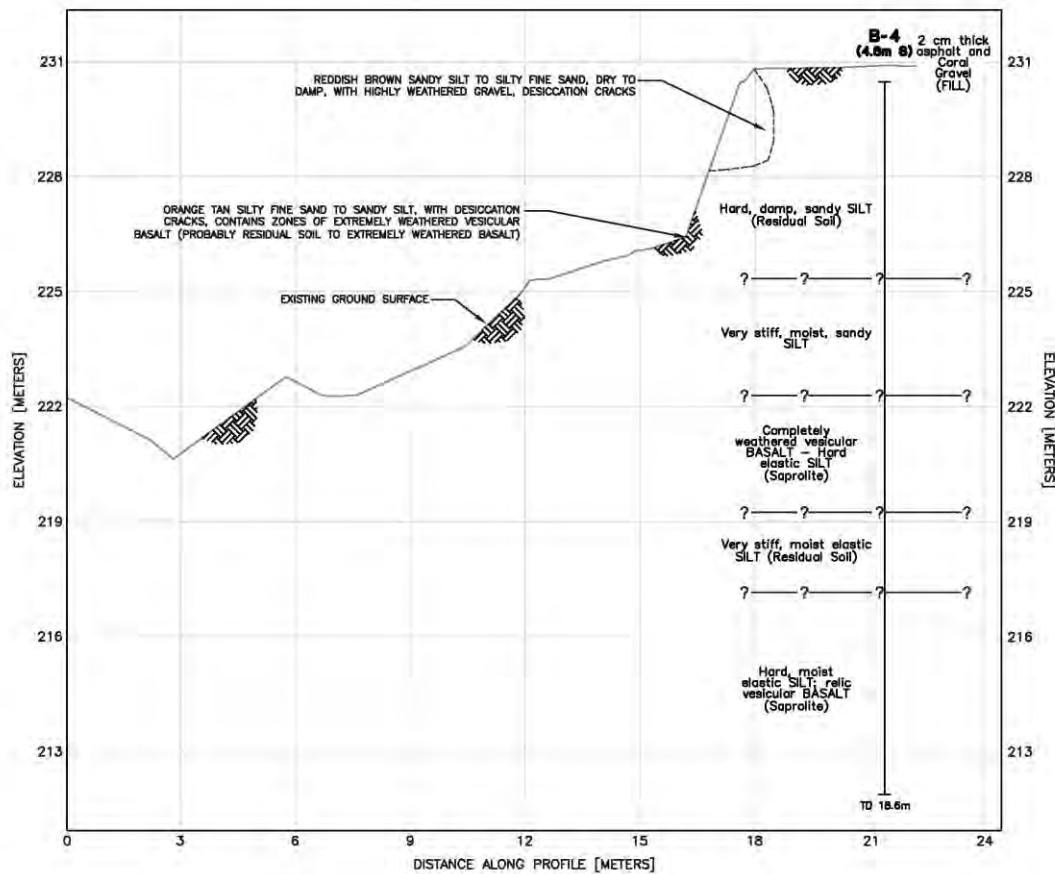


Figure1. Site 4 Geologic Cross-Section.

2.3 Groundwater Conditions

Explorations were drilled during both wet weather (January and February 2010 by others) and dry weather (October 2010) and none of the borings encountered groundwater. Groundwater was not encountered during construction (December 2011 and January 2012).

3. DESIGN

Three conceptual retaining wall options were included in the RFP for restoring the roads. The first concept used a cast-in-place concrete wall supported with micropiles; the second option used micropiles, a shotcrete wall face, and a cast-in-place concrete drive slab; and the third option used drilled shafts, steel H-beams as soldier piles, and pre-cast concrete panels for lagging (Figure 2).

The selected design-build team determined that pile structures were too expensive and too difficult to construct safely near the edge of the landslide scarps. Access would have been difficult for the large equipment needed for the steel pile and concrete wall concepts. The team decided that mechanically stabilized earth (MSE) walls could be constructed less expensively, quicker, and more safely. Rock slopes and reinforced soil slopes were also considered; however, the toe of the slopes would have extended beyond allowable construction limits into wetland areas for most of the sites. A rock slope was used to restore Site 6, the smallest of the landslides, with minimal site impacts. Gabion basket gravity walls were considered, but the baskets were not readily available on the island and they would have been susceptible to corrosion in the highly humid tropical environment. Stacked geocell facing with geogrid reinforcing layers were selected for their design advantages, constructability, and availability on the island for five areas.

The proposed walls were located close to the previous edge of the road shoulder due to the construction limits and access limitations. Furthermore, due to the depth of the landslides, a large amount of temporary excavation was necessary to access the base of the wall, allow room for the geogrid reinforcements and create a safe slope for workers (Photograph 2).

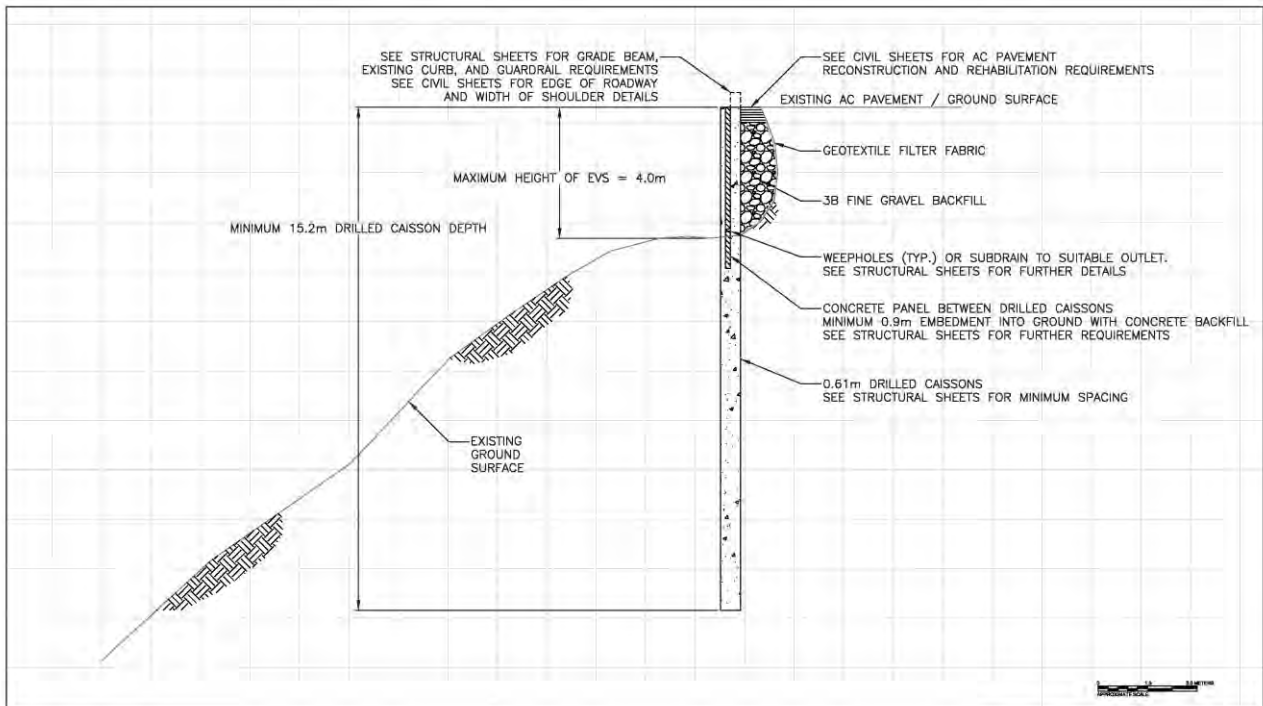


Figure 2. Conceptual Walls.



Photograph 2. Site 1 Excavation, Total Depth of 6.1 meters.

3.1 Slope Stability Analyses

The safety factors against sliding for trial failure surfaces were high for any deep-seated failures when the failed slopes were analyzed. Based on this evaluation, it appeared that the landslides that occurred at each of the six sites was the result of erosion, and there was no indication of deep-seated slope instability. This analysis gave the team confidence that the original concept of structural walls supported by piles was not necessary and an excessively costly repair given the site conditions. Our estimated values of internal friction angle, cohesion, and density for each soil layer are listed in Table 1 below. These conservative values are based on exploration information, laboratory testing, and slope stability calibration.

Table 1. Estimated Values of Internal Friction Angle, Cohesion, and Density for Each Soil Layer.

Geologic Name	Soil Type	Unit Weight (kN/m ³)	Internal Friction Angle (degrees)	Cohesion (kPa)
Fill, Colluvium and Slide Debris	Silt with gravel	16.5	28	0
Residual Soil	Highly plastic Silt	18	36	0
Saprolite	Highly plastic Silt	18	34	4.8

3.2 MSE Wall Design

Project specific external loads on the walls included a traffic live load on the road above the walls and seismic horizontal acceleration coefficient, as well as the lateral earth pressure from the retained soils. The traffic live load was modeled as an additional 0.61 m of soil (12 kPa) placed on the roadway, as specified by AASHTO (2002, 2010) and FHWA (2001) design manuals. A peak ground acceleration of 0.18g was used for the seismic stability analysis, as recommended by Hawaii Department of Transportation (HDOT, 2005). Global stability of the retaining walls determined the embedment depth of the wall and the minimum length of the geogrid reinforcement. Internal and external stability analyses determined the geogrid strength and spacing for the walls.

3.3 Wall Components

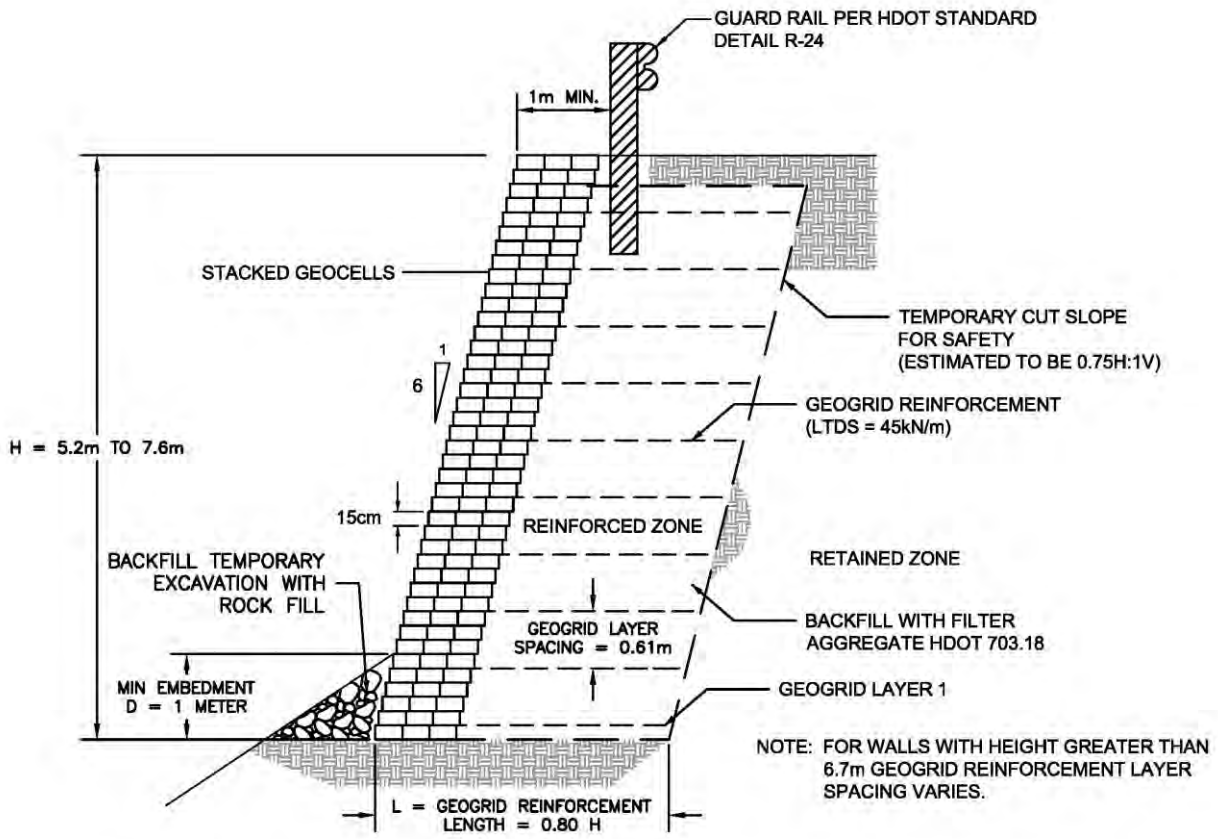
The geocells consisted of polyethylene, stabilized for ultraviolet light and corrosion, forming cells that were 27 cm long by 33 cm wide by 15 cm high when expanded. The geocells were delivered in sections 0.80 m wide by 2.6 m long. Each course of geocells were stacked with a 2.5 cm setback from the course below, to achieve a batter of 1H:6V. The geogrids consisted of polyester multifilament yarns woven in tension and finished with a PVC coating and had a long-term design strength (LTDS) of 45 kN/m. The LTDS is determined by reducing the ultimate tensile strength to account for potential material degradation. Both the geocell infill and the wall backfill material was a crushed and screened gravelly sand, meeting the HDOT 703.18 Filter Material specification (2005), which had a maximum grain size of 4 cm and less than 5 percent fines (Photograph 3).

Geogrid lengths were approximately 80 percent of the total wall height and spaced every 0.61 m (four stacked geocells), except for walls greater than 6 m tall, in which case the geogrid spacing was less for the lower portion of the wall.

The walls were embedded a minimum of 1 m into the intact soils. This embedment is deeper than typical installations due to the falling foreslope and desire to ensure global stability. The typical design cross-section (Figure 3) displays the wall components.



Photograph 3.Site 1 Backfilling.



TYPICAL REINFORCED GEOCELL RETAINING WALL SECTION
NTS

Figure 3. Design Cross-Section.

3.4 Other Design Considerations

This paper is focused on the use of geogrid reinforced geocell retaining walls, however it should be noted that there were other design and construction tasks. Surface water drainage improvements were an important component of the project in order to reduce the risk of future erosion. The project also included repairing electrical service that had been lost due to the landslides.

4. CONSTRUCTION

The advantages of geogrid reinforced geocell walls quickly became evident during construction. The light-weight materials are easier to transport; less expensive to ship to Hawaii, and easier for laborers to carry and assemble at the wall location than typical precast blocks or cast-in-place construction. The light-weight, flexible facing tolerates settlement better than heavier, rigid facing elements. It is also very easy to adjust the facing during construction to accommodate actual site conditions and the specified wall position tolerances. Since the geocells are 15 cm high, the backfill lifts are always 15 cm thick, never more. The thin lifts ensured that sufficient compaction (95%) could be achieved with relatively small equipment.

There were several advantages over the conceptual steel pile and concrete walls including:

- All of the materials could be easily and cost effectively transported;
- No need for a drill rig and a crane, and the contractor did not need to provide access for a concrete truck. The heaviest equipment near the edge of the landslides was the bucket of the tracked excavator.
- Geosynthetics are not corrosive, which was an important consideration in a tropical environment.

- The outer edge of the geocells will eventually become vegetated blending the wall into the tropical environment. In addition, the green colored geocells initially blended in with the lush vegetation of the ravine, even without becoming vegetated (Photograph 4).



Photograph 4. Site 4 Near the End of Construction.

5. COMPARING COSTS

The engineer's cost estimate for the design-build RFP was approximately \$5 million, based on the conceptual steel pile and concrete retaining walls. The selected design-build team completed the project for approximately \$2.9 million by constructing geocell faced walls with geogrid reinforcing and drainage improvements instead of the conceptual walls presented in the RFP. Excavation costs were about \$970 per square meter of wall face, and the wall construction with imported gravel backfill was \$3,200 per square meter of wall face. These unit costs will appear high compared with typical reported construction costs for MSE walls, which is due to the following factors:

- The project was on Oahu, an isolated island with limited competition, a high cost of living, and where all supplies and equipment must be shipped ahead of time.
- The project was competed under a federal contract that required contractors to be experienced with additional procedures and reporting requirements.
- Site access constraints allowed only one wall to be constructed at a time resulting in reduced economies of scale and concurrent activity scheduling instead of simultaneous.
- The five walls were tall, ranging from 5.2 m to 7.6 m deep, but short in length. The total wall face area for each wall ranged from 49 m² to 93 m², for a total of 330 m² of wall facing.

6. CONCLUSIONS

This case history demonstrates the advantages of using geosynthetics for retaining wall components in difficult access conditions, and the advantage of the design-build contracting process. The design-build team repaired the landslides using safer, lighter, greener and less expensive materials than the original concept of steel pile supported concrete walls, saving approximately \$1.5 million in the process.

Geocells reinforced with geogrids were the winning solution for repairing the landslides at these difficult access sites.

- The lightweight materials were easy to transport to the project and were easy to carry and place in position.
- Only small, light-weight equipment was needed to construct the walls.

- The geosynthetic materials allowed for flexibility in the layout of the walls and tolerance to differential settlement.
- Geosynthetics were non-corrosive, important in tropical environments.
- The green geocell facing blended into the tropical vegetation surrounding the walls.
- The materials and construction methods allowed for a cost effective method of repairing the failed slopes.

ACKNOWLEDGEMENTS

We would like to acknowledge design-build team leader and general contractor, Hal Hays Construction, who deserves credit for selecting, bidding and constructing a different wall design than shown in the RFQ. The earthwork contractor Koga Engineering did a terrific job of constructing their first reinforced Geoweb retaining walls. Presto Geosystems were very helpful with design and construction support, and they supplied Geoweb cellular confinement system components. Last but not least, we acknowledge the rest of the AMEC Environment & Infrastructure staff who worked on this project.

REFERENCES

- AASHTO LRFD Bridge Design Specifications, 5th Edition, 2010, American Association of State and Highway Transportation Officials, Washington D.C..
- AASHTO Standard Specifications for Highway Bridges, 17th Edition 2002, American Association of State Highway and Transportation Officials, Washington, D.C.
- FHWA Mechanically Stabilized Earth Walls and Reinforced Soil Slopes Design and Construction Guidelines, 2001, Publication No. FHWA-NHI-00-043.
- Hawaii Department of Transportation Standard Specifications, 2005.
- Sherrod, D., Sinton, J., Watkins, S., and Brunt, K. (2007) *Geologic Map of the State of Hawaii, Sheet 3 – Island of O’ahu*, U.S.G.S. Open File report 2007-1089.
- Turner, A. and Schuster R. Editors (1996) *Landslides Investigation and Mitigation*, Special Report 247, Transportation Research Board, National Academy Press, Washington D.C., USA.

Geomembrane Surficial Landfill Gas Collection Systems

C M. Richgels, P.E., Agru-America, Inc., USA, crichgels@agruamerica.com
M. Ayers, P.E., Closure Turf, Inc., USA, mayers@closureturf.com
D. Lewis, Closure Turf, Inc., USA, dlewis@closureturf.com

ABSTRACT

Typical final cover systems can be damaged by differential settlement during postclosure, can suffer from slope veneer failures, and experience strain of the geomembrane beyond allowable yield with development of excessive landfill gas (LFG) pressure beneath geomembrane barrier layers.

Given the risks with standard final cover systems, additional design elements have been recommended for use in final cover systems. For example, use of sub-barrier layer LFG collection has been recommended by Thiel (1998) and Richardson (2000) to control LFG pressure beneath geomembranes to improve stability. Exposed geomembranes have been suggested for consideration by Koerner (2010) as a temporary final cover system until the deleterious effects of landfill differential settlement, and LFG generation with the attendant slope stability risks, have reduced in the initial postclosure period. In addition, geosynthetic material can be used in substitution for typical LFG control devices being used today.

This paper discusses a new alternate final cover system which can best be described as a geosynthetic final cover system. It consists of a sand ballast layer placed on a specialized HDPE artificial grass tufted into a double layered polypropylene woven geotextile. This assembly is deployed across a structured geomembrane that provides a sub drainage layer beneath the turf component. This hybrid Final Cover system (trade name "Closure Turf®") can provide designers with an alternative LFG collection system that can significantly reduce requirements for more costly and easily damaged vertical LFG extraction wells for energy recovery projects. In combination with two other geosynthetic based LFG collection systems, an Integrated LFG Collection System can be deployed at modern sanitary landfills with geosynthetic materials.

1. INTRODUCTION

This surficial LFG collection system can be combined with vacuum application to geosynthetic leachate collection and removal systems (LCRS), and placement of geosynthetic LFG strip collectors in the active landfill areas. These geosynthetic applications may be used in substitution for typical vertical LFG extraction well systems. The location of these applications is depicted in Figure 1. There are three general locations where geosynthetic materials could be applied as LFG collection layers:

1. A surficial collection layer beneath the geosynthetic final cover system.
2. Geosynthetic collection strips in active landfill areas.
3. Geosynthetic leachate collection and removal system (LCRS) layer at the landfill base.

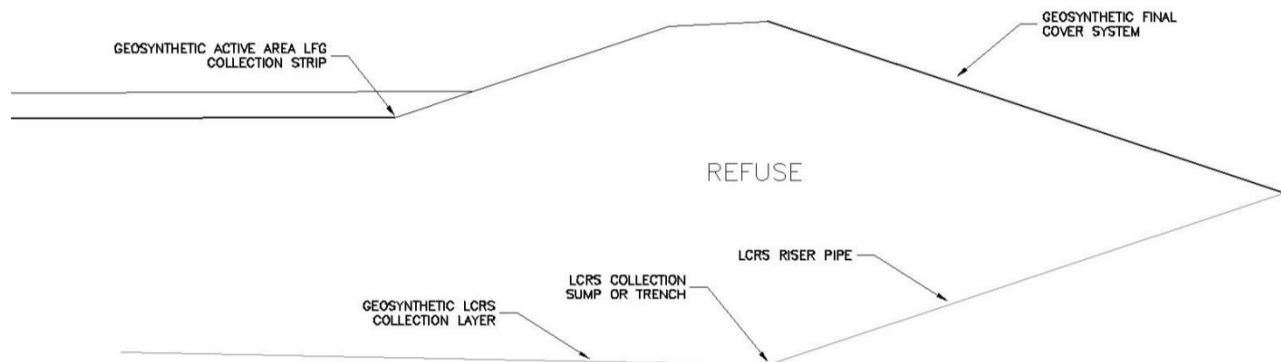


Figure 1. Locations for LFG collection with geosynthetic materials

These applications are discussed below.

2. GEOSYNTHETIC FINAL COVER SYSTEM

The geosynthetic final cover system can be placed in combination with geocomposite collection strips to control LFG beneath the final cover system. This practice has been recommended by Thiel (1998) and others to reduce the negative effects on LFG pressure build-up beneath final cover geomembranes on slope stability. The concept of this system is depicted in Figure 2.

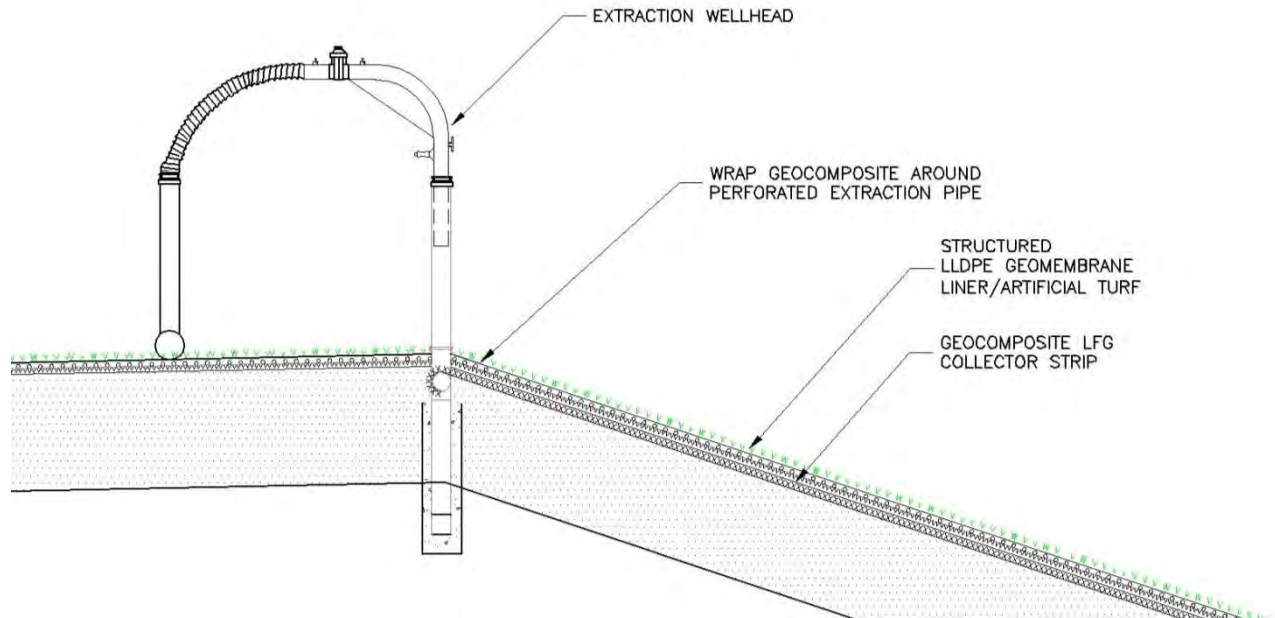


Figure 2. Surficial LFG collection beneath geosynthetic final cover system

In general, a geocomposite strip of an engineered width is placed along the length of the landfill slope. At the top of the slope, the geocomposite is connected to an extraction point - a typical LFG wellhead tapped to a perforated pipe manifold. The geocomposite is wrapped around the perforated pipe manifold and can be secured in place using a gravel backfill. The geosynthetic final cover system is then deployed over the geocomposite collector strip(s) to complete the surficial gas collection system. The configuration shown is proposed for incremental closure construction along the landfill sideslopes.

2.1 Geocomposite Collection Strip Spacing and Flow

Spacing of geocomposite collection strips can be determined based on allowable gas pressures beneath the final cover system. Using an interface shear strength accounting for gas uplift pressure (Equation 1), the allowable gas pressure ($u_{(g\text{-allow})}$) beneath the geosynthetic final cover system can be determined as 60 Pa (at $FS_{allow} = 1.5$).

$$u_{(g\text{-allow})} = h\gamma\cos\beta - \frac{FS_{allow}h\gamma\sin\beta - \alpha}{\tan\phi} \quad [1]$$

From Thiel, LFG flow to geocomposite collector strips can be estimated using Equation 2:

$$U_g x = \frac{Q_i}{A} \frac{1}{k_g t} \gamma_g Lx - \frac{x^2}{2} \quad [2]$$

Where,

- $U_{g(x)}$ = gas pressure, Pa (minimum applied vacuum in this scenario)
- Q_i = LFG flow rate, M^3/sec
- k_g = gas permeability of flow media, m/sec
- t = thickness of flow media, m
- γ_g = gas unit weight, N/m^3
- L = half distance between collection strips, m
- x = distance from collection strip, m

The LFG flow rate, Q_i , is related to the LFG generation rate and the volume of waste where gas is being generated. Q_i is estimated below.

$$Q_i = r_g(t \times L \times 1) \gamma_{\text{waste}} \quad [3]$$

Where r_g is the LFG generation rate and γ_{waste} is the unit weight of the in-place waste. Emcon (1980) estimated r_g at 7 ml/day/kg. Thiel recommended a value of 17 ml/day/kg. The variable t represents the depth of waste generating LFG to be collected by the geocomposite strip. The unit weight of waste can be taken 700 and 800 kg/m³.

The gas unit weight is essentially the combined unit weight of methane (6.54 N/m³) and carbon dioxide (17.9 N/m³). At a nominal mixture of 50/50 in a balanced extraction scenario, $\gamma_g = 12.2 \text{ N/m}^3$.

The gas permeability, k_g , of the flow media is derived from the refuse beneath the slope cover. Emcon reported an intrinsic permeability, k_s , for refuse between 13 and 20 Darcies. Intrinsic permeability is a function of the solid material structure. Gas permeability of the waste can be found by Equation 4.

$$k_g = ks(\gamma_g)/\mu_g \quad [4] \text{ (Kou)}$$

Converting to Darcies to SI units, and using a LFG dynamic viscosity, μ_g , as $1.15 \times 10^{-5} \text{ Ns/m}^2$ (Emcon), k_g can vary from $1.2 \times 10^{-5} \text{ m/sec}$ to $1.8 \times 10^{-5} \text{ m/sec}$.

The slope cover will be too variable in thickness to act as a gas relief layer with any reliability. A refuse thickness, t , of 5 meters is assumed as immediately affected by an applied vacuum from the geocomposite beneath the final cover system. Using an average landfill depth of 30 meters in sideslope areas, it can be assumed that half that depth is generating landfill gas that will be collected by the geocomposite strip before vacuum influence from an active area horizontal collector strip (Section 3), or the LCRS (Section 4 below) compete for the flow.

Substituting Equation 3 into Equation 2 and inserting the highest variable values, $U_g(x)$ every 1 meter along the collector strip can vary according to L as shown in Table 1

Table 1. Surficial LFG Collection System Pressure and Collector Spacing

Collector Strip Half-Distance L (m)	$U_g(x)$ (Pa)
5	3
10	28
15	93
20	220
25	430
30	743

Based on the estimated allowable gas pressure from Equation 1, geocomposite strips would be required every 20-30 meters for natural venting as was discussed by Thiel. For active extraction as considered here, the unit flow (per meter of strip length) towards geocomposite strips placed along a nominal 50 meter long slope spaced every 60 meters, can be calculated using Equation 3 as 71 ml/sec/m (with $r_g = 17 \text{ ml/day/kg}$, $t = 15 \text{ m}$). Or 7,080 ml/sec across the length of the strip (both sides) applying vacuum to an area of 3,000 m².

2.2 Actual Flow Conditions at an Active Landfill

In March 2011, the LFG surficial collection system described above was applied to a partial closure at an active landfill in Missouri. The partial closure area was approximately 40,490 m². The average slope (3H:1V) length in the closure area was 75 meters. A total of eight (8) 1.5-meter wide 5-mm thick single-sided geocomposite strips were placed on this slope at an average spacing of 60 meters. The strips were curled around a perforated pipe collector at the toe of the slope. The perforated pipe was connected to a typical LFG vertical well head as depicted in Figure 2. The well head delivered collected gas to a perimeter header pipe feeding an onsite flare. The lower end of LFG flow from this surficial LFG collection system was measure as of 4.1 ml/sec/m². Applied over an area of 3,000 m² as calculated above, this is equivalent to 12,250 ml/sec, or 1.7 times the estimated flow rate calculated above. Adjusting the calculation method by the actual data suggests applied vacuum from the geocomposite strip may reach as deep as 25 meters into the waste mass.

2.3 Laminar Flow within the Geocomposite Strip

As long as the Reynolds number for gas flow within the geocomposite strip is less than that for the equivalent of a pipe ($Re = 2,000$), laminar flow conditions are expected, therefore the equations above are expected to produce valid estimates. In the application at the Missouri site, the velocity for a 1.5 meter wide, 5-mm thick single-sided geocomposite (assuming very little geotextile intrusion due to the low overburden) is found from:

$$V = Q/A = 12,250/(1.5 \times .005) = 0.17 \text{ m/sec} \quad [5]$$

Reynolds number is then:

$$Re = \frac{\rho v d}{\mu} = (1.24 \text{ kg/m}^3)(0.17 \text{ m/sec})(.005 \text{ m})/(1.15 \times 10^{-5} \text{ N}\cdot\text{s/m}^2) = 92 \quad [6]$$

Use of these equations in the above scenarios is acceptable with this low of a Reynolds number.

3. HORIZONTAL COLLECTION STRIPS IN ACTIVE LANDFILL AREAS

The surficial collection system discussed above can also be expanded for use within the active landfill area to control surface emissions. Installation of horizontal LFG collection wells require landfill operations to move to another location in the landfill. The wells are excavated as trenches across the topdeck surface of the landfill. Excavation spoils and the trench itself release significant amounts of LFG exposing the construction workers and landfill operating staff to health risks that must be controlled with engineered controls and personal protective equipment. Horizontal collection wells can water in with leachate if the bottom of the trench is in contact with previous placed intermediate cover. To avoid these issues, geosynthetic collection strips could be used in lieu of vertical and horizontal LFG collection wells as shown in Figure 3.

A structured geomembrane is available for use in this application. The membrane is a 1.5 mm HDPE geomembrane with 3.3-mm studs on one side of the membrane sheet. The studs with a covering geotextile (underlying in this application) behave similar to a geocomposite collection layer. The horizontal collector strip would be placed over a completed daily refuse cell before daily or intermediate cover soil is placed. First a geotextile would be deployed to prevent fines intrusion into the drainage matrix of the structured geomembrane. The structured geomembrane would then be deployed with studs in contact with the geotextile strip to complete the horizontal collector strip. No seaming equipment would be needed. The materials would simply be rolled out by site labor crews before soil cover was placed. Site personnel would not be in contact with exposed waste as they would walk behind the rolls as they rolled them out.

This placement method would allow for the horizontal collector strip to draw LFG from the refuse lift below, out to a distance L , depending on the spacing of the strips and the refuse gas permeability. This construction technique also would reduce the potential for watering in the collector strip as percolating fluids from above lifts would be diverted to either edge of the collector strip and continue downward in contrast to fluid gathering in the gravel backfill of a horizontal collection well. No refuse excavation is required, and normal cover operations can be completed immediately after the geotextile and structured geomembrane collector strips are deployed.

Laboratory performance data for this material is typically reported only for hydraulic properties. This material has a tested hydraulic transmissivity value of $5.4 \times 10^{-3} \text{ m}^2/\text{sec}$ at an applied normal load of 250 KPa, and a flow gradient of 0.1 (applicable for a near horizontal application). The hydraulic permeability, k_w , of the material is simply the transmissivity divided by the stud height of 3.3-mm, or $k_w = 1.6 \text{ m/sec}$. The gas permeability of the structured drainage geomembrane can be found by Equation 7.

$$k_g = k_w \frac{\mu_w \gamma_g}{\mu_g \gamma_w} \quad [7]$$

With μ_w equal to $1.01 \times 10^{-3} \text{ N}\cdot\text{s/m}^2$ and γ_w at $9,797 \text{ N/m}^3$, k_g is found as 0.17 m/sec.

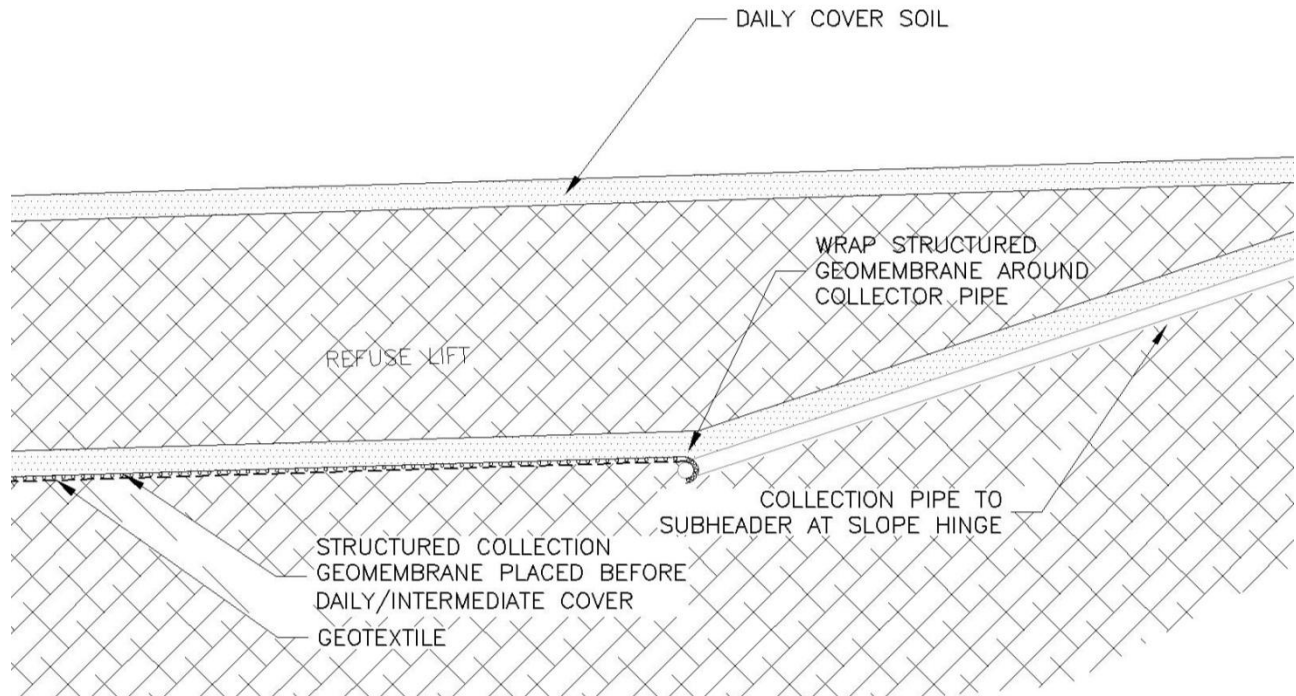


Figure 3. Conceptual Horizontal Geosynthetic Collection Strips

For flow within the refuse mass, Equation 2 is reapplied to create Table 2 for a 1.5-m wide, 90-m long horizontal structured geomembrane LFG collection strip, placed over a refuse lift 9-meters thick (t), approximately 30 meters below grade.

Table 2. Horizontal LFG Collection Strip Pressure and Collector Spacing

Collector Strip Half-Distance L (m)	Ug(x) (Pa)
5	1
10	8
15	26
20	63
25	122
30	212

The calculation in Table 2 assumed a lower intrinsic permeability in the waste mass of 13 darcies due to the much higher overburden stresses. From Equation 3, the corresponding flow in the horizontal strip collector will be 7,650 ml/sec.

3.1 Laminar Flow Conditions within the Horizontal Collector Strip

Using Equation 5 and substituting the values for this application, the flow velocity within the horizontal collector strip is found to be $v = (7,650 \text{ ml/sec}) / (1.5 \text{ m})(.0033 \text{ m}) = 1.5 \text{ m/sec}$.

Using Equation 6, the corresponding Reynolds number is 550 which is higher than the surficial collection strip discussed above. Still, this number suggests spacing between horizontal collector strips can be increased and still satisfy laminar flow requirements within the collector itself. Additionally, the collector strip could be widened to reduce flow velocity within the system, thus reducing losses due to turbulence. This geosynthetic system requires testing in an active landfill to measure actual performance against that predicted in this paper.

3.2 Horizontal Collection Strip Replacement

Horizontal collection strips will be temporary by their very nature. As succeeding lifts of waste are placed over them, additional collector strips are added in those overlying lifts reducing the importance (as well as function) of the initial

collector strip. Fortunately, the strips would be very cost effective in comparison to typical horizontal well construction. Also the topmost strip is what is required for surface emissions control. Deeper strips would have decreasing importance for this function as additional waste lifts are placed.

4. LCRS LFG EXTRACTION

Typical LCRS installations are either gravel collection layers above a primary geomembrane liner or geocomposite drainage layers replacing the gravel. A cross section of a collection trench in the LCRS is depicted in Figure 4.

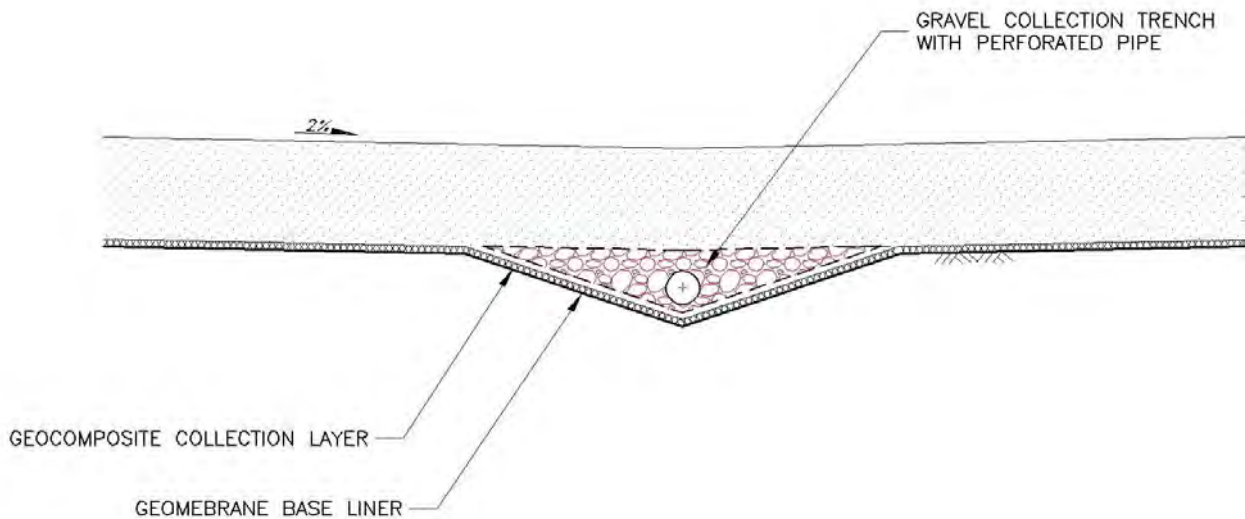


Figure 4. LCRS Collection Trench

Base liner grades are typically designed using a herringbone pattern with multiple ridges and troughs directing leachate flow to the troughs. The base liner grades are typically 2% towards the trench as depicted in Figure 4. The collection troughs are sloped at a nominal grade between 0.5% and 1% to a LCRS sump where leachate is mechanically removed. The typical design distances from trough to ridge can be approximately 30 to 45 meters.

As leachate begins percolating down through the waste mass, the saturation of the operations soil layer will increase thereby impeding landfill gas migration into the LCRS system. The operations layer will not become fully saturated, however, thereby allowing some buildup of LFG pressure in the LCRS system. This pressure can cause surface emissions near LCRS clean out pipes and extreme venting of LFG when the LCRS pipes are opened for system inspection, exposing maintenance workers to hazardous gases and vapors. Pressure build-up in the LCRS can also increase the risk of LFG migration out of the landfill into the surrounding soil. Migration of LFG through the geomembrane is a much more likely scenario for landfill contaminant release than that risk posed by leachate leakage. Fortunately, LFG risk is also easier to control with active application of LFG system vacuum to the LCRS (Richgels 2000).

To avoid hydraulic blockage in the LCRS sump, LFG collection system vacuum can be applied to LCRS system cleanout pipes that are placed in the collection troughs away from the sump. The flow characteristics allow that system vacuum to quite effectively spread applied vacuum across the entire floor of the base liner. The authors are aware of at least one such application that produced an average LFG flow of $0.25 \text{ m}^3/\text{min}/\text{ha}$ with an average applied vacuum of 6.35 KPa across a 0.3 meter thick gravel LCRS. Back-calculation of Equation 3 indicates gas collection under this scenario may only be from a refuse thickness, t , of 2.7 meters versus the initial assumption of 15 meters. Given the applied vacuum, this confirms the operations soil layer has a significant degree of saturation.

Geosynthetics, being thinner, may not perform as well. Using the flow and refuse thickness variables from the gravel LCRS scenario above, we can estimate the applied vacuum coverage from the LCRS clean-out pipes into the field of a geocomposite LCRS using Equation 2. For a 5-mm geocomposite, typical transmissivity values are reported as $1 \times 10^{-4} \text{ m}^2/\text{sec}$ with a 480 KPa normal load and a gradient of 0.1. These are appropriate conditions for a base liner application. Reducing the geocomposite thickness by a factor of 0.25 to allow for compressive loss in thickness, the resulting hydraulic conductivity of the geocomposite is $2.67 \times 10^{-2} \text{ m}/\text{sec}$. Using Equation 7 again to estimate gas permeability as

2.9×10^{-3} m/sec, and then substituting into Equation 2, distance from the trough to ridge for varying pressure is shown in Table 3.

Table 3. LCRS Trough-Ridge Distance, Applied Pressure, Geocomposite Thickness

Trough-Ridge Distance L (m)	Ug(x), 5-mm Geocomposite (Pa)	Ug(x), 7.5-mm Geocomposite (Pa)
5	7,799	584
10	62,394	4,675
15	210,579	15,780
20	499,149	37,404
25	974,901	73,055
30	1,684,628	126,238
35	2,675,127	200,462

This is too restrictive in some base liner designs with greater trough-ridge distances as noted above. If a 7.5-mm geocomposite is used as the LCRS, the gas permeability increases to 1.72×10^{-2} m/sec. This improves the vacuum “reach” across the LCRS, but is still beyond typical LFG extraction system vacuum (<12,450 Pa) for typical trough-ridge distances. By reducing the refuse thickness across which vacuum is applied (Equation 3), acceptable system vacuum levels can be eventually be found for a geocomposite LCRS. This is generally 10-percent of the vacuum influence distance for a gravel LCRS, or tenths of meters. This implies significant pressure can build within the waste mass above the LCRS. Geocomposite LCRS may be more effective at providing migration control from the landfill base than actual LFG extraction. This concept needs field evaluation from landfills with geocomposite based LCRS.

5. CONCLUSIONS

In general, geosynthetic materials can be used to extract LFG from municipal waste landfills. Geocomposite collection strips placed under the synthetic final cover system have been shown to be an effective LFG extraction system. Use of structured geomembranes collection strips to control LFG movement in active areas of the landfill could provide similar LFG control in active landfill areas as horizontal collection trenches. Placement of structured geomembrane collection strips could be more easily integrated into the landfill operations than installation of excavated trenches. However, this horizontal collector strip design needs to be tested in the field to verify the design assumptions presented in this paper. Horizontal collector strips are subject to a variety of destructive forces within the active landfill. At this time, no credible estimation of a strip service life can be made without application in the field. When compared to gravel based LCRS, a geocomposite LCRS may not be effective as an active LFG extraction system. However, they should be able to provide LFG migration control from the base of the landfill. This should be confirmed with data collection from landfills with existing geocomposite LCRS.

REFERENCES

- Emcon. (1980). *Methane Generation and Recovery from Landfills*, Ann Arbor Science Publishers, Inc., Ann Arbor, MI, USA.
- Kou, J. (1999), *Practical Design Calculations for Groundwater and Soil Remediation*, CRC Press LLC, Boca Raton, FL, USA
- Koerner, R.M., (2010). *Advances and Concerns in Geosynthetic Materials, Geosynthetics for Success*, GSE Technical Seminars, Walnut Creek, California, USA
- Thiel, R.S. (1998). Design Methodology for a Gas Pressure Relief Layer Below a Geomembrane Landfill Cover to Improve Slope Stability, *Geosynthetics International*, Vol. 5, No. 6.
- Richardson, (2000). Gas Transmission in Geocomposite Systems, *GFR Magazine*, Volume 18, Number 2, March 2000
- Richgels, C. (2000) , Reasonably Foreseeable Water Quality Risks From Lined Landfills, Leachate And Landfill Gas Releases, *5th Annual Landfill Symposium*, Solid Waste Association of North America, Austin, TX, USA

Geosynthetic Clay Liners – Accomplishments and Disappointments - The Do's and Don'ts of GCLs.

B. Herlin. Terrafix Geosynthetic Inc., Toronto, Ontario, Canada. bherlin@terrafixgeo.com

ABSTRACT

Geosynthetic Clay Liners (GCLs) are mainly used in landfill applications, however their use extends to a wide range of applications such as ponds, lakes, canals, dams, roads, railways, waterproofing of buildings, including out of the ordinary situations. When used wisely and effectively, GCLs, have proven to be an effective alternative to other types of liners in applications beyond landfills. This paper will summarize these applications with recent case studies including specific details on when to use them with confidence and when to avoid using them based on site conditions and parameters. Not all GCLs are identical and not all can be used on specific projects. As with all types of liners, when used improperly without any attention, the consequences are enormous to the industry as a whole, however when used properly, can have the complete opposite reaction with repeated success and a complete benefit to all in the Geosynthetic industry.

1. INTRODUCTION

1.1 Landfill Caps & Base Lining with GCLs – An abundance of documented research & case studies.

Since the late 1980s, Geosynthetic Clay Liners (GCLs) have been specified and used mainly in landfill applications such as a landfill caps and/or base seals in combination with and without geomembranes (HDPE) as shown in Figures 1 and 2. The main purpose of a GCL is to reduce/limit the flow of liquid through the GCL or barrier system. The performance of GCLs in landfill applications has been well documented in research papers to outperform Compacted Clay Liners (CCLs) to the point where engineers, government agencies, and landfill owners feel secure to incorporate them in their designs.

The marked increased in Geosynthetic Clay Liners as a whole appears to have been driven by the many advantages they have over traditional construction methods and materials, ie. CCLs. GCLs present numerous advantages over CCLs. They take up less airspace (5-10mm thickness), are resistant to freeze/thaw and wet/dry cycles, can be installed quicker at substantially lower costs, transported to site at a lower carbon footprint than CCLs, they reduce on site QA/QC, improved possibilities of steeper slope applications, and offer equivalent or better hydraulic characteristics depending upon the thickness and quality of the CCL being replaced.



Figure 1. GCL being used in a landfill cap application.



Figure 2. Landfill Base Liner (HDPE over GCL). GCL being used in a composite liner design used in lieu of a CCL component.

1.2 Available GCLs – Numerous GCLs are available – Specific projects require a specific GCL.

There are many types of GCLs available on the market. Not all are identical and everyone is unique to a specific application. Using a particular GCL may work well in one application, however the same GCL may have detrimental results when used in another application, ie. a complete debacle. The many types of GCLs are: stitched, glued, needlepunched, different bentonite content, different geotextile weight, scrim-reinforced, non scrim-reinforced, with thin geomembranes, enhanced polymer, etc. The list is long. Unfortunately over the years and through increased

competition, this area of Geosynthetics Engineering seem to see lower cost GCLs requested for projects. This usually means thinner textiles and/or less bentonite, almost to the point of becoming less a GCL than a double-layered textile. A design engineer should never use tradenames when specifying GCLs. Tradenames change over time and so do the actual properties and values attached to a specific tradename. An engineer should always provide a table of physical properties when requesting a particular GCL which includes basic information as shown in Figure 3.

Geotextile Properties	Test Method	Minimum Test Frequency	Value - SI -
Cap Fabric Mass/Unit Area	ASTM D 5261	1/20,000 sq. m	X g / m ² MARV Usually non-woven
Bottom Fabric Mass/Unit Area	ASTM D 5261	1/20,000 sq. m	X g / m ² MARV Woven or Non-woven or Scrim Non-woven With or without an added coating and/or thin liner.
Bentonite Properties			
Swell Index	ASTM D 5890	50,000 kg	X ml / X g min. Usually 24 ml min & 2 g
Moisture Content	ASTM D 4643	50,000 kg	X % max. Oven dried measurement
Fluid Loss	ASTM D 5891	50,000 kg	X ml max. Usually 18 ml
Finished GCL Properties			
Bentonite Mass Per Unit Area	ASTM D 5993	1/4,000 sq. m	X kg / m ² MARV
Grab Strength	ASTM D 4632	1/4,000 sq. m	X N MARV
Peel Strength	ASTM D 6768	1/4,000 sq. m	X kN/m MARV
	ASTM D 4632		X N min
Permeability	ASTM D 6496	1/10,000 sq. m	X N/m min
	ASTM D 5084		X cm/sec max
Index Flux	ASTM D 5887	1/Week	X m ³ /m ² /sec Max
Internal Shear Strength	ASTM D 6243	Periodic	X kPa Typical

Figure 3. Example of physical properties to list when requesting a GCL, ie. do not use tradenames.

One should never use a top fabric in a GCL to be less than 200 g/sqm, unfortunately as mentioned above, market forces with competition, GCLs with thinner and thinner top fabric weights are specified and used. The bottom fabric of a GCL should always contain a woven (scrim) fabric for numerous reasons (ie. avoid internal erosion, avoid shrinkage of the GCL in a double composite system). The amount of bentonite added to a GCL should not be lower than a certain amount (Maubeuge – Nuremberg 2002) yet from time to time one does see specified requested amount of 0.5 lbs/sqft which seems to be playing with fire. The swell index of a bentonite in a GCL should be above 24ml (min) while the fluid loss test should not exceed 18ml. As far as Peel and Grab Strength values of a GCL, these values can have a wide range depending on what is trying to be achieved in a project, ie. type of application, type of GCL required. Of course, one can never assume what is being requested on a project, is what is being supplied on a project, hence third party testing using samples from the site should be done by a project engineer. Numerous testing labs are available in this regard, however one must use a testing lab with Geosynthetic experience and knowledge of Geosynthetics.

2. GEOSYNTHETIC CLAY LINERS – USED IN PROJECTS BEYOND LANDFILLS

When using a GCL in a landfill application such as a base seal, one doesn't see visually if the liner is working or not. Research papers and data results over the last three decades have told us that GCLs work like a charm in landfill base seals with a High Density Polyethylene (HDPE) membrane, easily outperforming CCLs. However the research data beyond landfill applications is negligible. We do find some GCL related papers beyond landfills, however most of these are case study related papers. Case study papers are beneficial to the industry and most of the background to justify using a GCL in applications beyond landfills are based on findings done on landfill related research of

GCLs. For example, Scrim-Reinforced GCLs vs Non Scrim-Reinforced GCLs. Research done on Scrim-Reinforced GCLs vs Non Scrim-Reinforced GCLs has provided us information on the highest hydraulic head pressure that can be applied over these GCLs based on a certain subgrade below a GCL (Rowe and Orsini, 2002). A Scrim-Reinforced GCL can handle far greater hydraulic head pressures than a GCL which is not Scrim-Reinforced, ie. lacking a woven fabric (Scrim=woven; Scrim-Reinforced NonWoven = woven + nonwoven; Scrim-Reinforcement = needlepunching of a woven and nonwoven geotextile together).

All needlepunched GCLs have a nonwoven top geotextile. The bottom geotextile geotextile is either a required woven on its own and/or a scrim-nonwoven geotextile and/or a non scrim-reinforced geotextile. The thickness of the geotextiles in a GCL depend on the subgrade conditions and the application such as steep slope applications. The Geosynthetic Research Institute (GRI) recommends that the bottom geotextile of a GCL contain a scrim-reinforced nonwoven geotextile. Possible failures that may occur by not using a scrim-reinforced bottom geotextile are internal erosion of the bentonite through the geotextile in hydraulic head conditions as mentioned above, and possible shrinkage of the GCL itself in a composite lining system (GRI White paper, 2005). As per the GRI's White Paper of April 2005, do not use GCLs with needlepunched nowoven geotextiles on both sides of a GCL unless one of the geotextiles is scrim-reinforced. There are numerous possibilities in this regard, but all should have a woven component embedded within, or bonded to, the nonwoven component.

2.1 GCLs in Pond Applications – Storm Water Management Ponds to Golf Course Ponds.

This is an application where you know if it works or doesn't work. With any type of liner, your liner is only as good as the subgrade it's lying on. Pond lining applications require a hard subgrade for the liner to be resting on. If the General Contractor is unable to supply a hard subgrade, walk away until something solid is provided for the liner. Every GCL manufacturer has numerous types of GCL available on the market. Pond applications, as shown in Figures 4 and 5, require an onsite decision to be made once the pond cavity is done, once the subgrade conditions are seen, then the GCL selection is made. Local project engineers who know the subgrade conditions can make a decision well ahead of the project start. Standard regular GCLs such a top fabric nonwoven and bottom woven fabric for pond applications should be avoided unless the subgrade is a silty clay. A subgrade rough in nature such as a gravel base, a scrim-reinforced GCL should be used with the scrim-nonwoven fabric side of the GCL facing down to avoid internal erosion of the bentonite. Should the subgrade contain sand, a coated GCL or GCL containing a thin geomembrane should be used. Geosynthetic Clay Liners are an excellent liner choice for ponds larger than 2,000 sqm. A GCL should not be used for ponds less than 2,000 sqm. Ponds smaller than 2,000 sqm have sharp turns which a GCL is unable to perform. Another factor to avoid lining small ponds with a GCL is that the cover soil thickness of one feet over the GCL is hard to achieve and maintain.

Any General Contractor can install a GCL in a Storm Water Management (SWM) Pond. SWM Ponds are normally larger than 2,000 sqm. GCLs are easy to install and only require minimal start up assistance for the General Contractor. Lining a Golf Course Pond is a different matter entirely. A specialized GCL installer should be used for these types of applications. Golf Course Ponds tend to have awkward shapes like the boot of Italy, they contain pipe penetrations which SWM Ponds normally don't, and they require an aesthetic cover soil thickness over the liner. Using a GCL in pond applications is a lucrative market, however as mentioned, requires more attention up front with the subgrade conditions for the liner, on site assistance, and should allows have supervision during the cover soil placement. Most project engineers like to attend a lining project during the liner deployment, however they should also remain on site during the cover soil placement. Unfortunately, most of them stay in the trailer or are nowhere to be on seen on their own project. Most lining damages are caused during the cover soil placement.

Overlap of the GCL sheets/panels are normally recommended to be one feet (30cm). Over hard subgrade, which should always be provided. However if there's any doubt in the strength of the subgrade, the overlap should be increased to a more respectable value. GCLs are a great liner selection for winter installations. Most cavity holes done for SWM Ponds and/or other ponds have a high water table to deal with. In some cases, project engineers will use a dewatering system around the cavity. In situations where stubborn water (approx. 30cm) remains at the bottom of the cavity, the GCL overlap should be increased to at least three feet (90cm) to compensate for the soft subgrade which may exist below the water level. During winter installation work, stubborn water may exist as ice and the same should be done in these cases; Either remove the ice to an acceptable level or if the ice is at approximately 30cm from the subgrade then the ice can remain in place and the GCL installed with a greater overlap, ie. 90cm.



Figure 4. GCL being deployed for a SWM Pond in winter conditions. Note the ice (30cm thickness), ie. stubborn water (water table). Overlap increased from 30cm to 90cm over the ice.



Figure 5. Placement of the cover soil for any lining projects should always be supervised.

2.2 GCLs in the Mining Industry.

Beyond Municipal Landfills and Ponds, another attractive market for GCLs is the Mining Industry, as shown in Figures 6 and 7. Mostly used in capping applications, GCLs main advantage in this sector is the ease of installation they offer for local general contractors. Most mine sites are located in remote areas far from populated centres and of course specialized trades. Whereas other types of liners require specialized contractors, a GCL can be deployed using local labourers. Other advantages include the rate of deployment and the capability to deploy during winter months. Although the rate of deployment of a GCL can reach high deployment rates, the deployment is restricted by the cover soil placement over the GCL. One can deploy a GCL with specialized deployment techniques, however the need for a specialized machine to deploy a GCL is restricted to the fact that a GCL deployed during a construction day should be covered in that same construction day. Deployment of a GCL can simply be done with a spreader bar by a local contractor. Deployment rates with a simple maintenance free bar are normally between 10,000 sqm to 20,000 sqm in flat conditions during an eight hour work shift. Deployments rates can reach up to 30,000 sqm if the general contractor starts his/her cover soil placement immediately behind the GCL deployment crew.

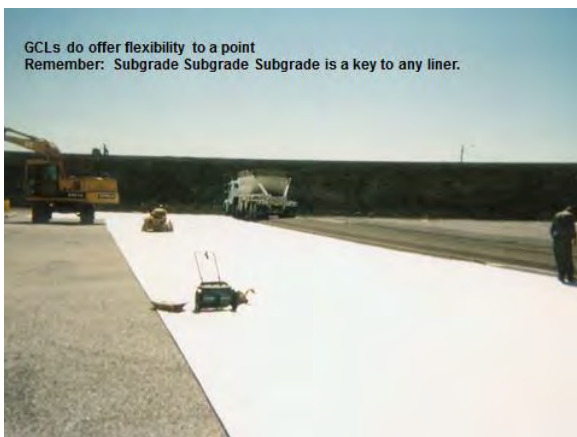


Figure 6. Note Belly dump trucks being used over the GCL for cover soil placement. Dry bentonite manufactured GCL, hard subgrade (no rutting), no sharp turns done by the truck (Mining industry).



Figure 7. GCL being deployed in a dam lining application (Mining industry).

2.3 GCLs in the Waterproofing industry.

GCLs are used extensively in the concrete industry for waterproofing lining applications, as shown in Figures 8 and 9. This type of application requires both the technical expertise at the design level as well as a specialized contractor. Whereas most GCL installation applications do not require any installation experience, this is one application sector that truly needs an experienced contractor. Connection details are paramount to this sector.



Figure 8. GCL used as a component in a waterproofing lining system for a new condominium building.



Figure 9. Concrete being poured over a GCL for a new concrete clarifier (Farming industry).



Figure 10. GCL being deployed inside a new production plant facility – lining underneath new machinery – Liquid Spills from equipment above (machine/equipment not shown).



Figure 11. GCL being used to line underneath a highway – groundwater protection against road salt – GCL containing a polymer.



Figure 12. Can you use a GCL in this application? Every project engineer has his/her needs. GCL being deployed in a SWM Pond containing a high water level. Bizarre situation but required by project engineer who had wanted a liner without dewatering the site.



Figure 13. GCL being used instead of a PVC liner under Storm Chambers due to winter temperatures.

2.4 GCLs in bizarre situations.

Every engineer has his/her projects which requires a solution to a bizarre situation, as shown in Figures 10 thru 13. Can a GCL work in this situation? Sometimes the answer is, I don't know? Can't see why it can't! In these situations, the project engineer or the designer in question has an extensive experience with prior applications with a GCL and/or other types of liners. As shown in Figure 10, the engineer may require a liner below the concrete surface of a new factory to prevent any potential leaks going through the concrete (cracks/expansion joints in the concrete) into the subgrade soil to prevent soil contamination. Figure 12 as you can see requires an excavator operator to wear a cowboy hat in this application. On a serious note, this application was a fast track project where the SWM pond required a liner as requested by local authorities. The SWM pond was required to be in place prior to winter arriving and the official opening date of a regional train service (train station parking lot). For these applications, an experienced lining contractor and an experienced crew is required to perform projects listed as "Can it be done?". Underwater applications with GCLs have been done in the past with success and of course flexibility to the standard guidelines must be altered to accommodate the project at task, ie. greater overlap of the GCL sheets/panels.

3. DON'TS OF GCLS – WHAT ON EARTH WERE THEY THINKING?!

Over the last decade being involved with Geosynthetic Clay Liners (GCLs) not one construction season goes by where I do say to myself "What on Earth were they thinking?!", it's a geotextile (don't leave exposed to the sun), it's clay (loves to crack when dried out), "where's the cover soil?". My favourite is the GCL left exposed without cover soil for weeks and/or months and either the GC or project engineer and/or someone deployed the GCL and called it "project done" without providing a cover soil over the GCL. As mentioned, a GCL is after all a product made of a geotextile and a clay both of which don't like the sun, and one of which needs a confining stress for it to do its function as a liner. Now either the GC and/or project engineer wasn't told to apply a cover soil or not, which hence could be the fault of the manufacturer and/or the distributor for not mentioning this point, but still, it still leaves me in shock to hear "your liner doesn't work". All liners work if done properly, however a GCL liner does need a cover soil, and for one to leave out the final instruction procedure of adding a cover soil is hard to stomach until everyone involved in the project comes to the fact that someone must take the fall for their errors. Alas the damage has been done and hence begins the game that a GCL does not work.



Figure 14. The GCL isn't working. No cover soil ! GCL left exposed for weeks/months. Incredible ! Last item in procedure, "place cover", not done.



Figure 15. GC leaving the site once the GCL has been deployed. No cover soil.

4. SUMMARY AND CONCLUSION

Based on over 20 years of production and application experience with needle-punched Geosynthetic Clay Liners (GCLs), numerous laboratory studies and case histories have shown the excellent performance capable with natural sodium bentonite GCLs. GCLs have shown to work quite effectively in numerous projects with success. The research done on GCLs is fairly extensive: hydraulic conductivity, effect of GCL structure on bulk void ratio, mine waste waters testing, hydrocarbon testing, freeze-thaw, hydration rate, internal erosion, shrinkage, desiccation, peel strength, diffusion, estimated service life, CCL vs GCL. If an engineer has a question, there's no doubt that the research has already been done on a GCL. For all the research done on GCLs, the true advantage of a GCL is the ease of deployment, which does not require any experience. However as mentioned, attention to the cover soil placement over a GCL is far more important than the actual deployment of the GCL itself and of course, your GCL is only as good as the subgrade it's resting on, ie. hard vs soft subgrade. Failure to understand the limitations of a

GCL based on previous research papers can lead to detrimental consequences. When used appropriately, GCLs offer an economical cost advantage to other liners.

ACKNOWLEDGEMENTS

The author would like to acknowledge first and foremost Mr. Kent von Maubeuge who in 2001 provided all the bells and whistles including all the warnings signs on the 5 Ws (What, Where, Why, When, Who) on Geosynthetic Clay Liner including how connections are made in this industry (the Skoda connection).

REFERENCES

- Bentofix Technologies Inc., "Fix – 412 Features of a Scrim-Reinforced GCL & Manufacturing Process", Barrie, Ontario, Canada, 1992, (*unpublished*).
- GRI – Geosynthetic Research Institute – Philadelphia, PA, USA. GRI-GCL3. Standard Specification for Test Methods, Required Properties, and Testing Frequencies of Geosynthetic Clay Liners (GCLs), Geosynthetic Research Institute, 2005.
- Herlin, B. and von Maubeuge, 2010. Geosynthetic clay liners – applications beyond landfills – case studies. GBR-C 2k10 3rd International Symposium on Geosynthetic Clay Liners, Wurzburg, Germany, 2010, pp. 301-307.
- Koerner, K.R. and Koerner, R.M., 2005. GRI White Paper #5 on In-Situ Separation of GCL Panels Beneath Exposed Geomembranes. Geosynthetic Research Institute.
- Maubeuge von, 2002. Investigation of bentonite requirements for Geosynthetic clay liners. International Symposium on Clay Geosynthetic Barriers, Nuremburg, Germany, 2002, pp 155-163.
- Rowe, R.K. and Orsini, C., 2002. Internal erosion of GCLs placed directly over fine gravel. International Symposium on Clay Geosynthetic Barriers, Nuremburg, Germany, 2002, pp. 199-207.
- Rowe, R.K. Quigley, R.M., Brachman, R.W.I., and Booker, J.R. (2004). *Barrier Systems for Waste Disposal Facilities*, 2nd ed., Spon Press, New York, NY, USA.

Geosynthetic Opportunities Associated With Shale Gas Extraction

R. M. Koerner, Ph.D., P.E., NAE., Geosynthetic Institute, USA, robert.koerner@coe.drexel.edu
G. R. Koerner, Ph.D., P.E., CQA, Geosynthetic Institute, USA, gkoerner@dca.net

ABSTRACT

While natural gas contained within shale rock is geologic by its very nature, the practice of its removal by horizontal drilling coupled with hydrofracing is quite recent. Indeed, these dual technologies are making possible the recovery of huge amounts of natural gas. So much so that one can envision natural gas as an energy source rivaling oil, coal and nuclear, while dwarfing all of the renewables combined. The potential in this regard is awesome particularly since it is worldwide in its availability and opportunities.

This white paper briefly describes shale gas drilling and extraction operations, along with its associated environmental concerns. Using this as a background, the paper then describes and illustrates many geosynthetic materials opportunities that exist in order to make the overall operations more efficient, economical, and environmentally acceptable.

1. SHALE GAS PLAYS

Shale is a fine-grained sedimentary rock which is formed by heat and pressure over geologic time. Many formations contain organic materials (they are then called *oil shales*), which upon decay, generates natural gas within the rock itself. The liberation, capture and transmission of this gas is at the heart of the technology. It should be mentioned that natural gas has traditionally accompanied oil drilling operations and has historically been a nuisance to oil drillers.

Shale gas plays are both nationwide and worldwide in their occurrence, e.g., see Figure 1 in which the data is in units of trillions of cubic meters. In the U.S., there is activity in many states as Figure 2 indicates. Of the locations shown, the Barnett formation in the Fort Worth basin is very significant since it was the first large-scale operation using these newer drilling and extraction technologies. By 2004, it had been explored by 15,000 deep wells, over 4000 in 2007 alone, and had produced 1.4 trillion cubic feet; TCF (0.04 trillion cubic meters, TCM) of natural gas in 2008. It appears as though horizontal drilling at great depths coupled with hydraulic fracturing was perfected in the Barnett shale of Texas.



Figure 1. Worldwide conventional and shale gas reserves (The Economist, August 6, 2011).



Figure 2. United States shale gas plays (compl. Wikipedia).

The most recent major gas play is in the Marcellus formation underlying major parts of Pennsylvania, New York, Ohio and West Virginia.

Financial incentives are enormous. For example, Professor Timothy Considine of the University of Wyoming estimates that a *typical Marcellus well* generates \$2.8 M in direct economic benefits, another \$1.5 M from workers and landowners, and \$2.0 M in federal, state and local taxes. This type of financial incentive is, of course, reflected in the present activity associated with shale gas extraction, transportation and eventual usage as an energy source.

2. REGULATIONS AND ENVIRONMENTAL CONCERNS

The U.S. Energy Policy Act of 2005 was, and is, the foremost federal regulatory act governing shale gas plays of the type described in this white paper. Two aspects of this legislation have attracted considerable scrutiny;

- hydrofracking was exempted from the Safe Drinking Water Act, and
- chemical additives to the water used for fracing were exempted from disclosure.

To gain some perspective in this regard a chemical analysis of the flowback fracwater (at a specific site) is of interest, see Table 1. Note should be made of the highlighted alkaline minerals which results in an extremely brackish liquid about five-times the salinity of sea water. Also to be noted is the number of heavy metals, although the quantities are felt to be relatively low.

Table 1. Chemical analysis of flowback water at a site near Williamsport, Pennsylvania (compl. CETCO).

Na, mg/Kg	25,930	Mg, mg/Kg	725	Ag, mg/Kg	12
K, mg/Kg	137	CL, mg/Kg	60,769	Au, mg/Kg	23
Ca, mg/Kg	6,896	HCO ₃ , mg/Kg	275	Ba, mg/Kg	5,145
Fe, mg/Kg	39	Hg, mg/L	<0.001	Cd, mg/Kg	0.12
Cr, mg/Kg	0.28	Pb, mg/Kg	0.80	Se, mg/Kg	1.4
Zn, mg/Kg	33	Cu, mg/Kg	1.6	TSS, mg/L	1.1

It should be noted that pending federal legislation, the so-called Frac Act of 2009, will require disclosure of fracking chemicals and place the entire process under U.S. Environmental Protection Agency regulations.

At the state-level in Pennsylvania, shale gas operations are regulated under various departments, for example;

- drilling via the state Oil & Gas Division,
- fracking water via the state Field & Stream Division, and
- waste disposal via the state Solid Waste Division.

In keeping with an emotionally-charged technology, such as natural gas plays, there are many environmental issues that have been raised by various concerned organizations, such as, federal, state and local regulatory groups, local water authorities, various industry groups, concerned citizens groups, etc. Some (but clearly not all) are mentioned below and have been selected because of the positive potential of using geosynthetic materials to solve, or at least mitigate, the issues listed:

- Containment and storage of large quantities of surface water for drilling and fracturing purposes.
- Storage and reuse of flow-back water from the hydrofracking process.
- Proper disposal of the “cuttings” from drilling operations (ca. 1000 tons per well).
- Drill pad site contamination (each being typically 3-5 acres in size).
- Frac-tank and storage area contamination.
- Access roads, parking and staging areas, and maintenance thereof.
- Minimizing site disturbance and providing level staging and working areas.
- Soil erosion and temporary containment so as to avoid stream and property contamination.

In order to appreciate some of these environmental issues it is helpful to view a composite drilling operation as well as the enormity of the drilling wells themselves, see Figures 3a and 3b.

Furthermore, some knowledge of the actual drilling operations are significant insofar as site development and maintenance. For example, a typical well site usually contains a number of vertical wells (3 to 6) which have horizontal branches going in different directions. Also, each well is generally hydraulically fractured several times. This iterative process depends upon the diminishing gas yield over time. Lastly, it is anticipated that a well pad should have a usable lifetime of approximately 20 to 30 years.

Furthermore, the following generalized goals with these shale gas extraction plays are interesting to keep in mind as we now go into geosynthetic opportunities and solutions;

- the drilling operations are large construction projects with considerable public and regulatory scrutiny,
- once permitted, fast mobilization and deployment is necessary,
- a “low profile” is advantageous particularly with minimization of truck traffic, and
- benefit/cost is always important but maximum benefit often outweighs minimum cost.



(a) Typical gas extraction operation in Marcellus Shale in Pennsylvania



(b) Several large gas well drill rigs

Figure 3. Site operations at natural gas plays (compl. Wikipedia).

3. GEOSYNTHETIC OPPORTUNITIES

This section describes some of the many geosynthetic solutions that can be applied to shale gas plays. The section is subdivided according to (i) the drilling operations themselves, (ii) opportunities at permanent locations, and (iii) opportunities at temporary locations.

3.1 Geosynthetics Associated with Drilling Operations

The first, and quite obvious, opportunity is the use of geomembranes for fresh water containment and subsequent use in the well drilling operations. The design stages are well known and consist of the following sequential steps:

- geometry (length, width, depth)
- cross section materials
- geomembrane type
- geomembrane thickness
- subgrade soil stability
- cover soil stability
- runout and anchor trench details

Perhaps the most overlooked design detail is the requirement of providing an underdrain system beneath the geomembrane. Shown in Figure 6 are the all-to-common “whales” lifting up the geomembrane via rising gases within the underlying soil subgrade. Various underdrain solutions that should be considered are the following:

- thick needlepunched nonwoven geotextiles
- drainage geocomposites (complete or strips)
- interconnected perforated pipe system
- geotextiles with small perforated pipes
- sand bedding layer (with pipe network)

The second, and also obvious, opportunity is the containment and re-use of the flow back water which was characterized in Table 1 and is seen to be quite contaminated. Presently, this water is generally being held in mobile holding tanks but geomembrane lined ponds or even underground storage systems offer attractive alternatives. Underground storage systems that are typically used for storm water runoff from industrial and private development sites. Both strategies should be considered in contrast to hundreds of holding tanks interconnected to one another.

A third opportunity for geosynthetics is the containment of cuttings from the drilling operation itself insofar as proper safe and secure disposal is concerned. In this regard, it should be mentioned that each well produces about 1000 tons (\approx 75 truckloads) of contaminated cuttings.

These cuttings can, of course, go to a licensed public or private landfill but alternatively can be placed in geotextile tubes at the site and can even have a decontaminant added such that the treated effluent can be released to the environment. The addition of charcoal, activated carbon, phosphoric rock, or organoclays is necessary and all are within decontamination technology that is associated with geotextile tubes.

3.2 Opportunities at Permanent Locations

Of first priority in this category are the roadways into and out of the drilling site which are necessary for the 20 to 30 years lifetime of the operations. Geotextiles and geogrids have been shown to save from 10 to 50% of the crushed stone thickness of base courses placed on soil subgrades. The functions of separation, stabilization and/or replacement are clearly indicated in the literature since this application has been ongoing for about 30-years. Not only is there a savings in stone base material, the distance from the quarry is significant in the total cost of the application.

A second way of reducing crushed stone thickness there is considerable economy offered by using geocells. They are filled with gravel, sand or locally available soil and their design (which uses a geotextile beneath them) is well established. Thicknesses saved are from 50 to 100% over the use of gravel by itself.

Thirdly, these same geocells in a less-thick format are ideal for parking and staging areas located adjacent to the drill pad.

Fourth, locally available soils (even silts and clays) can be meaningfully strengthened by the addition of discrete fibers or microgrids. Both types lead to major increases in shear strength in the upper 4 to 12 inches (100 to 300 mm) of surface. The technology is well advanced and mature at this point in time.

Fifth, the drill pad site along with adjacent parking and staging areas must be level. To accomplish this in hilly terrain (as is typical in the Marcellus shale area) one needs to create stable soil slopes or even vertical walls. The concept of mechanically stabilized earth (MSE) slopes and walls using geogrid or geotextile reinforcement is ideal in this regard. Not only are these situations the least expensive of all types of retaining structures (GRI Report #20), they are straightforward to construct, have no limitations as to curvature, height, or orientation, and have proven stable insofar as extreme surcharge loads are concerned.

Sixth, the drill pad itself should be lined so as to avoid contamination from spilled fracwater, hydrocarbons or other potential ground contaminants. This calls for a geomembrane, a geosynthetic clay liner, or both, as a composite liner. There are many choices in this regard and a designer should consider the generation of a benefit/cost ratio to select the appropriate liner material.

Seventh, natural gas plays are replete with plastic pipe. Such pipe as shown in Figure 17 is used for many purposes such as;

- fresh water transmission
- frac water transmission
- gas transmission
- surface water drainage

The pipe is generally HDPE or PVC and can be solid wall (for transmission) or corrugated with slots or holes (for drainage). Whatever the case, natural gas plays require the use of plastic pipe in a major way.

3.3 Opportunities at Temporary Locations

First of all, temporary roadways of weeks or months are necessary in connection with setup and eventual demobilization at natural gas plays. The geosynthetics industry has the capability of providing wearing surfaces placed directly on the ground. Shown in Figure 18 are light and heavy roadway systems developed by the Dutch Military for rapid deployment of heavy vehicles and equipment. They are typically 60 ft. long and 10 ft. wide and the weight varies with type. Obviously, they can be redeployed as often as necessary.

Secondly, temporary dams may be used for surface water control or for accidental spills associated with the drilling or containment operations. Figure 19 shows that geomembranes can readily provide such temporary containment and be adaptable to myriad applications.

Third, on sloping surfaces soil erosion is a concern and must be avoided so as to prevent silting of off-site areas and local streams and rivers. Geotextile silt fences have played an economical role in this regard for decades.

Fourth, rather than containing the site's erosion after it occurs it is better to control and stabilize it before it starts. This has been traditionally provided by geosynthetic-erosion control materials of which there are a great variety. The two major categories are slopes and channels/ditches, respectively. Designs are well advanced in both cases.

4. CLOSING COMMENTS

Natural gas plays (including actual drilling, the well pad, staging and parking areas, permanent and temporary roadways and access areas) are extremely large construction projects with enormous natural gas energy potential. They also have attracted considerable public and regulatory scrutiny. That said, once permits are obtained, fast mobilization, deployment and operations are necessary. Within the entire activity a low profile and exposure is always an advantage. All of these aspects can capitalize on geosynthetics in a major way. This White Paper has described many of these opportunities.

Of course, and within acceptable environmental criteria, benefit/cost analyses are always required for alternative and competing systems. We feel that in so doing, geosynthetic materials will invariably be the obvious choice for many of these applications.

For general information on geosynthetics see the following websites or contact the authors of this White Paper.

- Geosynthetic Institute www.geosynthetic-institute.org
- Geosynthetic Materials Association www.ifai.com
- GMA Techline at gmatechline@ifai.com
- Geosynthetics Magazine www.geosyntheticsmagazine.com
- Geosynthetica www.geosynthetica.net
- International Geosynthetics Society www.geosyntheticsociety.org
- North American Geosynthetics Society www.nagsigs.org

Geosynthetics in Drainage Systems

Barry R. Christopher, Ph.D., P.E., Christopher Consultants, barryc325@aol.com

ABSTRACT

This paper provides an overview of the historical uses of geosynthetics in drainage systems, including: trench drains, cutoff drains, retaining wall and building wall drains including toe drains, base drains and chimney drains, and roadway edge drains. The paper includes a brief description of each application of geotextile filters and prefabricated geocomposite drains used as alternates to graded granular materials. Design methods are reviewed for both geosynthetics and conventional drains and these systems are compared on the basis of performance, cost benefit and sustainability based on actual project cost data, case histories and past synthesis national practice.

1. BACKGROUND

In the United States, the use of geotextiles as filters can trace its development back to the late 1950s when Mr. Robert Barrett developed the concept of using geotextiles to replace graded aggregate filters beneath rip-rap along the coast of Florida. The first filtration tests and design criteria were developed around the successful performance of these early applications (Calhoun 1972; and Carroll 1983). The author was fortunate to directly evaluate the performance of several of these early applications (Christopher 1983) and has revisited one of the sites in the late 1980s and again in the 1990s (Christopher and Valero 1999) to confirm the performance of these materials. Because of these early successes as well as their comparable performance, improved economy, consistent properties, and ease of placement, the use of geotextile filters has extended to almost all drainage applications as a replacement for graded granular filters. Geotextiles are used as filters in trench and interceptor drains, blanket drains, pavement edge drains, structure drains, and beneath permeable roadway bases. In addition to geotextile filters, geocomposites consisting of a drainage core surrounded by a geotextile filter are often used as the drain itself in these applications. Geotextiles also continue to be used as filters beneath hard armor erosion control systems.

1.1 Geotextile Filter Applications

The Federal Highway Administration (FHWA) Geosynthetics Design and Construction Guidelines (Holtz et al. 2009) schematically presents the following geotextile filter applications.

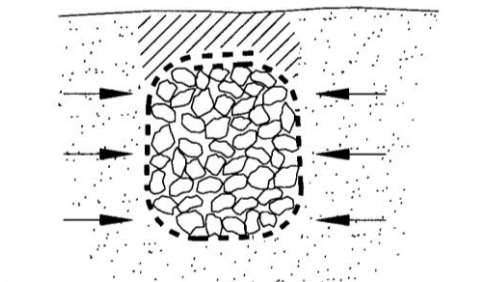


Figure 1. Filters around trench drains and edge drains – to prevent soil from migrating into the drainage aggregate or system, while allowing water to exit from the soil

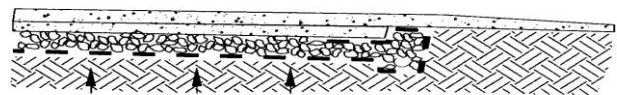


Figure 2. Filters beneath pavement permeable bases, blanket drains and base courses. (Prefabricated geocomposite drains are also used as horizontal drains in pavement systems.)

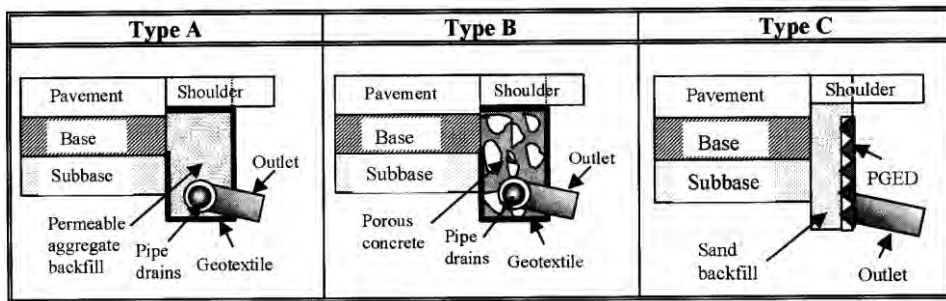


Figure 3. Geotextile filters and prefabricated geocomposite pavement edge drain applications (NCHRP 1-37A).

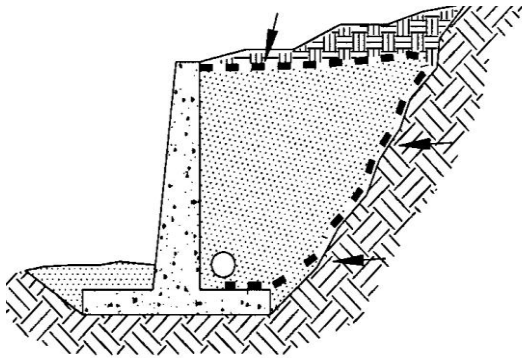


Figure 4. Drains for structures such as retaining walls and bridge abutments. (They separate the drainage aggregate or system from the backfill soil, while allowing free drainage of ground and infiltration water. Geocomposite drains are especially useful in this application.)

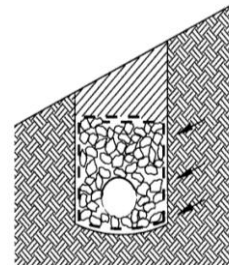


Figure 5. Interceptor, toe drains, and surface drains -- to aid in the stabilization of slopes by allowing excess pore pressures within the slope to dissipate, and by preventing surface erosion. (Again, geocomposites have been successfully used in this application.)

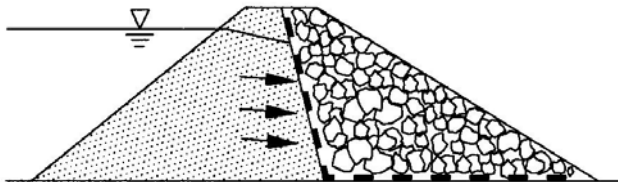


Figure 6. Chimney and toe drains for earth dams and levees to provide seepage control.

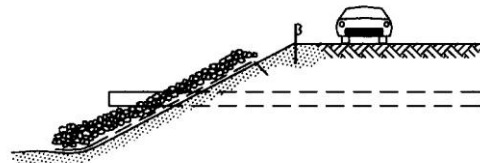


Figure 7. Hydraulic structures such as culverts, drop inlets, and artificial stream channels may require protection from erosion. (In such applications, if vegetation cannot be established or the natural soil is highly erodible, a geotextile can be used beneath armor materials to increase erosion resistance.)

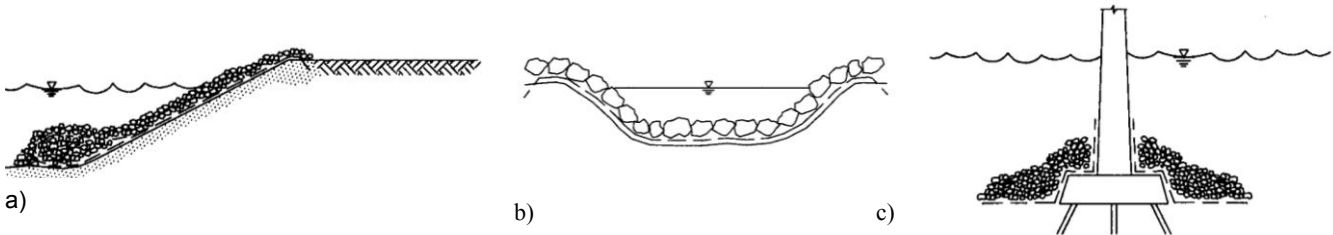


Figure 8. Geotextiles have been successfully used as a filter below: a) riprap for coastal and river bank protection; b) precipitation runoff collection, high-velocity diversion ditches, and slope protection; and, c) scour protection around structures.

1.2 Prefabricated Geocomposite Drains

The in-plane drainage ability of prefabricated geocomposite drains is potentially quite effective in several of the previously noted drainage applications. Virtually all of the drainage applications have a lateral transmission component (i.e., gravel is required to collect and drain infiltration water out of the system). Specific lateral drainage applications include interceptor trench drains on slopes, drains behind abutments and retaining structures, transmission of seepage water below pavement base course layers, pavement edge drains, vertical drains to accelerate consolidation of soft foundation soils, dissipation of pore water pressures in embankments and fills, dissipation of seepage forces in earth and rock slopes, chimney drains in earth dams, leachate collection and gas venting systems for waste containment systems, etc.

Thick nonwoven geotextiles alone can also provide suitable in-plane drainage for some of these applications; however, it should be realized that the flow quantities transmitted by in-plane flow of typical geotextiles (on the order of 2×10^{-5} m³/s/linear meter width of geotextile under a pressure equivalent to 0.6 m of soil) are relatively small when compared to the flow capacity of only 0.15 to 0.3 m of filter sand. Therefore, geotextiles alone should only be used to replace sand or other drainage layers in situations with small seepage quantities. Also the in-plane seepage quantities of geotextiles are highly affected by compressive forces, incomplete saturation, and hydraulic gradients. These considerations have led engineers to use geocomposite drains in most lateral drainage applications.

During the past 20 years or so, a large number of geocomposite drainage products have been developed, which consist of cores of extruded and fluted plastics sheets, three-dimensional meshes and mats, plastic waffles, and nets and channels to convey water, and geotextiles on one or both sides to act as a filter. Geocomposite drains may be fabricated on site although most are manufactured. They generally range in thickness from 5 mm to 25 mm or greater and have transmission capabilities of between 0.0002 and 0.01 m³/sec/linear meter width of drain.

Probably the most common uses for geocomposite drains in highways are pavement edge drains and drains behind retaining walls and abutments. However, the use prefabricated geocomposite edge drains (PGED) in pavements appears to have actually decreased over the past two decades. As noted in a national synthesis of practice on edge drains (Christopher, 2000), this reduction is attributed to a decrease in retrofit edge drain applications and reported problems that have discouraged the continued use of PGEDs by some agencies including "J" bending and crushing of the drain. These reports are somewhat contrary to the PGED research as reported in NCHRP Report 367 (*Koerner et al., 1994*), which found good performance of these materials and reported that most failures were predictable and related to either the absence of design, misapplication, or improper construction techniques. Extensive evaluation of installations in Canada (Raymond et al., 1999) also led to similar conclusions as the NCHRP Report 367. The industry has responded to the bending and crushing issue through the development of ASTM standard test methods (ASTM D6244 - 06(2011) Standard Test Method for Vertical Compression of Geocomposite Pavement Panel Drains) and a detailed guide specification for edge drain installation and specifications requirements (ASTM D6088 - 06(2011) Standard Practice for Installation of Geocomposite Pavement Drains and ASTM D7001 - 06(2011) Standard Specification for Geocomposites for Pavement Edge Drains and Other High-Flow Applications).

There are also issues with any type of edge drain that have discouraged their use, including confirmation of improved pavement performance, rigorous construction quality control to achieve performance (e.g., the use of video inspection), and maintenance requirements, especially at outlets to maintain flow (see Christopher et al., 2010 for a complete discussion of these issues). Another issue discouraging the use of edge drains is a perception by many of the northern agencies that edge drains do not work in cold regions. However, edge drain studies in Maine, Minnesota, Michigan, Ontario, and Wisconsin tend to strongly refute this claim. To the contrary, edge drains may have their greatest benefit in cold regions to rapidly remove water from the pavement during spring thaw. Separate studies of edge drains in Minnesota (*Hagen and Cochran, 1996*) and Maine (*Christopher et al., 1999*) found that more water comes out of the pavement section during the spring thaw than any rain event during the year.

Several states (e.g., Maine, Wisconsin, and Virginia) have also experimented with the use of horizontal geocomposite drains selected to be able to handle the estimated flow and support traffic loads. They are placed either below or above a dense graded base, used as a drainage layer beneath full depth asphalt, or placed between a "crack and seat" concrete surface and a new asphalt layer (e.g., see *Christopher et al., 1999*). In these applications, the drainage path is significantly reduced (i.e., vertically to the horizontal geonet composite versus laterally to the edge of the road), thus allowing the use of a lower drainage quality, lower cost, denser graded aggregate while maintaining very good to excellent drainage.

2. ADVANTAGES OF GEOSYNTHETICS

In most drainage and filtration applications, geosynthetic use can be justified over conventional graded granular filters and drainage aggregate material use because of cost advantages from:

- the use of less-costly drainage aggregate;
- the possible use of smaller-sized drains;
- the possible elimination of collector pipes;
- expedient construction;
- lower risk of contamination and segregation of drainage aggregate during construction;
- reduced excavation.

In addition, geosynthetics often increase drainage system reliability and, considering the value of drainage in geotechnical engineering, a significant cost-benefit can result when the designer is assured of a properly performing drain.

2.1 Cost Considerations

Determining the cost effectiveness of geotextile filters versus graded granular filters in drainage systems is a straightforward process. Simply compare the cost of the geotextile with the cost of a conventional granular filter layer, while keeping in mind the following:

- *Overall material costs including a geotextile versus a conventional system* - For example, the geotextile system will allow the use of poorly graded (less-select) aggregates, which may reduce the need for a collector pipe, provided the amount of fines is small (Q decreases considerably if the percent particles passing the No.200 (0.075 mm) sieve is greater than 5%, even in gravel).
- *Construction requirements* - There is, of course, a cost for placing the geotextile; but in most cases, it is less than the cost of constructing dual-layered, granular filters, for example, which are often necessary with fine-grained soils.
- *Possible dimensional design improvements* - If an open-graded aggregate is used (especially with a collector pipe), a considerable reduction in the physical dimensions of the drain can be made without a decrease in flow capacity. This size reduction also reduces the volume of the excavation, the volume of filter material required, and the construction time necessary per unit length of drain.

Geotextile filters in drainage applications will typically cost in the range of \$.80 to \$1.50 per square meter, depending upon the type specified and quantity ordered. Installation costs will depend upon the project difficulty and contractor's experience; typically, they range from \$0.50 to \$1.50 per square meter of geotextile. 2012 bid prices obtained from the web sites of several state agencies in preparation of this paper strongly support these costs. Higher costs should be anticipated for below-water placement. Labor installation costs for the geotextile are easily repaid because construction can proceed at a faster pace, less care is needed to prevent segregation and contamination of granular filter materials, and multilayered granular filters are typically not necessary. It should be noted that geotextile prices have not risen significantly in the last 20 years, however gravel cost has. The same web pages used for the cost of geotextiles also showed prices of select granular materials ranging from \$3.00 to \$10.00 in place for a 75 mm to 150 mm thick per sq meter layer (i.e., on the order of \$20 to \$30/metric ton) without consideration for special construction and dimensional requirements indicated above. This is typically the volume of gravel that will be replaced with the geosynthetic.

Prefabricated geocomposite drains are used to replace or support conventional drainage systems. According to Hunt (1982), prefabricated drains offer a readily available material with known filtration and hydraulic flow properties; easy installation, and, therefore, construction economies; and protection of any waterproofing applied to an adjacent structure's exterior. Cost of prefabricated drains typically ranges from \$7.50 to \$10.00 per square meter. The high material cost is usually offset by expedient construction and reduction in required quantities of select granular materials. For example, geocomposites used for pavement edge drains typically cost \$3.00 to \$10.00/linear meter installed while a conventional geotextile wrapped gravel drain with a pipe is on the order of \$30.00/linear meter installed.

Geotextile selection should not be based on cost alone. The cost of the geotextile is usually minor in comparison to the other components and the construction costs of a drainage system. Also, do not try to save money by eliminating laboratory soil-geotextile performance testing when such testing is required by the design procedure.

3. DESIGN

Geotextiles, like graded granular filters, require proper engineering design or they may not perform as desired. Unless

flow requirements, piping resistance, clogging resistance and constructability requirements (defined later) are properly specified, the geotextile/soil filtration system may not perform properly. In addition, construction must be monitored to ensure that materials are installed correctly. Thus, the geosynthetic materials must perform the same functions as graded granular filters that they replace:

- allow water to flow through the filter into the drain, and to continue doing this throughout the life of the project; and
- retain the soil particles in place and prevent their migration (*piping*) through the filter (if some soil particles do move, they must be able to pass through the filter without blinding or clogging the downstream media during the life of the project).

Designing with geotextiles for filtration is essentially the same as designing graded granular filters. A geotextile is similar to a soil in that it has voids (pores) and particles (filaments and fibers). However, because of the shape and arrangement of the filaments and the compressibility of the structure with geotextiles, the geometric relationship between filaments and voids is more complex than in soils. In geotextiles, pore size is measured directly, rather than using particle size as an estimate of pore size, as is done with soils. Since pore sizes can be directly measured, at least in theory, relatively simple relationships between the pore sizes and particle sizes of the soil to be retained can be developed. Three simple filtration concepts are used in the design process:

1. If the size of the largest pore in the geotextile filter is smaller than the larger particles of soil, soil particles that tend to move will be retained by the filter. As with graded granular filters, the larger particles of soil will form a *filter bridge* over the hole, which in turn filters smaller particles of soil, which then retain the soil and prevent piping.
2. If the smaller openings in the geotextile are sufficiently large enough to allow smaller particles of soil to pass through the filter, then the geotextile will not *blind* or *clog*.
3. A large number of openings should be present in the geotextile so that water flow can be maintained even if some of the openings later become plugged.

These simple concepts and analogies with soil filter design criteria are used to establish design criteria for geotextiles. Specifically, these criteria are the geotextile must retain the soil particles (*retention* criterion), while allowing water to pass (*permeability* criterion), throughout the life of the structure (*clogging resistance* criterion and *durability requirements*). To perform effectively, the geotextile must also survive the installation process (*survivability* or *constructability* criterion).

Specific criteria to meet these design requirements, design details and construction requirements are provided in the FHWA Design and Construction Guidelines (Holtz et al. 2009) and the text book by Koerner (2012). A National Cooperative Highway Research Program (NCHRP) study by Koerner et al. (1994) of the performance of geotextiles in drainage systems indicated that the FHWA design criteria developed by Christopher and Holtz (1985) were an excellent predictor of filter performance, particularly for granular soils (<50% passing a No.200 (0.075 mm) sieve). The hydraulic design requirements for geotextile filters used in pavement systems can also be evaluated using the FHWA computer program DRIP. The software was developed to evaluate the effectiveness of a drainage system in terms of the quality of drainage. It also provides tools for determining the design requirements for the permeable base, separator layers (i.e., geotextile or subbase), and edge drains, including the geotextile retention and permeability requirements for given natural and imported soil characteristics. The software can be purchased from <http://mctrans.ce.ufl.edu>.

3.1 Design Criteria for Geocomposite Drainage Systems

For the design and selection of geotextiles with in-plane drainage capabilities and geotextile filters for geocomposite drainage systems, there are four basic design considerations:

1. Adequate filtration without clogging or piping.
2. Adequate inflow/outflow capacity under design loads and field boundary conditions to provide maximum anticipated seepage during design life.
3. System performance considerations.
4. The two geotextile filters on the sides of geocomposites should not contact under load for capillary break applications.

Consideration should be given to system performance factors such as distance between drain outlets, hydraulic gradient of the drains, potential for blockage due to vegetation and siltation, small animals, freezing, etc. When using geosynthetics to drain earth retaining structures and abutments, drain location and pressures on the wall or abutment must be properly accounted for. It is important that the drain be located away from the back of the wall and be appropriately inclined so it can intercept seepage before it impinges on the back of the wall. Placement of a thin vertical drain directly against a retaining wall may actually increase seepage forces on the wall due to rainwater infiltration

(Terzaghi et al. 1996; and Cedergren 1989). For further discussion of this point, see Christopher and Holtz (1985).

4. SPECIFICATIONS

Guide specifications for geotextile filters can be found in AASHTO M288 (2006) geotextile material specification and its accompanying construction/installation guidelines; developed for routine drainage and filtration applications. For geocomposite edge drains, as previously mentioned, ASTM D7001 - 06(2011) provides detailed guide specifications. The actual hydraulic and physical properties of the geotextile filter or geocomposite drain must be selected by considering the nature of the project (critical/less critical), hydraulic conditions (severe/less severe), soil conditions at the site, and construction and installation procedures appropriate for the project.

5. CONCLUSIONS

After 50 years of successful practice, the author must conclude that geotextiles can effectively replace graded granular filters in drainage applications and beneath riprap or other hard armor materials in revetments and other erosion control systems. Numerous case histories have shown geotextiles to be very effective compared to graded granular filters in preventing fines. Furthermore, geotextiles and geocomposite drains have proven to be very cost effective in these applications. Indeed geotextile filters have become the standard of practice and geocomposite drainage systems are not too far behind, especially considering the recent increases in the cost of gravel.

ACKNOWLEDGEMENTS

This paper presents the state of the practice in geosynthetics used in drainage applications, a portion of which was extracted from the Federal Highway Administration *Geosynthetics Design and Construction Guidelines Manual* (Holtz et al. 2009). The author wishes to thank his co-authors of the FHWA manual, Dr. Robert Holtz and Ryan Berg for permitting the use of this material and, of course, their efforts in its development.

REFERENCES

- AASHTO (2006). *Standard Specifications for Geotextiles - M 288, Standard Specifications for Transportation Materials and Methods of Sampling and Testing*, 26th Edition, American Association of State Transportation and Highway Officials, Washington, D.C.
- ASTM (2012). *Annual Books of ASTM Standards*, American Society for Testing and Materials, West Conshohocken, PA:
- Volume 4.08 (I), Soil and Rock
- Volume 4.09 (II), Soil and Rock; Geosynthetics
- Carroll, R.G., Jr. (1983). Geotextile Filter Criteria, *Engineering Fabrics in Transportation Construction, Transportation Research Record 916*, Transportation Research Board, Washington, D.C., pp. 46-53.
- Calhoun, C., 1972, *Development of Design Criteria and Acceptance Specifications for Plastic Filter Cloths*, Technical Report S-72-7, U.S. Army Corps of Engineers, Waterways Experimental Station, Vicksburg, Mississippi, USA, 105 p.
- Cedergren, H.R. (1989). *Seepage, Drainage, and Flow Nets*, Third Edition, John Wiley and Sons, New York, 465 p.
- Christopher, B.R. (1983). Evaluation of Two Geotextile Installations in Excess of a Decade Old, *Transportation Research Record 916*, Transportation Research Board, Washington, DC, pp. 79-88.
- Christopher, B.R. and Holtz, R.D. (1985). *Geotextile Engineering Manual*, FHWA-TS-86/203, 1044 p.
- Christopher, B.R. and Valero, S.N. (1999). Thirty Year Performance Evaluation of a Geotextile Filter, *Proceedings of Geosynthetics '99*, Vol. 2, Boston, Massachusetts, March 1999, pp. 977-990.
- Christopher, B.R., Hayden, S.A., and Zhao, A. (1999). Roadway Base and Subgrade Geocomposite Drainage Layers, *Testing and Performance of Geosynthetics in Subsurface Drainage, ASTM STP 1390*, J.S. Baldwin and L.D. Suits, Eds., American Society for Testing and Materials, West Conshohocken, PA.
- Christopher, B.R. (2000) *Maintenance of Highway Edgedrains*, National Cooperative Highway Research Program, Synthesis of Highway Practice 285, Transportation Research Board, National Academy Press, Washington, D.C., 62 p.
- Christopher, B.R., Schwartz, C., and Boudreau, R., (2010) *Geotechnical Aspects of Pavements*, U.S. Department of Transportation, Federal Highway Administration, Washington DC, FHWA-NHI-10-092 (update of FHWA-NHI-05-037), 568 p.
- Hagen, M.G., and Cochran, G.R. (1996) *Comparison of Pavement Drainage Systems, Transportation Research Paper #960203*, Transportation Research Board, Washington, D.C.
- Hunt, J.R. (1982). The Development of Fin Drains for Structure Drainage, *Proceedings of the Second International*

- Conference on Geotextiles*, Las Vegas, NV, Vol. 1, pp. 25-36.
- Koerner, R.M., Koerner, G.R., Fahim, A.K. and Wilson-Fahmy, R.F. (1994). *Long Term Performance of Geosynthetics in Drainage Applications*, National Cooperative Highway Research Program Report No. 367, 54 p.
- Raymond, G.P., Bathurst, R.J. and Hajek, J. (1999). Evaluation and Suggested Improvements to Highway Edgedrains Incorporating Geotextiles, *Geotextiles and Geomembranes*, vol 17, No. 5.
- Terzaghi, K., Peck, R.B., and Mesri, G. (1996). *Soil Mechanics in Engineering Practice*, Third Edition, John Wiley & Sons, New York, pp 330-332.

Geosynthetics: The Solution for Managing Nuclear Power Generation Water Supply in an Arid Environment

C. Eichelberger, American Environmental Group, Ltd. (AEGL), USA, ceichelberger@aegl.net
G. Hersh, American Environmental Group, Ltd. (AEGL), USA, ghersh@aegl.net
S. Pittawala, Arizona Public Service (APS), USA

ABSTRACT

Nuclear power generation requires substantial amounts of water both in the power generating process and the subsequent cooling process. Of the 439 active nuclear facilities in the world, only the Palo Verde Nuclear Generating Station is not located adjacent to a lake, ocean or river. To the contrary, the Palo Verde facility is located in the desert of Arizona, and utilizes treated effluent from Phoenix as the plant's cooling water supply. This is made possible through the construction of more than 780 acres of specialty containment systems which incorporate more than 135 million square feet of various geosynthetic products and results in 4.4 billion gallons of storage capacity. These containment structures utilize state-of-the-art technology such as video monitoring of the leak detection zone, which provides protection of the underlying aquifer. As a result, the Palo Verde Generating Station is able to serve the energy needs of more than 4 million people, generating more electricity than any other facility in the United States.

1.0 INTRODUCTION

The Palo Verde Nuclear Generating Station is located 55 miles west of downtown Phoenix and is the largest power producer of any kind in the United States. Its three units are capable of generating more than 4,000 megawatts of electricity. The facility provides power to New Mexico, California, Texas and Arizona. Palo Verde's design, construction and operation is based upon very robust levels of containment for various materials and processes in compliance with federal and state regulations. On-site containment includes not just radioactive material but more than 4.4 billion gallons of water. This amount of storage is designed to provide sufficient cooling water for longer than one year in the unlikely event of a severe accident.

Given its desert location, Palo Verde is the only nuclear plant in the world that does not sit on a large body of water. Instead, it uses treated effluent from several area municipalities, primarily Phoenix, to meet its cooling water needs. It recycles approximately 20 billion gallons of wastewater annually. The site receives approximately 70-90 million gallons per day (MGD) of wastewater and handles the responsibility of tertiary treatment on site. The use of the wastewater preserves enough ground or surface water for hundreds of thousands of households each year.

2.0 WATER CONTAINMENT FOR TWO PROCESSES

Palo Verde Cooling Water Conveyance System

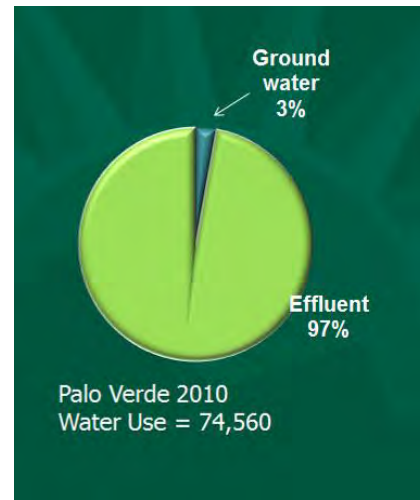
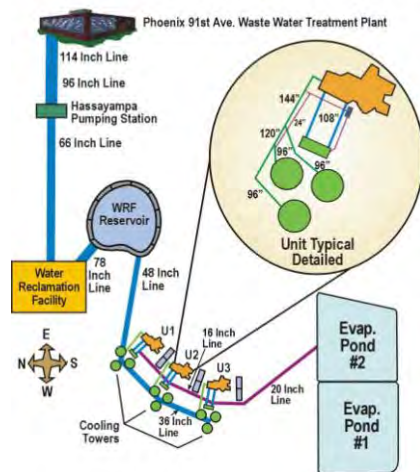


Figure 1. The Original Cooling Water Conveyance System, Evaporation Ponds 1 and 2, and water usage data are shown above. (Palo Verde Engineering Assessment PowerPoint)

2.1 The Water Reclamation Facility Reservoirs

The design of the massive treatment facility that accepts the 70-90 MGD of wastewater includes two lined reservoirs. The first reservoir was constructed in 1978 and is approximately 85 acres in size, with a second reservoir covering 45 acres being constructed in 2006.

The two storage reservoirs contain approximately a 14 day supply of the water required to operate the facility during normal operations.

2.2 Evaporation Ponds for Storage of Blow-down Water

The second use of geosynthetic lined containment on the site is to store “blow-down” from the cooling systems and to process waste. APS strives to maximize the amount of water that can be recycled through the energy production process. However, a certain percentage of blow-down water must be discharged to control the salinity of the water used in the power plant processes. The cooling water is able to be recirculated through the plant cooling system approximately 25 times, or until its salinity is 20 or more times the salinity of the source water, prior to its diversion to the evaporation ponds.

Regulations specific to the Palo Verde site do not allow discharging of blow-down to the aquifer. Therefore, APS receives 70-90 million gallons of water per day, but operates a “zero discharge” water management plan. To fulfill the requirements, Palo Verde operates three large evaporation ponds, totaling approximately 650 acres of lined area. The 650-acre footprint utilizes multiple layers of geosynthetics, as a means to ensure a BADCAT (Best Available Demonstrated Control Technology) leak-free system. The reservoirs allow the natural environment to evaporate approximately 60 inches / year of water across the 650 acres, which equates to about 1.1 billion gallons per year. Current research is on-going to provide more detail to the amount of water evaporated and the rate of evaporation across different months of the year.



Figure 2. Aerial view of the lined containment reservoirs for municipality wastewater and Evaporation Ponds. The 85-acre and the 45-acre reservoirs are shown above.

Water containment for both purposes on the site is subject to aquifer protection requirements. The following organizations apply oversight to Palo Verde water containment processes: Nuclear Regulatory Commission, Arizona Department of Environmental Quality / Environmental Protection Agency, Arizona Department of Water Resources Dam Safety, and the Maricopa County Flood District.

3.0 INITIAL CONSTRUCTION OF THE RESERVOIRS

The use of a geosynthetic liner material in a reservoir application is a common design/construction option for the storage of various liquids. The relatively impermeable characteristics of a geomembrane provides a cost-effective option, especially in areas with a lack of low permeability soil, and provides superior containment and a decreased construction schedule when compared to a compacted soil liner. Many factors are involved when designing an impoundment with a geomembrane. Key decisions for the Palo Verde facility include:

- Exposure of the geomembrane to the environment (UV rays, wind, etc)
- Expected lifetime of the product and system
- Expected performance of the system (Allowable Leakage Rates)
- Subgrade Preparation and armament of side slopes

3.1 Wastewater Reservoirs

The original design for containment of wastewater at the treatment facility included the construction of an 85-acre reservoir which can store up to 788 million gallons of cooling water. This was the first containment area constructed at the facility and was put into service in 1982. The design consisted of 3:1 side slopes and the chosen lining materials included a rubberized asphalt base liner on the floor and Hypalon on the side slopes.

The impoundment was single-lined and construction utilized state-of-the-art technology for that time. After more than 20 years of operation, the lining began to fail as it reached its operational end-life. The reservoir then was re-designed and reconstructed. Lessons learned from the operation of the first impoundment along with the use of BADCAT provided information that led to a complete redesign for all future impoundments to be constructed at the Palo Verde site.

The newly designed reservoir would need to be taken out of service in order to be relined; however, the plant could not afford to stop service. Therefore, construction of a second wastewater reservoir began in 2005 which allowed the plant to operate while the 85-acre reservoir was under construction. Most importantly, APS not only wanted to be compliant in

its new design, it wanted to set the bar for all future water containment. As with any innovative concept, the design of the next impoundment would incorporate “lessons learned” from the initial construction in order to minimize similar issues going forward. Major revisions included flattening the side slopes to 4:1 in order to reduce the forces of wave action. Additionally, the subgrade on the side slopes was enhanced with soil cement as an additional armament against wave action. This was a very innovative approach at the time and the project was recognized by the soil cement industry. This also would become the site’s first double-lined system with an extensive LCRS (Leak Collection Recovery System); hence, leading to the design of the future evaporation ponds. The redesign and reconstruction of the evaporation ponds is detailed in section 4.0 of the paper.

3.2 Evaporation Reservoirs for Storage of “Blow-down” Water

The initial site design included two large lined reservoirs for evaporation of the blow-down water. The first pond constructed for evaporation purposes was the 250-acre pond termed Evap Pond 1. Initial construction was completed in 1986. The reservoir now is in its third generation, in that the first liner system reached its design life and was replaced in 1991 and the third generation currently is under construction at the time of this paper (August 2012). Evap Pond 1 initially was constructed just after the 85-acre reservoir and utilized a very similar design of 3:1 sideslopes and an asphalt base liner on the floor and Hypalon on the side slopes.

Evap Pond 2 was the next reservoir to be constructed. It utilized high-density polyethylene (HDPE) geomembranes, which were gaining more acceptance within the industry. Construction began in 1988 and was completed in 1989. The surface area is approximately 220 acres and again was constructed with 3:1 side slopes, but utilized a more traditional liner profile, as recognized today. The liner system consisted of a geotextile cushion installed directly over the subgrade and a 60-mil black HDPE geomembrane was placed over the textile. The switch to an HDPE liner produced satisfactory results for the site; however, operational concerns arose regarding the use of 3:1 slopes and the lack of a detection system associated with a single-lined system. The large surface area of the pond allowed desert winds to produce wave action across the pond, thus colliding into the side slopes and eroding subgrade soil from beneath the geomembrane. Evap Pond 2 has since been redesigned and reconstructed with the alternative design addressing these operational issues. The details of the design, construction and operation are discussed in Section 4.0 of the paper.

The initial wastewater treatment (WWTP) reservoirs and evaporation ponds still are in service today, but new materials have been installed using a revised design that incorporates a sophisticated leak detection zone in a double-lined profile. Given the size and depth of the ponds, the minimum standard for leakage between the primary and secondary membrane layers is quite low by industry standards. To monitor this, a state-of-the-art leak detection system was designed which includes remote level sensors and video monitoring of the sumps (See Section 5.0). Additionally, the site includes the 45-acre Wastewater Storage Reservoir and Evap Pond 3 (180 acres) which were both constructed in order to provide operational water storage capacity during reconstruction of the existing ponds.

4.0 PHASE II REDESIGN AND RECONSTRUCTION OF RESERVOIRS AND EVAP PONDS

Construction Timeline - Palo Verde Water Reclamation Facility and Evaporation Ponds

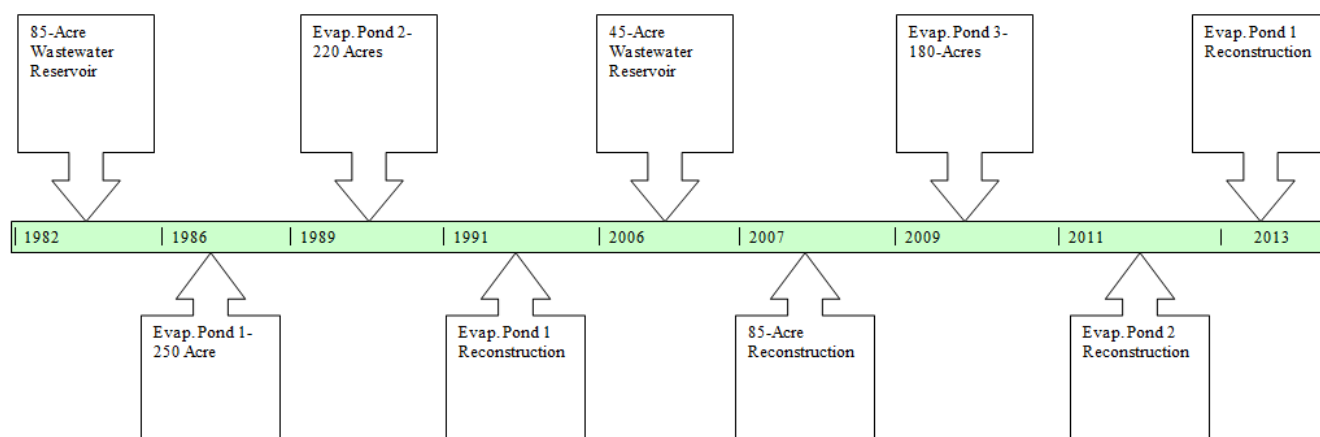


Figure 3 – Timeline of Initial and Reconstruction of Containment Projects.

The first pond that required redesign and reconstruction was Evap Pond 1 and the work was completed in 1991 (Figure 3). This pond consisted of 3:1 side slopes, rubberized-asphalt liner on the floor, and Hypalon on the side slopes. The subgrade beneath the Hypalon material had been eroded in areas due to the wave action across the large 250-acre surface area of the pond. The redesign / reconstruction sought to stabilize the side slopes and a BADCAT evaluation also provided a revised geomembrane material choice for the pond. To stabilize the side slopes, Palo Verde required soil cement armoring on the internal side slopes of the pond. To accomplish this work, the Hypalon material was removed from the slopes and the asphalt floor liner remained. The soil cement layer then was constructed on the side slopes, followed by a geotextile cushion layer and a 60-mil HDPE black geomembrane throughout the entire pond. This was the first project that included soil cement and HDPE geomembrane as the primary components for containment in the Palo Verde site. All additional construction and reconstruction of reservoirs and ponds now include soil cement armament and an HDPE geomembrane product.

The next project implemented by Palo Verde included the addition of a 45-acre reservoir for the water reclamation facility. The existing 85-acre reservoir had been in service since 1982 and was beginning to reach the end of design / service life. Closing the Water Reclamation Facility (WRF) during reconstruction of the 85-acre reservoir and ultimately ending the supply of cooling water to Palo Verde was not an option, so a second reservoir was to be constructed to allow operation of all facilities during construction and to add additional capacity when both reservoirs are operating. The 45-acre reservoir was completed in 2006 and included a cutting-edge design consisting of advanced geosynthetic products and a robust LCRS and monitoring infrastructure. Products included a geosynthetic clay liner (GCL), conductive white-surfaced geomembrane, primary and secondary geomembrane layers and LCRS. Major components of this next generation design for the Palo Verde site have been included in all subsequent projects.

The 45-acre reservoir located at the WRF was the first “new-excavation construction” project since Evap Pond 2, which initially was constructed in 1989. A major component of this new construction included the use of 4:1 side slopes, in contrast to the 3:1 design that had been used on all other projects. The 4:1 slope design, which included the soil cement requirement from Pond 1’s reconstruction, was utilized to combat and limit wave action on the surface of the reservoir (Figure 4).

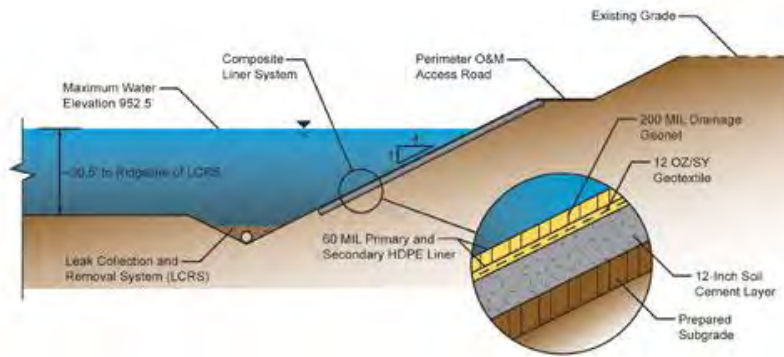


Figure 4. Side-slope armoring and liner profile used for the 45-acre WRF reservoir and reconstruction of the 85-acre WRF reservoir. (C. Wigginton, M Annala, J Mitchell, R Fongemie and S Pittalwala)

The profile of the liner system from top to bottom now included:

- 60-mil, white-surfaced, conductive, HDPE geomembrane (Primary)
- 200-mil HDPE geonet drainage product
- 60-mil, white-surfaced, conductive, HDPE geomembrane (Secondary)
- Non-woven geotextile cushion layer
- Soil cement subgrade

The addition of a second layer of geomembrane produced a leak detection zone or leak collection and recovery system (LCRS) for the reservoir. The dual-lined or primary and secondary geomembrane layers can be compared with the design and operation of a double-hull ocean vessel, when containment of liquids is discussed. The outer hull or primary geomembrane layer is the initial containment barrier and is subjected to large head pressures, especially in the case of the approximate 30 foot depth of the ponds. The head pressure may expand any imperfections in the primary geomembrane, thus providing a pathway for leakage into the detection zone or space between the two layers.

Detection zone piping then is utilized to pump out the liquid and redistribute it into the evaporation pond. Removing the liquid from the detection zone also removes or eliminates head pressure that could build on the secondary geomembrane. The absence of pressure on the secondary geomembrane greatly increases the overall performance of a liquid impoundment. The incorporation of conductive geomembrane provides for the use of spark testing of the installed geomembrane layers. This test adds an additional layer of quality control to ensure the best possible installation and performance of the system.



Figure 5. Photo of secondary 60-mil conductive white-surfaced HDPE geomembrane with LCRS piping and gravel drain. Geonet drainage layer (black) is installed over the piping.

Palo Verde increased the performance of the detection zone by adding two additional features into the 45-acre reservoir design. The first enhancement required intricate grading of the subgrade elevations. The design used varying elevations that would separate any flow of liquid within the detection zone to separate monitoring areas, or sumps. This now would create subsections in the 45-acre floor plan, thus allowing Operations personnel to determine which area of the primary liner may be leaking in the event that “action level flow values” are exceeded. Additionally, pipe trenches were constructed into the subgrade (above the secondary geomembrane) to quickly collect and transport any leakage to the detection sumps (Figure 5). The detection sumps are equipped with visual operation hatches, flow meters and video monitoring equipment focused on the detection pipe outlets.

With completion and operation of the 45-acre WRF reservoir, reconstruction of the 85-acre reservoir could begin. Reconstruction began in late 2006 and was completed in 2007. All design revisions included in the 45-acre reservoir were implemented into the 85-acre reconstruction project. Although the existing side slopes of the reservoir were 3:1, the reconstruction included removal of the existing Hypalon geomembrane and excavating the slope back to a 4:1, then installing the soil cement armament required on all pond side slopes. With both WRF reservoirs reconstructed and operational, focus was shifted to reconstruction of the evaporation ponds.

A new construction/excavation project now was necessary to address the eventual reconstruction of Evap Ponds 1 and 2. Evap Pond 2 had been in service for more than 20 years by this time and was reaching operational end-life. It was not possible to take Evap Pond 2 out of service and continue to have adequate volume for storage of blow-down, so plans were made to design and build Evap Pond 3, which would be two separate ponds (A and B). Each would create 90 acres of surface area. Evap Ponds 3A and 3B were completed in 2009 and utilized a similar design as the 45-acre WRF reservoir, with two significant exceptions. A GCL product was utilized in place of the geotextile cushion layer that was installed above the soil cement and below the secondary 60-mil HDPE geomembrane. The GCL material layer added a significant amount of increased performance, in terms of overall containment performance of the geosynthetic system. Additionally, Palo Verde installed a video monitoring system within the detection sumps to observe the outlets of the detection system piping. The amount of flow within the detection system is recorded via flow meters. However, the addition of the cameras increased monitoring efforts to a 24-hour “real time” situation (Figure 6). With the completion of Evap Pond 3 in 2009, the site began to focus on the reconstruction of Evap Ponds 1 and 2, as the geosynthetic products in those ponds were reaching their respective design lives.



Figure 6. Leak detection monitoring equipment

After 22 successful years of service life, Evap Pond 2 reconstruction began in 2010 and was completed in 2011. The single-lined containment system of a geotextile cushion layer and one layer of 60-mil HDPE geomembrane was completely removed from the pond (Figure 7). Then, subgrade contours were re-graded to create isolated areas of the LCRS on the floor of the pond (Figure 8). This would allow for more rapid identification of any areas that showed signs of leakage.



Figure 7. Removal of existing geomembrane material in Pond 2

The existing 3:1 sideslopes were reconstructed to 4:1, as has become the standard, and the soil cement armament was installed. Evap Pond 2 utilized the same geosynthetic profile from Evap Pond 3 (GCL, 60-mil conductive white HDPE, geonet drainage, 60-mil conductive white HDPE). One additional design revision was incorporated into Evap Pond 2 construction, however. The berm used to separate Evap Ponds 3A and 3B produced another deterrent to wave action across the full surface area of the pond by splitting the surface area in half from 180 acres to 90 acres for each area. For this reason, two berms were created within the 220 acres of surface area in Evap Pond 2, thus creating Evap Ponds 2A, 2B and 2C.



Figure 8. Regrading of pond floor subgrade in Pond 2. The subgrade elevations isolate identifiable areas and sumps.



Figure 9. Photo of installed primary geomembrane layer and deployment of geonet drainage layer over installed secondary geomembrane.

Reconstruction and the third generation of Evap Pond 1 currently is under construction as of August 2012 (Figure 9). Approximately 50 percent of the geosynthetic materials have been installed in Pond 1B, with plans to move directly into Evap Pond 1C. Evap Pond 1A will be completed during 2013 and with that will complete the redesign and reconstruction of all lined reservoirs and ponds at the Palo Verde site. Evap Pond 1 “third generation” has utilized the same design as the reconstruction of Evap Pond 2.

Accountable installation is required, expected and specified at the APS facility. An installation for a typical APS project will consist of 30 – 40 employees. The labor components of the crew include a production supervisor and additional “non-working” supervisors for each individual component of the work. For example, a “non-working” supervisor is required to oversee the unloading of geosynthetic materials from delivery trucks (Figures 10 and 11). An additional superintendent would be required if GCL was being deployed, while another superintendent would supervise the geomembrane installation over the GCL. A full-time certified safety officer is provided by the installer to oversee and manage all safety requirements at the site. Six to ten operators are required to operate the flatbed trucks, forklifts, bobcats, loaders and water truck.

Another step in providing the greatest level of liquid containment, APS requires that all welding personnel be a Certified Welding Technician as recognized by the International Association of Geosynthetic Installers (IAGI).



Figure 10 – Delivery of geonet drainage material



Figure 11 – Unloading of geonet drainage material using man-lift for attachment of roll straps to excavator.

In total, more than 3,120 acres of geosynthetic materials have been installed and are currently used in operation of the Palo Verde facility. The acreage converts to approximately 136,000,000 square feet of material, or 2,360 United States football fields. For reference, if all of the material was cut into a 12-inch wide strip, that strip would reach around the 24,900 miles of the earth's equator. Innovative state-of-the-art geosynthetic products and accountable highest-quality installation play a major role in the containment of Palo Verde's water resources in this arid environment.

REFERENCES

Wigginton, C., Annala, M., Mitchell, J., Fongemie, R., and Pittalwala, S. (2008) *Soil-Cement Plays Key Role in Protecting Large Water Impoundments at Nuclear Generation Station*. Portland Cement Association, Skokie, Ill.

Geosynthetic Reinforced Soil – Integrated Bridge Systems: Successful Private Sector Case Studies over the Last 20 Years.

Robert K. Barrett, P.G., TerraTask, USA, bbarrett33@aol.com
Albert C. Ruckman, P.E., Soil Nail Launcher, Inc., USA, Al@soilnaillauncher.com
Colby E. Barrett, E.I.T., Soil Nail Launcher, Inc., USA, Colby@soilnaillauncher.com

ABSTRACT

The recent FHWA initiative to expand the use of GRS-IBS technology offers a multitude of benefits over more traditional bridge construction, including reduced construction time, 25 to 60 percent cost savings over pile foundations, and the elimination of the “bump at the bridge” problem associated with uneven settlement of the superstructure and the approaching roadway. GRS technology is based on closely spaced, relatively lightweight layers geotextile reinforcement alternated between layers of compacted granular fill, with the bridge superstructure founded directly on the GRS composite. This flexible, simple, and generic technology is a viable option for many single-span bridges, but is often perceived as a “new” technology. This paper presents case studies from 5 bridges built using GRS-IBS technology in the private sector over the last 20 years including a 191-foot span bridge built in Montana, a historic bridge replacement project in one of California’s highest seismic zones, and an abutment constructed on 90 feet of zero blow count soils in Jamaica.

1. INTRODUCTION

1.1 GRS Technology – Ancient Roots

Thousands of years before the concept of “Reinforced Soil” became widely accepted, ancient people had already used soil with vegetative tensile inclusions to build structures. As early as 1000 B.C., early Mesopotamians used layers of reeds and packed clay to build the cores of their ziggurats. Portions of the Great Wall in China were reinforced using the twigs of tamarisks trees between layers of gravel and clay. An engineer named Pan in the Ming dynasty was well known for using willows to stabilize earth dikes in China (Barker, 1994). As recently as the 1960’s, tin miners in Malaysia placed grass stems in their mine tailings piles to prevent slope failures (Hengchaovaich, 1999). Adobe and bricks made from straw and clay have been used for thousands of years (and are still used) from the Southwestern United States to Egypt to Central China.

Modern reinforced soil can trace its roots to French architect Henri Vidal in the mid-1960’s. Vidal’s system, known as *Terre Armee* used a dense array of small steel strips to reduce lateral earth pressure in earthen retaining walls. The first Reinforced Earth wall in the United States was built on California State Highway 39 (Northeast of Los Angeles) in 1972. The technology then spread throughout the country. In the mid-1970’s, these structures began replacing reinforced concrete structures previously developed by the Colorado Department of Transportation (CDOT) along interstate 70 near Vail pass. As I-70 was constructed through Glenwood Canyon, Reinforced Earth walls were also constructed, again using steel as reinforcement (in the form of strips and mesh mats).

Around the same time the U.S. Forest Service in the Pacific Northwest began using geotextiles to enable heavy logging trucks to travel over soft materials (Steward, 1977). In 1974 John Steward of the U.S. Forest Service and Professor Dick Bell of Oregon State University expanded this technology by constructing the first GRS walls in the United States (Holtz, 2004). A 6-ft high wrapped-face wall using lightweight geotextile was constructed in Oregon and an 18-ft high counterpart was constructed in Washington State. Stewart and Bell analyzed the walls using the tieback-wedge analysis, an adaptation of the work of Professor Lee at UCLA in 1973 (Lee, 1973). This theory was based on the geotextiles acting as “tiebacks” and the soil mass acting as it would on a traditional externally reinforced retaining wall. The equivalent lateral earth pressure coefficient (K_A) is determined by assuming a horizontal backslope and no wall friction, given an active zone defined by the Rankine failure plane. The amount of earth pressure at each elevation must be resisted by the geosynthetic “tieback” at that elevation. The “tiebacks” could fail in two modes: pullout and rupture, and the theory analyzed each. The theory was simple and revolutionary, but also over conservative, neglecting any composite behavior of the reinforced soil mass. Although the technology was new, Professor Bell seemed to intuitively understand that close reinforcement spacing would play a key role in wall stability (although Bell was also worried about under compaction, which small spacing helped to prevent).

Once again, CDOT researchers picked up on the revolutionary work with geosynthetics coming out of the northwest. Bob Barrett, Al Ruckman, and J.R. Bell built an 18-ft high wrapped face non-woven geosynthetic demonstration reinforced

soil wall on I-70 in Glenwood Canyon, Colorado with onsite granular backfill and closely spaced (8 to 10-in) reinforcement layers (Bell, 1983). Using the models available at the time, portions of the wall had a calculated safety factor of 0.33, but no failure was observed. Massive earth surcharges were added that lowered the safety factor to 0.11, but again the wall remained unaffected. Even after differential settlement of the wall foundation of up to 2 feet, the wall was unaffected. Fabric was exhumed periodically to determine degradation in soil.

This research project demonstrated that current models were overly conservative and that internally reinforced structures could endure massive surcharges and differential settlement. For the first time, researchers saw that internally supported structures may be more than a low cost replacement for externally reinforced structures, they may actually be superior. What was not understood at the time was that close spacing was the key to this “better than expected” performance.

The capstone to the GRS research efforts (especially for bridge abutment applications) was a CDOT demonstration project carried out in the Havana Maintenance Yard in 1996 that demonstrated the tremendous loads that GRS systems were able to withstand. Shown in figure 1, piers as narrow as 8 feet and over 24 feet tall were subjected to 2,340 kN loads without showing signs of distress during the loading process. Later analysis of the structure demonstrated that these loads were sustained even though the compaction on the piers was sub-optimal (likely due to the difficulty involved in running a plate compactor on an 8 foot wide platform 24 feet above ground) (Abu-Hejleh et. al. 2001).



Figure 1. Havana Yard GRS Pier Demonstration.

Later research also demonstrated that GRS with select granular backfill and closely spaced geotextile was one of the most resilient systems to seismic loading (Wu, 2006).

1.2 Applications

Following these research efforts, the authors and others in the private sector began using closely spaced (12 inches or less), lightweight woven polypropylene geotextile sheets in a well compacted granular backfill matrix in a variety of applications including avalanche and debris-flow barriers, rockfall catchment structures and barriers, retaining walls, and, notably, bridge abutments. All of the case studies presented were completed using design-build contracting on private sector projects. This method of contracting lends itself to the versatile GRS technology. At the time, few bridge engineers were willing to try a “new” technology, so the relatively few design-build firms able to use the technology saw a distinct market advantage over competing firms. Bridges were routinely constructed for less than half what a traditional pile-founded bridge would cost, with construction times often 30% of the traditional option. Today, as more engineers understand the technology most GRS-IBS projects are completed through bid-build contracting, and the technology is much more prevalent in the public sector. Cost and time savings to the ultimate client are similar to design-build contracting once construction commences.

1.3 FHWA Design Methodology

Building on CDOT research efforts and the myriad of GRS abutments constructed starting in the late 1990s, FHWA researchers presented an interim implementation manual for Geosynthetic Reinforced Soil Integrated Bridge Systems (GRS-IBS) in early 2011 (Adams, et al., 2011). The manual identified the GRS-IBS technology as simple to design and construct, easy to modify in the field, and appropriate for construction in various weather conditions. The manual also notes that when compared to traditional bridges systems, GRS-IBS costs less (by 25-60%), can be completed in less time, requires less maintenance (primarily by eliminating the “bump at the bridge” due to differential settlement between the abutment and the superstructure) and is more durable (Adams, 2011).

As the cost savings associated with GRS-IBS would be in the billions if implemented nationwide, the technology was selected for deployment through the FHWA’s Everyday Counts (EDC) initiative. EDC is designed to identify and deploy innovation aimed at shortening project delivery, enhancing roadway safety, and protecting the environment. Selection by the EDC is evidence of how far GRS technology has come from its experimental roots in the 80’s and 90’s, as the program is focused on “taking effective, proven and market-ready technologies and getting them into widespread use” rather than “inventing the next ‘big thing.’”

Currently, the initiative has over 60 public bridges across the U.S at some stage of development and construction, including multiple on the interstate highway system. Ironically, FHWA researchers have had to overcome the incorrect assumption that GRS-IBS is a “new” or “experimental” technology, although, as the case studies below demonstrate, many of these structures are now entering their 15th year of service. Figure 2 shows a typical GRS-IBS abutment cross section.

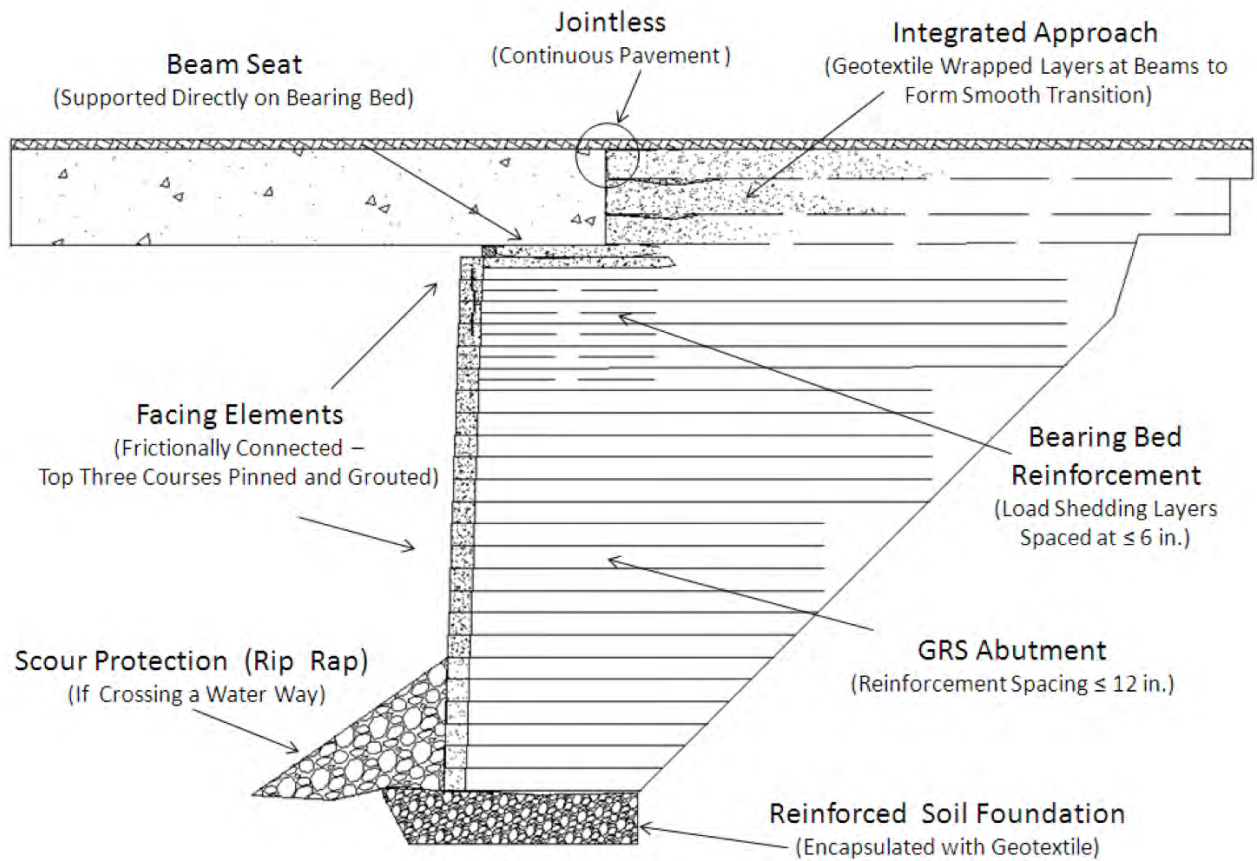


Figure 2. Typical Cross Section of GRS-IBS Abutment (Adams et al., 2011).

2. CASE STUDIES

2.1 Tied Arch Bridge near Black Hawk, CO (1998)

The abutments were constructed above the city of Black Hawk, Colorado, to support a 118 foot span steel arch bridge. The abutments were constructed with the on-site granular soil and reinforced with layers of a woven geotextile (Amoco brand 2044 fabric) on 12 inch spacing, with native rock as the facing element rather than the more traditional concrete blocks. As with blocks, the reinforcement sheet extended to the front face of the wall to provide a positive frictional connection between the facing and the abutment. Tie rods were drilled through the abutments into bedrock and tensioned to pre-load the abutment prior to bridge installation. Although this method is effective in reducing or eliminating settlement of GRS abutments, later research showed that vertical abutment strain without preloading is well below 0.5% at typical design loads (Adams, 2011). A view of the bridge is shown in figure 3 below.



Figure 3. Black Hawk Bridge, with mortared native stone facing.

2.2 Abutment near Green Island, Jamaica (1999)

A 30 foot tall abutment was constructed near Green Island, Jamaica as part of an island-wide highway upgrade initiative through design-build contracting. Initially, the West abutment of the bridge was to be founded on piling. The design-build contractor from Korea was unable to get the required equipment to the abutment site, which was in a mangrove swamp overlying 90 feet of zero blow count alluvial silt. Layers of geotextile and marl fill provided access to the site and also as the abutment material. Photographs of the construction process and the finished abutment are shown in figures 4 and 5. The abutment was constructed in lifts to allow pore water pressures to dissipate, and settled globally approximately 24 inches. A surcharge was added to simulate the load of the bridge deck. During the process, currency fluctuations and political factors resulted in a change in the international design-build contractor. The new design team was unfamiliar with GRS-IBS technology and opted to abandon the abutment and construct a traditional pile founded bridge at nearly 3 times the cost. This project demonstrated that with proper construction staging and surcharge loading, the GRS-IBS system can be installed on the weakest of soils.



Figure 4. Green Island bridge under construction. The construction was nearly all completed using local unskilled labor and hand tools.



Figure 5. View of abutment after completion of surcharge loading.

2.3 Bridge near Mammoth Lakes, CA

An historic bridge near Mammoth Lakes, CA required replacement due to structural deficiencies of the superstructure. Moreover, the abutments and pillars were of unknown quality but were required to be preserved for aesthetic and historic reasons. After the original superstructure was removed, the area behind the abutment walls was excavated and replaced with GRS composite. A new deck was placed on the GRS composite so that with full loading the deck would not touch the existing pillars (as shown in figure 6). The end result was a modern GRS-IBS bridge that appeared to be resting on historic abutments and piers. This project demonstrated the flexibility of the GRS-IBS system and the cost savings associated with leaving existing abutment walls in place.



Figure 6. Mammoth Lakes bridge. Note that the deck clears the historic piers by approximately 4 inches.

2.4 Private Development Access Bridge near Big Sky, MT (2001)

Access to a private development crossed a protected stream and terminated on an ancient landslide in one of Montana's highest seismic zones. Traditional bridge options required piling and post-tensioned ground anchors. The GRS-IBS approach shown in figure 7 spanned the gorge with a 191 foot single span steel girder bridge founded on GRS abutments, at approximately 25% the cost of the traditional solution. Post construction settlement has been negligible, even after the owners placed a 100,000 pound decorative timber cladding on the bridge in 2004. To the authors' knowledge, this is still the longest GRS-IBS bridge in the world.



Figure 7. Big E-Z bridge. At 191 feet, the longest GRS-IBS structure in the world.

2.5 Private Access Bridge, Sonoma County, CA (2011)

Access to a timber tract in Sonoma County required a single span bridge. The developer had traditionally installed railcar bridges founded on piling, but wanted to reduce the cost of construction. The on-site material was highly granular and met the specifications for GRS-IBS backfill. Figures 8, 9, and 10 show the relatively simple plan set, the site during construction, and the final product. The bridge was completed in approximately two weeks at significant cost savings over the traditional method. Although this case study demonstrates the cost savings associated with using on-site backfill, this would not be feasible in most parts of the United States. Notable exceptions would be mountainous areas in the Rockies, Sierras, and Pacific Northwest, as well as areas with clean sandy soils in the Southeast.

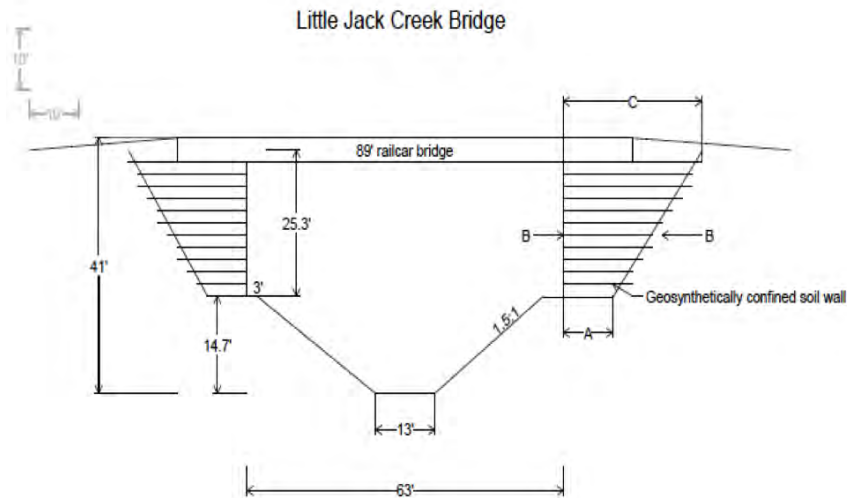


Figure 8. Typical elevation view of access bridge.



Figure 9. Abutments during construction. Using two crews cut construction time in half.



Figure 10. Completed railcar bridge.

3. GRS OBSERVATIONS

Following nearly 30 years of work with GRS, the authors have been continually impressed with the versatility and durability of the technology. However, many misperceptions about how the technology actually “works” remain. The FHWA GRS-IBS interim implementation manual makes great strides in dispelling myths associated with the technology, but a few notable ones continue to pervade the engineering community.

3.1 GRS Is Just a Subset of Mechanically Stabilized Earth (MSE)

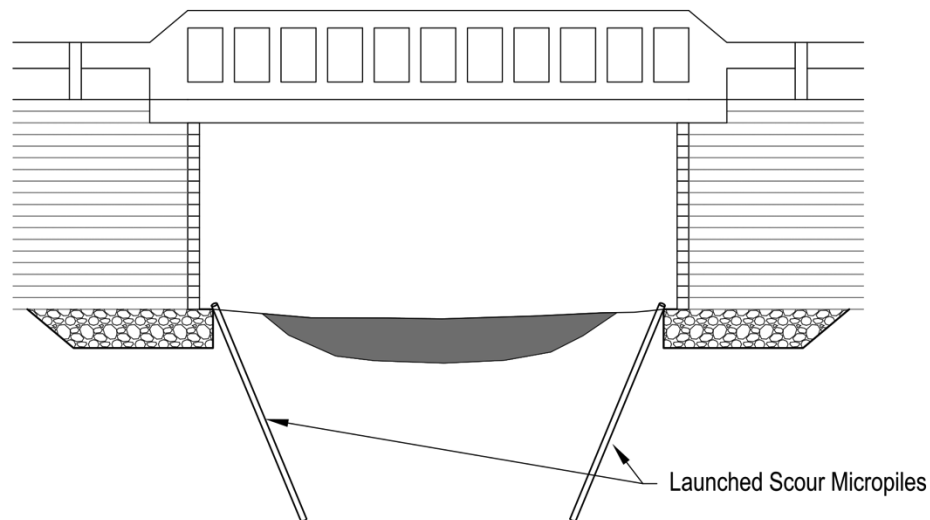
Although the components of MSE and GRS are identical (reinforcement, facing, and earth backfill) the similarities end there. The grids used in MSE are designed -- and performs as -- tiebacks. The load in the MSE system is carried by the reinforcement, with only negligible composite behavior. In contrast, GRS using close spacing performs as a unique composite system, where the performance of the structure cannot be accurately quantified by adding the properties of the constituent parts. The function of the reinforcement in GRS is not to carry load, but to confine the granular soil particles so they cannot dilate. If the individual particles are prevented from dilating, they must fail through shear. Shearing of bedrock particles is difficult, and explains why GRS test pillars require nearly 22,000 lbs/sf to fail. For this reason, the authors typically refer to the technology as Geosynthetically Confined Soil (GCS®) to be clear that the confined soil, rather than the confining inclusion, is doing the work in the system.

Unlike MSE, GRS is not reliant on the *quality* of the confining inclusion but the *quantity*. Closely spaced inclusions, 8 to 12 inches, provide significantly better confinement, causing the failure mode to divert to shear through the particles. 8 inch spacing with woven geosynthetics with wide strip tensile capacities of 100 to 400 pounds per foot is a common solution (Wu et al, 2006). Also unlike MSE, where low quality backfill can be used, GRS backfill must be a friction-controlled material (road base or other granular aggregate). On site soils (especially cohesive soils) are generally shunned for lack of consistency and propensity to creep. There are instances where local sands and gravels will meet structural fill requirements and can be used. The operative word here is structural; poor quality backfill will not demonstrate confinement and transition to particle shear failure modes. Compaction is absolutely critical for GRS particle confinement. Uncompacted backfill will not self-compact with loading; rather it will fail, failing the tensile inclusions.

The facing in GRS systems is the weakest part of the system. Unlike MSE, where large proprietary blocks with mechanical connections to the grids have been shown to positively affect global stability, GRS uses lightweight facing with friction connections more as a forming element and permanent erosion control facing. Indeed, if the facing is lost in a GRS system, the only structural issue is subsequent erosion of the actual load-carrying element – the granular backfill.

3.2 GRS Abutments Cannot be Used in Scour-prone Areas

As spread footings, GRS abutments are subject to scour undermining if improperly designed. However, any abutment is subject to scour, regardless of whether the superstructure is founded on deep foundations. The presence of scour should never preclude the use of GRS-IBS, rather, it should necessitate the use of appropriate and site-specific scour protection measures. These include founding the reinforced soil foundation below scour depth, installing riprap aprons, gabion mattresses, articulating concrete blocks, or other proven technologies. The authors have had good success with the use of scour micropiles (shown in figure 11) to protect GRS abutments from undermining. These are typically drilled or launched at a 30-45 degree sub-vertical angle. If the center-to-center spacing of the piles is 3 times the micropile diameter (or less) they will typically behave as a continuous wall.



BRIDGE ABUTMENT / CULVERT SCOUR PROTECTION

Figure 11. Typical Cross Section of scour pile installation.

3.3 GRS Abutments Settle, and Always Require Firm Foundation Soils

As shown in the FHWA Implementation manual, vertical strain in GRS abutments is less than 0.5% under typical design loads (Adams, 2011). Although the internal abutment settlement is negligible, there is always a possibility of settlement of the foundation soils under any bridge abutment. In the authors' experience, settlement of foundation soils for bridge replacements is generally negligible, as the existing abutment served as a long-term surcharge load. For new construction, settlement should be evaluated and taken into account in design, but in itself settlement is not a limiting factor. The abutment in Jamaica settled over 24 inches during construction and surcharge loading. Long-term foundation settlement in GRS-IBS structures is actually superior to that of conventional bridges. In both cases, the abutments settle. In GRS-IBS, this serves to lower the superstructure by a commensurate amount. In a traditional system, the superstructure remains rigid, causing the ubiquitous "bump at the bridge" phenomenon. The only issue with global settlement with GRS-IBS would be differential settlement, which can be mitigated by using a lightweight backfill, pre-loading, or other design measures.

3.4 GRS-IBS Span Length Should be Kept Below 140 Feet

According to the FHWA implementation manual, "[t]he demands of longer spans on GRS-IBS are not fully understood at this time, and it is recommended that engineers limit bridge spans to approximately 140 ft until further research has been completed." While the authors agree with the requirements to quantify loading for all bridges (especially longer spans), our experience with spans as long as 191 feet show that this arbitrary limitation on span length is not necessary and has precluded the use of GRS-IBS in otherwise appropriate sites.

4. CONCLUSIONS

Ancient peoples intuitively understood reinforced soils. In the modern era, this powerful technology was resurrected and quantified by researchers in the public sector. The private sector was the first to adopt the technology due to the significant competitive advantage conferred on early-adopters of the technology. The FHWA effort to bring this powerful technology to the public sector will save the transportation community billions of dollars and should be commended.

ACKNOWLEDGEMENTS

The authors would like to thank Mr. Mike Adams and Dr. J. T. H. Wu for their contributions in providing much of the background information and references for this paper.

REFERENCES

- Abu-Hejleh, Nasar et al., (2001) *Results and Recommendations of Forensic Investigation of Three Full-Scale GRS Abutment and Piers in Denver, Colorado*, Colorado Department of Transportation, Denver, CO, CDOT-DTD-R-2001-6
- Adams, M. T., Ketchart, K. and Wu, J.T.H. (2007) Mini Pier Experiments: Geosynthetic Reinforcement Spacing and Strength as Related to Performance, *Geo-Denver 2007: New Peaks in Geotechnics*, Denver, Colorado, USA.
- Athanasopoulos, G.A., (1993) On the Enhanced Confining Pressure Approach to the Mechanics of Reinforced Soil, *Geotechnical and Geological Engineering*, 12: 122-132.
- Barker, D.H., (1994) *Vegetation and Slopes*, Thomas Telford, London.
- Barrett, R.K., (1996) *Bedsheets as Earth Reinforcements?* Videotape, Colorado Transportation Institute.
- Barrett, R.K., (1993) Dispelling Myths, *Geotechnical Fabrics Report* 11:36-40
- Bell, J.R., Barrett, R.K., and Ruckman, A.C. (1983) Geotextile Earth-Reinforced Retaining Wall Test: Glenwood Canyon, Colorado, *Transportation Research Record*, National Academy Press, Washington, D.C. 916: 59-69.
- Christopher, B.R., and Holtz, R.D. (1985) *Geotextile Engineering Manual*, U.S. Federal Highway Administration, Washington, D.C., FHWA-TS-86/203.
- Haliburton, T.A., Lawmaster, J.D., and McGuffy, V.C., 1981, The use of Engineering Fabrics in Transportation Related Applications, Final report under contract No. DTFH-80-C-0094
- Hengchaovanich, D., (1999) 15 Years of BioEngineering in the Wet Tropics, *First Asia-Pacific Conference on Ground and Water BioEngineering*, Manila, Philippines
- Holtz, R.D., (2004) Geosynthetics R&D – The “Early” Days (1960s to Circa 1985) *Symposium Honoring the Research Achievements of Dr. Robert M. Koerner*, Folsom, PA, USA
- Lee, K. L., Adams, B. D., and Vagneron, J. J., (1973) Reinforced Earth Retaining Walls, *Journal, Soil Mechanics Division, ASCE*, 99: 745-764.
- Leshchinsky, D. and Vulova, C., (2001) Numerical Investigation of The Effects of Geosynthetic Spacing on Failure Mechanisms in MSE Block Walls, *Geosynthetics International*, Vol. 8, No. 4: 343-365.
- Steward, J., Williamson, R. and Mohny, J. (1977) Guidelines or Use of Fabrics in Construction and Maintenance of Low Volume Roads, USDA Forest Service, Portland, Oregon.
- Wu, J.T.H., (2001) Revising the AASHTO Guidelines for Design and Construction of GRS Walls, CDOT Research Branch, Report No. CDOT-DTD-R-2001-16.
- Wu, J.T.H., Lee, K.Z.Z., Helwany, S.B., and Ketchart, K. (2006) design and Construction Guidelines of Geosynthetic-Reinforced Soil Bridge Abutments with a Flexible Facing, NCHRP Report 556, Transportation Research Board, Washington, D.C.

Geotextile Constriction Size and Physical and Chemical Clogging Potential

Sangho Lee, Ph.D. and P.E., GESTRA Engineering Inc., slee@gestrainc.com

ABSTRACT

Geotextile constriction size is critical to estimate clogging/blinding potential of base soils planned for drainage or protection from internal erosion. Author updated polyhedra model adapted by Faure (1990) to produce reasonable opening size distribution examinable by bubble point method (ASTM D6767) or apparent opening size (ASTM D4751). Particle size comparison with geotextile constriction enables to analyze potential of either physical or chemical clogging fate. Probabilistic simulation using Markov Chain was conducted to predict the clogging fates of non woven geotextile depending on particle size of filtered soils and geotextile porosity.

1. INTRODUCTION

Geotextile has been used in many civil infrastructures (e.g., retaining wall drainage, road way underdrain and earth dam toe drain) replacing granular filters with advantages of convenient installation process and quality controlled material properties (porosity, constriction size distribution, thickness). However, piping, blinding and internal clogging can occur at geotextile filter as well as granular filters under an unfavorable site soil/hydraulic condition.

Past nationwide field investigation on the drainage systems employing geotextile filters revealed that current deterministic filter design format was incapable of predicting the filter clogging especially associated with non-cohesive fine soils (i.e. well graded silty sands) (Wilson-Fahmy *et al*, 1996). The failures of filter designs were considered from the subtle migration behaviors of the non-cohesive fine particles which is not explicitly explainable with a few deterministic parameters of the current design methods.

Geotextile fabric can be considered as multi layered sieves since seepage flows and soil migration directions are relatively uniform and consistently transverse to the geotextile plane compared to the retained granular layer where fine particle migration shows a more random direction and dispersive pattern. Both granular and geotextile filter regions are characterized with constriction features, but the constituent shapes are spheres for the soil and strings for the geotextile.

Rigo *et al* (1990) found the filter opening size (i.e. $O_f^* = O_{f,90}$ or $O_{f,95}$), the largest opening size of geotextile (GT), has the greatest influence on the filter performance among filter design parameters. This finding implies that fine particle migration in nonwoven GT should be explained with other than a filtration mechanism of granular filters, the retention performance of which is mainly controlled by the minimum constriction size as demonstrated by Giroud (1996). Later, Bhatia and Smith (1996) demonstrated with experimental works that the breadth of opening size distribution (OSD) of nonwoven GT is also related to the nonwoven GT filter performance. OSD presenting the effective pore channels (the smallest constriction sizes) of nonwoven GT can be successfully assessed by the bubble point method (ASTM D 6767) (Bhatia *et al*, 1996). At present, CSD of nonwoven GT is measurable using image analysis (Aydilek *et al*, 2005), or can be inferred from the OSD from the bubble point method (ASTM D 6767) and the filter opening sizes (O_f^*) with a reasonable probabilistic assumption (Giroud *et al*, 1998).

A new filter design is strongly demanded to overcome the limitation of existing deterministic designs which were proven ineffective for well graded and non-compacted soils. Probabilistic model is considered as an effective approach coping with the random features of geotextile CSD and soil GSD, and it enables to envision the behaviors of fine particle migration differentiated by the various filter performances. In this paper, probabilistic models, developed to explain the behaviors of fine particle migration inside geotextile filters, are introduced, and the methodology and basic assumptions of the models are reviewed, compared and modified as for feasibility study to predict physical and/or chemical clogging within geotextile filter.

2. REVIEW OF EXISTING PROBABILISTIC MODEL AND ITS MODIFICATION

2.1 Poissonian Polyhedra Model and Analogy Sieve Model for Geotextile Constriction Size

Probabilistic methods have been developed to predict the filtration behaviors of nonwoven GT associated with various types of soils (Giroud, 1996, Giroud *et al*, 1998, Faure *et al*, 1990 and Elsharief and Lovell, 1996). Faure's *et al* (1990) interpreted the pore structure of geotextile as a layered sieve model consisting of sub elementary sieves, the CSD feature of which can be described with a gamma distribution or Poisson distribution (Figure 1). In the model, fiber specific length, χ plays a critical role to the CSD change of Poissonian polyhedra model (Matheron, 1971).

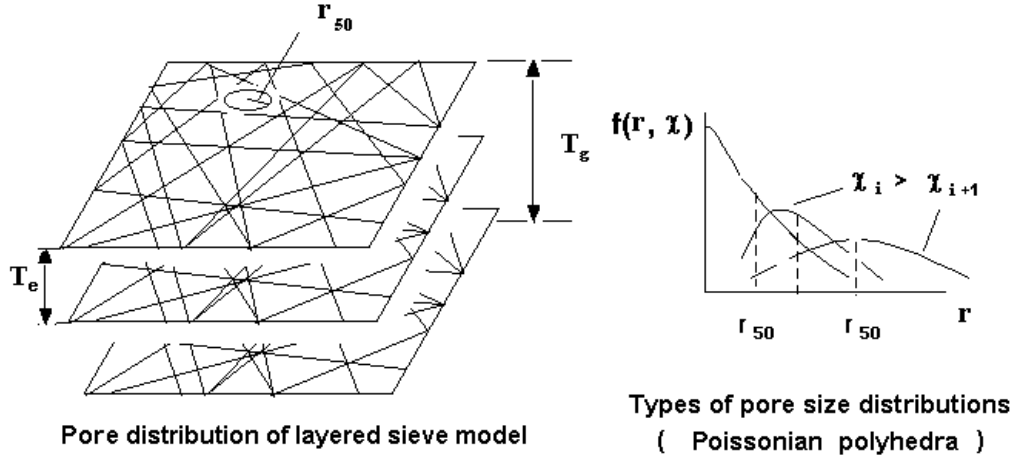


Figure 1 Layered sieve model presenting pore structure of non woven geotextile. (T_e : distance between sub elementary layers, T_g : geotextile thickness, χ : geotextile fiber specific length, r : constriction radius)

The random opening feature of nonwoven GT can be described with a cumulative probability, presented as $F(r, \chi)$, a function of input parameters of specific length, χ (fiber length per unit area) and inscribed constriction radius, r .

$$F(r, \chi) = 1 - [(1 + \chi r)^2 e^{-2\chi r}] \quad \text{from Matheron, 1971 [1]}$$

The probability density function (PDF) can be derived from taking the derivative of $F(r, \chi)$ with respect to constriction radius, r

$$f(r, \chi) = 2\chi^2 r (1 + \chi r) e^{-2\chi r} \quad [2]$$

In Figure 2 the transitions of PDF from Gaussian distribution to Poisson distribution are compared as specific length, χ increases.

The PDF feature of the Poissonian polyhedra model can be confirmed with an analogy model of wired mesh sieve. If $f(x)$ and $f(y)$ present the PDF of the wired mesh spans in x and y axes, respectively, the uniform $f(x)$ and $f(y)$ can represent the CSD of geotextiles with low fiber density and the declined wedge shapes can present the CSD of geotextiles with high fiber density (Figure 3).

Joint probability density function, $f(x,y)$ is calculated from the $f(xy)$ presenting the PDF of the opening area size. However, the $f(x,y)$ itself cannot depict the probabilities of the soil particles confronting the geotextile constrictions with different areas because the soil accessibility shall increase by the constriction area size as well as the constriction frequency. The redefined cumulative probability function, $F^*(z)$ accounting for constriction area where z is defined x times y , can be rewritten as the following formula. This is schematically depicted in Figure 3.

$$F^*(z) = \Pr\{d \leq z\} = \frac{\iint_0^z xyf(x, y) dx dy}{\iint_0^z xy dx dy} = \frac{\int_0^z \alpha f(\alpha) d\alpha}{\int_0^z \alpha d\alpha} \quad [3]$$

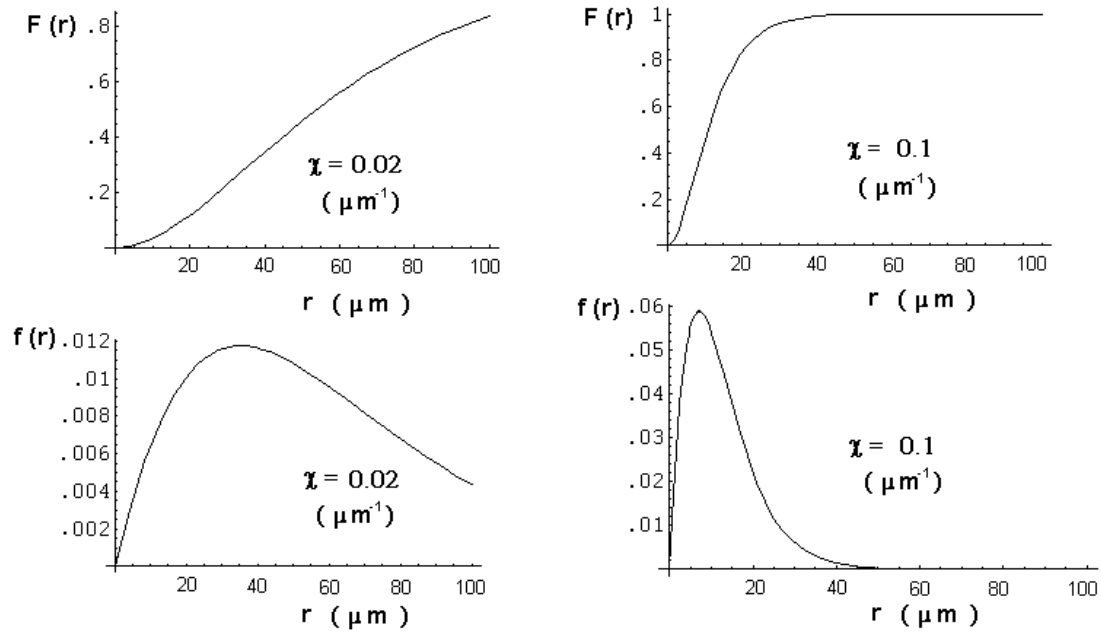


Figure 2 Transitional constriction size distributions of nonwoven geotextile with increase of the fiber specific length (χ) based on Matheron's model (1971). ($F(r)$ is cumulative probability function; $f(r)$ is probability density function where r is constriction radius)

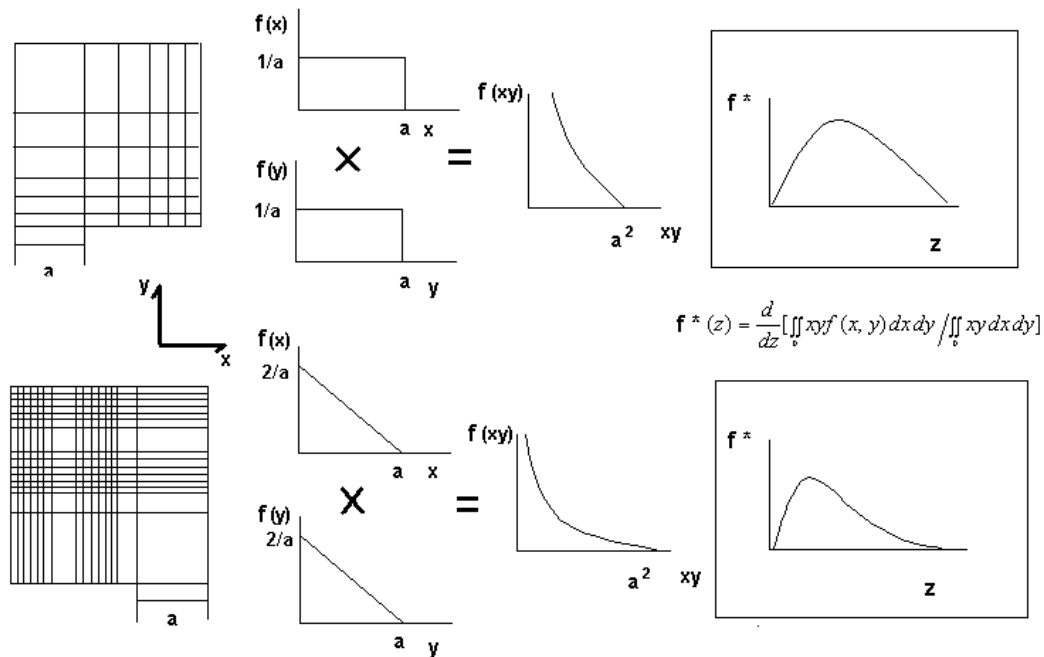


Figure 3 Analogy model of wired mesh openings to explain the constriction size distribution of non woven geotextile. (f is frequency, a is the maximum size of openings, and $z=xy$)

The associated PDF, $f^*(z)$ can be derived from taking the derivative of cumulative $F^*(z)$. Similar to Figure 2, the mesh opening CSD becomes closer to the Poisson distribution as the wire intensity increases (Figure 3).

Fiber diameter (d_f) was considered the sub elementary layer thickness (T_e) in the Faure's model (Faure *et al*, 1990). Thus, calculated $O_{f,95}$ values of the thick nonwoven GT were not compatible with sieve test results due to the excessive sub layer numbers.

Urashima and Vidal (1998 and 2002) investigated experimentally the unit step walk distance with which the geotextile pore structures can be considered consisting of multi sieve layers sharing a common CSD, estimated from a probabilistic model or semi-empirically method such as by image analysis. A greater unit walk distance was measured for geotextile filters from the laboratory experiments compared with the granular filter ones.

2.2 Faure Model Modification for Production of Reasonable Sub Layer Number of Geotextile

If aforementioned findings are acceptable, Faure's model can be modified with a variable T_e , unit sub layer thickness depending on the design parameter, O_f^* (i.e. $O_{f,90}$ or $O_{f,95}$) determined from dry/wet sieving test or OSD from bubble point method, which subsequently influence on the sub layer number defined as $N = T_g/T_e$ where T_g is geotextile thickness.

Passing probability function or complementary cumulative probability function of geotextile constriction inscribed diameter ($d = 2r$) can be calculated with Faure's formula,

$$P(d) = 1 - F(d) = \left(\frac{2 + \chi(d + d_f)}{2 + \chi d_f} \right)^2 \exp[-\chi d] \quad [4]$$

where d_f is nonwoven GT fiber diameter, from Faure *et al*, 1990

Specific length, χ can be determined by the relationship with other geotextile properties. At each sub elementary layer of geotextile, the following equation is satisfied.

$$(1 - n)A \cdot T_e = \frac{\pi}{4} d_f^2 \cdot L \quad [5]$$

where n : porosity of geotextile, A : area of geotextile, L : length of textile fiber within the coverage area of A , T_e : the unit step walk distance between sub elementary layers

Therefore, the specific length, χ ($= L/A$) can be estimated from a determined T_e

$$\chi = \frac{4 T_e (1 - n)}{\pi d_f^2} \quad [6]$$

from Faure *et al*, 1990

The relationship between geotextile CSD and OSD is illustrated in Figure 4. Layer number is a critical parameter in determining the CSD from the OSD which is experimentally estimable by the bubble point method (ASTM D6767). In case OSD information is not available, the CSD can be assessed by the Faure's model with a O_f^* value from dry sieving analysis.

The specific length, χ for an sub elementary layer can be estimated from the value of O_f^* ($=O_{f,95}$ or $O_{f,90}$) measured by sieving tests (e.g. AOS from dry sieving or FOS from wet sieving). The CSD of sub layers is considered more compatible with the AOS value since the AOS is presumably independent of geotextile thickness (T_g) under cyclic dynamic load to facilitate particle penetration.

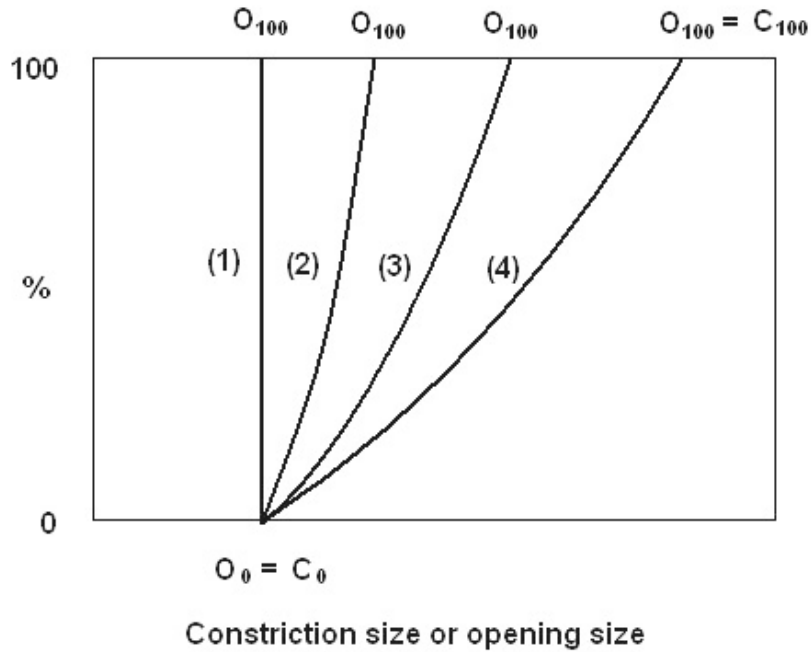


Figure 4 Opening size distribution curves of the four geotextile products from same nonwoven material, but with different thickness: (1) infinitely thick, (2) thick, (3) thin and (4) infinitely thin. (Curve (4) presents the constriction size distribution curves for the geotextiles.) from Giroud et al, 1998

$$P(O_{f,95}) = \left\{ \left(1 + \frac{O_{f,95}\chi}{2 + \chi d_f} \right)^2 \exp[-\chi O_{f,95}] \right\} = 0.05 \quad [7]$$

where O_f^* is based on $O_{f,95}$

The optimum value χ satisfying the experimental output (i.e. O_{95}) can be found by iterative method

$$2\text{Ln}\left(1 + \frac{O_{f,95}\chi}{2 + \chi d_f}\right) - \chi O_{f,95} = \text{Ln}(0.05) \quad [8]$$

Subsequently, the sub layer number, N can be determined from a relationship between T_e and χ (Equation 6). In comparison with original Faure's model (Faure et al, 1990), a CSD with smaller constriction size range was generated from the modified model for the same nonwoven GT porosity ($n=0.89$) and filtration opening size ($O_{f,95} = 0.21$ mm) (Figure 5).

For the nonwoven GT having 1 mm in thickness and 30 μm in fiber diameter, the sub layer number was calculated 6 by Equation 8, far less than 33 estimated by the original model. The modified CSD rendered a more realistic size range since unrealistic constriction sizes (i.e., over 1 mm) of the original CSD (Figure 5) was not produced. The OSD derived from the modified model also concurs with the lab experiment results of Bhatia et al (1996) in which the $O_{f,95}$ values of OSD are consistently smaller than AOS values for the tested geotextiles.

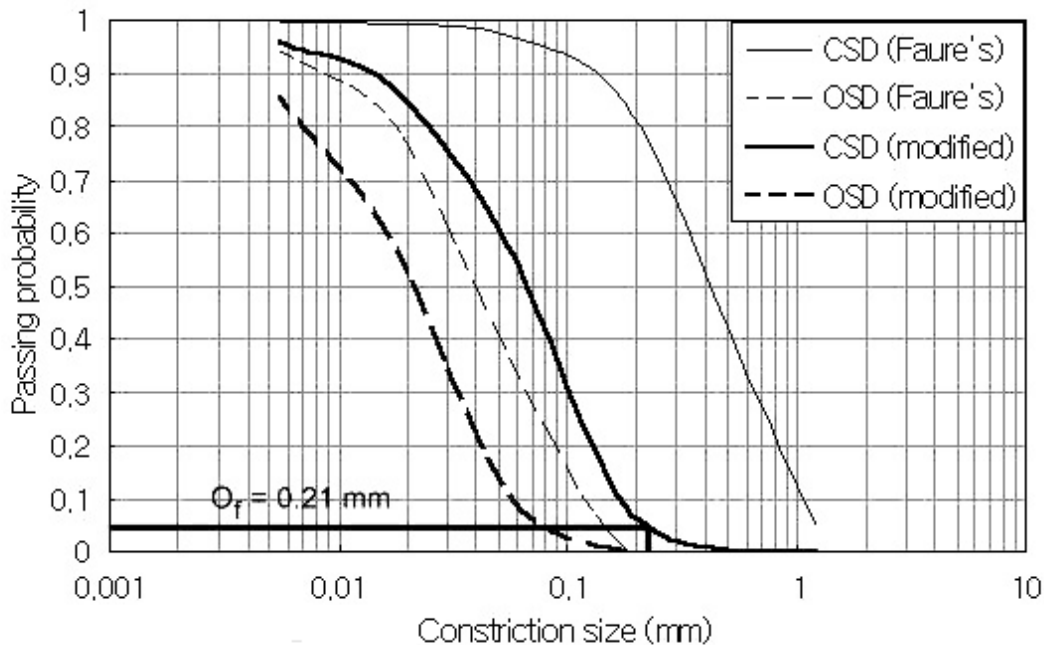


Figure 5 Constriction and opening size distributions of non-woven geotextile from the modified model proposed by author and original Faure's model (1990) where CSD: constriction size distribution; OSD: opening size distribution (detailed GT specifications are described in text contents).

3. PROBABILISTIC MODEL FOR FINE PARTICLE MIGRATION WITHIN GEOTEXTILE

Elsharief and Lovell (1996) developed an internal clogging model of nonwoven GT using the Markov chain theory. Their theory assumed three possible states of geotextile internal clogging exist such as the non-absorbing state when a particle size is smaller than the surrounding constrictions and two absorbing states when a particle size is larger than the constriction size or deposits onto the fiber surface. Even though their model took into account reduction in geotextile porosity under overburden pressure for the first time, Urashima and Vidal (2002) designated ignorance of additional non-absorbed state of small particles released from the fiber as the defect of the model.

In general, the porosity (n) of nonwoven GT influences on soil filtration performances primarily governed by seepage flow rate and capability of fine particle retention. A previous research indicated that the fine particle deposition onto geotextile fiber surface is less probable as the flow rate increases since the specific surface and the critical velocity producing particle deposition are much smaller than granular filter ones (Xiao and Reddi, 2000). However, the fine particle deposition will eventually occur inside nonwoven GT as the flow rate is attenuated by internal clogging process.

The pore sizes of nonwoven GT are more relevant to a physical clogging process, which prevails for non cohesive soils (e.g. fine sand and/or silt) whereas the fiber specific length of geotextile is more relevant to physicochemical process of fine particle deposition on the fiber surface, which prevails for cohesive soils (e.g. clay and/or bituminous soil). Therefore, both the constriction size and fiber specific length should be considered in the probabilistic model to explain the actual clogging behaviors of nonwoven GT influenced by both soil cohesiveness and particle sizes.

Porosity (n) needs to be associated with a retention probability, $1-P(d)$ in function of migrating particle size, d where $P(d)$ is a passing probability or cumulative probability function of constriction size, d since constriction areas are related to GT porosity. Meanwhile, the fiber density ($1-n$) needs to be considered in calculation of the particle deposit probability $q(d)$ (i.e., relative soil affinity to fiber material) in function of particle size, d (Figures 6 (a) and (b)). Hence, Markov chain formula used in the Elsharief and Lovell model (1996) needs to be expanded into including a non-absorb state of particle desorbed from geotextile fiber. Based on the four different cases of particle infiltration within geotextiles (Figure 7), the canonical form of the transition matrix can be reconstructed as following format.

$$\begin{matrix} & A & C & B & D \\
 A & \left[\begin{array}{cc|cc} 1 & 0 & 0 & 0 \\ 0 & 1 & 0 & 0 \\ \hline n(1-p) & (1-n)q & np & (1-n)(1-q) \\ n(1-p) & (1-n)q & np & (1-n)(1-q) \end{array} \right] & \equiv & \left[\begin{array}{c|c} I & O \\ \hline R & Q \end{array} \right] \\
 C & & & & \\
 B & & & & \\
 D & & & &
 \end{matrix} \quad [9]$$

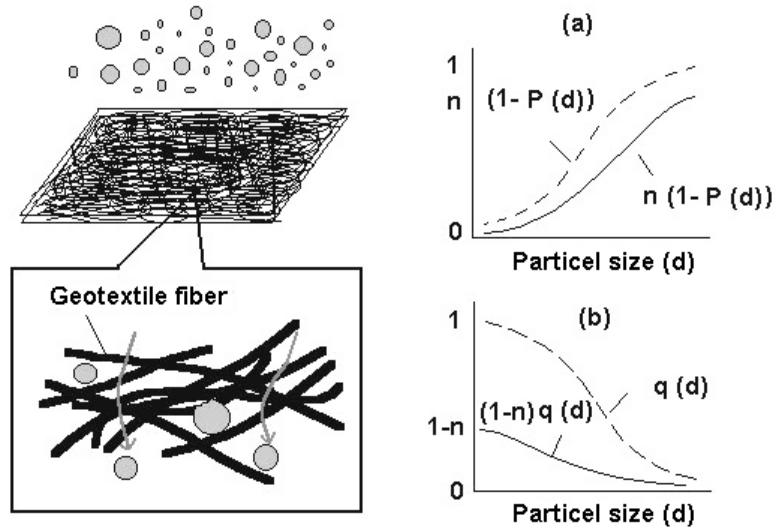


Figure 6 Retention and deposition probabilities of nonwoven GT clogging due to (a) the smaller constriction size and (b) particle affinity to fiber material where $(1-P)$ is cumulative CSD of geotextile ; q is the relative soil affinity strength to fiber material ; n is geotextile porosity

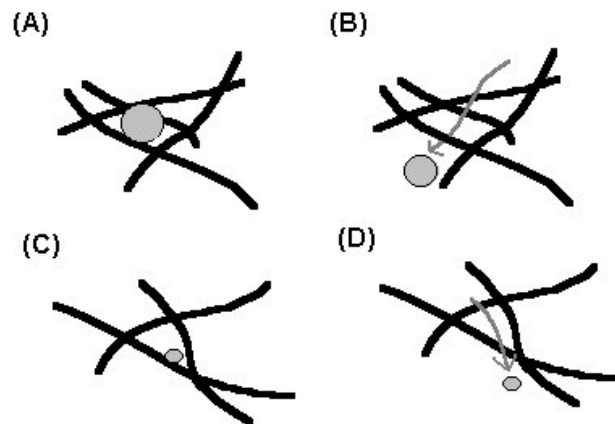


Figure 7 Possible scenarios of soil particle infiltration within nonwoven geotextile where (A) being retained by the smaller constriction; (B) passing across the larger constriction ; (C) being adsorbed to nonwoven GT fiber; (D) being desorbed from nonwoven GT fiber

From operation of the fundamental matrix, $(I-Q)^{-1}$ (Kemeny et al,1966), the probabilities of two ultimate absorbing states where state A is defined with particle retention by smaller constrictions and state C is defined with particle adsorption onto geotextile fiber can be assessed with the properties of geotextiles and soils (geotextile porosity (n), cumulative constriction size distribution $(1-p)$ and relative soil affinity to fiber material (q) where p and q are mutually independent functions of particle diameter, d).

$$\begin{aligned} \Pr\{A\} &= \hat{e}_1^T \cdot (I-Q)^{-1} \cdot R \cdot \hat{e}_1 \\ \Pr\{C\} &= \hat{e}_2^T \cdot (I-Q)^{-1} \cdot R \cdot \hat{e}_2 \end{aligned} \quad [10]$$

where $(I-Q)^{-1}$ and R are the fundamental and residual matrices defined in transition matrix. \hat{e}_1 and \hat{e}_2 are the column basis vectors- $\{1, 0\}$ and $\{0, 1\}$ respectively

The probability values for the ultimate absorbing states - cases A and C can be calculated as the p and q vary from 0 to 1 (Figure 8). Based on the simulation results, the physical pore obstruction by coarse particles will govern internal clogging process if the soil affinity to the fiber material is insignificant (i.e. q approaches to zero), and the particle deposition on the fiber will govern the clogging process especially for small porosity GT if the relative soil affinity is significant (i.e. q approaches to one).

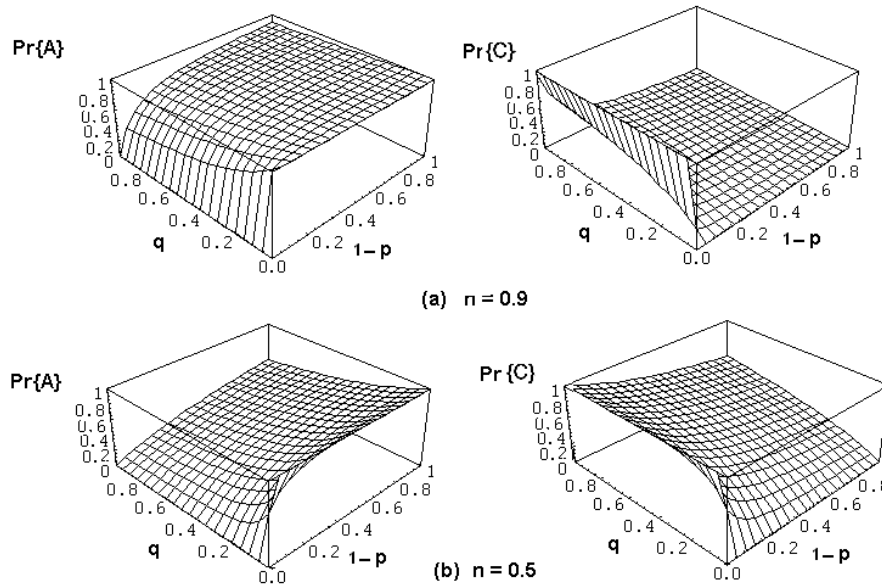


Figure 8 Joint probability distribution in functions of constriction size and soil affinity to filter fabric presenting the ultimate clogging states of non-woven geotextile (cf. $\Pr\{A\} + \Pr\{C\} = 1$) where n : geotextile porosity, $\Pr\{A\}$ and $\Pr\{C\}$: probability functions of cases A and C described in Figure 7

4. SUMMARY

Probabilistic modeling helps envision the subtle behaviors of fine soil particles associated with physical retention or chemical clogging inside geotextile filters. Proposed probabilistic methods showed satisfying results in characterizing of fabric constriction structure and estimating of the different geotextile filter performances subject to the various soil sizes. Due to limitation of existing experimental techniques to assess reliable and accurate pore/constriction size distribution of geotextile filter, these probabilistic approaches will help coping with the uncertainty of test outputs, inherited in the filter designs.

Many probabilistic modeling were conducted based on a best fitting probability function to delineate the features of filter pore/constriction and soil particle size distributions. However, a closer investigation is necessitated to check the feasibility of candidate probabilistic model, if the model has clearly defined the uncertainty of outputs and assumed realistic premise of probabilistic process. A further in-depth study should be followed to investigate whether advanced probabilistic models more relevant to the granular/geotextile filter design are available. The previous researches have already demonstrated that poor output reliability and productivity would be anticipated from the application of probabilistic models especially, if the probabilistic modeling was based on pre-mature assumptions of input parameters (e.g., soil/geotextile GSD and CSD), the authenticity of which could not be demonstrated by available advanced and reliable experimental techniques (image analysis with resin fixation).

5. NOMENCLATURE

AOS : apparent opening size of geotextile (measured by dry sieving)
CSD : geotextile constriction size distribution
 $F(r)$: cumulative probability function of constriction size, the inscribed circle radius, r
 $F^*(z)$: cumulative probability function accounting for the opening area, z ,
FOS : filtration opening size of geotextile (measured by hydrodynamic (wet) sieving)
GSD: soil grain size distributions, volume based
OSD : geotextile opening size distribution
 O_r^* : representative geotextile opening size specified for deterministic designs
 $O_{r,i}$: opening size of geotextile corresponding to i % in cumulative OSD
 $P(d)$, p : complementary cumulative probability function of constriction diameter, d presenting soil or non woven geotextile CSD or passing probability of particle size, d
 $1-p$: retention probability of soil particle due to limited constriction size
PDF : probability density function
 T_e : unit step walk distance between elementary sub layers of nonwoven geotextile
 T_g : geotextile thickness
 d : constriction inscribed diameter of nonwoven geotextile
 d_f : fiber diameter of nonwoven geotextile
 $f(r)$: probability density function of constriction size defined by the inscribed circle radius, r
 $f(xy)$: probability density function of the opening area (xy) associated with wire spans (x and y).
 $f^*(z)$: probability density function of the geotextile opening area (z), compensated for the constriction area ($z = xy$).
 n : porosity
 q : relative affinity of soil particle to geotextile fiber (0 is non- adhesive, 1 is fully adhesive)
 r : the inscribed circle radius of geotextile constriction
 ρ : soil specific density
 χ : fiber specific length in geotextile

ACKNOWLEDGEMENT

This research was performed as addendum part of author's Ph.D. research titled "Filter Performance and Design for Highway Underdrain" published by FHWA/IN/JTRP 2005/1, May, 2006.

REFERENCES

- Aydilek, A. H., Oguz, S. H. and Edil, T. B. (2005) Constriction Size of Geotextile Filters, *Journal of Geotechnical and Geoenvironmental Engineering*, 131 : 28-38
- Bhatia, S. K. and Smith J. L. (1996) Geotextile characterization and pore size distribution: part I. *A review of test methods and results*, Geosynthetics international , 3: 85-105
- Bhatia, S. K., Smith J. L. and Christopher, B. R. (1996) Geotextile Characterization and Pore Size Distribution: part III. *Comparison of Methods and Application to Design*, Geosynthetics international, 3:301-328
- Elsharief, A. M. and Lovell, C. W. (1996) A Probabilistic Retention Criterion for Nonwoven Geotextiles, *Geotextile and Geomembranes*, 14: 601-617
- Faure, Y. H., Gourc, J. P. and Gendrin, P. (1990) Structural Study of Porometry and Filtration Opening Size of Geotextiles, in: Peggs, I.D. (Ed.), *Geosynthetics: Microstructure and Performance*, ASTM STP, Philadelphia, 1076:102-119
- Giroud, J.P. (1996) Granular filters and geotextile filters, in: Proceedings of *GeoFilters '96*, Lafleur, J. and Rollin, A.L., Editors, Montréal, Canada, May, 565-680.
- Giroud, J.P., Delmas, P. and Artieres, O. (1998) Theoretical Basis for the Development of a Two-Layer Geotextile Filter, in: Proceedings of *Sixth International Conference on Geosynthetics*, Atlanta, Georgia, USA, March, 2:1037 – 1044
- Kemeny, J. G., Mirkil, H., Snell, J. L., and Thompson, G.L. (1966) *Introduction of Finite Mathematics*, 2nd Ed., Prentice-Hall Inc., Englewood Cliffs, NJ.
- Matheron, G. (1971) "Les Polyèdres possoniens isotropse"[Isotropic Poissonian Polyhedral], International Report from the Centre de Morphologie Mathématique, Fontainebleu.
- Rigo, J.M., Lhote, F., Rollin, A.L., Mlynarek, J. and Lombard, G. (1990) Influence of Geotextile Structure on Pore Size Determination, in: *Geosynthetics: Microstructure and performance*, Peggs, I.D. (Ed.), ASTM STP, Philadelphia, 1076: 90-101
- Urashima, D. C. and Vidal, D. (1998) Geotextiles Filter Design by Probabilistic Analysis, in: *Proceedings of Sixth International Conference on Geosynthetics*, Atlanta, Georgia, USA, March, 2:1013-1016

- Urashima, D. C. and Vidal, D. (2002) Analysis of Filtration System by Probabilistic Theory and Simulation Methods, in: Ph. Delmas and J.P. Gourc (Eds.), *Proceedings of 7th International Conference on Geosynthetics*, , Nice, France, 1015-1018
- Xiao, M. and Reddi, L. N. (2000) Comparison of Fine Particle Clogging in Soils and Geotextile Filters, in: J.G. Zornberg and B.R. Christopher, (Eds.), *Advances in Transportation and Geoenvironmental Systems Using Geosynthetics*, ASCE Geotechnical Special Publication, Proceedings of Geo-Denver 2000, Denver, Colorado, August, 103:176-185
- Wilson-Fahmy R.F., Koerner, G.R. and Koerner, R.M. (1996) Geotextile Filter Design Critique, in: Shobha K. Bhatia and L. David Suits (Eds.), *Recent Developments in Geotextile Filters and Prefabricated Drainage Geocomposites*, ASTM STP, American Society for Testing and Materials, 1281:132-164

Geotextile Tube Failures

Douglas A. Gaffney, P.E., Gahagan and Bryant Associates, dagaffney@gba-inc.com

ABSTRACT

This paper explores the various mechanisms responsible for the failure of geotextile tubes during filling. Geotextile tubes are designed to withstand the rigors of hydraulic filling. While failures are quite rare, they usually happen during filling or immediately after repeated pumpings. When tubes are used for dewatering slurries, they are generally subject to multiple fillings. Each filling subjects the tube to circumferential and axial stresses which cause elongation of the yarns. Repeated cycles can cause fatigue resulting in rupture. Six geotextile tube fabrics were tested using a modified ASTM D 4595 test which increased the tension to 325 pounds per inch in three cycles. During the third cycle, the geotextile was pulled to failure. The five polypropylene fabrics and one polyester fabric were tested in both the machine and cross machine directions. This paper will compare the stress - strain curves and relate the results to actual failures seen in full scale tube projects.

1. INTRODUCTION

1.1 Dewatering with Geotextile Tubes

A geotextile tube is simply a large tube sewn together from sheets of permeable high strength geotextile. Geotextile tubes have been used to dewater a wide variety of liquid wastes and dredged slurries since the early 1990's. While these high moisture content materials vary in viscosity and density, and range from organic to inorganic with widely ranging grain size distributions, they generally behave as a liquid, applying hydrostatic pressure to the geotextile shell. Water is released through the pores of the fabric leaving the solids in the tube. Over time, as the water drains, the percent solids within the tube increases.

Leshchinsky, et al (1996) formulate the shape of a geosynthetic tube filled with pressurized slurry on the equilibrium of an encapsulating flexible shell. The tube is analyzed as it lays on a flat surface and is inflated by the filling pressure. This analysis allows the determination of tensile forces in the axial and circumferential directions during the filling process. Parametric analyses provide two very important observations, namely: 1) circumferential stresses (hoop stresses) are always greater than axial stresses when filled on a flat surface and 2) when the tube circumference is known, the tube height can provide an accurate estimation of stresses in the geotextile and cross sectional area of the tube. Observation 1 is the reason that most geotextiles used in tubes have tensile strengths that are greater in the cross machine direction. Observation 2 allows filling to occur without monitoring the discharge pressure, since height alone has proven sufficient to monitor tensile forces in the tube. This second observation, however, does not account for changes in the geotextile yarns as a result of repeated fillings.

Multiple fillings are commonplace when the purpose is to dewater a high moisture content waste. Figure 1 shows an example of multiple fillings from a fixed volume storage tank into a small circumference tube (from Gaffney et al., 1999). The tube was filled every fourth day, on average. A characteristic curve is evident after each filling where the tube elevation decreases as the percent solids within the tube increases.

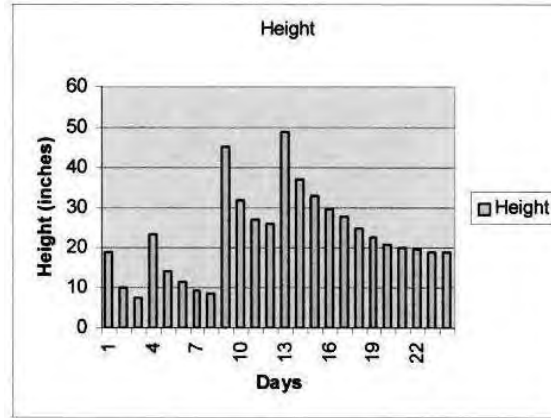


Figure 1. Time vs. height for a 15-ft circumference tube with sewage sludge (from Gaffney et al. 1999).

For larger dewatering projects, the usual procedure is to initially fill the tube to its prescribed fill height (note the dashed line in Figure 2), let it dewater, fill it again, and so on until the remaining capacity is too small to allow additional filling. A time history of fillings will resemble Figure 2 (Lawson, 2006). Each time the tube is filled it is pressurized. The pressure results in tensile forces on the yarns comprising the geotextile tube. The tensile forces elongate the yarns.

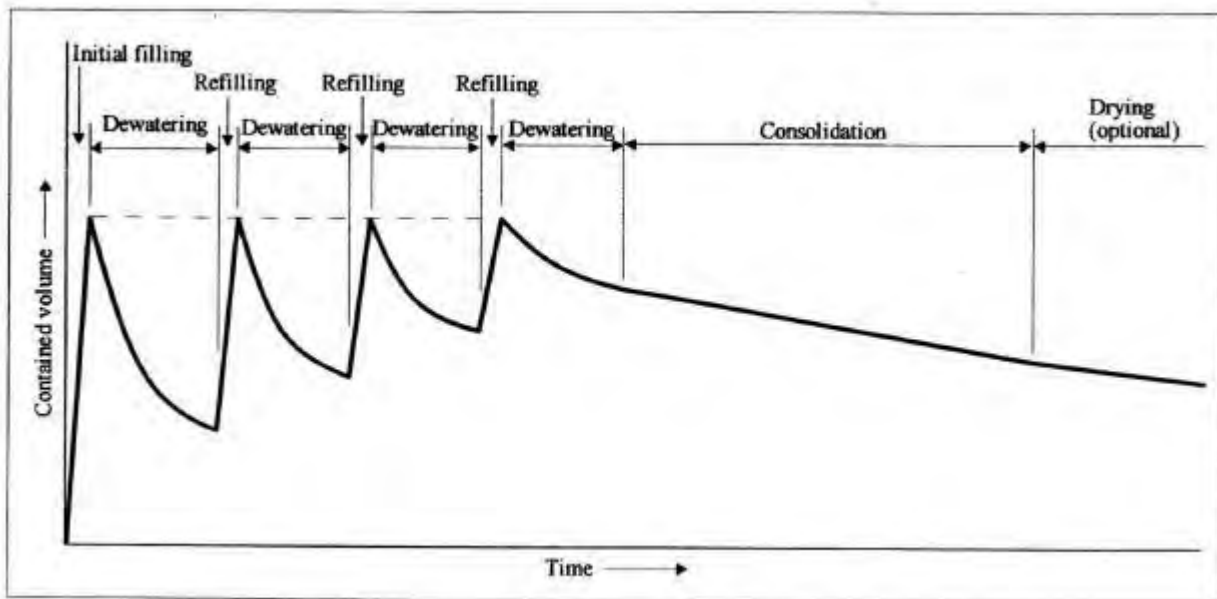


Figure 2. Filling, dewatering and consolidation stages when using geotextile tubes (from Lawson 2006).

1.2 Types of Failures

The vast majority of tubes are fabricated by sewing. A sewn seam is typically between 50 and 70 percent of the original tensile strength of the geotextile (ASTM D 4595). To account for this loss of strength, most geotextile tube fabrics are generally stronger in the cross machine (XD) direction. Since most tubes are sewn with a longitudinal seam(s) extending along the length of the tube, and since the highest predicted stresses on the tube are circumferential, it would stand to reason that failures would be most common at the longitudinal seam. This is, however, not the experience of the author.

Most tube failures are attributed to contractor error, pumping the tubes higher than the recommended fill height. In rare instances the failure will be along a longitudinal seam. The end seam can also fail for the same reason, although axial stresses are generally less than circumferential. If the tube is installed with the long axis on a slope, however, the low end will be subject to more hydrostatic pressure, and the end seam will experience axial forces greater than predicted. Another rare failure is due to a manufacturing flaw. Once a tube ruptures it can be very difficult to determine the cause

due to the difficulty exhuming the fabric. Sometimes a manufacturing defect can be determined if the failure is limited to one geotextile panel or the direction of failure does not correspond to the major stress direction.

The three most common failures are: 1) stresses induced at the fill ports that are located along the top of the tube, 2) a failure along the top centerline of the tube and 3) failure at the bottom of the tube when it is stacked above a “V” shaped gap between two bottom tubes. Stresses induced at the fill ports can be minimized by proper construction techniques related to the fill nozzle (or discharge pipe). It is good practice to suspend the discharge pipe over the fill port thus minimizing undue stresses on the fill port seam. When this is not practical, the rigid end of the discharge pipe should be minimal, and connected to flexible hose. Care should be taken during filling to adjust the fill line as the tube increases in height to minimize stress on the fill port seam. This paper will concentrate on the remaining two failure modes, namely the top centerline failure and failures when stacking.

2. TOP CENTERLINE FAILURE DUE TO CYCLICAL ELONGATION

2.1 Elongation

The wide width tensile strength test (ASTM D4595) places a load on a geotextile until it breaks. This test results in a stress strain curve similar to Figure 3. As the load is increased, the geotextile experiences elongation until it reaches a maximum elongation at failure. The fabric in figure 3 fails at a mean elongation of 17.34% and a load of 4,418.79 pounds per foot (552.35 pounds per inch).

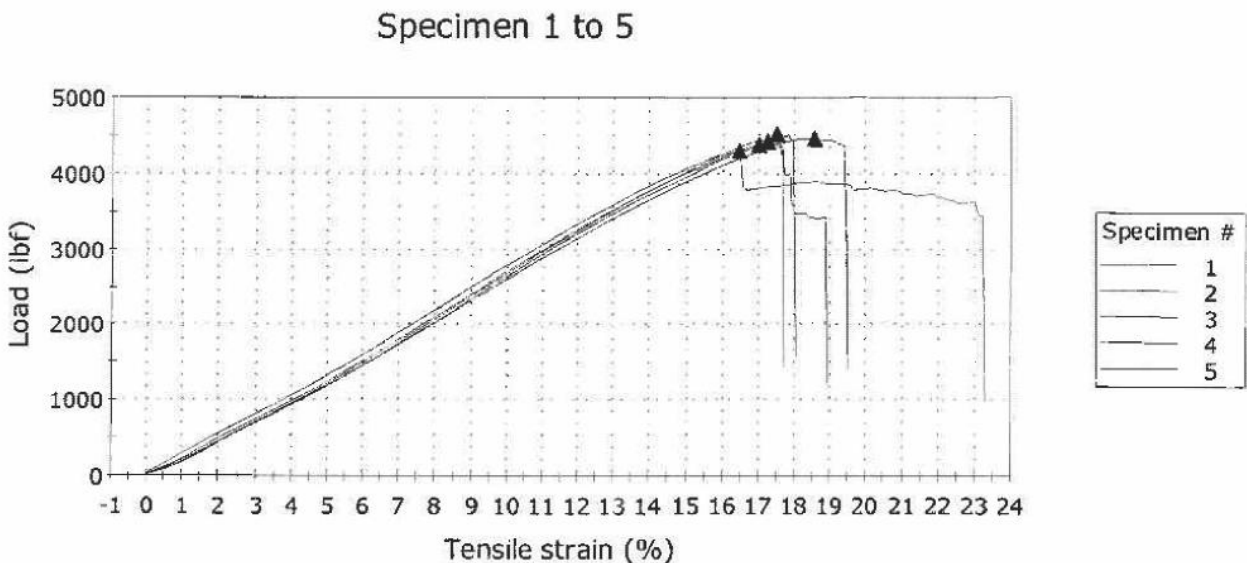


Figure 3. Stress-Strain curve for Geotextile E, machine direction (MD).

Loading a plastic material such as polypropylene yarns results in elongation. Repeated loading necessarily generates plastic deformations in the yarns. In the case of a tube, filling it once, then allowing the tube to dewater, will induce plastic deformation, that is, the yarns do not completely return to their original length, and presumably loses some tensile strength.

When the tube is allowed to relax during dewatering, the elastic component if the deformation is recovered. The next loading starts at new yarn length due to the plastic deformation generated in the first loading. Repeated loading will increase the plastic (permanent) deformation in the yarns and will eventually break at a certain specific plastic strain. In geosynthetics, if the plastic strain plus the elastic strain induced by the last loading exceeds a certain percentage, breakage will occur. In fact, the material will quickly creep leading to creep strain failure (Leshchinsky, 2012). A modified wide width tensile test was conducted to examine this phenomenon; the test results of which will be discussed in Section 4.

2.2 Example Failures

Actual geotextile tube failures are rather infrequent, and are not generally reported in the literature. Some examples do exist. Taylor, et al (2001) report a failure during “topping off” which started at one of the fill ports and ran the length of

the tube. The description implied repeated fillings, and also that the tube was on a sloped concrete pad. Post-failure testing indicated that there was a loss of tensile strength and this was attributed to UV degradation. Looking back in hindsight, the loss of tensile strength could have resulted from repeated fillings and resultant plastic deformation in the yarns.

In another dewatering project in Michigan, a 45-foot circumference polypropylene tube experienced catastrophic failure when the top of the tube split from one end to the other. Examination of the geotextile revealed telltale elongation of the yarns (see Figure 4).

It was determined that the tube had been filled twice prior to the failure. The fill material was a slurry containing both sand and fine-grained material (silt and clay). When the tube was full, it was allowed to relax during dewatering. During this time, the sand settled in a dense flat "pancake" on the bottom while the fines dewatered. During the second filling, the tube was inflated to normal height. To achieve the characteristic elliptical tube shape, the sides of the tube (now filled with sand) had to be raised off the ground by the tensile strength of the geotextile. The tube was again allowed to dewater and was filled a third time. Again, the sides of the tube had to be raised off the ground to allow the tube to reach its maximum fill height. At this point the stress in the yarns was concentrated in the top center of the tube where the failure occurred.



Figure 4. Elongated yarns at the location of failure.

To test this theory and to prevent future failures, a 10 inch long line was painted on the top of the tube in the circumferential direction. Each time the tube was filled, the line was measured. As expected, the line increased in length, conforming to the elongation. This procedure was so predictable and effective that the contractor used this method to allow filling to the maximum extent prior to planned failures (see Figure 5).



Figure 5. Controlled failure of tube.

3. BOTTOM CENTER FAILURE IN A STACKED CONFIGURATION

As dewatering projects have become larger, with larger circumference tubes and more dredged material to dewater, stacking tubes has become more commonplace. With stacking, a relatively new type of failure is seen at the bottom of the tube. Two examples were reported by Vine and Jury (2005). In both cases, the tubes were being filled on top of a row of previously filled tubes. The configuration is similar to Figure 6.

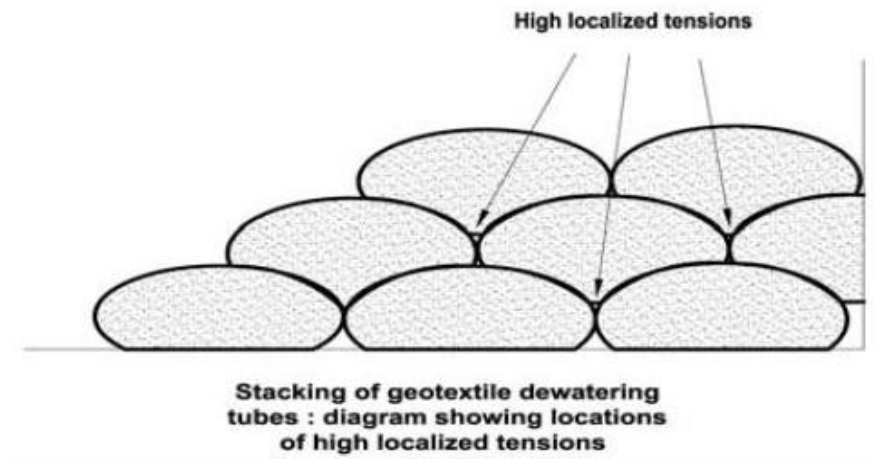


Figure 6. Schematic of stacked tubes.

In reality, tubes are often not stacked as neatly as Figure 6. Gaps can exist between the underlying tubes resulting in a “V” shaped void. The stresses on the geotextile within this void space can be examined as discussed in Plaut and Klusman (1999). Note the tensile force S_7 in Figure 7. Assuming that the coefficient of friction between the upper and lower geotextile surfaces is 1.0 (in a static condition), the force S_7 can be estimated using the analysis for a container filled with slurry exiting a split barge (see Pilarczyk ,2000). The two bottom tubes are presumed to be solid and the slurry in the top tube behaves as a liquid. The highest stresses are shown to occur when the fill material behaves as a liquid.

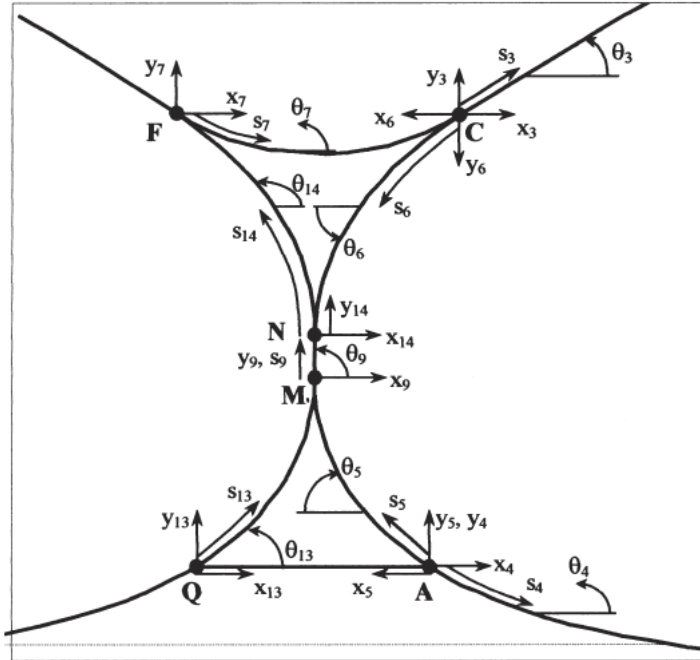


Figure 7. Geometry and coordinate systems for three tubes (from Plaut and Klusman, 1999)

The failures reported by Vine and Jury (2005) noted a gap and deep notch under the tube that failed. Figure 8 shows an example of a stacked tube configuration that has suffered this type of failure. In subsequent stacking operations by others, when the gap becomes too large, an attempt is made to fill it. One such method uses a small filler tube. It should be noted that when tubes are circumferentially sewn, there is a longitudinal seam in exactly this region of potential stress.



Figure 8. Example stacked tube configuration.

4. ANALYSIS OF GEOTEXTILE SUBJECT TO CYCLICAL STRESS

A modified ASTM D4595 test was conducted on a variety of geotextiles commonly used in the fabrication of geotextile tubes. In this procedure, the strain is fixed when the load reaches 325 pounds per inch (ppi), and cross head movement is stopped. This load was chosen as it represents a typical stress applied on a tube when filled to 6 feet in height. Then, after 15 minutes the load is completely removed for 15 minutes. This procedure is repeated, then loaded to ultimate. The geotextiles are described in Table 1 below. Geotextiles A, C, D, E and F are woven polypropylene while Geotextile B is woven polyester. Geotextiles A, D, E and F are most similar in terms of yarn type, weave and published MARV tensile strength.

Table 1. Geotextiles used in the modified wide width tensile test

Style	Type	Direction	Ultimate Cyclical Tensile Strength (ppi)	Ultimate Published Elongation (MARV) %	Ultimate Cyclical Elongation %
A	Woven PP	XD	651	9	10.2
A	Woven PP	MD	475	14	12.9
B	Woven PET	XD	1199	17	16.7
B	Woven PET	MD	1233	17	21.5
C	Woven PP	XD	960	18	21.6
C	Woven PP	MD	465	18	20.6
D	Woven PP	XD	639	20	13.4
D	Woven PP	MD	488	20	19.5
E	Woven PP	XD	615	n/a	14.8
E	Woven PP	MD	511	n/a	23.9
F	Woven PP	XD	645	16.5	12.2
F	Woven PP	MD	447	26.5	19.5

Figure 9 is an example of the cyclical stress test results for Geotextile E, machine direction (MD) which can be compared to the results shown earlier in Figure 3. From Figure 3, the average ultimate tensile strength of this geotextile is 552 ppi with the lowest value being 537 ppi. The ultimate tensile strength of the same fabric after the third cycle is less at 511 ppi (see Figure 9). Additionally, the total strain (elongation) is 23.9% in Figure 9, while the average elongation in Figure 3 is 17.34%. Results are similar for the same fabric in the cross machine direction (not shown). Standard stress-strain data was also available for geotextile D. Similar observations were observed, namely that the tensile strength of the fabric was higher when tested in a single pull, and the elongation was lower. To summarize, the act of placing the geotextile under cyclical stress tends to stretch or elongate the yarns making the tube larger in circumference, and slightly weaker over multiple fillings.

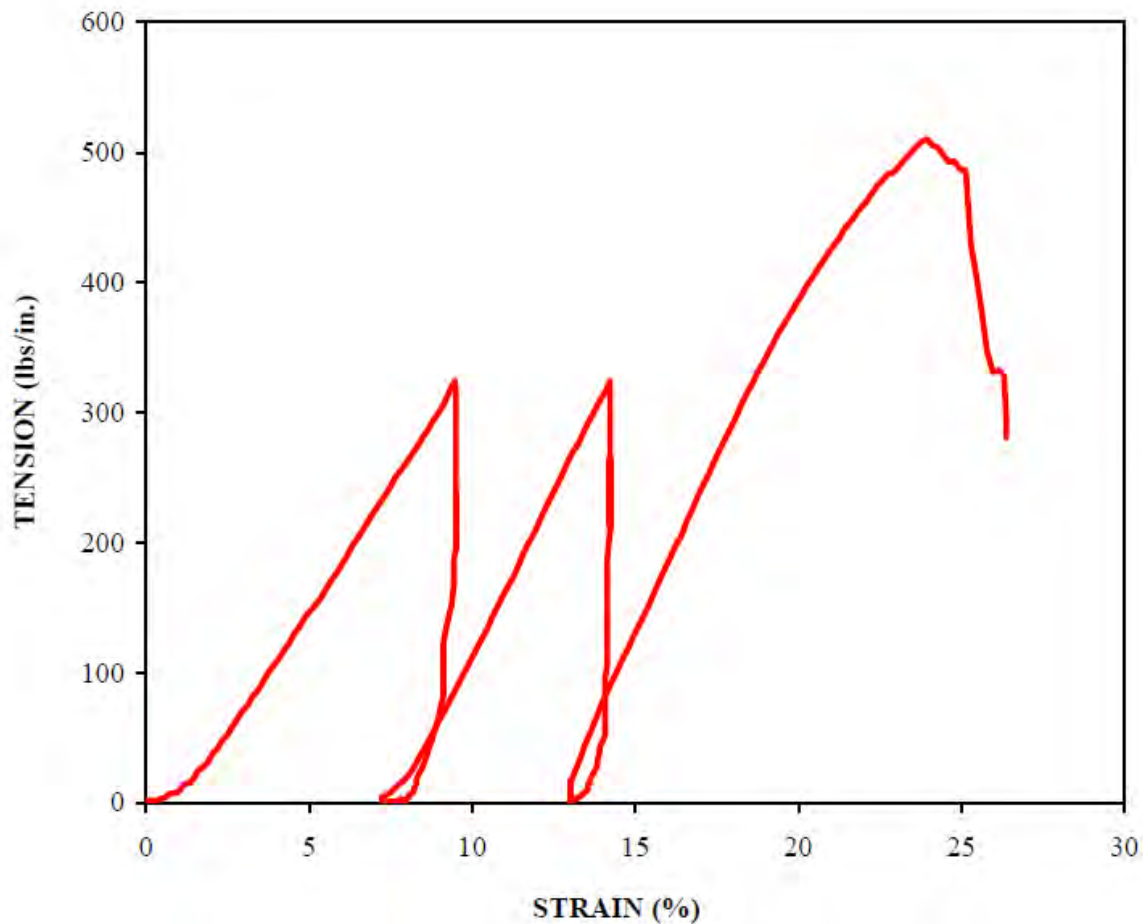


Figure 9. Cyclical Stress-Strain curve for Geotextile E, machine direction (MD).

5. SUMMARY AND CONCLUSIONS

In summary, while failures remain infrequent, they can be minimized even further through a better understanding of the physical properties of the geotextiles that make up the tubes. Standard tube geotextiles have been designed for the rigors of most filling applications, and this includes the seams, both longitudinal and circumferential. Actual field conditions, which include foundation slopes, dissimilar fill materials, and gaps under tubes can be accounted for in the design of the fabric and in the recommended fill height, or in the contractor's construction methodology. For example, when designing tubes to be stacked, the specified fill height should account for the possibility of a gap under the tube. In other words, either a factor of safety should be applied, or the additional step of determining that the tensile strength in the scenario of cyclical stress and void space under the tube is adequate.

A very small data set was used in the development of this paper. It is recommended that more testing be accomplished to increase the size of the data set. Based on the above test results which show a loss of tensile strength due to cyclical stress, further analysis should be done to establish a rule of thumb to account for this loss. At a minimum, project owners and engineers should ensure that the design of large dewatering projects, especially stacked tubes on contaminated sites, has addressed the potential for the types of failures identified.

ACKNOWLEDGEMENTS

This paper was made possible through the cooperation and support of Belton Industries, Geo-Synthetics Inc. (GSI) and Thrace Linq.

REFERENCES

- Gaffney, D.A., Toups, D.H., and Wynn, J.R. (1999). "The Future of Geotextile Tubes and Containment Systems" at the *13th Geosynthetic Institute Conference*, Philadelphia, PA, December 1999.
- Leshchinsky, D., Leshchinsky O., Ling, H. and Gilbert, P. (1996). Geosynthetic Tubes for Confining Pressurized Slurry: Some Design Aspects, *Journal of Geotechnical Engineering*, ASCE, August 1996.
- Leshchinsky, D. 2012. Personal Communication.
- Pilarczyk, K. (2000). Geosynthetics and Geosystems in Hydraulic and Coastal Engineering. A.A. Balkema, Rotterdam.
- Plaut, R., and Klusman, C. (1999). Two-dimensional analysis of stacked geosynthetic tubes on deformable foundations, *Thin Walled Structures*, 34 (1999) 179–194.
- Taylor, M., Sprague, C., Elliot, D., and McGee, S. (2001). Paper Mill Sludge Dewatering Using Dredge-filled Geotextile Tubes, *Proceedings of the 2001 International Conference TAPPI*, 2001.
- Vine, B., and Jury, M. (2006). Lower Fox River Operable Unit 1 2005 Remedial Action – Summary of Geotextile Tube Failures. Technical Memorandum, February 27, 2006.
- ASTM D 4595. Standard Test Method for Tensile Properties of Geotextiles by the Wide-Width Strip Method, *American Society for Testing and Materials*, West Conshohocken, Pennsylvania, USA

Granular Columns Reinforced with Geosynthetics: An Overview of Employment Trends

Santos, C.T., Aeronautics Institute of Technology, Brazil, caroline@ita.br
Vidal, D.M., Aeronautics Institute of Technology, Brazil, delma@ita.br
Queiroz, P.I.B., Aeronautics Institute of Technology, Brazil, pi@ita.br

ABSTRACT

Granular columns are vertical structural elements of dense interlocking aggregate or compacted sand, that are intended to increase the foundation overall bearing capacity and provide vertical drainage pathways to expedite the consolidation settlement. They are recognized as highly efficient and cost-effective ground improvement techniques. However the rigidity and load carrying capacity of the columns depend largely upon the amount of lateral restraint or confining stress that can be mobilized in the surrounding soft clay to avoid excessive radial deformation or even to keep the column's integrity. This additional restraint required could be provided by encapsulating the column granular backfilling in a geotextile wrapping, a technique that is referred to as geotextile-encased columns (or just GEC). The GEC represent the most wide-spread technique for improving poor ground using granular columns reinforced with geosynthetics, however other possibilities have been published, which can slightly or strongly differs from the current concept. According to some authors the reinforcement of a granular column can be also achieved by horizontal tensile elements (geosynthetic layers) either in full or partial column length, or by partial encasement of the upper column section that is prone to bulge. Another variation closely related to the conventional GEC technique is to encapsulate columns with geogrids or geocomposites. Hence, the aim of this paper is to present a broad review and a comparative analysis of the techniques proposed to reinforce granular columns with geosynthetics over the last 30 years, discussing the advantages and the feasibility of each method.

1. INTRODUCTION

Ground improvement methods using column-type techniques have been largely employed in construction over poor ground, especially when soft cohesive soils are involved. The current range of column-type techniques includes granular piles (stone columns and sand compaction piles), grout injected stone columns with load transfer mats constructed with geosynthetic reinforcement, combined soil stabilization with vertical columns (CSV-method), geotextile encased sand columns (GEC), cut-mix-injection method (FMI), lime and lime cement columns and friction piles in soft soils. Undoubtedly, granular columns (stone columns and sand compaction piles - or composer piles) represent the most wide-spread column-type technique for improving loose or weak soils (Kempfert 2003).

As the name implies, granular columns consist on the introduction of granular cylinders with intervening native soil which are disposed in a regular grid-pattern according to the soil profile and its mechanical characteristics. Depending to the execution process, the natural soil can be partially replaced by granular material infilled into holes made with the depth vibrator and compacted (vibro-replacement process).

Despite some similarities, granular columns differ from the classical foundation techniques like piles once they act over the terrain improvement and not only on the loads support. Considering that granular elements are stiffer then the local soil, the loads tent to concentrate over them; however, when loaded, the columns deform by bulging into the subsoil strata compressing the native soil. Furthermore, regarding the columns high permeability, the native soil water tends to migrate to them, allowing a faster dissipation of porewater pressures and, consequently, accelerating the consolidation settlements. Hence, the strengthening of the surrounded ground is accomplished and the bearing capacity of the composite ground is increased while its compressibility is reduced. With the development of the process the stress concentration over the columns tends to be relieved and the role of supporting loads is in part transferred to the native soil mass.

The range for granular columns applications includes not only the improvement of in-place soils with an appreciable content of fines. In fact, there are potential benefits in the application of granular columns for the densification of natural deposits or fills made of loose sands and gravels.

The feasibility of using any ground improvement approach in any given case depends on several factors, mainly on soil conditions. The granular columns performance is significantly related with the lateral support provided by the surrounding soil. To maintain the columns integrity, the lateral passive resistance mobilized in the surrounding soil must be at least equal to horizontal stresses exerted by the column, what can be many times impossible in very soft cohesive or organic

soils. It is worth noting that the horizontal support depends also on the vertical pressure over the soft soil, which magnitude can be much smaller than those acting over the columns.

One way to allow the application of granular columns in very soft soils could be made by the employment of some binder, like grout, cement, lime or quicklime, with the aim to confer some cohesion to keep the columns steady. On the other hand, this solution could affect the performance of the columns as drains, and consequently, their contribution on the soft soil improvement.

Another way to enable the employment of granular columns on very soft cohesive or organic soils is reinforcing the granular material with geosynthetics, both by confining the granular backfilling in geotextile, geocomposites or geogrids wrappings or by placing horizontal tensile elements (geosynthetic layers) either in full or partial column length. In the following, the particularities of each one of these solutions are discussed.

2. GEOTEXTILE ENCASED COLUMNS (GEC)

Geotextile-encased columns (GEC) system is a soft soil improvement technique that consists in confinement of granular material by geotextile wrappings. The idea of encasing granular columns with geotextile wrappings is commonly attributed to Van Impe (1986), however the technique devise is still not clear. Gray et al. (1982) were probably the first to recognize that columns could be encased by geosynthetic fabrics, however this work presented a particular concept of reinforcing sand columns internally and externally with geotextiles in a synergistic fashion. This proposal will be discussed in a future item.

Probably the first attempt on GEC employment was an improvement of containment dike foundation to Leitha river in the low Austria, between the cities of Rohrau and Pachfurth in 1991, which was reported by Strauch (2003). In the following Geuder & Bräu (1997) reports the execution of small diameter encased-ballast columns in 1993/1994 used to speed the consolidation of a clay stratum that should to be improved to the construction of railway line embankment. Similar attempt was reported to Kitazume et al. (1993) that presented results of centrifuge model tests of "fabric-packed sand drains" performed to investigate its effect on the improvement of dredged soft sea sediment to be used on the Haneda Airport reclamation in the Tokyo Bay area, which started in 1994. The aim of this study was to assess the effect of fabric encapsulation on sand drains integrity as well as to verify the evolution of the consolidation process and its influence over the effective terrain improvement.

In all of the three first attempts in adding an encasement to granular columns, non-woven geotextiles were employed. Despite columns did not performed as bearing elements in the last two referred projects Kitazume et al. (1993) reports that good results reached in mechanical terms in the Haneda Airport construction, which was confirmed both in laboratory and in the practical application.

It seems that the two following projects just happened 1996 on road embankments projects in Germany, which were reported by Kempfert (1996), Kempfert & Wallis (1997), Raithel & Henne (2000) and deeply analyzed by Raithel (1999). In all of these projects the encasement employed was fabricated using woven and non-woven geotextiles and geocomposites sewn in the radial direction and in the bottom end. However, the significant growth in using GEC system only came with by the development of a woven geotextile encasement manufactured seamlessly in the radial direction, what happened just in the end of nineties. This solution circumvented some problems related to joints in the main load-carrying direction and consequently improving, together with the use of the woven products, the confinement efficiency.

Hence, the GEC ideally suited to cope with extremely soft soils because the confinement and consequently the stiffness that the geotextile encasement adds to the granular columns. The high tensile stiffness and the lower radial strain of the products available to the encasement construction provide the increasing of a single column bearing capacity thus reducing settlements. However, it must be noticed that, despite geotextile encased columns being stiffer than the uncased ones, this solution is still more flexible than conventional piled embankments and its concept remains quite different, once the columns are aimed to improve the proper surrounding soil. Nevertheless, the benefits achieved by the use of the GEC technique are not limited to mechanical advantages that regards to the bearing behaviour. Because of the fine size particles and the low permeability of soft soils, the insertion of the GEC enhances a significant drainage in the foundation. The ability of the geotextile wrap to prevent particle migration while allowing the free passage of water provides the maintenance of the drainage properties of the column. In addition to having suitable filtration properties, the granular column encasement provides a further benefit of separation, i.e., it prevents the intermixing of poor in-situ soil with column backfilling. Lastly, the advantages of the GEC-system in comparison to similar techniques, in special to conventional granular columns, or piled embankments can be summarized as:

- Allow the execution of granular columns into extremely soft soils: in contrast to conventional techniques, geotextile-encased columns can be used as a ground improvement and bearing system in extremely soft soils,

for example peat or sludge with undrained shear strengths $S_u < 2 \text{ kN/m}^2$; uncased granular columns are usually limited to soft soils which possess undrained shear strength superior to 15 kPa.

- Might provide cost savings: studies proceeded by Short et al. (2005) have shown that GEC system was less costly than other methods such as deep mixing or augercast piles with pedestals for the analysed case. Also, in comparison to conventional granular columns, the encasement may allow higher columns spacing, since the bearing capacity of the single units are much higher (Kassem & Imai 2004), and demand smaller volume of filling since the material loose to the soft soil around is reduced due to confinement promoted (Mandal & Kamble 1999).
- Reduce post installation settlement compared to conventional granular columns and prefabricated vertical strip drains (wick drains).
- The encasement provides an uniformly shaped column - The varying diameter of the column over a certain length plays a vital role in load transfer (Muir-Wood, 1990). In addition, whereas geotextile-encased column surface are smoother than piles, they are hardly affected by negative shear stresses that might occur.
- Less time consuming: discard preloading requirement and allow immediate loading after installation avoiding delays with curing, for instance (Short et al. 2005).
- More flexible behaviour: special interesting in situations where secondary settlements will play an important role on the system behaviour, like in organic soils like peat which significant secondary settlements might occur regarding the organic matter decomposition.
- Environment friendly since the amount of backfilling material might be reduced and, when installed by the displacement method, no in-place soil needs to be removed and consequently it is not required off-site disposal, what can be specially interesting on dealing with contaminated soils.

By now, the GEC technique has been applied in almost 30 important projects, most of them in Germany, in which country the technique experimented the major part of its development. Raithel et al. (2005) tabulates all the 20 first projects executed in Germany from 1996 to 2004, Nevertheless GEC projects were also executed in Netherlands, Sweden, Brazil and Spain (Figure 1).



FIGURE 1 – (a) polder construction for EADS Industry enlargement in Germany (Source: Huesker); (b) first GEC Brazilian work – connection between SP-99 Rodovia dos Tamoios and BR-116 Rodovia Presidente Dutra. In details, installed columns.

Regarding installation, two execution procedures were developed to GEC-system: the displacement and the replacement method. The basic difference between them is that in the displacement method no local soil is removed and in the replacement method the soil within the open steel shaft (employed to support the column installation) is taken out by an auger boring. Regarding many advantages, the displacement method is being more employed. The scheme in Figure 2 describes this installation procedure by this method. Details of each of installation process, as well as their advantages, disadvantages and applications interval can be found in Kempfert and Gebreselassie (2006).

In terms of design, the project of GEC-systems has been done essentially on the basis of the design method proposed by Raithel (1999, 2000). Despite this design tool allows the forecast of total settlements with high confidence, but it does not provides a practical approach to the evaluation in terms of prediction and performance, especially regarding consolidation process development. Recently, Santos (2010,2011) a presented a series of analytic solutions which provide a basis for a rational prediction of the system consolidation response. This last method is also capable of addressing the effect of column installation and the stress concentration ratio over the consolidation. Due to the lack of

space, the design procedures are beyond the scope of this paper and we suggest to consult these two last authors to further information about this topic.

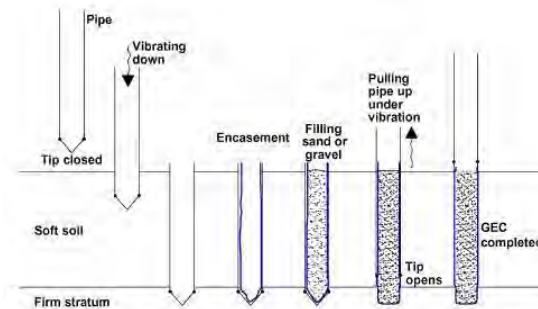


FIGURE 2 – Installation by the displacement method using end-closed pipe - from Alexiew et al. (2005).

3. GEOGRID ENCASEMENT

Another variation closely related with the last solution discussed (use of geotextile) is the columns encapsulated with geogrids. Similarly, this technique consist on encapsulating compacted mineral materials by a cylindrical-shaped encasement sleeve formed by a geogrid. The employment of geogrid wrappings are often related to coarse filling (crushes stones, gravel and aggregates) and for that reason the technique is frequently referred as geogrid-encased or geogrid reinforced stone column.

According to Gniel & Bouazza (2009), despite the obvious suitability of geotextile encased columns to certain applications, the technique can be limited by the relatively large settlements that occur as a result of minimal compaction received during installation and geotextile strain during loading. Moreover, according to Schuessler (2002) apud Trunk et al. (2004) sand columns encased by woven-geotextiles require relatively large lateral strains to mobilize the ring-tensile forces, which also can lead fairly large settlements of the overall system. Despite these statements being quite controversial, the idea of employing geogrids as granular columns encasement is to provide a more robust and perhaps stiffer alternative to geotextile and to broaden the appeal of geosynthetics in stone column ground improvement (Gniel & Bouazza, 2010).

According to Lee et al. (2008) another advantage of the geogrid-encased stone column technique in relation to the geotextile encased columns regards to the possibility to employ waste concrete and recycled aggregates as a filling material. Indeed, this range of filling may lend to this solution a series of potential site applications and also may provide economical and environmental benefits.

The use of geogrid encasement has been investigated for many authors like Smoltczyk (1999), Schuessler (2002), Paul & Schwedt (2003), Heerten (2004), Heerten & Ewert (2004), Trunk et al. (2004), Paul & Ponomarjow (2004), Malarvizhi & Ilamparuthi (2004), Gniel & Bouazza (2009), Gniel & Bouazza (2010). Smoltczyk (1999) describes a set of large-scale load tests performed on 5 columns in a field trial and Paul & Ponomarjow (2004) and Trunk et al. (2004) discuss a large-scale unconfined compression laboratorial testing. Malarvizhi & Ilamparuthi (2004) studied the load versus settlement response of geogrid-encased columns by small-scale modeling using three different types of geogrid net.

Regarding geogrid encasement confection, most of references like Heerten (2004) suggest as the construction technique rolling geogrid into a cylinder and mechanically welding a narrow section of overlap (about 30 mm wide) to form the encasement sleeve. According to Gniel & Bouazza (2010) the technique of welding provides an effective method for constructing geogrid encasement sleeves but it is unlikely to be used in practice. The technique requires either the shipment of a large welding frame to site or prefabrication of geogrid encasement sleeves away from site and both methods are unlikely to be cost effective. To overcome this problem Gniel & Bouazza (2010) investigated an alternative method of encasement construction that comprises overlapping the geogrid encasement by a nominal amount and relying on interlock between the stone aggregate and section of overlap. Based on a series of small-scale and medium-scale compression tests using different geogrids types - Figure 3 - Gniel & Bouazza (2010), concluded that the “method of overlap” provides a simple and effective method of encasement construction, providing a level of fixity similar to welding. However, still according to this author, a full circumference of overlap should generally be adopted to achieve adequate fixity. Hence, this solution to the encasement construction also seems to be economically disadvantageous and cost concerns appears as the greater obstacle on the geogrid as encasement adoption.

It must be also pointed out that the “window-mesh” type of the geogrid do not provide the adequate separation of the filling material and the surrounding soft soil as well as this solution fails on the drainage properties maintenance. Indeed, bisection of samples in small-scale laboratorial testing reported by Gniel & Bouazza (2009) showed significant ingress of surrounding clayey material into the prototypes, possibly reducing the columns performance as drains. To overcome problems associated with clogging, some authors suggest the use of a geogrid combined with a mechanically bonded non-woven geotextile (Trunk et al., 2004), creating a solution closer to the use of geocomposites.

With respect to installation, Trunk et al. (2004) also present some field trials regarding the installation using a bottom feed vibrator which, according to these authors, provide the filling with a high degree of density and what can consequently reduce the magnitude of deformations and settlements by loading. In this solution, the geogrid wrapping is positioned around the outside of the vibroflot before driven it down, like the displacement procedure using a depth vibrator to geotextile-encasement columns. On the other hand Gniel & Bouazza (2010) suggest the employment of the excavation method to perform the installation of the geogrid-encased columns - Figure 4.



FIGURE 3 – Medium-scale testing with columns encased by two types of geogrid and one geocomposite performed by Gniel & Bouazza (2010). Extracted from Gniel & Bouazza (2010)

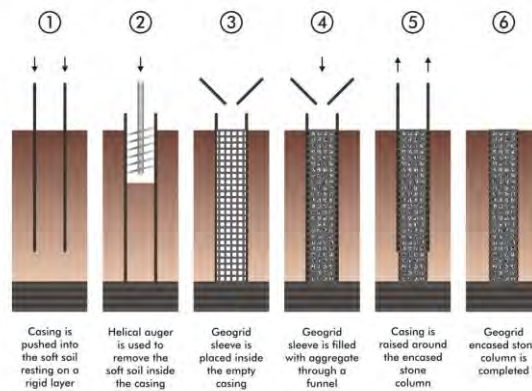


FIGURE 4 – Installation of the geogrid reinforced stone column - Adapted from Gniel & Bouazza (2010)

After all, it seems that the unique attempt on using geogrid-encased columns was reported by Trunk et al. (2004) in the foundation of a training center (Villa Borsig) in Berlin, however the geogrid encasement in this project was employed as a mold to concrete stone columns. More specifically, the geogrid wrapping was used in these project in order to prevent an uncontrolled leakage of the concrete into the soft underground and it had any further function after curing the column. However the effective application of the geogrid-encased stone column method to actual construction was not reported until the present moment, fact which was also outlined by Lee et al. (2008).

4. PARTIAL ENCASED COLUMNS

The lower lateral earth pressure and lower stiffness of near-surface soils may cause greater radial expansion on the upper section of granular columns. This phenomenon known as bulging is one of the most common failure mechanisms for granular piles.

According to some authors like Murugesan & Rajagopal (2006), Gniel & Bouazza (2009), Wu & Hong (2009) the partial encasement of only this zone prone to bulge may adequately reinforce the column. Murugesan & Rajagopal (2006) outlines that this innovative design solution are specially interesting when very long stone columns are involved.

An analytical procedure to determine the optimum column skirting length that prevents the granular column from bulging was presented by Wu & Hong (2009). Theoretical simulations proceeded by these authors indicates that the characteristics of the in situ soil and the stiffness and yield strength of the sleeve govern the optimum skirting length.

Murugesan & Rajagopal (2006) have investigated the performance of partial-encased columns through a parametric study carried out by finite element analysis. Analyses were carried out adopting an encasement stiffness of 2500 kN/m and 0.6 m as the column diameter. Varying the depth of the encasement from the ground level it was observed a settlement reduction over the uncased situation until a depth of encasement that corresponded about two diameters of the stone column (until 1 m) - see Figure 5. Based on these results, Murugesan & Rajagopal (2006) have concluded that this limit determines the optimum skirting length and the stretching of the encasement sleeve up to twice the diameter of the column does not lead to further improvement in performance.

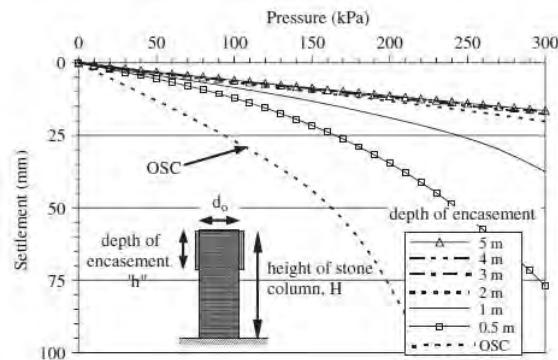


FIGURE 5 – Influence of encasement depth on the settlement response obtained by FEM analysis performed by Murugesan & Rajagopal (2006)

To investigate the impact of partial encasement on vertical and radial column deformation Gniel & Bouazza (2009) developed a laboratory scale model testing program where tests were undertaken on columns with 25 %, 50%, 75% and 100% encasement. In the obtained results for partially encased columns the entire non-encased length was observed to bulge. Still, radial bulging tended to increase in magnitude with increased encased length and the largest lateral deformations occurred directly below the base of the encasement. However, it is expected that by changing the length of encasement, the bulge zone can be transferred to depths able to offer a greater confinement, in a way that columns could be tailored to meet a range of settlement criteria. Hence partially encased columns could be a good alternative for sites with layered stratum, where a soft clay overly a relative firm layer or in profiles where shear strength monotonically increases with depth. Anyway, Gniel & Bouazza (2009) have observed that the fully-encased columns displayed a much stiffer response, contradicting the results obtained by Murugesan & Rajagopal (2006).

However, as many other alternative solutions, it seems that partial encased columns have been not employed in the practice. Still, careful consideration must be given to installation techniques and encasement material selection.

5. IMPROVEMENT BY HORIZONTAL REINFORCEMENT LAYERS

According to some authors the reinforcement of a granular column can be also achieved by placing horizontal tensile elements either in full or partial column length (Wu & Hong, 2009). In fact, it seems that the idea of reinforcing granular columns with geosynthetic layers preceded the encasement concept, as it is inferred by the pioneer Gray et al. (1982) work. In their proposal, Gray et al. (1982) introduced the concept that lateral restraint comes both from encapsulating the sand column with a woven geotextile used conjunctively with intercalated fabric layers (both woven or non-woven) within

the sand - Figure 6. In the following Gray et al. (1989) evaluated the performance of embedded granular structures reinforced independently with internal layered geotextile inclusions and externally encapsulated with a fabric skin.

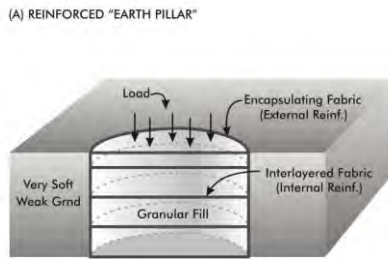


Figure 6 - Internally/ externally fabric reinforced columns - pioneering proposal of Gray et al (1982). - Adapted from Gray et al.(1982)

It seems that the original concept was to insert reinforcement layers evenly placed in whole column length, however, considering that the most common granular column failure mechanism is governed by bulging near the top portion, this technique is most frequently referred as a resource to prevent the excessive radial displacement in this region. Hence, following the same idea of partial encased columns technique, the idea consists in laying out a certain number of reinforcing sheets (most of times geogrid layers) up to a certain extent of the top region prone to bulge (Sharma 1998, Madhav et al. 1994, Sharma et al. 2004, Wu & Hong 2008). Figure 7 schematize this concept.

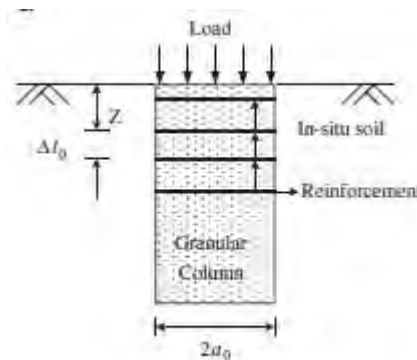


FIGURE 7 – Concept of the "laminated reinforced granular column"

In this technique the lateral restraint and the improvement of the column bearing capacity are achieved through the boundary shear stress developed in the granular material - reinforcement interface (Madhav et al. 1994). The inclusion of reinforcement layers results in redistribution of lateral deformation of granular column and, therefore, provides the transfer of lateral stresses from the column to the soft clay (Sharma, 1998).

The improvement provided by this technique depends on the number, spacing and the column length reinforced and also on interactive mechanism at the soil-inclusion interface (angle of shearing resistance of the granular medium and the coefficient of frictional resistance of reinforcement). It seems that all researches agree that the bearing capacity increasing is related to the increasing of the number of reinforcing layers and the spacing decrease among them (Gray et al.1982, Gray et al.1989, Sharma 1998, Madhav et al. 1994, Sharma et al. 2004, Wu & Hong 2008). However, Gray et al. (1982) have observed in a triaxial test programm with sand samples where reinforcements were evenly spaced that although reinforcement with synthetic fabrics increase ultimate strength, they tend to reduce overall stiffness of sand and this tendency is still pronounced as the number or reinforcement layers increase.

According to a parametric study using FEM presented by Sharma (1998) the optimum spacing of geogrid layers was found to be between 0.5 to 1.5 times the diameter of the stone column and the installation of geogrid layers at spacing closer than 0.5 times the diameter of stone column does not result in appreciable increase in column bearing capacity. Moreover, according to laboratorial tests conducted by Sharma et al. (2004) the column load-carrying capacity is further improved when the granular pile was reinforced by geogrids. However in the study presented by Sharma (1998), referred previously, it was concluded that is better to reinforce the stone column using a more flexible reinforcement spaced in smaller intervals than to employ a stiffer reinforcement more spaced apart because the column will evenly deform. Still

according to Sharma (1998) this would result in bulging being distributed over a greater length, thus preventing localized bulging failure and furnishing a better performance.

The stress-deformation response of sand columns reinforced with layers of both woven and non-woven geotextile inclusions was investigated by Gray et al. (1989) that developed a finite element model that was validated against results of triaxial tests. The results of this study showed that the stress-strain response of woven fabrics is best modelled as an elastic, polynomial function of strain, whereas that of non-woven fabric was best represented as a function of confining stress. Also with the aim to investigate the load carrying response of the “laminated reinforced granular column”, Madhav et al. 1994 presented an analytical approach to evaluate the ultimate bearing capacity by modifying the Hughes & Whithers (1974) model proposed to conventional granular columns. In the same line, Wu & Hong (2008) adopted models from Duncan & Chang (1970) and Wong (1990) to formulate the mechanical characteristics of the granular materials and establish analytical procedures to investigate the axial stress-strain response of an encapsulated granular column. The proposed analytical method was verified through laboratory triaxial tests carried out with sand columns reinforced with four layers of horizontal geotextile sheets (Figure 8). The evaluations of these two analytical analysis strongly agree with the studies run by Sharma (1998), Sharma et al. (2004) and, concerning to the triaxial tests proceeded by Wu & Hong (2008) it was observed that the slippage occurs for columns reinforced with stiffer inclusions, what also converge to the results obtained by Sharma (1998).

In addition, this technique does not appear to adequately prevent the clogging of the granular medium and keep the column drainage properties. Moreover, it can not prevents the lateral squeezing of the column backfilling embedded in very soft to extreme soft clays and the limits of the technique in terms of the undrained resistance of the soft soil. Indeed, in the triaxial tests performed by Gray et al. (1982) aforementioned the sand specimens failed by bulging or lateral spreading between reinforcements. In addition, it was observed that below a critical confining stress the reinforcements tended to slip or pullout as apposed to stretching

As the last solution presented (partial encased granular column), no field trial was reported to confirm the technique efficiency in the construction practice.

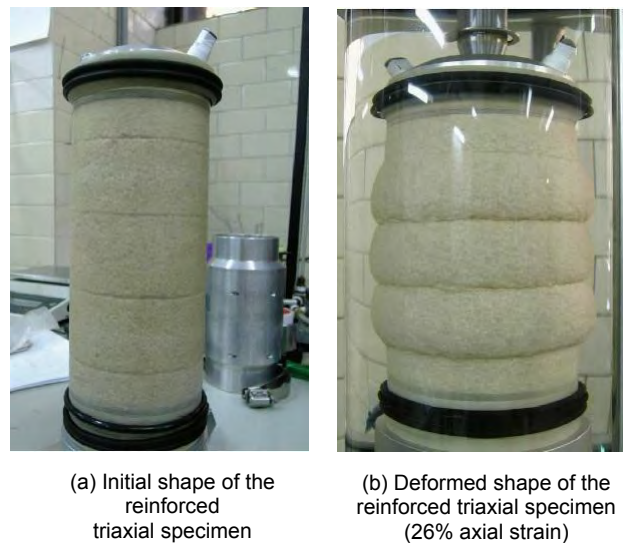


FIGURE 8 – Laboratory triaxial tests with four-layer reinforced specimen - from Wu & Hong (2008)

6. FINAL REMARKS

There is no doubt that the use of geosynthetics amplified the range of application of the granular columns, furnishing both economic and technical benefits.

Regarding the GEC, that is the most disseminated and employed technique to this aim, an important distinction needs to be drawn between the use of non-woven and woven geotextiles. There are important differences in the stress-deformation response of encased granular columns with relatively low modulus non-woven fabrics to the high modulus woven fabrics. The tensile modulus and allowable elongations in the reinforcement are important considerations and

high modulus reinforcement will greatly inhibit internal soil tensile strains, limit boundary deformations and increase strength. For this reason, when mechanical characteristics of the geotextile are important features in the project as in the cases where very soft soils are involved, woven products appear as the most appropriate choice.

On the other hand great benefits could be reached by the adoption of non-woven encasements when the geotextile reinforcement property is not required (soils in which additional lateral restraint is not necessary) as a separation and filter element in order to keep the good quality and the mechanical properties of the backfill as well as maintain the stability of the columns as drainage elements.

However, many of the techniques here discussed are only theoretical proposals; the feasibility of each technique in practice seems to rely more on the executive procedures and the characteristics of the in situ soil.

The solution of geogrid encapsulation appears to be suitable for relatively rigid clays when high loads are demanded, considering the column's backfilling is more prone to clog. Because of this limitation, the excavation method seems to be the more appropriate installation technique to geogrid reinforced stone column, as it was suggested to Gniel & Bouazza (2010).

To the case "laminated reinforced granular column", regarding the difficulties in constructive operations, the technique seems to be viable just for shallow and large diameter columns. Problems like clogging and the lateral squeezing could be avoided by the conjunctive use of encasement according the Gray et al. (1982) proposal, however the executive constrains remains the same.

ACKNOWLEDGEMENTS

The first author would like to gratefully acknowledge the financial support provided by the Brazilian Federal Agency for Support and Evaluation of Graduate Education (CAPES), the DAAD (German Academic Exchange Service) and Huesker Brazil.

REFERENCES

- Alexiew, D., Montez, F.T., Silva, A.E.F., Brokemper, D. (2003). Simplified Estimation and Graphs for Pré-Design of Geosynthetic-Encased Sand or Gravel Columns as Embankment Foundation. *Proc.4th. Brazilian Symposium of Geosynthetics*. IGS Brazil/ ABMS, Porto Alegre, Brazil, in cd-rom.
- Alexiew, D., Brokemper, D., Lothspeich, S. (2005). Geotextile encased columns (GEC): load capacity, geotextile selection and pre-design graphs. *Proceedings of Geo-Frontiers 2005*. ASCE, USA.
- Duncan, J.; Chang, C. (1970). Nonlinear analysis of stress and strain in soils. *Journal of Soil Mechanics and Foundations Divisions*, 96(5):1629–1652.
- Geuder, S.; Bräu, G. (1997). Geotextile Bauweisen beim Umbau der BAB A8 München-Salzburg im Bereich des Chiemsees. *Tiefbau*, 12: 748-753.
- Gniel, J.; Bouazza, A. (2009). Improvement of soft soils using geogrid encased stone columns. *Geotextiles and Geomembranes*, 27:167–175.
- Gniel, J.; Bouazza, A. (2010). Construction of geogrid encased stone columns: A new proposal based on laboratory testing. *Geotextiles and Geomembranes*, 28(1): 108–118.
- Gray, D. H.; Athanasopoulos, G.; Ohashi, H. (1982). Internal/ external fabric reinforcement of sand. *In: Proceedings of the Second International Conference on Geotextiles*. Las Vegas, USA: [s.n.]. p. 611–616.
- Gray, D. H.; Kaldjian, M.; Wu, C. (1989). Stress-deformation response of geotextile granular structures. *In: Geosynthetics'89 Conference Proceedings*. San Diego, USA: [s.n.], 1989. v. 2, p. 373–384.
- Heerten, G. (2004). Geogitterummantelte mineralstoffsäulen—ein neues system für gründung und baugrundverbesserung. *In: Proceedings of 28. Baugrundtagung*. Leipzig: Verlag Glückauf GmbH.
- Heerten, G.; Ewert, W. F. (2004). Welded geogrids as new generation of reinforcing products in geotechnical applications. *In: Proceedings of ECI International Conference on the Use of Geosynthetics in Soil Reinforcement and Dynamics*. Dresden, Germany: [s.n.] p. 85–102.
- Hughes, J. M. O.; Withers, N. J. (1974). Reinforcing of soft cohesive soils with stone columns. *Ground Engineering*. 7(3): 42–49.
- Kempfert, H.-G. (1996). Embankment foundation on geotextile-coated sand columns in soft ground. *In: Proc. First European Geosynthetics Conference - EUROGEO 1*. Netherlands: A. A. Balkema, p. 245–250.
- Kempfert, H.-G.; Wallis, S, P. (1997). Geokunststoffummantelte sandsäulen - ein neues gründungsverfahren im verkehrswegbau. *Geotechnik*, Sonderheft zur 5. Informationsveranstaltung über Kunststoffe in der Geotechnik in München, p. 41–46.

- Kempfert, H.-G.; Jaup, A.; Raithel, M. (1997). Interactive behaviour of a flexible reinforced sand column foundation in soft subsoil. In: *Proc. XIV International Conference on Soil Mechanics and Foundation Engineering*. Hamburg, Germany: [s.n.], 1997. v. 3, p. 1757–1760.
- Kempfert, H.-G. (2003). Ground improvement methods with special emphasis on column-type techniques. In: *Proc. International Workshop on Geotechnics of Soft Soils-Theory and Practice – SCMEP*.
- Kempfert, H.-G.; Gebreselassie, B. (2006). *Excavations and Foundations in Soft Soils*. [S.l.]: Springer-Verlag. 576 p.
- Kassem, A.M., Imai, G. (2004). Combined effects of geosynthetic cased sand compaction piles and preloading on the improvement of very soft ground. In: *Proceedings of the 3rd. Eurogeo*, Munich, Germany, pp. 53-59.
- Kitazume, M., Terachi, M., Aihara, N. (1993). Centrifuge model tests on the consolidation behavior of soft clay with fabric-packed sand drain. In: *Geosynthetics' 93 Conference Proceedings*, IFAI, Vancouver, Canada, 1: 393-406.
- Lee, D.; Yoo, C.; Park, S.; Jung, S. (2008). Field load tests of geogrid encased stone columns in soft ground. In: *Proceedings of the Eighteenth (2008) International Offshore and Polar Engineering Conference*. [S.l.: s.n.].
- Malarvizhi, S.; Ilamparuthi, K. (2004). Load versus settlement of claybed stabilized with stone and reinforced stone columns. In: *Proceedings of GeoAsia*. Seoul, Korea: [s.n.] p. 322–329.
- Mandal, J.N., Kamble, S.M. (1999). Geosynthetics Encased Stone Columns. In: *Geosynthetics'99 Conference Proceedings*, IFAI, Boston, USA, 1: 101-113.
- Madhav, M. R.; Alamgir, M.; Miura, N. (1994). Improving granular column capacity by geogrid reinforcement. In: *Proc. of Fifth International Conference on Geotextiles, Geomembranes and Related Products*. Singapore: [s.n.] p. 351–356.
- Muir Wood, D.; Hu, W., Nash, D.F.T. (2000). Group effects in stone column foundations: model tests. *Géotechnique*. ICE, 50(6):689-698.
- Murugesan, S.; Rajagopal, K. (2006). Geosynthetic-encased stone columns: Numerical evaluation. *Geotextiles and Geomembranes*, n. 24, p. 349–358, 2006.
- Paul, A.; Ponomarjow, A. (2004). The bearing behaviour of geogrid reinforced crushed stone columns in comparison to non-reinforced concrete pile foundations. In: *Proceedings of the Third European Geosynthetics Conference - 3rd. EUROGEO*. Munich, Germany: [s.n.]. v. 1, p. 285–288.
- Paul, A.; Schwedt, S. (2003). Untersuchungen zum tragverhalten vertikaler gründungselemente aus gelegten geogittern - perspektiven für neue anwendungsmöglichkeiten im tiefbau. In: *Proceedings of 3. Geokunststoff-Kolloquium der Fa. Naue*. [S.l.: s.n.], 2003.
- Van Impe, W.F., Silence, P. (1986). Improving of the bearing capacity of weak hydraulic fills by means of geotextiles. Proc. of the 3rd. International conference on geotextiles, Vienna, Austria, pp. 1411-1416. Balkema.
- Raithel, M. (1999). *Zum Trag- und Verformungsverhalten von geokunststoffummantelten Sandsäulen*. Schriftenreihe Geotechnik. Univesität Gh Kassel, Heft 6, Kassel, Germany.
- Raithel, M., Henne, J. (2000). Design and numerical calculation of a dam foundation with geotextile coated sand columns. In: *Proceedings of the 4th. International Conference on Ground Improvement Geosystems*. Helsinki, Finland, pp.153-161.
- Raithel, M.; Kempfert, H.-G.; Kirchner, A. (2005). Berechnungs-verfahren und bemessung von ummantelten säulen - entwircklung und aktueller stand. *Geotechnik*, 28(1): 20–31.
- Santos, C. T. Queiroz, P.I.B.; Vidal, D.M.; Alexiew, D. (2010). Assessment of a consolidation model issued to geotextile-encased columns based on field instrumentation data. In: *Geosynthetics for a challenging world - Proceedings of the 9th. International Conference on Geosynthetics*. [S.l.: s.n.].
- Santos, C. T. (2011). Rational Analysis of Consolidation in Geosynthetic-Encased Columns Foundation Systems. PhD thesis, Aeronautics Institute of Technology, Brazil.
- Schuessler, M. (2002). Anwendungen neuer, innovativer gründungslösungen - ist das risiko für den auftraggeber überschaubar? In: DGGT (Ed.). In: *Proceedings of 27th. "Baugrundtagung in Mainz"*. [S.l.: s.n.].
- Sharma, J. S. (1998). A study on the behaviour of geogrid reinforced stone column. In: IFAI, I. e (Ed.). In: *Proceedings of the Sixth International Conference on Geosynthetics*. Atlanta, USA: [s.n.], 1998. p. 877–882.
- Sharma, J. S.; Phanikumar, B. R.; Nagendra, G. (2004). Compressive load response of granular piles reinforced with geogrids. *Canadian Geotechnical Journal*, 41(1): 187–192.
- Short, R. D.; Prashar, Y.; Metcalfe, B. (2005). Repairing a railway spur roadbed failure using geotextile encased columns. In: *Proc. of 84th. Transportation Research Board Annual Meeting*. Washington D.C, USA: [s.n.], 2005.
- Smolczyk, U. (1999). Geogitter schafft biegesteife schotter säulen. *Bauen mit Textilien*, 1: 30–35, 1999.
- Strauch, N. S. und G. (2003) Herstellung geotextileummantelter kiestragsäulen mit keller-tiefenrüttler. In: *Tagungsbeiträge 4. Österreichische Geotechniktagung*. Vienna, Austria: [s.n.] p. 415–433.
- Trunk, U.; Heerten, G.; Paul, A.; Reuter, E. (2004). Geogrid wrapped vibro stone columns. In: *Proceedings of Third European Geosynthetic Conference*. Munich, Germany: [s.n.]. 289–294.
- Wong, C. (1990). A normalizing relation for granular materials. *Canadian Geotechnical Journal*, 27: 68–78.
- Wu, C.; Hong, Y. (2008). The behavior of a laminated materials reinforced granular column. *Geotextiles and Geomembranes*, 26(4): 302–316.
- Wu, C.-S.; Hong, Y.-S. (2009). Laboratory tests on geosynthetic-encapsulated sand columns. *Geotextiles and Geomembranes*, 27: 107–120.

High Density Polyethylene (HDPE) Lined Produced/Flow-back Water Evaporation Ponds

Neil C. Nowak, PE, Weaver Boos Consultants, LLC, USA, nnowak@weaverboos.com

ABSTRACT

The problem to be solved is the disposal of millions of gallons of production water (brine water) and flow-back water generated annually from the Rocky Mountain Region oil and gas industry in an environmentally safe, low cost, and efficient manner. A technology that is effective and safe is the evaporation of the water in lined containment ponds after separation and removal of the hydrocarbon component from the water.

Four projects are the case studies for this paper, located near the following cities:

- Cheyenne, Wyoming
- Cisco, Utah
- Dad, Wyoming
- Hobbs, New Mexico

They were designed to evaporate water in a series of geomembrane lined ponds.

1. INTRODUCTION

Some of the aforementioned projects are complete and have been operational for a number of years, while others are currently under construction. The production and flow back water from oil and gas wells in the area local to each site is trucked to the sites for disposal. The water is evaporated in ponds lined with high density polyethylene (HDPE) as the top layer by using a combination of factors that are favorable to the evaporative process, including the following:

- Natural characteristics of the site, including the arid climate, windy conditions, and numerous sunny days,
- The top liner in the ponds is black HDPE, which creates a hot surface,
- HDPE liner was chosen to protect the surface and ground waters of the area and to assist with the evaporation of the water (evaporation is enhanced due to the black color of the liner).

The projects are interesting in that each facility provides oil and gas production companies in the area with a large commercial alternative to production water and flow-back disposal versus numerous small ponds that may service only one well pad, or expensive re-injection wells, or even more expensive water recycle treatment facilities. The regulatory agencies like it for centralization and protection of the state's waters. The facilities protect surface waters in the area due to the large capacity of the ponds, 2 feet (Utah) and 3 feet (Wyoming and New Mexico) of freeboard, and secondary containment in case of catastrophic berm failure (Utah).

1.1 Project Location – Cheyenne, WY

1.1.1 Silo Field, Wyoming

The project is located in a semi-arid region of southeastern Wyoming in Laramie County, which is situated at approximately 5,900 feet above mean sea level (amsl). The site is located approximately 15 miles northeast of the intersection of Interstates I-80 and I-25 in Cheyenne, WY.

1.1.2 Background and Site Conditions

The ground surface is privately owned land primarily used for arid farming and stock grazing. No residences are located within 1 mile of the site. Access to the site is over unpaved roads used primarily for agriculture, oil and gas vehicles.

Topography: The topography at the site slopes gradually from elevation 5,910 ft amsl to 5,890 ft amsl to the east. There are no major watercourses on the site.

Geology and Hydrology: The site is located above the High Plains Formation underlain by Pierre Shale at approximately 5,700 feet thick which is dominant throughout the region. The primary aquifer includes the High Plains Aquifer, consisting of the Ogallala, Arikaree, and White River formations, which total approximately 1,480 feet thick. The Ogallala is the first instance of usable groundwater at approximately 160 to 300 feet below the site.

1.1.3 Climatological Data

According to the U.S. Department of Agriculture (USDA) Natural Resources Conservation Service (NRCS) map, the average annual precipitation is 15.17 inches. The climate survey for Cheyenne, WY (closest weather station to site) according to the Western Regional Climate Center (WRCC) is offered in the following table (re-created from WRCC information).

Table 1. Climate Survey, Cheyenne, WY

Parameter	Jan	Feb	Mar	Apr	May	Jun	Jul	Aug	Sep	Oct	Nov	Dec	Annual
Average Max. Temperature (F)	32.6	36.1	47.6	58.7	68.3	79.3	86.3	83.6	73.9	60.7	43.0	33.8	58.7
Average Min. Temperature (F)	5.2	8.9	20.7	27.9	34.7	41.5	48.1	46.4	37.9	27.6	16.8	7.4	26.9
Average Total Precipitation (in.)	0.44	0.39	0.51	0.87	1.44	0.85	1.16	0.92	1.19	1.35	0.66	0.51	10.29
Average Total Snowfall (in.)	8.4	5.4	5.3	1.9	0.2	0.0	0.0	0.0	0.0	2.0	6.1	8.8	38.2

1.1.4 Design Evaporation Data

The National Weather Service developed an isopleths map of the Free Water Surface Evaporation (shallow lake evaporation) based on 24 years of data. The free water surface evaporation rate is the amount expected to evaporate from the disposal ponds, which is 45 inches per year. Approximately 35 inches of that rate occurs from May to October. The remaining 10 inches would evaporate from November to April. This is based on a water containmentment that is not lined with black HDPE.

1.2 Project Location – Cisco, UT

1.2.1 Danish Flats, Utah

The project is located in an arid region of eastern Utah in the area known as Danish Flat, which is situated at approximately 4,610 feet above mean sea level (amsl). The site is located in Grand County approximately 3.5 miles north of Interstate 70 interchange exit number 214, and approximately 43 miles west of the Utah-Colorado state line.

1.2.2 Background and Site Conditions

The ground surface is privately owned land primarily used for stock grazing and oil and gas transmission piping. No residences are located within 10 miles of the site. Access to the site is over unpaved roads used primarily for oil and gas vehicles.

Topography: The topography at the site slopes gradually from elevation 4,615 ft amsl to 4,600 ft amsl to the southeast. There are no major watercourses on the site.

Geology and Hydrology: The site is located in the Mancos Shale lowland area including the Greater Cisco area. The Mancos Shale Formation is the predominant outcrop in this area. Due to the preponderance of fine-grained sediments and water soluble minerals found in this formation, it does not usually contain any fresh water. Groundwater that comes in contact with the Mancos Shale Formation almost always contains high levels of dissolved solids. Groundwater is usually limited to alluvial deposits along streams and drainages or to sandstone units, some of which are very localized with low recharge rates. Wells in the area are usually drilled with air with little or no water encountered until the Dakota Formation is penetrated (Hunt et al. 1996).

The underlying Mancos shale is a dark grey to black soft shale with sandstone beds at various horizons. The

maximum thickness of the Mancos shale is approximately 900 to 1,000 feet. The Mancos shale is considered a confining unit and is a thick barrier to vertical and lateral groundwater flow. Below the Mancos shale is the lower to upper Cretaceous Dakota Sandstone, which are a yellow-brown and gray friable to quartzitic sandstone and conglomerate sandstone and interbedded gray to black carbonaceous shale with occasional lenticular coal beds (Cashion et al. Map I-736). The Dakota Sandstone is considered to be the first aquifer in the area.

1.2.3 Climatological Data

According to the U.S. Department of Agriculture (USDA) Natural Resources Conservation Service (NRCS) map, the average annual precipitation is six inches. The climate survey for Cisco, UT (closest weather station to site) from 1952 to 1967 according to the Western Regional Climate Center (WRCC) is offered in the following table (re-created from WRCC information).

Table 2. Climate Survey, Cisco, UT

Parameter	Jan	Feb	Mar	Apr	May	Jun	Jul	Aug	Sep	Oct	Nov	Dec	Annual
Avg. Max Temp (F)	37.2	45.7	56.6	68.7	80.3	91.8	98.7	94.3	85.5	72.5	53.4	40.2	68.7
Avg. Min Temp (F)	8.8	17.7	24.0	33.5	43.7	52.1	60.7	58.4	47.3	35.2	22.5	12.5	34.7
Avg. Total Precip. (in.)	0.48	0.50	0.52	0.61	0.61	0.26	0.37	1.03	0.80	0.86	0.63	0.43	7.11
Avg. Total Snow (in.)	4.3	2.1	1.1	0.3	0.0	0.0	0.0	0.0	0.0	0.2	0.9	2.1	11.0

1.2.4 Design Evaporation Data

The National Weather Service developed an isopleths map of the Free Water Surface Evaporation (shallow lake evaporation) based on 24 years of data. The free water surface evaporation rate is the amount expected to evaporate from the disposal ponds, which is 50 inches per year. Approximately 35 inches of that rate occurs from May to October. The remaining 15 inches would evaporate from November to April. This is based on a water containment that is not lined with black HDPE.

1.3 Project Location – Dad, WY

1.3.1 Southern Cross, Wyoming

The project is located in an arid region of southwest Wyoming in the area known as Mexican Flat, which is situated at approximately 6,540 feet above mean sea level (amsl). The site is located in Carbon County approximately 5 miles west of Wyoming State Highway 789, approximately 30 miles south of the intersection of highway 789 and Interstate 80 at Wamsutter, and approximately 22 miles north of Baggs, Wyoming.

1.3.2 Background and Site Conditions

The ground surface is privately owned land primarily used for stock grazing and oil and gas transmission piping. No residences are located within 20 miles of the site. Access to the site is over unpaved roads used primarily for oil and gas vehicles.

Topography: The topography at the site slopes gradually from elevation 6,546 ft amsl to 6,536 ft amsl to the northeast. There are no major watercourses on the site.

Geology and Hydrology: The site is located in the Wasatch/Claron Formation. The Claron Formation also referred to as the "Pink Cliffs," and forms the highest "step" of the Grand Staircase. This formation is also known as the Wasatch Formation. The site is located in the Cathedral Bluffs Tongue of the Wasatch Formation. This outcropping consists of claystone, mudstone and sandstone. The field investigation and laboratory analysis confirmed the published description to the depth of the deepest boring.

The only known groundwater is at a depth of approximately 700 feet based on a recent boring by Devon Energy. This boring is on the north side of the property.

1.3.3 Climatological Data

According to the U.S. Department of Agriculture (USDA) Natural Resources Conservation Service (NRCS) map, the average annual precipitation ranges between ten and twelve inches. The climate survey for Baggs, WY (the closest weather station to site) from 1948 to 2007 according to the Western Regional Climate Center (WRCC) is offered in the following tables (re-created from WRCC information).

Table 3. Climate Survey, Baggs, WY

Parameter	Jan	Feb	Mar	Apr	May	Jun	Jul	Aug	Sep	Oct	Nov	Dec	Annual
Average Max. Temperature (F)	32.6	36.1	47.6	58.7	68.3	79.3	86.3	83.6	73.9	60.7	43.0	33.8	58.7
Average Min. Temperature (F)	5.2	8.9	20.7	27.9	34.7	41.5	48.1	46.4	37.9	27.6	16.8	7.4	26.9
Average Total Precipitation (in.)	0.44	0.39	0.51	0.87	1.44	0.85	1.16	0.92	1.19	1.35	0.66	0.51	10.29
Average Total Snowfall (in.)	8.4	5.4	5.3	1.9	0.2	0.0	0.0	0.0	0.0	2.0	6.1	8.8	38.2

1.3.4 Design Evaporation Data

The National Weather Service developed an isopleths map of the Free Water Surface Evaporation (shallow lake evaporation) based on 24 years of data. The free water surface evaporation rate is the amount expected to evaporate from the disposal ponds, which is 45 inches per year. Approximately 35 inches of that rate occurs from May to October. The remaining 15 inches would evaporate from November to April. This is based on a water containment that is not lined with black HDPE.

1.4 Project Location – Hobbs, NM

1.4.1 CRI, New Mexico

The project is located in an arid region of southeastern New Mexico in Lea County, which is situated at approximately 3,540 feet above mean sea level (amsl). The site is located approximately 25 miles west of Hobbs, NM.

1.4.2 Background and Site Conditions

The ground surface is privately owned land primarily used for oil and gas production. No residences are located within 10 miles of the site. Access to the site is over a paved highway.

Topography: The topography at the site slopes gradually from elevation 3,550 ft amsl to 3,530 ft amsl to the northwest. There are no major watercourses on the site.

Geology and Hydrology: The site is located above the Triassic Redbeds, consisting of Chinle Shale, Santa Rosa sandstone and the Dewey Lake formation. The Triassic Redbeds occur at 40 to 50 feet below the ground surface and are virtually impermeable and therefore prevent vertical seepage beyond the redbed level.

1.4.3 Climatological Data

According to the U.S. Department of Agriculture (USDA) Natural Resources Conservation Service (NRCS) map, the average annual precipitation is 15.6 inches. The climate survey for Duval Potash Mine, NM (closest weather station to site) according to the Western Regional Climate Center (WRCC) is offered in the following table (re-created from WRCC information).

Table 4. Climate Survey, Duval Potash Mine, NM

Parameter	Jan	Feb	Mar	Apr	May	Jun	Jul	Aug	Sep	Oct	Nov	Dec	Annual
Average Max. Temperature (F)	32.6	36.1	47.6	58.7	68.3	79.3	86.3	83.6	73.9	60.7	43.0	33.8	58.7
Average Min. Temperature (F)	5.2	8.9	20.7	27.9	34.7	41.5	48.1	46.4	37.9	27.6	16.8	7.4	26.9
Average Total Precipitation (in.)	0.44	0.39	0.51	0.87	1.44	0.85	1.16	0.92	1.19	1.35	0.66	0.51	10.29
Average Total Snowfall (in.)	8.4	5.4	5.3	1.9	0.2	0.0	0.0	0.0	0.0	2.0	6.1	8.8	38.2

1.4.4 Design Evaporation Data

The National Weather Service developed an isopleths map of the Free Water Surface Evaporation (shallow lake evaporation) based on 24 years of data. The free water surface evaporation rate is the amount expected to evaporate from the disposal ponds, which is 46 inches per year. Approximately 36 inches of that rate occurs from May to October. The remaining 10 inches would evaporate from November to April. This is based on a water containment that is not lined with black HDPE.

2. PROJECT DETAILS

2.1 Purpose

The main purpose of the projects is to evaporate the production water and flow back water as quickly as possible while maintaining environmental controls and containment. The projects were planned and built in order to service the oil and gas industry for the disposal of production water and flow back water from oil and gas production in the service areas local to each facility location.

Several water disposal options exist, including reinjection wells, frac injection, treatment for surface discharge, and evaporation. The evaporation technology was chosen for these projects due to the ideal site conditions for evaporation, including low precipitation, windy conditions, high ambient temperatures and sun. Other factors that made the project sites ideal include the following; little or no residences within several miles of the site (other than consenting land owners), easy access to/from a major highway, long distance to open water at several miles, deep groundwater, and impermeable formations below the sites.

2.2 Selection of Technology

To enhance the evaporative quality of the projects and to adequately contain the brine water, the top layer of the pond lining needs to be a durable long-lasting product that is cost-effective and helps to enhance evaporation while being acceptable to the regulatory agencies involved. Some of the liner technologies considered include compacted clay, geosynthetic clay liner (GCL), polyvinyl chloride (PVC), polypropylene (PPE), and high density polyethylene (HDPE). While several lining technologies exist and are allowed by the regulatory agencies, the HDPE liner was chosen for the top layer for several reasons, including, durability, resistance to ultraviolet (UV) degradation, chemical resistance, black color, and ease of construction.

HDPE is designed to be the top layer of ponds and be exposed to the elements (sun, freeze/thaw, and physical impact), therefore, the material needs to be resistant to UV degradation and be durable. The addition of the proper amount of high quality carbon black to the geomembrane during manufacturing is universally accepted as being resistant to significant deterioration caused by weathering. In addition to high quality carbon black, highly effective chemical UV stabilizers further extend the life of the liner. These additives absorb incident radiation and/or terminate free radical production, thus protecting the HDPE against thermal degradation and possible chemical reactions with surrounding materials. Other factors that affect the potential UV resistance of a material include average density, density range or dispersion, chemical stabilizer system, catalyst type and amount of residue, copolymer type, combined chemical exposures, and failure criteria (GSE 2003). HDPE was chosen for this application due to these characteristics.

2.3 Implementation

To enhance the evaporative quality of each facility, and to adequately contain the brine water, high density polyethylene (HDPE) was chosen as the top layer. The top or primary liner was designed and constructed with 60-mil thick textured HDPE to help ensure a durable long-lasting containment. The liner was textured to increase the safety factor for personnel using the facility (i.e. the textured surface increases traction and gripping to enable easier egress in case of someone falling into the pond).

The facilities were designed by Weaver Boos Consultants, LLC and have been or are currently being constructed. The facilities consist of the following components (refer to Figures 1 and 2 for details):

- Access road and truck off-loading pad
- Piping and valves
- Acceptance Pits (vaults) or advanced oil/water separation equipment
- Sludge Pond covered with bird control netting or no sludge pond if oil/water separation equipment used
- Evaporation ponds (constructed or planned):
 - Silo Field, WY has 3 ponds out of the permitted 10 ponds in the process of being built at approx. 5.2 acres each and 25 feet deep (double lined HDPE with leak detection in between the liners)
 - Danish Flats, UT has 14 ponds built at approx. 5.2 acres each and are 12 or 22 feet deep (single HDPE liner underlain by compacted clay layer)
 - Southern Cross, WY has 4 ponds built at approx. 5.2 acres each and are 12 feet deep (double lined HDPE with leak detection in between the liners)
 - CRI, NM will have 2 ponds at approx. 4.2 acres each and be 24-28 feet deep (double lined HDPE with leak detection in between the liners)

General: Production water and flow back water is delivered to the sites via tanker trucks from well sites located within the geographic area local to each site, and depends on transportation costs and disposal fees when compared to other alternatives for water disposal in the area. The tanker trucks are off-loaded and the water is sent through a treatment process, including separation vaults, gun-barrel tanks, or state-of-the art equipment.

The Silo Field and CRI facilities will include a truck off-loading area and the water will be treated prior to placement in the evaporation ponds, including the removal of hydrocarbons to a level below 30 parts per million (ppm).

The Danish Flats facility's plan view is shown on the following Figure 2. The operation units include one set of 14,000 gallon three-stage concrete receiving tanks, a sludge pond, and a series of five-acre evaporation ponds. All of the structures are connected via gravity or force-main fed via an underground piping system. The Southern Cross facility process is similar to the Danish Flats layout.

Pond Inlet: Various methods exist for the separation of the oil and water prior to placement in the ponds for evaporation, and the proper removal of the oil from the water will dictate whether or not the ponds should be covered with bird control netting.

The incoming water at the Silo Field and CRI facilities will flow through state-of-the-art oil/water separation equipment capable of removal of the hydrocarbons to a level of 30 ppm or less prior to moving the water to the ponds for evaporation. There will be no sludge ponds used for these facilities. Volatile organic compound (VOC) emissions from the separation equipment and ancillary tankage are controlled to maintain air quality.

The incoming water at the Danish Flats and Southern Cross sites flows through the three-stage concrete settling tank systems and pretreatment tanks (Danish Flats) or one of the three-stage concrete settling tank systems (Southern Cross) and each site uses a the sludge pond before entering the evaporation ponds. The pre-treatment facilities and the evaporation ponds have been designed to follow the topography, allowing for gravity flow throughout the system, and the Danish Flats site is equipped with force-mains to allow pumping of the water from the lower Phase 1 ponds to the upper Phase 2 ponds.

Shut-off valves have been installed on the crossover piping to allow for proper flow management. If necessary, portable gasoline powered pumps will be used to transfer liquid to ponds that are not in the gravity flow line or to empty a pond for maintenance or liner repair.

Slope Design: At Danish Flats and Southern Cross the sludge ponds and evaporation ponds have an interior slope of 3 horizontal to 1 vertical, and a maximum exterior slope of 2 to 1.

At Silo Field and CRI, the pond interior and exterior slopes were designed with 4 to 1 slopes.

The HDPE chosen has a textured surface, which will increase the safety characteristics of the facility by making it easier to walk on, especially on the interior slopes.

Berm Design: Surface water will not be allowed to enter the ponds because the constructed berms are several feet higher than the surrounding ground surface and also diversion and control ditches are used to direct the run-on and run-off for minimizing impact of storm water. The interior berm walls are covered with a protective layer of 60-mil high density polyethylene (HDPE). The HDPE will provide erosion control. The area between the evaporation ponds has been covered with HDPE or compacted clay to prevent erosion, control dust and enhance evaporation. The exterior sides of the berm have been seeded as necessary.

Leak Detection System: As described in the geology/hydrology section of this paper, each site is underlain by impermeable layers of shale or clay, including at Danish Flats approximately 1,200 feet thick of Mancos Shale, and at Southern Cross the Wasatch Formation. The first usable aquifers for human use are below these formations for these sites. The geological investigations did not detect perched groundwater.

At the Silo Field site the first usable aquifer will be protected by the three layers of liner in the pond, as well as natural clay aquitards below the pond bottoms at approximately 30 and 60 feet below the ground surface, which also includes the leak detection under the primary liner. At the CRI location, the geology and hydro geology is favorable including low permeable shale at 50 feet below the ground surface.

In addition to the ideal natural conditions at each site, a 60-mil HDPE liner has been installed as the top layer in all of the ponds. The pond floors slope toward sumps that are fitted with a riser monitoring pipe and leak detection equipment.

The leak detection system is inspected and data recorded as required. A summary of the inspections are reported to the regulatory agencies as needed. Liquid from the sump can be pumped back into the pond, if excessive amounts accumulate then specific protocols for repairing the liner are required if the volume of the leak exceeds certain thresholds.

Livestock/Wildlife Protection Measures: The entire facility area at each site has been fenced and gated to help prevent cattle or other animals from entering. Since the sludge ponds could have oily material on the surface, netting has been used to deter the entry of birds or other wildlife at the Danish Flats and Southern Cross sites.

Capacity: The volume of water able to be stored for evaporation in the ponds is as follows:

- Silo Field – Ponds 1 -3 are 25 feet deep of water holding capacity and nearly 582,000 barrels each for a total water holding capacity of approximately 1,746,000 barrels.
- Danish Flats - Ponds 1 through 8 are 12 feet of water holding depth and nearly 240,000 barrels each (at 42 gallons per barrel) for a total capacity of approximately 2,000,000 barrels. Ponds 9 through 13 are 22 feet of water holding depth at Danish Flats and nearly 632,000 barrels each for a total capacity of 3,160,000 barrels.
- Southern Cross - Ponds 1 through 4 are 12 feet of water holding depth and nearly 240,000 barrels for a total capacity of approximately 960,000 barrels.
- CRI – Ponds 1 and will be 22 feet deep with a total water holding capacity of approximately 650,000 barrels.

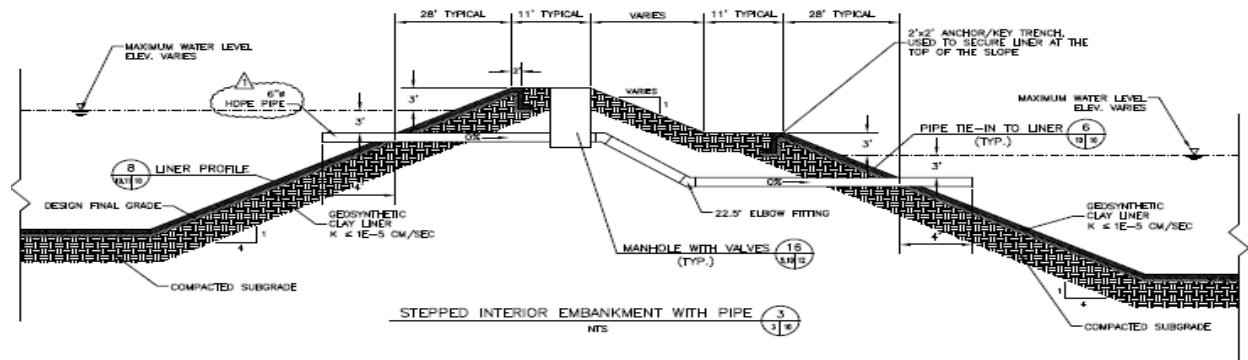


Figure 1. Silo Field Pond Liner Details

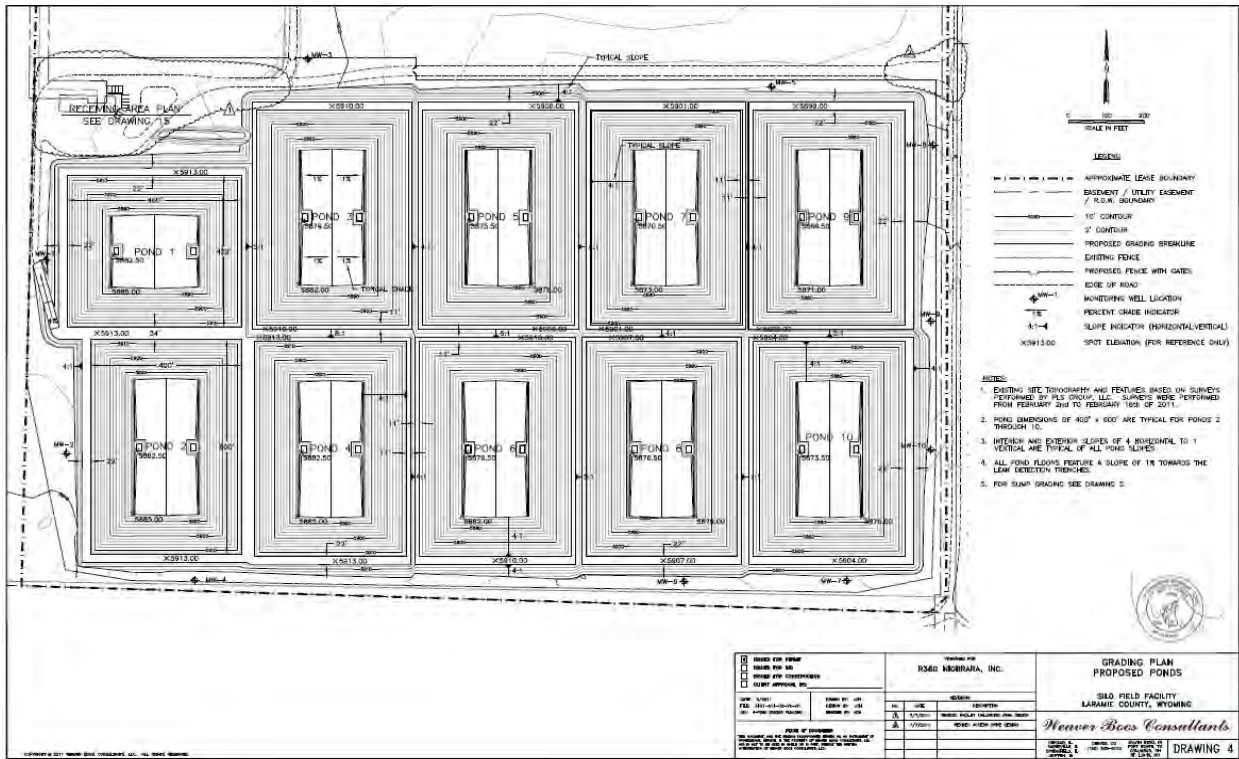


Figure 2. Silo Field - Facility Design Plan View – Permit Approved Layout



Figure 3. Aerial Photo of Completed Project at Danish Flats, UT

The partially completed and partially operational project at Danish Flats was photographed from the air on June 29, 2009 and is shown above. The water was distributed from the sludge pond to the Ponds 1 through 12, which appear as “black”. The Ponds 13 appears to have “brownish” water, which includes some construction water is shown in the background and was not yet approved for water disposal at the time of the photography, but has since been put into operation. Currently, 14 evaporation ponds are operational at Danish Flats.

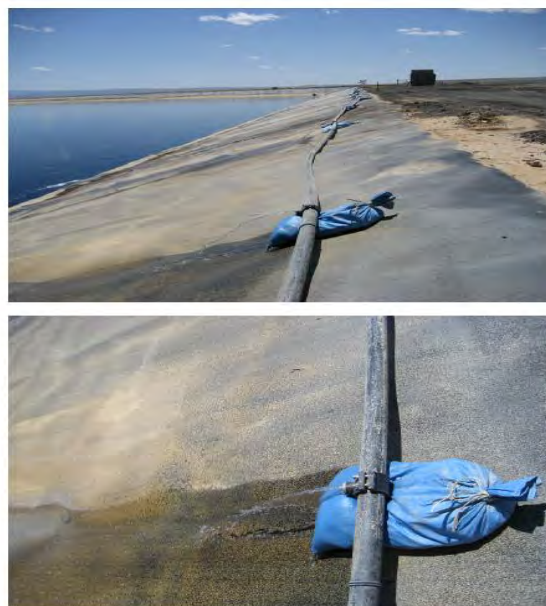
2.4 Operational Data

At Danish Flats they have experienced various quantities of water deliveries ranging from 10,000 barrels to 35,000 barrels per day. Each barrel is equal to 42 gallons. The water is moved from the off-loading area through the sludge pond and to the evaporation ponds by gravity or via force main for distribution to Phase 2. Each pond at Danish Flats, Utah has a free board requirement of 2 feet, and each pond for the projects in Wyoming at Southern Cross and Silo Field has a free board requirement of 3 feet. The free board at New Mexico is 3 feet.

When an individual evaporation pond was brought on-line, such as Ponds 5 through 8 at Danish Flats, and the water was allowed to flow into the empty pond lined with HDPE, the water was observed as “disappearing” due to the evaporative nature of the HDPE when in combination with the hot sun and arid climate in Utah in July and August.

In Cisco, UT in July and August the ambient air temperatures often exceeds 100 degrees Fahrenheit and the wind normally blows to some extent. The actual evaporation encountered during the months of July and August 2008 at the site was measured to be approximately 15 and 18 inches per day, respectively. The facility operators observed very favorable evaporation of the water and measured the total evaporation for the year 2008 above the estimate of 50 inches for approximately 6 months of operation. In year 2009, the Danish Flats facility was measured to have 60 inches of evaporation, which took place mostly in the months from April 1 to October 31, and again in year 2010 the evaporation total has exceeded 60 inches over the entire water surface of the ponds. The deeper ponds at Danish Flats experienced an approximately 30 percent lower evaporation rate due to the deeper water depth, therefore, the entire depth of water was not able to be achieve warmer temperatures as did the shallower ponds.

Each site is equipped or designed with leak detection systems that are monitored on a monthly basis or continuously, depending on the equipment chosen. Two ponds at Danish Flats were adversely affected by shifting ice at the HDPE pipe boots when the liquid level in the ponds were adjusted, which resulted in leaks at the pipe boots. The liner was easily repaired and there has not been a reoccurrence of any leaks at these ponds.



Figures 4 and 5. Weep system to enhance evaporation

In an effort to increase evaporation with low costs in mind, a “weep” system was added to the allow water to flow and fan out over the surface of the HDPE liner that is above the water line. This system utilizes the exposed HDPE liner to increase evaporation by using the heat generated from the exposed HDPE liner in combination with the increased surface area of the water fanning out over the liner. Please refer to the below photographs of the “weep” system.

This system will be used at Silo Field, CRI, and Danish Flats.

3. CONCLUSIONS

The use of HDPE as the primary liner in the ponds appears to be favorably enhancing the evaporation of the water. At Danish Flats, the estimate of 50 inches of evaporation per year was far exceeded given the 33 inches of evaporation experienced in only July and August 2008, which may have totaled 70 inches for 2008. In years 2009 and 2010, the evaporation rate was over 60 inches. In 2012, the evaporation rate was 42 inches from May through August. The “weep” system was an enhancement to increase evaporation, which was not quantitatively measurable, but may have been a factor in the total evaporation. The deeper ponds at Danish Flats experienced approximately a 30 percent lower evaporation rate due to cooler water at depth. Similarly, the actual evaporation experienced at the Southern Cross project was also more than the pan evaporation estimate based on ponds without the HDPE liner effects, including the increase in evaporation from the estimate of 45 inches per year to nearly 55 inches.

It is anticipated that the evaporation rates at Silo Field and CRI will also be enhanced with the use of the HDPE liner as the top layer and the use of the “weep” system along the exposed liner too.

The durability and resistance to UV degradation due to the proper amount of carbon black in the geomembrane and other factors as discussed above are the major reasons for the use of the HDPE geomembrane liner as the top layer. The increase with the rate of evaporation due to the black color of the HDPE has been a great benefit and in combination with the “weep” system has realized an increase with the total evaporation at each facility.

Some of the liner was installed during the summer months and due to the expansion and contraction of the liner with ambient air temperature gradients, the anchor trenches were only filled during the coolest part of the day to reduce bridging.

The leak detection system is used to capture leaks through the primary liner, which worked as designed at the Danish Flats site when a leak was propagated due to ice on the water and the level in the ponds changing which resulted in the ice grabbing onto the pipe and pulling on the pipe boot. The liner was repaired and the leak did not appear again.

An existing study was conducted on an HDPE liner installed at a site in Colorado after 20 years of service where the liner was not buried and exposed to weathering, UV light and cooling tower blow-down water. The material was tested for various properties and was found to have no significant reduction in the primary physical properties of the HDPE (Ivy 2002).

ACKNOWLEDGEMENTS

Thank you to R360 Environmental Solutions, Danish Flats Environmental Services, and Southern Cross Environmental Services for the use of their projects in this paper. Also, I'd like to recognize Gerald Knudsen, PE of AgriTech who provided his engineering expertise, during the design and permitting of two of these sites, and to John Heap of Colorado Lining, Inc. who provided his installation expertise and also performed the construction of the HDPE liners at the ponds in field, which all are performing exceptionally well and without leaks due to construction.

REFERENCES

- Cashion, W. B. Geologic and Structure Map of the Grand Junction Quadrangle, Colorado and Utah, USGS Miscellaneous Geologic Investigations, Map I-736.
- Gundle/SLT Environmental, Inc. (GSE). (2003). “Technical Note – HDPE, UV Resistance for GSE Geomembranes.” <http://www.truslate.com/grid/techspec.pdf> .
- Hunt, G. L. (1996). Environmental Handbook, Environmental Regulations for the Oil & Gas Exploration and Production Industry.
- Ivy, N (2002). HDPE geomembrane after 20 years of service, GFR Magazine June/July 2002.

Implications of MSE Connection Criteria for Frictionally Connected GRS Structures

J. Nicks, PhD, FHWA Turner-Fairbank Highway Research Center, McLean, VA, USA, jennifer.nicks@dot.gov

M. Adams, FHWA Turner-Fairbank Highway Research Center, McLean, VA, USA, mike.adams@dot.gov

D. Alzamora, P.E. FHWA Resource Center, Lakewood, CO, USA, daniel.alzamora@dot.gov

ABSTRACT

In the geosynthetic reinforced soil integrated bridge system (GRS-IBS), the facing is frictionally connected to the reinforced soil composite. This frictional connection method has performed well for closely-spaced ($\leq 0.3\text{m}$) GRS under both working and failure loads, leading to the removal of the connection criterion as a strength limit within the FHWA's design guidance for the GRS. Conversely, AASHTO LRFD Bridge Design Specifications require a check between the long-term strength, determined through connection testing, and the maximum load on the reinforcement. To investigate the impact this criterion has on the design of the GRS-IBS, connection testing was performed between hollow-core concrete modular blocks and geotextiles and compared to assumed lateral facing pressures. The results of large scale direct shear tests and block pull-out tests conducted at Turner Fairbank Highway Research Center were also compared. This paper describes the testing procedures, results, and implications for design of GRS.

1. INTRODUCTION

1.1 Current Practice

In many segmental reinforced soil walls and abutments, the reinforcement is connected to the facing element through various connection mechanisms. When geosynthetics are utilized as the reinforcement, the connection with the facing elements can be frictional, structural, or a combination of both (i.e. partial friction connection). Fully frictional connections rely solely on the friction between the geosynthetic reinforcement, the facing element, and sometimes the aggregate placed in the core of the unit (Figure 1), while structural connections physically tie the facing and reinforcement together, typically through pins, clips, or shear lips.



Figure 1. Cross-section of fully frictional connection.

Current design methods for mechanically stabilized earth (MSE) allow for any type of connection; however, the strength of the connection must equal the maximum factored tension in any reinforcement layer (AASHTO 2010, Berg et al. 2009). Recent Federal Highway Administration (FHWA) design guidance on geosynthetic reinforced soil (GRS) eliminates the criterion for connection strength, thus, no connection testing is required, provided that the reinforcement is closely spaced, less than 0.3m, and each course of block is frictionally connected to the reinforcement (Adams et al. 2011a). The fully frictional connection method is recommended because of its compatibility with the modular block units, cost, and time effectiveness; it has also been shown to perform well both at the service limit under working loads and at the strength limit under failure loads for GRS with close reinforcement spacing (Adams et al. 2011b). To date, no connection failures have ever been observed on a GRS wall or abutment.

1.2 Connection Testing

In MSE wall design, the connection strength for a particular reinforcement and facing element combination is found either through short- or long-term testing. Long-term testing requires a creep rupture envelope for the geosynthetic (ASTM D5262); this can take over 1 year. Short-term testing is much quicker (on the order of a few days) and is performed in accordance with ASTM D6638. To account for long term design strength, a creep reduction factor is then applied to the short-term ultimate connection strength. Both types of testing are conducted in-isolation (i.e. no soil-confinement effect); the procedures are described in FHWA's Geotechnical Engineering Circular (GEC) No. 11 (Berg et al. 2009).

To investigate the in-service connection strength of a GRS wall, FHWA's Turner-Fairbank Highway Research Center (TFHRC) developed the block pull-out test (Adams et al. 2011b). This test was devised in 1998 to quantify the amount of force required to mobilize or displace a modular block unit from the face of a GRS wall. The test is performed on blocks at different heights along a full-scale GRS test wall to determine the relationship between the normal force on top of the block and the required pull-out force (Figure 2). While the test should provide more realistic results than the standardized short- and long-term connection testing, a full-scale wall is needed to test the strength which is often not practical in design.



Figure 2. Block pull-out test on a GRS wall (Adams et al. 2011a).

1.3 Connection Load

In practice, connection testing provides short- and long-term strength which can then be compared to the estimated loads on the face to ensure adequate strength of the connection in-service. In MSE wall design, the thrust against the face is equal to the internal loads of the reinforced soil system, as calculated according to Equation 1 (AASHTO 2010, Berg et al. 2009). According to Soong and Koerner (1997), this design requirement was first recommended by an industry-wide group; however, it was not based on theoretical calculations.

$$T_{\max} = \sigma_h S_v \quad [1]$$

Where T_{\max} is the maximum tension in each reinforcement layer, σ_h is the average lateral earth pressure within the tributary area of the reinforcement layer under consideration, and S_v is the reinforcement spacing.

For closely spaced GRS, the thrust at the face is not equal to the internal lateral stress, as assumed in MSE wall design. Soong and Koerner (1997) and Wu (2007) conclude that the pressure at the face develops independently between each reinforcement layer and surcharge does not transfer to the face. Wu (2001) proposed that this distribution between closely spaced layers is based on the concept of bin pressure for frictionally connected segmental facing. Ideally, the pressure is zero at the depth of any reinforcement layer within a bin, increases linearly with depth before decreasing to zero at the next reinforcement layer. Because reinforcement may deform slightly at the soil reinforcement interface, the bin pressure diagram shown in Figure 3 was adopted, with the thrust calculated according to Equation 2. Measurements from large-scale test walls have shown the estimated bin pressure magnitudes to be similar to those assumed with bin pressure (Yogarajah and Saad, 1996; Andrawes and Yogarajah, 1994); however, additional research should look at the impact of spacing and thrust against the face to better verify this assumption. Soong and Koerner (1997) theoretically assume a typical active lateral earth pressure distribution between each layer to determine the thrust (Equation 3).

$$F_{bin} = 0.72\gamma S_v^2 K_a \quad [2]$$

$$F_{bin,R} = \frac{1}{2} \gamma S_v^2 K_a \quad [3]$$

Where F_{bin} is the thrust against the face assuming the proposed bin pressure diagram (Figure 3), $F_{bin,R}$ is the thrust against the face assuming a typical lateral earth pressure distribution between each reinforcement layer, γ is the unit weight of the soil, S_v is the reinforcement spacing, and K_a is the active earth pressure coefficient.

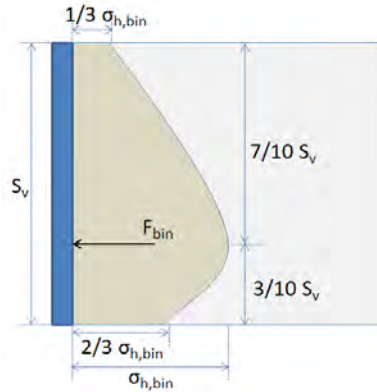


Figure 3. Assumed bin pressure diagram for GRS structures (After Wu 2007).

1.4 Objective

The full frictional connection method is not widely used for MSE applications; however, it is recommended for closely spaced GRS applications because of its demonstrated performance and efficiency of construction (Adams et al. 2011a). To date, very few fully frictional connection tests have been published (Bathurst and Simac 1998); testing has also been largely limited to geogrids, whereas geotextiles are widely used in GRS. To investigate the implications of the connection strength criterion on closely spaced GRS walls and abutments, frictional connection tests and large scale direct shear (LSDS) tests were performed at TFHRC and compared to the designed connection loads (i.e. lateral earth pressure acting at the face). The results of the block pull-out tests are also studied to determine the applicability of the connection tests for field applications.

2. CONNECTION STRENGTH TESTING AND RESULTS

2.1 Short-Term Connection Tests

A series of short-term connection tests were performed at Turner-Fairbank Highway Research Center (TFHRC) in accordance with ASTM D6638. The reinforcement tested is a woven polypropylene (PP) geotextile with an ultimate tensile strength (i.e. MARV value) of 70 kN/m; the facing element is a lightweight, approximately 0.2 kN, hollow-core concrete masonry unit (CMU) block with nominal dimensions of 0.2m x 0.2m x 0.4m.

2.1.1 Test Set-Up

A schematic of the test setup is shown in Figure 4. The free length of the geotextile reinforcement was set at 0.2 m for each test with the width of the geotextile specimens equal to two CMU widths, or 0.8m. To isolate the movement of the geotextile relative to the CMU facing, all components except the geotextile were braced to prevent external lateral movement of the test frame and facing elements due to the pull-out force of the geosynthetic connection. A jactuator was used to apply the tensile force to the geotextile; the rate of loading was 6% of the free length of reinforcement per minute, or 12.7 mm per minute. Displacement was measured using two LVDTs set at each end of the geosynthetic clamp. Normal load on the CMU blocks, to simulate additional wall height, was applied using dead weight placed on a 50 mm thick steel plate cushioned with a 6 mm rubber pad to uniformly distribute the load on the hollow-core CMUs.

2.1.2 Testing Schedule

Two sets of connection tests were performed; one with the hollow-core of the CMUs left voided (termed “hollow” throughout the paper) and the other with the hollow-core infilled with stone (termed “infilled” throughout the paper). The former is recommended in the FHWA guidelines for GRS abutments (Adams et al. 2011a), whereas the latter is standard

practice for MSE walls and abutments (Berg et al. 2009). The purpose of testing both methods is to determine the improvement in connection strength due to the additional friction caused by the aggregate infill in the core of the facing.

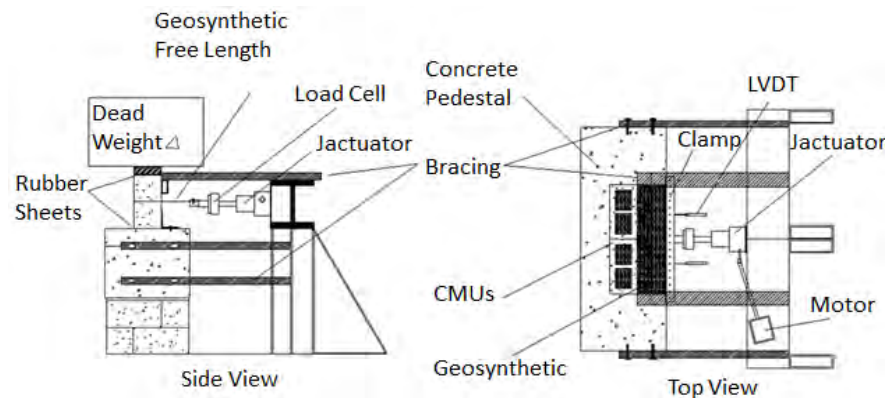


Figure 4. TFHRC Frictional Connection Test Schematic.

Seven unique tests were conducted for the hollow CMUs at different applied normal pressures: 12 kPa, 35 kPa, 69 kPa, 125 kPa, 147 kPa, 204 kPa, and 237 kPa; this corresponds to the 3rd, 7th, 14th, 25th, 30th, 40th, and 47th course of block from the top of a GRS structure, respectively, to simulate the connection capacity of a 9-m high wall. The test at 125 kPa was repeated 4 additional times and the test at 237 kPa was repeated 1 additional time to determine repeatability of the connection test method at different applied loads, as outlined in ASTM D6638.

In addition, five unique tests were conducted with the hollow cores of the CMUs infilled with AASHTO No. 57 aggregate (Figure 5). The applied pressures in these tests were 14 kPa, 37 kPa, 72 kPa, 128 kPa, and 150 kPa; this corresponds to the 3rd, 8th, 15th, 26th, and 30th course of block from the top of a GRS abutment, respectively, to simulate the connection capacity of a 6-m high wall. The test at 128 kPa was repeated 4 additional times. The slight difference in applied normal pressures between the two sets of tests (i.e. hollow and infilled) is related to the additional weight of the infilled aggregate.



Figure 5. TFHRC Frictional Connection Test with Hollow Core CMUs Infilled with No. 57 Aggregate.

2.1.3 Connection Strength Results

The results of the short-term connection tests conducted between the dry cast CMUs, both hollow and infilled, and the 70kN/m woven, PP geotextile are summarized in Table 1. For each test, the failure mode was pullout of the reinforcement, not rupture. An 11-point moving average was taken to filter the data and reduce noise (Figure 6); the peak ultimate connection force ($T_{ultconn}$) at each applied normal load was determined based on this average.

To determine the interface friction angle, the results presented in Table 1 were plotted and the linear best-fit envelope found (Figure 7). For the hollow and infilled CMUs, the friction angle was measured at approximately 38 degrees and 42 degrees, respectively. The addition of the aggregates in the voids provides increased connection strength; the infilling of the hollow-core CMUs produced a 10% increase in the interface friction angle.

Table 1. Short-Term Connection Strength Results.

Hollow CMUs			Infilled CMUs		
Applied Normal Load (kN/m)	Peak Connection Force (kN/m)	Interface Friction Angle (deg)	Applied Normal Load (kN/m)	Peak Connection Force (kN/m)	Interface Friction Angle (deg)
1.26	1.79	38	1.48	3.25	42
3.50	4.54		3.72	5.54	
6.93	7.51		7.16	9.67	
12.51	11.15		12.73	9.98	
12.51	13.65		12.73	10.65	
12.51	13.35		12.73	13.81	
12.51	11.76		12.73	17.22	
12.51	12.33		12.73	12.24	
14.75	14.98		12.73	11.76	
20.42	17.26		14.97	16.70	
23.72	19.66		-	-	
23.72	19.44		-	-	

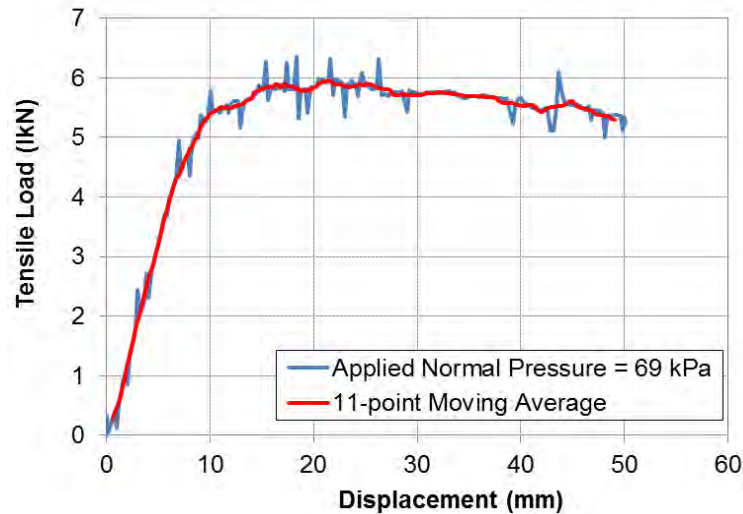


Figure 6. Short-Term Frictional Connection Test Results for hollow-core CMUs and 70 kN/m PP geotextile.

Note that Figure 7 does not show every test conducted. The repeated tests at 125 kPa and 237 kPa for the hollow CMUs and at 128 kPa for the infilled CMUs were averaged to arrive at a single value at each applied normal load. For the hollow CMUs, the results of the repeated tests were all within about 10% of the average indicating good repeatability. The results are somewhat more mixed for the infilled CMUs. Out of six tests, three were within 10% of the average; the largest difference was about 36%. The scatter in repeatability is likely attributed to the variability in placement of the aggregate for the infill conditions which can impact the interaction between the infilled aggregate and the geosynthetic.

2.2 Large Scale Direct Shear (LSDS) Tests

As an alternative to the set-up of the short-term connection test, a series of LSDS tests at various applied normal stresses was conducted to determine the interface friction angle between dry cast concrete and geosynthetic reinforcement. The testing was conducted with the LSDS device at TFHRC; the dimensions of the shear box are 0.3m x 0.3m x 0.2m.

To conduct the test, two 0.3m x 0.3m x 0.1 m solid concrete blocks were placed in the device; one in the top box and one in the bottom box of the LSDS device. A woven PP geotextile with a minimum average roll value (MARV) of 70 kN/m was clamped between the concrete blocks at the shear interface of the device. Note that the purpose of this test was to determine the interface friction angle between dry cast concrete and geotextile. The test could also be modified with hollow CMU blocks for conditions with and without gravel placed in the core of the block.

LSDS tests for the interface friction angle were conducted according to a modified ASTM D5321. The shear rate and gap size for the tests were set at 40 mm/min and 0.6mm, respectively. To determine the interface friction angle between the two materials, tests were performed dry at four applied normal pressures: 15 kPa, 25 kPa, 58 kPa, and 103 kPa. Note that the resulting friction angles are for the interface between the reinforcement and CMU blocks; similar tests can also be conducted to determine the interface friction angle at the base of the GRS wall or abutment for direct sliding analysis; however, this is outside the scope of this particular study

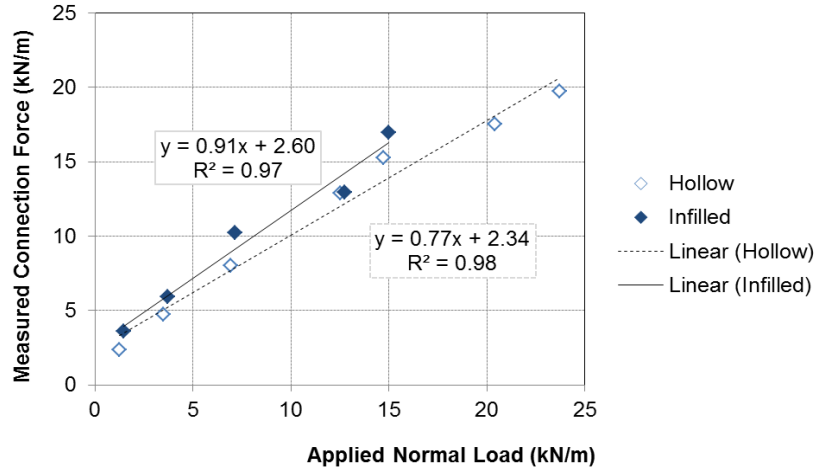


Figure 7. Short-Term Frictional Connection Test Results for hollow-core CMUs and 70 kN/m PP geotextile.

2.2.1 LSDS Results

The results of the LSDS tests indicated a measured interface friction angle of 37 degrees (Figure 8). Compared to the results of the short-term connection testing, the results are reasonably close, a 1 degree difference; this is within the variability of direct shear testing (Paikowsky et al. 2010), indicating that for fully frictional connections, the interface friction angle, if necessary for design, can be determined with a LSDS device as opposed to the more complicated short-term connection test set-up.

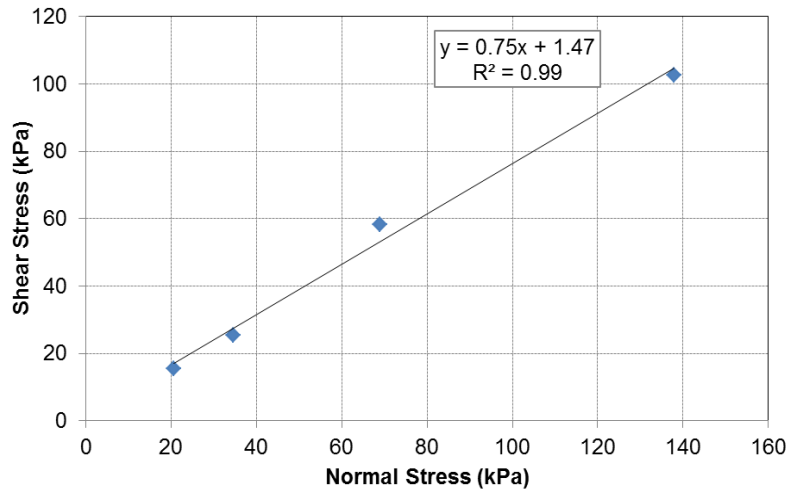


Figure 8. Large Scale Direct Shear Results between Dry Cast Concrete and 70 kN/m Geotextile.

2.3 In-service Wall Block Pull-Out Tests

The results of the block-pull out tests on a full-scale GRS wall, conducted by TFHRC in 1998, are compared to the results of the short-term connection testing (Figure 9). The interface friction angle for the block pull-out tests is about 37 degrees, the same as for the comparable LSDS tests. Note that for the block-pull out tests, heavier segmental retaining wall (SRW) block, infilled with aggregate, was used in the test wall with 70 kN/m woven, PP geotextile; however, the

resulting interface friction angle is comparable to that of CMUs because the SRW block is also made of dry-cast concrete. This suggests that the short-term connection test is applicable for real-world applications.

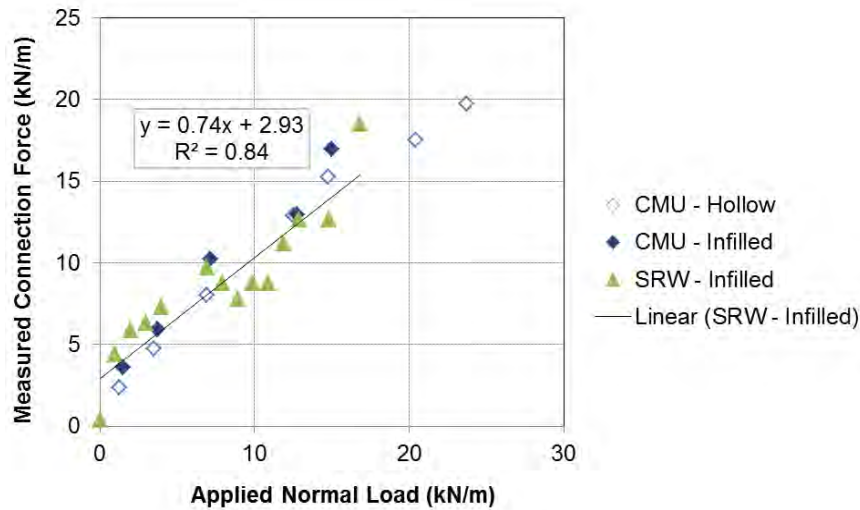


Figure 9. Results of Block Pull-Out Tests Compared to Short-Term Connection Tests.

2.4 Summary

Three types of tests were conducted by TFHRC to determine the strength of the frictional connection between a dry-cast modular block unit and geotextile reinforcement: (1) short-term connection testing, (2) large scale direct shear testing, and (3) block-pull out testing. The results are summarized in Table 2. Based on the three tests, the average interface friction angle for dry-cast, hollow CMUs is 37 degrees. Infilling CMUs may lead to an increase in the interface friction angle; however, the use of this friction angle in the design of an MSE wall may not be prudent, as compared to the case with the cores left hollow, because of the inexact nature of infilling aggregate in the facing blocks.

Table 2. Summary of Measured Interface Friction Angles.

Short-Term Connection Test		LSDS Test	SRW Block (Infilled)
Hollow	Infilled		Pull-Out Test
38	42	37	37

3. IMPLICATIONS ON DESIGN

According to current design practice for MSE walls and abutments, the results of connection testing are used to determine the long-term strength and ensure it is greater than the associated lateral loads at the connection (AASHTO 2010, Berg et al. 2009). The long-term connection strength is often computed from the results of short-term connection tests with reduction factors taken to account for durability and creep (Equation 4). The loads at the connection are assumed to equal the product of horizontal stress on the reinforcement due to active earth pressure conditions and the reinforcement spacing (Berg et al. 2009).

$$T_{alc} = \frac{T_{ult} \times \left(\frac{T_{ultconn}}{RF_{cr} T_{lot}} \right)}{RF_D} \quad [4]$$

Where T_{alc} is the nominal long-term connection strength, T_{ult} is the ultimate tensile strength of the geosynthetics reinforcement, defined as the minimum average roll value (MARV), $T_{ultconn}$ is the short-term connection strength, RF_{cr} is the geosynthetics creep reduction factor, T_{lot} is the ultimate wide width tensile strength of the reinforcement material roll/lot used for connection strength testing, and RF_D is the reduction factor to account for chemical and biological degradation.

For the facing, backfill and reinforcement conditions shown in Table 3, and assuming no surcharge or traffic loads, a GRS wall with frictional connections would fail the MSE requirement for connection when the height is more than 1.2 m or 1.6m in height, depending on if the facing is hollow or infilled, respectively (Figure 10). Applying the appropriate load and resistance factors, however, limits the height to less than 1m, effectively making the frictional connection infeasible for real-world application. Note that the connection load was determined according to Equation 1.

Figure 10 also extends the results to an abutment application assuming the same facing, backfill and reinforcement conditions shown in Table 3 and an applied surcharge load of 200 kPa, equivalent to typical bridge design loads. Note that the effect of block-soil friction due to compression of the reinforced soil mass is ignored. The results indicate that fully frictional connections would be prohibited at any height. Furthermore, even assuming no reduction in the short-term connection strength, the full frictional connection is not capable of withstanding the loads at the top of the wall (to about 1.8 m below for hollow CMUs) due to the bridge surcharge (Figure 10). Current MSE design therefore implies that a mechanical connection is required to prevent connection failure for a GRS wall or abutment, regardless of reinforcement spacing.

Table 3. Example Facing, Backfill, and Reinforcement Conditions.

Facing		Backfill		Reinforcement				
Type	Weight (kN)	Unit Weight, γ (kN/m ³)	Friction Angle, Φ (deg)	Spacing (m)	Ultimate Strength, T_{ult} (kN/m)	Lot Strength, T_{lot} (kN/m)	RF_{cr}	RF_D
CMU	0.2	17.3	40	0.2	70	77	4	1.15

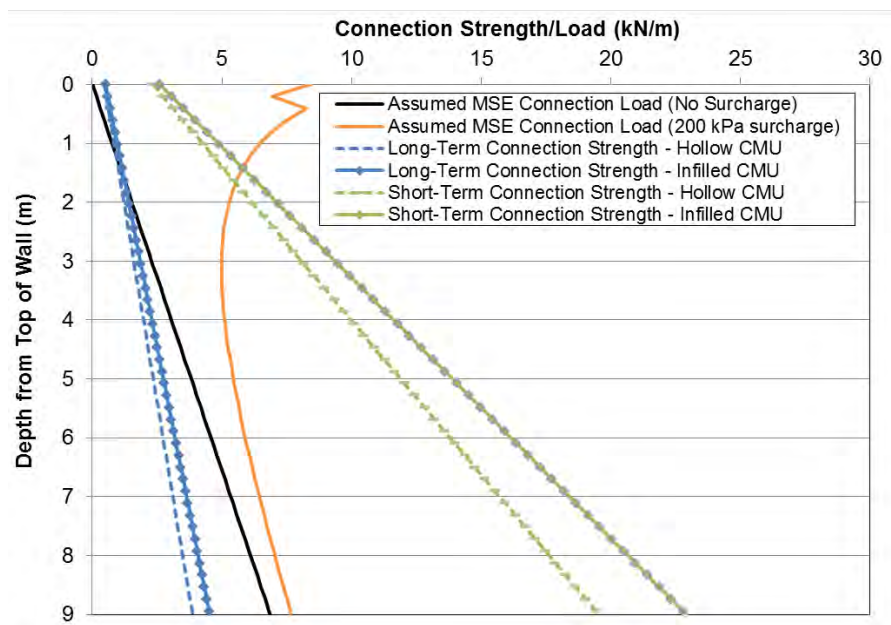


Figure 10. Frictional Connection Strength Requirement for MSE walls with geosynthetics.

The requirement of a mechanical connection rather than a simple, full frictional connection is not supported by the numerous examples, both published and unpublished, of closely spaced GRS walls and abutments that have frictionally connected facing elements which have excellent performance (Adams et al. 2011b, Wu 2007, Adams 1997, Adams et al. 2007, Ketchart and Wu 1997, Schiebel, et al., 1996, Barrett, 1997). Earthquake loads, up to 1g acceleration, on a GRS abutment produced no connection failure throughout testing, only some cracked blocks (Helwany et al. 2012). This was supported by a previous NCHRP study on the design of GRS abutments with flexible facings that concluded connection strength is not a design concern for well compacted, closely spaced (less than 0.2 m) systems (Wu et al. 2006). Connection failure is also not evident when GRS walls and abutments are loaded to failure (Adams et al. 2011a, Wu et al. 2006). FHWA design guidance for GRS abutments do not require a design check for connection strength when reinforcement spacing is less than 0.3 m (Adams et al. 2011a). This is because the observed loads at the face for closely spaced GRS are significantly smaller than that assumed in MSE design.

Assuming the more conservative bin pressure (Equation 3) and the conditions in Table 3, the thrust against the face is equal to 0.1 kN/m (Figure 11). By using the reduction factors for creep and durability for long-term strength, as is done in MSE design, the minimum factor of safety is 4 at the top of the wall against connection failure for bin pressure. The

results of this analysis, and the assumed bin pressures, therefore show that connection will not control the design of GRS, therefore supporting the removal of connection as a design calculation for closely spaced GRS, as recommended in FHWA’s design guidance (Adams et al. 2011a)

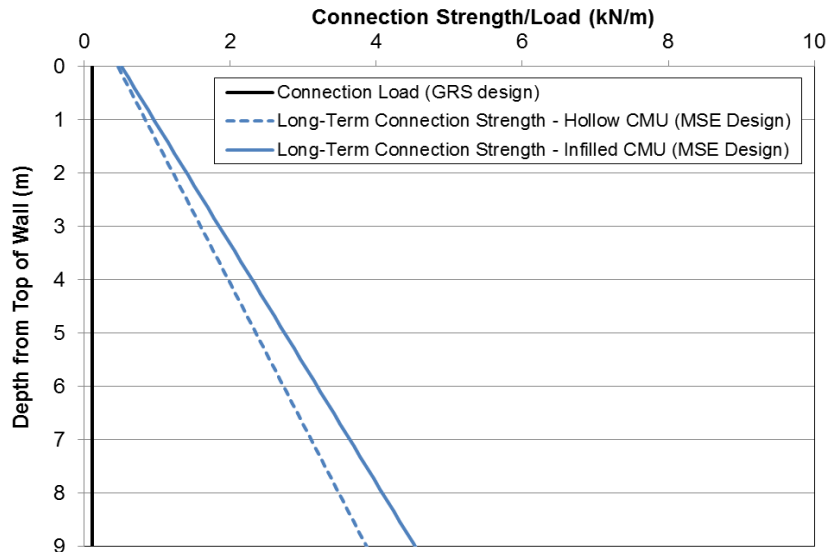


Figure 11. Comparison of thrust against the face (bin pressure) and assumed long-term connection strength.

4. CONCLUSIONS

The simple frictional connection method has successfully been used on numerous in-service GRS walls and abutments constructed with reinforcement spacing less than 0.3m for more than 20 years. In addition, this connection method has been shown to withstand extreme loading conditions without connection failure. The in-service performance of numerous walls and abutments built with the full frictional method, compared to the long-term connection strength, indicates that the loads at the face for closely spaced GRS are not equal to those assumed internally as in MSE design (AASHTO 2010, Berg et al. 2009). Rather, bin pressure is a more realistic assumption of the thrust against the face for service conditions. Additionally, considering the strength of the frictional connection is significantly greater than the thrust exerted at the face further supports the conclusion that the connection strength criterion does not control the design for closely spaced GRS walls and abutments. The implications of connection strength criterion on larger spaced (greater than 0.3 m) MSE systems, however, still needs to be further investigated.

ACKNOWLEDGEMENTS

The authors would like to acknowledge the support of Tom Stabile, Jan Li, and Moustafa Ibrahim for their assistance in the laboratory testing, and appreciate the review and advice of Dr. Jonathan Wu and Dr. Philip Ooi throughout this study.

REFERENCES

AASHTO. (2010). LRFD Bridge Design Specifications, Edition 5, American Association of State Highway and Transportation Officials.

Adams, M., Nicks, J., Stabile, T., Wu, J., Schlatter, W., and Hartmann, J. (2011a). *Geosynthetic Reinforced Soil Integrated Bridge System Interim Implementation Guide*. Report No. FHWA-HRT-11-026, Federal Highway Administration, McLean, VA.

Adams, M., Nicks, J., Stabile, T., Wu, J., Schlatter, W., and Hartmann, J. (2011b). *Geosynthetic Reinforced Soil Integrated Bridge System Synthesis Report*. Report No. FHWA-HRT-11-027, Federal Highway Administration, McLean, VA.

Adams, M.T., Schlatter, W. and Stabile, T. (2007). “Geosynthetic-Reinforced Soil Integrated Abutments at the Bowman Road Bridge in Defiance County, Ohio.” *Proceedings, GeoDenver 2007*, American Society of Civil Engineers, Denver, CO.

- Adams, M.T. (1997). Performance of a Prestrained Geosynthetic Reinforced Soil Bridge Pier, *Mechanically Stabilized Backfill*, Wu, J.T.H (ed.), Balkema, Rotterdam, Netherlands, 35-53.
- Andrawes, K.Z. and Yogarajah, I. (1994). "Effects of Connections on the Behaviour of Reinforced Soil Walls". *8th Intl. Conf. of the Assoc. for Computer Methods and Advances in Geomechanics*, Virginia, USA.
- ASTM D 5262. Standard Test Method for Determining Connection Strength Between Geosynthetic Reinforcement and Segmental Concrete Units (Modular Concrete Blocks), *American Society for Testing and Materials*, West Conshohocken, Pennsylvania, USA.
- ASTM D 4321. Standard Test Method for Determining the Coefficient of Soil and Geosynthetic or Geosynthetic and Geosynthetic Friction by the Direct Shear Method, *American Society for Testing and Materials*, West Conshohocken, Pennsylvania, USA.
- ASTM D 6638. Standard Test Method for Evaluating the Unconfined Tension Creep and Creep Rupture Behavior of Geosynthetics, *American Society for Testing and Materials*, West Conshohocken, Pennsylvania, USA.
- Barrett, R.K. (1997). *Research Pays Off with the Least Cost, Most Durable Retaining Walls and Bridges in U.S. History*, Colorado Department of Transportation, Denver, CO, USA.
- Berg, R., Christopher, B., and Samtani, N. 2009. *Design of Mechanically Stabilized Earth Walls and Reinforced Soil Slopes – Volume 1*. GEC-11, Report No. FHWA-NHI-10-024, National Highway Institute, Federal Highway Administration, Arlington, VA
- Helwany, S., Wu, J.T.H., Meinholz, P. (2012). *Seismic Design of Geosynthetic-Reinforced Soil Bridge Abutments with Modular Block Facing*. NCHRP Web-Only Document 187, Transportation Research Board, Washington, DC, USA.
- Ketchart, K. and Wu, J.T.H. (1997). *Loading Test of a GRS Wall Reinforced with a AMOCO Geotextile*. Research Report, Department of Civil Engineering, University of Colorado, Denver, USA.
- Paikowsky, S.G., Canniff, M.C., Lesny, K., Kisse, A., Amatya, S., and Muganga, R. (2010). LRF Design and Construction of Shallow Foundations for Highway Bridge Structures, NCHRP Report 651, Transportation Research Board, Washington, DC, USA.
- Schiebel, W.R., Ruckman, A.C., and Barrett, R.K. (1996). The Roles of Facing Connection Strength, Truncated Base, and Embedment in Mechanically Stabilized Backfill Walls. Report No. CDOT/CTI-96-3, Colorado Transportation Institute, USA.
- Soong, T-Y. and Koerner, R.M. (1997). On the Required Connection Strength of Geosynthetically Reinforced Walls. *Geotextiles and Geomembranes*, Elsevier Science Limited, 15:377-393.
- Wu, J.T.H., Lee, K.Z.Z., Helwany, S.B., and Ketchart, K. (2006). *Design and Construction Guidelines for Geosynthetic-Reinforced Soil Bridge Abutments with a Flexible Facing*, NCHRP Report 556, Transportation Research Board, Washington, DC, USA.
- Wu, J.T.H. (2007). Lateral Earth Pressure Against the Facing of Segmental GRS Walls, *Geosynthetics in Reinforcement and Hydraulic Applications*, Geotechnical Special Publication No. 165, ASCE, Reston, VA, USA.
- Yogarajah, I. and Saad, M.A. (1996). Development of Horizontal Pressures and Behavior of Single and Multi Segmented Walls," Proceedings, International Symposium on Earth Reinforcement, Fukuoka, Japan, A.A. Balkema Publisher, Rotterdam, Netherlands, pp. 553-558.

Importance of Variability in the Interface Shear Strength between Textured Geomembrane and Geocomposite Drainage Layer in Landfill Covers

Gregory Dellinger, The University of Texas at Austin, USA
Richard Lacey, TRI Environmental, USA
John Allen, TRI Environmental, USA
Robert Gilbert, The University of Texas at Austin, USA

ABSTRACT

A common interface in landfill covers is between a textured geomembrane and an overlying geocomposite drainage layer. The shear strength of this interface is particularly important for stability since it is subjected to water pressures that develop in the drainage layer. The shear strength of this interface can exhibit significant variability at the low effective normal stresses present in a landfill cover. The objective of this paper is to provide insight into how the variability of this interface affects the interpretation of laboratory test results and their use in stability analyses. Laboratory tests are presented and analyzed, leading to the following conclusions:

1. The texturing on blown-film textured geomembranes can be highly variable locally within a sheet as well as between rolls. The height and density of asperities, as well as their shapes, are variable.
2. This variability in texturing can lead to significant variability in the peak interface shear strength, with a coefficient of variation in the peak friction coefficient of about 0.15.
3. These local variations in texturing and interface shear strength are not generally important to the overall stability of a landfill cover slope because the area of the slip surface is typically much larger than the scale of variations. It is the average shear strength from test results and not the minimum tests result that is relevant.
4. In QA/QC, these local variations are important in establishing the number of tests and the criterion for accepting or rejecting material based on the test results. A minimum of five to ten tests are recommended to assess the average peak shear strength for this interface, and the criterion for accepting and rejecting material is best based on the average test result rather than the minimum result.

1. INTRODUCTION

A geocomposite drainage layer overlying a texture geomembrane is a common interface within landfill covers (Figure 1). In many designs, the peak shear strength of this interface will govern the stability of the slope due to the possibility of pore water pressures in the drainage layer. The peak shear strength of this interface can exhibit significant variability in testing due to variations in the roughness of a blown-film textured surface (e.g., Dove and Frost 1996, Stark et al. 1996 and Frost and Lee 2001). This variability could be important for design if relatively large areas of low shear strength are possible. This variability could also be important for Quality Assurance/Quality Control (QA/QC) programs in establishing the number of tests and the criterion for accepting or rejecting material based on the test results.

A recent project involved conducting a large number of shear tests on the interface between a textured geomembrane and a geocomposite drainage layer. The objective of this paper is to use this large data set to quantify the variability in the peak shear strength, to investigate potential sources of this variability, and to develop guidelines for interpreting shear test results for purposes of design and QA/QC.

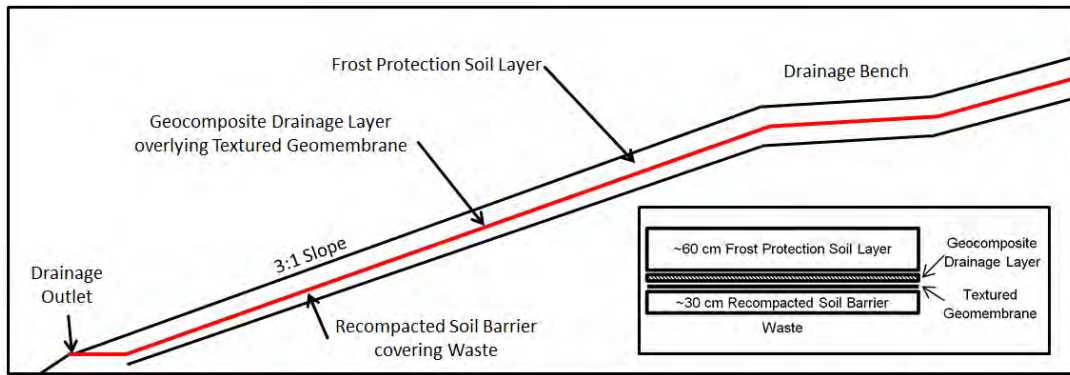


Figure 1. Typical Landfill Cover Schematic

2. TEST DATA

The shear strength data analyzed in this paper come from a series of testing programs to measure the shear strength of the interface between a textured geomembrane and a geocomposite drainage layer.

2.1 Interface Materials

The textured geomembrane is a 1.0-mm thick, LLDPE, blown-film textured geomembrane. The geocomposite drainage layer is a 6.86-mm thick geonet bonded to 203 g/m² non-woven polypropylene geotextiles on each side. Samples of these materials were obtained from a variety of sources but the same production run of material. First, samples were obtained directly from the manufacturer. Second, samples were removed from a construction project after the textured geomembrane and the geocomposite drainage layer were installed, but before they were covered with cover soil. Third, samples were obtained from a construction project after the installed geomembrane and geocomposite drainage layer were covered with about 0.61 meters of cover soil.

2.2 Shear Tests

A total of 75 shear tests were conducted on this interface between the textured geomembrane and the geocomposite drainage layer at the range of normal stresses typical in a cover system. Two types of test methods were used to measure the shear strength for the interface: 56 large-scale direct shear tests and 19 tilt table tests.

The large-scale direct shear tests were conducted according to ASTM D 5321 using a dead-load large-scale direct shear box. The textured geomembrane specimens were mounted in the bottom of the shear box. The geocomposite drainage layer specimens were mounted in the upper shear box, which reacted against a load cell; the non-burnished side of the geocomposite was in contact with the textured geomembrane. The interface was submerged in a bath of tap water for the duration of the testing. The applied normal stresses ranged from 12 to 24 kPa. The normal stress was applied for a 15 minute seating time before the interface was sheared. A shear rate of 0.5 centimeters per minute was used.

The tilt table consisted of a flat 61-centimeter by 46-centimeter tray on a hinge attached to a steel frame that used a strap with a gear hand crank to raise one side of the tray. A ratchet mechanism attached to the crank was used to hold the table at the desired inclination. A 46-centimeter long by 46-centimeter wide specimen of the textured geomembrane was clamped to the tray. A 20-centimeter long by 10-centimeter wide specimen of the geocomposite drainage layer was then placed on the geomembrane. A loading plate with a roughened surface was placed on top of the geocomposite specimen. Weights were then placed on the loading plate; the center of gravity for the weights was located so that there would be minimal eccentricity when the specimen sheared as the table was tilted. The specimens were placed into a bath of tap water for the duration of the test. A seating time of five minutes was imposed before the table was tilted and shearing stress was applied. The rate of lifting the table was set to give an approximate shear rate of 0.5 centimeters per minute. The applied normal stresses during shear ranged from 4 to 20 kPa.

3. MAGNITUDE OF VARIABILITY IN INTERFACE STRENGTH

The test results are plotted in Figure 2. For slope stability analyses, the quantity of interest is the tangent of the peak friction angle for the interface, $\tan \phi'_{peak}$, which is also sometimes referred to as the peak friction coefficient. A frequency

distribution plot is shown in Figure 3 and sample statistics are summarized in Table 1 for the peak friction coefficient. The frequency distribution is approximately normal. As a check on this approximation, a probability plot is shown in Figure 4. The linear trend in Figure 4, particularly in the vicinity of the smaller values of the peak friction coefficient that are of most concern from a design perspective, indicates that a normal distribution is a reasonable model for the variability.

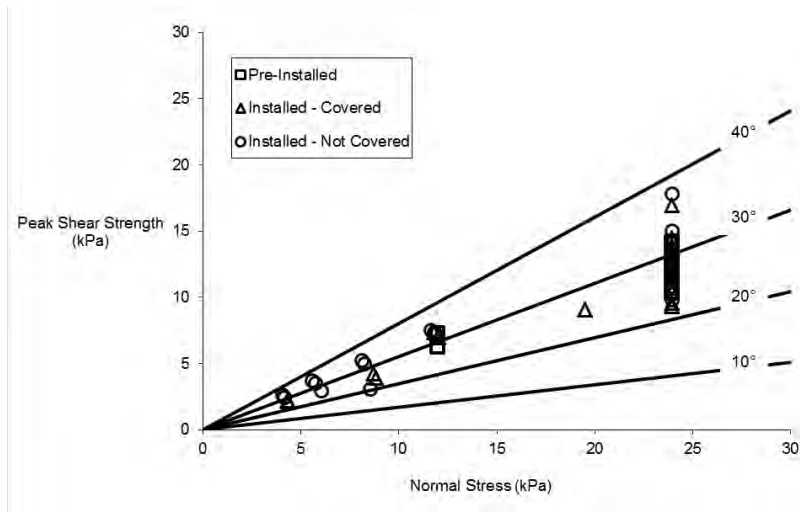


Figure 2. Peak Shear Strength versus Normal Stress for Shear Test Results

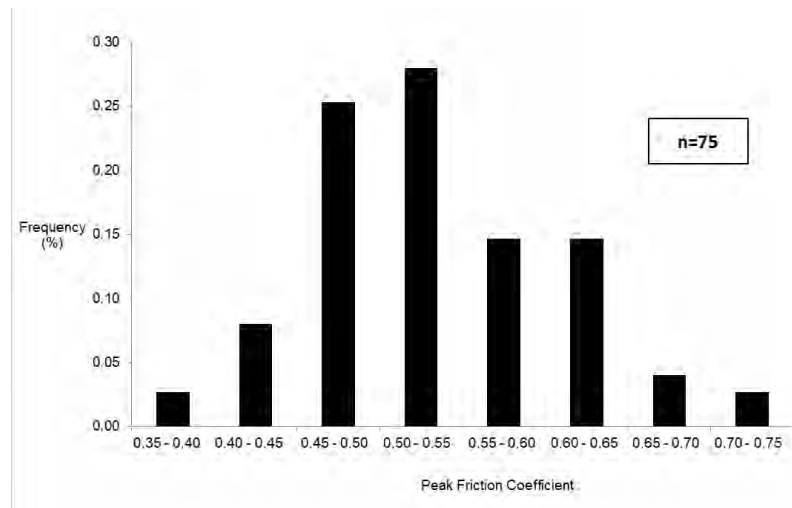


Figure 3. Frequency Distribution for Peak Friction Coefficient

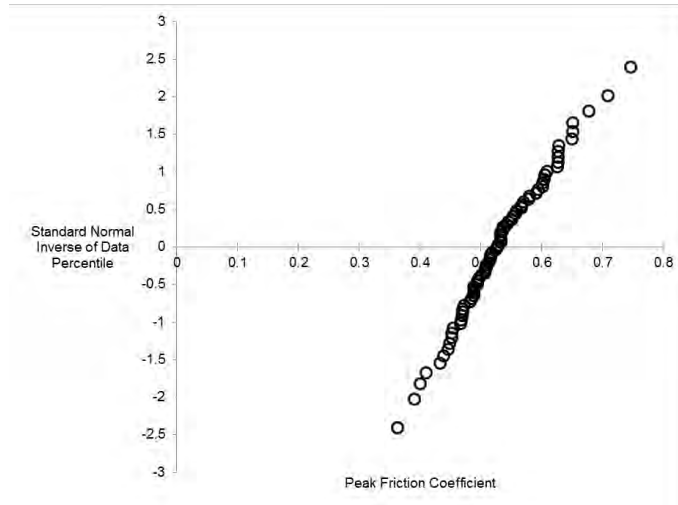


Figure 4. Standard Normal Inverse Plot for Peak Friction Coefficient

The magnitude of variability in peak friction coefficient is noteworthy. The coefficient of variation, the standard deviation divided by the mean, is about 0.15. For comparison, coefficient of variation in the friction coefficient for simple interfaces, such as that between a nonwoven geotextile and a smooth geomembrane or simply the sliding mechanism in the direct shear box, are typically less than 0.05 (e.g., Gilbert et al. 1995 and Allen and Gilbert 2002). Hence, the variability in Figures 2 and 3 is not a reflection of inherent variations in the test procedure itself; instead, it is real variations in the shear strength of the interface. Practical implications of this relatively large coefficient of variation are the following:

- Five percent of measurements will be outside of +/- 30 percent from the mean value;
- Ten percent of measurements will be smaller than 20 percent below the mean value and five percent will be smaller than 25 percent below the mean value; and
- The Minimum Average Roll Value (MARV), which is the 2.5 percentile value, is 30 percent below the mean value.

Therefore, considerable care is warranted in interpreting, comparing and evaluating interface shear results due to this relatively large variability.

4. SOURCES OF VARIABILITY

The following factors were first considered as potential sources of variability in the peak friction coefficient: the shear test method (large-scale direct shear box versus tilt table), the effects of pushing the soil cover over the interface before samples were exhumed for testing, and the effective normal stress during shear. The result of a statistical analysis considering the significance of each of these factors is summarized in Table 1. For conventional significance levels of 1 to 5 percent, none of these factors is a statistically significant source of the measured variability in the peak friction coefficient for this interface (that is, none of the P-values are smaller than 0.01 to 0.05).

Table 1 Summary of Statistical Analysis for Potential Factors affecting Peak Friction Coefficient

Factor	P-value ¹
Direct Shear Box versus Tilt Table	0.84
Before versus After Pushing 2-feet of Cover Soil over Interface during Construction	0.19
Effective Normal Stress	0.44

¹Probability of Obtaining Data Set from Testing if the Peak Friction Coefficient is Not Related (Linearly) to that Factor

The inference from Table 1 is that the variability in the shear strength of this interface is primarily due to variability in the material properties. One possible source of material variability is the effect of construction, such as fibres of the geotextile being strained or asperities on the geomembrane surface being damaged during installation. However, Figure 2 shows that there is no significant difference in the variability and average shear strengths between samples from the

manufacturer and samples obtained after installation. These results suggest that the variability is primarily due to variations in the as-manufactured materials. Previous research on a similar interface (Li and Gilbert 2006) indicates that this variability in interface shear strength is almost entirely due to spatial variability in the texturing of the geomembrane. To investigate this possibility further, the asperity height was measured in accordance with ASTM D 7466 on many of the specimens; the height was measured at nine locations within a 15-centimeter by 16-centimeter grid for each specimen. As with the peak friction coefficient, there is significant variability in the asperity height of the texturing; the coefficient of variation for the asperity height, 0.18, is as large as that for the peak friction coefficient. However, the peak friction coefficient is poorly correlated with the asperity height alone (Figure 5). This result is not surprising as many researchers, such as Dove and Frost (1996), have shown that the roughness of a textured geomembrane surface is a complex, three-dimensional object that cannot be easily represented by the height of the asperities alone. To illustrate this point with this interface, Figure 6 shows a rendering of the coverage of asperities for two different specimens of this geomembrane. These renderings were produced by coating the geomembrane surface with ink, placing the inked surface against a white poster board, and then rolling the poster board with a rigid roller. Both specimens have the same measured asperity height. However, Specimen A had a lower areal density of asperities and a smaller measured peak shear strength compared to Specimen B (Figure 6). Therefore, the variability in the peak interface shear strength is related both to the height and the coverage of the asperities in the test specimen.

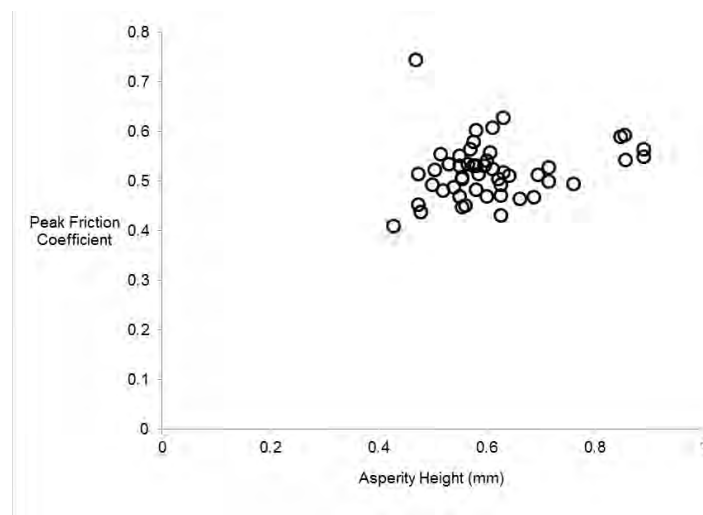


Figure 5. Peak Friction Coefficient versus Asperity Height

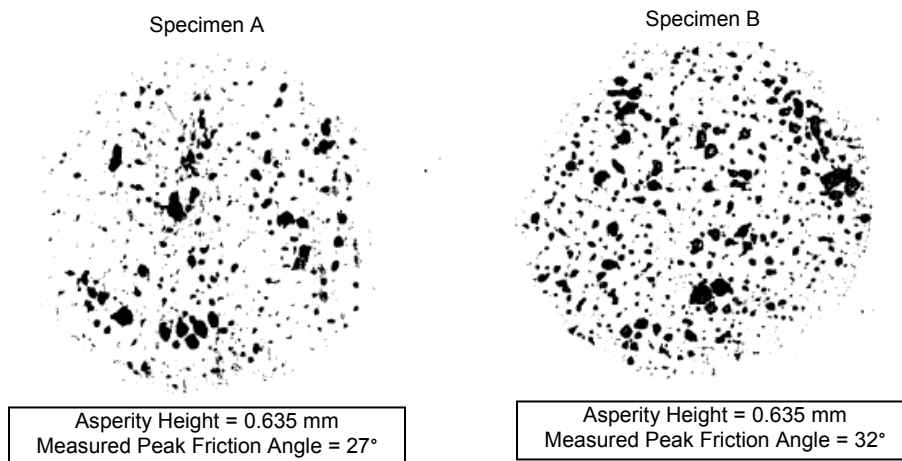


Figure 6. Example of Variations in Asperity Density based on Pressed Ink Images

This spatial variability in texturing exists over a relatively small area, on the order of the size of a 30-centimeter by 30-centimeter test specimen. Figure 7 shows a comparison of measured peak shear strength for specimens that came from within the same roll (and even the same location along the machine direction of the roll) with that for specimens that came from different rolls. If the spatial variations in texturing were over scales larger than the sizes of the specimens,

then there would be a different mean and a smaller standard deviation for the inter-roll specimens than the intra-roll specimens. However, the mean values and the standard deviation values are essentially the same, indicating that the spatial variability in texturing is over a small scale (centimeters).

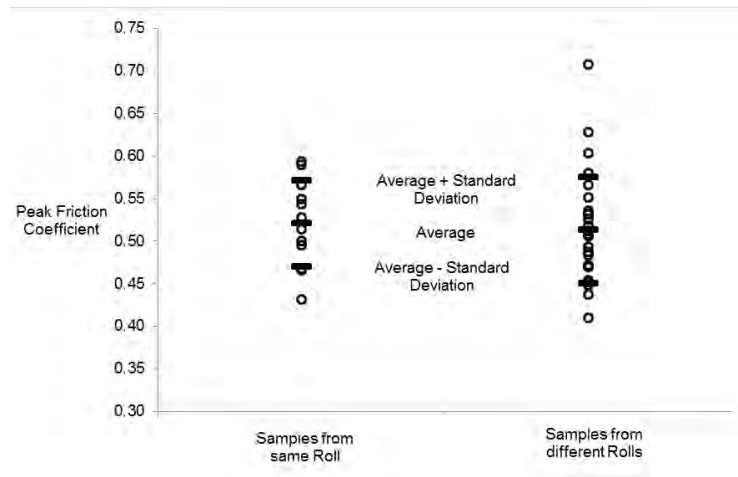


Figure 7. Comparison of Inter-Roll versus Intra-Roll Variability

5. PRACTICAL IMPLICATIONS OF VARIABILITY

Practical implications of the variability in the peak friction coefficient for this interface between a textured geomembrane and a geocomposite drainage layer include its effects on design and on Quality Assurance/Quality Control (QA/QC).

5.1 Slope Stability Design

The total shear resistance along a slip surface at this interface is proportional to the average peak friction coefficient over the area of the slip surface. The relatively large magnitude of variations in peak shear strength shown in Figures 2 and 3 occur over small areas on the order of 30 centimeters by 30 centimeters, while a typical slip surface would be tens to hundreds of meters in dimension. Therefore, there will be significant averaging of the small-scale variations in the peak friction coefficient over the area of the slip surface, and the uncertainty in the average peak friction coefficient for the slip surface will be markedly smaller than the small-scale variability. As a simple approximation, the coefficient of variation of the average peak shear strength for a slip surface that is L x W in dimension is related to the coefficient of variation measured in large-scale direct shear tests as follows:

$$\delta_{L \text{ by } W \text{ slip surface}} \cong \left[\sqrt{\left(\frac{30 \text{ centimeters}}{100xL} \right) \left(\frac{30 \text{ centimeters}}{100xW} \right)} \right] \delta_{30 \text{ centimeter by } 30 \text{ centimeter test specimen}} \quad [1]$$

where $\delta_{L \text{ by } W \text{ slip surface}}$ is the coefficient of variation in the average peak friction coefficient over the L x W area of the slip surface, $\delta_{30 \text{ centimeter by } 30 \text{ centimeter test specimen}}$ is the coefficient of variation in the small-scale shear test specimens, and L and W are in meters. As an example consider a potential 25-meter by 5-meter slip surface; the coefficient of variation in the average peak shear strength across this slip surface is approximately 3 percent of the coefficient of variation in the measured shear strength, or about 0.003. Therefore, it is the average and not the small-scale variations in peak shear strength that will be of practical concern for slope stability.

5.2 Quality Assurance/Quality Control

For QA/QC purposes, the practical significance of the relatively large variability in the measured shear strength for this interface is that it is difficult to assess the strength of the interface with a small number of shear tests. In addition, it is not useful to measure asperity height as a surrogate for peak shear strength (Figure. 7). Therefore, care is warranted both in deciding how many QA/QC shear tests are to be performed and in establishing reasonable criteria for accepting material based on these test results. One consideration is minimizing the possibility of rejecting material that is actually adequate, and the other consideration is minimizing the possibility of accepting material that is actually inadequate.

Since the average value for the peak friction coefficient is what is relevant for slope stability, it is most useful to evaluate QA/QC test results in terms of the average value. For accepting or rejecting material, a threshold will be specified. If the average peak friction coefficient from the test results is greater than this threshold, then the material will be accepted; otherwise, the material will be rejected. Figure 8 shows how this threshold is related to the number of test specimens and the probability of rejecting material that is actually adequate (Probability of Rejecting Good Material). For a given number of test specimens, the probability of rejecting good material decreases as the required minimum average threshold decreases (Figure 8). Also, for a given probability of rejecting good material, the required minimum average threshold decreases as the number of test specimens decreases.

As an example, consider that the required average value for the peak secant friction angle is 26.6° , a peak friction coefficient of 0.5. In order to achieve smaller than a 1-percent probability of rejecting good material, the specified minimum threshold would be

- 0.80 times the required average (a peak friction coefficient of 0.40 or a peak secant friction angle of 21.8°) for a QA/QC program with 3 test specimens;
- 0.84 times the required average (a peak friction coefficient of 0.42 or a peak secant friction angle of 22.9°) for a QA/QC program with 5 test specimens; and
- 0.89 times the required average (a peak friction coefficient of 0.44 or a peak secant friction angle of 24.0°) for a QA/QC program with 10 test specimens.

Note that even with 10 test specimens, it is not reasonable to specify that the average value from the test results be greater than the required average, 26.6° , without incurring a relatively large probability of rejecting good material.

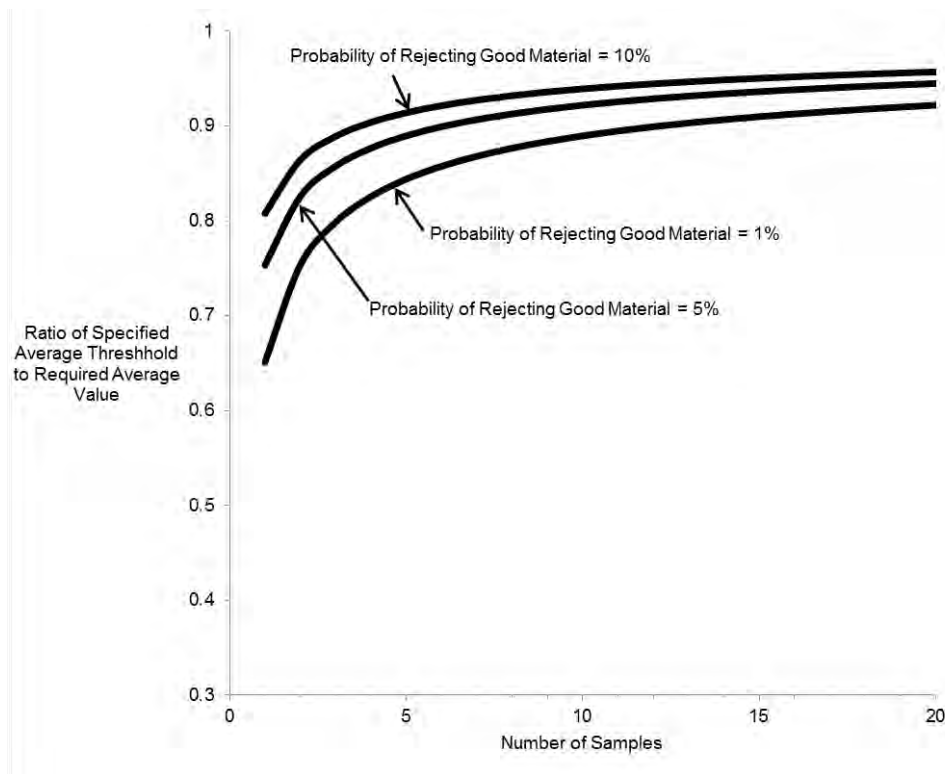


Figure 8. QA/QC Minimum Average Threshold versus Number of Test Specimens for Different Probabilities of Rejecting Good Material (assumed Coefficient of Variation of 0.15)

Figure 9 shows how the probability of accepting inadequate material is related to the specified average threshold from Figure 8 and the factor of safety between the required average and what is actually needed in the field. For a given number of test specimens, the probability of accepting inadequate material decreases as the design factor of safety increases. Also, for a given factor of safety, the probability of accepting inadequate material decreases as the number of test specimens increases.

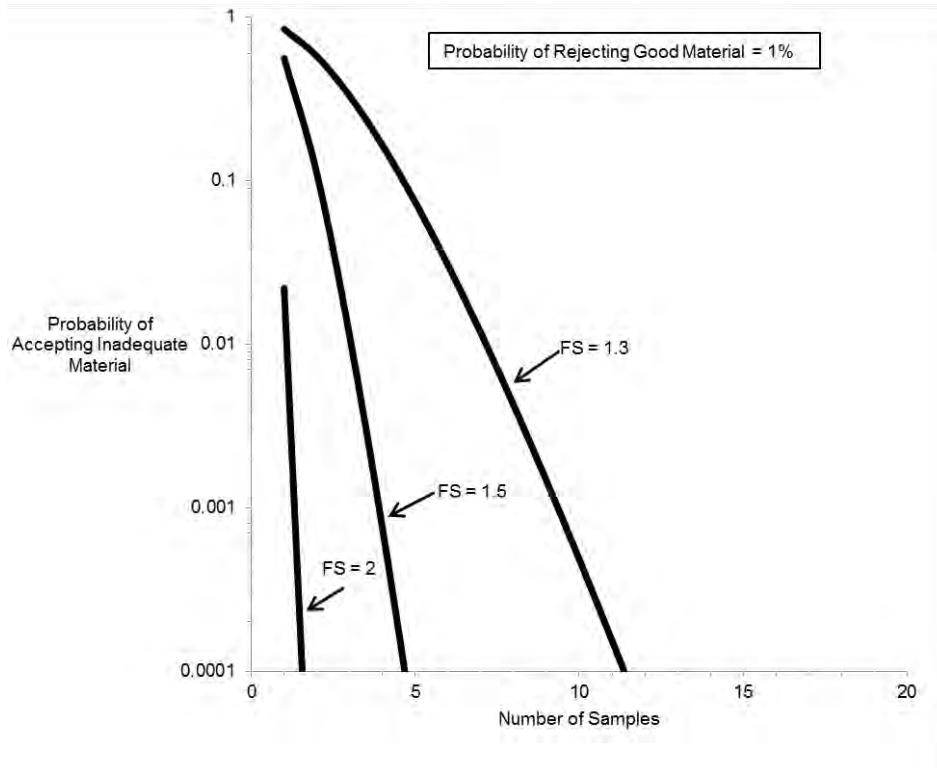


Figure 9. Probability of Accepting Material (based on Average Threshold) with an Average Peak Friction Coefficient less than the Required Average Divided by the Factor of Safety QA/QC versus Number of Test Specimens for Different Factors of Safety (assumed Coefficient of Variation of 0.15)

As an example, consider a 3H:1V cover slope (slope angle of 18.4°) with this interface. If the slope is designed with a factor of safety of 1.5 assuming no water pressure acting at the interface, then the required average peak friction coefficient is 0.5 (or a peak secant friction angle of 26.6°). If the probability of rejecting good material is kept below 1 percent, then the probability of accepting inadequate material (that is, an interface with an average peak shear strength corresponding to a friction angle less than the slope angle of 18.4°) is

- about 1 percent for a QA/QC program with 3 test specimens;
- about 0.01 percent for a QA/QC program with 5 test specimens; and
- considerably less than 0.01 percent for a QA/QC program with 10 test specimens.

Since the consequences of a cover slope failure can be substantial, the probability of a slope failure will typically be targeted to be smaller than 0.01 percent. Therefore, a QA/QC program would need to be based on 5 or more specimens in order to achieve this probability of accepting inadequate material.

In some projects, a QA/QC threshold has been established as the minimum value for all of the shear test results. For example, if a peak secant friction angle of 26.6° specified, then the material is accepted only if all shear test results produce a shear strength greater than this minimum. This approach is not recommended for three reasons. First, the average shear strength versus the minimum shear strength is what is of concern for slope stability. Second, it is very likely that adequate material will be rejected based on this approach unless the minimum threshold is set to be considerably smaller than the required average value. Figure 10 shows how this minimum threshold is related to the number of test specimens and the probability of rejecting good material. Unlike for a threshold based on the average value (Figure. 8), the required minimum threshold for a given probability of rejecting good material decreases as the number of test specimens increases because the chance of a smaller test results increases with the number of tests. Third and most importantly, the probability of accepting inadequate material is much higher using this approach (Figure 11).

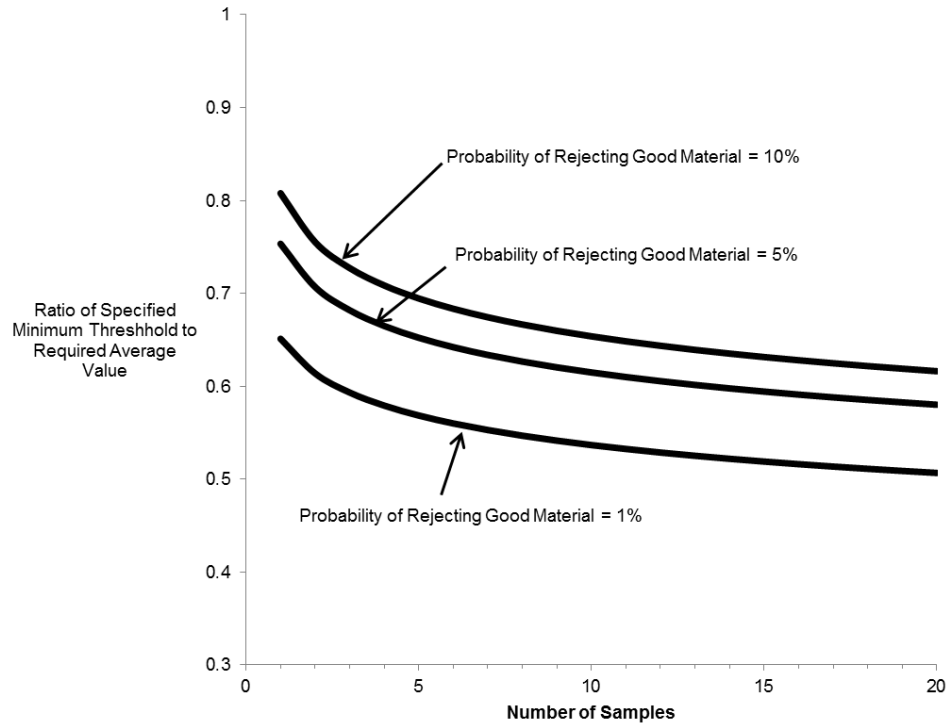


Figure 10. QA/QC Minimum Threshold versus Number of Test Specimens for Different Probabilities of Rejecting Good Material (Assumed Coefficient of Variation of 0.15)

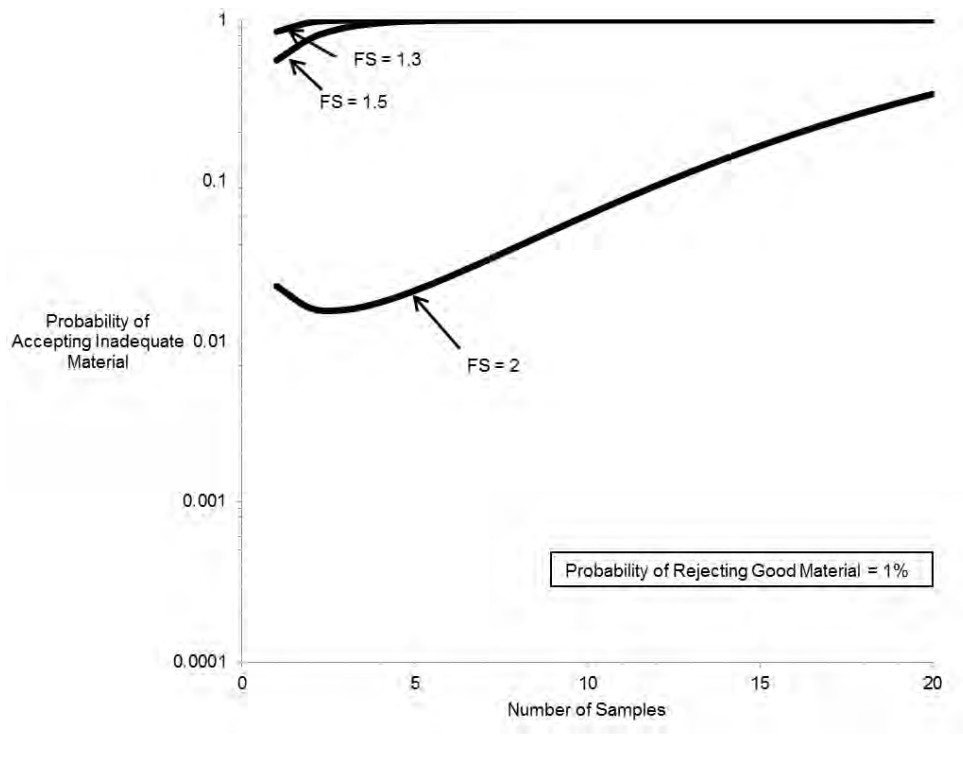


Figure 11. Probability of Accepting Material (based on Minimum Threshold) with an Average Peak Friction Coefficient less than the Required Average Divided by the Factor of Safety versus Number of Test Specimens for Different Factors of Safety (Assumed Coefficient of Variation of 0.15)

6. SUMMARY

A large number of shear tests on the interface between a blown-film textured geomembrane and a geocomposite drainage layer provided an opportunity to quantify the variability in the peak shear strength, investigate potential sources of this variability, and develop guidelines for interpreting shear test results for purposes of design and QA/QC. At a range of normal stresses typical for a landfill cover, 4.0 to 24 kPa, the variability in the peak friction coefficient, $\tan \phi_{peak}$, for this interface is approximately normally distributed with a coefficient of variation of about 0.15. This variability is due primarily to spatial variations in the texturing and it occurs at small scales, on the order of 1,000-square centimeter areas. This variability is not correlated strongly with asperity height alone; rather it reflects variations in the height, shape and density of asperities across the test specimens.

In cover slope stability design, these variations in the peak shear strength are not important because they are localized and will average out over a relatively large slip surface with an area of tens to hundreds of square meters. Therefore, it is the average value of the peak friction coefficient from multiple tests and not the individual values or the minimum value that is most relevant for design.

However in QA/QC, these variations are important in establishing the number of tests and the criterion for accepting or rejecting material based on the test results. In order to minimize the probability of rejecting adequate material and the probability of accepting inadequate material, a QA/QC test program should include at least five to ten tests taken from any rolls since the variability occurs over a small scale. In addition, the criterion for accepting or rejecting material should be based on the average test result versus the minimum test result. It should be noted that this criterion is specific to the type of materials tested in this study.

REFERENCES

- Allen, S. R. and Gilbert, R. B. (2002), "One Sigma in the Testing Geosynthetics Laboratory," *Proceedings*, 16th GRI Conference on Hot Topics in Geosynthetics III, Philadelphia, Pennsylvania, 19-43.
- ASTM D 5321. Standard Test Method for Determining the Coefficient of Soil and Geosynthetic or Geosynthetic and Geosynthetic Friction by the Direct Shear Method. *American Society for Testing and Materials*, West Conshohocken, Pennsylvania, USA.
- ASTM D 7466. Standard Test Method for Measuring Asperity Height of Textured Geomembranes. *American Society for Testing and Materials*, West Conshohocken, Pennsylvania, USA.
- Dove, J.E. and Frost, J.D. (1996). A Method for Measuring Geomembrane Surface Roughness, *Geosynthetics International*, Vol. 3, No. 3, pp. 369-392.
- Frost, J.D. and Lee, S.W. (2001). Microscale Study of Geomembrane-Geotextile Interactions, *Geosynthetics International*, Vol. 8, No. 6, pp. 577-597.
- Gilbert, R. B., Liu, C.-N., Wright, S. G. and Trautwein, S. J. (1995), "A Double Shear Test Method for Measuring Interface Strength," *Proceedings of Geosynthetics '95*, IFAI, Nashville, Tennessee, 1017-1029.
- Li, M. H. and Gilbert, R. B. (2006), "Mechanism of Post-Peak Strength Reduction for Textured Geomembrane-Nonwoven Geotextile Interfaces," *Geosynthetics International*, IGSIGS, Vol. 13, No. 5, 207-209.
- Stark, T.D., Williamson, T.A. and Eid, H.T., 1996, HDPE Geomembrane/Geotextile Interface Shear Strength, *ASCE Journal of Geotechnical Engineering*, Vol. 122, No. 3, pp. 197-203.

Improving the Stability of High Fill Load Structures Built on Low-Strength Geosynthetic Interfaces

Allan J. Breitenbach, P.E., Ausenco, USA, allan.breitenbach@ausenco.com
Chris Athanassopoulos, P.E., CETCO, USA, catha@cetco.com

ABSTRACT

Geosynthetic composite liner systems, consisting of geosynthetic clay liners (GCLs) underlying geomembrane liners, are seeing increased usage in large lined fill structures such as heap leach pads, tailings storage impoundments, and landfills, largely due to improved construction time and enhanced operational liquid containment compared to compacted clay composite liners. The improved hydraulic seepage barrier performance provided by geomembrane/GCL composite lining systems is well documented (Bonaparte et al, 2002). However, there is a concern by engineers and regulatory agencies over the stability of such composite liner systems, due to the low shear strength of hydrated bentonite.

This paper focuses on solving the liner engineer's ultimate long term slope stability challenge (or nightmare): high fill loads on planar composite liner surfaces with low-strength bentonite clays in direct interface contact with a smooth geomembrane liner surface. In particular, the focus will be on the slope stability of heap leach pads as the ultimate lined fill structure challenge due to a combination of several stabilization considerations, including large planar pad surfaces, controlled ore lift stacking to high wet density fill load conditions, downhill sloping gravity drainage surfaces to recover leach solutions in external ponds, and generally without any downhill toe buttress berm fill support. A summary of design and construction stabilization methods is presented to improve the long-term stability of worst-case composite liner strengths on planar surfaces.

1. INTRODUCTION

Textured geomembrane liners in direct contact with the nonwoven geotextile side of GCLs have been functioning successfully for more than 20 years in the mining and landfill industry. However, the primary question for long term closure of lined facilities is the worst-case condition where the GCL loses internal strength due to either rupture, pullout, or degradation of the needle-punched reinforcing fibers, leaving behind only hydrated unreinforced bentonite. Fox and Ross (2011) state that at high normal stress, a textured geomembrane/needle-punched reinforced GCL composite liner system can experience GCL internal failure, as the shear strength between the textured geomembrane and GCL exceeds the strength of the needle-punch reinforcement. The normal stress at which the failure plane transitions from textured geomembrane/GCL interface to GCL internal depends on the specific materials and testing conditions. McCartney et al. (2009) observed no GCL internal failures in a database of 534 geomembrane/GCL interface tests performed at normal stresses as high as 965 kPa (20,150 psf). Fox and Ross observed this transition occurring at normal stresses between 692 and 2,071 kPa (14,450 and 43,240 psf). These types of GCL internal failures appear to be limited to the laboratory however. Koerner (2012) and Fox and Ross (2011) report that there are no known cases of internal shear failure of needle-punched GCLs in the field. Another potentially problematic, but less severe, condition involves the extrusion of hydrated bentonite through the woven geotextile component of the GCL, resulting in a reduction in interface shear strength (Vukelic et al, 2008). This condition can be minimized by specifying GCLs with nonwoven geotextiles, which have a smaller opening size, on both sides of the bentonite clay layer.

If these conditions occur in the field, then large planar composite liner surfaces would approach the residual strength of the bentonite clay at the interface contact with a smooth geomembrane liner surface. Excess pore pressure conditions can be neglected for evaluating long term closure slope stability, assuming operational fill lift loads are placed before post-construction hydration and swell pressures can fully develop over time along large lined fill slope areas.

Traditional methods covered by previous literature and textbooks, such as earthen toe berms and flattened fill slopes (e.g., Abramson et al, 2002) or stabilized underliner toe grades and operational startup lift placement control (Breitenbach, 1997) have been used with success since the 1990's. Slope stability can also be improved through the use of non-planar features to improve liner shear strength. The earliest discussion of this technique is given by Poulter (1995), who presented two case studies. The first involved the addition of a small berm under the toe of a gold heap to stabilize a liner failure in 1990 in South Carolina, USA. The critical slip plane was a smooth HDPE geomembrane against a soft clay soil compacted at wet of optimum moisture content (calculated equivalent friction angle of 11 degrees at failure). The second case study involved the addition of two berms to compensate for low shear strength between a smooth VLDPE geomembrane and a nonwoven geotextile (calculated equivalent friction angle of 8 degrees at failure).

This paper builds on this previous work, and analyzes three basic types of non-planar liner interface stabilizing techniques used primarily in the mining industry on heap leach pads for downhill toe stability. Based on the non-planar slope stability analyses results for an idealized pad liner section and past leach pad experience, these non-planar stabilization techniques can be applied to lined dams and landfill structures as well, subject to low interface strength composite liner conditions during construction, operation or for long term closure scenarios.

2. INTERFACE STRENGTH SELECTION

2.1.1 General

The low interface strength between a composite clayey soil and geomembrane liner or synthetic geotextile to geomembrane liner has been proven by large scale laboratory direct shear testing, theoretical slope stability analyses and construction into operation practice to be the cause of numerous lined fill structure failures (Breitenbach, 1997, Koerner and Soong, 1999). Therefore the selection of the liner interface strength value for stabilized surface grades is the most important factor in designing stable fill structures to function for the life of the facilities to closure.

The general concerns for the GCL in a planar composite liner high load facility are 1) the loss of hydrated bentonite through the geotextile sheets, 2) interface friction strength in direct contact with the overlying geomembrane liner or underlying bedding fill surfaces, 3) loss of internal geotextile needle-punched and/or stitch-bond fabric strength in the reinforced GCL sheets, and 4) long term performance to resist soil creep movement at hydrated low residual strength conditions.

This section discusses GCL materials and a review of past test results for selecting a worst-case interface strength for analyses. The GCL laboratory test strengths provide a guideline for selection by the authors of a typical post-construction hydrated bentonite residual strength value in modeling the stabilization of a GCL composite lined planar leach pad in an idealized study section under high ore heap fill load conditions.

2.1.2 GCL Material

The natural deposits of montmorillonite sodium bentonite clays provide the lowest permeability clayey soil liner materials in the world with few exceptions. The permeability of fully hydrated thin sheets of bentonite clay under 0.6 m (2 ft) of load can achieve permeabilities less than 1×10^{-8} cm/sec (Estornell and Daniel, 1992). Along with the low permeability characteristics of bentonite, the clay material is expansive when wetted from a dry condition (excellent for sealing off local void spaces), however bentonite clay hydration also causes residual low strength conditions.

Geosynthetic clay liners (GCLs) use sodium montmorillonite (bentonite) clays sandwiched between different geotextiles. GCLs can be either unreinforced or reinforced with needle-punching or stitch-bonding. The reinforcement imparts increased shear strength and resistance to hydrated clay swelling. The sodium bentonite clays in Wyoming and Montana USA are formed from weathered or decomposed volcanic ash material deposited long ago in an ancient inland sea marine environment. The bentonite clay in the GCL sheet is essentially "dry" at 15 to 30 percent deployment moisture content for short term exposure before being covered by a geomembrane liner. When wetted from liner leakage or in contact with moist subgrade material, the bentonite clay absorbs water and swells to form a relatively impervious clay barrier. At the same time, the hydrated bentonite clay acts as a low strength planar material, when used in a composite geomembrane and GCL liner system for lined landfills, heap leach pads and tailings impoundments. The hydrated bentonite clay has low internal and interface peak friction strength, in addition to low residual strength after movement occurs. These lined containment facilities are subjected to a range of loading conditions requiring stabilization of the loaded structures for the life of the facility and long term into closure.

2.1.3 GCL Laboratory Test Strengths

Numerous laboratory tests have been conducted on unreinforced and reinforced, needle-punched, needle-punched and thermal bonded, and stitch-bonded GCL in dry to fully hydrated and low to high load conditions. The internal strength of the bentonite itself under hydrated conditions is the controlling factor, since the interface strength interlocking bond with a textured geomembrane liner surface or drain fill materials would be higher. The exception to this rule would be smooth and less flexible geomembrane liner surfaces in contact with hydrated bentonite extruded or squeezed through the GCL geotextile layer under high load conditions.

The numerous variables for the laboratory tests considered delaying loads to reduce pore pressure at failure, rate of shearing to failure, extent of hydration before or during test loading, peak versus large-displacement (residual) strengths, and test apparatus/testing variations. Changes in GCL hydration in conjunction with loading conditions over time were found to have the most influence on interface strengths under the same liner system design conditions. The equivalent

residual friction strength is defined throughout this paper as the straight line slope on the Mohr stress-strain failure envelope drawn through the zero cohesion intercept for ease in comparing the various total and effective stress friction and cohesion strengths to a single equivalent friction strength parameter. This technique is a useful tool for determining a general strength condition for an idealized section, however it has limitations for use in site specific design considerations such as changes in GCL loading and moisture conditions over time.

The GCL strengths are site-specific to the liner design and apply to changing conditions over time from construction to operation to closure of a lined facility. The general conclusion from over 300 laboratory test results on GCL in a single laboratory test environment (McCartney, et al 2002) is the following:

Peak equivalent friction angle:

- Needle-punched GCL = 33.5 degrees
- Needle-punched, thermal bonded = 28.9 degrees
- Stitch-bonded = 12.2 degrees
- Unreinforced = 6.6 degrees

Large-displacement equivalent friction angle (post-peak approach to residual strength):

- Needle-punched GCL = 13.7 degrees
- Needle-punched, thermal bonded = 12.9 degrees
- Stitch-bonded = 6.7 degrees
- Unreinforced = 5.9 degrees

Assuming that the geotextile fabric in GCLs will provide some residual strength reinforcement in the long term decomposition of the liner system, a lower bound worst-case interface strength was selected to be 7 degrees friction for the idealized study section analyses.

3. EVALUATION OF LOW STRENGTH PLANAR SURFACES

3.1 General

The evaluation of these low strength clays for stabilized composite liner design options included several steps: The first step is to select a bentonite clay strength representative of a fully hydrated GCL material with no residual strength excess pore pressures. This would best represent the worst-case long term closure conditions with minimal support from the geosynthetic geotextile materials in the sheet. The second step is to simplify the analyses with an equivalent friction strength only. Cohesive or adhesive strengths of clays in direct contact with geomembrane liners have a tendency to decrease with time, therefore the analyses for this paper considered an equivalent low interface friction strength only and neglected any additional strength from cohesion. The third step included using several techniques that demonstrate increasing the pad liner stability to acceptable factors of safety by breaking up the planar low strength liner interface conditions. These include stability berms, stability trenches and stability benches as discussed in this section and illustrated in Figures 2 to 9.

3.2 Heap Leach Pad Stability Analyses

This paper presents a series of stability calculations for a hypothetical ore heap study section containing a pad composite liner at an assumed very low bentonite clay to geomembrane liner interface friction strength equivalent to 7 degrees friction and no cohesion. An equivalent friction only interface strength was selected for simplification purposes and to represent long term residual strengths at low excess pore pressure conditions.

After preliminary calculations on the baseline planar pad liner surface condition (i.e., no non-planar slope stability improvement measures), a series of calculations were performed to evaluate the benefit of adding non-planar structures to the study section, including the use of stability berms, trenches, and benches.

The hypothetical heap study section used in this analyses was taken from Breitenbach and Thiel (2005). They considered a typical ore heap configuration, built on a planar 2 percent pad grade, with 2H:1V overall ore heap slopes above the pad liner, and no toe berm support, as shown on Figure 1.

Breitenbach and Thiel assumed that the heap leach pad liner system had an interface friction angle of 18 degrees, and that both the ore and subgrade soil had a density of 18.85 kN/m^3 (unit weight of 120 pcf) and a friction angle of 38 degrees. The phreatic surface was assumed to be 0.6 m (2 feet) above the liner throughout the structure. Under these conditions, the modified Janbu method in PCSTABL 5M was used to calculate a critical factor of safety (FS) of 1.44, which would be acceptable to regulatory agencies for a low risk heap leach structure that does not pond water.

The first step in our baseline analysis involved evaluating the same ore heap shown in Figure 1, using the same conditions as Breitenbach and Thiel, as a means of validating our calculation method. The authors employed XSTABL (Sharma, 1996), using the modified Janbu method, and found that, for the same geometry and material properties, the calculated FS was 1.44, the same value and the same critical surface reported by Breitenbach and Thiel.

After this initial baseline step, the liner interface shear strength was reduced from 18 degrees down to a very low strength of 7 degrees friction. This low strength represents an assumed worst-case scenario, where a GCL's internal needle-punch reinforcement has entirely ruptured, leaving behind a weak layer of unreinforced, hydrated sodium bentonite clay. All of the remaining study section parameters were left the same. The XSTABL calculations found that the same heap geometry, built on a layer of unreinforced hydrated bentonite, would be expected to have FS = 0.89, or in other words, be subject to an imminent sliding failure. This scenario now becomes our baseline for applying non-planar stabilization measures for improvements to the ore heap's stability, as discussed in the following section. (Please note that the calculated FS = 0.89 is conservatively based on an assumed friction angle 7 degrees across the entire liner area, regardless of normal stress. If the calculation is repeated to include a more realistic nonlinear Mohr-Coulomb failure envelope, using the large displacement shear strength values measured by Fox and Ross (2011) for a textured geomembrane/GCL interface, the FS increases to 1.16).

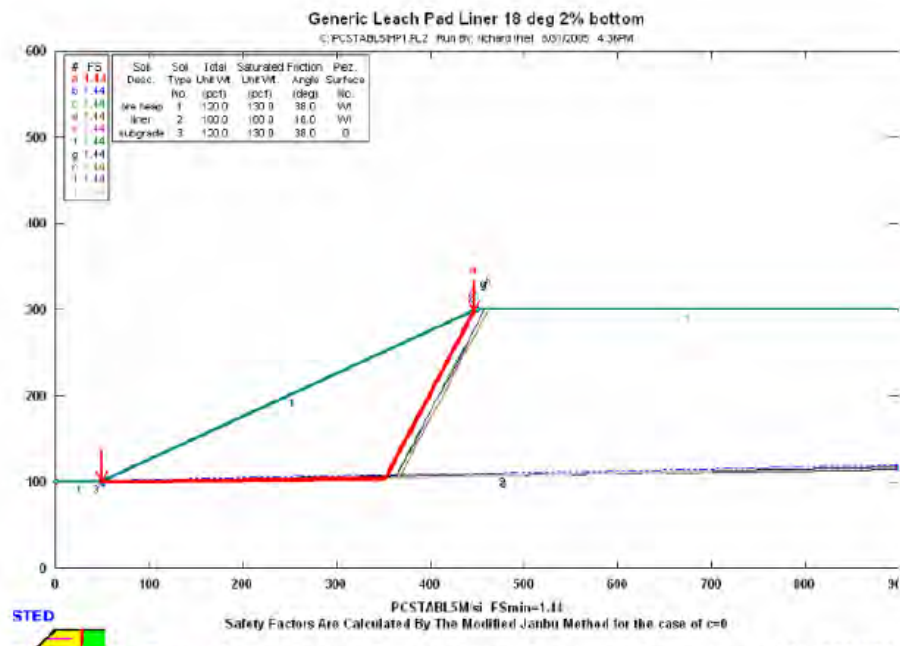


Figure 1. Hypothetical Ore Heap Section from Breitenbach and Thiel (2005) used as Baseline Starting Point for this Stability Analyses

3.3 Stability Berms

The first non-planar stability improvement method considered the use of stability berms along the baseline heap study section, as it was the first type of slope strengthening method used in the mining industry. The senior author had considered using what were called “speed bumps” in the analyses for planar leach pad liner surfaces in South Dakota and for a water storage dam upstream section with composite GCL and liner core in Nevada USA in the late 1980’s. Subsequently the speed bump concept was put into practice to remediate a pad liner failure in 1990 in South Carolina USA. The slide occurred along the composite liner interface on a planar 6.5 to 7.7 percent pad downhill toe grade under 15 m (45 ft) of ore lift load. The pad failure extended 60 m (200 ft) inward from the toe, and the non-leached dry ore lift was removed to make the repairs. Several low-level “speed bump” stability berms were suggested to the design engineer for remediation and were constructed in the slide area perpendicular to the direction of slide. Ore lift placement resumed with no further problems, which included multiple placed and leached ore lifts over the following year. The stability berms provide added sliding resistance and cause the critical slip plane to shear through an overall higher non-planar interface surface, thus improving overall stability. A photograph showing a past heap leach project that employed this technique is shown in Figure 2.

In this evaluation, the hypothetical example presented above ($\phi = 7$ degrees, FS = 0.89) was modified by introducing increasing numbers of stability berms along the 2 percent grade, and calculating the improvement to FS. The stability

berms were added in two different orders: (1) starting at the toe of the slope and moving deeper into the pad interior to the failure wedge plane; and (2) starting at the back failure wedge plane and moving towards the pad downhill toe. For the purposes of these analyses, the stability berms were assumed to be 0.5 m (1.5 feet) in height, 3 m (9 feet) wide crest and 1H:1V slopes. The stability berms were spaced 5 m (15 feet) apart to allow for vehicular access. The sensitivity analysis effects of varying stability berm height, width, and spacing are evaluated in a later section of this paper. \



Figure 2. Example stability berm configuration from a heap leach pad liner project (photo courtesy of Comanco)

3.3.1 Addition of Stability Berms (Starting at the Downhill Toe)

Scenarios involving the addition of 1 to 11 stability berms, starting from the toe of the pad inward, were evaluated, as shown in Figure 3. The different critical failure surfaces associated with selected stability berm values is shown in Figure 3. Figure 5 presents a summary of the relationship between FS and number of stability berms. The calculations showed that there was a gradual improvement in FS with the addition of up to four stability berms, with no change in the critical failure surface location. With the addition of the fifth stability berm, there was a corresponding shift in the critical failure surface to deeper within the ore heap. This intuitively makes sense, as the sliding resistance along the toe increases, a greater driving mass of ore would be necessary to overcome the non-planar change in pad interface strength. Nine stability berms were needed to improve the FS to greater than 1.3, and eleven berms were needed to improve the FS to greater than 1.4. The number of required stability berms is reduced as the interface strength is increased, like for a change from smooth to textured liner surfaces.

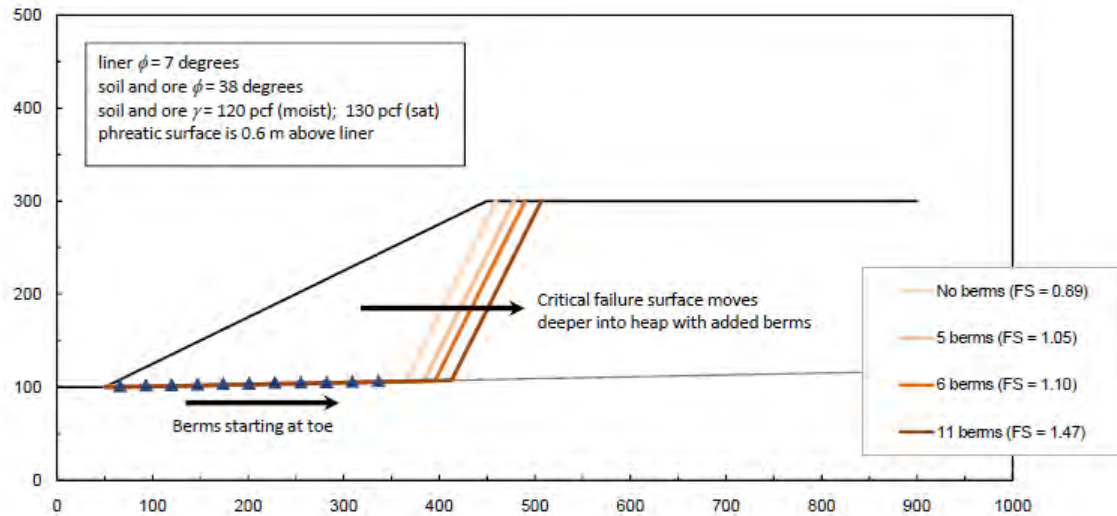


Figure 3. Critical Failure Surfaces associated with addition of stability berms along liner starting from the toe

3.3.2 Addition of Stability Berms (Starting at the Back of the Failure Wedge)

The evaluation above was then repeated, this time with the stability berms starting from the back of the failure wedge toward the downhill toe, as shown in Figure 4. Figure 5 presents a summary of the relationship between FS and number of stability berms for each of the two scenarios evaluated. Intuitively, one would expect the incremental benefit of each berm added at the back of the wedge would be greater, due to the greater normal stress on the failure plane, and therefore greater shear strength at this location. However, in this scenario, the expected sharp increase in FS was not realized, since the critical failure surface was forced outward, towards the toe of the pad, as shown in Figure 4. (Note that performing the analysis with a fixed failure surface showed that the addition of just one berm at the back of the wedge improved the FS of that fixed surface significantly from 0.89 to 1.14). This movement continued until the addition of eight berms finally forced the critical failure surface deeper into the ore heap. Eight berms were needed to improve the FS to greater than 1.3, and ten berms were needed to improve the FS to greater than 1.4.

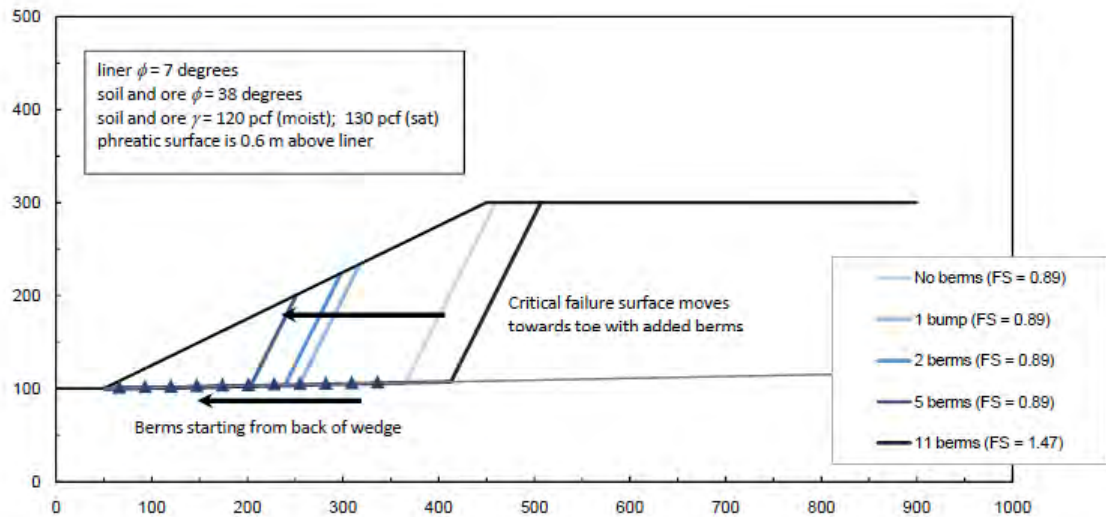


Figure 4. Critical Failure Surfaces associated with addition of stability berms along liner starting from the back of wedge

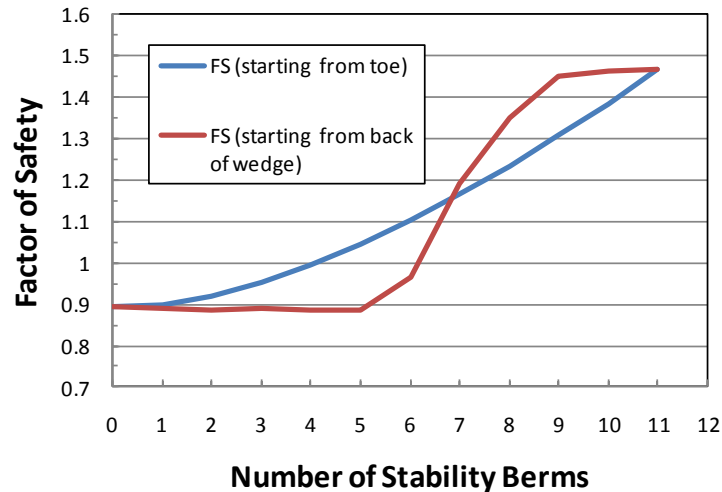


Figure 5. FS versus Number of Stability Berms

3.3.3 Stability Berm Size Sensitivity Analysis

The scenario with eleven stability berms and FS = 1.47 was selected for additional sensitivity analyses of the berm size, looking at variables such as the stability berm height, width, and spacing. As mentioned above, the standard stability berms were assumed to be 0.5 m (1.5 feet) in height, 3 m (9 feet) wide crest with 1H:1V side slopes, and spaced 5 m (15 feet) apart. The subgrade soil was assumed to have an internal friction angle of 38 degrees. With all other parameters kept constant, each of the stability berm variables were changed to evaluate its impact on the overall factor of safety. A constant number of stability berms over a given area was maintained. A summary of the sensitivity analysis is presented in Table 1.

This analysis shows that the stability berm height is not a critical parameter for the model geometry and strengths compared to the stability berm width and spacing. As expected, reducing the subgrade soil's internal friction angle decreased FS. Increasing the stability berm width improved FS, with the greatest improvement seen when combining increased stability berm crest width together with closer spacing. Conversely, reducing the stability berm crest width resulted in the largest observed reduction in FS.

Table 1. Stability Berm Sensitivity Analysis

<i>Parameter</i>	<i>FS</i>
Initial Condition, height = 0.5 m (1.5 feet), width = 3 m (9 feet), spacing = 5 m (15 feet)	1.47
Increase berm height to 1 m (3 feet)	1.55
Decrease subgrade soil friction angle to 25 degrees	1.23
Increase berm width to 5 m (15 feet), with 5 m (15 feet) spacing	1.75
Increase berm width to 5 m (15 feet) and decrease berm spacing to 2.5 m (7.5 feet)	1.73
Decrease berm width to 1 m (3 feet) and increase berm spacing to 7 m (21 feet)	1.17

3.4 Stability Trenches

A similar stability improvement method involves the use of stability trenches, also known as shear keys (Abramson et al., 2002), to provide additional sliding resistance along a planar surface. Stability trenches are sometimes used along with stability berms as a dozed cut to fill non-planar structure, however the trenches are more difficult to design and construct

for gravity drain systems to the downhill pad toe collection ditches and ponds versus leaving openings in key areas of the stability berms to facilitate drainage as shown in Figure 2 (ease in separation of operational solution cell flows). Stability trenches improve the non-planar surface strength depending on the width of the trench cut and steep wall trench cuts are preferred to cause passive wedge resistance to sliding.

Stability trenches were evaluated for the Breitenbach and Thiel baseline scenario. For ease of comparison, the trenches were assumed to be simply the “inverse” of the stability berms discussed previously (11 trenches, each with depth = 0.5 m, base width = 3 m, and spacing = 5 m). XSTABL calculations found that the FS against sliding was 1.45, almost identical to the stability berm case at FS = 1.47. The complex variables for stability trenches should be similar to stability berms with the exception that berms provide more stability in the case where the overlying containment fill strengths become low.

3.5 Stability Benches

Another stability improvement method for ore heaps and earthwork structures in steep terrain involves the use of interior “stair-step” stability benches, or terraces. To evaluate this method, the Breitenbach and Thiel baseline example was modified to include a 3H:1V backwall slope as shown in Figure 6. In this scenario, a base width of 40 m (130 feet) was used, leading up to a 15 m (50 feet) high 3H:1V graded slope, a 5 m (16.5 foot) wide bench, then another 3H:1V slope and bench, repeated until the top is reached. This is a common configuration encountered at sites with existing steep topography. An XSTABL analysis for this steep lined backwall scenario resulted in a very low calculated FS = 0.78 for an assumed 7 degree liner interface friction angle.

To improve the slope stability factor of safety, a series of stability benches was added to the lower portion of the backwall slope (the critical wedge failure area) as shown in Figure 7. Each bench was 5 m (16.4 feet) high and 5 m (16.4 feet) wide, with a 2H:1V slope. Using the geometry, the three benches create an overall 3H:1V slope. A photograph from a past project site where a similar configuration was used is shown in Figure 8. An XSTABL analysis of the scenario shown in Figure 7 resulted in a calculated FS = 1.32, a significant improvement, once again due to the creation of a non-planar feature along a critical planar failure surface.

3.6 Stabilization Combinations

A different approach to improving the slope stability factor of safety is shown in Figure 9. First, the 40-m base initially presented in Figure 6 was extended an additional 45 m (150 feet), resulting in a larger base area able to accommodate several stability berms. A total of eight berms were then added at the back of the wedge, resulting in an improved FS = 1.38. And finally, a series of three 5-m tall, 5-m wide, 2H:1V stability benches was added to the lower portion of the backwall slope. Together, the combination of increased base width, backwall slope benches, and stability berms was able to almost triple the factor of safety (from an undesirable FS = 0.78 to an acceptable FS = 2.01 for low risk fill structures that remain fully drained).

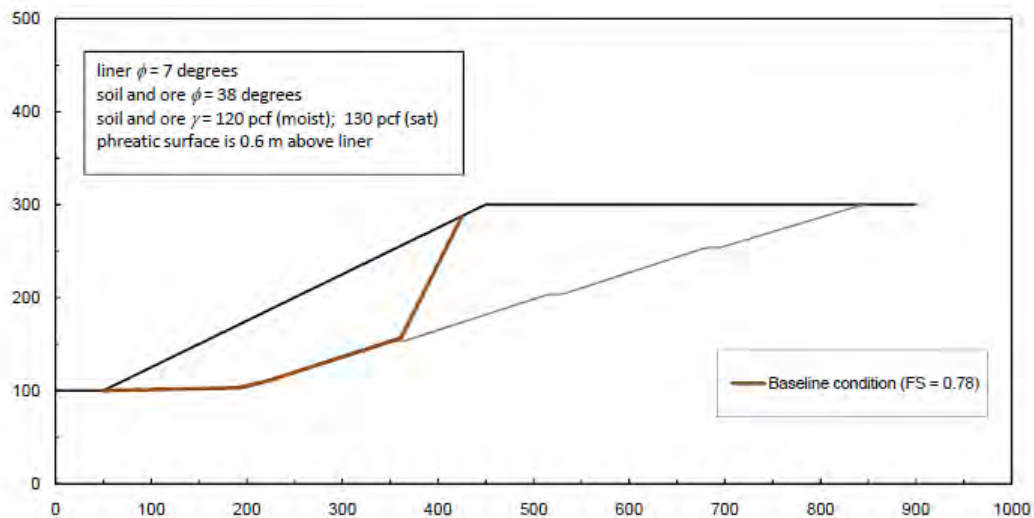


Figure 6. Modified baseline scenario with 3H:1V backwall slope

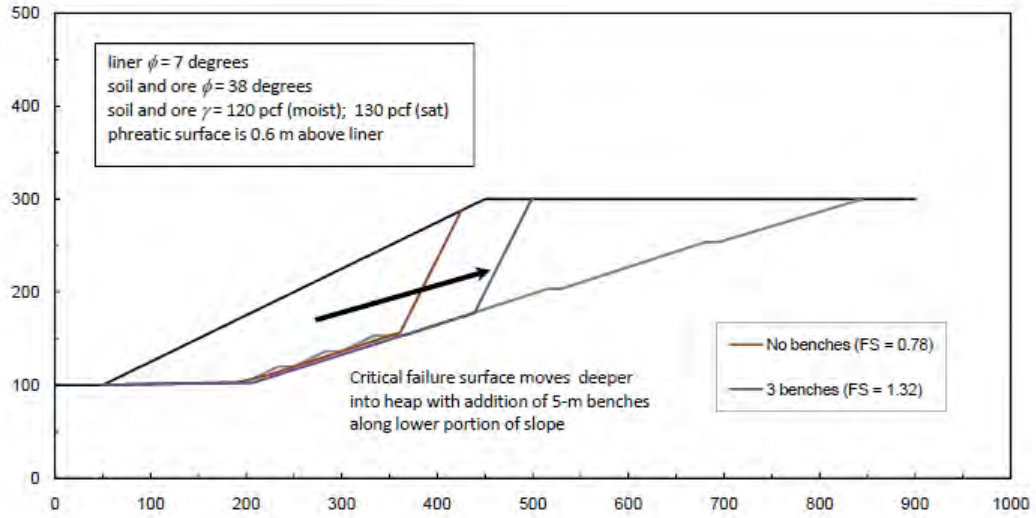


Figure 7. Critical Failure Surfaces associated with addition of “stair step” stability benches

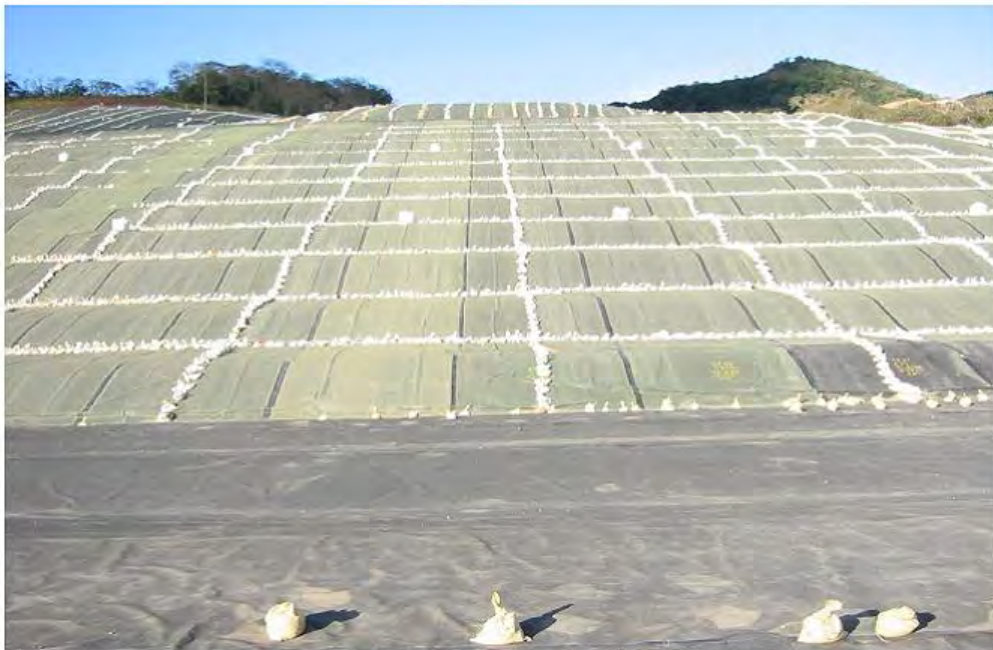


Figure 8. Example “stair step” stability bench configuration on a composite lined heap leach pad

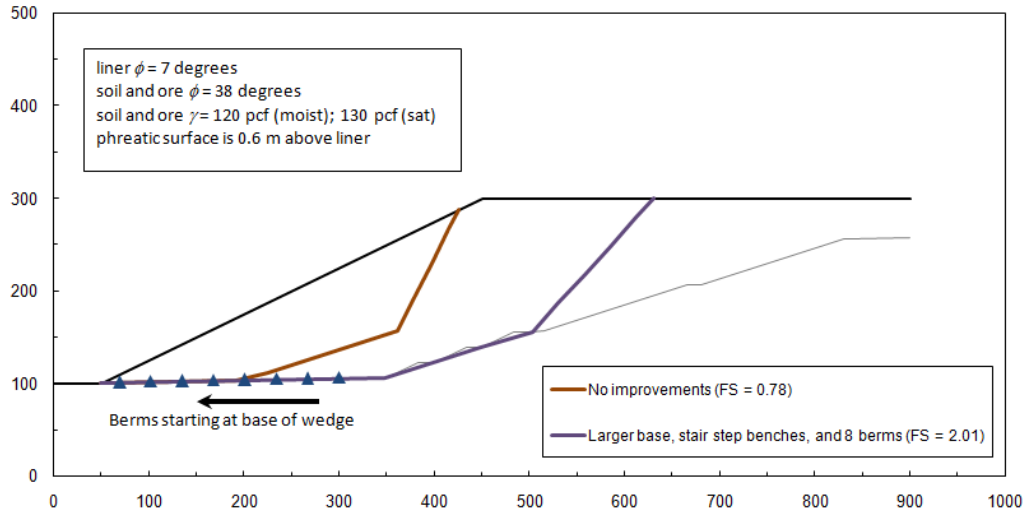


Figure 9. Critical Failure Surfaces associated with increased base width and addition of stability berms along liner starting from the back of wedge

4. CONCLUSIONS

Geosynthetic composite liner systems, consisting of GCLs underlying geomembrane liners, are seeing increased use in large lined fill structures such as heap leach pads, tailings storage impoundments, and landfills, largely due to improved construction time and operational liquid containment. However, there is a concern by engineers and regulatory agencies over the stability of such composite liner systems, due to the low shear strength of hydrated bentonite. Although Koerner (2012) and Fox and Ross (2011) report that there are no known cases of internal shear failure of needle-punched GCLs in the field, laboratory testing has shown that GCLs can experience internal failure at very high normal stresses, corresponding to low residual shear strength. Another consideration that could decrease liner interface strength involves the extrusion of hydrated bentonite through the woven geotextile component of the GCL (Vukelic et al, 2008).

This paper presents a series of stability calculations for a hypothetical ore heap study section containing a pad composite liner with a very low strength (friction angle = 7 degrees) bentonite clay to geomembrane liner interface. After preliminary calculations on the baseline condition (i.e., no non-planar slope stability improvement measures), a series of calculations were performed to evaluate the benefit of adding non-planar structures to the study section, including the use of stability berms, trenches, and benches. The benefit of each individual method alone was evaluated, as well as the combined benefit of multiple methods. For one example study section, employing a combination of methods (increased flat slope base width, backwall slope benches, and stability berms) was able to almost triple the factor of safety (from an undesirable FS = 0.78 to a very favorable FS = 2.01).

These findings have important design implications for lined fill structures with low planar interface strengths. The incorporation of non-planar structures in geosynthetic-lined slopes can improve overall stability and maintain an adequate factor of safety, even in worst-case loss of GCL internal strength due to either rupture, pullout, or degradation of the needle-punched reinforcing fibers, or reduction in geomembrane/GCL interface strength due to extrusion of hydrated bentonite through the woven geotextile component of the GCL. The non-planar liner designs can turn the liner engineer's worst nightmares into his best dreams for liquid containment and stability.

REFERENCES

- Abramson, L.W., Lee, T.S., Sharma, S., and Boyce, G.M. (2002). Slope Stability and Stabilization Methods. John Wiley & Sons, Inc. New York.
- Bonaparte, R., Daniel, D., and Koerner, R. (2002). Assessment and Recommendations for Improving the Performance of Waste Containment Systems. CR-821448-01-0, Environmental Protection Agency, Washington, DC, 1039 pp.
- Breitenbach, A.J. (1997), "Overview study of several geomembrane liner failures under high fill load conditions", Geosynthetics '97 Conference Proceedings, Industrial Fabrics Association International (IFAI), Long Beach, California, Vol. 2, pp. 1045 to 1062.

- Breitenbach, A.J. and Thiel, R.S. (2005), "A tale of two conditions: landfill versus heap leach pad liner strengths", GRI-19 Geosynthetics Conference, North American Geosynthetics Society (NAGS), Las Vegas, Nevada.
- Estornell, P. and Daniel, D. (1992). "Hydraulic Conductivity of Three Geosynthetic Clay Liners." *J. Geotech. Engrg.*, 118 (10), 1592–1606.
- Fox, P.J. and Ross, J.D. (2011), "Relationship between NP GCL Internal and HDPE GMX/NP GCL Interface Shear Strengths", *J. Geotech. Geoenviron. Eng.*, 137 (8), 743–753.
- Koerner, R.M. and Soong, T.Y (1999), "Stability analyses of ten landfill failures", Proceedings 2nd Austrian Geotechnical Congress, Austrian Engineering and Architects Society, Eschenbachgasse, Vienna, pp. 9 to 50.
- Koerner (2012), "Selected Topics on Geosynthetic Clay Liners", Keynote lecture at GCL University, Washington, D.C., April 12, 2012.
- McCartney J.S., Zornberg, J.G., and Swan Jr., R.H. (2002), "Internal and Interface Shear Strength of Geosynthetic Clay Liners (GCLs)", Geotechnical Research Report, Dept of Civil, Environmental and Architectural Engineering, University of Colorado.
- McCartney, J. S., Zornberg, J. G., Swan, R. H., Jr. (2009). "Analysis of a large database of GCL-geomembrane interface shear strength results." *J. Geotech. Geoenviron. Eng.*, 135 (2), 209–223.
- Poulter, D.A. (1995). "Leach Pad Liner Stability On Slopes - Two Case Histories." Presentation at the SME Annual Meeting, Denver, Colorado, March 6-9, 1995.
- Sharma, S. K. (1996). "XSTABL: An integrated slope stability analysis program for personal computers." Reference manual, Version 5, Interactive Software Designs, Inc., Moscow, Idaho. 213 p
- Vukelic, A., Szavits-Nossan, A., and Kvasnicka, P. (2008). "The Influence of Bentonite Extrusion on Shear Strength of GCL/Geomembrane Interface." *Geotextiles and Geomembranes* 26: 82–90.

Influence of Textile Structure in Relationship to Filtrate Quality in Dewatering Applications Using Geotextile Containers

Christopher Timpson, TenCate Water & Environment, USA

ABSTRACT

Geotextile containers offer a cost effective alternative to mechanical dewatering processes. Geotextile containers are constructed of a specially engineered textile which allows a high flow rate of effluent while restricting solid particles from passing through the textile. This technology reduces disposal costs by consolidating higher solids with very little maintenance when compared to mechanical dewatering processes. Chemical conditioners and polymers are used to promote flocculation and improve solids retention.

The dewatering performance is influenced by the type of sludge, pumping rate, chemical conditioning, and filtration properties of the specially engineered textile. All of these factors determine the quality of filtrate which filters through the engineered textile. The common assumption is that the filter cake building up inside of the geotextile container determines the filtrate quality, however this paper summarizes a study of how the textile structure can influence filtrate quality.

The GDT (Geotextile Dewatering Test) is a very efficient and effective test method for predicting dewatering performance and results. This test is conducted in an enclosed system which best simulates an actual geotextile container versus other bench test methods. The current GDT test method can be modified by applying a specific amount of discharge pressure during filling to better simulate actual project conditions. This improvement in the GDT test is known as the P-GDT (Pressurized Gravity Dewatering Test). With the P-GDT test set-up, several types of textile constructions can be evaluated for dewatering performance in a controlled environment using the same sludge, polymer dosage, and pressure.

This paper will address the development of a dewatering testing protocol, dewatering experiment, fabric weave construction analysis, and resultant filtrate quality in relation to textile structure of various weave constructions. The dewatering experiment was performed with contaminated river sediments and water treatment sludge.

1. INTRODUCTION

Geotextile containers have been used since the 1960's as shoreline protection in marine and river structures such as breakwaters, dikes, artificial islands, and jetties. Over the years, this technology has transferred into the dewatering of wastewater with the aid of chemical conditioning. Geotextile containers for dewatering applications have proven both reliable and efficient. There are three basic stages to dewatering with geotextile containers which are confinement, dewatering, and consolidation (See Figure 1). The specially engineered textile which the geotextile containers are fabricated allows confinement of the fine solids inside the container but allows water to filter for dewatering. As the water drains, the solids continue to densify inside the geotextile container and the volume inside the container continues to consolidate over time.

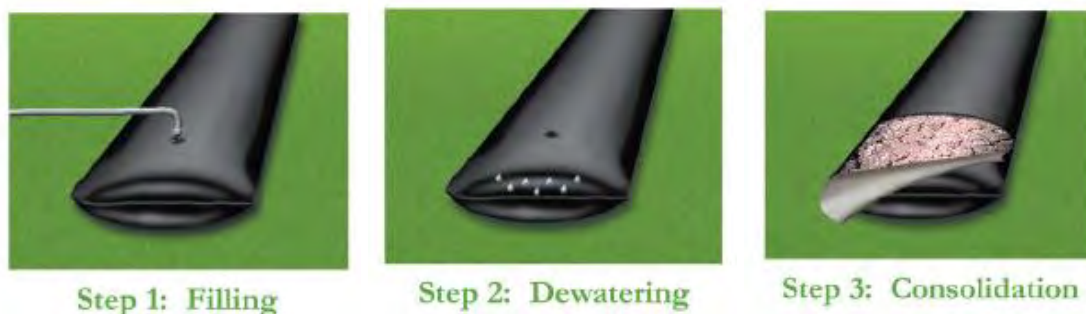


Figure 1. Three basic stages of geotextile container dewatering.

As their use becomes more prevalent, the overall knowledge of the technology advances along with the methods of testing to predict their suitability and efficiency for specific applications. Over the years there has been some evolution in the bench testing of sludge. The GDT is a very efficient and effective test method for predicting dewatering performance and results. This test is conducted in an enclosed system which best simulates an actual geotextile container versus other bench test methods like the cone test and hanging bag test.

With GDT testing, a large amount of sludge can be evaluated versus the smaller quantity used in cone test. Typically 20 to 40 gallons of sludge can be used in GDT testing. The hanging bag test can be conducted using a larger quantity of sludge, but the action of pouring the conditioned sludge in the hanging bag assembly may break down the floc formation of the suspended solids as shown in Figure 2.



Figure 2. Hanging Bag Testing

The current GDT test method can be modified to apply a specific amount of discharge pressure during filling to better simulate actual project conditions. This improvement in the GDT test is known as the P-GDT (Pressurized Geotextile Dewatering Test). The concept for this testing was developed by Jim Meagher of Mineral Processing Services, LLC. In this controlled environment the sludge, polymer dosing, and pressure during filling can all remain constant to allow for evaluation of dewatering performance. A three-phase filling cycle is conducted to simulate the filling, dewatering, and re-filling as seen in real world pumping of geotextile containers.

2. TEXTILE WEAVE CONSTRUCTIONS

The broken twill weave is the dominate textile construction used in the fabrication of geotextile dewatering containers, see Figure 3. A twill weave is produced by passing the weft yarns over or under two or more warp yarns which produces diagonal type pattern and appearance. This weave provides for the optimum performance to allow open area within the construction for free water to flow through the textile and interlacings to provide a filter media to restrict solid particles from passing.

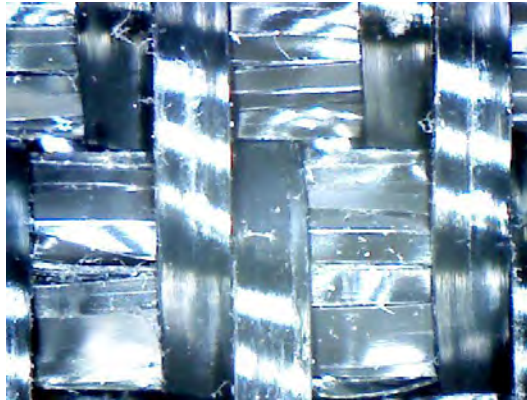


Figure 3. Typical Broken Twill

Although the broken twill weave construction is a major factor in determining the dewatering characteristics of the textile, the yarn constructions which build the weave influence the dewatering performance. Several variations of the broken twill weave construction were evaluated in this experiment, see Table 1. A double layer construction will be evaluated to understand any differences in filtration properties compared to a broken twill construction.

A tape yarn typically has a flat and wide cross-section. A fibrillated tape is a tape yarn which has been serrated, the slits in the cross-section allow the yarn to be flexible to fold and twist. A monofilament yarn typically has a rounded, cylindrical cross-section.

Table 1. Textile Weave Constructions Evaluated

Weft Yarn	Warp Yarn	Weave Construction
Fibrillated Tape	Monofilament	2x2 Broken Twill
Tape	Tape	2x2 Broken Twill
Fibrillated Tape	Fibrillated Tape	3x3 Broken Twill
Fibrillated Tape/Continuous Filament	Monofilament	Double Layer

The combination of these various yarn types in a broken twill weave construction can influence the permeability, percent open area of a textile, and porosity. The water flow results in Table 2 show the potential flow characteristics of each construction without any regard for potential filtration properties. Water flow was tested according to ASTM D4491. The P-GDT test will be used to evaluate the filtration characteristics of each weave operating under similar conditions with the same sludge, polymer dosing, and filling pressure.

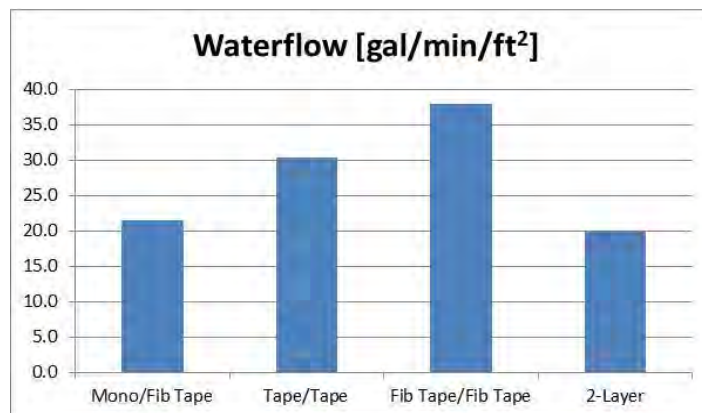


Table 2. Water Flow Results of Weave Constructions

3. TEST PREPARATION

This testing protocol was developed to provide best practices for fabrication of GDT bags, seam preparation, polymer conditioning, set-up of P-GDT test equipment, and sampling. This procedure was established based on the experiments conducted during this study with contaminated river sediments and water treatment sludge (alum).

All fabrics must be cut from a standard template to produce a 21-inch x 21-inch GDT bag. A 2-inch PVC flange port must be installed for filling. The sewn edges of the GDT must be sealed with a clear PVC cement to prevent leakage. Leakage at the seams during P-GDT testing will permit solid particles to pass through the seam which can influence test results.



Figure 4. GDT Test Bag Preparation

Bench scale testing must be conducted prior to P-GDT testing to determine the appropriate polymer and dosage required for the slurry or sludge to be tested. Before proceeding with P-GDT testing, conduct floc tests to guarantee equivalent polymer performance with the slurry or sludge which will be tested.

The amount of unconditioned slurry or sludge required is dependent on the number of products which will be tested. It is recommended to acquire a large quantity of unconditioned material in a sizeable tote. The tote must be continuously agitated to keep all particles in suspension and prevent settling at the bottom of the tote. This will provide consistency of unconditioned slurry across all GDT products tested.

Each GDT test requires a 30-gallon sample of unconditioned material. The unconditioned material will be chemically conditioned with polymer in individual batches of the same dosage and mixing rpm. Figure 5 illustrates the set-up of the P-GDT testing equipment. The discharge pressure required to fill the GDT bag is dependent on the circumference of a full size tube. The discharge pressure is calculated based on the dimension of the full size geotextile container which is simulated.



Figure 5. P-GDT Test Machine Set-up

To simulate the repetitive filling, dewatering, and consolidation phases, this testing using a three phase filling cycle for each GDT Test. This allows the GDT bags to simulate the filling and dewatering of full scale geotextile dewatering containers.

First Phase Fill

1. Weight empty GDT to determine initial weight.
2. Obtain sample of unconditioned slurry from 40-gallon container.
3. Add appropriate amount of polymer and mixing energy required for flocculation.
4. Fill GDT until discharge pressure is obtained.
5. Maintain discharge pressure for 60 secs, then stop pumping.
6. Allow GDT to drain for 20 mins. Collect filtrate sample underneath drainage tray while draining.
7. Record gallons of slurry pumped and volume of filtrate collected.

Second Phase Fill

1. Fill GDT until discharge pressure is obtained.
2. Maintain discharge pressure for 60 secs, then stop pumping.
3. Allow GDT to drain for 20 mins. Collect filtrate sample underneath drainage tray while draining.
4. Record gallons of slurry pumped and volume of filtrate collected.

Third Phase Fill

1. Fill GDT until discharge pressure is obtained.
2. Maintain discharge pressure for 60 secs, then stop pumping.
3. Allow GDT to drain for 20 mins. Collect filtrate sample underneath drainage tray while draining.
4. Record gallons of slurry pumped and volume of filtrate collected.
5. Weigh GDT to determine final weight.
6. Clean off test equipment prior to next sample.

For each GDT test, a sample of unconditioned slurry, first phase filtrate, second phase filtrate, and third phase filtrate must be collected. The dewatering performance of each textile construction will be evaluated on filtrate quality based on turbidity and total suspended solids (TSS). The turbidity is an indication of how clear and transparent the filtrate passing through the textile appears. The total suspended solids include all particles suspended in water and the greater the total suspended solids, the murkier the filtrate will appear. The percent dry solids of unconditioned slurry, turbidity, and TSS of filtrate for each phase will be measured. The percent dry weight solids must be calculated at 1-day, 3-day, and 7-day intervals.

In this study the filtrate samples, percent dry weight solids of unconditioned slurry, and percent dry weight solids of dewatered cake sample inside the GDT were measured according to U.S. EPA Methods 160.2 and 160.3. Turbidity was measured with a portable meter and TSS was measured with a HACH DR 2800.

4. WASTEWATER COMPOSITION

Two P-GDT tests were conducted to understand the dewatering performance of various textile constructions. The first test was conducted on-site at an active dewatering project and evaluated the dewatering performance of contaminated river sediments. A tote was filled with 250 gallons of unconditioned slurry and diluted to approximately 3% solids. A two-part chemistry was used for chemical conditioning. The P-GDT testing was performed with a discharge pressure of 3.5 psi. This testing was conducted outdoors at the project site.

The second test was conducted in a laboratory and evaluated the dewatering performance of water treatment sludge (alum). A tote was filled with 250 gallons of unconditioned water treatment sludge and continuously mixed. A cationic polymer was used for chemical conditioning. For the second test, the discharge pressure was reduced to 3.0 psi

5. CONCLUSIONS

The dewatering performance of fabrics is determined by of the rate of dewatering, filtration under stress, and filtrate quality. The rate of dewatering is the fabric's ability to allow flow through the fabric and this flow rate is most critical when the fabric is stressed. As the fabric is stressed, the pores of the fabric are closed off and pressure will build up inside of a geotextile container. As the pressure increases inside the tube and flow is restricted, the potential for rupture

is magnified. The dewatering performance was based on the clarity and quality of the filtrate exiting the textile structure. Tables 3 is an illustration of the filtrate quality of the P-GDT testing of sediments. Table 4 is an illustration of the filtrate quality of the P-GDT testing of alum sludge. In both tables, the data shows better performance in filtrate quality with monofilament and fibrillated tape constructions. The high clarity of the filtrate was visible versus the other weave constructions.

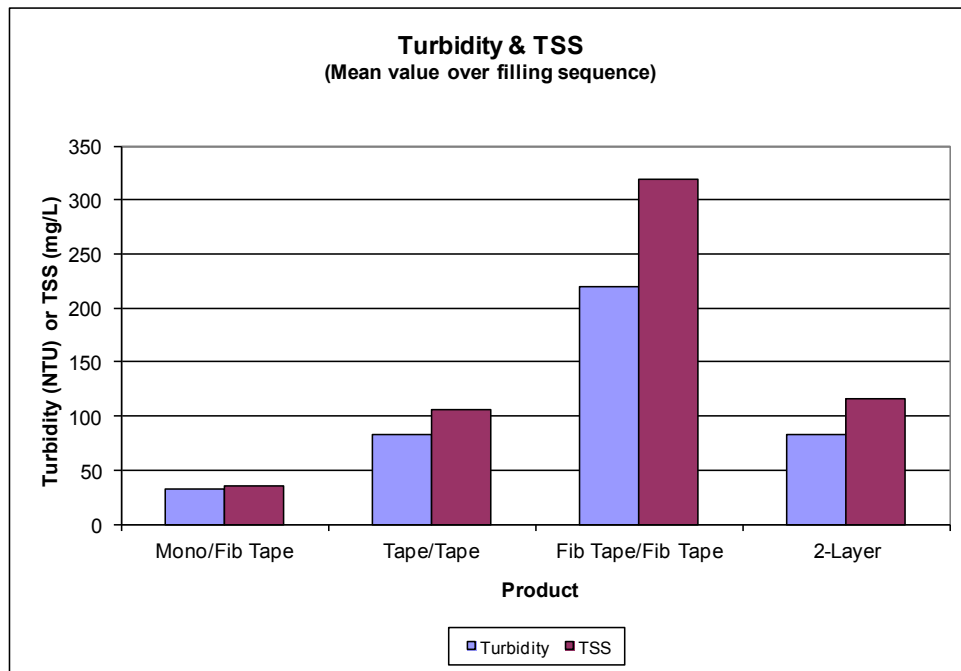


Table 3. P-GDT Results of Sediments

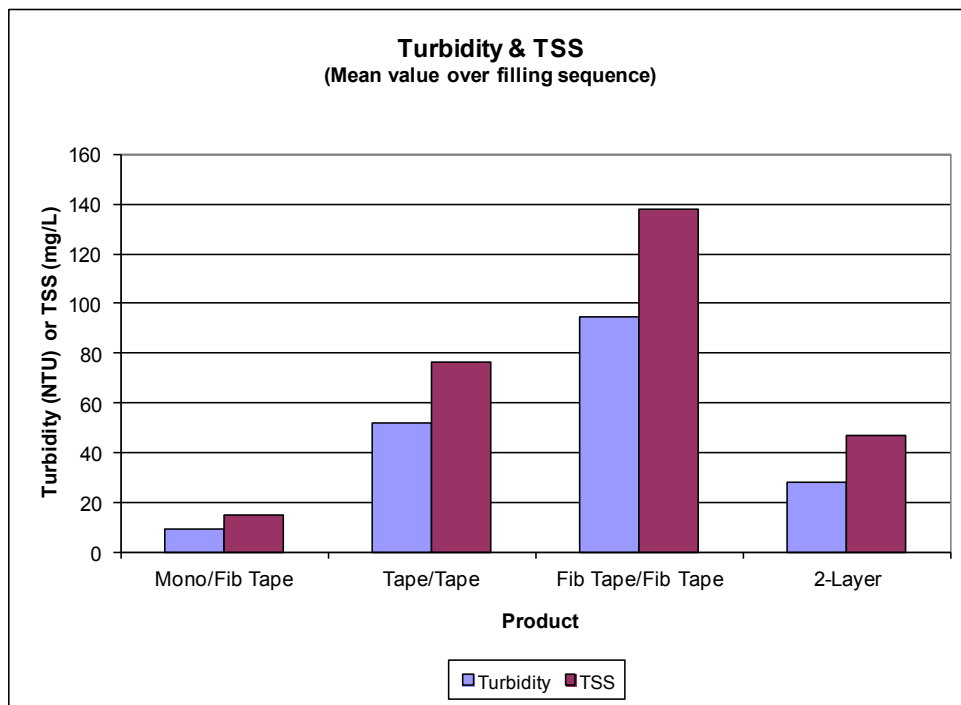


Table 4. P-GDT Results of Alum

Weave constructions using only tape yarns have a lower rate of dewatering which leads to a shorter time to blind off since the weave construction closes up under stress. Weaves which are only composed of fibrillated yarns allow for a high rate of dewatering but produce poor filtrate quality given that the more open structure allows for too many solid particles to flow through the fabric.

A double layer construction acts a good filter media but restricts the rate of dewatering. Although this construction has a lower rate of dewatering, it has a high rate of filtration under stress unlike the tape/tape and fibrillated yarn constructions. As the construction closes up while under stress, the double layer construction allows for depth filtration and yields a high retention of solid particles.

In these experiments, the monofilament and fibrillated tape construction produced the optimum dewatering performance. The monofilament warp yarn and fibrillated tape fill yarn create a structure which maintains a consistent rate of dewatering when the fabric is stressed and has a high retention of solid particles.

The three-phase filling cycle of the P-GDT demonstrates there are two distinct dewatering stages. The initial fill has the highest percentage of solid particles passing through the fabric which indicates initial filtration is based on the fabric construction. After a short time, a filter cake builds up and both the fabric and filter cake determine the dewatering performance. In the later filling stages, the filter cake is mostly responsible for dewatering and the rate of dewatering is greatly affected by the tendency of the fabric to blind off.

The turbidity and TSS data demonstrate this phenomenon as the filtrate quality consistently improves with subsequent filling stages with all weave constructions tested. This experiment shows that the monofilament and fibrillated tape construction produces a better quality filtrate versus other variations of the broken twill constructions. The ability of the textile construction to allow filtrate to flow yet retain solid particles will produce the optimum construction for dewatering.

Influence of the Protection Used for Installation Damage in Long Term Durability of Soil Reinforcement Elements

R. Lozano. Senior Geotechnical Engineer – Corporate Geosynthetics Specialist. The Reinforced Earth Company. USA

J. Sankey. Vice President of Engineering. The Reinforced Earth Company. USA

L. Naït-Ali. Materials Engineer Terre Armée Internationale. France

ABSTRACT:

Currently in Mechanically Stabilized Earth (MSE) technologies, there are two main families of reinforcing elements; metallic and polymeric. Depending on the material, the protection of such elements against the potential for damage during installation is critical to the long term performance of the structure. Reduction of available strength during the process of installation is well known to be one of the factors that affect soil reinforcement elements. Depending on the type of reinforcement selected, this factor could account for a large reduction of the available strength for MSE design. Inadequate means for protection against installation damage will have synergistic effects on the durability and long term performance of the reinforcement; these effects being hard to predict but in some cases could potentially accelerate degradation rates causing early failures. This paper explores 40 years of evidence for in service performance of reinforcement materials used in MSE structures and provides a corresponding guide for designers for the correct material selection and specification of reinforcing elements material selection and specification of reinforcement elements.

1. INTRODUCTION

The proper selection of a specific type of reinforcing element by owners and/or design engineers to is critical to the performance and stability of Mechanically Stabilized Earth (MSE) structures during the assigned design life. The current state of the practice for MSE structures is limited to two types of reinforcing materials; metallic and polymeric. Each of these reinforcing materials possess unique performance and behaviors in both short and long term. Indeed metallic and polymeric reinforcement are typically separated in terms of inextensible and extensible design methodologies (AASHTO LRFD 2010)

Common to both types of reinforcement are some level of protection, either active or passive, to mitigate and/or reduce the initial damage and stress caused by installation. The effectiveness of the protection is highly dependable on the type of material selected and the effective interaction of these barriers with the reinforcing element substrate.

Installation damage only affects the strength of the material immediate to the installation and will act synergistically to reduce or facilitate other ageing factors to further reduce the strength of the material during the service of the reinforcement. While installation damage does not depend directly on the material used as reinforcing element, the resistance to withstand and survive the installation depends directly on the protection provided to the reinforcement and the installation practices observed.

2. MECHANICS OF INSTALLATION DAMAGE.

MSE structures consist of reinforcement elements placed in intimate contact with compacted soil; in all cases the reinforcement will be subjected to the process of installation and construction induced stresses until the structure reaches completion. The basic construction consists of placing the reinforcement in to position followed by installing fill in compacted, discrete layers. The fill is normally spread by mechanized equipment, which requires vehicular traffic to pass over the working area underlain by reinforcement in areas of active installation. The construction process may physically damage the reinforcement by way of the physical characteristics of the fill, the construction practices employed and/or equipment used. These processes are used to form the basis to quantify the damage inflicted on the reinforcement.

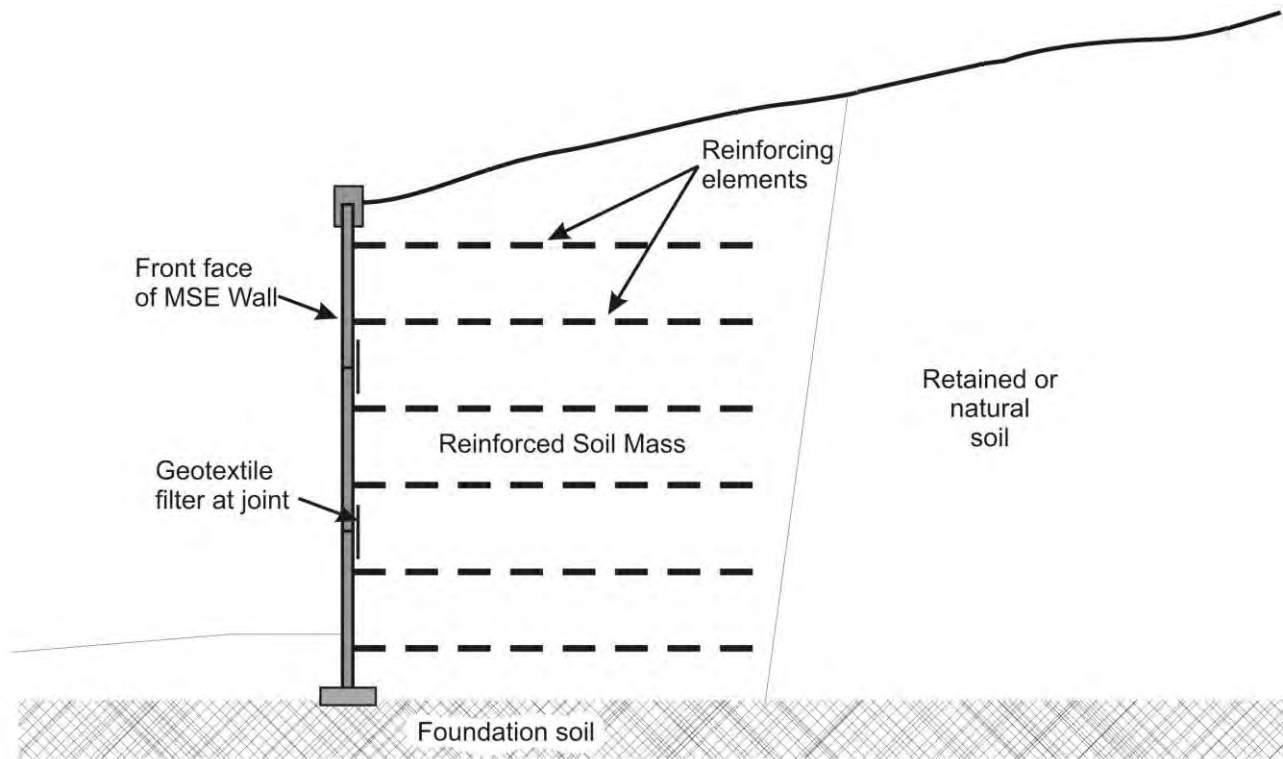


Figure 1 Reinforcing elements on a MSE structure

Aggressive means of install backfill directly related to the type of materials used in the MSE structure. The fill itself will be controlled by the physical properties of gradation, coefficient of uniformity, origin of the material and relative hardness, which serve as potential sources of damage inflicted upon the reinforcement members. It is well accepted that crushed, angular hard gravel from blasting quarries is more aggressive than rounded natural sand or silty sand materials, since coarse and hard aggregates rapidly transmit the mechanical efforts of compaction directly to the reinforcement causing damage.

The installation processes effectively reduce the strength of polymeric reinforcement by abrasion when the spreading of the backfill is moved against the reinforcement. Abrasion is highly dependent on the type of backfill, construction practices used to spread the aggregate and type of reinforcement were elements with wide exposed area and stiffer in nature are prone to higher damage.

Dynamic impact damage is caused by the compaction process when backfill particles are push against the reinforcement members; which are in turn placed over firm compacted substrates that score, cut or mar the available cross section and reduces the carrying loads in the reinforcement. Dynamic impact is more pronounced in coarse materials such as gravel and crushed aggregates, and attacks all the reinforcements (metallic and polymeric) in similar fashion.

Bending of the reinforcement is caused by unevenness of the substrate or incorrect compaction under the substrate receiving the reinforcing element, and if pronounced, can produce additional localized damage when the reinforcement moves and deforms to accept a forced contour. This type of damage is characteristic of soft soils, poorly compacted backfills but is more evident in connection points with blocks and other types of fascia.

The equipment selection ultimately provides the source of energy to produce the damage. While sheepsfoot rollers are considered one of the most damaging and aggressive type of equipment it is typically used in construction practice with finer grain silty sands which causes less damage potential (the use of sheepsfoot rollers are unusual in metallic MSE construction but less uncommon in polymeric MSE) practices .and soils that are low in injurious effects. Heavy smooth vibratory rolls are the most common equipment used with coarse materials; the transferred of energy from the equipment through the soil is almost direct and has a potentially harmful effect on the reinforcement unless construction practices are correctly selected to reduce damage. Hand held light weight equipment in almost all cases does not have deleterious effects on any type of reinforcement due to the low impact/energy applied.

2.1 Polymeric Reinforcements and Installation Damage.

All polymeric reinforcements are susceptible to lose a percentage of the ultimate tensile strength by the construction stresses imposed on the material. Installation damage as a reduction factor is the only immediate term that affects the nominal long term reinforcement design strength, since damages caused by installation reduce the effective available strength of the material when the material is installed.

$$T_{al} = \frac{T_{ult}}{RF_{ID} * RF_{CR} * RF_D} \quad [1]$$

Where

T_{al} = Nominal Long Term Reinforcement Design Strength
 T_{ult} = Minimum Average Roll Value of Ultimate Tensile Strength
 RF_{ID} = Reduction Factor for Installation Damage
 RF_{CR} = Reduction Factor for Creep
 RF_D = Reduction Factor for Durability

Equation 1 Nominal Long Term Reinforcement Design Strength equation (AASHTO LFRD 2010)

The assessment of this reduction was considered critical since early developments in polymeric reinforcement. A controlled trial for evaluation was proposed by Watts and Brady (1990) as methodology for assessing the installation damage to reinforcement under field conditions. This method was rapidly accepted as the best practice to obtain the reduction factor for installation damage to be used in design of MSE structures with polymeric reinforcement. Currently this method of exposing polymeric reinforcement is complemented with the ASTM D5818, "Standard Practice for Exposure and Retrieval of Samples to Evaluate Installation Damage of Geosynthetics" and the guidelines presented in FHWA-NHI-10-024/025, FHWA-NHI-090-87 and the protocols used in the National Transportation Product Evaluation Program (NTPEP) for polymeric reinforcement evaluation. The installation damage reduction RF_{ID} factor then is determined as the ratio of the initial Ultimate Tensile Strength (T_{ult}) of the reinforcement, to the Retained Tensile Strength ($T_{Exposed}$) after damage:

$$RF_{ID} = \frac{T_{ult}}{T_{Exposed}} \quad [2]$$

Equation 2 Ratio for obtaining the Reduction factor for installation damage

In AASHTO LFRD 2010, 11.10.6.4.2b-1 established the minimum criteria for acceptance of polymeric reinforcement for use in assigned default reduction factor for installation damage is required to have a mass per unit area of 270 grams per square meter. However, Section 11.10.6.4.3b also assigns a minimum value of this reduction factor as 1.10, even with site specific test available. The use of both of these values is highly conservative and does not reflect the current state of manufacturing geosynthetics using highly durable materials with high survivability against installation damage. It is noted in NTPEP reports that several manufacturers have products evaluation results reporting installation damage factors well below 1.10.

The ISO Installation damage approach is radically different. The objective of the test is to use a bench scale test focused on quality control to provide an index of the production. ISO 10722 has proven difficult to perform due to the lack of availability of the designated aggregate and low test reliability due to the of the high cyclic load use. This test is so aggressive that results obtained using ISO 10722 have reported losses over 90% of the ultimate tensile strength while the same material using full size installation damage trials with aggressive compaction, angular coarse aggregate have reported losses of 30 to 40 percent.

2.1.1 Extrusion Coated Polymeric Bars and Strips

The technology of extrusion coating of filaments and yarns with an extruded sheath was developed in the UK during the late 1960s. The process pulls yarns made from filaments through an extrusion die while a polymer with a lower melting point is extruded completely encapsulating the yarn. This process provides an integral barrier that, depending on the rate of extrusion of the selected polymer for the sheath and the resulting thickness, provides variable resistance to installation damage. This material was initially used as a reinforcement element in mid 70s showing exceptional survivability to installation at that time due to the particularly thick sheathing. Currently manufactured polymeric strips benefit from the use of compatible polymers and the latest technology on extrusion and resin developments, with reported values in

NTPEP and other publications showing the polymeric strips rarely exceed reduction factors higher than 1.10, even in conditions where coarse, angular and aggressive compaction is used.

2.1.2 Punch Drawn Grids

As reported by NTPEP, punch drawn geogrids in mid to mildly aggressive soils such as sandy gravel and sandy silt the installation damage values of this type of grids ranges from 1.12 to 1.02. While these value have been well documented in other sources and published papers, installation damage factors in coarser more aggressive fills were reported as high as 1.25 (Certificate No. RF 2/07 CEED Hong Kong 2007) for coarse gravels in aggressive conditions.

While loosely related to punch drawn grids, geogrids manufactured from extruded profiles that are then welded have being proved as excellent survivors for installation damage. As reported in some independent sources the reduction factors to this grids ranging from 1.15 to as low as 1.05.

2.1.3 Woven or Knitted Coated Grids

Most of the textile grids reviewed in this paper were polyester either woven PVC coated or knitted grids with PVC or acrylic polymeric coating. Early textile grids had low survivability on installation damage. Historically reported during the late 80's and later starting in the 90s by the Geosynthetics specifier's guide (formerly known as Geosynthetics Fabrics Report GFR) early PVC coated grids manufactured were prone to suffer higher damage than their modern versions. Reduction factors have consistently dropped from the upper 1.50 to mid 1.20 ranges on average. Current advancements in weaving and coating technology allows manufacturers to greatly improved the survivability of textile grids with reduction factors in the range between 1.30 to 1.05, depending on specifics such as strength of the grid and type of soil used during the installation damage trials. In the case of geogrids, the coating is an essential element for the stability of the material during handling. A great deal has being learned in the last years with regards to the effectiveness of PVC coatings being linked directly to viscosity, percentage of solids and dueling time for drying. Viscosity of the coating in liquid form is critical since it has a direct impact on the penetration of the fibers in the yarn bundles and interstitial spaces, effectively linking all the structure protecting the filaments from probable damaged caused by fine abrasive particulate and direct abrasion and impact during compaction. One of the largest consequences of the use of PVC in textile grids is the direct impact on the mass per unit area of the finished product versus the greige textile, the increase of mass per unit area ranges from 1/3 to 1/2 of the total mass per unit area of the finish geogrid, this also provide an indication how much the coating influence the survivability of the finished grid during installation damage.

The latest innovation in protection against installation damage of grids is the use of new polymeric coating that show great improvement in the protection of the yarns, some relative new materials use acrylic heat set polymers with high penetration and high abrasion resistance. The introduction of this new coating during the mid 2000s showed a great reduction of installation damage particularly in grids with less than 270 grams per square meter, where the coating accounted for less than 1/3 of the total weight.

2.1.4 Woven and Knitted Geotextiles

Geotextiles either from polyester or polypropylene have proven to be susceptible to damage during installation and only rely on mass of yarns to protect the fabrics. Other than modifying some of the traditionally patterns used for weaving the yarns non coated textiles, reduction factors are currently in the range of 1.5 and higher, with some examples of light weight woven polypropylene and some of the weft insertion polyester fabrics reporting factors in excess of 1.8.

2.2 Metallic Reinforcements and Installation Damage.

Metallic (typically carbon steel) reinforcements do not typically have deleterious effects due to installation damage. Metallic strips, bars and grids have a higher relative strength and hardness than the backfill used, hence the possibility of damage immediately reducing the strength of the members is relatively nonexistent. However while the effect of installation damage on metallic reinforcement is not directly related to losses of strength in the member, the effects of installation may still influence the durability depending on what is used to protect the metallic reinforcement against long term metal losses. The main objective of galvanic protection of metallic reinforcement is to increase the durability of the element by modifying the metal losses rates but this is ultimately dictated by the electrochemical environment present in the surrounding soils.

Hot dip galvanization is the common practice used as protection of metallic elements and has proved effective in extending the duration of the life of steel in soil reinforcement applications. It is important to note that the term galvanization term is sometimes incorrectly used to describe steel layered with zinc-rich paint, electro plated or mechanically applied zinc since all of these methods of applying zinc to steel for corrosion protection are different from

hot dip galvanizing and are inappropriate for reinforcement soil applications. Hot dip galvanization changes the external layers of the steel making an alloy with different electrolytic behavior of the base steel or the zinc alone.

The galvanic metallurgical process is more than a simple barrier to prevent metal losses; the barrier created by this process provides a layer integrally bonded to the surface of the steel element that is fully impermeable and uniform with variable hardness depending on the exact position on the thickness of the galvanic layer. The first 3 layers (Gamma, Delta and Zeta) are harder than steel providing excellent resistance to abrasion and hardness against impact. The last Eta layer is ductile providing one more layer of impact resistance by some dissipation of the impact.

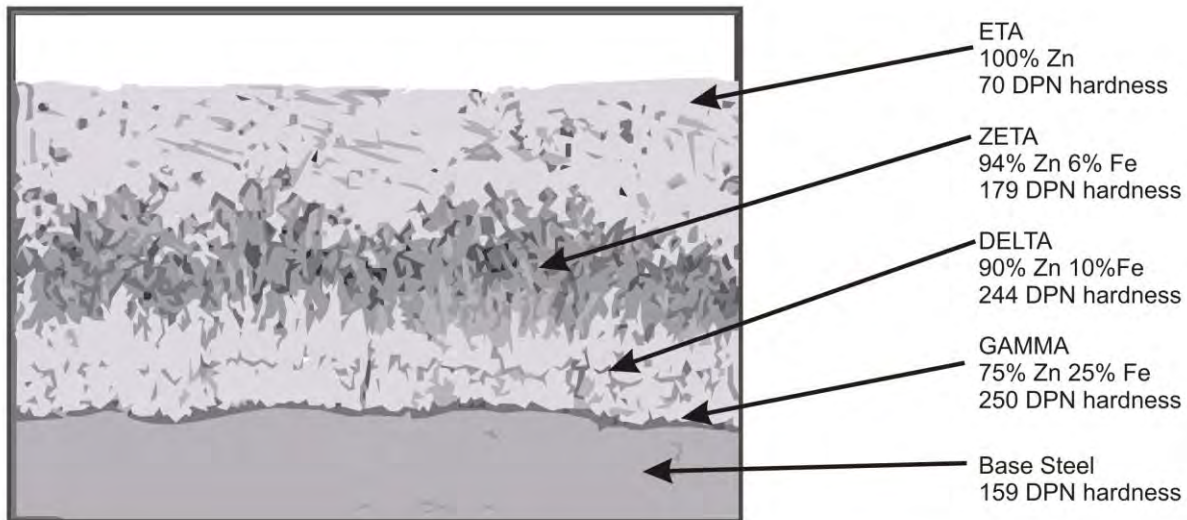


Figure 2 Representation of the alloy layers in hot dip galvanized carbon steel

Additionally, the intrinsic electrolytic behavior that zinc provides is extra protection in case of damage to the alloy protection. The dielectric exchanging electric current between the zinc rich outside layer to the bare steel will make zinc migrate to areas with less rich zinc, effectively protecting any exposed area. This self-healing ion exchange process takes place in the reinforcing member as long as the zinc is present.

Another alloy available for protection of metallic reinforcement elements is Galfan[®] (registered trade name by the International Lead Zinc Research Organization) Galfan is an alloy consisting of 95% zinc and 5% aluminum, ductile in nature and applied to steel using a hot dip bath. Galfan was originally engineered as protective coating against corrosion on cars and industrial equipment but its use has migrated as alternative for protection of soil reinforcement metallic elements. Any advantages of using the proprietary alloy versus pure zinc have not been demonstrated, particularly because the conditions of metallic reinforcement elements in prolonged soil burial are completely different than what Galfan was initially intended.

Other attempts of using paint, epoxy coatings or sheathing have been documented in the literature. While paint and fusion epoxy coatings are intended as barrier for corrosion, those offer no significant resistance against installation damage, negating any benefit gained as barriers. Polyolefin sheathing and PVC focus is commonly used as justification for thinner or no galvanic protection in wires with claims that this treatment will increase the durability and life span of the materials when used as soil reinforcement elements, these claims still are unsubstantiated with testing.

According to Berg et al (2009) in order for polymeric coating and sheathing to be effective, the coatings must be impermeable to gasses, moisture and free of microscopically thin gaps, but it is also critical to have a compatible hard bond to the base metal. Since current techniques in polymeric treatments use a softer-than-metal treatment, and there is no affinity with the metallic base intended to be protected, the sheathing has a higher probability to be breached by impact or abrasion. The lack of intimate contact between the sheathing and the metallic substrate also leaves a microscopic gap that will allow capillary flow of water creating an ideal environment to promote corrosion. In both cases the mechanism relative to the resistance of metallic reinforcement against installation damage changes. The potentially deleterious effect of the coating should be taken into consideration by site specific, long term testing under the same conditions of installation. Unless the use of metallic elements protected with co-extruded polymers is limited to non-aggressive installation practices with non-aggressive soils, the sheathing will have a high probability of being breached and negate any benefit of increasing durability on the reinforcing elements.

New developments in fusion epoxy bond coatings may have a promising future, particularly when combined with galvanization. Since new epoxy bond coatings are applied in controlled environments, outstanding adhesion to the metal substrate is achieved, compounding the survivability of the reinforcing elements against installation damage opening the possibility to achieve higher durability for the associated MSE structure. The composite use of hot dip galvanization with new fusion epoxy bonding is promising but long term testing is still unavailable.

3. SELECTION GUIDE OF REINFORCEMENT BY INSTALLATION DAMAGE RESISTANCE

While the selection of the specific type of reinforcement not only depends on the condition of installation but on the overall structure use, type of materials available, performance needed and design life; the intention of this paper is to present a general guide for designers of how have an informed decision on the effects of installation damage on the selected reinforcement. Table 1 provides a general guide for criteria on the selection of reinforcement members based on their performance in installation damage.

Table 1. Characteristics of reinforcement elements currently in use.

Type of reinforcement	Protection used	Effect	Recommendation
Metallic bars and wires	Galvanization ⁽¹⁾	No effect	Use with all soil gradations and compaction equipment
	Galfan	Unknown	Use with site specific testing. May affect durability. Test needs to be provided.
	Paint	No recommended	Not able to survive installation. Does not provide any survivability protection to base material. Deleterious effect on durability of the reinforcement
	Epoxy coating and polymeric sheathing	Deleterious	Only recommended with non-aggressive backfills and non-aggressive compaction equipment.
Polymeric bars and strips	Co-extrusion	Minimal	Use with all soil gradations and compaction equipment. Apply correct reduction factors depending on site conditions and gradation specific installation damage trials.
Punch drawn grids	Integral	Minimal to moderate	Use with all soil gradations and compaction equipment. Apply correct reduction factors depending on site conditions and gradation specific installation damage trials. Coarse gradation may be problematic
Woven textile coated grids	PVC or heat set acrylic	Minimal to moderate	Use with all soil gradations and compaction equipment. Apply correct reduction factors depending on site conditions and gradation specific installation damage trials. Coarse gradation may be too aggressive
Woven and knitted geotextiles	None	Moderate to Aggressive	Use with non-aggressive soil gradations and compaction equipment. Apply correct reduction factors depending on site conditions and gradation specific installation damage trials. Coarse gradation may be too aggressive to withstand installation

NOTES:

(1) Hot dip galvanization is not provided as protection for installation damage but for protection against metal losses

4. CONCLUSIONS

Polymeric reinforcement is susceptible to damage during installation. Correct assessment and application of the reduction factor for installation damage based on actual full scale tests and applied in the design is critical for the performance of the structure.

During the last 20 years the evolution of polymeric reinforcement manufacturing have reduce the sensitivity of the reinforcement to be damaged during installation, however current US codes of practices still uses conservative default values not updated to reflect this changes.

Installation damage depends greatly on the type of reinforcing element selected. While metallic reinforcements are generally immune to installation damage some process such painting and polymeric coatings are deleterious to the long term performance.

There is direct correlation between the compatibility of materials used for protection of metallic reinforcement and the substrate, incorrect selection of the protection on metallic reinforcement instead of increasing the long term durability of the metallic member by accelerating the rates of degradation.

Regardless of the type of reinforcement used in MSE structures, the use of reputable manufacturers with serious commitment to quality assurance, supporting reports from actual testing of materials intended to be provided are necessity for owners and designers.

REFERENCES

- Berg R.R. Christopher B.R. & Samtani N.C. (2009) Design and Construction of Mechanically Stabilized Earth Walls and Reinforced Soil Slopes – Volume I and II, FHWA-NHI-10-024/025 Washington DC, USA: Federal Highway Administration.
- Brady, K.C. (1987). Performance of reinforced earth bridge abutment at Carmarthen. Transport and Road Research Laboratory Report 111 United Kingdom.
- CEED Certificate No RF 2/07 Reinforced fill product certificate Government of Hong Kong special administrative region China.
- Elias, V. & Christopher, B. R. 1997. Mechanically stabilized earth walls and reinforced soil slopes design and construction guidelines. Report FHWA-SA-96-071. Washington DC, USA: Federal Highway Administration.
- Elias, V. 1997. Corrosion/degradation of soil reinforcements for mechanically stabilized earth walls and reinforced soil slopes. Report FHWA-SA-96-072. Washington DC, USA: Federal Highway Administration.
- Geoguide 6 (2002). Guide to reinforced fill structure and slope design. Geotechnical Engineering Office, Hong Kong.
- Greenwood J.H., Brady K.C. & Watts G.R.A., (2002) The Last Word on Reduction Factors for Soil Reinforcement? Geosynthetics: State of the Art - Recent Developments. Seventh International Conference on Geosynthetics, Nice, France. Volume 4
- Naughton, P.J., Balderson, T & Lozano, R. (2005). The properties of polyethylene encased high density linear elements. Geosynthetics and Geosynthetic-engineered soil structures: Contributions from the symposium honoring Professor Robert Koerner. Ed. Ling, H.I., Kaliakin, V.N. and Leshchinsky, D., pp 19-38.
- NTPEP Report 8502.1 - Laboratory Evaluation of Geosynthetic Reinforcement - Final Report for ACE Geosynthetics Reinforcement Products - 2005 Product Submissions. American Association of State Highway and Transportation Officials. Washington, DC USA
- NTPEP Report 8505.3 - Laboratory Evaluation of Geosynthetic Reinforcement - Final Product Quality Report for Miragrid XT Geogrid Product Line - 2005 Product Submissions. American Association of State Highway and Transportation Officials. Washington, DC USA
- NTPEP Report 8507.1 - Laboratory Evaluation of Geosynthetic Reinforcement - Final Product Qualification Report for Synteen SF Geogrid Product Line - 2007 Product Submissions (Revised 1/10). American Association of State Highway and Transportation Officials. Washington, DC USA
- NTPEP Report 8507.2 - Laboratory Evaluation of Geosynthetic Reinforcement - Final Product Qualification Report for Luckenhaus Raugrid Geogrid Product Line - 2007 Product Submissions. American Association of State Highway and Transportation Officials. Washington, DC USA
- NTPEP Report 8507.3 - Laboratory Evaluation of Geosynthetic Reinforcement - Final Product Qualification Report for Maccaferri Macgrid Product Line - 2007 Product Submissions. American Association of State Highway and Transportation Officials. Washington, DC USA
- NTPEP Report 8507.4 - Laboratory Evaluation of Geosynthetic Reinforcement - Final Product Qualification Report for Tensar UX-MSE/UX-HS Geogrid Product Line - 2007 Product Submissions. American Association of State Highway and Transportation Officials. Washington, DC USA

NTPEP Report 8508.1 - Laboratory Evaluation of Geosynthetic Reinforcement - Final Product Qualification Report for Linear Composites ParaWeb/ParaLink and ParaGrid Product Lines - 2008 product Submissions. American Association of State Highway and Transportation Officials. Washington, DC USA

NTPEP Report 8509.1 - Laboratory Evaluation of Geosynthetic Reinforcement - Final Product Qualification Report for Strata SG Geogrid Product Line - 2009 Product Submissions. American Association of State Highway and Transportation Officials. Washington, DC USA

Watts, G.R.A. & Brady, K.C. (1994). Geosynthetics: Installation damage and the measurement of tensile strength. Proc. 5th Int. Conf. on Geotextiles, Geomembranes and related Products, Singapore Sept 1994. Vol 3, pp1159-1164.

Watts, G.R.A. (2000). The durability of geosynthetics for retaining walls and slopes for long term performance. Proceedings of the International Symposium on Earth Reinforcement, Vol. 2, pp 895-918, Kyushu, Japan

Watts, G. R. A. & Brady, K. C. 1990. Site damage trials on geotextiles. 4th International Conference on Geotextiles, Geomembranes and Related Products, The Hague. Rotterdam: Balkema. 603-607.

D5818-06 Standard Practice for Exposure and Retrieval of Samples to Evaluate Installation Damage of Geosynthetics. American Society for Testing and Materials, West Conshohocken, Pennsylvania, USA

ISO 10722:2007 Index test procedure for the evaluation of mechanical damage under repeated loading. International Organization for Standardization

In Situ Deformation Measurements for Geomembranes in Landfill Liners

James L. Hanson, Ph.D., P.E., California Polytechnic State University, San Luis Obispo, CA, USA,
jahanson@calpoly.edu

Michael T. Onnen, California Polytechnic State University, San Luis Obispo, CA, USA,
onnen.michael@gmail.com

Nazli Yesiller, Ph.D., Global Waste Research Institute, San Luis Obispo, CA, USA, nyesille@calpoly.edu

ABSTRACT

A field investigation was undertaken to determine deformations and associated strains in bottom liners in municipal solid waste landfills. Data were obtained at landfills in New Mexico and Alaska. Geomembranes were instrumented with linear sensor arrays extending from the perimeter to the center of a cell with multiple monitoring points. Displacement measurements were taken using linear potentiometers installed at the perimeter of the cell. Temperatures were monitored along the strain measurement setups both below and above the liner systems. Data have been collected for 7 and 4 years for Alaska and New Mexico, respectively. Maximum tensile strains (approximately 2.6% and 0.4 for Alaska and New Mexico, respectively) were measured near the toe of the slopes at both sites. Compressive strains up to 1.3% were present along the slope and on the floor of the cells. Liner displacements reached stable levels relatively soon after overlying waste placement.

1. INTRODUCTION

Geomembranes are used extensively in waste containment facilities for providing barrier function to isolate wastes from the surrounding environment. While geomembranes have been demonstrated to be effective in reducing leakage and emissions from landfills, concerns remain related to the long-term performance of these materials (NRC 2007).

Stress-strain characteristics of geomembranes have been established in the laboratory, however data commonly are not available for field investigations for mechanical performance. Measurement of localized strain in geomembranes is complicated due to difficulties of attaching sensors to the polymeric materials, as adhesives typically are not available for bonding sensors to geomembranes particularly for polyolefin materials. In the case of thermal bonding, the properties of the geomembranes are potentially altered by the heat applied to the material. Similarly, adhesive and mechanical attachments also can affect the properties of the membrane. In addition, access to sensors and ability to conduct measurements is complicated by normal landfill operations and by presence of overlying wastes.

Numerical analyses have been reported to predict stress/strain characteristics or displacements of geomembranes used in bottom liners of landfill systems. The numerical analyses indicated:

- In a veneer analysis of cover soils, a buttressing effect at the toe of the slope was quantified and the response of the geomembrane liner to heavy equipment loads was determined to be a function of the travel characteristics of the heavy equipment (e.g., upslope or downslope backfilling) (Koerner and Soong 1998).
- Load-displacement analysis demonstrated that maximum geomembrane tension increases as the slope angle increases (Kodikara 2000).
- Local stability of liner systems due to waste settlement (and associated downdrag on the liner system) was documented as a valid concern (Jones and Dixon 2005), even though such analyses are not often employed in engineering practice (NRC 2007).
- Finite element analysis of liner systems conducted by Reddy et al. (1996) indicated that: displacements of smooth geomembranes were significantly greater than textured geomembranes, displacements increased with increasing waste placement height, minimum displacements occurred near the toe of the slope (i.e., connection point between base liner and side liner), displacements increased with increasing slope angle, and waste filling strategies could be used to minimize liner displacements.
- A number of the investigations demonstrated that limit equilibrium approach was not sufficient for describing displacement/strain behavior of liner system response to loading conditions (e.g., Reddy 1996, Kodikara 2000).
- Waves and wrinkles were analyzed numerically for localized effects and tensile stresses resulting from wrinkling strains are limited to approximately 5 to 8% (Soong and Koerner 1999, Gudina and Brachman 2011).

This investigation was conducted to directly determine field response of geomembranes in bottom liner systems. A novel measurement approach was developed to measure displacements and strains occurring in the geomembranes. Displacements were measured over a duration extending from initial waste placement onward for extended periods.

2. EXPERIMENTAL PROGRAM

2.1 Test Sites

The field investigation was conducted at two landfill sites, in Anchorage, Alaska and Las Cruces, New Mexico. The sites are Subtitle D municipal solid waste landfills. Basic statistics about the sites are presented in Table 1.

Table 1. Characteristics of Test Sites

Parameter	Alaska	New Mexico
Design volume (m ³)	32,360,000	11,754,000
Permitted area (m ²)	67 ha	79 ha
Waste intake rate (tonnes/year)	275,000	140,000
Slope ratio (Horizontal:Vertical)	3:1	5:1
Bottom liner components (from bottom to top)	Native subgrade (gravelly sand with clay), 150-300 mm compacted sand protection layer, GCL, 1.5-mm thick HDPE geomembrane (smooth on floor, textured on slopes), nonwoven geotextile, granular leachate collection and removal layer consisting of washed gravel, woven geotextile separator, 600-mm thick operations layer consisting of sandy gravel. On slopes, additional layers of nonwoven geotextile, geogrid, nonwoven geotextile reside between the GCL and geomembrane.	Native subgrade, 100-mm thick compacted caliche clay base, GCL (nonwoven geotextile, bentonite, woven geotextile), 1.5-mm thick HDPE geomembrane (smooth on floor, textured on slopes), 600 mm of sand.

2.2 Measurement System

Strain measurements were made using a custom fabricated system using displacement monitoring coupons attached to the HDPE geomembrane liners. The displacements were measured using linear potentiometers (i.e., stringpots), UniMeasure Model P420-50 (1250 mm range) that were connected to the coupons with extension wires. The linear potentiometers were placed at the crest of the slope, just outside the anchor trench. The displacement monitoring coupons were installed along a linear path extending over the length of the slope and out onto the floor of the landfill cell. Thermocouple arrays were installed along the same alignment to measure temperatures, both below and above the liner system. Details of the temperature array configurations were described in Hanson et al. (2010). The displacement monitoring coupons were placed at 10, 30, 50, 65, 75, and 100 m from the crest of the slope in Alaska (where the toe of the slope was 69.2 m from crest of slope) and at 5, 15, 25, 35, 45, and 55 m in New Mexico (where the toe of the slope was 38.9 m from the crest of the slope). Most coupons were placed on the slope and the two farthest coupons were placed on the floor of the landfill cells (Figure 1). Using this configuration, strains were calculated between consecutive coupons in the arrays. This method of measurement provides global geomembrane displacements and associated strains and therefore avoids the complications associated with localized measurements described above.

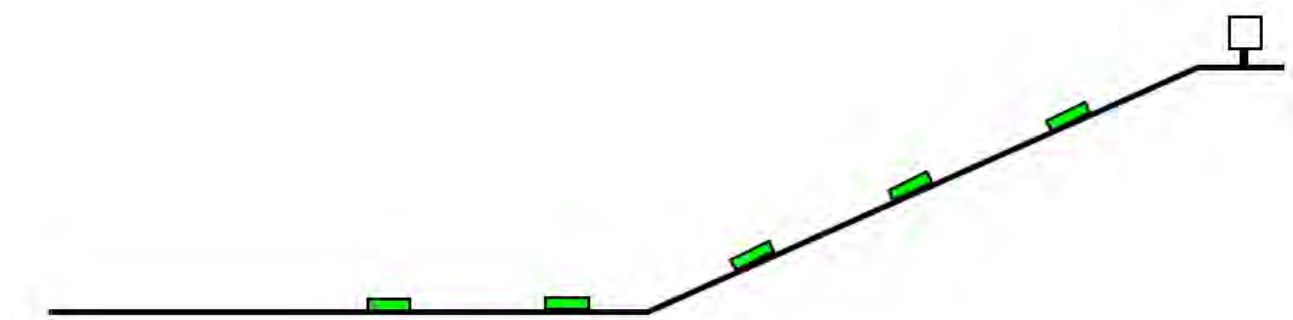


Figure 1. Schematic of displacement monitoring array.

A schematic of a displacement monitoring coupon is presented in Figure 2 and hardware details associated with anchorage mechanism is presented in Figure 3. Extension wires (stainless steel) were attached to the displacement monitoring coupon. The extension wire was placed inside a hard and smooth polyethylene tube that progressed up the slope from the monitoring coupon to a monitoring station, which was located at the perimeter of the cell (at the crest of the slope, directly outside the anchor trench). As the membrane slides up or down the slope due to loading of the heavy equipment or application of waste mass or alternatively due to thermal expansion/contraction, the wire responds to indicate the magnitude of the displacement of the coupon. Electrical current readings of the linear potentiometers were used to determine the distance traveled by the monitoring coupon. Corrections were applied to account for thermal expansion and contraction of the stainless steel extension wires. The coupons were installed in summer 2005 in Alaska and summer 2008 in New Mexico and have been monitored since. Some periods of limited measurements were present due to problems with the measuring equipment.

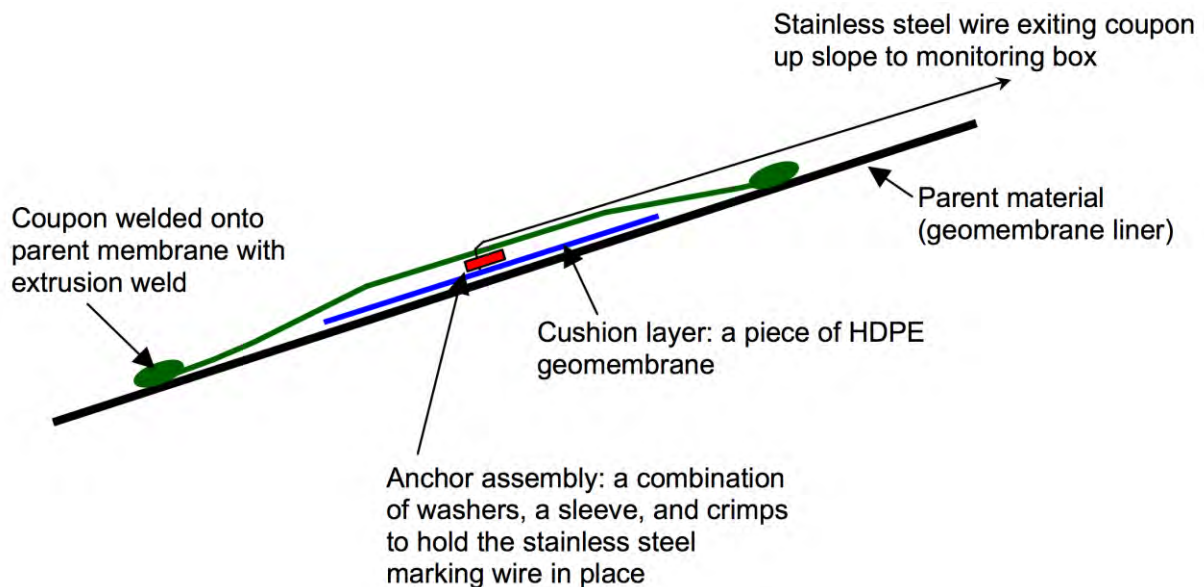


Figure 2. Monitoring sensor configuration.

- 1) HDPE Coupon (300 mm x 300 mm)
- 2) Cushion, HDPE (200 mm x 200 mm)
- 3) Stainless steel sleeve
- 4) Washers around sleeve to hold in place
- 5) Crimps on wire to hold in place
- 6) 0.34-mm-diameter braided stainless steel wire

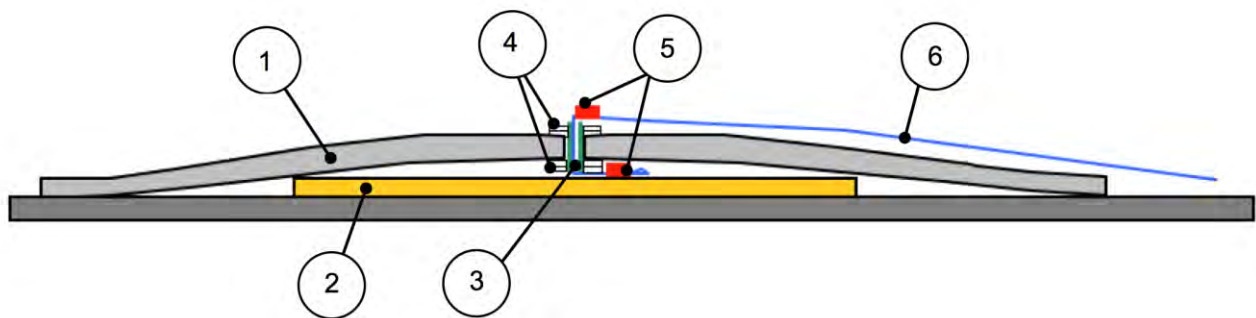


Figure 3. Cross section detail of anchor assembly (not to scale).



a) monitoring coupon



b) monitoring station at crest of slope

Figure 4. Photographs of test setup.

3. RESULTS AND DISCUSSION

Results of the investigation are presented as plots of displacement versus elapsed time (Figures 5 and 6). Downslope displacements (i.e., moving downhill or towards the center of the floor of the cell) are positive. Temperatures of the liner system near the perimeter of the cell and near the center of the cell (i.e., at the end of the measurement array) and waste height above the floor of the cell also are presented in Figures 5 and 6.

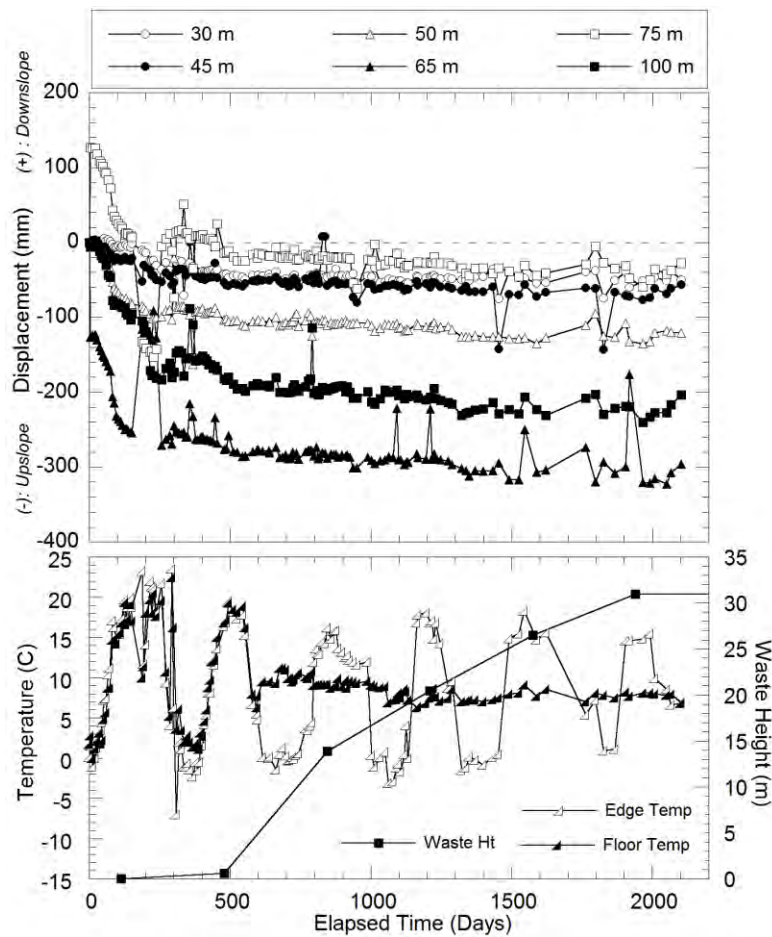
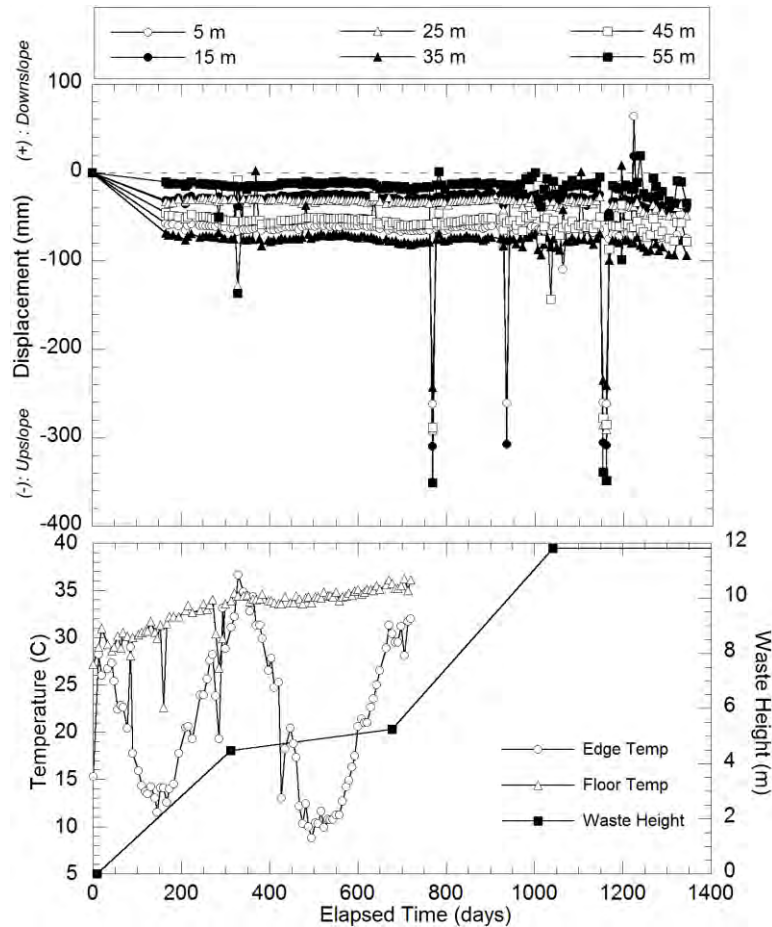


Figure 5. Geomembrane displacements at Alaska site.



(Only partial temperature results are presented due to sensor malfunction)

Figure 6. Geomembrane displacements at New Mexico site.

Strains were calculated for sections of geomembrane between the individual measurement coupons. The average stable strains are presented in Table 2. Variations of strains with time are presented in Figure 7 for both sites. Tensile strains are positive and compressive (i.e., wrinkling) strains are negative. Strains reached stable values after approximately 500 days in Alaska and after 200 days in New Mexico. The long-term strains in the geomembranes are presented graphically in Figure 8. Overall, the strains were greater at the Alaska site than at the New Mexico site. This was attributed to the steeper slope and greater waste height at the Alaska site. Overall, the measured displacements and strains were relatively low and do not represent levels of immediate concern for the two test sites. The long-term response of the liners (beyond approximately 1000 days at both sites) indicated onset of small and continued displacements, which may be resulting in wrinkling strains in the long term. Whereas the geomembranes are undergoing seasonal thermal fluctuations near the perimeters of the cells, a seasonal response of displacements or strains was not observed.

Table 2. Measured Long-Term Strains

Zone Number	Alaska Coupon Locations	Alaska Strain ¹	New Mexico Coupon Locations	New Mexico Strain ²
1	0-30 m	-0.16 %	0-5 m	-1.32%
2	30-45 m	-0.05%	5-15 m	+0.36%
3	45-50 m	-1.10%	15-25 m	-0.03%
4	50-65 m	-1.17%	25-35 m	-0.38%
5	65-75 m	+2.62%	35-45 m	+0.18%
6	75-100 m	-0.71%	45-55 m	+0.41%

¹tension is positive, calculated as average strain from day 500 to day 1500

²tension is positive, calculated as average strain from day 200 to day 1200

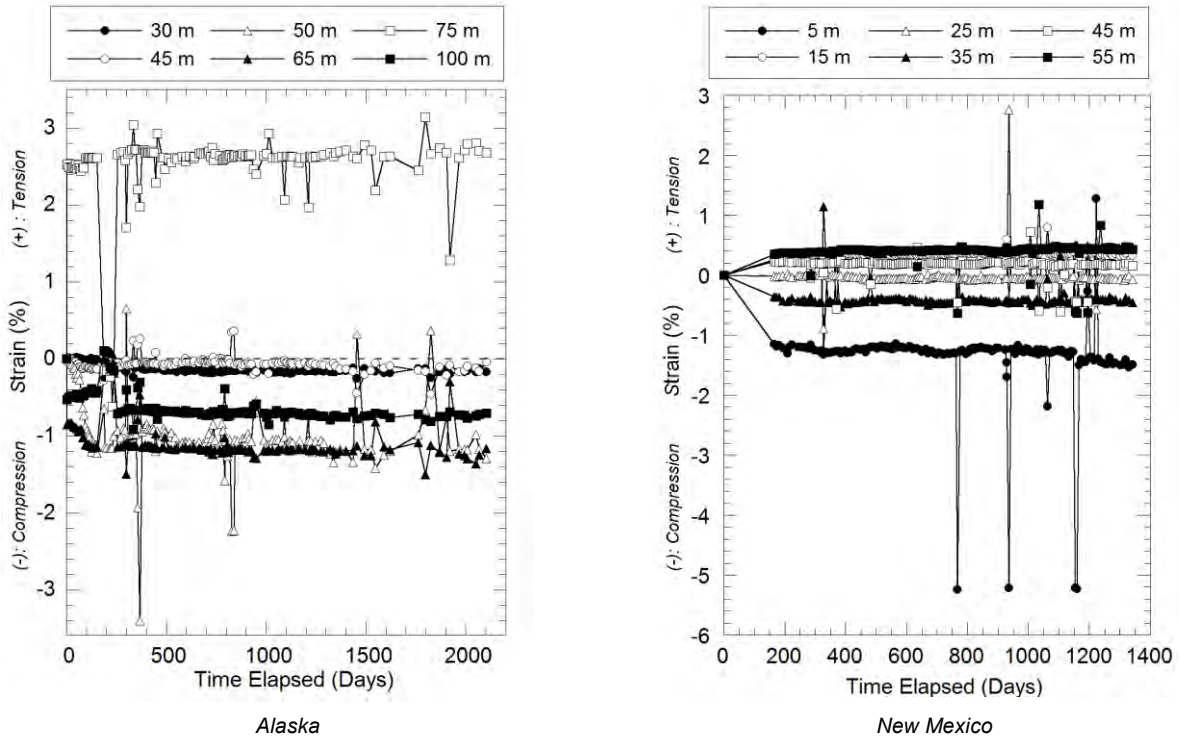


Figure 7. Geomembrane strains at the sites.

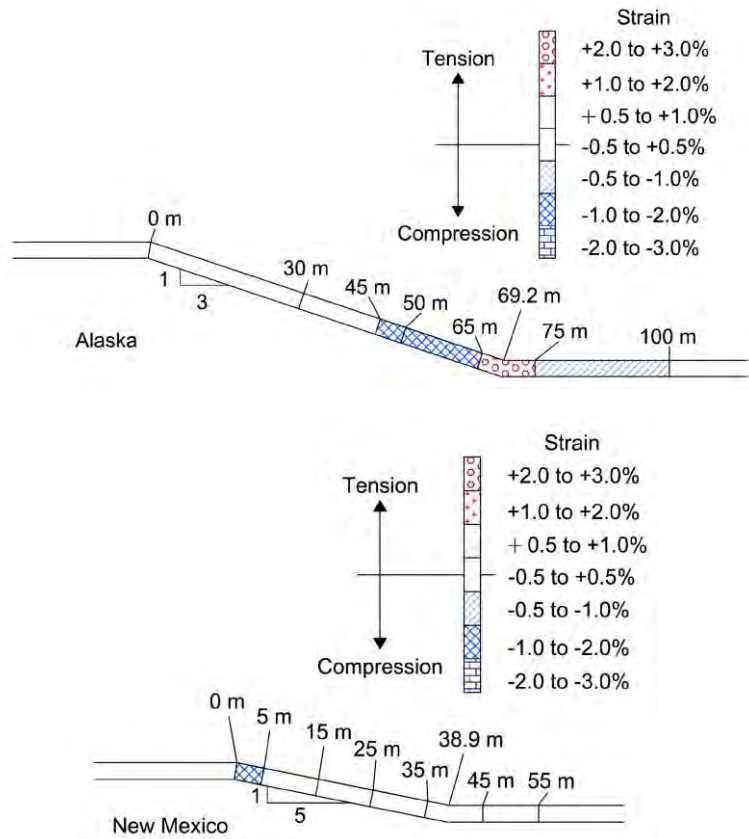


Figure 8. Graphical representation of measured strains.

The majority of the displacement monitoring coupons moved upslope. Upslope displacements were attributed to the following mechanisms: a) buttress effect of waste mass, b) thermal contraction of anchored geomembrane upon cooling relative to exposed conditions during installation of liner system and displacement monitoring coupons, c) translational movement, primarily in the machine direction, of the geomembrane in response to shrinkage strains of the underlying GCL (Hanson et al. 2012). The upslope movement of geomembranes with time and the associated compressive strains have not been widely reported through analytical or numerical investigations. Predictions of liner performance have generally indicated tensile displacements based on numerical analysis. The relatively large displacements observed in the field support the use of residual interface shear strength values for stability analyses.

4. SUMMARY AND CONCLUSIONS

Displacement monitoring systems were installed to measure response of geomembrane liners in municipal solid waste landfills in Alaska and New Mexico, USA. Displacements were monitored for extended durations from initial waste filling to several years after waste placement. Based on the investigation, the following conclusions were drawn:

- Displacements of geomembranes were observed in the field after construction, and prior to and during waste placement.
- The maximum displacements were on the order of 125 mm downslope and 300 mm upslope corresponding to strains on the order of between approximately -1.3% (compressive) to +2.6% (tensile) as calculated from sequential displacement monitoring coupons, supporting the use of residual interface shear strengths for stability analyses.
- Maximum tensile strains occurred near the toe of the slopes.
- The magnitudes of strains at the Alaska site were larger than at the New Mexico site, which was attributed to the steeper slope and greater waste height at Alaska.
- Maximum displacements occurred within 0.5 to 2 years after construction with limited further displacements occurring in the long-term.
- The long-term response of the liners (beyond approximately 1000 days at both sites) indicated onset of small and continued displacements, which may be resulting in wrinkling strains in the long term.
- Upslope displacements were common at the test sites and were attributed to buttress effect, thermal contraction, and translational movement between underlying GCLs and the geomembranes. In general, tension in geomembranes had been predicted in previous studies based on numerical analysis.

ACKNOWLEDGEMENTS

The cooperation and sponsorship of Anchorage Regional Landfill (Anchorage, Alaska) and the South Central Solid Waste Authority (Las Cruces, New Mexico) are acknowledged. Specifically, Mr. Mark Madden, Mr. Keith Howard, and Mr. Steve Cooper (Alaska), and Mr. Patrick Peck (New Mexico) facilitated the instrumentation installations and field monitoring. The Global Waste Research Institute provided additional support for the project. Mr. Raymond Ziegler and Mr. Wilson Wong assisted with the field installations. Mr. Nicolas Oettle assisted with analysis.

REFERENCES

- Gudina, S. and Brachman, R.W.I. (2011). Geomembrane strains from wrinkle deformations. *Geotextiles and Geomembranes*, Elsevier, 29: 181-189.
- Hanson, J.L., Yesiller, N., and Olsen, G.R. (2012). Factors Influencing Dimensional Stability of Multi-Component Geosynthetic Clay Liners. *STP1562 on Third Symposium on Current and Future Practices for the Testing of Multi-Component Geosynthetic Clay Liners*, June 27, 2012, San Diego, CA, in press.
- Hanson, J.L., Yesiller, N., and Oettle, N.K., (2010). Spatial and temporal temperature distributions in municipal solid waste landfills, *Journal of Environmental Engineering*, ASCE, 136:8, 804-814.
- Jones, D.R.V., and Dixon, N. (2005). Landfill lining stability and integrity: The role of waste settlement. *Geotextiles and Geomembranes*, 23:27-53.
- Kodikara, J. (2000). Analysis of tension development in geomembranes placed on landfill slopes. *Geotextiles and Geomembranes*, Elsevier, 18: 47-61.
- Koerner, R.M. and Soong, T.-Y. (1998). Analysis and design of veneer cover soils. *Proceedings, Sixth International Conference on Geosynthetics*, 1-23.
- National Research Council - NRC, (2007). *Assessment of the Performance of Engineered Waste Containment Barriers*, The National Academies Press, Washington D.C., USA.
- Reddy, K.R., Kosgi, S., and Motan, S. (1996). Interface shear behavior of landfill composite liner systems: A finite element analysis, *Geosynthetics International*, Industrial Fabrics Association International, 3:2, 247-275.
- Soong, T.-Y. and Koerner, R.M. (1999). Behavior of waves in high density polyethylene geomembranes: A laboratory study. *Geotextiles and Geomembranes*, Elsevier, 17: 81-104.

Interface Friction Testing Between Soil and a Bituminous Geomembrane

M. Lew, G.E., AMEC Environment and Infrastructure, Inc., USA, marshall.lew@amec.com
H. Ponnaboyina, P.E., AMEC Environment and Infrastructure, Inc., USA, hari.ponnaboyina@amec.com
C. A. Davis, G.E., Los Angeles Department of Water and Power, USA, craig.davis@water.ladwp.com
A. Perez, P.E., Los Angeles Department of Water and Power, USA, adam.perez@water.ladwp.com

ABSTRACT

The Los Angeles Department of Water and Power is planning to build two side-by-side reinforced concrete reservoir structures in the southeastern San Fernando Valley of Los Angeles. An important part of the operations of the reservoirs will be a detection system below the bottom of the reservoirs to determine if there are leaks or discharges of water. It is planned to use a bituminous geomembrane (BGM) beneath the reservoirs to collect any leakage and convey the water to a monitoring location outside of the reservoirs. Because of regulatory requirements, the design earthquake ground motions are quite high and there was concern that a plane of weakness would be present at the interface with either the predominantly granular soils beneath the BGM or the Class 2 permeable material above the BGM. Direct shear testing (ASTM D5321) was performed to determine the soil friction for these two interfaces.

1. INTRODUCTION

The Headworks Reservoir project will consist of two underground reservoirs. The east reservoir will have a capacity of 54 million gallons and the west reservoir will have a capacity of 56 million gallons. The reservoirs will be about 30 feet apart, about 40 feet high and will contain about 30 feet of water. The reservoirs will be covered with a 3-foot thick soil layer on the roof. The reservoirs are planned to be supported on mat foundations. At this time, the rough grading work for the east reservoir is complete and the construction of the east reservoir foundations will commence in the near future (at the time of this writing); the west reservoir will be constructed at a later date.

The upper on-site soils beneath the east reservoir were only medium dense and were subject to liquefaction settlement on the order of a few inches. To remediate the liquefaction settlement, the on-site soils were remediated in-place by removal and recompaction to a depth of about 20 feet below the mat foundation. Although the reservoir is designed not to leak, due to its critical function, a leak detection system is planned beneath the bottom of the reservoir structure. Above the compacted fill, it is planned to place a 3-foot thick drainage layer consisting of a series of perforated pipes in a parallel pattern surrounded by permeable material. The drainage layer will be placed above the compacted fill and the below reservoir mat foundation. The pipes are intended to collect any water leaked from the reservoir structure and transmit it to individual collection systems designed for each reservoir quadrant. The purpose of the leak detection system is to also trace the location(s) of the potential leaks at least to a quadrant-level to qualitatively assess the severity of the cracking in the reservoir foundation and plan for remedial work, if needed. In the unlikely event of an excessive leakage, the leak detection system would provide early warning to take timely actions for emptying the reservoir especially after a large magnitude earthquake. As part of this leak detection system, a relatively impermeable membrane is planned immediately beneath the drainage layer. The impermeable membrane layer is needed due to high permeability of the underlying sandy soil foundation materials and to allow increased spacing of the perforated pipes.

To meet the objectives of the leak detection system, a membrane underlying the drainage material was required to have a relatively low permeability. A bituminous geomembrane (BGM) was considered because of its relatively low permeability on the order of 10^{-10} to 10^{-13} centimeters per second (Koerner 1990) and long history of success in canal, reservoir and pond lining as well as in containment of industrial and nuclear wastes. The BGM is planned to be placed beneath the entire reservoir footprint.

2. BITUMINOUS GEOMEMBRANE

Bituminous geomembrane (BGM) is an asphalt-impregnated non-woven polyester geotextile. A typical cross-section of the BGM is shown on Figure 1. A BGM manufactured by Coletanche Limited is being considered for the project. Two types of products are available, namely the NTP and ES products. The NTP and ES products are manufactured in four different thicknesses varying from 140 to 240 mils (NTP 1 through NTP 4 and ES1 through ES-4). The weight of geotextile (which affects the thickness and its mechanical properties) varies for the different products from 200 to 400 grams per square meter. The NTP product contains blown (oxidized) bitumen and has lower resistance to ultraviolet (UV) exposure that could make the bitumen brittle and cause alligator cracking over time. The ES products are polymer-

based and contain elastomeric bitumen which is considered more stable to UV exposure and subject to less cracking (Coletanche, 2008). The non-woven polyester geotextile in both products provide the mechanical resistance and the bituminous binder provides waterproofing, chemical resistance and good aging behavior. The BGM is sanded and roughened on one side and has a shiny smoother texture on the other side (see Figure 2).

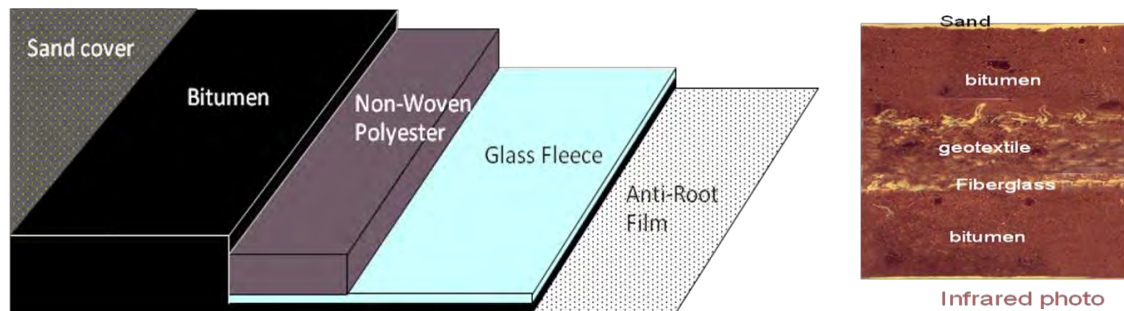


Figure 1. Typical cross-section of geomembrane.

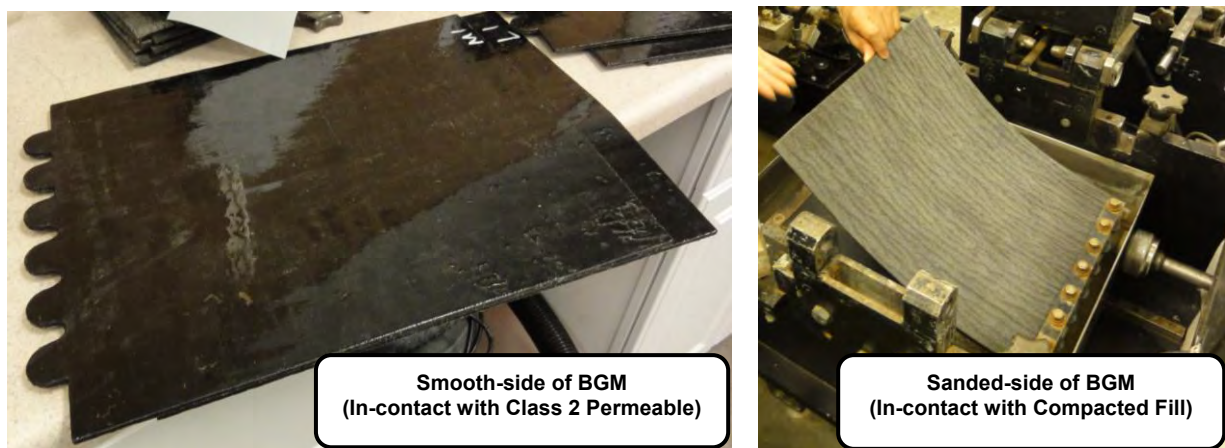


Figure 2. Smooth and sanded sides of BGM.

Five properties of the BGM were evaluated: physical properties (thickness), mechanical properties (tensile and puncture resistance), waterproofing (permeability) and interface frictional resistance achieved with the materials in contact. An ES-3 product with a thickness of 192 mil (4.8 millimeters) was selected for the project based on the prior experience with this product for similar applications.

3. BGM/FILL AND BGM/CLASS 2 PERMEABLE INTERFACES

The two materials that will be in contact with the BGM are (1) the overlying 3-foot thick drainage material consisting of permeable material and (2) the underlying subgrade consisting of compacted fill. The sanded/roughened surface of the BGM will be in contact with the compacted fill and the smoother surface with the drainage material. The drainage material consists of Class 2 permeable material as specified by California Department of Transportation (2006). The compacted fill material is the on-site soil that was overexcavated and recompacted to 95% of the maximum dry density obtainable using ASTM Designation D1557 test method. The particle size distributions of the Class 2 permeable material and the on-site fill are presented in Figure 3. According to Unified Soil Classification System, the compacted fill and Class 2 permeable materials classify as silty sand (SM) and poorly-graded gravel with sand (GP), respectively. The compacted fill is primarily a sandy material with about 10 percent fine gravel. The Class 2 permeable material contains about 65 percent fine to coarse gravel. The largest gravel size in the compacted fill is 12.7 millimeter (1/2 inch) whereas the Class 2 permeable material contains coarse gravel up to 19.1 millimeter (3/4 inch in size).

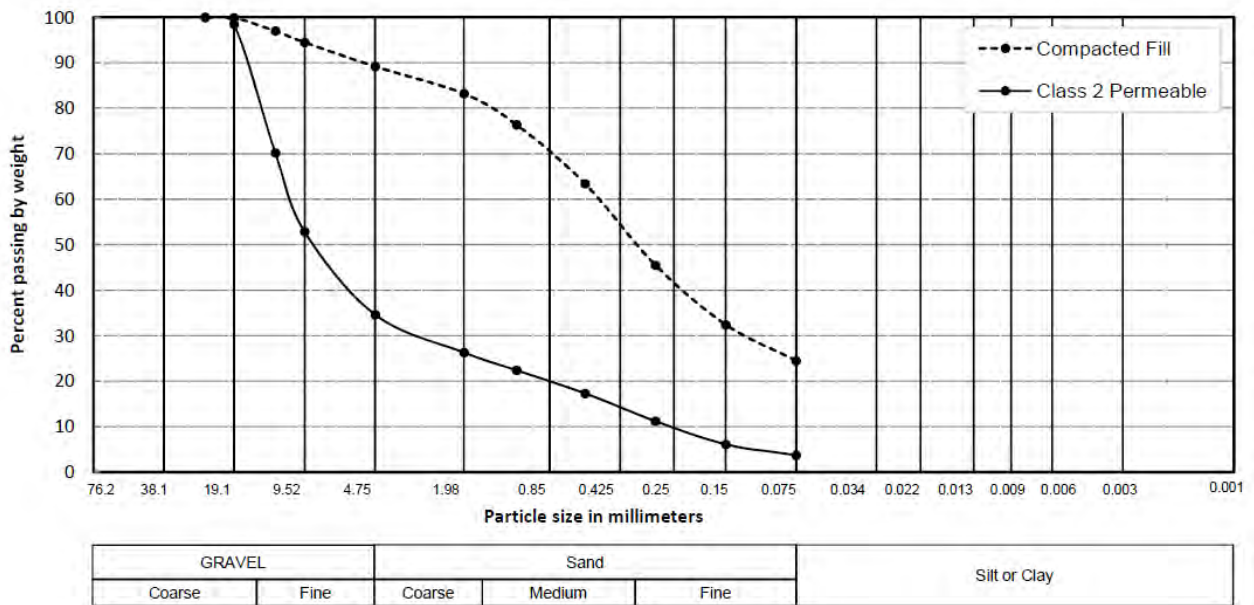


Figure 3. Particle size distribution of compacted fill and Class 2 permeable material.

The foundation improvements and grading work for the east reservoir site was completed in late 2011. Based on over 50 gradation tests performed during grading work, the compacted fill predominately consisted of silty sand with about 10 to 30 percent fines (passing No. 200 sieve). The compacted fill and Class 2 permeable materials beneath the mat foundation were specified to be compacted to at least 95% relative compaction. The maximum dry density for the compacted fill and Class 2 permeable materials were 21.2 kN/m^3 and 21.5 kN/m^3 , respectively; the optimum moisture content for both materials was about 8 percent. These maximum dry density and the optimum moisture content values were based on the compaction tests performed on the fill and Class 2 permeable samples used for interface friction testing.

For the seismic analysis of the reservoir, it is important to evaluate if a plane of sliding occurs at either the BGM/Fill interface or the BGM/Class 2 interface. Therefore, direct shear testing was planned to evaluate the frictional resistance for these two interfaces. A three-interface testing of Fill/BGM/Class 2 Permeable would simulate the field conditions better; however, for the dynamic soil-structure interaction (SSI) studies of the reservoir, strength parameters (cohesion and friction angle) for the two interfaces were required as separate input parameters. Therefore, separate tests were planned for the two-interface types. The direct shear test equipment used for the interface friction testing and the test procedure are presented in the following sections.

4. DIRECT SHEAR TEST EQUIPMENT

The interface friction between a soil and geomembrane or geotextile can be evaluated using an adapted version of direct shear test equipment typically used in geotechnical engineering (Koerner 1990). Other methods such as pull-out tests either in laboratory or field can be performed, if economically feasible, however, the elongation of the geomembrane could affect the usefulness of the test results. Therefore, conventional direct shear tests in the laboratory but with a larger shear box was used to evaluate interface friction.

The test equipment used for interface friction testing was a Brainard-Kilman LG-112 model with an effective test area (plan dimensions) of 305 millimeters by 305 millimeters (12 inches by 12 inches) and a depth of 51 millimeters (2 inches). The shear box consists of an upper rigid box and a lower moveable box as shown on Figure 4a. The upper box has plan dimensions of 305 millimeters by 305 millimeters whereas the lower box is slightly larger with plan dimensions of 305 millimeters by 406 millimeters (12 inches by 16 inches).

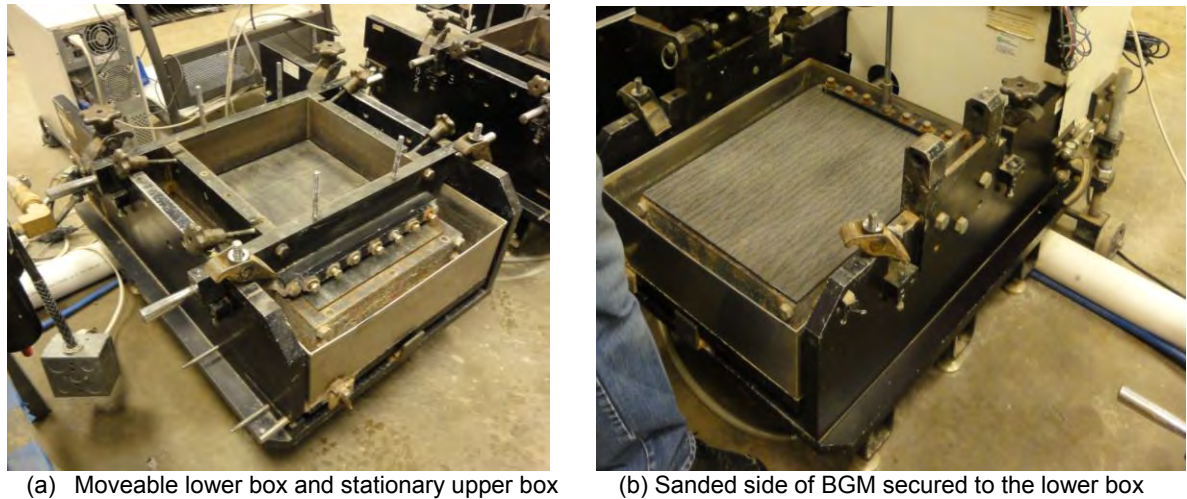


Figure 4. Direct shear test equipment.

A large-sized shear box was used considering the size of the material being tested, particularly the coarser gravel in the Class 2 permeable material. Per ASTM D 5321, the minimum dimension of the shear box should be at least 15 times the D_{85} (the size corresponding to which 85% of the sample is finer) of the coarser material and the depth of the box should be a minimum of 50 millimeters or six times of the maximum particle size of the coarser soil tested whichever is greater. The gravel in Class 2 material was coarser than that in compacted fill material. The estimated 15 times D_{85} for the Class 2 material is about 286 millimeters which is smaller than a 305-millimeter shear box used for the interface friction testing.

The BGM sheets received from the supplier were carefully inspected for surface defects prior to trimming them to 356 millimeters by 483 millimeters sample size for an effective test area of 305 millimeters by 305 millimeters. The thickness of the sample was also verified to be 4.8 millimeters for the ES-3 product specified for the project. If significant variation of BGM thickness was observed from the specification, the supplier was notified to resend the specified BGM material.

The BGM was secured to the lower box using flat bar clamping with seven pairs of bolts and nuts spaced at about 25.4 millimeters (1 inch) on centers on one end of the lower shear box as shown on Figure 4b. The surface of the lower box (substrate) has a roughened texture which assists in gripping the BGM in-place and avoids slippage of the BGM during testing. The material being tested against the BGM (compacted fill or Class 2 permeable) was compacted in the upper box to the specified density and moisture content. The on-site soil and Class 2 material was moisture conditioned to the optimum moisture content and with the known volume of the upper shear box, the soil was placed in relatively thin lifts and tamped to achieve the specified density. The upper shear box was weighed before and after placing the tested material to ensure that the material was compacted to the specifications.

5. INTERFACE FRICTION TEST PROCEDURE AND TEST CONDITIONS

The interface friction testing was performed by Precision Geosynthetic Laboratories (PGL) of Anaheim, California using the procedures stated in ASTM D 5321 (Determining the Coefficient of Soil and Geosynthetic or Geosynthetic and Geosynthetic Friction by Direct Shear Method).

Two test conditions were evaluated in the direct shear testing: (1) non-saturated condition—wherein the materials were compacted to 95% of the maximum dry density and at optimum moisture content, and (2) saturated condition—wherein the material was compacted at 95% of the maximum dry density at optimum moisture content and was inundated with water in the shear box for about 24 hours under a given normal load for consolidation and maintained inundated during shearing. Although the materials being tested were primarily granular (either SM or GP), it was desired to have the sample consolidate for about 24 hours and allow enough time to attain uniform moisture content throughout the sample. The BGM material itself has a low permeability on the order of 10^{-10} to 10^{-13} millimeters per second and was therefore not anticipated to absorb significant moisture content and undergo some reduction in strength. For the non-saturated condition, the normal load was sustained for about 15 minutes prior to applying the shear load. To evaluate the effects of sustained load, tests were also performed for the non-saturated condition but with normal load maintained for 24 hours before shearing.

The tests were performed at a constant rate of displacement of about 2.5 millimeter per minute (0.10 inch per minute) to ensure that pore pressures were not developed during testing. Although ASTM D 5321 suggests a shearing rate of 1 millimeter per minute (0.04 inch per minute), a higher rate was used considering the materials tested were primarily granular and would not develop excess pore pressures. For a maximum displacement of 76.2 millimeters (3 inches), a single test was completed in about one-half hour.

The normal load was applied on the shear box either using dead weights for lower test loads (less than 50 kN/m²) or hydraulically using a bladder for the higher test loads (50 to 250 kN/m²). The shear load was applied to the lower box with a pulling mechanism. The shearing process was carefully monitored to ensure that the shear load was applied in the horizontal direction with little or no tilting of the equipment to avoid applying torque which could cause non-uniform pressures on the interface. The displacement rate was monitored during testing through a digital readout unit. The normal pressure remained the same during testing due the constant shearing area. The cumulative horizontal shear displacement was also monitored; however vertical displacements were not monitored during the test. The test was continued until a maximum displacement of about 76 ± 0.5 millimeters (3 ± 0.2 inches) was reached. After the tests, the BGM specimen was usually inspected to determine if there were any shear strains (evidence of stretching) in the BGM or at the clamps. Tests were repeated if either excessive stretching (greater than 13 millimeters or 0.5 inches) of the BGM or slipping of the BGM over the substrate occurred.

The BGM has different surface textures on its two sides: (1) smooth side – which acts as a waterproofing membrane and is in contact with the Class 2 permeable material, and (2) rough/sanded side – which is in contact with the compacted fill. Direct shear tests were performed for both BGM surfaces depending on which material (compacted fill or Class 2 permeable) was being tested against. The BGM properties are reportedly uniform in both longitudinal and transverse directions on the same side. As stated by the manufacturer, the direction of testing did not have a significant impact on the test results. The tests were conducted using three normal pressures of about 50, 120, and 240 kN/m². The test loads were selected based on the range of pressures anticipated in the field for empty reservoir and full reservoir cases. All tests were conducted at the laboratory test conditions at a temperature of 71.6 ± 3.6 degrees Fahrenheit and 60 ± 10 percent relative humidity.

6. INTERPRETATION OF TEST RESULTS

The interface friction tests can be classified into four subgroups as listed below for the purpose of evaluating the results.

- BGM/Fill (non-saturated)
- BGM/Fill (saturated)
- BGM/Class 2 Permeable (non-saturated)
- BGM/Class 2 Permeable (saturated)

For each test, the peak shearing resistance of the stress-strain curve was used in the interface shear stress vs. normal load plots presented in this section. The designation “24-hour” on the plots means the sample was consolidated for 24 hours prior to shearing; the designation “15-minutes” means the sample was consolidated for 15 minutes prior to shearing.

To evaluate the interface resistance to sliding for the two interfaces, it was important to first evaluate the test results as presented in Figure 5 for the BGM/Fill and BGM/Class 2 Permeable interfaces for non-saturated condition. As evident from Figure 5, the BGM/Class 2 interface has higher shear resistance at low confining pressures, whereas the BGM/fill interface has higher shear strength at medium to high confining pressures. In addition, the cohesion and frictional components of the two interfaces are significantly different. The interface friction angle for BGM/fill interface is at least 15 degrees higher and the cohesion for the BGM/Class 2 interface is about five times higher than that for BGM/Fill interface.

The test results for the BGM/Class 2 interface for the non-saturated condition under 15-minute and 24-hour sustained load cases are presented in Figure 6. As clearly observed from the figure, the 24-hour sustained load conditions yields a significantly higher friction angle (10 degrees higher) compared to the 15-minute sustained load test. It is believed that the coarser gravel particles of the Class 2 permeable material are pushed into the outer layer of the bitumen at higher confining pressures thereby engaging the tensile strength of the BGM to result in a higher cohesion and frictional resistances. In contrast, a similar comparison of the test results for the BGM/Fill interface presented in Figure 7 indicates that the frictional angles are nearly the same. The 24-hour sustained load case does not seem to improve the frictional resistance for the BGM/Fill interface as the particle size of the fill is much smaller than the Class 2 permeable material resulting in less penetration of particles into the bitumen. It is also noted that the friction angle of the BGM/Fill interface ranges from 36 to 37.5 degrees, which is much higher than that obtained for the BGM/Class 2 interface. It appears that the shear failure for the BGM/Fill interface occurred within the fill material as noted from a thick soil film retained on the BGM after testing (see Figure 8).

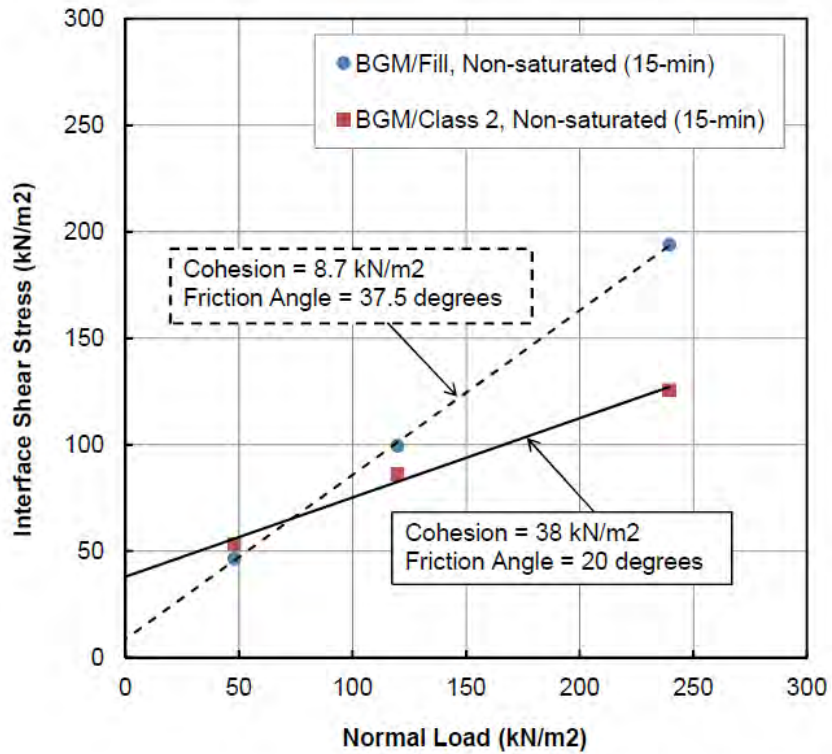


Figure 5. Test summary for BGM/fill and BGM/class 2 interface (non-saturated condition).

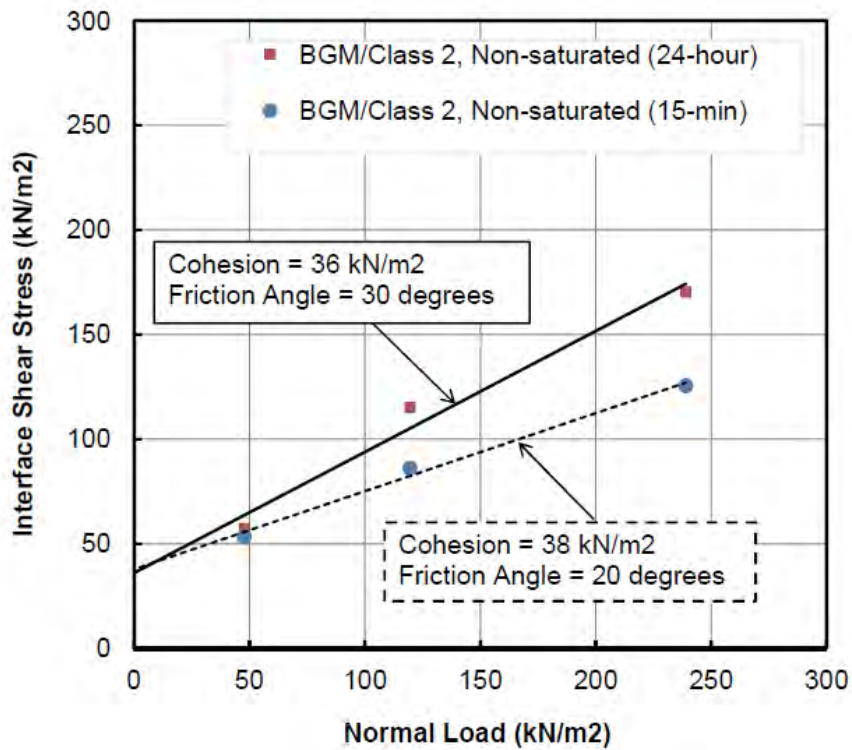


Figure 6. Test Summary for BGM/Class 2 interface (24-hr versus 15-min) for non-saturated condition.

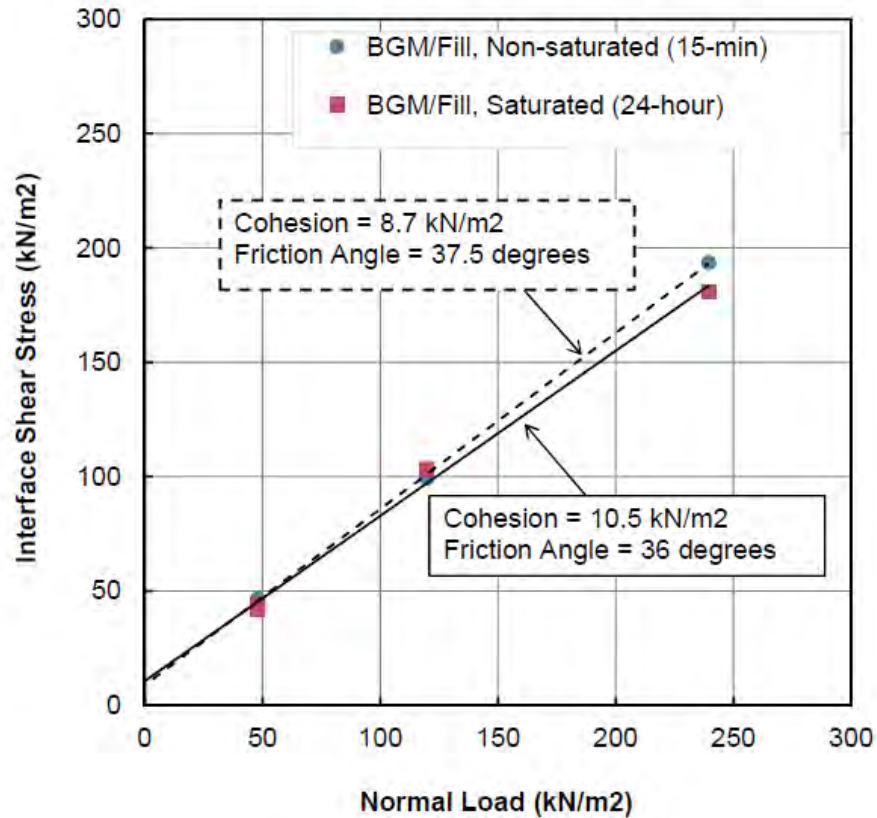


Figure 7. Test summary for BGM/Fill interface (24-hr versus 15-min).



Figure 8. Thick soil film retained on BGM/Fill Interface after testing (non-saturated condition).

To evaluate the effect of moisture content on the interface friction, tests were performed on the BGM/Class 2 interface but with 24-hour sustained load for both saturated and non-saturated conditions; the results are presented in Figure 9. The effect on saturation on the interface friction appears to be relatively small. In addition, the friction angles are the

same indicating that the effect of 24-hour sustained load is significantly higher than the increase in moisture content upon saturation for the granular material.

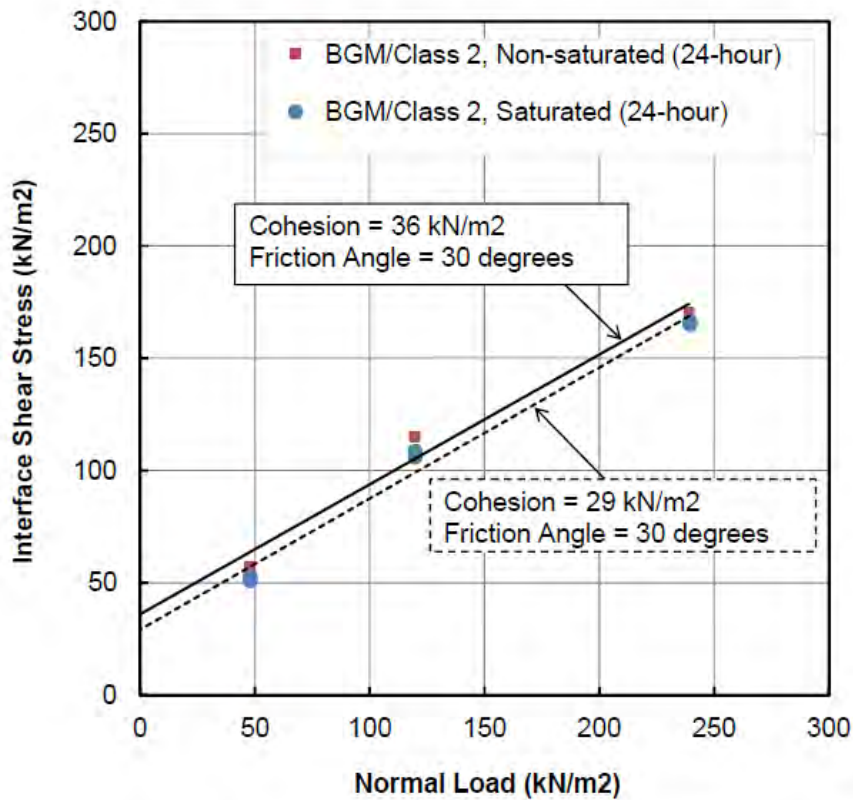


Figure 9. Test Summary for BGM/Class 2 (non-saturated condition versus saturated condition).

7. DESIGN FRICTION VALUES

The results of all tests performed for the BGM/Class 2 interface and BGM/Fill interface are shown on Figure 10. A lower-bound cohesion and friction angle were chosen as the design values for the two interfaces. The lower-bound of the 24-hour saturated versus 15-minute non-saturated condition test was used for the BGM/Class 2 interface and the lower bound of the BGM/Fill saturated condition versus non-saturated condition was used. The 15-minute versus 24-hour sustained load condition did not appear to improve the shear strength for the BGM/Fill due to shear failure within the fill material (i.e., the interface friction of BGM/fill was possibly higher than the frictional resistance of the fill material).

The design interface shear strength parameters (cohesion and friction angle) for the BGM/fill and BGM/Class 2 interfaces as well as anticipated governing sliding interface are shown in Figure 10. The design parameters estimated from the direct shear tests for these two interfaces were used in the SSI studies.

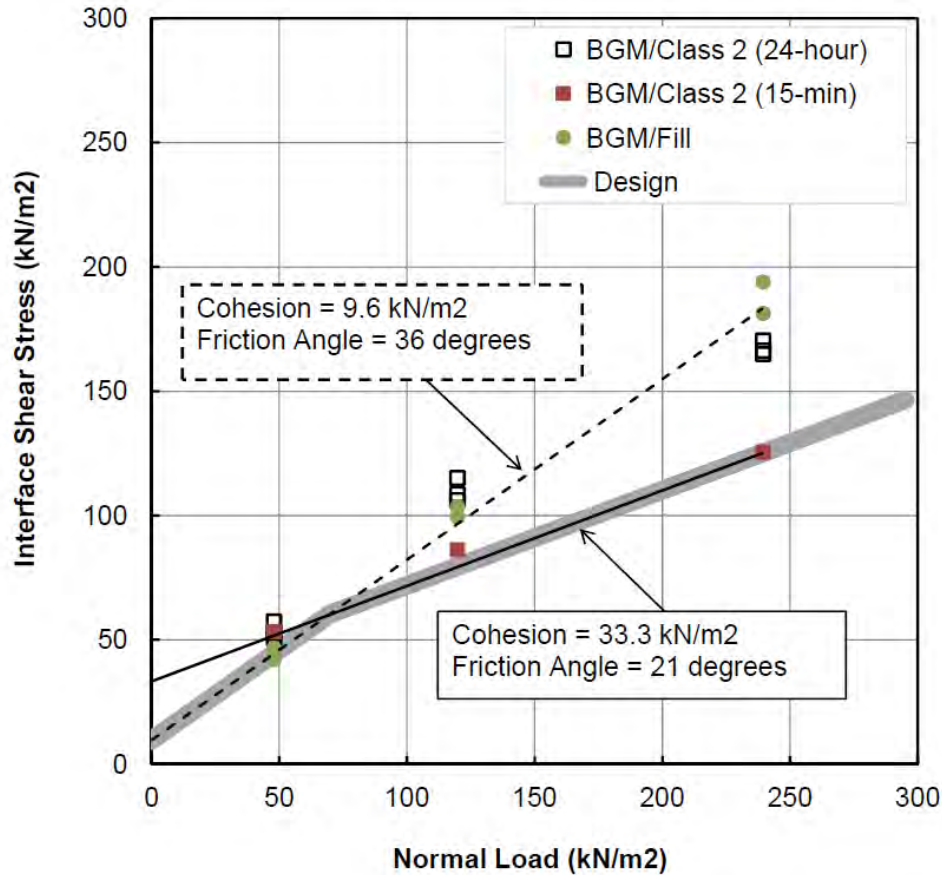


Figure 10. Test Summary for BGM/Class 2 and BGM/Fill interface and estimated design shear strength.

8. DETERMINATION OF CRITICAL SLIDING INTERFACE

As shown in Figure 10, the BGM/Fill interface has lower shear strength than the BGM/Class 2 interface at lower confining pressures (less than about 70 kN/m²), beyond which BGM/Class 2 interface has lower shear strength. In other words, the BGM/Fill interface is expected to be the weaker sliding plane for low confining pressures and the BGM/Class 2 interface would be the weaker sliding plane for medium to high confining pressures.

For the operating conditions of the reservoir, the BGM/Fill interface would govern the behavior for an empty reservoir condition (where confining pressures are low), whereas the BGM/Class 2 interface would govern the behavior of the full reservoir structure. It is noted again that at higher confining pressures, the tensile resistance of the BGM becomes engaged in resisting the shear load when in contact with Class 2 permeable material resulting in a higher cohesion with a lower contribution of the interface friction angle. If direct shear tests were to be performed on Class 2 material itself, a friction angle of at least 40 to 45 degrees would be expected. Therefore, for the full reservoir case, a greater shear displacement is expected to occur within the BGM material itself than in the overlying Class 2 permeable material or the underlying compacted fill. For the empty reservoir case, the greater shear displacement is expected to occur within the compacted fill or at the BGM/Fill interface.

The SSI studies of the east reservoir that were performed using design peak ground acceleration (PGA) of 1.0g indicated that sliding (i.e., permanent displacement after earthquake) was not expected at either interfaces. Since the reservoir is covered with 30-foot high compacted fill embankments on all four sides, the additional lateral resistance derived from these embankments likely assisted in resisting the sliding forces due to earthquake load. A discussion of the SSI studies and the modeling details of the BGM/Fill and BGM/Class 2 interfaces below the reservoir are provided in Hudson et al. (2012).

9. CONCLUSIONS

The test results indicate that the critical sliding plane is the BGM/Fill interface for low confining pressures (less than about 70 kN/m²) such as for empty reservoir case and the BGM/Class 2 interface for medium to high confining pressures (70 to 250 kN/m²) such as for full reservoir case. As expected, the Class 2 permeable material has sufficient frictional resistance within itself to be not the weakest sliding plane. The sustained loading condition (24-hour) as expected in the field would in-fact yield higher interface frictional strength than the design values. The tensile resistance of the BGM would be engaged for higher confining pressures such as when the reservoir is full. The maximum shearing resistance (load) on the BGM surface is expected to be about 192 kN/m² (4,000 pounds per square foot) for the full reservoir condition. In the event of excessive leakage through the reservoir or rise in groundwater level that could saturate the compacted fill, the interface friction tests indicate that the reduction in frictional strength upon saturation is relatively minor for both BGM/Fill and BGM/Class 2 interfaces.

ACKNOWLEDGEMENTS

We would like to thank Dr. Tarik Hadj-Hamou of Strategic Engineering and Science, Inc. for providing information regarding bituminous geomembrane and for providing geomembrane samples for testing. We also thank Ms. Cora Queja and Mr. Carmelo Zantua of Precision Geosynthetic Laboratories International for diligently performing the interface friction testing. We also acknowledge Mr. Alek Harounian and Dr. Marty Hudson of AMEC Environment and Infrastructure, Inc. for their help in reviewing the test results and Ms. Kelly Dudek of AMEC Environment and Infrastructure, Inc. for assisting with the figures.

REFERENCES

- ASTM D 1557, Standard Test Methods for Laboratory Compaction Characteristics of Soil Using Modified Effort (56,000 ft-lbf/ft³ (2,700 kN-m/m³), *American Society for Testing and Materials*, West Conshohocken, Pennsylvania, USA.
- ASTM D 5321. Determining the Coefficient of Soil and Geosynthetic or Geosynthetic and Geosynthetic Friction by Direct Shear Method, *American Society for Testing and Materials*, West Conshohocken, Pennsylvania, USA.
- California Department of Transportation (2006), Standard Specifications, State of California, Department of Transportation, Sacramento, California.
- Coletanche (2008), Design and Application Handbook for Bituminous Geomembrane.
- Hudson, Martin B., Craig A. Davis, Marshall Lew, Alek Harounian, and Liping Yan (2012), "Seismic Resilient Design of a Concrete Box Reservoir," Proceedings of the 6th China-Japan-United States Symposium on Lifeline Earthquake Engineering, ASCE Technical Council on Lifeline Earthquake Engineering, Chengdu, Sichuan, China.
- Koerner, R.M. (1990), *Designing with Geosynthetics*, 2nd ed., Prentice-Hall Inc., Englewood Cliffs, NJ, USA.

Investigation of a Gas Bubble in a Final Cover Constructed with a Geosynthetic Liner

B. Gao, Ph.D., P.E., Golder Associates, Inc., USA, bgao@golder.com
C. M. Moeller, P.E., Golder Associates, Inc., USA
K. S. Brown, P.E., Golder Associates, Inc., USA
G. H. Collison, P.E., Golder Associates, Inc., USA

ABSTRACT

During the final stages of construction of a composite landfill final cover cap, a gas bubble occurred at the toe of the final cover slope before the surface water diversion berms were constructed and the final cover was stabilized with vegetation. As the gas pressure in this area was relieved, several large wrinkles were noted in the geomembrane that extended over a lateral distance of approximately 73 meters. This paper presents the investigation of the gas bubble and the geomembrane wrinkles through the visual evidence found at the landfill, the geomembrane sample tests, and calculations modeling the actual construction sequence. The investigation indicated that two different situations may have contributed to the gas bubble and the wrinkles: first, placement of the soil cover from top to bottom with 40-ton haul trucks backing down the slope to dump soil on the slope; second, the combination of some stretching of the geomembrane in the area where the gas bubble developed and the accumulation of the stretched geomembrane and possibly some excess geomembrane being walked down the slope.

1. INTRODUCTION

The landfill is located in the Southeastern United States. In the latter months of 2006 and into early 2007, the final cover system was installed on approximately 2.4 hectares of the landfill.

Before the surface water diversion berms were constructed and the final cover stabilized with vegetation, high gas pressures caused the geomembrane cap to expand under the vegetative cover soils in the lower portions of the cover slope. At the toe of the slope (Figure 1a), the gas pressure was sufficiently high that the vegetative cover soils were pushed off the geosynthetics, resulting in a gas bubble approximately 3 meters high, 1.8 meters wide and 4.6 meters long.



a A Gas Bubble

b Geomembrane Wrinkles

Figure 1

The pressure was relieved by cutting through the geomembrane and directing the gas through a flexible pipe to the landfill gas collection system. As the gas pressure in this area was relieved, several large wrinkles were noted in the geomembrane (Figure 1b). Landfill personnel exposed the geomembrane to define the extent of the wrinkles, and found that they extended over a lateral distance of approximately 73 meters. Further investigation in the upper portion of the slope above the area where the gas bubble had occurred, indicated that the geomembrane had been stretched resulting in the thickness of the geomembrane being reduced to 60 to 90 percent of its original thickness.

This paper presents the investigation of the gas bubble and the geomembrane wrinkles through the visual evidence found at the landfill, the geomembrane sample tests, and calculations modeling the actual construction sequence. Based on the field investigation results and calculations, the paper discusses the mechanisms that contributed to the elongation of the geomembrane.

2. BACKGROUND

2.1 Final Cover Cross Section

The cross-section of the permitted final cover is as follows (from the bottom up):

- A 457-mm thick soil foundation layer;
- A geomembrane and drain layer combination of,
 - a 1.00 mm (40 mil) textured LLDPE with geocomposite above, or
 - a 1.50 mm (60 mil) textured HDPE with geocomposite above, or
 - a 1.25 mm (50 mil) Supergripnet™ drain liner with a 271 g/m² (8 oz./yd²) geotextile above;
- A 457-mm thick vegetative cover.

The partial closure included a 1.25 mm Supergripnet™ Drain Liner installed over the compacted soil foundation layer, topped by a 271 g/m² non-woven geotextile and the 0.45 meters thick vegetative soil cover. The final cover has a general slope of 3.0 horizontal to 1.0 vertical (3H:1V), with diversion berms located every 9.1 meters to control storm water and soil erosion.

During the design phase, the stability of the final cover against sliding along the interfaces of the different materials was evaluated. The stability analyses were conducted for the following conditions:

- Long-term static conditions, with no construction loading, and up to 0.15 meters of water within the cover drainage layer; and
- Short-term conditions to evaluate the slope during construction, specifically during placement of the vegetative cover layer.

The design of the slope was based on Factors of Safety (FOS) against sliding as follows (Koerner, et al. 1998):

- FOS = 1.6 for static conditions with no equipment loading;
- FOS = 1.2 for static conditions with seepage forces; and
- FOS = 1.3 for low ground pressure equipment loading during placement of the vegetative cover soil. Note that this analysis assumed that the vegetative cover soil would be placed upward from the bottom of the slope.

2.2 Conditions of Gas Collection and Control System in the Area of Interest

There were four extraction wells upslope from the area where the gas bubble developed designated as G1 through G4. The liquid level measurements in these wells taken in early January of 2007 showed that in all but one of these wells the liquid level was above the top of the well screen. Furthermore, well G1 had only about 25 percent of the screen above the liquid level. High liquid levels in the gas wells are generally indicative of perched zones of leachate or high condensate generation rates causing the well screen to become flooded with leachate. Historically, replacement wells have been installed within 9.1 meters of a well that was flooded without encountering saturated waste. However, it is possible that saturated conditions could have been present in the waste underlying the cover area.

Throughout the final cover construction period, the four extraction wells were monitored approximately every two weeks for gas quality, temperature, and pressure. These wells exhibited elevated oxygen concentrations and, in some cases, high positive pressures. This is a common occurrence with gas wells where the liquid level is high because the limited screen space available for the gas to enter the well increases the potential for the atmospheric intrusion (oxygen) through the fittings in the wellhead or sample ports when vacuum pressures are applied to extract the gas.

On October 19, 2006, when problems were noted with operation of the flare and/or gas header, a positive pressure of 1.2 meters of water was measured in one of the wells. Smaller positive pressures (less than 0.13 meters of water) were measured in the other wells in the investigation area during this same monitoring event.

The pressures measured in the flooded wells (wells with no screen available) were unlikely to represent the overall gas pressure within the landfill. When the wells are flooded with leachate, gas pressure typically increases in the headspace

of the well as gas "bubbles up" through the leachate. When the well is closed, positive pressures will continue to increase until they are allowed to vent. To measure the gas pressure in the landfill, it would be necessary to have a well with the screen properly exposed to the waste and that has been shut-off (i.e., not allowed to vent) for a period of time that would allow the gas pressure within the well to stabilize.

2.3 General Sequence of Construction and Discovery of Landfill Gas Bubble

The following summarizes the geomembrane and vegetative layers construction timeline:

- The geomembrane was installed over a period of 5 days. CQA conformance tests were conducted during the installation. The average geomembrane thickness at time of placement based on seven conformance tests was 1.4 mm with a standard deviation of 0.056 mm and the lowest interface friction angle was measured to be 25.6 degrees between the geomembrane and the underlying soil foundation layer. This is from laboratory testing of the interfaces between the geotextile and geomembrane and geomembrane and soil foundation layer using four different types of direct shear tests.
- Placement of vegetative cover began on December 12, 2006 according to the Contractor's records. Significant activity for vegetative cover placement began on December 18, 2006, with over 150 loads placed per day until December 21, 2006. Forty-ton trucks were used to haul and dump the vegetative cover material down the slope from the top.
- The vegetative cover material was placed over all of the final cover area and was compacted and smoothed with a smooth drum compactor prior to the beginning of a shut-down period from December 22, 2006 to January 2, 2007. The erosion control diversion berms along the slope were not installed prior to the shut-down.
- Approximately 63.5 mm of rainfall fell during the shut-down period with one event producing 37.3 mm of rainfall.

A bubble near the toe of slope was noticed by the landfill personnel on when they came back on site, but the exact date of when the bubble began to form is unknown. A gas extraction well located approximately 45.7 meters up the slope from the bubble was investigated due to an apparent vacuum leak. During the walk up the slope, several small (less than 25.4-mm wide) tension cracks were observed at irregular intervals up the slope. Several erosion rills running up and down the slope had formed.

In addition to the largest bubble near the toe of slope, several smaller bubbles were noticed in the area; including one immediately north of the largest bubble and another located approximately 23 meters further up the slope. The Contractor also observed a bubble near the tie-in with the adjacent closed area after returning from the shut-down period. The following lists information related to the bubbles.

- In preparation for the holiday shut down, the Contractor left the longitudinal anchor trench adjacent to the existing capped area open on December 21 to facilitate venting of the gas. On returning, Contractor noted that the anchor trench had been silted in and they uncovered the anchor trench. At this same time, the Site Superintendent also observed a gas bubble near this tie in. Upon cleaning the silt from the anchor trench, this bubble dissipated without having to lance the bubble.
- The largest bubble (Figure 1) was noted the same day and was lanced.
- Inspection of the bubble on January 2 revealed no obvious signs of a slope failure at the time.
- The largest bubble was estimated about 4.6 meters long, 1.5 to 1.8 meters tall, and 3 meters wide.
- The bubble located immediately north of the largest bubble appeared to have deflated when lancing the largest bubble. The smaller bubble located approximately 23 meters up the slope was covered and the soil was reworked.
- While attempting to repair the area surrounding the largest bubble, the geomembrane at the toe area near the bubble was exposed. Numerous wrinkles were noticed and the liner continued to be exposed over an area approximately 6 meters wide and 73 meters long to determine the extent of the wrinkles.

3. FIELD INVESTIGATION

3.1 General

After the gas "bubble" occurred, the author visited the site on several occasions and sampled the geomembrane to observe the soil under the geomembrane and for laboratory testing. The locations of the samples are shown on Figure 2. Note that the sample locations are described relative to the surface water benches designed on the slope, These benches were not installed before the bubble appeared and they did not have an impact on the wrinkling or the stretching of the liner. The design location of the storm water diversion benches are shown only as location markers. The samples were taken as follows:

- Twenty-nine geomembrane samples were taken at toe of slope in the area of the wrinkles one month after the contractor resumed work on the cover. These samples are marked with an “x” on Figure 2 and denoted as “S-1” to “S-29.” Among these samples, S-19 was taken next to the punched hole that was used to release the bubble.
- A few days after the initial sampling, four (4) geomembrane samples were taken higher up the slope. These were denoted as “Bench Sample 1” to “Bench Sample 4.”
- Eight (8) geomembrane samples were taken higher up the slope ten (10) days later and denoted as “# 1” to “# 8.”

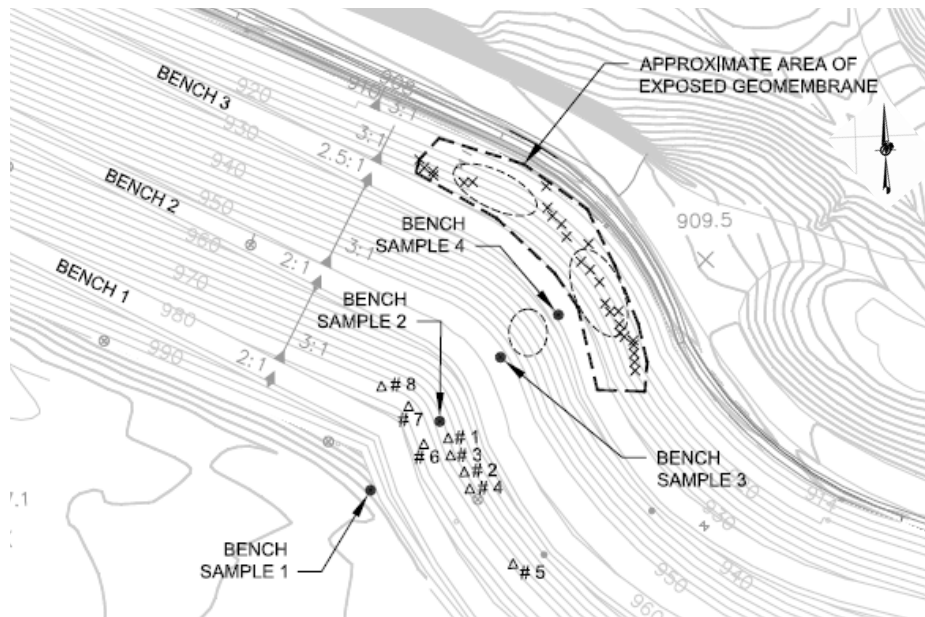


Figure 2 Geomembrane Sampling Locations

3.2 Field Observations

3.2.1 Observations in the Bubble Area at the Toe of the Slope

After the gas bubble was pierced and deflated, the geomembrane that had been uncovered was noticeably wrinkled. The width and length of the affected area was measured to be about 6 meters wide by 73 meters long. The increase in length of the geomembrane creating the wrinkles was measured along the wavy surface from top to the bottom of the exposed geomembrane at six different locations. The length of geomembrane ranged from approximately 6.9 meters to over 11 meters, averaging about 1.6 meters (141% of the original length) longer than should have theoretically been present at the exposed location. Several samples were cut from the geomembrane. The surface of the foundation soil under the geomembrane samples was relatively dry, but several areas were marked with downhill progressive penetrations (not continuous drag marks) caused by spikes in geomembrane as shown in Figure 3a.

3.2.2 Observations on the Slope

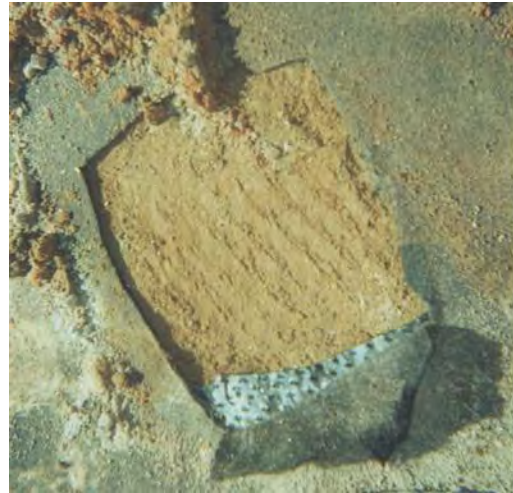
To further investigate the cause of the wrinkles, test pits were excavated on the slope from the top down (Bench Samples 1 through 4) and on the upper portion of the slope (samples #1 through #8) and samples were taken from the exposed geomembrane. Several geomembrane samples obtained in the upper portion of the slope were notably (visually) thinner than indicated by the conformance testing. Also, the geomembrane was under tension and separated easily when the samples were cut. The surface of foundation soils under several samples from the top of the slope showed clear “dragging” marks, as shown in Figure 3b.

Furthermore, the spikes on the bottom of the geomembrane sample taken between Benches 2 and 3 were bent, indicating that the geomembrane had been dragged down the slope, as shown in Figure 3c.

The soil beneath the sample taken between Benches 2 and 3 did not exhibit the same drag markings, as shown in Figure 3d.



a Markings under Sample Taken at the Toe of the Slope



b "Drag" Marks under the Geomembrane



c Spikes Bent in the Downslope Direction



d Markings on Soil under the Sample Taken between Benches 2 and 3

Figure 3

3.3 Laboratory Testing

3.3.1 Thickness Measurement

Table 1 Geomembrane Thickness Results from Conformance Tests

Sample ID	Sample Date	Average Sample Thickness (mm)	Minimum Thickness Reading (mm)
146101-06		1.55	1.33
146317-06		1.45	1.31
146433-06		1.43	1.25
146548-06	11/2006	1.46	1.31
146764-06		1.39	1.23
147104-06		1.38	1.24
147220-06		1.40	1.26
Average		1.44	

The thicknesses of the 41 samples obtained from the geomembrane were measured at multiple locations along the perimeter of each sample. The thickness test results are summarized in Tables 2, and 3. The thicknesses of samples taken for conformance testing during the installation are also included in Table 1 for reference. The thicknesses measured in the conformance tests ranged from 1.38 mm to 1.55 mm, with an average of 1.44 mm and a standard

deviation of 0.056 mm. The thicknesses of samples taken between Benches 1 and 2 ranged from 0.85 mm to 1.54 mm (Table 2). The thicknesses of samples taken from the toe of the slope in the area of the wrinkles ranged from 1.24 mm to 1.53 mm, averaging 1.38 mm (Table 3).

Table 2 Geomembrane Thickness Test Results on Slope Samples after Gas “Bubble” Occurred

Sample ID	Sample Date	Average Thickness (mm)	Sample Thickness Reading (mm)	Minimum Thickness Reading (mm)	Percent Deformation	Meet Specifications?	
						Min. Average (=1.25 mm)	Min. Value (=1.14 mm)
Bench Sample 1		1.54		1.46	0.0%	Yes	Yes
Bench Sample 2	2/7/07	1.03		0.76	28.0%	No	No
Bench Sample 3		1.47		1.39	0.0%	Yes	Yes
Bench Sample 4		1.29		1.22	9.9%	Yes	Yes
# 1		1.33		0.90	7.4%	Yes	No
# 2		0.87		0.66	39.3%	No	No
# 3		0.85		0.34	41.1%	No	No
# 4	2/18/07	1.09		0.86	24.1%	No	No
# 5		1.29		1.23	10.3%	Yes	Yes
# 6		1.24		0.91	13.8%	No	No
# 7		1.53		1.38	0.0%	Yes	Yes
# 8		1.18		0.95	18.1%	No	No

Note:

1. Percent deformation was calculated in comparison to the average sample thickness from conformance tests (=1.44 mm).

Table 3 Geomembrane Thickness Test Results on Samples from Toe of Slope

Sample ID	Average Sample Thickness (mm)	Minimum Thickness Reading (mm)	Percent Deformation	Meet Spec?		Sample ID	Average Sample Thickness (mm)	Minimum Thickness Reading (mm)	Percent Deformation	Meet Spec?	
				Min. Avg	Min. Value					Min. Avg	Min. Value
S-1	1.39	1.20	2.8%	Yes	Yes	S-16	1.44	1.34	0.0%	Yes	Yes
S-2	1.32	1.30	8.0%	Yes	Yes	S-17	1.32	1.24	8.3%	Yes	Yes
S-3	1.39	1.34	3.4%	Yes	Yes	S-18	1.30	1.22	9.7%	Yes	Yes
S-4	1.50	1.41	0.0%	Yes	Yes	S-19	1.42	1.33	1.1%	Yes	Yes
S-5	1.38	1.32	3.5%	Yes	Yes	S-20	1.35	1.27	5.8%	Yes	Yes
S-6	1.37	1.30	4.8%	Yes	Yes	S-21	1.25	1.18	12.6%	No	Yes
S-7	1.34	1.28	6.9%	Yes	Yes	S-22	1.32	1.26	8.0%	Yes	Yes
S-8	1.53	1.45	0.0%	Yes	Yes	S-23	1.49	1.40	0.0%	Yes	Yes
S-9	1.27	1.26	11.3%	Yes	Yes	S-24	1.41	1.28	1.8%	Yes	Yes
S-10	1.34	1.28	6.9%	Yes	Yes	S-25	1.31	1.25	8.5%	Yes	Yes
S-11	1.50	1.33	0.0%	Yes	Yes	S-26	1.34	1.24	6.5%	Yes	Yes
S-12	1.35	1.28	6.2%	Yes	Yes	S-27	1.31	1.23	8.8%	Yes	Yes
S-13	1.47	1.33	0.0%	Yes	Yes	S-28	1.34	1.30	6.5%	Yes	Yes
S-14	1.42	1.35	0.7%	Yes	Yes	S-29	1.24	1.18	13.3%	No	Yes
S-15	1.51	1.43	0.0%	Yes	Yes						

The thickness measurements of the samples indicate the following:

- The liner in the toe area appears to be slightly stretched.
- Sample S-19 was taken adjacent to the hole punched to release the gas. Samples S-20, S-21, and S-22 were taken adjacent to S-19, but away from the hole. S-19 was likely at the bottom or side of the bubble where elongation would be expected to be lower than along the upper part of the bubble. Since the thicknesses of samples S-20, S-21 and S-22 are less than that of S-19, it is inferred that the liner at the top of the bubble was likely stretched even more.
- The liner between the first bench and the second bench (top down) was stretched. The thicknesses of five of the eight samples, i.e. Bench Sample 2, and samples #1 to #8, were generally less than 1.27 mm (see Table 2).

- The liner immediately uphill from the liner exposed in the toe area may have been under slight tension, since the thickness of Bench Sample 4 was approximately 10% less than the conformance tests average.

3.3.2 Stress-strain Behavior of the Geomembrane

Wide Width Tensile Strength tests were also conducted on three 203-mm by 203-mm specimens cut from the samples # 1, # 2, and S-23, respectively. The tests were performed based on ASTM 4885, except that, instead of 12 specimens per sample, only one specimen was tested.

The Wide Width Tensile Strength tests indicated that samples # 1 and S-23 were not stretched or stretched very slightly, but sample # 2 was stretched significantly. Based on the results of the Wide Width tests, the geomembrane would behave elastically when the tensile stress is less than 15.8 newtons per millimeter (N/mm). Over 15.8 N/mm, the geomembrane will display plastic (permanent) deformation. The results of the Wide Width tests are shown on Figure 4 below:

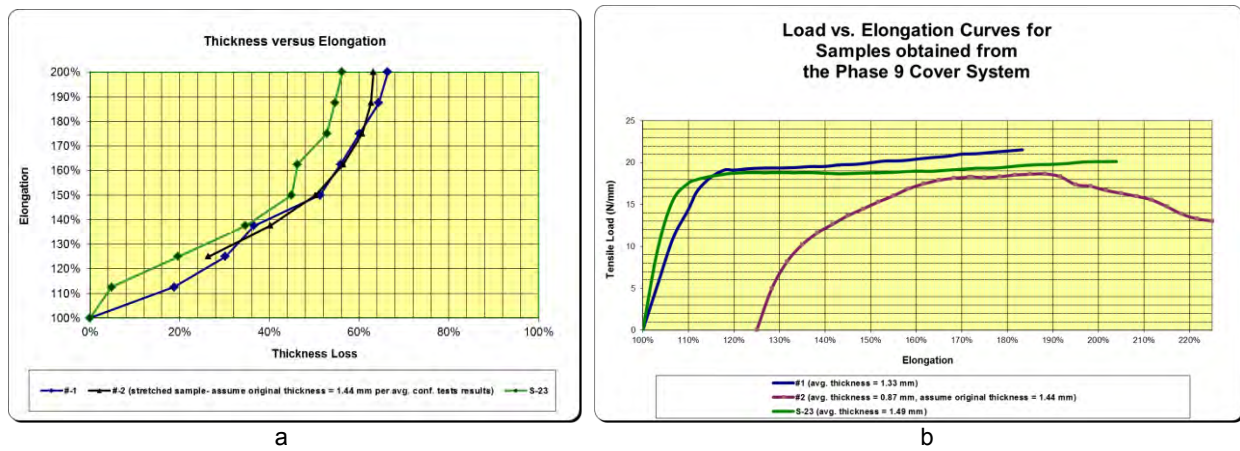


Figure 4

4. STABILITY ANALYSES

4.1 Cases Analyzed

For a landfill cover system, veneer stability is developed through the interface shear strength between the layers and the internal shear or tensile strength of the material in each layer. Veneer stability is typically evaluated using a two dimensional force balancing model (Koerner, et al. 1998; Qian, et al. 2002).

Calculations were performed to assess the difference in FOS between placing the vegetative cover layer on the geomembrane from the toe of the slope up (as designed and specified), and placing the vegetative cover layer from the top of the slope down (as constructed). Cases 1 and 2 are indicative of design conditions, as described above in Section 2.1, while Cases 3 and 4 represent the construction conditions. For Cases 3 and 4, Case 3 assumes that the geomembrane does not take any tension and Case 4 estimates the tension experienced by the geomembrane during construction. These calculations do not include the effect of gas pressure beneath the geomembrane.

A separate calculation (Case 5) was performed to estimate the magnitude of the gas pressure that would be required to counter the weight of the vegetative cover (after construction) such that the contact between the geomembrane and the underlying soil was broken (i.e., zero interface friction). Under these conditions, the down-slope component of the weight of soil above the geomembrane is essentially carried by tension in the geomembrane. This loading condition also estimates the length of soil along the slope that, when lifted by gas pressures, would cause sufficient tension to elongate the geomembrane past the yield point (transition point from elastic to plastic behavior), which is approximately 15.8 to 17.5 N/mm (see Figure 4b).

4.2 Veneer Stability Analyses Results

The results of the stability analyses for the conditions described in the previous section are summarized in the following table.

Table 4 Veneer Stability Analyses Results without Gas Pressures

Case	Construction Direction	Equipment On Slope	Tension on Geomembrane (ppi)	FOS	Comments
1	NA	No	0	1.6	As designed
2	Upslope	LGP Dozer	0	1.5	As designed
3	Downslope	LGP Dozer and Truck	0	0.9	As Built – assumes the equipment is on 9.1 m of the slope with no tension on the geomembrane.
4	Downslope	LGP Dozer and Truck	154	1	As Built – assumes the equipment is on 9.1 m of the slope and allows tension in the geomembrane.

Table 5 Veneer Stability Analyses Results with Gas Pressures

Case	Tension (N/mm)	Gas Pressure Under Membrane (H ₂ O mm) Needed to Overcome Weight of Soil	Comments
5	16.8	No	Assumes there is no contact between the geomembrane and the foundation soil layer along 1/3 of the slope, and no construction loads

The results of these analyses results are discussed in the following section.

5. DISCUSSIONS

5.1 General

The focus of the investigation was to assess what mechanisms would result in the elongation of the geomembrane along the upper and lower portion of the slope, and whether these elongations were related to each other and to the large gas bubble that occurred at the top of the slope.

The wrinkling of the geomembrane when uncovered at the toe of the slope raised the question of whether the geomembrane had been stretched along the entire slope and why this had occurred. The geomembrane is manufactured with low-density polyethylene which is an elastoplastic material, meaning that it exhibits both elastic and plastic behavior. Under lower tensile loading, the geomembrane deforms elastically and rebounds when the load is removed. Under higher loads, beyond the elastic (or yield) limit, the geomembrane deforms plastically; it will not fully rebound when the load is removed and if the load is maintained, the geomembrane will continue to deform without an increase in load (creep). Since it was known that the geomembrane had stretched and thus been under tension, the long-term creep (increase in deformation under constant load) resistance of the geomembrane on the slope was of concern. While the main focus was to assess what caused the problems identified and identifying potential ways to prevent future occurrence, one part of the investigation was geared towards assessing whether the geomembrane would continue to creep under the static load imposed by the vegetative cover soil layer and the diversion berms.

5.2 Potential Geomembrane Elongation Mechanisms

5.2.1 General

The results of the stability analysis summarized in Section 4 (Table 4 and 5) confirm that, as indicated by the physical state of the geomembrane samples taken from the investigation area, the geomembrane had been stretched, and therefore tensioned, during construction and by gas pressures that built up under the geomembrane. The following sections discuss, based on the stability analyses and field observations, how these mechanisms are likely to have occurred.

5.2.2 Discussion of Elongation During Construction

The effect of equipment loading was analyzed by performing the veneer stability analyses to compare design to construction conditions as described in Section 4.0. The design analyses of the slope (Cases 1 and 2 with no gas

pressure) result in factor of safety (FOS) greater than 1.0, indicating that the geomembrane on the slope would not be in tension during and/or after construction if the slope was properly drained, both externally and internally.

Case 3 uses construction loading conditions (soil placed from the top of the slope to the bottom) and assumes that there is no tension in the geomembrane; the resulting FOS of 0.9. This FOS is indicative of a condition where the cover materials would have slid along the geomembrane/soil interface had it not been for the increase in tensile strain (and stress relief) of the geomembrane. Case 4 was analyzed to quantify the tension (stress relief) that would have developed in the geomembrane to keep the cover materials on the slope.

Case 4 is representative of the cover conditions as evidenced from the geomembrane samples and the soil surface beneath the samples. There was no visually apparent indicator of mass sliding failure, such as a large tension crack in the soil surface or obvious visual evidence of significant elongation of the geomembrane below the soil placement area reported by the CQA personnel. However, the geomembrane was stretched in the area that the loaded haul trucks traversed and dumped the soil as indicated by the reduction in the thickness and tensile strength of the samples taken in the upper 1/3 of the slope (between Benches 1 and 2). This is the area where the forces from the construction loads would have been the greatest. Also, sliding of the geomembrane in this area is visually apparent from the striations observed in the soil surface exposed beneath the geomembrane when the samples were cut (see Figure 3b), as well as the direction of bending of the spikes observed in geomembrane (see Figure 3c).

Once the geomembrane had been tensioned, and despite the fact that the equipment was no longer on the slope, the friction resistance of the geomembrane/soil interface was reduced to a value less than the peak friction resistance and approaching the residual friction resistance of the interface. Consequently, the FOS against sliding for that portion of the slope that has been stretched was somewhat less than the original design FOS = 1.6, although it cannot be accurately estimated.

5.2.3 Discussion of Elongation Potentially Caused by Gas Pressures

The existence of the gas bubble at the toe of the slope is of significance because it brought to light the existence of wrinkles within the geomembrane in this location. As indicated on Table 5, the intent of the Case 5 veneer stability analyses was to quantify first, the gas pressure needed to counter the weight of the soil and thus “break” the contact between the soil and the geomembrane, and second, to estimate the tension in the geomembrane once there was no contact between these two components. Based on this analysis, the gas pressure necessary to lift the geomembrane when there is no equipment on the slope is about 762 mm of water (about 6.9 kPa). Given that the geomembrane bubble pushed the soil away and was exposed, this level of gas pressure is known to have occurred. As described in Section 4, if the soil on about 1/3 of slope length is lifted by gas pressure, the geomembrane would be in tension at approximately its yield point, which could cause some permanent elongation.

The samples indicate that there was elongation of the geomembrane in the vicinity of the largest gas “bubble,” but the elongation was not as severe as the elongation of the samples in the upper portion of the slope. The elongation of samples taken from what is inferred to be the top portions of the gas bubble has been estimated from the reduction in thicknesses of these samples that varies from 1.24 to 1.32 mm (i.e., an 8% to 13% reduction assuming an original average thickness of 1.44 mm). Given the reduction in thickness of the geomembrane, there would be a similar percentage elongation of the geomembrane within the exposed area as indicated by the graph included in Figure 4. Samples obtained from an area just upslope of the bubble would also be slightly elongated.

In addition to the slight elongation at the gas bubble area, it was noticed that the soil under the geomembrane samples had been marked by the geomembrane spikes in a pattern that indicated that the geomembrane had “jumped” downhill, rather than dragged downhill, as was observed in the upper portions of the slope. This can be seen in Figure 3a where the spike pattern clearly shows a series of individual spike holes without drag marks, indicating that the geomembrane was lifted off the soil and then re-set. The pattern of the spike marks also indicates that the movement was down the slope. These observations, together with the results of the stability analysis that includes gas pressure, leads to the explanation that it is likely that as the gas pressure built up in the lower portion of the slope the cover system components were lifted, breaking the contact between the soil and the membrane, and the down-slope component of the weight of the soil was transferred to the geomembrane, which carried the load in tension. As the bubble expanded, the gas pressure under the geomembrane temporarily decreased, allowing the cover to drop back down onto the foundation soil, but since the geomembrane was slightly stretched, the new contact location was slightly downhill from the original location. As the gas pressure built up again, the process repeated itself, several times as indicated by the pattern of the spike marks.

6. CONCLUSION

The evidence observed at this site, the geomembrane sample tests results, and the results of the calculations indicate that two different conditions, possibly unrelated, caused the final cover geomembrane to stretch. First, the stretching of the geomembrane between benches 1 and 2, in the upper part of the slope, occurred during construction and it is ascribed to placement of the soil cover from top to bottom of the slope with the 40-ton haul trucks backing down the slope to dump soil on the slope. Second, the wrinkles in the geomembrane noticed after the gas bubble had been deflated were likely a combination of some stretching of the geomembrane in the area where the gas bubble developed along with the accumulation of the geomembrane and the excess geomembrane being “walked” down the slope as landfill gas built up and dissipated over a short period of time. There is some excess geomembrane from small waves that occur during normal geomembrane deployment and with top-to-bottom construction, some of this excess would have also been walked down the slope. The excess geomembrane in the wrinkles near the toe of slope is not thought to be a result of the stretching upslope, since this amount of material would have been noticed during construction, which was not so recorded in the construction quality assurance records. Also, the excess geomembrane at the bottom of the slope was not the result of a mass slide of the cover down the slope pushing geomembrane to the bottom since there was no evidence of such sliding either in the soil cover or at the soil/geomembrane interface on the slope below midslope.

REFERENCES

- Koerner, R.M., Soong, T.Y. (1998). Analysis and Design of Veneer Cover Soils, Proceeding of the Sixth International Conference on Geosynthetics Roseville, MN, IFAL, pp 1-26.
- Qian, X., Koerner, R.M., Gray, D.H. (2002). *Geotechnical Aspects of Landfill Design and Construction*, Prentice Hall, New Jersey, USA.

Investigation of Temperature Variation in Soil Backfill and its Consequence to Tensile Strength of Geogrid

Andrew M. Kasozi, Department of Civil and Environmental Engineering, University of Nevada, Reno, USA, akasozi@gmail.com

Rajib Mahamud, Department of Mechanical Engineering, University of Nevada, Reno, USA, rajib.mahamud@gmail.com

Raj V. Siddharthan, Department of Civil and Environmental Engineering, University of Nevada, Reno, USA, siddhart@unr.edu

ABSTRACT

Use of geogrid reinforcement in Mechanically Stabilized Earth (MSE) walls can provide a feasible and economical alternative to using inextensible steel reinforcement. The latter can undergo elevated levels of corrosion, over time, such as was discovered in two well-documented field cases in Southern Nevada. Nevada DOT has used inextensible steel reinforcement for all of their MSE walls thus far. Therefore, use of geogrid reinforcement may become necessary since it also comes with relatively easier installation during construction. However, long term performance of geogrid reinforcement under elevated temperatures, such as those encountered in Southern Nevada, remains uncertain especially since polymeric materials exhibit temperature-sensitive behavior. Current design manuals (AASHTO 2002a and AASHTO-LRFD 2007) limit the design air temperature at the wall site to 30°C in long-term static design. This study showed that this threshold is exceeded in select cities in Southern Nevada, which presents a dilemma relative to undertaking geogrid reinforced soil wall designs in such locations. By evaluating laboratory and field data, an attempt has been made to develop a design framework to address the effect of elevated temperatures on long term performance of geogrid reinforcement. Arrhenius modeling to model strength degradation due to long term exposure to elevated temperatures, and thermal modeling to model soil backfill temperatures, are presented here as integral parts of the proposed design framework. Strength of geogrid was evaluated through the ultimate tensile strength test in accordance with ASTM D6637 under temperatures ranging from 20°C to 40°C.

1. PROBLEM STATEMENT

1.1 Introduction

Mechanically Stabilized Earth (MSE) wall is one of the least expensive earth retaining structures and it is used extensively in Nevada. Nevada DOT has used inextensible steel reinforcements for all of their MSE walls thus far. However, one major concern that has become apparent recently is the elevated corrosion of steel reinforcement. This is because within the last ten years, two well-documented field cases of substantially elevated corrosion have come to light in Southern Nevada. Across the United States there is a growing trend towards favoring use of geosynthetic reinforced soil (GRS) walls because of their improved performance capabilities and relative installation ease during construction.

Use of geosynthetic reinforcement can avoid the corrosive aspects of the degradation of reinforcing material. However, geosynthetic materials may have other potential degradation issues that are specific to the conditions in Nevada. Such issues include uncertainty of field performance at elevated temperatures along with wide swings that can substantially accelerate the degradation of strength and stiffness with aging (e.g., creep). Design manuals limit the design air temperature at the wall site to 30°C in long-term static design (AASHTO 2002a and AASHTO-LRFD 2007). The temperatures in many locations in Southern Nevada exceed this limit thereby presenting a dilemma relative to undertaking geosynthetic wall designs in such locations.

This paper presents a design framework, based on laboratory and field data to account for the effect of elevated temperatures on performance of geosynthetics in future MSE wall designs in Nevada. The ultimate tensile capacity, which is a critical design input to GRS wall design, was the focus of the laboratory investigation.

1.2 Design Temperature at Selected Sites in Southern Nevada

The effective design temperature is defined as the temperature which is halfway between the average yearly air temperature and the normal daily air temperature for the warmest month at the wall site and should not exceed 30°C for permanent applications (AASHTO LRFD, 2007). The cities of Las Vegas, Laughlin and Henderson were selected as being representative sites in Southern Nevada to first establish a historical temperature profile at each of these sites.

These data were then used to arrive at the effective design temperature. Use was made of the Mechanistic Empirical Pavement Design Guide (MEPDG; AASHTO 2002b) software in this effort. The MEPDG is a widely used and most recent AASHTO design procedure to undertake pavement design. One of the initial steps in this design procedure is to establish the pavement temperature based on air temperature at a given site. The MEPDG temperature analysis is undertaken with a climatic database containing hourly data from 800 weather stations across the United States. The data source embedded in MEPDG is from the National Climatic Data Center (NCDC). Given location e.g. latitude and longitude, the software computes and outputs interpolated air temperature distribution data, by month, from nearby weather stations. It interpolates across two or more weather stations that are closest to the user-defined location. Table 1 shows the stations used for the three cities identified above.

Table 1. Weather Stations used to determine design temperature in select Southern Nevada cities

City	Station	Latitude, Longitude	Distance from Selected Site, km	Complete Data Available, Months
Las Vegas ¹	McCarran Int. Airport, NV	36.05, -115.10	11.9	116
	North Las Vegas Airport, NV	36.13, -115.12	11.9	65
Laughlin ²	McCarran Int. Airport, NV	36.05, -115.10	95.6	116
	Needles Airport, CA	34.46, -114.37	62.4	62
Henderson ³	McCarran Int. Airport, NV	36.05, -115.10	15.4	116
	North Las Vegas Airport, NV	36.13, -115.12	27.4	65

¹Las Vegas latitude and longitude are 36.08, -115.17, respectively

²Laughlin latitude and longitude are 35.14, -114.62, respectively

³Henderson latitude and longitude are 36.03, -114.98, respectively

The Design Guide uses a base unit of one month (30 days), as the analysis period, in establishing the temperature history at a given site. In situations where freeze-thaw cycles are present, the analysis period is reduced to 15 days to account for rapid changes in the pavement material properties during the freeze-thaw period (AASHTO, 2002b). Due to lack of swing in temperature, a 30-day analysis period was considered to be appropriate for Southern Nevada. The software generates a table for average monthly quintile air temperatures at the pavement surface in accordance with the following steps. Quintile temperatures are simply temperatures that represent 20% of the temperature data in the analysis period.

- The analysis starts out with 720 hourly air temperature data points for each month (24 hrs x 30 days);
- The data points are rearranged in ascending order;
- Data is then split into 5 segments of 144 data points each i.e. quintiles;
- The average temperature in each quintile is then computed;
- Repeats the above steps for each corresponding month in every year for which data is available;
- Computes averages of each of the corresponding quintiles for the specific month;
- Finally computes mean of the quintiles in each month to obtain their corresponding mean surface temperatures.

The MEPDG uses these surface temperatures, among other data, to produce the temperature profile in the pavement. These data are then used in pavement performance models to predict pavement distresses. As a representative historical temperature data, only the computed average monthly quintile air temperature data for Las Vegas is reported in Table 2. The air temperature data used span from July 01, 1996 to February 28, 2006. In determining the effective design temperature, the average yearly air temperature was computed as the arithmetic mean of the monthly mean temperatures in Table 2. The normal daily air temperature for the warmest month was read off as the highest mean temperature. July was observed to be the warmest month at each of the three locations considered. The effective design temperature at the wall site was finally computed as the arithmetic mean of the average yearly air temperature and the normal daily air temperature for the warmest month. Table 3 summarizes the design temperature calculations for the three cities evaluated. The results in Table 3 show that the AASHTO threshold of 30°C is exceeded for all three cities. The approach discussed above is preferred to one that uses only maximum and minimum air temperature data because the latter skews the analysis and is bound to produce lower effective design temperatures. This approach therefore, ensures safer MSE wall designs in locations where temperature may be an issue.

1.3 Review of a Case Study

The Tanque-Verde GRS wall project located in Tucson, AZ is a well-instrumented wall site located in the Sonora desert whose conditions closely approximate those in Southern Nevada. The environmental conditions at the site provide an ideal case study to address many of the geosynthetic wall behavior concerns in Southern Nevada (Crouse et al. 2003).

Table 2. Quintile Air Temperatures-Las Vegas

Month	1 st Quintile, °C	2 nd Quintile, °F	3 rd Quintile, °C	4 th Quintile, °C	5 th Quintile, °C	Mean Temp., °C	Std. Dev., °C
January	3.6	7.4	10.6	14.4	20.6	11.3	-11.7
February	5.3	9.2	12.2	16.5	23.0	13.3	-11.4
March	8.8	13.5	17.7	23.7	32.9	19.3	-9.0
April	11.5	16.7	21.4	27.5	38.1	23.1	-8.2
May	18.6	24.2	29.2	36.3	45.1	30.7	-8.2
June	23.3	28.6	33.9	41.5	50.2	35.5	-8.0
July	27.2	31.6	36.7	43.7	51.6	38.1	-8.9
August	27.1	31.2	35.7	42.9	50.5	37.5	-9.2
September	21.0	25.6	29.9	37.2	45.9	32.0	-8.7
October	12.7	17.7	21.9	27.7	38.1	23.6	-8.6
November	7.0	10.7	14.1	18.8	26.4	15.4	-10.8
December	3.1	6.8	9.7	13.8	20.2	10.7	-11.6

Table 3. Effective Design Temperatures in select cities in Southern Nevada

City in Southern Nevada	Average Yearly Air Temperature, °C	Normal Daily Air Temp. (Warmest Month), °C	Effective Design Temperature, °C
Las Vegas	24.2	38.1	31.2
Laughlin	27.2	41.4	34.3
Henderson	23.2	37.6	30.4

The project was completed with full-height precast concrete wall facing in October 1985 and serves as a grade separation for a highway project (Fishman et al. 1991). The geosynthetic reinforcement used on this project featured the uniaxially oriented SR2 geogrid made of extruded high density polyethylene (HDPE) from Tensar International Corporation. This geogrid had a maximum tensile strength of 79 kN/m (Fishman et al. 1991).

The wall was instrumented with the goal to study the response of the wall system and compare it with design assumptions and calculations that were made. Instrumentation included resistance thermometers to determine the distribution of temperature within the reinforced soil backfill. Figure 1 shows temperature readings within the wall section taken in March 1986 at 11:00 am, June 1986 at 3:00 pm, and June 1996 at 8:30 am (FHWA 1989 and Wayne et al. 1998). The soil backfill temperatures observed in Figure 1 clearly reflect the influence of air temperature measurements shown on the wall face. The highest backfill temperature was 39°C recorded at 8:30 am in June 1996. At that time the average wall face temperature was 44°C. This represents a 5°C reduction in backfill temperature relative to wall face temperature. It should be noted that wall surface temperatures are directly influenced by air temperature fluctuations and presence of cloud.

Despite the high soil backfill temperature, the overall performance of the Tanque-Verde wall has been reported to be satisfactory over the last 25 years with no major issues (Berg et al. 2009). The applicability of this one observation to other geosynthetics, soils and environmental conditions would however be questionable. In addition, a large safety factor of 10 was used on this project (FHWA 1989). According to NOAA weather data presented for major US cities by Bonaparte (1987), the maximum and average air temperatures in Tucson, AZ were lower than those in Las Vegas, NV. The maximum and average air temperatures were reported as 37°C and 30°C, respectively, for Tucson, AZ whereas Las Vegas temperatures were reported as 40°C and 32°F, respectively. This observation, coupled with the soil backfill temperature trends in Figure 1 and the fact that design temperatures in Southern Nevada exceed the AASHTO threshold (Table 3), justify the GRS wall design concerns for Southern Nevada. Moreover the temperature immediately behind the facing could be higher than the air temperature for walls which face the sun (AASHTO 2002a, AASHTO-LRFD 2007).

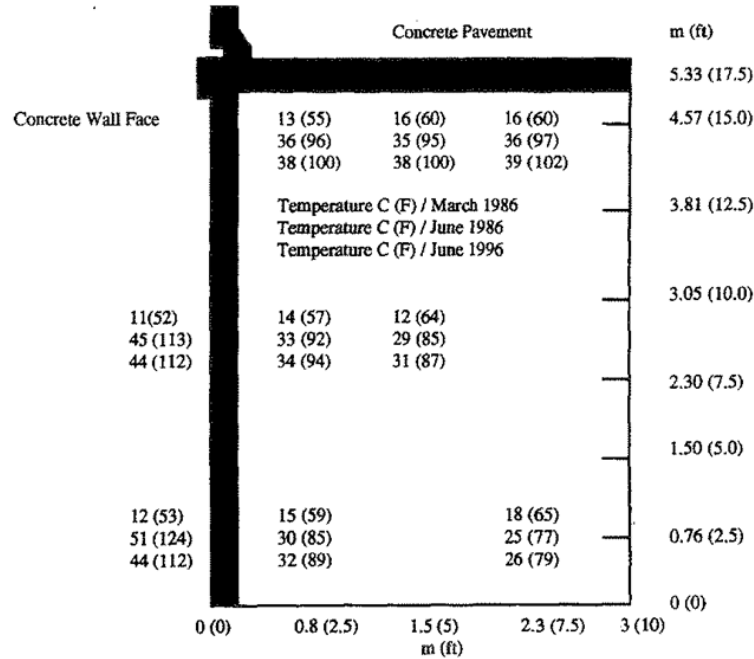


Figure 1. Temperature readings within wall section (Wayne et al. 1998).

1.4 Design Approach

According to AASHTO-LRFD (2007) wall design procedures, the allowable long-term reinforcement tensile strength (T_{all}) required to prevent rupture calculated on a load per unit of reinforcement width basis is defined as:

$$T_{all} = \frac{T_{ult_lot}}{RF} \quad [1]$$

where,

$$RF = RF_{ID} \times RF_{CR} \times RF_D \quad [2]$$

T_{ult_lot} is the average lot-specific ultimate tensile strength for the unaged (fresh) lot of material (ASTM D6637) and RF is a combined reduction factor to account for potential long-term degradation due to installation damage (ID), creep (CR) and rupture of reinforcement due to strength degradation (D). Representative values of RF_{ID} , RF_{CR} and RF_D have been suggested by Elias et al. 2009 and AASHTO 2002a, AASHTO-LRFD 2007, among others. Notably, elevated temperatures directly affect RF_{CR} and RF_D factors. The ultimate tensile capacity, which was the focus of the foregoing study, is reflected in the RF_D factor as shown in Equation 3 below;

$$RF_D = \frac{T_{ult_lot}}{T_D} \geq 1.1 \quad [3]$$

where, T_{ult_lot} is as defined before; and T_D is the extrapolated lot-specific tensile strength after degradation based on laboratory aging tests. Elias et al. (2009) propose that a Product-Specific Durability Study be undertaken to arrive at the appropriate design RF_D value. In such an undertaking, laboratory aging tests along with the use of Arrhenius modeling are recommended. Arrhenius modeling allows for time-temperature superposition and is widely used to forecast strength degradation in polymer science. Details on this are presented subsequently.

2. LABORATORY TESTING

This effort was geared towards evaluating the effect of elevated temperatures on the strength of geogrid. The ultimate tensile strength and failure strain of geogrid were measured in accordance with ASTM D6637.

2.1 Geosynthetic Material Evaluated

The uniaxial (UX1600MSE) HDPE geogrid from Tensar International Corporation was evaluated. A roll of the material, size 1.33 m x 61 m, was obtained and out of it, single rib samples were cut and used in the tensile testing. Industrial Fabrics Association International (2011) provides an ultimate tensile strength of UX1600MSE geogrid of 144 kN/m. This value is consistent with that reported on Tensar International Corporation's website. The recommended minimum RF_{ID} , RF_{CR} and RF_D values by Tensar International Corporation for the UX1600MSE geogrid are 1.05, 2.60 and 1.0, respectively.

2.2 Laboratory Test Temperatures

The temperature data in Table 2 was used to estimate representative test temperature ranges for use in laboratory testing. The following temperature ranges were selected arbitrarily: <27°C, 27 - 32°C, 32 - 38°C, 38 - 43°C, 43 - 49°C and >49°C. The average percentage of time, in days, for which a temperature range is exceeded in a year, was then computed and the results plotted in Figure 2(a). According to Figure 2(a), on average, the hourly air temperature in Las Vegas exceeds 30°C for 33% of the time in a year. This amount of exposure to elevated temperatures may not be trivial to GRS wall performance.

Further, using the results in Figure 2(a) the annual exposure time to the selected range of temperatures was computed and the results graphed are shown in Figure 2(b). A year was considered to have 360 days, consistent with 30-day month analysis periods in the MEPDG procedure. From the results in Figures 2(a) and 2(b) it was decided that the elevated temperatures for laboratory testing would be 20°C, 30°C and 40°C. 20°C was included as being on the lower end of the 30°C threshold and also because it is the standard test temperature as per ASTM D6637.

2.3 Laboratory Test Setup and Testing

The ASTM D6637 procedures were used with the higher test temperatures mentioned in the previous section. In other words, all other requirements of the test standard were adhered to except the test temperature. An environmental chamber to facilitate elevated and controlled temperature testing was constructed around the Universal Testing Machine (Figures 3(a) and 3(b)).

Preliminary testing included both unconditioned (fresh) and conditioned geogrid samples. The fresh samples represent strength properties at the early stages of service (i.e. immediately after construction) whereas conditioned geogrid represents the aged material in the field. Conditioning constituted hanging geogrid samples in a forced air draft oven (Figure 3(c)) at 91°C for durations of 1, 5, 10 and 30 days i.e. heat-aging. The conditioning temperature was selected as the high end of the range recommended for HDPE polymers by Elias et al. (2009) while the choice of conditioning durations was limited by project duration and budget. Different conditioning durations provide a simple means of evaluating tensile strength property changes with age in the field.

Testing was conducted on a single longitudinal rib cut from a grid sample. The effective length of rib under tension was 0.44 m. The test was conducted at a constant rate of extension of 10% per minute at 20°C, 30°C and 40°C. A total of 5 replicates were tested for each sample category.

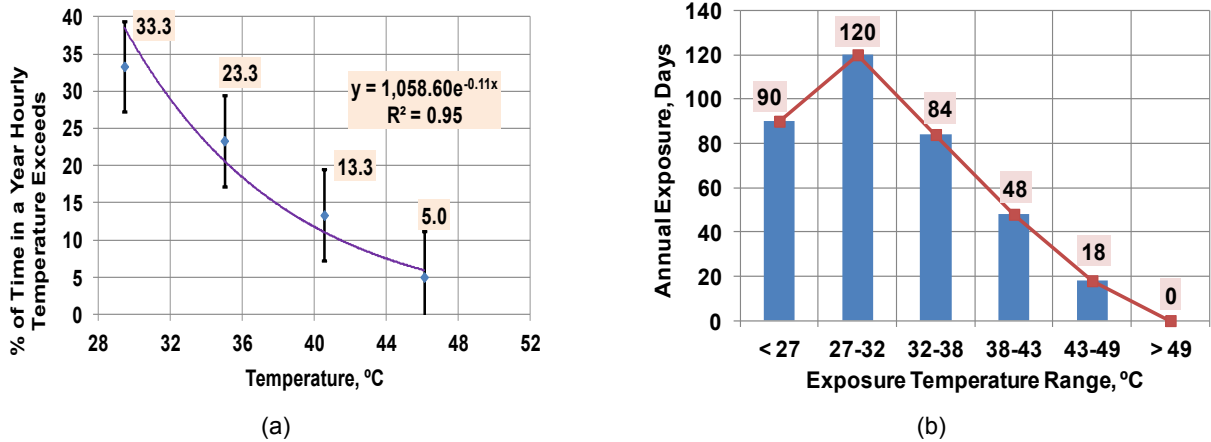


Figure 2. (a) Hourly air temperature distribution in Las Vegas (whiskers represent mean \pm 1 STD, while highlighted numbers represent means for the years of data considered); (b) Annual exposure time to specific temperature ranges in Las Vegas

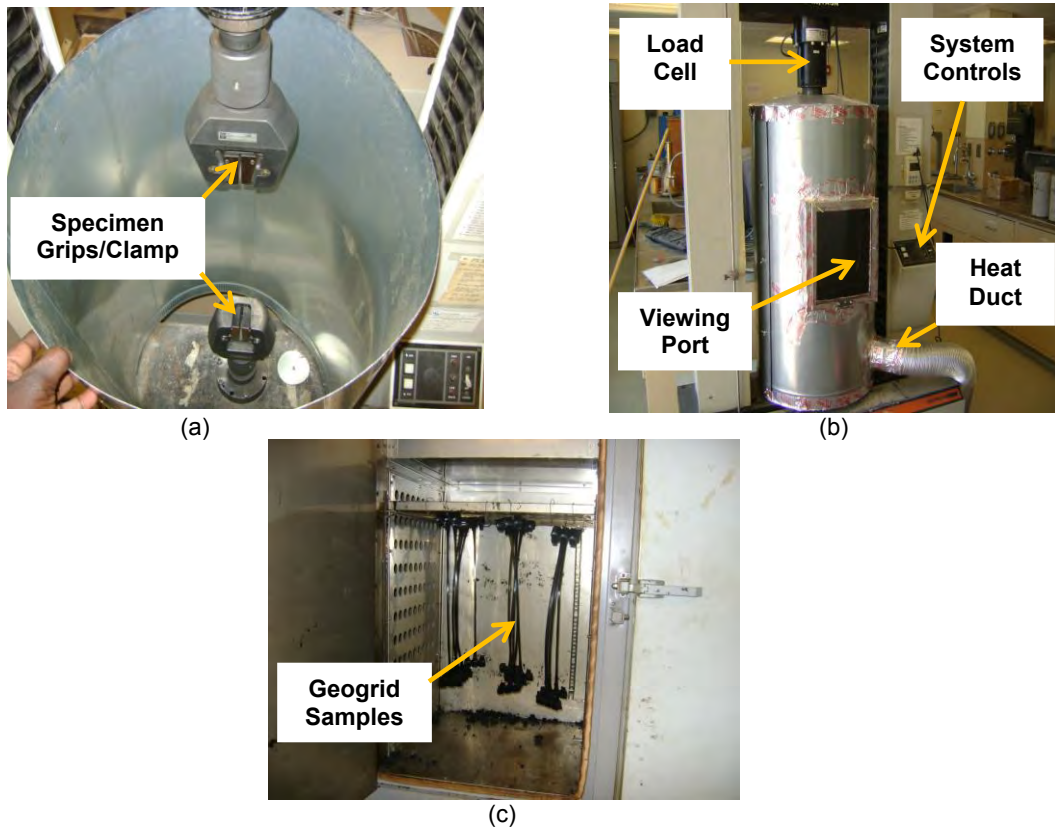


Figure 3. (a) Plan view inside chamber; (b) Chamber in front elevation view; (c) Oven conditioning of Geogrid samples

2.4 Results and Discussion

Table 4 shows a summary of the test results. Tensile strength ratios were calculated by normalizing the conditioned value at the test temperature with the unconditioned value at the same temperature. Failure strain ratios were calculated in a similar manner. When ratios are greater than 100%, the property is higher at the elevated test temperature.

The data obtained on fresh samples showed a decrease of 8% in ultimate tensile strength at 30°C and a further 15% decrease at 40°C. This is based on tensile strength ratios calculated by normalizing the value at elevated temperature

with that at 20°C. In a similar manner, the data showed a 12% increase in strain required to develop the peak tensile strength at 30°C and a further 13% increase when the temperature increased to 40°C. The latter is believed to be due to the geogrid becoming slightly more ductile as test temperature increased. This would most likely result in more distress in the form of higher MSE wall deformations before failure. Further investigation is necessary to address this issue. The data obtained on the heat-aged geogrid samples showed that overall, sample conditioning increased both the ultimate tensile strength and the failure strain of the geogrid at the elevated temperatures. However as expected, for a given conditioned sample (i.e. same conditioning duration) the ultimate tensile strength decreased as the test temperature increased. Additionally, for a given test temperature, both the ultimate tensile strength and failure strain generally increased with conditioning duration.

It is worth noting that results of tensile tests conducted in air are conservative compared to observed in-soil behavior. In-soil behavior is such that under load, both soil and geogrid deform and stresses develop within the geogrid. Upon load withdrawal, McGown et al (1995) report that the geogrid attempts to recover its original shape but this is resisted by the soil particles within the geogrid apertures. This results in locked-in stresses in the geogrid which are transmitted to the trapped soil as compressive stresses. It is the presence of residual tensile strains in the geogrid, as shown by McGown et al (1995) that indicates presence of these locked-in stresses. However, the in-air tensile test results discussed above are invaluable to defining overall trends in the material behavior under elevated temperatures.

3. PROPOSED DESIGN FRAMEWORK

In order to account for the effect of elevated temperatures on long term performance of geogrid reinforcement, a design framework was proposed as shown in Figure 4. The design framework is such that results from both Arrhenius and thermal modeling are required to modify the design. These are explained in the following sections.

Table 4. Results of tensile strength testing on both conditioned and unconditioned samples

Conditioning Time, days	Ultimate Tensile Strength, kN/m	Tensile Strength Ratio, %	Tensile Strain at Failure, %	Failure Strain Ratio, %
Testing Temperature = 20°C				
0	141.7	100	11.3	100
1	149.6	106	13.8	122
5	150.7	106	14.2	126
10	154.5	109	15.1	134
30	151.9	107	16.3	144
Testing Temperature = 30°C				
0	130.0	100	12.7	100
1	127.1	98	14.9	117
5	131.9	101	16.8	132
10	129.7	99	15.8	124
30	130.9	106	15.9	125
Testing Temperature = 40°C				
0	109.2	100	14.1	100
1	105.4	97	15.0	106
5	113.6	104	16.4	116
10	114.5	105	17.1	121
30	108.9	99	17.0	121

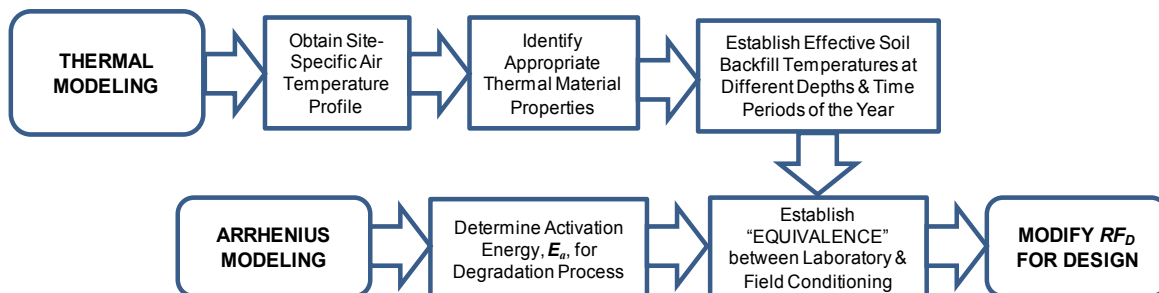


Figure 4. Elements of the proposed design framework to account for effect of elevated temperatures

3.1 Arrhenius Modeling

Arrhenius modeling, which is based on time-temperature superposition, is the predictive technique most widely used by industry for polymer degradation (Elias et al. 2009). It uses material behavior under predefined testing conditions (time and temperature) to predict similar behavior under field conditions and/or vice versa. The process involves conditioning the polymeric material at high temperatures, followed by laboratory testing to define physical or chemical properties so as to extrapolate the experimental behavior to a site-specific and lower temperature (Koerner et al. 1992). In the foregoing study, the ultimate tensile strength of geogrid was the physical property of interest. Arrhenius modeling is ideally suited to account for the effect of elevated temperatures on selection of design long-term tensile capacity of geogrid reinforcement.

The rate of polymer degradation is temperature-sensitive and can be modeled using the Arrhenius rate equation shown below in Equation 4.

$$K = Ae^{\frac{-E_a}{RT}} \quad [4]$$

Where: K is the rate constant at temperature, T, in Kelvin; A is the pre-exponential factor; E_a is the activation energy, or minimum energy required for intermolecular movement to occur, in Jmol^{-1} ; and R is the universal gas constant ($8.3136 \text{ Jmol}^{-1}\text{K}^{-1}$). Based on a melting point range of 120 – 130°C typical of medium and high density polyethylene, 116°C was selected as the highest conditioning temperature so as to ensure significant changes in the ultimate tensile strength of the geogrid. Subsequently, 93°C and 104°C were also selected since additional conditioning temperatures are required to complete the Arrhenius modeling scheme. The geogrid was conditioned at these temperatures in a forced draft oven for various exposure times.

Geogrid samples were retrieved from ovens after various exposure times and were immediately tested for ultimate tensile strength at 20°C in accordance with ASTM D6637. Table 5 shows the results of this effort. The percent reduction in strength is calculated with reference to the unconditioned value i.e. strength at zero days.

Table 5. Results of tensile strength testing on retrieved samples for Arrhenius modeling

Aging Time, days	T = 93°C		T = 104°C		T = 116°C	
	T _{ult} , kN/m	% Strength Reduction	T _{ult} , kN/m	% Strength Reduction	T _{ult} , kN/m	% Strength Reduction
0	141.7	0.0	141.7	0.0	141.7	0.0
1	141.0	0.5	139.2	1.8	135.4	4.5
10	-	-	136.0	4.1	-	-
15	-	-	-	-	92.9	34.5
20	-	-	-	-	89.5	36.8
30	138.1	2.6	128.4	9.4	82.1	42.1
50	-	-	118.6	16.3	-	-
60	136.4	3.8	-	-	-	-
72	134.6	5.1	-	-	-	-

Based on these results, linear regression analysis of percent strength reduction versus exposure time was used to compute the strength degradation rate constant, K for each of the conditioning temperatures. In such linear regression, K is simply the slope of the straight line as seen in Figure 5(a). Rearranging Equation 4 reveals that when the natural logarithm of K is plotted against the inverse of temperature, T, a straight line with slope, $-E_a/R$, is obtained (Figure 5(b)). This enabled determination of activation energy, E_a , as $16696.5 \text{ Jmol}^{-1}$, for the tensile strength degradation process evaluated. From Figure 5(b), Equation 6 provides the relationship that can be used to estimate the reduction rate in ultimate tensile strength at various temperatures.

$$\ln K = -20051 \left(\frac{1}{T} \right) + 51.97 \quad [6]$$

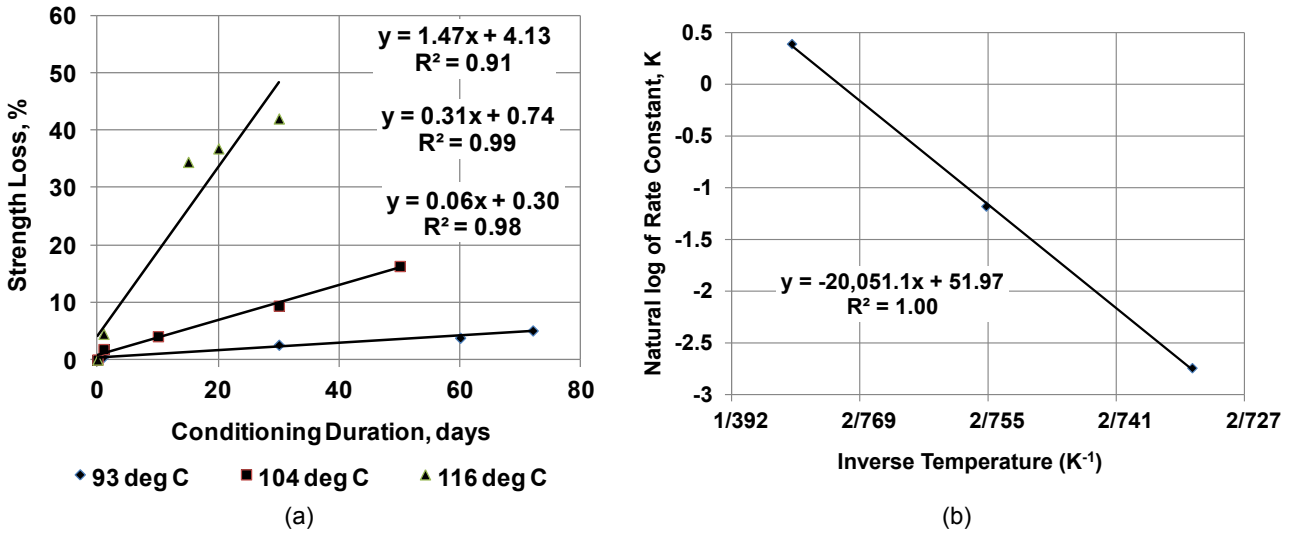


Figure 5. (a) Linear regression analysis of test data to determine strength degradation rate, K; (b) Determination of Arrhenius equation parameters

3.2 Thermal Modeling

3.2.1 ANSYS Modeling

In order to estimate soil backfill temperatures, a one-dimensional (1D) transient heat flow analysis was conducted using the finite element-based solver/software, ANSYS Fluent 12.1. The mid-section of the Tanque-Verde wall shown in Figure 1 was selected for modeling purposes. The trends of the concrete face panel and soil backfill temperature data in Figure 1 suggest that the soil backfill temperatures in the top section are influenced by the concrete pavement at the top while those in the bottom section are influenced by the absorptive nature of the in-situ soil acting as a heat sink along with presence of a hot mix asphalt layer to the bottom left of the wall. Focus was therefore given to the mid-section where 1D modeling may be appropriate. The model consists of a concrete face panel section and an adjacent soil backfill section, which is the primary area of interest. Figure 6 shows a schematic of the model with the appropriate dimensions. To make the problem 1D, the upper and lower boundaries of the mid-section were made insulated, as shown in Figure 6. An insulated boundary condition was also applied at the far end of the soil since temperature there remains relatively unchanged. It is believed that numerical modeling is an ideal tool for estimating soil backfill temperatures where no field data are available.

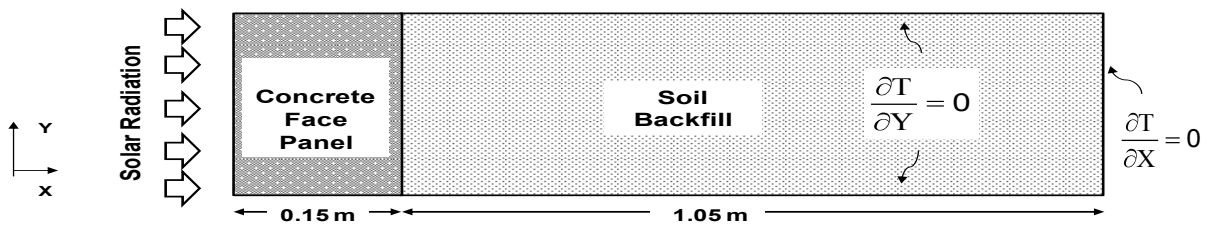


Figure 6. Schematic diagram of the 1D transient heat flow analysis model

The domain was uniformly meshed with square elements of size 0.005 m. A time increment of 450 s was selected as the time step size for the transient solution and a total of 20 iterations for every time step was used.

3.2.2 Thermal Material Properties

The thermal material properties of interest in heat flow analyses include thermal conductivity (K), density (ρ) and specific heat (C_p). These were carefully selected based on the collation presented in Table 6 which provides a summary from different sources. Medium weight concrete was used for the concrete face panel since it is typically non-structural. As such, its thermal conductivity was selected as 1.194 W/m $^{\circ}$ C which corresponds to a density of 1920 kg/m 3 (Neville 2009). Its specific heat was selected as 840 J/kg $^{\circ}$ C, resulting in a thermal diffusivity of concrete face panel of 7.4×10^{-7}

m²/s which is within the range (Neville 2009). Thermal diffusivity (ψ) is the ratio of thermal conductivity to the product of density and specific heat.

Table 6. Summary of relevant thermal material properties from different sources

Thermal Property	Concrete Face Panel	Soil Backfill (Sandy)	Source
Thermal Conductivity (K), W m ⁻¹ °C ⁻¹	0.1 – 0.7	0.15 - 2	Engineering Toolbox, 2012
	-	4.5 – 7.1	Geo Studio, 2010
	0.360 – 1.488	-	Neville, 2009
	-	0.25 – 2.5	Mitchell et al. 2005
Density (ρ), kg m ⁻³	-	0.23 – 2.8	Jumikis, 1966
	1120 - 2080	-	Neville, 2009
Specific Heat (C_p), J kg ⁻¹ °C ⁻¹	-	1900 - 2000	Jumikis, 1966
	895	830	Engineering Toolbox, 2012
	840 - 1170	710	Geo Studio, 2010
	-	-	Neville, 2009
	-	2.4 + 427 ω /100 g *	Mitchell et al. 2005
Thermal Diffusivity, (ψ), m ² s ⁻¹	653	837	Jumikis, 1966
	5.6 x 10 ⁻⁷ – 2.0 x 10 ⁻⁶	-	Neville, 2009

* ω is water content based on mass and g is acceleration due to gravity

Assuming 4% water content for the soil backfill and selecting a density of 1900 kg/m³ (Jumikis, 1966) as reasonable, the thermal conductivity of the soil backfill was selected as 1.5 W/m/°C and specific heat as 878 J/kg/°C (Mitchell et al. 2005). This gives a thermal diffusivity of soil backfill of 9.0 x 10⁻⁷ m²/s and this was used in the modeling.

3.2.3 Boundary and Initial Conditions

Equation 7 (Jumikis, 1966) is the governing equation for the 1D transient heat flow analysis with x as the horizontal distance from the exposed surface of the concrete face panel to the interior of the soil backfill.

$$\frac{\partial T}{\partial t} = \psi \frac{\partial^2 T}{\partial x^2} \quad [7]$$

Equations 8 – 11 show the boundary and initial conditions that were used in the modeling.

$$T(x = 0, t = 0) = T_{s,avg} \quad [8]$$

$$T(x > 0, t = 0) = T_{s,avg} \quad [9]$$

$$T(x = 0, t > 0) = T_s \quad [10]$$

$$\frac{dT(x = 1.2, t > 0)}{dx} = 0 \quad \text{(Boundary condition at right hand side or far-end of domain)} \quad [11]$$

where; $T_{s,avg}$ is the average surface temperature also assumed to be the initial temperature, and T_s , the concrete face panel surface temperature assumed to follow a sinusoidal function with time, t, as shown in Equation 12 and Figure 7. A similar sinusoidal temperature variation was also suggested by Bonaparte (1987).

$$T_s = T_{s,avg} + \Delta T_s \sin(\omega t - \phi) \quad [12]$$

where: $\Delta T_s = T_{s,max} - T_{s,avg} = T_{s,avg} - T_{s,min}$; $\omega = \frac{2\pi}{T}$, T = period = 24 hours; and ϕ is the phase shift.

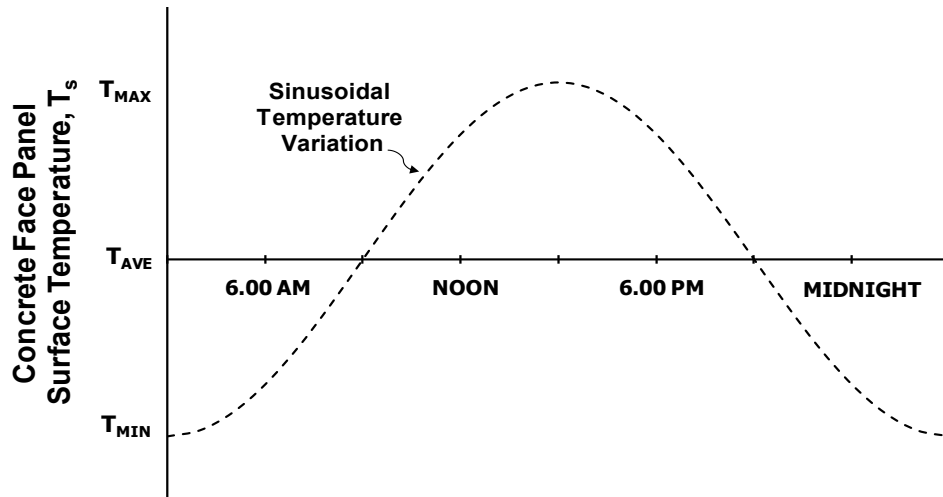


Figure 7. Sinusoidal temperature variation at the concrete face panel surface

Based on Figure 1, 45°C was used as the maximum surface temperature in the analysis, and $T_{s,avg}$ was taken as 29.4°C, which is the measured soil backfill temperature at the far end. In case surface temperature is unknown, it can be determined from air temperature (T_{air}) using Equation 13 in which ΔT is the increase due to solar radiation as suggested by Bonaparte (1987).

$$T_s = T_{air} + \Delta T \quad [13]$$

Obtaining site-specific data such as that shown in Table 2 would be helpful in obtaining T_{air} .

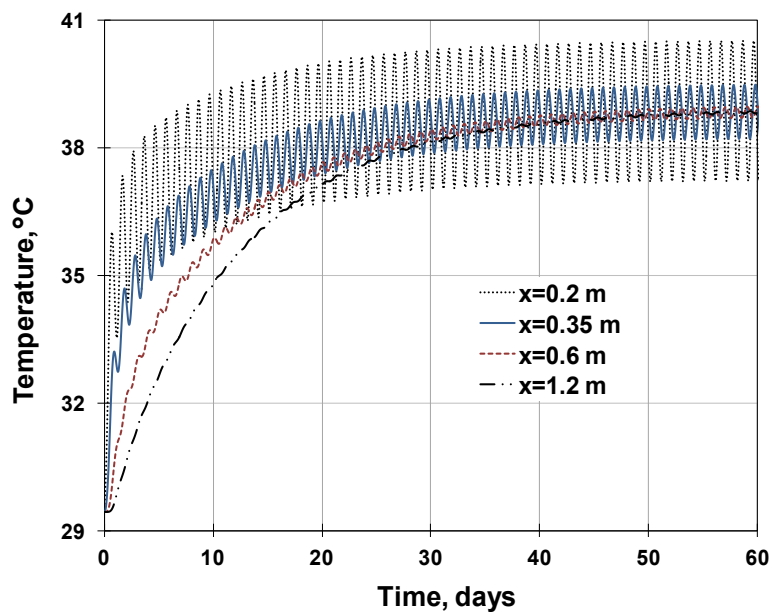


Figure 8. Transient temperature profiles at different soil backfill locations

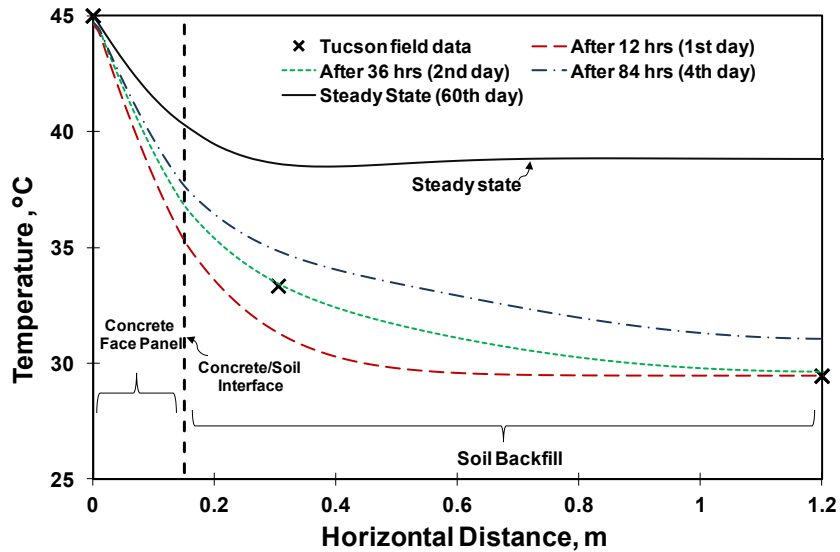


Figure 9. Comparison between Tucson, AZ field-measured data and computed data from ANSYS modeling

3.2.4 Thermal Modeling Results

In order to establish the time it takes for a steady state condition to occur, temperature-time histories were evaluated using ANSYS at different soil backfill locations as shown in Figure 8. According to Figure 8, steady state is reached after about 60 days. However the field measured temperature at $x = 0.35$ m, in the soil backfill, occurs between the first and third day. This is explained by the fact that the field data were taken in June, which is early summer, with yet more heating to occur in the latter parts of the summer. In addition, the initial temperature (29.4°C) was set high enough to match computed data with field data at an early stage of simulation. It is also worth noting that locations closer to the concrete face panel (i.e. $x = 0.2$ m and $x = 0.35$ m) exhibit significant temperature fluctuations compared to those that are deeper in the interior of the soil backfill. This is because the former are more influenced by air temperature fluctuations due to their proximity to the exposed surface. Figure 8 also shows that the temperature gaps between points reduce as the system approaches quasi steady state condition.

Based on the results from Figure 8, the spatial temperature distribution was plotted for different times of simulation as shown in Figure 9. In all cases since the backfill temperatures were measured at 3:00 pm on June 16, 1986, the computed temperature values also correspond to those at 3:00 pm. This time of day corresponds to the highest temperature value in the daily variation shown in Figure 7. It is clear from Figure 9 that the computed data matched well with the field data after about 36 hours of simulation, which falls on the second day.

3.3 Integration of Elements of Design Framework

As noted above in Figure 4, there are many elements that need to be integrated to account for the role of elevated soil backfill temperatures. The following steps outline the proposed design framework.

- a. Establish site-specific air temperature profile data, such as those shown in Table 2, for the selected site of interest (section 1.2);
- b. Undertake thermal modeling to establish the temperature profile within the soil backfill (section 3.2);
- c. Using Arrhenius modeling, determine the percent strength loss (or reduction) per day versus inverse of temperature relationship to evaluate the strength loss (section 3.1, Figure 5(b));
- d. Integrate the steps a and b above to evaluate the total strength loss, progressively as a function of time, over the entire life time of the geosynthetic reinforcement;
- e. Evaluate a conservative estimate for RF_D that can be used in design so that the role of elevated temperature is accounted for in future designs of GRS walls

The proposed design steps are consistent with the Product-Specific Durability Study proposed by Elias et al. (2009).

The ANSYS modeling conducted to establish the backfill temperature utilized a simple 1D model. Though this may be appropriate for the mid-section of the GRS walls, a more appropriate 2D model that allows for the role of the concrete pavement and other boundary conditions (e.g. in-situ or foundation soil conditions) may be required. In addition, this

study focused on tensile strength degradation only. Another design concern is creep and this also can be of importance, since geosynthetics undergo noticeable creep under elevated temperatures.

4. CONCLUSIONS

This study showed that limitation of long term static design air temperature to 30°C imposed by current design manuals (AASHTO 2002a and AASHTO-LRFD 2007) presents a dilemma relative to undertaking geogrid reinforced soil wall designs in Southern Nevada. Using laboratory and field data, a design framework to address this issue has been proposed. Both Arrhenius and thermal modeling are presented as integral parts of the proposed design framework. Following are the conclusions that were made from this study.

- a. Geogrid reinforcement exhibits temperature-sensitive behavior as evidenced by the ultimate tensile strength results conducted in accordance with ASTM D6637 under temperatures ranging from 20°C to 40°C on both fresh and conditioned samples. Conditioning, which was conducted under elevated temperatures ranging from 91°C to 116°C, constituted heat aging in an oven at various exposure times.
- b. Using Arrhenius modeling principles, the activation energy, E_a , of the evaluated geogrid material was established as 134522 Jmol^{-1} . This activation energy relates degradation of tensile strength with time and temperature.
- c. A one-dimensional heat flow analysis was undertaken using ANSYS Fluent 12.1 software to model soil backfill temperatures. By comparing computed data with field-measured data from the Tanque-Verde geogrid-reinforced soil wall in Tucson, AZ, it was shown that thermal modeling is capable of predicting soil backfill temperatures based on air temperatures. This is particularly useful where no field data are available.
- d. A major phase in the proposed design framework is the integration of laboratory-measured degradation of tensile strength and the elevated backfill temperature. This is helpful in predicting long term geogrid performance in the soil backfill. A step by step procedure to accomplish this undertaking is outlined in the paper.
- e. The paper addressed only the tensile strength degradation brought on by elevated temperatures and thermal modeling was limited to a 1D model using ANSYS. The investigation of the role of creep and 2D temperature modeling may be important.

ACKNOWLEDGMENTS

The authors acknowledge the Nevada Department of Transportation for funding this study and Tensar International Corporation for providing geogrid samples for testing.

REFERENCES

- American Association of State Highway and Transportation Officials (AASHTO), (2002a). Standard Specifications for Highway Bridges, 17th Edition, Washington D. C
- American Association of State Highway and Transportation Officials (AASHTO), (2002b). Mechanistic Empirical Pavement Design Guide (MEPDG)
- American Association of State Highway and Transportation Officials (AASHTO), (2007). LRFD Bridge Design Specifications, 4th Edition, Washington D. C
- ASTM D6637. Standard Test Method for Determining Tensile Properties of Geogrids by the Single or Multi-Rib Tensile Method, *American Society for Testing and Materials*
- Berg, R.R. and Anderson, R.P., (2009). Silver Anniversary: The Tanque-Verde Retaining Walls, http://geosyntheticsmagazine.com/articles/1009_f4_anniversary.html, Industrial Fabrics Association International (IFAI)
- Bonaparte, R., (1987). Influence of Temperature on Performance of Tensar Geogrid Reinforced Soil Retaining Walls, Geo Services Project No. 87-901-01
- Crouse, P.E., and Wu, J.T.H., (2003). Geosynthetic-Reinforced Soil Walls, Transportation Research Records, Vol. 1849, TRB Paper No. 03-4066, pp. 53 – 58, National Research Council, Washington D.C
- Elias, V., Fishman, K.L., Christopher, B.R., and Berg, R.R., (2009). Corrosion/Degradation of Soil Reinforcements for Mechanically Stabilized Earth Walls and Reinforced Soil Slopes, Report No. FHWA-NHI-09-087
- Federal Highway Administration, (1989). Tensar Geogrid-Reinforced Soil Wall Grade-Separation Structures on the Tanque-Verde-Wrightstown-Pantano-Roads Intersection Tucson, AZ, Report No. FHWA-EP-90-001-005
- Fishman, K.L., Desai, C.S., and Berg, R.R., (1991). Geosynthetic-Reinforced Soil Wall: A 4-Year History, Transportation Research Records, Vol. 1330, TRB, National Research Council, Washington D.C.
- Geo-Slope International Ltd, (2010). Thermal Modeling with TEMP/W 2007 Fourth Edition, Geo-Studio TEMP/W Software Manual

- Industrial Fabrics Association International (IFAI), (2011). Geosynthetics Specifier's Guide, Geogrids Product Data
- Jumikis, A.R., (1966). *Thermal Soil Mechanics*, Rutgers University Press, New Brunswick, New Jersey, USA
- Koerner, R.M., Lord, A.E. and Hsuan, Y.H., (1992). Arrhenius Modeling to Predict Geosynthetic Degradation, *Geotextiles and Geomembranes* 11
- McGown, A., Yogarajah, I., Andrawes, K.Z. and Saad, M.A., (1995). Strain Behavior of Polymeric Geogrids Subjected to Sustained and Repeated Loading in Air and in Soil, *Geosynthetics International*, Vol. 2, No. 1, pp. 341 - 355
- Mitchell, J.K., Soga, K., (2005). *Fundamentals of Soil Behavior*, 3rd ed., John Wiley and Sons, New York, USA
- Neville, A.M., (2009). *Properties of Concrete*, 4th ed., Pearson Education, Inc. and Dorling Kindersley Publishing, Inc., New Delhi, India
- Wayne, M.H., Bright, D., Berg, R.R., and Fishman, K.L., (1998). Tanque-Verde Retaining Wall Structure: Revisited after 11+ Years, Elsevier Science Limited

Laboratory Evaluation of the Performance of Geosynthetic-Reinforced Aggregate over Weak Subgrade

M. Abu-Farsakh, P.E., Louisiana Transportation Research Center, Louisiana State University, USA.
I. Akond, Department of Civil and Environmental Engineering, Louisiana State University, USA
Q. Chen, P.E., Louisiana Transportation Research Center, Louisiana State University, USA.
L. Mohammad, Louisiana Transportation Research Center, Louisiana State University, USA.

ABSTRACT

The objective of this study was to evaluate the performance of geosynthetic-reinforced aggregate bases for unpaved roads over soft subgrade using laboratory plate load test. The model tests were conducted in a 1.5 m long, 0.91 m wide, and 0.91 m deep steel test box. The load was applied through a 190.5-mm diameter steel plate. The parameters evaluated in this study included the thickness of aggregate base surfacing, the location and tensile modulus of geosynthetics, and the number of geosynthetic reinforcement layers. Test results indicated that the geosynthetic reinforcement resulted in appreciable reduction of surface deformation and increase of bearing capacity for unpaved aggregate base over soft subgrade. The test results also showed obvious effects of the geogrid arrangement/location on the unpaved test section's performance, with the double reinforcement location consistently yielding the largest improvement. Higher tensile modulus geosynthetics performed better than others. Greater improvement due to geosynthetic reinforcement was seen for test sections with thinner aggregate base surfacing.

1 INTRODUCTION

Weak subgrades are a common problem in road construction. Whether it is a temporary access road or a permanent road built over a weak subgrade, a large deformation of the subgrade can lead to deterioration of the paved or unpaved surface. The use of geosynthetic material in unpaved roads built over a weak subgrade is known to provide a reinforcing benefit to the roadway sections. Geogrids and geotextiles help distribute the loads more efficiently, increase the effective bearing capacity of the subgrade, and hence provide a better alternative to costly, conventional, stabilization methods. Geosynthetic materials have been widely used as reinforcement in structures with unbound materials, such as pavements, slopes, retaining walls, and embankments. Geosynthetic stabilization and reinforcement is a mechanical process. Geosynthetics placed either on top of the subgrade or within the base course layer, works with the soil and granular material to create a reinforced section through separation, confinement, and/or reinforcement functions. Several studies have shown that in a pavement system, the inclusion of geosynthetic materials at the interface between the pavement base course and subgrade can significantly improve the performance of the pavement structure on a weak subgrade, based on both laboratory tests and full-scale field experiments (Barksdale et al. 1989, Al-Qadi et al. 1994, 2007, Perkins 1999, Hufenus et al. 2006). Due to the soft nature of Louisiana soils, it is a common practice to stabilize the subgrade layer to create a working platform for pavement construction. For pavements built over weak subgrade, distresses are first identified along the wheel path, followed by top-down cracks (Tarefder et al., 2008). Advanced pavement distresses are inclusive of widening longitudinal cracks, side-by-side cracking, rutting, shoving, and potholes. Weak subgrade may be stabilized, using geosynthetic materials as an alternative to lime or cement stabilization, to create a working platform and to resist the surface vehicular load. Geosynthetic material (mainly geogrids) may also be used to reinforce the base layer within the pavement section.

2 OBJECTIVES AND SCOPE

The main objective of this research is to evaluate the performance of geosynthetics (geogrids and geotextiles) to stabilize subgrade and/or to reinforce base course layers in unpaved test sections. For this purpose, extensive small-scale in-box static plate load tests (PLTs) were conducted on several unreinforced and geosynthetic reinforced unpaved test sections. The parameters investigated in this study included the location of geosynthetic material, geosynthetic tensile modulus, number of geosynthetic layers, and base course layer thickness.

3 MATERIAL PROPERTIES AND TEST PROGRAM

3.1 Material Properties

Two different types of geomaterials (silty clay and Kentucky crushed limestone soils) were used in this research study. The silty clay soil used in this study is a marginal embankment soil with low to medium plasticity that is often encountered in embankments in southern Louisiana. The soil has a maximum dry density of 1,670 kg/m³ and an optimum moisture content of 18.75% as determined by the Standard Proctor test. From the Atterberg Limits test, the silty clay is classified as CL according to the Unified Soil Classification System (USCS), and A-6 according to the American Association of State Highway and Transportation Officials (AASHTO) classification systems. The crushed limestone has a maximum dry density of 2,418 kg/m³ and an optimum moisture content of 6.6%, as determined by a modified Proctor test. It is classified as GW and A-1-a according to the USCS and AASHTO classification system, respectively.

The small-scale laboratory PLTs were conducted inside a test box at the Geotechnical Engineering Research Laboratory (GERL) of the Louisiana Transportation Research Center (LTRC). The model tests were conducted inside a steel test box with dimensions of 1.5 m (length) × 0.91 m (width) × 0.91 m (height). The method of performing PLTs on subgrade soils and pavements are described by ASTM D1196-93. Nonrepetitive static plate load tests were performed on soils, as well as unbound base and subbase materials, in order to determine the modulus of subgrade reaction or to measure the shear strength of pavement components. A loading device, a hydraulic jack, bearing plates of 7.5-in. (190 mm) dia, dial gages (two or more), a reaction frame, and a deflection beam were used in the static plate load test.

Several types of geogrids and geotextiles were used in this research study. Biaxial geogrids BX1100, BX1200, BX1500, BXG10, BXG11, BXG12 with rectangular aperture shape, triaxial geogrids TX5, TX6, TX7 with triangular aperture shape, and geotextile RS580i and RS380i were used to stabilize the subgrade and/or reinforce the base material in unpaved test sections. The physical and mechanical properties of these reinforcements as provided by the manufacturers are listed in Table 1.

Table 1 Properties of reinforcements

Reinforcement	Polymer Type	T ¹ , kN/m		J ² , kN/m		Aperture Size (mm) & shape	Junction Efficiency (%)
		MD ³	XMD ⁴	MD ³	XMD ⁴		
Mirafi RS580i	Polypropylene	7	26.26	350	1313.3	-	-
Mirafi RS380i	Polypropylene	7	14.88	350	744	-	-
Tensar TX7	Polypropylene	2.375 ⁵		475		40×40	△
Mirafi BasXgrid12	Polyester	9.1	12.3	455	615	25×25	□
Tensar BX1500	Polypropylene	8.5	10	425	500	25×30.5	□
Tensar TX6	Polypropylene	2.15 ⁵		430		40×40	△
Mirafi BasXgrid11	Polyester	9.1		455		25×25	□
Tensar BX1200	Polypropylene	6	9	300	450	25×33	□
Tensar TX5	Polypropylene	7.5		375		40×40	△
Tensar BX1100	Polypropylene	4.1	6.6	205	330	25×33	□
Mirafi BasXgrid10	Polyester	4.1	6.6	205	330	25×25	□

¹Tensile Strength (at 2% strain), ²Tensile Modulus (at 2% strain), ³Machine Direction, ⁴Cross Machine Direction, ⁵Tensile Modulus (at 0.5% strain);

3.2 Section Preparation and Compaction Control

The subgrade soil was first placed and the required amount of water was added to achieve the desired moisture content. The soil was compacted inside the box, using a 203 mm × 203 mm plate, adapted to a vibratory jack hammer to a predetermined height to achieve the required density. The jackhammer delivers compaction energy of 58.3 m.N and blows at a rate of 1,400 per minute. The preparation of crushed limestone base layer followed the same procedure as the subgrade layer.

The crushed limestone was placed on top of the subgrade layer inside the test box with the required depth; then water was added. The compaction-quality control processes to achieve the required soil densities were accomplished by conducting three passes of vibrating compaction: the compaction effort was applied through the plate for approximately ten seconds in the first pass, five seconds in the second pass, and two seconds in the third pass at each location.

The dry densities measured by the nuclear density gauge varied from 1,570 to 1,630 kg/m³ for a subgrade, silty clay layer and the moisture contents varied from 21.5 to 22.5%, to achieve a weak subgrade of CBR≈1. The corresponding resilient modulus from geogauge stiffness moduli (EGG) ranged from 9.5 to 11.8 MPa, and from the light falling weight deflectometer stiffness moduli (ELFWD) ranged from 8.6 to 9.8 MPa.

The measured-in-place dry density and water content of the crushed limestone base course layer were 2,290 to 2,340 kg/m³ and 4.0 to 5.5%, respectively. The corresponding geogauge stiffness moduli (EGG) were in the range of 160 to 220 MPa. A Dynamic Cone Penetrometer test was also used in the crushed limestone base course layer, and the measured penetrometer values in mm/blow were in the range of 4 to 9 mm/blow. The corresponding resilient moduli from geogauge stiffness moduli (EGG) were in the range of 81 to 86 MPa. The corresponding resilient modulus from light falling weight deflectometer stiffness moduli (ELFWD) were in the range of 38 to 40 MPa for 305 mm, 46 to 47 MPa for 457 mm, and 35 to 38 MPa for 203 mm thick base course layer. The corresponding resilient moduli from DCPI were in the range of 34 to 41 MPa.

3.3 Experimental Testing Program

The in-box static plate load tests were conducted to evaluate the performance and benefits of geosynthetic stabilized subgrade and geosynthetic base reinforcement in unpaved test sections. A total of 47 tests were performed on unreinforced and geosynthetic stabilized/reinforced unpaved test sections. Three different thicknesses in base course layers were used in this research. The parameters investigated in this study included the number of geosynthetic reinforcement layers, the location and tensile modulus of the geosynthetics, and the thickness of aggregate surfacing layer. The test results showed that the inclusion of geosynthetic materials can significantly improve the performance of unpaved sections over weak subgrades [California Boring Ratio (CBR) ≤ 1%]. Table 2 summarizes the testing program and test variables.

4 TEST RESULTS AND ANALYSIS

The results of the in-box static plate load tests for unpaved test sections are summarized in Table 2. In this table, the BCR values were determined at 25 mm (1-in.) and 51 mm (2-in.). Table 2 presents the results for the 305 mm (12 in.) thick base course layer; Table 3 presents the results for the 203 mm (8 in.) thick base course layer; and Table 4 presents the results for the 457 mm (18 in.) thick base course layer.

4.1 Effect of Reinforcement Location

The location of geosynthetic reinforcement within the base course layer is one important factor on the performance of unpaved sections. For the 457 mm thick base course layer section, the use of reinforcement at interface is not so effective. From Table 4, one can see that for geosynthetic reinforcement at the interface location in 457 mm thick base course layer, the BCR values are not significant. Whereas, geosynthetic reinforcement located at mid depth or the upper one-third position shows better improvement than at the interface location. For example, at 51 mm settlement, the BCR increased from 1.06 to 1.11, with a layer of TX7 reinforcement placed at interface and at the upper one-third position of the base course layer, respectively. Also at 25 mm settlement, the BCR increased from 1.06 to 1.11, with a layer of TX7 reinforcement placed at interface and at the upper one-third position of the base course layer, respectively. Similar performance was observed for a layer of BXG11 reinforcement. Therefore, based on the laboratory test results of the unpaved test section, the optimum location of reinforcement is located at the upper one-third position of thick base course layer.

Table 2 Summary of unpaved test sections with 305 mm thick base course layer

Test No.	Reinforcement Configuration	Reinforcement Location	51 mm (2 in.) settlement		25 mm (1 in.) settlement	
			q* (kPa)	BCR	q* (kPa)	BCR
1	Unreinforced		2708	...	2000	...
2	N=1, BX1100		2804	1.04	2000	1.00
3	N=1, BX1200		2996	1.11	2300	1.15
4	N=1, BX1500		3275	1.21	2650	1.33
5	N=1, TX5		2948	1.09	2100	1.05
6	N=1, TX6		3092	1.14	2480	1.24
7	N=1, TX7	interface	3283	1.21	2540	1.27
8	N=1, BXG10		2756	1.02	2000	1.00
9	N=1, BXG11		2900	1.07	2350	1.18
10	N=1, BXG12		3246	1.20	2400	1.20
11	N=1, RS580i		3475	1.28	2550	1.28
12	N=1, RS380i		3379	1.25	2450	1.25
13	N=1, TX7		3379	1.25	2580	1.29
14	N=1, BXG11	middle	2899	1.07	2220	1.11
15	N=1, TX7		3379	1.25	2650	1.33
16	N=1, BXG11	upper one third	3091	1.14	2400	1.20
17	N=1, BX1200		3187	1.18	2500	1.25
18	N=2, BX1200		3859	1.43	2800	1.40
19	N=2, TX5		3763	1.39	2600	1.30
20	N=2, TX7		3955	1.46	2900	1.45
21	N=2, RS580i/ BXG11	Interface + upper one third	4146	1.53	3050	1.53
22	N=2, RS380i/ BXG11		4050	1.50	3000	1.50

* q = applied surface pressure

Table 3 Summary of unpaved test sections with 203 mm thick base course layer

Test No.	Reinforcement Configuration	Reinforcement Location	51 mm (2 in.) settlement		25 mm (1 in.) settlement	
			q* (kPa)	BCR	q* (kPa)	BCR
23	Unreinforced		1702	...	1300	...
24	N=1, BX 1200		2133	1.25	1500	1.15
25	N=1, TX 5		2085	1.23	1470	1.13
26	N=1, TX 7		2325	1.37	1700	1.31
27	N=1, BXG 10		1893	1.11	1370	1.05
28	N=1, BXG 11	interface	2037	1.20	1450	1.12
29	N=1, BXG 12		2229	1.31	1650	1.27
30	N=1, RS 580i		2421	1.42	1750	1.35
31	N=1, RS 380i		2373	1.39	1720	1.32

Table 4 Summary of unpaved test sections with 457 mm thick base course layer

Test No.	Reinforcement Configuration	Reinforcement Location	51 mm (2 in.) settlement		25 mm (1 in.) settlement	
			q* (kPa)	BCR	q* (kPa)	BCR
32	Unreinforced		4495	...	3600	...
33	N=1, BX1200	interface	4620	1.03	3600	1.00
34	N=1, TX5		4619	1.03	3650	1.01
35	N=1, TX7		4744	1.06	3800	1.06
36	N=1, BXG11		4619	1.03	3800	1.03
37	N=1, RS580i		4869	1.08	4000	1.11
38	N=1, TX7	middle	4869	1.08	3800	1.06
39	N=1, BXG11		4744	1.06	3800	1.06
40	N=1, TX7	upper one third	4994	1.11	4000	1.11
41	N=1, BXG11		4869	1.08	4000	1.11
42	N=1, BX1200		4869	1.08	4000	1.11
43	N=2, BX1200	Interface + upper one third	5743	1.28	4400	1.22
44	N=2, TX5		5493	1.22	4250	1.18
45	N=2, TX7		5868	1.31	4450	1.24
46	N=2, RS580i/ BXG11		6118	1.36	4800	1.33
47	N=2, RS380i/ BXG11		5993	1.33	4600	1.28

However, for a thin base course layer like 203 mm of thick crushed limestone base, placing geosynthetic reinforcement at the interface location is very effective (Table 3). The BCR values were also improved significantly in a 203 mm thick base course layer (up to 1.42) through the use of different types of reinforcements. For the 305 mm thick base course layer, the BCR value showed an increase from 1.21 to 1.25 by moving the TX7 reinforcement from the interface to the upper one-third position of base course layer. From Figure 1, one can see that when geogrid reinforcement is placed at the upper one-third position of a base course layer, rather than at an interface location, BCR values will increase.

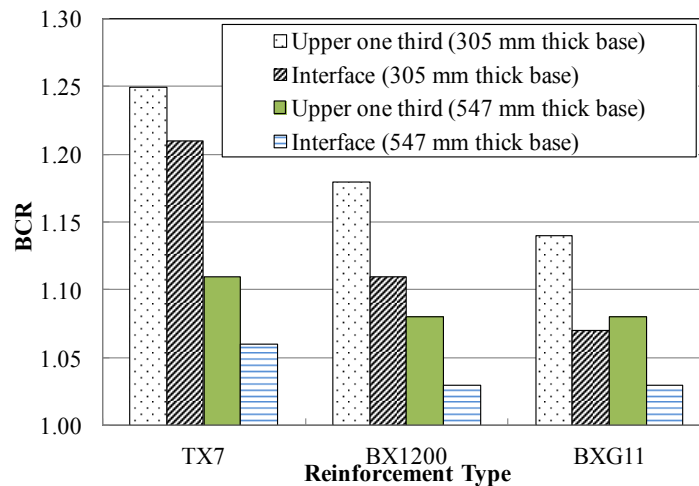


Figure 1 BCR values for unpaved test sections with geosynthetic reinforcements placed at different locations

4.2 Effect of Number of Reinforcement Layers

A series of in-box static plate load tests were conducted on unpaved test sections, where two layers of geosynthetic material were used. One geosynthetic layer (geogrid or geotextile) was placed at the base-subgrade interface and the other geosynthetic layer (geogrid only) was placed at the upper one-third of the base course layer. As expected, the BCR increased as the number of reinforcement layers increased. For example, at a 51 mm settlement for the 305 mm thickness base course layer, the BCR increased from 1.11 to 1.43 for the BX1200 geogrid; 1.09 to 1.39 for the TX5 geogrid; and 1.21 to 1.46 for the TX7 geogrid. The combination of RS580i and BXG11 gave the best performance in the 305 mm base course layer. By using the RS580i and BXG11, the BCR increased from 1.28 (only RS580i) to 1.53 (RS580i+BXG11). For the 457 mm thickness base course layer at a 51 mm settlement, the BCR

increased from 1.03 to 1.28 for the BX1200; 1.03 to 1.22 for the TX5; and 1.06 to 1.31 for the TX7. Again, the RS580i and BXG11 combination demonstrated the best performance in the 457 mm base course thick layer, where the BCR increased from 1.11 (only RS580i) to 1.33 (RS580i+BXG11). Figure 2 depicts the BCR values of 305 mm and 457 mm thick base course layer reinforcements. Using RS580i and BXG11 combination in these base course layers allowed a performance better than any other combination of reinforcement. Among the two-layer geogrids, the triangular TX7 geogrid performed better than BX1200 and TX5 geogrids. From this research, we obtained BCR values of 1.53 and 1.36 in 305 mm and 457 mm thickness base course layer sections respectively, by placing RS580i geotextile at interface and BXG11 at the upper one-third of the section.

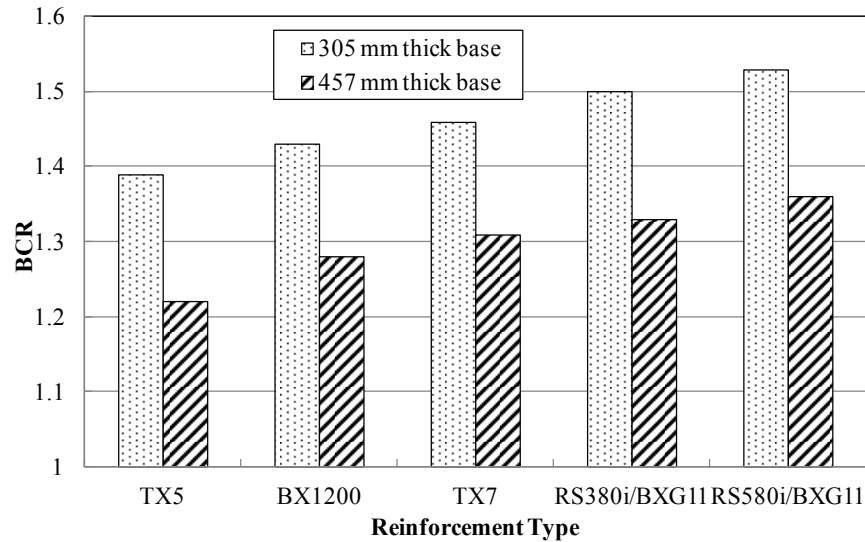


Figure 2 BCR values for unpaved test sections with double reinforcement layers

4.3 Effect of Tensile Modulus of Reinforcement

Eleven different types of geosynthetic reinforcements with different strength/modulus were used in the in-box, unpaved, static plate load tests. These include biaxial geogrids: BX1100, BX1200, BX1500; and BasXgrid10, BasXgrid11, BasXgrid12 geogrids; triaxial geogrids: TX5, TX6, TX7; and RS580i, RS380i geotextiles. The properties of these reinforcements were presented earlier in Table 1. The comparisons between the different types of geosynthetic reinforcement, in terms of bearing capacity ratio versus strength/modulus are described in Figure 3a and Figure 3b, for the 305 mm, and 203 mm thick base course layer sections with geosynthetic reinforcement placed at the base-subgrade interface. From the figures, one can see that the bearing capacity generally increases with the increase of the tensile modulus of the reinforcement. The tensile modulus-related increase in the BCR is more appreciable at low tensile modulus, and the effect gradually decreases as the tensile modulus increases. For the unpaved test section studied herein, the BCR increased almost linearly when the geosynthetic tensile modulus increased from 267.5 to 550 kN/m. After that, the BCR increased at a much lower rate and appeared to approach a limiting value at a tensile modulus of 750 - 800 kN/m.

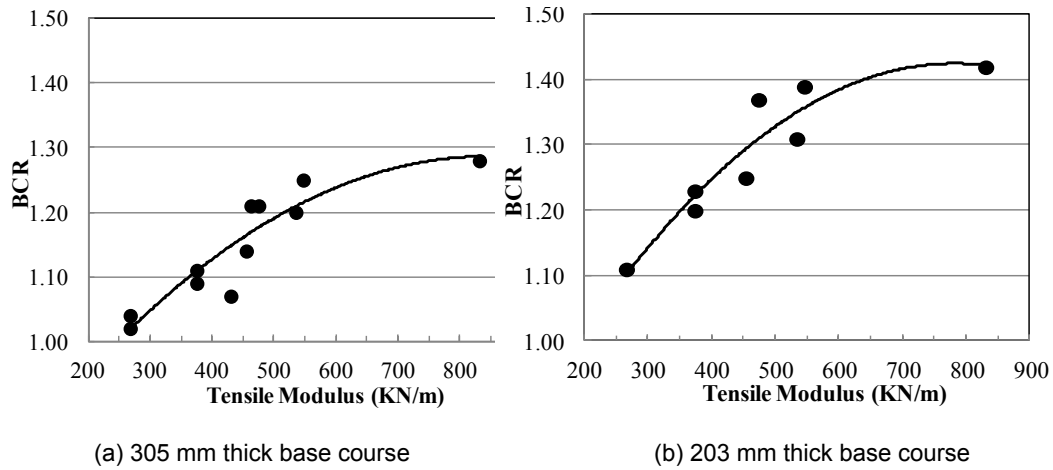


Figure 3 BCR versus tensile modulus for single layer reinforcement placed at the interface.

4.4 Effect of Different Thickness Base Course Layer in BCR

Figure 4 presents a comparison between the 203 mm, 305 mm, and 457 mm thick crushed limestone base course layer sections with different types of geosynthetic reinforcement placed at the base-subgrade interface. From the figure, one can see that for the 203 mm base course layer section, the improvement in bearing capacity values is the highest, when compared with the 305 mm and the 457 mm thick base course layer sections. The BCR values decreased as the thickness of base layer increased for all types of geosynthetic reinforcement. However, the BCR values were not the same for each base course thickness as discussed earlier, since the BCR also depends on location, geometry, and tensile modulus of geosynthetics.

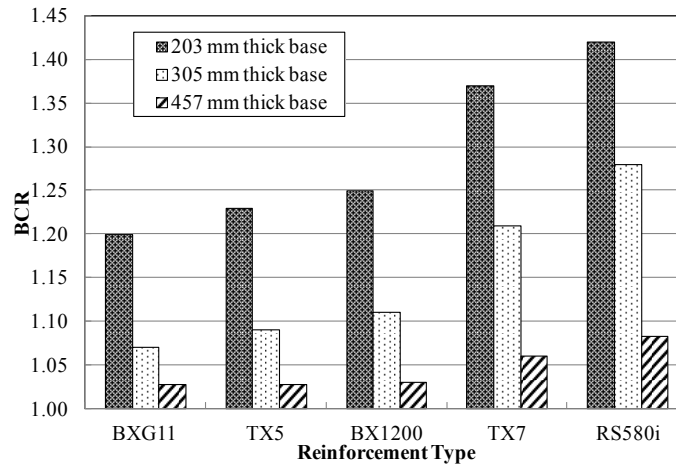


Figure 4 BCR values for 203 mm, 305 mm, and 457 mm thick base course layer sections with geosynthetic reinforcements placed at base-subgrade interface.

5 CONCLUSIONS

Based on the results of the present study, the following conclusions can be drawn:

1. The bearing capacity ratio (BCR) generally increases with the increase in tensile modulus of geosynthetic reinforcement (up to 1.53) and approaches a limit value as the tensile modulus of geosynthetic reinforcement exceeds 550 kN/m.
2. Placing the geosynthetic material in the double location yielded the largest improvement. For the single layer of reinforcement, the upper one third locations yielded highest improvements.

3. The geogrid benefits were more appreciable in sections with thin base course layer compared to those in sections with thick base course layer.

REFERENCES

- Al-Qadi, I. L., Brandon, T.L, Valentine, R J., Lacina, B.A., and Smith, T.E., 1994, "Laboratory Evaluation of Geosynthetic Reinforced Pavement Sections", Transportation Research Record 1439, pp. 25-31.
- Al-Qadi, I.L., et al., 2007. Accelerated full-scale testing of geogrid-reinforced flexible pavements. TRB 2007 Annual Meeting (CD-ROM). Washington, DC: Transportation Research Board, National Research Council.
- ASTM D1195-93 (2004). Standard Test Method for Nonrepetitive Static Plate Load Tests of Soils and Flexible Pavement Components, for Use in Evaluation and Design of Airport and Highway Pavements.
- Barksdale, R.D., Brown, S. F., and Chan, F., 1989, "Potential benefits of geosynthetics in flexible pavement systems", National Cooperative Highway research Program Report No. 315, Transportation Research Board, National Research Council, Washington, DC, USA, 56 p.
- Hufenus, R., Rueegger, R., Banjac, R., Mayor, O., Springman, S.M., and Bronnimann, R., 2006. "Full-scale field tests on geosynthetic reinforced unpaved roads on soft subgrade." *Geotextiles and Geomembranes* 24 (2006) 21–37.
- Perkins, S. W. 1999. "Geosynthetic Reinforcement of Flexible Pavements Laboratory Based Pavement Test Sections", Final Report FHWA/MT-99-001/8138, State of Montana department of transportation research, and development and technology transfer program, Bozeman, Montana, USA, 108 pp.
- Tarefder, R.A., Saha, N., Hall, J.W., and Ng, T.T.P., 2008. "Evaluating Weak Subgrade for Pavement Design and Performance Prediction: A Case Study of US 550." *Journal of GeoEngineering*, Vol. 3, No. 1, pp. 13-24, April 2008.

Lake Tahoe California Lake Shore Bluff Stabilization and Restoration

J.P. Chinchio, Landslide Solutions, Inc., United States of America

ABSTRACT

Restoring the natural look of an area following a landslide or severe erosion repair can often rank just as high a project priority as the actual stabilization. This paper presents a non-traditional biotechnical stabilization and restoration approach using ballistic soil nails, galvanized steel mesh and native plant impregnated coconut fiber geocells in an area prone to rotational slope failures along the western shore of Lake Tahoe, California. Working within stringent Tahoe Regional Planning Agency (TRPA) guidelines, the project produced a restored shoreline face with a walking path through a newly stabilized high bank waterfront property. In addition to preventing further rotational failures, the approach mitigated widespread surface erosion and sloughing of the shoreline face. Traditional methods of mechanical slope stabilization such as benching, shotcreting, or anchoring would have been effective at stabilizing the shoreline movement and accommodating a new walking path. However, those approaches would have substantially altered the appearance of the shoreline and would have been unacceptable to TRPA and the property owners. In this case study, the benefits of biotechnical stabilization were crucial to the acceptance of the project. A combination of ballistic soil nails and custom vegetated mats both stabilized the existing rotational failure and provided anchorage points for the vegetated mats. That concept allowed cuts up to six vertical feet in the unstable sandy silt shoreline material. Working close to a protected lake and establishing plantings in the semi-arid Lake Tahoe environment presented real challenges, but a biotechnical stabilization system using mechanical elements and appropriate high mountain desert native vegetation met both the structural and aesthetic demands of the project.

1. THE SITUATION

Bluff erosion and stability is an ever present problem along the shoreline of pristine Lake Tahoe and one such area presented itself during the planning phase of an estate reconstruction project along the west shore of Lake Tahoe. The inherent problem of an eroding unstable bluff is quite obvious. In this situation the problem was intensified by the desire to build a high end housing structure just feet from the top edge of the bluff while planning to restore the bluff face and construct a walking path to the beach below. In addition, because of tough environmental regulations, most of the work would need to take place from the top of the bluff thus requiring specialized equipment and construction techniques.

Stringent Tahoe Regional Planning Agency (TRPA) and local county permit requirements then made design and construction factors even more difficult and limited time for construction from May 1st to October 15th. The ultimate goal of the project was to protect, strengthen, support, preserve and provide global stability to the existing bluff surface all without noticeably changing the appearance of bluff.

If bluff surface erosion was not corrected at this site the bluff would have continued to erode back thus reducing usable property at the top of the bluff. If overall global stability of the slope was not corrected the housing structure would have had to be placed on a piling system sufficient enough to support the house should the bluff continue to fail.



Picture Sample of the Bluff before Construction

2. THE SOLUTION

Several stakeholders, agencies and industry professionals worked in harmony to develop the final bluff erosion and stability issue. Those entities included the owner, project architect, project civil engineer, permit specialist, geologist, landscape design / build contractor and specialty slope stabilization design / build contractor.

After considerable thought and consultation with erosion control vendors and consultants, it was decided that a hybrid biotechnical solution would be required - a smorgasboard of stabilization recipes. Ultimately, a combination of ballistic soil nails, steel wire mesh and a specialty custom vegetated coconut coir cellular confinement was chosen.

The ballistic nails were primarily chosen because of the ability to install them with minimal impact to the bluff, faster production rates relative to traditional nails and the ability to install the nails from the top of the bluff (no need for equipment on the beach). Cost was also an important factor with regards to the final decision to utilize ballistic soil nails.

Ballistic soil nails are long steel or fiberglass rods installed to reinforce or strengthen the existing ground. Ballistic soil nails are inserted using high-pressure air approaching 2500 psi (17.2 MPa) by a launcher that can be mounted on a hydraulic excavator (Figure 1). As the soil nail passes into the soil, the ground around the nail is displaced by compression at the nail tip. This forms an annulus of compression which reduces the soil drag on the nail. As the nail comes to rest, the soil rebounds onto and bonds with the nail. The soil nails reinforce the locally unstable soil mass by transferring the nail's tensile and shear resistance through the failure plane of the sliding soil. The nails maintain the resisting force because they are anchored beyond the slip plane.

In order to determine the length and spacing of the ballistic soil nails both a slope survey and a soils report were used. These documents were provided by the project geologist and information gleaned from them was imported into a commercially available slope stability software tool. The tool then calculated probable slide planes under varying circumstances and at a defined Factor of Safety (FoS). An appropriate FoS at this site was determined to be 1.5, effectively meaning that the repair is capable of handling 50% more than the maximum expected load. Without any stabilization measures the stability of the slope was approximated at a FoS 1.0. With the installation of ballistic nails on 5-ft x 5-ft spacing it was determined the slope could be augmented to reach the targeted FoS 1.5 (Figure 2).



Figure 1 - Installation of Ballistic Soil Nails

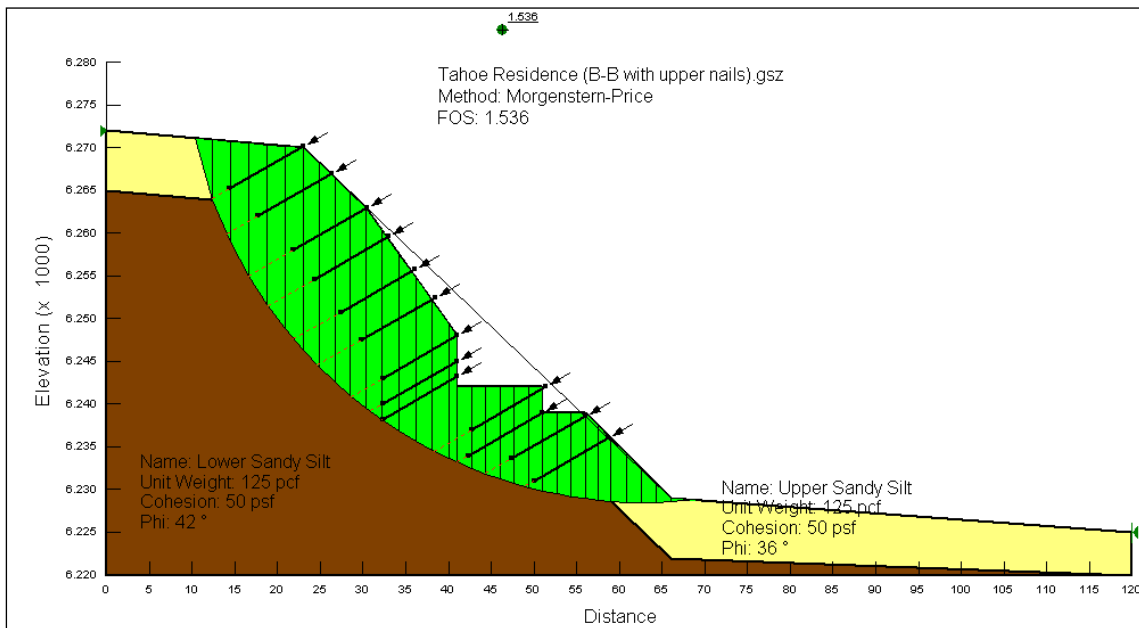


Figure 2 – Slope W Output File

Galvanized wire mesh was then attached to the tips of the nails with the purpose of providing cohesiveness to the ballistic soil nail system, a medium to attach the coir cellular confinement and a last defense for erosion in the event of localized coir failure (Figure 3, 4 and 5). The mesh was carefully tensioned across the entire slope face. At the bottom of the slope native rocks were hand selected and placed to provide slope buttressing and to protect against high water wave action (Figure 6). The wire mesh was installed prior to the placement of the rocks thus the rocks provided another source of tension as they were set in place.

The success of the entire stabilization system depended in large part on the erosion control and beautification provided by the vegetated surface treatment. The installation of custom vegetated cellular confinement surface treatment was installed immediately after the placement of the steel mesh and native rock. Vegetation selected for planting within the cellular confinement area included; large deeply rooted woody shrubs, forbs, sub-shrubs, ground-cover and grasses that were chosen based on esthetic appeal and ability to retain soil. In order to support these species amended soil was imported and placed within six inch deep honeycomb-configured coir cellular confinement. This biodegradable six inch deep blanket was securely anchored to the steel mesh and stretched in six foot stripes from top to bottom of the slope forming a continuous three dimensional form covering the slope.

Soil sources were tested and a biologically active green-waste composted soil formula was selected. The soil needed to hold and distribute moisture, rapidly germinate seed, grow healthy plants, texture and color to blend with native soil and adhesiveness. Soil was conveyed and packed into the coir layer.

A diverse mix of native plants was specified, ranging in size from 4" native grass plugs to 44" ball and burlap native trees. Larger tree species, Incense Cedar and Jeffery Pine were placed lower on slope to avoid being blown over by the wind. Smaller scale, slower growing native trees such as Mountain hemlock (*Tsuga mertensiana*) and Subalpine fir (*Abies larsiocarpa*) and other native shrubs were placed higher on the steepest exposed areas of bluff. The native shrubs provide shade, bird habitat and forage for fowl and small mammals. Boulder groupings pinned periodically in the slope with Launched Soil Nails™ also provided an opportunity for small mammal colonization and complimented the boulders throughout the rest of the property. Native ground covers and forbs like Squaw Carpet (*Ceanothus prostratus*) and Mountain Pride Penstemon (*Penstemon newberryi*) added color, attracting beneficial insects. Additionally, small burnet (*Sanguisorbia minor*) provided nitrogen fixing.

Five gallon and larger plants were installed in small openings cut through the cellular confinement and steel mesh. Inserting the root mass of these larger plants into the subsurface soil allowed space for root growth and trunk flare. A final mulch layer formulated with a matrix of long, medium and fine natural fibers was distributed throughout the entire area. The mulch layer was composted with a small amount of formulated soil for one week to activate microbial activity, and then firmly felted on the surface. After mulching, a seed mix of shrubs, forbs and native grass was broadcasted evenly over the mulch. A three foot wide path was constructed and surfaced with recycled rubber composite pavers. The construction process was completed by September 15, 2010. By October seed had begun to germinate and plant materials already exhibited growth. The entire planted area is now irrigated and controlled by a sophisticated irrigation controller that automatically turns the entire irrigation system off if any irrigation line breach is detected. The system controls an in-line drip irrigation system providing low volume, low impact supplemental irrigation for the first three growing seasons.

Late October 2010 brought an unusually strong rain event (4-inches within 24 hours). The stabilized area weathered the storm without an issue. Project monitoring and maintenance will continue through October 2015.

3. CONCLUSION

From conception to completion this project took more than three years. Construction took two and one half months with more than two years in planning and permitting negotiations. The project has met the expectation of all entities involved and provides an attractive natural looking footpath to the beach, stabilized slope suitable for a building above and a restored view from land and water (Figure 6).



Figure 3 - Tensioned Galvanized Wire Mesh



Figure 4 - Cedars and pines planted through keyholes in cellular confinement and steel mesh.



Figure 5 - 75% of the cellular confinement has been filled and planting has started.



Figure 6 - Native boulders to protect the toe of slope from wave action.



Figure 7 - Path surface and planting complete, irrigation is 80% complete.



Figure 8 - Planting is 90% complete and path surface installation has started.



Figure 9 - 100% Complete

REFERENCES

- GeoSlope International, Inc. Slope/W 2007.
FHWA. 2003 *Geotechnical Engineering Circular No. 7: "Soil Nailing."*

Layer Coefficient Ratio for Reinforced Pavements and the Influence of Pavement Thickness and Subgrade Strength

S.W. Perkins, P.E., PhD, Montana State University, USA, stevep@ce.montana.edu

B.R. Christopher, P.E., PhD, Christopher Consultants, USA, barryc325@aol.com

J. Klomp maker, BBG Bauberatung Geokunststoffe, GmbH & Co. KG, Germany, jklomp maker@bbgeo.com

ABSTRACT

Flexible pavement with geosynthetic reinforcement in the base course layer is typically designed using empirical techniques. The empiricism is developed from the construction of pavement test sections similar in cross section and materials to the expected design and observation of the improvement in pavement performance due to the reinforcement. Modified structural layer coefficients for the reinforced base course layer, expressed within the context of the AASHTO 1993 Pavement Design Guide, are sometimes used to express the improvements observed from these tests. However, design approaches based on these test results are often extended beyond the range of empirical evidence and often do not account for the influence of subgrade strength and overall thickness of the pavement cross section on structural improvement. Several mechanistic-empirical models for analysis and design of reinforced flexible pavements have recently been reported, which allow a thorough evaluation and confirmation of these postulated improved design values. One of these methods is used to analytically generate benefit values for a range of pavement design conditions. In this paper, the steps involved in this approach are presented. The results show the importance of the strength of the subgrade and the thickness of the proposed pavement cross section on the layer coefficient ratio.

1. INTRODUCTION

The design of flexible pavements with geosynthetic reinforcement in the base course layer is typically accomplished via empirical techniques involving the construction of pavement test sections similar in cross section and materials to the expected design and observation of the improvement in pavement performance (AASHTO, 2011). The results of these tests are often expressed in terms of an improvement in the structural layer coefficient of the base course layer, which is done within the context of the AASHTO '93 Pavement Design Guide (AASHTO, 1993) or a Traffic Benefit Ratio, *TBR*, which can then be related to an improvement in the base layer coefficient. *TBR* is defined as the ratio of traffic passes for a certain level of pavement rutting for a reinforced pavement compared to an otherwise identical unreinforced pavement. This approach requires an extensive research and testing program to establish benefit values for the range of variables known to be of influence. These variables include the subgrade strength, the thickness of the asphalt concrete, base aggregate and subbase, if present, the structural quality of these materials, the geosynthetic type and the placement position of the geosynthetic within the base layer (Berg et al., 2000).

Several mechanistic-empirical models for analysis and design of reinforced flexible pavements have recently been reported (Perkins et al. 2009, Perkins and Edens, 2003). These models have been calibrated against the type of pavement test sections suggested by AASHTO (2011). In this paper, the method by Perkins and Edens (2003) is used to analytically generate benefit values for a range of pavement design conditions involving differences in subgrade strength and overall pavement thickness. In a previous paper, Perkins et al. (2012) showed comparable results obtained by the two methods of Perkins et al. (2009) and Perkins and Edens (2003).

2. REVIEW OF DESIGN METHODS

Three empirical design methods for reinforced pavements, referred to as Manufacturer Method 1, 2 and 3, were identified that use improved structural base layer coefficients within the context of the AASHTO '93 Pavement Design Guide. References for these methods are Tenax (2001), TenCate (2010) and Tensar (2010), respectively. These methods are briefly reviewed and discussed in this section.

2.1 Manufacturer Method 1 (MM1)

MM1 was developed based on the AASHTO '93 pavement design equation and uses a Layer Coefficient Ratio (*LCR*) to modify the structural contribution of the base when reinforcement is added. *LCR* has a value greater than or equal to one and is used in Equation 1 to modify the structural number (*SN*) for use in the AASHTO '93 pavement design equation. Equation 1 can be used to calculate the required thickness of the asphalt layer (D_1) or the base layer (D_2).

$$SN = D_1 a_1 + D_2 a_2 m_2 LCR + D_3 a_3 m_3 \quad [1]$$

In Equation 1, a_1 , a_2 and a_3 are the layer coefficients for the asphalt concrete, base aggregate and subbase layers, respectively, D_3 is the subbase thickness, if present, and m_1 and m_2 are the drainage coefficients for the base aggregate and subbase layers. All layer thickness are in units of inches.

LCR was determined from test sections for a particular multilayer polypropylene extruded biaxial geogrid. Test sections were constructed in a pavement test box where a cyclic load was applied to a stationary plate (Cancelli et al. 1996). In these test sections, a fine sand subgrade was used. A subgrade with a CBR ranging from 1 to 18 was produced for different test sections by placing the sand at different dry densities. Placement of loose sand to produce low values of subgrade CBR results primarily in volumetric compaction when subject to traffic loads, which is considerably different from an undrained shear distortion pattern of deformation typical of weak soft subgrades.

From the results of the study a design chart was produced where LCR varied from 1.81 to 1.41 and was a function of subgrade CBR . The results indicated an LCR of over 1.4 for subgrade CBR values greater than 8, which corresponded to a TBR of 4.5.

Subsequent test sections were constructed in an outdoor test track and subjected to truck traffic (Cancelli and Montanelli, 1999). A clay subgrade was used in the outdoor test track and placed at a CBR ranging from 1 to 8. Results from this study were analyzed by Berg et al. (2000) and for the subgrade at a CBR of 8 a TBR of 1.6 was obtained. This produces an LCR considerably below 1.4 and is in conflict with the data presented in the design curve.

2.2 Manufacturer Method 2 (MM2)

MM2 was originally developed for reinforced pavements within the context of the 1972 AASHTO pavement design equation (Pearce, 1981). The approach is similar to that used in MM1 in that the AASHTO equation for structural number is modified by adding a term (M) to the structural contribution of the base course aggregate containing a geosynthetic (Equation 2). The design method was advanced for two woven polypropylene geotextiles. Values of M were given as a function of the CBR value of the subgrade and the design traffic for the roadway. Values of M ranged between 1.08 and 1.22. While reference was made to the use of theoretical behavior models for structural analysis (Thompson and Radd, 1979) and consideration for geosynthetics used for both separation benefits and confining effects, the basis for the M values used in the design method was not provided.

$$SN = D_1 a_1 + D_2 a_2 M \quad [2]$$

The method was recently updated and expressed within the context of the AASHTO '93 design equation for structural number. The parameter M was replaced by a Geosynthetic Structural Coefficient (GSC). Values of base course reduction (BCR) factors were provided for four polypropylene woven geotextiles and two coated polyester woven biaxial geogrids as a function of the CBR of the subgrade. Values of BCR ranged from 3.7 to 60.9 % for CBR values ranging from 20 to 0.5 with varying BCR values for each geosynthetic within that CBR range. The basis for these values was not provided. It can be shown that a relationship between BCR and LCR , which is the same as between BCR and GSC is given by Equation 3. For the BCR values listed above, GSC values ranging from 1.04 to 2.56 are obtained.

$$GSC = LCR = \frac{1}{1 - BCR} \quad [3]$$

2.3 Manufacturer Method 3 (MM3)

The MM3 design method for reinforcement of paved roads was originally developed for extruded polypropylene biaxial geogrids (Tensar, 1996). That method relied upon the use of Traffic Benefit Ratio (TBR), which is formally defined in Equation 4 as the ratio of the traffic passes carried by a reinforced and unreinforced pavement having otherwise identical pavement materials and layer thickness.

$$TBR = \frac{W_{18-R}}{W_{18-U}} \quad [4]$$

Results from tests sections by Collin et al. (1996) were used to express TBR as a function of the thickness of the base course and the allowable rut for the roadway. Results from other studies (Haas, 1985, Barksdale et al., 1989 and Webster, 1992) were used as support for the TBR values used from Collin et al. (1996). Design curves were provided for two extruded polypropylene biaxial geogrids. TBR values as a function of subgrade strength were not provided.

TBR was used to extend the performance period of the pavement by direct use of Equation 4 or to reduce the base thickness for an equivalent performance period as the unreinforced pavement. The latter was accomplished within the context of the AASHTO '93 pavement design equations by solving for the structural benefit of the base giving a particular *TBR* and using this benefit to reduce the base thickness to yield the same traffic level as the unreinforced pavement.

This approach has been updated for use with a new extruded polypropylene triangularly configured geogrid. MM3 describes how the structural layer coefficient, as used in the AASHTO '93 pavement design equation, for an aggregate base is modified for the geogrid and how it is dependent on the thickness of the asphalt concrete layer and the subgrade strength. The improvement factors for a given set of pavement design conditions are calculated from regression equations supported by various experimental studies involving the evaluation of laboratory-scale and full-scale test sections. The improvement factors are calculated within a licensed program (Tensar, 2012). The design method can be used for pavements with an asphalt thickness as great as 250 mm, however the method warns that empirical evidence for reinforcement benefit is available only up to asphalt thickness of 200 mm.

The improvement in the structural layer coefficient for various pavement design conditions was calibrated from several experimental studies, however only one study was documented and referenced. Jersey and Tingle (2010) showed results for a geogrid for a pavement with 50 mm of asphalt concrete and 200 mm of aggregate base on a subgrade with a *CBR* of 3. Other supporting studies are reported to be documented in internal reports.

The Tensar licensed program was used to evaluate *LCR* values for an unreinforced pavement cross section consisting of 75 mm of asphalt concrete and 300 mm of aggregate base and for a subgrade having a *CBR* ranging from 0.5 to 20. The program was used to evaluate *BCR* by decreasing the reinforced base thickness until a number of traffic passes equivalent to the unreinforced section was obtained. Equation 3 was then used to calculate *LCR*. Values of *LCR* ranging from 1.76 to 1.04 were obtained

2.4 Discussion of Design Methods

The three design methods reviewed predict an increase of benefit as the subgrade *CBR* decreases. The three methods predict different levels of benefit, which is partly due to each method being for a particular geosynthetic and partly due to each method being calibrated from different experimental studies. MM3 appears to limit the reinforcement benefit below a subgrade *CBR* of 3 whereas the other two methods show this benefit to continue to increase.

There are three principal limitations associated with these methods. The first involves the level of documentation associated with establishing the basis for the benefit values used in the methods. As discussed previously in this section, MM2 and MM3 do not provide adequate public documentation to allow the designer to judge the basis for the benefit values reported. MM1 provides sufficient documentation, however the use of an unrealistic subgrade and the lack of consistency with field test sections raises questions concerning the appropriateness of the benefit values reported.

A second limitation of MM1 and MM2 is the suggestion that a single benefit curve for a given geosynthetic product that is a function of the subgrade strength or modulus but is not dependent on other pavement variables. As discussed previously, reinforcement benefit is known to depend on the thickness of the pavement layers, the structural quality of these materials and the placement position of the geosynthetic within the base layer (Berg et al., 2000). MM3 accounts for layer thickness, however the basis for this accounting could not be established.

The third limitation with these methods concerns the relatively high values of benefit predicted for subgrade strengths approaching and exceeding a *CBR* of 8. Berg et al. (2000) reviewed available studies and showed conflicting results regarding expected reinforcement benefit for pavements on a subgrade with a *CBR* approaching 8. In general, the majority of studies tended to show diminishing benefit for subgrade strength approaching a *CBR* of 8. To the knowledge of the authors, no experimental test sections exist for clay or silt type subgrades with a *CBR* exceeding 8. At the time of the Berg et al. (2000) report, this led to a recommendation of a subgrade with a *CBR* of 8 being the typical limit for expected reinforcement benefit.

Since the Berg et al. (2000) report, a study by Henry et al. (2009) was conducted, which tends to support the above. In this study, eight test sections were constructed and loaded by a moving wheel load. The sections were constructed on a subgrade having a post construction resilient modulus ranging from 109 to 138 MPa (*CBR* = 10-13). Prior to trafficking, the subgrade was soaked with water. Subgrade resilient modulus was backcalculated from falling weight deflectometer tests and shown to range from approximately 55 to 75 MPa (*CBR* = 5-7). The test sections were constructed with an asphalt thickness of 100 and 150 mm and with a base thickness of 300 and 600 mm. *TBR* values for reinforced test sections were no greater than 1.5, however the results were difficult to interpret due to variable subgrade conditions. These results tend to support the conclusions in Berg et al. (2000) that low values of reinforcement benefit should be expected for higher values of subgrade strength and for thick pavement layers. The relatively high values of benefit for

subgrade *CBR* equal to and greater than 8 should be viewed with caution until they can be verified by a combination of analytical modeling validated by results from experimental test sections. In this paper, a process of analytical modeling is illustrated to provide an example for how this can be accomplished.

3. MECHANISTIC-EMPIRICAL MODEL

A mechanistic-empirical model for reinforced flexible pavements was used in this study to illustrate how analytical models can be used to generate benefit values for reinforced pavements. The model was previously calibrated against pavement test sections of the type recommended by AASHTO (2011). This calibration process was performed for several types of geosynthetics. This provides confidence in use of the model for other types of reinforcement products. This section provides background information on components contained in the model and how the model was formulated. The input parameters for the model used in this study are given in Section 4 along with model results.

The mechanistic-empirical model by Perkins and Edens (2003) is based on a project reported by Perkins (2001a,b). The mechanistic model consists of a three-dimensional (3-D) finite element model matching the nominal conditions for the pavement test facility described in Perkins (1999). This facility consisted of a 2 m by 2 m by 1.5 m deep reinforced concrete box in which the roadway cross section was constructed and loaded by 40 kN applied cyclically at a period of 1.5 seconds to a 304 mm diameter steel plate resting on a waffled rubber pad in turn resting on the asphalt concrete surface. A 3-D model was used to account for the potential influence of the box's square corners and for the geosynthetic inclusion that has direction dependent material properties. Symmetry of the box was recognized such that a model of one-quarter of the box was created. Figure 1 illustrates the geometry of the model. Layer thickness was varied for the parametric study performed.

The model used elasto-plastic constitutive models for the majority of the pavement layers. The bounding surface plasticity model described by Dafalias and Hermann (1986) was used to account for the positive effect of aggregate confinement on the increase in stiffness and strength of the base course aggregate. An orthotropic linear-elastic model was used for the geosynthetic. Anisotropy was included to account for differences in elastic modulus between machine and cross-machine directions and allowed for specification of the in-plane shear modulus and in-plane Poisson's ratio. The principal response parameters extracted from the finite element model include vertical strain in the top of the subgrade and bulk stress in the unbound base aggregate layer. These response parameters were used in empirical damage models for the prediction of long-term pavement performance and the definition of reinforcement benefit. Reinforcement benefit is defined in terms of an extension of service life of the pavement, a reduction in aggregate thickness for equivalent service life, or a combination of the two. The damage models were calibrated from reinforced and unreinforced pavement test sections. The model was shown to provide general descriptions of reinforcement mechanisms that are consistent with those previously observed in instrumented pavement test sections. Additional details are provided in Perkins and Edens (2002).

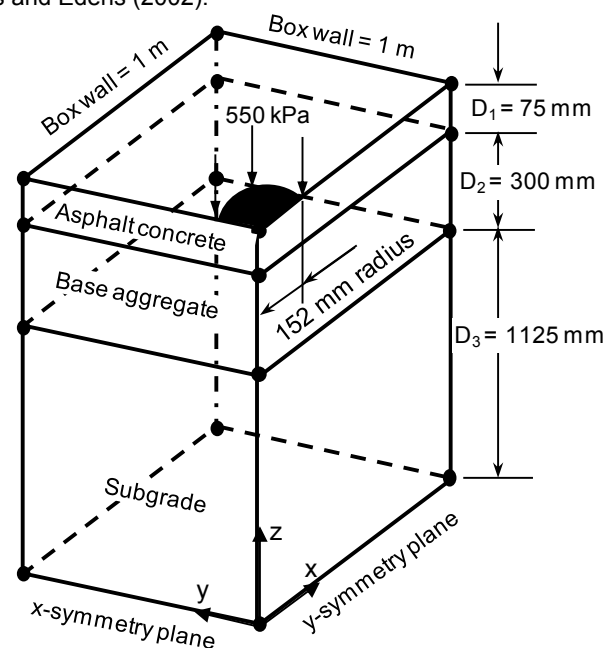


Figure 1. Finite element model for the Perkins and Edens (2002) model.

The mechanistic-empirical model was used in a parametric study to generate regression equations describing reinforcement benefit in terms of variables relating to pavement geometry, subgrade strength and geosynthetic properties. These parameters included asphalt concrete and unbound aggregate thickness, quality of these materials, subgrade strength and geosynthetic elastic properties. A total of 465 pavement design cases were analyzed. The model therefore consists of a series of regression equations used to predict reinforcement benefit for a given set of pavement design conditions.

4. PROJECT MODEL AND RESULTS

The Perkins and Edens (2003) model requires the input properties shown in Table 1 with the values listed as those used in this study. Quality of the asphalt concrete and base aggregate materials is defined in terms of layer coefficients defined in the AASHTO '93 method. The tensile stiffness of the geosynthetic is defined by a modulus at 2 % axial strain. Differences in modulus between the two principal directions of the geosynthetic are accounted for by the modulus ratio. The parametric study performed to originally develop the model was conducted by including geosynthetics having different classes of interaction properties and in-plane mechanical behavior as defined by an in-plane Poisson's ratio and an in-plane shear modulus.

Table 1. Input for Perkins and Edens (2003) model.

Property	Value
Asphalt concrete thickness, D_1 (mm)	75
Asphalt concrete layer coefficient, a_1	0.40
Base thickness, D_2 (mm)	Variable (150 – 1000)
Base layer coefficient, a_2	0.14
Base layer drainage coefficient, m_2	1.0
Subgrade CBR	Variable (0.5 – 8.0)
Geosynthetic modulus, $G_{SM-2\%}$ (kN/m)	1140
Geosynthetic modulus ratio, G_{MR}	0.995
Reduction factor for interface shear	1.0
Reduction for Poisson's ratio	Checked
Reduction for shear modulus	Unchecked

A range of pavement cross sections and subgrade strengths were used in the model, as noted in Table 1. The model produces a value of BCR , which is used in Equation 3 to determine LCR . For a pavement with a subgrade CBR of 2.0, the base course thickness was varied between 150 to 1000 mm to produce a range of values of structural number (SN) according to Equation 2. For each pavement cross section, the model was used to predict BCR , with corresponding LCR values shown against SN in Figure 2. The results show LCR to decrease with increasing base layer thickness and structural number. Reinforcement benefit becomes insignificant beyond a SN of approximately 5.

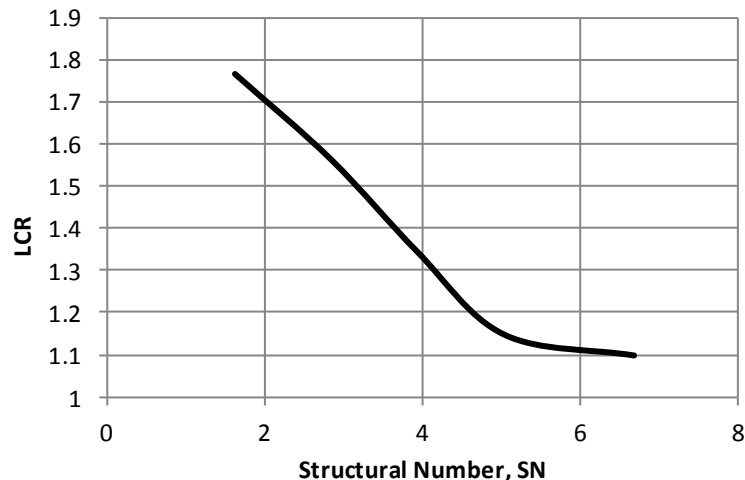


Figure 2. Effect of pavement structural number on LCR .

For a pavement with a base course thickness of 300 mm, the pavement subgrade *CBR* strength was varied between 0.5 and 8. The model was used to evaluate the *BCR* for each case with the resulting *LCR* shown against subgrade *CBR* in Figure 3. The results show that *LCR* decreases with increasing subgrade *CBR*. The results in Figures 2 and 3 show the ability of this model to account for two key components known to influence the benefit derived from geosynthetic reinforcement.

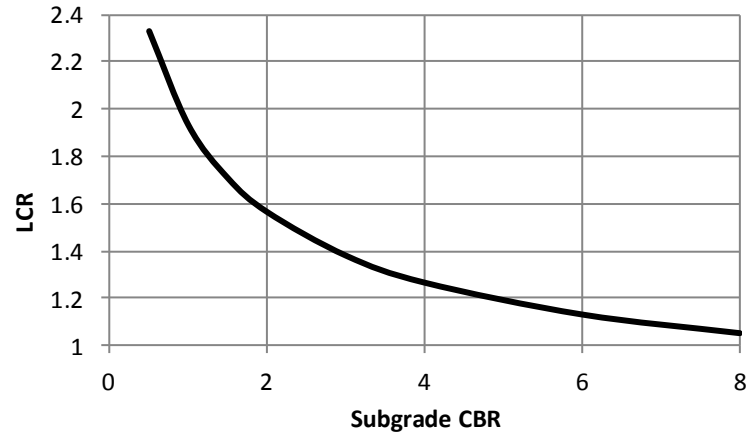


Figure 3. Effect of pavement subgrade *CBR* on *LCR*.

5. CONCLUSIONS

Three currently available proprietary methods for the design of geosynthetic reinforced pavements that rely upon the use of improved layer coefficients for the base course layer were reviewed and shown to have several limitations. The three methods are empirically based and rely upon the demonstration of benefit from reinforced test sections. Limitations of these methods involved: 1) the lack of documentation of benefit values derived from test sections; 2) the inability of some methods to account for the effect of pavement thickness on reinforcement benefit; and, 3) the tendency for all methods to produce relatively high values of benefit for subgrades with a *CBR* of 8 and greater, which is not supported by recent independent full scale test sections. These limitations should be considered when using these methods for the products that they support.

This paper outlined an approach for determining reinforcement benefit using analytically based models that have been previously calibrated against reinforced test sections. The benefit values for the model used produce reasonable results when compared to studies involving the construction of reinforced pavement test sections. This approach is considered favorable due to its ability to account for the variables that are known to influence reinforcement benefit values in a consistent manner that relies upon engineering materials testing and analytical modeling principles. This was illustrated by using the model to examine the influence of the pavement's structural thickness and the strength of the subgrade on layer coefficient ratio. Validation of this approach is needed for those conditions for which benefit values have not been clearly established. Those conditions include stronger subgrades and medium to thick pavement cross sections.

REFERENCES

- AASHTO (1993). AASHTO Guide for Design of Pavement Structures. American Association of State Highway and Transportation Officials, Washington, DC.
- AASHTO (2011). Standard Practice for Geosynthetic Reinforcement of the Aggregate Base Course of Flexible Pavement Structures. AASHTO Designation R 50, Standard Specifications for Transportation Materials and Methods of Sampling and Testing (31st ed.), American Association of State Highway and Transportation Officials, Washington, DC.
- Barksdale, R. D., Brown, S. F. and Chan, F. (1989). Potential Benefits of Geosynthetics in Flexible Pavement Systems, National Cooperative Highway Research Program Report No. 315, Transportation Research Board, National Research Council, Washington DC.
- Berg, R.R, Christopher, B.R. & Perkins, S.W. (2000). Geosynthetic Reinforcement of the Aggregate Base/Subbase Courses of Pavement Structures, GMA White Paper II, Geosynthetic Materials Association, Roseville, Minnesota, USA, 176 p.

- Cancelli, A., Montanelli, F., Rimoldi, P. and Zhao, A. (1996). "Full Scale Laboratory Testing on Geosynthetics Reinforced Paved Roads", Proceedings of the International Symposium on Earth Reinforcement, Fukuoka/Kyushu, Japan, November, Balkema, pp. 573-578.
- Cancelli, A. and Montanelli, F. (1999). "In-Ground Test for Geosynthetic Reinforced Flexible Paved Roads", Proceedings of the Conference Geosynthetics '99, Boston, MA, USA, Vol. 2, pp. 863-878.
- Collin, J. G., Kinney, T. C. and Fu, X. (1996). "Full Scale Highway Load Test of Flexible Pavement Systems With Geogrid Reinforced Base Courses", Geosynthetics International, Vol. 3, No. 4, pp. 537-549.
- Dafalias, Y.F. and Hermann, L.R. (1986). "Bounding Surface Plasticity. II: Application to Isotropic Cohesive Soils", Journal of Engineering Mechanics, ASCE, 112 (12), pp. 1263-1291.
- Haas, R. (1985). Final Project Report on Tensar Reinforced Granular Bases. Department of Civil Engineering, University of Waterloo, Ontario, Canada.
- Henry, K.S., Clapp, J., Davids, W., Humphrey, D., and Barna, L. (2009). Structural Improvements of Flexible Pavements Using Geosynthetics for Base Course Reinforcement. US Army Corp of Engineers, Cold Regions Research and Engineering Laboratory, Report Number ERDC/CRREL TR-09-11, 182p.
- Jersey, S.R. and Tingle, J.S. (2010). Full-Scale Accelerated Pavement Tests Geogrid Reinforcement of Thin Asphalt Pavements, Phase 1 Interim Report, USACE Engineer Research and Development Center, Vicksburg, MS.
- NCHRP (2004). NCHRP Project 1-37A Design Guide, Mechanistic-Empirical Design of New and Rehabilitated Pavement Structures, <http://www.trb.org/mepdg/>.
- Pearce, R. A. (1981) Guidelines for Design of Flexible Pavements Using Mirafix® Woven Stabilization Fabrics, Law Engineering, Houston, TX, 35p.
- Perkins, S.W. (1999). Geosynthetic Reinforcement of Flexible Pavements: Laboratory Based Pavement Test Sections. U.S. Department of Transportation, Federal Highway Administration, Washington, DC, Report No. FHWA/MT-99/8106-1, 140 p.
- Perkins, S.W. (2001a). Numerical Modeling of Geosynthetic Reinforced Flexible Pavements. U.S. Department of Transportation, Federal Highway Administration, Washington, DC, Report No. FHWA/MT-01-003/99160-2, 97 p.
- Perkins, S.W. (2001b). Mechanistic-Empirical Modeling and Design Model Development of Geosynthetic Reinforced Flexible Pavements. U.S. Department of Transportation, Federal Highway Administration, Washington, DC, Report No. FHWA/MT-01-002/99160-1, 170 p.
- Perkins, S.W. (2002). Evaluation of Geosynthetic Reinforced Flexible Pavement Systems Using Two Pavement Test Facilities. U.S. Department of Transportation, Federal Highway Administration, Washington, DC, Report No. FHWA/MT-02-008/20040, 120 p.
- Perkins, S.W. and Edens, M.Q. (2002). Finite Element and Distress Models for Geosynthetic-Reinforced Pavements. International Journal of Pavement Engineering, 3:4, 239-250.
- Perkins, S.W. and Edens, M.Q. (2003). A Design Model for Geosynthetic-Reinforced Pavements. International Journal of Pavement Engineering, 4:1, 37-50.
- Perkins, S.W., Christopher, B.R., Cuelho, E.V., Eiksund, G.R., Schwartz, C.S. and Svanø, G. (2009). A Mechanistic-Empirical Model for Base-Reinforced Flexible Pavements. International Journal of Pavement Engineering, Vol. 10, No. 2, pp. 101-114.
- Perkins, S.W., Christopher, B.R. and Klompaker, J. (2012). Reinforced Flexible Pavement Layer Coefficients Determined by Mechanistic-Empirical Modeling. To appear in the Proceedings of the Conference EuroGeo 5, the 5th European Geosynthetics Congress, Valencia, Spain, September 2012.
- Tenax (2001). Design of Flexible Pavements with Tenax Geogrids. Technical Reference GRID-DE-2, February. 14p.
- Tensar (1996). Design Guideline for Flexible Pavements with Tensar Geogrid Reinforced Base Layers. Technical Note TTN:BR96, April, 77p.
- Tensar (2010). SpectraPave4 PROTM v3, Tensar TriAx® Geogrid Paved Applications Design Method, June, 15p.
- Tensar (2012). SpectraPave4 PROTM Software User's Manual – Version 3.2, January, 31p.
- Thompson, M.R. and Raad, L. (1979). Fabric Utilization in Transportation Support Systems (Low- Deformation Criteria). Civil Engineering Studies, Department of Civil Engineering, University of Illinois, December, 40p.
- Webster, S. L., (1993) Geogrid Reinforced Base Courses For Flexible Pavements For Light Aircraft, Test Section Construction, Behavior Under Traffic, Laboratory Tests, and Design Criteria, Technical Report GL-93-6, USAE Waterways Experiment Station, Vicksburg, Mississippi, USA, 86p.
- White, D.J., Vennapusa, P.K.R., Gieselman, H.H., Douglas, S.C., Zhang, J. and Wayne, M.H. (2011). In-Ground Dynamic Stress Measurements for Geosynthetic Reinforced Subgrade/Subbase. Proceedings of the Conference Geo-Frontiers, ASCE, pp. 4663-4672.
- Ingold, T.S. and Miller, K.S. (1983). Drained axisymmetric loading of reinforced clay, *Journal of Geotechnical Engineering*, ASCE, 109: 883-898.

Leak Location Liner Performance Evaluation

Abigail Beck, M.S., P.E., TRI Environmental, Austin, TX (formerly of Geo-Logic Associates, Grass Valley, CA), email: abeck@tri-env.com

David Gallagher, GSE Lining Technology, Houston, TX, email: dgallagher@gseworld.com

Erik Kramer, PhD, College of the Redwoods, Eureka, CA 95501, erik-kramer@redwoods.edu

ABSTRACT

A new geomembrane product, Leak Location Liner, developed by GSE specifically for electrical liner integrity surveys (ELIS), enables leak detection surveys for otherwise unfeasible applications and improves leak detection sensitivity for common applications. The capability of this new geomembrane to enable leak detection surveys on the primary liner of a double-lined installation, sites with complete subgrade desiccation, holes at the peak of a wrinkle, under a seam flap, and in an area of poor contact with the subgrade were all tested and verified. In order to compare the leak detection sensitivity of a survey performed on Leak Location Liner to a survey performed on traditional geomembrane, comparative bench-scale testing on both was conducted. The ratio of a leak signal obtained on the Leak Location Liner setup relative to a leak signal obtained on the traditional geomembrane setup was calculated and is here-on referred to as the improvement factor for ease in interpreting the comparative data. This improvement factor was quantified for a spectrum of subgrade soil resistivity values by varying the moisture content of the subgrade soil. The results of comparison trials with the subgrade soil condition varying from near zero moisture content to saturation show the improvement in leak detection sensitivity as a function of subgrade resistivity when Leak Location Liner is used. The results of the testing include expected improvement factors for single-lined applications as a function of subgrade soil type and moisture content, as well as in a multitude of hole conditions.

1. INTRODUCTION

1.1 Background

The electrical liner integrity survey (ELIS) is currently the most effective and practical means of locating leaks in installed geomembranes, particularly after cover soil installation. This type of survey includes ASTM methods D7002, D7007 and D7703. However, a few boundary conditions are critical to its success. The technology functions along the principal that polyethylene geomembranes are electrically isolative and by applying an electrical potential across a geomembrane, an electrical current will flow only if a hole is present in the geomembrane. The various survey methods track the flow of electricity in order to pinpoint a leak. This is only possible if there is an electrically conductive medium both above and below the geomembrane. For geomembranes covered with soil, the soil provides the conductive medium above the geomembrane. Traditionally, subgrade soil acts as the conductive medium below the geomembrane when the application allows it. For single-lined applications using traditional liner there is typically no problem performing an ELIS, as long as the subgrade soil maintains natural moisture content. In applications featuring encapsulated geosynthetic clay liners (GCL) desiccation issues have been reported to preclude surveys on primary geomembranes (Peggs, 2007). Although hydrating encapsulated GCL has been suggested (Beck et. al., 2008), this idea has not been embraced by the industry and GCL desiccation is still an unresolved issue when performing an ELIS on traditional liner. Subgrade soil electrodes are sometimes placed in the subgrade before deployment of the geomembrane, in order to shorten the electrical path during an ELIS and thus increase survey sensitivity for soils with low conductivity. However, when using Leak Location Liner, the conductive layer in the geomembrane serves as the lower conductive medium and the aforementioned are no longer concerns. One solution to these issues has been conductive geotextile, which is quite expensive and requires the installation of an additional layer of material under the geomembrane to be tested and therefore has not been widely used.

Another issue that frequently arises during an ELIS is poor hole contact. An example of a hole with poor contact would be a hole that is located at the peak of a wrinkle. A hole on the peak of a wrinkle is unlikely to be detected by an ELIS on traditional liner because the electrical path is broken by the lack of intimate contact between the hole and the subgrade soil. Holes located under seam flaps are also difficult to locate due to the lack of intimate contact with the cover soil.

The recently improved Leak Location Liner features a conductive backing designed to carry sufficient current for a ELIS, acting as the conductive medium below the geomembrane. Successful pilot projects of the product have shown that the conductive backing sufficiently carries the required range of survey current and specialized wedge welders prevent false positives at the seams (Ramsey, 2012, Gallagher, 2012). Designed for enabling a survey where it was previously unfeasible or ineffectual, the product has also enhanced the overall quality of an ELIS on any application. A series of

tests were performed on a bench scale in order to quantify the increase in survey quality when Leak Location Liner is used in comparison with traditional geomembrane for single-lined applications, including situations with poor hole contact.

1.2 ELIS Quality

The essence of ELIS quality lies in the size and number of leaks that can be located in the geomembrane during a survey for subsequent repair. A higher quality survey will naturally locate more leaks in the geomembrane than a lower quality survey. The authors chose to employ ASTM method D7007 as the means to quantify survey quality. The measure of survey quality is taken to be the signal to noise ratio as calculated during the sensitivity test portion of ASTM method D7007.

The signal to noise ratio is expressed as:

$$R = (S+N)/N \quad [1]$$

Where R is the signal to noise ratio, (S+N) is the magnitude of the difference between the highest and lowest voltage potential readings when travelling across a hole location per the ASTM D7007 dipole spacing requirements and N is that magnitude when the hole is not there, otherwise known as the background noise of the survey area.

A higher signal to noise ratio means that smaller leaks can be located compared with a lower signal to noise ratio, based on the authors' field experience. Below a signal to noise ratio of 3:1, the leak is not considered to be locatable per ASTM D7007. As the sensitivity (i.e. signal to noise ratio) increases, smaller leaks become detectable, and therefore smaller leaks that would otherwise go undetected become detectable and more leaks are located during the survey.

2. TEST METHOD

The survey quality when using either traditional liner or Leak Location Liner was quantified in parallel, identical bench-scale test set ups. The signal to noise ratio, referred to henceforth as the leak signal, was measured for a given hole in both traditional geomembrane and Leak Location Liner.

2.1 Bench-scale Setup

A small-scale geomembrane-lined survey area was created for a bench-scale dipole testing apparatus. The dimensions of the bench-scale set up measured 61 cm (24") wide by 91 cm (36") long by 8.9 cm (3.5") tall. The dipole instrument used to take voltage potential readings employed a spacing of 7.6 cm (3"). The subgrade portion of the apparatus measured 6.3 cm (2.5") thick and the cover soil portion measured 2.5 cm (1") thick.

The subgrade consisted of a box of moisture-conditioned soil confined by a wooden frame. The soil type used in these tests was sandy clay. The wooden frame ensured the same depth of subgrade material for each trial. The subgrade soil box was covered by the geomembrane being tested. Holes in the geomembrane were carefully drilled out and a clay plug the thickness of the geomembrane was inserted into each hole to provide the same hole contact for each test run. Hole diameters of 1.6 mm (1/16"), 3.2 mm (1/8") and 6.4 mm (1/4") were used. For background noise measurements, electrical tape was placed over the holes. The cover soil was kept at a constant moisture content of approximately 18% for all tests and was the same material as the subgrade soil. This higher moisture content was chosen so that the effects of subgrade moisture content could be clearly measured, since drier cover soils were more susceptible to contact quality errors, both between the probes and soil and the hole and soil. The cover soil was placed with a wooden frame to ensure uniform compaction and depth throughout the testing, as shown in Figure 1. A voltage of 50V was applied to the cover soil in one corner of the box. The power source ground was placed in the opposite corner of the box in the subgrade soil for the traditional geomembrane trials and it was clamped directly to the conductive backing of the Leak Location Liner at approximately the same location for the Leak Location Liner trials.

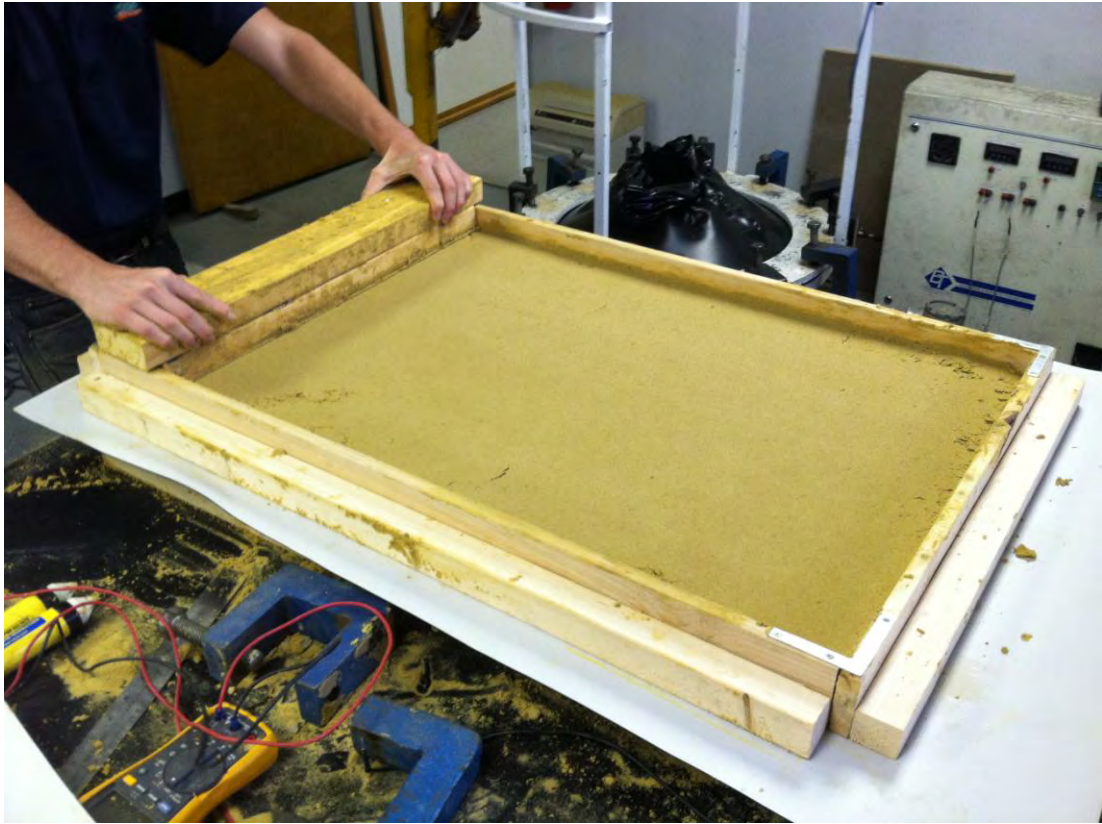


Figure 1. Bench-scale dipole test apparatus as cover soil is placed.

For each trial, two measurements of voltage potential were taken; one as the dipole approached the hole location and the second as the dipole was just past the hole location, with the position of the dipole relative to the hole placement as prescribed by ASTM D7007. A template was created to ensure the same dipole placements for each trial. The system current for each trial was recorded in tandem with the dipole voltage potential measurements for quality control.

2.2 Bench-scale Test Method Descriptions

Four series of tests were performed, referred to as Tests A through D. The test setups, results and discussion are reported in alphabetical order throughout this text.

Test A was designed to calculate the improvement factor when Leak Location Liner is used instead of traditional geomembrane in applications where historically traditional geomembrane would have been used. Hole diameters of 3.2 mm (1/8") and 6.4 mm (1/4") were used. A total of 34 trials were performed on each of the traditional and Leak Location Liner geomembranes. For each set up, at least two measurements were taken for each hole size, digging up the cover soil and recompacting it between trials to account for any variation in hole to cover soil contact. The moisture content of the subgrade material was measured after each test was performed using ASTM D2216. The soil resistivity value was measured while the subgrade soil was in place using the soil resistivity method developed by Erik Kramer, PhD (Beck et. al., 2008). The moisture content of the soil was varied from a desiccated condition (~0.5%) until saturation (~25%). Leak signals were measured for both the Leak Location Liner and traditional geomembrane and then the improvement factor was calculated by dividing the leak signal obtained from the Leak Location Liner setup by the leak signal obtained from the traditional liner setup.

Poor hole contact situations were simulated for Test B. Three different scenarios were tested; a hole at the peak of a wrinkle, a hole located above a slight depression in the subgrade, and a hole located underneath a seam flap. All holes for this test measured 3.2 mm (1/8") in diameter. The simulated wrinkle consisted of an 13 mm (1/2") diameter wrinkle molded into the geomembranes, as shown in Figure 2. The slight depression in the subgrade was made with an index finger and checked after the test to verify that there was no direct subgrade to hole contact, as shown in Figure 3. The hole drilled under the seam flap was similarly checked after the test to have maintained separation with the cover soil, as shown in Figure 4.

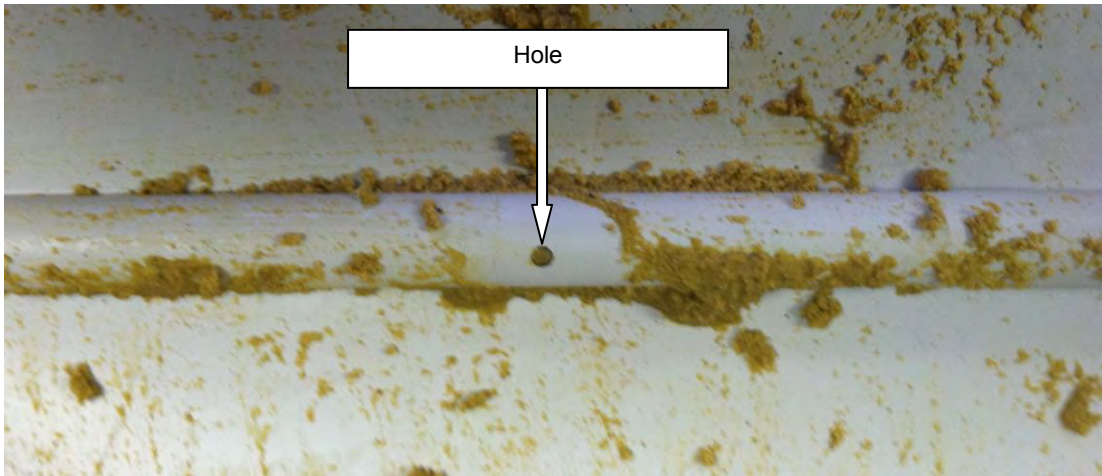


Figure 2. Hole at Peak of Simulated Wrinkle.



Figure 3. Hole Over Depression in Subgrade.

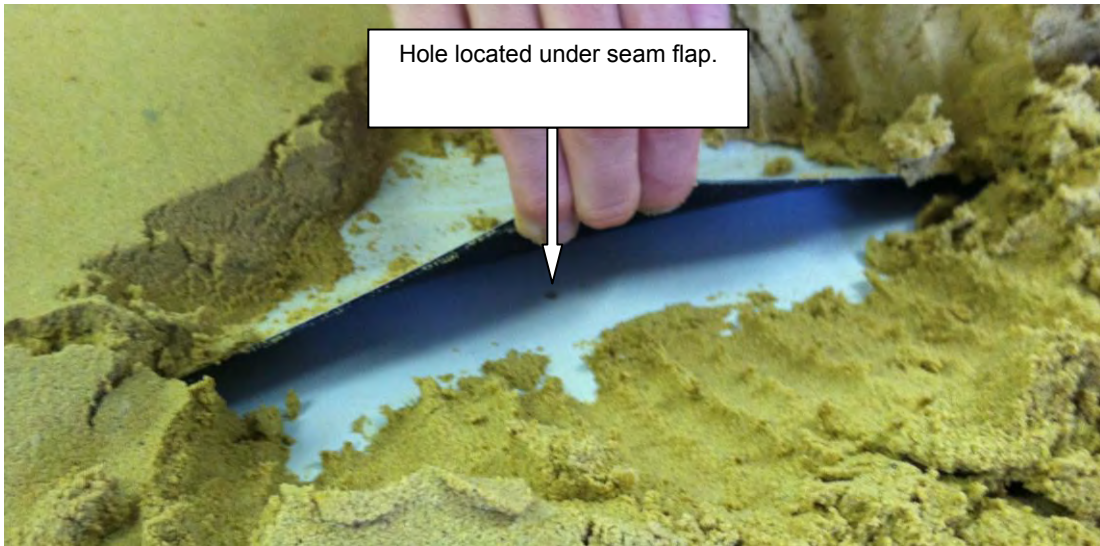


Figure 4. Hole Under Seam Flap.

The leak signal as a function of distance from the hole was investigated for Test C. The subgrade moisture content was 2% and the hole size was 1.6 mm (1/16") diameter. The first dipole readings were taken at the initial location as specified by ASTM D7007 and the subsequent readings were taken increasingly further away in 51 mm (2") increments. One trial was done on each geomembrane type for each distance point.

Test D was designed to evaluate the impact of the placement of the power source ground electrode on the leak signal. The electrical contact of the power source electrodes are very important for the current path of a ELIS. The series of improvement factor trials in Test A had been grounded to the subgrade soil for the traditional liner trials and clamped directly to the conductive backing of the Leak Location Liner for the Leak Location Liner trials. The ground placement trials were performed on Leak Location Liner at a subgrade moisture content of 25%. Leak signals were recorded on the same bench-scale set up for three different grounding positions; subgrade ground only, ground clamped to conductive backing, and grounded to both the subgrade and conductive backing. Each set up was tested twice, digging up and recompacting the hole locations between trials. It was a direct comparison test, which measured the leak signal as a function of ground placement.

3. RESULTS

3.1 Test A: Improvement Factors for Currently Used Applications

The most significant result of this test was that the traditional geomembrane setup did not produce a leak signal for the lowest moisture content tested. The improvement factor is exponential, with drastic increases in improvement at lower values of subgrade moisture content.

The observed improvement factors as a function of subgrade moisture content from 2% to 15% are presented in Figure 5. The reported moisture content is only valid for the type of soil used in the bench-scale test. Improvement factors for other soil types are reported in the discussion section of this paper. The data points represent an average of two or more trials. There is more data scatter at the lower moisture contents, likely because the electrical contacts become more difficult to control at lower moisture contents.

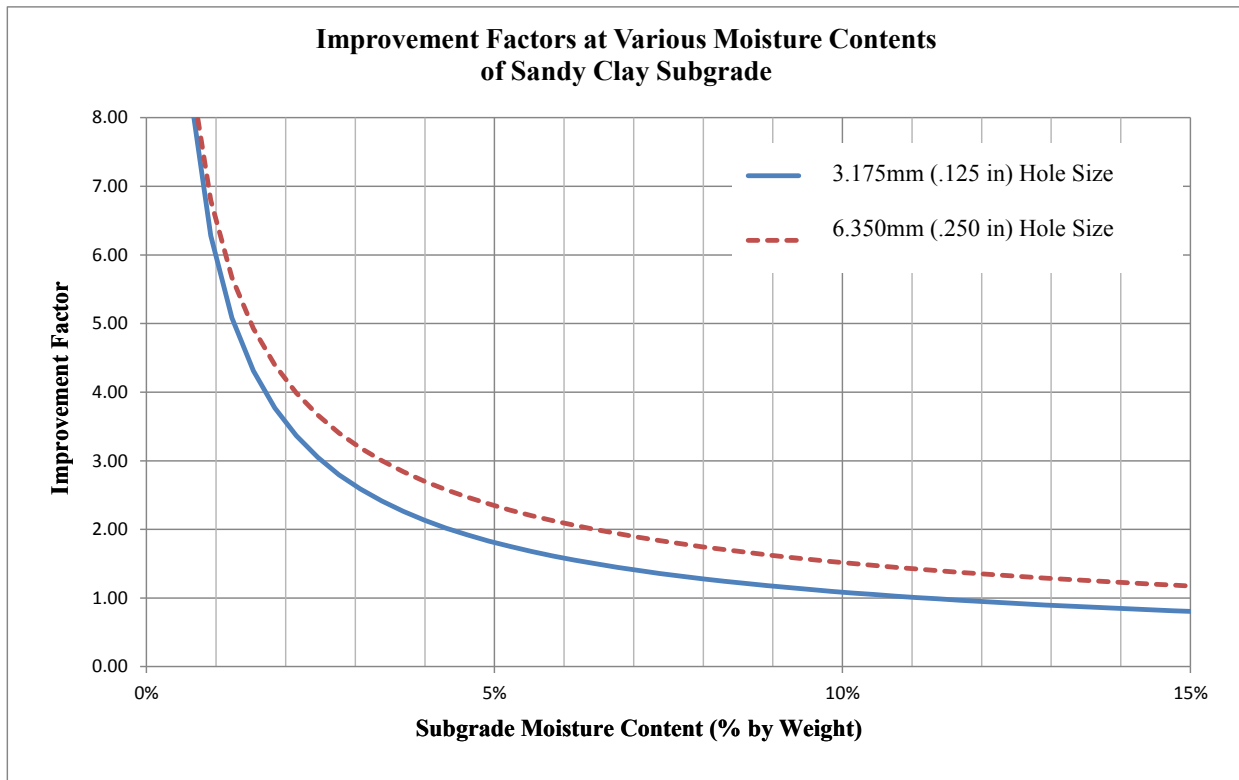


Figure 5. Observed Improvement Factors in Single-Lined Applications.

3.2 Test B: Poor Contact Situations

Leak signals were measured twice for each poor contact scenario on each geomembrane type. The average leak signals obtained are reported in Table 1. Leak signals are dimensionless and the following data is used as a comparison between leak signals in various conditions using each liner type.

Table 1. Leak Signals for Poor Contact Situations.

Geomembrane Type	Void Under Geomembrane	Hole Under Seam Flap	Hole on Wrinkle
Traditional	12	2	0.4
Leak Location Liner	86	21	91

3.3 Test C: Distance from Hole Testing

The measured leak signals are shown as a function of lateral distance from the hole location for both geomembrane types in Figure 6.

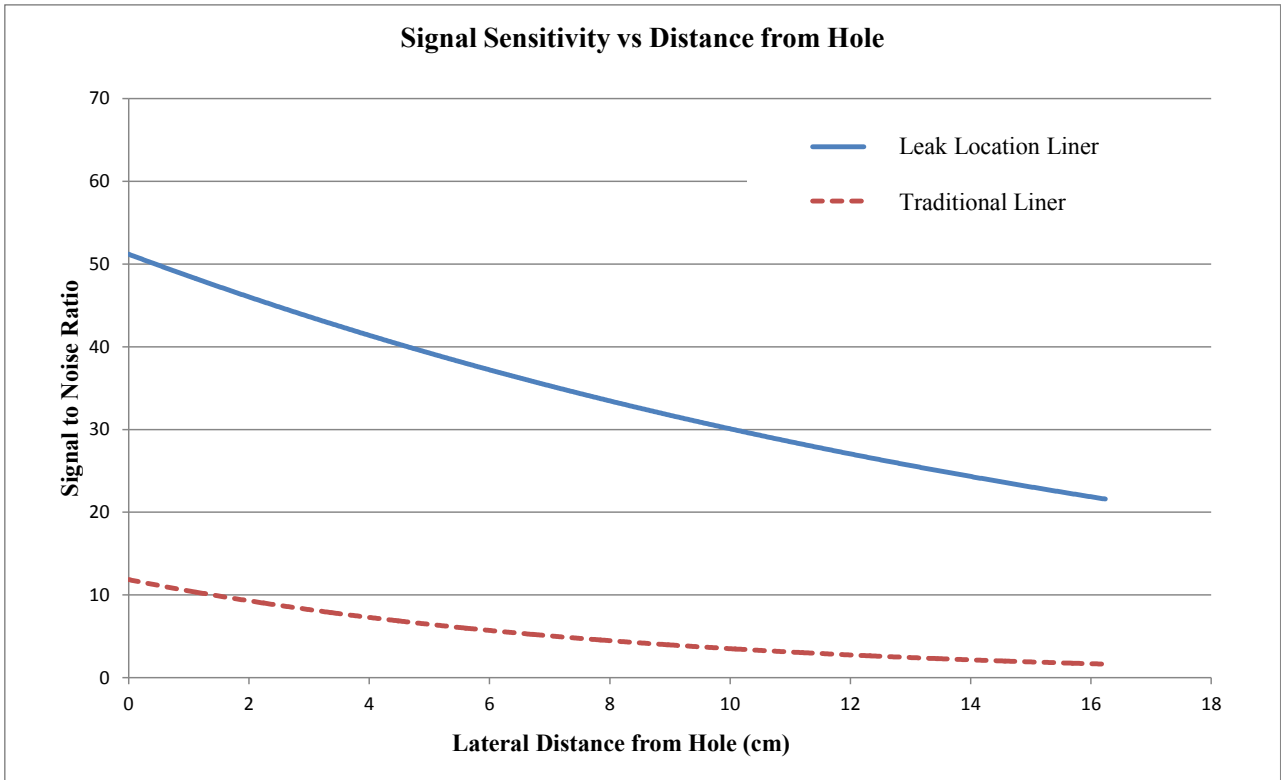


Figure 6. Leak Signals as a Function of Distance from Hole Location.

3.4 Test D: Ground Placement Investigation

The results of the ground placement investigation are reported as average values for the two trials measured for each condition.

Table 2. Average Leak Signals for Various Ground Placements.

Subgrade Ground Only	Sheet Ground Only	Multiple Grounds – Subgrade and Sheet
163	271	327

4. DISCUSSION OF RESULTS

The results of Test A showed that Leak Location Liner can provide a more sensitive survey than traditional liner, especially if the subgrade soil is placed at a lower moisture content or desiccates in the field before placement of the geomembrane. As the moisture content of the subgrade increases, the sensitivity of a survey on traditional liner also increases, which decreases the improvement in sensitivity that Leak Location Liner can provide.

The improvement factors calculated from the raw test data in Test A are shown as a function of moisture content of the specific soil used as the subgrade material for the bench-scale testing. Soil resistivity values were also measured at the various moisture contents of the soils in order to obtain results that could be applied to different soil types. Subgrade soils are generally placed at near optimum moisture content, which is a function of soil type. The resistivity value of the soil is a function of both soil type and moisture content, among other factors. A literature survey of resistivity values ranges for soil types and moisture contents was performed. Figure 7 shows values of resistivity for various soil types as a function of a range of values for moisture content. Potential improvement factors for a range of resistivity values are presented in Figure 8. These improvement factors apply if the Leak Location Liner is grounded to the power source by only the conductive backing. Greater improvement is expected when multiple grounds are used.

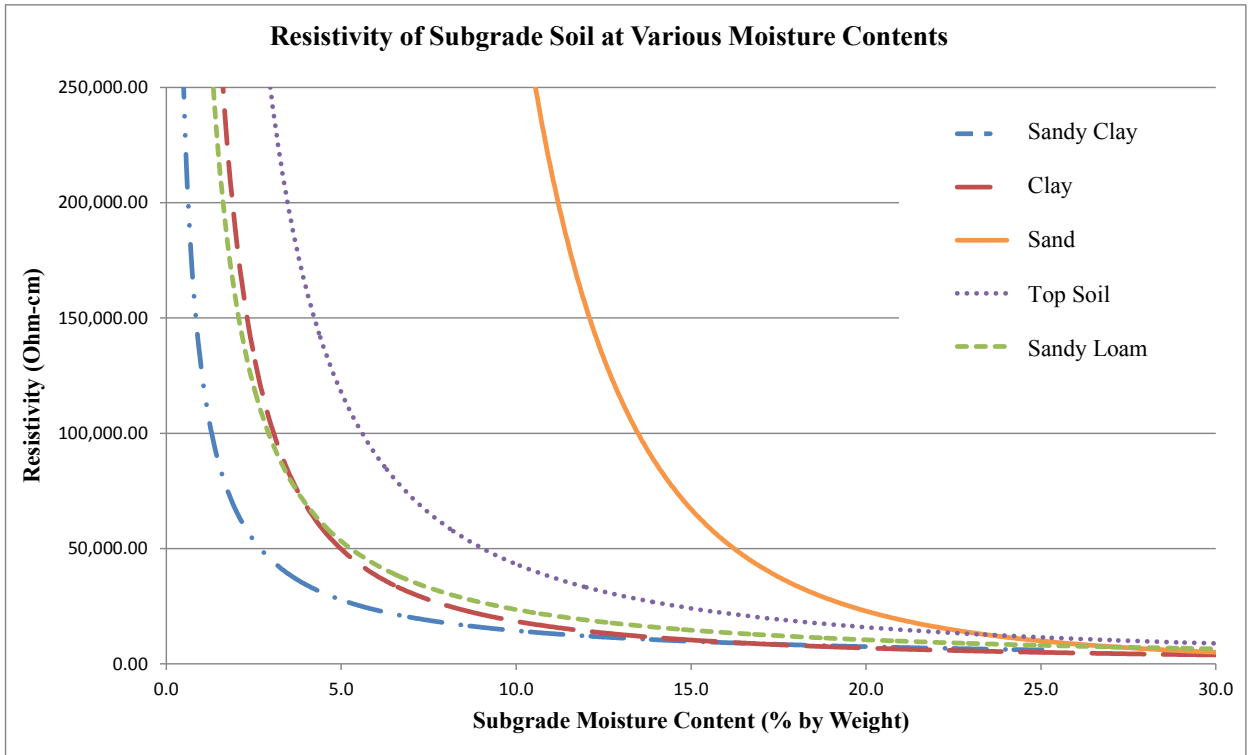


Figure 7. Subgrade Resistivity Values as a Function of Soil Type and Moisture Content.

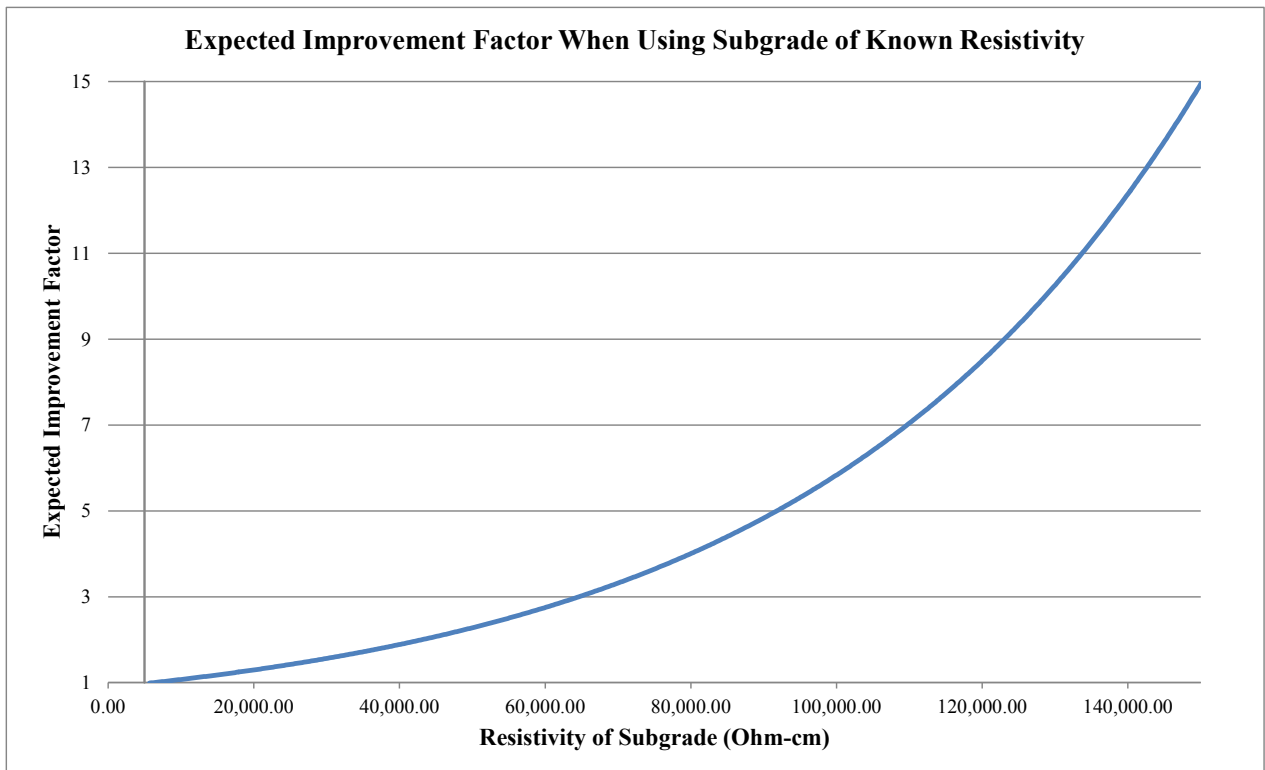


Figure 8. Improvement Factor as a Function of Subgrade Resistivity.

The values of the leak signals reported for Test B represent a bench-scale set up where the hole size and thickness of cover soil are not proportional to a field-scale set up. The leak signals reported cannot be compared directly to the ASTM D7007 requirement for a 3:1 signal to noise ratio as a limit for hole detection. The average leak signal value for the traditional geomembrane bench scale test was approximately 300, roughly five times a signal that would be considered excellent in field conditions. Therefore, the reported values should be scaled down by a factor of five to approximate a similar field condition, based on the author's field experience. The scaling down of the leak signal results in the approximations of signal strength and the likelihood of locating the hole in a field situation shown in Table 3.

Table 3. Approximated Field Signals and Hole Detection Evaluation in Poor Contact Situations.

Geomembrane Type	Void Under Geomembrane	Hole Under Seam Flap	Hole on Wrinkle
Traditional	Very weak signal; not likely to be detectable	Not detectable	Not detectable
Leak Location Liner	Very good signal; detectable	Weak signal; detectable	Very good signal; detectable

Holes that are difficult or impossible to detect on traditional geomembrane can be detected when Leak Location Liner is used. The reason why the Leak Location Liner enables the leak signal in the poor contact situations is because the conductive backing carries the current even in the absence or poor conductivity of the subgrade material. In the case of the hole located under the seam flap, the flap of the seam also has the conductive backing, which completes the circuit between the cover soil and the hole.

Test C directly illustrates how a stronger leak signal results in greater survey sensitivity. Due to the increase in signal strength relative to the background noise, the leak can be detected at a further distance from the hole. In terms of survey grid spacing for the bench-scale setup, the hole could be seen during multiple passes of the dipole equipment as it got closer and closer to the hole. The signal being seen on multiple passes decreases the likelihood of a dipole operator passing over a hole location.

As the moisture content of the subgrade soil increased beyond 15% in the Test A trials, it is theorized that the combination of the subgrade geometry and the lower resistivity value resulting from an increase in moisture content caused the subgrade to be a more preferential path for current flow than the conductive backing of the sheet. In addition, the grounding electrode contact in the subgrade improved as the moisture content increased. By grounding to both the sheet and the subgrade, the current is not only allowed to travel the path of least resistance, whichever it may be, but also travel the two paths at once. This is similar to the case when there are two resistors in parallel in a circuit. The overall resistance is diminished when a resistor is added in parallel, and the overall resistance is always less than just one of the resistors wired in series. Although Test A was not repeated with multiple grounds, the Test D results show that a substantial further increase in leak signal can be achieved by utilizing the multiple grounds in tandem with Leak Location Liner when the application allows it. This set up should cause the Leak Location Liner to show continued improvement over traditional liner at any subgrade moisture content and in any application.

4.1 Applicability to Large-scale Installations

A mathematical model was created and compared to the bench-scale test in order to extrapolate the performance of Leak Location Liner on a large-scale installation. The model used a single charge point to model the hole and appropriate image charges to model the boundaries. The model can calculate simulated improvement factors for the Leak Location Liner versus traditional geomembrane. As well, it can calculate simulated voltage signals of a given grid spacing and correct for input impedance.

Figure 9 shows that the model's calculated improvement factors compare well to the measured data for a 3.175 mm (1/8") hole from Test A, confirming the accuracy of the model in small scale. The theory curve was generated by the model's formula for improvement factor with geometric inputs matching those specified for Test A, cover soil conductivity matching measurements, and manufacturer data on liner conductivity and thickness.

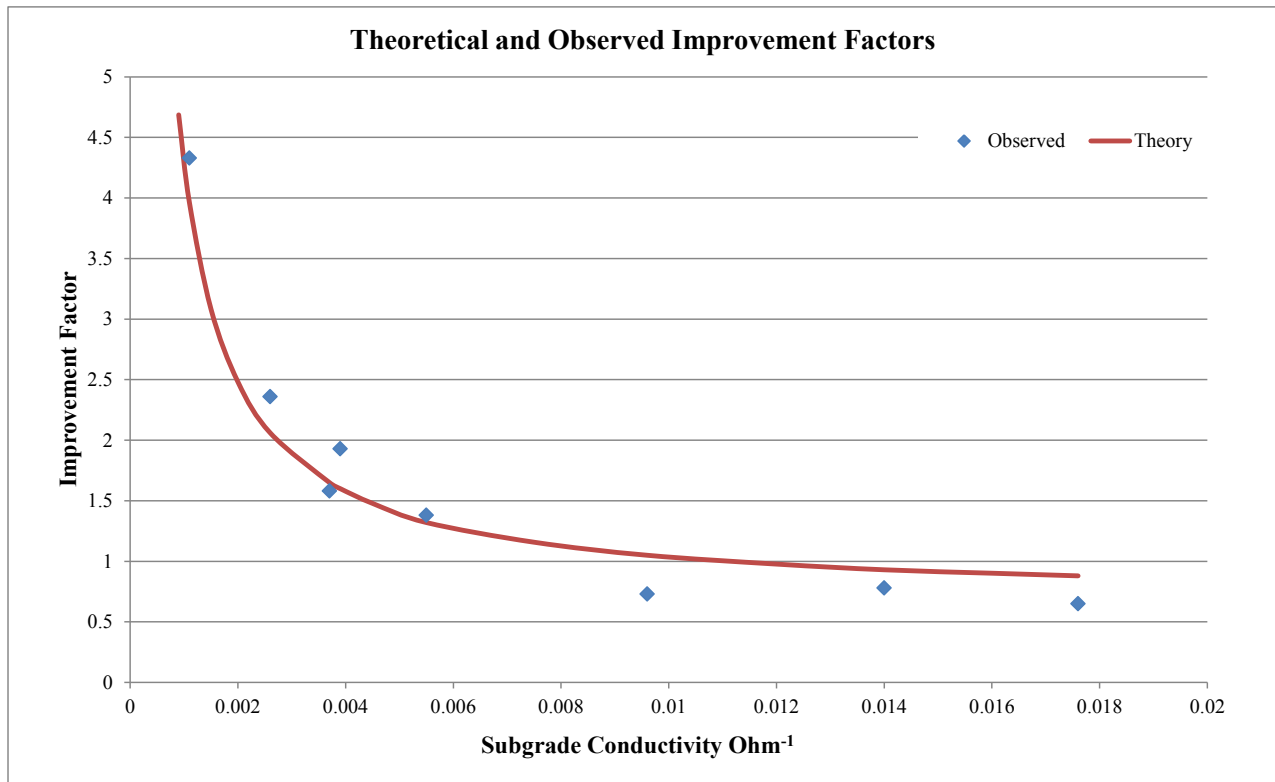


Figure 9. Observed Data and Theoretical Curve for 3.2 mm (1/8") hole.

Additionally, curves comparing the theoretical voltage signals and real data as measurements are taken over a hole from large installations showed that the theoretical signals matched field data in general form. This result means that the theoretical model still holds true when scaled up to real world site conditions and can be used to show expected improvement factors when Leak Location Liner is used in a full-scale application.

In applying this model, various common field geometries and site conditions were entered into the model to observe the performance of the Leak Location Liner. In each of the cases the model output showed that the improvements seen in small scale testing of the Leak Location Liner over traditional geomembrane were mirrored in large-scale field applications.

5. CONCLUSION

In addition to enabling an ELIS on the desiccated subgrade soil where the traditional liner could not be used, the results of the testing showed that the Leak Location Liner could also increase ELIS sensitivity on single-lined applications for a wide range of soil types and moisture contents. Leak Location Liner also makes it possible to locate holes in poor hole contact situations such as at the peak of a wrinkle, over a depression in the subgrade and under a seam flap. By increasing the signal strength, holes can be detected at further distances from the hole location, increasing the survey quality. The follow-up testing utilizing multiple grounds showed promise for an even greater improvement factor when Leak Location Liner is used. This should result in survey quality improvement no matter what the soil subgrade resistivity value.

For double-lined geomembrane applications, Leak Location Liner enables an ELIS where it would have previously been impossible. For sites with encapsulated GCL or large installations where subgrade conductivity might be an issue, Leak Location Liner can ensure the success of a ELIS where otherwise the results might range from marginal survey quality to a complete failure to perform the test.

REFERENCES

- ASTM D2216-05. Standard Test Method for Laboratory Determination of Water (Moisture) Content of Soil and Rock by Mass. *American Society for Testing and Materials*, West Conshohocken, Pennsylvania, USA.
- ASTM D5199-01. Standard Test Method for Measuring the Nominal Thickness of Geosynthetics. *American Society for Testing and Materials*, West Conshohocken, Pennsylvania, USA.
- ASTM D7007-03. Standard Practices for Electrical Methods for Locating Leaks in Geomembranes Covered with Water or Earth Materials. *American Society for Testing and Materials*, West Conshohocken, Pennsylvania, USA.
- ASTM G57-06. Standard Test Method for Field Measurement of Soil Resistivity Using the Wenner Four-Electrode Method. *American Society for Testing and Materials*, West Conshohocken, Pennsylvania, USA.
- ASTM F390. Standard Test Method for Sheet Resistance of Thin Metallic Films With a Collinear Four-Probe Array. *American Society for Testing and Materials*, West Conshohocken, Pennsylvania, USA.
- Beck, A., Kramer, E. and Smith, M.E. (2008). Specifications for Moisture Content of GCL to Perform Electrical Leak Location Surveys. *Proc. of the 4th European Geosynthetics Conference*, September 7-10, Edinburgh, Scotland.
- Dahlin, T. (2000). Short Note on Electrode Charge-up Effects in DC Resistivity Data Acquisition Using Multi-Electrode Arrays. *Geophys. Prospec.* 48: 181-187.
- Department of the Army. (1997). *Military Soils Engineering, US Army Field Manual 5-410*. Chapter 8, Soil Compaction.
- Gallagher D., Youngblood J., Ramsey B. (2012) New Electrically Conductive Geosynthetics in Support of Post Installation Liner Integrity Surveys. *Proc. of GeoAmericas 2012*, May 1-4, Lima, Peru.
- Fukue, M., Minatoa, T., Horibe, H., Taya, N. (1999). The microstructure of Clay Given by Resistivity Measurements. *Eng. Geol* 54: 43-53.
- Lightening & Surge Technologies. n.d. Earthing Techniques. Retrieved March 7, 2012, <<<http://www.lightningman.com.au/Earthing.pdf>>>.
- Megger. (2010). Getting Down to Earth. <<<http://www.biddlemegger.com/biddle-ug/GettingDownToEarth-MC.pdf>>>.
- Peggs, Ian D. (2007). Liner integrity/leak-location survey: The significance of boundary conditions. *Geosynthetics*, February-March 2007, pp. 34.
- Pozdnyakova, L.A. (1999). Electrical properties of soils. *PhD Dissertation, Univ. of Wyoming, Col of Agriculture, Laramie, WY*.
- Ramsey B. J., Peggs I., Gallagher D., et.al. (2012). New Electrically Conductive Geomembrane for Post Installation Liner Integrity Surveys. *Proc. of the 5th European Geosynthetics Conference*, September 16-19, Valencia, Spain.
- Samouelian, A., Cousin, I., Tabbagh, A., Bruand, A. and Richard, G. (2005). Electrical Resistivity Survey in Soil Science: A Review. *Soil & Tillage Research*, 83: 173-193.
- Sverko, Elvis R. (1999). Ground Measuring Techniques: Electrode Resistance to Remote Earth and Soil Resistivity. <<http://www.stu2.net/wiki/images/0/03/Grounding_Measurements-1.pdf>>.

Lifetime Prediction of Thin HDPE Geomembranes for the Shrimp Aquaculture Industry

Daniel Tan, Engr., Solmax International Asia Pacific Sdn Bhd, Malaysia, dtan@solmax.com

Robert Denis, P.E., Solmax International Inc., Canada, rdenis@solmax.com

Guy Elie, P.E., Solmax International Inc., Canada, gelie@solmax.com

David Cao, Solmax International Inc., Canada, dcao@solmax.com

ABSTRACT

High-density polyethylene (HDPE) geomembrane (GMB) is commonly specified as the preferred lining for shrimp aquaculture industry in South East Asia. Shrimp farms generally consist of extensive water canals surrounding grow-out, culture and treatment ponds. The water canals and ponds are relatively shallow in depth and commonly designed and constructed to 1.5m to 2.5m deep. Both the water canals and ponds are generally lined with thin gauge ($\leq 0.75\text{mm}$) HDPE GMBs mainly to maintain water level and control of water quality amongst other lining benefits. Due to the shallow depths, a significant section of the GMB lined canals and shrimp aquaculture ponds are therefore exposed to direct sunlight between the water freeboard level to the crest of bund and hence susceptible to UV degradation. The durability and lifetime prediction of HDPE GMBs particularly for the landfill industry where the common thicknesses range between 1.0mm to 2.5mm depending on the design and regulation of respective countries around the world have received much attention from engineers and researchers alike. However, there is a lack of information from the industry on the lifetime prediction of thin HDPE GMBs installed in the exposed environment particularly common to the shrimp aquaculture industry in South East Asia. Furthermore the properties of thin ($\leq 0.75\text{mm}$) HDPE GMBs are not covered by the industry standard of "GRI Test Method GM13" and needs to be extrapolated. This paper seeks to collate available information on the durability and lifetime prediction of GRI GM13 standard HDPE GMBs both in the exposed and buried environment and proposes a cautious extrapolation method in order to arrive at a reasonable lifetime prediction for the thinner gauge GMBs for the shrimp aquaculture industry.

1. INTRODUCTION

Aquaculture output has increased rapidly in Southeast Asia over the past 15 years resulting in six of its member countries namely Indonesia, Malaysia, Myanmar, Philippines, Thailand and Vietnam being ranked among the top 25 countries in the world in terms of aquaculture volume. Shrimp aquaculture is the largest farmed fish by species in Southeast Asia in terms of output as well as value where shrimp consists of 22% of the total 5.03 million tons of the regions' fish aquaculture output in 2005. Although the output by weight is only 1/5 of the total regional output, the value of shrimp aquaculture is US\$4.36 billion (46% of total farmed fish value) in 2005 (Hishamunda et al. 2009).

Youngblood and Ng (2008) states that HDPE GMB appears to be the liner of choice for shrimp farms due to its beneficial characteristics such as high chemical resistance, low permeability rate and superior UV resistance among other properties. Profitability of shrimp farmers are known to increase when HDPE GMB liners are used to line the ponds as it lowers the mortality rate of shrimps, promote growth and preferential color, reduce possible spreading of disease, ease of water quality control and faster harvest to culture turnover.

Commonly required HDPE GMB thicknesses for the shrimp aquaculture industry are 0.5mm, 0.65mm and 0.75mm. HDPE GMB thickness specified by the client are generally based on extensive observational experience of the site ground condition pertaining to installation and operational survivability rate of the liners and not subject to mechanics based engineering computation nor governed by regulatory requirements. The typical properties of thin gauge HDPE GMBs for shrimp aquaculture are ordinarily obtained by extrapolation from the internationally widely accepted Geosynthetic Research Institute's (GRI) specification no. 13 as illustrated in Table 1. The mechanical properties of HDPE GMBs as presented in Table 1 have been observed to meet the installation and operational requirements for the shrimp aquaculture industry.

However, the theory that thinner gauge GMBs have lower lifetimes when compared to thicker GMBs (Kay et al. 2004 and Koerner et al. 2012) compounded with the widely accepted fact that UV exposed GMBs have lower lifetimes compared with buried environments poses a significant issue of HDPE GMB durability for the aquaculture industry where a significant portion of the liners are exposed to UV from the water freeboard level to the crest of bund.

Islam and Rowe (2007), Rowe et al. (2010), Ewais and Rowe (2012) have carried out studies on the durability effect of HDPE GMB thickness in the buried environment exposed to synthetic landfill leachate. Tarnowski and Baldauf presented a case study on a sludge deposit pond in Galing, Germany where it was observed that the top layer of a 2.5mm HDPE GMB has lesser remaining OIT when compared to its middle layer and hence concluded that thickness has a major influence on antioxidant depletion which leads to lower liner durability. Apart from these, the authors find that there is at present a paucity of industry information with regards to thickness effect on the lifetime prediction of HDPE GMB and this pertinent issue remains a research needs especially for UV exposed thin gauge HDPE GMBs (Koerner et al. 2012).

Table 1. Typical thin gauge HDPE GMB properties extrapolated from GRI GM 13 for shrimp aquaculture.

Properties	ASTM Test Method	Units	0.5mm (20mil)	0.65mm (25mil)	0.75mm (30mil)
Thickness					
- Minimum average (Min. Avg.)		mm	0.50	0.65	0.75
- Lowest of 10	D5199	mm	0.45	0.585	0.68
Sheet Density (ρ), (Min.)	D792	g/cc	0.94	0.94	0.94
Tensile Properties (Min. Avg.)					
- Yield Strength, (T_{yield})		kN/m	8	9	11
- Yield Elongation, (ϵ_{yield})	D6693	%	12	12	12
- Break Strength, (T_{break})	Type IV	kN/m	14	18	20
- Break Elongation, (ϵ_{break})		%	700	700	700
Tear Resistance (TR), (Min. Avg.)	D1004	N	65	80	93
Puncture Resistance (PR), (Min. Avg.)	D4833	N	176	225	240
Stress Crack Resistance (SCR) ¹	D5397	hr.	300	300	300
Carbon Black Content (CBC)	D4218	%	2.0 – 3.0	2.0 – 3.0	2.0 – 3.0
Carbon Black Dispersion (CBD)	D5596	-	Cat.1/Cat.2	Cat.1/Cat.2	Cat.1/Cat.2
Oxidative Induction Time (OIT)					
- Standard (Std.) OIT (Min. Avg.)	D3895	min.	100	100	100
Oven Aging (% Retained)					
- High Pressure (HP) OIT (Min. Avg.)	D5885	%	80	80	80
UV Resistance (% Retained)					
- High Pressure (HP) OIT (Min. Avg.)	D5885	%	50	50	50

¹Precision is required to administer the 20% notch for SCR test on thin gauge HDPE GMBs

2. DEGRADATION MECHANISM OF HDPE GMBS AS POND LINERS IN SHRIMP AQUACULTURE

2.1 Buried Section

Degradation mechanism of HDPE GMB below water level could possibly come from chemical degradation and / or thermal degradation. The presence of oxygen below water level is also very low and hence yields an environment for lower oxidation.

Table 2 presents the optimum water quality conditions for cultured shrimp ponds recommended by ASEAN (2005). HDPE GMBs are found to be chemically resistant to these conditions.

Table 2. Optimum water quality conditions for cultured shrimp pond (ASEAN 2005).

Parameter	Value	Units
Dissolved Oxygen (DO)	> 4	mg/L
pH	7.5 – 8.5	-
Ammonia	< 0.1	mg/L
Transparency	30 – 45	cm

With regards to thermal degradation, the water temperature of the shrimp pond is generally only slightly higher than ambient due to conduction from sunlight as water is a low heat conductor. As such, the water temperature in shrimp aquaculture ponds does not pose a concern to thermal degradation effect on HDPE GMBs.

For HDPE GMBs buried in the anchor trench, the degradation mechanism is dependent on the soil type and moisture content as both sides of the liner are in direct contact with the soil.

Given the above, liner durability at sections below water level does not pose serious concerns for HDPE GMBs when compared to the UV exposed section.

2.2 Exposed Section

It has been widely published and generally accepted that GMBs constructed in the exposed environment has a lower durability compared to the buried environment due to detrimental degradation mechanisms such as lush presence of oxygen, photo-oxidation from UV degradation and thermo-oxidation due to increase in liner temperature (Rowe and Sangam 2002 and Koerner et al. 2012) as HDPE GMB is a good heat conductor. Moreover, the presence of oxygen for the exposed section has oxygen concentrations 8 times the section covered by water (Hsuan and Koerner 1995). As such, the section of GMB liner above the water level up to the crest of bund is exposed to severe degradation mechanism.

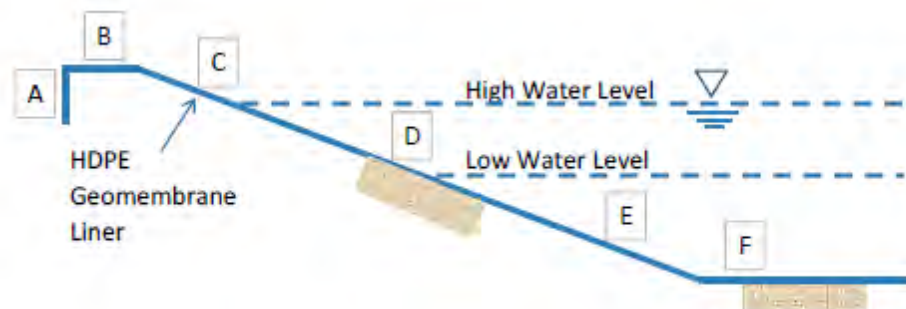
However, a point to note is that the UV radiation intensity as well as heat exposure is largely dependent on the geographical location of the shrimp aquaculture farm. Several world solar maps have been published such as Annual Irradiation Energy Isocurves in “kLy” after Van Wilk and Stoezer (1986) (Koerner et al. 2012), Average Annual Solar Radiation in “kWh/m².year” (Keller et al. 2009) and Local Noon Erythermal UV Irradiance in “mW/m²” after USA National Aeronautics and Space Administration (NASA) (Tencate 2010) and may be referred to for correlation purposes. Furthermore, the intensity of solar radiation is also dependent on the GMB liner facing direction in relation to the site geographical location (Martin 2005).

Given the above, liner durability at sections above water level is the critical section for liner durability and lifetime prediction of HDPE GMBs for shrimp aquaculture and is the main focus of this paper.

2.3 Summary of Various Liner Exposure Sections in Shrimp Aquaculture Ponds

Figure 1 schematically illustrates the various sections of HDPE GMBs exposed to different possible degradation mechanisms as discussed in Section 2.1 and 2.2 above. Table 3 summarizes the different possible degradation mechanisms for the various sections in a shrimp aquaculture pond as illustrated in Figure 1 and discussed in Section 2.1 and 2.2 above.

It is noted that for some applications where aggressive solutions are being contained, location D may be the most critical section in terms of durability of the GMB due to antioxidants leaching out by water when exposed to high temperature. This however is unlikely for the shrimp aquaculture application where the general water quality is as given in Table 2 above. As such, it is hypothesize that HDPE GMBs at location A, E and F are envisaged to have higher durability compared to location B, and C whereas location D is likely to have estimated durability in between the fully buried and fully exposed sections.



Note: A – Anchor trench; B – Horizontal runoff; C – Above high water level; D – Intermittent level; E – Below low water level; F – Pond bottom

Figure 1. Schematic diagram illustrating various sections of HDPE GMBs

3. CASE STUDY: 0.65MM HDPE GMB EXHUMED FROM A SHRIMP AQUACULTURE FARM IN MALAYSIA

3.1 Background

0.65mm HDPE GMB was selected as the pond liner for a shrimp aquaculture farm in Malaysia. Malaysia receives an average of about 7 hours of sunshine per day with maximum temperature of 34°C and minimum temperature of 23°C. The annual irradiance energy for Malaysia obtained after Van Wilk and Stoezer (1986) from Koerner et al. (2012) is 140 kLy.

Table 3. Summary of various exposure levels in respective liner sections.

GMB Liner Section (Ref. Fig. 1)	Exposure Level				
	Oxygen	UV Radiation (Photo-oxidation)	Heat (Thermal-oxidation)	Water (Chemical degradation)	Sludge/Waste (Chemical degradation)
A	Subjective ¹	No	No	No	No
B	High	High ²	High ²	No	No
C	High	High ²	High ²	No	No
D	Moderate	Moderate	Moderate	Moderate	No
E	Low	Low	Low	High	Low
F	Low	No	Low	High	High

¹Quantity of oxygen in saturated soil is dependent on the type of soil and moisture content (Hsuan and Koerner 1995);

²Intensity of UV radiation as well as heat exposure from sunlight is dependent on the geographical location of the shrimp farm as well as the facing direction of the liner.

Apart from water canals and water treatment ponds, the shrimp aquaculture farm has grow out ponds with an approximate area of 0.9ha and the slope gradient is 1V:1.5H with run-out length of 0.5m and nominal anchor trench depth.

The slopes and berms of the ponds were lined in year 2010. In year 2012, a 0.5m wide x 3.8m long GMB liner strip was exhumed from the run-out length to the toe of berm. The GMB liner strip was taken from a pond berm facing south-west. Figure 2 presents pictorial records of the GMB samples exhumed from site.



Figure 2. Photograph of field exhumed samples

3.2 Properties of 0.65mm HDPE GMB After 2 Years of Field Exposure

Four testing locations demarcated with reference to Figure 1 were identified on the exhumed GMB. Table 4 summarizes the results of index, mechanical and durability properties' tests carried out on the four locations of the exhumed GMB in

comparison with values extrapolated from GRI GM 13 as well as the original roll values. It was unfortunate that the exact roll number could not be identified at site and hence average values were tabulated for reference.

3.3 Discussion of Results

In general, with the exception of elongation at break on sample E (-3%), all other index and mechanical test properties from the aged GMB complied with or exceeded the specification of GRI GM 13 extrapolated values. The minor shortfall of -3% elongation at break (i.e. 0.4% short of specification value) for sample E is deemed to be within the normal testing variance and uncertainty of GAI-LAP geosynthetic tests (Koerner et al. 2006).

Table 4. Summary of 0.65mm HDPE GMB properties exhumed from site.

Aged Sample ID	D5199		D792	D6693 Type IV				D1004	D4833	D5397	D4218	D3895	D5885
	t _{GMB}			ρ	Yield		Break					OIT	
	Min.	Lowest	T		ε	T	ε	TR	PR	SCR	CBC	Std.	HP
	Avg.	of 10	Min.		Avg.	Avg.	Avg.	Avg.	Min.	Min.	Min.	Range	Min.
	mm	mm	g/cc	kN/m	%	kN/m	%	N	N	hr.	%	min.	min.
Original Values ¹	0.67	0.642	0.949	11.8	13.9	21.4	772	89	339	550 ³	2.54	122	300 ⁵
B	0.72	0.704	0.953	13.1	13.4	21.2	703	99	371	- ⁴	2.44	46	230
C	0.68	0.645	0.953	13.4	13.6	22.0	717	98	360	- ⁴	2.43	17	139
D	0.67	0.655	0.952	13.1	13.4	20.6	748	95	353	- ⁴	2.47	23	136
E	0.69	0.658	0.952	13.3	13.4	20.7	697	99	350	- ⁴	2.43	29	143
GRI GM 13 ²	0.65	0.585	0.94	9.0	12.0	18.0	700	80	210	300	2 – 3	100	400

¹Average original values from all HDPE GMB rolls ; ²GRI GM 13 extrapolated values; ³All samples did not break but test was ceased after reaching 550 hours; ⁴SCR was not carried out due to unavailability of equipment at time of testing; ⁵Actual test was not carried out as Std OIT was opted to be measured at time of production. Average HP OIT values were estimated from database.

Comparison of results and comments are listed as follows:

- Measured density values are similar for all locations;
- Tensile strength at yield is consistent for all locations and the values exceeds GRI GM 13 and average original values;
- Elongation at yield appears to be consistent, exceeds GRI GM 13 but is slightly lower than average original values for all locations;
- Tensile strength at yield is fairly consistent for all locations, exceeds GRI GM 13 but is slightly lower than average original values except for sample C. The variation from original is -3.7% to 2.8% which is deemed within testing variability;
- Tear and puncture resistances comfortably exceeds both GRI GM 13 as well as average original values for all locations;
- Measured carbon black content values are similar for all locations;
- With the exception of location B, the OIT depletion following ASTM D 3895 follows envisaged results where location C has undergone the greatest degradation due to UV exposed condition followed by location D where it is only intermittently exposed and location E in buried condition. The retained OIT value for location B is the highest when compared to the other three locations. This is counter intuitive as location B is supposed to have undergone greater degradation due to full UV exposure. It is hypothesized that location B may have been protected by collection of dust on the flat portion of the GMB whereas rain would have constantly washed the dust off the sloped areas. Further investigation is necessary to understand this condition;
- Results of OIT depletion following HP OIT test method is generally similar to the findings of standard OIT test where location B presents highest retained OIT values followed by sample E. The HP OIT values for sample C and D is similar likely due to inherent testing variability.

4. LIFETIME PREDICTION

4.1 General

The service life of a HDPE GMB is characterized by the duration before it reaches its 'half – life'. The notion of 'half-life' is ascertained by the 50% reduction of a specific design property of concern (Hsuan and Koerner 1995).

Lifetime prediction of HDPE GMBs have been expounded by Hsuan and Koerner (1995) and Sangam and Rowe (2002). In summary, the lifetime of HDPE GMBs undergoes three distinct stages namely A, B and C. Stage A is where the HDPE GMB is protected through the presence of antioxidants. Stage B also known as induction time to onset of polymer degradation starts when the HDPE resin is unstabilize through antioxidant depletion until the value of 0.5 minutes for standard-OIT and 20 minutes for HP-OIT (Hsuan and Koerner 1998). Stage C starts when the HDPE GMB begins to lose its properties until it reaches 50% of the specific design property of concern.

Stage A antioxidant depletion rate can be estimated through the following equation:

$$\ln(\text{OIT}) = \ln(P) - (S)(t) \quad [1]$$

where P = Initial value of OIT in the GMB (min.); S = antioxidant depletion rate (month⁻¹ or year⁻¹); t = ageing time (months or years); OIT = OIT at time t (min.)

Equation [1] can also be used to estimate the antioxidant depletion time once the antioxidant depletion rate is determined by rearrangement as follows:

$$t = [\ln(P) - \ln(\text{OIT})] / S \quad [2]$$

It should be noted that the above equations and findings were derived from simplifications and reductions after Hsuan and Koerner (1998) where black HDPE GMBs conforming but not exceeding GRI GM 13 specifications were used in the research. The proposed model by Hsuan and Koerner (1995) is adequate for the purpose of comparing GMBs but may not reflect actual long term degradation rate of the particular GMB due to the many variations such as different resins, antioxidants and exposure conditions.

Literature review on lifetime prediction and thickness sensitivities to antioxidant depletion of HDPE GMBs through laboratory studies and field performances of HDPE GMBs in the exposed environment have been carried out by Denis et al. (2012) and will not be repeated in this paper. Only published references where relevant data is required for comparison and careful extrapolation in this paper shall be summarized in the following sections.

4.2 Stage A Analysis

Conditions of a UV exposed 14 year old 1.5mm HDPE GMB used to line a lagoon storing nonhazardous leachate from industrial, municipal and commercial landfill in Ontario, Canada were studied by Rowe et al. (2003). Ivy (2002) reported on the performance of a 20 year 2.5mm HDPE GMB exposed to UV in a surface impoundment of a power plant in Colorado, USA. Tarnowski and Baldauf provided data on a 2.0mm HDPE GMB that was installed in a water reservoir in Levante, Spain where samples were tested after 11 years of outdoor weathering. Swihart and Haynes (2002) from the US Bureau of Reclamation reported the performance of an exposed 2.0mm HDPE GMB as part of its long term study to investigate the most suitable canal lining system. Hsuan et al. (1991) published data on the effects of a 1.5mm HDPE GMB 7 year outdoor exposure in a disused domestic solid waste leachate storage facility. OIT test results from these published references are summarized with the results obtained from the case study in Table 5 for sample location C and D as identified in Figure 1 only so that reasonable correlation may be carried out. Figure 3 illustrates the correlation of antioxidant depletion rate in the form of normalized OIT in natural logarithmic scale versus time.

Koerner et al. (2012) carried out extensive long term studies for lifetime prediction of laboratory UV exposed GMB. A correlation of 1200 light hours exposure at 70°C in ASTM D7238 device as equivalent to 1 year service life in a hot climate similar to West Texas and Southern California was established. Stage A period of 19 years was inferred from the graph of Strength retained (%) versus light hours for a 1.5mm HDPE GMB and included in Figure 3 a) for correlation with the other results.

Table 5. Summary of OIT depletion rates from published data for correlation with case study.

(References) HDPE GM thickness	Sample Location	t (years)	P (min.)	OIT ³ (min.)	S (year ⁻¹)
(Ivy 2002) 2.5mm (100mil)	C	20	50 ²	32	0.022
(Rowe et al. 2003) 1.5mm (60mil)	D	14		36	0.016
(Hsuan et al. 1991) 1.5mm (60mil)	C	7		1.8	0.237
Tarnowski and Baldauf ¹ 2.0mm (80mil)	D	11	145	3.3	0.194
Swihart and Haynes 2.0mm (80mil)	C	10	73	11	0.216
Shrimp Aquaculture 0.65mm (25mil)	C	2	122	25	0.099
	D			61	0.079
				108	0.027
				47	0.044
				17	0.985
				23	0.834

¹Values of OIT are based on DIN EN 728, 190°C; ²Value of P is estimated based on typical values for HDPE GMBs manufactured during period respective period of construction in North America (Ivy 2002; Rowe et al. 2003); ³Average values obtained from respective references.

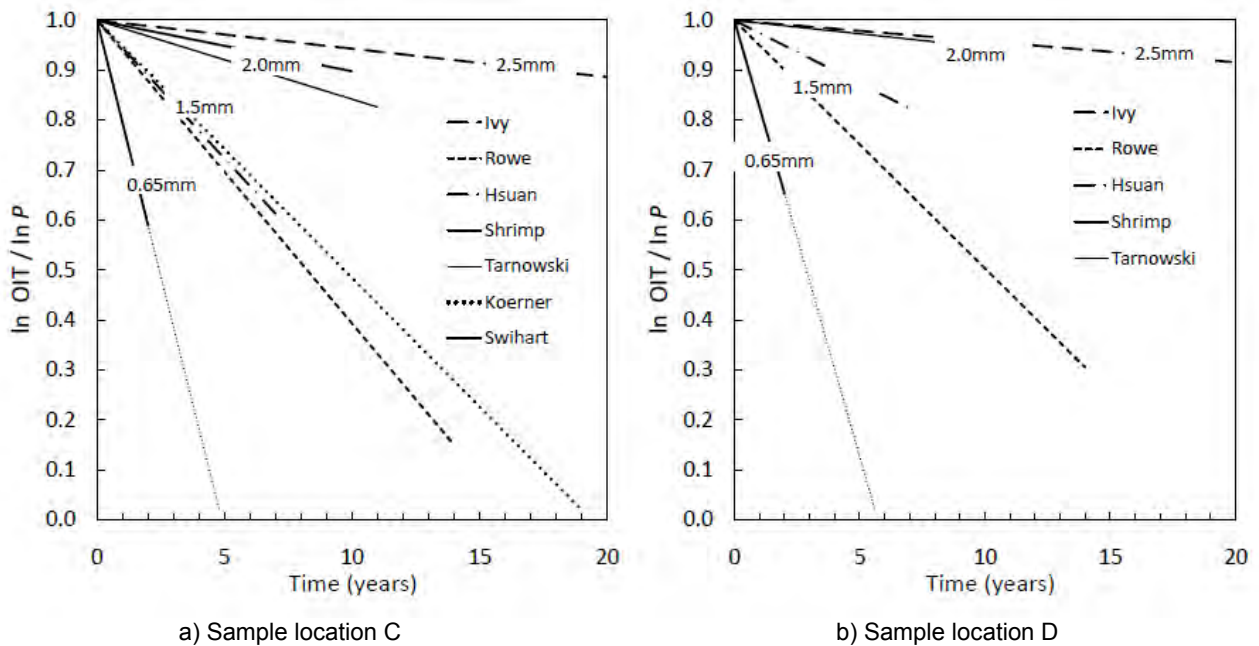


Figure 3. Normalized natural logarithm of standard OIT over natural logarithm of P against time for GMB thickness 2.5mm (100mil), 2.0mm (80mil), 1.5mm (60mil) and 0.65mm (25mil)

Good agreement was observed in Figure 3 a) for antioxidant depletion rate of 1.5mm HDPE GMB derived from data after Ivy (2002), Hsuan et al. (1991) and Koerner et al. (2012). Figure 3 a) also presents antioxidant depletion rate in the same order of magnitude for 2.0mm HDPE GMB. The slightly varying values between the two data would also be affected by the different test conditions employed between ASTM and DIN EN. Antioxidant depletion rate for sample location C was further analyzed for thickness sensitivity and the result is presented in Figure 4.

Antioxidant depletion rate for sample location D yielded similar trends as location C where the depletion rate for thicker HDPE GMB is lower compared to thinner gauge GMBs. However, no strong correlation was observed for HDPE GMB of similar thickness such as the 1.5mm HDPE GMB as published by Rowe et al. (2003) and Hsuan et al. (1991). Unlike sample location C where the degradation mechanisms are limited to exposed environment, sample location D is partly exposed to the pond liquid and hence antioxidant depletion could be affected by chemical degradation mechanism of the varying liquid at respective sites. As such, some degree of differences in the degradation mechanism is likely to occur from one application to the other.

4.3 HDPE GMB Thickness Sensitivity to Antioxidant Depletion Rate

Figure 4 plots the antioxidant depletion rate versus HDPE GMB thickness from data obtained in Table 5. From Figure 4, it was observed that antioxidant depletion rate for UV exposed HDPE GMBs increases exponentially with the decrease of GMB thickness. Data for sample location D (partially exposed) also shows similar trend to fully exposed sample denoted as location C.

Figure 4 a) extrapolates the data from commonly used HDPE GMB thickness to thinner gauge HDPE GMB. The coefficient of determination (R^2) for Figure 4 a) is 0.9482 and is statistically deemed a very good fit. Figure 4 b) includes the data obtained from the case study of 0.65mm HDPE GMB exhumed from a shrimp aquaculture site in Malaysia. The R^2 for Figure 4 b) is 0.9691 which is better than Figure 4 a). Figure 4 b) thus serves to validate that the extrapolation process done in Figure 4 a) is reasonable.

The trendline exponential equation given in Figure 4 a) and b) cannot be used for exact extrapolation / interpolation of antioxidant depletion rates of HDPE GMB but is presented for the sole purpose of illustrating that durability of HDPE GMB is sensitive to its thickness following the exponential trend and not linear.

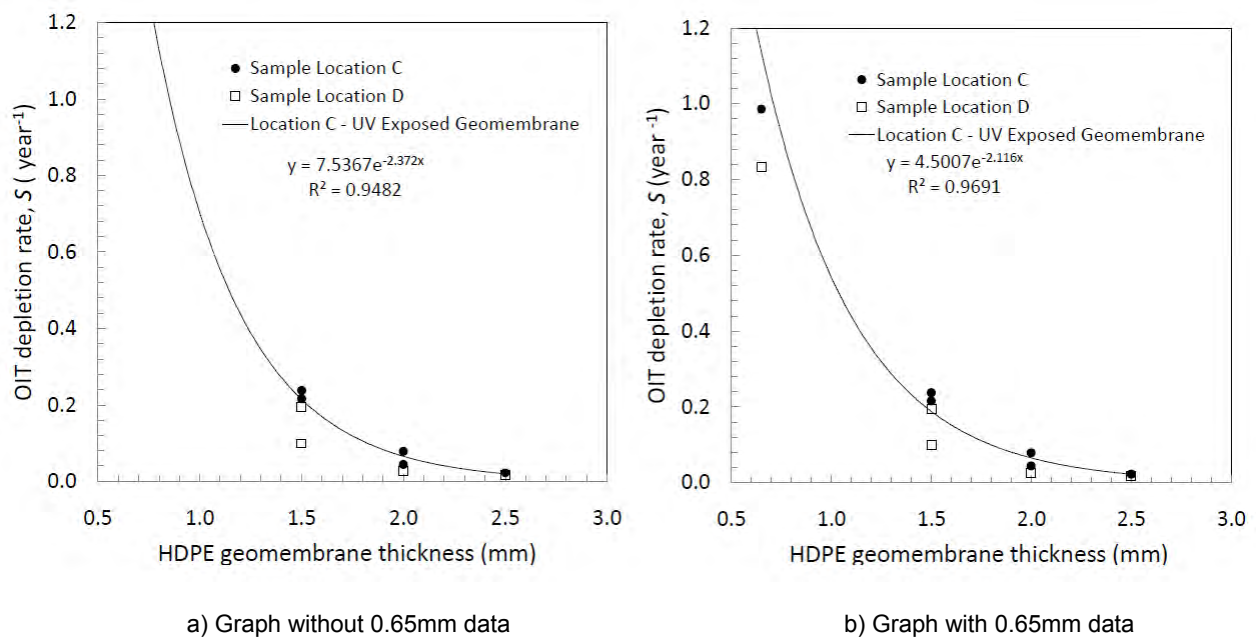


Figure 4. OIT depletion rate, S against HDPE GMB thickness.

5. DISCUSSION AND CONCLUSION

Correlation of antioxidant depletion rate versus thickness carried out in Section 4 took the following liberty:

- Initial OIT value, P were estimated at 50 minutes for data from Rowe et al. (2003), Ivy (2002) and Hsuan et al. (1991) following comments from Ivy (2002) and Rowe et al. (2003) in order to arrive at the estimated antioxidant depletion rate;
- Only 2 points were available or estimated for each set of data to compute the antioxidant depletion rate for all thicknesses;
- The likely variability of UV irradiation and differences in temperature for each respective sites were not taken into account in the correlation process;
- Data for 1.5mm HDPE GMB from Koerner et al. (2012) was inferred from published graph and not from OIT test results;
- OIT values for data from Tarnowski and Baldauf were obtained following DIN EN 728 instead of ASTM D 3895;
- Initial OIT value, P for the case study of 0.65mm HDPE GMB was estimated based on average values as the original roll could not be traced;

With regards to the above, the authors wish to express that at this juncture, there is limited information to fully validate the findings of antioxidant depletion rate and its correlation to HDPE GMB thickness in the exposed environment.

Furthermore, use of different HDPE GMB formulation, resin and antioxidants would result in varying behavior. As such, the data presented in this paper is an estimate at best and should be carefully interpolated or extrapolated with engineering judgment in order to predict the lifetime of UV exposed HDPE GMBs especially for thinner gauge liners.

However, the information obtained from this study clearly showed that antioxidant depletion rate does not increase linearly but exponentially with decreasing HDPE GMB thickness. It is therefore wise for stakeholders to be cautious in the lifetime estimates of thinner gauge HDPE GMBs in the exposed environment.

Tarnowski and Baldauf also reported that for thicker UV exposed HDPE GMB such as 2.5mm, remaining OIT at the top 0.9mm portion of the GMB is significantly lesser than the middle 0.9mm portion. As such, it can be hypothesized that thinner gauge HDPE GMB is fully exposed to UV radiation throughout its entire core whereas the middle portion of the thicker HDPE GMB is significantly protected from UV radiation.

Correlation for lifetime prediction for Stage B and C for thin UV exposed HDPE GMBs was not carried out at this moment as there are no available published data apart from the 1.5mm HDPE GMB from Koerner et al. (2012).

Lastly, the authors would also like to note that lifetime of HDPE GMBs in the field is also largely dependent on the quality of installation works. Better field workmanship is required as the GMBs get thinner especially for thicknesses of < 1.0mm.

ACKNOWLEDGEMENTS

The authors are grateful to their colleagues Simon Gilbert St-Pierre and Teoh Pei Ching who provided valuable critique of the paper and carried out the laboratory tests for samples obtained from the shrimp aquaculture farm in Malaysia.

REFERENCES

- ASEAN (2005). Manual of ASEAN Good Shrimp Farm Management Practice. *ASEAN Cooperation in Food, Agriculture and Forestry, Fisheries Publication Series No. 1*, Sisingamangaraja, Jakarta, Indonesia, Web reference: http://www.aseansec.org/aqr_pub/fi1.doc
- ASTM D 638. Standard Test Method for Tensile Properties of Plastics, *American Society for Testing and Materials*, West Conshohocken, Pennsylvania, USA. [do not include year since standards are re-published every year]
- ASTM D 792. Standard Test Method for Density and Specific Gravity (Relative Density) of Plastics by Displacement, *American Society for Testing and Materials*, West Conshohocken, Pennsylvania, USA.
- ASTM D 1004. Standard Test Method for Tear Resistance (Graves Tear) of Plastic Film and Sheeting, *American Society for Testing and Materials*, West Conshohocken, Pennsylvania, USA.
- ASTM D 3895. Standard Test Method for Oxidative-Induction Time of Polyolefins by Differential Scanning Calorimetry, *American Society for Testing and Materials*, West Conshohocken, Pennsylvania, USA.
- ASTM D 4218. Standard Test Method for Determination of Carbon Black Content in Polyethylene Compounds By the Muffle-Furnace Technique, *American Society for Testing and Materials*, West Conshohocken, Pennsylvania, USA.
- ASTM D 4833. Standard Test Method for Index Puncture Resistance of Geomembranes and Related Products, *American Society for Testing and Materials*, West Conshohocken, Pennsylvania, USA.
- ASTM D 5199. Standard Test Method for Measuring the Nominal Thickness of Geosynthetics, *American Society for Testing and Materials*, West Conshohocken, Pennsylvania, USA.
- ASTM D 5397. Standard Test Method for Evaluation of Stress Crack Resistance of Polyolefin Geomembranes Using Notched Constant Tensile Load Test, *American Society for Testing and Materials*, West Conshohocken, Pennsylvania, USA.
- ASTM D 5885. Standard Test Method for Oxidative Induction Time of Polyolefin Geosynthetics by High-Pressure Differential Scanning Calorimetry, *American Society for Testing and Materials*, West Conshohocken, Pennsylvania, USA.
- ASTM D 6693. Standard Test Method for Determining Tensile Properties of Non reinforced Polyethylene and Nonreinforced Flexible Polypropylene Geomembranes, *American Society for Testing and Materials*, West Conshohocken, Pennsylvania, USA.
- ASTM D 7238. Standard Test Method for Effect of Exposure of Unreinforced Polyolefin Geomembrane using Fluorescent UV Condensation Apparatus, *American Society for Testing and Materials*, West Conshohocken, Pennsylvania, USA.
- Denis, R., Tan., D. and Cao, D. (2012). A literature review on lifetime prediction of thin HDPE geomembranes in the exposed environment, *Geosynthetics Asia 2012*, IGS – Thailand Chapter, Bangkok, Thailand.
- DIN EN 728. Plastics Piping and Ducting Systems – Polyolefin Pipes and Fittings – Determination of Oxidation Induction Time, *German Institute for Standardization*, Berlin, Germany.
- Ewais, A.R.M. and Rowe, R.K. (2012). The effects of thickness on OIT depletion of HDPE geomembranes made from the same resin and immersed in synthetic leachate, *GeoAmericas 2012*, IGS – Perú Chapter, Lima, Perú.

- GRI GM 13. Test Methods, Test Properties and Testing Frequency for HDPE Smooth and Textured Geomembranes, *Geosynthetic Institute*, Folsom, PA, USA.
- Hishamunda, N., Bueno, P.B., Ridler, N. and Yap, W.G. (2009). Analysis of Aquaculture Development in Southeast Asia: A Policy Perspective, *FAO Fisheries and Aquaculture Technical Paper No. 59*, FAO, Rome, Italy.
- Hsuan, Y.G., Lord, A.E., Jr. and Koerner, R.M. (1991). Effects of outdoor exposure on a high density polyethylene geomembrane, *Geosynthetics '91*, IFAI, Atlanta, Ga., USA.; 287-302.
- Hsuan, Y.G. and Koerner, R.M. (1995). Long Term Durability of HDPE Geomembranes: Part I – Depletion of Antioxidants, *GRI Report #16*, Geosynthetic Research Institute, Drexel University, Philadelphia, PA, USA.
- Hsuan, Y.G. and Koerner, R.M. (1998). Antioxidant depletion lifetime in high density polyethylene geomembranes, *Journal of Geotechnical and Geoenvironmental Engineering*, ASCE, 124(6): 532-541.
- Islam, M.Z. and Rowe, R.K. (2007). Effect of HDPE geomembrane thickness on the depletion of antioxidants. *OttawaGeo 2007*, Ottawa, Canada.: 2129-2134.
- Ivy, N. (2002). HDPE geomembrane after 20 years of service. *Geotechnical Fabrics Report*, IFAI, June/July 2002: 18-20.
- Kay, D., Blond, E. and Mlynarek, J. (2004). Geosynthetic durability: A Polymer chemistry issue. *GéoQuébec 2004: 57th Canadian Geotechnical Conference and 5th Joint CGS/IAH-CNC Conference*, Québec, Canada, Session 4D: 1-14.
- Koerner, G.R., Hsuan, Y.G. and Koerner, R.M. (2006). Geosynthetic Accreditation Institute-Laboratory Accreditation Program (GAI-LAP), *GRI White Paper #7*, Geosynthetic Institute, Folsom, PA, USA.
- Koerner, R.M., Koerner, G.R. and Hsuan, Y.G. (2012). Lifetime Prediction of Laboratory UV Exposed Geomembrane: Part I – Using a Correlation Factor, *GRI Report #42*, Geosynthetic Institute, Folsom, PA, USA.
- Martin, D. (2005). UV resistance in thin film geomembranes accelerated and natural weathering studies. *GeoFrontiers 2005*, Geotechnical Special Publication 142, ASCE, Austin, Texas, USA.
- Rowe, R.K. and Sangam, H.P. (2002). Durability of HDPE geomembranes. *Geotextiles and Geomembranes*, Elsevier, 20: 77-95
- Rowe, R.K., Sangam, H.P. and Lake, C.B. (2003). Evaluation of an HDPE geomembrane after 14 years as a leachate lagoon liner. *Canadian Geotechnical Journal*, 40: 536-550.
- Rowe, R.K., Rimal, S. and Sangam H. (2009). Ageing of HDPE geomembrane exposed to air, water and leachate at different temperatures. *Geotextiles and Geomembranes*, Elsevier, 27: 137-151
- Rowe, R.K., Islam, M.Z. and Hsuan, Y.G. (2010). Effects of thickness on the aging of HDPE geomembranes. *Journal of Geotechnical and Geoenvironmental Engineering*, ASCE, 136(2): 299-309.
- Sangam, H.P. and Rowe, R.K. (2002). Effects of exposure conditions on the depletion of antioxidants from high-density polyethylene (HDPE) geomembranes. *Canadian Geotechnical Journal*, 39: 1221-1230.
- Swihart, J. and Haynes, J. (2002). Canal-Lining Demonstration Project Year 10 Final Report, R-02-03, *Bureau of Reclamation*, U.S. Department of the Interior, Denver, Colorado, USA.
- Tarnowski C. and Baldauf S. *Ageing Resistance of HDPE Geomembranes – Evaluation of Long-term Behavior under Consideration of Project Experiences*, GSE Lining Technology GmbH, Hamburg, Germany, Web reference: <http://www.gseworld.com/content/documents/articles/Ageing%20resistance%20of%20HDPE-geomembranes.pdf>
- Youngblood, J. and Ng, H.B. (2008). Geomembrane Shrimp Farm Liners in Indonesia, *GRI-21 Conference*, Geosynthetic Institute, Folsom, PA, USA.

Lining Systems for Shale Gas Drilling Activities

Theresa Andrejack Loux, Ph.D., InterGEO Services, USA, theresa@intergeoservices.com
Archie Filshill, Ph.D., InterGEO Services, USA, archie@intergeoservices.com

ABSTRACT

In the past several years, there has been an influx of oil and gas companies breaking ground in the Eastern United States and Canada for the purpose of natural gas extraction from the Marcellus and Utica formations. Geosynthetic lining systems have been utilized at many shale gas drilling sites as a solution to control environmental contamination and to contain large quantities of surface water; these applications include protection at drill pads and frack-tank storage locations, freshwater impoundments for drilling and fracking purposes, and stormwater control basins. The robustness of the geosynthetic lining systems that have been used at shale gas drilling sites varies widely by owner and location. There is also the potential for the use of geosynthetics in frack water surface impoundments and the proper management and disposal of drill cuttings.

This paper presents an overview of the geosynthetic lining systems that are, or could be, used for applications relating to shale gas drilling, a summary of the current regulations that exist for these applications, the concerns that face the engineers designing the lining systems, and finally, the challenges that are confronted by the geosynthetic contractors during installation.

1. INTRODUCTION

Natural gas has long been used to heat buildings, and more recently, it has been used to fuel internal combustion engines and power plants. With natural gas providing an alternative to oil, gasoline, and coal in these applications, it promises a marked decrease in the dependence of the U.S. on foreign oil. It is often seen as a “cleaner” fossil fuel and has been easier to harvest with the advancement of drilling techniques including horizontal drilling and hydraulic fracturing (also known as “fracking”). In 2008, studies were published citing the recoverable gas potential of the Marcellus Shale to be around 363 trillion cubic feet as a low estimate. It is not surprising this information set off a large prospecting rush throughout the Northeast (Wilber 2012). Gas has been extracted from shale basins worldwide; Figure 1 shows identified shale gas plays within the continental United States. The Marcellus Shale extends from Virginia to New York, with the distribution of Marcellus Shale Play as presented in Table 1.

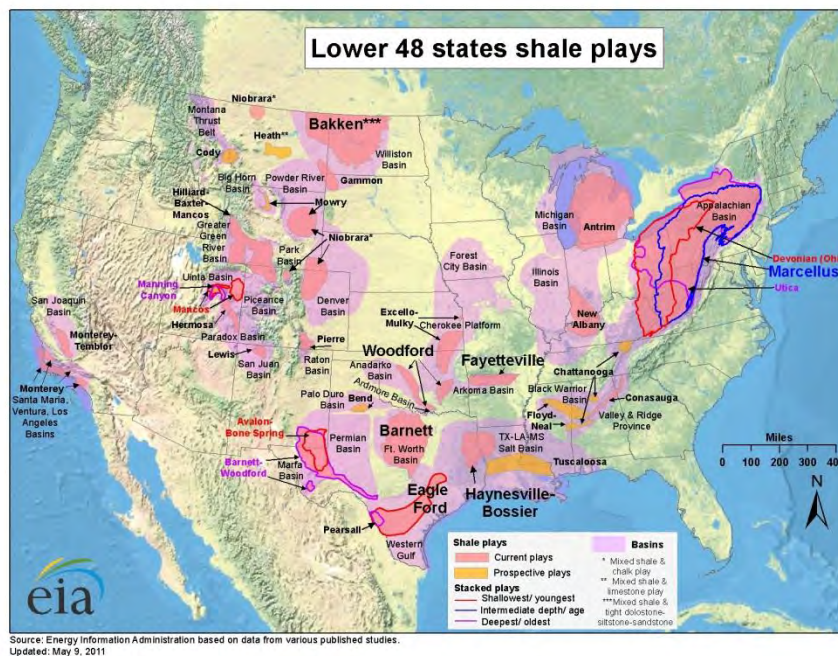


Figure 1. Shale Gas Plays in the Continental United States [U.S. Energy Information Administration (2011)].

Table 1. State Distribution of the Marcellus Shale Play [U.S. Energy Information Administration (2011)].

State	Area % of Marcellus
Pennsylvania	35.4
West Virginia	21.3
New York	20.1
Ohio	18.2
Virginia	3.9
Maryland	1.1

Fresh on the heels of the Marcellus Shale speculation is new information hypothesizing that the Utica Shale formation, covering a more extensive footprint in the Appalachian Basin and several thousand feet deeper, will rival the resource potential of the Marcellus play (Wilber 2012).

A large source of potential contamination during shale gas drilling activities is from the mixture of water, sand, and chemicals used during fracking operations. This mixture is forced under high pressure through the vertical and horizontal bore in order to split the rock and free the trapped gas (Wilber 2012). Without these additional pathways for gas to flow out, the shale rock would not be permeable enough to extract large quantities of gas. The chemicals that are added during fracking serve roles such as reducing friction or killing bacteria (Galbraith 2012). Additionally, the recovered water from fracking, also known as flowback or produced water, will contain these added chemicals as well as naturally occurring contaminants that exist within the subsurface profile. Thus, the contaminant profile of the flowback water is very site-specific. Commonly found contaminants in flowback water include mineral salts, heavy metals, and organic compounds, and naturally-occurring radioactive elements (U.S. Environmental Protection Agency 2000).

A complication to environmental protection during shale gas drilling is that only some U.S. states have disclosure laws requiring oil and gas companies to provide information on the chemical makeup of the fracking fluid additives that they are using. Even in states where disclosure laws exist, there is often a “trade secrets” clause that enables companies to prevent this information from ever entering the public sphere (Galbraith 2012).

2. APPLICATIONS OF LINING SYSTEMS IN SHALE GAS DRILLING

Geosynthetic lining systems have been vetted by the solid waste industry for the past 50 years to ensure the adequate protection of our groundwater sources and the surrounding environment from potential contamination. Other industries are quick to adopt these systems, including similar material types, configurations, and quality control techniques during construction, when confronted with the same goal. Similarly, the materials used to waterproof ponds for freshwater storage or stormwater control have been in existence for many years, and these lining systems are ubiquitous in modern E&S control plans.

2.1 Drill Pads and Frack Tank Storage

Typically, there exists three (3) to six (6) vertical well heads at a single well site. Large drill rigs are brought in to complete the vertical and horizontal drilling of each well. These wells are usually concentrated in an area onsite known as the drill pad. While the well heads are usually clustered together at a site, it should be noted that because of the existence of horizontal drilling, the “reach” of a single well site can extend radially outward for several miles from the drill pad. The pumps and pipe lines required for fracking are connected at these access points on the drill pad.

Frack tanks are often located in close proximity to the well heads, in many cases utilizing the same underlying lining system to protect against any spills or leaks from the tanks, piping network, or pump system.

2.2 Freshwater Impoundments and Stormwater Control Basins

During fracking operations, large quantities of fresh water are consumed. Thus, a reliable method of storing the required water is necessary and is often a geosynthetic-lined impoundment. The inclusion of lined stormwater control basins at shale gas drilling sites may be necessary depending on the BMPs that govern an individual site.

2.3 Frack Water Surface Impoundments and Drill Cutting Disposal

There are sites where frack water is stored in impoundments rather than onsite, above-ground tanks. These flow back pits may also serve as temporary storage facilities for drill cuttings that reside onsite during drilling operations. Eventually, these cuttings are normally sent to a nearby solid waste disposal facility for permanent removal.

3. GEOSYNTHETIC LINING SYSTEMS OVERVIEW

All geosynthetic lining systems acting as barriers are designed to be “impermeable”; that is, they are intended to prevent or restrict the transport of liquid or gas through them. Geosynthetic materials that function as barriers include geomembranes and geosynthetic clay liners. There are many types of geomembranes that vary with resin type (LLDPE, HDPE, PVC, etc.) and additives, texture, and thickness. The resin type and additives will be most critical when determining compatibility of the contaminants with the geomembrane. Geosynthetic clay liners are more expensive than most geomembranes and should be analyzed for compatibility issues if utilized to contain flow back water.

The design for a liner system includes specified items including: geometry of the liner, cross section including underlying and overlying materials, geosynthetic type and thickness, and runout and anchor trench details (Koerner 2005).

The design lifetime for the lining systems at shale gas drilling sites can vary greatly. Some of the freshwater impoundments are only required for the initial vertical and horizontal drilling at these sites which may take around one year to complete. Other applications, such as the liner system under the well pad itself will be in use for the lifetime of the wells (as long as 40 years). The applications detailed above can be divided into two categories: the first must prevent the migration of generally fresh water while the second must prevent the migration of contaminants.

3.1 Containment of Freshwater

Additionally, it is imperative to include an underdrain system in these freshwater impoundments to prevent gas “whales.” These whales are pockets of gas that get trapped beneath a geomembrane liner and have no pathway to escape. Common underdrain systems include: sand bedding layers, thick needle-punched nonwoven geotextiles, drainage geocomposites, and geotextiles outfitted with small perforated pipes within its cross section. A typical cross section and installation photograph is shown in Figures 2 and 3.

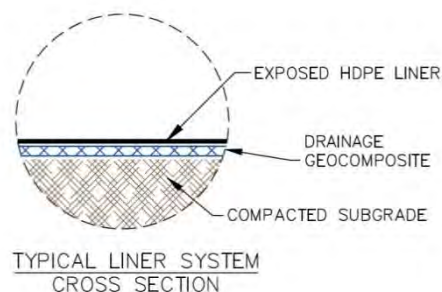


Figure 2. Typical liner system cross section.



Figure 3. Photograph of the installation of an exposed, 1.5 mm (60 mil) HDPE liner underlain by a draitube geocomposite.

While the freshwater impoundments described above are generally designed to balance cut-to-fill earthwork quantities, certain circumstances such as a high water table or permitting issues, lead to mobile impoundment construction. These mobile impoundments consist of fabricated steel trusses with a geomembrane liner overlying them (Figure 4). While generally more expensive than the in-ground impoundments, the only site requirement for these systems is a flat, competent subgrade. These systems also have the benefit of being able to be deconstructed and reused, giving them an economic advantage in cases where the impoundment will be in service for a relatively short period of time.



Figure 4. Photographs of an above-ground impoundment for water storage.

3.2 Containment of Contaminated Water and Waste

A more robust lining system would include both a primary and a secondary liner, with a collection system in between the two liners and a detection system beyond the secondary liner. While this type of system is common in landfills where leachate will be generated over hundreds of years, the containment of flow back water will only be necessary for the design life of the well pad (likely 20- to 30-years).

The author has seen a gamut of well pad designs. The minimum requirement is generally a single geomembrane or geosynthetic clay liner. Other designs combine the two materials to form a composite liner. Yet other systems that have been proposed include a geomembrane liner overlaid by a cushion geotextile and then topped with geocells or other specialty mat or cushioning product (Figure 5).

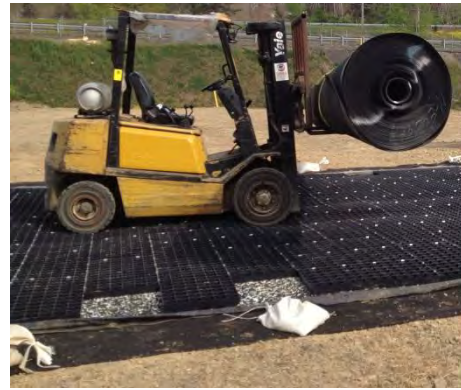


Figure 5. Photographs of a potential well pad system that consists of, from the bottom upwards: a 1.5 mm (60 mil) HDPE textured geomembrane, a 340 g/m² (10 oz./yd²) cushion geotextile, a 50 mm (2 in.) recycled foam product, and a durable, reusable specialty mat product.

4. REGULATIONS REGARDING LINING SYSTEMS IN SHALE GAS DRILLING

To attempt to summarize all of the regulations regarding shale gas drilling in the U.S. would be an onerous task as there is a fair amount of variation state-to-state.

Koerner and Koerner (2012) compiled survey results of 35 U.S. state environmental departments to determine how many departments were involved with the shale gas drilling permitting process. Alarming, 18 states responded to the survey indicating that two to four departments were involved in the permitting process. Many of these states are those that are relatively new to shale gas drilling activities. It should also be noted that currently, New Jersey has a ban on all fracking within the state and New York has had a moratorium on shale gas drilling for the past four years while the environmental impacts of hydraulic fracturing are evaluated.

As an example, a review of the Pennsylvania regulation (PA § 78.56) for pits and tanks required for the temporary containment of polluttional substances and wastes during and produced from drilling, the following requirements are set forth:

- Two (2) feet of freeboard should be maintained at all times.
- The synthetic liner should have a coefficient of permeability of less than 1×10^{-7} cm/s.
- The synthetic liner thickness should be greater than 0.75 mm (30 mils).
- The protective subbase should be greater than 150 mm (6 inches) thick.
- The bottom of the pit should be at least 20 inches higher than the seasonal high groundwater table.
- The pit or tank should be protected from third parties at all times.

Many companies with drilling operations in Pennsylvania have chosen to exceed the requirements listed above, most notably with an increase in the thickness of the synthetic liner. Also in Pennsylvania, there exist recommendations to provide a secondary containment system with a leak detection layer in between the secondary and primary liner system for flow back pits and drill pits.

5. CONCERNS

5.1 Engineering Perspective

In many cases, the state in which a given site is in will dictate the minimum lining system requirements in a freshwater or containment liner system. While the culture of the oil and gas company often contributes to the assent of increasing the robustness of the system that is designed and installed, many engineering firms should also be commended for their expert guidance that they have provided.

Those local engineering firms that are active in the solid waste sector and already experienced with all aspects of designing long-term containment solutions likely had an easier transition to providing oil and gas companies with lining system design and oversight services. Additionally, these companies would be familiar with the geology in the areas where drilling operations commenced. In some states, it might be an advantage to be familiar with the solid waste

regulators if shale gas drilling impoundments also fall under their jurisdiction. In other states, Pennsylvania included, many engineering firms deal with an entirely different department for shale gas impoundments and liner systems than they do for solid waste.

Best management practices (BMPs) influencing liner system design and selection include but aren't limited to: material strength (its resistance to tear and puncture), liner material compatibility with the contained medium, installation methods, quality control and inspection, and maintenance and repair procedures. The underlying geotextile or geocomposite should be designed to serve two primary roles: to provide drainage to prevent the formation of whales under the liner system and to provide puncture protection to the geomembrane liner from the subbase material. In any liner system design, the subgrade soil stability and cover soil stability should always be evaluated, and may affect the selection of the liner. Common geomembrane liner materials are 40- or 60-mil textured LLDPE or HDPE geomembranes.

Also, with regards to the regulatory hurdles, certainly those states with a single department that acts as the point of contact for all shale gas permitting has a more transparent and easier to navigate permitting process than those which do not.

5.2 Contractor Perspective

Some of the biggest challenges for geosynthetic and earthwork contractors working at Marcellus Shale sites are the locations themselves. The sites are generally rural, mountainous, and out of cell phone reception (Figure 6). Combined with the capricious weather in the Northeast U.S., contractors must be organized and prepared for adverse conditions, as well as somewhat flexible in their installation schedules. The pace of construction has slowed somewhat in the past year as natural gas prices reached all-time lows, but there are still many wells being permitted and drilled at this point in time.

Quality control is of utmost importance during the installation of the liner system itself. A fusion weld or extrusion weld is utilized to seam LLDPE or HDPE geomembranes. The more conscientious owners and engineers will insist that the field crew completing these welds should have sufficient training, experience, and qualifications. The geosynthetic contractor may be required to complete nondestructive field testing of every seam and weld in the liner system and document these and the panel locations in field as-built drawings. Additionally, destructive tests are completed at given intervals to ensure proper seam strength. There is usually a third-party CQA consultant present at all times during liner installation to ensure proper installation conditions and procedures. Once the liner system installation is complete, a leak-detection survey may be done before the pit is put into service.



Figure 6. Aerial photograph of a remote drilling site in Central Pennsylvania.

6. CONCLUSIONS

The regulations and governing agencies that influence lining system design at shale gas drilling sites varies by state within the U.S. Within a single U.S. state, the lining system requirements may differ for pits or tanks that will contain potentially polluted sediments or liquid compared to those that are constructed to hold freshwater reserves or stormwater

runoff. Geosynthetics offer versatile and cost-effective solutions in lining systems to minimize the impact of shale gas drilling activities on the surrounding environment.

REFERENCES

- Galbraith, K. (2012). "Seeking Disclosure on Fracking." *The New York Times*. 30 May 2012.
- Koerner, R.M. (2005). *Designing with Geosynthetics, 5th ed.* Pearson Prentice Hall, Upper Saddle River, NJ.
- Koerner R.M. and Koerner, J.R. (2012). "State Regulatory Departments Involved in Shale Gas Permitting." The Geosynthetic Institute, Folsom, PA.
- The Pennsylvania Code (2012). "§ 78.56. Pits and tanks for temporary containment." <<http://www.pacode.com/secure/data/025/chapter78/s78.56.html>> 31 July 2012.
- U.S. Energy Information Administration (2011). *Review of Emerging Resources: U.S. Shale Gas and Shale Oil Plays*. Washington, D.C.
- U.S. Environmental Protection Agency (2000). *Profile of the Oil and Gas Extraction Industry*. Washington, D.C.
- Wilber, T. (2012). *Under the Surface: Fracking, Fortunes, and the Fate of the Marcellus Shale*, Cornell University Press, Ithaca, NY, USA.

Market Impacts for Geosynthetics from the Regulation of the Storage of Coal Combustion Residuals

Authors: B. Ramsey, GSE Environmental LLC., Houston, Texas, USA, bramsey@gseworld.com
A. Aho, Director, Technical Markets, Industrial Fabrics Association International, Roseville Minnesota USA

ABSTRACT:

The Geosynthetic Materials Association (GMA) is a United States based industry and trade organization with the goal of expanding the marketplace for geosynthetics. GMA provides a forum for consistent and accurate information to increase acceptance and promote the correct use of geosynthetics. Activities center on five areas: engineering support, business development, education, government relations and industry recognition.

Arguably, the most important of these activities is government relations. GMA has operated an active government relations program with a firm working full time within Washington D.C. to pursue opportunities for geosynthetic materials. Working together with this firm, GMA has conducted lobbying efforts and engaged not only congressional offices, but multiple agencies including US Environmental Protection Agency (EPA), Department of Transportation, Bureau of Reclamation, the Department the Interior, the Army Corp of Engineers, the Council on Environmental Quality and other federal and state agencies. In each case, the overall goal of the discussions was the same; to promote the use of geosynthetic materials as cost effective, performance enhancing and environmentally friendly alternatives to traditional soil, sand, gravel and clay as construction materials. Coal ash storage has been an important issue in this effort.

Coal ash storage site failures at a power facility in Kingston, Tennessee in December 2008 and Oak Creek, Wisconsin in October 2011 and more than 50 documented cases of groundwater contamination near coal ash storage facilities all relate to the US EPA's issuance of a notice of proposed rulemaking in June 2010. These proposed rules outline new regulations for the storage of coal ash which will require the use of geosynthetic materials and expand the geosynthetic market significantly. This paper will present pertinent facts on the existing marketplace, discuss the current status of the regulatory, legislative and governmental processes and offer current opinions and projections on the potential effect of regulations on market size and impacts. The market growth will be reviewed in three segments: new site lining/barrier opportunities, capping and "normal" site closure opportunities and large scale site remediation and associated closures opportunities.

1. INTRODUCTION

It is difficult to present marketing information at a technical conference or via a technical journal. However, this paper aims to do exactly that. The written section of the presentation will largely contained historical information that is pertinent, presented chronologically. This is intended to provide context and an historical background. The "live" presentation portion of this paper will contain current information on the effects of the regulation of coal ash storage on the geosynthetic marketplace in North America.

2. HISTORY AND TIMELINE

The geosynthetics market as a whole and the geomembrane industry in particular received its first large growth spurt with the 1976 U.S. Congressional act known as RCRA [The Resource Conservation and Recovery Act]. RCRA created regulations to manage the store of both household and hazardous waste. The regulations were issued in two sections, the first specific to material deemed as hazardous waste, the second addressing the long-term fate of solid waste. Hazardous waste has since become known as "subtitle C" type waste and solid or most commonly household waste has become known by that specific section of the regulations "subtitle D." There is an additional waste stream known as construction and demolition waste or "C& D material" that is not regulated under RCRA but is instead addressed on a state-by-state or local regulatory basis.

The second significant regulatory impact waste management occurred in 1980 when the U.S. Congress passed the Comprehensive Environmental Response, Compensation and Liability Act more commonly known as "Superfund." Superfund was created to clean up uncontrolled hazardous waste sites. This regulation not only increased demand for geosynthetic materials but helped to spur on large growth in the capping applications, using geosynthetics as surface or near surface barriers to prevent rainwater infiltration.

3. COAL ASH, ITS REGULATION, OR LACK THEREOF, IN THE UNITED STATES

The proper place to begin this review is in calendar year 1980 with the passage by the U.S. Congress of what is known as the "Bevill Amendment," named for former Representative Tom Bevill (D-AL). This law amended RCRA by adding section 3001(b)(3)(A)(ii), known as the Bevill exclusion, to exclude "solid waste from the extraction, beneficiation, and processing of ores and minerals" from regulation as hazardous waste under Subtitle C of RCRA. It also required EPA to study the impact of coal ash on the environment. This study was completed and published in the Federal Register on May 22, 2000. The study reported "The Agency has concluded these wastes do not warrant regulation under subtitle C of RCRA and is retaining the hazardous waste exemption under RCRA section 3001(b) (3) (C). However, EPA has also determined national regulations under subtitle D of RCRA are warranted for coal combustion wastes when they are disposed in landfills or surface impoundments,..." However, the EPA determination for subtitle "D" regulation was not heeded and the absence of regulations of coal ash storage continued. Consequently just before 1 a.m. on Monday, December 22, 2008, a dike containing coal fly ash slurry ruptured at an 84-acre (0.34 km²) solid waste containment area at the TVA Kingston Fossil Plant in Roane County, Tennessee, USA. An estimated 1.1 billion U.S. gallons (4,200,000 m³) of coal fly ash slurry was released. Subsequent direct clean-up and remediation costs have been estimated at greater than 1.3 billion dollars.



Figure 1

This incident and other issues with groundwater contamination at or near coal combustion residual storage facilities has resulted in the US EPA considering new regulation of coal ash storage and significant companion actions on the legal, federal congressional and multiple governmental fronts.

Following the Kingston spill, on June 21, 2010 the EPA issued a "proposed rule" for the regulation of coal ash storage. . The proposed rule was actually at least three, perhaps as many as six unique and different regulatory schemes depending on how they were parsed. Two of the regulatory schemes were to regulate coal ash as a solid waste, under RCRA subtitle "D." or as a hazardous waste, using subtitle "C." Additionally, an option described as "D prime" but was also discussed in some detail. EPA held a series of nine public hearings on this topic. There have been volumes of comments, correspondence and information provided on this topic by participants across all range of the political spectrum. (In the opinion of this writer, EPA overreached in the attempt to obtain classification for coal ash as a hazardous waste material.) Further, EPA did itself and the United States a disservice by proposing multiple options rather than a single concise proposal.)

On October 12, 2011 after a period of internal consideration, EPA published a Notice of Data Availability [NODA] requesting additional comments and information on some selected topics pertinent to coal ash.

The U.S. EPA surveyed the operators and owners of coal-fired power generation facilities and received responses covering 240 facilities and 676 surface impoundments. Of the units that have been rated, 50 (of the 676) have been given the designation of "high hazard." This designation does not indicate a high probability of failure at a site; a site can receive a

“high hazard” designation based on its location-and the impact on the surrounding neighborhood or environment should a failure occur even if the estimated chances of failure are small.

On October 31, 2011 a failure occurred at a power generation facility owned by a WE Energies located on the shore of Lake Michigan in Oak Creek Wisconsin, south of Milwaukee.



Figure 2

This event resulted in a significant quantity of coal ash being released into Lake Michigan.

According to a report published by the State of Wisconsin Department of Natural Resources, the spill was the result of construction of a sediment retaining basin being constructed over old coal ash deposits. “...the FGD sediment basin would potentially be constructed in coal ash deposits (see figure 5). During construction, ash deposits were found in the western portion of the FGD sediment basin. These deposits were removed and replaced with suitable soil in accordance with the contaminated materials management plan. However, a liner plan was not submitted to the Department when ash deposits were discovered...” “A significant component of the bluff collapse material appears to be the coal ash deposited in a ravine in the 1950s – 1960s.”

4. CONGRESS ATTEMPTS TO ACT

On October 14, 2011 the U.S. House of Representatives passed H.R.2273 - Coal Residuals Reuse and Management Act, also known as the McKinley bill after the sponsor (Representative David McKinley (R-WV)). On October 20, 2011, Senator Hoeven (R-ND) and co-sponsors introduced to the 112th congress Senate resolution #1751, proposing legislation closely paralleling H.R. 2273; a modification of subtitle ‘D’ of the RCRA regulations, essentially regulating coal ash as a non-hazardous, solid waste. Multiple versions of legislation and regulatory schemes existed during this period and for several weeks, the regulation of coal ash was an active component of the 112th congress’s transportation bill, however, in the final negotiations, coal ash was dropped from that particular bill.

Subsequently, on August 3, 2012 the “Coal Ash Recycling and Oversight Act of 2012” (S.R.3512) was introduced to the Senate, sponsored by Senator Hoeven and 23 others (12 Republicans and 12 Democrats) . As of this writing, the congress is in recess, but it is anticipated that this bill may see action during the 112th congress. Clearly, some form of regulation for coal ash disposal will be propagated either through the legislative or regulatory pathway.

5. MARKET SIZE ESTIMATES

We further address the question of how much coal ash there is in existing storage facilities and how much is being produced and, what regulations might mean to the size of the North American geosynthetic marketplace.

Coal is used to supply approximately 45% of the annual demand for electricity in the U.S. It is estimated that 125 billion kilograms of coal ash is generated annually in United States. Of this quantity approximately 43% is “beneficially reused” or recycled into applications such as concrete, wallboard, pavement and other construction materials. Using an average bulk density for coal ash of 725 kilograms per cubic meter this equates to a volume of slightly greater than 172 million cubic meters per year total, with approximately 74 million cubic meters per year placed into long term storage/landfill operations. If one assumes a facility height of 15 meters, an annual area of just under 500 hectares (1235 acres) is needed for storage. While this is clearly a large number, the underlying assumptions are critical to understanding the market effect. One must settle on estimates for the following factors at a minimum; the number and capacity of existing facilities, an accurate bulk density of the specific ash in question, site selection, geotechnical, construction and other issues relative to the height/depth of the ash storage pile, additional land use and geometric concerns as well as a host of other factors, all highly variable.

The combination of this information and data set into an estimate of the effects of regulation on the geosynthetic marketplace is complex. Clearly regulation will expand the marketplace significantly. A critical unknown is the regulatory activity for existing facilities, both those currently receiving coal ash and those that are no longer receiving ash. Generally these sites have not been “closed” as thought of in the context of geotechnical, geosynthetic and environmental engineering. It is conceivable and in fact likely the regulators will concern themselves with the fate of the sites and locations where coal ash had been stored in the past. Consideration of the past performance of sites relative to groundwater contamination and the results of groundwater monitoring would lead one to anticipate regulation of older sites, even those that may not be currently accepting ash. A second equally important concern is the “stigma” attached with the potential designation of coal ash as a hazardous waste. During the recent short term, beneficial use has clearly declined and a designation of coal ash as hazardous waste would result in more materials diverted to landfill and storage operations..

Note to reviewers and readers: This is a fast moving topic where situations change as time and political positions evolve. It is the authors’ intent to report on the current situation and implications “at the time of the conference”; providing historical and background information to place the opinions and projections of the authors into context.

6. GEOSYNTHETICS IMPACT AND MARKET ESTIMATES

A brief snapshot of the past and more recent global geosynthetic marketplace is offered in the following paragraphs. Please note that all units presented in the following are either in U.S. dollars or percentages.

In calendar year 2001, the global demand for geosynthetics was \$3.2 billion. This was distributed geographically as follows: North America 42%, Europe 35%, Asia Pacific 16%, All Others 7%. Global sales by product type: geomembrane 45%, geotextile 22%, geogrid and high strength fabrics 17%, erosion control materials 10%, drainage materials 6%. Global sales by application; pavement 25%, erosion control 8%, drainage 11%, barrier products 22%, stabilization and reinforcement 22%.

In calendar year 2010, the global demand for geosynthetics was \$6.1 billion. This was distributed geographically as follows: North America 40%, Europe 18%, Asia Pacific 21%, All Others 21%. Global sales by product type; geomembrane 32%, geotextile 32%, geogrid and high strength fabrics 8%, erosion control materials 11%, drainage materials 17%. Global sales by application; pavement 18%, erosion control 13%, drainage 16%, barrier products 34%, stabilization and reinforcement 19%.

7. CONCLUSIONS

The combination of this information and data set into an estimate of the effects of regulation on the geosynthetic marketplace is complex. Clearly the regulation will expand the marketplace significantly. A critical unknown is the regulatory treatment for existing facilities, both those currently receiving coal ash and those that are no longer receiving ash. Generally these sites have not been “closed” as thought of in the context of geotechnical, geosynthetic and environmental engineering. It is conceivable and in fact likely the regulators will concern themselves with the fate of the sites and locations where coal ash had been stored in the past.

A second equally important concern is the “stigma” attached with the potential designation of coal ash as a hazardous waste. During the recent short term, beneficial use has clearly declined and a designation of coal ash as hazardous waste would result in more materials diverted to landfill and storage operations.

REFERENCES

- Bowne, T.R. (2002) Geosynthetics: Industry Study 1621, The Freedonia Group, Cleveland, Ohio, USA
- Fettig, D.R. (2002-2006) Geosynthetics Market Survey, Geosynthetic Materials Association, Roseville, Minnesota, USA
- Goss, D. (2010) "CCP Beneficial Use Shows Steady Growth", Ash at Work: Issue 1: 2010, American Coal Ash Association, Aurora, Colorado, USA
- Jones, M. and Behm, D. "Bluff Collapse at Wisconsin Powerplant Sends Dirt, Coal Ash Into Lake Michigan", Milwaukee Journal Sentinel/Engineering News Record, November 1, 2011 Accessed November 3, 2011
http://www.enr.com/yb/enr/article.aspx?story_id=165390983
- Koerner, R.M. (2004) Geosynthetics Survey, Geosynthetic Institute, Folsom, Pennsylvania, USA
- Lombardi, K. "The Hidden History" I watch News January 7, 2009. The Center For Public Integrity. Accessed 11/11/11
www.iwatchnews.org
- U.S.EPA (2002) 25 Years of RCRA: Building on Our Past To Protect Our Future, EPA-K-02-027, Washington D.C. USA
- "Regulatory Determination on Wastes from the Combustion of Fossil Fuels; Final Rule." Federal Register 65:99 (May 22, 2000) Page 32213-32237. Available from: US EPA, www.epa.gov; Accessed: 11/11/11.
- "Hazardous and Solid Waste Management System; Identification and Listing of Special Wastes; Disposal of Coal Combustion Residuals From Electric Utilities; Proposed Rule." Federal Register 75:118 (June 21, 2010) Page 35127-35264. Available from: The United States Government, www.regulations.gov; Accessed: 11/11/11.
- "Bevill Amendment Questions" US EPA Updated as of May 1, 2009. Accessed 10/23/11
<http://www.epa.gov/compliance/assistance/sectors/minerals/processing/bevillquestions.html>
- "Fossil Fuel Combustion (FFC) Waste Legislative and Regulatory Time Line". US EPA. Updated as of October 20, 2011. Accessed 10/24/11 <http://www.epa.gov/wastes/nonhaz/industrial/special/fossil/regs.htm>
- "Information Request Responses from Electric Utilities". US EPA. Updated as of August 16, 2011. Accessed 11/11/11
<http://www.epa.gov/epawaste/nonhaz/industrial/special/fossil/surveys/index.htm#databaseresults>
- "Kingston Fossil Plant coal fly ash slurry spill". Wikipedia. Updated as of September 19, 2011. Accessed 10/24/11
http://en.wikipedia.org/wiki/Kingston_Fossil_Plant_coal_fly_ash_slurry_spill
- "Summary of Bluff Failure We Energies Oak Creek Power Plant". State of Wisconsin Dept. of Natural Resources. Updated as of Dec. 14, 2011. Accessed 08/12/12 <http://dnr.wi.gov/topic/Spills/documents/oakcreek/nrbpresentation.pdf>
- "Lack of lining in pond blamed in bluff collapse at We Energies site". Milwaukee Wisconsin Journal Sentinel Online. Updated as of March 1, 2012. Accessed 08/12/12 <http://www.jsonline.com/news/milwaukee/lack-of-lining-in-pond-blamed-in-bluff-collapse-at-we-energies-site-f34ddln-141132423.html>
- "H.R.2273 - Coal Residuals Reuse and Management Act". OpenCongress.org. Accessed 08/12/12
<http://www.opencongress.org/bill/112-h2273/show>
- "S.1751 - Coal Residuals Reuse and Management Act". OpenCongress.org. Accessed 08/12/12
<http://www.opencongress.org/bill/112-s1751/show>
- "Coal Ash Recycling and Oversight Act of 2012". Association of State and Territorial Solid Waste Management Officials, ASTSWMO.org Accessed 08/12/12.
http://www.astswmo.org/Files/Announcements/2012-08-Senate_Coal_Ash_Recycling_and_Oversight_Act.pdf

Microbiological Resistance Properties of Various Synthetic and Natural Textiles.

Chiwan Wayne Hsieh, Professor, Department of Civil Engineering National Pingtung University of Science and Technology

Shih Kai Su, Graduate Student, Department of Civil Engineering National Pingtung University of Science and Technology

Ying-Wei Liu, Professor, Department of Civil Engineering National Pingtung University of Science and Technology

ABSTRACT

The EN 12225 standard test method was adopted to evaluate the microbiological resistance of several natural and synthetic textiles. The bio-active soil criterion is the test cotton fabric should reduce 75% of its tensile strength after 7 days after burial within the test bio-active soil under controlled humidity and temperature conditions. After several trial procedures a commercial organic soil was chosen for use as the bio-active incubation soil for the standard test. The cotton fabric strength reduction, test materials and the most probable number (MPN) for total bacteria and fungi test count were evaluated for each incubation period. The test materials included the natural jute temporary erosion control mat (TECM), a reinforced polypropylene permanent erosion control mat (PECM), a polypropylene silt film geotextile, a black and white PP multi-filament woven geotextile, a reinforced polyester nonwoven geotextile, and a PVC coated polyester geogrid. After 28-days incubation the strength of the natural jute fabric was reduced by 90%. Fifteen percent strength reduction was measured for the PP PECM after nearly 4 months incubation. However, only 1.3% to 5.9% strength reductions were determined for the other tested geosynthetic materials. The total amount of bacteria was generally higher than that for fungi. The MPN values for the tested PECM and TECM were decreased as the burial duration increased. However, the MPN values increased with the increase in burial duration.

Keywords: Microbiological resistance test, Geosynthetic, Geotextile, Microbiology.

1. INTRODUCTION

Many geosynthetic applications require burying the geosynthetic product within the soil. Natural soils generally contain of large amounts of bacteria and fungi. This phenomenon is especially true for the soils in tropical areas. The primary resin used in geotextiles is mixed with anti-oxidants, screening agents, filters and/or other materials for a variety of purposes. Some of these additives might be excellent foods for the fungi and bacteria within soils. Burying geosynthetics within bioactive soils could influence the geotextiles' engineering properties. In addition, the search for biodegradable materials has also become an important environmental topic. Understanding and evaluating the microbiological resistance of several locally used geosynthetic and natural erosion control products is the purpose of this study. The EN 12225 soil burial standard test method was adopted to evaluate the microbiological resistance of the tested materials. The most probable number (MPN) of total bacteria and fungi was also used as the evaluation criteria in this study.

1.1 Soil Burial Test

BS EN 12225, Geotextiles and geotextiles-related product – Method for determining the microbiological resistance using a soil burial test was used to evaluate the biological resistance behavior of the tested materials. An environmentally controlled room was built for this study as shown in Figure 1. The tested soil was cultivated for one month to ensure the bioactivity reached the standard requirement. The cultivated temperature was controlled at 28 ± 2 °C with the relative humidity kept at $97 \pm 2\%$. The water content of the tested soils was kept at around 100%. Cotton fabric strips were buried 100 mm deep within the cultivated soils for 7-days. The fabric strips were then retrieved and cleaned with an alcohol/water mixture. The cleaned and retrieved cotton samples were then stored at a temperature of 20 ± 2 °C with relative humidity of $65 \pm 5\%$ for 72-hours before checking the strength reduction rate. Strength reduction greater than 75% or not was the criteria. Five soil containers were used to evaluate the tested soil activity. The average reduction rate was 79.28%. A minimum of 18 test samples for each tested material were buried approximately 100 mm deep to ensure good contact with the test soil. The containers permitted free oxygen exchange. The incubation temperature was controlled at 26 ± 1 °C with the relative humidity maintained at $95 \pm 5\%$ during the test. The water content of the test soil was kept at around 60% and checked every 4 weeks. The test

containers with test samples were incubated for 16 weeks at the specified climate conditions before retrieving and cleaning the fiber strips under standard procedure for further evaluation tests. The tensile strength of the control and retrieved strip samples were tested according to the EN 12226 strip tensile test method or ASTM D6637 method A for geogrid single rib tensile test.



Figure 1. Setup of incubation room.

1.2 Most Probable Number (MPN) Test

The most probable number (MPN) of bacteria and fungi test was also conducted for all tested materials and incubation soils at each period. This test procedure involved retrieving 1 g soil sample from the soil container and adding 10 ml of 100% no bacteria polluted water. The soil was suspended in diluted water for 101, 102, ..., 1010 ratios. For each diluted ratio of suspended water, take 0.02 ml suspended water added to 0.18 ml TSB and PDB incubation agents and placed within 96 well-plates. Five samples were required for each diluted ratio water batch. The mixed TSB and PDB agents were placed in well plate and kept in 30 °C incubation chambers for 3 days. The total amount MPN of bacteria and fungi for each diluted ratio suspended water was then determined using the following Equation (1). The unit of analysis is Colong-Forming Units per gram (CFU/g) for the test sample.

$$\text{MPN (cfu / gm)} = \frac{\text{MPN chart reading}}{\frac{\text{diluted ratio}}{\text{amount of water sample (ml)}}} \quad [1]$$

2. TEST MATERIALS

Several natural and geosynthetic fabrics were used in this study. The control material was a cotton fabric with unit mass of 219.59 g/m² and tensile strength of 10.80 kN/m. A temporary erosion control material (TECM), a reinforced jute erosion control fabric was used as another natural test material. Five geosynthetic geotextiles and related products were used in this study. The synthetic test products included a PVC coated PET geogrid, a green polypropylene silt film woven geotextile, a black and white PP multi-filament woven geotextile, a white reinforced polyester nonwoven geotextile and a PE reinforced polypropylene erosion control mat. The mass per unit weight and tensile strength of the tested materials are summarized in Table 1.

Table 1. General properties of the test materials.

Type	Mass per unit area (g/m ²)	Base Material	Strength per unit width (kN/m)
Jute-TECM *	559.68	Jute	4.90
PECM (PP)	263.93	PP	3.40
W-GT1(PP)	323.95	PP	75.80
W-GT2(PP)	465.67	PP	81.20
NW-GT(PET)	594.70	PET	108.40
GG (PET)	1536.44	PET	190.97

3. TEST RESULTS AND DISCUSSIONS

Five soil containers were cultivated for one month and used to evaluate the test soil activity. The incubation durations for the reference cotton fabrics were seven days and 14 days. The retrieved 7-day cotton fabric samples were cleaned and conditioned according the standard procedure. Three samples were retrieved from each container. The retained tensile strengths of the retrieved samples were tested according to the EN 12226 test standard. The average reduction rate in tensile strength was 79.28%. A picture of the samples before the tensile test is shown in Figure 2. Two containers of cotton samples were extended to 14 days. Figure 3 shows the retrieved 14-day cotton samples. The fabric structure of the samples was completely destroyed by the bacteria and fungi within the test soils. The selected commercial organic soils and incubation procedure satisfied the biological activity requirement for EN 12225 test standard.



Figure 2. Picture of 7-day incubated cotton strip samples (significant rot was observed).



Figure 3. Picture of 14-day incubated cotton strip samples (samples were completely destroyed by rot).

The biodegradation properties of the five geosynthetic products and one natural jute fabric were studied. The incubation duration was 4 months or more. Incubated samples were retrieved from the test containers to evaluate the tensile strength and total MPN of bacteria and fungi. The typical retrieval times included 7, 28, and 112-days. The maximum incubation time for the natural jute fabric was 28 days. Some geogrid samples were embedded within the test soils for 168 days. A minimum of six 50-mm samples were used for the EN 12226 tensile strength tests. Single rib samples were used for the ASTM D6637 method A test. The average tensile strengths and associated strength retained rates for the reference group and 3 different incubation durations for each test materials are summarized in Tables 2 and 3. It is clear that only 10% strength was retained for the test jute fabric after only 28 days incubation time. Low tensile strength was retained for the 14-day jute samples as shown in Figure 4. The strength of the polypropylene PECEM reduced near 15% after 112 days incubation time. Only 1.3% to 5.9% strength reductions were observed for the geosynthetic products after 112-days incubation time. The total MPN of bacteria and fungi for the test materials incubation soils are summarized in Tables 4 and 5. The total MPN for bacteria was higher than that for fungi. The MPN values for the test PECEM and TECM were decreased as the incubation duration increased. However, the MPN values increased when the incubation duration was increased. Further analysis is required. Some bacteria and fungi grew on the PP geotextile samples as shown in Figure 5, However very low strength reduction was observed for the tested samples.

Table 2. Tensile strengths of reference group and various test material incubation groups. (kN/m)

Type	Reference group	7-day	28-day	112-day
Jute-TECM *	4.90	2.20	0.50	N/A
PECEM (PP)	3.40	3.30	3.30	2.90
W-GT1(PP)	75.80	76.00	75.6	74.8
W-GT2(PP)	81.20	79.40	77.20	76.40
NW-GT(PET)	108.40	107.20	107.40	105.60
GG (PET)	190.97	190.02	188.44	183.05

*Low tensile strength was observed for 14-day incubation jute fabric samples.

Table 3 Retained tensile strength ratios of various test material incubation periods. (%)

Type	7-day	28-day	112-day
Jute-TECM *	44.90	10.20	N/A
PECM (PP)	97.06	97.06	85.29
W-GT1(PP)	100.00	99.74	98.68
W-GT2(PP)	97.78	95.08	94.09
NW-GT(PET)	98.89	99.08	97.42
GG (PET)	99.50	98.67	95.85

*Low tensile strength was observed for 14-day incubation jute fabric samples.



Figure 4. Picture of 14-day incubated jute fabric samples (sample woven structure was damaged).

Table 4. Total MPN of bacteria for various test material incubation periods. (cfu/g)

Type	7-day	28-day	112-day
Jute-TECM *	7.701×10^8	4.559×10^7	1.227×10^7
PECM (PP)	4.964×10^9	1.824×10^8	3.570×10^7
W-GT1(PP)	1.261×10^8	4.604×10^9	2.215×10^8
W-GT2(PP)	7.468×10^8	2.545×10^8	7.231×10^7
NW-GT(PET)	7.547×10^7	1.179×10^8	3.473×10^9
GG (PET)	9.660×10^6	2.525×10^8	6.682×10^9

Table 5. Total amount MPN of fungi for various test material incubation periods. (cfu/g)

Type	7-day	28-day	112-day
Jute-TECM *	4.276×10^6	1.004×10^6	1.147×10^6
PECM (PP)	9.317×10^5	4.733×10^7	1.610×10^6
W-GT1(PP)	3.973×10^6	1.006×10^7	2.301×10^5
W-GT2(PP)	4.993×10^5	3.183×10^5	5.433×10^5
NW-GT(PET)	1.289×10^6	1.263×10^8	2.241×10^5
GG (PET)	4.192×10^5	3.659×10^7	9.112×10^6

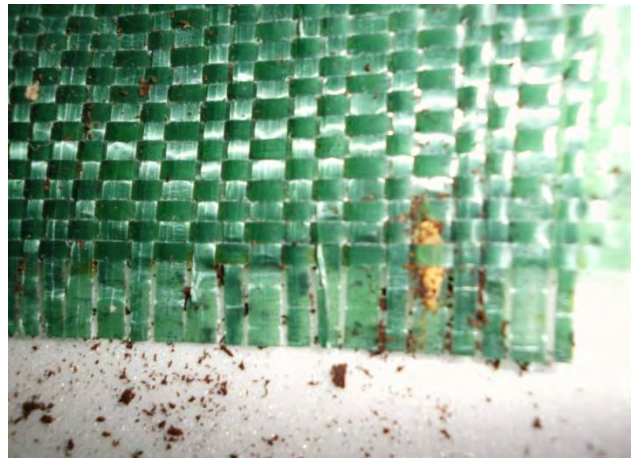


Figure 5. Picture of 112-day incubated polypropylene silt film geotextile sample (minor bacteria and fungi growth was observed).

4. SUMMARY AND CONCLUSIONS

The microbiological resistance of several locally used geosynthetic products and a natural erosion control product were studied. The BS EN 12225 testing method was used for the microbiological resistance evaluation using a soil burial test. The total most probable number (MPN) of bacteria and fungi for the test soils was used in this study. The retained tensile strengths of retrieved samples were tested according to the EN 12226 test standard and ASTM D6637 test method. A commercial organic soil was chosen as the bio-active soil for the standard test. Cotton fabric was used to evaluate the bio-activity of the cultivated test soils. The average strength reduction rate for the retrieved 7-day cotton fabric samples was 79.28%. The biodegradation properties of five geosynthetic products and one natural jute fabric were studied. The typical retrieval times included 7, 28 and 112-days. Only 10% tensile strength was retained for the 28-day incubation jute samples. The strength of the polypropylene PECM reduced to near 15% after 112 days incubation time. Only 1.3% to 5.9% strength reductions were observed for the remaining geosynthetic products after 112 days incubation time. In general, the total amount of bacteria was higher than that for fungi. The MPN values for the test PECM and TECM decreased as the incubation duration was increased. However, the MPN values increased with the increase in incubation duration.

ACKNOWLEDGEMENTS

This study is part of a generic research program on several natural and synthetic products by the Geosynthetic Laboratory of National Pingtung University of Science and Technology in Taiwan. The Geosynthetic Institute (USA)

recognized this laboratory as an accredited laboratory for BS EN 12225, BS EN 12226, and ASTM D6637 test methods. This study was partially supported by the National Science Council, Taiwan (NSC 99-2221-E-020-026). Mr. Chia-Shing Wu provided great support for the laboratory-testing program. The authors express their sincere appreciation to all members that contributed to this study.

REFERENCES

- ASTM D5261. Standard Test Method for Measuring Mass per Unit Area of Geotextiles, American Society for Testing and Materials, West Conshohocken, Pennsylvania, USA.
- ASTM D6637. Standard Test Method for Determining Tensile Properties of Geogrids by the Single or Multi-Rib Tensile Method, American Society for Testing and Materials, West Conshohocken, Pennsylvania, USA.
- ASTM G160. Standard Practice for Evaluating Microbial Susceptibility of Nonmetallic Materials by Laboratory Soil Burial, American Society for Testing and Materials, West Conshohocken, Pennsylvania, USA.
- BS EN12225:2000. Standard test of Geotextiles and geotextile-related products-Method for determining the microbiological resistance by a soil burial test, European Standard.
- BS EN12226:2000. Standard test of Geotextiles and geotextile-related products-General tests for evaluation following durability testing, European Standard.
- Chiwan Hsieh, Chiung- Hui Tseng. (2010). Microbiological Resistance Tests for Geosynthetics, Master thesis, National Pingtung University of Science and Technology, Taiwan, ROC .
- CNS13105. General rules for infrared spectrophotometric analysis, Chinese National Standard, Taiwan, ROC .
- Environmental Analysis Laboratory EPA, Executive Yuan, ROC. (2007, November 29). Detection of coliforms in water - multiple tube fermentation method, Announcement No. 0960091685, NIEA E201.54B, from the World Wide Web:
http://www.niea.gov.tw/analysis/method/methodfile.asp?mt_niea=E201.54B
- Environmental Analysis Laboratory EPA, Executive Yuan. (2008, October 2). Determination of soil pH (pH) - electrode method, Announcement No. 0970075579, NIEA S410.62C, from the World Wide Web:
<http://www.niea.gov.tw/niea/SOIL/S41062C.htm>
- Jadwiga Szostak-Kotowa. (2004). Biodeterioration of textiles, International Biodeterioration & Biodegradation, ELSEVIER, Vol.53, p.165~170.
- Koerner, R.M.. (2005). Designing with Geosynthetics, Fifth Edition, Prentice Hall, New Jersey, USA.
- L. Cosgrove, P. L. McGeehan, P. S. Handley, and G. D. Robson. (2010). Effect of Biostimulation and Bioaugmentation on Degradation of Polyurethane Buried in Soil, Applied and Environmental Microbiology. Vol. 76, No. 3, p.810~819.

Mine Water Treatment with Geotextile Tube System at Goldex Mine (Val d'Or, Qc, Canada)

Jocelyn Douh ret, ASDR Environment, Saint-Romuald, Quebec, CANADA
Andy Lister, TenCate, Toronto, Ontario, CANADA
Stephen Authier, ASDR Environment, Malartic, Quebec, CANADA

ABSTRACT

AGNICO Eagle operates Goldex Mine an underground gold mine in Val d'Or (Qc, CANADA) since April 2008. In 2009, Goldex decided to better handle mine water which was formerly directed to sumps. Solids from sumps were daily emptied mobilizing a full time scoop tram. Furthermore, water from the sumps was abrasive causing slurry pumps renewal.

A pilot test using a geotextile tube started in January 2010. High TSS mine water was conditioned in line with a coagulant and a flocculant prior dewatering with a geotextile tube. As results were convincing an automatic system was installed to feed two geotextile tubes in sequences.

Mine water average flow is about 60 m³ per hour with a 4 000 mg/L TSS level. Clean water comes out of the bags at a 10 mg/L TSS level. Once a geotextile tube is full, solids are removed by a scoop tram and reprocessed in the ore treatment process.

INTRODUCTION

AGNICO Eagle has been operating the Goldex underground Gold Mine in Val d'Or (QC, CANADA) since April 2008. The Mine is located in a semi-urban location at the west end of Val d'Or, QC. (Population 45 000).



In 2009, Goldex decided to better handle mine water. Mine water was formerly directed to sumps. Solids from sumps were regularly emptied mobilizing a full time scoop tram. Furthermore, water from the sumps was highly abrasive causing frequent slurry pumps renewal.

The gold mine extracts 8500 tons of ore per day. The Lowest level of the underground mine is situated at 2500 ft beneath the surface. Ore is extracted from the bottom of the gold reef.

Mine water comes from water infiltration at the surface as well as from the reef itself. This natural water is composed of 80% Mine Water. The water is also used for underground operations such as rock crushing, machinery cleaning as well as dust control. Mine water runs along the gallery eroding the mine shaft and transporting a high level of suspended solids. This water is collected in a sump located at the very bottom of the mine (level 76 under ground level).



Picture 2 : Sump collecting Mine Water



Picture 3: Sump pump

Mine Water is then pumped to the surface using high power pumps and booster pumps. This Mine Water is extremely abrasive, which increased the maintenance costs on the pumps. In addition the Mine Water was not clean enough to meet the discharge criteria into the local water course. Quebec regulation, Directive 019 from the Ministry of Environment, lists discharge criteria as shown in Table 1.

Table 1: Discharge Criteria under Quebec Regulation

PARAMETER	Monthly Average Concentration	Maximum Concentration
Arsenic	0,2 mg/l	0,4 mg/l
Copper	0,3 mg/l	0,6 mg/l
Iron	3 mg/l	6 mg/l
Nickel	0,5 mg/l	1 mg/l
Lead	0,2 mg/l	0,4 mg/l
Zinc extractible	0,5 mg/l	1 mg/l
Cyanures	1 mg/l	2 mg/l
Hydrocarbons (C10-C50)	-----	2 mg/l
TSS	15 mg/l	30 mg/l

Solids at the bottom of the sump were removed daily by a scoop tram dedicated to this full time.



Picture 4: Scoop Tram

With the above factors in mind, Goldex Mine decided to find a better solution to manage their mine water. Goldex Mine had one goal:

- Reduce mine water management cost by
 - o Reusing water
 - o Obtaining dryer solids

1.0 – PROPOSED SOLUTION AND PILOT TEST

A Rapid Dewatering Test (RDT) with a woven geotextile tube was conducted. The purpose of the RDT test is to identify the appropriate polymers, their dosage rate and the effectiveness of the woven geotextile. The chemical conditioning consisted of using a coagulant first to precipitate dissolved ions followed by a flocculant to create a strong flock that would allow the water to be released from the sediments and subsequently filter through the geotextile tube.

A pilot test was then proposed. The process consisted of:

- Constant Agitation of the slurry in the Sump
- Pump the Mine Water to the treatment station
- Coagulant injection
- Flocculant injection
- Static Mixer, mixes both coagulant and flocculant
- Treated mine water pumped to a geotextile tube
- Clean water is collected and recycled to the crusher



Picture 5: Chemical conditioning results

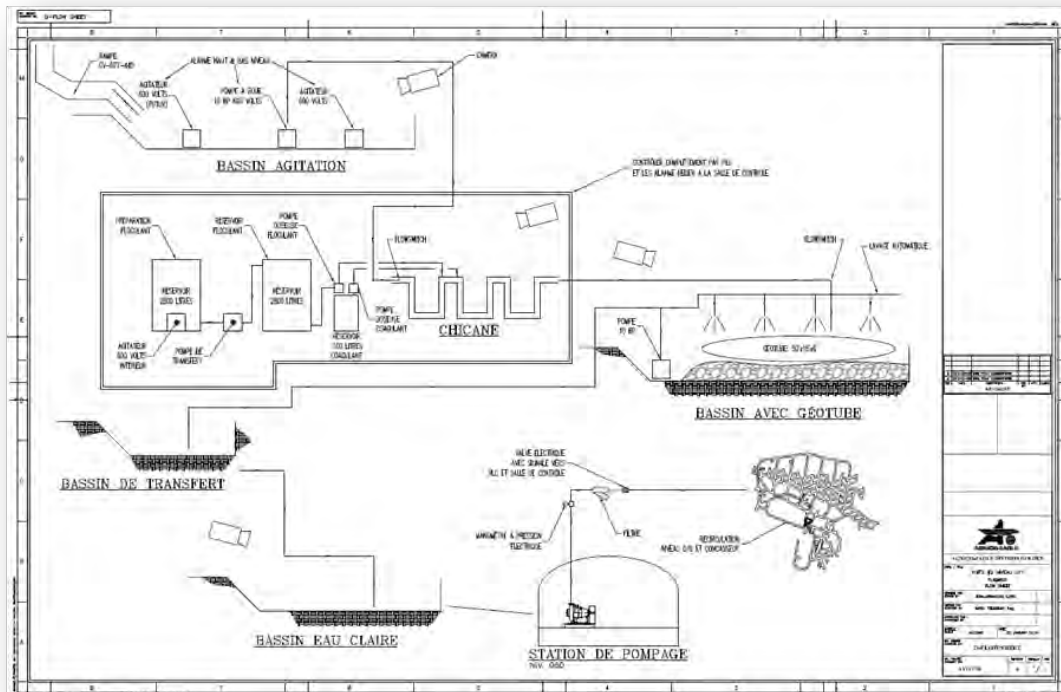


Figure 1: Principles of the process

A pilot test using a geotextile tube started in January 2010. High TSS mine water of 4000mg/l was conditioned in line with a coagulant and flocculent prior to pumping to the geotextile tube which was located in a nearby gallery (See Figure 1, Principles of the process). The dimensions of the geotextile tube were 30ft (9.14m) circumference X 50 ft(15.2m) long.



Picture 6: Chemical conditioning unit



Picture 7: Geotextile tube in a gallery

Water coming out of the geotextile tube was extremely clean with a TSS of 10mg/l



Picture 8: Clean water

2.0 – UNDERGROUND OPERATION

With the positive results of the pilot test an automatic polymer feed system was installed to feed in sequence two 30 ft (9.14m) circumference x 50 ft(15.2m) long geotextile tubes.

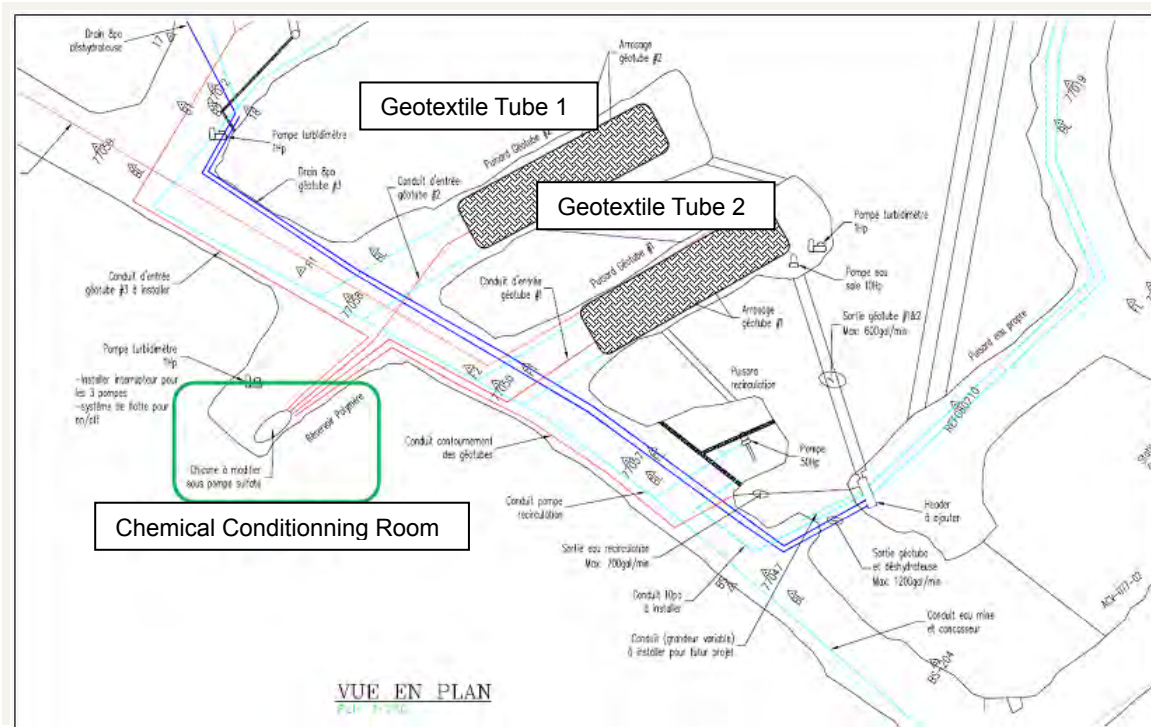


Figure 2 : Installation Plan

A more sophisticated and fully automated treatment unit was installed to ensure proper chemical conditioning of Mine Water prior to filtration and dewatering by the geotextile tube.



Picture 9: Polymer preparation unit



Picture 10 : Chemical dosing and mixing unit

Mine Water is pumped 40 minutes per hour at an average flow rate about 60 m³ per hour with a TSS level around 4 000 mg/L. Clean water comes out of the bags at a TSS level around 10 mg/L.

A sprinkler system was installed to spray water on the geotextile tube to prevent clogging.



Picture 11: Sprinkler System

Clean water coming out of the geotextile tube is used for crushing operation as well as equipment cleaning.

The geotextile tubes are filled 40 minutes every hour, 24 hours a day, 7 days a week during weeks. Solids are retained in the geotextile tubes. A complete fill cycle lasts approximately 1 month at which time the geotextile tubes are full holding 65 m³ of solids. The solids are then removed by the scoop tram and reintroduced into the ore treatment process. Table 2 shows performances of the geotextile tube solution regarding water treatment and solids dewatering.

Table 2: Performances of the geotextile tube solution

Parameters	Raw Water	Clean Water	Dewatered Solids
TSS Level (mg/L)	4000	10	n/a
Turbidity (NTU)			n/a
% solids	1 to 0,25	0,001	65
Specific Gravity (metric Tons/m ³)	1,6	1,0	3,5

3.0 - CONCLUSION

Geotextile tube solution with proper chemical conditioning allows for better Mine Water management.

Low maintenance clear water pumps then replaced the former slurry pumps. Clean water is re-used for mine operation and reduces the environmental impact of the mine on the local environment. The geotextile tube system also replaced a full time scoop tram with driver. Solids are removed once a month and follow the same mill process as ore extracted from the reef.

Using the geotextile tube solution, Mine water management costs were reduced by more than 50% compared to the previous manner.

Model Test of Stacked Permeable Geosynthetic Tubes

Jian Chu, Professor, Department Civil, Construction & Environmental Engineering, Iowa State University, USA, jchu@iastate.edu (Formerly Nanyang Technological University, Singapore)

Wei Guo, School of Civil and Environmental Engineering, Nanyang Technological University, Singapore, 639798, guowei@ntu.edu.sg

Shuwang Yan, Professor, School of Civil Engineering, Tianjin University, China, yanshuwang@tju.edu.cn

ABSTRACT

Geosynthetic tubes made of woven geosynthetic material provide an ideal medium for the dewatering of digested biosolids, dredged materials and industrial solid wastes and for the construction of levees. However, the dewatering process of a single permeable geosynthetic tube is time consuming. A better way is to stack permeable geosynthetic tubes one layer on top of another to use the weight of the tubes as surcharge. In order to improve the understanding of the performance of stacked permeable geosynthetic tubes, model tests of stacked permeable geosynthetic tubes resting on rigid foundation were carried out. A 2.0-mm-thick woven polypropylene geosynthetic sheet was used for the geosynthetic tubes. The deformation of the 2-layer geosynthetic tubes versus time curves are presented and analyzed in this paper. The time taken to achieve 80% dewatering efficiency for the stacking method is only 38% of that for the single tube method.

1. INTRODUCTION

In recent years, geotextile tubes have been used for dewatering waste sludge such as digested biosolids, sewage sludge, dredged materials, industrial solid wastes, fly ash and coal slurry. Traditionally, these high water content wastes are exposed to sunlight for the formation of desiccation crust. However, the process of sun drying is very slow and only effective for the top several centimeters. When geotextile tubes are used, the waste sludge is firstly filled into the geotextile tube by pumping. After that, water seeps through the permeable geosynthetic sheet and the water content of the solids inside the geosynthetic tube is reduced. In order to save space and accelerate the dewatering process, the geotextile tubes sometimes stacked together. The advantage and disadvantage of using permeable geosynthetic tubes for dewatering waste sludge have been summarized by Andrews (1999) and reproduced here as Table 1.

Table 1 Advantages and disadvantages of geotextile tube dewatering method (after Andrews, 1999)

Advantage	Disadvantage
<ul style="list-style-type: none"> • Able to dewater large quantities of sediments concurrently • Low operating costs • Can accommodate high flow rates and rapidly varying flows and solids concentrations, such as those produced from a hydraulic dredge • Provides immediate containment of material and reduces odors • Provides a method of increasing solids content quickly and efficiently • Replace small sludge lagoons, aerators and settling tanks, thus reducing the construction, maintenance and closing costs 	<ul style="list-style-type: none"> • Periodic removal of liquids required for maximum consolidation if sufficient drainage away from the tube is not provided • Water soluble contaminants can leach out over time.

In recent years, several analytical solutions for impermeable geosynthetic tubes have been proposed (Malik and Sysala, 2010; Cantré and Saathoff, 2010; Yan and Chu, 2010; Chu et al, 2011; Guo et al, 2011). The analysis of a permeable geosynthetic tube is more difficult than that of an impermeable one as the consolidation process of the soil in the tube during or after filling needed to be modeled too. One analytical method for single permeable tube proposed by Leshchinsky et al. (1996) was to assume that the consolidation process to be one-dimensional, that is, the width of the geosynthetic tube does not change during the consolidation process. The curve fitting methods to calculate the deformation of the permeable geosynthetic tube were also proposed by Shin and Oh, (2004), Yee et al. (2012) and Yee and Lawson, (2012). However, all these method were only applicable for single permeable geosynthetic tube. An easy and direct way to understand the performance of the stacked permeable geosynthetic tubes is by model test.

Usually model tests of permeable geotextile tubes were carried out in-situ because the field test considers the influence of weather and waves which are not easily simulated in laboratory. The engineering properties of dredged sediments ranged from beach sands to highly organic clays are usually indigenous to the environment from which they are dredged

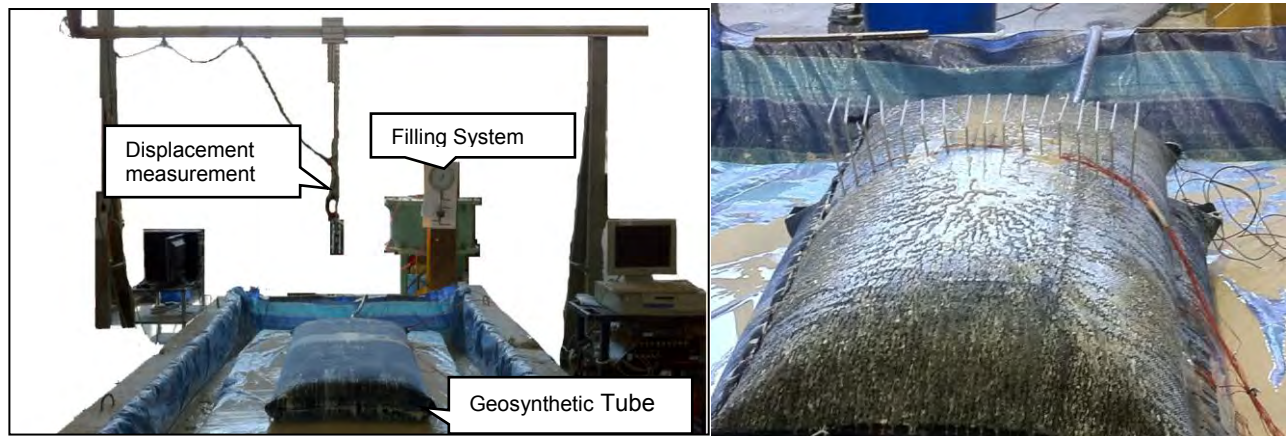
(Moo-Young and Tucker, 2002). Therefore, for coastal erosion projects, the model test of permeable geotextile tube was usually filled with dredge sand or silty clay materials on situ (Shin and Oh, 2003). However, the consolidated period will more or less be affected by the properties of the filling materials. Based on the field test conducted by Shin and Oh (2003), the dredge sand filled geotextile tube dropped off about 40% in height within 2 days from the time after being filled. But for silty clay, the tube dropped off 50% within a month after it has been filled. The basic engineering properties of consolidated soil after the model test such as water content and shear strength also have to be determined. The undrained shear strength of consolidated soil was usually tested by the laboratory vane shear test.

For dewatering sewage sludge using geotextile tubes, the dewatering time and the water content of consolidated soil are the two important dewatering performances. Normal dewatering operations require the dewatering time to be between one and two months (Lawson, 2008). The longer dewatering time constrains the speed and volume of waste that can be treated. Therefore, the acceleration of this dewatering process is necessary. Currently, there are two kinds of accelerate methods: 1) adding chemical dewatering accelerant; and 2) using electro-osmotic potential. The chemical dewatering accelerant can accelerate the dewatering time for the organic waste such as sewage sludge, lagoon solids but has no benefit with fly ash. The electro-osmotic potential dewatering acceleration method utilizes an electric potential between anode and cathode to accelerate the pore water moving through the fine-grained particles. The later method has been widely used in many kinds of sludge such as sewage sludge, waste water sludge, lagoon sewage and fine-grained residue from mine tailing.

A relatively large scaled model test of stacked permeable geosynthetic tubes resting on rigid basement was carried out in this paper. The permeable geosynthetic tubes are stacked together to use the weight of the tubes on top as surcharge to the tubes below. The tubes were made of 2-mm-thick, black color, polypropylene woven geosynthetic sheet supplied by Tok Si Engineering Co. Ltd, Taiwan. The tensile stress was 29kN/20cm and the maximum elongation was 20×27% tested by following ASTM D4595. The permeability of the geosynthetic was $1.00s^{-1}$ by ASTM D4491-99a, and apparent pore opening size (AOS) of O95 was 0.4mm by ASTM D4751. The slurry made from L2 Kaolin powder was used as filling material. Kaolinite was used because it had relatively high coefficient of consolidation. The deformation of the 2-layers geosynthetic tubes versus time curves were presented and analyzed.

2. MODEL TEST SET-UP

The experiments were performed in a box of 3.0 m wide, 4.0 m long and 0.4 m high as shown in Figure 1(a). The box was placed on the concrete floor. Two concrete beams and two wooden boards were used to form a box. Another flat wooden board was placed on the floor as the base for the geosynthetic tube. The box and the base were lined with double layers of plastic sheets to make it water proof and contain water that would seep out during the test.



(a) Panoramic view of the model setup

(b) Measurement of the surface between two tubes

Figure 1 Model test set up

The data loggers recorded the readings of strain gauges and water pressure transducers. The miniature pore water pressure transducers (PPTs) used in this model test was Druck® PDCR 81 type with an external diameter of 6.4 mm and height of 11.4 mm. Such a miniature size was necessary to minimize the influence of the measuring device to the overall soil behavior during model test. The PPTs has 5 m long and 2.3 mm diameter integral Teflon vented cable. Before a model test, all PPTs were calibrated by using water pressure generated in a triaxial cell. The reaction of the PPTs to the

applied pressure was linear and the capacity was 300 kPa. Two PPTs were used to test the pore water pressure during filling and dewatering stage. One was preinstalled on the inner top surface. Another was at the bottom.

The displacements of the HWG tubes during a test were measured by an automatic running scanner mounted on the frame. Two standing steel truss columns were fastened to the loading bearing concrete floor using bolts. A scanner was mounted on a horizontal track which was supported by the two columns. The scanner was attached to a motor so its movement could be controlled. The ILD1700-750 model laser sensor which was connected to a desktop computer recorded the time and the vertical distance to the top of the geosynthetic tubes at that time. The horizontal coordinate was calculated by the speed of scanner, 5 cm/s, multiply the recording time. Before the model test, the distance from wooden board to the laser sensor was scanned. Then the vertical coordinates of testing points on the HWG tube could be calculated as the difference between the distance to wooden board and the laser sensor readings. The contact surface between the two stacked geosynthetic tubes was determined by inserting a set of bended iron bars as shown in Figure 1(b). The bended right-angle part can be scanned by the laser sensor. The height of contact surface can then be calculated by the reading of the laser sensor subtracting the height of the iron bars. The iron bars were small enough so their disturbance to the top tube was negligible.

The kaolin powder was mixed with tap water into a slurry form. Firstly, the weighted dry kaolin powder and water were putted into a big mixer and blended for about 60 min. After mixing, the desired slurry was transferred from the mixer to a filling tank. This procedure was repeated several times until sufficient slurry was made. The filling tank had a height of 1.0 m and a diameter of 1.0 m.

Two sets of model tests on stacked permeable geosynthetic tubes (SPT) filled with slurry were tested. The details of the dimensions of the tubes and water content of the filling slurry are shown in Table.2.

Table.2 Information of stacked geosynthetic tube and filling slurry

Model test No.	Materials	Dimension of (W×L, m)		Water Content (%)
		Top tube	Bottom tube	
SPT1	HWG	0.70×1.35	1.0×2.0	71.6
SPT2	HWG	0.75×1.50	1.0×2.0	89.2

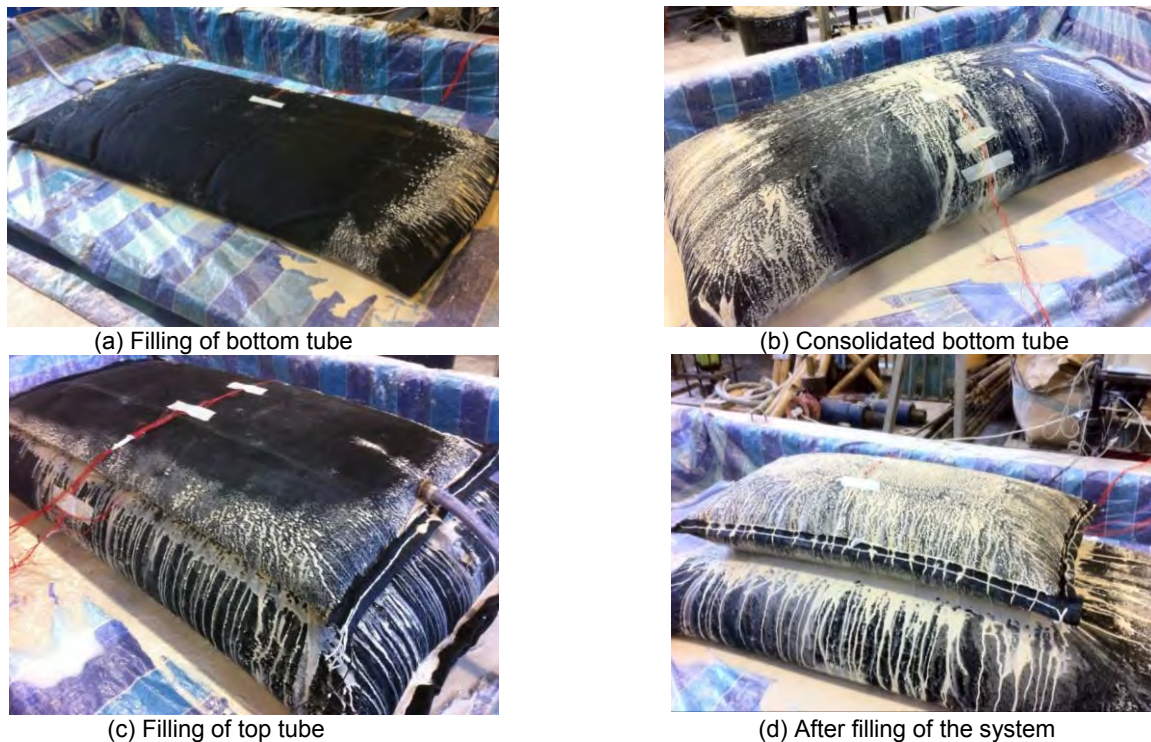


Figure 2 Filling process of Test SPT1

The model testing setup and testing procedure for Test SPT1 are shown in Figure 2. The bottom tube was filled and self-weight consolidated first in the same way as for the case of a single geosynthetic tube as shown in Figure 2(a) and (b). After the bottom tube was consolidated under self-weight, another tube was placed on top and fully inflated with the same type of slurry. The height of the tube after inflation was 0.677 m as shown in Figure 2(c) and (d).

3. TEST RESULTS

The measured cross-sections of the Test SPT1 are shown in Figure 3. Due to the limitation of the laser sensor, only the top profile of the each geosynthetic tubes could be recorded. The bottom geosynthetic tube of model SPT1 was inflated to almost sausage shape after filling for 4.51 hour as shown in Figure 3(a). Because of the dewatering process of the inflated slurry, the height of the bottom tube reduced until the top surface became flat as shown in Figure 3(a) by the profile measured at 44.6 h. At time of 99.03 h, a top tube was placed on to the bottom tube and inflated with slurry. The water content of the slurry was 71.2%. The height of the top tube after inflation was 0.677 m as shown in Figure 3(b). Under the weight of the top tube, the bottom tube compressed, but only by 2 cm, as shown in Figure 3 (b). The top tube consolidated till the top surface was flat as shown in Figure 3 (b) as the profile at time 113.2 h.

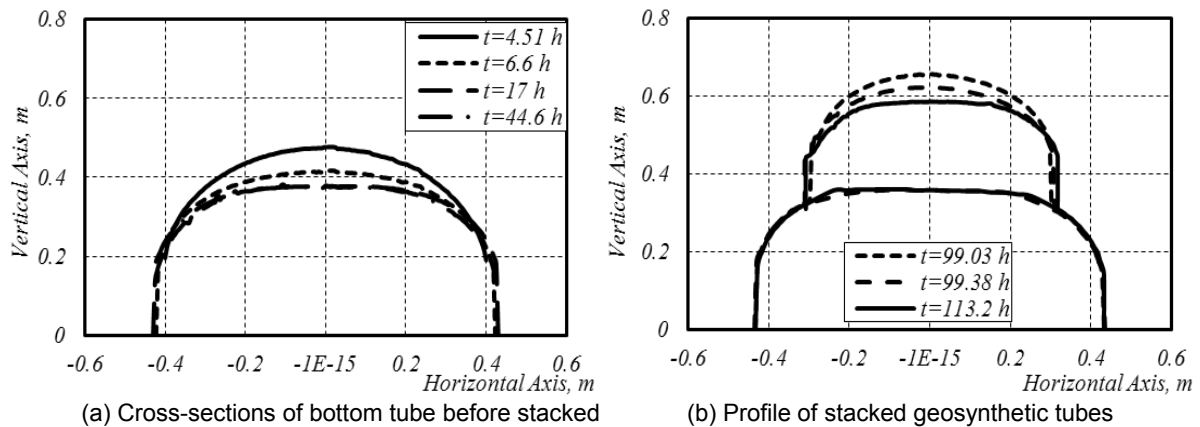


Figure 3 Cross-section changes with time for the Test SPT1

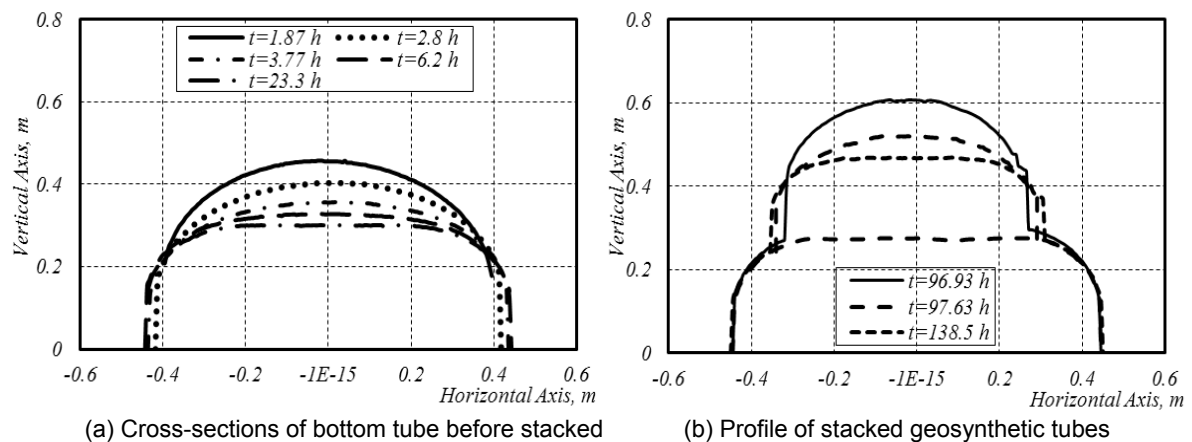


Figure 4 Cross-section changes with time for the Test SPT2

The displacements of the Test SPT1 tube versus time curve during filling and dewatering processes are presented in Figure 5. It can be seen that the self-weight consolidation of the bottom tube almost stopped 11h after filling. After the top tube was placed, the bottom tube settled about 2 cm in about 3h which was measured with the method discussed in

Figure 3. The small settlement of the bottom tube implies that the effect of the stacking of the top tube on the consolidation of the bottom tube was limited. Thus, stacking may not be effective in improving the dewatering effect of the bottom tube.

Test SPT2 was conducted using the same method as that for Test SPT1 except the water content of filling slurry of 89.2%. The measured cross-sections for Test SPT2 are shown in

Figure 4. The bottom tube in Test SPT2 was inflated in 1.87 hours and dewatered for 21.43 h (or total time 23.3 h) as shown in

Figure 4(a). At time of 96.93 h, the top tube was placed on top of the bottom tube and inflated till the total height of 0.606 m as shown in

Figure 4(b).

The displacements of the tube in Test SPT2 during filling and dewatering processes are shown in Figure 6. It can be seen that the self-weight consolidation process of the bottom tube were completed in about 6 hours after filling. After the placement of the top tube, the bottom tube settled about 1.9 cm in about 4 hours.

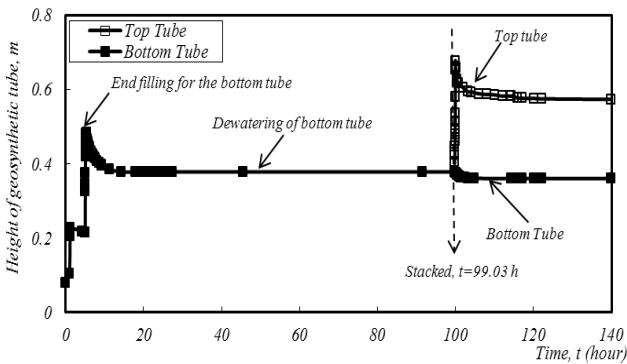


Figure 5 The height changing of Test SPT1

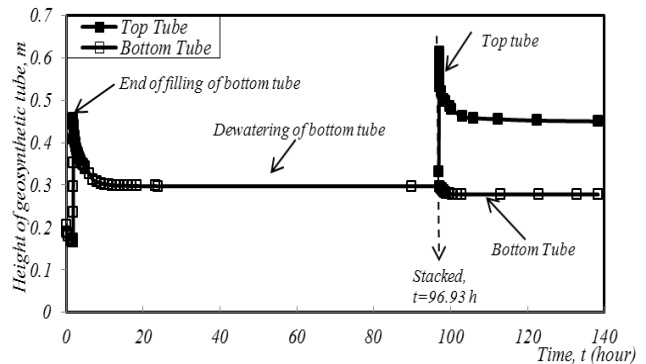


Figure 6 The height changing of the Test SPT2

4. DEWATERING EFFICIENCY

In fact, there is still no unified theory to predict the dewatering efficiency of permeable geosynthetic tube (Somasundaran, 2006). In this study, the dewatering efficiency, D_e , was calculated basing on the changes of displacement using Equation (8-1):

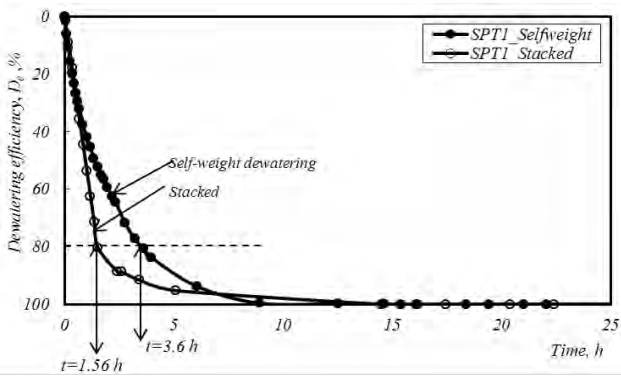
$$D_e = (H_0 - h) / (H_0 - H_{SF}) \quad (1)$$

where H_0 is the initial height of the bottom tube, h is the height at time t , H_{SF} is the final height of the bottom tube.

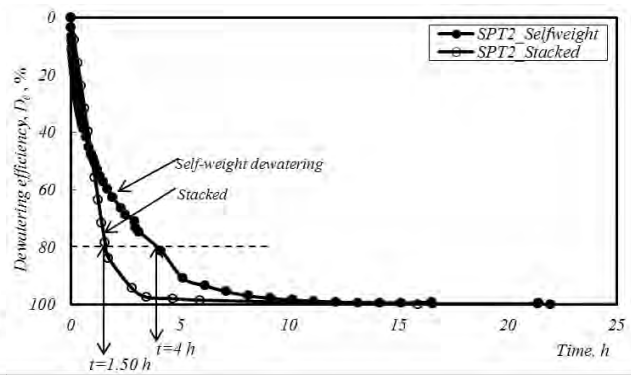
The dewatering efficiency for the Model Test SPT1 during self-weight dewatering stage was calculated with Equation (1) by taking H_0 = the height of bottom tube at the end of filling, and H_{SF} = the height of bottom tube before stacked. The dewatering time, t , was taken from the end of filling.

Figure 7(a) shows the dewatering efficiency versus time curve for Model Test SPT1 during self-weight dewatering stage. It takes about 3.6 hours for the 80% dewatering efficiency. Similar to the calculation of self-weight dewatering stage, the dewatering efficiency was calculated by taking H_0 = the height of bottom tube before stacked, and H_{SF} = the final height of bottom tube after test. The dewatering efficiency versus time curve for Model Test SPT1 during the stacking period is also shown in

Figure 7(a). The time was taken from the time when the top tube was placed. It can be seen that for the stacking method, only 1.56 hours was required to achieve 80% dewatering efficiency. Therefore, the stacking method is more efficient than the self-weight consolidation method as far as dewatering is concerned.



(a) Model Test SPT1



(b) Model Test SPT2

Figure 7 Dewatering efficiencies during self-weight dewatering and stacked periods

Figure 7(b) shows the dewatering efficiency versus time curves for Model Test SPT2 for both the self-weight dewatering and the stacking periods. The calculation method for Model Test SPT2 was the same as that used for Model Test SPT1. The time taken to achieve 80% dewatering efficiency was 4.0 hours for self-weight consolidation and 1.5 hours for the stacking period.

5. PROPERTIES OF KAOLIN AFTER TEST

After dewatering, the shear strength of the soil is improved as well. The engineering properties of the kaolin soil in the tube in the two model tests after dewatering were studied. At the end of the test, the permeable geosynthetic tube was cut off from one side in order to take soil samples for testing. The basic steps are shown in Figure 8 (a) to (d).



(a) Cut off the top tube



(b) Kaolin on top tube



(c) Remove the top tube



(d) Kaolin on bottom tube

Figure 8 Testing photograph of basic properties of Kaolin

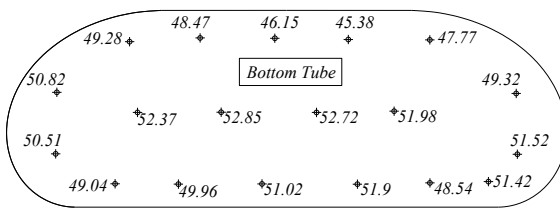


Figure 9 w/c of kaolin in the bottom tube of Test SPT1

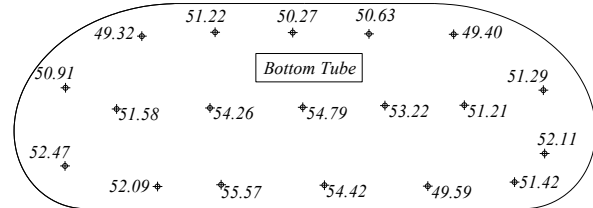


Figure 10 w/c kaolin in the bottom tube of Test SPT2

The water contents of the consolidated kaolin at different locations of the bottom tube from Test SPT1 are shown in Figure 9. It can be seen that water content distributions in the kaolin soil are not uniform. The values are higher in the center with an average of 52%, and lower on the two sides with an average of 50%. The water content of the soil along the top surface of the top tube had the lowest value of about 46%.

The water contents of kaolin in the bottom tube in Test SPT2 are shown in Figure 10. The average water content was 50.5% on the top, 52% on the two sides, and 54% at the center of the cross-section. The uneven water content distribution was due to not only the filter cake effect, but also the difference in the drainage length.

6. CONCLUSIONS

In this paper, the stacking method of permeable geosynthetic tubes is evaluated through laboratory model tests. The method uses the weight of the top tube as surcharge to the bottom tube. Through the model tests, the following conclusions can be drawn.

- (1) The stacking method is effective than the single layer of tube method. However, it is difficult to refill the bottom tube after consolidation.
- (2) The model tests results indicate that the time taken to achieve 80% dewatering efficiency for the stacking method is only 38% of that for the single tube method.
- (3) The water contents of the consolidated soil in the bottom tube were not uniform but with the higher values in the center and the lower ones at the boundary. In addition to the drainage length, the formation of filtration cake is another factor affecting the consolidation process of the soil in the tube.

REFERENCES

Andrews, D. B., Gaffney, D. A., and Martin, S. M. (1999). *Dewatering of high water content materials using geotextile tubes*, ASTM STP 1374, T.B. Edil and P.J. Fox, eds., American Society for Testing and Materials, West Conshohocken, PA.

- Cantré, S., & Saathoff, F. (2010). Design method for geotextile tubes considering strain - Formulation and verification by laboratory tests using photogrammetry. *Geotextiles and Geomembranes*, 29(3), pp. 201-210.
- Chu, J., Guo, W., & Yan, S. W. (2011). Geosynthetic Tubes and Geosynthetic Mats: Analyses and Applications. *Geotechnical Engineering Journal of the SEAGS & AGSSEA*, 42(1).
- Guo, W., Chu, J., & Yan, S. (2011). Effect of subgrade soil stiffness on the design of geosynthetic tube. *Geotextiles and Geomembranes*, 29(3), pp. 277-284.
- Lawson, C. R. (2008). Geotextile containment for hydraulic and environmental engineering. *Geosynthetics International*, 15(6), 384-427.
- Leshchinsky, D., Leshchinsky, O., Ling, H. I., and Gilbert, P. A. (1996). Geosynthetic Tubes for Confining Pressurized Slurry: Some Design Aspects. *Journal of Geotechnical Engineering*, 122(8): 682-690.
- Malik, J., & Sysala, S. (2010). Analysis of geosynthetic tubes filled with several liquids with different densities. *Geotextiles and Geomembranes*, 29, pp. 249-256.
- Moo-Young, H. K., and Tucker, W. R. (2002). Evaluation of vacuum filtration testing for geotextile tubes. *Geotextiles and Geomembranes*, 20(3): 191-212.
- Shin, E.C., Oh, Y.I., 2004. Consolidation process of geotextile tube filled with fine-grained materials. *International Journal of Offshore and Polar Engineering*, 14, 150-158.
- Shin, E. C., and Oh, Y. I. (2003). Analysis of geotextile tube behaviour by large-scale field model tests. *Geosynthetics International*, 10(4): 134-141.
- Somasundaran, P. (2006). *Encyclopedia of surface and colloid science*. New York: Taylor & Francis, 2: 6157.
- Yan, S. W., & Chu, J. (2010). Construction of an offshore dike using slurry filled geotextile mats. *Geotextiles and Geomembranes*, 28(5), pp. 422-432.
- Yee, T. W., Lawson, C. R., Wang, Z. Y., Ding, L. & Liu, Y. (2012). Geotextile tube dewatering of contaminated sediments, Tianjin Eco-City, China. *Geotextiles and Geomembranes*, 31, 39-50.
- Yee, T. W., Lawson, C. R. (2012). Modelling the geotextile tube dewatering process, *Geosynthetic international*, 19(5), pp. 339-353.

Numerical Modelling of Geogrid-reinforced Unpaved Roadways

Wen-Chao Huang, Ph.D., National Central University, Jhongli City, TAIWAN, wenchaoh@ncu.edu.tw
Hung-Yun Liao, Research Assistant, National Central University, Jhongli City, TAIWAN

ABSTRACT

A partial layer of subgrade is usually excavated and backfilled with aggregates when geogrid reinforcement is used as a treatment method for improving soft subgrade as a roadway foundation. Use of geogrid reinforcement produces an adequate platform for the planned roadway construction site, where heavy traffic loading is constantly moving. This study presents different numerical modeling methods to explore the reinforcing mechanisms of the geogrid-reinforced unpaved roadways. Numerical models include finite element method and discrete element method. The finite element analysis results show that most of the settlement comes from subgrade layer, and the use of geogrid reinforcement can indeed limit the zone of yielding in the subgrade layer. Discrete element analysis results show that the local stiffness can be enhanced in the reinforced case when a perfect interlocking is achieved.

1. INTRODUCTION

During a recent survey on geotechnical problems that create difficulty for highway engineers, the issue of soft subgrades was mentioned in every response provided by construction and maintenance units. Soft subgrades usually result in high deformability, low permeability and low shear strength. In consequence, the bearing capacity of these subgrades can be very low. If, at the time of construction of the roadway and throughout the life of the pavement, moisture control such as drainage or drying is not practical or is insufficient, the wet subgrade soil is difficult to compact, unable to sustain heavy construction equipment traffic, and the compaction effort of the overlaying aggregate is ineffective. For the pavements built on such poor foundations, this leads prematurely to excessive permanent deformation, rutting and cracking. Currently, the methods to address soft subgrade conditions include excavation-substitution, soil improvement with chemical additives, and mechanical reinforcement with geosynthetics. The method selection depends on location, volume of traffic expected in service, availability of local material and time-cost consideration.

As far as employment of geosynthetics is concerned, geosynthetic materials include geotextiles, geomembranes, geogrids and geocomposites. They all have in common of being made of plastic polymers (under the form of fibers, threads or extruded sheets). In roadway engineering they can have different functions depending upon their manufactured type and base polymer. For instance, geotextiles are fabrics that can be used as separation layer, drainage layer or filter. Geotextiles have been used successfully in unpaved roads constructed on soft subgrades. In such situations, they prevent subgrade material from intruding into the overlying aggregate layer and help dissipate excess pore pressure that may build up under repeated load. As a result, compaction of the aggregate base is more effective and shear failure of the subgrade is less likely. Structural reinforcement effect is also obtained using geotextiles in unpaved roads where large deformation is allowable. Geogrids are large aperture plastic meshes that are used only for their reinforcement function. These are placed horizontally on the subgrade and backfilled with compacted aggregate. As a tensile-resistant reinforcement, geogrids can provide mechanical support and added stiffness to the aggregate layer. Geogrid reinforcement spreads the load more broadly to the subgrade, thus improved performance in terms of bearing capacity and deflection are obtained.

The reinforcement mechanisms of geogrid in an unpaved roadway include (1) tensile effect of the geogrid, (2) aggregate interlocking and lateral restraint, and (3) enhanced compaction of the aggregate material. In this study, the mechanical performance of using geogrid reinforcement in an unpaved roadway was discussed through numerical modeling including finite element method and discrete element method. The use of finite element method is to obtain the stress and strain variation in the soil mass, while the use of discrete element method is to understand the qualitative improvement of the aggregate material under different reinforcement conditions.

2. REINFORCEMENT MECHANISMS OF GEOGRID IN UNPAVED ROADWAYS

2.1 Tensile Effect of Geogrid

The tensile effect of geogrid as shown in Figure 1 is a major mechanism when there is weak subgrade or the geogrid reinforcement develops high tension strength. Application of vertical load to the aggregate layer surface produces compression of the aggregate and subgrade layers. As a result, the geosynthetic deflects and tensile forces developed.

The under-tensioned geosynthetic provides additional vertical support and lightens pressure on the subgrade. Consequently, it decreases the potential of bearing capacity failure and possible settlements of the subgrade layer.

Previous analyses suggest the tensile effect would be maximized when high modulus geosynthetics are used with very soft subgrade according to Bourdeau (1989). Miura et al. (1990) also performed laboratory tests to investigate the influence of geogrid tensile modulus. According to their experimental results, improved performance was related to the magnitude of strain measured in the geogrid during loading. Field test results also showed that the improvement was obtained in terms of rut depth reduction when using higher modulus geogrids, although not to the same level as would be obtained from the laboratory tests.

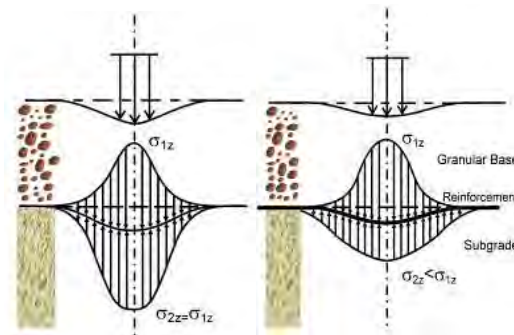


Figure 1 Unreinforced(left) and tensile effect in reinforced case(right)

2.2 Aggregate Interlocking and Lateral Restraint

Interlocking of aggregate and geogrid can be effective to improve the aggregate performance under cyclic loading. With repetitive loadings from the surface, the aggregate particles are rearranged and moved to a denser state. An appropriate size distribution of aggregate material and geogrid openings are needed such that the interlocking can be developed effectively.

Lateral restraint (Figure 2) is a reinforcement mechanism that does not require geosynthetic deflection. Under the vertical compressive pressure, particles in the aggregate layer and the soft subgrade tend to spread away from the loaded area. If the geosynthetic has sufficient interface shear resistance and tensile stiffness, friction or tangential interaction between soil and geosynthetic counteract this movement of the particles. This induces tension in the geosynthetic and enhances lateral confining stresses in the aggregate layer and the subgrade. Because confining stresses are increased, compressive stiffness and resistance of both the aggregate layer and the subgrade are improved by the lateral restraint mechanism.

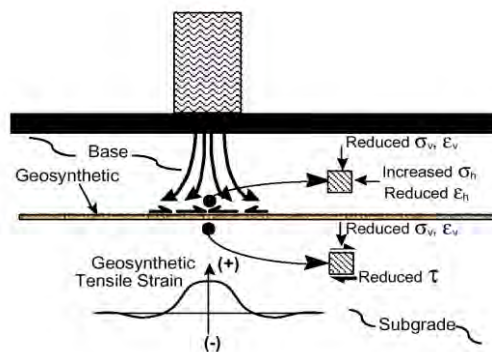


Figure 2 Principle of lateral restraint action (modified from Perkins, 1997)

2.3 Enhanced Compaction of the Aggregate Material

Nimmergern et al. (1991) has indicated that as geogrid reinforcement was used in a roadway, the repetitive loading can produce an additional compaction effect to the aggregate base layer, hence increase the stiffness of the aggregate layer. When there is no geogrid reinforcement, the compaction effect may be deteriorated due to the presence of the weak subgrade layer underneath.

3. NUMERICAL MODELING

To understand the mechanisms of the geogrid reinforcement in an unpaved roadway, different numerical models were employed. Finite element models were formulated to obtain the stress and strain variations in the soil mass, while the discrete element models were established to simulate the aggregate base material under simplified unreinforced and reinforced conditions. The following sections discuss the details about the numerical modeling.

3.1 Finite Element Analysis (FEA)

In this study, finite element models were formulated to simulate a two layer system (i.e., a subgrade layer overlaid by substituted aggregate base layer) including optional geogrid reinforcement at the interface of the two layer system. Figure 3 shows a simplified axisymmetric geometry and surface loading pattern.

The layout of the FEA model is shown in Figure 3, a replication of the model established by Love et al. (1987), which is the cross section of a 2D plane strain model or axis-symmetric models with two layer unpaved system. The reinforcement is installed at the interface of aggregate layer and subgrade layer for the axis-symmetric models. A loading of $\frac{1}{2}$ widths 0.0375m is applied at the top of the aggregate layer. The detailed geometry of the analyzed model is included in Figure 3. Most of the material properties shown in Table 1 were determined based on the reference by Love et al.(1987), however, for the purpose of finite analysis, the Poisson's ratio of subgrade were suggested based on the assumption that the clay is undrained condition. Since there is also no volume change, the Poisson's Ratio was also assumed to be 0.49.

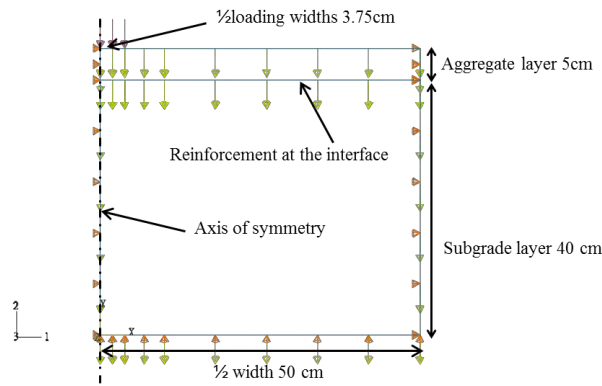


Figure 3 Layout of Finite Element Model

Table 1 Material Property in the Finite Element Model

Material	Young's Modulus (kPa)	Poisson's Ratio	Unit Weight (kN/m ³)	C_u (kPa)	ϕ (°)	Thickness (m)
Aggregate Layer	4000	0.35	19	1	36	0.05
Subgrade Layer	495	0.49	19	5.31	0	0.4
Geogrid Reinforcement	21000	0.49	-	-	-	0.001

3.2 Discrete Element Modeling (DEM)

Application of discrete element method to examine the mechanisms of geogrid reinforcement is also proposed. From the microscopic view of the aggregate particles in the sense of discrete element method, the reinforcing mechanisms such as lateral restraint, and the enhanced stiffness of the aggregate layer is the main purpose to be observed with the installation of geogrid reinforcement.

Because of the enhancement effect from geogrid reinforcements to the aggregate layer which consisted of mostly individual particles, it is of interest to investigate the effects through the application of discrete element method. The reinforcing mechanisms as mentioned previously are therefore to be investigated through the observation of aggregate movements qualitatively under either unreinforced or reinforced cases.

To simplify the unreinforced/reinforced condition in the discrete element model, the following models are established for analyses:

- (a) Aggregate particles rest on a given boundary wall.
- (b) Aggregate particles rest on pairs of smaller particles which is not subject to move in both the horizontal and vertical directions. This case is used to simulate the geogrid reinforced case.

The particles as mentioned above are simulated as cylinders (therefore simulating a 2D plane strain condition) in the models and generated randomly in a predetermined space (formed by boundaries – or walls), and then gravity force is applied to the system in order to simulate the effect of geostatic stress, another wall with limiting width simulating the foundation footing is moving downward at a certain velocity within a period of time until a given distance is achieved. The geometry of the discrete element model before loading is applied is illustrated in Figure 4. The aggregate layer consisted of 300 particles with radius ranging from 0.14 m to 0.28 m. The grids are assumed to be consisted of a series of two smaller particles with radius 0.1 m. The spacing of the grid is 1.2 m (center to center).

After the gravity force is applied to the system, it is found that the contact forces (shown in Figure 4 as black thick lines) are increasing with depth. In addition, the simulated reinforced case showed stress concentration above some “geogrid” locations. Due to this condition, the induced gravity force was also reduced in the locations adjacent to stress concentration areas, and thus the stress transferred to the subgrade layer is also reduced.

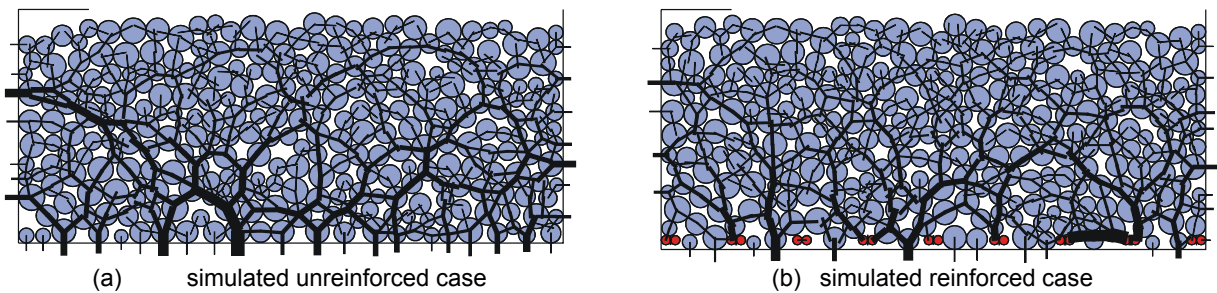


Figure 4 Discrete element model with gravity force applied

4. NUMERICAL MODELING RESULTS

4.1 Results of Finite Element Analysis

Figure 5 shows the surface and interface deformation, with a comparison between reinforced and unreinforced cases. It is found that the load plate settlement is reduced by around 40% (3.7mm to 2.2mm) with geogrid reinforcement. Also from the same figure it is noticed that most of the system deformation occurs in the subgrade layer, the settlement in the aggregate layer can be obtained by subtracting the total deformation at the top of the system by the deformation at the interface of aggregate and subgrade layer.

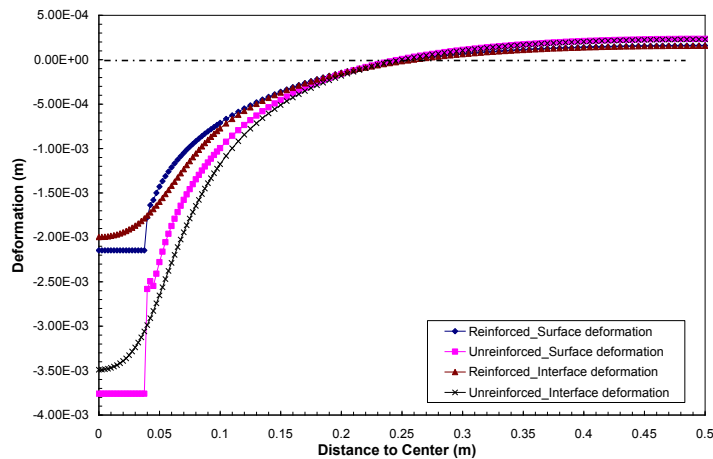


Figure 5 Aggregate layer surface deformation and aggregate-subgrade interface deformation for reinforced and unreinforced cases

From examination of the shear stress distribution above and below the reinforcement, it is found that the shear stress below the reinforcement is also reduced significantly by the presence of reinforcement as shown in Figure 6. The decrease in shear stress on the two sides of the reinforcement can be an advantage in the reinforced case, in that the induced shear stress in the subgrade is one source that made the system to reach failure. In addition, the vertical stress distribution also decreased from 19kPa (unreinforced) to 12kPa (reinforced) as shown in Figure 7, this result may also come from the geogrid reinforcement. Part of the vertical stress that needs to be developed in the subgrade layer in the unreinforced case now has been supported instead by the reinforcement due to the large stiffness of the geogrid reinforcement, therefore only a small amount deformation of the reinforcement is needed to mobilize this compensated vertical stress.

Figure 8 shows the development of the plastic strain in the system, it tells us what area in the system has reached the plastic deformation zone (blue zone represents yielding). From Figure 8, it is found that at the same loading step, the unreinforced case has a yielding zone both in the aggregate layer and the subgrade layer, while in the reinforced case, the yielding zone develops only in the aggregate layer and the boundary of the yielded zone has been limited as compared to the unreinforced case.

To summarize, the installation of the geogrid reinforcement in this case study plays an important role in decreasing the total deformation at the top of the roadway system, which is the main advantage of the installation of the reinforcement, the reason for that mostly comes from the compensation of stress reorganization of the geogrid reinforcement and therefore not only decrease the deformation in the subgrade layer from which most of the deformation comes, but also decrease the tendency of bearing capacity failure in the subgrade clay layer.

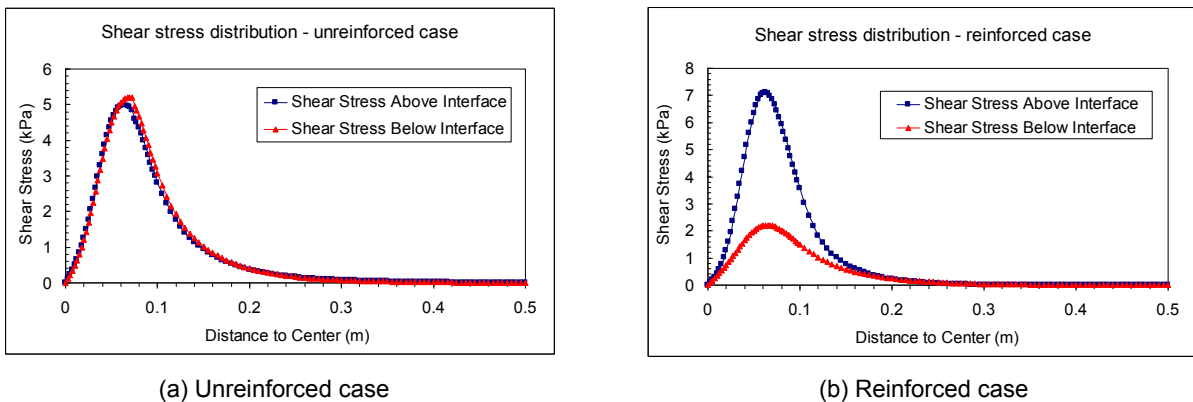


Figure 6 Shear stress distribution above (blue square) and below (red triangle) the aggregate-subgrade interface

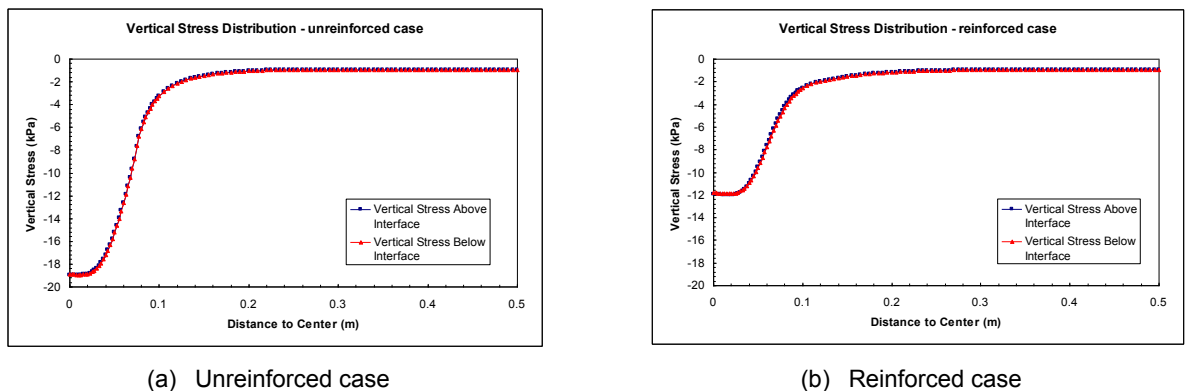


Figure 7 Vertical stress distribution above (blue square line) and below (red triangle line) the aggregate-subgrade interface

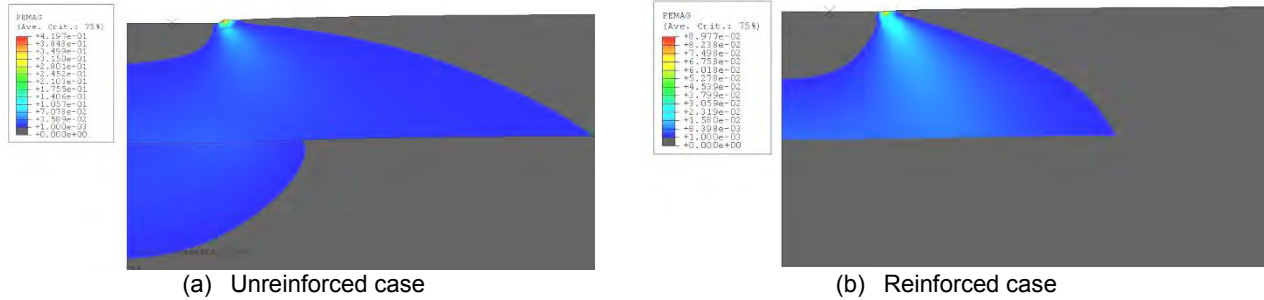


Figure 8 Yielding zone developments at the same loading stress. (grey zones represent “unyielding zone”, these two figures are at the same scale; blue zone represents yielding.)

One thing to note is that although the size of the FEM model is not realistic, however, the FEM model was established similar to a model proposed by former researchers. Once the FEM model was verified, the stress and strain fields can be observed and discussed in terms of its reinforcing mechanisms.

4.2 Results of Discrete Element Modeling

As mentioned in section 3.2, after force equilibrium is achieved in the gravity-applied system, the loading plate is then lowered at a constant speed and the development of contact forces between particles is recorded as shown in Figure 9. In the unreinforced case, the stress is distributed within a wider range and concentrated at the corner of the loading plate. In the reinforced case, the contact forces are more concentrated, especially under the loading plate. Most of the contact forces are balanced by the simulated geogrid reinforcement in the reinforced cases, while in the unreinforced case, the forces are balanced by the particle-wall friction which is not as effective as in the reinforced case.

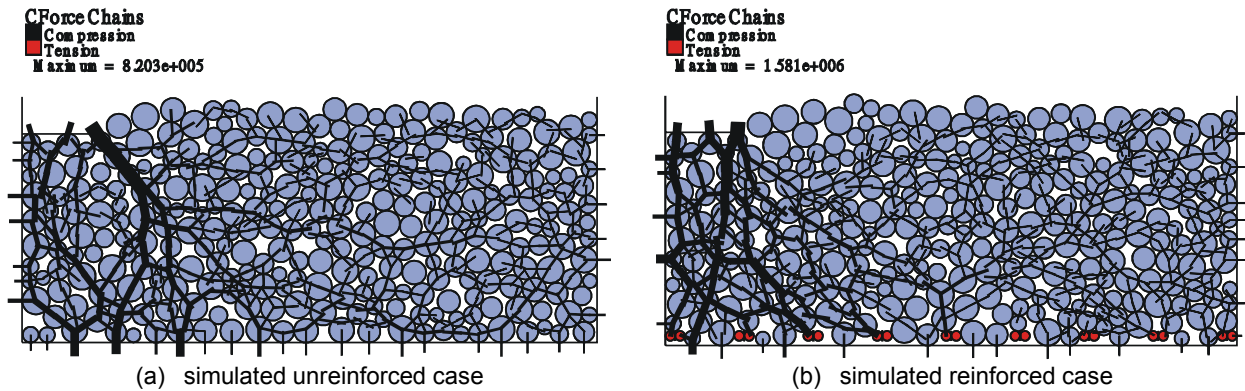


Figure 9 Contact forces in unreinforced (top) and reinforced cases (bottom)

The contact forces are recorded when similar plate displacements are achieved. In the unreinforced case, the maximum contact force is about 820 kN at the edge of the loading plate. In the reinforced case, the maximum contact force is 1581 kN, which is evenly distributed below the loading plate. From the examination of contact forces developed in the above cases, it is therefore understood that the induced stiffness (equivalent of force divided by displacement) in the reinforced case is much larger than that in the unreinforced case. In the reinforced case, due to the limitation of lateral movement of the geogrid particles, the forces are balanced by the reaction provided by the geogrid reinforcement.

From the above results, we have expected that the reinforcing mechanisms from geogrid reinforcements are therefore developed gradually. First of all, with gravity force before the external loading is applied to the system, some of the contact forces are already balanced by the geogrid reinforcement (Figure 4, the arching effect on the right). The location might be somewhat random; however, this condition can reduce the potential stress increment onto the subgrade layer. Secondly, as the loading plate is moving downward onto the aggregate layer, the contact forces are balanced by the geogrid with the particles directly above it. Since the local stiffness of the aggregate material is enhanced due to geogrid reinforcement, the propagation of enhanced stiffness of the aggregate material is moving upward to the area below the loading plate as the loading plate is pushed down further. This procedure creates a limited force-concentrated area compared to the unreinforced case. In this area, the local stiffness is enhanced significantly due to the geogrid reinforcement. The requirement for interlocking of aggregate particle and the geogrid reinforcement is needed to ensure

the effectiveness of geogrid reinforcement. Without effective interlocking of aggregate particles and geogrid aperture, lateral restraint and tensile effect cannot be activated sufficiently.

When taking a look at the displacement vector in the cases shown in Figure 10, it is found that for all the cases, the particles that are right outside the loading plate have a tendency to move counterclockwise, the only different phenomenon that has been observed is the range of the heaving of the particles close to the surface. In the unreinforced case, the overall heaving of the particles extends to a greater depth and extends more horizontally to the right (this can be observed from the vector at the bottom of the unreinforced case), while in the reinforced case, the moving particles extend to only half of the space and the remaining particles almost stay immobilized.

Although the particles used in this analysis are cylindrical, not the real shape of the gravel layer, the main purpose of this study was to observe the reinforcing mechanisms from a microscopic point of view, in addition, the geogrid was assumed to be constrained in the lateral direction to simulate the lateral constraint of the geogrid material, this assumption was made based on the full shear strength development when interlocking was formed in the aperture of the geogrid. It was known that the tensile strength may be mobilized with increasing tensile strain, however, in this study, the tensile strength was developed as the “contact force” between the particles and geogrid increases. (which can be converted to tensile strength of the geogrid)

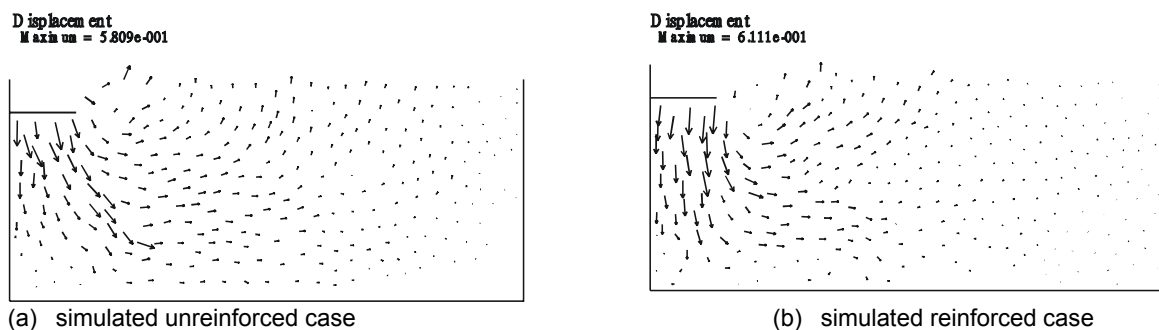


Figure 10 Displacement vectors of aggregate particles

The most important effect of the geogrid reinforcement can be observed in this analysis as well. From the vectors of the unreinforced case, it is found that at the bottom of the model, a noticeable horizontal displacement can be observed. In the reinforced case, it is found that the “lateral restraint effect” of the reinforcement has most significant effect below and right outside of the loading plate. Although the assumption of the “geogrid reinforcement” which is consisted of several “unmovable particles” may not be realistic in the actual practice, it provides us an insight from this extreme case.

When observing from the particle moving directions, it is shown that in the reinforced case, especially the rectangular area under the loading plate, most of the particles are confined horizontally, i.e. only vertical movements are permitted during loading. This condition explains the effect of lateral restraint and its consequences of enhanced confinement. As mentioned previously, the particles that are stuck in the geogrid apertures are confined laterally and vertically. As loading plate is moving downward, the lateral and vertical movement of the particles is less-limited such that particles below the loading plate started to express some degree of vertical and horizontal displacement. This condition can be observed apparently when comparing unreinforced and reinforced cases.

5. SUMMARY AND CONCLUSIONS

Geogrid reinforcement is a commonly used approach to deal with weak subgrade material in an unpaved roadway. The main reinforcing mechanisms of the geogrid reinforced unpaved roadway include (1) tensile effect of the geogrid, (2) aggregate interlocking and lateral restraint, and (3) enhanced compaction of the aggregate material. In this study, the mechanical performance of using geogrid reinforcement in an unpaved roadway was discussed through numerical modeling including finite element method and discrete element method. The conclusions are below:

- (1) Finite element analysis indicates that in an unpaved roadway, the settlement measured at the surface of the aggregate layer comes from the deformation of the aggregate layer and subgrade layer; however, most of the surface settlement comes from the settlement of the subgrade layer.
- (2) Finite element analysis indicates that the shear stress at the interface of the aggregate and the subgrade material is similar for the unreinforced case. However, for the reinforced case, the shear stress became smaller at the subgrade side of the geogrid reinforcement compared to the shear stress at the aggregate side of the geogrid reinforcement.

This indicated that the difference is compensated by the geogrid reinforcement and the induced shear stress in the subgrade layer subsequently decreased.

- (3) Discrete element analysis indicates that from the resultant contact forces recorded below the loading plate when comparing the unreinforced and reinforced cases, an approximate 50% increase of contact force to reach similar plate settlement is required for the reinforced case. Therefore, the local stiffness of the reinforced case was increased significantly when geogrid reinforcement is added. What was meant by local stiffness is that for reinforced case, most of the increased contact forces between particles were located right below the loading plate, only in the area below the loading plate and close to the geogrid reinforcement can we find the enhanced area extended slightly outward.
- (4) Discrete element analysis indicates that when checking from the movements of the particles, it is found that in the reinforced case, the aggregate particles tend to move within a limited range in the area under the loading plate both horizontally and vertically. Due to the assumption that the geogrid (which is consisted of unmovable particles) has very high stiffness, the aggregate particles are stuck (interlocked) in the apertures of the geogrid with very minor lateral deformation. When interlocking of aggregate material and geogrid aperture is formed at the interface, progressive interlocking between aggregate particles is initiated such that an enhanced confinement effect of the aggregate layer is appeared. The above condition explains that a higher resultant contact force may be required to reach similar plate settlement in the reinforced case.

REFERENCES

- Al-Qudi, I.L., Brandon, T.L., Valentine, R.L., Lacina, B.A., and Smith, T.E. (1994). "Laboratory Evaluation of Geosynthetic-Reinforced Pavement Sections." *Transportation Research Record*, Vol. 1439, pp 25-31.
- Al-Qadi, I.L., and Hughes, J.J. (2000). "Field Evaluation of Geocell Use in Flexible Pavement." *Transportation Research Record*, Vol. 1313, pp 26-35.
- Ashmawy, A.K., and Bourdeau, P.L. (1995). "Geosynthetic-Reinforced Soils under Repeated Loading: A Review and Comparative Design Study." *Geosynthetics International*, Vol. 2, No. 4, pp 643-678.
- Barksdale, R.D., Brown, S.F., and Chan, F. (1989). "Potential Benefits of Geosynthetics In Flexible Pavement Systems." National Coop. Highway Research Progress Report
- Bourdeau, P.L. (1989). "Modelling of membrane action in a two-layer reinforced soil." *Computers and Geotechnics*, 7, 19-36.
- Burd, H.J. (1995). "Analysis of Membrane Action in Reinforced Unpaved Roads." *Canadian Geotechnical Journal*, Vol. 32, pp 946-956.
- Giroud, J.P., and Noiray, L. (1981). "Geotextile-reinforced unpaved road design." *Journal of Geotechnical Engineering*, 107 (GT9), 1233-1254.
- Giroud, J.P., and Han, J. (2004). "Design method for geogrid-reinforced unpaved roads. I. Development of design method." *Journal of Geotechnical and Geoenvironmental Engineering*, 130 (8), 775-786.
- Giroud, J.P., and Han, J. (2004). "Design method for geogrid-reinforced unpaved roads. II. Calibration and Applications." *Journal of Geotechnical and Geoenvironmental Engineering*, 130 (8), 787-797.
- Huang, Wen-Chao (2007). "Numerical Modeling and Probabilistic Analysis of Subgrade Improvement Using Geosynthetic Reinforcement." Ph.D. Dissertation, Purdue University, West Lafayette, Indiana, USA
- Love, J.P., Burd, H.J., Milligan, G.W.E., and Houlby, G.T. (1987) "Analytical and Model Studies of Reinforcement of a Layer of Granular Fill on a Soft Clay Subgrade," *Canadian Geotechnical Journal*, Vol. 24, pp 611-622.
- Milligan, G.W.E., Jewell, R.A., and Houlby, G.T. (1989). "A new approach to the design of unpaved roads-part I." *Ground Engineering*, Vol. April 1989, pp 25-29.
- Milligan, G.W.E., Jewell, R.A., Houlby, G.T., and Burd, H.J. (1989). "A new approach to the design of unpaved roads-part II." *Ground Engineering*, Vol. November 1989, pp 37-42.
- Miura, N., Sakai, A., Taesiri, Y., Yamanouchi, T., and Yasuhara, K. (1990). "Polymer Grid Reinforced Pavement on Soft Clay Grounds," *Geotextile and Geomembranes*, Vol. 9, pp 99-123.
- Nimmegern, M., and Bush, D. (1991). "The Effect of Repeated Traffic Loading on Geosynthetic Reinforcement Anchorage Resistance." *Geosynthetics 91*, Atlanta, GA, USA, pp 665-672.
- Perkins, S. W., and Ismeik, M. (1997). "A Synthesis and Evaluation of Geosynthetic-Reinforced Base Layers in Flexible Pavements: Part 2." *Geosynthetics International*, Vol. 4, No. 6, pp 605-621.
- Webster, S.L. (1993). "Geogrid Reinforced Base Courses for Flexible Pavement for Light Aircraft, Test Section Construction, Behavior Under Traffic, Laboratory Tests and Design Criteria." Vicksburg, MS: USAE Waterways Experiment.

Numerical Simulation of Pullout Tests in Residual Clayey Silt

Leonardo D. B. Becker, Federal University of Rio de Janeiro, Brazil, leonardobecker@poli.ufrj.br
Alberto S.F.J. Sayao, Pontifical Catholic University of Rio de Janeiro, Brazil, sayao@civ.puc-rio.br
Anna Laura L. S. Nunes, Federal University of Rio de Janeiro, Brazil, alaura@coc.ufrj.br

ABSTRACT

This paper will present a comparison between results of field pullout tests and numerical simulations. The constitutive models and parameters used will be discussed. An earth dike was constructed in Poços de Caldas, Brazil, to contain 1,500,000 cubic meters of Bauxite residues. A geogrid-reinforced wall was built on the dike's top to reduce its width. PVA geogrids and local residual clayey silt were used. In order to verify the pullout behavior of the geogrid-soil system 16 large-scale pullout tests were conducted in an experimental fill. Pullout tests were simulated by finite element method. Hyperbolic elastoplastic model was used for the soil and linear elastic model was used for the geogrid. Soil parameters were determined by triaxial tests on undisturbed samples retrieved from the fill. An equivalent static distributed load was used to simulate compaction. Simulation results compare well to measured behavior.

1. INTRODUCTION

1.1 Description of the Dike

A dike was constructed in Poços de Caldas-MG, Brazil, by an aluminum company to contain 1,500,000 cubic meters of Bauxite residues. A nearby creek limited the space for the outer slope of the dike. To reduce the slope's width, a 5m high geogrid reinforced wall was built on the top of the dike. This solution led to significant reductions in volume of earth fills and in environmental impacts. Due to the high pH of the tailings material (NaOH contaminated sludge), special PVA geogrids were adopted, with a high chemical resistance. Figure 1 shows the dike and the reinforced soil wall.

Local clayey silt was excavated and used. Table 1 shows some properties of the soil. Heavy compaction equipment was used (roller and rammer compactors). Becker (2006) describes the construction details.

Two sections of the wall were monitored by telltales and topographic survey. A finite element analysis of the wall's construction was conducted (Sayao et al., 2010).



a) Aerial view during operation

b) Reinforced wall during construction

Figure 1. Dike for containment of bauxite residues.

1.1 Experimental Fill and Pullout Tests

An experimental fill was built at the construction site to verify the behavior of soil-geogrid system by means of field pullout tests. The fill was 2.6m high, 3.5m wide and 10.8m long, excluding the end access ramps. The same soil and the same compaction procedures of the wall were used. A vibratory CA-25 roller was used in the center and rammer compactors close to the sidewalls. To avoid variation of vertical stress due to slopes, the fill was laterally supported by vertical walls of lumber boards, held up by steel piles on both sides (Figure 2a). To reduce wall's interference, geogrid samples were passed through metallic sleeves. This procedure was adopted by several authors (Juran & Chen, 1988, Bonczikewicz et

al., 1988, Farrag et al., 1993 and Perkins & Edens, 2003) and is recommended in ASTM D 6707. The space inside sleeves was empty thus keeping the beginning of the sample 0.15m away from the wall. Sleeves were design to be robust in order to resist high compaction stresses and field conditions. Telltales were used to monitor sample displacements and load cells were used to monitor pullout forces. The load was applied in stages with an average pullout speed of 0.7mm/min at the beginning of the samples. In Figure 2b one can see metallic sleeve and geogrid sample with telltales.

Table 1. Average characteristics of compacted soil

Characteristics	Value
Percent passing in sieve #40	84.9
Percent passing in sieve #200	74.2
Plasticity index (%)	18
Optimum water content (%)	30.4
Maximum dry unit weight (kN/m ³)	13.83

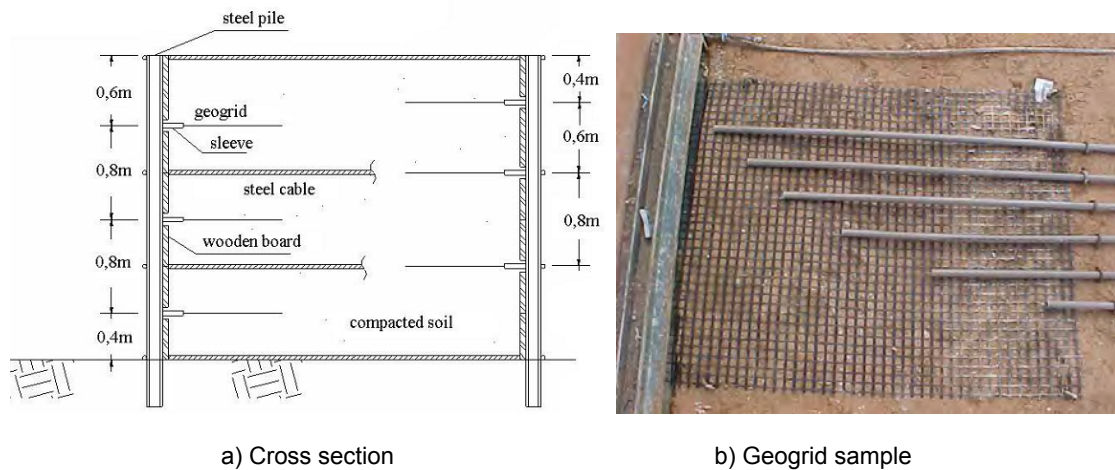


Figure 2. Experimental fill for pullout tests.

Three different types of polymeric geogrids were inserted in the fill (two of them were used in the wall). The samples were approximately 1.00 m long and 0.85m wide. Figure 3 shows results of tensile tests by manufacturer of geogrid Fortrac 55/25-20/30MP herein named 55A (ASTM D6637).

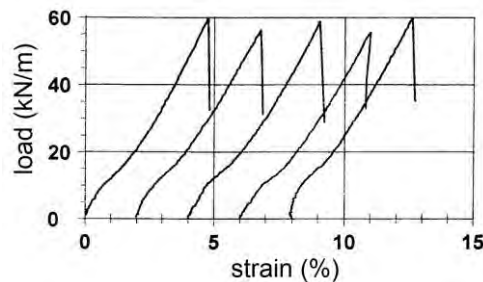


Figure 3. Load elongation curves of geogrid 55A (ASTM D6637).

Figure 4 presents the displacement distribution along the geogrid length, for tests with geogrid 55A. Some samples ruptured before pullout. Vertical stress and optimum water content of compacted soil are also shown. Strains were found to decrease along the specimen's length, due to geogrid flexibility. Consequently, the mobilized shear strength is non-uniform, being zero at the specimen's end. In many tests, slipping on the soil-geogrid interface occurred in the sample's initial portion while there was no displacement on the sample's end. Increase of vertical stress lead to a smaller mobilized length, as reported by Farrag et al (1993) and Lopes and Ladeira (1996).

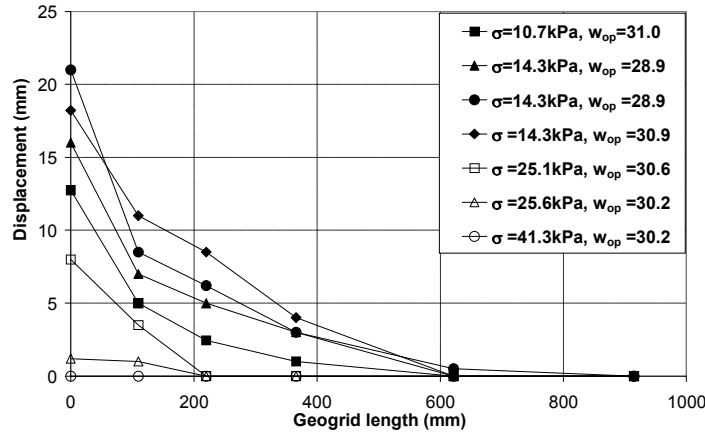


Figure 4. Distribution of displacements at maximum pullout load for geogrid 55A.

2. NUMERICAL ANALYSIS

The first objective of numerical simulation of pullout tests was verifying the performance of constitutive models and parameters because it has simpler boundary conditions, mesh, and construction sequence than the reinforced soil wall.

During pullout tests, the soil-geogrid interface may reach its resistance. In soil-reinforced walls the stresses and tensile forces (T) are usually much smaller and there is not slipping in the soil-geogrid interface. To overcome this difficulty, intermediate test phases were simulated.

2.1 Finite Element Mesh and Construction Sequence

The software Plaxis 2D v8.2 was used. A mesh of isoparametric triangular elements of 15 nodes was used for plane strain analysis. Figure 5 shows the test setup. Figure 6 shows the mesh and boundary conditions of the first simulation attempt. The metallic sleeve was simulated as rectangle of linear elastic material with steel modulus. Inside this rectangle there is a smaller one made of linear elastic material of negligible modulus in order to allow free displacement of geogrid. The geogrid samples begin beside the low modulus material (point "A" in Figure 6b).

The first attempt of simulation sequence was:

- generation of initial stresses without upper layers;
- activation of first soil layer on geogrid and compaction equivalent stress;
- deactivation of compaction equivalent stress and activation of second soil layer; the process goes on until full soil height; and
- application of tensile force.

The sleeve movements were free in early simulations (Figure 6a). The simulation was later simplified by eliminating compaction procedure and by restraining sleeve movements (Figure 6b) because the residual tensile load induced in geogrid by these procedures was negligible.

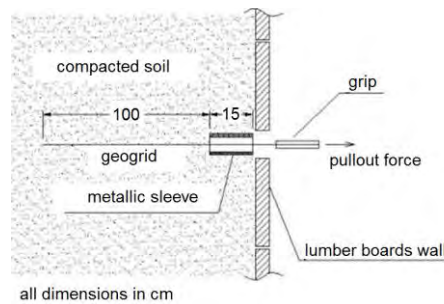
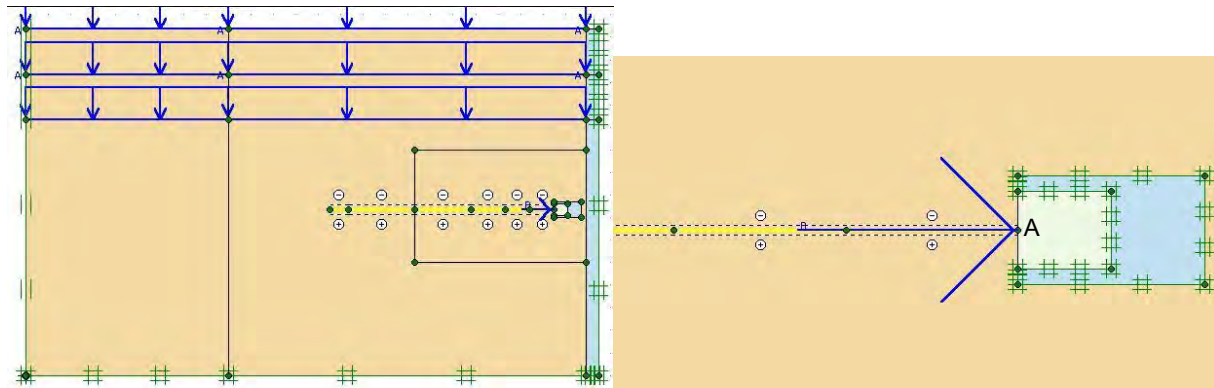


Figure 5. Typical pullout test setup.



a) First simulation: finite element mesh and fixities b) Last simulation: detail of metallic sleeve and load application

Figure 6. Plane strain analysis of pullout tests.

2.2 Material Models and Parameters

Soil behavior was simulated by hyperbolic elastoplastic model that accounts for stress dependency of stiffness moduli (Hardening Soil Model). Six undisturbed blocks of compacted soil were retrieved from different layers in the wall. Table 2 presents soil parameters of Hardening Soil model obtained from consolidated drained triaxial compression tests with saturated specimens from undisturbed block no. 1.

Table 2. Strength and deformability parameters of soil.

Unit weight (kN/m ³)	Friction angle (°)	Dilatancy angle (°)	Cohesion (kPa)	E_{50}^{ref} ¹ (MPa)	E_{oed}^{ref} ² (MPa)	E_{ur}^{ref} ³ (MPa)
17.9	34.2	2.7	10.0	9.5	9.5	28.5

¹ E_{50}^{ref} is the secant stiffness modulus corresponding to the reference confining pressure 100kPa;

² E_{oed}^{ref} is the tangent stiffness modulus for oedometer conditions corresponding to the reference confining pressure;

³ E_{ur}^{ref} is the secant Young's modulus for unloading and reloading corresponding to the reference confining pressure.

The soil in the fill was unsaturated and the shearing probably was partially drained. As a first approach to the problem, it was decided to model drained shearing with effective parameters because the saturation degree of soil was about 90% and unconsolidated undrained triaxial tests did not show significant generation of excess pore pressure.

Water content, optimum water content and degree of compaction of tests no. 9, no. 10 and no. 15 (vertical stress of 14.3kPa) was very similar to values of block no. 1. Therefore, the results of those tests were selected for comparison with numerical analysis results.

In the considered tests, slipping on soil-geogrid interface and failure of soil took place before tension failure of geogrids. However, the stress level of geogrids in well-designed walls is much lower than in pullout tests. In order to account for that difference, numerical simulation represented the intermediate steps of pullout tests. Figure 7 shows an averaged displacement distribution curve of considered tests.

Geogrids were represented as linear elements without flexure or compression stiffness. The effect of confinement in geogrid stiffness is small. Therefore, it was neglected. A linear elastic model was used and the only parameter is elastic stiffness $J = 1210\text{kN/m}$ obtained from load elongation curves (Figure 2):

$$J = \frac{T}{\Delta L/L_0} \quad [1]$$

Where T is the tensile force per unit length, ΔL is the change in geogrid length and L_0 is the initial length.

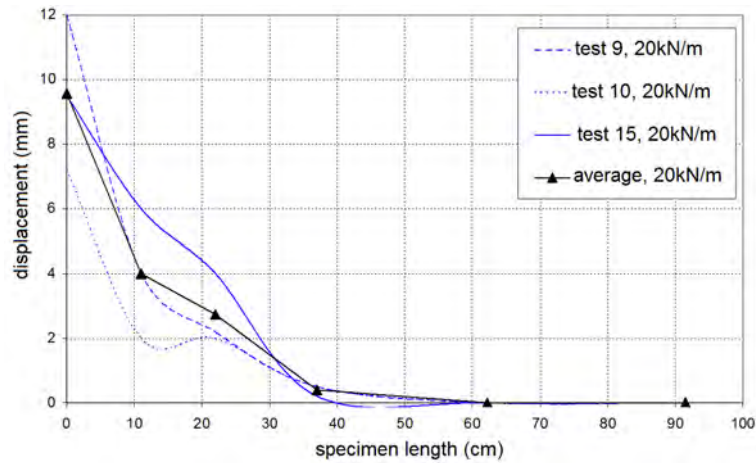


Figure 7. Pullout test results and average curve, $T=20\text{kN/m}$ and $\sigma'_v=14.3\text{kPa}$.

3. SIMULATION RESULTS AND ANALYSIS

Figure 8 shows regions of equal vertical stress before the application of tensile loads. The vertical stress varies along the geogrid length and decreases close to the walls. This reduction is caused by shear stresses acting on wall's surface. A high stiffness metallic sleeve was not effective to minimize this problem because of stress concentration around itself.

Figure 9 shows regions of equal horizontal stress after the application of 20kN/m tensile load. The sleeve minimizes the wall's interference but causes stress concentration.

Load application causes strains and displacements in geogrid and surrounding soil. Figure 10 shows displacement vectors after 20kN/m tensile load application. Directions of displacement vectors close to the initial part of geogrid sample show little interference of wall.

Figure 11 shows a comparison between average pullout test results and finite element method simulation for 20kN/m tensile load. The magnitude of predicted displacements is in good agreement with field test results. Finite element simulation curve shows smaller displacements along geogrid except for the sample's initial region. In field's curve, that region shows a concentration of displacements and strains.

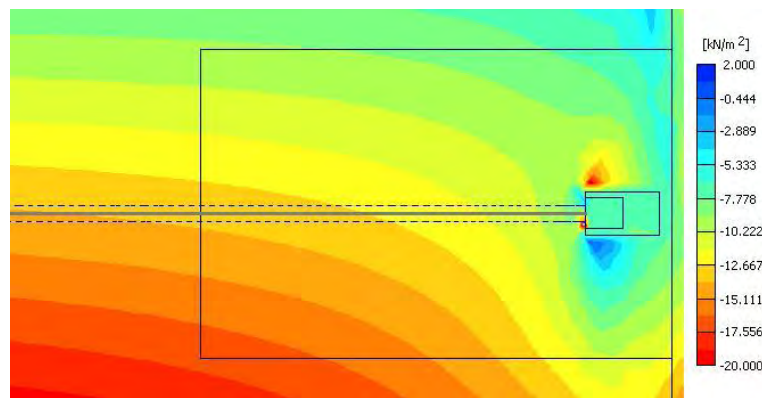


Figure 8. Regions of equal vertical stress before the application of tensile load.

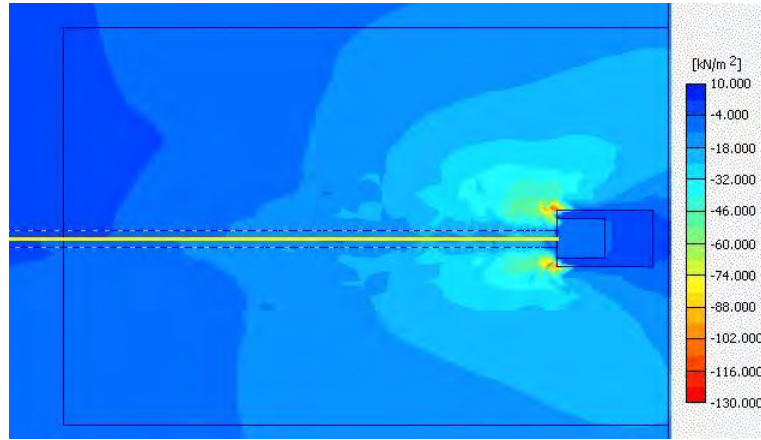


Figure 9. Regions of equal horizontal stress after tensile load application, $T=20\text{kN/m}$ and $\sigma'_v=14.3\text{kPa}$.

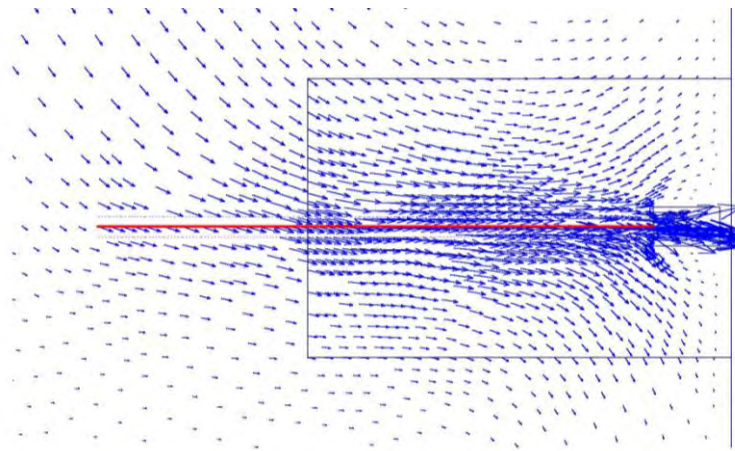


Figure 10. Displacement vectors after tensile load application, $T=20\text{kN/m}$ and $\sigma'_v=14.3\text{kPa}$.

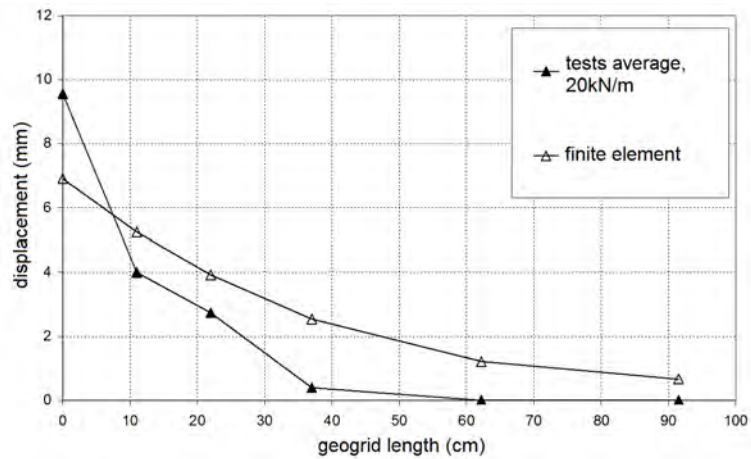


Figure 11. Displacement distribution along geogrid length, $T=20\text{kN/m}$ and $\sigma'_v=14.3\text{kPa}$.

Reducing geogrid stiffness and/or increasing shear resistance and stiffness of soil may cause strain concentration in pullout tests (Farrag et al., 1993, Lopes & Ladeira, 1996, Mallick et al., 1996 and Sugimoto et al., 2001). Several changes in parameters were made. Figure 12 shows predicted curves obtained by combinations of geogrid and soil stiffness increase and cohesion decrease. Although none of these sets of modified parameters resulted in significant

improvement of the displacement distribution curve, reducing geogrid stiffness and increasing cohesion and soil stiffness gave better results.

The constitutive model used for geogrid simulation is probably a significant cause of differences between experimental and predicted curves. In the finite element model, the geogrid is assumed to interact with surrounding soil only by transfer of shear stress by interface elements. The passive resistance developed against transverse ribs is neglected. In other words, the geogrid is represented like a geotextile.

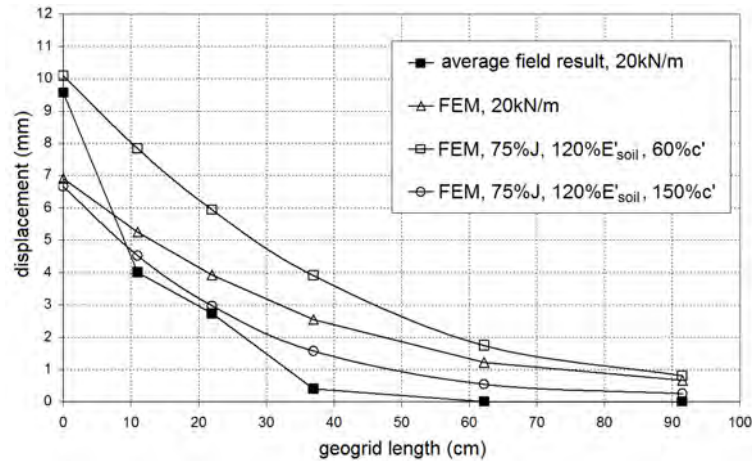


Figure 12. Displacement distribution curves for several sets of parameters, $T=20\text{kN/m}$ and $\sigma'_v=14.3\text{kPa}$.

The analysis of load level effects agrees with that conclusion. As the load increases the displacements also increase and the role of passive resistance becomes more significant for higher displacements. Figure 13 shows that increasing tensile loads lead to greater difference between predicted and experimental curves.

The low stiffness of geogrid's transverse ribs may have contributed to reduce the differences between test results and predictions.

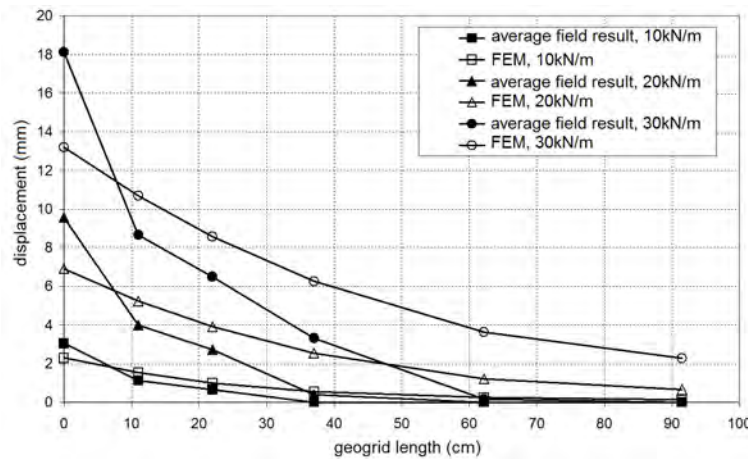


Figure 13. Effect of tensile load level on displacement distribution, $\sigma'_v=14.3\text{kPa}$.

4. CONCLUSIONS

Finite element simulation of field pullout tests was conducted. Constitutive models, parameters and boundary conditions were discussed. A Hyperbolic elastoplastic model was used for simulating soil behavior. For simulating geogrid behavior, a linear-elastic model that does not account for passive resistance on transverse ribs was used.

The constitutive model used for geogrid simulation is probably a significant cause of differences between experimental and predicted curves. The transfer of shear stress by interface elements is the only interaction between geogrid and surrounding soil. The passive resistance developed against transverse ribs is neglected. However, in spite of the fact that the numerical simulation was not able to reproduce stress concentration in the initial part of geogrid samples, overall predicted displacements compared well with test results. Therefore such model seems to be adequate for working stress conditions found in well designed walls and in early stages of pullout tests (particularly if transverse ribs have low stiffness), rather than for ultimate pullout conditions.

ACKNOWLEDGEMENTS

The authors express their gratitude to the sponsors of this research: HUESKER, LPS, ALCOA and National Counsel of Technological and Scientific Development - CNPq.
There was confusion.

REFERENCES

- ASTM D 6637. Standard Test Method for Determining Tensile Properties of Geogrids by the Single or Multi-Rib Tensile Method, American Society for Testing and Materials, West Conshohocken, Pennsylvania, USA.
- ASTM D 6706. Standard test method for measuring Geosynthetic pullout resistance in soil. American Society for Testing and Materials, West Conshohocken, Pennsylvania, USA.
- Becker, L.B. (2006). Behavior of geogrids in a reinforced wall and in pullout tests (in Portuguese). Doctoral thesis. PUC-Rio, Catholic University of Rio de Janeiro, Brazil, 322p.
- Bonczikiewicz, C. Christopher, B. R. Atmatzidis, D. K. (1988) Evaluation of soil-reinforcement interaction by large-scale pull-out tests. Transportation Research Record 1188. 1-18.
- Sayão, A. S. F. J. Becker, L. D. B. Nunes, A. L. L.S. and Costa Filho L. M. (2010). Behavior of a Geogrid Reinforced Soil Wall Built with Clayey Silt, 9th International Conference on Geosynthetics, Guarujá, SP, Brazil,
- Farrag, K., Acar, Y.B. e Juran, I. (1993) Pullout Resistance of Geogrids Reinforcements. Geotextiles and Geomembranes, v. 12: 133-159.
- Juran, I. Chen, C. L. (1988) Soil-geotextile pullout interaction properties: testing and interpretation. Transportation Research Record 1188: 37-47.
- Lopes M. L. Ladeira, M. (1996) Influence of the confinement, soil density and displacement rate on soil-geogrid interaction. Geotextiles and geomembranes. v. 14: 543-554.
- Mallick, S. B. Elton, D. J. Adanur, S. (1998). A new approach in modeling of soil-geotextile interface behavior in pullout tests. 6th International Conference on Geosynthetics: 729-732.
- Perkins, S. W. Edens, M. Q. (2003) Finite element modeling of a geosynthetic pullout test. Journal of Geotechnical and Geological Engineering. v. 21: 357-375.
- Sugimoto, M. Alagiyawanna, A. M. N. Kadoguchi, K. (2001) Influence of rigid and flexible face on geogrid pullout tests. Geotextiles and Geomembranes. v. 19: 257-277.

Observation and Numerical Modeling of MSE Test Wall Constructed Near Motorway 5C Section Drivusa-Gorica in Bosnia and Herzegovina

Skejic A., University of Sarajevo, Faculty of Civil Engineering, Sarajevo, Bosnia and Herzegovina
Balic A., University of Sarajevo, Faculty of Civil Engineering, Sarajevo, Bosnia and Herzegovina
Jasarevic H., University of Sarajevo, Faculty of Civil Engineering, Sarajevo, Bosnia and Herzegovina
Namas T., International University of Sarajevo, Faculty of Natural and Engineering Sciences, Sarajevo, Bosnia and Herzegovina
Selman S., International University of Sarajevo, Faculty of Natural and Engineering Sciences, Sarajevo, Bosnia and Herzegovina
Karamehmedovic E., International University of Sarajevo, Faculty of Natural and Engineering Sciences, Sarajevo, Bosnia and Herzegovina
Karic E., Public Company Motorways of Federation of Bosnia and Herzegovina Ltd., Mostar, Bosnia and Herzegovina
Bucu J., Public Company Motorways of Federation of Bosnia and Herzegovina Ltd., Mostar, Bosnia and Herzegovina

ABSTRACT

Observation and numerical modeling of MSE test wall is presented here. The 6m wide and 3.2m high wall with 10cm thick precast concrete face elements and reinforcement length of 2.15m was built on construction site of Motorway 5C in Bosnia and Herzegovina. Welded wire mesh Q335 was used as reinforcement. Compared to other MSE test walls, the presented work is unique due to the choice of backfill material consisting of course crushed stone aggregate ranging from ~0-100mm in size whereas most of other published studies used sandy backfill. Two weeks after the construction, the top of the wall was loaded with additional overburden weight 1.5m in height (~30 kPa). The forces in reinforcement were measured with a series of embedded sensors and deformation with an inclinometer installed in the middle of the wall length, including geodetic survey of wall face. Experimentally observed results are compared to the analysis results obtained from numerical model created using Plaxis software.

1. INTRODUCTION

The field monitoring of mechanically stabilized earth (MSE) wall behavior for work and ultimate stress states combined with numerical analysis can increase the cost-effectiveness and facilitate the ability to successfully predict the behavior of such structures. For this purpose, monitoring and numerical modeling of MSE test wall is presented. The 6m wide and 3.2m high wall with precast concrete elements face was built on construction site of Motorway 5C, section Drivusa-Gorica in Bosnia and Herzegovina. Welded wire mesh was used as reinforcement. Compared to other published test MSE walls, the work presented here is unique in the fact that the backfill material consists of course crushed limestone aggregate with D50=32mm, whereas the most of other published studies use sandy backfill.

The most comprehensive published research of behavior of flexible retaining structures was done by Allen and Bathurst (2003). They gave an overview of the results for 20 field structures made of reinforced soil as an official report published by Washington State Department of Transportation. Their results of measurements and conclusions along with the ones obtained on individual test walls made by other authors (see Allen et al. (2004) and Bathurst et al. (2002)), to a large extent, influenced the development of not only design codes, but also the development of innovative computation methods that enabled more rational reinforced earth structures (see Fannin and Holtz (2011), Koerner (2005), Palmeira, E. M. (2009), Rowe and Skinner (2001)). A practical example is semi-empirical "K Stiffness" method (Allen et al. (2003b, 2004)), which provides reinforcement forces prediction that are substantially smaller than the ones predicted by limit equilibrium based methods. In addition, Holtz and Lee (2002) made report on research conducted on the internal stability of reinforced soil walls. Using the results of monitoring of 6 walls with different reinforcement elements and types of backfill material, they made recommendations for improving the modeling techniques for the level of working stress. Carruba et al. (1999) analyzed the behavior of wall reinforced with flexible reinforcing elements (PE and PP geogrids), with monitoring done on application of surcharge load stage-wise. The authors used clayey gravel as backfill material. Back analysis was done using software package Abaqus, with the Drucker-Prager constitutive model and the associative flow rule. Bergado et al. (2003), analyzed the behavior of reinforced embankment built on soft soil. The embankment was reinforced with galvanized and PVC coated hexagonally shaped geogrids. Doing back analysis, authors analyzed the dominant mechanism of interaction for working stress state, with conclusion that dominant mechanism being direct shear. One of the interesting examples with different backfill material published is the detailed monitoring of reinforced

soil structures is 12.0 m high wall with backfill material of rammed clay, reinforced with HDPE geogrid (Yang, G. et al. 2009). Within this case study, the behavior of the wall for working stress condition was analyzed.

Practically, all studies mentioned above were made on the walls with fine grained (sandy) backfill material. The interaction of such material and reinforcement compared to the backfill composed of coarser granular material is significantly different, as confirmed by many of published articles dealing with research of interactions in various conditions (pullout, direct shear) (see Hsieh et al. (2011), Minazek et.al (2010)). Application of modern numerical methods in predicting stress-strain behavior and at the same time dealing with complex soil reinforcement interaction, cannot be considered satisfactory without confirming the results to measurements made on real structures. A wide variety of reinforcement elements and backfill material types further complicates this problem. As a result, the only way to reach reliable conclusions is to create sizeable databases of field wall case studies.

2. MATERIALS AND WALL GEOMETRY

The MSE test wall was constructed next to the slope of service road between two bridge piers on construction site of Motorway 5C, section Drivusa-Gorica in Bosnia and Herzegovina. It was placed on well-compacted coarse granular material ($\phi=45^\circ$ and $c=0$) with leveling pad consisting of C20/25 concrete beam 40x40cm, reinforced with 6 ($\phi=12\text{mm}$) longitudinal steel bars placed in corners and transverse reinforcement made of $\phi=8\text{mm}$ stirrups spaced 20cm c-c.

The wall face consisted of 10cm thick precast concrete panel elements 100x80cm (including half elements 50x80cm) as shown in Figure 1. Elements were made of high-strength concrete ($W/C=0.35$) with early strength of C30/37 achieved after one day. Self-compacting smart dynamic concrete (SDC) with admixtures based on polycarboxylate was used. Elements were reinforced with $\phi=8\text{mm}$ steel bars spaced 15cm c-c both placed in the midsection of thickness. In addition, two anchorage reinforcements in form of $\phi=12\text{mm}$ stirrups 25x80cm (extending 20cm out) were placed in each element to allow proper connection of facing with the soil reinforcement (see Figure 2).

Standard steel welded wire mesh (WWM) Q335 ($f_y=500/560\text{MPa}$) is used for soil reinforcement with 8mm bars spaced at 15cm c-c in both directions. They are fabricated as 6m long and 2.15m wide (see Figure 2). Course crushed limestone aggregate ($\phi=48^\circ$ and $c=0$), with grains ranging from ~0-100mm ($D_{50}=31.5\text{mm}$) was used as backfill material (Figure 3). The gradation test result is shown in Figure 4. The constructed wall was 6m long with reinforcement embedded 2.15m (to allow use of whole WWM) and 3.2m high (4 rows of prefabricated elements).



Figure 1. Erected MSE test wall



Figure 2. Q335 WWM with installed strain gauges, and strain gauge protection detail



Figure 3. Compaction of backfill material

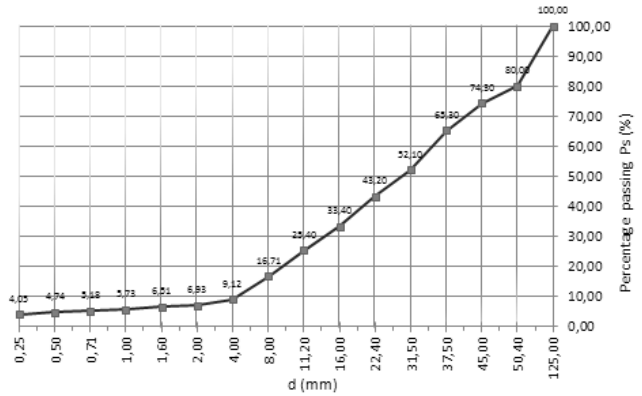


Figure 4. Backfill material gradation curve ($D_{50} = 31,5$ mm)

3. MEASUREMENTS AND CONSTRUCTION SEQUENCE

In order to measure soil stiffness after application and compaction of backfill material layer, circular plate, with 30cm diameter, was used (see Figure 5). The test was carried out in general accordance with HRN U.B1.046. The load was applied in five increments. Settlement readings were taken at 0.50 minute intervals for the first 2 minutes, and 1 minute intervals thereafter, until detectable movement of the plate has stopped, i.e. until the average settlement rate is less than 0.05mm per 3 minute interval. The Range of Pressures starts from 0 kPa to 250 kPa. Two tests were conducted on different heights of the wall. First one, for the height of 0,8 m (test 1), and second for 1,4 meters (test 2). The results of average settlements for 5 load increments are shown in Table 1 below.

Table 1 : Static load plate test results

Load and settl. Test No.	Load increments [kN/m ²]					
	0	50	100	150	200	250
	Settlements [mm]					
Test 1 [level 0,8 m]	0	0,09	0,44	0,825	1,36	1,8
Test 2 [level 1,4 m]	0	0,12	0,35	0,6	0,9	1,2

Note that the soil backfill reference deformation modulus for numerical model was obtained using back analysis results of this test.

An Interfels Standard Inclinator Casing is used for wall lateral displacements measurements (see Figure 5 and Figure 6). It was installed in the middle of wall length (to avoid boundary effects). Casing, which is 3,0m long, with outside diameter of 70mm, and inside one 65 mm was installed before wall construction. Casing is placed 1,5m below bottom of the wall in stiff foundation soil, in order to ensure prevention of movement of its base (fixed reference). Bottom cap is used to prevent fine particles infiltration, which may strongly affect the readings. Standard coupling unit 400mm long, with outside diameter of 77mm, and inside one 70 mm was used to connect extension casings during construction. Area around casing was protected by fine sand to avoid damaging (i.e. punching by courser grains). In addition to inclinometer, geodetic survey of vertical midsection of wall was performed using 8 fixed points spaced 40cm apart, in order to monitor horizontal displacements (see Figure 7).

The 4 rows of precast concrete elements were placed (6 elements in each row). The total of 8 WWM were used during wall construction (2 per element) placed 40cm apart. Each 40cm layer of backfill material between WWM was placed in 2 intervals (20cm each). After each interval, material was compacted using combination of 2 ton roller compactor (Figure 3) and vibratory plate compactor for difficult spaces (i.e. around inclinometer) to ensure proper stiffness of backfill.



Figure 5. Static load plate test



Figure 6. Inclinometer deformation measurements

A total of 16 strain gauges, were mounted to WWM bars on different locations (see Table 2) to measure forces. A total of 16 strain gauges (SGs), were mounted to WWM bars on different locations (see Table 2) to measure forces. The SGs were standard 350 Ohm gauges manufactured by HBM, put in a Whetstone bridge and amplifier system. After the wall was erected, two of the SGs malfunctioned and their readings were dismissed. The malfunction was probably due to mechanical damage caused during construction process. Calibration of the applied forces was conducted in the laboratory using tension loading frame. The error in measured forces is estimated to be up to 10% and can be, among other effects, due to slight differences in mounting of SGs on the mesh.

Two weeks after the wall was erected, 1.5m high overburden load (~30kPa) was added as shown on Figure 8. This load corresponds to the required design traffic load for regional roads in Bosnia and Herzegovina. Week after the loading was completed, inclinometer readings, geodetic survey of wall face and force measurements in reinforcement bars were performed again for comparison with the initial ones.



Figure 7. Geodetic survey of wall face



Figure 8. Wall with 1.5m overburden load (~30kPa)

4. OBSERVATIONS RESULTS

The results of force measurement without and with overburden load for 14 locations are listed in Table 2. They are compared with forces obtained by numerical analysis in the following section of the paper.

The geodetic survey of wall face as well as inclinometer readings show no horizontal displacements of the wall (only negligible values that are on the margin of error). The wall will be stepwise loaded with additional overburden load till its failure in future, and these results will be published elsewhere.

Table 2. Force measurement.

Sensor (height; depth [m])	Without overburden load kN/m	With overburden load kN/m
A1 (0,2; 0,4)	4,8	8,8
B1 (0,2; 1,15)	4,2	7,6
C1 (0,2; 1,90)	4,2	7,2
A2 (0,6; 0,4)	2,7	3,5
B2 (0,6; 1,15)	3,6	5,9
C2 (0,6; 1,90)	3,0	5,0
A3 (1,0; 0,4)	5,8	10,0
B3 (1,0; 1,15)	3,9	6,4
C3 (1,0; 1,90)	5,2	9,7
B5 (1,8; 1,15)	2,6	6,9
A6 (2,2; 0,4)	1,9	4,2
C6 (2,2; 1,90)	5,3	11,1
A8 (3,0; 0,4)	1,3	2,6
B8 (3,0; 1,15)	2,0	4,2

5. NUMERICAL MODELING

Numerical analysis was performed using Plaxis Geotechnical Software Package. A plane strain numerical model of reinforced earth wall built on stiff foundation soil is made of reinforcing element, soil elements and boundary conditions (loads and displacements). Triangular finite elements with 15 nodes, 12 Gauss integration points and average dimension of 10,0 cm were used. Soil geogrid contact was modeled by interface elements. Hu and L. Pu J. (2004) stated that use of interface elements in modeling is very important for obtaining realistic solutions to the many soil-structure interaction problems. Interaction coefficient of 1,3 was adopted according to pullout laboratory test conducted on similar reinforcement and backfill material (see Minazek (2010)). The soil is modeled by Mohr-Coulomb constitutive model with non associative flow. Table 3 defines the parameters of the granular backfill material and material supported by the wall as well as foundation soil. The foundation soil was considered as stiff with deformation modulus 5 times greater than the backfill one. Surcharge was modeled with 1 step of loading according to real constructive sequence.

Table 3. Soil parameters

Parameter	Granular backfill	MC (loose) – surcharge soil	Foundation soil
γ [kN/m ³]	22,0	21,0	24,0
φ'_p [°]	48	29	45,0
c' [kPa]	0,0	0,0	0,0
ψ [°]	15	0	0,0
E_{ref} [MPa]	60,0	15,0	300,0
E_{incr} [MPa/m']	2,0	-	-
ν [-]	0,3	0,3	0,2
R_i^*	1,3	-	-

*Note that $\varphi_i = R_i \cdot \varphi_{soil}$

The stiffness characteristics of the backfill material are determined by back analysis on numerical model of static plate load test. The axisymmetric numerical model of this test is shown in Figure 11b, and results in Figure 12. Dilatancy angle for modeling non associative flow was determined according to Bolton's empirical equation for plane strain conditions, which relates the mobilized friction angle (φ'_p) to the critical state friction angle (φ'_{cv}) and dilation angle (ψ): $0,8 \cdot \psi = \varphi'_p - \varphi'_{cv}$. Numerical model with finite element mesh is shown in Figure 11a. The reinforcement is modeled as an elastic geogrid slender element, with axial stiffness $EA = 1,11 \cdot 10^5$ kN/m', determined for maximum elastic strain of steel (in air tensile test).

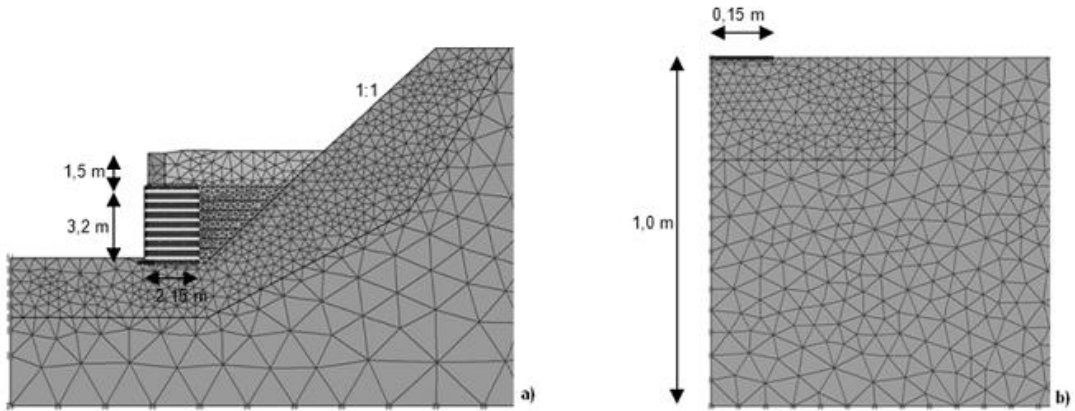


Figure 11. a) Numerical model and wall geometry;

b) Numerical model of plate load test

Facing elements are modeled as plate elements, with bending stiffness defined with thickness of the facing elements. For thickness of 10,0 cm, the stiffness is determined as: $EA = 3 \cdot 10^6 \text{ kN/m}$; $EI = 2500 \text{ kNm}^2/\text{m}$

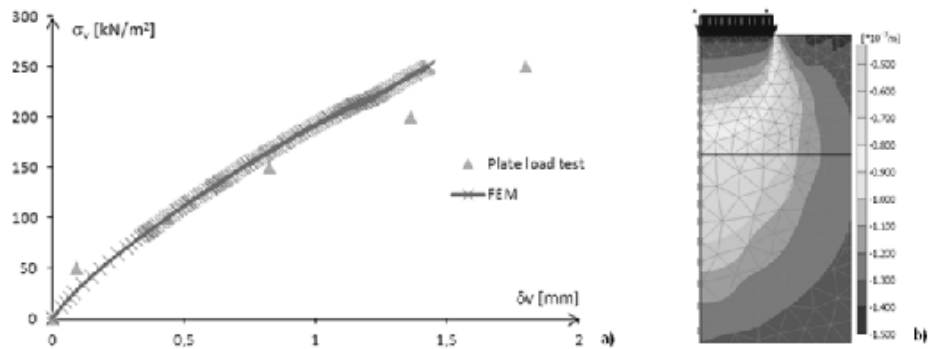


Figure 12. Results of plate load test numerical model : a) load – displacement curve; b) vertical displacements

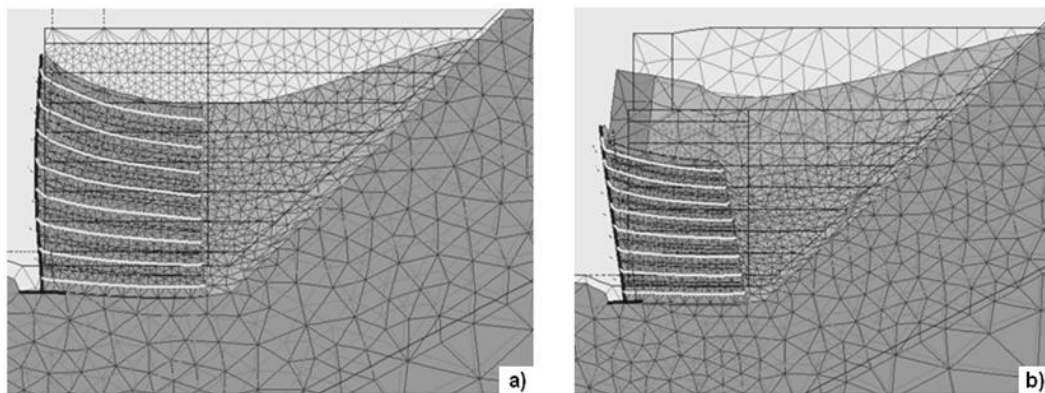


Figure 13. Deformed mesh (not in scale), a) Without overburden load; b) With overburden load

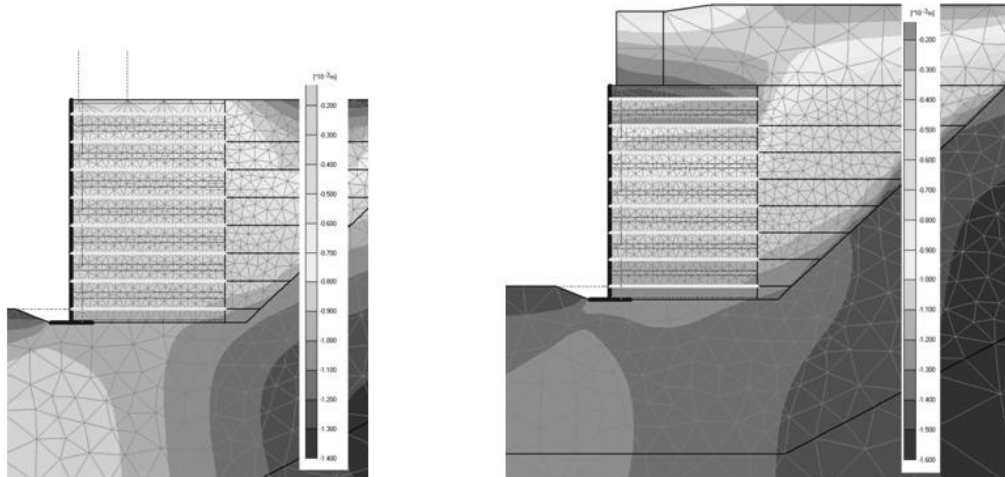


Figure 14. Lateral displacements, a) Without overburden load; b) With overburden load,

The trend of wall displacements is shown in Figure 13, while the magnitudes of lateral displacements are shown in Figure 14. Maximum horizontal displacement after placing overburden load is 1,0 mm, while the deformations of the wall self weight, range of about 0,5mm.

Table 4. Maximum reinforcement forces from numerical model.

Level (in meters from bottom of the wall)	Without overburden load kN/m	With overburden load kN/m
3,0	2,1	8,4
2,6	3,0	8,0
2,2	3,2	7,0
1,8	5,5	9,5
1,4	5,8	10,3
1,0	4,6	5,8
0,6	3,0	4,5
0,2	3,8	5,4

Finally a comparison between calculated and measured force distribution along geogrid was analysed. Figure 15 shows force distribution along geogrid calculated numerically, with indication of measured forces on the location of strain gauges.

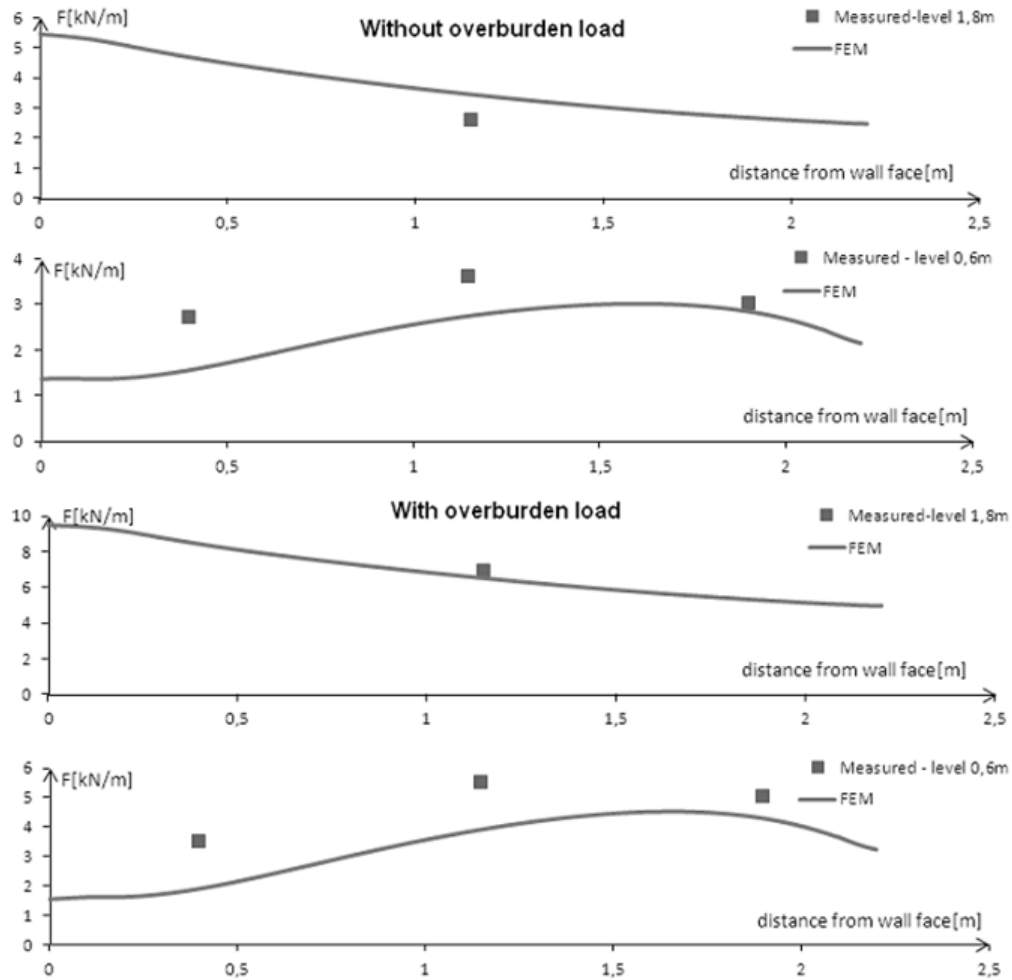


Figure 15 : Force distribution along reinforcement and comparison with measured values

6. CONCLUSIONS

Reinforced Earth Wall (REW) with WWM and course crushed limestone aggregate backfill was built in order to study the behavior of such structure under loading. The wall was surcharged with 1,5m of overburden load. Wall behavior was modeled by means of finite element analysis and comparison with actually measured values is showing fairly good agreement.

A very unique combination of WWM on relatively small vertical spacing, with course crushed limestone aggregate backfill makes the wall to behave as a stiff block with no internal displacements except the reinforcement elongation (which is less than 2,0mm). This fact, together with previous research results mentioned in introduction, can be used for analysis of two aspects of wall behavior. First one is the investigation of inclusions vertical spacing influence on REW behavior, and second one, for investigation of interaction mechanism between course crushed limestone aggregate and welded wire meshes.

A very simple Mohr-Coulomb soil constitutive model was able to predict the behavior of reinforced earth structure. The wall will be stepwise loaded with additional overburden load till its failure in future, and results obtained from that study will be published elsewhere

ACKNOWLEDGEMENTS

The authors would like to express deep gratitude to following companies for providing location, financial support, construction equipment and manpower for this project: PC Motorways of Federation of Bosnia and Herzegovina, Euro-Asfalt, STRABAG, SGS BH, BASF, Geokonzalting.

REFERENCES

- Allen, T. M. and Bathurst, R. J. (2003). *Prediction of Reinforcement loads in Reinforced Soil Walls*, Final Research Report, Washington State Department of Transportation and in cooperation with US Department of Transportation Federal Highway Administration.
- Allen, T.M., Bathurst, R.J, Holtz, R. D., Walters, D.L. and Lee, W.F. (2003). A new working stress method for predicting of reinforcement loads in geosynthetic walls. *Canadian Geotechnical Journal*, 40(5) : 976 – 994
- Bathurst, R.J., Allen, T., Walters, T. (2002). Reinforcement Loads in Geosynthetic Walls and the Case for a New Working Stress Design Method , *Geosynthetics International* , 9(5-6) : 525-566
- Bergado, D.T., Youwai, S., Teerawattanasuk, C. & Visudmedanukul, P. (2003). The interaction mechanism and behavior of hexagonal wire mesh reinforced embankment with silty sand backfill on soft clay, *Computers and Geotechnics* 30 517–534
- Brinkgreve, R.B.J. (2002). PLAXIS - Finite Element Code for Soil and Rock Analyses: Users Manual – Version 8, A.A. Balkema, Rotterdam, Netherlands.
- Carruba, P., Luchetta, F., Montanelli, F. & Moraci, N. (1999). Instrumented Reinforced Wall : Measurements and FEM Results, *Geosynthetics '99*, 271 – 291.
- Holtz, R. D. and Lee, F. (2002). *Internal Stability Analysis of Geosynthetic reinforced Retaining Walls*, Research Report, WA-RD 532.1, Department of Transportation and in cooperation with U.S. Department of Transportation Federal Highway Administration.
- Hsieh, C.W., Chen, G.H. & Wu, J-H. (2011). The shear behavior obtained from direct shear test and pullout test for different poor graded soil-geosynthetic system, *Journal of GeoEngineering*, Vol. 6, No. 1, pp. 15-26,
- Fannin, J and Holtz, R. (2011). *Geosynthetic Reinforced Soil Short Course*, Geo-Frontiers Conference, Dallas, Texas USA.
- Griffiths, D.V. & Lane, P.A. (1999). Slope stability analysis by finite elements, *Geotechnique* 49 (3): 387-403.
- Hu, L. & Pu, J. (2004). Testing and Modeling of Soil-Structure Interface, *Journal Of Geotechnical and Geoenvironmental Engineering* © ASCE /860
- Koerner, R. M. (2005). *Designing With Geosynthetics*, 5th ed., Pearson Education, New York, NY, USA.
- Minazek K. (2010). *Modelsko Ispitivanje interakcije geomreže i tla*, Phd thesis, University of Zagreb, Faculty of civil Engineering, Zagreb, Croatia.
- Palmeira, E. M. (2009). Soil–geosynthetic interaction: Modelling and analysis, *Geotextiles and Geomembranes* 27 368–390
- Yogarajah, I. & Yeo, K.C. (1994). Finite Element modeling of Pull-Out tests with the Load and Strain Measurements, *Geotextiles and Geomembranes* 13 43-54
- Rowe, R. K. and Skinner, G. D. (2001). Numerical analysis of geosynthetic reinforced retaining wall constructud of a layered soil foundation, *Geotextiles and Geomembranes* 19, 387-412.
- Skejic, A. (2012). Interface Formulation Problem in Geotechnical Finite Element Software, *The Electronic Journal of Geotechnical Engineering*, Volume 17, Bund. N. 2035–2041, ISSN: 10893032
- Sugimoto, M. & Alagiyawanna, A. M. N. (2003). Pullout Behavior of Geogrid by Test and Numerical Analysis, *Journal Of Geotechnical and Geoenvironmental Engineering* © ASCE / APRIL / 361-371
- Van Langen, H. & Vermeer, P. A. (1990). Automatic Step Size Correction for non-associated Plasticity Problems, *International Journal for Numerical Methods in Engineering*, Vol. 29, 579-598
- Yang, G., Zhang B., Ly and P. Zhou, Q. (2009). Behaviour of geogrid reinforced soil retaining wall with concrete-rigid facing, *Geotextiles and Geomembranes* 27, 350-356.

On the Role of Human Error in Failure of Three Geosynthetic Reinforced Earth Walls

Dhani Narejo, Ph.D., P.E., GSE Environmental LLC, USA, dnarejo@gseworld.com.

ABSTRACT

The paper presents three case histories of geosynthetic reinforced earth walls that failed due to human errors in their construction. "As-designed", "as-built" and "failed" scenarios are presented for each of the walls, emphasizing the connection between the error and the wall failure. In one case, the geogrid was installed in the wrong direction and incorrect soil was placed in the reinforced zone. In another case, surface runoff was directed into the drainage stone behind the wall face. In yet another case, a drainage swale shown on the plans was left out. Such human errors occur during construction when neither the design engineer nor a construction quality assurance inspector is engaged to ensure compliance with the wall plans and specifications. The failure mode varies depending on the nature of the error, but water is involved in all three walls as an additional cause of the failure. Noncompliance with the specifications may be intentional in a few cases in order to save money. Unintentional errors, however, are seen to occur in a majority of the cases. The cost of rebuilding the walls can be quite significant even when no lawsuits are involved. Most of the human errors can be easily prevented by requiring the presence of the design engineer or quality assurance inspector during the wall construction. A quality assurance inspection requirement is especially important for walls in the residential market, where errors are more common.

1. INTRODUCTION

Geosynthetic reinforced earth walls (GREWs) are one of the most popular soil retaining structures in the world and particularly in the USA. Ease of construction, aesthetic value, and lower construction cost are some of the important reasons for world-wide acceptance of GREWs. Well-designed and well-built GREWs are known to perform exceptionally well as one can see by visiting a few of the thousands of these walls in many towns and cities. The geosynthetic industry knows very well also that a small number of GREWs of questionable quality are built every year even in those markets that should be highly mature and sophisticated, such as the USA. This would indicate that similar problems would be more widespread in other emerging markets. Human errors should be a common factor in all types of projects such as buildings, roadways, landfills, bridges, and so on. An important difference is that these projects have a much stronger role of construction quality assurance than GREWs. Probably the ease of construction of GREWs, and the fact that this is a highly price-conscious industry, has contributed to lax standards for quality assurance. As a result, there are probably more problems, and even failures, of GREWs than highways, bridges and buildings. This state of affairs is less common in DOT (department of transportation) GREWs where construction quality assurance is already well established.

Retaining wall failures can be placed in two categories: those caused by deficiencies in design, and those caused by deficiencies in construction. The design procedures and construction materials are rarely ever to be blamed for the quality issues in GREWs. However, design practice of GREWs, especially in certain residential markets, is questionable with regard to remote designs, poor or no construction drawings, and little or no geotechnical investigation. The export of the design of GREWs by some manufacturers is a worrisome trend. Many contractors and project owners consider a detailed design and stability analysis to be unnecessary and a waste of money when walls are small and are located in residential areas. Design engineers are often happy to go along providing electronic designs all over the world without ever seeing the site. The entire industry must share the blame for the quality issues and take necessary actions to improve design and construction standards for GREWs. The recent inspector certification program by the Geosynthetic Institute is a welcome step in that direction. However, additional contractual standards are necessary to improve other aspects of GREWs such as the design practice. Certain minimum standards of quality for design and geotechnical investigation need to be established.

This paper presents case histories of three GREWs that failed due to one or more errors during construction. Later, the walls were rebuilt as before, except that the construction flaw(s) was removed. Therefore, these walls became like large-scale field experiments in the effect of the quality of construction on the performance of the walls. The paper emphasizes "designed", "built", "failed" sequence for each of the projects with the hope that others can benefit from such cases. Little emphasis is placed on an engineering analysis of the failures as the flaw is obvious in each case and the rebuilt walls – with the flaw(s) removed - are performing as expected. There are some interesting observations to be made about the endurance of these walls when challenged by adverse conditions. The purpose of this paper is to share these unintended experiments with the reader so that a consensus can be achieved about the need for construction quality

assurance of GREWs in residential and commercial construction where such a program is urgently needed. Fortunately, all three projects were settled amicably among the parties involved without a lawsuit.

2. CASE HISTORY 1

2.1 Description

This first case history is about a wall in a storm water detention pond in Houston, TX. Three sides of the detention basin were sloped while the fourth side required a wall due to right-of-way restrictions. The soil at the site is clayey silt or silty clay with a medium plasticity index. A 12 ft vertical cut for the wall was free-standing, showing the clayey soil being desiccated from the severe drought of 2011/2012 that occurred throughout Texas. The pond is to accept the surface water run-off from a large commercial building that is located in a mixed zoning community. The geotechnical investigation showed that the design engineer can use a ϕ' of 28° based on published relationships between friction angle and plasticity index of clayey soils. The engineer performed internal, external and global stability analysis using a commercially available slope stability and wall design software. With an ϕ of 34° for the reinforced soil and geogrid design strength of 2575 lbs/ft, factors of safety obtained for all failure modes were well above the required minimums. Other important features of the wall include a block fascia with a front batter of about 7° , 8" gravel drainage zone behind the blocks, 9 ft geogrid length at every 2 ft vertical spacing, and a low permeability cover soil to seal-off the top of the wall. A full set of drawings and design report was given to the wall contractor although these were not required by the contract agreement. The design engineer visited the site prior to the construction but no visit was performed during the construction as none was required and everyone agreed that the wall was quite simple. The wall was built during the peak drought season and the pond was put into service.

The wall failed after being in service for about six months. The engineer visited the site and took some photos as well as made some observations as summarized in Figure 1. Figure 1(a) shows a partial view of the design cross-section of the wall emphasizing only the differences with Figure 1(b) which shows as-built wall. Figure 1(c) shows the wall failure in one location while the rest of the wall, although distorted, did not fail. Note in Figure 1(a) that the design required the geogrid to be installed in the machine direction while the wall was built with the geogrid installed in the x-machine direction as seen in Figure 1(b). Note also that the reinforced soil required in the design is structural fill with zero percent fines while that used in the construction is the silty clay that was excavated from the pond. Interestingly, a third party quality assurance technician was at the site to monitor compaction of the backfill soil in the reinforced zone. The site geotechnical engineer – different from the wall design engineer – had also visited the site during the wall construction. The primary contractor for the site was closely involved with the wall construction.

The wall failed after a heavy rainstorm that was preceded by several months of drought. The failure mode was clearly block-geogrid connection rupture which took a triangular shaped zone of soil out, leaving the geogrid hanging in the air. While the strength of the clayey soil was great during the drought, the rainfall went right into the body of the wall due to the cracks, wetting the soil. Therefore, the strength of the reinforced soil decreased over time, caused by a dissipation of the negative pore water pressure. This could be easily seen from the failed section which was moist and showed large lumps of high plasticity clay. There was one area where the blocks actually sheared off from the geogrid. The rest of the wall showed a wavy deformation along the length, with severe cracks extending back to the end of the reinforced zone. It was decided by all the parties unanimously that the entire wall must be demolished and rebuilt according to the plans. The same wall-builder rebuilt the wall and the same soils inspector was hired to perform the wall inspection. The only difference was that the inspector and the design engineer ensured that the wall was built according to the specifications and plans.

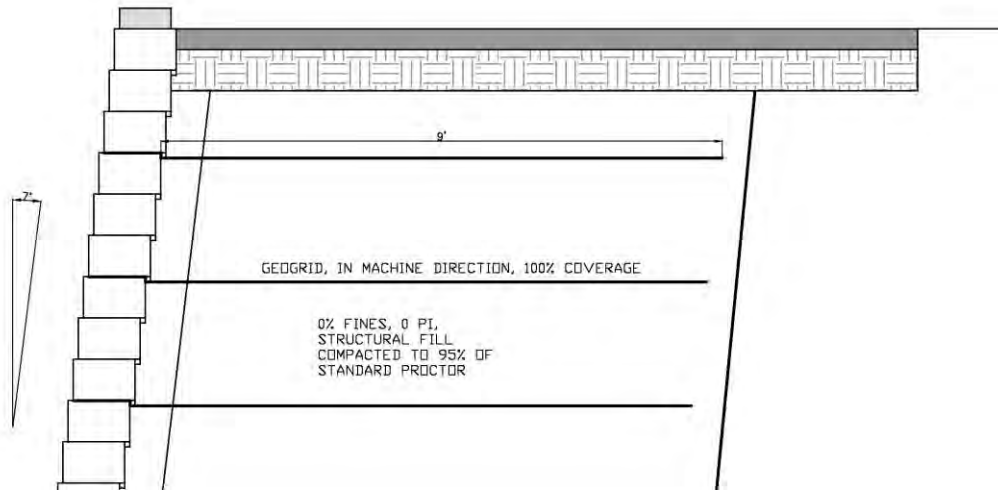
2.2 Lessons Learned

Several important lessons could be learned from this case history, among them the following:

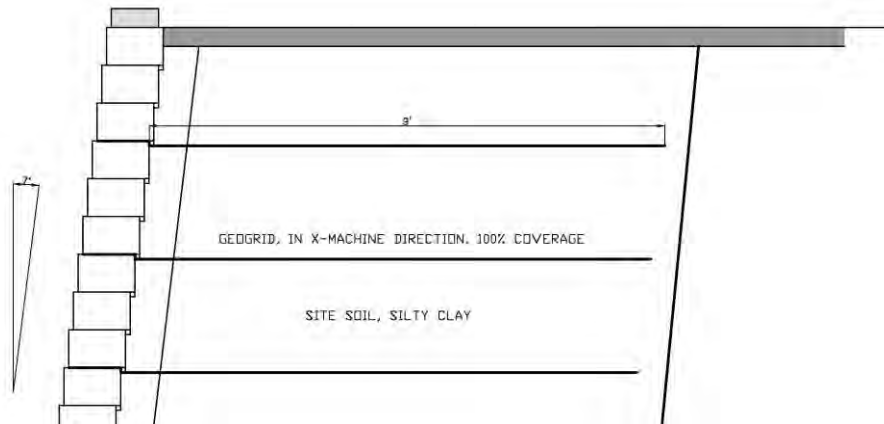
- i) This failure could have been easily prevented if a construction quality assurance inspector or the wall design engineer had been contracted to inspect the wall construction. Just one site visit could have sufficed in this particular case.
- ii) A soils compaction testing technician was at the site but was ineffective in this case. This shows that the wall inspection must be performed by parties given specific responsibility and training to perform this work.
- iii) Mistakes occurred despite the wall-builder, contractor, design engineer and soils inspector all having considerable experience in their respective areas of expertise.
- iv) It is possible that the problem could have been limited to deformation – but no failure – had the geogrid been installed in the correct direction. It appears that GREWs can be built with cohesive soil provided water is kept out and some deformation is accepted. The top and back of the walls built with clayey soil must be sealed against water. This can be achieved with a geosynthetic clay liner at the top and a drainage

geocomposite at the back.

- v) All parties quickly agreed to cooperate, thereby preventing an expensive lawsuit. Even then this was an expensive failure for several parties involved, whose insurance had to cover the reconstruction cost.



(a) As Designed



(b) As Constructed



(c) A Photo of the Failure

Figure 1 – For Case History 1, Wall As Designed, As Built and a Photo of the Failure.

3. CASE HISTORY 2

3.1 Description

The second case history is about a wall built in front of a large commercial building in Dallas, TX. The original ground had a slight negative slope in front of the building. A parking lot was built in front of the building that also accommodated heavy shipping and receiving traffic and one of the entrances to the building. It was necessary to build a small wall– 8 ft maximum height - in order to obtain the required grades for the pavement. The need for this wall was realized after the fill had already been placed. But it was easy enough to move the fill back slightly in order to make room for the wall. Ideally, the wall should have been built first, or at the same time as the placement of the fill. The engineer assumed a friction angle of 33° for the reinforced soil, 28° for the retained soil and 30° for the foundation soil based on the information available at the time of the design. Internal, external and global stability analyses were performed with a commercially available software and the effect of heavy truck traffic was considered in the design. The contractor agreed to use pea gravel for the entire reinforced zone of the wall. Adequate drainage pipe was placed behind the fascia blocks and day-lighted every 20 ft. The design engineer visited the wall during the construction but before the pavement was built. A geogrid with a long-term allowable design strength of 1918 lbs/ft was specified by the engineer with 2 ft vertical spacing and a minimum length of 5.5 ft. Since most of the wall was only 6 ft high, 5.5 ft geogrid length showed adequate factors of safety for all failure modes.

The pavement behind the wall failed about 18 months after the construction. Although the wall designer was relieved to hear that it was not the wall failure, the primary engineer for the project appeared to be quite concerned about the wall. The wall contractor had left the back of the wall open to receive surface flows from the parking lot. Figure 2(a) shows a partial cross-section of the design of the wall as submitted to the wall contractor while Figure 2(b) shows the same for the wall as constructed. Figure 2(c) shows a photo of the failure of the pavement behind the wall. Notice that the design called for extending the pavement all the way to behind the wall cap so that the surface flows would go over the wall face. The wall, as-built, collects all the flow from the parking lot in the gravel behind the blocks. Pea gravel has a limited capacity to handle fines that could have been brought in with vehicular traffic over time and entered the pea gravel. It is not difficult to visualize a scenario where the drainage/reinforced soil zone got contaminated over time with fines, preventing water flow outward and inducing seepage inward towards the parking lot. Truck traffic over wet and/or poorly compacted soil was likely the cause of the pavement failure. The wall remained intact and was able to resist load from trucks as close as 2ft to the wall face.

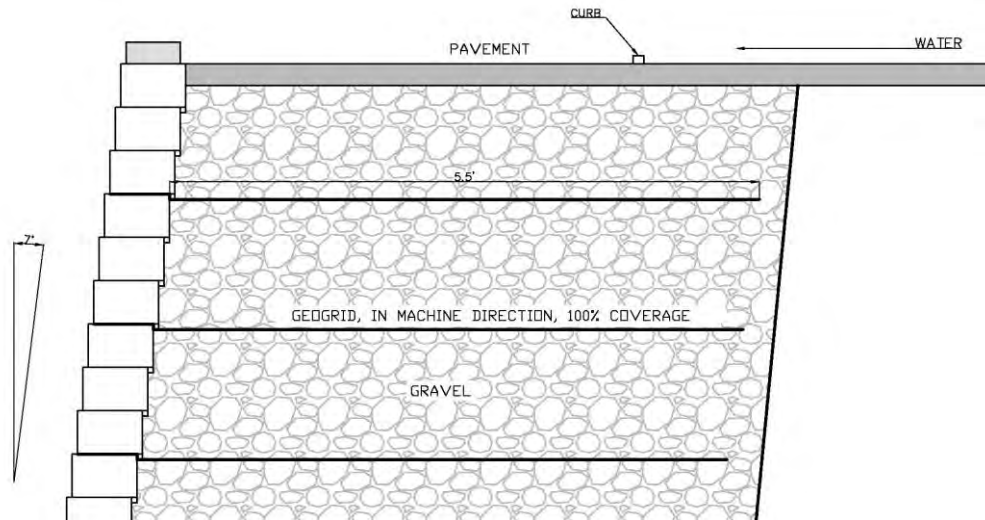
An independent civil engineer was hired by the primary contractor to investigate the pavement failure as well as the design of the wall. The engineer concluded that the pavement failure could have occurred due to several reasons including a poor compaction of the fill soil and seepage from the water entering the back of the wall. Leaving the back of the wall open to storm flows is an obvious flaw while the soil compaction is difficult to verify with the same level of

certainty. Had the wall contractor followed the plans, there could have been no doubt that he was not responsible for the problem with the pavement. Based on conversations with various parties, the author assumes that the wall and the adjacent pavement was removed completely and reconstructed. The reconstruction cost was very likely shared by the primary contractor and the wall contractor as in the case of the first case history. An experienced wall contractor made an error in his eagerness to be creative. The engineer made one visit to the site at his own expense as the agreement required no visit from the engineer.

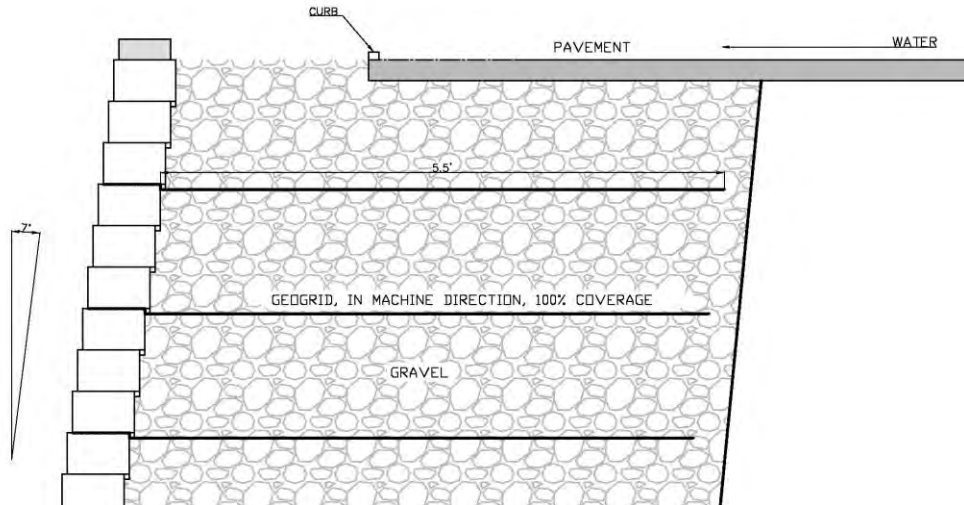
3.2 Lessons Learned

This case study reinforces the lessons learned from the previous case history about the role of human errors in GREW failures. However, one can never overemphasize the following:

- i) A construction quality assurance inspector could have easily noticed the problem with the wall construction and alerted the design engineer or the owner.
- ii) The design engineer visited the site only once during the wall construction, which does not appear to be enough. The design engineer should have also visited the wall after the construction of the building and the parking lot were completed.
- iii) Water is a common threat in many of the wall problems and should not be underestimated. Specifically, the top of the wall, and even the back of the wall, should be sealed from water by a combination of low permeability soil, GCL, and a drainage geocomposite.
- iv) Wall contractors assume a significant risk when building walls differently from the stamped plans. Even when a change is necessary, it is important to contact the design engineer and have the plans changed so that the plans and the construction are in complete agreement.
- v) Heavy truckloads immediately behind walls should be considered not only in the design process but also in construction details, including compaction requirements.



2.2(a) – As Designed



2.2(b) – As Built



2.2(c) – A Photo of Pavement Failure

Figure 2 – For Case History 2, Wall as Designed, As Built and a Photo of Failure.

4. CASE HISTORY 3

4.1 Description

The third case history is about a wall in a new residential development in San Antonio, TX. The hilly terrain at the site is characterized by about 6" of brown clay underlain by limestone with approximately 12 to 50 SPT blows per inch within the top seven feet. House building pads are developed at the site by extensive cut and fill operations requiring walls ranging from a few feet up to 40 feet in height. Since walls are founded in a competent limestone, global stability of the walls is not a concern. On the other hand, almost all the fill at the site is uncontrolled and obtained from either limestone blasting at the site or imported from adjacent sites with similar soils. The friction angle of these clayey gravels is more than 45 degrees and unsupported vertical cuts of up to 8 ft in these fill material can be observed at the site. However, these same soils are highly erodible when exposed to storm water flows. Therefore, ravines and gullies as deep as 5 ft could be observed at the site. The wall in question has a maximum height of 9 ft and occurs at the end of the property line which is also the toe of a 10-degree 500 ft upward slope. The depth of the fill ranges from about 9 ft at the wall to zero feet at about 200 ft up the slope. Even after the fill, there is a significant slope of about 10 degrees for about 500 ft in some areas. The wall was designed based on NCMA (National Concrete Masonry Association) guidelines for block walls with geogrid reinforcement. A friction angle of only 34 degrees was used for the reinforced soil which was the same as blasted limestone. For the retained and foundation soils, a friction angle of 30 degrees was used. A 3H:1V slope was assumed for the backfill. Therefore, the design was based on a highly conservative assumption of the soil properties.

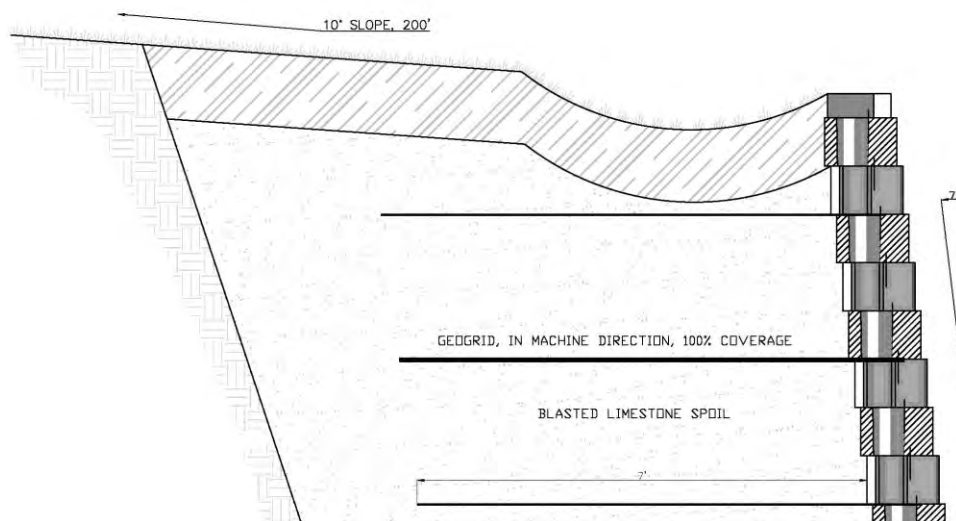
The wall failed gradually over a time period of two years due to the erosion of the reinforced and retained soil. The failure mode was an overtopping of the fascia due to water pressure. Although the wall was designed conservatively, one of the main problems at the site, that of the erosion, was not addressed by the wall contractor as required by the contract with the owner. Figure 3(a) shows a partial cross section of the wall as designed by the wall engineer. The reader may note in the figure a drainage swale that is intended to accommodate the surface water flows behind the wall. Figure 3(b) shows the way the wall was built, that is, without the drainage swale. In the absence of the drainage swale, small rills and ravines formed initially on the slope above the wall. The erosion then continued to worsen to the point where eventually entire wall sections got washed out as is shown in Figure 3(c). This was the only location at the entire site where the wall failed due to erosion. This was also the only place where there was a long slope above the wall without a drainage swale. At the other location with much higher walls, either slopes were short or there was a drainage swale with an erosion control mat. In this case, the drainage swale was skipped to save money. There was also a change in the ownership of the entire site involved during the peak of the housing crisis in the USA.

After a long back and forth, the property owner and the wall contractor reached an agreement to rebuild the wall with a drainage swale. The same materials and methods were used as in the original wall. The only difference was that a drainage swale was placed immediately behind the blocks as indicated on the original construction drawings. The author has seen the wall after being exposed to a few heavy rainfalls. The erosion that caused the failure of the wall seems to have stopped at least for now. It is expected that the plot above the wall will have a housing pad soon which will solve the erosion problem. The contractor had to remobilize the crew from a long distance and completely rebuild large sections of the wall at a significant expense and as per the plans. Building the wall right at the first time would have cost less money and maintained amicable relations with the site owner.

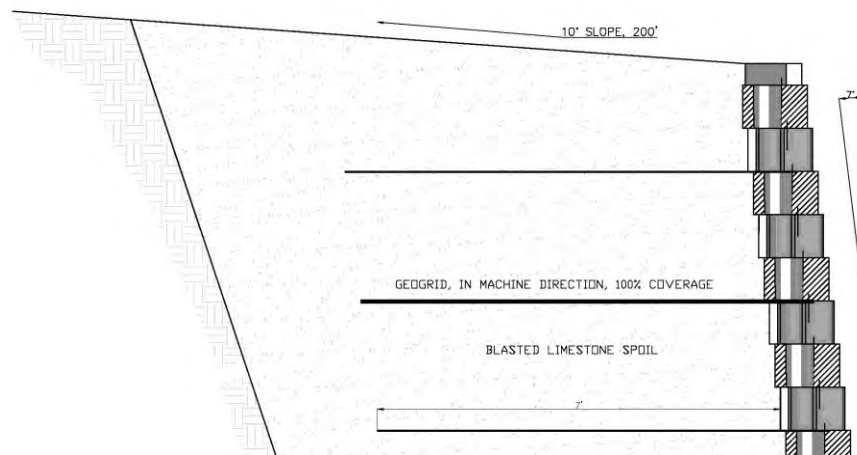
4.2 Lessons Learned

The lessons learned from this case history reinforce the same from previous two case histories, i.e., intentional or unintentional errors in wall construction can lead to wall failures. Here are some specific lessons from this case history:

- i) Water was involved in this failure as in the case of the previous two failures. Design engineers and wall contractors must consider surface and sub-surface water that may challenge a wall.
- ii) No design engineer ever visited the site in this case and no construction quality assurance inspector was hired to inspect the wall in order to ensure a compliance with the project specifications. Therefore, a noncompliance with the design went unchallenged until the wall failed completely.
- iii) Erosion of the backfill soil is a common problem in many walls and one that is often not properly considered at the design stage and during construction.
- iv) The cost of rebuilding the wall was many times higher than the cost of putting the drainage swale as required by the project specifications.
- v) Non-cohesive soils with very high shear strength, such as blasted limestone spoil, are also highly erodible requiring protection at the top of the wall.



3.3(a) – As Designed



3.3(b) – As Built



3.3(c) A Photo of the Wall Failure

Figure 3.3 – For Case History 3, the Wall as Built, as Designed and a Photo of the Failure.

5. CONCLUSIONS

Geosynthetic Institute has an ongoing program that tracks reinforced soil wall failures. The June 2012 newsletter (GSI, 2012) of the institute mentions 154 failures in the database. Several authors including Koerner & Koerner (2012) and Yoo & Jung (2009) present an analysis of reinforced soil wall failures. High seepage stress and poor drainage are two factors that are frequently associated with GREW failures. This paper emphasized the role of human errors and how water exploits weaknesses in walls. Errors in most cases are simple and can be easily prevented by requiring the engineer's representative or a quality assurance inspector to be present to monitor the wall construction. The following conclusions can be drawn based on the three case histories:

- Water was a factor in the failure of all three walls. This manifested in either poor surface drainage (case histories 2 and 3) or dissipation of negative pore pressures in the clayey reinforced soil.
- Two of the three cases (case histories 1 and 2) were of unintentional errors while one case (case history 3) involved cost savings as the motive.
- In all three cases, the walls were removed and rebuilt at a considerable cost to the parties involved in the construction. None of the cases resulted in a lawsuit which significantly lowered the overall cost of the resolution.

- Failures occurred after six to eighteen months of service under extremely adverse conditions of a defective construction. Even then the walls performed the intended function before giving in under additional loads from water.
- Surface water drainage and subsurface seepage are generally not adequately considered in the design and must be carefully designed and implemented.

REFERENCES

- Koerner, R.M. and Koerner, G.R., (2012). The importance of drainage control for mechanically stabilized earth reinforced walls. *Journal of GeoEngineering*, Vol. 6, No. 1, pp. 3-13, April 2011.
- The Geosynthetic Institute (2012). The GSI Newsletter/Report. www.geosynthetic-institute.org, Vol. 26, No. 2, June 2012.
- Yoo, C., and Jung, H.-Y., (2009). Case History of Geosynthetic Reinforced Segmental Retaining Wall Failure. *Journal of Geotechnical and GeoEnvironmental Engineering*, 132(12), pp. 1538-1548, August 2012.

Paving Fabric Interlayer Systems for Pavement Enhancement

Ray Myers, Asphalt Interlayer Association, USA, rmroads@gmail.com

ABSTRACT

Pavement interlayers represent one of the largest geosynthetic applications, in part due to the tremendous amount of research and documented proof of performance. However, much of this technical work was done 20-30 years ago and the commercial market for this technology peaked shortly thereafter. Today, because of transportation agencies personnel turn over and a lack of performance monitoring, much of the pavement life extension afforded by this technology has been overlooked, forgotten or misunderstood. This presentation will discuss the combination of benefits provided by geosynthetic pavement interlayers compared to other, less cost effective pavement construction and maintenance strategies. Many agencies are turning to open graded friction courses to reduce hydroplaning and road noise. This technology can result in added exposure to water in the pavement structure and more rapid pavement deterioration. It will be shown how interlayers can mitigate this issue. A geosynthetic interlayer remains a very attractive value proposition for pavement preservation, especially in light of the rapidly rising cost of road building materials. The presentation will redirect attention to this excellent pavement strategy for both new pavements and for pavement rehabilitation. The technology and the associated benefits of different geosynthetic pavement interlayers will be reviewed. Then, to allow designers and end users to make intelligent pavement design choices, the costs of the different systems are compared to the cost of traditional pavement strategies. It will be shown how geosynthetic pavement interlayers are more appropriate today than ever as public agencies and private owners try to meet their transportation/pavement maintenance needs with very limited dollars.

1. INTRODUCTION

The inclusion of a geosynthetic pavement interlayer system can address and mitigate many pavement distress factors. These systems may be used in both new pavements and those undergoing rehabilitation. The lowest cost and easiest to install system is the traditional nonwoven paving fabric, which is combined with asphalt cement to become a pavement membrane interlayer. More specialized geosynthetic interlayer systems are also available and will be briefly discussed at the end of this paper. The basic functions of geosynthetic interlayer systems will be discussed along with a brief explanation of how the systems are installed. These systems should be viewed like any other pavement enhancement tool—there are appropriate situations where they should be used to gain the optimum and most cost effective benefit for the pavement. Consistent with the theme of the conference session for which the paper is written, engineers should not forget the 40 plus years of successful application of the paving fabric interlayer system and the hundreds of thousand lane miles of pavement enhancement achieved. The usage is somewhat lower today than 15-20 years ago, but that is mainly due to the fact that the system was proven effective in the 80's and 90's and not a lot of research has been necessary since then. So, without so many current papers on the subject, the newer generation of pavement engineers forgets that this basic system is often the most cost effective pavement treatment available to them. However, the properties of the materials are the same, the installation is improved, and the pavement enhancement performance is the same or better. Also, with the current cost of asphalt concrete reaching very high levels and the paving fabric cost staying low, the paving fabric interlayer system is more cost effective today than any time in the past. With asphalt concrete cost now frequently rising above that of Portland cement concrete, those wishing to continue to use asphalt concrete should be looking for ways, like those discussed herein, to enhance the life of flexible pavements, to improve the life-cycle cost.

The history of modern paving fabric usage dates back to 1968 with the development of the nonwoven needle-punched fabric. This fabric was made using polypropylene fibers formed into a strong felt-like fabric structure of about 4.1oz./sq.yd.(140 gm./sq.m.). The way in which the fabric is applied to the pavement is 0.25 gal./sq.yd (1.14 l./sq.m.) of asphalt cement tack coat is uniformly sprayed onto an existing pavement and then the paving fabric is immediately laid into this tack coat.



Fig. 1 Paving fabric placed into fresh tack coat



Fig. 2 Asphalt concrete placed over paving fabric

Next, an asphalt concrete layer of at least 1.5 in.(38mm) is placed onto the fabric interlayer. There are two reasons for the minimum 1.5 in.(38mm) overlay thickness. First, the heat from the asphalt concrete re-melts the asphalt cement tack coat and draws it up to saturate the paving fabric and to bond to the overlay. Secondly, the 1.5 in. (38mm) thickness provides the necessary internal shear strength of the layer so that it will not shove or buckle in high shear stress areas of the pavement. Once the overlay is in place the interlayer becomes the thick, fabric reinforced asphalt cement layer that provides the functions of a moisture barrier and a stress absorbing interlayer. This paper will not go into the details of geosynthetic pavement interlayer installation. Please refer to the detailed installation instruction manuals available from every credible supplier of these materials. There is also the Asphalt Interlayer Association (AIA) with the website of www.aia-us.org where information on the specification and installation of these systems is readily available. Installation is not difficult, but all the considerations in the installation manuals must be followed to end up with a successful application. Admittedly, some areas of the country have more experience with the installation of geosynthetic pavement interlayer systems than other areas.

2. THE MOISTURE BARRIER FUNCTION

The first important function of the paving fabric is that of a pavement moisture barrier. When properly saturated with asphalt cement, the paving fabric interlayer is approximately four orders of magnitude less permeable than the pavement layers adjacent to it. The AASHTO M 288 paving fabric specification calls for a nonwoven fabric of 4.1oz./sq.yd.(140 gm./sq.m.), as it has been shown that this thickness and weight of fabric is required to absorb and reinforce the recommended asphalt cement tack coat of 0.25 gal./sq.yd (1.14 l./sq.m.), the amount necessary to form a proper moisture barrier. It is important to note here that the integrity of the moisture barrier is highly dependent on the good uniform application of the proper amount of asphalt cement tack that will saturate the paving fabric. Insufficient tack amount or a spotty spray application pattern will not result in a continuous moisture barrier with the system. As a pavement moisture barrier, the paving fabric interlayer, or any composite geosynthetic interlayer with a paving fabric, provides many benefits to the pavement. Pavements are quite permeable, with 30-40% of rainwater typically infiltrating asphalt concrete and 50-67% infiltrating Portland Cement Concrete pavements (Cedergren, 1974). The amount of water that infiltrates pavements is critical to pavement performance yet this information is not widely known or fully appreciated by most pavement engineers. Infiltrated water also frequently comes from over-zealous irrigation systems or washing systems that throw a lot of water onto pavements. The infiltrated water can cause significant damage to the pavement, dramatically shortening the pavement life. FHWA documents claim the road life can be shortened by up to 50% if the road section is saturated even 10% of the time (Cedergren, 1974). This damage can be pore water pressure that overrides the load spreading capability of the base and/or subbase aggregate support, limiting the vehicle loading to small areas and this exceeds the bearing capacity of the subgrade soil, failing the road. Free water in an aggregate can cause accelerated subgrade soil intrusion into the base aggregate and pumping of fines through cracks and joints to weaken and create voids under the road. Pumping action of water trapped within a pavement can also cause stripping of the lower asphalt concrete layers—an effect where the asphalt cement binder is mechanically scrubbed off the asphalt concrete stone and the layer can crumble apart. Also, water in the pavement support layers can cause damage due to the expansion and contraction associated with freezing and thawing in northern climates. Beyond these more obvious water related pavement concerns, when the subgrade and/or subbase layer has a higher moisture content, its strength and bearing capacity can be greatly compromised and, without the design bearing capacity support originally assigned to the subgrade, the road begins to fail rapidly.

The paving fabric membrane interlayer also minimizes the exposure of oxygen to the asphalt concrete layers below it. This keeps them from oxidizing, a primary cause of why older asphalt concrete layers become brittle and crack. In some areas of the United States, the subgrade soils beneath pavements are highly expansive clays. The incorporation of a paving fabric membrane interlayer within pavements over these soils, can maintain a constant moisture content in these soils year around, keeping them from experiencing pavement damaging shrinking and swelling.

There are other common sense ways to view the use of a paving fabric membrane interlayer “tool” as a pavement moisture barrier layer. In new pavements the incorporation of a pavement moisture barrier will prevent the infiltration of surface water down into the pavement structural support layers. Since this surface water is the primary source of moisture in pavements, the elimination of this source will take away the need to drain the infiltrated water from the pavement support layers. The paving fabric moisture barrier will therefore allow the designer to use base and/or subbase aggregates that are more dense-graded and more poorly drained as opposed to the more expensive aggregates with gradations designed to make them more free-draining.

To demonstrate this, look at how AASHTO assigns coefficients of drainage depending on the permeability of aggregate layers (AASHTO 1993):

<u>Quality of Drainage</u>	<u>Water Removed Within</u>	<u>Drainage Coefficient (Cd)</u>
Excellent	Two hours	1.20
Good	One day	1.00
Fair	One week	0.80
Poor	One month	0.60
Very Poor	Will not drain	0.40

The drainage coefficient is multiplied times the structural number of each aggregate layer. Therefore, as may be seen, aggregates that drain infiltrated water rapidly and keep the road base moisture levels low are, by AASHTO pavement design, assigned higher structural properties by applying high drainage coefficients (Cd). Conversely, dense-graded, slowly draining aggregates have their structural strength discounted by the assignment of low drainage coefficients. Examples of typical AASHTO pavement base designs are as follow:

Two different 10 inch thick aggregate base layers of moderately hard crushed stone with the same structural number (SN) of 0.12 per inch are multiplied times the drainage coefficient to show the dramatic effect of their ability to drain:

Excellent draining aggregate—10” X 0.12 SN X 1.2 Cd = 1.44 SN total structural contribution to the road

Poorly draining aggregate--10” X 0.12 SN X 0.6 Cd = 0.72 SN total structural contribution to the road

However, if the paving fabric moisture barrier never allows the water to saturate these aggregates, the highest drainage coefficients may be applied to even dense graded, low permeability aggregates. So, now instead of being discounted half their strength, the lower quality, poorly draining aggregates may be assigned as much strength as the more expensive free-draining aggregates. This provides not only a more cost effective way to utilize base aggregate layers, but it is also a green way to conserve resources since the aggregate fines are not screened and wasted at the quarry. It is difficult to design the ideal aggregate gradation where it is highly permeable yet dimensionally stable and easy to work with and compact. More dense graded aggregates, allowed when a paving fabric is incorporated, are more easily compacted and can be more stable layers for pavement construction. It is still very important to use a separation/stabilization geotextile beneath the aggregate base so that the subgrade soil does not contaminate and weaken any aggregate gradation. The separation/stabilization geotextile will also allow a lesser structural section since it improves the strength of both the subgrade soil and the aggregate base layers.

Another way common sense may be used is to potentially limit the use of highway edge drains. Edge drains are often built into new or rehabilitation highway projects to help control the moisture levels beneath pavements. If it is a groundwater problem, this needs to be addressed with geosynthetic cutoff drains and/or fairly deep edge drains. However, as discussed above, most of the water coming into the pavement structural layers is coming through the pavement surface. For a pavement edge drain system to work, the aggregate base needs to be open and free-draining to be able to rapidly move the infiltrated water to the edge of the highway. In new pavements this means using the more expensive, select graded aggregate. In pavement rehabilitation projects, the base aggregate is rarely

free-draining, by original design or due to subgrade soil contamination over the years. Therefore, transportation engineers are fooling themselves if they think retrofitting edge drains to these roads will pull the water out as rapidly as needed. Instead, the common sense alternative is to cap the pavement with a paving fabric membrane interlayer and never allow the water to enter the road structure in the first place. There is usually an overlay project accompanying a retrofit edge drain project anyway, so the low cost addition of the paving fabric interlayer is usually only one-third to one-fifth the cost of installing edge drains. The other problem this eliminates is the maintenance hassle with edge drains. They are difficult to keep functioning properly and many of these systems in roads right now are not working due to clogging, system collapse, overgrown or damaged outlet structures, etc.

A common pavement treatment today is mill and fill, where the existing pavement is milled down, often two to four inches, and a replacement layer of asphalt concrete is placed where the old layer was taken out. Obviously, there will be some short term benefit to the pavement, like an improved ride and a “younger” more flexible top pavement layer. However, using this methodology, the pavement engineer has not solved any of the real problems that made that original, same thickness pavement fail in the first place. So the agency is just inviting the same rapid deterioration cycle to repeat itself. If a paving fabric interlayer was placed at the bottom of this new, replacement asphalt concrete layer, a real structural benefit would be realized by the pavement as the pavement support layers would now be maintained at a lower moisture level and would thus have greater strength. This is the only way to effect a real positive change with a mill and fill strategy. The paving fabric interlayer may be placed at the bottom of the filler asphalt or up to half way from the bottom of the filling, if two overlay lifts are to be placed.

From a safety standpoint, many transportation agencies are using a highly drainable asphalt concrete surface layer. This keeps the surface drier to prevent hydroplaning and it also enables a quieter ride as less tire-to-road contact is made. These drainable layers are well suited for the inclusion of a paving fabric interlayer below to keep this rapidly infiltrated water from penetrating the entire pavement structure. The surface water is stopped at the paving fabric layer and routed to the edge of the pavement, instead of down through the pavement where the water can cause rapid pavement deterioration.

One inexpensive way to incorporate the benefit of a moisture barrier in a pavement is to apply the paving fabric interlayer beneath a chip seal surface treatment. The installation method is different because of no heat from an overlay, but instructions are readily available on how to accomplish this installation below a chip seal. This fabric reinforced chip seal maintains an effective moisture barrier for many years, whereby a plain chip seal surface treatment without the fabric interlayer, typically cracks back open within a couple of years negating any moisture barrier properties the chip seal might have had. An added benefit is the fabric forms a fibrous seat under the chip and actually holds the stone better for much less stone loss from the chip seal due to traffic. The fabric interlayer can also stop the surface bleed through of excessive crack filler from the underlying pavement to the new surface. Chip seal surface treatments over a paving fabric are reported to last two to four times as long as traditional chip seals and the moisture barrier properties are much better and longer lasting. Some agencies use chip seal surface treatments as interlayers, where they are immediately overlaid, or they are left to traffic for some time before the overlay is placed. Again, with no tensile strength to keep the moisture barrier from cracking open and without the fabric layer to create a stress absorptive layer, the chip seal does not work as well as a membrane interlayer as the paving fabric. The fabric and chip seal combination can be left for years and then overlaid to still realize its benefits beneath a future asphalt concrete overlay.

A comprehensive discussion on the effectiveness of paving fabric membrane interlayers as pavement moisture barriers may be found in the Electronic Circular 006 of the Transportation Research Board at <http://gulliver.TRB.org/publications/circulars/ec006.html> . This document discusses the research proving how impermeable the system is as well as the benefits to pavements.

3. THE STRESS ABSORPTION FUNCTION

The second major function of the paving fabric system is as a stress absorbing interlayer. The paving fabric system can absorb movements from cracks and joints in the underlying, existing pavement. This helps eliminate the hard contact/bond between the existing pavement and the overlay that can cause reflective cracking. Obviously, there are limitations to how much movement the paving fabric interlayer can absorb and dissipate. Looking at the 40 years of widespread, successful utilization of this system, it is extremely effective at mitigating slight to moderate fatigue cracking, and longitudinal cracking and joints, like highway widening cracks. The system is also effective at treating transverse cracks and joints, but these often have too much differential vertical movement associated with them to be mitigated for extended periods. The most difficult cracking to treat is thermal cracking, because it is generally not reflective, bottom up cracking. Instead, thermal cracking can reoccur within the new asphalt concrete overlay as it shrinks and expands. Thermal cracking needs to be addressed in the new overlay mix design.

It is interesting to hear the variety of opinions on the effectiveness of paving fabric interlayers at mitigating reflective and fatigue cracking. Most users understand the limitations of the system and are very happy with the performance they have seen. Notable transportation agencies consider the inclusion of a paving fabric interlayer equivalent to placing an additional 1.2 to 1.5 inches of asphalt concrete overlay thickness when looking at how long the overlay lasts before additional work is needed on the pavement (Smith, 1984 and Maxim, 1997). Another way the performance of the paving fabric has been measured is, agencies believe its inclusion doubles the life of an equivalent thickness overlay. Some agencies have mistakenly turned to using a paving fabric interlayer when they have an existing pavement that is so bad that they know their standard overlay will not work. Paving fabrics are not miracle layers and unfortunately, these agencies expected too much and became dissatisfied with the performance over these poor condition roads. Then when they are not satisfied with the performance where it should not have even been placed, they get a mindset that “paving fabrics do not work on our roads” although an agency next door may have very successful results properly applying these interlayers. Like any other pavement treatment, the earlier the treatment is applied in the deterioration cycle of the pavement, the longer the overlay will last—the whole idea behind pavement preservation. Paving fabrics placed over early to moderate fatigue cracking, block cracking, and longitudinal joints and cracks are extremely effective and many agencies have realized these benefits. Performance of the system is tied to suitable applications and pavement preparation. Many agencies forget about the importance of the moisture barrier function of paving fabrics and only measure their success by counting cracks. The paving fabric interlayer is quite flexible and durable and when cracking does eventually return to the overlay, the paving fabric interlayer typically remains intact and maintains its waterproofing capability. Even in areas of severe thermal cracking, it is reported that when thermal cracking occurs in the surface layer, the paving fabric membrane stays intact. Beyond maintaining its moisture barrier function, the intact interlayer does not allow foreign matter to fall into the crack to progressively wedge it wider, so the cracks stay smaller and more manageable.

Design guidelines, available from paving fabric manufacturers, describe which existing pavement conditions are suitable for the application of a paving fabric interlayer system. There are limitations as to how large of a crack the system may be installed over, as well as limitations on the vertical movement of adjacent sides of existing cracks or joints. Some crack filling preparatory work is recommended. If a pavement is not suitable for paving fabric placement, steps such as the placement of a leveling course of asphalt concrete can bring the existing pavement up to a condition where the paving fabric system will be the most effective. If there is rutting in the existing pavement, a leveling course or milling is required to establish a drainable surface on which the moisture barrier shall be placed. Milling to reshape a crown in a pavement, or to allow the new pavement elevation into an existing curb and gutter system is common, but, often, an excessive amount of milling is taking place that actually destroys pavement structure that could be supporting traffic. There is no problem placing a paving fabric interlayer system directly over a milled surface.

Often overlooked by pavement engineers is the tremendous benefit a flexible pavement may realize just by being layered as opposed to being a single thick, monolithic layer. Some of the earliest work on paving fabric interlayers showed that a layered pavement can withstand over 10 times the amount of flexural loading before the initial development of the typical bottom-up fatigue cracking (Maxim, 1997). This is because a thick, monolithic pavement generates a very high level of tensile stress at the bottom of this single layer every time the pavement flexes under load. A pavement made up of two layers, separated by the well bonded paving fabric interlayer, will experience much lower tensile stress at the bottom of each thinner layer. An analogous situation is how a piece of plywood may be flexed many more times than a clear wood board without cracking, simply because, even though the wood layers are well bonded together and strong, slight stress absorptive movement can occur between layers to minimize the tensile cracking stresses at the bottom of each layer. A highly effective, yet often overlooked application for paving fabric interlayers is their use within new asphalt concrete pavements or within thick pavement overlay layers, to greatly delay the development of the first fatigue crack development.

4. GENERAL PAVING FABRIC INFORMATION

4.1 Specifying the Paving Fabric Interlayer System

There are generally only three weight classes of paving fabric used in the US. The predominant style is what is recommended by the national guideline specification, AASHTO M 288, 2006, with a minimum weight of 4.1oz./sq.yd.(140 gm./sq.m.). A lighter version at 3.7oz./sq.yd.(125 gm./sq.m.) is used on some lighter duty roads, parking lots, and sometimes with a chip seal surface treatment over the fabric. Less frequently utilized are weights of about 5.0oz./sq.yd.(170 gm./sq.m.), and occasional fabrics up to 6.0oz./sq.yd.(203 gm./sq.m.). This heavier weight may provide more stress absorption but one must be careful to specify and install the heavier amount of asphalt cement tack consistent with this heavier fabric. If any weight fabric is not fully saturated to form the bond to the overlay, the new pavement could experience some shoving and the moisture barrier is not fully implemented. Ready

to use specifications are available to the engineer or owner and the author generally recommends the AASHTO M 288 specification be used.

4.2 Recycling the Paving Fabric Interlayer System

There are varying stories out there as far as the recyclability of an installed paving fabric interlayer when a pavement is milled. Large field trials have been run showing that paving fabric interlayers may be successfully milled and the resultant small pieces of paving fabric mixed back into a variety of asphalt concrete mixes. The system needs to have been installed properly, with the correct amount of tack coat so that all layers are well bonded and if the agency must mill through the interlayer, the milling should target $\frac{3}{4}$ to 1 in. (19 to 25mm) below the interlayer. This will mean the cutting is near vertical and there is no chance of going in and out of the interlayer level due to inconsistent overlay thickness over the interlayer. There have also been stories of milling operations where pieces of the paving fabric were milled up and later caused problems at the entrance screen to the secondary crushing operation. In these cases, it is probable that the fabric system was not installed properly and too little tack was used. This light tack causes poor layer bonding and pieces of partially dry fabric that could pull up during the milling. Some paving/milling contractors have solved the problem of handling these occasional larger pieces of fabric in their operations and are fine with milling through paving fabric layers. All that being said, the smart move is to **not** mill through the paving fabric interlayer, unless it is absolutely necessary. Not because of potential problems, but because the agency/owner has already paid for a stress absorbing and moisture barrier layer in their pavement. Asphalt concrete layers below the paving fabric are less oxidized and may not need replacement. Milling should stop at least 0.5 in. (12mm) above the interlayer so that it may remain intact and continue to offer its many benefits to the new overlay(s) placed over it. There seems to be far too much milling today, which may be partially because the paving contractor gets paid to mill it up, obtains the millings, generally for free, and then puts the millings back into new asphalt concrete that is sold on a project. If there is no grade problem, perhaps only enough milling should be done that is needed to reshape the road surface and not excessive milling that often destroys good existing pavement support structure that must then be replaced by new pavement at a high cost.

4.3 Paving Fabric Value Proposition

Looking at the cost benefit of paving fabric interlayers, the installed cost of the system varies somewhat based on the size of the project, location, etc. However, the installed system around the US in 2012 generally runs between \$1.50 and \$2.00 per square yard. The cost of asphalt concrete, which can also vary with the size of the project, is generally around \$4.00 to \$5.00 per inch thickness per square yard. Therefore, the fabric only costs about as much as 0.3 to 0.5 in. (7.5 to 12.5mm) of asphalt concrete yet it is widely proven to give the benefit of an additional 1.2 to 1.5 in. (30 to 38mm) of asphalt concrete. This shows how the paving fabric interlayers can greatly reduce or extend a transportation agency's overlay budget. If only a minimal, 1.5 in. (38mm) overlay is allowed, adding the low cost of the paving fabric can double the life of the overlaid pavement before additional maintenance treatments will be necessary. So, the agency/owner may choose to take the savings up front, or they may wish to lower the annual cost of the pavement. Transportation agencies frequently choose to save some up front, to pay for the paving fabric, **and** gain additional savings on extended pavement life.

5. SUMMARY OF PAVING FABRIC INTERLAYER BENEFITS

- The paving fabric interlayer system provides an effective, long lasting pavement moisture barrier and all the pavement benefits discussed.
- The moisture barrier function can be a very useful pavement design tool when the pavement structure and the hydraulic conditions are considered holistically.
- The moisture barrier function can solve some climatic problems and subgrade and base problems that typically shorten the life of pavements.
- As a moisture barrier, the system is more effective at preventing pavement moisture damage and saves money over the use of edge drains and over the use of select free-draining base aggregates.
- As a stress absorbing membrane the paving fabric interlayer can effectively minimize both the development of fatigue cracking in new and rehabilitated pavements and can retard the development of reflective cracking.
- A paving fabric interlayer is the most cost effective enhancement for flexible and composite pavements, considering all the benefits it provides.

--The paving fabric interlayer may be used beneath a chip seal surface treatment to create a pavement moisture barrier and to greatly extend the life and enhance the quality of the chip seal treatment.

--Paving fabrics may be recycled, but why destroy the existing interlayer that can go on helping a new overlay(s) and protecting the pavement from moisture.

--There is a large amount of reports on proof of performance, demonstrating both the crack retardation and moisture barrier benefits in pavements.

--There is also a vast amount of helpful design and installation information, including sample project specifications, available from the manufacturers of the products and from the Asphalt Interlayer Association.

6. OTHER GEOSYNTHETIC INTERLAYER SYSTEMS

This paper has focused on paving fabrics, the lowest cost interlayer with the longest history of use. There are other geosynthetic interlayers that have built on the success of the basic paving fabric system. One class of product is called paving mat and is made, at least partially, out of fiberglass fibers. These mats are somewhat thinner than a traditional paving fabric and require less tack coat to saturate.



Fig. 3 Paving Mat Installation the fabric

Therefore, the paving mats cannot absorb as much stress from the slight movements from underlying cracks and joints as the thicker, traditional paving fabric interlayer system. The paving mats can develop strength at lower elongation if they are placed into a pavement situation where that need occurs. Depending on the needs of the project, pavement engineers should consider this another interlayer tool, if they need higher modulus and generally lower impermeability and less stress absorption, compared to traditional paving fabrics. According to their manufacturers, these paving mats are more readily recycled, because they are more brittle, have lower tear strengths, and will shear apart easier upon milling. But, again, why mill the interlayer that was previously paid for and that could continue to benefit the new overlay(s). Paving mats are a bit more difficult to install and their initial cost is higher, so, the total installed cost may be twice or more than the traditional paving fabric, but this cost is still low compared to the additional amount of asphalt concrete that would be required to supply comparable pavement performance when all the interlayer benefits are considered.

Another class of geosynthetic interlayers is paving grids. These products are made with distinct opening sizes with the intent of interlocking with the asphalt concrete overlay. The grids are strong, made from fiberglass or polyester bundles of strands, so they have high strength at low strains. These products may have advantages in higher shear areas of pavements, such as at bus stops, before stop signs, toll booths, etc., because they add shear strength to the asphalt concrete overlay. Some paving grid manufacturers claim to have a higher degree of success than traditional paving fabrics at retarding reflective cracking, particularly over more aggressive cracks or joints. Some of these grids are composited with a traditional paving fabric so that the moisture barrier benefits discussed above may be realized as well. The project engineer has a choice of a waterproofing grid composite or a grid only that does not create a pavement moisture barrier. With the higher cost of these grid products and the higher cost to install these products, the overall installed product cost may be as much as 4 to 6 times the cost of an installed traditional paving fabric. However, the unique pavement situations where these grids or grid/fabric composites are applied can still make them cost effective solutions in pavement rehabilitation. This is because expensive, thick asphalt concrete overlays cannot overcome rapid failure in some pavement distress situations.



Fig. 4 Paving grid/paving fabric composite and overlay

There are two classes of strip membrane interlayers. The first is basically a paving fabric factory coated with rubberized asphalt, available up to 36 inch (0.9 meter) widths. This product class is used as strip stress absorption over cracks or joints and is used as a continuous bridge deck membrane waterproofing layer. A heavier, higher strength strip membrane is also available, and is used for treatment of more aggressive cracks and joints, generally beneath at least a 2 inch (50mm) overlay. These strip products are very effective at reflective crack retardation, but since they are generally not placed full width on the pavement, they are not an effective moisture barrier, other than how they seal the specific crack they are treating.



Fig. 5 Strip membrane over a joint before overlay



Fig.6 Strip membranes for a bridge deck waterproofing

Guideline specifications for all these more specialized geosynthetic pavement interlayers are available directly from the manufacturers and have not yet been published by AASHTO.

7. CONCLUSION

In summary, geosynthetic pavement interlayers are very useful tools that should always be considered both in analyzing new flexible pavement designs and in rehabilitation projects involving asphalt concrete overlays or chip seal surface treatments. It is important to note that although the discussion has been “pavements” and “roads”, these geosynthetic pavement interlayers are applied to parking lots, storage and commercial yards, all classes of roads, bike paths and trails, and airport pavements. Wide pavements, such as parking lots greatly benefit from the areal moisture barrier function of some of these systems. These interlayers should not be viewed as additional cost on a project. Instead, geosynthetic interlayers can save up front costs by getting the same performance out of thinner overlays. In addition, these interlayers can greatly extend the life of new asphalt pavements and asphalt concrete overlays, and traditional paving fabrics can greatly extend the life of chip seal surface treatments. Also, as shown, the moisture barrier function opens the door to the use of more cost effective construction materials, to lower the costs of new construction. Technical reports and installation guidelines are available for anyone wishing to further explore how these cost effective interlayer systems can save their pavement budget dollars. Many of the references below are provided as sources of information on these interlayer systems. Although most of the laboratory and in-pavement research was performed years ago on these interlayer products, the proof of their pavement enhancements is being realized every day by transportation agencies and private pavement owners. Over 250,000 lane miles of pavement have been enhanced by geosynthetic pavement interlayers and usage is still very strong, much of it by repeat users that have enjoyed how the interlayers have lowered the costs and extended the life of their pavements. Due to the frequent employment turnover by pavement engineers and administrators, the performance of roads with and without geosynthetic interlayers is rarely monitored and documented properly for the benefit of the

next engineer in that position. Current pavement engineers and administrators should take the time to investigate all the literature available on pavement interlayers and maybe even look into their own agency records to see why they have not had to invest as many maintenance and rehabilitation dollars on some of their roads—they might just have a geosynthetic interlayer below.

REFERENCES

- AASHTO, 1993. AASHTO Guide for Design of Pavement Structures, Vol. 2. American Association of State Highway and Transportation Officials, Washington, D.C., 1986 and 1993.
- Al-Qadi, I., *Petromat Evaluation in Kernersville, NC*, Communication Virginia Polytechnic Institute with Amoco Fabrics and Fibers, 1997
- American Association of State Highway and Transportation Officials, *Geotextile Specification for Highway Applications, AASHTO Designation M 288-06*, 2006.
- Cedergren, H. R., *Drainage of Highway and Airfield Pavements*, John Wiley and Sons, Inc., New York, 1974.
- C. Joel Sprague, P.E., *Flexible Pavement Rehabilitation using Paving Fabric – Quantifying the Benefit, 2002*
- Marienfeld, Mark L. and Baker, Thomas L., *Paving Fabric Interlayer System As A Pavement Moisture Barrier*, Transportation Research Board, Electronic Circular, 1999
- Maxim Technologies, Inc., *Nonwoven Paving Fabric Study, Final Report*, submitted to Industrial Fabrics Association International, 1997.
- Roschen, Theron J., (1997) "A Case Study into the Use of Pavement Reinforcing Grid, Mastic, and Membrane Interlayers on Asphalt Concrete Overlays", *Geosynthetics '97 Conference Proceedings*, Vol. 2, 725-748.
- Phillips, P., "Long Term Performance of Geotextile Reinforced Seals to Control Shrinkage on Stabilized and Unstable Clay Bases", *Reflective Cracking of Pavements*, RILEM, 1993, pp. 406-412.
- Predoehl, N.H., *Evaluation of Paving Fabric Test Installations in California*, FHWA/CA/TL-90/02, California Department of Transportation, 1990.
- Smith, Roger D., *Laboratory Investigation of Fabric Interlayers for Asphalt Concrete Paving (Final Report)*, FHWA/CA/TL-84-06, California Department of Transportation, 1984
- Sutherland, M., Phillips, P., "Geotextile Reinforced Sprayed Seal Roads in Rural Australia", *Proceedings of the Fourth International Conference on Geotextiles, Geomembranes and Related Products*, A.A. Balkema, Rotterdam, 1990, pp 209-212.

Permanent Geosynthetic Wrapped Face MSE Retaining Wall

Paul C. Frankenberger, P.E., TenCate Geosynthetics Americas, USA, p.frankenberger@tencate.com
John M. Lostumbo, P.E., TenCate Geosynthetics Americas, USA, j.lostumbo@tencate.com

ABSTRACT

Mechanically Stabilized Earth Retaining Walls (MSERWs) are commonplace on building sites and roadways. The typical MSERW uses a precast concrete facing panel or a masonry block facing unit. However, a new MSERW facing has been developed using geosynthetics. The first permanent geosynthetic wrapped face MSERWs using synthetic grass combined with structural geogrid soil reinforcement have been installed on a toll road construction project. MSERWs were needed to support the new roadway in limited access space. Although there are many types of MSERWs, geosynthetic wrapped face walls provide vertical grade separations at significantly lower cost. The long term design life of the geosynthetic face has always been the limiting factor in their use for permanent MSERWs. The benefit of using the synthetic grass geosynthetic wrapped face MSERWs was an economical, aesthetic and permanent structurally sound green wall face with no maintenance for the design life of the structure.

1. INTRODUCTION

Concrete and steel are standard materials in the construction of roads, bridges and retaining walls. With the introduction of MSERWs in North America in the early 1970s, concrete facing panels attached to steel soil reinforcements became the standard of practice. Later in the 1980s, concrete segmental block units were added as popular MSERW wall facing materials. Over the past 25 years, use of MSERWs with concrete segmental block units and geosynthetic reinforcement increased wall production and reduced overall wall costs. The development of polymer based geosynthetics such as geogrids offered a cost-effective, corrosion-free alternative to steel soil reinforcement. The use of MSERWs has been discussed and presented in several papers and the design methodology is well established. This paper expands beyond the limits of the concrete facing unit using geosynthetics composed of synthetic grass as the permanent wall face. A photo of one of the completed permanent geosynthetic wrapped face MSERWs is shown in Figure 1. The focus of this paper is on the synthetic grass facing as shown in Figure 2.



Completed permanent geosynthetic wrapped face MSERW.



Figure 2. Synthetic grass wall face.

2. WALL DESIGN

2.1 Project Overview

On the Nuevo Necaxa – Tihuatlan Toll Road Section of the Mexico DF – Tuxpan Highway in Puebla, Mexico, significant grade changes were encountered on the new highway alignment through beautiful mountainous terrain. Vertical retaining walls were needed to support the new roadway in the limited access space. Given the steep 70-degree terrain and large number of retaining walls required, MSERWs were designed to satisfy the project economics. A cross section of the

MSERW is shown in Figure 3.

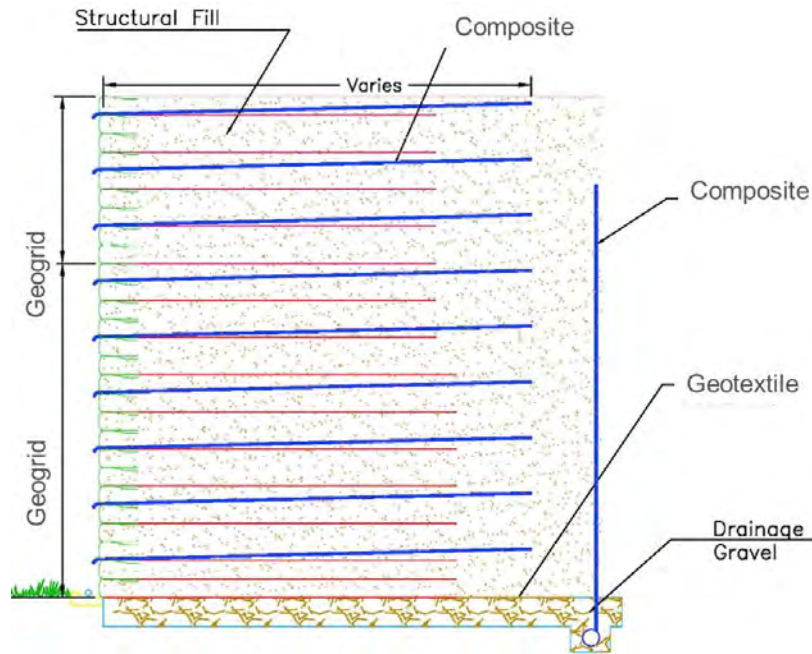


Figure 3. Cross section of MSERW.

Although there are many types of MSERWs, a geosynthetic wrapped face MSE retaining wall provides vertical grade separations at significantly less cost. However, the long term design life of the geosynthetic face has always been the limiting factor in their use. The solution on this project was an MSERW designed using TenCate Miramesh[®] SG (synthetic grass face geogrid mesh) attached to TenCate Miramesh[®] GR (green biaxial geogrid mesh) with Tencate Miragrid[®] XT (geogrid soil reinforcement). A typical section of the wall face is shown in Figure 4. The MSE wall is an economical and structurally sound permanent green wall face with no maintenance. Figures 3 and 4 show drainage composites used in the wall design. Drainage is an important factor in the MSERW design but is beyond the scope of this paper.

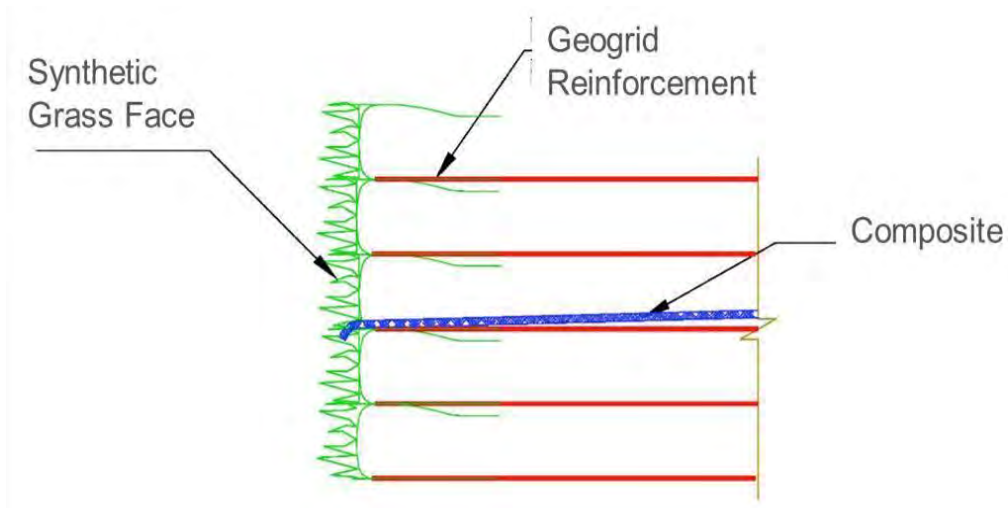


Figure 4. Typical section of synthetic grass wall face.

2.2 Soil Properties

The soil properties used in the MSERW design are shown in Table 1.

Table 1. Soil properties in MSE wall.

Soil Properties	Reinforced Zone	Retained Zone	Foundation Zone
Friction Angle (degrees)	38	38	35
Cohesion (psf)	0	0	333
Unit Weight (pcf)	128	128	128
USCS Classification	GW	GW	SM

2.3 Geosynthetic Properties

The long term design strengths of the geosynthetic reinforcements are shown in Table 2. The Primary Geogrid is the geogrid soil reinforcement. The Secondary Geogrid is the synthetic grass face geogrid mesh.

Table 2. Long term design strengths.

	Primary Geogrid	Secondary Geogrid
Ultimate Tensile Strength (lbs/ft)	9,500	1,790
Reduction Factor for Creep	1.6	3.16
Reduction Factor for Durability	1.1	1.1
Reduction Factor for Installation Damage	1.05	1.05
Long Term Design Strength (lbs/ft)	5,140	490

3. SYNTHETIC GRASS FACE GEOGRID MESH

3.1 Development

In the author's experience, the challenge in vegetated geosynthetic wrapped faced wall construction has been that over-seeding and hydro-seeding may not be as effective as desired. Many factors contribute to the complete vegetated geosynthetic wrapped face wall including; time to vegetation growth, homogeneous growth coverage, maintenance of irrigation system, direction of wall to sunlight exposure and seed mix selection (Tencate Geosynthetics North America, Miramesh... 2010). It takes time to achieve established grass growth especially in the case of a near vertical wall face. The typical pattern for grass growth is on top of the short ledges in the wall batter and then the grass cascades over the next lift. Initially, a geosynthetic was developed to provide high resistance to sunlight at the exposed vegetated face and also to satisfy the long term tensile strength needed as secondary reinforcement to prevent surficial slope failure. The material is a green biaxial geogrid mesh which is capable of permanently retaining soil at the wall face, yet open enough to promote vegetation growth. The mesh is coated and offers a 75 to 100 year design life exposed to sunlight. However, the goal was to create a geosynthetic wall facing that looked fully vegetated at the completion of wall construction.

A two-year development process was begun to develop a unique geosynthetic wall facing by tufting synthetic grass into a secondary reinforcement geogrid. Using TenCate's experience of grass yarn development, a review was conducted on high ultraviolet (UV) resistant fibers, new grass yarn, new tufter and capability of high pile height. The concept was to take the original green biaxial geogrid mesh and tuft in an 18-inch strip of synthetic grass which would represent the lift height of the face of an MSERW. The remaining material would not contain the synthetic grass, but extend back into the wall face to provide the necessary strength as secondary geogrid reinforcement at the wall face.

Initially, synthetic grass yarns were tufted in a backing geotextile attached to the green biaxial geogrid mesh but a typical coating to hold yarns in place cannot be applied as this would block all water flow and be detrimental to the design of the wall. However, the yarns were cut-pile and were not stable enough to maintain their relative position in the backing. The pile length of the yarn was increased and an additional substrate, a woven primary backing, was used to tuft the yarns for additional support. After testing, it was determined the flow rate of the 18-inch woven section that was tufted had insufficient water flow and could promote soil infiltration. In the final design a high flow heavy nonwoven was used that would not impeded water flow through the system but would adequately hold the synthetic grass tufts into place (see Figure 5). This resulted in synthetic grass face geogrid mesh, a composite product that would offer the necessary reinforcement for wall facing and provide a fully vegetated appearance immediately after completion. The nonwoven allows sufficient drainage and retains soil backfill, and the color of the grass can be changed depending on the desired color of the wall face.



Figure 5. Back of synthetic grass tufts in nonwoven geotextile.

The synthetic grass face geogrid mesh is a unique geosynthetic composite utilizing synthetic grass, nonwoven geotextile backing and green biaxial geogrid mesh as shown in Figure 6. The polymer for the backing is a homopolymer polypropylene, which offers one of the best combinations of UV stability and tenacity. The polymer for the grass blade is low density polyethylene and was chosen for its softness and drapability so that it more resembles the look and feel of actual grass. The synthetic grass yarn also provides significant UV protection to the geogrid. Both the synthetic grass and the nonwoven support membrane are made from inert polymer resins in the polyolefin family. They have hindered amine light stabilizers that are custom tailored for each specific polymer to allow the best weathering and color fastness properties over time.



Figure 6. Synthetic grass face geogrid mesh.

3.2 Laboratory Testing

The next stage was to test for UV durability of the geosynthetic when exposed to sunlight using fluorescent ultraviolet (QUV) testing. The data obtained from QUV testing at the Geosynthetics Institute, Folsom, PA, USA demonstrated that the synthetic grass significantly reduced damage of exposure to the reinforcing geogrid. The synthetic grass face geogrid mesh testing has shown 40 percent strength retained when exposed to high sustained UV levels approaching 40,000 hours of exposure (see Figure 7). We currently have more than 42,000 hours (almost 5 years) of accelerated UV test data with and without the tufted synthetic grass.

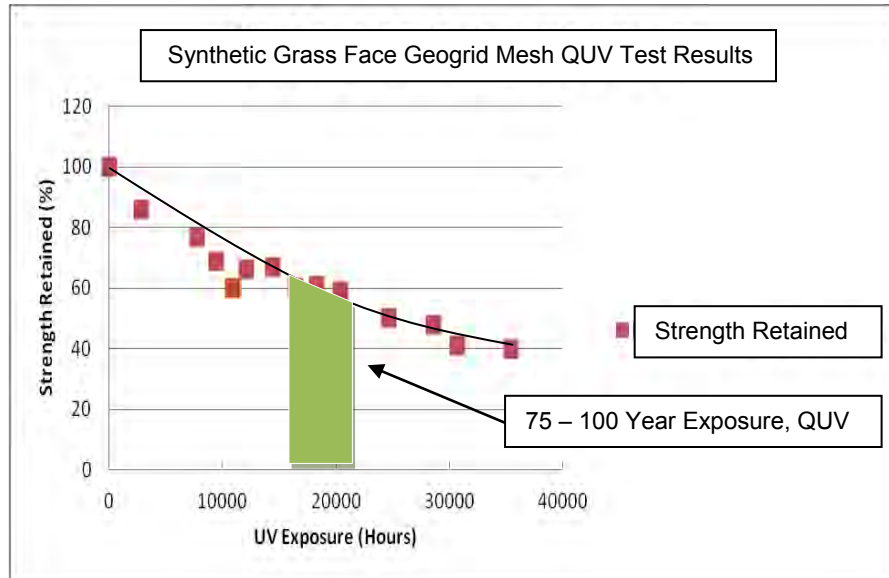


Figure 7. QUV test results on synthetic grass reinforcement (performed by Geosynthetic Institute, Folsom, PA, USA).

3.3 Design Life

Currently, the industry standard for measuring the UV resistance of geosynthetics is to use the xenon arc light source following ASTM D4355 or the fluorescent UV light with condensation to simulate weathering, ASTM D7238. For buried geosynthetics, the industry standard has been a minimum UV resistance of 70% strength retained after 500 hours per ASTM D4355. Correlating UV exposure from these test methods to field exposure is difficult. UV intensity and degradation rates are directly related to geographical location and other factors. However, it is possible to use the erythemal UV irradiance data of various geographic locations to develop a correlation between simulated UV exposure testing and field exposure (TenCate Geosynthetics North America, UV Durability... 2010).

Using the QUV simulated UV weathering (ASTM D7238), the intensity is about twice as much as using the xenon arc light source (ASTM D4355). Based on the intensity of the UV light source and the range of erythemal UV irradiances encountered in various geographic regions of North America, the equivalent exposure time for a design life of 75 years to 100 years ranges from about 18,000 hours to 23,000 hours. As shown in Figure 5, the result of the synthetic grass face geogrid mesh UV resistance is 62% strength retained at 18,000 hours and 59% strength retained at 23,000 hours per QUV testing. These are conservative values, since the irradiance levels are based on full sun exposure of a horizontal surface. Vertical surfaces, like a MSERW, will be shaded for a significant percentage of the day compared to a horizontal surface. This provides more strength than the LTDS of the material, so it may be used as a permanent wall face with design life of 75 to 100 years as shown in Table 3.

Table 3. Synthetic grass face geogrid mesh design strength.

Ultimate Tensile Strength (lb/ft)	LTDS (lb/ft)	Retained Strength at 75 year UV Exposure (lb/ft)	Retained Strength at 100 year UV Exposure (lb/ft)
1,790	490	1,110	1,056

4. WALL CONSTRUCTION

4.1 Project Overview

A total of six permanent geosynthetic wrapped face MSERWs were constructed by the general contractor, CONNET. The total wall area is 236,000 square feet with 105,000 square yards of geogrid soil reinforcement and 55,000 square yards of synthetic grass face geogrid mesh. The geogrid soil reinforcement was installed in 18-inch vertical lifts. The typical geogrid soil reinforcement length is 70 percent of the wall height. The tallest wall reaches a height of 40 feet with a maximum wall length of 984 feet and wall area of 39,370 square feet.

4.2 Facing Installation

Temporary forms were used at the wall face in the installation of the permanent geosynthetic wrapped face MSERW. The temporary form is required in order to achieve proper compaction at the wall face and is used to set the wall batter. On this project, some of the walls have a batter of 90°. The synthetic grass face geogrid mesh was placed vertically inside the temporary form with the green biaxial geogrid mesh extending back into the wall fill. The soil was placed in 8-inch vertical lifts and compacted to 95% modified proctor density. On this project, the contractor chose two different types of form systems: wire forms and wood forms.

4.2.1 Wire Forms

Wire forms typically consist of prefabricated L-shaped 18-inch high wire baskets that are 10-foot long and available through various steel fabricators. The detail of a typical wire basket form is shown in Figure 8. On this project, the contractor field-bent black steel wire mesh to create L-shaped wire baskets (see Figure 9.) Galvanized steel is not required since the wire basket is only considered a temporary form. The high pile height of the synthetic grass face geogrid mesh is designed to hide the wire basket form.

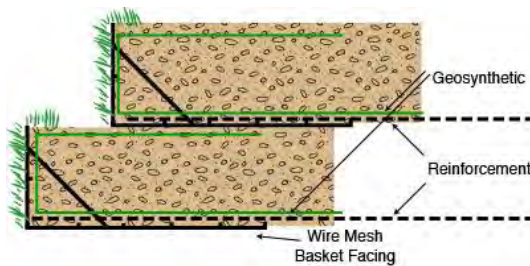


Figure 8. Detail of typical wire basket form.



Figure 9. Field-bent black steel wire basket form.

4.2.2 Wood Forms

Wood forms may be used to create the vertical wall face. The wood forms consist of 18-inch high sturdy wood members connected to steel brackets embedded in the wall (see Figure 10). As each lift is constructed, the wood forms are pulled from the wall face and moved up in consecutive wall lifts. Wood forms were used to construct many of the walls on the project as shown in Figure 11.

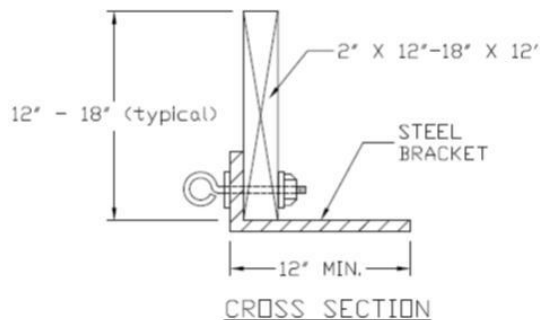


Figure 10. Detail of typical wood form.



Figure 11. Wood forms used at wall face.

5. CONCLUSION

MSERWs were constructed on a toll road project through mountainous terrain. These permanent MSERWs were constructed entirely of geosynthetic materials. The wall facing consists of synthetic grass face geogrid mesh to provide a design life beyond 75 years. The benefit is a structurally sound permanent geosynthetic wrapped face MSERW that is economical and aesthetic with no maintenance.

ACKNOWLEDGEMENTS

We wish to acknowledge the wall design and material supply services of TenCate Geosynthetics America's distributor, Geomembranas y Geosintéticos, S.A. de C.V. in Mexico City, and the research development data offered by TenCate Grass. We also wish to acknowledge the roadway owner Autovia Necaxa – Tihuatlan, S.A. de C.V. (AUNETI) and the general contractor Constructora Nuevo Necaxa – Tihuatlan S.A. de C.V. (CONNECT) a joint venture of ICA (Ingenieros Civiles Asociados SAB, Mexico) and FCC (Fomento de Construcciones y Contratas, Spain)

REFERENCES

- ASTM D 4355. Standard Test Method for Deterioration of Geotextiles by Exposure to Light, Moisture and Heat in Xenon Arc Type Apparatus, *American Society for Testing and Materials*, West Conshohocken, Pennsylvania, USA.
- ASTM D 7238. Standard Test Method for Effect of Exposure of Unreinforced Polyolefin Geomembrane Using Fluorescent UV Condensation Apparatus, *American Society for Testing and Materials*, West Conshohocken, Pennsylvania, USA.
- TenCate Geosynthetics North America, *UV Durability of TenCate Geosynthetics*, May 18, 2010.
- TenCate Geosynthetics North America, *Miramesh® GR for Vegetated Walls and Slopes*, May 18, 2010.

Polyester Geogrids as Asphalt Reinforcement - A Proven Technology

Bernd Thesseling, Applications Engineer, Huesker Synthetic GmbH, Germany, thesseling@huesker.de
Greg Kiggins, Product Manager, Huesker Inc., USA, gkiggins@hueskerinc.com

ABSTRACT

The conventional method for rehabilitation of cracked concrete or asphalt pavements is the installation of new asphalt layers. But a new overlay does not make the cracks disappear; they are still present in the old asphalt layers. Because bituminous bound materials are unable to withstand the high tensile stresses that result from external forces like traffic and temperature variations, these cracks rapidly propagate into the new asphalt overlay. This phenomenon, known as reflective cracking, is one of the major problems associated with the use of asphaltic overlays.

In order to tackle the problem of reflective cracking and to therefore prolong the service life of a pavement, a reinforcement grid made of high modulus polyester has proven to be a very effective solution. Geosynthetics as asphalt reinforcement have consistently shown outstanding results in addressing the issue of crack initiation and propagation, eliminating the damage caused by water intrusion that ultimately leads to the failure of the pavement structure. The increased pavement life achieved by the use of this technology not only prevents excessive disruption to traffic flow and local business, but it also demonstrates strong environmental and economic benefits.

Through basic theory and practical experiences this paper will demonstrate the success and extended pavement life that can be achieved in both highway and airfield applications. Special attention is given to the performance on site, e.g. the loss of tensile strength due to the paving procedure (influence of paver and truck passes), but also to milling of reinforced asphalt and its recycling.

1. INTRODUCTION

Asphalt reinforcement has been used worldwide for many years to delay or even prevent the development of reflective cracks in asphalt layers. Using asphalt reinforcement can clearly extend the fatigue life and therefore the maintenance intervals of rehabilitated asphalt pavements. Currently there are a number of different products and systems made of different raw materials (e.g. polyester, fiberglass, carbon fiber, polypropylene...) available in the market. It is not disputed that each of these systems has a positive effect in the battle against reflective cracking; however there are differences in the behavior and effectiveness of each system.

2. CREATING AN ASPHALT REINFORCEMENT OVER ALMOST 40 YEARS

The idea of a reinforcing fabric for asphalt road construction first emerged in the early 1970s (Figure 1). The first experiences with geogrids were in the construction of earthworks and foundations, so the idea to use them in asphalt pavements was a logical next step. The initial intention was that the embedded Geotextile layer was able to pick up the tensile stresses in the asphalt and prevent cracks from forming. However, it was soon realized that this principle did not work, but the product proved very useful at delaying the formation of reflection cracks in resurfaced roadways. Even then polyester was a preferred raw material because of the compatibility of its mechanical properties with the behavior of asphalt. Since then many products made from different raw materials have been developed.



Figure 1. One of the first attempts to use a Geogrid in asphalt pavements at the early 1970s.

3. BASICS REFLECTIVE CRACKING AND ASPHALT REINFORCEMENT

It is well known that cracks appear due to external forces, such as traffic loads and temperature variations. The temperature influence leads to the binder content in the asphalt becoming brittle; cracking starts at the top of a pavement and propagates down (top-down cracking). On the other hand, high stresses at the bottom of a pavement, from external dynamic loads, such as, traffic, lead to cracks that propagate from the bottom to the top of a pavement (bottom-up cracking).

A conventional rehabilitation of a cracked pavement involves milling off the existing top layer and installing a new asphalt course, but cracks are still present in the existing (old) asphalt layers. As a result of stress concentrations at the crack tips caused by external forces from traffic and natural temperature variations, the cracks will propagate rapidly to the top of the rehabilitated pavement.

Deteriorated concrete pavements are typically rehabilitated by installing new asphalt layers over the old concrete slabs. Temperature variations lead to a rapid crack propagation especially at the expansion joints to the top of the new asphalt overlay.

In order to delay the propagation of cracks into the new asphalt layers an asphalt reinforcement comprised of high tenacity polyester can be installed. The reinforcement increases the resistance of the overlay to high tensile stresses and distributes them over a larger area, thereby reducing the peak shear stresses at the edges of the cracks in the existing old pavement. The reinforcement also provides a normal load to the crack surfaces, thereby increasing the aggregate interlock (shear resistance) between both crack surfaces and thus increasing the resistance to reflective cracking.

High modulus polyester (PET) is a flexible raw material with a maximum tensile strain less than 12%. The coefficients of thermal expansion of polyester and asphalt (bitumen) are very similar. This leads to very small internal stresses between the PET fibers and the surrounding asphalt (similar to reinforced concrete). For this reason Polyester does not act as an extrinsic material in the asphalt package, however at this point it should be mentioned that the aim of a PET-grid as asphalt reinforcement is not to reinforce asphalt in such a way as one reinforces concrete. The installation of a PET-grid as asphalt reinforcement improves the flexibility of the structure and avoids peak-loads over a cracked existing layer into the overlay and through this mechanism reflective cracking is delayed.

As found by De Bondt (De Bondt 1999) the bonding of the material to the surrounding asphalt plays a critical role in the performance of an asphalt reinforcement. If the reinforcement is not able to sufficiently adopt the high strains from the peak of a crack, the reinforcement cannot be effective. In his research, de Bondt determined an equivalent "bond stiffness" in reinforcement pull-out tests on asphalt cores taken from a trial road section. The equivalent bond stiffness of a bituminous coated PET-grid was found to be, by far, the best of all the commercial products investigated.

Furthermore, asphalt reinforcement must resist as much damage as possible from the stresses and strains applied during installation and overlaying / compaction of the asphalt. Very high forces can also be applied to the individual strands of the reinforcement by aggregate movement in the hot blacktop during compaction.

In a research at the RWTH (Rheinisch-Westfaelische Technische Hochschule) Aachen University in Germany, called "Effectivity of asphalt reinforcement systems under consideration of installation damage" (Sakou 2011), it was found that products with a brittle raw material like fiberglass can lose a significant part of their tensile strength when trafficked by

asphalt delivery trucks and after the asphalt compaction. The results of the demonstrated research are also confirmed by results of tests performed according to EN ISO 10722-1 “Geosynthetics: Procedure for simulating damage during installation” (tBU 2003). In both tests Polyester as raw material exhibited a very good resistance to installation damage.

4. INFLUENCE OF DAMAGE DURING INSTALLATION ON THE TENSILE STRENGTH OF ASPHALT REINFORCEMENT PRODUCTS

The properties of asphalt reinforcement (e.g. tensile strength, tensile strain) are influenced during their installation, the paving procedure (paver and truck passes) and the compaction of the asphalt (Figure 2). The result, specifically the loss of tensile strength of the asphalt reinforcement grid during the paving procedure, is known as installation damage.

After an asphalt reinforcement product is placed, many asphalt delivery trucks have to pass over the grid. Additionally there is the compaction of the hot mix asphalt, during which the individual filaments or strands of the asphalt reinforcement are largely influenced by the movement of aggregates, in particular of coarse and sharp-edged aggregates. Next to the reinforcement characteristics (flexible or brittle raw materials), the degree of installation damage by roller compaction not only depends on the number of passes and the type of compaction (e.g. rubber tired, static, dynamic), but the weight of the compactor and the condition of the base layer (e.g. smooth, rough/milled) as well.

To successfully counteract reflective cracking, installed reinforcement products must resist the installation influences without damage and without significant loss of strength.

There is currently a lack of experience and knowledge concerning the real residual properties (what could be termed “effective tensile strength”) of asphalt reinforcement products following their installation and the subsequent paving installation procedure.

In the context of a diploma thesis at the RWTH Aachen University (Sakou 2011), a test procedure to describe installation damage was developed. One of the aims was to analyze and quantify the “effective tensile strength” for two different asphalt reinforcement products with different raw materials (polyester and fiberglass) after the influence of installation damage.



Figure 2. Influences on asphalt reinforcement products during the asphalt installation

4.1 Diploma Thesis at the RWTH Aachen University Considering Installation Damage

As part of the work to assess the resistance of asphalt reinforcement products to installation influences, site-appropriate tests were performed at the institute's installation test track. As one goal, comparable tensile strengths of the tested products after the following influences were intended to be achieved:

- Only the influence of trafficking asphalt trucks
- Only the asphalt compaction
- Combination: Trafficking of asphalt trucks and compaction of the asphalt

4.1.1 Test Procedure

To determine the impact of truck traffic only, undamaged specimens of the reinforcement products were placed on a clean and even road and loaded by a truck. The applied load was carried out by 35 passes with a speed of 20 ± 5 km/h without any steering movements or braking activity. Considering a truck with 5 axles who drives backwards to the paver and forward again this corresponds to 3.5 delivery trucks driving over the grid.

In preparation for the tests, an asphalt binder course (AC 16 B S) was installed on the base of the test track first. Onto the binder course, the reinforcement grids have been placed according to the manufacturer's installation guidelines. Some of the pre-damaged specimen (truck passes) have also been used in the test-track for further exposure to simulate the double load-effect, truck passes and compaction. To differ between undamaged, pre-damaged and the different loading types, the specimen had been placed into separate sections. Subsequent to the installation of the reinforcement specimen a 50mm asphalt wearing course was installed and compacted with 6 roller passes (2 static and 4 dynamic).

To test their tensile strength after the asphalt installation and compaction, some of the specimen had to be removed after the installation of the wearing course. For this reason these specimen have been wrapped into an aluminium foil and coated with a separating agent to create a very bad interlayer bond.

To investigate the different influences the test track was divided into different sections:

- A - An undamaged fiberglass reinforcement was installed, followed by the installation and compaction of an asphalt wearing course. (→ Load influence: Compaction only)
- B - A Polyester reinforcement was installed, followed by the installation and compaction of an asphalt wearing course. (→ Like „A“, load influence: Compaction only)
- C - A pre-damaged fiberglass grid was installed. Subsequently the asphalt wearing course was installed and compacted. (→ Load influence: Truck passes and compaction)
- D - A pre-damaged Polyester reinforcement was placed. Subsequently the asphalt wearing course was installed and compacted. (→ Like „C“, load influence: Truck passes and compaction)

4.1.2 Results

In the context of the research the final material characteristics (e.g. tensile strength) have been tested with the wide width tensile test according to EN ISO 10319. To compare the separate types of tests (variants) the property "residual strength" was chosen. The residual strength is defined as the maximum tensile strength after the installation damage tests, expressed as a percentage of the maximum tensile strength of the undamaged reference material.

The results revealed the considerable difference between the influence from truck traffic and asphalt compaction on the tensile strength of the specimens. It must be mentioned, however, that for the damaged fiberglass grids the test samples had to be taken from the side of the specimen, as the middle parts had been completely destroyed during the installation damage test, and were therefore impossible to test (Figure 3).

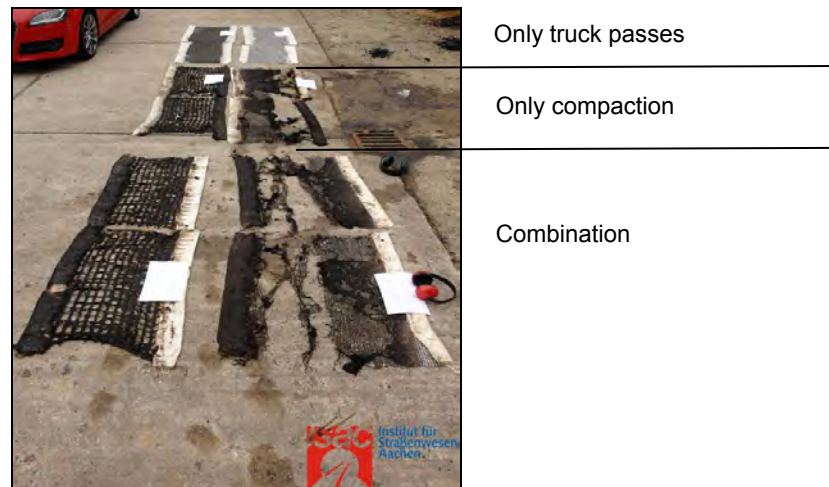


Figure 3. Results of installation damage test
Left: PET-Grid; Right: fiberglass grid

After the load influence "truck passes" only, the polyester grid showed a residual strength of 85%, while the fiberglass grid had only 44% residual strength. After the load influence "compaction" only, the polyester grid showed a residual strength of 71%, while the fiberglass grid had only 21%.

The polyester grid specimens which were subjected to both loading influences - asphalt compaction and truck passes - still had a residual strength of 70% while the fiberglass grid subjected to both loading influences revealed further damage with a residual strength of only 11% only (of the measurable areas, see Figure 3).

4.1.3 Summary

After a series of testing, it can be safely concluded that installation damage plays an important role on the "effective tensile strength" of asphalt reinforcement products. It was found that the polyester grid lost max. 30% of its tensile strength after loading from truck passes and asphalt compaction. In contrast to the performance of the polyester grid, the fiberglass grid showed a loss of strength up to approximately 90%. The fiberglass grid was damaged significantly more than the Polyester grid reinforcement.

4.2 Conclusion Regarding Installation Damage on Asphalt Reinforcement Products

As previously mentioned, asphalt reinforcement products must resist as much damage as possible from the stresses and strains applied during installation and compaction of the asphalt. Very high forces can also be applied to the individual strands of the reinforcement by aggregate movement within the hot asphalt during compaction.

From the research at the RWTH Aachen University, products with a brittle raw material (like fiberglass) can lose a significant part of their tensile strength when trafficked by asphalt delivery trucks and after the asphalt compaction. The results of the research are validated by results of tests performed according to EN ISO 10722-1 "Geosynthetics: Procedure for simulating damage during installation" (tBU 2003). Furthermore, it is expected that for fiberglass grids the results would be worse on a milled surface.

The tests reveal that polyester grids exhibit a very good resistance to installation damage compared to other products made with more brittle raw materials.

5. PRACTICAL EXPERIENCE: MUNICIPAL ROAD "ROSENSTRASSE" IN GERMANY

The following project shall give an example of the successful use of asphalt reinforcement in roads. The project is located in the Northwest German town of "Ochtrup". The road is a highly trafficked road. The majority of vehicles are trucks, because the road is one of the main connections to the nearby border of the Netherlands. Before rehabilitation, the road exhibited severe alligator cracking, longitudinal and transverse cracking in large scale. The original design called for milling, approximately 50 mm of the surface followed by installation of a new 50 mm asphalt surface course. Due to the problematic condition of the existing base, the expected lifetime of the new surface was only 2 years.

The more durable (but also much more expensive) solution would have been to remove the cracked binder and base course. An alternative to this solution was the installation of a Polyester Geogrid as asphalt reinforcement over the cracked binder course, where the thickness of the new wearing course would remain 50 mm. Therefore, the economical advantage had to be proven by a longer lifetime, which should be the main goal in most of these applications. The layers would have the same thickness, therefore the economical advantage results from the longer lifetime of the surface over the old cracked area.

After milling off the 50 mm surface course the asphalt reinforcement grid was installed, and covered again with a 50 mm 0/11 AC asphalt layer. The whole project was finished in the summer of 1996.

5.1 Project Update: June 2002

Six years after the repairs were carried out, the District's Chief Executive was asked for a condition report on the "Rosenstrasse". In his answer, he commented as follows: "I'm happy to inform you that the repairs have fully stood the test of time. The use of the asphalt reinforcement system under the 0/11 asphalt layer has meant that, to this day, no cracks have appeared in the asphalt-concrete surface. This method was chosen at the time to avoid the necessity of the additional work required for the binder and base course."

5.2 Project Update: September 2009; Assessment by TÜV Rheinland

The TÜV Rheinland is a leader in independent assessment services. In 2009, the TÜV Rheinland was commissioned to document the cracking and assess the condition of "Rosenstrasse" along the portion of the road that was repaired in 1996.

The appraisal compared the current condition with the condition that existed before repairs were carried out. This comparison allowed conclusions to be drawn about the effectiveness of the asphalt reinforcement system for delaying the occurrence of cracks propagated from the lower asphalt layers.

On August 24th 2009, a visual inspection was done in accordance with Working Paper No. 9 (by the German FGSV; Research Association for Transportation in Germany). The TÜV used the image documentation of the construction measures used in May 1996 as the basis for its assessment. The District's Chief Executive responsible at that time provided additional necessary information.

5.2.1 Result

After 13 years of use, the cracking condition value (ZWRIS) for the section of the road repaired with the Polyester grid in 1996 was determined to be excellent. The visual inspection of the road surface revealed almost no damage with the exception of two areas. The damage in these areas, however, was due to subsequent repair work on the drainage system. A few lateral cracks were discovered at one point on the outer edge of the road. Small cracks along the road surface were also found at a few other points on the outer edges (Figure 4).

The photos documenting the condition of the site in 1996 (Figure 5) show that the distance between the reinforcement system and the road edge was always around 150 - 300 mm. TÜV Rheinland also confirmed: "The entire remaining road area is free of cracks."



Figure 4. Lateral crack at the edge

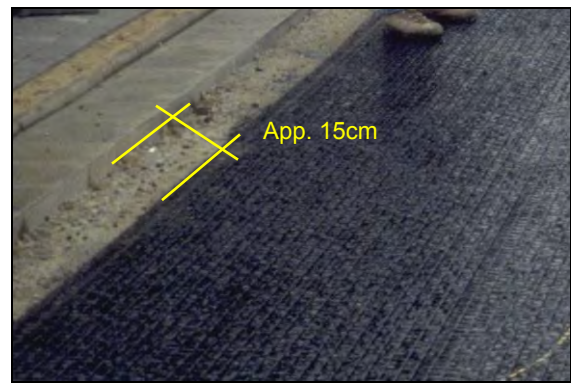


Figure 5. Fitted reinforcement (detail)

5.2.2 Conclusion

The condition assessment by TÜV Rheinland revealed that the "Rosenstrasse" in the city of Ochtrup has, in spite of constant heavy traffic, remained in good condition to this day. The deployment of the asphalt reinforcement system to effect repairs has completely stood the test of time. This measure has shown that a Polyester asphalt reinforcement can keep the condition of rehabilitated roads at a high level over extended periods of time.

6. PRACTICAL EXPERIENCE: SALGADO FILHO AIRPORT, PORTO ALEGRE (BRAZIL)

In 2001 the existing access to an aircraft maintenance hangar (used by aircraft as large as the Boeing 777, with a weight over 250 tons) had to be resurfaced after more than 40 years of use. The existing pavement was made of 5.0 × 3.5 m concrete slabs, 250 mm thick. The slabs were resting on a layer of gravel.

The rehabilitation design involved the installation of an asphalt leveling layer first. In order to prevent the propagation of the expansion joints from the concrete slabs into the new surface, an asphalt reinforcement made of high modulus polyester was to be installed. A 50 mm asphalt surface course was installed on top of the polyester reinforcement.

Because it was not possible to block the access for an extended period of time, the rehabilitation work had to be finished in just one night. In order to stay within this very tight time frame, it was decided to only reinforce the heavily loaded inner portion of the pavement. The outer portions, which are not typically subjected to the heavy loading of aircraft traffic, were left unreinforced.

What initially was thought to be a purely practical solution developed into an ideal demonstration of the effectiveness of an asphalt reinforcement grid. By only reinforcing a portion of the pavement and leaving the remainder unreinforced, a direct side-by-side comparison of the performance of the reinforced and unreinforced sections was possible.

In October 2007, approximately 7 years after the rehabilitation, the first assessment of the pavement took place. At that time the designer, the technical manager of the airport, and an employee of the reinforcement manufacturer were present.

The expansion joints in the concrete beneath the unreinforced pavement areas had already propagated to the top of the surfacing. The vegetation, visible in the developed cracks, led to the conclusion that these cracks had existed for some time. In contrast, the PET-grid reinforced areas did not show any indications of cracking (Figures 6 and 7). Because the unreinforced section was not subjected to aircraft traffic, the propagation of the expansion joints in these areas can be conclusively attributed to the horizontal stresses that resulted from changes in temperature. The areas reinforced with the polyester grid were subjected to both temperature-induced and aircraft traffic-induced stresses.

For further details the reader is referred to a paper prepared by Monser and Montestruque (Monser et al. 2010).

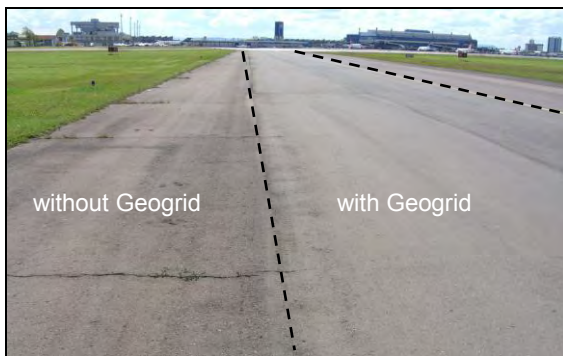


Figure 6. Overview of the studied section: view from the dockyards to the terminal.



Figure 7. Joints of the concrete slabs reflect in the area where no reinforcement was used

7. AN EYE ON SUSTAINABILITY

In the context of the construction industry, different construction techniques and designs for specific projects must be compared for their ECO_2 (Embodied carbon dioxide) emissions as an indicator for their sustainability. As a matter of fact, the ECO_2 is only one of the criterion for successful projects, along with social and economic considerations. However the request for sustainability is now appearing more and more important on both the client's and contractor's side.

7.1 Examples of ECO_2

The amount of ECO_2 per kg of material can vary significantly as seen in Table 1. The more processing and energy that is required to create the final product, the higher the ECO_2 emission. Processes that are especially energy intensive like the production of cement (for cement concrete) produce a high amount of CO_2 .

Cement manufacturing releases CO_2 into the atmosphere both directly and indirectly. Direct emissions of CO_2 occur when calcium carbonate is heated, producing lime and carbon dioxide. Indirect emission occurs if the energy used for cement manufacturing involves the emission of CO_2 .

Table 1. Examples of embodied carbon dioxide (ECO₂) in construction materials

Material	kg ECO ₂ / kg of material	Note
Aggregate	0.0052	gravel or crushed rock
Aluminium	9.16	-
Asphalt	0.076	6% binder content
Bitumen	0.55	-
Cement	0.74	UK weighted average
Concrete 16/20	0.10	unreinforced
Reinforced Concrete RC 40/50	0.188	high strength applications / precast
PVC General	3.10	-
Polyester	1.93	derived from HDPE
Steel	1.46	average UK recycled content
Steel	2.89	Virgin steel

Source: ICE Inventory of Carbon & Energy V2.0

7.2 Comparison of Embodied Energy for Reinforced and Unreinforced Asphalt Overlays

The report "Sustainable geosystems in civil engineering applications" commissioned by the Waste and Resource Action Plan (WRAP, 2010) has analyzed geosystems as alternatives to standard designs used by civil engineers. Parallel to geosystems for ground engineering the report has identified that:

"Reinforcement of the asphaltic or bound layers can increase the life of the surface layers, again by contributing to a strengthening of the bound layers. Such strengthening increases their ability to resist cyclic fatigue, thermal stresses during extremes of winter and summer temperatures, as well as increasing resistance to near surface crack propagation."

The report clearly identifies that asphalt reinforcements can extend pavement life by limiting reflective cracking and thus providing more sustainable pavements as a result. This paper aims to demonstrate the above referenced effect by comparing the ECO₂ based on the material consumption per year of lifetime of two construction techniques. One construction technique is the conventional rehabilitation of cracked overlays by milling and repaving; the second is a rehabilitation using a polyester asphalt reinforcement geocomposite in the same process.

The use of appropriate geosynthetic solutions in asphalt reinforcement applications can provide a reduced carbon footprint. Due to the reduction in fill/asphalt thicknesses there are related savings in carbon footprint, including a reduction in transport emissions and reduction in asphalt production emissions. A simple comparison between a reinforced and an unreinforced solution was done by Hessing (Hessing 2011). It was shown that, compared to the unreinforced overlay, savings up to of 60% ECO₂ can be achieved in the design life of a maintained reinforced asphalt pavement. Extending the pavement life and thus reducing the need for maintenance and the corresponding ECO₂ achieve this substantial savings.

8. MILLING AND RECYCLING

Even the best asphalt reinforcement cannot guarantee that an asphalt road will have an infinite life. The ease of removal of surfacing by milling is an increasingly frequent topic for discussion.

For this reason the impact of a polyester asphalt reinforcement on milling activities was investigated under defined conditions by the Institute of Road and Traffic Engineering at the RWTH Aachen University (RWTH 2008).

On the University's own 26m long, 1m wide test bed, RWTH staff can lay and remove lengths of road construction using ordinary methods typically employed on site. A rail-mounted paver machine with a high performance compacting screed installed the road materials. The surface was given its final compaction by a tandem vibratory roller.

For the milling tests a small milling machine with a milling drum width of 500mm was used.

The aim of the investigation was to analyze and evaluate the milling characteristics of the reinforced road construction in terms of process engineering and the machinery used. In addition to investigating particle size distribution and the type and size of reinforcement fibers in milled asphalt, the possibility of recycling the removed asphalt containing reinforcement fibers in the form of asphalt granulate in bitumen-bound layers was examined.

8.1 Test Procedure

A 60mm asphalt binder course (AB 0/16S) and an asphalt base were laid over a frost protection layer on the test bed. After a resting time of about one week, the PET asphalt reinforcement was installed in accordance with the manufacturer's installation instructions. This was then overlaid with a 40mm asphalt surface course (AB 0/11S).

8.2 Removal - Milling Tests

A milling depth of about 50mm was selected to ensure that the asphalt surface course and the first 10mm of the asphalt binder course (including reinforcement) were removed by the milling machine in a single milling operation (Figure 8). This procedure was recommended by the manufacturer for the removal of reinforced roads.

Result: During removal of the material no detrimental effect on the milling operation was observed. Over the full test length, the millings were finely graded. The fibers of asphalt reinforcement produced from the milling process were evenly distributed in the millings. The fibers had an average length of about 100mm.



Figure 8. Milling the asphalt including the reinforcement



Figure 9. Virtually no fibers on the milling drum

After completion of the milling operations, the milling drum was checked for adhering fibers. It was clear that over the whole test bed almost no (only 2) fibers had been trapped in the milling drum (Figure 9). During this test, no detrimental effects on the milling process were observed.

8.3 Recyclability: Effect of the Reinforcement Fibers on Marshall Stability

As part of tests on the recyclability of PET grid-reinforced asphalt, the effect of asphalt reinforcement fibers was investigated. Marshall test specimens were made from the asphalt binder layer material with and without asphalt reinforcement fibers and their Marshall stability and flow values were determined. The reference sample was defined as the asphalt binder course that was laid on the test bed. The asphalt reinforcement fiber content was the major difference between the two variants and the purpose of the test was to determine the effect of these fibers on Marshall Stability.

Result: There were only relatively small differences with respect to bulk density and void content between the Marshall test specimen used for the tests. The values for Marshall Stability and flow were virtually identical.

The results for the Marshall test parameters are shown in the following table.

Table 2. Results of Recyclability test

	Reference sample	With reinforcement fibers
Marshall Stability	8.4 kN	8.5 kN
Marshall Flow	3.6 mm	4.3 mm

No negative implications were observed in the course of the asphalt testing to determine the effect of asphalt reinforcement fibers on recyclability based on the Marshall Stability and Flow parameters.

9. LIMITS IN USING AN ASPHALT REINFORCEMENT GRID

There are limits in the types of asphalt problems that can be solved by using asphalt reinforcement. For example, the impact of asphalt reinforcement on the bearing capacity of a pavement has not been quantified. When a road has insufficient bearing capacity, it is necessary to carry out rehabilitation measures other than utilizing asphalt reinforcement, such as subgrade/base enhancement or increasing the asphalt thickness.

Another limitation of asphalt reinforcement involves large vertical movements in pavements. It is generally difficult to prevent crack propagation resulting from the large vertical movements that can be caused by concrete slabs which are not stable in their position or frost heave, even when using an asphalt reinforcement system.

In such cases, it is necessary to eliminate or minimize these movements prior to the installation of a reinforcement grid and the new asphalt layers (e.g. undertake injection below the slabs, or "crack and seat" the slabs to achieve a stress relief). One has to consider that reinforcement grids made of brittle raw materials (e.g. glassfibers) cannot resist shear forces. For this reason they tend to deteriorate quickly, especially when subjected to vertical movements (of concrete slabs, for example) that create shearing forces, even when they are minimal.

Manufacturers of grids made of brittle materials often point out that because of their fragility and brittleness (i.e. the low shear strength of fiberglass and the resulting high risk of damage) these grids should not be placed directly onto milled surfaces. The behavior of fiberglass reinforcements when placed directly over the sharp edges of cracks, especially during compaction, has not been clarified and requires further investigation.

10. CONCLUSION

Reflective cracking occurs in rehabilitated asphalt pavements. High tenacity Polyester as raw material is often chosen because of the high compatibility of its mechanical behaviour to the modulus of asphalt and its good behavior under dynamic loads. A bituminous coated Polyester asphalt reinforcement grid can show excellent results in delaying reflective cracking. This has been shown by numerous theoretical investigations and practical examples from the past several years.

Through research undertaken to complete a diploma thesis which analyzed and quantified the "effective tensile strength" for two different asphalt reinforcement products with different raw materials (polyester and fiberglass), it was shown that installation damage can have a noticeable influence on the properties of an asphalt reinforcement grid.

An investigation at the Institute of Road and Traffic Engineering of the RWTH Aachen University showed that milling and recycling of polyester grid-reinforced pavements does not negatively affect the milling process or the quality of the recycled asphalt.

REFERENCES:

- De Bondt, A.H., (1999), *Anti-Reflective Cracking Design of (Reinforced) Asphaltic Overlays*, Ph.D.-thesis, Delft, Netherlands.
- Helsinki University of Technology, Faculty of Civil Engineering and Surveying, (1992), Research Project Georeinforcements Part B: Laboratory Testing of Reinforcements, *Fifth International Conference on Geotextiles, Geomembranes and Related Products*
- Hessing C., Thesseling B., Alexander W. (2011), A sustainable maintenance method for cracked pavements using Polyester asphalt reinforcement, *14th International Flexible Pavements Conference*, Sydney, Australia
- ISO EN 10722-1. Geotextiles and geotextile-related products - Procedure for simulating damage during installation
- Knappenberg F., (1983) Report on Bruxelles/ Saventen Runway reinforcement
- Montestruque G. E., (2002), *Contribuição para a Elaboração de Método de Projeto de Restauração de Pavimentos Asfálticos Utilizando Geossintéticos em Sistemas Anti-Reflexão de Trincas (Contribution to the preparation of a method of a project for rehabilitation of asphaltic pavements using geosynthetics on anti-reflective crack systems)*. Ph.D.-thesis, Technological Institute of Aeronautics, São José dos Campos, Brazil.
- Montestruque G.E., Rodrigues R.M., Nods M., Elsing A., (2004), Stop of reflective crack propagation with the use of PET geogrid as asphalt overlay reinforcement, *Fifth International RILEM Conference*, Limoges, France.
- Monser C.A., Montestruque G.E., Silva A.E.F., (2010), Evaluation of an airport pavement after almost 8 years of overlay rehabilitation with a Polyester geogrid asphalt reinforcement, *9th International Conference on Geosynthetics*, Brazil.
- RWTH Aachen, (2008), Institute of Road and Traffic Engineering, Untersuchung der Asphaltbewehrung HaTelit® auf das Fräsverhalten von Asphalt und der Wiederverwertung des Ausbausphaltes.

Sakou L., (2011), Überprüfung der Wirksamkeit von Asphaltbewehrungssystemen unter Berücksichtigung der Einbaubedingungen, Diploma Thesis, RWTH Aachen, Institute of Road and Traffic Engineering
tBU (2003) Institut für textile Bau- und Umwelttechnik GmbH, Test Report Nr. 1.1/17810/493-2003e and 1.1/17810/494
2003e
WRAP Waste and Resource Action Plan (2010), *Sustainable Geosystems in Civil Engineering Applications*, UK

Prediction of Tensile Strength Behaviour of Coir Geotextiles

Dr .S. Chandrakaran, Professor, Department of Civil Engineering NIT Calicut
D.S.Shamla, Student, Department of Civil Engineering NIT Calicut

ABSTRACT

Tensile strength and elongation properties are the major requirements of geotextile used in various geotechnical applications. The present study deals with the prediction of the tensile strength behavior of the coir geotextiles by two empirical modeling methods- a multiple linear regression equation and an ANN (Artificial Neural Network) model. Warp yarn strength, warp yarn elongation, ends per metre (EPM), picks per metre (PPM) and scorage of the yarn were used as input parameters. Both the models were able to predict the geotextile strength with reasonably good precision although the ANN model demonstrated higher prediction accuracy. Warp yarn strength, number of warp yarns and ends per metre are the two most dominant factors determining the strength of geotextiles in warp direction. The scorage of the weft yarn and picks per metre have significant effect on the assistance and the strength of the geotextile in the warp direction.

1. INTRODUCTION

Geotextiles are woven / non-woven or knitted structures of natural /synthetic textile fibre used in various geotechnical, civil engineering and soil conservation applications. They can perform different functions like filtration, separation, drainage, reinforcement, erosion control etc.

Natural fibre geotextiles like jute and coir have recently gained increasing popularity in the field of geotechnical engineering all over the world, due to growing environmental concern. "Coir" is the agricultural fibre obtained from the husk of the coconut fruit which surrounds the base shell. It is a natural biodegradable material with a highly crystalline structure with the spiral angle of the micro fibres ranging between 30° - 45°. This leads to a greater extensibility than in most other natural fibres. Its high lignin content contributes to higher durability and slow bio-degradation compared to other natural fibres. It is also very long lasting, with infield service life of 4 to 10 years. Because of growing awareness of sustainable development coir geotextiles are increasingly used world over for various Civil Engineering applications such as slope stabilization, erosion control, sub-grade stabilization for low volume roads etc. Hence coir geotextile is recognized as an ideal material that is capable of offering an ecologically sustainable solution to many of the environment- related issues.

2. MATERIALS AND METHODS

For predicting the tensile strength of coir geotextiles two methods have been adopted- by developing a Linear Regression Equation and an Artificial Neural Network (ANN) model. The predicted results were compared with the existing experimental results.

3. MULTIPLE LINEAR REGRESSION

Multiple Linear Regression (MLR) is a well known statistical procedure trying to find a linear relationship between two or more explanatory variables and a dependent variable by observing data. It can be used for forecasting output values. Dependent variable (y) can be explained by the equation below:

$$y = a + \sum b x + \epsilon \quad [1]$$

Before using ANN, a multiple linear regression model is constructed. MLR is used as a verification and comparison model of ANN in the literature. It is claimed that ANN generally gives better results than MLR (Mithat Zeydan, 2010). Geotextile strength is defined as the dependent variable and explanatory variables are: number of warp yarns per fabric width, ends per metre (EPM), picks per metre (PPM), warp yarn strength, and scorage of the weft yarn.

4. STRENGTH PREDICTION BY ANN

Artificial Neural Network (ANN) is a very potent modelling tool, which mimics the functioning of biological neurons. The goal of this type of network is to create a model that can precisely map the functional relationship between inputs and outputs using historical data. Neural networks are composed of simple elements operating in parallel. These elements are inspired by biological nervous systems. As in nature, the connections between elements largely determine the network function, typically, neural networks are adjusted, or trained, so that a particular input leads to a specific target output. The figure below illustrates such a situation. There, the network is adjusted, based on a comparison of the output and the target, until the network output matches the target. Typically, many such input/target pairs are needed to train a network.

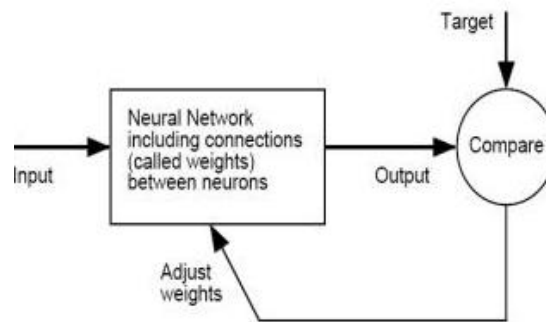


Fig .1Neural network model

The work flow for the neural network design process has six primary steps:

0. Collect data
1. Create the network,
2. Configure the network,
3. Initialize the weights and biases,
4. Train the network,
5. Validate the network and
6. Use the network.

In ANN, one or more hidden layers are positioned between one input layer and one output layer. Each layer is composed by a number of neurons or processing elements. Each neuron receives a signal from the neurons of the previous layer and each of these signals is multiplied by a separate weight known as synaptic weight. The weighted inputs are then summed up and passed through a transfer function, which converts the output to a fixed range of values. The output of the transfer function is then transmitted to the neurons of next layer. Finally the output is produced at the neurons of the output layer.

Back-propagation, a supervised learning algorithm, is the most popular among the existing ANN training algorithms namely forward pass and backward pass. In the forward pass, a set of data is presented to the network as input and its effect is propagated, in stages, through different layers of the network. Finally, a set of outputs is produced and the error vector is calculated. In the backward pass, this error signal is propagated backwards to the network and the synaptic weights are adjusted in such a manner that the error signal decreases in each iteration process. As the objective of the present endeavour is to predict the fabric strength, back-propagation algorithm was employed as it is apt for the prediction modelling. The algorithm uses the input-output data during training to optimize the synaptic weights, so that the error signal between actual and predicted output becomes minimum. Once the training is completed, the developed model can predict the output for any set of input pattern.

For ANN modelling, nn tool in MATLAB R2009a was used. 129 sample data had been collected for both multiple linear regression model and ANN, from the previous work done by Subaida et.al (2008). From the available 129 input-output data sets, 109 data sets were randomly chosen as training data and used for the development of ANN and linear regression models. Remaining 20 data sets were kept as testing data to evaluate the prediction performance of the models. ANN and regression predictions were done for various parameters of the coir geotextiles. By trial and error five parameters of the coir geotextiles were finally chosen for the prediction. Statistical parameters like mean absolute error% and coefficient of determination were used to judge the prediction performance of the developed models. Absolute error% was calculated by using the following expression.

$$\text{Absolute error\%} = \frac{\text{Actual value} - \text{Predicted value}}{\text{Actual value}} \times 100 \quad [2]$$

5. RESULTS AND DISCUSSION

5.1 Regression and ANN Models

The regression equation developed for the prediction of coir geotextile strength in warp direction is shown below

$$\text{Geotextile strength} = (0.1285 \times \text{No. of Warp Yarns}) - (0.9766 \times \text{Scorage}) + (0.2216 \times \text{Ends Per Metre}) - (0.1161 \times \text{picks Per Metre}) + (0.0472 \times \text{Warp Yarn Strength}) + 3.9611 \quad [3]$$

The summary of prediction performance of ANN and regression model is shown in Table1.

Table 1 Summary of fabric strip strength prediction results by ANN and regression models

Statistical Parameter	Training Data		Testing Data
	Co-efficient of Determination (R^2)	Co-efficient of Determination (R^2)	Mean Absolute Error (%)
ANN	0.98	0.94	1.9
Regression	0.91	0.94	2.4

It is noted that, in case of training data, the prediction performance of ANN model is better than that of regression model. The correlation coefficients between experimental and predicted values are 0.98 and 0.94 for regression and ANN models, respectively. Moreover, the absolute error of prediction was much lower for ANN model (1.90 %) as compared to that of regression model (2.4 %). It signifies superior modelling competency of ANN over the regression method. The scatter plot of experimental geotextile strength and predicted geotextile strength are depicted in figures 2 and 3.

It is observed that the actual and predicted geotextile strength values are more closely associated in case of ANN model. Table 2 shows the detailed prediction results of ANN and linear regression models in the testing data sets.

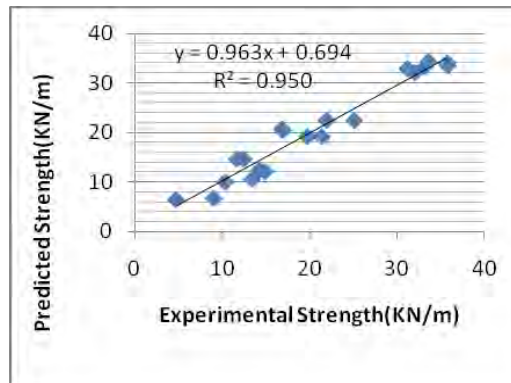


Fig 2 Scatter plot showing the experimental results and predicted geotextile strength by regression model

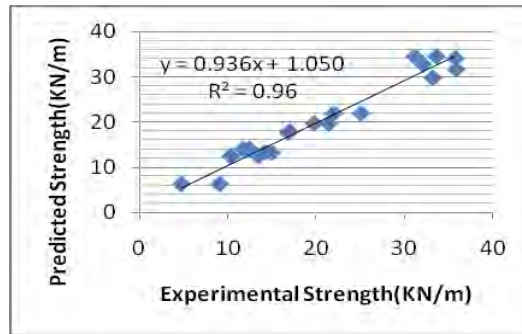


Fig 3 Scatter plot showing the experimental results and predicted geotextile strength by ANN

Table 3 Detailed fabric strip strength prediction results for testing data by ANN and regression models

Experimental Strength(KN/m)	Predicted Strength(KN/m)	
	ANN Model	Regression Model
10.33	12.4658	10.096
13.42	12.4792	10.61
14.91	13.2351	12.1762
14.16	13.314	12.4332
16.97	17.9458	20.4868
16.8	17.6161	20.7438
32.02	32.8168	32.0836
31.14	34.5435	32.8546
11.7	14.0295	14.714
12.42	14.0295	14.714
4.71	6.2618	6.5147
9.04	6.2799	6.7717
21.36	19.7181	19.2084
19.72	19.7181	19.2084
25.07	21.9174	22.4815
21.93	21.9174	22.4815
33.54	34.573	34.312
35.76	31.6971	33.541
33.15	29.8096	33.284
35.7	34.1469	34.055

It is observed that the performances of both the models are reasonably close to each other. Comparable prediction error shows that the ANN model was adequately trained and was able to achieve generalization.

5.2 Analyzing the Influence of Input Parameters

The influence of various input parameters on the geotextile strength was analyzed by curve fitting tool in Microsoft Excel and graphs were plotted with each parameter against the geotextile strength. All the parameters were kept at their middle value, except for the parameter whose influence is being estimated. Now, the parameter, whose importance is being evaluated, is varied from its minimum to maximum level and the corresponding change in the dependent variable or geotextile strength is noted. The influence of various parameters against the geotextile strength is shown in graphs plotted below.

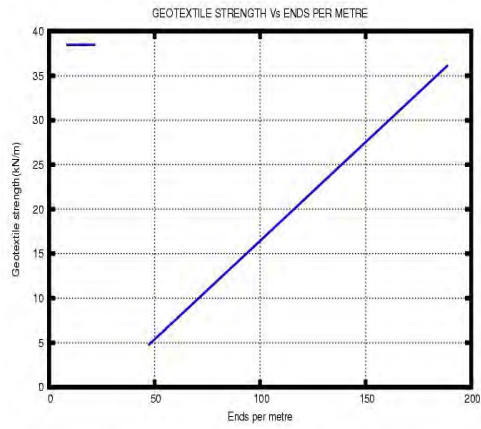


Fig 4 Effect of EPM on geotextile strength

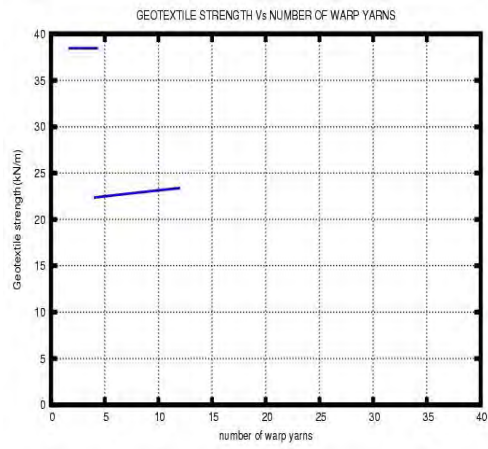


Fig 5 Effect of PPM on geotextile strength

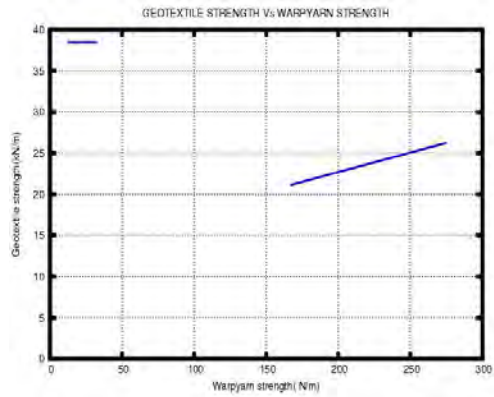


Fig 6 Effect of warp yarn strength on geotextile strength

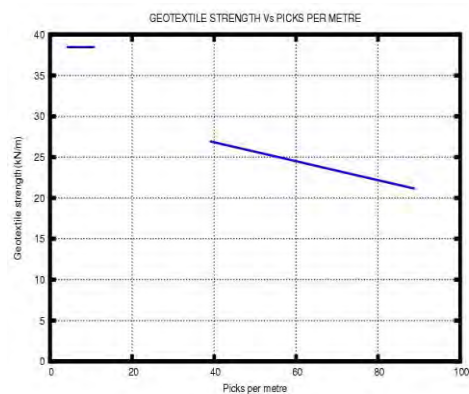


Fig 7 Effect of number of warp yarns on geotextile strength

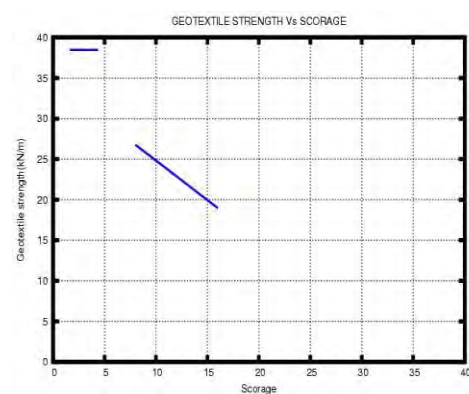


Fig 8 Effect of scorage of the weft yarn on geotextile strength

6. CONCLUSION

The tensile strength of coir geotextile has been predicted with two methods –by developing linear regression model and ANN model. Reasonably good accuracy was obtained by linear regression and ANN models using warp yarn strength, warp yarn number, ends per metre, picks per metre and weft yarn scorage as inputs. The prediction accuracy is consistent and better for ANN model than that of linear regression model. The absolute error in percentage obtained for the tested data was 2% for ANN model and 2.5% for multiple linear regression model. The co-efficient of determination for the trained data is 0.97 and 0.91 respectively for ANN and regression models. For the tested data the co-efficient of determination obtained are 0.97 and 0.95 for ANN and regression models correspondingly. From the analysis of various parameters show that warp yarn strength, no: of warp yarns and ends per metre are the two most dominant factors determining the strength of geotextile in warp direction. The scorage of the weft yarn and picks per metre have significant effect on the assistance and the strength of the geotextile in the warp direction.

REFERENCES

- Abhijit M, Anindya G, Anjan B, Ayan R ,Dhrubajyoti P, Shib Sankar S and Subir B : (2008) ,Empirical Modelling of Tensile Strength of Woven Fabrics , *Fibres and Polymers*, Vol.9, No.2:240-245
- Anwaruddin T , Tanveer H, Zulfiqar A M (2010) , Prediction of tensile strength of polyester/cotton blended woven Fabrics, *Indian journal of Fibre and Textile Research*, Vol.3:243-249
- ASTM D4595, Standard Test Method for Tensile Properties of Geotextiles by the Wide-Width Strip Method
- Cenk S, Onur B, R. Tugrul O, S. Noyan O (2006), The Prediction of Elongation and Recovery of Woven Bi-Stretch Fabric Using Artificial Neural Network and Linear Regression Models, *Fibres & Textiles*, Vol. 14, No. 2:46-49, www.fibtex.lodz.pl/56_14_46.pdf
- David B, Ning P (2000), Physical Properties of Twisted Structures.II. Industrial Yarns, Cords, and Ropes, <http://ningpan.net/Publications/51-100/72.pdf>

Howard B. D, Mark H B, Martin T. H: Neural Network Toolbox™ 7, User's Guide, www.mathworks.com/help/pdf_doc/nnet/rn.pdf

Maurizio G and Rocco F: Yarn Strength Prediction: A Practical Model Based on Artificial Neural Networks, (2010) *Advances in Mechanical Engineering*, Article ID 640103, 11 pages

Mithat Z: Prediction of Fabric Tensile Strength by Modelling the Woven Fabric (2010), *WovenFabricEngineering*, ISBN:978-953-307-194-7, www.intechopen.com/download/pdf/pdfs_id/12244

Savenije H. H. G, Balan K, Anil K. R., Van der Zaag P and Vishnudas S (2005), Experimental study using coir geotextiles in watershed management, *Hydrology and Earth System Sciences*, 2: 2327–2348,

Subaida. E.A., Sankar. N, Chandrakaran. S(2008), Prediction of Pullout Strength of Woven Coir Geotextiles from Yarn Pullout Resistances, 12th International Conference of International Association for Computer Methods and Advances in Geomechanics (IACMAG) 1-6 October,

Xungai W, Yuping Z (2002), Weibull analysis of the tensile behavior of fibres with geometrical irregularities, *Journal Of Materials Science* 37:1401 – 1406

Preliminary Assessment of the Mechanical Properties of Recycled-content Expanded Polystyrene (EPS) Block Geofoam

Chuanqi Wang, Graduate Research Assistant, The University of Memphis, USA, cwang1@memphis.edu
David Arellano, Associate Professor, The University of Memphis, USA, darellan@memphis.edu
Lee Ladely, EPS Development Scientist, NOVA Chemicals, Inc., USA, ladely@novachem.com
Dennis W. Koerner, Vice President of Technical Services, RAPAC, LP, USA, dennis.koerner@rapac.com

ABSTRACT

The unconfined compression strength test results performed on recycled-content expanded polystyrene (EPS) blocks indicate that EPS blocks consisting of recycled-content expandable polystyrene (PS) can be produced to meet the current ASTM D 6817 standard compressive resistance requirements. Additionally, the results also indicate that the overall recycled content may not significantly influence the compressive resistance values of recycled-content EPS blocks compared to virgin EPS blocks as demonstrated by the test results for a target density of 21.6 kg/m³, which showed compressive resistance values for 15% and 30% recycled-content blocks similar to the compressive resistance values obtained for a virgin EPS block with 0% recycled-content expandable PS. The compressive resistance results for the higher target density of 38.4 kg/m³ indicates the potential for an optimal recycled-content block that yields a higher compressive resistance than a virgin EPS block with 0% recycled-content expandable PS.

1. INTRODUCTION

Expanded polystyrene (EPS)-block geofoam made of virgin expandable PS is being successfully used in many civil engineering applications such as lightweight fill in roadway embankments over soft ground (Stark et al. 2004a, 2004b) and in landslide stabilization and repair (Arellano et al. 2010, Arellano et al. 2011a, 2011b); as a compressible inclusion to reduce lateral pressures on earth-retaining structures and earth pressures on underground utilities; as seismic buffers for building walls, bridge abutments, earth-retaining structures, and underground utilities; and as a buffer to reduce the increase in stresses due to thermal expansion of bridge integral abutments. At present, however, widespread use of recycled-content EPS is limited because no tool is available that can predict the key mechanical properties required to design recycled-content EPS blocks.

The primary obstacle to more widespread use of recycled-content EPS in civil engineering applications is the current lack of material prediction models that can provide the stress-strain-time-temperature behavior of recycled-content EPS. EPS blocks in civil engineering applications must typically support loads to prevent an ultimate limit state failure (collapse failure) as well as a serviceability limit state failure (failure due to excessive deformation). Therefore, the load-bearing capacity of EPS blocks is critical in civil engineering applications (Arellano and Stark 2009). The mechanical properties of EPS, which consist of the stress-strain-time-temperature behavior, are important in evaluating the load-bearing capacity of EPS blocks. Although recycled-content EPS is currently used in packaging material, this application is not as load-bearing critical as in civil engineering applications.

The overall goal of the research described herein is to develop stress-strain-time material prediction models for recycled-content EPS blocks that will allow engineers to perform structural response predictions in various civil engineering applications. Specifically, the proposed models will provide the stress-strain-time behavior of recycled-content EPS blocks thus allowing engineers to perform structural response predictions for various potential applications of recycled-content EPS, such as allowing engineers to determine the suitability of recycled-content EPS in lightweight fill applications that include roadway embankments, slope stabilization and repair, and levees.

This paper presents the preliminary results of unconfined compression strength tests completed for the purpose of evaluating the stress-strain properties of recycled-content EPS blocks. First, an overview of the recycled-content EPS manufacturing process and a description of the samples tested and tests performed are provided. After that, the unconfined compression test results of the recycled-content EPS samples are summarized and discussed. Lastly, conclusions based on the unconfined compression strength results are summarized.

2. OVERVIEW OF RECYCLED-CONTENT EPS BLOCK MANUFACTURING PROCESS

The recycled-content EPS block geof foam manufacturing process consists of the following primary steps: 1) recycling of pre- and post-consumer polystyrene (PS) and expandable PS, 2) pre-expansion of expandable PS beads, and 3) block molding. An overview of each step is subsequently provided.

Step1: Recycling of pre- and post-consumer polystyrene (PS) and expandable PS

Pre-consumer and post-consumer polystyrene (PS) and expandable PS material is sent into an extruder which melts and mixes the polystyrenic material, i.e., pre- and post-consumer PS and expandable PS. As the polystyrenic material exits the die of the extruder, it is cooled and solidified by water and the extruded polystyrenic material is cut into pellets by a pelletizer. Pre-extrusion and palletization of the recycled-content polystyrenic material facilitates mixing and further processing.

The polystyrenic material pellets undergo an additional extrusion process, whereby the pellets are impregnated with the blowing agent pentane and are transformed into recycled-content expandable PS beads. Virgin PS may also be added, but not required, during this additional extrusion process. Recycled-content expandable PS beads are defined herein to consist of the combination of polystyrenic material pellets and any virgin PS. The recycled-content expandable PS beads utilized in this research contain 60% recycled-content polystyrenic material (30% pre-consumer PS & expanded PS and 30% post-consumer PS & expanded PS) and 40% virgin PS.

Step2: Pre-expansion of recycled-content expandable PS beads

Before pre-expansion, the recycled-content expandable PS beads produced in Step 1 are combined with virgin expandable PS beads at the appropriate ratios to obtain a desired overall recycled-content block of 15% and 30%. The recycled-content expandable PS beads and virgin expandable PS beads are physically mixed together in a large ribbon blender. The overall recycled content of the block is defined as the ratio of the recycled-content expandable PS mass to the total (recycled-content and virgin) expandable PS mass used to mold the block. The 15% overall recycled content block was made by blending 25% of the recycled-content expandable PS beads produced in Step 1 with 75% of virgin expandable PS beads. The overall recycled content is calculated as $(25\% \times 60\% \text{ recycled-content PS beads}) + (75\% \times 0\% \text{ recycled-content virgin beads}) = 15\%$ overall recycled-content block. Similarly, the 30% overall recycled-content block was made by blending 50% of the recycled-content expandable PS beads produced in Step 1 with 50% of virgin expandable PS beads. The overall recycled content is calculated as $(50\% \times 60\% \text{ recycled-content expandable PS beads}) + (50\% \times 0\% \text{ recycled-content virgin expandable PS beads}) = 30\%$ overall recycled-content block.

The combined recycled-content and virgin expandable PS beads are placed in a pre-expander which injects steam to soften the PS beads and causes the blowing agent pentane within each bead to partially vaporize. The softened beads will expand to 50 times their original size due to the action of the blowing agent. The expanded beads are called pre-puff. The PS beads are pre-expanded to the appropriate pre-puff density needed to get an overall target EPS block density. In this stage, the steam properties, pressure in the expander, and expansion time will have an influence on the properties of the pre-puff and the final quality of the final EPS-block. The pre-puff is cured for 24 hours for physical stabilization.

Step 3: Block Molding

The stabilized pre-puff is moved into a molder and heated again with steam that is injected into the mold. "The residual blowing agent in the closed cells of each pre-puff particle causes some slight additional expansion of each particle. Because the outer skin of each pre-puff particle has been softened by the heat of the steam there will be thermal 'welding' (called bead fusion or simply fusion) at the contact points between the individual, expanding pre-puff particles (Horvath 2011). The fusion process transforms the pre-puff from individual grains to an EPS block with fused beads. In this stage, multiple factors, including the steam properties, pressure in the mold, molding time and the weight of pre-puff, will influence the final quality of the overall EPS-block.

As indicated in the summary of the block manufacturing process above, many variables such as steam temperature, steam pressure, pentane content, recycled content, density, curing time can impact the overall properties of the block. However, based on the experience with virgin EPS blocks, the primary variables that influence the mechanical properties of EPS blocks is the type (molecular weight) of PS used in the blend and overall EPS block density. Additionally, one hypothesis of this research is that the overall recycled content of an EPS block will have an influence on the mechanical properties. In this research, the pentane content was kept constant at 4%, and the other factors such as steam temperature, steam pressure and curing time were kept consistent throughout the study. Therefore, the results presented herein will focus on density and overall recycled content of the block.

3. DESCRIPTION OF SAMPLES AND TESTS PERFORMED

Unconfined compression, flexural, and creep tests will be conducted in order to obtain the mechanical properties of recycled-content EPS block geofoam. This paper presents the unconfined compression test results.

As previously noted, the recycled-content EPS block study focuses on the effect of density and overall recycled content on the stress-strain behaviour. ASTM D 6817 provides the physical property requirements for seven types of EPS blocks that are primarily based on density. However, this study is limited to evaluating the properties of recycled-content EPS blocks at two target densities of 21.6 kg/m³ and 38.4 kg/m³, which are the density requirements for ASTM types EPS22 and EPS39, respectively. ASTM 6817 provides minimum compressive resistance values for strains at 1%, 5%, and 10%. Therefore, the compression strength evaluation for recycled-content EPS blocks consists of comparing the recycled-content EPS block measured compressive resistance values to the ASTM required compressive resistance values.

Three different overall recycled-content EPS blocks were evaluated. As described in Step 2 of the manufacturing process, EPS blocks with an overall recycled content of 15% and 30% were tested. However, in order to provide a better comparison, blocks with only virgin expandable PS and no recycled-content expandable PS were also tested.

One 610 mm by 610 mm by 100 mm block sample was prepared for each combination of the two target densities and three overall recycled-content block types that were to be tested. Therefore, six different block samples were prepared for this study. The blocks were cured for 24 hours. ASTM C 165-05 recommends that a minimum of four specimens be tested and ASTM D 6817-11 recommends the use of 50 mm cube specimens. Therefore, four 50 mm cube specimens were prepared from each block sample for compression strength testing. The specimens were conditioned per ASTM D 1621.

Density measurements were obtained on each specimen based on the ASTM D 1622 procedure. The uniaxial unconfined compression test load frame S-610 manufactured by Durham Geo Slope Indicator was used to conduct the uniaxial unconfined compression tests. A displacement rate of 5.0 mm/min, which is equivalent to 10% strain per minute, was used in the compression tests based on the ASTM D 6817 procedure. WINSAS™ data acquisition software was used to record the compression platen displacement and the corresponding load during the tests. The “zero deformation point” method proposed in ASTM C 165-05 and ASTM D1621-10 was used to correct the compressive resistance values obtained from the tests. According to Horvath (2011), because platen-seating errors on an EPS test specimen surface that may not be perfectly smooth, planar and perpendicular to the direction of load application results in a slight concave-downward shape at the beginning of a stress-strain curve, correction of the stress-strain curve is required.

4. UNCONFINED COMPRESSION STRENGTH TEST RESULTS

Tables 1 through 6 show the measured densities and unconfined compression strength tests results as well as the average values obtained on the four specimens tested from each block sample and the corresponding standard deviation.

Table 1. Measured densities and compressive resistances of Sample A (15% recycled content, target density 21.6 kg/m³).

Specimen No.	Measured density (kg/m ³)	Compressive resistance (kPa)		
		1%	5%	10%
1	20.38	74	121	136
2	20.00	67	115	130
3	19.91	69	115	132
4	19.48	67	109	125
Avg.=	19.94	69.25	115	130.75
Std. Dev.=	0.32	2.86	4.24	3.96

Table 2. Measured densities and compressive resistances of Sample B (30% recycled content, target density 21.6 kg/m³).

Specimen No.	Measured density (kg/m ³)	Compressive resistance (kPa)		
		1%	5%	10%
1	19.14	56	108	124
2	20.51	61	114	135
3	20.29	62	116	133
4	20.49	64	119	137
Avg.=	20.11	61	114	132
Std. Dev.=	0.56	2.95	4.02	4.97

Table 3. Measured densities and compressive resistances of Sample C (0% recycled content, target density 21.6 kg/m³).

Specimen No.	Measured density (kg/m ³)	Compressive resistance (kPa)		
		1%	5%	10%
1	22.41	81	145	160
2	21.91	83	137	150
3	21.95	77	139	152
4	21.89	77	143	157
Avg.=	22.04	80	141	155
Std. Dev.=	0.21	2.60	3.16	3.96

Table 4. Measured densities and compressive resistances of Sample D (15% recycled content, target density 38.4 kg/m³).

Specimen No.	Measured density (kg/m ³)	Compressive resistance (kPa)		
		1%	5%	10%
1	38.25	224	322	347
2	38.02	229	329	354
3	38.28	229	335	360
4	38.27	216	319	346
Avg.=	38.21	225	326	352
Std. Dev.=	0.11	5.32	6.22	5.67

Table 5. Measured densities and compressive resistances of sample E (30% recycled content, target density 38.4 kg/m³).

Specimen No.	Measured density (kg/m ³)	Compressive resistance (kPa)		
		1%	5%	10%
1	38.04	183	297	326
2	36.43	179	288	317
3	36.38	182	286	315
4	38.25	180	298	327
Avg.=	37.27	181	292	321
Std. Dev.=	0.87	1.58	5.31	5.31

Table 6. Measured densities and compressive resistances of sample F (0% recycled content, target density 38.4 kg/m³).

Specimen No.	Measured density (kg/m ³)	Compressive resistance (kPa)		
		1%	5%	10%
1	36.89	194	299	326
2	38.85	198	314	343
3	38.63	201	308	337
4	36.91	202	299	327
Avg.=	37.82	199	305	333
Std. Dev.=	0.92	3.11	6.36	7.08

Because of limited experience molding recycled-content EPS blocks as well as inherent density variations that typically occur within a block, the measured densities obtained on the specimens are different from the target densities. Based on the experience with virgin EPS blocks, the density of an EPS block is related to the unconfined compression strength (Horvath 1995, Stark et al. 2004a). Therefore, in order to compare the unconfined compressive strength results obtained from the recycled-content EPS block specimens with the ASTM D 6817 compression strength requirements, linear regression analyses were performed to develop a relationship between the measured densities and compressive resistance values obtained from all specimens. Figures 1 through 3 provide the compressive resistance values at 1%, 5%, and 10%, respectively, versus density for the various overall recycled-content block samples tested. The linear regression relationships are also included in these figures as well as the requirements for ASTM types EPS22 and EPS39, which represent the two target densities of 21.6kg/m³ and 38.4 kg/m³ desired of the recycled-content EPS blocks.

From the linear regression relationships shown in Figures 1 through 3, normalized compressive resistance values were determined for each of the two ASTM target densities. Tables 7 and 8 provide the normalized compressive resistance values for target densities of 21.6kg/m³ and 38.4 kg/m³, respectively. As indicated by Tables 7 and 8 and as shown by Figures 1 through 3, the block samples met the ASTM minimum compressive resistance values for both target densities and for all overall recycled contents tested. Therefore, the unconfined compression strength test results indicate that recycled-content EPS blocks can be molded to meet the ASTM D 6817 compressive resistance requirements.

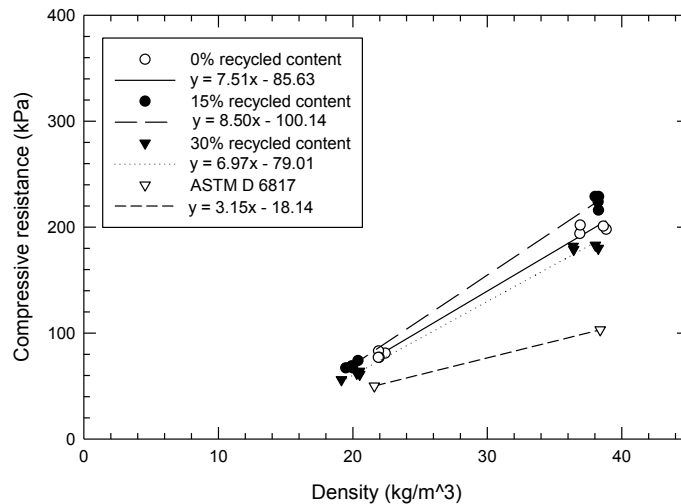


Figure 1. Regression relationships between density and compressive resistance at 1% strain.

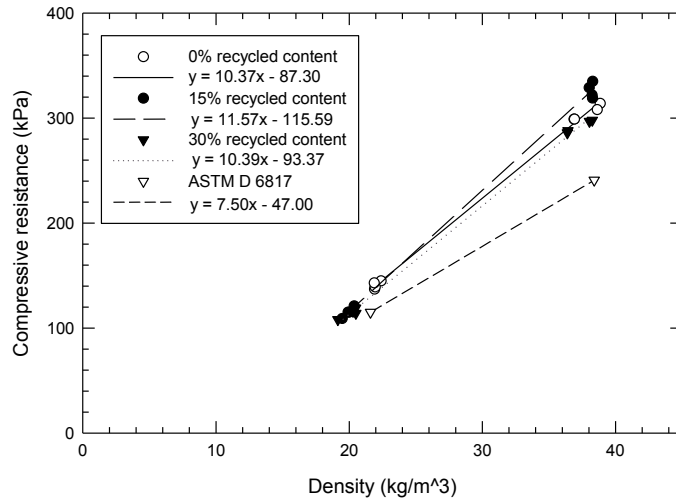


Figure 2. Regression relationships between density and compressive resistance at 5% strain.

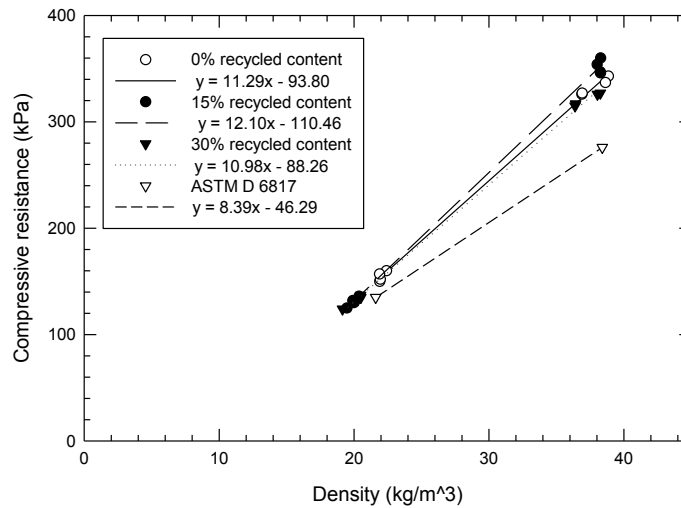


Figure 3. Regression relationships between density and compressive resistance at 10% strain.

Table 7. Normalized compressive values for target density of 21.6 kg/m³.

Sample	C (0%)	A (15%)	B (30%)	ASTM EPS22
Target density (kg/m ³)	21.6	21.6	21.6	21.6
Recycled content (%)	0	15	30	0
1% Compressive Resistance (kPa)	77	83	71	50
5% Compressive Resistance (kPa)	137	134	130	115
10% Compressive Resistance (kPa)	150	151	149	135

Table 8. Normalized compressive values for target density of 38.4 kg/m³.

Sample	F (0%)	D (15%)	E (30%)	ASTM EPS39
Target density (kg/m ³)	38.4	38.4	38.4	38.4
Recycled content (%)	0	15	30	0
1% Compressive Resistance (kPa)	203	226	189	103
5% Compressive Resistance (kPa)	311	329	304	241
10% Compressive Resistance (kPa)	340	354	333	276

Figure 4 shows a comparison of normalized compressive strength with recycled content variance. At the target density of 21.6 kg/m³, the compressive resistance behaviour is not very sensitive to recycled content because the compressive resistance values for recycled content of 0%, 15% and 30 % are similar for each strain range of 1%, 5%, and 10%. Therefore, the compressive resistance data at a target density of 21.6 kg/m³ indicates that blocks consisting of a higher recycled content than the blocks tested herein, i.e., greater than 30% recycled content, may also meet the ASTM D 6817 requirements.

At the target density of 38.4 kg/m³, the compressive resistance behaviour shows a greater compressive resistance at 15% recycled content compared to both 0% and 30% recycled content. Therefore, the compressive resistance data for the higher target density of 38.4 kg/m³ indicates a possible optimum recycled content that can produce a higher compressive resistance. As with the target density of 21.6 kg/m³ data, the 38.4 kg/m³ data also indicates that blocks consisting of a higher recycled content than the blocks tested herein may also meet the ASTM D 6817 requirements.

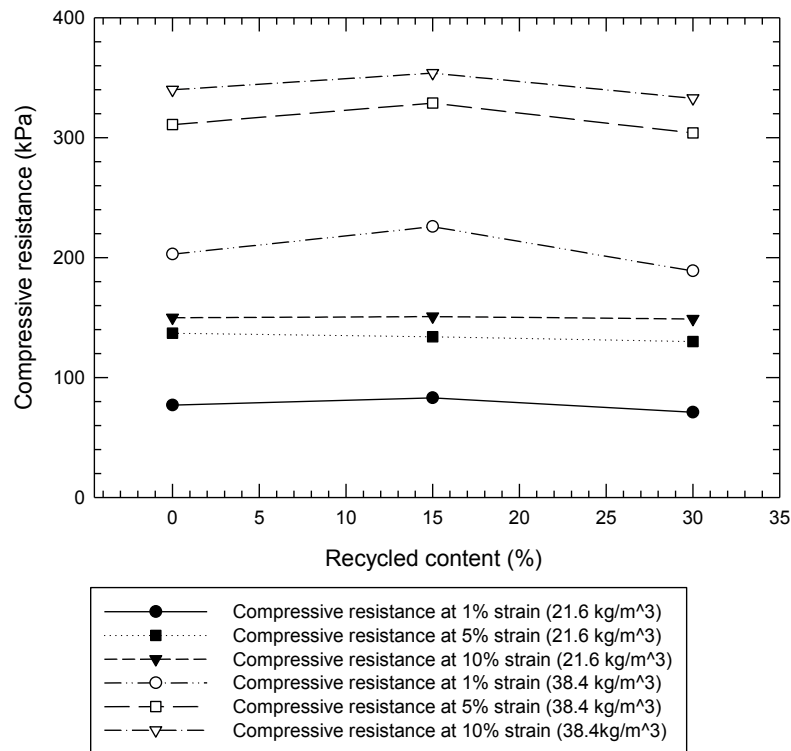


Figure 4. Comparison of normalized compressive strength with recycled content variance.

5. CONCLUSION

The unconfined compression strength test results performed on recycled-content EPS blocks indicate that EPS blocks consisting of recycled-content expandable PS can be produced to meet the current ASTM D 6817 standard compressive resistance requirements. Additionally, the results also indicate that the overall recycled content may not

significantly influence the compressive resistance values of recycled-content EPS blocks compared to virgin EPS blocks as demonstrated by the test results for a target density of 21.6 kg/m³, which showed compressive resistance values for 15% and 30% recycled-content blocks similar to the compressive resistance values obtained for a virgin EPS block with 0% recycled-content expandable PS. The compressive resistance results for the higher target density of 38.4 kg/m³ indicates the potential for an optimal recycled-content block that yields a higher compressive resistance than a virgin EPS block with 0% recycled-content expandable PS.

The research program includes supplemental compression resistance tests as well as flexural and creep tests. The results of these tests will facilitate accomplishment of the overall research goal, which is to develop stress-strain-time material prediction models for recycled-content EPS blocks that will allow engineers to perform structural response predictions in various civil engineering applications. Unlike traditional waste materials used in civil engineering applications, the benefit of the EPS recycling process is that it can be modified to achieve the desired engineering properties. Thus, the successful characterization and use of recycled-content EPS will contribute to wider acceptance of other recycled materials, such as plastics and glass that can be recycled in a controlled manner, in civil engineering applications. Importantly, extending the use of recycled-content EPS blocks to civil infrastructure applications will decrease the volume of polystyrene that ends up in landfills and will contribute to more sustainable infrastructure systems.

ACKNOWLEDGEMENTS

The authors thank Rapac, LP for providing the recycled-content expandable PS beads and NOVA Chemicals, Inc. for providing the virgin expandable PS beads and for molding the recycled-content EPS blocks.

REFERENCES

- Arellano, D., Stark, T.D. (2009). Load bearing analysis of EPS-block geofam embankments, *Proceedings of the 8th International Conference on the Bearing Capacity of Roads, Railways and Airfields*, Champaign, IL, USA, 981-990
- Arellano, D., Tatum, J.B., Stark, T.D., Horvath, J.S., and Leshchinsky, D. (2010). A framework for the design guideline for EPS-block geofam in slope stabilization and repair, *Transportation Research Record*, 2170, 100-108
- Arellano, D., Stark, T.D., Horvath, J.S. and Leshchinsky, D. (2011a). NCHRP Project 24-11(02), Guidelines for geofam applications in slope stability projects: final report, *NCHRP Project, No. 24-11(02)*, Transportation Research Board, Washington D.C.
- Arellano, D., Stark, T.D., Horvath, J.S. Leshchinsky, D., Kafash, M.H. and Wang, C. (2011b). Overview of the NCHRP design guideline for EPS-block geofam in slope stabilization and repair, *4th International Conference on Geofam Blocks in Construction Application (EPS 2011 Norway)*, Norway
- ASTM C 165-05. Standard Test Method for Measuring Compressive Properties of Thermal Insulations, *American Society for Testing and Materials*, West Conshohocken, Pennsylvania, USA.
- ASTM D 1621-10. Standard Test Method for Apparent Density of Rigid Cellular Plastics, *American Society for Testing and Materials*, West Conshohocken, Pennsylvania, USA.
- ASTM D 1622-08. Standard Test Method for Compressive Properties of Rigid Cellular Plastics, *American Society for Testing and Materials*, West Conshohocken, Pennsylvania, USA.
- ASTM D 6817-11. Standard Specification for Rigid Cellular Polystyrene Geofam, *American Society for Testing and Materials*, West Conshohocken, Pennsylvania, USA.
- Horvath, J.S. (1995), *Geofam Geosynthetic*, Scarsdale, New York, USA
- Horvath, J.S. (1998), Mathematical modeling of the stress-strain-time behavior of geosynthetics using the findley equation: general theory and application to EPS-blocks geofam, *Manhattan College Research Report No. CE/GE-98-3*, New York, USA
- Horvath, J.S. (2011), Manufacturing quality issues for block-molded expanded polystyrene geofam, *Manhattan College Research Report No. CEEN/GE-2011-2*, New York, USA
- NIST/SEMATECH. (2010), *e-handbook of statistical methods*. <<http://www.itl.nist.gov/div898/handbook/>>
- Stark, T. D., Arellano, D., Horvath, J. S., and Leshchinsky, D. (2004a). Geofam applications in the design and construction of highway embankments. *NCHRP Web Document 65 (Project 24-11)*, Available at http://trb.org/publications/nchrp/nchrp_w65.pdf, Transportation Research Board, Washington, D.C.
- Stark, T. D., Arellano, D., Horvath, J. S., and Leshchinsky, D. (2004b). Guideline and recommended standard for geofam applications in highway embankments. *NCHRP Report 529*, Available at http://trb.org/publications/nchrp/nchrp_rpt_529.pdf, Transportation Research Board, Washington, D.C.

Preliminary Evaluation of Thermally Induced Strains and Pressures Developed in a GRS Integrated Bridge System

K. A. Warren, University of North Carolina at Charlotte, USA, kawarren@uncc.edu

M. Whelan, University of North Carolina at Charlotte, USA, M.WheLAN@uncc.edu

M. Adams, Federal Highway Administration, USA, Mike.Adams@dot.gov

J. Nicks, Federal Highway Administration, USA, Jennifer.Nicks@dot.gov

ABSTRACT

An emerging technology that uniquely integrates commonly constructed bridge superstructures with geosynthetic reinforced soil bridge abutments is currently being promoted by the Federal Highway Administration. This technology enables rapid construction of single-span bridges without the expense of deep foundations, expansion joints, and approach slabs while eliminating the development of a “bump at the end of the bridge”, which generates long term maintenance costs. A 42.7 m long single-span bridge was constructed in Ohio using this integrated system approach. It is currently the longest GRS IBS in the US. To study the thermally induced interactions between substructure and superstructure, the bridge abutments and superstructure were heavily instrumented with vertical pressure cells, lateral pressure cells, strain gage, and survey targets. This paper provides a description of the construction process, a summary of the instrumentation utilized, and select data collected over a three year monitoring period.

1. INTRODUCTION

Since many of the existing single span bridges are reaching or have exceeded their expected service life, there is an increasing need to replace many of these bridges (Adams et al., 2007). Reducing the cost of construction is increasingly critical given the lack of funding at the county, state, and federal level to address the current bridge replacement need. Typically, bridges are constructed on deep foundations to minimize movement and vertical deformations, but deep foundation design and construction can be expensive due to the cost of the specialty contractors, among other things. Bridge abutments are typically designed using a conventional, integral, or semi-integral configuration in line with current practice, but each of these methods inherently has issues (Tatsuoka et al., 2009). The Federal Highway Administration (FHWA) at the Turner-Fairbanks Highway Research Center in McLean, Virginia developed and continues to refine Geosynthetic Reinforced Soil (GRS) Integrated Bridge System (IBS) technology (Adams et al., 2007, Adams et al., 2011a; Adams et al., 2011b), which uniquely integrates a commonly constructed bridge superstructure with a GRS abutment substructure. GRS IBS technology can potentially accommodate the construction or replacement of single span, low volume bridges without the need for deep foundations, expansion joints, or approach slabs, and without developing a “bump at the end of the bridge”.

While this project specifically targets GRS IBS technology, is important to note that conventional GRS bridge supporting structures have been constructed successfully in the U.S. and abroad for many years. Lee and Wu (2004) provide an excellent review of the configurations for and performance data collected on numerous GRS bridge-supporting structures. More recently, Adams et al. (2011b) summarized the performance of in-service GRS abutments (specifically GRS Integrated Bridge Systems between 2005 and 2010), and this report indicates that GRS IBS technology has the potential to advance the state of single span bridge design and construction. Also included in this report (Adams et al., 2011b) is a performance overview of several other bridges built with GRS abutments in the private and public sectors within the U.S. and Canada in addition to various case studies of GRS walls built during the past 20 years to validate the long-term performance of these structures. This paper will provide details regarding the construction of the largest GRS IBS to date and preliminary data collected during the first three years of this project. The long term goal of this research project is to evaluate the thermally induced interactions between the superstructure and the GRS approach behind it. There is some indication that the early-age substructure interactions are stable, which contrasts with the problematic ratcheting effect observed in conventional, integral, and semi-integral abutment bridge designs. Additionally, it is important to point out that this technology is constructed without the construction costs and long term maintenance expenses associated with deep foundations, expansion joints, and approach slabs.

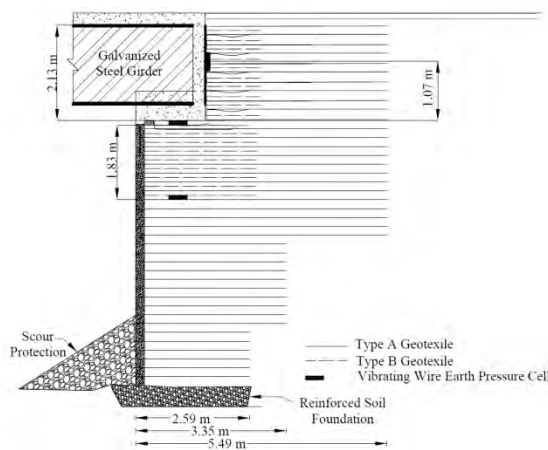
2. GEOSYNTHETIC REINFORCED SOIL (GRS) INTEGRATED BRIDGE SYSTEMS (IBS)

The structural components of a GRS IBS include a reinforced soil foundation, the GRS abutment, and the GRS integrated approach (Adams et al., 2011a). Each GRS abutment is constructed using 1) controlled fill between each reinforcement (a clean, crushed aggregate that meets AASHTO standards), 2) tight geosynthetic spacing (typically 20.3

cm with a 30.5 cm maximum), and 3) excellent compaction with special attention paid to the areas near the face of the wall since the load is placed directly behind of the face of the abutment. The tight spacing specified for a GRS IBS is non-negotiable to ensure the interaction between each geosynthetic reinforcement and soil layer is not compromised. The use of controlled, high quality fill material with excellent compaction also ensures that any movements are minimal and within the tolerable limits of the structure. In addition to the GRS abutment, the approach fill is also constructed using GRS techniques to minimize subsidence of the approach fill relative to the diaphragm wall.

When the superstructure design includes a reinforced concrete deck on steel girders (as was the case in this project), the girders are positioned on a reinforced concrete footing that is cast directly on the GRS abutment, and a diaphragm wall is formed at the beam ends similar to an integral or semi-integral abutment configuration. Because the concrete footing is cast directly on the GRS abutment, traditional bridge bearings between the superstructure and the GRS abutment are not installed. As a result, thermal movements of the superstructure induce some lateral movement in the upper portion of the GRS abutment with dissipation of the lateral stresses due to the flexibility of the system. Whether using steel or concrete superstructure elements, the GRS approach fill is compacted directly against the diaphragm wall. Based on performance monitoring of this arrangement conducted by the FHWA, there is no requirement of an expansion joint or approach slab. The specific requirements for the integrated approach are outlined by Adams et al. (2011a) in the most recent interim implementation guide for this technology. In addition to reduced construction cost and time, this design can easily be modified for unforeseen site conditions, construction is less dependent on weather conditions, and the IBS is easier to maintain because there are fewer components susceptible to deterioration (e.g. bearings). However, based on current field experience with this technology, GRS IBS should be limited to single span bridges with low scour potential if crossing over water.

As of January 2012, the FHWA reports that a total of 68 state DOT projects in 28 states are currently at some stage of development (conceptual to construction). In 2005, Defiance County, Ohio teamed up with the FHWA during the early stages of GRS IBS field deployment (Adams et al., 2007). As of 2011, the County Engineer in Defiance reports that they have constructed 25 single span bridges with span lengths ranging from 3.1 m – 42.7 m, and benefited from a 25% – 50% cost savings on these projects in comparison to more conventional technologies they have utilized in the past. Figure 1(a) displays the design profile of the GRS IBS constructed over the Tiffin River in Defiance, Ohio as part of this project. It is the largest single span GRS IBS constructed to date (42.7 m in length). Figure 1(b) displays a photograph of the actual bridge that was instrumented and is currently being monitored by UNC Charlotte as part of the research study.



a) design profile



b) constructed bridge in Ohio

Figure 1. Geosynthetic Reinforced Soil (GRS) Integrated Bridge System (IBS).

3. INSTRUMENTATION PLAN

Since this IBS does not include an expansion joint or approach slab in the design or construction of this bridge, one might expect surface cracks to develop in the same way the “bump at the end of a bridge” develops for more conventional designs. However, long term monitoring of GRS IBS bridges constructed over recent years indicates that cracking does not develop and the deformations measured post-construction are insignificant and within allowable deformation criteria. To evaluate the thermally induced interactions between the superstructure and GRS substructure,

both components were heavily instrumented with a network of sensors that measure strain, vertical pressure, lateral pressure, and abutment/footing deformation (Figure 2).

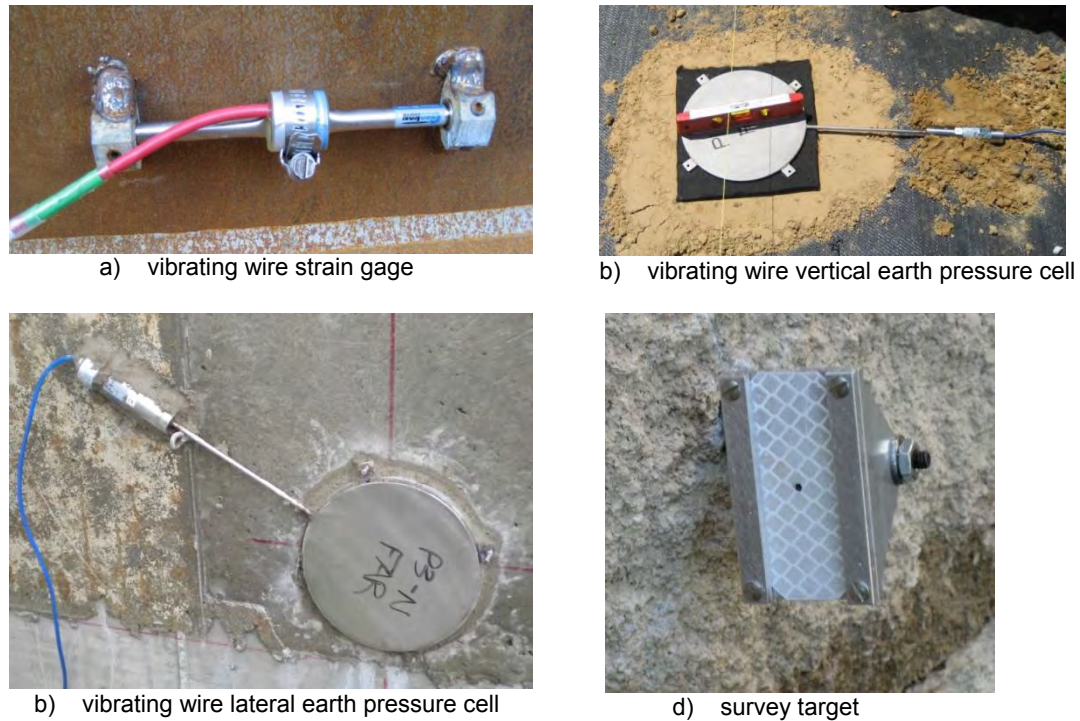


Figure 2. Project instrumentation.

Five steel girders were instrumented with 36 vibrating wire strain gages (Figure 2(a)) to measure the thermally induced deformations in the steel. It is important to note that vibrating wire technology was utilized for all sensors in this study to collect static measurements of strain and pressure as a result of thermal changes to the system. Dynamic loading conditions were not assessed and there are no stationary traffic loads that exist on this bridge, located on a rural county road. The mounting blocks for the strain gages were arc-welded to the girder sections at the steel fabrication plant, and the strain gages were installed just before the girders were erected on site. Strain gages were installed at the top and the bottom of the web on each girder as displayed on Figure 3. The 12 strain gage configuration displayed in Figure 3 was installed at the center of the bridge and approximately 1.7 m from the face of each GRS abutment. The gages were positioned on the inside of each girder to ensure they were not exposed to direct sunlight. The cables were aligned on the top surface of the bottom flange and fed into nonstructural pipe that was secured to the underside of the girders near the north abutment where the main data acquisition enclosure was located. Only one gage failed during the installation process (97% strain gage survivability).

At two elevations within each GRS abutment (see Figure 1(a)), three vibrating wire vertical pressure cells (Figure 2(b)) were installed. At each elevation, one cell was centrally located under the concrete footing and the other two cells were positioned approximately 2.7 m on either side of center. At each elevation, a small hole was drilled through one of the blocks on the side wing wall, and a pipe was fit through the hole to bring the cables from the inside of the abutment to the face of the wing wall. Plumbing was installed on the side of each abutment to protect these cables from vandalism and flood debris.

Three vibrating wire lateral earth pressure cells (Figure 2(c)) were installed on the back of the superstructure concrete diaphragm adjacent to the GRS reinforced approach fill to measure the horizontal soil pressure at each end of the bridge as the girders expand and contract with the normal thermal cycle. A layer of mortar was positioned between the cell and diaphragm wall to ensure a smooth transition between the bearing surface and the cell. A thick, nonwoven geotextile was glued to the face of the lateral pressure cells to protect the cells from excessive contact pressures as the stone backfill was compacted. These cables were also fed through a PVC pipe positioned inside the wing wall. One of the pipes installed on the wing wall of the south abutment is displayed in Figure 1(b).

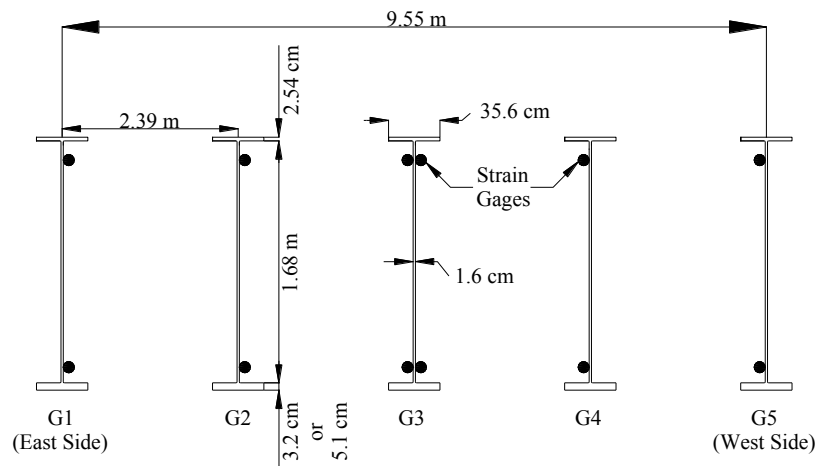


Figure 3. Strain gage installation configuration.

The Campbell Scientific data acquisition system includes a CR1000 data logger, three AVW200 vibrating wire spectrum analyzer modules, four AM16/32 multiplexers, an RF401 spectrum data radio modem, a Raven cellular modem, an Omni cellular antenna, and a power supply. All strain gages installed on the steel girders and all pressures measured on the north abutment were wired directly to the multiplexers connected to the logger on the north abutment. The remaining pressure cells on the south abutment were collected by a multiplexer on that side of the bridge, and the data was radioed to the logger on the opposing side of the bridge. Combined, these peripherals enabled UNC Charlotte to successfully establish a remote connection to the data acquisition system in Ohio and eliminated the need to implement a second data logger on the south abutment, which would have required a second cell phone connection. Deep cycle batteries charged by solar panels provide continuous power to the monitoring systems on site.

Three reflective survey targets (see Figure 2(d)) were mounted on each girder footing and nine targets were installed on the face of each GRS wall above the countermeasure (a total of 24 targets between the two sides of the bridge) to measure girder settlement, global GRS abutment settlement, and wall deflection. A permanent total station mount installed on site provides a fixed point of reference for the ongoing measurements collected by Defiance County (i.e. horizontal angle, horizontal distance, and vertical distance readings) to determine the three-dimensional coordinates for each target with time. Baseline readings were collected at the completion of each abutment and just prior to girder placement. Survey readings were recorded for all major loading events during the construction process and continue to be monitored.

4. GRS IBS CONSTRUCTION

The earth work and construction associated with the GRS abutments for this project was completed using a 4-6 man crew of county personnel, and it took them approximately 2 – 4 construction days to complete each GRS abutment. The abutments were constructed using 1) controlled fill between each reinforcement, 2) tight geosynthetic spacing, and 3) excellent compaction with special attention paid to the areas near the face of the wall since the load is placed directly behind the face of the wall. The FHWA recommends a setback distance of at least 20.3 cm (Adams et al., 2011a). The GRS abutment facing was constructed using solid core concrete masonry units (CMUs) on the bottom 1.5 m of the wall and hollow core CMUs for the remaining height. CMU dimensions were 20.3 cm by 20.3 cm by 40.6 cm. Figure 4(a) displays the construction of the initial reinforced layers.

The GRS layers were backfilled with AASHTO No. 89 crushed stone (Figure 4(a)) and compacted using method specifications (e.g. three passes with a vibratory plate tamper and a hand tamper along the edges) in accordance with Adams et al. (2011a). Compatible fill should be well graded or open-graded gravel to ensure excellent compaction directly behind the face of the wall, facilitate alignment of the facing, and limit post construction lateral deformation (Adams et al., 2011). At the completion of each compacted layer, a woven geotextile reinforcement (wide width tensile strength = 70 kN/m) was positioned between each course of block, creating a frictional connection that resulted in a vertical spacing equal to 20.3 cm.



a) GRS abutment construction



b) footing placement on GRS abutment



c) concrete footing



d) steel girders set on GRS abutment



e) constructed GRS approach



f) Concrete deck pour

Figure 4. Project construction phases.

The lengths of the primary reinforcement varied from 2.6 m (at the bottom) to 5.5 m at the top of the abutment, and a secondary geotextile reinforcement was installed to create the bearing bed for additional support beneath the footing, and within the approach fill behind the girders to minimize settlement (see Figure 1(a)). Due to the bearing loads on the top of each GRS abutment, the top three courses of the hollow core CMUs (just below the girder footing) were reinforced by filling their cores with concrete and installing rebar dowels. Before the footing was formed and poured, a layer of geofoam was placed on the top of the facing block and a single row of solid block was positioned behind it on top of the stone fill to help carry the front load of the footing without direct application to the facing (Figure 4(b)). The left side of the concrete footing in Figure 4(b) lines up with the front face of the wall. The geofoam is positioned between the CMU and the footing to the left of the solid block, and the top GRS layer is displayed behind the solid block in this photograph. Details of this general configuration are discussed in Adams et al. (2011). Figure 4(c) displays a photograph of the final footing cast directly on the GRS abutment with the exposed reinforcing steel for the back of the concrete diaphragm.

Using a large crane, local contractors positioned the steel girders on the reinforced concrete footing. The contractors attached the cross-bracing, installed the necessary steel reinforcement across the girder ends, and formed the concrete diaphragm with two additional concrete pours on top of the footing, encasing the ends of the girders (displayed in Figure

4(d)). The lateral pressure cells were installed mid-height on the back of the diaphragm before the construction of the GRS approach and wing walls was completed. Figure 4(e) displays the completed GRS approach, and Figure 4(f) displays the concrete cast in place deck. Two data acquisition enclosures were permanently installed on the north abutment (far abutment in Figure 4(f)) to handle all 36 strain gages and the nine pressure cells on the north side. A third data acquisition enclosure was installed on the south abutment to collect the pressure cell data on the opposing abutment and send it wirelessly to the logger on the north abutment. In both cases, these enclosures were conveniently located behind the guardrail for safety and accessibility. The anticipation of high flood waters prevented the positioning of these enclosures anywhere below the top of the abutments.

5. DISCUSSION OF PRELIMINARY RESULTS

Data continues to be collected from all 54 sensors at a two minute sampling rate. While considerable data has been collected and analyzed, the following figures have been selected for display in this paper due to space limitations. A more detailed evaluation of the full data set is in the process of being prepared for publication. All data displayed in the figures herein have been processed through a 30-day moving average digital filter to attenuate daily thermal fluctuations. This post-processing stage was performed to better illustrate the long term behaviors of the GRS IBS for the purpose of evaluating the interaction between the superstructure and the GRS integrated approach behind each end of the bridge.

Figure 5 displays the average ambient temperatures for both the top and bottom strain gages as a function of time over the three year monitoring period. The long term ambient temperatures clearly follow typical thermal cycles, and there is very little difference measured between the gages installed on the web near the top flange versus the gages installed on the web near the bottom flange (locations of these gages are displayed in Figure 3) throughout the majority of the year. During the summer months, a temperature differential of a few degrees Celsius (at most) develops throughout the depth of the girder (see the peaks of the curves displayed in Figure 5). This is consistent with expected temperature distributions in composite bridges, which are characterized by a linear profile in the deck and a near uniform temperature throughout the girder that only develops a significant nonlinear increase near the deck during summer months due to the substantial thermal gradient in the deck induced through intense solar radiation (Kennedy and Soliman, 1987).

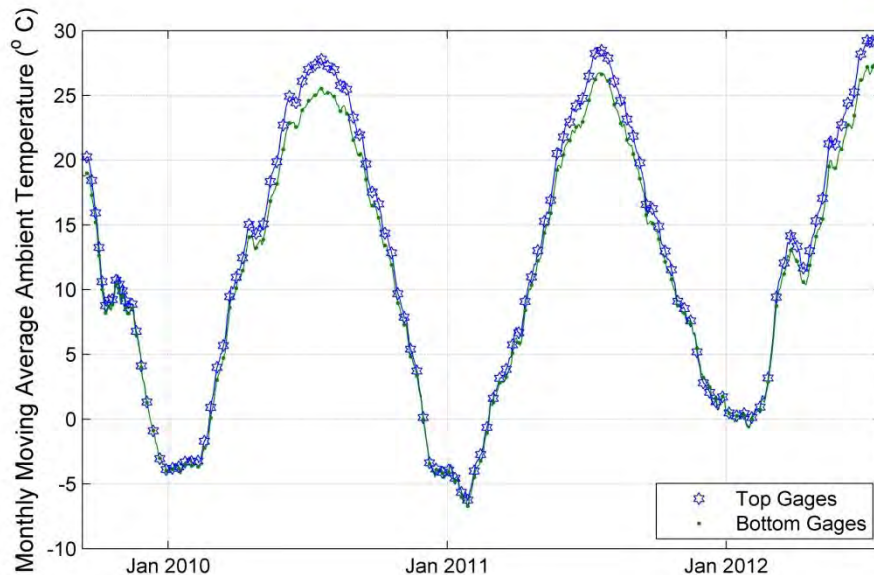


Figure 5. Ambient temperature as a function of time.

Figure 6 displays hysteresis curves for the average lateral pressure measured on the south abutment as a function of the average ambient temperature over a three year monitoring period. Each year of monitoring is labeled separately so the stress history of the lateral earth pressure cells installed on the south end of the superstructure is clearly illustrated in Figure 6. The stress history begins on the 2009-2010 curve at approximately 13°C (the initiation of data is indicated with a circle on Figure 6). The curves cycle over the three year time period with each year indicated by a different symbol. The yearly cycle transition occurs during the month of October, and each of the two transitions are indicated with a square on Figure 6 (e.g. the transition from 2009-2010 data to 2010-2011 data occurs at approximately 17°C when the average lateral pressure reads approximately 10 kPa). When the temperatures decrease, the abutments are

experiencing an 'active' state, and when the temperatures increase, the abutments are experiencing a 'passive' state of pressure. The equivalent figure for the north abutment displayed similar trends.

In general, Figure 6 displays the increase and decrease in lateral pressure as the steel expands and contracts with the thermal cycle, respectively. During the first two years, the steady decrease in lateral pressure was impacted by a spontaneous increase in lateral pressure after the average ambient temperature fell below freezing temperatures. This jump in lateral pressure developed during the 2009-2010 and 2010-2011 cycles between the temperatures of 0°C and -5°C in Figure 6. When ambient temperatures began to increase and they surpassed the freezing mark, the average lateral pressures displayed in Figure 6 re-established their initial trends. This behavior is illustrated by the large loops displayed on the left side of Figure 6.

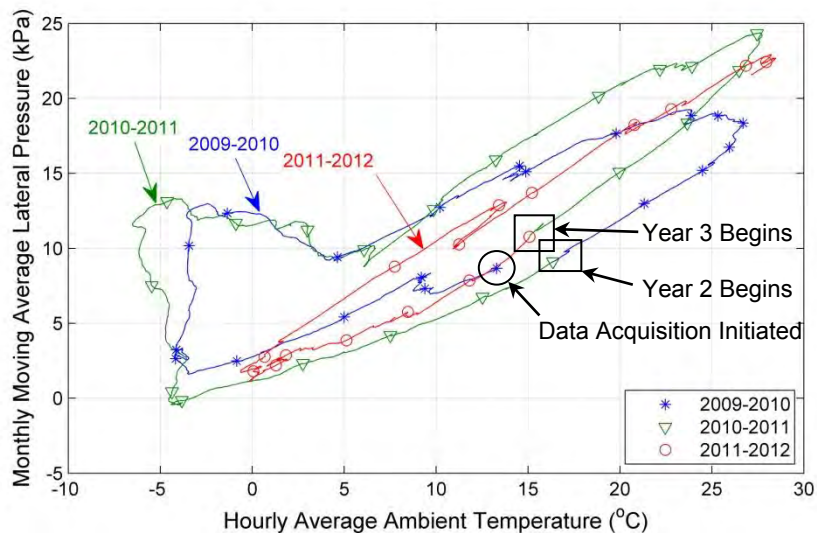


Figure 6. Average lateral pressure on south abutment as a function of ambient temperature.

There was a high density, nonwoven geotextile that was glued to the heads of the lateral earth pressure cells attached to the diaphragm wall before the backfill was placed. The geotextile was included to help prevent high contact pressures from developing between the stone and the stainless steel cell (i.e. it served as a bearing pad for the fill). It is hypothesized that the thickness of the geotextile enabled the material to retain moisture, and the geotextile exhibited freeze-thaw behaviors as the temperatures dropped below freezing and was then re-elevated above 0°C. The freeze-thaw behaviors of the geotextile created an increase in the lateral pressure that was likely not attributed to the thermally induced interactions between the superstructure and the substructure. During the 2011-2012 winter, the temperatures recorded were mild in comparison to the two previous years, which explains why the same trend did not occur during this cycle.

Since there is a gradual decrease in the average lateral pressure rather than a sharp elimination of lateral pressure when the temperatures decrease and the steel to contracts, the GRS approach fill appears to move with the superstructure within the limits of thermal deformation experienced by the steel. This would explain why long term monitoring of several GRS IBS bridges does not show surface cracking at the superstructure-substructure interface as one might expect. The two systems appear to be working together as thermally induced deformations take place.

Since the data indicates that the GRS fill remains in contact with the superstructure during these thermal cycles, one might be concerned about a 'ratcheting' effect that could develop during subsequent years. The geo-phenomenon referred to as 'ratcheting' is best defined by describing the behavior of a more common integral abutment configuration. For an integral abutment configuration constructed on deep foundations, rigid body rotation is experienced as the system moves inward during colder temperatures and outward during the warmer temperatures (Horvath, 2005). According to Horvath (2005), as the superstructure of a typical integral abutment configuration contracts during the winter, an active earth pressure wedge develops and follows the abutment inward. Due to the inelasticity of soil, the displacement is not fully recovered during the summer months, and at the end of each annual thermal cycle, a net inward displacement of each abutment commonly exists (Horvath, 2005). During the subsequent bridge expansion, increased lateral earth pressures can develop and more closely approach the theoretical passive state with dangers of exceeding the margin of safety built into the design (Horvath, 2005). This increase in lateral pressure with each thermal cycle is referred to as 'ratcheting', and the potential for structural failure increases with time even though it could take years to develop

(Horvath, 2005). In the case of the GRS IBS constructed as part of this project, the data does not show significant increases in lateral pressure from year to year. In fact, the lateral pressures displayed during the 2011-2012 cycle on this figure decrease relative to the 2010-2011 cycle. The authors will continue to monitor this interaction between the superstructure and the adjacent reinforced GRS approach.

Figure 7 displays the average thermal strain as a function of time for all top and all bottom gages over the three year monitoring period. Strain movement in the positive direction indicates tension and strain movement in the negative direction indicates compression. The data presented on this figure reflects actual strains in the steel girder computed using the manufacturer provided conversion displayed in Equation 1 (Geokon, 2012):

$$\mu\epsilon_{actual} = R_1 - R_0 B + T_1 - T_0 \alpha \quad [1]$$

Where: R_1 = the gage reading at time t
 R_0 = the initial gage reading at the chosen reference time t=0
 B = the gage factor of the sensor
 T_1 = the measured temperature at time t
 T_0 = the measured temperature at the reference time t=0
 α = the temperature coefficient of expansion for the instrumented material ($12.2\mu\epsilon/^\circ C$ for steel).

Since the purpose of this study is to determine the thermally induced interactions between substructure and superstructure, the theoretical thermal axial strain in an unrestrained steel girder was also calculated and displayed on the figure as an idealized reference model to characterize the relative end restraint in the superstructure over time. The ambient temperature and thermal expansion coefficient for steel were utilized to calculate the thermal strain for the theoretical unrestrained condition displayed. If the temperature of a fully unrestrained steel beam increased, the steel would expand without any internal stress in member. If, on the other hand, the same steel beam was fully restrained as the temperature increased, deformation would be prohibited, but the internal stress in the member would increase accordingly. Since composite action and the potentially large thermal gradient in the concrete deck are not accounted for in this reference model, comparison should be limited to only examining the relative behavior of the superstructure restraint over time. With each thermal cycle, the variance between the thermal strain measured at the top and bottom decreases. Additionally, the variance between the measured strain data (indicated with symbols on Figure 7) and the idealized reference model decreases with each thermal cycle. Initially, there is a large difference between the top and bottom strain, but these values converge with each thermal cycle. The convergence may be associated with drying shrinkage of the concrete deck. In general, the data presented on Figure 7 indicates that, contrary to ratcheting, the end restraint in the superstructure remains consistent and may even be experiencing slight relaxation over the first three seasons of operational service.

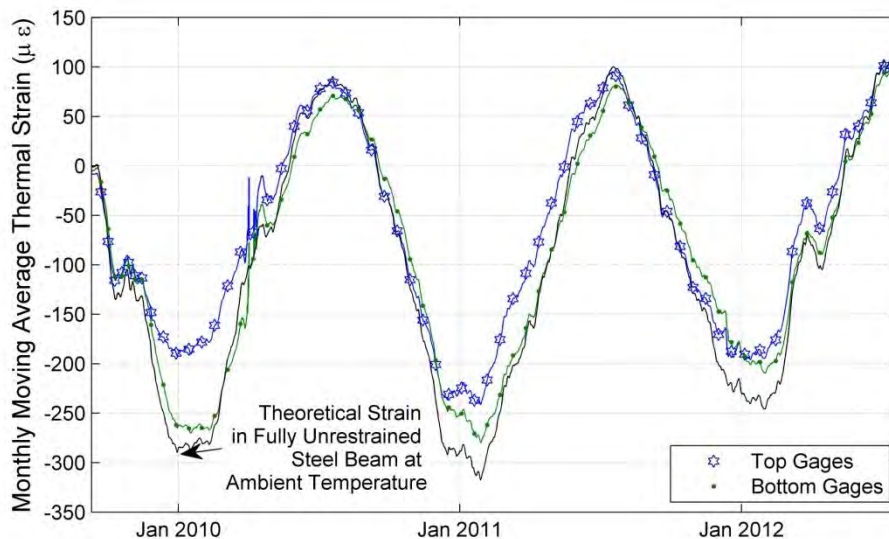


Figure 7. Thermal strain as a function of time.

Figure 8 displays the average thermal stress as a function of time for all top and all bottom gages over the three year monitoring period. Since a long-term static monitoring approach was taken, it is assumed that all stresses are thermal in

nature (i.e. they are not load induced). In the absence of load-induced stresses, thermal stress can be directly measured and calculated using vibration wire strain gage technology with Equation 2 (Geokon, 2012):

$$\sigma_{thermal}(t) = \sigma_{apparent}(t) = R_1 - R_0 BE \quad [2]$$

Where: E = the elastic modulus of the instrumented material

Note that the calculated thermal stresses are computed relative to the measured response on October 1, 2009. Although the data presented seems to show a bias toward higher tensile stresses in the winter months than compressive stresses in the summer, this is an artifact of the datum developed by the initial conditions. Similar to Figure 7, an idealized reference model was developed to provide the theoretical thermal axial stress associated with a fully restrained steel beam. The theoretical thermal axial stress is displayed in Figure 8 for comparative evaluation of end restraint behavior over time. An increase in stress indicates tension and vice versa. If a steel beam is fully restrained at the ends, any increase in temperature will cause an equivalent compressive axial stress in the beam and vice versa. Again, this reference model neglects the critical composite action between the concrete deck and steel girders as well as the thermal gradient in the superstructure so it should not be used as a direct means of evaluating superstructure performance. However, it can serve as a temperature-normalized baseline to compare the relative superstructure response over each thermal cycle. As noted for Figure 7, the variance between the top and bottom thermal stress responses decreases with time in Figure 8 as well. The difference in long-term thermally induced stresses and/or strains measured in the top and bottom gages throughout the superstructure are generally attributed to composite action and flexure. Over several thermal cycles, both the magnitude of stresses and the difference in thermal stress along the depth of the cross section is reduced, indicating a reduction in relative end restraint and flexure in the superstructure. Since the thermally induced stresses decrease over time relative to the fully restrained reference model, the end restraint in the superstructure is tending toward the idealized unrestrained response.

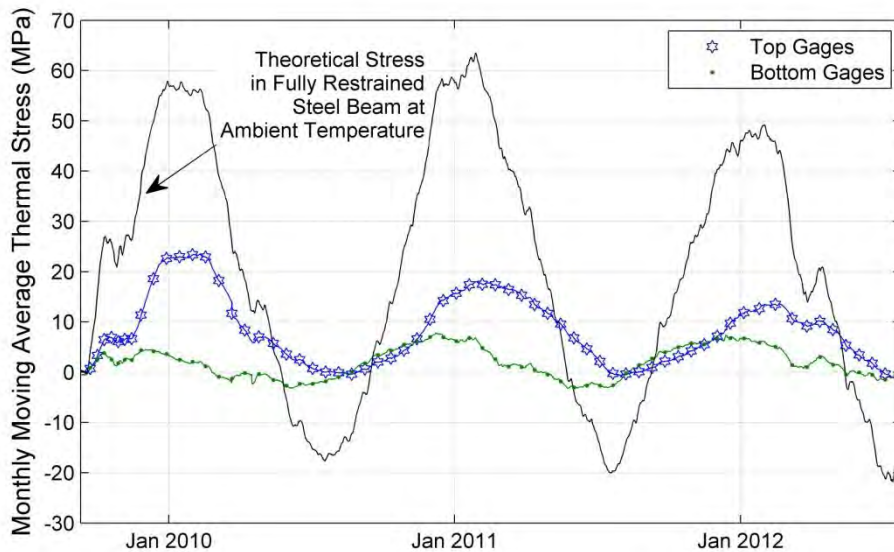


Figure 8. Thermal stress as a function of time.

6. CONCLUSIONS

1. The long term ambient temperatures clearly follow typical thermal cycles with minimal differences observed between the gages installed on the web near the top versus the bottom locations. A temperature differential equal to a few degrees Celsius (at most) develops during the summer months. This behavior is consistent with expected temperature distributions in composite bridges, which are characterized by a linear profile in the deck and a near uniform temperature throughout the girder that only develops a significant nonlinear increase near the deck during summer months due to the substantial thermal gradient in the deck induced through intense solar radiation.
2. The lateral pressures increase and decrease as the steel expands and contracts with the thermal cycle, respectively, but during the first two years, there was a spontaneous increase in lateral pressure when the average ambient temperature fell below freezing temperatures. When ambient temperatures re-elevated, the

average lateral pressures re-established their initial trends. The nonwoven geotextile installed between the pressure cell and reinforced fill was likely the cause of the erratic behavior observed. It is hypothesized that the geotextile retained moisture and exhibited freeze-thaw behaviors adjacent to the lateral earth pressure cells.

3. Since there is a gradual decrease in the average lateral pressure rather than a sharp elimination of lateral pressure when the temperatures decrease and the steel contracts, the GRS approach fill appears to move with the superstructure within the limits of thermal deformation experienced by the steel. The two systems appear to be working together as thermally induced deformations take place. This could explain why long term monitoring of several GRS IBS bridges does not show surface cracking at the superstructure-substructure interface as one might expect.
4. Since the data indicates that the GRS fill remains in contact with the superstructure during the thermal cycles, one might be concerned about a 'ratcheting' effect that could develop during subsequent summer months. The lateral end pressure data do not show significant increases from year to year as one might expect. In fact, the lateral pressures displayed during the 2011-2012 cycle on this figure decrease relative to the 2010-2011 cycle. However, these behaviors will continue to be monitored.
5. The variance between the thermal strain measured at the top and bottom of the web decreases with each thermal cycle. Additionally, the variance between the measured strain data and the idealized reference model decreases with each thermal cycle. Initially, there is a large difference between the top and bottom strain, but these values converge with each thermal cycle. The convergence may be associated with drying shrinkage of the concrete deck. Contrary to ratcheting behavior commonly experienced by an integral abutment configuration, the end restraint in this GRS IBS superstructure remains consistent and may even be experiencing slight relaxation over the first three seasons of operational service.
6. GRS IBS technology can potentially accommodate the construction or replacement of single span, low volume bridges without the need for deep foundations, expansion joints, or approach slabs, and without developing a "bump at the end of the bridge". As of 2011, Defiance County has constructed 25 single span bridges with span lengths ranging from 3.1 m – 42.7 m, and benefited from a 25% – 50% cost savings on these projects in comparison to more conventional technologies they have utilized in the past.

ACKNOWLEDGEMENTS

This research was funded by the Federal Highway Administration. Mike Adams (FHWA) and Warren Schlatter (Defiance County Engineer) should be recognized for their continued support and pursuance of innovative technology. We would like to thank the Defiance County personnel involved in this project for their hard work and cooperation during the construction process.

REFERENCES

- Adams, M., Nicks, J., Stabile, T., Wu, J., Schlatter, W. and Hartmann, J. (2011a). *Geosynthetic Reinforced Soil Integrated Bridge System, Interim Implementation Guide*. U.S. Department of Transportation, Federal Highway Administration, Report No. FHWA-HRT-11-026, Washington D.C., USA.
- Adams, M., Nicks, J., Stabile, T., Wu, J., Schlatter, W. and Hartmann, J. (2011b). *Geosynthetic Reinforced Soil Integrated Bridge System, Synthesis Report*. U.S. Department of Transportation, Federal Highway Administration, Report No. FHWA-HRT-11-027, Washington D.C., USA.
- Adams, M., Schlatter, W. and Stabile, T. (2007). Geosynthetic Reinforced Soil Integrated Abutments at the Bowman Road Bridge in Defiance County, Ohio. *Proceedings of the Geo-Denver 2007 Congress: Geosynthetics in Reinforcement and Hydraulic Applications, ASCE Geotechnical Special Publication 165*, Denver, Colorado, USA: 12 p.
- Geokon, Inc. (2012) *Instruction Manual: Model 4000 (and 4050) Vibrating Wire Strain Gage*. Doc. Rev W, 7/12, Lebanon, NH, USA.
- Horvath, J.S. (2005). Integral-Abutment Bridges: Geotechnical Problems and Solutions Using Geosynthetics and Ground Improvement. 2005 FHWA Conference on Integral Abutment and Jointless Bridges, Baltimore, Maryland, USA: 10 p.
- Kennedy, J.B. and Soliman, M.H. (1987). Temperature Distribution in Composite Bridges, *Journal of Structural Engineering*, ASCE, 113(3): 475-482.
- Lee, K.Z.Z. & Wu, J.T.H. (2004). A Synthesis of Case Histories on GRS Bridge-Supporting Structures with Flexible Facing, *Geotextiles and Geomembranes*, 22: 181-204.
- Tatsuoka, F., Hirakawa, D., Nojiri, M., Aizawa, H., Nishikiori, H., Soma, R., Tateyama, M. & Watanabe, K. (2009). A New Type of Integral Bridge Comprising Geosynthetic-Reinforced Soil Walls. *Geosynthetics International*, 16(4): 301-326.

Radial Load Tests for the Evaluation of Stress-Strain Relation of Geocells

Ansgar Emersleben, Dr.-Ing., Clausthal University of Technology, Institute for Geotechnical Engineering, GERMANY, Ansgar.emersleben@tu-clausthal.de

ABSTRACT

Geocells represent an alternative for the stabilization of soils with low bearing capacity. The use of geocells is recently increasing, especially in areas where good quality aggregate material is hard to find and/or expensive. The performance of geocell stabilized soils is mainly dependent on the stress-strain relation of the geocells. The stress-strain relation is commonly evaluated by tensile tests similar to other geosynthetics. This test method is unsuitable to evaluate the stress-strain relation of the geocell including the junctions or the cell geometry at construction site conditions. Therefore radial load tests were developed to determine the stress-strain relation of geocells for load support applications at in-situ conditions. In this paper the set up and the procedure of new radial load tests are described. Furthermore, the stress-strain relation of different geocells evaluated in tensile tests and in radial load tests are compared and analyzed. The influence of the geocell junctions on the stress-strain relation and the overall performance of geocells are presented.

1. INTRODUCTION

1.1 Geocells

According to DIN EN ISO 13426-1 (2003) geocells consist of single synthetic strips that are connected along specific lines or special points by different means in a way that a field of connected cells develops. Mainly polyethylene (PE), polypropylene (PP) and polyester (PET/PES) are used as raw materials. Polyvinyl alcohols (PVA) or Aramid (AR), which are sometimes used as raw materials for geogrids, are not of particular importance for the manufacturing of geocells. The connection between the single synthetic strips depends on the used raw material and can be realized by extrusion, thermal bonding, adhesive, hot melting or sewing. The connected cells build permeable expanded elements in a honeycomb shape. They are installed on site and filled with soil material which is finally compacted.

According to DIN EN ISO 10318 (2006) geocells are categorized as geotextile related products. In connection with a non-woven located below the geocells they can also be considered as geocomposite.

1.2 Application Areas of Geocells

Since their development in the seventies the application areas of geocells has increased significantly. Besides the classical soil stabilization, geocells are used for erosion control, retaining walls and other applications for example flood walls (Figure 1).

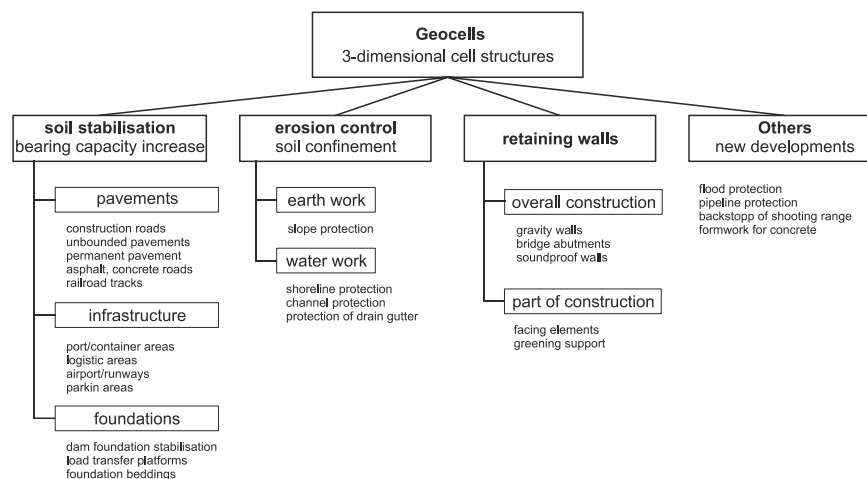


Figure 1. Geocell application areas (Emersleben 2010b).

1.3 Working Mechanism of Geocells

In a vertically loaded geocell horizontal earth pressure is activated due to the friction between infill material and geocell wall. The resulting strains in the cell walls mobilize hoop stresses in the cell walls and horizontal resistance in the adjacent cells. The amplitude of the activated hoop stresses depends on the type and magnitude of the applied load within the cell.

Due to the hoop stresses and the lateral passive earth resistance the horizontal deformation of the fill material is restricted and the stiffness of the fill material is increased. Mhaiskar et al. (1993) and Kazerani et al. (1987) determined (when verifying test results using the finite element method) a stiffness increase of a geocell stabilized soil compared to a non-stabilized sand by a factor of 2 to 3. Similar increase has been observed in field tests by Emersleben and Meyer (2010c).

The stiffness of the geocell composite results in a stiff plate effect which increases the load distribution angle. Due to this the vertical stresses are distributed on a larger area which reduces the vertical deformation (e.g. Dash et al. 2003; Chang et al. 2007; Sitharam et al. 2008) (Figure 2).

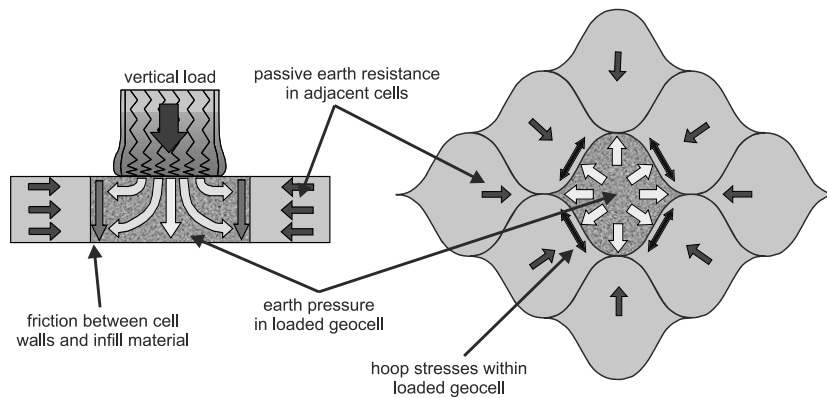


Figure 2. Working mechanism of geocells (Emersleben 2010b)

1.4 The Influence of Stress-strain Response on the Working Mechanism of Geocells

Regarding load support applications, the working mechanism and thereby the influence of geocells on the load distribution and load deformation behavior is dependent on many different factors, as for example geocell geometry, density of infill material, position of geocell within the pavement, cover thickness, loading geometry and material stiffness (Emersleben 2010b).

According to recent literature one of the most important factors is the tensile stiffness respectively the elastic modulus of the geocell material (e.g. Pokharel et al. 2009). An increase in elastic modulus of the cell material results according to Krishnaswamy et al. (2000), Mhaiskar et al. (1996) and Dash et al. (2003) in an increase of the measured bearing capacity.

According to Mhaiskar et al. (1996) especially the material stiffness in the small strain range is of importance as strains are mobilized already under small applied loads.

Krishnaswamy et al. (2000) investigated in tests with grid cells for dam foundations that with increasing material stiffness larger slip circles are developed.

Dash et al. (2003) however points out that the stiffness of the geocell material must be investigated in association with the surface structure of the geocell and the interconnected geocell system.

1.5 Evaluation of Stress-strain Response of Geocells

The stress-strain response of geocells is usually evaluated by standard tensile tests on the used raw material or on geocell strips according for example on DIN EN ISO 10319 or ASTM D 4595. Additional tests to evaluate the seam and peel strength of the junctions are usually carried out on basis of DIN EN ISO 13426-1 and ASTM D 4473 (Figure 3).

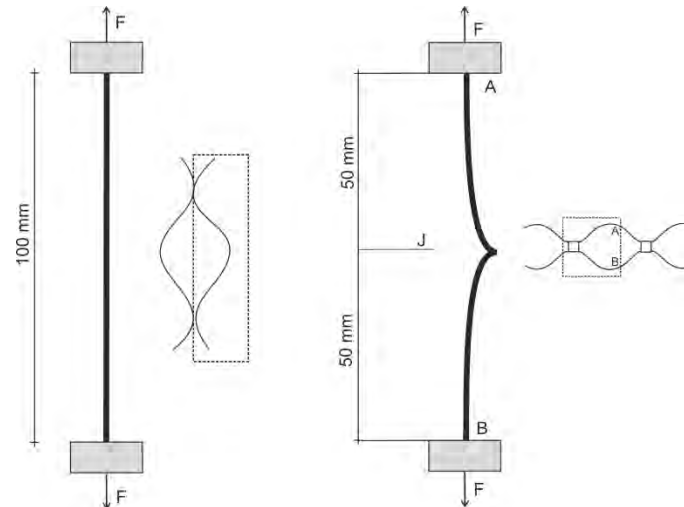


Figure 3. Wide strip tensile test and seam peel test according to European Standard DIN EN 10319 and DIN EN 13426-1

Both tests are adequate to evaluate the tensile strength of the raw material and the ultimate strength of the junction, as needed for example for erosion control applications, but do not simulate the in-situ situation of a geocell as presented in Figure 2. The radial load situation within the loaded cell is not considered in the tensile tests presented above.

Because of that an alternative test, called radial load test (RLT) was developed by the authors to evaluate the stress-strain relation of geocells at in-situ load conditions and to compare these relationships with stress-strain behavior of wide strip tensile and peel strength tests (Emersleben 2010b).

Used materials, conducted tests and results are described and analyzed in the following chapters

2. GEOCELL MATERIAL

Three different geocell types were used in the laboratory tests. The geocells can be differentiated by their manufacturing process as well as the used raw material. Geocells manufactured by a high density polyethylene (PEHD), a thermally bonded nonwoven and a mixture of PEHD and polyester (PES/PEHD) with different tensile strengths was used. The use of geocells manufactured by different raw materials was mainly considered for the variation of tensile stiffness. Besides the different stiffness, the used materials have a different surface texture. The rough structure of the surface of the PEHD geocells was achieved by a number of between 22 and 31, 0.35-0.85 mm deep sinkings per cm². Additionally perforated PEHD cells were tested, where holes with a diameter of 10mm were punched into the cell walls. The opening area of the holes represents 16 % of the whole cell area. The surface structure of the PES/PEHD cells is smooth while the geocells made of a non-woven (PES-V) is rough. An overview of the main geocell parameters are given in table 1.

Table 1. Basic parameters of tested geocells.

	PEHD perforated	PEHD non-perforated	Nonwoven PES-V	PES/PEHD (1)
Material surface	structured, perforated	structured	smooth	smooth
h^1 [cm]	15	15	15	15
h_{eff}^2 [cm]	8	15	15	15
t^3 [mm]	1.70	1.70	1.50	1.80
A^4 [cm ²]	1.36	2.55	2.25	2.7

¹ h = cell height; ² h_{eff} = cell height without perforations; ³ t = material thickness; ⁴ A = cross section area

For the determination of the stress-strain properties, tensile tests in accordance to DIN EN 10319 were conducted. The tests were conducted to determine the ultimate tensile strength of the raw material. For evaluation of the peel strength tensile tests on basis of DIN EN 13426-1 were conducted. The test results of both tests for a strain rate of 20 mm/min are given in Figure 4.

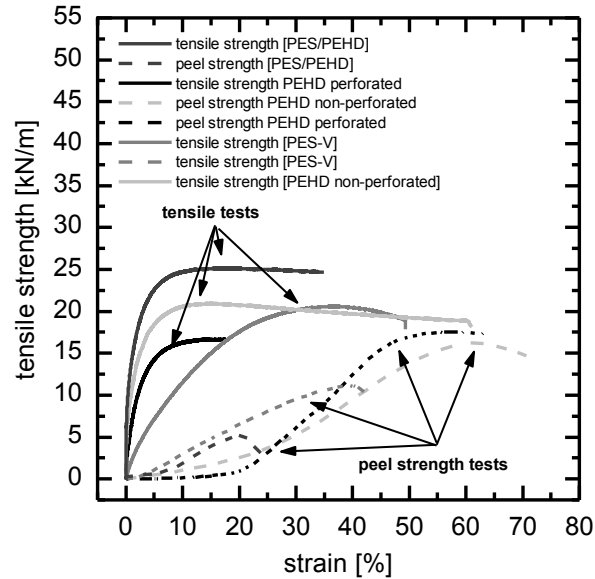


Figure 4. Comparison of tensile test and peel strength test results for different geocell materials.

Despite a comparable manufacturing process and identical raw material, the tested perforated and non-perforated PEHD geocells showed a significant difference in the stress-strain properties which was a result of the perforation within the geocell structure and the resulting stress distribution within the cell area.

Test results of the ultimate tensile strength for perforated PEHD cells in peel- and tensile tests are comparable. In contrast to this the measured peel resistance for the PES-V cells, the non-perforated PEHD cells and the PES/PEHD geocells resulted in smaller values than the measured material tensile strength (Fig. 4). Especially the PES/PEHD geocells showed a significant difference in peel resistance and tensile test data. Compared to the other geocells, the PES/PEHD geocells showed the highest tensile strength while their junction strength is least.

3. RADIAL LOAD TESTS

3.1 Basic Principal

Based on the overall accepted load transfer mechanism within a geocell system (Figure 2) used in load support applications, neither the tensile strength of the raw material nor the seam strength are sufficient to describe the stress-strain relationship of geocells at in-situ conditions. Both tensile tests and seam strength test are carried out two-directional, but at in-situ load situation the geocells are loaded in radial direction. In addition only the maximum seam strength of the geocells can be evaluated in the two-directional tests. Due to the missing consideration of the opening angle of the junctions in two-directional tensile tests, the influence of the junctions on the stress-strain behavior and with it the in-situ stress-strain behavior cannot be simulated adequate (Figure 5).

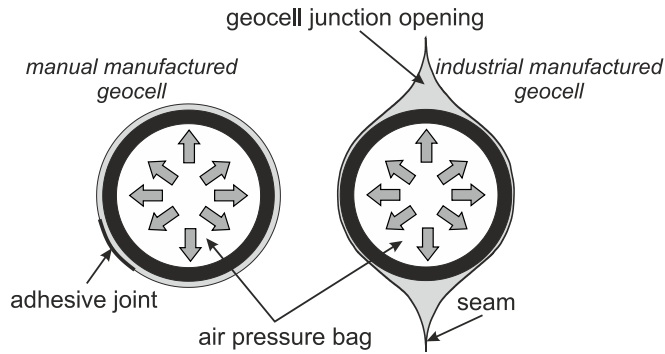


Figure 5. Radial load situation in single loaded geocell, manual manufactured geocell without junction (left side), industrial manual manufactured geocell with junction (right side).

3.2 Test Device

In the radial load tests a single geocell is loaded by a pneumatic pressure bag. The air pressure bag consists of an air filled membrane with an internal steel cylinder. The steel cylinder prevents internal stresses and ensured a uniform stress distribution on the geocell walls. The pressure bag has a height of 30 cm and diameter of 25 cm. The dimensions of the pressure bag were optimized to investigate 15 cm high cells with a diameter of 20 – 23 cm. The air pressure in the bag is controlled by an electronic valve with an automatic control program. Static tests can be executed in a load- or strain-controlled way up to 500 kPa. Dynamic loads tests can be executed with varying amplitudes and load frequencies up to 4 Herz (Emersleben and Meyer 2009).

Indirect strain sensors were incorporated by using a rotary potentiometer. Strains were measured by a string with plastic properties placed around the loaded cell. From the elongation the activated geocell strains were analyzed (Figure 6).

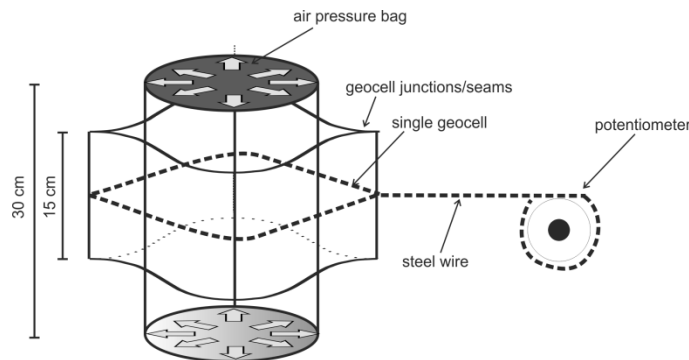


Figure 6. Schematic overview of radial load test on single geocell

3.3 Test Installation and Procedure

For the test setup the air pressure bag was installed in the centre of a test box. The box had a height of 30 cm and a width and length of 1.27 m.

The geocell is placed in the middle around the pressure bag. Afterwards the strain sensor was installed. The measurement wire was placed around the geocell in mid height, fixed and connected to the potentiometer located outside of the test box. To protect the measurement wire, the wire was placed in a plastic rod. To simplify the arrangement small holes were drilled in the cells through which the wires were taken to the potentiometer. Index tests indicated that this does not influence the test results. A preload was applied to the geocells to ensure a force-fit of single cells and the pressure bag. This also allowed control of the junction/seam opening angle (Figure 7).



Figure 7. Installed geocell on air pressure bag and connected strain measurement system

The static tests were used for the detailed investigation of interactions and load carrying mechanisms of different geocells. They were, compared to the tensile tests, deformation controlled based on the test specimen circumference and a strain rate of 20 mm/min. Load was applied until failure of the cells or strains exceeded values of 20 – 25 %.

4. RESULTS OF RADIAL LOAD TESTS

4.1 Interpretation of the Radial Load Test Results on Geocells Without Junctions

With a radial-symmetrical horizontal load of an unconfined single cell the horizontal loads must be taken by hoop forces in the geocell material. The mobilized hoop forces ($F_{rad,\epsilon}$) can be calculated on basis of a modified boiler formula ("Long Term Hydrostatic Pressure Resistance Formula" or "Barlow's Formula") according to DIN 2413 (German Institute for Standardization) (see Equation 1).

$$F_{rad(\epsilon)} = \frac{\sigma_{h(\epsilon)} \cdot d_{\epsilon,z(\epsilon)} \cdot A}{2 \cdot t} = F_{zug(\epsilon)} \quad (1)$$

where $F_{zug(\epsilon)}$ = measured tensile force in tensile test at strain level ϵ ; $F_{rad(\epsilon)}$ = calculated tensile force on basis of radial load test results at strain level ϵ ; $d_{\epsilon,z(\epsilon)}$ = diameter of the geocell at strain level ϵ ; t = material thickness of the geocell material; A = material cross section without consideration of perforations; $\sigma_{h(\epsilon)}$ = applied radial pressure on geocell.

Studies of Wesseloo (2009) under identical test conditions show that the stress-strain behavior of a plastic membrane is not influenced by the load direction (axially or radial).

Transferring the results from Wesseloo (2009) to the radial load and tensile tests presented in this paper leads to the conclusion that at the same stress level the mobilized strains within the geocell material should be identical. Figure 8 presents a comparison of the tensile strength measured in the tensile tests and the calculated hoop strength according to equation 1 for different geocells without junctions.

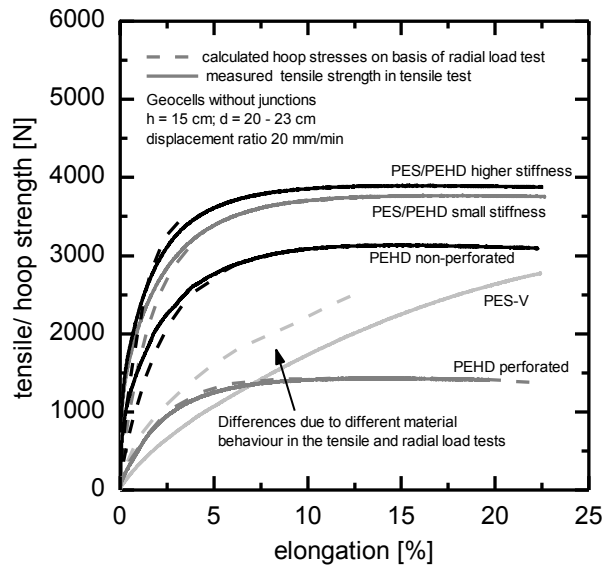


Figure 8. Comparison of measured tensile strength in tensile tests and back calculated tensile strength on basis of radial load test results for different circular manufactured geocells without junctions.

The results show that at similar strain level the calculated and measured forces/stresses in the geocell material are comparable. Minor deviations between the calculated and measured forces/stresses can only be observed for PES-V geocells. For these geocells a different material behavior was observed in radial load and tensile tests. In the tensile tests a material failure was observed as a result of creep behavior in the material. In radial load tests single nonwoven layers were separated, whereupon the materials cross section and hence the tensile strength decreased.

The results indicate that radial load tests on geocells without junction's leads to the same result as width tensile tests. Radial load tests are adequate to evaluate stress-strain behavior of geocells under in-situ load conditions.

4.2 Radial Load Test results on Geocells with Junctions

Radial load test results for different geocells are presented in Figure 9. Considering the junctions of the geocells and their opening angle at site conditions the non-perforated PEHD geocells shows the best stress-strain relationship while the non-perforated PES/PEHD geocells shows the worst stress-strain behavior. The difference between perforated PEHD geocells and nonwoven geocells made of PES-V is marginal.

The results show the huge influence of the junctions on the stress-strain behavior of geocells. This effect cannot be simulated in width tensile tests or seam tests.

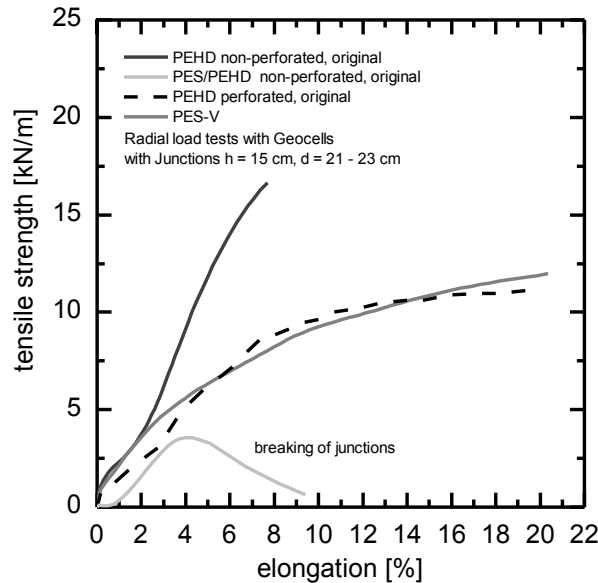


Figure 9. Results of radial load tests of single geocells with junctions.

4.3 Influence of Geocell Junctions and Their Opening Angle

The in-situ site installation process results in different opening angles of the geocell junctions/seams. The achievable opening angle for PEHD and PES/PEHD geocells is approx. 90° and for PES-V geocells approx. 130° . Varying opening angles even for similar geocell geometries are the result of material stiffness and the type of joint. Radial load tests on geocells with junctions (commercially manufactured) and without junctions (manually made geocells) were conducted to determine the influence of the junctions on the stress-strain behavior. Figure 10 indicates the influence of joints on the stress-strain behavior of the perforated and non-perforated PEHD geocells.

Geocell strains of industrial manufactured cells (with junctions) are larger than strains measured for manually made cells (without junctions), independent of the geocell material.

In contrast to the manually made geocells industrial manufactured geocells increase their opening angle during initial loading. Due to the continuous opening only small stresses are activated within the cells walls. Only for almost fully opened junctions, applied loads result in geocell strains accompanied by significant strength increase. In contrast handmade geocells without junctions are characterized by an immediate strain and stress activation. This result in improved stress-strain properties compared to industrial manufactured cells.

Perforated and non-perforated PEHD geocells and PES/PEHD geocells with similar opening area and opening angles (90°) were chosen to test the influence of the junctions. It was investigated that the joints have a large influence on the geocell stress-strain behavior (Fig. 10).

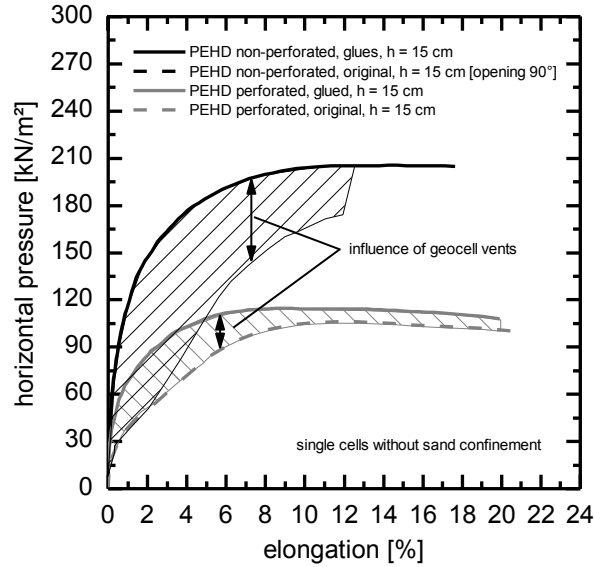


Figure 10. Comparison of pressure-strain behavior of circular manufactured (glued) geocells without junctions and industrial manufactured (original) geocells with junctions.

With increasing geocell material stiffness a higher influence of the joints was observed. The material stiffness is expressed as extensional stiffness according to equation 2. To consider the significant influence of the perforations of the geocell material (different cross section area) the extensional stiffness is expressed in the unit force (kN) which is different from the usually know expression according to ASTM.

$$J = E \times A \quad (2)$$

where J = extensional stiffness at strain ε ; E = Elastic modulus at strain ε based on tensile tests; A = material cross section.

The reduction of maximum applied pressure due to the junctions can be expressed up to a strain of 2 % by a linear function according to Figure 11. With increasing geocell stiffness the difference of the horizontal pressure which can be applied on the single geocell without and with junction, is significantly increasing. This is based on the fact that with increasing geocell material stiffness the achievable opening angle of the junction at site installation is smaller than for geocell materials with smaller material stiffness.

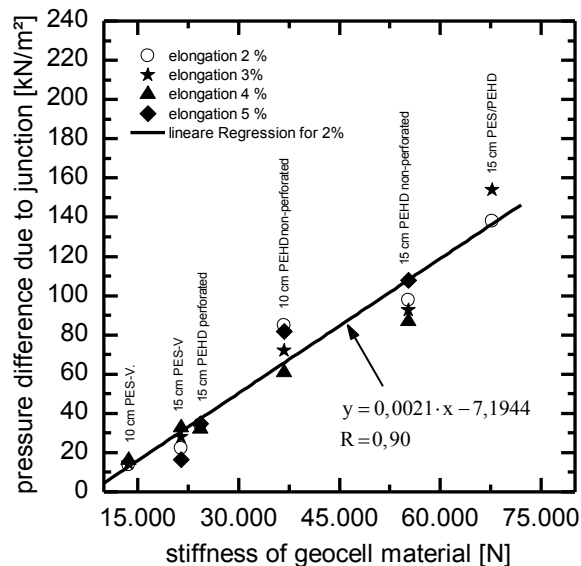


Figure 11. Influence of the junctions on the applied radial pressure dependent on the geocell stiffness.

5. COMPARISON OF TENSILE AND RADIAL LOAD TESTS

5.1 Comparison Between Wide Strip Tensile Tests and Radial Load Tests

Figure 12 shows a comparison between results of wide strip tensile tests according to DIN EN 10319 and radial load tests. Considering the geocell junctions/seam in the radial load tests and their influence on the stress-strain response the tensile strength measured in radial load tests is significantly smaller than the tensile strength measured in wide strip tensile tests. The consideration of the junctions leads to different results not only in the amount of tensile strength. Width tensile tests do not represent the stress-strain behavior of geocell at in-situ conditions and are therefore not representative to describe the stress-strain behavior of geocells in load support applications.

While the PES/PEHD geocells shows the highest tensile strength in the wide strip tensile test, the tensile strength was the smallest in the radial load test. As a result of the high material stiffness (based on width tensile tests) and the poor quality of the junctions the angle of the junction is not really high (Figure 10).

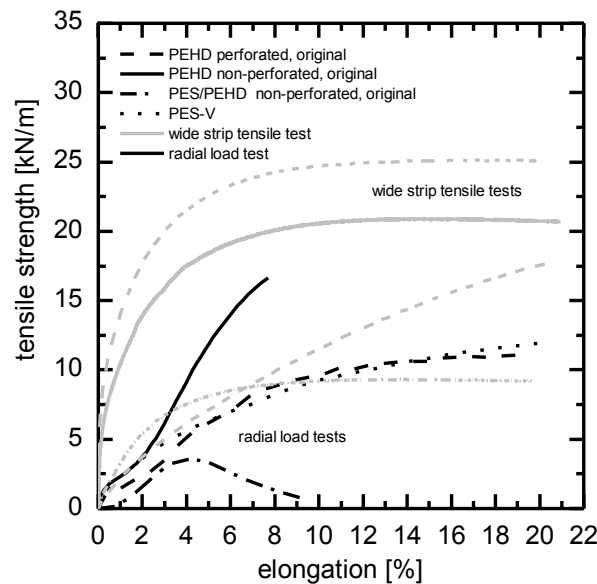


Figure 12. Comparison between wide strip tensile tests and radial load tests on different geocell materials.

5.2 Comparison Between Seam Peel Strength Tests and Radial Load Tests

Figure 13 shows a comparison between results of wide strip tensile tests according to DIN EN 13426-1 and radial load tests.

Compared to the radial load tests the tensile strength of the seam peel strength tests is smaller for all tested geocell materials. The main reason for this effect is the fact that the opening angle of the junction which occurred at side conditions cannot be sufficient simulated in seam peel strength tests. Because of that the stress-strain response of seam peel strength test is smaller than in radial load tests.

Results show that seam strength tensile tests do not represent the in-situ stress-strain behavior of geocell at in-situ conditions and are therefore not representative to describe the stress-strain behavior of geocell in load support applications.

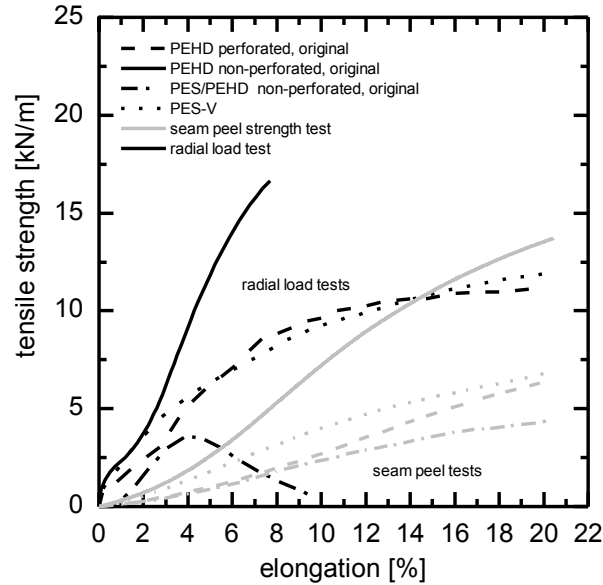


Figure 13. Comparison between seam peel strength tests and radial load tests on different geocell materials.

5.3 Influence of Different Tensile Tests on the Elastic/Stiffness Modulus of the Geocells

The influence of the conducted test on the tensile stiffness of the different geocell materials is presented in Table 2. The highest modulus can be observed for the tensile tests, because the influence of the junction is not considered. The smallest modulus can be observed for the radial load tests which represents the real in-situ conditions.

It can also be seen that the seam peel strength test is only adequate to measure the maximum peel strength but cannot be used to evaluate the stress-strain behavior in an exact way. The back calculated stiffness modules are more than four times smaller than those from the radial load tests.

Table 2. Tensile stiffness modulus of geocells at 5 % strain in kN.

test type	PEHD perforated	PEHD non-perforated	PES-V	PES/PEHD
Tensile test DIN EN 10319 [kN]	24.3	55.2	21.4	67.7
Seam peel strength test DIN EN 13426-1 [kN]	3.00	7.74	5.41	2.68
Radial load tests [kN]	18.4	35.6	19.0	9.8

6. SUMMARY

The paper presents a new test method called radial load tests to measure the stress-strain response of single geocells at site conditions. First time the opening angle of the geocells seams/junctions is considered in stress-stains measurement. The presented results show that especially the opening angle of the junction has a significant influence on the stress-strain behavior. Comparison of radial load test results with commonly known wide strip tensile and seam peel strength tests show that the measured radial tensile strength is smaller than the measured wide strip tensile strength but larger than the seam peel strength. This is based on the fact that the seams/junctions of the cells are not considered in width tensile strength and the opening angle of the junctions cannot be simulated adequate in the seam strength tests. Results show that the developed radial load tests are the first tensile test which really simulated in-situ conditions of installed geocells and thus leads to a stress-strain response, which simulated the in-situ behavior of geocells in the best way.

REFERENCES

- ASTM D4595 - 11 Standard Test Method for Tensile Properties of Geotextiles by the Wide-Width Strip Method
- ASTM D4437 - 08 Standard Practice for Non-destructive Testing (NDT) for Determining the Integrity of Seams Used in Joining Flexible Polymeric Sheet Geomembranes
- Chang, T.T.; Chang, C.H.; Pei, S.W. 2007. Investigation of the Bearing Capacity and dynamic elastic Behavior of Mechanical Stabilization of sandy Subgrade using Geocells. In: Transportation Research Board, 86th Annual Meeting 2007, Paper 07-1445, Transportation Research Board
- Dash S.K.; Kumar S.; Sireesh, S.; Sitharam, T.G. 2003. Model Studies on circular Footing supported on Geocell reinforced Sand underlain by soft Clay. In: Geotextiles and Geomembranes, Vol. 21, Issue: 4, June 2003, S. 197 - 219
- DIN EN ISO 10319 2008-08. Geosynthetics - Wide-width tensile test
- DIN EN ISO 13426-1 2003. Geotextiles and geotextile-related products - Strength of internal structural junctions - Part 1: Geocells
- DIN EN ISO 2413 2011-06. Seamless steel tubes for oil- and water-hydraulic systems - Calculation rules for pipes and elbows for dynamic loads
- DIN EN ISO 10318 2006. Geosynthetics - Terms and definitions.
- Sitharam, T.G., Sireesh, S., Dash, S.K. 2008. Bearing Capacity of circular Footings on Geocell Sand Mattress overlying Clay Bed with Voids. Geotextiles and Geomembranes, Vol. 27 (2). S. 89 - 98.
- Mhaiskar, S.Y., Mandal, J.N. 1993. Soft Clay Subgrade Stabilization Using Geocells: Experimental and Finite Element Investigations. Proceedings of the International Conference on Soft Soil Engineering, Guangzhou, November 1993, S. 785 - 791
- Emersleben A., Meyer M. 2009. Interaction between hoop stresses and passive earth resistance in single and multiple geocell structures. 1st African Regional Conference, GEO Africa 2009
- Emersleben A., Meyer M. 2010a. The influence of hoop stresses and earth resistance on the reinforcement mechanism of single and multiple geocells. 9th ICG 2010, Proceedings of the 9th International Conference on Geosynthetics, Guarujá, Brasilien, 23.-27. Mai 2010.
- Emersleben A. 2010b. Load transfer mechanism of geocells for the stabilization of mineral base courses at static and cyclic loading. PhD-Thesis at Clausthal University of Technology, ISBN 3-938924-13-6
- Emersleben A., Meyer M. 2010c. Verification of load transfer mechanism of geocell reinforced soil in large scale model tests and in-situ test fields. GeoFlorida 2010: Advances in analysis, modeling and design, Geotechnical Special Publications No. 199, Vol. 2/4, S. 1670-1680
- Kazerani, B.; Jamnejad, G.H. 1987. Polymer Grid Cell Reinforcement in Construction of Pavement Structures. In: Proceedings of the International Conference on Geosynthetics, Vol. 1, 1987, S. 58-68
- Krishnaswamy, N.R.; Madhavi Latha, G.; Karpurapu R. 2000. Model Studies on Geocell supported Embankments constructed over a soft Clay Foundation. In: Geotechnical Testing Journal, Vol. 23, Issues 1, 2000, S. 45 - 55
- Mhaiskar, S.Y.; Mandal, J.N. 1996. Investigations on soft Clay Subgrade strengthening using Geocells. In: Construction and Building Materials, Vol. 10, Issue: 4, June 1996, S. 281 - 286
- Pokharel, S.K.; Han, J.; Leshchinsky, D.; Parson, R.L.; Halahmi, I. 2009. Behaviour of geocell reinforced granular bases under static and repeated loads. Geotechnical special publication. Vol. 187
- Wesseloo, J., Visser, A.T., Rust, E. 2009. The Stress-Strain Behavior of multiple Geocell packs. Geotextiles and Geomembranes, Vol. 27, S. 31 - 38

Rehabilitation of Raw Water Reservoir for Franklin WTP

Bill Shehane, P.E., Seaman Corporation, USA, bshehane@seamancorp.com

ABSTRACT

The city of Franklin, Tennessee, a suburb of Nashville, initiated a rehabilitation project for their existing raw water reservoir to fix leaks caused by several deep fissures in the earthen basin. Because of the leaks, the reservoir ran complete dry during an extended drought season. When the Tennessee government released economic stimulus dollars, this site was among the top 10 projects earmarked to receive funding. After a failed attempt at using a natural clay liner, the city selected a potable water grade geomembrane to solve its water containment issues. This paper will go over the reservoir history, sizing options, liner material options, construction overview and lessons learned during the project.

1. INTRODUCTION

During the summer of 2007, the city of Franklin, Tennessee and its surroundings were experiencing a severe drought. Due to the high heat and low flows in the Harpeth River, Franklin struggled to meet water supply demands in the area. The city's raw water reservoir, which can hold 322 million liters (85 million gallons), was completely dry for several months. As a result, the 7.6 MLD (2.0 MGD) Franklin water treatment plant was inoperable for periods of time. Water is normally pumped from the Harpeth River into the raw water reservoir, where it is later treated before consumption.

Over the next 2 years, the drought officially ended and upgrades were put in the city's water distribution system. This helped to ease worries about Franklin's water system, except for the reservoir. It was estimated that up to 3.8 million liters (1 million gallons) of untreated water per day leaked from the reservoir, even after temporary installations of clay along the cracks in the bottom.



Figure 1: Reservoir in 2008 after the major drought of 2007

2. RESERVOIR HISTORY

The Franklin reservoir was originally built in the 1950's and during that time the water treatment plant was designed for only 3.8 million liters per day (1 million GPD). The reservoir served as a source of water during the warm summer months, where water was pumped from the Harpeth River. The reservoir was 121,000 square meters (30 acres) in size and designed to hold up to 380 million liters (100 million gallons) of water. During the 1960's, the water treatment plant was upgraded to handle 7.6 million LPD (2 million GPD). Over the years, volume within the reservoir was lost due to accumulated filter backwash solids reducing the capacity to only around 300 million liters (80 million gallons). Also, the original clay liner was no longer working and there were continuous leaks in the bottom.

The reservoir's problems had been common knowledge for years among past and current city officials, who had planned for the city to pay \$3.9 million on a rehabilitation project. However, in late 2009 Franklin received \$2.5 million from the Recovery Act/State Revolving Fund – a \$1.5 million loan to be paid over 20 years and \$1 million that will never have to be repaid. As a result, the city of Franklin only had to come up with \$1.4 million for the rehabilitation project.

3. SCOPE OF PROJECT

AECOM Engineers was hired to investigate and design alternatives, optimize sizing of the reservoir and recommend life cycle synthetic liner materials for an improved and enlarged reservoir for water conservation at the treatment source.

3.1 Liner System Alternatives

Eight different types of liner systems were evaluated and based on a design life of at least 20 years. They are as follows:

- Geosynthetic clay liner (GCL) with 30 cm (12") of soil cover
- HDPE liner left uncovered
- HDPE liner with 30 cm (12") of soil cover
- LLDPE liner with 30 cm (12") of soil cover
- Reinforced Chlorosulfonated Polyethylene (CSPE) left uncovered
- Reinforced Ethylene Propylene Diene Monomer (EPDM) left uncovered
- Reinforced Polypropylene (fPP-R) left uncovered
- Reinforced Ethylene Interpolymer Alloy (EIA-R) left uncovered

These eight alternatives were narrowed down to two, based on evaluations of long-term liner systems that had been in service for 20 years or more. In addition, it was decided that 30 cm (12") of soil cover on top of the geomembrane or GCL was too costly over a 142,000 SM (35-acre) site. The two options chosen were CSPE (Hypalon) and EIA-R (XR-3 PW/XR-5 PW). In addition, AECOM decided to specify a 36-mil thickness in the reservoir bottom and 45-mil thickness on the side slopes. A thicker geomembrane was recommended on the sides for higher abrasion resistance from potential wave action.

3.2 Resizing of the Reservoir

Alt.	Scope	Water Volume (MG)	Excavation C.Y.	Off-Site Spoil C.Y.	Avg MG/Yr WTP Production	Years @ 0.0 MGD WTP of past 31	Average Days per yr @ 0.0MGD WTP	Estimated Grading & Modifications Cost - No Liner	5yr savings (loss) including sludge/liner**
A.	Existing - Minimum Rehab	85.5	-	-	1,201	8	28.6	\$100,000	\$1,459,370
B.	Raise Spillway 1.0 ft	95	-	-	1,206	7	25.9	\$175,000	\$1,465,539
C.	Raise Spillway 1.5 ft	100	-	-	1,208	6	26.5	\$200,000	\$1,474,840
D.	Raise Spillway 2.0 ft, raise berm 8"	105	1500	-	1,211	5	27.8	\$250,000	\$1,474,613
E.	Raise Spillway 2.0 ft, raise berm 12" & cut for balanced cut/max spoil ~654	109	20,800	-	1,212	5	25.4	\$475,000	\$1,404,466
F.	Raise Spillway 2.0 ft & cut to "level" Bottom ~ 652.2 ft	113	40,600	20,000	1,214	5	22.8	\$700,000	\$1,334,418
G.	Raise Spillway 3.0 ft, add cut to berm, cut 4' below 652.2 "leveled bottom", & low	155	204,000	154,000	1,229	0	0	\$2,850,000	\$647,475

Figure 2: Seven alternatives to increase the water volume of the reservoir

AECOM looked at seven alternatives to increase the overall capacity of the reservoir from 300 million liters (80 million gallons) to a potential 590 million liters (155 million gallons) - see Figure 2. With a combination of raising the spillway 61 cm (2 feet), raising the berm 20 cm (8 inches) and excavating soil in the bottom, the optimum design volume came to be 400 million liters (105 million gallons) - Alternative D. This was based on the estimated grading and modifications cost at \$250,000 and only 1,150 cubic meters (1,500 CY) of excavation required.

3.3 Removal of the Filter Backwash Solids

Another means of increasing the capacity of the reservoir was removal of the existing filter backwash solids. There was a significant volume of material due to over four decades of use, with the solids now being diverted to the sanitary system. The filter backwash solids had high levels of aluminum and copper and was considered a "special waste" if taken outside the reservoir, since it was processed. The options were as follows:

- No action – poor bearing/volume soil
- Beneficial reuse for up to 24 million SM (6,000 acres) of cropland
- Take to a Class 1 landfill
- Take to a Construction and Demolition (C+D) landfill as a day cover

The option chosen was to haul the filter backwash solids to a C+D landfill, which required 1,900 dump truck loads or a total of 25,000 cubic meters (33,000 CY).



Figure 3: Disposal of filter backwash solids

During the solids removal, numerous areas of soft spots were found. To fix this, large rip rap from the side slopes was used in these areas for stabilization of the soil. This was a great use for the rip rap, since it had to be removed from the sides of the reservoir anyway before installation of the geomembrane liner and geoweb system. The haul off and rough grading of the reservoir bottom took approximately 3 months to complete.

3.4. Geomembrane Liner and Geoweb Installation

Even though the reservoir will be holding “raw water” from the Harpeth River, the facility owner wanted the liner system to be NSF 61 certified for potable water. After one month of fine grading the reservoir bottom, installation of the geomembrane liner started. Since the geomembrane was a heavily reinforced coated fabric with excellent physical properties such as puncture resistance, a geotextile below the liner was not needed.



Figure 4: Geomembrane liner installation

The EIA-R was prefabricated into panels 27.5 meters (90') wide by 55 meters (180') long, making them over 1,500 SM each (16,200 SF). Fabrication of the geomembrane was performed by Colorado Lining International's New Caney, TX facility and installation of liner and geoweb was by Geosynthetics, Inc. (GSI). A total of 95 prefabricated geomembrane panels were delivered to the job site. This allowed for only 2 field seams per acre required, which dramatically reduced the amount of CQA testing in the field.

A thicker 45-mil reinforced EIA-R was installed on the side slopes since they will experience greater exposure to the elements and a 36-mil reinforced EIA-R was installed on the reservoir bottom. Liner installation was completed in approximately 2 months and required over 142,000 square meters or 1.5 million square feet (35 acres). Sand tubes made out of the EIA-R were also placed along the bottom to prevent wind uplift when the reservoir is empty.

Due to concerns from potential wave action when the reservoir is full of water, AECOM recommended a geoweb with stone be installed along the top of the side slopes and on top of the geomembrane liner. After the geoweb was in place, a concrete anchor trench was installed. The geoweb with stone was also placed below the 61 cm (24") diameter influent pipe to prevent scouring and as a ramp down to the toe of slope for vehicle access when needed.



Figure 5: Installation of geoweb along the side slopes

To control any solids and sediment coming from the 61 cm (24") influent pipe, a 60-meter (200') long floating baffle system was installed. The baffle was also made out of an EIA-R potable grade geomembrane. A bench was installed inside the area of the baffle to help confine the sediment and also provide a specific area for clean out when needed.

4. CONSTRUCTION COMPLETION AND LESSONS LEARNED

The Franklin reservoir rehabilitation project went out for bid in December of 2009 and the notice to proceed was given on April 1, 2010. The reservoir was operationally complete in October of 2010, with the final construction cost being over budget by only 1% (\$3,946,762). The general contractor was Summit Construction based out of Nashville, TN. Once completed, the reservoir achieved a total of 430 million liters (113 million gallons) of storage which was 8% over the original design of 400 million liters (105 million gallons).

Some issues and lesson learned that came up during construction included:

- Subsurface conditions can vary greatly and were worse than expected in some areas
- Unit grading quantities can vary from design estimates
- Constructability of the geoweb "keyway" was more difficult than expected
- Geoweb needs concrete at the toe for more stable installation
- Baffle curtain should be anchored in some way at the bottom due to high flows

This rehabilitation project was able to improve and enlarge the raw water reservoir for water conservation at the treatment source by using a high performance geomembrane liner for leakage abatement. There was sustainable reuse of the filter backwash solids that were disposed of as a regulated solid waste and used as a daily cover at a C+D landfill. The project also had sustainable reuse of the interior rock rip rap, which was used as structural fill material to improve

low bearing soft spots in the reservoir bottom. The city of Franklin has potential plans to expand this water treatment facility and the impoundment for a future growth effort.



Figure 6: Completed reservoir rehabilitation shown now full of water

REFERENCES

- Stonecipher, P.E., Paul (2011). Rehabilitation of Franklin's WTP Raw Water Reservoir, *KY-TN Water Professionals Conference*, Covington, KY, USA.
- Walters, Kevin (2010). Franklin's leaky water reservoir to get help, *Tennessean* newspaper

Reinforced Soil Structures for Landfill Expansion

Veggi, S., Studio Geotecnico Italiano, Italy, s.veggi@studiogeotecnico.it
Poliero, E., Geotea, Italy, enrico.poliero@geotea.it
Terragni, T., Studio Geotecnico Italiano, Italy, t.terragni@studiogeotecnico.it
Testori, S., Studio Geotecnico Italiano, Italy, s.testori@studiogeotecnico.it

ABSTRACT

Due to the particular morphology of some Italian Regions, it is very difficult to find areas suitable for a new waste disposal site location. As a consequence, lots of waste disposal sites are in mountain areas and many of them have been enlarged with respect to their predicted dimensions.

The article describes the application of reinforced soil structures for the expansion of one mountain-located landfill and the use of geosynthetic materials for the lining systems.

A case history is presented: a needful embankment on the waste body for the construction of the upper new part of the landfill lining with natural and geosynthetic materials.

Because of the site conditions and other design requirements (stability, Italian regulations, lack of appropriate soil materials), realization of the works has been rendered very difficult in some circumstances; some problems could have been overcome thanks to the usage of geosynthetics materials as described in the paper.

1. INTRODUCTION

Due to the particular morphology of some Italian Regions (i.e. mountains very close to the sea, and basically the whole seaboard and flattish areas urbanized), it is very difficult to find areas suitable for a new waste disposal site location. As a consequence, many waste disposal sites are in mountain areas and many of them have been enlarged with respect to their predicted dimensions.

1.1 Main characteristics of the Facility

Bossarino landfill is located near the town of Savona in Liguria Region, in a small valley with lateral slopes that are very steep in some zones. The landfill is a non-hazardous solid waste (industrial waste) landfill. In the old part of the landfill, whose altitude ranges from about 80 m to about 200 m above sea level, waste disposal operations started in the 90s. Until 2009 about 2,100,000 m³ of waste materials had been placed.

At the bottom and at the slopes of the landfill, the subsoil is constituted of rock materials (mostly schists), weathered in the upper meters that were removed profiling the slope. Slopes can reach the inclination of 35° and more, and the mean inclination of the bottom, in the longitudinal axis, can vary from 7° to 14°.

An extension of about 1,500,000 m³ (1,100,000 m³ for waste) of the existing landfill, by superelevation up to 260 m above sea level, was authorized in 2007 (see Figure 1 and Figure 2).

1.2 Construction Problems and the New Project

In 2009, topographic surveying showed that the top plan of the existing plant was smaller than the designed one. This was caused by some settlements of the waste body larger than those expected. Principally these were due to chemical changes in stored waste over time: the increase of the biodegradable fraction and its decomposition.

The top plan of the existing landfill is the base of the new upper part, so a smaller base means a smaller quantity of waste.

As the maximum altitude of the expansion cannot be varied (it is a bond of the extension authorization), the only solution was to enlarge the existing top plan and obtain an area similar to the previous design, through the construction of an embankment on the waste body.

Because of the site conditions (very narrow operational spaces and impossibility to enlarge the landfill area) and the need to continue the waste disposal operations without involving extended areas that already have a vegetation cover,

the best engineering solution was to build the embankment with the technique of reinforced soil as described in the present paper.

This solution allowed to create an additional waste basin between the existing landfill and the new external slope of the landfill in the upper part of the embankment.

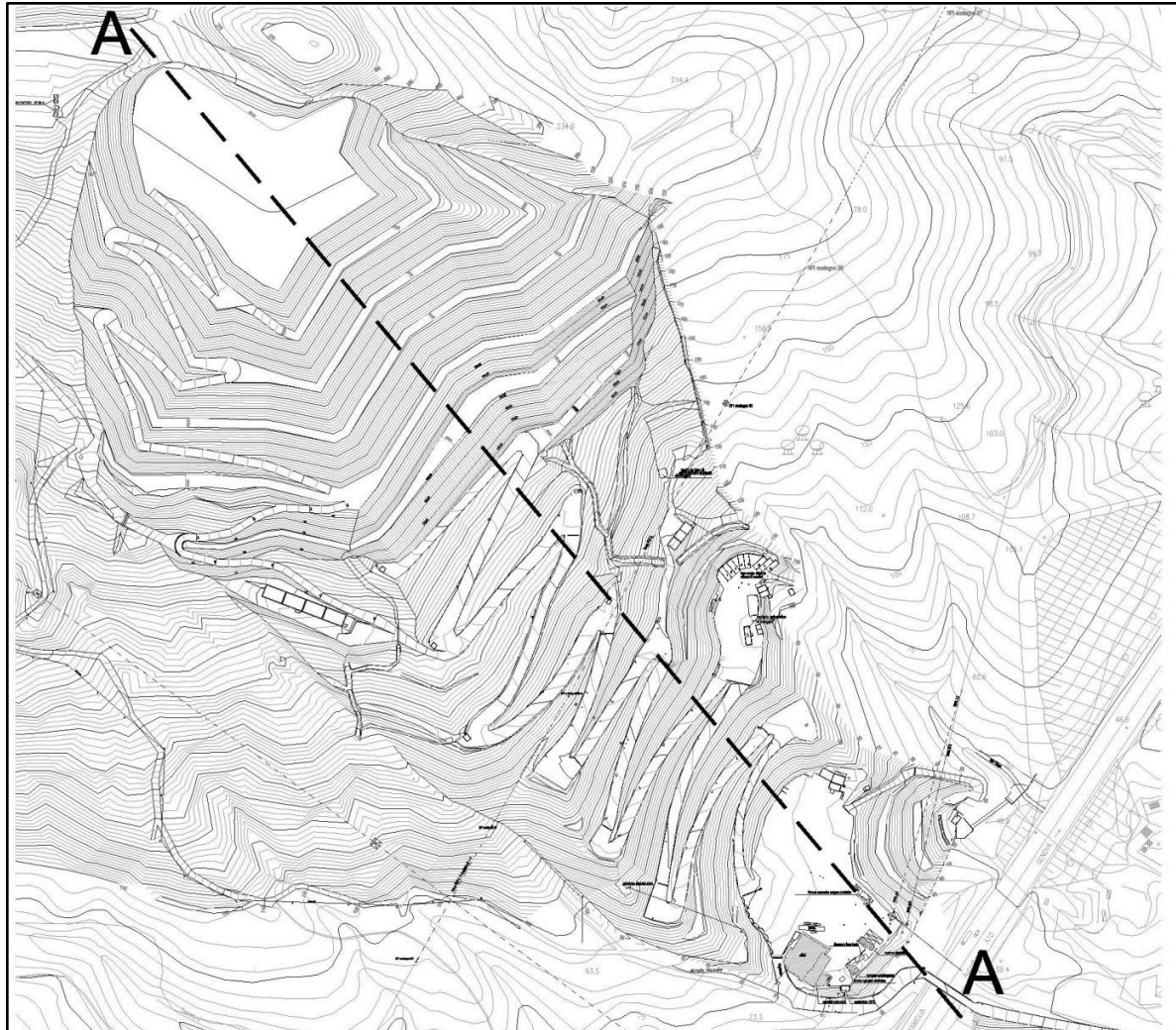


Figure 1. Plant of Bossarino landfill with the authorized superlevation

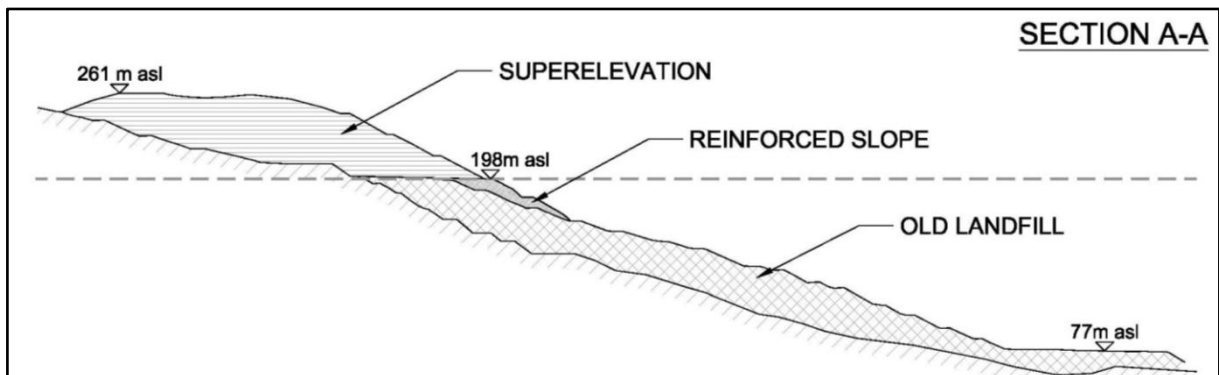


Figure 2. Cross section A-A

2. DESIGN CHARACTERISTICS

The choice of a reinforced soil structure instead of concrete retaining walls or non reinforced embankments is due to many reasons:

- Lack of external materials: soil derives only from excavation both from the cover of the existing waste and from the natural mountainside (on which the new upper part of the landfill will lay). This same material has to be used for daily cover, edge embankments, tracks, etc. The use of reinforced earth allows a reduction in materials for fill and backfill;
- Soil reinforced walls are flexible structures capable of bearing high differential settlements (typical of waste) without loss of functionality;
- Topographic surveying of the landfill showed a reduction of construction slopes due to settlements. The use of reinforcing elements allows the construction of steep slopes that, after settlement, are still steeper than the ones of non- reinforced natural soils, so the reduction of the top of the waste fill is lower with the same extent of landtake;
- Establishment of vegetation on reinforced slopes, like natural slopes can be easily achieved through the use of protection mats that increase the soil's resistance to erosion;
- An important aspect is the cost effectiveness of the system. Reinforced slopes allow considerable economies in earthworks by reducing the quantity of earth fill and the extent of landtake. Moreover in the upper part of the work, the backfill of the embankments is made by extra waste that means extra earnings for the plant.

2.1 Geometry

According to the morphology of the existing landfill, reinforced and non reinforced slopes were designed.

The total volume of the embankment is about 225,000 m³, of which 40,000 m³ is of waste placed in the basin in the upper part of the construction.

The maximum total height is about 40 m with stabilization berms in intermediate position along the slope. The construction angle of the slopes ranges from 45° to 60° for the reinforced soil structures and 35° for simple compacted soil.

Reinforcement is given by geogrids with characteristic strength of 80 kN/m, vertical spacing of 50 cm and length of 5 m (embankment toe) or 10 m.

There are also basal reinforcements with characteristic strength of 300 kN/m at the toe of each embankment. The length is variable according with the distance between the excavation profile and the edge of the embankment.

A plan view of the reinforced wall and a typical cross section are represented in Figure 3 and in Figure 4. It is important to point out that in the cross section is shown the final long term slope profile; the inclination angle is lower than the construction one due to consolidation settlements. These settlements are the product of mechanical (i.e.: self-weight and surcharge due to overlying landfill expansion) and biodegradation-related phenomena.

The evolution of settlements, as describes in the following, is monitored using benchmarks placed during construction activities and through periodic topographic surveyings.

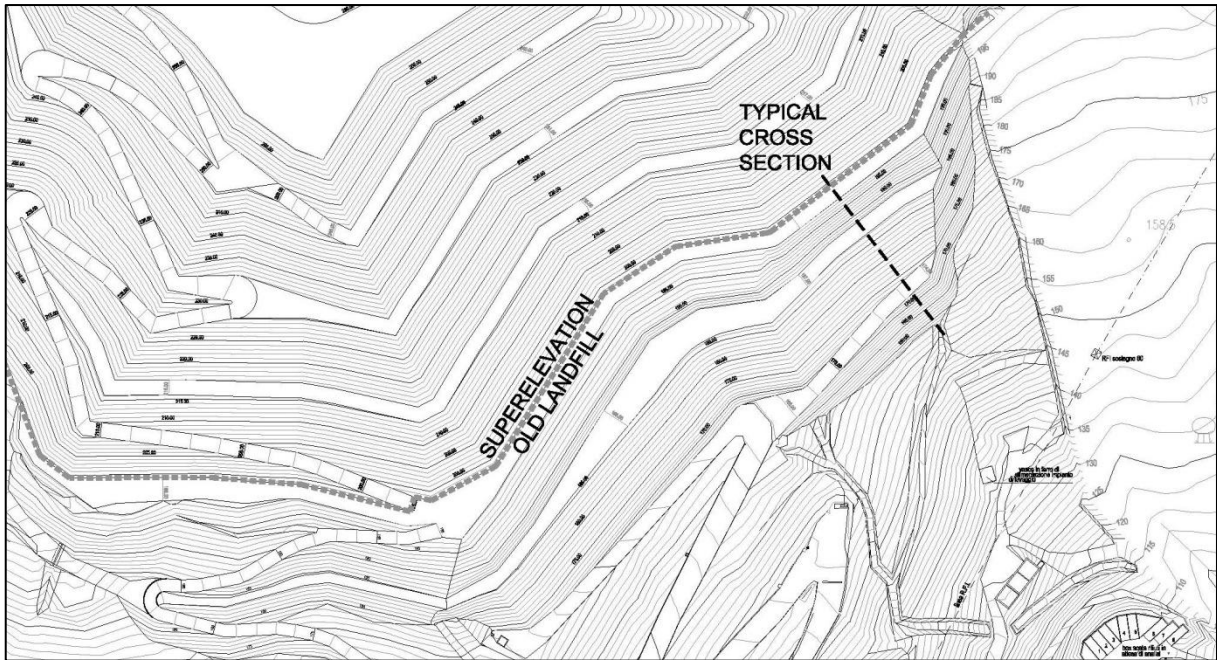


Figure 3. Plan view of the reinforced slope

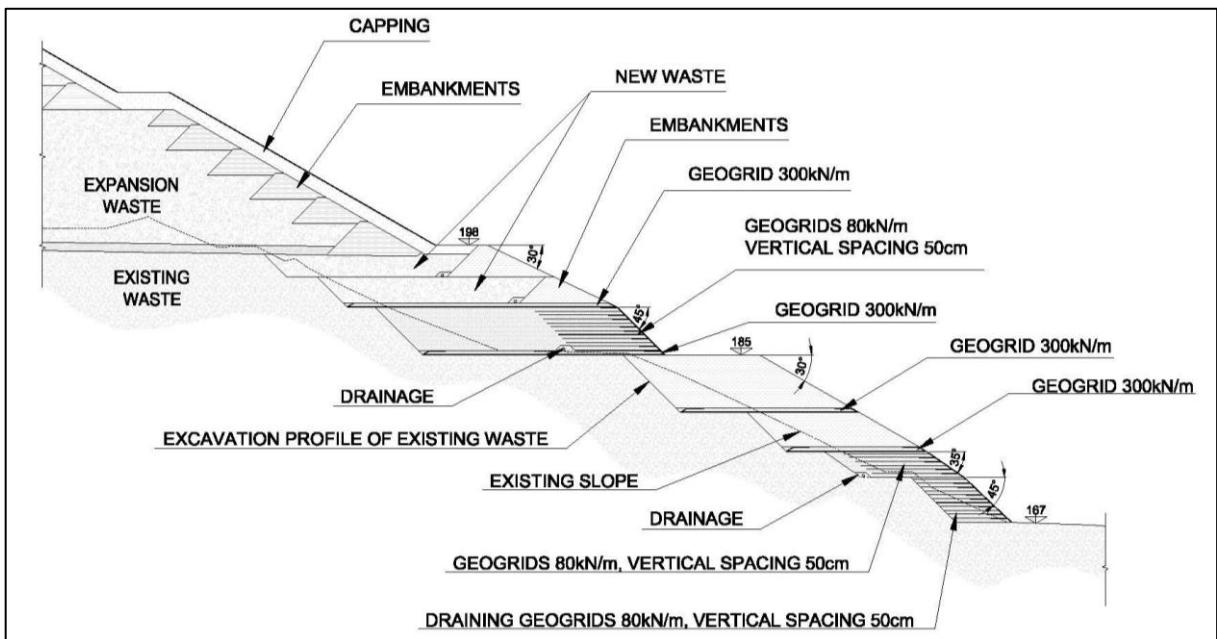


Figure 4. Typical cross section of the reinforced slope

To obtain maximum flexibility and better environmental integration, no hard facing was designed. Instead an external temporary formwork (a lightweight “climbing” shutter of tubes and boards) was erected to support the face during construction. The grids were turned up the face of the formwork and returned into the embankment directly below the next reinforcement layer.

In order to increase the soil’s resistance by providing immediate protection of exposed areas from the direct effects of wind and rainfall impact and by protecting seeded topsoil from washing out before vegetation grows, erosion protection mats are used in the external facing as shown in Figure 5.

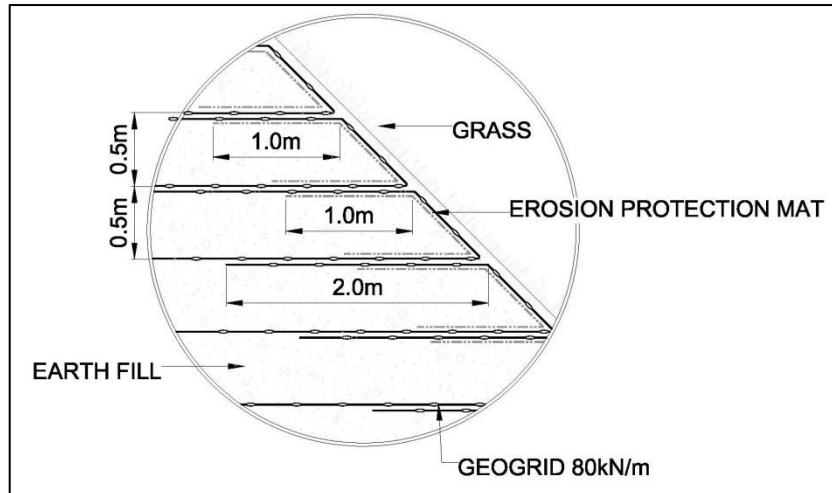


Figure 5. Detail section of the slope

2.2 Drainage System

Pore water pressures are controlled by drainage trenches at the back of the reinforced zone and by a particular underdrain.

The trenches are formed with a slotted HDPE pipe of 200 mm diameter, 30-70 mm size gravel and woven geotextile.

Besides, the toe of the slope is reinforced with a geogrid with built-in water drainage that quickly dissipates excess water pressures. This is a precautionary device as the soil used as fill material of the reinforced earth structure was predominantly coarse-grained with a little fraction of cohesive soil. Less than 15% of the particles should pass the U.S. No. 200 sieve according with U.S. Federal Highway Administration (2001).

In fact, such structures are negatively affected by the development of high excess pore water pressures caused by the applied load within the soil mass; the increase in pore pressures causes a reduction of short term strength characteristics. Besides, the effective stress reduction connected with the pore water pressure increase causes a reduction of pull-out resistance. In staged construction, such as that used in reinforced earth technique, pore pressure build-up can accumulate at each lift increasing the level of the risk as the construction proceeds. References on the behavior of draining geogrids embedded in cohesive soils are given in Zornberg & Mitchell (1994; 1995); Boardman, (1998); Zornberg & Kang (2005); Feng et al. (2008); Ghionna et al., (2010).

2.3 Lining of the Waste Basin

According to Italian regulation (D.Lgs. 36/2003), the waste basin in the upper part of the embankment is provided with sealing and drainage systems.

The sealing system is made up of the following layers (from bottom to top): GCL, HDPE geomembrane and a protection geotextile (mass per unit area of 600 g/m^2) and is laid on the bottom and on the sidewall and extended to the top of the lateral embankment (anchored under the culvert at the top).

The drainage layer is made up of a bottom gravel layer (0.5 m thick), slotted HDPE pipes and protection geotextile (areic mass of 125 g/cm^2).

It must be noted that the fabric encased GCL can substitute the mineral clay liner required by Italian regulation. In fact, it is said that particular solutions can be adopted in the realization of the lateral containment barrier provided, if they guarantee a performance equivalent to that of the mineral layer of 1 m with a permeability of 10^{-9} m/s .

However the GCL is a further lining in addition to the one at the bottom of the existing landfill.

The equivalence between the compacted clay liner (CCL) and the GCL liner can be easily demonstrated through the Darcy equation, which leads to the following:

$$k_{GCL} \times \frac{H+T_{GCL}}{T_{GCL}} = k_{CCL} \times \frac{H+T_{CCL}}{T_{CCL}} \quad [1]$$

where k_{GCL} and k_{CCL} are respectively the permeability of the geocomposite clay liner and mineral clay liner, T are their thicknesses and H is the height of the leachate above the liners (Koerner and Daniel, 1993).

2.4 Material Properties

There are two natural materials involved in the design of this work: fill and backfill of reinforced and non-reinforced slopes and waste.

The soil used in all models as the retained fill and backfill of reinforced earth was site material derived from excavation both of the cover of the existing waste and of the natural mountainside on which the new upper part of the landfill will lay. The waste material of the considered landfill is formed from the following main components: car fluff, industrial sludges, plastic fibers and fiberglass, contaminated soil from polluted sites and residues from waste treatment plants. The waste disposal operations contemplate, before compacting the waste, the mixing of different types of waste with hydraulic excavators or dozers in order to make the material homogeneous.

Unit weight and apparent frictional parameters were defined through back analyses, the composition of waste and specific site test such as unit weight site determination, standard penetration tests, field vane tests, surface seismic tests, and plate loading tests.

Beside natural materials, geosynthetics are involved in stability calculations. To assess the interface strength parameters (friction angle and cohesion), shear tests were made. In particular all the interfaces between geosynthetic materials and between natural material and geosynthetics present in the bottom and side sealing were investigated.

In Table 1 soil and waste characteristic parameters (average values) and interface characteristic parameters (minimum values) are shown.

Table 1. Characteristic parameters of materials

Material	γ [kN/m ³]	ϕ [°]	c' [kPa]
Fill and backfill of reinforced and non-reinforced slopes	19	31	0
Waste (industrial)	14	30	0
Natural subsoil (schists)	25	22	170
Lining (old landfill)	-	16	25
Slope lining (expansion)	-	22	0
Bottom lining (expansion)	19	27	0

Design parameters are obtained by reducing characteristic parameters by the appropriate partial coefficient given by Italian regulations (N.T.C. 2008).

2.5 Fabrics Properties and Design Strength

Three types of fabrics were selected for reinforced slopes:

- Draining geogrids with base tensile strength of 80 kN/m, with 50 cm vertical spacing;
- Geogrids with base tensile strength of 80 kN/m, with 50 cm vertical spacing;
- Geogrids with base tensile strength of 300 kN/m.

Grids are made of high tenacity polyester yarns encased in a durable sheath of polyethylene.

British Standards (BS 8006) were used to reduce reinforcement base strength as Italian regulations do not consider partial load factors. To define the reinforcement design strength, the unfactored strength of the reinforcement is reduced by the reinforcement material factor f_m which is the product of basic components:

$$f_m = f_{m1} \times f_{m2} \quad [2]$$

$$f_{m1} = f_{m11} \times f_{m12} \quad [3]$$

$$f_{m2} = f_{m21} \times f_{m22} \quad [4]$$

Where:

f_{m1} is a partial material factor related to the intrinsic properties of the material and is made up from the following component factors:

f_{m11} is related to the consistency of manufacture of the reinforcement and how strength may be affected by this and possible inaccuracy in assessment

f_{m12} is related to the extrapolation of test data dealing with base strength. This factor may vary with the required service life of the structure

f_{m2} is a partial material factor concerned with construction and environmental effects and is made up from the following component factors:

f_{m21} is related to the susceptibility of the reinforcement to damage during installation

f_{m22} is related to the environment in which the reinforcement is installed

2.6 Static Stability Analyses

Both internal stability of the embankment and global stability of landfill, taking into account also the geosynthetics interfaces and the foundation subsoil, were checked considering the ultimate limit states according to Italian regulations. Stability analyses were performed using traditional limit-equilibrium methods (2D).

The analyses helped to determine the characteristic strength of the reinforcements according to the strength parameters of the fill materials supplied.

References on the stability analyses of reinforced structures are given in Ghionna and Olivetta (2005) and in Ghionna and Veggi (2007).

2.7 Seismic Stability Analyses

The stability analyses were carried out taking into account seismic condition as well. According to Italian regulation, the analyses was performed considering the ultimate limit states and by simplified pseudo-static methods. For the purpose of the pseudo-static analysis, the seismic action shall be represented by a set of horizontal and vertical static forces equal to the product of the gravity forces and a seismic coefficient. Seismic coefficient is proportional to PGA (peak ground acceleration) that in this case is equal to 0.059 (g) as the part of Italy in which the landfill is located is lightly seismic.

Seismic coefficient takes into account also topography, soil stiffness and kind of structure. The use of a simplified method, like the pseudo- static one instead of a dynamic analysis, was considered adequate thanks to a low seismic action.

References about seismic stability analyses of landfills are given in Augello et al. (1995), Bray et al. (1995), Siegel et al. (1990), Singh et Murphy (1995).

3. CONSTRUCTION

The construction of the embankment began in May 2010. The waste basin on the upper part of the embankment was ready for waste disposal operations in June 2011 and the end of the whole embankment occurred in October 2011.

In situ and laboratory tests on the embankment and on the reinforcements (Proctor standard tests, Plate Load Tests, in situ density tests, pullout tests) were performed to ascertain if the final properties of the embankment match the design specifications. For reasons of shortness, the description of the tests conducted and the discussion of the results obtained are not included in the present paper, but they could be presented in the future.

Figure 6a) shows the beginning of the construction of the toe of the embankment with draining geogrids. Please note the utilization of removable climbing formwork. An intermediate phase of construction is shown In Figure 6b).



a) toe of the reinforced earth structures

b) intermediate phase of construction

Figure 6. Embankment construction

Figure 7 shows the embankment at the end of construction (October 2011) and during the construction of the toe of the superelevation of the landfill that is partly supported by the reinforced soil embankment.



Figure 7. Front photography; slope at the end of construction

According to the project, a monitoring system was built during construction (see Figure 8).

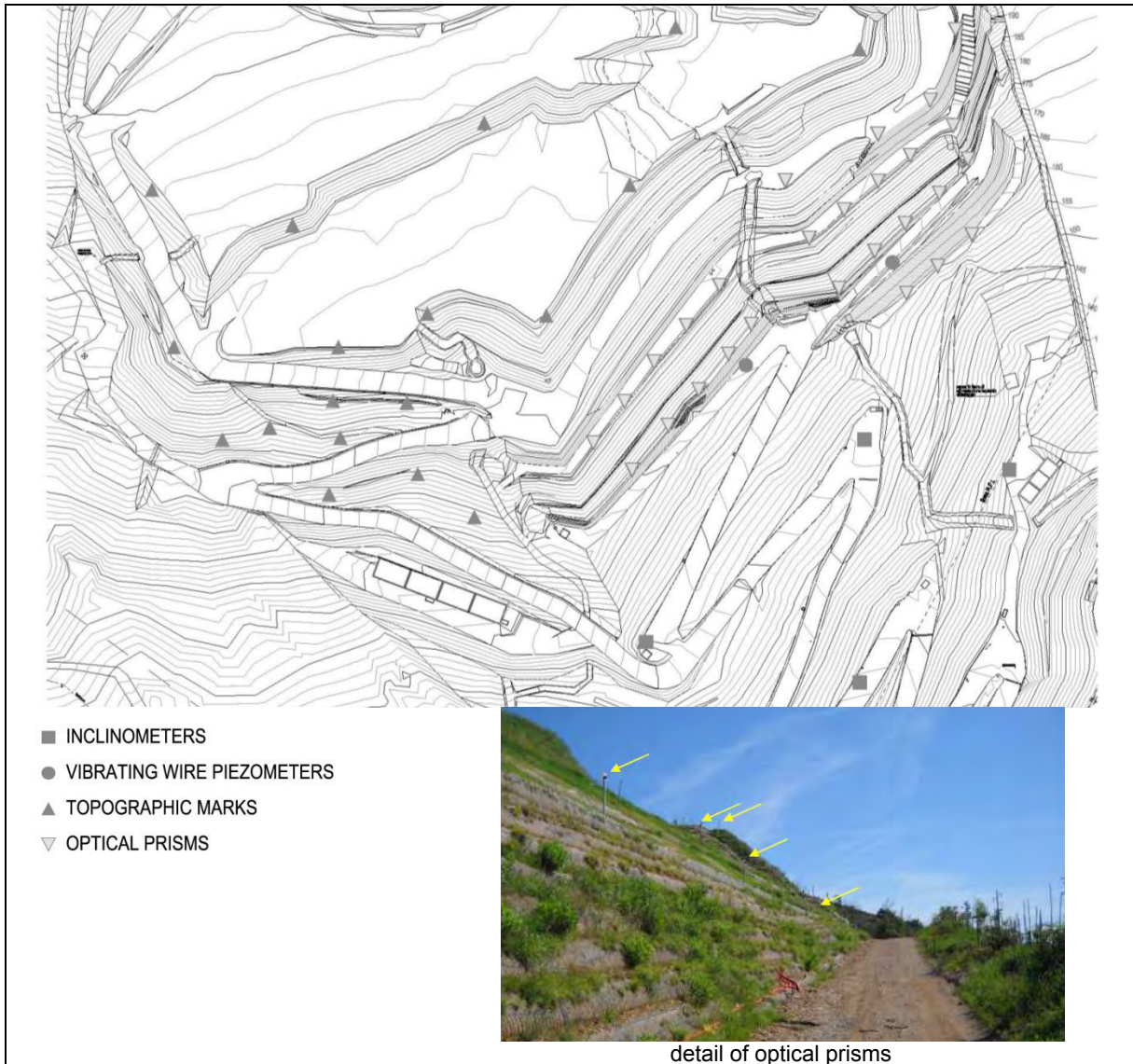


Figure 8. Plan of the landfill (2012) and monitoring system

The monitoring system had the function to check:

- vertical and horizontal settlements by means of about thirty topographic marks (optical prism) placed at the toe of the embankment, at intermediate positions and at the top. Topographic survey was planned once every fifteen days. Collected data were used to verify if the evolution of settlements and the velocity of deformation match the design calculated values. It was also programmed a topographic survey of the entire embankment and of the surroundings every three months.
- the increase of leachate pore pressure in the waste body under the embankment. For this purpose from street level at 170 m above sea level, two boreholes were drilled to a depth of 25 m and in each borehole two vibrating wire piezometers to a depth of 16 m and 25 m were placed. A data logger registered leachate pressure every 6 hours. The piezometers measured also the temperature of the leachate which is useful for understanding if some anaerobic biodegradation was ongoing.
- horizontal displacement along the base of the embankment through four vertical inclinometers installed in boreholes drilled to a variable depth of 20–30 m from the landfill surface. Surveying was programmed every fifteen days.

Surveying activities will be carried on up to landfill closure for a continuous check of stability conditions.

Today the superelevation is operational, the waste layers have a thickness ranging from 15 m to 20 m below the expansion bottom.

4. CONCLUSION

The article describes an example of the application of reinforced soil structures for the expansion of a mountain-located landfill and the use of geosynthetic materials for the lining systems.

In this case history the use of this kind of work allow the recovery of a volume for waste disposal with environmental and economic benefits.

In fact the use of reinforced soil structures is a typical application for solving problems due to particular morphology of the site or to different constraints (i.e. bonds of authorization, limits of properties, impossibility to find natural materials with proper geotechnical characteristic and so on).

It is also pointed out that the replacement of earth materials with geosynthetic, when the regulations allow that, provides many advantages: ease of construction, certainty of technical characteristics, landtake reduction and in some cases minor costs.

Others similar case histories with different purposes (solution to geotechnical problems) are known as described for example in Veggi and Parla (2009) or in Ghionna and Veggi (2007).

These examples confirm the validity of the application of reinforced soil structures in the environmental field.

REFERENCES

- Augello A.J.; Matasovic; Bray J.D.; Kavazanjian E. and Seed R.B. (1995) *Evaluation of solid waste landfill performance during the Northridge Earthquake* A.S.C.E. Geotechnical Special Publication N. 54 on "Earthquake Design and Performance of Solid Waste Landfills". ASCE Annual Convention San Diego (USA).
- Boardman, D.I. (1998), Investigation of the consolidation and pull out resistance characteristics of the Paradrain geotextile. University of Newcastle, UK (draft report).
- Bray, J.D., Augello, A.J., Leonards, G.A., Repetto, P.C. and Byrne, R.J. (1995), *Seismic stability procedures for solid waste landfills*. ASCE Journal of Geotechnical Engineering. Vol. 121 N. 2.
- Dixon, N., Jones, D.R.V. and Fowmes, G.J. (2006). Interface Shear Strength Variability and Its Use in Reliability-Based Landfill Stability Analysis, *Geosynthetics International*, 13, No 1, pp.1-14.
- Feng, X., Yang, Q. & Shoulong, L. (2008), *Pullout behavior of geogrid in red clay and the prediction of ultimate resistance*. *Electronic Journal of Geotechnical Engineering*, Vol. 13, Bund J.
- BS 8006 (1995). Code of practice for strengthened/reinforced soils and other fills.
- Fratilocchi, E., Pasqualini, E., Patacchini, C., Stella, M. and Veggi, S. (2003). Stabilità delle Discariche Controllate per Rifiuti Solidi Urbani, Proc. of XIX Turin Geotechnical Conference (CGT), Technical University of Turin.
- Ghionna, V.N. and Olivetta, M. (2005). La progettazione Geotecnica delle Opere in Terra Rinforzata con l'Approccio degli Eurocodici, Proc. of XX Turin Geotechnical Conference (CGT), Technical University of Turin.
- Ghionna, V.N. and Veggi, S. (2007). Stabilizzazione e rinforzo delle discariche, Proc. of XXI Turin Geotechnical Conference (CGT), Technical University of Turin.
- Ghionna, V. N., Parla, P., Scotto, M., Veggi, S., (2009). Pull-out behavior of a draining geogrid embedded in waste cohesive materials, Proc. Of the 9th International Conference of Geosynthetics, Brazil 23-27 may 2010.
- Koerner, R.M. and Daniel, D.E. (1993). Technical Equivalency Assessment of GCLs to CCLs, Proc. Seventh Annual GRI Seminar, Geosynthetic Research Institute, Philadelphia, PA, USA.
- Manassero, M., Parker, R., Pasqualini, E., Szabò, I., Almeida, M.S.S., Bouazza, A., Daniel, D.E. and Rowe, R.K. (1988). Controlled Landfill Design (Geotechnical aspects), Environmental Geotechnics, Sêco e Pinto ed., Balkema, Rotterdam.
- Mitchell, J.K. and Mitchell, R.A. (1991). Stability of Landfills, Proc. of XV Turin Geotechnical Conference (CGT), Technical University of Turin.
- Oweis, I.S. (1993). Stability of Landfills, *Geotechnical Practice for Waste Disposal*, Daniel Ed., Chapman & Hall, London.
- Siegel R.A.; Robertson R.J. & Anderson D.J. (1990), *Slope stability investigations at a landfill in Southern California*. A.S.T.M. Special Technical Publication STP 1070 "Geotechnics of waste fills - Theory and Practice.
- Singh S. and Murphy B. (1990) *Evaluation of the stability of sanitary landfills*. A.S.T.M. Special Technical Publication STP 1070 "Geotechnics of waste fills - Theory and Practice.
- Veggi, S. and Parla, P., (2009), Geosynthetics as a solution to geotechnical problems in a MSW landfill, *Geosynthetics 2009*, February 25-27 2009, Salt Lake City, Utah.

- Veggi, S., (2007). L'utilizzo di terre rinforzate per l'ampliamento di discariche. Convegno sul tema: Bonifica, messa in sicurezza ed ampliamento di vecchie discariche. Remtech 2007, 26-28 Settembre 2007, Ferrara, Italy.
- U.S. Federal Highway Administration (2001), *Mechanically stabilized earth walls and reinforced soil slopes – Design and construction guidelines*. Federal Highway Administration, Publication No. FHWA NHI-00-043.
- Zornberg, J. G., & Mitchell, J.K. (1994), Reinforced soil structures with poorly draining backfills. Part I: reinforcement interactions and functions. *Geosynthetics International*, vol. 1, no. 2, pp. 103-148.
- Zornberg, J. G., & Mitchell, J.K. (1995), *Reinforced soil structures with poorly draining backfills. Part II: case histories*. *Geosynthetics International*, vol. 2, no. 1, pp. 265-307.
- Zornberg, J. G., & Kang, Y. (2005), *Pullout of geosynthetic reinforcement with in-plane drainage capability*. *Geosynthetics Research and Development in Progress*, Eighteenth Geosynthetic Research Institute Conference (GRI-18), January 26, Austin, Texas.

Remediation of Industrial Wastewater Sludge by Electrokinetic Geobox

V. K. Tyagi, Managing Director, Hi-Tech Geosynthetics Pvt. Ltd., New Delhi, India, vipkolon@yahoo.com

ABSTRACT:

A pilot-scale study was conducted on in situ decontamination of industrial wastewater sludge containing relatively high concentrations of target metal contaminants such as cadmium (6.85 mg/kg), chromium (117.5 mg/kg), copper (335.7 mg/kg) and lead (64.1 mg/kg). A new type of geosystem (a cellular geobox) composed of geocomposites (electrokinetic geosynthetic, GEK) was developed for waste remediation. A low-level direct current results in physicochemical changes in the applied media, leading to species transport by coupled mechanisms, such as electromigration, electro-osmosis, electrophoresis and electrolysis of water. The modified geotextile and geocomposite with functions of filtration, drainage, conduction, and ion exchange capacity accelerated the contaminant removal rate. The electrokinetic removal efficiencies of abiotic heavy metals exceeded 85% for the mobile and weakly bound fractions, such as the exchangeable and carbonate fractions, and were higher than 69% for the strongly bound fractions, such as the organic/sulphide and residual fractions. The final product can be used as landfill material.

1. INTRODUCTION

The wastewater sludges obtained from industrial treatment plants often contain various contaminants, such as toxic heavy metals. They cannot be disposed of directly at landfill sites or reused as composts because of their toxicity. Furthermore, there may be the danger of a further significant increase in contamination potential and of the bioavailability of toxic heavy metals in the sludge because of the formation of more easily extractable forms of heavy metals from the less mobile forms originally present in the sludges (Lake 1987).

The use of electrokinetic techniques for remediation of low-permeability soils and sludges contaminated with heavy metals, organic compounds and radionuclides can be highly effective, efficient and economical (Acar and Alshawabkeh 1993; Acar et al. 1995). An electrically conductive geosynthetic, also known as an electrokinetic geosynthetic (GEK), is basically a geocomposite material combining the electrokinetic function with the existing conventional functions of geosynthetic materials. The superiority of GEK over conventional metallic electrodes lies in the absence of corrosion problems, permitting polarity reversal and providing required drainage. It can also act as ion exchange membrane by adding an ion exchange resin during the polymerisation process.

The conceptual scheme of electrokinetic remediation is shown in Figure 1. The geosynthetic material used for manufacturing the geosystem (i.e. the Geobox) was a woven geotextile made of composite multifilament yarns of inert polymeric (polyester), with carbon black added as impurity material. Traces of impurities of polymers from the family of polythiophenes, oligothiophenes and pentacene were also mixed to increase the conductive properties of the geotextile. The carbon black is mixed with polyester resin through 3D chaotic mixing. The percolation threshold of carbon black is 2.5%, which enables the polyester to decrease its resistivity from 1×10^8 ohm cm to a range between 1×10^3 and 1×10^2 ohm cm (1×10^3 ohmcm being the resistivity of steel). This final product is passed through a normal extrusion process to produce conductive polyester yarns. The yarn is then passed through weaving looms to make the woven geotextile. The same resin can be used to make nonwoven geotextiles or geocomposites.

The traces of polythiophenes, oligothiophenes and pentacene have been added to make the polyester intrinsically conductive. This has been done to impart a permanent conductivity effect to the geotextile. Passing the polyester resin through the electrochemical doping process does this. Normal polyester is an electrical insulator. The introduction of a charge carrier (by the addition or removal of electrons) into the conduction or valence bonds of polyester increases the electrical conductivity dramatically. The resin is suspended in an electrolytic solution (a mixture of tri-fluoroacetic acid, propionic acid and sulphonic acid) along with separate counter and reference electrodes. An electrical potential difference is created between the electrodes, which causes a charge (and the appropriate counter-ion from the electrolyte) to enter the polyester in the form of electron removal (p-doping). The woven geotextile was stitched to give a box shape with a three-chamber configuration, as shown in Figure 2. The stitching was done in such a manner that bodkins can be inserted in the grooves created to impart sufficient rigidity for box-type configurations. This box-type shape was configured to enhance the stability of the geosystem (as compared with geotubes) against the external environmental forces (wave, current and tidal forces) normally encountered in the field. The cellular configuration was envisaged to store sludge, provide anode purging and cathode electrolytic solution in separate compartments. The outer side was rendered impervious by applying a layer of bitumen coating. The objectives of this study were to monitor the effectiveness of the electrokinetic geosynthetic (GEK) system for the removal of contaminants in sludge, and to

investigate the factors that were most critical in determining the efficiency of electrokinetic processing for the removal of various contaminants in sludge.

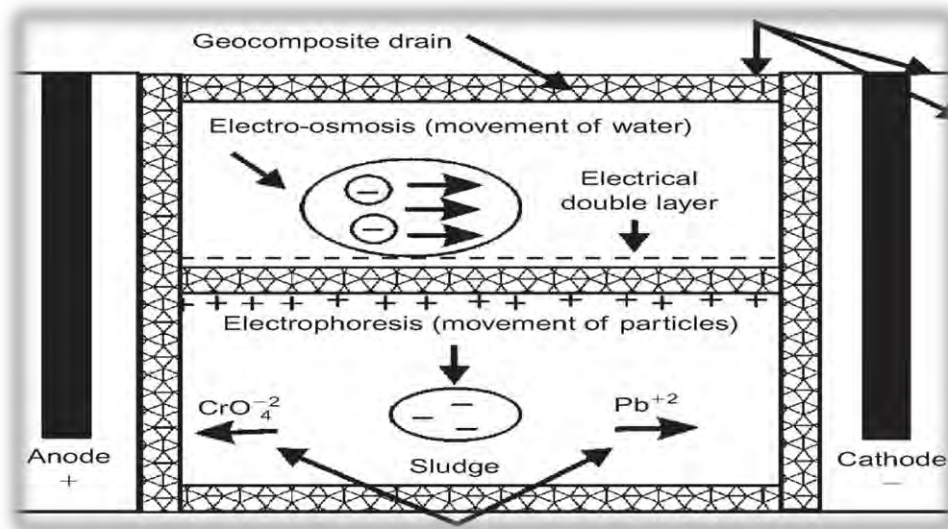


Figure 1. Conceptual scheme of electrokinetic remediation

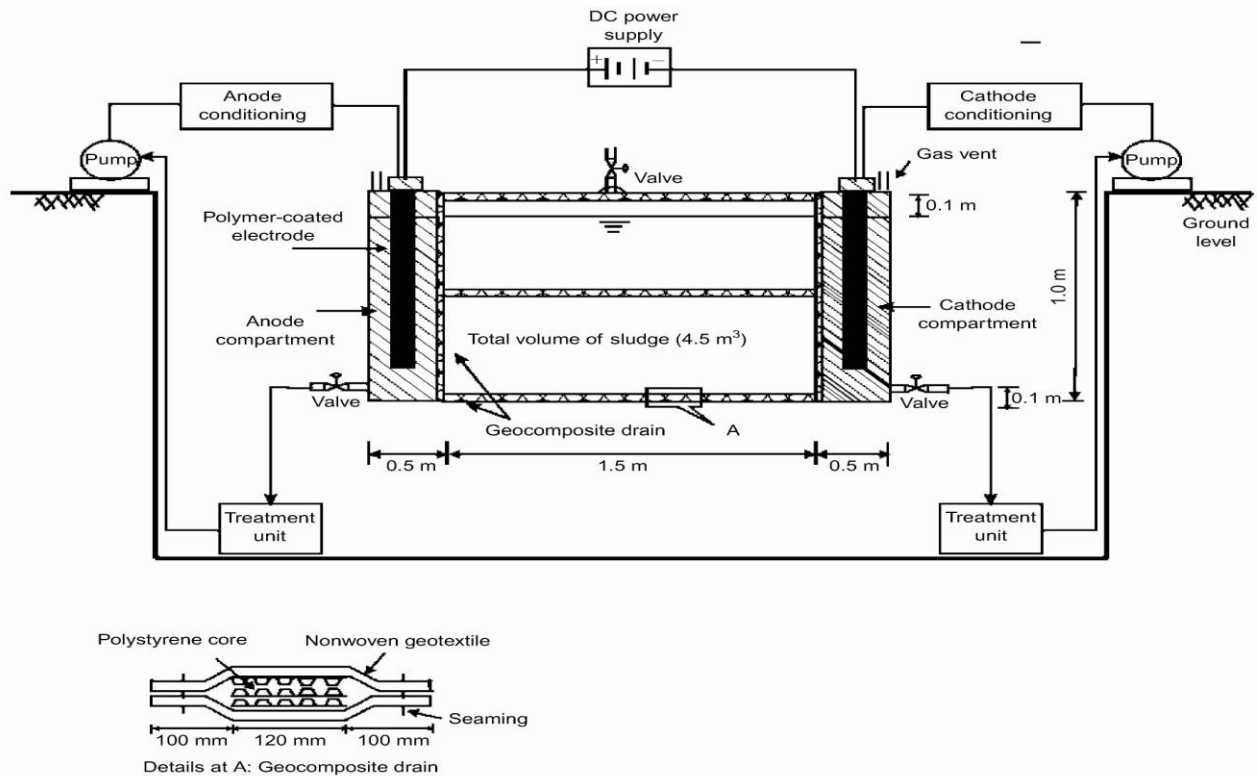


Figure 2. Schematic diagram of pilot-scale experiment on electrokinetic remediation

2. MATERIALS AND PROCEDURES

2.1. Experimental Set-Up

The experimental set-up consisted of five main components: the cellular geobox, the electrode chambers, the electrodes, the electrolyte solution containers and the power supply system. The geobox, made of woven geotextile, has overall dimensions 2.5 m x 3 m x 1 m. The properties of the woven geotextile are listed in Table 1. The central portion (1.5 m x 1 m x 1 m) formed the sludge chamber. At both sides of the sludge chamber, a woven geotextile acted as the semi-permeable ion-exchange membrane and also as secondary electrodes. In addition to the woven geotextile, conducting geocomposite drains (properties given in Table 2) were used. The apparent opening size (AOS) of the nonwoven geotextile was chosen to enhance the transport of ions towards the electrode compartments and to restrict the sludge particles from flowing into the electrode compartments. The experimental conditions maintained in the geobox are shown in Table 3.

Table 1. Properties of woven geotextile used for fabricating geobox

Property	Standard	Value (unit)
Grab tensile strength	ASTM D 4632	8130 N
Grab elongation	ASTM D 4632	30–40%
Trapezoidal tear strength	ASTM D 4533	2357 N
Puncture strength	ASTM D 4833	2067 N
Apparent opening size	ASTM D 4751	100 μ m
Permeability	ASTM D 4491	10^{-2} cm/s
Mass per unit area	ASTM D 5261	1000 g/m ²

Material: Polyester with traces of carbon black, polythiophene, oligothiophene and pentacene and ion exchange resin (di-vinyl benzene with styrene).

Table 2. Properties of geocomposite drain

Property	Standard	Value (unit)
Core:		
Mass per unit area	ASTM D 3776	850 g/m ²
Thickness	ASTM D 1777	9.5 mm
Compressive strength	ASTM D 6364	8500 N/100 cm ²
Filter:		
Grab tensile strength	ASTM D 4632	3000 N
Grab elongation	ASTM D 4632	60–90%
Trapezoidal tear strength	ASTM D 4533	1200 N
Puncture strength	DIN 54307	6000 N
Apparent opening size	ASTM D 4751	80 μ m
Permeability	ASTM D 4491	101 cm/s
Mass per unit area	ASTM D 5261	1000 g/m ²

Nonwoven geotextile material: Polyester with traces of carbon black, polythiophene, oligothiophene and pentacene and ion exchange resin (di-vinyl benzene with styrene). Core material: Polystyrene

The nonwoven geotextile component part of the drain intercepted finer soil particles before they entered the electrode compartment, and the drainage part ensured faster collection of contaminant in the main electrode compartment. This enhanced the efficiency of the removal system. Conductive geocomposite drains were also provided inside the sludge chamber to ensure free drainage of sludge in the extreme situation of sludge cake formation due to loss of moisture. They also acted as separate channels for electrokinetic removal of contaminants as they also acted as ion-exchange

membranes. One side of the geobox was used as the anode to prevent the electrode-electrolysis reaction, and other side was used as the cathode. The primary electrodes were composed of graphite and stainless steel cylinders. These cylinders were again coated with conductive high-density polyethylene (HDPE) polymer sheath through a p-doping process. Graphite and stainless steel were used to impart structural rigidity and to reduce the overall polymer coating thickness. The conductive polymer was provided to resist corrosion and chemical degradation. The electrode compartments contained electrolyte solutions in sufficient quantity to avoid sudden variations in electrolytic composition. Valves were provided to provide water for electroosmosis and to allow gas to escape from the electrodes. The outer sides of the geobox were made impervious by impregnating them using a bitumen spray. Two small cylinders were used as electrolyte solution reservoirs, which allowed the measurement of water transported from the anode side. The electrolytic solutions were passed through the treatment unit and were recirculated after conditioning in both electrode compartments by peristaltic pumps (1–250 rev/min, four heads), and a d.c. power supply (5–220 V, 0.01–2 A, 500 W) was used. Although electrolysis of water in an anode compartment naturally generates hydrogen ions, an anode-purging solution of 0.05N H₂SO₄ was used to boost the hydrogen level and enhance its reactivity with respect to the metal contaminants in the sludge bed. In the cathode compartment, hydroxides were precipitated by hydroxide ions derived from the electrolysis of water, and these precipitates inhibited the removal of contaminants in the sludge bed. A 0.5N H₂SO₄ solution was used as cathode electrolyte solution to buffer the effect of hydroxide ions produced in the cathode department. Constant current was applied to maintain the net rates of the electrolysis reactions at a constant level and to minimise complicated current boundary conditions during the experiments. The parameters are shown in Table 3.

Table 3. Experimental conditions in geobox for electrokinetic treatment

Parameters	Conditions
Target metal contaminants	Cd, Cr, Cu, Pb
Applied current (A)	2
Area of sludge bed (m ²)	1.5
Length of sludge bed (m)	1.5
Duration (h)	72
Anode purging solution	0.05N H ₂ SO ₄ solution 100 l
Cathode electrolyte solution	0.5 N H ₂ SO ₄ solution 100 l

The sludge chamber has been filled with industrial sewage in slurry form by hydraulic pumping through the inlet valve. The slurry was mechanically mixed to maintain water content of 80% by weight. 1300 l (1.3 m³) of sludge volume was maintained in the sludge chamber. The slurry level was at 0.9 m. The anode and cathode electrolyte solutions were pumped into the electrode compartments for 1 h, without electric current, for initial stabilisation of the system. The 0.9 m level was maintained for the electrolytes in the electrode compartments. As the experiment progressed, the overall voltage drop over the sludge and electrode compartments, pH variations and porewater volume transported by electro-osmotic flow were measured. After 7 days of operation, the electro-osmotic flow became constant, in line with the pH of the sludge bed. Samples were obtained from different locations of the sludge bed at regular intervals, and the residual concentrations of the various forms of metal contaminant in the sludge compartments were determined.

2.2. Contamination Measurement Methods

Heavy metals occur in sludge in various abiotic (physiochemical) forms, such as soluble, adsorbed, exchangeable, precipitated, organically complexed and residual phases. They may also exist in biotic forms, such as extracellular and intracellular species. The variety of heavy metal forms significantly influences their environmental mobility and bioavailability, and finally determines the potential for environmental contamination (McBride 1994). Heavy metals existing as loosely bound fractions, such as the adsorbed, soluble and exchangeable forms, tend to be easily moved and dispersed. Metals associated with organic ligands or embedded in crystal lattices are not easily separated or mobilised. Sequential extraction analysis has been suggested to determine the speciation of heavy metals in any given matrix (Tessier et al. 1979; Khalid et al. 1981; Bardi and Aston 1983; Gibson and Farmer 1986; Domingues and Silva 1990; Davidson et al. 1994).

2.3. Preparation of Sludge Samples

The sludges used in this experiment were anaerobically digested sludges taken from an industrial wastewater treatment plant in Mumbai, India. Sludges were collected at two different plant locations, i.e. before and after the dewatering process, and they were mechanically mixed to maintain a water content of 80% by weight. The sludge was hydraulically pumped through the inlet valve into the geobox at 65% of its volume.

2.4. Analysis of Sludge

The analytical procedure involved two extraction steps. The first step involved the sequential extraction of the abiotic fraction of the sludge heavy metals before and after the electrokinetic treatment. The sequential extraction method used in this experiment was suggested by Tessier et al. (1979) and later revised by the Environmental Biochemistry Research Group at Imperial College, UK (Li et al. 1995). The second step was based on an extraction scheme for determination of biotic speciation of the heavy metals. This method involved sieving, elutriation, EDTA extraction, washing and acid digestion, for determining the distribution of heavy metals, between their soluble, precipitated, extracellular and intracellular components (Hayes and Theis 1978). A volume of 100 ml of sludge was passed through a 150 mm sieve for separation of biomass and particulates; the sieve residue was washed with 500 ml of deionised water. A volume of 600 ml of diluted sludge was placed in a conical upflow clarifier for separation of the biomass from inert particulates. The overflow rate of the desired upflow clarifier was calculated using Stokes's law (specific gravity of sludge particle: 1.02). Elutriation was continued until the final elutriate volume collected from the upflow clarifier was about 5 l. As the chelating agent, EDTA is known to have a stronger affinity for heavy metals than for the extracellular polymers of the microbial cell wall, it was used to extract only the extracellular phase of the heavy metals from the biomass after elutriation. The procedure for subsequent extraction is shown in the flowchart in Figure 3, and the various chemical extractants used are shown in Table 4. The electrophoretic transport of microbial cells after electrokinetic treatment was examined by determining the number of microbial cells at different locations in the sludge.

3. ELECTROKINETIC PROCESS

3.1. Brief Overview

The electrical transport induced in the sludge is used for the removal of contaminants and the introduction and

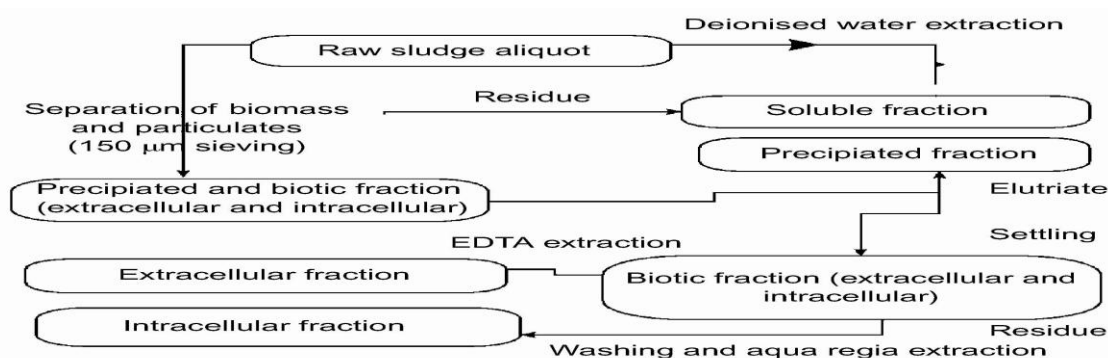


Figure 3. Subsequent fractionation scheme for analysis of biotic phases of heavy metal in the sludge

distribution of reagents into the sludge matrix. The reagents may be used for contaminant degradation, enhancement of contaminant solubility, immobilization of contaminant or attainment of an optimum pH in the sludge during the treatment process. The application of low-level direct current results in physicochemical changes in the medium, leading to species transport by coupled mechanisms, of electromigration, electro-osmosis, electrophoresis and the electrolysis of water. In the electrokinetic cell there is an anode half-cell and a cathode half-cell. Water undergoes electrolysis at each electrode.

At the anode, water is oxidised, producing an acid front and oxygen gas. Reduction of water occurs at the cathode, where a base is produced and hydrogen is released. The acid front migrates towards the cathode through the medium. This, in turn, causes contaminant to be desorbed and/or dissociated, resulting in the initiation of electrophoresis and electromigration, i.e. the transport of charged suspended solids and soluble ions under the influence of the applied potential gradient. The applied potential gradient also leads to electro-osmosis, i.e. the flow of an ionic liquid to a charged surface. Finally, the contaminants are transported towards the cathode and anode depending on their electrical charge

Table 4, Various chemical extractants used in sequential and subsequent extraction schemes for determination of abiotic and biotic speciations of heavy metals

Fractions	Chemical extractants
Abiotic	
Exchangeable	0.5 M MgCl ₂ + NH ₄ OH/HOAc (pH ¼ 7)
Bound to carbonate or specially adsorbed	1 M NaOAc + NH ₄ OH/HOAc (pH ¼ 5)
Bound to Fe and Mn oxides	0.04 M NH ₂ OH HCL in 25% HOAc
Bound to organics and sulphides	0.02 M HNO ₃ + 30% H ₂ O ₂ + 3.2 M NH ₂ OAc in 20% HNO ₃ (pH ¼ 2)
Residual	HF/HClO ₄ /HNO ₃ (4:2:15)
Total digestion	HF/HClO ₄ /HNO ₃ (4:2:15)
Biotic	
Soluble	Deionised water
Precipitated (insoluble)	Aqua regia; HNO ₃ /HCL (1:3)
Extracellular	10 ⁻⁴ M EDTA
Intracellular	Aqua regia
Total digestion	Aqua regia

(i.e. cationic or anionic), and the direction of porewater flow. Contaminants collected at the electrodes can then be extracted and subsequently treated for reuse. The dissolution and precipitation of ions may result from chemical reactions during electrokinetic treatment. These processes have a significant effect on contaminant removal. The acid front produced at the anode by electrolysis of water is able to dissolve most metal ions. However, relative dissolution of different species depends on the pH of the pore fluid and the solubility product of each species (Alshawabkeh and Acar 1994). Convective forces also contribute to front migration, but to a lesser extent. As precipitation of many metal ion species occurs at pH values greater than 6.0, and electrokinetic processing automatically raises the pH at the cathode, it becomes imperative to buffer the cathode compartment to facilitate the removal of contaminants (Alshawabkeh and Acar 1992). A reduction of pH to less than 4 results in the retention of cationic species in a stable form. It also facilitates the electrolysis of water, resulting in reduced production of OH ions. Cathode water electrolysis will also reduce the power requirement and overall treatment cost by decreasing the electrical potential difference applied across the mass (Acar and Alshawabkeh 1996). Electro-osmotic flow is important in some processes, such as removing organic contaminants and enhancing metal or radionuclide removal from the sludge.

3.2. Various Parameters for Electrokinetic Experiment

A possible range of electric potential to drive the electrokinetic remediation is from 10 V/m to about 250 V/m (but preferably from 20 V/m to 100 V/m). In this experiment, the voltage was varied between 25 V/m and 40 V/m. The current was maintained at a constant value of 2 A. The operating current was determined by measuring the temperature of the sludge chamber until constant chamber resistive heating was achieved owing to the passage of current. The electromigration of ions increases as the current increases, and the electro-osmotic flow enhances owing to the increase in voltage. The ionic current between the electrodes in the pore fluid depends on the voltage applied in the sludge. Depending on the type of ions being transported, the current and voltage induced in the sludge, and the sludge and pore fluid chemistry, the ion transport may vary between 0.5 and 5 cm/day.

4. RESULTS AND DISCUSSION

4.1. Initial Concentrations and Speciations

The initial concentrations of abiotic and biotic forms of metal contaminants present in the sludge are shown in Table 5. Figure 4 presents the relative availability of different phases of heavy metals. The total concentrations of target heavy metals were relatively high even though the sludges were taken from a industrial wastewater treatment plant. The recoveries of the sequential and subsequent extraction procedures were in the ranges 96–100% and 96–98%, respectively, as shown in Table 6. In line with the results of the abiotic heavy metal sequential extraction analysis, most of the heavy metals existed in the organic/ sulphide and residual fractions and resulted from the anaerobic digestion of the sludge in the wastewater plant prior to coagulation and settling (Lake 1987). The results of subsequent fractionation showed that the main portion of the biotic heavy metals was distributed between the precipitated (insoluble) and intracellular components of the sludge, with the exception of cadmium. Extracellular heavy metals (EDTA extractable) accounted for less than 6% of the total amount of the heavy metals present. Likewise, soluble metals were also insignificant fractions in all cases (less than 2.5%), again with the exception of cadmium, 10% of which was soluble. It may be presumed that microbial uptake actively competed with precipitation in the removal of heavy metals from the digester supernatant. This phenomenon has been verified by the demonstrated ability of microbes (and especially bacteria) to concentrate metal ions around the cell wall by complexing with proteins and acid grouping that serves as bonding sites (Hayes and Theis 1978). The inability to release these metals during EDTA extraction further suggested active transport of these metals to the cell interior.

4.2. Concentration of Metals After Electrokinetic Treatment

Figures 5 and 6 show, respectively, the concentration variations of abiotic and biotic heavy metals in the sludge compartment after electrokinetic treatment. The dissociation and desorption of metal species occurred continuously along the migration direction of the acid front during the treatment, and metal contaminants seemed to be gradually transported towards the cathode by electromigration and electro-osmotic purging. Charged polymers on the microbial cell surface contain ionisable groups, which result in an amphoteric surface. Their surfaces carry a net negative charge at high pH and a net positive charge at neutral pH (Ebersole and McCormick 1993; De Flaun and Condee 1997). Thus the microbial cells migrate towards the anode or the cathode in an electric field, depending on their surface charges, as

Table 5. Fractionation of heavy metals using two different extraction schemes

Extraction method	Fractions	Concentration (g/g)			
		Cd	Cr	Cu	Pb
Sequential extraction (abiotic fractionation)	Exchangeable	0.85	0.0	10.6	0.0
	Carbonates	1.1	1.4	5.0	5.1
	Fe/Mn oxides	4.0	2.7	15.9	2.9
	Organic/sulphides	0.0	38.2	245.0	33.4
	Residual	0.8	68.7	51.7	18.9
	Sum	6.75	111.0	328.2	60.3
	Total digestion(a)	6.85	117.5	335.7	64.1
	Recovery(b) (%)	98.5	94.4	97.7	96.7
Subsequent extraction (biotic fractionation)	Soluble	0.8	0.1	9.6	0.1
	Precipitated (insoluble)	5.3	77.7	246.7	36.3
	Extracellular	0.0	4.0	16.7	3.5
	Intracellular	0.4	11.6	28.6	10.6
	Sum	6.5	93.3	301.6	50.5
	Total digestion	6.7	94.6	308.7	52.4
	Recovery (%)	97.0	98.6	97.7	96.4

(a) The concentrations were determined by the final step of sequential extraction using HF/HClO₃/HNO₃ solution. (b) (Sum of concentrations of all fractions/concentration determined by total digestion) x 100%. (c) The concentrations were determined by the extraction of aqua regia solution.

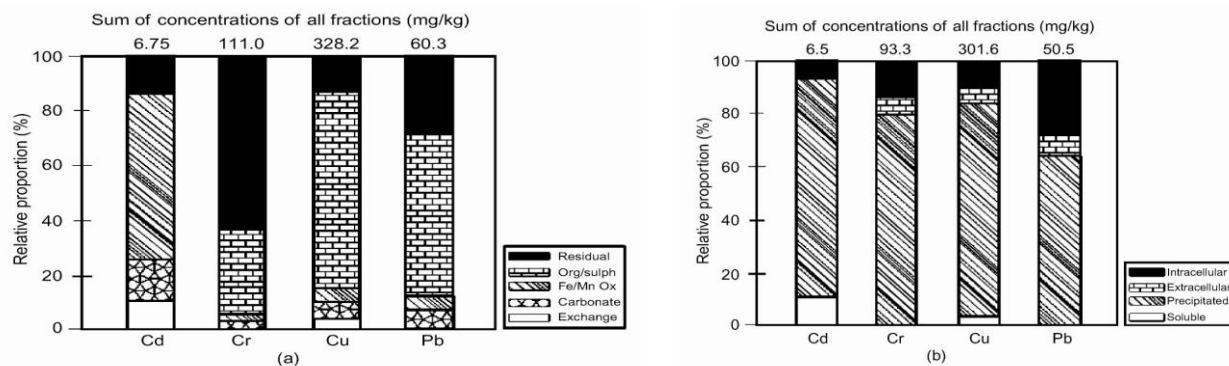


Figure 4. Relative proportioning of heavy metals in the untreated sludge: (a) abiotic speciations analyzed by sequential extraction: (b) biotic speciations analyzed by subsequent extraction

controlled by the surrounding pH. On the reverse side, the porewater in the sludge compartment flowed towards the cathode by electro-osmosis during the treatment period. Accordingly, the largest number of microbial cells appeared in the zone near the cathode rather than in the middle of the sludge compartment resulting from the coupled effect of the electrophoretic transport of microbial cells and the electro-osmotic flow. For this reason, the extracellular fractions of heavy metals accumulated in the same zone as the microbial. High effectiveness of the electrokinetic removal of metal contaminants is not expected on the basis of the sequential extraction analysis result, because 72–95% of most of the target metals (Cr, Cu and Pb) were predominantly partitioned in the strongly bound fractions, such as the organic/sulphide and residual fractions, again with the notable exception of Cd.

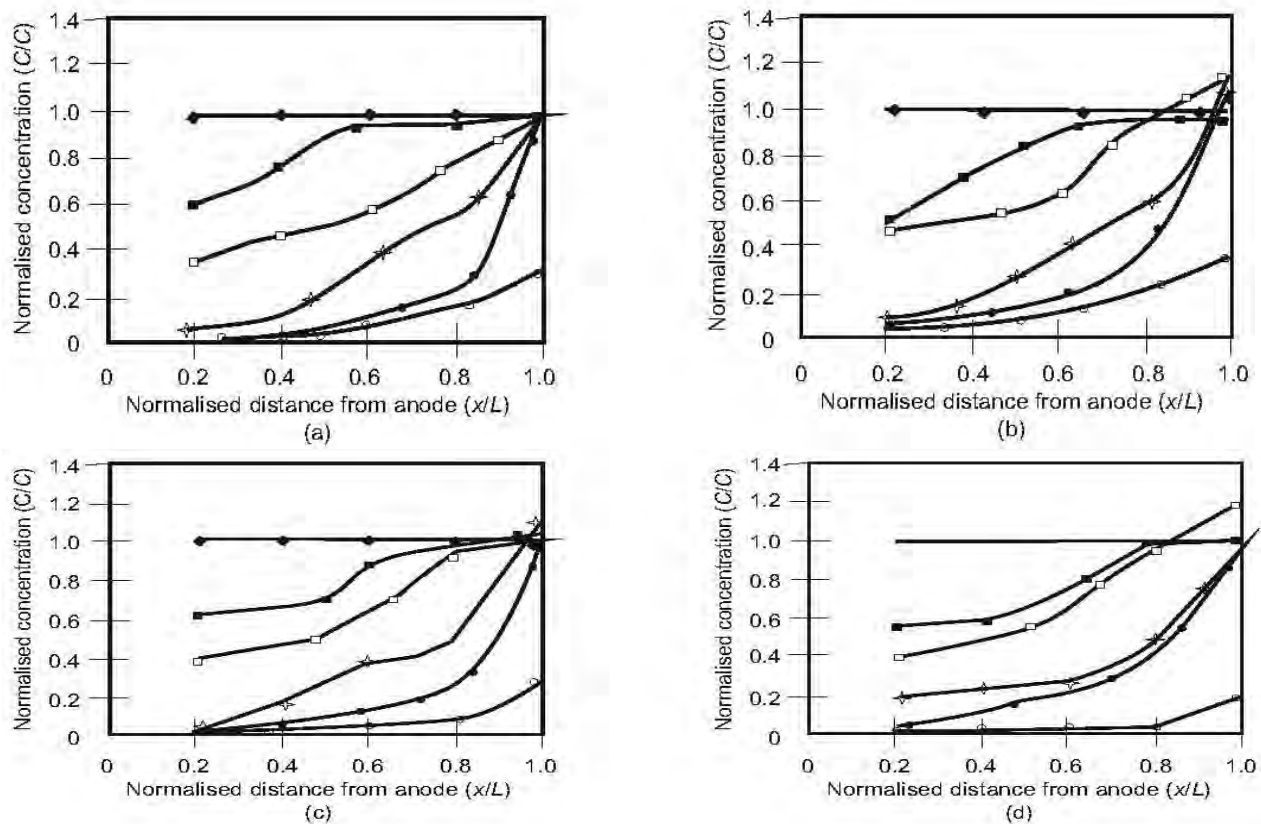


Figure 5. Concentration profile of abiotic metals in the sludge chamber after electrokinetic treatment (x distance from anode; L length of sludge chamber) for: (a) Cd; (b) Cr; (c) Cu; (d) Pb. r , initial; s , exchangeable fraction; d , carbonated fraction; Fe/Mn oxide fraction; h , organic/sulphide fraction; j , residual fraction

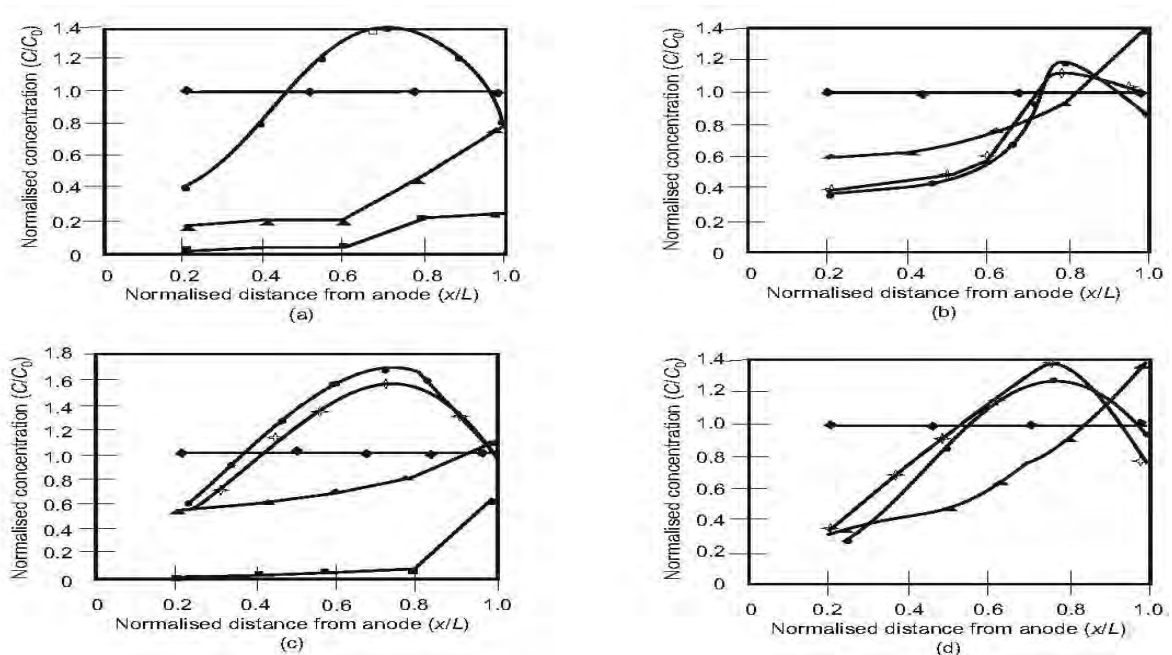


Figure 6. Concentration profile of biotic metals in the sludge chamber after electrokinetic treatment (x distance from anode; L length of sludge chamber) for: (a) Cd; (b) Cr; (c) Cu; (d) Pb. r, initial; j, soluble fraction; m, precipitated (insoluble) fraction; , extracellular fraction; d, intracellular fraction conditions.

5. CONCLUSIONS

From the results of a pilot-scale study on the electrokinetic removal of heavy metals from industrial wastewater sludges, using a geobox that included an electrokinetic geosynthetic (GEK), the following conclusions may be drawn:

Electrokinetic geosynthetic (GEK) materials offer a technically viable and efficient solution for remediation of contaminated wastewater sludge.

The sludge contained high concentrations of heavy metals in the chemical form of various speciations. To estimate the environmental impacts of metal contaminants in sludges, the concentrations and speciations of metal contaminants were determined by sequential and aqua regia extraction methods. Except for Cd, most target metals (Cr, Cu and Pb) exist predominantly in the organic/sulphide and residual fractions (72–95%).

The removal efficiencies of heavy metals were significantly dependent on their speciations in the sludge. The more strongly bound fractions, such as organic and residual fractions, were less effectively removed by electrokinetic treatment.

The variation of the sludge pH significantly influenced the removal efficiency of the electrokinetic technique. As the acid front generated by the electrolysis of water in the anode compartment migrated towards the cathode, the overall sludge pH decreased gradually. The complexed and/or adsorbed metal species were dissolved and desorbed along with the migration of the acid front.

REFERENCES

- Acar, Y. B. & Alshawabkeh A.N. (1993). Principles of electrokinetic remediation. *Environmental Science and Technology*, 27, No. 3, 2638–2647.
- Acar, Y. & Alshawabkeh, A. (1996). Electrokinetic remediation. II: Theoretical model. *Journal of Geotechnical Engineering*, ASCE, 122, No. 3, 186–196.
- Acar, Y. B., Gale, R. J., Alshawabkeh, A. N., Marks, R. E., Puppala, S., Bricka, M. & Parker, R. (1995). Electrokinetic remediation: basics and technology status. *Journal of Hazardous Materials*, 40, No. 2, 117–137.
- Alshawabkeh, A. & Acar, Y. (1992). Removal of contaminants from soils by electrokinetics: a theoretical treatise. *Journal*

- of Environmental Science and Health, 27, No. 7, 183.
- Alshawabkeh, A. & Acar, Y. (1994). Theoretical and Experimental Modeling of Multi Species Transport in Soils Under Electrical Field. Gulf Coast Hazardous Substance Research Center, Boston, MA, USA, No. 113LSU3225.
- ASTM D 1777. Standard Test Method for Thickness of Textile Materials. ASTM International, West Conshohocken, PA, USA.
- ASTM D 3776. Standard Test Methods for Mass Per Unit Area (Weight) of Fabric. ASTM International, West Conshohocken, PA, USA.
- ASTM D 4491. Standard Test Methods for Water Permeability of Geotextiles by Permittivity. ASTM International, West Conshohocken, PA, USA.
- ASTM D 4533. Standard Test Method for Trapezoid Tearing Strength of Geotextiles. ASTM International, West Conshohocken, PA, USA.
- ASTM D 4632. Standard Test Method for Grab Breaking Load and Elongation of Geotextiles. ASTM International, West Conshohocken, PA, USA.
- ASTM D 4751. Standard Test Method for Determining Apparent Opening Size of a Geotextile. ASTM International, West Conshohocken, PA, USA.
- ASTM D 4833. Standard Test Method for Index Puncture Resistance of Geotextiles, Geomembranes and Related Products. ASTM International, West Conshohocken, PA, USA.
- ASTM D 5261. Standard Test Method for Measuring Mass per Unit Area of Geotextiles. ASTM International, West Conshohocken, PA, USA.
- ASTM D 6364. Standard Test Method for Determining the Short-Term Compression Behavior of Geosynthetics. ASTM International, West Conshohocken, PA, USA.
- Bardi, M. A. & Aston S.R. (1983). Observation on heavy metal geochemical associations in polluted and non-polluted estuarine sediments. *Environmental Pollution*, 6, 181–193.
- Davidson, C. M., Thomas, R. P., McVey, S. E., Perala, R., David, L. & Ure, A. M. (1994). Evaluation of a sequential extraction procedure for the speciation of heavy metals in sediments. *Analytica Chimica Acta*, 291, No. 3, 277–286.
- De Flaun, M. F. & Condee, G. W. (1997). Electrokinetic transport of bacteria. *Journal of Hazardous Materials*, 55, No. 1–3, 263–277.
- Domingues, H. & Silva, J. M. V. (1990). Copper and zinc in sandy, granitic and schist soils. *Environmental Technology*, 11, No. 5, 463–468.
- Ebersole, R. C. & McCormick, R. M. (1993). Separation and isolation of viable bacteria by capillary zone electrophoresis. *Bio-Technology*, 11, No. 11, 1278–1282.
- Gibson, M. J. & Farmer, J. G. (1986) Multi-step sequential chemical extraction of heavy metals from urban soils. *Environmental Pollution*, 11, No. 2, 117–135.
- Hayes, T. D. & Theis, T. L. (1978). The distribution of heavy metals in anaerobic digestion. *Journal of Water Pollution Control Federation*, 50, No. 1, 61–72.
- Khalid, N. D., Gambrell, R. P. & Patrick, W. H. Jr (1981). Chemical availability of cadmium in Mississippi river sediment. *Journal of Environmental Quality*, 10, No. 4, 523–528.
- Lake, D. L. (1987). Chemical speciation of heavy metals in sewage sludge and related matrices. In *Heavy Metals in Wastewater and Sludge Treatment Processes*, Lester, J. N., Editor, Vol. 1. CRC Press, Boca Raton, FL, pp. 125–154.
- Li, X., Coles, B. J., Ramsey, M. H. & Thornton, I. (1995). Sequential extraction of soils for multi-element analysis by ICP-AES. *Chemical Geology*, 124, No. 1–2, 109–123.
- McBride, M. (1994). *Environmental Chemistry of Soils*, Oxford University Press, Oxford, pp. 308–341.
- Mitchell, J. K. & Yeung, T. C. (1991). Electrokinetic flow barriers in compacted clay. *Transportation Research Record*, No. 1289, National Research Council, Washington, DC.
- Tessier, A., Campbell, R. G. C. & Bisson, M. (1979). Sequential extraction procedure for the speciation of particular trace metals. 2nd edn. Wiley & Sons, Inc., New York, pp. 203–207. *Analytical Chemistry*, 51, No. 7, 844–851.

Removing Human Error from Geomembrane Leak Location Surveys

Matthew P. Kemnitz, Leak Location Services, Inc., USA, mkemnitz@llsi.com

ABSTRACT

Human error can drastically affect the accuracy, completeness and validity of geomembrane leak location surveys. Geomembrane leak location surveys have been commercially available since 1985 and industry standards have been developed for the various implementations. However, industry standards do not eliminate human error in applying the standards, taking the data and correctly interpreting the data. Proper use of technology, with extensive field experience and a thorough understanding of the technology, can reduce human error to a negligible level.

1. SURVEY DATA

At the heart of geomembrane leak location surveys is the process of taking the data, plotting the data and interpreting the data. If the data is taken incorrectly or inaccurately it can be useless. Without solid data acquisition, leak location surveys are often ineffective. The data must be read accurately, written correctly, and entered into the data plotting program correctly, each step entailing error. If the above can be done without errors there is still the aspect of interpreting the data. This takes time and experience that can only be fully mastered in the field. With a human interface, the human elements of reading a meter, writing down the data and interpreting tables of numbers or keyboarding the readings into the correct places in the data plotting software provide multiple opportunities for error.

1.1 Data Acquisition

One way data can become inaccurate is during the recording of the data. Simply writing down the information collected on a notepad is unreliable. There are multiple issues associated with this method that relate to human error. The data can be written down incorrectly, out of order or it can simply become destroyed or lost in certain field conditions. On an area of only 4,000 square meters (2-acres) there can be up to 6,000 readings to be recorded. This calculation is based on a grid pattern that accurately depicts a leak signal per the ASTM standard. Per ASTM D 7007 the leak signal shall be represented by five or more data points in the data. With larger grid spacing, leaks of smaller sizes can be missed. The likelihood of all of the readings to be written down accurately and in the correct order is very low. Assuming a one percent error on the copying of the data the number of errors increases with size and can be detrimental to the overall survey. (Table 1)

Table 1. Number of errors in relation to the size of the area surveyed.

Area(m ²)	Area(Acres)	# of Readings	1% Error
929	0.23	667	6.7
9,290	2.30	6,667	66.7
46,452	11.48	33,333	333.3
92,903	22.96	66,667	666.7
139,355	34.44	100,000	1,000.0

It can be expected that the larger the area the longer the survey will last and thus the potential for error increases even more due to fatigue and tediousness.

Pencil and paper recording of data from an instrument has long since been replaced by digital data acquisition systems and computers using microprocessors and software. Computer data acquisition systems as seen in Figure 1, take the reading, convert it to digital data and store the data practically instantaneously with no errors. The data is stored in the order that it was taken. The leak location technician does not have to concentrate on the physical recording of the data because it is automatically stored. Instead they can concentrate more on how they physically are taking the data and making sure their technique is sound and site conditions are ideal.



Figure 1. Leak location survey being performed on soil-covered geomembrane using a digital data acquisition system.

1.2 Plotting the Data

Once all of the data has been collected it should be plotted. This can be done many different ways, but the best way is the one with the least amount of human input. Inputting the data by keyboard increases the chance of error by incorrectly keying in the data and can lead to erratic data points and leak signals being missed. Without oversampling, one incorrect input can lead to a leak being missed. Using a computer system that automatically downloads the data and graphs it automatically eliminates the need for inputting the data by hand. By removing this extra step from the leak location survey process a significant amount of time is saved and the chance of the recorded data being input into the data plotting software incorrectly is eliminated.

1.3 Interpreting the Data

Using graphing software that accurately imports the data and converts it to easily understandable graphs can greatly aid in the interpretation of the data for leak signals. Since graphical representation of the data is the final step in the use of the data, it is important that the software being used is adaptable. Plotting the data on a fixed scale can cause larger signals to be off-scale, and suppress smaller signals. Figure 2 shows that the graphing software needs to be able to adjust in such a manner as to make the smaller leak signals visible. Figure 3 shows a plot of the same data on a better scale. By using graphing software and knowing how to fully use its capabilities, leaks similar to that shown in Figure 2 will be detected. Without the use of good graphing software the leak location surveyor would need to interpret all of the data by themselves. This can lead to complications and take much more time than is necessary. The idea is to be able to efficiently and effectively find leaks within a site. Being able to interpret the data onsite and to verify signals the same day greatly reduces the effect that site condition changes have and improve the accuracy of the leak signals locations. Data interpretation is a learned skill. It takes time to learn and cannot be fully understood in a few short weeks. Data must be viewed and interpreted consistently over multiple different surveys to better understand how each survey is different and how this relates to the data's interpretation. The operator must be thoroughly experienced in interpreting the data, knowing how site conditions can affect leak signals and knowing how to recognize false signals.

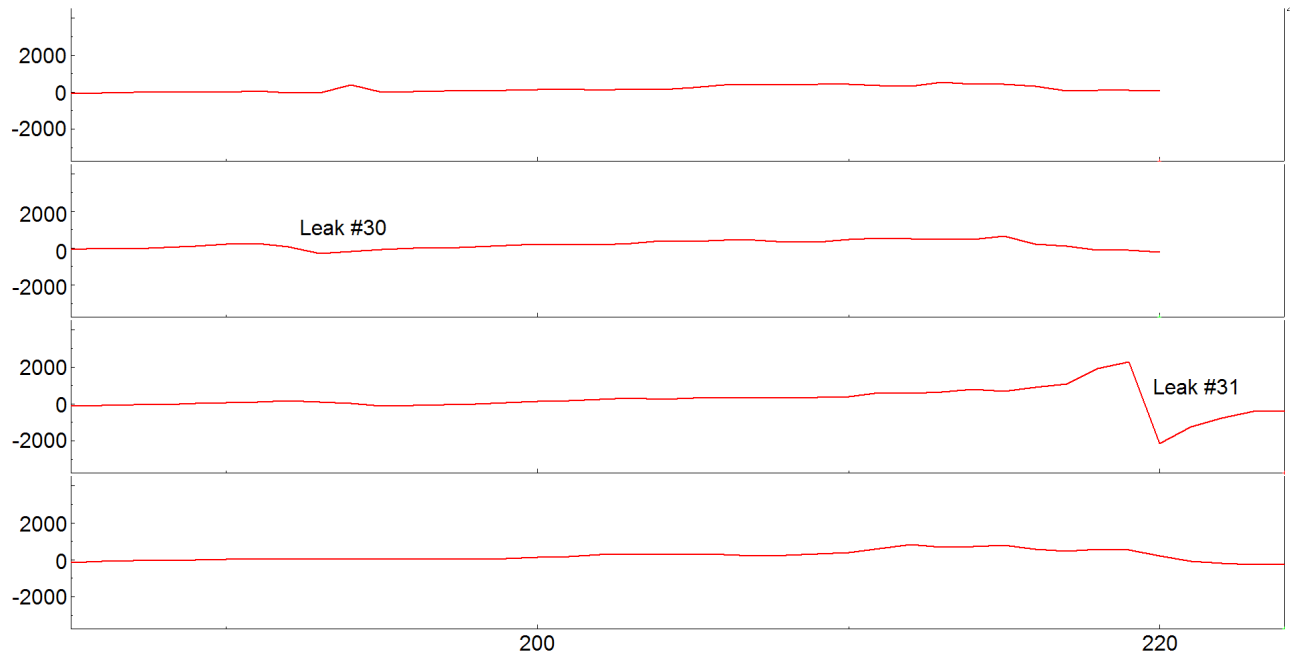


Figure 2. Leak location data showing two leak signals. The larger signal masks the smaller signal.

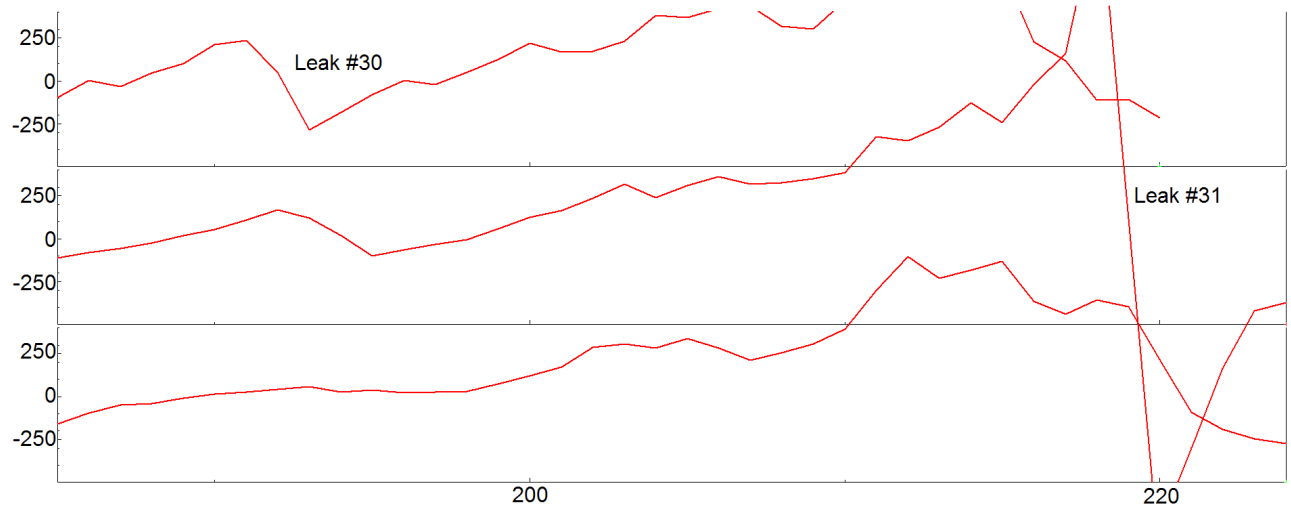


Figure 3. Leak location data showing two leak signals. The smaller signal is visible after adjusting the scale.



Figure 4. Leak #30 (Smaller leak signal.)



Figure 5. Leak #31 (Larger leak signal.)

2. FIELD EXPERIENCE

Lack of experience is another big factor that leads to human error. Simply understanding how to take the data correctly is not sufficient for finding all the leaks. The leak location surveyor also needs to thoroughly understand how to set up the survey to obtain the optimum results. Because of the many possible scenarios of landfill construction, this cannot be taught in a classroom. Extensive and frequent field experience is the only way to fully understand the intricacies of leak location surveys.

2.1 Survey Setup

Setting up for a leak location survey is actually done well before the leak location technician arrives onsite. Before arriving the technician should already know the layering sequence of the cell as well as the general geometry and possible grounding paths within the cell to be surveyed. They should also know how the cell will be surveyed and what equipment will be needed to perform a successful leak location survey. If grounding paths are present they will be able to advise the client on how to remove or greatly decrease the effect of the grounding path on the leak location survey. The intent is to best prepare for a leak location survey before arrival to the site. This is done so that when the survey is performed, every foreseeable detriment to the survey can be addressed in order to produce optimum results. This type of preparation greatly improves with field experience. Once the survey technician is onsite the remainder of the setup is just as important. Questions such as, "Are there pipes buried under the cover material?", "In which direction do they run?" and "What effect do they have on the survey?" all need to be answered so an optimum grid pattern can be placed for the best results.

2.2 Understanding the Technology

Equipment does become damaged whether it's from shipping or from day to day use. If the equipment is not working properly and the survey technician doesn't realize it, they can essentially be taking data for nothing. The ability to intimately understand how the equipment works will keep this from happening because they will know when something is not working properly. There are situations where there are multiple leaks in the near vicinity of each other. The graphing software may show what looks to be just noise or one leak signal to most technicians. An experienced leak location technician will know that this one signal can mask smaller nearby signals. This is remedied by exposing the leak signal shown in the data then testing the area around the initial leak signal to ensure there is no additional damage to the geomembrane. Figure 6 shows three leak signals which are relatively close to one another. The largest leak signal masks or distorts the first two leak signals as shown in Figure 6. It does not do any good to just find a leak at a site. It is far better to find all leaks of sizeable interest. The more experience someone has the more problems they have come across and the more solutions they have utilized. This helps the survey proceed correctly as well as reduce time to a minimum which always pleases the client.

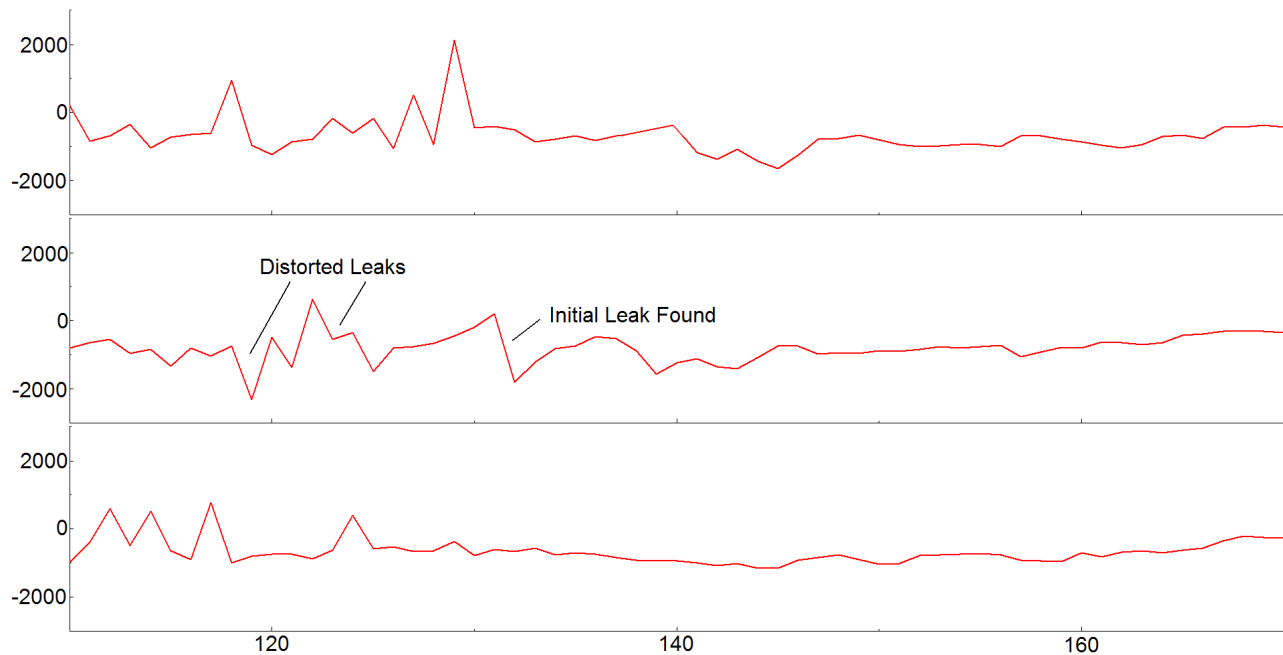


Figure 6. Leak location data showing what looks to be noise or one possible leak signal.

2.3 Continued Education

Continued education and further improvements on current technologies can help to reduce human error and further improve the effectiveness of leak location surveys. This can be done through training by frequently updating techniques to involve newer adaptations that advance survey techniques. Training is an on-going process that cannot be done once over a short time period if favorable results are to be expected. Frequently updated training topics and techniques will help to keep leak location surveys advancing along with the rest of the geosynthetics industry.

2.4 Review of Work

Openly sharing problems will help to avoid their reoccurrence and improve the quality of work of others. Peer review of work has been around for hundreds of years and can be used as a type of quality-control system. Through the review of work an increased awareness of possible pitfalls and complications can be better recognized and combated before they become an issue. Many instances have occurred where a leak location survey has been attempted by an initial company and the results have been inconclusive and no leak signals have been found for a specific cell. A second company was then called out to perform a leak location survey on the same cell and leak signals were found. This is due to an oversight where part of the setup was not done properly. Had the initial company had a peer review their work this setup error could have been avoided.

3. CONCLUSION

Removing human error in leak location surveys is imperative to the quality of landfills and surface impoundments throughout the world. Leak location surveys can be physically demanding and tedious and the likelihood of errors can be high. However there are ways to reduce these errors to a minimum that will not significantly affect leak location surveys. The proper application of industry standards coupled with sound technology and extensive field experience can minimize human error to an insignificant level.

REFERENCES

ASTM Standard D7007, "Standard Practices for Electrical Methods for Locating Leaks in Geomembranes Covered with Water or Earth Materials," ASTM International, West Conshohocken, Pa., www.astm.org.

Repeated Load Tests on Geocell Reinforced Sand Subgrades

Sireesh Saride, Assistant Professor, Dept. of Civil Engineering, Indian Institute of Technology Hyderabad, sireesh@iith.ac.in

Vijay Kumar Rayabharapu, Doctoral Student, Dept. of Civil Engineering, Indian Institute of Technology Hyderabad, vkraya@gmail.com

Suraj Vedpathak, Master's student, Dept. of Civil Engineering, Indian Institute of Technology, Hyderabad, vedpathaksd@gmail.com

Anand J Puppala, Professor, Department of Civil Engineering, The University of Texas at Arlington, anand@uta.edu

ABSTRACT

In this research, results from a series of large scale dynamic model tests on geocell reinforced and unreinforced homogeneous sand beds are presented. The placement density of sand in all the tests was maintained at 70%. The loading was applied through a circular steel plate which replicates the load application from a passenger car. A single axle wheel load of 40 kN was assumed on the pavement surface of which 7 kN was calculated to be applied on the subgrade layer. The influence of the width and height of the geocell reinforcement on the cyclic behavior of the loading system was studied and the performance improvement in terms of traffic benefit ratios and cumulative plastic deformations/rutting was determined. A traffic benefit ratio was observed to be as high as 45 for the case of geocell size $h/D=1$, $b/D=4$ at 10% plate settlement. The cumulative permanent deformations were reduced by 8 fold for the same case against the unreinforced case at 5% plate settlement.

1. INTRODUCTION

In India, a statistical survey by rural development of India shows that around 80% of road network is comprised of rural roads (Rural roads, 2012) whose performance is always inferior and questionable. Besides, engineers are often forced to seek alternative designs using inferior materials, commercial construction aids, and innovative practices for better performance of pavements. One such category of commercial construction aids is utilization of geosynthetics. Geosynthetics includes a large variety of products manufactured of different polymers are adopted in numerous geotechnical and transportation applications. Often, it is important to estimate the efficacy of such inclusions in natural ground to improve the design methodologies and construction practices prior to their utilization.

Research on geocell reinforcement for pavement applications started about five decades ago. This reinforcement technique was first adopted by the US Army Corps of Engineers for improving the bearing capacity of poorly graded sand by using it as a lateral confinement (Webster, 1979). Lateral confinement, increased bearing capacity, and tensioned membrane effects were identified as the important reinforcement mechanisms for geogrid and geocell reinforcement (Giroud and Noiray, 1981, Dash et al 2001, Han et al. 2008a). The geocell reinforced bases exhibit bending resistance, tensile strength, and shear strength, and intercept the failure planes from the subgrade (Zhou and Wen, 2008). Understanding these mechanisms originated from mostly static plate load tests, however, limited research has been focused on these mechanisms under cyclic loading. The following sections discuss the cyclic behavior of geosynthetic reinforcement and factors affecting the performance of the geosynthetics under repeated loading.

2. BACKGROUND

Ever since the reinforcement forms were used, many kinds of geosynthetics like geotextiles, geogrids and geocells have come into existence. Many researchers have studied these reinforcement forms (geogrids and geocells) under static loading for pavement applications, however, a very few studies are available on cyclic loading (Barksdale, 1989; Cancelli, 1999; Collin, 1996, Dash et al. 2001; Dash et al. 2003; Sitharam and Sireesh, 2005). Generally, geosynthetics are used as pavement base or subbase reinforcement. Base course lateral restraint is the main reinforcement mechanism of geosynthetics in paved roads as described by Bender and Barenberg (1980). Further, Kinney and Barenberg (1982) demonstrated that the geotextile-reinforcement can be used in unpaved roads. When the planar geosynthetic reinforcement is placed at the bottom of the asphalt concrete layer, it leads to the highest reduction in the vertical deflection (Hosseini et al., 2009). Hosseini et al. (2009) reported that the overall performance of the asphalt pavement was improved when an effective bonding was maintained between the asphalt concrete and the geogrid. The

settlement over the loading area of reinforced pavement was also reduced when compared with unreinforced pavement under cyclic loadings.

To quantify the benefits with geosynthetic reinforcements in pavements under cyclic loading, a non-dimensional term called traffic benefit ratio (TBR) has been introduced. TBR is expressed in terms of extension of life or by savings in base course thickness. TBR is defined as the ratio of the number of cycles necessary to reach a given rut depth for a test section containing reinforcement, divided by the number of cycles necessary to reach the same rut depth for an unreinforced section with the same section thickness and subgrade properties. This is in consistent with the non-dimensional parameter called improvement factor defined in the case of static loading system on geosynthetic reinforced beds (Dash et al. 2001; Dash et al. 2003; Sitharam and Sireesh, 2005).

Several researchers investigated the cyclic behavior of different forms of geosynthetic reinforcements and provided TBRs. Haas (1985) reported a TBR of about 3.3 for geogrid reinforced beds in a large test tank. Similarly Barker (1987) used geogrid reinforcement under a moving single wheel system and observed a TBR of 1.2. Al-Qadi (1994) studied a combination of geogrid and geocell reinforcements in a test tank and observed TBR ranging from 1.7 to 3.0. Similar observations were made by many other researchers where the TBR was observed to be ranged from 1 to 4 under single axle wheel loads (Barksdale, 1989; Cancelli, 1999; Collin, 1996). Recently, Pokharel (2010) performed large-scale cyclic plate loading tests on geocells and observed that the NEOLOY polymeric alloy (NPA) geocell improved the strength and life of the unpaved road sections over weak subgrade. The reinforced sections had much higher percentage of elastic deformation (more than 90%) as compared with the unreinforced sections and also the NPA geocell.

The effect of the properties of infill material on the performance of unpaved and paved road sections subjected to cyclic loading shows that both the strength of the subgrade and the quality of infill material play a vital role in improving the performance of the geocell-reinforced road sections (Kazerani and Jamnejad, 1987). Higher performance was observed with geocell reinforcement with dense infill on a good subgrade. Similar observations were reported by Han et al., (2008a). Han et al (2008b) also reported that the placement of geocell from the surface of loading is very crucial. In static load tests, it was observed that the depth of placement of geocell should be maintained about 1 to 5% of the width of the loading area (Dash et al., 2001; Sitharam and Sireesh, 2005).

Literature study reveals, based on the limited information available on geocells, that the cyclic behavior of geocell reinforced beds are not yet understood completely. Hence, in this study, an attempt has been made to understand the cyclic/repeated load response of the geocell reinforced sand subgrades.

3. MATERIALS AND METHODS

3.1 Sand

The soil used in this investigation was dry sand. The particle size distribution of the sand was determined by dry sieve analysis as per ASTM D 422. The particle size distribution of the sand is shown in Figure 1. The sand is classified as poorly graded sand with letter symbol SP according to the Unified Classification of Soil (UCS). The physical properties such as specific gravity, maximum and minimum void ratios of sand were determined according to ASTM D 854-00, ASTM D 4253 and ASTM D 4254 respectively. The properties of sand are depicted in Table 1.

3.2 Geocell

Geocell is a strong, lightweight, three dimensional honeycomb-like cellular confinement systems, which is made of ultrasonically-welded HDPE strips that are expandable on-site to form a honeycomb-like structure. It acts as a foundation reinforcement mat for improvement of bearing capacity of weak soils. It is a polymer of High density polyethylene (HDPE) material with a density ranging between 0.935-0.965 g/cm³ and with surface treatments of texturing which consists of a multiple of rhomboidal indentations over the entire strip area and material where the polyethylene strip shall be perforated with horizontal row of 10 mm diameter holes. The geocells used in this study are having weld at regular intervals of 400 mm and 75, 100 and 150 mm depths. A typical geocell mattress used in the present study can be seen in the Figure 2.

Table 1. Properties of sand used in investigation

Properties	Values
D 10 ,mm	0.20
D 30, mm	0.32
D 60, mm	0.48
C_u	2.40
C_c	1.07
Specific gravity	2.63
E_{max}	0.74
E_{min}	0.51

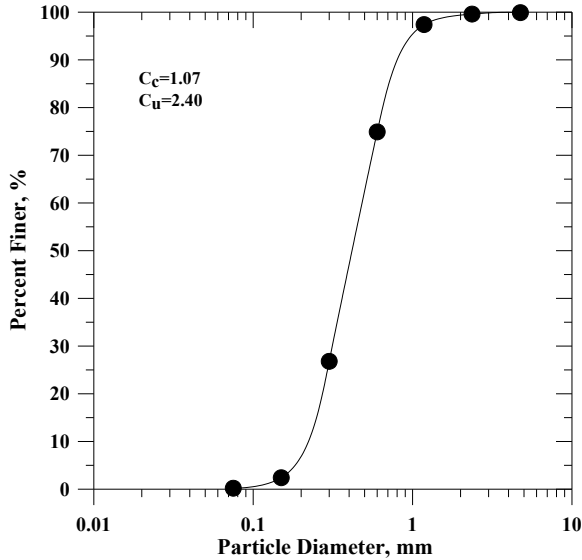


Figure 1. Particle size distribution curve for sand



Figure 2. Typical geocell used in the study

4. TEST SETUP

The sand beds with 70% relative density were prepared in a test tank measuring inner dimensions of 1m × 1 m x1 m (length x width x height). A rigid thin steel plate of 150 mm diameter (D) and 15 mm thickness was used to apply the repeated traffic loading. The size of the plate was chosen such a way that the area of the plate resembles the area of tire pressure. Loading was given by graphical user interfaced MTS MPT software with the help of hydraulic power unit (HPU), hydraulic service manifold (HSM) and sophisticated double acting linear dynamic 100 kN capacity actuator which is attached to a 3.5 m high, 20ton capacity reaction frame as shown in Figure 3.

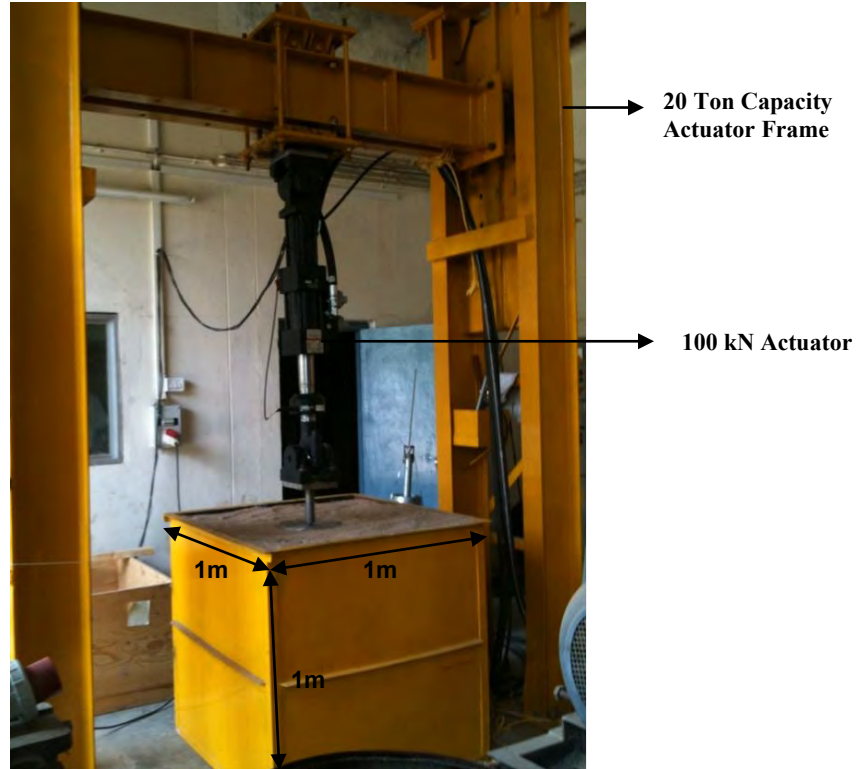


Figure 3. Test-cum-Loading system used in the present study

5. TESTING PROCEDURE

Test procedure can be explained under three sub topics:

1. Preparation of relative density calibration chart
2. Preparation of sand bed
3. Cyclic load tests

5.1 Preparation of Relative Density Calibration Chart

To determine the density with which sand is to be poured in the tank, a special technique called sand raining technique or sand pluviation technique was used. To achieve this, a special device is designed. This device has a hopper with a flexible pipe connected to its bottom. A 40 mm internal diameter and 300 mm long pipe with an inverted cone welded at its one end was intern attached to the bottom of the flexible pipe. The sand passes through the pluviator disperses at bottom by a 60° inverted cone. This pipe is fitted with a movable scale to arrange different heights shown in Figure 4.

Relative density calibration chart was obtained by conducting a series of tests with different heights of fall of sand pluviation. Natural densities were measured physically by collecting samples in small containers whose weights and volumes were known. With the known values of the minimum and maximum void ratios of sand used in the investigation, a calibration chart was prepared for the height of fall against the corresponding relative density. For any required relative density, the corresponding height of fall can be read directly from the calibration chart shown in Figure 5.

5.2 Sand Bed Preparation

The sand was placed in the test tank using pluviation technique as discussed above. In this study, the relative density of sand was maintained at 70 %. The test bed density was frequently monitored by taking samples at different depths during pluviation using flat cups. The densities were well within the range of 1% error. The modulus of the test beds were also examined with a 10 kg capacity Lightweight Deflectometer (LWD). From LWD tests, the average modulus of the test bed at 70% relative density was found to be 28.2 MPa. This modulus is compared with the pressure-settlement data obtained from an unreinforced bed which was found to be 27.8 MPa (average).



Figure 4. Devices used in the preparation of test beds

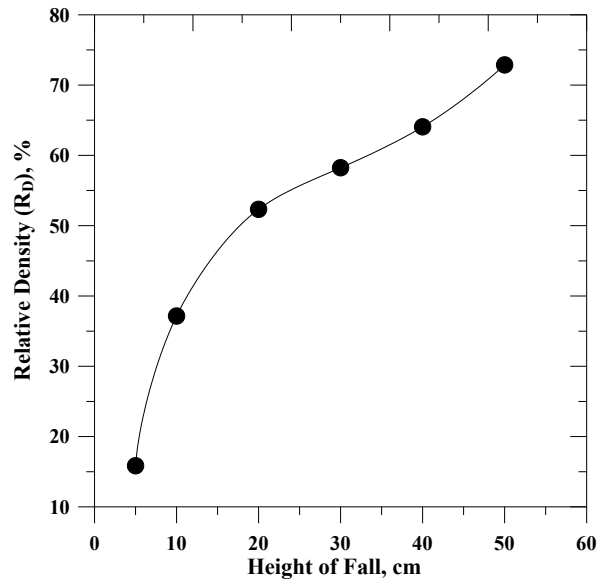


Figure 5. Calibration curve for the sand used in the study

5.3 Cyclic Load Tests

Upon filling the test tank up to the desired height, the fill surface was leveled and the loading plate was placed on a predetermined alignment such that the loads from the actuator applied would be transferred concentrically to the footing to avoid eccentricity. To facilitate this, a recess was made into the footing plate at its centre to accommodate a ball bearing through which vertical loads were applied to the plate. In the case of reinforced beds, upon ceasing the pluviation at predetermined depth, the geocell was stretched on the leveled subgrade and continued the sand pluviation to fill the geocell mattress.

The plate was located carefully at the centre of the actuator against the reaction frame to avoid eccentric loading. The cyclic load was applied to a loading plate using a computer-controlled servo hydraulic actuator, with a maximum load of 7 kN and a minimum on 0.7 kN using a continuous haversine loading pattern as shown in Figure 6. The load was estimated based on the field data using a strain type total pressure cells buried under subbase layer just above the subgrade. Similar loading pattern was also adopted by Edil et al (2007) for the case of geocell reinforced granular subbase layer. Since the intermediate layers have not been simulated in this model tests, the pressure exerted on to the subgrade was directly applied through a plate. A 10% of load (0.7 kN) was constantly applied on the plate to make the cycle a closed loop. The load form was applied at a frequency of 0.77 Hz. Multi-Purpose Test Ware (MPT) software was set up to control and acquire the applied load data as well as the deformation data.

A series of repeated load tests were conducted to verify the efficiency of the geocell layers in the subgrade. These tests include single geocell layers with different sizes with respect to the plate diameter. The width of geocell (b) was varied at 3 times the plate width (D) represented as geocell width ratio, b/D . Similarly the height of the geocell was varied as $h/D=0.5, 0.67$ and 1.0 . The relative density of the sand was maintained at 70% in all tests. The depth of the reinforcement layer from the bottom of the plate was maintained at 0.1 times the diameter of the plate according to Sitharam and Sireesh (2005) and Dash et al (2001). All the tests were conducted until reaching the settlement about 20% of the plate diameter. The equivalent diameter of geocell pockets, d_c was maintained at about $1.6D$ in all the tests.

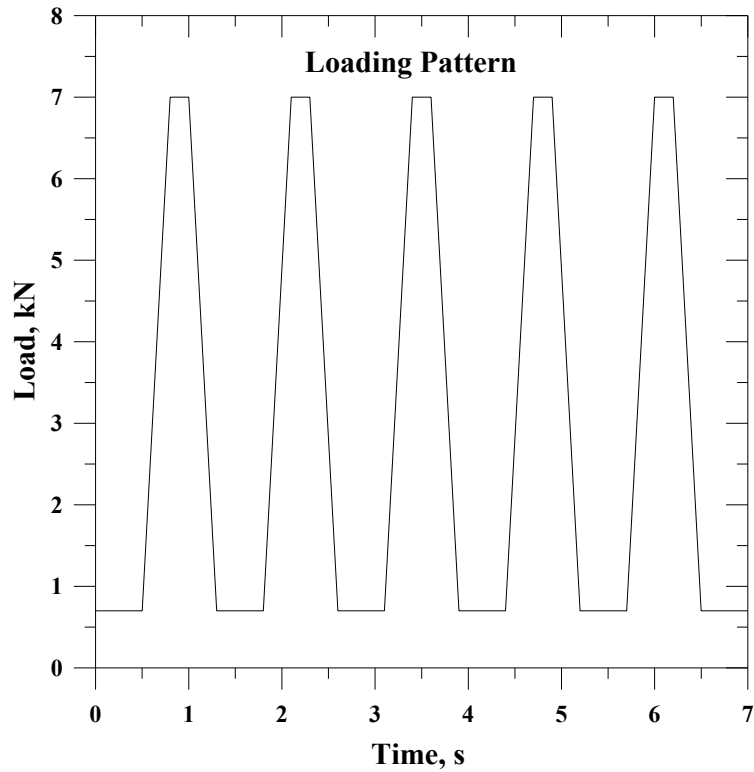


Figure 6. Loading pattern used in the study

6. RESULTS AND DISCUSSION

Figure 7 depicts the response of the geocell reinforced bed under cycling loading conditions. It can be observed that the total settlement ratios are large for the initial loading cycles, while their magnitude attenuates thereafter.

The settlement ratios are reduced as the amount of geocell reinforcement increases, hence, the unreinforced subgrade exhibits the highest settlement ratios. To quantify the reduction in settlement ratios and the efficacy of geocell, cumulative permanent deformations (CPDs) were calculated from a sequence of experiments. First, the permanent deformation was calculated for each loading cycle, by subtracting the elastic component of the settlement from the total settlement. The permanent deformations per loading cycle were then added cumulatively, to obtain the cumulative permanent deformations / settlements with increasing number of loading cycles. Figure 8 demonstrates the variation of cumulative permanent deformations with the number of loading cycles for all the cases considered in this study. The variation of the traffic benefit ratio, TBR, as defined earlier, for different geocell configurations is also presented in Figure 9.

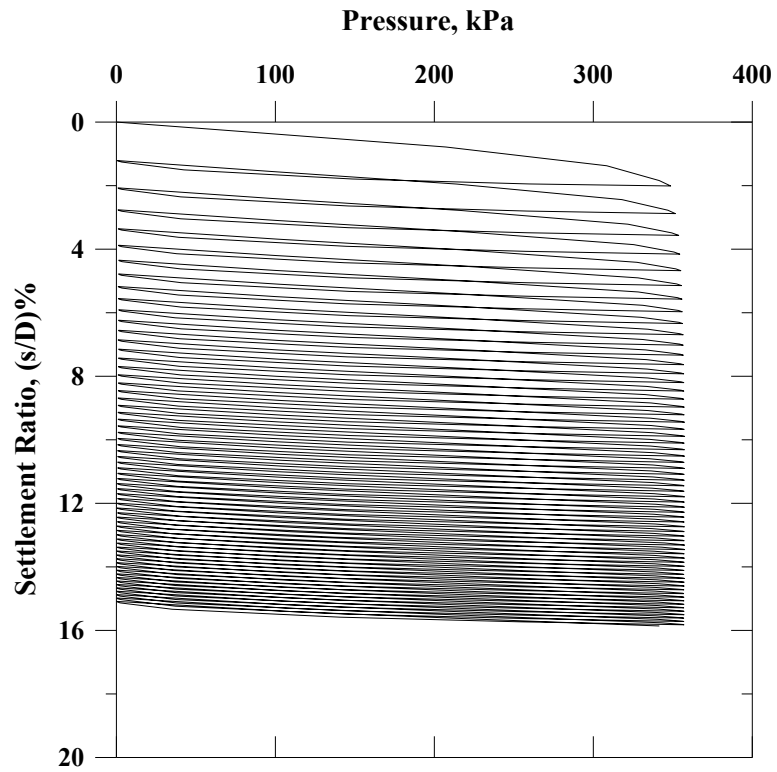


Figure. 7 Typical pressure-settlement pattern from repeated loading for the case of geocell reinforced bed ($h/D=1$, $b/D=4$)

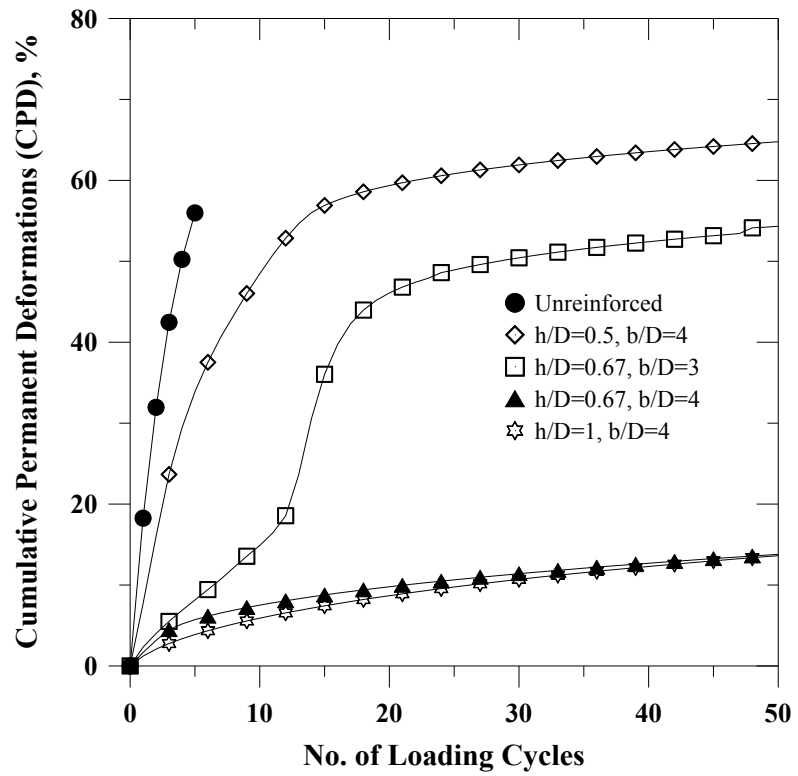


Figure 8. Variation of cumulative permanent deformations with number of loading cycles for various cases

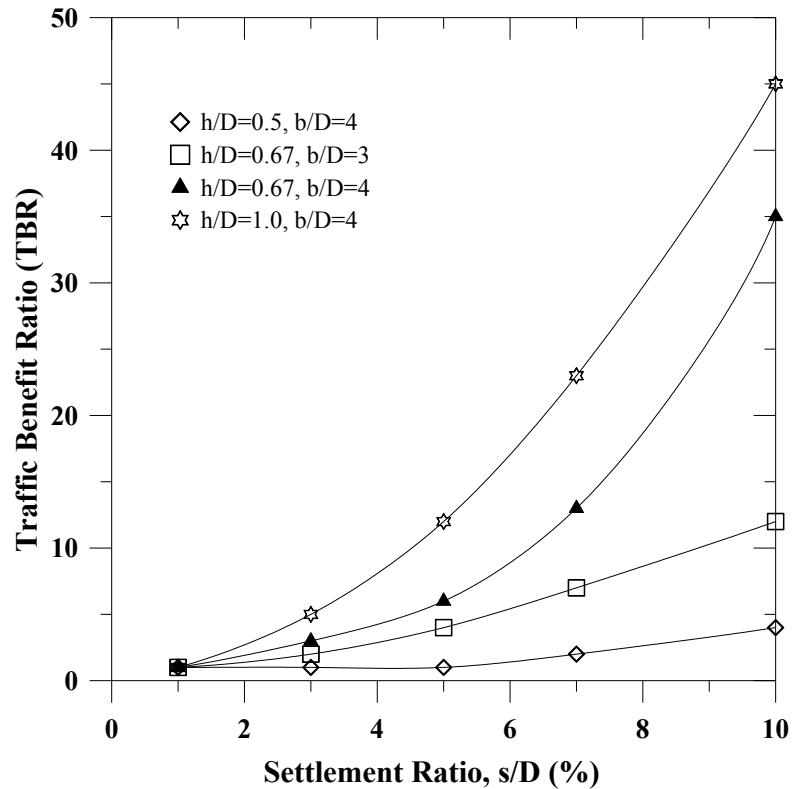


Figure 9. Variation of traffic benefit ratios with settlement ratios for different geocell sizes

The unreinforced subgrade was tested for only few loading cycles as the prescribed maximum amount of settlement ($s/D > 50\%$) was reached at this stage. It is clear from Figure 9 that the permanent deformations of geocell reinforced beds are much less when compared to the unreinforced subgrades. This reduction is as high as 8 fold between unreinforced case and geocell reinforced case ($h/D=1, b/D=4$). It is to be noted here that the permanent deformations are higher for the case of $h/D=0.5$ with $b/D=4$. The higher permanent deformations, in this case, can be attributed to the least flexural stiffness of the geocell mattress available compared to the other cases. It can also be inferred from this figure that for obtaining higher structural support for the pavement layers, the geocell height should be adequate enough to provide resilient behavior. The geocell with $h/D=1$ is providing highest resilient behavior during the repeated traffic loading in this study.

From Figure 9, the traffic benefit ratio (TBR) at 10% settlement ratio are observed to be as high as 45 for $h/D=1; b/D=4$ case; 35 for $h/D=0.67; b/D=4$ case, 12 for $h/D=0.67; b/D=3$ case and 8 for $h/D=0.5; b/D=4$ case of geocell reinforced sections. Hence, it can be summarized that the geocell of sufficient size (b) and thickness (h) will provide a higher traffic benefit ratio for a given level of traffic loading conditions.

Further study is required to understand the optimal benefits from the critical geocell geometry. It is also important to determine the depth of this kind of reinforcement and number of layers of reinforcement for optimum performance.

7. CONCLUSIONS

From a large scale cyclic model tests on unreinforced and geocell reinforced beds, following conclusions can be drawn:

1. Geocell can be used as reinforcement in pavement subgrade layers to increase the stiffness of the subgrade.
2. Geocell reinforcement reduces the plastic settlements, referred as rutting on the pavement surface by providing lateral confinement to the infill soil. The reduction in permanent deformation is observed to be as high as 8 fold for the case of geocell size $h/D=1, b/D=4$ versus the unreinforced bed at 5% plate settlement.

3. The traffic benefit ratio, TRB was observed to be as high as 45 for the case of geocell size $h/D=1$, $b/D=4$ versus 8 for the case of geocell size $h/D=0.5$, $b/D=4$ at 10% plate settlement. The lower TRB for the thin geocell layer is attributed to the flexural stiffness of the geocell mattress offered to support the cyclic loading. Hence, it is important to choose an optimum size geocell for higher structural support for a given traffic loading system.

4. Further systematic study is required to completely understand the geocell material in pavement layers such as base and subbase layers with aggregate infill.

ACKNOWLEDGEMENTS

The authors would like to express their appreciation to STRATA Geosystems India Pvt. Ltd. for providing the geocell material for this research.

REFERENCES

- Al-Qadi, I.L., Brandon, T.L., Valentine, R.J., Lacina, B.A. and Smith, T.E., (1994), "Laboratory Evaluation of Geosynthetic Reinforced Pavement Sections," In Transportation Research Record 1439, TRB, National Research Council, Washington DC, pp. 25-31.
- Barker, W.R., (1987), Open-Graded Bases for Airfield Pavements, Technical Report GL-87-16, USAE Waterways Experiment Station, Vicksburg, MS, USA, 76 p.
- Barksdale, R. D., Brown, S. F. and Chan, F., (1989), Potential Benefits of Geosynthetics in Flexible Pavement Systems, National Cooperative Highway Research Program Report No. 315, Transportation Research Board, National Research Council, Washington, DC.
- Bender, D.A. and Barenberg, E.J., (1980), "Design and Behavior of Soil-Fabric-Aggregate Systems," In Transportation Research Record 671, TRB, National Research Council, Washington, DC, USA, pp. 64-75.
- Cancelli, A., And Montanelli, F., (1999), "In-Ground Test For Geosynthetic Reinforced Flexible Paved Roads," Proceedings of the Conference Geosynthetics '99, Boston, MA, USA, Vol. 2, pp. 863-878.
- Collin, J. G., Kinney, T. C. and Fu, X., (1996), "Full Scale Highway Load Test of Flexible Pavement Systems with Geogrid Reinforced Base Courses," Geosynthetics Intentional, Industrial Fabrics Association International, Roseville, MN, Vol. 3, No. 4, pp. 537-549.
- Dash, S. K., Krishnaswamy, N. R., and Rajagopal K. (2001). "Bearing capacity of strip footings supported on geocell-reinforced sand." Geotextiles and Geomembranes, 19 (4), 235-256.
- Dash, S. K., Sireesh S., and Sitharam, T. G. (2003). "Model studies on circular footing supported on geocell reinforced sand underlain by soft clay." Geotextiles and Geomembranes, 21 (4), 197-219.
- Giroud, J.P. and Noiray, L. (1981). "Geotextile- reinforced unpaved road design." Journal of the Geotechnical Engineering Division, 107 (GT9), 1233-1254.
- Haas R., Wall, J., and Carroll, R.G., (1988), "Geogrid Reinforcement of Granular Bases in Flexible Pavements," In Transportation Research Record 1188, TRB, National Research Council, Washington, DC, USA, pp. 19-27.
- Han, J., Yang, X.M., Leshchinsky, D., and Parsons, R.L. (2008a). "Behavior of geocell-reinforced sand under a vertical load" Journal of Transportation Research Board, No. 2045, 95-101.
- Han, J., Yang, X.M., Leshchinsky, D., Parsons, R.L., and Rosen, A. (2008b). "Numerical analysis for mechanism of a geocell-reinforced base under a vertical load" Proceeding of 4th Asian Regional Conference on Geosynthetics, June 17-20, 2008 Shanghai, China, 741-746.
- Hosseini M., Kazemian, S, Arun P and Bujang B. K. Huat. (2009) "Effect of Geogrid Reinforcement Location in Paved Road Improvement" Electronic Journal of Geotechnical Engineering, Vol. 14.
- Kazerani, B. and Jamnejad, G. (1987). "Polymer grid cell reinforcement in construction of pavement structures. Section 1A, unpaved and paved roads." Geosynthetic'87 Conference, New Orleans, USA.
- Kinney, T.C. and Barenberg, E.J., (1982), "The Strengthening Effect of Geotextiles on Soil-Geotextile-Aggregate Systems," Proceedings of the Second International Conference on Geotextiles, Las Vegas, NV, USA, Vol. 2, pp. 347-352.
- Pokharel, S.K. (2010). "Experimental Study on Geocell-Reinforced Bases under Static and Dynamic Loading". Ph.D. Thesis, University of Kansas, USA.
- Rural Roads (2012), "Working Group on Rural Roads in the 12th Five Year Plan", Planning commission, Ministry of Rural Development, Government of India, Final Report, January 2012, pp 96.
- Sitharam, T. G., and Sireesh, S (2005), 'Behaviour of Embedded Footings Supported on Geocell Reinforced Foundation Beds'. Geotechnical testing Journal ASTM, Vol. 28, No. 5, pp 452-463.
- Edil, T. B, Kim, W.H, Benson, C. H, and Burak F. T. (2007). "Contribution of Geosynthetic Reinforcement to granular Layer Stiffness", Geo-Denver

- Webster, S. L. (1979a). Investigation of Beach and Trafficability Enhancement Using Sand-grid Confinement and Membrane Reinforcement Concepts. Report GL-79-20 (1), U.S. Army Engineer Waterways Experiment Station, Vicksburg, MS.
- Zhou, H. and Wen, X.(2008). "Model studies on geogrid - or geocell-reinforced sand cushion on soft soil." *Geotextiles and Geomembranes*, 26(3),231-238.
- Ingold, T.S. and Miller, K.S. (1983). Drained axisymmetric loading of reinforced clay, *Journal of Geotechnical Engineering*, ASCE, 109: 883-898.

Secondary Containment Retrofitting Using a Bituminous Geomembrane

Kurt Liebe, P.E., Chevron, USA, KLiebe@Chevron.com

Tarik Hadj-Hamou, Ph.D., P.E., Strategic Engineering and Science, THadj-Hamou@sesinonline.net

ABSTRACT

The City of Portland (OR) requires that bulk fuel terminals install impervious secondary containments (i.e. liners) around tanks or facilities built after 2004. To satisfy this requirement when planning to replace a group of tanks with two large tanks at its Willbridge Terminal in Portland, (Oregon) Chevron compared different liner options. The site is essentially flat and numerous tanks, pipelines, and ancillary structures exist within the secondary containment so any earthwork to cover a liner or promote drainage would have been very difficult. The number of penetrations, pipe support, and pipes crisscrossing the facility favored a liner that could be pieced together and seamed easily. An exposed liner consisting of a 160 mil Bituminous Geomembrane was ranked as the optimum solution. The City of Portland approved the design and the liner was installed in 2010 and has worked to the satisfaction of the Terminal operators. The paper describes the selection process, design, installation, and performance of the geomembrane thus far.

1. INTRODUCTION

1.1 Background

The Chevron Willbridge Terminal (the Terminal) is located in Portland, Oregon near the Willamette River and stores refined petroleum products. There are currently 11 light product tanks, 10 lube oil tanks of smaller diameter, and 3 waste tanks. In service for over a hundred years, the tanks at the Terminal are of varying sizes and fabrication styles (from riveted to welded plates as shown on Figure 1). Products are received and shipped via truck, pipeline, and marine vessels.

To manage inventories and dispense the products a large number of pipes crisscross the Terminal as shown on Figure 2. Drain inlets, pumps, electrical panels, electrical conduits and other appurtenances are also located with the secondary containment. The Terminal does not offer much topographical relief and is essentially flat. The stormwater drainage system consists of a series of drain inlets connected by pipes to an oil-water separator prior to connecting to the City of Portland sewer system. The soil at the Terminal is mostly sand and therefore stormwater rarely ponds around the tanks.

In 2008 Chevron decided to refurbish part of the Terminal and replace a series of small and relatively old tanks with two new tanks. The location of the two new tanks is shown on Figure 3. These two tanks (Tanks 163 and 163) were designed with the most current Chevron State of Practice and include double bottoms which mean that they are constructed on top of concrete slabs. However, replacing existing ASTs with new ones triggered the 2004 Stormwater Management of the City of Portland Department of Public Works and described in the next section.

1.2 Regulations

At the Federal level, secondary containment system for aboveground storage tanks (AST) at terminals and refineries are regulated by the Clean Water Act as amended by the Oil Pollution Act of 1990. The requirements are detailed in the Spill Prevention, Control, and Countermeasures (SPCC) and Facility Response Plan regulations.

At the state level, Oregon has adopted the International Fire Code that governs AST containing motor vehicle fuel. A permit from the state fire marshal is required for gasoline and diesel fuel tanks with a total storage capacity of more than 1,000 gallons (gal).

At the local level (City of Portland) the requirements for secondary containment are detailed in the City of Portland Stormwater Design Manual (2004). The requirements for bulk fuel terminals are:

- A secondary containment equal to 100 percent of the product's larger container or 10 percent of the total volume stored, whichever is larger;
- An impervious floor within all containment areas. Floors shall be sealed to prevent spill from contaminating the groundwater;

The local requirements are in fact more stringent than the Federal and State requirements for the secondary containment since they specify that an "impervious floor" shall be installed. To achieve this requirement, Chevron contemplated the options available to construct and or install an "impervious floor" around Tanks 163 and 164 at the Terminal and performed a feasibility analysis based on a set of criteria to select the optimum option.

2. SECONDARY CONTAINMENT SELECTION

2.1 Liner Options

Three main groups of liner options were considered for use at the Terminal:

- **Flexible Geomembranes.** These include resin-based geomembranes (HDPE, LLDPE, PVC, etc.), Bituminous Geomembrane, and Geosynthetic Clay Liner (GCL). Resin-based geomembranes are manufactured in a plant and brought to site for deployment and installation. They tend to be relatively thin (40-100 mil) sensitive to ultraviolet and cannot handle direct equipment traffic. Therefore they need to be protected with a soil cover. Bituminous geomembrane also manufactured in plant are very sturdy and resistant to ultraviolet and offer high penetration resistance. Consequently they do not need to be protected with a soil cover. GCL manufactured offsite and need to remain hydrated to be an effective barrier to petroleum product. They also need to be protected with a soil cover.
- **Structural Liners.** These include concrete, shotcrete, and asphalt concrete. These liners are constructed on site using mixes manufactured off-site. They are resistant and sturdy liner systems that do not require soil cover protection.
- **Soil based liner or soil treated liner.** These liners are all manufactured on site. The amendments (bentonite, cement, etc.) are brought to the Terminal and worked into the existing soil to create the liner system. The concept is to reduce the permeability of the soil in the secondary containment. They do not need a protective soil cover if thick enough and can fit the constraints of the site topography thereby not affecting drainage patterns.

Each liner present advantages and disadvantages and cost from few cents per square foot to few dollars per square foot. Therefore, to assess the benefit of each one and select the optimum liner for the Terminal, an evaluation process was established based on a set of selection criteria developed through review of available lining technologies and discussion with Chevron personnel.

2.2 Selection Criteria

A series of criteria were established for the Terminal and the project under consideration.

Three groups of criteria were established:

- Constructions and operational
- Performance
- Economic and regulatory

2.2.1 Construction and Operational Criteria

The Terminal is an operating facility and the new tanks will be constructed in an area previously developed and in the middle of existing ASTs. Therefore, the design and the construction must account for site conditions such as:

- Limited space to work and spread materials and equipment.
- Different activities ongoing at the same time: concrete, metal work, piping layout, electrical work, and liner installation.
- Presence of existing pipes, electrical conduct, and their supports.
- Numerous penetrations into the ground (conduits, pipes) that will need to be made water tight.
- Presence of appurtenances on the floor of the secondary containment system such as electrical control boxes, pumps, catwalks, concrete supports for pipes, etc.
- A topography almost "flat" which does not allow for easy regrading to facilitate drainage.
- Location of the drainage inlet at the ground surface.

The Terminal is a functioning revenue generating facility and this function should not be affected by the secondary containment system installed around the two new AST's. Therefore, operational flexibility and needs are a serious concern for the operator and must to be considered.

Some of those needs include:

- Possibility to get close to the tanks using standard equipment such as pick-up trucks and forklifts.
- Ability to easily and quickly repair any damage to the lining system, ideally using Chevron personnel or a local contractor.
- Improve or modify other portions of the Terminal and extend the new liner easily.
- Easy cleanup of any accidental spill.

Other criteria related to construction and operations include:

- Scheduling. The option selected must provide the contractor with flexibility so it can be installed in phases if needed and when possible based on weather, schedule of specialty subcontractors, and other factors. Ideally the liner should to require a specialty installer and could be installed by the general contractor.
- Ease of installation. To fit under the piping system, around penetration, around the tank foundation, and generally fit the complicated geometry the liner should be easy to cut and piece together.
- Stormwater management. Considering the weather conditions in Portland, a liner that can be installed in humid air or light rain conditions and that will facilitate drainage is preferred. Liners that need to be protected with a protective layer of soil will remain soggy and muddy and may even freeze during the winter. By contrast an exposed liner allows easy flow of water towards the drain system leaving the Terminal dry.
- Post spill clean-up. Following an accidental spill the operator needs to be able to clean-up the spill as quickly as possible and restore the functionality of the Terminal. Exposed liners are preferable over soil-protected liners since the product can be pumped rapidly and the area affected contained easily.

2.3 Performance Criteria

It is assumed herein that all the options will provide the degree of hydraulic control required by the regulation (i.e., "an impervious secondary containment"). However, other performance criteria are important to the operator namely trafficability, resistance to chemical and physical attacks, resistance to ultraviolet rays, and weather.

2.3.1 Financial and Regulatory Criteria

Financial considerations include capital costs and operations and maintenance costs. Capital costs are all the costs related to the design and installation of the liner system. Operations and maintenance cost include the anticipated cost related to maintaining the liner but also the extra cost associated with operating in a terminal with a liner system installed. For instance size and weight limitations for equipment that can circulate over a geomembrane may result in an increase in cost.

Regulatory approval is a critical element in designing a liner system. Some liner options are usually easier to get approved than other because of personal biases and experiences of the regulators.

2.4 Selection Matrix

The liner options and criteria were organized in a matrix where each column represents a liner option and each row is a criterion. Each criteria was assigned a number ranging from 1 (very good) to 4 (poor) and each option was 'graded' per each criterion. These grades were assigned based on both a qualitative and quantitative basis. For example, "construction costs" are quantifiable and the cheapest liner to purchase and install was given a '1' whereas the most expensive was given a '4'. By contrast "operational flexibility" is a subjective criterion and the grade assigned to each liner option was done using subjective and qualitative data based on personal experience and discussion with the operator. Therefore some criterion may vary from terminal to terminal and from operator to operator. To identify the optimum liner option the grade assigned to each criterion were summed and the optimum option was the option with the lowest grade.

Table 1 shows that the Bituminous Geomembrane was the optimum option for the project and was therefore selected.

3. DESIGN

As shown on Figure 3, Tanks 163 and 164 were constructed over the footprints of older smaller tanks that were decommissioned and demolished. Secondary containment of the Terminal is provided by a concrete wall that surrounds

it. However, this secondary containment provides for lateral containment per Federal and State regulations, as well as local regulations up to 2004. To provide for 2004 local regulations, a secondary containment had to be provided for Tanks 163 and 164. The areas corresponding to these volumes were lined with the Bituminous Geomembrane to provide the required “impervious floor”. A berm was laid out to provide for containment around the tank as shown on Figure 4 for Tank 163.

The areas within the berms were regraded to provide for drainage towards the existing drain inlets. Because of the overall flatness of the site, there was little latitude and the final slopes are on the order of ½ to 1 percent. However, because the subgrade is a firm gravelly sand (as seen on Figure 1) settlement is not expected and the slopes are expected to remain over time. Furthermore, the very low Manning coefficient of the Bituminous Geomembrane facilitates flow of stormwater toward the drain inlet. To address construction needs and the nature of the subgrade (gravelly sand) a 160 mil thick Bituminous Geomembrane was specified for the site.

A set of continuation documents, a Technical Specification, and a Construction Quality Assurance Plan was issued for grading and installation of the 160 mil thick Bituminous Geomembrane at the Terminal.

Table 1: Matrix of liner options and selection criteria

Liner Type	Flexible Membranes				Structural Liners					
	LLDPE or HDPE Geomembrane with cover	Geosynthetic Clay Liner with soil cover	Bituminous Geomembrane	Spray-On Liners	Asphalt	Shotcrete Concrete	Soil Bentonite	Soil Cement	Chemical Grouting	Compacted Clay Liner
CRITERIA	GRADE	GRADE	GRADE	GRADE	GRADE	GRADE	GRADE	GRADE	GRADE	GRADE
Construction and Operations Criteria										
Site Conditions	4	2	1	1	1	1	4	2	1	2
Terminal Geometry	3	3	1	1	4	4	3	1	1	4
Suitability for Penetrations	2	3	2	1	3	3	2	2	1	3
Operational Flexibility	2	3	1	2	2	2	1	1	3	3
Scheduling Flexibility	2	2	1	2	2	2	2	2	1	3
Stormwater Management	2	3	1	1	1	1	3	3	3	3
Ease of Installation	2	1	1	1	2	2	2	2	3	2
Post Spill Clean-Up	3	4	2	2	1	1	3	3	3	3
Performance Criteria										
Trafficability	2	2	1	2	1	1	4	1	2	4
Chemical Resistance	1	2	2	2	2	1	2	1	2	2
Dessication Resistance	1	3	1	1	1	1	3	1	2	4
Vegetation Control	2	3	1	1	1	1	3	2	2	3
Temperature Extremes	2	1	1	2	1	1	3	1	1	3
Ultraviolet Resistance	2	1	1	2	1	1	1	1	1	1
Economic and Political Criteria										
Regulatory Acceptance	1	2	1	1	1	1	2	3	2	2
Construction cost	1	3	2	3	4	4	2	2	4	3
Maintenance Costs	2	3	1	1	1	1	3	2	3	2
Total Grade	34	41	21	26	29	28	43	30	35	47

4. INSTALLATION

Chevron had retained a specialty industrial facilities contractor to construct Tanks 163 and 164. The work involved demolishing the old tanks and associated pipes and equipment, constructing the ring foundations for the new tanks (to install the standard "Chevron double bottom"), building the tanks, installing the new pipes, valves and other systems. Because of space limitations and time constraints, the work proceeded from one tank to the next with different activities performed depending upon availability, Terminal operations, and weather conditions.

The construction schedule was complex and installing the liner was not identified as a single task for each tank to be performed in one continuous period at a given time. Rather, lining was considered a "catch-up" task that would be started and stopped when time and other activities allowed. Because the 160 mil Bituminous Geomembrane is easy to cut and seam, is very sturdy, and has great resistance to puncture, its installation does not require specialty installer, it can remain exposed, and can be driven on it was the ideal geomembrane for this project. Relatively heavy weight vehicle traffic was permitted on the installed Bituminous Geomembrane as shown on Figure 5. This allowed the contractor to keep working in and around the tanks following placement of the Bituminous Geomembrane and gave him scheduling flexibility.

Workers from the contractor personnel were trained by the manufacturer to lay and seam the Bituminous Geomembrane. Because seaming Bituminous Geomembrane is similar to seaming roofing material, special equipment is not required. A roofing torch, trowels, and a weighted roller to press the seam are all that is required. A crew was trained and was very effective but they could also perform other activities when liner was not being installed and they were needed elsewhere.

During installation the same standards of quality assurances used for other geomembranes (HDPE, LLDDP, PVC, etc.) were followed. Panels were numbered and their location recorded. The seam consists of an 8 inch overlap welded together by melting together the bitumen over the overlap and pressing the two edges together and therefore does not have the air channel seen in HDPE or LLDPE seams. Integrity testing is different from other geomembranes. Continuity of the seam is monitored by CQA personnel. The integrity and water tightness are spot checked with either the vacuum box or an ultrasound sensor. The ultrasound sensor monitors the thickness and continuity of the weld across the 8 inch wide seam. The ultrasound monitor was used for this project and a one foot segment was tested every 50 ft. of seam. Every seam was tested at least once regardless of its length.

The Bituminous Geomembrane is easily connected to concrete or steel using a bitumen-sealant mix that is applied to the concrete or steel. The Bituminous Geomembrane is then attached by heating the asphalt as shown on Figure 6. An advantage of all geomembranes is their flexibility and the ease with which they can be laid under pipes and around penetrations. As shown in Figure 7, some areas of the Terminal were congested with pipe, concrete walls and supports.

The installation was performed in late 2009 and early 2010 during the rainy season but proceeded without problems. Figure 8 shows portions of the secondary containment at Tank 164 in July 2012.

5. CONCLUSIONS

To satisfy the requirement of the City of Portland for secondary containment around new petroleum product ASTs, Chevron evaluated different liner options when replacing a series of smaller tanks new with larger capacity tanks. An evaluation of options with respect to a set of criteria led to the choice of a Bituminous Geomembrane as the optimum solution. The 160 mil thick Bituminous Geomembrane selected and installed in 2009-2010 in the secondary containment has performed to the satisfaction of the operators since. Chevron is planning to retrofit another area of the Terminal this fall (2012) and will use the same Bituminous Geomembrane.



Figure 1: Tank 2 in foreground and Tank 141 in background prior to demolition – note Tank 2 is a riveted tank



Figure 2: Pipes across Terminal

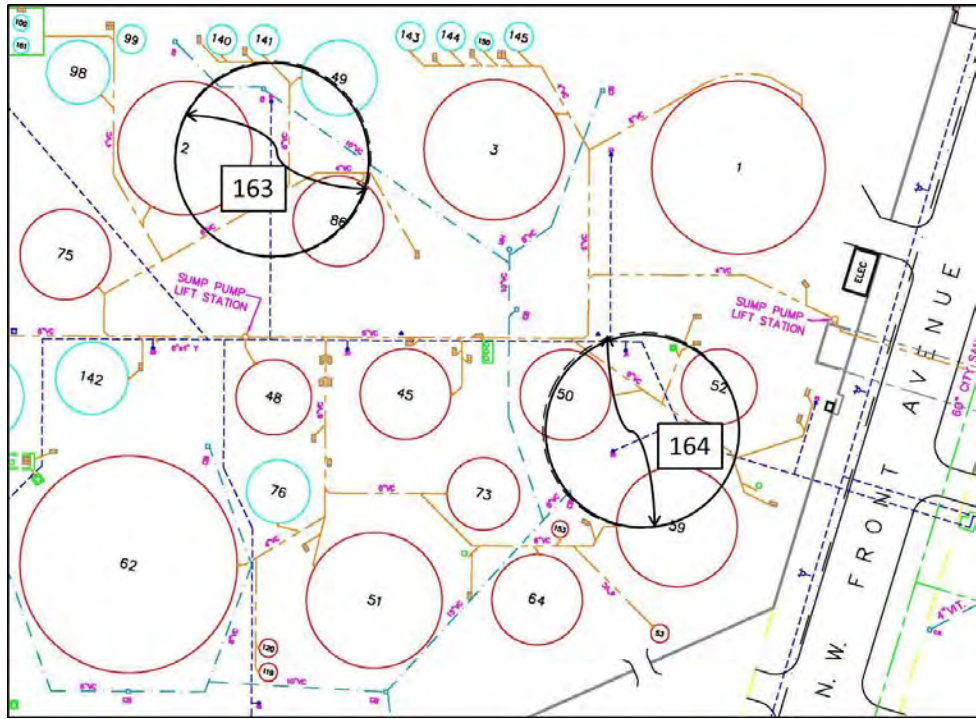


Figure 3: Replacement Tanks 163 and 164 at Willbridge Terminal

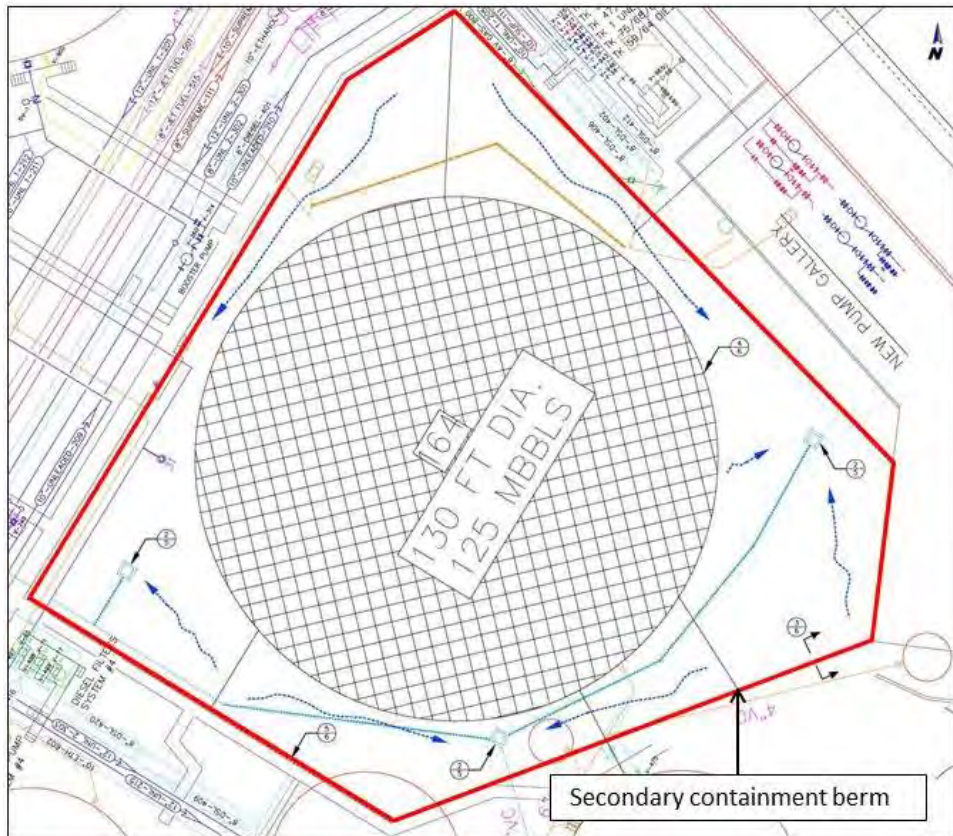


Figure 4: Design of containment for Tank 164



Figure 5: Vehicular Traffic on Top of Bituminous Geomembrane



Figure 6: Connection to concrete ring foundation of tank



Figure 7: Geomembrane under pipes and around penetrations

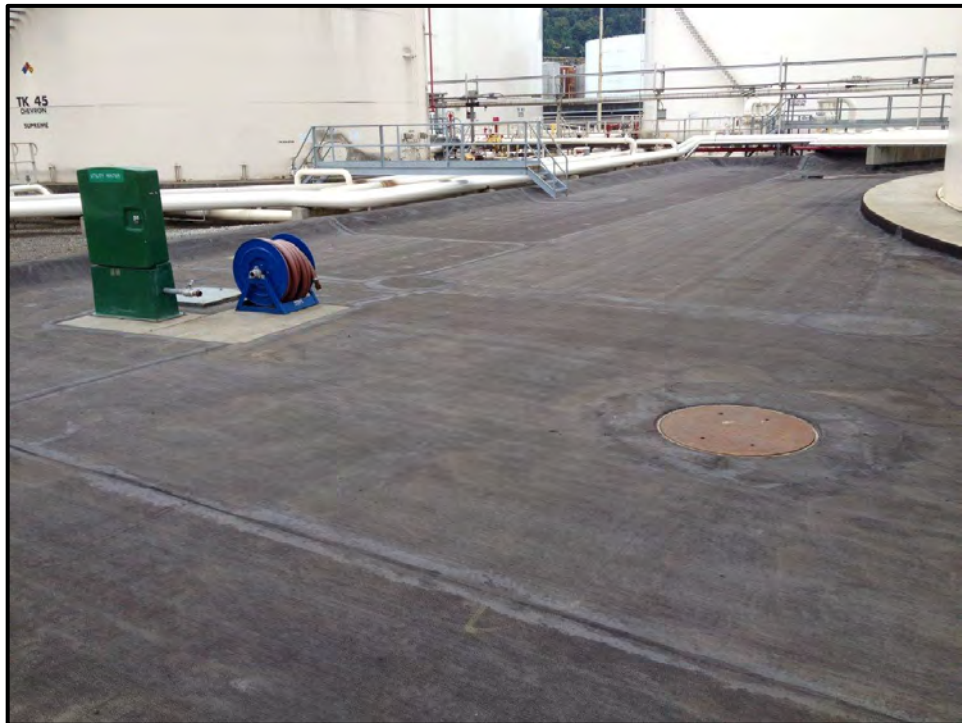


Figure 8: Lined secondary containment 2 years after installation

Seismic Behaviour of Hybrid Reinforced Soil High Walls and Slopes

P. Rimoldi, Geosynthetics International Specialist, Officine Maccaferri Spa, Zola Predosa, Italy.
pietro.rimoldi@gmail.com

A. D. Gharpure, Director & COO, Maccaferri Environmental Solutions Pvt. Ltd., India.
agharpure@maccaferri-india.com

R. R. Mahajan, Div. Manager-Technical, Maccaferri Environmental Solutions Pvt Ltd., India.
ratnwdc@maccaferri-india.com

ABSTRACT

Hybrid reinforced soil structures combine geogrids and steel meshes together to build high MSE walls or slopes, considering the geogrids as “primary reinforcement” and the wire mesh units (produced with an “integrated tail” of wire mesh) as a “secondary reinforcement” and “facing units”. In situ and laboratory results indicate that hybrid MSE structures afford high flexibility, strength and energy absorption capacity, making them ideal for the construction of structures with relevant heights in highly seismic areas. A case history is presented of a reinforced soil hybrid structure, over 80 m high, in Sikkim, India, which has recently withstood an earthquake with a 6.9 magnitude with no visible damage. The seismic resistance of the structures is analyzed while the design method in seismic conditions is compared with the actual acceleration withstood during the earthquake. Results indicate that hybrid reinforced soil structures afford very high factor of safety against seismic induced failure.

1. INTRODUCTION

Reinforced soil walls offer economic advantages over conventional mass gravity wall systems as the height of the wall increases. The cost of reinforcement constitutes an important part of the total cost of a reinforced soil retaining wall and can be as great as about 25% of the cost of the wall, depending on the wall height, backfill type, and design loading conditions. The present paper addresses the possibility of reducing the total cost of a reinforced soil wall by optimizing the vertical spacing of reinforcing geosynthetics elements, while ensuring the required Factor of Safety for the whole structure.

The reinforcement load in reinforced soil walls is commonly calculated from classic active earth pressure theory using the so-called contributory area approach. In this approach, the lateral earth pressure distribution from Rankine or Coulomb earth pressure theory is integrated over a distance equal to the spacing between reinforcement layers and the resultant load is assigned to the target reinforcement layer. In a tall retaining wall, the reinforcement load can vary with depth over a wide range of values. In such a case, more than one reinforcement type or spacing pattern along the wall height may be desirable.

Generally speaking a reinforcing geosynthetics elements with 200 kN/m ultimate tensile strength costs less than twice of a reinforcing geosynthetic with 100 kN/m ultimate tensile strength: hence a solution with half number of double strength reinforcing layers will cost less than a solution with a double number of half strength reinforcing layers.

International research and state-of-the-art practice have demonstrated that the former solution, if properly designed, ensures the same or even higher Factors of safety than the latter solution. In particular, very tall geogrid reinforced soil walls have been built with 2 – 3 m vertical spacing between the primary reinforcing layers, even in very highly seismic areas, with excellent results both in terms of total costs and structural safety.

2. HYBRID REINFORCED SOIL STRUCTURES

There is a long history of designing and providing reinforcement materials for mechanically stabilized earth (MSE) structures, through the use of double twisted wire mesh units able to provide “stone facings” or vegetated external facing.

Gabions are used since more than 100 years for the construction of gravity type retaining structures in all environments and climates. They are rectangular cages made of hexagonal woven steel wire mesh laced together and filled with stone. Gabions have been used for a variety of application in sectors of housing and commercial projects, roads and railways, bank stabilization, erosion control, architectural cladding and noise barriers, etc.

However when the height of the wall increases, gravity type retaining structures become soon impracticable, and there is the need to shift to MSE structures.

For building MSE structures it is possible to combine gabion units and wrap-around facing units (made up of double twisted wire mesh) with geogrids, considering in this case the geogrids as “primary reinforcement” and the “integrated tail” of the facing units as a secondary reinforcement (see Figure 1). In these “hybrid” structures the primary reinforcement is used to provide the tensile forces required to ensure global stability with the desired Factor of Safety; while the facing units, which are produced with a “integrated tail” of double twisted wire mesh as a secondary reinforcement, provide the local stability at the face, ensuring that no local mechanism of direct sliding, pullout or rotational failure can occur.

Figure 2 (from Hatami et Al, 2001) shows a typical tiered hybrid reinforced soil structure, with vertical gabion facing units at bottom and steep wrap-around facing units at top; it is possible to note that the primary reinforcing geogrids are always vertically spaced as a multiple of the height of the facing units.

Very tall hybrid structures have been built all over the world according to this approach; the reinforced soil hybrid structure under construction in Sikkim (India), later presented in this paper, is over 80 m high and it has recently withstood an earthquake with a 6.9 magnitude with no visible damage.

Hybrid structures usually include a vertical spacing of reinforcement that is typically multiple of 0.74 m (29 inches) - 1.00 meter (40 inches), i.e., multiple of the height of a wrap-around unit or of a gabion unit.

However, in USA, the FHWA and AASHTO limit the vertical spacing of the reinforcement to 0.80 m (32 inches). Such requirements have also affected international MSE practice as many countries follow the USA guidance. Research and state-of-the-art practice presented in this paper suggest that these limits have no real meanings and should be removed, at least for the hybrid reinforced soil structures described in this paper.

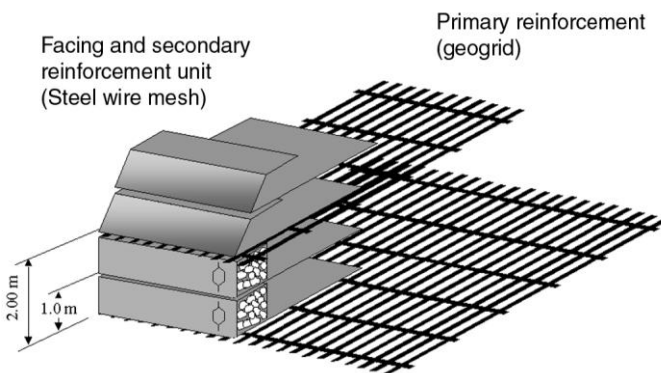


Fig. 1. Scheme of hybrid reinforced soil structures

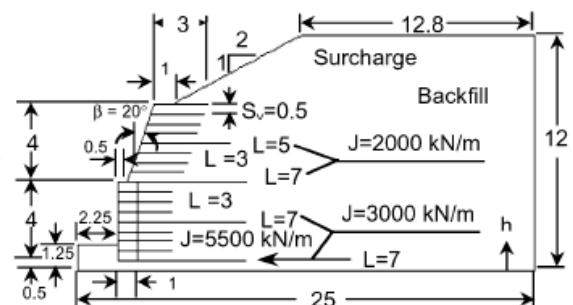


Fig. 2. Example of tiered wrap-around / gabion faced hybrid reinforced soil structure (from Hatami et Al, 2001)

Hybrid MSE structures are versatile modular system used for soil reinforcement applications such as mechanically stabilized earth (MSE) walls and reinforced slope systems (RSS). They are used for commercial and industrial projects, road works, erosion control and bank stabilization.

Hybrid MSE structures are the most detailed and complete reinforced soil system present on the market, with the possibility of using either just the double twist wire mesh reinforcement or of combining it with facing elements of high-strength polyester geogrids in the case of very high works which are subject to large loads. The numerous possibilities for construction of the outer face enables the best choices to be made in every situation both from a technical-environmental point of view and in consideration of the landscaping requirements.

For the selection of the most suitable solution, the fundamental aspects for the correct design of MSE hybrid structures with geogrid primary reinforcement shall be carefully considered: in order to carry out a structural analysis of such structures it is required to check a large number of load conditions and geometries in accordance with the most typical and frequent situations which occur in walls and slope stability analyses.

Hybrid structures rely upon the steel mesh and the geogrids placed horizontally within the slope or wall, with backfill compacted upon them. The gabion or wrap-around facing is fully integrated with the steel mesh reinforcement, which works based on the friction acting along the surface of the wire and, more importantly, on the mechanical interlocking properties of the backfill. Some proprietary hybrid MSE systems have been evaluated and approved by HITEC (with the collaboration of AASHTO and FHWA) for 75 years design.

Figure 3 shows in details the facing units used in MSE hybrid structures:

- the gabion unit comprises a continuous horizontal panel of woven wire steel mesh, faced at one end with a gabion box, formed from hexagonal, PVC-U coated, galvanized, double twist woven steel mesh; the front and top of the gabion box are folded during manufacture; the back and sides of the gabion box are formed from a separate piece of the mesh, which is folded and fixed to the horizontal panel during manufacture; additional, separate, diaphragm (partition) mesh panels can be fixed on site to the gabion box facing as required by the design; this creates rectangular shaped cells used for stone confinement; the gabion element is filled with hard durable rockfill, while the tail is then sandwiched between layers of compacted backfill material, thereby reinforcing it; having the tail as an integral part of the gabion box removes the need for any on-site connection or pinning, where errors during installation could occur due to incomplete connection, or reduced pinning frequency; hence the gabion facing unit is rapid to construct, and can even reuse site won materials when suitable; consecutive layers of gabion units are then constructed to form reinforced soil retaining structures of almost any height when used in conjunction with high strength geogrids.

- the wrap-around unit comprises a single length of double twist mesh that forms the base, the sloping face and the top part (that is the wrap-around length) of the unit; a bio-degradable or synthetic blanket is installed immediately behind the sloping faces of the unit to control erosion and to promote rapid vegetation establishment; a wedge of topsoil is placed behind and in contact with the blanket to provide a moisture and nutrient reservoir, essential for successful vegetation; no external support or shuttering is required when installing the wrap-around units, thus increasing considerably the speed of the installation; a steel reinforcement mesh is factory assembled to provide rigidity to the face; bioengineering techniques like live staking and brush layering can be used to create a more natural look to the structure.

Hybrid MSE structures afford important advantages:

- permeability of the front face, guaranteeing drainage of the backfill;
- flexibility, enabling the structure to tolerate differential ground settlement without compromising structural integrity;
- versatility, which allows the formation of a structure with vertical, battered or stepped front face as required and minimization of environmental impact.
- durability: testimonials of existing gabion structures built since 1894 and still in operation prove that such structures can be safely designed for 120 years design life;
- economy and simplicity: the ease of construction does not require specialist labour force or special equipment; gabions are filled with natural or quarried stones obtained locally, and minimum foundation preparation is needed;
- significant sound proofing characteristics (18-28 decibel);
- structural safety in case of fire near the front face;
- reduction of environmental impact through the use of vegetation incorporated into the front face of the structure.

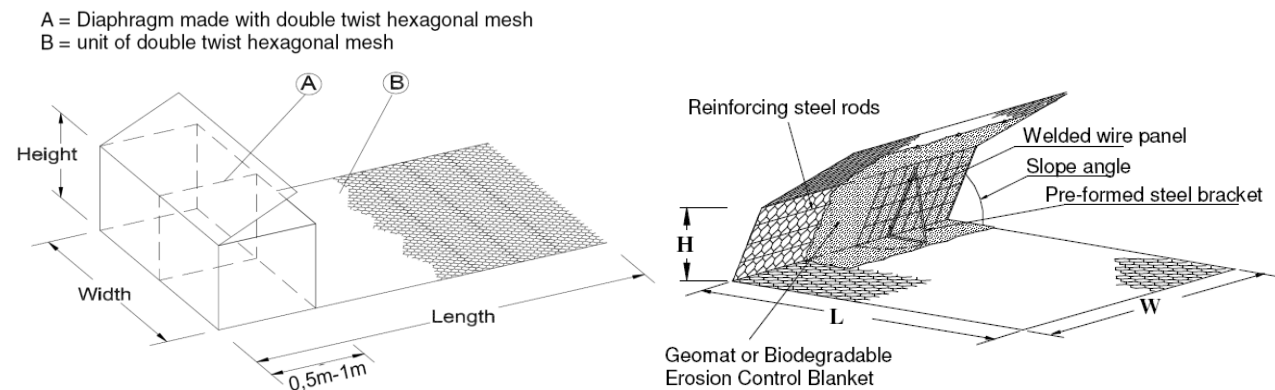


Fig. 3. Details of gabion facing units and wrap-around facing units used for MSE hybrid structures

3. BACKGROUND RESEARCH

The influence of a single reinforcement type with a given stiffness and length on wall response has been the subject of previous investigations.

Ho and Rowe (1996) and Ho et. al. (1996 and 1997) found that the reinforcement stiffness, vertical spacing and length to wall height ratio, L/H, are important parameters that influence the wall displacement response. Rowe and Ho (1996 and 1997) found little variation in the magnitudes of reinforcement load and soil stress for L/H values larger than 0.7. It is worth noting that the ratio L/H = 0.7 is the minimum reinforcement length ratio recommended by FHWA (1997)] and AASHTO (1998)] design guidelines for static stability of reinforced soil walls. A design chart to predict wall deformations as a function of L/H and reinforcement type (i. e., extensible geosynthetic or inextensible metallic) appears in the current FHWA (1997) and AASHTO (1998) guidelines.

Ho and Rowe (1996) concluded that placing equally spaced reinforcement layers with L/H = 0.7 is an efficient reinforcement distribution and recommended over other distribution patterns of reinforcement in reinforced soil walls. Rowe and Ho [13] showed that the magnitude of wall lateral displacement is influenced by the soil friction angle and a reinforcement stiffness factor, Λ , defined as

$$\Lambda = J / (K_a \gamma H S_v) \quad [1]$$

where:

J = reinforcement stiffness,

K_a = Rankine active earth pressure coefficient,

γ = soil unit weight,

H = wall height,

S_v = vertical spacing between reinforcement layers.

Helwany et al. (1999)] used a calibrated finite element model to investigate the effects of wall height, backfill type, and reinforcement stiffness on the response of reinforced soil walls with a hard facing. They found that the stiffness of geosynthetic reinforcement has an important influence on wall displacement response when the backfill shear strength and stiffness values are low.

Hatami et al. (2000) and Hatami et al. (2001), by using numerical simulations carried out with the assumption of plane-strain conditions, show that an alternating reinforcement scheme appears to be a more effective reinforcement arrangement, than grouped schemes with different stiffness combined together. The mixed reinforcement configurations with reduced stiffness toward the wall top did not result in significantly larger lateral wall displacements compared with walls with uniform reinforcement using the stiffest reinforcement type. Another interesting aspect for economic reinforced soil wall design is to reduce the length of every secondary reinforcement layer by 50% while maintaining the same stiffness value. This approach was found to be the best method to reduce the reinforcement supply requirement while maintaining wall serviceability and performance.

The authors demonstrated that the static and deformation behavior of hybrid MSE structures is depending on the following parameters:

1) Reinforcement stiffness and arrangement: the stiffness J of planar reinforcement materials (including geosynthetic products) is normally expressed in terms of the tensile force per unit width of reinforcement, T, for unit strain (i. e., units of kN/m) as (Figure 4):

$$J = T / \epsilon \quad [2]$$

where ϵ is the tensile strain in the reinforcement. The reinforcement is modeled as plane-strain sheets with the same cross-sectional area, perimeter and stiffness values as those of an equivalent number of cable elements per unit length of the wall (i. e., perpendicular to the wall plane). The reference reinforcement stiffness values are chosen from properties reported for woven wire mesh and polyester geogrid reinforcement products.

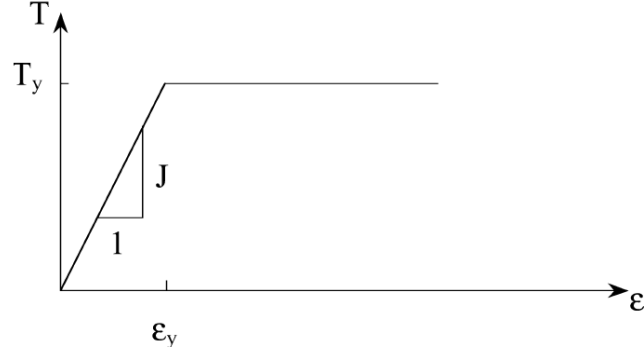


Figure 4. Mechanical response parameter definition for reinforcement.

2) Reinforcement quantity: the amount of reinforcement in each wall is quantified using the reinforcement stiffness J , length L , and vertical spacing S_v . The amount of reinforcement supply for a wall of given height, H , is proportional to the ratio $(J L / S_v)$. The demand from lateral earth pressure behind the wall is proportional to $(K_{ah} \gamma H^2)$, where γ is the backfill unit weight and K_{ah} is the horizontal component of the active Coulomb earth pressure coefficient given by:

$$K_{ah} = K_a \cos \left[\delta + \left(\alpha - \frac{\pi}{2} \right) \right] \quad [3]$$

Where

$$K_a = \frac{\sin^2(\alpha + \varphi)}{\sin^2 \alpha \sin(\alpha - \delta) \left[1 + \sqrt{\frac{\sin(\varphi + \delta) \sin(\varphi - \theta)}{\sin(\alpha - \delta) \sin(\alpha + \theta)}} \right]^2} \quad [4]$$

In equations (3) and (4), φ is the backfill soil friction angle, δ is the friction angle between the backfill and a hard facing, α is the wall batter angle from horizontal (i. e., $\alpha = \pi/2 + \beta$) and θ is the backfill surcharge slope. The active earth pressure coefficient is considered in the lateral earth pressure demand formulation because a plastic, active zone typically develops in reinforced zones with geosynthetic reinforcement materials due to their relatively low stiffness values (i. e., compared with metallic reinforcement stiffness).

The reinforcement ratio, R_λ , is introduced as a non-dimensional, single-valued parameter to quantify the reinforcement supply-to-demand ratio for a wall of given height H and backfill material as:

$$R_\lambda = \frac{\sum_{i=1}^n \frac{J_i l_{fi}(\lambda) L_i}{S_{vi}}}{K_{ah} \gamma H^2} \quad [5]$$

where J_i , L_i , and S_{vi} are the stiffness, length and vertical spacing (contributory height) of reinforcement layer i , respectively, and, n denotes the total number of reinforcement layers.

The length factor, l_{fi} , of the reinforcement layer i is defined as:

$$l_{fi}(\lambda) = 1 + \frac{L_i/H - \lambda}{L_i/H + \lambda} \quad [6]$$

where λ is a reference reinforcement length-to-wall height ratio that corresponds to an optimum L/H ratio value for the stability of reinforced soil walls. The value for λ is taken as 0.7 in accordance with the results of previous numerical and experimental studies, as above reported. However, a lower value for λ (i. e., optimum L/H ratio for wall stability) may be considered for higher backfill friction angles. The mathematical expression of equation (6) represents the direct influence of reinforcement length on wall stability for the range $L_i / H \leq \lambda$ and its reduced effect for $L_i / H > \lambda$.

The parameter R_λ defined in equation (5) includes both reinforcement supply and backfill friction angle which are the two most important parameters influencing the horizontal displacement of reinforced soil walls. Specifically, a higher

magnitude for the parameter R_x indicates a stronger backfill and/or greater reinforcement supply in the wall, both of which would result in lower wall lateral displacement. Equation (5) can be understood to be an indicator of the reinforcement cost.

Hatami et Al (2000) and Hatami et Al (2001) discuss the effect of the above listed parameters, coming to the following conclusions:

1) Effect of reinforcement stiffness arrangement:

uniformly stiff reinforcement over the entire height shows the smallest amount of lateral displacement, while replacing half of the reinforcement layers with a less stiff reinforcement material increases the wall lateral displacement.

However, the maximum displacement value and the displacement distribution pattern depend on the reinforcement arrangement: placing the less stiff reinforcement in the upper half of the wall results in local bulging of the facing in the upper half of the wall height; while the wall lateral displacement within the lower half does not increase noticeably; placing the less stiff reinforcement in the lower half of the wall height results in a considerable increase in wall lateral displacement in the lower half of the wall height.

Distributing the less stiff reinforcement material evenly between stiff reinforcement layers results in a wall displacement profile similar to the displacement response of uniformly reinforced wall but with larger lateral displacement magnitude at all reinforcement elevations; however the amount of displacement increase is uniform over the wall height and about half the maximum value observed in grouped reinforcement arrangements.

Therefore, an alternating reinforcement scheme appears to be a more effective reinforcement arrangement than grouped schemes with the same reinforcement ratio value to limit wall lateral displacement.

A comparison of displacement results shows the influence of using an alternating reinforcement arrangement with the same average reinforcement stiffness as an otherwise, identical configuration with uniform reinforcement: the alternating reinforcement configurations show only a slightly larger amount of deformation at end of construction compared with uniformly reinforced walls; accordingly, the deformation response of walls with alternating reinforcement stiffness arrangement can be considered to be practically the same as the response of uniformly reinforced walls with identical reinforcement ratio values.

For a wrapped-face wall the intuitive scheme of reducing reinforcement stiffness with height appears to be a cost-effective configuration that would not result in a significantly larger wall displacement compared to the alternating scheme. However, the reduction of reinforcement stiffness with elevation using an alternating reinforcement arrangement is more desirable (i. e., compared with grouped schemes) to avoid local, excessive deformation of the facing along the wall height.

2) Gabion facing vs. battered wrapped-face wall:

It is intuitive that an inclined wrapped face at 20° to the vertical usually generates less lateral displacement at the end of construction than a wall constructed with a vertical gabion facing. However the pattern of displacement profiles between wrapped-face and gabion facing walls is quite different: the maximum end-of-construction displacement occurs much higher up the face of the gabion wall (approx. at $0.75 H$) compared to the wrapped-face wall (approx at $0.35 H$). The displacement of the wrapped-face wall is considered to be due to lateral spreading of the backfill under soil self-weight, while the pattern of displacement for the vertical gabion wall is mainly due to rotation of the facing column about the toe.

3) Effect of reinforcement arrangement and vertical spacing:

the displacement response of a uniformly reinforced wall is practically indistinguishable from the response of a corresponding wall with grouped reinforcement configuration where the stiffness values of the two reinforcement groups are not substantially different (e.g. with a variation of J within 10% and difference in $R_{0.7}$ within 5%).

The combined influence of reduced reinforcement length and tiered wall construction results in greater facing displacements; however, the combined influence of tiered wall construction and reduced reinforcement length is more effective in controlling wall deformation than a battered wrapped-face structure constructed with a wider reinforcement spacing.

The above results suggest that reducing reinforcement stiffness with height while maintaining constant vertical spacing is recommended over increasing the spacing with height (as reported for a number of reinforced soil walls constructed in the past) to limit the facing lateral displacement and ensure the stability of the structure.

4) Effect of reinforcement length:

Different reinforcement schemes have been investigated, considering walls including primary reinforcement with $J = 8000 \text{ kN/m}$ and a less stiff secondary reinforcement with $J = 2000 \text{ kN/m}$:

- only primary reinforcement with uniform reinforcement length
- the secondary reinforcement is placed in an alternating scheme with the primary reinforcement; the length of every secondary reinforcement layer is equal to that of the primary reinforcement;
- the secondary reinforcement is to half length of the primary reinforcement and is placed alternating with the full-length, stiff primary reinforcement.

Results show that the magnitude and profile shape of lateral displacements of walls with the above reinforcement configurations are only marginally different.

It can be concluded that reducing the length of reinforcement for every secondary reinforcement layer is a viable strategy to reduce the required amount of reinforcement with little impact on the displacement response of the wall. The reduction in wall lateral displacement will be greater by adopting a long-stiff, short-secondary reinforcement scheme for the same total length of reinforcement material.

5) Effect of reinforcement ratio on wall displacement:

the maximum wall lateral displacement $(X_d)_{\max}$, normalized to reinforcement vertical spacing S_v , shows a consistent trend of reduction in magnitude with reinforcement ratio value (see Figure 5). The presence of S_v in the normalized parameter $(X_d)_{\max} / S_v$ emphasizes the significance of reinforcement spacing in the magnitude of wall lateral displacement compared with the influence of reinforcement length and stiffness. The alternating reinforcement length schemes provide the lowest wall displacement response magnitude for a given reinforcement ratio value. The magnitude of wall lateral displacement is less sensitive to reinforcement configuration for greater reinforcement ratio values.

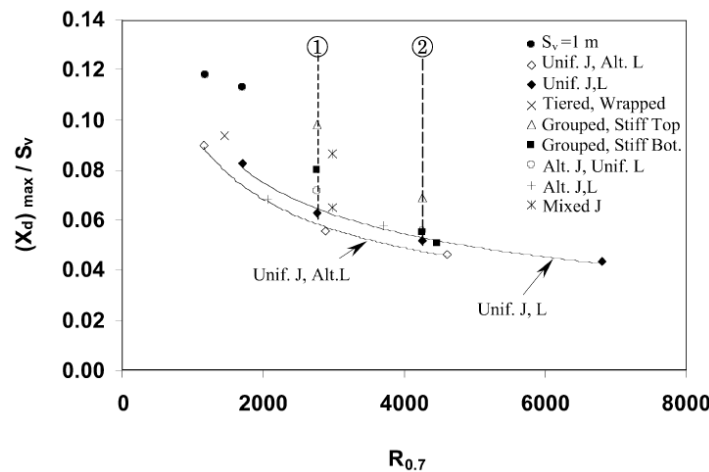


Figure 5. Variation of normalized wall lateral displacement with reinforcement ratio (from Hatami et Al, 2001)

From the above listed research it is evident that the design layout with long and stiff primary reinforcement alternated with short and less stiff secondary reinforcement (as shown in Figures 1 and 2) is the most effective option for hybrid MSE structures. The vertical spacing of the primary reinforcement equal to 2 – 3 times the height of the facing units (either gabion units or wrap-around units), with the secondary reinforcement spaced at each facing unit, affords an optimal distribution of reinforcement which minimizes the deformations of the structure, provided that the stiffness of primary reinforcement, the reinforcement ratio and length factor are properly designed.

This concept was extensively used in the design of two recent projects of high walls constructed in Sikkim and in Albania, where the use of combined reinforcement geometries provided an interesting cost saving benefit compared to the more conventional uniform reinforcement solution. They were designed using mixed reinforcement configurations with high strength geogrids as primary reinforcement and steel mesh as secondary reinforcement and facing unit.

Hence the FHWA and AASHTO limit of 32 inches (800 mm) for the vertical spacing of reinforcement layers should be revised and the vertical spacing should be limited only by design optimization, at least for the hybrid reinforced soil structures described in this paper.

4. CASE HISTORY: SIKKIM AIRPORT (INDIA)

Sikkim came into existence as a state of India in 1975. Due to its land locked scenario the state of Sikkim can only be approached by road. Sikkim is accessible via nearest airport at Bagdogra, which is 120 km from the capital city of Gangtok. Although Sikkim has ample scope of tourism development, due to non availability of an airport; the direct accessibility does not exist. Due to this reason, a new airport is now under construction at Pakyong, which is situated approximately 33 km from Gangtok. The work involves massive cutting and filling earth work. The site of the airport at Pakyong is on a hilly terrain having valleys and spurs with an acquired area of around 200 acres. When fully developed the project will have a 1700 x 30 m runway with turning pads at both ends, suitable for ATR type aircrafts.

The runway strip is planned along N-S direction and the hill is having a natural slope from West (uphill cutting portion) to East (downhill filling portion) as shown in the typical cross section in Figure 6. Since a plane surface is required for the construction of the runway, cutting of uphill portion was done and the same material was filled at downhill portion to get the required level of runway. The constraint that material from cutting should be used in filling was mandatory. As such the entire project was designed in such a way that total volume of cutting shall be equal to total volume of filling. The terrain at site is mainly a mixture of soil and rocks. In upper strata, rock is fragmented and highly weathered. But with depth weathering decreases and soft to hard rock is encountered. Therefore, uphill portion is cut and used for the filling operation. This filling was retained by providing a suitable retaining structure high enough to support and stabilize the filling. Sikkim receives a very high annual rainfall; hence proper drainage system has to be provided along with the conveying structures of the existing creeks. This has been achieved by providing series of catchwater drains and stepped intercepting drains along with gabion cascades. Water from these cascades is finally conveyed outside the site boundary by RCC box culverts, which follows the natural course.

4.1 Technical Considerations and Solution Adopted

Different types of solutions like PCC wall, Masonry wall, Soil Nailing, Gabion Walls, Hybrid MSE walls, were considered for toe walls. Following were the most important parameters specific to this project, based on which final selection of toe wall solution was chosen:

- a) Permeability: the region of Sikkim Airport Project witnesses high amount of rainfall through the year. Hence there will be lot of runoff generated and also the soil will be saturated most of the time; hence the permeability of the structure is very important to reduce the hydrostatic pressure behind the wall in the retained soil. The gabions of hybrid MSE structures are filled with cobbles or quarry stones to porosity in the range of 30% to 40%. This permeability of the front face ensures drainage of the backfill, resulting in less hydrostatic pressure and is thus a suitable option for this project.
- b) Environmental friendliness: one of the most specific requirements is to have an eco-friendly solution for the toe walls, as this area will have direct visibility from runway and terminal building. Hybrid MSE structures are very eco-friendly since they are made up of natural materials filled inside a wire mesh and can be easily vegetated.
- c) Flexibility: the Sikkim Airport Project area is in high seismic activity region. Any structure built will require inherent flexibility to absorb the shocks during seismic activity. Hybrid MSE structures are highly suitable as they are flexible structures which can take large amount of strain and settlements before failure. Flexibility of Hybrid MSE structures helps to accommodate ground settlement without any compromise in structural integrity.
- d) Speed of construction: the project needs to be completed within short duration of time and hence speed of construction is one of the major factors. Hybrid MSE structures can be assembled on site quickly and easily and, since locally available stone boulders are used, the speed of construction is very high.
- e) Cost of construction: use of locally available materials is highly important since it reduces the overall cost of the project by reducing the cost of transportation and delay; hybrid MSE structures are a cost effective solution as the installation is easy and do not require specialized labour and form works.
- f) Foundation considerations: hybrid MSE structures require lesser excavation effort as foundation depth requirement is smaller compared to RCC walls.

Based on all the above criteria, hybrid MSE structures have been selected as the best possible solution as retaining walls in the filling side.

4.2 Design and Construction

The design of hybrid MSE structures has been carried out according to BS: 8006 code, for the static load case, while the seismic load case has been designed as per FHWA code. Load combinations for static load case and seismic load case have been adopted with the appropriate material and loading factors, according to BS 8006 and FHWA, and corresponding loads for various load combinations. External checks like sliding and bearing capacity were performed, and internal checks like reinforcement rupture and pullout; internal stability have been checked according to the “slices method for slip circle analysis” (as per section 7.4.4.3 of BS 8006). Sliding stability at steel mesh and geogrid interface and bulging check at nearly vertical gabion blocks have been calculated for all sections: 3 m length of secondary reinforcement have been considered and all the specified factor of safety requirements were achieved.

Design of primary reinforcement has been based on the properties of bonded geogrids, manufactured with high strength polyester fibers encased in polyethylene coating, selected for the excellent creep characteristics and resistance to

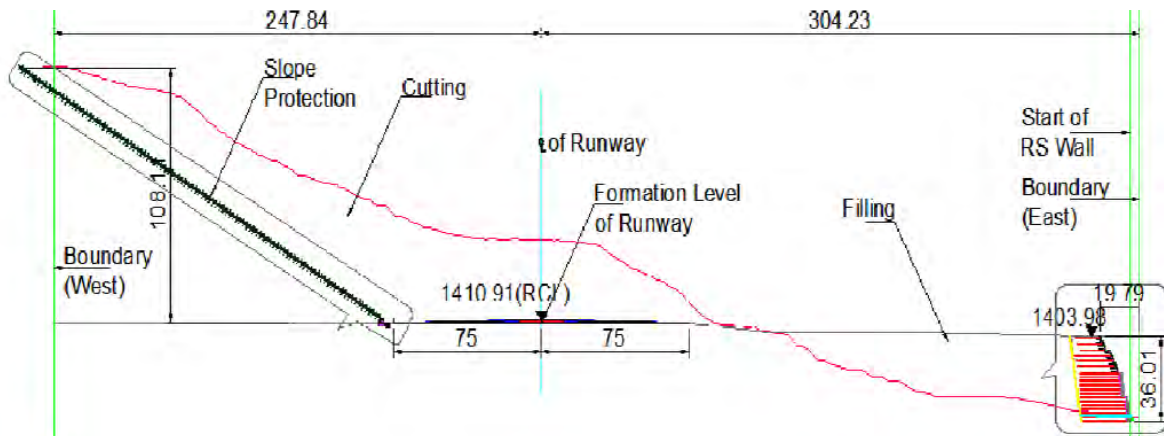


Figure 6. Typical cross section showing cutting and filling operations for Pakyong airport and the hybrid MSE structures for filling support at downstream edge

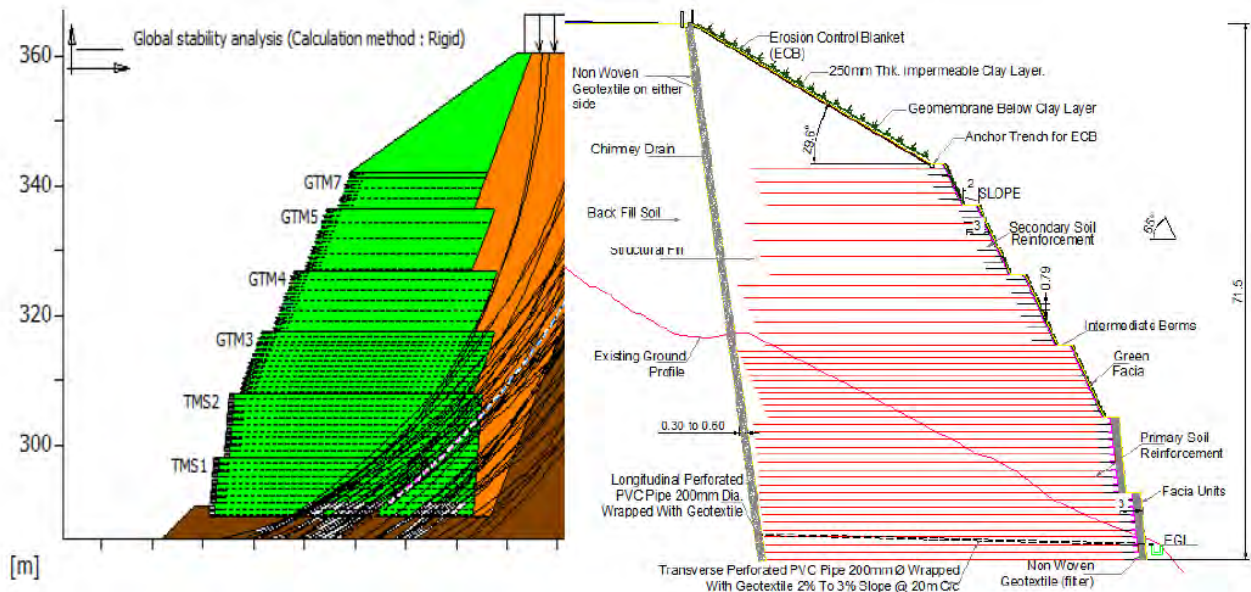


Figure 7. Design output and typical cross section for the highest hybrid MSE structure at chainage 1640

construction damages; geogrids with tensile strength from 200 kN/m to 800 kN/m have been designed, with vertical spacing up to 2.4 m. Totally 1.7 km length of hybrid MSE structures has been designed and built for supporting the airport runway. The most impressive structure is at Chainage 1640: the hybrid MSE structure consists of a 29 m high

wall with gabion facing at bottom and a 51.35 m wrap-around slope above; an embankment of 6.61m height is present above the structure; thus the total height of the structure, including the embankment, is 86.96m. Design output and typical cross section for the highest hybrid MSE structure are shown in Figure 7. To Authors' knowledge this is presently the highest reinforced soil structure in the world. Pictures of geogrids installation and of two finished hybrid MSE structures are shown in Figures 8 and 9.

5. SEISMIC DESIGN AND BEHAVIOUR

The good performance of MSE structures during earthquake has been documented by Koseki, et.al. (2006). In Japan; nowadays MSE walls are often the preferred construction technique compared to conventional retaining wall structures due to their good resistance to earthquake loading. Even MSE walls have been used to replace conventional structures damaged in earthquakes. Koseki et. al. (2006) presented case histories of different earthquakes from different parts of the world. From the case histories it can be noted that a flexible MSE structures performs better, and that MSE structure perform equally better with rigid structure with deep foundation. MSE structures fail progressively with warning displacements. The soil reinforcement immediately distributes stresses avoiding local concentration leading to ductile-like behavior of MSE structures.

India has been divided in four seismic zones viz. II, III, IV & V as per IS1893-1. Sikkim airport project lies in seismic zone



Figure 8. Geogrids installation at Sikkim airport project



Figure 9. Two finished hybrid MSE structures at Sikkim airport project

IV, classified as severe seismic intensity zone. For 70+m high structures located in seismic zone IV, the use of hybrid MSE structure is highly necessitated. Seismic design has been carried out as per pseudo static method described in FHWA manual. Reduction factors have been considered in calculating the long term design strength of primary geogrid reinforcement from its short term ultimate tensile strength. Seismic design has been carried out for considering load factors = 1.0 for all the loads. For seismic condition the target factor of safety for respective mode of failure is 75 % of static condition as per the guide lines of FHWA. In-house software was used for slip analysis and design. It is a software

developed to perform slope stability analysis using different types of reinforcement and complex design scenarios. The software uses conventional limit equilibrium approach (Bishop, Janbu, and Displacement Method). Internal stability checks like reinforcement rupture and pullout have been checked according to the slices method for slip circle analysis. Additionally hand calculations were performed to check the design. The structure was designed for horizontal seismic coefficient of 0.12.

September 18, 2011, earthquake of magnitude 6.9 was felt across northeastern India (Sikkim), Nepal, Bhutan, Bangladesh and southern Tibet. The earthquake centered within the Kanchenjunga Conservation Area, near the border of Nepal and the Indian state of Sikkim. At least 111 people were killed in the earthquake and most of the deaths occurred in Sikkim. The peak ground acceleration for the earthquake of 6.9 on Richter scale would be 0.354 g. Horizontal seismic coefficient can be worked out as half of ground acceleration (Kramer, 1996). Seismic analyses of full height structure with horizontal seismic coefficient of 0.175 shows that factor of safeties are just more than 1.0. Figure 10 presents the seismic analysis of typical cross section with horizontal seismic coefficient of 0.175, that is 45 % higher than the design seismic coefficient.

This means that hybrid MSE structures afford an inherent Factor of Safety which can be estimated to be approx. 50 % higher than the one resulting from design calculations with the present design Codes.

During earthquake major part of the structure attained more than 60% of height. Structure 1 from chainage 280 to 680 had attained height of 50m by September 2011. A rainfall was received at site before earthquake. It is worth to note that the hybrid MSE structure have withstood an earthquake of 6.9 magnitude with no visible damage. This clearly demonstrates the resilience of hybrid MSE structure in seismic loading condition with higher vertical spacing of primary reinforcement.

Hence it is the Authors' opinion that the limit of 32 inches (800 mm) for the vertical spacing of reinforcement layers, reported in the present AASHTO regulations, should be relooked and the vertical spacing should be limited only by design optimization, at least for the hybrid reinforced soil structures described in this paper.

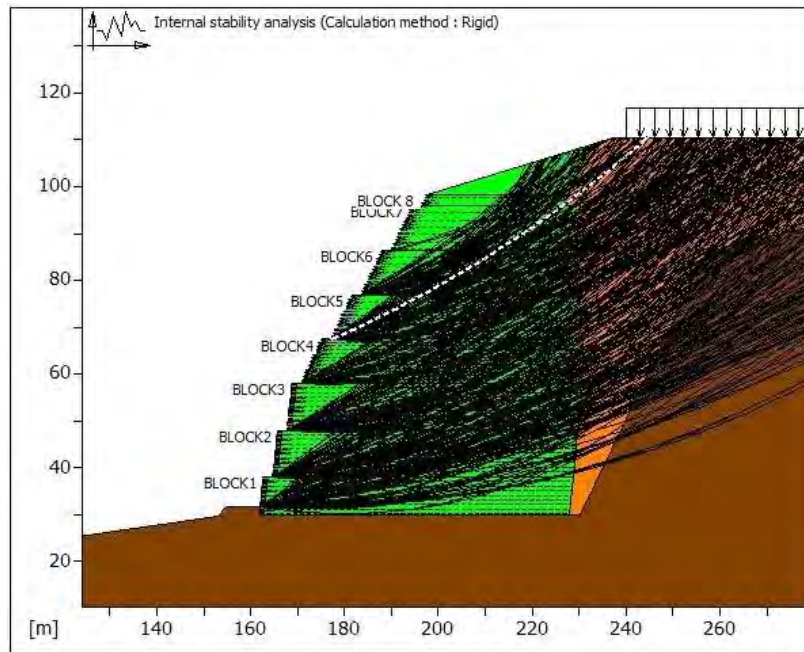


Figure 10. Seismic analysis of typical cross section with horizontal seismic coefficient of 0.175

6. SUMMARY AND CONCLUSIONS

Hybrid MES structures composed of gabion and wrap around facia with integrated tail can be used for construction of tall structures. The combination of facia made up of double twisted mesh and high strength geogrid are cost effective compared to other solutions. Locally available materials can be used for construction of hybrid MSE structure which reduces the overall cost of the project and delay. The integrated tail serves purpose of secondary reinforcement enabling use of vertical spacing of primary reinforcement up to 3m which is more than mentioned / recommended by FHWA with

due consideration of local stability of facia. Hybrid MSE structures are flexible structures which can bear seismic acceleration without any compromise in structural integrity.

REFERENCES

- AASHTO (1998). Interims: Standard Specifications for Highway Bridges, Am. Assoc. Sta. Highw. Trans. Offic. Washington, DC, USA.
- FHWA (1997). Mechanically Stabilized Earth Walls and Reinforced Soil Slopes Design and Construction Guidelines, Federal Highway Administration, Demonstration project 82, Washington, DC, USA.
- K.Hatami, R.J. Bathurst, P.Di Pietro (2001). Static Response of Reinforced Soil Retaining Walls with Nonuniform Reinforcement, *The international Journal of Geomechanics*, Vol. 1 No. 4, 477–506
- Hatami K., Bathurst R.J., Di Pietro P., Bianco P.M. (2000). Numerical Study of retaining walls with non-uniform reinforcement. *Proceedings of Eurogeo 2000: 219-224, Bologna*.
- Koseki, J., Bathurst, R.J., Guler, E., Kuwano, J. and Maugeri, M. (2006b). Seismic stability of reinforced soil walls, *Proc. of 8th International Conference on Geosynthetics, Yokohama, 1, 51-77*.
- Kramer S. L. (1996). *Geotechnical earthquake engineering*, Prentice-Hall Inc, New Jersey.
- S.M.B. Helwany, G. Reardon, and J.T.H. Wu (1999). Effects of Backfill on the Performance of GRS Retaining Walls, *Geotextiles & Geomembranes*, 17(1), pp. 1–16.
- S.K. Ho and R.K. Rowe (1996). Effect of Wall Geometry on the Behavior of Reinforced Soil Walls, *Geotextiles & Geomembranes*, 14(10), pp. 521–541.
- R.K. Rowe and S.K. Ho (1996). Some Insights into Reinforced Wall Behavior Based on Finite Element Analysis, in Earth Reinforcement, H. Ochiai, N.Yasufuku and K. Omine, Eds., *Proc. Int. Symp. Earth Reinf., Fukuoka, Kyushu, Japan, 1, pp. 485–490*.
- R.K. Rowe and S.K. Ho (1997). Continuous Panel Reinforced Soil Walls on Rigid Foundations, *ASCE J. Geotech. Geoenv. Eng.*, 123(10), pp. 912–920.

Seismic Performance of Mechanically Stabilized Earth Wall with Lightweight Aggregate (LWA) Backfill

M. Xiao, Department of Civil and Geomatics Engineering, USA, mxiao@csufresno.edu
D. Hartman, and M. Ledezma; Department of Civil and Geomatics Engineering, USA

ABSTRACT

The paper reports a shake table test on the seismic responses of mechanically stabilized earth (MSE) wall with lightweight aggregates (LWA) backfill. A section of a reduced-scale MSE wall was built in a box that was anchored on the shake table. The MSE wall dimensions were 1.5m high, 1.2m deep, and 1.5m long. Five layers of geogrid were used as the reinforcement. The LWA were compacted at 95% of the maximum dry unit weight at the optimum water content. Scaled 1989 Loma Prieta earthquake excitations were replicated by the shake table. The wrap-around MSE wall was instrumented with accelerometers, linear variable differential transformers (LVDT), linear potentiometers, and dynamic soil stress gauges to respectively record the accelerations, wall vertical settlements, horizontal deflections of wall face, and transient effective stresses during the shaking. The results revealed satisfactory seismic performance of the MSE wall with LWA backfill.

1. INTRODUCTION

Mechanically stabilized earth (MSE) walls are widely used in retaining embankments in highway systems. The MSE walls are easier to construct and more economical than the conventional reinforced concrete retaining walls. They have shown the advantage of safety, environmental friendliness, and savings in labor costs, equipment, and time. By and large, they performed well with no evidence of visual damage or with only minor damages during some of the past major earthquakes such as the 1989 Loma Prieta earthquake (M=7.1) (Collin et al. 1992), the 1994 Northridge earthquake (M=6.7) (Sandri 1994), and the 1995 Kobe earthquake (M=6.9) (Tatsuoka et al. 1996). However, major repairs or complete collapse were also reported for some MSE walls in the 1999 Chi-Chi earthquake (M=7.6) (Huang and Tatsuoka 2001), and in the 1995 Kobe earthquake (Tatsuoka et al. 1997).

Lightweight expanded clay and shale aggregates, also known as lightweight aggregates (LWA), are a type of alternative backfill for embankments and retaining walls. Their dry unit weight ranges from 7.1 to 11.0kN/m³ (45 to 70lb/ft³). They are produced in rotary kilns at temperatures over 1200°C. LWA provide excellent permeability and satisfactory internal friction as backfill materials. The durability and chemical neutrality of LWA can reduce corrosion of steel anchors and bars in MSE walls. Holm and Valsangkar(1993) reported the mechanical properties of LWA as backfill materials and discussed various case studies of such applications. Replacing conventional sand fills with the alternative LWA can reduce settlement on weak and compressible soils, reduce lateral loads on the MSE wall, and facilitate construction through the reduction of compaction needs. For example, the optimum water content of the LWA used in this research is 5%, much less than that of sand, and the compaction effort to reach 95% of the maximum dry unit weight is less than the sand as well. Therefore, the LWA may contribute to the mission of accelerated bridge construction (ABC) promoted by the Department of Transportation.

Shake table tests on MSE retaining walls have been conducted to study their seismic behaviors and to provide earthquake design recommendations for the past 35 years since Richardson and Lee (1975) pioneered the tests on metallic-reinforced earth walls. The recent studies included the large-scale shake table tests on 2.5m tall modular-blocks and geocell-reinforced soil retaining walls (Ling et al. 2005, 2008) and the centrifuge tests on bar mat MSE walls (Siddharthan et al. 2004). Ling et al. (2004) found through parametric study on the behavior of MSE retaining walls that the backfill soil properties, seismic motions, and reinforcement layouts are the three major design parameters (in the order of significance) under earthquake loading. Helwany et al. (2012) conducted a full-scale shake table test on geotextile-reinforced-soil bridge abutment, using a staged sinusoidal horizontal motion with increasing amplitude up to 1.0g. The abutment was 3.2 m tall and concrete masonry unit (CMU) blocks were used as the facing. Thorough data analyses of the tests indicated that the model safely withstood the bridge loads while being subject to ground accelerations up to 1.0 g at 3 Hz.

With the alternative backfill, however, the performances of MSE walls have yet to be fully tested and understood under seismic conditions. Specifically, the horizontal deflections of wall face, the dynamic vertical settlement of the MSE wall, the transient vertical effective stress within the wall, and the acceleration responses are unknown and therefore the focus of this research. The objective of this research is to quantify the seismic responses of an MSE wall with the LWA as backfill using reduced-scale shake table test.

2. MATERIALS CHARACTERISTICS, EXPERIMENTAL SETUP, AND INSTRUMENTATION

The lightweight aggregates were obtained from Utelite Corp (Coalville, UT). The grain size distribution curve of the lightweight aggregates is shown in Figure 1, and their properties are listed in Table 1.

Table 1. Properties of LWA

Optimum water content	5%
Maximum dry unit weight	10.8 kN/m ³ (68.9 lb/ft ³)
Cohesion	0
Internal friction angle	36.5°
Specific gravity	1.74
Coarse aggregate duability index (based on ASTM D3744)	93

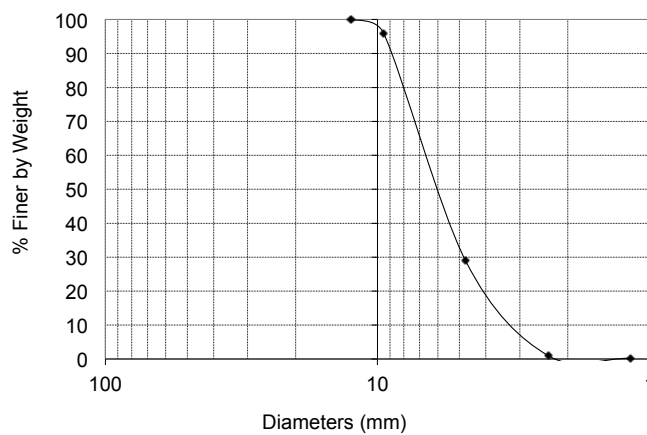


Figure 1. Size distribution of the lightweight aggregates



Figure 2. Shake table facility

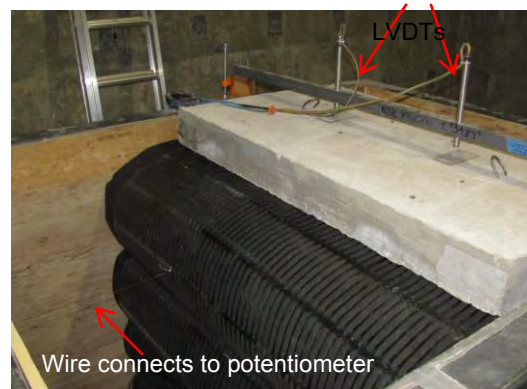


Figure 3. Completed MSE wall with surcharge

A section of reduced-scale MSE wall was built in a 1.5 m (wide) × 1.87 m (long) × 1.8 m (tall) rigid steel box that was anchored on a 2.4 m × 2.1 m one-dimensional shake table. The load capacity of the shake table is 177.9 kN (20.0 tons); the actuator provides 244.6 kN (55 kips) hydraulic fluid driving force; and the maximum travel distance of the table is ±12.7 cm (± 5 inch). The shake table is capable of replicating recorded historical earthquake motions that are within its allowable displacement range. Figure 2 is a photo of the shake table and the box with a retaining wall built inside. Figure 3 shows the constructed model MSE wall.

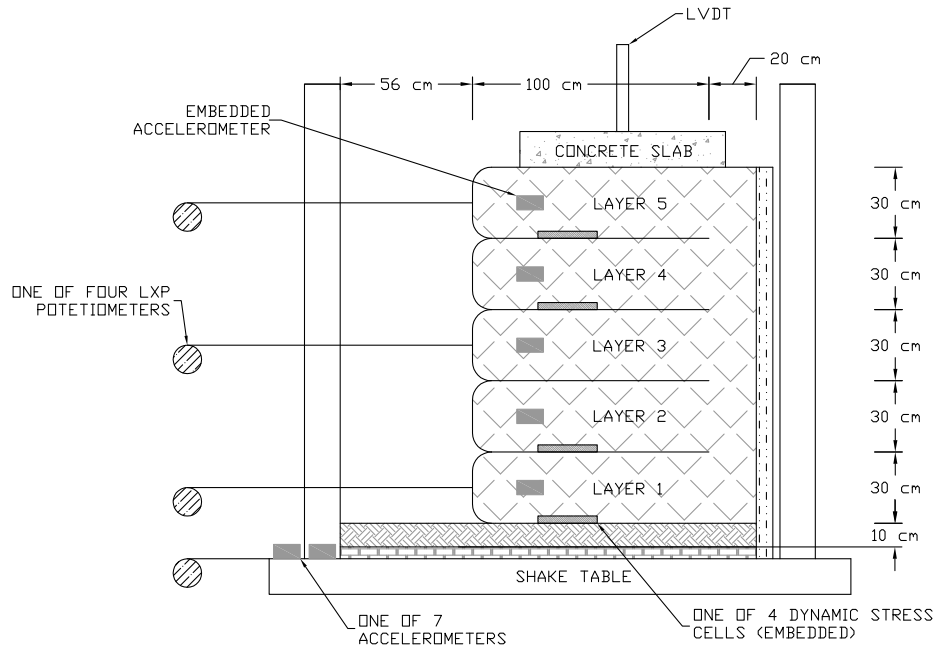


Figure 4. MSE wall configuration and instrumentation

The model MSE wall configuration is shown in Figure 4. The wall was 1.5 m high, 1.2 m deep, and 1.5 m long. The model MSE wall simulated an MSE wall of 4.5 m tall in the field. So the dimensional scale was chosen to be 1:3 (model:prototype). Five wrap-around layers of lightweight aggregates were used. Uniaxial geogrid was used as both reinforcement and containment of the lightweight aggregates. The geogrid installation followed the field practice recommended by Tensar International, Inc. The spacing and length of each reinforcement layer were determined according to the “Geosynthetic Design & Construction Guidelines Reference Manual” (FHWA 2008) and “Designing with Geosynthetics” (Koerner, 2005). The design parameters for geogrid reinforcement are listed as follows:

- Ultimate tensile strength, $T_{ult} = 54 \text{ kN/m}$, provided by Tensar International, Inc.
- Allowable tensile strength, $T_{all} = \frac{T_{ult}}{RF_{ID} \times RF_{CR} \times RF_{CBD}} = \frac{54}{1.2 \times 2.5 \times 1.2} = 15 \text{ kN/m}$
- Factor of safety for pullout failure: $FS = 1.5$
- Height of wall (prototype): $H = 4.5 \text{ m}$
- Effective external friction angle between geogrid and LWA, $\delta' = \phi'_{LWA} = 36.5^\circ$
- Effective adhesion between geogrid and LWA: $c_a = 0$.

It was determined from the design that five layers were needed, with minimum spacing as 0.9 m and the maximum reinforcement length as 3.0 m. In the model test, the dimensions were reduced by 3 times based on the 1:3 (model:prototype) ratio. To simplify the construction of the MSE wall in the lab, uniform spacing of 0.3 m and uniform length of 1.0 m were used, as shown in Figure 4. To prevent the LWA from seeping out of the geogrid, non-woven, needle-punched geotextile was used at the facing to contain the LWA. The geotextile covered the face of the wall and did not provide reinforcement. Beneath the first layer of LWA, a 10 cm sand layer was compacted to simulate the base soil. Formwork was used to hold the wall face in place as each layer was constructed. The LWA were premixed at the optimum moisture content of 5% using a concrete mixer and were transported by a crane into the box. A 15kg hand hammer with a long handle and 30 cm × 30 cm steel base was used to compact the LWA to reach the target dry unit weight of 10.3 kN/m³ (65.5 lb/ft³), or 95% of the maximum dry unit weight. The dry unit weight and water content relationship was derived using the modified Proctor test (ASTM D 1557). A concrete slab was placed at the top of the wall and anchored to the top layer with ten steel rebar, so that the slab did not move freely during the shaking. The concrete slab simulated a surcharge of 3.38 kN/m² in the model test.

Figure 4 also depicts the instrumentations used in the model test. Figures 5 and 6 show the accelerometer, dynamic stress cell, and the materials used in the model MSE wall. Three linear potentiometers were used to measure the horizontal deflections of the wall face at the bottom, middle, and the top layers. The potentiometers were fixed to an inertial frame outside of the shake table, and an inelastic wire connected each potentiometer to the geogrid at the three

designated levels. The fourth potentiometer was connected to the shake table in order to measure the actual seismic motions generated by the actuator. The potentiometers were spring-loaded, but the spring force was significantly smaller than the seismic force. Therefore, the spring stiffness did not affect the responses of the walls. The vertical settlements of the MSE wall during the shaking were measured by LVDT transducers that were anchored on the box above the concrete slab. The transient vertical effective stresses in the backfill were measured using dynamic soil stress cells, which were placed flat at the bottom of layers 1, 2, 4, and 5. The potentiometers, the LVDTs, and the dynamic stress cells were connected to the National Instrument data acquisition system, which automatically recorded the readings during the shaking. Wire-free accelerometers were embedded in each of the five layers and were close to the wall face in order to measure the acceleration responses of the backfill. One accelerometer was attached to the shake table and one to the box to measure their acceleration responses as well. A delayed-start timer was set in each accelerometer, and the data recording (100 data points per second) started automatically at a predetermined time when the shake table test was run.

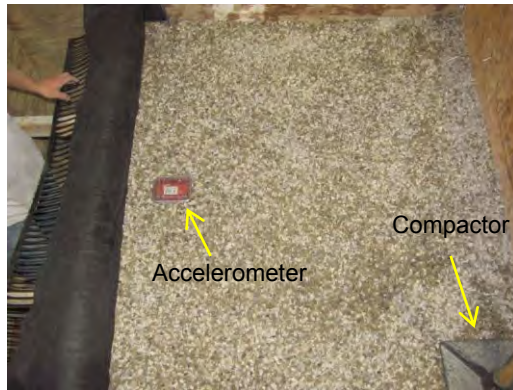


Figure 5. Accelerometer in each layer



Figure 6. Dynamic soil stress cell and geosynthetics

3. TEST PROGRAM

In this research, the 1989 Loma Prieta earthquake ($M = 7.1$) was simulated. The duration of the displacement-time history was 40 seconds. The earthquake's displacement-time history and acceleration-time history data were obtained from the Pacific Earthquake Engineering Research (PEER) Center Library of UC Berkeley and were implemented into the input file to the MTS® control system of the shake table. Trial shake table tests were run on the empty box, the input and measured displacements and accelerations matched well, respectively. In this research, the dynamic stress was scaled based on the dynamic scaling law for the "adequate model" that was presented by Moncarz and Krawinkler(1981). Equation (1) shows the principle of the dynamic scaling law:

$$a_r = \frac{a_{model}}{a_{field}} = L_r^{-1} = \left(\frac{L_{model}}{L_{field}} \right)^{-1} \quad [1]$$

Where a_r is the acceleration scaling factor between the model and the prototype (field), and L_r is the dimensional scaling factor and is 1/3 in this study. The dynamic stress provided by the shake table was represented by accelerations. Equation [1] shows that the acceleration scaling factor is the inverse of the dimensional scaling factor. So the input accelerations to the model test should be three times of the actually recorded accelerations in the field.

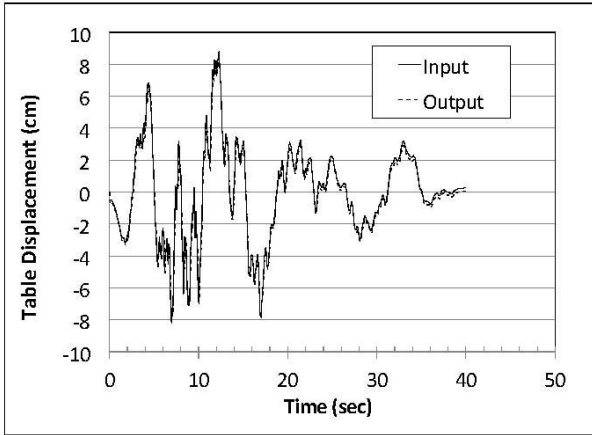


Figure 7. Displacement-time history of the shake table

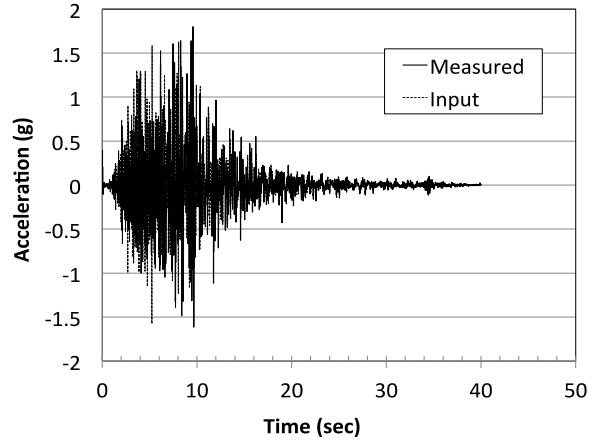


Figure 8. Acceleration-time history of the shake table

Figure 7 shows the match of the displacement-time histories of the input file and the measured displacements (output) of the shake table during the 40 seconds shaking. Figure 8 shows the match of the acceleration-time histories of the input file and the measured accelerations of the shake table during the 40 seconds shaking. The input files for both the displacements and accelerations were already scaled up based on the dynamic scaling law. For example, the maximum horizontal acceleration in the field was measured to be 0.54g, so the maximum horizontal acceleration in the model test was 1.62g (three times of the prototype value).

4. RESULTS AND DISCUSSION

During the simulated 40-second intense shaking, the MSE wall with LWA backfill did not show noticeable damage and failure. The MSE wall's seismic performances in terms of the lateral deflections of the wall face, vertical settlements of the wall, accelerations of the backfill, and the transient dynamic vertical soil stresses in the backfill are presented as follows.

The maximum accelerations and their time of occurrence are listed in Table 2. The maximum input acceleration was 1.62 g. But the measured maximum accelerations of the shake table and the box were slightly off the target value due to the following two reasons. (1) The actuator is controlled by the displacement-time history through the MTS® control system. The actuator that drives the shake table may not be able to move exactly as the input displacement-time history due to various software and hardware issues. But the input and the actual shake table movements were very close, as shown by Figure 7. (2) The weight of the MSE wall on the shake table affects the acceleration response. The weight of the MSE all was already taken into account during the shake table calibration, but tolerable errors may still occur in the calibration. From Figures 7 and 8 and Table 2, we conclude that the shake table was able to simulate the scaled Loma Prieta earthquake excitations. Table 2 also showed that the bottom layer had the least acceleration. But the maximum acceleration occurred in the middle layer (layer 3). The underlying mechanism is yet to be understood by the authors.

Table 2. Maximum input and measured accelerations of the table and the backfill

Location	Input	Shake table	Box	Layer 1 (bottom)	Layer 2	Layer 3	Layer 4	Layer 5 (top)
Max Acceleration (g)	1.62	1.8	1.55	1.37	1.85	2.74	2.22	2.03
Occurring time (sec)	8.07	9.57	8.28	9.45	8.84	9.44	6.15	6.12

Figure 9 shows the lateral deflections of the wall face measured by the linear potentiometers at the top, middle, and bottom layers. The deflections were relative to the table movements, i.e., the absolute movements of the layers minus the table movements at each time stamp. The lateral deflections showed an expected increasing trend from the bottom to the top layers. The bottom layer moved less than 0.5 cm relative to the underlying ground, and the top layer moved about 10 cm relative to the ground, or 6.7% of the wall height. The maximum deflections of the three locations occurred at approximately 10 seconds into the shaking when the maximum acceleration of the table occurred (refer to Figure 8

and Table 2). After that, the MSE wall maintained the maximum lateral deflections and moved together with the shake table.

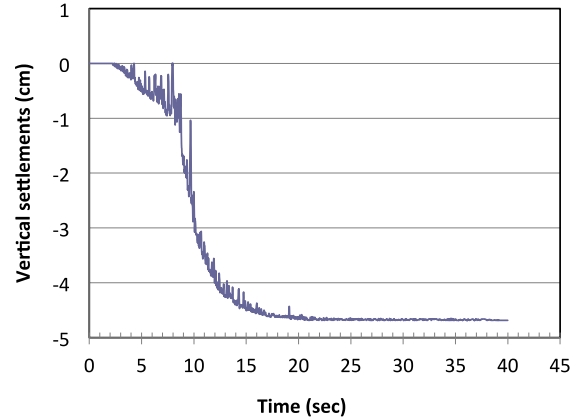
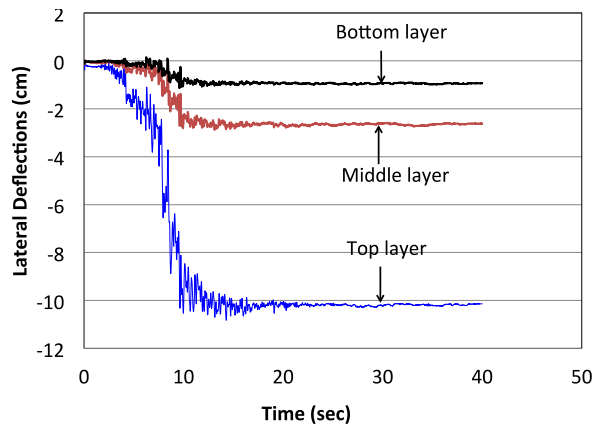


Figure 9. Lateral deflections of wall faces, relative to table movement Figure 10. Seismic settlements of MSE wall

Two LVDT transducers were positioned at the top of the concrete slab to record the dynamic settlements of the wall during the shaking. The two LVDT transducers recorded closely matched readings, showing good accuracy and reproducibility of the instrumentation. Figure 10 shows seismic settlements that were recorded by one of the LVDT transducers. The maximum settlement was approximately 4.7 cm, or 3.1% of the wall height. The settlements generally increased during the shaking with occasional upward bouncing. The occurrence of the maximum settlement also matched the time when the maximum horizontal acceleration occurred, at approximately 10 seconds. After 15 seconds into the shaking, no more settlement occurred.

As shown in Figure 4, four dynamic soil stress cells were embedded in layers 1, 2, 4, 5. The static stresses due to the weight of LWA and the concrete slab before shaking were determined to compare and verify the readings by the four stress cells. During the data analyses after shaking, we found erroneous readings by the stress cells in the very bottom and top layers (layer 1 and layer 5). The stress cell in layer 1 did not record continuous readings, and the stress cell in layer 5 recorded the initial readings that were more than three times of the static reading. We were unsure of the reason, and readings of these two stress cells are not included in the paper. Figures 11 and 12 show the dynamic vertical stresses at the bottom of layer 2 (lower layer) and layer 4 (upper layer). The initial readings are very close to the static stresses, as can be seen in the figures. The graphs showed three noticeable findings: (1) the maximum dynamic vertical stress in each layer occurred at approximately 8 to 10 seconds, the time when the maximum acceleration occurred; (2) the maximum dynamic vertical stresses doubled the initial static stresses; (3) toward the end of the shaking, the dynamic stresses stabilized and maintained at a higher level than the initial static readings, possibly due to the dynamic compaction effect. In this model test, horizontal stress was not measured.

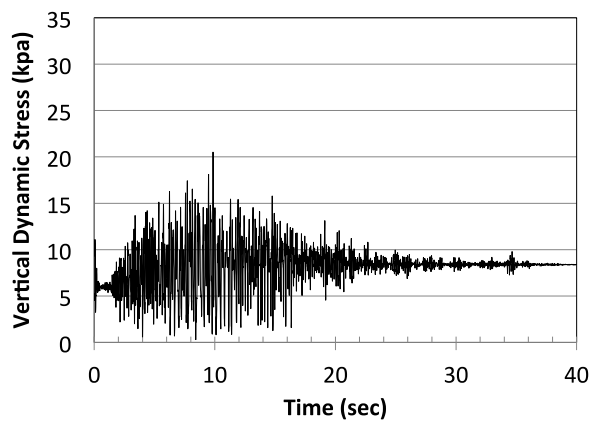


Figure 11. Dynamic vertical stresses in layer 2
(static stress = 9.9 kN/m²;
max dynamic vertical stress = 20.5 kN/m²)

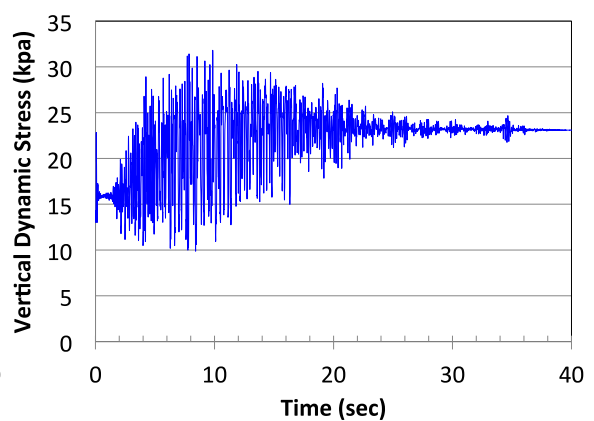


Figure 12. Dynamic vertical stress in layer 4
(static stress = 16.4 kN/m²;
max dynamic vertical stress = 31.8 kN/m²)

5. CONCLUSIONS AND LIMITATIONS OF THIS RESEARCH

This paper presented an experimental research on responses of a mechanically stabilized earth wall with lightweight aggregates backfill under simulated earthquake excitations. The research was conducted using scaled shake table test. Under the scaled earthquake excitations, the MSE wall showed no noticeable damage. This preliminary research showed promising potential of using lightweight aggregates as accelerated backfill for soil retaining walls in seismic regions.

This experimental study has several limitations. (1) The geogrid's tensile strength was not scaled and high reduction factors were used, this could result in an over-reinforced wall. (2) The reinforcement was based on static design. Seismic design using the methodologies presented by Helwany et al. (2012) and by National Concrete Masonry Association (NCMA 2010) may change the internal configuration of the MSE wall and consequently the seismic behavior. (3) The scaling law used in the model test should be improved to consider the scaling of the material properties. (4) External (global) stability, such as deep-seated rotational failure that can be caused by earthquakes, cannot be simulated in this test due to shallow soil depth. Because of these limitation, extrapolation of the model results to the field is premature at this stage. This research work is continued to address the limitations in (1), (2), and (3). Numerical model using Plaxis is being developed to simulate the laboratory conditions (including the boundary conditions, material properties, and seismic excitations). Using the same conditions, the numerical model can be calibrated using the model test results; then the numerical model can be used to predict the seismic performance in the field.

ACKNOWLEDGEMENTS

This project is funded by the California Department of Transportation (agreement number: 65A0449). Steve Scherer, research technician in the Department of Civil and Geomatics Engineering at CSU Fresno, helped the experimental setup. Mr. Darren Medeiros of Utelite Corp (Coalville, UT) provided the lightweight aggregate; Mr. Willie Liew of Tensar International provided the geogrid, and Dr. Mengjia Li of GSE World provided the geotextile. We appreciate these supports.

REFERENCES

- Collin, J. G., Chouery-Curtis, V. E., and Berg, R. R. (1992). Field observations of reinforced soil structures under seismic loading. *Proc., Int. Symp. on Earth Reinforcement Pract., Earth reinforcement practice*, H. Ochiai, N. Yasufuku, and K. Omine, eds., Vol. 1, Balkema, Rotterdam, The Netherlands, 223–228.
- Federal Highway Administration, U.S. Department of Transportation (2008). *Geosynthetic Design and Construction Guidelines Reference Manual*. Publication No. FHWA-NHI-07-092, by Holtz, R.D., Christopher, B.R., and Berg, R.R. National Highway Institute. Washington, DC. August 2008.
- Helwany, S., Wu, J.T.H., and Meinholz, P. (2012). *Seismic Design of Geosynthetic-Reinforced Soil Bridge Abutments with Modular Block Facing*. Final Report for NCHRP Project 12-59 (01). American Association of State Highway and Transportation Officials (AASHTO), Washington, D.C.
- Holm T. A., and Valsangkar A. J. (1993). *Lightweight Aggregate Soil Mechanics: Properties and Applications*. Transportation Research Board, National Research Council, Washington, D.C., *Transportation Research Record* 1422: Soils Geology and Foundations: Lightweight Artificial and Waste Materials for Embankments Over Soft Soils.
- Huang, C.C., and Tatsuoka, F. (2001). Stability analysis of the geosynthetic-reinforced modular block walls damaged during the Chi-Chi Earthquake. *Proc. Fourth Int. Conf. on Recent Advances in Geotech. Earthquake Engrg. and Soil Dyn.*, San Diego.
- Koerner, R.M. (2005). *Designing with Geosynthetics*. Fifth Edition. Pearson Prentice Hall. Upper Saddle River, NJ.
- Ling, H.I., Hohir, Y., Leshchinsky, D., Burke, C., Matsushima, K., and Liu, H. (2005). Large-scale shaking table tests on modular-block reinforced soil retaining walls. *ASCE J. Geotech and Geoenviron. Engrg.*, 131(4): 465-476.
- Ling, H.I., Leshchinsky, D., Wang, J.P., Hohri Y., and Rosen, A. (2008). Seismic responses of geocell retaining walls: experimental studies. *J. Geotech. and Geoenviron. Engrg.*, 135(4): 515-524.
- Ling, H.I., Liu, H., and Mohri, Y. (2004). Parametric studies on the behavior of retaining walls under earthquake loading. *J. Engineering Mechanics*, 131(10): 1056-1065.
- National Concrete Masonry Association (NCMA) (2010). *Seismic Design Of Segmental Retaining Walls*, TEK 19-5A. National Concrete Masonry Association, Herndon, Virginia.
- Moncarz, P., and Krawinkler, H. (1981). Theory and application of experimental model analysis in earthquake engineering. The John A. Blume Earthquake Engineering Center, Stanford University. A report on a research project sponsored by the National Science Foundation, Grants ENV75-20036 and ENV77-14444, June 1981.

- Richardson, G.N., and Lee, K.L. (1975). Seismic design of reinforced earth walls. *ASCE J. Geotech. Eng. Div.*, 101(2): 167-188.
- Sandri, D. (1994). Retaining walls stand up to the Northridge earthquake. *Geotech. Fabrics Rep.*, 12(4): 30-31.
- Siddharthan, R.V., Ganeshwara, V., Kutter, B. El-Desouky, M., and Whitman, R. (2004). Seismic deformation of bar mat mechanically stabilized earth walls. I: centrifuge tests. *ASCE J. Geotech. and Geoenviron. Engrg.*, 130(1): 14-25.
- Tatsuoka, F., Koseki, J., and Tateyama, M. (1997). Performance of reinforced soil structures during the 1995 Hyogo-ken Nanbu Earthquake. *Earth reinforcement*, H. Ochiai et al., eds., Balkema, Rotterdam, The Netherlands, 973–1008.
- Tatsuoka, F., Tateyama, M., and Koleski, J. (1996). Performance of soil retaining walls for railway embankments. *Soils and Foundations, Special Issue*, Japanese Geotechnical Society, 311-324.

Separation/Stabilization Geotextiles – The Underlying Solution that We Have Had All Along for More Resilient Roads

M. Grace, Propex Operating Company, LLC, United States

ABSTRACT

Far and away the largest geosynthetic application, the use of geotextiles in separation/ stabilization, is also one of the most cost effective. The proven performance of this technology has been widely published and implemented for decades. However, geotextiles remain under-utilized. This paper is not intended to present technical guidance for specific road design, but rather to review the technology comparing its low cost to that of traditional unpaved and paved roadway building technologies. Common mythical subject matters will be addressed, and barriers to implementation will be reviewed. An update will be given on recent U.S. government activity advocating change to achieve a sustainable transportation infrastructure by using separation/ stabilization geotextiles. Readers will be presented a clear message regarding the economic and technical reasons behind the application, and will be offered confidence to support a decision to employ geotextile policies. The intent is to provide stakeholders a tool to justify increased implementation of separation/ stabilization geotextiles, lower construction and maintenance costs, while confirming what is already known about geotextile use in roads is still relevant, and even more applicable today given the challenges at hand.

1. INTRODUCTION

1.1 The Challenge for a More Resilient National Infrastructure

“Do more with less” is a common theme amongst businesses and government agencies across the United States. Furthermore, extreme weather conditions, a declining economy, an increase in raw material costs, and the need to support a growing population with limited resources has made it painfully evident that our nation’s infrastructure needs improvement, and future infrastructure projects must follow the most cost effective and sustainable policies. These adaptation efforts are currently taking place nationwide and will continue, but immediate attention to roadway infrastructure must be undertaken to further economic development in the U.S. The challenge exists to make this critical infrastructure component stronger, longer lasting, and more durable than ever before to meet current demands, while holding costs down to enable a generation of economic growth.

Currently, there are 4.05 million miles of road in the 50 United States, according to the Federal Highway Administration (FHWA). At the core of the nation’s highway system lies 46,720 miles of Interstate Highways (comprising just over one percent of highway mileage) along with 116,948 miles of major roads that make up the National Highway System. This system carries a majority of the highway freight and traffic through the United States.

Of the remaining 3.9 million miles of roadway, about 2.6 million miles are paved, which includes most roads in urban areas. However, 1.3 million miles, or more than one-third of all road miles in the U.S. are still unpaved gravel or dirt roads. The majority of our nation’s roads are, surprisingly, low volume rural roads operated and maintained on a local level. Fortunately, this is also the type of roadway category that holds the largest opportunity for improved sustainability.

The trend for the future? Transportation use is outpacing population growth. Now is the time for policy makers and engineers to work together to implement new processes and procedures for overall reductions in initial construction and in maintenance costs. Fortunately, a proven technology to solve these challenges already exists; we just need to better understand and communicate the financial saving aspects. Although a non-traditional solution, but hardly an experimental technology, incorporation of a geotextile for separation and stabilization of a roadway section is a basic value proposition. Yet, for many reasons it is a surprisingly under-utilized solution. Geotextiles have been used in separation/ stabilization applications for decades, and must be embraced by transportation agencies as pressure to further implement life-cycle economics and pavement preservation practices continues to mount. Too much effort is expended on advanced, mechanistic-empirical pavement design methodologies while some of the basic shortcomings and failure mechanisms of roads are seemingly ignored. Increased forensic evaluations of failed paved and unpaved roads would give a better appreciation of how the road support structure loses its strength and bearing capacity due to subgrade soil contamination, aggregate loss, and adverse drainage conditions. Simple solutions to the most common pavement maladies are addressed herewith, and should become a fundamental basic for all pavement design methodologies. Getting back to the basics and understanding the use of geotextiles in separation/ stabilization will enable an engineer to implement impactful technology on infrastructure improvements, while avoiding the risks of unproven methodologies. Future sustainable infrastructure

improvements will undoubtedly incorporate geotextiles, and engineers and policy makers must be imparted with confidence to lead our nation in developing smarter, more cost-effective roadways into the future.

1.2 Roadway Geotextile Application Fundamentals

Before further discussion about roads with geotextiles and their most basic functionality, a review of the two most common mechanisms that contribute to premature road failure is offered. In every road without a geotextile, contamination and intermixing of the aggregate base at the subgrade soil/ aggregate interface occurs for the following reasons:

- Soil fines migrate into the stone aggregate voids
- Aggregate punches into the subgrade soil

These two failure mechanisms are major concerns for any roadway design engineer, and are thus compensated for in one way or another. It is how these failure mechanisms are most commonly addressed today that presents the greatest opportunity for improvement. Typically, traditional approaches are chosen to override these failure mechanisms, and introduce further design flaws, often unintended consequences, when trying to achieve sustainable future standards. Therefore, the greatest opportunity for improvement involves a positive shift in design methodology to incorporate more geotextiles. First, traditional methods will be reviewed in order to fully develop the separation/ stabilization geotextile value proposition.

The most common, traditional approaches to preventing contamination and intermixing at the aggregate/subgrade soil interface are:

- Designing a tight, well-graded base which, in theory, minimizes the migration of fines upward into the aggregate layer
- Increasing the design thickness of the aggregate base to account for “sacrificial aggregate” layer that will knowingly intermix into the subgrade soils in an attempt to still maintain a design structural thickness of a road support layer

Currently, agencies such as FHWA support design methodology where contamination of a road base aggregate is addressed by requiring an additional two (2) inches of aggregate atop the design thickness needed to achieve the desired structural performance of a road. Even though there is room to improve, these “safety factors” are not questioned or critiqued, and have become commonplace in the engineering community. However, in the effort to identify more sustainable roadway design and construction, the adverse effects of this methodology should be further examined. Implementation of a well-graded aggregate base decreases a road’s ability to drain water and results in a weaker base layer, thus increasing road costs. Holistically, the net result with either inadequate approach does not satisfy the nation’s need for more resilient roads, and requires the design engineer to choose between outdated and costly conventional technologies.

A third “alternative” approach is to use a geotextile to keep the intermixing and contamination from occurring at the subgrade soil/ aggregate interface for the life of the road. Simply put, geotextile separation is defined as the introduction of a flexible, porous textile placed between dissimilar materials so that the integrity and functioning of both materials can remain intact or be improved (Koerner,1994). Geotextiles are used for a broad array of applications, but for roadway construction, geotextiles primarily enhance unpaved and paved roads when placed in between the subgrade soil and the structural aggregate base. At this location within a road’s cross section, geotextiles serve two functions:

- To act as a long-term separator of the subgrade soil from the structural aggregate, permanently keeping the aggregate uncontaminated from the likely intrusion of subgrade soil particles over time
- To act as a stabilizer, contributing to the overall structural integrity of the road.

These two functions work concurrently; hence the application becomes known as “separation/ stabilization”.

A roadway system which includes a geotextile merely for separation keeps an aggregate base material under load from being forced into the subgrade at the soil/ aggregate interface, and keeps the subgrade soils from penetrating the clean aggregate layer. The migration of subgrade soil upward into the base aggregate is dramatically increased in the presence of moisture. While more investigative work to understand the mechanisms of premature road failure is warranted in hopes of being able to utilize new forensic technologies, it is intuitive to believe that preventing the aggregate layer from subgrade soil infiltration for the design life of a road will result in a more sustainable roadway. Typical base section loss beneath a pavement is four (4) inches sometimes even in the early stages of the design life. (Jorenby & Hicks, 1985) Aggregate loss can be even more significant in an unpaved road, and more rapid when above weak soils. Analyzing geotextiles providing separation in paved and unpaved roads is very non-technical and basic, while attempts to over engineer the application has limited its implementation. A geotextile providing separation in a roadway can be seen below in Figure 1:

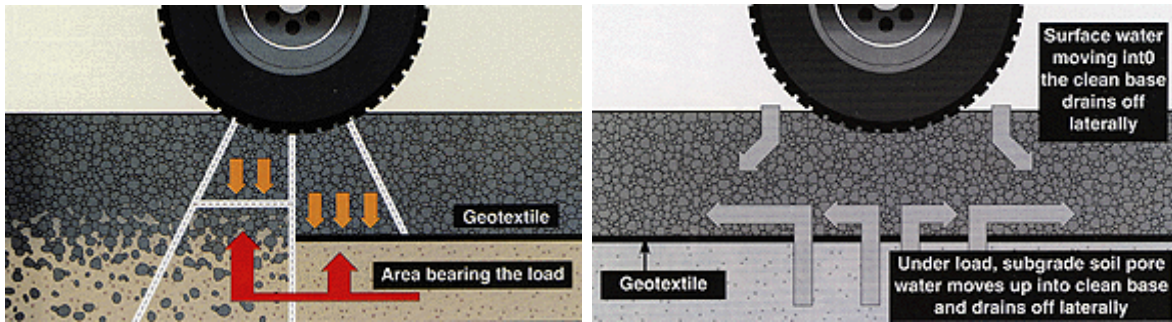


Figure 1: Geotextile placement in a roadway to provide separation and stabilization (Cyber North, 2012)

Geotextiles have functioned as separators for more than 30 years, but their implementation and acceptance is far less than the traditional approaches discussed above. A simplistic way to evaluate the cost benefit offered by a geotextile separator can be done because the cost of an installed geotextile equates to about one (1) inch of placed aggregate. Apply this rule to determine how much the traditional solutions used to prevent intermingling at the soil/aggregate interface cost and a geotextile results in at least a 50% cost savings. Another alternative view to consider is a geotextile that prevents at a minimum one (1) inch of aggregate base from being contaminated is a “break even” investment. These simple, conservative analyses do not capture all the benefits of using a geotextile, but alone justify the use of a geotextile beneath every road. Notable cost savings are also experienced after construction, specifically of unpaved roads since frequent and significant amounts of replacement aggregate are no longer needed for the duration of the road service.

An additional value-add proposition offered by geotextile separators is the potential to use a better, free draining aggregate for the structural layer of a road without fear of subgrade contamination. A more open aggregate drains faster, and is rewarded technically by often achieving twice the structural contribution per inch according to AASHTO design (AASHTO 1986 and 1993). As an aggregate base drains rapidly, there is less lingering free water to weaken the subgrade or cause freeze/ thaw cycles in extreme climates as depicted in Figure 1, right hand side.

In addition to separation, stabilization is the other significant value proposition offered by a geotextile used between the subgrade soil and the aggregate layer. Stabilization takes on more of an engineered evaluation when compared to the separation function since a composite road support system results. First, when the aggregate is compacted over the top of a geotextile for the first time, the individual stones directly above the geotextile become “seated” making impressions in the geotextile and the subgrade. This interaction locks the bottom of the aggregate into a fixed position, thus stabilizing the aggregate layer indefinitely. Secondly, the geotextile under load provides vertical confinement of the subgrade soil, making it more resistant to shear failures. It is widely proven that the incorporation of a geotextile changes the soil failure mode from local shear to general shear allowing 80% additional load before the soil’s strength is exceeded. This mechanism allows for a reduced structural section of between 15-25% over a subgrade stabilized with a geotextile, directly reducing the initial project cost of building both paved and unpaved roads. (Marienfeld, 2011) The membrane reinforcing affect makes it possible to reduce the thickness of the base course required for initial construction and is most significant when subgrade CBR values are less than 3%. (Barkdsdale,1989)

Whether evaluating the benefits provided by separation, stabilization or both, geotextiles are proven and recognized for reducing the need for several inches of aggregate required in the design of a conventional road section. Even if the decision is made to implement the traditional approach structural layer thicknesses, the incorporation of a separation/ stabilization geotextile will extend the life of a road by increasing allowable loadings, Equivalent Single Axle Loads (ESALs), by 50 to 75% (Al-Qadi, 1997) The decision should not be focused on whether or not to use a geotextile, but rather every road should incorporate a geotextile, and policy makers and engineers have to decide based on cost models, budgets, and goals when and how to reap the greatest cost benefit offered by a separation/stabilization geotextile—all savings up front to minimize construction cost, all savings through extended road life, or the commonly used method of saving just enough up front to pay for the geotextile and gaining extended road life.

To summarize, the separation/ stabilization geotextiles impact the overall approach to road design and when incorporated, they become no risk, high reward propositions because they:

- Reduce initial construction costs
- Reduce operation and maintenance costs
- Increase the lifecycle of a road by allowing additional traffic loading
- Separate aggregate from the subgrade soils

- Allow the use of free draining aggregate, for more strength and less freeze/thaw damage
- Reduce the aggregate thickness in a road by subgrade and base aggregate stabilization
- Increase subgrade soil bearing capacity; preventing vertical deformation of the road
- Distribute stress across a wider area limiting local failures which propagate to larger failures

2. FACT OR FICTION: THE TRUTH BEHIND THE SEPARATION/ STABILIZATION GEOTEXTILE

2.1 Using Geotextiles in a Road's Cross Section is a New Concept and a New Technology.

FICTION. The truth of the matter is that geotextiles used in separation/ stabilization applications started in the 1920s in the United States, and significant advancements have been made since. Nevertheless, even with advancement and now a better understanding as to the cost benefits that the technology provides, geotextile usage still has significant upside potential for increased usage. Geotextiles have been repeatedly proven to work, and numerous laboratory and field tests have been conducted and have documented positive results. Below is a list of just a few notable studies available:

Table 1. A list of references and a short summary of their contribution to the discussion of the benefits of incorporating a separation/stabilization geotextile (Narejo, 2005).

Reference	Type of Study	Results of Study
Jorenby & Hicks, 1985	Field Tests	Review of several pavements showed an average base aggregate loss of four inches due to subgrade soil upward migration.
US Army Corps, 1999	Field Tests	Separation geotextiles were found to be necessary to prevent oozing of fine subgrade soil into coarse base course.
Tsai, et. al., 1993	Field Tests	Control sections using no geotextiles were found to have significant fines in base course, whereas the sections with geotextiles were found to have significantly less fines.
Metcalf, et. al., 1995	Full scale projects	Twenty two pavements with geotextile separators were evaluated. Geotextiles were found to be successful in providing separation function at all of the sites.
Baldwin & Long, 1987	Full scale projects	A three year study found that free draining base courses obtained with geotextiles are effective in preventing water build up in pavements.
DeBerardino & Baldwin, 1996	Full scale project	Borings drilled through pavements with geotextiles, after thirteen years found no migration of fines.
Leu & Tasa, 2001	Full scale projects	Geotextiles were found to be successful in preventing contamination of the base course. At the end of ten year period, sections with geotextiles were found to have fifty percent less cracking than those without.
Guram, et. al., 1994	Field tests	Nine years later, separation geotextile and six inches of base aggregate were found to provide performance equivalent to 24 inches of lime treated subgrade, with the same pavement section at a much lower cost.
Faure & El Amir, 1982	Laboratory tests	Geotextiles were found to be successful in preventing fouling of aggregate by fines.
AL-Qadi, et. al, 1997	Laboratory tests	Geotextiles were found to be successful in preventing fouling of aggregate by fines.
Glynn & Cochrane, 1987	Laboratory tests	Geotextiles were found to be successful in preventing fouling of aggregate by fines.
DeBerardino & Hawkins, 1994	Full scale projects	After a period of twenty years, geotextile samples were dug. Geotextiles were found to adequately perform the separation function.
Bonaparte, et. al., 1988	Full scale projects	Geotextile excavated from seven sites after 1 to 12 years of burial proved that geotextiles provide adequate separation.

The studies cited above demonstrate the proven performance of separation/ stabilization geotextiles in actual applications. Additional information will be presented later in this paper when focus is on the separation/ stabilization application to lower initial construction costs and/or the lifecycle cost of a roadway.

2.2 Separation/ Stabilization Geotextiles Can Cause a Problem in a Road.

FICTION. Consider a road without a geotextile. It only takes about 20% by weight of subgrade soil mixed into the aggregate base to reduce the bearing capacity of the aggregate base to that of the subgrade soil.(Yoder, 1959) Thus, a road without a geotextile is at high risk to the mixing of aggregate and subgrade compromising the structural integrity of the road. There is no downside risk to using a geotextile, which makes it easy to implement in a road versus choosing not to use one. Even if the geotextile selected is not optimal for installation survivability or drainage, the geotextile will still function

as a separator maintaining the integrity of the initial road design, automatically extending the service life of a road. Plus, using geotextiles during construction promotes short-term separation allowing subgrade soils to consolidate. Studies by Austin and Coleman have shown that this short-term gain offered by a geotextile is more critical to unpaved roads rather than their long-term performance because of the subsequent strength gain of subgrade soils when a geotextile provides separation. (Austin and Coleman, 1993)

2.3 Understanding Which Geotextiles to Use for a Roadway Application is Simple and Geotextiles are Easy to Specify.

FACT. Specifying geotextiles in transportation projects is as simple as understanding their function, how they will be installed, and understanding the environment into which they will be installed. There are several methodologies and guidelines available for a designer to follow in order to include geotextiles in design, but the two specifications available from reputable major organizations, AASHTO M288-06 and FHWA FP-03, are invaluable resources and a design engineer needs to look no further. The performance properties needed from the geotextile, for most applications, are not complicated, and the user of the AASHTO M288-06 specification will make excellent geotextile choices based on knowledge of site-specific installation stresses and soil hydraulic properties for the project application.

AASHTO M288-06 categorizes the survivability of the geotextile into one of three different classes based on the intensity of installation conditions: Class 1 being the most severe and Class 3 being the least severe. The potential survivability of the geotextile within each class is determined by a standard set of properties generated from ASTM test methods. These properties are Grab Tensile Strength, Trapezoidal Tear Strength, CBR Puncture Strength, and Ultraviolet Stability. Why is there so much focus on the installation stresses of a geotextile? Installation is the point in a geotextile's design life that it will be subjected to the greatest stress, and maintaining the integrity of the geotextile through the installation process will ensure it performs as designed. In addition to evaluating the survivability of the geotextile, hydraulic properties are included based on the site soil conditions or percent fines. The properties associated with soil conditions are Permittivity and Apparent Opening Size. From a cost standpoint, there is actually very little difference between the lowest and the highest survivability class AASHTO recommended geotextile, so a default to Class 1 is often a reasonable approach.

To become an expert on the subject matter, understand the surface friction required and the CBR values of the soils present in the application. For example, the higher the surface friction desired, the more appropriate a nonwoven geotextile becomes. If lower CBR value soils are present, then a woven geotextile is more likely to provide the strength needed at lower strains to bridge over softer soils. But again, you cannot go wrong using AASHTO M288-06 and remember, even if the most optimal geotextile is not selected, there are no downside risks.

2.4 Geotextiles are Sensible Solutions to Lower Initial Project Costs and Maintenance.

FACT. From a cost-savings perspective, geotextiles make more sense now than they historically ever have, but still remain under-utilized. Their intrinsic value to supporting a more resilient national infrastructure is priceless. Diminishing transportation operational budgets and rising raw material costs have prompted owners and DOT officials to find other means and methods of roadway construction. Geotextiles provide solutions through short term and long term benefits.

The following is a hypothetical scenario to analyze the use of geotextiles in new road construction to reduce initial costs. For example, a high-level exploration of a state's DOT budget examines how geotextiles could be implemented to come in under budget while still improving the roadway system. Figure 2 below depicts two theoretical road cross sections equivalent in performance a) without a geotextile and b) with a geotextile. For comparison ease, the traditional method represents the average road cross section of all new roads that this state's DOT has budgeted to construct in 2012.

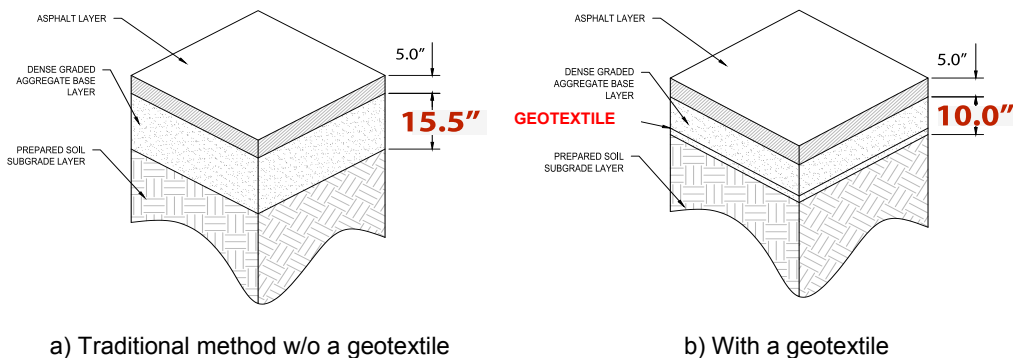


Figure 2: The differences in road cross sections w/o and with a separation/ stabilization geotextile

Comparing the construction costs associated with each, the traditional method utilizes 15.5" of a dense aggregate base which historically costs the DOT per 1" thickness \$1.64/ square yard. The geotextile costs on average about \$1.00/ square yard. Using this information, the state's DOT 2012 road budget can now be analyzed.

Table 2: Theoretical State Department of Transportation 2012 Road Budget and Volume

Budget Information	
Total Road Budget	\$1.817B
Spend Allocated to New Roads	\$732M
Estimated Total Lane Miles Built Annually	1600
Relate Lane Miles to Square Yards	
Lane Width (ft)	12
Surface Area per Lane Mile (ft ²)	63360
Total Square Yards/ Lane Mile	7040
Total Square Yards in the Budget	11.26MM
Savings Using a Geotextile (Figure 3)	
Amount of aggregate the geotextile displaces	5.5 inches
Cost for 1" thickness of dense aggregate	\$1.64/ square yard
Cost for 5.5" thickness of dense aggregate	\$9.02/ square yard
Cost for a geotextile	\$1.00/ square yard
Savings (per square yard)	\$8.02/ square yard
POTENTIAL BUDGET SAVINGS WITH A GEOTEXTILE	\$90.31MM

In this particular example, the geotextile displaces 5.5" of aggregate in the new road section, saving the DOT a minimum of \$90.31MM, or 12% of the total dollars allocated towards new road construction. Since geotextiles can reduce a minimum of 20 to 35 percent of the original required thickness of structural layers in a road and local raw material costs can fluctuate, the overall savings may vary. Yet, this example generally shows the potential for upfront cost savings provided by incorporating geotextiles and reducing other materials needed to build new roads.

Recall from earlier discussion that approximately one (1) inch of aggregate is equal to the cost of a geotextile covering the same surface area and that conventional FHWA design methodologies suggest a minimum of an additional two (2) inches of sacrificial aggregate be used to design the appropriate aggregate base thickness. We are seeing developing nations build their first real infrastructure and doing it correctly using geotextiles as part of state-of-the-art design. So, without being jaded by traditional, outdated design thinking, their infrastructure will be better built and require less maintenance than ours. The following chart demonstrates the geotextile value proposition compared to aggregate resources that are typically wasted.

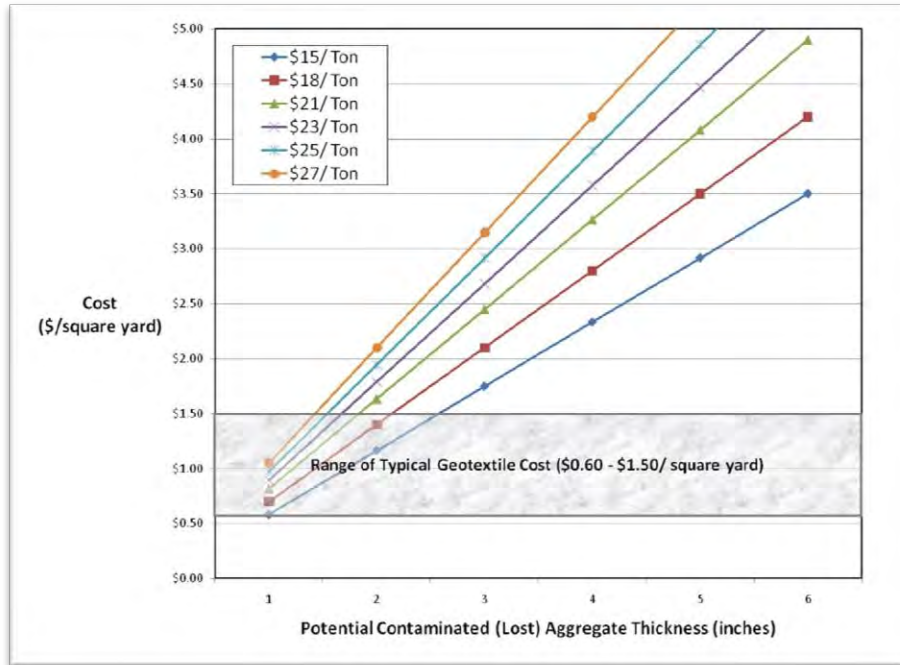


Figure 3: Comparison of cost of geotextile to the cost of contaminated, wasted base aggregate

The use of separation/ stabilization geotextiles in construction greatly reduces the need for future maintenance, especially for the municipalities with unpaved roads losing aggregate to subgrade soils every year. If all roads were built over geotextiles, maintenance budget spend today would be re-allocated and more tax dollars could go towards new or improved roads.

2.5 Geotextiles are Difficult to Install.

FICTION. Proper installation of a separation/ stabilization geotextile can be perceived as intimidating. Yet in reality, the installation is quite simple and may easily be explained to inexperienced laborers on the jobsite. The chief concerns surrounding installation include potential abuse of the fabric during deployment, and proper repair of the material if damaged. These concerns can be mitigated through proper training and common sense. Installation considerations and guidelines that address items such as overlap widths, direction of overlap, direction of application, and others are well established and easily obtained for any project. Detailed installation guidelines are available from product manufacturers for any geotextile application.

3. BARRIERS TO USE

If geotextiles are time proven, result in less expensive road construction when compared to traditional construction methodologies, contribute to longer lasting roads, are easy to design and are easy to install then why doesn't every road constructed in the United States utilize a geotextile for separation/ stabilization? One possibility is the lack of understanding of the economic benefit gained through such a simple technology. Another is that the technology is forgotten, undervalued, or overlooked by the engineering design community. Since the mid-1990's, manufacturers of geotextiles have focused promotional efforts towards other products, believing that there is little room for differentiation in this specific application. Conversely, the challenge(s) an engineer faces when designing a sustainable road are widespread, understood, easily defined, and must be compensated for in every road built today (yet still, they are not using a geotextile as a separator). Several barriers to use (explored below) were discussion points presented at GeoAmericas 2008. (Marienfeld, 2008) Since then, these barriers have compounded with deterioration of global economic conditions.

3.1 Lack of Understanding of the Root Causes of Road Failures

Agencies and owners generally fail to pursue the root causes of failure, such as; base aggregate contamination by subgrade soil intrusion, damage caused by the presence of water, and the loss of structural layer strengths and effective thicknesses. These discoveries are easily obtained by quick forensic analyses of failed roads before they are reconstructed. Unfortunately, the designer rarely sees the failure of their designs due to the loss of integrity of the originally

designed and installed structural layers. If they simply communicated with the people responsible for the maintenance and reconstruction of their roads, they would learn the root causes of why their designs failed and then simple inclusion of an inexpensive separation/stabilization would then seem absolutely necessary.

3.2 Comfort and Tendencies in Using the Traditional Technologies Outweigh the Rewards for Thinking Outside the Box.

The roadway design and construction industry of today does not readily reward those professionals that employ creative methodologies or push to implement innovative and cost-effective technologies. The litigious nature of the industry also makes the reduction of personal liability and risk a significant objective in the practice of engineering. Although using geotextiles in the design of roadways is proven and risk-averse, any deviation from conventional approaches is often met with hesitation. It is therefore critical to provide more education and promote the use of geotextile technology as a true solution to the crisis facing our national transportation infrastructure system. Focusing on lifecycle cost reduction and sustainable construction techniques must be a part of the next generation of engineering education.

3.3 There is a Mixed Message in the Industry about the Performance of Geotextiles.

Engineers that embrace innovation are unfortunately faced with the daunting task of deciphering mixed messages from the industry about geotextile performance. Manufacturers of geotextiles, contractors, owners, end users, and other design engineers all offer independent and often conflicting views of successes and failures when using geotextiles in road construction. In particular, a great deal of promotional effort is put into the marketing of the higher profit margin geogrids as superior products to geotextiles. Manufacturers often recommend geogrids for use in stabilization applications without an underlying geotextile, in an effort to minimize overall system costs. Geogrid market literature suggests separation and filtration is not generally needed, but the filter criteria they reference is not applicable to the dynamic pumping of subgrade soil fines into an aggregate base. Without an underlying geotextile, the geogrid cannot provide any separation function, and will lead to eventual contamination and intermixing of subgrade soils into the aggregate base above. (Al-Qadi, 2007). Testimonies of geotextile performance by entities that support competing technologies (e.g., manufacturers with incentives to promote alternative products, contractors that operate quarries that supply aggregate) can be inaccurate and misleading if the product was not installed properly. Many times owners of roadways and governing agencies don't understand the true performance of a road or the life cycle cost comparison with and without a geotextile, and therefore do not mandate the use of geotextile technology, even when there was a desire to implement change at the design level. Finally, engineers typically seek guidance from engineers with knowledge and experience in specific technologies. Equipping the engineering community with factual information and results of laboratory and field performance is critical to propagating the value-add message of geotextile technology success. All the competing product clutter can be bypassed simply by using the AASHTO M 288 national guideline specifications.

3.4 Lack of Supportive Policies Exists for Using Geotextiles.

While some agencies do provide guidance for using geotextiles to enhance road design, to the engineer who wishes to implement the technology, there are extremely few policies in existence that mandate the use of the technology in a road. The lack of supportive policies can be directly linked to the lack of data available that clearly defines the cost effectiveness of geotextiles in road construction for the entire life cycle of a road. Without this type of cost justification, agencies find it difficult to put policies in place that mandate or support geotextile usage. The development of a model to substantiate geotextile life cycle cost benefits for use as separators and stabilizers under roadways is greatly needed. Performance testing is not needed, since the technical merits of the system are widely proven. Existing studies and data are very good, just somewhat dated and not fresh in the mind of designers.

3.5 Geotextiles Don't Find Their Way from Design to Construction.

Contractors today find themselves fiercely competing for fewer projects, with more jobs having selection criteria based on low-bid proposals. Thus, many contractors find themselves struggling to obtain work and submit bids at break-even costs to preserve their businesses. In an effort to cut costs after winning a bid, contractors will often attempt to identify removal of items that are easier to justify than others. Unfortunately, geotextiles have become targeted items for removal due to the lack of understanding of its function and purpose. This bidding strategy for a contractor is high risk, but owners and agencies find themselves also limited on funds and are also often motivated to negotiate work after a bid that results in shared upfront cost reductions with the contractor.

Unfortunately, in this circumstance both parties are only thinking about short term gains, and many times the original intent of the design is lost. The owner or agency may not fully understand the value proposition of a geotextile, nor the intent of the design due to lack of education or exposure to the technology. Better communication with all stakeholders must be achieved at multiple levels, which results in knowledgeable agencies letting contracts to informed contractors. This is a key element in furthering sustainable infrastructure improvement.

3.6 Taxpayers Are Not Informed Enough to Demand Technologies that Result in Better, More Cost-Effective Roadways.

The responsibility for education about geotextiles and their use in roads to enhance road performance falls to the leading manufacturers within the industry. In recent years, manufacturers have placed too much focus on promoting specific product characteristics. Less emphasis should have been placed on the nuances of specific geotextile performance property discrepancies. More time should have been spent making the general public aware of the basics that the technology can do to make our nation’s infrastructure more sustainable. Geotextile education should be available through all channels within our society, with focus on college level education so the generic technology implementation becomes faster and easier into the future. Manufacturers have always directed marketing efforts at engineers, but frustration is moving them to approach transportation budget administrators.

4. RECENT GOVERNMENT DEVELOPMENTS AND TRENDS TO USE MORE GEOTEXTILES IN ROADWAYS

Below in Figure 4 is an excerpt of a letter to members of the Geosynthetics Materials Association (GMA) from Andrew Aho, managing director, explaining recent actions that our nation has taken towards making our roads more resilient. By suggesting geotextile usage is mandatory the net result will be responsible transportation spending and enhanced road performance:

Dear GMA Member,

Transportation Bill

On Friday, July 6, 2012, President Barack Obama signed into law H.R. 4348, the “Moving Ahead for Progress in the 21st Century Act” (MAP-21), a two-year, \$105 billion surface transportation bill that reauthorizes taxes that support the Highway Trust Fund through Sept. 30, 2016, and the authority to make expenditures from that Fund through Sept. 30, 2014. This law will provide states and the construction industry the needed funding certainty to continue work on existing projects and appropriately plan for future projects. States and the construction industry have been operating on nine short-term extensions of the surface transportation authorization since September 2009.

Fiscal Year 2013 Transportation, Housing and Urban Development Appropriations/Funding Bill (THUD).

On June 29, 2012, the U.S. House passed the THUD appropriations bill that provides funding to the U.S. Department of Transportation. From our perspective, the good news is that U.S. Rep. Jack Kingston (R-Ga.) and his staff worked with GMA to craft report language for the this bill that highlights the cost saving and environmental benefits of geosynthetics as well as the upcoming Government Accountability Office (GAO) study on innovative materials (see “GAO Study” below). The full Senate now needs to pass its THUD funding bill to move the appropriations process along. Directive language to the Federal Highway Administration (FHWA) in the bill reads:

Geosynthetics—The Committee directs the FHWA to continue assessing the use of geosynthetics in highway and civil infrastructure applications, especially potential cost savings and environmental benefits. The Committee also encourages FHWA to review and consider the recommendations in GAO’s upcoming report on geosynthetics and the associated life-cycle costs of incorporating innovative materials in pavement.

Figure 4: Letter excerpts from Andrew Aho of GMA to its members summarizing government interest in geotextile implementation (GMA, 2012).

These actions taken by the GMA advocating a higher degree of incorporation of geotextiles into roadways proves that the government is ready to listen. As discussed earlier, there is a defined need and high level of concern across the country when it comes to our aging infrastructure. In October 2011, GMA announced that two members of Congress sent a letter to the U.S. Government Accountability Office (GAO), requesting a study of geosynthetic materials in roadway systems. The coauthors of the letter were Rep. John Duncan (R-Tenn.) and Rep. Frank LoBiondo (R-N.J.), both members of the House Transportation and Infrastructure Committee. Rep. Duncan also serves as chairman of the Subcommittee on Highways and Transit, and Rep. LoBiondo serves as chairman of the Subcommittee on Coast Guard and Maritime Transportation. GMA has worked with GAO and Transportation Committee staff members to provide access to technical data and studies on the use of geosynthetics in transportation applications. The GAO was expected to complete the study by September 21, 2012 however the report back to Congress has been delayed. Preliminary speculation is positive; however more details will be available in 2013.

5. JUSTIFICATION TO USE SEPARATION/ STABILIZATION GEOTEXTILES IN ROADWAYS

The objective of this paper is to provide a reference tool for engineers, owners, and other stakeholders that desire the support for justifying the need to advocate geotextiles use in roadway applications. The material herein is not intended to provide in-depth technical analysis or design methodology, but rather to present a clear and precise message regarding the benefit of geotextile separation/ stabilization. Fundamental advantages exist when incorporating geotextiles into road design, and have become even more critical given the current climate and condition of the nation's economy and infrastructure, coupled with the rising cost of conventional roadway construction materials. A renewed emphasis must be placed on understanding geotextiles for use in roadway separation/ stabilization.

Looking ahead, the United States must find innovative ways to build roadways better, more durable, and at less cost. Geotextiles are tested and proven solutions that design engineers can rely on for better roads. In our search to develop more sound and sustainable infrastructure for the next generation, we must re-evaluate engineering practices and embrace change. Although the value proposition of a geotextile functioning as a separator and stabilizer in paved and unpaved roads is not new, reinforcement of the basic principles included herein provides a compelling reason to transition from outdated conventional approaches to sensible ones.

It is expected that the use of geotextiles will become increasingly routine, and that geotextiles will be the standard technology of choice for building better roads of the future. The wiser, most cost-conscious transportation agencies are already incorporating geotextiles under all roads as standard practice. Forward-thinking local agencies are also mandating the use of geotextiles under roads installed by private developers, so that eventual public operation and maintenance will require reduced costs. Yet more support in educating and highlighting the cost justification for separation/stabilization geotextiles is greatly needed, and will only result in a better spend of resources and money for a sustainable future.

REFERENCES

- Aho, Andrew. "Good News From Washington for Geosynthetics in the U.S. Transportation Market", Letter to GMA Members, Geosynthetics Materials Association, Roseville, Minn., Last Accessed August, 2012. <<http://geosyntheticsmagazine.com/posts/blog/1157>>
- Al-Qadi, I.L., Brandon, T.L., Bhutta, S.A., Lacina, B.A., "Geosynthetic Stabilized Flexible Pavements", Geosynthetics '97, pp. 647-661.
- American Association of State Highway and Transportation Officials AASHTO. *Guide for Design of Pavement Structures*. AASHTO, Washington, DC, 2006.
- American Association of State Highway and Transportation Officials AASHTO. *Guide for Design of Pavement Structures*. AASHTO, Washington, DC, 1986.
- Austin, D. N., and D. M. Coleman. "A Field Evaluation of Geosynthetic-Reinforced Haul Roads over Soft Foundation Soils", *Proceedings of Geosynthetic Conference*, Vancouver, BC, Canada. March 30- April 1, 1993, pp. 65-80.
- Christopher, B. R. and R.D Holtz. (1985). *Geotextile Engineering Manual*. Report FHWA-TS86/203 STS Consultants, Ltd, Northbrook, IL, for Federal Highway Administration, Washington, D.C.
- Due North Resources, "Geotextiles Can be Worth Their Cost in Aggregate". Last accessed August, 2012. <<http://www.cyber-north.com/geotextiles.html>>.
- Jorenby, N.B., & Hicks, R.G., "Base Course Contamination Limits", Transportation Research Record 1095, 1985.
- Koerner, R.M.. *Designing with Geosynthetics*. 4th Edition, Prentice Hall, 1998.
- Koerner, R. M., and G. R. Koerner. *Separation: Perhaps the Most Underestimated Geotextile Function*. Geotechnical Fabrics Report, Industrial Fabrics Association International, St. Paul, MN, 1994, pp. 4-10.
- Marienfild, M.L., "Separation Stabilization Geotextiles – Saving Transportation Agencies \$500 Million Per Year and Rising", *Proceedings of GeoAmericas 2008*, Cancun, Mexico, 2008.
- Marienfild, M.L., "Geotextiles: Sustainable building products that make roads last longer and conserve construction materials", *Proceedings of Geosynthetics Middle East 2011*, Hotel Park Rotana, Abu Dhabi, UAE, 2011.
- Narejo, D.N., Marienfild, M., Hawkins, W., Lacina, B.; "Ensuring Long Term Pavement Performance", *GFR Magazine*, 2005.
- Yoder, E.J. (1959). *Principles of Pavement Design*. John Wiley and Sons, Inc. New York. 21-32.

Settlement-compensating Connection of Geomembrane to Pile Caps for Structures Developed on Old Landfills

J. Weckmann, P.E., Tetra Tech, Inc., USA
M. Alvarran, The Barber-Webb Company, Inc. USA
J. Youngblood, GSE Lining Technology, Inc. USA
M. Czerniak, P.E., Tetra Tech BAS, Inc. USA

ABSTRACT

This paper presents the development and design of a settlement-compensating geomembrane connection between a non-settling fixed structure built on a landfill and the surrounding landfill cap geomembrane placed on the settling landfill surface. This paper addresses the design concept, design development process, full size prototype testing, field testing, final design and specifications, fabrication and installation quality assurance plans, and fabrication and installation experience.

1. INTRODUCTION

The former Cal Compact Landfill occupies 64 hectares in the City of Carson, California, of which approximately 55 hectares were used mainly for disposal of municipal solid waste and some hazardous waste from 1959 through 1964, with waste thickness up to 20 m. The site is being developed into a commercial/residential mixed use complex known as "The Boulevards at South Bay." All buildings will be on pile-supported structural slabs to eliminate the effect of settlement. When completed, there will likely be over 8,000 piles supporting over 140,000 m² of structural slab.

As part of the remedial systems at the site, a landfill cap will cover all waste areas, including under the pile-supported structural slabs consisting of, in most areas, a 1.5 mm linear low density polyethylene (LLDPE) geomembrane with 405 g/m² geotextile above and below. The approved remediation plan (DTSC 1995 and Brown & Root 1995) includes a requirement that the landfill cap be sealed to the piles and that a settlement-compensating connection be provided between the non-settling pile-supported structure and the landfill cap. A system was developed that includes a mechanical connection of the landfill cap geomembrane to the pile caps with an unfolding "boot" that allows slack for settlement compensation without relying solely on the elongation properties of the geomembrane material. The system is comprised of two parts: (a) an embedment "ring" that is installed into the pile cap at the time the pile cap concrete is placed, and (b) a boot made of LLDPE geomembrane that is connected to the pile cap at the ring and connected to the surrounding landfill cap geomembrane. Figure 1 shows how the landfill cap system transitions from the open area outside the buildings to under the building slab where the connection to the pile caps is made. Figure 2 shows a plan view of the boot final design.

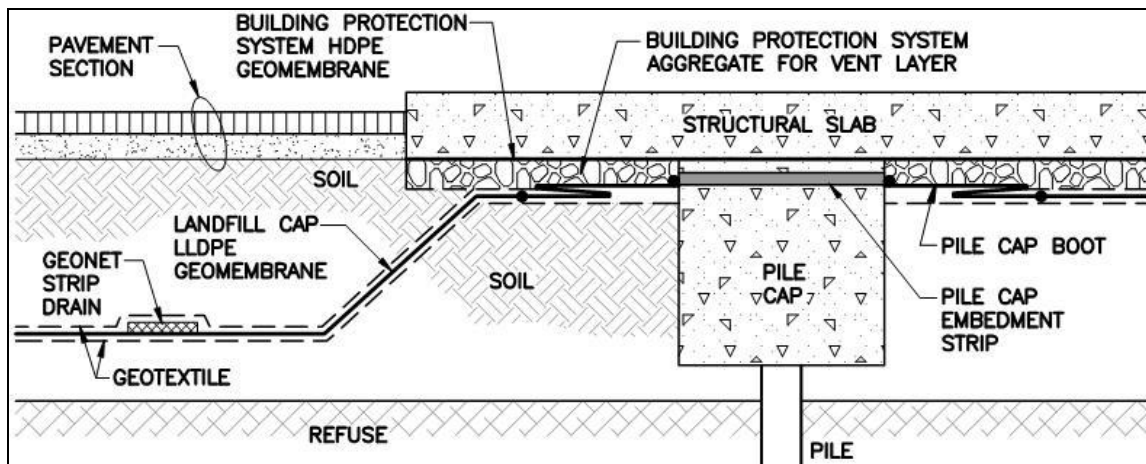


Figure 1: Boot-Ring settlement compensation system for a landfill cap under pile-supported structures

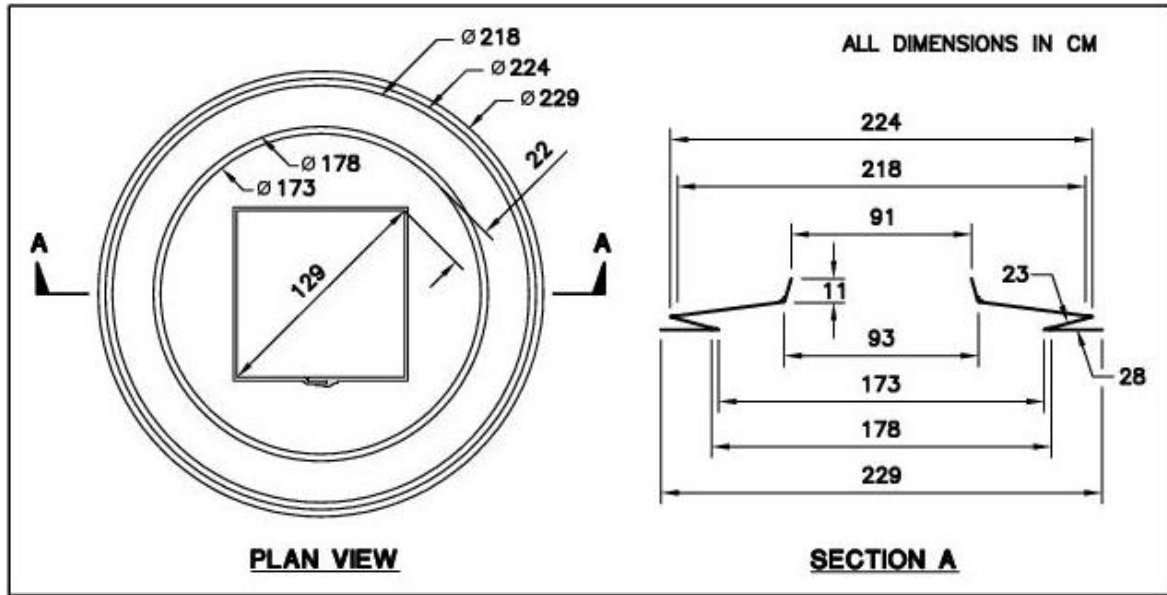


Figure 2: Final design of the single flap pile cap boot

2. DESIGN DEVELOPMENT

2.1 Design Goals

The design goals for the boot-ring system (Tetra Tech 2008) were:

- Develop a boot configuration that provided slack upon deployment to avoid excessive tension in the material and the welds and to avoid relying solely on the elongation properties of LLDPE.
- Develop a method (i.e., the embedment ring) by which the boot could be securely attached to the pile cap and form a reliable seal of the landfill cap geomembrane to the pile cap.
- Demonstrate that the boot-ring system would function reliably under building slabs to meet the design settlement.
- Develop rigorous specifications and quality assurance plans for fabrication and installation of the boot-ring system.
- Develop the boot and ring designs so that they could be fabricated offsite in a controlled and documented manner and be installed in the field as easily possible.

2.2 Design Settlement

Potential remaining settlement of the landfill was estimated (KFM Geoscience 2007) using the method proposed by Huitric (1981), and mapped to the site to illustrate the estimated settlement at all site locations, reflecting that the waste thickness varies around the site. The waste has been consolidating at the site since 1959. The maximum remaining settlement at the site was estimated to be 17 cm at the location of deepest waste (20 m). In the same location, the project Geotechnical Engineer of Record (Leighton Consulting 2008) specified a design settlement of 53 cm, thus incorporating a factor of safety of >3.

2.3 Early Concepts – Basic Geometry of the Boot

Early in the design process, a series of small models were constructed by The Barber-Webb Company to qualitatively explore the three-dimensional nature of how a boot of various shapes would function relative to square and round pile caps, and to explore relative dimensions, such as how large must the boot be relative to the pile cap to deliver satisfactory performance for the needed amount of settlement compensation. These models were constructed of wood, paper, and compressible foam. Settlement action was simulated by pressing down on a wood base, compressing the underlying foam, relative to the non-settling wood “pile cap.” Three configurations were investigated:

- a) Round boot on round pile cap
- b) Square boot on square pile cap

c) Round boot on square pile cap

The round boot on a round pile cap behaved as expected, with the boot opening in pure “accordion” fashion with no three-dimensional buckling of the boot geomembrane. However, the extra cost and complication of constructing 8000 round pile caps in the field, along with the greater difficulty and expense of a round embedment ring was judged to be countering factors to selecting this configuration.

The square boot on a square pile cap also opened in an accordion-like manner, but only to the an extent limited by the widths of the flaps of the boot, after which it was clear that the corners of square boots would experience high stresses on the welds. The square boot would also be difficult to fabricate and would need to be much larger than a round boot to achieve the same settlement compensation.

The round boot on a square pile cap allowed the use of standard square pile caps, square embedment rings, and provided satisfactory boot performance. As the boot opened with settlement, some three-dimensional distortion was induced, warping the boot surface, but the round shape served to allow for the distortion to be easily distributed and not concentrated. Thus, our fundamental concept was defined.

2.4 Full Size Boot Prototype Model and Testing

Going forward from the results of the small scale model that defined the general geometry of the pile cap boot, a series of full-scale prototype model tests were performed by GSE Lining Technology:

- Round boots were fabricated with 1.5 mm LLDPE geomembrane with an outer diameter of 2.3 m.
- A “single flap” boot and a “double flap” boot were fabricated and tested to be certain that the full range of the design settlement would be accommodated in the testing. The double flap boot incorporates more slack for settlement compensation.
- The top of the boot was secured to a simulated 0.9 m square pile cap (made of plywood).
- The pile cap and boot were centered in a 4.3 m square wooden box that would allow up to 30 cm of gravel to be placed over the boot (see Figures 3 and 4). Gravel was 1 cm rounded pea gravel.
- An electric jack was placed under the pile cap, allowing it to be raised in a controlled manner up to 71 cm.
- The box was lined with 1.5 mm LLDPE and the base of the boot was welded to the underlying geomembrane.
- The displacement of the pile cap relative to the base of the box (the settlement) was measured by a board calibrated in inches that was placed through the pile cap and visible in photographs and videos of the test.

Many tests of a variety of conditions were performed (Tetra Tech 2008), including redundancy tests, generally as follows:

- The functionality of the boots upon settlement was tested without the layer of gravel to see if the behavior of the boot at full size is the same as predicted in the small models. The full size boots were observed to behave in the same manner as in the small model.
- The functionality of the boots upon settlement was tested with the layer of gravel to see if the boots opened and provided slack for settlement by displacing the gravel. Upon settlement, the boot displaced the gravel to the side, leaving the gravel piled near in a circle surrounding the pile cap (Figures 5 and 6).
- The integrity of the boot extrusion welds was tested for leaks after deployment through the gravel layer. This was done with a blower and smoke generator to provide pressurized smoke into the boot through a sealed pile cap. In all cases, no leaks in the boots were observed. In all cases, the smoke exited the model from under the bottom geomembrane and was observed at the bottom and outside edge of the box.
- The boots were subjected to endurance tests without the gravel layer through 100 cycles of opening and closing, followed by a smoke test to confirm seam integrity. No boot failure occurred.
- Seam strength tests – upon completion of the tests, coupons were cut through the seams of the boots and tested for peel strength per ASTM D-6392. The extrusion welds used to fabricate the boot are subject to peel action upon deployment. The average peel seal strength after boot testing was 402 N/25mm, which exceeds the minimum of 290 N/25mm recommended by GRI-GM19 (2011) for extrusion welds in 1.5 mm LLDPE.
- Material tensile strength and elongation to break – upon completion of the tests, coupons were cut through the boot away from the seams and tested for tensile strength per ASTM D-6693. This was done to confirm that the material used for the boot met standard manufacturing specifications and had not been affected by the testing. As the boot deploys, it was observed that the material is subject to tensile forces as the boot pulls out from the gravel layer and displaces the gravel to the side.



Figure 3 – Prototype boot in test box without gravel layer



Figure 4 – Prototype boot in test box with 30 cm gravel layer



Figure 5 – Typical behavior of boot displacing 30 cm gravel layer upon differential settlement of 15 cm (approximately the maximum estimated remaining settlement of 17 cm). Dashed line added to show approximate location of base of cone of displaced gravel.

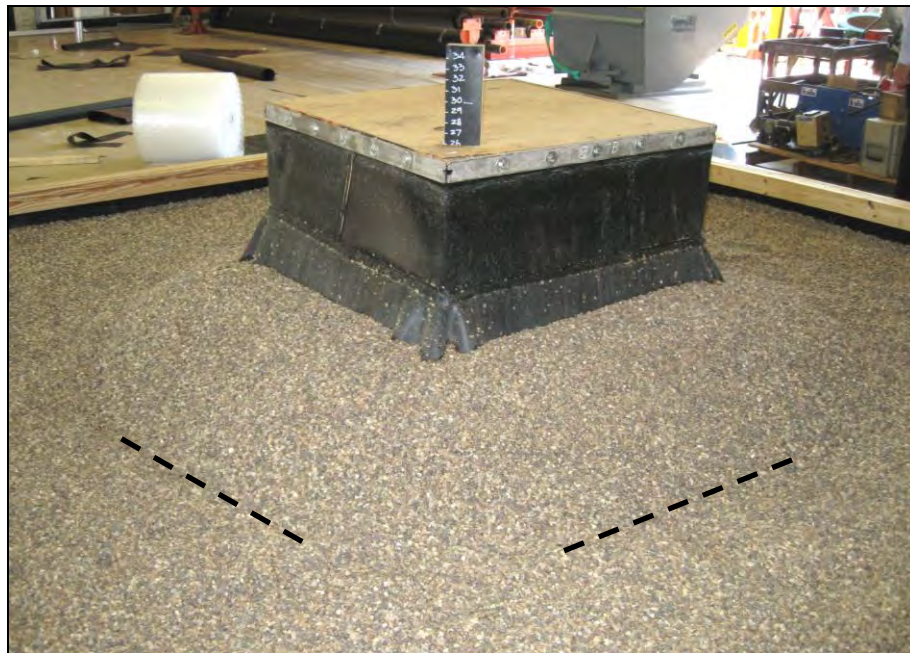


Figure 6 – Typical behavior of boot displacing 30 cm gravel layer upon differential settlement of 66 cm (exceeding the Design Settlement of 53 cm, which includes a factor of safety >3) Dashed line added to show approximate location of base of cone of displaced gravel.

2.5 Embedment Ring Development and Testing

The criteria for the development of the embedment ring in the pile cap to which the boot is welded were:

- The weld between the boot and the ring must provide a leak-proof seal.

- The extruded shape/profile of the ring material must provide a high pullout strength.
- The dimensions of the extruded shape/profile must be compatible with the structural design of the pile cap and anticipated location of attachment in the pile cap. Clearance from the reinforcing steel in the pile cap and distance from the edges of pile cap to the embedment ring were coordinated with the structural engineer.
- The extruded shape must be able to be reliably welded with a high production fabrication method into a square shape with strong welds to form a square ring.
- The ring must be easily installed into the pile cap forms by a concrete contractor.

Several manufactured embedment strips were evaluated and T-Lock material provided by EnviroCon Systems was selected (Tetra Tech 2010a). Pullout tests were conducted (TRI/Environmental 2009) to failure with forces applied to the embedment strip both perpendicular to the face of the pile cap (direct pull out) and parallel to the face of the pile cap (shear). 27.6 MPa concrete was used. In all tests, the failure occurred through the concrete around the embedment strip and not through the embedment strip itself.

2.6 Field Tests

Four test piles that were installed for geotechnical evaluation were also used to test and refine all steps needed from the time a pile is placed through the installation of the boot on the pile cap (Tetra Tech 2010b), including:

- Excavation around the pile for the pile cap, which may involve excavation and relocation of waste.
- Forming the pile cap, some below grade in a neat-cut excavation and some above grade with lumber. The height of the above-grade form corresponds to the thickness of the BPS aggregate vent layer shown in Figure 1. The required thickness of the aggregate layer was determined by the membrane protection needed to accommodate the method and equipment used to place and spread the aggregate in a thin layer over the membrane.
- Location of the embedment ring in the form (Figure 7), as previously coordinated with the structural engineer.
- Embedment rings of slightly varying size were tested to determine best fit and ease of installation.
- Methods of securing the embedment ring into the form that would provide a tight and unmovable connection to the pile cap form during concrete pouring and vibration without damage to the ring, and for ease of installation. Also of interest was minimizing the amount of concrete cream that worked into the space between the form and the embedment ring. That material must be removed in preparation for the installation of the boot.
- Placing concrete into the form and vibrating around the reinforcing steel and embedment strip.
- Stripping the forms without damage to the embedment strip, and cleaning and preparing the embedment strip for boot installation. Figure 8 shows the embedment strip in the finished pile cap.
- Placement of the prefabricated boots over the pile cap and protruding rebar, as previously coordinated with the structural engineer. Different neck designs of the boot were tested to determine best fit and ease of installation.
- Welding the boot neck to the embedment ring per the specifications. These field tests were done on test piles, so no surrounding landfill cap geomembrane was installed, and therefore the boots were not welded at the bottom for this test.

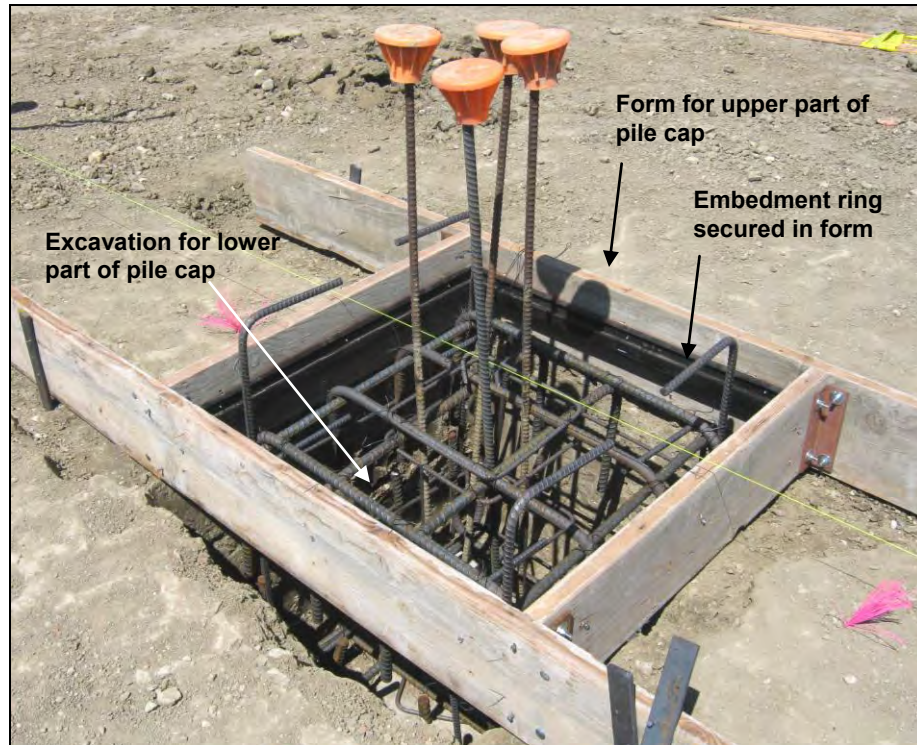


Figure 7: Embedment ring installed in pile Cap form

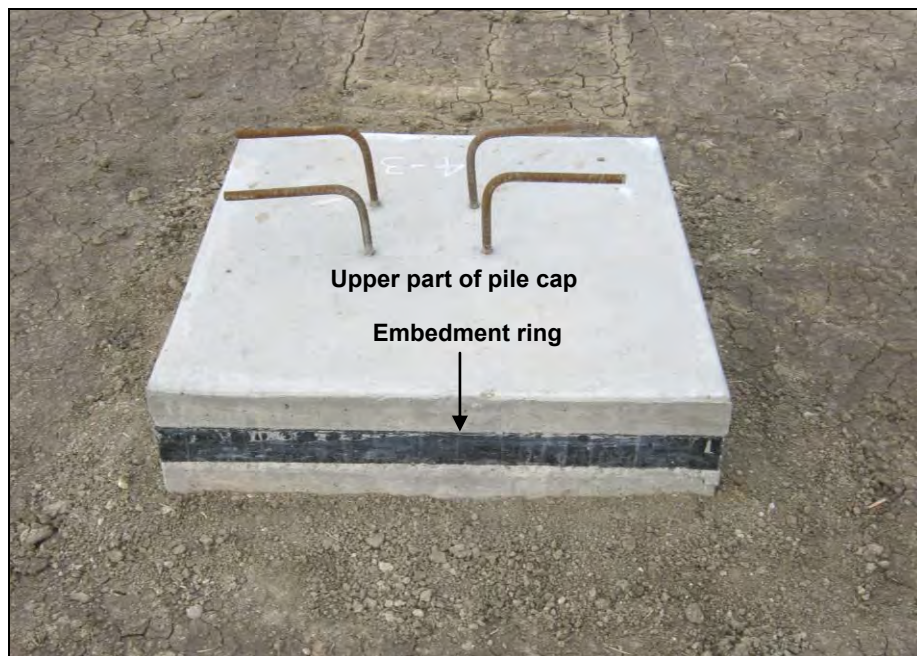


Figure 8: Finished pile cap with embedment ring for attachment of boot

2.7 Final Design

Based on all testing, field experience, and fabrication experience, the final design of the system was established:

- Thickness of BPS aggregate layer and above-grade portion of the pile cap form was selected at 18 cm (using 2x8 lumber for forms).

- Finalized the location of the embedment ring in the form (top edge of ring to be 5 cm from the top of form).
- The outside dimensions of the embedment ring were finalized at 91.1 cm square, which allowed easy insertion into a 91.4 cm square pile cap form, accommodating a certain amount of thermal expansion of the ring.
- The method of securing the ring into the form was finalized. Embedment ring would be secured with screws from the outside of the form, both above and below the midline of the embedment ring. This screw pattern held the ring close to the form, minimizing the concrete cream that worked between the ring and the form caused by vibrating the concrete around the reinforcing bar and embedment ring. This minimizes the effort needed to clean up the embedment ring for the attachment of the boot.
- Boot neck design was finalized to correspond to the final height of the above-grade form and final embedment strip location within the form.
- Specified that the boot neck would be welded to the embedment ring above the highest holes left in the embedment ring by the screws used to place it in the form.
- Boot dimensions were revised slightly to optimize the use of material based on best-fit layout of the boot pieces on 6.9 m wide geomembrane rolls. The final dimensions of the single flap boot are shown in Figure 2.
- Figure 9 shows the final single flap boot free-hanging by securing it at the neck and to a wooded pallet at the bottom, with the boot neck raised until the wood pallet lifted off the ground. Certainly more boot extension could be obtained by adding more weight hanging from the bottom of the boot, but it was judged that this boot extension would represent a settlement condition where the boot was not over-stressed. The extension of the single flap boot shown in Figure 9 is 76 cm, exceeding the maximum design settlement of 53 cm. This 76 cm extension yields a factor of safety of 4.5 relative to the estimated maximum remaining settlement of 17 cm. It should be noted that by using the same boot (with a 76 cm settlement compensation rating) in site areas where remaining settlement is less than 17 cm (i.e., where the waste prism is thinner) will result in a factor of safety even higher than 4.5.



Figure 9: Single flap boot on display at the site since April 2010; extended to compensate for 76 cm of settlement.

3. SPECIFICATIONS AND FQA AND CQA PLANS

The specifications for the fabrication and installation of the boots and rings, and the associated Fabrication Quality Assurance (FQA) Plan and Construction Quality Assurance (CQA) Plan were incorporated into the overall landfill cap Specifications and CQA Plan (Tetra Tech 2009a, 2009b), with appropriate adaptations pertinent to the boots and rings, as follows:

- All of the extrusion welds to fabricate the boots must have an embedded copper wire to allow spark testing of all seams for seam integrity.

- In field installation, the extrusion weld to fasten the boot to the embedment strip must have an embedded copper wire for spark testing. Either spark testing or vacuum box testing is approved for the extrusion weld of the base of the boot to the underlying landfill cap geomembrane.
- Trial welds are required for boot fabrication, with on-site seam strength testing. Trial weld seams are also sent out for lab destructive testing because cutting destructive seam samples from the boot can not be patched and the boot is destroyed. The trial weld logs and laboratory test logs allow any bad seam tests to be traced back to the specific boots represented by the failed seam test.
- A special boot fabrication QA form was developed that documented the provenance of the geomembrane used for each boot. The form records the roll number from which each panel of each boot is cut so that, with the geomembrane manufacturing and conformance test documentation, a complete paper trail for each boot is maintained. Each boot is uniquely numbered so that it's location of installation can be documented.
- The boot fabrication QA form also documents the seaming record of each seam on each boot, exactly like it is done in a field installation of geomembrane, providing a paper trail for any required follow up.
- Because boots and rings are fabricated off site, quality inspections are conducted prior to acceptance, which includes: (a) review and approval of all QA forms produced by the fabricator, and (b) complete inspection of a percentage of the boots and rings in the batch being inspected for acceptance and shipment to the site. In the boots inspected so far, this varied from 10% of the batch to 100% of the batch at the discretion of the inspector. The inspection includes complete spark-testing of every inch of every weld in any boot selected for inspection. The FQA plan also provides for unannounced inspection of the fabrication if deemed necessary.
- The acceptance inspection of the rings includes: (a) confirming integrity and sufficient squeeze-out of material at the welded corners, (b) confirming dimensions, (c) confirming squareness, and (d) manual strength test...can you pull it apart?

4. PRODUCTION FABRICATION

The fabricator implemented a boot and ring production process that resulted in a high degree of confidence that all of the boots and rings would be fabricated consistently and with detailed and complete documentation of quality control (Tetra Tech 2012). The production process included using cutting dies and jigs, fabrication forms, automated processes, color coding, unique numbering, forms, and full-time quality inspection. As of the publication of this paper, 2008 single flap boots and 1832 pile cap embedment rings have been fabricated.

5. INSTALLATION

Boots and rings have been installed on 68 pile caps for the first building developed at the site, as shown in Figure 10. Installation was routine, in accordance with the Specifications, and without problems, indicating that the design development process was effective.

ACKNOWLEDGEMENTS

The authors wish to thank Carson Marketplace, LLC, for permission to publish this paper. The authors also wish to acknowledge the contributions and valuable input provided by Thomas Cota, Ning-Wu Chang, Ph.D., P.E., Daniel Zogaib, and S. Steven Hariri, M.S., P.E., of the Department of Toxic Substances Control (DTSC) of the California Environmental Protection Agency. The Barber-Webb Company contributed to the conceptual design and the final design and fabricated and installed the boots and rings. GSE Lining Technology contributed to the conceptual design and designed and tested the prototype boot.



Figure 10: Boot-Ring system at first building on the site (boot welded to white geomembrane below)

REFERENCES

- ASTM D-6693. Standard Method for Determining the Integrity of Nonreinforced Geomembrane Seams Produced Using Thermo-Fusion Methods, *American Society for Testing and Materials*, West Conshohocken, Pennsylvania, USA.
- Brown & Root Environmental (1995). *Final Remedial Action Plan, Cal Compact Landfill (Upper Operable Unit)*, Carson, California.
- DTSC (1995). *Remedial Action Plan (RAP) Approval: Cal Compact Landfill, Upper Operable Unit, Carson, California*, Letter issued 25 October 1995 by Department of Toxic Substances Control, California Environmental Protection Agency.
- Geosynthetic Institute (2011). GRI Test Method GM19 - *Seam Strength and Related Properties of Thermally Bonded Polyolefin Geomembrane, Revision 6*.
- Huitric, R. (1981). Revised but unpublished in 2005. *Sanitary Landfill Settlement Rates, Verlängerung Der Nutzungsdauer Von Deponien (Conference on the Prolongation of the Capacity of Sanitary Landfills)*, Technische Universität Berlin.
- KFM Geoscience (2007). *Post Construction Refuse Settlement Evaluation*, The Boulevards at South Bay Project, Carson, California.
- Leighton Consulting (2008). *Geotechnical Investigation and Recommendations*, The Boulevards at South Bay Project, Carson, California.
- Tetra Tech (2008). *Design Report, Settlement-Compensating Connection of Geomembrane to Pile Cap Boots*, The Boulevards at South Bay Project, Carson, California.
- Tetra Tech (2009a). *Technical Specifications, Geosynthetic Landfill Cap*, The Boulevards at South Bay Project, Carson, California.
- Tetra Tech (2009b). *Construction Quality Assurance Plan, Geosynthetic Landfill Cap*, The Boulevards at South Bay Project, Carson, California.
- Tetra Tech (2010a). *Construction Quality Assurance Report, Geosynthetic Installer/Fabricator Pre-Construction Submittals*, The Boulevards at South Bay Project, Carson, California.
- Tetra Tech (2010b). *Project Report, Summary of Pile Cap Field Test*, The Boulevards at South Bay Project, Carson, California.
- Tetra Tech (2012). *Fabrication Quality Assurance Report – Pile Cap Boots 0001 through 2008 and Pile Cap Embedment Rings 0001 through 1832*, The Boulevards at South Bay Project, Carson, California.
- TRI/Environmental, Inc. (2009). *T-Lock Testing Program*, Letter report to EnviroCon Systems, Inc.

Soil Erosion Control Using Coir Geotextile – A Fuzzy Logic Modelling

1. Praseeja, A.V., IES College of Engineering, Thrissur, Kerala, India, prasiharee@gmail.com
2. Dr.K.Balan, College of Engineering Trivandrum, Kerala, India, drkbalan@gmail.com
3. Aswathy, J.S., Royal College of Engineering and Technology, Kerala, achoos14389@gmail.com

ABSTRACT

Soil erosion is a natural phenomenon enhanced by human activity which occurs in all landscapes under different land uses with climate and geology as the most important factors influencing them. Universal Soil Loss Equation (USLE) is widely accepted and designed for predicting long-term average annual soil losses. Slope stabilization using Coir Geotextile which is biodegradable can aid in vegetative turfing along the slopes and thereby reduce soil erosion. The objective of this paper is to develop and evaluate a Fuzzy Logic Model based on USLE empirical equation and thereby simulating the effects of Coir Geotextile on soil erosion during rainfall events. The Fuzzy model can be used for predicting soil erosion intensity in Kerala for different types of soil in various combinations of slope angle, crop cover, rainfall intensity etc., and also can be used to select the appropriate variety of coir geotextile for soil erosion control.

1. INTRODUCTION

Soil erosion is a complex dynamic process and is of great concern to humanity as it effects land degradation, limits the supply of hydropower, causes catastrophic floods damaging huge areas of low-lying fields, etc. Besides the influence of human activities, it can also be caused by morphometric characteristics of the land surface, the erosive forces of rainfall and the erodibility of soils (Lal, 2004). Conventional methods such as bench terracing, dry rubble packed bunds etc. have proven to be unsuitable in many of the steep slopes which are highly susceptible to erosion. A permanent and self-propagating vegetative cover is found to be an ideal solution to most of the erosion problems. Stabilization of soil along the hill slopes using natural and biodegradable materials such as Coir Geotextile is found to be a recent technique (Lekha, 2004).

Scientific planning for soil erosion reduction requires knowledge of the relations between those factors that causes soil erosion and those factors helps to reduce such losses. The Universal Soil Loss Equation (USLE) was designed to predict long-term average annual soil losses from sheet and rill erosion on given field slopes under specified land use and management (Wischmeier et al.1978). Soil loss calculations can also be made more reliable with the Revised Universal Soil Loss Equation (RUSLE) for some conditions that are not included in the USLE, if the fundamental information is available. This study is based on USLE, as the available data is more readily cope up with this equation.

Field surveys are however expensive, time consuming and difficult due to the complex interplay of many factors, such as climate, land cover, soil, topography, and human activities. There is a need in many emerging nations to develop simple methods for predicting areas of extensive soil erosion using imprecise, but real-world input data at low cost with considerable accuracy (Mitra et al.1998). This paper reports the application of Fuzzy logic modeling (Cohen et al. 2008) for predicting soil erosion intensity in Kerala for different types of soil in various combinations of slope angle, crop cover, rainfall intensity etc. Fuzzy logic model proved to be more realistic in the soil loss prediction and thereby used to select the appropriate variety of Coir geotextile for soil erosion control.

2. OBJECTIVES

- 1) To develop and evaluate Fuzzy Logic Model based on Universal Soil Loss Equation, thereby predicting soil erosion intensity in Kerala for different types of soil in various combinations of slope angle, crop cover, rainfall intensity etc.
- 2) To simulate the effects of Coir Geotextile on soil erosion by rainfall and runoff, and thereby select an appropriate variety of coir geotextile for soil erosion control.

3. DATA COLLECTION

3.1. For the Development of Fuzzy Logic Model

The Kerala state lies between 8° 18' and 12° 48' N and 74° 52' and 77° 22' E and covers an area of 38864 Sq.km. A major part of Kerala is in a very high rainfall and lower altitude zone with undulating topography and is highly susceptible to erosion. The average annual rainfall over the State is about 3000 mm (Lekha, 2004). Demographically, this state has three rain seasons, viz. pre-monsoon from February to May, monsoon from June to September and post-monsoon from October to January. Laterite soil, forest loams and coastal loams are the major soil types of the State. The land slope ranges from 5 % to over 40 %. Field bunding and terracing are the commonly adopted soil conservation practices in Kerala. (Balan, 1995)

The data set used in this study was obtained from existing study results in Kerala (Table1).

Table1.Description of data used in the study

Source	Project	Duration	Plot size	Data Collected
1. KAU ¹ , Thrissur, Kerala	Agrotechniques for soil conservation systems in Taungya systems	1984-1985 (2 years)	24 X 4 Sq.m	Rainfall intensity (EI values), Soil type, Slope details, Calculated C factor, Measured Soil loss.
2. KCAET ² , Malappuram, Kerala	a) Erodibility and Runoff potential of laterite soils under simulated rainfall conditions	1998-1999 (2 years)	20 x 5 Sq.m (each zone)	Rainfall intensity, 3 series of laterite soil, LS details, Calculated C factor, Measured Soil loss.
	b) Estimation of erosion and runoff project report	2003 (10 years)	40.25 hectares	Rainfall intensity, soil type, LS details, Calculated Soil loss as per USLE of 39 subdivided plots.

¹KAU : Kerala Agricultural University .Vellanikara, Thrissur, Kerala

²KCAET : Kelappaji College of Agricultural Engineering & Technology, Tavanur, Malappuram, Kerala

As per the data source (1) mentioned in table 1, the experiment was conducted in the College of Horticulture campus where the soil type is Sandy Clay Loam as per textural classification. They adopted seven types of treatments (T1 to T7) with different cultivations, of which the value of C factor ranges between 0.10 – 0.60. For the measurement of eroded soil, a multi-slot device with 47 slots of size 2.5 x 10 sq.cm each was fixed on the outer edge of the settling tank of dimension 3.4x0.75x0.35 cu.m.

As per the data source (2.a) mentioned in table 1, the experiment was conducted in three zones of laterite soils with different permeability, water holding capacity and drainage properties which are named as Mannamkulam series, Naduvattom series and Vellanikara series. The experiment was conducted in bare soils without any vegetation. Multi slot devices were used for the measurement of soil loss.

As per the data source (2.b) mentioned in table 1, the experiment was conducted in the college campus itself. The Plot size is about 40.25 ha. and the entire area is subdivided into 39 subareas which are mentioned in the report as L1 to L39. They adopted different types of vegetations for each plot for the estimation of soil loss through erosion and runoff. The value for cover management factor obtained from the report ranges between 0.2 to 0.7

3.2. For Simulating the Effects of Coir Geotextile

Coir geotextile is a natural geotextile made of coir applicable for erosion control which is more preferred to synthetic fibres on account of the fact that the material is environmental friendly and ecologically compatible as it gets degraded with the soil. It serves the purpose of protecting the seeds and surface soil from being washed away in the initial stage and the final stability of the slope is attained by the roots of vegetation and soil consolidation. This method is more appropriate in places where vegetation is considered to be the long-term answer to the slope stabilization (Lekha, 2004).

Table 2: Description of data used in the study

Source	Project	Duration	Plot size	Data Collected
1. NCRMI ¹ , Trivandrum, Kerala	Coir geotextiles as an effective erosion control measure in varying slopes of tropical humid condition	2000-2003 (3 years)	25 x 5 Sq.m	Rainfall intensity, Forest loam soil details, LS details (20%, 30%, 40% and 50% slope), Coir geotextile – 3types (1", 1/2", 1/4"), Measured annual soil loss.

¹NCRMI : National Coir Research and management Institute, Kudappanakkunnu

As per the data source (1) from NCRMI mentioned in table 2, the study was conducted at the Soil Conservation Research Station, Konni which is located at 9°51'20" and 9°51'44" North latitude and 76°13'54" East longitude, where the soil type is typical forest loam. The 11 slot multi-slot divisors known as Geib divisor were used to measure the runoff from the plot. The Coir geotextiles considered in this study (table 2) are woven types of three mesh sizes namely Less opening (1/4 inch), Medium Opening (1/2 inch) and High opening (1 inch). As the coir geotextiles has its role only up to the stage where vegetation starts sprouting, the data obtained were considered only up to the action of Geotextiles alone. The slope percentage considered ranges from 20% to 50%.

4. METHODOLOGY

4.1 Universal Soil Loss Equation (USLE)

USLE is a set of mathematical equations that estimate average annual soil loss and sediment yield resulting from interrill and rill erosion. It is derived from the theory of erosion processes, more than 10,000 plot-years of data from natural rainfall plots, and numerous rainfall-simulation plots. The Universal Soil Loss Equation (Wischmeier and Smith, 1978) is:

$$A = R * K * LS * C * P \quad [1]$$

- A - Annual soil loss (t/ha/yr)
- R - Rainfall erosivity factor (mm/yr)
- K - Soil erodibility (t/ha/mm)
- LS - Slope length and steepness
- C - Cover management
- P - Support practice factor

4.1.1. Rainfall Erosivity (R):

R factor represents the driving force for sheet/rill erosion. It is sum of individual storm erosivity values for qualifying storms over a time period. Storms of less than 0.5 inch and by more than 6 hours are not included in the computations. The R factor corresponds to USLE is found more appropriate as per the collected data (table 1). The R factor as per USLE (Wischmeier and Smith, 1978) is given by:

$$R = \sum_{i=1}^n \frac{EI}{100} \quad [2]$$

The variable EI is the product of the total energy for a storm and the storm's maximum 30-minute intensity and n represents the number of storms in the series.

4.1.2. Soil Erodibility (K):

K factor indicates a soil's inherent susceptibility to erosion. It is the rate of soil loss per unit of R for a specified soil as measured on a unit plot. The K values were usually estimated using the soil-erodibility nomograph (Das, 2009) method and is found more appropriate as per collected data (table 1). The K factor (Wischmeier and Smith, 1978) is given by:

$$K = 2.8 \times 10^{-7} M^{1.14} (12 - a) + 4.3 \times 10^{-3} (b - 2) + 3.3 \times 10^{-3} (c - 3) \quad [3]$$

- M - Particle size parameter
- a - Percent organic matter
- b - Soil structure code
- c - Profile permeability class

4.1.3. Topographical Factors (LS):

Two factors considered here are Slope length and Steepness. Slope length (L) represents the distance from the point of origin of overland flow to the point where the slope decreases sufficiently for deposition to occur. Slope steepness (S) is the field segment slope, expressed as percentage. The combined LS factor is given by (Wischmeier and Smith, 1978):

$$LS = (L_s/22.13)^m (65.41 \sin^2\theta + 4.56 \sin\theta + 0.065) \quad [4]$$

- L_s - Slope length in meters
- m - Exponent that depends on slope steepness ($m = 0.5$ for slope exceeding 5%)
- θ - Slope angle

4.1.4. Crop Management Factor(C):

The C cover-management factor is used to express the effect of plants and soil cover. The C-factor is defined as the ratio of soil loss from land cropped under specified conditions to the corresponding loss from clean-tilled, continuous, fallow land. To calculate the value of the C factor, the ratio of soil loss under a given crop stage period is given a weightage in accordance with the rainfall factor of that particular period (Das, 2009).

$$C = EI (\%) \times \text{Soil Loss Ratio} (\%) \quad [5]$$

4.1.5. Support Practice Factor (P):

It is the rate of soil loss caused by a specific support practice divided by the soil loss caused by row farming up and down the slope. It is used in USLE calculations only for row cropped land uses, and for all other land uses it is always taken as 1.00 (Das 2009). In this study, since no soil conservation practices were considered, a constant value of 1.00 is assigned

4.2. MATLAB – Fuzzy Logic Toolbox

MATLAB (short for MATrix LABoratory) is a computer program optimized to perform engineering and scientific calculations where problems and solutions are expressed in familiar mathematical notation (Overman, 2012). The design of the fuzzy system must include all of the four blocks in the block diagram (Fig 1). The singleton fuzzyfier will involve the smallest volume of calculations. The centroid defuzzyfier gives the best accuracy with the system output compared to other defuzzifiers (Wang, 1997). The Fuzzy Logic toolbox in MATLAB helps to model complex system behaviors using simple logic rules, and then implement these rules in a fuzzy inference system (Pazhouhesh et al. 2011).

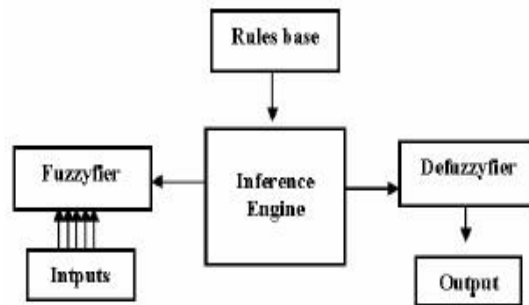


Fig 1- Block Diagram of the Fuzzy system

4.3. Results and Discussion

4.3.1. Development of Fuzzy Logic Model

Determination of Annual soil loss parameter (A) in the USLE model depends on five factors such as: Rainfall erosivity factor (R), soil erodibility factor (K), Length-Slope-gradient factor (LS), Cover management factor (C) and Support practice factor (P). The equations (Eq. 1 to 5) for each factor were developed in MATLAB programming through M-files, which can execute a series of statements. The collected data (table 1) such as Rainfall intensity, Soil type, Slope angle etc. is then substituted accordingly in M-files and obtained the range of values for R, K, LS, C and A factors.

The value obtained for R factor (Eq.2) is in the range between 0-4000. The values above 3000 are not considered in this study. The K factor (Eq.3) was based on Wischmeier's Nomograph (Das, 2009). The types of soil considered in this study are sandy loam, fine sand and Lateritic soil, of which the value for K factors ranges between 0.02 and 0.13. The value for slope length gradient (Eq.4) varies between 0.04-15 according to the slope angles of collected data. The C factor (Eq.5) value ranges between 0-2. The value greater than 1 is considered as severely high. The value for annual soil loss (Eq.1) ranges between 0-50. The range above 50 is considered as Very Severely High (VSH).

The range of values thus obtained are then sub categorized from very low (VL) to extremely high (EH) as shown in table 3 for creating Membership functions in Fuzzy logic.

Table 3: Range of values for each factors (VL= Very Low, ML = Moderately Low, L= Low, LM= Least Moderate, MM= Moderately Moderate, VM= Very Moderate, M= Moderate, LH= Least High, MH= Moderately High, H= High, VH= Very High, SH= Severely High, EH= Extremely High)

R		K		LS		C		A	
0-250	- VL	0-0.025	- VL	0-0.07	- VL	0-0.03	- VL	0-0.10	- VL
250-500	- ML	0.025-0.04	- ML	0.07-0.08	- ML	0.03-0.075	- ML	0.10-0.75	- ML
500-750	- L	0.04-0.06	- L	0.08-0.10	- L	0.075-0.20	- L	0.75-1.50	- L
750-1000	- LM	0.06-0.08	- LM	0.10-0.80	- LM	0.20-0.25	- LM	1.50-2.50	- LM
1000-1250	- MM	0.08-0.10	- M	0.80-1	- VM	0.25-0.30	- MM	2.50-3.50	- MM
1250-1500	- VM	0.10-0.115	- H	1-3	- M	0.30-0.40	- VM	3.50-5	- VM
1500-1750	- M	0.115-0.13	- VH	3-4	- LH	0.40-0.45	- M	5-7	- M
1750-2000	- LH			4-5	- H	0.45-0.50	- LH	7-9	- LH
2000-2250	- MH			5-8	- VH	0.50-0.70	- H	9-12	- MH
2250-2500	- H			8-13	- SH	0.70-0.80	- VH	12-16	- H
2500-2750	- VH					0.80-2	- SH	16-20	- VH
2750-3000	- SH							20-25	- SH
								25-40	- EH

Fuzzification plays a greater role for fuzzifying data, which is based on certain membership functions. Large number of membership functions with overlapping will increase the system accuracy (Pazhouhesh et al. 2011). Figures 2a to 2e show the trapezoidal membership functions with overlapping of all the five factors and annual soil loss in the Fuzzy system as per the range of values mentioned in table 3.

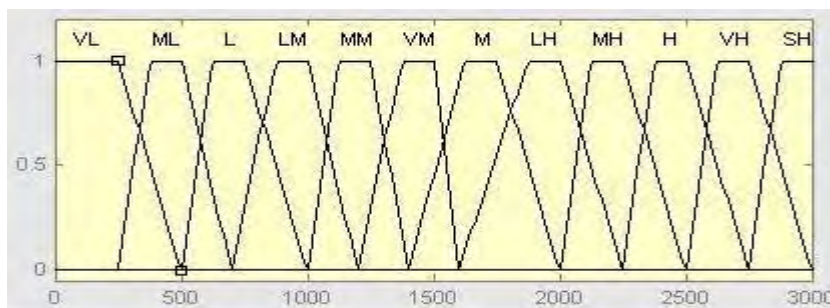


Fig 2a- Membership functions of 'R factor' (input 1)

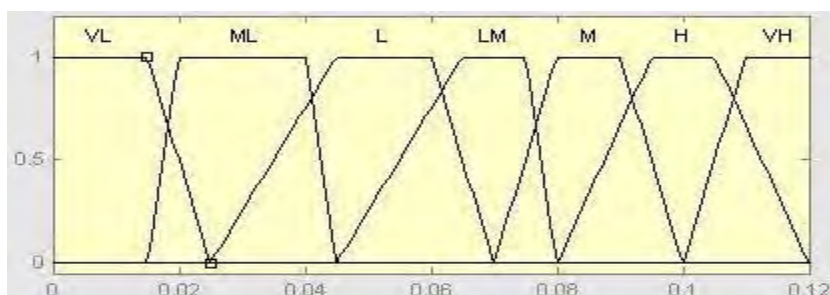


Fig 2b- Membership functions of 'K factor' (input 2)

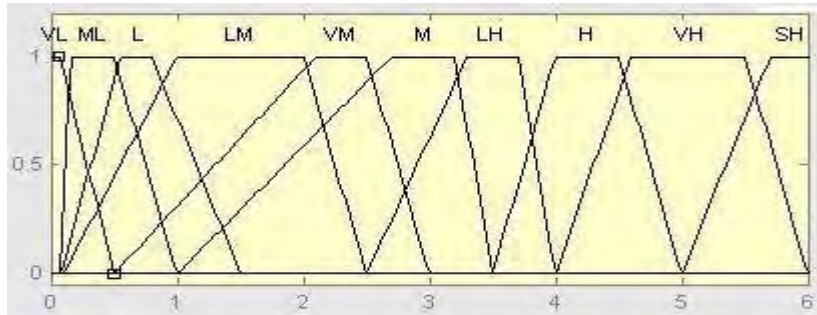


Fig 2c- Membership functions of 'LS factor' (input 3)

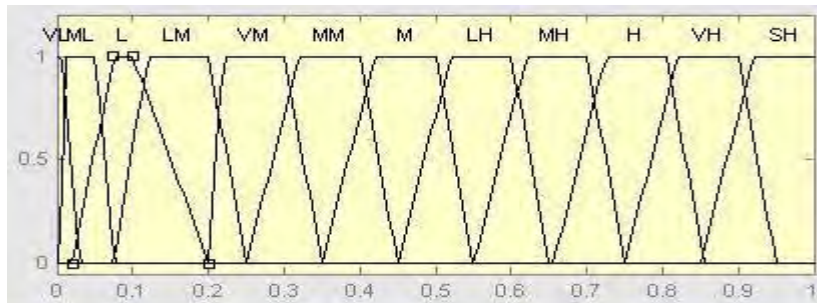


Fig 2d- Membership functions of 'C factor' (input 4)

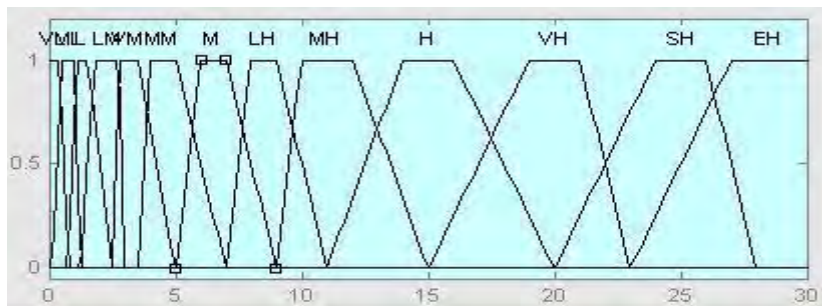


Fig 2e- Membership functions of 'Annual Soil loss' (output)

Fig 2- Membership functions of R, K, LS, C factors and Annual Soil Loss (A) as per table-3

After deriving the membership functions for the inputs and output, the rule base should be developed. So, many configurations using USLE empirical equation have been extracted to develop the rules in Fuzzy system. Three examples are shown in table 4a. Around 650 such configurations were obtained to get more refined output.

Table 4a: Rules extracted using USLE empirical equation

No	R	K	LS	C	A-USLE
1	317 - ML	0.026 - ML	3.43 - LH	0.097 - VL	2.74 - VM
2	213 - VL	0.043 - L	2.50 - M	0.04 - ML	0.916 - L
3	1520 - M	0.015 - VL	8.10 - SH	0.76 - H	140 - VSH

The most important step in the fuzzy system is the expression of the process in the IF-THEN logic. It is quite important to be able to determine which entry would produce the largest output with the smallest incremental change (Burrough et al. 1992). The example of three fuzzy rules relating to annual soil loss is summarized and shown in Table 4b.

Table 4b: Fuzzy rules relating to Annual Soil Loss

Rules	IF	R	IF	K	IF	LS	IF	C	THEN	A
1	IF	ML	IF	ML	IF	LH	IF	VL	THEN	VM
2	IF	VL	IF	L	IF	M	IF	ML	THEN	L
3	IF	M	IF	VL	IF	SH	IF	H	THEN	VSH

4.3.2. Evaluation of Fuzzy Logic Model

For evaluating the model, the fuzzy predicted annual soil loss values (A-Fuzzy) must be compared with actual field measured values (A-Field). The results from the fuzzy model (A-Fuzzy) were obtained from the “Rule Viewer” as shown in figure 3. The input and output tab is marked as ‘a’ and ‘b’ respectively in figure 3, which illustrates the example 1 in table 5. For verifying the performance of the designed fuzzy system, five experimental data sets have been chosen and applied to the model. Table 5 shows a summary of the results.

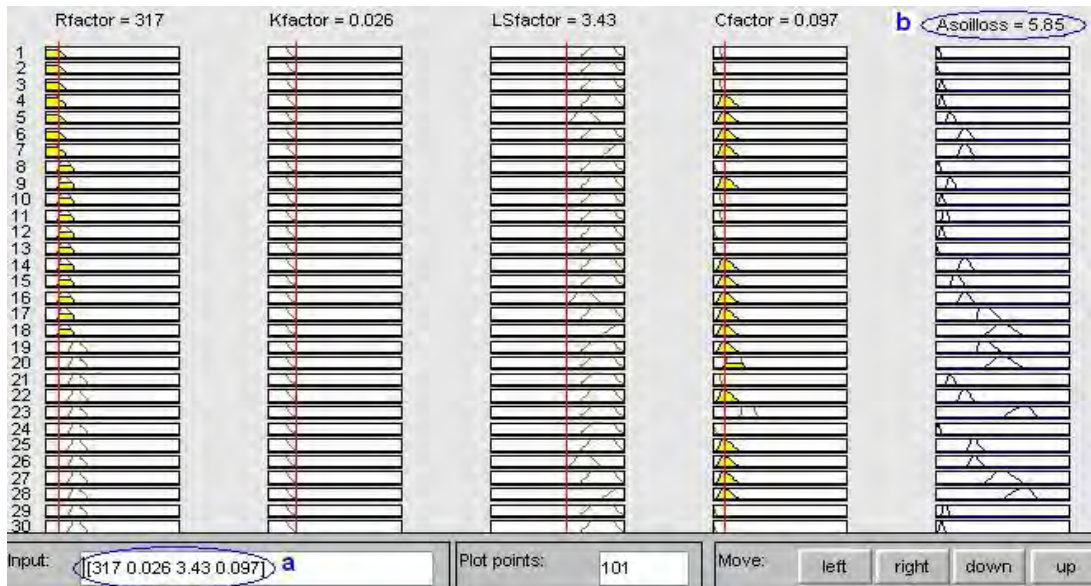


Fig 3- Rule Viewer in Fuzzy Logic

The comparison in Table 5 indicates that the values of the Annual Soil loss calculated by the fuzzy system are quite closer to the actual values obtained in the field (A-Field). Results showed that the fuzzy model performed better than USLE. Hence it can be presumed that the efficiency of the fuzzy model will be higher than USLE.

Table 5: The results of Annual Soil Loss obtained with the fuzzy system and with the USLE model

No	R	K	LS	C	A-Field	A-USLE	A-Fuzzy
1	317	0.026	3.43	0.097	5.10	2.74	5.85
2	213	0.043	2.50	0.04	1.20	0.916	1.49
3	697	0.030	7.10	0.20	25.30	21.92	26.70
4	689	0.065	0.22	0.70	2.60	5.90	2.10
5	742	0.065	0.22	0.70	4.30	7.50	3.80

4.3.3. Selection of Coir Geotextile Type

The collected data (table 2) such as rainfall intensity, soil type, slope angle etc. is substituted accordingly in the M-files of MATLAB programming and obtained the values of corresponding R, K and LS factors. Three types of Coir geotextiles were considered in this field study namely Less opening (LO), Medium opening (MO) and High opening (HO). The C factor of Coir Geotextile is thus obtained using the equation:

$$C = (\text{Measured Annual soil loss}) / (R * K * LS) \quad [6]$$

For various slope percentages, the range of values of C factor for coir geotextile is summarized in table 6.

Table 6: Range of C values depends on Slope percentage

Types	Mesh size	20%	30%	40%	50%
LO	0.25"	0.04-0.10	0.02-0.11	0.20-0.60	0.30-0.60
MO	0.50"	0.06-0.20	0.05-0.15	0.30-1.00	0.40-1.20
HO	1.00"	0.08-0.30	0.07-0.30	0.50-1.10	0.50-1.30

For predicting the type of geotextile for various combinations, soil type according to textural classification (Das, 2009) is considered which ranges from sandy soils (less erosive) to fine textured clayey and silty soils (highly erosive). The annual soil loss less than 5 (t/ha/yr) is considered as low erosion potential (Lal, 2004). Table 7 shows the range of values for each factor.

Table 7 – Range of values for each factors (EL=Extremely Low, VVL= Very Very Low, VL= Very Low, ML = Moderately Low, L= Low, LM= Least Moderate, VM= Very Moderate, M= Moderate, H= High, VH= Very High, SH= Severely High)

R	K	LS	A	C
0-250 – VL	0.01-0.03 – S (Sand)	0-1 – VL	0-1.5 – EL	0.03-0.2 – LO
250-400 – L	0.04-0.05 – LS (Loamy Sand)	1-5 – L	1.5-2.5 – VVL	0.2-0.6 – MO
400-600 – VM	0.06-0.09 – FS (Fine Sand)	5-10 – M	2.5-4 – VL	0.6-1 – HO
600-800 – M	0.12-0.14 – SL (Sandy Loam)	10-15 – H	4-5 – L	
800-1000 – H	0.15-0.2 – SCL(Sandy Clay Loam)	15-20 – VH		
1000-1500 – VH	0.16-0.23 – SC (Sandy Clay)			
1500-2000 – SH	0.2-0.25 – C (Clay)			
	0.25-0.27 – SiC (Silty Clay)			
	0.26-0.34 – L (Loam)			
	0.3-0.4 – SiCL (Silty Clay Loam)			
	0.35-0.45 – SiL (Silty Loam)			
	0.41-0.5 – Si (Silt)			

Accordingly membership functions for each factor were developed as per the values in table 7. Figures 4a to 4e shows the trapezoidal membership functions with overlapping of all the four factors (R, K, LS and A) for the prediction of C factor in the Fuzzy system.

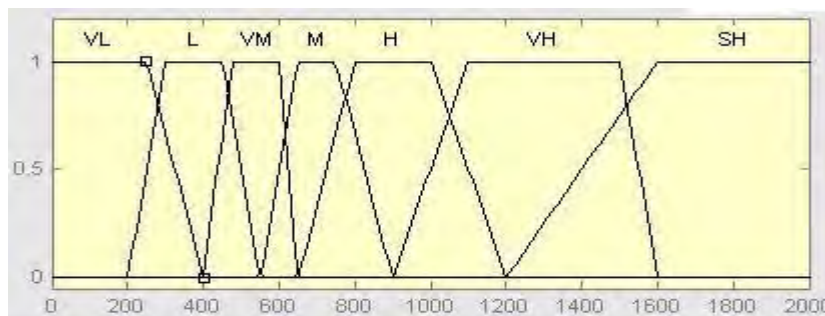


Fig 4a- Membership functions of 'R factor' (input 1)

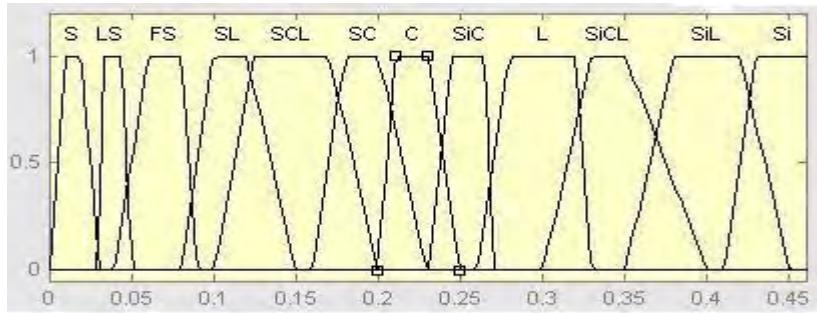


Fig 4b- Membership functions of 'K factor' (input 2)

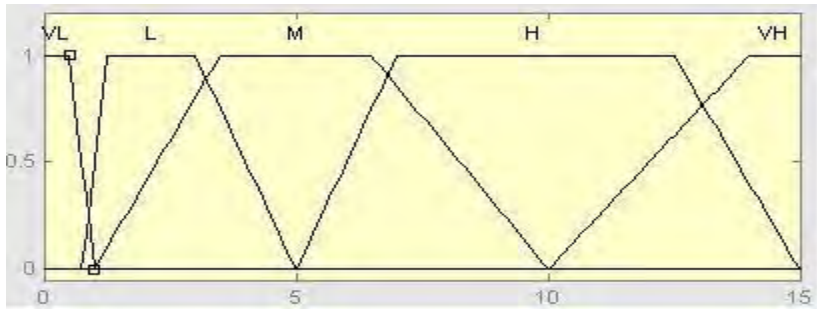


Fig 4c- Membership functions of 'LS factor' (input 3)

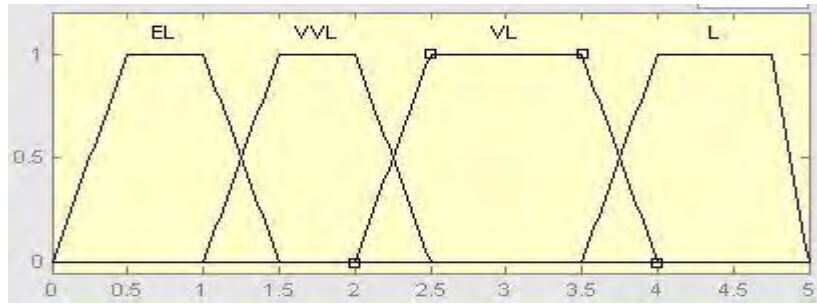


Fig 4d- Membership functions of 'Annual Soil Loss' (input 4)

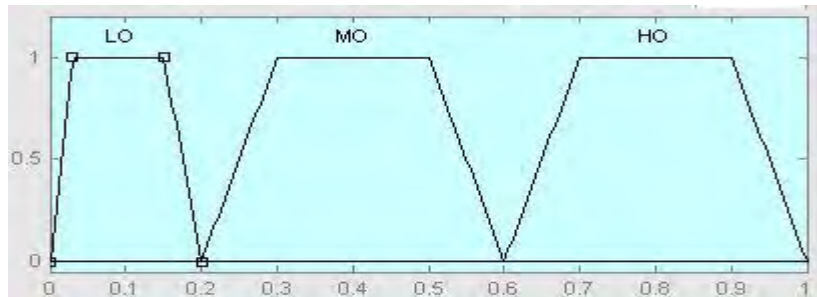


Fig 4e- Membership functions of 'C factor' (output)

Fig 4- Membership functions of R, K, LS factors and Annual Soil Loss (A) for the prediction of C factor as per table 7

After deriving the membership functions for the inputs and output, the next step is the development of rules using USLE empirical equation. First set of rules were created by considering the typical forest loam soil type ($K = 0.026$) for different slope percentages as per the collected data mentioned in table 2. The subsequent sets of rules were then created by considering all the soil types as per textural classification. Around 300 set of rules were developed for the prediction of

coir geotextile for various combinations. The example of three such fuzzy rules relating to the selection of the type of coir geotextile is summarized in Table 8.

For example, the first example shows that for a particular site where the soil type is Sandy (K factor = S) having very low (VL) R factor and LS factor, in order to reduce the annual soil loss to extremely low condition (A = 0 to 0.15), adopt High opening (HO) type of coir geotextile.

Table 8: Fuzzy rules relating to Coir geotextile selection

Rules	IF	R	IF	K	IF	LS	IF	A	THEN	C
1	IF	VL	IF	S	IF	VL	IF	EL	THEN	HO
2	IF	M	IF	SCL	IF	M	IF	VL	THEN	MO
3	IF	SH	IF	SiL	IF	H	IF	L	THEN	LO

Therefore for a particular combination of rainfall intensity, soil type and slope gradient, it become possible to select the appropriate type of coir geotextile for the minimum soil erosion potential.

5. CONCLUSIONS

Fuzzy logic method is shown to be a relatively easy way for determining soil erosion potential. Comparing the A values calculated using the designed fuzzy model with those obtained from the USLE model showed that the fuzzy logic modeling for determination of the Soil loss factor is more flexible and realistic procedure for describing the relationship with the five factors. Thus the evaluated model can then be used for the prediction of the type of coir geotextile for a particular combination of rainfall, soil type and slope gradient for the minimal soil loss. Due to changing weather conditions year by year, the dataset for minimum twenty years is required for different soil type, slope angle, cover factor etc. to have accurate prediction. One major advantage of fuzzy logic model is that they can be used in developing countries where digital data are not readily available and where simple and inexpensive techniques are useful for a preliminary reconnaissance survey of soil erosion potential.

REFERENCES

- Balan, K. (1995). "Studies on engineering behavior and uses of geotextiles with natural fibres", Ph.D thesis, Indian Institute of Technology, Delhi, India.
- Burrough, P.A., MacMillan, R.A., Deursen, W. (1992)." Fuzzy classification methods for determining land suitability from soil profile observations". *Journal of Soil Science* 43, 193–210.
- Cohen, S., Svoray, T., Laronne, J.B., and Alexandrov, Y. (2008). "Fuzzy based dynamic soil erosion model (FUDSEM): Modelling approach and preliminary evaluation". *Department of Geography and environmental, Journal of Hydrology*, 356,185-198.
- Das, G. (2009, January) "Hydrology and Soil conservation engineering", 2nd edition, Fourth Printing, Asoke K Ghosh Publishers, New Delhi.
- Grimm, M., Jones, R.A., Rusco, E., and Montanarella, L. (2003). "Soil erosion risk in Italy: a revised USLE approach", *European Soil Bureau*, research report No.11
- Lafren, J.M., and Moldenhaus. W.C. (2003)."Pioneering soil erosion prediction: The USLE story", *World association of soil and water conservation no.1*
- Lal, R. 2004. "Soil degradation by erosion". *Land Degradation & Development* 12: 519-539.
- Lekha, K.R. (2004) "Field Instrumentation and monitoring of soil erosion in coir geotextile stabilized slopes- A case study", *Geotextiles and Geomembrances* 22 : 399-413.
- Mitra, B., and Scatte, H.D. (1998)"Application of Fuzzy Logic to Prediction of Soil Erosion in Large Watershed". *Geoderma* 47: 12-21.
- Morgan, R.P.C., et al. (1998). "The European Soil Erosion Model: A dynamic approach for predicting sediment transport from fields and small catchment", *Earth Surface processes and Landforms* 23,527-544
- Overman. E. (2012) "A MATLAB Tutorial", *Department of Mathematics*, The Ohio State University
- Park, S.D., Lee, K.S., and Shin, S.S. (2012). "Statistical Soil Erosion Model for Burnt Mountain Areas in Korea- RUSLE Approach", *Journal of Geo environmental Engineering*, Vol.17, No.2, 292-304.
- Pazhouhesh, M., Gorji, M., Taheri, S.M., and Keshavarzi, A. (2011),"Determination of soil erodibility factor using fuzzy rule base system", *International Journal of Environmental Sciences* Vol.1, NO.7, ISSN 0976-4402
- Renard,K.G.,Foster,G.R.,Weesies,G.A.,McCool,D.K., and Yoder,D.C. (1997),"Predictiong soil erosion by water:A guide to conservation planning with the Revised Universal Soil Loss Equation(RUSLE)" *Handbook 703,USDA Agricultural Research Service*, Washington, DC.

- Smets T.,Borselli L.,Poesen J., and Torri D.,(2011),“Evaluation of the EUROSEM model for predicting the effects of erosion-control blankets on runoff and interill soil erosion by water”, ,Geotextiles and Geomembranes: 285-297
- Smitha, A.V., and Sobha, V. (2011), “Spatial Information Technology as a tool for soil erosion assessment using USLE- A study in the Shendurney wild life Sanctuary, South Kerala”, *International Journal of Environmental Sciences* Vol 1. Pg: 1978-1988
- Tayfur, G., and Singh, V.P. (2006). "ANN and Fuzzy logic models for simulating event based Rainfall Runoff", *Journal of Hydraulic Engineering*, ASCE 0733-9429, and Vol.132:12, 1321-1330
- Tran, L.T., Ridgley, M.A., Nearing, M.A., Duckstein, L. and Sutherland, R. (2001),”Using Fuzzy logic-based modeling to improve the performance of the RUSLE”, *International soil conservation organization*, 919-923.
- Wang, L.X. (1997). “A Course in Fuzzy Systems and Control”. Prentice Hall, N.Y, 572 pp.
- Wischmeier, W.H., and Smith, D.D. (1978). “Predicting rainfall erosion losses, a guide to Conservation planning” *USDA Agriculture Handbook* 537.58p

Specifying Allowable Geomembrane Leakage Rates Based on Available Technology

Glenn T. Darilek, P.E., Leak Location Services, Inc., San Antonio, Texas, USA, glenn@llsi.com
Daren L. Laine, Leak Location Services, Inc., San Antonio, Texas, USA

ABSTRACT

Engineering and regulatory specifications for allowable leakage through geomembranes should be consistent with state-of-the-art technologies for locating leaks. In many actual cases, surface impoundments are allowed to leak an order of magnitude more than what could be easily attained by locating leaks using currently available leak detection technologies. In some cases for landfills, if an allowable leakage rate is exceeded, there is no technology that can be used to locate the small leak or leaks for repair.

ASTM D7007, the established standard for geomembrane leak location with water or earth materials on the geomembrane, and a mathematical equation for leakage rate versus size of the leak are used to examine what is achievable and what is unrealistic for the specification of allowable leakage rates.

Specification writers and design engineers should specify low, but realistic allowable leakage rates that can be attained using geomembrane leak location surveys.

1. ALLOWABLE LEAKAGE RATES

Allowable Leakage Rates or Action Leakage Rates (ALRs) are specified for installed geomembranes to quantify the maximum allowable liquid leakage. If the ALR is exceeded, then corrective action must be taken to reduce the leakage rate below the set limit. To lower the leakage, the holes in the geomembrane must be located and repaired. In some cases, the allowable leakage rate can be set so low that if it is exceeded, there is no technology that can be used to locate the very small leak or leaks for repair. In other actual cases, surface impoundments are allowed to leak an order of magnitude more than what could be easily attained by locating and repairing leaks using currently available leak detection technologies.

When the U.S. Environmental Protection Agency promulgated the final rule for Action Leakage Rates (1992), it considered what was usually attainable with good construction quality assurance. They may not have considered what could be attained with the available leak location technologies, nor the consequences if it was not technologically possible to detect leaks that would cause the ALRs to be exceeded particularly for landfills. Paradoxically, the usual technical guidelines that geomembranes covered with water are allowed to leak 10 times more than geomembranes covered with earth materials is opposite than what is attainable with the technologies available today. The result is that some surface impoundments are allowed to leak 10 times more than necessary, and some landfills that may never meet their allowable leakage specification by a factor of about 10. So today, the capabilities of currently available technologies should be considered when specifying allowable leakage rates.

2. MEASURING LEAKAGE RATES

2.1 Rudimentary Leak Detection Systems

The concept of allowable leakage rates depends on being able to measure the leakage over time. In some instances, a relatively permeable earth drainage material layer with an underlying relatively impermeable clay layer are used to collect leakage and drain the leakage to a leak collection sump. Because of wide variations in the construction and performance of the layers, the quantity of leakage measured is less than the actual leakage. Actual leakages may be much more, so the measured leakages are more qualitative than quantitative.

2.2 Water Balance Testing

Water balance testing is another way to measure leakage in single-geomembrane liners. The methodology is to measure the water level over a period of time and compensate for evaporation, rainfall, geometry, and runoff.

The accuracy of water balance testing is questionable. Even using the best protocols, it is problematic to accurately read the water levels to the accuracy needed and make the corrections accurately. Compensating for rainfall must account for the rain that falls on the unflooded side slopes that drain into the pond. Any rainfall drainage that flows into the impoundment from the surrounding berms or road surfaces will cause error. The evaporation rate for a large body of water is not the same as that for the smaller control container used to measure the evaporation. If the evaporation pan used for measuring the evaporation and rainfall is disrupted unintentionally or by animals during the long period of measurement, the results will be invalidated.

The leak detection sensitivity for water balance testing is poor, and the method only detects the presence of leakage, and not the location of the leaks. Because of meniscus and wave effects, the water level usually cannot be read to an accuracy greater than about 2 mm. This allows an error in the measurement of 20 cubic meters per hectare (2,140 gallons per acre).

A significant amount of time and cost are needed to fill the impoundment, then empty the impoundment and dispose of the water. For sensitive leak detection, the water level monitoring must occur over a period of weeks. During that time, the test can be subject to disruption, vandalism, and tampering.

Most of the errors in the water balance test act in the favor of passing the test. The results of some water balance tests falsely indicate that water is created during the test! Some specifications for water balance testing allow evaporation ponds to leak more than they evaporate. Water balance testing results in questionable results, costs a lot, and takes a long time.

2.3 Double Geomembranes

The most accurate and common leakage detection system is to use double geomembranes with a drainage layer between the geomembranes. The drainage layer incorporates a geonet, earthen drainage material, or structured geomembrane. The drainage layer is sloped to a sump between the geomembranes, which is pumped out to determine the leakage. The cost of the secondary geomembrane and the drainage layer is significant, but often required by regulatory agencies.

Assuming proper design and construction, that the secondary geomembrane is intact, this method is very accurate for determining leakage rates. Leakages of a few liters per month can be gauged. Leakages can be measured as frequently as needed.

2.4 Geomembrane Leak Location Technologies

Geoelectric leak location technologies do not measure the leakage rates as such, but they are used to detect the leaks so once the leaks are found and repaired, the leakage rates can be expected to be very low. The various implementations are described in ASTM Standard D6747. Various methods are used to locate leaks in bare geomembranes, geomembranes covered with water, and geomembranes covered with earth materials. Various implementations are used to locate leaks in bare geomembranes, geomembranes covered with water, and geomembranes covered with earth materials. Other leak location methods include visual inspection, vacuum box testing, and pressure testing of seams, but these methods are usually limited to pre-service testing, and are not applicable after earth materials are installed on the geomembrane.

3. LOGICAL CRITERIA FOR SPECIFYING ALLOWABLE LEAKAGE RATES

Allowable leakage rates should be specified at a low level that is consistent with being able to detect leaks that would contribute significantly to the ALR. The best available technologies for locating leaks in geomembranes are geoelectric leak location methods. The practical approach is to specify allowable leakage rates that are achievable in all reasonable cases when currently available leak detection technologies are applied.

By this criteria, it does not make sense to specify a high allowable leakage rate if the leakage rate can be easily met using the available geomembrane leak location technology. Allowing a higher leakage rate allows inferior construction standards and possible future environmental damage.

It is usually possible to construct a facility with very low leakage rates, and that is certainly the goal. But specifying a leakage rate that can be exceeded by a leak that cannot be located using any technology is unrealistic and untenable. The logical criteria for specifying an allowable leakage rate is not whether a certain low leakage rate is achievable with good construction and quality assurance practices, but whether there is a practical solution if the low leakage rate is not achieved for some reason.

3.1 Approach

ASTM Standard D7007 for geomembrane leak location with water or earth materials on the geomembrane requires determining the distance from which an actual or artificial test leak of specified sizes can be found. Then the leak location surveys are conducted so that the leak detection probe passes within that distance of every point on the geomembrane. Leaks smaller than the actual or artificial leak are routinely found when the measurement probe passes closer to the leak, but one can expect to locate all leaks larger than the actual or artificial test leak. So one can assume the worst-case condition of free-flow through the leak of that size. The free-flow leakage rate can be calculated using an equation derived from Bernoulli's equation for free flow through an orifice (Giroud and Bonaparte, 1989).

$$Q = 0.6 a \sqrt{2 g h} \quad [1]$$

Where Q = leakage rate (m^3/s)
 a = area of the leak (m^2)
 g = acceleration of gravity (m/s^2)
 h = hydraulic head (m)

Then if one assumes one leak of this size for an assumed area, an allowable leakage rate can be assigned on this basis. For this paper, one leak is assumed for every 4,050 square meters (1 leak per acre).

3.2 Water-Filled Impoundments

Geoelectric leak location surveys with only water covering the geomembrane can very easily locate leaks that would contribute to a sometimes-suggested allowable leakage rate of 9,350 liters per hectare per day (1,000 gallons per acre per day). Figure 1 is a graph of the free flow leakage rate versus the leak size for surveys with water on the geomembrane using Equation 1. ASTM D7007 specifies a 1.4 mm (0.055 in.) test leak. The equipment and survey parameters are set up to be able to detect leaks this size under near worst case conditions. This diameter and the corresponding leakage rates are also indicated in Figure 1 for two depths of water above the leak. Assuming free flow, which is the case with a properly designed leak detection system, the graph shows that the leakage rate from such a leak is about 790 and 353 liters per day (80 and 180 gallons per day) for water depths of 1m (3.3ft) and 5m (16ft), respectively. Such a leak is very practical to detect, and those leakage rates are typically a fraction of the usual allowable leakage rates for water-filled impoundments.

This illustration is for only one leak. For large impoundments, it is reasonable to assume there would be multiple leaks. If one would expect maybe 2.5 leaks per hectare (1 leak per acre), the illustration can be extrapolated to larger impoundments. However, it is unsound to interpolate for smaller impoundments, because that would result in a leakage rate and leak size that may not be located using leak location methods.

In general, this analysis suggests that typical allowable leakage rates could be made more stringent for ponds larger than about one acre. Using the analysis and assumptions above, a more suitable allowable leakage rate of approximately 940 liters per hectare per day (100 gallons per acre per day) would be more suitable.

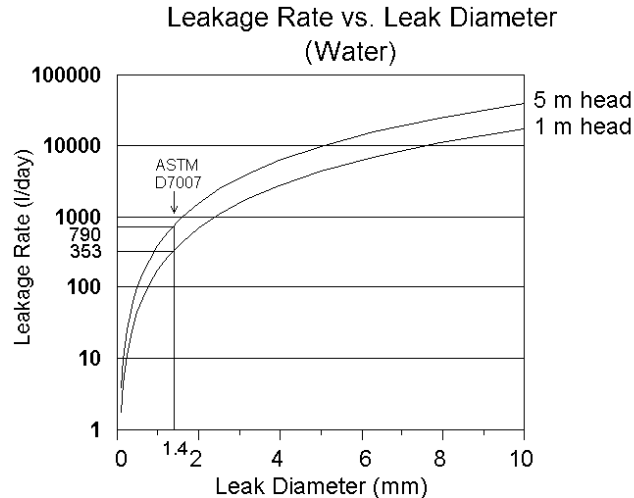


Figure 1. Free Flow Rate versus Leak Diameter with Water on the Geomembrane

3.2 Impoundments and Landfills with Earth Materials on the Geomembrane

The analysis for geomembranes with earth materials covering the geomembrane shows that increases in the allowable leakage rates may be warranted in some situations. Figure 2 shows a graph of the free flow leakage rate vs. leak size for surveys with earth materials on the geomembrane. ASTM D7007 specifies a 6.4 mm (0.25 in.) test leak. Again, as part of the leak location procedure, the equipment and survey parameters are set up to be able to detect leaks this size under near worst case conditions. This diameter and the corresponding leakage rates for water heads of 0.3 m (1 ft) and 1.0 m (3.3 ft) are also shown in Figure 2.

Assuming free flow, which would be essentially the case with granular drainage materials or geosynthetic drainage materials above and below the geomembrane; the graph shows the leakage rate from such a leak is about 4,045 and 7,385 liters per day (1,070 and 1,950 gallons per day) for typical hydrostatic heads of 0.3m (1ft) and 1m (3.3ft), respectively. A leak with this diameter is practical to detect, but these leakage rates are more than an order of magnitude higher than some allowable leakage rates for landfills.

This illustration shows that if an allowable leakage rate is set very low, then detection of the small leaks in the geomembrane that cause the leakage may not be possible. This unrealistic requirement can result in disastrous consequences that may prevent the permitting of the landfill cell.

Fortunately in some cases, when a very low allowable leakage rate is specified, a low-permeability layer such as a geosynthetic clay liner (GCL) is placed under the geomembrane to help meet the leakage criteria. A low-permeability layer greatly decreases the leakage rate if the geomembrane makes good contact with the layer. Therefore, larger holes can be located or tolerated. However, if the geomembrane is not in intimate contact with the low-permeability layer, such as on wrinkles or bridging, the unsolvable problem remains if there are leaks in these areas.

A common geoelectric leak location specification for landfills calls for detecting all leaks that could contribute to an allowable leakage rate of 187 liters per hectare per day (20 gallons per acre per day). This leakage will flow through a 0.86 mm (0.034 in.) diameter leak assuming free flow with only 0.3 m (1 ft.) of head. Meeting this low ALR depends almost entirely on the GCL or other leak-sealing layer having intimate contact with the geomembrane and not on the detection capabilities of the geoelectric leak location method. The analysis above shows that meeting that geoelectric leak location specification may be in conflict with the ASTM standard and the available technology.

4. SENSIBLE APPROACHES

4.1 Surveys of Bare Geomembranes

It may not be possible to detect smaller leaks, after the overlying earth layer is installed. To meet a low allowable leakage rate, and certainly if there is no low-permeability layer in contact with the geomembrane, a sensible approach is to test the bare geomembrane for leaks before the earth materials are placed. This can be easily accomplished using the water puddle method specified in ASTM Standard D 7002. This will detect the smaller geomembrane installation

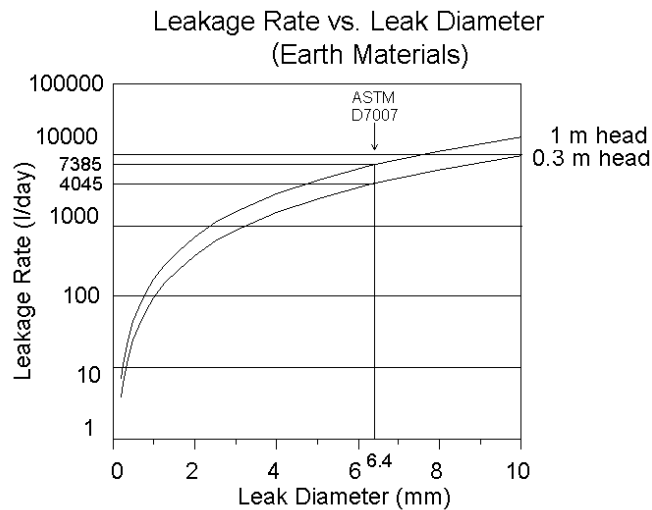


Figure 2. Free Flow Rate versus Leak Diameter with Earth Materials on the Geomembrane

leaks. Leaks that are caused by machinery placing the earth materials on the geomembrane are generally larger, and may be detected after the earth materials are being placed on the geomembrane.

4.2 The Misconception of Specifying Zero Leakage

Some engineers and owners are still specifying zero leakage or no leaks. Specifying zero leakage for a geomembrane is even more unreasonable than specifying an allowable leakage rate that is too low. A reasonable person could interpret zero leakage as never a drop. Although one strives to obtain the best attainable results with a specification, it is naive to specify something that cannot be remedied if the specification is not met. That is the case when specifying zero leakage in a geomembrane of any practical size. There have been several instances of this faulty specification, most notably in water storage reservoirs with many pipe penetrations and roof support columns with battens and other details. Sometimes, one is fortunate and the leakage is zero or ignorable. But specifying zero leakage or specifying that a liner has no leaks almost always results in disputes and sometimes unsolvable problems.

4.3 The Dilemma

The industry has been fortunate for the most part in installing geomembranes to meet low allowable leakage rates. However, that does not justify flirting with disaster by continuing to specify allowable leakage rates that are too low. Despite best efforts, for whatever reason, the primary geomembrane may have a leakage that is slightly above a specified low allowable leakage rate. A geoelectric leak location survey can be conducted in the hope that any leaks detected and repaired will lower the leakage rate. However, if the leaks are too small to be detected, the only alternative is to remove the cover material and geosynthetics from the geomembrane, remove and replace the geomembrane, and hope that the problem does not reoccur. All of this added expense and possible lost revenues and liquidated damages over a small amount of leakage through the primary geomembrane, and probably very negligible leakage through the secondary geomembrane! This can be avoided if a proper and reasonable allowable leakage rate is specified from the beginning.

4.4 Easily Attainable Better Performance

The prospect for water-filled impoundments is much more promising. In fact, in most cases, the allowable leakage rates can be made much lower. It does not make sense to install a geomembrane as an impermeable layer and tolerate easily detectable leaks. The technology is widely available to locate leaks that would contribute an order of magnitude less than some allowable leakage rates. If a lower allowable leakage rate is exceeded, there are easy ways to solve the problem.

5. CONCLUSIONS

Allowable leakage rates should be set according to what is easily attainable using existing technologies. Many ALRs for impoundments can be easily decreased by using geomembrane leak location technologies. But, particularly for geomembranes covered with earth materials, an important part of engineering and specification writing is to balance the desire for perfection with what is suitable for the purpose, at a reasonable cost, and attainable with existing technology.

Although perfection may be the goal, specifying perfection or the unattainable without regard to the technology and cost and consequences is not good engineering. The logical criteria for specifying low allowable leakage rates is not whether a certain low leakage rate is achievable with good construction practices, but whether there is a practical solution if the low leakage rate is not achieved. Specification writers and design engineers should consider what is attainable using the available technologies and understand the implications for their project if the ALR cannot be met.

REFERENCES

- ASTM D 6747. Standard Guide for Selection of Techniques for Electrical Detection of Leaks in Geomembranes, *ASTM International*, West Conshohocken, Pennsylvania, USA.
- ASTM D 7002. Standard Practice for Leak Location on Exposed Geomembranes Using the Water Puddle System. *ASTM International*, West Conshohocken, Pennsylvania, USA.
- ASTM D 7007. Standard Practices for Electrical Methods for Locating Leaks in Geomembranes Covered with Water or Earth Materials, *ASTM International*, West Conshohocken, Pennsylvania, USA.
- Bonaparte, R. and Giroud, J.P., (1989) Leakage Through Liners Constructed with Geomembranes, Part I: Geomembrane Liners", *Geotextiles and Geomembranes*, 8: 27-67.
- U.S. Environmental Protection Agency, Office of Solid Waste, "Action Leakage Rates for Leak Detection Systems," EPA 530-R-92-004, January 1992.

Storage of Coal Combustion Residuals with a Geosynthetic Liner – A 30 Year Forensic Study

B. Ramsey, GSE Environmental LLC, Houston, Texas, USA, bramsey@gseworld.com

B Betke, GSE Environmental LLC, Houston, Texas, USA

I. Peggs, I-CORP INTERNATIONAL, Inc., Ocean Ridge, FL, USA

ABSTRACT:

The storage of coal ash has become an increasing concern in recent years. The December 2008 failure at the power facility in Kingston, Tennessee, USA along with the October 2011 failure in Oak Creek, Wisconsin in addition to over 50 documented cases of groundwater contamination at or nearby coal ash storage facilities and consideration of the US EPA's issuance of new regulations for the storage of coal ash will require the use of geosynthetic materials as a critical part of the containment system.

This paper will present pertinent facts on a long term success story in the use of geomembranes as containment for coal combustion residuals. Recently material that has been in use in this exact application was exhumed from a power company site in Florida where the geomembrane had been used to successfully contain coal ash for over thirty years.

1. INTRODUCTION

1.1 Introduction and History

The geosynthetics market as a whole, and the geomembrane industry in particular, received its first large growth spurt with the 1976 U.S. congressional bill that is known as RCRA [The Resource Conservation and Recovery Act]. These regulations were issued in two sections, the first specific to material deemed as hazardous waste, the second addressing the long-term fate of solid waste. Hazardous waste has since become known as "subtitle C" type waste and solid or most commonly household waste has become known by that specific section of the regulations "subtitle D." There is an additional waste stream known as construction and demolition waste or "C& D material" that is not regulated under RCRA but is instead addressed on a state-by-state or local regulatory basis. The second significant regulatory impact occurred in 1980 with passage of the Comprehensive Environmental Response, Compensation and Liability Act more commonly known as "Superfund." This regulation not only increased demand for geosynthetic materials but helped to spur large growth in the capping applications, using geosynthetics as surface or near surface barriers to prevent rainwater infiltration.

The proper place to begin a review of coal ash and its regulation, and lack thereof, within the United States is in calendar year 1980 with the passage by the U.S. Congress of what is known as the "Bevill Amendment," named for former Representative Tom Bevill (D-AL). In passing the law, RCRA was amended by adding section 3001(b)(3)(A)(ii), known as the Bevill exclusion, to exclude "solid waste from the extraction, beneficiation, and processing of ores and minerals" from regulation as hazardous waste under Subtitle C of RCRA. Further, an EPA study of the impact of coal ash on the environment was mandated. This study was completed and published in the Federal Register on May 22, 2000. The report states "The Agency has concluded these wastes do not warrant regulation under subtitle C of RCRA and is retaining the hazardous waste exemption under RCRA section 3001(b) (3) (C). However, EPA has also determined national regulations under subtitle D of RCRA are warranted for coal combustion wastes when they are disposed in landfills or surface impoundments,..." However, the EPA determination for subtitle "D" regulation was not heeded and the absence of regulations of coal ash storage continued. Just before 1 a.m. on Monday, December 22, 2008, a dike containing coal fly ash slurry ruptured at an 84-acre (0.34 km²) solid waste containment area at the TVA Kingston Fossil Plant in Roane County, Tennessee, USA. An estimated 1.1 billion U.S. gallons (4,200,000 m³) of coal fly ash slurry was released. Subsequent direct clean-up and remediation costs have been estimated at greater than 1.3 billion dollars.

On October 31, 2011 a failure occurred at a power generation facility owned by a WE Energies located on the shore of Lake Michigan in Oak Creek Wisconsin, south of Milwaukee. This event resulted in a significant quantity of coal ash being released into Lake Michigan. According to a report published by the State of Wisconsin Department of Natural Resources, the spill was the result of construction of a sediment retaining basin over old coal ash deposits. "...the FGD sediment basin would potentially be constructed in coal ash deposits (see figure 5). During construction, ash deposits were found in the western portion of the FGD sediment basin. These deposits were removed and replaced with suitable soil in accordance with the contaminated materials management plan. However, a liner plan was not submitted to the Department when ash deposits were discovered..." "A significant component of the bluff collapse material appears to be the coal ash deposited in a ravine in the 1950s – 1960s."

This incident and other issues with groundwater contamination at or near coal combustion residual storage facilities has resulted in the US EPA considering new regulation of coal ash storage and significant companion actions on the legal, federal congressional and multiple governmental fronts.

In the absence of regulations, some coal burning power generation facilities and companies have voluntarily chosen, over the years, to apply the use of geosynthetic materials to the issues of coal ash storage. This paper addresses one such facility that was constructed in Hillsborough County near the city of Tampa, Florida. The facility was constructed in 1981/1982 and the barrier system consisted of a 2.0 mm (80 mil) High Density Polyethylene Liner (HDPE) which was manufactured by SLT (Schlegel Lining Technology) in Conroe, Texas. This facility of ~ 5.25 hectares, has operated successfully since the installation and has stored approximately 5.7×10^8 kilograms (~ 650,000 tons) of coal combustion residuals. Recently the decision was made, based on the age of the lining system, the appearance of a few stress cracks along extrusion welds at the tops of the slopes and the current legal and economic environment and significant costs associated with a leak or other containment failure, to replace the geomembrane with current, more advanced materials. This decision has offered a rare opportunity to obtain forensic samples for testing and evaluation and to document the performance of these materials subjected to real world aging and exposure conditions. Samples were obtained from multiple locations within the containment structure; at the bottom of the structure, along the side walls/slopes and at the freeboard level(s), from the upper sections of the side slopes which have seen a near continuous exposure and from the upper anchor trenches where the materials have only been exposed to soil and have neither had UV exposure, nor exposure to the stored ash materials.



Figure 1. Site overview during sample collection

1.2 Sample collection and Identification

Multiple samples were obtained for testing and evaluation. The samples are identified in the table below, which includes references to the sources of the sample and the existence or absence of field welds ("FW") within the sample.

Table 1. Sample Identification		
Sample Name	Field weld	Location
IC-2	N	South facing slope
IC-3-FW	Y	West slope at freeboard/waterline
IC-3	N	West slope at freeboard/waterline
IC-4-FW	Y	Floor sample
IC-4	N	Floor sample
IC-5	N	Toe of SE corner
AT	N	Anchor Trench

Data is presented on samples from 5 locations within the site. Descriptions are as follows: IC-2 is a sample from the southern facing (North) slope; this sample was above the evidence of waterline, near the anchor trench. IC-3 was taken from the western slope at the visible waterline deposits. It is presumed to have been exposed to the largest quantity of wet dry cycling. IC-4 was taken from the site floor and is assumed to have little UV exposure, but maximum chemical exposure. AT designates materials that were taken from the anchor trench on the upper perimeter of the site. These samples are presumed to have seen no UV, chemical exposure or highly variable moisture levels during the sites operation.

2. GEOMEMBRANE CONSTRUCTION AND HISTORICALLY COMPARABLE MATERIALS

Placing this material into proper context is important. In 1982, President Regan was still fighting the cold war, the Bell System provided telephone service, England and Argentina were at war over the Falkland islands, the Dow Jones Industrial Average was just over 800, and the USA Today newspaper premiered. A cell phone (the Nokia Senator model) and a computer (the Kaypro II) looked like this:



Figure 2.circa 1982 cell phone and computer

..and geomembranes were several generations earlier than current practice in performance and durability. Multiple advances have been made in machinery, process controls, and importantly, polymer characterization, dramatically reducing the residual catalyst levels within the polymer. New stabilizers that are more effective and more difficult to extract from the polymer matrix and other advances have rendered the exhumed geomembranes “ancient” in their overall composition and quality. Nevertheless the exhumed materials have done an excellent job of providing containment and protecting the environment.

The passage of three decades has also made it difficult to obtain comparative technical data for evaluation of the existing samples. The manufacturer does not have retained samples that are from the time period when the original materials were created and there is very limited data available. Three data sets are used in this paper for baseline comparison. Within a few years after the manufacture of this material, the National Sanitation Foundation (NSF) published NSF 54, a standard for minimum properties of geomembrane used to store potable water. NSF-54 has since been discontinued, however, during that general time period was the “standard” by which these materials could be expected to perform. Additionally, very limited test data from that time period has been found and can be used as a comparison. Also, the samples properties are (on a very unfair basis) compared with the existing materials standards (GM-13, Revision 10, date April 11, 2011). Again, in

historical context this would be similar to comparing the output of a secretary using an IBM Selectric Typewriter to the output from the Dell laptop that I used to write this paper.

Further, and perhaps most important, there was a major structural difference between the geomembrane that was exhumed and today's materials. This is the result of significant differences in the manufacturing equipment that was used to make the exhumed geomembrane and that which is used today. In the early 1980's equipment did not exist to manufacture geomembrane in the necessary widths in one continuous and uniform piece. In order to produce the needed widths, a geomembrane strip about 450 mm wide was extruded onto and across a large rotating drum about 6 m wide. This process was repeated and continued to produce a geomembrane ~ 6 meters in width and ~ 100 meters in length. The geomembrane thus contained hundreds of linear feet of "factory welds". These welds were, of course, present in the exhumed samples and are tested and compared with both the field welds and the un-welded "normal" sections of the geomembrane. In the following data, the sheet itself is given the designation from table one, where factory welds or field welds are tested, they are designated as such and peel and shear strength values are reported.

3. TESTING RESULTS

In the tables below, test results are reported and comparisons can be made between the four site locations that have been described above, where the geomembranes were exposed to the contained materials and the elements. Also included in the test results is geomembrane taken from the anchor trench which has the same age as the other four samples, but was not exposed to the contained materials or the elements. These results are compared with two industry standards of practice. The first is the National Sanitation Foundation (NSF) Standard 54 for materials in contact with potable water. The second the current version of the Geosynthetic Research Institute GM-13 "Standard Specification for Test Methods, Test Properties and Testing Frequency for High Density Polyethylene (HDPE) Smooth and Textured Geomembranes" and GM-19 "Standard Specification for Seam Strength and Related Properties of Thermally Bonded Polyolefin Geomembranes". Note the weld testing data is presented in English units as such units are representative of the methodology used when it was tested and in the opinion of this author, does not convert "cleanly" to SI units.

Table 3. Physical property comparisons Thickness, Tear, Puncture, Density, Dispersion								
Method	ASTM	D5199	D1004	D1004	D4833	D1505	D4218	D5596
		Thickness	Tear Strength		Puncture	Density	Carbon	Dispersion
	Direction		TD	MD			Black	# in Cat 1 & 2
Sample	Units	(mm)	(Kpa)	(Kpa)	(Kpa)	Gms/cm3	%	#
IC-2		2.02	0.0346	0.0349	0.0812	0.947	2.02	10
IC-3		2.04	0.0327	0.0329	0.0838	0.945	2.04	10
IC-4		2.08	0.0353	0.0364	0.0826	0.945	2.03	10
IC-5		2.07	-	-	-	0.947	2.04	10
AT		2.06	0.0331	0.0336	0.0853	0.948	2.08	10
NSF 54 requirement		2.03	0.0181	0.0181	N.S.	not listed	not listed	not listed
GM-13 requirement		2.03	0.0254	0.0254	0.0653	>0.940	2.0 to 3.0	9 or more

Table 4. Physical property comparisons Weld Strength Values					
Method D6392		Peel mode		Shear mode	
	mode	Strength	Separation	Strength	Separation
Sample	Units	(ppi)	(%)	(ppi)	(%)
IC-2 (factory weld)		-	-	221	1425
IC-3 (factory weld)		-	-	237	1335
IC-3-FW (field weld)		179	4	233	933
IC-4 (factory weld)		-	-	243	1194
IC-4-FW (field weld)		222	0	241	810
AT (factory weld)		-	-	223	750
NSF 54 requirement		FTB		108	
GM-19 requirment		121	25	160	50

Table 5. Chemical property comparisons OIT, NCTL				
Method	ASTM	D 3895	D 5885	D5397
		OIT	HP-OIT	NCTL
	Direction			
Sample	Units	(mins)	(mins)	(Hours)
IC-2		14	68	65
IC-3		6	106	64
IC-4		22	156	72
IC-5		12	131	90
AT		5	80	34
NSF 54 requirement		not listed	not listed	not listed
GM-13 requirement		>100	>400	>300

Additionally, samples of the materials were subjected to infrared analysis. The goal of this testing was to attempt to quantify the chemical degradation and oxidation of the geomembranes by observing the size of the peak(s) in the range of 1700-1750 cm^{-1} . The peaks in this range correspond to the quantity of carbonyl entities which are generated during the degradation of the geomembrane. The figure (2) below indicates some of the difficulty associated with that process. This figure presents results from three different scans from the same geomembrane sample (IC-4). The lowest (blue) line, labeled "smooth side" was taken from the underside of the sample and was in contact with the subgrade soils. The middle (green) line, labeled "rough side..." was taken from the top of the geomembrane in contact with the contained materials. The top (red) line labeled "below the exposed outside surface" was taken from the top of the geomembrane in contact with the contained materials after cleaning the surface of the geomembrane.

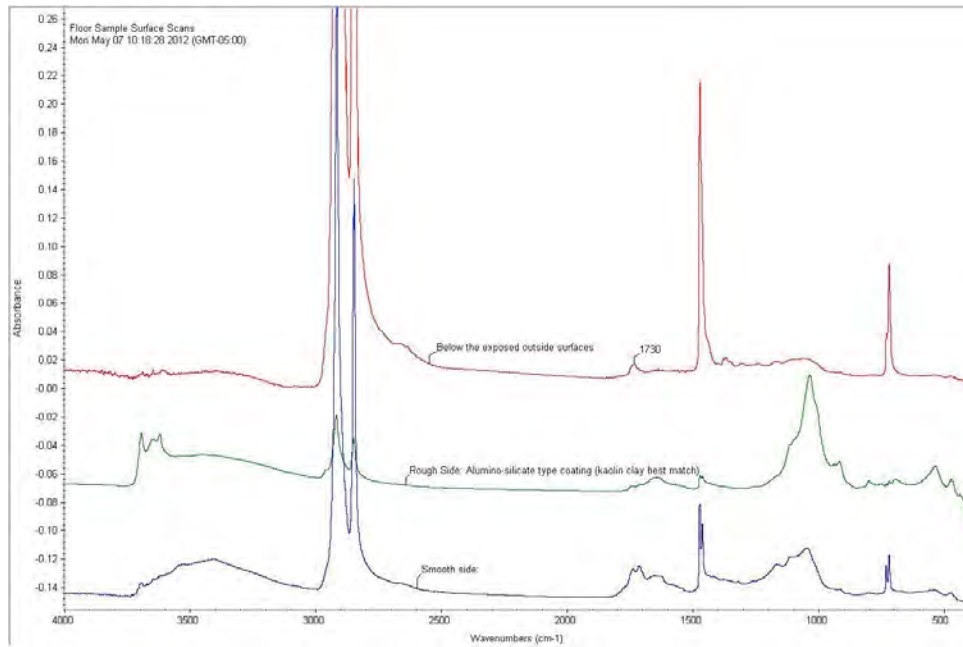


Figure 2. Infrared Spectrum of Sample IC-4 (floor)

The figure (3) below indicates the potential of this technique of investigation. This figure compares results from the same geomembrane sample (IC-4) with a sample taken from the anchor trench (AT). The now top (green) line, labeled “floor” was another scan of IC-4 taken from the top of the geomembrane in contact with the contained materials. The bottom (red) line labeled “anchor trench” was taken from the anchor trench and does shown qualitatively a lower degree of degradation and oxidation as compared to the other sample.

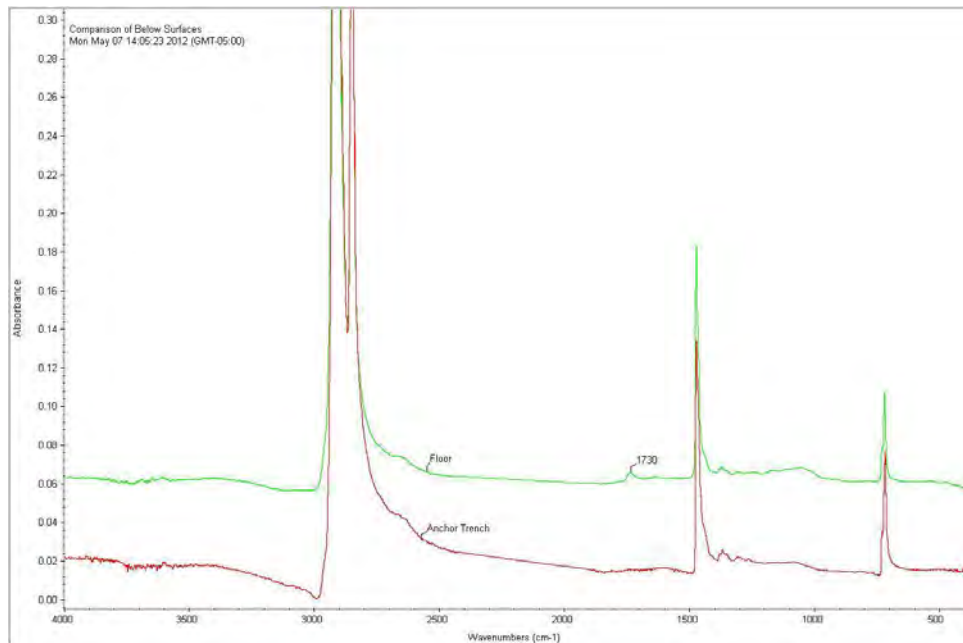


Figure 3. Infrared Spectrum of Sample IC-4 (floor) and AT (anchor trench)

The difficulty with the application of this technology is twofold. One issue is that the reading are taken on a very small portion of the sample and the selection of the specific area for testing can dramatically affect the results obtained, particularly if the degradation is not uniform in distribution as is often the case. Secondly, the deposition of foreign materials on the samples

and amount of cleaning that is done to the samples prior to testing can also strongly influence the test results. On the other hand degradation will first occur on the surface so it is important that surface changes be monitored.

4. CONCLUSION and ACKNOWLEDGEMENTS

Data has been presented on a 30 year old geomembrane that was used, successfully to contain coal ash. This data can be compared among the samples taken and evaluations and estimation of the further utility of the materials made. Clearly the geomembrane has 'aged" and suffered chemical oxidation and degradation. However the material's physical properties are still quite good even when compared to current standards. There are still stabilizers present in the aged materials as illustrated by the oxidative induction time (OIT) results. The performance of the geomembrane would appear to be in agreement with the scheme described in GRI report #16: "Long Term Durability of HDPE Geomembranes" and thus could be expected to supply containment service for several more decades. Admittedly the stress crack properties of the aged geomembrane being a legitimate concern; the "notched constant tensile load" (NCTL) properties are lower than current standards, but are consistent with the performance of geomembranes from that time period. As technology has advanced, the performance of this geomembrane clearly must be judged as inferior to current product. However, if one assumes that only the stress crack resistance was improved to current standards, the expected lifespan of currently produced materials would be in agreement or potentially exceed expected lifespan predictions. In short, even old geomembrane has done a good job of coal ash containment, there is every reason to expect current improved materials to offer improved performance.

In addition to recognizing the contributions of my co-authors, without whom this paper would have not come to realization, I should also offer thanks to Mr. David Barnett, Project Manager for COMANCO Environmental Corporation. Comanco was a key supporter of this effort; further inquiries regarding the installation can be addressed to David or to Mr. Mark Topp, President, COMANCO Environmental Corporation. Additionally Dr. Lili Cui, Plastics/Polymer Engineer for Chevron Phillips Chemical Company LP should be recognized for her and CP Chem's support of the IR/analytical portion of this work; their support is greatly appreciated.

REFERENCES

- Jones, M. and Behm, D. "Bluff Collapse at Wisconsin Powerplant Sends Dirt, Coal Ash Into Lake Michigan", Milwaukee Journal Sentinel/Engineering News Record, November 1, 2011 Accessed November 3, 2011
http://www.enr.com/yb/enr/article.aspx?story_id=165390983
- U.S.EPA (2002) 25 Years of RCRA: Building on Our Past To Protect Our Future, EPA-K-02-027, Washington D.C. USA
- "Regulatory Determination on Wastes from the Combustion of Fossil Fuels; Final Rule." Federal Register 65:99 (May 22, 2000) Page 32213-32237. Available from: US EPA, www.epa.gov; Accessed: 11/11/11.
- "Hazardous and Solid Waste Management System; Identification and Listing of Special Wastes; Disposal of Coal Combustion Residuals From Electric Utilities; Proposed Rule." Federal Register 75:118 (June 21, 2010) Page 35127-35264. Available from: The United States Government, www.regulations.gov; Accessed: 11/11/11.
- "Bevill Amendment Questions" US EPA Updated as of May 1, 2009. Accessed 10/23/11
<http://www.epa.gov/compliance/assistance/sectors/minerals/processing/bevillquestions.html>
- "Fossil Fuel Combustion (FFC) Waste Legislative and Regulatory Time Line". US EPA. Updated as of October 20, 2011. Accessed 10/24/11 <http://www.epa.gov/wastes/nonhaz/industrial/special/fossil/regs.htm>
- "Information Request Responses from Electric Utilities". US EPA. Updated as of August 16, 2011. Accessed 11/11/11
<http://www.epa.gov/epawaste/nonhaz/industrial/special/fossil/surveys/index.htm#databaseresults>
- "Kingston Fossil Plant coal fly ash slurry spill". Wikipedia. Updated as of September 19, 2011. Accessed 10/24/11
http://en.wikipedia.org/wiki/Kingston_Fossil_Plant_coal_fly_ash_slurry_spill
- "Long Term Durability of HDPE Geomembranes": GRI report #16 Geosynthetic Institute, Folsom, Pennsylvania, USA
- GM-13 "Standard Specification for Test Methods, Test Properties and Testing Frequency for High Density Polyethylene (HDPE) Smooth and Textured Geomembranes", Geosynthetic Institute, Folsom, Pennsylvania, USA
- GM-19 "Standard Specification for Seam Strength and Related Properties of Thermally Bonded Polyolefin Geomembranes", Geosynthetic Institute, Folsom, Pennsylvania, USA
- NSF 54-1993, Flexible Membrane Liners - WITHDRAWN - NSF International, 01-Nov-1993

Studies on Behaviour of Footings on Prestressed Geogrid Reinforced Granular Bed Overlaying Weak Soil

Jayamohan,J., Shivashankar,R., Aswathy,M.S. and Vigey Mary, W.
National Institute of Technology Karnataka, Surathkal, Mangalore, India 575025
jayamohan7@gmail.com, shivashankar.surathkal@gmail.com

ABSTRACT

This paper studies the effects of prestressing the reinforcement in granular bed on the load carrying capacity and settlement response of a geogrid reinforced granular bed (RGB) overlying weak soil. A series of laboratory scale bearing capacity tests are conducted to study the behaviour of unreinforced (GB), reinforced (RGB) and prestressed geogrid reinforced (PRGB) granular bed overlying weak soil. The parameters varied are strength of the underlying weak soil, thickness of the GB, magnitude of prestressing force applied and direction of prestressing forces. It is found that there is a significant improvement in bearing capacity and reduction in settlements, by addition of prestress to the geogrid reinforcement. Biaxial Prestressing is found to be better than uniaxial prestressing. A punching shear failure (numerical) model is envisaged. The BCR (Bearing Capacity Ratio) values predicted from the model are found to be in good agreement with the experimentally obtained BCR values.

1 INTRODUCTION

Over the past three decades, the beneficial use of various types of geosynthetics to increase the bearing capacity of soil has been clearly established. Extensive research has been carried out by several researchers to understand the role of reinforcement materials in improving the bearing capacity of foundation soils. The use of geosynthetic reinforced foundation bed over weak soil effectively reduces settlement and increases the bearing capacity of weak soil. Many experimental and analytical studies have been performed to investigate the behaviour of reinforced foundation beds for different soil types (eg. Binquet and Lee (1975), Shivashankar et al. (1993)). Several experimental and analytical studies were conducted to evaluate the bearing capacity of footings on reinforced soil (eg. Shivashankar et al. (1993); Shivashankar and Reddy (1998); Madhavilatha and Somwanshi (2009); Alamshahi and Hataf (2009); Vinod et al. (2009) etc).

Earlier studies have shown that geosynthetics demonstrate their beneficial effects only after considerable settlements, since the strains occurring during initial settlements are insufficient to mobilize significant tensile load in the geosynthetic. This is not a desirable feature since for foundations of certain structures; the values of permissible settlements are low. Thus there is a need for a technique which will allow the geosynthetic to increase the load bearing capacity of soil without the occurrence of large settlements. Lovisa et al. (2010) conducted laboratory model studies and finite element analyses on a circular footing resting on sand reinforced with prestressed geotextile. The improvement in bearing capacity due to prestressing the reinforcement was particularly studied. It was found that the addition of prestress to reinforcement resulted in significant improvement in the load bearing capacity and reduction in settlement of foundation.

The purpose of this paper is to study the effects of prestressing the reinforcement in granular bed on the load-bearing capacity and settlement response of a reinforced granular bed overlying weak soil. The study involved laboratory model tests on a square footing of size 100mm x 100mm x 20 mm thick. Numerical analysis is conducted using the improvised model of Shivashankar et al. (1993) and the results are compared with those obtained from the model tests. The parameters studied are the strength of the underlying weak soil, thickness of granular bed, magnitude of prestress, direction of prestress. The settlements at the interface between weak soil and GB are also measured.

2 EXPERIMENTAL PROGRAMME

The experimental programme mainly involved a series of laboratory scale bearing capacity tests (typically one-tenth scaled model tests) conducted on a model footing resting on a prestressed reinforced granular bed overlying weak soil. Details of the experimental programme, test procedures and analysis of test results are presented in the following paragraphs.

2.1 Materials

The material used for granular bed is well graded medium sand and its properties are given in Table 1 and particle size distribution is shown in Figure 1. Locally available soil termed as 'Shedi soil' is used as weak soil and its properties are also given in Table 1 and particle size distribution is shown in Figure 1. The Shedi soil is used in two conditions namely moist condition (termed as moist soil or weak soil 1) and also used in submerged condition (termed as submerged soil or weak soil 2). The reinforcement used is geogrid and its properties are given in Table 2. The geogrid used is a somewhat weak geogrid with a tensile strength of only 7.68 kN/m, for purpose of laboratory scale model tests.

Table 1. Properties of sand and weak soils used in the model tests

Property	Sand	Value	
		Weak soil 1 (Moist soil)	Weak soil 2 (Submerged soil)
Specific gravity	2.61	2.32	2.32
Average dry unit weight during model test (kN/m ³)	16.60	16.00	16.00
Void ratio during model test	0.54	0.42	0.42
Water content during model test (%)	0	10	31.5
Effective grain size D ₁₀ (mm)	0.50	0.11	0.11
D ₆₀ (mm)	1.30	0.155	0.155
D ₃₀ (mm)	0.80	0.125	0.125
Coefficient of uniformity C _u	2.60	1.41	1.41
Coefficient of curvature C _c	1.00	0.92	0.92
Friction angle Φ (degrees)	31.0	12	6
Cohesion (kPa)	0	10	5.5

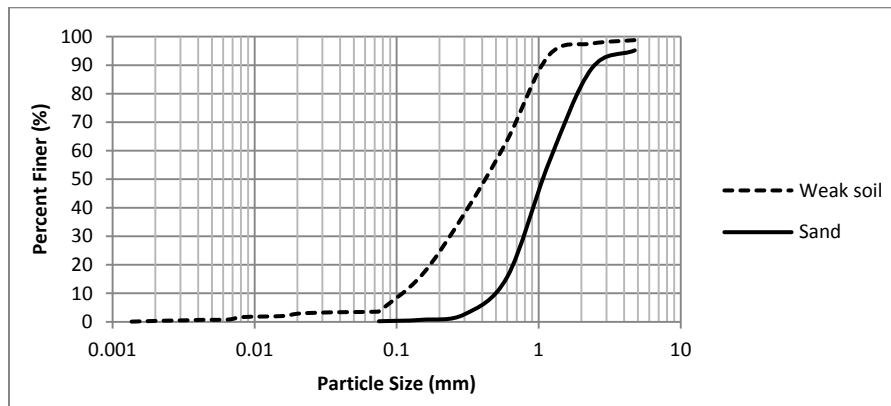


Figure 1. Particle size distribution of sand and weak soil used

Shedi soils are predominantly found in the west coast (Konkan coast) of southern peninsular India and most of the foundations are placed on this soil layer. These soils are problematic in the sense that their strength reduces drastically under saturation condition, which is the typical behaviour of dispersive type of soils. It has resulted in many foundation problems wherever it is met with in this area.

2.2 Test Setup

Laboratory scale bearing capacity tests are carried out on a square rigid footing made of mild steel. The dimensions of the model footing are 100mm x 100mm x 20 mm thick. The model footing is kept on the surface of soil during all the tests. The test tank is made of ferrocement having internal dimensions 0.75 m x 0.75m in plan (7.5 times size of footing and sufficient to nullify any edge effects) and 0.75m high (Figure 4). A single layer of reinforcement is used. The prestress applied is equal to 1%, 2% and 3% of the tensile strength of the geogrid and is distributed over three pulleys. In uniaxial prestressing the prestress is applied only in the X-direction whereas in biaxial prestressing it is applied in both X and Y directions as shown in Figures 2 & 3 respectively. The figure of the test setup is shown in Figure 4 and photograph of the same is shown in Figure 5.

The load is applied using a hydraulic Jack of 10 kN capacity. The load is measured using a proving ring and deformation using two dial gauges placed diametrically opposite to each other. Preparation of underlying soil in all the tests involved compaction

of soil using a rammer. In the preparation of foundation (granular) bed, the sand was compacted using a small plate vibrator. The densities to which the soils were compacted are indicated in Table 1.

Table 2. Properties of geogrid used in the model tests

Property	Value
Mass per unit area (gm/m^2)	730.00
Aperture size (mm)	8 x 6
Thickness (mm)	3.30
Tensile strength (kN/m)	7.68
Extension at maximum load (%)	20.20
Color	Black
Polymer	HD-Polyethylene

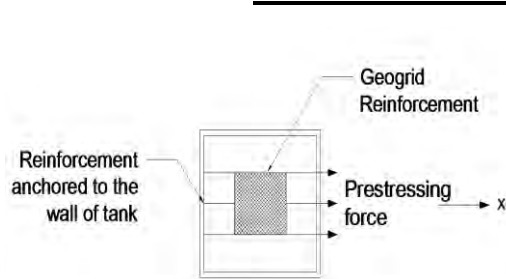


Figure 2. Uniaxial prestressing

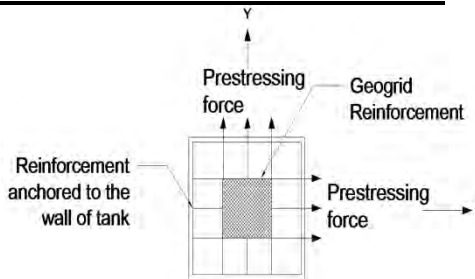


Figure 3. Biaxial prestressing

In the literature, it is reported that optimum depth of placement of the first layer of reinforcement is 0.2B to 0.5B (B is the width of footing) (Sharma et al. 2009). The depth of reinforcement from the base of footing is adopted as 0.5B for all the tests. Same procedure and same compactive effort are used in all the tests to maintain consistency and for sake of comparison.

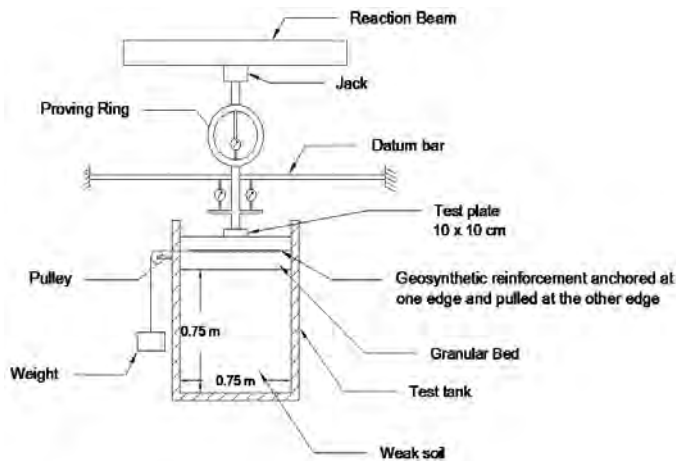


Figure 4. Test set up



Figure 5. View of test set up

2.3 Test Details

At first the weak soil is filled in the ferrocement tank to the required level with compaction done in layers, to achieve the pre-determined density. Then sand is filled up to the bottom level of reinforcement and compacted. The reinforcement is then placed with its centre exactly beneath the jack, and the prestress is applied. Then sand above the reinforcement is placed and compacted to the pre-determined density. Thus prestressing is applied before the top layer of granular fill is placed and compacted. In all the tests, reinforcement is kept at a depth of 50 mm (0.5 B) from the base of model footing. The compactive effort required to achieve the required density of both the soils is determined by trial and error. The settlement is measured using two dial gauges and their average value is adopted. The settlement at the interface between two soils is determined by measuring the levels at specified points at regular intervals on the surface of weak soil before and after each test. The test

tank is emptied and refilled for each test to ensure that controlled conditions are maintained throughout the investigation. The details of testing programme are given in Table 3.

Table 3. Testing programme

Series	Type	Thickness	Prestress
A	Weak soil 1 (Moist soil) (Unreinforced) Granular bed (GB) on weak soil 1	B & 2B	
B	Reinforced granular bed (RGB) on weak soil 1	B & 2B	
C	Prestressed reinforced granular bed (PRGB) on weak soil 1	B & 2B	Uniaxial 1%,2%&3%
D	Prestressed reinforced granular bed on weak soil 1	B & 2B	Biaxial 1%,2%&3%
E	Weak soil 2 (Submerged soil) (Unreinforced) Granular bed on weak soil 2	B & 2B	
F	Reinforced granular bed on weak soil 2	B & 2B	
G	Prestressed reinforced granular bed on weak soil 2	B & 2B	Uniaxial 1%,2%&3%
H	Prestressed reinforced granular bed on weak soil 2	B & 2B	Biaxial 1%,2%&3%

Under series A, tests are conducted on weak soil 1 (moist soil) and on weak soil 1 overlain with unreinforced granular bed of thickness B or 2B. Under series B, tests are conducted on weak soil 1 overlain with reinforced granular bed of thickness B or 2B. Under series C, tests are conducted on weak soil 1 overlain with prestressed reinforced granular bed. The prestress applied is uniaxial. The parameters varied are magnitude of prestress and thickness of granular bed. Series D is similar to series C except that prestress applied is biaxial. Series E, F, G and H are similar to series A, B, C and D respectively, except that the underlying soft soil is kept submerged (termed as weak soil 2). The level of water table in the test tank is monitored by installing four peizometers.

3 NUMERICAL ANALYSIS

In the present study, loading tests on unreinforced and reinforced granular beds are simulated numerically by improving the model proposed by Shivashankar et al. (1993). They proposed a punching shear failure mechanism in which both the footing and the portion of the reinforced granular bed directly beneath the footing are envisaged to act in unison to punch through the soft soil underneath. The improvement in bearing capacity of a reinforced granular bed is considered to comprise of three components namely Shear layer effect, Confinement effect and Surcharge effect. These effects are represented in Figures 6, 7 & 8(a), respectively. They proposed the following equations for computing Bearing Capacity Ratio (BCR).

$$BCR = 1 + \Delta BCR_{SL} + \Delta BCR_{CE} + \Delta BCR_{SE} \quad [1]$$

Where

ΔBCR_{SL} , ΔBCR_{CE} , ΔBCR_{SE} = Improvement in bearing capacity ratio due to Shear layer, Confinement and Surcharge effects respectively

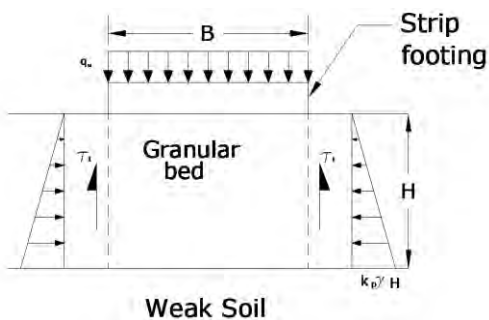


Figure 6. Shear layer effect for GB, RGB and PRGB (Shivashankar et al. 1993)

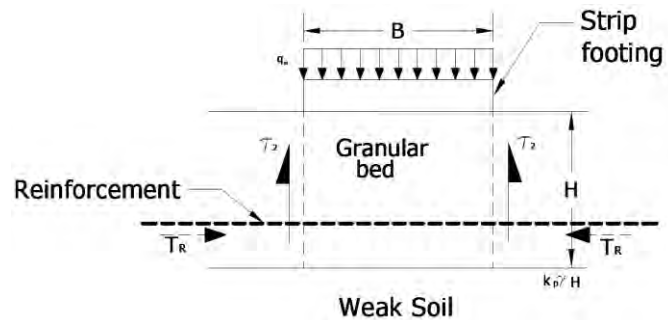


Figure 7. Confinement effect for GB, RGB and PRGB (Shivashankar et al. 1993)

3.1 Shear Layer Effect

In shear layer effect, the shear stress mobilized along the failure surface due to the passive pressure developed in soil is considered (Figure 6). The equation proposed for strip footings is

$$\Delta BCR_{SL} = 2 \tau_1 / Q \quad [2]$$

$$\tau_1 = P_p \tan \phi_s \quad [3]$$

$$\Delta q_{SL} = 2 \tau_1 / B \quad [4]$$

Where

Q = Bearing capacity of underlying weak soil

τ_1 = Total vertical force along the punching shear failure plane due to shear layer effect

P_p = Force due to passive pressure developed on the sides of failure surface, acting normally, per unit length

ϕ_s = Angle of shearing resistance.

The above equation was developed for a strip footing. In the present study, since a square footing is used, the equation is modified as given below

$$\tau_1 = P_p' \tan \phi_s \quad [5]$$

$$\Delta BCR_{SL} = 4 \tau_1 / Q \quad [6]$$

$$\Delta q_{SL} = 4 \tau_1 / B^2 \quad [7]$$

Where

P_p' = The passive pressure developed on each of four sides of square column of granular soil beneath the square footing of width 'B'

3.2 Confinement Effect

The tensile stress mobilized in the reinforcement will provide a confinement effect to the soil beneath the footing. The shear stress developed along the failure surface due to this confining stress is considered here (Figure 7). The equation proposed for strip footing was

$$\Delta BCR_{CE} = 2 \tau_2 / Q \quad [8]$$

$$\tau_2 = T_R \tan \phi_s \quad [9]$$

$$\Delta q_{CE} = 2 \tau_2 / B \quad [10]$$

Where

τ_2 = Total vertical force along the punching shear failure plane due to confinement effect of reinforcement

T_R = Tensile stress mobilized in the reinforcement = $2L\sigma_v \tan \delta$

L = Length of reinforcement beyond the failure surface

σ_v = Vertical stress at the level of reinforcement

δ = angle of friction between reinforcement and soil = ϕ_s for geogrid

The above equation was developed for a strip footing. In the present study, since a square footing is used, the equation is modified as given below

$$\tau_2 = T_R' \tan \phi_s \quad [11]$$

$$\Delta BCR_{CE} = 4 \tau_2 / Q \quad [12]$$

$$\Delta q_{CE} = 4 \tau_2 / B^2 \quad [13]$$

Where

T_R' = Tensile stress mobilized in reinforcement beyond each of the four sides of square column of granular soil beneath the square footing

B = Width of the square footing

In the case of PRGB, if the friction on reinforcement (on one side of the square prism, along plane of reinforcement) is less than the applied prestress, value of T_R' is taken as equal to the value of applied prestress. If the friction in reinforcement is more than applied prestress, the value of T_R' is taken as equal to value of frictional resistance over the reinforcement. The same principle applies also in the case of field application of PRGB. However the optimal value of prestress to be applied to the reinforcement in field will have to be investigated and is expected to be larger than laboratory optimal value due to larger vertical stress on reinforcement. Stronger geogrid will have to be used in field and strength of geogrid is not likely to influence the confinement effect.

3.3 Additional Surcharge Effect

The vertical stresses along the punching shear failure surface due to shear layer effect and confinement effect are envisaged to act as a surcharge stress on the underlying soft soil. There will be an improvement in bearing capacity due to this surcharge stress. The distribution of this surcharge stress was assumed to be exponential as shown in Figure 8(a) for a strip footing (Shivashankar et al. 1993). The improvement in bearing capacity due to this surcharge stress is given by

$$q_o = 0.84(\Delta BCR_{SL} + \Delta BCR_{CE}) \quad [14]$$

Where q_o = Intensity of surcharge stress at the edge of the failure plane due to shear layer and confinement effects

Surcharge stress was envisaged to decrease exponentially from q_o at edge of footing to $0.01q_o$ at end of reinforcement. In the present study, in case of PRGB, the additional surcharge stress is envisaged to be uniform over the reinforcement in the direction of prestressing (Figure 8(b)). This is also justified from the measured settlements. In case of Uniaxial prestressing, the surcharge stress is considered to decrease exponentially in the cross direction. Average surcharge stress is considered around the square footing and accordingly ΔBCR_{SE} is estimated.

$$\Delta BCR_{SE} = q_{avg} \times N_q \quad [15]$$

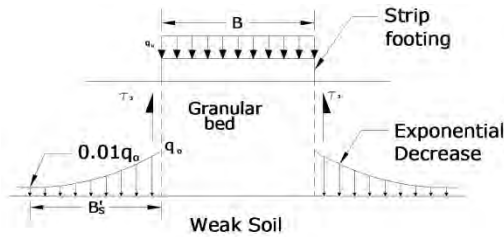


Figure 8(a). Surcharge effect for GB and RGB (Shivashankar et al. 1993)

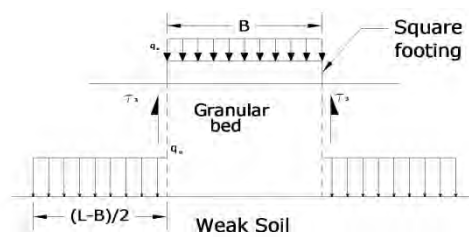


Figure 8(b). Surcharge effect for PRGB proposed in the present study

4 RESULTS AND DISCUSSION

4.1 Improvement in Bearing Capacity

Vertical stress (load per unit area) vs normalized settlement curves are shown in Figures 9 to 18. The footing settlement 'S' is expressed in non-dimensional form as 'S/B' (%). It is clearly observed that the addition of prestress significantly improved the settlement behaviour of soil. The load carrying capacity of footing is also significantly improved.

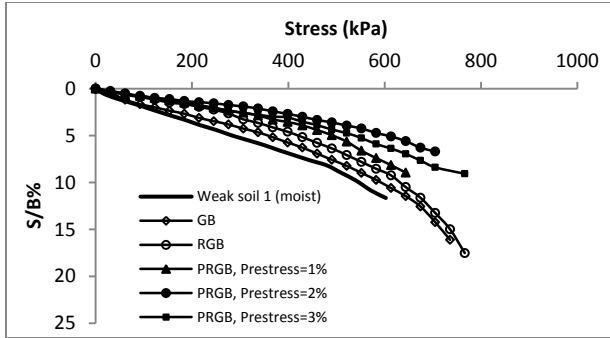


Figure 9. Stress vs normalized settlement curves for granular bed of thickness B with uniaxial prestressing overlying (moist) weak soil 1

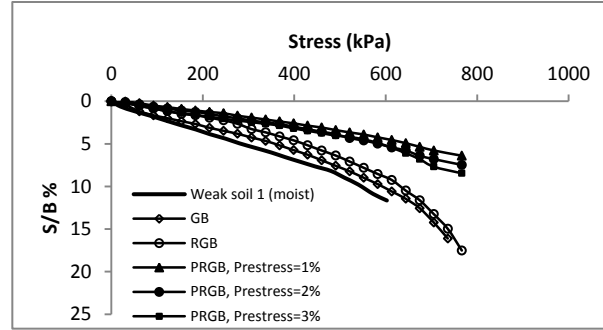


Figure 10. Stress vs normalized settlement curves for granular bed of thickness B with biaxial prestressing overlying (moist) weak soil 1

4.1.1 Effect of Magnitude of Prestress and Type of Weak Soil

4.1.1.1 Granular Beds Overlying (Moist) Weak Soil 1

From Figure 9 which represents the variation of bearing pressure with footing settlement of uniaxially prestressed granular bed of thickness B overlying (moist) weak soil 1, it can be seen that maximum improvement is observed when the magnitude of prestress is equal to 2% of the tensile strength of reinforcement. Further addition of prestress is not beneficial. However for a granular bed of thickness B with biaxial prestressing overlying (moist) weak soil 1, it is observed that the maximum improvement in settlement behaviour occurred when the magnitude of prestress is equal to 1% of the tensile strength of reinforcement. Further increase in prestress is not beneficial (Figure 10).

The results obtained from a granular bed of thickness 2B with uniaxial prestressing overlying (moist) weak soil 1 are shown in Figure 11. It is observed that the maximum improvement is when the magnitude of prestress is equal to 3% of the tensile strength of reinforcement. The results obtained from a granular bed of thickness 2B with biaxial prestressing overlying (moist) weak soil 1 (Figure 12) indicates that maximum improvement is also got when the magnitude of prestress is equal to 3% of the tensile strength of reinforcement.

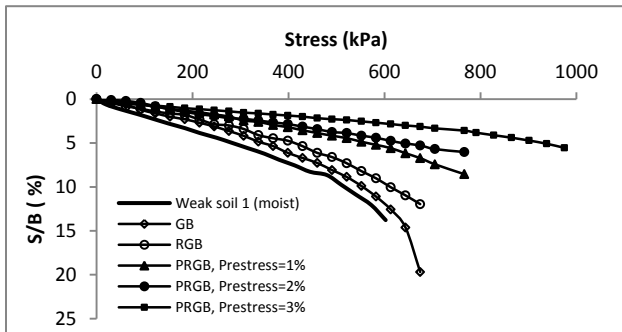


Figure 11. Stress vs normalized settlement curves for granular bed of thickness 2B with uniaxial prestressing overlying (moist) weak soil 1

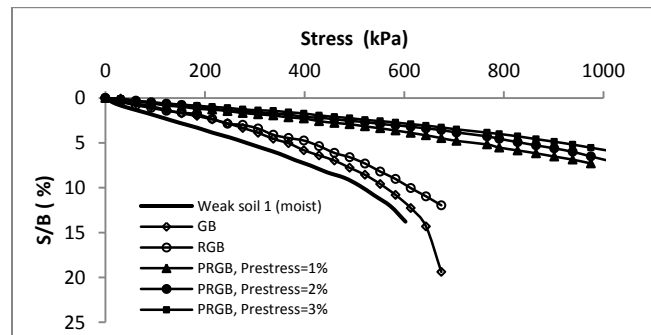


Figure 12. Stress vs normalized settlement curves for granular bed of thickness 2B with biaxial prestressing overlying (moist) weak soil 1

4.1.1.2 Granular Beds Overlying (Submerged) Weak Soil 2.

Figure 13 presents the variation of bearing pressure with footing settlement of uniaxially prestressed granular bed of thickness B overlying (submerged) weak soil 2. It can be seen that maximum improvement is observed when the magnitude of prestress is equal to 2% of the tensile strength of reinforcement. Further addition of prestress did not show any improvement. This is same as in case of weak soil 1. In case of granular bed of thickness B with biaxial prestressing overlying submerged weak soil2, from Figure 14, it is observed that the maximum improvement in settlement behaviour occurs when the magnitude of prestress is equal to 2% of the tensile strength of reinforcement. Further increase in prestress showed no gain.

This is unlike in case of weak soil 1, which peaked at 1% itself. With increased thickness of granular bed to 2B and with uniaxial prestressing overlying (submerged) weak soil 2, it is observed (Figure15) that the maximum improvement is observed when the magnitude of prestress is again equal to 2% of the tensile strength of reinforcement. Further increase in prestress caused a reduction in the improvement in bearing capacity.

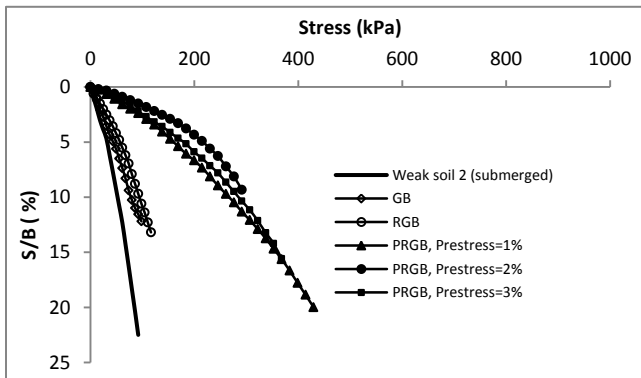


Figure 13. Stress vs normalized settlement curves for granular bed of thickness B with uniaxial prestressing overlying (submerged) weak soil 2

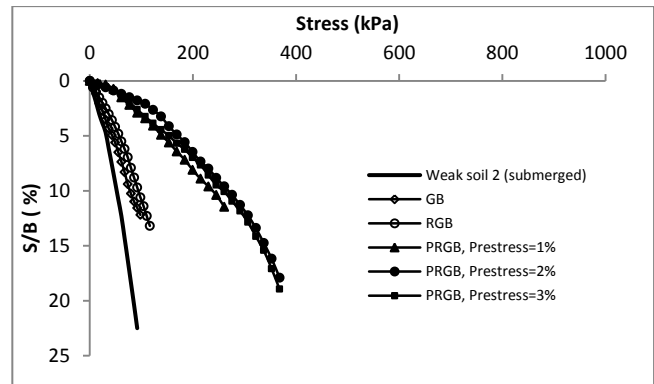


Figure 14. Stress vs normalized settlement curves for granular bed of thickness B with biaxial prestressing overlying (submerged) weak soil 2

It is also observed that the improvement in bearing capacity when the prestress was increased from 1% to 2% was only marginal. The results obtained from a granular bed of thickness 2B with biaxial prestressing overlying (submerged) weak soil 2, it is observed that the improvement in settlement behaviour with 3% prestress is less than that with 1% and 2% (Figure 16).

4.1.2 Effect of Thickness of Granular Bed

For moist soil (weak soil 1) experimental results indicate that greater prestress (of 3%) is optimal for thicker granular bed (Figure 17). However from Figures 13 to 16, for submerged soil (weak soil 2), 2% prestressing is found to be optimal for both B and 2B thickness of granular bed, for both uniaxial and biaxial prestressing.

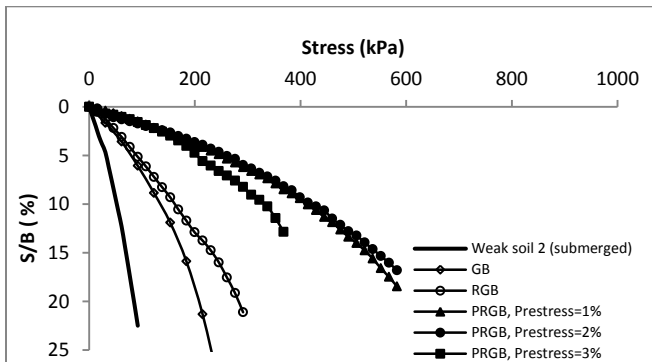


Figure 15. Stress vs normalized settlement curves for granular bed of thickness 2B with uniaxial prestressing overlying (submerged) weak soil 2

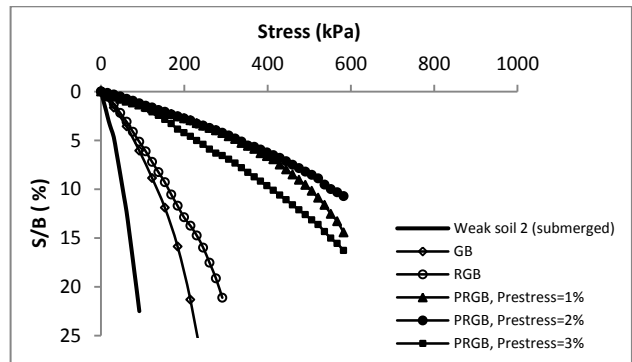


Figure 16. Stress vs normalized settlement curves for granular bed of thickness 2B with biaxial prestressing overlying (submerged) weak soil 2

4.1.3 Effect of Direction of Prestress

A comparison between the experimentally observed improvements in settlement behaviour of a granular bed of thickness B, overlying (moist) weak soil 1, due to uniaxial and biaxial prestressing is shown in Figure 18. Therein and from other figures it is observed that improvement in settlement behaviour is generally better when prestress is biaxial.

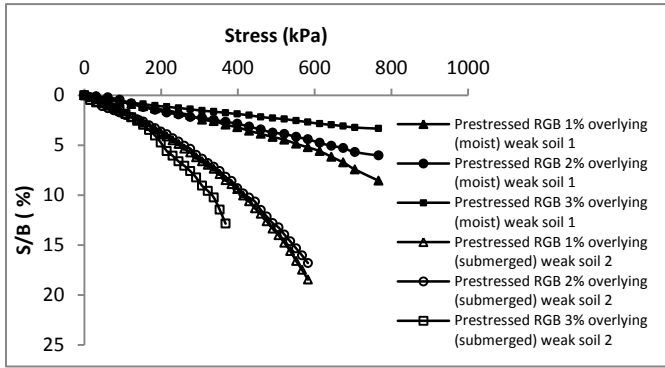


Figure 17. Comparison between stress vs normalized settlement curves for GB of thickness 2B overlying (moist) weak soil 1 and (submerged) weak soil 2 with uniaxial prestressing

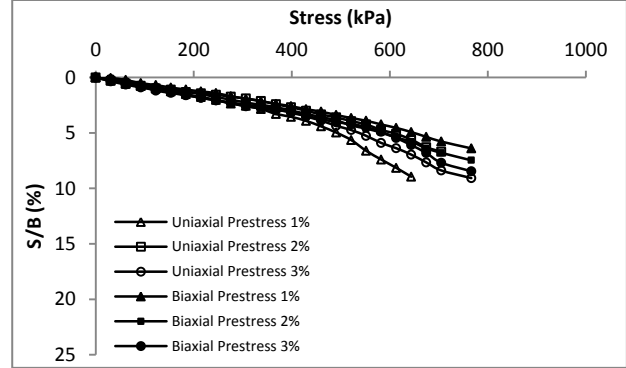


Figure 18. Comparison between stress vs normalized settlement curves for GB of thickness B overlying (moist) weak soil 1 with uniaxial and biaxial prestressing

4.1.4 Initial Stiffness Modulus

The initial stiffness modulus is defined as slope of initial part of the stress – strain curve, ie at origin. Strain is calculated as 'S/B' when the granular bed thickness is 'B' and as 'S/2B' when the granular bed thickness is '2B'. The variation of initial stiffness modulus with prestress for granular bed of thickness B is shown in Figure 19. It is observed from the figure that for weak soil 1 with uniaxial prestress, the initial stiffness modulus is maximum when the prestress is 2%, and for biaxial prestress, 1% prestress is found to be optimum. In weak soil 2, for both uniaxial and biaxial prestress, maximum initial stiffness modulus is at 2% prestress.

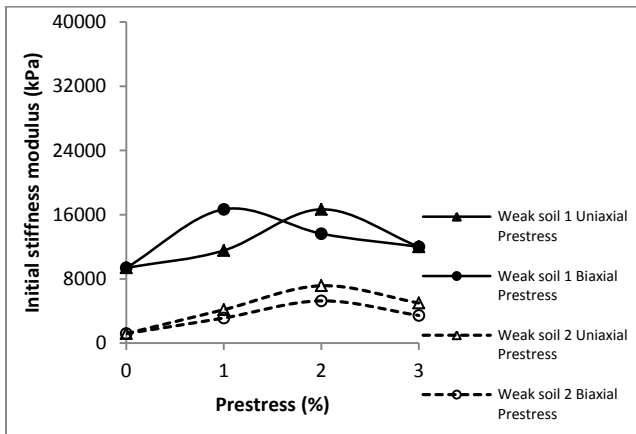


Fig 19. Prestress vs initial stiffness modulus curves for granular bed of thickness B

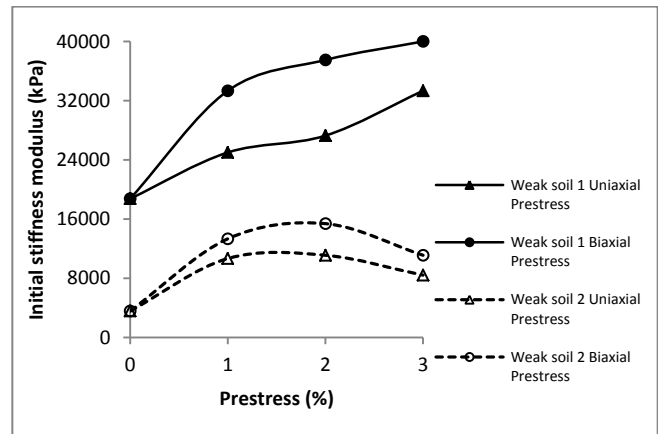


Fig 20. Prestress vs initial stiffness modulus curves for granular bed of thickness 2B

The maximum value of initial stiffness modulus for weak soil 1 with granular bed of thickness 2B for both uniaxial and biaxial prestressing is when the prestress is equal to 3%, whereas for weak soil 2, prestress of 2% is found to be most optimal (Fig 20).

4.2 Numerical Analysis

All the above various cases are analysed numerically using the 'improvised model' of Shivashankar et al. (1993) proposed in this paper. The Bearing Capacity Ratios (BCRs) obtained experimentally and those predicted by the model are shown graphically in Figure 21. It is observed that the model predicts the bearing capacity ratio with fairly good accuracy, especially for the moist soil (weak soil 1).

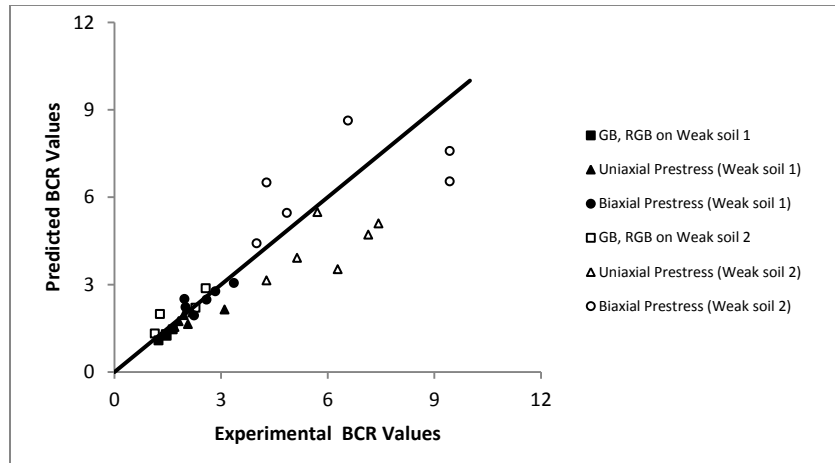


Figure 21. Comparison between observed and predicted values of bearing capacity ratios (BCRs) for GB, RGB and PRGB overlying (moist) weak soil 1 and (submerged) weak soil 2

5 CONCLUSIONS

Based on the results obtained from experimental and numerical studies, the following conclusions can be made on the behaviour of prestressed reinforced granular beds overlying weak soils.

1. The addition of prestress to geogrid reinforcement significantly improves the bearing capacity and settlement behaviour of the soil. Prestressing the geosynthetic reinforcement results in increased load bearing capacity of soil without the occurrence of large settlements, as compared to geosynthetics without any prestress. Improvement is more significant in case of submerged soil (weak soil 2) when compared to moist soil (weak soil 1).
2. The improvement in bearing capacity depends upon the thickness of granular bed, magnitude of prestress and the direction of prestress. The improvement in bearing capacity is found to be more with biaxial prestressing than uniaxial prestressing. The improvement in bearing capacity increases with the thickness of granular bed.
3. The proposed numerical model predicts the bearing capacity ratios for granular beds overlying weak soil with reasonably good accuracy.
4. Experimental results indicate that greater prestress of about 3% is optimal for thicker granular beds on moist soil (thickness of 2B).

REFERENCES

- Alamshahi, S. and Hataf, N. (2009). Bearing capacity of strip footings on sand slopes reinforced with geogrid and grid-anchor, *Geotextiles and Geomembranes*, 27 (2009) 217 – 226.
- Binquet, J. and Lee, K.L. (1975). Bearing capacity tests on reinforced earth slabs. *Journal of Geotechnical Engineering Division*, ASCE 101 (12), 1241–1255.
- Lovisa, J., Shukla, S.K. and Sivakugan, N. (2010). Behaviour of prestressed geotextile-reinforced sand bed supporting a loaded circular footing, *Geotextiles and Geomembranes*, 28 (2010) 23 – 32.
- Madhavilatha, G. and Somwanshi, A. (2009). Bearing capacity of square footings on geosynthetic reinforced sand, *Geotextiles and Geomembranes*, 27 (2009) 281 – 294.
- Sharma, R., Chen, Q., Farsakh, M.A. and Yoon, S. (2009). Analytical modeling of geogrid reinforced soil foundation, *Geotextiles and Geomembranes*, 27 (2009) 63 – 72.
- Shivashankar, R., Madhav, M.R. and Miura, N. (1993). Reinforced granular beds overlying soft clay, *Proceedings of 11th Southeast Asian Geotechnical Conference*, Singapore, 409 – 414.
- Shivashankar, R. and Reddy, A.C.S. (1998). Reinforced granular bed on poor filled up shedi ground, *Proceedings of the Indian Geotechnical Conference - 1998*, Vol.1, 301-304.
- Vinod, P., Bhaskar, A.B. and Sreehari, S. (2009). Behaviour of a square model footing on loose sand reinforced with braided coir rope, *Geotextiles and Geomembranes*, 27 (2009) 464 – 474.

Studies on the Engineering Behaviour of Coir Waste Mixed Soil

Balan K., Ph. D., College of Engineering Trivandrum, India, drkbalan@gmail.com

Jayasree P. K., Ph. D., College of Engineering Trivandrum, India, jayasreepk@yahoo.com

Nisha K. K., B. Tech., College of Engineering Trivandrum, India, nknishakk@gmail.com

Thushara T. S., B. Tech., College of Engineering Trivandrum, India, thusharathulasee@gmail.com

ABSTRACT

The State of Kerala, which is named after coconut tree, has the first place in the production of coir, in India. The waste generated during the process includes coir pith along with some baby fibers. For every 1 kg of coir fiber production 2 kg of coir pith is generated. The disposal of this coir waste becoming a major issue nowadays. Soil reinforcement using randomly distributed fibers has been proved fruitful. The use of natural fibers in soil stabilization is often advantageous as they are cost effective and locally available. No major studies are conducted on the influence of the coir waste in the engineering behavior of soil. The present study investigates the compaction characteristics of two types of soils mixed with different percentages of coir waste. The main objective of the present investigation is to assess the usefulness of coir waste as a soil admixture, especially for pavement construction.

1. INTRODUCTION

Coconut (*Cocos nucifera* Lignin) is one of the most useful palms to mankind amongst the various tropical palms. Coir pith is a biomass residue generated during the extraction of coir fiber from coconut husk and is a byproduct of the coir manufacturing industry. Normally, they are dumped as agricultural waste and become accumulated as a waste product in the form of heaps of coarse and fine particles with lots of baby fibre and short fibre. It is estimated that at present there is an accumulated stock of 10×10^6 metric tons of coir pith in Kerala. This waste has traditionally been disposed off by burning, which results in various environmental problems, including carbon deposits as well as the warming of the atmosphere. During the rainy season, the tannins and phenols of the coir pith are leached out into the soil and into the irrigation canals, thereby making agricultural lands unproductive. Moreover, the water pollution caused by such leaching is harmful to the aquatic and soil biological life. Therefore, finding out an alternate way to dispose the coir pith is of critical importance.

The concept of soil reinforcing with tensile elements has been widely accepted in engineering practice. It is the combination of soil and reinforcement, suitably placed, to withstand tensile stresses and also to improve the resistance of soil in the direction of greatest tensile strain. The basic principles of reinforced soil are demonstrated abundantly in nature by the action of tree roots. Reinforcement of soil is practiced to improve the mechanical properties of the soil by the inclusion of structural elements such as granular piles, lime or cement mixed soil, metallic or plastic strips, synthetic or natural fiber etc. The presence of reinforcement modifies the stress field giving a restraint mostly in the form of friction or adhesion so that less strain is induced and tension is avoided. Conventional methods of reinforcement include continuous inclusions of strips, fabrics, and grids into an earth mass. But as a modification technique, various types of fibers are also considered for reinforcing soil. Soil reinforcement using discrete randomly distributed fibers has been widely investigated over the last thirty years. The use of fibers, such as jute, coir, bamboo, polypropylene, nylon etc. as soil reinforcement materials, is prevalent for a long time and they are abundantly used.

The main advantage of using fibers as reinforcing material is that they are locally available and are very cost effective. Processing of these materials into usable form is an employment generation activity in rural areas of countries in which they are prevalent. Effective use of these materials uplifts the rural economy and its use in engineering construction reduces the construction cost.

Coir manufacturing units are mainly concentrated on the banks of back water in Kerala, near to the coastal areas, where the major portions of soil are lateritic soil or soft clay. The use of coir waste as soil admixture in these soils has been investigated in this paper. This paper presents the influence of coir waste on compaction and compressive strength of two types of soil viz., lateritic soil and soft Kuttanad clay.

2. LITERATURE REVIEW

The process of randomly mixing discrete fibres into the soil has become a proven technology to improve the strength of the soil as pointed out by various researchers. The fibers increase the cohesion among the soil particles. In addition

the interaction of the fibers among themselves and the flexibility of the fibers makes them behave as a structural mesh that holds the soil together increasing the soil structural integrity. Advantages of this method are: (i) there are several different materials that can be used to reinforce the soil, (ii) the machinery required is minimal, and (iii) the fibers are inexpensive and environmentally friendly. Disadvantages of this method are that, some of the fibers have less durability and can only be implemented in shallow depths. However, this characteristic of the reinforcement method allows it to be easily implemented in large areas (Babu & Vasudevan, 2008).

Several studies have been conducted to study the influence of natural fibres on different strength aspects of soft soils. Aggarwal and Sharma (2010) have proved that addition of natural fibres to expansive soils improves the California Bearing Ratio value. This is mainly because of the fact that the randomly distributed natural fibres prevent the development of weak failure planes in soil. But, Aggarwal and Sharma (2010), Ramesh et al. (2010), Prabakar and Sridhar (2002) and Jamellodin et al. (2010) are of the opinion that addition of randomly distributed natural fibres increases optimum moisture content and decreases maximum dry density. This is due to the fact that inclusion of materials with low specific gravity and unit weight replaces the soil mass and also due to the rearrangement of soil particles with reinforcing particles.

However, all other strength parameters are seen to improve as explained below. Ghavami et al. (1999), Ramesh et al. (2010), Bouhicha et al. (2005) and Marandi et al. (2008) showed that addition of randomly distributed natural fibres to expansive soils increases strain after reaching peak strength showing the ductile behaviour of the sample. Ghavami et al. (1999), Bouhicha et al. (2005) also reported that compressive strength of the soil also increases slightly. Chauhan et al. (2008) showed that the unconfined compressive strength value of poor soils increases with addition of natural fibres. Prabhakar and Sridhar (2002), Bouhicha et al. (2005), Huat et al. (2005), Babu et al. (2008) and Jamellodin et al. (2010) showed that the value of cohesion and shear stress of fibre reinforced soil improves due to the addition of natural fibres. Although, Babu et al. (2008) reported that friction angle also increases with increase in fibre content, this aspect is not highlighted in other works related to shear strength parameters on fibre reinforced soils.

The influence of natural fibres on the stress strain parameters of fibre reinforced soils were also studied with much significance. Nagrale et al. (2006) reported that inclusion of fibres in expansive soils improves the modulus of elasticity of soil and reduces the compressive strain. This reduction can be exploited either to reduce the thickness of intermediate layers of pavement sections or to increase the life of pavements. Marandi et al. (2008) showed that the secant modulus also increases with increase in fibre content. Babu and Vasudevan (2008), Babu et al. (2008) showed that stress – strain behaviour, deviator stress, stiffness and energy absorption capacity (hence toughness) increase with the inclusion of fibres. Chauhan et al. (2008) proved that the fibre reinforcement enhances the resilient response for soils, but the amount of enhancement depends on the type of soil. The author also concluded that resilient strain is less in soils reinforced with coir fibre than with synthetic fibre, indicating that coir fibre can help in delaying the failure of subgrade in pavement systems. It is also reported that fibres can reduce rut formations in the pavement structures depending on the fibre used as reinforcement. Coir fibre exhibits better responses than synthetic fibre. Also, coir fibre exhibits greater enhancements in resilient modulus or strength of the soil than the synthetic fibre.

Along with strength parameters, the swell / shrink behaviour of soils is also reported to improve. Ghavami et al. (1999) and Bouhicha et al. (2005) showed that inclusion of natural fibres in the soil matrix prevents the development of shrinkage cracks due to the drying process in expansive soils while Babu et al. (2008) reported that inclusion of fibres reduces the swell potential. Babu et al. (2008) reported that compression index also reduces due to fibre inclusion.

Among the natural fibres, coir is having the highest lignin content (46%) which provides the highest durability for coir fibre (Rao and Balan, 2000). Balan (1995) conducted accelerated durability studies on coir yarn and reported that the life of coir yarn is controlled by the type of embedded soil, climatic conditions, water content, organic content and the type of coir used. Coir degrades at a faster rate in sand with high organic content followed by clay with high organic content or burial, sand and finally clay where the degradation is least.

As seen from the literature review, fiber inclusion normally increases the strength of soils. In the coir fiber producing centres, coir baby fiber and coir pith become the industry waste which mixes up with the natural soil surrounding the production centres. In Kerala, the southernmost state of India, coir production units are all concentrated along the coastal belt and also near to the backwaters. The soil in these production centres are either of clay or of lateritic in nature. The main coir industry in Kerala is situated in the District of Alleppey, where in the highly soft clay commonly called as Kuttanad Clay is abundantly available. Hence based on the literature, it was decided to have a detailed study on the influence of coir pith on the engineering behaviour of Kuttanad Clay and lateritic soil. The study basically concentrated on the compaction and California Bearing Ratio behaviour of both the soils when coir pith was added as admixture.

3. EXPERIMENTAL WORK

Two different types of soil was used in this study, Lateritic soil and Kuttanad Clay. Indian Coir Industry is concentrated in Alleppey district of Kerala in India. Kuttanad in Alleppey district is a water logged area, which is below mean sea level and the predominant highly soft soil in this region is known as Kuttanad Clay. The physical properties of both the soils are given in Table 1. The coir waste used in this study was in a soaked state and it was then sun dried to reduce the water content to 0%. The saturated clay was also sundried to bring down the moisture content to 0% and it was then powdered (to a size less than 4.75 mm) using mallet, in order to mix the coir pith in a uniform manner. The coir pith was obtained by sieving the coir waste through 4.75 mm sieve, by this process medium to large fibres along with gravel sized coir waste are all removed. The sieved pith consisted of baby fibres which were difficult to separate manually. The coir pith was brown in colour and was light in weight (specific gravity was determined as 0.12). It has a property of imbibing water and swells 600 times more than its weight. This property of coir pith is advantageously being used in agriculture to replace peat moss.

The soil samples were prepared by mixing coir pith with soil in 0%, 0.5%, 1%, 1.5%, 2%, 2.5% and 3% by weight of soil. Standard Proctor Compaction test was conducted for each mix to find out maximum dry density and optimum moisture content. California Bearing Ratio tests, both soaked and unsoaked were also conducted in the above mix at their respective maximum dry density. The mix was filled in the CBR mould with a moisture content that was obtained in the compaction test conducted for corresponding mix.

Table 1. Characteristics of tested soils

PROPERTY OF SOIL	LATERITIC SOIL	KUTTANAD CLAY
Specific gravity	2.4	2.3
Liquid limit (%)	43	93
Plastic limit (%)	22	31
Plasticity index (%)	21	62
Maximum dry density (g/cc)	1.7	1.4
Optimum moisture content (%)	17.5	28
Unconfined compressive strength (kN/m ²)	49	24
Cohesion (kN/m ²)	11	12
Angle of internal friction (degrees)	24	0

4. RESULTS AND DISCUSSIONS

4.1 Effect of Coir Waste Content on Dry Density and Optimum Moisture Content (OMC)

4.1.1. Dry Density – OMC of Lateritic Soil Mixed with Coir Waste

The effect of coir waste addition on compaction shows that the shapes of the compaction curves are similar to that of unreinforced sample. For all samples, the dry density increases with increase in water content up to the point of optimum moisture content beyond which increase in water content reduces the dry density. The compaction curves of lateritic soil with and without coir waste addition are shown in Figure 1.

It was observed that dry density decreases and OMC increases with increase in coir waste content. The variation of dry density and OMC with coir waste content is shown in Figures 2 and 3 respectively. A sudden decrease in dry density and increase in OMC was found beyond 1.5% of coir waste content.

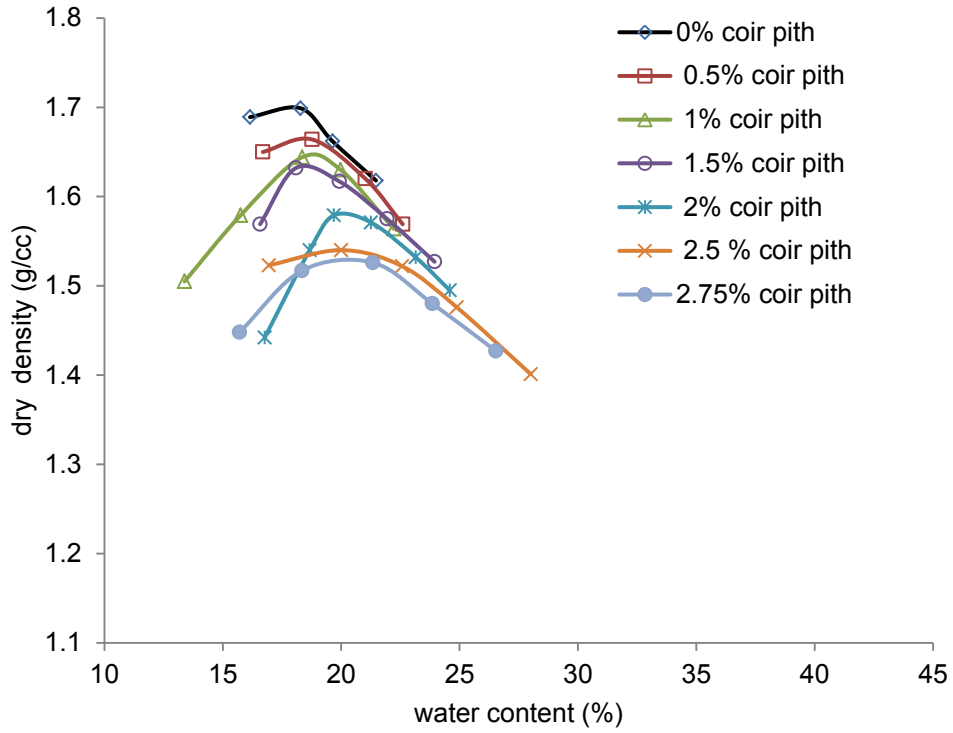


Figure 1. Compaction curves for lateritic soil with different percentages of coir pith

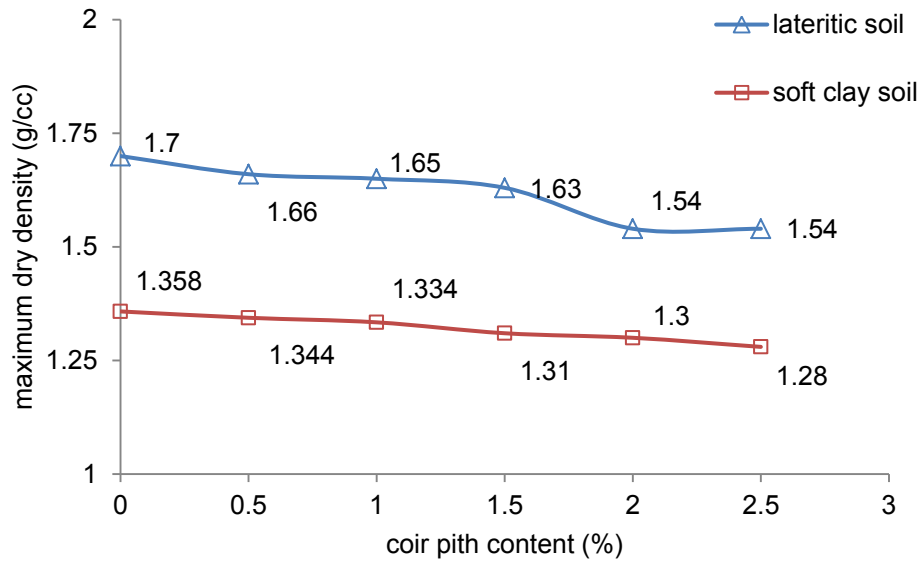


Figure 2. Variation of maximum dry density with coir pith content for lateritic soil and Kuttanad clay

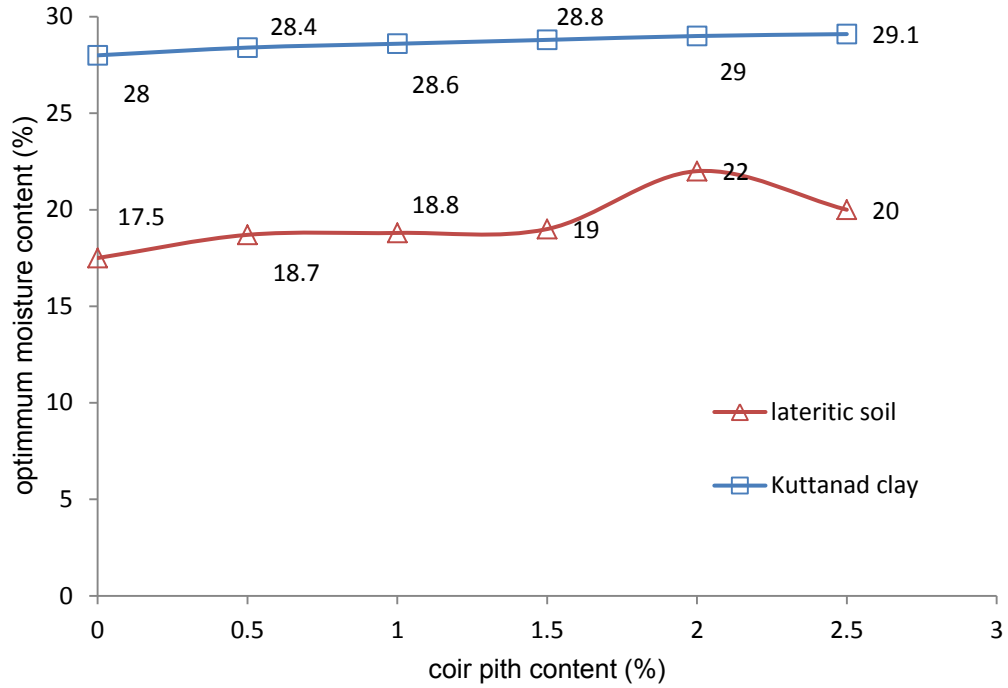


Figure 3. Variation of OMC with coir pith content for lateritic soil and Kuttanad clay

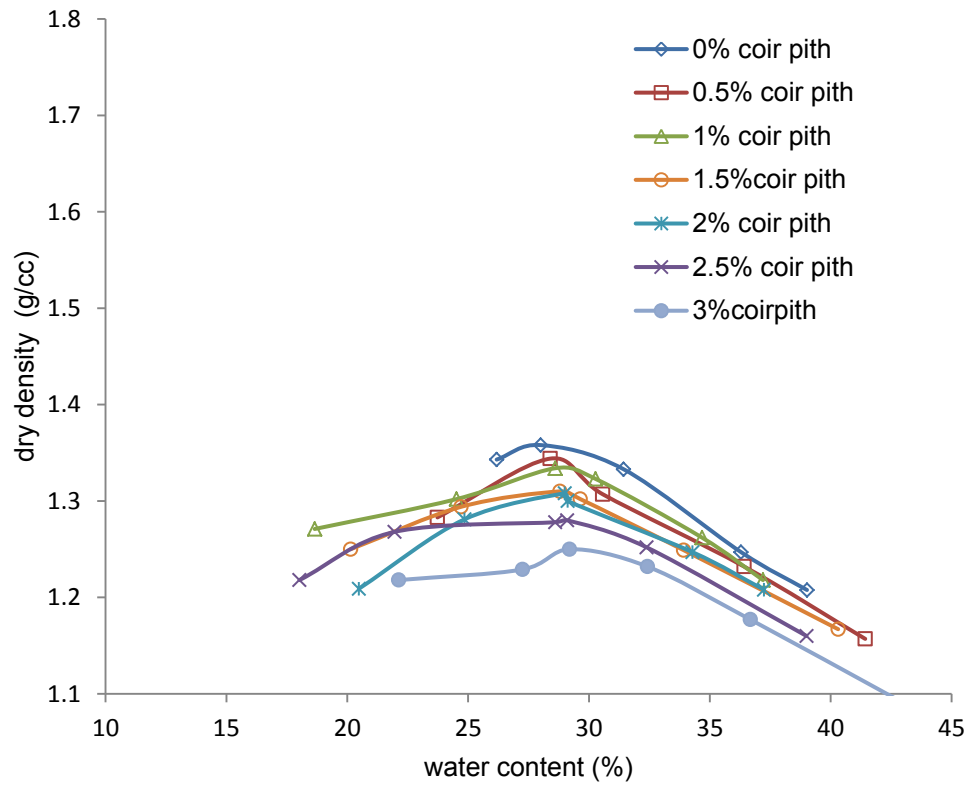


Figure 4. Compaction curves for Kuttanad clay with different percentages of coir pith

4.1.2 Dry Density – OMC of Kuttanad Clay Mixed with Coir Waste

The compaction curves for Kuttanad clay with and without coir waste are shown in Figure 4. The shape of the compaction curves for coir pith mixed soil is similar to that of raw sample without pith. Dry density decreases and the optimum moisture content increases with increase in coir waste content. The variation of dry density and OMC of Kuttanad clay with increase in coir waste content is shown in Figures 2 and 3 respectively.

Optimum moisture content of both types of soil increases with increase in percentage of pith content because of the absorption of water by coir pith. The decrease in dry density can be attributed to the low density of coir pith.

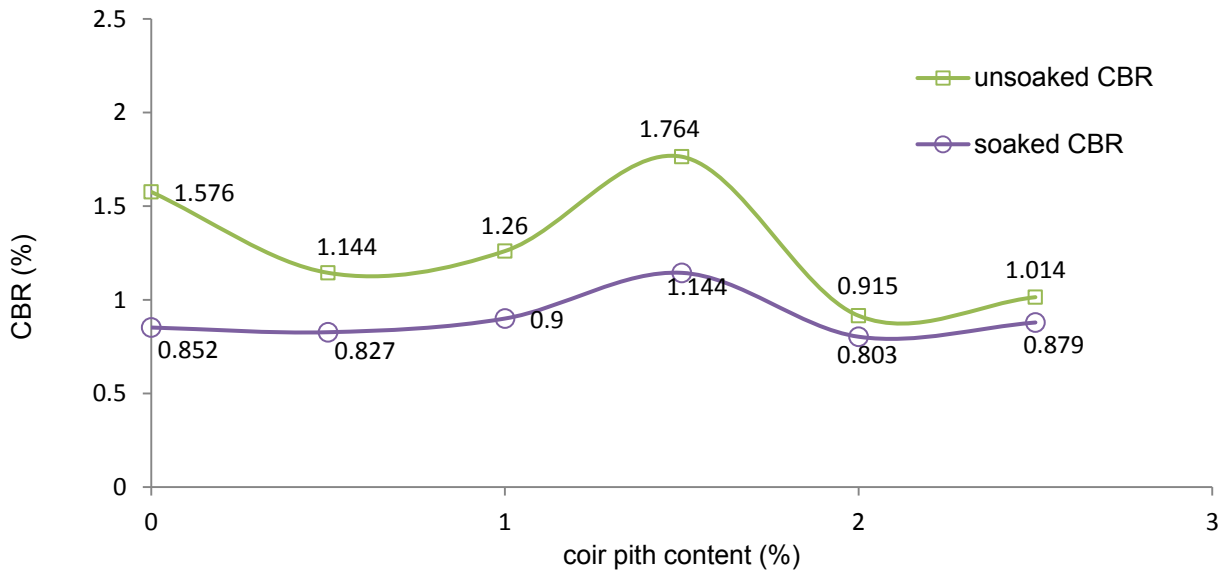


Figure 5. Variation of CBR value with coir pith content for lateritic soil

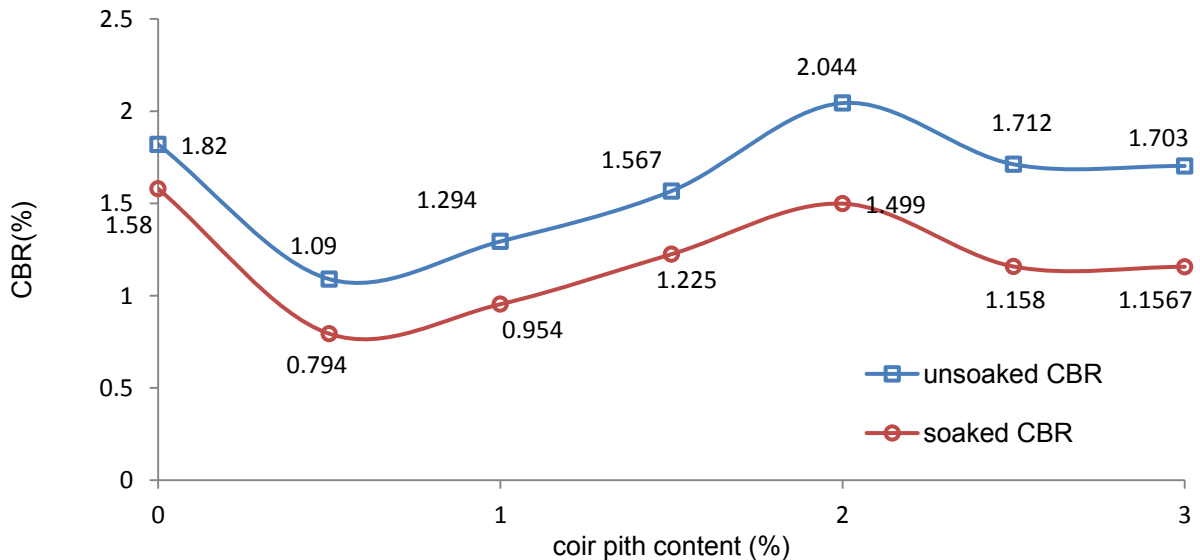


Figure 6. Variation of CBR value with coir pith content for Kuttanad clay

5.2. Effect of Coir Pith Content on California Bearing Ratio (CBR)

The variation of unsoaked and soaked CBR value with increase in coir pith content for lateritic soil and Kuttanad clay is shown in Figures 5 and 6 respectively. It is seen that the CBR value decreases at low coir pith content and then increases for both soaked and un-soaked conditions. Maximum CBR value is obtained at 1.5% of pith content for lateritic soil while for Kuttanad clay; it is obtained at 2% pith content. The variation of soaked and unsoaked CBR values shows the same trend.

In both the soil types, the unsoaked and soaked CBR value suddenly decreases with an inclusion of 0.5% of pith, there after an increase in the inclusion of pith to both types of soil increases the CBR value upto 1.5% and 2% respectively for lateritic soil and Kuttanad clay respectively. After that point, further increase in pith content decreases the CBR value. The initial decrease in the CBR Value may be due to insufficient adhesion between the soil and the pith. With an increase in the pith content there are sufficient pith particles to attain cohesive attraction between the pith particles and also the presence of baby fibers (the amount of which is higher in higher grams of pith) provides reinforcement effect. This is why the CBR value increases after 0.5% of pith content. Pith content of more than 1.5% and 2% respectively in lateritic soil and Kuttanad clay, decreases the CBR value. This may be due to the cushioning effect of pith and the higher replacement of soil by pith. The optimum value of pith content in lateritic soil is found to be 1.5% and the corresponding un-soaked and soaked CBR values are 1.764% and 1.144% respectively. For Kuttanad clay the optimum value of pith content is 2% and the corresponding un-soaked and soaked CBR values are found to be 2.044% and 1.499% respectively.

6. CONCLUSIONS

The results show that the addition of coir waste with baby fibres improved the engineering behavior of both lateritic soil and Kuttanad clay. The addition of coir waste increases optimum moisture content and decreases maximum dry density because of its water absorption capacity and low unit weight. In the case of lateritic soil, beyond 1.5% an abrupt increase in OMC and decrease in dry density is observed. For lateritic soil, a CBR value higher than plain soil is observed at 1.5% coir pith content and for Kuttanad clay at 2%. Kuttanad clay with 2% coir pith can be used for rural road subgrades since it gives a CBR value higher than 2.

In the coir waste in addition to baby fibres, medium to short fibres will also be present. The effect of these fibres at optimum coir waste content arrived from above has to be evaluated further.

REFERENCES

- Aggarwal P. and Sharma B. (2010), "Application of Jute Fibre in the Improvement of Subgrade Characteristics", *Proceedings of International Conferences on Advances in Civil Engineering*, Trivandrum, Kerala, India, 51 -53.
- Babu G. L. S., and Vasudevan A. K. (2008), "Strength and Stiffness Response of Coir Fiber- Reinforced Tropical Soil", *Journal of Materials in Civil Engineering*, 571-577.
- Babu G. L. S., Vasudevan A. K. and Sayida M. K. (2008), "Use of Coir Fibers for Improving the Engineering Properties of Expansive Soil", *Journal of Natural Fibers*, 5(1): 61-75.
- Balan K. (1995), "Studies on Engineering Behaviour and Uses of Geotextile with Natural Fibres", Ph. D. thesis, Indian Institute of Technology, Delhi, India.
- Bouhicha M., Aouissi F. and Kenai S. (2005), "Performance of Composite Soil Reinforced with Barley Straw", *Cement and Concrete Composites*, 27: 617-621.
- Chauhan M. S., Mittal S. and Mohanty B. (2008), "Performance Evaluation of Silty Sand Subgrade Reinforced with Fly Ash and Fibre", *Geotextiles and Geomembranes*, 26: 429 – 435.
- Ghavami K , Romildo D, Filho T and Normando P. (1999) "Behaviour of Composite Soil Reinforced with Natural Fibres," *Cement and Concrete Composites*, 39-48.
- Jamellodin Z, Talith Z A and Kolop Rosian (2010), "The Effect of Oil Palm Fibre on Strength Behaviour of Soil". *Proceedings of 32rd SANREM Conference 2010*
- Marandi S. M., Bagheripour M.H., Rahgozar R., and Zare H. (2008), "Strength and Ductility of Randomly Distributed Palm Fibers Reinforced Silty Sand Soils", *American Journal of Applied Sciences*, 5 (3): 209-220.
- Nagrale P P and Chandra S (2006) "Benefits of Fibre Reinforced Sub Grade Soils in flexible Pavemnts", 17: 53-57.
- Prabhakar J. and Sridhar R. S. (2002), "Effect of Random Inclusion of Sisal Fiber on Strength Behavior of Soil", *Construction and Building Materials*, 16: 123-131.
- Ramesh H. N., Manoj Krishna K. V., and Mamatha H. V. (2010), "Compaction and Strength Behavior of Lime-Coir Fiber Treated Black Cotton Soil", *Geomechanics and Engineering*, 2(1): 19-28.
- Venkatappa Rao G. and Balan K. (2000), "Coir Geotextiles Emerging Trends", Kerala State Coir Corporation Ltd., Alappuzha, Kerala, India.

Study on Geogrids for Improving Safety in Underground Mining

Martins, P.M., Pimenta de Ávila Consultoria Ltda, Brazil, paula.mello@pimentadeavila.com.br
Gontijo, A.A., DSI Fosminas Mining & Tunneling, Brazil, alexandre.gontijo@dsifosminas.com.br

ABSTRACT

To protect against the fall of small blocks between the mesh of anchors in the openings, meshes that are used today has been replaced by geogrids, due to its flexibility, resistance to oxidation, high strength, lightweight and due to decreased risks during the installation. This work will present technical considerations about this new geosynthetic application regarding the advantages presented, as well as a discussion of the actual requests these materials in various possibilities of application, executive considerations and test results in underground mining from Brazil.

1 INTRODUCTION

Among the methods of mining, underground mining is growing every day around the world due to high mineral commercialization that occurs today. The work in underground mines have essentially two major aspects of security: security structural of underground openings involving roofs, floors, walls and pillars; environmental safety, which refers to creating and maintaining a working environment and proper conditioning to perform the tasks relevant the enterprise. The environmental concern has a broad sense and includes this concern about safety.

Knowing that the mines is done by observing three fundamental principles, safety, economy and the best use of reserves, no one doubts that the first of these principles overlap to the other and has been extended beyond the great concern about loss of life. High investments in equipment and structures that have to be created to provide access to sites where the minerals are removed, they cannot be at the mercy of accidents, mainly caused by falls of small blocks.

So, to protect against the fall of small blocks between the mesh of anchors in the openings, meshes that are used today has been replaced by geogrids, due to its flexibility, resistance to oxidation, high strength, lightweight and due to decreased risks during the installation. This work will present technical considerations about this new geosynthetic application regarding the advantages presented, as well as a discussion of the actual requests these materials in various possibilities of application, executive considerations and test results in underground mining from Brazil.

2 CRITICAL AREAS RELATED TO FALLS OF SMALL BLOCKS

In underground mining, the redistribution of stresses can generate large deformation and ruptures of the rock mass, such as peeling, falling blocks, lateral movements and even subsidence as a result of the performance of tensions.

Generally the performance of tensions behaves according the Figures 1a and 2b, below.

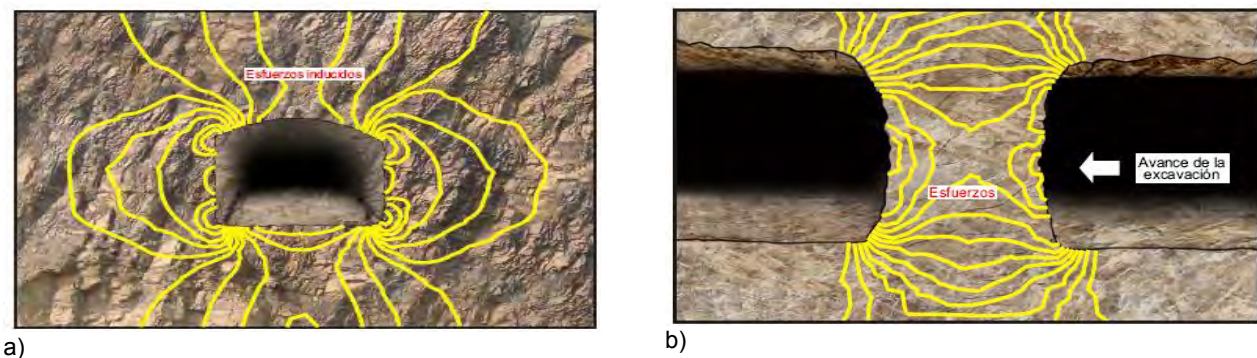


Figure 1: Performance of tensions.a) Stress induced an excavation simple.b) Stress concentration on the pillar.

The measure of tensions in the scale of engineering (m, km) is performed by tests performed on the same job site, with test methods and use of equipment that enables the data register of stresses acting on site, thereby defining the direction and intensity of the principal stress (σ_1), and secondary stresses (σ_2) e (σ_3).

These measures can be obtained from boreholes or surface areas exposed rock mass. For each type of measurement are, today, different techniques.

Stress concentrations in the excavation walls can be of great intensity, reaching mobilize resistance of the rock mass locally or at larger scales, often leading to rupture of the rock.

The major ruptures of larger scale are contained by anchors or systems appropriately designed to reach the safety of the work. But between these anchors still becomes necessary to use a system which protects the fall of small blocks.

In places where the redistribution of stresses resulting in an horizontal principal stress, we observe the occurrence of ruptures predominantly in the roof of the underground excavation, as shown in Figure 2.

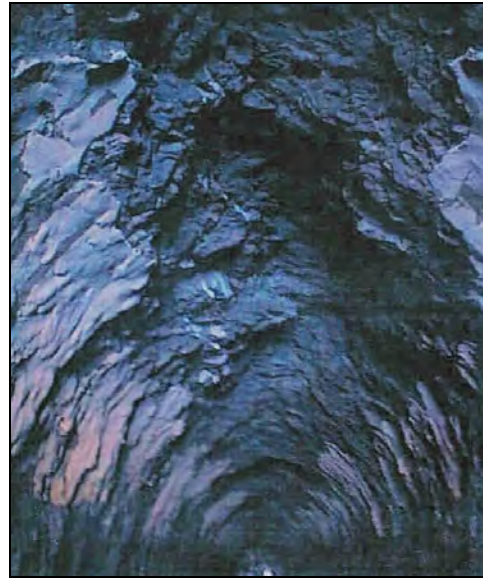


Figure 2: Higher horizontal stress, UHE – ITA, Brazil (Barton & Infanti, 2006, Quadros, 2010)

In places where the redistribution of stresses resulting in a vertical principal stress, we observe the occurrence of ruptures predominantly in the walls of the underground excavation, as shown in Figure 3.



Figure 3: Higher vertical stress, UHE – Jinping II, Sichuan - China (Hudson, 2009).

The pillars in room and pillar mining method (Figure 4) are subjected to vertical stress due to overburden rock mass and horizontal stress relieve due to entries excavation around them.



Figure 4: Partially benched pillar failing under elevated stress at the edge of bench mining (Esterhuizen, G.S. et al. 2011).

In Brazilian underground mining (coal and metals) that work with room and pillar mining method usually pillars design by the Salamon-Munro formulation (Salamon and Munro, 1967).

3 TRADITIONAL METHODS OF PROTECTION AGAINST FALLS OF SMALL BLOCKS

3.1 Introduction

In recent years, the meshes began to use more frequently in conjunction with roof bolts to prevent skin falls in weak roofs such as weathering-sensitive shale. Its function is to cover the roof area, and support and hold in place the broken roof between bolts, preventing injuries (Robertson and Hinshaw, 2002).

Some Mines are applying rock bolts and steel straps to improve the pillar strength and consequently to reducing the pillar size. The Figure 5, shown some examples the type of protection.



Figure 5: Examples of the traditional meshes to cover roofs and pillars.

3.2 Types of Meshes

The wire meshes and straps are usually used in underground mines to prevent the fall of small blocks of rock from the roof and pillars between roof bolts (Figure 6).

There are two types of wire meshes used in this application, chainlink mesh and weldmesh. Chainlink consists of an array of woven wire. The wire can be galvanized for corrosion protection, is flexible and strong. The weldmesh are used to strengthen the application of concrete and consist of a square mesh of steel wires, welded at their intersection points. They are more rigid and easier to install.

Another options are the straps, this system is used where the bolts cannot support alone roofs immediate formed by layers of small thickness.



Figure 6: Wire mesh and straps application.

4 THE GEOGRID APPLICATION

4.1 Introduction

Since 1994, longwall coal mines have used polymer geogrids during longwall recovery to control intrusion of gob material into shield/pan line area (Bailey, 2006).

Grids of different strengths and materials have been used in concert to answer the challenges of differing mine. Nowadays, it possible found geogrids from an average of ultimate strength of 55 kN/m to over 500 kN/m.

4.2 Geogrids

The main geogrids applies in underground mine are biaxial polypropylene an polyester geogrids.

The polypropylene geogrids (Figure 7) are manufactured by extrusion of a polypropylene sheet. Drawing is done under controlled temperatures and strain rates, so as to avoid fracture while allowing ductile flow of the molecules into an elongated condition. Besides, significant increases in modulus and strength, the creep sensitivity of the elongated ribs is greatly reduced by the drawing process. The resulting geogrids are referred to as homogeneous, utilized, or relatively stiff geogrids (Koerner, 1998).

The polyester geogrids (Figure 8) are made from high-tenacity polyester yarns, woven into an open structure with the junctions being knitted together or physically intertwined to link the transverse and longitudinal ribs, and coated with PVC (Koerner, 1998). This type of geogrid presents greater ultimate tensile strength and high-modulus than the polypropylene geogrids, therefore today should be the most applied.



Figure 7: Polypropylene geogrids extruded.

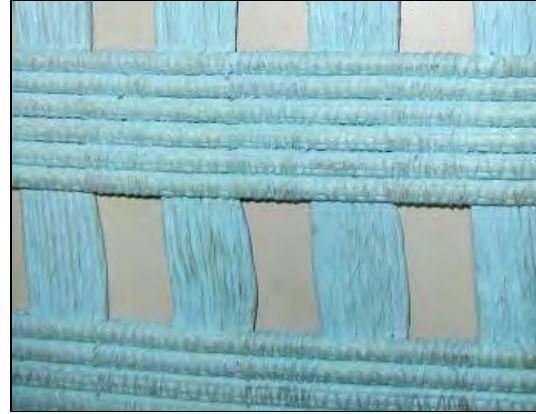


Figure 8: Polyester geogrids.

4.3 Case Studies

4.3.1 Dolinar (2006)

Dolinar (2006) presents a results of tests comparing same types of wire meshes and a geogrid. The author discusses in his paper a series of tests were conducted to evaluate the effects of various parameters such as bolt tension, the type of load bearing surface and the size of bearing plates.

The Figure 9 shown same results of these tests.

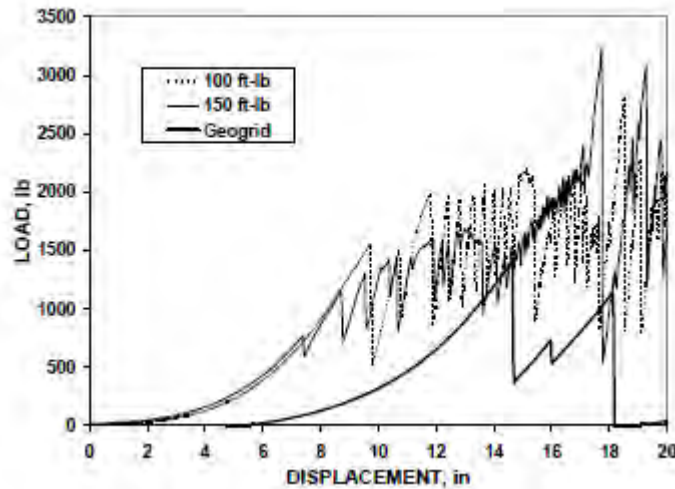


Figure 9: Dolinar (2006) results.

A very important note is, in the tests presented the geogrid used was polypropylene extruded geogrid with low ultimate tensile strength.

4.3.2 Applications in a Gold Mining from Brazil.

In July 2011, one gold mine from Brazil did a pilot test with polyester geogrids. Usually they used wire meshes to protect the underground excavation against fall of small blocks.

The geogrid was placed in the roof and attached by plates spaced at 1.5 to 1.5 m, as shown in Figure 10.



a) Area for geogrid application.



b) Manual installation.



c) Detail of anchor installation through the geogrid.



d) Geogrid installed and details of plates and its spacing.

Figure 10: Details of geogrid installation in a gold mining from Brazil in 2011.

These geogrids are working until today. During the application some considerations were shown by the worker:

- the geogrid rolls are lighter than wire meshes rolls, is easier to carry;
- easier installation;
- its minimum aperture size was enough to apply the anchor bolt;
- the geogrids has no sharp edges that compromise the safety of the worker.

5 INSTALLATION NOTES COMPARING GEOGRIDS AND WIRE MESH

Geogrids and wire meshes can be installed by manual or mechanized processes and there aren't a lot of differences between their installation processes, as shown in Figure 11.



a)



b)

Figure 11: a) Manual installation of wire mesh using rock bolts to fix in roof. b) Manual installation of geogrid using rock bolts to fix in roof.

During manual installation Geogrid or wire mesh has to be unrolled and pinned to anchors; the anchors are often installed first and the mesh is attached to the anchors afterwards using scissor lifts or baskets on tool carriers. When use the wire mesh the operation will be slow and labour intensive. Geogrid is easier to install them wire mesh

The mechanical system to installation of wire mesh was development to hard rock Mines seeking to reduces manual handling and personal exposure during the installation process reduces support cycle time, enables the mesh to follow the rock surface contours more closely, as shown in Figure 12.

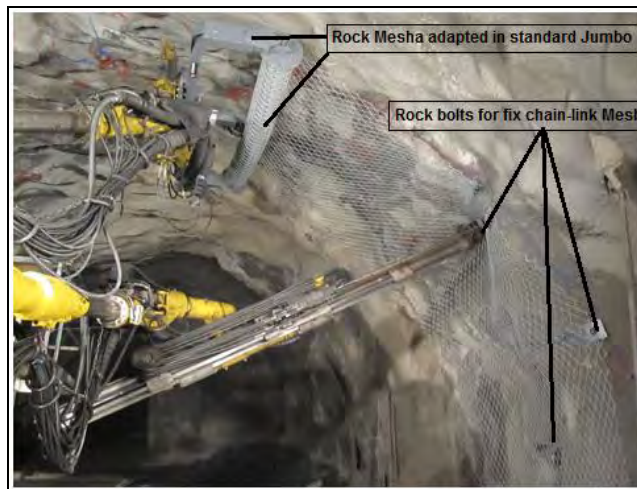


Figure 12: Automatic component installation of wire mesh adapted to standard jumbo.

The same system was developed to geogrids and has been used frequently, mainly in mining that use the longwall method, as shown in Figure 13.



Figure 13: USA and Australian Coal Mines working with Longwall method mining are using geogrid how surface control in underground mines .

6 DISCUSSION

As all geosynthetic products that start your application on the market, at first they are done empirically. Most considerations and comments are made on the field and people learn directly at the time of product application.

What this paper has as main objective is to highlight the need to develop requirements for design, specification and installation correct for these types of products in underground mining, from the survey of the state of the art current application.

Designing methods should be further elaborated, taking into consideration the size and weight of the blocks, average distance between the anchors and fixing points of geogrids.

Another issue to be significant also in relief is the chemical compatibility of geogrids to the environment of each type of underground mining. This guarantees the durability and effectiveness of the product.

In addition to, the development of methods and equipment adapted for underground installation also put to use in ideal operating conditions.

7 CONCLUSION

According to the previously presented, it was possible to conclude that the application of geogrids for protection with falling blocks in underground mining is an application more and more feasible.

Observations in the field show the following advantages of the product compared to traditional application of metallic screens, such as:

Advantages:

- It is light - reduces costs and operating time.
- No tip-sharp, these reduce the risk of injuries.
- Easily accommodates in the surface of underground excavation.
- Chemicals and Mechanicals properties anti-corrosive.

In relation to the minimum aperture size is important to note that this should remain larger than 60 x 60 mm, to enable the implementation of the anchors through the geogrid.

In relation to the spacing of the attachment plates, a general rule which can be used for deciding the spacing between support bolts is that the distance between the plates should be about equal to 3 times the average spacing of the planes of weakness of the rock mass. Therefore, if a set of planes layering together and create wedges or blocks with an average length of 0.5 m, the ideal spacing between screws should be about 1.5 m length of the bolt should be two times the spacing, i.e., 3 m.

In relation to the ultimate tensile strength of geogrids, further study should be done, considering biaxial geogrids with ultimate tensile strength greater than 200 KN / m and checking the influence of the high-modulus.

Geogrids with higher stiffness also facilitates product application.

REFERENCES

- Bucher, R., Roth, A., Roduner, A., Temiño, J. (2010) Ground Support in High stress mining with high-tensile chain-link mesh with high static and Dynamic load capacity, 5^o International Seminar on Deep and High Stress Mining , pp. 273 – 282 .
- Dolinar, D.R. (2006) Load Capacity and Stiffness Characteristics of Screen Materials Used for Surface Control in Underground Coal Mines, 25^o International Conference on Ground Control in Mining, pp. 152 – 158.
- DSI North American Presentation 2011 and Newsletter – December 2011.
- Esterhuizen, G.S. et al. (2011) Pillar strength in underground stone mines in the United States. Elsevier - Volume 48, Issue 1, January 2011, Pages 42–50
- Hoek, E., Kaiser, P.K., Bawden, W.F. (1995) Support of Underground Excavations in Hard Rock , pp. 194 .
- Koerner, R.M (1998) Design with Geosynthetics, Prentice Hall, Englewood Cliffs, N.J. 761 p.
- Murali M Gadde , John A. Rusnak , Jay W. Honse (2006) Behavior of Welded Wire Mesh used for Skin Control in Underground Coal Mines, 25^o International Conference on Ground Control in Mining, USA, pp. 142 - 151.
- Potvin, Y., Heal, D. (2010) Dynamic testing of High Energy Absorption, 5^o International Seminar on Deep and High Stress Mining , pp. 283 - 300 .
- Quadros, E.F. de (2010), Estado da Arte da Medida de Tensões In Situ, IPT, SG / LMHR, Brazil.
- SALAMON, M.D.G. and MUNRO, A.H. (1967) A study of the strength of coal pillars. J. S. Afr. Inst. Min. Metall. September
- Thompson, A. (2004) Support and rock mass reinforcement, Codelco – Chile.
- Villaescusa, E. (2004) Support and rock mass reinforcement, Codelco – Chile.
- Zingano. A.C., Koppe, J.C., Costa, J.F.C.L. (2006) Pilar Reinforcement or Rib Support? 25^o International Conference on Ground Control in Mining, USA, pp. 152 – 158.

Subgrade Improvement for Segmental Retaining Walls

James A. McKelvey, III, P.E., D.GE, Earth Engineering Incorporated, East Norriton, Pennsylvania, USA,
JayM@EarthEngineering.com

Corey D. Mislinski, E.I.T., Earth Engineering Incorporated, East Norriton, Pennsylvania, USA,
Corey.Mislinski@EarthEngineering.com

ABSTRACT

At a large development site in Malvern, Pennsylvania, twelve segmental retaining walls were required to achieve the proposed grades. The subgrade investigation in the karst geology underlying the site revealed a pinnacled bedrock surface underlying partially saturated overburden varying from low plasticity silts to silty sands. Blow counts within the overburden were generally less than 10, and many were observed to be weight-of-hammer. As part of the subsurface investigation a substantial laboratory testing was performed on recovered samples. Subsequent design analyses that subgrade improvement was required beneath six of the twelve retaining walls. Subgrade improvements selected included staged construction, subgrade surcharging, and surcharging with vertical strip drains.

For staged construction analyses, the maximum height of retaining wall that could be constructed with the initial undrained cohesion value and comply with required total stress safety factors were determined. The undrained shear strength required to adequately support the total height of the retaining wall under total stress conditions was then calculated where needed. The amount of strength gain and duration needed to develop the strength gain is a function of the distribution of the applied stress, the stress history, and consolidation parameters of the supporting soils. Considering the laboratory data, the anticipated anisotropic stress distribution and strength gain theory, a relationship was developed for undrained strength gain for the saturated fine-grained soils at the site. Finally, the duration to develop the required strength gain was calculated.

Monitoring of construction was performed using pore pressure transducers and settlement plates. This paper will discuss the subgrade investigation, laboratory testing and design analyses necessary to provide the necessary subgrade improvement beneath the segmental retaining walls.

1. INTRODUCTION

At a 42hectare brownfields site in Malvern Pennsylvania, a prominent developer envisioned revitalizing the former steel mill into a thriving town center featuring retail shops, restaurants, a bowling alley, a movie theatre, offices and residential units. The initial phase of the redevelopment involved demolition of the steel mill buildings and storage buildings and related structures. Figure 1 is an aerial photograph taken prior to redevelopment. Twenty four buildings were proposed to be constructed for the town center, along with three bridges to cross a stream that flows from the west to the east across the property. Twelve retaining walls were proposed at the property, with eight located along the stream to provide providing building geometries averaging 7m above the stream elevation.

An extensive subsurface investigation was performed at the site for each of the major structures proposed, followed by laboratory testing and development of geotechnical recommendations for each structure. The subgrade investigation revealed a pinnacled bedrock surface underlying partially saturated overburden varying from low plasticity silts to silty sands. The overburden soils were found to have a consistency ranging from very soft to firm. Subsequent laboratory testing and design analyses showed that subgrade improvement would be required beneath six of the twelve retaining walls.

Construction of site works began in 2007 and continued until 2009 when construction temporarily ceased due to funding issues. Additional funding for the project was obtained, however the project was reconfigured to accommodate economic criteria and different tenants from those who were identified for the initial planning for the project. A total of ten segmental retaining walls and one reinforced earth slope were constructed during the initial phase of construction. Currently, two retaining walls are being redesigned to accommodate the current reconfigured development.



Figure 1- Aerial view of the site prior to redevelopment, with north towards the top of the photograph. The building at the lower right is approximately 285m long (Google Earth, 2012).

2. SUBSURFACE INVESTIGATION

The site is primarily located above a karst geologic formation, known as the Conestoga Formation, which is particularly prone to the development of sinkholes. Along the southern end of the property there is a geologic contact with schist of the Octororo Formation. Over 285 borings were performed across the site during the subsurface investigation of the proposed buildings, bridges and retaining walls. Cone penetrometer testing (CPT) was initially performed at 25 locations across the site to provide estimates of average shear wave velocities of the overburden for seismic site classification. Figure 2 shows the overall site development and locations of completed borings and CPT locations.

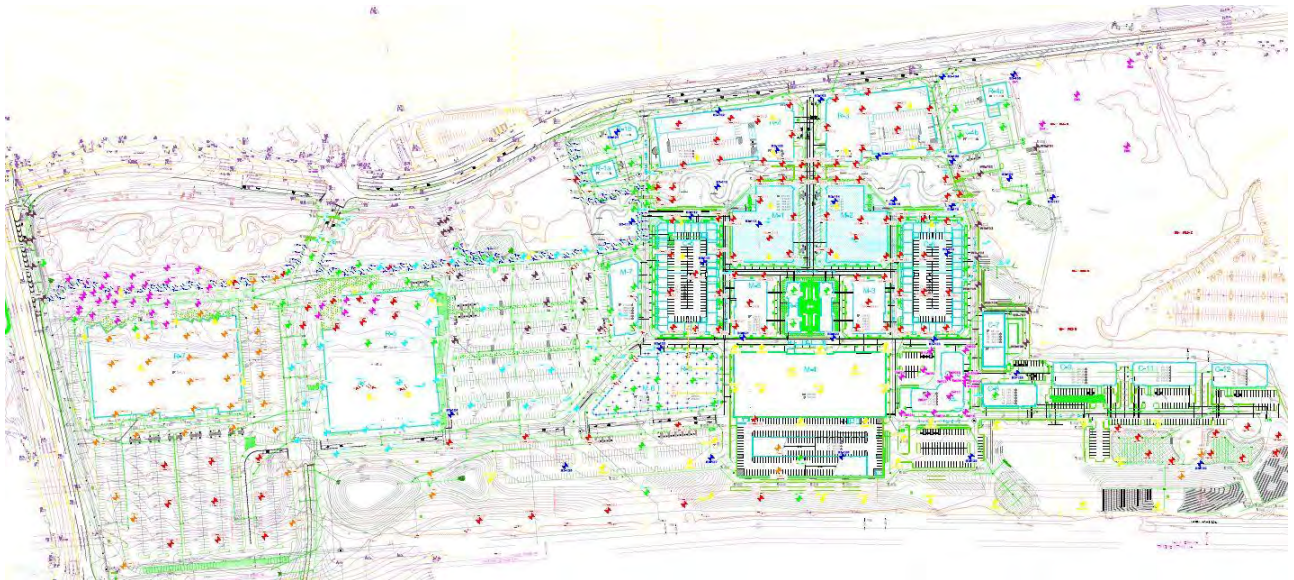


Figure 2- Plan view of 2006 development.

2.1 Field Investigation

The subgrade investigation in the karst geology underlying the northern portion of the site revealed a pinnacled bedrock surface underlying partially saturated overburden was relatively consistent, varying from low plasticity silts to silty sands. The consistency of the overburden overlying the karst was found to be very soft to firm, with blow counts observed to be generally less than 10, and many were observed to be weight-of-hammer. The CPT tip resistances observed correlated well with blow counts, with most observed below 2,394kPa. Numerous thin-walled tube samples were recovered during the subsurface investigation for subsequently laboratory testing. Along the southern portion of the site, the overburden was found to be much more competent, consisting of dense weathered schist. Groundwater was observed to be 6m to 8m within the overburden, generally coinciding with the elevation of the stream. The depth to bedrock was highly sporadic across the site, ranging from 1m to over 35m below the existing grades.

2.2 Laboratory Testing

Index testing of split-spoon samples was performed in the laboratory included classification, moisture content and organic content. Moisture content profiles were developed on continuous samples recovered in the field at many of the boring locations. Laboratory testing performed on recovered thin-walled soil samples included consolidation, unconsolidated-undrained (UU) triaxial shear and consolidated undrained (CU) triaxial shear. Direct shear tests and compaction testing were performed on bulk samples recovered from the site.

Considering the blow counts and CPT results observed in the field investigation, the results of the consolidation testing showed overconsolidation ratios (OCRs) ranging from 1.0 to 3.5 for the seven consolidation tests performed. The higher OCRs were noted in portions of the site previously supporting the steel mill buildings. The vertical coefficient of consolidation (c_v) ranged from 0.23cm²/min to 2.01cm²/min, averaging 0.83cm²/min. The compression index (C_c) of the overburden soil was very well behaved, varying only between 0.10 and 0.14. The average recompression index (C_r) was 0.014.

The peak undrained shear strengths observed in the UU tests were variable, with shear strengths ranging from 37kPa to 131kPa, depending on the applied normal stress. Strains to the peak stress generally exceeded 15%, introducing uncertainty to actual behavior in the field. To develop a high degree of certainty to field performance, the undrained shear strength at 5% strain was considered appropriate. Considering the erratic behavior of undrained shear strength observed in the laboratory, preference was given to the lowest value of undrained shear strength observed, 26kPa.

The consolidated undrained tests performed on recovered samples also had variable results. The effective stress internal angles of friction observed in the CU tests were 33° and 38°. The higher value is inconsistent with typical values associated with low plasticity silts and silty sands. The lower value showed reasonable agreement with the results of direct shear testing performed on remolded samples obtained from the site.

3. DESIGN ANALYSES AND RECOMMENDATIONS

Foundation design for the buildings varied substantially given the vast difference in building types and bearing pressures. Many of the buildings and the bridge abutments were recommended to be supported on mini-piles. Where possible, shallow foundations were recommended, however subgrade improvement would be required. As segmental retaining walls were envisioned to be constructed along the stream corridor and elsewhere on the site, the developer elected to have the design of the retaining walls designed by the contractor under a design-build contract. However, due to exclusions in the wall designer's contract, geotechnical support was required for the wall design.

3.1 Consolidation Analyses for North Town Center

One of the primary initiatives of the developer was to construct the entrance of the town center to attract tenants for the development. Specifically, the four buildings identified as M-1, M-2, R-2 and R-3 in Figure 3 would be the first buildings constructed. Along the stream, approximately 7m of fill would be required to achieve the building pad elevations. As these four buildings would be constructed largely on engineered fill, shallow foundations were recommended, provided consolidation of the underlying overburden soils could occur prior to building construction. The entire area was to have a 3m surcharge placed above the fill, which would remain for 9 months, which conformed to the initial development schedule. The stream had been previously diverted away from this area. Vertical deformation associated with consolidation of the overburden was estimated to be 155mm in response to the embankment and fill loading.

As with many projects, the developer's willingness to wait 9 months for the required consolidation to occur diminished as the onset of construction neared. Using wick drains spaced 1.5m apart in a triangular pattern and a 7m surcharge, the consolidation period was reduced to 30 days. This satisfied the revised schedule, however the expected costs for wick

drain installation was twice what the developer wanted to pay. The developer decided to accelerate the consolidation beneath the M-1 and M-2 buildings and wait 9 months for surcharge without wick drains consolidation. Figure 3 shows the limits of wick drains hatched in light blue. The surcharge would also benefit the subgrade beneath the retaining walls adjacent to the creek, driving out excess pore pressures prior to wall construction.

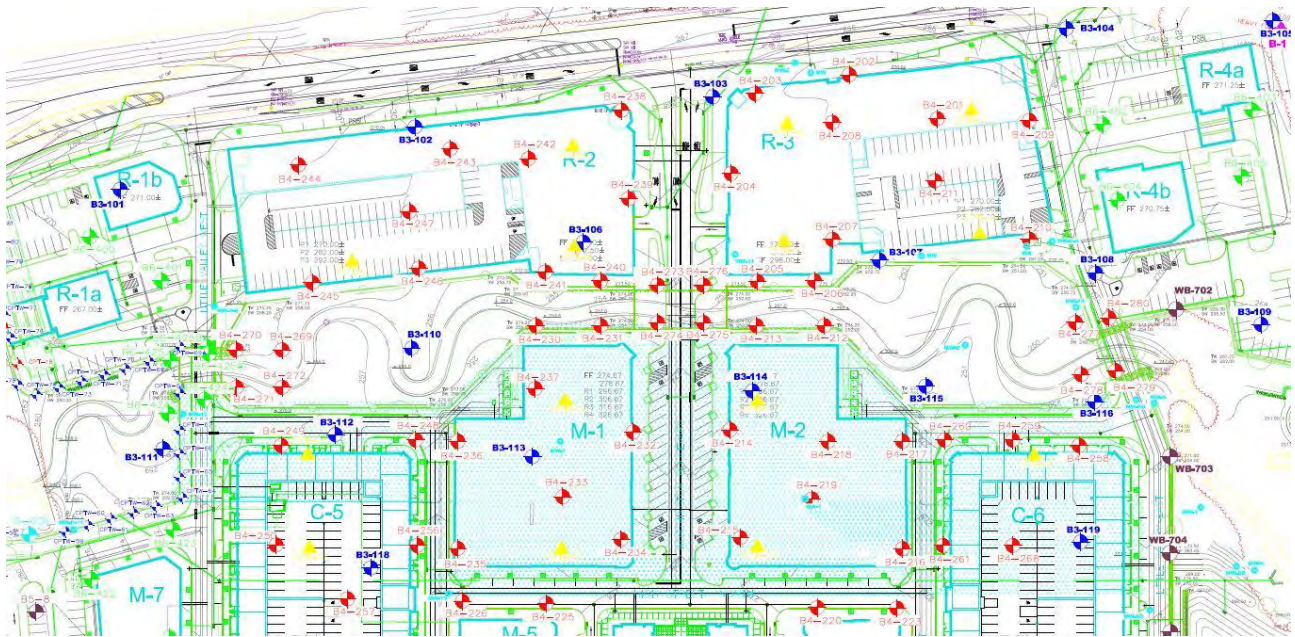


Figure 3- First buildings to be constructed at the north end of the town center.

3.2 Geotechnical Engineering for Segmental Retaining Walls

As typical in many design-build contracts for segmental retaining walls, the wall designer initially stipulated that the design of the segmental retaining walls only evaluated internal stability and that bearing capacity, settlement, and overall stability was the responsibility of the developer's geotechnical engineer. This stipulation was initially rejected, particularly for retaining walls along the stream outside the aforementioned surcharge area. It was later agreed that the geotechnical engineer would provide any additional data needed by the wall designer to evaluate all aspects of stability and vertical deformation.

As differential settlement beneath the retaining walls along the stream was anticipated to be problematic, the wall designer decided to incorporate joints in the retaining wall fascia every 8m. To provide wall designer the geotechnical information needed to support the design concept to address differential settlement, an additional subsurface investigation was performed gain a clear understanding of anticipated vertical deformation beneath the retaining walls adjacent to the stream. Cone penetrometer testing (CPT) was performed in 80 locations at approximate 8m on center locations along the alignment of the retaining walls. The results of the previously performed consolidation testing were used in subsequent analyses.

The bearing pressures beneath the wall fascia were then attenuated to the mid-point of the saturated fine-grained soils subject to consolidation in accordance with Newmark's attenuation relationship for rectangular flexible footings. No attenuation was considered at the rear of the reinforced zone of the retaining walls as the bearing soils would be subject to embankment loading at these locations. A 122 consolidation analyses performed in this study. Elastic settlement of the vadose zone soils was been neglected in these analyses as this vertical deformation would not be time dependent, and therefore assumed to occur during construction of the walls. Consolidation was calculated for the fascia and the reinforced zone of the retaining walls at each analysis point, as well as the anticipated duration for consolidation to occur. Results of these analyses showed that deformations in excess of 200mm and consolidation periods greater than 90days are anticipated in many locations along the proposed retaining walls along the stream. The retaining walls in the area of the surcharge area were excluded from this study.

The initial total stress global stability analyses suggested that in order to have adequate safety factors against instability, phasing of retaining wall construction would be required. It was identified that the fine-grained soils supporting the retaining wall would need to experience a gain in shear strength as consolidation to applied stress occurred. The amount of strength gain and duration needed to develop the strength gain is a function of the distribution of the applied stress,

the stress history, and consolidation parameters of the supporting soils. Considering the laboratory data, the anticipated anisotropic stress distribution and SHANSHEP theory (Ladd, 1986), a relationship was developed for undrained strength gain for the saturated fine-grained soils at the site.

To account for the varying thickness of overburden beneath the retaining walls, the largest drainage path beneath the retaining walls was considered in estimating the average degree of consolidation that would occur over a given period. Once the drainage paths were established, a time factor relationship was developed for each evaluation. The progress of construction the wall installer hoped to achieve was 600mm vertical over a 180m distance per day. The average degree of consolidation, excess pore water pressure and strength gain over this period was then determined. The maximum height of retaining wall that could be constructed with the initial undrained cohesion value and comply with the total stress safety factor against instability discussed above was determined. Safety factors considered appropriate in these analyses were in agreement with suggested values in the literature (Collin, et.al, 2007). Results of these analyses suggested that phased construction would be required in some areas of the proposed retaining walls. The undrained shear strength required to adequately support the total height of the retaining wall under total stress conditions was then calculated where needed. Finally, the duration to develop the required strength gain was calculated, which was estimated to be as much as 3 months. The maximum height of construction of the retaining walls and subsequent periods required for the strength gain were provided to the wall installer.

4. CONSTRUCTION OF INITIAL PHASE OF DEVELOPMENT

Demolition of the former steel mill began in the fall of 2006, followed by land development beginning in the spring of 2007. Grading necessary and installation of wick drains occurred first, followed by placement of the embankment and surcharge in the northern portion of the town center. Site grading and construction of retaining walls in other areas of the site began after construction of the surcharge.

4.1 Wick Drains and Surcharges

Once grading was completed for the wick drain field in the northern portion of the town center, 6,160 wick drains were installed at a spacing of 1.5m apart over the 1.43hectare area. Each wick drain was advanced to refusal at the bedrock surface, ranging in depth between 9m to 13.5m. Figure 4 is a photograph of the wick drain installation.



Figure 4- Installation of wick drains in the northern portion of the town center.

Once the wick drains were installed, a 305mm thick layer of free draining gravel was installed over the area to permit drainage of the wick drains. Twelve settlement places and pore pressure transducers were then installed in discrete locations across the entire area to be surcharged. Each pore pressure transducer was installed at the approximate mid-point of the fine grained strata subject to consolidation. Figure 5 shows construction of a settlement marker after a pore pressure transducer was installed. The 7m embankment and 3m surcharge was then constructed over the area.

Monitoring of the settlement markers and pore pressures was then performed daily for 38 days. The period required for dissipation of excess pore pressures within the saturated fine grained overburden was approximately 25% longer than that predicted during design analyses. Vertical deformation recorded in the settlement markers varied from 96mm to 150mm, compared to the 150mm predicted.



Figure 5- Settlement plate and pore pressure transducer cable.

4.2 Retaining Wall Construction

Once the surcharge and embankment were removed from the northern town center, construction of the segmental retaining walls along the stream began. Preparation of subgrade for the three bridges also began at this time. Construction of the retaining walls went rapidly, and the retaining walls soon reached either their full height or the height required for staged construction. As with the surcharge area, settlement plates and pore pressure transducers were installed where staged construction of the retaining walls was required.

Construction of the mini-pile foundations for the three bridges began after the subgrade was prepared, but due to the nature of the work, advanced at much slower rate in comparison to the retaining wall construction. The pile contractor elected to install the mini-piles by jetting them through the overburden. The jetting led to a localized issue where the surface soils liquefied, creating a 1m depression as shown in Figure 6. The surface depression created a loss of subgrade support for one of the retaining walls, as can also be seen in Figure 6. The wall yielded at this location, creating differential settlement, cracking the wall fascia approximately 5m from the surface depression. To remediate, the retaining wall was locally dismantled after completion of the mini-piles. The subgrade restored, and then the wall was rebuilt.

5. SUMMARY

Construction of the initial phase of development concluded in the fall of 2008, when funding for the project was interrupted. Two of the building pads on the western portion of the site were completed, allowing for construction of buildings by the two tenants who would occupy this portion of the site. Infrastructure and building pads were also completed for most of the town center. The retaining walls along the stream and the three bridges were completed. Figure 7 and Figure 8 show the completed retaining walls, bridges and completion of the stream bed.

Other than the opening of the two buildings at the western portion of the site, the project remained idle for three years while the developer secured alternative funding. In the fall of 2011, funding for the project became available. Unfortunately, many of the previously secured tenants had lost interest in the development. Furthermore, the project was required to be downsized from the initial development plan, which prompted redesign of the town center area. Two of the proposed retaining walls were not constructed, and are currently under design due to the reconfiguration. One of the retaining walls is over 300m long, and will have a maximum height approaching 15m. Construction of the

reconfigured town center is anticipated to begin in the spring of 2013, and should be completed in time to prepare a follow up paper for the next geosynthetics conference.



Figure 6- Loss of foundation due to mini-pile installation.



Figure 7- Completed retaining walls along the proposed stream.



Figure 8- Completed retaining walls along stream, view from stream.

REFERENCES

- Collin, J.G., Meyers, M. S., and Berg, R.R., (2007), "State-of-the-Practice Design of Segmental Retaining Walls; NCMA's Third Edition Manual", *Proc. Geosynthetics 2007*, Washington, District of Columbia: IFAI.
- Google Earth, (2012), aerial imagery dated June 17, 2010.
- Ladd, C.C., (1986), "Stability Evaluation During Staged Construction", 22nd Karl Terzaghi Lecture, *Jrnl. Of Geotechnical Engineering*, Volume 117, No. 4, New York, New York: ASCE.

Surface Analysis of Weathered HDPE Geomembrane Studied by LSCM and FTIR Spectroscopy

Wu, P., Yang, H.H., Luo, S.H., Zhu, T.G., Zhe, D.M., China Petroleum & Chemical Corporation Beijing Research Institute of Chemical Industry, China, wupeng.bjhy@sinopec.com

ABSTRACT

Surface of three high density polyethylene (HDPE) geomembrane (GM) samples was examined using laser scanning confocal microscope (LSCM) after artificial weathering test. Although no significant changes were observed on the surface of the GM samples, it was found that the variation of roughness value was different among the three samples due to differences in weathering resistance. Changes of surface chemistry were studied using Fourier transform infrared (ATR-FTIR) spectroscopy to monitor the development of photodegradation of GM samples. To estimate weathering resistance, tensile properties and oxidation induction time (OIT) of GM samples were also determined after artificial weathering. The results showed that surface roughness have correlation with weathering resistance, although the correlation is not strong. And it still needs to be further investigated.

1. INTRODUCTION

HDPE geomembranes are commonly used in geotechnical and civil engineering systems to provide barrier to advective and diffusive migration of contaminants (Rowe, 2005). Membranes can perform one or more functions such as liquid and gas barrier and stress crack resistance during long period (50 to >100 years). Many researches show that the properties of GM change with time due to ageing (Rowe et al. 2004; Rowe, 2005; Müller, 2007). Ageing of exposed geomembranes is mainly initiated by ultraviolet (UV) light, combined with heat, oxygen and other factors such as rain, oxides of nitrogen and sulphur. Generally, geomembranes are exposed to UV light for only a limited time. While for some special cases, geomembranes are used in exposed applications, without clay or vegetative covering layers. Thus, it is important that HDPE GM remain chemically and mechanically stable over its design life.

LSCM Confocal laser scanning microscopy (CLSM or LSCM) is a technique widely-used in numerous biological science disciplines, such as cell biology, microbiology, genetics and so on (Samuel et al. 2007). The main advantage of confocal microscopy is its ability to acquire high-resolution optical images with depth selectivity.

As the laser scans over the plane of interest, a single image is obtained pixel-by-pixel and line-by-line. Images of different focal planes can be collected by raising or lowering the microscope stage or objective lens. Finally, a three-dimensional picture of a specimen can be obtained by assembling a stack of these two-dimensional images using computer (Mathia, 2011).

Unlike atomic force microscopy (AFM) or scanning tunneling microscope (STM), LSCM doesn't need a probe scanning on the surface. The distance from the objective lens to the sample surface can be hundreds of micrometres to several millimeters.

In this paper, laser scanning confocal microscope (LSCM) and ATR-FTIR spectroscopy are mainly used to analyze surface changes of some exposed GM samples during ageing.

2. MATERIALS AND PROCEDURE

Three HDPE geomembranes were studied in this article: sample 1 for 1.5mm smooth geomembrane, sample 2 for 2.0mm single textured geomembrane and sample 3 for 2.0 mm smooth geomembrane.

The artificially simulated weathering was carried out using an Atlas UVTest, equipped with eight low-pressure Hg fluorescent lamps, with a maximum emission at 343 nm (type 1A UVA-340). Tests were performed for up to 1680 h in accordance with GRI Standard GM 11, tests consisted of 20h UV cycle at 75±3°C black panel temperature, followed by 4h condensation at 60°C. The intensity of the UV radiation sources was frequently verified with calibrated 340 nm radiometers. Black panel thermometer was checked to assure the accuracy during the test periods. The test pieces were placed in a similar position relative to the radiation source and any differences in the distribution of the weathering parameters were compensated by periodic change of position of the lamps. The samples were randomly distributed after each periodic LSCM analysis.

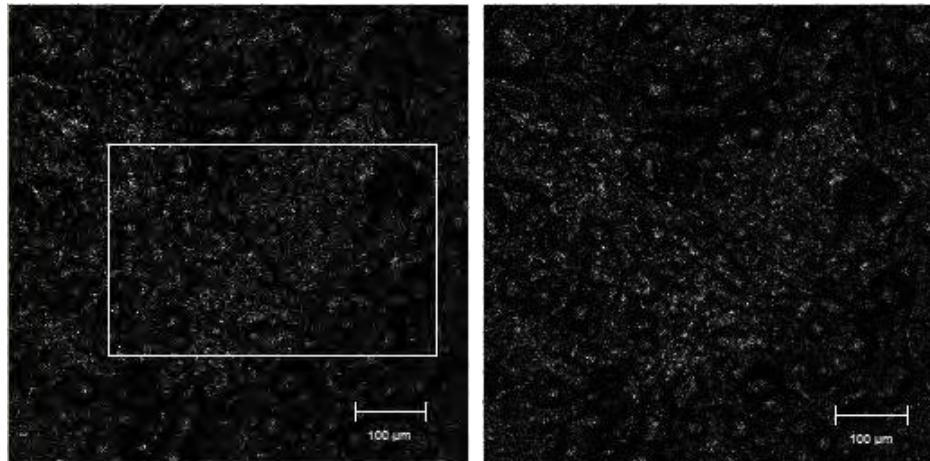
3. RESULTS AND DISCUSSION

3.1 Surface Roughness

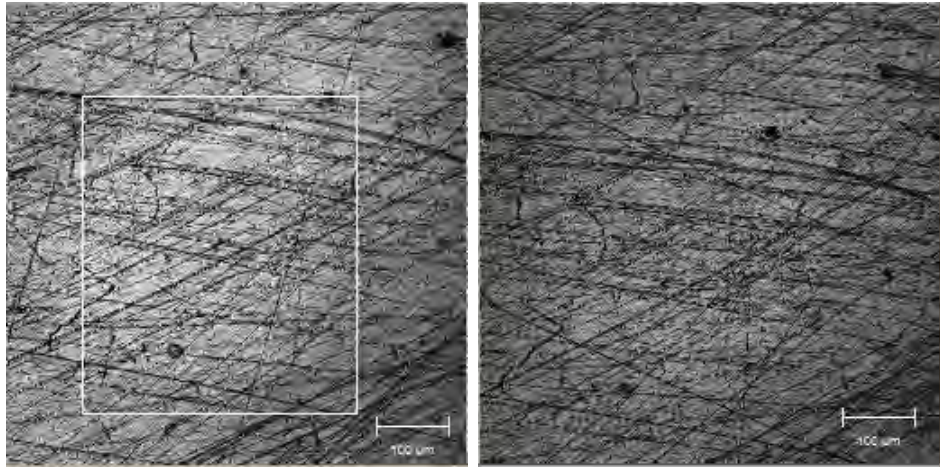
Surface roughness is a measurement of the texture of a surface. There are many different roughness parameters in use. By convention 2D roughness parameter is a capital R followed by additional characters in the subscript. Ra is the arithmetic average of the roughness profile. In this paper, Ra (2D surface roughness) was calculated based on DIN EN ISO 4287, using LSCM.

LSCM is useful for acquiring surface morphology of polymer materials. A Carl Zeiss LSM 700 laser scanning confocal microscope is used to examine surface morphology of three HDPE GM samples for roughness analysis. LSCM images showed in this paper are in 2D maximum intensity projection and 3D. They are representative of a series of overlapping optical slices (a stack of z-scan images) with a z-step of 0.05 μm . The laser wavelength used is 405nm.

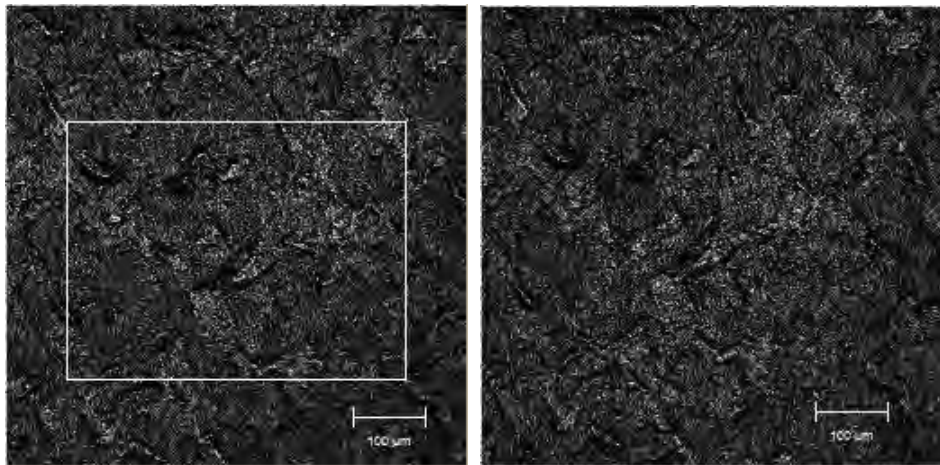
LSCM analysis was conducted on the three GM samples after every 168 hours' UV exposure. The LSCM images (Fig.1, Fig.3), in the form of 2D maximum intensity projection and 3D, show the topography of original GM samples and GM samples after 1680 hours' UV exposure respectively. From the LSCM images it can be seen that there are significant differences among these samples, but no obvious changes on the surfaces of aged GM compared with the original sample. Height information of the sample's surface could be obtained at the same time using LSCM, from which the roughness of the surface can be calculated. In the analysis of LSCM, the roughness of several dispersed positions of each sample was measured, and same trend of each sample was found. So in this paper, a fixed position of each geomembrane was chosen for the LSCM analysis to observe the changing of surface roughness under different exposure time. Roughness was calculated based on the same scan area marked out by the white rectangle, as shown in Fig. 1. Each scan area was chosen by some special points which could be easily recognized in the LSCM images.



(a) sample 1



(b) sample 2



(c) sample 3

Fig. 1 LSCM micrographs of the surface of the three samples before (left) and after 1680 hours' UV exposure (right)

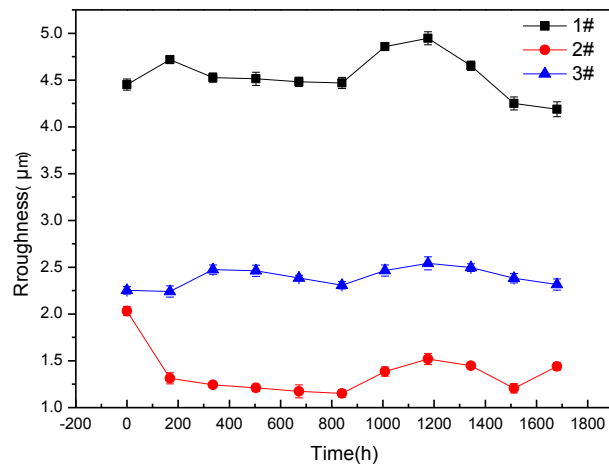


Fig. 2 Surface roughness change as a function of exposure time

The variation in roughness of three GM samples with respect to age time is shown in Fig. 2. The roughness of three GM samples was different from each other, which is consistent with the LSCM images. As shown in Fig. 2, three GM samples show different variation in roughness.

Sample 1 had the biggest original roughness. Roughness remained unchanged up to 800h and increased from 4.469 to 4.947 at 840h. Then the roughness subsequently decreased and the final value was 4.188, lower than the initial value 4.452.

During the initial aging period there was a sharp decrease in roughness of sample 2 from the original value 2.033 to 1.313. Then it kept decreasing slowly until 800h. After that the roughness values gradually increased until 1176h. During the whole ageing period, the roughness value was lower than the initial value. The roughness value after ageing for 1680h was 1.441, about 71% of its original value.

For sample 3, the roughness values were basically at a steady state. There was only a slight increase during the whole ageing period from the initial value of 2.254 to 2.316.

Based on the analysis of LSCM results, it could be deduced that the different changes of surface roughness among the three samples were caused by their different UV resistance. UV resistance of sample 2 was weaker compared with the other two samples, and sample 3 had the best UV resistance. In order to see if there is correlation between the surface roughness and UV resistance, GM samples were also tested for ATR-FTIR intensity changes, tensile properties and OIT after artificial weathering to estimate their UV resistance.

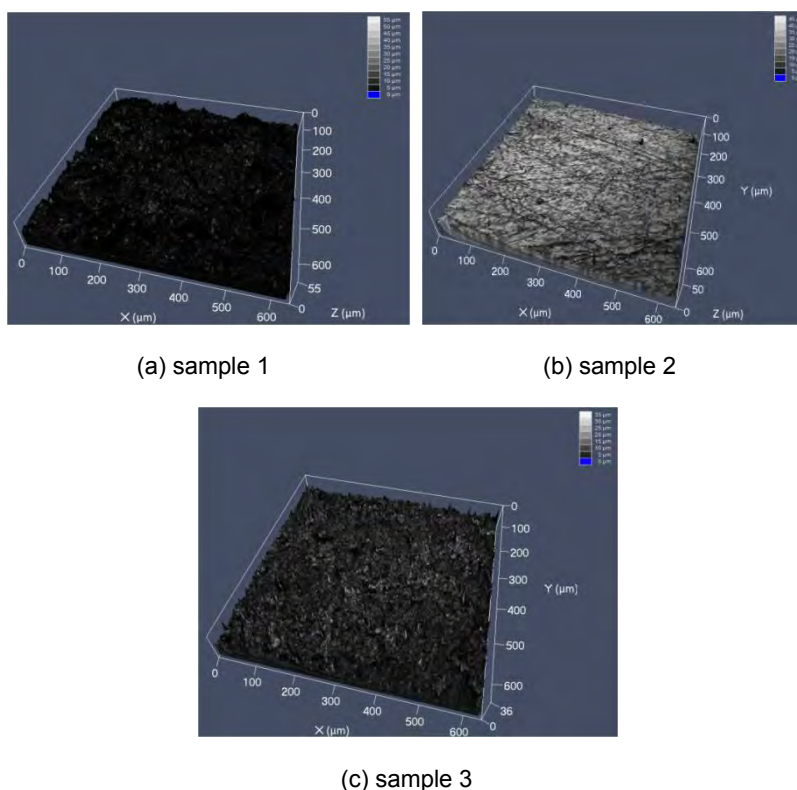


Fig. 3 LSCM images of three samples in the form of 3D

3.2 ATR-FTIR

ATR-FTIR is a well-established, nondestructive method implemented in various different studies for determining the chemical composition of materials based on their chemical bonding. In order to obtain a better identification of the functional groups present in the exposed samples, ATR-FTIR spectra were recorded with a Varian 1000 Fourier Transform IR spectrometer conducted in the ATR mode. Spectra were made up to 32 co-added scans and resolution was set to 4 cm^{-1} . Samples were analyzed as a function of exposure time. In this paper, the ATR-FTIR band selected for chemical degradation analyses was from strong absorption band and ATR-FTIR results will be used just to check weathering resistance of the three different samples.

Fig. 4 show ATR-FTIR intensity changes of a band at 1730cm^{-1} (due to C=O stretching of a ketone) for the 3 samples respectively. Each data point shown in Fig. 4 was obtained from approximately the same location. Intensities were obtained from the ATR-FTIR spectra at a specific exposure time after adjusting for the base line shift.

For sample 2, it can be seen that the intensity of band at 1730cm^{-1} increased with exposure time and it had the most significant changes due to photo oxidation. The intensity value increased from 0.004 to 0.025 after 1680h exposure. The rising of the value was rapid in the first 168h and appeared to be stable in the next 1344h. Compared with the results of LSCM, it can also be seen that the roughness of sample 2 had a sharp decrease in the first 168h, and then the value slowly went down until 840h. This means the variation of surface roughness have correlation with the ATR-FTIR intensity change. The intensity value of sample 1 and sample 3 had only slight changes. The trends were also in good agreement with the changes of surface roughness of sample 1 and sample 3.

From the ATR-FTIR results we can see that UV resistance of sample 2 was weaker than the other two samples, which also can be inferred from the analysis of LSCM results.

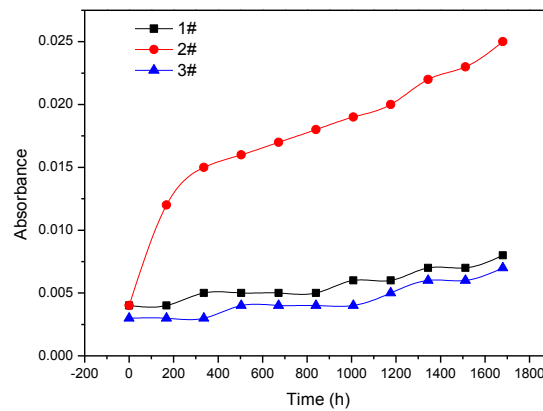


Fig. 4 Intensity change of 1730cm^{-1} as a function of exposure time

3.3 Tensile Properties

The tensile properties of a GM provide an index as to how it will respond to physical stress and are a useful means to assess the durability of the GM (Rowe and Sangam,2002). Generally, polymer degradation due to ageing leads to decreases in strength and strain at break while increases in tensile modulus and yield stress, which signifies the transition from a ductile material to a brittle one as a result of degradation. The tensile properties of the GM were obtained in accordance with ASTM D6693 using a Zwick Roell test machine equipped with load cell, crosshead measurements, and self-aligning wedge grips. The dumbbell shaped GM specimens were stretched at a speed of 50 mm/min until rupture. Tensile properties at yield and break were recorded.

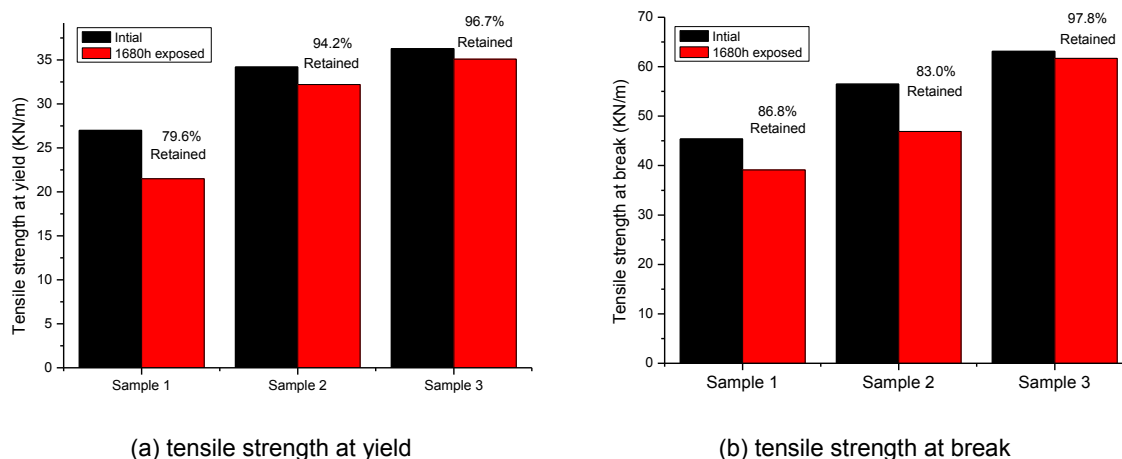


Fig. 5 Tensile properties change of three samples before and after 1680 hours' UV exposure

Fig. 5 respectively shows the tensile strength at yield and tensile strength at break of the three GM samples before and after UV radiation. From the histogram, it can be seen that the yield strength of sample 1 had dropped by 20% and tensile strength at break decreased by up to 13% of its original value during 1680 hours of testing. The tensile strength at break of sample 2 decreased by up to 17% while the yield strength only changed a little. Sample 3 was the most stable one compared with sample 1 and sample 2. There were only slight changes in tensile properties observed after the artificially simulated weathering (could be due to a small variability in tensile properties at different locations along the GM roll), which showed that sample 3 had the best weathering resistance.

3.4 Oxidation Induction Time (OIT)

Studies show that service life of HDPE GM can be divided into three stages (Hsuan and Koerner, 1998; Sangam and Rowe, 2002; Müller and Jakob, 2003). Stage I: Antioxidant depletion, Stage II: Induction time to the onset of polymer degradation, and Stage III: Polymer degradation. The sum of the three stages is regarded as the service life of GM. According to test method GM 13, the UV resistance of GM is based on percent retained value regardless of the original OIT value, which is initially controlled by the rate of antioxidant depletion in Stage I. Hindered amine light stabilizers (HALS) are not present in the GM samples. We use standard OIT tests to estimate UV resistance of three samples. Standard OIT tests were carried out following ASTM D3895 with differential scanning calorimeters (DSC) PE Diamond. The GM samples were heated to 200 °C in nitrogen, and then held isothermally at 200 °C and 35 kPa in an oxygen environment until the exothermic peak was detected. The time to the onset of exothermic peak resulting from oxidation was taken as the OIT value.

During UV exposure, antioxidants are lost by evaporation and chemical reactions with oxygen, free radicals and alkylperoxides at the polymer surface. Thus OIT value of the GM decreases as antioxidants are depleted with time.

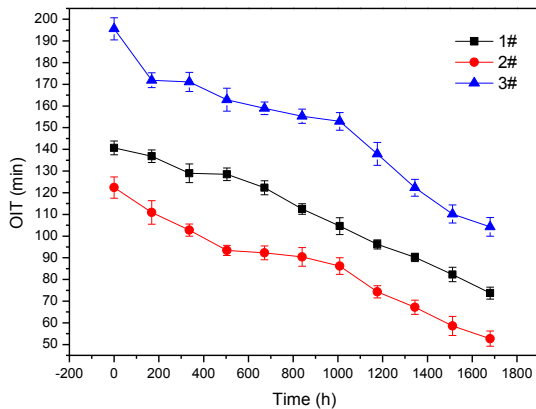


Fig. 6 OIT change as a function of exposure time

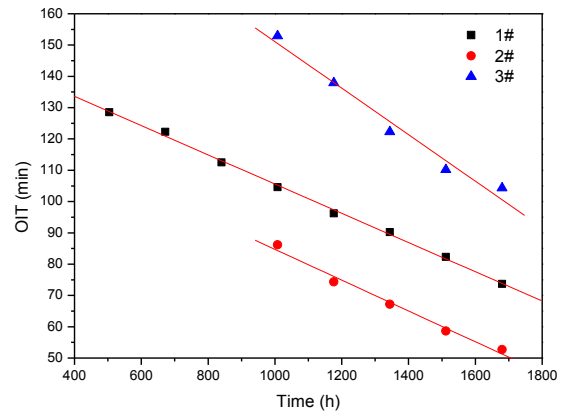


Fig. 7 Variation of OIT with ageing time using linear regression (from 504h to 1680h)

Fig. 6 presents typical plots of OIT with ageing time for three GM samples respectively. It can be seen from the figure that OIT value of the three samples decreased in varying degrees during the ageing test. For sample 1 and sample 3, the Std-OIT retained 52.4% and 53.3% of the original value respectively, both greater than 50%. There was most significant difference between the std-OIT value of the virgin GM and sample 2 being aged after 1680h with the Std-OIT retained being only 43.1% of the original value. It was also observed that the std-OIT value of three GM samples remained steady for a period of time during the ageing test. Then the OIT value began to decrease at a relatively higher rate.

By using linear regression through the data points (from 504h to 1680h for sample 1, from 1008h to 1680h for sample 2 and sample 3), it can be calculated that if the OIT value dropped down to zero, 3261 hours of ageing test would be needed for sample 1, 2721 hours for sample 2 and 3032 hours for sample 3. The coefficient of determination R^2 of the regression line ranged from 0.976 to 0.998. The results of OIT test showed that UV resistance of sample 2 was weaker than the other two samples, which also can be concluded from the result of ATR-FTIR and LSCM.

4. CONCLUSIONS

Surface roughness of a series of HDPE GM samples were analyzed using laser scanning confocal microscope (LSCM) after UV exposure. The exposed samples were also tested for OIT, ART-FTIR spectra and tensile properties. Due to the difference in UV resistance, sample 2 showed the most significant change in surface roughness, decline in tensile strength and OIT, while sample 3 remained stable in surface roughness, tensile properties, and had the highest retention of OIT. Based on the test results, the following conclusions were reached.

- (1) During the period of UV exposure, the change of surface roughness was consistent with the variation in tensile properties, OIT and ATR-FTIR results. So surface roughness can be used to evaluate the UV resistance of HDPE GM.
- (2) The value of surface roughness changed significantly with decreased UV resistance. The surface roughness remained stable for HDPE GM with better UV resistance.

It is proposed that surface roughness has correlation with weathering resistance when the geomembrane is still in the stage of antioxidant depletion (Stage 1). Maybe the roughness is not uniquely related to a single parameter but influenced by many factors, such as loss of antioxidants (by evaporation and chemical reactions) on the surface of GM, outward migration of antioxidants from the core to the surface, formation of low molecular weight polymers due to photo-oxidation. The correlation between surface roughness and weathering resistance, and the trends of roughness change during its entire service life cycle need to be further studied.

REFERENCES

- ASTM D6693. Standard test method for determining tensile properties of nonreinforced polyethylene and nonreinforced flexible polypropylene geomembranes, *American Society for Testing and Materials*, West Conshohocken, Pennsylvania, USA.
- ASTM D3895. Standard test method for oxidative-induction time of polyolefins by differential scanning calorimetry, *American Society for Testing and Materials*, West Conshohocken, Pennsylvania, USA.
- Gulec, S.B., Edil, T.B. and Benson, C.H. (2004). Effect of acidic mine drainage on the polymer properties of an HDPE geomembrane, *Geosynthetics International*, 11(2): 60–72.
- Hsuan, Y.G. and Koerner, R.M. (1998). Antioxidant depletion lifetime in high density polyethylene geomembranes, *Journal of Geotechnical and Geoenvironmental Engineering*, ASCE 124 (6): 532–541.
- Mathiaa, T.G. and Pawlus, P.M. (2011). Recent trends in surface metrology, *Wear*, 271: 494–508.
- Müller, W.W. (2007). *HDPE Geomembranes in Geotechnics*, Springer Verlag, Heidelberg, Germany.
- Müller, W. and Jakob, I. (2003). Oxidative resistance of high-density polyethylene geomembranes, *Polymer Degradation and Stability*, 79: 161–172.
- Rowe, R.K. (2005). Long-term performance of contaminant barrier systems. *Geotechnique*, 55: 631–678.
- Rowe, R.K., Quigley, R.M., Brachman, R.W.I. and Booker, J.R. (2004). *Barrier Systems for Waste Disposal Facilities*, 2nd ed., Spon Press, New York, NY, USA.
- Rowe, R.K. and Sangam, H.P. (2002). Durability of HDPE geomembranes, *Geotextiles and Geomembranes*, 20: 77–95.
- Samuel R.P., Joanne W., Peter T. and Colin D.M. (2007). Pharmaceutical applications of confocal laser scanning microscopy: The physical characterisation of pharmaceutical systems. *Advanced drug delivery reviews*, 59: 1434–1452.

Ten Years of Innovation in the Application of Piled Embankments in the Netherlands

A.E.C. van der Stoel, PhD., University of Twente / CRUX Engineering Netherlands, vanderstoel@cruxbv.nl

ABSTRACT

This paper describes the construction and some general aspects of the design and execution of several Load Transfer Platforms (LTPs) or piled embankments in the Netherlands over the past 10 years. In this period extensive innovations were carried out in both design and execution, resulting in a new design guideline and innovative applications. Because of the particularly poor soil circumstances, many specific challenges were encountered during construction of piles and geogrids.

The paper first briefly outlines the major design rules in Dutch Guideline CUR226 after which an extensive overview is given of the major characteristics of various executed projects for road and rail constructions. The paper concludes with two completely new and innovative applications: one for a cemetery (currently being realized) and one for the crane platforms of the biggest on-shore wind farm in the Netherlands (>7,5MW, >198m tip).

1. INTRODUCTION

Because of an emphasis on reducing construction time, lateral movements near existing structures (bridges, aqueducts) and reducing the disturbance to the surrounding area during the construction of embankments, several Load Transfer Platforms (LTPs) on piles or Piled Embankments (PEs) have been constructed in the Netherlands in the past 10 years. Piled embankments generally consist of a large number of piles, installed at a small spacing, overlain by geogrids in a platform of material with a high friction, the Load Transfer Platform (LTP). The general principle is illustrated in Figure 1: after applying a working platform of sand (1), the piles (2) and steel pile reinforcement (3) are installed, on which a pile cap (4) is placed (prefab) or casted. On top a mattress (5) consisting of geogrids and granular material is constructed. Finally, on top of this the embankment and (rail)road can be constructed without (piles in bearing layer) or with limited settlements (friction piles, *not* shown in Figure 1) any settlements occurring.

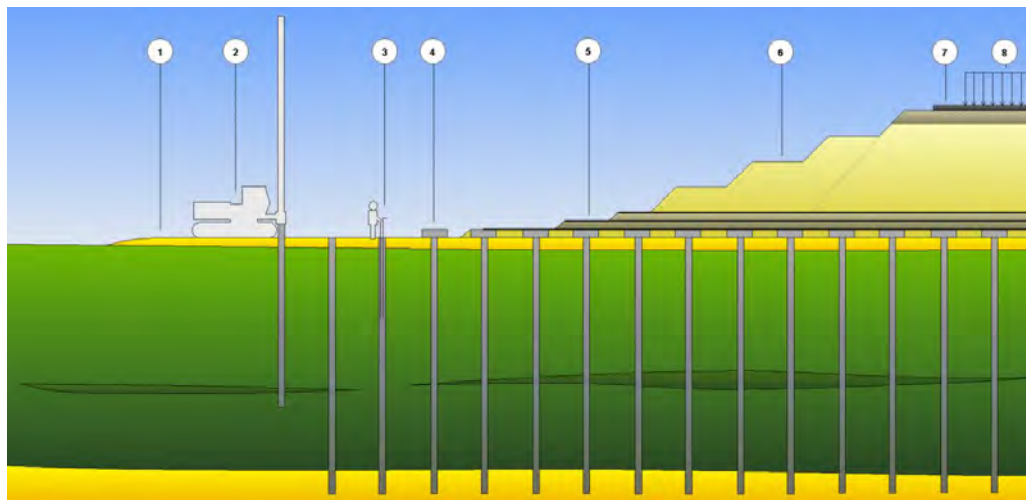


Figure 1: Principle of piled embankment installation

2. SOIL CONDITIONS IN THE NETHERLANDS

To sketch the typical circumstance in which piled embankments are applied in the Netherlands, two typical soil profiles are outlined. Most typical for the soil conditions is that the top meters consist of soft soils with a high groundwater table. In Figure 2 (left, Amsterdam) a soil profile, that is typical for the ground conditions in the western part of the Netherlands is shown. The top layer of the first meters below surface level consists of Anthropogenic sand. Below this top layer the

Holocene deposits are found until a depth of about 10-15 m below surface level. The Holocene formation can be divided (from top to bottom) into peat (Hollandveen), clay (Oude Zeeklei), silty sand (Wadzand), clay (Hydrobiaklei) and peat (Basisveen). The soft Holocene has been deposited on top of the stiff Pleistocene sands which are sometimes divided by an intermediate silty, clayey sand layer (Allerod). The phreatic water level is found about 0.4 m to 1.5m below surface level. The artesian water level in the Pleistocene sand layers usually lie 2 m below the phreatic water level.

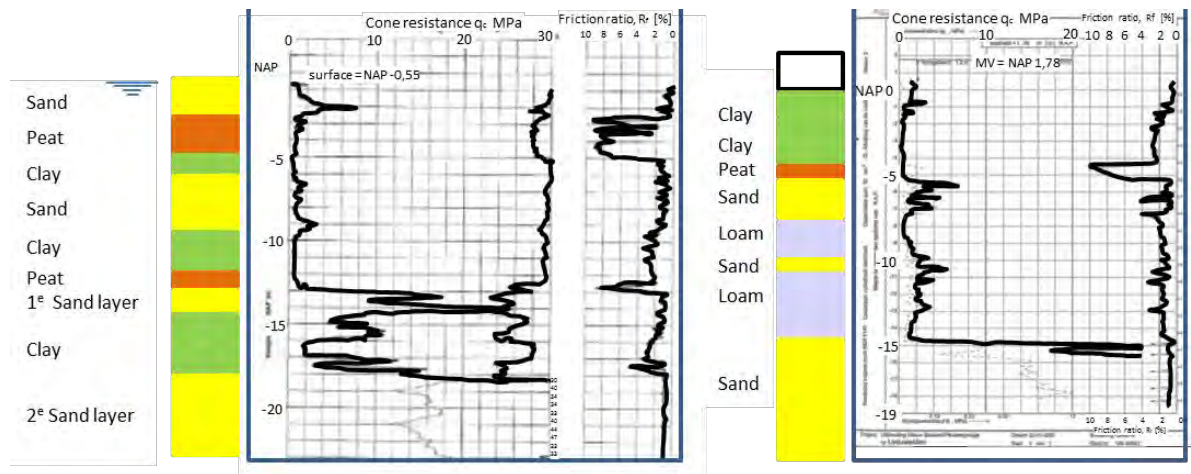


Figure 2: Characteristic soil profile for western part (left) and northern part (right) of the Netherlands

For the northern part of the Netherlands, the soil conditions are comparable with the western part of the Netherlands, only the Holocene layers are generally much more loamy, see Figure 2 (right, Leeuwarden). The phreatic water level is found about 1.0 m to 2.5m below surface level.

For the central and eastern part of the Netherlands, the soil consists of mainly medium dense to dense Pleistocene sand layers, locally overtopped by some Holocene clay or silt layers. The application of piled embankments for these profiles is generally less interesting compared to convention settlement reducing solutions.

3. MODELING PILED EMBANKMENTS

3.1 Introduction to CUR226

In 2010, the Dutch Design Guideline for the design of piled embankments CUR 226 (2010), has been introduced. The outlines of this Design Guideline are given by Van Eekelen et al (2010). The choices made within the Dutch Design Guideline are based on comparisons with and analyses of several field tests, finite element calculations, parameter studies, and work of several authors. The BS8006 (1995 and 2010) and the EBGEO (2010) have been discussed in great detail and the decision was made to adopt the design method of Zaeske (2010) / EBGEO.

The safety philosophy and the constraints of the EBGEO for the applicability of the design rules have been adapted for the Dutch situation.

In the first stage of the design of a piled embankment, the efforts can usually be limited to calculations for the grids and the bearing capacity of the piles. Lateral loads can however cause relatively large bending moments in the piles, and because the steel pile-reinforcement significantly contributes to the total costs, the determination of displacements, lateral forces and bending moments plays an important role in the design process. In the next paragraphs the design stages of the CUR 226 will be explained.

3.2 Analytical Grid Calculation

In the design of the geosynthetic reinforcement, several calculation steps are distinguished. After the material properties on load- and material factors are determined, all loads are converted to an uniformly distributed load and the force distribution within the piled embankment (piles, reinforcement & subsoil) is determined. The line loads that result from this are translated into a strain and membrane tensile force and the spreading perpendicular to the (rail)road axis is included. Because the tensile force depends on the tensile stiffness of the grid, this calculation is an iterative process.

In the past years much research has been performed by Van Eekelen et al. (2012a, 2012b, 2012c), which will probably be incorporated in a revised version of the CUR226 guideline.

3.3 Pile Calculation

The vertical bearing capacity of the piles is determined analytically using the Dutch design guidelines Eurocode 7 - NEN 9997-1 (2012). The LTP can be either considered as a Settlement Free Construction (SFC+ settlements < 3cm), where the end-bearing piles transfer the full load to the bearing layers, or as Settlement Reduction Construction (SRC), where a limited settlement of the LTP is accepted and part of the load is transferred to the subsoil between the pile(cap)s and the rest is transferred to (friction) piles.

3.4 Bending Moments in Piles

A major part of the design of the LTP is formed by the determination of the bending moments in the piles, caused by for example vehicle loads or asymmetry of the embankment. Because of the complicated deformation behavior of the LTP, this can generally not be done analytically. Therefore, Finite Element Method (FEM) calculations are used to calculate pile moments and deformations. The FEM computer program PLAXIS is very suitable for modeling LTPs (Slaats & Van der Stoel, 2009 & Van der Stoel et al 2007b).

Based on the SI the soil profile for the model geometry is determined. For modeling the soil layers the Hardening Soil or Soft Soil Creep model are most appropriate, because they are capable to describe reduction of stiffness as well as irreversible deviator strains due to deviatoric stress. In order to get appropriate parameters for the model, samples have to be taken from the (soft soil) layers that are considered to be most important regarding deformations. Besides determining the volumetric weight (γ), triaxial tests and oedometer tests should be performed for determining stiffness parameters (E_{50} , E_{oed}) and strength parameters (c' , ϕ'). Although complex geometries justify a 3D approach, 2D FEM is still preferred because of lower model complexity and limited calculation time.

The validity of the CUR226 approach has been verified Houten case (Table 1, #22), using Plaxis 3D Tunnel and Plaxis 2D v9 respectively, see also Figure 3. The bending moments in the piles have been compared for various cases with different traffic loads and soil support, from which the conclusion could be drawn that the bending moments generally occur at the same locations and the extreme bending moments per pile do not differ significantly. Therefore it was concluded that 2D calculations assess the maximum occurring bending moment quite accurately and some reserve should be made when using a 2D model to determine the exact location of the extreme bending moments.

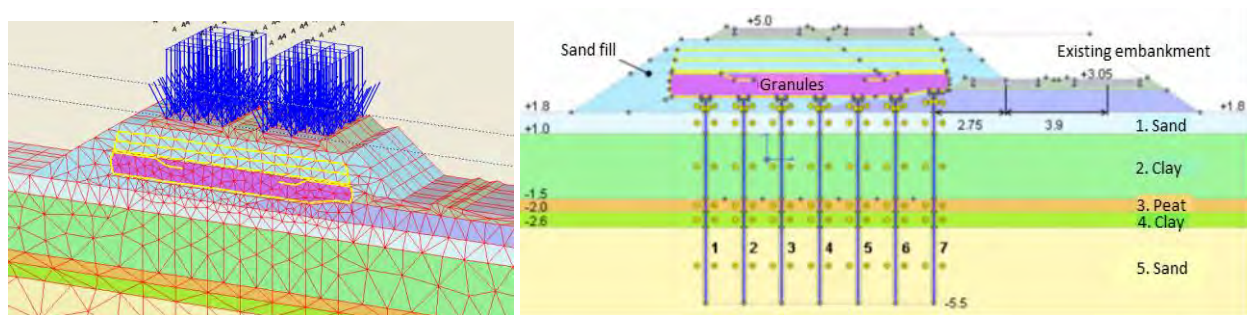


Figure 3: Example of 3D (left) and 2D model (right) based on CUR 226

Recently the calculations of the pile reinforcement and grids of the piled embankment of the highway A12 in Woerden (Table 1, #23), designed using PLAXIS 2D v9, was compared with PLAXIS 3DTunnel (2.4) and PLAXIS 3D 2011 calculations by Oskam (2012). The results, see Figure 4, confirm the CUR 226 findings.

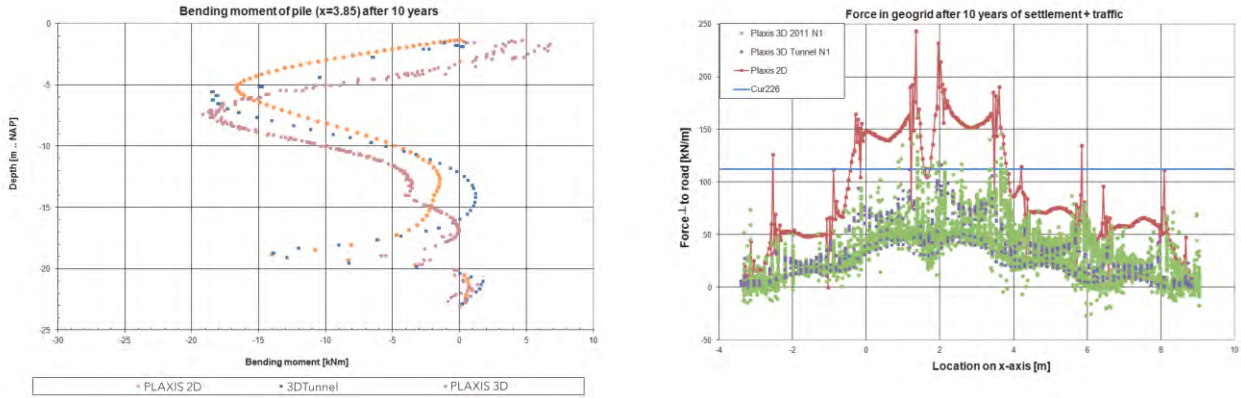


Figure 4: Bending moments and grid forces 2D vs. 3D after Oskam (2012)

4. OVERVIEW OF DUTCH PILED EMBANKMENTS

4.1 Realized Projects

In Table 1 an overview is given of the piled embankments that have been realized in the Netherlands over the past decennium; the numbers (#) of these projects are used as a reference in the next paragraphs. In the first years most designs were based on the British Standard 8006. From 2010 this formally (regulation) changed to the German Standard (EBGEO) and after since about 2010 the Dutch Standard CUR226. The embankment at Carnisselande (#5) was the first LTP for a light rail system (Van der Stoel et al, 2006) and the application with the highest embankment so far. Because of great variety in embankment height, width and pile center to center distances combined with little experience at that time, measurements were conducted, but also many problems were encountered that have led to many improvements in later projects. In the next paragraphs some characteristic and innovative features of these projects are outlined.

4.2 Almere, First LTP-Gabion Intergraded System (#10)

In Almere a noise barrier consisting of an integrated system of a LTP and a gabions wall was constructed on very soft and very heterogeneous soil, demanding specific execution measures for the High Speed Piles (HSP) and geotextile grids used for the system. The gabions consist of boxes made of twisted or welded steel wire filled with stones, and are anchored by geotextiles to ensure stability. The architectural demands require the gabions to appear nearly (visually) horizontal for a period of over 30 years, thus limiting the allowed settlements of the LTP significantly. Design and execution are outlined in Van der Stoel et al (2007a) and the main principle is shown in Figure 5.

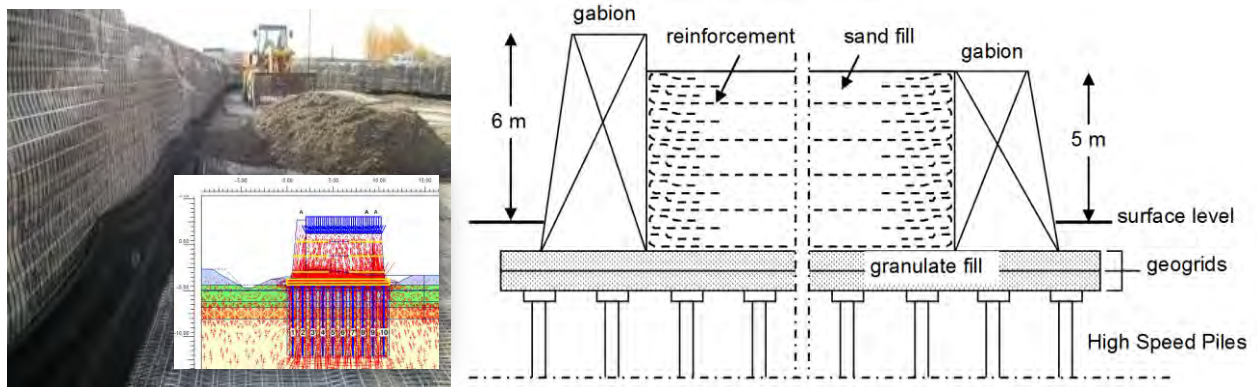


Figure 5: Execution, PLAXIS output stresses model gabions and LTP (left) and cross section LTP and gabions (right)

4.3 A2 Beesd 2x2 Abutments KW9 (#21)

In Figure 6 the first application for a major highway is shown. Special feature in the piled embankment was that it was constructed next to a very old bridge that had to stay in function during the construction of phase 1. Therefore lateral

displacements were a big issue and no consolidation time was available. Thus, the high abutment foundation was constructed before construction of the LTP. When the embankment and new bridge were completed, the old bridge was demolished and at this location also a piled embankment was constructed.

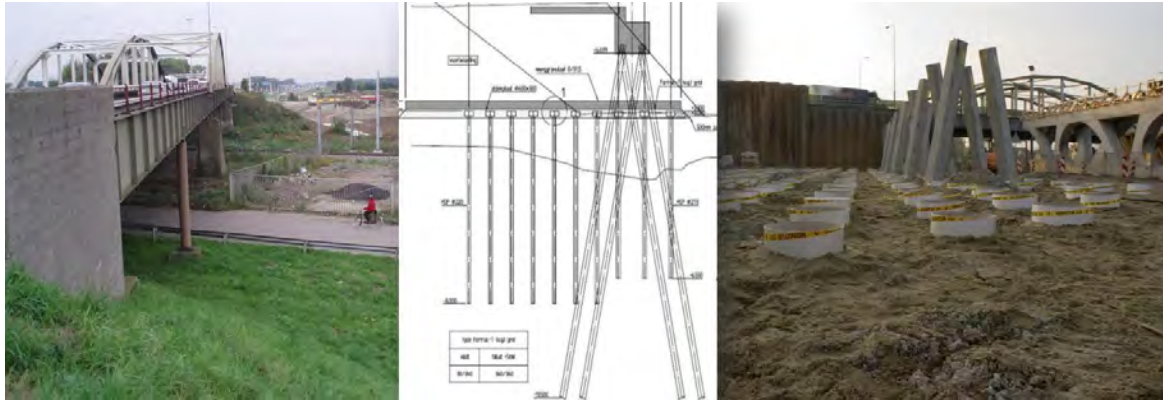


Figure 6: Existing bridge (old situation, left), LTP, sheet pile and abutment foundation (right)

Table 1 Overview of piled embankment projects in the Netherlands over the past 10 years (partially based on CUR226) *

Ref	Project	Area	Year	Pile	Pile	Principal / main	Pile	Max	Principal / main	Design calculation
#	[-]	[m ²]	finis- hed	Type	dimensions	center to center distance	length	embank. Height	Reinforcement type	for grids / geosynthetic reinf.
			[-]	[-]	[mm]	[m]	[m]	[m]	[-]	[-]
1	N247 Monnickendam Busbaan	3600	2002	Prefab	290	2.5 (triangular grid)	7	1.1-1.2	3 x Tensar SS30	BS 8006
2	Amsterdam Diemerzeedijk	250	2002	AuGeo	Ø174	1.0x0.8	14	0.8	Secugrid 120-40 R6 + Secugrid 200-40 R6	Enhanced arch
3	A15 Wijngaarden	1000	2003	Prefab	320	3.0 (triangular grid)	7.5	1.55	3 x Tensar LTP30	BS 8006
4	IJsselmonde Trampuslijn	7500	2003	AuGeo	Ø174	1.16x1.16	15-18	3	Fortrac-T 200/50 + Comtrac-T 110/50	BS 8006 + Plaxis
5	<i>Camisselande Trampuslijn</i>	8300	2004	HSP	Ø180.Ø273	0.8x0.8-1.6x1.6	15-17	1.2-8.7	<i>Enkagrid Pro 40 - 180 kN/m</i>	BS 8006
6	Nesseland	5800	2006	AuGeo	Ø174	1.2x1.2	8-11	1.05-1.25	Fortrac-T 200/50 total strength 660 kN	BS 8006
7	A15 Wijngaarden	2700	2004	AuGeo	Ø174	1.1x1.05	10-11.5	2.9	Fotrac-T 200/50 - Fotrac-T 250/50	BS 8006
8	A15 Sliedrecht	9500	2005	AuGeo	Ø174	1.18x0.90-1.18x1.20	10-18	1.6-4.1	Fortrac-T 150/50 to 500/50	BS 8006
9	A15 Hardinxveld Giesendam	12850	2006	AuGeo	Ø174	0.9-1.2	10-12	0.9-4.8	Fortrac-T 150/50 - Fotrac-T 350/50	EBGEO
10	<i>Almere Bastions 2J</i>	1600	2005	HSP	Ø 180	1.0x1.0	9.5-13.5	5.6	<i>Enkagrid Pro 180 kN/m</i>	BS 8006
11	A4 Hoogmade Toerit	3500	2005	AuGeo	Ø 174	0.9x0.9-1.1x1.1	10-12	2.8-5.4	Fortrac-T 150/50 to 500/50	EBGEO
12	Kyotoweg (pilot)	60	2005	Timber		1.15x1.15		1.15	Fortrac R 350-400/30-30 MP	BS 8006
13	Papendrecht Overtoom	520	2006	Prefab	290	2.0x2.0	13-16	1.5-4.5	Fortrac R 200/30-30 MP	BS 8006
14	Sliedrecht dikes	280	2006	AuGeo	Ø174	1.1x1.1	12-14	1.75	Fotrac-T 300/50	EBGEO
15	<i>Soundbarier/Coupure Almere</i>	600	2006	HSP	Ø 180	1.2x1.2	9.5-13.5	5.6	<i>Enkagrid Pro 180 kN/m</i>	BS 8006
16	Gorinchem Zuiderlingedijk	500	2007	Timber	tip150/180	1.1x1.1	4.5m+2m	2.0-3.6	Fortrac 80/30-20 T	BS 8006
17	Uithoorn Buitenhof	600	2008	Timber	Head 180	1.0x1.0+1.6x1.6	6	3.6	Fortrac R 300-400/30-30	BS 8006
18	<i>Nieuw Vennep Zuidtangent</i>	6000	2008	HSP	Ø220	1.75x1.75	6.2-12.5	1.6-5.5	<i>Tensar LTP40 + 2 x Tensar LTP30</i>	BS 8006
19	N210 Krimpen a/d IJssel	190	2010	Prefab	290	2.3x2.35	15-20	1.35	Stabilenka 2x350/50 Fortrac R 600/50-30T	EBGEO
20	<i>N201-N523 Turborotonde</i>	3000	2008	Prefab	220	1.0x1.0	6	1.2-1.5	<i>Fortrac R 450/50-30 MP</i>	EBGEO
21	<i>A2 Beesd 2x2 abutments KW9</i>	2700	2008	HSP	Ø220.Ø273	1.45x1.45	10.5-12	6.4	<i>Fortrac R 450 T</i>	EBGEO
22	<i>Houten railway track</i>	650	2009	HSP	Ø220	1.25x1.4 + 1.45x1.9	7.5-9	2.7	<i>Fortrac R 450 MP + Fortrac R 600 T</i>	CUR226
23	A12 - N204 Woerden	5000	2010	Prefab	290	2.25x2.25	10-25	1.6-3.4	Stabilenka 600/50 + Fortrac R 600/50T	CUR226
24	<i>Capelle a/d IJssel, access road</i>	700	2010	Timber	Head 0.14	1.25x1.25	13.5-18.5	≈1.50	<i>Stabilenka 600 en Fortrac 400 T</i>	EBGEO
25	<i>Zwolle Hanzenlijn railtrack</i>	1930	2011	HSP	Ø 273	1.15x1.15	10.5	7.6	<i>Fortrac T 1200. 800 and 600</i>	EBGEO
26	<i>Amsterdam Arena</i>	930	2012	HSP	Ø 220	1.2x1.2 + 1.5x1.5	4.5	3.3-5.8	<i>Fortrac-T 170/170 + 230/230</i>	EBGEO
27	<i>N201-A4-KW137</i>	3810	2012	HSP	Ø 273	1.75x1.75	8.5-11.5	8.1	<i>Fortrac-T 320/900</i>	CUR 226
28	<i>A2 Nieuwegein highway SpoedF</i>	7500	2011	Prefab	220	1.4x1.4	10	4.1-5.6	<i>Fortrac-T 275/460</i>	CUR 226
29	<i>Gouda Parkeerterrein</i>	5000	2011	VSP	Ø 273	2.35x2.35	14-15	1.5	<i>Fortrac-T 400/400</i>	CUR 226
30	<i>Gouda Jamessingel</i>	10000	2011	VSP	Ø 273	2.35x2.35	14-20	1.75	<i>Fortrac-T 400/400</i>	CUR 226
31	<i>Ablasserdam cemetery</i>	5400	2012	HSP	Ø 220	2.15x2.15	14.5-16.5	3.5	<i>Stabilenka 600 + Fortrac 500</i>	CUR 226

* please note that this table only shows the main properties of the piles, main center to center distances, pile lengths and types of reinforcements applied. Each construction has had special geometrical challenges in which tailor-made solutions were applied, mainly having to do with the overlap of the grids and the depth and center to center distance of the piles. In general more / deeper piles and heavier grids are applied for situations where the piles could not be applied in the general grid. In the transition zones between the regular LTP and conventional solutions (vertical drains, excess loads etc.) piles spacing is generally increased / depth is decreased and/or no piles (just grids) are applied.

** the author has been involved in / responsible for the design of the *italicized* projects

*** HSP = Voton High Speed Piles; VSP = *Verdingende Schroef Paal* (screw-push aside); AUGEO = tube pile installation by modified drain stitcher (see website references)

4.4 Houten, First Railway Application and Special Transition Zone (#22)

In Houten, the first LTP for a main railway system was applied (Van Duijnen et al, 2010 and Van der Stoel et al 2010). Because of the specific requirements that had to be met for the transition between a (rigid bridge) foundation on one side and a regular embankment on the other side, a LTP transition zone was applied, see Figure 7. After the regular LTP in zone 2, in zone 3A first the pile spacing was increased, after which in zone 3B this spacing was increased further and the length of the piles was reduced. Finally in zone 4 no piles were applied, thus creating a smooth transition.

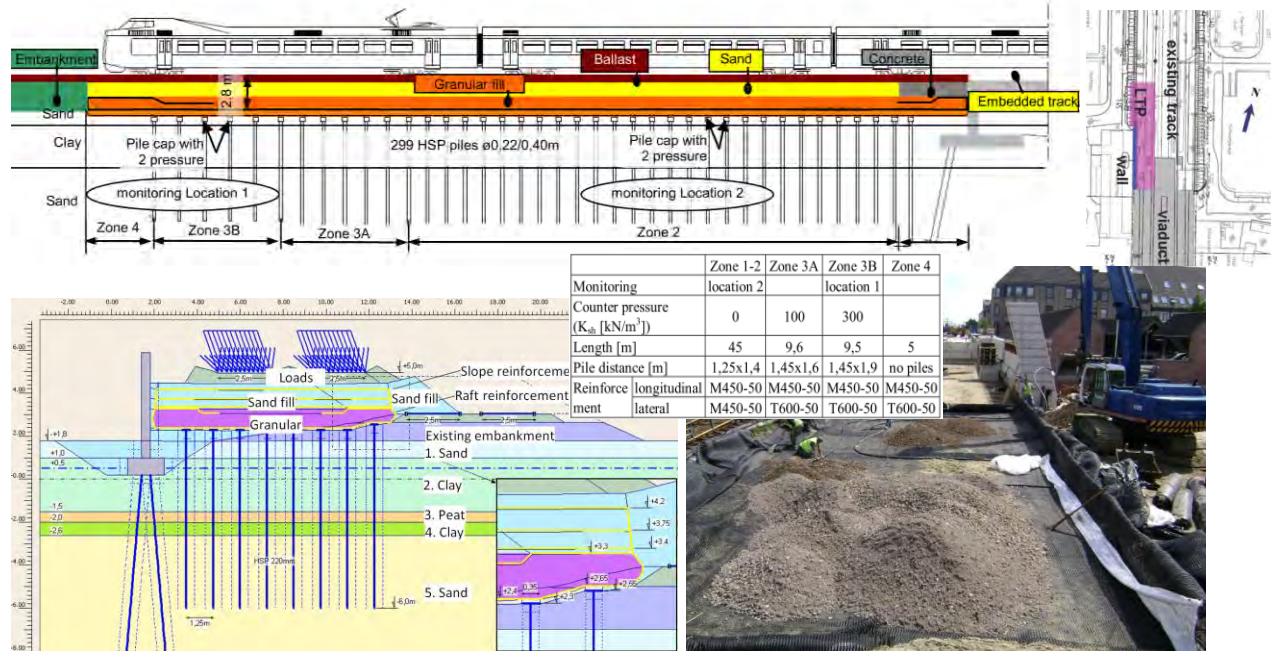


Figure 7: Houten Plaxis input model LTP and wall (left) and construction LTP next to operational railroad (right)

4.5 Zwolle Hanzelijn, Rail Crossing and Integrated System (#25)

Near Zwolle, the Hanzelijn, the new rail link between the central Randstad urbanization and the north of the Netherlands is constructed. Prior to constructing a railtunnel trough (see Figure 8), the surrounding area was partially preloaded with sand to limit the settlement caused by the fill alongside the tunnel. The need for a piled embankment for the railway lines around the intersection arises from the local geotechnical impact of connecting to the existing tunnel trough (Van der Stoel et al, 2012). The tunnel comprises a closed part with an open part at each end. The two lines cross at the closed part. The lateral loads on the walls of the open parts are relieved through the use of a reinforced soil construction for the fill (see Figure 9). The piled embankment at the intersection will help to reduce the horizontal soil pressure against the open trough and duct, and prevent excessive moments in the piles underneath the structure. This method also guarantees the stability of the reinforced soil construction. This solution, with high demands on differential settlements between the piled embankment and the rigid tunnel foundation, was the first application for a railway / tunnel crossing.

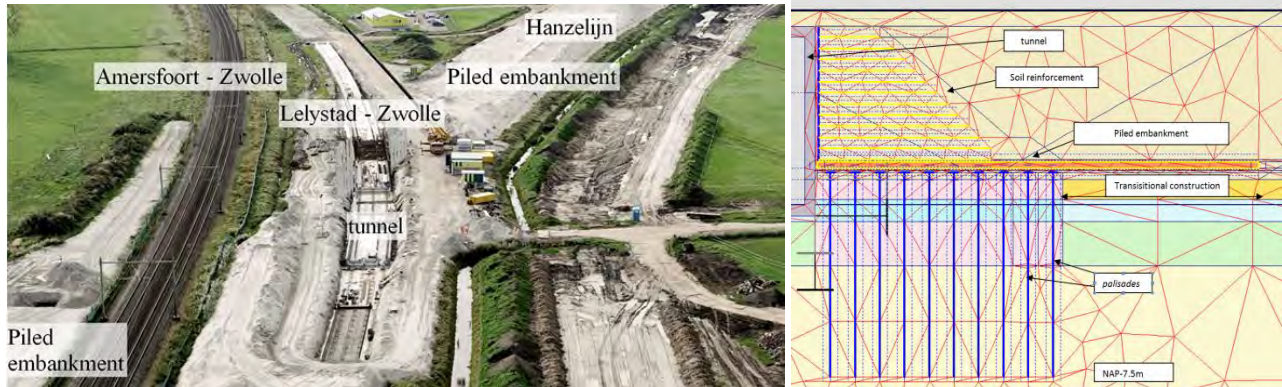


Figure 8: Overview Hanzelijn crossing tunnel (left) and Plaxis model LTP and soil reinforcement (right)



Figure 9: Hanzelijn pile installation (left), bottom grid (middle) and layered soil reinforcement (right)

4.6 Gouda, Very Low Embankment, Road and Parking (#29 & #30)

In Gouda, both a road and a large parking were constructed on very soft soil. Special circumstances were the possible presence of WWII explosives, so for the first time, vibration free screwed piles were used. To reduce the risk of hitting explosives during pile installation, high center to center distances were demanded. Combined with the very low embankment due to the necessary connection to existing roads, this led to the most 'slender' piled embankment system so far, see Figure 10. To be able to transfer the loads to the piles, relatively large pile caps had to be applied combined with a small excavation below water level before pile installation / construction.

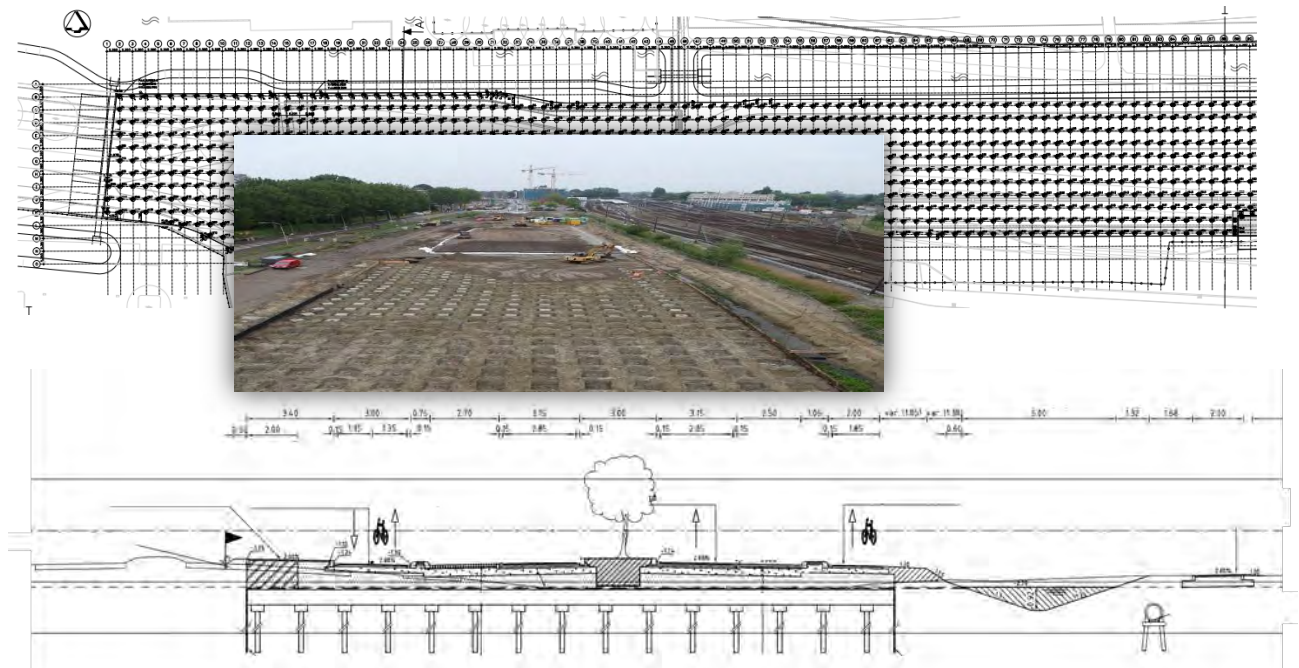


Figure 10: Gouda very slender LTP, pile grid and construction (upper) and cross section (lower)

4.7 Ablasterdam, Cemetery (#31; Still Under Construction)

In Ablasterdam the capacity of an existing cemetery had to be significantly increased. Because of the fact that the location for this expansion is positioned approximately 4m lower than the existing cemetery, the very soft soil and the high groundwater table, a solution was designed in which both 'sand graves' as well as 'concrete basement graves' are positioned on top of a piled embankment, see Figure 11. Because of the very low embankment this leads to a situation in which the arch of the LTP either goes through the sand grave or through the concrete shaft. In the case of the concrete basement graves, the center to center distance of the piles was therefore increased to fit the dimensions of the concrete U-shaped boxes (2,56mx2,15m). Because of the structural properties of the boxes, the grid forces could also be reduced. For the sand graves an uniform 2,15mx1,15m grid was applied.

This very innovative application of a piled embankment has the main advantage that the expansion could be realized without having to take into account long consolidation times that normally apply for these kind of locations in order to meet the strict settlement requirements. Also, the maintenance costs of the cemetery will be drastically reduced because of the settlement free solution and the flexibility of the application. Construction will be finished by the end of 2012.

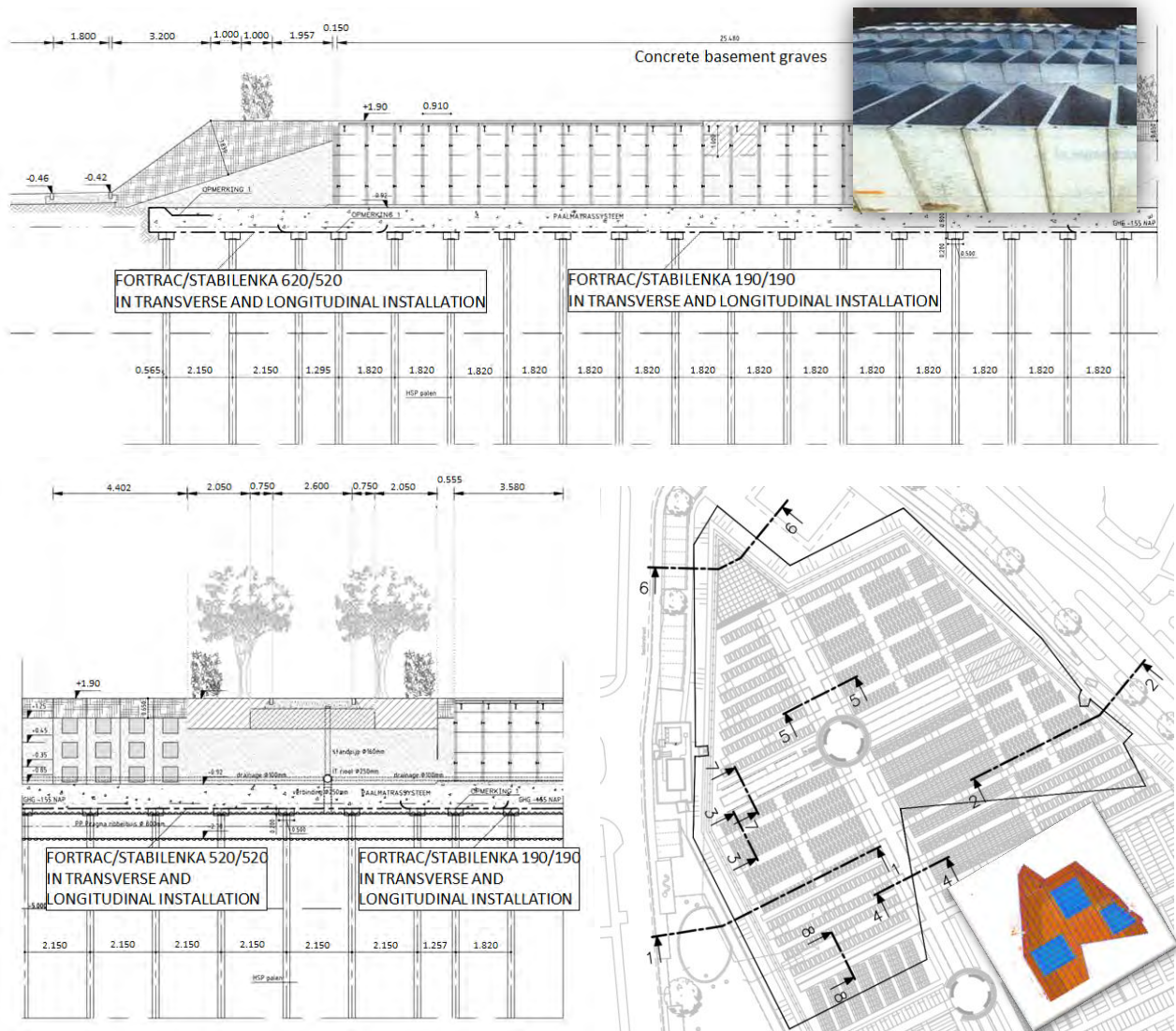


Figure 11: Two cross sections (1-1, upper & 5-5 lower) and plan view of cemetery with sand graves and tombs

4.8 Noordoostpolder, Wind Park (to Be Constructed Fall 2012/Spring 2013)

A partnership of more than 100 agricultural entrepreneurs from the North East Polder and energy company RWE/Essent are about to construct the largest wind farm in the Netherlands (website). It will be located on-shore and near-shore along the dikes of the IJsselmeer. The estimated total investment comprises about 1 billion euros. The 86 wind turbines (>7,5MW, >198m tip) of Windpark Noordoostpolder will generate 1.4 billion kWh of clean sustainable electricity per year in 2015, enough to power more than 400,000 households every day. This makes the North East Polder one of the leading European regions in modern wind energy.

In order to build the first 12 on-land wind turbines, a huge mobile crane is needed to place the generator on the tower. In order to build this crane, smaller (but still large) mobile cranes are needed. To position these cranes on the very soft soil and to be able to reach the needed positioning accuracy at hub height, settlement is not allowed at the platform. Therefore, piled embankments will be applied at each location, as shown in Figure 12. Because of the high load on the crane platform (260 kN/m²) and the surrounding platform (185 kN/m²), a HSP pile grid of 1,10x1,10m and 1,30x1,30m respectively will be used. The area of the platforms is 5000 m² each, adding up to about 60.000m² total, making it the largest application of a LTP in the Netherlands so far.

Special attention is required for the interface between the foundation of the turbines themselves and the crane platform. For this, special FEM interaction calculations have been made, which will be published in near future.

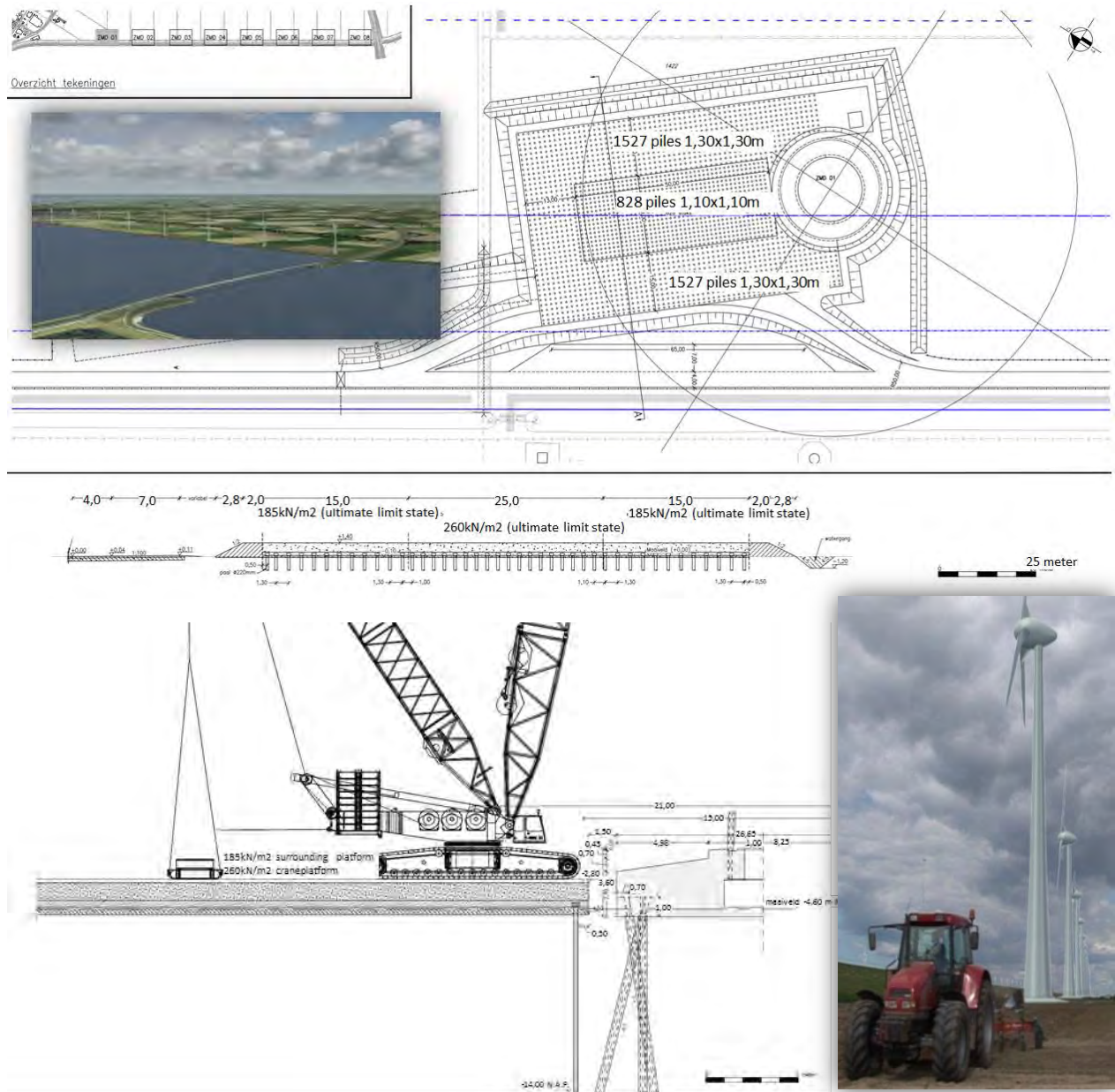


Figure 12: Two cross sections and plan view of wind mill construction LTP (and interaction with mill foundation)

5. CONCLUSION

The application of piled embankments has taken a huge flight in the Netherlands in the past ten years. Because of the work conducted by the CUR committee, the publication of the CUR226 guidelines, the many research projects and the fast experience that has been gained in multiple applications, design and execution have been brought to a next level, in which innovative applications, as for the cemetery and wind turbines, are made possible.

ACKNOWLEDGEMENTS

The author greatly acknowledges the permission of CUR committee 226 on piled embankments, Heijmans, Dura Vermeer, Voorbij Funderingstechnieken / TBI Infra, Huesker Geosynthetics, Koninklijke Sjouke Dijkstra and RWE Essent to use multiple photos and figures in this paper.

REFERENCES

- Duijnen, P.G. van, Eekelen, S.J.M. van, Stoel, A.E.C. van der, Monitoring of a Railway Piled Embankment, 2010, Proceedings of 9th International Conference on Geosynthetics, Brazil, 2010, pp 1461-1464
- van Eekelen, S.J.M., Jansen, H.L., Duijnen, P.G., van, De Kant, M., Dalen, J.H., van, Brugman, M.H.A., Stoel, A.E.C., van der, Peters, M.G.J.M., The Dutch design guideline for piled embankments, Proceedings of 9th International Conference on Geosynthetics, Brazil, 2010, pp 1911-1916
- van Eekelen, S.J.M., Bezuijen, A., Lodder, H.J., van Tol, A.F., 2012a and 2012b. "Model experiments on piled embankments" Geotextiles and Geomembranes 32 part I 69-81+ Part II."82-94
- van Eekelen, S.J.M. and Bezuijen, A., 2012c, Dutch Research on basal reinforced piled embankments, Geotechniek Special, English edition, pp. 12-17
- Oskam, E., Piled embankments in PLAXIS 2D, 3DTunnel and PLAXIS 3D 2011, Plaxis Bulletin Issue 31, March, 2012
- Slaats, H and Stoel, A.E.C. van der, Validation of numerical model components of LTP by means of experimental data, 17th International Conference on Soil Mechanics & Geotechnical Engineering, Alexandria, Egypt, 5-9 October 2009
- van der Stoel, A.E.C., De Lange, A.P., Bussert, F. & Meyer, N., Railway embankment on "high speed piles" - Design, installation and monitoring, Eighth International Conference on Geosynthetics, September 2006, Yokohama Japan
- van der Stoel, A.E.C., Vink, D., Ravensbergen, R.W., De Hertog M., Design and execution of an integrated LTP and gabions system, XIV European Conference on Soil Mechanics and Geotechnical Engineering, Madrid, 2007a
- van der Stoel, A.E.C., J.W. Dijkstra & H. Slaats, A comparative study on the design of LTP; XIV European Conference on Soil Mechanics and Geotechnical Engineering, Madrid, 2007b
- van der Stoel, A.E.C., Brok, C.A.J.M., De Lange, A.P., Van Duijnen, P.G., Construction of the first railroad widening in the Netherlands on a Load Transfer Platform, Proceedings of 9ICG, Brazil, 2010
- van der Stoel, A.E.C., Brok, C. A.J.M., De Lange, A.P., Piled embankments in the Netherlands: Lelystad-Zwolle (Hanzelijn) and Amersfoort-Zwolle rail intersection, EuroGeo 5, Proceedings of 5th European Geosynthetics Congress, Valencia, 2012
- Zaeske, D., 2001. Zur Wirkungsweise von unbewehrten und bewehrten mineralischen Tragschichten über pfahlartigen Gründungselementen. Schriftenreihe Geotechnik, Uni Kassel, Heft 10, February 2001 (in German).
- BS8006, Code of practice for strengthened/reinforced soils. Soil nail design (1995 & 2010)
- CUR 226, 2010, Ontwerprichtlijn paalmatrassystemen (Design Guideline Piled Embankments), ISBN 978-90-376-0518-1 (in Dutch).
- EBGEO (2010), Empfehlungen für den Entwurf und die Berechnung von Erdkörpern mit Bewehrungen aus Geokunststoffen
- NEN 9997-1 Geotechnical design of structures - Part 1: General rules ICS 91.080.01; 93.020, 2012

Websites (12th of October 2012):

<http://www.windkoepelnop.nl> (Dutch)

<http://www.voton-hsp.nl> (High Speed Piles)

<http://www.voorbijfunderingstechniek.nl/producten/paalsystemen/vsp.html> (VSP piles (Dutch))

<http://www.cofra.nl/product.asp?id=380505&mid=8747&pid=8738> (AUGEO piles)

Tensile Behavior of Triaxial Geogrid: Application of the Theoretical Method

Robert H. Swan, Jr., University of North Carolina at Charlotte, USA, rswan1@uncc.edu
Zehong Yuan, Ph.D., P.E., SGI Testing Services, LLC, USA, zyuan@sgilab.com

ABSTRACT

Questions have been raised as to the proper determination of the wide width tensile strength as well as strength versus strain behavior characteristics for triaxial geogrids. This paper details how single-rib tension tests can be used to determine the tensile properties of triaxial geogrids. Laboratory testing of single-ribs are used in conjunction with a theoretical analysis developed by the authors using a technical approach based in structural mechanics. Using this approach, the wide width tensile strength behavior of two triaxial geogrids are presented. This analysis will be based on the classical approach for a two dimensional truss due to the slenderness ratio of the geogrid ribs. An analysis of the tensile behavior for a number of geogrid orientations ranging in rotation from MD to TD using both force equilibrium and deformation compatibility will allow for the determination of the wide width tensile strength of the two triaxial geogrids.

1. INTRODUCTION

Over the past thirty plus years, geosynthetic materials have been used in both bound and unbound layers of pavement structures for a wide range of applications. In unbound layers, geosynthetics have been used within the subbase and/or base material or at the interface between the unbound base or subbase layer and subgrade for separation, stabilization, drainage, reinforcement and as moisture barrier, as discussed by Koerner (1984) and Holtz et al. (1998). In bound wearing courses such as hot-mix asphalt (HMA), geosynthetics have been utilized for tensile reinforcement and as stress absorption membrane interlayers to reduce the potential of reflective cracking (Koerner, 1984). When designing and specifying pavement structures incorporating geosynthetics an understanding of the geosynthetic products' wide width tensile behavior in particular the tensile modulus is useful. Traditionally these applications have used geogrids, which have had orthogonal tensile elements in the machine and transverse directions (i.e., geogrids with square or rectangular apertures). Therefore, the wide width tensile strength and strength vs. strain behavior have been determined using either ISO 10319 or ASTM D 6637 standard test methods. Both of these test methods are conventional uni-directional tensile tests. ISO 10319 is solely a wide width test having a test specimen with a minimum width of 200 mm and a width to length ratio 2:1. ASTM D 6637 allows for three types of test specimens, which include: a) minimum 200 mm wide width multi-rib specimen b) single-rib specimens or c) multi-layer specimens. As written, both of these test methods only use test specimens, which are orthogonal in the machine and transverse directions of a geogrid.

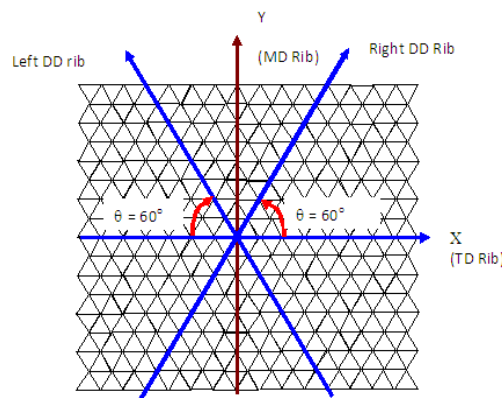
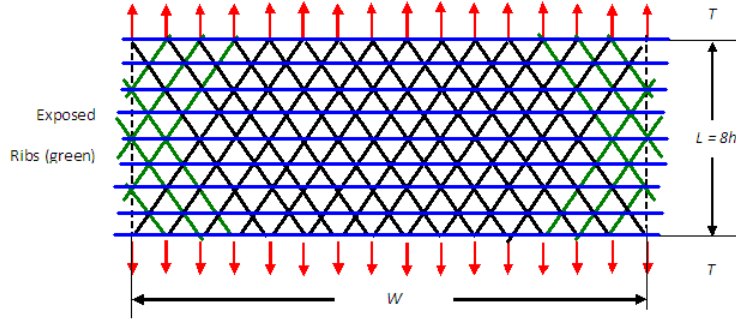


Figure 1. A schematic diagram of a triaxial geogrid where MD is the machine direction, TD is the cross-machine direction, DD is the diagonal direction, and θ is the angle of equilateral triangle.

With the recent introduction of triaxial geogrids, questions have been raised by design professionals and testing agencies as to the proper determination of the appropriate ultimate wide width tensile strength as well as strength versus strain behavior characteristics (tensile modulus) for these products. For definition purposes, a triaxial geogrid is a geogrid consisting of three sets of tensile elements (ribs) to form a grid-like structure with equilateral triangular apertures as schematically shown in Figure 1.

For a given triaxial geogrid consisting of three sets of ribs forming junctions with equilateral triangular apertures, there are a couple basic questions, which need to be addressed before these new types of geogrids can be used in any soil or base reinforcement application. They are: 1) what is the tensile force–strain relationship in the MD, TD and DD directions and 2) what is the tensile strength of the triaxial geogrid in MD, TD, and DD? Naturally one would attempt to answer the above two questions simply by running a wide width (multi-rib) tensile test in accordance with ASTM D 6637 as schematically shown Figure 2. However, due to the unique geometric construction of triaxial geogrids, there exists a boundary effect in testing the triaxial geogrid by the multi-rib method. This boundary effect defined as the effect of those ribs with one end clamped and other end free are herein referred to as exposed ribs. Figure 2, shows these exposed ribs as the “green” DD ribs. These exposed ribs cannot mobilize their full strengths in this type of wide width tensile test; therefore, a multi-rib triaxial geogrid specimen with exposed ribs may significantly underestimate the tensile strength of the triaxial geogrid in the direction it is tested. Therefore, requiring a complex structural analysis to precisely quantify the exposed rib effect on the tensile behavior of the triaxial geogrid.



Swan et al. (2013) developed a theoretical approach to determine the wide width tensile strength of a triaxial geogrid based on the single-rib tensile properties of a triaxial geogrid. This theoretical approach was based on structural mechanics using both force equilibrium and deformation compatibility based on small deformation theory. In this analysis for a triaxial geogrid, the slenderness ratio was defined as the distance between the two adjacent nodes divided by the rib width. For a typical triaxial geogrid, the slenderness ratio is in the range of 35 to 40. Based on structural mechanics, the bending stress in a tensile element (rib) having a slenderness ratio of that magnitude is negligible. Therefore, they made a reasonable assumption that DD and TD ribs were simple tensile elements, which could only carry tensile force. Based on this assumption a classical approach for analyzing a 2-D truss was adopted for the theoretical analysis of the triaxial geogrid using both force equilibrium and deformation compatibility. This paper will detail how the single-rib tension method of ASTM D 6637, can be utilized in conjunction with the theoretical analysis to determine the tensile properties of triaxial geogrids in MD, TD, and DD directions as well as the strength versus strain behavior characteristics of these types of geogrids.

2. DETERMINATION OF ULTIMATE WIDE WIDTH STRENGTH

Based on the work of Swan et al. (2013) the wide width tensile force–strain relationships have been fully defined for: (i) the MD direction by Equations 1 and 2, (ii) the TD by Equations 3 and 4; (iii) the 60-degree direction by Equations 5 and 6; and (iv) the 30-degree direction by Equations 7 and 8. Where T_{WMD} is the wide width tensile force (kN/m) in the MD direction, T_{D-RIB} is the tensile force (kN) in the two DD ribs, h is the rib pitch (m), θ is equal to 60° , ε_{MD} is the wide width tensile strain in the MD direction, ε_{RIB} is the tensile strain in the DD ribs, T_{WTD} is the wide width tensile force (kN/m) in the TD direction, T_{T-RIB} is the tensile force (kN) in the TD rib, ε_{D-RIB} is the tensile strain in the DD rib, ε_{T-RIB} is the tensile strain in the TD rib, T_{W60} is the wide width tensile force (kN/m) in the 60-degree direction, T_{D-60} and T_{D-120} are the tensile forces (kN) in the two DD ribs, ε_{D-60} and ε_{D-120} are the tensile strains in the DD ribs, T_{W30} is the wide width tensile force (kN/m) in the 30-degree direction, $T_{DRIB-60}$ is the tensile force (kN) in the DD rib in the 60-degree direction, and ε_{30} is the wide width tensile strain in the 30-degree direction.

$$T_{WMD} = 2T_{D-RIB} \frac{1}{h} \sin^2 \theta \quad [1]$$

$$\varepsilon_{RIB} = \varepsilon_{MD} \sin^2 \theta \quad [2]$$

$$T_{WTD} = T_{T-RIB} \frac{1}{h} + 2T_{D-RIB} \frac{\cos \theta}{2h} \quad [3]$$

$$\varepsilon_{D-RIB} = \frac{\cos\theta}{2} \varepsilon_{T-RIB} \quad [4]$$

$$T_{W60} = T_{D-60} \frac{1}{h} + (T_{D-120} + T_{T-RIB}) \frac{\cos\theta}{2h} \quad [5]$$

$$\varepsilon_{T-RIB} = \varepsilon_{D-120} = \frac{\cos\theta}{2} \varepsilon_{D-60} \quad [6]$$

$$T_{W30} = (T_{DRib-60} + T_{T-RIB}) \frac{1}{h} \sin^2 \theta \quad [7]$$

$$\varepsilon_{RIB} = \varepsilon_{30} \sin^2 \theta \quad [8]$$

It should be noted that the wide width tensile properties of the triaxial geogrid in the 120-degree direction (i.e., parallel to the left DD rib) are the same as those in the 60-degree direction if the left and right DD ribs have approximately the same tensile properties. Therefore, Equations 5 and 6 can also be used to determine the wide width tensile force-strain relationships in the 120-degree direction. Similarly, the wide width tensile properties of the triaxial geogrid in the 150-degree direction are the same as those in the 30-degree direction if the left and right DD ribs have approximately the same tensile properties. Therefore, the wide width tensile force-strain relationship in the direction of 150 degree can also be determined by Equations 7 and 8. Also for a given direction (MD, TD, or DD, etc), establishing the wide width tensile force-strain curve requires calculating a large number of force-strain data points. However, it becomes a single data point calculation if the focus is to define a characteristic strength, for example, the ultimate tensile strength of a triaxial geogrid in MD.

For this study single-rib tensile tests were conducted in accordance with ASTM D 6637 on two styles of integrally formed (punched and drawn) Polypropylene (PP) triaxial geogrids with equilateral triangular apertures which are referred to as Triaxial A and Triaxial B geogrids. Testing was conducted in both the TD and DD for each geogrid. A total of five (5) single-rib tensile tests were conducted in each direction for each geogrid under a strain rate of 10% per minute using mechanical face grips. A summary of the average tensile strength test results are presented in Table 1. The tensions vs. strain plots for each geogrid are presented in Figures 3 and 4. This data will be used to complete the various calculations throughout the remainder of this paper.

Table 1. Average Single-rib tensile test results for triaxial A and B geogrids in both the TD and DD.

Geogrid Style	Test Direction	Rib Pitch (ft)	Angle of Equilateral Triangle (°)	Tension at 0.5% (lb)	Tension at 2% (lb)	Tension at 5% (lb)	Ultimate Rib Strength (lb)	Strain at Ultimate Strength (%)
Triaxial A	DD	0.1275	60	16.5	50.6	99.0	132.4	8.5
Triaxial A	TD	0.1275	60	9.3	43.4	95.5	137.6	9.9
Triaxial B	DD	0.1283	60	17.5	53.1	102.8	135.8	8.5
Triaxial B	TD	0.1283	60	20.6	60.1	115.0	150.2	8.9

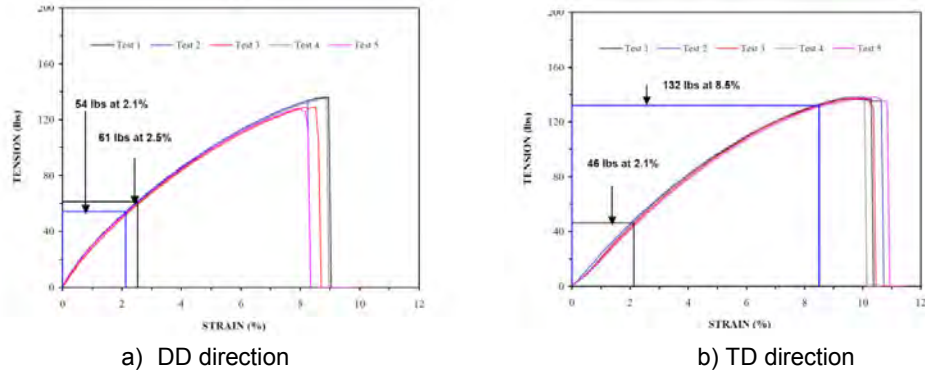


Figure 3. Single-rib tensile test results for Triaxial A geogrid in both the TD and DD directions.

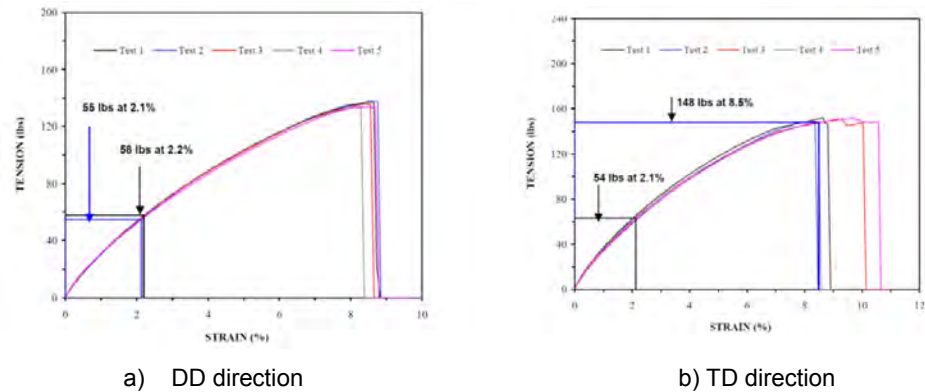


Figure 4. Single-rib tensile test results for Triaxial B geogrid in both the TD and DD directions.

2.1 Tensile Strength In The Machine Direction

The procedures to calculate the ultimate wide width tensile strength of a triaxial geogrid in the machine direction (T_{WMD}) are as follows:

- Conduct single-rib tensile testing on both the left and right DD ribs in accordance with ASTM D 6637 and determine the average ultimate strength of the right and left DD ribs;
- Measure the rib pitch; and
- Calculate the ultimate wide width tensile strength in the MD direction using Equation 1.

Therefore the ultimate wide width tensile strength of the Triaxial A geogrid in the MD direction was calculated to be 1558 lb/ft using the values of $T_{D-RIB} = 132.4$ lb, $h = 0.1275$ ft, and $\theta = 60^\circ$ from the DD single-rib test results presented in Table 1. For the Triaxial B geogrid in the MD direction the ultimate wide width tensile strength was calculated to be 1588 lb/ft using the values of $T_{D-RIB} = 135.8$ lb, $h = 0.1283$ ft, and $\theta = 60^\circ$ from the DD single-rib test results presented in Table 1. The sample calculations are presented in Equations 9 and 10.

$$T_{WMD} \text{ (for Triaxial A geogrid)} = 2(132.4 \text{ lb}) \frac{1}{0.1275 \text{ ft}} \sin^2(60^\circ) = 1558 \text{ lb/ft} \quad [9]$$

$$T_{WMD} \text{ (for Triaxial B geogrid)} = 2(135.8 \text{ lb}) \frac{1}{0.1283 \text{ ft}} \sin^2(60^\circ) = 1588 \text{ lb/ft} \quad [10]$$

2.2 Tensile Strength In The Transverse Direction

The procedures to calculate the ultimate wide width tensile strength of a triaxial geogrid in the transverse direction (T_{WTD}) are as follows:

- Conduct single-rib tensile testing on both the left and right DD ribs in accordance with ASTM D 6637 and determine the average ultimate strength of the right and left DD ribs;
- Conduct single-rib tensile testing on TD ribs in accordance with ASTM D 6637 and determine the average ultimate strength of the TD ribs;
- Measure the rib pitch;
- Determine the rupture (ultimate) strain of TD ribs;
- Calculate the mobilized strain in DD ribs using Equation 4;
- From the measured DD rib force-strain curve, determine the mobilized strength in DD ribs using the mobilized strain; and
- Calculate the ultimate wide width tensile strength in the TD using Equation 3.

Therefore, for the Triaxial A geogrid, when the TD ribs reach their ultimate strain of 9.9% (see Table 1), the mobilized strain in the DD ribs in the TD orientation were calculated to be 2.5%. From the DD rib tensile-strain curves (Figure 3a) the value of T_{D-RIB} was determined to be 61.0 lb at the mobilized strain of 2.5%. The ultimate wide width tensile strength of the Triaxial A geogrid in the TD was then calculated to be 1318 lb/ft using the values of $T_{T-RIB} = 137.6$ lb, $h = 0.1275$ ft, and $\theta = 60^\circ$ from the TD single-rib test results presented in Table 1. The sample calculations are presented in Equations 11 and 12.

$$\varepsilon_{D-RIB} \text{ (for Triaxial A geogrid)} = \frac{\cos 60^\circ}{2} (9.9\%) = 2.5\% \quad [11]$$

$$T_{WTD} \text{ (for Triaxial A geogrid)} = 137.6 \text{ lb} \frac{1}{0.1275 \text{ ft}} + 2(61.0 \text{ lb}) \frac{\cos 60^\circ}{2(0.1275 \text{ ft})} = 1318 \text{ lb/ft} \quad [12]$$

For the Triaxial B geogrid, when the TD ribs reach their ultimate strain of 8.9% (see Table 1), the mobilized strain in the DD ribs in the TD direction were calculated to be 2.2%. From the DD rib tensile-strain curves (Figure 4a) the value of T_{D-RIB} was determined to be 58.0 lb at the mobilized strain of 2.2%. The ultimate wide width tensile strength of the Triaxial B geogrid in the TD direction was then calculated to be 1397 lb/ft using the values of $T_{T-RIB} = 150.2$ lb, $h = 0.1283$ ft, and $\theta = 60^\circ$ from the TD single-rib test results presented in Table 1. The sample calculations are presented in Equations 13 and 14.

$$\varepsilon_{D-RIB} \text{ (for Triaxial B geogrid)} = \frac{\cos 60^\circ}{2} (8.9\%) = 2.2\% \quad [13]$$

$$T_{WTD} \text{ (for Triaxial B geogrid)} = 150.2 \text{ lb} \frac{1}{0.1283 \text{ ft}} + 2(58.0 \text{ kN}) \frac{\cos 60^\circ}{2(0.1283 \text{ ft})} = 1397 \text{ lb/ft} \quad [14]$$

2.3 Tensile Strength At 60-Degree

The procedures to calculate the ultimate wide width tensile strength of a triaxial geogrid in the 60-degree direction (T_{W60}) are as follows:

- Conduct single-rib tensile testing on both the left and right DD ribs in accordance with ASTM D 6637 and determine the average ultimate strength of the right and left DD ribs;
- Conduct single-rib tensile testing on TD ribs in accordance with ASTM D 6637 and determine the average ultimate strength of the TD ribs;
- Measure the rib pitch;
- Determine the rupture (ultimate) strain of the DD ribs;
- Calculate the mobilized strain in the left DD and TD ribs using Equation 6;
- From the measured DD rib force-strain curve, determine the mobilized strength in the left DD ribs using the mobilized strain;
- From the measured TD rib force-strain curve, determine the mobilized strength in TD ribs using the mobilized strain;
- Calculate the ultimate wide-width tensile strength in 60 degree using Equation 5.

Therefore, for the Triaxial A geogrid, when the DD ribs reach their ultimate strain of 8.5% (see Table 1), the mobilized strain in the left DD and TD ribs in the 60-degree direction were calculated to be 2.1%. From the DD and TD rib tensile-strain curves (Figures 3a and 3b) the value of T_{D-120} and T_{T-RIB} were determined to be 54.0 lb and 46.0 lb respectively at the mobilized strain of 2.1%. The ultimate wide width tensile strength of the Triaxial A geogrid in the 60-degree direction was then calculated to be 1235 lb/ft using the values of $T_{D-60} = 132.4$ lb, $h = 0.1275$ ft, and $\theta = 60^\circ$ from the DD and TD single-rib test results presented in Table 1. The sample calculations are presented in Equations 15 and 16.

$$\varepsilon_{T-RIB} \text{ (for Triaxial A geogrid)} = \varepsilon_{D-120} = \frac{\cos 60^\circ}{2} (8.5\%) = 2.1\% \quad [15]$$

$$T_{w60} \text{ (for Triaxial A geogrid)} = 132.4 \text{ lb} \frac{1}{0.1275 \text{ ft}} + (54.0 \text{ lb} + 46.0 \text{ lb}) \frac{\cos 60^\circ}{2(0.1275 \text{ ft})} = 1235 \text{ lb/ft} \quad [16]$$

For the Triaxial B geogrid, when the DD ribs reach their ultimate strain of 8.5% (see Table 1), the mobilized strain in the left DD and TD ribs in the 60-degree direction were calculated to be 2.1%. From the DD and TD rib tensile-strain curves (Figures 4a and 4b) the value of T_{D-120} and T_{T-RIB} were determined to be 55.0 lb and 54.0 lb respectively at the mobilized strain of 2.1%. The ultimate wide width tensile strength of the Triaxial B geogrid in the 60-degree direction was then calculated to be 1271 lb/ft using the values of $T_{D-60} = 135.8$ lb, $h = 0.1283$ ft, and $\theta = 60^\circ$ from the DD and TD single-rib test results presented in Table 1. The sample calculations are presented in Equations 17 and 18.

$$\varepsilon_{T-RIB} \text{ (for Triaxial B geogrid)} = \varepsilon_{D-120} = \frac{\cos 60^\circ}{2} (8.5\%) = 2.1\% \quad [17]$$

$$T_{w60} \text{ (for Triaxial B geogrid)} = 135.8 \text{ lb} \frac{1}{0.1283 \text{ m}} + (55.0 \text{ lb} + 54.0 \text{ lb}) \frac{\cos 60^\circ}{2(0.1283 \text{ ft})} = 1271 \text{ lb/ft} \quad [18]$$

2.4 Tensile Strength At 30-Degree

The procedures to calculate the ultimate wide width tensile strength of a triaxial geogrid in the 30-degree direction (T_{w30}) are as follows:

- Conduct single-rib tensile testing on both the left and right DD ribs in accordance with ASTM D 6637 and determine the average ultimate strength of the right and left DD ribs;
- Conduct single-rib tensile testing on TD ribs in accordance with ASTM D 6637 and determine the average ultimate strength of the TD ribs;
- Measure the rib pitch;
- Determine the rupture (ultimate) strains of the DD and TD ribs from the single-rib test results;
- Determine the mobilized ultimate strain in the right DD and TD ribs based on the fact that the mobilized ultimate strain is equal to the ultimate strain of the DD or TD rib, whichever is smaller;
- From the measured DD and TD rib force-strain curves, determine the mobilized tensile forces in the right DD and TD ribs using the mobilized ultimate strain; and
- Calculate the ultimate wide-width tensile strength in 30 degree using Equation 7.

Therefore, for the Triaxial A geogrid, when the DD and TD ribs mobilize their ultimate strain of 8.5% and 9.9% (see Table 1), the mobilized strain in the left DD and TD ribs in the 30-direction will be limited to 8.5% due to the DD ribs. From the DD and TD rib tensile-strain curves (Figures 3a and 3b) the value of $T_{DRib-60}$ and T_{T-RIB} were determined to be 132.4 lb and 132.0 lb respectively at the mobilized strain of 8.5%. The ultimate wide width tensile strength of the Triaxial A geogrid in the 30-degree direction was then calculated to be 1555 lb/ft using the values of $h = 0.1275$ ft, and $\theta = 60^\circ$ from the DD and TD single-rib test results presented in Table 1. The sample calculations are presented in Equation 19.

$$T_{w30} \text{ (for Triaxial A geogrid)} = (132.4 \text{ lb} + 132.0 \text{ lb}) \frac{1}{0.1275 \text{ m}} \sin^2(60^\circ) = 1555 \text{ lb/ft} \quad [19]$$

For the Triaxial B geogrid, when the DD and TD ribs mobilize their ultimate strain of 8.5% and 8.9% (see Table 1), the mobilized strain in the left DD and TD ribs in the 30-direction will be limited to 8.5% due to the DD ribs. From the DD and TD rib tensile-strain curves (Figures 4a and 4b) the value of $T_{DRib-60}$ and T_{T-RIB} were determined to be 135.8 lb and 148.0 lb respectively at the mobilized strain of 8.5%. The ultimate wide width tensile strength of the Triaxial B geogrid in the 30-

degree direction was then calculated to be 1659 lb/ft using the values of $h = 0.1283$ ft, and $\theta = 60^\circ$ from the DD and TD single-rib test results presented in Table 1. The sample calculations are presented in Equation 20.

$$T_{W30} \text{ (for Triaxial B geogrid)} = (135.8 \text{ lb} + 148.0 \text{ lb}) \frac{1}{0.1283 \text{ ft}} \sin^2(60^\circ) = 1659 \text{ lb/ft} \quad [20]$$

2.5 Development Of A Wide Width Force vs. Strain Curve

The procedures to develop a wide width force vs. strain curve of a triaxial geogrid in the any of the calculated directions (0, 30, 60, 90, 120, 150, 180, 210, 240, 270, 300, 330-degrees) are as follows:

- Conduct single-rib tensile testing on the TD and DD ribs in accordance with ASTM D 6637 and plot force-strain curves for each set of ribs;
- Calculate average rib force and strain data to develop an average force-strain response for each set of ribs. The average curve should contain at least 15 points ranging from 0 strain to the ultimate rib strain in increments of 0.5% strain;
- Calculate the wide width tensile force using the average rib data and the specific equations related to the orientation of interest as discussed in Sections 2.1 through 2.4; and
- Plot the calculated wide width tensile force-strain data to develop the average wide width force vs. strain curve.

For example to develop a wide width force vs. strain curve in the MD orientation for a triaxial geogrid one would need to first run the single-rib tensile tests on both the left and right DD ribs. Then develop the average force-strain response for each set of ribs as shown in Figure 5a. Rearrange Equation 2 to determine the strain in the MD direction (ϵ_{md}) for each of the 0.5% increments of rib strain (ϵ_{rib}). Then use Equation 1 to calculate the wide width strength T_{WMD} for each increment of rib strain (ϵ_{rib}). Finally plot the results of T_{WMD} vs. ϵ_{rib} to develop the average wide width force vs. strain curve as shown in Figure 5b.

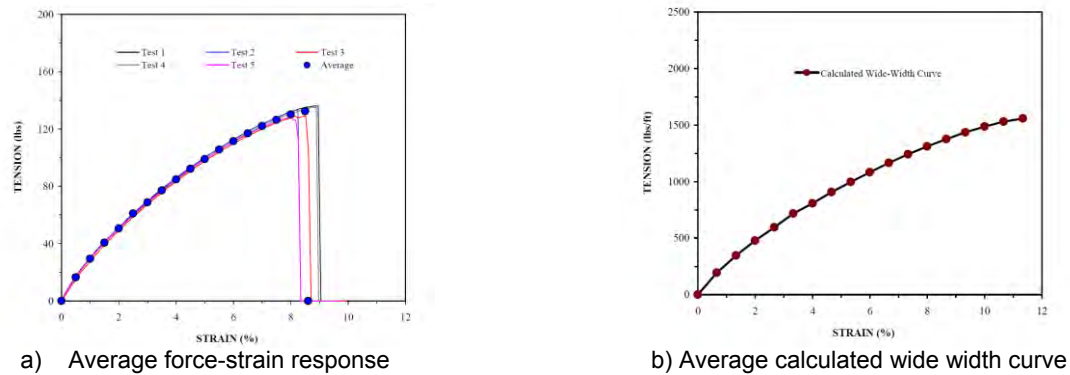


Figure 5. Examples of average single-rib and wide width strength curves in MD direction.

3. DISTRIBUTION OF ULTIMATE WIDE WIDTH TENSILE STRENGTH

The calculated ultimate wide width tensile strengths in directions of 0, 30, 60, 90, 120, 150, 180, 210, 240, 270, 300, 330-degrees are summarized in Table 2 for the Triaxial A geogrid and Table 3 for the Triaxial B geogrid. The distributions of the calculated ultimate wide width strengths along the z-axis with the direction of θ are graphically presented in Figure 6 for the Triaxial A geogrid and Figure 7 for the Triaxial B geogrid.

Table 2. Summary of calculated ultimate width tensile strengths for triaxial A geogrid.

Direction Θ (°)	Ultimate Strength $T_{W\Theta}$ (lb/ft)	X $T_{W\Theta} \cos \Theta$ (lb/ft)	Y $T_{W\Theta} \sin \Theta$ (lb/ft)	R $\text{Sqrt}(x^2 + y^2)$ (lb/ft)
0	1318	1318	0	1318
30	1555	1347	777	1555
60	1235	618	1069	1235
90	1558	0	1558	1558
120	1235	-618	1069	1235
150	1555	-1347	777	1555
180	1318	-1318	0	1318
210	1555	-1347	-777	1555
240	1235	-618	-1069	1235
270	1558	0	-1558	1558
300	1235	618	-1069	1235
330	1555	1347	-777	1555

Table 3. Summary of calculated ultimate width tensile strengths for triaxial B geogrid.

Direction Θ (°)	Ultimate Strength $T_{W\Theta}$ (lb/ft)	X $T_{W\Theta} \cos \Theta$ (lb/ft)	Y $T_{W\Theta} \sin \Theta$ (lb/ft)	R $\text{Sqrt}(x^2 + y^2)$ (lb/ft)
0	1397	1397	0	1397
30	1659	1437	829	1659
60	1271	636	1100	1271
90	1587	0	1587	1587
120	1271	-636	1100	1271
150	1659	-1437	829	1659
180	1397	-1397	0	1397
210	1659	-1437	-829	1659
240	1271	-636	-1100	1271
270	1587	0	-1587	1587
300	1271	636	-1100	1271
330	1659	1437	-829	1659

4. CONCLUSIONS

Based on the application of the theoretical method, developed by Swan et al. (2013), presented in this paper, one can clearly see that the ultimate wide width strength of triaxial geogrids can be established through the use of single-rib tensile testing in accordance with ASTM 6637. From the distribution plots of the calculated ultimate wide width strengths presented in Figures 5 and 6 for each triaxial geogrids, the actual ultimate wide width strength can be established for each geogrid based on the minimum calculated wide width strength measured in the 60, 120, 240, and 300-degree directions. Therefore, the actual ultimate wide width strength for the triaxial A geogrid would be 1235 lb/ft and for the triaxial B geogrid would be 1271 lb/ft. Though higher strengths can be calculated for each geogrid, the geogrid must act as a system of connected ribs and nodes (junctions) whose strength is limited by the weakest rib or junction. Using this analogy, triaxial geogrids can be considered to have homogeneous and isotropic behavior when they are constructed of equilateral triangular apertures. In order to establish the wide width tensile force-strain curves for any given direction (MD, TD, or DD, etc), requires calculating a large number of force-strain data points. However, it becomes a single data point calculation if the focus is to define a characteristic strength for a specific direction.

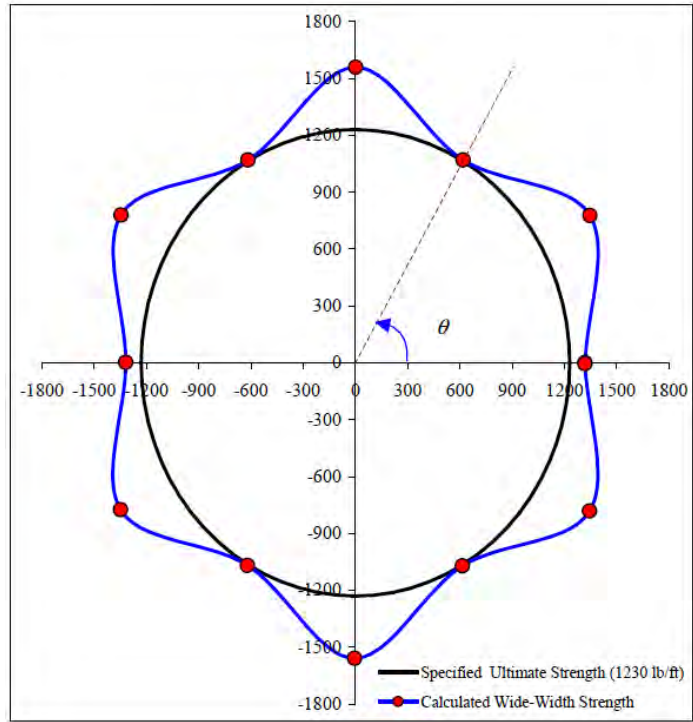


Figure 6. Distribution of calculated ultimate wide width tensile strengths (unit lb/ft) for triaxial A geogrid.

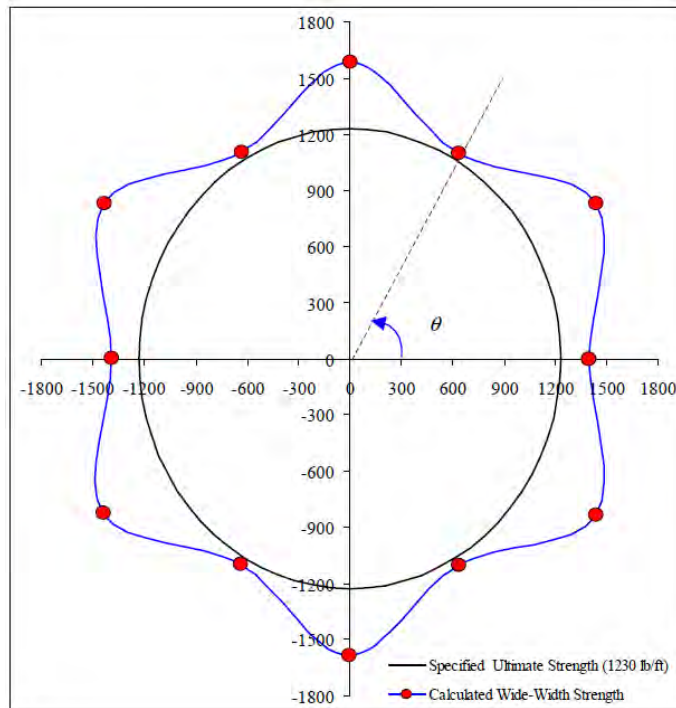


Figure 7. Distribution of calculated ultimate wide width tensile strengths (unit lb/ft) for triaxial B geogrid.

REFERENCES

- ASTM D 6637. Standard Test Method for Determining Tensile Properties of Geogrids by the Single or Multi-Rib Tensile Method, *American Society for Testing and Materials*, West Conshohocken, Pennsylvania, USA.
- Holtz, R., Christopher, B. and Berg, R. (1998). Geosynthetic design and construction guidelines. FHWA HI-95-038. Course No. 13213.
- ISO 10319. Geosynthetics: Wide-width Tensile Test, *International Organization for Standardization*, Geneva, Switzerland
- Koerner, Robert, "Construction and Geotechnical Methods in Foundation Engineering," McGraw-Hill, 1984.
- Swan, Jr., R.H, Yuan, Z. and Wayne, M.H., (2013), Tensile Behavior of Triaxial Geogrid: Development of a Theoretical Method, *Geosynthetics 2013*, IFAI, Long Beach, California, USA, X: pp – pp.

Tensile Behavior of Triaxial Geogrid: Development of a Theoretical Method

Robert H. Swan, Jr., University of North Carolina at Charlotte, USA, rswan1@uncc.edu
Zehong Yuan, Ph.D., P.E., SGI Testing Services, LLC, USA, zyuan@sgilab.com

ABSTRACT

Questions have been raised as to the proper determination of the wide width tensile strength and strength versus strain behavior characteristics for triaxial geogrids. For traditional type (uniaxial and biaxial) geogrids, this can be determined using ASTM International (ASTM) D 6637. The single-rib method within ASTM D 6637 is applicable to triaxial geogrids; however there is a boundary effect that occurs due to the unique geometric construction of the triaxial geogrid when the multi-rib method is performed. Therefore, the multi-rib method may significantly underestimate the tensile stiffness and strength of the triaxial geogrid. Using a technical approach based in structural mechanics for a two-dimensional truss, the wide width tensile response of triaxial geogrids in varying orientations is analyzed. The results of the analysis show that the wide width tensile strength of the triaxial geogrid in a specific orientation can be determined based on single-rib tensile properties of the triaxial geogrid.

1. INTRODUCTION

Over the past thirty plus years, geosynthetic materials have been used in both bound and unbound layers of pavement structures for a wide range of applications. In unbound layers, geosynthetics have been used within the subbase and/or base material or at the interface between the unbound base or subbase layer and subgrade for separation, stabilization, drainage, reinforcement and as moisture barrier, as discussed by Koerner (1984) and Holtz et al. (1998). In bound wearing courses such as hot-mix asphalt (HMA), geosynthetics have been utilized for tensile reinforcement and as stress absorption membrane interlayers to reduce the potential of reflective cracking (Koerner, 1984). When designing and specifying pavement structures incorporating geosynthetics an understanding of the geosynthetic products' wide width tensile behavior in particular the tensile modulus is useful. Traditionally these applications have used geogrids, which have had orthogonal tensile elements in the machine and transverse orientations (i.e., geogrids with square or rectangular apertures). Therefore, the wide width tensile strength and strength vs. strain behavior have been determined using either ISO 10319 or ASTM D 6637 standard test methods. Both of these test methods are conventional uni-directional tensile tests. ISO 10319 is solely a wide width test having a test specimen with a minimum width of 200 mm and a width to length ratio 2:1. ASTM D 6637 allows for three types of test specimens, which include: a) minimum 200 mm wide width multi-rib specimen b) single-rib specimens or c) multi-layer specimens. As written, both of these test methods only use test specimens, which are orthogonal in the machine and transverse directions of a geogrid.

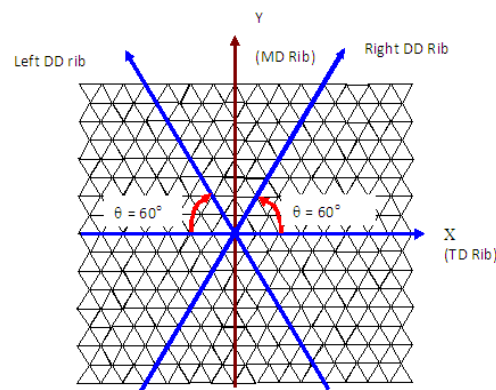


Figure 1. A schematic diagram of a triaxial geogrid where MD is the machine orientation, TD is the cross-machine orientation, DD is the diagonal orientation, and θ is the angle of equilateral triangle.

With the recent introduction of triaxial geogrids, questions have been raised by design professionals and testing agencies as to the proper determination of an appropriate ultimate wide width tensile strength as well as strength versus strain (tensile modulus) behavior characteristics for these products for acceptance and design purposes. For definition purposes, a

triaxial geogrid is a geogrid consisting of three sets of tensile elements (ribs) to form a grid-like structure with equilateral triangular apertures as schematically shown in Figure 1. In the following analysis, the triaxial geogrid is considered structurally symmetric in three principal orientations (0, 60, and 120 degree) in the coordinate system as shown in Figure 1.

For a given triaxial geogrid consisting of three sets of ribs forming junctions with equilateral triangular apertures, there are a couple basic questions, which need to be addressed before these new types of geogrids can be used in any soil or base reinforcement application. They are: 1) what is the tensile force–strain relationship in the MD, TD and DD orientations and 2) what is the tensile strength of the triaxial geogrid in MD, TD, and DD? Naturally one would attempt to answer the above two questions simply by running a wide width (multi-rib) tensile test in accordance with ASTM D 6637 as schematically shown Figure 2. However, due to the unique geometric construction of triaxial geogrids, there exists a boundary effect in testing the triaxial geogrid by the multi-rib method. This boundary effect defined as the effect of those ribs with one end clamped and other end free are herein referred to as exposed ribs. Figure 2, shows these exposed ribs as the “green” DD ribs. These exposed ribs cannot mobilize their full strengths in this type of wide width tensile test; therefore, a multi-rib triaxial geogrid specimen with exposed ribs may significantly underestimate the tensile strength of the triaxial geogrid in the orientation it is tested. It is difficult, if not impossible, to precisely quantify the exposed rib effect on the tensile behavior of the triaxial geogrid, and correct the directly measured test data in the test (Figure 2) to define the true tensile response of the triaxial geogrid.

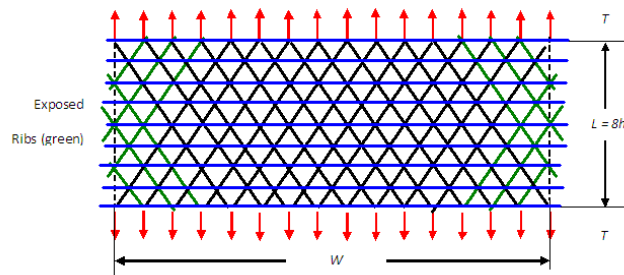


Figure 2. A uniform tensile load applied to a wide specimen in MD.

It should be obvious to those familiar with testing uniaxial and biaxial geogrids that if any active tensile element (rib) parallel to the orientation of the applied tensile force is precut prior to testing then the tensile properties obtained from the test will not characterize the actual tensile behavior of the geogrid. Figure 3 describes such a condition.

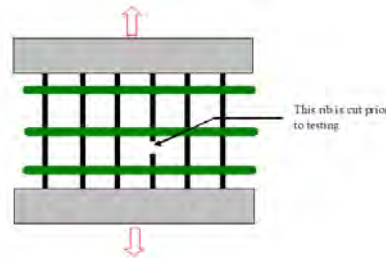


Figure 3. An orthogonal (biaxial) geogrid tensile test with an active rib precut.

Similarly when testing a triaxial geogrid, the same principle of “no active tensile element should be precut” should be applied to the testing procedures. Practically speaking, can one maintain that all the active tensile elements are intact in the wide width tensile test on the triaxial geogrid? In order to answer this question, consider a wide width test on a triaxial geogrid similar to that shown in Figure 2. For a given test specimen length, the number of exposed ribs is fixed. In Figure 2, the test specimen length is $8h$ (with h being the height of an equilateral triangle), therefore there are six (6) exposed “green” DD ribs on each side of the test specimen. One would expect that the impact of these six exposed DD ribs on the measured tensile strength will decrease as the specimen width increases, and will increase as the specimen width decreases. Theoretically, one would need to test a specimen with an infinite width in order not to have the exposed rib effect. In practice, we can only test a specimen with a limited width. It would be difficult and probably cost prohibitive to

conduct tensile testing on a very wide triaxial geogrid specimen. Therefore, there is a need to develop a theoretical approach to determine the wide width tensile strength of a triaxial geogrid based on the single-rib tensile properties of the triaxial geogrid. This paper will present such an analysis based in structural mechanics using both force equilibrium and deformation compatibility.

2. TECHNICAL APPROACH

2.1 Basis of Theory

In structural mechanics, there are two major types of structural components (members) within a structure. These members are classified as beams and trusses based on their slenderness ratios. The slenderness ratio is defined as the length of a structural member divided by the dimension of its cross-section (width or diameter). When this ratio is sufficiently large, the structural member is considered as a truss member. By definition, a truss member can only carry axial force (tension or compression). When the ratio is sufficient small, the structural member is considered as a beam. By definition, a beam can carry axial forces and moments. Further, a truss is simply a very long beam, which carries little or no moment. (Laursen (1978) and Timoshenko and Gere (1972)). In this analysis for a triaxial geogrid, the slenderness ratio is defined as the distance between the two adjacent nodes divided by the rib width. For a typical triaxial geogrid, the slenderness ratio is approximately in the range of 35 to 40. Based on structural mechanics, the bending stress in a tensile element (rib) having a slenderness ratio of that magnitude is negligible. Therefore, it is reasonable to assume that DD and TD ribs are simple tensile elements that can only carry tensile force. Based on the above assumption a classical approach for analyzing a 2-D truss has been adopted for the theoretical analysis of the triaxial geogrid using both force equilibrium and deformation compatibility.

2.2 Relationship of Axial And System Deformation

In order to define the deformation compatibility for this analysis, small strain theory was used in order to develop a relationship between the axial strain and system deformation, as is discussed in this section. Let us assume a 2-rib system is subjected to a vertical load at node C as shown in Figure 4 and the two ribs (i.e., AC and BC) have the same tensile properties and the same length (i.e., structurally symmetric in the orientation of applied tensile force).

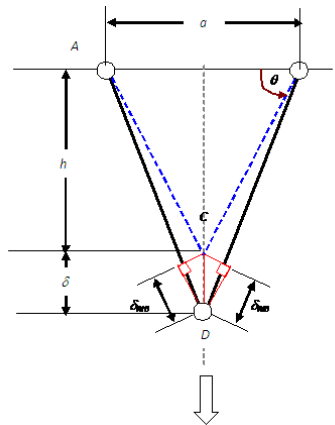


Figure 4. Deformation in a 2-rib system.

Under the action of the vertical load, node C displaces vertically to point D. From the Pythagorean Theorem, the axial deformation (i.e., change in the length) in the two ribs is presented in Equation 1. In Equation 1, δ_{RIB} is the axial deformation (i.e., net stretch) of the rib AB or rib AC, a is the initial distance between nodes A and B, h is the height of equilateral triangle, and L is the initial length of the rib AB or rib AC. Further L can be expressed in terms of “ a ” and “ h ” as shown in Equation 2.

$$\delta_{RIB} = \sqrt{0.25a^2 + (h + \delta)^2} - L \quad [1]$$

$$L = \sqrt{0.25a^2 + h^2} \quad [2]$$

Equation 1 can then be rewritten as Equation 3.

$$\delta_{RIB} = \frac{2h\delta + \delta^2 - \delta_{RIB}^2}{2L} \quad [3]$$

If the displacements of δ and δ_{RIB} are small in magnitude then they can be defined as small deformations, and terms involving the square of the displacements can be neglected. Equation 3 can then be reduced to Equation 4 and by further substituting $\sin \theta$ for h/L yields the final relationship between axial strain and system deformation as shown in Equation 5.

$$\delta_{RIB} = \frac{h}{L} \delta \quad [4]$$

$$\delta_{RIB} = \delta \sin \theta \quad [5]$$

The general conclusion from the above analysis is that, for small displacements, each deformed rib can be considered parallel to its original position, and the axial displacement of the deformed rib can be calculated using Equation 5.

3. TENSILE BEHAVIOR

The tensile behavior of a triaxial geogrid will be theoretically analyzed using both force equilibrium and deformation compatibility based on the technical approach discussed previously. Analyses will be discussed with respect to the MD and TD orientation as well as 60° and 30° parallel to the orientation of loading of the diagonal orientation (DD) ribs.

3.1 With Respect to the Machine Direction

3.1.1 Force Equilibrium

Assume a representative area from a triaxial geogrid is subjected to a uniform tensile load in the MD orientation as shown in Figure 5. For the analysis, the uniform load, is applied along the top and bottom rows of nodes and is distributed to each of the nodes evenly.

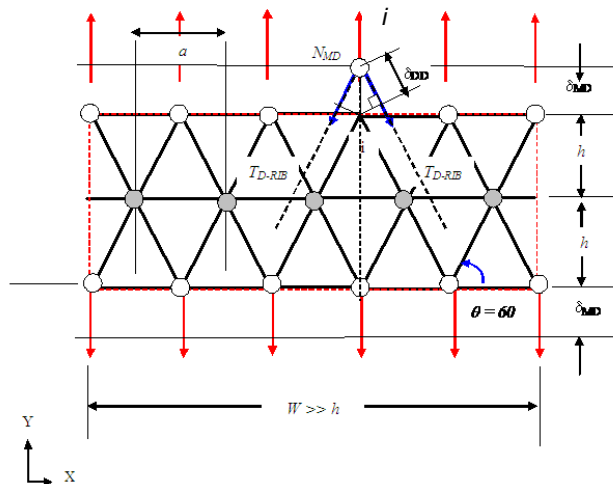


Figure 5. A uniform tensile load applied in MD orientation.

Further, assume the tensile properties of the left and right DD ribs are the same. Therefore, at an arbitrary node i , the force equilibrium in the MD orientation can be expressed in Equation 6. Where N_{MD} is the tensile force (kN) in the MD orientation at the arbitrary node i , T_{D-RIB} is the tensile force (kN) in the two DD ribs, and θ is equal to 60°.

$$N_{MD} = 2T_{D-RIB} \sin \theta \quad [6]$$

The corresponding wide width tensile force in the MD orientation is expressed in Equation 7. Where T_{WMD} is the wide width tensile force (kN/m) in the MD orientation and a is the center to center distance (m) between two adjacent nodes. Furthermore, a is the related the distance between two adjacent ribs (i.e., rib pitch) where h equals $a \sin \theta$. Therefore, Equation 7 can be further reduced to Equation 8.

$$T_{WMD} = 2T_{D-RIB} \frac{1}{a} \sin \theta \quad [7]$$

$$T_{WMD} = 2T_{D-RIB} \frac{1}{h} \sin^2 \theta \quad [8]$$

Equation 8 is strictly derived from the force equilibrium in the MD orientation at an arbitrary node i . Whether or not the DD rib has a linear or nonlinear force-strain relationship, Equation 8 is valid for determining the wide width tensile force in the MD orientation from a given DD rib force. Since the triaxial geogrid described in this analysis is symmetric along the y -axis (MD), it is expected that the triaxial geogrid will reach its ultimate wide width strength in the MD when both the right and left DD ribs reach their ultimate single-rib strengths simultaneously.

3.1.2 Deformation Compatibility

Assuming uniform tensile load acting on the upper and lower boundary, a $2h$ long triaxial geogrid deforms to a final length of $2h + 2\delta_{MD}$ as shown in Figure 5. If δ_{MD} is $\ll h$, then the above geogrid structure can be analyzed in the frame of small deformation theory, as discussed previously. Following the principle of small deformation analysis, a deformed rib can be considered parallel to its original position for determining the relationship between the nodal and axial displacement. At node i , the MD displacement is related to the DD displacement as shown in Equation 9.

$$\delta_{DD} = \delta_{MD} \sin(\theta) \quad [9]$$

The wide width tensile strain (ϵ_{MD}) of the triaxial geogrid in the MD orientation can then defined in Equation 10.

$$\epsilon_{MD} = \frac{\delta_{MD}}{h} \quad [10]$$

The tensile strain in the DD ribs (ϵ_{RIB}) can then be defined in Equation 11.

$$\epsilon_{RIB} = \frac{\delta_{RIB}}{a} \quad [11]$$

Further substituting Equation 9 into Equation 11 results Equation 12:

$$\epsilon_{RIB} = \frac{\delta_{MD} \sin \theta}{a} \quad [12]$$

Substituting Equation 10 and $h = a \sin \theta$ into Equation 12 results in Equation 13 that relates the tensile strain in DD ribs to the wide-width tensile strain in the MD:

$$\epsilon_{RIB} = \epsilon_{MD} \sin^2 \theta \quad [13]$$

Equation 13 shows that the mobilized tensile strain in the DD ribs is 75% of the wide width tensile strain in the machine direction. For the analysis, the two sets of DD ribs (i.e., left and right DD ribs) of the triaxial geogrid were considered to be the same strength and symmetrical along machine direction. Further, it was assumed that the left and right DD ribs would

reach their ultimate strain and/or strength simultaneously. Therefore, the triaxial geogrid would reach its ultimate wide width strength in MD when both DD ribs reach their ultimate strengths simultaneously.

3.2 With Respect to the Transverse Orientation

3.2.1 Force Equilibrium

Assume a representative area from a triaxial geogrid is subjected to a uniform tensile load in the traverse (TD) orientation as shown in Figure 6. For the analysis, the uniform load, is applied along left and right rows of nodes and is distributed to each of the nodes evenly. Therefore, at an arbitrary node j , the force equilibrium in the TD can be expressed in Equation 14. Where N_{TD} is the tensile force (kN) in the TD at the arbitrary node j , T_{D-RIB} is the tensile force (kN) in the two DD ribs, T_{T-RIB} is the tensile force (kN) in the TD rib, and θ is the equal to 60° .

$$N_{TD} = T_{T-RIB} + 2T_{D-RIB} \cos\theta \quad [14]$$

The corresponding wide width tensile force in the TD is expressed in Equation 15. Where T_{WTD} is the wide width tensile force (kN/m) in the traverse orientation and h is the rib pitch (m).

$$T_{WTD} = T_{T-RIB} \frac{1}{h} + 2T_{D-RIB} \frac{\cos\theta}{2h} \quad [15]$$

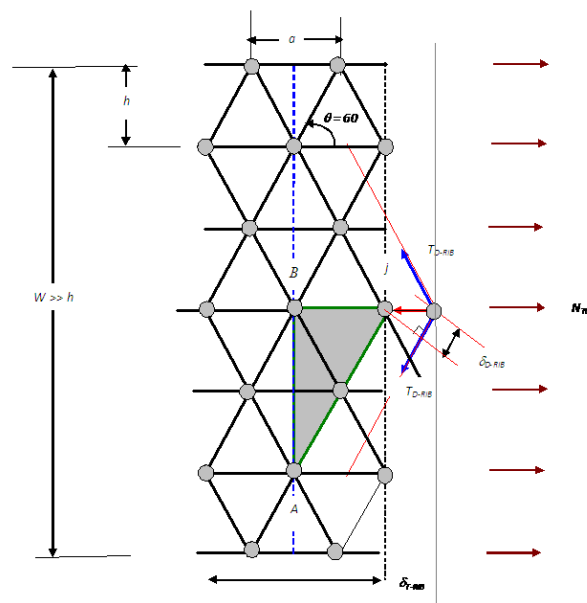


Figure 6. A uniform tensile load applied in TD.

Equation 15 is strictly derived from the force equilibrium in the TD at an arbitrary node j . Whether or not the TD and DD ribs have the linear or nonlinear force-strain relationships, Equation 15 is valid for determining the wide width tensile force in the traverse direction from given single-rib forces in the DD and TD ribs.

3.2.2 Deformation Compatibility

Using Figure 6, at node j , and assuming small deformation conditions, the displacement compatibility of the triangle AjB is shown in Equation 16. Where δ_{T-RIB} is the displacement of node θ in the TD orientation and δ_{D-RIB} is the change in the length of the DD rib over an initial length $2a$. It should be noted that δ_{T-RIB} is the same as the TD rib length increase over the initial length a . Therefore, Equation 17 defines the strain in the TD orientation, Equation 18 defines the strain in the diagonal direction, and Equation 19 relates the strain in the DD rib to the strain in the TD rib.

$$\delta_{D-RIB} = \delta_{T-RIB} \cos\theta \quad [16]$$

$$\varepsilon_{T-RIB} = \frac{\delta_{T-RIB}}{a} \quad [17]$$

$$\varepsilon_{D-RIB} = \frac{\delta_{D-RIB}}{2a} \quad [18]$$

$$\varepsilon_{D-RIB} = \frac{\cos\theta}{2} \varepsilon_{T-RIB} \quad [19]$$

Equation 19 shows that the mobilized strain in DD ribs is 25% of that in TD ribs when the triaxial geogrid is subjected to a uniform tensile load in the TD orientation. It should be noted that the mobilized strains in the TD orientation and DD ribs are not the same when the triaxial geogrid is subjected a uniform tensile load in the TD orientation. Under the loading conditions as shown in Figure 6, the tensile strain in TD rib will always be 4 times the strain in DD ribs. Therefore, when the TD rib reaches its ultimate strain and/or strength, the mobilized tensile strain in the DD ribs will only be 25% of that in the TD rib and the mobilized strength in DD ribs will be significantly less than its ultimate rib strength. Therefore, it is expected that the triaxial geogrid reaches its ultimate wide width strength in TD when the TD ribs reach their ultimate strengths. The contribution of the DD ribs to the wide width tensile strength in TD orientation is the mobilized tensile force in DD ribs at a strain level equal to 25% of the wide width rupture strain (i.e., rupture tensile strain in TD ribs).

3.3 With Respect to 60 Degree Orientation

3.3.1 Force Equilibrium

Knowing that the triaxial geogrid is geometrically symmetric along three principal orientations, we can use the coordinate system shown in Figure 7, to define these three principal orientations as: (i) TD (0 -180 degree); (ii) right DD (60-240 degree); and (iii) left DD (120-300 degree).

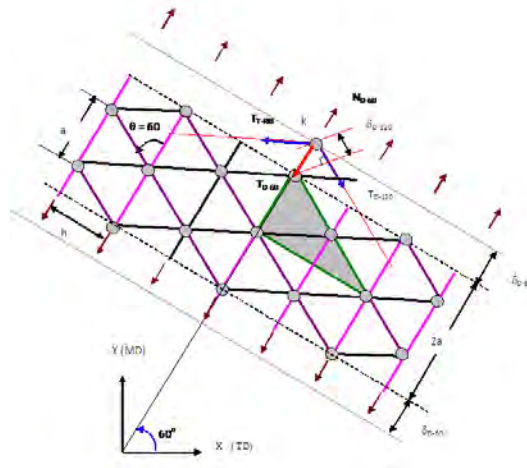


Figure 7. A uniform load applied in 60 degree.

When a uniform load is applied in the orientation parallel to the right DD rib, at an arbitrary node k , Equation 20 can be used to define the force equilibrium in the 60-degree orientation (right DD rib). Therefore, the corresponding wide width tensile force in the TD orientation is shown in Equation 21. Where T_{W60} is the wide width tensile force (kN/m) in the 60-degree orientation and h is the rib pitch (m).

$$N_{D-60} = T_{D-60} + (T_{D-120} + T_{T-RIB}) \cos\theta \quad [20]$$

$$T_{W60} = T_{D-60} \frac{1}{h} + (T_{D-120} + T_{T-RIB}) \frac{\cos\theta}{2h} \quad [21]$$

3.3.2 Deformation Compatibility

Using Figure 7, at node k , and assuming small deformation conditions, the displacement compatibility can be expressed in Equations 22 and 23. Where δ_{D-60} is the displacement of node k in the orientation of 60-degree orientation (right DD rib), δ_{D-120} is the change in the length of the left DD rib over an initial length $2a$, and δ_{T-RIB} is the change length of the TD rib over an initial length $2a$. Therefore, Equation 24 relates the strain in the left DD rib to the strain in the right DD rib and Equation 25 relates the strain in the TD rib to the strain in the right DD rib.

$$\delta_{D-120} = \delta_{D-60} \cos\theta \quad [22]$$

$$\delta_{T-RIB} = \delta_{D-60} \cos\theta \quad [23]$$

$$\varepsilon_{D-120} = \frac{\cos\theta}{2} \varepsilon_{D-60} \quad [24]$$

$$\varepsilon_{T-RIB} = \varepsilon_{D-120} = \frac{\cos\theta}{2} \varepsilon_{D-60} \quad [25]$$

Equation 25 shows that the mobilized strain in either the TD or left DD rib is 25% of that in the right DD rib. It should be noted that the mobilized strains in the TD (0 degree) and left DD (120 degree) ribs are different from that in the right (60 degree) rib when the triaxial geogrid is subjected to a uniform tensile load in the 60-degree orientation. Under the loading conditions as shown in Figure 7, the tensile strains in the TD and left DD ribs are the same. When the right DD rib reaches its ultimate strain and/or strength, the mobilized tensile strain in the TD and left DD ribs are only 25% of that in the right DD rib, and the mobilized strength in the TD and left DD ribs are significantly less than the ultimate single rib strength. Therefore, it is expected that the triaxial geogrid reaches its ultimate wide width strength in the right DD when the right DD ribs reach their ultimate strengths. The contribution of the TD and left DD ribs to the wide width tensile strength in the 60-degree orientation is the combined mobilized tensile force in the TD and left DD ribs at the strain equal to 25% of the wide width rupture strain (i.e., rupture tensile strain in the right DD ribs).

3.4 With Respect to 30 Degree Orientation

3.4.1 Force Equilibrium

In the coordinate system as shown in Figure 8, when a uniform load is applied in the 30-degree orientation and is distributed to each of the nodes evenly, at an arbitrary node m , Equation 26 defines the force equilibrium in the 30-degree orientation of a triaxial geogrid. Therefore, the corresponding wide width tensile force in the 30-degree orientation is shown in Equation 27. Where T_{W30} is the wide width tensile force (kN/m) in the 30-degree orientation and h is the rib pitch (m).

$$N_{30} = (T_{DRib-60} + T_{T-RIB}) \sin\theta \quad [26]$$

$$T_{W30} = (T_{DRib-60} + T_{T-RIB}) \frac{1}{h} \sin^2\theta \quad [27]$$

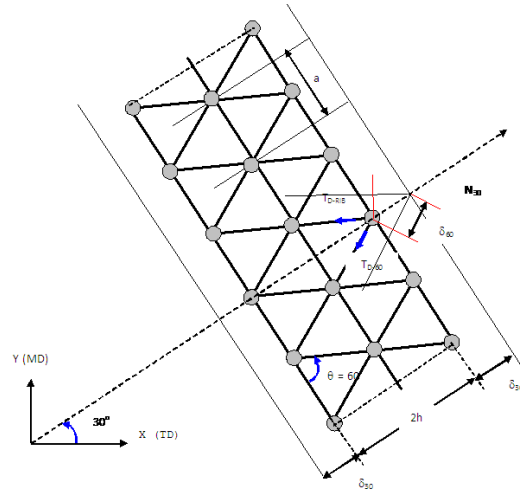


Figure 8. A uniform load applied in 30 degree.

3.4.2 Deformation Compatibility

Under a uniform tensile load acting in the 30-degree orientation, a $2h$ long triaxial geogrid deforms to a final length of $2h + 2\delta_{30}$ as shown in Figure 8. If δ_{30} is $\ll h$, then the geogrid structure can be analyzed in the frame of small deformation theory. Following the principle of small deformation analysis, a deformed rib can be considered parallel to its original position for determining the relationship between the nodal and axial displacement. At node m , the displacement in the 30-degree orientation is related to the displacement in the right DD and TD ribs as shown in Equation 28.

$$\delta_{DRib-60} = \delta_{T-Rib} = \delta_{30} \sin \theta \quad [28]$$

Equation 29 defines the wide width tensile strain (ϵ_{30}) of the triaxial geogrid in the 30-degree orientation.

$$\epsilon_{30} = \frac{\delta_{30}}{h} \quad [29]$$

The tensile strain in the right DD and TD ribs (ϵ_{RIB}) is defined in Equation 30, where δ_{RIB} is the strain in the right DD and TD ribs.

$$\epsilon_{RIB} = \frac{\delta_{RIB}}{a} \quad [30]$$

Substituting Equation 28 into 30 results in Equation 31:

$$\epsilon_{RIB} = \frac{\delta_{30} \sin \theta}{a} \quad [31]$$

Further substituting $h = a \sin \theta$ into Equation 31, The relationship between the tensile strain in the right DD or TD rib and wide width tensile strain in the 30-degree orientation is presented in Equation 32.

$$\epsilon_{RIB} = \epsilon_{30} \sin^2 \theta \quad [32]$$

Equation 32 shows that the mobilized tensile strain in the right DD or TD ribs is 75% of the wide width tensile strain in the 30-degree orientation. Theoretically, the tensile behavior of the triaxial geogrid in the 30-degree orientation should be identical to that in the MD orientation if the TD and DD ribs have the same tensile properties and $\theta = 60^\circ$.

4. CALCULATION OF ULTIMATE WIDE WIDTH STRENGTH

Based on this theoretical analysis on the triaxial geogrid, the wide width tensile force-strain relationships have been fully defined for: (i) the MD by Equations 8 and 13, (ii) the TD by Equations 15 and 19; (iii) the 60° orientation by Equations 21 and 25; and (iv) the 30° orientation by Equations 27 and 32. It should be noted that the wide width tensile properties of the triaxial geogrid in the 120-degree orientation (i.e., parallel to the left DD rib) are the same as those in the 60-degree orientation if the three sets of ribs have approximately the same tensile properties. Therefore, Equations 21 and 25 can also be used to determine the wide width tensile force-strain relationships in the 120-degree orientation. Similarly, the wide width tensile properties of the triaxial geogrid in the 150-degree orientation are the same as those in the 30-degree orientation if the three sets of ribs have approximately the same tensile properties. Therefore, the wide width tensile force-strain relationship in the orientation of 150 degree can also be determined by Equations 27 and 32.

In summary, when the tensile properties of DD and TD ribs are known, the wide width tensile force-strain relationships can be determined in 0, 30, 60, 90, 120, 150, 180, 210, 240, 270, 300, 330-degree orientations.

5. CONCLUSIONS

Based on the theoretical analysis presented in this paper, the following conclusions can be drawn:

- Due to the unique geometric construction, there exists an “exposed-rib” effect in testing a triaxial geogrid by the multi-rib method (ASTM D 6637).
- The wide width tensile test on a triaxial geogrid specimen with a limited specimen width will underestimate the ultimate tensile strength of the triaxial geogrid due to the effect of the exposed ribs.
- In traverse direction, analysis shows that the DD ribs carry a portion of applied tensile load in TD and contribute to the ultimate strength of the triaxial geogrid in traverse direction. However, in the typical wide width test in TD (ASTM D 6637), almost all of the DD ribs are exposed. Therefore, the wide width test as it exists today cannot properly measure the contribution of DD ribs to the ultimate wide width strength in the traverse direction.
- The typical triaxial geogrid as manufactured have slenderness ratios in the range of 30 to 50. The DD and TD ribs can be defined as simple tensile elements which carry tensile forces only (no moments).
- Under the small deformation conditions, the wide width tensile properties of a triaxial geogrid in 0, 30, 60, 90, 120, 150, 180, 210, 240, 270, 300, 330-degree orientations can be determined based on the tensile properties of DD and TD ribs by using this proposed theoretical method.

REFERENCES

- ASTM D 6637. Standard Test Method for Determining Tensile Properties of Geogrids by the Single or Multi-Rib Tensile Method, *American Society for Testing and Materials*, West Conshohocken, Pennsylvania, USA.
- Holtz, R., Christopher, B. and Berg, R. (1998). Geosynthetic design and construction guidelines. FHWA HI-95-038. Course No. 13213.
- ISO 10319. Geosynthetics: Wide-width Tensile Test, *International Organization for Standardization*, Geneva, Switzerland
- Koerner, R.M., “Construction and Geotechnical Methods in Foundation Engineering,” McGraw-Hill, 1984.
- Laursen, H.I., (1978). *Structural Analysis*, 2nd ed., McGraw Hill, New York, NY, USA.
- Timoshenko, S.P. and Gere, J.M., (1972). *Mechanics of Materials*, Litton Educational Publishing, Inc., Monterey, California.

Test Field for Monitoring Geocomposite Reinforcement Behavior in a Crane Working Platform at a Wind Farm

L. Batali, Technical University of Civil Engineering Bucharest, Romania, loretta@utcb.ro

N. Butnarciuc, Technical University of Civil Engineering Bucharest, Romania,
natalia_butnarciuc@yahoo.com

J. Klomp maker, BBG Bauberatung Geokunststoffe GmbH & Co. KG, Germany, ijklompmaker@bbgeo.com

ABSTRACT

The development of wind farms requires heavy cranes to erect the wind turbines under very severe safety working conditions. Often the ground conditions are not meeting the safety conditions in terms of settlement, bearing capacity etc., which requires the necessity to reinforce the crane working platform with geosynthetics. The design of such working platforms is often based on practice and empirical methods; one of these methods is described in BR470. In order to be able to verify and improve the design methodology a good knowledge of the real behavior of the reinforcement geosynthetic is required. The paper presents some aspects about the platform design and the first results of a test field carried out for a geocomposite reinforced crane working platform at a wind farm project in the Dobrogea area, which is located in the South-Eastern part of Romania.

1. INTRODUCTION

1.1 Reinforced Working Platforms

The foundation ground with weak soil layers can cause severe damages upon the structures that are built on it. Working platforms are geotechnical structures that provide a stable working surface for mobile cranes and other heavy construction equipment, these structures are critical for plant stability. Many of these are built on soft, compressible subgrades with low shear strength, providing weak support for the expected loads. The incidents involving overturning of piling rigs and cranes have led to an increased awareness of the importance of providing a stable working platform and to achieve an acceptable level of safety. Conventional improving methods involve replacing part of the weak soil with a layer of granular fill. An alternative is the use of geosynthetic materials for improving the soft soils (Figure 1). The resulting reinforced soil mass provides better stress distribution on top of the underlying weak soil and reduces the settlements.

The benefits that can be realized are as follows:

- reduction of the quantity of granular material required for working platforms through the incorporation of suitable geosynthetic reinforcement;
- bearing capacity increasing, particularly important if heavy plants are used;
- smaller quantity of higher quality material resulting in cost savings both in procurement and avoidance of transport costs;
- reduced maintenance, better response of the working platform under heavy loads and improved working conditions for heavy plant;
- as the principle of sustainable construction is requiring, the excavation should be minimised and the use of waste by-product materials should be maximized; also, a considerable reduction in transport requirements can be obtained, resulting in significant avoidance of greenhouse gas emissions.

The geotechnical properties of the subgrade have a substantial effect on the design of the working platform.

For construction of a working platform the granular materials such as gravel or crushed rock are generally used. The reinforcement can be a nonwoven or woven geotextile, geogrids or geocomposites. Geofabrics are used to separate a granular platform from a cohesive subgrade, these acting as a filter. Geogrids has the function of strengthening the platform. Geosynthetics are generally placed between the subgrade and the working platform.

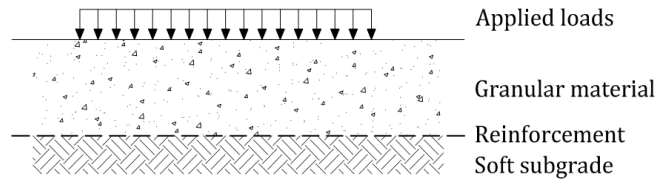


Figure 1 – Reinforced working platform scheme

1.2 Design Calculation Guidance

Recommendation for the design of working platforms given in BR470 “Working platforms for tracked plant” (2004) was prepared by the British Research Establishment (BRE) and provides a good practice guidance on the design, installation, maintenance and repair of ground supported working platforms. In case of cohesive subgrades BR470 is applicable only for soils with an undrained shear strength $20\text{kPa} < c_u < 80\text{kPa}$.

The design calculation given in BR470 is based on an analysis by Meyerhof (1953), Valsangkar and Meyerhof (1979), Hanna and Meyerhoff (1980) and Hanna (1981) for a footing punching through a strong platform material overlying a weak subgrade

The bearing resistance of a platform on soft soil is considered to be the sum of the shear required to punch through a vertical plane in the granular platform material and the bearing capacity of the subgrade (see Figure 2).

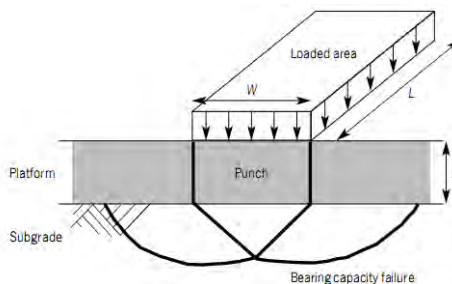


Figure 2 – Punching failure mechanism.

The geotechnical parameters that are used in design calculations are:

- density, γ of the natural soil and of the granular material [kN/m^3];
- angle of friction, ϕ' [$^\circ$] of the platform fill material;
- undrained shear strength, c_u [kPa];
- angle of shear resistance, ϕ' [$^\circ$].

According to BR470, the loading operations can be divided into two loading cases:

Case 1 Loading - Standing, Traveling, Handling;

Case 2 Loading - Installing casing, Drilling, Extracting an auger, bucket or casing, Traveling.

The first one may be applied when the crane operator is unable to avoid an imminent platform failure. The second one is applicable when the crane operator can control the load safely.

The first step is to determine the bearing resistance of the subgrade, if this is large enough, only a running surface would be required. If the bearing resistance is too low, a working platform is required and the bearing capacity is calculated taking into account both subgrade and working platform. If the bearing capacity is still too low, a platform material with higher shear strength (higher ϕ') needs to be used. Then the platform thickness (unreinforced) is calculated.

In order to decrease the thickness of the granular working platform and/or for a more uniform repartition of the loads, a geosynthetic reinforcement can be used. When a load is applied on the geosynthetic reinforced granular layer, the horizontal tensile stresses developed in the geogrid are transferred to the base. As stresses at the base increase, aggregate interlock becomes stronger and the base becomes more rigid. Consequently, the base spreads the loads over a larger area of the subgrade. This allows building a thinner, but stronger geogrid-reinforced granular base. The stress

on the subgrade is held constant while the base is thinned, due to the increased strength of the reinforced granular base (Figure 3).

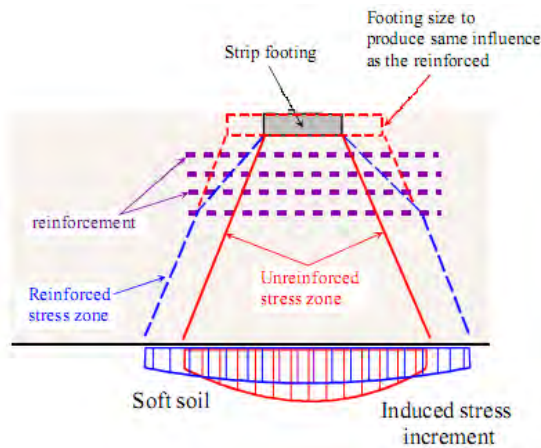


Figure 3 - Reinforced soil foundation, stress distribution (Binquet, Lee 1975)

The aggregate is inter-locking with the geogrid and thus the tensile forces are transferred to the geosynthetic (Figure 4).

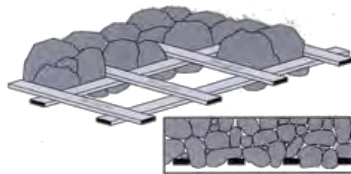


Figure 4 – Interlocking mechanism between aggregate and geogrid

When a load is applied to the subgrade, the bearing resistance can be calculated using known bearing capacity factors (N_q , N_v , N_c), while for calculation of the bearing resistance of a two-soil system (the case of the working platform which is placed on the natural soil) demands deep analysis.

The distribution of pressure under machine tracks should be calculated and the maximum track pressures can be estimated by static calculation for critical jib positions, according to Annex B of SR EN 996+A3:2009 - "Calculation of piling equipment stability and ground pressure". In order to calculate equipment stability, the following characteristics have to be estimated: angle of stability, dumping lines, barycenter, partial security factors, working load, static moment, centrifugal moment (if is applicable) etc. For the worst combinations of the operating conditions, the maximum ground pressure should be established. This pressure can be introduced in the design of the working platform.

2. TESTING PROGRAM

2.1 The Sălbatica Wind Farm, Romania

The main objective of this experimental test is to determine the real behavior of the reinforcement geocomposite within the working platform during the loading. The further objective is to determine what the benefits are of using reinforced soil foundations to improve the bearing capacity and reduce settlements of working platforms and also to improve the design methods.

The Sălbatica Wind Farm is located in Romania's Dobrogea region, near Tulcea city. From an energy generation perspective, Dobrogea is one of the best places in Europe for the construction and operation of a wind farm. Its open lands are characterized by some of the continent's most dependable, strong winds. The Sălbatica Wind Farm involved the construction of 35 turbines in the first stage, followed by another 35 in the second stage, each producing 2 MW of power. The annual production of the site is 85.5 million kWh/year. This is enough to power 29,000 households. Equally important, from an environmental standpoint, is the reduced carbon footprint. Sălbatica's turbines produce power that if

produced by traditional means would have released 48,000 metric tons of CO₂ per year. That pollution is prevented through Sălbatica's renewable energy approach.

The cranes used for lifting the wind turbines are of 750 tones and require special measures of working safety. As the natural ground on site was not meeting the geotechnical requirements, a working platform of crushed stone was provided and reinforced by one layer of laid-and-welded geocomposite (Figure 5), whose material properties are described below. With regard to the project specific requirements a working platform thickness of 60 cm would have required to distribute the crane loadings to acceptable rates for the available strength of the in-situ subgrade. An alternative design using a biaxial laid-and-welded geogrid allowed the reduction of the working platform thickness to 40cm.

2.2 Natural Soil and Platform Characteristics

The subgrade on site is mainly composed of loess – yellow silty clays and clayey silts, stiff – solid, sensitive to wetting. The soil in its natural state has an oedometric modulus of approx. 9000kPa, an undrained cohesion (c_u) of about 25kPa, an additional settlement to wetting, $i_{m3} = 1.1 - 9.74 \%$ (according to Romanian regulations, for more than 2% the soil is considered sensitive to wetting).

A working platform has been built using 40 cm of compacted crushed stone (0/63 mm) for each of the 4 pads of the crane. One of these 4 working platforms was instrumented with strain gauges and pressure cells attached to the geocomposite. All 4 pads were treated identically.

In order to determine the strength of the in-situ soil, a plate loading test according to DIN 18134 was carried out using a loading plate with 300 mm diameter. The plate tests performed on natural soil after compaction showed values of $E_{V1} = 19 - 34 \text{ MPa}$ and $E_{V2} = 35 - 62 \text{ MPa}$.

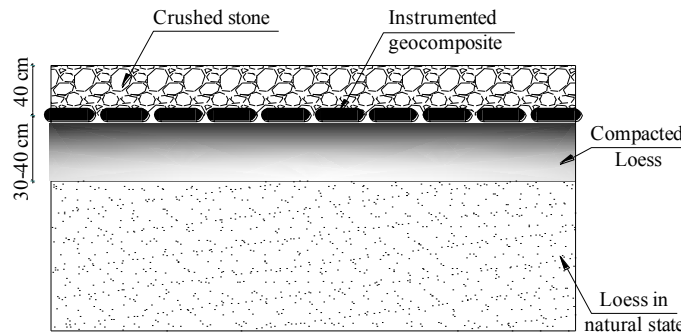


Figure 5. Cross – section through the working platform

2.3 Reinforcement Geocomposite

The reinforcement geocomposite is a laid-and-welded geocomposite made of a welded biaxial geogrid (PP) with mass of 240 g/m² and a nonwoven needle punched geotextile (PP) with mass of 150 g/m², firmly bonded between the longitudinal and transversal ribs. This material is used for stabilization, separation and filtration applications in various civil engineering fields. The tensile strength of the reinforcement in longitudinal and transverse direction is 30 kN/m; the strain level at failure is $\leq 8\%$.

Strains taken by the geocomposite reinforcement are measured by linear strain gauges (max. elongation 100,000 $\mu\text{m/m}$ ($\pm 10 \%$) and max. allowable bridge supply voltage of 8V, nominal resistance of 120 Ω) which were glued onto the geogrid reinforcement bar (Figure 6.a).



Figure 6 - Application of strain gauges (a) and pressure cells (b) on geocomposite

2.4 Field Test

The geocomposite was instrumented with 8 strain gauges attached to the geogrid and 3 pressure cells placed between the geocomposite and the granular layer to measure the applied load (Figure 6.b). The scheme of the installation is presented in Figure 8. The load is applied in the center of the platform of the crane. Only one of the 4 crane pads were instrumented.

Once the Lucas plate test was completed, the instrumented 4,75m x 10m geocomposite was installed over the test platform. The strain gauges, pressure cells and all the cables were covered with sand taken from the site to protect them from deterioration (Figure 6.b). From that moment on, the recordings of each gauge and cell data started. Finally, the geosynthetic reinforcement was carefully covered with 400 mm of crushed stone (grading: 0/63 mm) and compacted using a 7.5t drum roller.

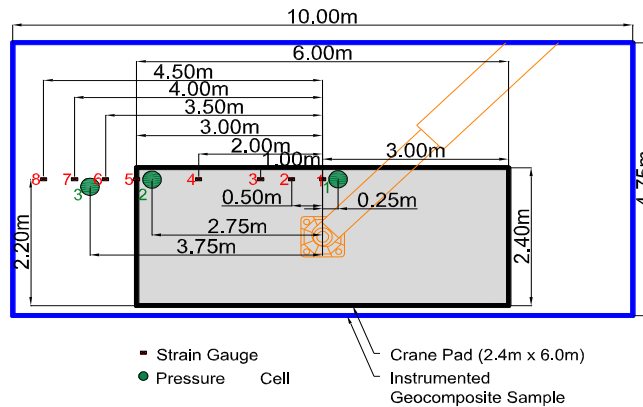


Figure 7 - Instrumentation scheme

Settlements under the crane pad were determined using a wireless laser level.

2.5 Recording Data

The recording of the strains, stresses and settlements under the crane pad started with the installation of the 400 mm thick working platform and covered the complete construction steps to assemble the 750 t mobile crane. In total, 22 measurements were performed during the several stages of the construction, the measurement being singular or continuous recording in time. The assembly of the crane in the working platform area took a full working day. The maximum load in the area of the crane pad was expected when the full counterweight of 225t was directly positioned over the crane pad without having a lifting weight at the boom (Figure 8).

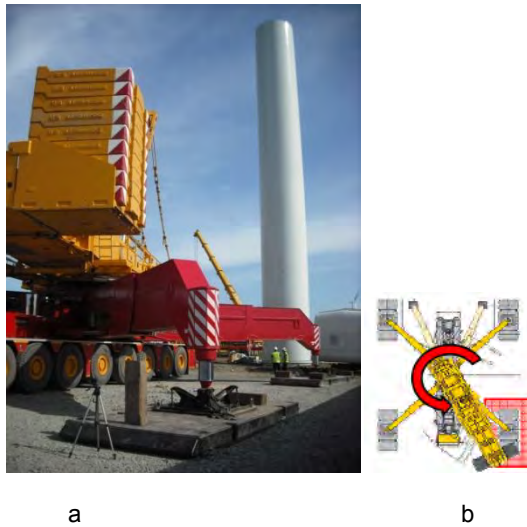


Figure 8 - Most critical load scenario over crane pad in situ (a) and scheme (b)

First measurement (single type measurement) was performed after the geocomposite was covered with the crushed stone layer. The 2nd measurement (continuous type measurement) corresponds to the static compaction of the instrumented platform. The 3rd measurement was performed during the dynamic compaction of the working platform using a 7.5 t drum roller. In Figures 9 and 10 are presented the results for the 3rd measurement in terms of strain vs. time and pressure vs. time. These results, corroborated with the 2nd stage ones prove that the gauges are working correctly.

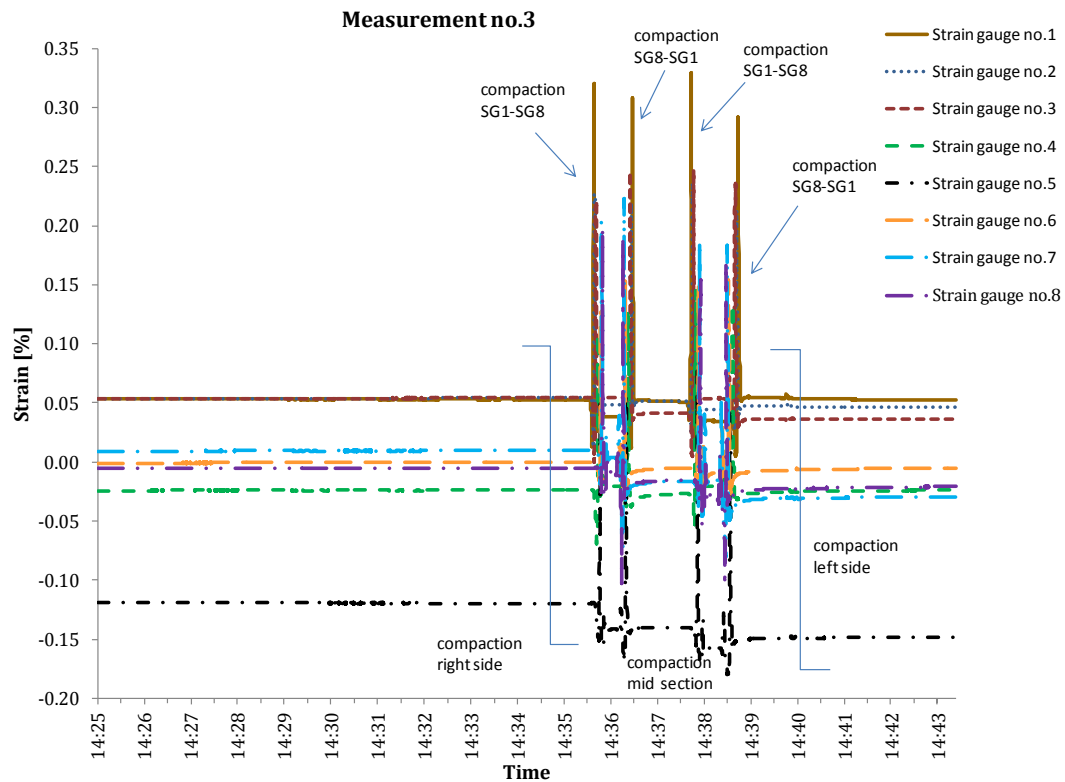


Figure 9 - Strain versus time during the dynamic compaction of the working platform (3rd measurement).

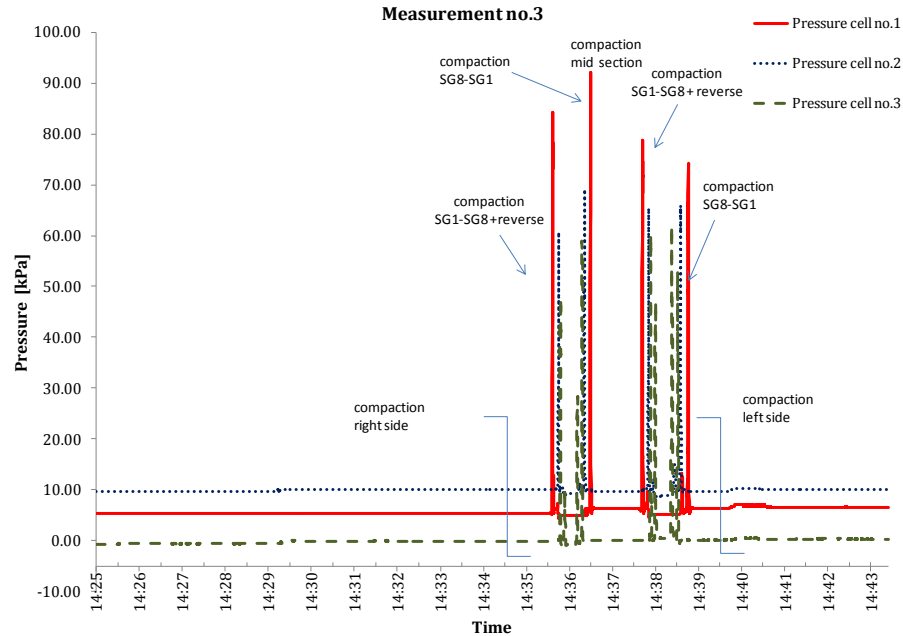


Figure 10 - Pressure versus time during the dynamic compaction of the working platform (3rd measurement).

2.6 Monitoring Results

The results for stages 16 and 22 were chosen to be presented in this paper; the 16th measurement is corresponding to the application of the counterweights to the crane (maximum load scenario), while the 22nd measurement is corresponding to assembling of crane lattice jib.

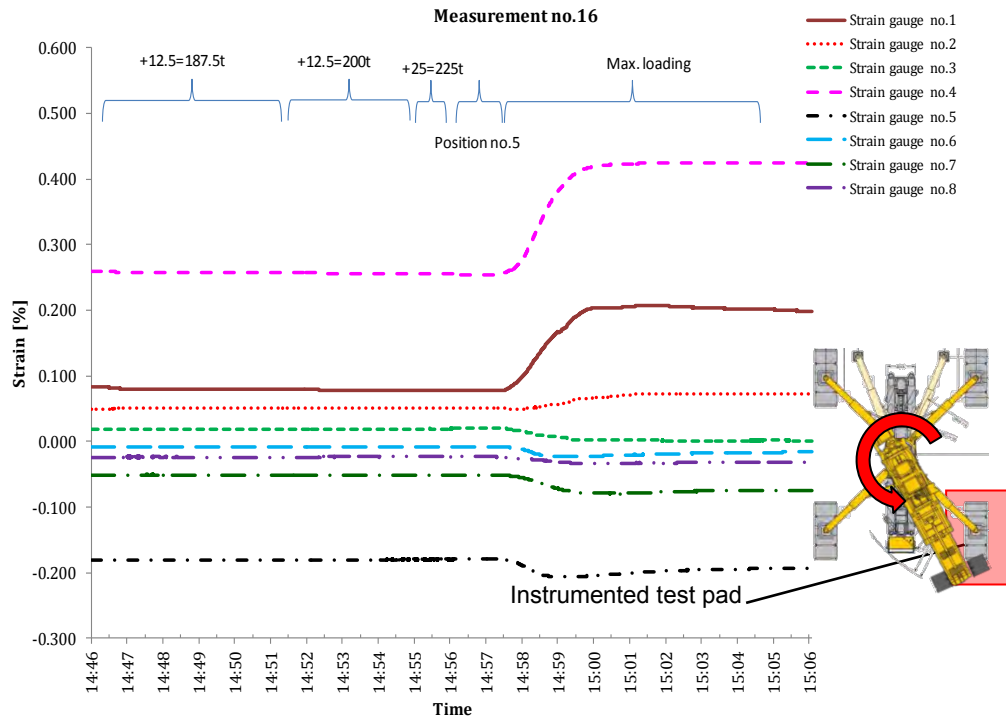
Figure 11.a presents the recorded strains in the reinforcement geocomposite during stage 16, for each strain gauge (SG), in the crane position showed in Figure 8.b. A maximum strain of 0.42 % was recorded for strain gauge no. 4.

Figure 11.b shows the strain vs time graph for stage 22. During this stage a maximum strain of 0.45% was recorded for the same strain gauge, no. 4.

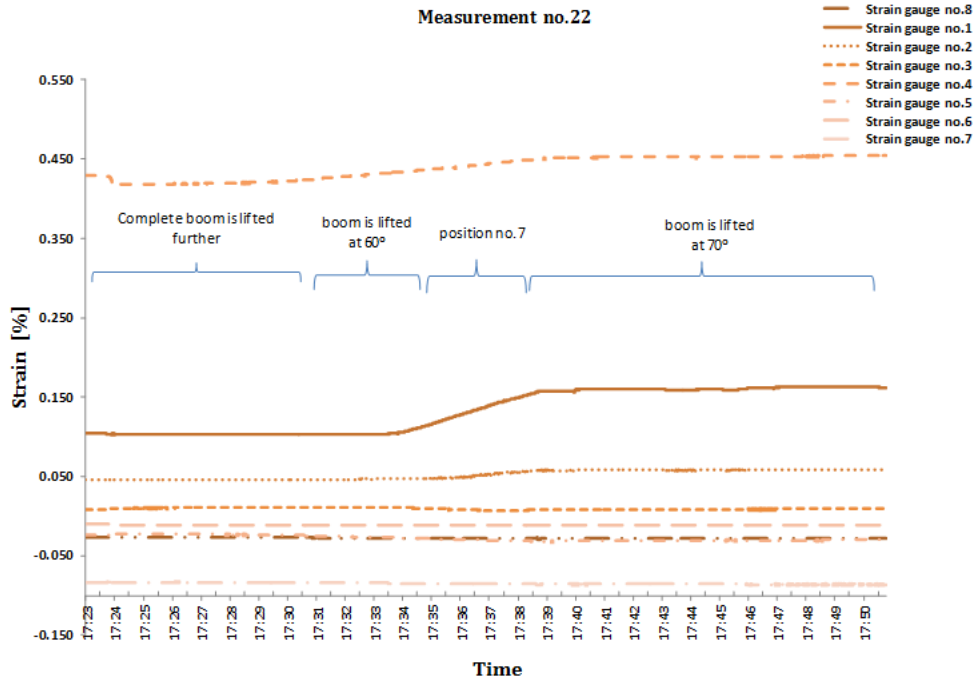
In Figure 12.a and 12.b are presented the variation of the strains (12.a) and pressures (12.b) with the distance from the center of crane pad, for stages 16 and 22 of measurement. For stage 16, the maximum value of the pressure was of 143.52kPa, while for stage 22, the maximum pressure was of 121.20kPa.

Figure 13 shows the real level of the stress and strain in the geosynthetic compared with the overall stress – strain curve of the material.

The maximum measured settlement was about 9.5mm (final loading and positioning).

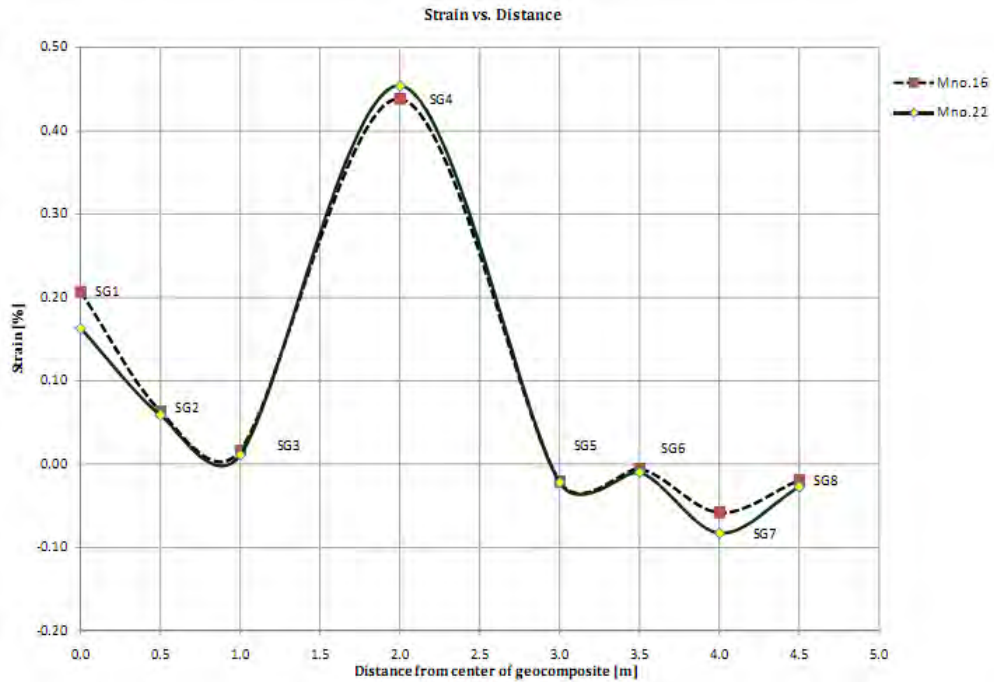


a

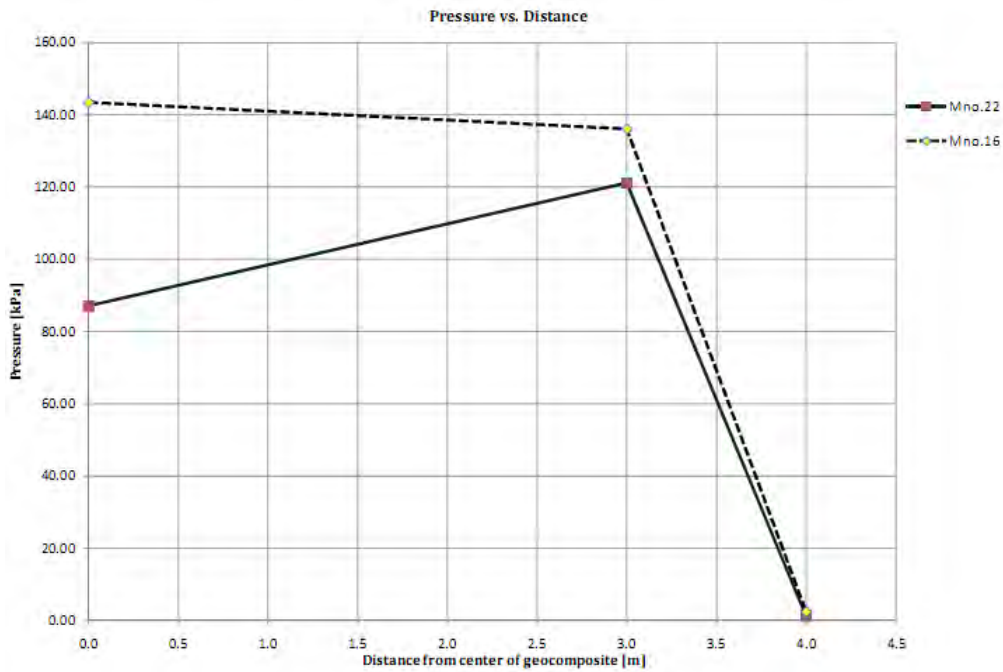


b

Figure 11 - Strain vs. time - stage 16 (a) and stage 22 (b)



a



b

Figure 12 - Strain vs distance (a) and pressure vs distance (b) from center of crane pad – stages 16 and 22

3. CONCLUSIONS

Working platforms are used for offering a safe and stable support for heavy equipment. They are often built on soft soils which cannot provide the adequate bearing capacity and the required safety conditions. One of the common solutions is to reinforce the platform using geosynthetics, this resulting in increased safety and durability, lower maintenance, less thick platforms and also environmental benefits.

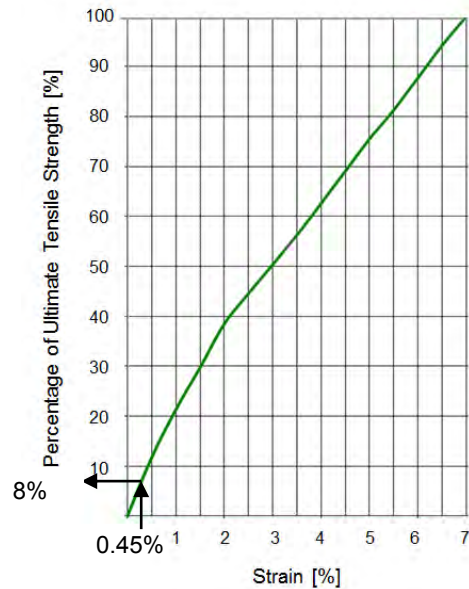


Figure 13. Level of stress and strain for the reinforcement geosynthetic

Working platforms are usually designed based on BR470, which uses mainly practice and empirical methods.

The paper presents a field test from a Romanian wind farm, where a working platform for a heavy crane was reinforced with an instrumented geocomposite, together with the performed measurements and the main obtained results. The geosynthetic reinforcement was monitored using 8 strain gauges and 3 pressure cells.

The objective of the field test is to assess more exactly the behavior of the geosynthetic reinforcement in order to improve the design methods. The paper presents only the results of the monitoring performed on site. These results will be used in the near future for calibrating a numerical model and to further improvement of the design methods (aspects which will be published latter).

The working platform used for this test field was made of 40 cm thick crushed stone reinforced with a geocomposite at its base. If no geosynthetic had been used for reinforcement, the overall thickness of the required working platform would have been 60cm, which allowed savings in the range of approx. 30%.

REFERENCES

- Binquet, J. and Lee, K. L. (1975). Bearing Capacity Analysis of Reinforced Earth Slabs, *Journal of Geotechnical Engineering Division*, ASCE, Vol. 101, No. GT12, 1975: 1257-1276.
- BR470 (2004). Working platform for tracked plant. *Building Research Establishment*, ISBN: 1 86081 700 9.
- Hanna, A.M. (1981). Foundation on strong sand overlying weak sand, *Journal of Geotechnical Engineering Division*, ASCE, Volume 107 No. GT7: 915-927.
- Hanna, A.M. and Meyerhoff, G.G. (1980), Design charts for ultimate bearing capacity of foundations on sand overlying soft clay, *Canadian Geotechnical Journal*, Volume 17 No.2: 300-303.
- Meyerhoff, G.G. (1953). The bearing capacity of foundations under eccentric and inclined loads, *Proceedings of 3rd International Conference on Soil Mechanics and Foundation Engineering*, Zurich, Volume 1: 440-445.
- Valsangkar, A.J. and Meyerhof, G.G. (1979). Experimental study of punching coefficients and shape factors for two-layered soils, *Canadian Geotechnical Journal*, Volume 16: 802-805.

Testing and Specifying Rolled Erosion Control Products

C. J. Sprague, TRI/Environmental, Inc., United States
J. E. Sprague, TRI's Denver Downs Research Facility, United States

ABSTRACT

Sediment continues to be a major pollutant of public water resources even though erosion control best management practices, BMPs, are now commonly used. In order to help protect water quality as it relates to sediments, regulatory agencies and site designers are increasingly asking how well specific BMPs will perform quantitatively relative to alternatives. While a large amount of information on erosion control products (ECPs) has been available for quite some time, the information has too often been non-standard, out-of-date, insufficient, or unable to be compared to alternative products, making it difficult for users to create generic construction specifications or qualified product listings of comparable products.

Standardized test procedures have been recognized as the means to develop comparable product data. Thus, a two decade effort by industry professionals has produced recognized tests for measuring relevant material properties as well as performance capabilities of ECPs – with most effort focused on rolled erosion control products (RECPs).

This paper discusses the details of these now commonly used standardized index, bench-scale, and large-scale tests for RECPs, along with a review of data from hundreds of independent tests performed on a range of RECPs under the auspices of the National Transportation Product Evaluation Program (NTPEP). Along with an assessment of the relevance and correlation of the various tests, recommendations will be made on the appropriate use of these test results in specifications for RECPs.

1.0 MANUFACTURED EROSION CONTROL PRODUCTS AND ASSOCIATED TESTING

1.1 Manufactured Erosion Control Product Types

While conventional erosion control materials ranging from loose straw to rock riprap continue to be used extensively, new developments in erosion control systems are being used, including the following types of rolled erosion control products (RECPs):

- Temporary RECPs - For applications where natural vegetation alone will provide sufficient permanent erosion protection.
 - Open Weave Textile (OWT). OWTs are a degradable product composed of processed natural or polymer yarns woven into a matrix. The most common of these are comprised of jute or coir.
 - Erosion Control Blanket (ECB). ECBs are composed of processed natural or polymer fibers mechanically, structurally or chemically bound together to form a continuous matrix.
- Permanent RECPs - For applications where natural vegetation alone will not sustain expected flow conditions and/or provide sufficient long-term erosion protection.
 - A turf reinforcement mat (TRM) is a permanent RECP composed of non-degradable synthetic fibers, filaments, nets, wire mesh and/or other elements, processed into a permanent, three-dimensional matrix of sufficient thickness.

1.2 Quality Control, Quality Assurance and Performance Testing of RECPs

Basic index tests are typically needed to assure manufacturing quality control of RECPs. Not only are these tests useful for manufacturing quality control, but when used on the same materials deployed in bench-scale and large-scale performance tests, they serve to “bench-mark” the performance results to specific material properties. A variety of performance tests have been developed over the years to answer designers’ and specifiers’ questions regarding performance among different products and product categories.

Since 2003, the National Transportation Product Evaluation Program (NTPEP) has provided a program for independent testing of RECPs. The program has included both index tests and bench-scale “indexed performance” tests. The goal of the program is to minimize duplicative testing of erosion control products done by individual State Departments of Transportation (DOTs) by providing a process where manufacturers and suppliers submit their products to the NTPEP

for independent index and bench-scale testing. The results of the testing are then shared with participating DOTs. The results of the testing may be used for assessing product conformance to material specifications. Further, the testing results provide quantitative material data necessary for placing specific products on, or removing specific products from a DOT's qualified products list (QPL). The NTPEP program is intended to serve as a nationwide quality assurance (QA) program for the DOTs.

Additionally, in 2009, NTPEP began offering independently verified large-scale performance testing to complement ongoing index and bench-scale testing. NTPEP (2011) describes the purpose and rationale for exclusive use of standardized test procedures in the programs.

1.2.1 Index Testing

Index tests are standard tests that may be used for manufacturing quality control and to compare the relative material properties of several different RECPs. Quality Control tests are index tests which are performed on a production basis to evaluate product integrity, quality and continuity, and to assess the impact of changes in production methodology on product properties. Quality control test results can be reported with statistical relevance when they are run with sufficient frequency. Recently, ASTM D4354, "Standard Practice for Sampling of Geosynthetics for Testing", has been revised to include appropriate sampling frequencies to achieve a 95% confidence level for RECP quality control, quality assurance, and conformance testing. Following are the index test methods used for RECPs:

Mass per Unit Area: ASTM D 6475, "Standard Test Method for Measuring Mass per Unit Area of Erosion Control Blankets"; ASTM D 6566, "Standard Test Method for Measuring Mass per Unit Area of Turf Reinforcement Mats". The mass per unit area, also known as the "weight" per square yard of a sample, is an important quality control property. The ECB test uses ten 8"x8" specimens at ambient laboratory conditions. The TRM test uses five larger, typically 12"x14", specimens that have been dried at 50° overnight.

Thickness: ASTM D 6525, "Standard Test Method for Measuring Nominal Thickness of Permanent Rolled Erosion Control Products". Thickness is another important quality control property which is measured after application of a 6-inch diameter presser foot under a 0.029 psi pressure.

Tensile Strength: ASTM D 6818, "Standard Test Method for Ultimate Tensile Properties of Turf Reinforcement Mats". The ASTM tensile test method for RECPs uses at least 5 inch-wide grips.

Light Penetration: ASTM D 6567, "Standard Test Method for Measuring the Light Penetration of a Turf Reinforcement Mat (TRM)". Within a light box, a calibrated meter measures the amount of light that is able to pass through the specimen from a 150 watt light source on the other side of the specimen. The inverse of the percent of light passing through the specimen is termed the "% cover".

Water Absorption: ASTM D 1117 Section 5.4 and ECTC-TASC 00197, "Standard Guide for Evaluating Nonwoven Fabrics – Absorptive Capacity Test (for Larger Test Specimens)". Water absorption is a measure of a material's capacity to absorb water and is generally applicable to organic RECPs.

Specific Gravity: ASTM D 792, Method A, "Standard Test Methods for Density and Specific Gravity (Relative Density) of Plastics by Displacement". Specific gravity is the ratio of the unit weight of a material to that of water.

1.2.2 Bench-scale Testing

Bench-scale "indexed" performance tests are a class of tests that have been developed to focus on testing the RECP/soil system under carefully controlled "standard" conditions. Bench-scale tests have been developed for slope erosion, channel erosion, and vegetation enhancement for RECPs. Variations in the mass per unit area, raw materials, manufacturing processes, and other product and production components are a constant challenge to manufacturers of RECPs. Since performance of RECPs relies on the complex interaction of the RECP structure with the soil and the water impact/flow, it is helpful and beneficial to a quality assurance program to be able to examine the effects of product variability without having to rerun large-scale tests. Bench-scale testing facilitates lower costs and quicker testing for evaluating product conformance. However, it is critical to emphasize that bench-scale testing is not appropriate for use in design models unless correlated to large-scale testing. Bench-scale tests do not reflect product installation techniques or site conditions to which these materials are typically subjected. Therefore the results of these tests may not be indicative of a RECPs actual field performance.

Slope Erosion and Runoff Reduction: ASTM D 7101, "Standard Index Test Method for Determination of Unvegetated Rolled Erosion Control Product (RECP) Ability to Protect Soil from Rain Splash and Associated Runoff under Bench-Scale Conditions". This test method evaluates the ability of RECPs to protect soil from rain splash and immediate

runoff-induced erosion. The critical element of this protection is the ability of the RECP to absorb the impact force of raindrops, thereby reducing soil particle loosening through “splash” mechanisms. The test method utilizes containers of both bare and RECP-protected soil that are exposed to simulated rainfall and immediate runoff for 30 minutes in the test apparatus. It is a sloped table enclosed by a curtain. Rainfall is simulated using a laboratory drip-type simulator capable of creating uniform drops with a median diameter of 3.0 to 3.5 mm from a drop height of 2.0 ± 0.1 m and producing rainfall intensities as high as 150 mm/hr. The amount of soil that splashes or is washed out of the containers is collected and weighed. From this data, an appropriate soil loss ratio (SLR) can be calculated by comparing the RECP-protected soil loss to the control. The inverse of the SLR is comparable to the C-factor which is more commonly used to relate to performance, but should not be used as a true measure of performance without verification from large-scale testing.

Permissible Shear and Channel Erosion: ASTM D 7207, “Standard Test Method for Determination of Unvegetated Rolled Erosion Control Product (RECP) Ability to Protect Sand from Hydraulically-Induced Shear Stresses under Bench-Scale Conditions”. This test method evaluates the ability of RECPs to protect soils from flow-induced erosion. The test method utilizes containers of RECP-protected soil that are immersed in water and subjected to shear stresses caused by the rotation of a three-blade impeller for 30 minutes in the test apparatus. The shear stress test apparatus includes a tank, test well, motor, plastic lid, and impeller. The three-blade impeller is mounted in the cylindrical tank so that the lower edge of the blades is slightly above the floor of the tank. The sample test well is a recession in the floor of the tank that holds the pots of soil prepared for testing. When the pots are placed in the well, the test surface is flush with the floor of the tank. Pots holding soil and test specimens are normally 200 mm diameter plastic pipe sections with height of 100 mm. The amount of soil that erodes is found by weighing the containers under water. The results of the testing include the amount of soil lost at various shear stresses. From this data, an appropriate permissible shear can be calculated by assuming a critical amount of soil loss, typically 13 mm (1/2-inch). The index limiting shear stress value obtained is comparable to the “permissible shear stress” commonly used to relate to performance, but should not be used as a true measure of performance without verification from large-scale testing.

Germination/Vegetation Growth: ASTM D 7322, “Standard Test Method for Determination of Rolled Erosion Control Product (RECP) Ability to Encourage Seed Germination and Plant Growth under Bench-Scale Conditions”. This test method established procedures for evaluating the ability of RECPs to enhance the rate and quantity of seed germination and facilitate subsequent establishment of vegetation. Containers of soil are sown with a single indexed seed mix and then covered with an RECP. Additional containers are left uncovered as controls. Testing is conducted within a growth chamber where the light, water, and temperature are regulated and documented. The rate of germination is measured periodically throughout the test, and the weight of vegetation is calculated at the conclusion of the test. The testing results include the rate and total weight of germination after 21 days. From this data, a percent enhancement can be calculated by comparing results from the RECP-protected soil to the control.

1.2.3 Large-scale Testing

Large-scale performance tests have been developed to simulate expected field conditions to report performance properties of “as installed” RECPs. Large-scale tests have been developed for slope erosion and channel erosion. The channel erosion test may be conducted un-vegetated or vegetated. Performance of RECPs relies not only on material properties but also on the installation techniques. Products are installed on the test slope or channel per manufacturer installation recommendations. The results of these tests are more indicative of actual field performance of RECPs and are acceptable for use in design calculations.

Slope Erosion: ASTM D 6459, “Standard Test Method for Determination of Rolled Erosion Control Product (RECP) Performance in Protecting Hillslopes from Rainfall-Induced Erosion”. This large-scale test is conducted on one bare soil control and three replicate RECP-protected soil 3:1 slopes. Rainfall is simulated at target intensities of 2, 4, and 6 inches per hour which are applied in sequence for 20 minutes each. Runoff from each slope is collected and soil loss is measured. From this data, an appropriate soil loss ratio and associated C-factor can be calculated by comparing the RECP-protected soil loss to that of the control.

Channel Erosion: ASTM D 6460, “Standard Test Method for Determination of Rolled Erosion Control Product (RECP) Performance in Protecting Earthen Channels from Stormwater-Induced Erosion”. This large-scale test is conducted in a rectangular flume with at least four sequential increasing flows applied for 30 minutes each. Unvegetated RECP-protected soil is tested on a 10% slope flume. Vegetated RECP-protected soil is tested on a 20% slope flume. The limiting or permissible shear stress is defined as the shear stress necessary to cause an average of 0.5 inch of soil loss over the entire channel.

2. NTPEP TESTING TO-DATE.

As noted earlier, the NTPEP's nationwide quality assurance program for RECPs began in 2003 and uses three bench-scale "indexed performance" tests; as well as several index tests, including mass per unit area, thickness, tensile strength, percent cover (i.e. inverse of % light penetration), and water absorption (for ECBs) or specific gravity (for TRMs) to provide member DOTs with independent data on the RECPs entered into the program. Sprague and Nelson (2009) reported on the testing and how it is useful in identifying a hierarchy of product types for each performance measurement. Additionally the data can be used by the individual states to identify products that are excessively outside the expected average for a particular product class.

2.1 NTPEP Index and Bench-scale Testing To-date

As noted earlier, the NTPEP's nationwide quality assurance program for RECPs began in 2003 and uses the index and bench-scale tests discussed above to provide member DOTs with independent data on RECPs entered into the program. Table 1 shows the number and types of the most commonly tested RECPs and the average index and bench-scale test results (and associated standard deviations) for each type of RECP. All the products, except the 2NFF (double net polyfiber matting), are ECBs. The 2NFF is a TRM. None of the few tested OWTs are included.

2.2 NTPEP Large-scale Testing To-Date

Not available until recently, large-scale performance testing information has now been added to the voluminous amount of index and bench-scale data found at www.ntpep.org to better characterize and differentiate between various RECP types. Table 2 shows the results of independent large-scale slope and channel testing done under the NTPEP program and the index property results that "bench-mark" the large-scale results. Also included in Table 2 are the index and bench-scale results for testing from 2009 thru early 2012 – the same years as the large-scale testing results. These are the data that will be reviewed and compared herein.

Table 1. Index and Bench-scale Results for NTPEP Testing 2003-2011+

Product Type**	Number of Products Tested	Mass/Area (osy)	Tensile Str. (lb/in)		Tensile Elongation (%)		Thickness (mils)	% Cover Perm. Shear	Absorption / Sp. Gravity	Channel Permissible Shear, psf	Slope Average SLR*	Average C-Factor*	Germination Improvement, %
			MD	XD	MD	XD							
1NS	59	8.0	9.6	5.6	26.3	24.1	396.7	1.5	426.9	1.5	9.2	0.108	306
	Std Dev	1.7	2.8	3.2	9.1	8.7	468.9	0.3	81.3	0.3	2.2	-	128.8
2NS	67	8.1	14.1	9.7	25.4	25.3	358.4	1.8	410.0	1.8	11.5	0.087	341.6
	Std Dev	1.5	4.1	4.2	9.0	10.4	308.2	0.4	69.4	0.4	5.6	-	132.0
1NX	16	8.8	8.4	5.3	20.8	21.5	353.4	2.1	236.2	2.1	7.2	0.139	381.3
	Std Dev	2.1	1.9	1.8	6.9	11.1	96.3	0.3	40.1	0.3	1.9	-	123.4
2NX	27	12.4	16.6	13.3	23.7	23.7	430.0	2.7	230.9	2.7	11.2	0.089	384.7
	Std Dev	4.1	8.7	11.5	11.6	7.4	120.6	0.6	55.0	0.6	7.1	-	90.7
2NSC	34	9.0	19.1	13.6	21.2	22.8	294.0	2.2	359.5	2.2	15.1	0.066	415.3
	Std Dev	1.8	7.6	9.4	8.8	8.0	63.5	0.3	109.0	0.3	5.4	-	131.4
2NC	37	8.8	24.7	17.8	22.6	27.2	250.4	2.7	242.8	2.7	19.9	0.050	361.8
	Std Dev	2.0	12.9	7.2	11.6	11.2	64.9	0.4	81.5	0.4	18.4	-	120.0
2NFF	40	11.8	33.4	27.5	25.9	29.8	380.4	2.8	0.9	2.8	11.1	0.090	329.4
	Std Dev	3.2	16.2	17.0	5.6	16.4	108.6	0.5	0.018	0.5	15.4	-	114.9

* SLR = soil loss ratio; C-Factor calculated as $1/(\text{average of soil loss ratios at 50, 100, and 150 mm/hr})$

**Product Type Key:

1NS = single net straw blanket;
 2NS = double net straw blanket;
 1NX = single net excelsior blanket;

2NX = double net excelsior blanket;
 2NSC = double net straw-coconut blanket;
 2NC = double net coconut blanket;
 2NFF = double net polyfiber matting;

Table 2. Index, Bench-scale, and Large-scale Results for NTPEP Testing 2009-2011+

Product Type	# of Tests	Statistic	Mass/Area (osy)	Tensile Str. (lb/in)		Tensile Elongation (%)		Thickness (mils)	% Cover	Absorption / Sp. Gravity	Channel Perm. Shear	Slope Avg C-Factor	Germination Improvement, %
				MD	XD	MD	XD						
1NS Bench-scale	18	AVG	8.6	10.1	4.9	25.2	24.2	308	86.0	418	1.6	0.110	334.7
		STDDEV	1.3	1.4	1.6	6.6	6.0	97	6.3	93	0.2	0.036	103.9
		MIN	7.0	8.1	3.2	10.9	11.1	217	75.3	296	1.2	0.071	186.0
		MAX	12.9	12.9	9.1	36.1	33.1	529	95.9	606	2.1	0.189	565.0
1NS Large-scale	4	AVG	8.1	8.7	3.7	34.5	27.1	430	88.0	391	1.8	0.028	
		STDDEV	0.5	1.9	0.8	4.4	3.0	77	8.6	61	n/a	0.022	
		MIN	7.7	6.7	2.6	28.0	22.7	355	75.6	344	1.8	0.012	
		MAX	8.7	10.3	4.5	37.8	29.1	496	95.6	471	1.8	0.053	
2NS Bench-scale	20	AVG	8.7	15.0	8.8	25.3	25.3	296	86.8	403	2.0	0.089	406.4
		STDDEV	1.3	4.0	3.1	6.8	5.8	81	5.3	60	0.3	0.033	104.7
		MIN	6.9	8.0	4.1	11.2	13.5	221	80.1	288	1.5	0.042	194.0
		MAX	12.3	28.9	17.4	38.0	35.2	548	99.1	523	2.9	0.154	590.0
2NS Large-scale	9	AVG	8.0	11.4	8.1	30.4	28.9	365	80.6	371	2.1	0.020	
		STDDEV	0.8	1.7	2.7	7.2	7.6	41	9.0	88	0.2	0.011	
		MIN	6.2	9.3	3.2	15.9	11.9	319	63.6	218	1.9	0.005	
		MAX	9.2	14.3	12.6	38.3	37.5	410	90.8	445	2.3	0.035	
1NX Bench-scale	4	AVG	9.0	9.3	4.8	21.2	33.0	241	63.4	266	2.1	0.139	419.0
		STDDEV	1.5	1.4	1.7	8.8	12.4	37	1.7	10	0.0	0.044	69.1
		MIN	8.0	7.4	3.2	12.8	15.7	216	61.1	258	2.1	0.113	361.0
		MAX	11.3	10.8	7.3	33.7	45.2	295	65.2	281	2.2	0.205	498.0
1NX Large-scale	1	AVG	8.5	6.7	2.3	28.5	22.9	391	55.1	189		0.039	
		n/a	n/a	n/a	n/a	n/a	n/a	n/a	n/a	n/a		n/a	
		MIN	8.5	6.7	2.3	28.5	22.9	391	55.1	189		0.039	
		MAX	8.5	6.7	2.3	28.5	22.9	391	55.1	189		0.039	
2NX Bench-scale	6	AVG	12.9	19.3	16.3	24.0	29.7	376	78.7	244	2.8	0.087	356.2
		STDDEV	3.5	11.8	18.5	7.8	4.7	111	7.3	59	0.6	0.034	68.6
		MIN	8.3	9.3	5.4	15.6	23.8	234	65.2	157	1.6	0.066	298.0
		MAX	17.1	42.5	52.8	36.7	36.4	560	87.3	314	3.2	0.159	481.0
2NX Large-scale	2	AVG	8.6	10.6	4.2	32.7	25.1	417	55.7	185	2.2		
		STDDEV	1.6	1.0	0.0	5.0	4.5	22	7.8	6	0.1		
		MIN	7.5	9.9	4.2	29.1	21.9	401	50.1	181	2.1		
		MAX	9.7	11.3	4.2	36.2	28.2	432	61.2	189	2.3		
2NSC Bench-scale	10	AVG	8.5	17.2	11.8	21.7	23.9	255.6	85.7	423.4	2.2	0.071	464.6
		STDDEV	0.9	4.0	3.3	6.9	6.9	43.2	4.2	90.4	0.3	0.017	126.7
		MIN	7.0	11.6	5.7	11.5	12.4	206.0	78.5	271.0	1.5	0.044	321.0
		MAX	9.8	22.1	15.6	31.8	32.0	349.0	93.4	523.0	2.8	0.098	763.0
2NSC Large-scale	4	AVG	8.0	14.0	10.8	31.6	27.8	314	89.8	353	2.1	0.019	
		STDDEV	0.8	2.5	3.2	2.3	3.4	32	3.1	56	0.1	0.018	
		MIN	7.2	10.8	6.3	30.1	24.0	286	86.5	295	2.0	0.006	
		MAX	8.8	16.6	13.5	35.0	32.1	359	92.6	429	2.2	0.031	
2NC Bench-scale	12	AVG	8.9	24.8	17.5	22.2	25.8	235	83.9	295	2.9	0.040	404.4
		STDDEV	2.0	7.1	5.6	8.7	8.6	45	5.1	62	0.3	0.022	139.2
		MIN	7.2	13.1	12.1	11.3	12.9	160	75.2	139	2.4	0.008	111.0
		MAX	14.5	39.8	31.2	40.0	39.5	309	97.0	379	3.5	0.086	583.0
2NC Large-scale	5	AVG	9.8	25.8	16.9	21.5	25.9	264	82.8	274	2.9	0.007	
		STDDEV	1.8	6.0	4.8	6.0	9.3	36	6.1	60	0.9	0.003	
		MIN	7.0	19.2	12.3	11.6	14.5	232	73.7	205	2.3	0.004	
		MAX	11.4	33.9	23.1	26.5	38.5	326	88.3	356	3.6	0.010	
2NFF Bench-scale	15	AVG	11.8	37.2	29.4	28.7	28.2	345	74.5	0.9	2.8	0.125	317.8
		STDDEV	2.9	23.4	25.2	4.1	7.4	78	15.6	0.0	0.4	0.023	71.9
		MIN	7.9	24.0	11.6	23.1	18.8	203	36.5	0.9	2.2	0.093	165.0
		MAX	19.9	119.7	119.0	37.2	40.8	468	90.1	0.9	3.7	0.168	428.0
2NFF Large-scale	4	AVG	10.3	35.6	20.6	28.0	29.9	316	68.1	0.9	2.4		
		STDDEV	1.0	7.9	5.3	3.4	11.5	70	20.0	0.0	0.4		
		MIN	9.0	24.5	14.5	24.9	18.4	231	38.3	0.9	2.0		
		MAX	11.5	41.4	25.2	32.4	45.9	384	79.8	0.9	2.8		

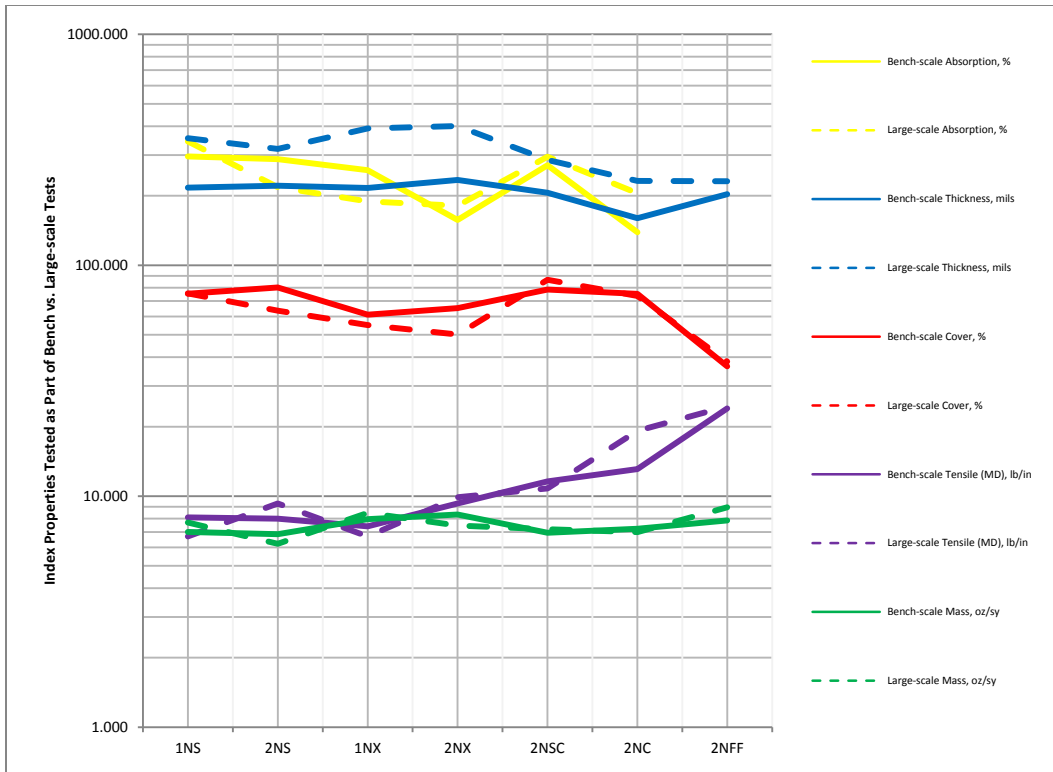


Figure 1. Comparison of Average Index Properties Measured on Products used for Bench-scale vs. Large-scale Testing

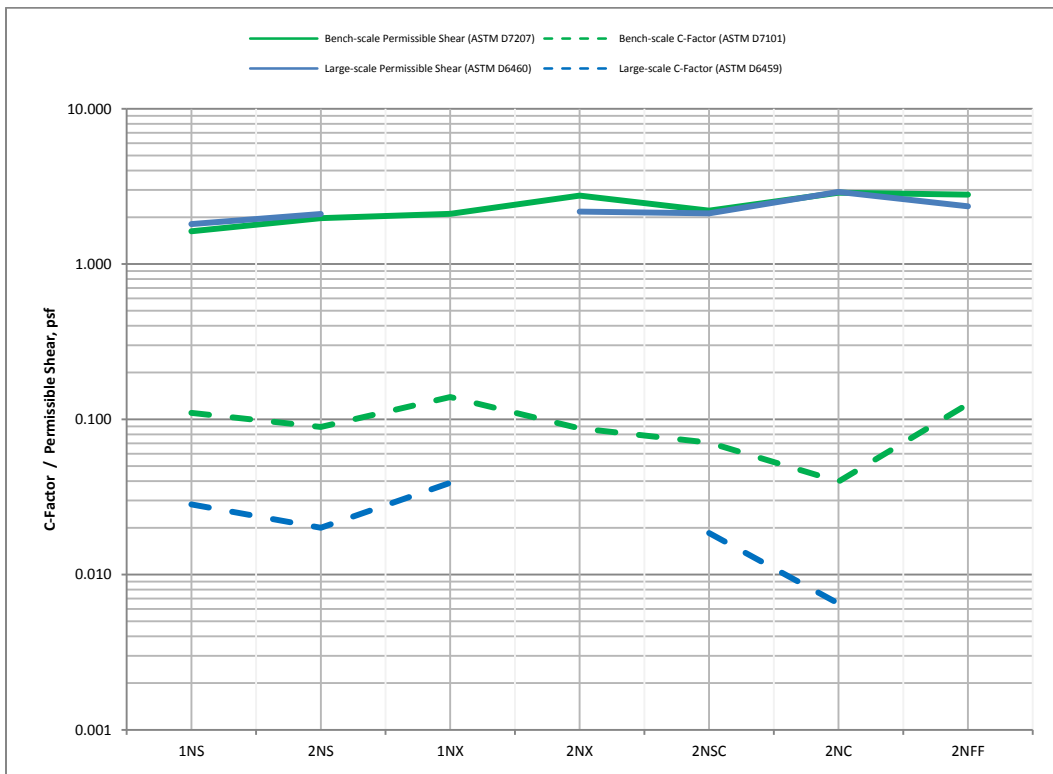


Figure 2. Comparison of Average Bench-scale vs. Large-scale Performance Results

2.3 Review of Index, Bench-scale and Large-scale Testing

The data presented in Table 2 has been graphically presented in Figures 1 and 2 to facilitate a visual comparison of the data. Figure 1 suggests that sufficient uniformity exists in associated index test results from products used in both the bench-scale and large-scale tests to support comparing performance results as shown in Figure 2. Still, one index property – thickness – demonstrates a clear bias toward lower values when tested as part of the index/bench-scale program. This may be because the index properties for the large-scale tests are performed on samples that have been removed from the roll at the large-scale laboratory, repackaged (but not tightly re-rolled) and shipped to the index laboratory, where they are once again unpackaged and cut into specimens. This likely allows the RECPs to “rebound” or even loosen leading to greater thickness and lower % cover.

The data was further evaluated to attempt to identify any meaningful correlation(s) between index (QC) tests and associated bench-scale and large-scale performance tests. If a correlation between properties, or at least a consistent relationship between properties and product types could be found, it would be easier to develop generic specifications for the range of products studied. To this end, possible relationships between index, bench-scale, and large-scale results were explored and are summarized in Table 3.

It quickly becomes clear, based on the correlation coefficients, that no strong credible correlations exist between any of the index properties and product performance as measured by the bench-scale and large-scale tests used. Still, there are “hints” that mass/area, thickness, and % cover may be related to performance. Yet, the correlations are spotty. All correlations are shown in Table 3.

Fortunately, Figure 2 demonstrates quite convincingly that there is a hierarchy of performance among the commonly available RECPs. Additionally, Figure 1 presents the typical index properties for each of these RECPs. Used together, the index and performance data facilitates the preparation of generic specifications that include performance criteria as well as minimum property “thresholds” to assure that only proven materials are used.

Table 3. Possible Index, Bench-, and Large-scale Correlations

Index Test	vs. Bench-scale Test	vs. Large-scale Test	Best Fit Equation	Correlation Coefficient, R ²
Mass/Area, D6475	Slope Erosion, D7101		$C = -0.0021X + 0.1087$	0.0161
		Slope Erosion, D6459	$C = -0.0084X + 0.0937$	0.3011
	Channel Erosion, D7207		$\tau = 0.227X + 0.0869$	0.6053
		Channel Erosion, D6460	$\tau = 0.2513X + 0.0254$	0.4877
Thickness, D6525	Slope Erosion, D7101		$C = -0.0003X + 0.0006$	0.2880
		Slope Erosion, D6459	$C = -0.0002X - 0.0322$	0.6960
	Channel Erosion, D7207		$\tau = -0.0014X + 2.7388$	0.0260
		Channel Erosion, D6460	$\tau = -0.0046X + 3.858$	0.6531
Tensile Strength, D6818	Slope Erosion, D7101		$C = -0.0019X + 0.1235$	0.3425
		Slope Erosion, D6459	$C = -0.0015X + 0.0422$	0.8478
	Channel Erosion, D7207		$\tau = 0.0462X + 1.4293$	0.6121
		Channel Erosion, D6460	$\tau = 0.0214X + 1.8589$	0.3819
Light Penetration, D6567 (% Cover)	Slope Erosion, D7101		$C = -0.0024X + 0.2755$	0.4776
		Slope Erosion, D6459	$C = -0.0006X + 0.0678$	0.4397
	Channel Erosion, D7207		$\tau = -0.0179X + 3.681$	0.0852
		Channel Erosion, D6460	$\tau = -0.0023X + 2.4177$	0.0069

3. SPECIFICATIONS FOR RECPs

Many different specifications for RECPs are in circulation, including proprietary specifications promoted by product suppliers, broad product “categorizations” published by industry groups, and generic specifications used by public agencies. To insure free and fair competition, there are at least three critical elements to a material specification for use on public projects – the focus of this effort. The elements include:

1. The specification must be generic. That is, it must be completely comprised of requirements that are not exclusive to a single product.
2. The specification requirements must be relevant. That is, that each requirement must be shown to relate to how the product is expected to perform or must be critical to assuring product quality.
3. Specification conformance must be verifiable. That is, it must be possible to corroborate every requirement within the specification via independent sampling and verification (a.k.a. conformance) testing. For properties requiring long-term testing, a test report from an independent, accredited laboratory may be acceptable.

3.1 Existing Specs

The most widely circulated “generic” specifications for RECPs are the categorizations presented by the ECTC (2006) and the Federal Highway Administration’s FP-03 (2003) and are reproduced in Tables 4 and 5.

Table 4. Temporary Rolled Erosion Control Product (RECP) Specifications (per FP-03, Table 713-3)

Property	1.A ⁽¹⁾	1.B	1.C	1.D	2.A ⁽¹⁾	2.B	2.C	2.D	3.A ⁽¹⁾	3.B	4	Test Method
Typical functional longevity ⁽²⁾ (months)	3	3	3	3	12	12	12	12	24	24	36	N/A
Minimum tensile strength ⁽³⁾ (lb/ft)	5	5	50	75	5	50	50	75	25	100	125	ASTMD 4595
Maximum “C” factor ⁽⁴⁾	0.10 at 1V:5H	0.10 at 1V:4H	0.15 at 1V:3H	0.20 at 1V:2H	0.10 at 1V:5H	0.10 at 1V:4H	0.15 at 1V:3H	0.20 at 1V:2H	0.10 at 1V:5H	0.25 at 1V:1½H	0.25 at 1V:1H	ASTM D6459 ⁽⁷⁾
Minimum permissible shear stress ⁽⁵⁾⁽⁶⁾ (lb/ft ²)	0.25	0.50	1.50	1.75	0.25	0.50	1.50	1.75	0.25	2.00	2.25	ASTM D6460 ⁽⁷⁾

(1) Obtain max “C” factor and allowable shear stress for mulch control nettings with the netting used in conjunction with pre-applied mulch material.

(2) Functional longevity are for guidance only. Actual functional longevity may vary based on site and climatic conditions.

(3) Minimum average roll values, machine direction.

(4) “C” factor calculated as ratio of soil loss from rolled erosion control product protected slope (tested at specified or greater gradient, v:h) to ratio of soil loss from unprotected (control) plot in large-scale testing. These performance test values should be supported by periodic bench scale testing under similar test conditions and failure criteria using ASTM D7101.

(5) Minimum shear stress the rolled erosion control product (unvegetated) can sustain without physical damage or excess erosion (> 1/2-inch soil loss) during a 30-minute flow event in large-scale testing. These performance test values should be supported by periodic bench scale testing under similar test conditions and failure criteria using ASTM D7207.

(6) The permissible shear stress levels established for each performance category are based on historical experience with products characterized by Manning’s roughness coefficients in the range of 0.01 to 0.05.

(7) Or other qualified independent large scale test method determined acceptable by the CO.

Categories of Temporary RECPs : 1.A, 2.A, 3.A = mulch control nets; 1.B, 2.B = netless ECBs; 1.C, 2.C = single net ECBs and Open Weave Textiles; 1.D, 2.D = double net ECBs; 3.B, 4 = ECBs & Open Weave Textiles

Table 5. Turf Reinforcement Mat (TRM) Specifications (per FP-03, Table 713-4)

Properties ⁽¹⁾	Rolled Erosion Control Product Type			Test Method
	5.A	5.B	5.C	
Minimum tensile strength ⁽²⁾⁽³⁾ (lb/ft)	125	150	175	ASTM D4595
UV stability (minimum % tensile retention)	80	80	80	ASTM D 4355 (500-hr exposure)
Minimum thickness ⁽²⁾ (inches)	0.25	0.25	0.25	ASTM D 6525
Minimum permissible shear stress ⁽⁴⁾ (lb/ft ²)	6.0	8.0	10.0	ASTM D6460 ⁽⁵⁾

(1) For TRMs containing degradable components, obtain all property values on the non-degradable portion of the matting alone.

(2) Minimum average roll values, machine direction only.

(3) Field conditions with high loading and high survivability requirements may warrant the use of turf reinforcement mats with tensile strengths of 3,000 pounds per foot or greater.

(4) Minimum shear stress the turf reinforcement mat (fully vegetated) can sustain without physical damage or excess erosion (>1/2-inch soil loss) during a 30-minute flow event in large-scale testing. These performance test values should be supported by periodic bench scale testing under similar test conditions and failure criteria using ASTM D7207.

(5) Or other qualified independent large scale test method determined acceptable by the CO.

3.2 Proposed Generic Specs

Table 6 is a proposed specification that includes all of the critical specification elements listed above, reflects as much as possible the generally accepted specification requirements of Tables 4 and 5, and incorporates new knowledge gained (and discussed above) from the NTPEP program. This includes using minimum “thresholds”, or lower limits, to

protect against deficiently manufactured or underperforming product being furnished to the project. Shaded values in Table 2 are used to guide the choice of minimum “thresholds” recommended in Table 6.

Table 6. Proposed Generic Specification for RECPs

RECP Classification		Type 1	Type 2	Type 3	Type 4	Type 5	Type 6	Type 7
Typical RECP Type (for guidance only)		1NS, 1NX (ECB)	2NS, 2NX (ECB)	2NSC (ECB)	2NC (ECB)	2NFF (TRM)	Other TRM	Other TRM
Durability (for guidance only)		Ultra Short-Term	Short-term	Extended Term	Long-Term	Permanent	Permanent	Permanent
		3 to 6 mos.	6 to 12 mos.	12 to 24 mos.	> 24 mos.			
C-Factor - ASTM D 6459		C ≤ 0.10	C ≤ 0.05	C ≤ 0.05	C ≤ 0.025	C ≤ 0.10	C ≤ 0.05	C ≤ 0.05
Max. Slope Gradient	Max. Slope Length (ft)	Permitted Use on Slopes (X)						
< 5:1	100	X	X	X	X	X	X	X
5:1 ≤ ___ < 4:1	80	X	X	X	X	X	X	X
4:1 ≤ ___ < 3:1	60		X	X	X	X	X	X
3:1 ≤ ___ < 2:1	40			X	X	X	X	X
2:1 ≤ ___ < 1:1	20				X	X	X	X
Permissible Shear, Unvegetated - ASTM D 6460		1.50	1.75	2.0	2.25	2.5	2.5	2.5
Permissible Shear, Fully Vegetated - ASTM D 6460		Not req'd	Not req'd	Not req'd	Not req'd	6.0	8.0	10.0
Tensile Strength (MD), lb/in	ASTM D6818	7.0	8.0	10.0	12.0	20.0	TBD	TBD
Tensile Elongation (MD), %	ASTM D6818	10	10	10	10	20	TBD	TBD
Tensile Strength (XD), lb/in	ASTM D6818	3.0	4.0	6.0	10.0	12.0	TBD	TBD
Tensile Elongation (XD), %	ASTM D6818	10	10	10	10	20	TBD	TBD
Mass / Unit Area, osy	ASTM D6475	7.0	7.0	7.0	7.0	8.0	TBD	TBD
Thickness, mils	ASTM D6525	200	200	200	200	200	TBD	TBD
Ground Cover, %	ASTM D6567	60	65	70	75	60	TBD	TBD
Water Absorption, % (ECBs); Sp. Gravity (TRMs)	ASTM D1117	200	200	200	200	0.9	TBD	TBD
Bench-scale Slope, Avg Soil Loss Ratio	ASTM D7101	5.0	6.0	10.0	10.0	5.0	TBD	TBD
Bench-scale Shear Permissible Shear, psf	ASTM D7207	1.25	1.5	1.75	2.0	2.25	TBD	TBD
Bench-scale Germination, % Improvement	ASTM D7322	200	200	200	200	200	TBD	TBD
UV Stability, % Retained at 500 hrs	ASTM D4355	n/a	n/a	n/a	n/a	80%	80%	80%
QC Data from daily testing must be provided with certification.		Product must be listed at www.ntpep.org .			Reports for large-scale testing must be provided from accredited independent laboratory.			

4. CONCLUSIONS

Commonly used index, bench-scale, and large-scale standardized tests have been discussed along with a review of results from independent testing performed on a range of rolled erosion control products (RECPs) under the auspices of the National Transportation Product Evaluation Program (NTPEP).

Using results to-date, potential correlations have been identified between commonly measured index properties and the ability of specific product types to protect against both rainfall-induced erosion and erosion associated with concentrated flows. Based on these identified relationships a generic specification has been presented for consideration.

REFERENCES

- ASTM D 792, Method A, "Standard Test Methods for Density and Specific Gravity (Relative Density) of Plastics by Displacement," ASTM, West Conshohocken, PA.
- ASTM D 1117, Section 5.4 and ECTC-TASC 00197, "Standard Guide for Evaluating Nonwoven Fabrics – Absorptive Capacity Test (for Larger Test Specimens)," ASTM, West Conshohocken, PA.
- ASTM D 6459, Standard Test Method for Determination of Erosion Control Blanket (ECB) Performance in Protecting Hillslopes from Rainfall-Induced Erosion," ASTM, West Conshohocken, PA.
- ASTM D 6460, Standard Test Method for Determination of Erosion Control Blanket (ECB) Performance in Protecting Earthen Channels from Stormwater-Induced Erosion," ASTM, West Conshohocken, PA.
- ASTM D 6475, "Standard Test Method for Measuring Mass per Unit Area of Erosion Control Blankets," ASTM, West Conshohocken, PA.
- ASTM D 6525, "Standard Test Method for Measuring Nominal Thickness of Permanent Rolled Erosion Control Products," ASTM, West Conshohocken, PA.
- ASTM D 6566, "Standard Test Method for Measuring Mass per Unit Area of Turf Reinforcement Mats," ASTM, West Conshohocken, PA.
- ASTM D 6567, "Standard Test Method for Measuring the Light Penetration of a Turf Reinforcement Mat (TRM)," ASTM, West Conshohocken, PA.
- ASTM D 6818, "Standard Test Method for Ultimate Tensile Properties of Turf Reinforcement Mats," ASTM, West Conshohocken, PA.
- ASTM D 7101, "Standard Index Test Method for Determination of Unvegetated Rolled Erosion Control Product (RECP) Ability to Protect Soil from Rain Splash and Associated Runoff under Bench-Scale Conditions," ASTM, West Conshohocken, PA.
- ASTM D 7207, "Standard Test Method for Determination of Unvegetated Rolled Erosion Control Product (RECP) Ability to Protect Sand from Hydraulically-Induced Shear Stresses under Bench-Scale Conditions".
- ASTM D 7322, "Standard Test Method for Determination of Rolled Erosion Control Product (RECP) Ability to Encourage Seed Germination and Plant Growth under Bench-Scale Conditions," ASTM, West Conshohocken, PA.
- ECTC (2006), "ECTC Standard Specification for Temporary Rolled Erosion Control Products," Erosion Control Technology Council, www.ectc.org.
- ECTC (2006), "ECTC Standard Specification for Permanent Rolled Erosion Control Products," Erosion Control Technology Council, www.ectc.org.
- FHWA (2003), "Standard Specifications for Construction of Roads and Bridges on Federal Highway Projects", FP-03 (U.S. Customary Units), U.S. DEPARTMENT OF TRANSPORTATION, Federal Highway Administration.
- NTPEP (2011), "ECP User Guide," National Transportation Product Evaluation Program, AASHTO, www.ntpep.org.
- Sprague, C.J. and Nelson, J. (2009), "Correlation of Bench-scale and Large-scale Performance Testing of RECPs", Conf. XXXX, International Erosion Control Assoc., Reno, NV, (digital proceedings).

The Comparison and Analysis of International Tensile Test Methods and Results

K. Lin, A. Tang, B. Lai, W. Yu, ACE Geosynthetics, Taichung city, Taiwan

ABSTRACT

One of the most fundamental tests on the geosynthetics materials is tensile property. By means of tensile test, the ultimate tensile strength, elongation, initial tensile modulus, et cetera could be acquired, which are not only the good index for design works but also the fine reference for conformity checks.

Test specimen preparation, conditioning atmosphere, procedures, as well as apparatus such as types of clamps and jaw faces are specified and declared thoroughly in individual literatures. All these elements have certain influences upon the test result. By far it is inappropriate to cite values from random or unassociated tests. However, when tests are carried out by the one method, it still might explore variances in results due to dissimilar setups without violating the norms. Focusing upon the differentiation among the international tensile test methods, this article illustrates the variation of principles and analyzes reciprocal effects resulted from multiplicity test settings.

1. FOREWARD

Many geosynthetic materials, for instance geogrid, geotextile and geostrip are suitable for reinforcement. However, when properties of reinforcement materials are varied, optional testing methods are required. Among mechanical, physical and hydraulic properties, tensile strength testing which is found in numerous national standard test methods is taken as the most significant indicator to assess the quality. The obtained results of tensile strength test, an index test, are taken into consideration when it comes to design the reinforcement structure or to contract for the merchantability and goods conformity criteria. Although all test methods are designed to calculate the tensile strength, the test setups and conditions are not necessary in line with each other. At any rate, it is not allowed to grab the testing results of method A to represent or support an outcome carried out by method B. In order to read the relationship between conditions and test results, a condition-permutation project covering 3 grades of flexible geogrid examined by 5 international and national test methods – ISO, ASTM, JIS, GB, CNS (legalized in Taiwan) as well - is thus conducted.

2. ANALYSIS

Common tensile strength test methods consisting in ISO 10319 (EU and international), ASTM D6637 (America), JIS L 1096, JIS L 1908 (Japan), GB/T 15788, GB/T 17689 (China) and CNS 13330 (Taiwan) are summarized in terms of scope, apparatus, strain rate, specimen dimension, as well as pretension. Please refer to Table 1(I) and (II).

Table 1. Test method comparison (I)

Test method	ASTM D6637	ISO 10319	CNS 13300
Version	2011	2008	1993
Test specimens	Single rib & Multit-rib	Wide-width	Wide-width
Scope	Geogrid	Most Geosynthetics, including woven & nonwoven geotextiles, geocomposites, knitted geotextiles, felts, geogrids, similar open-structure geotextiles, not applicable to polymeric or bituminous geosynthetic barriers	Most geotextiles that include woven & nonwoven fabrics, layered fabrics, knit fabrics, and felt that are used for geotextile application.
Tensile testing machine	CRE	CRE	CRE
Testing clamp	Fixed & roller grip clamping system	Wedge, compressive, capstan	Wedge
Gauge length (mm)	Minimum 60	≥60	NA
Strain rate (%/min)	10±3	20±5	10±3 (10±3 mm/min)
Length between the clamps (mm)	Greater distance of 3 junctions or 200±3 mm	100±3	100±3
Number of test specimens	5 for MD & CD	5 for MD & CD	3 for MD & CD
Dimensions of test specimens	<ul style="list-style-type: none"> ●Method A: contain 3 junctions long in test direction. ●Method B: a min. 200 mm wide and contain 5 ribs by at least 3 junctions or 300 mm long in test direction. 	<ul style="list-style-type: none"> ●GT: 200 × sufficient length. ●GG: 200 × sufficient length (at least 100 mm), contain at least one row of junction, excluding the junctions held in the jaws. For products of pitch < 75 mm, at least 4 complete ribs in the width. For products of pitch 75 ~ 120mm, at least 2 complete ribs in the width. 	<ul style="list-style-type: none"> ●200×200 ●the exhibit strengths approx. 100 kN/m, 100 mm width specimens may be substituted for 200 mm width specimens.
Preload	●1.25% of max. load or 225N	1% of the max. load	NA

Table 1. Test method comparison (II)

Test method	JIS L1908	JIS L1096	GB/T 15788	GB/T 17689
Version	2000		2005	2008
Test specimens	Wide-width	Strip	Wide-width	Single rib & Multi-rib
Scope	Geotextiles, nonwoven, geogrids, geonet	General characteristics of woven fabrics	Most Geosynthetics, including woven & nonwoven geotextiles, geocomposites, knitted geotextiles, felts, geogrids, similar open-structure geotextiles, not applicable to polymeric or bituminous geosynthetic barriers	PP & HDPE plastic geogrids, not applicable to chemical and glass fiber weave geogrids
Tensile testing machine	CRE	CRE, CRT, CRL	CRE	NA
Testing clamp	NA	The jaw at least 60 mm wide by 20 mm length	Wedge, compressive, capstan...	no
Gauge length (mm)	NA	NA	≥60	no
Strain rate (%/min)	20±5% of length between the clamps	50% or 100% of length between the clamps	20±5% of length between the clamps	20% of length between the clamps
Length between the clamps (mm)	•100 •Geogrid & Geonet >200 mm, at least 3 junctions.	200	100, except geogrid	NA
Number of test specimens	5 for MD & CD	3 for MD & CD	5 for MD & CD •GT: 200 × sufficient length. •GG or geocomposites: 200 × sufficient length, contain at least one row of junction, excluding the junctions held in the jaws. For products of pitch < 75 mm, at least 5 complete ribs in the width. For products of pitch < 120mm, at least 2 complete ribs in the width.	10 for single rib, 5 for multi-rib •single rib method: contain 3 junctions long in test direction. •multi-rib method: a min. 200 mm wide and contain 5 ribs by at least 2 junctions or at least 100 mm long in test direction.
Dimensions of test specimens	•woven & nonwoven geotextile: 50 or 200 mm wide. •Geogrid & Geonet: at least 200 mm wide.	•Ordinary fabric: approx. 50 or 25 × approx. 300 •Heavy fabric : 30 × approx. 300		
Preload	1% of the max. load	test specimen of 10 m	1% of the max. load	1% of nominal strength

2.1 Scope

Test methods necessarily specify the applicable materials and fields and point out the purposes. Standard test methods ISO 10319, ASTM D6637, GB/T 15788, GB/T 17689 and JIS L 1908 all plainly identify that the geogrid is one of the applicable materials to be tested. The method JIS L 1908 states it is suitable for geogrid and geonet which are more properly categorized as one of stiff materials. Even though the method JIS L 1096 is designed for woven fabrics, the reality is that in Japan, it is definitely to be applied for geogrid. Similarly, the method CNS 13300, Method of Test for Tensile Properties of Geotextiles by the Wide-Width Strip, is actually used to test not only woven fabrics but also geogrid in Taiwan as there is not a specific method for geogrid drawn up. A series of 7 methods are brought into this discussion, thus.

2.2 Apparatus

2.2.1 Tensile Testing Machine

Doubtlessly, constant rate of extension type (CRE), constant rate of traverse type (CRT) and constant rate of loading (force) type (CRL) tensile machines have found as the most accepted equipments to conduct the index test of tensile strength. CRE type tensile machine is recommended to apply in the rest 5 methods with the exception of methods JIS L 1096 which individually establishes unlike setups per 3 different testing apparatus and GB/T 17689 which does not precisely denote a suitable machine type. There is no evidence to link test results derived from CRE and CRT type machine. Providing any disagreement is raised, it is suggested settle by arranging a test by CRE type machine as judgment.

2.2.2 Testing Clamp

It is understandable the choice of clamp is quite depending on the features and strength of materials to be tested. Wedge jaws and compressive jaws and capstan grips are employed to perform this type of testing when we narrow down to 7 tensile strength test methods discussed in this essay. The fact is that only the methods ISO 10319 and GB/T 15788 have directly indicated the use of clamp. Generally speaking, wedge jaw is appropriate to test low-grade specimen; either capstan grip or compressive jaw high-grade specimen. It is worth noting that confined to grasping strength, compressive jaw is incapable of performing very high strength testing.

2.2.3 Extensometer

Extensometer is mandatory to measure the movement of the reference points from the point of view of test methods ISO 10319, ASTM D6637 and GB/T 15788; yet this device is not mentioned in the rest methods. In the test method JIS L 1096, the elongation is counted by reading the movement of length between clamps.

2.3 Set-Up Conditions

2.3.1 Strain Rate

Strain rate of $(20\pm 5)\%$ per minute is given in the methods ISO 10319, GB/T 15788, JIS L 1908 as well. The method JIS L 1096 determines the strain rate by calculating the length between clamps. In the method GB/T 15788, the strain rate is determined in accordance with 20% per minute of Ge-ju length (隔距長度) which lacks the definition. Since the framework of GB/T 15788 was derived from the method ISO 10319:1993, the author presumes Ge-ju length means the length between clamps. Yet the strain rate in ISO 10319:2008 has clarified as $(20\pm 5)\%$ per minute in the gauge length of the specimen. The method GB/T 17689 declares 20% per minute of clamping distance for strain rate. Methods ASTM D6637 and CNS 13300 both share the same strain rate $(10\pm 3)\%$ per minute of the gauge length; however, the method JIS L 1096 states to take 50% or 100% of clamping distance per minute. Evidently, different strain rate shall bring dissimilar results. The gauge length, assert the methods ISO 10319 and ASTM D6637, is meant to compute the elongation, instead of being straight taken as strain rate. The method ISO 10319 apparently organizes the setup as thorough as possible compared with the rest that produce extra variances in the events.

2.3.2 Width of Specimen

With the exception of JIS L 1096, all methods spell the specimen with 200 mm wide. When it comes to the classification of geogrid, at least 5 nodes have to be included in the width. When the tensile strength of woven fabrics exceeds 100kN/m, 100 mm wide specimen is allowed, says the method CNS 13300, to replace 200 mm wide specimen. In a similar system, the method JIS L 1096 states either 5 cm or 2.5 cm wide specimen is for general woven fabrics and 3 cm wide specimen for high strength specimen. The tensile strength usually is expressed in kilonewtons per meter (kN/m) but it pretty much is calculated based on the strength per the width of tested specimen. The specimen coupon is on a quite small scale contrast to the sheet of reinforcing materials installed in the engineering structure. Therefore, there is a possibility to overestimate the real tensile strength through the conversion of unit measurements. ISO 10319 defines how to calculate strength based on the number of ribs in the sample and the number of ribs in a metre of product to avoid this over-estimate.

2.3.3 Length Between Clamps

Once wedge jaws are assigned, the length between clamps is set at 100 mm as the methods ISO 10319 and GB/T 15788 indicate. The method JIS L 1908 also adopts the above operation when it involves neither geogrid testing nor a capstan operation. The method ASTM D6637 requests a length of greater distance of three junctions or 200 mm. Likewise, a length of 200 mm is given by the method JIS L 1096. The method GB/T 17689 is in absence of this discussion.

2.3.4 Gauge Length

An initial distance of at least 60 mm is agreed by methods ISO 10319, ASTM D6637, GB/T 15788 as well. In ISO 10319 the gauge length must be a whole number of rib pitches with measurement from rib centre to rib centre across at least one junction

2.3.5 Pretension

A major reason to set up a preload is to eliminate the errors in the act of operation among testers and ensure the effectiveness of test results. The method CNS 13300 is missed in this section. A preload of 1% of the estimated maximum load is shared and agreed by method ISO 10319, JIS L 1908 and GB/T 15788. On the other hand, the method GB/T 17689 has the same opinion to the preload but it is on nominal strength basis. The method ASTM D6637 comes up to a strict requirement to be limited to 1.25% of the peak tensile strength or 225N (50 lbf). The method JIS L 1096 takes a preload by assessing the tensile strength of a 10 cm specimen.

2.4 Test Results and Applications

By means of a tensile test, all associated values including ultimate tensile strength, ultimate elongation, strain strength, initial tensile modulus, offset tensile modulus and secant tensile modulus are obtained to set out the practical engineering design. In the scope of the civil engineering, long term strength and stress-strain are two key factors to design reinforced structures such as retaining wall, embankment, and so on; meanwhile, they are valuable figures to evaluate the feasibility of the design. Furthermore, since tensile testing is an index test, it commercially turns a basic and important indicator for merchantability.

2.5 Comparison

A summery is made to list the scope of each test method. Please refer to Table 2. The author uses the flexible geogrid to conduct a program in accordance with several methods and is going to details in the following paragraphs.

Table 2. Test methods and products

Test method	Geogrid	Geotextile	Woven fabrics
ASTM D6637	●		
ISO 10319	●	●	
CNS 13300	○	●	
JIS L1096	○	○	●
JIS L1908	●	●	
GB/T 15788	●	●	
GB/T 17689	●		

Note: ● suitable method; ○ not suitable method but adopted in the country where issues the method

3. DISCUSSION

3.1 Conditions

Three grades of geogrids are selected to perform tensile testing program, as schemed. The conditions of strain rate, length between grips, gauge length, width of specimens and the use of clamps are all given as per methods in Table 3. Since GB/T 15788 and JIS L 1908 have quite similar instructions on many terms, they are taken as one same method to perform in this program. In order to lessen variances, the following elements had been categorized. Distance between the clamps is set up at 30 cm from centerline to centerline of rollers when capstan is applied and 20 cm to wedge jaws. Typically, 60 mm and 100 mm gauge lengths are adapted by standards. In aspect of the setting of test speed, a trial test is required beforehand in order to calculate the test speed in accordance with requirements of the standards as the extensometer is to determine the gauge length for use in elongation calculations and not test speed. Please refer to Table 4.

Table 3. Conditions

Item(s)	ISO 10319	ASTM D6637-A	ASTM D6637-B	CNS 13300	GB/T 15788 JIS L 1908
Strain rate (%/min)	20	10	10	10 mm/min	20 ¹
Pretension (%)	1%	NA	1.25%	NA	1%
Gauge length (mm)	60 &100	60 &100	60 &100	60 &100	60 &100
Width of specimen	Wide width	Single rib	Multi-rib	Wide width	Wide width
Type of grip	Capstan	Capstan & Compressive wedge jaws	Capstan	Capstan	Capstan

¹ 20 %/min of the length between 2 grips

Table 4. Speed (Type of grip: Capstan)

Item	ISO 10319		ASTM D6637-A & B		CNS 13300	GB/T 15788 JIS L 1908
Testing speed	%/min	mm/min	%/min	mm/min	mm/min	mm/min ¹
GG1	20.1	180	9.1	90	10	60
GG2	19.7	185	9.1	90	10	60
GG3	19.3	200	9.6	100	10	60

¹20 %/min of the length between 2 grips

3.2 Results

Test results are tabled in Table 5 – 10. Gauge length of 60 mm or 100 mm gives negligible difference in the results when rest conditions remain. The readings of tensile strength of Type 1 and Type 2 are not very unlike whether capstan grips or compressive wedge jaws are applied. However, when it comes to Type 3 group, the tensile strength carried out by capstan grip appears higher. A better performance of strength at 2% and 5% strain is observed while compressive wedge jaws are used. Given that the strain rate is accelerate, the tensile strength and strain strength go higher without raising the elongation.

Table 5. Type 1 tensile strength result (Gauge length: 60mm)

Item	ISO 10319	ASTM D6637-A	ASTM D6637-B	CNS 13300	GB/T 15788 JIS L1908	ASTM D6637-A ¹
Tensile strength (kN/m)	69.10	70.86	68.29	63.84	68.16	69.45
Elongation (%)	8.36	11.16	8.21	8.04	8.70	10.19
2% strain (kN/m)	14.28	10.42	14.31	11.70	12.57	11.11
5% strain (kN/m)	39.65	27.98	43.11	36.14	37.67	30.08

¹Compressive wedge jaws

Table 6. Type 1 tensile strength result (Gauge length: 100mm)

Item	ISO 10319	ASTM D6637-A	ASTM D6637-B	CNS 13300	GB/T 15788 JIS L1908	ASTM D6637-A ¹
Tensile strength (kN/m)	69.17	71.31	68.05	65.42	65.71	68.31
Elongation (%)	8.20	10.70	8.20	8.39	7.87	9.61
2% strain (kN/m)	14.04	10.97	14.11	11.68	14.10	11.52
5% strain (kN/m)	41.95	31.5	41.54	37.16	40.71	32.74

¹Compressive wedge jaws

Table 7. Type 2 tensile strength result (Gauge length: 60mm)

Item	ISO 10319	ASTM D6637-A	ASTM D6637-B	CNS 13300	GB/T 15788 JIS L1908	ASTM D6637-A ¹
Tensile strength (kN/m)	161.22	162.94	160.7	150.50	155.07	161.91
Elongation (%)	8.38	10.91	8.44	8.86	8.43	9.24
2% strain (kN/m)	38.57	24.15	40.19	30.30	35.42	35.29
5% strain (kN/m)	97.91	70.90	99.70	84.03	93.83	96.36

¹Compressive wedge jaws

Table 8. Type 2 tensile strength result (Gauge length: 100mm)

Item	ISO 10319	ASTM D6637-A	ASTM D6637-B	CNS 13300	GB/T 15788 JIS L1908	ASTM D6637-A ¹
Tensile strength (kN/m)	160.61	163.74	160.34	147.59	154.62	162.77
Elongation (%)	8.41	10.44	8.53	7.52	8.23	9.22
2% strain (kN/m)	36.34	27.05	39.22	34.85	36.52	36.54
5% strain (kN/m)	99.62	78.83	98.22	96.05	95.01	93.01

¹Compressive wedge jaws

Table 9. Type 3 tensile strength result (Gauge length: 60mm)

Item	ISO 10319	ASTM D6637-A	ASTM D6637-B	CNS 13300	GB/T 15788 JIS L1908	ASTM D6637-A ¹
Tensile strength (kN/m)	217.92	231.18	216.75	207.95	214.98	212.59
Elongation (%)	9.67	12.18	9.68	10.12	9.78	9.55
2% strain (kN/m)	44.75	31.81	42.67	41.15	47.04	45.47
5% strain (kN/m)	98.97	81.83	99.89	94.99	99.58	102.67

¹Compressive wedge jaws

Table 10. Type 3 tensile strength result (Gauge length: 100mm)

Item	ISO 10319	ASTM D6637-A	ASTM D6637-B	CNS 13300	GB/T 15788 JIS L1908	ASTM D6637-A ¹
Tensile strength (kN/m)	219.31	225.18	217.25	210.00	212.54	212.35
Elongation (%)	9.40	11.54	9.33	9.69	9.42	9.58
2% strain (kN/m)	50.25	34.22	50.20	43.07	45.95	48.51
5% strain (kN/m)	108.20	85.25	109.41	98.94	102.31	104.05

¹Compressive wedge jaws

4. CONCLUSION

- Strain rate interferes with tensile strength and elongation. High strain rate produces high strength, including strength at 2% and 5% strain, initial tensile modulus, setoff tensile modulus and secant tensile modulus, at lower elongation.
- The selection of gauge lengths influences upon the elongation quite slightly as far as remaining conditions are not changed.
- Capstan grip earns a better performance in the strain strength at lower elongation. This phenomenon seems not noticeable in tests of low-grade geogrid though it is easier to observe the efforts in tests of high-grade geogrid. Compared with capstan grips, the mechanism of wedge jaws is relevantly limited to the grasping strength so often slippage or jaw breaks are occurred.
- A flexible geogrid greater than 200 kN/m is recommended to be executed tensile tests with capstan grips.
- Without violating the normative procedure of test method, either the form of clamps or the length between clamps possibly controls the test results. Any controversy in inspection activity could be raised so long as an ambiguity is found in the explanation of procedures, testing setup and conditions.
- A requirement of strain rate appears missed or imprecise in many test methods. A strain rate is at 20% of Ge-ju length (隔距長度) as per GB/T 15788, which could be defined as length between clamps or length of gauge. According to the method ASTM D6637, the strain rate is at 10% per minute of the gauge length based on the gauge length so the dependence of strain rate and gauge length is seen. A strain rate is at 10±3%/min (10±3 mm/min) as far as the length between clamps is 10±3 mm as per CNS 13300.

REFERENCES

- ISO 10319. Geosynthetics – wide-width tensile test, *International Organization for Standardization*,
- ASTM D4595. Standard test method for tensile properties of geotextiles by the wide-width strip method, *American Society for Testing and Materials*, West Conshohocken, Pennsylvania, USA.
- ASTM D6637. Standard test method for determining tensile properties of geogrids by the single or multi-rib tensile method,

American Society for Testing and Materials, West Conshohocken, Pennsylvania, USA.
JIS L 1096. Testing methods for woven fabrics, *Japanese Industrial Standard*, Japan.
JIS L 1908. Test methods for geotextiles, *Japanese Industrial Standard*, Japan.
CNS 13300. Method of Tensile Properties of Geotextiles by the Wide-Width Strip, *Chinese National Standards*, Taiwan.
GB/T 15788. Geotextiles and geotextile-related products – wide-width tensile test, *China Standards*, China.
GB/T 17689. Geosynthetics – plastic geogrids, *China Standards*, China.

The Impact of Site Conditions on the Electrical Surveying of Pond Liner Installations

Bennett, Phillip. Managing Director. Geotest Pty Ltd. Australia. pbennett@geotest.net.au

ABSTRACT

Contractors, with over six year's experience, were engaged to survey and report on the condition of a HDPE liner in Queensland, Australia. The 35,000m² pond was a clay lined, cut and fill construction with a trench anchored, 2.0mm HDPE liner with no appurtenances or perforations. All fill and discharge was undertaken over the top of the basin. The pond contained a solution of 7000ppm saline water, a by-product of coal seam gas extraction.

In the course of preparing the survey equipment (in accordance with ASTM.D7002¹, ASTM D.7007² and ASTM D7703³), it became evident that the voltage was unstable and the contractors were unable to electrically identify the calibration puck, thus making it impossible to identify the parameters for the equipment settings, or to successfully carry out the requirements of the test regime. Further extensive investigation eventually identified a set of conditions peculiar to the site, and which impacted on the surveyors' ability to undertake effective testing.

This paper intends to explore this specific incident, in which several major site related factors, including:

1. Salinity levels of contained liquid;
2. Substrate conditions;
3. Metallic properties of contained pond sediment, and
4. Ambient meteorological conditions

The above contributed directly to the detrimental effect on the electrical surveying of a pond liner. The subsequent importance of understanding site conditions and nuances when undertaking electrical survey is highlighted within.

1. INTRODUCTION

Integrity surveys are increasingly being used as a process to test the integrity of installed geomembrane throughout Australia. The success of such a process has given rise to specifiers requiring, now more often as a matter of course, that the liner be electrically tested.

The installation of geomembranes to prevent leakage from storage ponds into the environment has been in longstanding and successful use worldwide, and as the industry has developed, so have the materials and the installation techniques peculiar to their construction. These developments have not only been in the materials themselves, and their properties in resisting chemical and environmental attack, but so have the techniques relating to the installation and the subsequent verification of the installation.

Traditionally the materials have been well tested and verified, as have the techniques of installation and the construction of the liner as a completed product, but final inspection has traditionally been restricted to a visual methodology, incorporating the finished surface of the liner. This particular methodology has the potential to overlook hidden damage or holes that are not readily detectable with the naked eye.

The use of electrical integrity testing has now given the industry a tool with which it can verify the completed installation, both on the surface and deep within it. This process has not been recognised by the industry and has proven itself as an extremely valuable tool for locating voids, thus allowing repairs, and improving the overall quality of the installation.

The basic outline of the integrity test is to use the geomembrane itself as an electrical insulator; between the water within the pond and the ground beneath the pond. When an electrical potential is applied to the surface of the pond, either via a wetted surface, or the water stored in the pond, the geomembrane (if intact) acts as an electrical insulator. In this manner, if the and the overall circuit is not connected, it means that there will be no flow of current. Is however, there are holes present in the geomembrane, the circuit will not be completed, and a flow of current will therefore exist. The amount of current in existence will generally be proportionate to the resistance of the geomembrane; the higher the number and/or the size of the holes, the lower the resistance will be, and the greater the current flow. If there are holes in the liner, the electrical current passes through the hole, and this can then be measured by sensitive equipment.

The potential applied to the pond is a DC current, which has direction , thus enabling traceability of the current to as a means of locating the holes in the pond. (Refer to FIG 1-6 below)

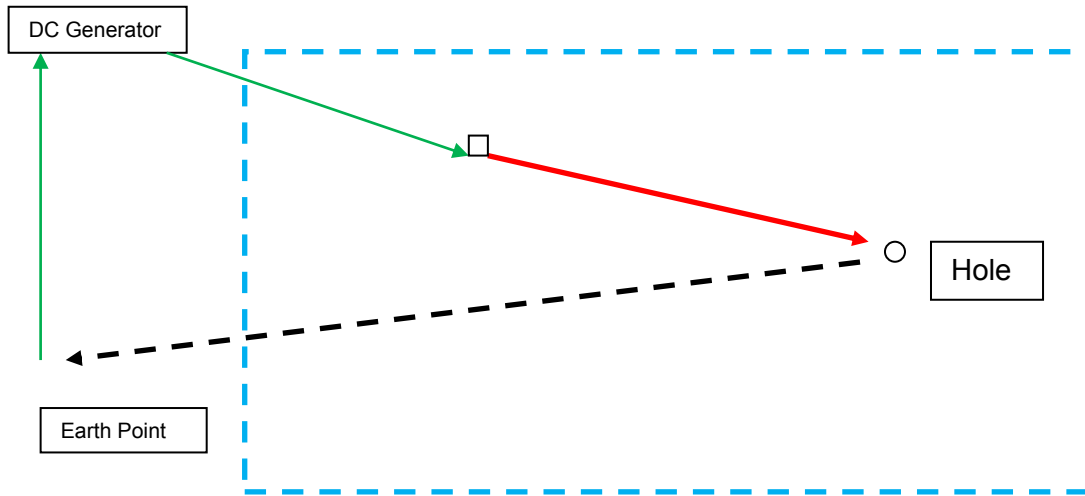


Fig 1. Schematic of basic setup for electrical surveying and flow of the current (in one direction)

KEY

- Connection to the earth peg and energiser plate within the pond to the DC energiser
- Direction of the current with the pond
- - - ← Direction of the current through the hole and return to the energiser via the ground.

As with the testing of any engineered product, and especially those products which are containment solutions, the process of electrical testing and liner verification should be undertaken by an experienced operator. Given the risks involved with the containment of solutions and the fallout associated with possible liner integrity failure, such an operator should be totally au fait with all aspects of the equipment, including its purpose.

The process of electrical surveying has been used for many years and has been successfully applied around the world by Specialist Companies. Such companies have been on an exponential learning curve as they have developed their systems and garnered a complete understanding of the process. Such understanding is often the result of having been exposed to a wide variety of site conditions.

While Electrical Surveying is based on a process of applying a potential to the surface of a membrane, measuring the return current and using a mathematical formula to calculate the approximate area of damage to the membrane, site conditions have the propensity to significantly affect outcomes. The complexity of site conditions, which range from the geotechnical through to metallurgic and atmospheric, are much more complicated than is generally perceived.

Simple circuitry equations bear little significance in the field. The process is very effective in simple applications, particularly when the elements of the circuit are simple, but when the complexity of circuit is affected by the introduction of multiple components (some of which act differently and change resistance when a potential is applied), it is then that changes occur within the process. The test has, under such circumstances, the potential to evolve from a simple test to a complex situation which requires a greater analytical skill.

The industry now faces significant risk to its integrity. Currently, the impartation of small amounts of knowledge to a handful of people with little or no specialist experience, has resulted in such individuals promoting themselves as having the skills to understand and undertake the necessary tasks. Sadly, where results are often open to interpretation, as is the case in the electrical testing of liner integrity, small amounts of knowledge and limited experience can often count for nought when site conditions vary as constantly as they have been known to do.

As a consequence, the industry is in danger of a growing misinterpretation of testing results, and such a situation has the potential to damage the reputation of the process itself as a result, to say nothing of the possible ramifications to in situ products and the solutions contained within them.

Recently, I encountered a lining contractor who advised his client that his company had ***“bought the equipment, and the process is so simple that we will undertake all of our own testing and save money”*** (sic) The contractor likened the electrical surveying process to that of simply throwing a wire into a pond and wandering around, with the equipment locating any holes by itself This attitude of those uninformed contractors can be challenged by asking them if welding was simply a matter of putting metal together and glueing it with a machine. Ignorance is no excuse, as the likelihood of irreparable damage to the industry is high and the effect this can have on the industry as a whole is of great concern.

As geomembranes are applied to a growing variety of complex installations, which in turn have their own idiosyncratic requirements for performance owners and regulators are continually being challenged to ensure testing is appropriate and exhaustive.

In our consistently evolving world of scientific geomembrane testing, we are duty bound to ensure that the applied technology takes all complexities into consideration, and that Research and Development must include the knowledge and experience of those operators who are well aware that there is far more to their profession than throwing a wire into liquid and allowing a machine to do the rest.

2. CASE HISTORY

2.1 Background

Phillip Bennett is an Australian geomembrane consultant, with over 30 years experience in the design, construction and installation of liners and floating covers in the Asia Pacific region. He has been at the coal face of the geomembrane installation industry since its infancy and was responsible for the majority of pioneering design solutions throughout that period. For the past four years, he has worked as a geomembrane consultant, specialising in the electrical survey testing of lined containment installations. Part of his work in this field has involved the research and development of cutting edge survey equipment in Australia, Europe and the USA.

The focus of this paper is on one particular situation, wherein the client required verification of a pond's integrity in order to satisfy regulatory license conditions.

2.2 Site Description

The site, situated in remote northern Queensland, Australia, comprised a 35,000m² lined pond, which was a process storage pond for coal seam gas extraction, containing a saline solution of approximately 7000ppm. The pond's construction was a cut and fill with both a clay liner and 2.00mm HDPE liner, the latter being buried in an anchor trench. There were no perforations, appurtenances or liner incursions and all fill and discharge took place over the perimeter of the pond. The installation itself was similar to numerous other installations, all of which had been undertaken without any difficulty in locating potential holes. in the membrane..

The liner was installed by a reputable company, which has previous experience in the installation of the material. The specifications were written by a large consulting engineering company and were compliant with GRI Test Method GM 13⁴ and GRI Test Method GM19⁵ standards. Additionally, all appropriate CQA paperwork was in order.

2.3 Problematic Set-Up

Initial set-up for the survey was expected to be 'text book', in accordance with ASTM 7002 and ASTM.D 7007. Generally, the survey would consist of the application of a potential into the solution or onto the surface of geomembrane liner and, and mapping the electrical currents. A calibration puck was used to set the parameters and to represent the electrical fields that could be generated from a hole in the liner. Once the signals were established, standard procedure was to proceed in a methodical fashion to detect any anomalies or leaks in the geomembrane. Due to the exacting nature of the work and the size of the installation, it was realistic to expect the process to take approximately five days.

It became clear almost immediately that the survey equipment was unable to locate the calibration puck and could not maintain a stable voltage, thus disabling the entire process. Following a Standard Operating Procedure in the first instance, the survey equipment was checked to ensure it was in functioning order and that operator fault was not the cause.

2.4 Site Anomalies

Once it was established that the survey equipment was functioning within normal parameters, the site itself was considered as the most likely contributor to the situation, and the entire installation required forensic investigation to determine the solution. Methodical investigation revealed a number of abnormalities both in the installation and in the site conditions, each of which fell outside the parameters of what could be considered a 'text book' installation. Each of these abnormalities contributed to the overall problem, these being:

- The contained solution was of a high saline concentration (5500ppm);
- The contained solution also carried a high mineral content (Soil conductivity-1-2Ohms/m;
- Sedimentation in the base of the pond had a very high mineral content;
- The liner's sub grade contained a high mineral content;
- The combined high saline and mineral content in the pond as a whole produced an electrical potential of its own (acting as a battery);
- The configuration and assembly of the pond itself resulted in the installation acting as a capacitor, the result of the presence of conductive material on both sides, with insulation material between;
- Holes within the geomembrane;
- At the time of construction, liner installation technicians had discarded a roll remnant (which contained metal staples) under the liner itself which, when compounded by the pressure of the contained solution, resulted in 12 small holes.

3. SOLUTION

Initially the potential applied to the pond was relatively low approx 30 volts and at this level the voltage was relative stable but it was impossible to locate the artificial puck , the voltage was slowly increased in 10 volt DC increments and the calibration was attempted and in each instance location of the puck was impossible unless you were almost directly over the puck.

As the potential was increased the ability to locate the puck became better but not sufficient to allow a survey. When the potential reached just over 100 volts DC the voltage became very unstable.

The potential was increased through a range of voltages until just over 300 Volts DC which did allow better ability to see the calibration puck but the signals on the meters were also very unstable and not suitable to carry out a survey.

Once all contributing factors were identified, compensatable measures were taken with the survey equipment. The resistance on the earth return to the DC power supply was increased and the circuitry was altered to accommodate the capacitor effect created by the pond, thus achieving a stable voltage and current. At this point, it was possible to locate the artificial calibration puck and commence the survey.

Following the achievement of a stable voltage, surveyors discovered a relatively low voltage present with a high current, indicating the liner had been compromised with a number of small holes or a large hole. This was due to the presence of the abovementioned 12 staples in the discarded liner off cut. The metal staples under the liner were systematically located and subsequently sealed, thus negating their effect on the installation and making it possible to complete the survey and certify the liner's integrity.

4. CONCLUSION

The situation was brought about by a culmination of anomalies at the site, rather than one specific problem. Addressing the first anomaly identified and accepting it as the sole cause would have resulted in a failure to correctly diagnose and rectify the low voltage/high current situation. It was only through the systematic application of a logical, diagnostic procedure that the surveyors were able to arrive at both a conclusion and a solution to what may have been an insurmountable problem. The invaluable experience has subsequently led to the formulation of a procedural diagnostic regime that will assist in the field in future endeavours.

Photos



Fig 2. Typical HDPE lined CSG water pond



Fig 3. DC Generator and leads for applying electrical potential to the pond



Fig 4. Mobile recording and monitoring equipment on site



Fig 5. Testing utilising ASTM 7007 wading probe method



Fig 6. Testing utilising ASTM 7703 water lance method .

REFERENCES

- ASTM D7002-10, Standard Practice for Leak Location on Exposed Geomembranes Using Water Puddle System.
- ASTM D7007-09, Standard Practice for Electrical Methods for Locating Leaks in Geomembranes Covered with Water or Earth Materials.
- ASTM D7703-11, Standard Practice for Electrical Leak Location of Exposed Geomembranes Using the Water Lance System.
- GRI Test Method GM19, Seam Strength and Related Properties of Thermally Bonded Polyolefin Geomembrane, Revision 6, October 2011, The Geosynthetic Institute.
- GRI Test Method GM13, Test Methods, Test Properties and Testing Frequency for High Density Polyethylene (HDPE) Smooth and Textured Geomembranes, Revision 11, December 2012, The Geosynthetic Institute.

The Mechanics of Filter Cake Formation on a Geotextile

J. Richard Weggel, Ph.D., P.E., Department of Civil, Architectural and Environmental Engineering, Drexel University, USA, weggel@drexel.edu

Nicholas D. Ward, Ph.D., Otago Computational Modeling Group Ltd, New Zealand, nick@ocmo.co.nz

ABSTRACT

A numerical model describing the accumulation of suspended sediment on a geotextile is developed for both a colloidal suspension and for sediment that includes larger settleable particles. The model is solved using an Excel spreadsheet and is presented for a sediment comprised of 5 separate size components; however, the model can be easily expanded to more components. The time-varying rate of flow through the geotextile/sediment system is predicted along with the rate of accumulation of filter cake. The permeability of the two layer system is given as a function of time as it increases in thickness. The model has been verified experimentally using a settling tube by measuring the rate of discharge from the tube with time. Verification of the model is presented for three sediments: Ottawa sand, a fine sand and Plasti-grit, a low density plastic abrasive used for sand blasting. The model also allows the size distribution of the sediment at various levels in the filter cake layer to be estimated. A parametric analysis of the model investigates: (a) the occurrence of a clear water interface in the slurry, (b) the application of a vacuum to increase the rate of filtration and sediment deposition and dewatering, and (c) the effect of flocculants on the dewatering process. The relative importance of the geotextile vis-à-vis the sediment in the dewatering process indicates that sediment characteristics are usually more important than geotextile characteristics.

1. INTRODUCTION

Large geotextile bags are increasingly being used to dewater dredged material and mine tailings (Gaffney, et al., 1999; Gaffney & Wynn, 2004 and Weggel et al., 2010). As the water passes through the geotextile, solids in the slurry are retained on the surface of the geotextile. As the thickness of the accumulating filter cake increases the dewatering rate decreases. Thus, as time passes, the dewatering efficiency of the system decreases. The rate of flow through the filter cake depends on the permittivity of the geotextile, the permeability of the filter cake and its thickness. At the start of the dewatering process the permittivity of the geotextile can be important; however, as the filter cake's thickness increases, the permeability of the filter cake controls the dewatering rate. Weggel & Ward (2011) presented a numerical model that describes the accumulation of filter cake on a geotextile. The equations are solved numerically using an Excel spreadsheet to give the discharge through the geotextile-filter cake layers, the decrease in head, the cumulative discharge and the thickness of the filter cake, all as functions of time. In addition, the distribution of sediment grain size at various layers in the filter cake can be determined given the size distribution of the sediment in suspension at the start of the process. Thirty-four experiments were conducted with two geotextiles and three different sediments to verify the theory. The geotextiles used were Propex 135ST (Geotextile A) and Propex 315ST (Geotextile B), both with permittivities reported by the manufacturer as 0.05 s^{-1} . Table 1 presents the hydraulic properties of the geotextile as reported by the manufacturer. The sediments used were a well-sorted Ottawa sand, a fine sand and a well-graded, light weight plastic material (Plasti-grit).

2. THEORY

Details of the theory are presented in Weggel & Ward (2011). A summary is presented here along with the explicit numerical equations.

Application of Darcy's law to vertical flow through a two layer system gives the permeability of a geotextile/filter cake system, K_{system} , as,

$$K_{system} = \frac{z}{\left\{ \frac{1}{\Psi} + \frac{z}{K} \right\}} \quad [1]$$

in which z = the thickness of the filter cake, K = the permeability of the filter cake and Ψ = the permittivity of the geotextile. Hence the flow through the two layer system is,

$$q = \frac{h}{\left\{ \frac{1}{\Psi} + \frac{z}{K} \right\}} \quad [2]$$

where q = the flow through the geosynthetic/filter cake system per unit area and h = the head. See Figure 1 for a definition of terms. Note that the head is measured from the top of the filter cake and not from the top of the geotextile; therefore the head decreases because both the slurry level drops and because the filter cake thickness increases.

Table 1 Hydraulic Properties of Geotextiles

Property	Test Method	Geotextile A	Geotextile B
Material		Polypropylene	Polypropylene
Permittivity	ASTM D-4491	0.05 s-1	0.05 s-1
Water Flow Rate	ASTM D-4491	160 l/min/m ²	160 l/min/m ²
AOS	ASTM D-4751	0.6 mm	0.425 mm

Table 2 Sediment Characteristics

Ottawa Sand, SG = 2.65, ρ = 2650 kg/m³		
Geometric Mean (mm)	%	Settling Velocity (cm/s)
0.7140	97	7.875
Fine Sand, SG = 2.62, ρ = 26.20 kg/m³		
Geometric Mean (mm)	%	Settling Velocity (cm/s)
0.1057	20.2	0.0834
0.1930	76.0	2.2440
0.2725	3.0	3.4753
0.3532	0.6	4.5424
Plasti-grit, SG = 1.17, ρ = 1170 kg/m³		
Geometric Mean (mm)	%	Settling Velocity (cm/s)
0.0690	10.8	.00119
0.2470	26.7	0.00151
0.3615	35.8	0.03219
0.5288	20.5	0.06767
0.7736	3.2	0.13780

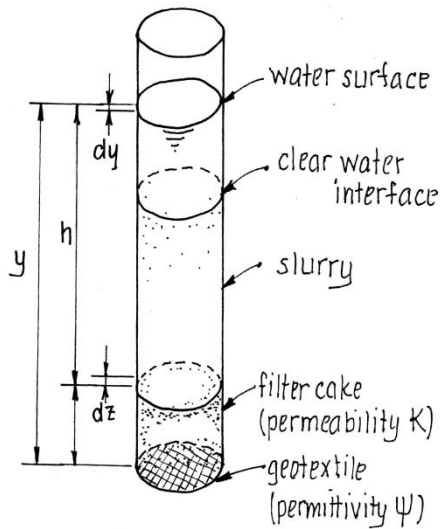


Figure 1 Definition of Terms

Filter cake thickness increases because of advection (the downward fluid flow carries sediment) and because the sediment settles. Advective transport depends on the rate of downward flow while the particle settlement rate depends on grain size. In the present numerical solution sediments have been characterized by six discrete size classes; however, the model can be expanded to accommodate any number of size classes. The six sizes used here include a "colloidal" component which does not settle but is transported only by the downward flow (advection) and five sizes which are transported by both advection and settlement. The solution progresses by stepping through time in Δt steps with successive values of the variables calculated from values at the preceding time step.

The flow through the system at the start of filtration is given by,

$$q_0 = \frac{h_0}{\left\{ \frac{1}{\Psi} + \frac{z_0}{K} \right\}} = \frac{y_0 - z_0}{\left\{ \frac{1}{\Psi} + \frac{z_0}{K} \right\}} \quad [3]$$

in which q_0 = the initial flow rate, h_0 = the initial head, y_0 is the initial height of the slurry level above the geotextile, z_0 = the initial thickness of the filter cake, Ψ = the permittivity of the geotextile and K = the permeability of the filter cake. The initial head is the height of the slurry surface above the top of the filter cake. The initial cumulative discharge is,

$$q_{cum0} = 0 \quad [4]$$

The initial water level in the tube is y_0 and the water level one time step, Δt , later is,

$$y_n = y_{n-1} - q_{n-1} \Delta t \quad [5]$$

The rate at which the thickness of the filter cake increases is given by,

$$\frac{dz}{dt} = \left\{ \frac{\alpha_o}{\varepsilon} + \sum_i \frac{\alpha_i}{\varepsilon} \right\} q + \sum_i \frac{v_i \alpha_i}{\varepsilon} \quad [6]$$

in which α_i = the volumetric solids concentration of the i^{th} component in the slurry, ε = the solids fraction of the accumulated filter cake (1 – porosity), v_i = the settling velocity of the i^{th} component of the slurry material. The first term on the right hand side of Eq. 6 is the advective transport while the second term is the particle settlement term. Taking a finite difference discretization, Eq. 6 becomes,

$$z_n = z_{n-1} + \left\{ \frac{\alpha_o}{\varepsilon} + \sum_i \frac{\alpha_i}{\varepsilon} \right\} q_{n-1} \Delta t + \sum_i \frac{v_i \alpha_i}{\varepsilon} \Delta t \quad [7]$$

where the subscript $n-1$ indicates a value at the previous time step and n the value Δt later. The flow rate is given by,

$$q_n = \frac{(h_n + h_{n-1})}{2} \left\{ \frac{1}{\frac{1}{\Psi} + \frac{(z_n + z_{n-1})}{2K}} \right\} \Delta t \quad [8]$$

where

$$h_{n-1} = y_{n-1} - z_{n-1} \quad [9]$$

and

$$h_n = y_n - z_n \quad [10]$$

which can be evaluated using values obtained from equations [5] and [7]. The cumulative discharge through the two-layer system is,

$$q_{cum(n)} = q_{cum(n-1)} + \frac{q_n + q_{n-1}}{2} \Delta t \quad [11]$$

The final thickness of the filter cake after all i components have accumulated is,

$$z_{\infty} = h_0 \sum_i \frac{\alpha_i}{\varepsilon} + z_0 \quad [12]$$

Given initial conditions for y_0 and z_0 (and thus h_0), equations [3] through [11] can be solved successively to yield the change in discharge and filter cake thickness with time. The dimensionless parameters, $\Psi y_0/K$, $g\Psi^2/y_0$ and the values of α_i/ε for the sediment components characterize the solution. $\Psi y_0/K$ is a measure of the relative importance of the geotextile's permittivity compared with the filter cake's permeability and $g\Psi^2/y_0$ is a dimensionless permittivity.

The model assumes that the size components comprising the slurry are completely mixed and uniformly distributed throughout the column at the start of the process.

3. EXPERIMENTS

3.1 Geotextiles

Two woven polypropylene geotextiles (Geotextile A and Geotextile B) were used for the experiments. They were selected for their low permittivities. Their hydraulic characteristics, as reported by the manufacturer, are given in Table 1.

3.2 Sediments

Three sediments were used in the experiments: Ottawa sand, a fine quartz sand and Plasti-grit. (Plasti-grit is a commercially available plastic material with a specific gravity of 1.17 used for sand blasting.) The Ottawa sand was characterized by a single size, the fine sand by four sizes and the Plasti-grit by five sizes. The size characteristics of the three sediments are given in Table 2. Of the three sediments, Plasti-grit most closely approximates the size and sedimentation rates characteristic of sediments being dewatered. The Plasti-grit size distribution is given in Figure 2 and the five sizes used to characterize it are shown in the histogram of Figure 3. Settling velocities were determined from the Rubey (1933) equation,

$$v_i = \left\{ \sqrt{\frac{2}{3} + \frac{36v^2}{gd_i^3(\rho_s/\rho - 1)}} - \sqrt{\frac{36v^2}{gd_i^3(\rho_s/\rho - 1)}} \right\} \sqrt{gd_i(\rho_s/\rho - 1)} \quad [13]$$

in which v_i = the settling velocity, d_i = the particle diameter, ρ_s = the density of the sediment, ρ = the fluid density and g = the acceleration of gravity. The equation is valid for any consistent set of units.

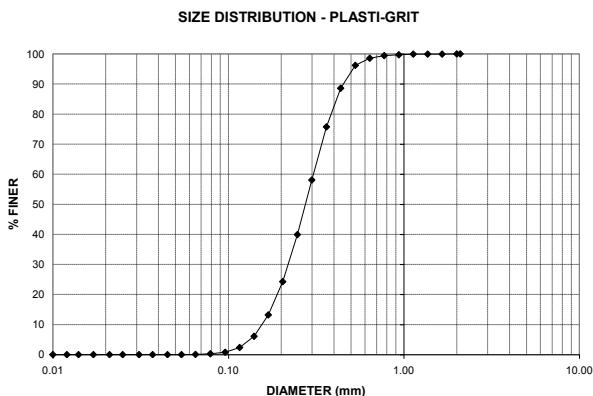


Figure 2 Plasti grit Size Analysis for Plasti-grit



Figure 3 Histogram for Plasti-grit

3.3 Experiment Protocol

Details of the experiments are given in Weggel & Dortch (2011) and are summarized here. The experiments were conducted using a 4.46-cm (1.756-inch) inside diameter Plexiglas settling tube approximately 1.37 meters (4.5 feet) long. See Figures 4 and 5. A scale graduated in inches was taped to the side of the tube. The geotextile was fastened to the bottom of the tube with a hose clamp. Initial experiments were conducted without sediment in order to determine the permittivity of the geotextile. The bottom of the tube was placed on the floor on a large diameter rubber stopper and filled

with water. (The stopper diameter was larger than the outside diameter of the tube.) The stopper and tube were picked up and placed over a receiving basin, the stopper was removed and the time for the water surface to pass various levels on the graduated scale recorded. In effect, the system was a falling head permeameter. While this is not a standardized test for determining permittivity, it was deemed appropriate to determine the permittivity *in situ* rather than in a separate test. Permittivity was determined by plotting water level against time with water level on a logarithmic scale. An exponential curve was fitted to the data with the permittivity found from the exponent. Figure 6 presents a typical plot for Geotextile A for four tests. Permittivity values found for Geotextile A ranged from $\Psi = 0.0532$ to 0.0585 s^{-1} and from $\Psi = 0.1571$ to 0.1613 s^{-1} for Geotextile B.

Essentially the same procedure was used in subsequent experiments with sediment; however, an additional stopper with a hole was inserted into the top of the tube. The bottom of the tube was placed on the large stopper; a measured quantity of sediment placed in the tube and water added to fill the tube. The tube and stoppers were picked up and the system shaken until the sediment appeared to be evenly distributed throughout the water column. It was difficult to achieve a uniform distribution of sediment through the fluid for the Ottawa sand because of its high settling velocity. It was somewhat difficult for the fine sand but the distribution was observed to be more uniform than for the Ottawa sand. A uniform distribution was achievable with the Plasti-grit. The tube was placed over the receiving basin, the bottom stopper removed and the time for the water surface to pass various levels on the graduated scale measured. After water stopped draining from the system, the weight of water released was recorded and the thickness of the sediment in the bottom of the tube measured to the nearest 0.25 cm (0.1 inch). The thickness of the accumulated sediment filter layer was sensitive to any subsequent disturbance of the tube. If, following a test, the tube was disturbed, the sediment consolidated and its thickness decreased; consequently, for some tests, several sediment thicknesses were recorded. The basic data obtained from each test was: the water level as a function of time, the weight of the sediment introduced, the weight of the water released and the final thickness of the sediment layer. Some small amount of water was retained in the pores of the accumulated sediment at the end of a test; however, the amount of water remaining in the filter cake was small relative to the amount in the initial water column.

4. EXPERIMENTAL RESULTS

Thirty-four experiments were conducted, 18 with Geotextile A and 16 with Geotextile B. Of these, 13 were conducted with only water to determine the permittivity of the geotextile while 21 were conducted with sediment.

4.1 Permeability of the Geotextile/Filter Cake System

The permeability of the accumulating filter cake sediment was determined from the final permeability of the geotextile/filter cake system and the permittivity of the geotextile using the equation,

$$K = \frac{z}{\left\{ \frac{z}{K_{sys}} - \frac{1}{\Psi} \right\}} \quad [14]$$

which is the inverse of Eq. [1]. K_{sys} was determined from the rate of water level decline near the end of a test when all of the sediment had accumulated.



Figure 4 Experimental Setup

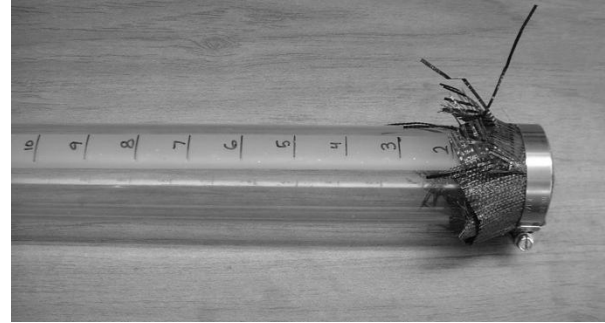


Figure 5 Settling Tube

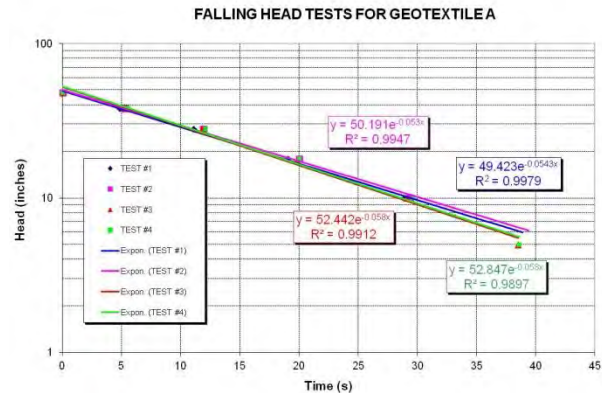


Figure 6 Settling Tube Permittivity Measurements

Figures 7 through 9 present typical experimental results compared with theory for three tests. Figure 7 is for Ottawa sand and Geotextile A; Figure 8 is for the fine sand and Geotextile B while Figure 9 is for the Plasti-grit and Geotextile A. The figures show the variation with time of y = the water level in the tube, q = the flow through the system, q_{cum} = the cumulative volume of flow through the system and z = the thickness of the accumulating filter cake. Only theoretical values for z are given since only the final thickness of the filter cake was measured.

Agreement between theory and experiment is generally very good; however, the agreement for Ottawa sand is not as good as for the fine sand and Plasti-grit due to the speed at which the Ottawa sand settled during the experiments. Initially, comparisons were made assuming that the initial sediment thickness was zero; however, the rapidity with which the Ottawa sand settled and the likelihood that it was not completely mixed throughout the water column at the start of the experiment made it necessary to assume an initial sediment thickness. The Ottawa sand settled so quickly that a significant amount accumulated before the first timing interval - in some cases the entire amount in suspension. The fine sand also accumulated relatively quickly while the Plasti-grit, because of its low specific gravity and fine size distribution, accumulated slowest. In plotting the data and theory, several variables were adjusted to give the observed fit: (a) the permittivity of the geotextile (although it was close to the value reported by the manufacturer), (b) the permeability of the filter cake and (c) the initial thickness of the filter cake. For Figure 7 (Ottawa sand), $\Psi = 0.070 \text{ s}^{-1}$, $K = 0.610 \text{ cm/s}$ and $z_0 = 5.80 \text{ cm}$. For Figure 8 (fine sand), $\Psi = 0.05 \text{ s}^{-1}$, $K = 0.0290 \text{ cm/s}$ and $z_0 = 1.52 \text{ cm}$. For Figure 9 (Plasti-grit), $\Psi = 0.050 \text{ s}^{-1}$, $K = 0.0152 \text{ cm/s}$ and $z_0 = 2.13 \text{ cm}$.

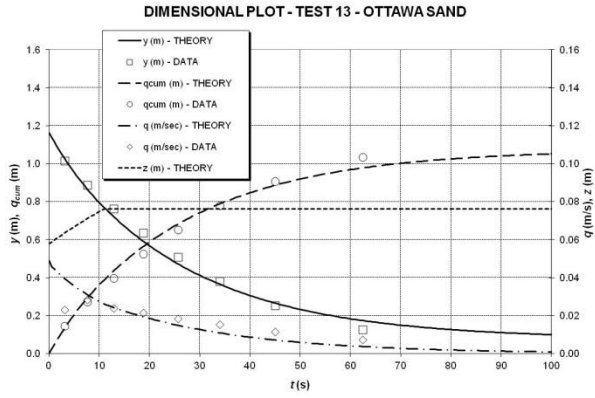


Figure 7 Experimental Results for Ottawa Sand and Geotextile A, $\Psi = 0.07 \text{ s}^{-1}$, $K = 0.610 \text{ cm/s}$, $z_0 = 5.79 \text{ cm}$.

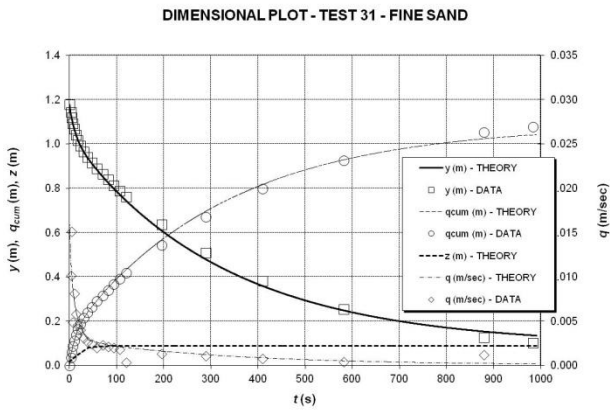


Figure 8 Experimental Results for Fine Sand and Geotextile B, $\Psi = 0.05 \text{ s}^{-1}$, $K = 0.029 \text{ cm/s}$, $z_0 = 1.52 \text{ cm}$.

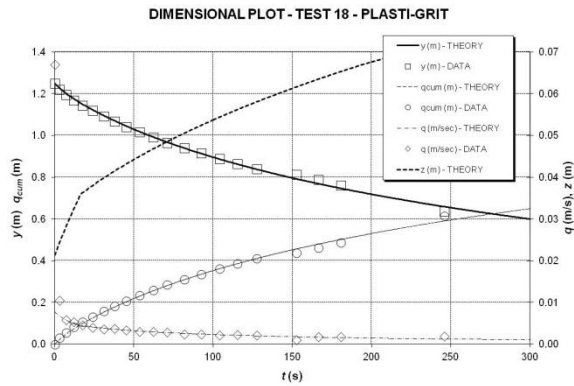


Figure 9 Experimental Results for Plasti-grit and Geotextile A, $\Psi = 0.05 \text{ s}^{-1}$, $K = 0.0152 \text{ cm/s}$, $z_0 = 2.13 \text{ cm}$.

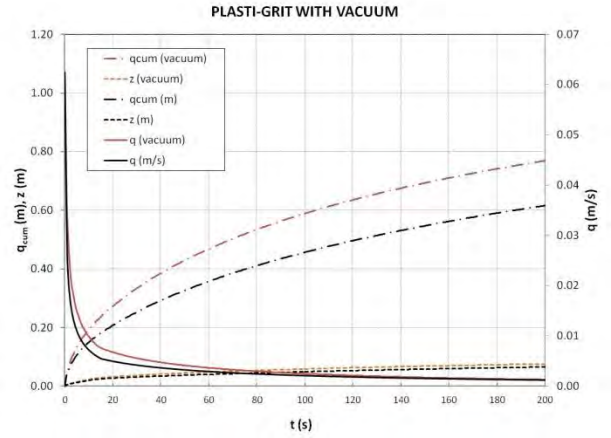


Figure 11 Simulated Effect of a Vacuum on Dewatering Rate

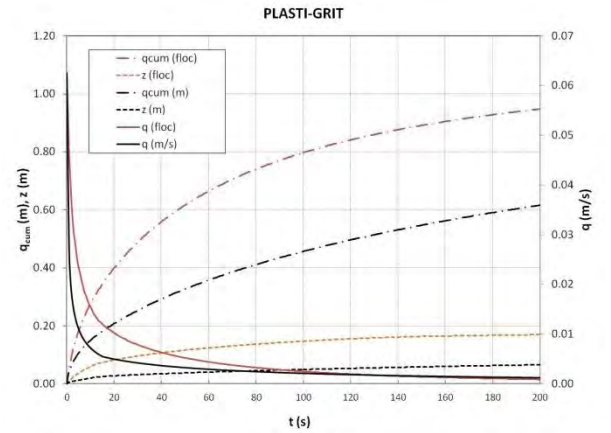


Figure 12 Effect of a Flocculant on Dewatering Rate

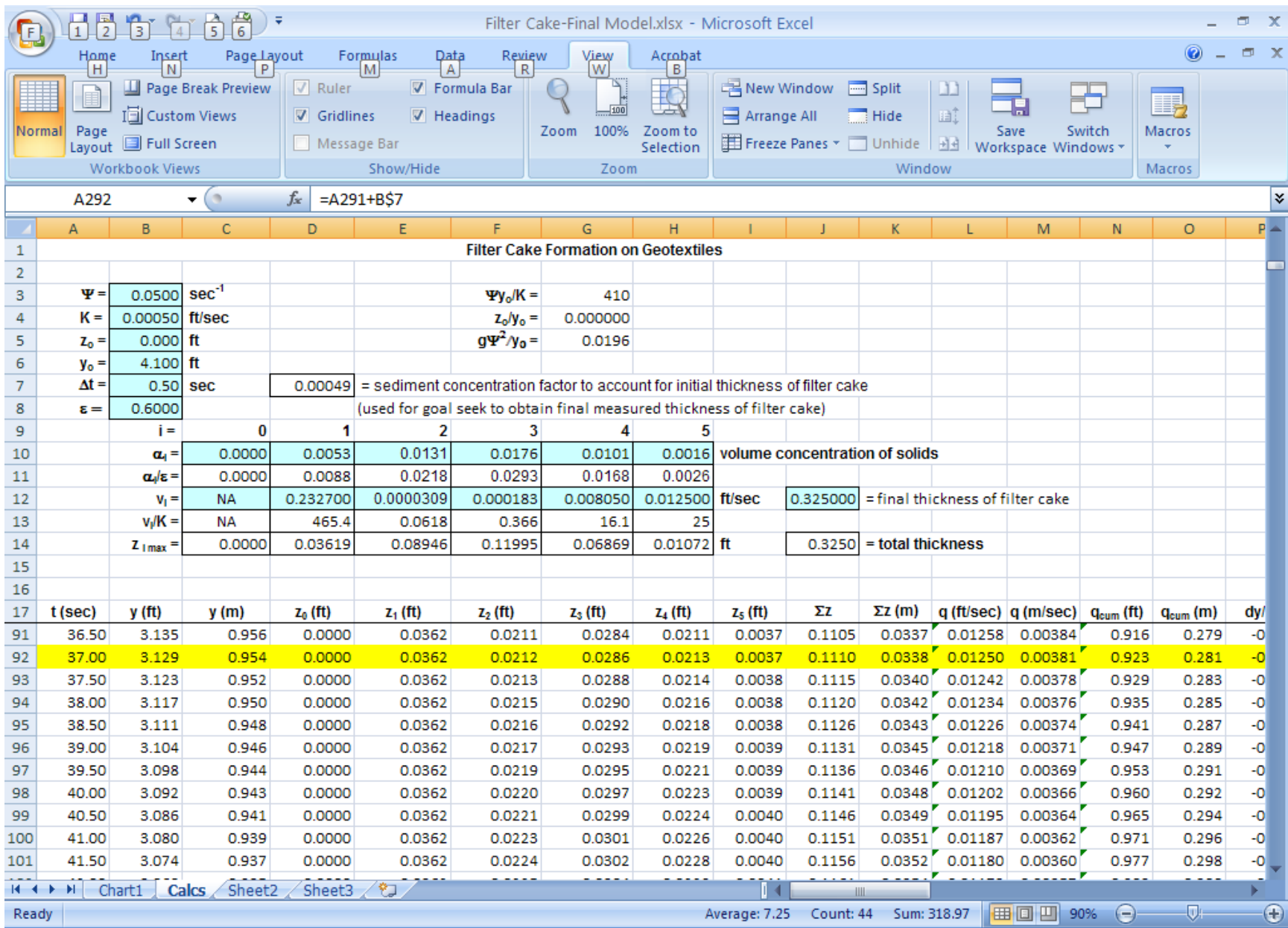


Figure 10 Screen Shot of Excel Program – Plasti-grit Example

5. PARAMETRIC STUDY OF PLASTI-GRIT RESULTS

The Excel model used for Plasti-grit is used here to demonstrate the capabilities of the model. Figure 10 presents a screen shot of the Excel spreadsheet for Plasti-grit. The shaded cells at the top of the sheet are input data. For the example, $\Psi = 0.005 \text{ s}^{-1}$, $K = 0.0005 \text{ ft/s}$ (0.000152 m/s) and $z_0 = 0$. (Figures 2 and 3 present the size distribution for the Plasti-grit and the five components used to characterize it.) Settling velocities shown in cells C12 through H12 were approximated using Eq. 13 (Rubey, 1933).

5.1 Size Distributions in Sediment Layers

The model allows the size distribution of sediments to be determined for various sediment layers. For example, with reference to Figure 10, the cumulative thickness of sediment is given in column J. Between $t = 37 \text{ s}$ and $t = 41.5 \text{ s}$ (rows 92 and 101 of the spreadsheet) the total accumulation of sediment is $0.0352 - 0.0338 = 0.0046 \text{ ft}$ (1.402 mm). The accumulation of size Class 1 (Column E) is $0.0362 - 0.0362 = 0 \text{ ft}$ (0 mm) since this entire size component settled in less than 30 s. The percent accumulation in size Class 2 (column F) is $0.0224 - 0.0212 = 0.0012 \text{ ft}$ (0.366 mm). Similarly the accumulation in size Class 3 (Column G) is $0.0302 - 0.0286 = 0.0016 \text{ ft}$ (0.488 mm), size Class 4 (Column H) is $0.0228 - 0.0213 = 0.0015 \text{ ft}$ (0.457 mm) and size Class 5 (Column I) is $0.0040 - 0.0037 = 0.0003 \text{ ft}$ (0.091 mm). Thus the percent of the total in size Class 1 is 0%, size Class 2 is $(0.0012/0.0046) \times 100 = 26\%$; size Class 3 is $(0.0016/0.0046) \times 100 = 35\%$; size Class 4 is $(0.0015/0.0046) \times 100 = 33\%$ and size Class 5 is $(0.0003/0.0046) \times 100 = 6\%$. These percentages can be compared with the original size distribution given in Table 2. (Class 1 is the coarsest fraction.) Note that the bottom layers of sediment are near the top of the spreadsheet since that accumulate first. For the example, the layer is 0.1110 ft (0.0338 m) above the geotextile.

5.2 Clear Water Interface

A clear water interface will occur in the slurry when the settling rate of the finest sediment component exceeds the rate at which the slurry level is declining. A clear water interface will generally occur for filter cakes with low permeabilities and/or high settling rates. The time when the clear water interface arises can be estimated by calculating the rate of the slurry surface decline, $q = dy/dt$, and comparing it with the settling rate of the finest component of the sediment. When q becomes less than v_i , where v_i is the settling velocity of the finest sediment, the clear water interface appears. The height of the clear water interface at any time can be calculated as the difference between the two velocities q and v_i times the elapsed time.

For the Plasti-grit example of Figure 10, the settling velocity of the finest component is 0.00381 m/s (0.0125 ft/s, cell H12). The rate of slurry level decline equals this velocity when $y = 0.953 \text{ m}$ (3.129 ft, cell B92) and $t = 37.0 \text{ s}$ (cell A92); hence the clear water interface arises at this time. One hundred seconds later, at $t = 137 \text{ s}$ the slurry surface has declined from 0.953 m (3.129 ft) to 0.708 m (2.323 ft) = 0.245 m (0.803 ft) while the clear water interface has declined $(0.00381 \text{ m/s}) \times (100 \text{ s}) = 0.381 \text{ m}$ (1.25 ft) giving the height of clear water as $0.953 - 0.245 = 0.708 \text{ m}$ (3.129 - 0.803 = 2.326 ft).

5.3 Vacuum Filtration

The model can be “tweaked” to yield results if a vacuum is applied downstream of the geotextile to increase the filtration rate. This can be done by artificially increasing the permeability of the system. The effect of applying a vacuum is to increase the head driving the flow without increasing the travel distance of the sediments through the slurry to the filter cake. The vacuum-induced rate of flow can be simulated by increasing the permeability of the geotextile/filter cake system. Since Darcy’s law is linear in head and permeability, the permeability can be increased to simulate an increase in head. Thus,

$$\frac{K_v}{K} = \frac{h_2}{h} \quad [15]$$

where K_v = the “artificial” permeability for the vacuum head (the increased head due to applying the vacuum), h = the actual head without the vacuum, and K = the actual permeability of the system. Letting $h_2 = h_v + h$ where h_v is the added head due to the vacuum,

$$K_v = K \left(1 + \frac{h_v}{h} \right) \quad [16]$$

It is not possible to allocate the increased permeability between geotextile and sediment without assigning a thickness to the geotextile. Fortunately, however, the greatest impedance to flow is usually due to the filter cake. Thus K can be increased assuming Ψ remains the same. This introduces some error at the start of the calculations until a small layer of filter cake

accumulates. (Note that if z/K_v approaches $1/\Psi$ for typical values of z , errors may be substantial. Normally this only occurs at the start of filtration.) For example, using the Plasti-grit model in Figure 10 and applying a vacuum head of 1 meter of water with an upstream head of 1.25 m (4.10 ft) and $K = 0.000152$ m/s (0.0005 ft/s). Applying Eq. 16, $K_v = 0.000152(1 + 1/1.25) = 0.000274$ m/s (0.0009 ft/s). The effect of the vacuum on the flow rate and cumulative flow is shown in Figure 11. The effect is to increase the dewatering rate, q_{cum} , shown as the light colored lines in the figure.

5.4 The Role of Flocculants in Dewatering

Chemical flocculants are often added to slurries to accelerate the dewatering process. Flocculants impact the process in several ways. The permeability of the accumulating floc is usually much greater than the slurry itself hence increasing the rate of flow (Koerner & Koerner, 2010). The rate at which the filter layer thickens increases and its final thickness is greater; however, its porosity and permeability are also greater. The settling velocity of the floc is greater than the original fine particles. Increased thickness decreases the rate of flow but this is compensated for by the increase in permeability. For successful flocculation, the benefit of increased permeability and porosity overcomes the increase in filter cake thickness and results in more rapid dewatering. Consequently, appropriately chosen flocculants accelerate the dewatering process. Figure 12 for the Plasti-grit example illustrates the effect of increasing the porosity from 0.4 to 0.7 (reducing ε from 0.6 to 0.3) and increasing the permeability by one order of magnitude from 0.0005 ft/s (0.000152 m/s) to 0.005 ft/s (0.00152 m/s). The thickness of the filter layer is doubled due to the increase in porosity which by itself would decrease the dewatering rate; however, the increase in permeability results in a net increase in the dewatering rate as shown by the light lines on Figure 12.

6. DISCUSSION & CONCLUSION

The equations describing the accumulation of filter cake on a geotextile were developed and solved numerically using an Excel spreadsheet with an explicit Euler finite difference scheme. The solution considers both a colloidal suspension that is transported to the geotextile by advection and sediments with finite settling velocities. The solution gives the head, discharge, cumulative discharge and filter cake thickness as a function of time. The dimensionless parameters that characterize a solution are $\Psi y_o/K$, a measure of the relative importance of the permittivity of the geotextile to the permeability of the accumulating filter cake, $g\Psi^2/y_o$, a dimensionless permittivity, and the values of α/ε , measures of the contribution of each size class to the filter cake's thickness per unit discharge. The rate of filter cake accumulation depends on the flow velocity (discharge) and the settling velocities of the various particles. The size distribution is considered by selecting a number of particle sizes with different settling velocities and different concentrations to approximate the actual size distribution. Coarser particles form the bottom layers of the filter cake while finer particles accumulate in the upper layers. The model allows the size distribution in the various layers of the filter cake to be determined. (Note that a Runge-Kutta numerical solution may also be used to solve the equations. Such an R-K solution has been developed using Matlab; however, the simpler finite difference Excel/Euler numerical version presented herein gives essentially the same results.)

The solution assumes that the colloidal filter cake material does not pass through the geotextile/filter cake but accumulates on it. Depending on the characteristics of the geotextile, it is likely that some or all colloidal material will pass through it at least initially. However, coarser settle-able components of the filter cake will accumulate first and subsequently retain any colloidal material. Thus, at the start of the process some colloidal and very fine sediment may escape through the geotextile while later the accumulating filter cake will retain the fines. Polymer additives are typically used to flocculate and capture colloidal materials. Experiments with various size materials including colloids are needed to further verify the model and establish its limitations. Furthermore, application of the model to the geometry of the geotextile tubes used for dewatering needs to be explored.

Agreement between the numerical theory and the experiments is very good and indicates the success of the theory and numerical model for describing filter cake accumulation on geotextiles. The experiments also indicate that for fine sediments, such as those usually dewatered using geotextile tubes, the model gives excellent results and indicates that the permittivity of the geotextile is normally of secondary importance; the permeability of the accumulating filter cake dominates the process. For coarse, rapidly settling, highly permeable sediments such as Ottawa sand, the permittivity of the geotextile plays a more significant role, at least at the beginning of the process.

In the experiments reported here, the Plasti-grit most closely approximates the type of sediments dewatered because of its relatively slow setting velocity; however, additional experiments need to be performed with finer, more slowly settling sediments to confirm the theory's validity for them. Also, experiments that measure where and when a clear water interface occurs should be conducted to verify the results of the model; experiments with flocculants and experiments with a vacuum application also need to be conducted.

In the present analysis the permeability of the filter cake has been assumed independent of z . It is likely that as filter cake accumulates its overall permeability will decrease. The upper layers of the filter will have a lower permeability since they will

be comprised of finer materials deposited later in the process. Consequently, K will be a function of z and the size distribution of the materials. Also, the solids fraction, ε , or equivalently the porosity, $1 - \varepsilon$, of the accumulating filter cake has been assumed constant in the present analysis with $\varepsilon = 0.6$. However, the solids fraction will vary somewhat depending on grain shape and grain size distribution. It is, however, independent of sediment size.

REFERENCES

- Gaffney, D.A., S.M. Martin, M.H. Maher & T.A. Bennert (1999) "Dewatering Contaminated, Fine-Grained Materials Using Geotextiles" Geosynthetics '99, Boston, MA, April 1999.
- Gaffney, D.A. & J.R. Wynn (2004) "Bag Tests are a Good Field Measurement of Geotextile Tube Performance," International Dredging Review, May/June, 2004. pp 8.
- Koerner, R.M. & G.R. Koerner (2010) "Performance Tests for the Selection of Fabrics and Additives when used as Geotextile Bags, Containers and Tubes," *Geotechnical Testing Journal*, Vol. 33, No. 3, Paper GTJ102686.
- Rubey, W.W. (1933) "Settling Velocities of Gravel, Sand and Silt Particles," *American Journal of Science*, 5th Series, Vol. 25, No. 148, pp 325-338.
- Weggel, J.R., J. Dortch & D. Gaffney, 2010, Analysis of fluid discharge from a hanging geotextile bag, *Geotextiles and Geomembranes*, Vol. 29, pp 65-73.
- Weggel, J.R., & N.D. Ward (2011) "A model for filter cake formation on geotextiles: Theory," *Geotextiles & Geomembranes* 31 (2012) 51-61.
- Weggel, J.R. & J. Dortch (2011) "A model for filter cake formation on geotextiles: Experiments," *Geotextiles and Geomembranes* 30 (2012) 62-68.

Upper Chiquita Reservoir Floating Cover and Liner

Andrew Mills, Layfield Environmental Systems Corp, USA, amills@layfieldgroup.com
Sven Falk, Layfield Environmental Systems Corp, USA, sfalk@layfieldgroup.com

ABSTRACT

The Upper Chiquita Reservoir is a large potable water reservoir located in Rancho Santa Margarita in Orange County California. The reservoir contains 244 million gallons of domestic water and covers an area of 18 acres. The reservoir was constructed on the western slope of the Chiquita Canyon by creating an earthen dam across the canyon. The reservoir is lined and covered with geosynthetic barrier materials with a defined-sump style cover. This case history details the construction of the reservoir lining and cover system including some of the unusual design details caused by the shape and size of the project. The paper also covers the difficulties caused by the excessive rainfall and the solutions to a leakage issue that developed after construction.

1. INTRODUCTION

1.1 Background

The Upper Chiquita Reservoir is a large reservoir that is part of the Santa Margarita Water District in Southern California. The Santa Margarita Water District (SMWD) is the second largest water district in Orange County covering 52,000 acres of land just east of Mission Viejo and San Juan Capistrano. The SMWD provides water to about 155,000 residents and businesses in Mission Viejo, Rancho Santa Margarita, Coto de Caza, Las Flores, Ladera Ranch, and Talega.

All domestic water supplied to the SMWD has to be purchased from outside sources as there are no local water sources. Most of the region's water is piped from the Diemer Filtration Plant in Yorba Linda. In the past few years the district has experienced major supply disruptions with the unplanned break in the district supply pipeline in 1999, and the additional planned outages of the Diemer Filtration Plant in several recent years. Any disruption in water supply was requiring immediate and severe water conservation measures in the district.



Figure 1: Aerial view of the Upper Chiquita Reservoir under construction.

The main purpose of the Upper Chiquita Reservoir was to increase reserve storage capacity to ensure water security to the customers served by the SMWD. The total installed cost for the investigation, design, and construction of the reservoir was \$53 million and was a shared project between a number of local agencies. These agencies included the SMWD, the City of San Clemente, San Juan Capistrano, Moulton Niguel Water District (Laguna Niguel), and South Coast Water District (Dana Point). The reservoir is operated by the SMWD.

2. THE RESERVOIR



Figure 2: Site visit during the construction of the dam.

the lengthy slopes and contained a drain system to monitor leakage for dam safety purposes.

The Upper Chiquita Reservoir is one of the first large emergency potable water reservoirs to be built in Orange County in decades. It has a design capacity of 244 million gallons (750 acre-feet) and has a surface area of approximately 18 acres. The reservoir is of new construction being built into the side slopes of the Chiquita Canyon. The reservoir was formed by constructing an earthen dam across the mouth of a section of the canyon to create a roughly triangular containment. At its deepest point it is 120 feet deep with side slopes ranging from 3 to 1 up to about 2 to 1. The construction of the reservoir began in June of 2009 and was put into service in October of 2011.

The reservoir has a number of interesting details. The first is the depth and the steepness of the slopes. This led to safety concerns during construction and led to problems in removing rainwater during an exceptionally rainy season.

The second issue was the irregular shape of the containment. Designing a defined-sump floating cover on an unusual shape requires some different techniques. In this case a bench was built into the side slopes at the half-way point. This earthen bench provided a flat surface on which to construct the floats and weights that tensioned the cover. The bench also acted as an intermediate anchor for

3. THE GEOSYNTHETICS

3.1 Geosynthetic Under Drain

A geosynthetic under drain was placed as the first layer of material underneath the entire reservoir. This underdrain was placed to monitor the performance of the lining system and to provide drainage during construction. The underdrain also provided drainage for the earthen dam section. The underdrain consisted of a tri-planar double-sided geocomposite. The core of the geocomposite was 300 mil (7.6mm) thick and was sandwiched between two layers of 8 oz/yd² (270 g/m²) non-woven polypropylene geotextile.

3.2 Geomembrane Lining System

The original specification for the primary geosynthetic barrier system (geomembrane) called for the use of a three-ply 60 mil (1.5mm) Chlorosulphonated Polyethylene (CSPE) geomembrane. During the time of construction there were challenges in the supply of CSPE materials and the lining was changed to a flexible polypropylene material in order to get both the lining and the cover materials delivered on time. The final liner material selected was a 60 mil (1.5mm) thick three-ply fabric-reinforced flexible polypropylene geomembrane (fRPP).



Figure 3: Placement of the geocomposite underdrain.

The fRPP materials for the liner were prefabricated prior to installation according to a detailed panel layout. All seams were welded using a 3" wide wedge welder that bonded the materials together edge to edge without leaving a flap of

material at the seams. In order to reduce creases in the lining material the fabricator on this project used a 36' wide winder to create rolls of fabricated materials that did not require any folds in the material. There is some thought that creases in fRPP materials can lead to stress concentrations that can initiate failures. This is especially problematic in thicker materials such as a 60 mil material. By fabricating without folds this particular fabricator was eliminating this area of potential problems.



Figure 4: 36 ft wide prefabricated liner panels

The liner was anchored to the perimeter of the containment using a concrete stub wall and steel battens. This concrete wall went around the entire perimeter.

Once the lining system was in place the entire area was surveyed using an electrical leak location method. Weather problems prevented the reservoir from being installed in a straight-forward fashion and earthworks, lining installation, and cover installation all took place at the same time in different parts of the reservoir. In order to test areas that couldn't be filled with water the leak location survey was performed with the Water Puddle Method (ASTM D7002). In this method a flow of water is delivered to the survey probe which is directed at the liner. The water is swept across the liner surface and penetrates any defects that are present. Contact with the ground below the liner generates a signal that the operator can use to locate the defect.

3.3 Floating Cover System

The Upper Chiquita Reservoir is one of the larger covered reservoirs in California and also one of the most irregular. The irregular shape is a challenge when designing the method in which the cover will rise and fall in response to water level changes. The design of this cover used the "defined sump" method of construction as first described in US Patent 3,991,900 (1976). A defined sump floating cover uses a series of weighted sumps and floats to maintain tension on the cover material as it changes elevation with water movement. The design of the cover layout needs to maintain continuous tension on the cover at all times to prevent wind damage.

The material used for the cover was a Chlorosulphonated Polyethylene (CSPE) three-ply fabric-reinforced 60 mil (1.5mm). During the construction period for this project the primary supplier of CSPE resins chose to close their plant and supplies of the CSPE resin were restricted. This resulted in allocations of resin which would have impacted the construction schedule. There was sufficient available material for the cover but not for the cover and the liner. That led to the change in the liner from a CSPE to an fRPP material. Note that since the time of this project the secondary manufacturers of CSPE resin have increased capacity to meet demand. CSPE has been used for many floating covers in the California area and has a strong performance record. The CSPE for this project was issued with a 30-year weathering warranty.

The cover system was factory prefabricated to match a detailed panel layout prior to deployment in the field. The normal sequence of operations for cover construction is to complete the liner installation and then to start placing the cover. The cover is usually installed over the entire area of the containment before floats, sump weights, and other details are added. In this project the excessive rain forced changes to this sequence. Since the base of the containment could not be kept free of water the liner and then the cover were advanced down the side slopes with the base remaining open. Only when the base was finally dried out could the liner, and then the cover, be completed.

Layout and location of floats and sump weights is usually accomplished on site once the cover panels are installed and tested. A special bench was included in the earthworks of this project to provide a flat area about half-way down the slopes where the main floats and sump weights for the cover could be constructed. Much of the detail work on the cover took place on this bench while the base of the containment was still too wet for construction. Another adaptation to the weather was to transfer the construction of appurtenances back to the factory. This moved a significant amount of the field labor inside when the weather was poor.

The final cover design covered an area of 900,000 ft² (84,000 m²) and included 18 hatches, 71 air vents, and 40 rainwater removal pumps. Once the cover was completed it was inflated with air using fans on the access hatches. Because of the size of this cover it was inspected in sections. Sand bags were used to isolate sections so that each area was inflated in turn. This reduced the risk of damage in the event of unexpected winds. The cover was 100% inspected from the inside for any defects (defects show as pinholes light). Once the cover inspection was completed the air was released and the cover was ready for service.

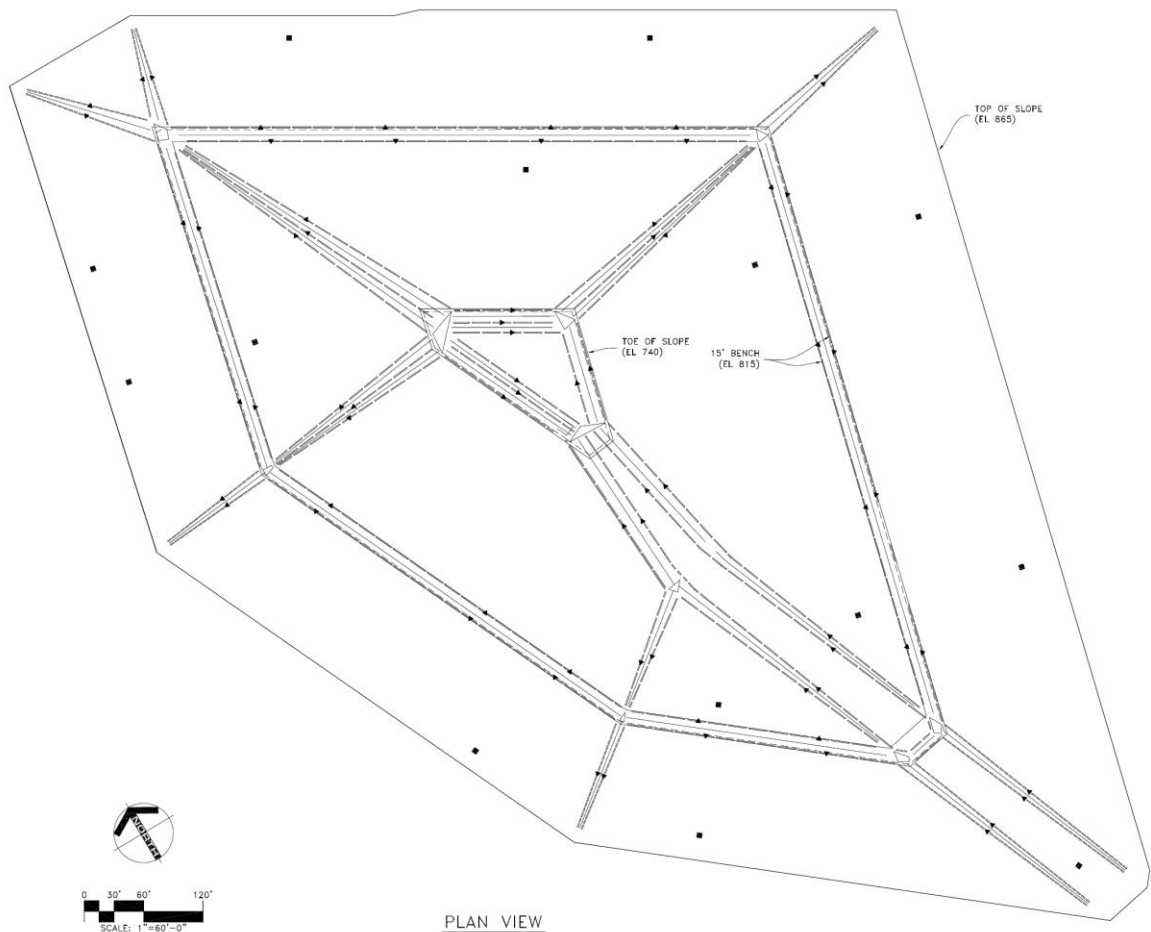


Figure 5: Plan view of cover system showing location of sump channels. Vents are indicated by black squares.

4. THE PROJECT

The Upper Chiquita Reservoir project had actually been started nearly 20 years earlier as part of the long range plans for the water district. There were a number of sites located that were deemed suitable for a large reservoir and environmental studies were begun. These environmental and planning studies started in the 80's and took many years to work their way through the system until this site was selected and approved for a reservoir.

The design of the reservoir has a number of interesting features. The first is the large earth-fill dam that encloses the canyon to create the containment. This dam is designed for stability in the strong earthquake environment of California. The other noticeable detail is the bench about half-way down the slopes. This bench and a road to access the bench was a design feature to improve access for maintenance. The bench lets the operators reach much of the reservoir surface without having to drain the reservoir completely. Part of the design was a concrete trough over 400 feet long from the top of the slope to the toe of the slope. This trough held the pneumatic lines that were used to operate the valves in the bottom of the reservoir. A final feature of the project was consideration given to the construction of the berms so that the reservoir is not normally visible from the nearby busy highway.

The construction of the reservoir started in the summer of 2009 and progressed well until the winter of that year. The winter of 2009/2010 was very rainy and there were many project delays. The large volumes of water kept the base of the reservoir very wet so that the earthworks could not be completed and the lining could not cover the base of the reservoir. The winter of 2010/2011 was even wetter with one particular week seeing over 10 inches of rain. "The rain gauges overflowed three days in a row" said Bart Lantz, project manager for SMWD. This rain event washed out a portion of the

subgrade underneath the liner and a large section of liner had to be removed and the subgrade repaired. Over 200,000 ft² of liner was pulled back to access this repair area. It took more than a month for the earthworks contractor to dry out the site after this rain event.

Finally after many weather delays and significant effort in repairs the liner and cover were complete. The reservoir went into service in October 2011.

5. LEAKAGE

As soon as the reservoir started to fill there was leakage observed in the leak detection system. The leakage started as soon as the reservoir had been filled to the 2 ft level and increased in intensity as the water head increased. The leak was approximately 90 gallons a minute which was higher than the specified leakage rate for this structure. The reservoir was put into service while the leak was evaluated.

The first steps were to send divers into the reservoir to see if they could spot any obvious leakage. Immediately they detected leakage in the concrete trough area that carried the pneumatic lines to the base of the pond. Using underwater epoxy the divers attempted to stop the leaks however there appeared to be too many leaks to stop effectively with this technique.



Figure 7: Pneumatic tubing in concrete trough



Figure 6: Subgrade damage after a significant rainfall event.

At this point the reservoir was needed in service and the leakage repairs had to wait for a suitable opportunity.

6. REPAIR

The opportunity to repair the reservoir occurred in 2012 when the Metropolitan Water District did a week-long shut-down of the Diemer Filtration Plant. This type of shut-down is precisely why the Upper Chiquita Reservoir was built and it supplied water to the region throughout this time. Once the shut-down was completed the reservoir was at a very low level so this was the opportunity to make repairs.

The reservoir was drained and the cover and the liner were cut back to expose the concrete trough. The trough was completely filled with additional concrete and then matched to the surrounding the subgrade. The geocomposite and liner materials were then extended over this sealed trench. The operators of the facility were concerned about the maintenance implications of sealing the pneumatic lines in concrete so a secondary set of pneumatic lines were placed on top of the liner in case they are needed in the future. The facility will operate with the encapsulated pneumatic lines until they malfunction and then a diver can switch the lines over to the newer lines on top of the liner using valves in the reservoir. Once the new lines were completed the cover was repaired and the reservoir brought back into service.

Since the repair the leakage rate fallen to between 9 and 10 gallons per minute which is within the design limits for a project of this size.

7. CONCLUSION

The Upper Chiquita Reservoir is the culmination of a long range plan to ensure water security to Santa Margarita Water District and area users. The reservoir is operating as designed and is not experiencing any further issues. The reservoir is an excellent example of a large covered potable water reservoir typical of the California area.



Figure 8: The Upper Chiquita Water Reservoir of the Santa Margarita Water District filled and in service.

ACKNOWLEDGEMENTS

We would like to acknowledge the participation of the following organizations in this project:

The Santa Margarita Water District
AECOM
Sukut Construction Inc.
Burke Industries Inc.
Carlisle SynTec Inc.

Special thanks to Bart Lantz from SMWD for his contributions to this paper.

REFERENCES

ASTM D 7002. Standard Test Method for Tensile Properties of Plastics, *American Society for Testing and Materials*, West Conshohocken, Pennsylvania, USA. [do not include year since standards are re-published every year]
Volzke, Jonathan (July 7, 2011). Securing the Water Supply, *The San Clemente Times*, Capistrano Beach, CA, USA.
Burke, N. Kutnewsky, D. Price, V. Gerber, D. (1976). Reservoir cover and canalizing means, US Patent #3,991,900, US Patent and Trademark Office, Alexandria, VA, USA.

The Use of a Concrete Composite for a Boat Ramp Extension

John Paulson, P.E. – DISON C & S, LLC, Alpharetta, GA USA, Johnp@rediengineering.com
Rich Pilston - Milliken & Company, Spartanburg, SC USA, Rich.Pilston@Milliken.com

ABSTRACT:

A boat ramp for a recreational lake had outlived its useful life. Constructed in the 1970s this ramp was no longer adequate for the larger and longer boats and recreational craft using the facility in the 21st century. Longer boat trailers would drop off the end of the ramp, requiring specialized equipment to lift and remove trapped trailers. Additionally, the recent drought had magnified the problem with the resulting lower lake levels.

The City had addressed the problem in past years by simply dumping gravel at the ramp end. This solution was temporary, as the gravel would eventually be pushed away from the end of the ramp and build up down below the ramp end. This required frequent maintenance (re-grading the gravel and filling with additional gravel) on an ongoing basis.

As a result, the City began investigating permanent alternatives to solve this problem. The City intended to perform this extension effort using a portion of a state grant. A Geosynthetic Concrete Composite Mat (GCCM) was used to extend the ramp without dewatering.

1. BACKGROUND:

The East Fork Lake in the City of Olney, IL, is a significant recreational draw for boating and fishing enthusiasts. The lake has only one public access boat ramp, which was built in the 1970's to accommodate small fishing boats and recreational watercraft. Over time, as recreational and fishing boat sizes increased, the city found that the ramp was not long enough to accommodate longer boat trailers, especially when water levels in the lake dropped. (Figure 1)

A Conventional solution considered required the construction of a temporary dewatering cofferdam, then construction in the dry. Bids from contractors revealed the cost was in excess of the grant funds provided by the State of Illinois. Faced with a spiraling cost above the grant amount, the city searched for an alternative solution that could be constructed within the budgeted amount. The Geosynthetic Concrete Composite Mat option was identified as an alternative to the conventional approach.



Figure 1 – Boat ramp

2. LITERATURE REVIEW

The published literature was searched to determine past practices in boat ramp construction and enhancement. The following was found.

- a. Design of recreational areas and Facilities – Access and circulation – This engineering manual was developed by the US Army Corps of Engineers and discusses boat ramp construction. Section 4.1 refers to ramps for Existing impoundments stating: “Where additional ramps are required for existing impoundments and it is not feasible or economical to permit construction in the dry, ramps may be constructed on a bank and shoved into the water on a temporary base course.” A figure follows with details of this cast then shoved into place solution. This option was not considered during the evaluation phase.
- b. Extension kits are also a solution, but primarily for temporary extensions that were not considered. Several companies offer these, which consist mainly of parallel rails that are deployed so the boat may be deployed. (Roll N Go website)
- c. Mississippi Agricultural and Forestry Equipment Station publication – describes several means of boat ramp extension including the use of both cast in place and push slabs options. Little detail is provided.

The city of Olney selected two alternatives for further consideration as detailed below.

3. RAMP EXTENSION OPTIONS CONSIDERED:

3.1 Extend the Ramp with Additional Poured Concrete (Dewatering and Casting in the Dry Condition).

The City solicited bids for extending the ramp with poured concrete. This approach required that the contractor build a cofferdam, dewater the area around the ramp, build forms and pour the concrete in the dry, and then allow the concrete to cure for 1-2 weeks. The result would close the lake for 2-3 weeks at a minimum (with the potential for a one-month closure). Bids for this work ran approximately \$58,000, far exceeding the grant budget.

3.2 Extend the Ramp with a GCCM (Construct in the “Wet”).

An alternative approach was to extend the ramp with a prepared gravel bed, capped by a layer of GCCM to provide the hard, trafficking surface, and to protect the prepared gravel subgrade. This approach was estimated to take ~1-2 days to place the composite with the direct material costs expected to be ~\$7,000. With two days of surface contractor (excavator) work and one day of underwater contractor work, the approach appeared to be less costly than extending the ramp with poured concrete, especially since the work could be done under water. In addition, it was expected that the lake would be open within ~1 week of starting the project.

4. DECISION:

The City of Olney chose to extend the ramp using the Geosynthetic Concrete Composite Mat. This would reduce the time the ramp had to be closed, and was estimated to be less costly. The comparison of the two alternatives is listed below.

APPROACH USING COFFERDAM - DEWATERING, FORMING & POURING CONCRETE IN THE DRY	APPROACH USING CONCRETE CLOTH COMPOSITE ALTERNATIVE PERFORMED UNDERWATER
Time the ramp would be closed: 2 weeks	Time the ramp would be closed: 1 week
Cost of dewatering and construction in the dry: \$58,000	Cost of dewatering and construction in the wet: \$27,000

The attached figures 5 and 6 presented after the conclusions show the cross section and plan view of the existing ramp.

5. DESIGN CONSIDERATIONS:

Design considerations were driven by the need to provide a flat, hard underwater surface for the far end of boat trailers when dropping and retrieving boats launched. Note that the beginning of the GCCM extension occurred when the existing boat ramp was under about 1.2m of water. As such, high loads from the trailers were not expected. Regardless, the use of the CC13 material, the thickest of the GCCM product offerings was deemed sufficient to support the required loads.

Properties of concrete cloth composite, CC13				
<i>Thickness</i>	<i>Compressive Strength</i>	<i>Weight (unset)</i>	<i>Roll Width</i>	<i>Roll Length</i>
13 mm	>40 MPa	19kg/sm	1.1 m	6.7 m

6. THE GEOSYNTHETIC CONCRETE COMPOSITE MAT PRODUCT:

The GCCM material is a three dimensional fiber matrix into which specially formulated dry concrete mix is placed. This material hardens upon hydration to form a high strength fiber reinforced protection layer. Product compressive strengths of over 40 MPa are achieved once hydration is complete. (See Figure 2)



Figure 2 - Samples of Hardened 5mm, 8mm and 13mm thick GCCM, with fabric side showing (side with PVC attached is down).

7. CONSTRUCTION PLANNING:

The project consisted of three elements:

- the earthwork contractor and earthwork construction (including the divers),
- the Geosynthetic Concrete Composite Mat supplier, Milliken & Company, and
- design and drawings by the city engineer, Roger Charleston, P.E., of Charleston Engineering.
-

The Olney City engineer and Milliken staff developed this unique installation plan which is depicted in the attached figures.

8. INSTALLATION:

Day 1 - Site Preparation took one day to complete, and consisted of excavation and removal of the old stone and muck from past the end of the ramp, and grading to the final grades determined for the new extension. This excavation was performed in the wet, with the excavated material removed from the site. This was followed by deposition of stone backfill beyond the end of the ramp, out to the fullest extent of the new ramp extension, about 6 meters. The contractor used a long reach backhoe for this preparation work, necessitated by the need to reach some 12 meters into the lake.

Day 2- Divers arrived in the morning and inspected the underwater grading. They directed the contractor to place and spread additional stone to achieve a reasonably smooth, consistent surface. Concurrently, the GCCM, prefabricated into 6.5 meter long custom-length rolls, was fastened side by side to form two 5 meter wide panels. Panel fabrication consisted of hog ringing adjacent panels at approximately .5 meter centers down the 6.7 meter length of roll. The completed panels were then clamped at the leading edge with C clamps using 5 by 50 cm lumber on each side of the leading edge for support, and attached to the bucket for deployment (See Figure 3).



Figure 3 – Leading Edge Fabrication Concrete Cloth Composite

The backhoe then walked down the ramp dragging the panel with it and out into the lake for final placement (Figure 4). Divers assisted in the panel placement and guided the operator. Once the panel was positioned in the correct location with .3 meter of overlap with the existing concrete ramp, a second roll of GCCM was laid transverse to the ramp direction, bridging the junction between the existing concrete and the stone base. This was another support layer for this location.

Finally, a galvanized hold down bar was bolted underwater to the existing concrete ramp effectively holding down the two layers of GCCM and affixing them to the existing slab.

Once the installation was completed, sandbags were placed along the edges to confine the roll edge during the curing process. The sandbags were removed the following day. This process was repeated for the two sides of the boat ramp. Complete installation of both sides was accomplished by about 3:00 pm on day two.



Figure 4– Panel Installation Concrete Cloth Composite Mat

9. CONCLUSIONS:

The challenge of extending an old boat ramp was met using a Geosynthetic Concrete Composite Mat solution. The ability to fabricate a panel and then install it underwater without the cost and construction time that a dewatering construction required drove the decision by the city staff.

This option utilized a Geosynthetic Concrete Composite Mat product that cured underwater and accomplished the objective of ramp extension in two days using conventional construction equipment at half the cost of the conventional alternative.

REFERENCES

- EM 1110-2-410 “DESIGN OF RECREATION AREAS AND FACILITIES –ACCESS AND CIRCLATION”
1982, Department of the Army, Corps of Engineers, Office of the Chief of Engineers
“Roll n Go” Temporary Ramp Extension Kits www.roll-n-go.com 2012
Boat Ramps, Wildlife & Fisheries Extension-Mississippi State University Extension Service
www.msucare.com/wildfish/fisheries/farmpond/building/ramps3.html Oct. 2010

Figure 5 Plan view of the Boat Ramp Extension

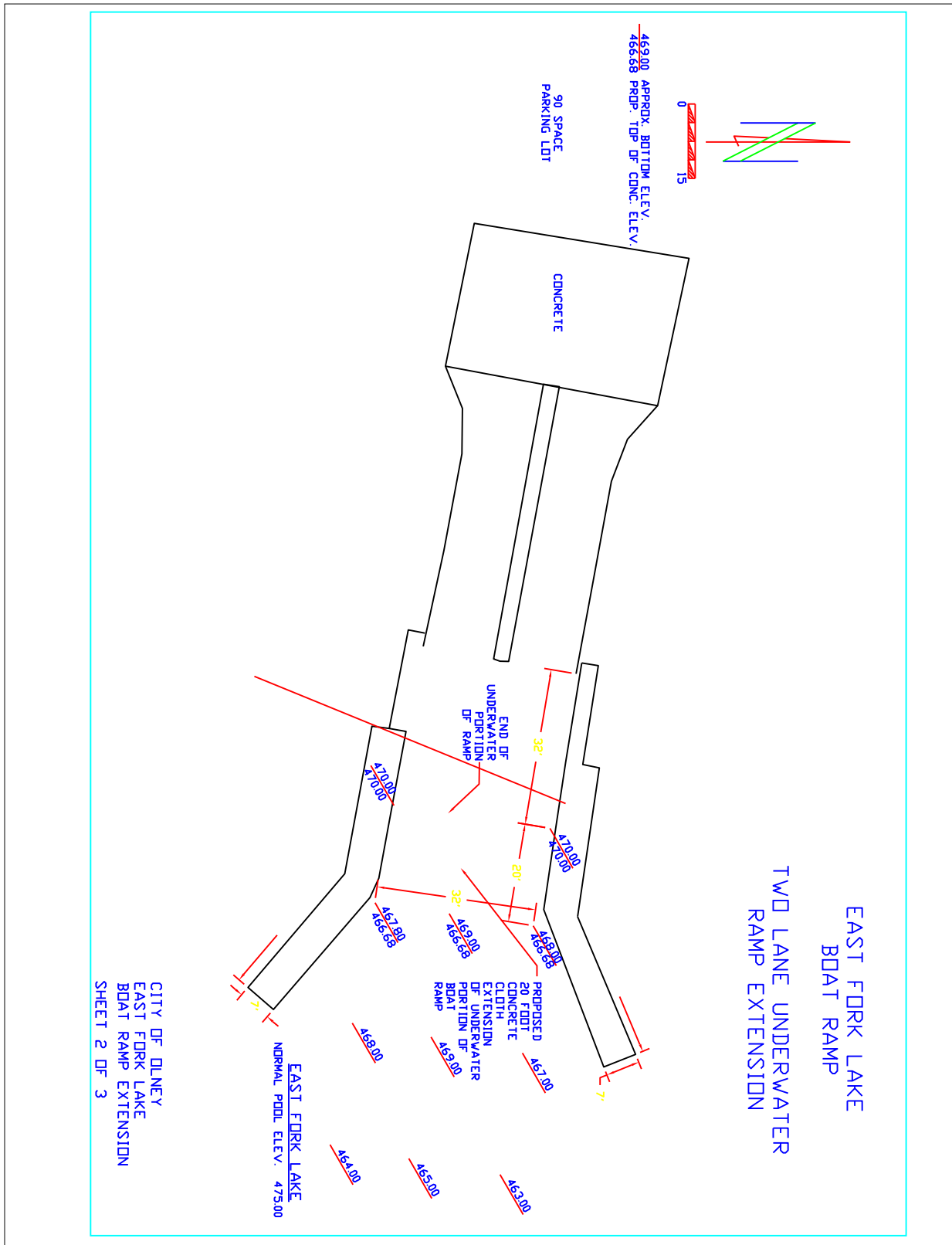
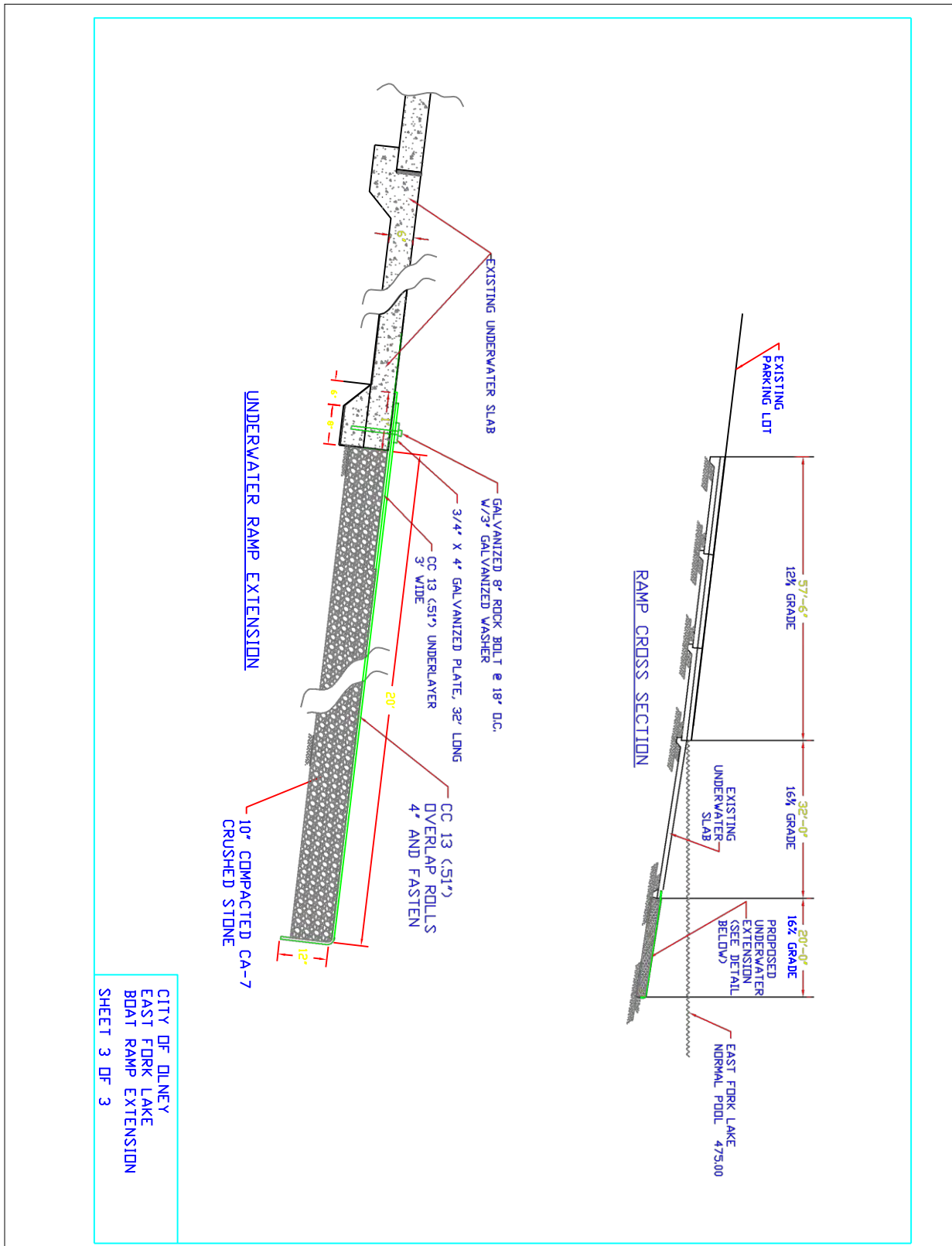


Figure 6 – Cross Section View of the Ramp Extension



The Use of Cationic Starch-based Polymers in Geotextile Tube Dewatering Applications

Mahmoud M. Khachan, M.S., Department of Civil and Environmental Engineering, Syracuse University, Syracuse, NY, USA, mmkhacha@syr.edu

Shobha K.Bhatia, Ph.D., Department of Civil and Environmental Engineering, Syracuse University, Syracuse, NY, USA, skbhatia@syr.edu

Erin Zeqja, B.S., Department of Civil and Environmental Engineering, Syracuse University, Syracuse, NY, USA, ezeqja@syr.edu

Elizabeth Y-S. Maio, B.S., State University of New York, College of Environmental Science and Forestry, Syracuse, NY, USA, eymaio@syr.edu

ABSTRACT

Polyacrylamide-based (PAM) conditioners have become an essential component of the geotextile tube dewatering processes. These conditioners act as flocculants, binding fine sediments through charge neutralization and particle bridging, resulting in faster dewatering rates and greater retention of fines and contaminants. Recently, however, momentum has begun to shift towards the use of sustainable materials. Natural polymers, such as starch and chitosan, are increasingly being tested as an attractive alternative to synthetic polymers. Researchers have identified a number of natural flocculants, polysaccharides and polysaccharide derivatives in particular, as candidates for dewatering applications. In this study, the dewatering performance of four cationic starch-based polymers with degrees of substitution ranging from 0.3% to 0.9% and molecular weights ranging from 4.6×10^4 to 6.9×10^4 g/mole were compared with four cationic acryl-amide based polymers. The synthetic polymers were selected among several synthetic cationic polymers and proved to be very effective in flocculating Tully fines. The optimum dose for each polymer was determined and compared and pressure filtration tests (PFT) were used to determine and compare retention and dewatering indices, such as dewatering rate and filter cake solids content. Furthermore, centrifuge tests were performed to determine the compressibility of the filter cakes. The test results showed that the dewatering properties of the slurries conditioned with starch based polymers are comparable to those conditioned by synthetic polymers. Further, the degree of substitution in starch polymers plays a significant role in minimizing the optimum dose. The optimum dose of starch polymers (~500 ppm for 33% solids) was about 5 times that of the synthetic polymer (~100 ppm for 33% solids). These findings were echoed in the centrifuge tests, the results of which were found to be in agreement with the PFT results.

1. INTRODUCTION

Polyacrylamide-based flocculants have become an essential component of the geotextile tube dewatering process. Depending on their molecular weights and the charge densities, the critical characteristics of polyacryl-amide (McLaughlin and Bartholomew 2007), flocculation of fine particles may occur by polymer bridging, charge neutralization, polymer-particle surface complex formation and depletion flocculation, or by a combination of these mechanisms (Nasser and James 2006). This can result in faster dewatering rates and better retention of fines and contaminants (Maurer et al. 2012).

Flocculants can be categorized according to their charge type. Positive charge carrying polymers are cationic, negative charge polymers are anionic, and polymers with no charge are non-ionic. Cationic polymers are more commonly used as flocculants for a wide variety of soils when compared to anionic and the non-ionic polymers due to the negative nature of soils and colloids. However, several studies (Satyamurthy and Bhatia 2009, Koerner and Koerner 2010, Maurer et al. 2012) have shown that anionic and cationic polyacryl-amide based polymers can be successfully used in geotextile tube dewatering projects. Further, these studies showed that polymer conditioning yielded significant improvements in dewatering time and fines retention. Moreover, additional studies have shown that polyacrylamide polymers are also very effective in dewatering wastes other than soils, such as municipal wastes (Fowler et al. 2005) and fly ash wastes (Maurer et al. 2012, Khachan et al. 2012). Although PAM based polymers have succeeded in dewatering high water content slurries, concerns regarding the safety of synthetic polymers, including their non-biodegradability, aquatic toxicity (Letterman and Pero 1990), and the potential risks associated with toxic residual monomers due to additives and incomplete synthesis (Semsar et al. 2007), should be addressed. By contrast, starch-based polymer derivatives are biodegradable and their degradation intermediates are harmless to humans and the environment. Additionally, cationic starch polymers are believed to be effective flocculants over a wide range of pH (Brostow et al. 2009); they are non-toxic and can be used to treat organic and inorganic matter in negatively charged wastewater (Heinze et al. 2004; Pal et al. 2005). Furthermore, natural polymers are

less expensive and do not depend on non-renewable resources (Sharma et al 2006). Therefore, this research investigates natural polymers, such as starch, as an alternative for dewatering applications.

The current study builds on previous studies that demonstrate the viability of using starches for flocculation. For example, Oelmeyer et al. (2002) studied the systematic optimization of dual flocculant systems using cationic starches and various polymers on dredged sediments and found that the starches were economically competitive with synthetic alternatives. Further, Semsar et al. (2007) compared cationic starch to synthetic PAM polymers as flocculants for harbor sludge. Five different cationic starches were characterized by their flocculation and turbidity measurements, in addition to conducting zeta potential measurements. The flocculation and dewatering measurements demonstrated that synthetic cationic flocculant PAM can be substituted by cationic starches. Finally, Wang et al (2010) used starch-based cationic copolymer flocculant to flocculate wastes obtained from gas and oil exploration projects. According to Wang et al., starch-based polymer yielded better flocculation results than several commercially available synthetic polymers. Although these studies showed that starch-based polymers were successfully used as flocculants, studies in this field are still limited; none of the studies explored the behavior of starch polymers in geotextile tube environments. Moreover, the effect of starch polymers on dewatering time, floc structure, and filter cake strength has not been addressed.

Geotextile tube researchers (e.g., Moo-Young et al., 2002; Liao and Bhatia, 2005; Satyamurthy and Bhatia, 2009, Khachan et al. 2012) have found that filter cake properties such as floc structure and compressibility, not the geotextile properties alone, ultimately control dewatering performance. They have thus concluded that understanding the filter cake structure is critical to improving performance. Given these findings, it is believed that changes to the floc structure and related changes to the filter cake will positively impact the overall success of geotextile tube dewatering, including improvements in the dewatering rate, final solids content, retention of fines, and total volume of retained material in the geotextile tube.

This study evaluated the effects of differing polymer molecular weights, charge densities, and dosage variations on dewatering performance. Four cationic polyacryl-amide based polymers and four cationic starch based polymers were used to evaluate the dewatering performance of Tully fines along with a high strength woven geotextile typically used in geotextile tube dewatering projects. The optimum doses were determined by jar tests and preliminary pressure filtration tests. Determining optimum doses is important due to the negative effect of over-dosing and under-dosing for dewatering projects (Satyamurthy and Bhatia 2009, Khachan et al. 2010). Furthermore, centrifuge tests were performed to determine the effect of polymer properties on the compressibility of the filter cakes. The compressibility of the filter cake is a major concern in this study due to its direct impact on dewatering time and the final volume of solids in the geotextile tubes. Pressure filtration tests (PFT) were also performed to determine and compare dewatering indices, such as filtration efficiency (FE), dewatering efficiency (DE), fines retention, dewatering rate, and filter cake solids content (PS). The dewatering indices were determined for slurries conditioned with polyacryl-amide, starch- based polymers, and for unconditioned slurries.

2. MATERIALS

2.1 Tully Fines

Tully fines were obtained from Clarks Gravel Pit in Tully, NY. The soil is wet sieved through No. 200 standard US sieve. The fine fraction ($d_{85} = 0.062$ mm) is collected and oven dried. Hydrometer analysis showed that Tully fines have about 7% clay size particles and 93 percent silt size particles. Tully silt fines classify as silt (ML), as per ASTM D2487. Tully fines have a liquid limit (LL) of 23.6, plastic limit (PL) of 21.2, and Plasticity Index of 2.4. Figure 1 shows the particle size distribution of Tully silt fines.

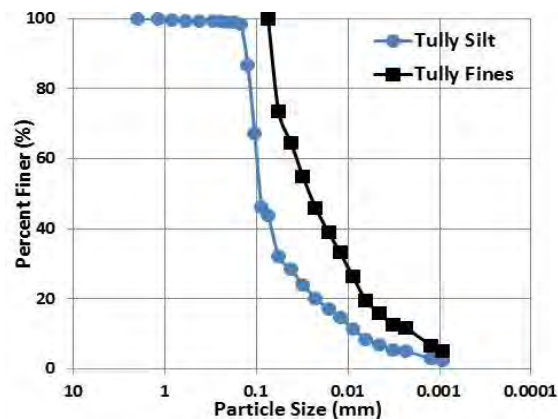


Figure 1. Particle size distribution.

2.2 Geotextile

High strength monofilament woven geotextile (W1) made of polypropylene (PP) was used in this study, a geotextile commonly used in geotextile tube dewatering applications. W1 has an apparent opening size (AOS) of 0.25 mm. Table 1 shows the physical and hydraulic properties of the geotextile.

Table 1. Geotextile physical and hydraulic properties as obtained from the manufacturer.

Geotextile Properties	W1
Polymer Type	PP ¹
Fabric Structure	W ² , MF ³
AOS ⁴ (mm)	0.42 (0.25 ⁵)
Permittivity (s ⁻¹)	0.37
Mass per Unit Area (g/m ²)	585
Thickness (mm)	1.04
Tensile Strength (kN/m)	96x70

¹PP: polypropylene; ²W: woven; ³MF: monofilament; ⁴AOS: apparent opening size; ⁵According to Khachan et al. 2012

2.3 Polymers

Four commercially available cationic polyacryl-amide polymers with varying charge densities and molecular weights were selected from sixteen different cationic polymers known to be the most effective flocculants for Tully fines based on turbidity analysis. Additionally, four commercially available starch-based cationic polymers were also selected to compare their flocculation efficiency to synthetic polymers. The cationic starch polymers have varying charge densities, but similar molecular weights. Polymacryl-amide based polymers are dry powders that need to be dissolved in de-ionized water in order to be used for flocculation. The synthetic polymer concentration in this study is 0.25% polymers by mass. Starch-based polymers are prepared by placing the starch in a boiling water bath at 3% concentration by mass, except for N1, which is prepared by mixing in cold water. Table 2 shows a list of the polymers used in this study along with their properties.

Table 2. Polymers types and properties.

Polymer Type	Charge Density	Molecular Weight	Preparing Method
S1 (Synthetic)	Very Low	High	CWM ¹
S2 (Synthetic)	Med.-High	High	CWM
S3 (Synthetic)	High	Medium	CWM
S4 (Synthetic)	Very High	Low-Medium	CWM
N1 (Natural)	Very Low	Medium	CWM
N2 (Natural)	Low	Medium	BWB ²
N3 (Natural)	Low	Medium	BWB
N4 (Natural)	Medium	Medium	BWB

¹CWM: Cold Water Mixing; ²BWB: Boiling Water Bath

3. TEST METHODS

3.1 Supernatant Turbidity Test

The optimum doses of polymers were determined through turbidity tests. In this test, 500 ml of slurry at concentration of 5% by mass is added to a 500 ml graduated cylinder. 5% concentration by mass was selected to allow for visual observation of the flocculation of the fine particles. Polymers are then added in increments and the cylinder is manually inverted and rotated to assure the complete mixing of polymers and slurry. The turbidity of supernatant at each dose is measured using a turbidity meter (Hach 2100N Turbidimeter). The turbidity was measured for samples that were taken from the middle of the cylinder after allowing 2 min of settling time. The dose versus turbidity is then plotted and analyzed, and the optimum dose is estimated to be the lowest possible dose that yields minimum turbidity.

3.2 Centrifuge Test

The strength and compressibility of the filter cake can have significant effects on dewatering time and the geotextile tube solids content. Filter cakes with high compressibility are susceptible to decrease in their dewatering ability due to the decrease in void volume. In this study, filter cake compressive yield stress measurements were made using a batch centrifuge (Ample Scientific S-50D) with 4 x 50 ml swinging bucket rotor. The polycarbonate centrifuge tubes used in these measurements held 50 ml and had a diameter of 29.3 mm. The diameter of the tube was maximized to limit side friction in accordance with the findings of Green and Boger (1997). Rotational speeds in the range of 300-1000 rpm were used in

accordance with Glover et al. (2004), giving centrifugal accelerations of 10-140g. Centrifuge tests were conducted at slurry samples with 33% solids content by mass (15.8 % by volume) in order to determine the change in solids volume fraction (ϕ) and the compressive yield strength ($P_y(\phi)$). The solids volume fraction represents the packing of solids under the effect of applied pressure (centrifugal force), and the compressive yield strength ($P_y(\phi)$) is the force needed for a certain volume fraction to be compressed into a denser network. Therefore, when the applied pressure exceeds the yield stress of the network at the original volume fraction, the network collapses to a denser concentration that has sufficient strength to carry the applied load (Eckert et al. 1996). Buscall et al. (1987) defined $P_y(\phi)$ and ϕ and as follows:

$$P_y(\phi) = (\rho_p - \rho_f) h_0 \left(1 - \frac{h}{2R}\right) \quad [1]$$

and

$$\phi = \frac{\rho_f h_0 \left[1 - \left(\frac{h + s}{2R}\right)\right]}{(h + s) \left(1 - \frac{h}{R}\right) + \frac{h^2}{2R}} \quad [2]$$

Where:

P_y	=	Compressive Yield Strength (kPa)
ϕ	=	solid volume fraction
ϕ_0	=	initial solid volume fraction
$\rho_p - \rho_f$	=	difference in density between the particle and fluid (g/cm^3)
g	=	centrifugal acceleration ($g = \omega^2 R$)
h_0	=	initial sediment bed height (cm)
h	=	equilibrium sediment bed height (cm)
R	=	distance between the center of the centrifuge and bottom of sediment bed (cm)
s	=	$\frac{dh}{d \ln(g)}$

3.3 Pressure Filtration Test

The Pressure Filtration Tests (PFTs) were used to simulate geotextile tube dewatering in the lab. The PFT consists of a cylindrical reservoir (72 mm diameter and 170 mm tall) holding 600 mL of slurry and a threaded base plate that secures the geotextile specimen and directs effluent flow. For the test, 575 mL of 33% by mass solids slurry was mixed using a jar test apparatus for 180s; optimum doses were then added to the slurry mix. The slurry was mixed in manual rotational movement to assure flocculation of the soil. The flocculated slurry was then immediately transferred into the testing apparatus. A top cap with pressure inlet was secured atop the testing chamber with pressure applied at 34.5 kPa using a lab supply of compressed air. This pressure is representative of the internal pressure during geotextile tube dewatering (Gaffney 2001; Moo-Young et al. 2002). Volume measurements of the effluent were taken frequently for the first 10 to 15 minutes and additional readings were taken at 5 minute intervals. Upon completion of the test, percent solids retained, flow rate, filter cake strength, and the soil piping were evaluated. A photograph and schematic of the PFT apparatus are shown in Fig. 2.

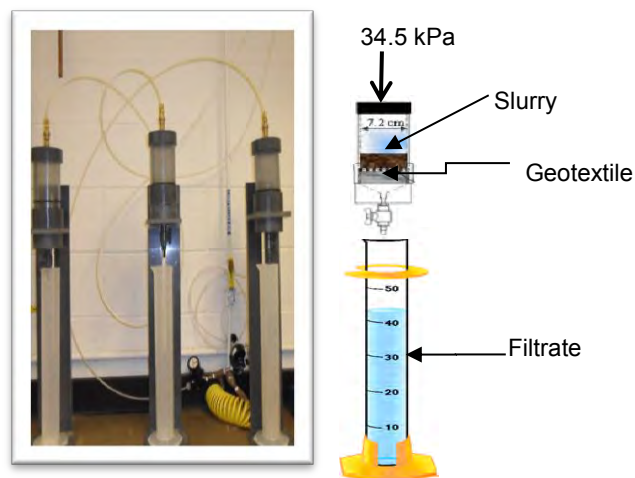


Figure 2. Pressure filtration test setup.

4. RESULTS AND DISCUSSION

4.1 Optimum Dose Analysis

The optimum doses needed to flocculate Tully fines were determined from the supernatant turbidity versus polymer dose curves of the synthetic and natural polymers. Figure 3 (a, b) presents the turbidity versus dose curves for the eight polymers used in this study. Figure 3(a) shows that the four synthetic polymers yielded relatively similar behaviors and reached turbidities as low as 15 NTU at doses between 20 and 40 ppm for slurries with 5% solids content. On the other hand, the starch-based polymers, as shown in Figure 3(b), were also able to yield turbidity values as low as 15 NTU. However, it required a minimum of 40 to 120 ppm dose, which is two to three times higher than the dose obtained from the synthetic polymers. Moreover, Figure 3(a, b) shows that over-dosing of synthetic and of starch-based polymers leads to an increase in turbidity, which is demonstrated by the U-shape curves in the figure. Therefore, the optimum dose from the supernatant turbidity method does not give a clear cut result for the optimum dose value, but it gives a dose range where polymers are yielding minimum turbidity values.

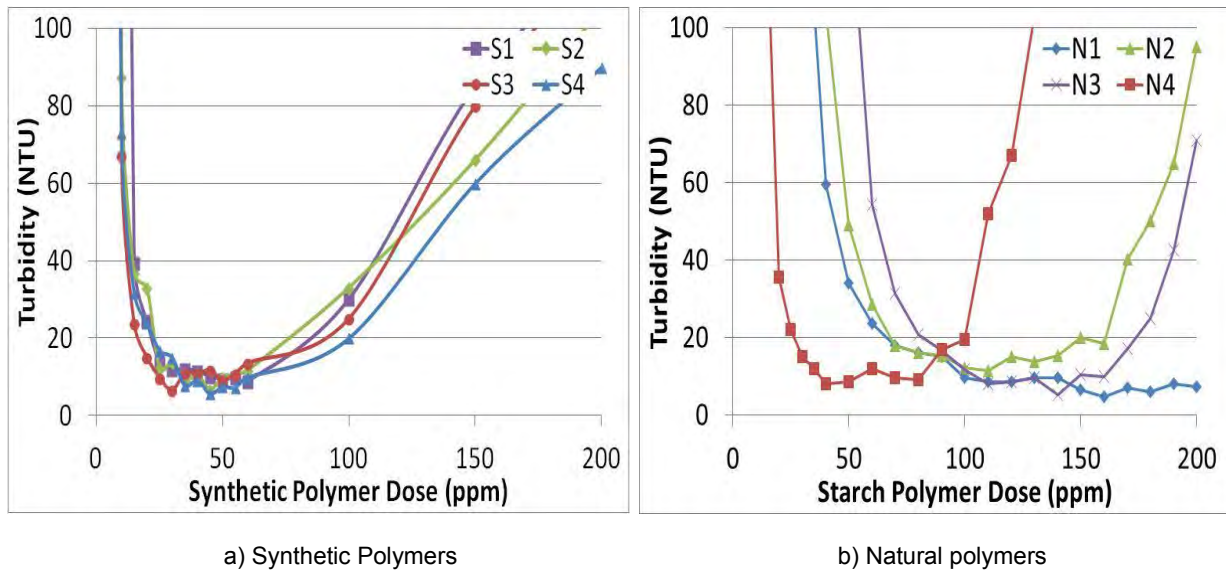


Figure 3: Turbidity versus dosage.

The dosing results obtained from the turbidity tests were used to determine the optimum dose needed in dewatering applications. Since this method yielded varying dosage ranges for the two types of polymer groups, preliminary pressure filtration test were conducted to determine the required dose for successful soil retention in a dewatering performance test. The initial doses were selected to correspond with a turbidity value of 15 NTU for all the polymers. The doses were determined for soil slurry at 5% and 33% solids concentrations, where a linear relationship is found between polymer dose and slurry solids concentration. The determined doses at 33% fines concentration were used to flocculate soil slurries; the test was then repeated with higher doses until successful soil retention (minimum soil loss) was obtained. For most of the tests, the optimum doses were higher than the minimum dose that gives a turbidity of 15 NTU. Table 3 shows the comparison between the minimum doses that yielded low turbidity and the optimum doses obtained from preliminary PFT.

Table 3. Optimum doses determined from different tests at 5% and 33% solids concentration.

Polymer Type	Turbidity method (concentration = 5%) (ppm)	Turbidity method (Concentration = 33%) (ppm)	Optimum dose from PFT (Concentration = 33%) (ppm)
S1	30	198	220
S2	26	170	150
S3	20	130	145
S4	30	198	220
N1	80	520	660
N2	80	520	990
N3	100	660	1180
N4	36	240	530

As can be seen in Table 3, the optimum doses determined from PFT were generally higher than the minimum dose that yielded low turbidity values. This indicates that performance tests are necessary to determine the optimum doses needed in application. Furthermore, Table 3 shows that synthetic polymers S1 (very low charge density and high molecular weight), and S4 (very high charge density and low molecular weight) yielded similar and the highest optimum doses, while S2 (high charge density and high molecular weight) and S3 (high charge density and medium molecular weight) yielded the lowest optimum dose. For the natural polymers that have almost equal molecular weights to each other (see Table 2), the increase in charge density helped in decreasing the optimum dose needed for dewatering tests. Therefore, such comparisons show that polymers properties play an important role in determining the dose necessary for successful fines flocculation and retention.

4.2 Compressive Yield Strength of Filter Cakes

The previously determined optimum doses from PFT were used to perform centrifuge test on Tully fines slurries at 33% fines concentration in order to measure filter cake compressibility and compressive yield strength. Since the permeability of the filter cakes decreases with the increase in compressibility of filter cake, performing the centrifuge test allowed for better understanding of filter cake strength and dewatering behavior in geotextile tube dewatering applications. Equations 1 and 2 were used to determine the compressive yield strength $P_y(\phi)$ and the solid volume fraction (ϕ). Figure 4 presents the soil volume fraction (ϕ) versus compressive yield strength of the filter cake $P_y(\phi)$ results.

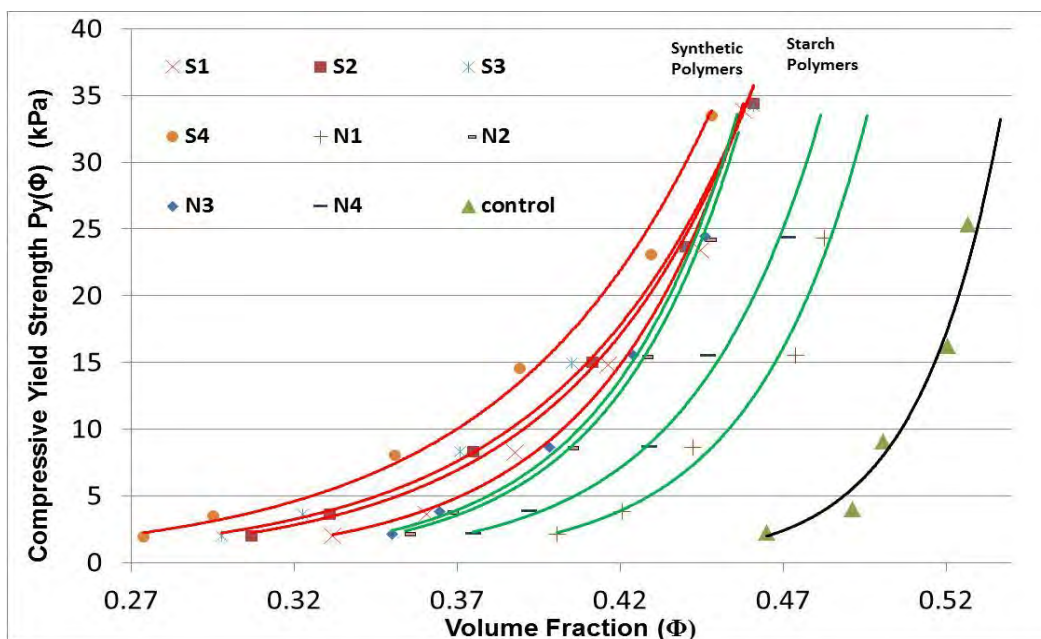


Figure 4: Volume fraction versus compressive yield strength.

Figure 4 shows that the centrifugal pressure that was applied to unconditioned (control) and polymer conditioned slurries yielded varying resistance to compressibility for all the tested samples. For example, the control sample needed a pressure as low as 2 kPa to yield and reach solid volume fraction of 0.47, while at the same pressure the slurries conditioned with synthetic polymers had solids volume fraction ranging from 0.27 to 0.33 only. On the other hand, the samples conditioned with starch polymers reached volume fraction ranging from 0.35 to 0.40. This indicates that the samples conditioned with synthetic polymers are more resistant to compression than natural polymers. However, both synthetic and natural polymers were more resistant to the external compressive pressures than the control sample. The same trend was noticed for all $P_y(\phi)$ values that ranged from 2 to 35 kPa. Therefore, synthetic and natural polymers filter cakes were able to resist applied loads as high as 35 kPa while they still have less packed floc structure than the control sample. This indicates that they can attain larger void ratios which allows for higher permeability in the filter cake. The results obtained of centrifuge test can be further studied by comparing them with the dewatering indices obtained from pressure performance tests.

4.3 Dewatering Indices

The dewatering performance of Tully fines conditioned with synthetic and starch based polymers were evaluated by performing PFT. The dewatering rate, dewatering indices such as filtration efficiency (FE) and dewatering efficiency (DE),

and filter cake properties such as the solids content, water content, and height can also be determined from PFT. Figure 5 shows the dewatering time versus effluent volume obtained from the eight polymers in this study.

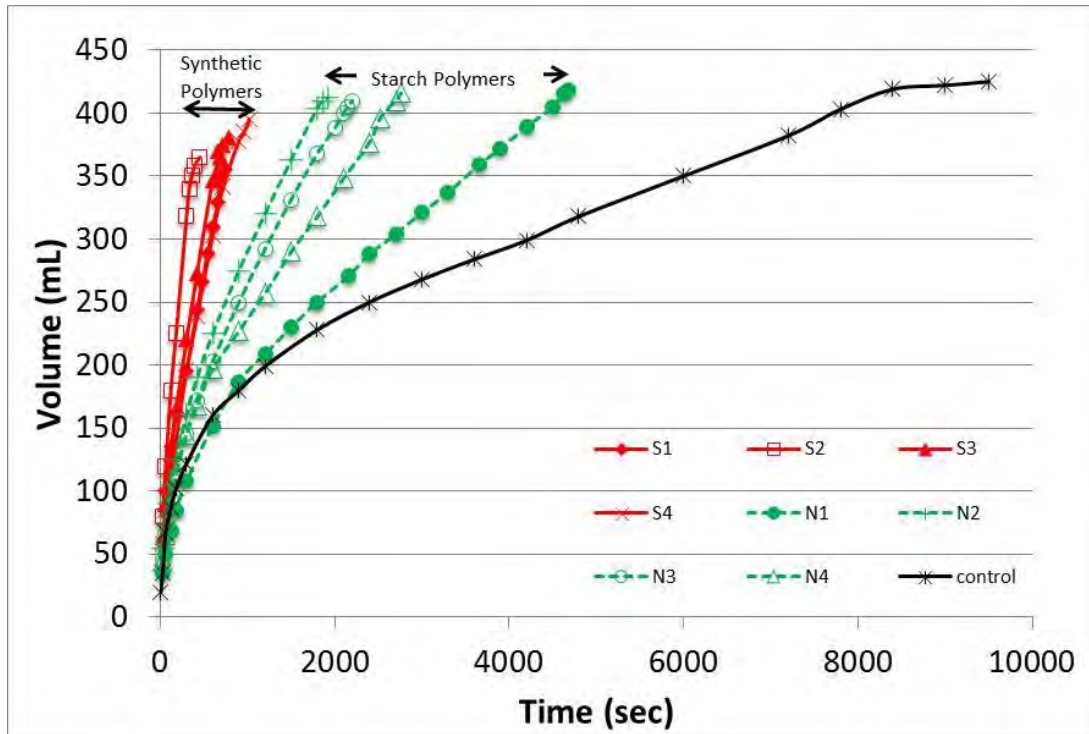


Figure 5: Dewatering time versus effluent volume

The PFT tests results showed that all starch-based polymers resulted in slower dewatering rate than the synthetic polymers, but the difference was not significant except for polymer N1, which has a very low charge density and medium molecular weight. Synthetic polymers yielded a dewatering rate that was 12 times faster than the unconditioned sample, and the starch based polymers had a dewatering rate six times faster than the unconditioned sample. These conclusions agree with the results obtained from centrifuge testing. Centrifuge test results showed that all tested slurries that were conditioned with synthetic polymers are more resistant to compression because they have smaller solid volume fraction and larger void ratios than all the ones conditioned with starch polymers and the control sample. This trend can be observed in Figure 5, where synthetic polymers yielded the lowest dewatering time (~15 min), starch-based polymers allows for relatively close dewatering time (~35 min) to that of the synthetic polymers, and the control sample shows significantly higher dewatering time (~150 min). Therefore, it is believed that the centrifuge test can be a useful tool to assess the effect of polymers on filter cake properties and dewatering performance.

Moreover, PFT results were used to determine filter cake properties and dewatering indices for the eight polymers as shown in Table 4. Filter cake properties such as filter cake height and water content were determined after the completion of the PFT, and dewatering indices include FE, DE, and PS and can be defined as follows.

$$FE = \frac{TS_i - TSS_f}{TS_i} \times 100(\%) \quad [3]$$

$$DE = \frac{PS_f - PS_i}{PS_i} \times 100(\%) \quad [4]$$

$$PS = \frac{W_s}{W_T} \quad [5]$$

Where:

TS_i : initial total solids (g/l)

TSS_f : final total suspended solids in the filtrate (g/l)

PS_i : initial percent solids of the slurry by weight (%)

PS_f : final percent solids of the retained material by weight (%)

W_s : weight of retained solids (g)

W_T : total weight of the filter cake before drying.

Table 4. Filter cake properties and dewatering indices.

Polymer	Ch ¹ (mm)	Cw ² %	Piping g/m ²	FE	DE	PS
S1	55	52.5	118	99.8	100.7	66.2
S2	58	55.1	95	99.9	101.2	66.4
S3	65	62.9	450	99.1	91.3	63.1
S4	68	71.1	780	98.8	87.3	61.8
N1	41	36.1	651	98.9	134.4	78.1
N2	49	41.5	677	98.8	115.9	71.2
N3	44	39.2	1040	98.3	125.6	74.7
N4	43	37.8	651	98.9	128.3	76.3
No Polymer (Control)	40	28.2	6238	78.9	125.3	83.2

¹Ch: Filter cake height; ²Cw: Filter cake water content

As is shown in Table 4, the filter cake heights for the samples conditioned with synthetic polymers were 35% to 65% higher than those conditioned with starch-based polymers. The same conclusion can be applied to the water content of the filter cakes. These results are in agreement with the results obtained from centrifuge test showing that the filter cakes conditioned with synthetic polymers are less compressible than those conditioned with starch polymers and the control sample, yielding larger filter cake heights and higher water contents. Moreover, starch-based polymers allowed for higher DE values indicating that the filter cakes with higher DE hold less water and have higher solids content (PS) and thinner filter cakes. Therefore, starch-based polymers allow for more fillings of the geotextile tubes, which can help in decreasing dewatering costs. Piping, on the other hand, was not significant in any of the conditioned samples where the maximum piping amount of 1040 g/m² was only 1.5% of the initially tested solid amount. For FE, it was almost equal for all the tested polymers, which indicates that both the natural and the synthetic polymers successfully retained the soil particles.

The PFT results indicate that cationic starch polymer is comparable to synthetic polymers for use in dewatering high water content slurries. Furthermore, although synthetic polymers yield faster dewatering rate, the cationic starches allowed for more compressible filter cakes, higher dewatering efficiency, and higher filter cake solids content.

To further assess the validity of starch polymers in dewatering applications, this study will be extended to include flocculation and dewatering properties of soils that have high organics and clay contents. Furthermore, due to the significant effect of polymers properties on dewatering performance, future work will include testing starches with varying ranges of molecular weights and charge densities.

5. CONCLUSIONS

A total of 72 turbidity, centrifuge, and PFT tests were conducted using four PAM-based polymers, four starch-based polymers, Tully fines, and woven geotextile (W1). The tests were conducted to determine polymers optimum dosage, filter cake strength and compressibility, and dewatering properties. The optimum dose was verified by performing centrifuge tests and PFTs. Based on the results of this study on Tully fines, the following conclusions can be drawn:

- Polymers properties such as molecular weights and charge densities have significant effects on the dose amounts and on overall dewatering performance.
- The supernatant turbidity test allows for determining the minimum dose for separating fine soils from water. However, such doses were found to be slightly less than the optimum dose needed for dewatering applications.
- Centrifuge tests allows for determining the compressibility and strength of the filter cake which cannot be determined from PFT. Moreover, centrifuge test proved to be successful in predicting the filter cake behavior in dewatering applications, where less compressible filter cake allowed for higher dewatering rate and vice versa.
- Tests results showed that cationic starch polymers yielded a thinner filter cake and higher solids content. Additionally, PFT results showed that the dewatering time decreased from 150 minutes for the unconditioned sediments to about 15 minutes and 35 minutes for the synthetic and natural polymers respectively.
- Generally, the performance of the cationic starch polymer was comparable to that of the synthetic polyacrylamide polymer, indicating good potential for future use in geotextile tube dewatering applications.

ACKNOWLEDGEMENTS

This study was supported by the National Science Foundation (NSF) (CMMI 1100131), Geosynthetic Institute (GSI), and Wen-Hsiung and Kuan-Ming Li Graduate Fellowship of Syracuse University. The authors would like to thank P. Kaye and V. Ginter of TenCate for providing geotextiles, D. Hunter of BASF Corporation for providing the synthetic polymers flocculant, and National Starch Company for providing the cationic starch-based polymers. The authors would also like to thank Prof. Bandaru V. Ramarao for his contribution to this paper.

REFERENCES

- ASTM D2487. Standard Practice for Classification of Soils for Engineering Purposes (Unified Soil Classification System). ASTM International, West Conshohocken, PA, USA.
- Buscall, R., McGowan, I.J., Mills, P.D.A., Stewart, R.F., Sutton, D., White, L.R., and Yates, G.E. (1987). The rheology of strongly flocculated suspension. *Journal of Non-Newtonian Fluid Mechanics*, 24: 183-202.
- Brostow, W., Lobland, H.E., Pal, S., and Singh, R.P. (2009). Polymeric flocculants for wastewater and industrial effluent treatment, *Journal of Materials Education*, 31(3-4): 157–166.
- Eckert, W.F., Masliyah, J.H., Gray, M.R., and Fedorak, P.M. (1996). Prediction of sedimentation and consolidation of fine tails, *AIChE Journal*, 42(4): 960-972.
- Fowler, J., Larkins, K., and Duke, M. (2005). Dredging aerobic digested biosolids into geotextile tubes for dewatering, New Orleans east municipal sewage treatment plant, New Orleans, LA, *Geotec Associates*, www.geotec.biz.
- Gaffney, D.A. (2001). Geotextile tube dewatering: Part 1 – design parameters, *GFR Magazine*, 19(7):1-5.
- Glover, S.M., Yan, Y.D., Jameson, G.J., and Biggs, S. (2004). Dewatering properties of dual-polymer-flocculated systems. *Int. J. Miner Process.* 73: 145-160.
- Green, M.D., and Boger, D. (1997). Yielding of suspensions in compression. *Ind. Eng. Chem. Res.* 36:4984-4992.
- Heinze, T., Haack, V., and Rensing, S. (2004). Starch derivatives of high degree of functionalization. 7. preparation of cationic 2-hydroxypropyltrimethylammonium chloride starches, *Starch-Starke*, 56(7): 288-296.
- Khachan, M.M., Bader, R.A., Bhatia, S.K., and Maurer, B.W. (2010). Comparative dewatering performance of slurries conditioned with synthetic polymers vs. eco-friendly polymers, *Geotechnical Special Publication*, Geo-Frontiers 2011, Dallas, TX. 3050-3058.
- Khachan, M.M., Bhatia, S. K., Maurer, B.M., and Gustafson, A.C., (2012). Dewatering and Utilization of Fly Ash Slurries Using Geotextile Tubes, *Indian Geotechnical Journal*. 42(3): 194-205.
- Koerner, R.M., and Koerner, G.R. (2010). Performance tests for the selection of fabrics and additives when used as geotextile bags, containers, and tubes, *Geotechnical Testing Journal*, 33(3): 1-7.
- Letterman, R. D., and Pero, R. W. (1990). Contaminants in Polyelectrolytes Used in Water Treatment, *Journal AWWA*, 82(11): 87-97.
- Liao, K. and Bhatia, S.K., (2005). Geotextile tube: Filtration performance of woven geotextiles under pressure. *Proceedings of NAGS 2005/GRI – 19 Cooperative Conference*, Las Vegas, NV, USA, 1:1-15.
- Maurer, B.W., Gustafson, A.C., Bhatia, S.K., and Palomino, A.M. (2012). Geotextile Dewatering of Flocculated, Fiber Reinforced Fly-Ash Slurry, *Fuel*, 97:411-417.
- McLaughlin, R.A. and Bartholomew, N. (2007). Soil factors influencing suspended sediment flocculation by polyacrylamide, *Soil Science Society of America Journal*, 71(2): 537-544.
- Moo-Young, H.K., Gaffney, D.A., and Mo, X. (2002). Testing procedures to assess the viability of dewatering with geotextile tubes, *Geotextiles and Geomembranes*, 20(5): 289-303.
- Nasser, M.S. and James, A.E. (2006a). Settling and sediment bed behavior of kaolinite in aqueous media, *Separation and Purification Technology*, 51: 10-17.
- Oelmeyer, G., Krentz, O., and Kulicke, W.M. (2002). Combined flocculant systems with cationic starches in the solid/liquid separation of harbor sediments, *Chemical Engineering Technology*, 25(1): 47-50.
- Pal, S., Mal, D., and Singh, R.P. (2005). Cationic starch: an effective flocculating agent, *Carbohydrate Polymers*, 59(4): 417-423.
- Satyamurthy, R. and Bhatia, S.K. (2009). Effect of polymer conditioning on dewatering characteristic of fine sediment slurry using geotextiles, *Geosynthetics International*, 16(2): 83-96.
- Semsar, M. S., Scholz, S., and Kulicke, W. M. (2007). Cationic starches as substitute for synthetic cationic flocculants in solid-liquid separation of harbor sludge, *The Journal of Physical Chemistry*, 111: 8641–8648.
- Sharma, B.R., Dhuldhoya, N.C., and Merchant, U.C. (2006). Flocculants—an Ecofriendly Approach. *J Polym Environ*, 14: 195-202.
- Wang, F., Zou, J., Zhu, H., and Fan, J. (2010). Preparation of high effective flocculant for high density waste drilling mud, *Journal of Environmental Protection*, 1: 179-182.

Time-dependent Impact of RECPs on Surface Water Quality

J.L. Smith, Sustainable Construction Management and Engineering, SUNY College of Environmental Science and Forestry, Syracuse, NY, USA

S.K. Bhatia, Civil and Environmental Engineering, Syracuse University, Syracuse, NY, USA

ABSTRACT

Geosynthetic rolled erosion control products (RECPs) are often used by engineers to manage and protect surface water quality by providing ground cover protection for bare soil slopes and channels. Although many studies have been published documenting the successful use of RECPs in reducing soil losses, few studies have considered the contributions of RECPs to protecting surface water quality in terms of the turbidity of runoff over time. Knowledge of runoff turbidity is important because it is commonly used by regulators to assess the effectiveness of best management practices (BMPs) and downstream surface water quality. This paper presents the results of a laboratory rainsplash study that compares runoff turbidity for three different RECPs (coconut, straw, and wood excelsior) over time. This paper demonstrates that turbidity can be used as a measure to assess the performance of RECPs and that RECPs can have an immediate positive impact on downstream surface water quality.

1. INTRODUCTION

Soil erosion from construction sites is a significant concern to downstream surface water quality. Soil erosion can lead to high sediment loads, decreased water clarity, and increased levels of contaminants, such as nitrogen and phosphorus, in surface waters. These effects can negatively impact the health and survival of fish, wildlife, and their habitat, the cost to treat surface waters for industrial and domestic uses, and the recreational value of downstream water bodies.

State and federal regulations have been enacted to regulate construction sites in efforts to protect downstream surface water quality. Regulations, such as the United States Environmental Protection Agency (USEPA) National Pollutant Discharge Elimination System (NPDES) program, typically require engineers and contractors working on construction sites to obtain permits, implement best management practices (BMPs), and monitor downstream water quality to prevent storm water pollution (USEPA 2007). The effectiveness of BMPs is typically based on downstream measurement of turbidity, similar to Safe Drinking Water Act (SDWA) standards which specify turbidity limits (USEPA 2012a).

Turbidity is a measure of the cloudiness of water that is caused by the presence of suspended solids, measured as the amount of light that is scattered by suspended particles in a sample as compared to a clear sample (USEPA 2009). Turbidity is commonly used because it is easy to measure, is relatively inexpensive, and can be continuously measured, unlike time-consuming laboratory total suspended solids (TSS) or suspended sediment concentration (SSC) tests. Relationships have been found between turbidity, measured in nephelometric turbidity units (NTUs), and TSS (e.g. Sims and Cotching 2000, Packman et al. 2002, Holliday et al. 2003.) Work by Holliday et al. (2003) suggests that NTU measurements can be used to estimate sediment concentrations of fine soil fractions, but underestimate total sediment concentrations when sand-size fractions are present. This is because sand and silt-clay particles rapidly fall from suspension, substantially decreasing NTU values within the first 12 hours; clay-sized particles stay in suspension for longer periods, typically more than 24 hours (Holliday et al. 2003.)

Recently, the USEPA has expressed interest in specifying turbidity limits in their NPDES permits to limit downstream impacts from construction site erosion (USEPA 2012b). However, the establishment of absolute turbidity limits has been difficult due to the lack of turbidity data from commonly used BMPs (USEPA 2012b). Rather than specifying an upper turbidity limit, many states evaluate turbidity violations by comparing turbidity increases relative to absolute or relative background levels. Background turbidities typically range from 25 to 75 NTUs; whereas, surface water turbidity downstream from construction sites can exceed several hundred to several thousand NTUs, even with the effective use of BMPs (Minton and Benedict 1999.)

Geosynthetic rolled erosion control products (RECPs) are BMPs that are broadly used by engineers and contractors to minimize soil erosion from bare soil slopes and channels. RECPs are temporary degradable or long-term non-degradable materials manufactured or fabricated into rolls designed to reduce soil erosion and assist in the growth, establishment, and protection of vegetation (ECTC 1998.) RECPs work by providing immediate ground cover protection against raindrop impact and stabilizing seed and soil within their structures, allowing vegetation to grow. Many field (e.g. Bhatia et al. 2002, Smith et al. 2005, Sutherland and Ziegler 2006), large-scale (e.g. Clopper et al. 2001, Kelsey et al. 2004), and bench-scale laboratory (e.g. Rickson 2002, Smith and Bhatia 2006, 2009, Smith et al. 2007) studies have

been conducted, documenting the successful use of RECPs in minimizing soil erosion. The majority of these studies, however, focus on RECP performance in terms of total soil losses measured by gravimetric methods. Although gravimetric methods are accurate, they are time-consuming and tedious. Regulators are typically more interested in evaluating downstream water quality, where turbidity can be quickly and inexpensively monitored, so that problems can be readily identified and addressed.

Few studies have been conducted that focus on downstream measurements of water quality from RECPs. One study by Babcock and McLaughlin (2011) evaluated the runoff water quality from three different erosion control methods (excelsior blankets, straw, and straw with polyacrylamide (PAM)) on four different sites with two horizontal to one vertical (2H:1V) bare slopes. The soils at the sites were mostly sand, with some silt and a trace of clay. Runoff was collected at the base of 10- to 30-ft wide by 29.5-ft long plots and analyzed for turbidity and TSS. Based on average data, the straw with PAM reduced mean runoff turbidity at three of the four sites by a maximum of 81% and TSS at two of the four sites by a maximum of 56%, in comparison to straw alone. Slopes covered with excelsior blankets had significantly lower turbidity and TSS than straw alone in one of the three sites; however, had significantly higher turbidity at two of the three sites in comparison to straw with PAM.

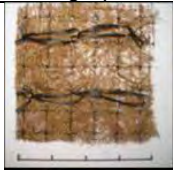


This paper presents the results of a laboratory rainsplash study that evaluates the contributions of RECPs to protecting downstream surface water quality in terms of turbidity. This paper demonstrates that turbidity can be used as a measure to assess the performance of RECPs and vegetative cover and that RECPs can have an immediate impact on downstream surface water quality. Attempts are also made to correlate turbidity, based on subsamples, with SSCs, based on whole samples from rainsplash tests. The role and contribution of RECPs to managing and protecting surface water quality are assessed.

2. MATERIALS AND METHODS

2.1 RECPs

This study, which is part of a larger study that included thirteen different RECPs, focuses on the performance of three different RECPs. The selected RECPs are erosion control blankets (ECBs), temporary degradable RECPs composed of processed natural or polymer fibers mechanically, structurally, or chemically bound to form a continuous matrix (ECTC 2001). The ECBs are made of three different fiber types: coconut (C2), straw (S1), and wood excelsior (W1). The ECBs range in light penetration from 20.5% to 41.5% and water absorption from 228% to 1218%, properties noted by several researchers (e.g. Ziegler et al. 1997, Rickson 2002, Smith et al. 2010) to be important to their rainsplash erosion performance. A summary of the RECPs and their average measured physical properties is given in Table 1.

Table 1. RECP properties.

RECP	Fiber type	Properties	Photograph ⁵
C2	Coconut	Mass/Area Thickness Light penetration Water absorption	
S1	Straw	Mass/Area Thickness Light penetration Water absorption	
W1	Wood excelsior	Mass/Area ¹ Thickness ² Light penetration ³ Water absorption ⁴	

¹ASTM D6475; ²ASTM D6525; ³ASTM D6567; ⁴ASTM D1117; ⁵4-in by 4-in specimens

2.2 Rainsplash Erosion

A laboratory rainsplash simulator was used to simulate rainfall events over different combinations of RECPs, soil, vegetated soil, and vegetated RECPs. The simulator was constructed in accordance with ASTM D7101. The simulator is approximately 2-m tall and produces 2.2-mm diameter raindrops that fall onto a 3 horizontal to 1 vertical (3H:1V) slope table, simulating a 15.24 cm/hr rainfall intensity. The slope table consists of three channels 89-cm long by 25-cm wide. Soil containers, 20-cm diameter and 10-cm deep, were placed in recessed holes at the base of the outside channels. Only the outside channels were used so that consistent rainfall conditions could be produced. Bare soil was compacted in the containers to $90\pm 3\%$ of standard dry density at an optimum moisture content of $\pm 2\%$. RECP specimens were placed along the length of the channels and covered the prepared soil containers. Runoff and eroded sediment were collected in buckets at the base of the channels. Photographs of the rainsplash simulator and examples of vegetated soil tests and RECP tests are shown on Figure 1.

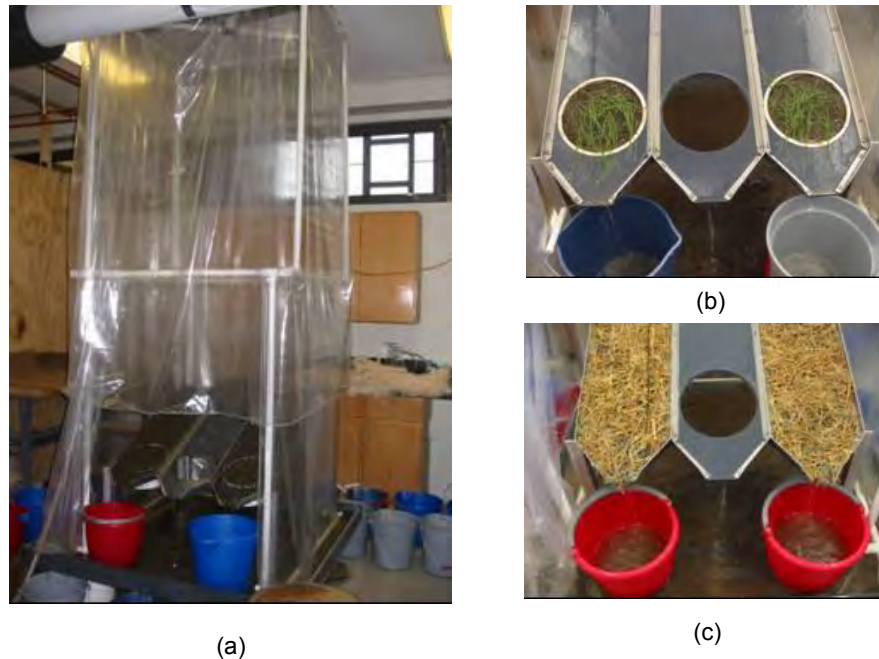


Figure 1. (a) Rainsplash simulator and testing with (b) vegetated soil containers and (c) RECP-covered soil containers.

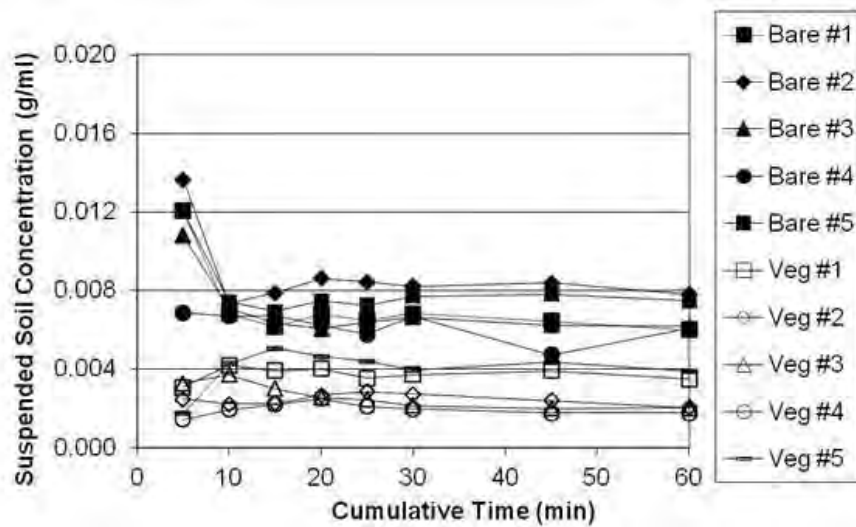
Soil. A well-graded silty sand (SM) consisting of 27% non-plastic fines and 73% sand (ASTM D2487) was used for the tests. The soil has an average organic matter content of 4.66%, based on the Loss-on-Ignition (LOI) method (Nelson and Sommers 1996). The maximum dry density of the soil is 1670 kg/m^3 at an optimum moisture content of 19.6% (ASTM D698).

Vegetation. For the vegetated tests, the soil was sown with Kentucky 31 tall fescue grass seeds and watered. For the vegetated RECP tests, RECP was then placed above the seeded soil. Seeds were placed at a rate of 0.75 g per container, which is equal to approximately 350 seeds. This amount of grass seed is twice the rate specified in ASTM D7322 for encouraging seed germination and plant growth under bench-scale conditions to ensure that an adequate stand of grass would be established after 21 days. The soil containers were placed in an environmental chamber capable of sustaining conditions at $27\pm 2^\circ\text{C}$, $45\pm 5\%$ relative humidity, and $9687 \text{ lumens/m}^2 \pm 1076 \text{ lumens/m}^2$. The soil containers were watered twice per week with 100 ml of water. The vegetated specimens were tested for rainsplash performance after 21 days of growth.

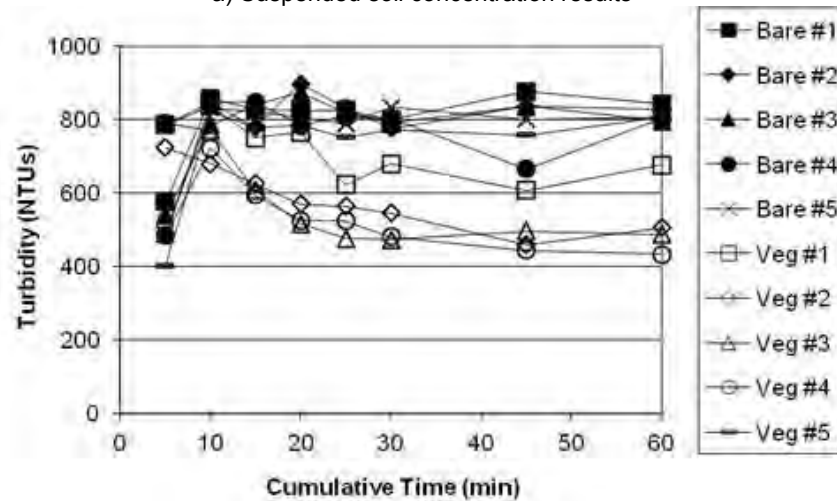
Turbidity. The mass of eroded soil, runoff volume, and turbidity were measured every 5 minutes through 30 minutes and at 45 and 60 minutes for each rainsplash test. A 30-ml grab sample of the runoff water was collected for each time increment and measured for turbidity using a laboratory turbidity meter (HF Scientific, Inc., HF - Micro 100 Laboratory Turbidimeter). The turbidity meter was calibrated with 0.02 and 10 NTU calibration standards and had an accuracy of $\pm 2\%$ of the reading plus 0.01 NTU. Once the eroded soil was dry, its weight was determined. SSCs of whole samples were calculated based on measured weights of eroded soil divided by runoff volume for each time increment. Five tests were performed for the bare soil and each RECP. Three tests were performed for the bare soil with vegetation and each RECP with vegetation tests.

3. RESULTS AND DISCUSSION

Runoff SSC and turbidity results are presented for the bare soil and soil with vegetation tests on Figure 2. As shown on Figure 2a, SSCs were relatively high over a large range (approximately 0.007 to 0.014 g/ml) within the first 5 minutes of the bare soil tests, but decreased and leveled off 10 minutes into the tests, to an average SSC of around 0.007 g/ml for the remainder of the tested time. Turbidity results (Figure 2b) also varied over a relatively wide range initially, from 487 to 790 NTUs for the bare soils tested; however, unlike the SSC results, the turbidity results continued to increase for 10 minutes then leveled off at an average turbidity of 815 NTUs. This level of turbidity is within the range of values given by Minton and Benedict (1999) of typical surface water turbidity downstream from construction sites.



a) Suspended soil concentration results



b) Turbidity results

Figure 2. Runoff water quality results for bare and vegetated soil.

It is believed that during the initial 5 to 10 minutes of the tests, loose coarse and fine soil particles present on the soil surface were dislodged and transported with the runoff. The coarse soil particles rapidly fell out of suspension and did not significantly contribute to the turbidity of the runoff (Figure 2b), similar to observations by Holliday et al. (2003), who found that higher concentrations of eroded sediment did not necessarily translate into increased turbidity. After 10 minutes, both the SSC and turbidity results stabilized, with SSCs decreasing and turbidity increasing then leveling off. This indicates that once the coarse soil particles eroded from the soil surface, it was the eroded fine soil fraction along with organics that dominated runoff water quality results, eroding at a fairly constant rate, for the remainder of the tests. The eroded soil surface is shown on Figure 3a.

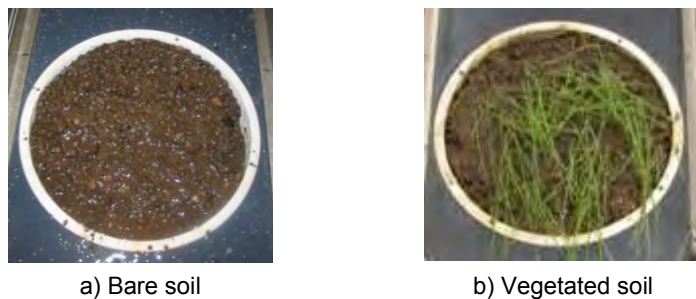


Figure 3. Comparison of eroded soil surfaces (20-cm diameter containers).

The SSC results for the vegetated soils fell within a relatively narrow range of 0.00248 and 0.0028 g/ml for the initial 5 minutes, then slightly increased and leveled off to an average of 0.00295 g/ml within 10 minutes (Figure 2a). Although the average initial vegetated SSC was 78% less than the bare soil SSC, turbidity results (Figure 2b) for the vegetated tests (404 to 793 NTUs) were initially similar to the bare soil tests (487 to 790 NTUs), with turbidity sharply increasing to bare soil levels at 10 minutes. After 10 minutes, however, the turbidity of the vegetated samples decreased to an average of 590 NTUs, approximately 28% less than bare soil turbidity levels. The effectiveness of the vegetation continued to increase as the tests progressed, due to the shoots falling down from vertical to horizontal, providing increased ground cover protection (Figure 3b), stabilizing within 20 to 30 minutes. The vegetation also provided root reinforcement, which minimized the detachment of soil particles. The relatively wide range in turbidity results can be attributed to the varying densities of ground cover provided by the vegetation. Table 2 shows the wide range of biomass results that can be obtained under controlled conditions (ASTM D7322).

Table 2. Vegetation results at 21 days (ASTM D7322).

RECP	No. of Shoots	Plant Height (cm)	Biomass (mg)
Vegetation alone	0-42	0-13	0-42
W1	36-44	1-16	65-70
S1	34-46	1-16	30-70
C2	31-36	2-14	45-65

Establishing vegetation is a common BMP for stabilizing bare soil slopes. Although the vegetation was effective in reducing the turbidity of the runoff in comparison to the bare soil tests, the turbidity levels were still higher than typically acceptable limits (typically 5 to 10 NTUs above background levels of 25 to 75 NTUs). The vegetation also provided a delayed response in minimizing turbidity. In these tests, turbidity did not start to decrease relative to bare soil conditions until 10 minutes into the tests (Figure 2a.) The quality and density of vegetation can also vary significantly, even under controlled conditions. Difficulties establishing vegetation in the field have been noted by several researchers (e.g. Fifield et al. 1988; Rickson and Morgan 1988.)

RECPs were developed to address some of the limitations of seeding or mulching alone. RECPs are manufactured into rolls that can be easily installed on a slope to provide immediate ground cover protection. RECPs also stabilize soil and seed within their structures, allowing seeds to germinate quickly and vegetation to grow, reinforcing vegetation once it is established. Figure 4 presents photographs of the three ECBs included in this study, coconut fiber C2 (Figure 4a), straw fiber S1 (Figure 4b), and wood excelsior fiber W1 (Figure 4c) during a rainsplash test.

The runoff SSC and turbidity results for the coconut (C2), straw (S1), and wood excelsior (W1) ECBs are given on Figure 5. The coconut ECB SSCs (Figure 5a) were in a relatively narrow range (between 0.00026 and 0.0029 g/ml) within the first 5 minutes, and leveled off to an average of 0.000511 g/ml within 15 to 20 minutes, approximately 92% lower than bare soil and 82% lower than the vegetated tests. Turbidity (Figure 5b) ranged between 186 and 500 NTUs within the first 5 minutes. Turbidity continued to decrease and leveled off at an average of 131 NTUs, 84% less than bare soil and 78% less than vegetated soil. It is believed that the long, randomly placed, dense fibers of the coconut ECB, coupled with its high ground cover percentage of 79.5% (light penetration of 20.5%), allowed the ECB to effectively intercept and reduce the kinetic energy of the majority of raindrops. The high water absorption value of 1218% also allowed the ECB to uptake water, increasing the weight of the ECB, allowing it to conform to the soil surface, reducing the energy of the runoff beneath the ECB. Vegetating the ECB further increased its effectiveness. Once the coconut ECB was vegetated, turbidity decreased to an average of 95 NTUs. This value is within 20 NTUs of typical upper limit background values.



Figure 4. Photographs of the ECBs (C2, S1, W1) during a rainsplash test.

The straw ECB SSCs (Figure 5c) ranged from 0.00238 to 0.00482 g/ml and decreased to an average of 0.00125 g/ml, approximately 82% less than bare soil and 58% less than vegetated soil SSCs. Turbidity (Figure 5d) varied within a relatively wide range within the first 5 minutes of the tests (between 556 and 929 NTUs.) Turbidity was actually higher for one straw ECB test than the bare soil tests (Figure 2b). However, unlike bare soil and vegetated tests, turbidity did continually decrease beyond this point, and stabilized to an average turbidity of 314 NTUs, 61.5% lower than bare soils and 47% lower than vegetated soil turbidity. Once the straw ECB was vegetated, turbidity decreased to an average of 94 NTUs, similar to C2.

The wood excelsior fiber ECB SSCs (Figure 5e) ranged from 0.00301 to 0.00504 g/ml and decreased to an average of 0.00111 g/ml, approximately 84% less than bare soil and 62% less than vegetated soil SSCs. Turbidity (Figure 5f) varied from 534 to 759 NTUs during the first 5 minutes, again similar to the bare soil tests (Figure 2b). However, as with the straw ECB, turbidity continued to decrease beyond 5 minutes and leveled off at an average value of 289 NTUs, 65% lower than bare soils and 52% lower than vegetated soil turbidity. Once the wood excelsior ECB was vegetated, turbidity decreased to an average of 73 NTUs, slightly lower than C2 and S1.

As with the coconut fiber ECB (C2), both the straw (S1) and wood fiber (W1) ECBs work by providing ground cover and conforming to the underlying soil surface. Although the wood fiber ECBs contained relatively long wood fibers, visible openings were observed in the ECB. Similar observations were made for the straw ECBs, which contained loose fibers between two nets. The straw fibers easily moved during the tests, creating clear openings through the ECB. The straw and wood fiber ECBs provided ground cover of 73% and 59%, respectively. The wood fiber and the straw fiber ECBs also have relatively low water absorption capacities, 228% and 556%, respectively, in comparison to the coconut fiber ECB (1218%). Although the fibers absorbed some water, the contribution of water by the straw and wood ECBs did not seem to make a significant contribution to the ability of the ECBs to conform to the underlying soil surface. RECPs are particularly effective when they are vegetated. The vegetation provides a second layer of defense, further reducing the impact of raindrops and runoff on the soil surfaces.

4. CONCLUSIONS AND RECOMMENDATIONS

This paper demonstrates that turbidity can be used as a measure to assess the performance of RECPs and that RECPs can have an immediate positive impact on downstream surface water quality. Although vegetation alone is commonly used to stabilize slopes, results from this study indicate that the use of vegetation alone may not be sufficient in meeting downstream water quality requirements, only reducing turbidity levels by 28% in comparison to bare soil turbidity. Although turbidity results for some RECPs were initially high, in the range of bare soil levels, turbidity continued to decrease and reached an average of 70% below turbidity levels for bare soil and 60% lower than vegetated turbidity levels, for the RECPs. This behavior was unlike that for the bare and vegetated soil, where turbidity levels increased before leveling off. Overall, fiber type plays an important role in an RECP's ability to absorb water, which assists RECPs in conforming to and adhering to the soil surface. RECPs are particularly effective in reducing downstream water quality once vegetated, providing downstream turbidities in the range of 73 to 95 NTUs, as compared to 815 NTUs for bare soil and 590 NTUs for vegetated soil.

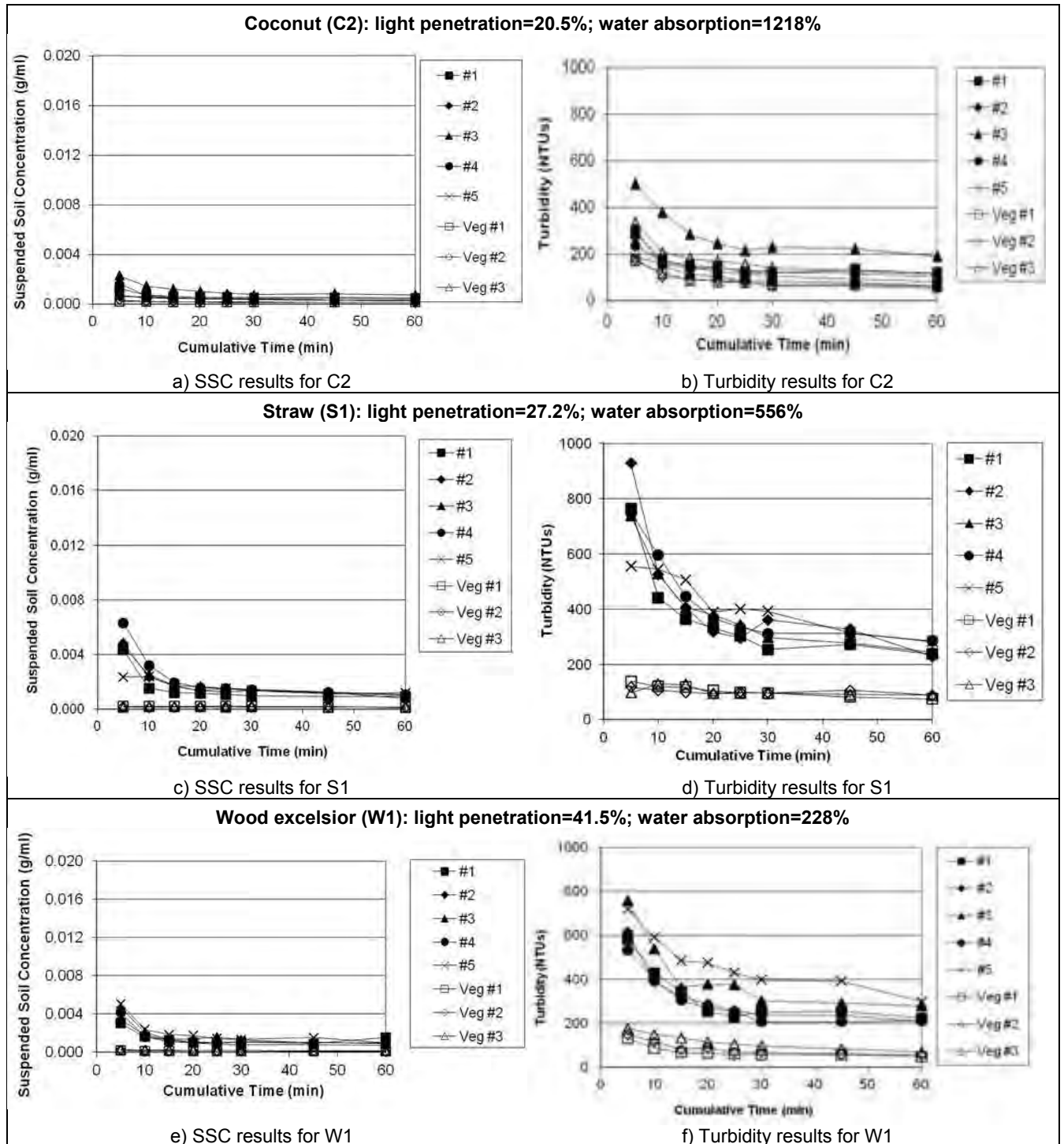


Figure 5. Runoff (a) SSC and (b) turbidity results for bare and vegetated soil.

ACKNOWLEDGEMENTS

The authors would like to acknowledge support received from the National Science Foundation (Award #3535848), the Department of Education (Foreign Language and Area Studies Fellowship in South Asia), and the Syracuse University Graduate School (University Fellowship Award), and the State University of New York College of Environmental Science and Forestry (SUNY-ESF) (Award #43263). The authors would also like to gratefully acknowledge Tony Johnson (American Excelsior Company), Bob Moran (Belton Industries), Roy Nelsen (North American Green), and Marc Theisen (Profile Products) for providing materials used in this study.

REFERENCES

- ASTM D 698. Standard Test Methods for Laboratory Compaction Characteristics of Soil Using Standard Effort (12 400 ft lbf/ft³ (600 kN m/m³)), *American Society for Testing and Materials*, West Conshohocken, Pennsylvania, USA.
- ASTM D 1117. Standard Guide for Evaluating Nonwoven Fabrics, *American Society for Testing and Materials*, West Conshohocken, Pennsylvania, USA.
- ASTM D 6475. Standard Test Method for Measuring Mass Per Unit Area of Erosion Control Blankets, *American Society for Testing and Materials*, West Conshohocken, Pennsylvania, USA.
- ASTM D 6525. Standard Test Method for Measuring Nominal Thickness of Permanent Rolled Erosion Control Products, *American Society for Testing and Materials*, West Conshohocken, Pennsylvania, USA.
- ASTM D 6567. Standard Test Method for Measuring the Light Penetration of a Turf Reinforcement Mat (TRM), *American Society for Testing and Materials*, West Conshohocken, Pennsylvania, USA.
- ASTM D 7101. Standard Index Test Method for Determination of Unvegetated Rolled Erosion Control Product (RECP) Ability to Protect Soil from Rain Splash and Associated Runoff Under Bench-Scale Conditions, *American Society for Testing and Materials*, West Conshohocken, Pennsylvania, USA.
- ASTM D 7322. Standard Test Method for Determination of Rolled Erosion Control Product (RECP) Ability to Encourage Seed Germination and Plant Growth Under Bench-Scale Conditions, *American Society for Testing and Materials*, West Conshohocken, Pennsylvania, USA.
- Babcock, D.L., and McLaughlin, R.A. (2011). Runoff water quality and vegetative establishment for groundcovers on steep slopes, *Journal of Soil and Water Conservation*, 66(2): 132-141.
- Bhatia, S.K., Smith, J.L., Lake, D., and Walowsky, D. (2002). A technical and economic evaluation of geosynthetic rolled erosion control products in highway drainage channels," *Geosynthetics International*, 9(2):125-148.
- Clopper, P., Vielleux, M., and Johnson, A. (2001). Quantifying the performance of hillslope erosion control best management practices, *Proceedings of Bridging the Gap: Meeting the World's Water and Environmental Resources Challenges*, World Water Congress 2001, 1:351.
- Fifield, J.S., Malnor, L.K., Richter, B and Dezman, L.E. (1988). Field testing erosion control products to control sediment and to establish dryland grasses under arid conditions, *Erosion Control - Stay in Tune: Proceedings of XIX IECA Annual Conference*, Louisiana, 327-341.
- Holliday, C.P., Rasmussen, T.C., and Miller, W.P. (2003). Establishing the relationship between turbidity and total suspended sediment concentration, *Proceedings of the 2003 Georgia Water Resources Conference*, held April 23-24, 2003 at The University of Georgia, Kathryn J. Hatcher, editor, 3pp.
- Kelsey, K., Johnson, T., and Vavra, R. (2004). Which degradable rolled erosion control product (RECP) should I use for slope protection? *StormCon*, 2004.
- Minton, G.R., and Benedict, A.H. (1999). Use of polymers to treat construction site stormwater, *Proceedings of the International Erosion Control Association (IECA) Conference 30*, IECA, Steamboat Springs, CO, 177-188.
- Nelson, D.W. and Sommers, L.E. (1996). Total carbon, organic carbon, and organic matter, *Methods of Soil Analysis, Part 3, Chemical Methods*, Soil Science Society of America Book Sec. 5, D.L. Sparks (ed.), Madison, Wisconsin, 961-1010.
- Packman, J.J., Comings, K.J., and Booth, D.B. (2002). Using turbidity to determine total suspended solids in urbanizing streams in the Puget Lowlands, <http://depts.washington.edu/cuwr/research/tssturb.pdf>.
- Rickson, R.J. (2002). Salient properties of erosion control geotextiles, *Proceedings of 33rd Annual Conference*, IECA, Orlando, Florida, February 2002, 499-506.
- Rickson, R.J. and Morgan, R.P.C. (1988). Approaches to modeling the effects of vegetation on soil erosion by water, *Geomorphology in Environmental Planning*, J.M. Hooke, ed., Wiley, Chichester, 51-62.
- Sims, C., and Cotching, B. (2000) "Erosion and water quality turbidity and sediment loads from selected catchments in north-west Tasmania," *Natural Resources Management Journal*, 3:1, 8-14.
- Smith, J.L. and Bhatia, S.K. (2006). The use of index and bench-scale tests for the characterization of RECPs, *Proceedings of Eighth International Conference on Geosynthetics*, September 18-22, 2006, Yokohama, Japan, 2:741-746.
- Smith, J.L. and Bhatia, S.K. (2009). Bioimprovement of soils for highway applications using rolled erosion control products, *Transportation Research Record: Journal of the Transportation Research Board*, No. 2108, Transportation Research Board of the National Academies, Washington, D.C., 117-126.

- Smith, J.L., Bryz-Gornia, C.J., Bhatia, S.K., and Walowsky, D. (2005). A comparative study of RECPs: lab testing and field performance, *Proceedings of GeoFrontiers 2005*, Austin, Texas.
- Smith, J.L., Davieau, M.R., and Bhatia, S.K. (2007). Evaluation of soil erosion using the rainsplash technique, *Proceedings of ASCE Geo-Denver 2007 Conference*, February 18-21, 2007, Denver, CO.
- Smith, J.L., Bhatia, S.K., and Sprague, C.J. (2010). Comparison of geosynthetic rolled erosion control product (RECP) properties between laboratories, *Scour and Erosion*, Ed. by S.E. Burns, S.K. Bhatia, C.M. Avila, and B.E. Hunt, *Proceedings of the Fifth International Conference on Scour and Erosion, Geotechnical Special Publication No 210*, American Society of Civil Engineers, 212-221.
- Sutherland, R.A. and Ziegler, A.D. (2006). Hillslope runoff and erosion as affected by rolled erosion control systems: a field study, *Hydrological Processes*, 20, 2839-2855.
- USEPA. (2007). *Developing Your Stormwater Pollution Prevention Plan*, EPA-833-R-06-004, May 2007.
- USEPA. (2009). *Drinking Water Glossary: A Dictionary of Technical and Legal Terms Related to Drinking Water*, Office of Water/Office of Ground Water and Drinking Water, http://ofmpub.epa.gov/sor_internet/registry/termreg/searchandretrieve/glossariesandkeywordlists/search.do?details=&glossaryName=Drink%20Water%20Tech/Legal%202009, updated February 17, 2009, accessed August 1, 2012.
- USEPA. (2012a). *Safe Drinking Water Act (SDWA)*, <http://water.epa.gov/lawsregs/rulesregs/sdwa/index.cfm>, updated March 6, 2012, accessed August 1, 2012.
- USEPA. (2012b). *Construction and Development, Status of Rulemaking to Revise Numeric Turbidity Limit*, <http://water.epa.gov/scitech/wastetech/guide/construction/index.cfm>, updated April 19, 2012, accessed August 1, 2012.
- Ziegler, A.D., Sutherland, R.A., and Tran, L.T. (1997). Influence of rolled erosion control systems on temporal rainsplash response – a laboratory rainfall simulation experiment, *Land Degradation & Development*, 8:139-157.

Trending Applications in Landfill Closure: Case Studies and Data on Exposed, Trenchless Covers

C.A. Eichelberger, American Environmental Group Ltd., USA
C.S. Kelsey, Geosynthetica, USA

ABSTRACT

This presentation will profile the United States' first large-scale designs and installations of exposed geomembrane covers that utilize a non-traditional, trenchless ballast approach. Four case histories and data from these sites will provide practical but forward-thinking design information on this new concept in geosynthetics and the solid waste industry. Data from these sites indicate that the design offers cost savings when compared to a ballast trench method, and provides a system that is more aesthetically pleasing and UV resistant than current ballast alternatives, such as ropes and sandbags. Cost savings are realized through construction methods and increased efficiencies, required equipment on-site, productivity of geosynthetic installation, and geosynthetic material quantities. Significant project schedule efficiencies are offered and provide a methodology that allows late-season construction and even construction during winter months in cooler climates.

1.0 INTRODUCTION: EMBRACING NEW TECHNOLOGY

The waste management field in the United States has routinely received the highest infrastructure grades in the American Society of Civil Engineers' (ASCE) *Report Card for America's Infrastructure*. The industry has benefited from deep interaction between all its key partners, resulting in dependable regulation, refined design, better construction, advanced waste stream management, beneficial reuse of former waste cells, improved operations and management practices on site, and the incorporation of renewable energy technologies. One thing that connects all aspects of the industry's consistent performance is an openness to new technologies and approaches that can improve environmental performance and the economic health of waste management facilities.

A new wave of exposed geomembrane covers (EGC) is one such technology that is giving numerous buried waste facilities a more flexible design and operational approach to save money on construction, create long term site value, and even reduce the carbon footprint of waste cell/closure construction practices.

Two types of EGC systems of note have emerged in the past few years:

- Exposed, trenchless ballast covers that utilize percussive driven earth anchors
- "Solar" EGCs, in which flexible thin-film photovoltaic laminates are adhered to the exposed geomembrane and provide long-term renewable energy generation that may be combined with landfill gas (LFG) to energy collection systems

The solar EGC systems have been well-publicized and discussed at major waste management engineering conferences; but the trenchless approach is a new and complementary process. Exposed, trenchless ballast systems will be the focus of this paper.

2.0 EGC ADVANTAGES

Exposed geomembrane cover systems offer a number of advantages over traditional, thick soil-covered systems. Of note:

- Greater cover stability
- No establishment / maintenance of vegetation above the cover soil (O & M advantages for the site)
- Reduction of hydraulic head
- Easier to spot/handle repairs
- Shorter construction time
- Much lower cap construction cost
- Potential for increased air space for waste after years of expected settlement

- Efficient stormwater control
- Improved odor/gas containment performance

Traditional thick soil cover layers, which already must have a geosynthetic system beneath them, are heavy and present a number of potential engineering problems, such as sliding of the soil along the membrane on a saturated slope or due to landfill gas pressure from beneath the cap. Slipping soil can tear the membrane as well, forcing not just a rebuild of the slope's vegetated soil-cover system but significant repair of the membrane cover and any affiliated system that might be affected (landfill gas, leachate management, etc.).

Removing the soil cover component and using only the geosynthetic membrane eliminates these types of cover stability concerns. Also, without soil to hold precipitation, potential hydraulic head acting upon the membrane has been neutralized. Stormwater runoff is cleaner and easier to manage in terms of sedimentation concerns. A tear in the geosynthetic cover, no matter the cause, is far easier to identify because it is on the surface and the repairs can be handled quickly.

In terms of cost, the absence of the earthworks necessary for thick cover soil placement and vegetation establishment is avoided. Furthermore, there are no long-term maintenance costs for mowing and re-seeding. Significant cost savings are also recognized due to the lack of trenching required to ballast the membrane system. (See section "ADVANTAGES OF TRENCHLESS BALLAST DESIGNS.")

3.0 EXPOSED COVER CHALLENGES

Exposed geomembrane caps, like all engineered systems, do have challenges that need to be overcome. Challenges have been addressed in various ways as the designs have advanced through lessons learned in the field. Exposed membrane challenges include:

- Wind uplift risk / membrane movement
- Landfill gas (LFG) system uplift
- UV exposure and thermal oxidation
- Less natural appearance
- Run-off volume management
- Animal/human traffic damage

Wind uplift and membrane movement concerns can be mitigated through proper selection of the geomembrane and anchoring systems (e.g., traditional anchor trenches and soil berms or the newer trenchless, geosynthetically anchored methods).

While exposed cover projects are gaining popularity as "voluntary closures" by landfill owners, many are still constructed in response to a site condition, such as odor, extreme leachate generation, etc. Therefore, a landfill gas collection system and more importantly a surface gas collection system, installed directly under the exposed cover membrane, is necessary for construction and performance of the system. The surface collection systems are not similar to the highly engineered primary gas collection systems, in that they typically consist of perforated plastic pipe in very shallow trenches beneath the membrane. Other examples include strips of geocomposite material that lead to the top of the closure with gas extraction ports where vacuum can be applied to the areas along the top of the cap.

Runoff management can be handled through normal bench, channel, and swale design and through other standard runoff controls on waste management sites. Sites with exposed covers generate more stormwater runoff, but the additional water is typically sediment free.

Most geosynthetic membrane formulations are tailored to specific performance goals, including UV resistance and protection against oxidation. Proper membrane selection can match the correct membrane to the site's conditions and the client's performance expectations of the system. Membrane material choice will vary based upon the expected lifetime of the exposed cover.

Standard landfill site security—such as fencing—can reduce, as much as possible, animal and human access onto the exposed membrane. Sites with exposed covers typically report little animal traffic on the membrane, as previous food and water sources are sealed with a membrane product that is not attractive to most wildlife.

And in terms of the site's aesthetics, the pigment of a membrane can be adjusted to take on visual characteristics of the area. There have been "camouflage" floating covers installed on reservoirs, for example, and green tinted membranes installed as an exposed cover on landfills (Figure 1).



Figure 1. The 40-mil textured high-density polyethylene (HDPE) exposed cap on the first use of the trenchless ballast approach in the United States used a green-tinted membrane to help the cap blend into the surrounding environment.



Figure 2. “Solar” exposed geomembrane cap on Hickory Ridge Landfill, Georgia.

4.0 EVOLUTION OF THE EXPOSED COVER DESIGN

Exposed geomembrane covers are not new solutions for landfill cell closure (see, for example, Gleason et. al), but they have not been utilized widely. Aesthetics (bare membrane vs. grass and vegetation) and questions about susceptibility to wind uplift and overall durability across a standard 30-year post-closure monitoring period have slowed both the acceptance of this application and innovation within this sector of design. But recent high-profile exposed cover systems (e.g., the “solar” membranes on the Tessman Road Landfill in San Antonio, Texas and Hickory Ridge Landfill, Atlanta, GA – Figure 2) and a new wave of R&D support have helped demonstrate the engineering, aesthetic, environmental and economic benefits of exposed geomembrane caps.

Adhering thin-film photovoltaic cells to the surface of exposed membranes has quickly moved from pilot projects to full-scale integration. A system that joins a surface layer of synthetic grass to the capping membrane has been developed. And, as this paper focuses on, a trenchless ballast system has been developed.

The trenchless system design has grown out of standard geotechnical anchoring solutions. At the four landfills cited in the case studies below, a percussive driven earth anchor installation system has been used—an approach commonly used for anchoring with sheet piles, gabions, tunnel liners, rockfall retention netting, bridges and in other applications. Applying them securely to membrane has been quickly successful.



Figure 3. The anchor installation requires only a small penetration of the membrane. Lightweight, common equipment is used to drive the corrosion-resistant anchors.

The anchors being used on these landfill covers are percussive driven earth anchors as used in other geotechnical applications. Corrosion-resistant steel cables are used and produce an overall 907KG load rated system, though they are not stressed to that level. The anchors are installed at typical depths of 1.2 – 1.8m and driven into the waste through a small penetration in the exposed membrane (Figure 3). While flexible membranes rated for long-term exposure (e.g., 45-mil EPDM) have been used for the cover membrane, the plates are connected to the membrane via a membrane patch (that matches the installed membrane, much as a normal penetration, such as a gas pipe penetration, would be dealt with) and an additional scrim-reinforced patch has been placed beneath the percussive anchors so that while the membrane may flex slightly the anchor point remains firmly in place.

IN PLACE LOAD TESTING OF EACH ANCHOR INSTALLED

The two-patch approach has resolved questions of resealing the geomembrane after driving in the anchor and securing the anchor plate to the geomembrane. The logical next question has concerned the waste, and it has quickly been confirmed that standard waste compaction practices have made the waste an ample medium for the anchor head to lock into inside of a few feet. The anchor installation equipment is lightweight, so it has not impacted equipment usage specifications on site, and allows easy readings of the load resistance of the installed anchor.

For HDPE geomembranes, the anchor load plate is adhered directly to the membrane surface.

Spacing of the anchors has varied based upon site characteristics (e.g., slope angle, expected wind/precipitation runoff conditions) and the specified material type (e.g., 40-mil HDPE, 45-mil EPDM, etc.).

5.0 ADVANTAGES OF TRENCHLESS BALLAST DESIGNS

The advantages of a trenchless approach include all of the advantages of an exposed geosynthetic cover as well as additional and considerable time and material-saving expense during installation. In the author's experience, traditional ballast trenches cost \$3.00 – \$4.50/m. The discussed ballast trenches should not be confused with typical landfill anchor trenches around the perimeter of new cell construction. Ballast trench excavation will encounter previously placed solid waste. The excavation of the solid waste produces odor and is typically constrained to daytime working hours of the site. The removed waste then needs to be replaced with suitable backfill materials that can be compacted to a specified density required for ballast of the exposed membrane cover. The excavated solid waste must then be transported to the active workface or to an offsite disposal location if the site is closed for waste acceptance. Additional hauling efforts are then required to supply suitable backfill material to be compacted into the excavated trenches. Offsite borrow material may be required for backfill of trenches if material of adequate quality and quantity is not available onsite.

Consider that standard ballast trench design requires the exposed membrane to be buried down and through the bottom of the trench, thus adding additional material to the order quantity. A ballast trench will require 1.5 – 2.1 meters of additional membrane (on a plan sheet detail), per LF of trench. Experience shows that excavating a defined trench through solid waste materials is difficult given the variations in solid waste. Therefore, trenches are usually much larger in the field and will utilize more material than anticipated. A 2.02 hectare exposed cover closure will contain approximately 2,285 – 3,050 meters of ballast trenching. When you add that to standard overlapping of membrane panels on site, overlap of trench-covering membrane welded to the previously installed membrane, and the oversized trenches caused by irregular waste materials, you then may be installing close to 3.6 hectares of membrane on that 2.2

hectare cell—with the lionshare of material “waste” being in the ballast trenches. This is a significant source of cost and carbon footprint increase due to materials used, labor, CQA and inspection, equipment, time, etc.

Trenches must be closed at the conclusion of every day, and liner material may not be left exposed without being anchored. As such, it is common to find liner installation crews waiting for trench crews to finish backfilling the most recently installed and seamed liner panels. Waiting on trench construction and backfilling adds to construction costs by forcing slower construction. A final item of significant cost / labor / and schedule associated with the trench ballast design includes the need to seam installed geomembrane to the geomembrane that was buried in a ballast trench. An extrusion seam is necessary in this application and is performed with hand welding equipment. Costs range between \$1.65 - \$2.25 / m and would be necessary for each meter of ballast trench, or \$55,000 - \$75,000 in the above 2.2 hectare example.

Excavation through cover soil / solid waste materials can also create additional factors to consider. The materials encountered when trenching through a landfill are not consistent and make a consistently sized trench difficult to impossible to construct. The irregular shapes of sidewalls and varying widths of trenches will create wrinkles in the geomembrane after backfilling of the trenches. Geomembrane wrinkles resulting from trenching activities are not a new concept to the landfill industry, but they can cause concern in exposed applications (such as when power generation from adhered photovoltaic cells is involved).

Table 1. Koerner’s (2011) analysis shows an exceptional advantage for exposed cap designs.

	Total Cost	Total CO₂ Footprint
Traditional Cap	\$916,000 / ha	652,400 Kg CO ₂ /ha
Exposed Geomembrane Cap	\$273,000 / ha	131,200 Kg Co ₂ /ha
Exposed Cap Savings	\$643,000 / ha	521,200 Kg Co₂/ha

The quick installation record for a trenchless ballast system reduces time spent running trucks and equipment on site. (In one of the case studies below, for example, the work window was reduced from 4-5 months to 1.5 months). While the carbon footprint reduction here is not on the scale that will make or break a project, it is a very healthy step for the construction field and another benefit for the waste management industry, which already invests considerable resources in environmental performance, R&D, and documentation. As such, whenever CO₂ issues can be reduced, they should be—especially when these strategies do not cost more and, in fact, save money.

For a detailed examination of the larger cost and sustainability benefits of exposed geomembrane caps, see Koerner (2011) and Ramsey (2011) (Table 1).

The following case studies summarize some of the project details, data and benefits the author has found at four early uses of the trenchless ballast EGC engineering strategy in the US waste management industry.

6.0 CASE STUDY #1: THE FIRST INSTALLATION

A large, municipal solid waste landfill needed to reduce landfill odors and chose to install an exposed geomembrane cover and landfill gas (LFG) collection system to manage this odor issue. Community complaints about the site’s odors and a desire to preserve their positive image had heightened the time-sensitivity of response to the odor and gas management issues. A seven-day work week program was established, but meeting all of the project’s fast-tracked goals, and finishing the work within budget, was made possible largely by two factors:

- The project utilized the first soil anchor ballast geomembrane cover design in the United States
- The contract used a single provider for all essential services (installation of geosynthetics, LFG design and construction, and primary operations and maintenance [O&M] services)
-

The trenchless, anchored ballast approach allowed for faster installation and lower job costs because it did not require nearly as large of a crew or suffer the delays commonly associated with trenching. The installation schedule was decreased dramatically, and the job cost was decreased. In this case, an installation of this size may have taken roughly

4 months, but ultimately took only 1.5 months due to using this geosynthetically anchored system. The owner selected to utilize a non-traditional approach in hopes of completing the work prior to winter, which would not have been achievable utilizing a trenching option, but also in hopes of creating a case study for the new technology and advancing the use of exposed covers to additional sites. The time savings, lesser need for heavy equipment, decreased quantity of geosynthetic material required, translated roughly to a 35% cost reduction for the project when compared to a trenched exposed cover design. In addition to the gas system installation and calibrating, only the liner then needed to be installed, anchored and inspected; versus, the trench-ballast approach which would have called for alternating stages of earthworks, liner installation, ballast trench excavation/backfill and inspection/compaction testing of the trenches. Also, if trenches had been used, open trenches during non-work hours would have been forbidden due to the sensitivity of odor emissions and safety concerns. All which would have led to a much longer construction schedule.

The installation involved roughly 186,000 m2 of 40-mil textured high-density polyethylene (HDPE) geomembrane. Because it was to be an exposed geomembrane, the material was tinted green by the manufacturer to better blend the special cover into the surrounding landscape. More than 4,290 meters of tie-in to the existing HDPE lined area was installed with 1,975 anchors installed to secure the liner in place without a need for the traditional trench. Some portions of the liner did not require anchors.

Additionally, more than 186,000 m2 of nonwoven geotextiles were installed for protection, drainage, and collection of gas beneath the geomembrane.

The trenchless ballast system approach allowed the LFG system to be installed with the liner installation and anchoring crews following close behind. This coordination was key to finishing the project quickly and successfully.

The odor issues were controlled by the combination of the covering anchored-membrane and the LFG system. Subsequent analysis has confirmed heightened performance of the gas collection system (Table 2). Off-site odor complaints ceased and the issue was controlled using the cover and operations and maintenance of the LFG collection system.

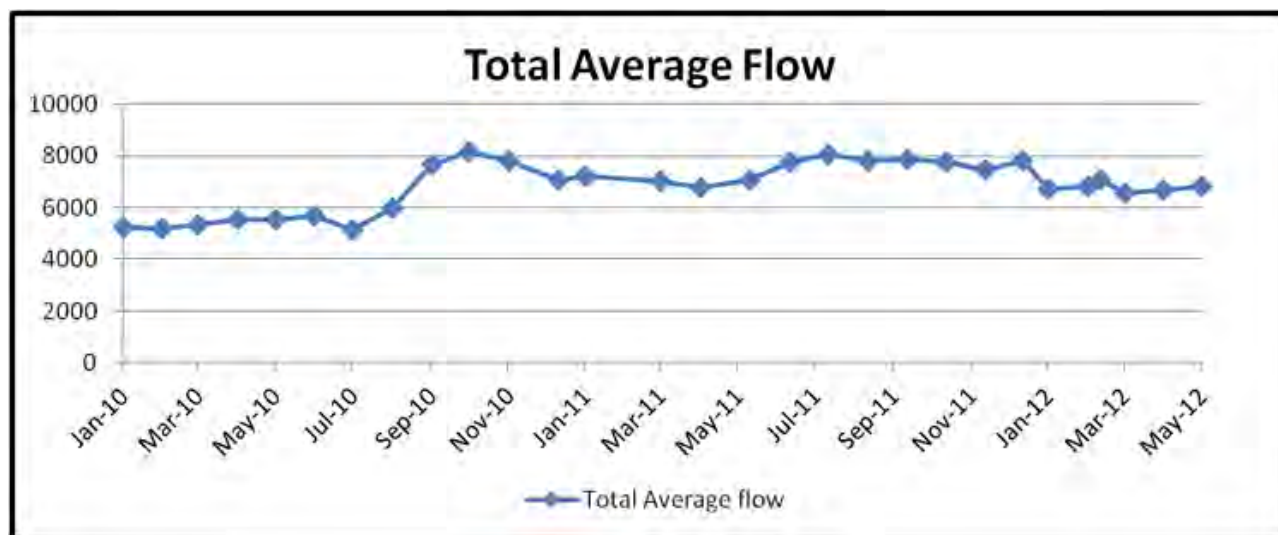


Table 2. Prior to the installation of Case Study #1's exposed cap (January 2010), the site gas flow was measured at 5228 CFM. As cap installation began (July 2010), gas capture increased, spiking in October 2010 (8150 CFM) when the last section of cap was installed.

7.0 CASE STUDY #2: RAPID RESPONSE TO ODOR CONCERNS

A municipal solid waste landfill in the southeastern United States installed a 40-mil high-density polyethylene (HDPE) exposed geomembrane cap with a trenchless ballast system that was tied into the existing HDPE cover system. The solid waste facility involved here was proactively addressing an odor concern from the site's landfill gas. The cover needed to be installed as quickly as possible and the geosynthetically anchored option provided a schedule of two weeks. A traditional trench-ballast response would have necessitated a two-month schedule.

As this work was ordered in October, the two-month schedule (associated with the ballast trench design) would have pushed construction too far into the winter/high moisture months to guarantee project completion.

The “trenchless anchor method” was chosen and the project was completed in two weeks. Work accomplished by the crew in those two weeks included the installation of:

- 81,290 m² of 40-mil textured HDPE over subgrade
- 10,405 m² of geocomposite with a 200-mil net
- 730 meters of tie-in seam to the existing HDPE-lined area
- Approximately 750 geomembrane anchors
- (15) 15 cm to 25 cm pipe penetrations
- 66 additional pipe penetrations

The scope of this work helped the site immediately address the landfill gas concerns, and the site operators have since reported (July 2012) nearing 100% on gas collection as estimated by their twice-daily gas readings.

The site operators have not attempted to quantify the leachate reduction, but when surveyed they estimated it to be “sizable.”

Importantly, they note that one of the greatest impacts of the exposed cap on their site has been in regards to their relationship with the community they serve. It has historically been a well-regarded site; the installation of the cap in a rapid-response manner has helped the operators quickly and economically maintain their community position while gaining additional long-term benefits to the site’s operations.

8.0 CASE STUDY #3: MORE EFFICIENT & ECONOMICAL

When a northern Midwestern landfill began an expansion plan simultaneously with relocating 1,000,000 ft.³ of waste from its original cell, the site operators looked to more efficiently manage stormwater runoff, control erosion, and reduce maintenance costs.

The site’s multiple cells have taken primarily municipal solid waste, though one ash pile—with a separated leachate and water management stream—is located on site.



Figure 4. 45-mil EPDM exposed cover installed in northern Midwest, with Phase I completed in November 2011 and Phase II in June 2012.



Figure 5. Percussion anchor installed on 45-mil EPDM exposed cap. An additional reinforced scrim patch is installed over the non-reinforced geomembrane to provide a significantly stronger attachment and pull-through resistance of the anchor to the geomembrane.

Two sections have recently been closed with an exposed interim cap. Totalling more than 46,500 m² of space, the choice to go with an exposed geomembrane cap and a trenchless ballast approach has replaced more than 3,000 m of ballast trench with roughly 1,000 percussion anchors. Both phases use 45-mil EPDM geomembrane with a 20+ year exposed service life.

A June 2012 installation secured roughly 0.4 ha of exposed membrane per day (Figure 4). Combined with other site activities (such as additional LFG pipe installation and maintenance checks) and a slight weather delay, the construction team was on site for only one week. A reinforced EPDM material was utilized in the areas of anchor attachment to provide a significant increase in strength of the anchor / geomembrane attachment (Figure 5).

The site does not currently convert landfill gas to energy, but the increased retention of LFG with the cap in place has drawn the interest of a developer with whom the site owner plans to work in 2013 on upgrading the gas collection system to an energy-generating operation. New gas header pipe is already being installed (July 2012). The site owner also reports an interest in converting another section of the landfill to an exposed cap in 2013.

9.0 CASE STUDY #4: USE OF NON-TRADITIONAL LANDFILL CLOSURE GEOMEMBRANE

For a northwest United States municipal solid waste landfill, more than 8 ha were secured with a 45-mil EPDM exposed geomembrane cap (79,000 m²). The site also incorporated a small amount of 40-mil green-tinted HDPE geomembrane (4,925 m²), to an existing exposed closure (Figure 6). Prior to this project, the site had installed previous exposed covers with varying degrees of success in terms of material performance and ballast option performance. The high amounts of precipitation allow for the financial expenditure on an exposed cover, given the cost savings on leachate treatment and the benefit of increased LFG collection.



Figure 6. Picture of Northwestern US exposed cap (Case History #4)

Various other geosynthetics were also incorporated into the construction, such as geomembrane for a rain flap and berms, geocomposite for gas collection and subgrade cushion, and geosynthetic clay liners for a tie-in anchor trench impermeable layer. The use of EPDM geomembrane provides the Owner the opportunity to make repairs / modifications to the liner given the ease of seaming and lack of specialty equipment required. The seaming supplies and techniques are shown below (Figure 7).

The trenchless ballast approach—the first of its type in the region—involved the installation of just under 2,000 geosynthetic anchors (Figure 8). These anchors replaced what would have been more than 6,000 m of ballast trenches. When considering the wider extent of work on the site, that trenching would have added a considerable amount of time and expense to the contract.



Figure 7. EPDM seaming procedure



Figure 8. Anchor installed to EPDM Geomembrane

In summary, the geosynthetically anchored ballast solution for exposed geomembrane covers offers a cost effective and “schedule enhancing” alternative to conventional ballast trenching of the geomembrane. A project can be completed in less than half the time and offer an additional advantages to those already recognized by exposed membrane covers.

REFERENCES

- Gleason, M. H., Houlihan, M. F. and Giroud, J.-P., 1998, “An Exposed Geomembrane Cover System for a Landfill,” Proceedings of the 6th ICG Conference, Atlanta, Georgia, Industrial Fabrics Association International, Roseville, Minn. pp. 211-213.
- Hullings, D. E., 2009, “Exposed Geomembrane Cover Details,” Proceedings GRI-22 Conference, Salt Lake City, Geosynthetic Institute, Folsom, Pa. pp. 77-85.
- Kelsey, C., 2009, “Geotechnical Applications of Solar Cells and Geomembranes,” Presentation from Waterproof Membranes 2009, Duesseldorf, Germany, AMI Conferences, Bristol, United Kingdom.
- Koerner, R., 2011, “Traditional Versus Exposed Geomembrane Landfill Covers: Cost and Sustainability Perspectives,” Proceedings GRI-24 Conference, Geosynthetic Institute, Folsom, Pa. pp. 182-197.
- Ramsey, B. and Eichelberger, C., 2011, “Reduced CO2 Emissions and Energy Consumption with Geosynthetic Installations,” Proceedings of GRI-24, Geosynthetic Institute, Folsom, Pa. pp. 159-162.

Unconfined Compressive Strength Behaviors of Fiber-fly Ash-soil Mixtures

Yuksel Yilmaz, Ph.D., Gazi University, Turkey, yyuksel@gazi.edu.tr

ABSTRACT

An experimental program was undertaken to investigate the effects of discrete polypropylene fibers and class C fly ash on the unconfined compressive strength (UCS) behaviors of the clayey soil. Two types of polypropylene fiber (fibrillated and multifilament) in two different lengths and two fiber dosages were utilized. The effect of the fly ash content on the UCS is superior compared to the effect of fibers. Inclusion of fiber without fly ash decreases the UCS of the compacted fiber-clay mixtures. On the other hand, when combined with the fly ash, the fiber inclusion increases the UCS depending on fiber type, length and dosage, and the higher the dosage of fiber the higher the UCS for both fiber types and fiber lengths are. At the end of 28 days curing period, the increase in UCS is up to 218% for 30% fly ash content and 1.0% 19 mm long fibrillated polypropylene fiber.

1. INTRODUCTION

Fine grained soils with high plasticity are not desirable for use as a structural support unless their engineering properties are improved significantly in an economic manner. For many years, extensive research has been carried out on the usability of some additives (lime, cement, fly ash, cement kiln dust, chemicals, fibers, etc.) to improve the engineering properties of fine grained soils.

The modification of fine grained soils with fly ash to improve their engineering properties is well recognized and widely practiced. Through stabilization, the plasticity of soil is reduced, and its compressive strength properties are improved. Several factors such as plasticity of soil, types and amounts of fly ash, mixing and compaction methods, curing conditions, gradation and pulverization, etc., affect the performance of stabilized soil. These issues have been previously discussed by several authors (Goktepe et al., 2008; Buhler and Cerato, 2007; Kate, 2005; Aydilek and Arora, 2004; Kumar and Sharma, 2004; Prabakar et al., 2004; Cokca, 2001; Misra, 1998; Sivapullaiah et al., 1996; Chu and Kao, 1993; Ferguson, 1993; Keshawarx et al., 1993).

In addition, a number of studies have been conducted for several years to investigate the influence of randomly oriented discrete fibers on the engineering behavior of mainly coarse grained or cohesionless soils. Discrete fibers are simply added and mixed with soil, similar to traditional additives.

Several studies have been carried out on the effect of randomly oriented discrete fibers on the geotechnical behavior of fine grained or cohesive soils. In these attempts, various types of discrete fibers are used (Jadhao and Nagarnaik, 2008; Kumar et al., 2007; Ozkul and Baykal, 2007; Rafalko et al., 2007; Ozkul and Baykal, 2006; Heineck et al., 2005; Loehr et al., 2005; Ang and Erik Loehr, 2003; Iasbik et al., 2002; Nataraj and McManis, 1997; Maher and Ho, 1994; Freitag, 1986).

In the present investigation, the effect of various fly ash contents, fiber types, fiber lengths and fiber dosages on UCS behavior has been investigated.

2. PROPERTIES OF MATERIALS

Various types of material (the Ankara clay, the Cayirhan fly ash and polypropylene fibers) used in the present study have been described below.

2.1 Clay

The soil used in this study was obtained from an open-cut excavation in Ankara, the capital of Turkey. The particle size distribution curves of the clay and the fly ash are shown in Fig. 1. Some of the basic characteristics of the Ankara clay and the Cayirhan fly ash are also summarized in Fig. 1.

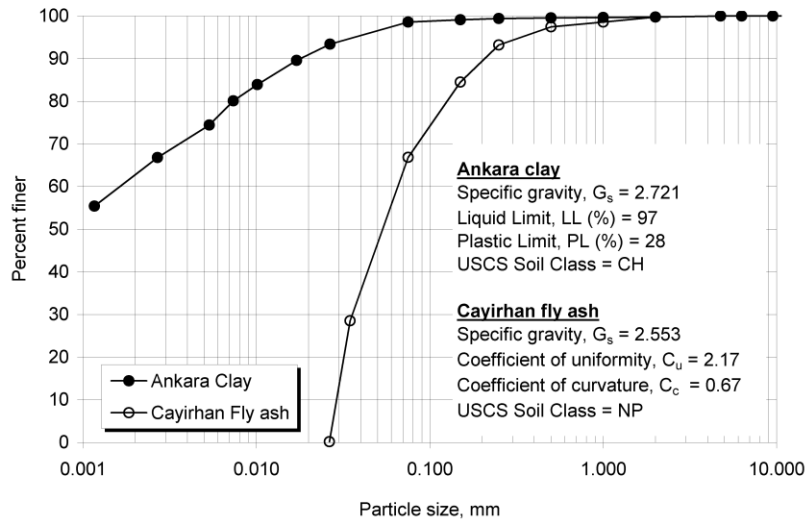


Figure 1. Particle size distribution curves and basic characteristics of Ankara clay and Cayirhan fly ash.

2.2 Fly Ash

The fly ash used for this study was obtained from Cayirhan thermal power plant in Ankara and it is referred to as the Cayirhan fly ash throughout the text. The chemical composition of the Cayirhan fly ash is presented in Table 1. Cayirhan fly ash classified as Class C fly ash (ASTM C 618-05).

Table 1. Chemical compositions of the Cayirhan fly ash and the chemical requirements for Class C fly ash according to ASTM C 618 standard.

Chemical Composition	Content (%)	Chemical Requirements for Class C fly ash, (%)
SiO ₂	49.72	-
Al ₂ O ₃	15.15	-
Fe ₂ O ₃	9.30	-
SiO ₂ + Al ₂ O ₃ + Fe ₂ O ₃	74.17	min. 50.0
CaO	13.1	-
MgO	2.97	-
SO ₃	2.60	max. 5.0
K ₂ O	2.00	-
Na ₂ O	2.37	-
Free CaO	0.74	-
Loss on ignition	1.00	max. 6.0

2.3 Fiber

Two different types of polypropylene fibers, namely fibrillated polypropylene fibers and multifilament polypropylene fibers, with two different lengths (6 mm and 19 mm) were used in the study. The fibrillated polypropylene fibers in length of 6.0 mm and 19.0 mm are denoted as F06 and F19, respectively. In a similar manner, the 6.0 mm and 19.0 mm long multifilament polypropylene fibers are denoted as M06 and M19, respectively. Table 2 shows some of physical characteristics of the polypropylene fibers provided by the manufacturer.

Table 2. The physical characteristics of the fibres (Ployfibres, 2009)

Properties	Fibrillated polypropylene fibre	Multifilament polypropylene fibre
Appearance	Fully oriented collated fibrillated (network) form	Fully oriented multifilament fibrous form
Content	100% virgin homopolymer Polypropylene(C ₃ H ₆)N	100% virgin homopolymer Polypropylene(C ₃ H ₆)N
Compliance	ASTM C 1116-1997 Type III	ASTM C 1116 1997 Type III
Density (g/cm ³)	0.91	0.91
Tensile strength (MPa)	400	700
Young Modulus (MPa)	2,600	3,500
Elongation at yield, %	15 %	20 %
Elongation at yield, %	15 %	20 %

3. COMPOSING FIBER-FLY ASH-CLAY MIXTURES

The design of fiber and/or fly ash mixtures was based on dry weight percentages of the fiber and the fly ash in the clay matrix. The proportions of dry mass of the fly ash to dry mass of the clay were predetermined as 0% (no fly ash) for the lower bound, 10% to representative for conventional range, and 30% for the upper bound. These three percentages of fly ash content were chosen to clearly reflect the effect of fly ash in a very wide range although the upper bound of 30% fly ash content is not practical in application. The proportions of dry mass of the fiber to dry mass of the clay were designated as 0.5% and 1.0%.

Standard Proctor compaction tests were conducted on 3 different fly ash-clay mixtures (0%, 10%, and 30% by dry mass of the fly ash to dry mass of the clay) without fiber inclusions according to ASTM D 698-00a standard. The maximum dry unit weight and the optimum moisture content of fiberless fly ash-clay mixtures were also used to prepare samples for strength tests of the fiber-fly ash-clay mixtures for all fiber inclusions.

The effect of polypropylene fiber type (fibrillated polypropylene fiber and multifilament polypropylene fiber), fiber length (6.0 mm and 19.0 mm) and fiber dosage (0.5% and 1.0% by dry weight of the clay) on the UCS was examined at the end of 28-days curing period.

4. PREPARATION OF FIBER-FLY ASH-CLAY SAMPLES FOR STRENGTH TESTS

A compaction mold was used to prepare cylindrical compacted samples of different fiber-fly ash-clay mixtures at optimum moisture content and maximum dry unit weight. The compaction mold was designed for specimens of the unconfined compression testing with a height-to-diameter ratio of 2.01 (50.0 mm in diameter and 100.50 mm in height).

5. UNCONFINED COMPRESSION TESTS

Unconfined compression tests were performed on the specimens using strain-controlled application of the axial load in accordance with ASTM D 2166-00 standard. In order to test all the mixtures under similar conditions and to isolate the effect of strain rate on the strength behavior, the strain rate was kept constant at 0.5 mm/min in the course of the testing program. Minimum three specimens were prepared for each combination of variables for the unconfined compression tests.

6. RESULTS AND DISCUSSION

6.1 Compaction Characteristics

The compaction curves of 3 different fly ash-clay mixtures (fly ash content from 0% to 30%) are shown in Fig. 2. With increasing fly ash content, the compaction curve shifted upward and toward the left, which indicates that the clay was stabilized by addition of the fly ash even at low water contents (Fig. 2). Furthermore, at given water content, the dry unit weight increases with increase in the fly ash content.

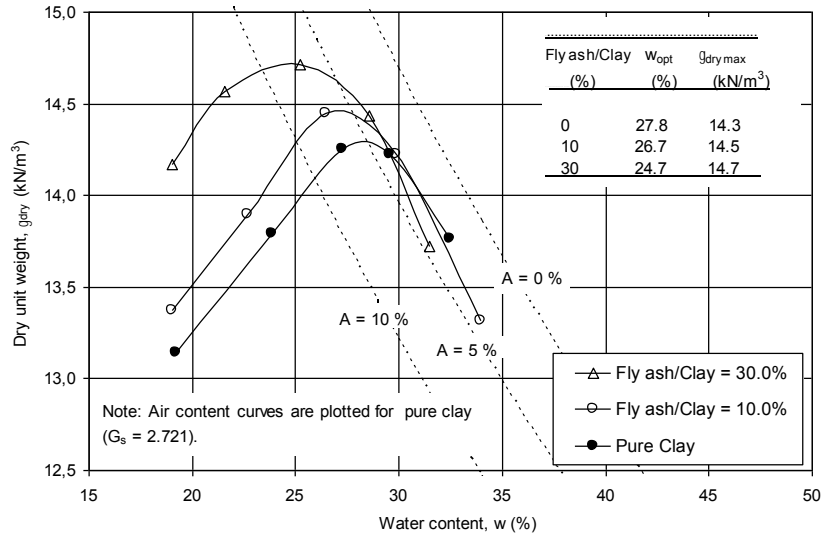


Figure 2. Standard Proctor compaction curves, maximum dry unit weight and the optimum moisture content of the fly ash-clay mixtures.

The maximum dry unit weight and the optimum moisture content of the mixtures are also shown in Fig. 2. As the fly ash content in the mixture increases from 0% to 30%, the maximum dry unit weight gradually increases from 14.3 kN/m³ to 14.7 kN/m³ while the optimum moisture content tends to decrease from 27.8% to 24.7% (Fig. 2).

6.2 Unconfined Compression Characteristics

The UCS of the compacted fiber-fly ash-clay samples was plotted with reference to fiber type and fiber length in Fig. 3 for each fly ash content and fiber dosage, separately. For determination of the UCS the failure deviator stress was taken as the peak deviator stress for the strain softening specimens and as the deviator stress at 15% axial strain for the strain hardening specimens. It is clearly seen from Fig. 3 that in spite of some exceptions, the higher the dosage of fiber the higher the UCS for both fiber types and fiber lengths is. For the mixtures with 10% and 30% fly ash contents (Fig. 3b and Fig 3.c) the effect of 0.5% M06 fibers on UCS is slightly greater than that of 1.0% M06.

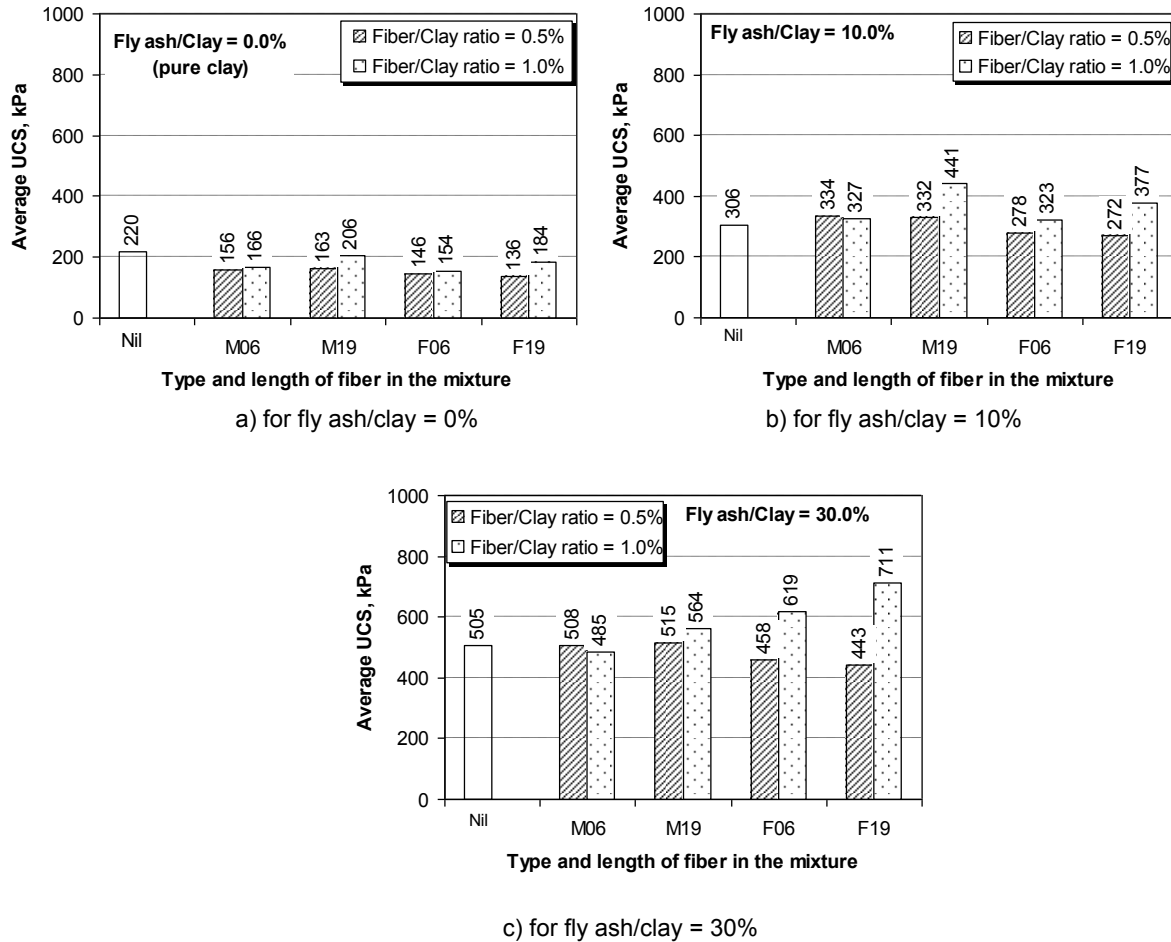


Figure 5. Variation of average UCS of 28 days cured fiber-fly ash-clay mixtures with respect to type and length of fiber in the mixtures

For the mixture with 10% fly ash content, the effect of multifilament polypropylene fibers (M06 and M19) is significantly higher than that of fibrillated polypropylene fibers (F06 and F19) at 1.0% fiber dosage. Moreover, the effect of 19 mm long fibers at 1.0% fiber dosage is slightly greater. Among the other fiber types, lengths and dosages, 1.0% M19 and 1.0% F19 give the highest increase and the second increase in the UCS, respectively. Addition of 1.0% M19 and 1.0% F19 further increased the UCS from 306.1 to 441.1 kPa (44%) and from 306.1 to 377.0 kPa (23%), respectively.

For the mixture with 30% fly ash content, the effect of the dosage on UCS is not significant for multifilament polypropylene fibers (M06 and M19) whereas the effect of fibrillated polypropylene fibers (F06 and F19) at 1.0% dosage significantly increases the UCS. While the 1.0% M19 gives the highest increase, 1.0% F06 and 1.0% M19 give the second and third highest increase in the UCS, respectively. Addition of 1.0% F19 and 1.0% F06, and 1.0% M19 further increased the UCS from 505.2 to 710.6 kPa (41%), 505.2 to 619.0 kPa (23%) and from 563.5 to 710.6 kPa (12%), respectively.

For the mixture with 0% fly ash content, inclusion of fiber reduces UCS except for 1.0% M19. Thus it may be concluded that addition of fiber alone does not improve the UCS of the clayey soil in fact it tends to decrease the UCS. Addition of fiber reduces the contact area of the clay-to-clay cohesive forces and increases the fiber-to-clay contact area at the failure plane. It is thought that depending on the soil plasticity, addition of fiber alone does not provide sufficient frictional resistance and addition of fiber tends not to improve the UCS. During shear, the fiber at the failure plane forced to orient in the direction of rupture in Fig. 4.

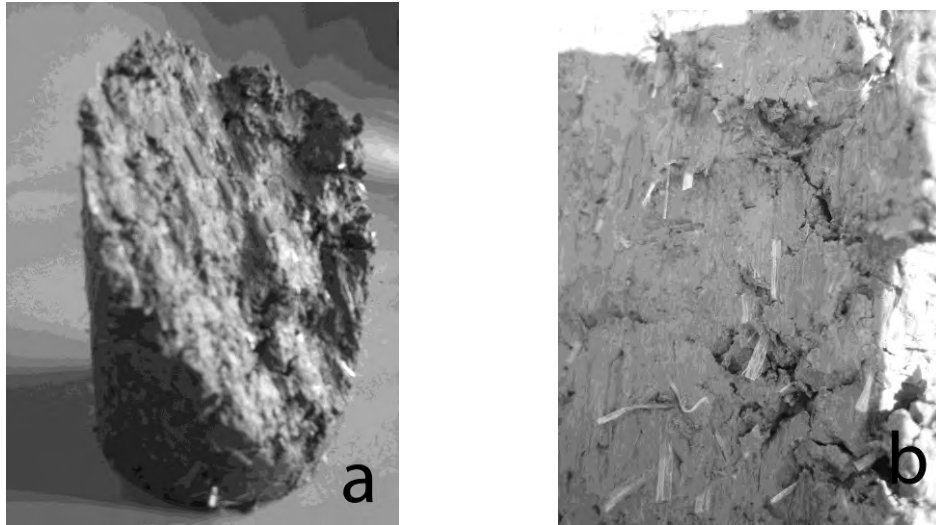


Figure 4. Typical failure surface for 0.5% F06 fiber-fly ash mixture a) parallel orientation of the fibers in the direction of rupture b) magnified photo of the failure surface.

7. CONCLUSIONS

An experimental study was conducted to investigate the influence of the fly ash (Class C) and randomly oriented polypropylene fiber (fibrillated and multifilament) inclusions on the stress-strain behavior and unconfined compressive strength (UCS) of high plasticity clay. The study results show that fibers have little effect on UCS for the soil tested. The conclusions of the study are as following.

1. This study showed that with an increase in the fly ash content the optimum moisture content decreases and the maximum dry density increases.
2. The frictional resistance between the fiber-to-clay contact areas is strongly improved by the fly ash inclusion and is proportional with fiber length and dosage. The effect of fiber type on the frictional resistance is less important.
3. Addition of the fly ash alone increased the UCS but inclusion of fiber alone (with no fly ash inclusion) negatively affects the UCS of clay. When combined with the fly ash, addition of the fiber increases the both UCS and residual strength considerably depending on fiber dosage, type and length. The effect of fiber type seems to be not significant on the UCS but the dosage and length of fiber considerably affect the UCS. The higher the dosage of the fiber and the longer the fiber length the higher the degree of improvement in UCS is.

ACKNOWLEDGMENTS

Financial support for this work was partially provided by Gazi University Scientific Research Project Grant No. BAP 06/2010-15.

REFERENCES

- ASTM C 618-05, 2006. Standard Specification for Coal Fly Ash and Raw or Calcined Natural Pozzolan for Use in Concrete. *Annual Book of ASTM Standards*, West Conshohocken, Pennsylvania, USA.
- ASTM D 698-00a, 2006. Standard Test Methods for Laboratory Compaction Characteristics of Soil Using Standard Effort (12,400 ft-lbf/ft³ (600 kN-m/m^{3Annual Book of ASTM Standards, West Conshohocken, Pennsylvania, USA.}
- ASTM D 2166-00, 2006. Standard Test Method for Unconfined Compressive Strength of Cohesive Soil. *Annual Book of ASTM Standards*, West Conshohocken, Pennsylvania, USA.
- Ang, E. C. and Erik Loehr, J. 2003. Specimen size effects for fiber-reinforced silty clay in unconfined compression. *Geotechnical Testing Journal*, 26(2), 191-200.
- Aydilek, A.H. and Arora, S. 2004. Fly ash amended soils as highway base materials. *Geotechnical Special Publication*, ASCE, n 126, 1032-1041.

- Buhler, R.L. and Cerato, A.B. 2007. Stabilization of Oklahoma expansive soils using lime and Class C Fly ash. *Geotechnical Special Publication, ASCE*, n 162, 1-10.
- Chu, S.C. and Kao, H.S. 1993. Study of engineering properties of a clay modified by fly ash and slag. *Geotechnical Special Publication, ASCE*, n 36, 89-99.
- Cokca, E. 2001. Use of class C fly ashes for the stabilization of an expansive soil. *Journal of Geotechnical and Geoenvironmental Engineering, ASCE*, 127(7), 568-573.
- Ferguson, G. 1993. Use of self-cementing fly ashes as a soil stabilization agent. *Geotechnical Special Publication, n 36, ASCE*, 1-14.
- Freitag, D.R. 1986. Soil randomly reinforced with fibers. *Journal of geotechnical engineering, ASCE*, 112(8), 823-826.
- Goktepe, A.B., Sezer, A., Sezer, G.I. and Ramyar, K. 2008. Classification of time-dependent unconfined strength of fly ash treated clay. *Construction and Building Materials*, 22(4), 675-683.
- Heineck, K. S., Coop, M. R., and Consoli, N. C. 2005. Effect of microreinforcement of soils from very small to large shear strains. *Journal of Geotechnical and Geoenvironmental Engineering, ASCE*, 131(8), 1024-1033.
- Iasbik, I., De Lima, D. C., Carvalho, C. A.B., Silva, C. H.C., Minette, E., and Barbosa, P. S.A. 2002. Geotechnical Characterization of a Clayey Soil Stabilized with Polypropylene Fiber Using Unconfined Compression and Resilient Modulus Testing Data." *ASTM Special Technical Publication, STP 1437*, 114-125.
- Jadhao, P.D. and Nagarnaik, P.B. 2008. Influence of polypropylene fibers on engineering behavior of soil-fly ash mixtures for road construction. *Electronic Journal of Geotechnical Engineering*, v 13 C.
- Kate, J.M. 2005. Strength and volume change behavior of expansive soils treated with fly ash. *Geotechnical Special Publication, n 130-142 & GRI-18, ASCE*, 1851-1865.
- Keshawarx, M.S. and Dutta, U. 1993. Stabilization of south Texas soils with fly ash. *Geotechnical Special Publication, n 36, ASCE*, 30-42.
- Kumar, B.R.P and Sharma, R.S. 2004. Effect of fly ash on engineering properties of expansive soils. *Journal of Geotechnical and Geoenvironmental Engineering, ASCE*, 130(7), 764-767.
- Kumar, A., Walia, B.S. and Bajaj, A. 2007. Influence of fly ash, lime, and polyester fibers on compaction and strength properties of expansive soil. *Journal of Materials in Civil Engineering, ASCE*, 19(3), 242-248.
- Loehr, J.E., Romero, R.J., and Ang, E.C. 2005. Development of a strain-based model to predict strength of geosynthetic fiber-reinforced soil. *Geotechnical Special Publication, n 130-142, ASCE*, 4037-4043.
- Maher, M.H., and Ho, Y.C. 1994. Mechanical properties of kaolinite/fiber soil composite. *Journal of geotechnical engineering, ASCE*, 120(8), 1381-1393.
- Misra, A 1998. Stabilization characteristics of clays using Class C fly ash. *Transportation Research Record*, n 1611, 46-54.
- Nataraj, M.S., McManis, K.L. 1997. Strength and deformation properties of soils reinforced with fibrillated fibers. *Geosynthetics International*, 4(1), 65-79.
- Ployfibers, 2009. Polyfibers analysis certificate. Ployfibers Micro Reinforcement Fibers Catalogue, Polipropilen Elyaf® Industry and Trade Co.
- Prabakar, J., Dendorkar, N. and Morchhale, R.K. 2004. Influence of fly ash on strength behavior of typical soils. *Construction and Building Materials*, 18(4), 263-267.
- Sivapullaiah, P.V., Prashanth, J.P. and Sridharan, A. 1996. Effect of fly ash on the index properties of black cotton soil. *Soils and Foundations*, 36(1), 97-103.
- Ozkul, Z. H., and Baykal, G. 2007. Shear behavior of compacted rubber fiber-clay composite in drained and undrained loading. *Journal of Geotechnical and Geoenvironmental Engineering, ASCE*, 133(7), 767-781.
- Ozkul, Z.H., and Baykal, G. 2006. Shear strength of clay with rubber fiber inclusions. *Geosynthetics International*, 13(5), 173-180.
- Rafalko, S. D., Brandon, T. L., Filz, G. M., and Mitchell, J. K. 2007. Fiber reinforcement for rapid stabilization of soft clay soils. *Transportation Research Record*, n 2026, 21-29.

Unique Approach to Dewatering of Mine Wastewater Residuals Using Geotextile Containers

Christopher Timpson, TenCate Water & Environment
Vicki Ginter, TenCate Water & Environment
TenCate Water & Environment, 3680 Mt. Olive Rd., Commerce, GA 30529

ABSTRACT

Mining and mineral processing is vast and complex industry. There are a variety of applications requiring the management of waste streams from the processing of raw coal, removal of tailings and fines from settling ponds, and treatment of thickened wastewater sludge. As in remediation projects, governmental regulations dictate what mines can and cannot do in terms of handling their waste streams. In some areas underground storage of process waste is allowed, in other states there is a moratorium on underground storage. Sometimes in states that allow underground storage, there may be temporary situations that require an alternative storage.

This paper will address how geotextile containers offer a unique high volume, low cost de-watering system to provide a very effective way of dewatering wastewater residuals in mining applications.

1. GEOTEXTILE CONTAINER DEWATERING TECHNOLOGY

Geotextile containers have been used since the 1960's as shoreline protection in marine and river structures such as breakwaters, dikes, artificial islands, and jetties. Over the years, this technology has transferred into the dewatering of wastewater with the aid of chemical conditioning. There are three basic stages to dewatering with geotextile containers which are confinement, dewatering, and consolidation (See Figure 1). The specially engineered textile which the geotextile containers are fabricated allows confinement of the fine solids inside the container but allows water to filter for dewatering. As the water drains, the solids continue to densify inside the geotextile container and the volume inside the container continues to consolidate over time.



Figure 1. Three basic stages of geotextile container dewatering.

A dewatering cell must be constructed to hold the geotextile containers (See Figure 2). In most cases the available area for construction of a dewatering cell is limited but geotextile containers can be manufactured in many configurations and sizes to maximize the available footprint. Creating a slight grade with the slope in the length direction of the geotextile containers promotes drainage of the filtrate for better collection. An advantage of geotextile containers is that they can be stacked in a pyramid configuration several layers high depending on the consolidated characteristics of the dewatered solids.



Figure 2. Geotextile containers inside dewatering cell

Generally this cell has an impermeable membrane installed to help control the volume of effluent which drains through the containers. Typically the effluent is returned back into a body of water, and in some instances can be directly discharged if the filtrate quality meets reporting limits. The wastewater can be dredged or pumped directly into geotextile containers.

If the flow of wastewater is extremely high, a manifold system can be installed which allows multiple containers to be filled at one time to maximize dredging output. The primary feature of a geotextile container is to retain solids and contaminants while permitting effluent to drain through the pores of the woven engineered filtration textile. During all phases of the dewatering process (filling, dewatering and consolidation), the filtration textile must provide excellent tensile properties, efficient effluent drainage, and effective retention of solids to guarantee optimum slurry dewatering. The filtration properties of the engineered textile permit the containers to capture the solids, while water drains out. The moisture will continue to filter out and solids will continue to dry over time promoting more volume consolidation. Using the appropriate polymer for chemical conditioning will allow for the solids in the wastewater stream to create an agglomeration and release free water for drainage. Figure 3 shows typical results of geotextile container dewatering with a depiction of filtered effluent, conditioned slurry, and in-situ slurry.



Figure 3. Results of dewatering with geotextile containers showing filtrate, conditioned slurry, and in-situ slurry.

Chemical conditioning optimizes the dewatering performance of geotextile containers, increasing the dewatering rate, improving effluent quality, and achieving higher dry mass. The chemical conditioning of the wastewater occurs before the slurry is pumped into geotextile containers to accelerate dewatering

Once the solids are fully consolidated or have met minimum requirements for transport, several options are available for disposal. Typically after consolidation, the geotextile containers can be cut open and solids transported to landfill or land applied. In some applications, the containers can be buried in place allowing the dewatering area to be reclaimed.

2. PROCESSING OF RAW COAL PROCESSING

Conventional disposal methods of surface impoundment or injection into abandoned underground mine workings is not always possible. Regulatory restrictions, available area, and construction scheduling can create possible interruptions to the primary disposal methods for mining refuse. Geotextile containers can offer an alternative disposal method for wastewater and allow for the coal processing to continue operation without disruption.

A coal processing plant faced an issue where it was facing a possible interruption of its operation which involved a waste stream of almost 1.5 million gallons of slurry per day. Continued production of coal was needed in order to meet shipment demands, and geotextile containers were chosen as an alternative to prevent any shutdown.

The plant's normal operation created two waste streams from the impurities of processing raw coal, which were composed of rock and fire clay. Both coarse rock and fine rock particles are produced during the process, the coarse rock is sent to a refuse disposal area by conveyor and fine rock particles are slurried and disposed.

Due to the volume of slurry to be processed, the coal mine needed a safe and efficient plan that would allow the containers to be reclaimed in place instead of opening them up and transporting the material to the coarse refuse disposal area. In order to maximize utilization of the available dewatering area, a stacked pyramid of four layers of geotextile containers was designed for one particular dewatering area. The additional layers were installed and stacked once the consolidated material reached 35% dry weight solids. The complete project required three dewatering cells. Figure 4 is an illustration of the dewatering cell and progression of the stacked containers.



Figure 4. Dewatering cell and stacking progression.

A manifold system, along with a polymer tank and pumps was implemented to fill and manage the flow to multiple containers at once. A swinging ladder 8-inch dredge was placed into the slurry pond to pump the slurry into the containers. The dredge was initially operated on a 24-hour basis with two 12-hour shifts. A crew of five to six men operated the dredge plus managed the filling and dewatering of the containers.

This set-up was capable of pumping 1,750 cubic yards per 24-hour day. The completed project utilized 240 geotextile containers, and a total of 200,000 cubic yards were pumped and dewatered. The average holding capacity of the geotextile containers was 5 cubic yards of solids per linear foot of container.

Once all the containers in the dewatering cell were fully dewatered, the site was then ready for reclamation. Eventually, the containers were covered with earth and then topsoil. Once reclamation was complete, the entire dewatering cell was mulched and seeded. All three dewatering cells were covered and reclaimed. During the reclamation process, a layer of

sand was first applied to cover the containers and provide a filter medium. Next a layer of limestone was installed for drainage, and then containers were covered with earth and topsoil.

3. REMOVAL OF TAILINGS & FINES FROM SETTLING PONDS

Many aggregate plants experience high equipment and manpower costs associated with the handling and removing of tailings and fines from settling ponds. The costs of maintaining pond operations can vary significantly from plant to plant. Not only is valuable space tied up during gravity settling and thickening the materials in the settling ponds, but the ability to calculate the overall costs for mechanical dewatering, removal, and disposal costs of fines can be difficult.

Smaller plants face a more difficult challenge since the capital, maintenance, and operating expense of mechanical dewatering equipment for the removal of clays and fines from plant effluent is beyond their budgetary means. Aggregate plants find it necessary to explore and evaluate other dewatering options.

Several states are revising permits aimed at protecting water quality from the pollution discharged by sand and gravel operations. These facilities can include sand and gravel mines, rock quarries, clay mines, concrete batch plants, and asphalt plants. Federal and state laws require a permit because these operations discharge water that may be polluted, such as sediment from gravel washing, oil and grease from trucks and heavy equipment, and alkaline wastewater from concrete plants. The permit requires companies to take steps to ensure that surface and ground waters are protected and to monitor water quality on a regular basis.

Dewatering with geotextile containers is a cost effective alternative to mechanical processes. Plant effluent can be pumped directly from the process or, if a clarifier/thickener is used, effluent from the underflow can be diverted through a geotextile container, eliminating the requirement for expensive mechanical dewatering units. Table 1 illustrates the effectiveness of dewatering aggregate tailings with geotextile tubes.

Table 1. Effectives of Dewatering with Geotextile Containers with Aggregate Tailings

<i>Material Type</i>	<i>% Solids During Pumping</i>	<i>Dry Solids after 1-Day</i>	<i>Dry Solids after 3-Days</i>	<i>Dry Solids after 15-Days</i>
Clarifier inflow with Polymer	8%	27%	45%	71%
Clarifier outflow with Polymer	31%	43%	55%	70%
Aggregate Tailings with Polymer	26%	42%	67%	86%
Pond Material with no polymer addition (high solids in filtrate)	26%	NA	36%	79%

Geotextile containers can be used to capture fines, silts, and clays from the tailings effluent prior to discharge into the ponds or directly into streams. The containers will separate and dewater the fines and allow disposal without expensive dredging and transporting operations.

4. DEWATERING OF ACID MINE DRAINAGE

A mining company was faced with a challenge to reopen a pit mine which had been converted into a tailings pond for nearly a decade. The mining company desired to extract zinc from the former pit mine, now a tailings pond since the value of zinc had increased. Restarting the operation also required refurbishment of the waste water treatment plant. Figure 5 shows the condition of the open pit mine at the start of the project.



Figure 5. Former pit mine converted into tailings pond.

The challenge of the operation required the removal of 392,000 cubic yards of zinc-contaminated water from the pit mine and dewatering 41,000 cubic yards of sludge. Of the potential options to either dewater the sludge with mechanical systems or build a storage pond on-site; geotextile containers were chosen for dewatering and temporary containment. The project began by adding lime to the tailings pond to raise the pH and precipitate metal ions. The addition of the lime to precipitate zinc created a need to inject CO₂ to balance the pH of the water during removal. This process left the need to dewater 41,000 cubic yards of sludge comprised tailings and addition of lime with geotextile containers. The limited area to construct a dewatering cell required two layers of containers in a pyramid stack to maximize the area, see Figure 6.



Figure 6. Two layer pyramid to maximize available area.

There was an additional benefit of the geotextile containers which allowed the mine to contain the sludge onsite for transport and disposal at a later time. Filtrate results showed that the geotextile containers in conjunction with proper chemical conditioning produced zinc leachate concentrations below the discharge limit of 250 ppb.

5. TREATMENT OF THICKENED WASTEWATER SLUDGE

Typically, thickened wastewater sludge from underground mines is pumped back underground. West Virginia has discontinued issuing new permits for underground wastewater storage. Geotextile containers can contain and dewater the thickened sludge and provide an efficient alternative to liquid hauling of the sludge to the refuse pile.

A particular coal mine produced approximately 2 million gallons of raw mine water per day which is pumped out of the underground mine. The wastewater containing coal fines, iron, and manganese salts is pumped to a neutralization tank where it is treated with hydrated lime and oxygen. The treated water in the neutralization tank overflows into the thickener. Flocculants are added in the overflow trough and thickened solids settle to the bottom of the tank, allowing clear water to overflow from the top to the discharge.

Rakes direct the solids at the bottom of the tank to a center well pump. From there, the solids at 15% by dry weight are pumped to geotextile containers. A dewatering cell was constructed near the wastewater treatment plant and containers were placed on an aggregate base for good drainage. Clean filtrate is collected in a pond and a submersible pump returns the filtrate to the thickener.

After one week the dewatered solids typically reach 33% dry weight solids and continue to consolidate over additional weeks to 67% dry weight solids.

6. CONCLUSIONS

As in remediation projects, governmental regulations dictate what mines can and cannot do in terms of handling their waste streams. In some areas, underground storage of process waste is allowed but in other states there is a moratorium on underground storage. Sometimes in states that allow underground storage there may be temporary situations that require an alternative storage. Likewise, the mines are accountable for contaminants in their waste streams. Case in point is a metals mine where a pond had to be closed pond. For several years wastewater had been stored in the pond due to nitrate contamination.

Acid mine drainage is heavily regulated in all mining areas and all these issues create opportunities for dewatering in geotextile containers. These opportunities may not have existed if not driven by regulations. Mining and mineral processing offer a variety of applications where geotextile containers offer a unique solution to dewatering of wastewater residuals.

REFERENCES:

- Watts, Mike. Trainer, Edward. 2009. *Disposal of Coal Slurry Waste Using Geotextile Containers at the North River Mine. Case Study.*
- Douheret, Jocelyn. Trainer, Edward. Lister, Andy. Hauthier, Stephen. 2009. *The Use of Geotube® Bags for Dewatering The Restigouche Open Pit Zinc Mine and Settling Pond Basin in, New Brunswick, Canada.* Geosynthetics 2009, Salt Lake City Utah.

Use of an Innovative Geocomposite to Construct a Reinforced Soil Slope using Marginal Fill Soils in Canada

Michael Simons, P.Eng., Maccaferri Canada Ltd., Canada, msimons@maccaferri.ca

ABSTRACT

The use of clayey and silty soils (marginal fill soils) in reinforced soil slopes and walls is usually avoided due to the low shear strength of these soils and the buildup of excessive pore pressures within the reinforced soil mass during compaction operations. On sites where these soils predominate and it is necessary to construct reinforced soil structures, it is not uncommon to import higher quality soils for use in the construction of these structures, usually at considerable cost to the project.

An innovative geocomposite reinforcement grid has been developed that combines reinforcement and drainage characteristics into a single geocomposite geogrid that allows for marginal fill soils to be used in reinforced soil applications. Significant cost savings were realized by using readily available marginal fill soil for the construction of an earth embankment in a large urban area in Southern Ontario. This paper will discuss the first use of this innovative geocomposite in North America.

1. INTRODUCTION

Many construction sites in urban areas are generators of excavated earth materials that may be unsuitable for reuse on site as structural backfill due to high fines and possible contamination. Some of this material may be used for general landscaping or other non-structural applications. Generally, most of these excavated soils are disposed of offsite. Increasingly, these soils are being exported to dump sites or new developments located at increasing distances from the source. This results in an increase in the amount of transit time for each load to be disposed, as well as a cost for disposal.

Reinforced soil structures consist of a series of planar tensile elements arranged in horizontal planes placed at a defined vertical spacing within a mass of engineered backfill. They are conventionally designed (FHWA 2009) and constructed using free draining granular soils. These soils have relatively high shear strength and are able to rapidly dissipate pore water pressures that develop in the reinforced soil mass. The use of high quality soils provides a material that is well understood, easily worked and minimizes post construction movement of the soil mass. When available at a reasonable cost, these high quality soils can provide a cost effective solution for the construction of soil retaining structures. Sources of high quality fill soils are increasing located at greater distances from urban construction site, resulting in longer transit times for truckloads of material.

A reinforced soil slope is a form of reinforced soil structure with an outward face of the reinforced soil mass that is typically inclined at greater than 26° from the horizontal, but usually no steeper than 70°. The facing is typically a flexible system that will tolerate movement and deformation, usually vegetation, but it may also consist of some form of flexible armor. With a flexible facing, these structures are capable of tolerating movement and deformations. The use of cohesive and marginal fill soils within reinforced soil slope is possible, but not commonly done in Canada.

Due to the high content of fine grained particles, cohesive and marginal fill soils are usually low permeability materials. When low permeability soils are subjected to loading, excess pore pressures can develop. This increase in excess pore pressure can lead to a reduction in the available shear strength of the soil. The bond between a soil reinforcement and the soil may also be reduced, requiring more reinforcement in order to provide adequate bond length. The dissipation of the excess pore pressure over a period of time will result in consolidation and settlement of the reinforced structure. This consolidation may result in unacceptable deformation of the reinforced soil structure.

Research (Zornberg & Mitchell 1994, Kempton et al 2000) has shown that cohesive and marginal soils can be used effectively in the construction of reinforced soil structures provided that adequate drainage has been incorporated into the design. With cohesive and marginal fill soils, the friction angle is generally lower than a high quality fill soil. A lower friction angle and the presence of pore pressures within the soil mass can significantly reduce the interaction between the soil and reinforcing elements. Dissipating the pore pressures locally around the soil reinforcement has been shown (Kempton et al 2000) to increase the interaction with the reinforcement and increasing the overall stability of the soil mass.

As long term post construction movement and deformations are a possibility with the use of lower quality soils, the use of cohesive and marginal fill soils is usually limited to reinforced soil slopes. Marginal or poor quality soils are usually defined as soil having more than 15% passing the 0.075mm sieve and with plasticity index of greater than 6 for walls, and greater than 20 for slopes (FHWA, 2009).

An innovative geocomposite has been developed that combines the functions of soil reinforcement and drainage for use in stabilizing steep slopes in conjunction with marginal and cohesive soils. This paper will discuss the first usage in North America of this innovative geocomposite, or draining geogrid, that has been designed solely for use as reinforcement for cohesive and marginal fill soils.

2. GEOCOMPOSITE REINFORCEMENT GEOGRID

2.1 Description of Innovative Geocomposite

The geocomposite soil reinforcement consists of high tenacity multifilament polyester yarns that are placed in tension and then co-extruded with a polyethylene sheath into strips. The combination of polyester and polyethylene polymers in a single strip provides high tensile strength and superior creep performance of the polyester while having the superior installation damage resistance of the polyethylene.

The polyethylene sheath is profiled to provide a shaped drainage channel. The drainage channel is oriented parallel to the load bearing axis of the polyester yarns, providing drainage along the direction of tensile loading in the reinforced soil zone. The profiled element has a thermally bonded nonwoven geotextile strip bonded on the shoulders of the drainage channel. The geotextile allows excess pore water pressure to dissipate while retaining the cohesive soil. The profiled strips are either 24mm or 33mm wide. The thickness of the strips varies from 2.1mm to 2.6mm, depending upon the strength of the strips.



Figure 1. Multiple extruded elements welded into geogrid roll (after Linear Composites)

Multiple polymeric strips are laid flat in the machine direction and a secondary member is laid in the cross direction and heat welded across the full width of the strip cross section at a 75mm centre to centre spacing. The geocomposite is available in a range of strengths from 50 kN/m up to 200kN/m (machine roll direction). The transverse strength of the material is constant at 15kN/m.

2.2 Geocomposite Concept

The laboratory performance of the geocomposite has been studied and reported by numerous authors (Kempton et al 2000, Naughton & Kempton 2004, Zornberg & Kang 2005, O'Kelly & Naughton 2008). A geogrid that is manufactured in a very similar manner to the geocomposite, but without a drainage profile, has been used for comparison purposes in these studies to quantify the improvement in interaction. Pullout resistance in testing improved 20% or more in various studies (Zornberg & Kang 2005, Clancy & Naughton 2010). Kempton *et al.* (2000) reported that when tested with English China Clay (coefficient of consolidation 1.3 to 2.3m²/year; permeability 1.07x10⁻¹⁰ to 2.43x10⁻¹⁰ m/s), excess pore water dissipated to 20% of the initial value in 32 hours, pore pressures measured at various distances from the geocomposite did not reach the applied confining stress, nor did there appear to be a difference in pore pressure dissipation above or below the geocomposite even though the drainage channel was only on one side. A good correlation between the volume of water displaced from the test cell and the measured dissipation of pore pressures was found. No clogging or washing through of fines into the drain was noted.

These studies have demonstrated that the geocomposite is effective in dissipating excess and increasing the shear strength of soils that would traditionally have been classified as cohesive or marginal fills and that would not have been normally used to construct a reinforced soil embankment.

Naughton et. al (2001) proposed a design methodology that incorporates dissipation times and settlements during the construction of reinforced slopes. The vertical spacing of geocomposite is determined based upon the consolidation behaviour of the fill soils. The goal of the design method is to dissipate any excess pore water pressures present in the slope during the construction stage to control vertical and horizontal deflections so as to occur during construction. A target of 80% as an average degree of consolidation is desirable at the end of construction of each lift. A vertical spacing of 0.5m between layers of the geocomposite is recommended as an initial starting spacing. A vertical spacing of 0.5m would facilitate construction of a maximum fill thickness in a period of approximately 24 hours. This time period would allow for the placement and compaction in one day of 0.5m of fill, making the construction of a reinforced marginal or cohesive soil embankment efficient.

2.3 Usage of Geocomposite

The use of geocomposite has been documented by Naughton & Kempton (2004) for the reconstruction of a slope failure in Taiwan in 1999, and by Veggi & Parla (2009) to construct part of the capping layer for a municipal solid waste landfill in Italy. The geocomposite has also been used to construct a berm in the United Kingdom (Maccaferri, 2001). These projects have used poor quality soils reclaimed from the site, or used imported cohesive soils.

3. NORTH AMERICAN USAGE

3.1 Site Location and History

The multi-phase conversion of a former industrial site within the City of Toronto, Ontario, Canada, into a residential infill development has been ongoing since 2005. The site is bounded along the north by Davenport Road, Lansdowne Road along the east and an active railway line along the western boundary. The three previous phases of redevelopment at the site required the staged construction of an earth berm aligned parallel to the railway line to act as a noise and crash berm. Reinforced soil embankment structures have been used for the construction of the berm in order to minimize the footprint of the berm. These reinforced soil berms were all constructed using imported fill soils that ranged from gravelly sands to silty sands, depending upon the type of material that was available during construction.

3.2 Phase IV Original Embankment Design

The fourth phase of development and the associated earthworks for the construction of the berm began in 2011. The berm was originally designed to be built as a 4.2m high, vegetated reinforced soil slope inclined at 60° from the horizontal. Imported gravelly sand fill was to be used to construct the berm. A PVC coated, double twisted galvanized woven wire mesh ($T_{ult}=50\text{kN/m}$) geogrid was to be used as the tensile reinforcement. The design of the reinforced slope used 6 layers of woven wire geogrid at 4m lengths, vertically spaced at 0.7m. The soil reinforcement was to be wrapped at the face of the slope. A synthetic turf reinforcement mat was used to secure a layer of topsoil at the face. The volume of fill required to construct the reinforced soil zone within the embankment was estimated to be 2,800m³ compacted, or 3,400m³ loose (1.225 bulking factor). The original embankment required a wooden sound fence to be installed at the crest of the embankment. This would require the installation of circular footing forms for the pouring of concrete footings for the fence during the construction of the reinforced embankment.

At the time of construction, the project Owner was developing another site located within close proximity to the project site. This site was generating significant quantities of sandy silt soils that had to be disposed of offsite, some of which was allocated for use for landscaping purposes on the project site. A contractor that had built two of the three previous reinforced berms was retained to construct the current phase. The project Owner requested that the contractor develop a method to use this sandy silt soil as structural fill within the reinforced soil zone of the berm. The reuse of the sandy silt soil as engineered fill on the project provided the Owner with a number of benefits: i.) A close disposal site (30 minute round trip); ii.) Elimination for the need to purchase and import high quality granular fill; iii.) Significant reduction in disposal fees (only costs associated with transportation between sites); and iv.) A reliable source of imported fill material for the construction of the Phase IV berm, thereby minimizing disruptions to the earthworks.

The sandy silt soil had a unit weight of 18 kN/m^3 and an angle of internal friction of 23° . The sandy silt soil had approximately 50% passing $75\mu\text{m}$. The optimum moisture content of the sandy silt fill was 11.3%. Figure 2 shows the gradation envelope of the gravelly sand fill compared to the gradation of the proposed sandy silt fill.

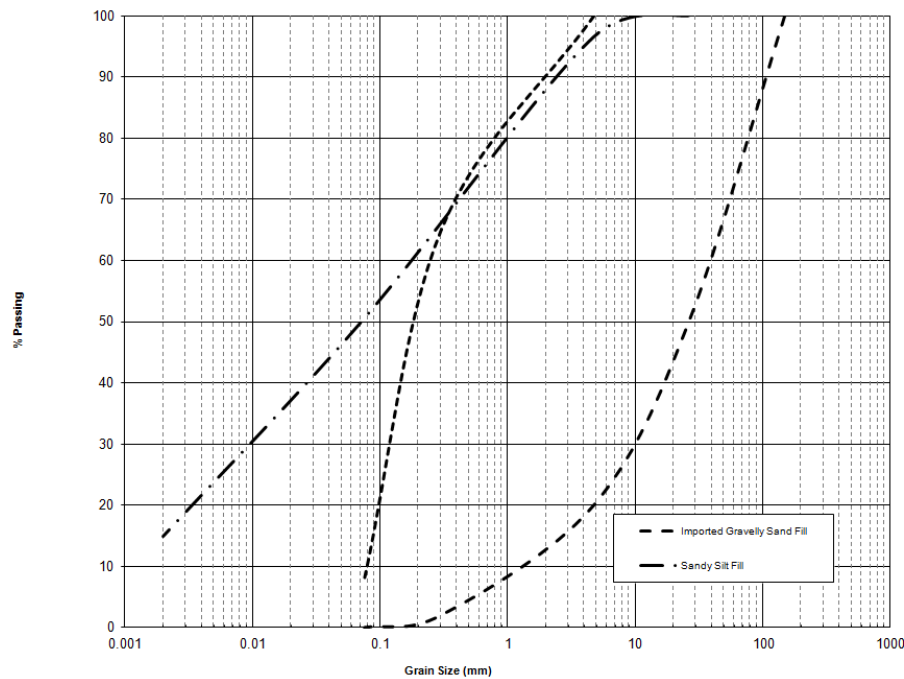


Figure 2. Comparison of backfill soil gradations

3.3 Redesign Embankment Using Draining Geogrid

After reviewing the limited soils information available for the project site and literature on the geocomposite, it was decided that the reinforced embankment could be redesigned to incorporate sandy silt fill. The redesign utilized 8 layers of the draining geogrid at 0.56m vertical spacing. The length of the geogrid was increased to 5m. The vertical spacing was selected based upon use of woven wire mesh forms at the slope face and the necessity to provide a reduced drainage path for the poor quality silt fill. Correspondence with authors of several reference papers (Naughton, pers. comm., 2011; Scotto, pers. comm., 2010) indicated that a vertical spacing of between 500mm and 600mm was typical of projects using different types of marginal and cohesive soils and no issues with performance had been observed.

The additional layers of geogrid in the redesigned structure did act to slightly decrease the speed at which the contractor could place reinforcement and fill. The increased installation time was offset by the efficiencies gained through the use of a steady, reliable source of imported fill material. The crew constructing the reinforced slope had extensive experience building similar structures using other types of geogrids and found no special accommodations were required to work with the draining geogrid. As per the original embankment design, the placement of circular forms for concrete fence post footings was required.

The placement and compaction of the sandy silt fill was monitored during the construction of the reinforced soil berm. The sandy silt fill was placed at 96% to 100% SPMDD. Moisture content of the fill ranged from 6.9% to 12.9%.

The circular forms were installed during the placement upper portion of the reinforced embankment. The footings were 1.5m deep, requiring adjustments in the 3 layers of reinforcement.

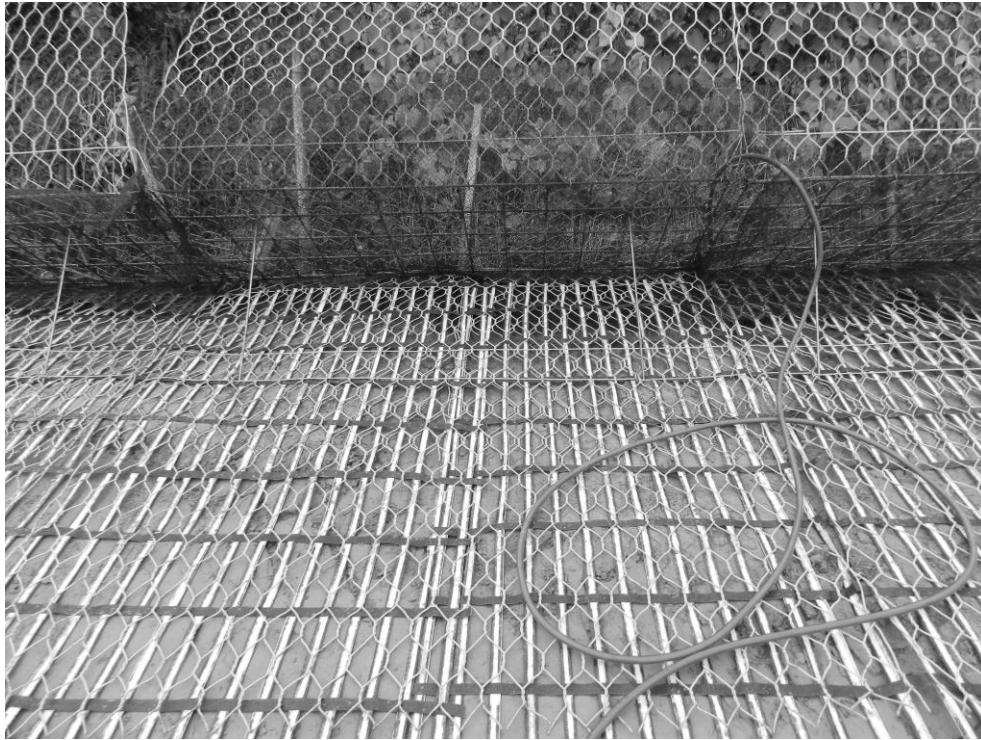


Figure 3. Geocomposite with woven wire mesh facing



Figure 4. Reinforced slope after 6 months



Figure 5. Circular forms for wooden fence

A visual inspection done one year after the start of construction showed no signs of tensile cracking along the crest of the berm or settlement. No bulging of the wire mesh facing panels was observed. A vegetated cover of primarily annual and perennial ryegrasses was present. The vegetation is estimated to cover approximately 85% to 90% of the area of the reinforced slope face.

The wooden fence was installed 10 to 11 months after completion of the reinforced berm. No signs of horizontal or vertical displacement were observed in the alignment of the fence.

3.4 Cost Comparison of Designs

It is possible to compare the cost of constructing the embankment as originally designed using imported granular fill against the redesigned embankment using marginal fill. The cost to supply the materials associated with the use of the geocomposite was approximately 10% higher than the material supply cost for the original reinforced slope design using the woven wire geogrid.

The embankment as original designed required approximately 2,200m³ of imported granular fill and 1,200m³ of marginal fill. The price presented to the owner to construct the embankment as originally designed was \$237,654, or \$486/m². This cost included the supply and installation of the woven wire mesh reinforcement. The costs associated with the disposal of 2,200m³ of the sandy silt soil were calculated to be \$62,700.

The embankment as constructed with the geocomposite utilized approximately 3,400m³ of marginal fill. The cost to build the redesigned embankment was \$160,881 or \$329/m². This cost included the supply and installation of the woven wire forms and geocomposite. There were no extra costs associated with the off-site disposal of the marginal fill.

4. CONCLUSION

Constructing reinforced soil structures using high quality granular fill soils is becoming increasingly difficult due to the high cost of these soils. Many construction sites in urban areas generate excavated spoil soils that are historically considered

as waste and transported off site. These exported soils are not normally considered for reuse in the construction of reinforced soil structures.

Soil reinforcement that is capable of dissipating excess pore pressure for cohesive and marginal fill soils may afford an opportunity on some projects to mitigate the off-site disposal these materials. The reduction and re-use of materials will have obvious economic benefits for the project.

The use of an innovative geocomposite geogrid in conjunction with sandy silt soil that was to be wasted from a nearby construction site allowed for the construction of a steep, reinforced soil slope using soils that would normally be used for landscaping purposes or bulk engineering fill. The reuse of the marginal soil in a reinforced soil slope resulted in a significant cost savings to the project owner.

REFERENCES

- Clancy, J., Naughton, P.J., 2008. Design of Steep Slopes Using Fine Grained Fills and Novel Multifunctional Geocomposites. *Proc. of the Fourth European Geosynthetics Conference, EuroGeo4*, Edinburgh, Scotland. IGS. Paper 131.
- Federal Highways Administration (FHWA) 2009. Design and Construction of Mechanically Stabilized Earth Walls and Reinforced Soil Slopes – Volume I, Publication No. FHWA-NHI-1024, Washington DC
- Federal Highways Administration (FHWA) 2009. Design and Construction of Mechanically Stabilized Earth Walls and Reinforced Soil Slopes – Volume II, Publication No. FHWA-NHI-1025, Washington DC
- Ghionna, V.N., Parla, P., Scotto, M., Veggi, S., 2010. Pull-out behavior of a draining geogrid in waste cohesive materials, *Proc. of the 9th International Conference on Geosynthetics of the IGS*, Brazil
- Kempton, G.T. Jones, C.J.F.P. Jewell, R.A. & Naughton, P.J., 2000. Construction of slopes using cohesive fills and a new innovative geosynthetic material. *EuroGeo 2*, Bologna: 825 - 828.
- Linear Composites Ltd., 2009. *ParaDrain™ 50/15 Technical Data Sheet*, West Yorkshire, UK
- Maccaferri Limited , 2001. Berry Hill Case Study (SR/0010), Oxford, UK
- Naughton, P.J., Jewell, R.A., Kempton, G.T., 2001. The design of steep slopes constructed from cohesive fills and a geogrid. *Proc. of the International Symposium on Soil Reinforcement*, IS Kyushu, Japan
- Naughton, P., Kempton, G., 2004, Construction of Steep Slopes Using Cohesive Fill and an Innovative Geogrid. *Proc. Int. Conf. on Geosynthetics and Geo-environmental Engineering ICGGE 2004*, Bombay, India: 407-410.
- Naughton, P., Scotto, M., Prelovsky, B., 2010 Reusing Excavated Soil Waste in Reinforced Steep Slopes and Embankments, *Proc. 14th Danube-European Conference on Geotechnical Engineering "From Research to Design in European Practice"*, Bratislava, Slovakia
- O'Kelly, B.C., Naughton, P.J., On the interface shear resistance of a novel geogrid with in-plane drainage capability. *Geotextiles and Geomembranes 2008*, doi:10.1016/j.geotextmem.2007.12. 006
- Simons, M., Cameron, N., 2012, A reinforced soil slope built using marginal fill soil and an innovative geocomposite reinforcement geogrid in Southern Ontario . 2012 *Proc. of 65th Canadian Geotechnical Conference, GeoManitoba 2012*, Winnipeg, Manitoba, Canada, Paper 371.
- Veggi, S., Parla, P., 2009. Geosynthetics as a solution to geotechnical problems in a MSW landfill. *Geosynthetics 2009*. Salt Lake City, UT, USA, Paper 1116.

Use of Bituminous Geomembranes in Harsh Conditions

Bertrand Breul, Montreal Canada, BBreul@axtercoeltancehe.com
Bernard Breul, Axter Coletanche, Irvine USA, Breul@eirnet.com

ABSTRACT

This paper presents two mining applications of bituminous geomembrane. At the Diavik Diamond Mine in the 'Lac de Gras' area in the Northwest Territories of Canada, the diamonds are extracted from the Kimberlite ore, and the rejected material is permanently stored in a diked containment facility lined with a geomembrane. The initial stages of the embankment construction used HDPE geomembrane, which meant that geomembrane lining could not be done for many months of the year. The design was changed to bituminous geomembrane, which can be installed at very low temperature. This increased the construction period by several months each year. At the Furioso Mine in the Chilean Patagonia region, the waste rock pile was closed using a bituminous geomembrane covered with 20 cm of soil. The driver for liner selection was the ability to install the bituminous geomembrane in winds up to 50 km/h.

1. INTRODUCTION

Over the past two decades the use of geosynthetics in the mining industry has grown. Geotextiles, geomembranes, geosynthetic clay liner, and geocomposite to name a few have been used to line dams, heap leach pads, tanking storage facilities, tailings ponds and water ponds and to cover mine waste facilities at closure. Bituminous geomembranes have been part of this growth and have been deployed in numerous mines worldwide over the past few years. Bituminous geomembrane offers specific advantages over other geomembrane that have led to their usage in parts of the world characterized by harsh weather and some very difficult access conditions. Bituminous geomembranes are manufactured by impregnating a non-woven geotextile with bitumen. The thickness of the bituminous geomembrane is controlled mostly by the thickness (mass) of the geotextile. Bituminous geomembrane exhibits the strength and deformation characteristics of the non-woven geotextile and the very low permeability of the bitumen. They are therefore well suited for applications that require strong geomembrane such as tailings facilities, mine waste rock piles, process water ponds, and areas where equipment must traffic over the lined area. Because of the high melting point of bitumen, asphalt can be laid on top of bituminous geomembranes to create hard impervious surfaces.

Bituminous geomembranes are:

- Heavier than most polymeric geomembranes, and can be installed in very windy conditions.
- Denser than water so they do not flood.
- Have a low coefficient of thermal expansion, and so do not expand and contract and develop wrinkles as the temperature changes daily after deployment.
- Thick (at least 3.5 mm) and therefore, extremely resistant to puncture.

The balance of this paper highlights two projects where bituminous geomembranes were used to address weather related constraints.

2. COLD WEATHER SITE

2.1 Location

The Diavik Diamond Mine (DDM) is located on East Island, a 17 km² island in Lac de Gras, NWT, approximately 300 km northeast of Yellowknife (64°31' North, 110°20' West) as shown in Figure 1.

2.2 Climate

The DDM site lies within the Arctic Climatic Region where daylight reaches a minimum of 4 hours per day in winter and a maximum of 20 hours per day in summer. The climate is extreme, with long, cold winters and very short, cool summers. The mean monthly temperature in July is 10 °C and that in January is -31 °C. The mean annual air temperature at the site is approximately -10 °C. On average, there are 260 days per year with temperatures below zero degrees Celsius. Snow falls every month, although rain generally only occurs between May and October.



Figure 1: Diavik Diamond Mine Location

2.3 Permafrost

The DDM site is located in the area of continuous permafrost, with permafrost depths confirmed to 150 m at the mine site. The active layer is about 1.5 m to 2.0 m deep in till deposits, 2.0 m to 3.0 m deep in well-drained granular deposits (eskers) and about 5 m in bedrock. In poorly drained areas including bogs, with thicker vegetation cover, the active layer is less than 1 m in depth. Thermistor data shows that the mean annual ground temperatures range from about -3°C to -6°C .

2.4 Water Management Ponds

Protection of the quality of water in Lake Lac de Gras is a priority for the mining company. Water management at the DDM site involves collecting all surface water runoff from areas affected by the mining operations. This water is used in the diamond processing operations or is treated and discharged to Lac de Gras. Water collection ponds are built as mining operations expand. During the initial construction of the mine facilities in 2001 and 2002, the water collection ponds were lined with using an HDPE geomembrane.

A new pond (Pond 14) was required for the spring-melt period in 2005 and two additional ponds (Ponds 2 and 13) were required for 2006. Due to other construction activities at the mine site, the construction of Pond 14 was scheduled for the second quarter of 2005, before the onset of the spring thaw and surface water runoff. This meant that construction would be carried out completely in freezing conditions. In addition, the locally borrowed fine sand that was used as liner bedding and cover would not be available during this time. Therefore, both the liner bedding and cover materials would be angular materials produced by crushing and screening granitic rock. Alternative designs of the dike section and pond liner system sections were evaluated to allow efficient cold weather construction and to minimize the amount of crushing and screening required. A section incorporating a bituminous geomembrane liner in the upstream section was selected.

The decision to use a bituminous geomembrane liner was based on the fact that the elastomeric bitumen in the geomembrane remains flexible at temperatures lower than -20°C and exhibits a low coefficient of thermal expansion ($1 \times 10^{-6} \text{ cm/cm/}^{\circ}\text{C}$). This meant that the material would be relatively insensitive to temperature changes during installation and service. In addition, the 4mm thick bituminous geomembrane is much heavier than the HDPE geomembrane previously used in these ponds (3.9 kg/m^2 vs 1.4 kg/m^2), and not is prone to being lifted by light winds during installation. This type of liner had been installed at other sites at temperatures down to about -20°C and productivity during installation at low temperatures was reported to be similar to productivity at temperature above zero degrees Celsius. A 50 mm minus crushed gravel was initially selected as the liner bedding and cover material. Tests during construction showed that a crushed 150 minus cobble, gravel and sand material could be used without damage to the liner, if surface

of the bedding was smoothed and raked to remove protrusions from the surface. The grain size distribution for the fine and coarse liner bedding materials are shown in Table 1.

Table 1. Liner bedding and cover grain size limits

Coarse Liner Bedding and Cover				Fine Liner Bedding and Cover			
Grain (mm)	Size	% Passing (Minimum)	% Passing (Maximum)	Grain (mm)	Size	% Passing (Minimum)	% Passing (Maximum)
200		100	100	50		100	100
75		45	100	19		80	100
19		24	56	9.5		60	90
4.75		13	34	4.75		40	70
2		7	28	0.85		18	38
0.42		0	16	0.075		3	15
0.075		0	12				

Pond 14 was constructed during April and May 2005, with 12,700 m² of liner installed in a 6 day period in early May 2005. During this period the temperature varied from -18 °C to -4 °C, winds were typically in the range of 10 km/hr to 20 km/hr and 1 to 2 cm of snow fell on a number of days. The rate of liner installed varied from 1,300 m²/day to 2,400 m²/day. Quality control testing and quality assurance testing involved vacuum box and ultrasound testing of seams to confirm the quality of the welds. Vacuum box testing proved to be more effective than ultrasound testing in the cold conditions during installation. Anti-freeze is required in the testing water to prevent the vacuum box from freezing to the liner.

To assess the performance of exposed bituminous geomembrane, and select a thickness for future design, a test pad was built with panels of 3.5, 4.0, and 4.8 mm thick bituminous geomembrane. The test pad was left uncovered and exposed to the elements (Figure 2). After exposure for four winters there were no changes in the appearance of any of the panels.



Figure 2: Bituminous geomembrane liner exposed for long term weathering assessment

Ponds 2 and 13 were designed with the same lining system as as Pond 14. Construction of Pond 2 was started in May 2005, but stopped in June 2005 when warm temperatures caused ice-rich permafrost exposed in the cut off trench excavations to melt and create unstable excavations. The construction of Pond 2 was finished in November and December 2005. Twenty-five thousand square meters of liner were installed in Pond 2, with 1,000 to 2,000 m² being installed per day. The temperature during installation in June 2005 ranged from about 3 °C to 14 °C, while the temperature during installation in November and December 2005 ranged from -4 °C to -32 °C. Some sections of the liner was successfully installed at a temperature of -25 °C, not including the effect of wind chill. Heavy snowfall occurred on a number of days, which required snow to be removed from the face of the dike on the already installed sections before installation could continue. The upper surface of the bituminous geomembrane has a sand coating, which provides good traction for the workers walking and working on the liner even in the presence of a thin cover of snow.

Pond 13 was constructed during April and May 2006. Ten thousand square meters of liner were installed. Temperatures during liner installation were in the range from -15 °C to -5 °C.

The water management ponds now have been in operation for 7 years. Each of the ponds has experienced some seepage. Investigations into the cause of each area of seepage have identified foundation issues, most likely melting of ice lenses in soil or ice within fractures in the bedrock beneath the cut-off level of the liner. The performance of the ponds indicate that after the dam and foundation re-establish a stable temperature regime, with the foundation refrozen, seepage does not occur. Planning for the construction of new ponds incorporates construction of a pond at least one year in advance of when the pond is required to allow the foundation to refreeze.



Figure 3: Snow clearing during bituminous geomembrane liner installation in Pond 2

2.5 Processed Kimberlite Containment Facility

The Processed Kimberlite (PK) that remains after diamond recovery is permanently stored in the Processed Kimberlite Containment (PKC). At DDM, the diamond recovery process results in two by-products, Coarse PK consisting of kimberlite particles with grain size between 1 mm and 6 mm, and Fine PK consisting of kimberlite particles with grain size less than 1 mm. The Coarse PK is trucked from the process plant to the PKC facility and the Fine PK is transported as low-density slurry in a pipeline to the PKC facility. The PKC facility design provides for storage of both streams of PK within geomembrane-lined rock fill perimeter dams. The perimeter dams now completely surround the PKC facility. The process water pond is maintained in the center of the facility by discharging fine PK from each of the perimeter dams. A rockfill berm constructed into the center of the facility is used to access the barge mounted pumps that recycle water to the process plant.

The perimeter dams are all wide rockfill embankments with the seepage control elements on the upstream face. Till and HDPE geomembranes were used on the initial stages of the dams, but this was changed to a bituminous geomembrane to allow lining to be carried out in colder temperatures. The bituminous geomembrane also allowed the use of coarser bedding material, which reduces the amount of crushing and screening required, and hence fuel consumption.

A typical section with bituminous geomembrane including the coarse liner bedding material, a sand liner cover material, and a layer of rock fill for erosion protection shown on Figure 4. Bedding materials used for various stages have been a coarse till material, the coarse material shown in Figure 4 and a 50 mm minus crushed material. Liner cover materials have been sand, and processed sand and gravel materials.



Figure 4: Typical dam section with coarse bedding and sand cover

Seepage has occurred from the PKC dams into the water management ponds located downstream of each dam. Investigations show three causes of the seepage. The first is related to winter construction and the difficulty of controlling the fine grained materials used in the liner anchor trench at the toe of the dams. If these fills freeze before or during placement and then subsequently thaw, soft and open zones can develop across the trench and allow seepage. This is a problem common to all winter construction. The second cause is melting of ice in the permafrost foundation. This either creates flow paths in the foundation, or creates voids in the foundation supporting the dam fills and liner bedding materials. Settlement of the fills into these voids results in liner damage. This is a foundation issue, and common to all liner types. The third cause is related to the discharge of the fine PK slurry into the facility. If the slurry erodes the liner cover and is directed against the liner, erosion of the liner occurs resulting in holes. Again, this mechanism is common to all liner types.

2.6 Joining Bituminous Geomembrane to HDPE

One of the technical aspects of the PKC Dam construction was joining the HDPE liner used in earlier stages of construction with the bituminous geomembrane liner. The process involved thoroughly cleaning the HDPE by sweeping and then washing with water (Figure 5). A primer was applied to the HDPE to enhance adhesion and then a peel and self-adhesive elastomeric membrane (commonly known as Flam Stick) was applied to the HDPE (Figure 6). Careful rolling of the Flam Stick was required to ensure a good bond. Sand and gravel liner bedding material was then placed over the HDPE to the edge of the Flam Stick to prevent excessive heating of the HDPE when the bituminous geomembrane was welded to the Flam Stick using the roofing torch. Tensile testing of samples taken of the joint showed that failure occurred within the Flam Stick and separation of the HDPE from the Flam Stick did not occur.



Figure 5: Primer being applied to HDPE



Figure 6: Flam Stick attached to HDPE

3. WINDY REGION SITE

3.1 Background

The Furioso Mine is approximately 46 miles (75 km) southwest of Chile Chico at an elevation of about 4,600 ft. (1,400m) above sea level in Chilean Patagonia and is essentially non-accessible during the winter months (between mid-March through December) due to the high snowfall and poor road conditions.

Following cessation of operation, the mine owner started closing the facilities including the waste rock facility which covers approximately 6.5 ha.

3.2 Weather

Daytime temperatures in the winter can be as low as -25°C with wind speed in excess of 80 km/h. Snow fall can occur just about any day of the year slowing down construction activities.

3.3 Closure Design

The closure plan called for a geomembrane protected by 1 meter of soil and an erosion protection layer consisting of 50 cm minus rock.

- Facing the potential of high wind and cold temperatures, the design team was looking for a geomembrane that:
- Could be installed when wind speed could in near 50 km/h;
- Would provide the contractor with flexibility in installation;
- Could sustain some vehicular traffic and could remain exposed to the element for a few weeks;
- Did not need a cushion geotextile or a fine grained subgrade; and
- Could be covered with a thinner soil cover than originally planned.

The designer selected a bituminous geomembrane because it could satisfy the needs expressed above, namely:

Weighting up to 3,900 g/m² the 4 mm bituminous geomembrane can sustain winds up to 60 km/h. Following deployment, minimum ballast was placed over the geomembrane that would remain exposed and subjected for the placement of the soil cover.

The installation and seaming process, similar to roofing material does not require a specialty subcontractor. A roofing torch is all that is need to weld the seam which consists of a 20 cm overlap of one panel over the other. This allowed the mine operator to use his own forces (local Patagonians resident) to do the closure work.

The 4 mm thick bituminous geomembrane could be deployed directly on the support that includes protrusion up to 2.5 cm in diameter as shown on Figure 7.

It was decided at design time that a 20 cm thick sand and gravel cover was enough to protect the geomembrane.

The design including the 4 mm bituminous geomembrane and the 20 cm cover was approved by the regulatory agencies and implemented.



Figure 7 Support for the bituminous geomembrane (note particle size of the support)

3.4 Construction

Work started on 11 January 2012, a mid-summer day in the Southern Hemisphere but a snow fall delayed construction for two days (Figure 8). The procedure followed was to prepare and line small areas as weather permitted. Because the bituminous geomembrane is heavier than most geomembrane with a low thermal coefficient it remains flat on the ground support with no wrinkles, waves, or kinks and therefore the cover soil can be pushed over without problem at any time during the day even when the temperature increases.



Figure 8: Snowy cold day in Chilean Patagonia

Nearly 65,000 m² of bituminous geomembrane including 12,000 m of welding and all the Construction Quality Assurance activities (Ultrasound and vacuum box) were installed and performed in 45 days. The bituminous geomembrane was then covered with 20 cm of sand and gravel as shown in Figure 9. The waste rock facility is now considered closed.



Figure 9: Placement of sand and gravel cover

4. CONCLUSION

Bituminous geomembranes have been successfully used at two sites with very harsh weather: extremely cold at the Diavik Diamond Mine in the Northwest Territory (Canada) and very windy and susceptible to quick changes in weather at the Furioso Mine in Chilean Patagonia. The use of bituminous geomembrane provided several benefits to the two mines namely:

- The possibility to install the geomembrane in difficult weather conditions: liner can be efficiently installed at nearly any time of the year. Only when temperatures dip below $-30\text{ }^{\circ}\text{C}$ is liner installation not possible.
- The installation does not require a specialty contractor so it offers employment opportunities for local workforces. The owner at Furioso mine was able used Patagonian residents whereas at Diavik first Nation People were employed.
- Economically viable when balancing the initial higher capital cost with the facts the cushion geotextile are not needed, not using a specialty contractor provide full schedule flexibility, and coarser bedding and cover material can be used.

Use of Chemically Modified Geotextiles to Selectively Remove Metallic Impurities from Potable Water

Jamil S.F., Textile Institute of Pakistan, Pakistan, syedafaizajamil@gmail.com

Ariadurai, S.A., Open University of Sri Lanka, Sri Lanka, saari@ou.ac.lk

Shah, T., University of Bolton, UK, T.H.Shah@bolton.ac.uk

Bandukda, Z., Textile Institute of Pakistan, Pakistan, zubair.bandukda@tip.edu.pk

ABSTRACT

The paper provides an overview of the areas in which geosynthetics are traditionally employed for “Sustainable Water Management” and then goes on to shed light into a new application area of “Geotextiles based ion exchangers (GTIX)”. When compared to the conventional resinous form, GTIX offer comparative advantages such as high rate of sorption and osmotic stability, and the possibility of the textile being spun into various forms such as filters, cloth, moving bands etc. The paper also offers insights on research investigations that have been undertaken on how a geotextile could be modified to remove selective metal ions so as to provide clean potable water to everyone, especially the rural dwellers. The source of water could be open water sources or groundwater. Water treatment is done either in-situ, or ex-situ where groundwater can be pumped out and filtered through these chemically modified textiles before usage.

1. WATER AS A SCARCE COMMODITY

More than 1.1 billion people in the world do not have access to clean drinking water- this is one person in every six. There are 4 billion cases of diarrhea each year, causing 2.2 million deaths (5 000 every day), mostly of children under the age of five. (Coping with Water Scarcity, UN 2007) Over 260 river basins are shared by two or more countries mostly without adequate legal or institutional arrangements. (World Water Council, Marseille 2002) Many women, throughout the world and particularly in developing countries, suffer permanent skeletal damage from carrying heavy loads of water over long distances day after day.

While water scarcity is linked to obvious problems such as hunger, poverty and disease, its far reaching effects exacerbate such issues as gender inequality, denial of education to children, pollution and environmental sustainability, and even regional and global conflicts.

Fortunately, there is heightened awareness about the global water crises that confronts us today and threatens to risk our survival even more in near future. The incorporation of sustainable access to clean drinking water and sanitation in Millennium Development Goals of 2005 was a pointer to this increased realization. Even more encouraging are the reports that convey that the MDG on clean drinking water has been met, halving the proportion of the world's population without access to safe drinking water, five years before the deadline of 2015.

Before going any further however, a word of clarification and caution is important here. While defining water as a scarce commodity, it is important to note that the term ‘Scarcity’ does not imply shortage of water from global perspective. In fact, if all the freshwater resources of the world are divided equally among the global population, there would be 5 000–6 000 m³ of water available per year, per person. According to this per capita calculation, the volume of water lies quite above the threshold value of 1700 m³/person, giving an impression of excess rather than scarcity.

Therefore, from the global perspective, there is no water shortage at all. The World Health Organization and Unicef Joint Monitoring Programme admit this dilemma in their report on ‘Progress on drinking water and sanitation 2012’. Almost half of the 2 billion people who have gained access to drinking water since 1990 live in China or India. Meanwhile, many countries in Africa are not on track to meet the target by 2015, with some countries actually falling back to pre-1990 rates of coverage. More than 40% of all people globally who lack access to drinking water live in sub-Saharan Africa.

The appropriate scale to understand scarcity is, therefore, at the local or regional level. It is also the appropriate level to address the water scarcity issues. Comprehensive Assessment of Water Management in Agriculture, 2007 has listed ‘small-scale, individually managed water management technologies’ as one of the pathways for reducing poverty and vulnerability in rural areas. These technologies can provide water at lower unit costs than large-scale hydraulic infrastructures and can be easily implemented locally.

It is in this context that chemically active geotextiles offer promising potential to provide clean drinking water solutions to rural areas or other water stressed regions.

2. GEOTEXTILES FOR SUSTAINABLE WATER MANAGEMENT

Before embarking on this relatively new area of chemically active geotextiles, it is only befitting to review the traditional role of geotextiles and how they have been used extensively in various hydraulic applications for sustainable water management. Historically, geotextiles have been used in the following ways in water conservation and conveyance systems.

2.1 Canal Lining

Geotextiles and their composites are used for lining of canals. They are known to prevent water loss due to seepage. Additionally, canals can also be covered to reduce evaporation. Their efficiency is known to be as high as 95% in preventing seepage loss.

As a fabric layer, this system is extremely easy to install. Geo composites can be used, depending on the requirement of the project, either in membrane-grid-textile or grid-textile combinations. In these composites, while the grid eliminates the requirement of graded filter for drainage, the textile layer prevents the fines from interfering with the drainage path. The geo composites are used in canal lining system with the water proof membrane in contact with the cover (required to weigh down the geo composite on the slope) and the geo textile is laid against the well graded slope.

Geotextiles also serve to protect the membrane layer on top side walls of the canals. The exposed membranes are susceptible to being damaged either due to intentional or unintentional vandalism; birds that pick at the seams, or animal hoofs when animals approach canals for drinking water.

2.2 Dams

Geotextiles and their composites are employed in dams both for erosion control and reinforcement purposes. To prevent erosion caused by atmospheric agents such as rain, the entire downstream facing and the upper portion of the upstream facing are covered with geotextile; whereas erosion of the dam caused by overtopping can be prevented by protecting the downstream face of the dam. This is a more technically viable and economically feasible solution than protection using concrete slabs. Geotextiles are also used to reinforce dams to give them more stability; this is even more essential in areas prone to high seismic activity.

2.3 Coastal Protection

Geotextile Tubes are used to prevent coastal erosion by simply filling the bags or tubes with readily available fill material such as sand; and strategically placing these tubes on the banks or shores to dissipate or absorb wave energy. These tubes can either be left exposed, which can be a risk to its integrity, or incorporated into the environment as part of a manmade dune or riverbank. They can also be placed in the water to serve as jetties and groins.

2.4 Landfill Liners

In modern landfills, the waste is contained by a geotextile lining system which serves to prevent the movement of small soil and refuse particles into the leachate collection layers and to protect geomembranes from punctures. These materials allow the movement of water but trap particles to reduce clogging in the leachate collection system. In this way they help to protect the soil and ground water/ aquifers from pollution originating in the landfill.

3. CHEMICALLY MODIFIED GEOTEXTILES- A WAY FORWARD TO TACKLE WATER SCARCITY PROBLEMS

Textile materials made of polymers with chemically active functional groups have a unique combination of properties. On one hand, they can fulfill functions of conventional textile materials such as cloths, non-woven fabrics, filters etc., and on the other hand, they can function as chemical agents, such as ion exchangers, complexones, reductants or oxidants and catalysts.

This section will elaborate the function of textiles as ion exchangers to remove metallic impurities from potable water, the possibility of either using this technology as small scale water purification units or as active materials in groundwater barriers; and most importantly, the edge that the fibrous ion exchangers provide over conventional resinous ion exchangers. It is important to begin this subject by revisiting the basic definitions and concept of ion exchange.

3.1 Basic Concept of Ion Exchange

Ion-exchange is a chemical reaction between two substances (each consisting of positively and negatively charged species called ions) that involves an exchange of one or more ionic components. Ion exchange usually transpires between a material carrying a fixed ion and a solution carrying mobile ions. The solution must be permeable in the material in order to allow the exchange to take place.

Materials with fixed negative charges exchange positive ions, or cations, and the process is called cation exchange. Those having fixed positive charges correspondingly exchange negative charges, or anions, and are said to undergo anion exchange. Typical ion-exchange reactions can be written as follows:



Where Fix^- is an ion fixed in the resin or other type of exchanger, A^+ and B^+ are univalent cations and C^{2+} is a divalent cation.

3.2 Treatment of Water

Ion exchange technique is extensively used for purification of water from ionic impurities. These may include poisonous ions such as arsenic and silver or ions such as calcium and magnesium that are responsible for causing hardness in water. Hard water is a nuisance as it causes scaling and also forms insoluble precipitates with soaps. Excess calcium and magnesium in water also leads to increase chances of cardiovascular disease. Arsenic, on the other hand, is known for affecting the gastrointestinal tract (nausea, vomiting), and in more severe cases even the cardiovascular system (hypotension, shock).

In order to remove calcium and magnesium ions from water, hard water is made to pass through a column densely packed with resins such as natural aluminosilicates or synthetic resins. These resins have sodium ions fixed on the surface. As the water comes into contact with the resin, magnesium and calcium ions are exchanged by the sodium ions; and the water leaving the column is free from the Ca/Mg impurities. After the column has been in use for some time, calcium and magnesium begin to appear in the water leaving the column. The column must then be regenerated by passing a concentrated solution of brine slowly through the column.

Removal of other poisonous metallic ions such as silver and arsenic from water can also be explained using similar principles of ion exchange. However for every metal, different kinds of fixed ions are required based on the preference attraction of the resin for the particular mobile ion.

4. GTIX ADVANTAGES

Though resinous ion exchangers are extensively used all over the world for water purification, there are possibilities to make it even more efficient and easier to handle or operate. Inconvenience is particularly caused owing to its large size, especially if large quantity of water needs to be purified. Chemically active textiles, also known as geotextiles based ion exchangers (GTIX), offer promising alternative to resinous counterparts in this context. Some of their advantages over conventional ion-exchange beads include:

GTIX can be easily fabricated into various textile forms such as cloth, conveyer belts, non-woven materials, staples, nets, felts, papers, etc. This opens many possibilities for new configurations for mounting the materials. The increased surface area of textiles provides opportunity for better accessibility of the mobile ions to the active sites. This leads to shorter diffusion time and the sorption rates can be as much as a hundred times faster than that of the conventional granular resins. They also allow column designing with pressure drops much lower than in reactors using granular materials. Furthermore, GTIX do not lose their shapes on successive absorption and desorption of water, for example, during cyclic sorption/regeneration processes.

Figure 2 shows the comparison of typical behavior of fibrous and resinous ion exchangers with the same chemistry of ion exchange sites. As is seen in the figure, a considerable part of GTIX graph shows complete absence of metallic ions in the beginning, giving credence to the extremely high sorption rates of GTIX. This also implies that GTIX can be used for efficient purification in thin layer beds. Both these advantages make geotextiles based ion exchangers a suitable technology for small scale water purification systems.

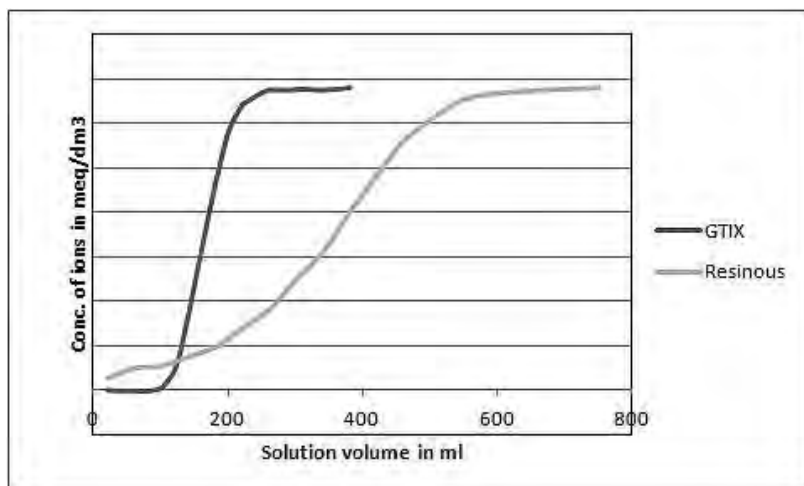


Figure 01. Schematic of fibrous and granular ion exchangers' performance.

5. SYNTHESSES AND FABRICATION METHODS OF GEOTEXTILES BASED ION EXCHANGERS

Essentially, there are two steps for formation of textile based ion exchangers. The first is related to the formation of fiber itself, and the second to its functionalization. However, in more cases than not, the two steps are not discrete but may overlap in a variety of methods. Several researchers have experimented with innovative routes to obtain a chemically active textile. A general classification of these methods is given below. These methods are by no means exhaustive, but they serve to give some basic understanding of the principles of synthesis of GTIX.

5.1 Suspension of Resinous Beads into Fiber Forming Solutions or Melts

This can be done either directly by dispersing fine particles of resinous ion exchangers into an inert fiber forming solution, or indirectly when two polymer solutions are mixed whereupon the ionizable group is formed upon mixing of the two solutions.

This method is quite appealing because of its universality in which any form of resins can be incorporated into the fibers. However, its limitation lies in the size and quantity of the resin beads being dispersed. Particle size of more than 3-5 μm , and resin quantity more than 35% of the solution leads to deterioration in the mechanical strength of the resultant fiber.

5.2 Graft Polymerization via Radiation or Chemical Means

Grafting is the process of joining or incorporating a copolymer into the chains of a main or principal polymer. This requires activation of sites on the main polymer in the form of free radicals or ions. The stimulus for this activation can either be by means of chemicals or direct radiation.

5.2.1 Irradiation Technique

Irradiation technique can proceed in three different ways: preirradiation, peroxidation and simultaneous irradiation.

In the pre-irradiation technique, the principal polymer is first irradiated in vacuum or in the presence of an inert gas to form free radicals. The modified polymer is then grafted with the monomer. One limitation of this methodology is the formation of homopolymer, which results in the loss of chemicals, and involves tedious task of washing off the homopolymer from the final product.

Peroxidation technique is carried out in the presence of air, resulting in the formation of peroxides or hydroperoxides. These intermediate products are rather stable in ambient conditions and can be stored for days. When treated with monomer at higher temperature, the peroxides decay spontaneously to initiate grafting.

In the mutual irradiation technique, the polymer and the monomers are irradiated simultaneously, to form free radicals and subsequent graft. Since, the backbone polymer is not irradiated separately, this technique, unlike the preirradiation one, does not cause the problem of homopolymerization.

5.2.2 Chemical Technique

Chemical grafting is done by means of initiator, the type and quantity of which determines whether the reaction would proceed via free radicals or ions. In chemical method, unlike the irradiation method where the free radicals are formed directly on the polymer, the radicals are first formed on the initiator and then transferred to the monomer.

Both the chemical and irradiation grafting have their own pros and cons. From the process control aspect, irradiation grafting yields purer products. Higher degrees of penetration of radiation can be used to access the inside of polymers resulting in greater depths of grafting. Furthermore, it's easier to control the molecular weight of the polymer via irradiation grafting as opposed to chemical grafting. On the other hand, the biggest limitation of irradiation grafting lies in its feasibility on industrial scale; it also poses health hazards associated with exposure to radiation.

6. TRANSLATING THE SCIENCE INTO TECHNOLOGY

Textile materials can be functionalized either by means of radiation or chemicals to introduce ion exchange sites into their matrix. These sites can exchange the metallic impurities from water on the same principle as the resinous ion exchangers do. This, with the added advantages of overall simplification of the process and greater efficiency, makes GTIX a promising aspect to look into for research and development.

The science can either be incorporated into water purification filters (ex situ method) or become a part of underground permeable barriers (in situ method) to prevent groundwater from contamination.

6.1 Water Purification Filters

There are several water purification techniques available in the market and the degree of their sophistication varies from nanofiltration and reverse osmosis (RO) to ultra and micro filtration. By principle of filtration, only reverse osmosis and nanofiltration are capable of *filtering out* ionic impurities.

While nanofiltration blocks out multivalent ions, it is largely permeable to monovalent ionic impurities. On the other hand, reverse osmosis blocks out virtually all the dissolved ions. This, itself, is a disadvantage, since the process removes even the recommended level of certain minerals. Water purified by RO plants must be treated with calcium and magnesium beds, for example, to make them suitable for drinking purposes. Furthermore, both nanofiltration and RO are expensive processes and are particularly not feasible for small scale purification units in rural areas.

An alternative is to modify the ultra filtration technique (which in its basic form does not block out ionic impurities) by assisting it with geotextiles based ion exchangers. GTIX assisted membrane filtration can remove metallic species from water. Metallic species are retained after binding with the fixed ion on the textiles, and the replaced ions pass through the membranes. The process is depicted in Figure 02. The advantages of this process are the low energy requirement involved in UF processes and the high binding capacity of the water soluble polymers.

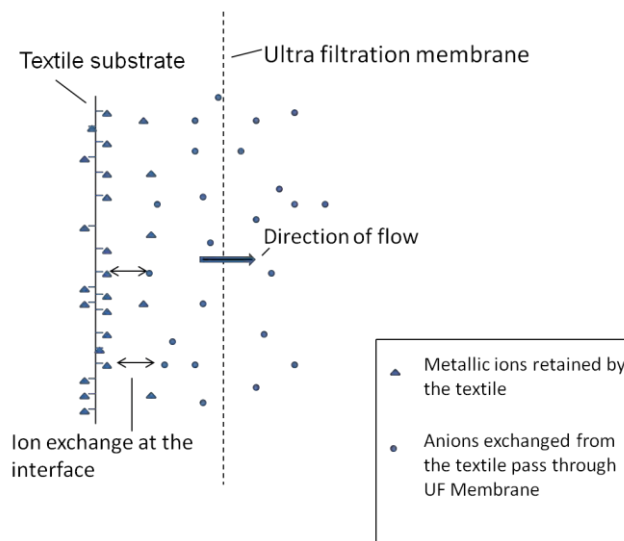


Figure 02. Schematic of GTIX assisted Ultra filtration

6.2 Permeable Reactive Barriers

Physical barriers constructed in a contaminated groundwater system that intercept and degrade or remove soluble pollutants yet allow groundwater to flow through are called permeable barriers. PRB is just one of the groundwater remediation techniques amongst other techniques such as containment of contaminants, removal of contaminated soil and its subsequent disposal or treatment, and removal of pollutants and their subsequent neutralization.

However, other remediation methods have several disadvantages over the PRBs. These include water supply disruptions for long time periods, producing undesirable by products such as contaminated soil or sludge, and institutional obstacles pertaining to pumping large volumes of groundwater such as requirements for discharge permits and possible purchase of ground water.

Nevertheless, in order for the PRB's to perform effectively there are several factors that should be taken into proper consideration. These include

- **Depth of groundwater:** This should be only as much as would make the aquifer feasibly accessible by trenching or boring equipments.
- **Contaminant transport:** The groundwater should flow through the barrier with sufficient velocity so as to enable the contaminants to come into contact with the activated barriers.
- **Barrier performance:** The barrier must be swift and effective in removal of the particular impurities of water. Chemically active geotextiles can be used as barriers to remove harmful metallic impurities by intercepting and exchanging the mobile ions with non hazardous ones. GTIX various advantages such as the ease with they can be made into any shape or form, their osmotic stability and swifter sorption rates make them a suitable candidate for PRBs.
- **Construction and operating cost:** The construction and operating cost should be reasonable when compared to other groundwater remediation techniques. Since most GTIX can be manufactured by cheap or recycled polymers or fibers as the backbone, and inexpensive copolymers; they are poised to give cost effective products for groundwater restoration.

Though chemically modified textiles are being manufactured and used, at least to a limited extent, for water purification in ex-situ situations; their applicability and usage in in-situ environments has not been touched upon by researchers as yet. The in-situ scenarios maybe difficult to explore in terms of logistics, but the successful incorporation of this technology in PRBs has the potential to solve myriad of groundwater contamination problems.

7. CONCLUSION

Geotextiles are used extensively in a variety of sustainable water management systems in the world. However, their traditional use is limited to their important but passive properties such as strength and permeability. The possibility of modifying their structures so that they play an active role in the purification of water presents exciting opportunities for further research and subsequent product development. The concept of GTIX introduced in this paper is a step in this direction. GTIX offers superior performance when compared to resinous counterparts; and the technology can be employed for either in-situ or ex-situ for water purification.

ACKNOWLEDGEMENTS

The author acknowledges the British Council, Pakistan for funding the presentation of this paper through "International Strategic Partnership for Research and Education- INSPIRE, Strategic Partnership Award" Programme.

REFERENCES

- Bhattacharya, A., and Misra, B.N., (2004). Grafting: a versatile means to modify polymers techniques, factors and applications, *Progress in Polymer Science*, 29: 767-814.
- Inamuddin and Luqman, M. (2012). *Ion Exchange Technology I, Theory and Materials*, Springer, New York, USA
- Juang, R.S., and Chiou, C.H. (2001). Feasibility of the use of polymer-assisted membrane filtration for brackish water softening, *Journal of Membrane Science*, 187, 119-127
- Novoselova, L.Y. and Sirotkina, E.E. (2006). Polyolefinic fibrous ion exchange materials: properties and application (Review), *Chemistry for Sustainable Development*, 14, 199-213

- Soldatov, V.S., (2008). Syntheses and main properties of FIBAN fibrous ion exchangers, *Solvent Extraction and Ion Exchange*, 26-5, 457-513
- Soldatov, V.S., Shunkevicha, A.A., Elinsona, I.S., Johannc, J. and Iraushekc, H. (1999) Chemically active textile materials as efficient means for water purification, *Desalination*, 124, 181-192
- Soldatov, V.S., Shunkevich, A.A and Martsinkevich, V.V (2001). Comparative study of water softening with granular and fibrous ion exchangers, *Russian Journal of Applied Chemistry*, 74, 1521-1524.
- Thomson, B.M., Finrock, D.J., McHaley, C.P. (1999) Development of permeable barriers for groundwater remediation: Air stripping of methyl tertiary-butyl ether (MTBE). *Journal of Environmental Science and Health, Part A: Toxic/Hazardous Substances and Environmental Engineering*. 34:2, 263-287
- Ulbricht, M., (2006) Advanced functional polymer membranes. *Polymer*, 47, 2217-2262
- Varshney, K.G. (2003) Synthetic ion exchange materials and their analytical applications: past, present and future, *Solid State Phenomenon*, 90-91, 445-450
- Yalala, B.N. (2009) Ion Exchange Resins and Functional Fibers: A Comparative Study for the Treatment of Brine Waste Water, University of the Western Cape, Cape Town, South Africa.

Use of Coir Fiber Reinforcement Technique to Improve Strength of Cement Kiln Dust Treated Black Cotton Soil Subgrade

Amadi A. A. *, Department of Civil Engineering, Federal University of Technology, Minna, Nigeria.
agapitusahamefule4@yahoo.com

Eberemu, A. O., Department of Civil Engineering, Ahmadu Bello University Zaria, Nigeria.
aeberemu@yahoo.com

Momoh, O. H., Department of Civil Engineering, Federal University of Technology, Minna, Nigeria.
happiness2k3@yahoo.com.au

ABSTRACT:

In this study, the use of coir fiber reinforcement to improve the strength properties of black cotton soil subgrade stabilized with cement kiln dust (CKD) was investigated. Black cotton soil was mixed with optimum of CKD along with different proportions of discrete coir fibers (0%, 0.25%, 0.5%, 0.75% and 1.0% by dry weight of soil cut to 25mm size). Compaction properties and unconfined compressive strength (UCS) values were determined for soil mixtures compacted using British Standard Light (BSL) effort. Test results indicated that the inclusion of fiber in stabilized specimens resulted in reduced maximum dry unit weight, higher optimum moistures as well as UCS and therefore enhanced load carrying capacity of the subgrade. The results further demonstrated that randomly distributed coir fibers can be used to reduce the brittleness of stabilized soil which is the drawback associated with high lime content stabilizers. Thus, strength of black cotton soil can be successfully improved by the combined action of CKD and coir fiber.

Keywords: Black cotton soil, Cement kiln dust, Coir fiber reinforcement, unconfined compressive strength

1.0 INTRODUCTION

Black cotton soil is an expansive clay soil that constitutes a major group of soils found in tropical latitudes. It is however considered a problem soil due to its small load bearing capacity, high swelling characteristics, excessive shrinkage properties with the resultant large cracks and long term settlement under external load as moisture content fluctuates (Ola, 1983; Warren and Kirby, 2004; Osinubi, 2006). Consequently, roads running through regions covered with these clays are subjected to severe distress resulting in poor performance and increased maintenance cost. These behaviors are attributed to the presence of clay minerals with expanding lattice structure. Among them, montmorillonite, the most common of all the clay minerals in expansive clay soils. The mineral is made up of gibbsite sheet sandwiched between two silica sheets (Morin, 1971, NBBRI, 1983; Chen, 1988).

Thus, in natural states, the soil is not suitable for subgrade construction but can be used as subgrade material only after stabilization by means of admixtures.

Over the years, progress has been made as different types of stabilizers have achieved different levels of performance. Cement and lime are still among the most effective stabilizers in use, although many studies have been made for nontraditional stabilizers, such as fly ash, cement kiln dust, blast furnace slag, baggase ash, reinforcing fibers or the combination of these materials with varied degree of success (Osinubi and Medubi, 1997; Peethamparan and Olek, 2008; Liman, 2009; Oriola and Moses, 2011).

Unfortunately, the increase in compression resistance associated with lime or related stabilizers is always accompanied by brittle failure and consequently the possibility of hazardous failures under any unexpected load condition.

The technique of soil stabilization by admixtures and reinforcement in form of discrete fibers is known to cause significant improvement in strength characteristics of soils. The main reasons of using randomly oriented fibers as additional additive is to increase tensile strength, solve the problem of brittle failure of stabilized soils as well as to maintain strength isotropy (Gray and Ohasi, 1983; Al Refeai, 1991; Ranjan et al., 1996; Consoli, et al., 1998; Prabhakar and Sridhar, 2002; Kumar et al., 2005; Rafalko et al., 2006).

In the present study, the use of eco-friendly coir fiber with high initial tensile strength and excellent durability derived from yarns of coconut husk to improve strength properties of black cotton soil subgrade treated with cement kiln dust was investigated by measuring strength in terms of unconfined compression strength.

2.0 EXPERIMENTAL PROGRAM

2.1 Materials

The soil used in this study was collected at shallow depth from Adamawa state, Nigeria. It is a blackish grey clayey silt of intermediate plasticity normally classified as black cotton (BC) soil.

Fresh CKD sample used as primary stabilizer in this study was collected from Benue Cement Company, Gboko, Nigeria. The coir fiber which is abundantly available in some parts of south and coastal regions of Nigeria was used as secondary stabilizer. For the present study, brownish coir fiber obtained from processed coconut husk, was collected from Minna.

2.2 Method

2.2.1 Sample Preparation and Testing

British standards (BS 1990a, b) were used to determine the particle size distribution, Atterberg limits and specific gravity of black cotton soil as well as mixture of soil and CKD. The effect of fiber content was evaluated by testing specimens in which the fiber weight fraction related to dry weight of the soil was varied, but all other significant test variables were controlled. The fiber content selected were 0, 0.25, 0.5, 0.75 and 1% by dry weight of soil cut to 25mm size and were randomly mixed with soil. The maximum dosage rate was limited to 1% of dry weight of soil because of possible mixing difficulties at greater dosages. The composite soil specimens (soil, stabilizer and fiber) were prepared by dry blending soil and the optimum CKD content together with fiber for fiber reinforced mixtures. The samples were mixed manually with proper care to get homogeneous mix and then the required amount of water was added. Compaction test was conducted using British Standard Light (BSL) compactive effort as per BS 1377 (1990a, b) and unconfined compressive strength tests were conducted for various combinations of soil sample compacted to their optimum moisture content – maximum dry unit weight. Treated specimens for UCS tests were cured for 7 days before testing. A 7-day curing period was adopted to simulate the relatively short period between subgrade preparations to pavement construction activities in practice.

3.0 RESULTS AND DISCUSSION

3.1 Index Properties

The grain size distribution curve (Figure 1) indicates that the study soil was primarily fine grained with specific gravity of soil solids as 2.67. The index properties of the natural soil are summarized in Table 1. The soil is classified under the A – 7 – 6 subgroup of the AASHTO classification system and CH in accordance with USCS system. Liquid limit and plasticity index values of 52% and 37%, respectively were established and this indicates that the soil is highly plastic. The dominant clay mineral is montmorillonite which is consistent with results of previous research findings on black cotton soil samples from the region (Ola, 1983, Osinubi, 1999). From these results, the soil would not meet the standard specification for most geotechnical works including pavement subgrade construction.

On application of optimum CKD, the liquid limit and plasticity index of soil mixture were lowered to 49% and 34% respectively. The concentrations of the major detected oxides in the black cotton soil together with that of the CKD analyzed using X-ray fluorescence (XRF) are summarized in Table 2, while some properties of coir fiber used are reported in Table 3.

Table 1 Summary of study soil index properties

Property	Value
Natural moisture content	8
Liquid limit (%)	52
Plastic limit (%)	15
Plasticity index (%)	37
Linear shrinkage (%)	15
USCS classification	CH
AASHTO classification	A-7-6
Specific gravity	2.67
Maximum dry unit weight (kN/m ³)	13.7
Optimum moisture content (%)	33.6
Swelling potential	High
pH	7.2
Color	Blackish grey

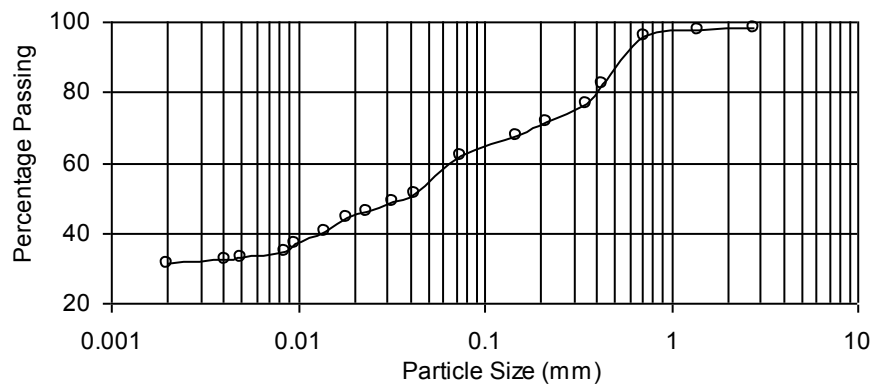


Figure 1 Particle size distribution of study soil

Table 2: Oxide composition of study soil and Cement Kiln Dust

Oxide	(%)	
	Soil	Cement kiln dust (CKD)
CaO	0.35	43.69
SiO ₂	46.84	12.18
Al ₂ O ₃	23.40	2.97
Fe ₂ O ₃	5.80	2.46
MgO	0.22	0.89
SO ₃	0.93	-
Mn ₂ O ₃	2.00	-
K ₂ O ₃	-	0.40
Loss on ignition	14.8	37.54

Table 3: Some properties of coir fiber used in the study

Properties	Value
Color	Brown
Average diameter (mm)	0.25
Average length (mm)	25
Aspect ratio	100
Average tensile strength (N/mm ²)	405.9
Density (g/cm ³)	1.45
Young modulus (kN/m ²)	4.0x10 ⁶
Elongation (%)	15

3.2 Compaction Characteristics

The maximum dry unit weight (γ_{max}) decreased and the optimum moisture content (OMC) increased with the addition of optimum cement kiln dust. The decrease in the maximum dry unit weight of the treated soil mixtures is reflective of increased resistance offered by the flocculated soil structure while the increase in optimum moisture content is probably a consequence of additional water held within the flocculated soil structure resulting from CKD reactions (Osinubi, 2000). This trend did not change even after the addition of coir fiber. The optimum moisture content of soil - CKD mixtures reinforced with coir fiber varied between 1 to 6% above the OMC stabilized soil. Similarly, the variation in maximum dry unit weight of coir fiber reinforced soil – CKD mixtures is between 18.56kN/m^3 and 16.9kN/m^3 which again represents up to 10% that of stabilized soil. The reduction in dry unit weight of stabilized soil specimen reinforced with coir fiber is due to the fact that lighter material replaces heavy soil particles. The compaction characteristics of untreated and treated soils with CKD and different percentages of fibers are shown in figure 2.

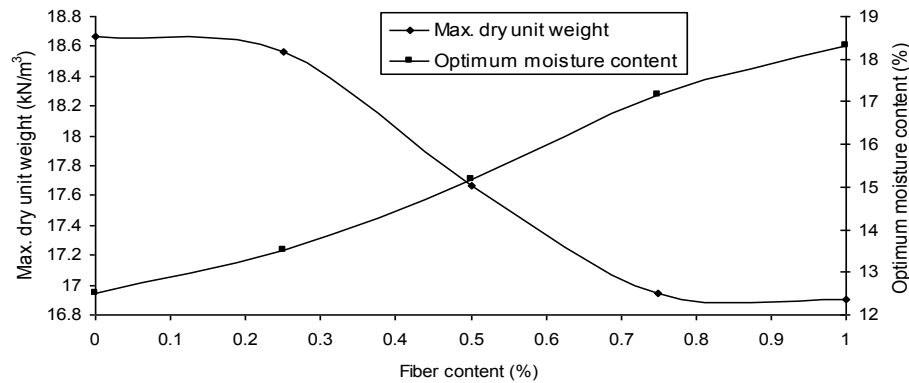


Figure 2: Compaction characteristics of reinforced stabilized soil specimens

3.3 Strength of Stabilized Unreinforced and Stabilized Reinforced Specimens

The addition of optimum CKD increased the UCS nearly 2.5 times that recorded by the untreated soil. For reference, the maximum value of UCS (q_u) of the natural soil was 48 kN/m^2 , while that of stabilized soil was 118 kN/m^2 . The increase in strength of soils with CKD is well established (Liman, 2009; Oriola and Moses, 2011; Amadi and Eberemu, 2012). The increase in unconfined compressive strength after CKD application is as a result of flocculation, cation exchange and the formation of various cementitious compounds i.e., calcium silicate hydrates and calcium aluminate hydrates due to pozzolanic reaction between silica present in soil and lime in the CKD in the soil matrix.

Reinforcement of CKD-stabilized soil with varying fiber contents produced slightly higher strengths than exhibited by the chemically stabilized black cotton soil without fibers. Figure 3 reports the normalized UCS of composite soil. The normalization was by the unreinforced soil – CKD UCS of 118 kN/m^2 . In general, the UCS gain increased with an increase in fiber content achieving an increase of 1.3 times the value of unreinforced soil – CKD on addition of highest dosage level of 1% fiber.

In terms of the general relationship between UCS and the quality of the sub-grade soils used in pavement applications (Das, 1994), the natural soil was upgraded from soft subgrade to stiff subgrade by the integrated effects of the chemical stabilizer and coir fiber.

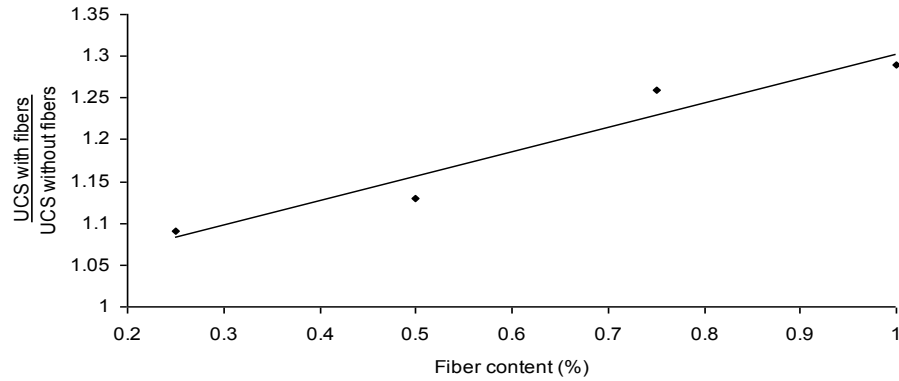


Fig. 3 Normalized UCS vs. fiber content of stabilized soil

In addition to increase in UCS, one of the main reasons for fiber inclusion to soils with chemical stabilizers is to increase their energy absorbing capacity or toughness, so that the composite materials (soil, stabilizer and fiber) will exhibit a more ductile post peak behavior. Toughness is important because chemically stabilized soils without fibers exhibit brittle stress-strain curves and have relatively little toughness, which may cause the treated soil to crack and fail suddenly (Consoli et al., 1998; Rafalko et al., 2006). At 0% fiber, the soil – CKD mixture was friable, although high strength was achieved. Figure 4 presents the normalized toughness index values for stabilized soil reinforced with the fiber dosage used in this study. As in UCS, toughness index was normalized by taking the ratio of the reinforced soil – CKD toughness index and the toughness index of mixtures with 0% fiber. From the figure, soil mixtures in reinforced state exhibits slightly higher toughness than in unreinforced condition. The results indicate that the toughness index increased by as much as 1.2, 1.9, 2.08 and 2.15 times due to the inclusion of 0.25, 0.5, 0.75 and 1% coir fiber respectively compared to unreinforced sample. Similar to UCS results, the soil stabilized with 8% CKD and 1% of the fiber produced the highest toughness index. It is likely that the bond strength and friction at the interface seem to be the dominant mechanism controlling the reinforcement benefit.

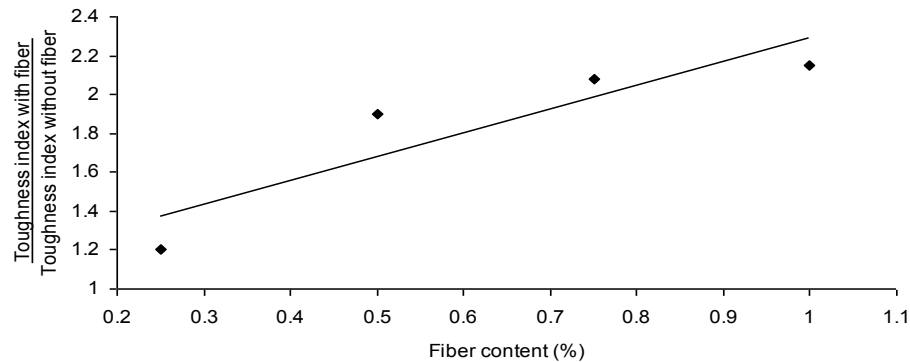


Fig. 4 Normalized toughness index vs. fiber content of stabilized soil

The increment in the peak stress and the corresponding decrease of the failure axial strain (ϵ_f) associated with the addition of optimum CKD content is also noteworthy. This brittle behavior of CKD stabilized soil was however reduced with the inclusion of randomly distributed coir fibers which increased the failure axial strain (ϵ_f) as reported in Table 4. It is observed that the soil alone attained a peak strength at about 9.52% axial strain while the stabilized soil reinforced with different coir fiber contents increased the axial strain and failure occurred at higher strains around 10% and above exhibiting a more ductile behavior of composite soil (Karimi et al., 2010; Ramesh et al., 2010).

Table 4: Peak stress and axial failure strain of unstabilized, stabilized and reinforced stabilized specimens

Mixture	Peak strength (kN/m ²)	Axial strain at failure (ϵ_f)
Unstabilized soil (Natural)	48	9.52
Stabilized soil (soil + 8% CKD)	118	5.7
Soil + 8% CKD + 0.25% fiber	128.62	6.4
Soil + 8% CKD + 0.5% fiber	133.27	8.6
Soil + 8% CKD + 0.75% fiber	148.67	9.5
Soil + 8% CKD + 1% fiber	152.42	11.66

4.0 SUMMARY

Black cotton soil has been identified as one of the major groups of soils found in the tropical latitudes. Roads running through regions covered with these clays are subjected to severe distress resulting in poor performance and high maintenance cost. Different stabilization techniques to achieve suitable performance and provide required service life for the expected traffic intensity have been adopted in the past.

In the present study, representative sample of black cotton soil chemically stabilized with optimum cement kiln dust content (8%) was reinforced with varying percentages of coir fiber (0, 0.25, 0.5, 0.75 and 1% by weight of soil) cut to 25mm size to evaluate its suitability for pavement subgrade construction. Laboratory tests carried out included Atterberg limit test, compaction test as well as unconfined compressive strength tests. All specimens for UCS tests were compacted at optimum moisture content using British Standard Light (BSL) compactive effort.

Test results indicated that the maximum dry unit weight decreased marginally while the optimum moisture content and UCS increased on application of optimum CKD content. Although, CKD treatment of soil improved the compressive strength but it imparted brittleness in soil specimens. Coir fiber inclusion in stabilized samples resulted in further reduction of maximum dry unit weight as well as higher optimum moistures together with the UCS and therefore the load carrying capacity of the subgrade. Evaluation of the toughness index established an increasing trend with higher fiber content. An increased toughness index is desirable, as the longevity of the pavement would be expected to increase with increasing toughness.

Overall, stabilization with the optimum stabilizer content and the fiber at the highest dosage of 1% increased the strength and toughness index of the study soil the most. Based on these results, it can be concluded that tropical black cotton soil can be successfully stabilized by the combined action of CKD and coir fiber.

REFERENCES

- Al Refeai, T. (1991). Behaviour of granular soils reinforced with discrete randomly oriented inclusions, *Geotextiles and Geomembranes*, 10: 319-333.
- Amadi, A. A. and Eberemu, A. O. (2012) Performance of Cement Kiln Dust in Stabilizing Lateritic Soil Contaminated with Organic Chemicals. *Advanced Materials Research*, Trans Tech Publications, Switzerland, 367: 41 – 47. doi: 10.4028/www.scientific.net/AMR367.41
- British Standard Institute. (1990a). Methods of testing soils for civil engineering purposes. *BS1377*, London.
- British Standard Institute (1990b). Methods of tests for stabilized soils. *BS 1924*, London.
- Chen, F. H. (1988). *Foundations on Expansive Soils*, Elsevier Scientific Pub. Co. Amsterdam.
- Consoli, N.C., Prietto, P.D.M. and Ulbrich, L.A (1998). Influence of fiber and cement addition on the behavior of sandy soil. *Journal of Geotechnical and Geoenvironmental Engineering*, ASCE, 124(12): 1211-1214.
- Das B. (1994). *Principles of Geotechnical Engineering*. PWS-Kent Publishing Company, Boston, 3 rd ed.
- Gray, D.H., and Ohashi, H. (1983). Mechanics of fiber-reinforcement in sand. *Journal of Geotechnical Engineering*, 109: 335-353.
- Karimi, M., Salemnia, A. and Ahadiyan, J. (2010). Evaluation of strength parameters of stress – strain development in clay soil and clay sand soil. *International Journal of Civil and Structural Engineering*, 1(3): 644 – 660.
- Kumar, A., Wakia, B. S. and Mohan, J. (2005). Compressive strength of fibre reinforced highly compressible clay”, *Journal of Construction and Building Materials*, 20:1063- 1068.
- Liman, A. (2009). Evaluation of Compacted Lateritic Soil Treated with Cement Kiln Dust as Hydraulic Barriers in Municipal Solid Waste Containment Systems. *Unpublished MSc Thesis*, Department of Civil Engineering, Ahmadu Bello University, Zaria, Nigeria.
- Morin, W.J. (1971). Properties of African tropical black clay soils. 5th Reg. Conf. for African on Soil Mech. and Foundation Engrg. Luanda, 1: 51-59.
- NBRRI, (1983). Engineering properties of black cotton soils of Nigeria and related Pavement design. *Nigerian Building*

- and Road Research Institute, 3: 1 – 20.
- Ola, S.A. (1983). The geotechnical properties of black cotton soils of North Eastern Nigeria In: S.A. Ola (Ed.). *Tropical soils of Nigeria in Engineering Practice*, A.A. Balkema, The Netherlands, Rotterdam, 155-171.
- Oriola, F. and Moses, G. (2011). Compacted black cotton soil treated with cement kiln dust as hydraulic barrier material. *American Journal of Scientific and Industrial Research*, 2(4): 521-530. doi:10.5251/ajsir.2011.2.4521.530.
- Osinubi, K.J. and Medubi, A.B. (1997). Evaluation of cement and phosphatic waste admixture on tropical black clay road foundation. *Proc. of 4th Int. Conf. on Structural Engineering (SEAM 4)*, Accra, 2: 297-307.
- Osinubi, K.J. (2006). Influence of compactive efforts on lime-slag treated tropical black clay. *Journal of Materials in Civil Engineering*, ASCE, 18(2): 175- 181.
- Osinubi, K.J. (2000). Stabilization of tropical black clay with cement and pulverized coal bottom ash admixture. In: *Advances in Unstaturated Geotechnics*. Edited by Charles D. Shackelford, Sandra L.H and Nien-Yui Chang. ASCE Geotechnical Special Publication, 99: 289-302.
- Osinubi, K.J. (1999). Evaluation of admixture stabilization of Nigerian black cotton soils. *NSE Technical Transaction*, 34(3): 88-96.
- Peethamparan, S. and Olek, J. (2008). Study of the effectiveness of cement kiln dusts in stabilizing N-montmorillonite clays. *Journal of Materials in Civil Engineering*, 20(2): 137-146.
- Prabhakar, J. and Sridhar, R.S. (2002). Effect of random inclusion of sisal fibre on strength behaviour of soil, *Journal of Construction and Building Materials*, 16:123-131.
- Rafalko, S. D., Brandon, T. L., Filz, G. M. and Mitchell, J. K. (2006). Fiber Reinforcement for Rapid Stabilization of Soft Clay Soils. <http://www.dtic.mil>. Accessed June, 2012.
- Ranjan, G. Vasan, R.M. and Charan, H.D. (1996) Probabilistic Analysis of Randomly Distributed Fiber Reinforced Soil. *Journal of Geotechnical Engineering*, ASCE 122 (6): 419-426.
- Ramesh, H.N., Manoj Krishnaa, K.V. and Mamatha, H.V. (2010). Compaction and Strength behavior of Lime-Coir Fiber treated Black Cotton soil. *Geomechanics and Engineering*, 2(1): 19-28
- Warren, K.W. and Kirby, T.M. (2004) Expansive Clay Soil a Wide Spread and Costly Geohazard, Geostra, Geoinstitute of The American Society Of Civil Engineers.

Use of Electronic Leak Detection System in 24/7 On-line Mode to Control Construction and Operation of Lined CAL Lagoons

Vladimir Nosko, RNDr., PhD., Sensor spol. s r.o., Slovakia, nosko@sensorgroup.com
Petar Razdorov, MSc., Consultant, Canada, PetarRazdorov@gmail.com

ABSTRACT

The latest Covered Anaerobic Lagoon (CAL) equipped with Electronic Leak Detection System (ELDS), with permanently fixed position sensors (to monitor integrity of geomembrane) was built in 2011/2012 in UK. A new improved CAL design was implemented. Advancements incorporated into the new design were based on experiences from previous installations and operation of permanent ELDS, now incorporating sophisticated Continuous Monitoring Station (CMS), allowing real time monitoring of geomembrane integrity 24/7 and providing leak alarms and positioning of damage in the event of any leak. Special conductive geotextiles are used providing consistent current distribution and in the latest application a new conductive geotextile incorporating a unique signal layer was introduced. The presented article describes the use of ELDS to further perfect and continuously improve CAL construction. The 24/7 electronic monitoring and processing unit is described to help promulgate the understanding of the process of on-line geomembrane integrity testing of CAL facilities.

1. INTRODUCTION

The concept or requirement for leak detection monitoring of geomembrane lined tanks filled with liquid are as old as the use of geomembrane lining itself. The options for leak monitoring and detection of damage have historically been restricted to passive solutions. Such solutions have provided only indicative information that a tank or lagoon is 'probably' free of any damage. This unacceptable level of uncertainty is as a result of the nature of passive systems utilising drainage pipes or drainage composites. Prior to this indicative bore holes were used as integrity indicators, especially for tanks filled with toxic material or contaminants where the presence / absence of the stored material in a tank or lagoon was controlled. In both cases if the presence of the material in bore holes or the drainage system was positive, the leak was detected however it was never possible to detect the exact position of any geomembrane damage. In many cases having found that a tank was leaking, the only solution was the installation of an additional layer of the geomembrane. Unfortunately many lagoons were still found to be leaking even after a number of additional layers were installed.

The installation of five or more geomembrane layers has been seen on sites where there were still leakage problems. There have been many experiments using indication chemicals and similar tracing solutions, but none have adequately resolved the inherent problems.

2. DESCRIPTION OF APPLICATION

Resolution of the root cause of the problem (a leak through damaged geomembrane) required the use of an electronic monitoring system in order to mitigate the huge costs associated with unserviceable tanks, which could have resulted in the closure of a factory. The data from the electronic monitoring system was used to create a report of geomembrane integrity, which was issued to the inspection office at the Environmental Bureau in order to get approval to use the lagoon.

The cost of suspended production on the site was the dominant consideration and after consultations with the Client an ELDS off-line system was designed. As a result, when testing of the geomembrane was carried out with the installed system it was found that the impact of 'the electrical bridges' and ELDS electric signal formation itself, caused very complicated data analysis and their evaluation / interpretation, was practically impossible without the input of highly experienced engineers.

2.1 Europe

The first Covered Anaerobic Lagoon (CAL) to be equipped with permanently installed ELDS with sensors in fixed positions (to monitor integrity of geomembrane), was built in 2001 in Europe. Three different types of leak detection and location systems were applied prior to filling the lagoon with water. To enable function of the pre-filling tests a conductive geotextile was installed. The physical make up of the sealing layers (reading from bottom to top) were: HDPE

geomembrane; geosynthetic drainage layer; conductive geotextile; ELDS; upper HDPE geomembrane. Both HDPE geomembranes were tested prior to filling the lagoon using an electro acoustic test method as well as wading and water lance surveys. These techniques revealed a number of leaks, which were then repaired prior to the filling process. During the filling process the permanent ELDS was used to monitor the integrity of the lagoon. Data from the ELDS was recorded and analysed in-situ requiring the permanent presence of an engineer throughout the filling process. Since then over the period of 11 years service zero leakage has been recorded. This first application was published and presented by group of authors I.D.Peggs, V.Nosko, P.Razdorov and P.Galvin at Eurogeo 2004.

2.2 North America

Based on the abovementioned success, the Client wanted the system adapted in order to monitor the integrity of geomembrane layers automatically both during the construction and during the operational life of a lagoon. **The main requirement was to have information available 24/7 in the control centre for the site (via SCADA)** where all information about the function of a lagoon is coordinated (pumps, mixers, liquid levels, etc). At the time, the only system available was an off-line version, but driven by the client's desire for innovation and a culture of continuous improvements based on experiences since, a new type of system was developed. In 2008 in North America the iterative technical improvements made through continuous improvement allowed for a technological leap to a much more sophisticated electronic leak detection system which was installed complete with an on-line 24/7 testing mode. The photographs 1 and 2 below show the installation of sensors and cables to the geogrid that is to be contained along with the conductive geotextile between two layers of geomembrane.

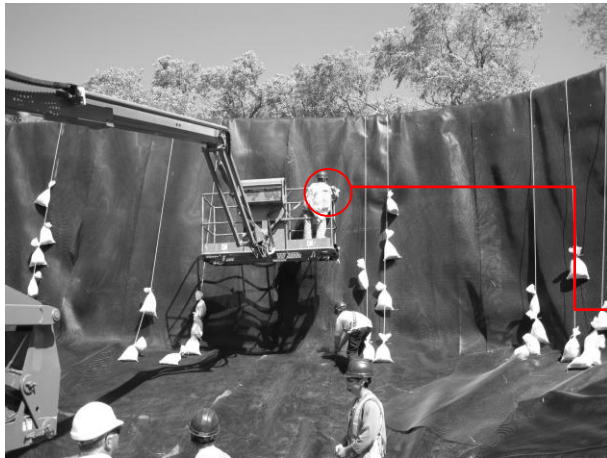


Photo 1. Installation of ELDS.

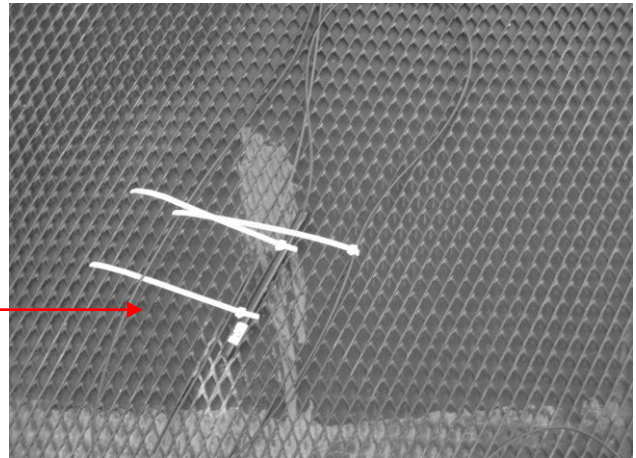


Photo 2. Detail of sensor installation.



Photo 3. General view of the tested lagoon



Photo 4. ELDS remote analysing centre

Unlike previous experiences, earlier involvement in the design stage made it possible to influence the process. This allowed the client eliminate the impact of 'electrical bridges' and to eliminate false signals in data scanning. In this case

two geomembrane layers were installed with a conductive geotextile between in order to maintain consistent signal transfer from any damage. The sealing layers comprised (in order from bottom to top): a compacted clay base; thick protective geotextile; lower HDPE geomembrane; drainage geocomposite; conductive geotextile; ELDS; and finally the top layer of HDPE geomembrane.

2.3 Europe

After the successful implementation of ELDS incorporating the 24/7 monitoring concept in 2011 in Europe the same system was installed (Photo 3) but adapting the installation to work with only one geomembrane layer. 24/7 monitoring was included but **we also added a new 'Watchdog function' (a leak alarm)**. The sealing layers comprised (in order from bottom to top): clay subsoil; thick protective geotextile; drainage geocomposite; **new type of conductive geotextile with integrated the signal layer (for watchdog alarm function)**; ELDS; and on the top the HDPE geomembrane. There were 400 sensors installed for monitoring the integrity of lagoon, the area monitored is 10,200m². The aim of the project was achieved with 100% integrity in the construction phase of the lagoon. The main aims of the project in relation to the ELDS implementation was set out as:

1. Integrity testing of a geomembrane before filling;
2. 24/7 Integrity testing during the filling lagoon with water;
3. Integrity testing during the use of the lagoon.

In order to ensure that the ELDS was able to achieve aim 3 above it was necessary to develop a system that could filter the electrical noise generated by the production processes. The methodology adopted to test during the operational lifespan of the CAL was the use of the Watchdog system during periods of sustained production process 'noise', then to switch to scanning mode during low noise periods. This method enabled the elimination the false signals, or damaged data caused by 'noise' and was achieved by implementing a high level of data coordination through the client's SCADA system. This system and other similar systems installed around the world are monitored remotely from our monitoring (Photo 4 above). These developments took more than **10 years Research & Development** by teams of highly educated engineers.

It is very important to clearly state that the unambiguous aim was that 100% geomembrane integrity be maintained during lagoon construction process and its fluent transfer from construction to operational service. This aim was achieved by maintaining the team whose close coordination and shared experience of such installations enabled familiarity to be translated into success. Cooperation between the individual companies started on the earlier applications developing the collective intelligence as each project was completed. This intelligence is both built and capitalised by the repetitious deployment of the same installers, manufacturers and consultants on each project. The combined and thorough knowledge of all processes involved in the construction process resulted in a successfully delivered project.

The key measure of the success of the whole project was the coordination of all processes without the need to repair the geomembrane which would cause construction delay. In 2001 there were 7 anomalies; in 2007 there were only 3 anomalies; and in the year 2011 there were none (the functionality of the ELDS monitoring system was proven by successful detection of 2mm diameter test holes, shown in Photo 5 and Photo 6). This is the most important result validating the approach of learning from mistakes during the construction process and in order to achieve this the importance of maintaining the same team of companies cannot be overstated.



Photo 5. Position of test hole.

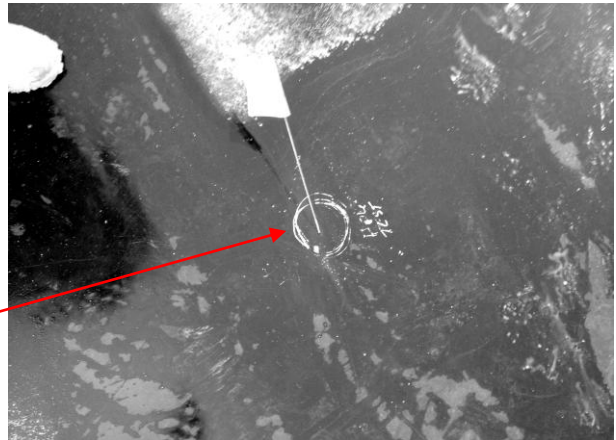


Photo 6. Detail of the test hole.

3. CONCLUSION

The latest installation was carried out during 2011/2012 where another improved CAL design was implemented to make ELDS more effective. The advancements incorporated into the design were based on the experiences from previous installations and the operation of the permanent ELDS, now incorporating the sophisticated Continuous Monitoring Station (CMS) which allows real time control of geomembrane integrity 24/7.

In each case special conductive geotextiles were used, the latest of these textiles enable CMS to provide a leak alarm in the event of a leak. The prescribed ELDS testing process has two modes:

- Watchdog monitoring mode to warn clients immediately that the integrity of the geomembrane is broken;
- Measuring mode when liner is scanned and the position of any damage / leak can be precisely located.

The abovementioned functions of the ELDS CMS system, provide 24/7 geomembrane integrity monitoring during each phase of the CAL's life, these phases are summarised as:

1. Construction Phase (pre-filling);
2. Water Filling Phase (up to maximum capacity);
3. Operational Phase.

Each of these phases present their own challenges as the dynamic forces applied to liner shift the installed system is continuously and automatically reporting to the client through their SCADA system, confirming the integrity of the protective geomembrane.

The presented article describes the use of ELDS with permanently installed sensors in fixed positions to assist in the further and continuous evolution of CAL construction perfection.

The full electronic monitoring and processing unit in 24/7 mode are described to help promulgate the understanding of the process of on-line testing of geomembrane integrity within a CAL facility.

ACKNOWLEDGEMENT

As authors we would like to thank Jon Crowther from Sensor UK for his valuable input.

REFERENCES

Peggs, I.D., Nosko, V., Razdorov, P. and Galvin, P. (2004). Leak monitoring for a double liner separated by a novel conductive geotextile, *EUROGEO 3*, Proceedings of the 3rd European Geosynthetics Conference, Munich, Germany, pp: 515-518.

Use of Geocomposite as an Internal Drain in Levees Subjected to Seepage: Centrifuge Model Study

Rishabh Kumar Saran¹, Research Scholar, Dept. of Civil Engineering IIT Bombay, India. rishabhsaran@iitb.ac.in
B.V.S. Viswanadham² Professor, Dept. of Civil Engineering, IIT Bombay, India. viswam@civil.iitb.ac.in

ABSTRACT

The main objective of this paper is to investigate the performance of levee sections at the onset of flooding and subsequent seepage with the help of centrifuge model tests at 30 gravities. Three levee sections were modeled viz. levee section without drainage layer, with horizontal sand drain and with horizontal geotextile drainage layer. The flood was simulated with the help of remotely operated in-flight flood simulator. Levee section without any horizontal drain or clogged drain was observed to experience a catastrophic failure. Horizontal sand drainage layer was found to be very effective to dissipate pore water pressure leading to the stability of a levee. The analysis of centrifuge test results shows that horizontal geotextile drainage layer is effective in ensuring stability of the levee section at the onset of flooding and subsequent seepage. An attempt has also been made to compare results obtained from centrifuge studies with seepage and stability analyses using SEEP/W and SLOPE/W software. Finally, this paper concludes the use of geotextile horizontal drainage layer as an internal drain in place of conventional sand drainage layer as a viable option for imparting economy to construction projects.

1. INTRODUCTION

Levees are earthen embankments that run along the river or canal banks, which protect land side area containing agricultural, industrial, urban and rural areas. Any breach in levee section can trigger catastrophic consequences to cities situated in the vicinity of rivers. Construction material used in levees greatly varies from silty sand to clayey soil according to availability of borrow materials locally. Preferably, less permeable soil is used in hearting zone in order to contain water and relatively permeable soil is used in the casing zone of a levee section, which is not subjected to cracking in the case of direct exposure to atmosphere. One of the most acute problems in designing levees is to control seepage of the water. In the absence of appropriate seepage control measures, it may lead to various types of failures, such as: i) downstream side face/base failure, ii) piping, boiling failure, iii) excessive hydrostatic pressure below the hard stratum etc. An earthen embankment has various components such as cut-offs, trenches, drainage layers and reinforcement layers etc. All these components address numerous functions such as, drainage, resistance to piping and erosion control in order to maintain stability and facilitate the functionality of levee. Horizontal drains serve to dissipate pore water pressure in the downstream side. In this study internal drainage system in the form of horizontal drain embedded in downstream side was considered. BIS 9429(1990) suggests guidelines for drainage system for earth and rockfill dams where it is illustrated that geometry of drains are essentially affected by water level at upstream side, height of embankment both in upstream and downstream sides, permeability of embankment and drainage material, gradation of embankment and drainage materials and angle of discharge face. Additionally, several regulations recommend different thicknesses of horizontal drains. US Army Corps of Engineers EM 1110-2-1913 (2000) suggests a minimum thickness of horizontal drain layers of about 457.2mm for construction purposes. BIS 9429(1990) proposes a minimum 1.0 m thick horizontal drain in earthen dams. Geometry of horizontal drain is also affected with the availability of well graded material, as per filter requirements. Due to rapid expansion of infrastructure in developing countries in the world like India, lack of availability of suitable material for drainage imposes economic burden on projects. Hence, there is a need to explore avenues for replacing conventional drainage layer with an appropriate material, which can cater the basic requirements of internal drain.

Several researchers adopted different approaches for understanding the hydraulic behavior within the levee section, such as analytical, numerical, large-scale and small-scale studies. Iryo and Rowe (2003) studied the applicability of Van Genuchten equation for estimating unsaturated/ saturated water flow within soil-geotextile system and simulated the phenomenon using SEEP/W. Further, Iryo and Rowe (2004) examined the hydraulic response of a geotextile layer embedded in sandy soil subjected to 1-dimensional infiltration. Jia et al.(2009) evaluated the stability of the slope model constructed using sandy silt (12% sand, 80% silt, less than 5% clay) subjected to rising and lowering water level by conducting large-scale model tests at normal gravity. Ubilla et al. (2008) investigated the failure and non-failure conditions of levees subjected to Katrina hurricane with help of centrifuge studies on the London Avenue and Orleans Canal South. Das and Viswanadham (2010) proposed an experimental set up for examining the piping behavior of silty sand soil type with and without discrete and randomly distributed geofibers. Raisinghani and Viswanadham (2010) presented the effect of geosynthetic layers in enhancing the in-plane permeability of fine-grained soils in the laboratory by using custom made permeameter tests. It was reported that the use of a permeable geosynthetic layer in the form of

a geocomposite (which is combination of woven geotextile and non-woven geotextile or geogrid and non-woven geotextile) helps in lowering phreatic surface and reducing generated pore water pressures by draining water in the plane of geocomposite layers. Successful application of using geocomposite materials for pavement, behind retaining walls, reinforced soil walls and slopes was reported by Raisinghani and Viswanadham (2011).

However, very few attempts have been made to understand the stability and deformation behavior of levee sections without and with conventional or geocomposite drainage layer as internal drain using a centrifuge modeling technique. Hence this forms the research interest of the present study.

In this present study, hydraulic behavior of horizontal drainage layer of sand and geotextile at the toe of the embankment constructed with low permeable embankment material was evaluated using centrifuge tests at 30 gravities. For this purpose three levee model sections with and without horizontal drainage layers subjected to flooding were considered as shown in Table 1. Sand and geotextile were used as internal drain materials separately in the horizontal direction located at toe towards downstream side. A set-up has been developed to induce in-flight flooding at 30g. Material properties of levee section, upstream and downstream slopes, levee height, top width and base layer thickness were kept constant. The effect of inclusion of drainage layer and replacement of sand with a non-woven geotextile material on the stability and deformation behavior of levee, pore water pressure distribution, phreatic surface development has been evaluated. Further an attempt was made to compare observed centrifuge model test results with the help of finite element based SEEP/W and limit equilibrium based SLOPE/W (Geostudio, 2007).

Table 1. Details of centrifuge model tests

Test Legend	Drainage material	H (mm)	Upstream slope angle (α)	Downstream slope angle (β)	Drainage length (mm)	Thickness of drainage layer (mm)
RL-1	- ^a	200 (6000)	45 ⁰ (1V:1H)	56.3 ⁰ (1.5V:1H)	- ^a	- ^a
RL-2	Sand	200 (6000)	45 ⁰ (1V:1H)	56.3 ⁰ (1.5V:1H)	185 (5550)	20 (600)
RL-3	NW Geotextile	200 (6000)	45 ⁰ (1V:1H)	56.3 ⁰ (1.5V:1H)	185 (5550)	0.66

^a Not relevant; Prototype dimensions are given within parentheses; NW = Non-woven.

2. SCALING CONSIDERATIONS FOR MODELING NON-WOVEN GEOTEXTILE

In the present study, centrifuge modeling technique was adopted to achieve stress similarity at homologous points by subjecting a model reduced by 1/N times to N time's gravity. The use of centrifuge modeling technique was considered relevant because of the requirement of simulation of stress conditions and pore water pressure variation at the onset of flooding and subsequent seepage through a levee section as that of in the prototype. In addition, climatic events like simulation of flooding at full-scale are difficult.

In order to scale-down a geocomposite layer, three criteria are required to be satisfied: i) Scaling down of tensile-load strain characteristics, ii) Scaling of in-plane permeability characteristics, and iii) Soil-geocomposite interface friction. Detailed discussion on modeling of geocomposites in a centrifuge was reported by Raisinghani and Viswanadham (2011). Based on the scaling considerations, there is requirement of having a geocomposite layer with reduced thickness, tensile load and secant stiffness reduced by 1/N times that of the commercially available geocomposites and with identical soil-geocomposite interface friction. However, in order to satisfy scaling requirements from hydraulic properties point of view, the geocomposite shall have identical transmissivity as that of in the commercially available geocomposites and shall possess N times more in-plane permeability characteristics in the model. Although geocomposite can have reinforcement and drainage functions, considering the requirement of drainage function, only non-woven geotextile was considered and referred as geocomposite in the present study.

3. CENTRIFUGE MODEL TESTS ON LEVEES SUBJECTED TO FLOODING

3.1 Model Materials

Three types of model materials are involved. They are; i) Model soil for constructing a levee; ii) Sand as an internal drain; iii) Non-woven geotextile as an internal drain and as a replacement for conventional sand drainage layer. Generally, levees are constructed by using low to very low permeable materials. By blending 80% of locally available fine sand with 20% of commercially available kaolin (by dry weight), silty sand type model soil was formulated. The model soil was found to have maximum dry unit weight $\gamma_{d, \max}$ of 18.75 kN/m³ and optimum moisture content (OMC) of

8% according to standard Proctor compaction. The value of coefficient of permeability of the model soil moist-compacted at $\gamma_{d, \max}$ and OMC is 1.54×10^{-6} m/s. The model soil (moist-compacted at $\gamma_{d, \max}$ and OMC and saturated) was found to have a cohesion of 11.9 kN/m^2 and angle of internal friction of 27° obtained by conducting drained direct shear box test. The sand used in the present study is classified as SP according to Unified Soil Classification System and has an effective particle size $d_{10} = 0.10 \text{ mm}$. The sand was found to have a maximum void ratio of 0.89 and minimum void ratio of 0.58. The coefficient of permeability of sand placed at 85% relative density is 1.49×10^{-4} m/s.

Based on the above set scaling considerations for modeling non-woven geotextile, a non-woven geotextile having thickness of 0.66 mm, a mass per unit area of 46 g/m^2 , transmissivity θ of $0.38 \times 10^{-6} \text{ m}^2/\text{s}$ at 20 kPa normal stress, and coefficient of in-plane permeability of 5.757×10^{-4} m/s (ASTM D6574, 2006) was used.

3.2 Model Test Package

The 4.5 m radius large beam centrifuge facility having 2500 g-kN capacity available at Indian Institute of Technology Bombay was used in the present study. The specifications were discussed by Viswanadham and Mahajan (2007). Identical stress-strain behavior can be simulated by subjecting the scaled down model to N-times gravity level in controlled environment. Centrifuge models tests reported in this study were carried out at 30g. The internal dimensions of strong box were 760 mm in length, 200 mm in breadth and 410 mm in height. Model was constructed in strong box having three steel walls with honey-comb structure and one wall with thick Perspex glass sheet. Fig. 2 shows cross-section of a model test package. Plane strain conditions were maintained by applying white petroleum grease on inner surfaces of front and rear walls of strong box. Perspex sheet was used to ensure clear view of front elevation of the model to the digital photo camera mounted in front of the container. A rectangular grid of 430 mm x 210 mm with four permanent markers was glued on to the Perspex surface in contact with the soil to serve as reference points for image analysis. Movable markers were embedded in the soil at different elevations as along the downstream face to traced displacement vectors at the onset of flooding. Relative positions of movable markers were captured and recorded with help of high resolution digital photo camera. Four pore water pressure transducers (PPT) were embedded at the levee bottom to evaluate the variation in pore water pressure with respect to seepage time. Two linear variable differential transformers (LVDT) were housed at both side of crest to obtain crest deformations with respect to seepage time.

To induce in-flight flooding, a remotely operated DC-pump based flood simulator has been developed. As shown in Fig. 1, there are three main components of set-up: a) water reservoir b) Pump assembly and c) voltage controller. Water reservoir having dimensions (650 mm x 160 mm x 140 mm) was placed by the side of strong box. Firstly, this water reservoir constantly receives water supply from one of the slip rings provided in centrifuge. Thus, this reservoir acts as constant head reservoir catering a continuous source of water to the inlet of pump. Secondly, pump was housed vertically over the water reservoir. A mild-steel frame was used to fasten pump firmly to avoid any sort of damage to pump during flight. This frame was firmly attached to backside of the strong box. Finally, power supply to this pump was regulated remotely with help of DC-voltage controller. Thus, for a given g-level, voltage level and levee section, a particular flood rate could be generated. One PPT was also placed in upstream side of levee in order to monitor and evaluate flood level with seepage time.

3.3 Model Test Program and Test Procedure

Base layer was comprised of two layers viz. 60 mm thick with silty sand and 40 mm thick with kaolin. Kaolin layer was overlaid the base layer of silty sand (80:20 mix). Kaolin having very less permeability was intentionally selected as a model soil to be placed just beneath the levee section in order to induce potential seepage through levee section only. In model RL-2, Goa sand was placed as a horizontal drainage layer at downstream. The sand was placed at 85% relative density with a dry unit weight of 15.5 kN/m^3 . Angle of internal friction for the sand in dry sand placed at 85% relative density was found to be 32° . In Model RL-3, sand layer was replaced with a model needle punched nonwoven geotextile to serve as an internal drain.

Model Levee sections were constructed with a height of 200 mm, top width of 100 mm, upstream slope 1V:1H and downstream slope 1.5V:1H. Geometry of levee was selected such that factor of safety at the onset of seepage is close to one. In this paper, results of three centrifuge model tests are presented. They are: i) without drainage layer (RL-1), ii) with horizontal sand drainage (RL-2) and iii) with horizontal geotextile drainage layer (RL-3), as shown in Table 1. Levee models were constructed in layers of 30 mm thickness moist-compacted at $\gamma_{d, \max}$ and OMC according to standard Proctor compaction. L-shaped movable plastic markers were also placed at the top of each compacted layer horizontally at a centre to centre spacing of 20 mm from downstream slope face. External side of one leg of the movable markers was lubricated with grease in order to reduce friction between Perspex sheet and marker surfaces. Positions of the movable markers were traced with help of image analysis of front elevation images of levee section captured during the centrifuge test. At selected locations, food dye was placed to trace the movement of water at the onset of flooding through a levee section during centrifuge test.

In model RL-2, a 20 mm thick horizontal sand drainage layer was placed at toe of the levee section towards downstream side. The length of the sand drainage layer was maintained constant throughout the width of the levee and it was laid from vertical projection of midpoint of top width to the toe in the downstream side. The drainage layer was constructed by pluviating the sand in dry state and desired density was controlled by performing density checks. The sand layer was confined with a thin layer of geotextile fabric was wrapped with an anchor length of 20 mm at toe to prevent washing of sand particles at the onset of seepage. In model RL-3, horizontal drainage layer with sand was replaced with a model non-woven geotextile layer having same length and width as that of in model RL-2. It was positioned vertically 10 mm above the base layer, embedded in levee material to ensure no clogging of geotextile with kaolin particles from the base layer.

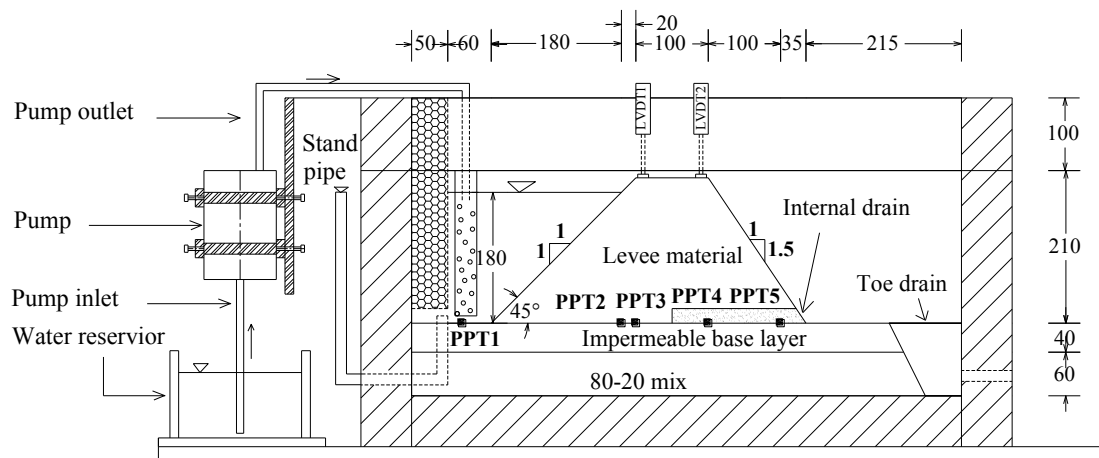


Figure 1. Schematic cross-section of model test package (All dimensions are in mm)

All levee models were instrumented with 5 no's PPTs and 2 no's LVDTs to evaluate variations in pore water pressure and settlement behavior of levee crest respectively. As shown in Fig. 1, PPT1 was placed above the base layer towards upstream to monitor the flood level and another four PPTs were embedded along the levee bottom at a distance of 180 mm (PPT2), 200 mm (PPT3), 300 mm (PPT4) and 400 mm (PPT5) from the upstream toe. PPT3 was placed at different position at 250 mm from upstream toe of levee in both model RL-2 and RL-3. In models RL-2 and RL-3, PPT3 was placed right below the mid-point of top width of the levee section to capture pore water pressure variations at the junction of levee material and horizontal drainage layer. LVDTs were housed at both left and right side of the crest at a horizontal distance 210 mm and 290 mm from upstream side toe. After completion of the model, in-flight simulator was mounted along with the model and initial checks were performed.

For all the models, 30 gravities was induced by rotating a model with 81 revolutions per minute. On reaching 30g, in-flight flood was commenced by activating pump remotely from the control room. Once the pump started, flood level kept on increasing due to constant pumping of water into the enclosure in front of the upstream face, as shown in Fig. 1. In order to prevent early seepage of water into levee section, the upstream side slope surface was coated with a thin layer of bentonite up to desired flood height. Constant High flood level could be maintained with the help of a stand pipe connected to the enclosure in front of the upstream slope face, as shown in Fig. 1. At the onset of flooding and subsequent seepage, seepage of water into levee section could be easily traced with help of diffused colored food dye. The seepage phenomenon through levee section was captured with the help photographs triggered at every 30 seconds from the time of commencement of flooding.

4. ANALYSIS AND INTERPRETATION OF CENTRIFUGE MODEL TESTS

4.1 General

Based on Pore water pressure data obtained from PPTs and corresponding variation of pore water pressures, head development and development of phreatic surfaces were calculated for all centrifuge models carried-out in the present study. Deformation behavior of levee sections was evaluated with the help of LVDTs data and image analysis. The following sections present analyses and interpretation of results of centrifuge tests.

4.2 Simulation of Flood

Figure 2 shows the variation of flood level with seepage time in prototype dimensions. This figure was plotted by considering the time in prototype dimensions, right after commencement of flooding at 30g. This was calculated by using $t_m/t_p = 1/30^2$ (where t_m = time in model dimensions and t_p = time in prototype dimensions). As shown in Fig. 2, maximum flood level could be achieved within four days for all the models. Efforts were made to simulate ideally identical flood levels for all the levee section, but due to limitation of pump capacity in high gravity environment water head slightly dipped and flood level fluctuations were observed. However, hydraulic response of levee sections in the form of pore water pressure and phreatic surfaces were evaluated with respect to function of flood level for individual levee sections.

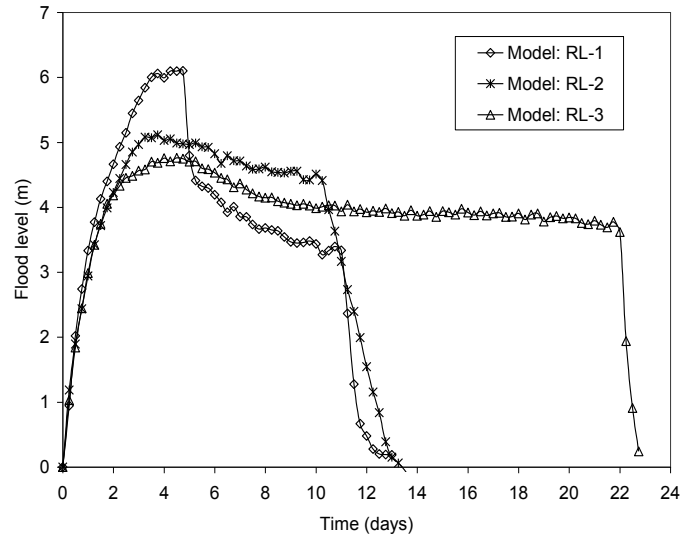


Figure 2. Simulated flood function with respect to time in centrifuge models

4.3 Deformation Behavior of Levees

Crest deformations were measured with help of LVDTs placed at both sides of crest viz. landside crest and riverside crest, as shown in Fig. 1. Measured deformations of landside crest (i.e. towards downstream side) with respect to time in days for all the centrifuge tests are shown in Fig. 3. It can be seen from Fig. 3 that levee model RL-1 has undergone catastrophic failure right after attaining highest possible flood level. However, levee sections RL-2 and RL-3 with horizontal drainage layer were observed to experience only very negligible crest settlements. Values of normalized pore water pressures ($u/\gamma H$) are also marked in different stages of test in Fig. 3. Normalised pore water pressure is defined herein as a ratio of the measured pore water pressure with the help PPT3 to the product of bulk unit of the soil (γ) and height of levee section H. At the onset of seepage, normalized pore water pressure within levee section for model RL-1 was observed to increase up to 0.665 at 5 days after initiation of flood. In comparison, steady state seepage conditions were found to establish in models RL-2 and RL-3. This demonstrates the importance of un-clogged or proper drainage layer at the toe of levee section.

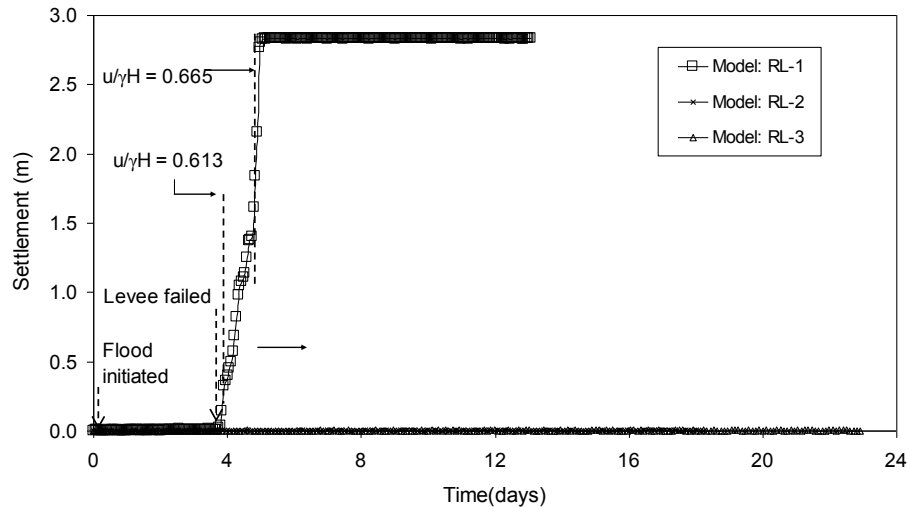
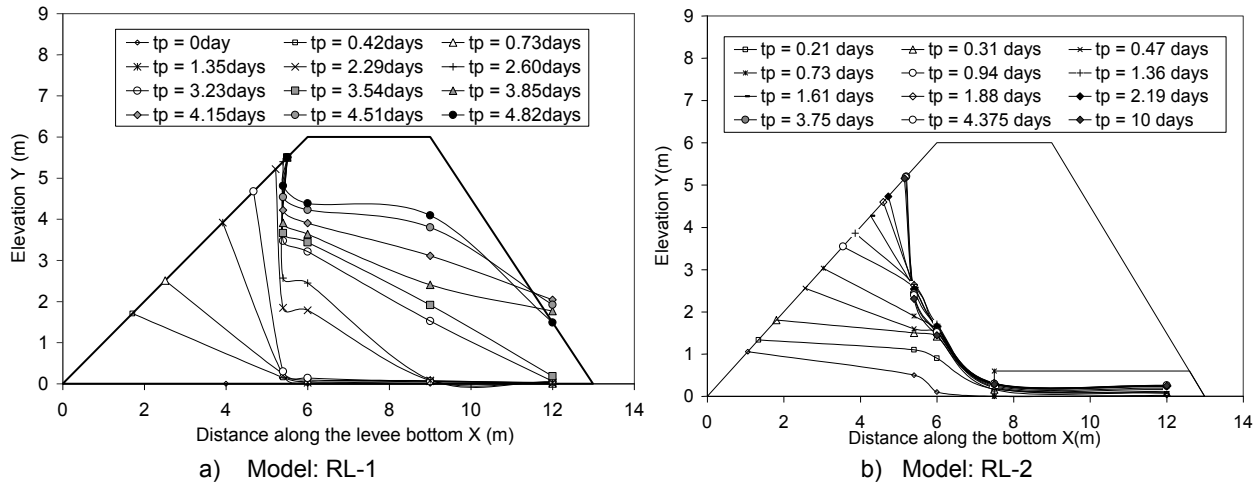


Figure 3. Measured variation in surface settlements of land side crest with respect to time

4.4 Development of Pore Water Pressure Within Levee Section

Phreatic surfaces during various stages of centrifuge after commencement of initiation of flooding were evaluated with the help of pore water pressure data obtained from PPTs embedded along the levee bottom. Figs. 4a-c present development of phreatic surfaces in levee sections with prototype time in days for models RL-1, RL-2 and RL-3 respectively. Three different types of phreatic surface development patterns can be observed for all the models presented in this paper. Relatively higher elevation of phreatic surfaces was observed in case of model RL-1. This is attributed to the absence of horizontal drainage layer at the toe or the presence of clogged drainage layer. In the case of model RL-2, the flow path of the water changed considerably and significant drop in pore water pressure drop within the levee section was observed. Depletion in the elevation of phreatic surfaces indicates efficiency of sand horizontal drainage layer in model RL-2. As depicted in Fig. 4c, a considerable dip in phreatic surfaces was observed for model RL-2 when compared with RL-1 without any drainage layer. However, development of pore water pressures in the drain zone for model RL-3 was found to be relatively higher than those in model RL-2.



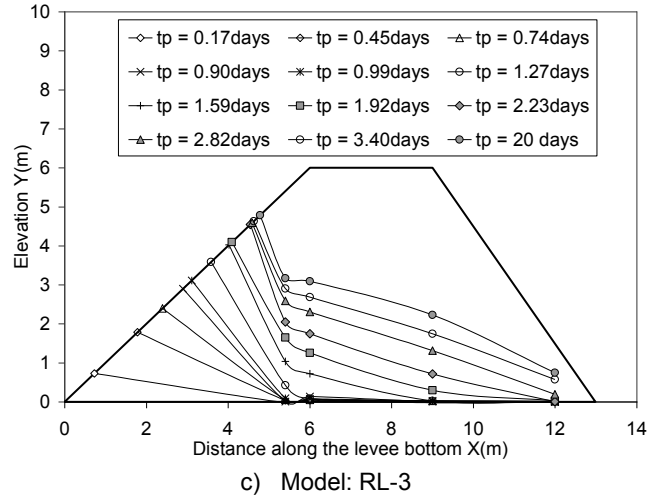


Figure 4. Development of phreatic surface with seepage time within time (days)

Figs. 5a-b present variations in normalized pore water pressure with respect to prototype time for models RL-1, RL-2 and RL-3 respectively. In Fig. 5a, variation of $u/\gamma H$ obtained from PPT3 was used and in Fig. 5b, variation $u_{toe}/\gamma H$ obtained from PPT5 placed at the toe was presented. As shown in Fig. 5a, relatively high peaks of normalised pore water pressures both within the levee section and the toe were observed for model RL-1. These high values of pore-water pressures lead to the catastrophic failure immediately at the onset of maximum flood level for model RL-1. In comparison, lower values of $u/\gamma H$ and $u_{toe}/\gamma H$ were recorded for models RL-2 and RL-3 reflecting stability of levee models. Moreover, interestingly, distinct peaks were not observed for models RL-2 and RL-3 and this indicates the need of an appropriate internal drain in levee sections. The decrease in normalized pore water pressure values at the toe ($u_{toe}/\gamma H$) essentially depicts efficiency of drainage layer either in the form sand as well geotextile layer. In the case of RL-2 and RL-3, centrifuge tests were terminated after attaining steady state conditions in terms of pore water pressures. Long term hydraulic behavior of drainage measures is beyond the scope of this study.

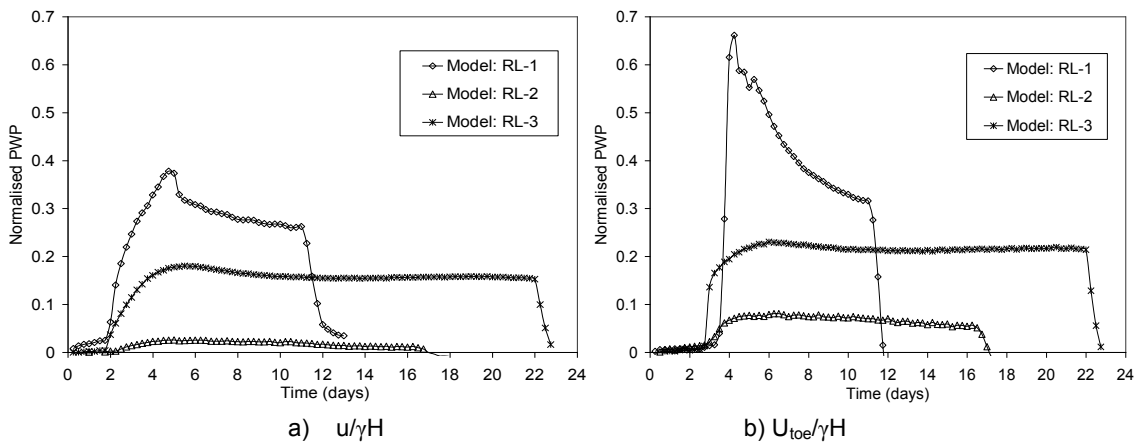


Figure 5. Variation of $u/\gamma H$ and $u_{toe}/\gamma H$ with time in days

4.5 Digital Image Analysis of Centrifuge Models

Images of front elevation of levee models captured with the help of on-board digital cameras at 30g for various stages of seepage were used to arrive at displacement vectors of markers embedded within the levee body and along with the downstream slope face. Image processing software, ImageJ (Version 1.44, 2011) was used for evaluation of relative positions of movable markers. For each image, global co-ordinates were fixed with reference to a grid of permanent markers. This was adopted for analyzing each and every image to prevent any error due to monitor resolution. After fixing global coordinates, positions of all the markers were registered for each image. Fig. 6 shows displacement vectors from the time of initiation of flooding and up to penultimate stage of the stage. Fig. 6 also depicts levee geometries of model RL-1 at both pre and at failure states. Levee model RL-1 was observed to experience a catastrophic failure at 5.1

days after initiation of flooding. A clear and distinct failure surface extending from the crest towards water side to the toe of the levee section can be observed. However, in case of levee models RL-2 and RL-3, negligible movements were recorded and hence digital image analysis was not performed.

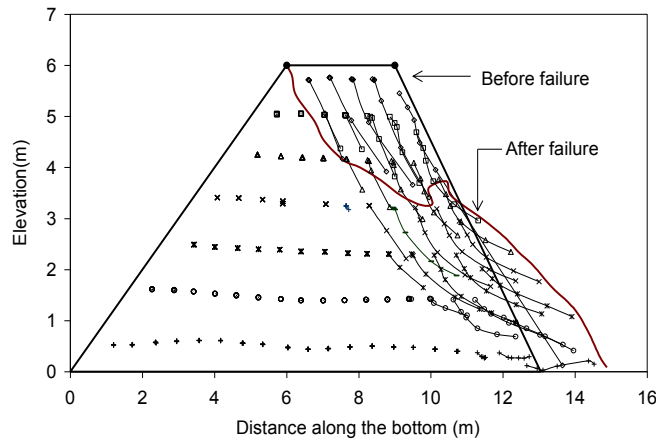


Figure 6. Displacement vectors for model RL-1

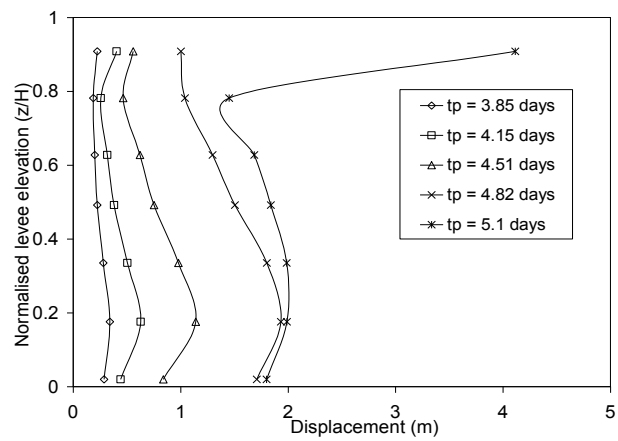


Figure 7. Variation of face movements at the onset of seepage for model RL-1

Figure 7 presents variation of face movements for different durations of time (both in horizontal and vertical direction) with normalized height (which is defined as a ratio of height z from the top surface of impervious layer to the levee height in vertical direction) for model RL-1. The face movements could be obtained with the help of tracking movements of markers glued on to down stream slope surface. As can be noted from Fig. 7, downstream slope face was observed to move considerably immediately after completion of $t_p = 5.1$ days and experiencing a catastrophic failure. Further, relatively large movements at the toe (i.e. at $z/H = 0.2$) due to higher values of higher values of normalized pore water pressures at downstream slope lead to toe failure and is attributed mainly due to the absence of horizontal drainage layer or clogged drainage layer.

5. SEEPAGE AND STABILITY ANALYSIS OF CENTRIFUGE MODELS

Seepage analyses and stability analyses were also carried-out for all the three models with the help of finite element based software package SEEP/W and limit equilibrium method based SLOPE/W (GEO-SLOPE, 2007) softwares. For all models, dimensions of models were maintained in their corresponding prototypes having identical soil properties. As per the scaling considerations, hydraulic properties of geotextiles were scaled-up corresponding to 30 gravities. Geotextile tensile load characteristics were not considered while performing SLOPE/W analysis. Boundary conditions in numerical modeling were kept similar to those adopted in centrifuge model tests. Boundary conditions were assigned in the form of total head on the upstream side, total head on the downstream side and transient seepage time span. Flood functions were kept identical to simulated flood in a centrifuge test with the help of flood simulator, as shown in Fig. 2. Soil water characteristics curve (SWCC) was obtained with the help of grain size distribution curve to consider unsaturated-saturated properties of levee material (Geoslope, 2007). Drainage materials sand and geotextile were modeled as saturated materials and interface model respectively. Foundation layer was modeled as an impermeable material to ensure potential seepage through levee section only. For stability analyses, slip surfaces were specified to pass through toe at the downstream side. Special geometrical points were specified in numerical models to represent various PPT positions along the levee bottom of centrifuge models. Pore water pressure contours and phreatic surfaces were obtained from the seepage analysis. Variations in pore water pressure at levee bottom were plotted for the special geometrical points.

Figs. 8a-c present variations of pore water pressure for all centrifuge model tests. For comparison purposes, measured pore water pressure with seepage time for models RL-1, RL-2 and RL-3 is shown in Figs. 8a-c. Model RL-1 without any drainage measure registered high pore water pressures along levee bottom in comparison to RL-2 and RL-3. In all the levee sections the delay in pore water pressures built-up at levee bottom was found to be about by 2 days immediately after initiation of flooding, which can be attributed to unsaturated-saturated properties of levee material. PPT2 placed just vertically below the water level interacts with upstream levee face experienced highest pore water pressure. Measured pore water pressures by PPT2 in models RL-1, RL-2 and RL-3 were 48 kPa, 27 kPa and 32 kPa respectively. In comparison, computed pore water pressures from the seepage analysis of models RL-1, RL-2 and RL-3 at PP2 location were found to be 46 kPa, 27 kPa, and 32 kPa respectively. Measured pore water pressure at PPT5 (near toe) was found

to be 22 kPa in case of RL-1, whereas in the case of models RL-2 and RL-3, it was found to be the order of only 3 kPa and 7 kPa. Identical trend could be obtained from the seepage analysis of levee models. Relatively high pressures at the downstream toe in RL-1 caused instability to levee section. Whereas, proximity of reduced pore water pressure in models RL-2 and RL-3 at PPT5 indicates the efficiency of horizontal drainage layer to dissipate pore water pressure constructed with sand as well as non-woven geotextile as a drainage material.

Figs. 8a-c exhibit identical pattern of pore water pressure variation as obtained in centrifuge tests. Pore water pressure in model RL-2 near the downstream was found as 5 kPa from the centrifuge test and 4 kPa through SEEP/W respectively. In the case of model RL-3, it is 7 kPa and 11 kPa respectively. The consistencies in variations of pore water pressures demonstrate a good agreement with observed phenomenon in centrifuge model tests.

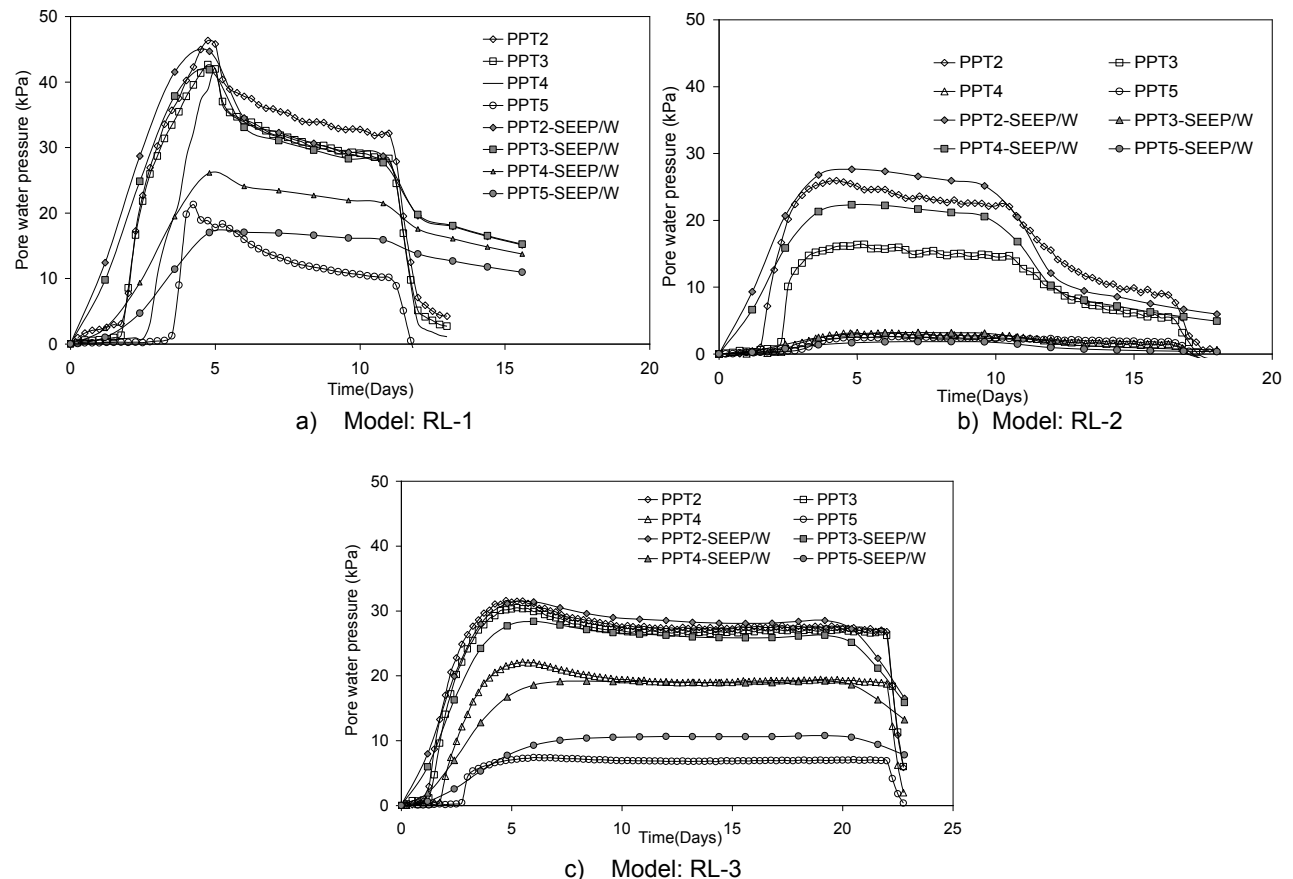


Figure 8. Comparison of pore water pressure variation in centrifuge tests and seepage analysis

Figs. 9a-c depict stability analyses carried out using Bishop's simplified method of slices with help of SLOPE/W (Geoslope, 2007) based on limit equilibrium analysis. While performing stability analysis, phreatic surfaces recorded during penultimate stages of centrifuge tests were used. As depicted in Fig. 9a model RL-1 was found to have a factor of safety 0.933. This is found to represent the observed failure for model RL-1 immediately after 5.1 days of seepage time. Whereas, for models RL-2 and RL-3, the computed factor of safeties were found to be of the order of 1.1 and 1.107 respectively. Marginal increase in factor of safety shows the efficiency of drainage layers to enhance stability of levee sections in high flood conditions.

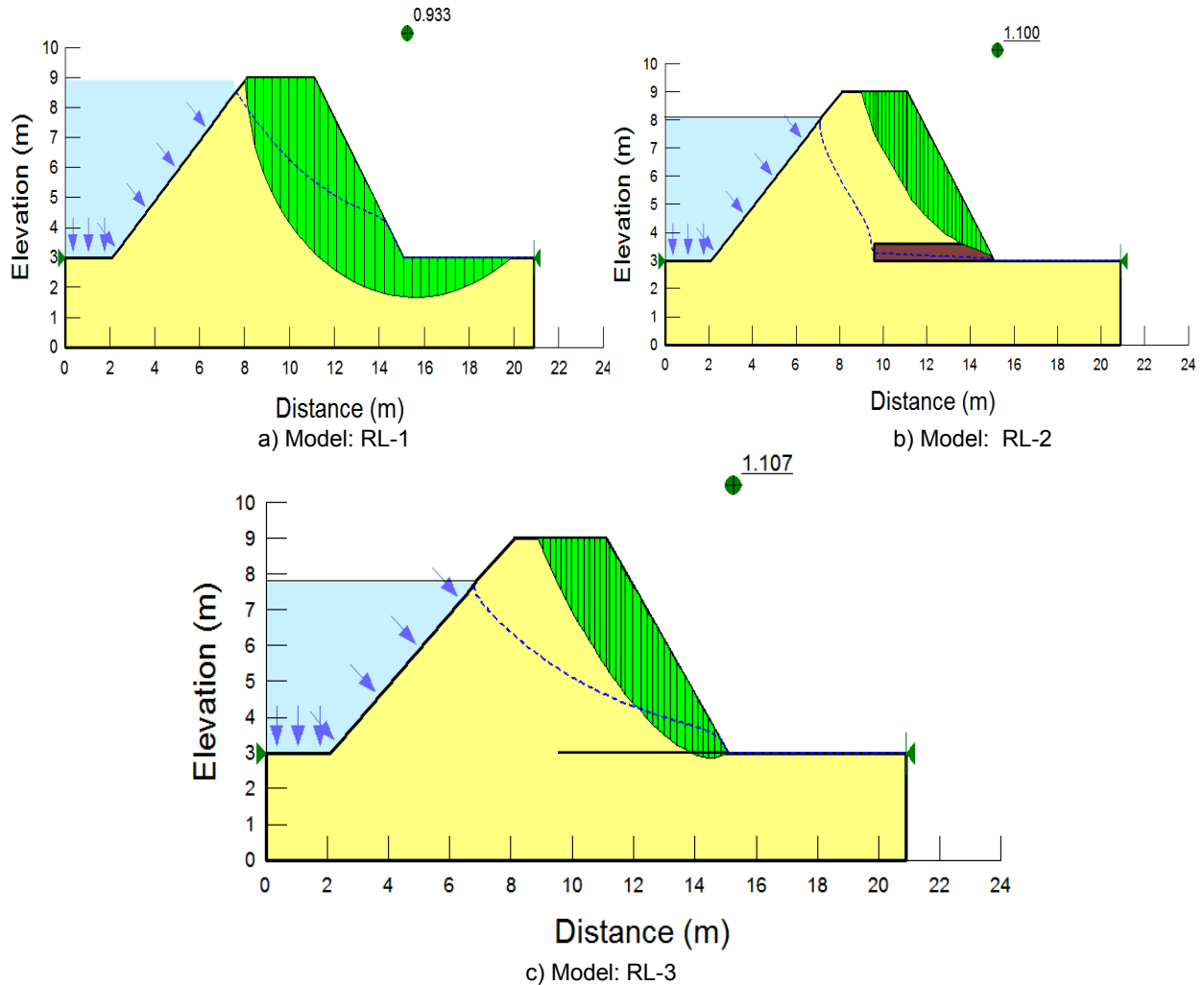


Figure 9. Stability analysis of centrifuge models using SLOPE/W.

6. CONCLUSIONS

This paper evaluates performance of an internal horizontal drainage layer (with sand or nonwoven geotextile) positioned at the levee bottom in the downstream side at the onset of flooding and subsequent seepage. For this purpose, three centrifuge model tests were performed. Furthermore, centrifuge model tests were also replicated with numerical experiments using finite element method based SEEP/W and limit equilibrium based SLOPE/W software. Finally, Influence of inclusion of drainage layer and replacement of sand with a non-woven geotextile layer was examined. Based on analyses and interpretation of centrifuge model tests and seepage and slope stability analyses, the following conclusions can be drawn:

1. Levee section without any horizontal drainage layer or clogged drainage layer experienced a catastrophic failure at the onset of flooding and subsequent seepage. The normalized water pressure ($u/\gamma H$) was registered as high as 0.665 and in the case of models with internal drain either in the form sand or non-woven geotextile, it is 0.08 and 0.24 respectively. Further, reduced values of maximum pore water pressures at the toe of the order of 3 kPa and 7 kPa were recorded for models with sand and non-woven geotextile as an internal drain. In comparison, the maximum pore water pressure recorded at the toe for the model without any drainage layer was 22 kPa. This indicates the efficacy of provision of drainage layer in the horizontal direction in levee sections.
2. Movement of displacement vectors from the time of initiation of flooding to penultimate stages of the test indicates a catastrophic failure for the levee section without any drainage layer. On the other hand, levee sections with sand and geotextile layers as an internal drain was not noticed experience any notable movements.

3. Results of transient seepage and stability analyses were found to be very consistent with those in physically observed centrifuge model test results.
4. Finally, hydraulic response of geotextile layer was found to be almost identical to sand drainage layer in order to improve the stability of levees. This study indicates that the conventional drainage layer constructed with sand as an internal drain can be replaced with a suitable geosynthetic layer which can impart economy in levee/earth dam construction projects.

However, further studies are warranted to have a better insight into the hydraulic behavior of geotextile embedded in levee sections, especially under long-term conditions.

REFERENCES

- ASTM D6574(2006), Standard Test Method for Determining the (In-plane) Hydraulic Transmissivity of a Geosynthetic by Radial Flow. American Society for Testing and Materials, West Conshohocken, Pennsylvania, USA.
- Viswanadham, B.V.S., and Mahajan, R. R. (2007) Centrifuge model tests on geotextile reinforced slopes. *Geosynthetics International Journal*, Vol. 14(6): 365- 379.
- Das, A. and Viswanadham, B.V.S. (2010). Experiments on the Piping Behavior of Geofiber-Reinforced Soil, *Geosynthetics International*, Thomas Telford Ltd, 17(4): 171-182
- EM 1110-2-1913 (2000), Manual for Design and Construction of Levees, Department of the Army, U.S. Army Corps of Engineers Washington, DC 20314-1000.
- Geo-Slope (2007). SLOPE/W and SEEP/W Ver. 7.15 User's Guide. Geo-Slope International Ltd, Calgary, Canada.
- Iryo, I., and Rowe, R.K. (2003). On the Hydraulic Behavior of Unsaturated Non-woven Geotextile, *Geotextiles and Geomembranes*, Elsevier Ltd, 21: 381-404
- Iryo, T., and Rowe, R. K., (2004). Numerical Study of Infiltration into a Soil-Geotextile Column, *Geosynthetics International*, Thomas Telford Ltd., 11(5): 377-388
- BIS 9429(1999), Drainage System for Earth and Rockfill Dams-Code of Practice, Bureau of Indian Standards.
- Jia, G.W., Zhan Tony L.T., Chen Y.M., Fredlund D.G. (2009). Performance of a Large-Scale Slope Model Subjected to Rising and Lowering Water Levels, *Engineering Geology*, Elsevier B.V., 106(1), 92–103.
- Raisinghani, D.V. and Viswanadham, B.V.S. (2011). Centrifuge model studies on low permeable slope reinforced by hybrid geosynthetics, *Geotextiles and Geomembranes*, 29(6), 567-580.
- Ubilla, J., Abdoun, T., Sasanakul, I., Sharp, M., Steedman S., Vanadit-Ellis W. and Zimmie T., (2008). New Orleans Levee System Performance during Hurricane Katrina: London Avenue and Orleans Canal South, *Journal of Geotechnical and Geoenvironmental Engineering*, ASCE, 134(5): 668-680.

Use of Geotextile Reinforced Slope for Containment Facility Dike

M. Surendra, Findling, Inc., 3401 Carlins Park Drive, Baltimore, MD 21215, USA,
surisurendra@findlinginc.com

ABSTRACT

Geotextiles have been used successfully in the construction of retaining structures and in order to make fill slopes steeper. This paper presents a case history where a reinforced slope section was incorporated into the design cross section of a dike around a dredged material containment facility (DMCF). The paper provides a brief discussion of the dike that was designed to retain dredged materials that will be pumped in to the containment facility periodically. The alignment of the dike was located in the area of previous shoreline and contained remnants of previous structures. This necessitated the need for a slope cross section that would remain stable in the event the existing previous remnants were to collapse and induce a ground loss condition. The dike that was constructed encompassing the stabilized portion of the slope and the overall stability of the dike is also briefly discussed.

1. INTRODUCTION

The site of the Masonville DMCF is located in Baltimore, Maryland, USA as shown on Figure 1: Site Vicinity Map. The dredged material that will be generated during the maintenance dredging operations by the Maryland Port Administration (MPA) will be placed inside the containment facility. The DMCF is about 38 ha in plan and is approximately rectangular in plan. The west and north sides of the facility consist of earthen dike constructed in water, the east side consists of a steel cellular cofferdam that will be used as a pier and the south side consists of existing shoreline.

The site is located to the south of the Patapsco River and consists of several existing piers on the east and a containment facility to the southwest and several previously used slips. Several barges and other vessels were also encountered at various parts of the site in the southeast portion. A layout of the proposed DMCF is shown on Figure 1.

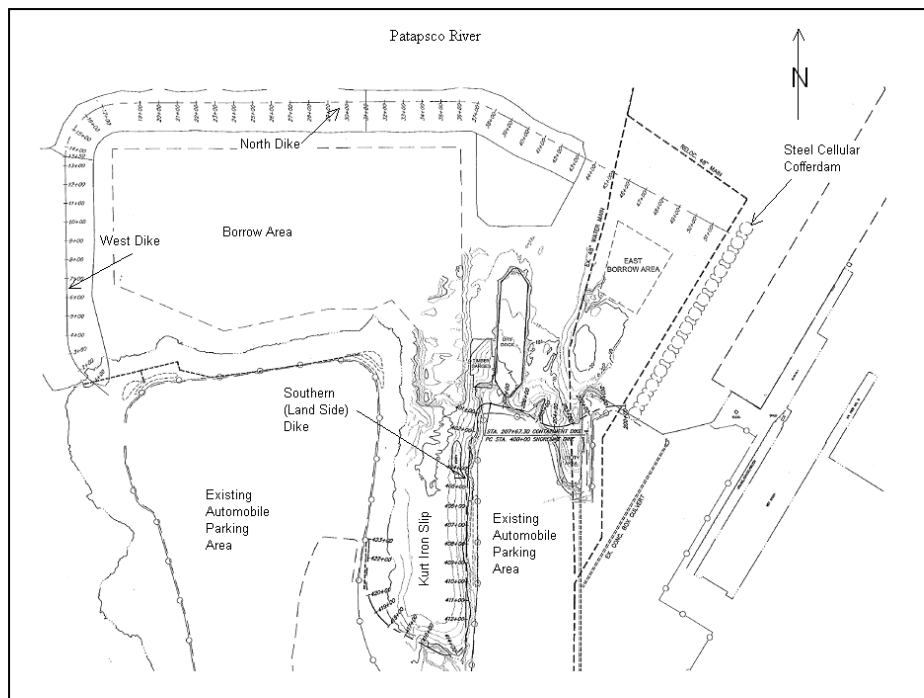


Figure 1. Layout of DMCF

2. SITE AND SUBSURFACE CONDITIONS

Geologically, the site is located in the Western Shore Lowland Region of the Atlantic Coastal Plain Province. The Coastal Plain Deposits generally consist of Sand, Silt and Clays that have been deposited by the receding seas. The site is located on the southern bank of Patapsco River and was previously used as a borrow area for sand and gravel. The area to the east of the site consists of active piers and remnants of old piers. During the past use, this portion of the site was used where ships were repaired and later was used as a salvage yard in the 1970's. Steel and wooden dry-docks and barges were abandoned in shallow waters along the then existing shoreline following the completion of the repair and salvage operations at the site. The site surrounding the subject DMCF has been developed for use by the port as a storage facility for automobiles by placing fill over the shallow portions along the previous shore line. During this process, many structures were buried underneath the currently used parking areas.

Test borings were drilled along the alignment using a truck-mounted drill rig from a barge. The depth to mud line (i.e., the depth of water) at the site ranges from 4.5 m to 6 m below Mean Lower Low Water (MLLW). The tidal change in water level is about -0.2 m to +1.2 m. The near surface soil beneath the water was Muck consisting of very loose and soft organic SILT. The Muck layer extends to a depth of 9 m to 12 m below MLLW. Below the Muck layer, relatively soft Silty CLAY stratum was encountered. Thickness of the clay layer ranged from 1 m to 3 m. Below the Silty CLAY stratum, a Silty SAND stratum with varying percentages of Gravel was encountered. This Sand stratum extended to a depth of 20 m to 23 m below MLLW. Below the Silty SAND stratum a hard CLAY or dense SAND and Gravel stratum was encountered to the maximum depths explored (i.e., to 30 m below MLLW).

A summary of the subsurface conditions and typical properties of the stratum encountered and design parameters used in the analysis of the dike (Findling, 2010) is summarized on the following table:

Table 1. Summary of Subsurface Conditions

Stratum	Elevation, m	USCS Classification	Natural Moisture Content, %	% Passing No 200 Sieve	Atterberg Limits (LL, PL, PI)	Undrained Shear Strength, kPa	Angle of internal Friction, degrees	Total Unit Weight, kN/m ³
Water	0 to -6	--						
Muck	-6 to -12	MH	>100	90	70, 40, 30	4.78	--	17.28
Silty CLAY	-12 to -15	CL	36	95	29, 20, 9	4.78 – 19.20	--	18.06
SAND	-13 to -23	SM	12	10 – 30	--	--	30	18.85
CLAY	-23 to -30	CH	20	95	50, 20, 30	95.6	--	19.63
SAND & Gravel	-23 to -30	GM-SM	12	10 – 30	--	--	35	19.63

3. DESIGN OF CONTAINMENT DIKE

The initial design of the dike was considered to extend to a height of El +3.66 m. The cross section of the dike consisted of a 6.1 m wide crest and side slopes of 3 Horizontal to 1 Vertical. The dike was planned to be constructed using SAND obtained from dredging the area inside the containment facility. The dike was designed to be constructed using the sand from the borrow area (within the containment facility) by hydraulic placement. The dike was also planned to be raised in the future to El +12.8 m in stages using the dried crust materials generated from the crust management program of the dredged materials within the containment facility.

Slope stability analysis was performed using PCSTABL computer program. The subsurface conditions and the cross section of the dike used in the analysis of the inside slope is shown on Figure 2 in the Appendix. Based on initial analysis of the cross section, it was determined that the muck layer will have to be displaced by the fill for the new dike or undercutting of the muck layer is required in order to obtain adequate factor of safety for the proposed dike cross section. The muck layer was replaced with Sand fill, and the analysis was repeated. The resulting factor of safety after the replacement of the muck is about 1.27.

In order to obtain an adequate factor of safety against global failure, undercutting (i.e., excavation and disposal) of the muck stratum was required. Therefore, during the construction operations, a pre-dredging program was used to excavate and remove the muck stratum along the proposed footprint of the dike on the west and north sides of the proposed dike.

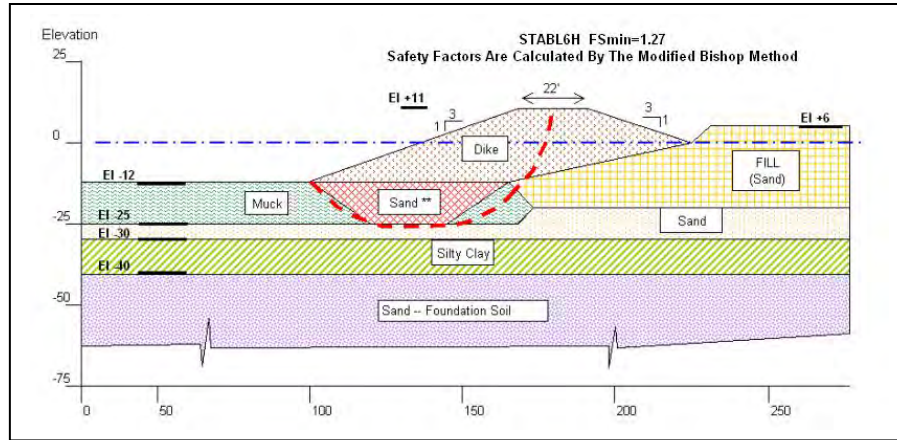


Figure 2. Slope Stability Analysis of landside Dikes

3.1 Landside Dike

The landside dikes are located in the southern portion of the site as shown on Figure 3. In the area of the southern portion, the shoreline adjacent to the previous slips had been previously filled to create the parking lot that is currently being used to park automobiles. The containment dike in this area is located along the current shoreline. The existing parking lot is near El +7 and the dike is designed to extend towards the water. Due to the limited access and to minimize disturbance to the operations of the existing parking lot, undercutting of the muck stratum was not performed. The dike was constructed in this portion of the site by displacing the muck by placing sand over the existing muck stratum.

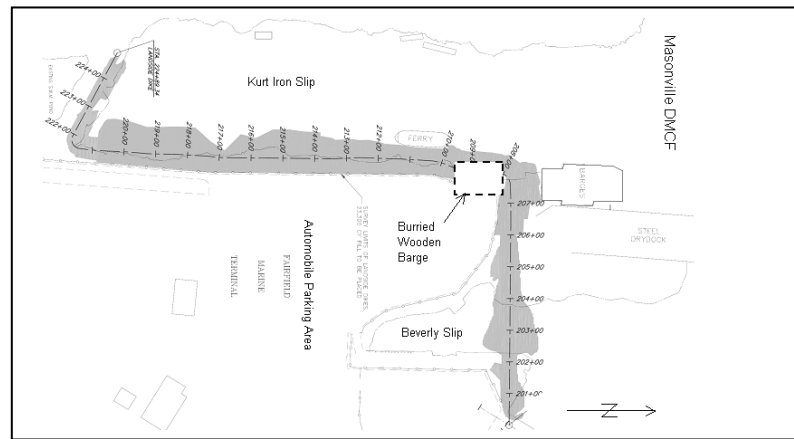


Figure 3. Location of Landside Dike

During the subgrade preparation operations, prior to the placement of the sand for the construction of the dike, the existing subgrade was cleared of surface vegetation and remnants of previous construction (such as concrete slabs, asphalt pavement, etc.). During this subgrade preparation, remnants of a previous barge structure were encountered near the northern portion of the Kurt-Iron Slip. Approximate limits of the buried barge in relation to the cross section of the proposed dike are shown on Figure 4.

After clearing the surficial materials, the timber planks and beams that constituted the barge were encountered. A portion of this wooden barge structure was removed and disposed of off-site. The excavation and removal was stopped at the property line and the structure was noted to extend under the active parking lot. The dimensions of the barge structure and the limits of the structure under the existing parking lot are not known.

Slope stability analysis was performed using PCSTABL computer program (Achilleos, 1988). A typical cross section that was used in the slope stability analysis is shown on Figure 5. The results of the slope stability analysis indicated that the stability of the new dike constructed on top of the remnant of the wooden barge structure was marginal. In order to

increase the factor of safety of the dike, the barge structure that is empty (i.e., filled with water and not soil) would have to be grouted with flowable fill (that consists of a Sand, fly ash and cement mix). However, due to cost associated with grouting the barge with flowable fill and other project constrains it was decided by the owner that the grouting would not be performed at this time.

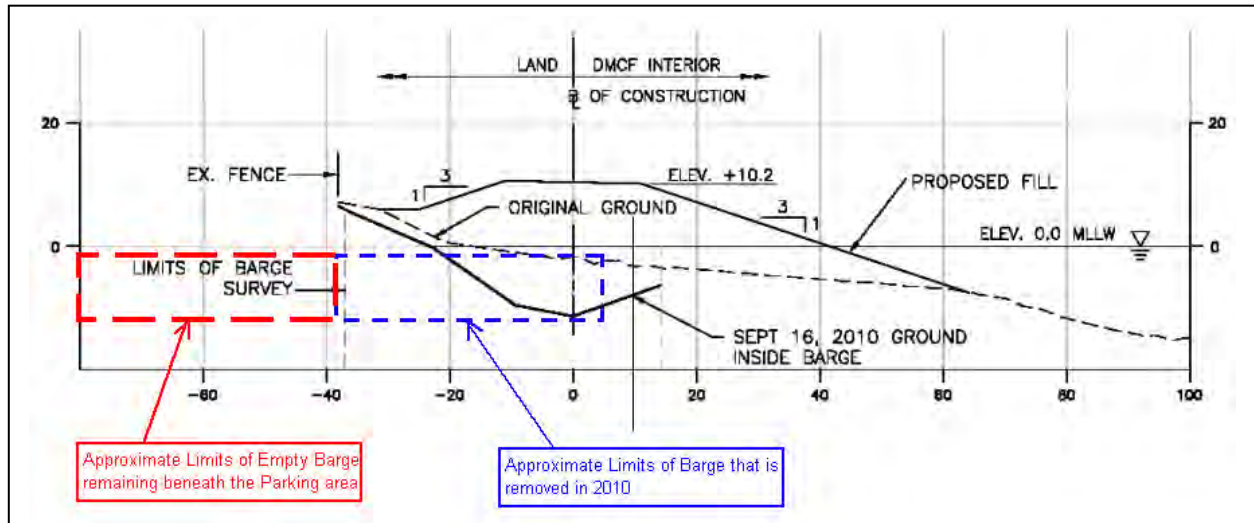


Figure 4. Typical Cross Section of Dike at the location of the Buried barge

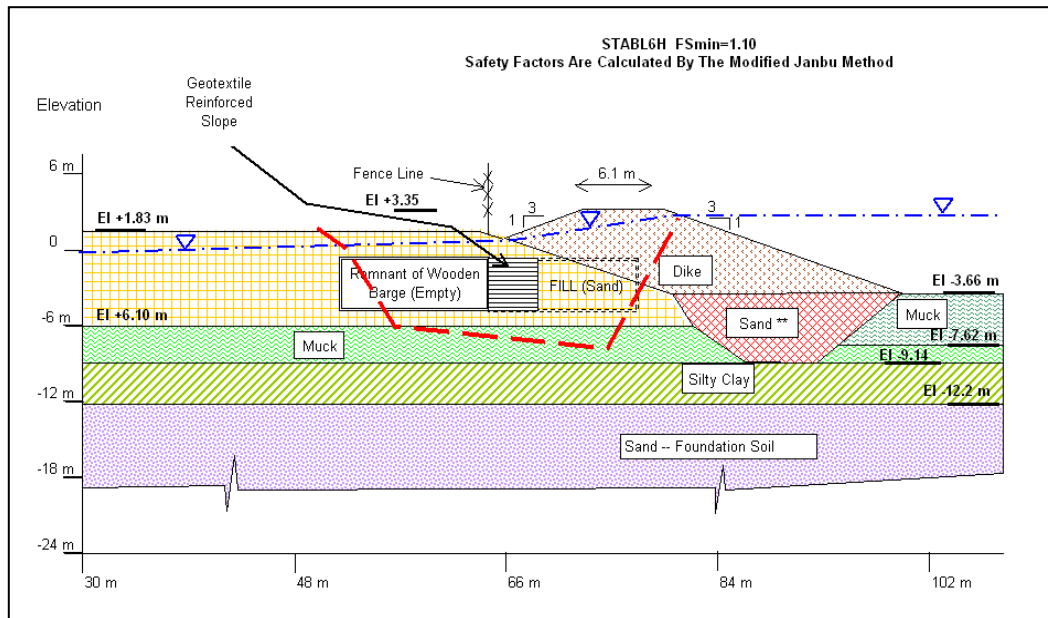


Figure 5. Slope Stability Analysis at Location of Barge

3.2 Geotextile Reinforced Slope within the Dike

The wooden barge structure that extends under the current parking lot and that will be incorporated into the body of the containment dike in this area extends from EI +0 to EI -3.66 m. A dewatering operation was performed to lower the water inside the containment facility to facilitate the first inflow of the dredged materials into the containment facility. At the time the site preparation was performed, the water inside the containment facility had been lowered to about EI -4.0 m. The dike in this area had to be completed before the first inflow of the dredged material was scheduled for placement

into the containment facility. A view of the wooden barge structure that was encountered along the alignment of the proposed landside dike is shown on Figure 6.



Figure 6. Slope Stability Analysis at Location of Barge

The barge structure extends from El +0 to El -3.66 m and about 45 m along the alignment of the dike. The exposed vertical face of the barge structure along the property boundary is an interior partition of the barge. The vertical exposed face contained several openings in to the interior compartments that are located beneath the active parking lot. The construction of the dike along its planned alignment would require placement of Sand fill against the vertical face of the remnants of the barge structure. The sand fill could migrate into the open voids of the interior compartments (beneath the parking lot). Also the wooden structure could collapse under the lateral load of the new sand fill of the dike and thus create a ground loss condition. The ground loss condition will cause the dike to become unstable.

The geotextile reinforced slope was designed to meet the following requirements:

- a. Prevent Fill material from being infiltrating into the open voids of the barge
- b. Confine the fill materials in front of the remnant of the barge
- c. Reduce lateral pressures on the walls of the remnant of barge structure

In order to prevent the migration of sand into the open voids and to reduce the lateral earth pressures on the exposed face of the wooden barge structure, a Geotextile reinforced slope was designed (DM7.2, 1982). Active earth pressure of sand backfill was used in computing the horizontal design load and surcharge load from the fill above the reinforced zone was used in the design of geotextile required for the slope. The Geotextile used consisted of Mirafi 600x and the sand material used consisted of Silty SAND with about 20 % of fines. Typical properties of Geotextiel Mirafi 600x are summarized on Table 2 below. This Geotextile was selected based on its adequate strength to retain the fill behind it and also prevent migration of the sand material into the voids of the adjacent barge structure. In addition, this Geotextile had been used at the site for other purposes and was readily available for use for this application (Koerner, 1986).

Table 2. Physical Properties of Geotextile Mirafi 600X

Mechanical Properties	Test Method	Unit	Minimum Average Roll Value	
			MD	CD
Grab Tensile Strength	ASTM D4632	lbs (N)	315 (1402)	315 (1402)
Grab Tensile Elongation	ASTM D4632	%	12	
Trapezoid Tear Strength	ASTM D4533	lbs (N)	113 (503)	113 (503)
CBR Puncture Strength	ASTM D6241	lbs (N)	900 (4005)	

¹ ASTM D4751, AOS is a Maximum Opening Diameter Value

The Geotextile was extended to a distance of 3.05 m from the face and consisted of 0.46 m to 0.30 m lifts. The face consisted of wrapping the Geotextile back for a distance of 1.22 m. The annular space between the Geotextile reinforced earth structure and the vertical face of the wooden barge structure was filled with crushed stone aggregate (of

ASTM gradation No. 57). A typical cross section of the Geotextile reinforced slope is shown on Figure 7. The geotextile reinforced slope was incorporated into the cross section of the dike in this area. This enabled the completion of the dike in time for the first inflow of the dredged material into the containment facility. The performance of the dike will be monitored by surveying the crest elevation during the operation of the facility.

4. CONCLUSION

The paper provides a brief discussion of the background information that required the need for a stabilized slope within a dike section. The dike was designed to retain dredged materials that will be pumped periodically in to the containment facility. The alignment of the dike was located in the area of previous shoreline and contained various obstructions. This necessitated the need for a slope cross section that would remain stable in the event the existing previous remnants were to collapse and induce a ground loss condition. The design methodology used for the construction of a Geotextile stabilized slope cross section adjacent to the previous remnants at the site is discussed. The dike was constructed to encompass the stabilized portion of the slope.

The construction operation was completed in September 2011. Based on the performance of the dike in the last 6-months, it appears that there is no measurable settlement or loss of ground condition that has occurred in the vicinity of the Geotextile stabilized portion of the dike adjacent to the buried barge. Field observations will continue on a periodic basis. The use of the Geotextile reinforced slope within the dike cross section enabled the completion of the containment dike to receive the placement of dredged materials in time.

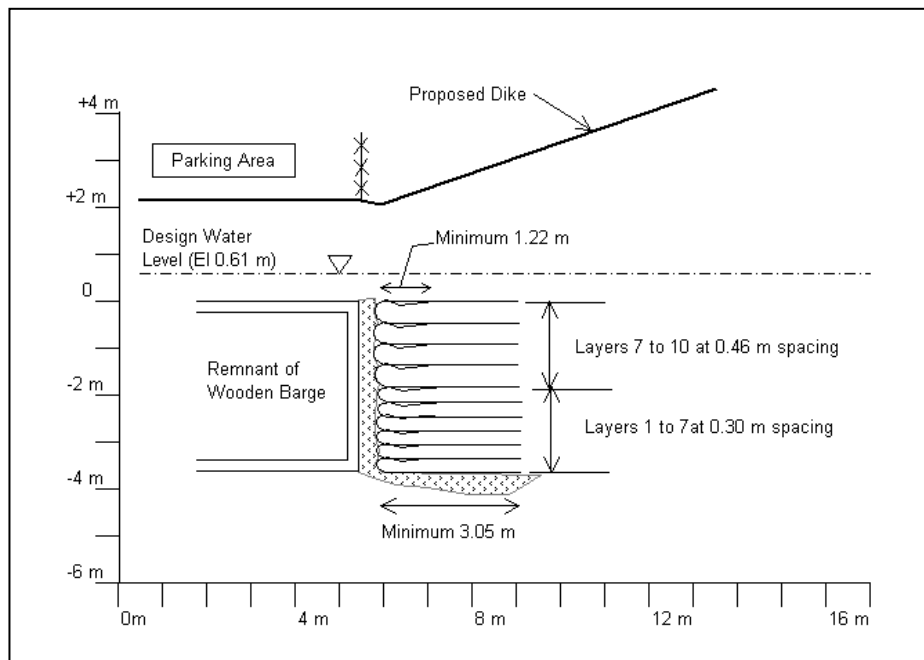


Figure 7. Typical Cross Section of Geotextile Reinforced Slope

ACKNOWLEDGEMENT

The author would like to thank Mr. Steve Storm with the Maryland Port Administration for allowing use of the data from which this paper is prepared. Mr. Dennis Urso and Mr. Tim Donegan with Gahagan, Bryant and Associates provided the design of the containment facility. Mr. Mike Miller with Maryland Environmental Services, Inc. provided the assistance in the implementation of the Geotextile reinforced section into the dike. Mr. Amsalu Duressa and Mr. John Tallman with Findling, Inc. provided assistance in the preparation of this paper.

REFERENCES

- Achilleos, E. (1988), User Guide For PC STABL 5M, School Of Civil Engineering, Purdue University, West Lafayette, Indiana.
- DM 7.2, Foundations and Earth Structures (1982), Design Manual 7.2, NAVFAC DM 7.2, Department of the Navy, Naval Facilities Engineering Command, Alexandria, VA.
- Findling, Inc. Internal Reports and Design Memorandum, 2010
- Koerner, R. M. (1986), Design with Geosynthetics, Prentice Hall, USA

What Value of Interface Friction to Select for Geosynthetic Liner on Landfill Slopes?

Carbone L., MECMAT, Italy, LTHE, France, laura.carbone@unirc.it
Gourc J.P., LTHE, France, jean-pierre.gourc@ujf-grenoble.fr
Brianchon L., CNAM, France, laurent.brianchon@cnam.fr
Moraci N., MECMAT, Italy, nicola.moraci@unirc.it
Carrubba P., IMAGE, Italy, paolo.carrubba@unipd.it

ABSTRACT

To characterize the geosynthetic friction, the Inclined Plane is recognized as a very suitable and versatile device, since it allows to test large samples with variable relative tangential displacements under low normal stress. According to different studies carried out in France, the procedure proposed by the European Standard could provide non-conservative results. For this reason, two alternative procedures are proposed: the "Displacement Procedure" and the "Force Procedure". In this study a full description of the two procedures is presented and an application to a typical landfill barrier interface is carried out. Furthermore, several values of the interface friction angles are determined from the two methods and a comparison with the "standard" value is provided.

1. INTRODUCTION

Geosynthetics barriers in landfill are frequently arranged on slopes. Consequently, the stability of these systems is a key issue. Despite a lot of research on this topic, quite often sliding of the barriers is observed on slope (Girard et al. 1990). This kind of dramatic event could be attributed in many cases to a not proper assessment of the friction at the different interfaces.

As different studies demonstrated (Izgin & Wasti 1998, Lalarakotoson et al. 1999, Wasti & Özdüzgün 2001, Palmeira et al. 2002, Palmeira 2009, Reyes Ramirez & Gourc 2003, Wu et al. 2008, Brianchon et al. 2011), the main advantage of the Inclined Plane test is to allow testing the materials with variable relative tangential displacements under low normal stress (<10 kPa) typically present during the construction of the lateral barriers and in the landfill covers.

The test procedure is ruled by the European Standard EN ISO 12957-2 (2005); since it is not rigorous method as other researches underlined (Gourc & Reyes Ramirez 2004, Pitanga et al. 2009, Brianchon et al. 2011), Gourc and Reyes Ramirez (2004) and Brianchon et al. (2011) proposed two alternative test procedures in order to improve the evaluation of the interface friction angles.

The three test procedures are carried out to assess and to compare the friction angles of a typical landfill cover interface. In particular, the present study investigates, as an example, the behavior of the geocomposite drain (GCD) in contact with a geomembrane (GMB) which is likely to be a critical interface in the geocomposite systems. Furthermore, the influence of the two geosynthetics (geotextile (GTX) and geonet (GNT)) which constitute the GCD, are separately tested in direct contact with the geomembrane in order to assess their influence in the geocomposite drain performance.

2. THE INCLINED PLANE TEST

2.1 Generalities

The Inclined Plane Test permits to determine the friction angle between soil-geosynthetic and geosynthetic-geosynthetic interface at very low normal stress (5.0 ± 0.1 kPa). The test is ruled by the European Standard EN ISO 12957-2 (2005), that describes both the apparatus and test procedure.

The normal stress must be applied to obtain a regular distribution on the entire surface of the specimen and the plane tilts slowly and at a constant rate, i.e. $d\beta/dt = 3.0 \pm 0.5^\circ/\text{min}$ where β is the plane angle related to the longitudinal position.

According to EN ISO 12957-2 (2005), the device is composed by two boxes for the upper and the lower layer respectively. The minimum dimensions of the boxes are: $l_u = 0.3$ m in length along the displacement direction, and $b_u =$

0.3 m in width for the upper box; while $l_1 = 0.4$ m, $b_1 = 0.325$ m for the lower box. In the case of geosynthetic – geosynthetic contact, the upper geosynthetic is fastened to the upper box while the lower is fixed to the inclined support in order to limit any relative movement between the layer and the plane.

The techniques used to fix the lower geosynthetic are: sewing, gluing, using a rough support to increase the adherence between the geosynthetic and the plane, or anchoring the layer outside the contact area.

2.2 Standard Procedure

The European Standard proposes a specific interpretation of test results, here called “Standard Procedure”. According to this interpretation, the interface friction angle is a plane inclination angle β corresponding to a conventional displacement of the upper box $u = 50$ mm. The relative friction angle ϕ_{stan} is calculated considering a static equilibrium along the plane direction, as follows:

$$W \cdot \sin\beta_{50} - N \cdot \tan\phi_{\text{stan}} = 0 \quad [1a]$$

$$W \cdot \cos\beta_{50} = N \quad [1b]$$

where, N is the reactive force balancing the normal component of the weight, W , of the upper box.

The value of the standard interface friction angle, ϕ_{stan} , is obtained combining Equations 1a and 1b to yield the following:

$$\tan\phi_{\text{stan}} = \tan\beta_{50} \quad [2]$$

2.3 Displacement Procedure

The interface friction angle ϕ_{stan} calculated following Equation 2, is obtained from a static approach. Gourc & Reyes Ramirez (2004), modifying the standard inclined plane device (Figure 1), demonstrated that during the sliding the uniformly accelerated movement takes place and the equilibrium equations should take into account this dynamic condition.

For this purpose, the modified apparatus presents a sufficient length in the slope direction ($l_1 = 1.3$ m, $b_1 = 0.8$ m) to measure the acceleration of the upper box during the motion. The initial normal stress is applied using metal plates as overload.

Using this modified setup, Gourc & Reyes Ramirez (2004) proposed a new interpretation, here called “Displacement Procedure” where the sliding behavior could be divided into three characteristic phases (Figure 2), as follows:

- Phase 1 (Static Phase): The upper box is practically motionless (the displacement of the upper box equals zero) over the inclined plane until a critical angle, β_0 , is reached,
- Phase 2 (Transitory Phase): With increasing inclination beyond β_0 , the upper box moves gradually downward, and the acceleration γ of the upper box is not constant, and
- Phase 3 (Stabilized - Sliding Phase): At $\beta = \beta_s$, the upper box undergoes stabilized sliding with constant acceleration γ_c , and the speed progressively increases.

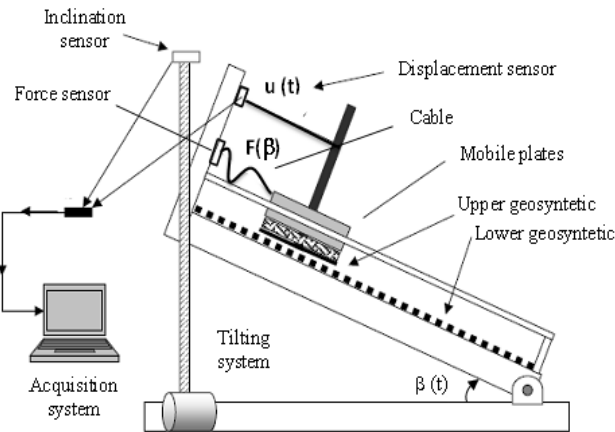


Figure 1. Inclined Plane apparatus geosynthetic – geosynthetic configuration.

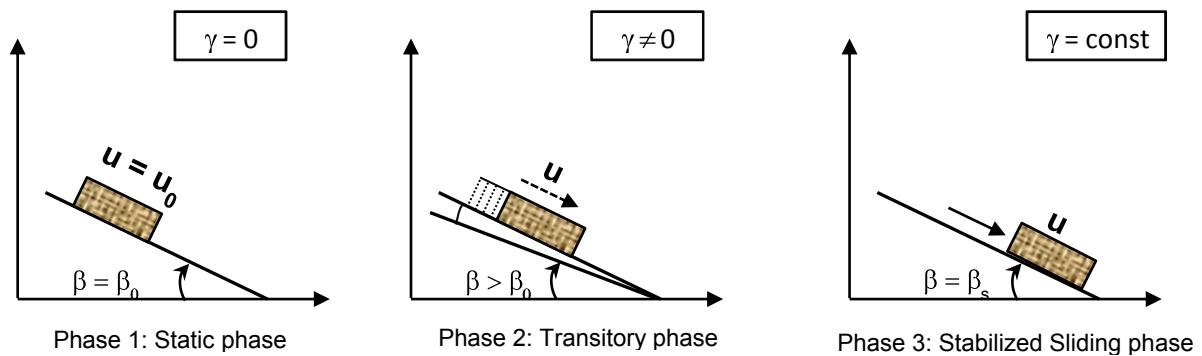


Figure 2. Different phases of the "Displacement Procedure" Test.

Here, β_0 is defined as the plane inclination angle before the initialization of the sliding corresponding to the static interface friction angle, ϕ_0 , at the end of the Phase 1 and β_s is the plane inclination angle when the acceleration γ of the upper box could be considered constant for the stabilized sliding.

As already found by (Pitanga et al. 2009), Phase 2 may be of two types:

- Sudden sliding: abrupt displacement of the upper box with $\beta_0 \sim \beta_s$, and
- Gradual sliding: displacement u increases with inclination β , progressively or as a stick-slip mode.

The Phase 3 starts when the acceleration reaches a constant value γ_c ; under this condition, the relations (Equations 1a and 1b) should be replaced by the Equations 3a and 3b:

$$W \cdot \sin\beta_s - N \cdot \tan\phi_s = W \cdot \frac{\gamma_c}{g} \quad [3a]$$

$$W \cdot \cos\beta_s = N \quad [3b]$$

The value of the actual friction angle, ϕ_s , in place of ϕ_{stan} , is similarly obtained by combining Equations 3a and 3b to give:

$$\tan\phi_s = \tan\beta_s - \frac{1}{\cos\beta_s} \cdot \frac{\gamma_c}{g} \quad [4]$$

where γ_c is the constant acceleration of the upper geosynthetic component of the interface during the stabilized-sliding phase.

2.4 Force Procedure

The “Force Procedure” was recently proposed by Briançon et al. (2011) since evaluating the acceleration during the motion in the “Displacement procedure” could be very complex for some interfaces.

This method consists in determining the interface friction angle, here denoted as δ , through the inclined plane apparatus by measuring the force required to restrain the upper box after reaching a limiting value of the sliding displacement u_{lim} .

To perform the Force Procedure, the inclined plane device is modified linking the upper box by means of a loose cable (Figure 1) to a force sensor fixed to the device frame.

After reaching a predetermined displacement value, u_{lim} , corresponding to an inclination $\beta = \beta_{lim}$, the cable is stretched and the force $F(\beta)$ required to hold back the upper box is measured (Briançon et al. 2011).

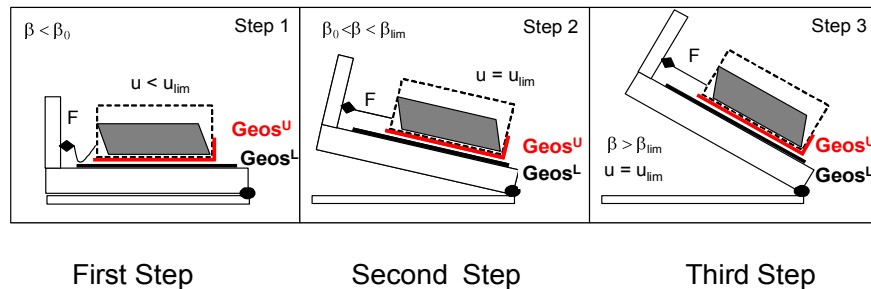


Figure 3. Schematization of the different steps during the “Force Procedure” test.

The test consists of three steps (Figure 3):

- Step 1: corresponds to the static state of the upper box with respect to the lower plane during the tilting process ($\beta < \beta_0$),
- Step 2: corresponds to the transitory state where the upper box slides, gradually or suddenly, it is in the dynamic state until the cable is stretched for a displacement u_{lim} ($\beta_0 \leq \beta \leq \beta_{lim}$), and
- Step 3: the upper box reaches the end of the slide ($u = u_{lim}$) and it could be considered in a static state because the only possible movement is due to the elongation of the cable that could be neglected. Here, the variation of F is monitored during the test, in particular it increases with the continuous tilting process of the plane ($\beta > \beta_{lim}$).

During the Step 1 (where $F(\beta) = 0$) and the Step 3 ($F(\beta) > 0$) the equilibrium analysis is achieved by the following equations:

$$W \cdot \sin\beta - N \cdot \tan\delta - F(\beta) = 0 \quad [5a]$$

$$W \cdot \cos\beta = N \quad [5b]$$

$$\tan\delta = \frac{W \cdot \sin\beta - F(\beta)}{W \cdot \cos\beta} \quad [6]$$

where W is the total weight of the upper box and $F(\beta)$ is the force required to hold back the upper box.

During Step 2, the equilibrium should take into account the acceleration during the sliding and it is not considered in this method.

Thus, for convenience the whole test may be represented in terms of the parameter λ as follows:

$$\tan\lambda = \frac{W \cdot \sin\beta - F(\beta)}{W \cdot \cos\beta} \quad [7]$$

In particular, $\tan \lambda$ could be characterized during all the test as follows:

During Step 1:

$$\tan \lambda_0 = \tan \bar{\delta}_0 = \tan \beta_0 \quad [8]$$

During Step 2:

$$\tan \lambda = \tan \bar{\delta} - \frac{\gamma}{g \cos \beta} \quad [9]$$

During Step 3:

$$\tan \lambda_{\text{lim}} = \tan \bar{\delta}_{\text{lim}} = \tan \beta - \frac{F(\beta)}{W \cdot \cos \beta} \quad [10]$$

If the acceleration γ is not measured during the Step 2, in the analysis of test results, it is possible to calculate only two different values of the interface friction angles corresponding to the Step 1 and Step 3. In particular, as found by Briançon et al. (2011), $\bar{\delta}_{\text{lim}}$, is considered the key parameter of this method because it is not sensitive to the test conditions.

3. TESTING PROGRAM

The study is carried out on a wide range of geosynthetic interfaces typically present in landfill liners. In particular, the present work investigates the behavior of the geocomposite drain – geomembrane interface since its use is very widespread in the composite systems.

The geocomposite for drainage (GCD) consists of a thermobonding rhomboidal shape HDPE geonet (GNT) with two nonwoven geotextiles (GTX) on both sides, working as separation, filtration and protection layers. The geomembrane is a smooth high density polyethylene (HDPE) geomembrane (GMB) representing, in all the tests, the lower layer (here denoted as Geos^L) while the other geosynthetics are glued to the upper box (Geos^U). The physical properties of the materials are given in Table1 and all the tests are performed using specimens obtained from virgin samples, in the machine direction.

To examine the geocomposite drain–geomembrane interface, the influence of the different materials which constitute the geocomposite system is also assessed; thus, during the experimental program the three different interfaces are tested:

- geotextile (GTX^U) – geomembrane (GMB^L);
- geonet (GNT^U) – geomembrane (GMB^L);
- geocomposite drain (GCD^U) – geomembrane (GMB^L).

For the Inclined Plane tests program, the Standard Procedure, the Displacement Procedure and the Force Procedure are carried out in order to compare the results.

It is worth noting that, the behavior of each interface is standard and replicable; the friction results are determined as an average value of at least three tests where the deviation is less than 0.5°.

Table 1. Characteristics of tested geosynthetics.

Type of geosynthetic	Material	Thickness (mm)	Mass per Unit Area (g/m ²)
Geotextile (GTX)	Thermally bonded nonwoven	1	130
Geonet (GNT)	Thermobonding rhomboidal shape High Density Polyethylene	3.5	520
Geocomposite drain (GCD)	External filter + Drainage core	5.5	780
Geomembrane (GMB)	High Density Polyethylene	2	/

4. RESULTS AND DISCUSSION

The Figure 4a shows the displacement (u) versus time for the three different interfaces, according to the “Displacement Procedure”.

In the case of the GTX^U-GMB^L interface, the upper box starts to slide for a plane inclination β_0 corresponding to 15.8°. In this case, the upper box moves gradually downward with a very low velocity.

Considering test results about GNT^U – GMB^L interface, it could be seen that the interface shows a stick-slip behavior characterized by an abrupt initial displacement ($\phi_0 = 15.2^\circ$) followed by a braking phase where the upper box slides slowly, up to a very fast sliding until the end of the plane. In this case, determining the dynamic interface friction angle is not simple because it changes during the sliding.

Finally, the GCD^U - GMB^L interface is tested; the direct contact is between the geotextile GTX^U and the geomembrane GMB^L but, as it could be noticed by the Figure 4b, the influence of the geonet core is clearly highlighted.

In fact, the sliding remains gradual and constant until the end of the test as in the case of GTX^U -GMB^L interface even if there is a sudden initial displacement as for GNT^U – GMB^L interface.

Regarding the Displacement Procedure, ϕ_s is calculated in the range of the displacement curve (Figure 4b) where the velocity increases linearly. It could be noticed that all the interfaces are characterized by a gradual sliding of the upper box at a very low velocity. This kind of behavior indicates that the resisting force (friction) gradually increases respect the value at rest during the slide. Consequently, in all the cases the dynamic friction angle ϕ_s is greater than the ϕ_0 corresponding to the beginning of the movement.

In the Force Procedure the force $F(\beta)$, the displacement, u , of the upper box and the plane inclination angle, β , are measured. In Figure 5a, the force F mobilized during the entire test procedure is presented and, subsequently the parameter λ is calculated (Equation 7) and plotted versus the plane inclination β (Figure 5b).

At the beginning of the test, during Step 1, ($\beta < \beta_0$) the mobilization of static friction is partial and, the value of λ increases linearly according to the Equation 8.

At the end of Step 1, at the initialization of the sliding for $\beta = \beta_0$, the corresponding measured friction angle is δ_0 that corresponds to the interface friction angle also determined in the Displacement Procedure ϕ_0 . Subsequently, the force F increases fast (Figure 5a) and β rises from β_0 to β_{lim} . During this transitory state (Step 2), as the interface friction angle depends on the acceleration of the upper box (Equation 9), its representation is only qualitative. Finally, at the end of the sliding ($u = u_{lim}$ and $\beta = \beta_{lim}$) Step 3 begins; the driving forces are higher than the friction resistant forces and there is a full mobilization of the friction corresponding to a displacement u_{lim} .

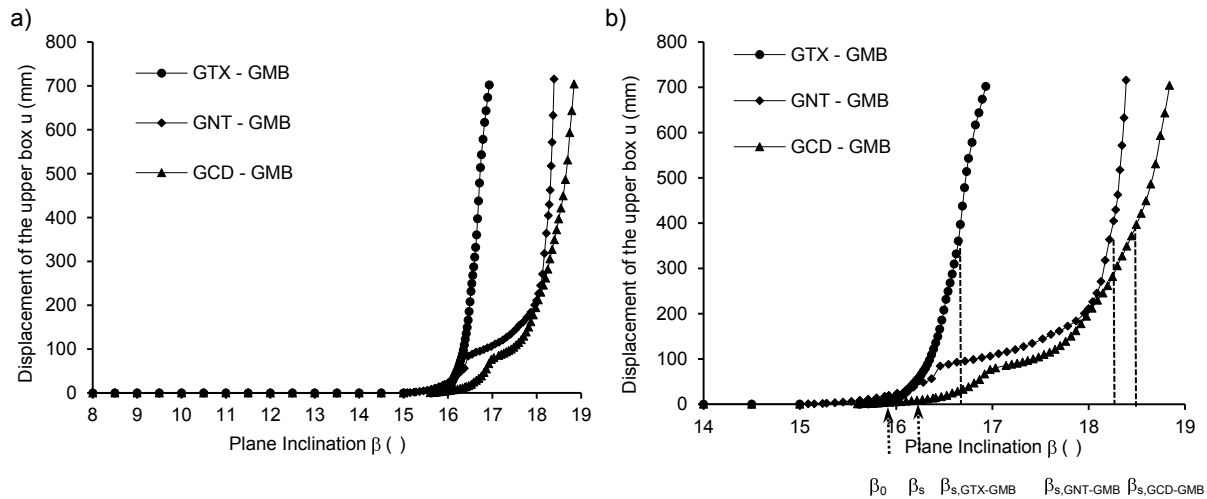


Figure 4. Inclined Plane test according to the “Displacement Procedure”: a) Displacement of the upper box against the plane inclination angle β ; b) Zoom on the initial sliding phase of GTX-GMB, GNT-GMB and GCD-GMB interfaces, plotting all the characteristic plane inclination angles used for the “Standard” and the “Displacement” procedures interpretations.

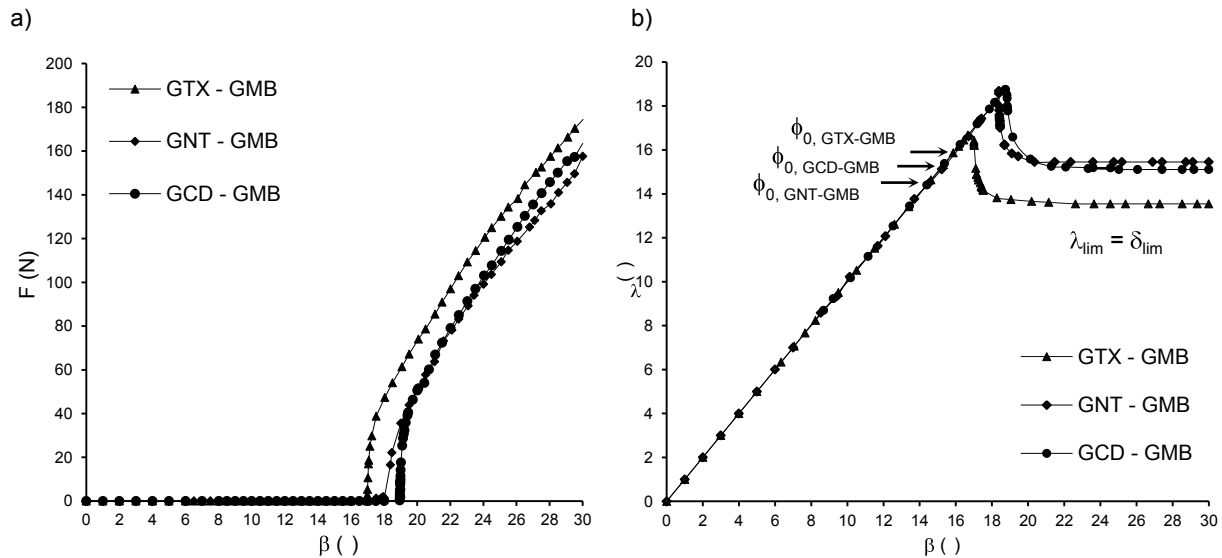


Figure 5. Force Procedure test results: a) The force F mobilized against the plane inclination angle β during the entire test; b) The parameter λ versus β plotted during the three steps.

At this stage, as it could be noticed in Figure 5b, λ versus β reaches a constant value and the characteristic parameter corresponding to the static phase, can be determined after the stabilization of the system ($\delta_{lim} = \lambda_{lim}$ for $\beta > \beta_{lim}$). Thus, the limit interface friction angle, δ_{lim} is the only parameter of the interface that could be determined according to the Force Procedure.

In this experimental program, the length of the cable is adjusted to perform the test at large displacement before the cable stretching, $u_{lim} = 715$ mm.

It is worth noting that, also in this method, the performance of GCD^U-GMB^L interface is influenced by the combination of the geotextile and the geonet and the resulting limit interface friction angle is between the two values: $\delta_{lim}^{GTX} < \delta_{lim}^{GCD} < \delta_{lim}^{GNT}$.

The results of the interface friction angles determined with the three different approaches are presented in Table 2.

From test results it could be noticed that the Standard Interpretation is not consistent with the real friction mobilization because a static approach is proposed for a kinematic condition. Furthermore, the conventional reference displacement $u = 50\text{mm}$ could lead to an overestimation of the interface friction compared to the static angles ϕ_0 and δ_{lim} as also found in other studies concerning other geosynthetic interfaces (Brianchon et al. 2011; Pitanga et al. 2009).

Thanks to the Displacement Procedure results, it is possible to understand the evolution of the interface friction if a slip occurs. In particular, in the studied cases, the dynamic friction angle increases ($\phi_s > \phi_0$) as soon as the stabilized sliding is attained.

Table 2. Friction angles at the Inclined Plane test applying the Standard, the Displacement and the Force Procedures.

INTERFACE TESTED	STANDARD PROCEDURE	DISPLACEMENT PROCEDURE		FORCE PROCEDURE
	ϕ_{stan} (°)	ϕ_0 (°)	ϕ_s (°)	δ_{lim} (°)
GTX^U - GMB^L	16.3	15.8	16.3	13.5
GNT^U - GMB^L	16.3	15.2	18.3	15.4
GCD^U - GMB^L	16.8	15.7	18.0	15.1

The static interface friction angle δ_{lim} could represent the minimum mobilized friction after a large relative displacement between the two layers in contact.

At last, regarding the ϕ_s and δ_{lim} angles, a similar trend of test results is found in other studies (Pitanga et al. 2011; Brianchon et al. 2011) even if the friction angles could be different depending on the materials properties.

However a question is still pending: what kind of the interface friction value should be selected to represent appropriately the interface behaviour? Additional tests program on many different interfaces are in progress in order to fit test results belonged to different kinematics conditions with the actual field situations.

5. CONCLUSIONS

Nowadays, the use of geosynthetics is a common practice in landfill barriers. Since the landfill liner systems are even steeper, an appropriate characterization of the mechanical properties of the interfaces is required for their stability analysis. In this contest, the appropriate determination of the interfacial frictional properties is necessary.

In this work, the mechanical characterization of a typical interface found in landfill barriers is presented and discussed. In fact, the experimental assessment of geocomposite drain (GCD) – geomembrane (GMB) interface is particularly important since its use is become even more widespread. To assess its performance, also the effect of the two different materials which form the composite layer (geonet and geotextile) is examined separately. For this purpose, the three procedures “Standard”, “Displacement” and “Force” are carried out.

The results shown in Figure 4a and 4b, indicate that all combinations of geosynthetics tested with HDPE smooth geomembrane, exhibit a typical behavior of gradual sliding and, in particular, a stick-slip behavior for GNT - GMB and GCD - GMB interfaces.

Following the test sets on GNT-GMB and GTX-GMB, it could be deduced that the behavior of GCD-GMB interface, where the Geotextile GTX is in direct contact with the Geomembrane GMB, is influenced by the Geonet GNT support. In conclusion, based on test results, it could be noticed that:

- “Standard Procedure” is not rigorous because a static approach is proposed for kinematic conditions. Moreover, this interpretation overestimates the interface friction angle, overall in the case of gradual sliding, compared to the static ones.
- Thanks to the “Displacement” and the “Force” Procedures it is possible to study accurately the interface friction during different phases of the test. Anyway, it is worth noting that the corresponding friction angles are calculated in different kinematics conditions. In particular, the interface friction angle ϕ_s is determined taking into account the acceleration during the slide (dynamic conditions of the upper box) while δ_{lim} corresponds to a static

state of the upper box after large displacements. Test results show that the kinematic conditions could influence the interface friction angles. For this purpose it is important to relate the conditions found during the laboratory tests with the existing situations on site. Finally, it is necessary to answer to the outstanding question about the selection of the interface friction angle that could lead to an appropriate value for a safe design.

ACKNOWLEDGEMENTS

The authors acknowledge the European Commission, European Social Found (FSE) and the Regione Calabria for the co-funding grant.

REFERENCES

- Briançon, L. Girard, H. and Gourc, J.P. 2011. A new procedure for measuring geosynthetic friction with an inclined plane. *Geotextiles and Geomembranes*, 29: 472-482.
- Briançon, L. Girard, H. and Poulain, D. 2002. Slope stability of lining systems - Experimental modelling of friction at geosynthetic interfaces. *Geotextiles and Geomembranes*, 20 (3): 147-172.
- EN ISO 12957-2, 2005. Geosynthetic - Determination of friction characteristics, Part 2: Inclined Plane test. Brussels: European Committee for Standardization.
- Girard, H. Fischer, S. Alonso, E. 1990. Problems of friction posed by the use of geomembranes on dam slopes - examples and measurements. *Geotextiles and Geomembranes*, 9 (2): 129-143.
- Gourc, J. P. & Reyes Ramirez, R. 2004. Dynamics-based interpretation of the interface friction test at the inclined plane. *Geosynthetics International*, 11 (6): 439-454.
- Izgin, M. & Wasti, Y. 1998. Geomembrane-sand interface frictional properties as determined by inclined board and shear box tests. *Geotextiles and Geomembranes*, 16 (3): 207-219.
- Lalarakotoson, S. Villard, P. and Gourc, J.P. 1999. Shear strength characterization of geosynthetic interfaces on inclined planes. *Geotechnical testing journal*, 22 (4): 284-291.
- Palmeira, E.M. 2009. Soil-geosynthetic interaction: modeling and analysis. *Geotextiles and Geomembranes*, 27(5): 368-390.
- Palmeira, E.M. Lima, Jr. N.R. Mello, L.G.R. 2002. Interaction between soils and geosynthetic layers in large-scale ramp tests. *Geosynthetics International*, 9(2) (IFAI, USA): 149-187.
- Pitanga, H.N. Gourc, J.P. and Vilar, O.M. 2009. Interface shear strength of geosynthetics: evaluation and analysis of inclined plane test. *Geotextiles and Geomembranes*, 27 (6): 435-446.
- Pitanga, H.N. Gourc, J.P. Vilar, O.M. 2011. Enhanced measurement of Geosynthetic Interface Shear strength using a Modified Inclined Plane Device. *Geotechnical Testing Journal*, 34, 6.
- Reyes Ramirez, R. & Gourc, J.P. 2003. Use of the in-clined plane test in measuring geosynthetic interface friction relationship. *Geosynthetic International*, 10 (5): 165-175.
- Wasti, Y. & Ozduzgun, Z. B. 2001. Geomembrane-geotextile interface shear properties as determined by inclined board and shear box tests. *Geotextiles and Geomembranes*, 19 (1): 45-57.
- Wu, W. Wang, X.T. and Aschauer, F. 2008. Investigation on failure of a geosynthetic lined reservoir. *Geotextiles and Geomembranes*, 26 (4): 363-370.